

# COVID-19: Integrating artificial intelligence, data science, mathematics, medicine and public health, epidemiology, neuroscience, and biomedical science in pandemic management

## Edited by

Reza Lashgari, Atefeh Abedini, Babak A. Ardekani, Arda Kiani,  
Seyed Alireza Nadji and Ali Yousefi

## Published in

Frontiers in Medicine

Frontiers in Public Health

Frontiers in Big Data

Frontiers in Artificial Intelligence

Frontiers in Human Neuroscience





## FRONTIERS EBOOK COPYRIGHT STATEMENT

The copyright in the text of individual articles in this ebook is the property of their respective authors or their respective institutions or funders. The copyright in graphics and images within each article may be subject to copyright of other parties. In both cases this is subject to a license granted to Frontiers.

The compilation of articles constituting this ebook is the property of Frontiers.

Each article within this ebook, and the ebook itself, are published under the most recent version of the Creative Commons CC-BY licence. The version current at the date of publication of this ebook is CC-BY 4.0. If the CC-BY licence is updated, the licence granted by Frontiers is automatically updated to the new version.

When exercising any right under the CC-BY licence, Frontiers must be attributed as the original publisher of the article or ebook, as applicable.

Authors have the responsibility of ensuring that any graphics or other materials which are the property of others may be included in the CC-BY licence, but this should be checked before relying on the CC-BY licence to reproduce those materials. Any copyright notices relating to those materials must be complied with.

Copyright and source acknowledgement notices may not be removed and must be displayed in any copy, derivative work or partial copy which includes the elements in question.

All copyright, and all rights therein, are protected by national and international copyright laws. The above represents a summary only. For further information please read Frontiers' Conditions for Website Use and Copyright Statement, and the applicable CC-BY licence.

ISSN 1664-8714  
ISBN 978-2-88976-601-7  
DOI 10.3389/978-2-88976-601-7

## About Frontiers

Frontiers is more than just an open access publisher of scholarly articles: it is a pioneering approach to the world of academia, radically improving the way scholarly research is managed. The grand vision of Frontiers is a world where all people have an equal opportunity to seek, share and generate knowledge. Frontiers provides immediate and permanent online open access to all its publications, but this alone is not enough to realize our grand goals.

## Frontiers journal series

The Frontiers journal series is a multi-tier and interdisciplinary set of open-access, online journals, promising a paradigm shift from the current review, selection and dissemination processes in academic publishing. All Frontiers journals are driven by researchers for researchers; therefore, they constitute a service to the scholarly community. At the same time, the *Frontiers journal series* operates on a revolutionary invention, the tiered publishing system, initially addressing specific communities of scholars, and gradually climbing up to broader public understanding, thus serving the interests of the lay society, too.

## Dedication to quality

Each Frontiers article is a landmark of the highest quality, thanks to genuinely collaborative interactions between authors and review editors, who include some of the world's best academicians. Research must be certified by peers before entering a stream of knowledge that may eventually reach the public - and shape society; therefore, Frontiers only applies the most rigorous and unbiased reviews. Frontiers revolutionizes research publishing by freely delivering the most outstanding research, evaluated with no bias from both the academic and social point of view. By applying the most advanced information technologies, Frontiers is catapulting scholarly publishing into a new generation.

## What are Frontiers Research Topics?

Frontiers Research Topics are very popular trademarks of the *Frontiers journals series*: they are collections of at least ten articles, all centered on a particular subject. With their unique mix of varied contributions from Original Research to Review Articles, Frontiers Research Topics unify the most influential researchers, the latest key findings and historical advances in a hot research area.

Find out more on how to host your own Frontiers Research Topic or contribute to one as an author by contacting the Frontiers editorial office: [frontiersin.org/about/contact](https://frontiersin.org/about/contact)

# COVID-19: Integrating artificial intelligence, data science, mathematics, medicine and public health, epidemiology, neuroscience, and biomedical science in pandemic management

## Topic editors

Reza Lashgari — Shahid Beheshti University, Iran

Atefeh Abedini — Shahid Beheshti University of Medical Sciences, Iran

Babak A. Ardekani — Nathan Kline Institute for Psychiatric Research, United States

Arda Kiani — Shahid Beheshti University of Medical Sciences, Iran

Seyed Alireza Nadji — Shahid Beheshti University of Medical Sciences, Iran

Ali Yousefi — Worcester Polytechnic Institute, United States

## Citation

Lashgari, R., Abedini, A., Ardekani, B. A., Kiani, A., Nadji, S. A., Yousefi, A., eds. (2023). *COVID-19: Integrating artificial intelligence, data science, mathematics, medicine and public health, epidemiology, neuroscience, and biomedical science in pandemic management*. Lausanne: Frontiers Media SA.  
doi: 10.3389/978-2-88976-601-7

# Table of contents

- 14 **Association of Cigarette Smoking, COPD, and Lung Cancer With Expression of SARS-CoV-2 Entry Genes in Human Airway Epithelial Cells**  
Junping Yin, Brigitte Kasper, Frank Petersen and Xinhua Yu
- 24 **Temporary “Circuit Breaker” Lockdowns Could Effectively Delay a COVID-19 Second Wave Infection Peak to Early Spring**  
Thomas Rawson, Chris Huntingford and Michael B. Bonsall
- 28 **Increased Red Cell Distribution Width Is Associated With Disease Severity in Hospitalized Adults With SARS-CoV-2 Infection: An Observational Multicentric Study**  
Theodoros Karampitsakos, Karolina Akinosoglou, Ourania Papaioannou, Vassiliki Panou, Athanasios Koromilias, Petros Bakakos, Stelios Loukides, Demosthenes Bouros, Charalampos Gogos and Argyrios Tzouvelekis
- 32 **Diagnosis of COVID-19 Pneumonia Based on Graph Convolutional Network**  
Xiaoling Liang, Yuexin Zhang, Jiahong Wang, Qing Ye, Yanhong Liu and Jinwu Tong
- 45 **Follow-Up Study of the Chest CT Characteristics of COVID-19 Survivors Seven Months After Recovery**  
Mengqi Liu, Fajin Lv, Yang Huang and Kaihu Xiao
- 53 **Analysis of the Tradeoff Between Health and Economic Impacts of the Covid-19 Epidemic**  
Samson Lasaulce, Chao Zhang, Vineeth Varma and Irinel Constantin Morărescu
- 66 **A Novel BrainHealth Index Prototype Improved by Telehealth-Delivered Training During COVID-19**  
Sandra Bond Chapman, Julie M. Fratantoni, Ian H. Robertson, Mark D’Esposito, Geoffrey S. F. Ling, Jennifer Zientz, Stacy Vernon, Erin Venza, Lori G. Cook, Aaron Tate and Jeffrey S. Spence
- 88 **Simulation of COVID-19 Propagation Scenarios in the Madrid Metropolitan Area**  
David E. Singh, Maria-Cristina Marinescu, Miguel Guzmán-Merino, Christian Durán, Concepción Delgado-Sanz, Diana Gomez-Barroso and Jesus Carretero
- 109 **Combination of Angiotensin (1-7) Agonists and Convalescent Plasma as a New Strategy to Overcome Angiotensin Converting Enzyme 2 (ACE2) Inhibition for the Treatment of COVID-19**  
Hawraa Issa, Ali H. Eid, Bassam Berry, Vahideh Takhviji, Abbas Khosravi, Sarah Mantash, Rawan Nehme, Rawan Hallal, Hussein Karaki, Kawthar Dhayni, Wissam H. Faour, Firas Kobeissy, Ali Nehme and Kazem Zibara

- 126 **Thymidine Phosphorylase Is Increased in COVID-19 Patients in an Acuity-Dependent Manner**  
Wei Li and Hong Yue
- 133 **Neuropsychiatric Symptoms of COVID-19 Explained by SARS-CoV-2 Proteins' Mimicry of Human Protein Interactions**  
Hale Yapici-Eser, Yunus Emre Koroglu, Ozgur Oztot-Cakmak, Ozlem Keskin, Attila Gursoy and Yasemin Gursoy-Ozdemir
- 149 **Three-Dimensional CT for Quantification of Longitudinal Lung and Pneumonia Variations in COVID-19 Patients**  
Qiuying Chen, Lv Chen, Shuyi Liu, Luyan Chen, Minmin Li, Zhuozhi Chen, Jingjing You, Bin Zhang and Shuixing Zhang
- 158 **End-to-End AI-Based Point-of-Care Diagnosis System for Classifying Respiratory Illnesses and Early Detection of COVID-19: A Theoretical Framework**  
Abdelkader Nasreddine Belkacem, Sofia Ouhbi, Abderrahmane Lakas, Elhadj Benkhelifa and Chao Chen
- 171 **Detection of SARS-CoV-2 Infection in Human Nasopharyngeal Samples by Combining MALDI-TOF MS and Artificial Intelligence**  
Meritxell Deulofeu, Esteban García-Cuesta, Eladia María Peña-Méndez, José Elías Conde, Orlando Jiménez-Romero, Enrique Verdú, María Teresa Serrando, Victoria Salvadó and Pere Boadas-Vaello
- 183 **The Diagnostic Yield of the Multidisciplinary Discussion in Patients With COVID-19 Pneumonia**  
Fiorella Calabrese, Federica Pezzuto, Chiara Giraudo, Luca Vedovelli, Francesco Fortarezza, Claudia Del Vecchio, Francesca Lunardi, Anna Sara Fraia, Elisabetta Cocconcelli, Stefania Edith Vuljan, Dario Gregori, Andrea Crisanti, Elisabetta Balestro and Paolo Spagnolo
- 195 **Case Report: Chemotherapy Indication in a Case of Neurofibromatosis Type 1 Presenting Optic Pathway Glioma: A One-Year Clinical Case Study Using Differential Tractography Approach**  
Amir Mohammad Pajavand, Guive Sharifi, Amir Anvari, Farahnaz Bidari-Zerehpooosh, Mohammad A. Shamsi, Saeedeh Nateghinia and Tohid Emami Meybodi
- 208 **Advancing Risk Analysis of COVID-19 Clinical Predictors: The Case of Fasting Blood Glucose**  
Hamad Ali, Abdullah A. Al-Shammari, Barrak Alahmad and Fahd Al-Mulla
- 211 **Frequency and Risk Factors for Spontaneous Pneumomediastinum in COVID-19 Patients**  
Tania Guadalupe Rodriguez-Arciniega, Erick Sierra-Diaz, Jesus Armando Flores-Martinez, Maria Elena Alvizo-Perez, Irlanda Nataly Lopez-Leal, Ana Luisa Corona-Nakamura, Hermes Ernesto Castellanos-Garcia and Alejandro Bravo-Cuellar

- 216 **Contact Tracing in Healthcare Settings During the COVID-19 Pandemic Using Bluetooth Low Energy and Artificial Intelligence—A Viewpoint**  
Guanglin Tang, Kenneth Westover and Steve Jiang
- 219 **How Genetics Might Explain the Unusual Link Between Malaria and COVID-19**  
Marta Rusmini, Paolo Uva, Antonio Amoroso, Manlio Tolomeo and Andrea Cavalli
- 233 **False Negative Mitigation in Group Testing for COVID-19 Screening**  
Amir Reza Alizad-Rahvar, Safar Vafadar, Mehdi Totonchi and Mehdi Sadeghi
- 241 **Clinical and Laboratory Findings of COVID-19 in High-Altitude Inhabitants of Saudi Arabia**  
Mostafa Abdelsalam, Raad M. M. Althaqafi, Sara A. Assiri, Taghreed M. Althagafi, Saleh M. Althagafi, Ahmed Y. Fouda, Ahmed Ramadan, Mohammed Rabah, Reham M. Ahmed, Zein S. Ibrahim, Dalal M. Nemenqani, Ahmed N. Alghamdi, Daifullah Al Aboud, Ahmed S. Abdel-Moneim and Adnan A. Alsulaimani
- 251 **Unknown Disease Outbreaks Detection: A Pilot Study on Feature-Based Knowledge Representation and Reasoning Model**  
Rui Feng, Qiping Hu and Yingnan Jiang
- 261 **Data-Driven and Machine-Learning Methods to Project Coronavirus Disease 2019 Pandemic Trend in Eastern Mediterranean**  
Wenbo Huang, Shuang Ao, Dan Han, Yuming Liu, Shuang Liu and Yaojiang Huang
- 270 **Investigation of Knowledge, Attitude and Practice of Personal Protection Among Different Types of Workers Returning to Work Under COVID-19 Epidemic**  
Zhaoya Fan, Yuanlin Mou, Rui Cheng, Yong Zhao and Fan Zhang
- 278 **High Infection Fatality Rate Among Elderly and Risk Factors Associated With Infection Fatality Rate and Asymptomatic Infections of COVID-19 Cases in Hong Kong**  
Jun Tao, Xiaoyu Zhang, Salihu S. Musa, Lin Yang and Daihai He
- 286 **Noninvasive Ventilation in Patients With COVID-19-Related Acute Hypoxemic Respiratory Failure: A Retrospective Cohort Study**  
Yingyun Fu, Lili Guan, Weibo Wu, Jing Yuan, Shanshan Zha, Junmin Wen, Zhenghao Lin, Chen Qiu, Rongchang Chen and Lei Liu
- 293 **Follow-Up SARS-CoV-2 PCR Testing Outcomes From a Large Reference Lab in the US**  
Adam Sullivan, David Alfego, Brian Poirier, Jonathan Williams, Dorothy Adcock and Stan Letovsky



- 299 **SARS-CoV-2 Gastrointestinal Infection Prolongs the Time to Recover From COVID-19**  
Zhijie Xu, Meiwen Tang, Ping Chen, Hongyu Cai and Fei Xiao
- 307 **A Coronavirus Outbreak Linked to a Funeral Among a Romani Community in Central Italy**  
Giancarlo Ripabelli, Michela Lucia Sammarco, Fabio Cannizzaro, Carmen Montanaro, Guido Vincenzo Ponzio and Manuela Tamburro
- 316 **Monitoring Coronavirus Disease 2019: A Review of Available Diagnostic Tools**  
Shanshan Liu, Qiuyue Li, Xuntao Chu, Minxia Zeng, Mingbin Liu, Xiaomeng He, Heng Zou, Jianghua Zheng, Christopher Corpe, Xiaoyan Zhang, Jianqing Xu and Jin Wang
- 330 **Can Clinical Symptoms and Laboratory Results Predict CT Abnormality? Initial Findings Using Novel Machine Learning Techniques in Children With COVID-19 Infections**  
Huijing Ma, Qinghao Ye, Weiping Ding, Yinghui Jiang, Minhao Wang, Zhangming Niu, Xi Zhou, Yuan Gao, Chengjia Wang, Wade Menpes-Smith, Evandro Fei Fang, Jianbo Shao, Jun Xia and Guang Yang
- 340 **Radiomics Is Effective for Distinguishing Coronavirus Disease 2019 Pneumonia From Influenza Virus Pneumonia**  
Liaoyi Lin, Jinjin Liu, Qingshan Deng, Na Li, Jingye Pan, Houzhang Sun and Shichao Quan
- 348 **Differential Diagnosis of COVID-19 Pneumonia From Influenza A (H1N1) Pneumonia Using a Model Based on Clinicoradiologic Features**  
Wei-Ya Shi, Shao-Ping Hu, Hao-Ling Zhang, Tie-Fu Liu, Su Zhou, Yu-Hong Tang, Xin-Lei Zhang, Yu-Xin Shi, Zhi-Yong Zhang, Nian Xiong and Fei Shan
- 358 **CT Quantification of COVID-19 Pneumonia at Admission Can Predict Progression to Critical Illness: A Retrospective Multicenter Cohort Study**  
Baoguo Pang, Haijun Li, Qin Liu, Penghui Wu, Tingting Xia, Xiaoxian Zhang, Wenjun Le, Jianyu Li, Lihua Lai, Changxing Ou, Jianjuan Ma, Shuai Liu, Fuling Zhou, Xinlu Wang, Jiaying Xie, Qingling Zhang, Min Jiang, Yumei Liu and Qingsi Zeng
- 370 **Identification of Variable Importance for Predictions of Mortality From COVID-19 Using AI Models for Ontario, Canada**  
Brett Snider, Edward A. McBean, John Yawney, S. Andrew Gadsden and Bhumi Patel
- 378 **Corrigendum: Identification of Variable Importance for Predictions of Mortality From COVID-19 Using AI Models for Ontario, Canada**  
Brett Snider, Edward A. McBean, John Yawney, S. Andrew Gadsden and Bhumi Patel

- 380 Sero-Prevalence and Sero-Incidence of Antibodies to SARS-CoV-2 in Health Care Workers in Israel, Prior to Mass COVID-19 Vaccination**  
Khitam Muhsen, Mitchell J. Schwaber, Jihad Bishara, Elias Kassem, Alaa Atamna, Wasef Na'amni, Sophy Goren, Anya Bialik, Jameel Mohsen, Yona Zaide, Nimrod Hazan, Ortal Ariel-Cohen, Regev Cohen, Pnina Shitrit, Dror Marchaim, Shmuel Benenson, Debby Ben-David, Bina Rubinovitch, Tamar Gotessman, Amir Nutman, Yonit Wiener-Well, Yasmin Maor, Yehuda Carmeli and Dani Cohen
- 389 Comparison of Residual Pulmonary Abnormalities 3 Months After Discharge in Patients Who Recovered From COVID-19 of Different Severity**  
Mei Zhou, Juanjuan Xu, Tingting Liao, Zhengrong Yin, Fan Yang, Kai Wang, Zhen Wang, Dan Yang, Sufei Wang, Yi Peng, Shuyi Peng, Feihong Wu, Leqing Chen and Yang Jin
- 401 Clinical Outcomes of Severe COVID-19 Patients Admitted to an Intermediate Respiratory Care Unit**  
Guillermo Suarez-Cuartin, Merce Gasas, Guadalupe Bermudo, Yolanda Ruiz, Marta Hernandez-Argudo, Alfredo Marin, Pere Trias-Sabria, Ana Cordoba, Ester Cuevas, Mikel Sarasate, Albert Ariza, Joan Sabater, Nuria Romero, Cristina Subirana, Maria Molina-Molina and Salud Santos
- 411 Comparison of the Filtration Efficiency of Different Face Masks Against Aerosols**  
Connor Stahl, Kevin Frederick, Sachin Chaudhary, Christopher J. Morton, Douglas Loy, Krishna Muralidharan, Armin Sorooshian and Sairam Parthasarathy
- 416 Using Proper Mean Generation Intervals in Modeling of COVID-19**  
Xiujuan Tang, Salihu S. Musa, Shi Zhao, Shujing Mei and Daihai He
- 423 Original Hosts, Clinical Features, Transmission Routes, and Vaccine Development for Coronavirus Disease (COVID-19)**  
Ting Wu, Shuntong Kang, Wenyao Peng, Chenzhe Zuo, Yuhao Zhu, Liangyu Pan, Keyun Fu, Yaxian You, Xinyuan Yang, Xuan Luo, Liping Jiang and Meichun Deng
- 440 Digital Technology-Based Telemedicine for the COVID-19 Pandemic**  
Yu-Ting Shen, Liang Chen, Wen-Wen Yue and Hui-Xiong Xu
- 463 Traditional Chinese Medicine Enema Therapy in a Patient With a Confirmed Negative SARS-CoV-2 Test in the Respiratory Tract but Positive in the Intestinal Tract: A Case Report**  
Yuzhu Dai, Zhiyou Zhao, Huajun Zhou, Dedong Huang, Jianjun Luo, Cunhai Zhang, Qingyong Chen, Xingcan Chen, Yuan Yao, Xiaoxiao Jiang and Jun Cheng

- 472 **The Prognostic Accuracy of National Early Warning Score 2 on Predicting Clinical Deterioration for Patients With COVID-19: A Systematic Review and Meta-Analysis**  
Kai Zhang, Xing Zhang, Wenyun Ding, Nanxia Xuan, Baoping Tian, Tiancha Huang, Zhaocai Zhang, Wei Cui, Huaqiong Huang and Gensheng Zhang
- 483 **Probable Causes and Risk Factors for Positive SARS-CoV-2 Testing in Recovered Patients: Evidence From Guangzhou, China**  
Lei Luo, Dan Liu, Zhoubin Zhang, Zhihao Li, Chaojun Xie, Zhenghe Wang, Zongqiu Chen, Peidong Zhang, Xiru Zhang, Yujie Zhang, Wenfang Zhong, Wenting Zhang, Pei Yang, Qingmei Huang, Weiqi Song, Hui Wang and Chen Mao
- 493 **Exploring the Clinical Characteristics of COVID-19 Clusters Identified Using Factor Analysis of Mixed Data-Based Cluster Analysis**  
Liang Han, Pan Shen, Jiahui Yan, Yao Huang, Xin Ba, Weiji Lin, Hui Wang, Ying Huang, Kai Qin, Yu Wang, Zhe Chen and Shenghao Tu
- 509 **Network Analysis of Outpatients to Identify Predictive Symptoms and Combinations of Symptoms Associated With Positive/Negative SARS-CoV-2 Nasopharyngeal Swabs**  
Hervé Spechbach, Frédérique Jacqueroiz, Virginie Prendki, Laurent Kaiser, Mikaela Smit, Alexandra Calmy, François Chappuis, Idris Guessous, Julien Salamun and Stéphanie Baggio
- 517 **Prolonged Active Prone Positioning in Spontaneously Breathing Non-intubated Patients With COVID-19-Associated Hypoxemic Acute Respiratory Failure With  $\text{PaO}_2/\text{FiO}_2 >150$**   
Paola Pierucci, Nicolino Ambrosino, Valentina Di Lecce, Michela Dimitri, Stefano Battaglia, Esterina Boniello, Andrea Portacci, Onofrio Resta and Giovanna Elisiana Carpagnano
- 525 **COVID-19 as a Research Dynamic Transformer: Emerging Cross-Disciplinary and National Characteristics**  
Ryosuke L. Ohniwa, Joji Kijima, Mizuho Fukushima and Osamu Ohneda
- 534 **Laboratory Testing Implications of Risk-Stratification and Management of COVID-19 Patients**  
Caidong Liu, Ziyu Wang, Wei Wu, Changgang Xiang, Lingxiang Wu, Jie Li, Weiye Hou, Huiling Sun, Youli Wang, Zhenling Nie, Yingdong Gao, Ruisheng Zhang, Haixia Tang, Qianghu Wang, Kening Li, Xinyi Xia, Pengping Li and Shukui Wang
- 545 **Containing the Transmission of COVID-19: A Modeling Study in 160 Countries**  
Yan Niu, Jia Rui, Qiupeng Wang, Wei Zhang, Zhiwei Chen, Fang Xie, Zeyu Zhao, Shengnan Lin, Yuanzhao Zhu, Yao Wang, Jingwen Xu, Xingchun Liu, Meng Yang, Wei Zheng, Kaixin Chen, Yilan Xia, Lijuan Xu, Shi Zhang, Rongrong Ji, Taisong Jin, Yong Chen, Benhua Zhao, Yanhua Su, Tie Song, Tianmu Chen and Guoqing Hu

- 557 **Development of an Early Warning Model for Predicting the Death Risk of Coronavirus Disease 2019 Based on Data Immediately Available on Admission**  
Hai Wang, Haibo Ai, Yunong Fu, Qinglin Li, Ruixia Cui, Xiaohua Ma, Yan-fen Ma, Zi Wang, Tong Liu, Yunxiang Long, Kai Qu, Chang Liu and Jingyao Zhang
- 565 **Mapping Trends and Hotspots Regarding Clinical Research on COVID-19: A Bibliometric Analysis of Global Research**  
Demeng Xia, Renqi Yao, Sheng Wang, Gaoqi Chen and Yin Wang
- 578 **Regional COVID-19 Dynamics: Surrogate Synchrony in Case Infection Rates**  
Samantha Robinson
- 585 **Follow-Ups on Persistent Symptoms and Pulmonary Function Among Post-Acute COVID-19 Patients: A Systematic Review and Meta-Analysis**  
Qiuyue Long, Jiwei Li, Xiaoyi Hu, Yangyuyan Bai, Yali Zheng and Zhancheng Gao
- 596 **Longitudinal Characterization of Cytokine Overproduction: A Case Report in Critically Ill COVID-19 Patients With Hyperinflammation in Bronchoalveolar Lavage**  
Zhen Luo, Chengliang Zhu, Zhihui Ruan, Xianghua Cui, Muhammad Adnan Shereen, Pan Pan, Jingtao Huang, Fubing Wang, Hanwen Su, Yuchen Xia and Jianguo Wu
- 607 **The Association Between Risk Perception and COVID-19 Vaccine Hesitancy for Children Among Reproductive Women in China: An Online Survey**  
Min Du, Liyuan Tao and Jue Liu
- 617 **Predicting Severe/Critical Outcomes in Patients With SARS-CoV2 Pneumonia: Development of the prediction severe/critical outcome in COVID-19 (CRITIC) Model**  
Fausto Salaffi, Marina Carotti, Marco Di Carlo, Luca Ceccarelli, Massimo Galli, Piercarlo Sarzi-Puttini and Andrea Giovagnoni
- 626 **Asthma Patients Benefit More Than Chronic Obstructive Pulmonary Disease Patients in the Coronavirus Disease 2019 Pandemic**  
Ruoyan Xiong, Zhiqi Zhao, Huanhuan Lu, Yiming Ma, Huihui Zeng and Yan Chen
- 634 **Elaboration of a Radiomics Strategy for the Prediction of the Re-positive Cases in the Discharged Patients With COVID-19**  
Xiao-Hui Wang, Xiaopan Xu, Zhi Ao, Jun Duan, Xiaoli Han, Xing Tang, Yu-Fei Fu, Xu-Sha Wu, Xue Wang, Linxiao Zhu, Wenbing Zeng and Shuliang Guo
- 643 **The Similarities and Distances of Growth Rates Related to COVID-19 Between Different Countries Based on Spectral Analysis**  
Ray-Ming Chen

- 652 **Pneumonia Patients Caused by Co-infection With SARS-CoV-2 and Human Adenovirus in China**  
Shaofu Qiu, Ge Zeng, Peihan Li, Xiaohui Li, Hongbo Liu, Xinying Du, Hongbo Liu, Heng Zhang, Xingyu Xiang, Hui Wang, Xiangbing Chen, Guangyao Yang, Sai Tian, Ligui Wang, Mingjuan Yang, Chaojie Yang, Lidong Gao, Shixiong Hu, Hongbin Song and Zhifei Zhan
- 660 **Prevalence of Covid-19 Associated Symptoms, Their Onset and Duration, and Variations Among Different Groups of Patients in Bangladesh**  
Md. Tanzilul Amin, Mahmud Hasan and N. M. Mahmudul Alam Bhuiya
- 673 **Artificial Intelligence for COVID-19: A Systematic Review**  
Lian Wang, Yonggang Zhang, Dongguang Wang, Xiang Tong, Tao Liu, Shijie Zhang, Jizhen Huang, Li Zhang, Lingmin Chen, Hong Fan and Mike Clarke
- 688 **A Novel Matrix Profile-Guided Attention LSTM Model for Forecasting COVID-19 Cases in USA**  
Qian Liu, Daryl L. X. Fung, Leann Lac and Pingzhao Hu
- 701 **BNT162b2 and ChAdOx1 SARS-CoV-2 Post-vaccination Side-Effects Among Saudi Vaccinees**  
Ahmed N. Alghamdi, Mohammed I. Alotaibi, Adel S. Alqahtani, Daifullah Al Aboud and Ahmed S. Abdel-Moneim
- 711 **Changes in Incidence of Notifiable Infectious Diseases in China Under the Prevention and Control Measures of COVID-19**  
Bizhen Chen, Meiling Wang, Xun Huang, Maokun Xie, Liting Pan, Huiwen Liu, Zhenguo Liu and Pengcheng Zhou
- 723 **Longer Prehospitalization and Preintubation Periods in Intubated Non-survivors and ECMO Patients With COVID-19: A Systematic Review and Meta-Analysis**  
Kenji Funakoshi, Takayoshi Morita and Atsushi Kumanogoh
- 740 **Intermediate- vs. Standard-Dose Prophylactic Anticoagulation in Patients With COVID-19 Admitted in Medical Ward: A Propensity Score-Matched Cohort Study**  
David M. Smadja, Guillaume Bonnet, Nicolas Gendron, Orianne Weizman, Lina Khider, Antonin Trimaille, Tristan Mirault, Charles Fauvel, Jean-Luc Diehl, Delphine Mika, Aurelien Philippe, Théo Pezel, Guillaume Goudot, Willy Sutter, Benjamin Planquette, Victor Waldmann, Olivier Sanchez, Ariel Cohen and Richard Chocron for the Critical COVID-19 France Investigators
- 747 **Investigating Fungi-Derived Bioactive Molecules as Inhibitor of the SARS Coronavirus Papain Like Protease: Computational Based Study**  
Aweke Mulu Belachew, Asheber Feyisa, Seid Belay Mohamed and Jerusalem Fekadu W/Mariam
- 757 **COVID-19 Risk Assessment for the Tokyo Olympic Games**  
Wenhui Zhu, Jie Feng, Cheng Li, Huimin Wang, Yang Zhong, Lijun Zhou, Xingyu Zhang and Tao Zhang



- 785 **Epidemiologic Characteristics of and Prognostic Factors for COVID-19 Among Hospitalized Patients: Updated Implications From Hubei Province, China**  
Xiang Liu, Linzhi Zhu, Tingjuan Lu, Xibang Liu, Demin Jiao, Xiali Tang, Jun Chen, Yu Chen, Wenya Yu and Qingyong Chen
- 795 **Adapting the Surveillance Platform for Enteric and Respiratory Infectious Organisms at United States Veterans Affairs Medical Centers (SUPERNOVA) for COVID-19 Among Hospitalized Adults: Surveillance Protocol**  
Elissa Meites, Kristina L. Bajema, Anita Kambhampati, Mila Prill, Vincent C. Marconi, Sheldon T. Brown, Maria C. Rodriguez-Barradas, David O. Beenhouwer, Mark Holodniy, Cynthia Lucero-Obusan, Cristina Cardemil, Jordan Cates, Diya Surie and The SUPERNOVA COVID-19 Surveillance Group
- 805 **Early Detection of COVID-19 Waves From Cases in a Neighboring Country With an Open Border**  
Anil Kamat and Amrita Sah
- 813 **Leveraging of SARS-CoV-2 PCR Cycle Thresholds Values to Forecast COVID-19 Trends**  
Nicolas Yin, Simon Dellicour, Valery Daubie, Nicolas Franco, Magali Wautier, Christel Faes, Dieter Van Cauteren, Liv Nymark, Niel Hens, Marius Gilbert, Marie Hallin and Olivier Vandenberg
- 822 **Prevalence and Impact Factors of COVID-19 Vaccination Hesitancy Among Breast Cancer Survivors: A Multicenter Cross-Sectional Study in China**  
Xin Peng, Ping Gao, Qiong Wang, Hong-ge Wu, Yun-li Yan, Ying Xia, Jian-ying Wang, Fang Lu, Hong Pan, Yi Yang, Fan Liang, Lei Zhao and Jing Cheng
- 831 **Bibliometric Analysis and Systematic Review of Global Coronavirus Research Trends Before COVID-19: Prospects and Implications for COVID-19 Research**  
Peijing Yan, Meixuan Li, Jing Li, Zhenxing Lu, Xu Hui, Yuping Bai, Yangqin Xun, Yongfeng Lao, Shizhong Wang and Kehu Yang
- 847 **Chest-Related Imaging Investigations During Multiple Waves of COVID-19 Infection in Hong Kong**  
Kei Shing Ng and Varut Vardhanabhuti
- 853 **Knowledge, Attitude, and Practice Toward COVID-19 Among Sherubtse College Students in Bhutan: A Web-Based Cross-Sectional Study**  
Thinley Dorji, Karma Wangmo, Yezer, Tashi Wangchuk, Tshokey and Kinley Wangdi
- 862 **Abnormal Respiratory Sounds Classification Using Deep CNN Through Artificial Noise Addition**  
Rizwana Zulfiqar, Fiaz Majeed, Rizwana Irfan, Hafiz Tayyab Rauf, Elhadj Benkhelifa and Abdelkader Nasreddine Belkacem

- 878 **Automatic Classification Between COVID-19 and Non-COVID-19 Pneumonia Using Symptoms, Comorbidities, and Laboratory Findings: The Khorshid COVID Cohort Study**  
Hamid Reza Marateb, Farzad Ziaie Nezhad, Mohammad Reza Mohebian, Ramin Sami, Shaghayegh Haghighi Javanmard, Fatemeh Dehghan Niri, Mahsa Akafzadeh-Savari, Marjan Mansourian, Miquel Angel Mañanas, Martin Wolkewitz and Harald Binder
- 892 **Assessment of Sequelae of COVID-19 Nearly 1 Year After Diagnosis**  
Fangyuan Zhou, Meihui Tao, Luorui Shang, Yuhuan Liu, Guangtao Pan, Yan Jin, Li Wang, Shaoke Hu, Jinxiao Li, Mengqi Zhang, Yu Fu and Shenglan Yang
- 901 **Clinical Applicable AI System Based on Deep Learning Algorithm for Differentiation of Pulmonary Infectious Disease**  
Yu-han Zhang, Xiao-fei Hu, Jie-chao Ma, Xian-qi Wang, Hao-ran Luo, Zi-feng Wu, Shu Zhang, De-jun Shi, Yi-zhou Yu, Xiao-ming Qiu, Wen-bing Zeng, Wei Chen and Jian Wang
- 911 **The Second Wave of COVID-19 in South and Southeast Asia and the Effects of Vaccination**  
Haitao Song, Guihong Fan, Yuan Liu, Xueying Wang and Daihai He
- 918 **Modeling COVID-19 Transmission Dynamics With Self-Learning Population Behavioral Change**  
Tsz-Lik Chan, Hsiang-Yu Yuan and Wing-Cheong Lo
- 932 **Developing a Screening Procedure During the COVID-19 Pandemic: Process and Challenges Faced by a Low-Incidence Area**  
Wei Tang, Fei Wang, Jian-Wei Wang, Yao Huang, Li Liu, Shi-Jun Zhao, Xin-Ming Zhao and Ning Wu
- 945 **Impact of Workplace on the Risk of Severe COVID-19**  
Tsuyoshi Nakamura, Hiroyuki Mori, Todd Saunders, Hiroaki Chishaki and Yoshiaki Nose
- 957 **Differential COVID-19 Symptoms Given Pandemic Locations, Time, and Comorbidities During the Early Pandemic**  
Yang Wang, Fengwei Zhang, J. Brian Byrd, Hong Yu, Xianwei Ye and Yongqun He
- 972 **Staffing and Capacity Planning for SARS-CoV-2 Monoclonal Antibody Infusion Facilities: A Performance Estimation Calculator Based on Discrete-Event Simulations**  
Çaglar Çaglayan, Jonathan Thornhill, Miles A. Stewart, Anastasia S. Lambrou, Donald Richardson, Kaitlin Rainwater-Lovett, Jeffrey D. Freeman, Tiffany Pfundt and John T. Redd
- 984 **Understanding the Geography of COVID-19 Case Fatality Rates in China: A Spatial Autoregressive Probit-Log Linear Hurdle Analysis**  
Hanchen Yu, Xin Lao, Hengyu Gu, Zhihao Zhao and Honghao He

- 996 **An Unsupervised Machine Learning Clustering and Prediction of Differential Clinical Phenotypes of COVID-19 Patients Based on Blood Tests—A Hong Kong Population Study**  
Kitty Yu-Yeung Lau, Kei-Shing Ng, Ka-Wai Kwok, Kevin Kin-Man Tsia, Chun-Fung Sin, Ching-Wan Lam and Varut Vardhanabhuti
- 1007 **Research on Spatial-temporal Spread and Risk Profile of the COVID-19 Epidemic Based on Mobile Phone Trajectory Data**  
Qi Zuo, Jiaman Du, Baofeng Di, Junrong Zhou, Lixia Zhang, Hongxia Liu and Xiaoyu Hou
- 1018 **Medication Non-adherence and Condomless Anal Intercourse Increased Substantially During the COVID-19 Pandemic Among MSM PrEP Users: A Retrospective Cohort Study in Four Chinese Metropolises**  
Yangyang Gao, Qinghai Hu, Sequoia I. Leuba, Le Jia, Hongyi Wang, Xiaojie Huang, Yaokai Chen, Hui Wang, Jing Zhang, Zhenxing Chu, Lukun Zhang, Zixin Wang, Hong Shang, Junjie Xu and CROPrEP Study Team



# Association of Cigarette Smoking, COPD, and Lung Cancer With Expression of SARS-CoV-2 Entry Genes in Human Airway Epithelial Cells

Junping Yin, Brigitte Kasper, Frank Petersen\* and Xinhua Yu\*

Division of Pulmonary Immune Diseases, Department of Asthma and Allergy, Research Center Borstel, Leibniz Lung Center, Borstel, Germany

## OPEN ACCESS

### Edited by:

Babak A. Ardekani,  
Nathan Kline Institute for Psychiatric  
Research, United States

### Reviewed by:

Renat Shaykhiev,  
Cornell University, United States  
Eduardo Luis De Vito,  
University of Buenos Aires, Argentina

### \*Correspondence:

Frank Petersen  
fpetersen@fz-borstel.de  
Xinhua Yu  
xinhuayu@fz-borstel.de

### Specialty section:

This article was submitted to  
Pulmonary Medicine,  
a section of the journal  
Frontiers in Medicine

**Received:** 20 October 2020

**Accepted:** 09 November 2020

**Published:** 04 December 2020

### Citation:

Yin J, Kasper B, Petersen F and Yu X  
(2020) Association of Cigarette  
Smoking, COPD, and Lung Cancer  
With Expression of SARS-CoV-2 Entry  
Genes in Human Airway Epithelial  
Cells. *Front. Med.* 7:619453.  
doi: 10.3389/fmed.2020.619453

SARS-CoV-2 enters into human airway epithelial cells via membrane fusion or endocytosis, and this process is dependent on ACE2, TMPRSS2, and cathepsin L. In this study, we examined the expression profiles of the three SARS-CoV-2 entry genes in primary human airway epithelial cells isolated from smokers, non-smokers, patients with chronic obstructive pulmonary disease or lung cancer. An exhaustive search of the GEO database was performed to identify eligible data on 1st June 2020. In total, 46 GEO datasets comprising transcriptomic data of 3,053 samples were identified as eligible data for further analysis. All meta-analysis were performed using RStudio. Standardized mean difference was utilized to assess the effect size of a factor on the expression of targeted genes and 95% confidence intervals (CIs) were calculated. This study revealed that (i) cigarette smoking is associated with an increased expression of ACE2 and TMPRSS2 and a decreased expression of cathepsin L; (ii) significant alternations in expression of ACE2, TMPRSS2, and cathepsin L were observed between current smokers and former smokers, but not between former smokers and never smokers; (iii) when compared with healthy controls with identical smoking status, patients with COPD or lung cancer showed negligible changes in expression of ACE2, TMPRSS2, and cathepsin L. Therefore, this study implicates cigarette smoking might contribute to the development of COVID-19 by affecting the expression of SARS-CoV-2 entry genes, while smoking cessation could be effective to reduce the potential risk.

**Keywords:** COVID-19, SARS-CoV-2, human airway epithelial cells, ACE2 (angiotensin converting enzyme-2), smoking, transmembrane serine protease 2, cathepsin L

## INTRODUCTION

In December 2019, a cluster of viral pneumonia cases which is featured by pulmonary parenchymal opacities at chest radiography was reported in Wuhan, China (1). Analysis of lower respiratory tract samples from patients identified a novel beta-coronavirus termed severe acute respiratory syndrome coronavirus 2 (SARS-CoV-2) as the casual pathogen for the pneumonia (2). On 11 March 2020, the World Health Organization (WHO) declared coronavirus disease 2019 (COVID-19) as a pandemic (3). As of Oct 15, 2020, there have been over 40 million laboratory-confirmed

cases of COVID19 worldwide with more than one million deaths (4). SARS-CoV-2 shares ~80% sequence identity to SARS-CoV and both viruses use the same cell entry receptor, namely angiotensin converting enzyme 2 (ACE2) (5, 6). As the receptor of SARS-CoV and SARS-CoV-2, ACE2 mediates the viral entry via two major pathways, cathepsin L-dependent endocytosis and transmembrane serine protease 2 (TMPRSS2) dependent membrane fusion (7–9). Since COVID-19 is an acute disease resulted from respiratory tract infection of SARS-CoV-2, the interaction between the spike protein (S protein) of the virus and the ACE2 on human airway epithelial cells could be a crucial step for the development of the disease (10, 11).

Although SARS-CoV-2 can infect individuals of any age, most of the severe cases have been reported in older adults or patients with significant comorbidities including chronic respiratory diseases (12). For example, a study with large case series reported a higher prevalence of COPD in patients with severe COVID-19 (12), and this finding was confirmed by several subsequent studies (13–15). Meta-analysis revealed that COPD is associated with a significant, roughly 5-fold increased risk for the development of severe COVID-19 infections (16, 17). Understanding the molecular mechanisms behind the increased risk for severe COVID-19 in patients with chronic respiratory diseases would provide clues toward their pathophysiology and the identification of therapeutic targets. Since ACE2 might play an important role in protecting the host against lung injury (18), one hypothesis is that the expression of ACE2 in airway epithelial cells of patients with chronic respiratory diseases might

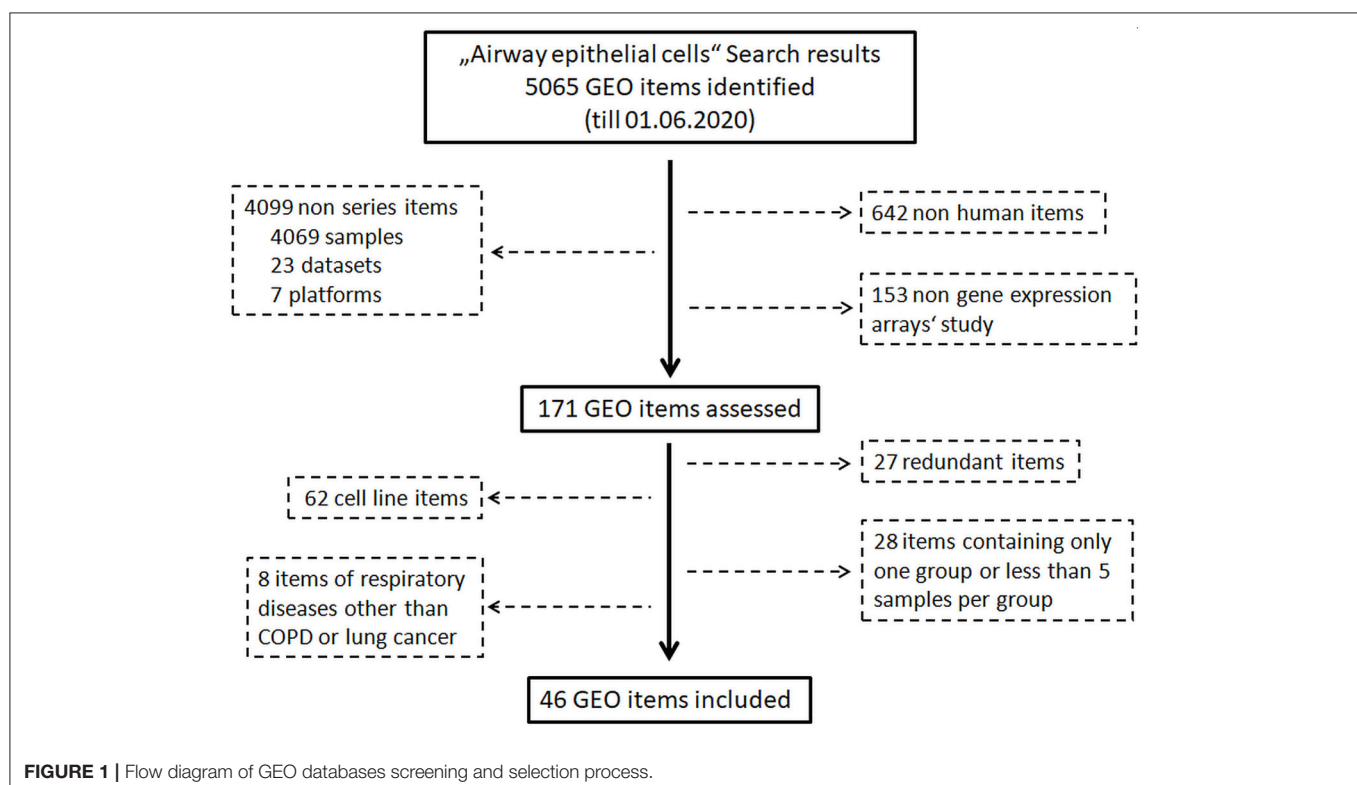
be upregulated, which enhances the infection of SARS-CoV-2. This notion is partially supported by a recent study, in which Leung et al. reported that smokers and patients with COPD show a higher levels ACE 2 than healthy non-smokers (19).

In this study, our objective is to explore the effect of on the expression of three genes essentially involved in SARS-CoV-2 entry, namely ACE2, TMPRSS2, and cathepsin L in human airway epithelial cells isolated from non-smoker, smoker, and patients with cigarette smoking (CS)-induced diseases. To reach this aim, we retrieved previously published transcriptomic datasets of human airway epithelial cells of healthy subjects with different status of cigarette smoking as well as patients with COPD or lung cancer.

## MATERIALS AND METHODS

### Data Retrieval

An exhaustive search of the Gene Expression Omnibus (GEO) database (<https://www.ncbi.nlm.nih.gov/geo/>) was performed to identify eligible data on 1st June 2020. The procedure of identification of eligible data is shown in **Figure 1**. First of all, the key word “Airway epithelial cells” was used for the search without any limitations. In a second step, non-human datasets, non-series datasets, and non-gene expression array datasets were filtered out. Finally, datasets from step two were reviewed carefully, and the following datasets were excluded: (a) datasets of cell line(s), (b) redundant dataset, (c) datasets containing only one group, (d) datasets of respiratory diseases other than COPD and





lung cancer, and (e) datasets containing <5 samples per group. Healthy groups consisted of asymptomatic subjects with normal pulmonary functions, while pathological conditions including COPD and lung cancer were defined using criteria described in original studies.

## Data Correction, Normalization

For affymetrix microarrays, CEL files were uploaded into RStudio (Version 1.3.959, based on R version 4.0.1) using package “affy” (20). Subsequently, background correction and normalization were applied to the raw data using “Robust Multichip Average (RMA)” method (21). For agilent microarray data, raw expression profiling files were uploaded into RStudio using package “limma” (22). By using the “limma” package, background correction and normalization were performed using “normexp” and “quantile” methods, respectively. Background corrected, normalized and log2 transformed signal intensities of ACE2, TMPRSS2, and cathepsin L were outputted and used for further analysis.

## Meta-Analysis

All meta-analysis were performed using “meta” package in RStudio. Standardized mean difference (SMD) was utilized to assess the effect size of a factor on the expression of targeted genes, and 95% confidence intervals (CIs) of SMD were calculated (23). According to the guideline proposed by Cohen (24), the magnitude of the SMD is interpreted as below: small, SMD = 0.2; medium, SMD = 0.5; and large, SMD = 0.8. To evaluate the influence of pack-years of smoking in current smokers on the gene expression, meta-analysis was performed to determine correlation coefficients and *p*-values. Fixed or random effect model was applied to pool the effect size depending on the heterogeneity across the datasets determined by inconsistency ( $I^2$ ) statistics and Cochran's Q test. random effect model was applied when there was significant heterogeneity among datasets ( $I^2$  value > 50% or *P*-value of Q-test < 0.05), otherwise fixed effect model was utilized (25, 26).

## Statistics

All statistical analyses were conducted using RStudio. Statistical significance between two groups was calculated using Student's *t*-test or Mann Whitney U-test depending on the normality test of the data. Linear regression model was generated to evaluate the correlation of age or lung function index of COPD patients and healthy controls with gene expression of SARS-CoV-2 entry genes. To assess the correlation between pulmonary function parameters and gene expression, multiple linear regression was used and age was added as a covariate. A *P* < 0.05 was considered as statistical significance.

## RESULTS

### Study Selection and Data Retrieval

A search of the Gene Expression Omnibus (GEO) database with the key word “Airway epithelial cells” resulted in 5,065 hits. In the next step, 642 non-human items, 4,099 non-series items, and 153 items of non-gene expression array were filtered

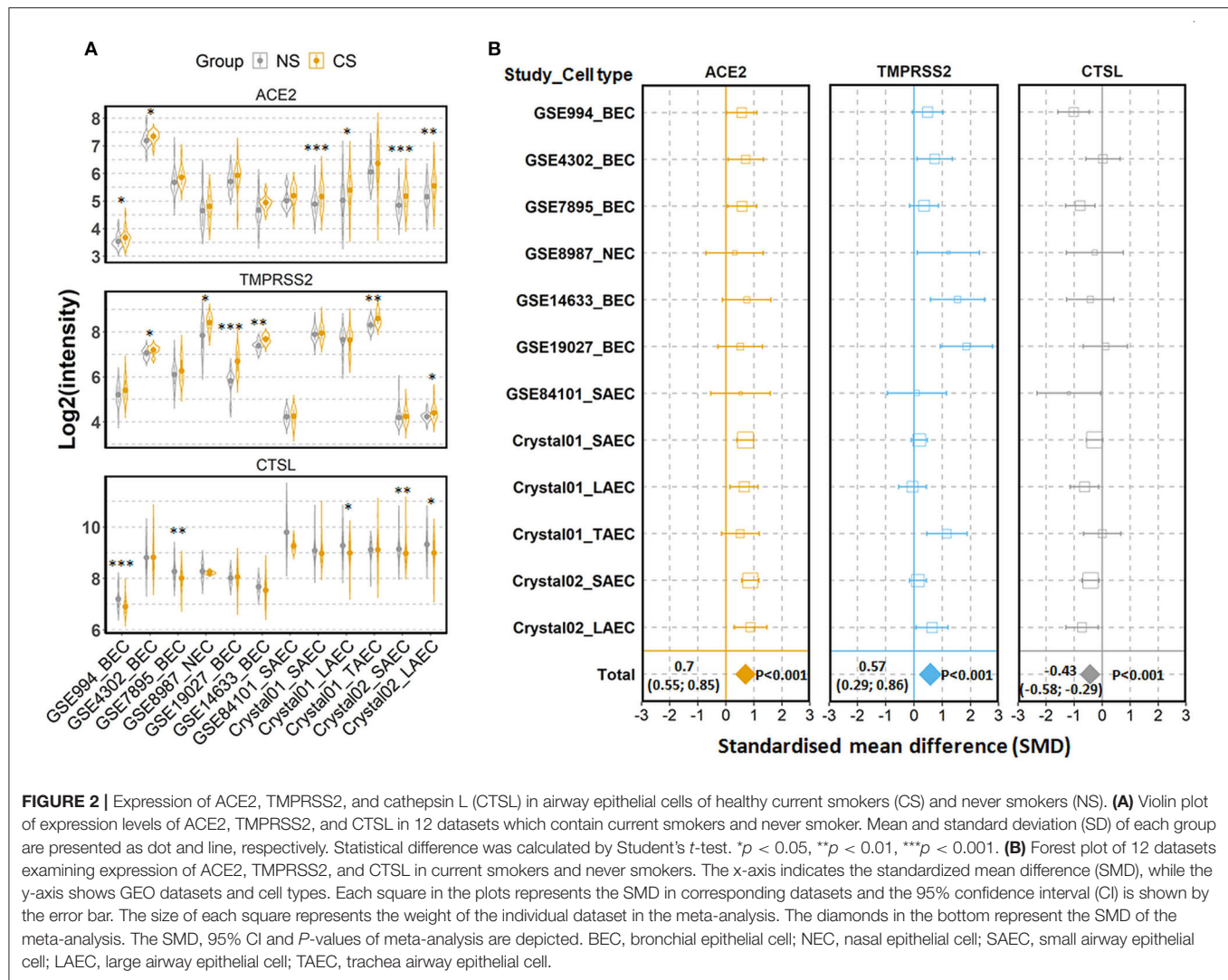
out. Subsequent assessment further excluded 125 items which were transcriptomic data of cell lines, redundant data, other respiratory diseases or datasets containing only one group or <5 samples per group. Finally, 46 GEO datasets comprising 3,053 transcriptomic data of human airway epithelial cells were identified (Figure 1, Supplementary Figure 1). Microarray data of each dataset were retrieved from the GEO database. After combining datasets generated by same research group with identical platforms, 20 transcriptomic datasets were generated and used for further analysis (Supplementary Table 1). After background correction and normalization of each transcriptomic dataset, expression levels of ACE2, TMPRSS2, and cathepsin L were used for further analysis.

### Effect of Age, Gender, and Cell Type on Expression of ACE2, TMPRSS2, and Cathepsin L

Before proceeding to the comprehensive meta-analysis, we evaluated the effect of age, gender and cell type on the expression of the three SARS-CoV-2 entry genes. As shown in Supplementary Figure 2, no significant correlation was observed between age and gene expression of ACE2, TMPRSS2, and cathepsin L in healthy smokers or patients, with an exception of a weak correlation between age and expression of cathepsin L in patients with lung cancer. Negligible association was also observed between gender and expression of the three SARS-CoV-2 entry genes (Supplementary Figure 3). In contrast to age and gender, cell type showed a great impact on expression of ACE2 and TMPRSS2. As shown Supplementary Figure 4, trachea airway epithelial cells (TAEC) expressed significantly higher levels of ACE2 and TMPRSS2 than both small airway epithelial cells (SAEC) and large airway epithelial cells (LAEC) (Supplementary Figure 4).

### Expression of ACE2, TMPRSS2, and Cathepsin L in Never Smoker, Former Smoker, and Current Smokers

To examine the expression of the three genes in airway epithelial cells under physiological conditions, we performed comparisons among healthy individuals according to their status of cigarette smoking. The first comparison was performed between current smokers and never smokers. In total, 12 comparisons were performed, with 594 current smokers and 329 never smokers (27–43). As shown in Figure 2A, mean values of expression levels of ACE2 in current smoker were consistently higher than those in never smokers in all 12 comparisons, and differences in 6 out of 12 were statistically significant. Meta-analysis for the standardized mean difference (SMD) showed a moderate effect of smoking on ACE2 expression (SMD = 0.70, *P* < 0.001) (Figure 2B). Similar to ACE2 expression, the expression of TMPRSS2 was also significantly increased in airway epithelial cells of current smoker as compared to never smokers (SMD = 0.57, *P* = 0.001) (Figures 2A,B). By contrast, smoking affected the expression of cathepsin L in the opposite direction. As compared to never smokers, current smokers expressed significantly



lower levels of cathepsin L (SMD =  $-0.43$ ,  $P < 0.001$ ) (Figures 2A,B).

We next investigated whether the effect of cigarette smoking on the three genes reflects a chronic or an acute response of the tissue. Six datasets which contain expression data of former smokers and current smokers were recruited for this comparison (28, 35, 41, 44–46). Notably, the differences in the expression of the three genes between current smokers and former smokers follow the same pattern observed between current smokers and never smokers. As compared to former smokers, current smokers showed a moderate increased expression levels of ACE2 and TMPRSS2, which was found to be significant only for the latter protein (ACE2; SMD =  $0.58$ ,  $P = 0.11$  and TMPRSS2; SMD =  $0.27$ ,  $P = 0.003$ , respectively). By contrast, decreased levels were seen for cathepsin L (SMD =  $-0.31$ ,  $P = 0.046$ ) (Figure 3). In line with this observation, a comparison between never smokers and former smokers (28, 35, 41) revealed no significant differences between

these group with regard to the expression of these genes (Figure 4).

Thus, these results suggest that the effect of cigarette smoking on expression of ACE2, TMPRSS2, and cathepsin L is more likely an acute reaction than a chronic alteration of the tissue. The acute effect of cigarette smoking on ACE2 was confirmed in a further dataset (47). In this study, current smokers were asked to refrain from cigarette smoking for at least 2 days and then subjected to acute smoking exposure. As shown in **Supplementary Figure 5**, the acute smoking exposure increased the expression of ACE2, but showed no effect on TMPRSS2 or cathepsin L.

To further examine the effect of cigarette smoking on expression of SARS-CoV-2 entry genes, we next determined whether smoking intensity was correlated with expression of ACE2, TMPRSS2 and cathepsin L. Meta-analysis with seven datasets showed that there was no significant correlation between the pack-years of smoking and expression of any of the three genes (**Supplementary Figure 6**).

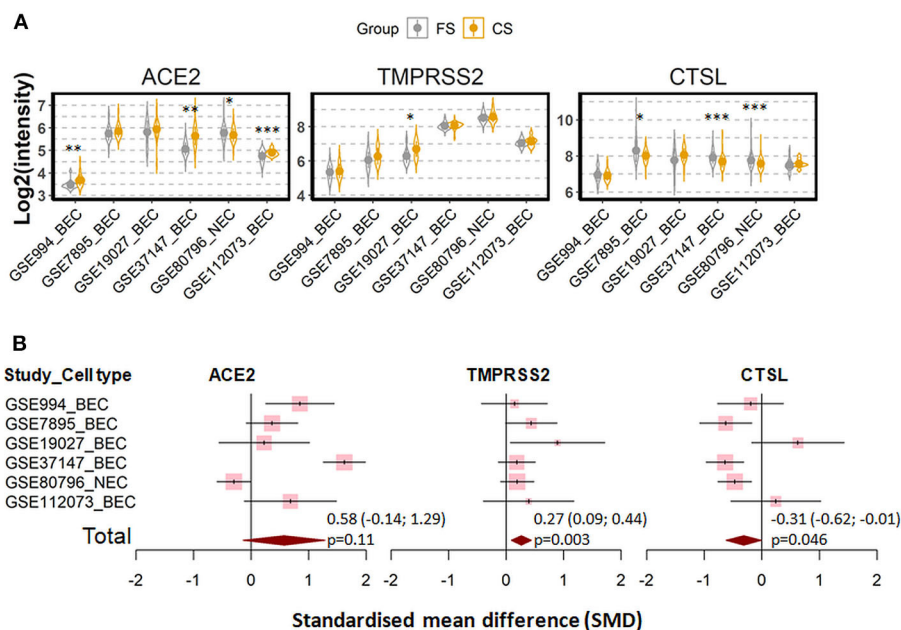


**FIGURE 3 |** Expression of ACE2, TMPRSS2, and cathepsin L (CTSL) in airway epithelial cells of healthy current smokers (CS) and former smokers (FS). **(A)** Violin plot of expression levels of ACE2, TMPRSS2, and CTSL in six datasets which contain current smokers and former smoker. The mean and standard deviation (SD) of each group were presented as dot and line, respectively. BEC, bronchial epithelial cells; NEC, nasal epithelial cells. Statistical differences were calculated by Student's *t*-test. \**p* < 0.05, \*\**p* < 0.01, \*\*\**p* < 0.001. **(B)** Forest plot of six datasets examining expression of ACE2, TMPRSS2, and CTSL in current smokers and former smokers. The x-axis indicates the standardized mean difference (SMD), while the y-axis shows GEO datasets and cell types. Each square in the plots represents the SMD in corresponding datasets and the 95% confidence interval (CI) is showed by the error bar. The size of each square represents the weight of the individual dataset in the meta-analysis. The diamonds in the bottom represent the SMD of the meta-analysis. The SMD, 95% CI and *P*-values of meta-analysis are depicted.

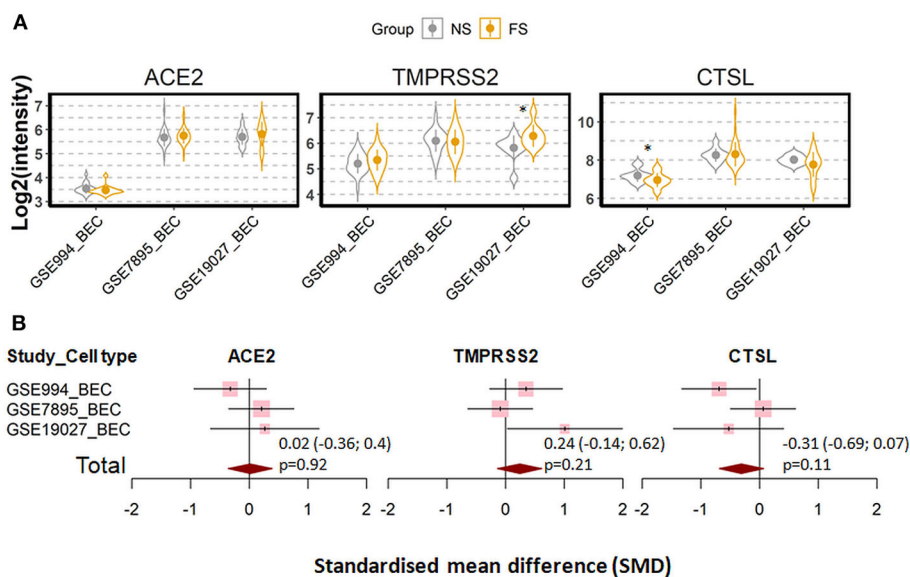


**FIGURE 4 |** Expression of ACE2, TMPRSS2 and cathepsin L (CTSL) in the airway epithelial cells of healthy never smokers (NS) and former smokers (FS). **(A)** Violin plot of expression levels of ACE2, TMPRSS2, and CTSL in three datasets which contain current smokers and former smoker. BEC, bronchial epithelial cells. Statistical difference was calculated by Student's *t*-test. \**p* < 0.05. **(B)** Forest plot of three datasets examining expression of ACE2, TMPRSS2, and CTSL in never smokers and former smokers. The x-axis indicates the standardized mean difference (SMD), while the y-axis shows GEO datasets and cell types. The SMD, 95% CI and *P*-values of meta-analysis are depicted.

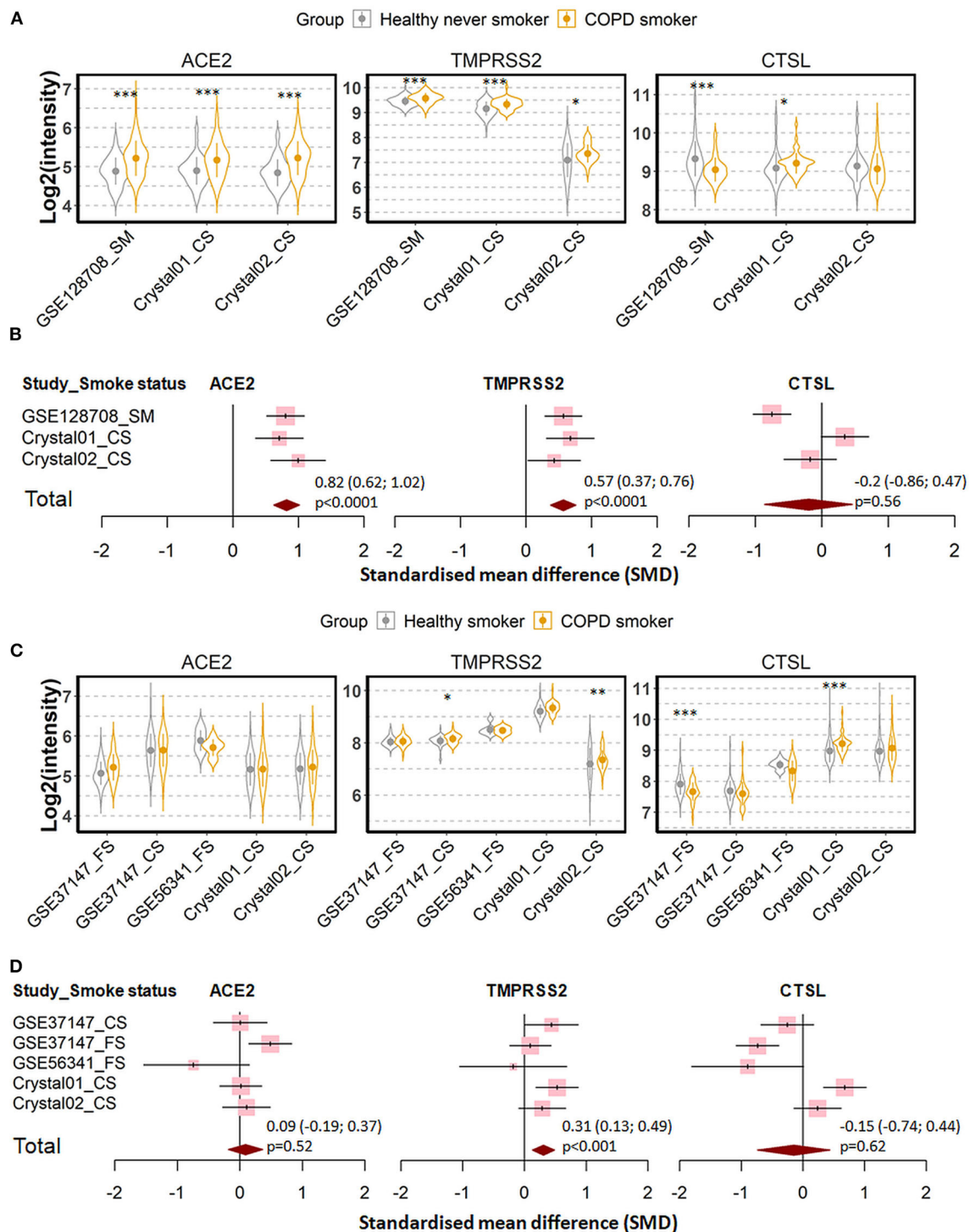


**FIGURE 5 |** Expression of ACE2, TMPRSS2, and cathepsin L (CTSL) in airway epithelial cells of healthy subjects and COPD patients. **(A)** Violin plot of expression levels of ACE2, TMPRSS2, and CTSL in three datasets which contain healthy never smokers and patients with COPD. Statistical difference was calculated by Student's *t*-test. \* $p < 0.05$ , \*\* $p < 0.01$ , \*\*\* $p < 0.001$ . **(B)** Forest plot of three datasets examining expression of ACE2, TMPRSS2, and CTSL in healthy never smokers and patients with COPD. The SMD, 95% CI and *P* values of meta-analysis are depicted. **(C)** Violin plot of expression levels of ACE2, TMPRSS2, and CTSL in five datasets which contain healthy smokers and patients with COPD. **(D)** Forest plot of five datasets examining expression of ACE2, TMPRSS2, and CTSL in healthy smokers and patients with COPD. CS, Current smokers; FS, Former smokers.



## Expression of ACE2, TMPRSS2, and Cathepsin L in Patients With COPD

Consequently, we compared in the next step expression profiles of the three SARS-CoV-2 entry genes of epithelial cells derived from none-diseased subjects with those of patients with different respiratory disorders. Since smoking has a major impact on the expression of these genes, we focused on COPD as a smoking-related disease in a first approach.

Three datasets were recruited to compare never smoker control and COPD patients (27, 29–33, 37, 38, 40, 43, 48). Expression of ACE2 and TMPRSS2 were found to be increased, while the expression of cathepsin L was decreased in COPD patients as compared to never smoker controls (**Figures 5A,B**). Meta-analysis revealed a strong effect of COPD on ACE2 expression ( $SMD = 0.82$ ,  $P < 0.0001$ ), a moderate effect on TMPRSS2 ( $SMD = 0.57$ ,  $P < 0.0001$ ), and no significant effect on cathepsin L.

Since most the COPD patients were smokers, we next determined whether the effect of COPD on expression of our target genes is due to cigarette smoking by comparing COPD patients with healthy smokers (27, 29–33, 37, 38, 40, 43, 46, 49). As shown in **Figures 5C,D**, expression levels of ACE2 and cathepsin L are similar between both groups. The only difference between the two groups could be assigned to the expression of TMPRSS2, where COPD patients showed moderately higher RNA levels than healthy smokers ( $SMD = 0.31$ ,  $P < 0.001$ ). According to these results, the observed difference in the expression of the three SARS-CoV-2 entry genes between COPD patients and healthy controls is mainly due to cigarette smoking but not to disease manifestation.

To substantiate these findings, we examined the relationship between the lung function of COPD patients and gene expression by data from a further study in which lung function parameters were included (46). Expression levels of ACE2, TMPRSS2 and cathepsin L were not correlated with the first second of forced expiration (FEV1) or FEV1/FVC (Forced vital capacity) suggesting that the impairment of lung function does not affect the expression SARS-CoV-2 entry genes (**Supplementary Figure 7**).

## Expression of ACE2, TMPRSS2, and Cathepsin L in Patients With Lung Cancer

Cigarette smoking does not only promote COPD but represents also a main cause for lung cancer. Therefore, we evaluated next the expression the three genes in patients with lung cancer and in corresponding healthy controls. In total, seven datasets were recruited for the comparison, including 1,003 patients and 540 healthy controls (41, 44, 50–54). Of note, healthy control subjects and patients in each dataset were identical in smoking status, either never smokers, former smokers or current smokers. Meta-analysis showed that lung cancer is associated with a very mild effect on modulation of expression of ACE2 ( $SMD = -0.16$ ,  $P = 0.0038$ ) and cathepsin L ( $SMD = -0.18$ ,  $P = 0.0011$ ) (**Figure 6**).

Finally, we determined whether types of cancers and cancer-related mutation affected the expression of SARS-CoV-2 entry genes. No significant difference in expression of ACE2,

TMPRSS2, or cathepsin L between patients with adenocarcinoma and squamous cell carcinoma (**Supplementary Figure 8**), suggesting types of lung cancer show no effect on expression of SARS-CoV-2 entry genes. However, cancer-related mutations affected expression of SARS-CoV-2 entry genes in adenocarcinoma patients from a previous study (55), where the Kirsten Rat Sarcoma virus (*KRAS*) mutation was associated with slight but significant decrease in expression of ACE2 and TMPRSS2, and the epidermal growth factor receptor (*EGFR*) mutation was associated with increased expression of ACE2 and TMPRSS2 and decreased expression of cathepsin L (**Supplementary Figure 9**).

## DISCUSSION

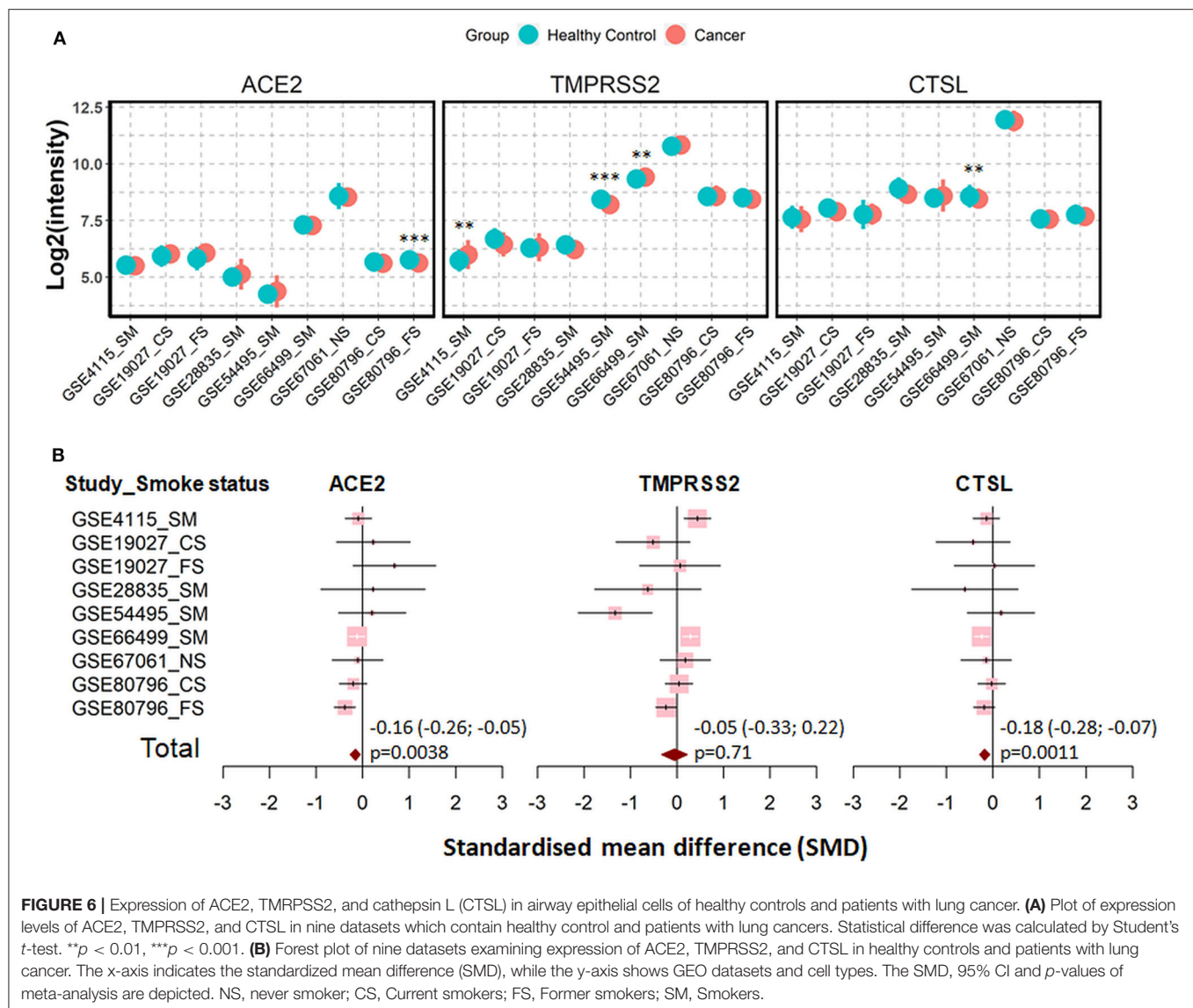
In this study, we examined expression levels of ACE2, TMPRSS2, and cathepsin L in human airway epithelial cells derived from never smokers, former smokers, current smokers, patients with COPD, or lung cancer. By performing comprehensive meta-analysis, we generated a complete picture of expression profiling of the three SARS-CoV-2 entry genes.

In our current study we could demonstrate that current smokers show a highly significant increase in ACE2 expression as compared to never smokers, which is in line with previous findings (19). Moreover, our study extends the analysis to two other SARS-CoV-2 entry genes, TMPRSS2 and cathepsin L. Unexpectedly, smoking exerts antagonistic effects on the expression of TMPRSS2 and cathepsin L in airway epithelial cells by increasing the expression of the former but decreasing the latter. Accordingly, it is conceivable that smoking might enhance the entry of SARS-CoV-2 via membrane fusion but decrease the entry via endocytosis. In several recent meta-analysis it was reported that smoking is associated with an approximately 2 fold increase in the risk of developing severe COVID-19 (17, 56, 57), and it has been hypothesized that this increase may be caused by an elevated expression of ACE2 in smoking subjects (19). Therefore, cigarette smoking-associated changes in the expression of SARS-CoV-2 entry genes might explain the COVID-19-promoting effect.

Irrespective of the unclear pathomechanism of smoking on SARS-CoV-2 infection, our study uncovered an unexpected difference in the expression of the three genes between current smokers and former smokers, but not between former smokers and never smokers. This result indicates an enormous acute effect of smoking on the expression of SARS-CoV-2 entry genes. In contrast to many chronic and irreversible changes in the lung, smoking cessation could be effective to reduce the potential risk emanating from the alternation of the viral entry associated genes.

According to our findings, COPD, a chronic respiratory disease mainly caused by cigarette smoking, is also associated with an increased expression of ACE2 in human airway epithelial cells. However, the effect seems largely related to smoking rather than the disease itself since (i) the differences of the gene expression become visible only between COPD patients and never-smoker healthy controls, but do not appear between





COPD patients and healthy smoker controls, (ii) the variations in the expression of the three genes between COPD patients and never smoker controls follow the same pattern as that between healthy smokers and never smokers, and (iii) lung function is not correlated with the expression of the three genes. Similar to COPD, patients with lung cancer also do not show higher levels of the three SARS-CoV-2 related genes than healthy controls with identical smoking status. Therefore, these results indicate that the high susceptibility to severe COVID-19 in patients with COPD or lung cancer is unlikely due to the alternations in expression of SARS-CoV-2 entry genes.

Although this study provides an overview of the expression profile of SARS-CoV-2 entry genes in human airway epithelial cells in healthy smoker and patients, three major limitations of the study need to be mentioned. First of all, this study only investigated the gene expression at the mRNA level, without providing protein data. Secondly, since the gene expression

were detected by microarray, it is not possible to distinguish transcripts of a gene generated by alternative splicing. Finally, the definition of pathological conditions including COPD and lung cancer in different datasets was not always consistent, which might also affect the findings in the current study.

In conclusion, the results from this study implicate that cigarette smoking affect the expression of SARS-CoV-2 entry genes, and thus might contribute to the development of COVID-19. However, this potential risk could be reduced by smoking cessation.

## DATA AVAILABILITY STATEMENT

The datasets generated for this study can be found in online repositories. The names of the repository/repositories and accession number(s) can be found in the article/Supplementary Material.

## AUTHOR CONTRIBUTIONS

XY: study design. JY: literature search and data analysis. BK, FP, and XY: data interpretation and writing. All authors contributed to the article and approved the submitted version.

## FUNDING

This study was supported by the Deutsche Forschungsgemeinschaft via DFG-27260646 and GRK1727

## REFERENCES

- Huang C, Wang Y, Li X, Ren L, Zhao J, Hu Y, et al. Clinical features of patients infected with 2019 novel coronavirus in Wuhan, China. *Lancet*. (2020) 395:497–506. doi: 10.1016/S0140-6736(20)30183-5
- Zhu N, Zhang D, Wang W, Li X, Yang B, Song J, et al. A novel coronavirus from patients with pneumonia in China, 2019. *N Engl J Med*. (2020) 382:727–33. doi: 10.1056/NEJMoa2001017
- WHO characterizes COVID-19 as a pandemic. (2020). Available online at: <https://www.who.int/emergencies/diseases/novel-coronavirus-2019/events-as-they-happen>
- COVID-19 Coronavirus Pandemic. (2020). Available online at: <https://www.worldometers.info/coronavirus/>
- Lu R, Zhao X, Li J, Niu P, Yang B, Wu H, et al. Genomic characterisation and epidemiology of 2019 novel coronavirus: implications for virus origins and receptor binding. *Lancet*. (2020) 395:565–74. doi: 10.1016/S0140-6736(20)30251-8
- Zhou P, Yang XL, Wang XG, Hu B, Zhang L, Zhang W, et al. A pneumonia outbreak associated with a new coronavirus of probable bat origin. *Nature*. (2020) 579:270–3. doi: 10.1038/s41586-020-2012-7
- Heurich A, Hofmann-Winkler H, Gierer S, Liepold T, Jahn O, Pohlmann S. TMPRSS2 and ADAM17 cleave ACE2 differentially and only proteolysis by TMPRSS2 augments entry driven by the severe acute respiratory syndrome coronavirus spike protein. *J Virol*. (2014) 88:1293–307. doi: 10.1128/JVI.02202-13
- Hoffmann M, Kleine-Weber H, Schroeder S, Kruger N, Herrler T, Erichsen S, et al. SARS-CoV-2 cell entry depends on ACE2 and TMPRSS2 and is blocked by a clinically proven protease inhibitor. *Cell*. (2020) 181:271–80. doi: 10.1016/j.cell.2020.02.052
- Ou X, Liu Y, Lei X, Li P, Mi D, Ren L, et al. Characterization of spike glycoprotein of SARS-CoV-2 on virus entry and its immune cross-reactivity with SARS-CoV. *Nat Commun*. (2020) 11:1620. doi: 10.1038/s41467-020-15562-9
- Othman H, Bouslama Z, Brandenburg JT, da RJ, Hamdi Y, Ghedira K, et al. Interaction of the spike protein RBD from SARS-CoV-2 with ACE2: similarity with SARS-CoV, hot-spot analysis and effect of the receptor polymorphism. *Biochem Biophys Res Commun*. (2020) 527:702–8. doi: 10.1016/j.bbrc.2020.05.028
- Ziegler CGK, Allon SJ, Nyquist SK, Mbano IM, Miao VN, Tzouanas CN, et al. SARS-CoV-2 receptor ACE2 is an interferon-stimulated gene in human airway epithelial cells and is detected in specific cell subsets across tissues. *Cell*. (2020) 181:1016–35. doi: 10.1016/j.cell.2020.04.035
- Guan WJ, Ni ZY, Hu Y, Liang WH, Ou CQ, He JX, et al. Clinical characteristics of coronavirus disease 2019 in China. *N Engl J Med*. (2020) 382:1708–20. doi: 10.1056/NEJMoa2002032
- Wang D, Hu B, Hu C, Zhu F, Liu X, Zhang J, et al. Clinical characteristics of 138 hospitalized patients with 2019 novel coronavirus-infected pneumonia in Wuhan, China. *JAMA*. (2020) 323:1061–9. doi: 10.1001/jama.2020.1585
- Wang Z, Yang B, Li Q, Wen L, Zhang R. Clinical features of 69 cases with coronavirus disease 2019 in Wuhan, China. *Clin Infect Dis*. (2020) 71:769–77. doi: 10.1093/cid/ciaa272

Modulation of Autoimmunity as well as the Bundesministerium für Bildung und Forschung (BMBF) via the German Center for Lung Research (DZL).

## SUPPLEMENTARY MATERIAL

The Supplementary Material for this article can be found online at: <https://www.frontiersin.org/articles/10.3389/fmed.2020.619453/full#supplementary-material>

- Zhang JJ, Dong X, Cao YY, Yuan YD, Yang YB, Yan YQ, et al. Clinical characteristics of 140 patients infected with SARS-CoV-2 in Wuhan, China. *Allergy*. (2020) 75:1730–41. doi: 10.1111/all.14238
- Lippi G, Henry BM. Chronic obstructive pulmonary disease is associated with severe coronavirus disease 2019 (COVID-19). *Respir Med*. (2020) 167:105941. doi: 10.1016/j.rmed.2020.105941
- Zhao Q, Meng M, Kumar R, Wu Y, Huang J, Lian N, et al. The impact of COPD and smoking history on the severity of COVID-19: a systemic review and meta-analysis. *J Med Virol*. (2020) 92:1915–21. doi: 10.1002/jmv.25889
- Zhang M, Gao Y, Zhao W, Yu G, Jin F. ACE-2/ANG1-7 ameliorates ER stress-induced apoptosis in seawater aspiration-induced acute lung injury. *Am J Physiol Lung Cell Mol Physiol*. (2018) 315:L1015–27. doi: 10.1152/ajplung.00163.2018
- Leung JM, Yang CX, Tam A, Shaipanich T, Hackett TL, Singhera GK, et al. ACE-2 expression in the small airway epithelia of smokers and COPD patients: implications for COVID-19. *Eur Respir J*. (2020) 55:2000688. doi: 10.1183/13993003.00688-2020
- Gautier L, Cope L, Bolstad BM, Irizarry RA. Affy-analysis of Affymetrix GeneChip data at the probe level. *Bioinformatics*. (2004) 20:307–15. doi: 10.1093/bioinformatics/btg405
- Irizarry RA, Hobbs B, Collin F, Beazer-Barclay YD, Antonellis KJ, Scherf U, et al. Exploration, normalization, and summaries of high density oligonucleotide array probe level data. *Biostatistics*. (2003) 4:249–64. doi: 10.1093/biostatistics/4.2.249
- Ritchie ME, Phipson B, Wu D, Hu Y, Law CW, Shi W, et al. Limma powers differential expression analyses for RNA-sequencing and microarray studies. *Nucleic Acids Res*. (2015) 43:e47. doi: 10.1093/nar/gkv007
- Faraone SV. Interpreting estimates of treatment effects: implications for managed care. *P T*. (2008) 33:700–11.
- Cohen J. *Statistical Power Analysis for the Behavioral Sciences*, 2nd ed. Lawrence Erlbaum Associates, Publishers (1988).
- He RQ, Wu PR, Xiang XL, Yang X, Liang HW, Qiu XH, et al. Downregulated miR-23b-3p expression acts as a predictor of hepatocellular carcinoma progression: a study based on public data and RT-qPCR verification. *Int J Mol Med*. (2018) 41:2813–31. doi: 10.3892/ijmm.2018.3513
- Higgins JP, Thompson SG. Quantifying heterogeneity in a meta-analysis. *Stat Med*. (2002) 21:1539–58. doi: 10.1002/sim.1186
- Ammous Z, Hackett NR, Butler MW, Raman T, Dolgalev I, O'Connor TP, et al. Variability in small airway epithelial gene expression among normal smokers. *Chest*. (2008) 133:1344–53. doi: 10.1378/chest.07-2245
- Beane J, Sebastiani P, Liu G, Brody JS, Lenburg ME, Spira A. Reversible and permanent effects of tobacco smoke exposure on airway epithelial gene expression. *Genome Biol*. (2007) 8:R201. doi: 10.1186/gb-2007-8-9-r201
- Butler MW, Fukui T, Salit J, Shaykhiyev R, Mezey JG, Hackett NR, et al. Modulation of cystatin A expression in human airway epithelium related to genotype, smoking, COPD, and lung cancer. *Cancer Res*. (2011) 71:2572–81. doi: 10.1158/0008-5472.CAN-10-2046
- Carolan BJ, Heguy A, Harvey BG, Leopold PL, Ferris B, Crystal RG. Up-regulation of expression of the ubiquitin carboxyl-terminal hydrolase L1 gene in human airway epithelium of cigarette smokers. *Cancer Res*. (2006) 66:10729–40. doi: 10.1158/0008-5472.CAN-06-2224
- Carolan BJ, Harvey BG, De BP, Vanni H, Crystal RG. Decreased expression of intelectin 1 in the human airway epithelium of

- smokers compared to nonsmokers. *J Immunol.* (2008) 181:5760–7. doi: 10.4049/jimmunol.181.8.5760
32. Hessel J, Heldrich J, Fuller J, Staudt MR, Radisch S, Hollmann C, et al. Intraflagellar transport gene expression associated with short cilia in smoking and COPD. *PLoS ONE.* (2014) 9:e85453. doi: 10.1371/journal.pone.0085453
  33. Raman T, O'Connor TP, Hackett NR, Wang W, Harvey BG, Attiye MA, et al. Quality control in microarray assessment of gene expression in human airway epithelium. *BMC Genomics.* (2009) 10:493. doi: 10.1186/1471-2164-10-493
  34. Schembri F, Sridhar S, Perdomo C, Gustafson AM, Zhang X, Ergun A, et al. MicroRNAs as modulators of smoking-induced gene expression changes in human airway epithelium. *Proc Natl Acad Sci USA.* (2009) 106:2319–24. doi: 10.1073/pnas.0806383106
  35. Spira A, Beane J, Shah V, Liu G, Schembri F, Yang X, et al. Effects of cigarette smoke on the human airway epithelial cell transcriptome. *Proc Natl Acad Sci USA.* (2004) 101:10143–8. doi: 10.1073/pnas.0401422101
  36. Sridhar S, Schembri F, Zeskind J, Shah V, Gustafson AM, Steiling K, et al. Smoking-induced gene expression changes in the bronchial airway are reflected in nasal and buccal epithelium. *BMC Genomics.* (2008) 9:259. doi: 10.1186/1471-2164-9-259
  37. Strulovici-Barel Y, Omberg L, O'Mahony M, Gordon C, Hollmann C, Tilley AE, et al. Threshold of biologic responses of the small airway epithelium to low levels of tobacco smoke. *Am J Respir Crit Care Med.* (2010) 182:1524–32. doi: 10.1164/rccm.201002-0294OC
  38. Tilley AE, O'Connor TP, Hackett NR, Strulovici-Barel Y, Salit J, Amoroso N, et al. Biologic phenotyping of the human small airway epithelial response to cigarette smoking. *PLoS ONE.* (2011) 6:e22798. doi: 10.1371/journal.pone.0022798
  39. Walters MS, Salit J, Ju JH, Staudt MR, Kaner RJ, Rogalski AM, et al. Waterpipe smoking induces epigenetic changes in the small airway epithelium. *PLoS ONE.* (2017) 12:e0171112. doi: 10.1371/journal.pone.0171112
  40. Wang R, Ahmed J, Wang G, Hassan I, Strulovici-Barel Y, Salit J, et al. Airway epithelial expression of TLR5 is downregulated in healthy smokers and smokers with chronic obstructive pulmonary disease. *J Immunol.* (2012) 189:2217–25. doi: 10.4049/jimmunol.1101895
  41. Wang X, Chorley BN, Pittman GS, Kleeberger SR, Brothers J, Liu G, et al. Genetic variation and antioxidant response gene expression in the bronchial airway epithelium of smokers at risk for lung cancer. *PLoS ONE.* (2010) 5:e11934. doi: 10.1371/journal.pone.0011934
  42. Woodruff PG, Boushey HA, Dolganov GM, Barker CS, Yang YH, Donnelly S, et al. Genome-wide profiling identifies epithelial cell genes associated with asthma and with treatment response to corticosteroids. *Proc Natl Acad Sci USA.* (2007) 104:15858–63. doi: 10.1073/pnas.0707413104
  43. Zhou H, Brekman A, Zuo WL, Ou X, Shaykhiev R, Gosto-Perez FJ, et al. POU2AF1 functions in the human airway epithelium to regulate expression of host defense genes. *J Immunol.* (2016) 196:3159–67. doi: 10.4049/jimmunol.1502400
  44. Perez-Rogers JF, Gerrein J, Anderlind C, Liu G, Zhang S, Alekseyev Y, et al. Shared gene expression alterations in nasal and bronchial epithelium for lung cancer detection. *J Natl Cancer Inst.* (2017) 109:djw327. doi: 10.1093/jnci/djw327
  45. Corbett SE, Nitzberg M, Moses E, Kleerup E, Wang T, Perdomo C, et al. Gene expression alterations in the bronchial epithelium of e-cigarette users. *Chest.* (2019) 156:764–73. doi: 10.1016/j.chest.2019.05.022
  46. Travis WD, Brambilla E, Nicholson AG, Yatabe Y, Austin JHM, Beasley MB, et al. The 2015 world health organization classification of lung tumors: impact of genetic, clinical and radiologic advances since the 2004 classification. *J Thorac Oncol.* (2015) 10:1243–60. doi: 10.1097/JTO.0000000000000630
  47. Billatos E, Faiz A, Gesthalter Y, LeClerc A, Alekseyev YO, Xiao X, et al. Impact of acute exposure to cigarette smoke on airway gene expression. *Physiol Genomics.* (2018) 50:705–13. doi: 10.1152/physiolgenomics.00092.2017
  48. Zhang H, Rostami MR, Leopold PL, Mezey JG, O'Beirne SL, Strulovici-Barel Y, et al. Expression of the SARS-CoV-2 ACE2 receptor in the human airway epithelium. *Am J Respir Crit Care Med.* (2020) 202:219–29. doi: 10.1164/rccm.202003-0541OC
  49. Vucic EA, Chari R, Thu KL, Wilson IM, Cotton AM, Kennett JY, et al. DNA methylation is globally disrupted and associated with expression changes in chronic obstructive pulmonary disease small airways. *Am J Respir Cell Mol Biol.* (2014) 50:912–22. doi: 10.1165/rcmb.2013-0304OC
  50. Beane J, Vick J, Schembri F, Anderlind C, Gower A, Campbell J, et al. Characterizing the impact of smoking and lung cancer on the airway transcriptome using RNA-Seq. *Cancer Prev Res.* (2011) 4:803–17. doi: 10.1158/1940-6207.CAPR-11-0212
  51. Silvestri GA, Vachani A, Whitney D, Elashoff M, Porta SK, Ferguson JS, et al. A bronchial genomic classifier for the diagnostic evaluation of lung cancer. *N Engl J Med.* (2015) 373:243–51. doi: 10.1056/NEJMoa1504601
  52. Spira A, Beane JE, Shah V, Steiling K, Liu G, Schembri F, et al. Airway epithelial gene expression in the diagnostic evaluation of smokers with suspect lung cancer. *Nat Med.* (2007) 13:361–6. doi: 10.1038/nm1556
  53. Tong R, Feng L, Zhang L, Zhang J, Mao Y, Zhang K, et al. Decreased interferon alpha/beta signature associated with human lung tumorigenesis. *J Interferon Cytok Res.* (2015) 35:963–8. doi: 10.1089/jir.2015.0061
  54. Tsay JC, Li Z, Yie TA, Wu F, Segal L, Greenberg AK, et al. Molecular characterization of the peripheral airway field of cancerization in lung adenocarcinoma. *PLoS ONE.* (2015) 10:e0118132. doi: 10.1371/journal.pone.0118132
  55. Schabath MB, Welsh EA, Fulp WJ, Chen L, Teer JK, Thompson ZJ, et al. Differential association of STK11 and TP53 with KRAS mutation-associated gene expression, proliferation and immune surveillance in lung adenocarcinoma. *Oncogene.* (2016) 35:3209–16. doi: 10.1038/onc.2015.375
  56. Guo FR. Active smoking is associated with severity of coronavirus disease 2019 (COVID-19): an update of a meta-analysis. *Tob Induc Dis.* (2020) 18:37. doi: 10.18332/tid/121915
  57. Zheng Z, Peng F, Xu B, Zhao J, Liu H, Peng J, et al. Risk factors of critical & mortal COVID-19 cases: a systematic literature review and meta-analysis. *J Infect.* (2020) 81:e16–25. doi: 10.1016/j.jinf.2020.04.021

**Conflict of Interest:** The authors declare that the research was conducted in the absence of any commercial or financial relationships that could be construed as a potential conflict of interest.

Copyright © 2020 Yin, Kasper, Petersen and Yu. This is an open-access article distributed under the terms of the Creative Commons Attribution License (CC BY). The use, distribution or reproduction in other forums is permitted, provided the original author(s) and the copyright owner(s) are credited and that the original publication in this journal is cited, in accordance with accepted academic practice. No use, distribution or reproduction is permitted which does not comply with these terms.



# Temporary “Circuit Breaker” Lockdowns Could Effectively Delay a COVID-19 Second Wave Infection Peak to Early Spring

Thomas Rawson<sup>1\*</sup>, Chris Huntingford<sup>2</sup> and Michael B. Bonsall<sup>1</sup>

<sup>1</sup> Mathematical Ecology Research Group, Department of Zoology, University of Oxford, Oxford, United Kingdom, <sup>2</sup> UK Centre for Ecology and Hydrology, Wallingford, United Kingdom

**Keywords:** mathematical modeling, COVID-19, lockdown, health policy, Circuit Breaker (CB) interruption

## INTRODUCTION

This opinion submission is based upon the modeling framework previously published in *Frontiers in Public Health*: “How and When to End the COVID-19 Lockdown: An Optimization Approach” (1).

To curb an initial rapid increase in COVID-19 cases, the UK entered a nationwide “lockdown” on March 23rd 2020, where people were instructed to stay in their homes except for essential journeys. This generally proved successful, decreasing the  $R_0$  value to approximately 0.81 (2) during this period. The UK has since begun to ease these lockdown measures, with businesses being allowed to operate and social gatherings permitted subject to certain limitations. However, infection numbers have since started to grow again, with the UK government reporting on September 25th 2020 a new  $R_0$  value between 1.2 and 1.5 across the country (3).

With growing concern that a second wave of COVID-19 infections could place stress on the National Health Service (NHS) during the busy winter months (4), there has been discussion as to the potential for shorter, temporary, “circuit breaker” lockdowns (5). These lockdowns could be enacted with the intention to reduce  $R_0$  briefly, slowing transmission and delaying a peak in infections. Alternatively, lowered infections could be followed by revised social distancing measures to keep  $R_0$  below the critical value of 1. These “circuit breaker” measures are considered an undesirable last resort, with current limitations already causing an estimated 12.4% loss to the UK’s GDP (6), and have been met with growing public displeasure. As such there is a need to investigate more formally what will be gained from the use of “circuit breaker” lockdowns.

In June 2020, we published a model to simulate the impact of multiple lockdown and subsequent release strategies upon the UK (1). It was concluded that a gradual easing of lockdown measures was vital to ensure that any increase in infection numbers could be observed, constrained, and appropriate action taken. The model considered two separate Susceptible-Exposed-Infected-Recovered (SEIR) compartmental cascades, one for those in a state of lockdown, and one for those who were not, so as to simulate the need for shielding certain areas or sub-populations. We have now used this model framework to simulate the effect of a “circuit breaker” lockdown, and to assess the impact of such a lockdown on the infection dynamics.

## Circuit Breaker Modeling

We set the initial states of the system in accordance with the latest reports from the Real-time Assessment of Community Transmission (REACT) programme. They found approximately 0.089% of the population to currently be infected as of September 7th 2020 (7), and 3.6 million people in the UK are estimated to have contracted COVID-19 as of the end of June 2020 (8).

## OPEN ACCESS

### Edited by:

Babak A. Ardekani,  
Nathan Kline Institute for Psychiatric  
Research, United States

### Reviewed by:

Arni S. R. Srinivasa Rao,  
Augusta University, United States

### \*Correspondence:

Thomas Rawson  
thomas.rawson@zoo.ox.ac.uk

### Specialty section:

This article was submitted to  
Infectious Diseases - Surveillance,  
Prevention and Treatment,  
a section of the journal  
*Frontiers in Public Health*

**Received:** 07 October 2020

**Accepted:** 18 November 2020

**Published:** 07 December 2020

### Citation:

Rawson T, Huntingford C and  
Bonsall MB (2020) Temporary “Circuit  
Breaker” Lockdowns Could Effectively  
Delay a COVID-19 Second Wave  
Infection Peak to Early Spring.  
*Front. Public Health* 8:614945.  
doi: 10.3389/fpubh.2020.614945



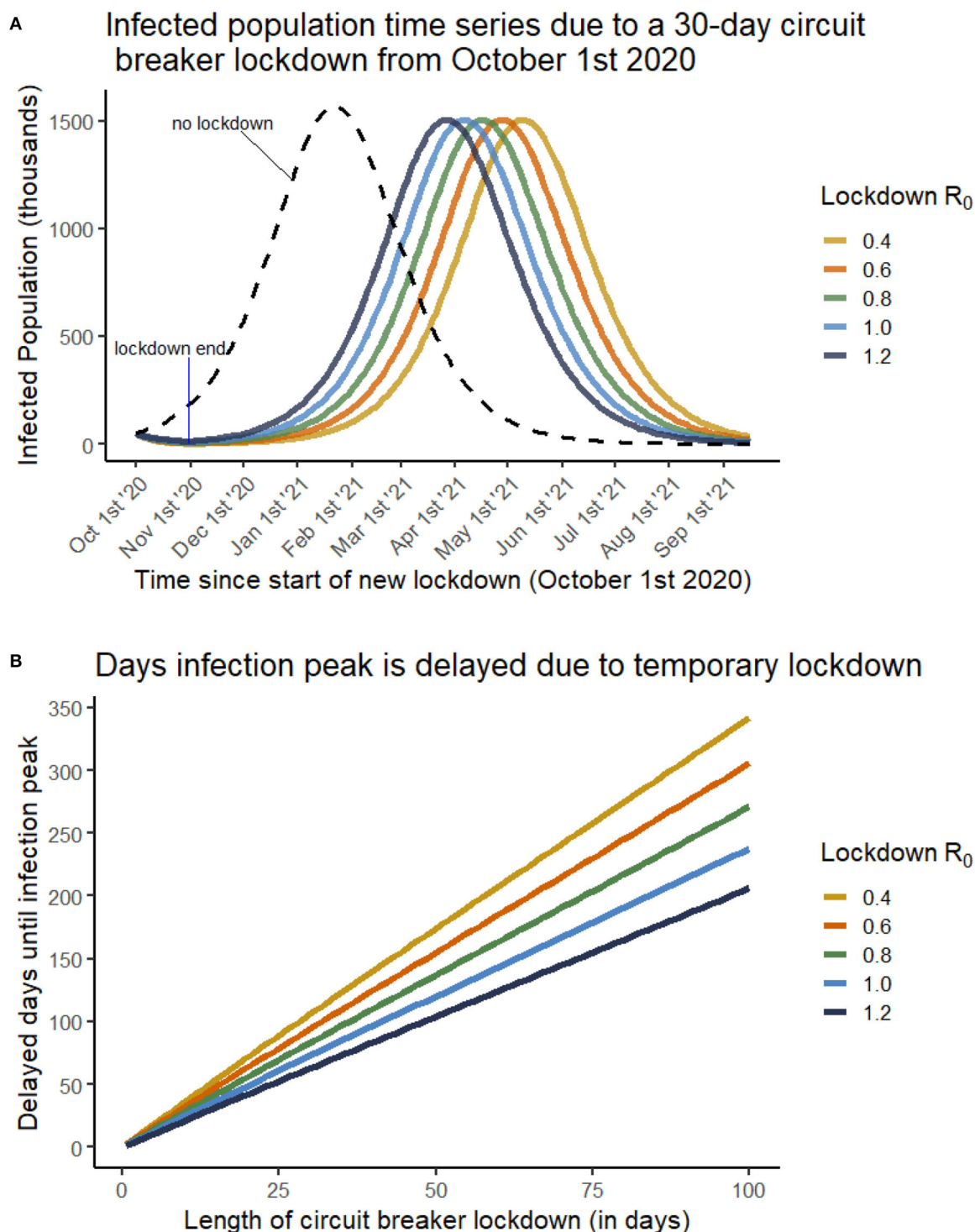


**FIGURE 1 | (A)** The infected population through time if a 30-day circuit breaker lockdown is enacted from October 1st 2020. Each curve is for a different  $R_0$  value during the lockdown phase, as given in the legend. Once lockdown is ended, an  $R_0$  of 1.6 is considered. The dashed line depicts a scenario where no circuit breaker lockdown is enacted, and an infection peak is reached in late January 2021. **(B)** The number of days that infection peak is delayed by (y-axis) as a result of a temporary lockdown of variable duration (x-axis). Each curve is for a different  $R_0$  value during the lockdown phase, as given in the legend. Multiple lockdown effectiveness are considered, including cases where the lockdown does not succeed in lowering  $R_0$  below 1.

Adding to this the new estimated cases (9), we assumed an initial recovered population of 4 million. The transmission rate ( $\beta$ ; infected people per day from an infected individual) of the disease was reduced to 0.35 to represent the impact of continued social distancing measures, to reflect the reported  $R_0$  value of approximately 1.6 (3, 7). Lockdown measures were then assumed to halve transmission, reducing  $R_0$  to approximately 0.8 as reported in Grant (2). All other model parameters were kept as reported in the original study, including a fraction of “key workers” who would not be under circuit breaker restrictions. All code used in this assessment is provided at [osf.io/tfcdw/](https://osf.io/tfcdw/).

Without lockdown (i.e., no “circuit breaker”), our model reports an infection peak reached in 114 days (late January 2021). We considered the scenario where, from an initial time  $t = 0$  corresponding to October 1st 2020, the UK was entered into a lockdown of variable duration. It was then recorded how many days from initialization it would take for the infection peak to occur as a result of an initial lockdown (Figure 1).

Figure 1A shows that lockdowns have very little impact on the magnitude of the infection peak. This is due to very few new infections occurring within a lockdown, meaning that roughly the same susceptible population is exposed following the end of lockdown. The peak is delayed due to a vastly reduced infected population under a stricter (or longer) lockdown, requiring substantially more time for the virus to re-establish itself within the population.

We see from Figure 1B that a near-linear relationship is always observed between duration of circuit-breaker lockdown and the delay of infection peak. In the case of an especially strict lockdown ( $R_0 = 0.4$ ) a 20-day circuit-breaker would result in moving the infection peak back roughly 75 days (to early April 2021), however in a weakly effective lockdown ( $R_0 = 1.2$ ), the 20 day circuit breaker would only delay the peak by roughly 40 days (to late February 2021). In each case, however, a benefit is still observed, suggesting that a temporary lockdown, of even low effectiveness, would be successful in delaying a second wave of COVID infections, providing a buffer to health services from simultaneously dealing with multiple, severe winter infections.

## Discussion

These results support the implementation of circuit breaker lockdowns as effective strategies to delay infection peaks,

however they also argue that little impact will be seen in the total infection load and infection peak. As such, we advise policy makers to consider multiple factors when ultimately deciding upon resorting to such restrictions. Even in our simulations with only modest reductions in  $R_0$ , the significant changes to dynamics will likely have considerable impact on the timings associated with other common upper respiratory infections such as the seasonal flu. Focusing on disrupting infection peaks will prevent overburdening health services through the next few months. It is also important to consider how a circuit-breaker is announced, and which measures are implemented before its commencement. For instance, during the days before implementation, there may be alterations to behavior (e.g., additional levels of shopping for essentials and socializing), bringing people into closer contact than may have otherwise happened.

On October 23rd 2020, Wales began a 17-day “fire breaker” lockdown, while the rest of the UK has implemented a tiered system of restrictions depending on infection levels within individual regions. Should this circuit breaker lockdown show significant effectiveness at reducing  $R_0$  in Wales, we would argue that central and other devolved administrations in the UK should similarly consider the use of circuit breaker lockdowns; implementation of these lockdowns needs to be predicated on critical planning for additional public health measures that will be available after the lockdown period, such as pharmaceutical (e.g., vaccines), or further non-pharmaceutical (e.g., altered social distancing) interventions.

## AUTHOR CONTRIBUTIONS

TR built the model and generated the figure. All authors contributed to writing the manuscript.

## FUNDING

This work was supported through an Engineering and Physical Sciences Research Council (EPSRC) (<https://epsrc.ukri.org/>) Systems Biology studentship award (EP/G03706X/1) to TR. The funders had no role in study design, data collection and analysis, decision to publish, or preparation of the manuscript.

## REFERENCES

1. Rawson T, Brewer T, Veltcheva D, Huntingford C, Bonsall MB. How and when to end the COVID-19 lockdown: an optimization approach. *Front Public Health*. (2020) 8:262. doi: 10.3389/fpubh.2020.00262
2. Grant A. The reproduction number R for COVID-19 in England: why hasn't “lockdown” been more effective? *medRxiv*. (2020). doi: 10.1101/2020.07.02.20144840
3. The R Number and Growth Rate in the UK. Available online at: <https://www.gov.uk/guidance/the-r-number-in-the-uk> (accessed September 30, 2020).
4. The Academy of Medical Sciences. *Preparing for a Challenging Winter 2020/21*. Available online at: <https://acmedsci.ac.uk/file-download/51353957> (accessed September 30, 2020).
5. Regular UK Lockdowns Could Help Control Covid, Says Sage Expert. Available online at: <https://www.theguardian.com/world/2020/sep/27/regular-uk-lockdowns-could-help-control-covid-says-sage-expert-coronavirus> (accessed September 29, 2020).
6. OBR (Office for Budget Responsibility). *Coronavirus Analysis*. (2020). Available online at: <https://obr.uk/coronavirus-analysis/> (accessed September 29, 2020).
7. Riley S, Ainslie KE, Eales O, Walters CE, Wang H, Atchison CJ, et al. Resurgence of SARS-CoV-2 in England: detection by community antigen surveillance. *medRxiv*. (2020). doi: 10.1101/2020.09.11.20192492

8. Ward H, Atchison CJ, Whitaker M, Ainslie KE, Elliot J, Okell LC, et al. Antibody prevalence for SARS-CoV-2 in England following first peak of the pandemic: REACT2 study in 100,000 adults. *medRxiv*. (2020). doi: 10.1101/2020.08.12.20173690
9. Coronavirus (COVID-19) Infection Survey Pilot: England, Wales and Northern Ireland, 25 September 2020. Available online at: <https://www.ons.gov.uk/peoplepopulationandcommunity/healthandsocialcare/conditionsanddiseases/bulletins/coronaviruscovid19infectionsurveyspilot/englandwalesandnorthernireland25september2020> (accessed September 29, 2020).

**Conflict of Interest:** The authors declare that the research was conducted in the absence of any commercial or financial relationships that could be construed as a potential conflict of interest.

Copyright © 2020 Rawson, Huntingford and Bonsall. This is an open-access article distributed under the terms of the Creative Commons Attribution License (CC BY). The use, distribution or reproduction in other forums is permitted, provided the original author(s) and the copyright owner(s) are credited and that the original publication in this journal is cited, in accordance with accepted academic practice. No use, distribution or reproduction is permitted which does not comply with these terms.





# Increased Red Cell Distribution Width Is Associated With Disease Severity in Hospitalized Adults With SARS-CoV-2 Infection: An Observational Multicentric Study

Theodoros Karampitsakos<sup>1</sup>, Karolina Akinosoglou<sup>2</sup>, Ourania Papaioannou<sup>1</sup>, Vassiliki Panou<sup>3</sup>, Athanasios Koromilias<sup>3</sup>, Petros Bakakos<sup>3</sup>, Stelios Loukides<sup>4</sup>, Demosthenes Bouros<sup>3</sup>, Charalampos Gogos<sup>2</sup> and Argyrios Tzouvelekis<sup>1\*</sup>

<sup>1</sup> Department of Respiratory Medicine, University Hospital of Patras, Patras, Greece, <sup>2</sup> Department of Internal Medicine, University General Hospital of Patras, Patras, Greece, <sup>3</sup> First Academic Department of Pneumology, Hospital for Diseases of the Chest, "Sotiria," Medical School, National and Kapodistrian University of Athens, Athens, Greece, <sup>4</sup> Second Academic Department of Respiratory Medicine, ATTIKON General Hospital, National and Kapodistrian University of Athens, Athens, Greece

## OPEN ACCESS

### Edited by:

Reza Lashgari,  
Institute for Research in Fundamental  
Sciences, Iran

### Reviewed by:

Koji Sakamoto,  
Nagoya University, Japan  
Jose Herazo-Maya,  
University of South Florida,  
United States

### \*Correspondence:

Argyrios Tzouvelekis  
atzouvelekis@upatras.gr;  
argyrios.tzouvelekis@flaming.gr

### Specialty section:

This article was submitted to  
Pulmonary Medicine,  
a section of the journal  
Frontiers in Medicine

**Received:** 11 October 2020

**Accepted:** 25 November 2020

**Published:** 11 December 2020

### Citation:

Karampitsakos T, Akinosoglou K, Papaioannou O, Panou V, Koromilias A, Bakakos P, Loukides S, Bouros D, Gogos C and Tzouvelekis A (2020) Increased Red Cell Distribution Width Is Associated With Disease Severity in Hospitalized Adults With SARS-CoV-2 Infection: An Observational Multicentric Study. *Front. Med.* 7:616292. doi: 10.3389/fmed.2020.616292

**Background:** There is an amenable need for clinically applicable biomarkers in patients with SARS-CoV-2 infection. Red Cell Distribution Width (RDW) has been recently suggested as a prognostic biomarker for COVID-19.

**Methods:** This was an observational study enrolling patients between February 26 and May 15 2020. We aimed to validate the association of the previously published RDW threshold of 14.5% with markers of disease progression and mortality.

**Results:** A total number of 193 hospitalized patients with COVID-19 were enrolled and analyzed. Median age was 61 years (95% CI: 58–64). Patients with baseline RDW  $\geq 14.5\%$  ( $n = 41$ , 19.2%) presented with more progressive disease compared to patients with baseline RDW  $< 14.5\%$  ( $n = 156$ , 80.8%) as indicated by significant differences in maximum FiO<sub>2</sub> during hospitalization (median: 100, 95% CI: 45.2–100, vs. 35, 95% CI: 31–40,  $p = 0.0001$ , respectively). Values of RDW  $\geq 14.5\%$  were also strongly associated with increased risk of mortality (HR: 4.1, 95% CI: 0.88–19.23), ( $p = 0.02$ ).

**Conclusion:** Our study provides evidence to support reproducibility and validity of a specified cut-off threshold of RDW as biomarker of disease severity and mortality in patients with COVID-19.

**Keywords:** SARS-CoV-2, COVID-19, biomarkers, mortality, red cell distribution width (RDW)

## INTRODUCTION

The role of red cell distribution width (RDW) as a prognostic biomarker in various chronic lung diseases has gained much of attention (1, 2). Recently, our study group demonstrated that increased RDW is associated with poor clinical outcomes in chronic lung diseases, including chronic obstructive pulmonary disease and idiopathic pulmonary fibrosis (2, 3). RDW reflects the variation of red blood cell volumes and represents a relatively reproducible biomarker, considering

the relatively prolonged lifespan of red blood cells. Nonetheless, underlying mechanisms of RDW elevation remain to be addressed. It has been suggested that arterial hypoxemia leads to increased erythropoietin secretion and thus to increased RDW through mechanisms that involve regulation of erythrocyte maturation and survival (2). Studies have shown that in patients with Coronavirus Disease 2019 (COVID-19), the severity of hypoxemia is independently associated with in-hospital mortality and can reliably predict admission to the intensive care unit (4). Unfortunately, oxygen saturation is often dissociated from arterial hypoxemia as well as the sense of dyspnea in patients with COVID-19 (5, 6). To this end, additional determinants of hypoxemia that are minimally invasive and clinicians' friendly are urgently needed for patients with COVID-19 (7). RDW has been suggested, in combination with hemoglobin and neutrophil to lymphocyte ratio, as a diagnostic and prognostic biomarker of COVID-19 (7–10). Recently, a large prospective study by Foy et al. demonstrated that elevated baseline RDW ( $>14.5\%$ ) levels were independently associated with worse clinical outcomes in hospitalized patients with COVID-19 (11). Despite relative enthusiasm, peripheral blood biomarkers, including RDW, need to be validated and reproduced in multiple cohorts from different institutions to support their widespread clinical applicability. To this end, we aimed to further validate in a completely different cohort of patients with COVID-19 (validation cohort), derived from a low incidence and mortality country (Greece), the association of RDW threshold of 14.5%, previously published by Foy et al. (derivation cohort) with markers of disease progression and mortality (11).

## METHODS

This was an observational, multicentric study enrolling patients from six reference centers for COVID-19 in Greece. From February 26 to May 15 2020 epidemiological and laboratory data from patients hospitalized for COVID-19 were collected on a prospective basis. The study was approved by the Institutional Review Board and the Local Ethics Committee (Protocol Number: 8681/1-4-20). Diagnosis of COVID-19 was based on a positive real-time reverse transcriptase polymerase chain reaction of an upper respiratory nasopharyngeal (or oropharyngeal) swab. Disease progression and severity was estimated by maximum  $\text{FiO}_2\%$  during hospitalization and mortality. We applied the suggested cut-off threshold of 14.5% for RDW and divided patients into high group ( $\text{RDW} \geq 14.5\%$ ) and low group ( $\text{RDW} < 14.5\%$ ). The cut-off threshold for RDW in our laboratories was 14.8%. Nonetheless, RDW is calculated based on a standardized technique involving the width of red cells' distribution curve and mean cell size. In particular, it is calculated by dividing the standard deviation of the mean cell size by the mean corpuscular volume of red cells and multiplying by 100 to convert to a percentage. Mann-Whitney test was applied to assess differences in maximum  $\text{FiO}_2\%$  during hospitalization between high and low RDW group. Kaplan-Meier method was used to analyze survival for patients stratified

**TABLE 1 |** Baseline characteristics.

| Characteristics          | (N, %)                   |
|--------------------------|--------------------------|
| Total number of patients | 193                      |
| Age median (%95 CI)      | 61 (58 to 64)            |
| Males/Females            | 139/54                   |
| Current/ Ex-smokers      | 83 (43%)                 |
| Never smokers            | 110 (57%)                |
| RDW (%) median (95% CI)  | 12.8 (95%: 12.6 to 13.1) |
| Inpatient                | 193/193 (100%)           |
| Mechanical ventilation   | 38/193 (19.7%)           |
| Hypertension             | 62/193 (32.1%)           |
| Diabetes mellitus        | 17/193 (8.8%)            |
| Cancer                   | 13/193 (6.7%)            |
| Hypothyroidism           | 9/193 (4.7%)             |
| Atrial fibrillation      | 8/193 (4.1%)             |
| Heart failure            | 5/193 (2.6%)             |
| COPD                     | 4/193 (2.1%)             |
| Asthma                   | 2/193 (1.0%)             |

COPD, Chronic Obstructive Pulmonary Disease; RDW, Red cell distribution width.

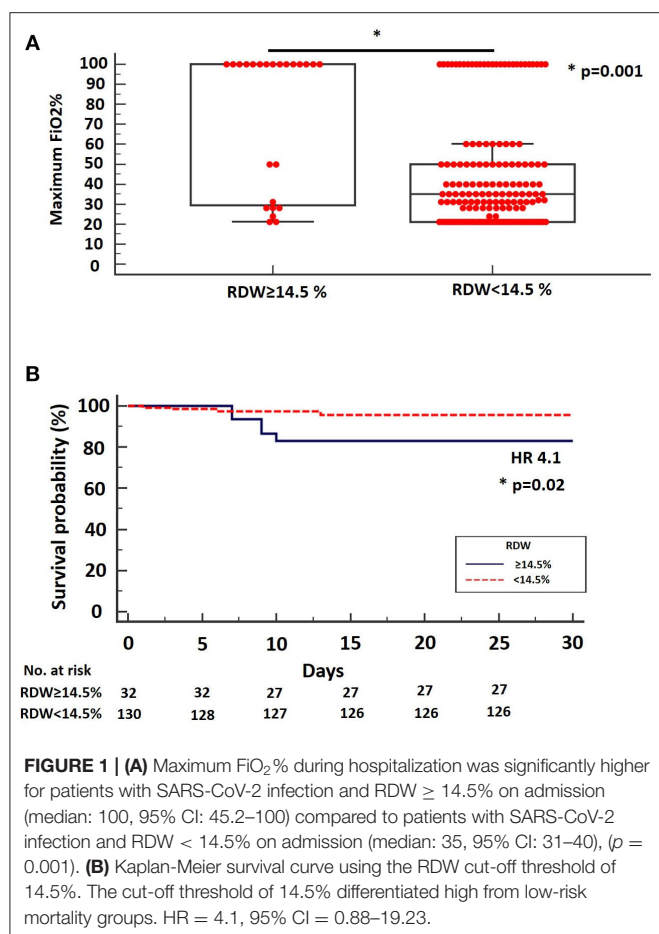
**TABLE 2 |** Therapeutic compounds administered to study population.

| Characteristics                                  | (N, %)          |
|--|-----------------|
| Azithromycin                                     | 175/193 (90.7%) |
| Hydroxychloroquine                               | 170/193 (88.1%) |
| Low molecular weight heparin (prophylactic dose) | 166/193 (86.0%) |
| Other antibiotics                                | 163/193 (84.4%) |
| Lopinavir/Ritonavir                              | 33/193 (17.1%)  |
| Colchicine                                       | 9/193 (4.7%)    |
| Tocilizumab                                      | 5/193 (2.6%)    |
| Remdesivir                                       | 3/193 (1.6%)    |
| Anakinra   | 2/193 (1.0%)    |

by RDW on admission.  $p$ -values  $< 0.05$  were considered statistically significant.

## RESULTS

A total number of 193 hospitalized patients with COVID-19 were enrolled and analyzed (**Table 1**). Median age was 61 years (95% CI: 58–64). Patients were mostly males ( $n = 139$ , 72%) and never smokers ( $n = 110$ , 57%). Thirty eight patients ( $n = 38$ , 19.7%) required mechanical ventilation at any time during hospitalization. There were no patients under the status—“Do Not Attempt Resuscitation”—in this study group of the first wave of the pandemic. Comorbidities of the study group are summarized in **Table 1**. All patients were hospitalized and the majority of them received the standard of care at the time of the first wave (azithromycin, hydroxychloroquine, prophylactic dose of low molecular weight heparin). Treatment regimens were relatively homogeneous based on the national protocol. Further details for treatment modalities are presented in **Table 2**.



We reported a median RDW on admission of 12.8% (95%: 12.6–13.1). By applying RDW cut-off threshold of 14.5%, as suggested by Foy et al. we managed to identify a subgroup of patients with more advanced disease (high group,  $n = 41$ , 19.2%) compared to the low group ( $n = 156$ , 80.8%) as indicated by significant differences in maximum  $\text{FiO}_2\%$  during hospitalization (median: 100, 95% CI: 45.2–100, vs. 35, 95% CI: 31–40,  $p = 0.0001$ , respectively) **Figure 1A**. Interestingly, values of  $\text{RDW} \geq 14.5\%$  were strongly associated with increased risk of mortality in the unadjusted analysis (HR: 4.1, 95% CI: 0.88–19.23), ( $p = 0.02$ ), (data for mortality available for 162 patients) (**Figure 1B**). RDW was not an independent risk factor for mortality when adjusted for age, gender, body mass index and comorbid conditions. However, in the unadjusted analysis, RDW was associated with higher risk of mortality. Finally, RDW could not determine ICU admission in our cohort (data not shown).

## DISCUSSION

Our study demonstrated that baseline RDW is associated both with disease severity and mortality in patients with COVID-19. Our findings exhibit a number of significant attributes that need to be outlined. To our knowledge, this is the first study in the

literature that reproduces prognostic accuracy of a previously published threshold of RDW in a completely independent cohort of patients with COVID-19. The reproducibility and concordance of our data support the notion that RDW may serve as a reliable prognosticator and a clinician's friendly biomarker accessible to almost every physician in the world, for patients with COVID-19 (11).

Interestingly, our cohort exhibited lower median RDW levels (12.8%) compared to Foy et al. (survivors: 13.8%, non-survivors: 15%) (11). In addition, our cohort exhibited higher percentage of patients ( $n = 156$ , 80.8%) below the suggested cut-off threshold for RDW (14.5%) compared to Foy et al. ( $n = 1173$ , 71.5%) (11). These differences might be explained by different stages of disease severity between two cohorts. Given that RDW has been suggested as a biomarker of hypoxia, low RDW on admission in Greece may reflect timely implementation of lockdown and meticulous application of prophylactic measures from patients with chronic lung diseases during the first wave of the pandemic (3.1% of our cohort,  $n = 6$ ) (12). However, exact association of RDW with hypoxia remains to be addressed and elevation of RDW might be associated with alternative pathways. The design of this study cannot lead to definite conclusions. Thus, RDW might instead reflect the severity of lung injury or the underlying comorbid conditions of each cohort.

Despite these attributes, our study exhibited a number of limitations that need to be addressed. We chose maximum  $\text{FiO}_2$  instead of  $\text{PaO}_2/\text{FiO}_2$  due to the fact that  $\text{PaO}_2/\text{FiO}_2$  was not available from all centers. We acknowledge that maximum  $\text{FiO}_2$  required does not directly reflect patients' physiological status, but is also partly dependent on institutional strategy of respiratory support. Moreover, RDW was not an independent risk factor for mortality when adjusted for age, gender, body mass index and comorbid conditions. However, in the unadjusted analysis, RDW was associated with higher risk of mortality. Furthermore, our study was not designed to delineate potential mechanisms underlying RDW increases in the context of COVID-19. SARS-CoV-2 infection has been associated with altered turnover in all white blood cells lineages, as well as with altered platelet dynamics (13). Increases in RDW may not only reflect compensatory upregulation due to excessive blood hypoxemia but also counterregulatory changes of red blood cells turnover due to increased white blood cells and platelet kinetics (14–16). However, the concept that RDW is a non-specific biomarker of general illness and is affected by many confounding factors particularly in the setting of the multi-systemic inflammatory reaction of SARS-CoV-2 infection seems reasonable (11). We believe that a causal -effect relationship between SARS-CoV-2 infection and elevated RDW is highly unlikely. Instead, it is more likely that increased RDW is indicative of patients' comorbidome and thus may identify those patients at increased risk for mortality.

In conclusion, our study provides evidence to support reproducibility and validity of a specified cut-off threshold of RDW as biomarker of disease severity and mortality in two independent cohorts of COVID-19 patients. Further investigation of the exact role of RDW in SARS-CoV-2-infection may reveal mechanisms of potential

therapeutic interest. Longitudinal epidemiological studies and population-based analyses are sorely needed to prove these concepts.

## DATA AVAILABILITY STATEMENT

The raw data supporting the conclusions of this article will be made available by the authors, without undue reservation.

## ETHICS STATEMENT

The studies involving human participants were reviewed and approved by Institutional Review Board and the Local

Ethics Committee (Protocol Number: 8681/1-4-20). The patients/participants provided their written informed consent to participate in this study.

## AUTHOR CONTRIBUTIONS

TK and AT were involved in study conception, statistical analysis, and drafting of the initial version of the manuscript. KA, OP, VP, and AK were involved in data collection. KA, PB, SL, DB, CG, and AT supervised the work and offered significant intellectual contribution. All authors offered significant intellectual contribution for the last version of the manuscript and approved the final form.

## REFERENCES

- Nathan SD, Reffett T, Brown AW, Fischer CP, Shlobin OA, Ahmad S, et al. The red cell distribution width as a prognostic indicator in idiopathic pulmonary fibrosis. *Chest*. (2013) 143:1692–8. doi: 10.1378/chest.12-1368
- Karampitsakos T, Dimakou K, Papaioannou O, Chrysikos S, Kaponi M, Bouros D, et al. The role of increased red cell distribution width as a negative prognostic marker in patients with COPD. *Pulm Pharmacol Ther*. (2019) 60:101877. doi: 10.1016/j.pupt.2019.101877
- Karampitsakos T, Bouros E, Anagnostopoulos A, Cholidou K, Panou V, Korba A, et al. Increased red cell distribution width and absolute number of monocytes represent negative prognostic markers in patients with idiopathic pulmonary fibrosis. In: American Thoracic Society 2020 International Conference. Philadelphia, PA (2020). p. A3377. doi: 10.1164/ajrcm-conference.2020.201.1\_MeetingAbstracts.A3377
- Xie J, Covassin N, Fan Z, Singh P, Gao W, Li G, et al. Association between hypoxemia and mortality in patients with COVID-19. *Mayo Clinic Proc*. (2020) 95:1138–47. doi: 10.1016/j.mayocp.2020.04.006
- Tobin MJ, Laghi F, Jubran A. Why COVID-19 silent hypoxemia is baffling to physicians. *Am J Respir Crit Care Med*. (2020) 202:356–60. doi: 10.1164/rccm.202006-2157CP
- Dhont S, Derom E, Van Braeckel E, Depuydt P, Lambrecht BN. The pathophysiology of ‘happy’ hypoxemia in COVID-19. *Resp. Res.* (2020) 21:198. doi: 10.1186/s12931-020-01462-5
- Wang C, Deng R, Gou L, Fu Z, Zhang X, Shao F, et al. Preliminary study to identify severe from moderate cases of COVID-19 using combined hematology parameters. *Ann Transl Med*. (2020) 8:593. doi: 10.21037/atm-20-3391
- Pan Y, Ye G, Zeng X, Liu G, Zeng X, Jiang X, et al. Can routine laboratory tests discriminate SARS-CoV-2-infected pneumonia from other causes of community-acquired pneumonia? *Clin Transl Med*. (2020) 10:161–8. doi: 10.1002/ctm2.23
- Gong J, Ou J, Qiu X, Jie Y, Chen Y, Yuan L, et al. A tool for early prediction of severe coronavirus disease 2019 (COVID-19): a multicenter study using the risk nomogram in Wuhan and Guangdong, China. *Clin Infect Dis*. (2020) 71:833–40. doi: 10.1093/cid/ciaa443
- Lu G, Wang J. Dynamic changes in routine blood parameters of a severe COVID-19 case. *Clin Chim Acta*. (2020) 508:98–102. doi: 10.1016/j.cca.2020.04.034
- Foy BH, Carlson JCT, Reinertsen E, Padros I, Valls R, Pallares Lopez R, et al. Association of red blood cell distribution width with mortality risk in hospitalized adults with SARS-CoV-2 infection. *JAMA Netw Open*. (2020) 3:e2022058. doi: 10.1001/jamanetworkopen.2020.22058
- Epstein D, Nasser R, Mashlach T, Azzam ZS, Berger G. Increased red cell distribution width: a novel predictor of adverse outcome in patients hospitalized due to acute exacerbation of chronic obstructive pulmonary disease. *Respir. Med.* (2018) 136:1–7. doi: 10.1016/j.rmed.2018.01.011
- Spiezia L, Boscolo A, Poletto F, Cerruti L, Tiberio I, Campello E, et al. COVID-19-related severe hypercoagulability in patients admitted to intensive care unit for acute respiratory failure. *Thromb Haemost.* (2020) 120:998–1000. doi: 10.1055/s-0040-1710018
- Higgins JM, Mahadevan L. Physiological and pathological population dynamics of circulating human red blood cells. *Proc Natl Acad Sci USA*. (2010) 107:20587–92. doi: 10.1073/pnas.1012747107
- Patel HH, Patel HR, Higgins JM. Modulation of red blood cell population dynamics is a fundamental homeostatic response to disease. *Am J Hematol*. (2015) 90:422–8. doi: 10.1002/ajh.23982
- Chaudhury A, Miller GD, Eichner D, Higgins JM. Single-cell modeling of routine clinical blood tests reveals transient dynamics of human response to blood loss. *Elife*. (2019) 8:e48590. doi: 10.7554/eLife.48590

**Conflict of Interest:** The authors declare that the research was conducted in the absence of any commercial or financial relationships that could be construed as a potential conflict of interest.

Copyright © 2020 Karampitsakos, Akinosoglou, Papaioannou, Panou, Koromilias, Bakakos, Loukides, Bouros, Gogos and Tzouveleakis. This is an open-access article distributed under the terms of the Creative Commons Attribution License (CC BY). The use, distribution or reproduction in other forums is permitted, provided the original author(s) and the copyright owner(s) are credited and that the original publication in this journal is cited, in accordance with accepted academic practice. No use, distribution or reproduction is permitted which does not comply with these terms.





# Diagnosis of COVID-19 Pneumonia Based on Graph Convolutional Network

Xiaoling Liang<sup>1,2</sup>, Yuexin Zhang<sup>3\*</sup>, Jiahong Wang<sup>4</sup>, Qing Ye<sup>5,6</sup>, Yanhong Liu<sup>7</sup> and Jinwu Tong<sup>8</sup>

<sup>1</sup> Department of Marine Engineering, Dalian Maritime University, Dalian, China, <sup>2</sup> Department of Electrical and Computer Engineering, National University of Singapore, Singapore, Singapore, <sup>3</sup> School of Instrument Science and Engineering, Southeast University, Nanjing, China, <sup>4</sup> Department of Electrical and Computer Engineering, University of Illinois at Urbana-Champaign, Champaign, IL, United States, <sup>5</sup> Division of Life Sciences and Medicine, Department of Pathology, The First Affiliated Hospital of USTC, University of Science and Technology of China, Hefei, China, <sup>6</sup> Division of Life Sciences and Medicine, Intelligent Pathology Institute, University of Science and Technology of China, Hefei, China, <sup>7</sup> Department of Pathology, Nanjing Drum Tower Hospital, The Affiliated Hospital of Nanjing University Medical School, Nanjing, China, <sup>8</sup> School of Innovation and Entrepreneurship, Nanjing Institute of Technology, Nanjing, China

## OPEN ACCESS

### Edited by:

Reza Lashgari,  
Institute for Research in Fundamental  
Sciences, Iran

### Reviewed by:

Saeed Reza Kheradpisheh,  
Shahid Beheshti University, Iran  
Seyed Mohammad Sadegh Movahed,  
Shahid Beheshti University, Iran

### \*Correspondence:

Yuexin Zhang  
smileyuexin1314@gmail.com

### Specialty section:

This article was submitted to  
Pulmonary Medicine,  
a section of the journal  
Frontiers in Medicine

**Received:** 01 October 2020

**Accepted:** 11 December 2020

**Published:** 21 January 2021

### Citation:

Liang X, Zhang Y, Wang J, Ye Q, Liu Y  
and Tong J (2021) Diagnosis of  
COVID-19 Pneumonia Based on  
Graph Convolutional Network.  
Front. Med. 7:612962.  
doi: 10.3389/fmed.2020.612962

A three-dimensional (3D) deep learning method is proposed, which enables the rapid diagnosis of coronavirus disease 2019 (COVID-19) and thus significantly reduces the burden on radiologists and physicians. Inspired by the fact that the current chest computed tomography (CT) datasets are diversified in equipment types, we propose a COVID-19 graph in a graph convolutional network (GCN) to incorporate multiple datasets that differentiate the COVID-19 infected cases from normal controls. Specifically, we first apply a 3D convolutional neural network (3D-CNN) to extract image features from the initial 3D-CT images. In this part, a transfer learning method is proposed to improve the performance, which uses the task of predicting equipment type to initialize the parameters of the 3D-CNN structure. Second, we design a COVID-19 graph in GCN based on the extracted features. The graph divides all samples into several clusters, and samples with the same equipment type compose a cluster. Then we establish edge connections between samples in the same cluster. To compute accurate edge weights, we propose to combine the correlation distance of the extracted features and the score differences of subjects from the 3D-CNN structure. Lastly, by inputting the COVID-19 graph into GCN, we obtain the final diagnosis results. In experiments, the dataset contains 399 COVID-19 infected cases, and 400 normal controls from six equipment types. Experimental results show that the accuracy, sensitivity, and specificity of our method reach 98.5%, 99.9%, and 97%, respectively.

**Keywords:** COVID-19, graph convolutional network, 3D convolutional neural network, equipment types, chest computed tomography

## INTRODUCTION

The first case of COVID-19 was described in China in December 2019, and then COVID-19 has spread all over the world rapidly. So far, it has infected over 31 million people and has resulted in over 0.9 million deaths as of September 23, 2020. With the numerous cases needed to be tested, most countries and regions face a shortage of testing kits and medical resources.

For this issue, a series of automatic diagnosis methods based on deep learning models are proposed to relieve the medical burden (1). Unlike the reverse-transcription polymerase chain reaction (RT-PCR) based on a patient's respiratory samples, automatic diagnosis methods based on deep learning models usually accomplish the diagnosis task by using chest radiography images (2). Various published research articles indicate that chest scans are useful in detecting COVID-19 (3, 4). The lungs of the infected cases have visual marks like ground-glass opacity or hazy darkened spots, which help to differentiate infected cases from normal controls (5). With good sensitivity (SEN) and speed, chest computed tomography (CT) has been widely used in automatic diagnosis methods (6–9).

For the existing automatic diagnosis methods of COVID-19 based on medical images, structures based on a convolutional neural network (CNN) are widely used. For example, the DarkNet model (10) with 17 convolutional layers is used as a classifier for COVID-19 diagnosis based on X-ray images, and its accuracy (ACC) reaches 98.08%. A transfer learning neural network (11) based on the inception network is proposed to fit in few-shot CT datasets, and it achieved a total ACC of 89.5%. A deep three-dimensional (3D)-CNN (12) is applied to detect COVID-19 from CT volumes reaching 90.8% ACC. Additionally, ResNet50 (13), ResNet152 (14), LSTM (15), GAN (16, 17), and some other structures are successively used for COVID-19 diagnosis. Limited by the insufficient training samples and the great number of parameters in deep learning structures, the ACC of the above methods based on 3D-CT images is not satisfied. Besides, in most of the existing automatic diagnosis methods, the differences between image standards from different equipment types and hospitals are ignored, which further deteriorates the final diagnosis performance. As COVID-19 widely spreads, it is of great significance to exploit a robust diagnosis method to adapt to different acquired equipment types all over the world.

A graph convolutional network (GCN), which integrates phenotypic information into a graph to establish interactions between individuals and populations, can achieve an excellent filtering effect by graph theory. Nevertheless, there are no related works to study its application for COVID-19 diagnosis. Therefore, we propose a novel COVID-19 graph in GCN, which considers the image differences between different equipment types and hospitals. Specifically, we first employ the popular 3D-CNN structure to extract image features from 3D-CT images. In this process, a transfer learning method based on predicting equipment type is used to initialize the parameters of 3D-CNN. After this process, every subject on the graph is represented by a feature vector. Besides, every subject gets an initial diagnosis score from 3D-CNN. Second, we design a COVID-19 graph in GCN to consider the differences between different equipment types, hospital information, and disease statuses of those training samples. We also combine the extracted features and the scores from 3D-CNN to construct edge weights. Third, we input our COVID-19 graph into a GCN model for the final diagnosis.

Overall, we apply a 3D-CNN to extract image features from CT images and then design a COVID-19 graph in GCN to complete the diagnosis. The main contributions are described as follows:

- (1) We propose a transfer learning method by predicting equipment type to initialize the parameters of the 3D-CNN structure for extracting features from CT images.
- (2) We design a COVID-19 graph in GCN, which considers the information of equipment type, hospital, and disease status. We compute edge weights based on the correlation distance of extracted features and the score differences of subjects from the 3D-CNN structure.
- (3) We analyze the feature differences between different equipment types. Experimental results show that our method has a good diagnosis performance.

The rest of the paper is organized as follows. The related works of 3D-CNN and GCN are introduced in section Related Works. In section Methodology, our methodology is presented. The results of our experiments and analysis of feature differences between different equipment types are given in section Experiments and Results. Finally, this paper is concluded.

## RELATED WORKS

### 3D-CNN for Feature Extraction

As deep CNN can filter noise and reduce parameters, it is widely studied. The most popular CNN methods include LeNet-5, AlexNet, VGG-16, Inception-v1, ResNet-50, Inception-ResNet, and so on, which are successfully applied in semantic segmentation (18), object detection (19, 20), and image recognition and segmentation (21).

As CNNs usually contain numerous parameters to achieve good ACC, it is necessary to explore simple and efficient network architectures, especially for our time series CT scan images, which can be regarded as 3D images. Multitask learning incorporates the benefits from several related tasks to excavate features better. It can take the underlying common information that may be ignored by single-task learning. Eventually, it improves the performance, the robustness and stability of disease detection, or image segmentation (22, 23). Transfer learning can be used to improve a learner from one domain by transferring information from a related domain (24) and is widely used to initialize the parameters of a system (25–27). As the equipment information is usually acquired and is an essential feature to images, we propose to utilize the task of predicting equipment type to initialize the parameters of the 3D-CNN structure and finally employ it to improve the extracted features.

### GCN

A graph neural network (GNN) was proposed in 2009 (28), which is based on the graph theory (29), building the foundation of all kinds of graph networks (30–33). As one of the most famous graph networks, GCN mainly applies the convolution of Fourier transform and Taylor's expansion formula to improve filtering performance (34). With its excellent performance, GCN has been widely used in disease classification (34–38).

For graph theory, a node on the graph represents a subject's imaging data, and the edges establish interactions between each pair of nodes. Sarah et al. (35) integrated similarities between imaging information and distances between phenotypic

information (e.g., sex, equipment type, and age) into edges for the prediction of autism spectrum disorder and the conversion to Alzheimer's disease (AD). Zhang et al. (36) combined an adaptive pooling scheme and a multimodal mechanism to classify Parkinson's disease (PD) status. Kazi et al. (37) designed different kernel sizes in spectral convolution to learn cluster-specific features for predicting mild cognitive impairment and AD. All these studies validate the effectiveness of GCN and show that the convolution operation is the key to prediction performance. On a graph, edges and edge weights determine the convolution operation. According to the characteristic of COVID-19 datasets, we design a COVID-19 graph to establish edges by considering equipment types, hospitals, and disease statuses. Current edge weights are roughly computed based on the correlation distance between image feature vectors, which is inaccurate and may affect the convolution performance. Therefore, we propose a combination mechanism, which combines the correlation distance of extracted features and the scores from 3D-CNN, to better compute the edge weights.

## METHODOLOGY

The proposed method in this paper consists of two key parts. Using 3D-CNN, we extract image features from 3D-CT images and get an initial score for every subject. By designing our COVID-19 graph in GCN, we accomplish the COVID-19 diagnosis task. We first introduce the proposed 3D-CNN framework for feature extraction. Then we present the proposed COVID-19 graph and GCN. The overview of the proposed diagnosis mechanism is shown in **Figure 1**.

### Feature Extraction by Using 3D-CNN

The paper applies a 3D-CNN network (39, 40) to extract features from 3D-CT images. We first use z-score standardization to process the initial CT scans. Since the acquired datasets are not uniform and the 3D-CT images are of different sizes, we converted all the 3D-CT images into the same size of  $64 \times 64 \times 32$ . Specifically, the 3D-CNN model has six convolutional layers and six max-pooling layers with a rectified linear unit (ReLU) as its activation function. The details of the 3D-CNN structure are shown in **Figure 2**. In the first layer, C30@ $3 \times 3 \times 3$  denotes there are 30 convolution kernels and the kernel size is  $3 \times 3 \times 3$ . P2  $\times$  2 denotes the size of the pooling layer is  $2 \times 2 \times 2$ .

Transfer learning is a widely used machine learning technique especially for comparatively little data in many fields (41, 42), which enables scientists to benefit from the knowledge gained from a previously trained model for a related task. Specifically, by applying transfer learning, we can exploit the valuable information that has been learned in one task to improve generalization in another. The popularly used machine learning transfers the weights that a network has learned at "task A" to a new "task B."

As there are more than millions of parameters in our 3D-CNN and <1,000 samples for training 3D-CNN, it has great significance to applying transfer learning on our COVID-19 diagnosis task. In view of the fact the equipment type is an important factor that affects acquired images and is easy

to acquire, we design a transfer learning method to transfer the weights of 3D-CNN based on the known equipment type, as shown in **Figure 1**. There are two tasks, including predicting equipment type and diagnosing COVID-19. We first employ 3D-CT images and their corresponding equipment type labels to train the first system of predicting equipment type. Then we transfer the weights of the 3D-CNN in the first system to the second system of diagnosing COVID-19. Finally, we adopt 3D-CT images and their corresponding COVID-19 labels in a training set to train the COVID-19 diagnosis system.

After the above processes, we get a well-trained COVID-19 diagnosis system by using transfer learning. Further, we utilize the trained COVID-19 diagnosis system to score every subject and extract all samples' features from the 3D-CNN structure. As shown in **Figure 1**, we finally get a  $150 \times 1$  feature vector and a score value for every subject. Every extracted feature vector composes a node on the graph in GCN, and score values are used to establish edges between nodes. High-dimensional feature vectors will increase the burden on the following GCN, and we use recursive feature elimination (RFE) (43) to select features from the  $150 \times 1$  feature vector to reduce the feature vector's dimensions. In detail, given an estimator (e.g., ridge classifier) that assigns weights to features, RFE selects features by recursively considering smaller and smaller sets of features. First, the estimator is trained on the initial set of features, and the importance of each feature is obtained. Then the least important features are pruned from the current set of features. This procedure is recursively repeated on the pruned set until the desired number of features to be selected is eventually reached (44–46).

## GCN

Compared with traditional neural networks, GCN makes use of graph theory to improve performance, and the graph in GCN plays the role of filtering noise. On a graph, a node represents the feature vector of a subject, and an edge denotes the interaction between corresponding pair nodes. Graph theory takes all nodes on the graph to perform convolution, and edge weights are the key to the performance as they are the corresponding convolution coefficients. Thereby, they attract much attention (47, 48). The description of graph theory is shown in **Figure 3**. As shown, a node represents a subject, and there are total of  $n$  subjects, and everyone is represented by a  $1 \times m$  feature vector. In mathematical form, a graph with  $n$  nodes can be described as an  $n \times m$  feature matrix pre-multiplied with an  $n \times n$  adjacency matrix, where the adjacency matrix is composed of all edge weights. The  $n \times n$  adjacency matrix plays the role of filtering noise. For example, for subject 1, the filtered feature 2 is computed as  $\hat{x}_{12} = \sum_{i=1}^n a_{1i} \times x_{i2}$ . The convolution coefficients determine the filtering effect, and improving them is our main contribution in this paper. There are usually millions of parameters in 3D-CNN, whereas only thousands of COVID-19 infected and non-infected subjects in the training process, and the insufficiency of samples introduces



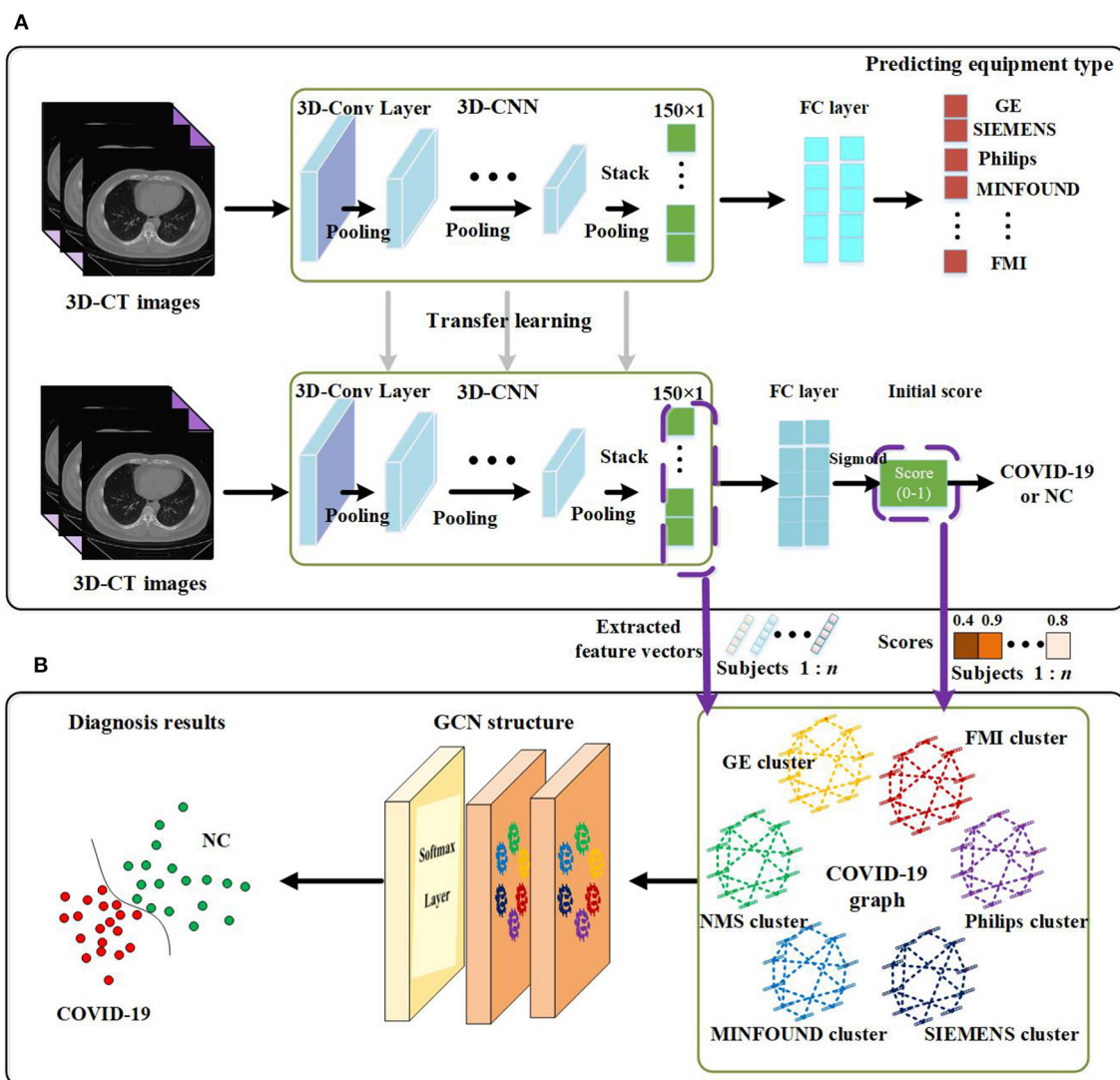


**FIGURE 1** | Overview of the proposed coronavirus disease 2019 (COVID-19) diagnosis framework. **(A)** Feature extraction. **(B)** GCN structure for final diagnosis.

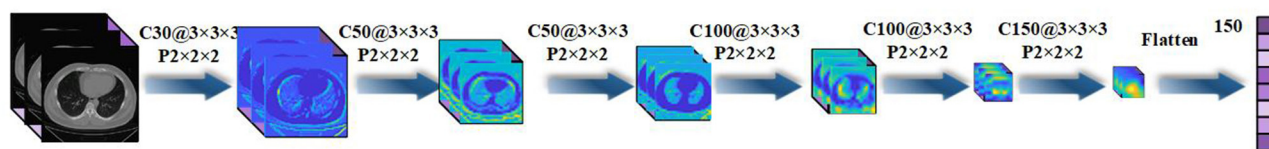


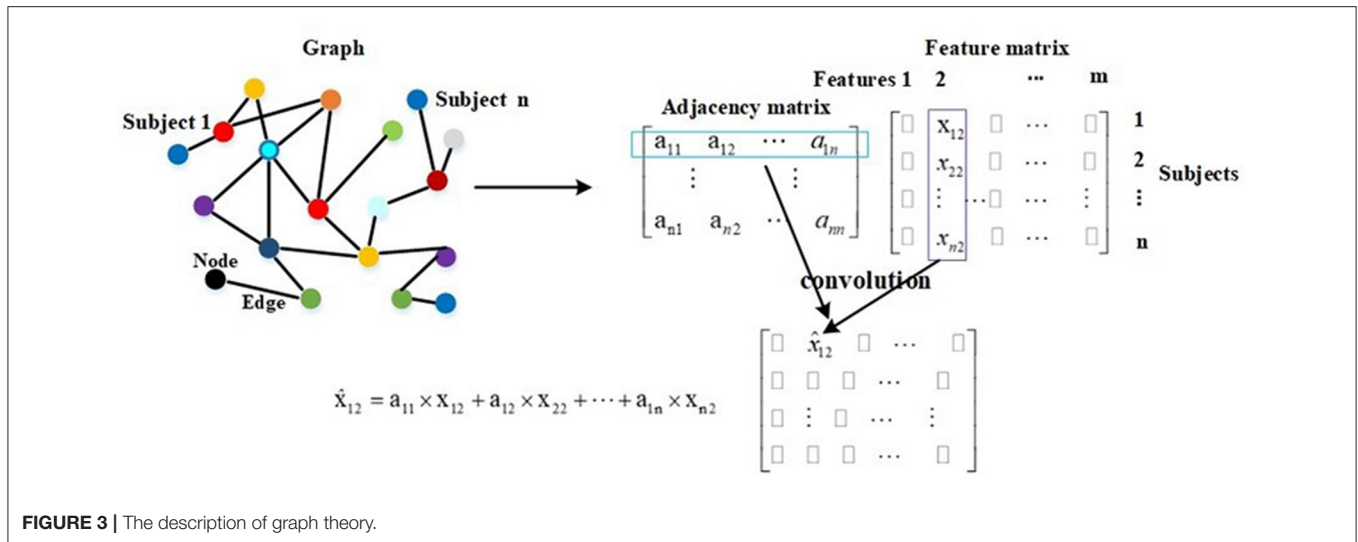
**FIGURE 2** | Details of the three-dimensional convolutional neural network (3D-CNN) structure for feature extraction.

noise in extracted features, which further deteriorates the final diagnosis performance. The existing noise is given in **Figure 6**.

In this subsection, we propose a COVID-19 graph in GCN to establish edges to fit in the characteristics of the diagnosis task, which finally plays the role of improving the adjacency matrix.

### COVID-19 Graph

We first consider the differences in the equipment types in our datasets, so we divide all nodes on the COVID-19 graph into several clusters. Those subjects with the same equipment type compose a cluster, which means the number



of clusters matches the number of equipment types in our datasets. There are six clusters, including SIEMENS cluster, Philips cluster, NMS cluster, Minfound cluster, FMI cluster, and GE cluster. Every cluster corresponds to one equipment type. We do not establish the connections between nodes in different clusters, which can also be regarded as zero-weight edges. For nodes in the same cluster, we propose a novel method to establish their edges, which considers the hospital information and disease status of those training samples. On our COVID-19 graph, the proposed edge weights between two subjects in the same cluster are calculated as follows:

$$A(v, u) = \text{Sim}(F_v, F_u) \times (1 + r_H(H_v, H_u) + r_S(S_v, S_u)) \quad (1)$$

$$r_H(H_v, H_u) = \begin{cases} 1, & H_v = H_u \\ 0, & H_v \neq H_u \end{cases} \quad (2)$$

$$r_S(S_v, S_u) = \begin{cases} 1, & S_v = S_u \\ 0, & S_v \neq S_u \\ 0, & S_v \text{ or } S_u \text{ is unknown} \end{cases} \quad (3)$$

where all edge weights compose adjacency matrix  $A$ .  $A(v, u)$  is the edge weight between subject  $v$  and subject  $u$ ,  $\text{Sim}(\cdot)$  denotes the similarity of imaging information,  $F_v$  and  $F_u$  represent the feature vectors of subject  $v$  and subject  $u$ , respectively.  $r_H$  represents the distance between hospitals,  $r_S$  represents the distance of disease status (the statuses of those training samples on the graph are known),  $S_v$  and  $S_u$  are the subjects' disease statuses (COVID-19 infected case or healthy case), and  $H_v$  and  $H_u$  denote their corresponding hospital. For example, if the images of subject  $v$  and subject  $u$  are acquired from the same hospital, we set  $H_v = H_u$ . If subject  $v$  and subject  $u$  are all COVID-19 infected cases (or healthy cases), we set  $S_v = S_u$ .

#### Edge Weights Based on Correlation Distance

The popular method for evaluating the similarity of imaging information is based on the correlation distance as follows (35):

$$\text{Sim}(F_v, F_u) = \exp\left(-\frac{[\rho(F_v, F_u)]^2}{2\sigma^2}\right) \quad (4)$$

where  $\rho(\cdot)$  is the correlation distance function and  $\sigma$  is the width of the kernel. We compute the correlation distances between each pair of nodes, and the  $\sigma$  is set as the mean value of the correlation distances according to the work in Zhang et al. (36).

By Equations (1)–(4), we can get an adjacency matrix  $A_f$ , which represents the adjacency matrix constructed based on the correlation distance of extracted feature vectors.

#### Edge Weights Based on Scores

Using correlation distance to compute similarities as in Equation (4) is rough and deteriorates convolution performance to some extent. We propose a method to compute the similarities in view that the 3D-CNN has good capability to excavate in-depth features. Employing 3D-CNN to extract features from CT images, we also get a diagnosis score for every subject, as shown in **Figure 1**. Based on these scores, the proposed similarities are calculated as follows:

$$\text{Sim}(F_v, F_u) = \exp\left(-\frac{[\text{Score}_v - \text{Score}_u]^2}{2\sigma^2}\right) \quad (5)$$

where  $\text{Score}_v$  and  $\text{Score}_u$  denote the scores of subject  $v$  and subject  $u$  from 3D-CNN diagnosis system, respectively, and  $\sigma$  is also the width of the kernel and is set as the mean value of the correlation distances according to the work in Zhang et al. (36). Based on Equations (1)–(3), (5), we can also get an adjacency matrix  $A_s$ .

#### Combined Adjacency Matrix

After getting an adjacency matrix  $A_f$  based on correlation distance and an adjacency matrix  $A_s$  based on initial scores, we

further design a method to combine the two adjacency matrices to get a robust adjacency matrix. The combined adjacency matrix  $A_c$  is calculated as follows:

$$A_c = a \times A_f + b \times A_s \quad (6)$$

where  $a$  and  $b$  are corresponding coefficients, and we set the two coefficients as 0.5 in this paper.

Then we can form our COVID-19 graph, which includes the extracted features from 3D-CT images and the edges represented by the combined adjacency matrix.

### Spectral Theory and GCN Structure

In GCN series methods, the adjacency matrix is processed to achieve a better filtering effect and computational efficiency (49). The spectral convolution can be described as the multiplication of a signal  $x \in \mathbb{R}^n$  (a scalar for every node) with a filter  $g_\theta = \text{diag}(\theta)$  by

$$g_\theta * x = U g_\theta(\Lambda) U^T x = \sum_{k=0}^K \theta_k T_k(\tilde{L}) x \quad (7)$$

where  $U$  is the matrix of eigenvectors and is computed from the formula  $L = I_N - D^{-(1/2)} A_{ac} D^{-(1/2)} = U \Lambda U^T$ .  $I_N$  is the identity matrix, and  $D$  represents the diagonal degree matrix.  $g_\theta(\Lambda)$  is well-approximated by a truncated expansion in terms of Chebyshev polynomials to the  $K$ th order.  $\theta_k$  is a vector of Chebyshev coefficients, and  $T_k$  is the Chebyshev polynomial function,  $\tilde{L} = \frac{2}{\lambda_{\max} \Lambda - I_N}$ .

After the above spectral convolution is applied, combined adjacency matrix  $A_c$  is approximated by  $\sum_{k=0}^K \theta_k T_k(\tilde{L})$ . When polynomial order  $K$  is adjusted, a different filtering effect can be obtained. It is worth mentioning that the adjacency matrix is computed according to Equations (1)–(7).

As shown in **Figure 1**, there are two graph convolutional layers with a ReLU function as the activation function and one softmax function as the final output layer. Let  $\hat{A} = \sum_{k=0}^K \theta_k T_k(\tilde{L})$ , and the formula of the two-layer GCN is as follows:

$$Z = \text{softmax}(\hat{A} \text{ReLU}(\hat{A} X W^{(0)}) W^{(1)}) \quad (8)$$

The GCN model is trained and tested using the whole graph as input. Let  $F_i$  and  $F_j$  represent the feature vectors of subject  $i$  and subject  $j$ , respectively.  $X = [F_1; F_2; \dots; F_n]$  represents the feature vectors of all subjects. In the training and test processes, the feature vector  $F_i$  is approximated by  $\sum_{j=1}^{j=n} \hat{A}_{i,j} F_j$  in every layer, and this is described by  $\hat{A}X$ . It is also embodied in **Figure 3**. In Equation (8),  $Z$  represents the labels of training and test samples. In the training process, the input is  $X$ , the feature vector of every training sample is approximated by  $\sum_{j=1}^{j=n} \hat{A}_{i,j} F_j$  in every layer, and the labels of test samples in  $Z$  are masked. The training samples and their labels are used for training GCN. In the test

**TABLE 1** | The equipment type information in the dataset.

| Equipment type | Number |
|----------------|--------|
| SIEMENS        | 176    |
| Philips        | 108    |
| NMS            | 154    |
| FMI            | 160    |
| MINFOUND       | 100    |
| GE             | 101    |

process, the input is also  $X$ , the feature vector of every test sample is approximated by  $\sum_{j=1}^{j=n} \hat{A}_{i,j} F_j$  in every layer, and after a two-layer trained GCN, we get their prediction results. In other words, in the training process, the feature vectors of test samples are used to help update the feature vectors of training samples. In the test process, the feature vectors of training samples are also used to help update the feature vectors of test samples. This is the meaning of graph theory for classification, and this is presented in **Figure 3** and Equation (8). In adjacency matrix  $\hat{A}$ , every row of elements corresponds to the convolution coefficients (convolution kernel) of a subject. For example, the  $i$  row of elements in  $\hat{A}$  represents the convolution coefficients of subject  $i$  as shown in **Figure 3**.

## EXPERIMENTS AND RESULTS

The proposed methodology is implemented on a database of CT scan images from open sources (50–53). The dataset contains 399 COVID-19 infected cases and 400 normal controls with six equipment types. The equipment type information is shown in **Table 1**.

The parameters of the proposed GCN structure are as follows: learning rate is 0.005, dropout rate is 0.1,  $l_2$  regularization is  $5 \times 10^{-4}$ , the number of epochs is 200, the number of neurons per layer is 64, and the number of extracted features is 20. Classification ACC, SEN, specificity (SPE), and area under receive operation curve (AUC) are selected as evaluation metrics.

This section is divided into seven parts. First, we evaluate the performance of the proposed transfer learning method on the 3D-CNN structure. Second, we test the performance of our GCN structure by comparing it with traditional methods. Third, we present the effect of different equipment types on extracted features. Fourth, we analyze the influence of the number of extracted features. Fifth, we analyze the effect of the width of kernel. Sixth, we analyze the performance of the GCN method on other public datasets. Last, we compare our methods with related works.

### Performance of the Proposed Transfer Learning Method

In the proposed feature extraction framework, the task of predicting equipment type is utilized to initialize the parameters of the 3D-CNN structure, as shown in **Figure 1**. The transfer learning method improves the performance of 3D-CNN, and

**TABLE 2 |** Performance of the 3D-CNN, 3D-ResNet18, and PENet diagnosis frameworks with and without our transfer learning method (5-fold cross validation).

| Model                           | ACC (%)    | SEN (%)    | SPE (%)    | AUC (%)     |
|---------------------------------|------------|------------|------------|-------------|
| 3D-CNN                          | 94.3 ± 0.8 | 90.1 ± 1.1 | 98.7 ± 0.5 | 98.7 ± 0.03 |
| 3D-ResNet18                     | 93.1 ± 1.4 | 93.9 ± 1.9 | 92.4 ± 1.2 | 97.9 ± 0.04 |
| PENet                           | 94.5 ± 1.2 | 90.7 ± 1.5 | 97.7 ± 0.7 | 98.2 ± 0.01 |
| 3D-CNN + transfer learning      | 95.6 ± 1.0 | 96.2 ± 1.6 | 95.1 ± 0.6 | 99.6 ± 0.02 |
| 3D-ResNet18 + transfer learning | 94.9 ± 1.5 | 95 ± 1.8   | 98 ± 0.9   | 99.4 ± 0.03 |
| PENet + transfer learning       | 95.2 ± 1.8 | 98.4 ± 2.1 | 96.2 ± 1.4 | 99.9 ± 0.03 |

**Table 2** shows the method's effectiveness on the diagnosis performance of the 3D-CNN diagnosis framework.

As shown in **Table 2**, with our transfer learning method, the ACC of the 3D-CNN diagnosis framework increases by 1.3%, SEN increases by 6.1%, and AUC increases by 1.1%, whereas SPE decreases by 3.6%. The ACC of the 3D-CNN diagnosis framework reaches 95.6%. These improvements support us getting better extracted features with our transfer learning method. In addition, we also test our transfer learning method on 3D-ResNet18 and PENet (54). **Table 2** shows that our transfer learning method can improve ACC by 1.8 and 0.7%. Compared to 3D-CNN, PENet has a little effect on performance improvement whereas 3D-ResNet18 deteriorates performance, and they consume much more time. In our paper, we use the simplest 3D-CNN structure to extract features as its stable performance.

## Performance of Our GCN Diagnosis Framework

To integrate equipment type information, hospital information, and disease status information, we design our GCN structure to accomplish the diagnosis task based on the extracted features and initial scores from the 3D-CNN framework. In this subsection, we compare our novel GCN structure with some other classifiers based on the extracted features. The compared classifiers include multiple layer perception (MLP), support vector machine (SVM), random forest (RF), gradient boosting decision tree (GBDT), and traditional GCN (35). The results of the performance comparison are shown in **Table 3**. **Figure 4** shows the performance comparison by histograms, and it shows our GCN has better performance than others. **Figure 5** describes the ROC curves of different methods, and it shows that our GCN has better AUC values.

As shown in **Table 3**, compared to the diagnosis performance of the 3D-CNN framework with transfer learning in **Table 2**, there is virtually no performance improvement by using the 3D-CNN extracted features and then using traditional classifiers (MLP, SVM, RF, and GBDT) for the final diagnosis. The traditional GCN (35) has slight performance improvement, with mean ACC increasing by 1.7% and mean SEN increasing by 3.5%. Nonetheless, with our proposed COVID-19 graph in GCN, mean

**TABLE 3 |** Diagnosis performance of different classifiers based on the extracted features (5-fold cross validation).

| Model | ACC (%)     | SEN (%)     | SPE (%)     | AUC (%)     |
|-------|-------------|-------------|-------------|-------------|
| MLP   | 95.5 ± 0.27 | 99.3 ± 0.05 | 91.2 ± 0.2  | 99.8 ± 0.01 |
| SVM   | 96.1 ± 0.81 | 98.9 ± 0.05 | 92.5 ± 1.25 | 99.9 ± 0.01 |
| RF    | 96 ± 0.94   | 99.3 ± 0.05 | 92.2 ± 1.62 | 99.7 ± 0.02 |
| GBDT  | 95.6 ± 0.44 | 99.1 ± 0.09 | 91.5 ± 0.55 | 99.9 ± 0.01 |
| GCN   | 97.3 ± 0.27 | 99.7 ± 0.05 | 95 ± 0.1    | 99.9 ± 0.02 |
| Ours  | 98.5 ± 0.96 | 99.9 ± 0.04 | 97 ± 1.73   | 99.9 ± 0.01 |

ACC increases by 2.9%, mean SEN increases by 3.7%, and mean SPE increases by 1.9%. These results show that our COVID-19 graph can improve performance significantly. In short, with our COVID-19 graph in GCN, the performance of GCN gets significant improvement, with final mean ACC, SEN, SPE, and AUC reaching 98.5, 99.9, 97, and 99.9%.

## Effect of Equipment Type on Extracted Features and the Filtering Effect of Our Graph on Features

As there are no related works to evaluate the filtering effect of GCN series methods for disease prediction, we propose to describe it by comparing  $X$  with  $\hat{A}X$ .  $X$  represents the feature matrix that is composed by all subjects' feature vectors,  $\hat{A}$  is our adjacency matrix, and  $\hat{A}X$  represents the feature matrix after filtering. As there are no real feature values, we propose to use mean values to represent real feature values and use standard deviation to describe noise level in this subsection. **Figure 6** visualizes the filtering effect of the different-equipment-type graph on the extracted features by comparing  $X$  with  $\hat{A}X$ , and the detailed effect on mean and standard deviation is given in **Table 4**. **Figure 7** shows t-SNE visualization results of feature maps where we compare  $X$  with  $\hat{A}X$ .

As shown in **Figure 6** and **Table 4**, there is much difference in the mean values of the same feature between different clusters. For example, the mean values of feature 1 with  $X$  in our six clusters are 1.03, 1.03, 1.96, 1.48, 1.42, and 0.93. The mean values of feature 2 with  $X$  in our six clusters are 0.69, 0.64, 1.22, 0.96, 1.00, and 0.66. These results validate that there are differences in images between different equipment types. Based on the big differences, we design our COVID-19 graph to divide all samples into several clusters (a cluster includes those samples acquired by one kind of equipment type) and establish edge connections between those samples from the same cluster. By pre-multiplying with adjacency matrix  $\hat{A}$ , the noise in extracted features is well-suppressed, as shown in **Figure 6**, where red lines have a small fluctuation and blue lines have a big fluctuation.

In **Table 4**, it is also shown that there are different noise levels between different features in the same cluster and also different noise levels between the same features in different clusters. For example, for feature 1, the standard deviations of our six clusters



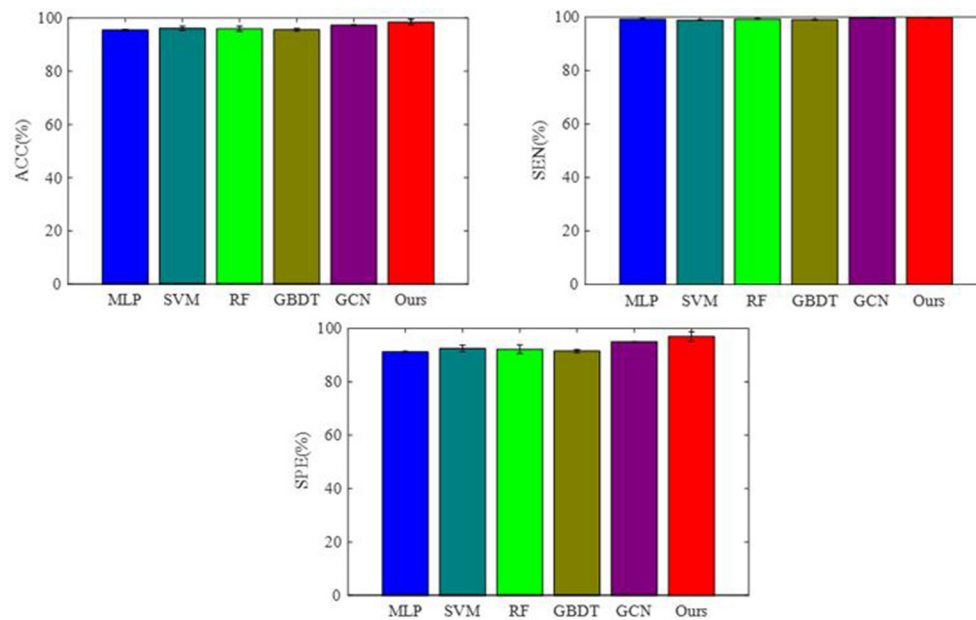


**FIGURE 4 |** Performance of the different classifiers based on the extracted features.

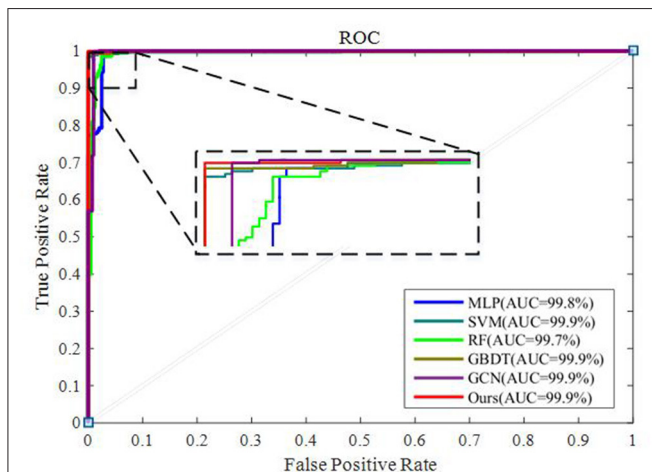


**FIGURE 5 |** ROC curves of the different classifiers based on the extracted features.

with  $X$  are 0.32, 0.32, 0.86, 0.70, 0.12, and 0.23. For feature 2, the standard deviations of our six clusters with  $X$  are 0.16, 0.15, 0.48, 0.37, 0.08, and 0.14. These results show that there is much noise on the extracted features in the NMS cluster and the FMI cluster. Furthermore, the comparison of the mean values and standard deviations of  $\hat{A}X$  with those of  $X$  shows that mean values were kept stable, whereas standard deviations reduced significantly. For example, for all features, the standard deviations of four clusters (i.e., SIEMENS, NMS, MINFOUND, and GE) are very small. These results show that the GCN has an excellent filtering effect.

## Effect of the Number of Extracted Features

The discriminative features are extracted from CT images by using 3D-CNN and initially form a  $150 \times 1$  feature vector for every subject. Further, we apply RFE to select the principal features. The effect of the number of final selected features on diagnosis ACC is shown in **Figure 8**, where the number of extracted features varies from 0 to 150.

As shown in **Figure 8**, the ACC value increases to a stable value rapidly and maintains stability after the number exceeds 10. As a large number can increase the burden on GCN, we set the number of the extracted features as 20 in this paper.

## Effect of the Width of Kernel

The width of kernel  $K$  in Equation (7) means the filter learned for neighbors  $K$  hops away from the node at the center of the receptive field, and it affects classification performance according to a previous study (35). We test the effect of  $K$  on performance in this subsection. Here, we test  $K \in \{1, 2, 3, 4, 5, 6\}$ . By setting different  $K$  values in our GCN method, we get their corresponding ACC as {97.9, 98.3, 98.5, 98.3, 98.1, 98.1%}.

As the above results shows, there are a few variations on ACC with different  $K$  values. Specifically, with  $K$  set as 3, the best ACC is reached, and this result is consistent with the work in Parisot et al. (35) and Ktena et al. (38). Therefore, we set  $K = 3$  in our experiments.

## Performance of the GCN Method on Other Public Datasets

There are several large public datasets available, but no equipment type information is included. In this subsection, we further test the GCN method by combining other datasets. The experiment includes the dataset from <http://ncov-ai.big.ac.cn/>

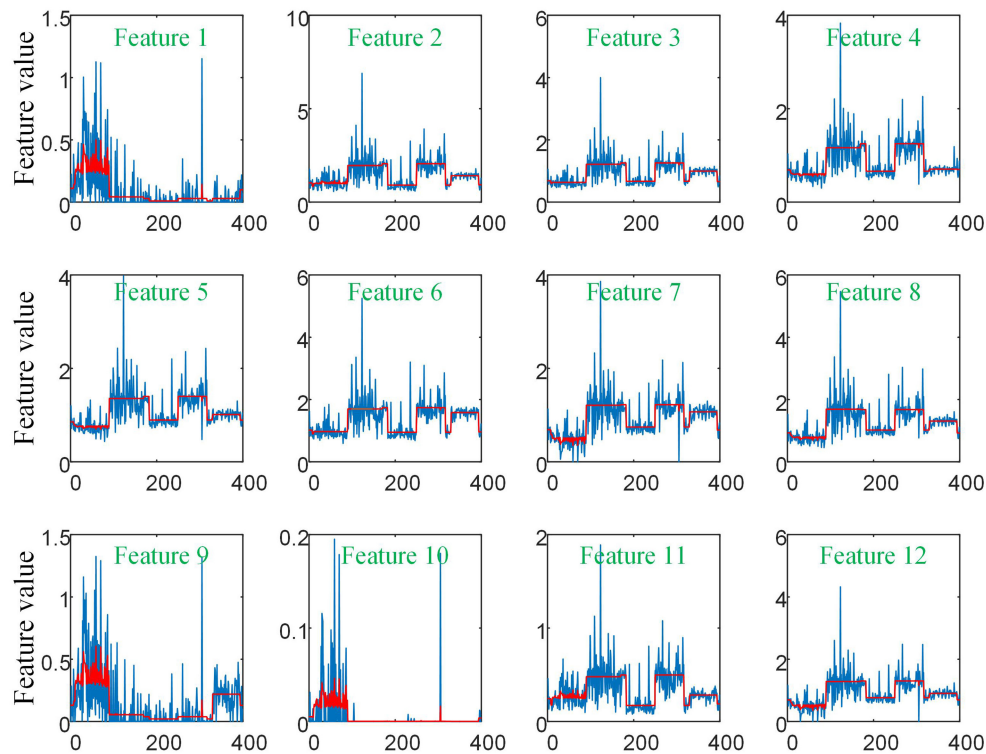


**FIGURE 6 |** The filtering effect of the different-equipment-type graph on the extracted features by comparing  $X$  with  $\hat{A}X$ .  $X$  is the original feature matrix of all equipment types' subjects, which is represented by the blue line, and  $\hat{A}X$  represents the filtered features by pre-multiplying with the adjacency matrix  $\hat{A}$ , which is represented by the red line.

**TABLE 4 |** The mean values and standard deviations of the top nine most discriminative features in our six clusters.

| Top 9 features |            | SIEMENS, mean $\pm$ SD | Philips, mean $\pm$ SD | NMS, mean $\pm$ SD | FMI, mean $\pm$ SD | MINFOUND, mean $\pm$ SD | GE, mean $\pm$ SD |
|----------------|------------|------------------------|------------------------|--------------------|--------------------|-------------------------|-------------------|
| Feature 1      | $X$        | 1.03 $\pm$ 0.322       | 1.03 $\pm$ 0.322       | 1.96 $\pm$ 0.863   | 1.48 $\pm$ 0.702   | 1.42 $\pm$ 0.123        | 0.93 $\pm$ 0.234  |
|                | $\hat{A}X$ | 1.03 $\pm$ 0.002       | 1.02 $\pm$ 0.053       | 1.96 $\pm$ 0.003   | 1.48 $\pm$ 0.574   | 1.42 $\pm$ 0.001        | 0.93 $\pm$ 0.002  |
| Feature 2      | $X$        | 0.69 $\pm$ 0.163       | 0.64 $\pm$ 0.154       | 1.22 $\pm$ 0.481   | 0.96 $\pm$ 0.378   | 1.00 $\pm$ 0.084        | 0.66 $\pm$ 0.146  |
|                | $\hat{A}X$ | 0.69 $\pm$ 0.001       | 0.63 $\pm$ 0.002       | 1.22 $\pm$ 0.002   | 0.96 $\pm$ 0.304   | 1.00 $\pm$ 0.002        | 0.66 $\pm$ 0.001  |
| Feature 3      | $X$        | 0.69 $\pm$ 0.155       | 0.59 $\pm$ 0.166       | 1.16 $\pm$ 0.452   | 0.95 $\pm$ 0.372   | 0.71 $\pm$ 0.086        | 0.70 $\pm$ 0.153  |
|                | $\hat{A}X$ | 0.69 $\pm$ 0.001       | 0.60 $\pm$ 0.013       | 1.16 $\pm$ 0.001   | 0.96 $\pm$ 0.297   | 0.71 $\pm$ 0.001        | 0.70 $\pm$ 0.001  |
| Feature 4      | $X$        | 0.85 $\pm$ 0.166       | 0.75 $\pm$ 0.154       | 1.35 $\pm$ 0.453   | 1.14 $\pm$ 0.331   | 1.01 $\pm$ 0.082        | 0.89 $\pm$ 0.122  |
|                | $\hat{A}X$ | 0.86 $\pm$ 0.001       | 0.75 $\pm$ 0.024       | 1.36 $\pm$ 0.001   | 1.15 $\pm$ 0.259   | 1.01 $\pm$ 0.001        | 0.89 $\pm$ 0.001  |
| Feature 5      | $X$        | 1.02 $\pm$ 0.263       | 0.97 $\pm$ 0.222       | 1.70 $\pm$ 0.637   | 1.34 $\pm$ 0.512   | 1.58 $\pm$ 0.123        | 0.96 $\pm$ 0.175  |
|                | $\hat{A}X$ | 1.02 $\pm$ 0.002       | 0.97 $\pm$ 0.015       | 1.70 $\pm$ 0.002   | 1.34 $\pm$ 0.404   | 1.58 $\pm$ 0.002        | 0.96 $\pm$ 0.001  |
| Feature 6      | $X$        | 0.69 $\pm$ 0.227       | 0.48 $\pm$ 0.217       | 1.21 $\pm$ 0.466   | 0.98 $\pm$ 0.328   | 1.07 $\pm$ 0.104        | 0.68 $\pm$ 0.137  |
|                | $\hat{A}X$ | 0.69 $\pm$ 0.003       | 0.48 $\pm$ 0.053       | 1.21 $\pm$ 0.003   | 0.98 $\pm$ 0.247   | 1.07 $\pm$ 0.002        | 0.68 $\pm$ 0.001  |
| Feature 7      | $X$        | 0.93 $\pm$ 0.286       | 0.78 $\pm$ 0.204       | 1.69 $\pm$ 0.663   | 1.34 $\pm$ 0.449   | 1.31 $\pm$ 0.101        | 0.93 $\pm$ 0.158  |
|                | $\hat{A}X$ | 0.93 $\pm$ 0.003       | 0.78 $\pm$ 0.035       | 1.69 $\pm$ 0.001   | 1.35 $\pm$ 0.334   | 1.31 $\pm$ 0.003        | 0.93 $\pm$ 0.002  |
| Feature 8      | $X$        | 0.24 $\pm$ 0.103       | 0.37 $\pm$ 0.332       | 0.48 $\pm$ 0.255   | 0.33 $\pm$ 0.213   | 0.28 $\pm$ 0.042        | 0.19 $\pm$ 0.064  |
|                | $\hat{A}X$ | 0.24 $\pm$ 0.001       | 0.36 $\pm$ 0.091       | 0.48 $\pm$ 0.001   | 0.33 $\pm$ 0.162   | 0.28 $\pm$ 0.001        | 0.19 $\pm$ 0.002  |
| Feature 9      | $X$        | 0.69 $\pm$ 0.221       | 0.49 $\pm$ 0.227       | 1.28 $\pm$ 0.535   | 1.03 $\pm$ 0.371   | 0.90 $\pm$ 0.103        | 0.70 $\pm$ 0.131  |
|                | $\hat{A}X$ | 0.69 $\pm$ 0.002       | 0.50 $\pm$ 0.053       | 1.28 $\pm$ 0.001   | 1.03 $\pm$ 0.275   | 0.90 $\pm$ 0.003        | 0.70 $\pm$ 0.003  |

We compare features' mean values and standard deviations with or without pre-multiplication with the adjacency matrix  $\hat{A}$ .



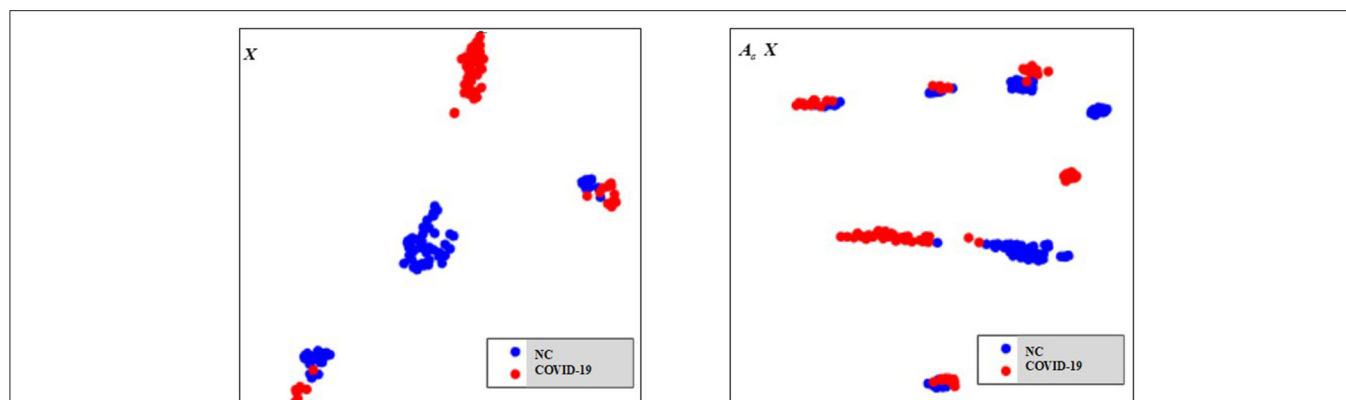


**FIGURE 7 |** The t-SNE visualization results of feature maps, where we compare  $X$  with  $A_x X$ .

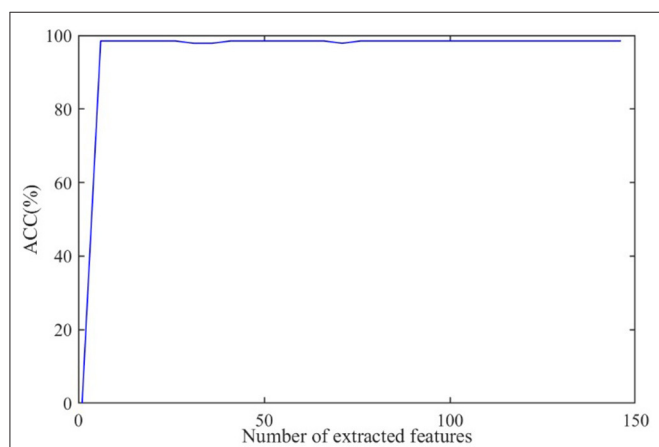


**FIGURE 8 |** The effect of the number of extracted features on diagnosis accuracy.

download?lang=en (55) and the dataset from [https://mosmed.ai/datasets/covid19\\_1110](https://mosmed.ai/datasets/covid19_1110) (56). Constrained by our computer memory, we selected a total of 1,560 COVID-19 cases and 1,560 NC cases randomly from the above datasets. As there is no equipment type information in the above datasets, we use 3D-CNN to extract features, ignoring the transfer learning method, and we treat all samples as one cluster in the COVID-19 graph. The experimental results are listed in **Table 5**.

As shown in **Table 5**, with a large dataset, the performance of COVID-19 diagnosis is satisfactory with an ACC reaching 99.5% by using the MLP method. Compared to the ACC with the MLP method, the ACC by using our GCN method increases by 0.3%. Compared to the 1.7% ACC improvement in **Table 3**, the little performance improvement validates that our GCN method relatively adapts to the few-shot learning task.

## Comparison With Related Works

**Table 6** shows the diagnosis performance of our method and related methods. It is observed that our method achieves the best

**TABLE 5 |** Diagnosis performance of the GCN method on the large dataset (5-fold cross validation).

| Model | ACC (%)     | SEN (%)     | SPE (%)    | AUC (%)     |
|-------|-------------|-------------|------------|-------------|
| MLP   | 99.5 ± 0.12 | 99.1 ± 0.02 | 100 ± 0.1  | 99.5 ± 0.04 |
| SVM   | 99.1 ± 0.31 | 99.3 ± 0.02 | 98.4 ± 0.7 | 99.6 ± 0.02 |
| RF    | 99 ± 0.12   | 98.9 ± 0.03 | 99.1 ± 0.1 | 99.6 ± 0.02 |
| GBDT  | 98.7 ± 0.11 | 97.1 ± 0.02 | 99.2 ± 0.2 | 99.4 ± 0.01 |
| GCN   | 99.6 ± 0.17 | 100 ± 0.03  | 99.3 ± 0.1 | 99.8 ± 0.01 |
| Ours  | 99.8 ± 0.36 | 99.6 ± 0.01 | 100 ± 0.5  | 100 ± 0.02  |

ACC, with it reaching 98.5%. Compared to related works, our method improves the ACC by 2.6–13.6%. In terms of SEN and SPE, our method also shows the best performance.

## Discussion

Diagnosis of COVID-19 utilizing 3D-CT images is a few-shot learning task. Specifically, there are more than millions of parameters in our 3D-CNN and <1,000 samples for training 3D-CNN. Although we propose a transfer learning method by predicting equipment type to initialize the 3D-CNN parameters, which improves the performance to some extent, there are still much noise existing in the extracted features as shown in **Figure 6**. It is also shown that there is much difference on the same features between different clusters. This difference shows that equipment type has a big effect on images and supports the good performance of our transfer learning method. In view of the big difference, we propose our COVID-19 graph, which divides all samples into several clusters and samples with the same equipment type composing a cluster, to suppress the existing noise in extracted features. The purpose of our COVID-19 graph is to improve the filtering effect, and the filtering principle is shown in **Figure 3**. With the application of our COVID-19 graph, **Figure 6** shows that the noise is well-suppressed, and this is the key for our performance improvement.

Our main contribution is analyzing the effect of equipment type on images. By analyzing its effect on the extracted features,

**TABLE 6 |** Algorithm comparison with the related works.

| References            | Data type | Method  | Database size              | ACC (%) | SEN (%) | SPE (%) |
|-----------------------|-----------|---|----------------------------|---------|---------|---------|
| Sun et al. (9)        | CT        | Transfer learning, CNN                        | 325 COVID-19, 740 others   | 89.5    | 87      | 88      |
| Abbas et al. (57)     | X-ray     | Decompose, transfer, compose, CNN             | 105 COVID-19, 80 NC        | 95.12   | 97.91   | 91.87   |
| Shi et al. (58)       | CT        | Infection size aware random forest            | 1,658 COVID-19, 1,027 CAP  | 87.9    | 90.7    | 83.3    |
| Sethy and Behera (59) | X-ray     | ResNet50, SVM                                 | 158 COVID-19, 158 others   | 95.38   | 97.29   | 93.47   |
|                       |           | DenseNet201, SVM                              |                            | 93.88   | 94.35   | 93.41   |
|                       |           | XceptionNet, SVM                              |                            | 93.91   | 94.76   | 93.06   |
| Narin et al. (60)     | X-ray     | Inception-ResNetV2                            | 50 COVID-19, 50 CAP        | 87      | 84      | 90      |
| Jin et al. (61)       | CT        | CNN   | 497 COVID-19, 1,385 others | 94.1    | 90.19   | 95.76   |
| Butt et al. (62)      | CT        | ResNet18, location attention                  | 219 COVID-19, 399 others   | 86.7    | 98.2    | 92.2    |
| Bai et al. (63)       | CT        | EfficientNet-B4, two-layer fully connected NN | 521 COVID-19, 655 others   | 96      | 95      | 96      |
| Ours                  | CT        | 3D-CNN, transfer learning, GCN                | 399 COVID-19, 400 NC       | 98.5    | 99.9    | 97      |

we proposed a transfer learning method and a GCN classifier for COVID-19 diagnosis. It is worth mentioning that there are still some limitations. Our GCN method is limited to a binary classification task, where the more important and difficult challenge is discriminating COVID-19 from other abnormal cases (e.g., pneumonia) and normal controls, and we will study this issue in our future work. Our work relatively adapts to a few-shot learning task as the advantage of GCN lies in its filtering effect.

## CONCLUSIONS

In this study, we proposed a novel method based on 3D-CNN and GCN for COVID-19 diagnosis. The proposed method considers three pieces of information: the equipment type, hospital information, and the disease status of the training samples. Comparing the diagnosis results of our method with the results of using 3D-CNN for diagnosis shows that using GCN with the three pieces of information can result in a 4.2% improvement on ACC. The comparison result validates that the three pieces of information are essential to CT images and effective for ACC improvement. The excellent performance of using the task of predicting equipment type to initialize the parameters of 3D-CNN also validates that the equipment type is a key information of CT images. The analysis of the extracted features from 3D-CNN in different clusters shows diversified noise levels across different

clusters. We can conclude that there exists disparate imaging quality with the use of different CT equipment. Finally, our method achieves excellent performance, with a diagnosis ACC reaching 98.5%.

## DATA AVAILABILITY STATEMENT

The dataset used in this study is from the open sources and can be downloaded from the following links: <https://github.com/ahmadhassan7/Covid-19-Datasets>, <https://www.medrxiv.org/>, <https://www.biorxiv.org/>, <https://www.kaggle.com/mohammadrahimzadeh/covidctset-a-large-covid19-ct-scans-dataset>, and <http://ncov-ai.big.ac.cn/download?lang=en>, [https://mosmed.ai/datasets/covid19\\_1110](https://mosmed.ai/datasets/covid19_1110).

## AUTHOR CONTRIBUTIONS

Conception, design, and statistical analysis were performed by XL and YZ. Drafting the manuscript and editing were performed by JW, QY, YL, and JT. All authors read and approved the final manuscript.

## FUNDING

This work was supported by the Jiangsu Biobank of Clinical Resources (BM2015004).

## REFERENCES

- Elgendi M, Fletcher RR, Howard N, Menon C, Ward R. The performance of deep neural networks in differentiating chest X-rays of COVID-19 patients from other bacterial and viral pneumonias. *Front Med.* (2020) 7:550. doi: 10.3389/fmed.2020.00550
- Yoo SH, Geng H, Chiu TL, Yu SK, Cho DC, Heo J, et al. Deep learning-based decision-tree classifier for COVID-19 diagnosis from chest X-ray imaging. *Front Med.* (2020) 7:427. doi: 10.3389/fmed.2020.00427
- Bernheim A, Mei X, Huang M, Yang Y, Fayad ZA, Zhang N, et al. Chest CT findings in coronavirus disease-19 (COVID-19): relationship to duration of infection. *Radiology.* (2020) 295:685–91. doi: 10.1148/radiol.2020200463
- Xie X, Zhong Z, Zhao W, Zheng C, Wang F, Liu J. Chest CT for typical 2019-nCoV pneumonia: relationship to negative RT-PCR testing. *Radiology.* (2020) 296:E41–5. doi: 10.1148/radiol.2020200343
- Fang Y, Zhang H, Xie J, Lin M, Ying L, Pang P, et al. Sensitivity of chest CT for COVID-19: Comparison to RT-PCR. *Radiology.* (2020) 296:E115–7. doi: 10.1148/radiol.2020200432
- Zu Z, Jiang M, Xu P, Chen W, Ni Q, Lu G, et al. Coronavirus disease 2019 (COVID-19): a perspective from China. *Radiology.* (2020) 296:E15–25. doi: 10.1148/radiol.2020200490
- Chung M, Bernheim A, Mei X, Zhang N, Huang M, Zeng X, et al. CT imaging features of 2019 novel coronavirus (2019-nCoV). *Radiology.* (2020) 295:202–7. doi: 10.1148/radiol.2020200230

8. Pan Y, Guan H. Imaging changes in patients with 2019-nCoV. *Eur Radiol.* (2020) 30:3612–3. doi: 10.1007/s00330-020-06713-z
9. Sun L, Mo Z, Yan F, Xia L, Shan F, Ding Z, et al. Adaptive feature selection guided deep forest for COVID-19 classification with chest CT. *arXiv.* (2020) 2005.03264. doi: 10.1109/JBHI.2020.3019505
10. Mahmud T, Rahman MA, Fattah SA. CovXNet: a multi-dilation convolutional neural network for automatic COVID-19 and other pneumonia detection from chest X-ray images with transferable multi-receptive feature optimization. *Comput Biol Med.* (2020) 122:103869. doi: 10.1016/j.combiomed.2020.103869
11. Wang S, Kang B, Ma J, Zeng X, Xiao M, Guo J, et al. A deep learning algorithm using CT images to screen for corona virus disease (COVID-19). *medRxiv.* (2020). doi: 10.1101/2020.02.14.20023028
12. Zheng C, Deng X, Fu Q, Zhou Q, Feng J, Ma H, et al. Deep learning-based detection for COVID-19 from chest CT using weak label. *medRxiv.* (2020). doi: 10.1101/2020.03.12.20027185
13. Hall L, Paul R, Goldgof DB, Goldgof GM. Finding covid-19 from chest x-rays using deep learning on a small dataset. *arXiv.* (2020) 2004.02060. doi: 10.36227/techrxiv.12083964.v4
14. Kumar R, Arora R, Bansal V, Sahayashela VJ, Buckchash H, Imran J, et al. Accurate prediction of COVID-19 using chest X-Ray images through deep feature learning model with SMOTE and machine learning classifiers. *medRxiv.* (2020). doi: 10.1101/2020.04.13.20063461
15. Kolozsvari LR, Berczes T, Hajdu A, Gesztelyi R, Tiba A, Varga I, et al. Predicting the epidemic curve of the coronavirus (SARS-CoV-2) disease (COVID-19) using artificial intelligence. *medRxiv.* (2020). doi: 10.1101/2020.04.17.20069666
16. Khalifa NEM, Taha MHN, Hassanien AE, Elghamrawy S. Detection of coronavirus (COVID-19) associated pneumonia based on generative adversarial networks and a fine-tuned deep transfer learning model using chest X-ray dataset. *arXiv.* (2020) 2004.01184.
17. Loey M, Smarandache F, Khalifa NEM. Within the lack of chest COVID-19 X-ray dataset: a novel detection model based on GAN and deep transfer learning. *Symmetry.* (2020) 12:651. doi: 10.3390/sym12040651
18. Chen L, Papandreou G, Kokkinos I, Murphy K, Yuille AL. Semantic image segmentation with deep convolutional nets and fully connected crfs. *arXiv.* (2014) 1412.7062.
19. Lin T, Goyal P, Girshick R, He K, Dollár P. Focal loss for dense object detection. *arXiv.* (2017) 1708.02002v2. doi: 10.1109/ICCV.2017.324
20. Ren S, He K, Girshick R, Sun J. Faster R-CNN: towards real-time object detection with region proposal networks. *arXiv.* (2016) 1506.01497v3.
21. Han K, Guo J, Zhang C, Zhu M. Attribute-aware attention model for fine-grained representation learning. In: *Proceedings of the 26th ACM International Conference on Multimedia*, Seoul (2018). p. 2040–8. doi: 10.1145/3240508.3240550
22. El-Sappagh S, Abuhmed T, Islam SR, Kwak KS. Multimodal multitask deep learning model for Alzheimer's disease progression detection based on time series data. *Neurocomputing.* (2020) 412:197–215. doi: 10.1016/j.neucom.2020.05.087
23. Tam CM, Zhang D, Chen B, Peters T, Li S. Holistic multitask regression network for multiapplication shape regression segmentation. *Med Image Anal.* (2020) 65:101783. doi: 10.1016/j.media.2020.101783
24. Weiss K, Khoshgoftaar TM, Wang D. A survey of transfer learning. *J Big Data.* (2016) 3:9. doi: 10.1186/s40537-016-0043-6
25. Wang Y, Liu Y, Chen W, Ma Z, Liu T. Target transfer Q-learning and its convergence analysis. *Neurocomputing.* (2020) 392:11–22. doi: 10.1016/j.neucom.2020.02.117
26. Lin J, Zhao L, Wang Q, Ward R, Wang Z. DT-LET: Deep transfer learning by exploring where to transfer. *Neurocomputing.* (2020) 390:99–107. doi: 10.1016/j.neucom.2020.01.042
27. Taherkhani A, Cosma G, McGinnity TM. AdaBoost-CNN: an adaptive boosting algorithm for convolutional neural networks to classify multi-class imbalanced datasets using transfer learning. *Neurocomputing.* (2020) 404:351–66. doi: 10.1016/j.neucom.2020.03.064
28. Scarselli F, Gori M, Tsoi AC, Hagenbuchner M, Monfardini G. The graph neural network model. *IEEE Trans Neural Netw.* (2009) 20:61–80. doi: 10.1109/TNN.2008.2005605
29. Bapat RB. *Graphs and Matrices*. New York, NY: Springer (2010).
30. Shuman DI, Narang SK, Frossard P, Ortega A, Vandergheynst P. The emerging field of signal processing on graphs: extending high-dimensional data analysis to networks and other irregular domains. *IEEE Signal Proc Mag.* (2013) 30:83–98. doi: 10.1109/MSP.2012.2235192
31. Zhao M, Chan RH, Chow TW, Tang P. Compact graph based semi-supervised learning for medical diagnosis in Alzheimer's disease. *IEEE Signal Proc Lett.* (2014) 21:1192–6. doi: 10.1109/LSP.2014.2329056
32. Defferrard M, Bresson X, Vandergheynst P. Convolutional neural networks on graphs with fast localized spectral filtering. *arXiv.* (2016) 1606.09375.
33. Duvenaud D, Maclaurin D, Aguilera-Iparraguirre J, Gomez-Bombarell R, Hirzel T, Aspuru-Guzik A, et al. Convolutional networks on graphs for learning molecular fingerprints. *arXiv.* (2015) 1509.09292v2.
34. Kipf TN, Welling M. Semi-supervised classification with graph convolutional networks. *arXiv.* (2016) 1609.02907.
35. Parisot S, Ktena SI, Ferrante E, Lee M, Guerrero R, Glocker B, et al. Disease prediction using graph convolutional networks: application to autism spectrum disorder and Alzheimer's disease. *Med Image Anal.* (2018) 48:117–30. doi: 10.1016/j.media.2018.06.001
36. Zhang Y, Zhan L, Cai W, Thompson P, Huang H. Integrating heterogeneous brain networks for predicting brain disease conditions. In: *International Conference on Medical Image Computing and Computer-Assisted Intervention*. Shenzhen (2019). p. 214–22. doi: 10.1007/978-3-030-32251-9\_24
37. Kazi A, Shekarfroush S, Krishna SA, Burwinkel H, Vivar G, Kortüm K, et al. InceptionGCN: Receptive field aware graph convolutional network for disease prediction. In: *International Conference on Information Processing in Medical Imaging*. Hong Kong (2019). p. 73–85. doi: 10.1007/978-3-030-20351-1\_6
38. Ktena SI, Parisot S, Ferrante E, Rajchl M, Lee M, Glocker B, et al. Metric learning with spectral graph convolutions on brain connectivity networks. *Neuroimage.* (2018) 169:431–42. doi: 10.1016/j.neuroimage.2017.12.052
39. Ji S, Xu W, Yang M, Yu K. 3D convolutional neural networks for human action recognition. *IEEE Trans Pattern Anal.* (2013) 35:221–31. doi: 10.1109/TPAMI.2012.59
40. Kumawat S, Raman S. LP-3DCNN: unveiling local phase in 3D convolutional neural networks. In: *Proceedings of the IEEE Conference on Computer Vision and Pattern Recognition*. Long Beach, CA (2019). p. 4903–12. doi: 10.1109/CVPR.2019.00504
41. Li Y, He K, Xu D, Luo D. A transfer learning method using speech data as the source domain for micro-Doppler classification tasks. *Knowl Based Syst.* (2020) 209:106449. doi: 10.1016/j.knsys.2020.106449
42. Yang X, Zhang Y, Lv W, Wang D. Image recognition of wind turbine blade damage based on a deep learning model with transfer learning and an ensemble learning classifier. *Renew Energy.* (2021) 163:386–97. doi: 10.1016/j.renene.2020.08.125
43. Guyon I, Weston J, Barnhill S, Vapnik V. Gene selection for cancer classification using support vector machines. *Mach Learn.* (2002) 46:389–422. doi: 10.1023/A:1012487302797
44. Song X, Elazab A, Zhang Y. Classification of mild cognitive impairment based on a combined high-order network and graph convolutional network. *IEEE Access.* (2020) 8:42816–27. doi: 10.1109/ACCESS.2020.2974997
45. Shao Z, Yang S, Gao F, Zhou K, Lin, P. A new electricity price prediction strategy using mutual information-based SVM-RFE classification. *Renew Sust Energy Rev.* (2017) 70:330–41. doi: 10.1016/j.rser.2016.11.155
46. Sahran S, Albashish D, Abdullah A, Abd Shukor N, Pauzi, SHM. Absolute cosine-based SVM-RFE feature selection method for prostate histopathological grading. *Artif Intell Med.* (2018) 87:78–90. doi: 10.1016/j.artmed.2018.04.002
47. Xu K, Li C, Tian Y, Sonobe T, Kawarabayashi KI, Jegelka S. Representation learning on graphs with jumping knowledge networks. *arXiv.* (2018) 1806.03536.
48. Liu Z, Chen C, Li L, Zhou J, Li X, Song L, et al. Geniepath: graph neural networks with adaptive receptive paths. In: *Proceedings of the AAAI Conference on Artificial Intelligence*. Honolulu, HI (2019). p. 4424–31. doi: 10.1609/aaai.v33i01.33014424
49. Defferrard M, Bresson X, Vandergheynst P. Convolutional neural networks on graphs with fast localized spectral filtering. *arXiv.* (2016) 1606.09375.

50. *Github*. Available online at: <https://github.com/ahmadhassan7/Covid-19-Datasets/tree/master/AHP-covid19-ctscans/Anonymized20200225> (accessed April 18, 2020).
51. *Medrxiv*. (2020). Available online at: <https://www.medrxiv.org/> (accessed September 20, 2020).
52. *Biorxiv*. (2020). Available online at: <https://www.biorxiv.org/> (accessed September 20, 2020).
53. *Kaggle*. Available online at: <https://www.kaggle.com/mohammadrahimzadeh/covidctset-a-large-covid19-ct-scans-dataset> (accessed August 27, 2020).
54. Huang SC, Kothari T, Banerjee I, Chute C, Ball RL, Borus N, et al. PENet-a scalable deep-learning model for automated diagnosis of pulmonary embolism using volumetric CT imaging. *NPJ Digit Med*. (2020) 3:1–9. doi: 10.1038/s41746-020-00310-6
55. Zhang K, Liu X, Shen J, Li Z, Sang Y, Wu X, et al. Clinically applicable AI system for accurate diagnosis, quantitative measurements and prognosis of covid-19 pneumonia using computed tomography. *Cell*. (2020) 181:1423–33. doi: 10.1016/j.cell.2020.04.045
56. Morozov SP, Andreychenko AE, Pavlov NA, Vladzmyrskyy AV, Ledikhova NV, Gomboleviskiy VA, et al. MosMedData: chest CT scans with COVID-19 related findings dataset. *arXiv*. (2020) 2005.06465. doi: 10.1101/2020.05.20.20100362
57. Abbas A, Abdelsamea MM, Gaber MM. Classification of COVID-19 in chest X-ray images using DeTraC deep convolutional neural network. *arXiv*. (2020) 2003.13815. doi: 10.1101/2020.03.30.20047456
58. Shi F, Xia L, Shan F, Wu D, Wei Y, Yuan H, et al. Large-scale screening of covid-19 from community acquired pneumonia using infection size-aware classification. *arXiv*. (2020) 2003.09860.
59. Sethy PK, Behera SK. Detection of coronavirus disease (COVID-19) based on deep features. *Preprints*. (2020) 2020030300. doi: 10.20944/preprints202003.0300.v1
60. Narin A, Kaya C, Pamuk Z. Automatic detection of coronavirus disease (COVID-19) using X-ray images and deep convolutional neural networks. *arXiv*. (2020) 2003.10849.
61. Jin C, Chen W, Cao Y, Xu Z, Zhang X, Deng L, et al. Development and evaluation of an AI system for COVID-19 diagnosis. *medRxiv*. (2020). doi: 10.1101/2020.03.20.20039834
62. Butt C, Gill J, Chun D, Babu BA. Deep learning system to screen coronavirus disease 2019 pneumonia. *Appl Intell*. (2020). doi: 10.1007/s10489-020-01714-3. [Epub ahead of print].
63. Bai HX, Wang R, Xiong Z, Hsieh B, Chang K, Halsey K, et al. AI augmentation of radiologist performance in distinguishing COVID-19 from pneumonia of other etiology on chest CT. *Radiology*. (2020) 296:201491. doi: 10.1148/radiol.2020201491

**Conflict of Interest:** The authors declare that the research was conducted in the absence of any commercial or financial relationships that could be construed as a potential conflict of interest.

Copyright © 2021 Liang, Zhang, Wang, Ye, Liu and Tong. This is an open-access article distributed under the terms of the Creative Commons Attribution License (CC BY). The use, distribution or reproduction in other forums is permitted, provided the original author(s) and the copyright owner(s) are credited and that the original publication in this journal is cited, in accordance with accepted academic practice. No use, distribution or reproduction is permitted which does not comply with these terms.



# Follow-Up Study of the Chest CT Characteristics of COVID-19 Survivors Seven Months After Recovery

Mengqi Liu<sup>1\*</sup>, Fajin Lv<sup>1</sup>, Yang Huang<sup>1</sup> and Kaihu Xiao<sup>2\*</sup>

<sup>1</sup> Department of Radiology, The First Affiliated Hospital of Chongqing Medical University, Chongqing, China, <sup>2</sup> Department of Cardiology, Chongqing University Three Gorges Hospital, Chongqing, China

## OPEN ACCESS

### Edited by:

Reza Lashgari,  
Institute for Research in Fundamental  
Sciences, Iran

### Reviewed by:

Eduardo Luis De Vito,  
University of Buenos Aires, Argentina  
Kamran Avanaki,  
University of Illinois at Chicago,  
United States

### \*Correspondence:

Mengqi Liu  
dany0714@163.com  
Kaihu Xiao  
xiaokh1@163.com

### Specialty section:

This article was submitted to  
Pulmonary Medicine,  
a section of the journal  
Frontiers in Medicine

**Received:** 01 December 2020

**Accepted:** 09 February 2021

**Published:** 01 March 2021

### Citation:

Liu M, Lv F, Huang Y and Xiao K  
(2021) Follow-Up Study of the Chest  
CT Characteristics of COVID-19  
Survivors Seven Months After  
Recovery. *Front. Med.* 8:636298.  
doi: 10.3389/fmed.2021.636298

**Background:** It has remained a concern whether any long-term pulmonary sequelae exist for COVID-19 survivors.

**Methods:** Forty-one patients (22 men and 19 women,  $50 \pm 14$  years) confirmed with COVID-19 performed follow-up chest CT and cardiopulmonary exercise testing at 7 months after discharge. Patients were divided into fibrosis group and non-fibrosis group according to the evidence of fibrosis on follow-up CT. The clinical data and the CT findings were recorded and analyzed.

**Results:** The predominant CT patterns of abnormalities observed at 7 months after discharge were parenchymal band (41%), interlobular septal thickening (32%), and traction bronchiectasis (29%). Sixty-one percent of the patients achieved complete radiological resolution, and 29% of patients developed pulmonary fibrosis. Compared with the patients in the non-fibrosis group, the patients in the fibrosis group were older, with a longer hospital stay, a higher rate of steroid and mechanical ventilation therapy, lower levels of lymphocyte and T cell count, higher levels of D-dimer and lactic dehydrogenase, and higher quantitative CT parameters (opacity score, volume of opacity, and percentage of opacity) at discharge. Besides, oxygen consumption and metabolic equations were decreased and ventilatory equivalent for carbon dioxide was increased in patients in the fibrosis group. Logistic regression analyses revealed that age, steroid therapy, presence of traction bronchiectasis on chest CT at discharge, and opacity score at discharge, were independent risk factors for developing pulmonary fibrosis at 7 months after discharge. Receiver operating characteristic analysis revealed that the combined clinical-radiological model was better than the clinical-only model in the prediction of pulmonary fibrosis.

**Conclusions:** The chest CT lesions could be absorbed without any sequelae for most patients with COVID-19, whereas older patients with severe conditions are more prone to develop fibrosis, which may further lead to cardiopulmonary insufficiency. The combined clinical-radiological model may predict the formation of pulmonary fibrosis early.

**Keywords:** coronavirus disease 2019, computed tomography, follow-up, pulmonary fibrosis, cardiopulmonary exercise testing



## INTRODUCTION

Since late December 2019, coronavirus disease 2019 (COVID-19) has emerged and promptly spread throughout the world. As of 1 February 2021, there have been over 102.3 million confirmed cases and 2.2 million deaths reported globally since the start of the pandemic (1). Thin-section chest CT scans have been making a significant contribution to the disease assessment. Currently, the radiological characteristics of COVID-19 have been extensively studied. The typical chest CT features of COVID-19 include ground glass opacities (GGO), consolidation, and interlobular septal thickening with peripheral distribution (2–4). To date, many patients have been recovered and discharged. It has remained a concern to the public whether any pulmonary sequelae exist for COVID-19 survivors. Wang and colleagues reported that clinical sequelae of patients on 3-month follow-up were common, including respiratory symptoms, cardiovascular-related symptoms, and psychosocial symptoms (5). Besides, recent studies have shown that pulmonary fibrosis may develop in patients with COVID-19 short term after discharge (6–8). However, the number of discharged COVID-19 patients keeps increasing worldwide but the definite long-term radiological outcomes of the patients after discharge are scarcely described in the literature. Herein, we present the results of the 7-month follow-up chest CT in patients discharged with COVID-19.

## METHODS

### Patients

This is a prospective observational study performed in patients discharged with COVID-19 from Chongqing University Three Gorges Hospital between February 10, 2020 and March 23, 2020. This study was approved by the local institutional review board. Written informed consents were obtained from all the patients enrolled in the study. The diagnostic and discharge criteria of COVID-19 pneumonia followed the latest guideline of Diagnosis and Treatment Program of COVID-19 released by the National Health Commission of the People's Republic of China (9). Clinical data of the patients were reviewed.

### Image Acquisition and Radiological Follow-Up

All the patients were imaged with a multi-detector CT scanner (uCT 510, United Imaging, China) using the following parameters: 120 kVp, 150 mA, 1.5 mm collimation, reconstruction matrix of  $512 \times 512$ , and slice thickness of 1.0 mm. All the patients were scanned in a supine position with a single inspiratory phase. The scanning range included the whole chest from the first ribs to the diaphragm. All the patients were examined without injection of contrast media. Images were obtained with mediastinal (width, 400 HU; level, 30 HU) and parenchymal (width, 1600 HU; level, -600 HU) window settings. We reviewed three chest CT scans for each patient: the CT examination at discharge, the CT examination at 3 months after discharge, and the CT examination at 7 months after discharge.

## Image Interpretation

Three thoracic radiologists (with 8, 12, and 25 years of experience, respectively) blinded to the clinical data reviewed the CT images independently, and the discrepancies were resolved by discussion and consensus. The CT images of each patient were assessed and compared for the presence of the following features: GGO, consolidation, crazy paving pattern, air bronchogram, nodules, interlobular septal thickening, irregular interfaces, reticular pattern, parenchymal bands, and traction bronchiectasis. All the above glossaries were defined according to the Fleischner Society (10). In addition, an artificial intelligence software (CT Pneumonia Analysis, Siemens Healthineers, Siemens, Erlangen, Germany) was employed to automatically identify and quantify hyperdense areas of the lung (**Figure 1**), and the following quantitative parameters were calculated for each CT scan: opacity score, volume of opacity, and percentage of opacity (the ratio of volume of opacity to lung volume). Each of the 5 lung lobes was scored automatically 0–4 as 0 ( $\leq 1\%$  involvement), 1 (2–25%), 2 (26–50%), 3 (51–75%), and 4 ( $> 75\%$ ). The total opacity score was the sum of the five lobar scores and ranged from 0 to 20. Patients were divided into two groups according to the evidence of fibrosis on the 7-month follow-up CT imaging: fibrosis group and non-fibrosis group. Fibrosis on chest CT was defined as a combination of findings including parenchymal bands, reticular pattern, and traction bronchiectasis (8, 11, 12). Clinical and radiological data between the two groups were subsequently compared.

## Cardiopulmonary Exercise Testing

Cardiopulmonary exercise testing was performed at the latest follow-up. Forced expiratory volume in 1 s (FEV1) and forced vital capacity (FVC) were measured using a turbine spirometer (Cosmed, Quark CPET, Rome, Italy). The incremental exercise was done on a treadmill (Cosmed, Quark CPET, Rome, Italy). Patients were encouraged to exercise until symptoms were intolerable. Peak oxygen uptake ( $\text{VO}_2$ ), minute ventilation (VE), and carbon dioxide production ( $\text{VCO}_2$ ) were measured using a Cosmed Face Mask (Quark CPET, Rome, Italy). The anaerobic

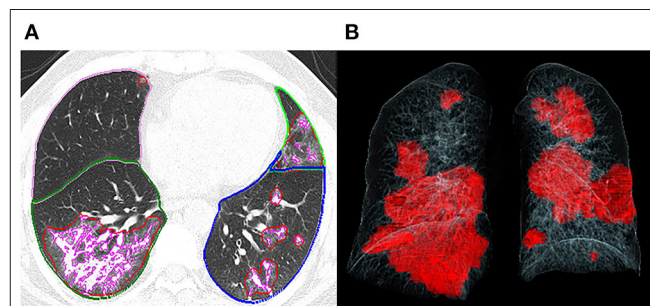


**FIGURE 1** | Representative postprocessing result of chest CT scan performed with Siemens CT Pneumonia Analysis. A 56-year-old male with COVID-19 (Opacity score = 5, volume of opacity = 671.6 ml, percentage of opacity = 15.1%). **(A)** Axis plane of chest CT shows bilateral ground glass opacities. **(B)** 3D-visualization of CT volume rendering technique shows the diffuse extent of opacities.



threshold (AT) was defined as the  $\text{VO}_2$  level where the  $\text{VE}/\text{VCO}_2$  decreased or remained constant while the ventilatory equivalent to oxygen ( $\text{VE}/\text{VO}_2$ ) persistently increased. Finally, the following parameters were recorded for each object: FEV1/FVC, Peak  $\text{VO}_2$  (mL/min/kg),  $\text{VO}_2$  at AT (mL/min/kg), peak metabolic equations (METs), and  $\text{VE}/\text{VCO}_2$  slope.

## Statistical Analysis

Statistical analyses were performed with the SPSS for Windows software package (version 17.0, SPSS Inc) and MedCalc statistical software (Med-Cale Software, Mariakerke, Belgium). The normality of the distribution was checked using a Kolmogorov-Smirnov test. Continuous variables were expressed as mean  $\pm$  standard deviation (SD) or median [interquartile range (IQR)] and compared with independent *t*-test or Mann-Whitney U test. Categorical variables were expressed as absolute and relative frequencies (%) and compared by the  $\chi^2$  test or Fisher's exact test between groups. Spearman's correlations were performed to evaluate the relationship between the three quantitative CT parameters (opacity score, volume of opacity, and percentage of opacity) and the laboratory results. Logistic regression analyses were performed to identify independent risk factors for developing pulmonary fibrosis at 7 months after discharge. Besides, receiver operating characteristic curves (ROCs) were constructed for the independent risk factors for predicting pulmonary fibrosis. Optimum cut-off point, sensitivity, specificity, and area under the curve (AUC) of each indicator were calculated. Then, comparisons of ROC curves between clinical characteristics alone and combined clinical-CT characteristics were performed using the non-parametric approach of DeLong et al. A *P*-value < 0.05 was considered statistically significant.

## RESULTS

### Clinical Characteristics of Patients

A total of 41 COVID-19 survivors (male: 22, female: 19) were enrolled in the present study, including 26 patients of moderate type and 15 patients of severe type (including 13 severe diseases and 2 critical diseases). Of these patients, 12 patients (29%, male: 7, female: 5) with evidence of fibrosis on the 7-month follow-up CT were designated as the fibrosis group, and the remaining 29 patients (71%, male: 15, female: 14) without evidence of fibrosis as the non-fibrosis group. The average age was 50 years old. The average days from symptom onset to admission were 6 days. The most prevalent initial symptoms were fever (66%) and cough (56%). Less common symptoms were sputum, dyspnea, headache, dyspnea, and muscle ache. Hypertension (7%) and chronic obstructive pulmonary disease (5%) were the most common concomitant diseases. Steroid hormone was given to 7 (17%) patients at a median of 5 days (IQR 4–10 days, prednisolone 40 mg b.i.d.), while 7 patients received mechanical ventilation at a median of 7 days (IQR 3–7 days). The patients were ventilated with continuous positive airway pressure (CPAP) via facemask at 10–12 cm  $\text{H}_2\text{O}$  at a fraction of inspired oxygen ( $\text{FIO}_2$ ) of 40–60%. The average hospital stay was 18 days. Subgroup analysis revealed that patients in the

fibrosis group were older ( $63 \pm 12$  years) than those in the non-fibrosis group ( $45 \pm 11$  years) ( $p < 0.001$ ). Besides, patients with severe type were more likely to develop pulmonary fibrosis at 7 months follow-up ( $p = 0.010$ ). There were no obvious differences in the clinical symptoms and the proportion of patients with comorbidities between the two groups. However, compared with the non-fibrosis group, the fibrosis group had lower levels of lymphocyte count ( $p = 0.019$ ) and T cell count ( $p = 0.022$ ) at discharge, and had higher levels of D-dimer ( $p < 0.001$ ) and lactic dehydrogenase (LDH,  $p = 0.037$ ). In addition, more patients in the fibrosis group were mechanically ventilated ( $p < 0.001$ ), and more patients were treated with steroids ( $p < 0.001$ ). The details are summarized in **Table 1**.

### Chest CT Evaluation

We reviewed three CT scans for each patient. The average interval between discharge and latest follow-up was 219 days, and the average intervals of the two subgroups did not differ statistically ( $p = 0.066$ ). The dynamic changes of chest CT features were listed in **Table 2**. As shown in **Table 2**, the predominant chest CT features observed at discharge included parenchymal band (73%), GGO (71%), interlobular septal thickening (68%), consolidation (46%), and irregular interface (46%). The less common CT features included reticular pattern (39%) and traction bronchiectasis (29%). The rare CT features were air bronchogram (7%) and crazy paving pattern (5%). Quantitative CT parameters calculated by the artificial intelligence software revealed that the median opacity score was 4.0 (IQR 2.0–5.0), the median volume of opacity was 178.0 ml (IQR 41.4–422.0 ml), and the median percentage of opacity was 4.3% (IQR 1.0%–12.4%). After discharge, all the quantitative CT parameters gradually decreased with time. The median opacity score, volume of opacity, and percentage of opacity on the latest follow-up CT (7 months after discharge) were decreased to 0.0 (IQR 0.0–1.0), 0.9 (IQR 0.0–12.8) ml, and 0.0% (IQR 0.0–0.3%), respectively. Twenty-five patients (61%) achieved complete radiological resolution on the 7-month follow-up CT. GGO (12%) and consolidation (10%) were almost resolved on the 7-month follow-up CT, while evidence of fibrosis, such as parenchymal band (41%), interlobular septal thickening (32%), reticular pattern (12%), and traction bronchiectasis (29%), were still obvious (**Figures 2, 3**).

The imaging features on chest CT at discharge were further compared between the fibrosis group and the non-fibrosis group (**Table 2**). Compared with the non-fibrosis group, the fibrosis group had higher levels of opacity score ( $p = 0.002$ ), volume of opacity ( $p = 0.009$ ), and percentage of opacity ( $p = 0.007$ ). Moreover, more patients in the fibrosis group manifested interlobular septal thickening ( $p = 0.005$ ), irregular interface ( $p = 0.018$ ), reticular pattern ( $p < 0.001$ ), parenchymal band ( $p = 0.013$ ), and traction bronchiectasis ( $p < 0.001$ ).

### Correlations of CT Quantitative Parameters With Laboratory Tests

Spearman's correlations were performed to explore the relationship between the three quantitative CT parameters and the laboratory results at discharge. As shown in **Table 3**, all

**TABLE 1 |** Clinical and laboratory characteristics of the patients included in the present study.

| Characteristics   | Total (N = 41)      | Fibrosis group (N = 12) | Non-fibrosis group (N = 29) | P-value          |
|---|---------------------|-------------------------|-----------------------------|------------------|
| <b>Sex</b>  |                     |                         |                             |                  |
| Male  | 22 (54%)            | 7 (58%)                 | 15 (52%)                    | 0.259            |
| Female  | 19 (46%)            | 5 (42%)                 | 14 (48%)                    |                  |
| Age (years)   | 50 ± 14             | 63 ± 12                 | 45 ± 11                     | <b>&lt;0.001</b> |
| <b>Severity</b>   |                     |                         |                             |                  |
| Moderate  | 26 (63%)            | 4 (33%)                 | 22 (76%)                    | <b>0.010</b>     |
| Severe  | 15 (37%)            | 8 (67%)                 | 7 (24%)                     | <b>0.010</b>     |
| <b>Comorbidity</b>  |                     |                         |                             |                  |
| Diabetes  | 1 (2%)              | 1 (8%)                  | 0 (0%)                      | 0.116            |
| Hypertension  | 3 (7%)              | 2 (17%)                 | 1 (3%)                      | 0.139            |
| Chronic obstructive pulmonary disease                             | 2 (5%)              | 1 (8%)                  | 1 (3%)                      | 0.509            |
| Cardiovascular disease  | 1 (2%)              | 1 (8%)                  | 0 (0%)                      | 0.116            |
| Hepatic disease   | 1 (2%)              | 0 (0%)                  | 1 (3%)                      | 0.505            |
| ≥1 comorbidity  | 7 (17%)             | 4 (33%)                 | 3 (7%)                      | 0.075            |
| <b>Symptoms</b>   |                     |                         |                             |                  |
| Fever   | 27 (66%)            | 8 (67%)                 | 19 (66%)                    | 0.944            |
| Cough   | 23 (56%)            | 6 (50%)                 | 17 (59%)                    | 0.613            |
| Sputum  | 9 (22%)             | 2 (17%)                 | 7 (24%)                     | 0.599            |
| Fatigue   | 10 (24%)            | 5 (42%)                 | 5 (17%)                     | 0.127            |
| Dyspnea   | 5 (12%)             | 3 (25%)                 | 2 (7%)                      | 0.107            |
| Headache  | 10 (24%)            | 3 (25%)                 | 7 (24%)                     | 0.953            |
| Muscle ache   | 12 (29%)            | 3 (25%)                 | 9 (31%)                     | 0.699            |
| <b>Lab test at discharge</b>                                      |                     |                         |                             |                  |
| White blood cell count ( $3.5\text{--}9.5 \times 10^9/\text{L}$ ) | 5.59 ± 1.95         | 5.58 ± 2.26             | 5.59 ± 1.85                 | 0.988            |
| Lymphocyte count ( $1.1\text{--}3.2 \times 10^9/\text{L}$ )       | 1.22 ± 0.49         | 0.97 ± 0.43             | 1.32 ± 0.48                 | <b>0.019</b>     |
| T cell count ( $699\text{--}2,540 \times 10^6/\text{L}$ )         | 784.57 ± 248.75     | 635.00 ± 190.61         | 844.40 ± 246.95             | <b>0.022</b>     |
| B cell count ( $90\text{--}660 \times 10^6/\text{L}$ )            | 112.74 ± 60.14      | 89.60 ± 43.34           | 122.00 ± 64.09              | 0.153            |
| NK cell count ( $90\text{--}590 \times 10^6/\text{L}$ )           | 135.09 ± 116.39     | 91.51 ± 57.53           | 152.52 ± 129.77             | 0.164            |
| D-dimer (0–0.55mg/L)  | 0.41 (0.22–0.89)    | 1.02 (0.42–2.96)        | 0.31 (0.20–0.72)            | <b>&lt;0.001</b> |
| Lactic dehydrogenase (120–250 IU/L)                               | 192.96 ± 56.42      | 220.25 ± 80.41          | 182.46 ± 41.42              | <b>0.037</b>     |
| C-reactive protein (0–11 mg/L)                                    | 3.21 (1.83–8.79)    | 3.91 (2.28–13.68)       | 3.08 (1.45–7.68)            | 0.523            |
| Procalciton (<0.046 ng/mL)  | 0.031 (0.025–0.050) | 0.030 (0.020–0.069)     | 0.032 (0.025–0.043)         | 0.883            |
| Interleukin-6 (0–7 pg/mL)   | 4.97 (0.00–22.26)   | 13.81 (0.00–46.45)      | 3.13 (0.00–9.79)            | 0.383            |
| <b>Treatment</b>  |                     |                         |                             |                  |
| Steroid   | 7 (17%)             | 6 (50%)                 | 1 (3%)                      | <b>&lt;0.001</b> |
| Mechanical ventilation  | 7 (17%)             | 4 (33%)                 | 3 (7%)                      | <b>&lt;0.001</b> |
| Days from onset to admission                                      | 6 ± 4               | 6 ± 3                   | 6 ± 4                       | 0.947            |
| Days from discharge to last follow-up                             | 219 ± 11            | 213 ± 11                | 220 ± 10                    | 0.066            |
| Hospital stay (day)   | 18 ± 7              | 23 ± 8                  | 17 ± 6                      | <b>0.008</b>     |

Data are expressed as mean ± standard deviation, median (interquartile range), and n (%). Bold values indicate  $p < 0.05$ .

three quantitative CT parameters were positively correlated with white blood cell count, C-reactive protein, D-dimer, and LDH.

## Logistic Regression and ROC Curve Analysis

Logistic regression analyses revealed that age (odds ratio = 1.078,  $p = 0.049$ ), steroid therapy (odds ratio = 12.880,  $p = 0.010$ ), opacity score at discharge (odds ratio = 1.565,  $p = 0.034$ ), and presence of traction bronchiectasis at discharge (odds ratio = 13.570,  $p = 0.012$ ), were independent risk factors for

developing pulmonary fibrosis at 7 months after discharge, while other clinical or CT indicators (sex, disease severity, lymphocyte count, T cell count, D-dimer, LDH, hospital stay, volume of opacity, percentage of opacity, parenchymal band, reticular pattern, ventilation therapy, days of ventilation) were not independent risk factors associated with fibrosis. For the prediction of pulmonary fibrosis at 7 months after discharge, ROC analysis yielded AUC values of 0.770, 0.782, 0.848, and 0.871 for age (cutoff point: >48 years), steroid therapy, traction bronchiectasis at discharge, and opacity score at discharge (cutoff

**TABLE 2** | Chest CT findings in the patients with COVID-19.

|                                | At discharge          |                            |                                   | P-value          | 3 months after discharge |                               |                                   | 7 months after discharge |                               |                                   |
|--------------------------------|-----------------------|----------------------------|-----------------------------------|------------------|--------------------------|-------------------------------|-----------------------------------|--------------------------|-------------------------------|-----------------------------------|
|                                | Total<br>(N = 41)     | Fibrosis group<br>(N = 12) | Non-fibrosis<br>group<br>(N = 29) |                  | Total<br>(N = 41)        | Fibrosis<br>group<br>(N = 12) | Non-fibrosis<br>group<br>(N = 29) | Total<br>(N = 41)        | Fibrosis<br>group<br>(N = 12) | Non-fibrosis<br>group<br>(N = 29) |
| Opacity score                  | 4.0 (2.0–5.0)         | 6.7 (5.0–9.0)              | 2.9 (1.0–4.8)                     | <b>0.002</b>     | 0.0 (0.0–2.0)            | 2.0 (0.0–3.0)                 | 0.4 (0.0–0.8)                     | 0.0 (0.0–1.0)            | 1.7 (0.5–3.0)                 | 0.2 (0.0–0.3)                     |
| Volume of opacity (ml)         | 178.0<br>(41.4–422.0) | 602.0<br>(156.0–1080.0)    | 183.0<br>(6.0–249.0)              | <b>0.009</b>     | 1.4 (0.0–19.0)           | 51.0<br>(1.0–67.0)            | 20.0<br>(0.0–33.0)                | 0.9 (0.0–12.8)           | 33.0<br>(3.0–41.0)            | 5.0 (0.0–18.0)                    |
| Percentage of opacity          | 4.3 (1.0–12.4)        | 19.4 (3.5–32.5)            | 5.3 (0.1–8.8)                     | <b>0.007</b>     | 0.0 (0.0–0.5)            | 1.7 (0.0–1.9)                 | 0.7 (0.0–0.8)                     | 0.0 (0.0–0.3)            | 1.1 (0.0–1.6)                 | 0.2 (0–1.0)                       |
| GGO                            | 29 (71%)              | 11 (92%)                   | 18 (62%)                          | 0.058            | 11 (27%)                 | 7 (58%)                       | 4 (14%)                           | 5 (12%)                  | 4 (33%)                       | 1 (3%)                            |
| Consolidation                  | 19 (46%)              | 8 (67%)                    | 11 (38%)                          | 0.093            | 6 (15%)                  | 4 (33%)                       | 2 (7%)                            | 4 (10%)                  | 3 (25%)                       | 1 (3%)                            |
| Crazy paving pattern           | 2 (5%)                | 1 (8%)                     | 1 (3%)                            | 0.509            | 0 (0%)                   | 0 (0%)                        | 0 (0%)                            | 0 (0%)                   | 0 (0%)                        | 0 (0%)                            |
| Air bronchogram                | 3 (7%)                | 2 (17%)                    | 1 (3%)                            | 0.139            | 0 (0%)                   | 0 (0%)                        | 0 (0%)                            | 0 (0%)                   | 0 (0%)                        | 0 (0%)                            |
| Interlobular septal thickening | 28 (68%)              | 12 (100%)                  | 16 (55%)                          | <b>0.005</b>     | 17 (41%)                 | 12 (100%)                     | 5 (17%)                           | 13 (32%)                 | 12 (100%)                     | 1 (3%)                            |
| Irregular interface            | 19 (46%)              | 9 (75%)                    | 10 (34%)                          | <b>0.018</b>     | 6 (15%)                  | 6 (50%)                       | 0 (0%)                            | 5 (12%)                  | 5 (42%)                       | 0 (0%)                            |
| Reticular pattern              | 16 (39%)              | 12 (100%)                  | 4 (14%)                           | <b>&lt;0.001</b> | 10 (24%)                 | 10 (83%)                      | 0 (0%)                            | 5 (12%)                  | 5 (42%)                       | 0 (0%)                            |
| Parenchymal band               | 30 (73%)              | 12 (100%)                  | 18 (62%)                          | <b>0.013</b>     | 22 (54%)                 | 12 (100%)                     | 10 (34%)                          | 17 (41%)                 | 12 (100%)                     | 5 (17%)                           |
| Traction bronchiectasis        | 12 (29%)              | 10 (83%)                   | 2 (7%)                            | <b>&lt;0.001</b> | 14 (34%)                 | 12 (100%)                     | 2 (7%)                            | 12 (29%)                 | 12 (100%)                     | 0 (0%)                            |

Data are median (interquartile range) or n (%). Bold values indicate  $p < 0.05$ .

point:  $>4$ ), respectively (**Table 4**). When combined the above clinical and CT indicators, the AUC value of the combined model was increased to 0.945 (**Figure 4**), which was significantly different from that of age ( $p = 0.031$ ), but not significantly different from that of opacity score ( $p = 0.109$ ).

## Cardiopulmonary Exercise Testing

There was no significant difference in FEV1/FVC and  $VO_2$  AT between the fibrosis group and the non-fibrosis group. However, compare with the non-fibrosis group, the fibrosis group had decreased  $VO_2/kg$  and METs and increased  $VE/VCO_2$ . The details are summarized in **Table 5**.

## DISCUSSION

After severe acute respiratory syndrome (SARS) outbreak in 2003, plenty of patients recovered. However, radiological abnormalities were detected in more than 70% of patients who recovered from SARS at 4–6 months after admission to the hospital (13, 14), and long-term pulmonary sequelae were also reported in previous studies (15, 16). So this may raise an important question for doctors: are there any long-term pulmonary sequelae in patients recovering from COVID-19? Up to now, few reports have described the sequelae of COVID-19 survivors (5–7, 17–20), and the long-term radiological changes have not been well-studied. In our study, we presented the results of 7-month follow-up chest CT in patients with COVID-19, and we compared clinical data and chest CT between patients with or without pulmonary fibrosis.

Clinically, patients in the fibrosis group were older than those in the non-fibrosis group, similar to SARS (11), which was in line with a previous study (8). Besides, the fibrosis group had a longer time of hospital stay. Moreover, more patients in the fibrosis group were severe type and treated with steroids and ventilator, and the fibrosis group had lower levels of lymphocyte count and T cell count and higher levels of D-dimer and LDH at discharge, which indicated that the patients with fibrosis may have more severe conditions with COVID-19. Furthermore, we found all the three quantitative CT parameters were positively correlated with white blood cell count, C-reactive protein, D-dimer, and LDH, which demonstrated that these quantitative CT parameters were reliable indicators of disease severity.

In our study, the chest CT abnormalities were still apparent at discharge. However, the pulmonary lesions had been gradually absorbed after discharge. Compared with the abnormalities found on the CT scans at discharge, the cases with GGO, consolidation, and air bronchogram were reduced from 71, 46, and 7%, to 12, 10, and 0% of cases on the 7-month follow up CT, respectively. Correspondingly, the median opacity score, volume of opacity, and percentage of opacity, were reduced from 4.0, 178 ml, and 4.3%, to 0.0, 0.9 ml, and 0.0%, respectively. Up to 66% of patients (86% of patients in the non-fibrosis group) achieved complete radiological resolution. Similarly, it was reported that the pulmonary lesions of 53.0% of COVID-19 patients would be fully absorbed at 3 weeks after discharge (18). Our results demonstrated that pulmonary lesions in the majority of COVID-19 patients could be reversible without any sequelae.



**FIGURE 2 |** Follow-up chest CT images of a 52-year-old male with COVID-19. **(A)** At discharge, CT imaging shows parenchymal bands, irregular interfaces, and traction bronchiectasis in left upper lobe and right lower lobe. The lesions are almost resolved on the 3-month follow-up **(B)** and 7-month follow-up **(C)** CT. This patient was enrolled in non-fibrosis group.

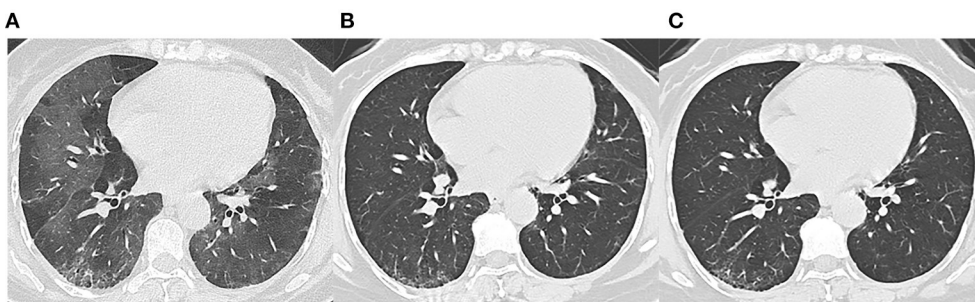


**FIGURE 3 |** Follow-up chest CT images of a 48-year-old female with COVID-19. **(A)** At discharge, CT imaging shows crazy paving pattern, parenchymal bands, irregular interfaces, and reticular pattern in bilateral lungs. **(B)** 3-month follow-up CT shows parenchymal bands, irregular interface, and traction bronchiectasis in the right lower lobe, which indicates fibrosis. **(C)** The lesions on 7-month follow-up CT are still present. This patient was enrolled in fibrosis group.

**TABLE 3 |** Correlations of CT quantitative parameters with laboratory tests.

|                       |                                  | WBC   | CRP   | PCT    | DD    | LDH   | Lymphocyte | T cell |
|-----------------------|----------------------------------|-------|-------|--------|-------|-------|------------|--------|
| Opacity score         | Correlation coefficient <i>r</i> | 0.401 | 0.337 | −0.195 | 0.343 | 0.720 | −0.214     | −0.254 |
|                       | <i>p</i> -value                  | 0.014 | 0.042 | 0.248  | 0.035 | 0.000 | 0.197      | 0.124  |
| Volume of opacity     | Correlation coefficient <i>r</i> | 0.401 | 0.397 | −0.184 | 0.344 | 0.604 | −0.079     | −0.114 |
|                       | <i>p</i> -value                  | 0.014 | 0.015 | 0.276  | 0.035 | 0.000 | 0.636      | 0.495  |
| Percentage of opacity | Correlation coefficient <i>r</i> | 0.464 | 0.409 | −0.104 | 0.348 | 0.722 | −0.181     | −0.218 |
|                       | <i>p</i> -value                  | 0.004 | 0.012 | 0.540  | 0.032 | 0.000 | 0.276      | 0.188  |

WBC: white blood cell; CRP: C-reactive protein; PCT: procalcitonin; DD: D-dimer; LDH: lactic dehydrogenase.

**TABLE 4 |** ROC analysis results for independent variables for predicting pulmonary fibrosis at 7 months after discharge.

| Variable                   | AUC (upper and lower limit) | SE     | Se    | Sp    | Optimal cut point |
|----------------------------|-----------------------------|--------|-------|-------|-------------------|
| Age                        | 0.770 (0.612–0.887)         | 0.0828 | 91.67 | 55.17 | >48               |
| Steroid therapy            | 0.782 (0.625–0.895)         | 0.0767 | 66.67 | 89.66 |                   |
| Traction bronchiectasis    | 0.848 (0.701–0.941)         | 0.0649 | 83.33 | 86.21 |                   |
| Opacity score at discharge | 0.871 (0.729–0.955)         | 0.0549 | 91.67 | 65.52 | >4                |
| Combined clinical and CT   | 0.945 (0.826–0.992)         | 0.0329 | 91.67 | 82.76 |                   |

AUC: area under curve; SE: Standard error; Se: sensitivity; Sp: specificity.

However, the CT manifestations of pulmonary fibrosis (interlobular septal thickening, irregular interface, parenchymal band, and traction bronchiectasis) were still apparent on the 7-month follow-up CT. As reported, pulmonary fibrosis may

develop in the early stage in discharged patients with SARS (11), and the fibrosis may be long-persistent (15), whereas the pulmonary fibrosis in discharged COVID-19 patients may be absorbed with time (6), which was consistent with our study



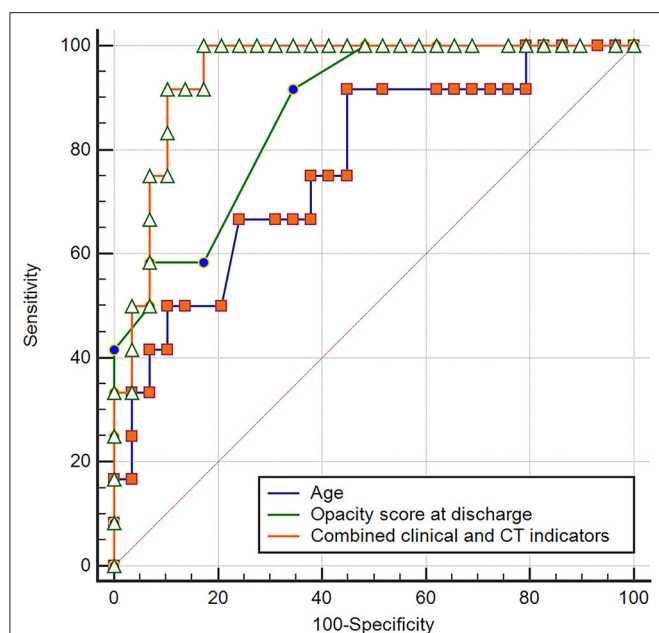


**FIGURE 4 |** Receiver operating curve for pulmonary fibrosis prediction in patients with COVID-19 using age or opacity score at discharge alone and combined clinical-CT indicators.

**TABLE 5 |** Results of cardiopulmonary exercise testing on patients with COVID-19.

|                     | Fibrosis group | Non-fibrosis group | P-value |
|---------------------|----------------|--------------------|---------|
| FEV1/FVC            | 98.0 ± 6.8     | 99.0 ± 8.1         | 0.741   |
| VO <sub>2</sub> /Kg | 16.4 ± 3.6     | 20.2 ± 3.7         | 0.009   |
| VO <sub>2</sub> AT  | 14.6 ± 3.7     | 16.0 ± 3.5         | 0.317   |
| METs                | 4.7 ± 1.0      | 5.8 ± 1.0          | 0.010   |
| VE/VCO <sub>2</sub> | 30.6 ± 4.0     | 26.3 ± 3.2         | 0.003   |

Data are presented as mean ± standard deviation.

FEV1, forced expiratory volume in 1 second; FVC, forced vital capacity; VO<sub>2</sub>, oxygen consumption; AT, anaerobic threshold; METs, metabolic equivalents; VE/VCO<sub>2</sub>, ventilatory equivalent for carbon dioxide.

(Figure 2). The reversibility of fibrosis probably indicated that the pulmonary fibrosis on chest CT did not signify actual pathologic fibrosis (14), and thus whether these lesions would completely disappear required further observation.

In our cohort, logistic regression analyses revealed that age, steroid therapy, presence of traction bronchiectasis, and opacity score at discharge, were independent risk factors for developing pulmonary fibrosis on 7-month follow-up CT. We could speculate that the above four indicators might be early predictors of pulmonary fibrosis in patients recovered from COVID-19. Further ROC analysis revealed that the combined clinical-radiological model was better than the clinical-only model in the prediction of pulmonary fibrosis. Our result should be validated by further large-scale studies.

Zhao and colleagues reported that lung function abnormalities were detected in 25% of COVID-19 patients at 3 months

after discharge (21). Cardiopulmonary exercise testing provides integrated data about cardiovascular, ventilatory and gas exchange, metabolic, and skeletal muscle response to the physical effort (22). So cardiopulmonary exercise testing can provide more physiological information than lung function tests. We found VO<sub>2</sub>/kg and METs were decreased and VE/VCO<sub>2</sub> was increased in patients in the fibrosis group, which may imply cardiopulmonary insufficiency resulting from fibrosis.

Our study had several limitations. Firstly, the sample size was quite small. However, our further studies will consider increasing the sample size of discharged patients on the 1-year follow-up. Secondly, pulmonary fibrosis had not been confirmed by pathology even though the CT manifestations were typical. We will continue to follow up these patients to confirm whether the radiological fibrosis could be further absorbed. Finally, we included very few patients with critically severe type, which may underestimate the incidence rate of pulmonary fibrosis. We will try to enroll more patients with severe type in future studies.

In conclusion, the most common imaging patterns of COVID-19 pneumonia at 7 months after discharge are interlobular septal thickening, parenchymal band, traction bronchiectasis, and reticular pattern. The chest CT lesions could be absorbed without any sequelae for most patients with COVID-19, whereas older patients with severe conditions are more prone to develop fibrosis, which may further lead to cardiopulmonary insufficiency. The quantitative CT parameters (opacity score, volume of opacity, and percentage of opacity) are reliable indicators of disease severity. Age >48 years old, steroid therapy, presence of traction bronchiectasis on chest CT at discharge, and opacity score at discharge >4, are the independent risk factors associated with fibrosis. The combined clinical-radiological model may be better than the clinical-only model in the prediction of developing pulmonary fibrosis on the 7-month follow-up.

## DATA AVAILABILITY STATEMENT

The raw data supporting the conclusions of this article will be made available by the authors, without undue reservation.

## ETHICS STATEMENT

The studies involving human participants were reviewed and approved by The First Affiliated Hospital of Chongqing Medical University. The patients/participants provided their written informed consent to participate in this study.

## AUTHOR CONTRIBUTIONS

ML and KX: conception and design. YH and KX: collection and assembly of data. ML, YH, and FL: analysis and interpretation of the data. ML: statistical expertise. ML and FL: drafting of the manuscript. ML and KX: critical revision of the article for important intellectual content. All authors had full access to all of



the data in the study and take responsibility for the integrity of the data and the accuracy of the data analysis.

## FUNDING

This work was supported by the Joint Project of Chongqing Science and Technology Commission and Chongqing Public Health Commission (2021MSMX062), the Emergency Research

Project of Chongqing Medical University (CQMUNCP0201), and the Wanzhou District COVID-19 Emergency Technology Research Project (wzstc-2020025).

## ACKNOWLEDGMENTS

ML wants to thank his wife, Jia Li, for her understanding, support, and infinite love.

## REFERENCES

- Coronavirus disease 2019 (COVID-19) situation report (<https://www.who.int/emergencies/diseases/novel-coronavirus-2019/situation-reports>).
- Wu J, Wu X, Zeng W, Guo D, Fang Z, Chen L, et al. Chest CT findings in patients with coronavirus disease 2019 and its relationship with clinical features. *Invest. Radiol.* (2020) 55:257–61. doi: 10.1097/RLI.0000000000000670
- Liu M, Zeng W, Wen Y, Zheng Y, Lv F, Xiao K. COVID-19 pneumonia: CT findings of 122 patients and differentiation from influenza pneumonia. *Eur. Radiol.* (2020) 30:5463–9. doi: 10.1007/s00330-020-06928-0
- Zu ZY, Jiang MD, Xu PP, Chen W, Ni QQ, Lu GM, et al. Coronavirus disease 2019 (COVID-19): a perspective from China. *Radiology.* (2020) 296:E15–E25. doi: 10.1148/radiol.2020200490
- Xiong Q, Xu M, Li J, Liu Y, Zhang J, Xu Y, et al. Clinical sequelae of COVID-19 survivors in Wuhan, China: a single-centre longitudinal study. *Clin. Microbiol. Infect.* (2020) 27:85–95. doi: 10.1016/j.cmi.2020.09.023
- Fang Y, Zhou J, Ding X, Ling G, Yu S. Pulmonary fibrosis in critical ill patients recovered from COVID-19 pneumonia: preliminary experience. *Am. J. Emerg. Med.* (2020) 38:2134–8. doi: 10.1016/j.ajem.2020.05.120
- Wei J, Yang H, Lei P, Fan B, Qiu Y, Zeng B, et al. Analysis of thin-section CT in patients with coronavirus disease (COVID-19) after hospital discharge. *J. Xray Sci. Technol.* (2020) 28:383–9. doi: 10.3233/XST-200685
- Yu M, Liu Y, Xu D, Zhang R, Lan L, Xu H. Prediction of the development of pulmonary fibrosis using serial thin-section CT and clinical features in patients discharged after treatment for COVID-19 pneumonia. *Korean J. Radiol.* (2020) 21:746–55. doi: 10.3348/kjr.2020.0215
- National Health Commission of the People's Republic of China. *Diagnosis and Treatment Protocols of Pneumonia Caused by a Novel Coronavirus (Trial Version 7)*. (2020). Available online at: <http://www.nhc.gov.cn/xcs/zhengcwj/202008/0a7bdf12bd4b46e5bd28ca7f9a7f5e5a/files/a449a3e2c94d9a856d5fae2ff0f94.pdf>
- Hansell DM, Bankier AA, MacMahon H, McLoud TC, Muller NL, Remy J. Fleischner society: glossary of terms for thoracic imaging. *Radiology.* (2008) 246:697–722. doi: 10.1148/radiol.2462070712
- Antonio GE, Wong KT, Hui DS, Wu A, Lee N, Yuen EH, et al. Thin-section CT in patients with severe acute respiratory syndrome following hospital discharge: preliminary experience. *Radiology.* (2003) 228:810–5. doi: 10.1148/radiol.2283030726
- Raghu G, Remy-Jardin M, Myers JL, Richeldi L, Ryerson CJ, Lederer DJ, et al. Diagnosis of idiopathic pulmonary fibrosis. an official ATS/ERS/JRS/ALAT clinical practice guideline. *Am. J. Respir. Crit. Care Med.* (2018) 198:e44–e68. doi: 10.1164/rccm.201807-1255ST
- Ng CK, Chan JW, Kwan TL, To TS, Chan YH, Ng FY, et al. Six month radiological and physiological outcomes in severe acute respiratory syndrome (SARS) survivors. *Thorax.* (2004) 59:889–91. doi: 10.1136/thx.2004.023762
- Chang YC, Yu CJ, Chang SC, Galvin JR, Liu HM, Hsiao CH, et al. Pulmonary sequelae in convalescent patients after severe acute respiratory syndrome: evaluation with thin-section CT. *Radiology.* (2005) 236:1067–75. doi: 10.1148/radiol.2363040958
- Zhang P, Li J, Liu H, Han N, Ju J, Kou Y, et al. Long-term bone and lung consequences associated with hospital-acquired severe acute respiratory syndrome: a 15-year follow-up from a prospective cohort study. *Bone Res.* (2020) 8:8. doi: 10.1038/s41413-020-0084-5
- Ngai JC, Ko FW, Ng SS, To KW, Tong M, Hui DS. The long-term impact of severe acute respiratory syndrome on pulmonary function, exercise capacity and health status. *Respirology.* (2010) 15:543–50. doi: 10.1111/j.1440-1843.2010.01720.x
- Denina M, Pruccoli G, Scolaro C, Mignone F, Zoppo M, Giraudo I, et al. Sequelae of COVID-19 in Hospitalized Children: a 4-months follow-up. *Pediatr. Infect. Dis. J.* (2020) 39:e458–9. doi: 10.1097/INF.0000000000002937
- Liu D, Zhang W, Pan F, Li L, Yang L, Zheng D, et al. The pulmonary sequelae in discharged patients with COVID-19: a short-term observational study. *Respir. Res.* (2020) 21:125. doi: 10.1186/s12931-020-01385-1
- Wang X, Xu H, Jiang H, Wang L, Lu C, Wei X, et al. Clinical features and outcomes of discharged coronavirus disease 2019 patients: a prospective cohort study. *Qjm.* (2020) 113:657–65. doi: 10.1093/qjmed/hcaa178
- Rogliani P, Calzetta L, Coppola A, Puxeddu E, Sergiacomi G, D'Amato D, et al. Are there pulmonary sequelae in patients recovering from COVID-19? *Respir. Res.* (2020) 21:286. doi: 10.1186/s12931-020-01550-6
- Zhao YM, Shang YM, Song WB, Li QQ, Xie H, Xu QF, et al. Follow-up study of the pulmonary function and related physiological characteristics of COVID-19 survivors three months after recovery. *EClinicalMedicine.* (2020) 25:100463. doi: 10.1016/j.eclinm.2020.100463
- Mezzani A. Cardiopulmonary exercise testing: basics of methodology and measurements. *Ann. Am. Thorac. Soc.* (2017) 14:S3–S11. doi: 10.1513/AnnalsATS.201612-997FR

**Conflict of Interest:** The authors declare that the research was conducted in the absence of any commercial or financial relationships that could be construed as a potential conflict of interest.

Copyright © 2021 Liu, Lv, Huang and Xiao. This is an open-access article distributed under the terms of the Creative Commons Attribution License (CC BY). The use, distribution or reproduction in other forums is permitted, provided the original author(s) and the copyright owner(s) are credited and that the original publication in this journal is cited, in accordance with accepted academic practice. No use, distribution or reproduction is permitted which does not comply with these terms.



# Analysis of the Tradeoff Between Health and Economic Impacts of the Covid-19 Epidemic

Samson Lasaulce<sup>1</sup>, Chao Zhang<sup>2\*</sup>, Vineeth Varma<sup>1</sup> and Irinel Constantin Morărescu<sup>1</sup>

<sup>1</sup> Université de Lorraine, CNRS, CRAN, Nancy, France, <sup>2</sup> School of Mathematics and Statistics, Central South University, Changsha, China

## OPEN ACCESS

### Edited by:

Babak A. Ardekani,  
Nathan Kline Institute for Psychiatric  
Research, United States

### Reviewed by:

Juliette Unwin,  
Imperial College London,  
United Kingdom  
Didier Georges,  
Grenoble Institute of Technology,  
France

### \*Correspondence:

Chao Zhang  
zhangchaohust@gmail.com

### Specialty section:

This article was submitted to  
Infectious Diseases - Surveillance,  
Prevention and Treatment,  
a section of the journal  
Frontiers in Public Health

**Received:** 27 October 2020

**Accepted:** 11 February 2021

**Published:** 05 March 2021

### Citation:

Lasaulce S, Zhang C, Varma V and  
Morărescu IC (2021) Analysis of the  
Tradeoff Between Health and  
Economic Impacts of the Covid-19  
Epidemic.  
Front. Public Health 9:620770.  
doi: 10.3389/fpubh.2021.620770

Various measures have been taken in different countries to mitigate the Covid-19 epidemic. But, throughout the world, many citizens don't understand well how these measures are taken and even question the decisions taken by their government. Should the measures be more (or less) restrictive? Are they taken for a too long (or too short) period of time? To provide some quantitative elements of response to these questions, we consider the well-known SEIR model for the Covid-19 epidemic propagation and propose a pragmatic model of the government decision-making operation. Although simple and obviously improvable, the proposed model allows us to study the tradeoff between health and economic aspects in a pragmatic and insightful way. Assuming a given number of phases for the epidemic (namely, 4 in this paper) and a desired tradeoff between health and economic aspects, it is then possible to determine the optimal duration of each phase and the optimal severity level (i.e., the target transmission rate) for each of them. The numerical analysis is performed for the case of France but the adopted approach can be applied to any country. One of the takeaway messages of this analysis is that being able to implement the optimal 4-phase epidemic management strategy in France would have led to 1.05 million of infected people and a GDP loss of 231 billions € instead of 6.88 millions of infected and a loss of 241 billions €. This indicates that, seen from the proposed model perspective, the effectively implemented epidemic management strategy is good economically, whereas substantial improvements might have been obtained in terms of health impact. Our analysis indicates that the lockdown/severe phase should have been more severe but shorter, and the adjustment phase occurred earlier. Due to the natural tendency of people to deviate from the official rules, updating measures every month over the whole epidemic episode seems to be more appropriate.

**Keywords:** epidemic, COVID-19, SARS-CoV2, SEIR model, epidemic management strategy, behavior model

## 1. INTRODUCTION

One of the goals of this work is to provide a simple but exploitable model to measure the quality of the epidemic management strategy implemented by a government to mitigate the health and macro-economic impacts of the Covid-19 epidemic. The quality is measured in terms of the tradeoff between the total number of infected people over a given period of time and the Gross Domestic Product (GDP) loss, under a constraint of the total number of infected people requiring

Intensive Care Units (ICU). To reach this objective, we propose a behavioral model for governmental decision-making operations. Although we assume a simple measure for the quality of the lockdown measures and a simple dynamical model (namely, a classical susceptible-exposed-infected-removed (SEIR) model), the proposed approach is seen to be sufficient to constitute a first step into capturing and quantifying the tradeoff under consideration. In contrast with most studies conducted on the Covid-19 epidemic analysis where the primary goal is to refine the SEIR model [see e.g., (1–5)] or employ the SEIR model by accounting for local variations [by using a given SEIR model per geographical region—see e.g., (6)] or for the impact of class type [by age, sex, risk level—see e.g., (7)] our approach is to use the standard SEIR model for an entire country and choose a simple economic model to focus on the study of the tradeoff between health and economic aspects.

Although there have been many several interesting studies on the economic impact of Covid-19 [see e.g., (8–12)], the pursued goal of these studies is not to model the behavior of the government. As a consequence, the proposed tradeoff has not been analyzed, at least formally. In fact, the closest contribution to this direction would be given by (13) where generic discrete-time epidemics over multiple regions are considered, the particular 4-phase structure is not considered, the focus is not on Covid-19, and the key aspect of the tradeoff analysis is neither developed nor analyzed. Additionally, the numerous studies available on the problem of the transmission rate control generally concern the continuous-time control approach. In this work, the focus is on a multiple phase approach (namely, 4 phases). In the literature dedicated to epidemic control, one can for instance find that some recent studies on how the lockdown strategies and quarantine can be planned in an optimal fashion (14–17). A common feature to all these works on optimal control and lockdown planning is that the policies under consideration, vary over time in a continuous manner, i.e., the lockdown policy is continuously evolving based on the infected population or just on time. However, from the perspective of a government, implementing such policies is not practical since daily changes of the epidemic control measures are difficult to be implemented and to be followed by people.

Summarizing, compared to the existing literature on epidemics modeling and control of epidemics, the main contribution of our work is four-fold:

- A model for capturing the tradeoff between health and economic aspect and therefore for the government decision-making operation is proposed and studied;
- The focus is on multiple phase control policies and not on general continuous-time control policies (to be precise, 4 phases are assumed, see **Figure 1**);
- The problem of finding the optimal features of the optimal epidemic management policy (i.e., the target severity level for each phase and the switching time instants) is stated and solved exhaustively. Additionally, to refine the analysis, we assume a simple model for the natural time drift in terms of behavior of people;

- The numerical analysis of the tradeoff is dedicated to the Covid-19 epidemic and a case study for France.

## 2. METHODS

### 2.1. Epidemic Model

To model the dynamics of the Covid-19 epidemic globally i.e., over an entire country, we assume a standard SEIR model. Let us, respectively, denote by  $s$ ,  $e$ ,  $i$ , and  $r$  the fractions of the population: being susceptible to be infected by the SARS-Cov2 virus, having been exposed to it, being infected, and being removed (including recoveries and deceases). The epidemic is assumed to obey the following continuous-time dynamics:

$$\left\{ \begin{array}{lcl} \frac{ds}{dt}(t) & = & -\beta(t)i(t)s(t) \\ \frac{de}{dt}(t) & = & \beta(t)i(t)s(t) - \gamma e(t) \\ \frac{di}{dt}(t) & = & \gamma e(t) - \delta i(t) \\ \frac{dr}{dt}(t) & = & \delta i(t) \\ s(t) + e(t) + i(t) + r(t) & = & 1 \end{array} \right. \quad (1)$$

where:

- $\beta(t)$ ,  $t \in \mathbb{R}$ , represents the **time-varying** virus transmission rate;
- $\gamma$  denotes the rate at which the exposed subject develops the disease (this includes people presenting symptoms and asymptomatics). The period  $\frac{1}{\gamma}$  is called the incubation period;
- $\delta$  denotes the removal rate and  $\frac{1}{\delta}$  is called the average recovery period.

We assume that the control action  $u(t)$  taken by the decision-maker (the government or possibly a more local decision-maker) has a **linear effect** on the transmission virus rate. Additionally, the effectiveness of this action is assumed to undergo a non-controllable drift or attenuation effect due to the observed fact that people tend to relax their effort over time (18, 19), hence the presence of the attenuation factor  $a(t)$  yields:

$$\beta(t) = R_0\delta - u(t)a(t) \quad (2)$$

where  $R_0$  is the natural reproduction number (namely, without any control or population awareness),  $u(t) \in [0, U]$  is the control action or severity level of the lockdown measures. Note that  $U$  corresponds to the most drastic or severe control action (in theory it could reach the value  $R_0\delta$  and make the reproduction number vanishing). In this work,  $u(t)$  is a piecewise-constant function. For the numerical analysis, we will assume  $a(t)$  to be a linearly decreasing function of time (as detailed in the next

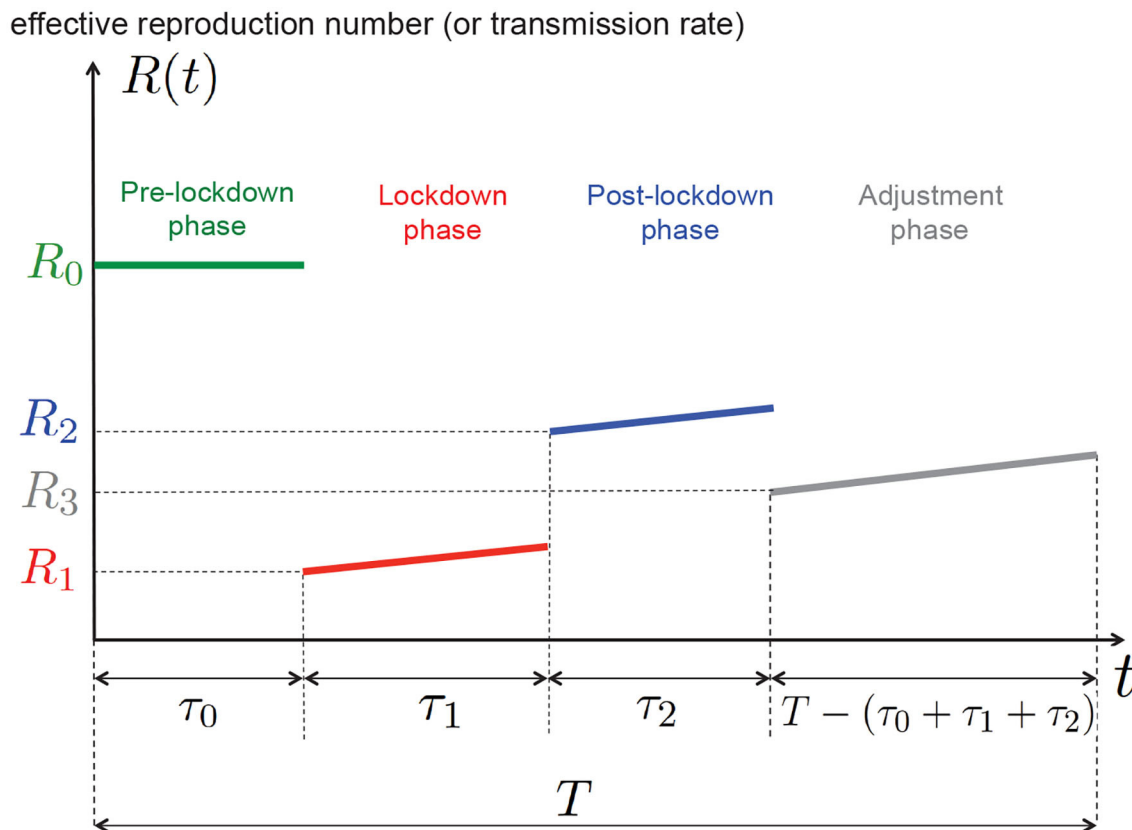


**FIGURE 1** | One of the goals of this work is to determine numerically, for a given tradeoff between health and economic costs, the best 4-phase epidemic management policy that is, the best values for  $\tau_0$ ,  $\tau_1$ ,  $\tau_2$ ,  $R_1$ ,  $R_2$ ,  $R_3$  (the epidemic time horizon  $T$  and the natural reproduction number  $R_0$  being fixed).

section). Therefore, one can define the time-varying effective reproduction number:

$$R(t) = \frac{\beta(t)}{\delta} = R_0 - \frac{u(t)a(t)}{\delta}. \quad (3)$$

As illustrated by **Figure 1**, we are solving an epidemic control problem in which determining the function  $u(t)$  or  $R(t)$  amounts to jointly determining the switching instants  $\tau_0$ ,  $\tau_1$ ,  $\tau_2$  and the targeted reproduction numbers  $R_1$ ,  $R_2$ ,  $R_3$ ;  $T$  is a given period of time for the epidemic analysis. In particular, we will determine the best duration of the lockdown phase  $\tau_1$  and the corresponding targeted reproduction number  $R_1$ . **Figure 1** shows for instance that if the lockdown measures taken are such the reproduction number is  $R_1$  at the beginning of the lockdown phase, then, because of the drift induced by the typical human behavior, the effective reproduction number increases over time.

## 2.2. Time Drift or People Behavior Model

We propose here a model for the attenuation function  $a(t)$ , which quantifies the degree to which people relax their effort to implement the government management measures. As the attenuation effect is negligible when a new policy is released, we consider that  $a(t) = 1$  when  $t \in \{\tau_0, \tau_1, \tau_2\}$ . The attenuation factor is assumed to increase over time in each phase, and we

assume the following piecewise linear behavior between phases:

$$a(t) = \begin{cases} 1 & \text{for } t < \tau_0, \\ 1 - a_1(t - \tau_0) & \text{for } \tau_0 \leq t < \tau_1, \\ 1 - a_2(t - \tau_1) & \text{for } \tau_1 \leq t < \tau_2, \\ 1 - a_3(t - \tau_2) & \text{for } t \geq \tau_2. \end{cases} \quad (4)$$

where  $a_1$ ,  $a_2$ , and  $a_3$ , respectively, represent the attenuation coefficients during the lockdown phase, after the lockdown phase, and during the adjustment phase.

## 2.3. Decision-Maker Behavior Model

The proposed model for the behavior of the decision-maker is based on the fact that it wants to obtain a given tradeoff between economic and health aspects. For the cost related to the economics loss, we assume the simplest reasonable model. That is, we assume that economic cost is quadratic in the control action. For the health cost, we assume that it is given by the number of infected people over the given period of time. Therefore, the proposed overall cost consists of a convex combination of these two costs. By minimizing the overall cost, one realizes the desired tradeoff between economic and health

aspects. On top of this we impose the number of patients requiring intensive care to be under a given threshold  $N_{\max}^{\text{ICU}}$ . Thus, the corresponding minimization is performed under a constraint on the number of people infected at any time  $t \in [0, T]$ :  $\sigma Ni(t) \leq N_{\max}^{\text{ICU}}$ ,  $N$  being the population size,  $N_{\max}^{\text{ICU}}$  the maximum number of ICU patients, and  $0 \leq \sigma \leq 1$  is the percentage of infected people requiring intensive care. In France, official records state that the maximum cumulated number of ICU patients has reached 7,148 (on April 8, 2020) but the capacity over the whole territory has been evaluated to be greater than 15,000. By denoting  $\alpha \in [0, 1]$  the weight assigned to the macroeconomic impact of the epidemic and  $K_e > 0$ ,  $K_h > 0$ ,  $\mu > 0$  some constants (parameters) defined below, obtaining the desired tradeoff amounts to finding a solution of the following optimization problem (OP) while fixing  $\alpha$  to a given value:

$$\underset{u(t)}{\text{minimize}} \left\{ \alpha K_e \left\{ \int_0^{\tau_0+\tau_1} u^2(t) dt + \frac{1}{\mu_1^2} \int_{\tau_0+\tau_1}^{\tau_0+\tau_1+\tau_2} u^2(t) dt + \int_{\tau_0+\tau_1+\tau_2}^T u^2(t) dt \right\} + (1-\alpha) K_h [s(0) - s(T)] \right\} \quad (5)$$

subject to  $\forall t \in [0, T], \sigma Ni(t) \leq N_{\max}^{\text{ICU}}$   
 $\tau_1 \geq T_{\min}$   
 Equations (1) and (2)

where:

- $K_e > 0$  and  $K_h > 0$  are constants that weight the economic and health cost functions (they also act as conversion factors allowing one to obtain appropriate units and orders of magnitude);
- $\tau_0$  and  $\tau_1$  represent the lockdown starting time and duration, respectively.  $T_{\min}$  is the minimum lockdown duration to make the lockdown policies effective. The quantity  $\tau_2$  represents the duration of the post-lockdown phase;
- the parameters  $\mu_1, \mu_2 \geq 1$  accounts for possible differences in terms of economic impact between the lockdown and post-lockdown phases;
- $s(0)$  and  $s(T)$  are, respectively, the fractions of the population susceptible at the beginning and the end of the analysis.

We would like to make additional comments concerning the parameter  $\mu_1, \mu_2$ . The motivation for introducing  $\mu_1, \mu_2$  is two-fold. First, after lockdown, people are more aware and act more responsibly than before lockdown. This means that automatic and costless population distancing typically occurs (8, 20, 21). Taking  $\mu_1, \mu_2 \geq 1$  precisely amounts to having a smaller reproduction number without any cost for the government. Additionally, as people typically tend to relax their effort to implement the epidemic management measures as time passes, it makes sense to assume that  $\mu_1 \geq \mu_2$  in our model. It also allows

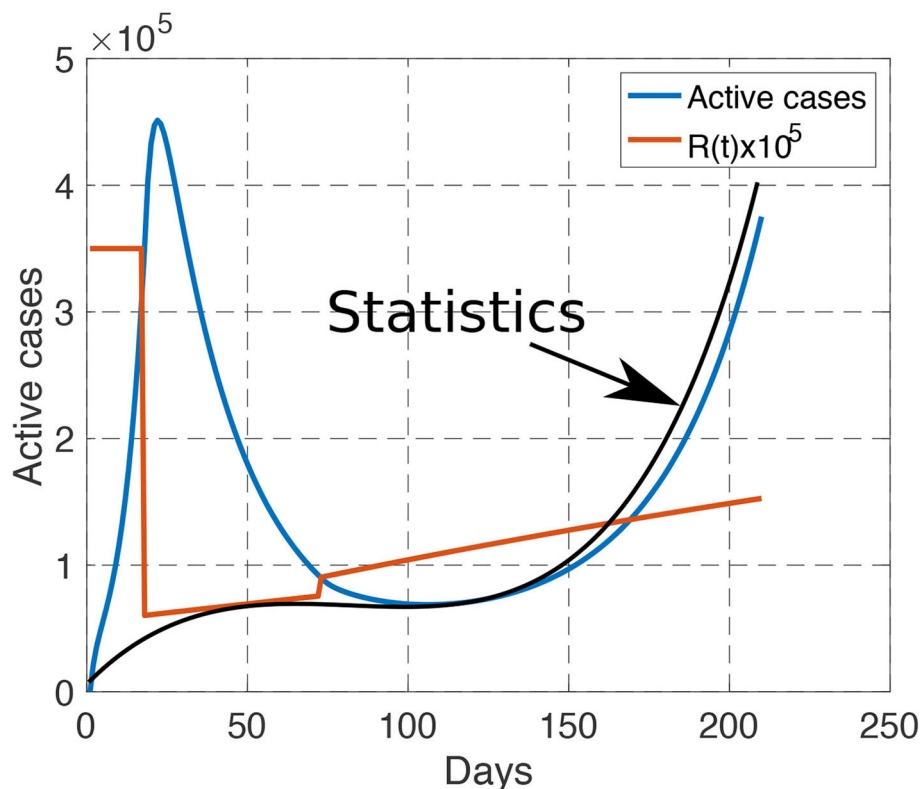


**FIGURE 2 |** Comparison between our model (blue curve) and the reported statistics (black curve) from March 1st to September 30th. When the number of tests are sufficiently large, our model matches well with the reported statistics. The reproduction number is linearly increasing during each phase, and is discontinuous during the transition between phases.



one to account for the fact that, after lockdown, the economic activity grows after the lockdown and the effects of the pandemic starts vanishing. This means that, in some sense we ignore memory effects due to lockdown measures. Further refinements of the proposed model might be considered to account for the lockdown memory effects. This is out of the scope of the present paper but we believe that, this would correspond to assuming  $\mu_i < 1$ .

## 2.4. 4-Phase Optimal Control With Piecewise Constant Control Actions

Solving analytically the optimization problem given by (5) is not trivial. However, since we restrict our attention to a certain class of control policies, the problem turns out to be solvable through exhaustive search. Assuming the attenuation factor  $a(\tau_0) = a(\tau_1) = a(\tau_2) = 1$  (no attenuation at the beginning of each phase) and a constant control action in each phase, by using the relation  $u(t) = \delta[R_0 - R(t)]$ , the OP (5) can be rewritten under a

more convenient form for numerical purposes:

$$\underset{(\tau_0, \tau_1, \tau_2, R_1, R_2, R_3)}{\text{minimize}} \left\{ \begin{aligned} &\alpha K_e \delta^2 (R_0 - R_1)^2 \tau_1 + \frac{\alpha K_e \delta^2 (R_0 - R_2)^2 \tau_2}{\mu_1^2} + \\ &\frac{\alpha K_e \delta^2 (R_0 - R_3)^2 [T - (\tau_0 + \tau_1 + \tau_2)]}{\mu_2^2} + \\ &(1 - \alpha) K_h [s(0) - s(T)] \end{aligned} \right\} \quad (6)$$

subject to  $\forall t \in [0, T], \sigma Ni(t) \leq N_{\max}^{\text{ICU}}$   
 $\tau_1 \geq T_{\min}$   
 $R_2 > R_1 + 0.2$   
 Equations (1) and (2).

where  $R_i$  represents the desired or target reproduction number over Phase  $i \in \{1, 2, 3\}$  without considering the attenuation factor (also, it is the reproduction number at the start of  $i$ -th phase). The second constraint is introduced here as there is a gap between lockdown reproduction number and after lockdown reproduction number. Finally, the conversion factors  $K_e$  and  $K_h$

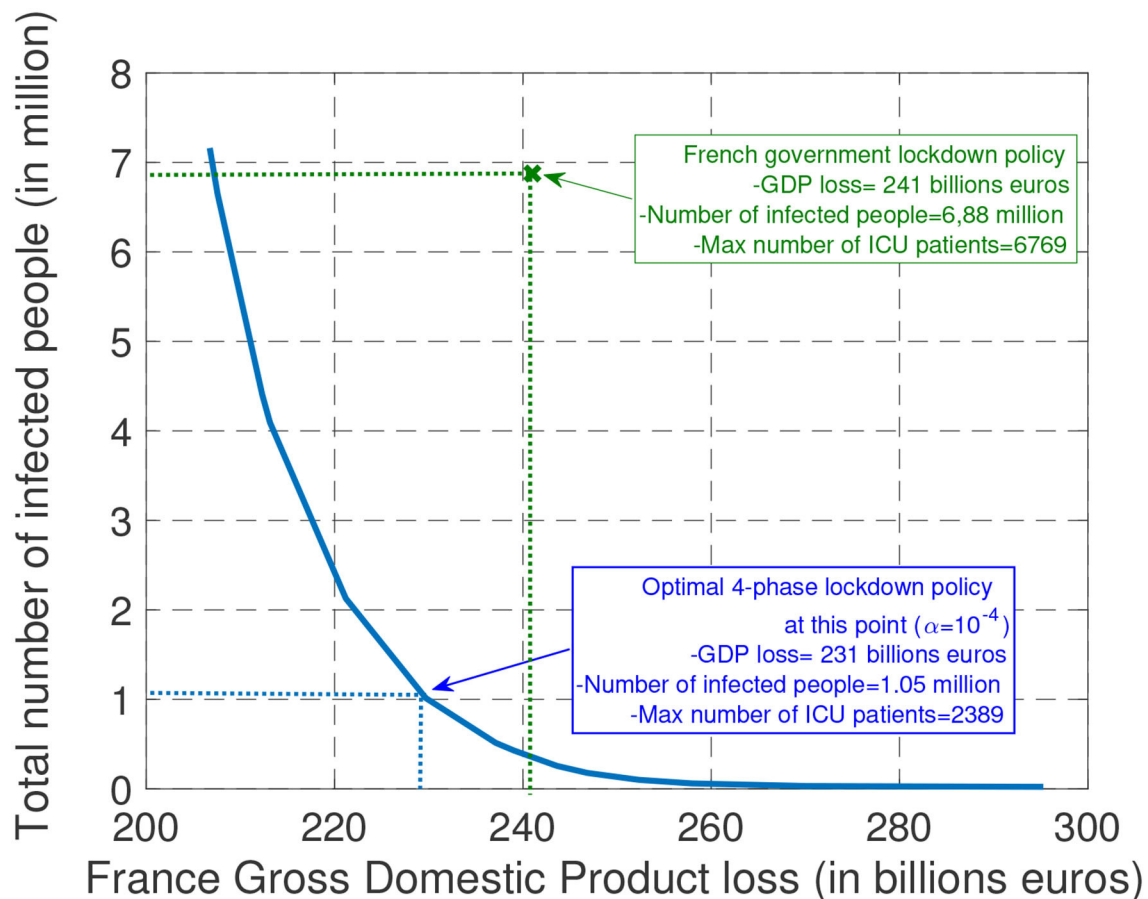


**FIGURE 3 |** The plots represent the possible tradeoffs between health cost (measured in terms of the total number of infected people) and economic cost (measured in terms of GDP loss) that can be obtained (by choosing the best epidemic management policy). In particular, with the assumed model, it is seen, in retrospect, that it would have been possible to divide the number of infected people by about 6 while saving about 10 billions € in terms of GDP with the optimal 4-phase strategy.

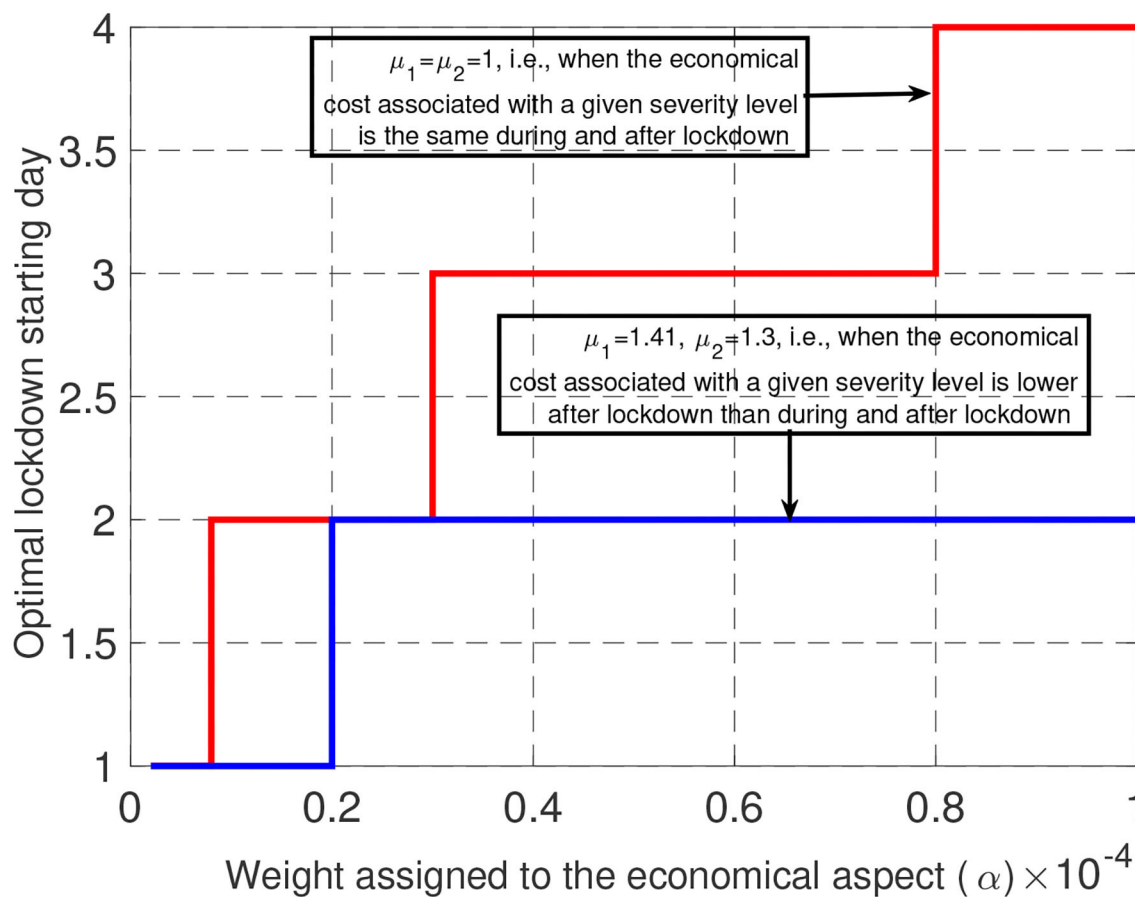


**FIGURE 4 |** When economic losses are assumed to be uniform over time ( $\mu = 1$ ), there is some economic incentive to delay the lockdown, but this delay is seen to be at maximum 4 days. When economic losses are lower after lockdown than during it, it is beneficial to start the lockdown faster, up to 3 days delay.

are chosen as follows. The rationale behind the choice of  $K_e$  is that when choosing  $\alpha = 1$  the GDP loss should correspond to the best estimations made by economists. The GDP loss over the lockdown period for a given country is denoted by  $\Delta\text{GDP}$ , the conversion factor  $K_e$  is chosen as follows:

$$K_e \delta^2 (R_0 - R_1)^2 \tau_1 = \Delta\text{GDP}. \quad (7)$$

For France for example, the GDP loss during the lockdown has been evaluated (on April 20) to be around 120 billions € according to the OFCE (22). At last, the constant  $K_h$  is merely chosen as  $K_h = N$ , that is, when  $\alpha = 0$  the cost function corresponds to the number of people infected over the considered period of time.

### 3. RESULTS

#### 3.1. General Simulation Setup

To perform exhaustive search over the sextuple of variables  $(\tau_0, \tau_1, \tau_2, R_1, R_2, R_3)$ , time and amplitudes are quantized; we thus use hat notations to indicate corresponding values are quantized.

Time is discretized with a step of 24 h (that is, one sample for each day) and a time horizon of  $\hat{T} = 300$  days (which approximately corresponds to 10 months that is the interval [March 1st, December 31st], for the tradeoff figure presented in section 3.4, for computational convenience, we take  $\hat{T} = 210$  days corresponding to 7 months from March 1st to September 30th) is assumed. The sets for the possible lockdown starting days, the lockdown duration (in days), post-lockdown phase duration, and the reproduction numbers are as follows:  $\hat{\tau}_0 \in \{1, 2, \dots, 30\}$ ,  $\hat{\tau}_1 \in \{T_{\min}, T_{\min} + 1, \dots, 90\}$ ,  $\hat{\tau}_2 \in \{1, 2, \dots, 120\}$ ,  $\hat{R}_1 \in \{0.4, 0.2, \dots, 1.5\}$ ,  $\hat{R}_2 \in \{0.4, 0.2, \dots, 1.5\}$ ,  $\hat{R}_3 \in \{0.4, 0.2, \dots, 1.5\}$ . Excluding **Figure 5**, due to the physical characteristics of the epidemics in France, we set  $T_{\min} = 30$  because the lockdown duration is at least 4 weeks or 1 month to make the lockdown effective in real systems (23, 24)<sup>1</sup>. The SEIR model parameters are as follows:  $\frac{1}{\delta} = \frac{1}{0.1857} = 5.4$  days,  $\frac{1}{\gamma} = \frac{1}{0.16} = 6.25$  days; these choices are consistent with many works and in particular the studies performed for France (25) and Italy (16). The population size is set to  $N = 66.10^6$ , the maximum number of patients

<sup>1</sup>Santé Publique France. Available online at: [www.santepubliquefrance.fr](http://www.santepubliquefrance.fr).

requiring intensive care is set to  $N_{\max}^{\text{ICU}} = 15.10^3$ , and  $\sigma = 1.5\%$  (23, 24)<sup>1</sup>. Notice that this number is only reached for very small values of  $\alpha$  (for which the total number of people infected over the analysis duration would be around 9 millions). The exposed population on March 1 2020 is initialized to  $Ne(0) = 1.33.10^5$ . This number is obtained from analyzing the data provided in (23). We consider the number of reported deaths at a given time to be a more reliable way of tracking the evolution of the pandemic rather than the reported number of infected people. Indeed, as soon as one examines absolute values, they typically become irrelevant. For example, during lockdown, because of the lack of tests and measurements, the real number of infected people was much higher than the official number. Now, even when tests were performed intensively, because of false positives, the absolute number of infected were again completely unreliable. For a prevalence of 1/1,000 and a test reliability of 5% of false positives we see that the number of infected for 1,000 people is declared to be about 50 whereas the actual number of infected

is only 1. Motivated by these critical issues, we have considered figures which are much more reliable such as the number of deaths due to Covid-19 in France (23, 25). From the number of deaths and the global average rate (worldwide) of the mortality rate (in the range 0.3–0.5% when averaged over classes of ages and countries), the reconstructed number of infected people turns out to be more accurate. Therefore, by fixing the mortality rate to a given value [in (25) for instance, the mortality rate averaged over all the classes of infected people is evaluated to be around 0.53% for France], one can estimate the exposed and infected population size 3–4 weeks before the measured number of deaths due to Covid-19. For our computation, the initial conditions of the ordinary differential equations (ODE) equations are chosen as  $s(0) = 1 - e(0)$ ,  $i(0) = r(0) = 0$ , and the ODE is solved by using the Matlab ode45 solver. Concerning the economic cost for France related to Covid-19, the GDP loss over the lockdown period is estimated by the OFCE (22) to be 120 billions € and we have, as reliable figures, that  $\tau_1^{\text{France}} = 55$  days with  $R_0^{\text{France}} = 3.5$

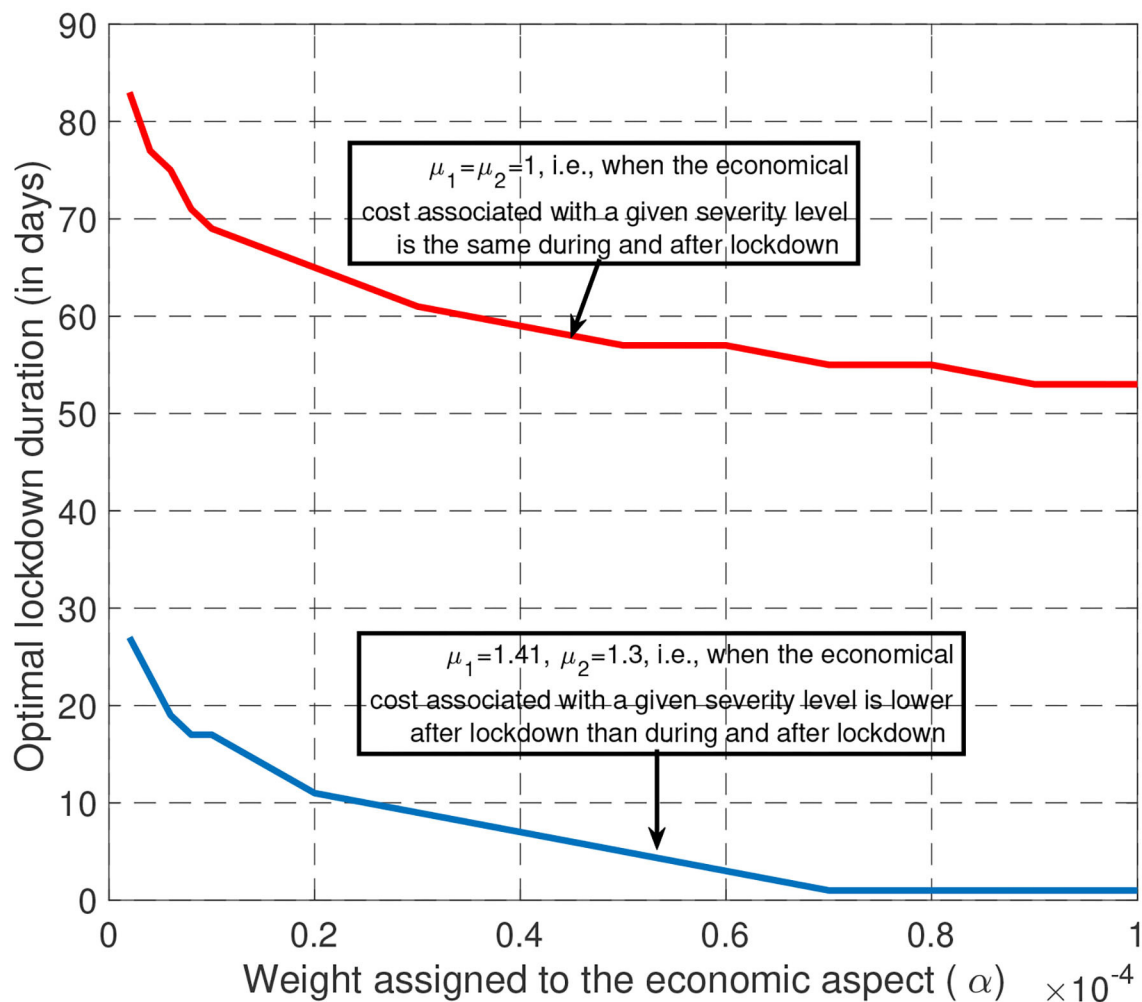


**FIGURE 5** | When economic losses are assumed to be uniform over time ( $\mu = 1$ ), it is optimal to have a long lockdown (typically between 60 and 80 days) whatever the tradeoff desired. But, if the economic losses of the third phase are less than during lockdown, the lockdown phase should be shorter.

and  $R_1^{\text{France}} = 0.6$ . We therefore take  $K_e = 7.379 \cdot 10^9$  €/day. Values of the reproduction number for the first two phases come from past and quite accurate evaluations [see e.g., (24)]. The value  $R_2^{\text{France}} = 0.9$  is less accurate and corresponds to the assumption that the government has been aiming at giving as much as freedom to the population while avoiding a second wave. Based on available statistics on Covid-19 in France<sup>1</sup>, the attenuation coefficients of the drift model have been chosen as follows:  $a_1 = 0.1\%$ ,  $a_2 = 0.2\%$ ,  $a_3 = 0.2\%$ . Unless stated otherwise, the economic impact parameters are chosen as  $\mu_1 = 1.41$  (i.e.,  $\mu_1^2 \sim 2$ ) and  $\mu_2 = 1.3$ . Also, when  $\alpha$  is assumed to be fixed, it is set to  $10^{-4}$ .

To justify the choice of the attenuation parameters, that is,  $a_1 = 0.1\%$ ,  $a_2 = 0.2\%$ ,  $a_3 = 0.2\%$ , we apply the French policy into our model. By comparing the active cases obtained from our model and the official data, it can be illustrated in **Figure 2** that our model matches well with the real data, especially in the second-half of the plot, where the number of tests conducted are sufficiently large. This validate the choice of our model and parameters. The mismatch on March and April are mainly due to the lacking number of tests that were taken during the early outbreak of the pandemic, leading to a much lower reported number of active cases.

### 3.2. Optimal Tradeoff Between Economic and Health Impacts

With the proposed government decision-making model, implementing a desired tradeoff between the health cost and economic cost merely amounts to choosing a given value for the parameter  $\alpha$ . **Figure 3** depicts for various values of  $\alpha$  in the interval  $[10^{-7}, 10^{-4}]$  the total GDP loss and number of infected people that is obtained after choosing the (quantized version of the) sextuple  $(\tau_0, \tau_1, \tau_2, R_1, R_2, R_3)$  that minimizes the combined cost given by Equation (6). At one extreme, when  $\alpha$  is relatively large ( $\alpha = 10^{-4}$ ) (that is, when the government aims at minimizing the economic cost in the first place—always under the ICU capacity constraint) we see that the best epidemic management strategy leads to a GDP loss over the entire study period [March 1, September 30] is about 206 billions € with 7.16 millions infected, and 15,000 patients requiring intensive care. At the other extreme, when  $\alpha$  is relatively small ( $\alpha = 10^{-7}$ ), the GDP loss reaches values as high as 295 billion € with a total number of newly infected people over the period [March 1, September 30] as low as 23,162. To evaluate the efficiency of the epidemic management strategy of the French government policy, we have represented the point corresponding to the estimated number of infected people and GDP loss by September

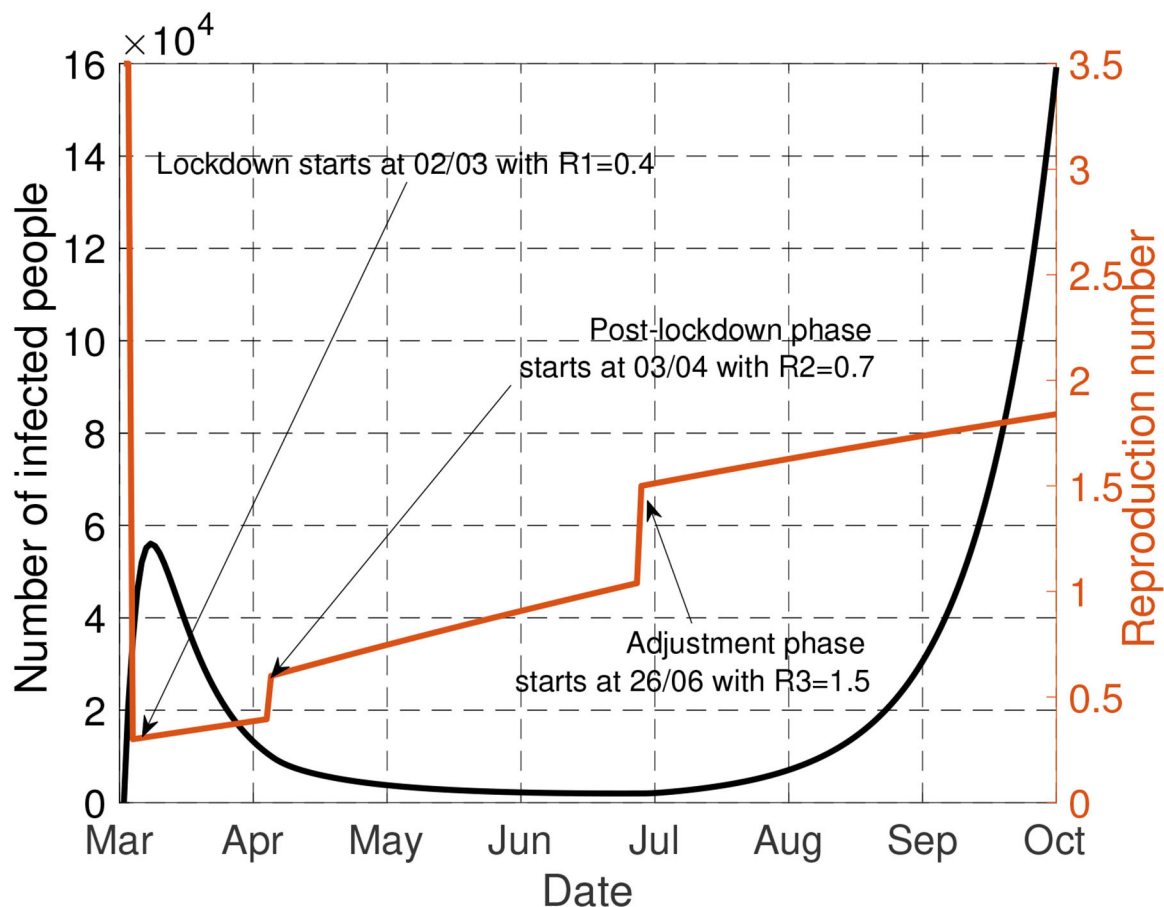


**FIGURE 6 |** This figure represents the evolution of number of infected people  $[N_i(t)]$  and the transmission rate when the optimal policy is adopted.

30; with our model, the GDP loss over the period of time of interest is 241 billion € and the total number of infected people is about 6.88 million. What the best tradeoff curve indicates is that there were management policies that would allow the French government to have a better “performance” both in terms of GDP loss and the number of infected people. For instance, we indicate a point for which it would have been possible to have about 1.05 million people infected (that is, about 6 times less than what is estimated with the current policy) while ensuring a total GDP loss of 231 billions €. Which type of epidemic management strategy should be used to have such an outcome? The next sections provide a detailed analysis of the features of the optimal strategy.

### 3.3. Optimal Features of the Optimal Epidemic Management Strategy

One of the important features for controlling the Covid-19 epidemic which has been well-commented in newspapers in various countries is the lockdown starting time. To minimize the health cost, the answer is ready: the lockdown phase should always start as soon as possible. But when one wants to realize a tradeoff between health and economic costs, the answer is less immediate. For different values for  $\mu_1$  and  $\mu_2$ , **Figure 4** provides the best day to start locking down the population, for

one hundred values of  $\alpha$  ranging from  $10^{-4}$  to  $10^{-6}$ . The main message of this figure is that, even for (relatively) large values for  $\alpha$  (that is, when the economic cost dominates the health cost), the optimal lockdown starting day should be before March 4th (i.e.,  $\tau_0 \leq 4$ ). This clearly shows that, once an epidemic has been declared, invoking economic damages to delay the lockdown phase is not acceptable. Note that this conclusion holds when economic losses are assumed to be uniform over time ( $\mu_1 = \mu_2 = 1$ ). When the economic cost associated with a given intensity or severity level is lower after lockdown than during it (here  $\mu_1 = 1.41$  and  $\mu_2 = 1.3$ ), it is always optimal to start locking down as soon as possible. Note that our model does not capture the possible fact that population needs to be psychologically prepared to follow the lockdown measures. In France, by March 17, there were official figures about the epidemic which were sufficiently critical to make the population accept the measures whereas, starting on March 4 (the optimal starting date for  $\mu_1 = \mu_2 = 1$ ) the situation might have not been critical enough to create full adhesion to government measures.

A second key feature of the Covid-19 epidemic control strategy was the lockdown phase duration namely, the value of  $\tau_1$ . To better explore the relationship between  $\tau_1$  and  $\alpha$  (the tradeoff), we relax the lockdown duration constraint here and set  $T_{\min} = 1$ . For  $(\mu_1, \mu_2) = (1, 1)$  and  $(\mu_1, \mu_2) = (1.41, 1.3)$ ,

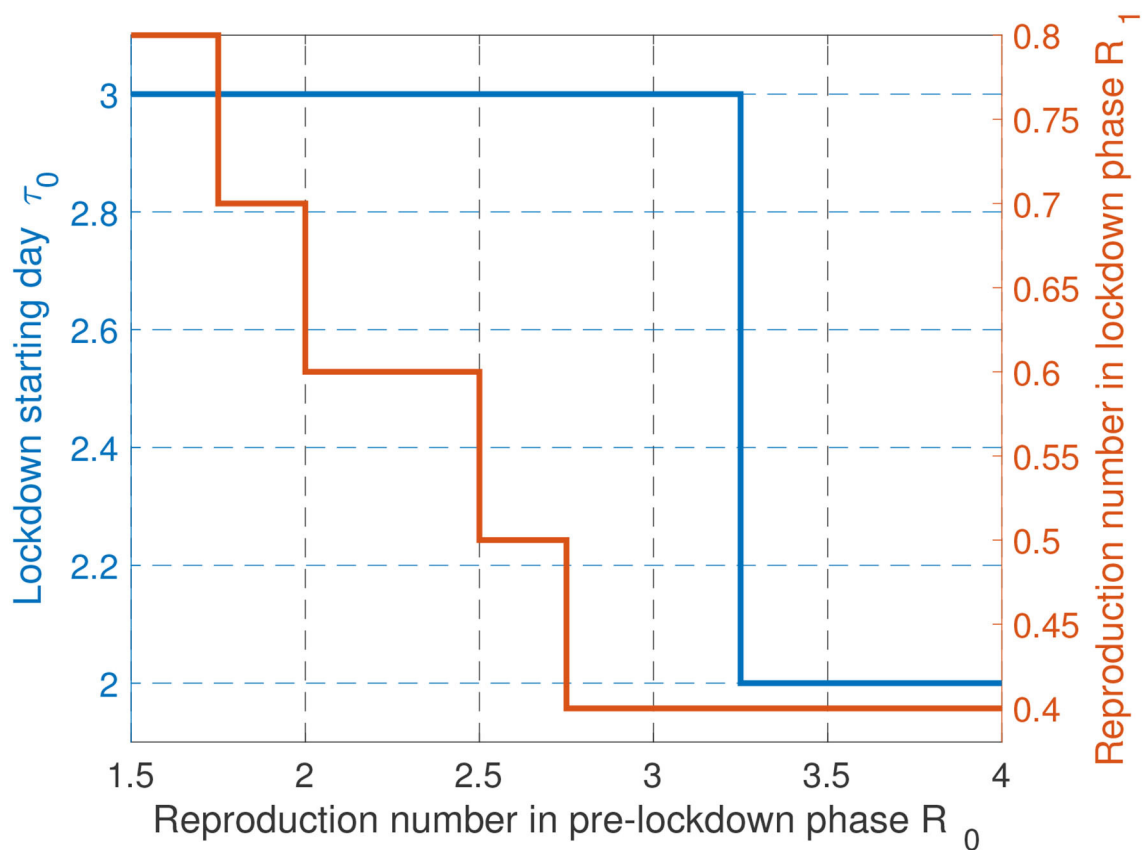


**FIGURE 7** | Comparison of lockdown policies with different  $R_0$ . When the situation is worse, a sooner and more strict lockdown strategy should be applied.



**Figure 5** provides the optimal lockdown duration (in days) for values of  $\alpha$  ranging from  $10^{-4}$  to  $10^{-6}$ . For  $(\mu_1, \mu_2) = (1, 1)$  (i.e., when economic losses are uniform over time), the optimal duration ranges from 53 to 83 days for a large fraction of the considered interval for  $\alpha$ . Interestingly, we see that these values are relatively close to the lockdown duration effectively imposed in France namely 55 days. For larger values of  $\mu_1$  and  $\mu_2$ , the optimal lockdown duration is seen to be much smaller. Therefore, if economic losses are uniform over time, the French government policy seems to be very coherent. On the other hand, if the economic impact is smaller after lockdown, our study suggests shorter lockdown durations. In fact, our results show the existence of a critical value for the tradeoff parameter  $\alpha$  above which the second phase of the management of the epidemic should not be present. This means that the optimal control consists of three phases instead of four.

To conclude this section, let us consider **Figure 6**. For the by default scenario studied in this paper  $[(\mu_1, \mu_2) = (1.41, 1.3), \alpha = 10^{-4}]$ , the figure represents the evolution of number of infected people, that is,  $Ni(t)$ , and the transmission rate when the optimal policy is adopted. First, it is seen that for the health-economic tradeoff corresponding to  $\alpha = 10^{-4}$ , there is no interest in delaying the lockdown phase. By “lockdown” phase, the authors mean that it might be any type of phase for which

the reproduction number is as low as 0.4 (vs. the estimated 0.6 in France); very efficient digital tracing and intensive use of face masks is also an option which has been successfully adopted in countries such as South Korea [see e.g., (26)]. The optimal lockdown phase duration is seen to be about 1 month (instead of 2 for France). We see that the existence of an adjustment phase is part of the optimal policy. For this point, we see that the adjustment phase should have occurred much before in France (end of June vs. end of September). The next section is precisely dedicated to the impact of the adjustment phase.

### 3.4. Lockdown Policies With Different $R_0$

Since the natural reproduction number  $R_0$  depends on temperatures, population density, may vary over time due to mutation effects, and in any case is not known perfectly, it is of interest to study the impact of  $R_0$  on the obtained characteristics for the optimal epidemic management policy. This is what **Figure 7** represents. It is seen that large variations on  $R_0$  do not involve large variations on the starting day. For instance, moving from  $R_0 = 2$  to  $R_0 = 3.5$  only changes the optimal date by 1 day (Day 2 instead of Day 3), which confirms the need to act fastly even when the transmission is more limited (e.g., thanks to higher temperatures or lower population density). Note that this holds even if the economic impact is accounted for. It is

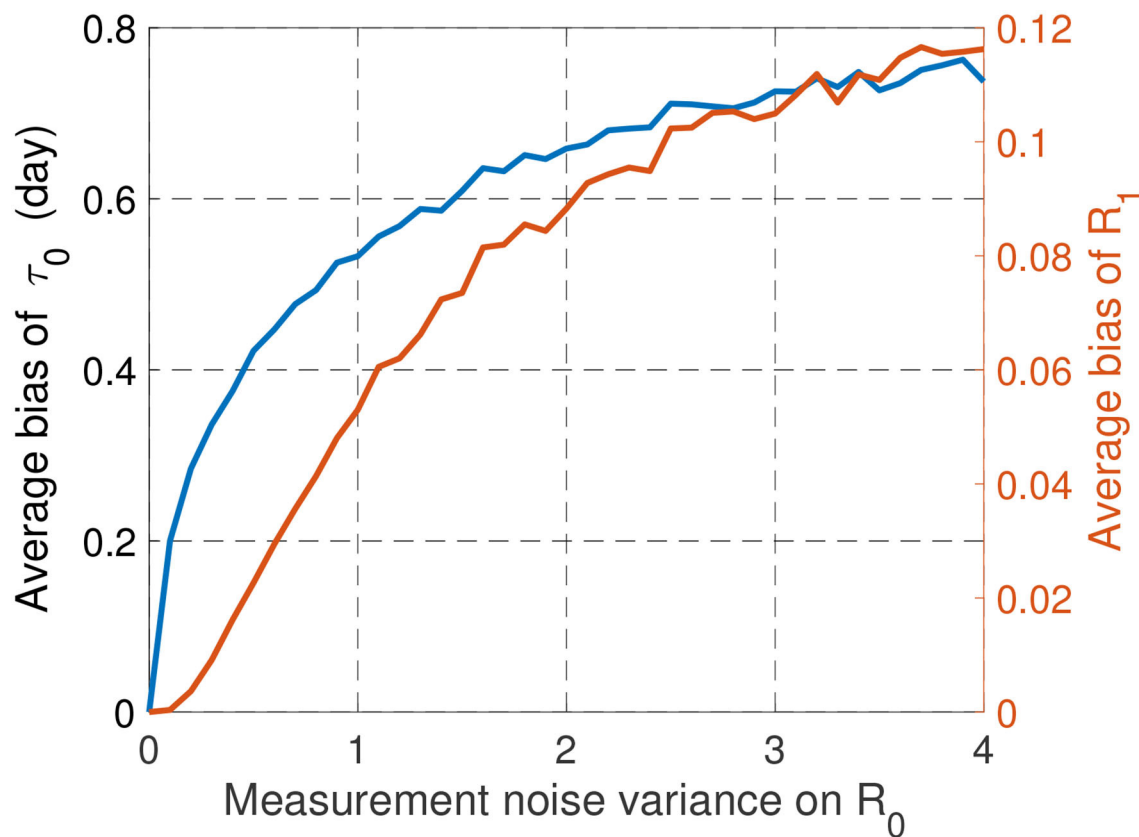


**FIGURE 8** | Influence of uncertainties on  $R_0$  on the optimal values for  $\tau_0$  and  $R_1$ .

also good for economical aspects to react fastly to an epidemics. For the optimal reproduction number during lockdown (namely,  $R_1$ ) it is also seen that moving a scenario in which  $R_0 = 2$  to  $R_0 = 3.5$  does not change very significantly the results: the target severity (or freedom) level would correspond to  $R_1 = 0.4$  instead  $R_1 = 0.6$ , which shows that the severity should be high during lockdown even in countries or regions where transmission is more limited.

Alternatively, the impact of  $R_0$  uncertainty can be evaluated by adding a perturbation on  $R_0$ . It is assumed that what is known to determine the optimal parameters is  $\hat{R}_0 = R_0 + \Delta$ ,  $\Delta$  being a Gaussian noise  $\Delta \sim \mathcal{N}(0, \sigma^2)$ . The reproduction number have to stay in a given interval of physical relevance of the form  $[R_{\min}, R_{\max}]$ . Thus, the noise is imposed to stay in the interval  $[-R_0 + R_{\min}, -R_0 + R_{\max}]$ . With  $R_0 = 3.5$ ,  $R_{\min} = 1$  and  $R_{\max} = 4$ , **Figure 8** depicts the average bias for  $\tau_0$  and  $R_1$  induced by uncertainty on  $R_0$ . The average biases for  $\tau_0$  and  $R_1$  are defined by  $\mathbb{E}_\Delta[|\hat{R}_1 - R_1|]$  and  $\mathbb{E}_\Delta[|\hat{\tau}_0 - \tau_0|]$ , where  $\hat{R}_1$  and  $\hat{\tau}_0$  are obtained with the noisy reproduction number  $\hat{R}_0$ . Remarkably, the impact of the corresponding noise on the results is seen to be very reasonable and does not affect the main conclusions

drawn in the first version of the paper. This indicates that the conducted analysis is robust against some forms of uncertainties. But of course, as mentioned previously, a deeper analysis would be required to state more general conclusions.

In addition, a more global sensitivity analysis to other SEIR model parameters, i.e.  $\delta$  and  $\gamma$ , have been conducted by simulations. A similar conclusion can be drawn. This shows that our conclusions are quite robust to effects such as parameter uncertainties. This is in part due to the fact that we are mostly seeking discrete parameters and not continuous parameters, which creates a form of robustness.

### 3.5. Impact of the Adjustment Phase

Always for the typical scenario presented in the general setting part, **Figure 9** depicts the evolution of the number of infected people (in France) for the policy effectively implemented over the period [March 1, September 30]. Here, only the adjustment phase is assumed to be optimizable. The figure allows one to quantify the impact of the severity level of the adjustment phase. Without the adjustment phase, the fraction of infected people is such that the number of people requiring intensive care exceeds

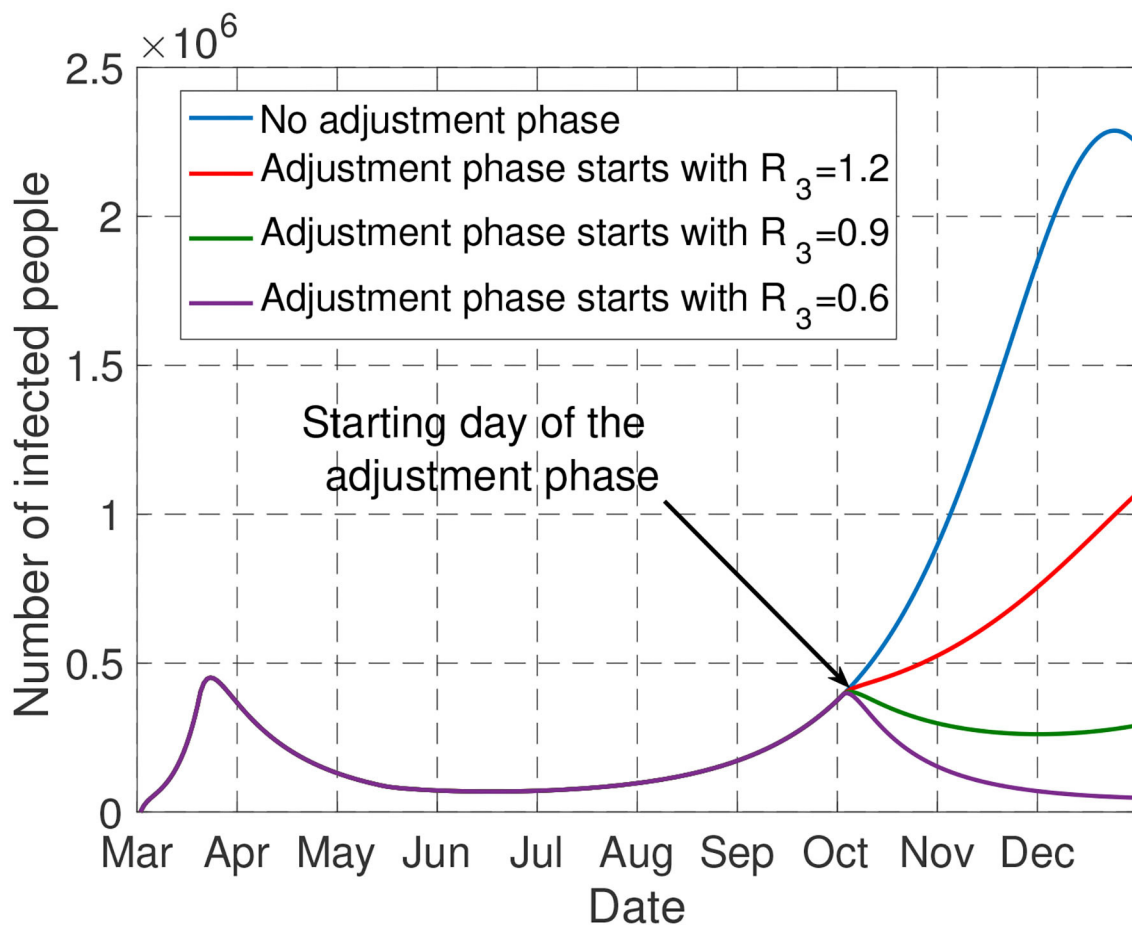


**FIGURE 9 |** The figure shows the impact of the adjustment phase. Only by imposing  $R(t) < 1.2$  over this phase, the number of people admitted in ICU does not exceed the capacity of France by the end of 2020.

the double of the maximum ICU capacity of France. However, by implementing measures such that  $R(t) < 1.2$  over the adjustment phase, the constraint on the ICU capacity is not violated by the end of 2020. Furthermore, to avoid the overwhelming health service for a longer time, it is better to implement measures such that  $R(t) < 1$  over the adjustment phase since the fraction of infected people will be non-increasing with  $R(t) < 1$ .

## 4. DISCUSSION

In this work, we propose to model the behavior of a government as far as the epidemic control is concerned. The proposed model, despite its simplicity, has the merit of being able to capture the fundamental tradeoff between economic and health aspects. Obviously, to capture other effects such as the psychological effects of measures on people, a more general model should be considered. The proposed model allows one to provide quantitative answers to issues which have been well-commented in the media. For example, even when a government chooses to assign a high value to the economic aspect, it is seen that the best strategy is almost always to implement a severe phase as soon as possible. This severe phase involves locking the population down, as most countries did, or to make intensive use of digital tracing and face masks as South Korea did. In the latter case, a loss in terms of privacy is the price to be paid for having more freedom. When inspecting the obtained numerical results performed for France, it is seen that the optimal features for the lockdown/severe phase require targeting a **reproduction number smaller** than the one achieved in France (0.4 vs. 0.6), while having a **shorter duration for the severe phase** (1 month instead of 2). Note that some countries adopted measures which were more severe than France. For instance, China has been imposing the use of a given food supply system which was very efficient in terms of epidemic mitigation (27–29). Then, by planning an adjustment phase at the right time, we have seen that as a final result, the number of infected people can be reduced by

a factor of 6 when compared to the current French policy (1.05 million of infected instead of 6.88 millions for the current policy) while having similar GDP losses (231 billions € instead of 241 billions €). We have seen that by considering a simple model as we have studied, the need for an adjustment phase could have been anticipated. Such a phase is necessary to avoid the number of patients under intensive care exceeding the capacity of the ICUs. Also, because of the natural tendency of humans to deviate from rules over time, it appears that measures should be **updated about every month** and not less frequently.

## DATA AVAILABILITY STATEMENT

The original contributions presented in the study are included in the article/supplementary material, further inquiries can be directed to the corresponding author/s.

## AUTHOR CONTRIBUTIONS

SL, CZ, VV, and IM designed the proposed model. SL and CZ conducted the review of the related literature. SL collected the data to calibrate the assumed model. CZ and SL performed the simulations. All authors contributed to the writing of the manuscript.

## FUNDING

This work was partially supported by ANR via the grant NICETWEET, number ANR-20-CE48-0009.

## ACKNOWLEDGMENTS

The authors acknowledge the support of the French National Research Agency ANR and the French National Research Center CNRS. Part of this manuscript has been released as a pre-print at medRxiv (30).

## REFERENCES

- Peng L, Yang W, Zhang D, Zhuge C, Hong L. Epidemic analysis of COVID-19 in China by dynamical modeling. *arXiv [Preprint]*. *arXiv:2002.06563*.
- Pribylova L, Hajnova V. SEIAR model with asymptomatic cohort and consequences to efficiency of quarantine government measures in COVID-19 epidemic. *arXiv [Preprint]*. *arXiv:2004.02601*.
- Victor A. Estimation of the probability of reinfection with COVID-19 coronavirus by the SEIRUS model. *medRxiv*. (2020). doi: 10.1101/2020.04.02.20050930
- Giordano G, Blanchini F, Bruno R, Colaneri P, Di Filippo A, Di Matteo A, et al. A SIDARTHE model of COVID-19 epidemic in Italy. *arXiv [Preprint]*. *arXiv:2003.09861*.
- Roques L, Klein EK, Papaix J, Sar A, Soubeyrand S. Impact of lockdown on the epidemic dynamics of COVID-19 in France. *Front Med*. (2020) 7:274. doi: 10.3389/fmed.2020.00274
- Di Domenico L, Pullano G, Coletti P, Hens N, Colizza V. *Expected impact of school closure and telework to mitigate COVID-19 epidemic in France*. Report #8. March 14, (2020). Available online at: [https://www.epicx-lab.com/uploads/9/6/9/4/9694133/inserm\\_covid-19-school-closure-french-regions\\_20200313.pdf](https://www.epicx-lab.com/uploads/9/6/9/4/9694133/inserm_covid-19-school-closure-french-regions_20200313.pdf) (accessed April 28, 2020).
- Khawaja AP, Warwick AN, Hysi PG, Kastner A, Dick A, Khaw PT, et al. Associations with Covid-19 hospitalisation amongst 406,793 adults: the UK Biobank prospective cohort study. *medRxiv [Preprint]*. (2020). doi: 10.1101/2020.05.06.20092957
- Atkeson A. *What Will Be the Economic Impact of Covid-19 in the US? Rough Estimates of Disease Scenarios*. National Bureau of Economic Research (2020). doi: 10.3386/w26867
- Eichenbaum MS, Rebelo S, Trabandt M. *The Macroeconomics of Epidemics*. National Bureau of Economic Research (2020). doi: 10.3386/w26882
- Baldwin R, Di Mauro BW. *Economics in the time of COVID-19*. VOX CEPR Policy Portal (2020).
- Fernandes N. *Economic effects of coronavirus outbreak (COVID-19) on the world economy*. Social Science Research Network (2020). doi: 10.2139/ssrn.3557504
- McKibbin WJ, Fernando R. The global macroeconomic impacts of COVID-19: seven scenarios. *CAMA Working Paper No. 19/2020* (2020). doi: 10.2139/ssrn.3547729
- Zakary O, Rachik M, Elmouki I. On the analysis of a multi-regions discrete SIR epidemic model: an optimal control approach. *Int J Dyn Control*. (2017) 5:917–30. doi: 10.1007/s40435-016-0233-2

14. Alvarez FE, Argente D, Lippi F. *A Simple Planning Problem for Covid-19 Lockdown*. National Bureau of Economic Research (2020). doi: 10.3386/w26981
15. Boujakjian H. Modeling the spread of Ebola with SEIR and optimal control. *SIAM Undergrad Res.* (2016) 9:299–310. doi: 10.1137/16S015061
16. Casella F. Can the COVID-19 epidemic be managed on the basis of daily data? *arXiv [Preprint]*. arXiv:2003.06967.
17. Rawson T, Brewer T, Veltcheva D, Huntingford C, Bonsall MB. How and when to end the COVID-19 lockdown: an optimization approach. *Front Public Health.* (2020) 8:262. doi: 10.3389/fpubh.2020.00262
18. Dagnall N, Drinkwater KG, Denovan A, Walsh RS. Bridging the gap between UK Government strategic narratives and public opinion/behavior: Lessons from COVID-19. *Front Commun.* (2020) 5:71. doi: 10.3389/fcomm.2020.00071
19. Anzum R, Islam MZ. Mathematical modeling of coronavirus reproduction rate with policy and behavioral effects. *medRxiv [Preprint]*. (2020). doi: 10.1101/2020.06.16.20133330
20. Greenstone M, Nigam V. *Does Social Distancing Matter?* University of Chicago, Becker Friedman Institute for Economics Working Paper (2020). doi: 10.2139/ssrn.3561244
21. Andersen M. *Early evidence on social distancing in response to COVID-19 in the United States*. Social Science Research Network (2020). doi: 10.2139/ssrn.3569368
22. Observatoire français des conjonctures économiques (OFCE). Évaluation au 20 avril 2020 de l'impact économique de la pandémie de COVID-19 et des mesures de confinement en France. *OFCE Policy Brief* (2020).
23. Open Stats Coronavirus. *Covid-19 Statistiques/France*. Technical report (2020). Available online at: <https://www.coronavirus-statistiques.com/stats-globale/covid-19-par-pays-nombre-de-cas/>
24. Delfraissy JF, Atlani-Duault L, Benamouzig D, Bouadma L, Casanova JL et al. *Sortie Progressive de Confinement: Prérequis et mesures Phares*. Conseil Scientifique Covid-19 (2020).
25. Salje H, Kiem CT, Lefrancq N, Courtejoie N, Bosetti P, Paireau J, et al. Estimating the burden of SARS-CoV-2 in France. *Science.* (2020). doi: 10.1126/science.abc3517
26. Park YJ, Choe YJ, Park O, Park SY, Kim YM, Kim J, et al. Contact tracing during coronavirus disease outbreak, South Korea, 2020. *Emerg Infect Dis.* (2020) 26:2465–8. doi: 10.3201/eid2610.201315
27. Wu Z, McGoogan JM. Characteristics of and important lessons from the coronavirus disease 2019 (COVID-19) outbreak in China: summary of a report of 72 314 cases from the Chinese Center for Disease Control and Prevention. *JAMA.* (2020) 323:1239–42. doi: 10.1001/jama.2020.2648
28. Lau H, Khosrawipour V, Kocbach P, Mikolajczyk A, Schubert J, Bania J, et al. The positive impact of lockdown in Wuhan on containing the COVID-19 outbreak in China. *J Travel Med.* (2020) 27:taaa037. doi: 10.1093/jtm/taaa037
29. Fang H, Wang L, Yang Y. *Human Mobility Restrictions and the Spread of the Novel Coronavirus (2019-ncov) in China*. National Bureau of Economic Research (2020). doi: 10.3386/w26906
30. Lasaulce S, Varma VS, Morarescu C, Siying L. How efficient are the lockdown measures taken for mitigating the Covid-19 epidemic? *medRxiv.* (2020). doi: 10.1101/2020.06.02.20120089

**Conflict of Interest:** The authors declare that the research was conducted in the absence of any commercial or financial relationships that could be construed as a potential conflict of interest.

Copyright © 2021 Lasaulce, Zhang, Varma and Morărescu. This is an open-access article distributed under the terms of the Creative Commons Attribution License (CC BY). The use, distribution or reproduction in other forums is permitted, provided the original author(s) and the copyright owner(s) are credited and that the original publication in this journal is cited, in accordance with accepted academic practice. No use, distribution or reproduction is permitted which does not comply with these terms.



# A Novel BrainHealth Index Prototype Improved by Telehealth-Delivered Training During COVID-19

Sandra Bond Chapman<sup>1\*</sup>, Julie M. Fratantoni<sup>1</sup>, Ian H. Robertson<sup>1,2</sup>, Mark D'Esposito<sup>3</sup>, Geoffrey S. F. Ling<sup>4</sup>, Jennifer Zientz<sup>1</sup>, Stacy Vernon<sup>1</sup>, Erin Venza<sup>1</sup>, Lori G. Cook<sup>1</sup>, Aaron Tate<sup>1</sup> and Jeffrey S. Spence<sup>1</sup>

<sup>1</sup> Center for BrainHealth®, School of Behavioral and Brain Sciences, The University of Texas at Dallas, Dallas, TX, United States, <sup>2</sup> Institute of Neuroscience, Global Brain Health Institute, Trinity College Dublin, Dublin, Ireland, <sup>3</sup> Department of Molecular and Cell Biology, Helen Wills Neuroscience Institute, University of California, Berkeley, Berkeley, CA, United States, <sup>4</sup> Department of Neurology and Neuroscience, School of Medicine, Johns Hopkins University, Baltimore, MD, United States

## OPEN ACCESS

### Edited by:

Atefeh Abedini,  
Shahid Beheshti University of Medical  
Sciences, Iran

### Reviewed by:

Christos Frantzidis,  
Aristotle University of  
Thessaloniki, Greece  
Michael Matthews,  
United States Military Academy,  
United States

### \*Correspondence:

Sandra Bond Chapman  
schapman@utdallas.edu

### Specialty section:

This article was submitted to  
Infectious Diseases - Surveillance,  
Prevention and Treatment,  
a section of the journal  
Frontiers in Public Health

**Received:** 14 December 2020

**Accepted:** 15 February 2021

**Published:** 16 March 2021

### Citation:

Chapman SB, Fratantoni JM,  
Robertson IH, D'Esposito M,  
Ling GSF, Zientz J, Vernon S, Venza E,  
Cook LG, Tate A and Spence JS  
(2021) A Novel BrainHealth Index  
Prototype Improved by  
Telehealth-Delivered Training During  
COVID-19.  
Front. Public Health 9:641754.  
doi: 10.3389/fpubh.2021.641754

**Introduction:** Brain health is neglected in public health, receiving attention after something goes wrong. Neuroplasticity research illustrates that preventive steps strengthen the brain's component systems; however, this information is not widely known. Actionable steps are needed to scale proven population-level interventions.

**Objectives:** This pilot tested two main objectives: (1) the feasibility/ease of use of an online platform to measure brain health, deliver training, and offer virtual coaching to healthy adults and (2) to develop a data driven index of brain health. Methods: 180 participants, ages 18–87, enrolled in this 12-week pilot. Participants took a BrainHealth Index™ (BHI), a composite of assessments encompassing cognition, well-being, daily-life and social, pre-post training. Participants engaged in online training with three coaching sessions. We assessed changes in BHI, effects of training utilization and demographics, contributions of sub-domain measures to the BHI and development of a factor analytic structure of latent BrainHealth constructs.

**Results:** The results indicated that 75% of participants showed at least a 5-point gain on their BHI which did not depend on age, education, or gender. The contribution to these gains were from all sub-domains, including stress, anxiety and resilience, even though training focused largely on cognition. Some individuals improved due to increased resilience and decreased anxiety, whereas others improved due to increased innovation and social engagement. Larger gains depended on module utilization, especially strategy training. An exploratory factor analytic solution to the correlation matrix of online assessments identified three latent constructs.

**Discussion/Conclusion:** This pilot study demonstrated the efficacy of an online platform to assess changes on a composite BrainHealth Index and efficacy in delivering training modules and coaching. We found that adults, college age to late life, were motivated to learn about their brain and engage in virtual-training with coaching to improve their brain health. This effort intends to scale up to thousands, thus the pilot data, tested by an impending imaging pilot, will be utilized in ongoing machine learning



(ML) algorithms to develop a precision brain health model. This pilot is a first step in scaling evidence-based brain health protocols to reach individuals and positively affect public health globally.

**Keywords:** brain health, digital health, mental health, neuroplasticity, pandemic, personalized care, prevention, resilience

## INTRODUCTION

Public health policies can profoundly benefit people at all levels of society to flourish around the world (1). There is however, a notable void in policies for the health of the most crucial organ in the human body—the brain. This absence is starkly highlighted by the COVID pandemic where rapidly deteriorating mental clarity and psychological well-being (2) have accompanied sudden adverse changes in economic markets, employment, and social systems. These detrimental effects are magnified by health, social, and economic disparities.

### Brain Health Is a More Policy-Ready Concept Than Mental Health

As a concept, the term “mental health” is widely used, but is a rather limited term focusing narrowly on emotional well-being. To date, the term mental health fails to capture broad aspects of the “mind” and the interdependencies of other mental capabilities and dimensions. The term “brain health” is less familiar, but, we argue, is more useful for public health policy action, for a number of reasons. First, the term mental health does not address cognitive abilities—or “cognitive capital,” i.e., the summated cognitive capacities of a population. This is crucially important because greater cognitive capital has been shown to predict higher levels of health generally, both physical and mental [e.g., (3)]. The cognitive capital of a country is also crucial for its economic prosperity because it enables populations to pivot more adeptly and adaptively in the face of economic shocks, rapid technological change, and environmental challenges (4, 5). An absence or reduction of such a flexible mindset leads to economic and social deterioration that will worsen mental and physical well-being (6).

A second reason that brain health is more policy-ready as a concept than mental health is that it encompasses what is predicted to be one of the greatest health challenges facing the world, one that particularly impacts low and middle income countries (7). This health challenge is the spiraling prevalence of dementia linked to the accelerating proportion of older people in all countries in the world, secondary to impressive lengthening of life expectancy (8). Additionally, impaired well-being is associated with dementia, but is often ignored in treatment considerations as the interrelationships are disregarded (9). Mental health as a concept does not afford policy implications for this enormous health challenge that, if unchecked, will swamp the resources and finances of health providers and services. Brain health, on the other hand, is “oven-ready” as a concept to be tested, with clear implications for policy, some of which we will describe in this paper.

Thirdly, the concept of brain health has positive connotations that avoid a certain stigma that attaches to mental health brought on due to the large focus on diagnosing deficits rather than considering individual potential. Brain health, on the other hand, organizes around capacity-building principles of neuroplasticity. Therefore, it affords vast opportunities for policymakers to advance population-scale interventions to millions of people, which could make headway in mitigating fear of being stigmatized, and to replace such concerns with individual empowerment. Brain health offers a positive message that is similar to successful heart-healthy interventions such as those advocating the value of aerobic exercise (10, 11). In sum, the semantics of mental health, as a concept, do not extend plausible multifaceted pathways to motivate desirable behavior change.

Fourthly, mental health has a confusing definition, because it combines “absence of mental illness” and imprecisely-defined ideas of emotional well-being (<https://www.merriam-webster.com/dictionary/mental%20health>). Such ambiguity makes mental health difficult to measure and hence fails to motivate behavioral change aimed at building it and intercepting issues before they become clinically significant deficits. Behavior change needs clear metrics to incentivize progress. Indeed, we manage what we measure. The absence of such metrics deters the sort of learning and behavior change we know to be essential to improve healthy habits (12). Yet the lack of a clear index of the health of the brain—the most important organ in the body, subserving all emotions, cognition, and behavior—is a major void for public health policy.

The concept of brain health lends itself to the creation of such an index, because it is a less confused term than mental health: It avoids the false dichotomies underpinning “mental health,” namely between mind and brain on the one hand, and emotion and cognition on the other. In this paper, we define, establish, and begin to validate a newly developed BrainHealth Index. We acknowledge that improvements in this index will require increased data over larger populations and longer time intervals of years. Nonetheless, this effort catalyzes that progress toward utilization of sophisticated data analytical methods, including, for example, machine learning.

Finally, brain health is a high-level category of health and actually incorporates the emotional and behavioral phenomena that comprise the concept of mental health. Brain health, in contrast to mental health, lends itself to wider public acceptability and greater opportunities for proactive, preventive interventions to potentially intercept concerns before they become clinically debilitating. Thus, it follows that population-scale policies will have tremendous impact if they improve not only the cognitive

capacity and flexibility of individuals but also the well-being and social connectedness of millions of people, particularly in the context of global challenges such as a health pandemic, e.g., COVID19.

## Measuring Brain Health

Our existing health systems have a limited scope of brain health, viewing it through the lens of disorder and disease rather than optimal function. For example, the National Institutes of Health (NIH) does not have its own definition of brain health and instead, uses one provided by the National Institute on Aging (13). Yet identifying brain health with aging ignores the centrality of brain health to the well-being and physical health of all ages, and risks misclassifying the concept as a problem of aging. Furthermore, the primary old-age-focus of the NIA definition of brain health results in only four elements being included, namely cognitive health, motor function, emotional function, and tactile function. This NIA definition of brain health is limited in the breadth and scope of what the brain is capable of and responsible for achieving. Specifically, the NIA definition leaves out components of social interaction (social support, social engagement, compassion), daily life (nutrition, exercise, mindset, sleep, responsibilities), and well-being (resilience, mood, quality of life). The fact that brain health is multifaceted and complex dictates a more integrated approach, rather than the current fragmented, siloed approach where domains are either not assessed at all or only as separate entities. Our preliminary BrainHealth Index encompasses all of these components—cognition, well-being, social interaction, and daily life. This is the first time these components have been combined to capture a single measure of the brain in an inter-related, holistic sense. There is a need to shift our existing thinking and definitions to include all of these domains in order to better care for the brain and understand the multiple pathways to strengthen overall brain health capacity. By integrating large-scale data across multiple domains and time intervals, we can evaluate, interpret, and perhaps even predict how components interact to achieve maintained, increased, or diminished brain health, at both group and individual levels. For example, emotions such as anxiety and depression affect cognitive function (14–18) while strong cognitive functions—particularly executive and attention processes—aid emotional regulation and build resilience (19, 20). Social isolation has negative effects on emotional well-being and cognitive function (21, 22). Sleep (23), diet (24), and physical activity (25) all mutually interact and affect these other emotional, cognitive, and social functions (26–28). Furthermore, all of these different processes both depend on, and influence the structure and function of brain networks and systems (29, 30). Brain health depends on the complex, interwoven interactions of these multifaceted processes (cognition, well-being, social, life habits/responsibilities) and therefore should not be addressed independently of each other. For this reason, a composite brain health measure is needed. As stated above, this study represents the first attempt to create such a holistic composite, which we label the BrainHealth Index, deliverable on an online platform.

## Scalable, Policy-Relevant Brain Health Interventions

To our knowledge, there have been no scalable interventions developed and tested to increase synergistically the multifaceted aspects of brain health across all age groups in a population. Moreover, definitely none exists that is delivered entirely remotely through a telehealth platform. The most prominent and successful attempt at a scalable multi-faceted intervention was directed at older individuals at risk of dementia, known as the Finnish “FINGER” trial. The FINGER trial showed how a multi-modal intervention delivering vascular risk monitoring, cognitive training, and dietary and exercise advice, could significantly improve cognition (27). This important study has seeded a worldwide network of similar trials (see an overview at <https://alz.org/wwfingers/overview.asp>).

The present intervention protocols differs in two main ways from the FINGER intervention. First, this pilot study targets all adults, ranging in age from 18 to 90, with the aim to test group and individual ability to improve brain health for a range of outcomes including mental well-being, innovative thinking, work performance, and social connection at one of the most difficult economic times in our history. Additionally, the current effort lays the foundation to assess effectiveness in reducing, postponing, or halting dementia risk as individuals are followed over time from health to diagnosis. Secondly, and crucially in the context of the COVID-19 pandemic, the current pilot was delivered entirely remotely which is a key factor in making such efforts scalable at a global level. The FINGER protocol is labor-intensive and, in contrast to the very low cost of a remote program, very expensive.

Our work complements and builds on decades of positive findings of the possibility of enhancing cognitive and emotional function using verbal and/or procedural protocols ranging from teaching strategy aimed at improving efficiency of frontal-lobe-based executive networks (31–35) to enhancing mood and reducing anxiety through methods such as cognitive behavior therapy (35). The ability to scale such methods using web-based technology has led to their now being available entirely remotely to millions of users across the globe. Most online offerings do not have strong published evidence of their efficacy. One exception to this are the BrainHQ ([www.brainhq.com](http://www.brainhq.com)) online training programs that have shown positive cognitive effects in a range of populations across many studies (36–42). One such study showed impressive gains in certain cognitive processes of older adults with real-life benefits maintained up to 10 years later with just a few booster sessions (39, 43). Their work has also shown to be associated with lowering driving accidents in older adults, and improvements in daily life independence (36, 38, 39). In larger, follow-up interventions, our goal is to include a range of evidence-based training methods, such as BrainHQ, selecting those with strong empirical support. We aim to test the extent to which participants can achieve gains on the holistic BrainHealth Index as we expand the study to larger enrollment with 10-year or longer follow-up in the BrainHealth Project.

Today more than ever, we need a global brain health strategy translatable across the lifespan (5). Fortunately, heart healthy

practices, established by decades of observational and more recently interventional studies (44), lay out a roadmap for how to increase public awareness and health practices. Over the past five decades, the Framingham study has delivered tremendous knowledge regarding preventive lifestyle habits, annual objective measurements, and medical interventions when necessary (45, 46). The good news is that people everywhere have access to: (a) clear indices of their heart health and (b) science-driven information on what they need to do to improve their heart health (47).

## Pilot Study Goals

The present study offers professional-quality video-based interventions aimed at teaching tactical cognitive strategies previously shown to improve brain health, including stress management and cognitive strategy training. Additional informational videos on diet, exercise, and sleep hygiene were provided. Remotely-delivered, individualized coaching sessions with a trained coach helped participants understand and integrate this information. Our prior work has shown that cognitive strategy training can generalize beyond the trained domains to neural signatures underpinning brain health, such as increased brain blood flow, connectivity, and cortical thickness, with the brain changes linked to improved complex cognition, psychological well-being, real life functions, and social adeptness (31, 32, 48–52).

We want to acknowledge at the outset, that this pilot study is the first element of a planned three-phase BrainHealth project (<https://brainhealth.utdallas.edu/programs/the-brainhealth-project/>). The first major goal of the present pilot study was to test an online system for: (1) remote delivery and collection of assessments; (2) remote delivery of a set of training modules; and (3) the feasibility of virtual coaching sessions with individual participants. The second major goal of this pilot study was to develop an exploratory factor model of a BrainHealth Index derived from the assessments in the domains of cognition, well-being, real life, and social interaction.

## METHODS

This study was performed in accordance with the standards provided by The University of Texas at Dallas IRB. All participants were informed about the study protocol before obtaining written informed consent.

## Recruitment

Participants were recruited for the study through word of mouth and email advertising. As the primary aim was to study the brain in health we recruited generally healthy adults. Participants completed an online screening form to determine if they qualified for the study. Inclusion criteria consisted of being: 18 years or older, able to access the internet (including access to a computer/smartphone/tablet), and being a proficient English speaker. Potential participants were excluded for any of the following reasons: being under age 18, having a diagnosed neurological disorder, diagnosed psychotic disorder or uncontrolled psychiatric disorder, history of brain injury, or any

uncontrolled health issues. It is important to note participants were not excluded for general health risk factors (ex: obesity, diabetes, and autoimmune conditions).

Two hundred people took the screener and 180 qualified for the study (**Figure 1**). One hundred eighty participants completed the baseline assessments for the BHI. Of those 180, 174 engaged in the online training and coaching. The six participants who did not engage in training were unresponsive to email prompts and reminders. One hundred and forty four participants took the Time 2 BHI. The 30 participants who did not complete the Time 2 BHI were sent reminders via email and phone. Most reported they were too busy and did not have time to take the assessments.

## Study Protocol

This pilot study consisted of online assessments, coaching, and training over a period of 12 weeks (**Figure 2**).

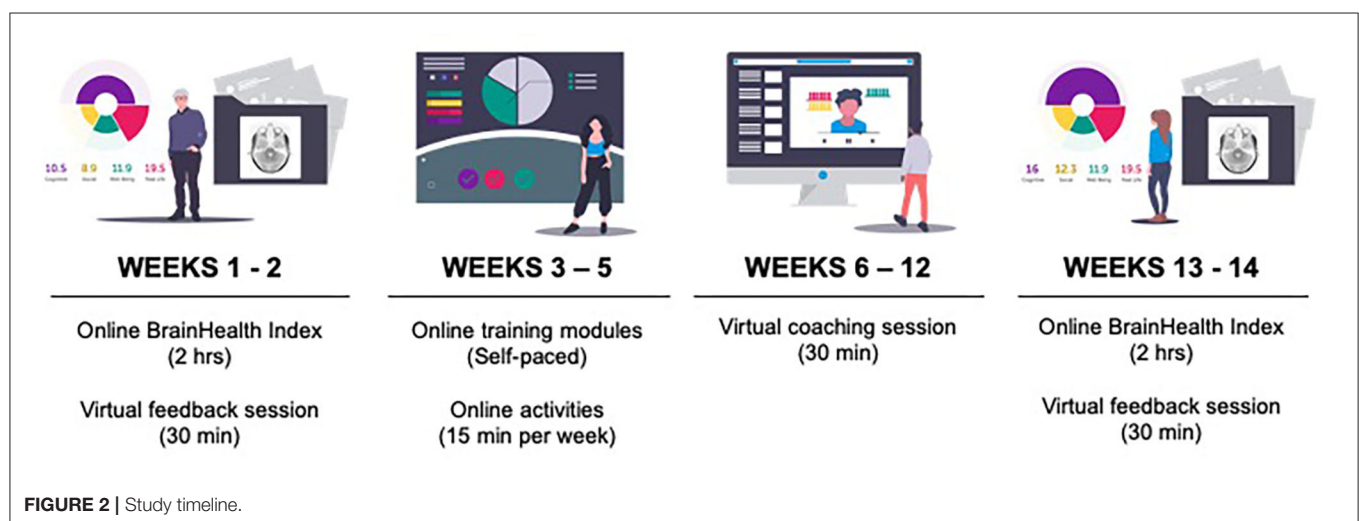
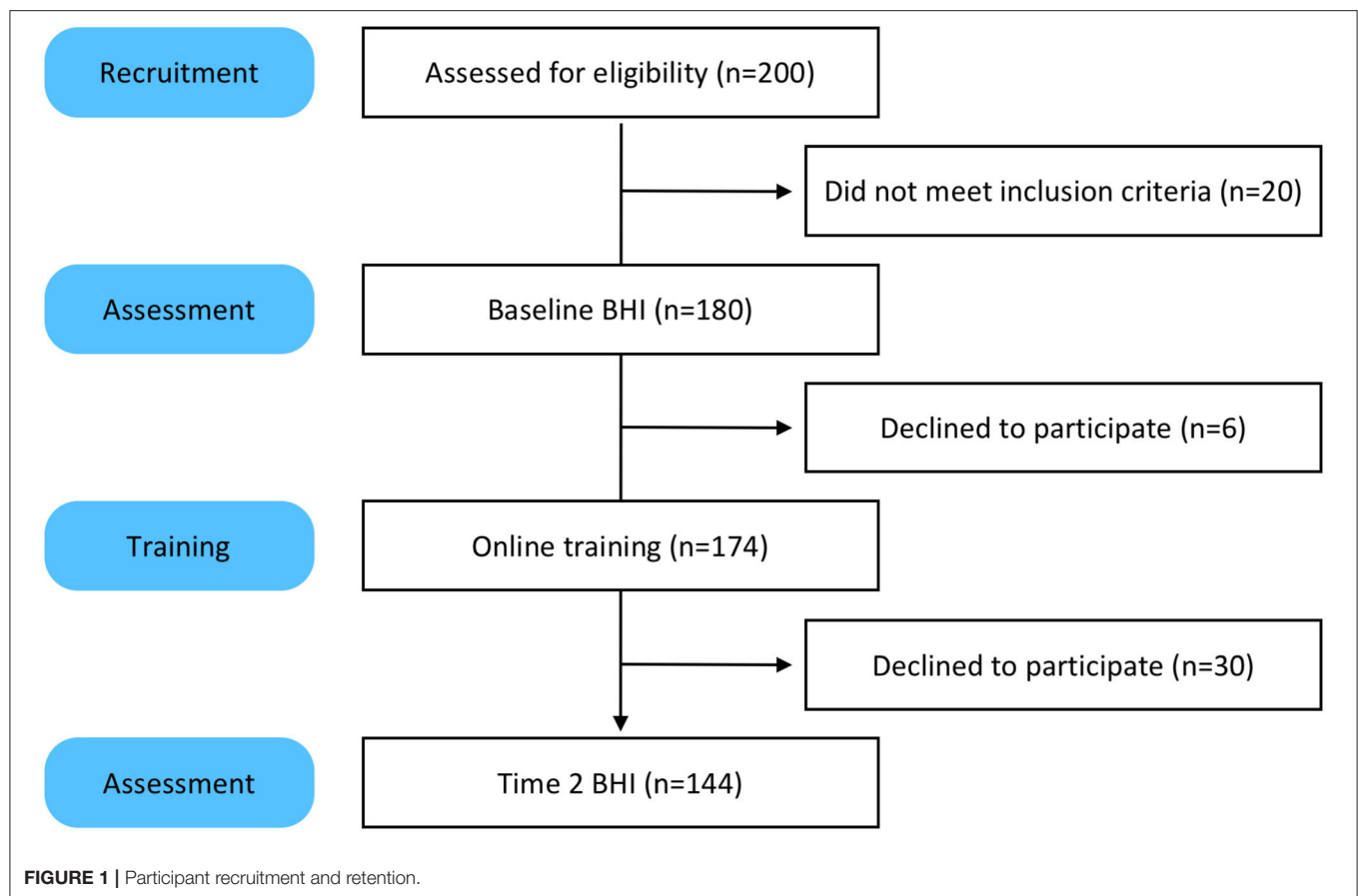
First, participants completed the online assessments and then received their BrainHealth Index score. Week 2, participants had their first coaching call with a BrainHealth coach to discuss their BrainHealth Index results and get personalized recommendations for interacting with the online training based on those results. The BrainHealth coaches were all masters-degree level clinicians who were well-versed in the implementation of the content found in the training modules. Weeks 3–5, participants were directed to complete self-paced online training modules (described below). Week 6 was a halfway-point coaching call intended to motivate participants to continue implementing what they learned in training into real-life. Weeks 7–10, participants continued working through training modules. Week 11, participants took the assessments for the BrainHealth Index a second time. Week 12, participants had their third coaching call where they were able to learn about and compare the changes in their BrainHealth Index score.

## Assessments

Participants completed a series of online assessments that tapped into our four critical hypothesized domains of brain health: (1) cognition, (2) well-being, (3) social interaction, and (4) daily life (**Table 1**).

The cognitive assessments consist of a battery of measures of complex text, which do not have ceiling effects and are a robust measure of cognitive aging. The cognitive evaluation looks at complex thinking capacities—such as reasoning, innovation, strategy, and memory. The well-being evaluation taps into an individual's emotional sense of self. This includes questions about quality of life, level of happiness, levels of stress and sadness, and emotional resilience. The social interaction evaluation looks at an individual's social vibrancy and quality of relationships, specifically, how they feel about their social support networks and the meaningfulness of their social engagements. The daily life evaluation monitors the complexity (depth and breadth) of daily responsibilities, habits, and challenges. These questions seek to understand how individuals optimize life circumstances and habits.

Whereas, many of these individual components of the BrainHealth Index are not novel, what has not been done before is integrating and interpreting these aspects as a single



composite index. The BrainHealth Component Wheel illustrates the complexity of these domains (Figure 3) and lays a foundation to build a model illustrating the interrelated, dynamic nature of the components.

The Component Wheel was designed not only to clarify the assessment domains, but also to educate participants regarding the myriad of paths to increase their brain health literacy. The

goal is for participants to embrace a perspective that brain health encompasses habits and behaviors working in concert across the above-mentioned domains and that strength building in one domain may generalize to gains in other dimensions. On the downside, participants also learn that losses may follow a similar but reverse pattern with decrements in one domain having a deleterious effect on others.



**TABLE 1** | List of online assessments.

| Domain      | Measure   | References                          | Time   |
|-------------|---|-------------------------------------|--------|
| Cognition   | Strategic attention: visual selective learning task     | (53)                                | 30 min |
|             | Innovation: pictures                                    | Developed at Center for BrainHealth |        |
|             | Innovation: high-level interpretation (TOSL)*           | (54)                                |        |
|             | Abstraction: proverbs                                   | Developed at Center for BrainHealth |        |
|             | Integrated reasoning: high-level summary of text (TOSL) | (54)                                |        |
| Well-being  | Memory for detail (TOSL)                                | (54)                                | 15 min |
|             | Happiness: Oxford Happiness Questionnaire               | OHQ; (55)                           |        |
|             | Depression, Anxiety, Stress Scale                       | DASS-21; (56)                       |        |
|             | Resilience: Connor-Davidson resilience scale            | CD-RISC-25; (57)                    |        |
| Interaction | Life satisfaction: Quality of life scale                | QOLS; (58)                          | 8 min  |
|             | Social support: Social Support Survey Index             | (59)                                |        |
|             | Compassion  | Adapted from (60, 61)               |        |
| Daily life  | Social engagement: Social BrainHealth Scale             | (48)                                | 20 min |
|             | Engagement in Meaningful Activities Survey              | EMAS; (62)                          |        |
|             | Sleep: Pittsburgh Sleep Quality Index                   | PSQI; (63)                          |        |
|             | Metabolic Equivalents: Cardiorespiratory Fitness        | CFEQ; (64)                          |        |
|             | Estimate Questionnaire                                  |                                     |        |
|             | Outlook: BrainHealth Appraisal Questionnaire            | Developed at Center for BrainHealth |        |

\*Test of Strategic Learning.

## Coaching

Three, 30-min individual coaching sessions with a clinician were offered to participants using video conference or telephone calls. The objectives of the coaching sessions were to review the participant's BrainHealth Index, provide awareness to improve literacy regarding the brain's potential to be modified by experience and habits, and to provide direction, guidance, and support related to the online cognitive training, stress solutions, and sleep advice.

## Training Protocol

This was a non-randomized, phase one pilot intervention trial designed to examine the neurocognitive and real-life (emotional well-being, social interaction, and daily function) benefits from an online training protocol. The current offerings were selected based on three decades of scientific investigations, including reported clinical trials showing that strategy training can yield significant gains in the multiple aspects contributing to brain health [e.g., (33, 65)]. These areas of positive change after in-person delivery of *Strategic Memory Advanced Reasoning Training* (SMART, described below) include: cognition (i.e., strategic attention, integrated reasoning, innovation), well-being (reduced depression, stress, anxiety), and real life function (increased quality of life and complexity of life work). These positive behavioral changes were correlated with significant changes in cerebrovascular brain metrics such as brain blood flow, neural connectivity, and neural efficiency (31, 32, 49–51, 66–68).

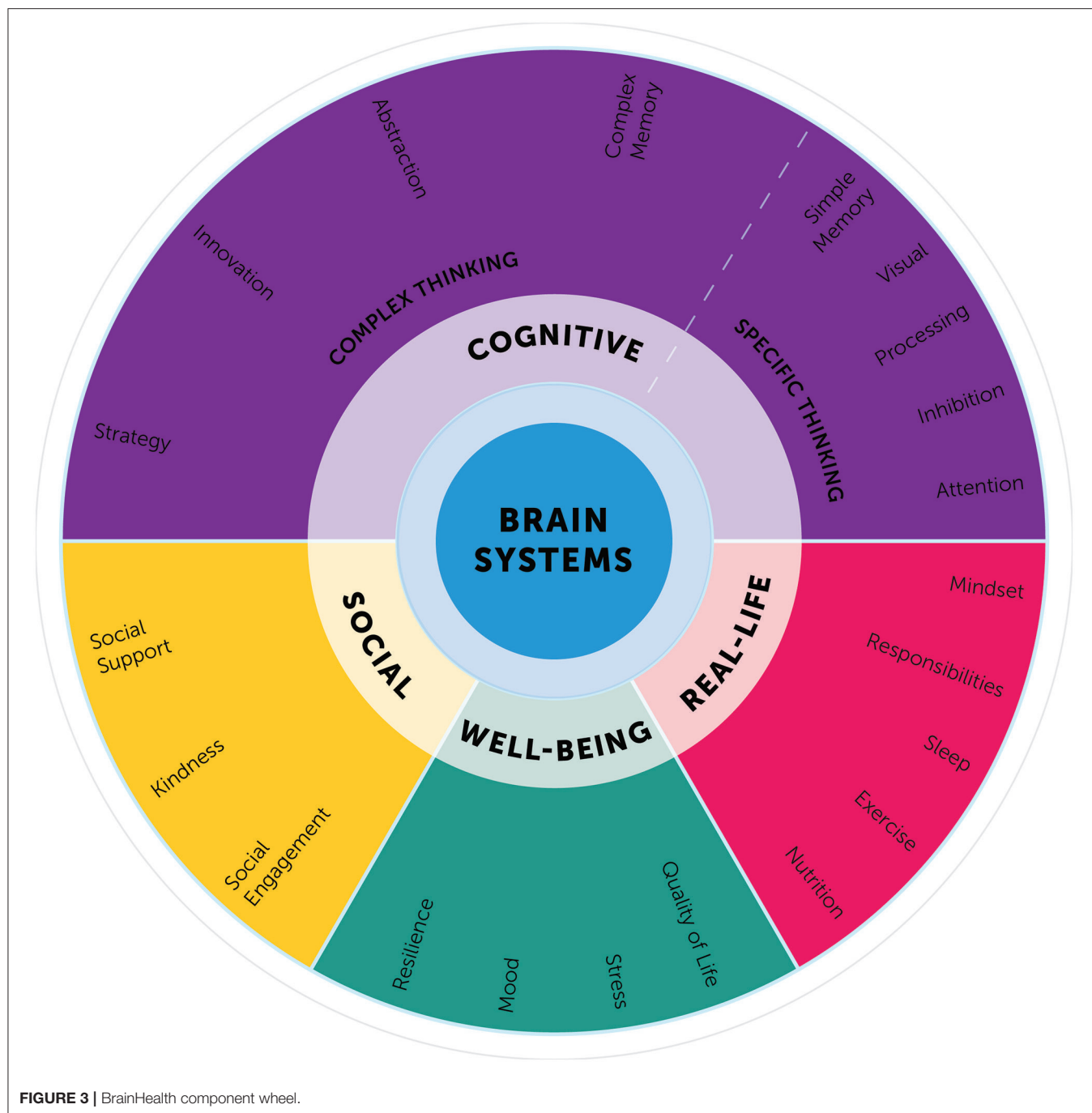
What was not tested in prior trials was whether the BrainHealth Index and strategy trainings could be delivered

through an online platform with similar efficacy and ease of use across the lifespan from teens to late life. The limitations of in-person assessments and trainings include reduced accessibility and high costs—factors that reduce the ability to meet public health demands. A dynamic online platform affords not only increased accessibility to the personalized information and tools provided but also facilitates greater adoptability (i.e., continued engagement) and scalability.

Training consisted of tactical brain strategies that are applicable to a multitude of circumstances, decisions, and goals. Participants completed 9 self-paced training modules over the 12-week period (**Table 2**). Modules 1–4 were the online, self-paced version of SMART, an evidence-based cognitive training protocol that is strategy-based, rather than content-specific (31, 32, 65). SMART includes tactical brain strategies of Strategic Attention, Integrative Reasoning, and Innovation as a guide for engaging in deeper-level innovative thinking across real-life activities.

Strategic attention strategies help reduce information overload and improve one's ability to block out irrelevant information to better focus and prioritize what really matters. Integrated reasoning strategies target the ability to abstract meanings from specific key details (be it from a situation or information), to interpret them within a broader context of world knowledge, and to create global themes and take away messages that remain relevant to the information or task at hand. Innovation strategies guide people to generate multiple, diverse perspectives and seek multiple solutions to better inform decision-making. Participants are provided exercises to practice real life tasks that incorporate strategic





attention, integrated reasoning, and innovation strategies as often as possible within the context of their own daily responsibilities and relationships. The goal is to make this type of thinking habitual by processing information at a focused, calm, and deeper level and to make innovative cognition intentional.

After engaging with the tactical brain strategies delivered via the online SMART modules, participants progressed to training modules 5-7 (Stress Solutions), which linked

the SMART principles with stress management research and techniques. Specifically, the Stress Solutions modules expand upon the SMART strategies to manage stress, build resilience, and make healthier lifestyle choices. Participants learn and practice skills in awareness, self-regulation, and emotion regulation through attentional focus exercises grounded in mindfulness meditation. Module 8 focused on information about sleep and how to improve one's sleep hygiene. Module 9 was an informational message

**TABLE 2 |** Description of self-paced training modules.

| Module                  | Description   | Time   |
|-------------------------|---|--------|
| 1. SMART 1              | Provides strategies and interactive activities on how to block irrelevant information and focus on key priorities (strategic attention). Example: Prioritize how you spend your time based on cognitive effort—each day identify top two tasks that require the most deeper level thinking.   | 30 min |
| 2. SMART 2              | Includes strategies and interactive activities on how to abstract big-picture concepts from information to better inform real life decisions (integrated reasoning). Example: Extract key concepts from incoming information vs. trying to take in and remember everything.   | 30 min |
| 3. SMART 3              | Includes strategies and interactive activities on how to generate multiple and diverse perspectives/interpretations to strengthen mental flexibility (innovation). Example: Identify multiple alternative ideas/perspectives on divisive issues.  | 30 min |
| 4. SMART 4              | Consists of real-life application scenarios where participants can practice dynamic implementation of the strategies from SMART 1-3 (strategic attention, integrated reasoning, and innovation) in a cohesive manner. Example: Think about and prepare for a difficult conversation with someone you care about (considering their perspective, identifying the real issue at hand etc.). | 30 min |
| 5. Stress Solution 1    | Presents the physiological and neurological response to stress, as well as cognitive strategies (linking with SMART) to manage and reframe stressors. Example: Reframe your perception of your response to a difficult situation from anxiety to excitement.  | 20 min |
| 6. Stress Solution 2    | Includes accessible techniques to help “recharge your battery” in times of stress or fatigue, as well as education on lifestyle factors that can positively impact our overall health. Example: Take several short breaks throughout your day.  | 20 min |
| 7. Stress Solution 3    | Provides research on the benefits of mindfulness, meditation, and healthy sleep habits, as well practical tips on how to practice each one (linking with SMART). Example: Participate in a meditation exercise.   | 20 min |
| 8. Sleep                | Presents research from Dr. Russell Foster on the science behind sleep, the brain impact of poor sleep, and practical tips for improving one's sleep habits.   | 20 min |
| 9. COVID-19 Information | Safety tips from an emergency medicine physician on how to protect ourselves and others during the COVID-19 pandemic.   | 5 min  |

*Modules 1-7 consisted of videos teaching tactical brain strategies and application exercises. Modules 8-9 were informational videos only.*

from an emergency medicine physician about what steps to take to protect self and others from contracting or spreading COVID-19.

## A BrainHealth Index Prior to Pilot Data Collection

As it was necessary to deliver a quantifiable measure of BrainHealth to our participants at two time points throughout the study, we developed a preliminary Index that would be meaningful to both participants and coaches. By doing so, we could evaluate our online system and real-time coaching and participant feedback without the need to wait until the end of our pilot study. To reiterate, this was an important aspect of the first major goal of the pilot study itself. Therefore, prior to data collection, our preliminary BrainHealth Index was a composite of the measures listed in **Table 1**, covering the four broad domains of brain health—cognition, well-being, social interaction and daily life. Each measure,  $z_i$ , was first converted to a common percentile scale  $z_i \rightarrow P_i$  and the Index was calculated as  $\sum_{i=1}^m w_i P_i$ , such that  $\sum_{i=1}^m w_i = 1$ . That is, our preliminary BrainHealth Index was a weighted average of transformed sub-domain measures from the BrainHealth component wheel (**Figure 2**). The transformations were derived as  $\{P_i = 100p_i : \Phi(z_i) = p_i\}$ , where  $\Phi(z_i)$  is the cumulative distribution function of  $z_i$ . Each of the  $\Phi(z_i)$  was determined by one of three methods: (1) Within the cognitive domain the  $\Phi(z_i)$  were estimated empirically, as we have over 1,000 individuals who have taken BrainHealth physicals at the Brain Performance Institute, University of Texas at Dallas; (2) For measures in the other domains, with the exception of the Cardiorespiratory Fitness Estimate Questionnaire [CFEQ; (64)], the  $\Phi(z_i)$  were obtained theoretically using either Gaussian, gamma, or negative binomial distributions whose respective parameters yielded  $z_i$  to match distribution statistics given in the references that described or utilized the measure; and (3) Finally, we obtained  $\Phi(z_i)$  for metabolic equivalents, derived in the CFEQ, from a bootstrap distribution obtained using the sufficient statistics of the individual variables that contribute to the model-based calculation of metabolic equivalents.

Because we had no preliminary data prior to the start of the pilot study, the weights,  $w_i$ , were fixed by clinical consensus of clinicians working on the project. The consensus of three clinicians with over 10 years of experience in BrainHealth Physicals assigned 50% of the weight to the cognitive domain, as these measures have been studied extensively at the Center for BrainHealth, University of Texas at Dallas, showing associations of functional brain changes with training utilization and the measures in the cognitive domain. Daily life and social domains were also assigned relatively higher weight, as these domains represent long term function. However, as noted above, one important goal of our Phase 2 and Phase 3 studies that will follow this pilot is to obtain data-driven calculations of brain health indices. As the raw data emerge from the factors mentioned above, from additional measures of cognition (e.g., processing speed, working memory, sustained attention, inhibition) and from other experimental measures being collected, we will be afforded the opportunity to discover those particular measures that provide the best contribution to, and assessment of, brain health. Importantly, these discoveries will be grounded in a

neurobiological and biophysical basis, as a large percentage of participants will also have measures from wearables and from functional and structural brain imaging. Machine learning will guide the mapping of these physical measures onto the space of our online assessments, which will serve both to calculate relevant indices of brain health and to justify the calculation based on physiology.

## Development of a BrainHealth Index From the Pilot Data

Our preliminary BrainHealth Index served an important function for our pilot study. It enabled our participants to receive immediate feedback from their assessments, and it enabled our coaches to offer personalized coaching sessions to participants in real time. Both of these were essential for an engaging user experience and the development of a successful online platform with which we can proceed to Phases 2 and 3 of the BrainHealth Project.

To address our second major goal of Phase 1 of the BrainHealth Project, the data collected from this pilot study was used to develop a modified BrainHealth Index, one that does not rely on fixed  $w_i$  by consensus but, rather, one that allows estimated  $w_i$  for variables on a natural scale. This was accomplished by fitting an exploratory factor model of the inter- and intra-domain correlations of online assessments. Specifically, we were interested in the relationships of 3-month change measures for each assessment since we posited that measures adaptable to change following training and coaching are those most relevant to plasticity changes in the brain over time. Therefore, a latent factor model of the correlations among change measures was estimated and utilized to obtain appropriate variable weights to transform individual assessments to factors.

## RESULTS

### Demographics

Our initial pilot sample contained 180 participants who completed their online baseline Assessments; 174 were assigned the set of training modules through the dashboard portal. The completion rates of training modules are recorded (described in more detail below), in brief, 144 participants completed their 3-month follow-up assessments, whether or not they completed the training modules. Our retention rate was 80% (see **Figure 1**).

**Table 3** lists some of the demographic characteristics of our initial sample of 180. The age of participants ranged 18–87 with a median of 55.9 and interquartile range (IQR) 33–78.8. Although our sample contained a large proportion of women (72%) and a highly educated cohort (87% with at least a Bachelor's degree and 41% with post-baccalaureate degrees), the age distributions were similar across gender and higher-education categories. For 13% of our sample without at least a Bachelor's degree, the age distribution was bimodal with a median 21.3 for the sub-cohort who are still in college and a median of 63.5 for those who are not in college.

### Preliminary BrainHealth Index

We first assessed whether or not the baseline BrainHealth Index and the change in the BrainHealth Index over 3 months depended on demographic sub-groups, which could indicate potential confounds in our analyses. Baseline characteristics of the preliminary BrainHealth Index by demographics are shown in **Figure 4**. The median value was 54 overall (IQR 45–61), and the distribution of the baseline Index was similar across age, education, and gender (**Figure 4**).

After 3 months following self-paced training and engaged, personalized coaching sessions, the change in the BrainHealth Index ( $\Delta$  BHI) had an average gain of 10.3 points across the entire sample (**Figure 5A**,  $p < 0.001$ ,  $d = 1.03$ , 95% CI 0.83–1.25). Moreover, 75% of participants showed at least a 5-point gain in the BrainHealth Index over 3 months. As with the baseline BHI values, the change in the BrainHealth Index also did not depend on age ( $p = 0.55$ ), education ( $p = 0.11$ ), or gender ( $p = 0.45$ ). **Figure 5B** demonstrates the regression of  $\Delta$  BHI on age. The average change in the BrainHealth Index is near 10 units across the age range and for both male and female participants.

All participants were assigned the training modules (**Table 2**) as well as informational content about sleep and COVID-19 for a total of 9 assignments, taken sequentially. Of the 80% of participants who completed their second assessments after 3 months, not all of them completed the training modules. We expected that there would be considerable variability in the amount of training participants were willing to complete. Therefore, another important question that we asked was whether the gains in the BrainHealth Index depended on self-paced training utilization, which also served to indirectly assess two potential confounds, namely practice effects and participant motivation.

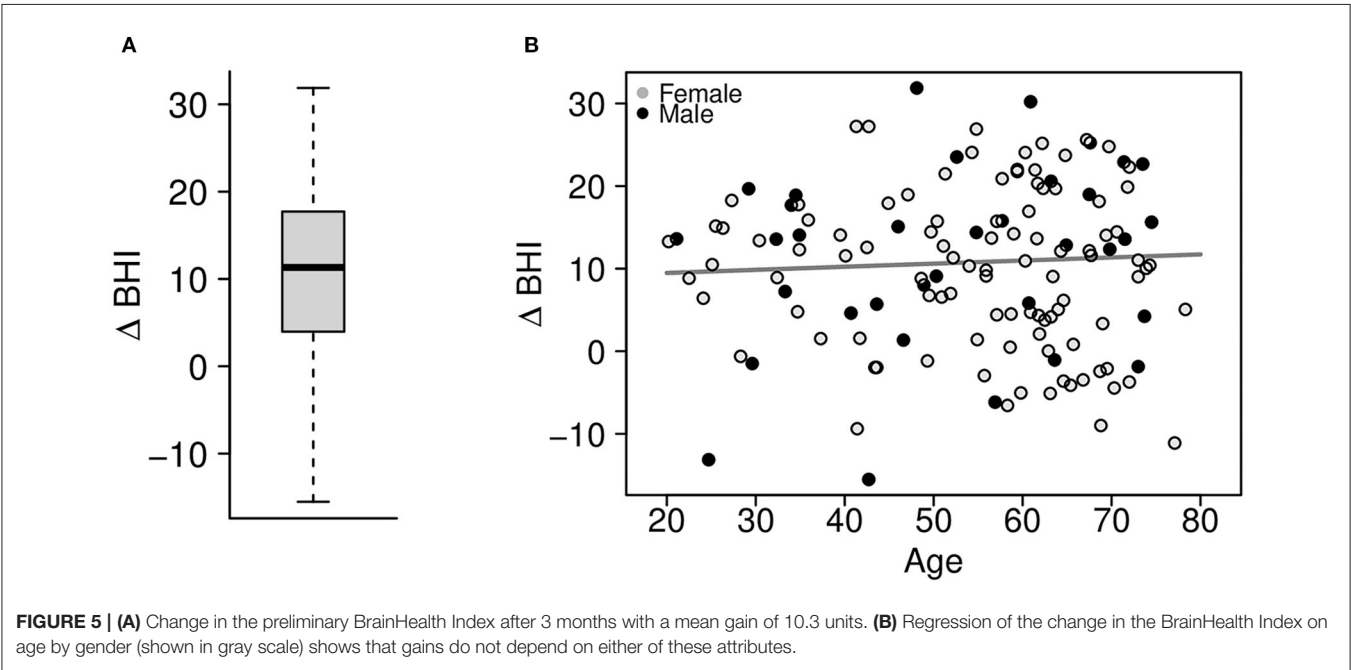
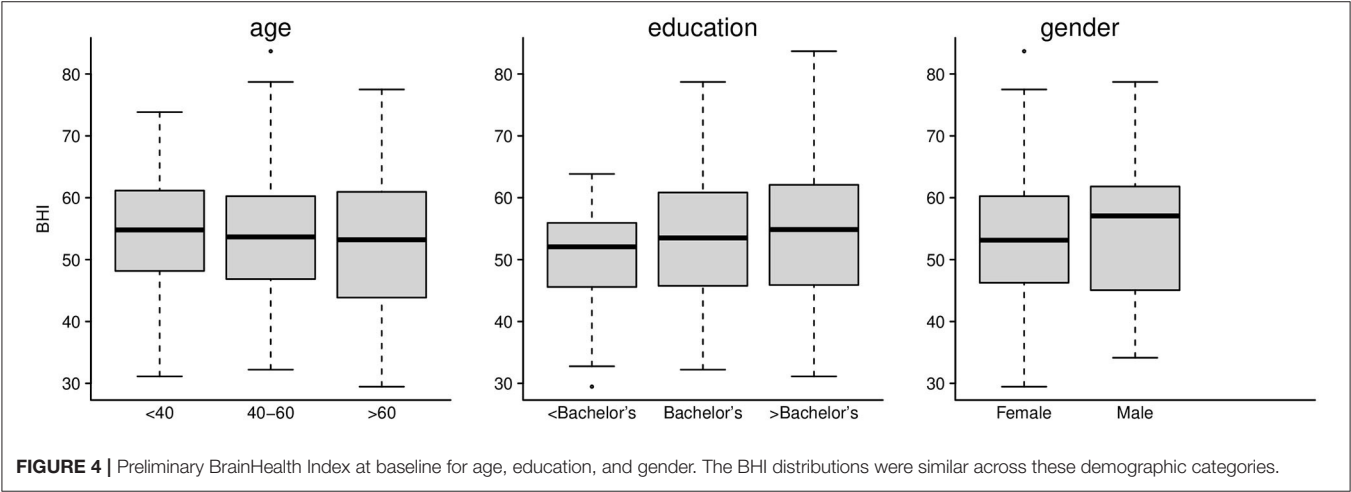
**Figure 6** shows change in the BrainHealth Index as a function of training utilization, which was estimated by the number of cumulative training modules completed, beginning with the four cognitive training modules and followed by the stress modules, then informational content. There are fractional values for the number of cumulative training modules completed because many participants did not fully complete modules (all activity, including time spent, was recorded).

Superimposed on the scatterplot in **Figure 6**, we show a conditional average, which was estimated by a regression of the change in the BrainHealth Index on a 3-degree-of-freedom natural cubic spline basis. The curve shows that there is no increase in the BrainHealth Index on average when participants completed none of the training assignments. Conversely, for those that completed the cognitive training modules and nothing further (i.e., 4 modules completed), the average increase in the BrainHealth Index was 8 units ( $p = 0.005$ ,  $d = 0.98$ , 95% CI 0.79–1.21). If participants, additionally, completed the stress modules (dashed red line at 7 modules completed), the average increase in the BrainHealth Index improved 4 units further ( $p < 0.001$ ,  $d = 0.43$ , 95% CI 0.25–0.61). However, if participants completed the rest of the training assignments beyond the first seven, there was no additional increase in the BrainHealth Index on average, as seen in **Figure 6** by the flattening of the regression curve.

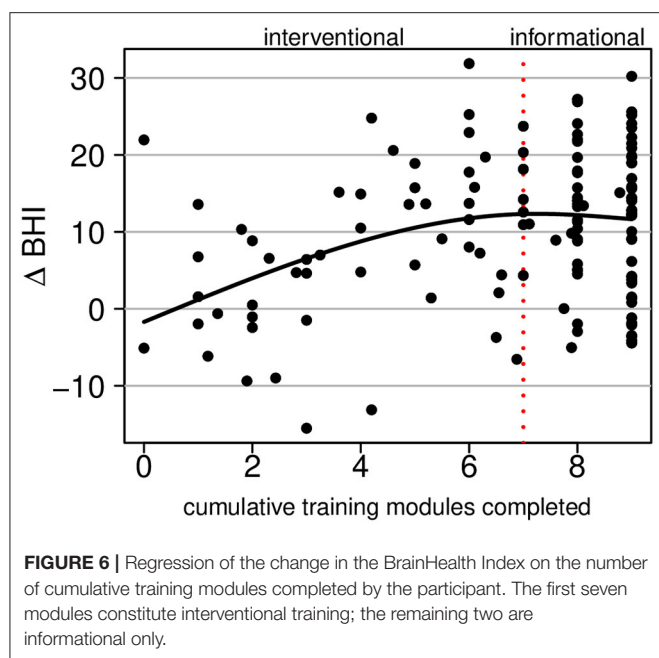
**TABLE 3 |** Demographic characteristics of our sample (*n* = 180).

|             |             | Age* x Gender |  | Age* x Education |           | Gender x Education |      |
|-------------|-------------|---------------|--|------------------|-----------|--------------------|------|
| Age*        | 55.9 (22.9) |               |  |                  |           |                    |      |
| Female      | 129 (0.72)  | 57.4 (20.6)   |  |                  |           |                    |      |
| Male        | 51 (0.28)   | 49.6 (31.7)   |  |                  |           |                    |      |
|             |             |               |  |                  |           | Female             | Male |
| <Bachelor's | 23 (0.13)   |               |  | 31.8 (41.3)      | 14 (0.61) | 9 (0.39)           |      |
| Bachelor's  | 83 (0.46)   |               |  | 56.9 (20.3)      | 58 (0.70) | 25 (0.30)          |      |
| >Bachelor's | 74 (0.41)   |               |  | 56.8 (24.1)      | 57 (0.77) | 17 (0.23)          |      |

*n* (proportion) except \*median (IQR).



The fact that the regression curve in **Figure 6** is relatively linear between the values 0 and 6 (training modules completed) suggests that gains in the BrainHealth Index are likely not solely due to practice effects. If gains were solely due to practice effects, one would expect a horizontal line at the overall average change in the BrainHealth Index (10.3 units), regardless of training



utilization. Moreover, if the increase in the change Index were due only to participant motivation, independently acting upon the change Index and the training utilization, one would expect an increase over the entire interval of training modules completed. However, this is not the case. There is no additional increase in the BrainHealth Index on average beyond 70% of the training assignments completed. Importantly, this observation cannot be explained by a ceiling on potential change because there exists a much larger range of potential change beyond that which is represented by our sample in **Figure 6**.

## Components of the BrainHealth Index

The contribution to the increase in the BHI over 3 months was due not only to measures in the cognitive domain, as one might expect following cognitive training, but also from the rest of the measures in all domains of the BrainHealth wheel. These included those measures within the domains of well-being, daily life and social interaction, even though training and coaching strategies focused largely on the cognitive components. **Figure 7** shows box plots of individual measures within each of the BrainHealth wheel domains on scaled axes. Many of these measures demonstrate improvements—some as much as 75% of the participants showing improvements—including the sleep index and the depression, anxiety, and stress indices from the DASS-21. Improvement for these measures is indicated by a decrease from baseline (although we reversed their sign in **Figure 7** so that change would be commensurate with the other measures).

These observations are important because not all individuals improve their BrainHealth Index by a similar route. Some showed gains due to increased resilience and decreased anxiety, for example, whereas others improved due to increased cognitive flexibility and social engagement. One of the primary goals of the BrainHealth Project (through Phase 3) is to enable individuals

to understand their own capacity to improve brain health, by a route that may be specific to each participant and encouraged by tailored coaching. Indeed the mechanism by which an individual achieves improved brain health is multifaceted, and we intend to leverage that variability as we utilize our pilot data and, subsequently, the imaging data we will collect in Phase 2 of the BrainHealth Project to develop individual prediction models and build BrainHealth indices based on biomarker validation.

## A Factor Analytic Model: Toward an Improved BrainHealth Index

The correlation matrix of change measures, shown in **Figure 8**, suggests that a data-driven BrainHealth Index can be built upon a factor structure from the relationships among the wheel-domain components.

Although many of the stronger correlations are within-domain, as expected, there are also strong across-domain correlations (e.g., across cognitive and social interaction domains; across well-being and daily life domains) that may be important to latent constructs of brain health. These constructs allow for a natural reduction in components and a model-derived set of weights for each component.

A factor solution for the correlation matrix in **Figure 8** was estimated by maximum likelihood using the R statistical computing language (<http://r-project.org>). We used varimax rotation to find simple structure, if one existed, and we utilized Horn's parallel analysis to estimate the appropriate number of factors for a solution. **Figure 9** shows the eigenvalues (EV) from the factor analysis, along with the 95th percentile of the eigenvalue distribution from random factor structure.

The difference between these are the “adjusted” eigenvalues. Those adjusted eigenvalues greater than zero are retained (adjusted EV retained in black; adjusted EV unretained in white). This analysis suggests that a 3-factor solution is sufficient. To assess the adequacy of the fit of the factor solution to the observed correlation matrix, we show the following common fit statistics: RMS of residuals = 0.058; Tucker Lewis Index (TLI) = 0.912; RMSEA Index = 0.036 (95% CI [0.0,0.061]); Fit (off-diagonal) = 0.912.

The likelihood Chi square was 158.14 on 133 df ( $p = 0.067$ ). RMS of residuals and RMSEA index both  $< 0.08$ ,  $p > 0.05$  from likelihood Chi square, TLI and fit statistics both  $> 0.90$  were all taken together as an indication of good fit of the factor solution to the observed correlation matrix as suggested in the factor analysis literature.

The BrainHealth wheel components that contribute to each of the three factors are shown in **Table 4**. The factor loadings have been normalized and those measures whose loadings are at least 0.200 in absolute value are highlighted in **Table 4** to identify the BrainHealth wheel measures that contribute most to each factor. The cut-off of 0.200 leads to the largest loadings, which comprise at least 80% of the normed length for each factor.

**Table 4** reveals a near simple structure for the factor solution: Only the measures of happiness and compassion load on more than one factor by the criteria described above, but the



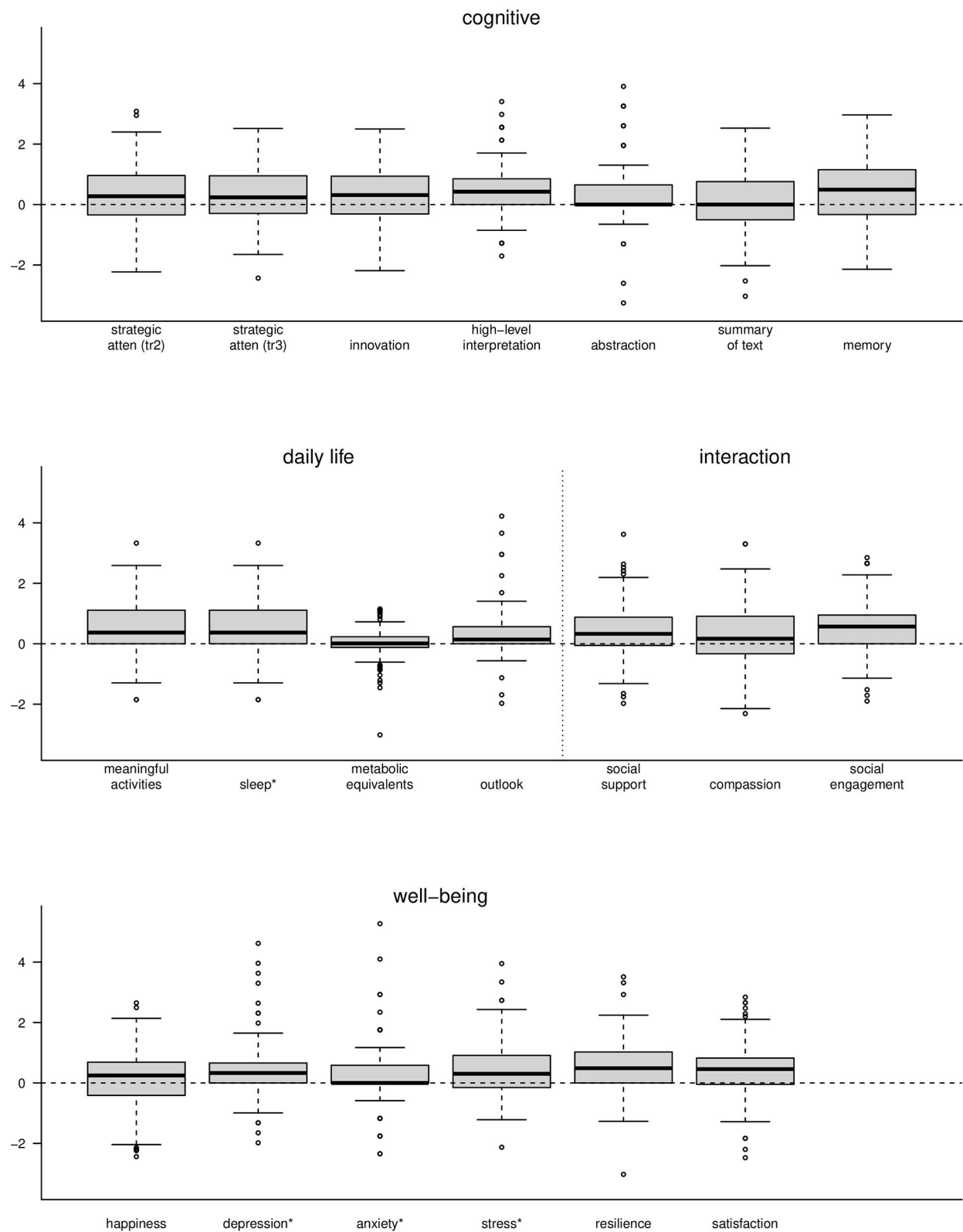
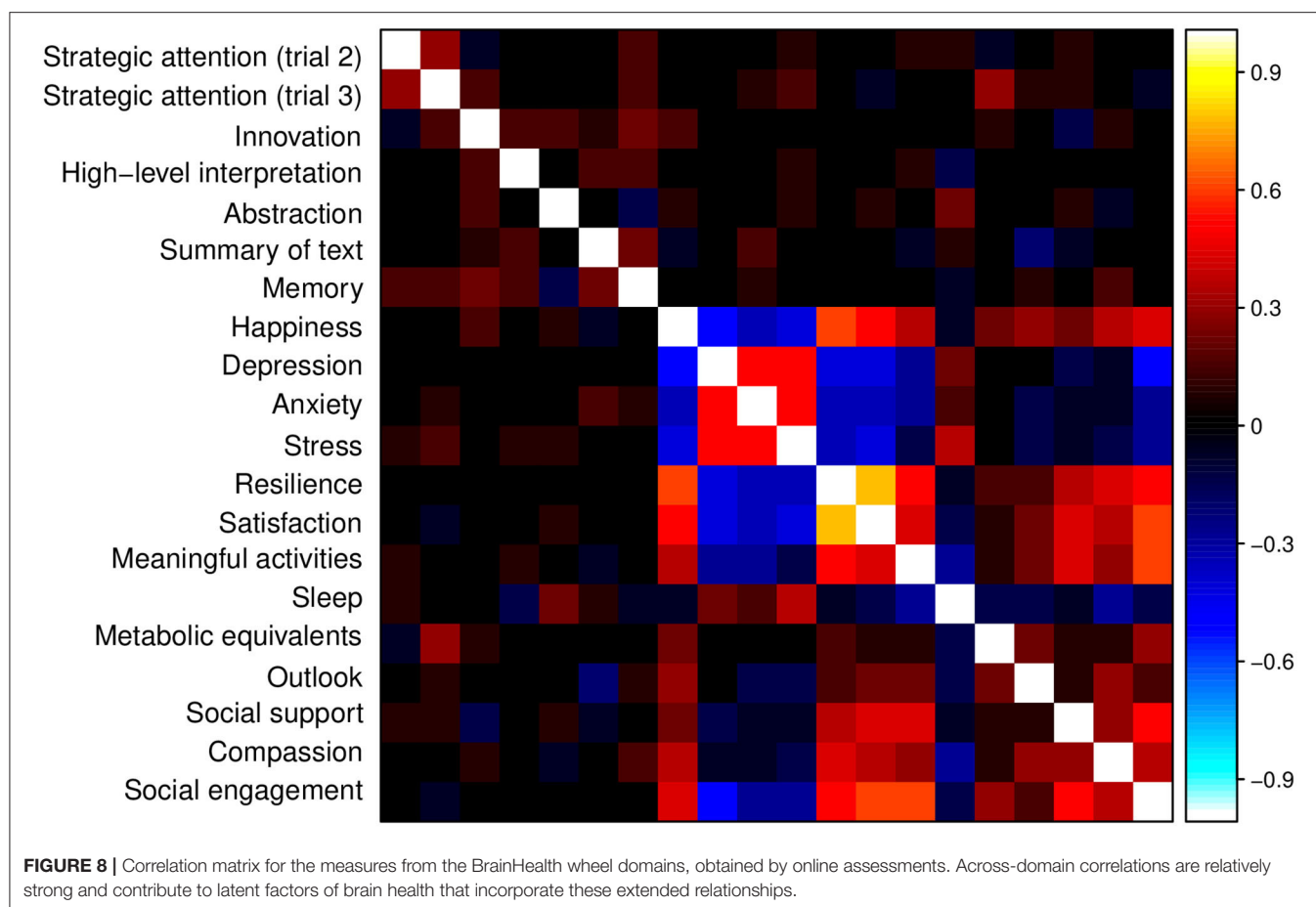


**FIGURE 7 |** Boxplots of change measures for each of the components of the BrainHealth wheel. Each measure was scaled for presentation on a common axis. \*The measures for sleep, depression, anxiety, and stress are shown with opposite sign.



simple structure is not the wheel domain structure themselves. Factor 1 is dominated by the measures in the social interaction BrainHealth-wheel domain and those measures in the well-being domain that constitute mental fortitude (e.g., resilience and satisfaction). Factor 2 is derived almost exclusively from mood assessments in the well-being domain—assessments of depression, anxiety, stress, and happiness constituting factor 2. Finally, factor 3 is comprised of cognitive components that measure strategy, innovation, and memory; but contributions from sleep and outlook within the daily life domain and, especially, compassion within the social interaction domain are equally as important to factor 3. The structure implied by this factor solution, then, suggests that a BrainHealth index can be derived from three latent constructs, which we will utilize as testable constructs. This factor structure is the first step to derive a data-driven BrainHealth Index. From this latent structure, we can now calculate a new Index based on combining construct scores for Phase 2 of the BrainHealth Project.

## Participant Responses and Case Illustrations

In this section, we provide examples of participant feedback and two case studies exemplifying the personalized nature of

the BrainHealth Index and training response. **Table 5** provides a sample of participant quotes regarding the feasibility and ease of use of the online platform. Also displayed are sample participant responses regarding whether the training and information provided impacted their understanding of brain health and their sense of agency related to their brain health.

The following two case studies illustrate how the BrainHealth Index was represented for the user with interpretation provided by the coach to achieve clarity in understanding their results. The case studies show how pre- to post-training performance may be reflected in overall change in BrainHealth Index scores, and how similar change in pre/post scores may be due to changes in different contributing brain health components. Additionally, these case studies are presented to illustrate the opportunities machine learning creates to refine data gleaned from the BrainHealth Index and increase the individual precision and predictions of the various trainings and recommendations offered based on the BrainHealth Index outcomes, especially possible as more data is collected. Refer to **Figure 10** for an illustration of the BHI scores and changes from Time 1 to Time 2 for both case studies.

Case study one is a 55-year-old female with a bachelor's degree. She is currently a homemaker. She enrolled in the BrainHealth Project because of her interest in improving her own

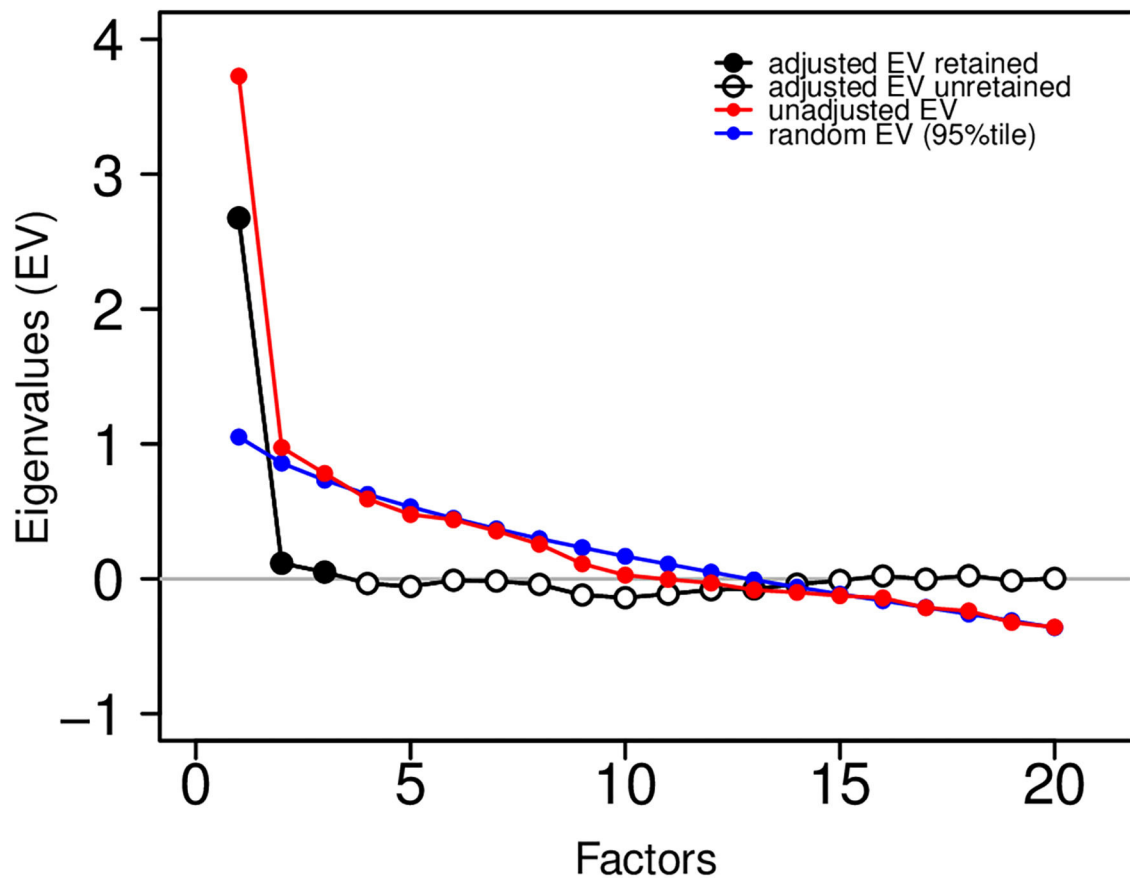


**FIGURE 9 |** Eigenvalue plot showing unadjusted eigenvalues (in red) and adjusted eigenvalues (in black and white). The factor solution was based on three retained (three adjusted eigenvalues greater than zero). Adjustments were based on the 95th percentile of a random eigenvalue distribution (in blue).

as well as her family members' brain health and performance. At Time 1, her performance on the Cognitive component of the BrainHealth Index (score of 49.72) reflected difficulty with strategic thinking and fluency of novel ideas. On the Daily Life (score of 33.26), Social Interaction (score of 40.68), and Well-being (score of 44.89) components of the BrainHealth Index (overall score = 44.67), her responses showed reduced purpose, difficulty with sleep, feelings of isolation, and missing her social network despite having good friends and family, and some elevated stress, all due to pandemic circumstances. She reported feeling overwhelmed and having trouble seeing possibilities that existed within the COVID-19 pandemic environment. Her BHI scores mirrored her subjective experience. At Time 2, her BrainHealth Index scores reflected the application of her learnings: in the Cognitive component (score of 79.14), her strategic blocking of unnecessary information improved, as did her fluency for novel, meaningful ideas; in the Daily Life component (score of 43.83), she felt greater purpose and her sleep improved; in the Social Interaction component (score of 72.82), she felt more satisfied with her social networks; and in the Well-being component (score of 75.33), her resilience improved as did symptoms of stress. She stated that she had developed

a more strategic approach to tasks in all of the BrainHealth components (overall score = 71.57). She started to prioritize regular contact with family members using video calls and spending uninterrupted time each day with her husband. She also learned how to better process and control her reactions to difficult situations. The overall change from Time 1 (44.67) to Time 2 (71.57) was a 26.9 point gain.

Case study two is a 20-year-old male, with a bachelor's degree, who is working as a full-time teacher. He enrolled in the BrainHealth Project because of his desire to improve his critical thinking skills and to help his students do the same. At Time 1, his Cognitive component score (40.03) showed some reduced abstract thinking despite having good ideas and some reduced memory function. He reported dissatisfaction with his thinned social network but overall satisfaction with his life considering the pandemic environment. At Time 2, his Social Interaction component score increased (from 72.82 to 97.07), as did his Cognitive component score (86.2) related to abstraction, synthesis, and memory performance. He found his BHI scores to accurately represent his subjective report or increased confidence in his abilities. He was engaging in abstract thinking more routinely, and applying those concepts to his life. He had moved

**TABLE 4 |** Normalized factor loadings.

| Measure                       | F1           | F2            | F3            |
|-------------------------------|--------------|---------------|---------------|
| Strategic attention (trial 2) | 0.046        | −0.100        | 0.139         |
| Strategic attention (trial 3) | 0.009        | −0.128        | <b>0.322</b>  |
| Innovation                    | −0.036       | 0.017         | <b>0.344</b>  |
| High-level interpretation     | 0.037        | −0.086        | <b>0.209</b>  |
| Abstraction                   | 0.083        | −0.061        | −0.176        |
| Summary of text               | −0.060       | −0.007        | 0.178         |
| Memory                        | −0.044       | −0.043        | <b>0.605</b>  |
| Happiness                     | <b>0.240</b> | <b>0.245</b>  | 0.186         |
| Depression                    | −0.086       | <b>−0.463</b> | 0.036         |
| Anxiety                       | −0.021       | <b>−0.506</b> | 0.099         |
| Stress                        | 0.024        | <b>−0.568</b> | −0.040        |
| Resilience                    | <b>0.368</b> | 0.156         | 0.119         |
| Satisfaction                  | <b>0.392</b> | 0.157         | 0.030         |
| Meaningful activities         | <b>0.385</b> | −0.036        | −0.017        |
| Sleep                         | −0.054       | −0.151        | <b>−0.200</b> |
| Metabolic equivalents         | 0.166        | −0.102        | 0.149         |
| Outlook                       | 0.134        | 0.017         | <b>0.205</b>  |
| Social support                | <b>0.390</b> | −0.145        | −0.103        |
| Compassion                    | <b>0.274</b> | −0.057        | <b>0.317</b>  |
| Social engagement             | <b>0.451</b> | 0.009         | −0.094        |
| Cumulative variance           | 0.144        | 0.229         | 0.275         |
| Proportion explained          | 0.524        | 0.309         | 0.167         |

*Highlighted are those contributing most to each factor.*

in with his partner and felt more socially supported. The overall change in his BHI score was a gain in 27.3 points (from 47.5 to 74.84). We chose to present these two case studies as an example of how similar point value changes can be due to gains in different aspects of brain health, but also to reinforce the value of a holistic measure. Individuals may advance their brain health over the lifetime building different competencies to thrive in the current life context.

## DISCUSSION

This Phase 1 pilot study had two main objectives. The primary goal was to test the efficacy of an online delivery platform across the adult life span (18+ years of age), which entailed three sub-aims. The first sub-aim sought to determine use of a remote/Telehealth-Delivery platform to administer the compendium of tests that comprise the BrainHealth Index. The second sub-aim was to assess how feasible and usable a set of training modules would be when delivered through the same remote platform as the BrainHealth Index, as measured by dose response (i.e., percentage of training sessions utilized). We evaluated the utility of online offerings in this Phase 1 pilot trial to complement our previous decades of research that identified positive gains when the majority of components comprising the BrainHealth Index and the trainings were delivered in person. For the third sub-aim, we wanted to evaluate how effective brief “live” virtual coaching sessions would be in guiding participants

**TABLE 5 |** Participant responses on feasibility and utility survey.

|                        |   |
|------------------------|---|
| Ease of use            | Everything taught was well-grounded and presented in a concise, easy manner. If someone is serious about improving their brain health, they can easily pick up on one or more of the cues and pursue it more in-depth elsewhere.<br><br>Everyone will learn some things that will improve the quality of their lives. And it's so easy to do.<br><br>I believe that the content was helpful, information, and laid out in a clear and concise way. I was able to easily understand the strategies and apply the ones I believed to be beneficial to my life.<br><br>There are concrete steps that can be taken to measurably improve brain health.<br><br>I like the conceptual framework that seems to suggest that brain health can be developed and nurtured through skills-based training and practice. |
| Brain health literacy  | This is not about playing games to train the brain this is about putting in place lifestyle changes that put you in a position to succeed<br><br>I learned the importance of balancing all of the areas of brain health due to their interdependence on each other. That was very eye opening.<br><br>The relationship between cognitive capacities performance on the well-being and daily life activities. The importance of not ignoring those areas.<br><br>How important good sleeping habits are to my overall brain health.<br><br>Having new/different perspectives is an important part of cognition and brain health as much as things like memory  |
| Agency in brain health | I learned so much about how I can make or break my brain health. I learned specific strategies that I can implement in my everyday life that help my brain stay healthy.<br><br>Overall, I feel a little more relaxed, confident and happier. In addition to sharpening my focus and broadening my perspective, the Brain Health project provided me with some tools that enhance my well-being.<br><br>I can keep improving my brain health no matter how old I am.<br><br>The SMART strategies I learned about and applied during my experience greatly improved my cognitive abilities.<br><br>Individuals who participate have an opportunity to improve their lives through better understanding of how their brain functions and how it can possibly be improved.                                     |

how to interpret the novel outcomes from the BrainHealth Index, and make progress toward individualized brain health goals. The second main objective of this pilot study was to develop a data-driven BrainHealth Index from an exploratory factor model of BrainHealth constructs that could be tested and validated in the next phase of our BrainHealth Project. Our ultimate goal was to lay the groundwork for a subsequent large-scale effort to establish an objective, repeatable, and interpretable framework to evaluate how the components combine and co-vary to contribute to holistic gains or losses in brain health metrics, at both group and individual levels.



## Efficacy of Online Platform Delivery

The results provide evidence that an integrated measure of brain health, reflected by a BrainHealth Index, can be meaningfully delivered online to individuals across the adult lifespan. The preliminary results and feedback from the participants suggest the composite has the potential to measure changes (whether gains or losses) as well as to chart performance stability over time with or without intervention protocols. As discussed in Methods, the weights used in the preliminary BrainHealth Index for this pilot effort was derived from clinical judgment/experience with a combination of previously validated and standardized measures of cognitive, emotional, social and everyday life function. The provision of a single index, comprised of four components, may have been a factor in motivating participants to engage in this entirely remotely-administered program. We suggest that individuals have different curiosities that may be self-motivating when they have multiple routes to improve global level of brain performance. These different metrics of human brain function typically have not been measured at all and if they were, the domains were assessed by different experts and never integrated or interpreted as to their covariance despite the fact that a strong interdependence exists. The combination of a multitude of measures into a single index in this effort is entirely novel.

Typically, efficacy of intervention protocols, including pharmacological and neurobehavioral treatments, are assessed primarily with cognitive measures, whereas those aimed at emotional problems, such as mood or anxiety, do not typically measure cognitive function. Yet, many studies have shown that

emotional, cognitive, social, and everyday behaviors mutually interact and influence each other to such a degree that the combination of components into a single index is entirely appropriate and perhaps more instructive. Anxiety, for example, degrades attentional capacity (14), and low mood and depression also worsen cognitive function, including attention, and executive and memory processes (17). Poor cognitive abilities, particularly low attentional control, on the other hand, lead to emotional regulation problems (20). People tend to experience problems in life in a holistic way, not one compartmentalized into somewhat arbitrary domains such as emotion and cognition. This means that having a single derived index representing this overall state may not only be meaningful, but also potentially motivating, as was implicated by the 80% adherence rates during this study. Real-life examples include an individual who, by learning to reframe her stressors, improved her sleep and cognitive flexibility, and another individual who improved her social interactions, stress, and resilience by utilizing cognitive tools to increase innovative capacity and become a stronger “possibility thinker.”

Simple measures related to heart health such as blood pressure or blood cholesterol are widely understood in peoples’ minds and as such serve as motivating targets for improvement through lifestyle changes such as exercise, nutrition, and stress. As we make progress in evaluating the BrainHealth Index in larger samples over longer periods, we may find that individual or combined parameters from the Index may be predictive and targeted as preventive measures, at either a group or individual



level. The creation of a single BrainHealth Index offers a systematic way to start exploring such possibilities in the domain of brain health. The provisional Index developed in this study met the objective of being deliverable, repeatable, and acceptable. Its promising scalability with an online delivery platform is of particular importance to meet the first aim of the study, namely whether we can address brain health status and overcome in-person challenges of participation that were brought to the forefront during the COVID-19 pandemic.

## Usage and Acceptability of Training Modules

The training offered in this program was also unique because, unlike other methods, it focused entirely on training tactical brain strategies (e.g., integrated reasoning, innovation) that can be directly adopted in real-life activities rather than training of isolated domains of specific cognition processes (e.g., attention, working memory). Similarly, the stress modules of the program used low-demand, micro-learning video instruction of tactical strategies with a highly positive tone unlike more clinically-oriented stress programs. The cognitive training was entirely focused on “top-down” strategic approaches to thinking, i.e., innovation, big-idea synthesis and strategic memory. We acknowledge the potential advantage of incorporating additional “bottom-up” training programs aimed at enhancing functions such as speed of processing (41, 69). Promising data from these latter approaches suggest that the effectiveness of the current program could be further enhanced by adding these to the menu of modules. We will address this additive value as our participants continue to be followed and these modules are added.

A majority of participants, regardless of age, gender, or education, showed significant gains in the BrainHealth Index based on training usage. Specifically, the results showed a significant training dose-response relationship on BrainHealth Index gains. The more training modules individuals completed, the higher were their gains on the BrainHealth Index, at least for the tactical training modules vs. the purely informational modules. The fact that there was no such dose-response relationship for the purely informational modules completed offers a partial quasi-experimental control which we cautiously interpret as a real training effect on the BrainHealth Index. Pre-existing motivation could have been a confounding variable explaining both the BrainHealth Index increase and the high program engagement. However, had that been the case, then engagement with the informational modules should have continued the rise in the Index gains—but the gain curve flattened for these, so motivation is unlikely to be a factor.

One might argue that the gain could be due to practice effects. Practice effects can be cautiously ruled out as a second potential confound because of the dose-response relationship between active training-module utilization and brain health gain. Had improvements in BrainHealth Index been entirely practice-related, then they would have increased independently of module usage.

## Live Virtual Coaching

No previous endeavor has combined online cognitive, emotional, and lifestyle interventions with real-person, virtual coaching. The ability of the coaches to incentivize participation by feeding back strengths and weaknesses in the components of the BrainHealth Index is an additional factor that may help explain the high compliance rate of 80%.

The role of coaching in these possible training-mediated brain health improvements cannot be underestimated. Combined with a simple, incentivizing metric to work toward, and training modules with very high face validity and real-life relevance, the coaches were able to motivate and direct participants to call upon areas of relative strength to shore up and strengthen areas of weakness with only two 30-min sessions. The first session served to help ensure the participants make sense of the personalized BrainHealth Index and set goals. The second was for the coach and participant to work together to find ways to apply the tactical brain strategies to their individualized life context. The quality/experience of the coaches will be a major factor to address as the number of coaches increase nationally and, eventually, internationally. We have developed a coach training manual/process that is being tested to determine the level of expertise necessary for a coach to be effective, recognizing that quality will vary across coaches just as it exists for physicians. We will also create different exercises and train coaches that are appropriate to different cultural groups.

We propose that these pilot data and participant responses support the simplicity and clarity of the BrainHealth Index. Furthermore, the accessibility and acceptability of the online training modules across the adult age span suggests that the relatively low-cost of training the large cohort of coaches needed to scale this program, for the millions of people who would benefit from it, is entirely possible. We estimate that one coach can work with ~500 participants a year, which is a small expense compared to the cost savings in keeping a person's brain functioning at fuller capacity longer. The major hurdle will be training, monitoring, and managing the large numbers of coaches needed to scale the BrainHealth Project.

## Application During a Pandemic to Strengthen Brain Health

The timing of this pilot trial came at an opportune moment, given it coincided with the outbreak of the COVID-19 pandemic, necessitating remote participation. Smith et al. (5) argue that the COVID pandemic is causing global misery with social isolation, loss of jobs, and livelihoods, unpredictable forces exacerbating stress, depression, and anxiety. Indeed, the majority of our participants reported notable deleterious impacts from the pandemic ramifications, even though few had contracted the virus. Smith and the international team of authors claim that the time is urgent to catalyze proactive efforts to invest and focus attention on brain health to help strengthen brain health, intercept early concerns and vulnerabilities, and develop measurable strategies for brain skills to rebound from losses given COVID has created a brain health crisis. We are beginning to

realize that resilience from massive disruptions can occur when brain health is foregrounded as a key driver and solution.

These pilot data offer promise that steps can be taken to reinforce brain skills even under times of unprecedented stress and unpredictability. The fact that 75% of the participants from ages 18 to 80 showed at least a 5-point increase, with a mean gain of 10 points in their BrainHealth Index, during one of the worst times in our global economy and public health crisis offers hope. This upward potential on a quantifiable BrainHealth Index composite suggests that individuals may be able to build resilience and perhaps even intercept losses before they become clinically full-blown. Intercepting losses will require longitudinal follow-up, which is already underway. This pattern of comparable baseline and gains across the lifespan challenges the long-standing perspective that peak brain years are in the 30s and that neuroplasticity weakens with age. Clearly, certain aspects of cognition, such as speed of processing and working memory, decline with age (70, 71). However, we suggest that a holistic approach to brain health will be fruitful. This approach takes into account the vast reservoir of brain capacities (such as social adeptness, innovative thinking, and life purpose to mention a few) and provides individuals guidelines to engage multiple, not singular, pathways to strengthen brain health to thrive in life. A siloed/segmented approach to brain health fails to take into account the complexity and vastness of capacities to adapt and continue to thrive.

It is often times of crisis that spark an openness to new approaches that improve life. Because of the isolation brought about by the pandemic, people have become much more open to e-health platforms. If we had tried this online aspect of the BrainHealth Project just 1 year ago, it may have met with resistance from different groups. In issues of the brain, the online offerings may provide a more anonymized way to seek help rather than ways that reinforce the stigma of identifying deficits and labeling something as wrong, instead empowering participants to be proactive about building their brain capacity.

## Validation Using Machine Learning

With the exploratory latent constructs of BrainHealth developed in this pilot study, which is part of Phase 1 of the BrainHealth Project, we will now proceed to the second phase of the Project to incorporate brain-imaging metrics in an independent sample of 200 participants. All aspects of Phase 2 will mimic Phase 1, including training modules and personalized coaching sessions, but the BrainHealth Index will be calculated using the three latent structures developed in this pilot. Most importantly, we will add imaging metrics using MRI such as regional brain volume, regional blood flow, functional connectivity, and structural connectivity. Brain imaging metrics will be collected at baseline and 6 months post-training, in addition to the online assessments from Phase 1. The purpose of adding the imaging metrics is to validate the BrainHealth constructs (and hence the Index itself) by finding the set of metrics that can best predict the construct domains.

Although much is known about associations between various imaging metrics and clinical measures, these are predominantly in the context of pathology (e.g., clinical depression, dementia).

Far less is known about these associations for healthy individuals with a goal of maintaining or improving their brain health, similar to the goal of maintaining or improving physical fitness as we age. This is a Big Data problem. With the success of machine learning in many different fields of study, including imaging-based prediction, we plan to leverage learning algorithms to help us find those relevant biomarkers that can best predict our testable constructs of BrainHealth.

Our first plan of attack is to develop locally connected deep learning networks that will take in imaging metrics across different modalities as features and propagate those through several layers, at the end of which is an output that represents one of the BrainHealth constructs. There will be a network for each of the BrainHealth constructs, and the algorithm will learn the imaging features that predict, as closely as possible, the measured construct. How the final Index is weighted from the construct domains will depend on how robust each set of learned features predicts the network outputs. More weight is given to the more efficient network-based prediction, as there would be more evidence of a physiological basis for the construct itself in that situation.

The strategy briefly described above will serve two important goals of the BrainHealth Project. First, to fulfill the goal of Phase 2, it will validate the BrainHealth Index as a quantifiable measure of a state of an individual's brain health that can be reliably tracked over time. Secondly, successful prediction models of BrainHealth constructs will allow a tailored approach to improving brain health for individuals. Just as physical health for different individuals can be improved by tailored means (i.e., precision health), the same would be true for brain health. Coaching strategies could be tailored to individuals for maximal benefit.

## Limitations

The BrainHealth Index is a dynamically-adapting tool for reflecting to an individual their level of functioning and motivating them to make changes to improve it. The BrainHealth Index will also change over time as machine-learning analysis of accumulating multi-dimensional data refines it. This unique strength of the BrainHealth Index also limits its use as a conventional static biomarker, at least during the first period of its iterative development. We regard the advantages of our approach to the BrainHealth Index to outweigh this limitation, however.

The trainings offered in the BrainHealth Project represent a relatively small proportion of the interventions that could and will be offered on this unique, coaching-facilitated platform. For example, the cognitive training consists of "top-down" training focused on high-level executive and attentional abilities and does not yet include some of the robust and effective "bottom-up" training of the type offered, for example by BrainHQ (41, 69). Similarly, our advice on important functions such as sleep, exercise and diet, could be complemented as we integrate reliable data from wearable devices and provide targeted behavior-change focused programs in these domains.

The acceptability of, and adherence to, this training and assessment program to a wide range of socio-economic and

cultural groups is not yet established. This serious limitation of the present pilot study is one we propose to address with alacrity.

Finally, this is an “open-label” trial and not a randomized controlled trial. We must therefore be cautious in ascribing cause-and-effect relationships between the training and the observed improvements in the BrainHealth Index. Whereas, this is a significant limitation, the results offer promise as supported by the compelling dose-response relationships between training engagement and BrainHealth Index improvement. Perhaps, this type of clinical trial may offer promise in the future to interventions that show no harm but have been shown in smaller, carefully controlled, randomized trials to be effective. Even more important is to document the persistence of the gains over time. One fact of neuroplasticity is that the brain never stays the same; just as gains are possible, so are losses. Therefore, keeping the brain fit will require continued effort on behalf of individuals. What is promising is that 95% of the people in this pilot signed up for the 10-year study to continue to measure, monitor, and take advantage of trainings to maintain or improve their brain health.

## Future Studies

The current Phase 1 pilot study lays a foundation for the next critical Phase 2 of the BrainHealth Project, which will include the addition of functional and structural imaging measures. In this second phase, we will incorporate machine learning models to map the imaging metrics onto our exploratory factor model space as described above. The purpose of this phase will be to refine and validate the factor structure and to obtain a data-driven BrainHealth Index measure that relates to brain biomarkers.

These two trials, Phase 1 and 2, will inform our scientific efforts as we prepare to launch Phase 3 of the BrainHealth Project with the goal of reaching hundreds of thousands of participants across demographic domains. This larger effort requires multi-institutional collaborations to show reliability and validity of measures as larger numbers of participants are followed over 10 years with semi-annual BrainHealth Index metrics, semi-annual physiologic measurements from wearable data on 20% of the participants, and semi-annual imaging metrics on 10% of the participants.

Future efforts need to greatly extend the demographic, socio-economic, and cultural reach of the populations addressed, to test whether high levels of acceptability are maintained, and if not, how these can be achieved. Finally, future studies should incorporate new evidence-based interventions and incorporate them into the platform. Such an approach is clearly antithetical to a classic randomized-controlled trial where the “treatment” must be fixed before the trial begins and not change as new validated interventions appear. The limitations of current practice randomized trial efforts are that the longer the follow-up periods are, the more likely the treatments evaluated will have been improved or even superseded by new ones. Hence, the apparent limitation of the present study—its open-label structure—may in fact be an advantage for the reasons just given. Sophisticated machine learning methods will be essential for increasing confidence in adducing cause-effect

relationships between training and BrainHealth Index in such an approach.

## CONCLUSIONS

In summary, the primary contribution of this pilot study was the development and online testing of the first composite BrainHealth Index to measure and monitor brain health in a holistic framework across the adult lifespan. The key goal of the BrainHealth Index was not to detect or diagnose problems, but rather to motivate individuals to take charge of adopting healthy habits to elevate their brain performance, regardless of the level at which they started. Our findings provide promising evidence that people found the information gleaned from the personalized online BrainHealth Index useful and applicable to their everyday lives. In support of this view, 95% of the individuals signed up to participate in the BrainHealth Project for the next 10 years. Moreover, with greater access to brain health literacy and tactical brain strategies to deploy this information, healthy adults took steps to be proactive about their brain health.

We recognize that the findings yield at least as many questions as they answer. It is important to note that these positive brain health gains were achieved at a time when individuals were burdened with dramatic life changes due to the pandemic. The results offer preliminary evidence to support the perspective that taking time to focus on building brain capacity and resilience during tough times may be especially relevant, instead of waiting until life returns to a more “normal state,” a better choice is perhaps to intercept problems before they worsen. This possibility warrants careful attention. We suggest that resilience is only possible with brain health.

Incorporating machine learning and other sophisticated data analytic methods into the large comprehensive data over the lifespan will help explore the vast opportunities to apply the science of neuroplasticity to unlock human potential. Promoting brain health entails making the most of the brain’s capacity to thrive in different contexts and involves strengthening capacities rather than simply remedying deficits when they manifest themselves. This pilot study paves the way for larger-scale efforts to determine whether monitoring and promoting brain health will achieve greater lifelong capacities to build resilient brain systems that respond to life’s unknowns and constant changes while averting decline by fine-tuning the brain’s complex highly synchronized circuits.

## DATA AVAILABILITY STATEMENT

The raw data supporting the conclusions of this article will be made available by the authors, without undue reservation.

## ETHICS STATEMENT

The studies involving human participants were reviewed and approved by University of Texas at Dallas IRB. The patients/participants provided their written informed consent to participate in this study.

## AUTHOR CONTRIBUTIONS

SC designed the study, interpreted the results, and wrote the manuscript. JF assisted with study design, directed study operations, assisted with development of the online platform, contributed to the manuscript, and edited manuscript. IR contributed content the online training modules, advised on some of the measures comprising the BrainHealth Index, interpreted the results, and wrote the manuscript. MD'E revised the manuscript. GL assisted with study design. JZ performed oversight of training delivery design and execution, collected and scored data, and contributed to manuscript. SV supervised coaching, collected and scored data, and contributed to manuscript. EV designed training protocol, collected and scored data, assisted with the literature review, and contributed to the manuscript. LC collected and scored data, assisted with the literature review, and reviewing of the manuscript. AT supervised and contributed to the development of the online training platform and training modules. JS performed analyses, interpreted results, wrote and edited the manuscript. All authors contributed to the article and approved the submitted version.

## FUNDING

This work was funded by private philanthropy: The Baldrige Foundation, Jean Ann Brock, The Joshua M. and Inette S. Brown Family Foundation, Peggy Dear, Estate of Alice Janet DeSanders,

Teresa and David Disiere, Folsom Charitable Foundation, Kozmetsky Family Foundation, The J. Willard and Alice S. Marriott Foundation, J. Willard Marriott, Jr. Foundation, John R. McCune Charitable Trust, Ellen and John McStay, Marlane Miller, and Jennifer and Peter Roberts.

## ACKNOWLEDGMENTS

We express sincere gratitude to the donors whose generous support allowed us to scale our work and develop a new model of precision brain health: Estate of Alice Janet DeSanders, Jean Ann Brock, Jennifer and Peter Roberts, Teresa and David Disiere, Kozmetsky Family Foundation, Peggy Dear, The Baldrige Foundation, The Joshua M. and Inette S. Brown Family Foundation, Folsom Charitable Foundation, Ellen and John McStay, Marlane Miller, John R. McCune Charitable Trust, The J. Willard and Alice S. Marriott Foundation, and J. Willard Marriott, Jr. Foundation. We recognize and applaud the coaches of The BrainHealth Project pilot study for guiding participants every step of the way with exceptional care and enthusiasm: Jill Hill, Katie Hinds, Audette Rackley, Janet Koslovsky, Tandra Allen, Kathleen Shaffer, and Shelly Gordon. Additionally, we must thank the team at Dialexa for their tremendous work creating the innovative and user-friendly online platform. Finally, we are immensely grateful for the pilot participants who chose to be pioneers in brain health and invested their time in this research.

## REFERENCES

- Zolotor AJ, Yorkery B. Public policy approaches to population health. *Prim Care*. (2019) 46:575–86. doi: 10.1016/j.pop.2019.07.015
- Torales J, O'Higgins M, Castaldelli-Maia JM, Ventriglio A. The outbreak of COVID-19 coronavirus and its impact on global mental health. *Int J Soc Psychiatry*. (2020) 66:317–20. doi: 10.1177/0020764020915212
- Richards M, Stephen A, Mishra G. Health returns to cognitive capital in the British 1946 birth cohort. *Longit Life Course Stud*. (2010) 1:281–96. doi: 10.14301/lcs.v1i3.94
- Rindermann H, Kodila-Tedika O, Christainsen G. Cognitive capital, good governance, and the wealth of nations. *Intelligence*. (2015) 51:98–108. doi: 10.1016/j.intell.2015.06.002
- Smith E, Ali D, Wilkerson B, Dawson WD, Sobowale K, Reynolds C, et al. A brain capital grand strategy: towards economic reimagination. *Mol Psychiatry*. (2020) 26:3–22. doi: 10.1038/s41380-020-00918-w
- Stephan BC, Pakpahan E, Siervo M, Licher S, Muniz-Terrera G, Mohan D, et al. Prediction of dementia risk in low-income and middle-income countries (the 10/66 Study): an independent external validation of existing models. *Lancet Glob Health*. (2020) 8:e524–35. doi: 10.1016/S2214-109X(20)30062-0
- Ferri CP, Jacob K. Dementia in low-income and middle-income countries: different realities mandate tailored solutions. *PLoS Med*. (2017) 14:e1002271. doi: 10.1371/journal.pmed.1002271
- Abbott A. Dementia: a problem for our age. *Nature*. (2011) 475:S2–4. doi: 10.1038/475S2a
- Diniz BS, Butters MA, Albert SM, Dew MA, Reynolds CF. Late-life depression and risk of vascular dementia and Alzheimer's disease: systematic review and meta-analysis of community-based cohort studies. *Br J Psychiatry*. (2013) 202:329–35. doi: 10.1192/bjp.bp.112.118307
- Gallagher KM, Updegraff JA. Health message framing effects on attitudes, intentions, and behavior: a meta-analytic review. *Ann Behav Med*. (2012) 43:101–16. doi: 10.1007/s12160-011-9308-7
- Notthoff N, Carstensen LL. Positive messaging promotes walking in older adults. *Psychol Aging*. (2014) 29:329–41. doi: 10.1037/a0036748
- Bailey RR. Goal setting and action planning for health behavior change. *Am J Lifestyle Med*. (2017) 13:615–8. doi: 10.1177/1559827617729634
- National Institute on Aging (NIA). *Cognitive Health and Older Adults*. (2020). Available online at: <https://www.nia.nih.gov/health/cognitive-health-and-older-adults> (accessed December 10, 2020).
- Eysenck MW, Derakshan N, Santos R, Calvo MG. Anxiety and cognitive performance: attentional control theory. *Emotion*. (2007) 7:336–53. doi: 10.1037/1528-3542.7.2.336
- Marvel CL, Paradiso S. Cognitive and neurological impairment in mood disorders. *Psychiatr Clin North Am*. (2004) 27:19–36. doi: 10.1016/S0193-953X(03)00106-0
- Park J, Moghaddam B. Impact of anxiety on prefrontal cortex encoding of cognitive flexibility. *Neuroscience*. (2017) 345:193–202. doi: 10.1016/j.neuroscience.2016.06.013
- Rock P, Roiser J, Riedel W, Blackwell A. Cognitive impairment in depression: a systematic review and meta-analysis. *Psychol Med*. (2014) 44:2029–40. doi: 10.1017/S0033291713002535
- Shimada H, Park H, Makizako H, Doi T, Lee S, Suzuki T. Depressive symptoms and cognitive performance in older adults. *J Psychiatr Res*. (2014) 57:149–56. doi: 10.1016/j.jpsychires.2014.06.004
- Hofmann W, Schmeichel BJ, Baddeley AD. Executive functions and self-regulation. *Trends Cogn Sci*. (2012) 16:174–80. doi: 10.1016/j.tics.2012.01.006
- Killingsworth MA, Gilbert DT. A wandering mind is an unhappy mind. *Science*. (2010) 330:932. doi: 10.1126/science.1192439
- Boss L, Kang DH, Branson S. Loneliness and cognitive function in the older adult: a systematic review. *Int Psychogeriatr*. (2015) 27:541–53. doi: 10.1017/S1041610214002749



22. Shankar A, Hamer M, McMunn A, Steptoe A. Social isolation and loneliness: relationships with cognitive function during 4 years of follow-up in the English Longitudinal Study of Ageing. *Psychosom Med.* (2013) 75:161–70. doi: 10.1097/PSY.0b013e31827f09cd
23. Sutter C, Zöllig J, Allemand M, Martin M. Sleep quality and cognitive function in healthy old age: the moderating role of subclinical depression. *Neuropsychology.* (2012) 26:768–75. doi: 10.1037/a0030033
24. Lourida I, Soni M, Thompson-Coon J, Purandare N, Lang IA, Ukoumunne OC, et al. Mediterranean diet, cognitive function, and dementia: a systematic review. *Epidemiology.* (2013) 24:479–89. doi: 10.1097/EDE.0b013e3182944410
25. Angevaren M, Aufdemkampe G, Verhaar H, Aleman A, Vanhees L. Physical activity and enhanced fitness to improve cognitive function in older people without known cognitive impairment. *Cochrane Database Syst Rev.* (2008) 2:CD005381. doi: 10.1002/14651858.CD005381.pub3
26. Clare L, Wu YT, Teale JC, MacLeod C, Matthews F, Brayne C, et al. Potentially modifiable lifestyle factors, cognitive reserve, and cognitive function in later life: a cross-sectional study. *PLoS Med.* (2017) 14:e1002259. doi: 10.1371/journal.pmed.1002259
27. Ngandu T, Lehtisalo J, Solomon A, Levälähti E, Ahtiluoto S, Antikainen R, et al. A 2 year multidomain intervention of diet, exercise, cognitive training, and vascular risk monitoring versus control to prevent cognitive decline in at-risk elderly people (FINGER): a randomised controlled trial. *Lancet.* (2015) 385:2255–63. doi: 10.1016/S0140-6736(15)60461-5
28. Strober LB, Becker A, Randolph JJ. Role of positive lifestyle activities on mood, cognition, well-being, and disease characteristics in multiple sclerosis. *Appl Neuropsychol Adult.* (2018) 25:304–11. doi: 10.1080/23279095.2018.1458518
29. Coelho FG, Gobbi S, Andreatto CA, Corazza DI, Pedrosa RV, Santos-Galduróz RF. Physical exercise modulates peripheral levels of brain-derived neurotrophic factor (BDNF): a systematic review of experimental studies in the elderly. *Arch Gerontol Geriatr.* (2013) 56:10–5. doi: 10.1016/j.archger.2012.06.003
30. Mintzer J, Donovan KA, Kindy AZ, Lock SL, Chura LR, Barracca N. Lifestyle choices and brain health. *Front Med.* (2019) 6:204. doi: 10.3389/fmed.2019.00204
31. Chapman SB, Aslan S, Spence JS, Hart JJ Jr, Bartz EK, Didehban N, et al. Neural mechanisms of brain plasticity with complex cognitive training in healthy seniors. *Cereb Cortex.* (2015) 25:396–405. doi: 10.1093/cercor/bht234
32. Chapman SB, Aslan S, Spence JS, Keebler MW, DeFina LF, Didehban N, et al. Distinct brain and behavioral benefits from cognitive vs. physical training: a randomized trial in aging adults. *Front Hum Neurosci.* (2016) 10:338. doi: 10.3389/fnhum.2016.00338
33. Vas A, Chapman S, Aslan S, Spence J, Keebler M, Rodriguez-Larain G, et al. Reasoning training in veteran and civilian traumatic brain injury with persistent mild impairment. *Neuropsychol Rehabil.* (2016) 26:502–31. doi: 10.1080/09602011.2015.1044013
34. Levine B, Schweizer TA, O'Connor C, Turner G, Gillingham S, Stuss DT, et al. Rehabilitation of executive functioning in patients with frontal lobe brain damage with goal management training. *Front Hum Neurosci.* (2011) 5:9. doi: 10.3389/fnhum.2011.00009
35. Stamenova V, Levine B. Effectiveness of goal management training® in improving executive functions: a meta-analysis. *Neuropsychol Rehabil.* (2019) 29:1569–99. doi: 10.1080/09602011.2018.1438294
36. Ball K, Edwards JD, Ross LA, McGwin G Jr. Cognitive training decreases motor vehicle collision involvement of older drivers. *J Am Geriatr Soc.* (2010) 58:2107–13. doi: 10.1111/j.1532-5415.2010.03138.x
37. Bamidis PD, Fissler P, Papageorgiou SG, Zilidou V, Konstantinidis EI, Billis AS, et al. Gains in cognition through combined cognitive and physical training: the role of training dosage and severity of neurocognitive disorder. *Front. Aging Neurosci.* (2015) 7:152. doi: 10.3389/fnagi.2015.00152
38. Edwards JD, Delahunt PB, Mahncke HW. Cognitive speed of processing training delays driving cessation. *J Gerontol A Biol Sci Med Sci.* (2009) 64:1262–7. doi: 10.1093/gerona/glp131
39. Edwards JD, Xu H, Clark DO, Guey LT, Ross LA, Unverzagt FW. Speed of processing training results in lower risk of dementia. *Alzheimers Dement.* (2017) 3:603–11. doi: 10.1016/j.trci.2017.09.002
40. Frantzidis CA, Ladas AKI, Vivas AB, Tsolaki M, Bamidis PD. Cognitive and physical training for the elderly: evaluating outcome efficacy by means of neurophysiological synchronization. *Int J Psychophysiol.* (2014) 93:1–11. doi: 10.1016/j.ijpsycho.2014.01.007
41. Shah TM, Weinborn M, Verdile G, Sohrabi HR, Martins RN. Enhancing cognitive functioning in healthy older adults: a systematic review of the clinical significance of commercially available computerized cognitive training in preventing cognitive decline. *Neuropsychol Rev.* (2017) 27:62–80. doi: 10.1007/s11065-016-9338-9
42. Harvey PD, Balzer AM, Kotwicz RJ. Training engagement, baseline cognitive functioning, and cognitive gains with computerized cognitive training: a cross-diagnostic study. *Schizophr Res.* (2020) 19:100150. doi: 10.1016/j.scog.2019.100150
43. Tennstedt SL, Unverzagt FW. The ACTIVE study: study overview and major findings. *J Aging Health.* (2013) 25(Suppl. 8):3S–20. doi: 10.1177/0898264313518133
44. Steinberg D, Bennett GG, Svetkey L. The DASH diet, 20 years later. *JAMA.* (2017) 317:1529–30. doi: 10.1001/jama.2017.1628
45. Andersson C, Johnson AD, Benjamin EJ, Levy D, Vasan RS. 70-year legacy of the Framingham heart study. *Nat Rev Cardiol.* (2019) 16:687–98. doi: 10.1038/s41569-019-0202-5
46. Bitton A, Gaziano TA. The Framingham heart study's impact on global risk assessment. *Prog Cardiovasc Dis.* (2010) 53:68–78. doi: 10.1016/j.pcad.2010.04.001
47. Kishore SP, Heller DJ, Vasan A. Beyond hypertension: integrated cardiovascular care as a path to comprehensive primary care. *Bull World Health Organ.* (2018) 96:219–21. doi: 10.2471/BLT.17.197996
48. Allen TT, Ashmore L, Gordon S, Tate A, Cook LG, Chapman SB. Charisma™: a virtual reality training to promote social brain health in adults. In: Nangle DW, Erdley CA, Schwartz-Mette R, editors. *Social Skills Across the Life-Span: Theory, Assessment, and Intervention.* London: Academic Press (2020). p. 295–309.
49. Han K, Chapman SB, Krawczyk DC. Neuroplasticity of cognitive control networks following cognitive training for chronic traumatic brain injury. *Neuroimage Clin.* (2018) 18:262–78. doi: 10.1016/j.nicl.2018.01.030
50. Han K, Davis RA, Chapman SB, Krawczyk DC. Strategy-based reasoning training modulates cortical thickness and resting-state functional connectivity in adults with chronic traumatic brain injury. *Brain Behav.* (2017) 7:e00687. doi: 10.1002/brb3.687
51. Motes MA, Yezhuvath US, Aslan S, Spence JS, Rypma B, Chapman SB. Higher-order cognitive training effects on processing speed-related neural activity: a randomized trial. *Neurobiol Aging.* (2018) 62:72–81. doi: 10.1016/j.neurobiolaging.2017.10.003
52. Yang YJD, Allen T, Abdullahi SM, Pelphey KA, Volkmar FR, Chapman SB. Neural mechanisms of behavioral change in young adults with high-functioning autism receiving virtual reality social cognition training: a pilot study. *Autism Res.* (2018) 11:713–25. doi: 10.1002/aur.1941
53. Hanten G, Li X, Chapman SB, Swank P, Gamino J, Roberson G, et al. Development of verbal selective learning. *Dev Neuropsychol.* (2007) 32:585–96. doi: 10.1080/87565640701361112
54. Vas AK, Chapman SB, Cook LG (editors). Language impairments in traumatic brain injury: a window into complex cognitive performance. In: *Handbook of Clinical Neurology: Traumatic Brain Injury Part II.* Amsterdam: Elsevier (2015). p. 497–510.
55. Hills P, Argyle M. The Oxford Happiness Questionnaire: a compact scale for the measurement of psychological well-being. *Pers Individ Differ.* (2002) 33:1073–82. doi: 10.1016/S0191-8869(01)00213-6
56. Lovibond PF, Lovibond SH. The structure of negative emotional states: comparison of the Depression Anxiety Stress Scales (DASS) with the beck depression and anxiety inventories. *Behav Res Ther.* (1995) 33:335–43. doi: 10.1016/0005-7967(94)00075-u
57. Connor KM, Davidson JRT. Development of a new resilience scale: the Connor-Davidson Resilience Scale (CD-RISC). *Depress Anxiety.* (2003) 18:76–82. doi: 10.1002/da.10113
58. Burckhardt CS, Anderson KL. The quality of life scale (QOLS): reliability, validity, and utilization. *Health Qual Life Outcomes.* (2003) 1:60. doi: 10.1186/1477-7525-1-60
59. Sherbourne CD, Stewart AL. The MOS social support survey. *Soc Sci Med.* (1991) 32:705–14. doi: 10.1016/0277-9536(91)90150-b



60. Strauss C, Lever Taylor B, Gu J, Kuyken W, Baer R, Jones F, et al. What is compassion and how can we measure it? A review of definitions and measures. *Clin Psychol Rev.* (2016) 47:15–27. doi: 10.1016/j.cpr.2016.05.004
61. Johnson LKD. *The Light Triad Scale: developing and validating a preliminary measure of prosocial orientation (Master's thesis)*. [Electronic Thesis and Dissertation Repository: 5515], The University of Western Ontario (2018). Available online at: <https://ir.lib.uwo.ca/etd/5515>
62. Eakman AM. Convergent validity of the engagement in meaningful activities survey in a college sample. *OTJR.* (2011) 30:23–32. doi: 10.3928/15394492-20100122-02
63. Buysse DJ, Reynolds CF, Monk TH, Berman SR, Kupfer DJ. The Pittsburgh Sleep Quality Index (PSQI): a new instrument for psychiatric research and practice. *Psychiatr Res.* (1989) 28:193–213. doi: 10.1016/0165-1781(89)90047-4
64. Jurca R, Jackson AS, LaMonte MJ, Morrow JR, Blair SN, Wareham NJ, et al. Assessing cardiorespiratory fitness without performing exercise testing. *Am J Prev Med.* (2005) 29:185–93. doi: 10.1016/j.amepre.2005.06.004
65. Chapman SB, Mudar RA. Enhancement of cognitive and neural functions through complex reasoning training: evidence from normal and clinical populations. *Front Syst Neurosci.* (2014) 8:69. doi: 10.3389/fnsys.2014.0006
66. Chapman SB, Spence JS, Aslan S, Keebler MW. Enhancing innovation and underlying neural mechanisms via cognitive training in healthy older adults. *Front Aging Neurosci.* (2017) 9:314. doi: 10.3389/fnagi.2017.00314
67. Cook LG, Chapman SB, Elliott AC, Evenson NN, Vinton K. Cognitive gains from gist reasoning training in adolescents with chronic-stage traumatic brain injury. *Front Neurol.* (2014) 5:87. doi: 10.3389/fneur.2014.00087
68. Han K, Martinez D, Chapman SB, Krawczyk DC. Neural correlates of reduced depressive symptoms following cognitive training for chronic traumatic brain injury. *Hum Brain Mapp.* (2018) 39:2955–71. doi: 10.1002/hbm.24052
69. Edwards JD, Fausto BA, Tetlow AM, Corona RT, Valdés EG. Systematic review and meta-analyses of useful field of view cognitive training. *Neurosci Biobehav Rev.* (2018) 84:72–91. doi: 10.1016/j.neubiorev.2017.11.004
70. Kerchner GA, Racine CA, Hale S, Wilhelm R, Laluz V, Miller BL, et al. Cognitive processing speed in older adults: relationship with white matter integrity. *PLoS ONE.* (2012) 7:e50425. doi: 10.1371/journal.pone.0050425
71. Wang M, Gamo NJ, Yang Y, Jin LE, Wang XJ, Laubach M, et al. Neuronal basis of age-related working memory decline. *Nature.* (2011) 476:210–3. doi: 10.1038/nature10243

**Conflict of Interest:** The authors declare that the research was conducted in the absence of any commercial or financial relationships that could be construed as a potential conflict of interest.

Copyright © 2021 Chapman, Fratantoni, Robertson, D'Esposito, Ling, Zientz, Vernon, Venza, Cook, Tate and Spence. This is an open-access article distributed under the terms of the Creative Commons Attribution License (CC BY). The use, distribution or reproduction in other forums is permitted, provided the original author(s) and the copyright owner(s) are credited and that the original publication in this journal is cited, in accordance with accepted academic practice. No use, distribution or reproduction is permitted which does not comply with these terms.



# Simulation of COVID-19 Propagation Scenarios in the Madrid Metropolitan Area

David E. Singh<sup>1\*</sup>, Maria-Cristina Marinescu<sup>2</sup>, Miguel Guzmán-Merino<sup>1</sup>, Christian Durán<sup>1</sup>, Concepción Delgado-Sanz<sup>3,4</sup>, Diana Gomez-Barroso<sup>3,4</sup> and Jesus Carretero<sup>1</sup>

<sup>1</sup> Department Computer Science, Universidad Carlos III de Madrid, Leganés, Spain, <sup>2</sup> Barcelona Supercomputing Center, Barcelona, Spain, <sup>3</sup> CIBER en Epidemiología y Salud Pública (CIBERESP), Madrid, Spain, <sup>4</sup> National Centre for Epidemiology, Carlos III Institute of Health, Madrid, Spain

## OPEN ACCESS

### Edited by:

Babak A. Ardekani,  
Nathan Kline Institute for Psychiatric  
Research, United States

### Reviewed by:

Cliff C. Kerr,  
The University of Sydney, Australia  
Fazle Hussain,  
Texas Tech University, United States

### \*Correspondence:

David E. Singh  
dexposit@inf.uc3m.es

### Specialty section:

This article was submitted to  
Infectious Diseases - Surveillance,  
Prevention and Treatment,  
a section of the journal  
Frontiers in Public Health

**Received:** 30 November 2020

**Accepted:** 11 February 2021

**Published:** 16 March 2021

### Citation:

Singh DE, Marinescu M-C,  
Guzmán-Merino M, Durán C,  
Delgado-Sanz C, Gomez-Barroso D  
and Carretero J (2021) Simulation of  
COVID-19 Propagation Scenarios in  
the Madrid Metropolitan Area.  
Front. Public Health 9:636023.  
doi: 10.3389/fpubh.2021.636023

This work presents simulation results for different mitigation and confinement scenarios for the propagation of COVID-19 in the metropolitan area of Madrid. These scenarios were implemented and tested using EpiGraph, an epidemic simulator which has been extended to simulate COVID-19 propagation. EpiGraph implements a social interaction model, which realistically captures a large number of characteristics of individuals and groups, as well as their individual interconnections, which are extracted from connection patterns in social networks. Besides the epidemiological and social interaction components, it also models people's short and long-distance movements as part of a transportation model. These features, together with the capacity to simulate scenarios with millions of individuals and apply different contention and mitigation measures, gives EpiGraph the potential to reproduce the COVID-19 evolution and study medium-term effects of the virus when applying mitigation methods. EpiGraph, obtains closely aligned infected and death curves related to the first wave in the Madrid metropolitan area, achieving similar seroprevalence values. We also show that selective lockdown for people over 60 would reduce the number of deaths. In addition, evaluate the effect of the use of face masks after the first wave, which shows that the percentage of people that comply with mask use is a crucial factor for mitigating the infection's spread.

**Keywords:** COVID-19, simulation, social distancing, mitigation policies, face mask

## 1. INTRODUCTION

At the beginning of March, when the number of infections started to escalate sharply in Italy and the first deaths occurred in Europe, the medical community did not yet fully understand the details of how the SARS-CoV-2 virus propagates. A few weeks later, more than 250 million people were in lock-down in Europe; it had started to become clear that this was an exceptional situation. At that point, the need to understand the evolution of the epidemic and the means to contain and mitigate its propagation became a priority for the health authorities. Many researchers started to work on how to better tackle these challenges. EpiGraph (1) is an already existing epidemic simulator that we had developed some years ago and was able to perform large scale, realistic stochastic simulations of the propagation of the influenza virus. During the past months we have adapted our simulator to COVID-19, we added more components, and we increased the detail level and accuracy of the simulations. The current version of EpiGraph has more than 12,000 lines of code written in the

C language and parallelized using the MPI library. The simulations we present in this work were executed on the Marenostrum4 supercomputer at the Barcelona Supercomputing Center.

EpiGraph consists of four different modules that work together to capture the transmission between different individuals based on social interconnections, mobility patterns, and climate factors (2). The simulator implements a sophisticated social interaction model, in which the individuals are realistically represented through different characteristics such as age and occupation. Besides the epidemiological and social interaction components, EpiGraph also models people's movements between different urban areas. In this work we have reproduced the mitigation policies taken by the Spanish government and we replicated the behavior of the first infection wave in the Madrid metropolitan area. Starting from this initial scenario, we present an analysis of the effect of potential mitigation policies, such as age-dependent social distancing and mobility restrictions and face mask use.

This work was developed in the context of the project *Medium and Long-term Simulation of Covid-19* funded by the Institute of Health Carlos III, for providing support to the Spanish health authorities, both for the forecast of the current COVID-19 propagation, as well as the evaluation of possible future scenarios. The main contributions of this work are the following:

- We provide a fully detailed description of the EpiGraph simulator and how it is adapted to COVID-19. As part of this, we show how EpiGraph was configured to reproduce the first COVID-19 wave (in Spring of 2020) for the Madrid metropolitan area.
- We evaluate the propagation of the virus under the different mobility restriction policies adopted at different times during the epidemic, including the de-escalation period.
- We analyze the effectiveness of selective social distancing measures and the impact of mask use considering different protection levels.

Section 2 contains a detailed description of the simulator, including its validation comparing both real and simulated values. In section 3, we analyze different mitigation scenarios. Section 4 provides a discussions of the findings as well as the limitations of the work; section 5 describes related work. Finally, section 6 presents the main conclusions of our work.

## 2. MATERIALS AND METHODS

### 2.1. Background

Algorithm 1 shows an outline of EpiGraph's simulation algorithm. The iterative algorithm discretizes the total simulation time in time steps of 10 min (line 1). In each time step, the algorithm considers each city in the simulated territory (line 2). A city has a given population which is modeled based on the Spanish census data<sup>1</sup>, with the associated social connections between the individuals. Line 5 updates the health status of each infected individual of each city, as indicated by the epidemic

**Algorithm 1:** EpiGraph transmission algorithm. Variable *simulation\_time* represents the simulation duration, *simulated\_territory* is the simulated area including several cities, each one of them with a social interaction model for the population, and *status* contains characteristics and health status of each individual for each city.

```

1: for timestep = 1  $\rightarrow$  simulation_time do
2:   for city  $\in$  simulated_territory do
3:     for individual  $\in$  city do
4:       if status[individual] is infectious then
5:         UpdateStatus(status[individual])
6:         ComputeSpread(individual, city)
7:       end if
8:     end for
9:     Individual_Interventions(status)
10:    Social_Interventions(city)
11:    Transportation(city, simulated_territory)
12:  end for
13: end for

```

model used by the simulator. The next step (line 6) computes how the infectious agent spreads via the social model, starting from every infected individual and evaluating the probability of transmission to each of their contacts. This probability depends on the type of connection, the time of day, and the characteristics of the individual potentially being infected, such as their age or the use of face masks.

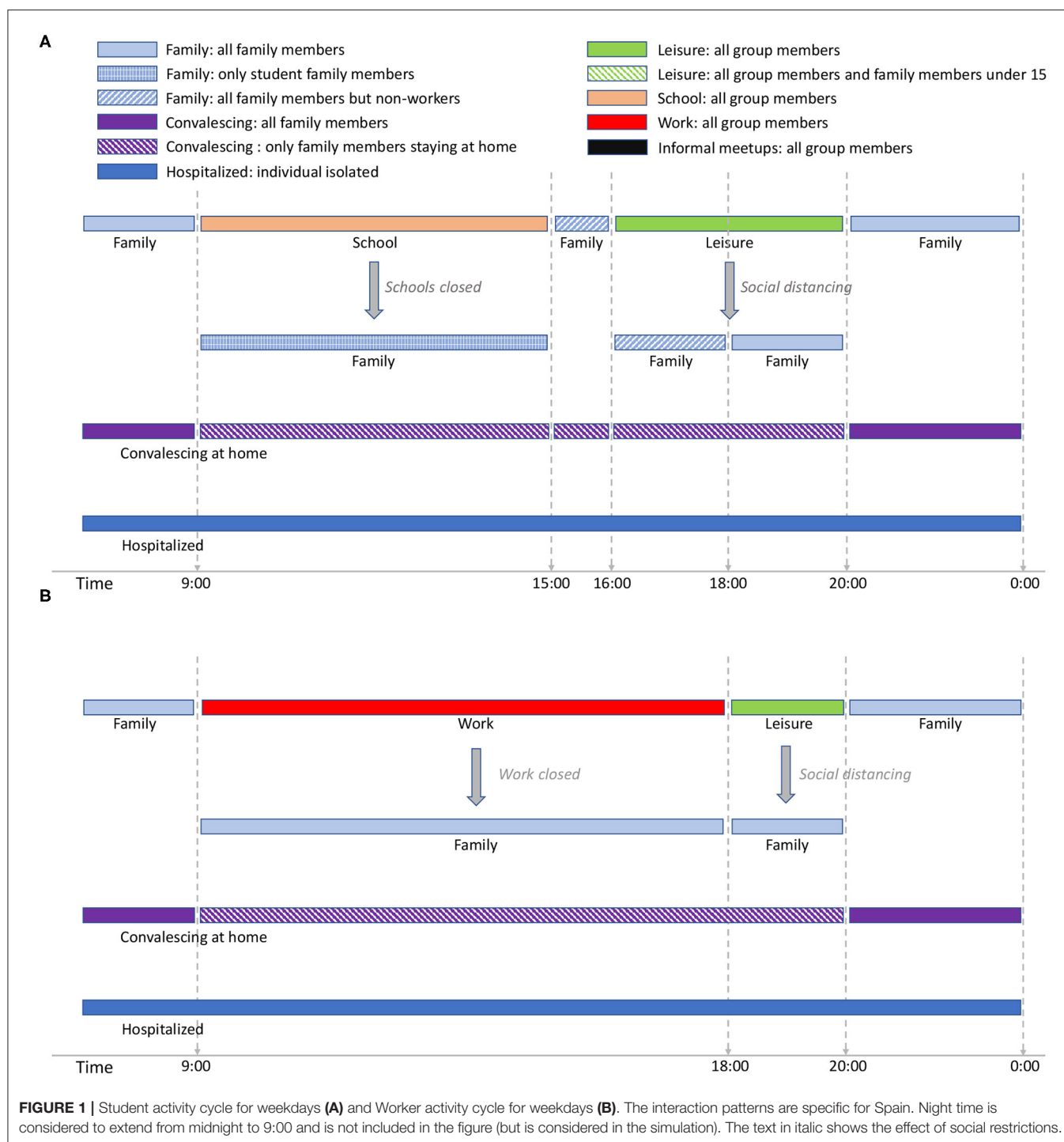
We call an individual intervention (line 9) an action taken by the individual to mitigate the propagation of the infectious disease. In EpiGraph these actions are activated or deactivated based on defined policies. One example of intervention is that at simulation day 30, a certain individual starts using surgical face masks at work, but not at family time. We call a social intervention (line 10) those interventions—such as school closing or social distancing—that are imposed (or lifted) by the health authorities at a certain time of the simulation. Finally, in the propagation of the infection via the transportation model (line 11), some individuals move between their city and another, depending on the city sizes and the geographical distance between them. This allows us to model the medium and long distance travel of people. The following sections describe each one of these components in greater detail.

### 2.2. Social Model

This section describes how EpiGraph models individuals' characteristics and their social interactions within the region under study. The simulator considers independently every single individual in the population. In this work we simulate the metropolitan area of Madrid with 5,018,241 individuals. In other experiments (not included in this work) we have been able to carry out European-level simulation with up to 198 million inhabitants.

EpiGraph's social model is an agent-based model that captures individual attributes and specifies the way that the individuals interact based on patterns extracted from social networks (Facebook) and from companies (Enron Email Corpus). Attributes include age, gender, and race, which are instantiated based on real census data. We use demographic information to reproduce social habits for four different group

<sup>1</sup>National Statistics Institute (INE). Available online at: <http://www.ine.es/> (2021).

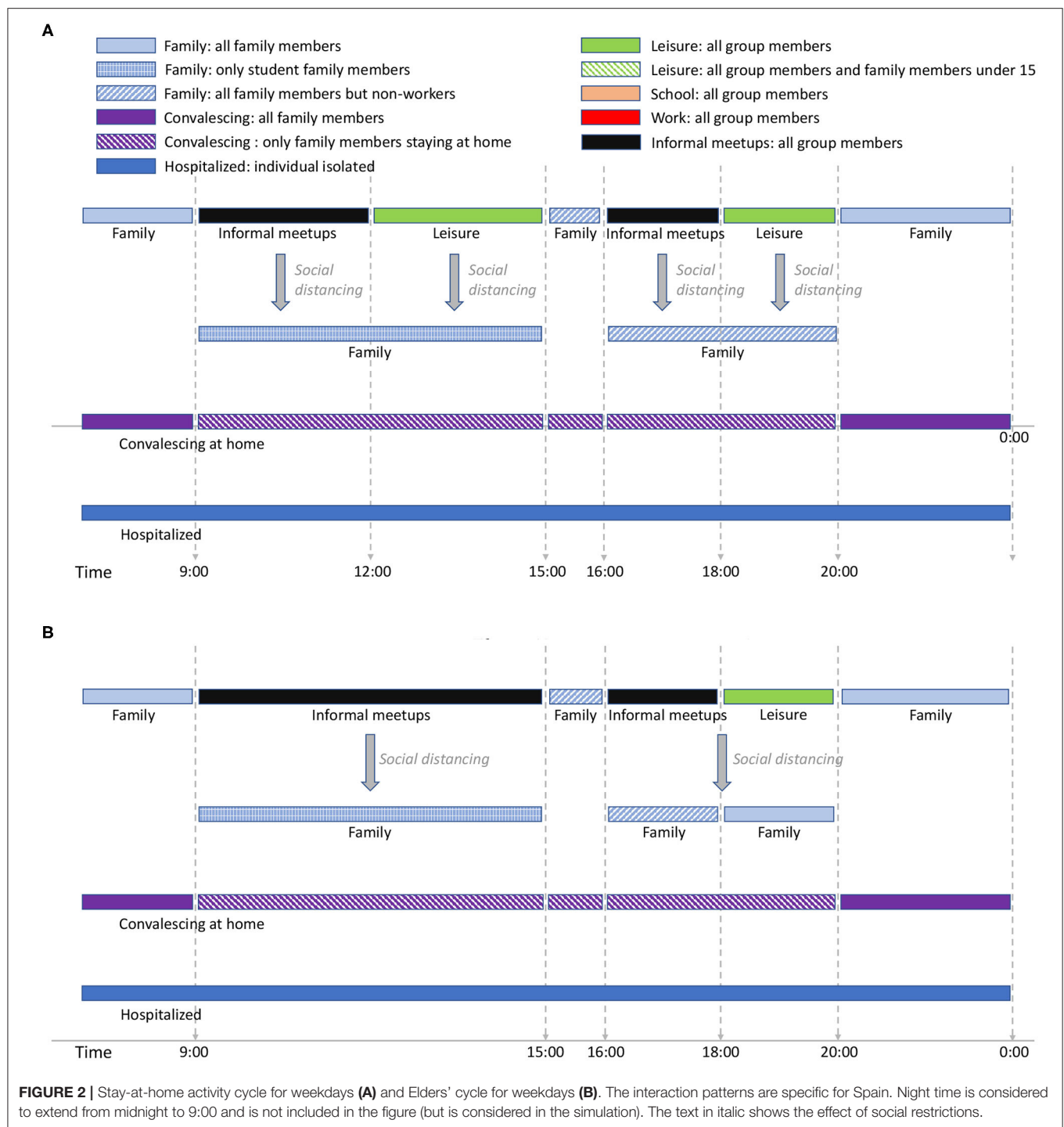


types (also called collectives): students, workers, stay-at-home people, and elders. The way the individuals establish social contacts<sup>2</sup> is time-dependent in order to realistically reflect the temporal nature of the different classes of interactions that each

individual has throughout the day. For each one of the group types we consider three different temporal distribution of the individual's activities, those related to weekdays, Saturdays, and holidays (including Sundays).

**Figure 1** shows the activity cycles for students and workers during weekdays while **Figure 2** shows the activity cycles for stay-at-home and elderly collectives. An activity cycle determines the contacts that are active at a certain time, i.e., the individual

<sup>2</sup>We define a social contact (also called contact or interaction) between two individuals a co-location in time (and space) at a distance that is small enough to make transmission possible.



interactions with other individuals that may produce a disease transmission. These patterns are specific to the place being modeled; in Spain, for instance, breakfast is around 8:00, lunch time around 14:00, and dinner time starts at 20:00. The period ranging from 0:00 until 9:00 (not shown in the figures) corresponds to family time (i.e., only family connections are active). Note that family time includes all the activities carried out at home (dinner time, family time and night sleep).

For the student group type (**Figure 1A**), school time is considered to be from 9:00 to 15:00<sup>3</sup>. We assume that school time is followed by a short period of family time, after which there is a leisure period in which the students are in contact

<sup>3</sup>This time interval is an average value obtained from public and private school timetables, and takes into account that some students leave school before lunch while others stay on during the afternoon.



with other individuals different from those belonging to the same school group. There are two social distancing policies applied for students: school closure, and social distancing in which school and leisure times are replaced by family time. In EpiGraph, we distinguish between different levels of family-time interactions, based on the family members that are at home at each time of the day, as follows; at night-time each individual is in contact with all family members; when schools are closed, the family-time for this period takes into account only those family members that are at home. For instance, if work places are opened, family time will not include the working members. On the other hand, when social distancing is not imposed, social contacts with stay-at-home and elderly family members are not taken into account during this time period because we assume that these two group types are not at home at this time. For the same reasons, during the family time slot from 15:00 to 16:00, stay-at-home persons and elderly family members are included in the interactions, while working members are not.

EpiGraph can model that a certain percentage of infected individuals stay at home during part of the infectious period. We call this the *convalescing at home* period, in which sick individuals have symptoms that, although not being severe, force them to remain in bed, canceling work, study and social activities. For convalescing individuals, the only contacts are within the family. That is, the infection can only be propagated within the family. In this work we have considered that 20% of the population are convalescing at home after being infected. The simulation also considers individuals with severe symptoms that are hospitalized. In this case, we assume that the patients are isolated in the hospital and do not transmit the disease. The probability of being hospitalized is age-dependent, as described in section 2.4.

The activity cycle for the remaining group types (workers, stay-at-home people, and the elders) are shown in **Figures 1B, 2A,B**. Each worker has an associated work time slot followed by a short period of leisure time. For stay-at-home individuals and elderly, we define *informal-meetup* as the contacts that a person belonging to these group types creates via typical weekday activities. This includes shopping, retirement home meetings, and social activities related to peer meetings belonging to the same group. In addition, individuals also have leisure periods in which they interact with other groups that may belong to the same or to a different collective.

**Supplementary Material** includes the activity cycles for Saturdays and Sundays/holidays. For students above 15 years old, we model leisure time on Saturday-night between 20:00 and 0:00. Younger students have assigned family time during this period. In our experiments, 35% of the total of workers work on Saturdays, while the rest don't. For those who do, leisure time ranges from 20:00 to midnight and is shared with the family group. For the stay-at-home and elders' groups there are no contacts within the informal-meetup groups during Saturdays and holidays. We assume that informal-meetup contacts are only related to weekday activities and not performed on weekends.

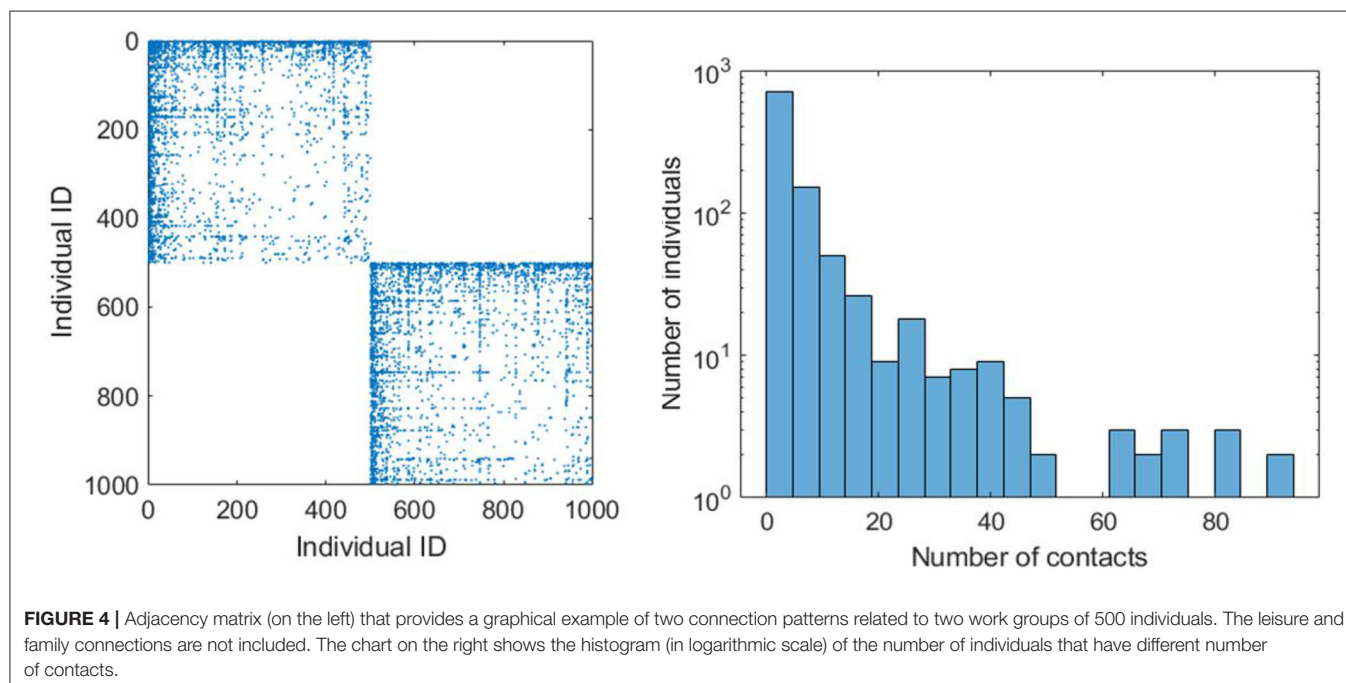
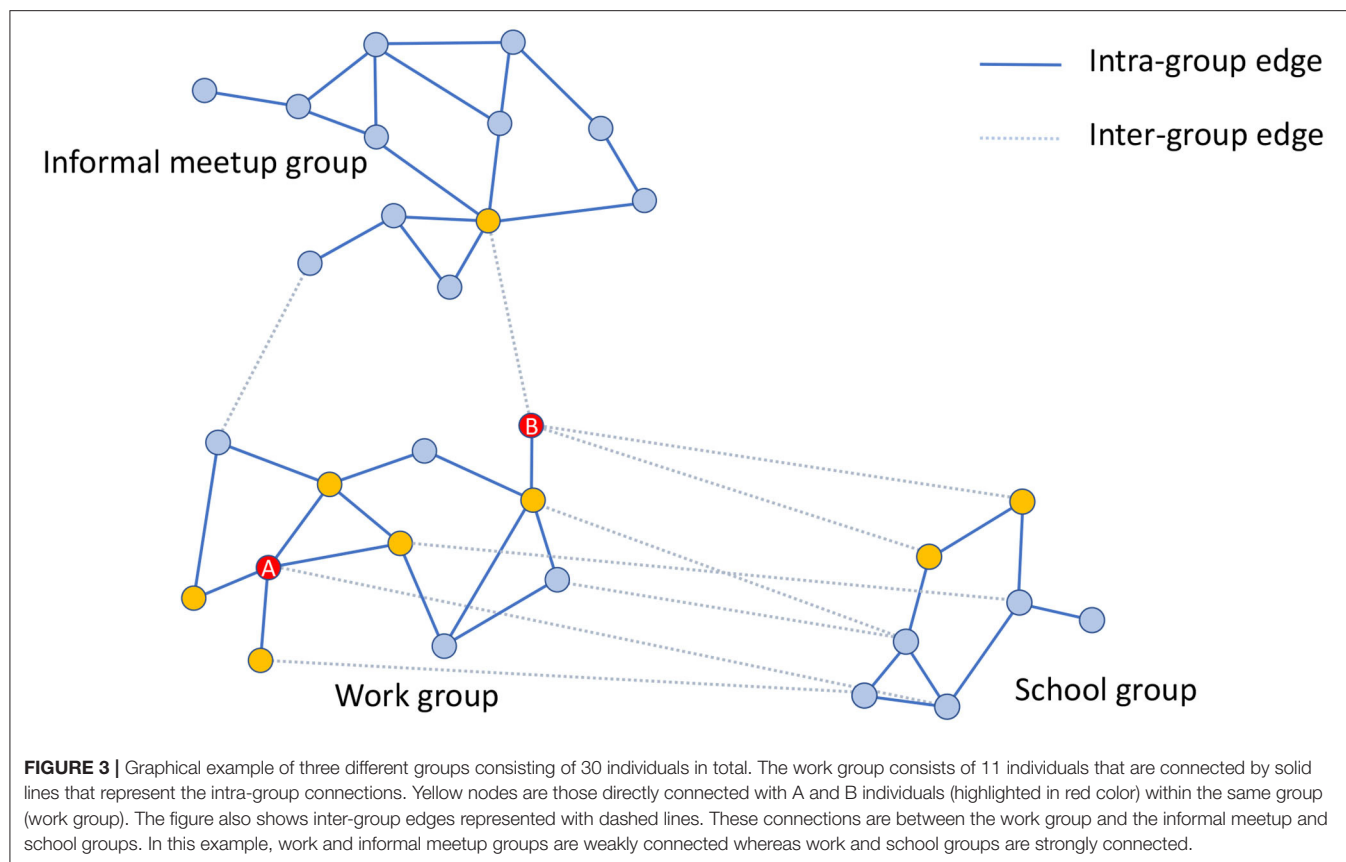
**Figure 3** shows an example of a work group consisting of 11 individuals. All the interactions, -denoted as intra-group contacts- and connected by solid lines are between individuals belonging to the same group and occur during the daily activities

of this group. The number of interconnections of each individual may be different, e.g., individual A has four connections while B only has one within the same group (work group). This reflects the nature of a real social graph used to generate the groups, where different persons have different connection degrees (3). If individuals A and B are infected, then the people susceptible to being infected within the group will be the nodes displayed in yellow. In this case, individual A has more chances of propagating the disease within the group than individual B. Section 2.4 describes how EpiGraph simulates the propagation of the infectious pathogen throughout the network.

EpiGraph creates different graphs for each work group, school group, stay-at-home (informal meetup) group, and elderly (informal meetups) group. **Supplementary Table 1** shows the parameters used for modeling each of these groups. Rather than assuming a distribution or generating synthetic interaction graphs, we use real information from social networks to model the social interaction patterns. Each group has a different size, in between *MinSize* and *MaxSize*. We have used the Enron Email Corpus (70,578 nodes and 312,620 edges) for generating the work and informal-meetup groups while the Facebook (250,000 edges and 3,239,137 edges) network was used to generate the school groups. The adjustment to the desired target size is done using a graph-scaling algorithm based on Random Walk (4). This algorithm selects as many nodes as the group size (i.e., number of individuals in the group) in a random fashion, creating a sampled graph with similar structure to the original one but with a smaller number of nodes. This procedure creates different connection patterns for each group, while maintaining certain graph-related properties such as the distribution of the number of contacts per individual (3). The resulting contact network has an average connectivity of  $\langle k \rangle = 6.4$ . This value is obtained according to Equation (1). Where,  $N$  is the total number of simulated individuals,  $K_{i,1}$ ,  $K_{i,2}$ , and  $K_{i,3}$  represent the number of connections of type 1 (work, school and informal meetups), 2 (leisure) and 3 (family) of each individual  $i$ , respectively. On the other hand,  $P_{i,1}$ ,  $P_{i,2}$ , and  $P_{i,3}$  represent the duration in hours of each of each connection during a day for individual  $i$ . **Figure 4** shows a graphic example of an adjacency matrix  $A$  for two groups of 500 individuals each and the histogram (in logarithmic scale) with the distribution of the number of contacts. In this representation, a matrix entry  $A_{i,j} \neq 0$  means that individual  $i$  and  $j$  have a contact. Note that the family and leisure contacts are not included, thus the figure only shows the contacts within the group. We can observe that the connection pattern is different for each group and that the histogram follows an exponential distribution, which is the usual connection distribution of social networks.

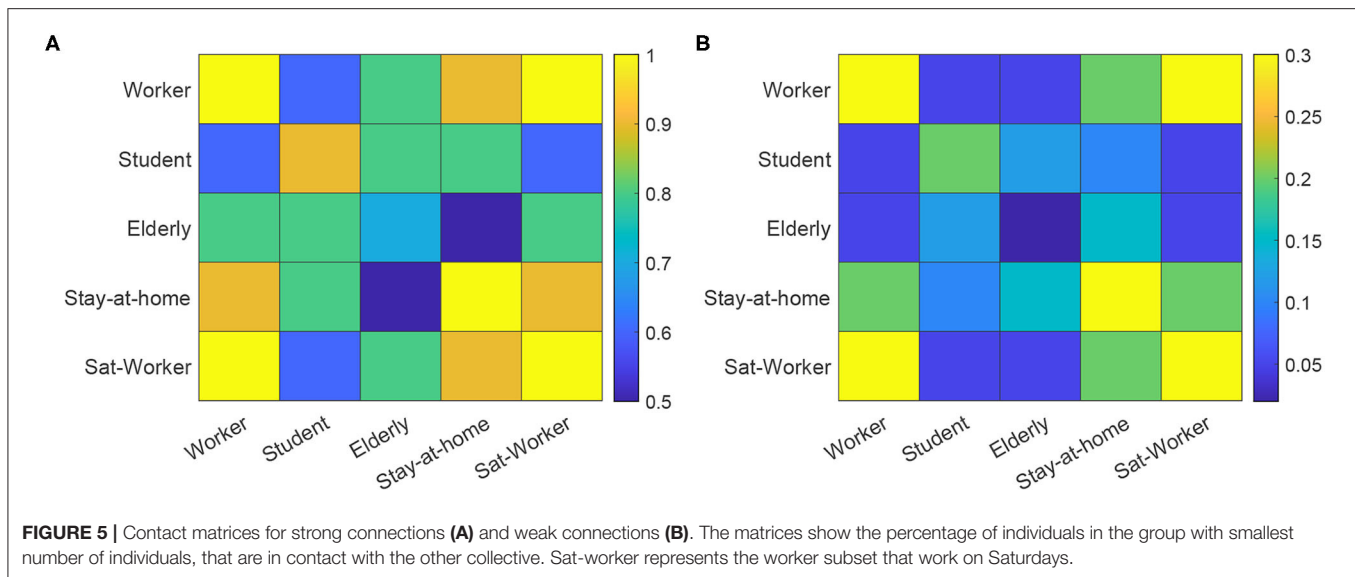
$$\langle k \rangle = \frac{\sum_{i=1}^N K_{i,1}P_{i,1} + K_{i,2}P_{i,2} + K_{i,3}P_{i,3}}{24} \quad (1)$$

Existing work such as (5) analyzes the relationship between the structure of the connection network and the propagation of an epidemic, concluding that there exists a direct relationship between the network structure and both the size of the epidemic (as the number of infected individuals) and the timing of the



propagation. These findings imply that the use of connection networks based on actual social interactions (3) can contribute to enhancing the simulation accuracy.

The social model includes two more types of social contacts for leisure and family activities. Leisure contacts are modeled by means of inter-group contacts. These contacts are between



individuals belonging to different groups (for instance, work and school groups) and occur mostly after the main daily activity and before family time, as well as during the weekends. These contacts represent interactions with friends as well as casual contacts with unknown people. In dashed lines, **Figure 3** shows the leisure contacts of the work group with a school and an informal-meetup groups. Note that now, individual B has more inter-group contacts than A. Leisure contacts provide heterogeneity of connections between groups, given that a certain individual can be connected with others belonging to different collectives, for instance, young people with elders, workers with unemployed, etc.

EpiGraph distinguishes two classes of inter-group connections: strong and weak. Groups that are strongly inter-related are tightly coupled, which means that there is a high percentage of individuals that have inter-group connections. This is the case of the work and school groups in the figure. In contrast, weakly inter-related groups, like the work and informal meetup groups in **Figure 3**, have a small percentage of inter-group connections. This reflects the asymmetry of daily interactions, where some groups (for instance, two different classes sharing the same playground, or two different informal meetup groups sharing the same leisure space) are strongly coupled while in others, that more weakly-related, only few people are involved in the inter-group interactions. The exact percentage of inter-group contacts is given by the contact matrices shown in **Figure 5**. These matrices show for each pair of collectives, the percentage of individuals that are in contact, either within a strong or a weak inter-relation. For instance, two strongly inter-related work groups will have a large fraction of the individuals with inter-group contacts<sup>4</sup>. Note that, in general,

only a small fraction of any group is either strongly or weakly connected. In our experiments, each group is connected strongly with 0.1% and weakly with 2.42% of the total number of existing groups. The inter-related groups are randomly selected, as well as the individuals with inter-group connections.

The third class of contacts are family contacts, interactions with family members who may or may not be part of the same group. The family connections graph is completely connected. However, connections are time-dependent. **Supplementary Table 2** shows the distribution of the number of family members, obtained from the INE<sup>1</sup>. Please note that we include single-member family units, where the individual lives alone.

### 2.3. Transportation Model

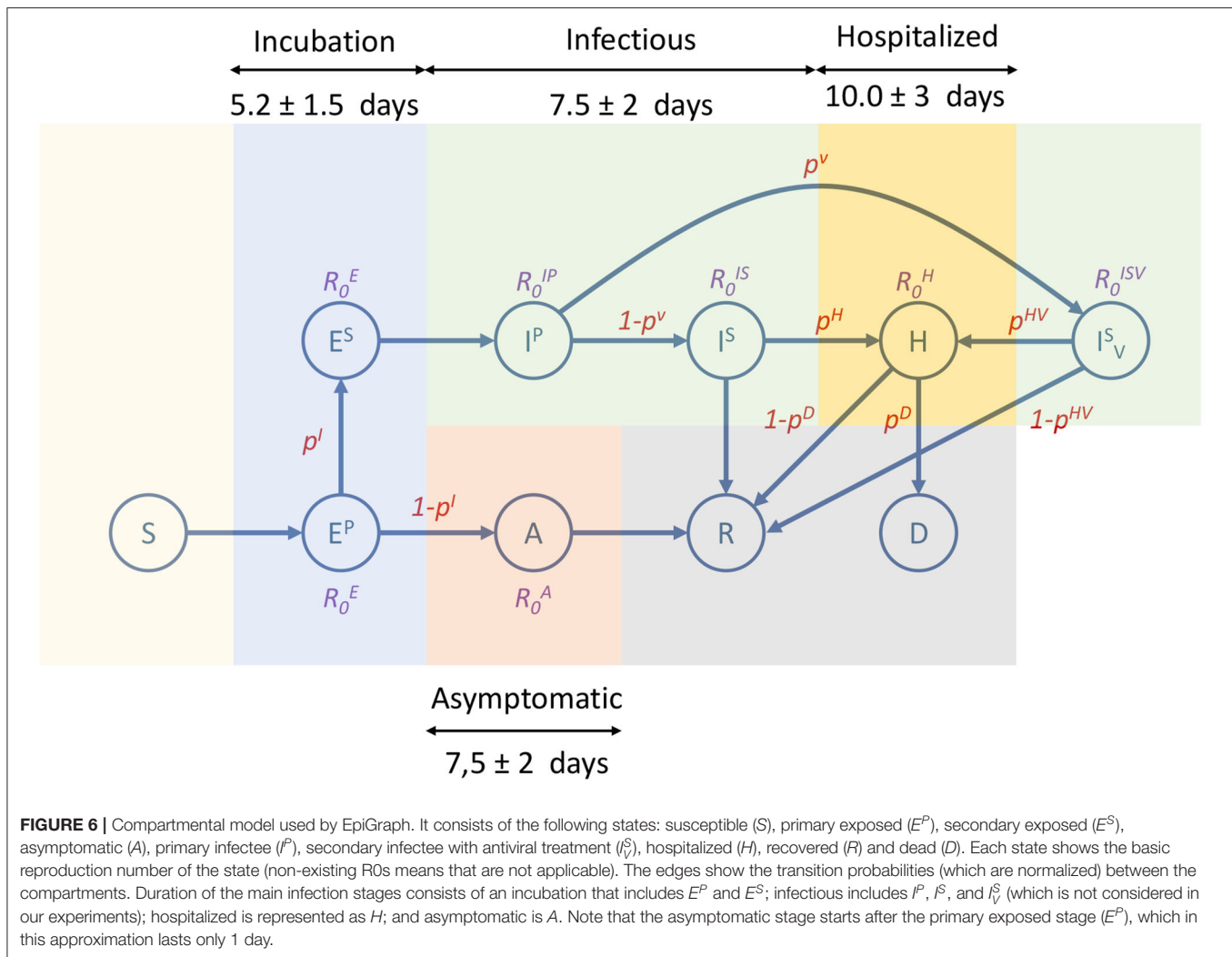
The transportation model reflects the movement of people between cities for work, study, or vacation, and it is based on the gravity model proposed by Viboud et al. (6). Note that the movement of people within a city is already captured by the social model. The transportation model serves the purpose of moving individuals between different cities, allowing for disease transmission over large areas. The geographical information that EpiGraph takes into account includes latitude, longitude, and distance between urban regions, and was extracted from the Google Maps web service using the Google Distance Matrix API<sup>5</sup>.

$$(d_{ij} < 120\text{Km}) \quad \Delta P_{ij} = \frac{P_i^{0.30} P_j^{0.64}}{d_{ij}^{3.05}} \quad (2)$$

$$(d_{ij} \geq 120\text{Km}) \quad \Delta P_{ij} = \frac{P_i^{0.24} P_j^{0.14}}{d_{ij}^{0.29}} \quad (3)$$

<sup>4</sup>For groups with different sizes, the maximum number of available inter-group connections is the size of the smaller group. For instance, two groups with 50 and 100 individuals that are strongly connected with 90% contacts, will have 45 inter-group connections between them.

<sup>5</sup>Google Maps API. Available online at: <https://developers.google.com/maps> (2021).



This model considers the exchange of individuals between cities, for each pair of cities  $i$  and  $j$ . This number ( $\Delta P_{i,j}$ ) depends on the population size in both locations ( $P_i$  and  $P_j$ ) as well as the distance between them ( $d_{i,j}$ ). Equation (2) refers to travel distances of less than 120 Km—which reflects the daily commute of students and workers to neighboring cities. Equation (3) refers to the long-distance commute of workers that need to reside at a different location for several days in a row. Additionally, we consider people from any group type that move at any distance for several days for vacation purposes. Once the volume of inter-city commuters is calculated, we randomly select individuals from specific group types within the populations and move them for a specific period of time to other locations. In our experiments, for the short distance commuters, 85% are workers and 15% are students; for the long-distance commuters the percentages are 50% workers, 30% students, 15% retired individuals, and 5% unemployed people.

## 2.4. COVID-19 Model

The epidemic model implemented in EpiGraph is a compartmental stochastic SEIR model extended to include

compartments for incubation, asymptomatic, and dead, as well as an additional hospitalized state. However, instead of being an analytic model based on differential equations, EpiGraph follows an approach based on probabilities using randomness to determine the duration and transitions between the compartments. In addition, the basic reproduction numbers  $R_0$ s are different for each compartment. **Figure 6** shows the infection phases, which are described below; **Table 1** shows the  $R_0$  values for each compartment, as well as the transition probabilities for the compartments that can transit to different states (like  $E^P$ ). The different infection stages are:

- Incubation stage.** At the beginning of this stage individuals are infected but symptoms are not present and they are not yet able to transmit the virus. This stage is represented as primary exposed  $E^P$ . From this stage the infection can enter one of two phases, based on a probability  $p^{EI}$ : a secondary exposed stage  $E^S$  where slight symptoms appear and the individual becomes infectious with a certain  $R_0^{ES}$ , or an asymptomatic stage (described below). We assume that  $R_0^{ES}$  is the same as the asymptomatic  $R_0^A$ .



**TABLE 1** |  $R_0$  Values and transition probabilities for each compartment state.

| Compartment state | $R_0$ values    | References | Probability          |
|-------------------|-----------------|------------|----------------------|
| $E^P$             | $R_0^{EP}$ 0    |            | $P^A$ 25%            |
| $E^S$             | $R_0^{ES}$ 1.42 |            | N/A                  |
| $A$               | $R_0^A$ 1.42    | (7)        | N/A                  |
| $I^P$             | $R_0^{IP}$ 4.5  | (8)        | $P^{IS}$ 100%        |
| $I^S$             | $R_0^{IS}$ 3.38 | (9, 10)    | $P^H$ <b>Table 2</b> |
| $I_V^S$           | $R_0^{IVS}$ N/A |            | N/A                  |
| $H$               | $R_0^H$ 0.34    |            | $P^D$ <b>Table 2</b> |

In this work we have not considered the use of antivirals, thus  $I_V^S$  state is not reached and the associated  $R_0^{IVS}$  value is not applicable.  $E^S$  and  $A$  states do not have a related transition probability because there is only a destination state.

- In the **asymptomatic stage** (compartment  $A$ ), infected individuals do not notice symptoms but are able to transmit the disease with a certain  $R_0^A$  reproduction number. After a certain time, they pass to the recovered compartment in which the subject acquires viral immunity.
- In the first **symptomatic stage**—called primary infection state  $I^P$ —symptoms appear and a certain fraction of the individuals (given by a probability  $P^V$ ) seek medical attention. This may imply initiating antiviral therapy ( $I_V^S$  state)—which is not considered in this work. In our experiments, all infected individuals will transition from  $I^P$  to  $I^S$ . In addition,  $I^P$ ,  $I^S$ , and  $I^V$  have associated basic reproduction numbers of  $R_0^{IP}$ ,  $R_0^{IS}$ , and  $R_0^{IV}$ .
- A certain fraction of the individuals are hospitalized (**hospitalized stage**). The probability of entering this stage is given by the parameter  $P^H(\text{age})$ , which is age-dependent. **Table 2** shows the values for  $P^H(\text{age})$ , obtained from (11). Note that this probability increases with age. From this state, an individual may transition to either the recovered or the dead stage. During hospitalization, we use  $R_0^H$  for modeling the transmission in hospitals. In this work we assume that due to the controlled conditions of hospitalized individuals, the transmission risk is reduced to 10% compared to a non-hospitalized person, and we use  $R_0^H = 0.34$  as a result. For the purpose of this work, we assume that a recovered individual acquires indefinite immunity to the virus.
- The individuals that reach the **dead stage** are removed from the simulation. The transition probability, denoted as  $P^D(\text{age})$ , is also age-dependent. **Table 2** shows these probabilities, which have been obtained from (11). Note that this probability is applied over the portion of hospitalized individuals.

The time spent in a given state is generated following a normal distribution to simulate the time ranges specific to each stage of the infection and the fact that each individual may go through phases of different lengths. **Figure 6** shows an overview of the different infection stages. We also consider that a percentage of the sick individuals stay in bed, thus reducing the number of people that they interact with.

While the EpiGraph model implements all the necessary phases and variables, it needs to be fine-tuned for COVID-19.

We adopt most of the concrete values for the model parameters from the existing literature. More specifically, (12) reports on an incubation period of 5 in mean. We considered that of these, 3 days correspond to the primary and 2 days to the secondary incubation phases (13). The difference between these phases is that in the primary phase there is no risk of transmitting the disease. We used a normal distribution to associate a different stage duration to each infected individual. We took the standard deviation for the incubation period to be 1.5 days, and we distribute it proportionally between stages. We assume that the related  $R_0^{ES}$  is the same as the asymptomatic  $R_0^A$  (described below).

We adopt an average infectious period of 5.90 days; a similar value to that reported in (14). This period is divided into two phases: the primary infection period that we assume to last for only 1 day, while the secondary infection lasts the remaining 4.9 days (14). We adopt a standard deviation for the infectious period of 2 days, which was proportionally distributed between the first and second periods. We found studies that pointed to higher virulence at infection onset, which we understood as the primary infectious stage. We therefore take the higher number in the literature (4.5) as the  $R_0^{IP}$  at the onset of the infection (8), i.e., for the primary infectious stage. For the rest of the period, i.e., the secondary infection period,  $R_0$  is taken to be 3.38 (9, 10).

Based on a study of the Diamond Princess cruise ship (15), 322 of 621 people on board tested positive but showed no symptoms. Given the controlled environment and fact that it was easy to test the passengers in their entirety, we believe that the percentage of people that go from incubation to asymptomatic is actually quite large. For lack of other data, we set it to roughly half the percentage on this cruise ship. This is also coherent with the ECDC reported values (16). Consequently, we assume that 25% of the infected individuals become asymptomatic. We used an asymptomatic phase duration of 5 days (13). According to (7), asymptomatic individuals were 42% less likely to transmit the virus than symptomatic people. Consequently, we take this basic reproductive number  $R_0^A$  to be 42% of  $R_0^{IS}$ .

In (17, 18), it is mentioned that the median number of days from first symptoms to death was 13. Given that the average duration of the  $E^S$ ,  $I^P$ , and  $I^S$  stages is 8 days<sup>6</sup> and an individual only dies after a hospitalization period, we adopt the mean time of being in hospital of 5 days. The simulator evaluates the risk of being hospitalized and dying based on the age of each individual. The age distribution among the existing group types was extracted from the INE (the Spanish National Statistical Institute).

## 2.5. COVID-19 Mitigation Strategies

Given that the simulator considers every single individual and their connections, it is possible to model in detail the different social distancing and mitigation policies imposed by the authorities. We developed a new component called the *mitigation model* that links these policies with the social and the mobility models. The policies that we are considering are:

<sup>6</sup>Note that here we are not considering the  $E^P$  stage because we assume that individuals in this stage have not developed symptoms.



**TABLE 2** | Values of  $P^H$  and  $P^D$  based on age.

|           | Age interval |       |       |       |       |       |       |       |      |
|-----------|--------------|-------|-------|-------|-------|-------|-------|-------|------|
|           | < 10         | 10–19 | 20–29 | 30–39 | 40–49 | 50–59 | 60–69 | 70–79 | ≥ 80 |
| $P^H$ (%) | 0.4          | 0.4   | 3.4   | 9.0   | 19.6  | 31.4  | 40.8  | 49.8  | 45.2 |
| $P^D$ (%) | 0.0          | 0.4   | 0.8   | 0.8   | 1.2   | 2.0   | 4.7   | 12.2  | 30.0 |

$P^H$  is the probability an infected person has of becoming hospitalized and  $P^D$  is the probability a hospitalized person (a fraction of the total infected) of dying.

- Social distancing. EpiGraph distinguishes four classes of contacts between individuals: at school, at work, with family, and during leisure time. We leverage this distinction to evaluate social distancing policies that can apply differently to the contact types, for instance the closure of the schools and work places. We have considered both essential and non-essential workers—which represent 35 and 65% of company employees—as well as the interruption of leisure activities.
- Mobility restrictions. The transportation model of EpiGraph includes long and short-distance movements of individuals between cities. In this work, we have introduced policies that restrict each one of them independently.
- Face-masks. We have introduced the use of surgical and ffp2-grade face-masks, which we evaluate when used by the general population or by targeted groups, such as the elderly.

## 2.6. Setting Up the Simulator Configuration

For the experiments presented in this work, we focus on results for the metropolitan area of Madrid, which includes the city of Madrid and the following surrounding satellite cities: Alcalá de Henares, Alcobendas, Alcorcón, Fuenlabrada, Getafe, Leganés, Móstoles and Parla—for a total of 5,018,241 inhabitants according to the census data<sup>1</sup>. The baseline scenario we modeled reproduces the social distancing measures that were applied in the Madrid metropolitan area in Spring of 2020. The simulation starts on March 3rd with a certain percentage of infected individuals, rather than with a patient zero. In our experiments, 0.6% of the population of each city was initially infected at this time. The lockdown occurred on simulation day 13 (equivalent to March 16th), when partial enforcement policies were applied, which include school closure, working from home for 65% percent of the businesses, social distancing (where all leisure connections are disabled), and travel restrictions—all reflecting the real-life policies that were enforced in Spain on that very date. On week before lockdown (March 9th) we introduced partial social distancing with a reduction in the number and duration of leisure contacts. This reflects the existing change in the behavior of the population just before lockdown. On simulation day 27 (which corresponds to the 30th of March), 100% of the companies closed or instated 100% work-from-home policies. At this point only the family connections are active. Finally, on day 41 (13rd of April), 35% of the companies reopen, activating the corresponding work connections. In this baseline scenario the rest of the population remains confined indefinitely in order to avoid creating a second wave of infection.

EpiGraph has to be initially calibrated to reproduce precisely the COVID19 spread. For each contact between a pair of infected

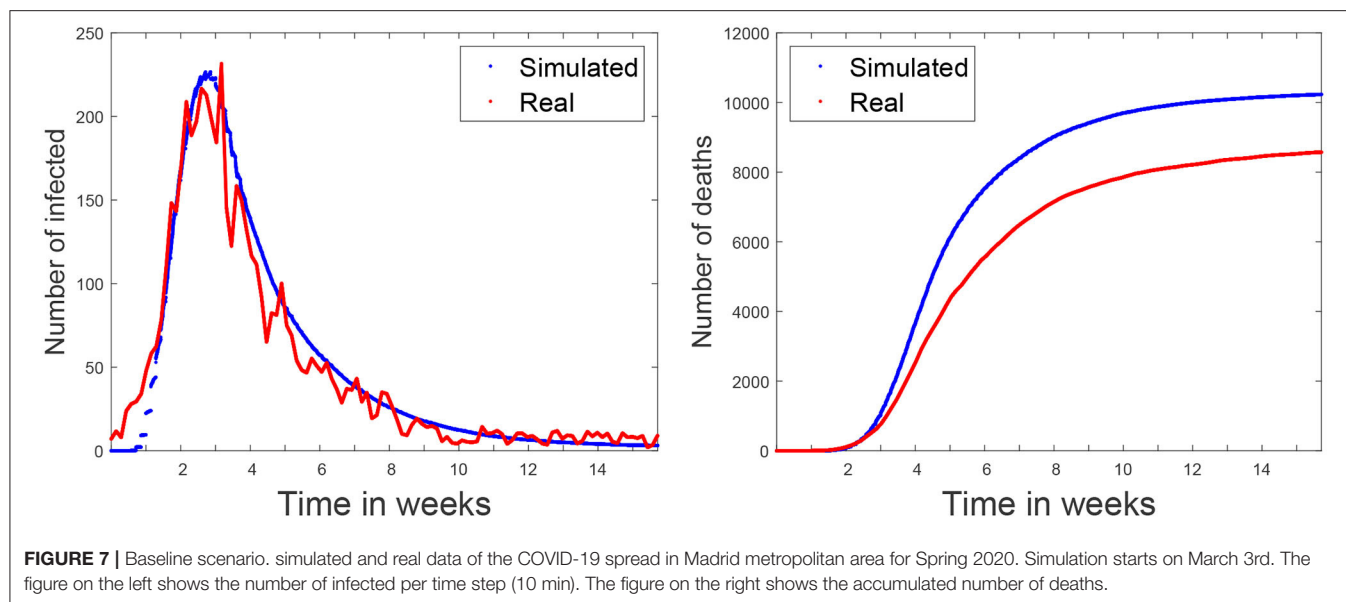
and susceptible individuals, the transmission probability depends on the infected individual's  $R_0$  value in the current infection phase and the duration of the contact. We have used a scale factor that increases or decreases this probability in order to produce realistic infection spreads. In total, three configuration parameters need to be specified: the scale factor, the initial number of infected individuals and the simulation starting time. In this work, the calibration was performed using the first wave in Spain. The goal was to replicate the shapes of the curves using the distributions of the number of daily infections and deaths (see details below), as well as to achieve the same prevalence value as the one in Spain after this first wave. After the calibration process the best fitting values were 7.14 for the scale factor, 0.6% for the initial percentage of infected population and March 3rd for the simulation start time. Note that these parameters are constant and will be used in all the experiments shown in this paper.

In the simulation outcome, an average percentage of 12.2% of the population becomes infected in the period until the simulation ends (on June 26th), a percentage similar to the one obtained from the prevalence study carried out in Spain (19), which predicts a prevalence of 11.7% for the metropolitan area of Madrid at this time, and a 5% as the average value for the country.

**Figure 7** (left) shows both the real (in red) and simulated (in blue) distributions of infected cases. The simulated values are the average of five independent simulation and have been scaled to the current population of the community (6.6 million, which includes the inhabitants of other smaller urban and rural areas). The daily reported cases of infections were obtained from<sup>7</sup>. Our aim is to compare the temporal distribution of infections for the reported and simulated cases. Note that the reported cases do not precisely reflect the actual number of infected individuals at a certain time, given that an important fraction of the cases are unaccounted for, including most of the asymptomatic cases and the unreported infections. In order to compare the two curves, in **Figure 7** (left) we scaled each one according to their prevalence percentages (11.7 and 12.2% for the real and simulated distributions, respectively) on June 26th (which corresponds to the end of the simulated scenario). The area under the red curve corresponds to the 11.7% of Madrid's population, while the area under the blue curve represents 12.2% of the population<sup>8</sup>. We can observe that the curves have a similar shape, with a rapid

<sup>7</sup>Red Nacional de Vigilancia de la Salud Publica. Available online at: <https://cnecovid.isciii.es/covid19/> (2021).

<sup>8</sup>In the figures, we have represented the values using the same time step (for the x-axis values) used by the simulator (10 min). This makes the graphics more detailed and smooth.



initial increase in the number of cases and a long decreasing infection tail.

The last validation was carried out using the number of officially reported deaths. **Figure 7** (right) shows with a red line the accumulated official number of deaths<sup>7</sup>. Note that, due to the uncertainty of the data, it is impossible to know if all the COVID19 deaths have been reported. For this reason, this curve represents a lower bound of the deaths. The blue line represents the simulated values that are the average of five independent simulations. According to (17, 18), the average time between the first symptoms and death is 13 days, which is the same that the simulations takes to go through the incubation, infectious, and hospitalized stages (see **Figure 6**). Empirically, the time difference between the simulated and the real deaths is 7 days (in the figure the simulated values have been already shifted by this value). This discrepancy is likely related to delays in the reporting of the deaths.

**Figure 8** shows the age distribution of the simulated population as well as the distribution of infection and death cases. We can observe that the elderly suffer a higher death toll, as expected.

### 3. RESULTS

In this section, we present results for different scenarios, including different lockdown alternatives, the impact of the use of face masks, social distancing measures, and the use of testing for the quarantine of early-detected infected individuals. All experiments start on the 7th of March with 0.01% of the population being infected; we apply the calibration described in section 2.6. The simulation captures as infected individuals not only the reported cases, but also those individuals that are not reported, as well as the asymptomatic cases.

On 18th of May, Madrid entered Phase 0.5 and most of the lockdown restriction were lifted. The first alternative

scenario represents the worst-case scenario, in which at this time (simulation week 11) all the restrictions are lifted, including social distancing measures and travel restrictions, and schools open. No masks were used at this time.

The idea of this scenario is to evaluate the maximum virus spread. **Figure 11A** shows that under these conditions, 95.7% of the population becomes eventually infected, and the death toll rises to 70,000. In this scenario, the effect of school closure on the disease propagation is minimal; we have simulated the same scenario keeping schools closed, while the rest of the restrictions are lifted, and 93.5% of the population becomes infected.

#### 3.1. Evaluating Face Mask Effectiveness

In this section, we evaluate the mitigation capabilities of different types of face masks, while considering different percentages of the population that use each type. The effectiveness of masks and face covers remains uncertain and depends on diverse and complex aspects including, among others, the ability to reduce the outward particle emission rates for the different transmission modes (droplet spray or aerosol) (20), the way this effectiveness is degraded after using or washing the mask, and the lack of experience in using them correctly, all of them resulting in increasing the risk of infection. EpiGraph models face mask effectiveness as a scale factor over the probability of transmitting the infection. For example, an effectiveness of 90% means that the probability of contagion using masks is reduced to 10% with respect to the case of not using them. Note that the way we define mask effectiveness is different from that of existing studies: instead of representing the capability of the mask to prevent the infection, we consider its effectiveness as a whole, which includes not only the protection provided by the mask by itself but also the change that taking this measure triggers in the individual habits; for instance, keeping a safe security distance with other people or the use of hygienization measures, e.g., hand washing or using hydro-alcoholic gels after contact with others. With this

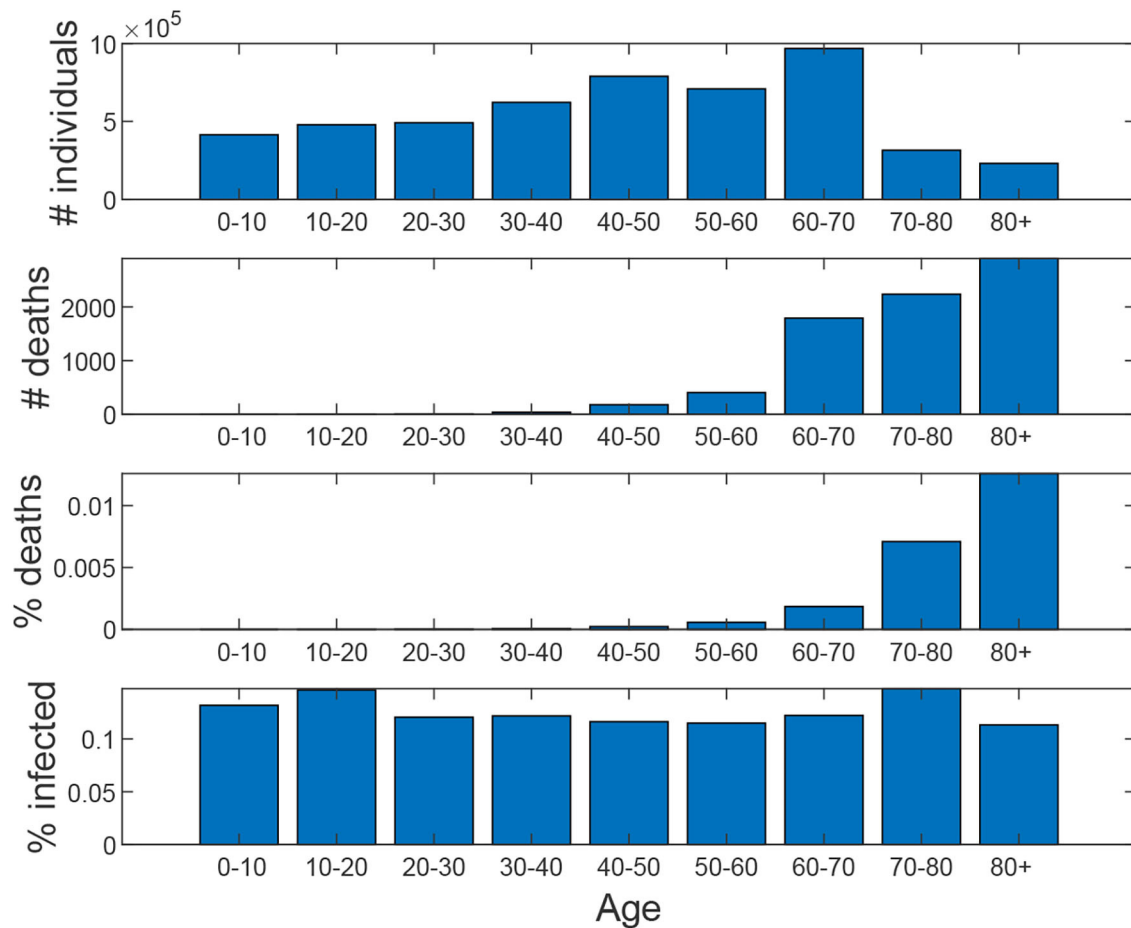


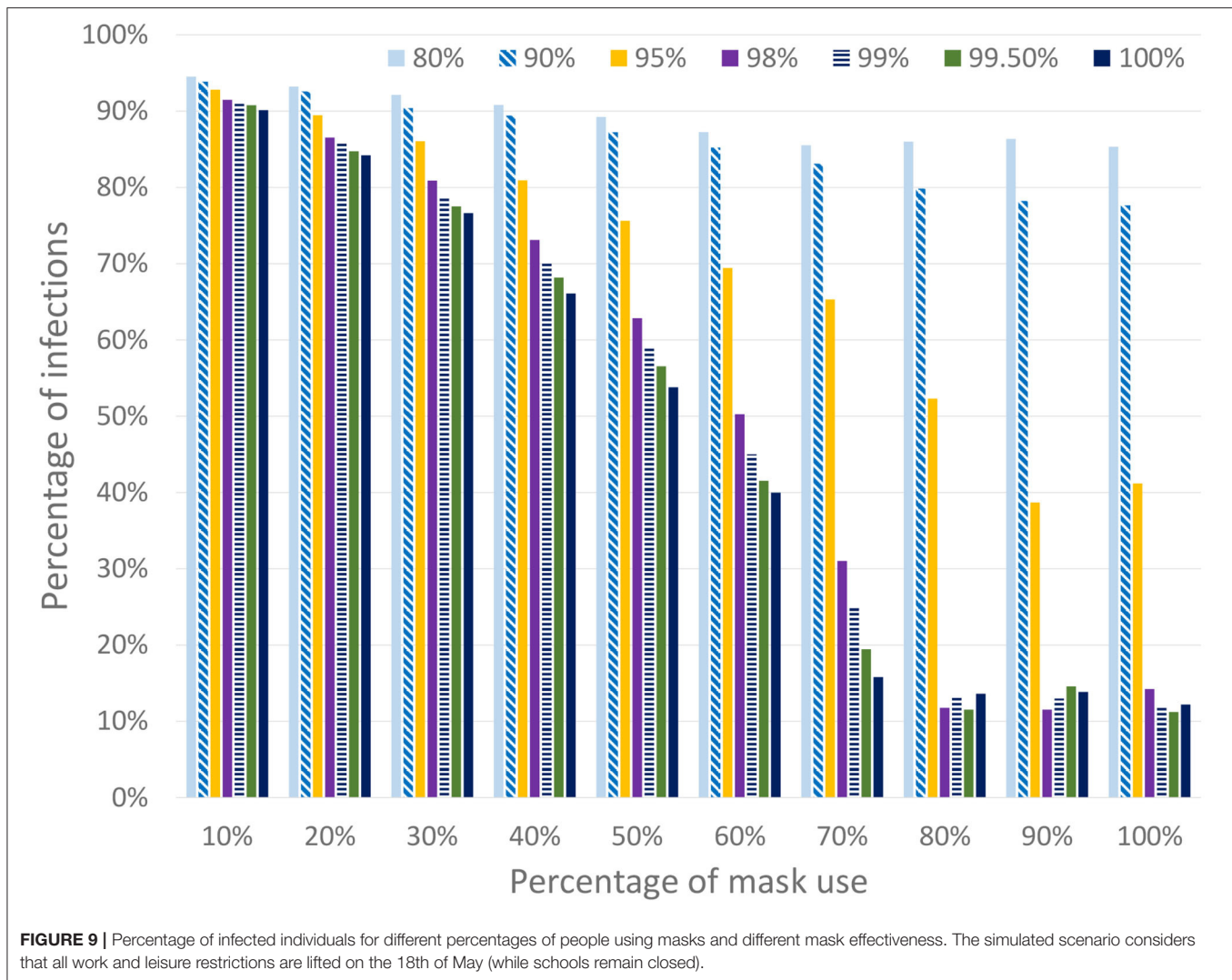
**FIGURE 8 |** Baseline scenario. From top to down: age distribution of the population, age distribution of the number of deaths, percentage of deaths for each age interval, percentage of infected for each age interval.

definition, we believe that the actual effectiveness provided by a mask may be larger than the actual reported one.

For the sake of simplicity, and in order to focus on the effect of face masks, all the scenarios in this section use the worst-case baseline shown in **Figure 11**, in which all the work and leisure restrictions are lifted on the 18th of May. Note that this scenario is similar to the existing condition in Spain at this time. At this time we assume that a certain percentage of the population starts using masks during outdoor activities but not during family time (which is to be expected), thus the transmission risk between cohabiting individuals (i.e., family contacts) is not avoided. EpiGraph considers distinct effectiveness with regard to preventing an infected individual from transmitting the disease or a susceptible individual from becoming infected. In this first part of the experiments we assume that both effectiveness are the same, thus the mask protects both infected and susceptible individuals. **Figure 9** shows the final number of infected individuals for different usage percentages (x-axis) and mask effectiveness. We can observe that both parameters are strongly related with the infection spread. EpiGraph performs the simulations using a stochastic approach

in which the results of different executions may differ. This may create small fluctuations in the results. We think that these fluctuations are the reason of having non-monotonic decreasing values when the percentage of mask use is larger than 70% and the mask effectiveness are larger than 95%.

The second study that we have performed, shown in **Figure 10**, consists of three scenarios that distinguish the mask protection between infected and susceptible individuals and considers different mask effectiveness. In the first one, denoted that the mask protects both of them, is similar to the previous ones where the masks have the same effectiveness for both infected and susceptible individuals. In the second one (where the mask protects the susceptible individuals) we consider that the masks are only effective for susceptible individuals. In this case, a mask does not reduce the transmission risk from the infected individual but protects a susceptible from being infected. In the third scenario (where the mask protects the infected individuals) the opposite is true: the mask prevents the transmission from infected individuals but it does not protect the susceptible. Note that these hypotheses, although unrealistic, are included as limits to represent the most extreme scenarios



where the protection is completely biased to only infected or only susceptible individuals. A real mask would produce an intermediate protection between these limits. In the figure, we can observe that these scenarios produce a significant decrease in the final number of infected individuals.

### 3.2. Policies Targeting the Elderly

The mobility strategies we consider relate to different work and free movement restrictions for people above 65 years of age, school closing, and travel restrictions. We refer to people above 65 as the elderly. Given that this group has the highest mortality levels, in this section we evaluate the effectiveness of specific targeted lockdown policies. In order to simplify the analysis, the use of face masks is not initially considered in this section.

Scenario 2 is an ideal (and rather unrealistic) case in which the elderly keep social distancing indefinitely since March 16th. This is defined as disabling contacts of all types, including with their families. Starting from the baseline scenario, work and free movement restrictions are lifted for people under 60 on 18th of May. Schools remain closed and travel restrictions are

maintained. **Figure 11B** shows the simulation results. Note that the number of infected individuals is slightly reduced when compared to the first scenario (now is 76%) but the total number of deaths is reduced to nearly one third (23,800 deaths). The reason is that the most vulnerable population group is prevented from getting infected, thus reducing the number of hospitalized and death cases.

Scenario 3 reflects a less restricted case, in which the elderly keep social distancing until simulation week 20 (17th of July). At this time they are allowed to return to normal life using mask with a protection of 99.8%. The aim of this scenario is to isolate the effect of the confinement of the elderly, while the rest of the population does not take any special measures to avoid transmission. Results show the same percentage of infections and 23,900 that the number of infections does not increase significantly due to herd immunity being already reached at the time the confinement of the elderly ends. Note that in these experiments we assume that a recovered individual acquires indefinite immunity to the virus and that the virus does not mutate during the simulation time.



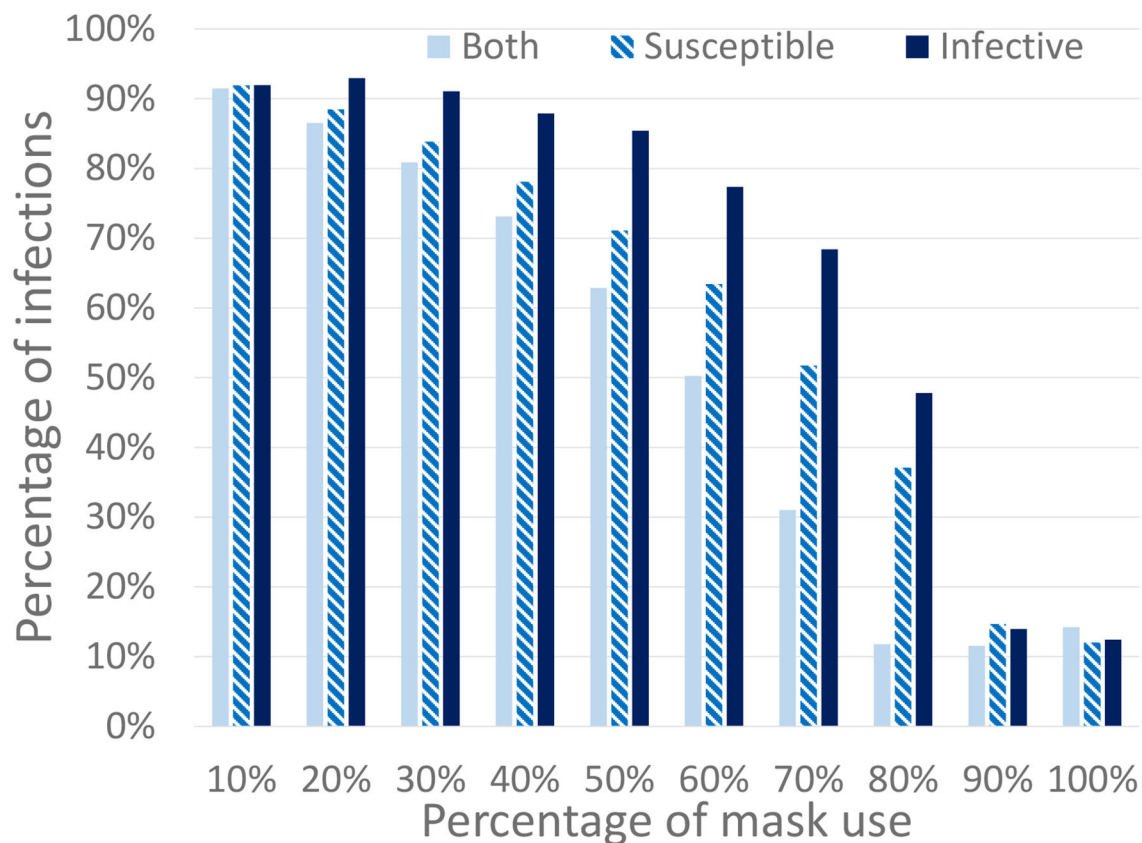


**FIGURE 10 |** Percentage of infected individuals for different percentages of the population using masks. We consider three different mask protection levels: protecting the infected, the susceptible, or both of them. All work and leisure restrictions are lifted on the 18th of May (schools remain closed).

Scenario 4 is a variation of Scenario 3 in which the elderly keep social distancing until the 18th of May (instead of the 17th of July). From this date on, they use masks with a protection of 99.8% at all times except during family connections. In this scenario, the number of infections increases to 88.7% and the deaths to 57,000. Note that, despite of mask use by the elderly, now they are not isolated during the second infection peak and thus suffer a significant number of deaths.

In order to represent a more realistic scenario we have modeled Scenario 5 (shown in **Figure 12A**) in which 70% of the population (picked at random) uses masks with an effectiveness of 99.5%. In this scenario a second infection wave occurs and, at the end of the simulation (week 38 corresponding to November 24th), 19.0% of the population is infected and results in 15,000 deaths. Note that the infection percentage is similar to the prevalence study for Madrid (21), which rounds 18.6% of Madrid population and that was carried out between the 16th and the 29th of November. The aim of this scenario is not to precisely reproduce the second infection wave in Madrid, but rather to evaluate different policies under a similar percentage of infections as the real one.

Scenario 6 (shown in **Figure 12B**) corresponds to a variation of Scenario 5 where people over 60 restrict themselves from all contacts but the familiar ones (where no masks are used). In this

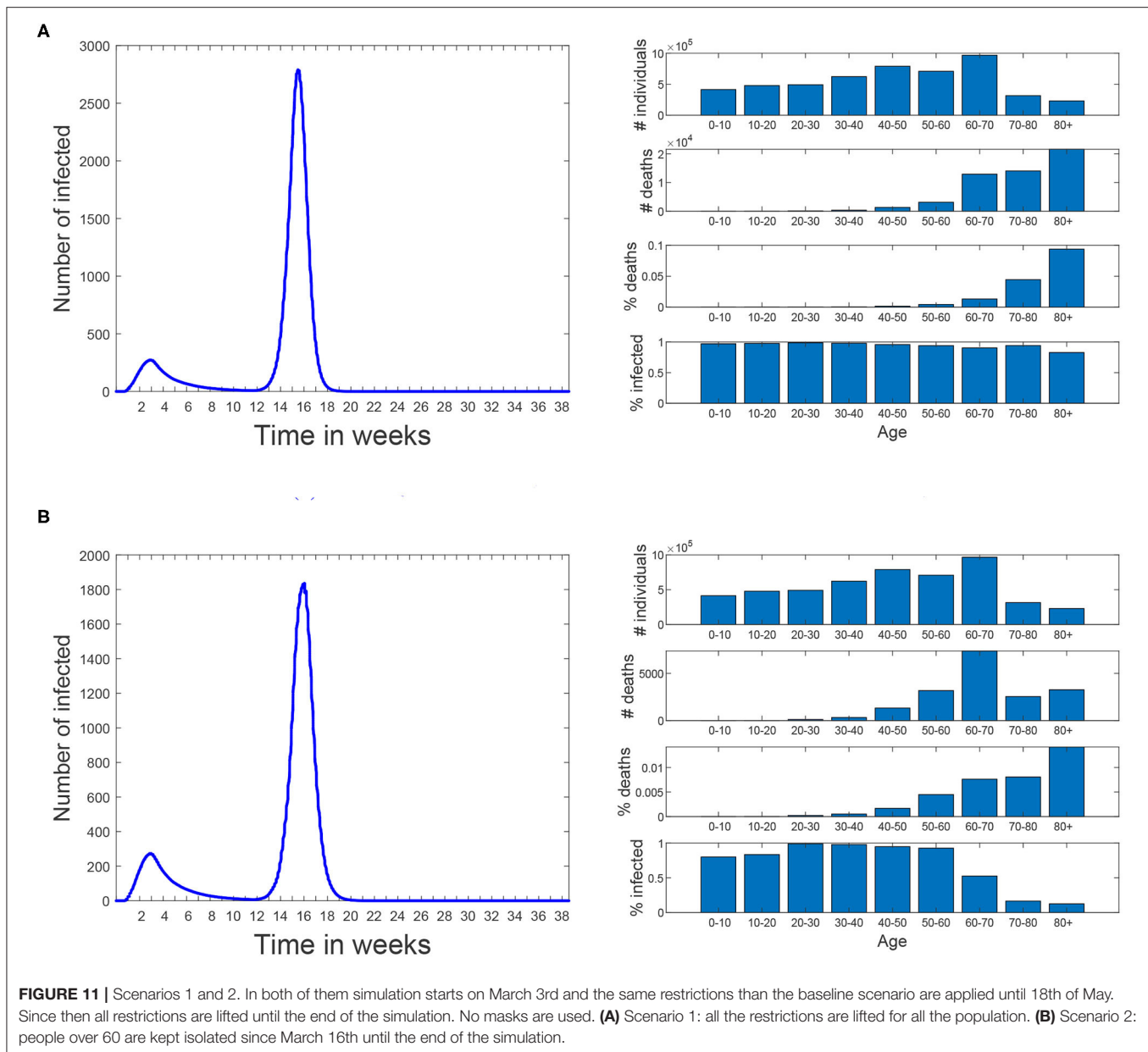
case the percentage of infections is reduced to 16.0% and the number of deaths is reduced in a greater proportion, all the way down to 11,600.

The last scenario (Scenario 7) has the same social distancing restrictions for the elderly as Scenario 6. In addition, workers over a certain age threshold are isolated from all contacts but the familiar ones. When this threshold was set to 60 years, the percentage of infections and number of deaths is similar to Scenario 6 (15.7% and 11,400), but when this threshold is reduced to 50 years, these values are reduced to 12.9% and 10,900.

## 4. DISCUSSION

This work presents the first results of the simulations using EpiGraph, for the Madrid metropolitan area and the first COVID-19 wave of Spring 2020. After creating an accurate social model of Madrid and reproducing the same mitigation measures as those taken by the authorities we first validated the simulator by comparing the predictions with the real values. Here we faced the problem related to the uncertainty of the real data, which is based on reported cases. Given that the reported cases are only a fraction of the real ones and that it is impossible to determine precisely how big this fraction is, we first compared the final number of infected individuals with the seroprevalence study





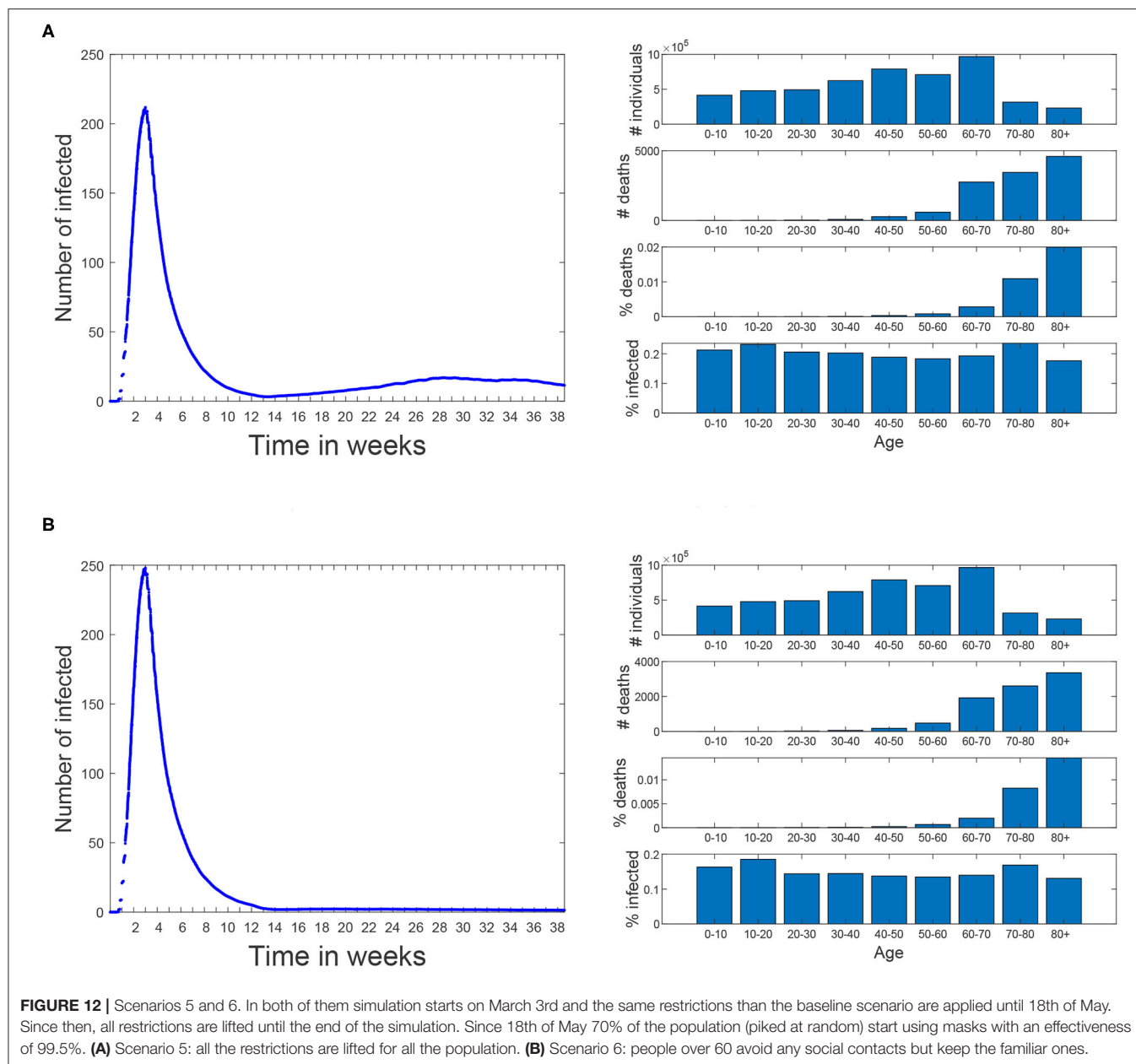
provided in (22). These values were similar enough, at 15 vs. 12%. The second validation was comparing the number of reported and simulated deaths (shown in **Figure 8**). Again, here there is also an uncertainty because the reported death cases related to COVID-19 that are provided by the health authorities smaller than the total number of deaths reported by the civil registry. Here, the simulated values are higher than the reported cases.

Once the validation was completed, we used the simulator to evaluate different scenarios after the real lockdown situation of the region and related to social distancing of the elderly and the impact of masks use. The information provided by these simulations represent a two-fold contribution. On the one hand, they were used to assess different social distancing policies; on the other hand, they evaluate different protection levels of mask use

among different percentages of the population. In total, both of them provide examples of the simulator features.

EpiGraph is a thoroughly validated simulator that models in detail most of the important factors in the propagation of an epidemic. It does nevertheless have certain limitations, some that have to do with the modeling of a new virus which is not 100% understood. The first limitation is that in the current version of EpiGraph, a recovered individual acquires indefinite immunity to the virus, which makes it impossible to be re-infected for the duration of the simulation. If the simulated time is long, this assumption may no longer hold. We are currently working on implementing this feature in the simulator.

Another limitation is that the current transportation model is a gravity model based only on the distance between the cities



and the population size. Having real knowledge about mobility patterns, for instance about those individuals using public transportation means, would provide a much more realistic approximation than the gravity model. It is also worth to mention that in the context of this work (with a prolonged lockdown) the influence of the transportation is reduced.

We currently assume 25% percent of the infected people to be asymptomatic. Research such as (23) assumes that the transmission rate of the virus is constant during the exponentially growing phase, and they use a time-dependent exponentially decreasing transmission rate to model the change in  $R_0$  after the early exponentially increasing phase. There is an attempt to examine the number of asymptomatic infectious cases and

unreported infectious cases; this type of approximation may be useful to perform a more precise calibration of the simulator. A last limitation is that EpiGraph uses contact matrices based on group types. We are currently working on a more detailed model based on contact matrices for age ranges, which will increase the accuracy of the social model.

Finally, it is necessary to refine the social model in order to include different collectives, among others, health and social-health workers and elderly people at nursing homes. This would produce more realistic forecasts. In this work, health care facilities are modeled as informal meetup groups for the elderly, which allow social gatherings. Besides that, leisure contacts also provide heterogeneity by allowing contacts with

different collectives in which individuals may belong to different age groups.

## 5. RELATED WORK

There are a vast number of publications on Covid since the beginning of the pandemic, a lot of them treating the same problem as we do—simulating the propagation of the virus under different scenarios of intervention on part of the governments. Friedman et al. (24) identifies 383 published or publicly released COVID-19 forecasting models.

DELPHI (Differential Equations Leads to Predictions of Hospitalizations and Infections) (25) is a compartmental model that is based on the widely successful SEIR model, with additional features such as modeling under-detected cases and governmental response measures. To model the response, the authors multiply an initial infection rate with an arc tan curve, along with an exponential jump correction to model the resurgence in cases in many places. They model the potential impact of various policies on future infections by estimating the average effect of each measure as implemented across states, via training.

Youyang Gu's COVID-19 model (26) applies machine learning to derive the basic reproduction number ( $R_0$ ) from data published by Johns Hopkins University's Center for Systems Science and Engineering (CSSE), and hooks this to a compartmental model. Their infection estimates include all infected individuals of the SARS-CoV-2 virus, not just those that took a COVID-19 test and tested positive.

The COFFEE model from Los Alamos National Laboratory (27) produces “forecasts, not projections; meaning it does not explicitly model the effects of interventions or other ‘what-if’ scenarios. We distinguish forecasts as attempts to predict what will happen vs. projections as attempts to describe what would happen given certain hypotheses.” COFFEE is probabilistic and it is fit to geographic regions independently, facilitating parallelization for fast computations. The method fits weighted regressions to the training data and compute Joint Probability Distributions over tuning parameters.

Imperial College London has several planning tools in place. Of these, Flaxman et al. (28) describes an extension of a semi-mechanistic Bayesian hierarchical model that infers the impact of interventions and estimates the number of infections over time. This approach works under the assumption that changes in the reproductive number are an immediate response to interventions rather than broader gradual changes in behavior, and are calculated backward from temporal data. The authors use the discrete renewal equation as a incubation process for the modeling of infections and propose a generative mechanism to connect infections to death data. They use this joint Bayesian hierarchical model to produce short-term predictions, and they apply their model to 11 different countries.

In (29), the authors use a deterministic SEIR framework to model the propagation of the virus and the effect of non-pharmaceutical interventions (social distancing mandates and mask use) until the Spring of 2021. The model also uses

projections of pneumonia seasonality, mobility, testing rates, and mask use per capita to predict infections, deaths, and hospital demand. In terms of social distancing, they include the following measures: (1) severe travel restrictions, (2) closing of public educational facilities, (3) closure of non-essential businesses, (4) stay-at-home orders, and (5) restrictions on gathering size. Based on data from Facebook, Google, SafeGraph, and Descartes Labs, the authors use a Bayesian, hierarchical meta-regression model with random effects by location to approximate the expected change in mobility. Based on data from February to September, they fit relationships between changes in the rates at which infectious individuals may come into contact and infect susceptible individuals and mobility, testing, masks, pneumonia seasonality and others. Some of the limitations of this approach are the exclusion of movement between locations, the absence of age structure and mixing within location (assumption of a well-mixed population), and the inability to model super-spreader-like events.

In (30), the authors focus on a better description of sojourn time, the duration before clinical symptoms become apparent but during which it is detectable by a screening test. Its clinical relevance is that it represents the duration of the temporal window of opportunity for early detection. The authors conduct a simple sensitivity analysis to determine the most important parameters in the model, which turn out to be the fraction of cases that are asymptomatic. Contrary to simple SLIR (or SEIR) models, this model allows to consider infection by asymptomatic individuals. Their predictions are over the short term, about 1 month. Other works, such as (23), also hone on identifying the unreported asymptomatic infectious cases (in mainland China). Their objective is to identify numbers for these individuals from specific time data of reported symptomatic infectious cases.

Also from the Centre for the Mathematical Modeling of Infectious Diseases COVID-19 working group, paper (31) tackles the problem of contact matrices. This work updates synthetic contact matrices that were published for Europe in 2017, with the most recent data and extends this analysis to 177 geographical locations. These matrices were constructed based on information that is more widely available than diary-based contact surveys and considers setting-specific survey data on household, school, classroom, and workplace composition combined with empirical data on contact patterns in Europe.

Authors in (32) discuss the “fundamental social causes” of disease, a factor that was up until now largely neglected when analyzing and predicting the effectiveness of prevention and mitigation measures. They argue that “inequitable social conditions lead to both more infections and worse outcomes” and expand the definition of “most at risk” to prioritize populations with social conditions and thus obtain more effective control of the epidemic.

The European Centre for Disease Prevention and Control (ECDC) (16) has built a Monte-Carlo based model of COVID that they use for forecasting. To model the behavior of the people and how well they are responding to the measures, they compare the predictions with Google data about mobile phone use. The most recent data on daily confirmed COVID-19 cases and daily

deaths are inserted into the model to calibrate it. It currently works well for some countries but not for others.

There exist other COVID simulators based on the SEIR model (33), but they compute the number of infected, recovered, and dead individuals based on a mathematical model—solving the differential equations with a forward Euler scheme—on the basis of the number of contacts, probability of disease transmission, incubation period, recovery rate, and fatality rate. More complex versions of the SEIR model include, for instance, a quarantine class and a class of isolated (hospitalized) members (34). In (35), the authors use spatial diffusion of the virus, an alternative to contact networks. De la Sen et al. (36) propose an SEIADR model, where A are asymptomatic infectious and D are dead-infective. In other models, recovered can become susceptible again [e.g., (37)], and, in addition, there are stochastic models (38), although the calibration becomes extremely difficult with incomplete data.

In (39), the authors hypothesize—and discover evidence for—the order of symptom occurrence in COVID-19 vs. other respiratory diseases, to help patients and medical professionals more quickly distinguish between them. Although orthogonal, these findings may be used to improve testing and filter cases to more precisely record actual infections by Covid—in those cases where testing is not an option. This would give us more precise data to test on, which may help to calibrate our tool more precisely.

In general, simulation approaches based on agents are able to model the spread of infections more realistically and in detail, although they tend to suffer from scalability problems. We discuss a few of these approaches below. OpenABM-Covid19 (40) explores different ways in which contact tracing, in particular digital contact tracing via mobile phone apps can contribute to epidemic control, while emphasizing larger population simulations and computational efficiency. CPU time is spent mostly on rebuilding the daily interaction networks and updating the individual's interaction diaries. Individuals move daily between networks representing households and either workplaces, schools, or regular social environments for older people. The occupation networks are modeled as small-world networks. Individuals also interact through random networks representing public transport, transient social gatherings etc. Network parameters are chosen such that the average number of interactions match age-stratified data from reports. The current version of the model does not currently include events in hospitals, care-home settings, non-hospital deaths, gender, or co-morbidities. Different from us, the authors create daily contact networks based on actual mobile phone data. Occupation networks, on the other hand, are assumed to be of the small-world type and they are created as such rather than from interconnection patterns.

Covasim (41) includes demographic information about age structure and population size; realistic transmission networks in different social layers, including households, schools, workplaces, and communities; age-specific disease outcomes; and intra-host viral dynamics, including viral-load-based transmissibility. In terms of the contact network they use, Covasim is capable of generating three alternative types: random networks, SynthPops

networks, and hybrid networks; in addition users have the option of defining their own networks. The SynthPops algorithm first chooses a reference individual for the specific layer, e.g., a school, to infer the school type, and then uses age the mixing contact matrix in the school setting to infer the likely ages of the other students in the school. Students are drawn from an ordered list of households. To deal with scalability issues, once a certain threshold in population number is reached, the non-susceptible agents in the model are downsampled and a corresponding scaling factor is introduced. Calibration to existing time-series data is performed externally to Covasim. One difference from our work is that the contacts are not based on existing patterns; scalability issues are partly sidestepped by dynamic scaling. On the other hand, their approach models critical patients, hospital capacity and ICU beds.

In (42), the authors integrate anonymized, geolocalized mobility data with census and demographic data to build a detailed agent-based model of Covid-19 transmission in the Boston metropolitan area. Their approach defines a weighted network with layers for the network of social interactions at (1) workplace and community level, (2) households, and (3) schools. Connections between two agents in the workplace and community layer are estimated from the data by the probability of both being present in a specific place weighted by the time they have spent in the same place. They do not include specific co-morbidities or pre-existing conditions of the specific population. Different from us, the authors construct the interaction network based on co-location at the same time, starting from mobility data. Interactions are considered well-mixed in school environments, while in our simulator every individual has its own characteristics and interaction patterns.

The work in (43) calibrates the simulator based on daily ICU admissions, ICU-bed occupancy, daily mortality and cumulative mortality. They approximate the value for the  $R_0$  from the observed average number of new individuals infected by each single infected individual from the beginning of the epidemic until about 30 days after. The numbers of infected and infecting people were estimated using the model. We, on the other hand, use the  $R_0$ s from the literature for each of the infection phases. One of their conclusions is that, in the absence of a vaccine, emphasis should be placed on policies that protect the most-vulnerable population while herd immunity is hoped to be achieved in the less vulnerable people. The social contact network among the individuals in the population is based on the geolocalized activity sequence over the day, taking into account co-location probability and duration, another difference with our work.

Koo et al. (44) uses FluTE, an agent-based influenza epidemic simulation model, which accounts for demography, host movement, and social contact rates in workplaces, schools, and homes. Individuals are allocated to workplaces or educational facilities on the basis of local transportation data and home addresses according to 2010 census data in Singapore. They conclude that spread control is feasible provided that  $R_0$  is low ( $\leq 1.5$ ), with a combination of quarantine, school closure, and workplace distancing, assuming a low percentage

of asymptomatic of 7.5%. The preventive effect of these interventions reduces considerably when higher asymptomatic proportions are assumed (all under 50%), when quarantining and treatment of infected individuals becomes more important and also unfeasible when the number of infected individuals exceeds the capacity of health-care facilities. This work relies on detailed data in Singapore, which is feasible given the size and infrastructure of the country. The study focuses on the types of measures that enable controlling the infection spread, although the values they use for some of the parameters seem unrealistically small.

Lau et al. use in (45) a dataset that contains demographic information of 9,559 symptomatic cases in Georgia, US, including age, sex, and race, and symptom onset times. It also contains geo-location information of the residences of all these recorded cases. Aggregate mobility data are used to characterize the average change of movement distance before and after the implementation of social distancing measures. Their framework infers the transmission paths among all cases and therefore generates the offspring distribution of each case; it also allows the computation of population-level epidemiological parameters such as  $R_0$  and quantify the degree of super-spreading over space and time. This is a very different type of work from ours, as it relies on concrete and detailed data from about 10K cases, based on which the authors can tackle the issue of superspreaders.

The work presented in (46) uses an ABM model specifically calibrated to reproduce the reproductive number, the length of incubation and generation periods, age-dependent fractions of the symptomatic cases and the probability of transmission from asymptomatic/pre-symptomatic agents in Australia. Contact and transmission rates were set to differ across distinct social contexts such as households, household clusters, local neighborhoods, schools, classrooms and workplaces. To infer a directed transmission link from the simulation results, the model connects any two infected individuals with the same household identifier, same neighborhood (household cluster) label or same wider community (SLA) index. The authors compare the findings using the ABM with genomic surveillance based on near real-time genome sequencing of Covid-19 in a sub-population of infected patients during the first 10 weeks of containment in Australia. The approach has limitations, e.g., the genomic study did not describe transmissions from asymptomatic carriage, while the ABM did not explicitly simulate transmissions in hospitals, residential age care facilities, or introduced by maritime traffic, for example, cruise ships. The results compare favorably, but including genomic sequencing allows to find potential sources of infections that cannot be identified using conventional epidemiological methods. Differently from other work we have seen, this work relies on genomic surveillance data to confirm the results obtained by their ABM simulator.

In (47), Silva et al. emulated a closed society living on a shared environment, consisting of agents that represent people, houses, businesses, the government and the healthcare system, each one with specific attributes and behaviors. The ABM proposed by the authors also models the economy in this society of agents, which helps them estimate the economic impact under different types

of interventions. Their model considers that a contact happens when the distance between any two agents is less than or equal to a defined threshold; this contact can be epidemiological or economical. This is a rare example of an approach that also models the behavior of other entities that are not individuals and thus can help understand the impact of the pandemic both on citizens and the economy.

## 6. CONCLUSION

This work was developed in the context of the project *Medium and Long-term Simulation of Covid-19* funded by the Spanish Health Ministry. The results we obtained provided support to the health authorities for the forecasting of the first wave and in the evaluation of possible future scenarios. The work targets the metropolitan area of Madrid, which we model in detail to take into account social aspects such as age distribution and occupation, size of family units, percentage of workers, school children, unemployed, and stay home parents. The epidemiological model is updated with the COVID-specific values, including the  $R_0$ s of each state and the time spent in each infection phase, as well as the probabilities for hospitalization and death depending on age (which we use in conjunction with existent mortality data for calibration of the simulator).

The main conclusions of this work are that EpiGraph is able to reproduce both the existing infected and death curves for Madrid metropolitan area in the Spring 2020. Regarding the elderly confinement, this social distancing policy would help to lower the number of deaths (not the number of infections), which, although reduced, would have remained important. We also evaluated that school opening after the lock down, which has a minor impact on the infection spread. In terms of mask use, the percentage of people that comply becomes a crucial factor for mitigating the infection spread. In the longer term, our tool could help to plan for a more resilient and efficient approach to epidemics, and study how to flexibly respond and adapt to this type of unexpected situations.

## DATA AVAILABILITY STATEMENT

The dataset supporting the conclusions of this article is available in the repository (doi: 10.3389/fpubh.2021.636023).

## AUTHOR CONTRIBUTIONS

DS, M-CM, and JC designed and implemented EpiGraph simulator. All authors conceived and designed the experiments. DS, MG-M, and CD processed the input data and ran the experiments. DS, JC, and M-CM wrote the paper. CD-S and DG-B provided insights on the validity of our assumptions, recommended additional related work, and contrasted the results with their own findings. All authors review the different manuscript drafts and approved the final version for submission.



## FUNDING

This work has been supported by the Spanish Instituto de Salud Carlos III under the project grant 2020/00183/001 Medium and long-term forecast of the spread of COVID-19, the project grant BCV-2020-3-0008 Simulating COVID-19 propagation at a European-level of the Spanish Supercomputing Network (RES), and the EU project 'ASPIDE: Exascale Programming Models for Extreme Data Processing under grant 801091. The role of both funders was limited to financial support and did not imply participation of any kind in the study and collection, analysis, and interpretation of data, nor in the writing of the manuscript.

## REFERENCES

- Martin G, Singh DE, Marinescu MC, Carretero J. Towards efficient large scale epidemiological simulations in EpiGraph. *Parallel Comput.* (2015) 42:88–102. doi: 10.1016/j.parco.2014.09.004
- Singh DE, Marinescu MC, Carretero J, Delgado-Sanz C, Gomez-Barroso D, Larrauri A. Evaluating the impact of the weather conditions on the influenza propagation. *BMC Infect Dis.* (2020) 20:265. doi: 10.1186/s12879-020-04977-w
- Martin G, Marinescu MC, Singh DE, Carretero J. Leveraging social networks for understanding the evolution of epidemics. *BMC Syst Biol.* (2011) 5:S14. doi: 10.1186/1752-0509-5-S3-S14
- Lovasz L. Random walks on graphs: a survey, combinatorics, paul erdos is eighty. *Bolyai Soc Math Stud.* (1993) 2:1–46.
- Keeling M, Eames K. Networks and epidemic models. *J R Soc Interface.* (2005) 2:295–307. doi: 10.1098/rsif.2005.0051
- Viboud C, Bjornstad ON, Smith DL, Simonsen L, Miller MA, Grenfell BT. Synchrony, waves, and spatial hierarchies in the spread of influenza. *Science.* (2006) 312:447–51. doi: 10.1126/science.1125237
- Byambasuren O, Cardona M, Bell K, Clark J, McLaws ML, Glasziou P. Estimating the extent of asymptomatic COVID-19 and its potential for community transmission: systematic review and meta-analysis. *Off J Assoc Med Microbiol Infect Dis Canada.* (2020) 5:223–34. doi: 10.3138/jammi-2020-0030
- Katul GG, Mrad A, Bonetti S, Manoli G, Parolari AJ. Global convergence of COVID-19 basic reproduction number and estimation from early-time SIR dynamics. *PLOS ONE.* (2020) 15:e0239800. doi: 10.1371/journal.pone.0239800
- Yousef A, Maryam T, Mojtaba S. Estimate of the basic reproduction number for COVID-19: a systematic review and meta-analysis. *J Prev Med Public Health.* (2020) 53:151–7. doi: 10.3961/jpmph.20.076
- Liu Y, Gayle AA, Wilder-Smith A, Rocklöv J. The reproductive number of COVID-19 is higher compared to SARS coronavirus. *J Travel Med.* (2020) 27:Taaa021. doi: 10.1093/jtm/taaa021
- COVID19-team. *Informe sobre la situacion de COVID-19 en Espana. Informe COVID-19 n 21. RENAVE.* Technical report. Centro Nacional de Epidemiologia, Instituto de Salud Carlos III Spain (2020).
- H N, NML, AR A. Serial interval of novel coronavirus (COVID-19) infections. *Int J Infect Dis.* (2020) 93:284–6. doi: 10.1016/j.ijid.2020.02.060
- Davies NG, Klepac P, Liu Y, Prem K, Jit M, Eggo RM. Age-dependent effects in the transmission and control of COVID-19 epidemics. *Nat Med.* (2020) 28:1205–11. doi: 10.1038/s41591-020-0962-9
- He X, Lau E, Wu P, Deng X, Wang J, Hao X, et al. Temporal dynamics in viral shedding and transmissibility of COVID-19. *Nat Med.* (2020) 26:1491–3. doi: 10.1038/s41591-020-1016-z
- Mizumoto K, Kagaya K, Zarebski A, Chowell G. Estimating the asymptomatic proportion of 2019. Novel Coronavirus onboard the Princess Cruises Ship. *Euro Surveill.* (2020) 25:2000180. doi: 10.2807/1560-7917.ES.2020.25.10.2000180

## ACKNOWLEDGMENTS

We would like to thank to Diego Fernandez Olombrada for his support in the early collection of part of the data of this work.

## SUPPLEMENTARY MATERIAL

The Supplementary Material for this article can be found online at: <https://www.frontiersin.org/articles/10.3389/fpubh.2021.636023/full#supplementary-material>

- European Centre for Disease Prevention and Control. *Transmission of COVID-19.* Stockholm: ECDC (2020). Available online at: <https://www.ecdc.europa.eu/en/covid-19/latest-evidence/transmission>
- Berenguer J, Ryan P, Rodríguez-Baño J, Jarrín I, Carratalà J, Pachón J, et al. Characteristics and predictors of death among 4035 consecutively hospitalized patients with COVID-19 in Spain. *Clin Microbiol Infect.* (2020) 26:1525–36. doi: 10.1016/j.cmi.2020.07.024
- Chen Y, Li T, Ye Y, Chen Y, Pan J. Impact of fundamental diseases on patients with COVID-19. *Disaster Med Public Health Prepared.* (2020) 1–15. doi: 10.1017/dmp.2020.139
- Pollán M, Perez-Gomez B, Pastor-Barriuso R, Oteo J, Hernán MA, Perez-Olmeda P, et al. Prevalence of SARS-CoV-2 in Spain (ENE-COVID): a nationwide, population-based seroepidemiological study. *Lancet.* (2020) 396:535–44. doi: 10.1016/S0140-6736(20)31483-5
- Asadi S, Cappa CD, Barreda S, Wexler AS, Bouvier NM, Ristenpart WD. Efficacy of masks and face coverings in controlling outward aerosol particle emission from expiratory activities. *Sci Rep.* (2005) 10:15665. doi: 10.1038/s41598-020-72798-7
- COVID19-Team. *Estudio ENE-COVID: Cuarta Ronda Estudio Nacional de Sero-Epidemiología de la Infección por SARS-Cov-2 en España.* Instituto de Salud Carlos III (2020).
- COVID19-Team. *Estudio ENE-COVID: Informe Final Estudio Nacional de Sero-Epidemiología de la Infección por SARS-COV-2 en España.* Instituto de Salud Carlos III Spain (2020).
- Liu Z, Magal P, Seydi O, Webb G. A COVID-19 epidemic model with latency period. *Infect Dis Modell.* (2020) 5:323–337. doi: 10.1016/j.idm.2020.03.003
- Friedman J, Liu P, Troeger CE, Carter A, Reiner RC Jr., Barber RM, et al. Predictive performance of international COVID-19 mortality forecasting models. *medRxiv [Preprint].* (2020) 1–20. doi: 10.1101/2020.07.13.20151233
- Li ML, Bouardi HT, Lami OS, Trichakis N, Trikalinos T, Zarandi MF, et al. *Overview of DELPHI Model V3 - COVIDAnalytics.* (2020). Available online at: [https://www.covidanalytics.io/DELPHI\\_documentation\\_pdf](https://www.covidanalytics.io/DELPHI_documentation_pdf)
- Gu Y. *COVID-19 Projections Using Machine Learning.* (2020). Available online at: <https://covid19-projections.com>
- Castro L, Fairchild G, Michaud I, Osthus D. *COFFEE: COVID-19 Forecasts Using Fast Evaluations and Estimation.* Los Alamos National Laboratory, LA-UR-20-28630 (2020).
- Flaxman S, Mishra S, Gandy A, Unwin HJT, Mellan TA, Coupland H, et al. Estimating the effects of non-pharmaceutical interventions on COVID-19 in Europe. *Nature.* (2020) 584:257–61. doi: 10.1038/s41586-020-2405-7
- Team IHME COVID, Reiner RC, Barber RM, Collins JK. Modeling COVID-19 scenarios for the United States. *Nat Med.* (2020) 27:94–105.
- Arino J, Portet S. A simple model for COVID-19. *Infect Dis Modell.* (2020) 5:309–15. doi: 10.1016/j.idm.2020.04.002
- Prem K, van Zandvoort K, Klepac P, Eggo RM, Davies NG, Cook AR, et al. Projecting contact matrices in 177 geographical regions: an update and comparison with empirical data for the COVID-19 era. *medRxiv [Preprint].* (2020) 1–37. doi: 10.1101/2020.07.22.20159772

32. Afifi RA, Novak N, Gilbert PA, Pauly B, Abdulrahim S, Rashid SF, et al. 'Most at risk' for COVID19? The imperative to expand the definition from biological to social factors for equity. *Prevent Med.* (2020) 139:106229. doi: 10.1016/j.ypmed.2020.106229
33. Carcione JM, Santos JE, Bagaini C, Ba J. A simulation of a COVID-19 epidemic based on a deterministic SEIR model. *Front. Public Health.* (2020) 8:230. doi: 10.1101/2020.04.20.20072272
34. Brauer F, Castillo-Chavez C. *Mathematical Models in Population Biology and Epidemiology*. New York, NY: Springer (2012). doi: 10.1007/978-1-4614-1686-9
35. Naheed A, Singh M, Lucy D. Numerical study of SARS epidemic model with the inclusion of diffusion in the system. *Appl Math Comput.* (2014) 229:480–98. doi: 10.1016/j.amc.2013.12.062
36. la Sen MD, Ibeas A, Alonso-Quesada S, Nistal R. On a new epidemic model with asymptomatic and dead-infective subpopulations with feedback controls useful for Ebola disease. *Discrete Dyn Nat Soc.* (2017) 1–22. doi: 10.1155/2017/4232971
37. Xia W, Kundu S, Maitra S. Dynamics of a delayed SEIQ epidemic model. *Adv Diff Equat.* (2018) 336:1–21. doi: 10.1186/s13662-018-1791-8
38. Allen L. A primer on stochastic epidemic models: formulation, numerical simulation, and analysis. *Infect Dis Modell.* (2017) 2:128–42. doi: 10.1016/j.idm.2017.03.001
39. Larsen JR, Martin MR, Martin JD, Kuhn P, Hicks JB. Modeling the onset of symptoms of COVID-19. *Front Public Health.* (2020) 8:473. doi: 10.3389/fpubh.2020.00473
40. Hinch R, Probert WJ, Nurtay A, Kendall M, Wymatt C, Hall M, et al. OpenABM-Covid19-an agent-based model for non-pharmaceutical interventions against COVID-19 including contact tracing. *medRxiv [Preprint]*. (2020) 1–23. doi: 10.1101/2020.09.16.20195925
41. Kerr CC, Stuart RM, Mistry D, Abeysuriya RG, Hart G, Rosenfeld K, et al. Covasim: an agent-based model of COVID-19 dynamics and interventions. *medRxiv [Preprint]*. (2020) 1–29. doi: 10.1101/2020.05.10.20097469
42. Aleta A, Martin-Corral D, y Piontti AP, Ajelli M, Litvinova M, Chinazzi M, et al. Modeling the impact of social distancing, testing, contact tracing and household quarantine on second-wave scenarios of the COVID-19 epidemic. *medRxiv.* (2020) 4:964–71. doi: 10.1101/2020.05.06.20092841
43. Hoertel N, Blachier M, Blanco C, Olsson M, Massetti M, Rico MS, et al. A stochastic agent-based model of the SARS-CoV-2 epidemic in France. *Nat Med.* (2020) 26:1417–21. doi: 10.1038/s41591-020-1001-6
44. Koo JR, Cook AR, Park M, Sun Y, Sun H, Lim JT, et al. Interventions to mitigate early spread of SARS-CoV-2 in Singapore: a modelling study. *Lancet Infect Dis.* (2020) 26:1417–21. doi: 10.1016/S1473-3099(20)30162-6
45. Lau MS, Grenfell B, Thomas M, Bryan M, Nelson K, Lopman B. Characterizing superspreading events and age-specific infectiousness of SARS-CoV-2 transmission in Georgia, USA. *Proc Natl Acad Sci USA.* (2020) 117:22430–5. doi: 10.1073/pnas.2011802117
46. Rockett RJ, Arnott A, Lam C, Sadsad R, Timms V, Gray KA, et al. Revealing COVID-19 transmission in Australia by SARS-CoV-2 genome sequencing and agent-based modeling. *Nat Med.* (2020) 26:1398–404. doi: 10.1038/s41591-020-1000-7
47. Silva PC, Batista PV, Lima HS, Alves MA, Guimarães FG, Silva RC. COVID-ABS: an agent-based model of COVID-19 epidemic to simulate health and economic effects of social distancing interventions. *Chaos Solitons Fractals.* (2020) 139:110088. doi: 10.1016/j.chaos.2020.110088

**Conflict of Interest:** The authors declare that the research was conducted in the absence of any commercial or financial relationships that could be construed as a potential conflict of interest.

Copyright © 2021 Singh, Marinescu, Guzmán-Merino, Durán, Delgado-Sanz, Gomez-Barroso and Carretero. This is an open-access article distributed under the terms of the Creative Commons Attribution License (CC BY). The use, distribution or reproduction in other forums is permitted, provided the original author(s) and the copyright owner(s) are credited and that the original publication in this journal is cited, in accordance with accepted academic practice. No use, distribution or reproduction is permitted which does not comply with these terms.



# Combination of Angiotensin (1-7) Agonists and Convalescent Plasma as a New Strategy to Overcome Angiotensin Converting Enzyme 2 (ACE2) Inhibition for the Treatment of COVID-19

Hawraa Issa<sup>1,2</sup>, Ali H. Eid<sup>3,4</sup>, Bassam Berry<sup>5</sup>, Vahideh Takhviji<sup>6</sup>, Abbas Khosravi<sup>6</sup>, Sarah Mantash<sup>1</sup>, Rawan Nehme<sup>1</sup>, Rawan Hallal<sup>1</sup>, Hussein Karaki<sup>1</sup>, Kawthar Dhayni<sup>1,7</sup>, Wissam H. Faour<sup>8</sup>, Firas Kobeissy<sup>9</sup>, Ali Nehme<sup>10</sup> and Kazem Zibara<sup>1\*</sup>

## OPEN ACCESS

### Edited by:

Reza Lashgari,  
Institute for Research in Fundamental  
Sciences, Iran

### Reviewed by:

Dongdong Li,  
Sichuan University, China  
Scott Wesley Long,  
Houston Methodist Hospital,  
United States

### \*Correspondence:

Kazem Zibara  
kzibara@ul.edu.lb

### Specialty section:

This article was submitted to  
Infectious Diseases - Surveillance,  
Prevention and Treatment,  
a section of the journal  
Frontiers in Medicine

**Received:** 26 October 2020

**Accepted:** 22 February 2021

**Published:** 18 March 2021

### Citation:

Issa H, Eid AH, Berry B, Takhviji V, Khosravi A, Mantash S, Nehme R, Hallal R, Karaki H, Dhayni K, Faour WH, Kobeissy F, Nehme A and Zibara K (2021) Combination of Angiotensin (1-7) Agonists and Convalescent Plasma as a New Strategy to Overcome Angiotensin Converting Enzyme 2 (ACE2) Inhibition for the Treatment of COVID-19. *Front. Med.* 8:620990. doi: 10.3389/fmed.2021.620990

<sup>1</sup> PRASE and Biology Department, Faculty of Sciences - I, Lebanese University, Beirut, Lebanon, <sup>2</sup> College of Public Health, Phoenicia University, Zahrani, Lebanon, <sup>3</sup> Department of Basic Medical Sciences, College of Medicine, QU Health, Qatar University, Doha, Qatar, <sup>4</sup> Biomedical and Pharmaceutical Research Unit, QU Health, Qatar University, Doha, Qatar, <sup>5</sup> Institut Pasteur, Paris 6 University, Paris, France, <sup>6</sup> Transfusion Research Center, High Institute for Research and Education in Transfusion, Tehran, Iran, <sup>7</sup> EA7517, MP3CV, CURS, University of Picardie Jules Verne, Amiens, France, <sup>8</sup> School of Medicine, Lebanese American University, Byblos, Lebanon, <sup>9</sup> Department of Biochemistry and Molecular Genetics, Faculty of Medicine, American University of Beirut, Beirut, Lebanon, <sup>10</sup> Department of Human Genetics, McGill University, Montreal, QC, Canada

Coronavirus disease-2019 (COVID-19) pandemic caused by severe acute respiratory syndrome coronavirus 2 (SARS-CoV-2) is currently the most concerning health problem worldwide. SARS-CoV-2 infects cells by binding to angiotensin-converting enzyme 2 (ACE2). It is believed that the differential response to SARS-CoV-2 is correlated with the differential expression of ACE2. Several reports proposed the use of ACE2 pharmacological inhibitors and ACE2 antibodies to block viral entry. However, ACE2 inhibition is associated with lung and cardiovascular pathology and would probably increase the pathogenesis of COVID-19. Therefore, utilizing ACE2 soluble analogs to block viral entry while rescuing ACE2 activity has been proposed. Despite their protective effects, such analogs can form a circulating reservoir of the virus, thus accelerating its spread in the body. Levels of ACE2 are reduced following viral infection, possibly due to increased viral entry and lysis of ACE2 positive cells. Downregulation of ACE2/Ang (1-7) axis is associated with Ang II upregulation. Of note, while Ang (1-7) exerts protective effects on the lung and cardiovascular system, Ang II elicits pro-inflammatory and pro-fibrotic detrimental effects by binding to the angiotensin type 1 receptor (AT1R). Indeed, AT1R blockers (ARBs) can alleviate the harmful effects associated with Ang II upregulation while increasing ACE2 expression and thus the risk of viral infection. Therefore, Ang (1-7) agonists seem to be a better treatment option. Another approach is the transfusion of convalescent plasma from recovered patients with deteriorated symptoms. Indeed, this appears to be promising due to the neutralizing capacity of anti-COVID-19 antibodies. In light of these considerations, we encourage the adoption of Ang (1-7) agonists and

convalescent plasma conjugated therapy for the treatment of COVID-19 patients. This therapeutic regimen is expected to be a safer choice since it possesses the proven ability to neutralize the virus while ensuring lung and cardiovascular protection through modulation of the inflammatory response.

**Keywords: ACE2, SARS-CoV-2, COVID-19, lung pathology, cardiovascular pathology, convalescent plasma (CP), Angiotensin 1-7 (Ang1-7), combination therapy**

## INTRODUCTION

Starting November 2019, several cases of pneumonia of unknown etiology were reported in Wuhan, China (1). The causal agent was identified as severe acute respiratory syndrome coronavirus-2 (SARS-CoV-2). The newly identified betacoronavirus differs from severe acute respiratory syndrome coronavirus (SARS-CoV-1) and Middle East respiratory syndrome coronavirus (MERS-CoV); however, it causes similar symptoms associated with pneumonia (2–4). In contrast to SARS-CoV-1, which caused the 2002 outbreak, SARS-CoV-2 exhibits a higher risk of transmission as evident from the rapid global rise in the number of Coronavirus disease 2019 (COVID-19) cases (2–4). As of mid February 2021, more than 110 million cases have been confirmed, and nearly 2,400,000 deaths were reported globally, with the rapid increase of numbers in many countries.

SARS-CoV-2 is mainly transmitted from person to person through respiratory droplets, contact, aerosol, or oral-fecal transmission (5, 6). While most reported COVID-19 cases present mild to moderate pathology, 20% of infected patients may develop severe disease and need intensive care (7–12). Severe cases progress to acute respiratory distress syndrome (ARDS) after 8–9 days of symptoms onset (1). ARDS seen in severe COVID-19 cases is characterized by difficulty in breathing and low blood oxygen level, leading to respiratory failure, which is the main cause of death in 70% of fatal COVID-19 cases (8–10). Plasma analysis of severe cases showed a massive release of cytokines by the immune system (cytokine storm) in response to the viral infection and/or potential secondary bacterial and fungal infections (8, 9). This uncontrolled inflammation induced by SARS-CoV-2 infection results in multi-organ damage, leading to organ failure (10).

**Abbreviations:**  $\alpha 7$ -nAChR,  $\alpha 7$  subtype of the nicotine acetylcholine receptor; ARDS, Acute respiratory distress syndrome; Ang I, angiotensin I; Ang (1-7), angiotensin (1-7); Ang (1-9), angiotensin (1-9); Ang II, angiotensin II; ACE, angiotensin converting enzyme; ACE2, angiotensin converting enzyme 2; ACEIs, angiotensin converting enzyme inhibitors; AT1R, angiotensin type 1 receptor; AT2R, angiotensin type 2 receptor; ARBs, angiotensin type 1 receptor blockers; Abs, antibodies; CV, cardiovascular; CVD, cardiovascular disease; CFR, case fatality rate; CCI, Charlson comorbidity index; COPD, chronic obstructive pulmonary disease; CP, convalescent plasma; COVID-19, coronavirus disease-2019; CRP, C-reactive protein; DPP4, dipeptidyl peptidase 4; FP, fusion peptide; MasR, G-coupled receptor Mas; GPCR, G protein-coupled receptors; HR1, heptad repeat region 1; HR2, heptad repeat region 2; HT, hypertension; MERS-CoV, Middle East respiratory syndrome coronavirus; NS, non-specified; PCT, pro-calcitonin; RBD, receptor-binding domain; rhACE2, recombinant human ACE2; RAS, renin angiotensin system; RASIs, renin angiotensin system inhibitors; SARS-CoV-1, severe acute respiratory syndrome coronavirus; SARS-CoV-2, severe acute respiratory syndrome coronavirus 2; S protein, spike protein; S1, S protein subunit 1; S2, S protein subunit 2; TMPRSS2, transmembrane protease serine 2.

Certain groups of the population are more susceptible to SARS-CoV-2 infection (11–14). The case fatality rate (CFR) seems to be age-dependent, with a higher percentage in the elderly, especially men. SARS-CoV-2 may have a higher transmissibility than SARS-CoV-1 and MERS-CoV (1, 8, 15, 16). Patients with pre-existing comorbidities such as chronic obstructive pulmonary disease (COPD), cardiovascular diseases, hypertension and type 2 diabetes mellitus, are more likely to display a severe course and to have higher mortality rates (13–18).

Initial research on SARS-CoV-2 demonstrated that it binds to host cells using the angiotensin-converting enzyme 2 (ACE2), similar to SARS-CoV-1. SARS-CoV-2 binds to ACE2 proteins as a receptor in bats, civet cats, swine, cats, ferrets, non-human primates, and humans (16–18).

The binding affinity of SARS-CoV-2 RBD to ACE2 seems stronger than that of SARS-CoV-1. Besides, SARS-CoV-2 has evolved to use a wide array of host proteases (transmembrane protease serine 2 (TMPRSS2), cathepsin L/B, furin, trypsin, etc.) for S-protein priming, thus facilitating cell entry following receptor binding. This may explain the considerably larger global influence of COVID-19 than the initial SARS epidemic of 2003 (19–21). It is worth noting that new SARS-CoV-2 strains, namely the British (B.1.1.7) and South African variants (B.1.351), that emerged toward the end of 2020 show increased transmission capacity, associated with increased interaction force between Spike and ACE2 proteins due to viral mutations (22, 23). In addition, the RBD/ACE2 mediated SARS-CoV-2 entry into cells is followed by subsequent downregulation of surface ACE2 expression (24). Several reports indicate that the reduction in ACE2 function influences blood pressure, perturbs fluid/electrolyte balance, enhances inflammation, and vascular permeability in the airways, and facilitates the development of multiorgan damage from SARS-CoV-2 infections (25–29). Consequently, ACE2 appears as a critical factor in understanding COVID-19 pathology and a potential target for COVID-19 treatment.

## ACE2 IS PART OF A COMPLEX SYSTEM

ACE2 is a membrane-bound glycoprotein of 805 amino acids that exhibits 40% identity and 61% similarity to human angiotensin converting enzyme (ACE). Full-length ACE2 consists of a heavily glycosylated N-terminal signal sequence containing the active site, a hydrophobic transmembrane sequence, and a short C-terminal cytoplasmic tail. A soluble and catalytically active form of ACE2 can be also produced by several mechanisms, including the action of ADAMs family members of zinc metalloproteases



(30–33). ACE2 is the main enzyme involved in the production of the Ang (1-7) peptide of the renin-angiotensin system (RAS) (**Figure 1**). The latter comprises successive enzymatic reactions that regulate multiple biological processes, including cellular growth, proliferation, migration, extracellular matrix remodeling, and inflammation. While RAS includes multiple enzymatic axes leading to the production of different bioactive peptides, local tissue effects of RAS are driven mostly by the balance between the pro-inflammatory/pro-fibrotic and anti-inflammatory/anti-fibrotic actions of Ang-II and Ang (1-7), respectively (34, 35) (**Figure 1**).

Ang II is produced by the cleavage of Ang I by the angiotensin-converting enzyme (ACE), and it exerts its pro-inflammatory/pro-fibrotic effects by binding to its angiotensin type 1 receptor (AT1R) (**Figure 1**). On the other hand, ACE2 is the most potent Ang (1-7) generating enzyme. By its single catalytic domain, ACE2 can produce Ang (1-7) directly by cleaving one amino acid from the C-terminal domain of Ang II or indirectly through two successive cleavage reactions from Ang I (36) (**Figure 1**). Of note, Ang II is the preferred substrate for ACE2, with an affinity of 400-fold higher than that of Ang I (37). Hence, Ang-(1-7) production is based on both ACE2 levels and the ACE/ACE2 ratio.

Ang (1-7) exerts its effects by binding to and activating the G-coupled receptor Mas (MasR), which opposes the pro-inflammatory and pro-fibrotic actions of Ang II through AT1R activation (38, 39). Moreover, MasR can inhibit Ang II-mediated actions by hetero-oligomerization and inhibition of AT1R. Ang (1-7) can also exert its protective effects by binding directly to the angiotensin type 2 receptor (AT2R) (40, 41). Interestingly, the AT2R can exert similar protective effects when bound by Ang II (34, 35). Thus, the crucial role of ACE2 in RAS stems from the fact that it cleaves and opposes the action of Ang II (**Figure 1**). Consequently, it has a beneficial role in many diseases such as diabetes and cardiovascular diseases (CVD) (33), as well as in COVID-19 (42).

## ROLE OF THE ACE2/ANG (1-7)/MASR AXIS IN PULMONARY PHYSIOLOGY AND PATHOLOGY

RAS gained an increased complexity and appreciation with the identification of local RAS in different tissues, including the brain, kidneys, heart, ovary, pancreas, and the vascular wall, independent of the well-known traditional circulatory RAS. Also, the discovery of additional RAS components (alternative enzymes, receptors, and bioactive angiotensin peptides) has extended the system's role far beyond blood pressure regulation and body electrolyte balance. Indeed, novel actions for each member of the RAS are continuously discovered in physiology and diseases (43).

ACE2 is expressed in human airway epithelia and lung parenchyma, suggesting a role in the regulation of pulmonary physiology (44, 45). A large body of evidence has shown the protective role of the ACE2/Ang (1-7)/MasR axis in several models of lung injury, including SARS-CoV-1 mediated injury

(25, 46). In fact, to protect from severe lung failure, ACE2 is known to inhibit Ang II production, ACE activity, and AT1R activation. Of note, the anti-inflammatory and anti-fibrotic responses of ACE2 are mediated by the production of Ang (1-7) bioactive peptide, which protects against acute lung failure via activation of MasR and AT2R. More specifically, Ang (1-7)/MasR exerts its beneficial effects by inhibiting ERK1/2 and NF- $\kappa$ B signaling pathways in a rat model of ARDS (47) and a mouse model of chronic allergic lung inflammation (44, 48). Magalhaes et al. also showed that MasR knockout mice failed to attenuate inflammation and pathological lung remodeling and presented aggravated asthma due to disruption of the protective arm of the RAS (49). The same research group confirmed that Ang (1-7) infusion resolved inflammation through correction of eosinophile defective apoptosis leading to lung damage (48). Ang (1-7) drug was also demonstrated to prevent bronchial responsiveness, a hallmark sign of chronic asthma (44).

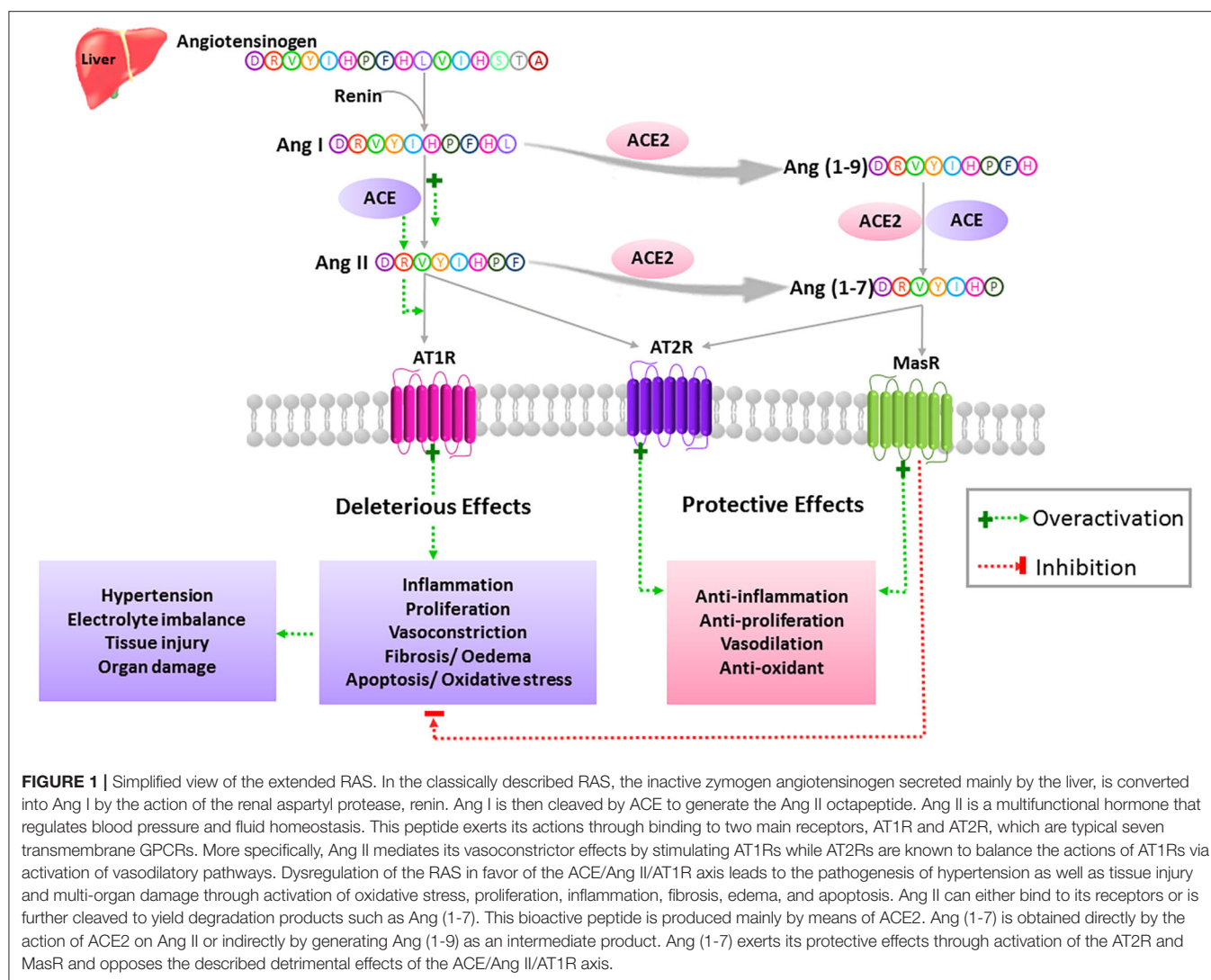
Dysregulation of ACE/ACE2 balance leads to impaired lung function due to inflammation, fibrosis, and lung edema. The latter phenomenon is most probably induced via increasing pulmonary blood vessels' permeability (25, 46, 47). Elevated ACE concentrations have been detected in many potentially fibrotic lung diseases, including idiopathic pulmonary fibrosis (50) and ARDS (51, 52). Similar pro-fibrotic effects were also observed in a mouse model of ARDS using the MasR antagonist A779 (53). Moreover, Ang II has been shown to stimulate lung fibroblast proliferation and procollagen production by stimulating AT1R and the autocrine action of TGF $\beta$ . Of interest, *losartan* (AT1R blocker) and *ramipril* (ACE inhibitor), and Ang (1-7) were shown to reduce lung collagen deposition in the same study (53, 54). Thus, the protective effects of ACE2 on the lungs can be attributed to the inactivation of the ACE/Ang II/AT1R axis in favor of the ACE2/Ang (1-7)/MasR-AT2R axis (25).

## ROLE OF ACE2 IN THE PATHOLOGY OF COVID-19

The expression of ACE2 in human airways and lung tissues highlights its role in respiratory infections, including SARS-CoV-1 and the related human respiratory coronavirus NL63 (55). Although ACE2 is the main door for virus entry, the total ACE2 activity seems to be protective. In fact, several reports mentioned that ACE2 could be downregulated after virus entry and/or host cell lysis, as in SARS-CoV-1. The latter is reported to reduce ACE2 expression at the cell surface as well as the release of active ACE2 ectodomains (56, 57). This fact may further accentuate the pathogenesis of COVID-19, as ACE2 is shown to be protective in several models of lung injury, including SARS-CoV-1 mediated injury (25, 46).

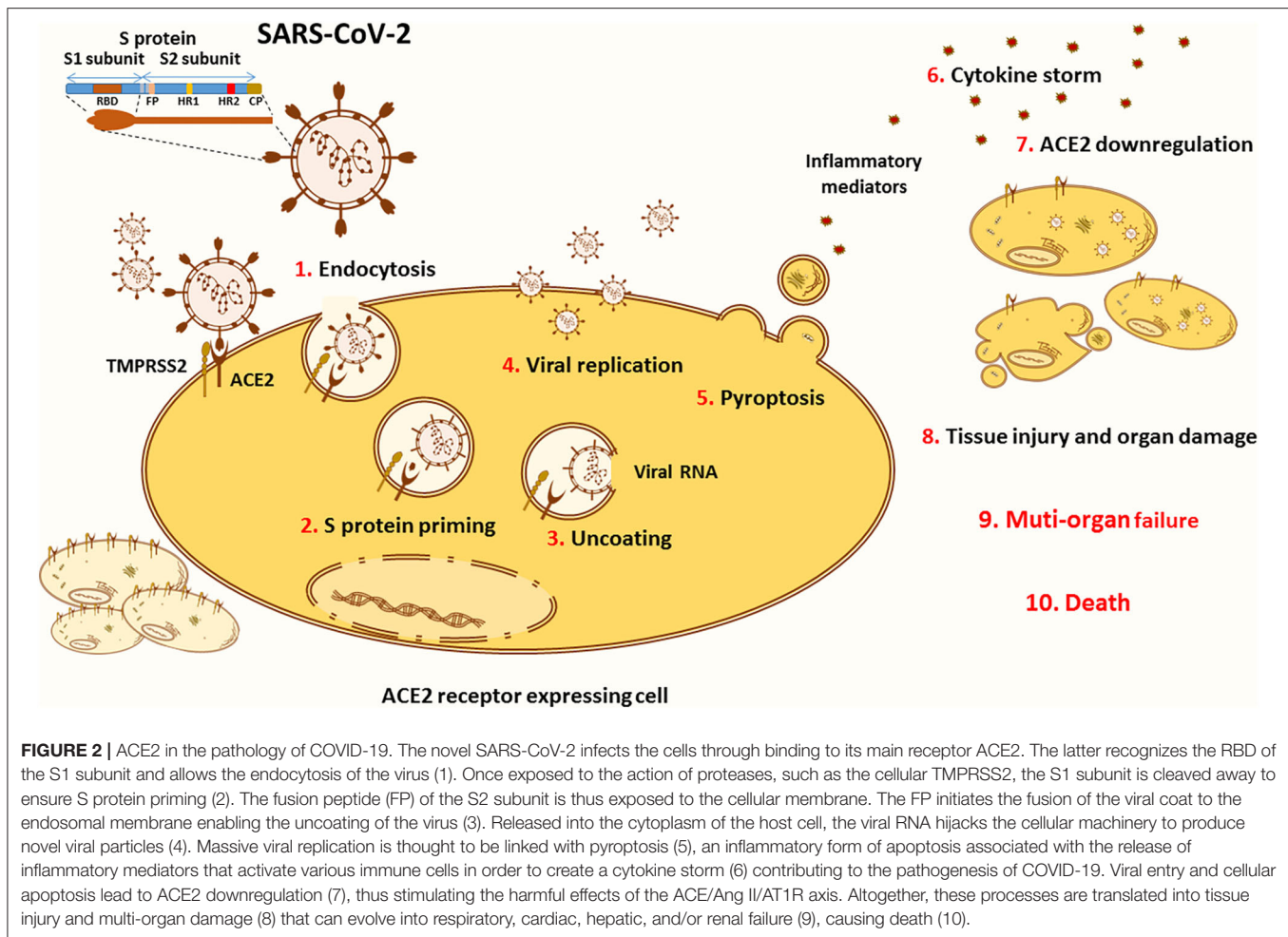
Both SARS-CoV-1 and SARS-CoV-2 use the same receptor, ACE2, to infect cells. Interestingly, SARS-CoV-2 was shown to have a higher affinity for ACE2 than SARS-CoV-1 (58–60). Higher affinity values could be related to the dynamic of infection and the rapid spread that characterize this virus (61). For instance, mutations that increase the infectivity on





RBD could explain why SARS-CoV-2 is more infectious than SARS-CoV-1 (62). Notably, mutations affecting SARS-CoV-2 have also been reported. In fact, by the end of August 2020, the C.1 lineage of SARS-CoV-2 presenting one amino acid substitution, D614G, on the spike protein, among 16 other nucleotide mutations, became the predominant lineage in South Africa (63). Analyses of over 28,000 SARS-CoV-2 spike protein gene sequences revealed that the D614G amino acid substitution facilitates the binding to ACE2 receptor and thus enhances viral replication in human lung epithelial cells and primary human airway tissues. This might account for its increased virulence to the respiratory system (64, 65). In addition, the 501Y.V2 variant that appeared in South Africa in December 2020 showed three important mutations in RBD (K417N, E484K, and N501Y) that are most probably correlated with functional significance (66). Another study on the B.1.1.7 British lineage revealed that the N501Y mutation of the SARS-CoV-2 spike protein is linked with increased interaction with ACE2 receptor, which explains its high infectivity rate (23).

The SARS-CoV-2 entry into target cells is initiated by the binding of the surface unit, S1, of the spike (S) protein to the ACE2 cellular receptor (**Figure 2**). The entry then requires S protein priming by TMPRSS2 serine proteases, which entails S protein cleavage and allows the fusion of viral and cellular membranes (67). Of note, several studies highlighted TMPRSS2 implication as a critical factor for the spread of clinically relevant viruses, including influenza A and other coronaviruses (68–70). One study conducted on a cohort of Italian patients announced that COVID-19 susceptibility is determined by genetic variability of TMPRSS2 known to be involved in SARS-CoV-2 entry into target cells. In this context, the data showed that in comparison to other European populations, Italians might have a higher level of TMPRSS2 or activity since they show a significant decrease in the deleterious variants of this protein. This can be considered as a risk factor for a more severe illness course (71). TMPRSS2 mediated activation of S protein priming enables viral infection of ACE2 positive cells. This initial phase is associated with viral replication and leads to pyroptosis, an inflammatory form of



apoptosis, inducing lung injury. Of note, the formation of new viruses is also correlated with the induction of a cytokine storm via activation of various immune cells (56, 72).

## DIFFERENTIAL RESPONSE TO COVID-19 COULD BE RELATED TO ACE2 EXPRESSION

Severe COVID-19 cases are mostly observed among elderly patients, with males suffering from chronic comorbidities such as cardiovascular and cerebrovascular diseases, diabetes, and others. Recently, it was established that risk factors including age, male sex, and hypertension provide a convenient tool to identify high-risk individuals. Hypertension elucidates the involvement of RAS in the pathogenesis of COVID-19 due to the interplay between SARS-CoV-2 and ACE2 (73–75). It is believed that ACE2 expression pattern in different organs, tissues, and cell types is permissive for the susceptibility of SARS-CoV-2 infection since ACE2 receptor permits coronavirus entry, replication, spread, and pathogenesis (76).

In order to identify the initial reservoirs of SARS-CoV-2, ACE2 expression levels were assessed within the lung and the

upper/lower airway epithelium. ACE2 was expressed at low levels in the respiratory tract, and it was expressed in multiple epithelial cell types across the lower airway, with the highest expression being observed in club epithelial cells in comparison with basal and ciliated epithelial cells (77). ACE2 expression was also detected in alveolar type II cells in the lung parenchyma (77). In fact, alveolar type II cells, which account for only 5% of the alveoli, are essential to maintain lung elasticity and act as progenitors for alveolar type I cells responsible for gas exchange. Thus, SARS-CoV-2 might be responsible for depletion of the alveolar stem cells leading to the development of irreversible lung injury (56, 76). Remarkably, in the upper airway, nasal epithelial cells, including goblet and ciliated cells, showed the highest expression of ACE2 among all investigated cells in the respiratory tree; thus, highlighting their role in facilitating initial viral entry, transmission, and clearance (45, 77). Moreover, ACE2 expression is dynamic and depends on the differentiation status of epithelial cells. For instance, it is worth noting that differentiated epithelial cells expressing a higher level of ACE2 are readily infected in comparison to undifferentiated cells with low ACE2 expression (55). These findings may raise the theoretical assumption that the differential response to COVID-19 in patients could be in some aspects attributed to changes in ACE2 expression.

In this context, it has been reported that long term smokers express high levels of ACE2 receptor (78), namely in type-2 pneumocytes and alveolar macrophages (79), making them at high risk of infection by SARS-CoV-2 (78). This elevated expression occurs through activation of the  $\alpha 7$  subtype of the nicotine acetylcholine receptor ( $\alpha 7$ -nAChR) (80). This is further highlighted in a recent meta-analysis revealing that patients with a history of smoking, as well as active smokers, recorded a significant severity of COVID-19 (81). In fact, cigarette smoking promotes alterations in the respiratory tract that might increase the risk of viral infections through multiple mechanisms such as impairment of mucociliary clearance, mucus hypersecretion, fibrosis, and dysfunction of the epithelial barrier. These mechanisms are accompanied by alterations in the immune response, eventually harming the function of the lungs, including gas exchange (82–86).

Although different studies have reported the upregulation of ACE2 expression in the lungs of cigarette smokers (78, 87), surprisingly, a very recent study revealed a decrease in the levels of ACE2 receptor in both alveolar and bronchial epithelial cells of mice exposed to cigarette smoking. Additionally, an *in vitro* study on Calu3 human lung cancer cell line treated with cigarette smoke showed no effect on ACE2 levels but effectively inhibited SARS-CoV-2 replication (88). These conflicting results urge for more work to clarify the role of cigarette smoking on ACE2 expression, SARS-CoV-2 infection and its severe respiratory complications.

## DIFFERENTIAL RESPONSE TO COVID-19 AND ACE2 EXPRESSION IN CARDIOVASCULAR PATIENTS

RAS dysregulation, highlighted by Ang II upregulation, is associated with the pathogenesis of CVD. RAS inhibitors, such as ACE inhibitors (ACEI) and AT1R blockers (ARBs), are commonly used for the treatment of CVD patients. ACEI are known to downregulate the expression of Ang II, whereas ARBs are known to block Ang II-mediated detrimental effects (41). Due to the beneficial effects for the activation of the ACE2/Ang (1-7) axis, there has been substantial interest in considering the effect of RAS inhibitors on ACE2 expression in patients with CVD. Previous evidence in several animal models indicated that certain ARBs and ACEIs exhibit the ability to increase ACE2 mRNA and protein expression levels in the heart (89, 90). More importantly, ARBs were shown to alter the expression of ACE2 more consistently than ACEI (91). Although some animal studies displayed an elevation in ACE2 expression under the effect of RAS inhibitors (92), other studies did not. In this context, it has been reported that ACEI did not alter the activity of ACE2 *in vitro* (93). In another study, the use of the ACEI *ramipril* or of the ARB *valsartan* did not increase cardiac ACE2 expression in a rat model of myocardial infarction (94).

In contrast to animal models, limited investigation has been conducted in humans to consider the influence of RAS inhibition on the expression of ACE2 (95). In fact, a human study involving patients with hypertension showed higher urinary ACE2 levels

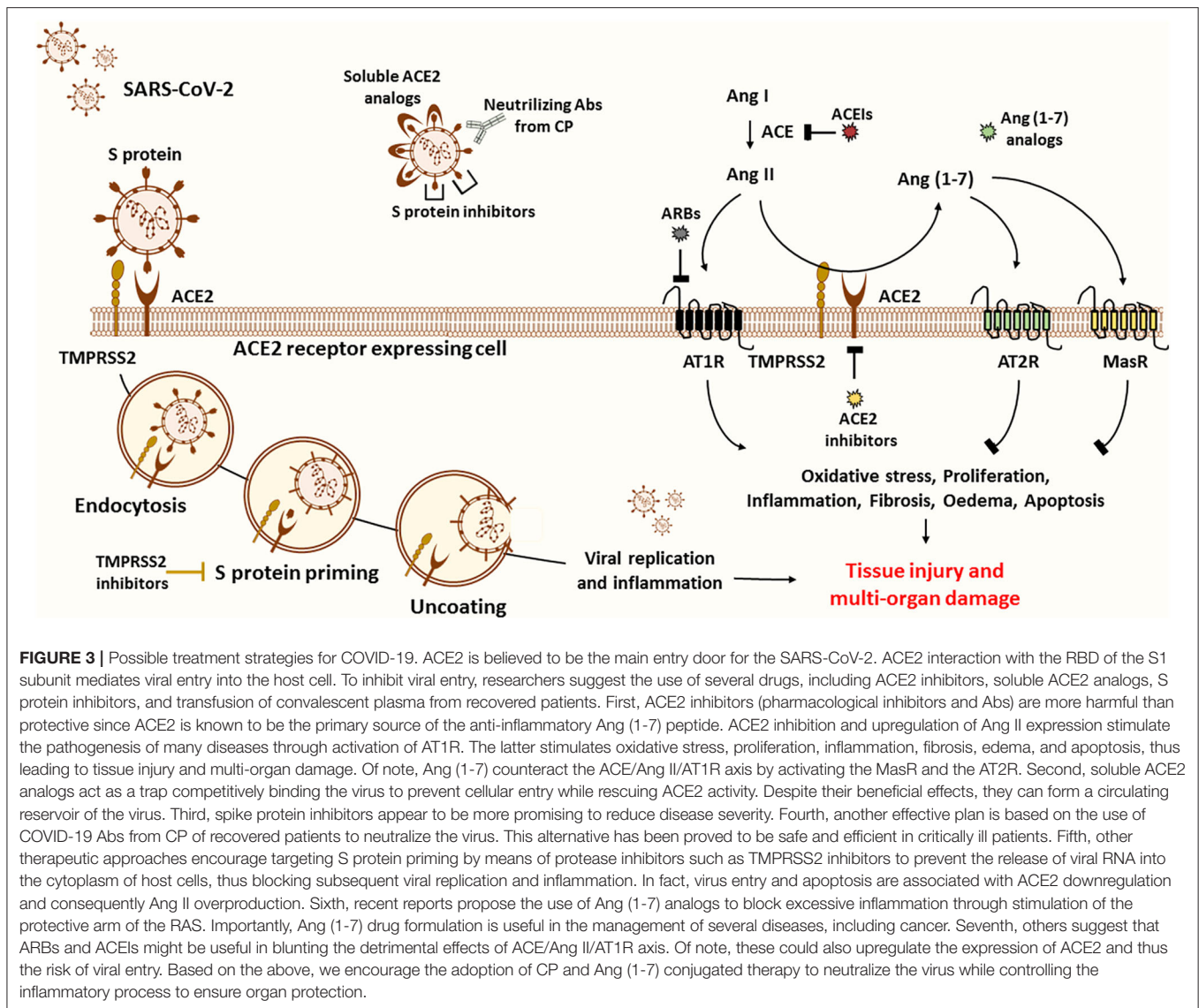
in patients treated with the ARB *olmesartan*, but not with other ARBs or the ACEI *enalapril* (96). Importantly, ACE2 upregulation has been mostly noticed in renal vasculature and in cardiac tissue. However, the outcomes differed depending on the RAS inhibitors used (97). Furthermore, most human studies relied on measuring the soluble ACE2 levels in the blood. It's worth noting that measuring the membrane-bound ACE2 expression *in vivo* is technically challenging. In this regard, an increase in soluble ACE2 levels may refer to a decrease in the membrane-bound form of ACE2. Therefore, the distinction between soluble and membrane-bound ACE2 must be clear (97).

Overall, upregulation of ACE2 expression in CVD patients under ARBs or ACEIs raised several theoretical assumptions that these treatment regimens might put them at a greater risk of infection by SARS-CoV-2 (60, 95).

## POSSIBLE SCENARIOS ON USING ACE2-BASED TREATMENTS FOR COVID-19

ACE2 appears as a potential target for COVID-19 treatment based on the fact that it is an entry receptor critically involved in mediating SARS-CoV-2 infection and on its central role in cardiac pathology as well as in lung damage (98). Some reports suggested introducing ACE2 blockers, such as the MLN-4760 chemical inhibitor, or targeted antibodies to disrupt the viral entry into cells (99, 100). This approach could be detrimental to the risk of reducing ACE2 protective and anti-inflammatory activity, which further increases the susceptibility of lungs for more damage. Instead, viral entry could be impaired by protease inhibitors targeting TMPRSS2 protease implicated in SARS-CoV-2 cell entry, without risking the endogenous ACE2 activity (98) (Figure 3).

A better alternative to attenuate the viral load and infection, in comparison with ACE2 antibodies and pharmacological inhibitors, would be to deliver excessive soluble viral receptor analogs in order to intercept the viral binding to the membrane-bound ACE2. The conceptual principle is that soluble ACE2 may act as a trap, competitively binding and neutralizing the virus while rescuing cellular ACE2 activity and protecting the lungs from injury (99). In fact, a fusion protein of recombinant human ACE2 (rhACE2) was reported to show high affinity to SARS-CoV-2 binding domain and to neutralize the virus *in vitro* (101). Furthermore, Monteil et al. recently demonstrated that a clinical-grade rhACE2 is capable of reducing the viral load of SARS-CoV-2 infection in Vero-E6 cells and of blocking its entry into the cells. This study revealed that rhACE2 could inhibit SARS-CoV-2 infections in human organoids, such as the kidneys, during early stages of viral infection (102). Moreover, a clinical pilot study was planned (NCT number: NCT04287686) to deliver soluble rhACE2 infusions in a small COVID-19 patient cohort in China. Nevertheless, this study was withdrawn for non-stated reasons. Regardless, a large phase II clinical trial has been initiated at the beginning of April by the Austrian pharmaceutical company APEIRON to treat COVID-19 patients with APN01-rhACE2, in Austria,



Germany, and Denmark (98). On the other hand, soluble ACE2 appears to have a short half-life and may lack the capacity to overcome massive virus infection. This agent could form a reservoir of circulating viruses, thus increasing its propagation (103–105) (**Figure 3**).

Altogether, clinical trials using ACE2-based treatments are eagerly awaited to exclude possible adverse effects and to prove their promising potential to enhance the positive outcomes in patients infected with COVID-19.

## ARBs TO REDUCE THE SIDE EFFECTS OF ACE2 INHIBITION BY COVID-19

It is believed that SARS-CoV-2 infection may cause an increase in lung injury and severe acute respiratory failure due to ACE2/Ang (1-7) downregulation. In addition, since Ang II is the major substrate of ACE2, inhibition of ACE2 following

viral entry is generally associated with Ang II upregulation as well as activation of the AT1R. In fact, elevated levels of Ang II were reported in the plasma of SARS-CoV-2 infected patients, which were positively correlated with viral load and lung injury. Thus, the harmful effects of COVID-19 could be achieved by inhibiting Ang II-mediated harmful effects (25, 26, 47, 56, 106). Due to its anti-fibrotic and anti-inflammatory properties, ARBs effectively block Ang II-mediated AT1R activation and reduce acute lung injury in patients diagnosed with pneumonia, sepsis, and influenza (107–109). Therefore, ARBs blocking Ang II/AT1R pathway could overcome the adverse effects of ACE2 downregulation by SARS-CoV-2. On the other hand, several studies reported that ARBs beneficial effects could be correlated to the increase of ACE2 expression and activity in patients. Despite the beneficial properties of ACE2/Ang (1-7) axis (96, 110, 111), ACE2 upregulation after ARB treatment may open the door for viral entry, thus increasing the susceptibility of patients to SARS-CoV-2 infection.



Since the treatment of CVD patients is based on ARBs, their discontinuation in COVID-19 patients has been proposed to reduce ACE2 expression and, thus, the risk of a more severe infection associated with the increased viral entry. In fact, interruption of treatment may be more harmful than protective. For instance, discontinuing RAS inhibitors, including ARBs, in patients with an unstable clinical state (hypertension, heart failure, myocardial infarction), may result in a decline in clinical status and higher risks of mortality (60, 95). In fact, ARBs are reported to block Ang II/AT1R axis and to reduce acute lung injury pathogenesis. Interruption of ARBs might increase lung injury since Ang II-mediated AT1R activation is associated with vasoconstriction, oxidative stress, increased fibroproliferative, and inflammatory responses as well as lung oedema (54, 60, 112, 113). Importantly, studies have shown that these drugs can be protective against lung injury in SARS-CoV-1 patients by enhancing the protective arm of RAS (114). Also, retrospective studies showed that patients using ACEIs and ARBs present a lower risk of mortality and develop less severe cases as compared with those using other hypertensive drugs. On the other hand, these treatment regimens do not increase the risk of SARS-CoV-2 infection nor disease severity, as summarized in **Table 1**.

Taken together, more evidence is needed to support the proper use of ARBs for the treatment of COVID-19 and to exclude the risk of an increased viral entry. ARBs play a protective role in CVD patients by reducing the harmful effects of Ang II/AT1R axis while enhancing ACE2/Ang (1-7) protective axis. Therefore, ARB withdrawal can be potentially harmful rather than protective.

## COMBINED THERAPY OF ANTI-COVID-19 ANTIBODIES AND ANG (1-7) AGONIST FOR THE TREATMENT OF COVID-19 PATIENTS

Several therapies are being investigated for the treatment of COVID-19 (124). Passive immunotherapy has also been reported as a treatment option to reduce mortality in many infectious viral diseases, including SARS-CoV-1 and severe influenza-related pathologies (125). Transfusion of anti-COVID-19 antibodies from recovered patients appears to be promising in severe patients. Recent studies showed that transfusion of convalescent plasma (CP) containing anti-COVID-19 neutralizing antibodies to COVID-19 critically ill patients, along with the conventional antiviral treatment, is associated with improvement in fever, inflammatory markers, lymphocyte count, viral clearance, and CT findings (126–128). In fact, Shen et al. conducted the first study describing the use of CP in COVID-19 patients. Indeed, 5 ARDS critically ill patients received CP from recovered healthy donors along with antiviral agents and methylprednisolone. All patients showed improvement of inflammatory markers, and the viral load became negative 12 days post transfusion (126). In another trial performed by Ye et al., 5 of 6 COVID-19 patients treated with CP demonstrated decreased pulmonary lesions based on their CT scan (129). Similar findings were reported by two other studies, revealing an overall improvement in clinical outcomes with no single death recorded during the treatment

procedure (128, 130). Noteworthy, all the preliminary studies mentioned in **Table 2** did not have control groups receiving CP alone, and the sample size of patients was generally limited in number. However, these studies established the safety and efficacy of anti-COVID-19 antibodies transfusion in critically ill patients. Therefore, CP was finally approved last August by the FDA as an investigational new drug for patients with life-threatening SARS-CoV-2 infection (144). On this basis, an FDA-initiated study on a cohort of 20,000 COVID-19 patients confirmed the safety of CP with low incidence of adverse events associated with transfusion (142). Recently, CP infusion was recommended during early stages of infection by Zeng et al. In this trial, 6 COVID-19 patients with respiratory failure received standard care along with CP treatment at a median of 21.5 days post-infection. Eventually, all patients tested negative for SARS-CoV-2 at 3 days post-infusion; however, 5 out of these 6 patients died, suggesting that CP is ineffective in reducing mortality in end-stage COVID-19 patients and should be initiated earlier (140). These findings were confirmed by Salazar et al., who reported a higher reduction in mortality rate in patients receiving CP transfusion within 44 hours of their hospitalization (143). These observations might be due to the late clinical deterioration observed in COVID-19 patients, related to hyper-immune attacks and inflammatory reactions, rather than a direct viral-effect since the peak of viral load is observed during the first week of infection (131). All clinical trials using CP for patients infected with SARS-CoV-1 or SARS-CoV-2 are presented in **Table 2**.

On the other hand, it is tempting to propose the use of Ang (1-7) agonists to overcome the harmful effects of SARS-CoV-2 infection in patients. Ang (1-7) has been reported to oppose the harmful effects of Ang II/AT1R axis by binding to MasR or to AT2R. In addition, it was shown to be cardiopulmonary protective through its anti-hypertensive, anti-thrombotic, anti-arrhythmic, and vasodilatory effects (145–147). Moreover, animal studies demonstrated that ARDS is associated with low Ang (1-7) levels and that Ang (1-7) upregulation reduces reactive oxygen species production and inhibits pulmonary fibrosis to control tissue damage. Besides, data showed that Ang (1-7)/MasR axis exhibits anti-inflammatory effects by inhibiting the NF- $\kappa$ B pathway and by reducing the production of pro-inflammatory cytokines such as TNF- $\alpha$  and IL-6 (53, 113, 148–151). In this context, Ang (1-7) oral formulation was also proved to attenuate the rupture of alveolar walls and behavioral changes in a mice model of elastase-induced emphysema (152).

The pathogenesis of SARS-CoV-2 infection is mediated through over-activation of the inflammatory response and an increased cytokine production (113, 148, 149). This could be related to the inhibition of the anti-inflammatory ACE2/Ang (1-7)/MasR axis by binding of the virus. Therefore, the severity of COVID-19 could be attenuated by Ang (1-7) administration, which may restore the anti-inflammatory response via MasR activation (153). Several Ang (1-7) agonists are available such as AVE-0991 (154), hydroxypropyl  $\beta$ -cyclodextrin (HP $\beta$ CD)/Ang (1-7) (155, 156), cyclic angiotensin (1-7) (157), CGEN-856, and CGEN-857 (158). In animal models, these agonists exert their



**TABLE 1 |** The effect of ACEIs and ARBs on COVID-19 patients with CVD.

| Study design                        | Patient population   | Outcomes   | Institutes   | References |
|-------------------------------------|--|--|--|------------|
| Multicenter, retrospective study    | <i>N</i> = 476 COVID-19 patients with moderate ( <i>n</i> = 352), severe ( <i>n</i> = 54), or critical cases ( <i>n</i> = 70)<br>HT group ( <i>n</i> = 113)<br>ACEIs/ARBs (51/113)<br>Other drugs (62/113)<br>Non-HT group ( <i>n</i> = 363) | Higher incidence of comorbidities in the severe and critical groups as compared to the moderate group<br>Patients receiving ACEIs or ARBs were more likely assigned to the moderate group than to the severe and critical groups                         | Three hospitals in Wuhan, Shanghai, and Anhui, China                               | (115)      |
| Multicenter, retrospective study    | <i>N</i> = 1128 COVID-19 patients with HT<br>ACEI/ARB group ( <i>n</i> = 188)<br>Other drugs group ( <i>n</i> = 940)   | The use of ACEIs and ARBs in COVID-19 patients with HT is associated with a lower risk of all-cause mortality  | Nine hospitals in Hubei, China   | (116)      |
| Multicenter, retrospective study    | <i>N</i> = 609 COVID-19 patients<br>HT group ( <i>n</i> = 311)<br>No treatment (60/311)<br>ARB (76/311)<br>ACEI (99/311)<br>Other drugs (76/311)<br>Non-HT group ( <i>n</i> = 298)   | Overall in-hospital mortality was 29%<br>42% among HT patients died in-hospital, after a median of 6 days from admission<br>Patients receiving anti-HT drugs other than RASIs had a higher CCI, with a higher prevalence of COPD and CV comorbidities    | Ten Italian hospitals  | (117)      |
| Single-center, retrospective study  | <i>N</i> = 417 COVID-19 patients<br>HT group ( <i>n</i> = 51)<br>No treatment (9/51)<br>ACEI/ARB (17/51)<br>Other drugs (25/51)<br>Non-HT group ( <i>n</i> = 366)  | RASIs improve the clinical outcomes of COVID-19 patients with HT<br>HT patients could benefit from the persistent or preferential usage of ACEIs and ARBs  | Shenzhen Third People's Hospital, Shenzhen, China                                  | (118)      |
| Single-center, retrospective study  | <i>N</i> = 251 COVID-19 patients<br>HT group ( <i>n</i> = 126)<br>ACEI/ARB (43/126)<br>Other drugs (83/126)<br>Non-HT group ( <i>n</i> = 125)  | ARB/ACEI group had significantly lower concentrations of CRP and PCT<br>ARB/ACEI group had a lower non-significant proportion of critical patients, and death rate<br>This study supports the use of ARBs/ACEIs in COVID-19 patients with preexisting HT | Hubei Provincial Hospital of Traditional Chinese Medicine (HPHTCM) in Wuhan, China | (119)      |
| Single-center, retrospective study  | <i>N</i> = 1,8472 patients<br>COVID-19 positive group ( <i>n</i> = 1735)<br>ACEI (116/1735)<br>ARB (98/1735)<br>COVID-19 negative group ( <i>n</i> = 16,737)<br>ACEI (1206/16737)<br>ARB (884/16737)   | This study supports various guidelines to continue current ACEIs or ARBs treatments during the COVID-19 pandemic<br>This study found no association between ACEIs or ARBs use and COVID-19 test positivity   | Cleveland Clinic Health System in Ohio and Florida, USA                            | (120)      |
| Single-center, retrospective study  | <i>N</i> = 1,178 COVID-19 patients<br>HT group ( <i>n</i> = 362)<br>ACEI/ARB (115/362)<br>Non-HT group ( <i>n</i> = 816)   | ACEIs/ARBs are not associated with COVID-19 severity or increased mortality rates<br>This study supports current guidelines and societal recommendations for treating HT during the COVID-19 pandemic  | The Central Hospital of Wuhan, China   | (121)      |
| Population based case-control study | <i>N</i> = 3,7031 patients<br>COVID-19 positive group ( <i>n</i> = 6,272)<br>ARBs (1394/6272)<br>ACEI (1502/6272)<br>COVID-19 negative group ( <i>n</i> = 30,759)<br>ARBs (5910/30759)<br>ACEI (6569/30759)                                  | The use of ACEIs and ARBs was more frequent among patients with COVID-19 than among controls<br>No evidence that ACEIs or ARBs affected the risk of COVID-19   | Lombardy region, Italy   | (122)      |
| Single-center, retrospective study  | <i>N</i> = 12,594 patients<br>COVID-19 positive group ( <i>n</i> = 5,894)<br>HT (2573/5894)<br>COVID-19 negative group ( <i>n</i> = 6,700)<br>HT (1784/6700)   | No substantial increase in the likelihood of a positive test for COVID-19 or in the risk of severe COVID-19 among patients who tested positive in association with five common classes of anti-HT medications including ACEIs and ARBs                   | New York University (NYU) Langone Health system, New York, USA                     | (123)      |

This table summarizes different retrospective studies evaluating the effect of ACEIs and ARBs on the risk of SARS-CoV-2 infection and disease severity in patients with preexisting HT. Altogether, the results showed that ACEIs and ARBs do not appear to be associated with a higher risk of SARS-CoV-2 infection, neither with disease severity and mortality. This evidence supports the current guidelines that discourage the discontinuation of ACEIs and ARBs in CVD patients infected with SARS-CoV-2. Of note, patients using ACEIs and ARBs are more likely to develop less severe symptoms and show improved clinical outcomes, reduced concentration of inflammatory markers as well as a lower risk of mortality compared to those using other antihypertensive drugs. In this context, recommendations are addressed toward the preferential use of RASIs for the management of hypertension in COVID-19 patients, all along with standard anti-viral medication. ACEI: angiotensin converting enzyme inhibitors; ARB, angiotensin receptor type 1 blockers; CCI, Charlson comorbidity index; COPD, chronic obstructive pulmonary disease; COVID-19, coronavirus disease-2019; CRP, C-reactive protein; CV, cardiovascular; CVD, cardiovascular disease; HT, hypertension; PCT, pro-calcitonin; RASI, renin-angiotensin system inhibitors; SARS-CoV-2, severe acute respiratory syndrome coronavirus 2.

**TABLE 2 |** The effect of convalescent plasma-based therapy on SARS and COVID-19 patients.

| Infectious agent | Study design                                      | Patient population  | Outcomes  | Institutes   | References |
|------------------|---|---|---|--|------------|
| SARS-CoV-1       | Case series                                       | <i>N</i> = 80 SARS patients with radiographic progression and hypoxemia<br>Group 1: patients given CP before day 14 of illness ( <i>n</i> = 48)<br>Group 2: patients given CP after 14 days of illness ( <i>n</i> = 32)<br>No control group   | A higher day 22 discharge rate was observed among patients who were given CP before day 14 of illness (58.3 vs. 15.6%)<br>Overall mortality rate among 80 patients was 12.5%  | Prince of Wales Hospital, Hong Kong, China             | (131)      |
| SARS-CoV-1       | Single-center, retrospective non-randomized study | <i>N</i> = 40 SARS patients having clinical and radiographic deterioration despite methylprednisolone treatment<br>Intervention group: patients given 3 doses of methylprednisolone steroids with CP ( <i>n</i> = 19)<br>Control group: patients given 4 or more doses of methylprednisolone ( <i>n</i> = 21) | Discharge rate in intervention group was 73.4 vs. 19% in control group<br>Mortality rate in intervention group was 0 vs. 23.8% in control group   | Prince of Wales Hospital, Hong Kong, China             | (132)      |
| SARS-CoV-1       | Case series                                       | <i>N</i> = 40 SARS patients with pneumonia or ARDS<br>Intervention group: patients receiving CP ( <i>n</i> = NS)<br>Control group: patients receiving other types of therapy ( <i>n</i> = NS)   | No mortality cases are reported in the intervention group<br>Three mortality cases are reported in the control group  | Medical College of Hong Kong Chinese University, China | (133)      |
| SARS-CoV-1       | Case series                                       | <i>N</i> = 8 SARS patients<br>Intervention group: patients receiving CP with antivirals and steroids ( <i>n</i> = 3)<br>Control group: patients receiving only antivirals and steroids treatments ( <i>n</i> = 5)   | Intervention group presents improved serial chest radiographs and decreased body temperature<br>Viral load was no longer detectable after 24h of CP treatment   | Taipei Municipal Hoping Hospital (TMHH), Taiwan        | (134)      |
| SARS-CoV-1       | Cases report                                      | <i>N</i> = 29 SARS patients<br>Intervention group: 74 years old patient receiving CP after antivirals and steroids treatments ( <i>n</i> = 1)<br>Control group: younger SARS patients receiving antivirals and steroids treatments only ( <i>n</i> = 28)  | The patient receiving CP recovered from SARS within 21 days and have a shorter disease course than the control group  | Beijing hospital, China                                | (135)      |
| SARS-CoV-1       | Case report                                       | <i>N</i> = 1 SARS patient<br>Intervention group: 57 years old patient receiving CP, antivirals and steroids treatments ( <i>n</i> = 1)<br>No control group  | Patient showed improved Chest X-ray and decreased body temperature following CP treatment<br>The patient made uneventful recovery   | Prince of Wales Hospital, China                        | (136)      |
| SARS-CoV-2       | Cases report                                      | <i>N</i> = 5 COVID-19 patients with ARDS, severe rapid progression pneumonia and continuously high viral load despite antiviral treatment<br>Intervention group: patients receiving CP ( <i>n</i> = 5)<br>No control group  | Body temperature normalized within 3 days, viral load became negative after 12 days and ARDS resolved in 4 patients out of 5  | Shenzhen Third People's Hospital in Shenzhen, China    | (126)      |
| SARS-CoV-2       | Multicenter, randomized clinical trial            | <i>N</i> = 103 COVID-19 patients with severe ARDS, hypoxemia or life-threatening organ failure<br>Intervention group: patients receiving CP in addition to standard treatment ( <i>n</i> = 52)<br>Control group: patients receiving standard treatment alone ( <i>n</i> = 51)                                 | 51.9% of the intervention group showed clinical improvement (defined as patients discharged alive, or reduction in disease severity) vs. 43.1% in the control group<br>Two patients from the intervention group experienced adverse events within hours after transfusion | Seven medical centers in Wuhan, China                  | (137)      |
| SARS-CoV-2       | Cases report                                      | <i>N</i> = 2 COVID-19 patients with severe pneumonia and ARDS<br>Intervention group: patients receiving antivirals and steroids treatments with CP ( <i>n</i> = 2)<br>No control group  | The patients showed improved oxygenation and chest X-rays with decreased inflammatory markers and viral loads after CP infusion   | Yonsei University College of Medicine, Seoul, Korea    | (127)      |

(Continued)

TABLE 2 | Continued

| Infectious agent | Study design                  | Patient population  | Outcomes   | Institutes  | References |
|------------------|-------------------------------|---|--|---|------------|
| SARS-CoV-2       | Cases report                  | <i>N</i> = 10 COVID-19 patients with severe symptoms, respiratory distress, or hypoxemia<br><br>Intervention group: patients receiving CP in addition to antiviral therapy and supportive care ( <i>n</i> = 10)<br>No control group   | All patients achieved negative viral load, accompanied with an increase of oxygen saturation, improvement of liver function and alleviation of the overreaction of the immune system after plasma transfusion  | Three participating hospitals in Wuhan, China                         | (128)      |
| SARS-CoV-2       | Cases report                  | <i>N</i> = 6 Critically ill COVID-19 patients with deteriorated symptoms after standard treatment<br>Intervention group: patients receiving CP with anti-viral drug arbutol ( <i>n</i> = 6)<br>No control group   | No adverse reactions were observed after plasma infusion<br>After CP transfusion 5 of 6 patients showed improvement in the CT scan results<br>All patients were discharged after achieving negative viral load   | Wuhan Huoshenshan Hospital, Wuhan, China                              | (129)      |
| SARS-CoV-2       | Cases report                  | <i>N</i> = 4 COVID-19 patients with severe symptoms including ARDS<br>Intervention group: patients receiving anti-viral and interferon-based drug in addition to CP ( <i>n</i> = 4).<br>No control group  | All 4 patients achieved negative RT-PCR test results after 3-22 days of transfusion<br>2 of the 4 patients produced anti-SARS-CoV-2 IgG 14 days after CP transfusion   | Dongguan Ninth People's Hospital and Xiangtan Central Hospital, China | (130)      |
| SARS-CoV-2       | Single-arm, multicenter trial | <i>N</i> = 46 COVID-19 patients with severe symptoms, including ARDS, low oxygen saturation levels and markedly elevated laboratory bio- markers<br>Intervention group 1: one unit of CP in addition to standards treatment ( <i>n</i> = 24)<br>Intervention group 2: two units of CP in addition to standard treatment ( <i>n</i> = 21)<br>Intervention group 3: three units of CP in addition to standard treatment ( <i>n</i> = 1)<br>No control group | 3 patients with important comorbidities died within 7 days of plasma transfusion<br>23% of survivors showed a clear chest X-ray, and 100% of them had improvement in laboratory biomarkers (C-reactive protein, ferritin and lactate dehydrogenase levels all decreased) after 7 days of transfusion<br>All 43 patients achieved negative viral-load at the end of the study | Two university hospitals and one general hospital in northern Italy   | (138)      |
| SARS-CoV-2       | Retrospective cohort study    | <i>N</i> = 80 Critically ill Covid-19 patients with severe symptoms<br>Intervention group: patients receiving CP along with standard care (including hydroxychloroquine, azithromycin, and lopinavir-ritonavir) ( <i>n</i> = 40).<br>Control group: patients receiving standard care only ( <i>n</i> = 40)  | Improvement in respiratory status achieved in 77.5% of intervention group vs 65% of control group<br>Viral clearance achieved after 28 days of CP infusion in 65% of intervention group vs 55% in the control group<br>Overall survival was 65% with no difference between the two groups  | Hamad Medical Corporation (HMC), Qatar                                | (139)      |
| SARS-CoV-2       | Cases report                  | <i>N</i> = 21 COVID-19 patients with respiratory failure and required intensive care unit admission<br>Intervention group: critically ill patients receiving CP transfusion at a median of 21.5 days' post infection in addition to standards treatment ( <i>n</i> = 6)<br>Control group: patients receiving standards treatment only ( <i>n</i> = 15)  | All the patients in the intervention group tested negative for SARS-CoV-2 RNA by 3 days after infusion<br>5 out of 6 patients in the intervention group died eventually  | First Affiliated Hospital of Zhengzhou University, China              | (140)      |
| SARS-CoV-2       | Cases report                  | <i>N</i> = 25 COVID-19 patients with severe and/or life-threatening disease<br>Intervention group: patients receiving anti-inflammatory treatment (including tocilizumab and steroids) and anti-viral drugs, in addition to CP transfusion at median of 10 days' post symptom onset ( <i>n</i> = 25)<br>No control group  | 36% of patients had improvement in the clinical markers after 7 days of transfusion<br>76% of patients improved from baseline or been discharged after 14 days of transfusion<br>Only one patient from the 25 died from a condition not caused by plasma transfusion   | Houston Methodist hospitals, USA                                      | (141)      |

(Continued)

TABLE 2 | Continued

| Infectious agent | Study design   | Patient population   | Outcomes  | Institutes  | References |
|------------------|--|--|---|---|------------|
| SARS-CoV-2       | Multicenter, single arm trial  | <i>N</i> = 20 000 COVID-19 patients with severe life-threatening disease<br>Intervention group: patients receiving CP in addition to standard care ( <i>n</i> = 20,000)<br>No control group  | Overall 7 days' mortality rate was 12.96%<br>The incidence of all serious adverse events related to plasma transfusion are low  | FDA-initiated trial including multicenter /national hospitals | (142)      |
| SARS-CoV-2       | Multicenter, retrospective, non-randomized, propensity score-matched study | <i>N</i> = 5297 COVID-19 patients<br>Intervention group 1: patients receiving CP with an anti-RBD IgG titer $\geq 1:1350$ ( <i>n</i> = 321)<br>Intervention group 2: patients receiving CP with an anti-RBD IgG titer $> 1:150$ but $< 1:1350$ ( <i>n</i> = 24)<br>Intervention group 3: patients receiving CP with an anti-RBD IgG titer $< 1:150$ ( <i>n</i> = 6)<br>Control group: propensity score-matched controls receiving standard treatment ( <i>n</i> = 594) | Mortality was significantly decreased in patients who received plasma with an anti-RBD IgG titer of $\geq 1:1350$ within 72 hours of admission<br>44 hours after hospitalization is optimal for transfusing COVID-19 patients with high-titer CP in order to prevent mortality<br>0.6% of patients developed significant adverse events related to plasma transfusion, including allergic reactions | Eight Houston Methodist hospitals, USA                        | (143)      |

This table summarizes the majority of clinical trials using CP from recovered patients to treat critically ill patients infected with SARS-CoV-1 or SARS-CoV-2. As reported by several research groups, it seems that CP based therapy is generally associated with a higher discharge rate and a lower mortality risk. Also, this treatment plan is showed to be linked to improved clinical outcomes (body temperature, chest X-ray, oxygen saturation), decreased viral load, and a faster recovery. Growing evidence supports early administration of a high titer anti-COVID-19 antibodies within 72 h post-hospitalization. Analyses regarding the efficacy of CP as a standalone treatment strategy might be limited by the lack of control groups in some human trials and by the co-administration of standard care drugs (anti-inflammatory and anti-viral formulations) together with CP. Even though attention was directed toward the incidence of serious adverse events that can be related to plasma transfusion, it was FDA approved that the risk is low. ARDS, acute respiratory distress syndrome; COVID-19, coronavirus disease-2019; CP, convalescent plasma; NS, non-specified; RBD, receptor binding domain; SARS, severe acute respiratory syndrome; SARS-CoV-1, severe acute respiratory syndrome coronavirus 1; SARS-CoV-2, severe acute respiratory syndrome coronavirus 2.

protective effects, such as vasodilation and improved cardiac remodeling, by binding to MasR, thus mimicking Ang (1-7) effects with high *in vivo* stability (158, 159). Unfortunately, not all Ang (1-7) agonists have been evaluated in human subjects; thus, the safety data is lacking for some of these drugs. Importantly, FDA has granted a pharmaceutical formulation of Ang (1-7), called TXA127, an orphan drug for the treatment of several conditions, including Duchenne muscular dystrophy and pulmonary arterial hypertension (160). Several clinical trials on TXA127 were announced since 2008, some of which were terminated or withdrawn for unknown reasons. For instance, phase I/II clinical trials conducted on cancer patients showed that Ang (1-7) drug is safe, well-tolerated, with no mortality rate and low-grade adverse events such as fatigue, injection site reaction, and flu-like symptoms (161, 162). Interestingly, two double-blind, placebo-control, randomized clinical trials are currently being conducted in Brazil (NCT04633772), Israel (NCT04605887), and New York (NCT04401423) on patients with severe COVID-19 cases. The purpose of these studies is to test the safety and efficacy of TXA127 and to determine whether Ang (1-7) infusions prevent respiratory failure, acute kidney injury, and multi-organ damage due to the management of inflammation. Considering the increasing spread and number of deaths due to COVID-19, it is extremely urgent to evaluate TXA127 and other Ang (1-7) agonists as possible treatments for seriously ill patients.

In the light of the vital role of Ang (1-7) in lung protection and the promising results of anti-COVID-19 antibodies based therapy, combination treatment of Ang (1-7) agonists along

with anti-COVID-19 antibodies may be the ideal therapeutic intervention to alleviate COVID-19 severity (Figure 3).

## CONCLUSION AND LIMITATIONS

This review summarizes the treatment strategies targeting ACE2 viral receptor, either directly or indirectly, in the context of COVID-19. Combination therapy using Ang (1-7) and CP in patients infected with SARS-CoV-2 appear to be the most promising alternative. Although the clinical potential of Ang (1-7) agonists has been evidenced in numerous human trials (161, 162); however, its use is limited due to the absence of studies validating its safety and efficacy in COVID-19 patients. In addition, a stable oral Ang (1-7) compound covering a broad range of patients is still lacking (163). Importantly, prolonged exposure to other immuno-suppressor drugs such as corticosteroids might increase the occurrence of secondary infections; thus, evaluating the risk of opportunistic infections in patients treated with Ang (1-7) appear to be of great value (164, 165). Furthermore, steroids possess salt retention activities that might increase the stress over the cardiovascular system.

On the other hand, CP therapy may encounter several challenges that should be taken into consideration despite its proven benefits. One such limitation is its availability; in fact, a shortage in the number of plasma donors could be seen in situations of rapid disease spread resulting in an increased number of infected patients compared to those that have recovered. This would be especially significant and serious for the rare blood group patients. In addition, potential risks can be

directly associated with CP regimen. These risks include, among others, the transmission of harmful pathogens such as HIV, hepatitis B/C, and syphilis. Moreover, other transfusion-related events may occur following CP treatment, including allergic, anaphylactic, or hemolytic reactions, fever, and transfusion circulatory overload (166). Furthermore, transfusion can be associated with transfusion-related acute lung injury (167). Although this complication is not common; however, this possibility should not be ignored since COVID-19 patients are at high risk of developing pulmonary disease (168). Importantly, all studies on CP transfusion as a COVID-19 treatment showed that these severe adverse reactions are infrequent.

The presence of a confounding variable in most CP studies makes it difficult to prove the efficacy of CP transfusion as a stand-alone treatment because patients are mostly receiving a standard care treatment such as anti-viral and anti-inflammatory drugs along with anti-COVID-19 antibodies (128, 141). In addition, the safety and efficiency of CP in pregnant women

and pediatric patients have not been evaluated yet. Noteworthy, several ongoing studies are covering both population groups (169). Finally, since the immune-competent population contributed to the generation of new viral strains in South Africa and the United Kingdom, new adaptations of the virus raise the concern about the possibility of escaping viral neutralization by convalescent antibodies. In this context, a very recent study reported that SARS-CoV-2 has the ability to generate new mutations in its viral spike, which is typically recognized by antibodies, thus facilitating the escape from neutralization (170).

Taken together, more clinical trials are warranted to prove the safety and efficacy as well as the synergistic therapeutic effects of this combination treatment procedure.

## AUTHOR CONTRIBUTIONS

AN and KZ proposed the hypothesis and originated this work. All authors listed have made a substantial, direct and intellectual contribution to the work, and approved it for publication.

## REFERENCES

- Huang C, Wang Y, Li X, Ren L, Zhao J, Hu Y, et al. Clinical features of patients infected with 2019 novel coronavirus in Wuhan, China. *Lancet Lond Engl*. (2020) 395:497–506. doi: 10.1016/S0140-6736(20)30183-5
- Coronaviridae Study Group of the International Committee on Taxonomy of Viruses. The species severe acute respiratory syndrome-related coronavirus: classifying 2019-nCoV and naming it SARS-CoV-2. *Nat Microbiol*. (2020) 5:536–44. doi: 10.1038/s41564-020-0695-z
- Wu F, Zhao S, Yu B, Chen Y-M, Wang W, Song Z-G, et al. A new coronavirus associated with human respiratory disease in China. *Nature*. (2020) 579:265–9. doi: 10.1038/s41586-020-2008-3
- Zhu N, Zhang D, Wang W, Li X, Yang B, Song J, et al. A novel coronavirus from patients with pneumonia in China, 2019. *N Engl J Med*. (2020) 382:727–33. doi: 10.1056/NEJMoa2001017
- Zhang W, Du R-H, Li B, Zheng X-S, Yang X-L, Hu B, et al. Molecular and serological investigation of 2019-nCoV infected patients: implication of multiple shedding routes. *Emerg Microbes Infect*. (2020) 9:386–9. doi: 10.1080/22221751.2020.1729071
- van Doremalen N, Bushmaker T, Morris DH, Holbrook MG, Gamble A, Williamson BN, et al. Aerosol and surface stability of SARS-CoV-2 as compared with SARS-CoV-1. *N Engl J Med*. (2020) 382:1564–7. doi: 10.1056/NEJMc2004973
- Kolifarhood G, Aghaali M, Mozafar Saadati H, Taherpour N, Rahimi S, Izadi N, et al. Epidemiological and clinical aspects of COVID-19; a narrative review. *Arch Acad Emerg Med*. (2020) 8:e41.
- Chen N, Zhou M, Dong X, Qu J, Gong F, Han Y, et al. Epidemiological and clinical characteristics of 99 cases of 2019 novel coronavirus pneumonia in Wuhan, China: a descriptive study. *Lancet Lond Engl*. (2020) 395:507–13. doi: 10.1016/S0140-6736(20)30211-7
- Wong CK, Lam CWK, Wu AKL, Ip WK, Lee NLS, Chan IHS, et al. Plasma inflammatory cytokines and chemokines in severe acute respiratory syndrome. *Clin Exp Immunol*. (2004) 136:95–103. doi: 10.1111/j.1365-2249.2004.02415.x
- Chu KH, Tsang WK, Tang CS, Lam MF, Lai FM, To KF, et al. Acute renal impairment in coronavirus-associated severe acute respiratory syndrome. *Kidney Int*. (2005) 67:698–705. doi: 10.1111/j.1523-1755.2005.67130.x
- Li Q, Guan X, Wu P, Wang X, Zhou L, Tong Y, et al. Early transmission dynamics in Wuhan, China, of novel coronavirus-infected pneumonia. *N Engl J Med*. (2020) 382:1199–207. doi: 10.1056/NEJMoa2001316
- Porcheddu R, Serra C, Kelvin D, Kelvin N, Rubino S. Similarity in Case Fatality Rates (CFR) of COVID-19/SARS-COV-2 in Italy and China. *J Infect Dev Ctries*. (2020) 14:125–8. doi: 10.3855/jidc.12600
- Remuzzi A, Remuzzi G. COVID-19 and Italy: what next? *Lancet Lond Engl*. (2020) 395:1225–8. doi: 10.1016/S0140-6736(20)30627-9
- Lu X, Zhang L, Du H, Zhang J, Li YY, Qu J, et al. SARS-CoV-2 infection in children. *N Engl J Med*. (2020) 382:1663–5. doi: 10.1056/NEJMc2005073
- Guan W-J, Zhong N-S. Clinical characteristics of Covid-19 in China. *Reply*. *N Engl J Med*. (2020) 382:1861–2. doi: 10.1056/NEJMc2005203
- Zhou P, Yang X-L, Wang X-G, Hu B, Zhang L, Zhang W, et al. A pneumonia outbreak associated with a new coronavirus of probable bat origin. *Nature*. (2020) 579:270–3. doi: 10.1038/s41586-020-2012-7
- Letko M, Marzi A, Munster V. Functional assessment of cell entry and receptor usage for SARS-CoV-2 and other lineage B betacoronaviruses. *Nat Microbiol*. (2020) 5:562–9. doi: 10.1038/s41564-020-0688-y
- Wan Y, Shang J, Graham R, Baric RS, Li F. Receptor Recognition by the novel coronavirus from Wuhan: an analysis based on decade-long structural studies of SARS Coronavirus. *J Virol*. (2020) 94:e00127-20. doi: 10.1128/JVI.00127-20
- Yan R, Zhang Y, Li Y, Xia L, Guo Y, Zhou Q. Structural basis for the recognition of SARS-CoV-2 by full-length human ACE2. *Science*. (2020) 367:1444–8. doi: 10.1126/science.abb2762
- Matsuyama S, Nao N, Shirato K, Kawase M, Saito S, Takayama I, et al. Enhanced isolation of SARS-CoV-2 by TMPRSS2-expressing cells. *Proc Natl Acad Sci USA*. (2020) 117:7001–3. doi: 10.1073/pnas.2002589117
- Millat JK, Whittaker GR. Host cell proteases: critical determinants of coronavirus tropism and pathogenesis. *Virus Res*. (2015) 202:120–34. doi: 10.1016/j.virusres.2014.11.021
- Wang P, Liu L, Iketani S, Luo Y, Guo Y, Wang M, et al. Increased resistance of SARS-CoV-2 Variants B.1.351 and B.1.1.7 to antibody neutralization. *BioRxiv Prepr Serv Biol [Preprint]*. (2021) doi: 10.1101/2021.01.25.428137
- Santos JC, Passos GA. The high infectivity of SARS-CoV-2 B.1.1.7 is associated with increased interaction force between Spike-ACE2 caused by the viral N501Y mutation. *Bioinformatics. [Preprint]*. (2021) doi: 10.1101/2020.12.29.424708
- Walls AC, Park Y-J, Tortorici MA, Wall A, McGuire AT, Veesler D. Structure, function, and antigenicity of the SARS-CoV-2 spike glycoprotein. *Cell*. (2020) 181:281–92.e6. doi: 10.1016/j.cell.2020.02.058
- Imai Y, Kuba K, Rao S, Huan Y, Guo F, Guan B, et al. Angiotensin-converting enzyme 2 protects from severe acute lung failure. *Nature*. (2005) 436:112–6. doi: 10.1038/nature03712
- Kuba K, Imai Y, Rao S, Gao H, Guo F, Guan B, et al. A crucial role of angiotensin converting enzyme 2 (ACE2) in SARS coronavirus-induced lung injury. *Nat Med*. (2005) 11:875–9. doi: 10.1038/nm1267



27. Wang K, Gheblawi M, Oudit GY. Angiotensin converting enzyme 2: a double-edged sword. *Circulation*. (2020) 142:426–8. doi: 10.1161/CIRCULATIONAHA.120.047049
28. Imai Y, Kuba K, Penninger JM. The discovery of angiotensin-converting enzyme 2 and its role in acute lung injury in mice. *Exp Physiol*. (2008) 93:543–8. doi: 10.1113/expphysiol.2007.040048
29. Kuba K, Imai Y, Penninger JM. Angiotensin-converting enzyme 2 in lung diseases. *Curr Opin Pharmacol*. (2006) 6:271–6. doi: 10.1016/j.coph.2006.03.001
30. Tipnis SR, Hooper NM, Hyde R, Karran E, Christie G, Turner AJ. A human homolog of angiotensin-converting enzyme: cloning and functional expression as a captopril-insensitive carboxypeptidase. *J Biol Chem*. (2000) 275:33238–43. doi: 10.1074/jbc.M002615200
31. Lambert DW, Yarski M, Warner FJ, Thornhill P, Parkin ET, Smith AI, et al. Tumor necrosis factor- $\alpha$  convertase (ADAM17) mediates regulated ectodomain shedding of the severe-acute respiratory syndrome-coronavirus (SARS-CoV) receptor, angiotensin-converting enzyme-2 (ACE2). *J Biol Chem*. (2005) 280:30113–9. doi: 10.1074/jbc.M505111200
32. Turner AJ, Hooper NM. Angiotensin-converting enzyme 2. In: Barrett AJ, Rawlings ND, Woessner JF, editors. *Handbook of Proteolytic Enzymes*. Elsevier (2004). p. 349–51. doi: 10.1016/B978-0-12-079611-3.50092-6
33. Tikellis C, Thomas MC. Angiotensin-Converting Enzyme 2 (ACE2) is a key modulator of the renin angiotensin system in health and disease. *Int J Pept*. (2012) 2012:256294. doi: 10.1155/2012/256294
34. Unger T, Steckelings UM, Santos RS dos. *The Protective Arm of the Renin Angiotensin: Functional Aspects and Therapeutic Implications*. Academic Press (2015). p. 316.
35. Simões e Silva AC, Pinheiro S, Pereira R, Ferreira A, Santos R. The therapeutic potential of Angiotensin-(1-7) as a novel renin-angiotensin system mediator. *Mini-Rev Med Chem*. (2006) 6:603–609. doi: 10.2174/138955706776876203
36. Turner AJ, Tipnis SR, Guy JL, Rice G, Hooper NM. ACEH/ACE2 is a novel mammalian metallopeptidase and a homologue of angiotensin-converting enzyme insensitive to ACE inhibitors. *Can J Physiol Pharmacol*. (2002) 80:346–53. doi: 10.1139/y02-021
37. Rice GI, Thomas DA, Grant PJ, Turner AJ, Hooper NM. Evaluation of angiotensin-converting enzyme (ACE), its homologue ACE2 and neprilysin in angiotensin peptide metabolism. *Biochem J*. (2004) 383:45–51. doi: 10.1042/BJ20040634
38. Ferrario CM, Ahmad S, Nagata S, Simington SW, Varagic J, Kon N, et al. An evolving story of angiotensin-II-forming pathways in rodents and humans. *Clin Sci*. (2014) 126:461–9. doi: 10.1042/CS20130400
39. Santos RAS, Simoes e Silva AC, Maric C, Silva DMR, Machado RP, de Buhr I, et al. Angiotensin-(1-7) is an endogenous ligand for the G protein-coupled receptor Mas. *Proc Natl Acad Sci USA*. (2003) 100:8258–63. doi: 10.1073/pnas.1432869100
40. Kostenis E, Milligan G, Christopoulos A, Sanchez-Ferrer CF, Heringer-Walther S, Sexton PM, et al. G-Protein-coupled receptor mas is a physiological antagonist of the Angiotensin II Type 1 receptor. *Circulation*. (2005) 111:1806–13. doi: 10.1161/01.CIR.0000160867.23556.7D
41. Nehme A, Zibara K. Efficiency and specificity of RAAS inhibitors in cardiovascular diseases: how to achieve better end-organ protection? *Hypertens Res*. (2017) 40:903–9. doi: 10.1038/hr.2017.65
42. Wehbe Z, Hammoud S, Soudani N, Zaraket H, El-Yazbi A, Eid AH. Molecular insights into SARS COV-2 interaction with cardiovascular disease: role of RAAS and MAPK signaling. *Front Pharmacol*. (2020) 11:836. doi: 10.3389/fphar.2020.00836
43. Paul M, Poyan Mehr A, Kreutz R. Physiology of local renin-angiotensin systems. *Physiol Rev*. (2006) 86:747–803. doi: 10.1152/physrev.00036.2005
44. Magalhães GS, Rodrigues-Machado MG, Motta-Santos D, Silva AR, Caliar MV, Prata LO, et al. Angiotensin-(1-7) attenuates airway remodelling and hyperresponsiveness in a model of chronic allergic lung inflammation. *Br J Pharmacol*. (2015) 172:2330–42. doi: 10.1111/bph.13057
45. Nehme A, Cerutti C, Dhauadi N, Gustin MP, Courand P-Y, Zibara K, et al. Atlas of tissue renin-angiotensin-aldosterone system in human: a transcriptomic meta-analysis. *Sci Rep*. (2015) 5:10035. doi: 10.1038/srep10035
46. Imai Y, Kuba K, Penninger JM. Angiotensin-converting enzyme 2 in acute respiratory distress syndrome. *Cell Mol Life Sci CMLS*. (2007) 64:2006–12. doi: 10.1007/s00018-007-6228-6
47. Li Y, Zeng Z, Cao Y, Liu Y, Ping F, Liang M, et al. Angiotensin-converting enzyme 2 prevents lipopolysaccharide-induced rat acute lung injury via suppressing the ERK1/2 and NF- $\kappa$ B signaling pathways. *Sci Rep*. (2016) 6:27911. doi: 10.1038/srep27911
48. Magalhães GS, Barroso LC, Reis AC, Rodrigues-Machado MG, Gregório JF, Motta-Santos D, et al. Angiotensin-(1-7) promotes resolution of eosinophilic inflammation in an experimental model of asthma. *Front Immunol*. (2018) 9:58. doi: 10.3389/fimmu.2018.00058
49. Magalhães GS, Rodrigues-Machado MG, Motta-Santos D, Alenina N, Bader M, Santos RA, et al. Chronic allergic pulmonary inflammation is aggravated in angiotensin-(1-7) Mas receptor knockout mice. *Am J Physiol Lung Cell Mol Physiol*. (2016) 311:L1141–8. doi: 10.1152/ajplung.00029.2016
50. Specks U, Martin WJ, Rohrbach MS. Bronchoalveolar lavage fluid angiotensin-converting enzyme in interstitial lung diseases. *Am Rev Respir Dis*. (1990) 141:117–23. doi: 10.1164/ajrccm/141.1.117
51. Fourrier F, Chopin C, Wallaert B, Mazurier C, Mangalaboyi J, Durocher A. Compared evolution of plasma fibronectin and angiotensin-converting enzyme levels in septic ARDS. *Chest*. (1985) 87:191–5. doi: 10.1378/chest.87.2.191
52. Idell S, Kueppers F, Lippmann M, Rosen H, Niederman M, Fein A. Angiotensin converting enzyme in bronchoalveolar lavage in ARDS. *Chest*. (1987) 91:52–6. doi: 10.1378/chest.91.1.52
53. Chen Q, Yang Y, Huang Y, Pan C, Liu L, Qiu H. Angiotensin-(1-7) attenuates lung fibrosis by way of Mas receptor in acute lung injury. *J Surg Res*. (2013) 185:740–7. doi: 10.1016/j.jss.2013.06.052
54. Marshall RP, Gohlke P, Chambers RC, Howell DC, Bottoms SE, Unger T, et al. Angiotensin II and the fibroproliferative response to acute lung injury. *Am J Physiol Lung Cell Mol Physiol*. (2004) 286:L156–64. doi: 10.1152/ajplung.00313.2002
55. Jia HP, Look DC, Shi L, Hickey M, Pewe L, Netland J, et al. ACE2 receptor expression and severe acute respiratory syndrome coronavirus infection depend on differentiation of human airway epithelia. *J Virol*. (2005) 79:14614–21. doi: 10.1128/JVI.79.23.14614-14621.2005
56. Rivellese F, Prediletto E. ACE2 at the centre of COVID-19 from paucisymptomatic infections to severe pneumonia. *Autoimmun Rev*. (2020) 19:102536. doi: 10.1016/j.autrev.2020.102536
57. Wu Y. Compensation of ACE2 function for possible clinical management of 2019-nCoV-Induced acute lung injury. *Virol Sin*. (2020) 35:256–8. doi: 10.1007/s12250-020-00205-6
58. Hirano T, Murakami M. COVID-19: a new virus, but a familiar receptor and cytokine release syndrome. *Immunity*. (2020) 52:731–3. doi: 10.1016/j.immuni.2020.04.003
59. Wrapp D, Wang N, Corbett KS, Goldsmith JA, Hsieh C-L, Abiona O, et al. Cryo-EM structure of the 2019-nCoV spike in the prefusion conformation. *Science*. (2020) 367:1260–3. doi: 10.1126/science.abb2507
60. Rossi GP, Sanga V, Barton M. Potential harmful effects of discontinuing ACE-inhibitors and ARBs in COVID-19 patients. *eLife*. (2020) 9:e57278. doi: 10.7554/eLife.57278
61. Ortega JT, Serrano ML, Pujol FH, Rangel HR. Role of changes in SARS-CoV-2 spike protein in the interaction with the human ACE2 receptor: an *in silico* analysis. *EXCLI J*. (2020) 19:410–7. doi: 10.17179/excli2020-1167
62. Chen J, Wang R, Wang M, Wei G-W. Mutations strengthened SARS-CoV-2 infectivity. *J Mol Biol*. (2020) 432:5212–26. doi: 10.1016/j.jmb.2020.07.009
63. Korber B, Fischer WM, Gnanakaran S, Yoon H, Theiler J, Abfalterer W, et al. Tracking changes in SARS-CoV-2 spike: evidence that D614G increases infectivity of the COVID-19 virus. *Cell*. (2020) 182:812–27.e19. doi: 10.1016/j.cell.2020.06.043
64. Plante JA, Liu Y, Liu J, Xia H, Johnson BA, Lokugamage KG, et al. Spike mutation D614G alters SARS-CoV-2 fitness and neutralization susceptibility. *BioRxiv Prepr Serv Biol [Preprint]*. (2020) doi: 10.1101/2020.09.01.278689
65. Zhang L, Jackson CB, Mou H, Ojha A, Rangarajan ES, Izard T, et al. The D614G mutation in the SARS-CoV-2 spike protein reduces S1 shedding and increases infectivity. *BioRxiv Prepr Serv Biol [Preprint]*. (2020) doi: 10.1101/2020.06.12.148726

66. Tegally H, Wilkinson E, Giovanetti M, Iranzadeh A, Fonseca V, Giandhari J, et al. Emergence and rapid spread of a new severe acute respiratory syndrome-related coronavirus 2 (SARS-CoV-2) lineage with multiple spike mutations in South Africa. *Epidemiology MedRxiv [Preprint]*. (2020) doi: 10.1101/2020.12.21.20248640
67. Hoffmann M, Kleine-Weber H, Schroeder S, Krüger N, Herrler T, Erichsen S, et al. SARS-CoV-2 cell entry depends on ACE2 and TMPRSS2 and is blocked by a clinically proven protease inhibitor. *Cell*. (2020) 181:271–80.e8. doi: 10.1016/j.cell.2020.02.052
68. Gierer S, Bertram S, Kaup F, Wrensch F, Heurich A, Krämer-Kühl A, et al. The spike protein of the emerging betacoronavirus EMC uses a novel coronavirus receptor for entry, can be activated by TMPRSS2, and is targeted by neutralizing antibodies. *J Virol*. (2013) 87:5502–11. doi: 10.1128/JVI.00128-13
69. Glowacka I, Bertram S, Müller MA, Allen P, Soilleux E, Pfefferle S, et al. Evidence that TMPRSS2 activates the severe acute respiratory syndrome coronavirus spike protein for membrane fusion and reduces viral control by the humoral immune response. *J Virol*. (2011) 85:4122–34. doi: 10.1128/JVI.02232-10
70. Iwata-Yoshikawa N, Okamura T, Shimizu Y, Hasegawa H, Takeda M, Nagata N. TMPRSS2 contributes to virus spread and immunopathology in the airways of murine models after coronavirus infection. *J Virol*. (2019) 93:e01815-18. doi: 10.1128/JVI.01815-18
71. Muruato AE, Fontes-Garfias CR, Ren P, Garcia-Blanco MA, Menachery VD, Xie X, et al. A high-throughput neutralizing antibody assay for COVID-19 diagnosis and vaccine evaluation. *Nat Commun*. (2020) 11:4059. doi: 10.1038/s41467-020-17892-0
72. Li G, He X, Zhang L, Ran Q, Wang J, Xiong A, et al. Assessing ACE2 expression patterns in lung tissues in the pathogenesis of COVID-19. *J Autoimmun*. (2020) 112:102463. doi: 10.1016/j.jaut.2020.102463
73. Shi Y, Yu X, Zhao H, Wang H, Zhao R, Sheng J. Host susceptibility to severe COVID-19 and establishment of a host risk score: findings of 487 cases outside Wuhan. *Crit Care Lond Engl*. (2020) 24:108. doi: 10.1186/s13054-020-2833-7
74. Singh AK, Gupta R, Misra A. Comorbidities in COVID-19: outcomes in hypertensive cohort and controversies with renin angiotensin system blockers. *Diabetes Metab Syndr*. (2020) 14:283–7. doi: 10.1016/j.dsx.2020.03.016
75. Lipi G, Wong J, Henry BM. Hypertension in patients with coronavirus disease 2019 (COVID-19): a pooled analysis. *Pol Arch Intern Med*. (2020) 130:304–9. doi: 10.20452/pamw.15272
76. Zou X, Chen K, Zou J, Han P, Hao J, Han Z. Single-cell RNA-seq data analysis on the receptor ACE2 expression reveals the potential risk of different human organs vulnerable to 2019-nCoV infection. *Front Med*. (2020) 14:185–92. doi: 10.1007/s11684-020-0754-0
77. Sungnak W, Huang N, Bécavin C, Berg M, Queen R, Litvinukova M, et al. SARS-CoV-2 entry factors are highly expressed in nasal epithelial cells together with innate immune genes. *Nat Med*. (2020) 26:681–7. doi: 10.1038/s41591-020-0868-6
78. Cai G, Bossé Y, Xiao F, Kheradmand F, Amos CI. Tobacco smoking increases the lung gene expression of ACE2, the Receptor of SARS-CoV-2. *Am J Respir Crit Care Med*. (2020) 201:1557–9. doi: 10.1164/rccm.202003-0693LE
79. Kashyap VK, Dhasmana A, Massey A, Kotnala S, Zafar N, Jaggi M, et al. Smoking and COVID-19: adding fuel to the flame. *Int J Mol Sci*. (2020) 21:6581. doi: 10.3390/ijms21186581
80. Russo P, Bonassi S, Giacconi R, Malavolta M, Tomino C, Maggi F. COVID-19 and smoking: is nicotine the hidden link? *Eur Respir J*. (2020) 55:2001116. doi: 10.1183/13993003.01116-2020
81. Gülsen A, Yigitbas BA, Uslu B, Drömann D, Kilinc O. The effect of smoking on COVID-19 symptom severity: systematic review and meta-analysis. *Pulm Med*. (2020) 2020:7590207. doi: 10.1101/2020.08.15.20102699
82. Lawrence H, Hunter A, Murray R, Lim WS, McKeever T. Cigarette smoking and the occurrence of influenza - systematic review. *J Infect*. (2019) 79:401–6. doi: 10.1016/j.jinf.2019.08.014
83. Duffney PF, Embong AK, McGuire CC, Thatcher TH, Phipps RP, Sime PJ. Cigarette smoke increases susceptibility to infection in lung epithelial cells by upregulating caveolin-dependent endocytosis. *PLoS ONE*. (2020) 15:e0232102. doi: 10.1371/journal.pone.0232102
84. Duffney PF, McCarthy CE, Nogales A, Thatcher TH, Martinez-Sobrido L, Phipps RP, et al. Cigarette smoke dampens antiviral signaling in small airway epithelial cells by disrupting TLR3 cleavage. *Am J Physiol Lung Cell Mol Physiol*. (2018) 314:L505–13. doi: 10.1152/ajplung.00406.2017
85. Staudt MR, Salit J, Kaner RJ, Hollmann C, Crystal RG. Altered lung biology of healthy never smokers following acute inhalation of E-cigarettes. *Respir Res*. (2018) 19:78. doi: 10.1186/s12931-018-0778-z
86. Shastri MD, Shukla SD, Chong WC, Kc R, Dua K, Patel RP, et al. Smoking and COVID-19: what we know so far. *Respir Med*. (2020) 176:106237. doi: 10.1016/j.rmed.2020.106237
87. Leung JM, Yang CX, Tam A, Shaipanich T, Hackett T-L, Singhera GK, et al. ACE-2 expression in the small airway epithelia of smokers and COPD patients: implications for COVID-19. *Eur Respir J*. (2020) 55:2000688. doi: 10.1101/2020.03.18.20038455
88. Tomchaney M, Contoli M, Mayo J, Baraldo S, Shuaizhi L, Cabel CR, et al. Paradoxical effects of cigarette smoke and COPD on SARS-CoV2 infection and disease. *BioRxiv Prepr Serv Biol [Preprint]*. (2020) doi: 10.1101/2020.12.07.413252
89. Ishiyama Y, Gallagher PE, Averill DB, Tallant EA, Brosnihan KB, Ferrario CM. Upregulation of angiotensin-converting enzyme 2 after myocardial infarction by blockade of angiotensin II receptors. *Hypertension*. (2004) 43:970–6. doi: 10.1161/01.HYP.0000124667.34652.1a
90. Wang X, Ye Y, Gong H, Wu J, Yuan J, Wang S, et al. The effects of different angiotensin II type 1 receptor blockers on the regulation of the ACE-AngII-AT1 and ACE2-Ang(1-7)-Mas axes in pressure overload-induced cardiac remodeling in male mice. *J Mol Cell Cardiol*. (2016) 97:180–90. doi: 10.1016/j.yjmcc.2016.05.012
91. Ferrario CM, Jessup J, Chappell MC, Averill DB, Brosnihan KB, Tallant EA, et al. Effect of angiotensin-converting enzyme inhibition and angiotensin II receptor blockers on cardiac angiotensin-converting enzyme 2. *Circulation*. (2005) 111:2605–10. doi: 10.1161/CIRCULATIONAHA.104.510461
92. Kow CS, Zaidi STR, Hasan SS. Cardiovascular disease and use of renin-angiotensin system inhibitors in COVID-19. *Am J Cardiovasc Drugs Devices Interv*. (2020) 20:217–21. doi: 10.1007/s40256-020-00406-0
93. Burrell LM, Risvanis J, Kubota E, Dean RG, MacDonald PS, Lu S, et al. Myocardial infarction increases ACE2 expression in rat and humans. *Eur Heart J*. (2005) 26:369–75; discussion 322–324. doi: 10.1093/eurheartj/ehi114
94. Burchill LJ, Velkoska E, Dean RG, Griggs C, Patel SK, Burrell LM. Combination renin-angiotensin system blockade and angiotensin-converting enzyme 2 in experimental myocardial infarction: implications for future therapeutic directions. *Clin Sci Lond Engl*. (2012) 123:649–58. doi: 10.1042/CS20120162
95. Vaduganathan M, Vardeny O, Michel T, McMurray JJV, Pfeffer MA, Solomon SD. Renin-angiotensin-aldosterone system inhibitors in patients with Covid-19. *N Engl J Med*. (2020) 382:1653–9. doi: 10.1056/NEJMs2005760
96. Furuhashi M, Moniwa N, Mita T, Fuseya T, Ishimura S, Ohno K, et al. Urinary angiotensin-converting enzyme 2 in hypertensive patients may be increased by olmesartan, an angiotensin II receptor blocker. *Am J Hypertens*. (2015) 28:15–21. doi: 10.1093/ajh/hpu086
97. Danser AHJ, Epstein M, Battle D. Renin-angiotensin system blockers and the COVID-19 pandemic: at present there is no evidence to abandon renin-angiotensin system blockers. *Hypertension*. (2020) 75:1382–5. doi: 10.1161/HYPERTENSIONAHA.120.15082
98. Groß S, Jahn C, Cushman S, Bär C, Thum T. SARS-CoV-2 receptor ACE2-dependent implications on the cardiovascular system: from basic science to clinical implications. *J Mol Cell Cardiol*. (2020) 144:47–53. doi: 10.1016/j.yjmcc.2020.04.031
99. Zhang H, Penninger JM, Li Y, Zhong N, Slutsky AS. Angiotensin-converting enzyme 2 (ACE2) as a SARS-CoV-2 receptor: molecular mechanisms and potential therapeutic target. *Intensive Care Med*. (2020) 46:586–90. doi: 10.1007/s00134-020-05985-9
100. Abassi ZA, Skorecki K, Heyman SN, Kinaneh S, Armaly Z. Covid-19 infection and mortality: a physiologist's perspective enlightening clinical features and plausible interventional strategies. *Am J Physiol Lung Cell Mol Physiol*. (2020) 318:L1020–22. doi: 10.1152/ajplung.00097.2020

101. Lei C, Qian K, Li T, Zhang S, Fu W, Ding M, et al. Neutralization of SARS-CoV-2 spike pseudotyped virus by recombinant ACE2-Ig. *Nat Commun.* (2020) 11:2070. doi: 10.1038/s41467-020-16048-4
102. Monteil V, Kwon H, Prado P, Hagelkrüys A, Wimmer RA, Stahl M, et al. Inhibition of SARS-CoV-2 infections in engineered human tissues using clinical-grade soluble Human ACE2. *Cell.* (2020) 181:905–13.e7. doi: 10.1016/j.cell.2020.04.004
103. Dimitrov DS. The secret life of ACE2 as a receptor for the SARS Virus. *Cell.* (2003) 115:652–3. doi: 10.1016/S0092-8674(03)00976-0
104. Alhenc-Gelas F, Druke TB. Blockade of SARS-CoV-2 infection by recombinant soluble ACE2. *Kidney Int.* (2020) 97:1091–3. doi: 10.1016/j.kint.2020.04.009
105. Ciaglia E, Vecchione C, Puca AA. COVID-19 infection and circulating ACE2 levels: protective role in women and Children. *Front Pediatr.* (2020) 8:206. doi: 10.3389/fped.2020.00206
106. Liu Y, Yang Y, Zhang C, Huang F, Wang F, Yuan J, et al. Clinical and biochemical indexes from 2019-nCoV infected patients linked to viral loads and lung injury. *Sci China Life Sci.* (2020) 63:364–74. doi: 10.1007/s11427-020-1643-8
107. Mentz RJ, Bakris GL, Waeber B, McMurray JJV, Gheorghiadu M, Ruilope LM, et al. The past, present and future of renin-angiotensin aldosterone system inhibition. *Int J Cardiol.* (2013) 167:1677–87. doi: 10.1016/j.ijcard.2012.10.007
108. Saavedra JM. Angiotensin receptor blockers and COVID-19. *Pharmacol Res.* (2020) 156:104832. doi: 10.1016/j.phrs.2020.104832
109. Fedson DS. Treating the host response to emerging virus diseases: lessons learned from sepsis, pneumonia, influenza and Ebola. *Ann Transl Med.* (2016) 4:421. doi: 10.21037/atm.2016.11.03
110. Fang L, Karakiulakis G, Roth M. Are patients with hypertension and diabetes mellitus at increased risk for COVID-19 infection? *Lancet Respir Med.* (2020) 8:e21. doi: 10.1016/S2213-2600(20)30116-8
111. Jakovac H. COVID-19: is the ACE2 just a foe? *Am J Physiol-Lung Cell Mol Physiol.* (2020) 318:L1025–6. doi: 10.1152/ajplung.00119.2020
112. Jia H. Pulmonary Angiotensin-Converting Enzyme 2 (ACE2) and inflammatory lung disease. *Shock Augusta Ga.* (2016) 46:239–48. doi: 10.1097/SHK.0000000000000633
113. Wösten-van Asperen RM, Lutter R, Specht PA, Moll GN, van Woensel JB, van der Loos CM, et al. Acute respiratory distress syndrome leads to reduced ratio of ACE/ACE2 activities and is prevented by angiotensin-(1-7) or an angiotensin II receptor antagonist. *J Pathol.* (2011) 225:618–27. doi: 10.1002/path.2987
114. Tan WSD, Liao Y, Zhou S, Mei D, Wong W-SF. Targeting the renin-angiotensin system as novel therapeutic strategy for pulmonary diseases. *Curr Opin Pharmacol.* (2018) 40:9–17. doi: 10.1016/j.coph.2017.12.002
115. Feng Y, Ling Y, Bai T, Xie Y, Huang J, Li J, Xiong W, et al. COVID-19 with different severities: a multicenter study of clinical features. *Am J Respir Crit Care Med.* (2020) 201:1380–8. doi: 10.1164/rccm.202002-0445OC
116. Zhang P, Zhu L, Cai J, Lei F, Qin JJ, Xie J, et al. Association of inpatient use of angiotensin converting enzyme inhibitors and angiotensin ii receptor blockers with mortality among patients with hypertension hospitalized with COVID-19. *Circ Res.* (2020) 126:1671–81. doi: 10.1161/CIRCRESAHA.120.317134
117. Tedeschi S, Giannella M, Bartoletti M, Trapani F, Tadolini M, Borghi C, et al. Clinical impact of renin-angiotensin system inhibitors on in-hospital mortality of patients with hypertension hospitalized for COVID-19. *Clin Infect Dis.* (2020) 71:899–901. doi: 10.1093/cid/ciaa492
118. Meng J, Xiao G, Zhang J, He X, Ou M, Bi J, et al. Renin-angiotensin system inhibitors improve the clinical outcomes of COVID-19 patients with hypertension. *Emerg Microbes Infect.* (2020) 9:757–60. doi: 10.1080/22221751.2020.1746200
119. Yang G, Tan Z, Zhou L, Yang M, Peng L, Liu J, et al. Effects of ARBs and ACEIs on virus infection, inflammatory status and clinical outcomes in COVID-19 patients with hypertension: a single center retrospective study. *Hypertension.* (2020) 76:51–8. doi: 10.1161/HYPERTENSIONAHA.120.15143
120. Mehta N, Kalra A, Nowacki AS, Anjewierden S, Han Z, Bhat P, et al. Association of use of angiotensin-converting enzyme inhibitors and Angiotensin II receptor blockers with testing positive for coronavirus disease 2019 (COVID-19). *JAMA Cardiol.* (2020) 5:1020–6. doi: 10.1001/jamacardio.2020.1855
121. Li J, Wang X, Chen J, Zhang H, Deng A. Association of renin-angiotensin system inhibitors with severity or risk of death in patients with hypertension hospitalized for coronavirus disease 2019 (COVID-19) infection in Wuhan, China. *JAMA Cardiol.* (2020) 5:825–30. doi: 10.1001/jamacardio.2020.1624
122. Mancía G, Rea F, Ludergrani M, Apolone G, Corrao G. Renin–Angiotensin–aldosterone system blockers and the risk of Covid-19. *N Engl J Med.* (2020) 382:2431–40. doi: 10.1056/nejmoa2006923
123. Reynolds HR, Adhikari S, Pulgarin C, Troxel AB, Iturrate E, Johnson SB, et al. Renin–Angiotensin–aldosterone system inhibitors and risk of Covid-19. *N Engl J Med.* (2020) 382:2441–8. doi: 10.1056/nejmoa2008975
124. Kaddoura M, Albrahim M, Hijazi G, Soudani N, Audi A, Alkalamouni H, et al. COVID-19 therapeutic options under investigation. *Front Pharmacol.* (2020) 11:1196. doi: 10.3389/fphar.2020.01196
125. Mair-Jenkins J, Saavedra-Campos M, Baillie JK, Cleary P, Khaw F-M, Lim WS, et al. The effectiveness of convalescent plasma and hyperimmune immunoglobulin for the treatment of severe acute respiratory infections of viral etiology: a systematic review and exploratory meta-analysis. *J Infect Dis.* (2015) 211:80–90. doi: 10.1093/infdis/jiu396
126. Shen C, Wang Z, Zhao F, Yang Y, Li J, Yuan J, et al. Treatment of 5 Critically Ill patients with COVID-19 with convalescent plasma. *JAMA.* (2020) 323:1582–9. doi: 10.1001/jama.2020.4783
127. Ahn JY, Sohn Y, Lee SH, Cho Y, Hyun JH, Baek YJ, et al. Use of convalescent plasma therapy in two COVID-19 patients with acute respiratory distress syndrome in Korea. *J Korean Med Sci.* (2020) 35:e149. doi: 10.3346/jkms.2020.35.e149
128. Duan K, Liu B, Li C, Zhang H, Yu T, Qu J, et al. Effectiveness of convalescent plasma therapy in severe COVID-19 patients. *Proc Natl Acad Sci USA.* (2020) 117:9490–6. doi: 10.1073/pnas.2004168117
129. Ye M, Fu D, Ren Y, Wang F, Wang D, Zhang F, et al. Treatment with convalescent plasma for COVID-19 patients in Wuhan, China. *J Med Virol.* (2020) 92:1890–901. doi: 10.1002/jmv.25882
130. Zhang B, Liu S, Tan T, Huang W, Dong Y, Chen L, et al. Treatment with convalescent plasma for Critically Ill patients with severe acute respiratory syndrome Coronavirus 2 infection. *Chest.* (2020) 158:e9–e13. doi: 10.1016/j.chest.2020.03.039
131. Cheng Y, Wong R, Soo YOY, Wong WS, Lee CK, Ng MHL, et al. Use of convalescent plasma therapy in SARS patients in Hong Kong. *Eur J Clin Microbiol Infect Dis.* (2005) 24:44–6. doi: 10.1007/s10096-004-1271-9
132. Soo YOY, Cheng Y, Wong R, Hui DS, Lee CK, Tsang KK, Ng MH, et al. Retrospective comparison of convalescent plasma with continuing high-dose methylprednisolone treatment in SARS patients. *Clin Microbiol Infect.* (2004) 10:676–8. doi: 10.1111/j.1469-0691.2004.00956.x
133. Nie QH, Luo XD, Hui WL. Advances in clinical diagnosis and treatment of severe acute respiratory syndrome. *World J Gastroenterol.* (2003) 9:1139–43. doi: 10.3748/wjg.v9.i6.1139
134. Yeh KM, Chiueh TS, Siu LK, Lin JC, Chan PK, Peng MY, et al. Experience of using convalescent plasma for severe acute respiratory syndrome among healthcare workers in a Taiwan hospital. *J Antimicrob Chemother.* (2005) 56:919–22. doi: 10.1093/jac/dki346
135. Zhou X, Zhao M, Wang FS, Jiang TJ, Li YG, Nie WM, et al. Epidemiologic features, clinical diagnosis and therapy of first cluster of patients with severe acute respiratory syndrome in Beijing area. *Zhonghua yi xue za zhi.* (2003) 83:1018–22.
136. Wong VW, Dai D, Wu AK, Sung JJ. Treatment of severe acute respiratory syndrome with convalescent plasma. *Hong Kong Med J.* (2003) 9:199–201.
137. Li L, Zhang W, Hu Y, Tong X, Zheng S, Yang J, et al. Effect of convalescent plasma therapy on time to clinical improvement in patients with severe and life-threatening COVID-19: a randomized clinical trial. *JAMA.* (2020) 324:460–70. doi: 10.1001/jama.2020.10044
138. Perotti C, Baldanti F, Bruno R, Del Fante C, Seminari E, Casari S, et al. Mortality reduction in 46 severe Covid-19 patients treated with hyperimmune plasma. a proof of concept single arm multicenter trial. *Haematologica.* (2020) 105:2834–40. doi: 10.3324/haematol.2020.261784
139. Omrani AS, Zaqout A, Baiou A, Daghfal J, Elkum N, Alattar RA, et al. Convalescent plasma for the treatment of patients with severe coronavirus



- disease 2019: a preliminary report. *J Med Virol.* (2020) 93:1678–86. doi: 10.1002/jmv.26537
140. Zeng Q-L, Yu Z-J, Gou J-J, Li G-M, Ma S-H, Zhang G-F, et al. Effect of convalescent plasma therapy on viral shedding and survival in patients with coronavirus disease 2019. *J Infect Dis.* (2020) 222:38–43. doi: 10.1093/infdis/jiaa228
  141. Salazar E, Perez KK, Ashraf M, Chen J, Castillo B, Christensen PA, et al. Treatment of Coronavirus Disease 2019 (COVID-19) patients with convalescent plasma. *Am J Pathol.* (2020) 190:1680–90. doi: 10.1016/j.ajpath.2020.08.001
  142. Joyner MJ, Bruno KA, Klassen SA, Kunze KL, Johnson PW, Lesser ER, et al. Safety update. *Mayo Clin Proc.* (2020) 95:1888–97. doi: 10.1016/j.mayocp.2020.06.028
  143. Salazar E, Christensen PA, Graviss EA, Nguyen DT, Castillo B, Chen J, et al. Significantly decreased mortality in a large cohort of coronavirus disease 2019 (COVID-19) patients transfused early with convalescent plasma containing high-titer anti-severe acute respiratory syndrome Coronavirus 2 (SARS-CoV-2) spike protein IgG. *Am J Pathol.* (2021) 191:90–107. doi: 10.1016/j.ajpath.2020.10.008
  144. Recommendations for Investigational COVID-19 Convalescent Plasma/FDA.7. Available online at: <https://www.fda.gov/vaccines-blood-biologics/investigational-new-drug-ind-or-device-exemption-ide-process-cber/recommendations-investigational-covid-19-convalescent-plasma>
  145. Nehme A, Zouein FA, Zayeri ZD, Zibara K. An update on the tissue renin angiotensin system and its role in physiology and pathology. *J Cardiovasc Dev Dis.* (2019) 6:14. doi: 10.3390/jcdd6020014
  146. Santos RA. Angiotensin-(1-7). *Hypertension.* (2014) 63:1138–47. doi: 10.1161/HYPERTENSIONAHA.113.01274
  147. Shenoy V, Ferreira AJ, Qi Y, Fraga-Silva RA, Diez-Freire C, Dooies A, et al. The angiotensin-converting enzyme 2/angiogenesis-(1-7)/Mas axis confers cardiopulmonary protection against lung fibrosis and pulmonary hypertension. *Am J Respir Crit Care Med.* (2010) 182:1065–72. doi: 10.1164/rccm.200912-1840OC
  148. Rodrigues Prestes TR, Rocha NP, Miranda AS, Teixeira AL, Simoes-e-Silva AC. The anti-inflammatory potential of ACE2/Angiotensin-(1-7)/Mas receptor axis: evidence from basic and clinical research. *Curr Drug Targets.* (2017) 18:1301–13. doi: 10.2174/1389450117666160727142401
  149. Chakraborty C, Sharma AR, Sharma G, Bhattacharya M, Lee SS. SARS-CoV-2 causing pneumonia-associated respiratory disorder (COVID-19): diagnostic and proposed therapeutic options. *Eur Rev Med Pharmacol Sci.* (2020) 24:4016–26. doi: 10.26355/eurrev\_202004\_20871
  150. Gwathmey TM, Pendergrass KD, Reid SD, Rose JC, Diz DI, Chappell MC. Angiotensin-(1-7)-Angiotensin-Converting Enzyme 2 attenuates reactive oxygen species formation to Angiotensin II within the cell nucleus. *Hypertension.* (2010) 55:166–71. doi: 10.1161/HYPERTENSIONAHA.109.141622
  151. Klein N, Gembardt F, Supé S, Kaestle SM, Nickles H, Erfinanda L, et al. Angiotensin-(1-7) protects from experimental acute lung injury. *Crit Care Med.* (2013) 41:e334–43. doi: 10.1097/CCM.0b013e31828a6688
  152. Bastos AC, Magalhães GS, Gregório JF, Matos NA, Motta-Santos D, Bezerra FS, et al. Oral formulation angiotensin-(1-7) therapy attenuates pulmonary and systemic damage in mice with emphysema induced by elastase. *Immunobiology.* (2020) 225:151893. doi: 10.1016/j.imbio.2019.12.002
  153. Magalhaes GS, Rodrigues-Machado M da G, Motta-Santos D, Campagnole-Santos MJ, Santos RAS. Activation of Ang-(1-7)/Mas receptor is a possible strategy to treat coronavirus (SARS-CoV-2) infection. *Front Physiol.* (2020) 11:730. doi: 10.3389/fphys.2020.00730
  154. Carvalho MBL, Duarte FV, Faria-Silva R, Fauler B, da Mata Machado LT, de Paula RD, et al. Evidence for Mas-mediated bradykinin potentiation by the angiotensin-(1-7) nonpeptide mimic AVE 0991 in normotensive rats. *Hypertension.* (2007) 50:762–7. doi: 10.1161/HYPERTENSIONAHA.107.094987
  155. Zhang F, Liu J, Li S-F, Song J-X, Ren J-Y, Chen H. Angiotensin-(1-7): new perspectives in atherosclerosis treatment. *J Geriatr Cardiol JGC.* (2015) 12:676–82. doi: 10.11909/j.issn.1671-5411.2015.06.014
  156. Marques FD, Ferreira AJ, Sinisterra RDM, Jacoby BA, Sousa FB, Caliar MV, et al. An oral formulation of angiotensin-(1-7) produces cardioprotective effects in infarcted and isoproterenol-treated rats. *Hypertension.* (2011) 57:477–83. doi: 10.1161/HYPERTENSIONAHA.110.167346
  157. Durik M, van Veghel R, Kuipers A, Rink R, Haas Jimoh Akanbi M, Moll G, et al. The effect of the thioether-bridged, stabilized Angiotensin-(1-7) analogue cyclic ang-(1-7) on cardiac remodeling and endothelial function in rats with myocardial infarction. *Int J Hypertens.* (2012) 2012:536426. doi: 10.1155/2012/536426
  158. Saverini SQ, Beiman M, Lautner RQ, de Paula-Carvalho V, Allahdadi K, Pessoa DC, et al. Vascular relaxation, antihypertensive effect, and cardioprotection of a novel peptide agonist of the MAS receptor. *Hypertension.* (2010) 56:112–20. doi: 10.1161/HYPERTENSIONAHA.110.152942
  159. Povlsen AL, Grimm D, Wehland M, Infanger M, Krüger M. The vasoactive mas receptor in essential hypertension. *J Clin Med.* (2020) 9:267. doi: 10.3390/jcm9010267
  160. National Center for Advancing Translational Sciences. ANGIOTENSIN 1-7. Available online at: <https://drugs.ncats.io/substance/IJ3FUK8MOF> (accessed March 04, 2021).
  161. Savage PD, Lovato J, Brosnihan KB, Miller AA, Petty WJ. Phase II Trial of Angiotensin-(1-7) for the treatment of patients with metastatic sarcoma. *Sarcoma.* (2016) 2016:4592768. doi: 10.1155/2016/4592768
  162. Rodgers KE, Oliver J, diZerega GS. Phase I/II dose escalation study of angiotensin 1-7 [A(1-7)] administered before and after chemotherapy in patients with newly diagnosed breast cancer. *Cancer Chemother Pharmacol.* (2006) 57:559–68. doi: 10.1007/s00280-005-0078-4
  163. Machado-Silva A, Passos-Silva D, Santos RA, Sinisterra RD. Therapeutic uses for Angiotensin-(1-7). *Expert Opin Ther Pat.* (2016) 26:669–78. doi: 10.1080/13543776.2016.1179283
  164. van Paassen J, Vos JS, Hoekstra EM, Neumann KMI, Boot PC, Arbous SM. Corticosteroid use in COVID-19 patients: a systematic review and meta-analysis on clinical outcomes. *Crit Care Lond Engl.* (2020) 24:696. doi: 10.1186/s13054-020-03400-9
  165. Use of Angiotensin-(1-7) in COVID-19 (NCT04633772). Available online at: <https://clinicaltrials.gov/ct2/show/NCT04633772> (accessed March 04, 2021).
  166. Piyush R, Rajarshi K, Khan R, Ray S. Convalescent plasma therapy: a promising coronavirus disease 2019 treatment strategy. *Open Biol.* (2020) 10:200174. doi: 10.1098/rsob.200174
  167. Mora-Rillo M, Arsuaga M, Ramírez-Olivencia G, de la Calle F, Borobia AM, Sánchez-Seco P, et al. Acute respiratory distress syndrome after convalescent plasma use: treatment of a patient with Ebola virus disease contracted in Madrid, Spain. *Lancet Respir Med.* (2015) 3:554–62. doi: 10.1016/S2213-2600(15)00180-0
  168. Gajic O, Rana R, Winters JL, Yilmaz M, Mendez JL, Rickman OB, et al. Transfusion-related acute lung injury in the critically ill: prospective nested case-control study. *Am J Respir Crit Care Med.* (2007) 176:886–91. doi: 10.1164/rccm.200702-271OC
  169. COVID-19 Treatment Guidelines. Available online at: <https://www.covid19treatmentguidelines.nih.gov/immune-based-therapy/blood-derived-products/convalescent-plasma/> (accessed March 04, 2021).
  170. Andreano E, Piccini G, Licastro D, Casalino L, Johnson NV, Paciello I, et al. SARS-CoV-2 escape *in vitro* from a highly neutralizing COVID-19 convalescent plasma. *BioRxiv Prepr Serv Biol [Preprint].* (2020) doi: 10.1101/2020.12.28.424451

**Conflict of Interest:** The authors declare that the research was conducted in the absence of any commercial or financial relationships that could be construed as a potential conflict of interest.

Copyright © 2021 Issa, Eid, Berry, Takhviji, Khosravi, Mantash, Nehme, Hallal, Karaki, Dhayni, Faour, Kobeissy, Nehme and Zibara. This is an open-access article distributed under the terms of the Creative Commons Attribution License (CC BY). The use, distribution or reproduction in other forums is permitted, provided the original author(s) and the copyright owner(s) are credited and that the original publication in this journal is cited, in accordance with accepted academic practice. No use, distribution or reproduction is permitted which does not comply with these terms.



# Thymidine Phosphorylase Is Increased in COVID-19 Patients in an Acuity-Dependent Manner

Wei Li\* and Hong Yue

Department of Biomedical Sciences, Joan C. Edwards School of Medicine of Marshall University, Huntington, WV, United States

## OPEN ACCESS

### Edited by:

Atefeh Abedini,  
Shahid Beheshti University of Medical  
Sciences, Iran

### Reviewed by:

Tarek A. Ahmad,  
Bibliotheca Alexandrina, Egypt  
Reza Lashgari,  
Institute for Research in Fundamental  
Sciences, Iran

### \*Correspondence:

Wei Li  
liwe@marshall.edu

### Specialty section:

This article was submitted to  
Infectious Diseases - Surveillance,  
Prevention and Treatment,  
a section of the journal  
Frontiers in Medicine

**Received:** 15 January 2021

**Accepted:** 01 March 2021

**Published:** 22 March 2021

### Citation:

Li W and Yue H (2021) Thymidine  
Phosphorylase Is Increased in  
COVID-19 Patients in an  
Acuity-Dependent Manner.  
Front. Med. 8:653773.  
doi: 10.3389/fmed.2021.653773

Coronavirus disease 2019 (COVID-19), caused by the severe acute respiratory syndrome coronavirus 2 (SARS-CoV-2), is a human respiratory disease. Hitherto, there is no effective treatment has been established. Patients with cardiovascular or diabetes comorbidities are a high-risk cohort. COVID-19 is accompanied by excessive systemic thrombotic events, but the mechanism is not yet known. Recent studies have indicated that thymidine phosphorylase (TYMP) plays an important role in platelet activation, thrombosis, and TYMP expression is increased in diabetic patients. By using data provided by the MGH (Massachusetts General Hospital) Emergency Department COVID-19 Cohort with Olink Proteomics, here we show that plasma TYMP level is correlated with the COVID-19 associated thrombotic event, inflammation, and organ damage, as evidenced by the positive correlations with plasma D-dimer, CRP (C reactive protein), and LDH (lactate dehydrogenase), as well as Interferons (IFN). Plasma TYMP is also positively correlated with COVID-19 patients who had respiratory symptoms. TYMP thus could be an acuity marker for COVID-19 diagnosis. Targeting TYMP with tipiracil, a selective TYMP inhibitor, which has been approved by the Food and Drug Administration for clinical use, could be a novel effective medicine for COVID-19.

**Keywords:** COVID-19, SARS-CoV-2, thymidine phosphorylase, thrombosis, acuity, tipiracil

## BACKGROUND

COVID-19 is a respiratory illness caused by severe acute respiratory syndrome coronavirus 2 (SARS-CoV-2) (1). Large-scale reports have characterized the symptoms, comorbidities, and clinical outcomes, and patients with cardiovascular- or diabetes-associated comorbidities are at a higher risk to develop advanced COVID-19 and need admission to intensive care (ICU) (2–5). While COVID-19 vaccines are distributing around the world, the long-term efficiency is unknown. We still do not know when we are able to achieve herd immunity and control morbidity and mortality at an acceptable rate. Currently, no effective regimen for the COVID-19 has been established, and an interim WHO (World Health Organization) solidarity trial report indicated that remdesivir, hydroxychloroquine, lopinavir, and interferon regimens have little or no effect on the hospitalized COVID-19 patients (6). Patients with advanced COVID-19 often die from acute respiratory distress syndrome or multiorgan failure (7). Accumulating evidence implicates that inflammatory cytokine storm plays an important role in the COVID-19 milieu (8). About 71% of the non-surviving COVID-19 patients had disseminated intravascular coagulation (9). SARS-CoV-2 positive individuals have an increased risk of heart attack and stroke (10). These data suggest that



some types of thrombotic events happened concurrently with the COVID-19. However, the cause of COVID-19-associated thrombotic events is uncertain.

TYMP catalyzes the reversible conversion of thymidine to thymine and 2-deoxy-D-ribose-1 phosphate and plays an important role in the pyrimidine salvage pathway (11). TYMP is also known as platelet-derived endothelial cell growth factor and is highly expressed in human platelets (11, 12). Our recent study, for the first time, demonstrated that TYMP has a signaling function in platelets and plays a mechanistic role in platelet activation and thrombosis (12, 13). Inhibition of TYMP with tipiracil hydrochloride (TPI), a selective, potent, and Food and Drug Administration-approved TYMP inhibitor, dramatically inhibits thrombosis in mice without increasing the risk of bleeding (13). Several inflammatory cytokines, including TNF $\alpha$ , IL-1, IL-6, IL-8, and IFN- $\gamma$  induce TYMP expression (11, 14–16). TYMP also enhances the expression of IL-8 and CXCL10 (15, 17). All of these cytokines form the component of inflammatory cytokine storm associated with COVID-19 (8, 18, 19). TYMP expression was increased in diabetic patients (20, 21), which are a high-risk cohort to develop severe COVID-19. Based on these pre-clinical and clinical studies, we tested the hypothesis that TYMP plays an important role in the SARS-CoV-2-induced inflammation and the COVID-19 associated thrombosis.

## METHODS

We used the database provided by the MGH (Massachusetts General Hospital) emergency department COVID-19 Cohort (Filbin, Goldberg, Hachohen) with Olink Proteomics (22), which includes four 384-plex panels focused on inflammation, oncology, cardiometabolic, and neurology proteins. TYMP was only found in the cardiometabolic panel. Totally, 733 TYMP data points were extracted. The TYMP data were stratified based on the final diagnoses: COVID-19 negative or positive. Both groups were further stratified based on age, BMI (body mass index), days after hospitalization, acuity assessed based on WHO Ordinal Outcomes Score, levels of plasma D-dimer, absolute counts of nucleated cells, plasma CRP (C-reactive protein), and LDH (lactate dehydrogenase) levels, as well as fever. The data were also stratified based on the presence or absence of pre-existing disease and respiratory symptoms, including sore throat, congestion, productive or dry cough, shortness of breath or hypoxia, or chest pain. See **Supplementary Materials** for detailed information. TYMP expression was then analyzed and compared among the defined groups. The data were analyzed using the 2-tailed Student's *t*-test with GraphPad Prism (version 9.0.0) and expressed as mean  $\pm$  SD. The Pearson correlation coefficient was used for analyzing the correlation between TYMP and IFNs. A *p*  $\leq$  0.05 was considered statistically significant.

## RESULTS

In the MGH study, totally, 384 patients with acute respiratory distress, which was defined with at least one of the following symptoms: (1) tachypnea ( $\geq$ 22 breaths per minute), (2) oxygen

saturation  $\leq$ 92% on room air, (3) a requirement for supplemental oxygen, or (4) positive pressure ventilation, were enrolled in the Emergency Department from 3/24/2020 to 4/30/2020 (22). Among them, 78 patients were confirmed SARS-CoV-2 negative and 306 were positive. These 78 non-COVID-19 patients were categorized as controls. Samples collected from 358 patients (284 are COVID-19) on day 0, 202 patients (197 are COVID-19) on day 3, and 131 patients (all are COVID-19) on day 7, as well as 42 patients who died from COVID-19 within 28 days, were extracted for analyzing TYMP expression. We found plasma TYMP were significantly increased in COVID-19 patients on day 0, 3, and 7 when compared with non-COVID-19 patients (**Figure 1A**). Patients who died from COVID-19 also had a higher level of plasma TYMP compared with non-COVID-19 patients. Since we do not know when these patients died and when their plasma samples were harvested, we excluded this group from the following analysis.

By stratifying patients by acuity levels on day 0, 3, and 7, based on the WHO Ordinal Outcomes Score, we found TYMP expression showed an acuity-dependent manner on day 0 (**Figure 1B**). In comparing with non-COVID-19 patients, COVID-19 patients, even those who were discharged from the emergency department (A6) had a significantly high level of plasma TYMP (*p* = 0.0003, **Figure 1B**). Among the hospitalized patients, patients who did not need supplemental oxygen (A5) had the lowest, patients who needed oxygen support (A3/4) had the middle level, and patients who received intubation (A2) had the highest level of plasma TYMP. On day 3, patients who received intubation still have a higher plasma TYMP when compared with patients without the need of supplementary oxygen (**Supplementary Figure 1A**). The acuity-associated TYMP expression was the same on day 7 (**Supplementary Figure 1B**). These data suggest that plasma TYMP are positively correlated with the acuity of COVID-19, especially in the early phase. We thus further analyzed the correlation between TYMP and COVID-19 associated severity markers on day 0.

COVID-19 patients have reduced platelet counts and elevated plasma D-dimer (9), suggesting that an excessive thrombotic event occurred. Since TYMP plays a mechanistic role in platelet activation and thrombosis (11–13), we analyzed the correlation between plasma TYMP and D-dimer. We found that the higher the D-dimer concentration the patients had, the more plasma TYMP were detected (**Figure 2A**). These data suggest that TYMP is correlated with the COVID-19 associated thrombotic event. TYMP is also expressed in nucleated cells (23), we thus further analyzed TYMP expression based on the absolute counts of monocyte, lymphocyte, and neutrophil. As shown in **Supplementary Figures 2A–C**, TYMP expression was not associated with the count of these nucleated cells. TYMP expression was also not associated with fever in COVID-19 either positive or negative patients (**Supplementary Figure 2D**).

Among the MGH COVID-19 Cohort, TYMP expression was not associated with age and BMI in both COVID-19 positive and negative patients (**Supplementary Figures 3A–D**). Primary kidney diseases, hypertension, and pre-existing immunocompromised conditions, as well as pre-existing

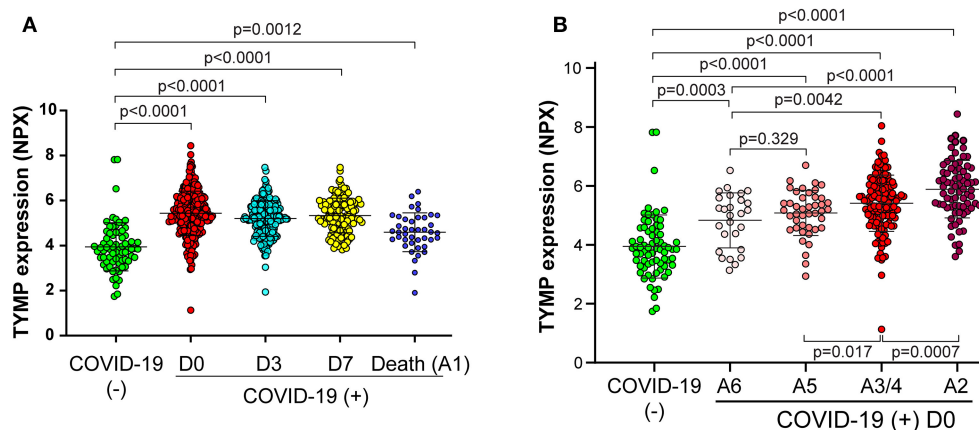


**FIGURE 1** | Plasma TYMP level is correlated with the acuity of patient with COVID-19. TYMP data were extracted from the original database provided by the MGH (Massachusetts General Hospital) Emergency Department COVID-19 Cohort with Olink Proteomics. Data were sorted based on days after hospitalization **(A)** and acuity **(B)**, and then TYMP expression was analyzed among the defined groups. Day (D) 0, 3, and 7 = enrollment plus 1 day, 3 days, and 7 days. Acuity (A) 1 = Death within 28 days, A2 = Intubated, ventilated, survived to 28 days, A3 = Non-invasive ventilation or high-flow nasal cannula, A4 = Hospitalized, supplementary O<sub>2</sub> required, A5 = Hospitalized, no supplementary O<sub>2</sub> required, and A6 = Not hospitalized.

gastrointestinal diseases and diabetes also did not affect TYMP expression in both COVID-19 positive and negative patients (**Supplementary Figures 3E–I**). These data suggest that TYMP expression is not affected by age or the presence of some diseased conditions. In non-COVID-19 patients, TYMP expression was similar between patients with and without heart or lung disease. However, TYMP expression at day 0 was lower in the COVID-19 patients who had primary heart or lung diseases (**Supplementary Figures 4A,B**). The acuity assessed using the WHO Ordinal Outcomes Score for day 0 was not different between patients with and without heart or lung disease, suggesting that the primary lung or heart disease associated low-TYMP expression in the patients with COVID-19 does not reflect the acuity. TYMP expression was similar in SARS-CoV-2 negative patients when they were divided into two groups based on whether they have respiratory symptoms or not (**Figure 2B**). However, TYMP expression was significantly increased in COVID-19 patients with respiratory symptoms when compared with COVID-19 patients without respiratory symptoms (**Figure 2B**). These data suggest that in addition to the thrombotic event, lung injury is also associated with plasma TYMP levels.

CRP is a critical component of the immune system and is a predictive factor for inflammation and future risk of cardiovascular events. We found patients who had a higher CRP level also had a higher plasma TYMP (**Figure 2C**). In the non-COVID-19 patients, even their plasma level of CRP was above 60–180 mg/L, their TYMP expression was still significantly lower than in the COVID-19 patients with CRP < 20 mg/L (**Figure 2C**,  $p = 0.025$ ). Similar to CRP, TYMP expression was also significantly correlated with the plasma level of LDH, an indicator of tissue damage (**Figure 2D**).

By searching GEO (Gene Expression Omnibus) profile using keywords “TYMP + virus,” we found that TYMP was also

upregulated in several other viral infections, including influenza virus H1N1 infected bronchia epithelial cells (**Figure 3A**) (24) and Sendai-virus infected monocytes (**Figure 3B**) (25). IFN- $\gamma$ , which was upregulated by SARS-CoV-2 infection (8, 18), significantly increased TYMP mRNA expression in the primary cultured bronchial epithelial cells (**Figure 3C**). The IFN- $\gamma$ -induced TYMP expression was inhibited by dexamethasone, an anti-inflammatory steroid (26). We thus further analyzed the correlation between plasma IFN and TYMP levels. INF was found in the inflammation panel, and only IFN- $\gamma$  and IFN- $\lambda$  were detected. As shown in **Supplementary Figure 5**, there was no correlation between plasma TYMP with either IFN- $\gamma$  or IFN- $\lambda$  in the non-COVID-19 patients on day 0. However, in the COVID-19 patients, a positive correlation was found between IFN- $\gamma$  and TYMP on day 0 (**Figure 4A**), and between IFN- $\lambda$  and TYMP on day 0, 3, and 7 (**Figures 4B,D,F**). There was no correlation between IFN- $\gamma$  and TYMP on day 3 and 7 (**Figures 4C,E**). These data indicate that TYMP does play a role in virus-mediated reactions and may be a mediator of IFN. Additional studies are needed to understand the detailed mechanism and the cellular sources that are responsible for the SARS-CoV-2 increased TYMP expression.

## DISCUSSION

COVID-19 pandemic is continually threatening our life and has globally affected more than 89 million individuals and caused more than 1.9 million global deaths by January 10, 2021 (<https://coronavirus.jhu.edu/>). Based on WHO's International Clinical Trials Registry Platform (WHO ICTRP), 3,369 COVID-19 associated clinical trials are undergoing or were finished ([https://clinicaltrials.gov/ct2/who\\_table](https://clinicaltrials.gov/ct2/who_table), January 10, 2021 data). Unfortunately, no effective therapeutic strategy has been established (6). By using the MGH Emergency Department

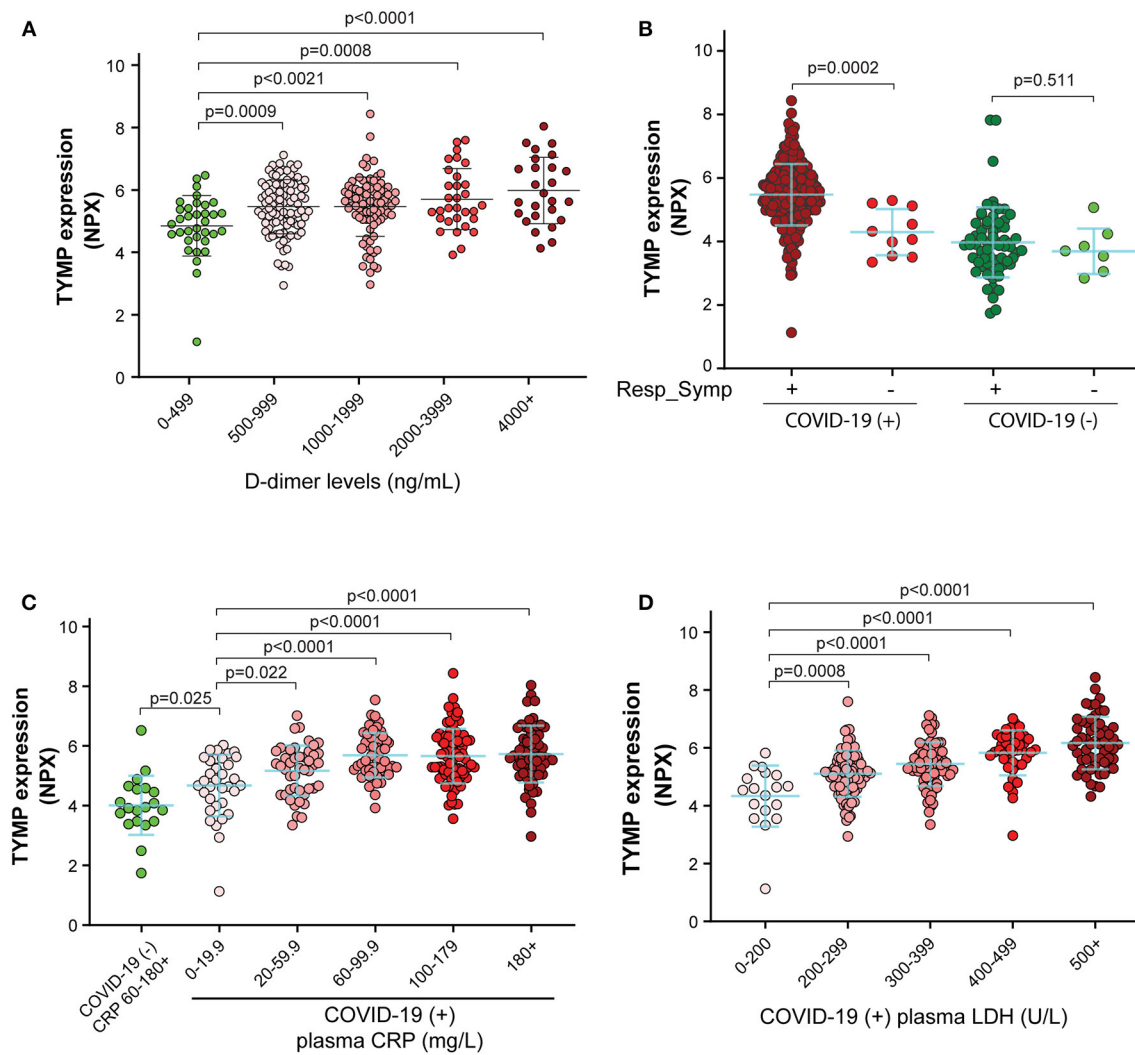


**FIGURE 2 |** Plasma TYMP level is correlated with the thrombotic event, the presence of respiratory symptoms, inflammation, and tissue damage in patients with COVID-19. TYMP data were sorted based on plasma levels of D-dimer (**A**), the presence or absence of respiratory symptoms (**B**), CRP (C-reactive protein) (**C**), and LDH (lactate dehydrogenase) (**D**), and then TYMP expression was analyzed based on the defined groups.

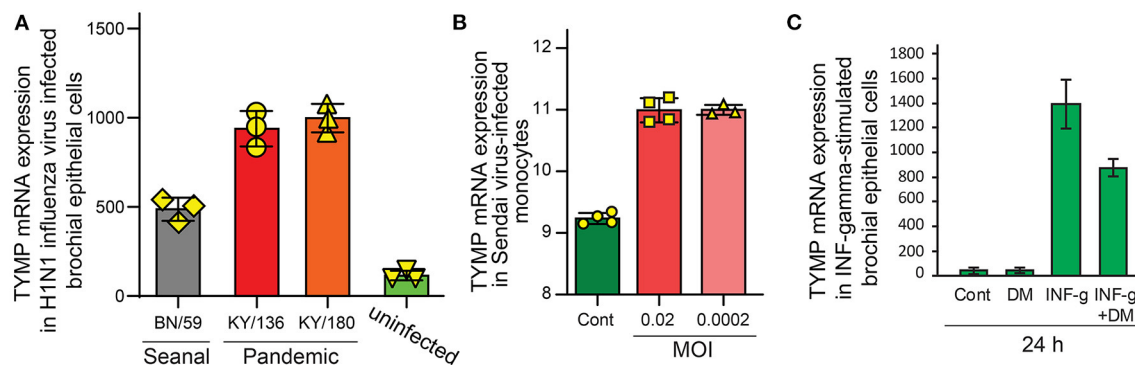


**FIGURE 3 |** TYMP expression is upregulated by virus infection and is associated with inflammation. GEO profile data were searched using keywords “TYMP + Virus.” (**A**) (GDS4855). Human bronchial epithelial cells were infected with seasonal influenza virus (BN/59), H1N1 pandemic virus isolated from two individuals (KY/136 and KY/180), and uninfected cells were used as control. (**B**) (GSE67198). U937 cells were uninfected or infected with either 0.02 or 0.0002 multiplicity of infection (MOI) Sendai virus for 24 h. (**C**) (GDS1256). Human bronchial epithelial cells were treated with IFN- $\gamma$ , dexamethasone, or their combination for 24 h.

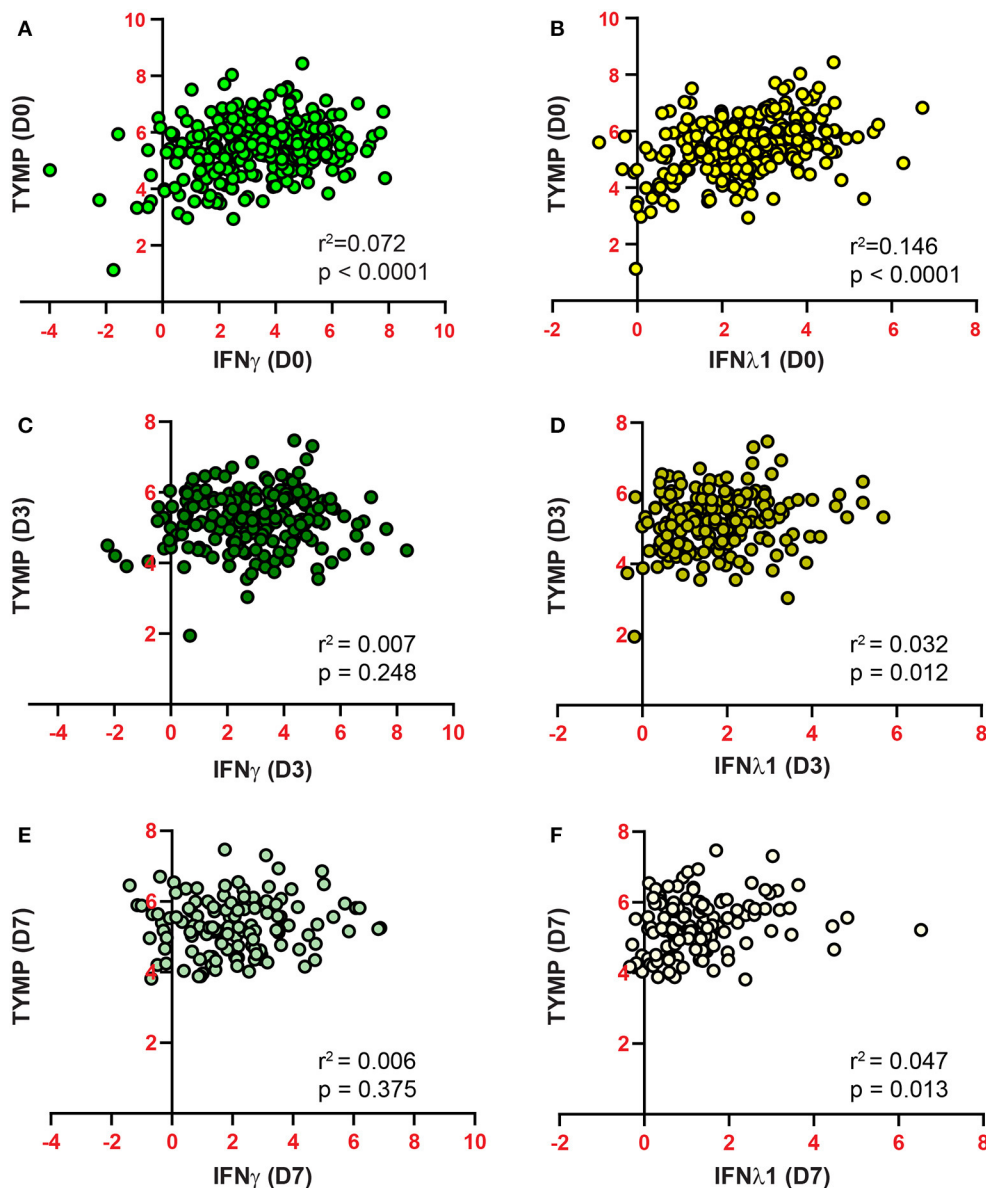


**FIGURE 4 |** Plasma TYMP levels are correlated with the expression of IFN- $\gamma$  (A,C,D) and IFN- $\lambda$  (B,D,F) in COVID-19 patients. TYMP, IFN- $\gamma$ , and IFN- $\lambda$  data on day 0 (A,B), 3 (C,D), and 7 (E,F) were extracted and the correlation between plasma TYMP levels and IFN- $\gamma$  or IFN- $\lambda$  was analyzed, respectively.

COVID-19 Cohort with Olink Proteomics database (22), this study, for the first time, unbiasedly demonstrated that plasma TYMP level is significantly increased and correlated to the acuity, inflammation, D-dimer (evidence of thrombotic events), and organ damage in the COVID-19 patients. Our findings suggest that TYMP is a more sensitive and specific marker for COVID-19 because in the COVID-19 patients with the lowest CRP ( $< 20$  mg/L), their TYMP expression was significantly higher than the non-COVID-19 patients, even they have a very high level of plasma CRP ( $> 60$ – $180$  mg/L, **Figure 2C**). This finding is in line with a platelet gene expression study in patients with COVID-19 (27), in which TYMP mRNA was 1.83-fold

increase in ICU patients, but it was only 1.45-fold increase in non-ICU patients. The absolute counts of nucleated cells are not associated with TYMP, suggesting that the change of plasma TYMP has not resulted from these cells. However, in a dual-center, two-cohort study, TYMP levels in monocytes of COVID-19 patients were increased in a range of 2.0- to 35-fold, in a monocyte-type dependent manner (**Supplementary Table 1**) (28). The CD163<sup>hi</sup> monocytes, which are M2 macrophage-skewed, had the highest TYMP expression (35-fold increase) and the HLA-DR<sup>hi</sup>CD83<sup>hi</sup> monocytes, which are M1-skewed, had the second high TYMP levels (15.5-fold increase). Interestingly, a recent study indicated that SARS-CoV-2 infects both M1 and M2



macrophages with the same permissivity, but elicits an M2-type genes-enriched response in transcriptional levels (29). These data further indicate that TYMP does participate in the systemic immune response to SARS-CoV-2 infection. However, since the numbers of classical, intermediate, and non-classical monocytes decreased in COVID-19 patients (29), the increase of TYMP in these particular monocyte populations may not account for the increased plasma TYMP. The detailed pathophysiological mechanism behind this should be further studied. Since red blood cells do not express TYMP and TYMP is not a secreted protein (11, 12), we consider that the increased plasma TYMP in COVID-19 patients was from either thrombolysis of the platelet-rich thrombi or organ damage. Both platelet and lung have high TYMP expression.

While there have been no extensive studies clarifying how SARS-CoV-2 affects bone marrow cells, several studies found that SARS-CoV-2 is detectable in the bone marrow (30, 31). Based on the study from Manne et al. (27), we speculate that SARS-CoV-2 can infect megakaryocytes and leads to the production of TYMP-overexpressing platelets. As mentioned above, our recent studies demonstrated that TYMP deficiency or inhibition significantly inhibited thrombosis in mice (12, 13). Currently, no human study has been conducted to clarify the role of TYMP on thrombosis. However, TYMP expression is high in several systemic diseases that are associated with a high risk of thrombosis. It has been reported that increased TYMP expression in human hepatocellular carcinoma correlates with a high incidence of portal vein tumor thrombosis (32). Aspirin, an anti-platelet drug, inhibits TYMP production in a monocyte cell line, THP1 (33), suggesting that aspirin may achieve its anti-thrombotic effect *via* inhibition of TYMP production in platelets. Perfusion of erythrocyte-encapsulated TYMP to mice resulted in thrombus formation in the lungs (34). All these data suggest that TYMP has a mechanistic role in platelet activation and aggregation toward thrombosis.

The rate of thrombosis and hemorrhage in COVID-19 patients is as high as 53 and 16%, respectively (35). Studies have demonstrated that microthrombi present in the lung of COVID-19 patients, and full-dose anticoagulation has been considered as a preventive treatment. Administration of antiplatelet drugs to critical COVID-19 patients has achieved some clinical benefits (35). Our recent study has demonstrated that TPI is a rapid-acting, safe antiplatelet medicine (13). As an auxiliary component of a novel anticancer drug, Lonsurf, TPI was approved by the FDA for clinical use. Lonsurf contains trifluridine and TPI. Trifluridine is a nucleoside analog and has been used as an anti-herpesvirus drug, in addition to its anti-cancer role, in which it acts as a thymidine-based nucleoside metabolic inhibitor. Since

TYMP plays an important role in platelet activation, thrombosis, and inflammation, and inhibition of TYMP with TPI significantly inhibited thrombosis in mice without causing bleeding, our study suggests that targeting TYMP with TPI could be a novel regimen for reducing COVID-19-associated thrombotic risk and inflammation. This hypothesis is supported by a recent study, in which TPI was found to bind to the uridine site and inhibited SARS-CoV-2 Nsp15 endoribonuclease function (36).

Taken together, our study, for the first time, indicates that plasma TYMP is correlated with thrombotic events, inflammation, and tissue damages in COVID-19 patients. TYMP may be a novel and sensitive acuity marker for patients with COVID-19. Targeting TYMP with TPI could be a potentially effective therapy for COVID-19.

## DATA AVAILABILITY STATEMENT

The original contributions generated in the study are included in the article/**Supplementary Material**, further inquiries can be directed to the corresponding author.

## AUTHOR CONTRIBUTIONS

HY found the MGH COVID-19 Cohort study, extracted TYMP-related data, conducted statistical analyses, literature search, and participated in writing the paper. WL acquired MGH Emergency Department COVID-19 Cohort raw data from Olink, generated figures based on HY's analyses, and wrote the paper. All authors contributed to the article and approved the submitted version.

## FUNDING

This study was supported by the Marshall University Institute Fund (to WL), the National Institutes of Health (R15HL145573 to WL), the West Virginia IDeA Network of Biomedical Research Excellence WV-INBRE (P20GM103434 to Gary Rankin), and the West Virginia Clinical and Translational Science Institute-Pop-Up COVID-19 Fund supported by the National Institute of General Medical Sciences (U54GM104942). The content is solely the responsibility of the authors and does not necessarily represent the official views of the National Institutes of Health.

## SUPPLEMENTARY MATERIAL

The Supplementary Material for this article can be found online at: <https://www.frontiersin.org/articles/10.3389/fmed.2021.653773/full#supplementary-material>

## REFERENCES

- Zhu N, Zhang D, Wang W, Li X, Yang B, Song J, et al. A novel coronavirus from patients with pneumonia in China, 2019. *N Engl J Med.* (2020) 382:727–33. doi: 10.1056/NEJMoa2001017
- Wu Z, McGoogan JM. Characteristics of and important lessons from the coronavirus disease 2019 (COVID-19) outbreak in China: summary of a report of 72314 cases from the chinese center for disease control and prevention. *JAMA.* (2020) 323:1239–42. doi: 10.1001/jama.2020.2648
- Richardson S, Hirsch JS, Narasimhan M, Crawford JM, McGinn T, Davidson KW, et al. Presenting characteristics, comorbidities, and outcomes among 5700 patients hospitalized with COVID-19 in the New York City Area. *JAMA.* (2020) 323:2052–9. doi: 10.1001/jama.2020.6775



4. Wu Q, Zhou L, Sun X, Yan Z, Hu C, Wu J, et al. Altered lipid metabolism in recovered SARS patients twelve years after infection. *Sci Rep.* (2017) 7:9110. doi: 10.1038/s41598-017-09536-z
5. Huang C, Wang Y, Li X, Ren L, Zhao J, Hu Y, et al. Clinical features of patients infected with 2019 novel coronavirus in Wuhan, China. *Lancet.* (2020) 395:497–506. doi: 10.1016/S0140-6736(20)30183-5
6. Pan H, Peto R, Henao-Restrepo AM, Preziosi MP, Sathiyamoorthy V, Abdool Karim Q, et al. Repurposed antiviral drugs for covid-19—Interim WHO solidarity trial results. *N Engl J Med.* (2020) 384:497–511. doi: 10.1056/NEJMoa2023184
7. Pedersen SF, Ho YC. SARS-CoV-2: a storm is raging. *J Clin Invest.* (2020) 130:2202–5. doi: 10.1172/JCI137647
8. Mehta P, McAuley DF, Brown M, Sanchez E, Tattersall RS, Manson JJ, et al. COVID-19: consider cytokine storm syndromes and immunosuppression. *Lancet.* (2020) 395:1033–4. doi: 10.1016/S0140-6736(20)30628-0
9. Tang N, Li D, Wang X, Sun Z. Abnormal coagulation parameters are associated with poor prognosis in patients with novel coronavirus pneumonia. *J Thromb Haemost.* (2020) 18:844–7. doi: 10.1111/jth.14768
10. Oxley TJ, Mocco J, Majidi S, Kellner CP, Shoirah H, Singh JP, et al. Large-vessel stroke as a presenting feature of covid-19 in the young. *N Engl J Med.* (2020) 382:e60. doi: 10.1056/NEJMc2009787
11. Li W, Yue H. Thymidine phosphorylase: a potential new target for treating cardiovascular disease. *Trends Cardiovasc Med.* (2018) 28:157–71. doi: 10.1016/j.tcm.2017.10.003
12. Li W, Gigante A, Perez-Perez MJ, Yue H, Hirano M, McIntyre TM, et al. Thymidine phosphorylase participates in platelet signaling and promotes thrombosis. *Circ Res.* (2014) 115:997–1006. doi: 10.1161/CIRCRESAHA.115.304591
13. Belcher A, Zulfiker AHM, Li OQ, Yue H, Gupta AS, Li W. Targeting thymidine phosphorylase with tipiracil hydrochloride attenuates thrombosis without increasing risk of bleeding in mice. *Arterioscler Thromb Vascular Biol.* (2021) 41:668–682. doi: 10.1161/ATVBAHA.120.315109
14. Waguri Y, Otsuka T, Sugimura I, Matsui N, Asai K, Moriyama A, et al. Gliostatin/platelet-derived endothelial cell growth factor as a clinical marker of rheumatoid arthritis and its regulation in fibroblast-like synoviocytes. *Br J Rheumatol.* (1997) 36:315–21. doi: 10.1093/rheumatology/36.3.315
15. Toyoda Y, Tabata S, Kishi J, Kuramoto T, Mitsuhashi A, Saijo A, et al. Thymidine phosphorylase regulates the expression of CXCL10 in rheumatoid arthritis fibroblast-like synoviocytes. *Arthritis Rheumatol.* (2014) 66:560–8. doi: 10.1002/art.38263
16. Rahmati M, Petitbarat M, Dubanchet S, Bensussan A, Chaouat G, Ledee N. Granulocyte-colony stimulating factor related pathways tested on an endometrial *ex-vivo* model. *PLoS ONE.* (2014) 9:e102286. doi: 10.1371/journal.pone.0102286
17. Nakajima Y, Gotanda T, Uchimiya H, Furukawa T, Haraguchi M, Ikeda R, et al. Inhibition of metastasis of tumor cells overexpressing thymidine phosphorylase by 2-deoxy-L-ribose. *Cancer Res.* (2004) 64:1794–801. doi: 10.1158/0008-5472.CAN-03-2597
18. Tay MZ, Poh CM, Rénia L, MacAry PA, Ng LFP. The trinity of COVID-19: immunity, inflammation and intervention. *Nat Rev Immunol.* (2020) 20:363–74. doi: 10.1038/s41577-020-0311-8
19. Xiong Y, Liu Y, Cao L, Wang D, Guo M, Jiang A, et al. Transcriptomic characteristics of bronchoalveolar lavage fluid and peripheral blood mononuclear cells in COVID-19 patients. *Emerg Microbes Infect.* (2020) 9:761–70. doi: 10.1080/22221751.2020.1747363
20. Hamed EA, Zakary MM, Abdelal RM, Abdel Moneim EM. Vasculopathy in type 2 diabetes mellitus: role of specific angiogenic modulators. *J Physiol Biochem.* (2011) 67:339–49. doi: 10.1007/s13105-011-0080-8
21. Barrachina MN, Sueiro AM, Izquierdo I, Hermida-Nogueira L, Guitian E, Casanueva FF, et al. GPVI surface expression and signalling pathway activation are increased in platelets from obese patients: elucidating potential anti-atherothrombotic targets in obesity. *Atherosclerosis.* (2019) 281:62–70. doi: 10.1016/j.atherosclerosis.2018.12.023
22. Filbin MR, Mehta A, Schneider AM, Kays KR, Guess JR, Gentili M, et al. Plasma proteomics reveals tissue-specific cell death and mediators of cell-cell interactions in severe COVID-19 patients. *bioRxiv [Preprint].* (2020). doi: 10.1101/2020.11.02.365536
23. van Kuilenburg AB, Zoetekouw L. Determination of thymidine phosphorylase activity in human blood cells and fibroblasts by a nonradiochemical assay using reversed-phase high-performance liquid chromatography. *Nucleosides Nucleotides Nucleic Acids.* (2006) 25:1261–4. doi: 10.1080/15257770600889006
24. Gerlach RL, Camp JV, Chu YK, Jonsson CB. Early host responses of seasonal and pandemic influenza A viruses in primary well-differentiated human lung epithelial cells. *PLoS ONE.* (2013) 8:e78912. doi: 10.1371/journal.pone.0078912
25. Zaritsky LA, Bedsaul JR, Zoon KC. Virus multiplicity of infection affects type I interferon subtype induction profiles and interferon-stimulated genes. *J Virol.* (2015) 89:11534–48. doi: 10.1128/JVI.01727-15
26. Pawliczak R, Logun C, Madara P, Barb J, Suffredini AF, Munson PJ, et al. Influence of IFN-gamma on gene expression in normal human bronchial epithelial cells: modulation of IFN-gamma effects by dexamethasone. *Physiol Genomics.* (2005) 23:28–45. doi: 10.1152/physiolgenomics.00011.2005
27. Manne BK, Denorme F, Middleton EA, Portier I, Rowley JW, Stubben C, et al. Platelet gene expression and function in patients with COVID-19. *Blood.* (2020) 136:1317–29. doi: 10.1182/blood.2020007214
28. Schulte-Schrepping J, Reusch N, Paclik D, Baßler K, Schlickeiser S, Zhang B, et al. Severe COVID-19 is marked by a dysregulated myeloid cell compartment. *Cell.* (2020) 182:1419–40.e1423. doi: 10.1016/j.cell.2020.08.001
29. Boumaza A, Gay L, Mezouar S, Bestion E, Diallo AB, Michel M, et al. Monocytes and macrophages, targets of SARS-CoV-2: the clue for Covid-19 immunoparalysis. *J Infect Dis.* (2021) jia044. doi: 10.1093/infdis/jia044
30. Issa N, Lacassin F, Camou F. First case of persistent pancytopenia associated with SARS-CoV-2 bone marrow infiltration in an immunocompromised patient. *Ann Oncol.* (2020) 31:1418–9. doi: 10.1016/j.annonc.2020.06.016
31. Deinhardt-Emmer S, Wittschieder D, Sanft J, Kleemann S, Elschner S, Haupt KE, et al. Early postmortem mapping of SARS-CoV-2 RNA in patients with COVID-19 and correlation to tissue damage. *bioRxiv [Preprint].* (2020). doi: 10.1101/2020.07.01.182550
32. Guo L, Kuroda N, Toi M, Miyazaki E, Hayashi Y, Enzan H, et al. Increased expression of platelet-derived endothelial cell growth factor in human hepatocellular carcinomas correlated with high Edmondson grades and portal vein tumor thrombosis. *Oncol Rep.* (2001) 8:871–6. doi: 10.3892/or.8.4.871
33. Zhu GH, Schwartz EL. Expression of the angiogenic factor thymidine phosphorylase in THP-1 monocytes: induction by autocrine tumor necrosis factor-alpha and inhibition by aspirin. *Mol Pharmacol.* (2003) 64:1251–8. doi: 10.1124/mol.64.5.1251
34. Levene M, Coleman DG, Kilpatrick HC, Fairbanks LD, Gangadharan B, Gasson C, et al. Preclinical toxicity evaluation of erythrocyte-encapsulated thymidine phosphorylase in BALB/c mice and Beagle dogs: an enzyme replacement therapy for mitochondrial neurogastrointestinal encephalomyopathy. *Toxicol Sci.* (2012) 131:311–24. doi: 10.1093/toxsci/kfs278
35. Bickdeli B, Madhavan MV, Jimenez D, Chuich T, Dreyfus I, Driggin E, et al. COVID-19 and thrombotic or thromboembolic disease: implications for prevention, antithrombotic therapy, and follow-up. *J Am Coll Cardiol.* (2020) 75:2950–73. doi: 10.1016/j.jacc.2020.04.031
36. Kim Y, Wower J, Maltseva N, Chang C, Jedrzejczak R, Wilamowski M, et al. Tipiracil binds to uridine site and inhibits Nsp15 endoribonuclease NendoU from SARS-CoV-2. *bioRxiv [Preprint].* (2020). doi: 10.1101/2020.06.26.173872

**Conflict of Interest:** The authors declare that the research was conducted in the absence of any commercial or financial relationships that could be construed as a potential conflict of interest.

Copyright © 2021 Li and Yue. This is an open-access article distributed under the terms of the Creative Commons Attribution License (CC BY). The use, distribution or reproduction in other forums is permitted, provided the original author(s) and the copyright owner(s) are credited and that the original publication in this journal is cited, in accordance with accepted academic practice. No use, distribution or reproduction is permitted which does not comply with these terms.



# Neuropsychiatric Symptoms of COVID-19 Explained by SARS-CoV-2 Proteins' Mimicry of Human Protein Interactions

Hale Yapici-Eser<sup>1,2\*</sup>, Yunus Emre Koroglu<sup>2,3</sup>, Ozgur Oztop-Cakmak<sup>2,4</sup>, Ozlem Keskin<sup>2,5</sup>, Attila Gursoy<sup>2,6\*</sup> and Yasemin Gursoy-Ozdemir<sup>2,4</sup>

<sup>1</sup> Department of Psychiatry, School of Medicine, Koç University, Istanbul, Turkey, <sup>2</sup> Research Center for Translational Medicine, Koç University, Istanbul, Turkey, <sup>3</sup> Graduate School of Sciences and Engineering, College of Engineering, Koç University, Istanbul, Turkey, <sup>4</sup> Department of Neurology, School of Medicine, Koç University, Istanbul, Turkey, <sup>5</sup> College of Engineering, Chemical and Biological Engineering, Koç University, Istanbul, Turkey, <sup>6</sup> Department of Computer Science and Engineering, College of Engineering, Koç University, Istanbul, Turkey

## OPEN ACCESS

### Edited by:

Reza Lashgari,  
Brain Engineering Research Center,  
Institute for Research in Fundamental  
Sciences, Iran

### Reviewed by:

Çiçek Hocaoglu,  
Recep Tayyip Erdogan University,  
Turkey  
Arash Mowla,  
Shiraz University of Medical Sciences,  
Iran

### \*Correspondence:

Hale Yapici-Eser  
hyapici@ku.edu.tr  
Attila Gursoy  
agursoy@ku.edu.tr

### Specialty section:

This article was submitted to  
Health,  
a section of the journal  
Frontiers in Human Neuroscience

**Received:** 20 January 2021

**Accepted:** 23 February 2021

**Published:** 23 March 2021

### Citation:

Yapici-Eser H, Koroglu YE,  
Oztop-Cakmak O, Keskin O,  
Gursoy A and Gursoy-Ozdemir Y  
(2021) Neuropsychiatric Symptoms  
of COVID-19 Explained by  
SARS-CoV-2 Proteins' Mimicry  
of Human Protein Interactions.  
*Front. Hum. Neurosci.* 15:656313.  
doi: 10.3389/fnhum.2021.656313

The first clinical symptoms focused on the presentation of coronavirus disease 2019 (COVID-19) have been respiratory failure, however, accumulating evidence also points to its presentation with neuropsychiatric symptoms, the exact mechanisms of which are not well known. By using a computational methodology, we aimed to explain the molecular paths of COVID-19 associated neuropsychiatric symptoms, based on the mimicry of the human protein interactions with SARS-CoV-2 proteins.

**Methods:** Available 11 of the 29 SARS-CoV-2 proteins' structures have been extracted from Protein Data Bank. HMI-PRED (Host-Microbe Interaction PREDiction), a recently developed web server for structural PREDiction of protein-protein interactions (PPIs) between host and any microbial species, was used to find the "interface mimicry" through which the microbial proteins hijack host binding surfaces. Classification of the found interactions was conducted using the PANTHER Classification System.

**Results:** Predicted Human-SARS-CoV-2 protein interactions have been extensively compared with the literature. Based on the analysis of the molecular functions, cellular localizations and pathways related to human proteins, SARS-CoV-2 proteins are found to possibly interact with human proteins linked to synaptic vesicle trafficking, endocytosis, axonal transport, neurotransmission, growth factors, mitochondrial and blood-brain barrier elements, in addition to its peripheral interactions with proteins linked to thrombosis, inflammation and metabolic control.

**Conclusion:** SARS-CoV-2-human protein interactions may lead to the development of delirium, psychosis, seizures, encephalitis, stroke, sensory impairments, peripheral nerve diseases, and autoimmune disorders. Our findings are also supported by the previous in vivo and in vitro studies from other viruses. Further in vivo and in vitro studies using the proteins that are pointed here, could pave new targets both for avoiding and reversing neuropsychiatric presentations.

**Keywords:** COVID-19, SARS-CoV-2, neuropsychiatric, delirium, mimicry, autoimmune

## INTRODUCTION

First identified in December 2019, coronavirus disease 2019 (COVID-19) has been announced as a pandemic and as of August 26th, 2020, more than 23 million confirmed cases, and more than 815,000 confirmed deaths around 216 countries have been announced<sup>1</sup>.

Accumulating evidence points to its presentation with neuropsychiatric symptoms. The patients may present with delirium due to unknown etiology (Alkeridy et al., 2020; Beach et al., 2020; Hosseini et al., 2020). A retrospective analysis of 214 patients diagnosed with COVID-19, revealed that 36.4% of patients experience a neurological symptom (Mao et al., 2020). In an analysis of 58 patients admitted to intensive care unit, agitation (69%) and cranial MRI lesions as either mini-strokes or decreased cerebral blood flow in 8 patients were reported (Helms et al., 2020). Higher incidence of embolism (Poissy et al., 2020) and risk for coagulation (Xiong et al., 2020), ischemic and hemorrhagic stroke (Beyrouiti et al., 2020; Ellul et al., 2020; Gonzalez-Pinto et al., 2020; Paterson et al., 2020), confusion, encephalopathy, and seizures (Hosseini et al., 2020; Karimi et al., 2020), ataxia, headache, dizziness, and sensory impairment (Herman et al., 2020; Mao et al., 2020), cranial neuropathies (Dinkin et al., 2020), decreased smell function (Moein et al., 2020) and anosmia (Boscolo-Rizzo et al., 2020; Hopkins et al., 2020; Lechien et al., 2020; Pallanti, 2020), decreased taste dysfunction (Boscolo-Rizzo et al., 2020) and encephalitis (McAbee et al., 2020), and parainfectious peripheral nerve-related effects as Guillain Barre (Ottaviani et al., 2020; Padroni et al., 2020; Paterson et al., 2020; Sedaghat and Karimi, 2020; Toscano et al., 2020; Zhao et al., 2020), and Miller Fisher syndromes (Gutierrez-Ortiz et al., 2020) have also been reported as individual cases. Also presentation with stroke in 3 patients, resembling antiphospholipid antibody syndrome, showed an increased risk for neural autoimmunity (Zhang et al., 2020).

In a recent follow-up study of 125 patients in the United Kingdom, 57 ischaemic strokes, 9 intracerebral hemorrhages, 1 central nervous system (CNS) vasculitis, 39 altered mental status, 9 unspecified encephalopathies, 7 encephalitis, 21 new psychiatric diagnoses with altered mental state change, 10 new-onset psychosis, 6 neurocognitive (dementia-like) syndrome, and 4 affective disorder were reported (Varatharaj et al., 2020). A report of 43 patients followed due to COVID-19 diagnosis also replicated the high emergence of delirium, psychosis, and encephalitis (Paterson et al., 2020). Previous coronavirus infections also point to increased risk of depression, anxiety, and dysexecutive syndrome in the follow up of infected patients (Rogers et al., 2020; Varatharaj et al., 2020).

The observed neurological presentations could be a direct result of the SARS-CoV-2 virus or secondary to the hypoxic and inflammatory or embolic process triggered by SARS-CoV-2. Viruses have compact and small genomes, therefore they utilize the host cells' machinery to establish critical functions by hi-jacking their host cellular mechanisms. They evolved to target and intervene host molecular mechanisms with their

limited number of proteins. While doing this, viruses may mimic host protein interaction motifs and host proteins' interaction pathways and hijack host cell's proteins for their own needs while causing a loss or gain of function in host proteins (Elde and Malik, 2009; Halehalli and Nagarajaram, 2015; Guven-Maiorov et al., 2016). They target to alter signaling pathways to change the fate of the cells, activate inflammation-related pathways, and alter the host cell's immune responses.

Some viruses as coronavirus may demonstrate a neurotrophic activity and they may infect the nervous tissue by a hematological route through various mechanisms such as infecting the epithelial cells and lymphocytes that can migrate to the brain, or a neural route as infection of olfactory neurons and retrograde transport, anterograde transport through axon bundles, transsynaptic passage and passing through the meningeal, blood brain barrier and blood-cerebrospinal fluid barrier (Ludlow et al., 2016; Desforges et al., 2019).

SARS-CoV virus, which affected several countries in 2003, was isolated from the postmortem brain of SARS-CoV patients (Ding et al., 2004; Xu et al., 2005) and was shown to enter the brain and infect multiple brain areas through olfactory nerves including the thalamus, cerebrum, and brainstem in a mice model (Netland et al., 2008). SARS-CoV proteins were reported to interact with claudin, myelin basic protein, and mitochondria in humans (Vojdani and Kharrazian, 2020). Human Coronavirus (HCoV) OC43 was also shown in the brain tissue of an immunocompromised infant who experienced encephalitis (Morfopoulou et al., 2016). HCoV RNA was previously detected in both gray matter and white matter of the postmortem brain tissue or cerebrospinal fluid of Multiple Sclerosis patients and HCoV had the ability to infect glial cells like astrocytes and microglia (Arbour et al., 2000) and caused necrosis of the neurons (Xu et al., 2005). Mice infected with HCoV-OC43 containing the Y241H mutation in the spike glycoprotein exhibited hind-limb paralysis by leading to glutamate excitotoxicity (Brison et al., 2011, 2014).

For COVID-19, only one study so far investigated cerebrospinal fluid of SARS-CoV-2 positive patients presenting with stroke and subarachnoid hemorrhage and the result was negative (Al Saiegh et al., 2020). Most researchers focus on angiotensin converting enzyme 2 (ACE-2) receptor binding for the access of the SARS-CoV-2 to CNS (Calcagno et al., 2020), however, considering the large profile of neurological symptoms associated and different neurobiological pathways, and inconsistent findings of cerebrospinal fluid (CSF) positivity, it is necessary to search other candidate pathways for the coronavirus association with CNS.

Based on the clinical observations of neuropsychiatric manifestations of COVID-19 and previous knowledge on other coronavirus types' neurotrophic effects, understanding virus-host interactions is critical to show the path of the virus to invade host cells and end up with CNS dysfunction. We hypothesized that mimicry of human protein interactions by SARS-CoV-2 proteins may help to understand the neurobiological pathways that underlie the neuropsychiatric manifestations of COVID-19. To do so, in this study, we first listed the available SARS-CoV-2 protein structures. Secondly, we utilized HMI-PRED tool

<sup>1</sup><https://www.who.int/emergencies/diseases/novel-coronavirus-2019>



to detect mimicry of human protein interactions by SARS-CoV-2 proteins, and lastly we classified these interactions for the molecular paths of COVID-19 associated neuropsychiatric symptoms. Our purpose was also to generate a list of protein targets that can guide researchers for further studies in *in vivo* and *in vitro* research.

## METHODS

This study used a four step approach. At the first step, all known structures of SARS-CoV-2 proteins by May 2020, have been extracted from Protein Data Bank (PDB). The list of proteins and their known functions are listed in below 'SARS-CoV-2 proteins' section. Secondly, HMI\_Pred is used to find the possible interactions between SARS-CoV-2 and human proteins based on binding site mimicry. This algorithm requires the structures of SARS-CoV-2 and human proteins (**Figure 1**). Detailed explanation of HMI-PRED tool is given in 'HMI\_PRED Algorithm' section. Thirdly, the list of human proteins predicted to interact with SARS-CoV-2 was loaded to PANTHER Classification System version 15.0 released on 2020-02-14<sup>2</sup> (Mi et al., 2019), which is a comprehensive classification system of the whole genes and proteins, where data is presented for locations, pathways, and reactome, in addition to a functional classification list (Section 'Classification of the found interactions'). PANTHER was developed in 2003 and then continuously updated for the needs of researchers. Fourth, the list of involved proteins in each category has been investigated and additional proteins that could take part in these pathways and that could be responsible for the neuropsychiatric representations of SARS-CoV-2 have been added by the researchers, based on the lists presented by the PANTHER analysis, authors' knowledge and literature search for the direct and indirect impact on the CNS, to generate the hypothesis. As most of the molecules are shared between different neurotransmitters' pathways, we grouped these proteins into synapse and neurotransmission related molecules, as well as pathways for growth factors, mitochondria, coagulation and hemostasis, blood-brain barrier elements and metabolic pathways.

## SARS-CoV-2 Proteins

First, the SARS-CoV-2 proteome has been investigated for finding their structures. Its proteome has a total of 29 proteins consisting of 16 nonstructural (NSP), 4 structural proteins (SP), 9 open reading frames (ORF) (Gordon et al., 2020). Four structural proteins are spike (S), membrane (M), envelope (E), and nucleocapsid (N) proteins. Spike (S) is a glycoprotein that forms homotrimers protruding from the virus capsid surface (Walls et al., 2020). It is responsible for the recognition and binding of the virus to the host cell ACE-2 receptor. It also mediates the entry into the host cell. The envelope (E) protein of SARS-CoV-2 oligomerizes to create an ion channel (Verdia-Baguena et al., 2012). It is thought to have several roles in viral pathogenesis including viral assembly (Lim and Liu, 2001), and virion release (Ruch and Machamer, 2012).

M is an integral membrane glycoprotein, it is one of the main components of the envelope mainly functioning in viral assembly (Neuman et al., 2011). This protein interacts with the N protein to encapsulate the RNA genome (Siu et al., 2008). The nucleocapsid (N) is a phosphoprotein that takes part in stability (Grunewald et al., 2018).

Non-structural protein (NSP) genes constitute almost 60% of the viral genome and are translated into a large overlapping polyprotein 1a (NSP1-NSP11) and 1b (NSP12-NSP16). These proteins are essential for viral replication and translation. NSPs constitute of polymerases, helicases, exonucleases, and papain-like and chymotrypsin-like proteases. Nonstructural protein 1 (NSP1) might be a potent inhibitor of host gene expression (Yoshimoto, 2020). In SARS-CoV, it inactivates translation by binding to the 40S ribosome of the host cell, leading to host mRNA degradation selectively (Huang et al., 2011). In SARS-CoV, NSP2 interacts with two host proteins: prohibitin 1 and prohibitin 2 (PHB1 and PHB2) (Cornillez-Ty et al., 2009). Prohibitins take part in cell cycle progression, migration, differentiation, apoptosis, and mitochondrial biogenesis. Therefore, NSP2 might be important to alter the host cell environment. NSP3 is the papain-like proteinase which includes ssRNA binding, ADPr binding, G-quadruplex binding, protease (papain-like protease), and NSP4 binding, and transmembrane domains. NSP4 might have a membrane arrangement function in SARS-CoV and is essential for viral replication. NSP6 was shown to induce membrane vesicles. Nsp3-Nsp4-Nsp6 form a complex involved in viral replication (Angelini et al., 2013). NSP5 is the main protease (3C-like). It cleaves 11 distinct sites to yield mature and intermediate nonstructural proteins (NSPs) in MERS (Tomar et al., 2015). The Nsp7-Nsp8 complex is part of the RNA polymerase. This NSP7-NSP8 complex then binds to NSP12 which is the RNA-dependent RNA polymerase (Gordon et al., 2020). NSP8 protein alone may also complex with NSP12, forming the RNA polymerase complex. NSP9 has an ssRNA binding domain and might function in viral replication (Egloff et al., 2004). NSP10 interacts with NSP14 for its stimulation and NSP16 which are methyltransferases, in SARS-CoV (Ma et al., 2015; Wang et al., 2015). NSP13 is a helicase that unwinds duplex RNA, it also acts as a triphosphatase. NSP12 binds to NSP13 increasing its helicase activity (Jia et al., 2019). NSP14 has an exoribonuclease activity and N7-methyltransferase activity (Ivanov et al., 2004). NSP15 of SARS-CoV was shown as an endoribonuclease cleaving RNA at uridylates (Bhardwaj et al., 2006). It can specifically target and degrade the viral polyuridine sequences to hide the virus from the host immune system (Hackbart et al., 2020). NSP16 is a methyltransferase also acting in mRNA translation, and preventing the viral RNA from being recognized by host immunity. SARS-CoV-2 also comprises nine viral accessory proteins that form complexes with the structural proteins. SARS-CoV's ORF3a protein is an ion channel protein involved in NLRP3 inflammasome activation. ORF6 is believed to be involved in virus-induced apoptosis. It interacts with NSP8. SARS-CoV ORF7a is an accessory protein that is transmembrane (Kumar et al., 2007). Other accessory proteins do not have assigned functions yet.

<sup>2</sup><http://www.pantherdb.org/>

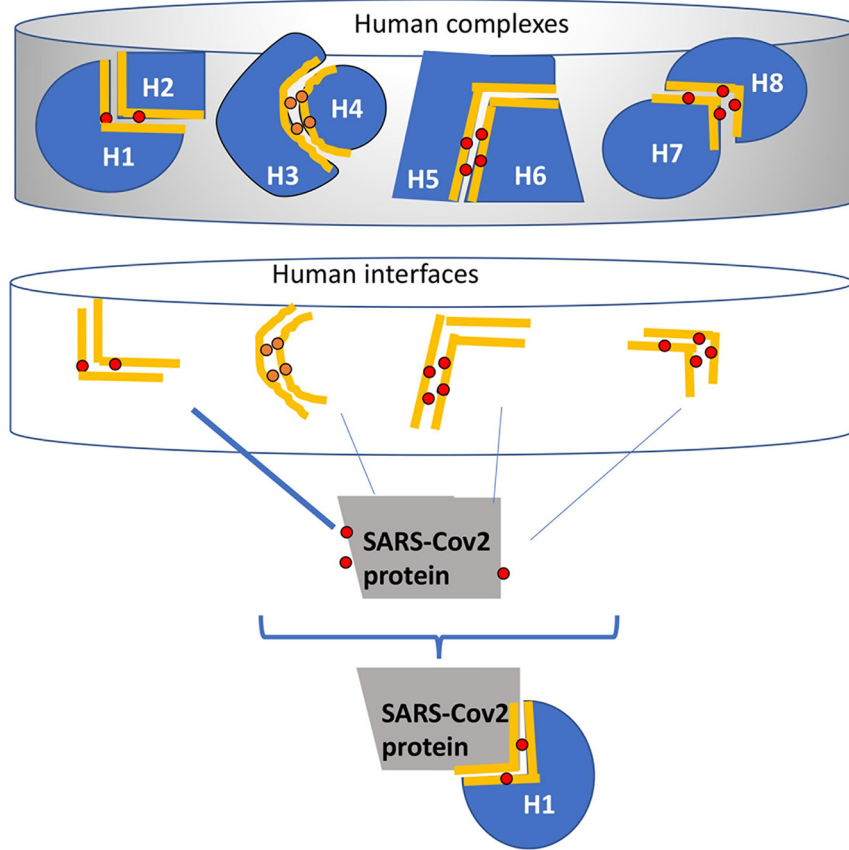


**FIGURE 1** | A schematic example of the HMI-Pred (human-virus protein interaction prediction) method. The initial set (Upper part) is all available structures of human protein-protein complexes extracted from Protein Data Bank. Interfaces that correspond to the binding sites on these complexes are extracted and form the template dataset (middle part). The red dots are the critical residues (hotspots) on these interfaces found by HotPoint (Tuncbag et al., 2010; Cukuroglu et al., 2012). The gray protein is the SARS-CoV-2 structure. In this example, the surface of the SARS protein has similar regions to the one side of the human interfaces (i.e., H2 side of the H1-H2 interface). The HMI-Pred algorithm assumes that since H1 forms a complex with H2 and SARS is similar to H2, SARS protein can complement and interact with H1. The same hotspots are found at the same location as the new complex formed between the SARS-CoV-2 and human proteins.

## HMI\_PRED Algorithm

Host-Microbe Interaction PREDiction (HMI-PRED) (Güven-Maiorov et al., 2020) is a recently developed web server for structural PREDiction of protein-protein interactions (PPIs) between host and any microbial species, including bacteria, viruses, fungi, and protozoa. HMI-PRED is a modified version of our PRISM server (Tuncbag et al., 2011; Baspinar et al., 2014). HMI relies on “interface mimicry” through which the microbial proteins hijack host binding surfaces. Interface mimicry is defined as the structural similarity of the protein-protein binding sites and conservation of at least one hotspot residue (critical residues for interaction, if mutated the interaction is disrupted). Given the structure of a microbial protein of interest, HMI-PRED will provide the list of host-microbe interactions together with structural models of these potential host-microbe interactions (HMI). HMI\_PRED is available at <https://interactome.ku.edu.tr/hmi/>. **Figure 1** describes how HMI-PRED works. In the upper panel, there are the human protein-protein complexes derived from known PDB (Berman et al., 2000). This example figure displays only four complexes,

in the HMI-Pred total number of human complexes (as of 2019) is around 53,000. Then, interface regions between two human proteins are extracted in these complexes (middle panel). The final template interface set includes 17351 structurally non-redundant interfaces. The user input is a (or a set of) microbial protein structure(s). HMI-Pred structurally compares the surface of the microbial proteins to the 17351 human interfaces. HMI-Pred uses two thresholds: TMscore (Zhang and Skolnick, 2005) (for interface mimicry, taken as 0.25 in HMI-Pred, however, mostly interactions with a score of 0.4 or above are considered in our study) and Rosetta  $I_{sc}^3$  (representing the interface binding energy, taken as -5 or better in HMI-Pred).

In this study, the host is the human and the microbe is the SARS-CoV-2. 11 of the 29 SARS-CoV-2 proteins have structures available, the list of SARS-CoV-2 proteins, their functions, and the PDB IDs for available structures are given in **Supplementary Table 1**.

<sup>3</sup><http://www.rosettacommons.org>



## Classification of the Found Interactions

All human proteins from HMI-Pred predictions (SARS-CoV-2 protein- human protein interactions) have been uploaded to panterdb, and a functional classification for homo sapiens has been generated. Two bar graphics have been produced for the molecular function and secondly, cellular components of the proteins by selecting PANTHER-GO-Slim ontology. In addition, the pathways associated with the proteins have been determined by selecting PANTHER-Pathway ontology. Pathways represented more than expected has been analyzed using PANTHER statistical overrepresentation in the Homo Sapiens all genes database with Fisher's exact test with Bonferroni correction for multiple testing.

## RESULTS

The full list of human proteins interacting with different protein structures of the SARS-CoV-2 is given in **Supplementary Table 2**. Of the 2256 genes that hit 1874 molecular functions, 33.1% showed a binding molecular activity, 30.1% was related to catalytic activity, whereas 2.8% was related to a transporter activity, based on the PANTHER classification (**Figure 2A**). When the cellular components of the human interactome with the SARS-CoV-2 proteins are analyzed, around 32 of the proteins were localized in the synapse, in addition to those localized to cell junction, cell part, and membranes of the cells (**Figure 2B**). When the pathways associated with the human proteins interacting with different protein structures of the SARS-CoV-2 are analyzed, 140 pathways were listed as given in **Supplementary Table 3**. Among these pathways, 33 pathways were found to be statistically overrepresented than expected in the SARS-CoV-2 proteins' mimicry list of human protein interactions (**Supplementary Table 4**).

When the molecular functions, cellular localizations, and pathways related to human proteins are analyzed, it was found that SARS-CoV-2 may affect the brain both by a central effect and by indirect vascular and inflammatory effects.

### SARS-CoV-2 Mimics Synaptic Vesicle Priming, Fusion, Docking, and Endocytosis Related Proteins

The results are presented in **Figures 3, 4** and **Supplementary, Table 5**. Among these molecules, AP-2, synaptojanin family, dynamins, and calcineurin related proteins mainly take part in endocytosis, whereas SNAP-25, SNAP-29, syntaxin, and VAMP2 take part in vesicle trafficking (Turner et al., 1999). AP-2 interactions may specifically be mimicked by nucleocapsid, spike, and NSP7 of SARS-CoV-2. SNAP-25 and SNAP-29, VAMP2 and VAMP8, which are all strongly mimicked by SARS-CoV-2 proteins, are also shared molecules for 5-HT, glutamate, acetylcholine, adrenaline, and noradrenaline, oxytocin neurotransmission, corticotropin-releasing factor receptor, and thyrotropin-releasing factor signaling, enkephalin release, GABA B receptor II signaling, opioid-prodynorphin/

proenkephalin/proopiomelanocortin pathways (**Supplementary Table 3** sublists) (Turner et al., 1999).

### SARS-CoV-2 Mimics Neurotransmission and Neuronal Excitability Related Proteins

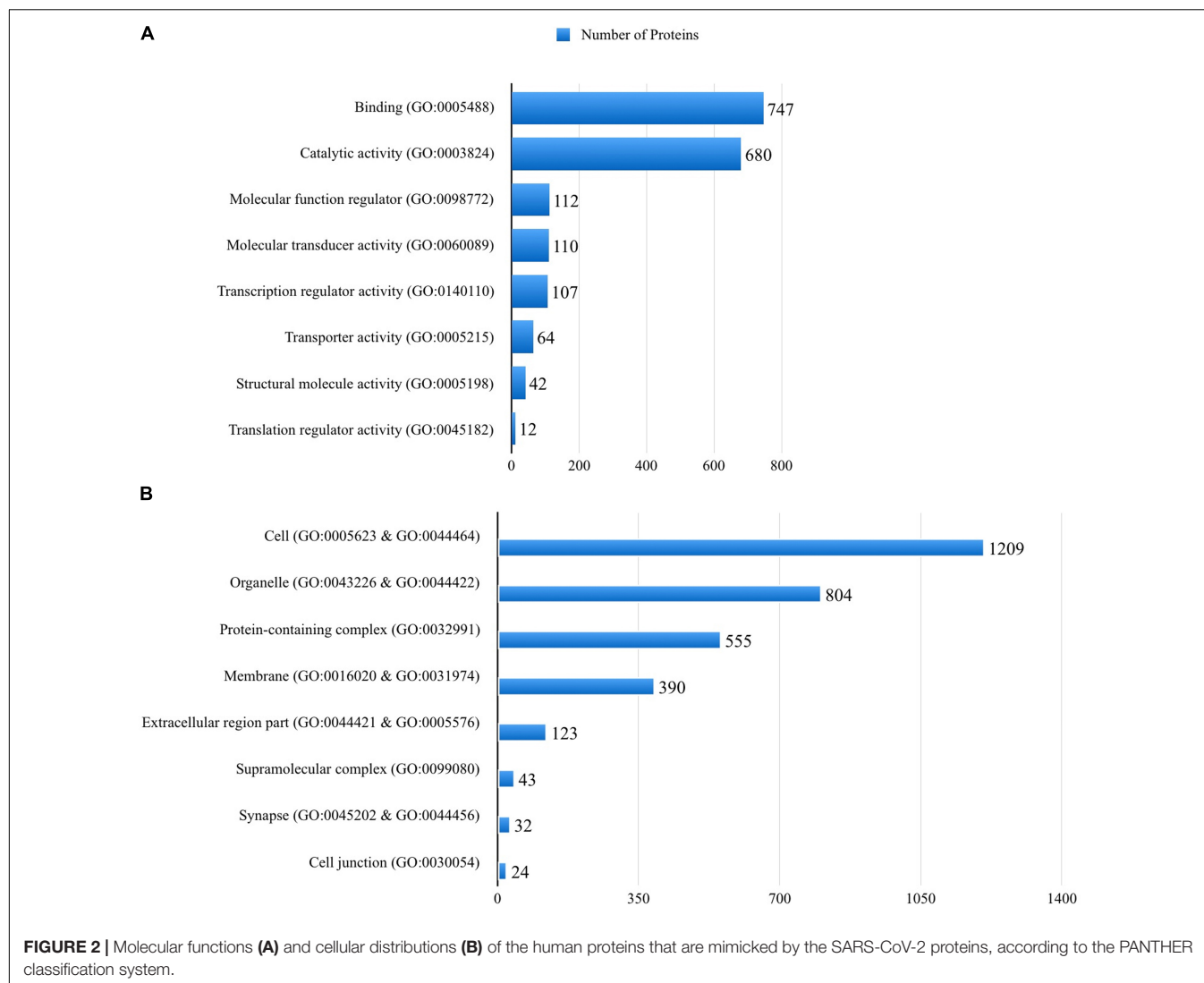
The results are presented in **Figure 4** and **Supplementary Tables 2, 3, 6**. Mainly spike, NSP7 and NSP8, also, some other NSP proteins mimic potassium voltage-gated channel subfamily KQT member 1 and 2, gamma-aminobutyric acid type A and B receptor subunits, glycine receptor subunits, metabotropic glutamate receptors, neuronal acetylcholine receptor subunits, dopamine D2 receptor, and adenosine receptor A2a. In addition to direct receptor interactions, SARS-CoV-2 proteins may mimic multiple proteins in both Gs, Gi, and Gq secondary messenger systems, which mediate metabotropic neurotransmission through both glutamatergic, adrenergic, histaminergic, cannabinoidergic, opioidergic, and serotonergic systems. In addition to histamine, serotonin, and acetylcholine synthesis and degradation (**Supplementary Tables 2, 3, 6**). Tryptophan 5-hydroxylase 2, which is an important enzyme for serotonin synthesis, also has a strong mimicry with the spike protein of SARS-CoV-2. Among these proteins, calmodulin-2 presents the strongest interaction with SARS-CoV-2 proteins (**Supplementary Table 2**). It is well established that increased intracellular calcium levels cause Nitric oxide synthase (NOS) enzyme activation through Ca-calmodulin. Both neuronal and endothelial NOS are activated with similar mechanisms. From our list, we have detected calmodulin as a strong interactor with viral protein (possible 3D model shown in **Figure 5**) and simulates NOS-Calmodulin binding (Aoyagi et al., 2003; Spratt et al., 2011).

### SARS-CoV-2 Mimics Major Growth Factors

The results are presented in **Figure 3** and **Supplementary Tables 2, 7**, as FGF1, FGF2 and FGF4, VEGF2, GDNF, EGF, GLP-1, insulin-like growth factor, insulin and estrogen receptor, ciliary neurotrophic factor, that take a role in neuroprotection, cell growth and survival both in the brain and spinal cord neurons and astrocytes. These neurotrophic factors are coupled to Ras-MAPK pathways, PI3 kinase pathways, PLCγ pathways, in addition to JAK-STAT signaling (**Supplementary Table 3**), whose associated proteins are not discussed specifically here.

### SARS-CoV-2 Mimics Mitochondrial Electron Transport and Mitochondrial Protein Import Related Proteins

The results are presented in **Figure 3** and **Supplementary Tables 2, 3, 8**. SARS-CoV-2 proteins mimic human proteins that take a role in ATP synthesis, apoptosis, and oxidative stress where mitochondrial proteins are also involved (**Supplementary Table 3**). In addition to these pathways, SARS-CoV-2 proteins interact with many structural mitochondrial proteins and enzymes (**Supplementary Table 8**). Among these enzymes, NSP8 strongly mimics NADH dehydrogenase [ubiquinone] 1 beta



subcomplex subunit 10 (Supplementary Table 2) interaction. Mitochondria also take an active role in glutamate-glutamine transmission by glutamate dehydrogenase which is also listed in the interactions, and this pathway is important in the lactate shuttle to neurons.

## SARS-CoV-2 Mimics Miscellaneous Proteins in the Brain

SARS-CoV-2 proteins mimic 17 proteins linked with Alzheimer's disease- amyloid secretase pathway and 25 proteins linked with Alzheimer's disease-presenilin pathway like beta-secretase, presenilin-1, amyloid-beta precursor and binding proteins, gamma-secretase subunit-2; 43 proteins linked to Parkinson's disease pathways including alpha-synuclein (Supplementary Table 3), 26 axon guidance proteins (Supplementary Table 9), axonal transport proteins like cytoplasmic dynein 1 intermediate chain 2, dynein light chain roadblock-type 1, tubulin alpha-1A chain, tubulin alpha-1B chain, tubulin beta-3 chain, kinesin-like protein KIF1A and KIF21A (Figures 3, 4) and numerous other

proteins linked to the central nervous system, as glia-derived nexin, glial fibrillary acidic protein, neural cell adhesion molecule 2 and survival motor neuron protein (Supplementary Table 2).

When the panther ontology database pathways that have been listed in Supplementary Table 3 are analyzed, it is found that SARS-CoV-2 may affect the brain through various indirect mechanisms such as thrombosis, vascular interactions involving BBB, and inflammation.

## SARS-CoV-2 Mimics Proteins in the Blood-Brain Barrier

The results are presented in Figure 6 and Supplementary Tables 2, 10. We chose the vascular pathway from panther ontology which showed 188 possible interactions and from the HMI list, 21 proteins that may interact with several parts of the SARS-CoV-2 virus were chosen. For example both spike and NSP9 show mimicry for most prominent extracellular basement membrane protein collagen type IV. Interestingly, C-type lectin domain family members important in blood-brain

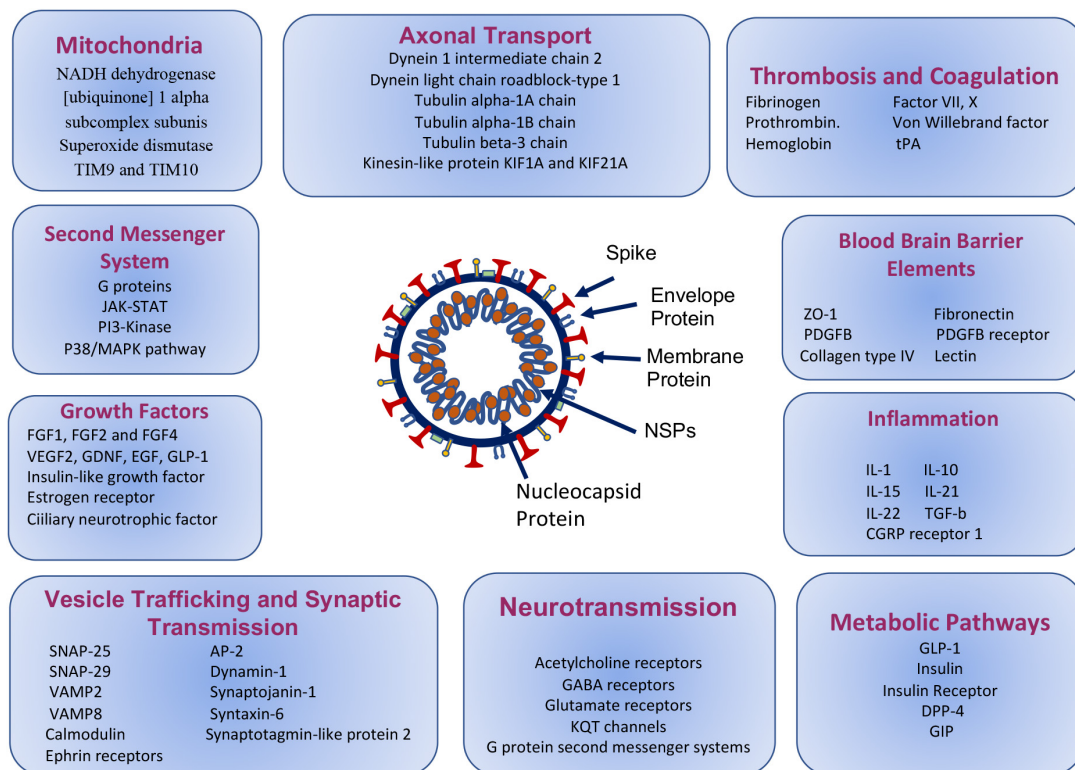


**FIGURE 3 |** Molecular paths of COVID-19 associated neuropsychiatric symptoms, based on the mimicry of the selected human protein interactions with SARS-CoV-2 proteins.

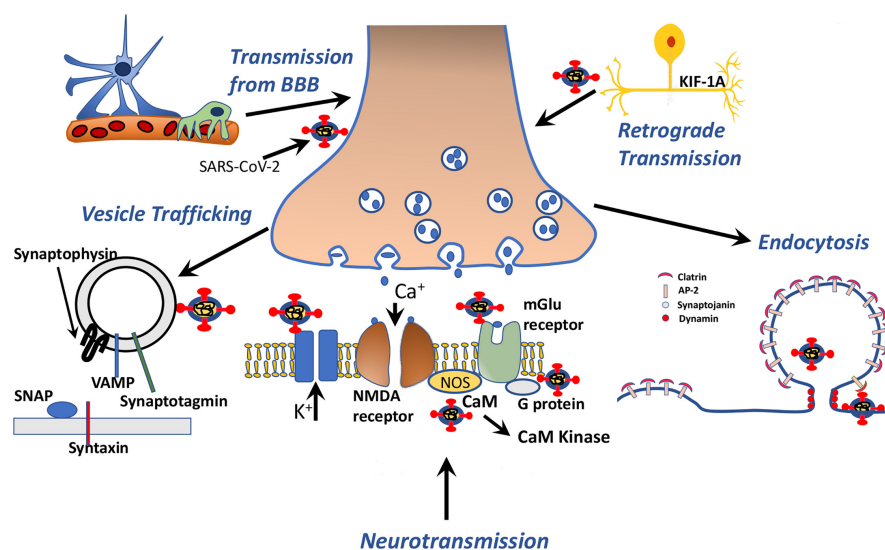
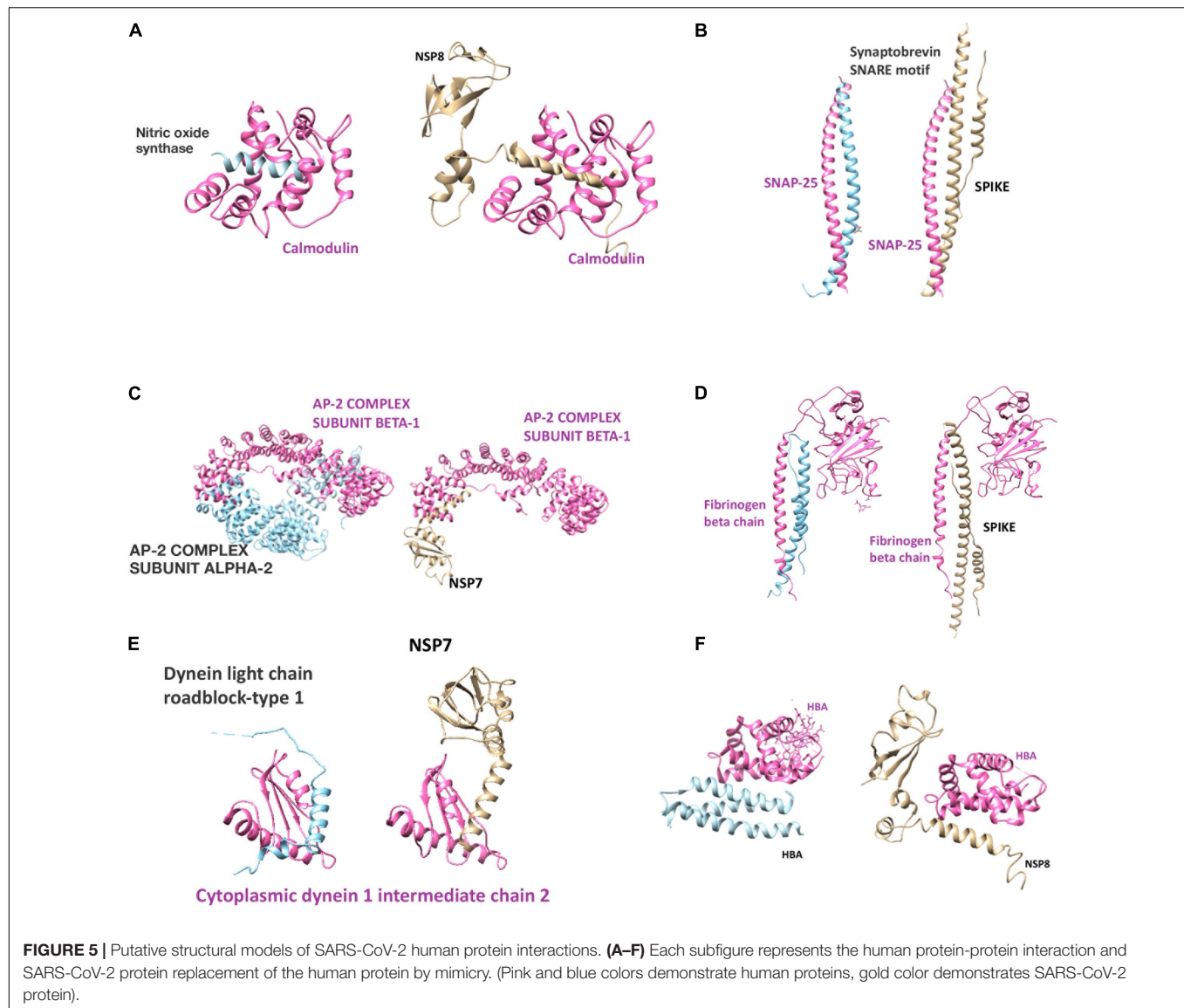


**FIGURE 4 |** Schematic drawing representing SARS-CoV-2 protein-human proteins interactions associated with vesicle transport, neurotransmission, endocytosis and axonal transport.

barrier integrity may interact nearly all proteins of the virus (Kim Y. et al., 2020). Fibronectin mimicry goes with NSPs, GFAP with spike, solid carrier proteins with NSPs mainly, insulin receptor with spike and NSP9, integrins with several

NSPs, laminin subunits with mostly spike, MMP13 with mainly 3CL-like protease, spike protein especially interacts with Zonula occludens-1, vimentin, protein S-100, laminin and collagen subunits, in addition to actin (**Supplementary Tables 2, 10**).



PDGF beta and its receptor as well as eNOS calmodulin interaction were mimicked by viral proteins.

gamma have demonstrated molecular mimicry with viral proteins (Supplementary Tables 2, 11).

## SARS-CoV-2 Mimics Various Proteins That Increase the Vulnerability of Thrombosis

SARS-CoV-2 proteins mimic human proteins that are involved in blood coagulation and hemostasis. Both elements of prothrombotic and antithrombotic pathways show mimicry with viral particles. According to PANTHER ontogene pathways analysis, 24 proteins for blood coagulation and from HMI lists 20 manually chosen coagulation related proteins demonstrated molecular similarity. Proteins that are involved in coagulation are listed in Figure 3 and Supplementary Table 11 and schematically drawn in Figure 6. Fibrinogen and laminin may interact with spike protein. Interestingly hemoglobin subunit alpha, beta, and

## SARS-CoV-2 Mimics Various Factors That Increase Peripheral Inflammatory Responses

The results are presented in Figure 3 and Supplementary Tables 2, 12. Some of these inflammatory proteins like IL-1, IL-10, IL-15, IL-21, and IL-22, may have roles in neural immune responses. Additionally, TGF-beta which is a strong stimulator of neural, pericyte, and endothelial immune responses may interact with different proteins of SARS-CoV-2. They may be involved in the inflammation mediated by chemokine and cytokine signaling pathways and T cell activation (Supplementary Table 3). Additionally, there is possible interaction and mimicry with CGRP receptor 1 and SARS-CoV-2.



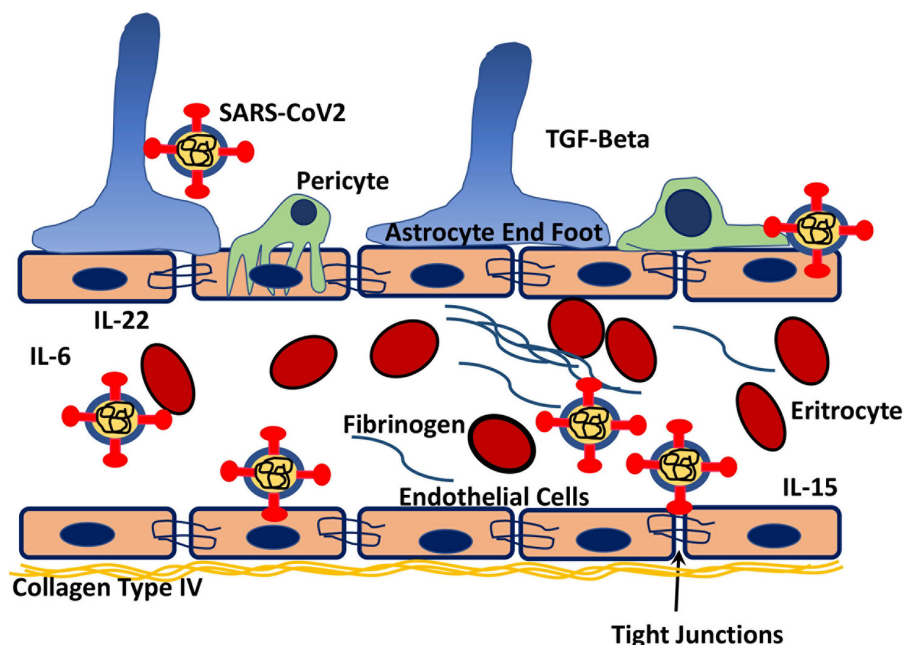


**FIGURE 6 |** Schematic drawing of possible interactions of the virus with both blood coagulation elements as well as components of the blood-brain barrier. By interacting with tight junction protein ZO-1, extracellular matrix elements of BBB like fibronectin, collagen it might cause BBB dysfunction. Reacting and with possible blockage of PDGF $\beta$  released from endothelium and its receptor on pericytes may disrupt the integrity of BBB. Also interacting with fibrinogen and factor VII may lead to coagulopathy, and reaction with hemoglobin subunits may cause decreased oxygenation of the brain tissue due to decreased oxygen-binding capacity. Decreased binding of endothelial NOS to calmodulin hence less activation of NOS with decreased NO production may lead to disturbances in vascular reactions.

## SARS-CoV-2 Mimics GLP-1, Insulin, DPP-4, and GIP

SARS-CoV-2 interacts with both insulin/IGF pathways (Supplementary Table 2) both by directly with insulin and its receptors and through its secondary effectors, also, it mimics GLP-1, GIP, and DPP-4 which affects GLP-1 levels. These molecules work together in the regulation of blood glucose levels (Foley, 2019). They have their receptors in the brain which will also be discussed for their direct effects.

## DISCUSSION

Here, we demonstrate the human protein interactions of 11 SARS-CoV-2 proteins via a computational approach. SARS-CoV-2 proteins mimic the interactions of proteins on the blood-brain barrier, synapse, and glial structures. These findings support the fact that SARS-CoV-2 may be affecting the brain and leading neuropsychiatric symptoms.

In COVID-19 cases with neurological symptoms onset, the presence of viral particles in the frontal lobe, in small vesicles of endothelial cells and the neural cell bodies, confirming a transendothelial passage to the brain, was detected, while cerebrospinal fluid (CSF) SARS-CoV-2 RT-PCR was negative (Paniz-Mondolfi et al., 2020). Coronaviruses may interact with tight junction proteins as zonula occludens-1 for viral entry and pass to the brain by decreasing the integrity of tight junctions, in addition to spreading around the body through the bloodstream

and invading the brain, as shown for other viruses (Torres-Flores and Arias, 2015). Olfactory epithelium and bulb were shown to be infected by the virus in postmortem investigation (Cantuti-Castelvetri et al., 2020). It is very well known that other viruses and some bacteria may modify blood brain barrier (BBB) components and induce inflammation leading to leakiness of BBB and passage to the brain and they may directly interact components of BBB like endothelial cells, pericytes, tight junction proteins, astrocyte end-feet, and matrix proteins. Viruses may interact with BBB endothelium through various receptors like insulin receptors, VEGF receptors, amino acid transport proteins. Particles may interact with adhesion molecules located on endothelium like integrins, also with tight junction proteins like ZO-1, claudin, and occludin as well. It was demonstrated that retroviruses leading to neural involvement like HIV and HTLV-1 can cause tight junction disintegration (Miller et al., 2012). Similarly, the Zika virus has been shown to alter BBB structure especially the tight junctions (Ljubin-Sternak et al., 2019). Additionally, the virus has an important interaction with ACE-2 receptors located on both endothelium as well as brain vascular pericytes. He et al. hypothesized that pericytes might be a key player in vascular complications of COVID-19 since they have a high-level expression of ACE-2 receptors (He et al., 2020). In addition to these findings, the virus may interact and block the effects of growth factors important in the maintenance of BBB, like PDGF beta and VEGF. We have also detected similarities of viral particles with extracellular matrix elements important in BBB structure and function like collagen, fibronectin, MMP



inhibitors. Additionally, at the level of the endothelium, the interaction of viruses with calmodulin may block the activation of endothelial NOS leading to decreased physiological responses and functions of the endothelium (Cirino et al., 2003).

After invasion into the brain, SARS-CoV-2 may use endocytosis pathways through its interaction with AP-2, dynamin and other endocytosis related proteins and enter the neuron. Clathrin coated endocytosis is an evolutionary reserved process regulated by adaptor proteins as AP-2 and mediator proteins as dynamin and ephrin, which can be used by both the host cells and also viruses for entry (Rappoport et al., 2006). We found that both spike and other SARS-CoV-2 proteins may mimic endocytosis proteins as AP-2, dynamin-1, and calmodulin located in the synapse. Zika virus, which is found to affect the development of the brain significantly, was also found to interact with dynamin (Agrelli et al., 2019). Rabies virus, which is transmitted to humans after bite of the infected animals, and presenting with agitation, hydrophobia, and mortal consequences, uses dynamin-1 and AP-2 for endocytosis (Guo et al., 2019). Pharmacological targeting of the dynamin was found effective in avoiding the neural entry of the virus (Xu et al., 2015). Mutations in dynamin protein in humans and upregulation in rat models were found to be related to seizures (Li and Kavalali, 2017). Dynamin-1 is a large GTPase, that is used by many other viruses as adenovirus, hepatitis C virus, herpes simplex virus, influenza A virus, HIV-1, and others as listed in Sun and Tien (2013). Even though there are different types of dynamin and dynamin-like proteins, dynamin-1, whose interactive sites which were found to be mimicked by SARS-CoV-2 proteins, are more abundant in the brain (Sun and Tien, 2013).

Knowledge from the previous viruses may point to clathrin non-dependent cell entry pathways as through caveolin, flotillin-dependent or macropinocytosis can be used by SARS-CoV-2 in cell entry (Glebov, 2020). Our computational analysis also reveals a mimicry of binding motifs to endophilin-A1 and endophilin-A3 by the SARS-CoV-2 proteins (**Supplementary Tables 2, 5**). Endophilin both interacts with dynamin and  $\beta$  adrenergic receptors (Zhang et al., 2012). Endophilin may also be responsible for fast non-clathrin dependent, dynamin-dependent uptake of EGFR, VEGF, and PDGF like G protein-coupled receptors (Walpole and Grinstein, 2020).

Our analysis reveals that SARS-CoV-2 proteins may also mimic important proteins for synaptic vesicle cycling. After invading the neuron, it may use intracellular replication pathways for its reproduction and later use vesicular trafficking pathways through SNAP-29, SNAP-25, and other vesicle trafficking proteins (Li and Kavalali, 2017; Kadkova et al., 2019). By occupying the named proteins, it may also cause their loss of function due to occupation and lead to a disrupted vesicle trafficking that may indirectly affect 5-HT, glutamate, acetylcholine, adrenaline and noradrenaline, oxytocin neurotransmission, corticotropin-releasing factor receptor, and thyrotropin-releasing factor signaling, enkephalin release, GABA B receptor II signaling, and opioid-prodynorphin/proenkephalin/proopiomelanocortin pathways that use these molecules. Dysfunctions of these pathways may explain the observed reversible changes in mental state as delirium, hallucinations, and smell function in COVID-19 patients. This

effect may also mimic the effect of botulinum toxin, which acts by entering the cytosol and cleaving the SNARE proteins (Rossetto et al., 2020). VAMP2, syntaxin-1, and SNAP-25 take a role in both spontaneous and active neurotransmitter release (Kadkova et al., 2019). Synaptotagmin on the vesicle membrane acts as a calcium sensor, and upon binding of Ca, it interacts with syntaxin-1 and SNAP-25 for the release of the neurotransmitters from the vesicles (Li and Kavalali, 2017).

VAMP2, tyrosine hydroxylase, and dopamine transporter are important molecules for dopamine neurotransmission in the striatum (Faustini et al., 2018). VAMP2 is also in interaction with alpha-synuclein and modulated alpha-synuclein aggregates (Faustini et al., 2018). VAMP2 increases insulin-stimulated GLUT4 translocation, which carries glucose into adipocytes, cardiac and skeletal muscles (Olson et al., 1997). A significant number of proteins in our analysis were linked with Parkinson's disease pathways. Dopaminergic pathways could be more vulnerable to the infection of SARS-CoV-2 and possible neurodegeneration.

On the other hand, VAMP2 was shown on the T-lymphocytes and related to granule exocytosis in mice (Matti et al., 2013) and SNAP-29 in cytokine secretion from keratocytes (Meng et al., 2019). Therefore, it is possible in humans as well that interaction of SARS-CoV-2 with SNARE proteins could also have an immune function. Among the SNARE proteins, SNAP-29 may also affect both Golgi secretosome pathways, in addition to endosome/lysosome pathways (Kadkova et al., 2019). A previous study from China found that 22 (12.02%) of the 183 hospitalized children with clinically suspected acute encephalitis, were identified with a coronavirus infection and these patients expressed higher GM-CSF compared to coronavirus cases with respiratory symptoms (Li et al., 2016).

SARS-CoV-2 might also be using axonal transport proteins for its spread and infection in the neuron, as demonstrated by the mimicry of tubulin, KIF1A, KIF21A, and dynein. HCoV OC43 was also shown to use axonal transport pathways, which lead to neuron to neuron propagation and spread of the virus in the brain (Dube et al., 2018). In addition to accelerating the spread of the virus, it may disrupt the transport of major proteins and structures through the axon, as seen in the HIV-1 disruption of mitochondrial transport (Wang et al., 2017).

As for its postsynaptic effects, SARS-CoV-2 proteins interact both directly with receptors of GABA (mainly GABA B) and glutamate (mainly NMDA and metabotropic glutamate receptors) leading to change in the membrane resting-state potential and action potential, in addition to secondary messenger systems that may indirectly affect membrane resting-state potential, in addition to intracellular protein functioning. At the cellular level, there is a possibility that SARS-CoV-2 affects not only the neurons, but also it may affect astrocytes due to its affinity for Glial Fibrillary Acidic Protein (GFAP) which has a strong interaction potential.

SARS-CoV-2 may also use the receptors for entry to cells. Rabies virus was shown to use nicotinic acetylcholine receptors for entry into the brain (Guo et al., 2019). Especially K<sup>+</sup>, Na<sup>+</sup>, Cl<sup>-</sup> and Ca<sup>2+</sup> channels are shown to be used by several viruses to enter the cell, and pharmaceutical targeting of viral entry through

ion channels has shown promise in avoiding viral effects (Hover et al., 2017). On the other hand, by interacting with these ion channels, viruses may change neuronal firing through loss or gain of function of the ion channel, as seen in Rabies and Varicella Zoster infections (Hover et al., 2017). An in vitro study also pointed that SARS-CoV-2 is different from other coronavirus types for involving a unique S1/S2 cleavage site, which mimics a peptide on the human epithelial sodium channel  $\alpha$ -subunit (ENaC- $\alpha$ ) (Anand et al., 2020). The neuroinvasive potential of SARS-CoV-2 and its interaction with both ion channels and vesicle trafficking may also be effective in the peripheral nervous system and as suggested by Li Y. C. et al. (2020), may contribute to the respiratory failure by both invading to central respiration centers and peripheral nerves that innervate the lungs.

SARS-CoV-2 can affect the survival of the CNS cells through multiple pathways. An in vitro analysis of SARS-CoV-2 spike proteins with human tissue also found increased interactions with mitochondria-related proteins (Vojdani and Kharrazian, 2020). Viruses target mitochondrial dynamics as fusion and fission, change mitochondrial membrane potential and target various mechanisms of mitochondrial metabolism, as  $\beta$ -oxidation and the TCA cycle, for their virulence capacity as replication and persistence (Tiku et al., 2020). Dynamin-1-like protein is responsible for the fragmentation of mitochondria into smaller components, known as mitochondrial fission. When this mechanism is blocked, it is also shown to block cell to cell spread of some bacteria (Tiku et al., 2020). HIV-1 infected patients with neurobehavioral symptoms were also investigated for dynamin-like protein-1 expression in the frontal cortex and its expression level was found to be decreased around 50% (Fields et al., 2016). NADH dehydrogenase [ubiquinone] 1 beta subcomplex subunit 10 is one of the proteins that have the highest mimicry and it is located in the complex I of mitochondria. Viruses may use mitochondrial energy pathways for their own bioenergetic and biosynthesis needs (Combs et al., 2020). Mitochondrial complex I activity is also linked with dementia in Parkinson's disease (Gatt et al., 2016) and bipolar disorder (Callaly et al., 2015).

SARS-CoV-2 proteins interact with growth factors and their receptors. FGF1 is also one of the interactions of SARS-CoV-2. FGF family uses Ras/MAPK, PI3, and PLC $\gamma$  pathways (Diez Del Corral and Morales, 2017), through which it helps for neuroprotection, cell survival, and neural differentiation during embryonic development, it is also linked with epileptogenesis, mood disorders and autoimmunity in the brain (Turner et al., 2016). Compared to other types of FGF, FGF 2 not only increases the cell survival, but they also help the maturation of the astrocytes and alter glutamate transport by the astrocytes through interaction with glutamate transporter 1 in mouse (Savchenko et al., 2019). By this effect, they contribute to neuroprotection in two ways, increasing cell survival and avoiding excitotoxicity induced by accumulated glutamate. EGFR is also a target of SARS-CoV-2 proteins. When ligands bind to EGFR receptors, they activate tyrosine kinase pathways and increase intracellular signaling through MAPK pathways (Novak et al., 2001). Other coronaviruses as MERS-COV and SARS-CoV were shown to interact with P38/MAPK and JAK-STAT pathways and their replication were inhibited

when these pathways are inhibited (Lim et al., 2016). SARS-CoV virus was shown to activate both p38/MAPK, PI3, and JNK pathways in Vero E6 cells (Mizutani, 2007). JNK and p38/MAPK were upregulated in the transfected cells, whereas ERK and Akt were downregulated (Surjit et al., 2004; Mizutani, 2007). Through its downstream effects, it was suggested to take a role in both cell survival and apoptosis (Mizutani et al., 2004). JNK and PI3 pathways were also found to be important for the persistence of the virus in the cell (Mizutani, 2007). PI3 pathway is important for autophagy (Wong and Sanyal, 2020). SARS-CoV's M protein-induced apoptosis through mitochondrial cytochrome c release (Chan et al., 2007). In vitro studies also proved the modulation of the ERK/MAPK and PI3K/AKT/mTOR pathways by MERS-COV for its replication (Kindrachuk et al., 2015). By affecting the autophagy pathways, mitochondrial dysfunction related to ROS production, increasing endoplasmic reticulum stress and protein misfolding, SARS-CoV-2 may increase vulnerability for neurodegeneration (Lippi et al., 2020).

The observed changes by the virus as increased chronic inflammation, mitochondria-related increased reactive oxygen species, and neurodegeneration, in addition to alteration in growth factors and second messenger system and neurodevelopmental effects on axonal guidance and neuronal growth, are shared mechanisms in the neurobiology of autism, schizophrenia, bipolar disorder and epilepsy (Konradi et al., 2012). Maternal infections are also known to increase the vulnerability of neurodevelopmental disorders, and its mechanism is not solely dependent on the mother's fever and high inflammatory responses (Simanek and Meier, 2015; Flinkkila et al., 2016; Al-Haddad et al., 2019; Gustavson et al., 2019). Persistent viral infection and epitope spreading may cause chronic inflammation and neurodegeneration (Smatti et al., 2019). Placental passage of viruses, persistence in the brain, and mild chronic inflammation are also discussed for the development of psychiatric disorders. Although in 9 newborn from COVID-19 positive mothers were negative (amniotic fluid, cord blood, neonatal throat swab tested), another pathway of transmission in addition to respiration and entry through the mouth and nose, the placental passage of SARS-CoV-2 (Dong et al., 2020) is also discussed in a case report where the nasal swab of the newborn was negative but IgM levels were high and newborn was showing COVID-19 symptoms. Therefore, intrauterine infection of the fetus and its neurological and psychiatric outcomes are also questioned. As another neuroinvasive virus, HIV-1 may produce a protected viral reservoir in the brain and neuropsychiatric manifestations are thought to result from the direct cytopathic effects of the virus (Schroecksnadel et al., 2012). We found that SARS-CoV-2 proteins also significantly interact with axon guidance molecules, neuronal growth, and survival. In the case of a placental passage and latent infection in the brain, SARS-CoV-2 could also be linked to neurodevelopmental disorders. As an example, genetic variations in SNAP-29 are also linked with neurodevelopment disorders as observed in 22q11.2 deletion syndrome (di George syndrome) which is linked with schizophrenia and bipolar disorder (Kadkova et al., 2019).

Other than the direct effects on the brain, SARS-CoV-2 may indirectly affect the brain. From clinical cases, it is well defined that thrombosis formation and vascular occlusion are troublesome for especially patients in ICU and going through ventilation-intubation. In a recent article, the authors described the pathophysiology of SARS-CoV-2 induced stroke in a pericyte based approach. They have demonstrated that, in CNS, BBB pericytes are the only cells with high expression of ACE-2 receptors and endothelial cells do not express ACE-2 receptors at all (He et al., 2020). They hypothesize that in the elderly, especially having diabetes mellitus and hypertension, endothelia become leaky, leading to easy passage of viruses (He et al., 2020). From our analysis on coagulation factors, it is evident that the virus can target coagulation pathways in multiple ways like affecting either blood coagulation factors as prothrombin, fibrinogen, coagulation factors VII, X, XI and von Willebrand factor or inhibition of coagulation like tissue plasminogen activator, plasminogen activator inhibitor. Additionally, we have detected that several viral particles may interact with subunits of hemoglobin. These similarities may explain decreased tissue oxygenation due to viral interference if this interaction leads to the decreased oxygen-binding capacity of hemoglobin. Interaction of viral proteins with fibrinogen in plasma may lead to activation of fibrinogen leading to fibrin polymer generation hence coagulation. On top of it, it may interact with factor VII, anti-thrombin, and other our listed coagulation related proteins leading to either loss of function or gain of function. Hence, it is not surprising that coagulopathy is one of the hallmark clinical presentations. Since here we describe computationally based similarities, all the proposed interactions must be studied in wet lab setups to establish direct effects of interactions.

In contrast to direct invasion and vascular reactions, most of the neurological involvement of viral-induced diseases may have CNS consequences due to systemic inflammatory conditions. This is mostly due to inflammatory responses induced by virus changes in BBB and a vicious circle leading to an inflammatory response in immune-privileged brain tissue like lymphocyte, neutrophil passage to brain, and induction of microglia-macrophage response of CNS. Systemic inflammatory molecules like IL-6 may have these effects but especially some interleukins might be involved, especially in CNS. From the list of proteins taking part in inflammation, IL-21, IL-22, IL-1B are important proteins that are involved in MS, Parkinson's disease, and other viral-bacterial CNS infections (Wang et al., 2012; Perriard et al., 2015; Xin et al., 2015). TGF-beta is known as an inducer of inflammation and vascular reaction in BBB and it is a strong stimulator of pericytes and macrophages (Rustenhoven et al., 2016) and may lead to pericyte to myofibroblast transformation and fibrosis generation in other organs.

The mimicry of human protein interactions by SARS-CoV-2 may also be linked to the development of autoimmune disorders. The emergence of autoimmune disorders affecting distinct tissues has been reported and the immune response produced to cope with SARS-CoV-2 may interact with human proteins due to molecular mimicry (Rodriguez et al., 2020). Latent viral infections of the long-living neurons may cause its spread to other glial cells like astrocytes and oligodendrocytes

and coronavirus infections in rats and cats are linked with autoimmune demyelinating disorders (Cohen, 2020). Many other viruses as measles, Epstein-Barr, and HTLV-1 have been linked with the emergence of autoimmune disorders like MS and this has been explained by bystander activation and molecular mimicry (Getts et al., 2013).

Additionally, we have detected that Calcitonin gene-related peptide type 1 receptor may have an interaction with spike protein. It is also interesting that this protein has a role in headache generation as well as gastrointestinal functions. Hence, if there is possible interaction, this may explain headache and some of the gastrointestinal symptoms of COVID-19.

Lastly, SARS-CoV-2 also targets insulin pathways and GLP-1 related regulation of blood glucose control. Literature supports this finding by reporting a 37-year-old previously healthy man with normal BMI that was diagnosed with diabetic ketoacidosis at the time of COVID-19 diagnosis (Chee et al., 2020). Another 54-year-old man with no diabetic history also was reported to present to the emergency room with hyperglycemia and shortness of breath and diagnosed COVID-19 (Heaney et al., 2020). COVID-19 diagnosed patients also presented with non-diabetic ketoacidosis in addition to the worsening of diabetic ketoacidosis (Kim N. Y. et al., 2020; Li J. et al., 2020). Diabetes is also known to increase the mortality of COVID-19 cases (Huang et al., 2020). The DPP-4 molecule was also used by MERS-COV as a receptor (Iwata-Yoshikawa et al., 2019; Widagdo et al., 2019). These molecules not only take part in glucose regulation, but they may have both indirect and direct effects in the brain, as especially GLP-1 has its receptors in the brain and it is related to neuroprotection (Erbil et al., 2019) and reward processing (Yapici-Eser et al., 2020).

This study has several limitations. First of all, our analysis is based on a computational model, therefore it may represent some false-positive results and the current possible interactions need to be assessed in cell culture and animal models for an in vivo interaction's existence and further biological effects. Secondly, our analysis involves only 11 of the 29 proteins of SARS-CoV-2, as these are the only proteins whose protein structures are known. The involvement of other SARS-CoV-2 proteins in the analysis may change the statistical overrepresentation of involved pathways. The pathways associated with the interaction list and subcategory lists have been generated using PANTHER classification, in addition to authors' knowledge and literature search. There may still be some proteins missed for inclusion in the **Supplementary Tables 5–12**. This study needs to be supported by clinical studies with large sample sizes and longer follow up durations to observe a wider outcome of the SARS-CoV-2 mimicry of human interactions on the nervous system.

In conclusion, we represent here the candidate proteins that are most likely to affect the neuropsychiatric representations of COVID-19. SARS-CoV-2 proteins mimic the human protein interactions for blood-brain barrier formation, synaptic vesicle trafficking, endocytosis, axonal transport, neurotransmission, apoptosis and also coagulation, inflammation, and metabolic control, which may result in the development of delirium,



psychotic features, seizures, encephalitis, stroke, sensory impairments, peripheral nerve diseases, and autoimmune disorders. With different personal risk factors, different pathways may be triggered, and may cause a different phenotype for COVID-19 clinical presentation. Our findings are also supported by the previous in vivo and in vitro studies from other viruses. Similar studies can be conducted to better understand SARS-CoV-2 pathology. Further in vivo and in vitro studies using the proteins that we pointed to, could pave new targets both for avoiding and reversing neuropsychiatric presentations.

## CONCLUSION

SARS-CoV-2 proteins mimic the human protein-protein interactions. Among the human proteins mimicked by SARS-CoV-2 proteins, many are linked to synaptic vesicle trafficking, endocytosis, axonal transport, neurotransmission, growth factors, mitochondrial and blood-brain barrier elements, in addition to its peripheral interactions with proteins linked to thrombosis, inflammation and metabolic control. Mimicry of human protein interactions by SARS-CoV-2 may explain the development of delirium, psychosis, seizures, encephalitis, stroke, sensory impairments, peripheral nerve diseases, and autoimmune disorders.

## REFERENCES

- doi: 10.1016/j.meegid.2019.01.018 Agreli, A., De Moura, R. R., Crovella, S., and Brandao, L. A. C. (2019). ZIKA virus entry mechanisms in human cells. *Infect. Genet. Evol.* 69, 22–29.
- Al Saiegh, F., Ghosh, R., Leibold, A., Avery, M. B., Schmidt, R. F., Theofanis, T., et al. (2020). Status of SARS-CoV-2 in cerebrospinal fluid of patients with COVID-19 and stroke. *J. Neurol. Neurosurg. Psychiatry* 91, 846–848.
- Al-Haddad, B. J. S., Oler, E., Armistead, B., Elsayed, N. A., Weinberger, D. R., Bernier, R., et al. (2019). The fetal origins of mental illness. *Am. J. Obstet. Gynecol.* 221, 549–562.
- Alkeridy, W. A., Almaghlouth, I., Alrashed, R., Alayed, K., Binkhamis, K., Alsharidi, A., et al. (2020). A unique presentation of delirium in a patient with otherwise asymptomatic COVID-19. *J. Am. Geriatr. Soc.* doi: 10.1111/jgs.16536 [Epub ahead of print].
- Anand, P., Puranik, A., Aravamudan, M., Venkatakrishnan, A. J., and Soundararajan, V. (2020). SARS-CoV-2 strategically mimics proteolytic activation of human ENaC. *eLife* 9:e58603.
- Angelini, M. M., Akhlaghpour, M., Neuman, B. W., and Buchmeier, M. J. (2013). Severe acute respiratory syndrome coronavirus nonstructural proteins 3, 4, and 6 induce double-membrane vesicles. *mBio* 4:e00524–13. doi: 10.1128/mBio.00524-13
- Aoyagi, M., Arvai, A. S., Tainer, J. A., and Getzoff, E. D. (2003). Structural basis for endothelial nitric oxide synthase binding to calmodulin. *EMBO J.* 22, 766–775. doi: 10.1093/emboj/cdg078
- Arbour, N., Day, R., Newcombe, J., and Talbot, P. J. (2000). Neuroinvasion by human respiratory coronaviruses. *J. Virol.* 74, 8913–8921. doi: 10.1128/jvi.74.19.8913-8921.2000
- Baspinar, A., Cukuroglu, E., Nussinov, R., Keskin, O., and Gursoy, A. (2014). PRISM: a web server and repository for prediction of protein-protein interactions and modeling their 3D complexes. *Nucleic Acids Res.* 42, W285–W289.
- Beach, S. R., Praschan, N. C., Hogan, C., Dotson, S., Merideth, F., Kontos, N., et al. (2020). Delirium in COVID-19: a case series and exploration of potential

## AUTHOR CONTRIBUTIONS

HY-E, OK, AG, and YG-O designed and conceived the study. YK prepared the HMI-PRED protein interaction data. HY-E conducted the PANTHER analysis. HY-E, YG-O, and OO-C generated the supplementary lists of proteins distributed for functions. All authors contributed significantly to writing the draft and approved the final version of the manuscript.

## FUNDING

The authors gratefully acknowledge use of the services and facilities of the Koç University Research Center for Translational Medicine (KUTTAM), funded by the Republic of Turkey Ministry of Development. HY-E's studies are partially funded by The Science Academy's Young Scientists' Award Program (BAGEP). The content is solely the responsibility of the authors and does not necessarily represent the official views of the Ministry of Development or The Science Academy.

## SUPPLEMENTARY MATERIAL

The Supplementary Material for this article can be found online at: <https://www.frontiersin.org/articles/10.3389/fnhum.2021.656313/full#supplementary-material>

- mechanisms for central nervous system involvement. *Gen. Hosp. Psychiatry* 65, 47–53. doi: 10.1016/j.genhosppsych.2020.05.008
- Berman, H. M., Westbrook, J., Feng, Z., Gilliland, G., Bhat, T. N., Weissig, H., et al. (2000). The protein data bank. *Nucleic Acids Res.* 28, 235–242.
- Beyrouiti, R., Adams, M. E., Benjamin, L., Cohen, H., Farmer, S. F., Goh, Y. Y., et al. (2020). Characteristics of ischaemic stroke associated with COVID-19. *J. Neurol. Neurosurg. Psychiatry* 91, 889–891.
- Bhardwaj, K., Sun, J., Holzenburg, A., Guarino, L. A., and Kao, C. C. (2006). RNA recognition and cleavage by the SARS coronavirus endoribonuclease. *J. Mol. Biol.* 361, 243–256. doi: 10.1016/j.jmb.2006.06.021
- Boscolo-Rizzo, P., Borsetto, D., Spinato, G., Fabbris, C., Menegaldo, A., Gaudioso, P., et al. (2020). New onset of loss of smell or taste in household contacts of home-isolated SARS-CoV-2-positive subjects. *Eur. Arch. Otorhinolaryngol.* 277, 2637–2640. doi: 10.1007/s00405-020-06066-9
- Brison, E., Jacomy, H., Desforages, M., and Talbot, P. J. (2011). Glutamate excitotoxicity is involved in the induction of paralysis in mice after infection by a human coronavirus with a single point mutation in its spike protein. *J. Virol.* 85, 12464–12473. doi: 10.1128/jvi.05576-11
- Brison, E., Jacomy, H., Desforages, M., and Talbot, P. J. (2014). Novel treatment with neuroprotective and antiviral properties against a neuroinvasive human respiratory virus. *J. Virol.* 88, 1548–1563. doi: 10.1128/jvi.02972-13
- Calcagno, N., Colombo, E., Maranzano, A., Pasquini, J., Keller Sarmiento, I. J., Trogu, F., et al. (2020). Rising evidence for neurological involvement in COVID-19 pandemic. *Neurol. Sci.* 41, 1339–1341. doi: 10.1007/s10072-020-04447-w
- Callaly, E., Walder, K., Morris, G., Maes, M., Debnath, M., and Berk, M. (2015). Mitochondrial dysfunction in the pathophysiology of bipolar disorder: effects of pharmacotherapy. *Mini Rev. Med. Chem.* 15, 355–365. doi: 10.2174/138957515666150324122026
- Cantuti-Castelvetri, L., Ojha, R., Pedro, L. D., Djannatian, M., Franz, J., Kuivanen, S., et al. (2020). Neuropilin-1 facilitates SARS-CoV-2 cell entry and provides a possible pathway into the central nervous system. *bioRxiv [Preprint]* doi: 10.1101/2020.06.07.137802

- Chan, C. M., Ma, C. W., Chan, W. Y., and Chan, H. Y. (2007). The SARS-Coronavirus Membrane protein induces apoptosis through modulating the Akt survival pathway. *Arch. Biochem. Biophys.* 459, 197–207. doi: 10.1016/j.abb.2007.01.012
- Chee, Y. J., Ng, S. J. H., and Yeoh, E. (2020). Diabetic ketoacidosis precipitated by Covid-19 in a patient with newly diagnosed diabetes mellitus. *Diabetes Res. Clin. Pract.* 164:108166. doi: 10.1016/j.diabres.2020.108166
- Cirino, G., Fiorucci, S., and Sessa, W. C. (2003). Endothelial nitric oxide synthase: the Cinderella of inflammation? *Trends Pharmacol. Sci.* 24, 91–95. doi: 10.1016/s0165-6147(02)00049-4
- Cohen, I. R. (2020). *Perspectives on Autoimmunity*. Boca Raton, FL: CRC Press.
- Combs, J. A., Norton, E. B., Saifudeen, Z. R., Bentrup, K. H. Z., Katakam, P. V., Morris, C. A., et al. (2020). Human cytomegalovirus alters host cell mitochondrial function during acute infection. *J. Virol.* 94:e01183-19. doi: 10.1128/JVI.01183-19
- Cornillez-Ty, C. T., Liao, L., Yates, J. R. III, Kuhn, P., and Buchmeier, M. J. (2009). Severe acute respiratory syndrome coronavirus nonstructural protein 2 interacts with a host protein complex involved in mitochondrial biogenesis and intracellular signaling. *J. Virol.* 83, 10314–10318. doi: 10.1128/jvi.00842-09
- Cukuroglu, E., Gursoy, A., and Keskin, O. (2012). HotRegion: a database of predicted hot spot clusters. *Nucleic Acids Res.* 40, D829–D833.
- Desforages, M., Le Coupanec, A., Dubeau, P., Bourgouin, A., Lajoie, L., Dube, M., et al. (2019). Human coronaviruses and other respiratory viruses: underestimated opportunistic pathogens of the central nervous system? *Viruses* 12:14. doi: 10.3390/v12010014
- Diez Del Corral, R., and Morales, A. V. (2017). The multiple roles of FGF signaling in the developing spinal cord. *Front. Cell Dev. Biol.* 5:58.
- Ding, Y., He, L., Zhang, Q., Huang, Z., Che, X., Hou, J., et al. (2004). Organ distribution of severe acute respiratory syndrome (SARS) associated coronavirus (SARS-CoV) in SARS patients: implications for pathogenesis and virus transmission pathways. *J. Pathol.* 203, 622–630. doi: 10.1002/path.1560
- Dinkin, M., Gao, V., Kahan, J., Bobker, S., Simonetto, M., Wechsler, P., et al. (2020). COVID-19 presenting with ophthalmoparesis from cranial nerve palsy. *Neurology* 95, 221–223. doi: 10.1212/wnl.00000000000009700
- Dong, L., Tian, J., He, S., Zhu, C., Wang, J., Liu, C., et al. (2020). Possible vertical transmission of SARS-CoV-2 from an infected mother to her newborn. *JAMA* 323, 1846–1848.
- Dube, M., Le Coupanec, A., Wong, A. H. M., Rini, J. M., Desforages, M., and Talbot, P. J. (2018). Axonal transport enables neuron-to-neuron propagation of human coronavirus OC43. *J. Virol.* 92:e00404-18. doi: 10.1128/JVI.00404-18
- Egloff, M. P., Ferron, F., Campanacci, V., Longhi, S., Rancurel, C., Dutartre, H., et al. (2004). The severe acute respiratory syndrome-coronavirus replicative protein nsp9 is a single-stranded RNA-binding subunit unique in the RNA virus world. *Proc. Natl. Acad. Sci. U.S.A.* 101, 3792–3796. doi: 10.1073/pnas.0307877101
- Elde, N. C., and Malik, H. S. (2009). The evolutionary conundrum of pathogen mimicry. *Nat. Rev. Microbiol.* 7, 787–797. doi: 10.1038/nrmicro2222
- Ellul, M. A., Benjamin, L., Singh, B., Lant, S., Michael, B. D., Easton, A., et al. (2020). Neurological associations of COVID-19. *Lancet Neurol.* 19, 767–783.
- Erbil, D., Eren, C. Y., Demirel, C., Kucuk, M. U., Solaroglu, I., and Eser, H. Y. (2019). GLP-1's role in neuroprotection: a systematic review. *Brain Inj.* 33, 734–819. doi: 10.1080/02699052.2019.1587000
- Faustini, G., Longhena, F., Varanita, T., Bubacco, L., Pizzi, M., Missale, C., et al. (2018). Synapsin III deficiency hampers alpha-synuclein aggregation, striatal synaptic damage and nigral cell loss in an AAV-based mouse model of Parkinson's disease. *Acta Neuropathol.* 136, 621–639. doi: 10.1007/s00401-018-1892-1
- Fields, J. A., Serger, E., Campos, S., Divakaruni, A. S., Kim, C., Smith, K., et al. (2016). HIV alters neuronal mitochondrial fission/fusion in the brain during HIV-associated neurocognitive disorders. *Neurobiol. Dis.* 86, 154–169. doi: 10.1016/j.nbd.2015.11.015
- Flinkkila, E., Keski-Rahkonen, A., Marttunen, M., and Raevuori, A. (2016). Prenatal Inflammation, infections and mental disorders. *Psychopathology* 49, 317–333. doi: 10.1159/000448054
- Foley, J. E. (2019). Insights into GLP-1 and GIP actions emerging from vildagliptin mechanism studies in man. *Front. Endocrinol. (Lausanne)* 10:780. doi: 10.3389/fendo.2019.00780
- Gatt, A. P., Duncan, O. F., Attems, J., Francis, P. T., Ballard, C. G., and Bateman, J. M. (2016). Dementia in Parkinson's disease is associated with enhanced mitochondrial complex I deficiency. *Mov. Disord.* 31, 352–359. doi: 10.1002/mds.26513
- Getts, D. R., Chastain, E. M., Terry, R. L., and Miller, S. D. (2013). Virus infection, antiviral immunity, and autoimmunity. *Immunol. Rev.* 255, 197–209. doi: 10.1111/immr.12091
- Glebov, O. O. (2020). Understanding SARS-CoV-2 endocytosis for COVID-19 drug repurposing. *FEBS J.* 287, 3664–3671. doi: 10.1111/febs.15369
- Gonzalez-Pinto, T., Luna-Rodriguez, A., Moreno-Estebanez, A., Agirre-Beitia, G., Rodriguez-Antiguedad, A., and Ruiz-Lopez, M. (2020). Emergency room neurology in times of COVID-19: malignant ischaemic stroke and SARS-CoV-2 infection. *Eur. J. Neurol.* 27, e35–e36.
- Gordon, D. E., Jang, G. M., Bouhaddou, M., Xu, J., Obernier, K., O'meara, M. J., et al. (2020). A SARS-CoV-2-human protein-protein interaction map reveals drug targets and potential drug-repurposing. *Nature* 583, 459–468.
- Grunewald, M. E., Fehr, A. R., Athmer, J., and Perlman, S. (2018). The coronavirus nucleocapsid protein is ADP-ribosylated. *Virology* 517, 62–68. doi: 10.1016/j.virol.2017.11.020
- Guo, Y., Duan, M., Wang, X., Gao, J., Guan, Z., and Zhang, M. (2019). Early events in rabies virus infection-Attachment, entry, and intracellular trafficking. *Virus Res.* 263, 217–225. doi: 10.1016/j.virusres.2019.02.006
- Gustavson, K., Ask, H., Ystrom, E., Stoltenberg, C., Lipkin, W. I., Suren, P., et al. (2019). Maternal fever during pregnancy and offspring attention deficit hyperactivity disorder. *Sci. Rep.* 9:9519.
- Gutierrez-Ortiz, C., Mendez, A., Rodrigo-Rey, S., San Pedro-Murillo, E., Bermejo-Guerrero, L., Gordo-Manas, R., et al. (2020). Miller Fisher Syndrome and polyneuritis cranialis in COVID-19. *Neurology* 95:409. doi: 10.1212/wnl.0000000000010405
- Guyen-Maiorov, E., Hakouz, A., Valjevac, S., Keskin, O., Tsai, C. J., Gursoy, A., et al. (2020). HMI-PRED: a web server for structural prediction of host-microbe interactions based on interface mimicry. *J. Mol. Biol.* 432, 3395–3403. doi: 10.1016/j.jmb.2020.01.025
- Guyen-Maiorov, E., Tsai, C. J., and Nussinov, R. (2016). Pathogen mimicry of host protein-protein interfaces modulates immunity. *Semin. Cell Dev. Biol.* 58, 136–145. doi: 10.1016/j.semcdb.2016.06.004
- Hackbart, M., Deng, X., and Baker, S. C. (2020). Coronavirus endoribonuclease targets viral polyuridine sequences to evade activating host sensors. *Proc. Natl. Acad. Sci. U.S.A.* 117, 8094–8103. doi: 10.1073/pnas.1921485117
- Halehalli, R. R., and Nagarajaram, H. A. (2015). Molecular principles of human virus protein-protein interactions. *Bioinformatics* 31, 1025–1033. doi: 10.1093/bioinformatics/btu763
- He, L., Mae, M. A., Sun, Y., Muhl, L., Nahar, K., Liebanas, E. V., et al. (2020). Pericyte-specific vascular expression of SARS-CoV-2 receptor ACE-2 – implications for microvascular inflammation and hypercoagulopathy in COVID-19 patients. *bioRxiv* doi: 10.1101/2020.05.11.088500
- Heaney, A. I., Griffin, G. D., and Simon, E. L. (2020). Newly diagnosed diabetes and diabetic ketoacidosis precipitated by COVID-19 infection. *Am. J. Emerg. Med.* 38, 2491.e3–e2491.e4.
- Helms, J., Kremer, S., Merdji, H., Clere-Jehl, R., Schenck, M., Kummerlen, C., et al. (2020). Neurologic features in severe SARS-CoV-2 infection. *N. Engl. J. Med.* 382, 2268–2270. doi: 10.1056/nejmc2008597
- Herman, C., Mayer, K., and Sarwal, A. (2020). Scoping review of prevalence of neurologic comorbidities in patients hospitalized for COVID-19. *Neurology* 95, 77–84. doi: 10.1212/wnl.00000000000009673
- Hopkins, C., Surda, P., Whitehead, E., and Kumar, B. N. (2020). Early recovery following new onset anosmia during the COVID-19 pandemic – an observational cohort study. *J. Otolaryngol. Head Neck Surg.* 49:26.
- Hosseini, A. A., Shetty, A. K., Sprigg, N., Auer, D. P., and Constantinescu, C. S. (2020). Delirium as a presenting feature in COVID-19: neuroinvasive infection or autoimmune encephalopathy? *Brain Behav. Immun.* 88, 68–70. doi: 10.1016/j.bbi.2020.06.012
- Hover, S., Foster, B., Barr, J. N., and Mankouri, J. (2017). Viral dependence on cellular ion channels - an emerging anti-viral target? *J. Gen. Virol.* 98, 345–351. doi: 10.1099/jgv.0.000712
- Huang, C., Lokugamage, K. G., Rozovics, J. M., Narayanan, K., Semler, B. L., and Makino, S. (2011). SARS coronavirus nsp1 protein induces template-dependent



- endonucleolytic cleavage of mRNAs: viral mRNAs are resistant to nsp1-induced RNA cleavage. *PLoS Pathog.* 7:e1002433. doi: 10.1371/journal.ppat.1002433
- Huang, L., Lim, M. A., and Pranata, R. (2020). Diabetes mellitus is associated with increased mortality and severity of disease in COVID-19 pneumonia – a systematic review, meta-analysis, and meta-regression. *Diabetes Metab. Syndr.* 14, 395–403. doi: 10.1016/j.dsx.2020.04.018
- Ivanov, K. A., Thiel, V., Dobbe, J. C., Van Der Meer, Y., Snijder, E. J., and Ziebuhr, J. (2004). Multiple enzymatic activities associated with severe acute respiratory syndrome coronavirus helicase. *J. Virol.* 78, 5619–5632. doi: 10.1128/jvi.78.11.5619-5632.2004
- Iwata-Yoshikawa, N., Okamura, T., Shimizu, Y., Kotani, O., Sato, H., Sekimukai, H., et al. (2019). Acute respiratory infection in human Dipeptidyl Peptidase 4-transgenic mice infected with middle east respiratory syndrome coronavirus. *J. Virol.* 93:e01818-18. doi: 10.1128/JVI.01818-18
- Jia, Z., Yan, L., Ren, Z., Wu, L., Wang, J., Guo, J., et al. (2019). Delicate structural coordination of the Severe Acute Respiratory Syndrome coronavirus Nsp13 upon ATP hydrolysis. *Nucleic Acids Res.* 47, 6538–6550. doi: 10.1093/nar/gkz409
- Kadkova, A., Radecke, J., and Sorensen, J. B. (2019). The SNAP-25 protein family. *Neuroscience* 420, 50–71. doi: 10.1016/j.neuroscience.2018.09.020
- Karimi, N., Razavi, S. A., and Rouhani, N. (2020). Frequent convulsive seizures in an adult patient with COVID-19: a case report. *Iran. Red Cres. Med. J.* 22:e102828.
- Kim, N. Y., Ha, E., Moon, J. S., Lee, Y. H., and Choi, E. Y. (2020). Acute hyperglycemic crises with coronavirus disease-19: case reports. *Diabetes Metab. J.* 44, 349–353. doi: 10.4093/dmj.2020.0091
- Kim, Y., Lee, S., Zhang, H., Lee, S., Kim, H., Kim, Y., et al. (2020). CLEC14A deficiency exacerbates neuronal loss by increasing blood-brain barrier permeability and inflammation. *J. Neuroinflamm.* 17:48.
- Kindrachuk, J., Ork, B., Hart, B. J., Mazur, S., Holbrook, M. R., Frieman, M. B., et al. (2015). Antiviral potential of ERK/MAPK and PI3K/AKT/mTOR signaling modulation for Middle East respiratory syndrome coronavirus infection as identified by temporal kinase analysis. *Antimicrob. Agents Chemother.* 59, 1088–1099. doi: 10.1128/aac.03659-14
- Konradi, C., Sullivan, S. E., and Clay, H. B. (2012). Mitochondria, oligodendrocytes and inflammation in bipolar disorder: evidence from transcriptome studies points to intriguing parallels with multiple sclerosis. *Neurobiol. Dis.* 45, 37–47. doi: 10.1016/j.nbd.2011.01.025
- Kumar, P., Gunalan, V., Liu, B., Chow, V. T., Druce, J., Birch, C., et al. (2007). The nonstructural protein 8 (nsp8) of the SARS coronavirus interacts with its ORF6 accessory protein. *Virology* 366, 293–303. doi: 10.1016/j.virol.2007.04.029
- Lechien, J. R., Hopkins, C., and Saussez, S. (2020). Sniffing out the evidence; it's now time for public health bodies recognize the link between COVID-19 and smell and taste disturbance. *Rhinology* 58, 402–403.
- Li, J., Wang, X., Chen, J., Zuo, X., Zhang, H., and Deng, A. (2020). COVID-19 infection may cause ketosis and ketoacidosis. *Diabetes Obes. Metab.* 22, 1935–1941. doi: 10.1111/dom.14057
- Li, Y., Li, H., Fan, R., Wen, B., Zhang, J., Cao, X., et al. (2016). Coronavirus infections in the central nervous system and respiratory tract show distinct features in hospitalized children. *Intervirology* 59, 163–169. doi: 10.1159/000453066
- Li, Y. C., Bai, W. Z., and Hashikawa, T. (2020). The neuroinvasive potential of SARS-CoV-2 may play a role in the respiratory failure of COVID-19 patients. *J. Med. Virol.* 92, 552–555. doi: 10.1002/jmv.25728
- Li, Y. C., and Kavalali, E. T. (2017). Synaptic vesicle-recycling machinery components as potential therapeutic targets. *Pharmacol. Rev.* 69, 141–160. doi: 10.1124/pr.116.013342
- Lim, K. P., and Liu, D. X. (2001). The missing link in coronavirus assembly. Retention of the avian coronavirus infectious bronchitis virus envelope protein in the pre-Golgi compartments and physical interaction between the envelope and membrane proteins. *J. Biol. Chem.* 276, 17515–17523.
- Lim, Y. X., Ng, Y. L., Tam, J. P., and Liu, D. X. (2016). Human coronaviruses: a review of virus-host interactions. *Diseases* 4:26. doi: 10.3390/diseases4030026
- Lippi, A., Domingues, R., Setz, C., Outeiro, T. F., and Krisko, A. (2020). SARS-CoV-2: at the crossroad between aging and neurodegeneration. *Mov. Disord.* 35, 716–720.
- Ljubic-Sternak, S., Mestrovic, T., Ivkovic-Jurekovic, I., Kolaric, B., Slovic, A., Forcic, D., et al. (2019). The emerging role of rhinoviruses in lower respiratory tract infections in children – clinical and molecular epidemiological study from Croatia, 2017–2019. *Front. Microbiol.* 10:2737. doi: 10.3389/fmicb.2019.02737
- Ludlow, M., Kortekaas, J., Herden, C., Hoffmann, B., Tappe, D., Trebst, C., et al. (2016). Neurotropic virus infections as the cause of immediate and delayed neuropathology. *Acta Neuropathol.* 131, 159–184.
- Ma, Y., Wu, L., Shaw, N., Gao, Y., Wang, J., Sun, Y., et al. (2015). Structural basis and functional analysis of the SARS coronavirus nsp14–nsp10 complex. *Proc. Natl. Acad. Sci. U.S.A.* 112, 9436–9441.
- Mao, L., Jin, H., Wang, M., Hu, Y., Chen, S., He, Q., et al. (2020). Neurologic manifestations of hospitalized patients with coronavirus disease 2019 in Wuhan, China. *JAMA Neurol.* 77, 683–690.
- Matti, U., Pattu, V., Halimani, M., Schirra, C., Krause, E., Liu, Y., et al. (2013). Synaptobrevin2 is the v-SNARE required for cytotoxic T-lymphocyte lytic granule fusion. *Nat. Commun.* 4:1439.
- McAbee, G. N., Brosigol, Y., Pavlakis, S., Agha, R., and Gaffoor, M. (2020). Encephalitis associated with COVID-19 infection in an 11-Year-old child. *Pediatr. Neurol.* 109:94.
- Meng, J., Wang, J., Buddenkotte, J., Buhl, T., and Steinhoff, M. (2019). Role of SNAREs in atopic dermatitis-related cytokine secretion and skin-nerve communication. *J. Invest. Dermatol.* 139, 2324–2333.
- Mi, H., Muruganujan, A., Huang, X., Ebert, D., Mills, C., Guo, X., et al. (2019). Protocol update for large-scale genome and gene function analysis with the PANTHER classification system (v.14.0). *Nat. Protoc.* 14, 703–721.
- Miller, F., Afonso, P. V., Gessain, A., and Ceccaldi, P. E. (2012). Blood-brain barrier and retroviral infections. *Virulence* 3, 222–229.
- Mizutani, T. (2007). Signal transduction in SARS-CoV-infected cells. *Ann. N. Y. Acad. Sci.* 1102, 86–95.
- Mizutani, T., Fukushima, S., Saijo, M., Kurane, I., and Morikawa, S. (2004). Phosphorylation of p38 MAPK and its downstream targets in SARS coronavirus-infected cells. *Biochem. Biophys. Res. Commun.* 319, 1228–1234.
- Moein, S. T., Hashemian, S. M. R., Mansourafshar, B., Khorram-Tousi, A., Tabarsi, P., and Doty, R. L. (2020). Smell dysfunction: a biomarker for COVID-19. *Int. Forum Allergy Rhinol.* 10, 944–950.
- Moropoulou, S., Brown, J. R., Davies, E. G., Anderson, G., Virasami, A., Qasim, W., et al. (2016). Human coronavirus OC43 associated with fatal encephalitis. *N. Engl. J. Med.* 375, 497–498.
- Netland, J., Meyerholz, D. K., Moore, S., Cassell, M., and Perlman, S. (2008). Severe acute respiratory syndrome coronavirus infection causes neuronal death in the absence of encephalitis in mice transgenic for human ACE-2. *J. Virol.* 82, 7264–7275.
- Neuman, B. W., Kiss, G., Kunding, A. H., Bhella, D., Baksh, M. F., Connelly, S., et al. (2011). A structural analysis of M protein in coronavirus assembly and morphology. *J. Struct. Biol.* 174, 11–22.
- Novak, U., Walker, F., and Kaye, A. (2001). Expression of EGFR-family proteins in the brain: role in development, health and disease. *J. Clin. Neurosci.* 8, 106–111.
- Olson, A. L., Knight, J. B., and Pessin, J. E. (1997). Syntaxin 4, VAMP2, and/or VAMP3/cellubrevin are functional target membrane and vesicle SNAP receptors for insulin-stimulated GLUT4 translocation in adipocytes. *Mol. Cell Biol.* 17, 2425–2435.
- Ottaviani, D., Boso, F., Tranquillini, E., Gapeni, I., Pedrotti, G., Cozzio, S., et al. (2020). Early Guillain-Barre syndrome in coronavirus disease 2019 (COVID-19): a case report from an Italian COVID-hospital. *Neurol. Sci.* 41, 1351–1354.
- Padroni, M., Mastrangelo, V., Asioli, G. M., Pavolucci, L., Abu-Rumeileh, S., Piscaglia, M. G., et al. (2020). Guillain-Barre syndrome following COVID-19: new infection, old complication? *J. Neurol.* 267, 1877–1879.
- Pallanti, S. (2020). Importance of SARS-Cov-2 anosmia: from phenomenology to neurobiology. *Compr. Psychiatry* 100:152184.
- Paniz-Mondolfi, A., Bryce, C., Grimes, Z., Gordon, R. E., Reidy, J., Lednický, J., et al. (2020). Central nervous system involvement by severe acute respiratory syndrome coronavirus-2 (SARS-CoV-2). *J. Med. Virol.* 92, 699–702.
- Paterson, R. W., Brown, R. L., Benjamin, L., Nortley, R., Wiethoff, S., Bharucha, T., et al. (2020). The emerging spectrum of COVID-19 neurology: clinical, radiological and laboratory findings. *Brain* 143, 3104–3120.
- Perriard, G., Mathias, A., Enz, L., Canales, M., Schluep, M., Gentner, M., et al. (2015). Interleukin-22 is increased in multiple sclerosis patients and targets astrocytes. *J. Neuroinflamm.* 12:119.

- Poissy, J., Goutay, J., Caplan, M., Parmentier, E., Duburcq, T., Lassalle, F., et al. (2020). Pulmonary embolism in COVID-19 patients: awareness of an increased prevalence. *Circulation* 142, 184–186.
- Rappoport, J. Z., Kemal, S., Benmerah, A., and Simon, S. M. (2006). Dynamics of clathrin and adaptor proteins during endocytosis. *Am. J. Physiol. Cell Physiol.* 291, C1072–C1081.
- Rodriguez, Y., Novelli, L., Rojas, M., De Santis, M., Acosta-Ampudia, Y., Monsalve, D. M., et al. (2020). Autoinflammatory and autoimmune conditions at the crossroad of COVID-19. *J. Autoimmun.* 114:102506.
- Rogers, J. P., Chesney, E., Oliver, D., Pollak, T. A., McGuire, P., Fusar-Poli, P., et al. (2020). Psychiatric and neuropsychiatric presentations associated with severe coronavirus infections: a systematic review and meta-analysis with comparison to the COVID-19 pandemic. *Lancet Psychiatry* 7, 611–627.
- Rossetto, O., Pirazzini, M., Fabris, F., and Montecucco, C. (2020). Botulinum neurotoxins: mechanism of action. *Handb. Exp. Pharmacol.* 263, 35–47.
- Ruch, T. R., and Machamer, C. E. (2012). The coronavirus E protein: assembly and beyond. *Viruses* 4, 363–382.
- Rustenhoven, J., Aalderink, M., Scotter, E. L., Oldfield, R. L., Bergin, P. S., Mee, E. W., et al. (2016). TGF- $\beta$ 1 regulates human brain pericyte inflammatory processes involved in neurovasculature function. *J. Neuroinflamm.* 13:37.
- Savchenko, E., Teku, G. N., Boza-Serrano, A., Russ, K., Berns, M., Deierborg, T., et al. (2019). FGF family members differentially regulate maturation and proliferation of stem cell-derived astrocytes. *Sci. Rep.* 9:9610.
- Schroeksnadel, S., Kurz, K., Weiss, G., and Fuchs, D. (2012). Immune activation and neuropsychiatric symptoms in human immunodeficiency virus type 1 infection. *Neurobehav. HIV Med.* 4, 1–13.
- Sedaghat, Z., and Karimi, N. (2020). Guillain Barre syndrome associated with COVID-19 infection: a case report. *J. Clin. Neurosci.* 76, 233–235.
- Simanek, A. M., and Meier, H. C. (2015). Association between prenatal exposure to maternal infection and offspring mood disorders: a review of the literature. *Curr. Probl. Pediatr. Adolesc. Health Care* 45, 325–364.
- Siu, Y. L., Teoh, K. T., Lo, J., Chan, C. M., Kien, F., Escrioni, N., et al. (2008). The M, E, and N structural proteins of the severe acute respiratory syndrome coronavirus are required for efficient assembly, trafficking, and release of virus-like particles. *J. Virol.* 82, 11318–11330.
- Smatti, M. K., Cyprian, F. S., Nasrallah, G. K., Al Thani, A. A., Almishal, R. O., and Yassine, H. M. (2019). Viruses and autoimmunity: a review on the potential interaction and molecular mechanisms. *Viruses* 11:762.
- Spratt, D. E., Duangkham, Y., Taiakina, V., and Guillemette, J. G. (2011). Mapping the binding and calmodulin-dependent activation of nitric oxide synthase isozymes. *Open Nitric Oxide J.* 3, 16–24.
- Sun, Y., and Tien, P. (2013). From endocytosis to membrane fusion: emerging roles of dynamin in virus entry. *Crit. Rev. Microbiol.* 39, 166–179.
- Surjit, M., Liu, B., Jameel, S., Chow, V. T., and Lal, S. K. (2004). The SARS coronavirus nucleocapsid protein induces actin reorganization and apoptosis in COS-1 cells in the absence of growth factors. *Biochem. J.* 383, 13–18.
- Tiku, V., Tan, M. W., and Dikic, I. (2020). Mitochondrial functions in infection and immunity. *Trends Cell Biol.* 30, 263–275.
- Tomar, S., Johnston, M. L., St John, S. E., Osswald, H. L., Nyalapatla, P. R., Paul, L. N., et al. (2015). Ligand-induced dimerization of middle east respiratory syndrome (MERS) Coronavirus nsp5 Protease (3CLpro): implications for Nsp5 regulation and the development of antivirals. *J. Biol. Chem.* 290, 19403–19422.
- Torres-Flores, J. M., and Arias, C. F. (2015). Tight junctions go viral! *Viruses* 7, 5145–5154.
- Toscano, G., Palmerini, F., Ravaglia, S., Ruiz, L., Invernizzi, P., Cuzzoni, M. G., et al. (2020). Guillain-barre syndrome associated with SARS-CoV-2. *N. Engl. J. Med.* 382, 2574–2576.
- Tuncbag, N., Gursoy, A., Nussinov, R., and Keskin, O. (2011). Predicting protein-protein interactions on a proteome scale by matching evolutionary and structural similarities at interfaces using PRISM. *Nat. Protoc.* 6, 1341–1354.
- Tuncbag, N., Keskin, O., and Gursoy, A. (2010). HotPoint: hot spot prediction server for protein interfaces. *Nucleic Acids Res.* 38, W402–W406.
- Turner, C. A., Eren-Kocak, E., Inui, E. G., Watson, S. J., and Akil, H. (2016). Dysregulated fibroblast growth factor (FGF) signaling in neurological and psychiatric disorders. *Semin. Cell Dev. Biol.* 53, 136–143.
- Turner, K. M., Burgoyne, R. D., and Morgan, A. (1999). Protein phosphorylation and the regulation of synaptic membrane traffic. *Trends Neurosci.* 22, 459–464.
- Varatharaj, A., Thomas, N., Ellul, M. A., Davies, N. W. S., Pollak, T. A., Tenorio, E. L., et al. (2020). Neurological and neuropsychiatric complications of COVID-19 in 153 patients: a UK-wide surveillance study. *Lancet Psychiatry* 7, 875–882.
- Verdia-Baguena, C., Nieto-Torres, J. L., Alcaraz, A., Dediego, M. L., Torres, J., Aguilera, V. M., et al. (2012). Coronavirus E protein forms ion channels with functionally and structurally-involved membrane lipids. *Virology* 432, 485–494.
- Vojdani, A., and Kharrazian, D. (2020). Potential antigenic cross-reactivity between SARS-CoV-2 and human tissue with a possible link to an increase in autoimmune diseases. *Clin. Immunol.* 217:108480.
- Walls, A. C., Park, Y. J., Tortorici, M. A., Wall, A., McGuire, A. T., and Veesler, D. (2020). Structure, function, and antigenicity of the SARS-CoV-2 Spike glycoprotein. *Cell* 181, 281–292.e6.
- Walpole, G. F. W., and Grinstein, S. (2020). Endocytosis and the internalization of pathogenic organisms: focus on phosphoinositides. *F1000Res* 9:368.
- Wang, P., Bai, F., Zenewicz, L. A., Dai, J., Gate, D., Cheng, G., et al. (2012). IL-22 signaling contributes to West Nile encephalitis pathogenesis. *PLoS One* 7:e44153. doi: 10.1371/journal.pone.0044153
- Wang, Y., Santerre, M., Tempera, I., Martin, K., Mukerjee, R., and Sawaya, B. E. (2017). HIV-1 Vpr disrupts mitochondria axonal transport and accelerates neuronal aging. *Neuropharmacology* 117, 364–375.
- Wang, Y., Sun, Y., Wu, A., Xu, S., Pan, R., Zeng, C., et al. (2015). Coronavirus nsp10/nsp16 methyltransferase can be targeted by nsp10-derived peptide in vitro and in vivo to reduce replication and pathogenesis. *J. Virol.* 89, 8416–8427.
- Widagdo, W., Okba, N. M. A., Li, W., De Jong, A., De Swart, R. L., Begeman, L., et al. (2019). Species-specific colocalization of middle east respiratory syndrome coronavirus attachment and entry receptors. *J. Virol.* 93:e107–e119. doi: 10.1128/JVI.00107-19
- Wong, H. H., and Sanyal, S. (2020). Manipulation of autophagy by (+) RNA viruses. *Semin. Cell Dev. Biol.* 101, 3–11.
- Xin, N., Namaka, M. P., Dou, C., and Zhang, Y. (2015). Exploring the role of interleukin-22 in neurological and autoimmune disorders. *Int. Immunopharmacol.* 28, 1076–1083.
- Xiong, M., Liang, X., and Wei, Y. D. (2020). Changes in blood coagulation in patients with severe coronavirus disease 2019 (COVID-19): a meta-analysis. *Br. J. Haematol.* 189, 1050–1052.
- Xu, H., Hao, X., Wang, S., Wang, Z., Cai, M., Jiang, J., et al. (2015). Real-time imaging of rabies virus entry into living vero cells. *Sci. Rep.* 5:11753.
- Xu, J., Zhong, S., Liu, J., Li, L., Li, Y., Wu, X., et al. (2020). Detection of severe acute respiratory syndrome coronavirus in the brain: potential role of the chemokine mig in pathogenesis. *Clin. Infect. Dis.* 41, 1089–1096.
- Yapici-Eser, H., Appadurai, V., Eren, C. Y., Yazici, D., Chen, C. Y., Ongur, D., et al. (2020). Association between GLP-1 receptor gene polymorphisms with reward learning, anhedonia and depression diagnosis. *Acta Neuropsychiatr.* 32, 218–225.
- Yoshimoto, F. K. (2020). The proteins of severe acute respiratory syndrome Coronavirus-2 (SARS CoV-2 or n-COV19), the cause of COVID-19. *Protein J.* 39, 198–216.
- Zhang, J., Fan, J., Tian, Q., Song, Z., Zhang, J. F., and Chen, Y. (2012). Characterization of two distinct modes of endophilin in clathrin-mediated endocytosis. *Cell Signal* 24, 2043–2050.
- Zhang, Y., and Skolnick, J. (2005). TM-align: a protein structure alignment algorithm based on the TM-score. *Nucleic Acids Res.* 33, 2302–2309.
- Zhang, Y., Xiao, M., Zhang, S., Xia, P., Cao, W., Jiang, W., et al. (2020). Coagulopathy and antiphospholipid antibodies in patients with Covid-19. *N. Engl. J. Med.* 382:e38.
- Zhao, H., Shen, D., Zhou, H., Liu, J., and Chen, S. (2020). Guillain-Barre syndrome associated with SARS-CoV-2 infection: causality or coincidence? *Lancet Neurol.* 19, 383–384.

**Conflict of Interest:** The authors declare that the research was conducted in the absence of any commercial or financial relationships that could be construed as a potential conflict of interest.

Copyright © 2021 Yapici-Eser, Koroglu, Oztop-Cakmak, Keskin, Gursoy and Gursoy-Ozdemir. This is an open-access article distributed under the terms of the Creative Commons Attribution License (CC BY). The use, distribution or reproduction in other forums is permitted, provided the original author(s) and the copyright owner(s) are credited and that the original publication in this journal is cited, in accordance with accepted academic practice. No use, distribution or reproduction is permitted which does not comply with these terms.



# Three-Dimensional CT for Quantification of Longitudinal Lung and Pneumonia Variations in COVID-19 Patients

Qiuying Chen<sup>†</sup>, Lv Chen<sup>†</sup>, Shuyi Liu, Luyan Chen, Minmin Li, Zhuozhi Chen, Jingjing You, Bin Zhang\* and Shuixing Zhang\*

Department of Radiology, The First Affiliated Hospital of Jinan University, Guangzhou, China

## OPEN ACCESS

### Edited by:

Reza Lashgari,  
Institute for Research in Fundamental  
Sciences, Iran

### Reviewed by:

Soroush Arabshahi,  
Columbia University, United States  
Kamran Avanaki,  
University of Illinois at Chicago,  
United States

### \*Correspondence:

Bin Zhang  
xld\_jane\_eyre@126.com  
Shuixing Zhang  
shui7515@126.com

<sup>†</sup>These authors have contributed  
equally to this work

### Specialty section:

This article was submitted to  
Pulmonary Medicine,  
a section of the journal  
Frontiers in Medicine

Received: 19 December 2020

Accepted: 04 February 2021

Published: 25 March 2021

### Citation:

Chen Q, Chen L, Liu S, Chen L, Li M,  
Chen Z, You J, Zhang B and Zhang S  
(2021) Three-Dimensional CT for  
Quantification of Longitudinal Lung  
and Pneumonia Variations in  
COVID-19 Patients.  
Front. Med. 8:643917.  
doi: 10.3389/fmed.2021.643917

**Objectives:** Visual chest CT is subjective with interobserver variability. We aimed to quantify the dynamic changes of lung and pneumonia on three-dimensional CT (3D-CT) images in coronavirus disease 2019 (COVID-19) patients during hospitalization.

**Methods:** A total of 110 laboratory-confirmed COVID-19 patients who underwent chest CT from January 3 to February 29, 2020 were retrospectively reviewed. Pneumonia lesions were classified as four stages: early, progressive, peak, and absorption stages on chest CT. A computer-aided diagnostic (CAD) system calculated the total lung volume (TLV), the percentage of low attenuation areas (LAA%), the volume of pneumonia, the volume of ground-glass opacities (GGO), the volume of consolidation plus the GGO/consolidation ratio. The CT score was visually assessed by radiologists. Comparisons of lung and pneumonia parameters among the four stages were performed by one-way ANOVA with *post-hoc* tests. The relationship between the CT score and the volume of pneumonia, and between LAA% and the volume of pneumonia in four stages was assessed by Spearman's rank correlation analysis.

**Results:** A total of 534 chest CT scans were performed with a median interval of 4 days. TLV, LAA%, and the GGO/consolidation ratio were significantly decreased, while the volume of pneumonia, GGO, and consolidation were significantly increased in the progressive and peak stages (for all,  $P < 0.05$ ). The CT score was significantly correlated with the pneumonia volume in the four stages ( $r = 0.731, 0.761, 0.715$ , and  $0.669$ , respectively,  $P < 0.001$ ).

**Conclusion:** 3D-CT could be used as a useful quantification method in monitoring the dynamic changes of COVID-19 pneumonia.

**Keywords:** coronavirus disease 2019, computed tomography, CT score, CAD system, low attenuation areas

## INTRODUCTION

Rapid and accurate diagnosis is urgently needed for the coronavirus disease 2019 (COVID-19) pandemic. In addition to real-time fluorescence polymerase chain reaction (RT-PCR), chest CT has been extensively used as a convenient and highly sensitive tool for screening, diagnosis, and follow-up of COVID-19 since its outbreak (1). Bilateral peripheral ground-glass opacities (GGO)

with or without consolidation are the most common lung appearance of COVID-19 (2). Some recent studies have depicted typical CT manifestations of COVID-19 pneumonia during disease course into the early, progressive, peak, and absorption stages (3–6). Semiquantitative CT score may reflect the severity of the disease, which is a simple marker in daily practice (7). However, radiologist-interpreted chest CT is limited by larger interobserver variability, time-consuming, and inefficient.

The serial lung changes in addition to pneumonia lesions were not taken into account in the follow-up plan of COVID-19 patients. The percentage of low-attenuation lung tissues can be used to describe the severities of the lung disease; low attenuation areas (LAAs) represent individual areas of emphysematous destruction (8). Previous studies failed to consider the coexisting chronic pulmonary abnormalities in COVID-19 patients, for instance, emphysema and interstitial lung diseases (7). Colombi et al. found that well-aerated lung volume on initial CT may indicate the severity of disease and was a predictor of intensive care unit (ICU) admission or death in patients with COVID-19 pneumonia (9). To date, no lung functional data are available for COVID-19 patients during hospitalization except for Mo et al. who found the impairment of lung volume in COVID-19 patients prior to discharge, especially in severe cases (10). Previous studies have shown that some recovered patients with other coronavirus pneumonias [e.g., severe acute respiratory syndrome (SARS) and Middle East respiratory syndrome (MERS)] may be left with persistently damaged lungs, which could last for months or even

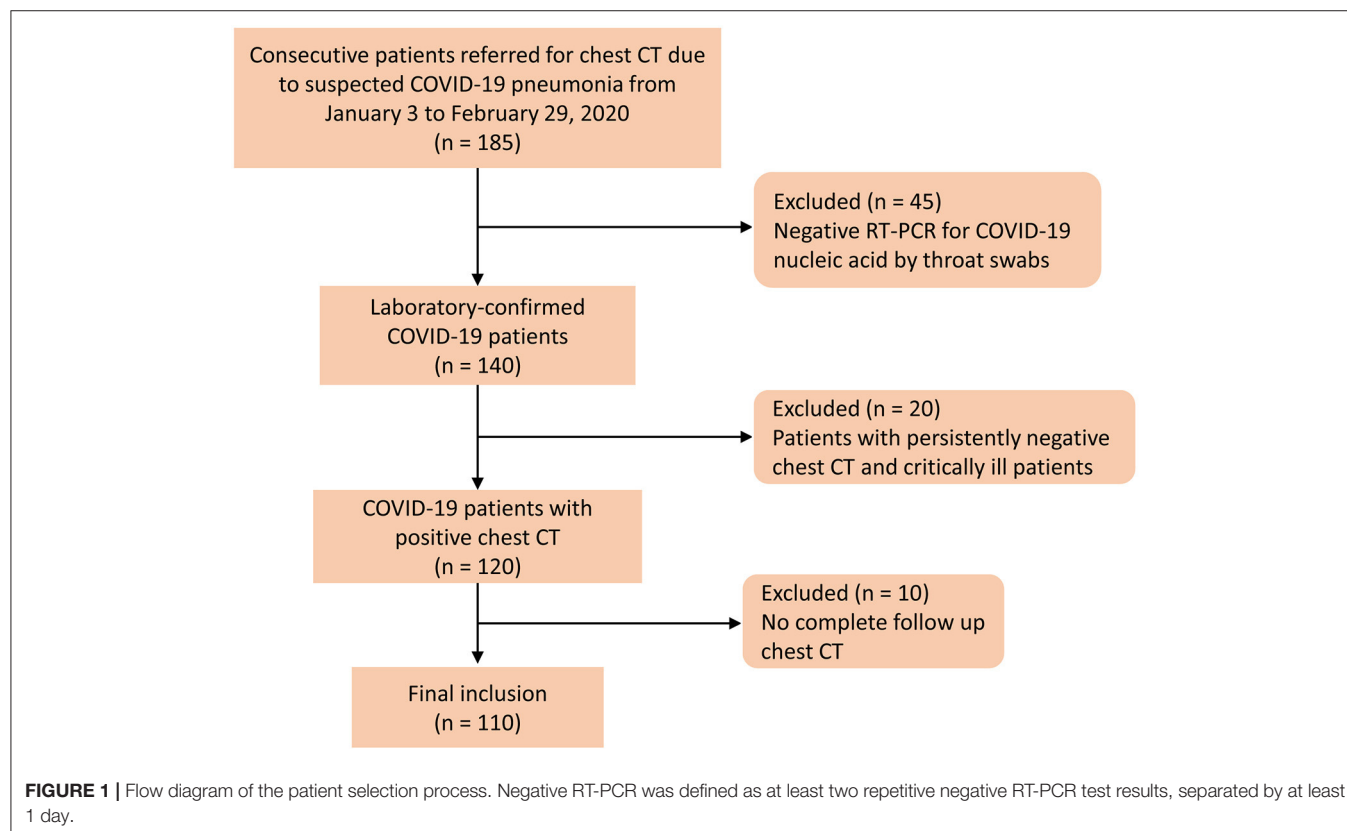
years (11–14). It would be of clinical importance to monitor the dynamic change of lung in COVID-19 patients after treatment and might determine the necessity for subsequent pulmonary function test and pulmonary rehabilitation.

In this study, we aimed to quantify the serial changes of lung and pneumonia on three-dimensional CT (3D-CT) in COVID-19 patients using a computer-aided diagnostic (CAD) system, which provides the imaging means for medical professionals to rapidly and accurately evaluate disease severity and treatment response of COVID-19 patients. This may play an important role in disease monitoring, early intervention, and determination of the timing of admission.

## MATERIALS AND METHODS

### Study Population

The retrospective study was approved by an ethics committee of our institution, and the informed consent was waived. A total of 185 patients were admitted to a designated hospital due to suspicion of COVID-19 between January 3 and February 29, 2020. The inclusion criteria were as follows: (1) patients were positive for COVID-19 through RT-PCR for COVID-19 nucleic acid by throat swabs (at least two samples were taken, at least 24 h apart); (2) patients had at least one positive chest CT during hospitalization; and (3) patients had follow-up chest CT. The disease severity of COVID-19 was categorized into mild, moderate, severe, and critical illness on the basis of the





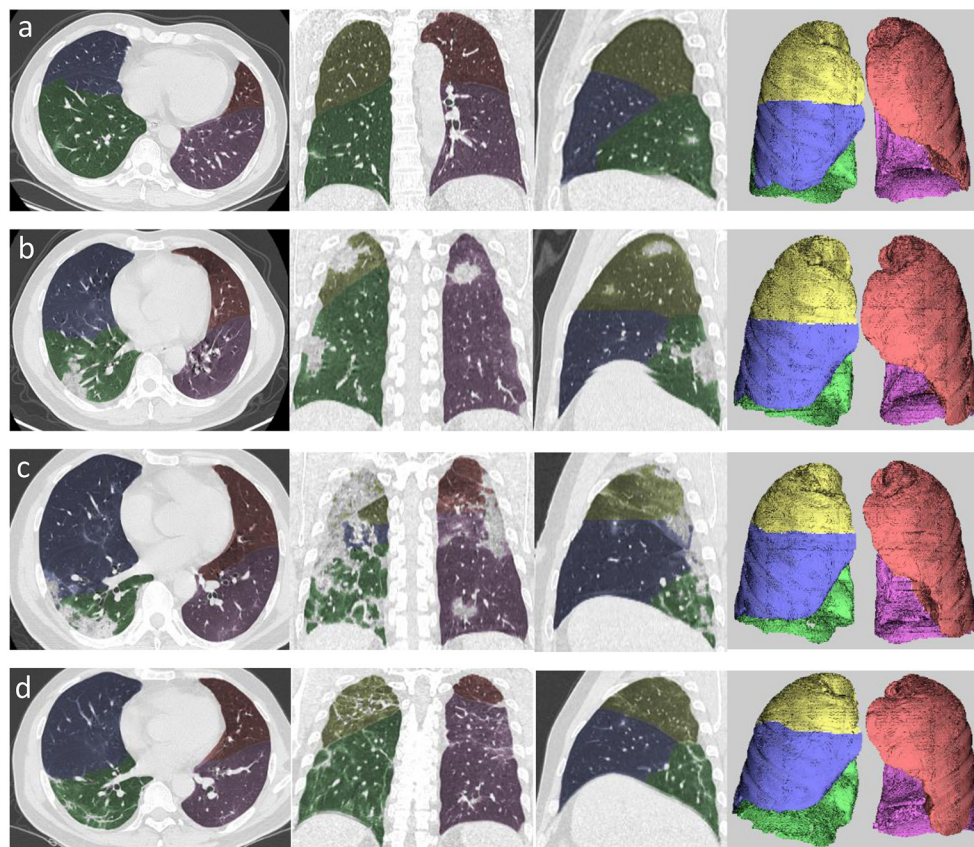


**FIGURE 2 |** Example of segmentation using automated computer-aided diagnosis in the four stages of COVID-19 pneumonia. **(a)** Axial, coronal, and sagittal multiplanar reconstruction views and volume rendering in the early stage. **(b)** Axial, coronal, and sagittal multiplanar reconstruction views and volume rendering (left to right) in the progressive stage. **(c)** Axial, coronal, and sagittal multiplanar reconstruction views and volume rendering (left to right) in the peak stage. **(d)** Axial, coronal, and sagittal multiplanar reconstruction views and volume rendering (left to right) in the absorption stage. Yellow area denotes right upper lobe, blue area denotes right middle lobe, green area denotes right lower lobe, orange area denotes left upper lobe, and pink area denotes left lower lobe.

newest COVID-19 guidelines released by the National Health Commission of China (15). Patients had persistently negative chest CT, and critically ill patients who underwent X-rays were excluded. **Figure 1** shows the patients' enrollment flowchart. Finally, 110 COVID-19 patients were included for analysis.

## CT Examinations

All patients underwent unenhanced chest CT scans by a Siemens Emotion 16 scanner (Siemens Healthineers; Erlangen, Germany), a CT 64 scanner (GE Medical System), or an ICT 128 scanner (Philips Healthcare, Netherlands). No contrast agent was administered. CT acquisition of the GE 64 scanner was executed as follows: tube voltage, 120 kV; tube current, 260 mAs; pitch, 0.984; and slice thickness reconstructions of 0.625 mm. CT acquisition of the Siemens 16 scanner was executed as follows: tube voltage, 130 kV; automatic tube current; pitch, 1.5; and slice thickness reconstructions of 1.0 or 0.6 mm. CT acquisition of the ICT 128 scanner was executed as follows: tube voltage, 120 kV; automatic tube current; pitch, 0.7; collimation, 0.625 mm and slice thickness reconstructions of 1.0 or 0.67 mm.

## Quantitative CT Analysis

According to a previous study (3), early, progressive, peak, and absorption stages on chest CT were defined as 0–4, 5–8, 9–13, and  $\geq 14$  days after the onset of the initial symptoms, respectively. A CT scoring system was used to assess the involvement area/degree of pneumonia for each lung lobe: 0 for 0%; 1 for 1–25%; 2 for 26–50%; 3 for 51–75%; and 4 for 76–100% (2). A CT score (range, 0–20) was assigned by summarizing the total scores for the five lobes. All the chest CT images were reviewed independently by two radiologists (with more than 10 years of experience), who were blinded to clinical and laboratory results. Any discrepancy was resolved by a consensus viewing.

The chest CT images were transferred to a workstation (Synapse Image Intelligence™ Vincent version 4.4; Fujifilm Medical Systems, Tokyo, Japan). This workstation implemented a lobar CAD system that was showed to accurately measure lobar volumes (16). This system automatically extracted both lungs, recognized lobar bronchi, and determined the locations of fissures (**Figure 2**). Subsequently, the CAD system semi-automatically extracted pneumonia regions after simply dragging both ends of the infected regions. Two cardiothoracic radiologists



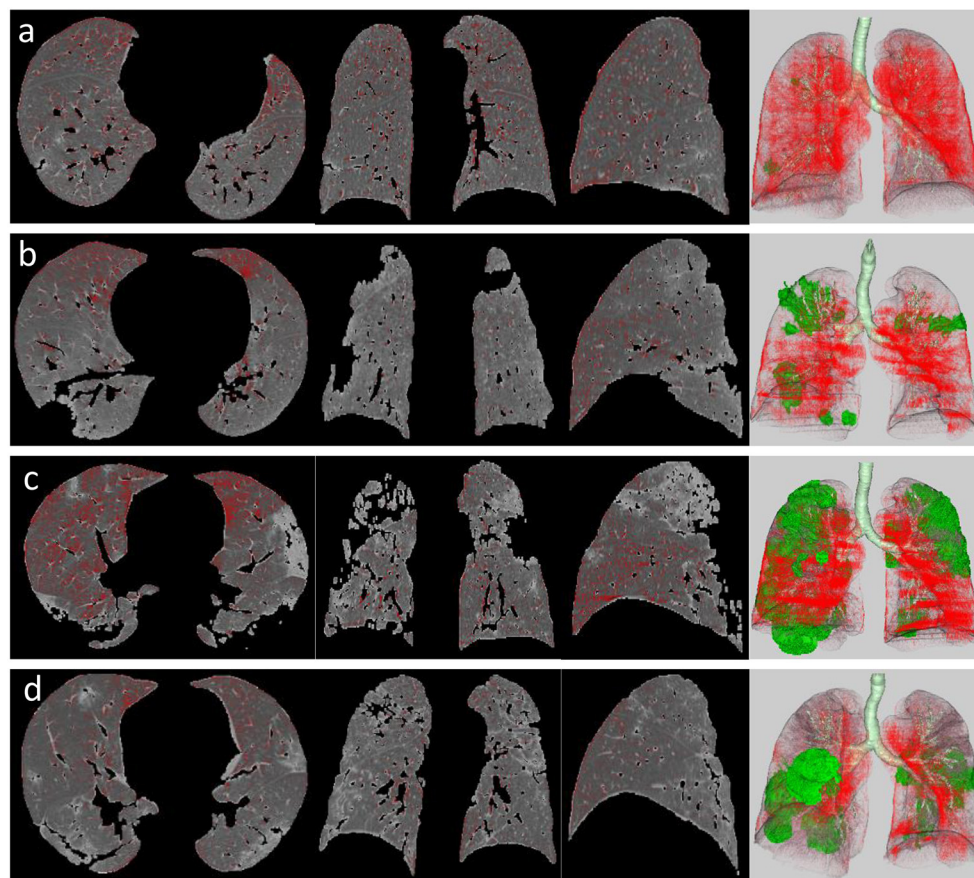


**FIGURE 3 |** LAA views of the four stages in a patient with COVID-19 pneumonia, which was defined as the lung field area with attenuation values < -950 HU of threshold (red areas). It shows axial, coronal, and sagittal two-dimensional (2D) displays and three-dimensional (3D) image (left to right) of LAA distribution in the early stage (a), progressive stage (b), peak stage (c), and absorption stage (d). Green area on 3D image represents pneumonia lesions.

checked the lesion segmentation by CAD and made manual corrections by delineating fissures and contour of infected regions when the CAD system failed to properly identify these.

A quantitative analysis procedure was performed based on the segmentation results. The lung field area with attenuation values < -950 Hounsfield Unit (HU) of thresholds was considered as LAAs (**Figure 3**). The proportion of LAAs (LAA%) for total lung volume was calculated automatically. By thresholding on CT values in the pneumonia lesions, GGO and consolidation were identified with the value range of -800 to -300 HU and -300 to 50 HU, respectively (17) (**Figure 4**). The volume and percentage of GGO and consolidation were calculated, accordingly. The ratio of GGO to consolidation was also computed.

## Statistical Analysis

Total lung volume, LAA%, the volume of pneumonia, the volume of consolidation, the percentage of GGO, the percentage of consolidation, and the GGO/consolidation ratio obtained at the four stages were compared using one-way ANOVA with *post-hoc* LSD multiple comparison tests at a level of significance  $P < 0.05$ . Spearman's rank correlation analysis was used to assess the correlation between the CT score and the volume of pneumonia.

All statistical analyses were performed using the SPSS statistical software package (version 23, SPSS Inc., Chicago, IL, USA).

## RESULTS

### Clinical Characteristics

The mean age of the 110 patients was  $45.2 \pm 12.8$  years (range, 14–80 years) and 65 (59.1%) were males. A total of 100 patients (90.9%) had moderate illness, and 10 patients (9.1%) had severe illness. A total of 534 chest CT scans were conducted with a median of 4 scans (interquartile range, 3–5) per patient. The total CT scans for the early, progressive, peak, and absorption stages were 91 (17.0%), 188 (35.2%), 39 (7.3%), and 216 (40.4%), respectively. A total of 62 (56.4%), 89 (80.9%), 18 (16.4%), and 95 (86.4%) patients experienced early, progressive, peak, and absorption stages, respectively.

### Comparison of Lung and Pneumonia Parameters Generated by the CAD System

**Table 1** shows the comparison of lung and pneumonia parameters among the four stages. As compared with the CT score of early stage, CT scores of the progressive stage ( $7.6 \pm 3.2$

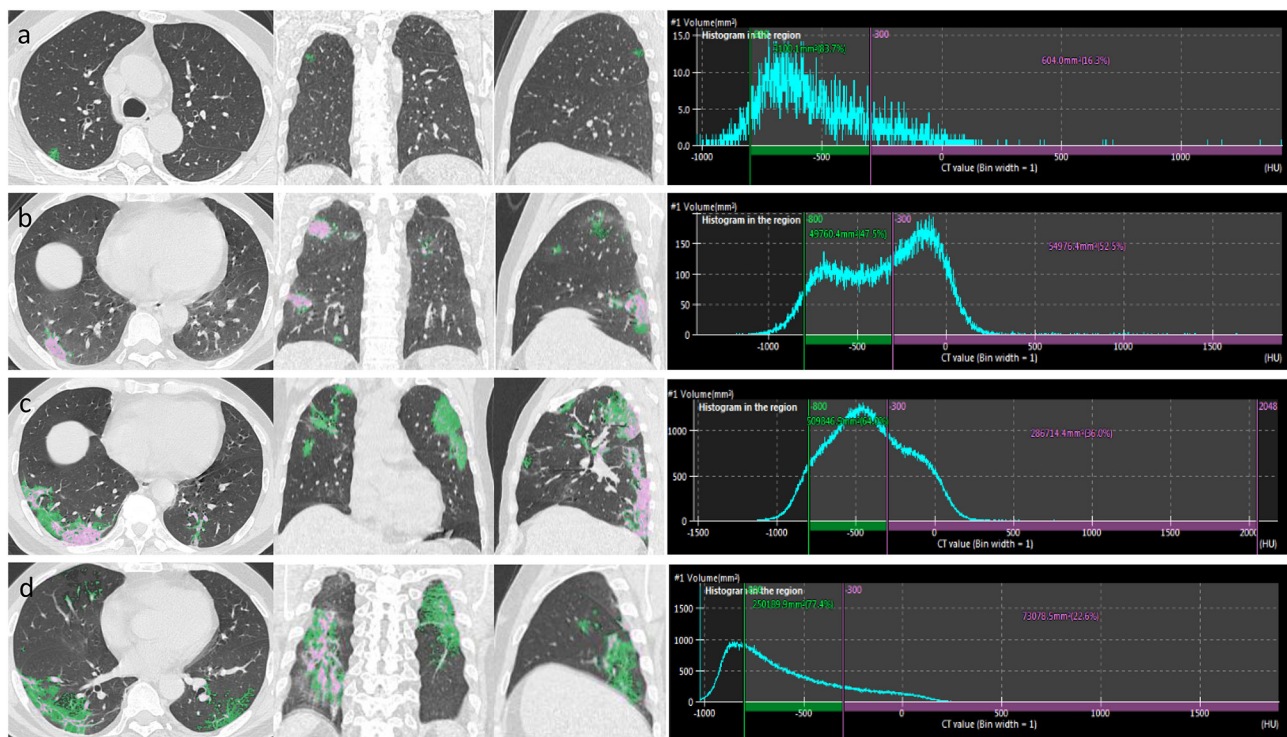


**FIGURE 4 |** After the segmentation of infected regions, automatic extraction of GGO and consolidation was performed in a patient with COVID-19 pneumonia. By thresholding on CT values in the pneumonia lesions, GGO (green area) and consolidation (pink area) were identified with the value range of  $-800$  to  $-300$  and  $>-300$  HU, respectively. The figure shows axial, coronal, and sagittal multiplanar reconstruction views (left to right) of GGO and consolidation in the early stage (a), progressive stage (b), peak stage (c), and absorption stage (d).

vs.  $3.2 \pm 2.1$ ,  $P < 0.001$ ) and the peak stage ( $10.3 \pm 4.4$  vs.  $3.2 \pm 2.1$ ,  $P < 0.001$ ) were significantly higher. **Table 1** shows that the total lung volume significantly decreased in the progressive stage ( $3.5 \text{ L} \pm 1.1$  vs.  $4.2 \text{ L} \pm 1.2$ ,  $P < 0.001$ ) and the peak stage ( $3.1 \text{ L} \pm 0.9$  vs.  $4.2 \text{ L} \pm 1.2$ ,  $P < 0.001$ ) and then recovered in the absorption stage ( $3.8 \text{ L} \pm 1.1$  vs.  $4.2 \text{ L} \pm 1.2$ ,  $P = 0.008$ ). The bilateral lower lobes were the most infected. The volume of pneumonia was significantly increased in the progressive stage ( $431.5 \pm 409.3 \text{ cm}^3$  vs.  $73.8 \pm 96.0 \text{ cm}^3$ ,  $P < 0.001$ ) and the peak stage ( $568.1 \pm 470.6 \text{ cm}^3$  vs.  $73.8 \pm 96.0 \text{ cm}^3$ ,  $P < 0.001$ ) and then decreased in the absorption stage ( $291.0 \pm 404.6 \text{ cm}^3$  vs.  $73.8 \pm 96.0 \text{ cm}^3$ ,  $P < 0.001$ ). The mean time to peak of the pneumonia volume was  $5.2 \pm 4.8$  days. In the early stage, 22 patients (20%) had LAA% of  $<5\%$ , 78 patients (70.9%) had LAA% of  $5-24\%$ , and 10 patients (9.1%) had LAA% of  $25-49\%$ . LAA% decreased in the progressive stage ( $10.1 \pm 6.6\%$  vs.  $13.7 \pm 8.0\%$ ,  $P < 0.001$ ), the peak stage ( $10.3 \pm 5.7\%$  vs.  $13.7 \pm 8.0\%$ ,  $P < 0.01$ ), and the absorption stage ( $9.8 \pm 6.1\%$  vs.  $13.7 \pm 8.0\%$ ,  $P < 0.001$ ). GGO volume increased in the progressive stage ( $230.6 \text{ cm}^3 \pm 231.0$  vs.  $41.4 \text{ cm}^3 \pm 59.2$ ,  $P < 0.001$ ), peak stage ( $328.3 \text{ cm}^3 \pm 299.0$  vs.  $41.4 \text{ cm}^3 \pm 59.2$ ,  $P < 0.001$ ), but decreased in the absorption stage ( $155.4 \text{ cm}^3 \pm 204.7$  vs.  $41.4 \text{ cm}^3 \pm 59.2$ ,  $P < 0.001$ ). Consolidation volume increased in the progressive stage ( $125.6 \text{ cm}^3 \pm 122.1$  vs.  $21.6 \text{ cm}^3 \pm 30.9$ ,  $P < 0.001$ ), peak stage ( $157.7 \text{ cm}^3 \pm 124.4$  vs.  $21.6 \text{ cm}^3 \pm 30.9$ ,  $P < 0.001$ ), but decreased in the absorption stage ( $49.4 \text{ cm}^3 \pm 71.5$  vs.  $21.6 \text{ cm}^3 \pm 30.9$ ,  $P < 0.05$ ). GGO:

consolidation ratio was significantly reduced in the progressive stage ( $3.0 \pm 4.0$  vs.  $31.2 \pm 160.5$ ,  $P < 0.01$ ), peak stage ( $2.6 \pm 2.7$  vs.  $31.2 \pm 160.5$ ,  $P < 0.05$ ) but increased in the absorption stage ( $9.5 \pm 36.2$  vs.  $31.2 \pm 160.5$ ,  $P < 0.05$ ).

## Relationship Between CT Score and Volume of Pneumonia

**Figure 5** shows the association between the visual CT score and the volume of pneumonia measured by the CAD system in the four stages. The CT score was found to be significantly correlated with the volume of pneumonia in the early stage ( $r = 0.731$ , 95% CI:  $0.614-0.816$ ,  $P < 0.001$ ), the progressive stage ( $r = 0.761$ , 95% CI:  $0.692-0.817$ ,  $P < 0.001$ ), the peak stage ( $r = 0.715$ , 95% CI:  $0.508-0.844$ ,  $P < 0.001$ ), and the absorption stage ( $r = 0.669$ , 95% CI:  $0.585-0.738$ ,  $P < 0.001$ ).

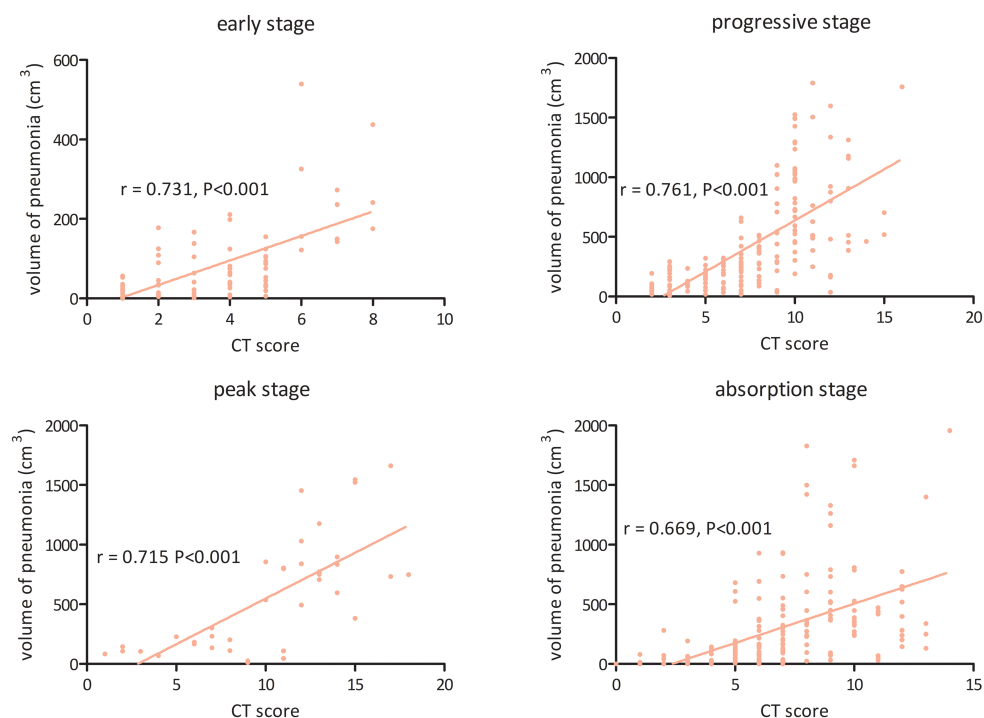
## DISCUSSION

In this study, we quantified the dynamic changes in lung and pneumonia on 3D-CT in patients with COVID-19 during hospitalization. The results showed that the lung volume and LAA% significantly decreased in the progressive, peak, and absorption stages. The volume of pneumonia lesions, GGO, and consolidation continually increased in the progressive and peak stages. The GGO/consolidation ratio was significantly reduced in the progressive and peak stages and then recovered a little in the

**TABLE 1** | Comparison of lung and pneumonia parameters generated by the CAD system among the four stages.

| Parameters                               | Early stage (n = 91) | Progressive stage (n = 188) | Peak stage (n = 39) | Absorption stage (n = 216) | P-value <sup>#</sup> |
|--|----------------------|-----------------------------|---------------------|----------------------------|----------------------|
| Total lung volume, L                     | 4.2 (1.2)            | 3.5 (1.1)+++                | 3.1 (0.9)+++        | 3.8 (1.1)++                | <0.001               |
| Volume of left lung, L                   | 1.9 (0.6)            | 1.7 (0.5)+++                | 1.5 (0.5)+++        | 1.8 (0.5)+                 | <0.001               |
| Volume of LUL, L                         | 1.1 (0.3)            | 1.0 (0.3)                   | 0.9 (0.3)+          | 1.0 (0.3)                  | 0.102                |
| Volume of LLL, L                         | 0.9 (0.3)            | 0.7 (0.3)+++                | 0.6 (0.3)+++        | 0.8 (0.3)+++               | <0.001               |
| Volume of right lung, L                  | 2.2 (0.6)            | 1.9 (0.6)+++                | 1.6 (0.4)+++        | 2.0 (0.6)++                | 0.013                |
| Volume of RUL, L                         | 0.9 (0.3)            | 0.9 (0.3)                   | 0.8 (0.3)+++        | 0.9 (0.3)                  | <0.001               |
| Volume of RML, L                         | 0.4 (0.2)            | 0.4 (0.2)                   | 0.4 (0.2)           | 0.4 (0.2)                  | 0.957                |
| Volume of RLL, L                         | 0.9 (0.4)            | 0.7 (0.4)+++                | 0.5 (0.3)+++        | 0.8 (0.3)+++               | <0.001               |
| LAA% of total lung                       | 13.7 (8.0)           | 10.1 (6.6)+++               | 10.3 (5.7)++        | 9.8 (6.1)+++               | <0.001               |
| LAA% of left lung                        | 14.0 (8.2)           | 10.5 (6.8)+++               | 10.6 (5.6)++        | 10.3 (6.3)+++              | <0.001               |
| LAA% of LUL                              | 16.6 (8.6)           | 13.1 (7.8)                  | 12.2 (5.9)          | 15.1 (33.8)                | 0.586                |
| LAA% of LLL                              | 11.6 (8.0)           | 7.5 (6.2)+++                | 7.6 (5.3)+++        | 7.0 (5.5)+++               | <0.001               |
| LAA% of right lung                       | 13.4 (8.0)           | 9.8 (6.4)+++                | 10.0 (5.9)++        | 9.3 (5.9)+++               | <0.001               |
| LAA% of RUL                              | 14.9 (8.3)           | 11.4 (7.1)+++               | 10.4 (5.6)+++       | 11.0 (6.6)+++              | <0.001               |
| LAA% of RML                              | 16.3 (8.6)           | 12.7 (7.9)+++               | 12.7 (7.3)+         | 12.0 (7.1)+++              | <0.001               |
| LAA% of RLL                              | 11.3 (8.1)           | 6.8 (6.1)+++                | 7.2 (5.5)+++        | 6.3 (5.4)+++               | <0.001               |
| Volume of pneumonia, cm <sup>3</sup>     | 73.8 (96.0)          | 431.5 (409.3)+++            | 568.1 (470.6)+++    | 291.0 (404.6)+++           | <0.001               |
| Volume of GGO, cm <sup>3</sup>           | 41.4 (59.2)          | 230.6 (231.0)+++            | 328.3 (299.0)+++    | 155.4 (204.7)+++           | <0.001               |
| Volume of consolidation, cm <sup>3</sup> | 21.6 (30.9)          | 125.6 (122.1)+++            | 157.7 (124.4)+++    | 49.4 (71.5)+               | <0.001               |
| GGO: consolidation ratio                 | 31.2 (160.5)         | 3.0 (4.0)++                 | 2.6 (2.7)+          | 9.5 (36.2)+                | 0.015                |

Values are expressed as mean (SD). <sup>#</sup>One-way ANOVA with post-hoc LSD multiple comparison tests was used to test the differences between data at early, progressive, peak, and absorption stages. The early stage was used as a reference. +P < 0.05, ++P < 0.01, and +++P < 0.001. LUL, left lower lobe; LUL, left upper lobe; RLL, right lower lobe; RML, right middle lobe; RUL, right upper lobe; LAA%, percentage of low attenuation areas; GGO, ground-glass opacities.

**FIGURE 5** | The association between visual CT score and volume of pneumonia measured by the computer-aided diagnosis system in the four stages of COVID-19 pneumonia.



absorption stage. In addition, we found a moderate association between the visual CT score and the volume of pneumonia in the early, progressive, and absorption stages.

The lung is the most involved organ by COVID-19 (18), and typical pathological findings consist of diffuse alveolar epithelium destruction, alveolar septal fibrous proliferation, hyaline membrane formation, and capillary damage/bleeding (19). The pathological changes are the basis of typical CT findings of COVID-19 pneumonia. Previous studies observed the time-dependent changes of COVID-19 pneumonia in the extent and severity of lesions (3, 20, 21), which could be classified as four stages. In the early stage, bilateral GGO with subpleural distribution was the primary manifestation. Subsequently, the infection rapidly progressed to diffuse GGO with crazy-paving pattern, air bronchogram sign, and consolidation. After that, infections in some patients increased to peak involvement in regard to size, number, and density. After the infection was controlled by supportive treatment, the consolidation was absorbed gradually with fibrosis, but GGO appeared due to the absorption of consolidation. Our quantitative analyses perfectly reflected the time course of lung changes on chest CT. We observed a significantly increased volume of pneumonia lesions, GGO, and consolidation in the progressive stage, which slowly increased in the peak stage and significantly decreased in the absorption stage. The mean time to peak of the pneumonia volume was  $5.2 \pm 4.8$  days. The GGO/consolidation ratio was persistently reduced in the progressive and peak stages and then recovered a little in the absorption stage. Timely monitoring the changes of total pneumonia, GGO, and consolidation would be beneficial for the evaluation of treatment response and adjustment of the clinical staging of COVID-19 patients.

The semiquantitative CT score can assess the disease severity of COVID-19 according to the area or degree of lung involvement (3). This marker is simple and readily available in a clinical setting without any need of post-processing. However, it is somewhat subjective when the COVID-19 pneumonia lesions are multiple and irregular. CAD-based quantitative CT might outperform the traditional semiquantitative method based on the visual CT score. Despite the limitation of the CT score, we found a moderate correlation between the visual CT score and the volume of pneumonia measured by our CAD system, indicating that the CT score could be safely and effectively used in clinical practice. Our study showed that the CT scores of progressive and peak stages were significantly higher than those of the early and absorption stages, which may be correlated with elevated inflammation-related biomarkers (22). Yang et al. showed that the CT score was higher in severe cases as compared to mild cases (23). They found that using the CT score of larger than 19.5 could predict severe COVID-19, with high sensitivity (83%) and specificity (94%), which was consistent with the study of Liu et al. (24). Mahdjoub et al. found that the admission CT score was an independent predictor for a 5-day outcome (i.e., mechanical ventilation or death) of COVID-19 patients (25). Therefore, the CT score may help risk stratification and identify those patients at high risk of rapid progress who need timely treatment.

To the best of our knowledge, this study firstly demonstrated that the lung volume of COVID-19 significantly decreased in the progressive and peak stages and then slowly increased in the absorption stage on chest CT, which may suggest the impairment of pulmonary function in COVID-19 patients; but, in the future, a pulmonary function test (PFT) is needed to confirm. Previous studies showed that a significant correlation between lung volume and PFT results in interstitial lung diseases (26–28). Since the outbreak of this disease, its impact on lung function remains unknown. Previous studies have demonstrated that recovered patients with SARS-CoV and MERS-CoV may be left with persistently damaged lung function (11–14). Mo et al. revealed that, in COVID-19 survivors, the most common abnormality of lung function is the reduced diffusion capacity, followed by restrictive ventilatory defect, which is associated with the disease severity (10). A recent case report might suggest that older patients with COVID-19 were more likely to have residual radiological changes and impaired lung function after discharge (29). These preliminary findings might suggest that lung function monitoring and rehabilitation in patients who recovered from COVID-19 is necessary. Our study may provide a possibility to evaluate lung volume without additional health costs.

Our study also has some limitations. First, it is a retrospective study. Second, our selection criteria might have introduced selection bias since we excluded mild and critical illness. Third, the different CT scan parameters might have a potential impact on software-based quantification. Fourth, some patients could not hold well their breath, especially severe cases, which may pose an impact on the calculation. Fifth, the sample size is relatively small, specifically for the peak stage; more subjects are needed to better understand the infection's underlying mechanism and its spread pattern. Sixth, the impact of other patient demographics, such as smoking status and preconditioned respiratory disease wasn't identified, which may play as a confounder. Finally, the effect of other lung structures, such as airways, vessels, and fissures, wasn't observed for analysis.

In summary, quantitative 3D-CT could be used as a useful complementary method to conventional CT in the follow-up of COVID-19 patients. Quantitative assessment of the dynamic changes in lung and pneumonia in patients with COVID-19 may be useful for routine patient management.

## DATA AVAILABILITY STATEMENT

The original contributions generated in the study are included in the article/supplementary material, further inquiries can be directed to the corresponding authors.

## ETHICS STATEMENT

The studies involving human participants were reviewed and approved by the Ethics Committee of The First Affiliated Hospital of Jinan University. Written informed consent for participation was not required for this study in accordance with the national legislation and the institutional requirements.



## AUTHOR CONTRIBUTIONS

QC and LC contributed to the conception and design of the study, the analysis and interpretation of data, and the work drafting. SL, LC, and ML participated in the data extraction and analysis. ZC and JY designed figures. BZ and SZ offered guidance in study design and revised the article critically for important intellectual content. All authors read the revision of the article as well as final approval of the version to be submitted.

## FUNDING

This work was supported by a grant from the National Natural Science Foundation of China (Grant Numbers:

81571664, 81871323, and 81801665); the National Natural Science Foundation of Guangdong Province (Grant Number: 2018B030311024); the Scientific Research General Project of Guangzhou Science Technology and Innovation Commission (Grant Number: 201707010328); and the China Postdoctoral Science Foundation (Grant Number: 2016M600145).

## ACKNOWLEDGMENTS

Thanks to Fujifilm (China) Investment Co. Ltd. MIBD team for providing Synapse 3D technical support. Thanks to all the medical workers for their fight against COVID-19 and to the people of the country and the world for their contributions to this campaign.

## REFERENCES

- Rubin GD, Ryerson CJ, Haramati LB, Sverzellati N, Kanne JP, Raoof S, et al. The role of chest imaging in patient management during the COVID-19 pandemic: a multinational consensus statement from the Fleischner society. *Radiology*. (2020) 296:172–80. doi: 10.1148/radiol.2020201365
- Chung M, Bernheim A, Mei X, Zhang N, Huang M, Zeng X, et al. CT imaging features of 2019 novel coronavirus (2019-nCoV). *Radiology*. (2020) 295:202–7. doi: 10.1148/radiol.2020200230
- Pan F, Ye T, Sun P, Gui S, Liang B, Li L, et al. Time course of lung changes at chest CT during recovery from coronavirus disease 2019 (COVID-19). *Radiology*. (2020) 295:715–21. doi: 10.1148/radiol.2020200370
- Li HW, Zhuo LH, Yan GW, Wang JS, Huang GP, Li JB, et al. High resolution computed tomography for the diagnosis of 2019 novel coronavirus (2019-nCoV) pneumonia: a study from multiple medical centers in western China. *Ann Transl Med*. (2020) 8:1158. doi: 10.21037/atm-20-5731
- Salehi S, Abedi A, Balakrishnan S, Gholamrezaezhad A. Coronavirus disease 2019 (COVID-19): a systematic review of imaging findings in 919 patients. *AJR Am J Roentgenol*. (2020) 215:87–93. doi: 10.2214/AJR.20.23034
- Zhou Z, Guo D, Li C, Fang Z, Chen L, Yang R, et al. Coronavirus disease 2019: initial chest CT findings. *Eur Radiol*. (2020) 30:4398–406. doi: 10.1007/s00330-020-06816-7
- Li K, Fang Y, Li W, Pan C, Qin P, Zhong Y, et al. CT image visual quantitative evaluation and clinical classification of coronavirus disease (COVID-19). *Eur Radiol*. (2020) 30:4407–16. doi: 10.1007/s00330-020-06817-6
- Mondoñedo JR, Sato S, Oguma T, Muro S, Sonnenberg AH, Zeldich D, et al. CT imaging-based low-attenuation super clusters in three dimensions and the progression of emphysema. *Chest*. (2019) 155:79–87. doi: 10.1016/j.chest.2018.09.014
- Colombi D, Bodini FC, Petrini M, Maffi G, Morelli N, Milanese G, et al. Well-aerated lung on admitting chest CT to predict adverse outcome in COVID-19 pneumonia. *Radiology*. (2020) 296:E86–96. doi: 10.1148/radiol.2020201433
- Mo X, Jian W, Su Z, Chen M, Peng H, Peng P, et al. Abnormal pulmonary function in COVID-19 patients at time of hospital discharge. *Eur Respir J*. (2020) 55:2001217. doi: 10.1183/13993003.01217-2020
- Xie L, Liu Y, Fan B, Xiao Y, Tian Q, Chen L, et al. Dynamic changes of serum SARS-coronavirus IgG, pulmonary function and radiography in patients recovering from SARS after hospital discharge. *Respir Res*. (2005) 6:5. doi: 10.1186/1465-9921-6-5
- Xie L, Liu Y, Xiao Y, Tian Q, Fan B, Zhao H, et al. Follow-up study on pulmonary function and lung radiographic changes in rehabilitating severe acute respiratory syndrome patients after discharge. *Chest*. (2005) 127:2119–24. doi: 10.1378/chest.127.6.2119
- Hui DS, Joynt GM, Wong KT, Gomersall CD, Li TS, Antonio G, et al. Impact of severe acute respiratory syndrome (SARS) on pulmonary function, functional capacity and quality of life in a cohort of survivors. *Thorax*. (2005) 60:401–9. doi: 10.1136/thx.2004.030205
- Hui DS, Wong KT, Ko FW, Tam LS, Chan DP, Woo J, et al. The 1-year impact of severe acute respiratory syndrome on pulmonary function, exercise capacity, and quality of life in a cohort of survivors. *Chest*. (2005) 128:2247–61. doi: 10.1378/chest.128.4.2247
- Guidelines for the Diagnosis and Treatment of Novel Coronavirus (2019-nCoV) Infection (trial version 7) (in Chinese)*. National Health Commission of the People's Republic of China (2020).
- Iwano S, Kitano M, Matsuo K, Kawakami K, Koike W, Kishimoto M, et al. Pulmonary lobar volumetry using novel volumetric computer-aided diagnosis and computed tomography. *Interact Cardiovasc Thorac Surg*. (2013) 17:59–65. doi: 10.1093/icvts/ivt122
- Cheng Z, Qin L, Cao Q, Dai J, Pan A, Yang W, et al. Quantitative computed tomography of the coronavirus disease 2019 (COVID-19) pneumonia. *Radiol Infect Dis*. (2020) 7:55–61. doi: 10.1016/j.rid.2020.04.004
- Zhou F, Yu T, Du R, Fan G, Liu Y, Liu Z, et al. Clinical course and risk factors for mortality of adult inpatients with COVID-19 in Wuhan, China: a retrospective cohort study. *Lancet*. (2020) 395:1054–62. doi: 10.1016/S0140-6736(20)30566-3
- Xu Z, Shi L, Wang Y, Zhang J, Huang L, Zhang C, et al. Pathological findings of COVID-19 associated with acute respiratory distress syndrome. *Lancet Respir Med*. (2020) 8:420–2. doi: 10.1016/S2213-2600(20)30076-X
- Ojha V, Mani A, Pandey NN, Sharma S, Kumar S. CT in coronavirus disease 2019 (COVID-19): a systematic review of chest CT findings in 4410 adult patients. *Eur Radiol*. (2020) 30:6129–38. doi: 10.1007/s00330-020-06975-7
- Vancheri SG, Savietto G, Ballati F, Maggi A, Canino C, Bortolotto C, et al. Radiographic findings in 240 patients with COVID-19 pneumonia: time-dependence after the onset of symptoms. *Eur Radiol*. (2020). doi: 10.21203/rs.3.rs-22623/v1
- Zhang B, Zhang J, Chen H, Chen L, Chen Q, Li M, et al. Novel coronavirus disease 2019 (COVID-19): relationship between chest CT scores and laboratory parameters. *Eur J Nucl Med Mol Imaging*. (2020) 47:2083–9. doi: 10.1007/s00259-020-04854-3
- Ran Y, Xiang L, Huan L, Yanling Z, Xianxiang Z, Qiuxia X, et al. Chest CT severity score: an imaging tool for assessing severe COVID-19. *Radiol Cardiothorac Imaging*. (2020) 2:e200047. doi: 10.1148/rct.2020200047
- Liu J, Chen T, Yang H, Cai Y, Yu Q, hen J, et al. Clinical and radiological changes of hospitalised patients with COVID-19 pneumonia from disease onset to acute exacerbation: a multicentre paired cohort study. *Eur Radiol*. (2020) 30:5702–8. doi: 10.1007/s00330-020-06916-4
- Mahdjoub E, Mohammad W, Lefevre T, Debray MP, Khalil A, Study Group. Admission chest CT score predicts 5-day outcome in patients with COVID-19. *Intensive Care Med*. (2020) 46:1648–50. doi: 10.1007/s00134-020-06118-y

26. Kitano M, Iwano S, Hashimoto N, Matsuo K, Hasegawa Y, Naganawa S. Lobar analysis of collapsibility indices to assess functional lung volumes in COPD patients. *Int J Chron Obstruct Pulmon Dis.* (2014) 9:1347–56. doi: 10.2147/COPD.S72616
27. Robbie H, Wells AU, Jacob J, Walsh SLF, Nair A, Srikanthan A, et al. Visual and automated CT measurements of lung volume loss in idiopathic pulmonary fibrosis. *AJR Am J Roentgenol.* (2019) 213:318–24. doi: 10.2214/AJR.18.20884
28. Ungprasert P, Wilton KM, Ernste FC, Kalra S, Crowson CS, Rajagopalan S, et al. Novel assessment of interstitial lung disease using the “computer-aided lung informatics for pathology evaluation and rating” (CALIPER) software system in idiopathic inflammatory myopathies. *Lung.* (2017) 195:545–52. doi: 10.1007/s00408-017-0035-0
29. Zha L, Shen Y, Pan L, Han M, Yang G, Teng X, et al. Follow-up study on pulmonary function and radiological changes in critically ill

patients with COVID-19. *J Infect.* (2021) 82:159–98. doi: 10.1016/j.jinf.2020.05.040

**Conflict of Interest:** The authors declare that the research was conducted in the absence of any commercial or financial relationships that could be construed as a potential conflict of interest.

Copyright © 2021 Chen, Chen, Liu, Chen, Li, Chen, You, Zhang and Zhang. This is an open-access article distributed under the terms of the Creative Commons Attribution License (CC BY). The use, distribution or reproduction in other forums is permitted, provided the original author(s) and the copyright owner(s) are credited and that the original publication in this journal is cited, in accordance with accepted academic practice. No use, distribution or reproduction is permitted which does not comply with these terms.



# End-to-End AI-Based Point-of-Care Diagnosis System for Classifying Respiratory Illnesses and Early Detection of COVID-19: A Theoretical Framework

Abdelkader Nasreddine Belkacem<sup>1\*</sup>, Sofia Ouhbi<sup>2</sup>, Abderrahmane Lakas<sup>1</sup>, Elhadj Benkhelifa<sup>3</sup> and Chao Chen<sup>4</sup>

<sup>1</sup> Department of Computer and Network Engineering, College of Information Technology, UAE University, Al Ain, United Arab Emirates, <sup>2</sup> Department of Computer Science and Software Engineering, College of Information Technology, UAE University, Al Ain, United Arab Emirates, <sup>3</sup> Cloud Computing and Applications Research Lab, Staffordshire University, Stoke-on-Trent, United Kingdom, <sup>4</sup> Key Laboratory of Complex System Control Theory and Application, Tianjin University of Technology, Tianjin, China

## OPEN ACCESS

### Edited by:

Reza Lashgari,  
Institute for Research in Fundamental  
Sciences, Iran

### Reviewed by:

Muder Almiani,  
University of Bridgeport, United States  
Brij Gupta,  
National Institute of Technology,  
Kurukshetra, India  
Yinlai Jiang,  
The University of  
Electro-Communications, Japan

### \*Correspondence:

Abdelkader Nasreddine Belkacem  
belkacem@uaeu.ac.ae

### Specialty section:

This article was submitted to  
Infectious Diseases - Surveillance,  
Prevention and Treatment,  
a section of the journal  
Frontiers in Medicine

**Received:** 21 July 2020

**Accepted:** 08 March 2021

**Published:** 31 March 2021

### Citation:

Belkacem AN, Ouhbi S, Lakas A,  
Benkhelifa E and Chen C (2021)  
End-to-End AI-Based Point-of-Care  
Diagnosis System for Classifying  
Respiratory Illnesses and Early  
Detection of COVID-19: A Theoretical  
Framework. *Front. Med.* 8:585578.  
doi: 10.3389/fmed.2021.585578

Respiratory symptoms can be caused by different underlying conditions, and are often caused by viral infections, such as Influenza-like illnesses or other emerging viruses like the Coronavirus. These respiratory viruses, often, have common symptoms: coughing, high temperature, congested nose, and difficulty breathing. However, early diagnosis of the type of the virus, can be crucial, especially in cases, such as the COVID-19 pandemic. Among the factors that contributed to the spread of the COVID-19 pandemic were the late diagnosis or misinterpretation of COVID-19 symptoms as regular flu-like symptoms. Research has shown that one of the possible differentiators of the underlying causes of different respiratory diseases could be the cough sound, which comes in different types and forms. A reliable lab-free tool for early and accurate diagnosis, which can differentiate between different respiratory diseases is therefore very much needed, particularly during the current pandemic. This concept paper discusses a medical hypothesis of an end-to-end portable system that can record data from patients with symptoms, including coughs (voluntary or involuntary) and translate them into health data for diagnosis, and with the aid of machine learning, classify them into different respiratory illnesses, including COVID-19. With the ongoing efforts to stop the spread of the COVID-19 disease everywhere today, and against similar diseases in the future, our proposed low cost and user-friendly theoretical solution could play an important part in the early diagnosis.

**Keywords:** COVID-19, intelligent learning, respiratory illness, health diagnosis, e-health

## 1. INTRODUCTION

People usually take breathing and respiratory health for granted and often forget that their lungs are vital organs, which are vulnerable to infections and injury. Respiratory diseases are, according to the World Health Organization (WHO), among the leading causes of disability and death in the world (1). Respiratory diseases include “acute respiratory infections as well as chronic respiratory diseases,

such as asthma, chronic obstructive pulmonary disease, and lung cancer” (2). Multiple factors can aggravate respiratory conditions, such as: tobacco smoke exposure either direct or indirect; heavy exposure to air pollution; occupational related disorders; malnutrition and low birth weight, but most commonly by exposure to viruses, such as the influenza virus or the Coronavirus (3). Making a timely and accurate diagnosis is essential for treatment as symptoms of respiratory illnesses are often very similar to each other (4), which can cause confusions that can lead to misdiagnosis. This may result in catastrophic consequences of further spread of the infection, particularly during pandemics, such as COVID-19 pandemic. Therefore, ensuring a diagnostic differentiator is highly crucial for timely and accurate prognosis and appropriate actions (5).

Cough is considered a key symptom of respiratory diseases (6). Cough is considered a key pulmonary disease symptom and a natural defense mechanism of the human body to protect the respiratory system (7). In normal conditions, a cough is a result of a contraction of respiratory muscles which compress the air in the lungs. This contraction follows the glottis closure after an inspiration of air (8) and occurs immediately before the sudden glottis reopening, which leads to a rapid air expulsion from the lungs to clear breathing passages. Cough properties are unique and repeatable for a given subject (9). A cough can be either productive or non-productive (10). A productive cough produces phlegm or mucus, clearing it from the lungs, while a non-productive cough, also known as a dry cough, does not produce phlegm or mucus. Analyzing the cough sound during therapy can give relevant information about the coughing pathophysiological mechanisms that result in specific cough patterns (11). Information on the glottis behavior in different respiratory conditions could also be retrieved from the cough sound (11). Change in cough sound is considered a critical indicator of the respiratory disease progress and the effectiveness of a therapy (11).

Characteristics of voluntary and involuntary (i.e., spontaneous or reflex) coughs have increasingly been analyzed to detect and characterize lung disease (12). Automated real-time and reliable lab-free tools for cough characterization and classification could be valuable for timely and accurate diagnosis and differentiating between different respiratory illnesses, which is crucial for correct treatment (13). This can be particularly useful in parts of the world with limited access to laboratory resources (14). Coughs are often seasonal events, therefore a cough classifier or detector shall have an extremely low false alarm rate to be considered clinically reliable. Moreover, this system shall be highly sensitive to changes in cough sounds to detect any infrequent event (15). To the best of our knowledge, there is no standard approach to evaluate cough sounds automatically that has been implemented, despite the fact that several approaches have been proposed in literature (11, 16). We also recognize that to achieve accurate diagnosis, data of other accompanying symptoms, such as temperature, must be used in conjunction with the cough data.

This paper proposes a theoretical end-to-end point-of-care system, supported by artificial intelligence (AI) module for classifying and diagnosing different respiratory illnesses,

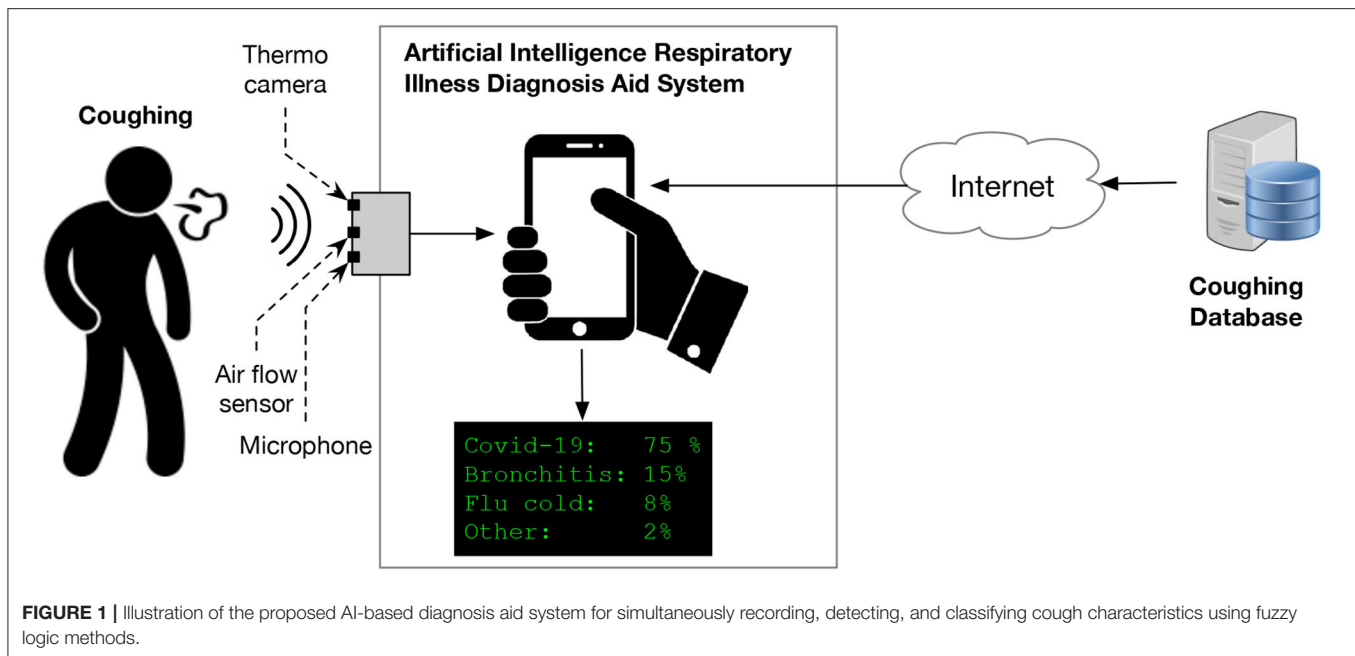
including early detection of COVID-19. The novel proposed theoretical system is composed of hardware and software components. The system will be able to record patients' or users' symptoms, including body temperature, cough sound, and airflow, using sensors. The recorded data will then be translated to health data, which will be processed by a machine learning module, to find patterns and classify the combined symptoms for different respiratory conditions, including COVID-19. A customized mobile application (app) will be developed and used for data processing and visualization. The app will allow the users to interact with the system's parameters, including the option to submit their results to physicians electronically. Patients' data will be stored securely in the cloud. **Figure 1** provides a high level illustration of the proposed system. The remainder of this theoretical framework paper is as follows: section 2 presents related works identified in the literature. In section 3, we explain the main components of the proposed system and its detailed architecture. In section 4, we conclude by discussing the perspective of the proposed framework, the challenges and the limitations.

## 2. RELATED WORK

Several studies have been conducted to classify and detect lung-related diseases using AI. Liu et al. (17) proposed a classification algorithm of lung sounds based on multilayer perceptron network and Hilbert-Huang transform features for non-invasive diagnosis of pulmonary diseases. The algorithm was tested using the R.A.L.E. database with a multi-layer perceptron classifier and achieved an averaged classification accuracy of 95.84%. Aykanat et al. (18) proposed a non-invasive classification method of recorded respiratory sounds using an electronic stethoscope. They recorded with this device 17,930 lung sounds from 1,630 subjects. Their results showed that by using convolutional neural network (CNN) and support vector machine (SVM), they could accurately classify respiratory sounds. Azam et al. (19) presented a scheme to detect respiratory patterns that are irregular due to respiratory diseases. They used 255 breath cycles captured using a smartphone under natural setting. Their experiments showed an accuracy around 75% using SVM for asthmatic inspiratory cycles and complete respiratory sounds.

Few AI systems have been proposed and/or developed to detect respiratory illnesses (20). Among them, *FluSense* (21), which is a contactless platform for syndromic surveillance of influenza-like illness used in waiting areas of hospitals. *FluSense* captures bio-clinical signals related to physical symptoms of influenza-like illness of individuals waiting in hospitals in privacy-sensitive and an unobtrusive manner. *FluSense* uses a thermal camera, a microphone array and a neural computing engine to characterize cough sound changes of individuals waiting in hospitals in a real-time manner. The researchers conducted a 7-month study in four public waiting areas equipped with *FluSense* within the hospital of a large university from December 2018 to July 2019 (21). In that study, *FluSense* collected and analyzed 21 million non-speech audio samples





and around 350,000 waiting room thermal images. The study (21) showed that *FluSense* accurately predicted the patient daily counts (Pearson correlation coefficient = 0.95). The *FluSense* platform did not take into consideration all respiratory illnesses nor additional health data. Cough data is important and relevant features but not sufficient one to be used for all respiratory illnesses.

With the recent rise in the new Coronavirus pandemic, early and accurate testing has been crucial due to the fast spreading feature of COVID-19, which caused more than 113 million confirmed cases and more than 2.5 million deaths up to late Feb 2021 (22). Among the important factors for the spread of COVID-19 have been lack of testing and erroneous diagnosis, which might be due to inaccurate testing or confusion with flu-like symptoms (23). Two main mechanisms to detect the Coronavirus disease were adopted at the beginning of the pandemic (24): (i) clinical scan images analysis of chest computed tomography (CT), and (ii) results of blood tests. COVID-19 patients, commonly, manifest persistent fever, tiredness, and dry cough. Although little peer-reviewed research existed on the diagnosis of COVID-19 during the first months of its spread worldwide, there has been a rapid response in the research community toward COVID-19 diagnoses and prediction using AI-based software on medical imaging (25–27). Chen et al. (28) have developed an engine to detect COVID-19 disease using high resolution CT images and deep learning. It has been deduced in Wynants et al. (27) that the prediction models for COVID-19 diagnosis are not well-reported with a high risk of bias. There is therefore a need to combine these models with other diagnostic methods, such as lab tests. However, these methods are costly and time consuming, which was problematic for many countries which do not have the capacity to accommodate tests for large populations. Cheaper rapid tests have emerged recently

to increase the testing capacity of many countries (29). However, these low-cost and rapid tests are often non-trusted, with many cases of false positives or false negatives. For this reason, several researchers have started looking into alternative solutions to detect COVID-19.

Some researchers have proposed a novel framework on how to detect COVID-19 using on-board smartphone sensors (30). However, their idea is still in the conceptualization phase and has not yet been implemented. The proposed solution is designed for certain types of smartphones, which may not be available and affordable to a large number of people. In addition their proposed framework is designed for COVID-19 diagnosis only. Imran et al. (31) have proposed *AI4COVID-19*, an AI-based app, that can diagnose and distinguish COVID-19 coughs from other non-COVID-19 coughs, such as pertussis and bronchitis. A similar tool has been proposed by Faezipour and Abuzneid (32), who have highlighted the benefits of developing a self-testing app using breathing sounds for COVID-19 diagnosis. They suggested that using an AI-based app using solely breathing sounds could estimate the user's lung volume and oxygenation, and diagnose healthy and unhealthy cases, including COVID-19. Laguarda et al. (33) have discriminated the asymptomatic COVID-19 infections through cellphone-recorded coughs using four biomarker patterns—vocal cord strength, sentiment, lung and respiratory performance, and muscular degradation—that are specific to COVID-19. Brown et al. (34) have analyzed a large-scale crowdsourced dataset of respiratory sounds that were collected to assist in diagnosis of COVID-19. They have concluded that it is possible to distinguish COVID-19 cough sounds from healthy cough using a simple binary machine learning classifier. This points to the potential of using cough sounds to diagnose COVID-19 (35–37). The cough sound can also be used to detect other respiratory illnesses. Moschovis et al.

(38) used a smartphone app, *SMARTCOUGH-C 2*, to collect and analyze cough sounds to detect respiratory diseases in children. Analyzing the sound cough to classify respiratory disorders other than COVID-19 has also been investigated by Taqee and Bhateja (39). To the best of our knowledge, there is no end-to-end solution proposed to diagnose COVID-19 and other respiratory disorders using cough sound in combination with other health data. Hence the need for our contribution. The aim of this paper is to develop an end-to-end point-of-care diagnosis device, that can collect data of combined common symptoms in respiratory illnesses (e.g., cough, body temperature, and airflow) and classify them as a diagnostic differentiator, detecting even asymptomatic COVID-19. The system has also the potential to be adaptable to early diagnosis of newly emerging respiratory illnesses.

### 3. THE PROPOSED SYSTEM

The objective of cough classification is to develop an automatic system that is capable of classifying various attributes of coughs, such as the intensity of the cough, time-frequency, energy distributed, or whether the cough is wet or dry. Different respiratory diseases, such as Bronchitis, Tuberculosis, Asthma, may have different effects on the pulmonary system, and therefore, are identifiable through the changes observed on the cough sound. For instance, coughs from asthmatic patients tend to have different energy signatures than that from non-asthmatic patients. In particular, asthmatic coughs exhibit more energy in the low frequency (40). On the other hand, the study of the cough phases reveals that dry coughs have lower intensity than wet coughs in phase two. In addition, during this phase, most of the signal intensity of the wet coughs is found to be within 0–750 Hz range, whereas that of the dry coughs is within 1,500–2,250 Hz range (41). Thus, most of cough recording experiments have been using a sampling frequency between 48,000 and 22,050 Hz to cover all cough types. Before designing the architecture of proposed system, it is important to first understand the cough audio preprocessing phase, which is described below.

#### 3.1. Cough Audio Preprocessing

##### 3.1.1. Cough Audio Analysis

The acoustic sound of a cough is generated by the contractions of the respiratory muscles. The cough, with its typical sound, is the result of the sudden opening of the glottis opening suddenly due to a rapid exhalation of air from the lungs. A typical cough sound signal consists of three phases as shown in **Figure 2**:

1. a rapid explosive phase which is recognized by an initial burst of emerging sound yielding a high frequency due to the vibrations resulting from the air flowing in the narrow bronchial airways.
2. an intermediary phase which decays as air is flowing in a steady-state while the glottis is fully open. This phase gives the duration to the whole cough. When the sputum is present a higher frequency component may be added to the signal.
3. a phase named voiced and that is not present in most coughs. This phase is characterized by a narrowing of the glottis again leading the vocal cords to get close to each other.

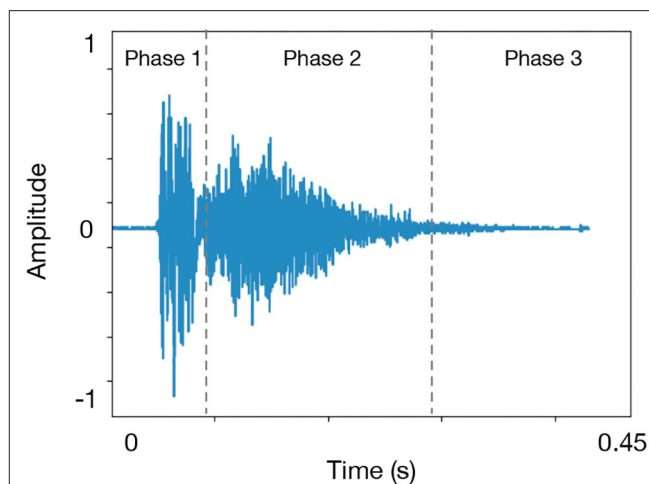


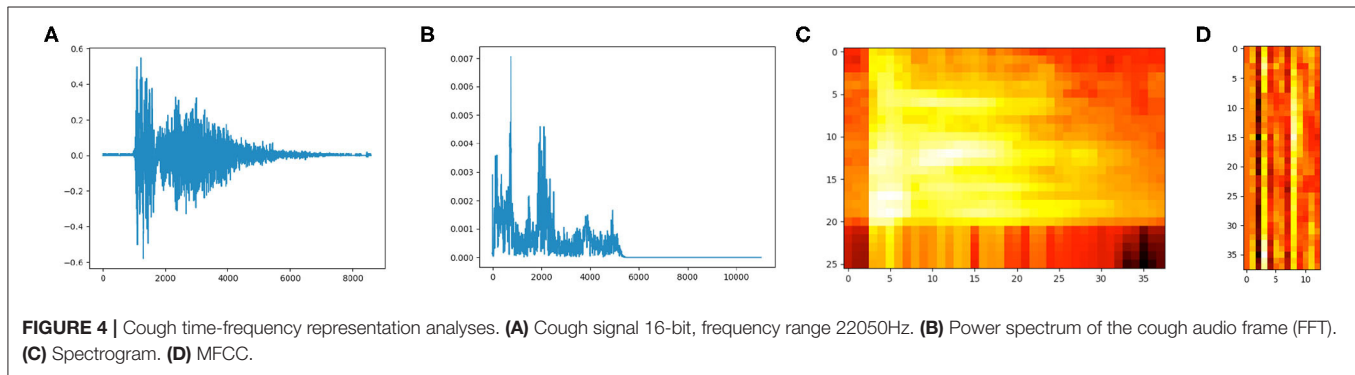
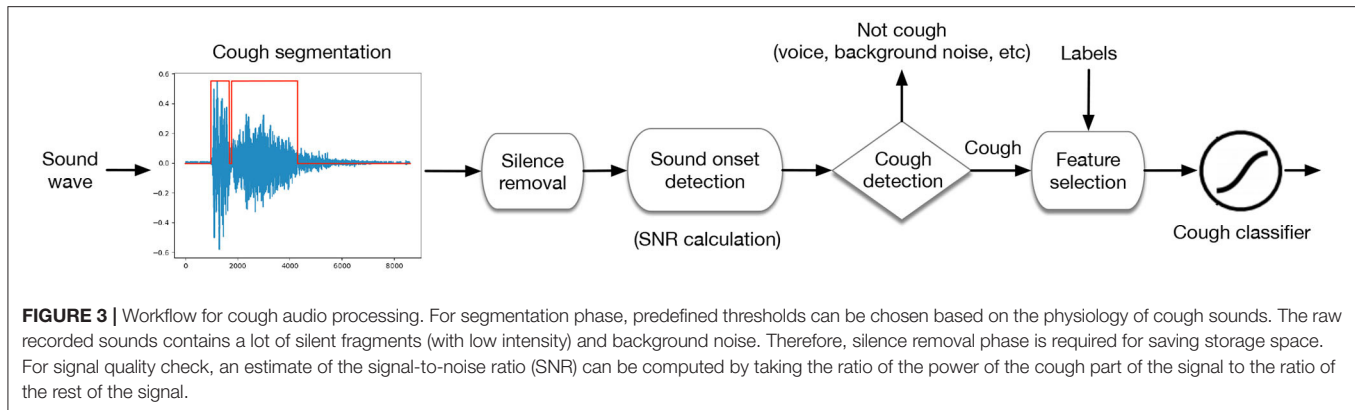
**FIGURE 2** | A typical cough sound structure. There are three common patterns of cough based on the number of phase, such as three-phase cough, two-phase cough, and peal cough.

The first two phases are ubiquitous across all coughs and will be useful in determining the start and end of a cough using an energy-based criteria. The majority of the coughs duration is around 400 ms (Here we chose 50 ms) (42). For instance a dry cough is characterized by the absence of any mucus or sputum (10). That is, all the three phases are visible in a dry cough signal. Initially, a burst of high energy is observed followed by less energy in the second phase at higher frequencies. However in the case of a wet cough sound signal more energy is observed in Phase 2 at higher frequencies. Typically, a wet cough, symptomatic of bronchitis, asthma, and pneumonia, is produced by inflammation and secretion of mucus and sputum in the lower airways caused by either a bacteria or a virus (10).

##### 3.1.2. Cough Segmentation and Detection

One of the first tasks of cough audio analysis is to be able to detect and identify a cough signal then classify it using some biomarkers (see **Figure 3**). Several research studies have addressed cough detection using different methods. For instance, in Barry et al. (43), the authors used Linear Predictive Coding and Mel-Frequency Cepstral Coefficients to model the sound of coughs, and used a Probabilistic Neural Network to classify time windows as containing or not a cough. Other researchers have used Hidden Markov Model (HMM) with Mel-Frequency Cepstral Coefficients (MFCCs) to be fed as input (44).

This process consists of cleaning the cough sounds dataset by filtering out all the interferences and the environmental noise from the audio frames and keeping only the relevant frames to the cough. of audio separation consists of extracting the cough sounds. There are several methods for source separation including Independent Component Analysis (ICA) (45), Blind Source Separation (BSS) (46), and Informed Source Separation (ISS) (47).



### 3.1.3. Feature Selection and Discriminant Analysis

Feature extraction is an important step toward classification of cough sounds. However, creating a classification model with from a dataset with high-dimensionality is time consuming and may converge to a local minima given the large search space. Therefore, selecting a reduced set of relevant features in an audio sample can improve immensely the performance generating a classification model (48). There are many techniques for feature selection including Shannon Entropy (SH), Fisher score, Mel-Frequency Cepstral Coefficients, and Zero Crossing Rate (ZCR). However, MFCC method has gained popularity due to its efficiency in the analysis of speech and sound signals in general, and is therefore opted for in the analysis of cough sounds. Features selection during the pre-processing of cough sounds is 2-fold: first, reducing the dimensionality for the feature matrix classification, and second, extracting the most dominant information present in the cough sound. Prior to feature extraction, any noise must be filtered out of the cough sound. The quality and performance of the classification process depends strongly on how well the process of features extraction has been done (see Figure 4).

### 3.1.4. Mel-Frequency Cepstral Coefficients

MFCCs are commonly used in audio processing for sound pattern recognition. In this method assumes that a sound is produced during the passage of small glottal pulses through vocal channel filter. Therefore, it only makes sense to exploit a small

set of features in the signal. That is, for MFCCs, usually about 10–20 are enough to represent the overall spectral envelope of the cough signal. MFCC analysis shows the power spectrum of the signal, and is often used to describe its timber. MFCCs are obtained after putting the signal spectrum on a non-linear Mel-scale of frequency, then obtaining the log-power spectrum from the result and finally applying a cosine transform. A cough sound has a complex signal structure carrying critical information that can contribute to the discrimination between various phases of the signal. The use of Mel scale is motivated by the fact that the features of an audio signal are better discerned by a human ear at low frequencies than they are at high frequencies. Therefore, Mel scale ensures that signal features match more closely what humans hear. The Mel scale is obtained using the following conversion formula:

$$M(f) = 1125 \ln \left( 1 + \frac{f}{700} \right) \quad (1)$$

$$M^{-1}(m) = 700 \left( \exp \frac{m}{1125} \right) - 1 \quad (2)$$

MFCCs calculated following few steps starting by framing the signal into shorter frames (20–40 ms frames). That is, for a signal sampled at  $f_s$  Hz, and a standard 25 ms, the frame length is equal to  $0.0025 \times f_s$  samples. For each sample, the periodogram estimate of the power spectrum is calculated. The Mel filter bank is then applied to the power spectra and the sum of the energy in

each filter is calculated. The next step consists of calculating the logarithm of all the filter bank energies, and the discrete cosine transform (DCT) of the result. From the computed DCT, only coefficients 2–13 are retained as Mel coefficients.

### 3.1.5. Cough Classification and Machine Learning

Classification of cough sounds is a helpful tool for identifying the underlying cause of coughs. Several methods for automatic cough classification have been developed to identify various cough types and the thus the pulmonary disease. The most common used classifiers are Gradient boosted decision trees (XGBoost), Deep Neural Network (DNN), Convolutional Neural Network (CNN), Recurrent Neural Network (RNN), and Fuzzy Deep Neural Network (FDNN).

## 3.2. Proposed System Architecture

Does cough sound contain sufficient information to be used for distinguishing among all respiratory illnesses? Is it possible to detect and classify COVID-19 infection through cough sounds using artificial intelligence algorithms? In this concept paper, a medical hypothesis of classifying respiratory illnesses using cough data from a forced-cough device recording is discussed with some proposed explanations made on the basis of limited evidence as a starting point for further investigation. We propose a theoretical design of reliable user-friendly AI based system for early detection of COVID-19 and other respiratory illnesses. This integrated hardware-software system will have two main components:

1. A novel hardware composed of several sensors (e.g., microphone, and thermal imaging tool, and a cough sound-recording device),
2. An AI software for cough classification and flu type recognition.

**Figure 5** shows all necessary hardware components to collect health data from healthy and unhealthy participants. In the following paragraphs, we will explain each component in details.

### 3.2.1. Collecting Data

Collecting data strategy is one of critical phases to build a trusted diagnosis model. The data can be collected using specific sensors for each input. For example, collecting cough sound requires a simple microphone for recording the sound via smartphone app or a web browser (49, 50). However, it is still a challenge to record big data for each respiratory illness. One way is to kindly ask people over the world to volunteer their cough sounds via online platforms. We may also collect basic demographics, medical history, and a few seconds of reflex and voluntary coughing samples. The participants should ensure that recording the sounds was in a quiet environment to avoid noisy sounds. The participant's anonymity and privacy are protected and no personal information is collected. If agreed on by the participant, the location may be collected as location information is particularly useful to draw a map of respiratory illnesses. The collected data may be made available as open source to be used for promoting science and fighting respiratory diseases. Therefore, a process of ethical approval and

clear informed consent from the participants may be required before and during the collection. **Table 1** shows recent online cough recording platforms. For developing an trusted AI model-based respiratory illnesses' diagnosis, many information can be recorded as inputs, such as cough sound, body temperature, airflow, EMG, ECG, and mucus. The COVID-19 pandemic has proved that it is time for everyone to contribute to public-cough datasets development which can include all cough types for each respiratory illness. The action can get sped up by encouraging patients, hospitals, and healthcare companies for donating their medical records to science. **Figure 6** shows an example of large public cough database [COUGHVID (49), the Embedded Systems Laboratory (ESL) at École polytechnique fédérale de Lausanne (EPFL), Switzerland].

### 3.2.2. Cough Sound Recording

The proposed system architecture is designed in order to extract useful clinical information from many inputs, such as cough sounds. For recording audio of people coughing, breathing (which indicate labored or irregular breathing) or even talking, we need a microphone to convert acoustical energy (sound waves) into electrical energy (the audio signal). Then, we need amplifier, analog to digital converter (ADC), and digital signal processing (DSP) for preprocessing phase. Cough characteristics and its acoustic features depend on the velocity of airflow, dimensions of the vocal tract and airways, and location of sound generated. Amplitude of the cough sound, intensity, duration, frequency, time-frequency representation (spectrogram which is a visual representation of the spectrum of frequencies of a signal as it varies with time), the mel frequency cepstral coefficients, the constant-Q cepstral coefficients (CQCC), and so on can be used for feature extraction phase as cough sound pattern. However, if the cough sound was not recorded in quiet room then blind source separation and independent component analysis can be used to find the right signal. **Figure 7** shows signals of three cough types (healthy, symptomatic, and COVID-19). Some researchers have already started using cough database for classifying some cough statues, such as healthy, symptomatic, asymptomatic, and COVID-19 coughs (33, 53).

### 3.2.3. Spirometer

A spirometer is an apparatus for measuring the volume of air inspired and expired by the lungs of healthy or unhealthy participants. It measures ventilation, the movement of airflow into and out of the lungs which a high indicator for early diagnosis of any respiratory illnesses. For this subsystem, the input is airflow and the outputs could sound pressure, aerosol volume, and cough flow rate.

### 3.2.4. Thermal Camera

The infrared thermal imaging camera can be used for detecting elevated body temperatures which may indicate the presence of a fever, a symptom of many respiratory illnesses, such as COVID-19. Detecting people with a potential fever may contain or limit the spread of many contagious respiratory illnesses through identification of infected individuals showing fever



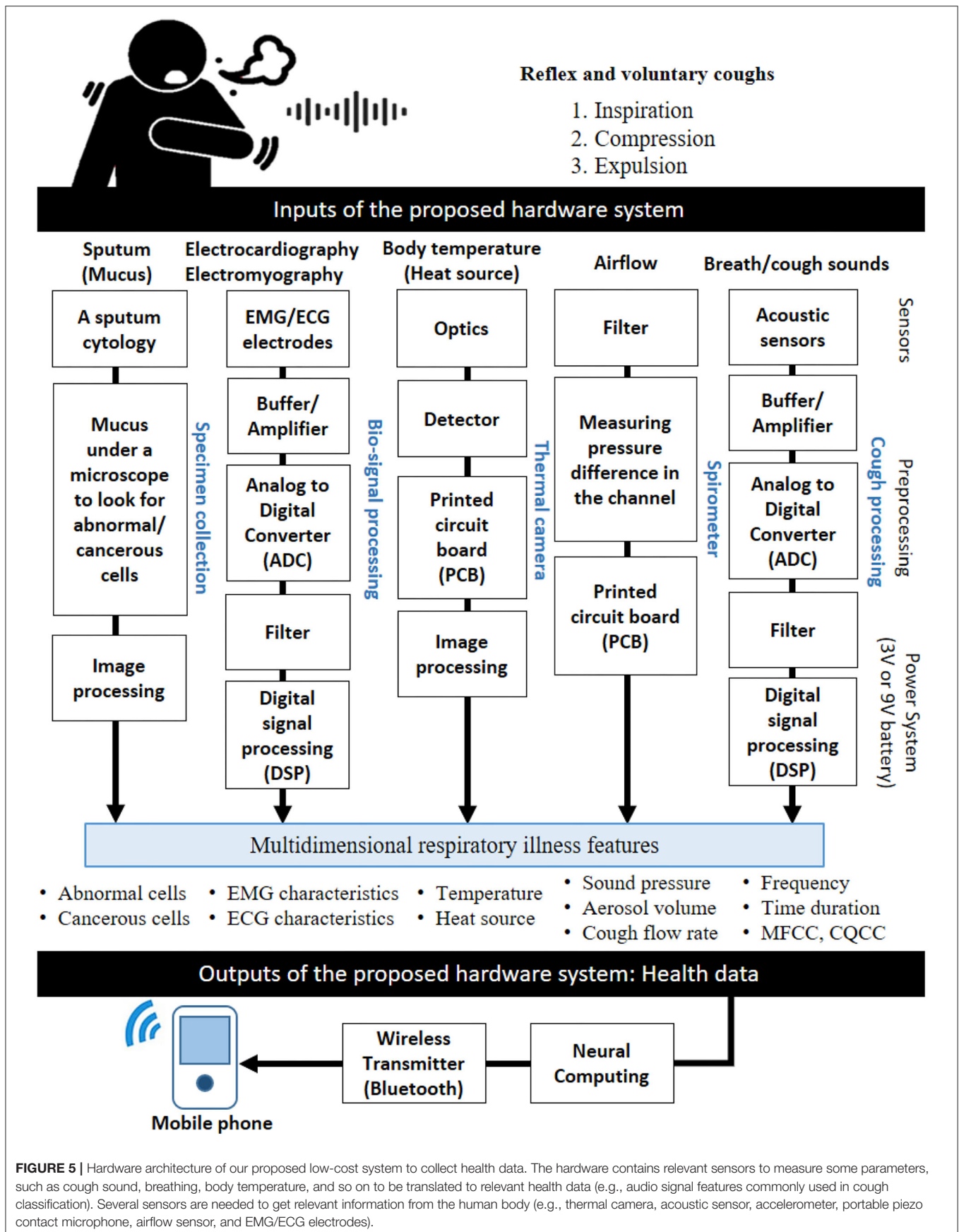
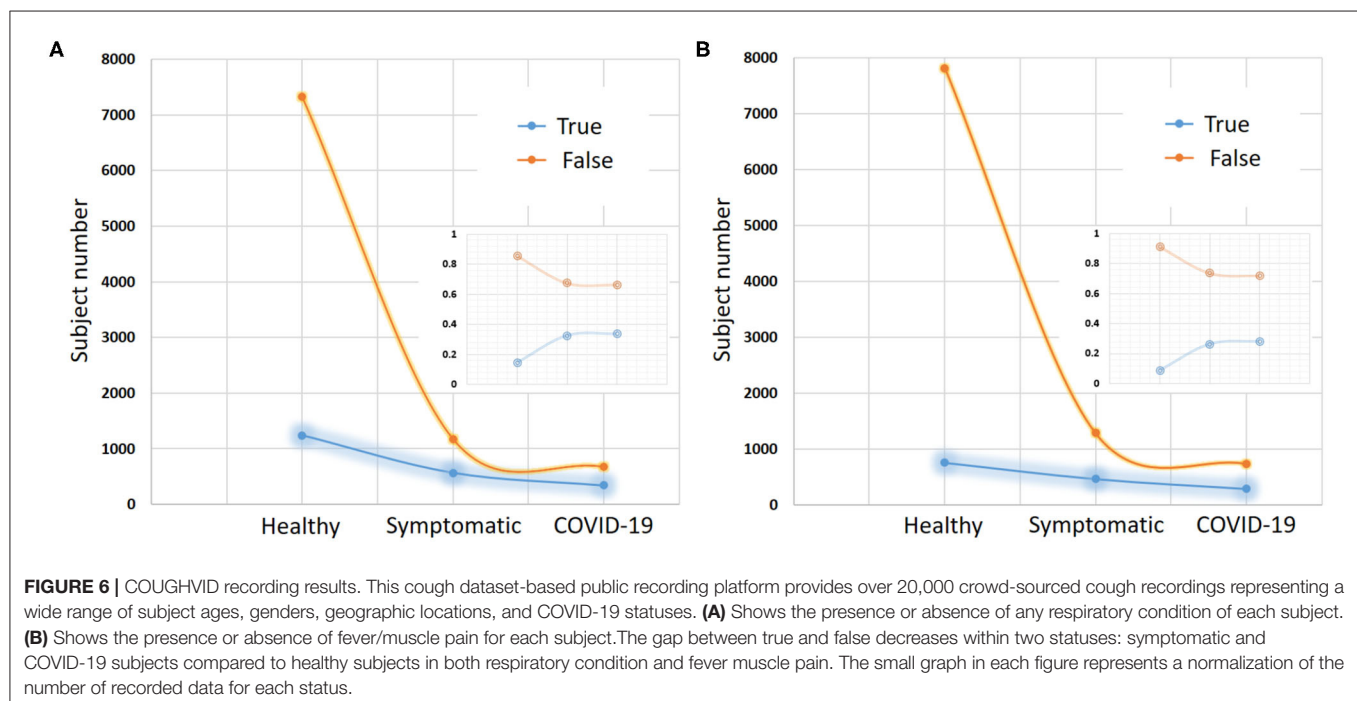


**TABLE 1** | A list of some online recording platform-based cough databases.

| Dataset            | Source   | Recording platform  | Recording type   | References |
|--------------------|--|---|--|------------|
| Cambridge database | University of Cambridge, UK                                  | <a href="https://www.covid-19-sounds.org/">https://www.covid-19-sounds.org/</a>                               | Short recordings of cough and breathing and report symptoms (healthy and non-healthy participants).                        | (34)       |
| MIT database       | Massachusetts Institute of Technology (MIT), USA             | <a href="https://opensigma.mit.edu/">https://opensigma.mit.edu/</a>   | Cough sounds from healthy and COVID-19 subjects, including asymptomatics.  | (33)       |
| NYU database       | New York University (NYU), USA                               | <a href="https://www.breatheforscience.com/">https://www.breatheforscience.com/</a>                           | Studying the link between respiratory diseases and breathing patterns in the US population.                                | (51)       |
| Virufy             | Stanford COVID-19 Response Innovation Lab, USA               | <a href="https://virufy.org/data">https://virufy.org/data</a>   | Virufy is a global applicability of crowdsourced and clinical datasets for AI detection of COVID-19 from cough.            | (52)       |
| NOCOCODA           | Carleton University's Institutional Repository, USA          | From online interviews with COVID-19 patients (e.g., published interviews on social media and YouTube videos) | This coronavirus coughs database contains cough events obtained from online interviews with COVID-19 positive individuals. | (50)       |
| COUGHVID           | École Polytechnique Fédérale de Lausanne (EPFL), Switzerland | <a href="https://coughvid.epfl.ch/">https://coughvid.epfl.ch/</a>   | Cough sounds from healthy, symptomatic, and COVID-19 participants.   | (49)       |

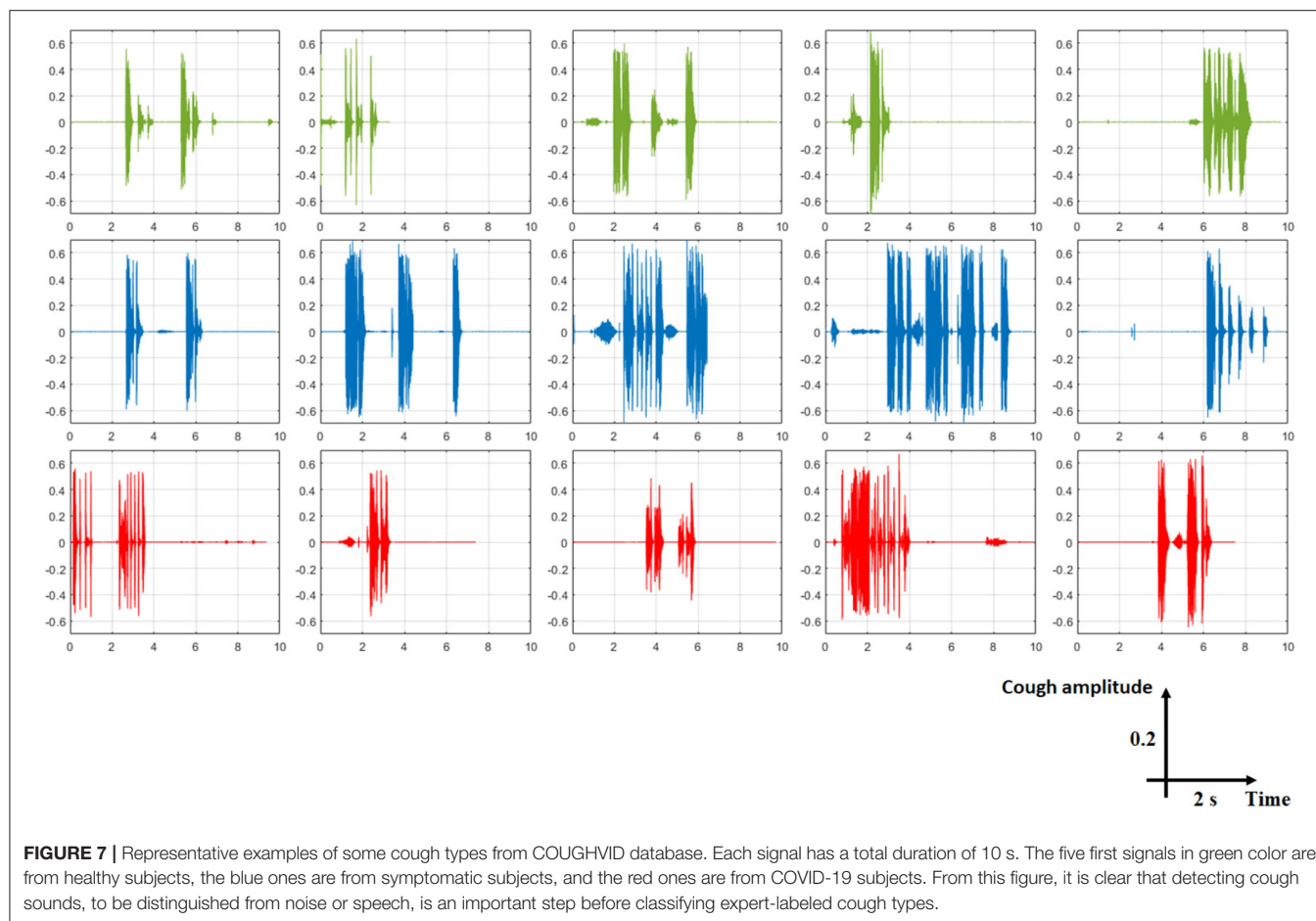


symptoms. Thermal cameras are passive devices that don't emit any radiation, rather they use infrared radiation emitted from objects (human body in this case) to deliver high-resolution images without the need of any additional illumination. These cameras provide a visual map of skin temperatures in real time. They allow the operator of a critical public infrastructure (e.g., airports, train stations, and schools) to non-invasively scan the crowd or individuals to avoid the spread of some infectious disease.

### 3.2.5. EMG/ECG Processing

COVID-19 and many respiratory illnesses may cause trouble breathing, liver problems or damage, heart problems, and kidney damage. In most cases, the lungs might become inflamed, making

it tough for patients to breathe. This can lead to pneumonia, an infection of the tiny air sacs (called alveoli) inside the lungs where the blood exchanges oxygen and carbon dioxide. However, during respiratory biofeedback, we can place some sensors or electrodes around the abdomen and chest to monitor the breathing patterns and respiration rate. Electrocardiogram (ECG) can be used for measuring the heart rate and how your heart rate varies (e.i., atrial and ventricular depolarization and repolarization are represented on the ECG as a series of waves PQRST: the P-wave, the QRS complex, and the T wave). In addition, electromyogram (EMG) can be also used for monitoring the electrical activity that causes muscle contraction around heart or chest wall movements or even for getting cough sound from the throat.



### 3.2.6. Sputum Cytology

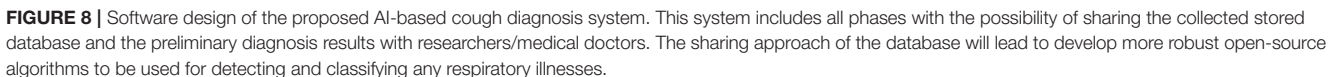
A sputum cytology is used for testing lung secretions or phlegm to look if there are some cancerous cells. The patient coughs up a sample of sputum (mucus), which is checked under the microscope to identify possible cancer cells or determine whether abnormal cells are present. However, using automated sputum cytometry, such as LungSign test for lung cancer, lung ultrasound for pneumothorax, or optical automation for sputum cytology can be also useful compared to the conventional cytology.

### 3.2.7. Artificial Intelligence Based Algorithm

After extraction some relevant patterns from system inputs and building a feature vector or matrix, we will give the data to some machine learning or deep learning methods [e.g., support vector machine (SVM), artificial neural network (ANN), convolutional neural network (CNN)]. However, machine learning algorithms almost always require structured data, while deep learning networks rely on layers of ANN. **Figure 8** shows cough diagnosis-based software design from collecting data until sending the health data with the preliminary diagnosis to the patients and/or physicians. This proposed software design can be used for all relevant collected health data, such as breathing instead of coughing inputs. The proposed software design has two phases: offline and online. For offline analysis, all collected data will

be used for building a classification model by dividing the data into 80–90% training data and 20–10% test data. For classification method, deep learning is the best choice for big raw data. However, the number of class of respiratory illnesses is very high. Therefore, fuzzy logic might be an option to give a percentage of truth of each class. The model will be made based on many participants' data to be able to generalize it later in the testing phase. In addition, normalization of the data is also important. After fixing all parameters of the supervised classifier and building the model, we will test it on new data to check its performance. For real-time analysis, an online classification algorithm based on offline model (or dynamic model) is needed. The classification result of any respiratory illnesses will be displayed for the user on the smartphone and it can be sent to experts via cloud service. Further details on the implementation of different machine learning algorithms for cough classification is presented in the subsequent sections.

1. Deep neural networks are feed-forward networks that are characterized by an input layer and an output layer and multiple hidden layers, through which information is typically processed by a logistic function. The total input at a given layer is mapped and sent forward to the next layer. In the case of signal classification, the audio input, represented by



2. Convolutional neural networks, like in neural networks, learnable kernels (filters) receive the audio spectral features as input, over which a weighted sum is computed and passed through an activation function. A CNN is typically made of a series of convolutional layers on top of which pooling layers are added for the purpose of down-sampling the learned feature maps. These layers are usually followed by one or more dense layers (see **Figure 9**). A fully convolutional network (FCN) is a variant of CNN extended with fully connected layers. For feature extraction, we use a logarithmic (log)-scaled mel-spectrogram with an appropriate number of components (bands) covering the audible frequency range of a cough (0–22,050 Hz), using a window size and a hop size

3. Recurrent Neural Networks (RNNs) allow cyclical connections in a feed-forward neural networks, which allows them to incorporate contextual information from previous input, and remember past input values in the layers' internal state. This property makes RNNs an attractive choice for sequence to sequence learning. Compared to CNNs, RNNs adopt a different approach for representing the temporal features of information. At each time-step, RNNs compute the output based on the current input and the result of the hidden state at the previous time-step. By doing so, RNNs embed in their processing the temporal dependency of the inputs across the time-steps of the past. That is for bidirectional RNNs, the same process can be employed in reversed order by extending the receptive field into the future. Long short-term memory networks (LSTMs) are a variant of RNNs that exploit the contextual information over longer



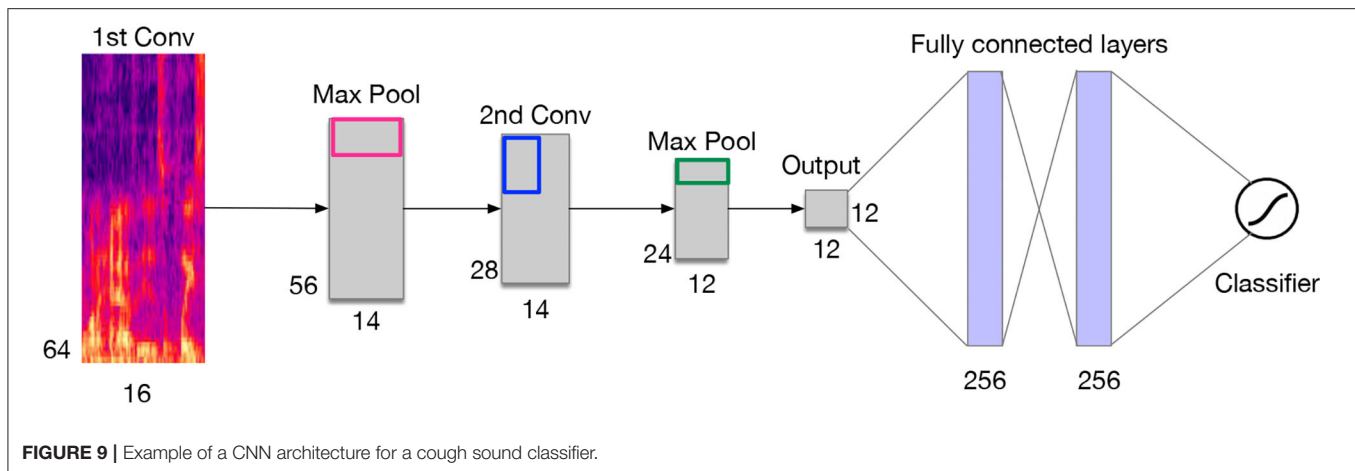


**FIGURE 9** | Example of a CNN architecture for a cough sound classifier.

time intervals to map the input sequence to the output. LSTMs known to be efficient at learning temporal dependencies, and they are applied in a variety of areas, such as speech recognition and synthesis. They are also used with some success when combined with CNN as front-end (CRNN), for video classification. Although, the applicability of LSTM for sound classification has not been fully investigated, they can be very beneficial given the temporal properties embedded in a cough sound.

4. Integrating fuzzy inference systems into deep learning networks is one of hybrid classification approaches that have proven to be effective methods for making highly accurate predictions from complex data sources in the fuzzy logic domain (i.e., fuzzy sets, fuzzy rules). This combination aims to model vague notions with rigorous mathematical tools and rejects the principle of bivalence for pattern recognition, classification, regression or density estimation. Based on this aspect, many methods can be produced, such as combining convolutional neural network with fuzzy logic which called the Fuzzy Convolutional Neural Network (FCNN). Both neural networks and fuzzy systems have no mathematical model necessary. Neural networks are able to learn from scratch using several learning algorithms but fuzzy systems are based on *a priori* knowledge and not capable to learn. Neural networks based on black-box behavior but fuzzy systems are based on simple interpretation and implementation. Therefore, combining both approaches aims to unite advantages and exclude disadvantages.

### 3.3. Cloud Hosting Solutions

Cloud is important for storing collected raw data and/or useful information using internet of medical thing (54) to improve the decision-making of the physicians and/or monitor the quarantined patients through the proposed digital device. The main benefit of this approach is to extend the use of our proposed system to facilities that people with respiratory illnesses to send their health data and early diagnosis to medical experts with high confidentiality.

## 4. CONCLUSIONS

The architectural design of the proposed theoretical framework is composed of two major components. The first one consists of devising a process of collecting the data related to the vital signs of the patient and the recorded cough sound, breathing, and so on. The second part consists of building an integrated hardware/software system for end-users intended to capture a patient's vital signs along with the sound of the coughing. The hardware part of this system includes all the sensing devices whereas the software part contains the data processing as well as the prediction algorithms, which predicts the type of the respiratory illness including COVID-19. The prediction algorithm relies on the state of the art AI model available in the respiratory illness database in the cloud. For the proposed system to gain traction in the market and be adopted by the public and healthcare systems, a number of KPIs need to be achieved and maintained, including efficient use of our proposed system, effectiveness and timeliness of early diagnosis, diagnosis costs, patient wait time, data transparency, decision-making errors of the used classifier, and patient safety and satisfaction. However, identifying the right KPIs, track them, and organize them in a logical, coherent and useful way, is critical step to achieve a good system evaluation, especially for developing medical devices. To evaluate this kind of systems, we shall conduct a pilot study and/or recruit volunteers (beta testers) to test the usability of the device and its software. Many other quality aspects, such as reliability and performance efficiency can be assessed in the of evaluation process, where the involvement of medical experts will form a crucial role in this process.

The effective and efficient use of our proposed theoretical system is based on the collection of a combination of relevant health data for creating a feature vector to differentiate between multi-class respiratory illnesses. A timely diagnosis is a critical criteria for evaluating such a system; using advanced deep learning methods and dimensionality reduction lead for big data analysis will minimize the classification and diagnosis time. The proposed system is designed to be a portable and low cost diagnostic tool, supported with AI. Many countries in the

world have limited resources, where this lab-free device will be handy. In addition, this system will increase data transparency between the patients and the physicians, and the ability to share data and diagnosis by the proposed system, with the medical experts via the cloud would improve timely intervention and reduce any false-positives of false-negatives. Advanced machine learning algorithms with public large-scale datasets are the key to speed up the realization of the proposed system for understanding the relationship between respiratory conditions and coughing patterns.

## DATA AVAILABILITY STATEMENT

The original contributions presented in the study are included in the article/supplementary material, further inquiries can be directed to the corresponding author/s.

## REFERENCES

1. FIRS. *The Global Impact of Respiratory Disease*. 2nd ed. Geneva: Forum of International Respiratory Societies (2017).
2. EMRO. *Respiratory Tract Diseases*. (2020). Available online at: <http://www.emro.who.int/health-topics/respiratory-tract-diseases/index.html>
3. Smith KR. Fuel combustion, air pollution exposure, and health: the situation in developing countries. *Annu Rev Energy Environ*. (1993) 18:529–66. doi: 10.1146/annurev.eg.18.110193.002525
4. Badnjević A, Cifrek M, Koruga D. Integrated software suite for diagnosis of respiratory diseases. In: *Eurocon 2013*. Zagreb: IEEE (2013). p. 564–8. doi: 10.1109/EUROCON.2013.6625037
5. Tang YW, Schmitz JE, Persing DH, Stratton CW. Laboratory diagnosis of COVID-19: current issues and challenges. *J Clin Microbiol*. (2020) 58:e00512–20. doi: 10.1128/JCM.00512-20
6. Cho SH, Lin HC, Ghoshal AG, Muttalif BA, Razak A, Thanaviratnanich S, et al. Respiratory disease in the Asia-Pacific region: cough as a key symptom. *Allergy Asthma Proc*. (2016) 37:131–40. doi: 10.2500/aap.2016.37.3925
7. Korpáš J, Tomori Z. Cough. In: *Cough and Other Respiratory Reflexes*. Vol. 12. Karger Publishers (1979). p. 15–188.
8. Abaza AA, Day JB, Reynolds JS, Mahmoud AM, Goldsmith WT, McKinney WG, et al. Classification of voluntary cough sound and airflow patterns for detecting abnormal pulmonary function. *Cough*. (2009) 5:8. doi: 10.1186/1745-9974-5-8
9. Day J, Goldsmith T, Barkley J, Day J, Afshari A, Frazer D. Identification of individuals using voluntary cough characteristics. In: *Biomedical Engineering Society Meeting*. Vol. 97. Philadelphia, PA (2004).
10. Murata A, Taniguchi Y, Hashimoto Y, Kaneko Y, Takasaki Y, Kudoh S. Discrimination of productive and non-productive cough by sound analysis. *Intern Med*. (1998) 37:732–5. doi: 10.2169/internalmedicine.37.732
11. Korpáš J, Sadloňová J, Vrabec M. Analysis of the cough sound: an overview. *Pulmon Pharmacol*. (1996) 9:261–8. doi: 10.1006/pulp.1996.0034
12. Everett CF, Kastelik JA, Thompson RH, Morice AH. Chronic persistent cough in the community: a questionnaire survey. *Cough*. (2007) 3:5. doi: 10.1186/1745-9974-3-5
13. Larson EC, Lee T, Liu S, Rosenfeld M, Patel SN. Accurate and privacy preserving cough sensing using a low-cost microphone. In: *Proceedings of the 13th International Conference on Ubiquitous Computing*. Beijing (2011). p. 375–84. doi: 10.1145/2030112.2030163
14. World Health Organization. *Acute Respiratory Infections in Children: Case Management in Small Hospitals in Developing Countries, A Manual for Doctors and Other Senior Health Workers*. Geneva: World Health Organization (1990).
15. Amoh J, Odame K. DeepCough: A deep convolutional neural network in a wearable cough detection system. In: *2015 IEEE Biomedical Circuits and Systems Conference (BioCAS)*. Atlanta, GA: IEEE (2015). p. 1–4. doi: 10.1109/BioCAS.2015.7348395

## AUTHOR CONTRIBUTIONS

AB conceived the topic and conducted the conceptual design for the hypothesis and theory. All authors listed have made a substantial, direct and intellectual contribution to the work, and approved it for publication.

## FUNDING

This work was supported by the United Arab Emirates University (UAEU grant no G00003270 31T130).

## ACKNOWLEDGMENTS

The first version of this work has been published as preprint version on server ArXiv (<https://arxiv.org/abs/2006.15469v1>).

16. Korpas J, Vrabec M, Sadlonova J, Salat D, Debreczeni L. Analysis of the cough sound frequency in adults and children with bronchial asthma. *Acta Physiol Hung*. (2003) 90:27–34. doi: 10.1556/APhysiol.90.2003.1.4
17. Liu YX, Yang Y, Chen YH. Lung sound classification based on Hilbert-Huang transform features and multilayer perceptron network. In: *2017 Asia-Pacific Signal and Information Processing Association Annual Summit and Conference (APSIPA ASC)*. Kuala Lumpur: IEEE (2017). p. 765–8. doi: 10.1109/APSIPA.2017.8282137
18. Aykanat M, Kılıç Ö, Kurt B, Saryal S. Classification of lung sounds using convolutional neural networks. *EURASIP J Image Video Process*. (2017) 2017:65. doi: 10.1186/s13640-017-0213-2
19. Azam MA, Shahzadi A, Khalid A, Anwar SM, Naeem U. Smartphone based human breath analysis from respiratory sounds. In: *2018 40th Annual International Conference of the IEEE Engineering in Medicine and Biology Society (EMBC)*. Honolulu, HI: IEEE (2018). p. 445–8. doi: 10.1109/EMBC.2018.8512452
20. Jiang X, Coffee M, Bari A, Wang J, Jiang X, Huang J, et al. Towards an artificial intelligence framework for data-driven prediction of coronavirus clinical severity. *Comput Mater Contin*. (2020) 63:537–51. doi: 10.32604/cmc.2020.010691
21. Al Hossain F, Lover AA, Corey GA, Reich NG, Rahman T. FluSense: a contactless syndromic surveillance platform for influenza-like illness in hospital waiting areas. In: *Proceedings of the ACM on Interactive, Mobile, Wearable and Ubiquitous Technologies*, Vol. 4 (2020). p. 1–28. doi: 10.1145/3381014
22. Visual and Data Journalism Team. *Coronavirus Pandemic: Tracking the Global Outbreak*. (2020). Available online at: <https://www.bbc.com/news/world-51235105>
23. Wu Z, McGoogan JM. Characteristics of and important lessons from the coronavirus disease 2019 (COVID-19) outbreak in China: summary of a report of 72,314 cases from the Chinese Center for Disease Control and Prevention. *JAMA*. (2020) 323:1239–42. doi: 10.1001/jama.2020.2648
24. Kang S, Peng W, Zhu Y, Lu S, Zhou M, Lin W, et al. Recent progress in understanding 2019 novel coronavirus associated with human respiratory disease: detection, mechanism and treatment. *Int J Antimicrob Agents*. (2020) 55:105950. doi: 10.1016/j.ijantimicag.2020.105950
25. Sedik A, Hammad M, Abd El-Samie FE, Gupta BB, Abd El-Latif AA. Efficient deep learning approach for augmented detection of coronavirus disease. *Neural Comput Appl*. (2021) 1–18. doi: 10.1007/s00521-020-05410-8. [Epub ahead of print].
26. Shi F, Wang J, Shi J, Wu Z, Wang Q, Tang Z, et al. Review of artificial intelligence techniques in imaging data acquisition, segmentation and diagnosis for covid-19. *IEEE Rev Biomed Eng*. (2020) 14:4–15. doi: 10.1109/RBME.2020.2987975
27. Wynants L, Van Calster B, Bonten MM, Collins GS, Debray TP, De Vos M, et al. Prediction models for diagnosis and prognosis of covid-19

- infection: systematic review and critical appraisal. *BMJ*. (2020) 369:m1328. doi: 10.1136/bmj.m1328
28. Chen J, Wu L, Zhang J, Zhang L, Gong D, Zhao Y, et al. Deep learning-based model for detecting 2019 novel coronavirus pneumonia on high-resolution computed tomography: a prospective study. *medRxiv*. (2020). doi: 10.1101/2020.02.25.20021568
  29. Al-Muharraqi M. Testing recommendation for COVID-19 (SARS-CoV-2) in patients planned for surgery-continuing the service and 'suppressing' the pandemic. *Br J Oral Maxillofac Surg*. (2020) 58:503–5. doi: 10.1016/j.bjoms.2020.04.014
  30. Maghdid HS, Ghafoor KZ, Sadiq AS, Curran K, Rabie K. A novel ai-enabled framework to diagnose coronavirus covid 19 using smartphone embedded sensors: design study. *arXiv*. (2020) 200307434. doi: 10.1109/IRI49571.2020.00033
  31. Imran A, Posokhova I, Qureshi HN, Masood U, Riaz MS, Ali K, et al. AI4COVID-19: AI enabled preliminary diagnosis for COVID-19 from cough samples via an app. *Inform Med Unlock*. (2020) 20:100378. doi: 10.1016/j.imu.2020.100378
  32. Faezipour M, Abuzneid A. Smartphone-based self-testing of COVID-19 using breathing sounds. *Telemed e-Health*. (2020) 26:1202–5. doi: 10.1089/tmj.2020.0114
  33. Laguarda J, Huetto F, Subirana B. COVID-19 artificial intelligence diagnosis using only cough recordings. *IEEE Open J Eng Med Biol*. (2020) 1:275–81. doi: 10.1109/OJEMB.2020.3026928
  34. Brown C, Chauhan J, Grammenos A, Han J, Hasthanasombat A, Spathis D, et al. Exploring automatic diagnosis of COVID-19 from crowdsourced respiratory sound data. In: *Proceedings of the 26th ACM SIGKDD International Conference on Knowledge Discovery & Data Mining*. (2020). p. 3474–84. doi: 10.1145/3394486.3412865
  35. Schuller BW, Schuller DM, Qian K, Liu J, Zheng H, Li X. COVID-19 and computer audition: an overview on what speech & sound analysis could contribute in the SARS-COV-2 corona crisis. *arXiv. arxiv-2003.11117*. (2020) 200311117.
  36. Sharma N, Krishnan P, Kumar R, Ramoji S, Chetupalli SR, Ghosh PK, et al. Coswara—a database of breathing, cough, and voice sounds for COVID-19 diagnosis. *arXiv*. (2020) 200510548. doi: 10.21437/Interspeech.2020-2768
  37. Vijayakumar DS, Sneha M. Low cost Covid-19 preliminary diagnosis utilizing cough samples and keenly intellectual deep learning approaches. *Alexandr Eng J*. (2021) 60:549–57. doi: 10.1016/j.aej.2020.09.032
  38. Moschovis PP, Sampayo EM, Cook A, Doros G, Parry BA, Lombay J, et al. The diagnosis of respiratory disease in children using a phone-based cough and symptom analysis algorithm: the smartphone recordings of cough sounds 2 (SMARTCOUGH-C 2) trial design. *Contemp Clin Trials*. (2021) 101:106278. doi: 10.1016/j.cct.2021.106278
  39. Taqee A, Bhateja V. Cough sound analysis in transform domain for classification of respiratory disorders. In: Satapathy S, Bhateja V, Janakiramaiah B, Chen YW, editors. *Intelligent System Design*. Springer (2021). p. 865–72. doi: 10.1007/978-981-15-5400-1\_82
  40. Al-khassawneh M, Bani Abdelrahman R. A signal processing approach for the diagnosis of asthma from cough sounds. *J Med Eng Technol*. (2013) 37:165–71. doi: 10.3109/03091902.2012.758322
  41. Pramono RXA, Imtiaz SA, Rodriguez-Villegas E. A cough-based algorithm for automatic diagnosis of pertussis. *PLoS ONE*. (2016) 11:e0162128. doi: 10.1371/journal.pone.0162128
  42. Amoh J, Odame K. Deep neural networks for identifying cough sounds. *IEEE Trans Biomed Circuits Syst*. (2016) 10:1003–11. doi: 10.1109/TBCAS.2016.2598794
  43. Barry SJ, Dane AD, Morice AH, Walmsley AD. The automatic recognition and counting of cough. *Cough*. (2006) 2:8. doi: 10.1186/1745-9974-2-8
  44. Matos S, Birring SS, Pavord ID, Evans H. Detection of cough signals in continuous audio recordings using hidden Markov models. *IEEE Trans Biomed Eng*. (2006) 53:1078–83. doi: 10.1109/TBME.2006.873548
  45. Naik GR, Kumar DK. An overview of independent component analysis and its applications. *Informatica*. (2011) 35:63–81. doi: 10.5772/3084
  46. Naik GR, Wang W. *Blind Source Separation*. Berlin: Springer (2014).
  47. Liutkus A, Durrieu JL, Daudet L, Richard G. An overview of informed audio source separation. In: *2013 14th International Workshop on Image Analysis for Multimedia Interactive Services (WIAMIS)*. Paris: IEEE (2013). p. 1–4. doi: 10.1109/WIAMIS.2013.6616139
  48. He Y, Fataliyev K, Wang L. Feature selection for stock market analysis. In: *International Conference on Neural Information Processing*. Lake Tahoe, NV: Springer (2013). p. 737–44. doi: 10.1007/978-3-642-42042-9\_91
  49. Orlandic L, Teijeiro T, Atienza D. The COUGHVID crowdsourcing dataset: a corpus for the study of large-scale cough analysis algorithms. *arXiv. arXiv:2009.11644*. (2020) 200911644.
  50. Cohen-McFarlane M, Goubran R, Knoefel F. Novel coronavirus cough database: Nococoda. *IEEE Access*. (2020) 8:154087–94. doi: 10.1109/ACCESS.2020.3018028
  51. Tang R, Nogueira R, Zhang E, Gupta N, Cam P, Cho K, et al. Rapidly bootstrapping a question answering dataset for COVID-19. *arXiv. arXiv:2004.11339*. (2020) 200411339.
  52. Chaudhari G, Jiang X, Fakhry A, Han A, Xiao J, Shen S, et al. Virufy: global applicability of crowdsourced and clinical datasets for AI detection of COVID-19 from cough. *arXiv. arXiv:2011.13320*. (2020) 201113320.
  53. Agbley BLX, Li J, Haq A, Cobbinah B, Kulevome D, Agbefu PA, et al. Wavelet-based cough signal decomposition for multimodal classification. In: *2020 17th International Computer Conference on Wavelet Active Media Technology and Information Processing (ICCWAMTIP)*. Chengdu: IEEE (2020). p. 5–9.
  54. Masud M, Gaba GS, Alqahtani S, Muhammad G, Gupta B, Kumar P, et al. A lightweight and robust secure key establishment protocol for internet of medical things in COVID-19 patients care. *IEEE Internet Things J*. (2020). p. 1. doi: 10.1109/JIOT.2020.3047662

**Conflict of Interest:** The authors declare that the research was conducted in the absence of any commercial or financial relationships that could be construed as a potential conflict of interest.

Copyright © 2021 Belkacem, Ouhibi, Lakas, Benkhalifa and Chen. This is an open-access article distributed under the terms of the Creative Commons Attribution License (CC BY). The use, distribution or reproduction in other forums is permitted, provided the original author(s) and the copyright owner(s) are credited and that the original publication in this journal is cited, in accordance with accepted academic practice. No use, distribution or reproduction is permitted which does not comply with these terms.



# Detection of SARS-CoV-2 Infection in Human Nasopharyngeal Samples by Combining MALDI-TOF MS and Artificial Intelligence

Meritxell Deulofeu<sup>1,2</sup>, Esteban García-Cuesta<sup>3,4</sup>, Eladía María Peña-Méndez<sup>5</sup>, José Elías Conde<sup>5</sup>, Orlando Jiménez-Romero<sup>1,2</sup>, Enrique Verdú<sup>1</sup>, María Teresa Serrando<sup>1,2</sup>, Victoria Salvadó<sup>6\*</sup> and Pere Boadas-Vaello<sup>1,2\*</sup>

## OPEN ACCESS

### Edited by:

Reza Lashgari,  
Institute for Research in Fundamental  
Sciences, Iran

### Reviewed by:

Armand Pauw,  
Netherlands Organisation for Applied  
Scientific Research, Netherlands  
Minjin Wang,  
Sichuan University, China

### \*Correspondence:

Pere Boadas-Vaello  
pere.boadas@udg.edu  
Victoria Salvadó  
victoria.salvado@udg.edu

### Specialty section:

This article was submitted to  
Infectious Diseases – Surveillance,  
Prevention and Treatment,  
a section of the journal  
Frontiers in Medicine

**Received:** 30 January 2021

**Accepted:** 11 March 2021

**Published:** 01 April 2021

### Citation:

Deulofeu M, García-Cuesta E,  
Peña-Méndez EM, Conde JE,  
Jiménez-Romero O, Verdú E,  
Serrando MT, Salvadó V and  
Boadas-Vaello P (2021) Detection of  
SARS-CoV-2 Infection in Human  
Nasopharyngeal Samples by  
Combining MALDI-TOF MS and  
Artificial Intelligence.  
Front. Med. 8:661358.  
doi: 10.3389/fmed.2021.661358

<sup>1</sup> Research Group of Clinical Anatomy, Embryology and Neuroscience (NEOMA), Department of Medical Sciences, University of Girona, Girona, Spain, <sup>2</sup> ICS-IAS Girona Clinical Laboratory, Santa Caterina Hospital, Parc Sanitari Martí i Julià, Salt, Spain, <sup>3</sup> Science, Computation, and Technology Department, School of Architecture, Design, and Engineering, European University of Madrid, Madrid, Spain, <sup>4</sup> Instant Biosensing Technologies, Carson, NV, United States, <sup>5</sup> Analytical Chemistry Division, Department of Chemistry, Faculty of Science, University of La Laguna, La Laguna, Spain, <sup>6</sup> Department of Chemistry, Faculty of Science, University of Girona, Girona, Spain

The high infectivity of SARS-CoV-2 makes it essential to develop a rapid and accurate diagnostic test so that carriers can be isolated at an early stage. Viral RNA in nasopharyngeal samples by RT-PCR is currently considered the reference method although it is not recognized as a strong gold standard due to certain drawbacks. Here we develop a methodology combining the analysis of from human nasopharyngeal (NP) samples by matrix-assisted laser desorption/ionization time-of-flight mass spectrometry (MALDI-TOF MS) with the use of machine learning (ML). A total of 236 NP samples collected in two different viral transport media were analyzed with minimal sample preparation and the subsequent mass spectra data was used to build different ML models with two different techniques. The best model showed high performance in terms of accuracy, sensitivity and specificity, in all cases reaching values higher than 90%. Our results suggest that the analysis of NP samples by MALDI-TOF MS and ML is a simple, safe, fast and economic diagnostic test for COVID-19.

**Keywords:** MALDI-TOF MS analysis, machine learning, SARS-CoV-2, NP samples, viral transport media

## INTRODUCTION

The COVID-19 pandemic not only represents a major health crisis, but has also had unprecedented economic repercussions. According to the most recent available report of the World Health Organization (1), the cumulative number of reported cases of SARS-CoV-2 infections worldwide has now reached over 98 million people and over 2 million people have died of the disease since the start of the COVID-19 pandemic in December 2019. Moreover, it has been estimated that the gross domestic product may drop by more than 10-15% in some countries (2). Taking into consideration how rapidly the COVID-19 pandemic has spread, often through the transmission of SARS-CoV-2 by asymptomatic individuals (3), fast and economic diagnostic tools are essential for the control of this devastating pandemic.



While several diagnostic and surveillance technologies for SARS-CoV-2 have been either developed or used during the COVID-19 pandemic (4–6), real-time reverse transcription polymerase chain reaction (RT-PCR) is currently still the validated assay for early diagnosis in patients with suspected SARS-CoV-2 infection (7). However, there are certain concerns regarding RT-PCR (8) as the gold standard analytical methodology for pandemic control. PCR-based strategies are costly, require a lot of technical personnel and laboratories, and the analysis time is relatively long, limiting the number of samples that can be processed daily. Although some of these problems can be overcome by using saliva for COVID-19 diagnosis and a dual RT-qPCR test, the time needed to obtain results remains high (9, 10). Moreover, most countries do not have sufficient laboratory resources and, due to the enormous global demand, are not able to obtain a sufficient supply of PCR kits. Given this situation, new alternative methodologies need to be developed.

A useful bioanalytical methodology that would allow most of these limitations to be overcome is matrix-assisted laser desorption/ionization mass spectrometry coupled to a TOF analyzer (MALDI-TOF MS). This technique is the current tool for rapid, accurate, and cost-effective identification of cultured bacteria and fungi in clinical microbiology (11, 12) and even though it is not routinely used in hospitals to identify viruses, it has been shown to be useful for this purpose (13, 14). Although some MALDI-TOF MS methodologies need time-consuming sample preparation, such as protein or nucleotide extraction, simpler protocols are possible. For example, protocols that consist only of the mixing of a diluted sample with the matrix have been successfully applied to differentiate samples from myeloma patients and healthy subjects (15). In that study, the analyses of biological samples by MALDI-TOF MS allowed the patterns or fingerprints of different biological samples to be obtained, which could be further used to differentiate between samples (e.g., control vs. disease samples).

The large amount of data obtained using MS spectra fingerprints requires the combination of powerful statistical strategies (13) and artificial intelligence methods in order to be able to identify the diagnostic pattern. These strategies have been successfully applied in medicine and biomedicine (15, 16). The fingerprint (pattern recognition) approach avoids tedious biological sample work and eliminates the need to identify biomarkers, so considerably reducing the analysis time (17). With regards to the use of biomarkers, it should also be noted that single biomarkers are generally considered as insufficient and so it is often necessary to search for a combination of several different biomarkers to perform effective clinical diagnosis (18, 19).

A method based on recording the MALDI mass spectra of nasal swab samples previously tested for SARS-CoV-2 by RT-qPCR and their subsequent analysis by machine learning (ML) has recently been proposed for large-scale SARS-CoV-2 testing (20). In this study, samples were analyzed after adding a CHCA solution as a matrix and irradiating the MALDI plates with an ultraviolet light for 20 min to inactivate the viruses. However, in addition to the problems regarding this methodology discussed

by SoRelle et al. (21), other aspects such as the application of safer sample inactivation protocols, the use of different viral transport media and the development of more robust machine learning protocols have required further progress.

In light of the above, the present work has aimed to develop a new methodology based on MALDI-TOF MS analyses of nasopharyngeal samples coupled to methods of artificial intelligence, allowing COVID-19 to be identified. We have employed a variety of machine learning approaches to analyze the pattern spectra (fingerprint) of nasopharyngeal samples in the two most widely used types of virus transport media. The methodology developed as a result of these approaches is a promising tool not only in the battle to control the spread of COVID-19 but also for post-pandemic testing in local settings to prevent future major outbreaks.

The hypothesis of the present work was that there is a MALDI-TOF mass spectral pattern (fingerprint) that can be assigned as a signature accurately characterizing negative and positive samples for SARS-CoV-2 infection. The application of a machine learning (ML) approach to the fingerprint mass spectra of positive and negative samples of SARS-CoV-2 infection will allow the development of a fast and efficient approach to support clinical decisions.

## MATERIALS AND METHODS

### Chemicals

Sinapinic acid was used as a matrix for MALDI-TOF MS analysis and was purchased from Bruker Daltonics (Bremen, Germany; #8201345). Trifluoroacetic acid (TFA) was purchased from Scharlab (#AC31420100; peptide synthesis grade) and acetonitrile (mass spectrometry grade) was purchased from VWR (#83640.29). Protein Calibration Standard I (#8206355) was used for MALDI-TOF MS calibration and was purchased from Bruker Daltonics (Bremen, Germany).

### Sample Collection

A total of 237 nasopharyngeal samples were provided by the ICS-IAS Girona Clinical Laboratory (Parc Sanitari Martí i Julià; Salt, Catalonia, Spain), according to IDIBGI Biobank (Biobanc IDIBGI, B.0000872) agreement, to carry out the present study, which was approved by the Clinical Research Ethics Committee of the Doctor Josep Trueta Hospital in Girona (ref#2020.088). A consecutive non-probabilistic model was chosen since samples were provided when available at several time points during the first COVID19 wave (April–July of 2020). Such samples were provided either in DeltaSwab ViCUM (#304273; DeltaLab) or DeltaSwab Virus (#304295; DeltaLab) virus transport medium. Concretely 149 samples were provided in DeltaSwab ViCUM and 88 in DeltaSwab Virus. Before delivering, they were processed in the Molecular area of the territorial laboratory of Girona under biosafety II conditions to perform both the chemical inactivation and the PCR diagnostics. The sample inactivation was performed using Ribospin vRD Buffer VL (GeneAll, Korea), which its principal component is guanidine thiocyanate in a concentration of 60–70%, by mixing 300 µl of the buffer with 300 µl of the transport medium where the NP sample was

collected. The RT-PCR diagnosis was performed using two different methodological platforms which detect 2 targets (N and E qRT-PCR methodology, Xpert SARS-CoV-2, Cepheid, US) or 4 targets (N, E, S and RpRd genes, Allplex 2019-nCoV assay, Seegen, South Korea). After sample inactivation and the RT-PCR analysis samples were sent to the laboratory of NEOMA research group.

## Sample Preparation for MS

Inactivated samples, previously tested by RT-PCR in the ICS-IAS Girona Clinical Laboratory, were then processed for MS analysis in the laboratory of NEOMA research group of the University of Girona.

All samples were first diluted 10 times with Milli-Q water. They were then mixed in 1:1 ratio with a solution of sinapinic acid (SA) containing 20 mg SA/mL in 60%:40% (v/v) acetonitrile (ACN): milli-Q water with 0.3% trifluoroacetic acid (TFA). TFA was added in order to increase the ionization. Finally, 1  $\mu$ l of the mixture was spotted on a purified stainless-steel target plate (MTP 384 target ground steel; Bruker Daltonics, Bremen, Germany) in triplicates and allowed to dry at room temperature before being analyzed by MALDI-TOF MS. To avoid carry-over contamination, the target plate was regularly cleaned in an ultrasonic bath using a specific cleaning procedure with ultrapure solvents sequentially in this order: 2-propanol, MilliQ water, 2-propanol and TA30 (350 ml ACN: 350 ml TFA 0.1%).

## Acquisition of Mass Spectra

Mass spectra were acquired using Autoflex maX with Time-Of-Flight (TOF) analyzer from Bruker Daltonics (Bruker Daltonics, Bremen, Germany). Ionization was achieved by irradiation with a solid phase laser (with patented Smartbeam technology) operating at 2,000 Hz. All spectra were acquired automatically using a regular raster (in random walk mode) and 20 shots were made in each raster spot; locations were calibrated prior to each run. Sample mass spectra was the sum of 1,800 satisfactory shots taken in 300 shots steps. All measurements were carried out in a positive linear mode and each spectrum was externally calibrated using a standard mixture of peptides (Standard Protein I, Bruker Daltonics). All mass spectra were acquired using FlexControl software (Bruker Daltonics, Germany) and each spectrum consisted of more than 25,000 m/z values with the corresponding intensities in the mass range from 5 to 20 kDa. The smoothing of mass spectra by Savitzky-Golay method, the baseline subtraction by Top-Hat method and the recalibration of each mass spectrum was performed using the FlexAnalysis 3.4 software (Bruker Daltonics, Germany). The same software was used to export all the m/z values with the corresponding intensities into ASCII format for its further analysis using machine learning approaches.

## Machine Learning

To classify the positive and negative samples a machine learning approach was adopted. The learned model represents the best solution given the data samples obtained by MALDI-TOF MS.

To study the performance, two of the most well-known and successfully applied techniques were selected. Extreme Gradient Boosting Trees (XBOOST) (22) and Support Vector Machines (SVMs) (23) were tested using different parameters to obtain their best results to the problem. A cross-validation (CV) was applied to study the performance of both XBOOST and SVM. In standard CV, instances are distributed randomly into CV partitions. But our study involved three replicas of the same sample and they were related. Therefore, in this study we considered the 3 replicas of the same individual as a unique sample in the CV phase. Also, a number of  $K = 10$ -folds was used because the number of samples was small, but a minimum of four positive and negative examples were added as a constraint for each fold to ensure that there are samples of at least two different individuals. Note that previous to the CV process, 10% of the samples were randomly separated to perform the test using the best model selected using CV. The test was done 20 times to avoid bias in the results and guarantee that the results are independent of the samples selected in the training phase (double-blind test).

Because the number of available features was large (29,393 m/z values) it is expected that many of them were highly correlated and some of them may contain irrelevant information. To overcome some of the problems that arise using high-dimensional data, all the experiments were performed using principal component analysis (PCA) as dimensionality reduction technique. Then, to analyze what was the optimal number of dimensions, the SVM and XBOOST methods were evaluated for 5, 10, and 50 projected features.

Both SVM and XBOOST have some hyper-parameters that require tuning in order to improve results. Three hyperparameters were fitted:

- Number of estimators (XBOOST): 50 and 10
- Tree depth (XBOOST): 5 and 10
- Subsample (XBOOST): between 50 and 80% in steps of 10%
- Learning rate (XBOOST): 0.01 and 0.05
- Kernel (SVM): radial base and linear functions
- Gamma (SVM): 0.01, 0.001 and 0.0001
- C-penalty parameter (SVM): 1 and 10

In order to tune the hyper-parameters, a systematic procedure known as grid-search was used. This method tries all possible combinations of hyper-parameter values. Models for each hyper-parameter combination are trained with the training partition and evaluated with the validation partition. The best combination on the validation set is selected.

Finally, F1-Score was used as a performance measure (Equation 1) to select the most suitable developed model. This criterion is very appealing when the positive and negative classes are unbalanced and we are interested in minimizing the probability that a random positive sample is included into the negative sample classification area and vice versa.

$$F1\text{-score} = 2 * \text{Precision} * \text{Recall} / (\text{Precision} + \text{Recall})$$

$$\text{Precision} = \text{TP} / (\text{TP} + \text{FP})$$

$$\text{Recall} = \text{TP} / (\text{TP} + \text{FN}) \quad (1)$$

## RESULTS AND DISCUSSION

Based on the hypothesis of differences in the fingerprints of positive and negative samples, a machine learning (ML) approach was adopted to build a model for the fast and efficient classification of these two groups of samples. Different experiments were designed to test the ability of MALDI-TOF MS to extract these spectral patterns from the data obtained from human nasopharyngeal (NP) and enable it to detect patients infected by SARS-CoV-2.

### The Optimization of the MALDI Parameters

It is well-known that several factors can influence the results obtained by MALDI-TOF MS, including matrix and sample preparation (24). Moreover, finding the mass range in which the most relevant information can be found is also an important step. Therefore, the optimization of the methodology was first carried out with the objective to find the optimal matrix, sample dilution and mass range in order to develop a simple procedure that would allow the maximum number of peaks to be obtained with acceptable resolutions and intensities. Firstly, undiluted samples were analyzed but no signals at different mass-to-charge ( $m/z$ ) values were observed in the mass spectra. When samples were diluted 10 times, rich mass spectra with acceptable resolution and

intensities were obtained. Since the idea was to develop a simple and fast methodology, the analysis of the low mass range ( $<1,000$  Da) was discarded due to the high background noise generated by the matrix (25, 26). Finally, we selected the mass spectra in the 5 to 20 kDa range. This mass spectra range was also used by Nachtigall et al. (20) in developing a similar methodology. In contrast we decided to use Sinapinic Acid (SA) for MALDI TOF MS sample analysis as this is particularly recommended for larger mass range (27).

### First Experiment: Using All Collected Samples

Initially, the transport media in which the nasopharyngeal (NP) samples were collected was not considered as a main experimental criterion. In other words, all spectra acquired from samples collected in either DeltaSwab-ViCUM or DeltaSwab-Virus transport media were used without splitting samples by the transporter. Therefore, different strategies of ML analysis were performed using the whole dataset composed of the  $m/z$  values, in the 5 to 20 kDa range, and their corresponding intensities for each sample. A total of 708 mass spectra were obtained by MALDI-TOF analysis, corresponding to samples that were previously analyzed by

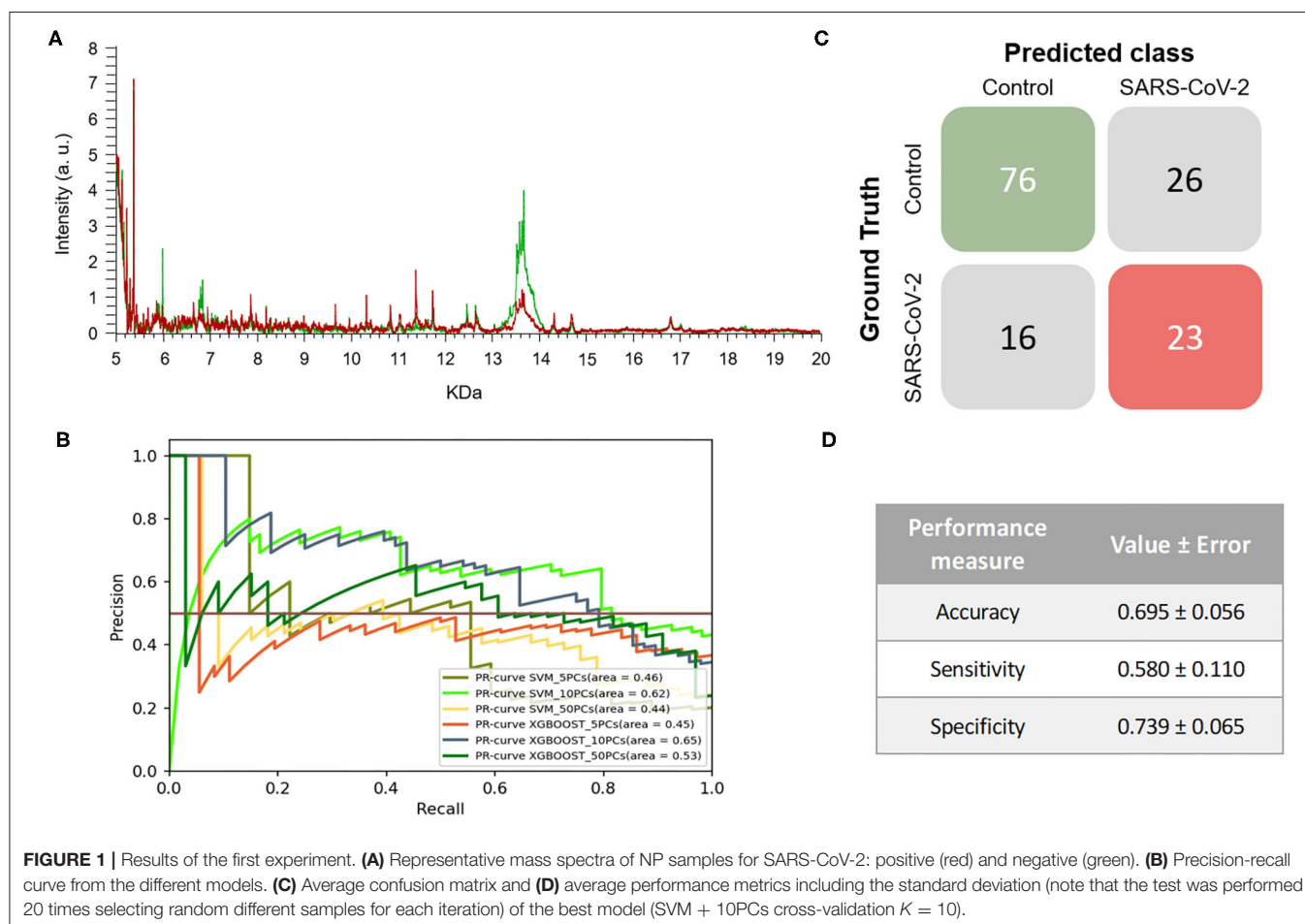


**TABLE 1** | Model learning (cross validation results  $K = 10$ ) of all the models tested in the different experiments.

| PCs used                       |          | F1-Score          |                                     | Sensitivity (TPR) |                   | Specificity (TNR) |                   | Accuracy          |                   |
|--------------------------------|----------|-------------------|-------------------------------------|-------------------|-------------------|-------------------|-------------------|-------------------|-------------------|
|                                |          | XGBOOST           | SVM                                 | XGBOOST           | SVM               | XGBOOST           | SVM               | XGBOOST           | SVM               |
| Experiment 1                   | $n = 5$  | $0.625 \pm 0.041$ | $0.595 \pm 0.073$                   | $0.658 \pm 0.093$ | $0.780 \pm 0.115$ | $0.684 \pm 0.062$ | $0.580 \pm 0.113$ | $0.677 \pm 0.043$ | $0.626 \pm 0.078$ |
|                                | $n = 10$ | $0.620 \pm 0.043$ | <b><math>0.639 \pm 0.056</math></b> | $0.580 \pm 0.084$ | $0.580 \pm 0.110$ | $0.716 \pm 0.066$ | $0.739 \pm 0.065$ | $0.678 \pm 0.043$ | $0.695 \pm 0.056$ |
|                                | $n = 50$ | $0.587 \pm 0.045$ | $0.558 \pm 0.057$                   | $0.283 \pm 0.098$ | $0.238 \pm 0.094$ | $0.890 \pm 0.055$ | $0.891 \pm 0.033$ | $0.679 \pm 0.065$ | $0.703 \pm 0.048$ |
| Experiment 2<br>(VTM1 results) | $n = 5$  | $0.749 \pm 0.066$ | $0.759 \pm 0.086$                   | $0.538 \pm 0.168$ | $0.525 \pm 0.150$ | $0.946 \pm 0.033$ | $0.950 \pm 0.051$ | $0.852 \pm 0.039$ | $0.832 \pm 0.070$ |
|                                | $n = 10$ | $0.793 \pm 0.116$ | <b><math>0.826 \pm 0.088</math></b> | $0.646 \pm 0.242$ | $0.652 \pm 0.176$ | $0.939 \pm 0.070$ | $0.969 \pm 0.031$ | $0.884 \pm 0.069$ | $0.879 \pm 0.065$ |
|                                | $n = 50$ | $0.754 \pm 0.132$ | $0.700 \pm 0.160$                   | $0.548 \pm 0.275$ | $0.487 \pm 0.319$ | $0.961 \pm 0.058$ | $0.937 \pm 0.071$ | $0.876 \pm 0.075$ | $0.845 \pm 0.080$ |
| Experiment 2<br>(VTM2 results) | $n = 5$  | $0.433 \pm 0.080$ | $0.418 \pm 0.104$                   | $0.273 \pm 0.081$ | $0.285 \pm 0.200$ | $0.618 \pm 0.119$ | $0.588 \pm 0.196$ | $0.494 \pm 0.082$ | $0.491 \pm 0.139$ |
|                                | $n = 10$ | $0.482 \pm 0.106$ | <b><math>0.515 \pm 0.110</math></b> | $0.241 \pm 0.162$ | $0.381 \pm 0.206$ | $0.762 \pm 0.138$ | $0.688 \pm 0.133$ | $0.581 \pm 0.111$ | $0.594 \pm 0.107$ |
|                                | $n = 50$ | $0.511 \pm 0.120$ | $0.476 \pm 0.093$                   | $0.158 \pm 0.172$ | $0.135 \pm 0.148$ | $0.914 \pm 0.063$ | $0.925 \pm 0.075$ | $0.711 \pm 0.083$ | $0.654 \pm 0.098$ |
| Experiment 3                   | $n = 5$  | $0.891 \pm 0.109$ | <b><math>0.979 \pm 0.048</math></b> | $0.922 \pm 0.127$ | $0.974 \pm 0.076$ | $0.872 \pm 0.157$ | $0.988 \pm 0.054$ | $0.897 \pm 0.109$ | $0.980 \pm 0.044$ |
|                                | $n = 10$ | $0.950 \pm 0.050$ | $0.947 \pm 0.066$                   | $0.930 \pm 0.070$ | $0.987 \pm 0.040$ | $0.970 \pm 0.090$ | $0.918 \pm 0.110$ | $0.981 \pm 0.052$ | $0.950 \pm 0.063$ |
|                                | $n = 50$ | $0.868 \pm 0.109$ | $0.968 \pm 0.055$                   | $0.911 \pm 0.106$ | $0.989 \pm 0.484$ | $0.832 \pm 0.214$ | $0.941 \pm 0.118$ | $0.882 \pm 0.093$ | $0.972 \pm 0.045$ |
| Robustness<br>analysis         | $n = 5$  | 0.647             | <b>0.964</b>                        | 0.956             | 1.000             | 0.377             | 0.923             | 0.687             | 0.964             |
|                                | $n = 10$ | 0.609             | 0.945                               | 0.922             | 0.964             | 0.346             | 0.923             | 0.654             | 0.945             |
|                                | $n = 50$ | 0.690             | 0.902                               | 0.956             | 1.000             | 0.446             | 0.795             | 0.719             | 0.902             |

Bold values represent the best model for each experiment using the selected metric F1-score.

RT-PCR, resulting in 180 positive and 528 negative samples for SARS-CoV-2 infection.

The mass spectra assigned by PCR as positive samples presented differences both in the intensity of signals and the  $m/z$  values in comparison to the spectra of PCR negative samples. Despite the differences exhibited, no specific biomarkers for any of the positive or negative PCR sample groups were found (Figure 1A). The ML approach was then applied to analyze the data from the entire range of the selected  $m/z$  pattern (fingerprint) without applying any variable selection method. Six models were constructed using both XGBOOST and support vector machine (SVM) algorithms with different numbers of principal components (PCs) (5, 10 or 50 PCs) to identify the conditions that would tend toward lower variance. When training the different models, performance analyses showed that the models' accuracies, sensitivities, and specificities did not vary significantly between the different number of PCs. Based on the metric F1-score, which is the harmonic-mean of precision and recall, the best model for this experiment was obtained by SVM + 10PCs. The model was able to perform better than baseline (F1-Score =  $0.639 \pm 0.056$ ) (Table 1), showing the existence of a general pattern associated to the mass spectra. These results can also be observed in the precision-recall (PR) curve (Figure 1B), providing insights that suggest the best model. Overall, the resulting model reached an  $0.580 \pm 0.110$  and  $0.739 \pm 0.065$  of sensitivity and specificity, respectively. This model was then applied to perform the test process. Figures 1C,D shows the matrix confusion of this experiment with the summary of the predicted results for all the samples used to perform the test.

The results demonstrated that the developed a methodology, without considering the viral transport media, enables SARS-CoV-2-positive and -negative samples to be discriminated with around 70% accuracy, 60% sensitivity and 74% specificity. Although these percentages may be lower than the expectations, it is worth noting that RT-PCR for COVID-19 diagnosis only

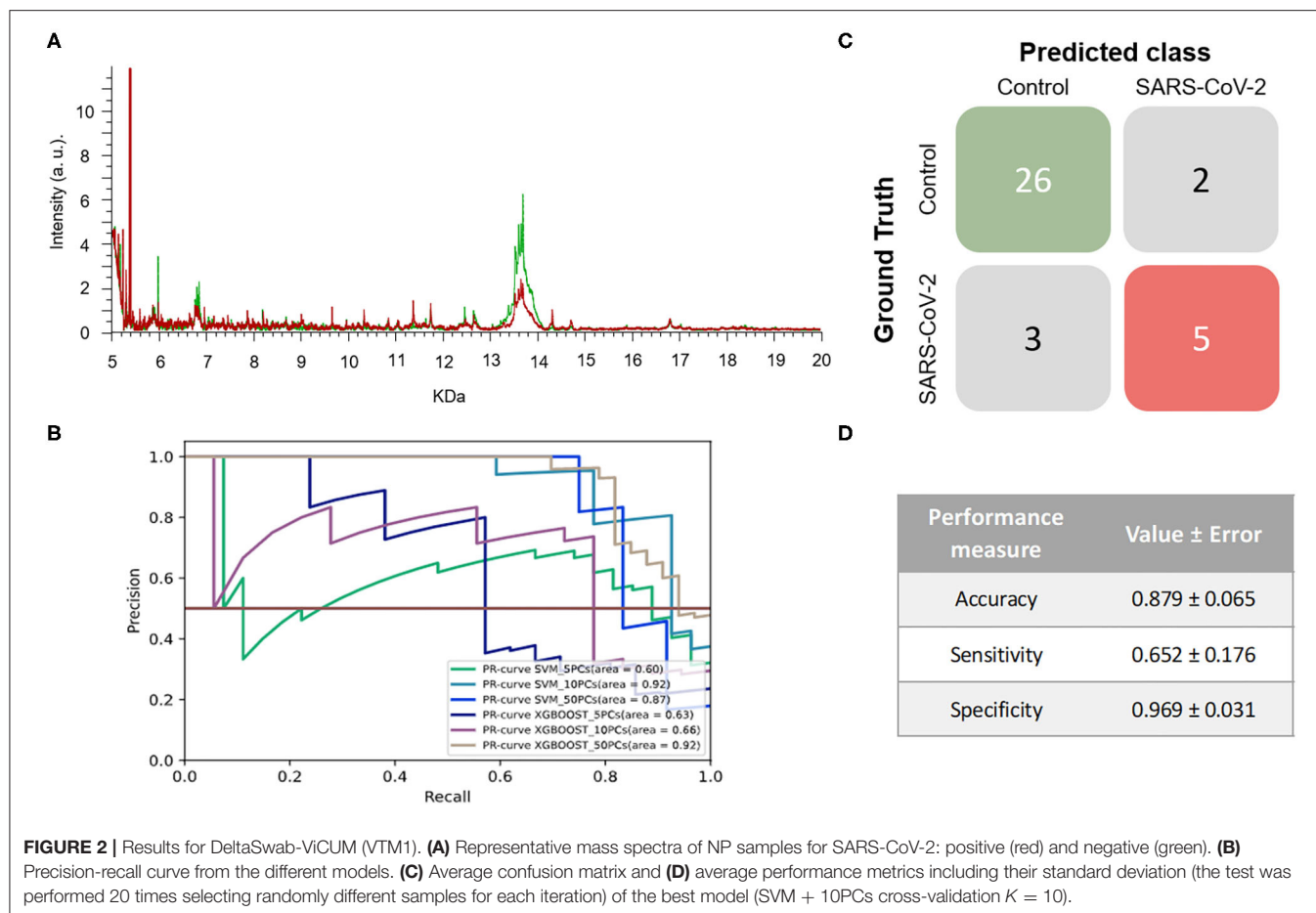
reaches clinical sensitivities of between 38 and 78% (28, 29). In the case of RT-PCR in nasopharyngeal swabs, sensitivity has not been found to exceed 70% (30, 31). Therefore, our first developed model using two different transport media would be as useful as RT-PCR in monitoring the spread of COVID-19 during a pandemic in which both incidence and prevalence are high. It is important to note that the mass spectra of the samples used to train and develop the different ML models were classified in the control group and in the COVID-19 group based on the previous RT-PCR result. However, there is a high rate of false negatives in RT-PCR results, estimated at between 2 and 29% by Arevalo-Rodriguez et al. (32), which may hinder the learning, validation and testing steps of the classification model. The drawbacks of RT-PCR as a diagnostic test for COVID-19 and the lack of a clear gold-standard complicates the evaluation of new methodologies (8, 33, 34).

Interestingly, the optimized model for the prediction of SARS-CoV-2-positive and negative samples shows a greater ability to detect negative samples than positive ones (despite the standard deviation of the sensitivity being quite large for the different tests performed). These results may indicate that the developed model has a dependence on factors such as the heterogeneity of the samples and the noise of the data. This heterogeneity of the data in this first experiment may be caused by the different viral transport media used for sample collection. The high demand during the COVID-19 pandemic for the specific transport media for SARS-CoV-2, resulted in the use of alternative viral transport media, following the recommendations of the FDA, that had the effect of increasing the heterogeneity of the samples received in the laboratories (35).

## Second Experiment: Splitting Samples by the Viral Transport Media

To test the hypothesis that the heterogeneity of the data was a result of the different viral transport media that were used, the





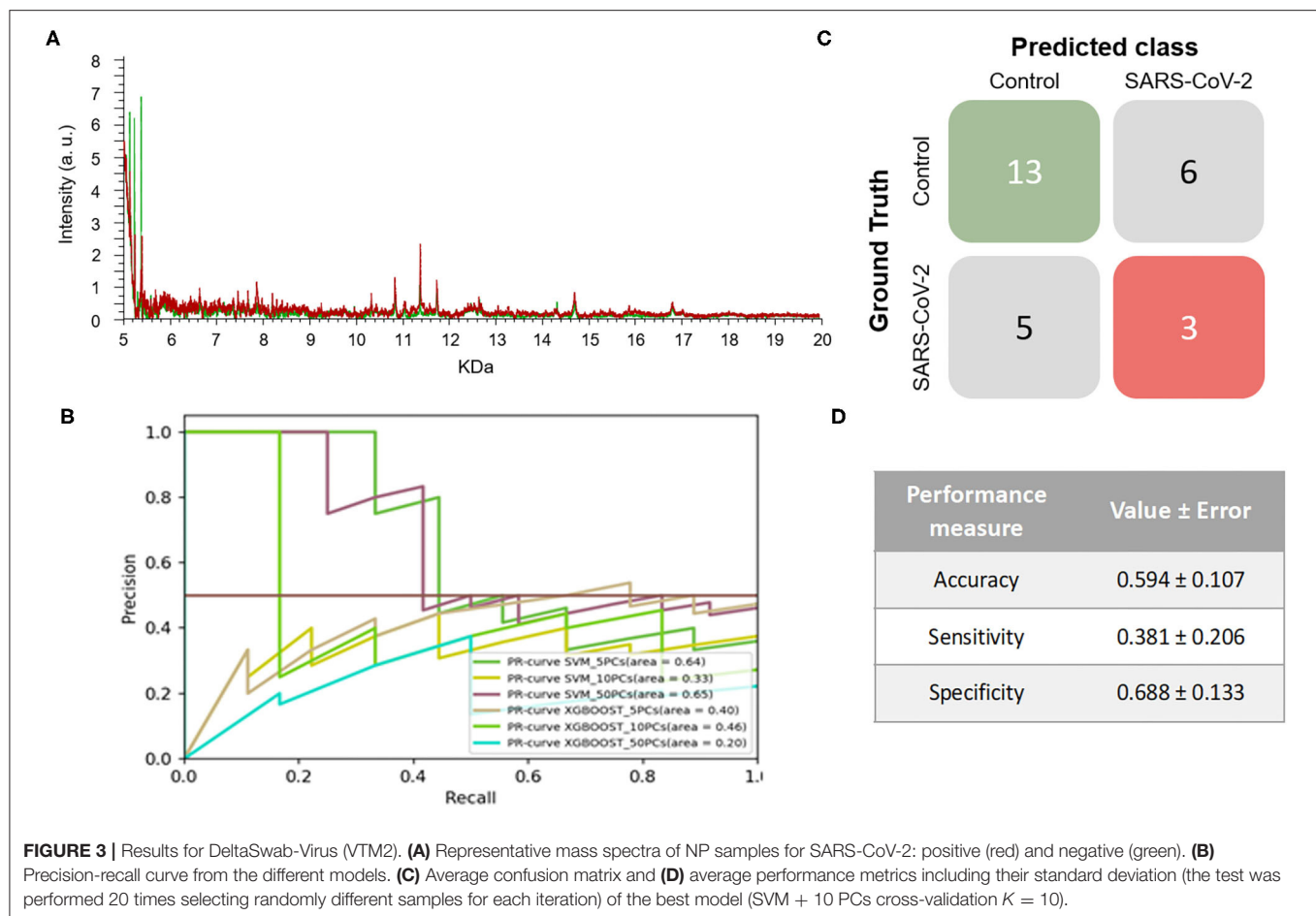
dataset was split by DeltaSwab-ViCUM (viral transport medium 1, VTM1) and DeltaSwab-Virus (viral transport medium 2, VTM2).

As for VTM1, 443 mass spectra (111 and 332 from samples that were positive and negative for SARS-CoV-2, respectively) were obtained from NP samples collected in this viral transport media. As observed in the first experiment, the spectra of the two groups present differences in certain regions (**Figure 2A**). The same ML strategy as was used in the previous section was then applied to analyze the information from the corresponding pattern of the mass spectra (fingerprint). The results did not vary substantially between the different ML models applied to perform the analysis (**Figure 2B** and **Table 1**). However, of the different models tested the best results in terms of the F1-score were obtained when the SVM using 10 PCs (F1-score = 0.826  $\pm$  0.088) was applied (**Table 1**).

On the other hand, 264 mass spectra [69 positive and 195 negative for SARS-CoV-2, respectively] were obtained from NP samples collected in VTM2. In this case, no clear differences were observed between the spectral pattern of positive and negative samples (**Figure 3A**). After analyzing the spectral data by the different ML models, the best model was obtained for SVM using 10PCs (F1-score = 0.515  $\pm$  0.110) (**Figure 3B** and **Table 1**).

The results obtained relating to the performance of the two best models clearly differed. Accuracy (VTM1 = 0.879  $\pm$  0.065 vs. VTM2 = 0.594  $\pm$  0.107), sensitivity (VTM1 = 0.652  $\pm$  0.176 vs. VTM2 = 0.381  $\pm$  0.206), and specificity (VTM1 = 0.969  $\pm$  0.031 vs. VTM2 = 0.688  $\pm$  0.133) all varied significantly between the two transport media (**Figures 2C,D, 3C,D**). The model that gave the best results was the one with VTM1, reaching 88, 65, and 97% for accuracy, sensitivity and specificity, respectively. The results prove that these two virus transporters behave differently and that VTM1 is better suited for the detection of SARS-CoV-2 infected samples. This finding that the model is reagent-dependent is unsurprising as the use of different analytical platforms in clinical laboratories require specific sample collectors and reagents in order to obtain accurate results.

Analyzing the results more deeply, it can be seen that despite the promising results related to VTM1 in this second experiment, there was still a significant standard deviation value in the sensitivity ( $\pm 0.176$ ), suggesting either internal VTM1 heterogeneity and noisy samples. This heterogeneity might be due to the nucleic acid amplification technique used for their analysis since different PCR platforms were used in the clinical laboratory. The main difference between the used platforms in this study lies in the number of the targets detected by PCR amplification related to viral structural proteins. At that time of



the pandemic that we collected the samples, two targets (N and E qRT-PCR methodology, Xpert SARS-CoV-2, Cepheid, US) or four targets (N, E, S and RpRd genes, Allplex 2019-nCoV assay, Seegen, South Korea) were detected, considering both platforms methodologically equivalents. However, these platforms provide positive or negative results for the SARS-CoV-2 detection by using different diagnostic algorithms (true positive is considered when we observe at least two targets amplified). It has to be highlighted that the sensibility and the specificity of the RT-PCR is assay-dependent (6, 30, 33, 36). So, it is important to remark that the analytical sensitivity and specificity of these platforms, which are both qualitative, can change due to the difference in the number of the targets detected.

Despite this methodological platform variability, we hypothesize that the greatest source of heterogeneity might be the moment during the pandemic at which the samples were collected. It is known that disease prevalence plays an important role in the accuracy of a specific test (33, 37, 38). The prevalence of COVID-19 was different during the peak of the pandemic than at the beginning of the de-escalation phase when the incidence of infections was much lower. Remarkably, the available number of SARS-CoV-2-positive samples for analysis was extremely low when compared with the negative ones. As a result, the class imbalance observed in the dataset was due to

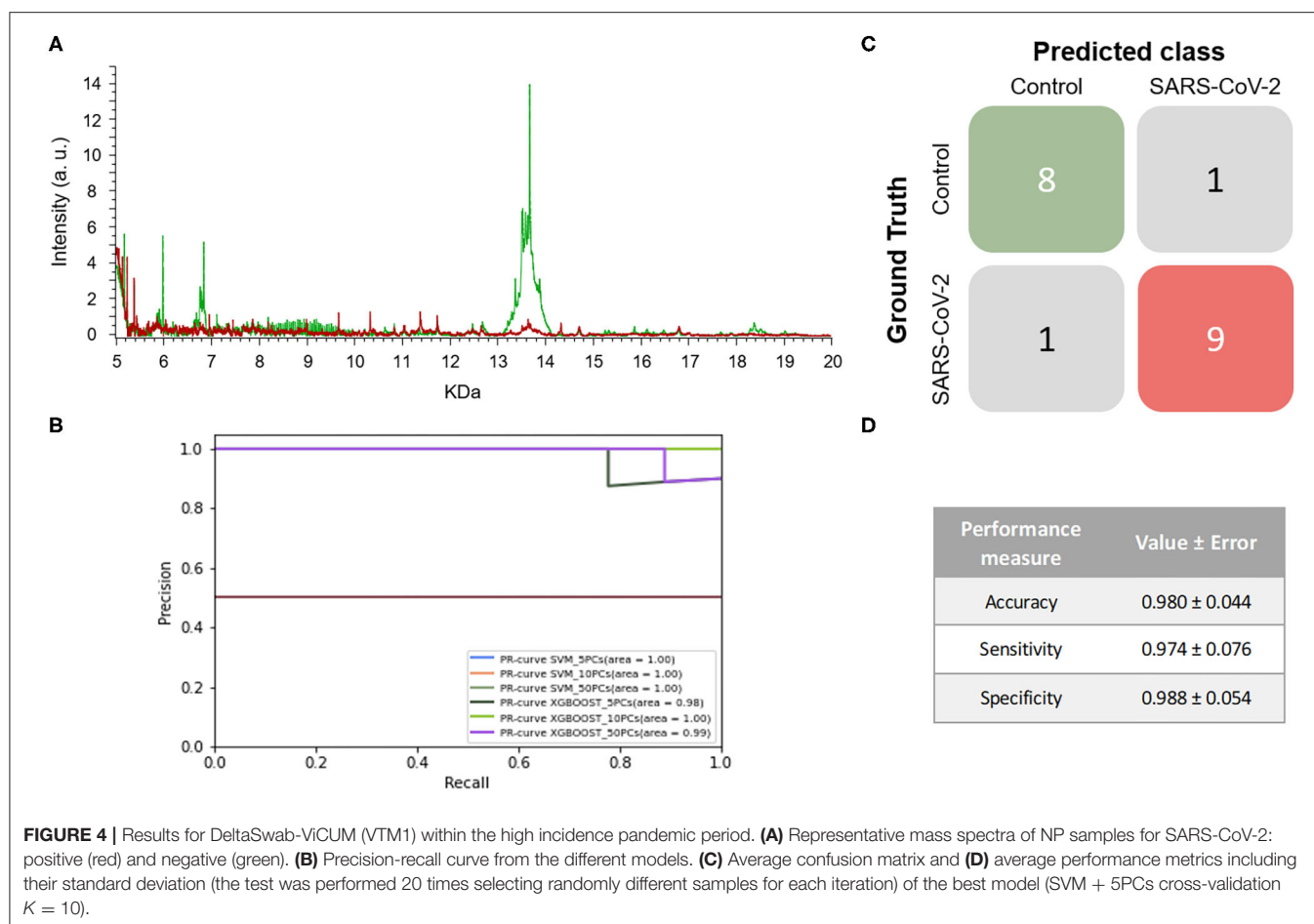
the low number of samples collected at the beginning of the de-escalation phase.

In light of the above, we decided to split the samples collected in viral transport media 1 into two groups based on the moment during the pandemic at which they were collected. Hence, in a third experiment, samples collected during the peak of the pandemic period were used for ML calculations due to their greater homogeneity, while those collected later during the de-escalated phase when the incidence of infections was much lower were discarded for this purpose.

### Third Experiment Focusing on DeltaSwab-ViCUM Transport Media

For this third experiment, NP samples collected in VTM1 between April and the beginning of May were analyzed. A total of 173 mass spectra (89 and 84 from samples that were positive and negative for SARS-CoV-2, respectively) were obtained and analyzed in this experiment.

When the mass spectra of positives NP samples were compared with the mass spectra of the negative ones, noticeable differences were observed in the profile of the mass spectra (Figure 4A). None of the performance measures varied significantly with the different numbers of PCs selected nor



with the different ML approaches. Although all of the models showed good results, the one with the highest F1-score was the SVM using 5 PCs (F1-score =  $0.979 \pm 0.048$ ) and so this was considered to be the best model (Figure 4B and Table 1). These results were not only highly precise but also had low variability, demonstrating that the learned models are independent of the training data selected and valid for SARS-CoV-2 infection detection in future samples. The average confusion matrix (Figures 4C,D) shows the high performance obtained for both negative and positive samples in terms of accuracy, sensitivity and specificity, in all cases reaching values higher than 90% ( $0.981 \pm 0.052$ ,  $0.993 \pm 0.040$ , and  $0.974 \pm 0.085$ , respectively).

Considering the promising results obtained in this third experiment, a final experiment was performed to evaluate the robustness of the methodology in which the results of an independent set of samples were tested.

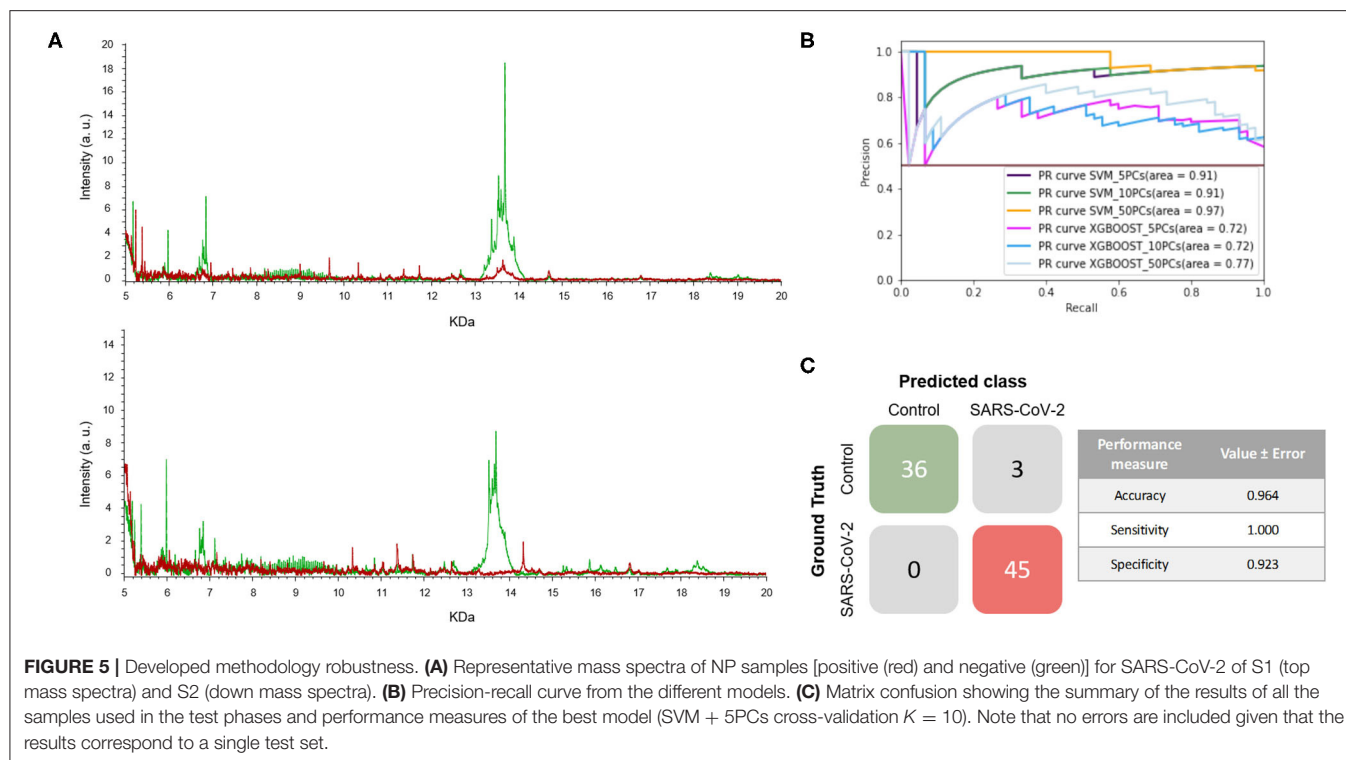
## Robustness Analysis and Applicability

As has been said, two different sample sets were acquired during the peak of the pandemic. Since the final objective is to develop a methodology that is able to discriminate between a SARS-CoV-2-positive and -negative sample, we needed to test whether an independent data set was

correctly classified using the model that was built using a different sample set.

With all the previous results described above, we decided to test the methodology using the same samples as in the third experiment, consisting of NP samples collected in VTM1 during the peak of the pandemic but selecting different time periods to train and test. Thereof, these group of samples consists of two independent sample sets. The first set (Set 1; S1) consisted of NP samples collected in VTM1 at the end of April 2020 while the second set (Set 2; S2) corresponded to those samples collected in the same transport media at the beginning of May. Unlike the third experiment where all samples were considered as a single group, in this experiment the 89 mass spectra (45 positive and 44 negative) of the samples of set 1 (S1) were used to train a model and the 84 mass spectra (45 positive and 39 negative) of set 2 were used to test it.

The mass spectra of the two sets of samples are shown in Figure 5A. As can be seen, the positive and negative samples for SARS-CoV-2 infection have clearly distinct fingerprints. In this experiment, the best model, which was the SVM using 5 PCs, had a F1-score of 0.964 (Figure 5B and Table 1). Excellent results were obtained in terms of accuracy, sensitivity and specificity, reaching values of 97, 100 and 92%, respectively (Figure 5C). Moreover, these high values with low variation errors showed



the robustness of the developed methodology when used for the detection of SARS-CoV-2-positive samples.

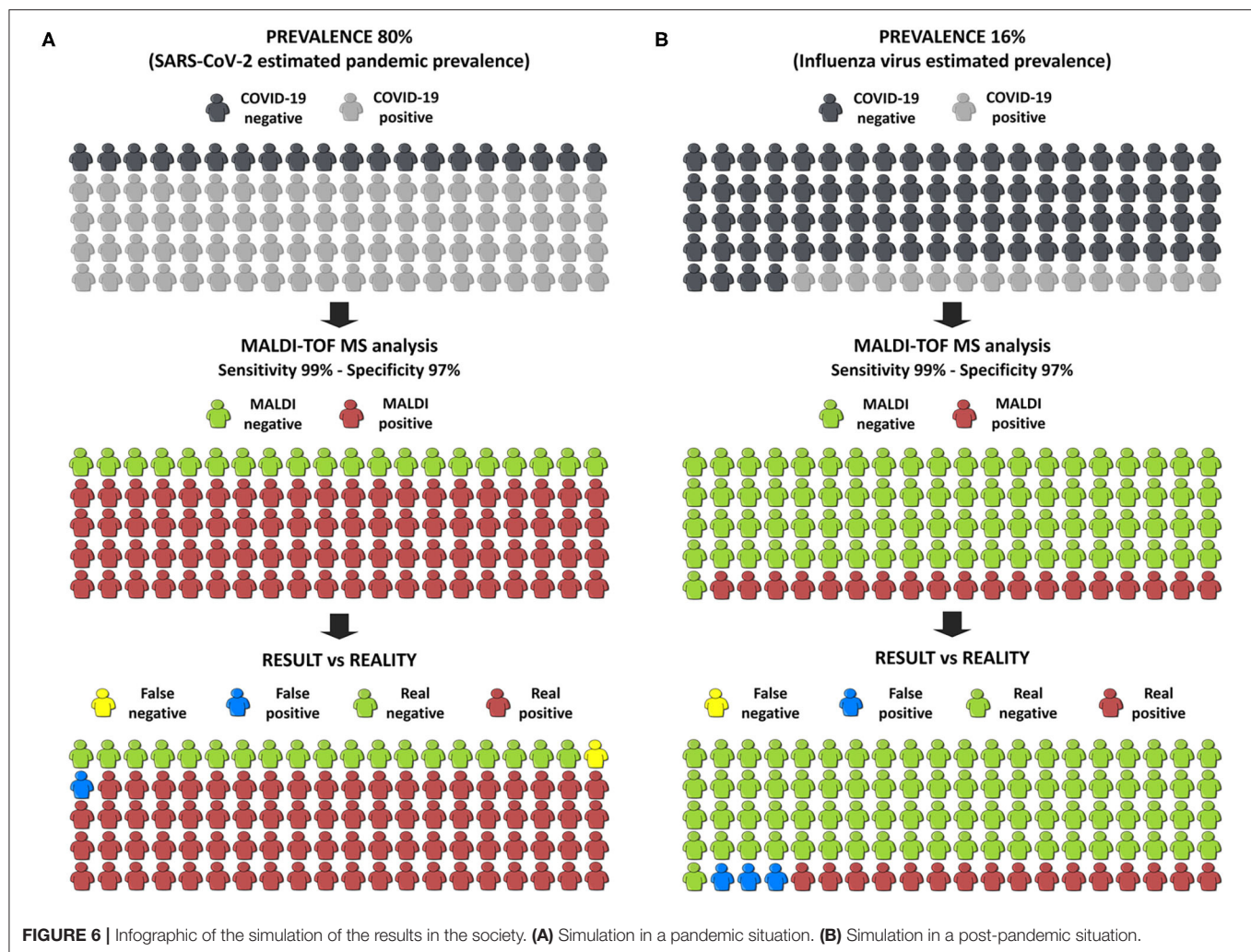
Overall, our results demonstrate that the developed method represents a promising method for the detection of SARS-CoV-2-positive samples. As it can be seen, the best results are achieved using the VTM1. However, a similar methodology was also described by Nachtigall et al. (20) where another viral transport media (Cary-Blair transport medium) was used. In contrast to what we have undertaken here, they did not study neither the effect that the use of different viral transport media might have in the results nor performed double-blind test in the ML. Another difference is that the samples used in our study were chemically inactivated whereas only ultraviolet irradiation was performed in their study. This detail is of great significance given that SARS-CoV-2 is extremely infectious and working with inactivated samples not only reduces the risk of in-lab infection during the experimental procedure but also reduces the mental stress that could be experienced by laboratory staff (39). In line with our results, an earlier study has also found that using inactivated samples does not interfere with RT-PCR results (40).

Due to the high infectivity rate of SARS-CoV-2, an accurate and rapid diagnosis of both symptomatic and asymptomatic patients is needed to reduce the spread of the virus (31, 40). Different diagnostic methodologies have been developed, each with its own specific applications as well as its own advantages and drawbacks (5). However, all these methodologies share certain limitations: low sensitivity, high rate of false negatives, high dependence on the moment of the diagnostic window in

which the sample is collected, etc. (8, 28, 30, 34, 41). Given that asymptomatic infected people can also spread the virus, a rapid and economic screening test is needed to detect those SARS-CoV-2-positive patients without symptoms (3, 5, 42). Considering the cost of materials per specimen, we estimate that the cost of MALDI-TOF MS will be no more than 25% of the cost of RT-PCR analysis. With regards to the length of time required to receive results, the turn-around-time of a conventional RT-PCR in which an RNA extraction phase is also needed is around 6 h (40) whereas the analysis of the NP samples by MALDI-TOF MS takes less than a third part of this. Therefore, the use of MALDI-TOF-MS analysis, which is widely available in clinical laboratories, as a screening technique for SARS-CoV-2 infection detection will offer enormous savings both in time and cost.

As said, community prevalence and pre-test probability have an important effect on the positive and negative predictive value of a diagnostic test (37, 38). Under a clinical point of view, this pandemic situation has been one of the most challenging experiences in the laboratories; recruiting resources, reagents, methodological platforms and personal staff has been the most difficult goal to achieve for the very last months. Nowadays, this new situation is extremely demanding due to the high incidence and prevalence in the general population. Vaccines are ready to be used as immunological protection against SARS-CoV-2 (43) so we will probably notice shortly a descent of the cases. In this future and new scenario and with lower prevalence in the population, we will need a strong and accurate methodology that provides results requiring less time and investment. MALDI-TOF is the best option available in





clinical laboratories that can reach this purpose. Moreover, this equipment is commonly found in clinical laboratories also in the developing countries, which means that the implementation of the developed methodology would not require a huge economic cost.

Finally, in order to estimate the benefit to society of this innovation, we have used the online calculator of the BMJ (33) applying our best developed model. Firstly, a pandemic situation was simulated taking an estimated prevalence of COVID-19 in Europe of 80%, which was a pre-test probability calculated by the WHO. If 100 people were tested, and only 1 false negative and 1 false positive were obtained (Figure 6A), the probability of having COVID-19 if the test is negative is only 5%. To simulate the results in a post-pandemic situation, the pre-test probability was set at 16% which is the estimated prevalence of the influenza virus in Europe. In this case, only 3 false positives and no false negatives were obtained (Figure 6B). These two simulations strongly support our own conclusion that the developed methodology, consisting in the analysis NP samples by MALDI-TOF-MS in combination

with machine learning approaches, is suitable to diagnose COVID-19 patients not only in pandemic situations but also in an epidemic situation as a screening tool in the first steps of diagnosis.

## DATA AVAILABILITY STATEMENT

The datasets presented in this article are not readily available because the data that support the findings of this study are available from the corresponding author upon reasonable request. Requests to access the datasets should be directed to Pere Boadas-Vaello, pere.boadas@udg.edu.

## ETHICS STATEMENT

The studies involving human participants were reviewed and approved by Clinical Research Ethics Committee of the Doctor Josep Trueta Hospital in Girona (ref#2020.088). Written informed consent for participation was not required for this

study in accordance with the national legislation and the institutional requirements.

## AUTHOR CONTRIBUTIONS

PB-V, MD, and VS conceived the experiments, supported by EV and MS. OJ-R and MS were in charge of the NP samples inactivation and management. MALDI-MS experiments were carried out by MD and PB-V. Spectra analyses were carried out by MD, EP-M, and JC. Machine learning analyses were performed by EG-C and MD. All authors were involved in interpretation of the data and they contributed to both critical discussion of the results and elaboration of the manuscript. All authors listed above have contributed sufficiently to be included as authors.

## REFERENCES

- World Health Organization (WHO). Coronavirus disease (COVID-2019) situation reports. 29 December, 2020. Available online at: <https://www.who.int/publications/m/item/weekly-epidemiological-update---27-january-2021> (accessed January 30, 2021).
- Zaman KT, Islam H, Khan AN, Shweta DS, Rahman A, Masud J, et al. COVID-19 pandemic burden on global economy: a paradigm shift. *Preprints* (2020). doi: 10.20944/preprints202005.0461.v1
- Bai Y, Yao L, Wei T, Tian F, Jin DY, Chen L, et al. Presumed asymptomatic carrier transmission of COVID-19. *JAMA*. (2020) 323:1406–7. doi: 10.1001/jama.2020.2565
- Ji T, Liu Z, Wang G, Guo X, Akbar Khan S, Lai C, et al. Detection of COVID-19: A review of the current literature and future perspectives. *Biosens Bioelectron*. (2020) 166:112455. doi: 10.1016/j.bios.2020.112455
- Wu SY, Yau HS, Yu MY, Tsang HF, Chan LWC, Cho WCS, et al. The diagnostic methods in the COVID-19 pandemic, today and in the future. *Expert Rev Mol Diagn*. (2020) 20:985–93. doi: 10.1080/14737159.2020.1816171
- Udugama B, Kadhiresan P, Kozłowski HN, Malekjahani A, Osborne M, Li VYC, et al. Diagnosing COVID-19: the disease and tools for detection. *ACS Nano*. (2020) 14:3822–35. doi: 10.1021/acsnano.0c02624
- World Health Organization (WHO). Laboratory testing for coronavirus disease 2019 (COVID-19) in suspected human cases: interim guidance, 2 March 2020. Available online at: <https://apps.who.int/iris/handle/10665/331329> (accessed December 20, 2020).
- Tahamtan A, Ardebili A. Real-time RT-PCR in COVID-19 detection: issues affecting the results. *Expert Rev Mol Diagn*. (2020) 20:453–4. doi: 10.1080/14737159.2020.1757437
- Williams E, Bond K, Zhang B, Putland M, Williamson DA. Saliva as a non-invasive specimen for detection of SARS-CoV-2. *J Clin Microbiol*. (2020) 58:e00776–20. doi: 10.1128/JCM.00776-20
- Pasomsab E, Watcharananan SP, Boonyawat K, Janchompoo P, Wongtabtim G, Suksuwan W, et al. Saliva sample as a non-invasive specimen for the diagnosis of coronavirus disease 2019: a cross-sectional study. *Clin Microbiol Infect*. (2020) 27:285.e1–285.e4. doi: 10.1016/j.cmi.2020.05.001
- Reeve MA, Bachmann D. MALDI-TOF MS protein fingerprinting of mixed samples. *Biol Methods Protoc*. (2019) 4:bpz013. doi: 10.1093/biomethods/bpz013
- Welker M, van Belkum A, Girard V, Charrier JB, Pincus D. An update on the routine application of MALDI-TOF MS in clinical microbiology. *Expert Rev Proteomics*. (2019) 16:695–710. doi: 10.1080/14789450.2019.1645603
- Majchrzykiewicz-Koehorst JA, Heikens E, Trip H, Hulst AG, de Jong AL, Viveen MC, et al. Paauw, Rapid and generic identification of influenza A and other respiratory viruses with mass spectrometry. *J Virol Methods*. (2015) 213:75–83. doi: 10.1016/j.jviromet.2014.11.014
- Calderaro A, Arcangeletti MC, Rodighiero I, Buttrini M, Montecchini S, Vasile Simone R, et al. Identification of different respiratory viruses, after

## FUNDING

The present work was supported by SAUN—Santander Universidades-CRUE, grant PEDIEC from FONDO SUPERA COVID-19 call.

## ACKNOWLEDGMENTS

The authors would like to thank the ICS-IAS Girona Clinical Laboratory staff for the RT-PCR assessments and we want to particularly acknowledge the patients and the IDIBGI Biobank (Biobanc IDIBGI, B.0000872), integrated in the Spanish National Biobanks Network, for their collaboration. Also we thank the staff of the Universitat de Girona Research Technical Services where the MALDI-TOF MS measurements were performed.

- a cell culture step, by matrix assisted laser desorption/ionization time of flight mass spectrometry (MALDI-TOF MS). *Sci Rep*. (2016) 6:36082. doi: 10.1038/srep36082
- Deulofeu M, Kolárová L, Salvadó V, María Peña-Méndez E, Almási M, Štokr M, et al. Rapid discrimination of multiple myeloma patients by artificial neural networks coupled with mass spectrometry of peripheral blood plasma. *Sci Rep*. (2019) 9:7975. doi: 10.1038/s41598-019-44215-1
- Amato F, López A, Peña-Méndez EM, Vanhara P, Hampel A, Havel J. Artificial neural networks in medical diagnosis. *J Appl Biomed*. (2013) 11:47–58. doi: 10.2478/v10136-012-0031-x
- Marchetti-Deschmann M, Allmaier G. Mass spectrometry — one of the pillars of proteomics. *J Proteomics*. (2011) 74:915–9. doi: 10.1016/j.jpro.2011.04.024
- Bäckryd E, Ghafouri B, Carlsson AK, Olausson P, Gerdle B. Multivariate proteomic analysis of the cerebrospinal fluid of patients with peripheral neuropathic pain and healthy controls—a hypothesis-generating pilot study. *J Pain Res*. (2015) 8:321–33. doi: 10.2147/JPR.S82970
- Sisignano M, Lötsch J, Parnham MJ, Geisslinger G. Potential biomarkers for persistent and neuropathic pain therapy. *Pharmacol Ther*. (2019) 199:16–29. doi: 10.1016/j.pharmthera.2019.02.004
- Nachtigall FM, Pereira A, Trofymchuk OS, Santos LS. Detection of SARS-CoV-2 in nasal swabs using MALDI-MS. *Nat Biotechnol*. (2020) 38:1168–73. doi: 10.1038/s41587-020-0644-7
- SoRelle JA, Patel K, Filkins L, Park JY. Mass spectrometry for COVID-19. *Clin Chem*. (2020) 66:1367–8. doi: 10.1093/clinchem/hvaa222
- Friedman JH. Greedy function approximation: a gradient boosting machine. *Ann Stat*. (2001) 29:1189–232. doi: 10.1214/aos/1013203451
- Boser BE, Guyon IM, Vapnik VN. A training algorithm for optimal margin classifiers. In: *Proceedings of the fifth annual workshop on Computational learning theory (COLT '92)* (Pittsburgh, PA). (1992).
- Albalat A, Stalmach A, Bitsika V, Siwy J, Schanstra JP, Petropoulos AD, et al. Improving peptide relative quantification in MALDI-TOF MS for biomarker assessment. *Proteomics*. (2013) 13:2967–75. doi: 10.1002/pmic.201300100
- Hossain M, Limbach PA. A comparison of MALDI matrices. In: Cole RB, editor. *Electrospray and MALDI Mass Spectrometry. Fundamentals, Instrumentation, Practicalities, and Biological Applications*. New Jersey, NJ: Wiley (2010). p. 214–244.
- Chen Y, Gao D, Bai H, Liu H, Lin S, Jiang Y. Carbon dots and 9aa as a binary matrix for the detection of small molecules by matrix-assisted laser desorption/ionization mass spectrometry. *J Am Soc Mass Spectrom*. (2016) 27:1227–35. doi: 10.1007/s13361-016-1396-y
- Harvey DJ. Mass spectrometry: ionization methods overview. In: Worsfold P, Townshend A, Poole C, Miró M, editors. *Encyclopedia of Analytical Science*. Amsterdam: Elsevier (2013). p. 350–9.
- Zitek T. The appropriate use of testing for COVID-19. *West J Emerg Med*. (2020) 21:470–2. doi: 10.5811/westjem.2020.4.47370
- Waller JV, Kaur P, Tucker A, Lin KK, Diaz MJ, Henry TS, et al. Diagnostic tools for coronavirus disease (COVID-19): comparing CT and

- RT-PCR viral nucleic acid testing. *AJR Am J Roentgenol.* (2020) 215:834–8. doi: 10.2214/AJR.20.23418
30. Lippi G, Mattiuzzi C, Bovo C, Plebani M. Current laboratory diagnostics of coronavirus disease 2019 (COVID-19). *Acta Biomed.* (2020) 91:137–45. doi: 10.23750/abm.v91i2.9548
  31. Basso D, Aita A, Navaglia F, Franchin E, Fioretto P, Moz S, et al. SARS-CoV-2 RNA identification in nasopharyngeal swabs: issues in pre-analytics. *Clin Chem Lab Med.* (2020) 58:1579–86. doi: 10.1515/cclm-2020-0749
  32. Arevalo-Rodriguez I, Buitrago-Garcia D, Simancas-Racines D, Zambrano-Achig P, Del Campo R, Ciapponi A, et al. False-negative results of initial RT-PCR assays for COVID-19: a systematic review. *PLoS ONE.* (2020) 15:e0242958. doi: 10.1371/journal.pone.0242958
  33. Watson J, Whiting PF, Brush JE. Brush, interpreting a covid-19 test result. *BMJ.* (2020) 369:m1808. doi: 10.1136/bmj.m1808
  34. Feng W, Newbigging AM, Le C, Pang B, Peng H, Cao Y, et al. Molecular diagnosis of COVID-19: challenges and research needs. *Anal Chem.* (2020) 92:10196–209. doi: 10.1021/acs.analchem.0c02060
  35. Rogers AA, Baumann RE, Borillo GA, Kagan RM, Batterman HJ, Galdzicka MM, et al. Evaluation of transport media and specimen transport conditions for the detection of SARS-CoV-2 by use of real-time reverse transcription-PCR. *J Clin Microbiol.* (2020) 58:e00708–20. doi: 10.1128/JCM.00708-20
  36. Axell-House DB, Lavingia R, Rafferty M, Clark E, Amirian ES, Chiao EY. The estimation of diagnostic accuracy of tests for COVID-19: a scoping review. *J Infect.* (2020) 81:681–97. doi: 10.1016/j.jinf.2020.08.043
  37. Shyu D, Dorroh J, Holtmeyer C, Ritter D, Upendran A, Kanna R, et al. Laboratory tests for COVID-19: a review of peer-reviewed publications and implications for clinical use. *Mo Med.* (2020) 117:184–95.
  38. Tu YP, O'Leary TJ. Testing for severe acute respiratory syndrome-coronavirus 2: challenges in getting good specimens, choosing the right test, and interpreting the results. *Crit Care Med.* (2020) 48:1680–9. doi: 10.1097/CCM.0000000000004594
  39. Wang Y, Song W, Zhao Z, Chen P, Liu J, Li C. The impacts of viral inactivating methods on quantitative RT-PCR for COVID-19. *Virus Res.* (2020) 285:197988. doi: 10.1016/j.virusres.2020.197988
  40. Long C, Xu H, Shen Q, Zhang X, Fan B, Wang C, et al. Diagnosis of the Coronavirus disease (COVID-19): rRT-PCR or CT? *Eur J Radiol.* (2020) 126:108961. doi: 10.1016/j.ejrad.2020.108961
  41. Bohn MK, Lippi G, Horvath A, Sethi S, Koch D, Ferrari M, et al. Molecular, serological, and biochemical diagnosis and monitoring of COVID-19: IFCC taskforce evaluation of the latest evidence. *Clin Chem Lab Med.* (2020) 58:1037–52. doi: 10.1515/cclm-2020-0722
  42. Gao Z, Xu Y, Sun C, Wang X, Guo Y, Qiu S, et al. A systematic review of asymptomatic infections with COVID-19. *J Microbiol Immunol Infect.* (2020) 54:12–6. doi: 10.1016/j.jmii.2020.05.001
  43. Polack FP, Thomas SJ, Kitchin N, Absalon J, Gurtman A, Lockhart S, et al. Safety and efficacy of the BNT162b2 mRNA Covid-19 vaccine. *N Engl J Med.* (2020) 383:2603–15. doi: 10.1056/NEJMoa2034577

**Conflict of Interest:** The authors declare that the research was conducted in the absence of any commercial or financial relationships that could be construed as a potential conflict of interest.

Copyright © 2021 Deulofeu, García-Cuesta, Peña-Méndez, Conde, Jiménez-Romero, Verdú, Serrando, Salvadó and Boadas-Vaello. This is an open-access article distributed under the terms of the Creative Commons Attribution License (CC BY). The use, distribution or reproduction in other forums is permitted, provided the original author(s) and the copyright owner(s) are credited and that the original publication in this journal is cited, in accordance with accepted academic practice. No use, distribution or reproduction is permitted which does not comply with these terms.



# The Diagnostic Yield of the Multidisciplinary Discussion in Patients With COVID-19 Pneumonia

Fiorella Calabrese<sup>1\*</sup>, Federica Pezzuto<sup>1</sup>, Chiara Giraudo<sup>2</sup>, Luca Vedovelli<sup>1</sup>, Francesco Fortarezza<sup>1</sup>, Claudia Del Vecchio<sup>3</sup>, Francesca Lunardi<sup>1</sup>, Anna Sara Fraia<sup>2</sup>, Elisabetta Cocconcelli<sup>1</sup>, Stefania Edith Vuljan<sup>1</sup>, Dario Gregori<sup>1</sup>, Andrea Crisanti<sup>3</sup>, Elisabetta Balestro<sup>1†</sup> and Paolo Spagnolo<sup>1†</sup>

<sup>1</sup> Department of Cardiac, Thoracic, Vascular Sciences, and Public Health, University of Padova, Medical School, Padova, Italy, <sup>2</sup> Department of Medicine, University of Padova, Medical School, Padova, Italy, <sup>3</sup> Department of Molecular Medicine, University of Padova, Medical School, Padova, Italy

## OPEN ACCESS

### Edited by:

Reza Lashgari,  
Institute for Research in Fundamental  
Sciences, Iran

### Reviewed by:

Ilias Papanikolaou,  
General Hospital of Corfu, Greece  
Atfeh Abedini,  
Shahid Beheshti University of Medical  
Sciences, Iran

### \*Correspondence:

Fiorella Calabrese  
fiorella.calabrese@unipd.it

<sup>†</sup>These authors share last authorship

### Specialty section:

This article was submitted to  
Pulmonary Medicine,  
a section of the journal  
Frontiers in Medicine

Received: 04 December 2020

Accepted: 03 March 2021

Published: 01 April 2021

### Citation:

Calabrese F, Pezzuto F, Giraudo C,  
Vedovelli L, Fortarezza F, Del  
Vecchio C, Lunardi F, Fraia AS,  
Cocconcelli E, Vuljan SE, Gregori D,  
Crisanti A, Balestro E and Spagnolo P  
(2021) The Diagnostic Yield of the  
Multidisciplinary Discussion in Patients  
With COVID-19 Pneumonia.  
Front. Med. 8:637872.  
doi: 10.3389/fmed.2021.637872

**Purpose:** The hypothesis of the study was that a multidisciplinary approach involving experienced specialists in diffuse parenchymal lung disease might improve the diagnosis of patients with COVID-19 pneumonia.

**Methods:** Two pulmonologists, two radiologists, and two pathologists reviewed 27 patients affected by severe COVID-19 pneumonia as the main diagnosis made by non-pulmonologists. To evaluate whether the contribution of specialists, individually and/or in combination, might modify the original diagnosis, a three-step virtual process was planned. The whole lung examination was considered the gold standard for the final diagnosis. The probability of a correct diagnosis was calculated using a model based on generalized estimating equations. The effectiveness of a multidisciplinary diagnosis was obtained by comparing diagnoses made by experienced pulmonologists with those made by non-pulmonologists.

**Results:** In 19% of cases, the diagnosis of COVID-19-related death was mainly incorrect. The probability of a correct diagnosis increased strikingly from an undedicated clinician to an expert specialist. Every single specialist made significantly more correct diagnoses than any non-pulmonologist. The highest level of accuracy was achieved by the combination of 3 expert specialists ( $p = 0.0003$ ).

**Conclusion:** The dynamic interaction between expert specialists may significantly improve the diagnostic confidence and management of patients with COVID-19 pneumonia.

**Keywords:** diagnostic yield, multidisciplinary approach, COVID-19, COVID-19 pneumonia, SARS-CoV-2

## INTRODUCTION

Coronavirus disease 19 (COVID-19) was first identified in Wuhan, China, in December 2019 and is now on its second wave. Genetic sequencing of the virus determined that it is a beta coronavirus named severe acute respiratory syndrome-related coronavirus 2 (SARS-CoV-2) (1). Although most patients have a favorable prognosis, pneumonia, and severe hypoxemia secondary to SARS-CoV-2 infection can lead to acute respiratory failure (ARF) and death (2). Elderly male



patients with comorbidities such as obesity, hypertension, diabetes, cardiac disease, and neoplasm also have an increased risk for severe disease and death and need distinct management and higher surveillance levels (3–6). Management remains suboptimal with high mortality rates, particularly among patients admitted to the intensive care unit (ICU).

The integration of all available data from each patient has proven crucial in the management of diffuse parenchymal lung disease (DPLD). Indeed, the international guidelines suggest health professionals with experience in DPLD be involved in patient diagnosis and management in a multidisciplinary approach to achieve the most confident diagnosis and optimize treatment (7). The sudden onset and rapid spread of the COVID-19 pandemic with the high number of infections and deaths have led to a global health emergency. Since this was an unknown disease, the priority has been stemming the infection, which inevitably has limited interaction among experts. As COVID-19 is an extremely complex disease, it would potentially benefit from a multidisciplinary approach even during the pandemic. The hypothesis of this study was therefore that a multidisciplinary approach involving specialists experienced in DPLD (pulmonologists, radiologists, and pathologists) may improve the diagnosis and management of patients with COVID-19 pneumonia, following a decision-making approach similar to what is used in DPLD.

## MATERIALS AND METHODS

### Study Subjects

The present study was a critical re-evaluation of deceased patients by an expert team of specialists (pulmonologists, radiologists, and pathologists) routinely involved in multidisciplinary meetings of mainly DPLD (8) but also with robust experience in COVID-19 diagnosis and management (9, 10). We retrospectively studied 27 patients who consecutively died from March to May 2020 in our hospital whose death certificate indicated SARS-CoV-2 infection (detected at least once on nasopharyngeal swab) and severe COVID-19 pneumonia as the main diagnosis made by non-pulmonologists (i.e., emergency room clinicians, general practitioners, specialists in infectious diseases, and anaesthesiologists).

The autopsy was performed according to national and international protocols, as previously described (11). At autopsy, the whole lungs were macroscopically examined. A small sample was taken from the most representative area of lung injury. The sample was in part preserved in RNA later and processed for molecular analyses (see below for molecular processing details) and in part fixed in formalin for routine histology, before and independently from the other additional fragments. Pathological features suggestive of COVID-19 pneumonia (alveolar injury as well as vascular lesions) were quantitatively described using a scoring system, as previously reported (10). Other associated lesions (neoplasia, infectious diseases, aspiration pneumonia, etc.) were also reported. To confirm the pathological diagnosis of COVID-19 pneumonia, the fragment preserved in RNA

later was also processed by real time reverse transcriptase-polymerase chain reaction (RT-PCR) for SARS-CoV-2 [SARS-CoV-2 (2019-nCoV) Centers for Disease Control and Prevention (CDC) Emergency Use Authorized (EUA) Authorized qPCR probe assay primer/probe mix]. An additional fragment was analyzed by culture. Briefly, virus isolation was performed using African green monkey kidney (Vero) cells. When a diffuse, refractile, rounding, cytopathic effect was noted, the Vero cell culture supernatant was passaged to a fresh Vero cell culture tube to ensure reproducibility of the cytopathic effect. SARS-CoV-2 in the supernatant was further confirmed by reverse transcription polymerase chain reaction using primers described previously (12).

In order to define the levels of certainty for a diagnosis of COVID-19 pneumonia, two expert pathologists (FC, FP) scored all cases independently and blinded to clinical and autopsy data. Several parameters, distinguishing distinct anatomic areas (airways, alveolar wall, alveolar space, pleura) and any additional findings were recorded, as previously described (13). Based on morphological/virologic evaluation, four distinct levels of diagnostic certainty were defined: (1) Definite COVID-19 pneumonia: all lung samples showing lesions typical of COVID-19 pneumonia (thrombosis, vascular injury, and/or diffuse alveolar damage/organizing pneumonia), confirmed SARS-CoV-2 lung positivity (both molecular and culture), with no other associated or pre-existing lesions (e.g., foci of bacterial pneumonia, neoplasia), (2) Probable COVID-19 pneumonia: lung samples displaying mainly features of COVID-19 pneumonia (+/- lung SARS-CoV-2 infection) with other associated lesions (e.g., foci of bacterial infection), (3) Possible COVID-19 pneumonia: lung samples showing only focal changes of COVID-19 pneumonia (+/- lung SARS-CoV-2 infection, etc.) with more extensive features consistent with alternative diagnoses (i.e., lung cancer/metastasis, etc.), (4) Non-COVID-19 pneumonia: lung samples not showing any typical lesions, no evidence of SARS-CoV2 infection, and presence of features consistent with alternative diagnoses.

During the autopsy, additional fragments were sampled from both lungs (at least 20 samples for each case) and systematically analyzed, as previously described (13, 14).

Clinical evaluation was performed by two experienced pulmonologists (PS, EB) based on the following data: past and recent medical history including comorbidities, respiratory and systemic signs, and symptoms (type and duration) before hospital admission, imaging, laboratory findings, gas exchange values (FiO<sub>2</sub>, pO<sub>2</sub>, and pO<sub>2</sub>/FiO<sub>2</sub>) and their changes during hospitalization, and oxygen supplementation. Based on this data, patients were classified as follows: (1) Definite COVID-19 pneumonia: clinical findings typical of COVID-19 such as severe acute respiratory illness (i.e., fever, cough, shortness of breath, hypoxemia) in the absence of an alternative diagnosis that could explain the clinical presentation (15, 16), (2) Probable COVID-19 pneumonia: features of COVID-19 pneumonia associated with findings suggestive of alternative diagnoses (e.g., pleural effusion, clinical and laboratory findings in keeping with heart failure, or signs of bacterial pneumonia), (3) Possible COVID-19 pneumonia: features of COVID-19 pneumonia associated

with prevalent findings consistent with alternative etiologies (e.g., lung cancer, pulmonary metastases, pulmonary edema, heart failure), (4) Non-COVID-19 pneumonia: absence of typical signs/symptoms and laboratory findings of COVID-19 pneumonia in the presence of features consistent with alternative

diagnoses (e.g., neoplasm, interstitial lung disease, ischemic heart disease, pulmonary edema).

With regard to the radiological assessment, all chest X-rays and, when available, chest computed tomography (CT) images were assessed by two expert thoracic radiologists (CG,

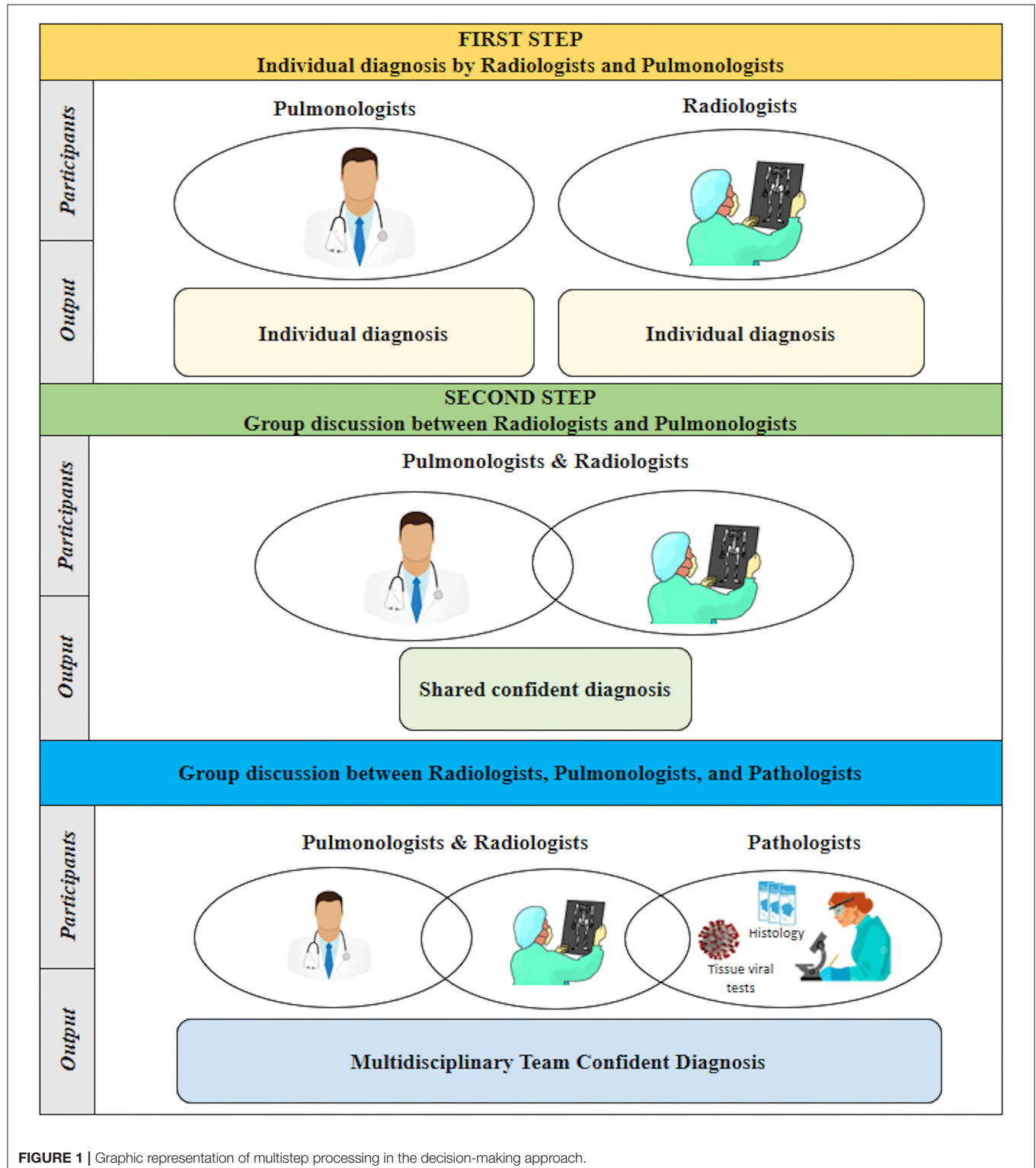


**FIGURE 1** | Graphic representation of multistep processing in the decision-making approach.

AF). According to the radiological findings, patients were classified as follows: (1) Definite COVID-19 pneumonia: typical findings of COVID-19 pneumonia, such as bilateral ground-glass opacities and/or consolidations (17), without any signs of alternative diagnoses, (2) Probable COVID-19 pneumonia: features of COVID-19 pneumonia associated with abnormalities such as pleural effusion, cardiomegaly, or Kerley B lines suggestive of cardiac failure, or lobar consolidation suggestive of bacterial pneumonia, (3) Possible COVID-19 pneumonia: features of COVID-19 pneumonia associated with predominant findings of alternative diagnoses (e.g., unilateral pulmonary lesions due to lung cancer, pulmonary bilateral metastatic nodules), (4) Non-COVID-19 pneumonia: no typical signs of COVID-19 with features suggestive of alternative diagnoses (e.g., unilateral pulmonary lesions due to lung cancer, reticular changes secondary to interstitial lung disease).

Data regarding demographics, smoking history, symptoms, comorbidities, treatment, disease duration, serology, radiological, and pathological findings were included in a dedicated database in REDCap. Informed consent was granted by a relative/legal representative of each deceased patient. The study was approved by the local clinical institutional review Board.

## Study Designs

To evaluate whether the contribution of pulmonologists, radiologists, and pathologists individually and/or in combination, could change the diagnosis originally made by non-pulmonologists, we planned a three-step process, modifying the methodology previously used in the evaluation of patients with DPLD (18).

Briefly, in the first step, two pulmonologists (PS, EB) and two radiologists (CG, AF) independently reviewed clinical and radiological data for each patient, without pathological data, and recorded their individual diagnoses and confidence levels. In the second step, pulmonologists and radiologists discussed their diagnosis and again recorded their individual or shared (in case of disagreement) confidence level. During the third step, pathologists entered the arena and reported the pathological diagnosis performed on a single lung fragment. The final diagnosis derived from the whole lung examination and full organ autopsy and was considered the diagnostic gold standard. Virtual meetings via the Zoom platform were set to allow pulmonologists, radiologists, and pathologists to discuss their interpretation with mutual collaboration (Figure 1).

## Analysis

All patients were evaluated by pulmonologists and pathologists. One case was not evaluated by radiologists due to lack of radiological data. Specialist scores (for single specialist and for combinations of different specialists) were compared with the full autopsy diagnosis, that was considered to be the true diagnosis, and were recorded as “correct” or “wrong”. Probability of a correct diagnosis (95% confidence interval) was calculated with the method of Wilson using the `binconf` function of the R package {Hmisc} (19). To explore the effectiveness of a multidisciplinary diagnosis we compared specialist diagnoses

with the non-pulmonologist using a model based on generalized estimating equations (GEE) (20) which expand the application of generalized linear models, providing a framework for analyzing correlated data, especially from repeated measures studies where multiple observations are collected from a specific sampling unit (21). In particular, we used a first-order autoregressive correlation structure and a robust standard error estimation to fit our small sample size. The R package {geepack} was used for the analysis (20). We exponentiated GEE results to obtain an odds ratio (95% CI) for each specialist (or combination of specialists) on their ability to formulate a correct diagnosis. All analyses and plotting were conducted on R software v.4.0.2 (22). The full code used for the analysis is available upon request.

## RESULTS

### Study Population

For all patients, demographic, clinical, and laboratory data are summarized in Table 1.

The patient population included 15 males (56%) and 12 females (44%) with a median age of 82 years (overall range 42–97 years, interquartile range, 75.5–87.5 years). At disease onset, the main common complaints were dyspnea (89%), fever (74%), and cough (67%). On admission, white blood cells (WBC), and lymphocytes showed a median value of  $2 \times 10^9/L$  (overall range  $0.99\text{--}20.36 \times 10^9/L$ , interquartile range  $4.14\text{--}12.90 \times 10^9/L$ ) and  $0.79 \times 10^9/L$  (overall range  $0.4\text{--}1.69 \times 10^9/L$ , interquartile range  $0.6425\text{--}1.0375 \times 10^9/L$ ), respectively. D-dimer levels were available for 19 patients, with a median value of  $497 \mu g/L$  (overall range  $150\text{--}3250 \mu g/L$ , interquartile range  $281\text{--}1216 \mu g/L$ ). Overall, the radiologists assessed 97 chest X-rays and four CTs. On average, for each patient four chest X-rays were available.

### Multistep Process and Interobserver Agreement

During the first step (Individual diagnosis by Radiologists and Pulmonologists), pulmonologists categorized 11 cases as definite (41%), nine cases as probable (33%), three cases as possible (11%), and four as non-COVID-19 pneumonia (15%). Radiologists classified 11 patients as definite (42%), 11 patients as probable (42%), two patients as possible (8%) and two patients as non-COVID-19 pneumonia (8%). The radiological data of one patient was not available. The overall diagnoses with their corresponding level of confidence are reported in Table 2.

During the second step (Discussion between Radiologists and Pulmonologists), a confident diagnosis was reached in 23 out of 26 cases (88%) with definite COVID-19 pneumonia in eight cases (30%). Following discussion, the diagnosis was changed in six cases, three changes for each specialist group (changes indicated with arrows in Table 2).

In the third step (Group discussion involving Radiologists, Pulmonologists, and Pathologists), the pathologists reported a diagnosis of definite COVID-19 pneumonia in 12 cases (45%), probable COVID-19 pneumonia in nine cases (33%), and possible COVID-19 pneumonia in three cases (11%). Three cases were classified as non-COVID-19 pneumonia (11%) (Table 3). A

**TABLE 1 |** Main clinical, epidemiological, and laboratory data available for all patients.

| ID | Epidemiological data |         |        |                          | SARS-COV-2-RT-PCR | Symptoms |       |         | Laboratory tests       |                       |      |          | Symptoms before admission | Ward    |
|----|----------------------|---------|--------|--------------------------|-------------------|----------|-------|---------|------------------------|-----------------------|------|----------|---------------------------|---------|
|    | Sex                  | Age yrs | Smoke  | Number of comorbidities* |                   | Fever C° | Cough | Dyspnea | WBC 10 <sup>9</sup> /L | LY 10 <sup>9</sup> /L | LY % | D-D µg/L | Days                      |         |
| 1  | M                    | 82      | No     | 2                        | Positive          | 39.5     | Yes   | Yes     | 15.17                  | 0.79                  | 5.2  | 311      | 5                         | ICU     |
| 2  | F                    | 69      | Na     | 2                        | Positive          | 37.9     | No    | Yes     | 8.94                   | 1.09                  | 12.2 | 2063     | 5                         | ICU     |
| 3  | M                    | 76      | Na     | 3                        | Positive          | 38       | No    | Yes     | 9.14                   | 1.02                  | 7.9  | 736      | 3                         | ICU     |
| 4  | M                    | 71      | No     | 1                        | Positive          | 38       | Yes   | No      | 17.98                  | 1.69                  | 9.4  | 684      | 14                        | ICU     |
| 5  | F                    | 87      | Former | 4                        | Positive          | 39       | No    | Yes     | 13.15                  | 0.65                  | 4.9  | 2929     | 3                         | Non-ICU |
| 6  | M                    | 79      | Yes    | 3                        | Positive          | 37.6     | Yes   | Yes     | 2.68                   | 0.62                  | 23.1 | 450      | 2                         | ICU     |
| 7  | M                    | 85      | Former | 5                        | Positive          | 38       | Yes   | Yes     | 18.09                  | 0.79                  | 4.4  | 772      | 4                         | Non-ICU |
| 8  | M                    | 76      | No     | 2                        | Positive          | 38       | No    | Yes     | 5.28                   | 1.36                  | 25.8 | 150      | 0                         | ICU     |
| 9  | F                    | 86      | No     | 5                        | Positive          | <37      | No    | Yes     | 12.16                  | 0.83                  | 6.8  | na       | 5                         | Non-ICU |
| 10 | M                    | 96      | No     | 5                        | Positive          | <37      | No    | Yes     | 4.99                   | 1.63                  | 32   | 150      | 2                         | Non-ICU |
| 11 | M                    | 86      | No     | 4                        | Positive          | 38.6     | Yes   | Yes     | 2.7                    | 0.4                   | 14.3 | 3250     | 3                         | Non-ICU |
| 12 | M                    | 77      | No     | 3                        | Positive          | 39       | Yes   | Yes     | 4.08                   | 0.81                  | 19.9 | 497      | 18                        | ICU     |
| 13 | F                    | 90      | No     | 4                        | Positive          | 39       | Yes   | Yes     | 17.83                  | 0.77                  | 4.3  | Na       | 7                         | Non-ICU |
| 14 | M                    | 80      | No     | 4                        | Positive          | 38.5     | Yes   | Yes     | 0.99                   | Na                    | Na   | Na       | 2                         | Non-ICU |
| 15 | F                    | 73      | Na     | 1                        | Positive          | 37.8     | No    | Yes     | 5.52                   | 0.67                  | 12.2 | 345      | 2                         | ICU     |
| 16 | M                    | 61      | Yes    | 3                        | Positive          | <37      | No    | Yes     | 3.02                   | Na                    | Na   | Na       | 5                         | ICU     |
| 17 | M                    | 82      | Former | 6                        | Positive          | 38       | Yes   | Yes     | 3.72                   | 0.46                  | 12.4 | 1711     | 3                         | Non-ICU |
| 18 | M                    | 75      | No     | 0                        | Positive          | 38.5     | Yes   | Yes     | 5.48                   | 0.49                  | 9.8  | 370      | 7                         | ICU     |
| 19 | M                    | 95      | Former | 3                        | Positive          | <37      | Yes   | Yes     | 20.36                  | 1.24                  | 6.1  | 176      | 2                         | Non-ICU |
| 20 | F                    | 88      | No     | 5                        | Positive          | 38.5     | Yes   | Yes     | 6.45                   | 0.94                  | 14.6 | 251      | 4                         | Non-ICU |
| 21 | F                    | 74      | Former | 3                        | Positive          | 38       | Yes   | Yes     | 5.2                    | 0.8                   | 15.4 | 150      | 10                        | ICU     |
| 22 | F                    | 87      | No     | 3                        | Positive          | 37       | Yes   | Yes     | 2.6                    | 0.49                  | 18.6 | 644      | 8                         | Non-ICU |
| 23 | F                    | 92      | Na     | 2                        | Positive          | 38.5     | No    | No      | 16.37                  | 0.95                  | 5.8  | 1660     | 2                         | Non-ICU |
| 24 | F                    | 90      | Na     | 3                        | Positive          | 37.7     | Yes   | Yes     | Na                     | Na                    | Na   | Na       | 1                         | Non-ICU |
| 25 | M                    | 83      | Former | 1                        | Positive          | <37      | Yes   | Yes     | 5.78                   | 0.61                  | 10.6 | Na       | 6                         | Non-ICU |
| 26 | F                    | 97      | Na     | 3                        | Positive          | 37.9     | Yes   | No      | 7.37                   | 1.49                  | 75.4 | Na       | 0                         | Non-ICU |
| 27 | F                    | 42      | Na     | 1                        | Positive          | <37      | No    | Yes     | 4.32                   | 0.70                  | 16.2 | Na       | 33                        | Non-ICU |

Yrs, years; na, not available; WBC, white blood cells; Ly, lymphocytes; D-D, d-dimer; ICU, intensive care unit; RT, reverse transcriptase; PCR, polymerase chain reaction; NF, nasopharyngeal. \*List of the most common comorbidities detected: Arterial hypertension, cardiovascular diseases (atrial fibrillation, valvular heart disease, cardiac failure, vasculopathy, angiodysplasia, chronic cerebral vasculopathy, pulmonary embolism, aortic aneurysm), kidney diseases (chronic renal failure, kidney transplant), chronic conditions (diabetes, dyslipidemia, dementia, chronic obstructive pulmonary disease, hyperthyroidism, and connective tissue diseases).



**TABLE 2 |** Confident diagnoses achieved step by step.

| ID | First step  |              | Second step  |               |           | Third step  |              |              | MDT confident diagnosis | Final diagnosis (after the evaluation of all lung specimens and full autopsy) |
|----|---|--------------|--|---------------|-----------|---|--------------|--------------|-------------------------|---|
|    | Individual diagnosis of pulmonologists and radiologists |              | Group discussion between pulmonologists and radiologists |               |           | Group discussion between pulmonologists, radiologists, and pathologists |              |              |                         |   |
|    | Pulmonologists  | Radiologists | Pulmonologists   | Radiologists  | Agreement | Pulmonologists + Radiologists   | Pathologists | Agreement    |                         |   |
|    | Output  | Output       | Output   | Output        |           | Output  | Output       |              |                         |   |
| 1  | Definite  | Definite     | Definite   | Definite      | Yes       | Definite  | Definite     | Yes          | Definite                | COVID-19 pneumonia  |
| 2  | Definite  | Definite     | Definite   | Definite      | Yes       | Definite  | Definite     | Yes          | Definite                | COVID-19 pneumonia  |
| 3  | Definite  | Definite     | Definite   | Definite      | Yes       | Definite  | Definite     | Yes          | Definite                | COVID-19 pneumonia  |
| 4  | Other   | Probable     | Other  | Probable      | No        | Other/Probable  | Other        | Yes, partial | Other                   | Iatrogenic pneumonia  |
| 5  | Probable  | Probable     | Probable   | Probable      | Yes       | Probable  | Definite     | No           | Probable                | COVID-19 pneumonia & edema  |
| 6  | Definite  | Definite     | Definite   | Definite      | Yes       | Definite  | Definite     | Yes          | Definite                | COVID-19 pneumonia  |
| 7  | Other   | Probable     | Other  | Probable      | No        | Other/Probable  | Probable     | Yes, partial | Probable                | COVID-19 pneumonia & squamous cell carcinoma                                  |
| 8  | Definite  | Definite     | Definite   | Definite      | Yes       | Definite  | Definite     | Yes          | Definite                | COVID-19 pneumonia  |
| 9  | Other   | Other        | Other  | Other         | Yes       | Other   | Probable     | No           | Probable                | COVID-19 pneumonia & bacterial pneumonia                                      |
| 10 | Other   | Probable     | Other  | Probable      | No        | Other/Probable  | Other        | Yes, partial | Other                   | COVID-19 pneumonia & bacterial pneumonia                                      |
| 11 | Probable  | Definite     | Probable   | Definite→Prob | Yes       | Probable  | Definite     | No           | Definite                | COVID-19 pneumonia  |
| 12 | Possible  | Possible     | Possible   | Possible      | Yes       | Possible  | Possible     | Yes          | Possible                | Squamous cell carcinoma & foci of COVID-19 pneumonia                          |
| 13 | Definite  | Probable     | Definite→Prob  | Probable      | Yes       | Probable  | Definite     | No           | Definite                | COVID-19 pneumonia  |
| 14 | Probable  | Probable     | Probable   | Probable      | Yes       | Probable  | Probable     | Yes          | Probable                | COVID-19 pneumonia & bacterial pneumonia                                      |
| 15 | Possible  | Possible     | Possible   | Possible      | Yes       | Possible  | Possible     | Yes          | Possible                | Malignant SFT & foci of COVID-19 pneumonia                                    |
| 16 | Probable  | Probable     | Probable   | Probable      | Yes       | Probable  | Probable     | Yes          | Probable                | COVID-19 pneumonia & Aspergillus bronchopneumonia                             |
| 17 | Probable  | Probable     | Probable   | Probable      | Yes       | Probable  | Probable     | Yes          | Probable                | COVID-19 pneumonia & bacterial pneumonia                                      |
| 18 | Definite  | Definite     | Definite   | Definite      | Yes       | Definite  | Definite     | Yes          | Definite                | COVID-19 pneumonia  |
| 19 | Definite  | Other        | Definite→Other   | Other         | Yes       | Other   | Other        | Yes          | Other                   | Aspiration and bacterial pneumonia  |
| 20 | Probable  | Probable     | Probable   | Probable      | Yes       | Probable  | Probable     | Yes          | Probable                | COVID-19 pneumonia & necrotizing granulomas                                   |
| 21 | Definite  | Definite     | Definite   | Definite      | Yes       | Definite  | Definite     | Yes          | Definite                | COVID-19 pneumonia  |
| 22 | Probable  | Definite     | Probable   | Definite→Prob | Yes       | Probable  | Probable     | Yes          | Probable                | COVID-19 pneumonia & aspiration pneumonia                                     |
| 23 | Probable  | Definite     | Probable   | Definite→Prob | Yes       | Probable  | Probable     | Yes          | Probable                | COVID-19 pneumonia & bacterial pneumonia                                      |
| 24 | Definite  | Na           | Definite   | Na            | Na        | Na  | Possible     | Na           | Possible                | Bacterial pneumonia & foci of COVID-19 pneumonia                              |
| 25 | Possible  | Probable     | Possible→Prob  | Probable      | Yes       | Probable  | Definite     | No           | Definite                | COVID-19 pneumonia  |
| 26 | Definite  | Definite     | Definite   | Definite      | Yes       | Definite  | Definite     | Yes          | Definite                | COVID-19 pneumonia  |
| 27 | Probable  | Probable     | Probable   | Probable      | Yes       | Probable  | Probable     | Yes          | Probable                | COVID-19 pneumonia & breast cancer metastasis                                 |

na, not available; MDT, multidisciplinary team; Prob, probable; SFT, solitary fibrous tumor.

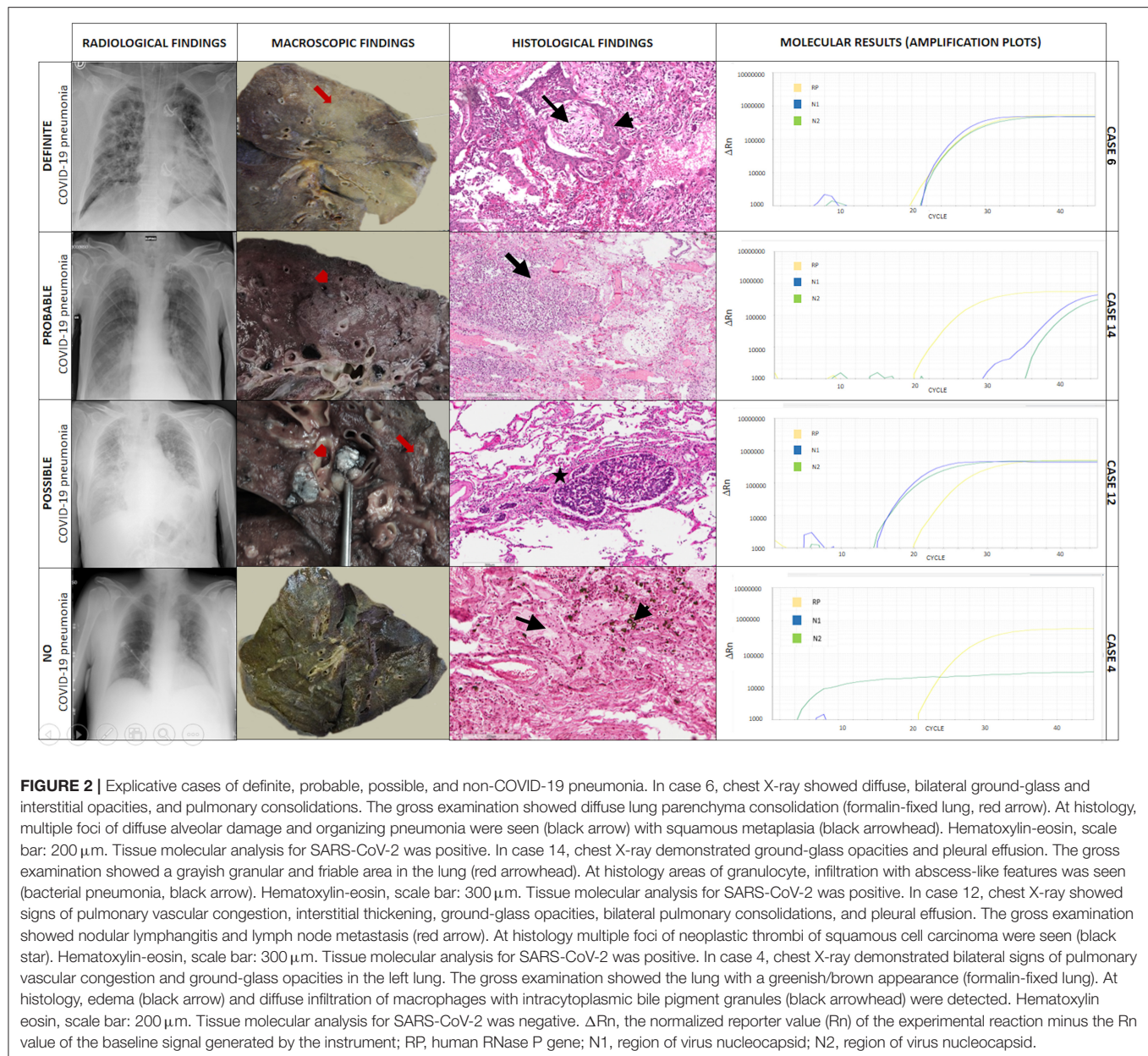
**TABLE 3 |** Results of lung histological examination, molecular tissue and cultural analyses.

| ID | Histological findings   |  | Molecular tests         |         | Pathological diagnosis |
|----|---|--|-------------------------|---------|------------------------|
|    | COVID-19 related lesions*   | Other lesions                                | Tissue real time RT-PCR | Culture |                        |
| 1  | Diffuse alveolar damage/organizing pneumonia and vascular injury                  |  | +                       | +       | Definite               |
| 2  | Diffuse alveolar damage/organizing pneumonia and vascular injury                  |  | +                       | Na      | Definite               |
| 3  | Diffuse alveolar damage/organizing pneumonia and vascular injury                  |  | +                       | +       | Definite               |
| 4  | No lesions  | Iatrogenic paracetamol injury                | –                       | Na      | Other                  |
| 5  | Diffuse alveolar damage/organizing pneumonia                                      |  | +                       | +       | Definite               |
| 6  | Diffuse alveolar damage/organizing pneumonia                                      |  | +                       | +       | Definite               |
| 7  | Multiple foci of diffuse alveolar damage/organizing pneumonia and vascular injury | Bronchial squamous cell carcinoma            | +                       | +       | Probable               |
| 8  | Diffuse alveolar damage/organizing pneumonia                                      |  | +                       | Na      | Definite               |
| 9  | Multiple foci of diffuse alveolar damage/organizing pneumonia and vascular injury | Bacterial pneumonia                          | –                       | Na      | Probable               |
| 10 | No lesions  | Bacterial pneumonia                          | +                       | Na      | Other                  |
| 11 | Diffuse alveolar damage/organizing pneumonia and vascular injury                  |  | +                       | Na      | Definite               |
| 12 | Foci of diffuse alveolar damage/organizing pneumonia and vascular injury          | Diffuse squamous cell carcinoma              | +                       | Na      | Possible               |
| 13 | Diffuse alveolar damage/organizing pneumonia and vascular injury                  |  | +                       | Na      | Definite               |
| 14 | Multiple foci of diffuse alveolar damage/organizing pneumonia and vascular injury | Bacterial pneumonia                          | +                       | +       | Probable               |
| 15 | Foci of diffuse alveolar damage/organizing pneumonia and vascular injury          | Malignant pleural solitary fibrous tumor     | +                       | –       | Possible               |
| 16 | Multiple foci of diffuse alveolar damage/organizing pneumonia and vascular injury | Aspergillus invasive bronchopneumonia        | +                       | +       | Probable               |
| 17 | Multiple foci of diffuse alveolar damage/organizing pneumonia and vascular injury | Bacterial pneumonia                          | +                       | –       | Probable               |
| 18 | Diffuse alveolar damage/organizing pneumonia and vascular injury                  |  | +                       | –       | Definite               |
| 19 | No lesions  | Aspiration/bacterial pneumonia               | –                       | –       | Other                  |
| 20 | Multiple foci of diffuse alveolar damage/organizing pneumonia and vascular injury | Necrotizing granulomas                       | +                       | +       | Probable               |
| 21 | Diffuse alveolar damage/organizing pneumonia                                      |  | +                       | –       | Definite               |
| 22 | Multiple foci of diffuse alveolar damage/organizing pneumonia and vascular injury | Aspiration pneumonia                         | +                       | +       | Probable               |
| 23 | Multiple foci of diffuse alveolar damage/organizing pneumonia and vascular injury | Bacterial pneumonia                          | +                       | –       | Probable               |
| 24 | Foci of diffuse alveolar damage/organizing pneumonia and vascular injury          | Bacterial pneumonia                          | +                       | –       | Possible               |
| 25 | Diffuse alveolar damage/organizing pneumonia and vascular injury                  |  | +                       | –       | Definite               |
| 26 | Diffuse alveolar damage/organizing pneumonia and vascular injury                  |  | +                       | +       | Definite               |
| 27 | Multiple foci of diffuse alveolar damage/organizing pneumonia and vascular injury | Breast cancer metastases/bacterial pneumonia | +                       | –       | Probable               |

RT, reverse transcriptase; PCR, polymerase chain reaction; na: not available. \* List of the most common histological findings detected. Diffuse alveolar damage/organizing pneumonia: hyaline membrane, edema, and hemorrhage (acute exudative phase); type 2 pneumocyte hyperplasia, organizing pneumonia, and squamous metaplasia (organizing/proliferative phase). Vascular injury: capillary inflammation, neutrophilic capillaritis, microthrombi and macrothrombi.

multidisciplinary discussion led to a confident diagnosis in 18 cases (69%), a partial agreement in three cases (12%), and no agreement in five cases (19%) (Table 2).

Additional data derived from examination of the entire lungs and other organs allowed us to finally reach a shared confident diagnosis in all cases. In two cases (8%), COVID-19 pneumonia



was ruled out, while in three cases (11%), COVID-19 pneumonia was only a marginal pathological process compared to other pathological lesions (Table 2). Examples of definite, probable, possible, and non-COVID-19 pneumonia are given in Figure 2.

The comparison between the diagnosis made by each specialist and the diagnosis made by the team following discussion and with the availability of the autopsy data showed that the ability to formulate a correct diagnosis increased strikingly from a non-pulmonologist to expert specialists, becoming progressively more accurate at different steps (Table 4).

The GEE model showed that every single specialist was able to make a significantly more accurate diagnosis than a non-pulmonologist. Hence, a radiologist and pulmonologist were

able to make a diagnosis about six times more accurate than a non-pulmonologist [OR: 6.33 (95% CI: 1.63–24.5);  $p = 0.0075$ ]. Of note, the highest level of accuracy was achieved by the combination of three expert specialists ( $p = 0.0003$ ) who made diagnoses that were about 35 times more accurate [OR: 35.2 (95% CI: 5.07–244)] than a single non-pulmonologist (Table 5, Figure 3). Indeed, in only one case (4%, case number 10) the multidisciplinary team diagnosis was wrong when compared to the gold standard (full autopsy diagnosis) (Table 5, Figure 3). In contrast, the diagnosis formulated by a non-pulmonologist was incorrect in over half of the cases (59%), whereas, the diagnosis formulated by a pulmonologist or a thoracic radiologist was not correct in seven (26%) and six cases (23%), respectively. After discussion, radiologists and pulmonologists incorrectly

**TABLE 4 |** Right and wrong diagnoses by each individual specialist and their combination.

|  | Overall    | 95% CI     |
|--|------------|------------|
| <b>Non-specialist</b>                            |            |            |
| Wrong  | 16 (59.3%) |            |
| Right  | 11 (40.7%) | 24.5–59.3% |
| <b>Pulmonologist</b>                             |            |            |
| Wrong  | 7 (25.9%)  |            |
| Right  | 20 (74.1%) | 55.3–86.2% |
| <b>Radiologist</b>                               |            |            |
| Wrong  | 6 (23.1%)  |            |
| Right  | 20 (76.9%) | 57.9–88.9% |
| <b>Pathologist</b>                               |            |            |
| Wrong  | 2 (7.4%)   |            |
| Right  | 25 (92.6%) | 76.6–97.9% |
| <b>Pulmonologist + radiologist</b>               |            |            |
| Wrong  | 5 (19.2%)  |            |
| Right  | 21 (80.8%) | 62.1–91.5% |
| <b>Pulmonologist + radiologist + pathologist</b> |            |            |
| Wrong  | 1 (3.8%)   |            |
| Right  | 25 (96.2%) | 81.1–99.8% |

CI, confidence interval.

diagnosed five cases (19%). After a full autopsy and whole lung examination, pathologists misinterpreted two cases (7%).

## DISCUSSION

In this study, we showed that the diagnostic accuracy of a multidisciplinary approach involving dedicated DPLD physicians is significantly higher than that of non-pulmonologists in a subset of patients infected by SARS-CoV-2 who died at the University Hospital of Padova and who underwent autopsy. We demonstrated that the dynamic interaction among DPLD experts influenced the level of confidence for the final diagnosis, which improved step by step. In two cases (8%), the diagnosis of COVID-19-related death was incorrect (final diagnosis: no COVID-19 pneumonia), while in three cases (11%), COVID-19 pneumonia was only a marginal feature compared to other pathological lesions. Thus, in 19% patients the diagnosis was mainly incorrect with consequent inappropriate management. This was the case in two patients, one with severe aspiration pneumonia and the other with carcinomatous lymphangitis who would have required different monitoring and management of care. Inappropriate treatment might have impacted on patient survival and outcome.

The global spread of the SARS-CoV-2 infection was quite unexpected, rapidly leading to a worldwide health emergency. As with any pandemic, patient care has been affected by staffing shortages, a chaotic work environment, and high levels of clinician stress. Clinicians had no choice but to provide care in an extraordinary setting. Moreover, the ICUs rapidly became saturated, and their overcrowding led to the recruitment of non-specialist medical staff, potentially exposing critically ill

**TABLE 5 |** GEE model for estimating the relative correctness of specialists in respect to the non-specialist diagnosis.

|   | Estimate | Standard error | p-value | 95% CI    |
|---|----------|----------------|---------|-----------|
| Pulmonologist                             | 4.14     | 0.540          | 0.0084  | 1.44–12.0 |
| Radiologist                               | 4.80     | 0.574          | 0.0063  | 1.56–14.8 |
| Pathologist                               | 20.5     | 0.821          | 0.0002  | 4.09–102  |
| Pulmonologist + radiologist               | 6.33     | 0.691          | 0.0075  | 1.63–24.5 |
| Pulmonologist + radiologist + pathologist | 35.2     | 0.989          | 0.0003  | 5.07–244  |

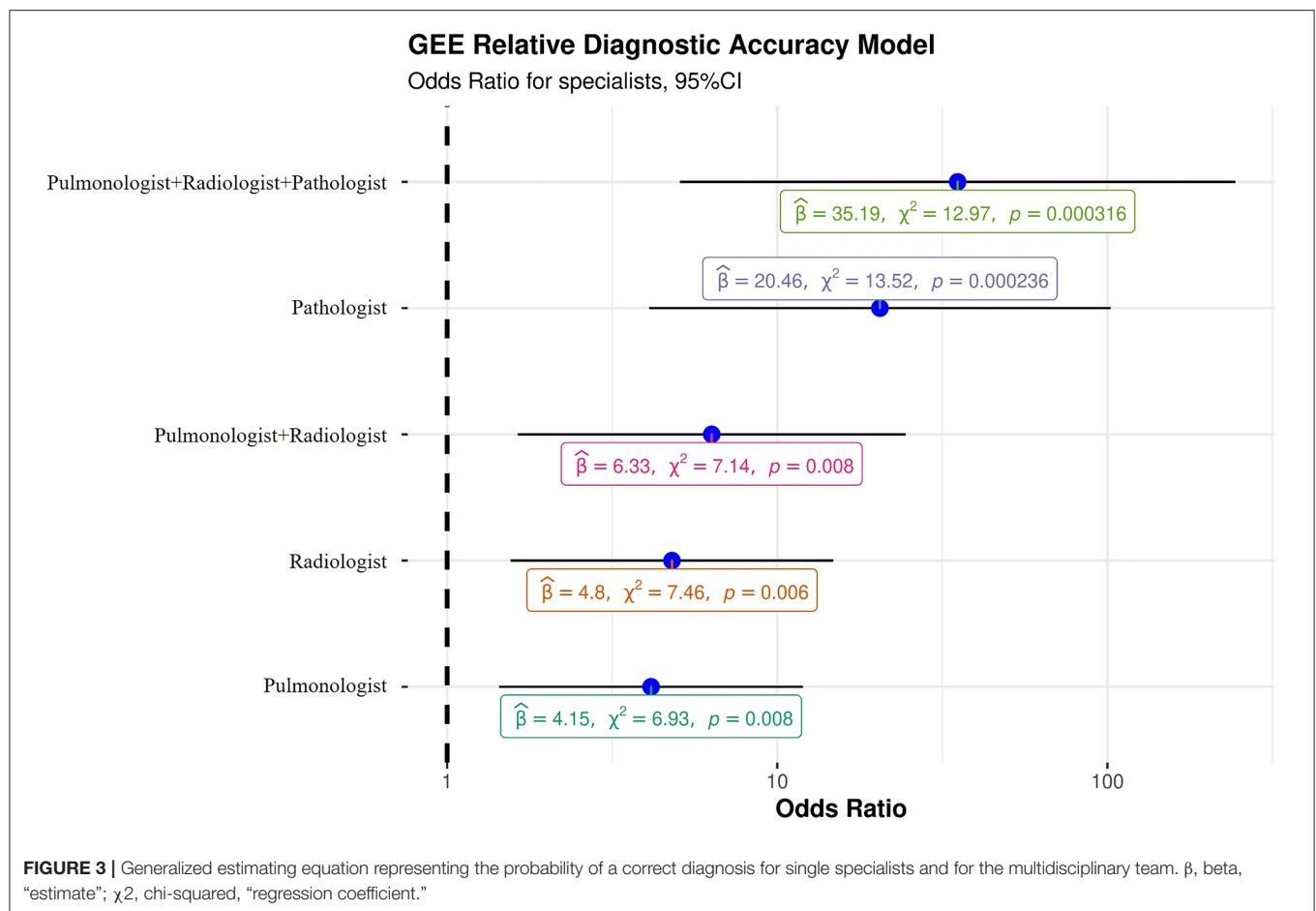
CI, confidence interval.

patients to mismanagement. Based on this distressing experience, COVID-19 health care should be planned adequately during the current second global wave. Today, the challenge is to establish a correct diagnosis taking into consideration several pathological conditions that may mimic and/or overlap with COVID-19 pneumonia, with the aim of optimizing patient management and, consequently, reducing mortality. Although our study consisted of a retrospective analysis (i.e., “a backward path by an expert team”), we believe a multidisciplinary approach involving specialists with experience in DPLD diagnosis and management can be highly beneficial to patient care. The multidisciplinary evaluation has become the diagnostic gold standard for DPLD, as it improves diagnostic confidence and interobserver agreement compared to individual components of the multidisciplinary team in isolation (18, 23), as was the case in our study.

An expert team should be involved in patient evaluation at the very time of hospital admission, particularly when patients are fragile and have severe respiratory failure. The chaotic work environment and the stressful conditions of emergency medical staff, which may make a face-to-face multidisciplinary approach non-realistic, might be successfully overcome by using newer digital technologies. Indeed, during the COVID-19 pandemic, multi-specialist meetings have been suspended and converted into virtual meetings, as occurred in our case.

In the multidisciplinary team of DPLD specialists, radiologists play a key role in that HRCT is largely recognized as a very sensitive and highly specific tool (23–25). During the early phase of the pandemic, CT was seldom performed in COVID-19-positive patients for safety reasons (26, 27). Although chest X-ray proved to be an accurate and reliable method to assess patients with COVID-19, even allowing the development of dedicated scores [CARE referral score] (27), CT plays a crucial role in recognizing alternative diagnoses, especially in patients with pre-existing pulmonary diseases (28–30). Moreover, as recently demonstrated by Borakati and colleagues, it has a higher sensitivity for COVID-19 and its use should be especially promoted in the initial assessment of suspected cases (31). The use of a diagnostic modality other than the gold standard may account for the higher agreement between pathologists and pulmonologists than radiologists in cases of partial agreement. Learning from the difficulties encountered in the first wave of the pandemic, most hospitals worldwide have recently adopted organizational models, which guarantee safe pathways to CT scanners that will surely increase the use of this technique and





are expected to have a significant impact on the quality of the delivered care (32, 33).

After discussion, pulmonologists and radiologists achieved a correct diagnosis in 81% of cases and were about six times more accurate than a single non-pulmonologist emphasizing their acceptable diagnostic yield even when histology is not available. These findings are of particular importance since, in some patients with COVID-19 pneumonia, severe respiratory failure could hamper invasive procedures (such as bronchoscopy) and consequently limit the pathologist's contribution. However, we then demonstrated that radiologists and pulmonologists incorrectly diagnosed five cases (19%) which could have influenced the decision-making process inducing a different treatment approach, monitoring, and setting of care. Indeed, in the scenario of an overcrowded intensive care unit, extra effort should be made to seek additional opinions by MDT to obtain greater confidence in the diagnostic impression and to improve the management and outcome of these patients.

In our study, as expected, pathologists showed the highest level of confidence between the first diagnostic impression on a single lung fragment compared to the final diagnosis on whole lung examination, with an incorrect diagnosis being made in only two cases. The lung fragments used by pathologists to perform the first diagnosis were similar in size to those obtained by video-assisted thoracic surgery (VATS) that is suggested to be the gold standard tool for the histological diagnosis of DPLD/ILD (23).

Invasive procedures such as VATS carry a high risk of mortality, particularly in patients with severe respiratory dysfunction and under mechanical ventilation (34). During the SARS-CoV-2 pandemic, invasive diagnostic procedures involving sampling of the lung parenchyma were discouraged. However, given the critically important contribution that pathologists could provide in the diagnosis of COVID-19 pneumonia, minimally invasive procedures, such as transbronchial lung biopsy/cryobiopsy could be reconsidered in the diagnostic work-up of COVID-19 pneumonia in doubtful cases, when radiological and/or clinical findings suggest the existence of an additional or alternative pathological condition. This is in line with recent expert recommendations (35) suggesting that bronchoscopy, if opportune, can be safely performed in patients with COVID-19, prioritizing minimization of the risk of viral transmission.

Information coming from a full autopsy of COVID-19 patients with the evaluation of numerous lung samples was considered the gold standard for final diagnosis in our case series. Data provided by the most recent autopsy studies have been crucial in improving our knowledge of the pathological substrates of COVID-19. Indeed, because of the contribution of autopsy studies, COVID-19 pneumonia is now recognized as a complex disease involving not only the lung parenchyma but also the vascular compartment with features that include vasculitis, angiogenesis, capillaritis, and micro/macrothrombi (10, 14, 36).

The present study has several limitations. First, the study is monocentric, and the study population is relatively small. However, despite this, we were able to implement a GEE model that is robust and provides reliable results even with small sample sizes. Moreover, this is one of the largest monocentric European case series wherein the same lung sampling methodology and analysis was consistently applied.

A multidisciplinary approach to diagnosis and management of patients with COVID-19 requires extra effort by the healthcare providers involved but, if it should be validated, it would have the potential to consistently improve the outcome of this often-fatal disease.

## DATA AVAILABILITY STATEMENT

The raw data supporting the conclusions of this article will be made available by the authors, without undue reservation.

## ETHICS STATEMENT

The studies involving human participants were reviewed and approved by The Local Ethics Committee of the University

Hospital of Padova (4853/A0/20). The patients/participants provided their written informed consent to participate in this study.

## AUTHOR CONTRIBUTIONS

FC, EB, and PS: conceptualization, writing—reviewing and editing, and supervision. FP, FF, and CG: writing original draft—preparation, visualization, and investigation. FL, EC, LV, SV, CD, and AF: resources and investigation. DG and AC: resources, investigation, visualization, and supervision. All authors have wrote, read, and approved the final version of the manuscript.

## FUNDING

This research was partially supported by a fellowship from the University of Padova/ Intesa San Paolo Vita bank (2020A08).

## ACKNOWLEDGMENTS

The authors thank Dr. Judith Wilson for English-language revision.

## REFERENCES

1. Coronaviridae Study Group of the International Committee on Taxonomy of Viruses. The species severe acute respiratory syndrome-related coronavirus: classifying 2019-Ncov and naming it SARS-Cov-2. *Nat Microbiol.* (2020) 5:536–44. doi: 10.1038/s41564-020-0695-z
2. Yang X, Yu Y, Xu J, Shu H, Xia J, Liu H, et al. Clinical course and outcomes of critically ill patients with SARS-Cov-2 pneumonia in Wuhan, China: a single-centered, retrospective, observational study. *Lancet Respir Med.* (2020) 8:475–81. doi: 10.1016/S2213-2600(20)30079-5
3. Rello J, Storti E, Belliato M, Serrano R. Clinical phenotypes of SARS-Cov-2: implications for clinicians and researchers. *Eur Respir J.* (2020) 55:2001028. doi: 10.1183/13993003.01028-2020
4. Grasselli G, Tonetti T, Protti A, Langer T, Girardis M, Bellani G, et al. Pathophysiology of COVID-19-associated acute respiratory distress syndrome: a multicentre prospective observational study. *Lancet Respir Med.* (2020) 8:1201–8. doi: 10.1016/S2213-2600(20)30370-2
5. Figliozzi S, Masci PG, Ahmadi N, Tondi L, Koutli E, Aimo A, et al. Predictors of adverse prognosis in COVID-19: a systematic review and meta-analysis. *Eur J Clin Invest.* (2020) 50:E13362. doi: 10.1111/eci.13362
6. Porcheddu R, Serra C, Kelvin D, Kelvin N, Rubino S. Similarity in case fatality rates (CFR) of COVID-19/SARS-COV-2 in Italy and China. *J Infect Dev Ctries.* (2020) 14:125–8. doi: 10.3855/jidc.12600
7. Raghu G, Remy-Jardin M, Myers JL, Richeldi L, Ryerson CJ, Lederer DJ, et al. Diagnosis of idiopathic pulmonary fibrosis. An official ATS/ERS/JRS/ALAT clinical practice guideline. *Am J Respir Crit Care Med.* (2018) 198:E44–68. doi: 10.1164/rccm.201807-1255ST
8. Cocconcelli E, Balestro E, Biondini D, Barbiero G, Polverosi R, Calabrese F, et al. High-resolution computed tomography (HRCT) reflects disease progression in patients with idiopathic pulmonary fibrosis (IPF): relationship with lung pathology. *J Clin Med.* (2019) 8:399. doi: 10.3390/jcm8030399
9. Cocconcelli E, Biondini D, Giraudo C, Lococo S, Bernardinello N, Fichera G, et al. Clinical features and chest imaging as predictors of intensity of care in patients with COVID-19. *J Clin Med.* (2020) 9:2990. doi: 10.3390/jcm9092990
10. Borczuk AC, Salvatore SP, Seshan SV, Patel SS, Bussell JB, Mostyka M, et al. COVID-19 Pulmonary pathology: a multi-institutional autopsy cohort from Italy and New York City. *Mod Pathol.* (2020) 33:2156–68. doi: 10.1038/s41379-020-00661-1
11. Basso C, Calabrese F, Sbaraglia M, Del Vecchio C, Carretta G, Saieva A, et al. Feasibility of postmortem examination in the era of COVID-19 pandemic: the experience of a Northeast Italy University Hospital. *Virchows Arch.* (2020) 477:341–7. doi: 10.1007/s00428-020-02861-1
12. Lavezzo E, Franchin E, Ciavarella C, Cuomo-Dannenburg G, Barzon L, Del Vecchio C, et al. Suppression of a SARS-Cov-2 outbreak in the Italian Municipality of Vo'. *Nature.* (2020) 584:425–9. doi: 10.1038/s41586-020-2488-1
13. Calabrese F, Pezzuto F, Fortarezza F, Boscolo A, Lunardi F, Giraudo C, et al. Machine learning-based analysis of alveolar and vascular injury in SARS-CoV-2 acute respiratory failure. *J Pathol.* (2021). doi: 10.1002/path.5653. [Epub ahead of print].
14. Calabrese F, Pezzuto F, Fortarezza F, Hofman P, Kern I, Panizo A, et al. Pulmonary pathology and COVID-19: lessons from autopsy. the experience of European pulmonary pathologists. *Virchows Arch.* (2020) 477:359–72. doi: 10.1007/s00428-020-02886-6
15. Huang C, Wang Y, Li X, Ren L, Zhao J, Hu Y, et al. Clinical features of patients infected with 2019 novel coronavirus in Wuhan, China. *Lancet.* (2020) 395:497–506. doi: 10.1016/S0140-6736(20)30183-5
16. Guan WJ, Ni ZY, Hu Y, Liang WH, Ou CQ, He JX, et al. Clinical characteristics of coronavirus disease 2019 in China. *N Engl J Med.* (2020) 382:1708–20. doi: 10.1056/NEJMoa2002032
17. Kanne JP, Little BP, Chung JH, Elicker BM, Ketani LH. Essentials for radiologists on COVID-19: an update-radiology scientific expert panel. *Radiology.* (2020) 296:E113–4. doi: 10.1148/radiol.2020200527
18. Flaherty KR, King TE Jr, Raghu G, Lynch JP III, Colby TV, Travis WD, et al. Idiopathic interstitial pneumonia: what is the effect of a multidisciplinary approach to diagnosis? *Am J Respir Crit Care Med.* (2004) 170:904–10. doi: 10.1164/rccm.200402-147OC
19. Harrell FE, with contributions from Dupont C and many others. *Hmisc: Harrell Miscellaneous.* (2020). Available online at: <https://CRAN.R-project.org/package=Hmisc>
20. Højsgaard S, Halekoh U, Yan J. The R package geepack for generalized estimating equations. *J Stat Softw Artic.* (2015) 15:1–11. doi: 10.18637/jss.v015.i02
21. Hardin JW. Generalized Estimating Equations (GEE). In: Everitt BS, Howell DC, editors. *Encyclopedia of Statistics in Behavioral Science* (2005). doi: 10.1002/0470013192.bsa250

22. R Development Core Team. *R: A Language and Environment for Statistical Computing*. Vienna: R Foundation for Statistical Computing (2019).
23. Raghu G, Collard HR, Egan JJ, Martinez FJ, Behr J, Brown KK, et al. An official ATS/ERS/JRS/ALAT statement: idiopathic pulmonary fibrosis: evidence-based guidelines for diagnosis and management. *Am J Respir Crit Care Med*. (2011) 183:788–824. doi: 10.1164/rccm.2009-040GL
24. Desai SR, Prosch H, Galvin JR. Plain film and HRCT diagnosis of interstitial lung disease. In: Hodler J, Kubik-Huch RA, Von Schulthess GK, editors. Chapter 4: *Diseases of the Chest, Breast, Heart, and Vessels 2019-2022: Diagnostic and Interventional Imaging*. Cham: Springer (2019).
25. Lynch DA, Sverzellati N, Travis WD, Brown KK, Colby TV, Galvin JR, et al. Diagnostic criteria for idiopathic pulmonary fibrosis: a fleischner society white paper. *Lancet Respir Med*. (2018) 6:138–53. doi: 10.1016/S2213-2600(17)30433-2
26. Fichera G, Stramare R, De Conti G, Motta R, Giraudo C. It's not over until it's over: the chameleonic behavior of COVID-19 over a six-day period. *Radiol Med*. (2020) 125:514–6. doi: 10.1007/s11547-020-01203-0
27. Giraudo C, Cavaliere A, Fichera G, Weber M, Motta R, Pelloso M, et al. Validation of a composed COVID-19 chest radiography score: the CARE project. *ERJ Open Res*. (2020) 6:00359-2020. doi: 10.1183/23120541.00359-2020
28. Larici AR, Cicchetti G, Marano R, Merlino B, Elia L, Calandriello L, et al. Multimodality imaging of COVID-19 pneumonia: from diagnosis to follow-up. A comprehensive review. *Eur J Radiol*. (2020) 131:109217. doi: 10.1016/j.ejrad.2020.109217
29. Rubin GD, Ryerson CJ, Haramati LB, Sverzellati N, Kanne JP, Raoof S, et al. The role of chest imaging in patient management during the COVID-19 pandemic: a multinational consensus statement from the Fleischner Society. *Chest*. (2020) 158:106–16. doi: 10.1016/j.chest.2020.04.003
30. Akl EA, Blazic I, Yaacoub S, Fria G, Chou R, Appiah JA, et al. Use of chest imaging in the diagnosis and management of COVID-19: a WHO rapid advice guide. *Radiology*. (2020) 30:203173. doi: 10.1148/radiol.2020.03173
31. Borakati A, Perera A, Johnson J, Sood T. Diagnostic accuracy of X-ray versus CT in COVID-19: a propensity-matched database study. *BMJ Open*. (2020) 10:e042946. doi: 10.1136/bmjopen-2020-042946
32. Mossa-Basha M, Medverd J, Linnau KF, Lynch JB, Wener MH, Kicska G, et al. Policies and guidelines for COVID-19 preparedness: experiences from the University of Washington. *Radiology*. (2020) 296:E26–31. doi: 10.1148/radiol.2019201326
33. Cester G, Giraudo C, Causin F, Boemo DG, Anglani M, Capizzi A, et al. Retrospective analysis of a modified organizational model to guarantee CT workflow during the COVID-19 outbreak in the Tertiary Hospital of Padova, Italy. *J Clin Med*. (2020) 9:3042. doi: 10.3390/jcm9093042
34. Ghatol A, Ruhl AP, Danoff SK. Exacerbations in idiopathic pulmonary fibrosis triggered by pulmonary and non-pulmonary surgery: a case series and comprehensive review of the literature. *Lung*. (2012) 190:373–80. doi: 10.1007/s00408-012-9389-5
35. Luo F, Darwiche K, Singh S, Torrego A, Steinfert DP, Gasparini S, et al. Performing bronchoscopy in times of the COVID-19 pandemic: practice statement from an international expert panel. *Respiration*. (2020) 9:417–22. doi: 10.1159/000507898
36. Calabrese F, Fortarezza F, Giraudo C, Pezzuto F, Faccioli E, Rea F, et al. Two sorts of microthrombi in a patient with coronavirus disease 2019 and lung cancer. *J Thorac Oncol*. (2020) 15:1782–5. doi: 10.1016/j.jtho.2020.08.008

**Conflict of Interest:** The authors declare that the research was conducted in the absence of any commercial or financial relationships that could be construed as a potential conflict of interest.

Copyright © 2021 Calabrese, Pezzuto, Giraudo, Vedovelli, Fortarezza, Del Vecchio, Lunardi, Fraia, Cocconcelli, Vuljan, Gregori, Crisanti, Balestro and Spagnolo. This is an open-access article distributed under the terms of the Creative Commons Attribution License (CC BY). The use, distribution or reproduction in other forums is permitted, provided the original author(s) and the copyright owner(s) are credited and that the original publication in this journal is cited, in accordance with accepted academic practice. No use, distribution or reproduction is permitted which does not comply with these terms.



# Case Report: Chemotherapy Indication in a Case of Neurofibromatosis Type 1 Presenting Optic Pathway Glioma: A One-Year Clinical Case Study Using Differential Tractography Approach

Amir Mohammad Pajavand<sup>1,2</sup>, Guive Sharifi<sup>2\*</sup>, Amir Anvari<sup>3</sup>,  
Farahnaz Bidari-Zerehpoo<sup>4</sup>, Mohammad A. Shamsi<sup>2</sup>, Saeedeh Nateghinia<sup>2</sup> and  
Tohid Emami Meybodi<sup>5\*</sup>

## OPEN ACCESS

### Edited by:

Reza Lashgari,  
Institute for Research in Fundamental  
Sciences, Iran

### Reviewed by:

Vicky Yamamoto,  
University of Southern California,  
United States  
Habib Ganjgahi,  
University of Oxford, United Kingdom

### \*Correspondence:

Guive Sharifi  
drsharifiguive@gmail.com  
Tohid Emami Meybodi  
tohid.emami.meybodi@gmail.com

### Specialty section:

This article was submitted to  
Health,  
a section of the journal  
Frontiers in Human Neuroscience

**Received:** 22 October 2020

**Accepted:** 01 March 2021

**Published:** 06 April 2021

### Citation:

Pajavand AM, Sharifi G, Anvari A,  
Bidari-Zerehpoo F, Shamsi MA,  
Nateghinia S and Meybodi TE (2021)  
Case Report: Chemotherapy  
Indication in a Case of  
Neurofibromatosis Type 1 Presenting  
Optic Pathway Glioma: A One-Year  
Clinical Case Study Using Differential  
Tractography Approach.  
Front. Hum. Neurosci. 15:620439.  
doi: 10.3389/fnhum.2021.620439

<sup>1</sup> Institute for Cognitive and Brain Sciences, Shahid Beheshti University Government College University, Tehran, Iran, <sup>2</sup> Skull  
Base Research Center, Loghman Hakim Hospital, Shahid Beheshti University of Medical Sciences, Tehran, Iran,

<sup>3</sup> Department of Radiation Oncology, Shahid Beheshti University of Medical Sciences, Tehran, Iran, <sup>4</sup> Department of  
Pathology, Loghman Hakim Hospital, Shahid Beheshti University of Medical Sciences, Tehran, Iran, <sup>5</sup> Functional  
Neurosurgery Research Center, Shohada Tajrish Hospital, Shahid Beheshti University of Medical Sciences, Tehran, Iran

Neurofibromatosis type 1 (NF1) is associated with peripheral and central nervous system tumors. It is noteworthy that the regions in which these tumors frequently arise are the optic pathways (OPs) and the brainstem. Thus, we decided to trace the procedure of diffusion Magnetic Resonance Imaging (dMRI) alterations along with Short-Wavelength Automated Perimetry (SWAP) examinations of the OPs after surgery and chemotherapy over 1 year, which enabled us to evaluate chemotherapy's efficacy in an NF1 patient with an OP tumor. In this study, a 25-year-old woman with NF1 and left optic radiation (OR) glioma underwent surgery to remove the glioma. Immunohistochemistry (IHC) revealed a Pilocytic Astrocytoma (PA) WHO grade I. Post-operation chemotherapy done using nine treatment cycles of administering Temozolomide (TMZ) for 5 days every 4 weeks. Applying the region of interest (ROI) differential tractography method and SWAP four times every 3 months allowed us to follow the patient's visual acuity alterations longitudinally. The differential deterministic tractography method and statistical analyses enabled us to discover the white matter (WM) tracts anisotropy alterations over time. Furthermore, statistical analyses on the SWAP results along time illustrated possible alterations in visual acuity. Then, we could compare and associate the findings with the SWAP examinations and patient symptoms longitudinally. Statistical analyses of SWAP tests revealed a significant improvement in visual fields, and longitudinal differential tractography showed myelination and dense axonal packing in the left OR after 1 year of treatment. In this study, we examined an old hypothesis suggesting that chemotherapy is more effective than radiotherapy for NF1 patients with OP gliomas (OPGs) because of the radiation side effects on the visual field, cognition, and cerebrovascular complications. Our longitudinal clinical case study involving dMRI and SWAP on a single NF1-OPG patient showed that chemotherapy did not suppress the OP myelination over time.



However, it should be noted that this is a clinical case study, and, therefore, the generalization of results is limited. Future investigations might focus on genetic-based imaging, particularly in more cases. Further, meta-analyses are recommended for giving a proper Field Of View (FOV) to researchers as a subtle clue regarding precision medicine.

**Keywords:** neurofibromatosis type 1, diffusion tensor imaging, optic pathway glioma, immunohistochemistry, short-wavelength automated perimetry, temozolomide, low-grade glioma, visual field index

## INTRODUCTION

The incidence of NF1 as a tumor suppressor syndrome has occurred in ~1 out of every 2500–3000 people worldwide (Huson et al., 1988; Compston, 1994; Hughes, 1999; Margaret, 2000). NF1 is associated with peripheral and central nervous system tumors. Most NF1 tumors occur in children, and most of these tumors arise within the OPs and hypothalamus (Korf, 2000; Albers and Gutmann, 2009).

The most frequent tumors associated with NF1 are PAs, WHO grade I tumors (Szudek et al., 2000); this is supported by other studies in the past decade, wherein 100 tumor patients with NF1 were evaluated in 2008, and 49% of the cases under 20 years old revealed PA tumors, while only 27% of adults exhibited other tumors (WHO grade II, III, and IV) (Rodriguez et al., 2008). Furthermore, in another study of 23 high-grade and 32 low-grade gliomas in NF1 patients, 77% of pediatric gliomas were low-grade while 78% of adult tumors were high-grade (D'Angelo et al., 2019).

Following the literature, the surgical resection of NF1 glioma tumors is not feasible due to their location and vision loss or hydrocephalus (Listernick et al., 2007). In addition, radiation therapy might lead to Moyamoya syndrome in NF1 patients (Ullrich et al., 2007). Also, radiotherapy in NF1 OPGs correlated with poor visual outcomes, increased mortality (Sievert et al., 2013), and the occurrence of secondary brain tumors and vasculopathy (Sharif et al., 2006; Merchant et al., 2009; Helfferich et al., 2016).

As a consequence of these risks, chemotherapy is considered an alternative approach for NF1 OPGs characterized by diminishing visual acuity. In this respect, chemotherapeutic agents used in the treatment include vincristine, carboplatin, vinblastine, vinorelbine, and TMZ (Packer et al., 1997; Bouffet et al., 2012; Cappellano et al., 2015). However, the use of chemotherapeutic agents barely recovers any premorbid visual acuity (Dalla Via et al., 2007; Kalin-Hajdu et al., 2014).

In this study, a 25-year-old young adult woman with a left OR PA was studied longitudinally. According to the literature, the patient is considered a rare NF1-OPG patient. Because

of the involvement of the left OR's large glioma with its massive edema, surgery was performed, and the tumor resected. We decided to utilize previously proposed hypotheses and experiences for the post-operation strategy, which led us to implement chemotherapy instead of radiation to avoid visual loss, cognitive problems, and vasculopathy.

To evaluate this hypothesis, we decided to use longitudinal DTI connectometry and SWAP examinations for 1 year. Differential statistical analyses were also performed to assess the outcomes of this investigation.

## MATERIALS AND METHODS

### Medical History and Treatment Strategy

A 25-year-old woman was referred to the hospital due to visual impairment. The MRI scan revealed multiple lesions, including a left Thalamus cyst, a right lesion of the pons, and a WM OR glioma with massive edema (see **Figure 1**).

Clinical diagnosis requires at least two of seven criteria (Gutmann, 1988; Gutmann et al., 1997) to confirm the presence of NF1.

Our patient presented with significant signs of several criteria, including the presence of eight or more café au lait macules (>1.5 cm) (see **Supplementary Figures 1A,B**), the presence of 15 or more cutaneous/subcutaneous neurofibromas (see **Supplementary Figures 1A,B**), axillary freckling (see **Supplementary Figure 1C**), and OP glioma (see **Supplementary Figure 1D**). The patient did not exhibit any oral manifestation of the ailment and demonstrated no balance problems or scoliosis.

Usually, after surgery, LGG patients receive systemic chemotherapy, such as PCV (Procarbazine, CCNU, and Vincristine) or TMZ. PCV and TMZ provide similar response rates (45–62%) and durations (10–24 months), with the toxicity profile favoring temozolomide in terms of tolerability (reduced myelotoxicity) (Quinn et al., 2003; Soffietti et al., 2010).

This idea has extended to national guidelines that list single-agent TMZ and multi-agent PCV as equally appropriate options (Ziu et al., 2015). Based on the available evidence and Duke University's clinical trial (NCT00003466<sup>1</sup>), we chose a single-agent TMZ agent for post-surgery chemotherapy surgery. Thus, the patient received TMZ orally (200 mg/m<sup>2</sup> per day) for 5 days every 4 weeks. The patient also received nine treatment cycles for the PA WHO grade I as a progressive LGG.

**Abbreviations:** DTI, Diffusion Tensor Imaging; MRI, Magnetic Resonance Imaging; dMRI, diffusion MRI; IHC, Immunohistochemistry; NF1, Neurofibromatosis type 1; OP, Optic Pathway; OPG, Optic Pathway Glioma; LGG, Low-Grade Glioma; PA, Pilocytic Astrocytoma; SWAP, Short-Wavelength Automated Perimetry; OR, Optic Radiation; WM, White Matter; TMZ, Temozolomide; FDR, False Discovery Rate; FA, Fractional Anisotropy; MD, Mean Diffusivity; RD, Radial Diffusivity; AD, Axial Diffusivity; ROI, Region Of Interest; VFI, Visual Field Index; MD, Mean Deviation; RGCs, Retinal Ganglion Cells Death; PCV, Procarbazine, CCNU and Vincristine.

<sup>1</sup>NCT00003466, N. N. Temozolomide in Treating Patients With Progressive Low-Grade Glioma, <https://ClinicalTrials.gov/show/NCT00003466>.

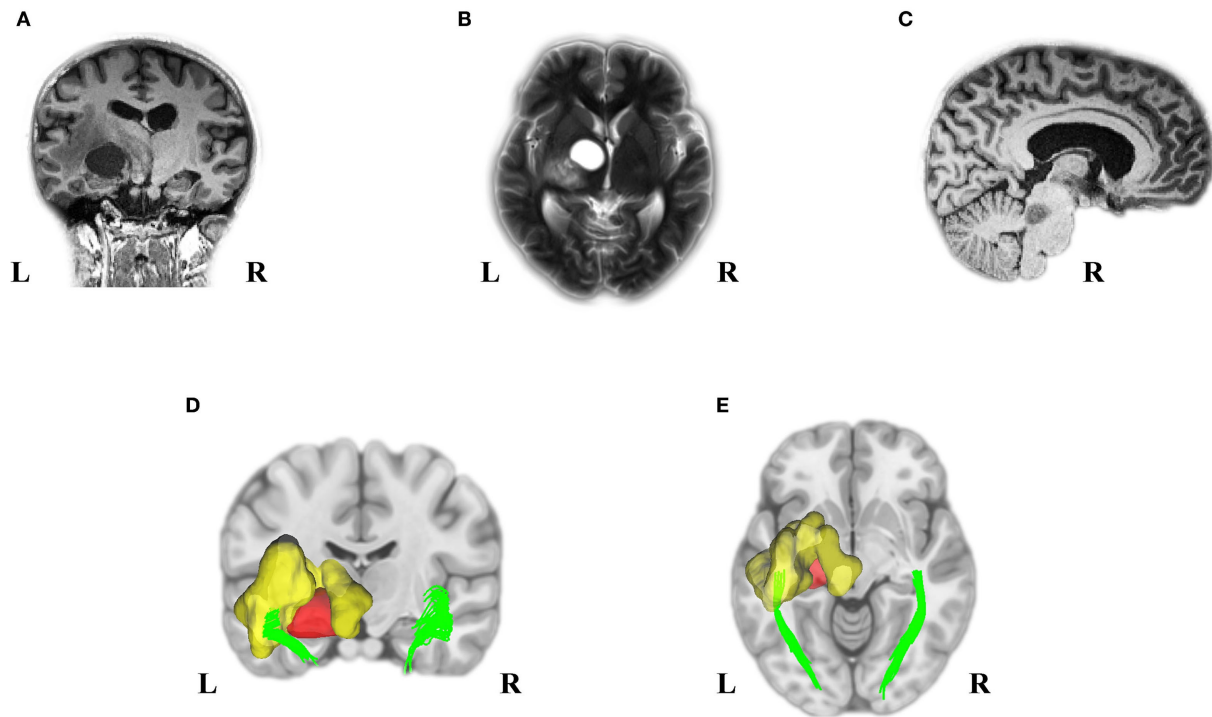


**FIGURE 1 |** Pre-Operation MRI and analyzed DTI scans displayed multiple tumors in our young adult NF1 patient. It is not uncommon for NF1 patients to have more than one CNS tumor. As the MRI presented, the NF1 brain showed a left OR glioma (A), Left thalamus cyst (B), and a right midbrain tumor (C). Deterministic tractography demonstrated the left OR involvement because of the left WM OR glioma with its massive edema (D,E). MRI, magnetic resonance imaging; DTI, diffusion tensor imaging; NF1, neurofibromatosis type 1; CNS, central nervous system; OR, optic radiation; WM, white matter.

## ASSESSMENTS

### Short-Wavelength Automated Perimetry (SWAP)

SWAP is a visual field examination designed to assess the short-wavelength-sensitive color system (Drance et al., 1981; Flammer and Drance, 1984). According to our strategy, we decided to utilize SWAP four times every 3 months for 1 year to examine the visual field. The data from each SWAP test were extracted and analyzed (see **Figure 2**) via the polynomial regression method (Ostertagová, 2012).

### Structural and Microstructural MRI Data Acquisition

#### DTI Data Acquisition

All structural MRI scans were acquired from 3T MRI scanners (Siemens Prisma). 3D T1 MPRAGE anatomic acquisitions were made [1 mm slice,  $256 \times 256$  matrices, echo time (TE) = 3.74 ms, repetition time (TR) = 1,810 ms, flip angle =  $30^\circ$ ] and used to superimpose DTI images. A diffusion-weighted imaging (DWI) brain scan was also done with the same scanner with a 64-channel head coil. Other acquisition parameters were as follows: number of slices, 68; diffusion directions, 30; FOV,  $256 \times 256$  mm<sup>2</sup>; voxel size,  $2 \times 2 \times 2$  mm<sup>3</sup>; TR/TE, 9,000/90 ms.

#### DTI Data Processing

To preprocess the DTI data, we utilized the FMRIB Software Library, FSL 6.0 (Woolrich et al., 2009; Jenkinson et al., 2012). At first, all diffusion-weighted images were checked visually for any visible artifacts and then corrected for B0 inhomogeneities and eddy-current distortion. Each subject's DWI was registered to the corresponding  $b = 0$  images via affine transformation.

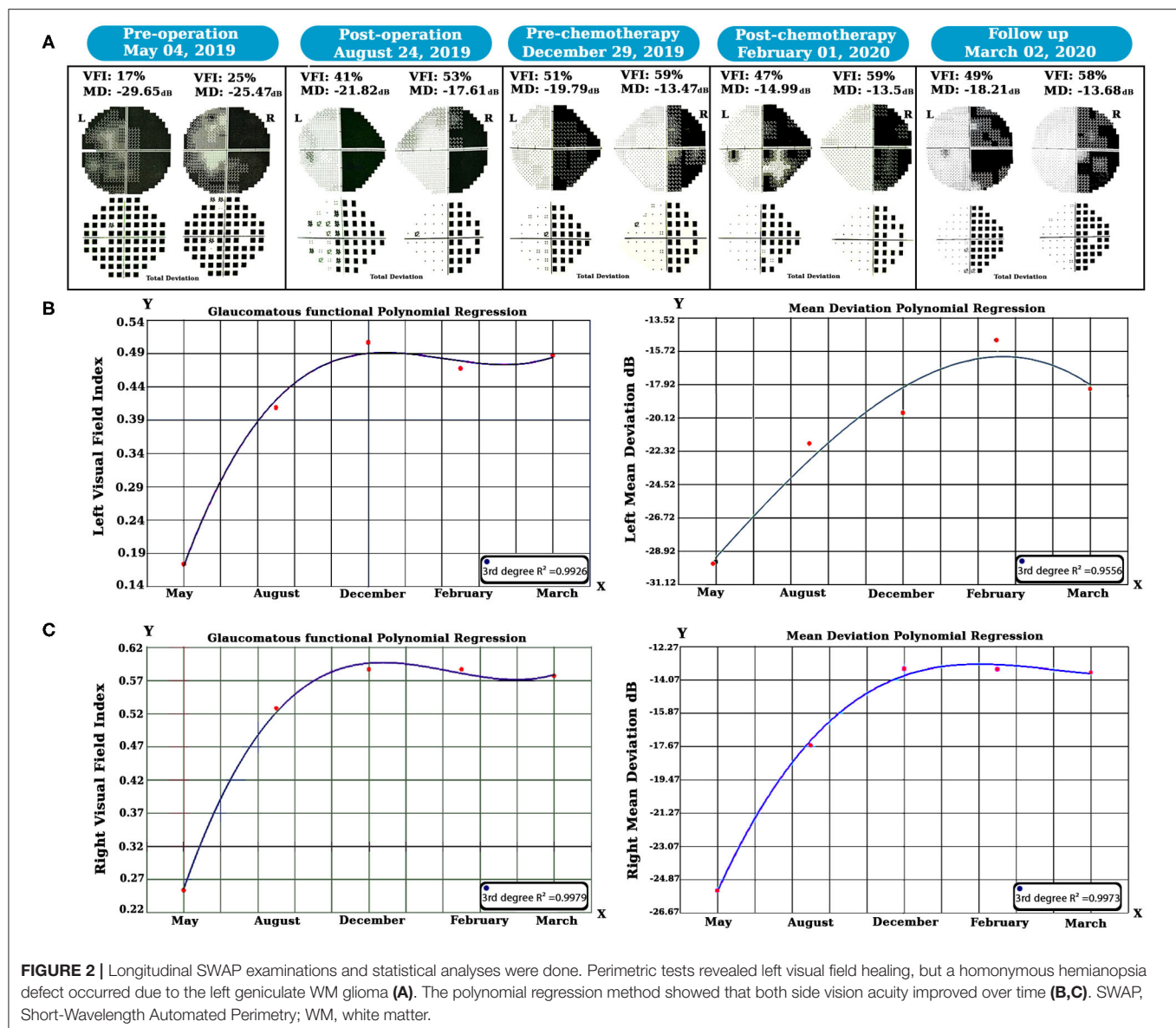
Second, the case's DWI data were reconstructed via Q-Space Diffeomorphic Reconstruction (QSDR), a method for calculating the directional distribution of the water diffusion density in standard space using DSI Studio software (Yeh and Tseng, 2011; Yeh et al., 2013).

To perform ROI-based individual connectometry, three normal age- and sex-matched individuals were added to the study for the analyses. Notably, just three structural MRI and dMRI scans were collected for our research, and no longitudinal data acquisition was performed for the normal subjects.

## Statistical Analyses

### Differential Tractography

We used differential tractography to track the anisotropy difference along WM tracts over time. This technique was developed to compare the dMRI scans of a single patient at different times by mapping the DTI data into a common space and tracing the connectivity alterations through all or specific WM fiber tracts (Yeh et al., 2019). By focusing on the



anisotropy difference, we can examine the tracking's stability across two periods.

The initial tracts for differential tractography were generated to create a series of 100,000 seeds with the same initial tracking parameters. We then used quantitative anisotropy (QA) instead of normalized quantitative anisotropy (NQA) to extract the connectivity percent change based on QA.

We determined that the initial QA threshold was 10% of the actual QA values. We looked at the QA changes with three different thresholds (+10%, +20%, and +30%) to make connectivity comparisons between time points.

### False Discovery Rate Estimation

Per our strategy, the patient underwent dMRI scans four times every 3 months. We used this method to

illustrate the WM tracts with increased anisotropy. **Supplementary Figure 2** demonstrates our experimental design, wherein true-positive and false-positive findings were obtained that enabled us to estimate the false discovery rate (FDR).

To estimate the false-positive findings using this approach, we needed to obtain a sham scan on the same day as the baseline scan. Any positive results from the sham scan would be considered false-positive findings.

Then, the sham scan was compared with the baseline scan. As presented in **Supplementary Table 1**, the false and true positive findings were estimated, and the FDR was calculated. We then used our dataset to find the pre-chemotherapy and post-chemotherapy dMRI changes. We used the pre-chemotherapy scan as the baseline and the post-chemotherapy scan as the study scan; the sham scan was also included. Moreover, to evaluate

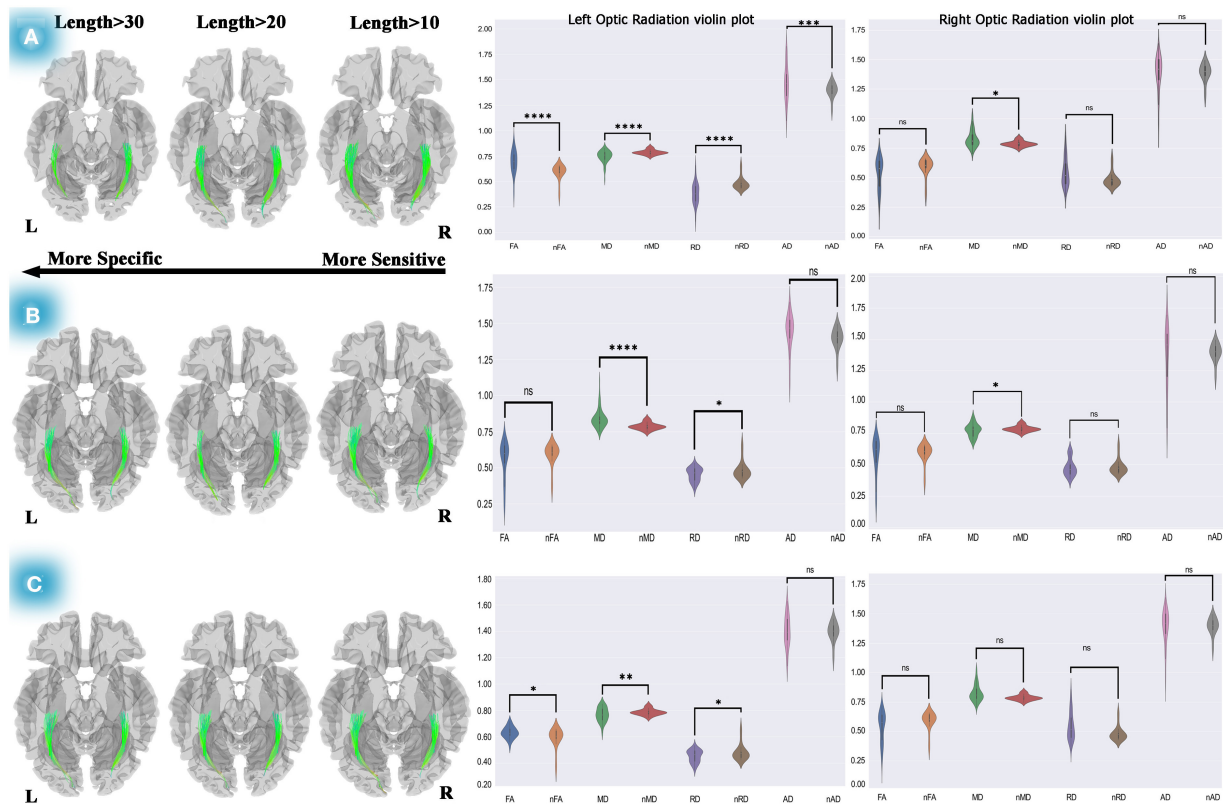


**FIGURE 3 |** Differential tractography approach and statistical analyses to discover the ORs connectivity and diffusion metric alterations. The analyses on pre-chemotherapy compared with pre-operation showed increased connectivity in the left and right OR. Furthermore, violin plots showed fiber maturation according to increased FA, decreased MD, and RD (A). This method used for post-chemotherapy vs. pre-chemotherapy revealed increased connectivity in the left and right OR, and statistical analyses on diffusion metrics showed no pathological indication (B). This method also revealed increased connectivity of both ORs after 1-year of post-operation compared to the pre-operation, and statistical analyses presented increased FA, decreased MD, and RD, which could be a picture of myelination and dense axonal packing in the left OR (C). Statistics performed on the diffusion metrics by two-tailed sample *t*-test, \**P* < 0.05; \*\**P* < 0.01; \*\*\**P* < 0.001; \*\*\*\**P* < 0.0001. OR, optic radiation; FA, fractional anisotropy; MD, mean diffusivity; RD, radial diffusivity; AD, axial diffusivity; nFA, normal FA; nMD, normal MD; nRD, normal RD; nAD, normal AD.

the pre-operation and post-chemotherapy DTI changes, the same method was used.

### Diffusion Metric Alterations Overtime and Illustration

To trace the diffusion changes over time, diffusion metric (FA, MD, RD, and AD) values were extracted; a two-tailed sample *t*-test was done between the patient's and normal subjects' diffusion metrics at each stage, and the results were displayed as violin plots (see **Figures 3, 4; Supplementary Figure 3**). All statistical analyses were done using Python 3.7.3 (Rossum and Drake, 2014).

### Spearman's and Pearson's Correlation Coefficient Tests

Spearman's correlation coefficient test was performed to determine the possible association between DTI metrics and perimetric parameters. We chose Spearman's correlation test because it does not keep any assumptions about distributing the data. It is the most appropriate correlation analysis when the

variables are measured on a scale that is at least ordinal, which is true of our dataset.

Moreover, we used a Python data visualization library (based on Matplotlib) to visualize significant perimetric parameter changes among dMRI metrics. Doing this allowed us to create a Pearson's correlation coefficient matrix heatmap, a two-dimensional graphical data representation wherein the matrix values are represented as colors (Bedre, 2020) and used to compute pairwise correlations of columns (excluding null values).

## RESULTS

### Immunohistochemistry (IHC) Examinations

According to the IHC results (see **Supplementary Figure 4**) and based on previous studies, significant attributes of the PA were revealed in which case bright red corkscrew-shaped Rosenthal fibers (RFs) are often found in compact regions (A), as they are biphasic with alternating compact and microcystic areas displayed (B). The existence of Mulberry-shaped eosinophilic



granular bodies (EGBs) is also regular in the loose fraction (C) (Collins et al., 2015; Perry and Wesseling, 2016).

## Perimetry Analyses

We examined the SWAP for visual field evaluation overtime after surgery and chemotherapy. As shown in **Figure 2A**, pre-operation SWAP examination showed the complete involvement of both visual fields due to the left hemisphere PA and its massive edema with substantial pressure on the left OPs.

After 6 months of follow-up, right homonymous hemianopia (RHH) displayed as predicted due to the PA pressure on the left side geniculate WM tracts. Based on our hypothesis, treatment was maintained by chemotherapy, and SWAP examinations remained in place for post-chemotherapy until March 2020. Visual Field Index (VFI) and Mean Deviation (MD) properties were compared over time using the polynomial regression method.

Our longitudinal polynomial regression on the left VFI (see **Figure 2B**) showed a significant improvement (third-degree  $R^2 = 0.9926$ ,  $P < 0.001$ ) as well as left MD, which increased over time as revealed by the third-degree polynomial regression analysis (third-degree  $R^2 = 0.9775$ ,  $P < 0.01$ ).

Additionally, the same method was also used for the right visual field (see **Figure 2C**); in this case, the third-degree longitudinal polynomial regression on VFI was significant (third-degree  $R^2 = 0.9979$ ,  $P < 0.001$ ). Moreover, the right side MD showed a considerable increase over time, and the (third-degree  $R^2 = 0.9973$ ,  $P < 0.001$ ).

As described, we calculated Spearman's rank correlation coefficients between dMRI metrics and perimetric parameters. We found only a significant association (see **Supplementary Tables 2, 3**) between the left OR's FA and the left VFI along time ( $r_s = 0.976$ ,  $P$  (2-tailed)  $< 0.001$ ). Interestingly, Pearson's correlation analysis also showed a significant association (see **Figure 4A**) between the left side OR's FA and the VFI ( $R^2 = 0.7011$ ,  $P = 0.0025$ ). However, no association was found in the right OR's diffusion metrics and perimetric parameters (see **Supplementary Tables 2, 3; Supplementary Figure 5**).

## Differential Tractography and Statistical Findings

### Three Months Post-operation vs. Pre-operation

Using differential tractography, left OR showed 0 to 15 % increased connectivity in 3 months after surgery and a two-tailed sample  $t$ -test showed significant FA reduction ( $t = -5.23$ ,  $P < 0.00001$ ), increased MD ( $t = 3.75$ ,  $P < 0.0001$ ), RD ( $t = 2.42$ ,  $P = 0.017$ ), and AD ( $t = 2.13$ ,  $P = 0.033$ ) relative to normal controls, which could be a reflection of cerebrospinal fluid (CSF) adjoining to the left OR (see **Supplementary Figure 3A; Supplementary Table 4A**). Additionally, no significant changes in the right OR's diffusion metrics were observed in the statistical analyses.

### Post-chemotherapy Relative to Three Months Post-operation

The same method was used for post-chemotherapy versus post-operation, shown in **Supplementary Figure 3B**. Our longitudinal differential tractography showed a 10–30% increased connectivity in the left and right ORs, and our statistical analyses on the left OR's diffusion metrics also showed no significant alteration of FA. However, a significant decrease was observed in MD ( $t = -3.39$ ,  $P < 0.01$ ) and RD ( $t = -4.451$ ,  $P < 0.0001$ ), and no significant changes were observed in the left OR's AD.

The statistical analyses on the right OR showed no significant diffusion metrics changes except for MD ( $t = 3.12$ ,  $P < 0.01$ ) in which depletion was observed. However, following the lack of changes in the other diffusion metrics, no pathological reflection could be considered for both sides of the ORs (see **Supplementary Table 4B**).

### Pre-operation in Comparison With Pre-chemotherapy

The individual connectometry (see **Figure 3A**) showed 10–30% and 10–20% increases in connectivity in the left and right ORs.

Interestingly, our statistical analyses (see **Figure 3A; Supplementary Table 4C**) showed fiber maturation in the left OR in which case a significant increase in FA ( $t = 4.13$ ,  $P < 0.001$ ) and AD ( $t = 2.195$ ,  $P < 0.05$ ) was observed. Moreover, MD ( $t = -3.62$ ,  $P < 0.01$ ) and RD ( $t = -4.59$ ,  $P < 0.0001$ ) showed a significant decrease. Also, no meaningful changes were seen in the right OR's diffusion metrics (see **Supplementary Table 4C**) except for in MD ( $t = -2.428$ ,  $P < 0.05$ ), which would not reflect any pathological properties.

### Post-chemotherapy Relative to Pre-chemotherapy

**Figure 3B** shows increased connectivity in the left (10–30%) and right (0–10%) ORs. Our two-tailed sample  $t$ -test displayed significant MD reduction ( $t = -4.403$ ,  $P < 0.0001$ ) and RD ( $t = -2.242$ ,  $P < 0.05$ ) in the left OR. Moreover, a significantly increased MD ( $t = 2.49$ ,  $P < 0.05$ ) on the right OR was observed. Subsequently, in this period (10 months after operation), no remarkable pathological variation was detected in both ORs according to our statistical analyses (see **Supplementary Table 4D**).

### Post-chemotherapy vs. Pre-operation

Concerning evaluating the changes in the OR's diffusion metrics over time, the differential tractography approach was used to measure our treatment strategy outcome. We decided to compare the pre-operation and post-chemotherapy diffusion properties (see **Figure 3C**). This comparison indicated crucial changes during 10 months of DTI follow-up.

Our statistical analyses which are presented as the violin plots demonstrated a significant increase in FA ( $t = 2.63$ ,  $P = 0.01$ ), remarkable decreased MD ( $t = -2.98$ ,  $P < 0.01$ ), RD ( $t = -2.24$ ,  $P < 0.05$ ), and a non-significant change in AD (see **Supplementary Table 4E**). These findings could indicate myelination and dense axonal packing of the left OR. Also, no diffusion metric changes were observed in the right OR.

## Whole-Brain Differential Tractography: Connectivity Alterations Over One Year

Our study focused on using ROI-based differential tractography to illustrate conventional chemotherapy's efficacy for the NF1-OPG. To this end (and to better understand the treatment strategy), we used a non-specific region-based differential tractography approach. This process provides a picture of the whole-brain WM connectivity alterations over 1 year.

We created a connectometry database from post-operation DTI scans and used the individual connectometry approach. This method allowed us to compare pre-operation and post-operation whole-brain WM integrities over time. As shown in **Supplementary Figure 6**, the left and right cingulum's connectivity, genu, and body of the corpus callosum increased by 10–30% over 10 months.

## DISCUSSION

In the present study, a 25-year-old female was diagnosed with NF1 adjacent to a left hemisphere glioma with massive edema for which the left OR was under high pressure. Based on the clinical examinations and SWAP test, limited visual acuity was an obvious consequence.

To eliminate the pressure of the glioma on the OPs, the patient underwent surgery, and, based on our hypothesis, to prevent adverse effects like OPs injury, neurocognitive dysfunctions, and cerebrovascular complications, the post-operation treatment was done by chemotherapy rather than radiation. Differential tractography adjoining SWAP tests were done for 1 year following surgery to evaluate the visual field and DTI metrics alterations of the OPs to evaluate this treatment strategy.

In addition to our experience with NF1 patients, PA was also revealed by IHC analyses, and the study was designed based on neuroimaging data and SWAP examinations. This information was obtained longitudinally four times every 3 months, and the VFI changes were demonstrated over time using the polynomial regression method.

On the other hand, differential tractography was used to evaluate the diffusion metrics of the OPs over time. This procedure was divided into five parts. Individual connectometry was performed to find out the possibility that the OP's diffusion would increase over time. Also, statistical analyses illustrated the longitudinal diffusion alterations relative to normal subjects.

The ORs showed diffusion alterations during the post-operation treatment, reflecting myelination dense axonal packing (see **Figure 4**; **Supplementary Table 4E**). Also, the SWAP examinations revealed significant improvements over time (see **Figure 2**). Moreover, the association between the left side OR's FA and the left VFI was substantial, as indicated by Spearman's and Pearson's correlation analyses (see **Figure 4A**, **Supplementary Tables 2, 3**).

Based on our hypothesis that post-operation chemotherapy could be more effective than radiation therapy for preventing OPs injury, ROI-based differential tractography and SWAP examinations adjacent to statistical analyses on diffusion metrics

were done over ten months. To the best of our knowledge, this study was the first to use these approaches.

## Optic Pilocytic Astrocytoma (PA) and Neurofibromatosis Type 1 (NF1)

OPGs affect 15–20% of NF1 patients, and they are not usually biopsied. Consequently, the most common tumors in NF1 patients are of the glioma type. Further, most of the NF1-OPGs are categorized as PAs (Lewis et al., 1984; Listernick and Charrow, 1990; Campen and Gutmann, 2018).

PAs can occur in different brain regions and are frequently found within the OP and the brainstem. About 66% of gliomas are located in the OP and the brainstem in NF1 patients (Guillamo et al., 2002).

Our case was a young adult NF1 patient with a PA located on the left white matter OR. Following the imaging details, the OR's glioma was observable, and no biopsy was needed. The post-operation IHC analyses revealed OR-PA.

According to the literature, low-grade OPGs are not confounding, and the post-operation treatment strategy was the main point of our study. Hence, chemotherapy (rather than radiation) was selected for the post-operation treatment to prevent OR injury, cognitive disorders, and cerebrovascular complications which the treatment strategy was examined via longitudinal differential tractography and SWAP tests.

## SWAP Feasibility in an NF1 Patient With Optic Radiation Glioma

Several perimetric tests can be applied to an individual patient with the glaucomatous progression that they might detect, such as short-wavelength automated perimetry (SWAP) (Drance et al., 1981; Flammer and Drance, 1984), standard automated perimetry (SAP) (Anderson and Patella, 1999), and frequency-doubling technology (FDT) perimetry (Johnson et al., 1999). A comparative study on glaucoma progression utilized these methods and observed no statistically significant difference between SAP, SWAP, and FDT via the pointwise linear regression (PLR) method (Hu et al., 2016).

Previously, SAP, FDT, and SWAP were compared to identify glaucomatous visual loss utilizing the Swedish interactive thresholding algorithm. However, no significant differences were found in their diagnostic performance (Tafreshi et al., 2009).

New special diagnostic instruments such as optical coherence tomography (OCT) and ganglion cell layer–inner plexiform layer (GCL-IPL) thickness have provided new FOV that can be used to investigate the ophthalmic indications of NF1 patients with optic nerve glioma (Gu et al., 2014; Abdolrahimzadeh et al., 2016). As previously described, our case is a young woman with optic radiation PA, not optic nerve glioma. Subsequently, as recommended by previous investigations, we decided to use SWAP to make longitudinal observations of her visual field.

Previous investigations revealed no differences between the abilities of SAP, SWAP, and FDT to monitor glaucomatous progression. However, in a study based on PLR analyses, FDT sensitivity was detected faster than SAP and SWAP in a cohort

of glaucoma patients (Liu et al., 2014). Such comparative studies are ongoing. Nevertheless, SWAP could be disadvantageous for observing our patient's perimetry alterations over time.

Meanwhile, in a recent study on perimetric anomalies, the researchers utilized FDT instead of SWAP in NF1 patients. A significant alteration was found in the transmission of visual impulse and FDT analyses, representing a significant reduction in all observed parameters, including (central sensitivity (CS), mean deviation (MD), pattern standard deviation (PSD), and glaucoma hemifield test (GHT). These findings point to the involvement of the visual pathway (Nebbio et al., 2020).

Optic neuropathy is characterized by damaged optic pathway axons, which could cause retinal ganglion cell (RGC) death. The primary damage areas are the optic nerve head (ONH) and the lateral geniculate pathways (Vrabec and Levin, 2007). This is relevant to our study, as our case is an NF1 patient with left geniculate pathway PA.

SWAP is designed to detect visual losses caused by optic neuropathy. In this perimetry method, short-wavelength sensitive (sws) cones are used, as humans' vision is most susceptible to this wave-length. These sws signals are sent to the blue-yellow retinal ganglion cells and will detect the target at any given retinal location when the blue-yellow cells are damaged (Sample, 2000).

Based on the neurobiology of RGCs due to the damaged OPs and the power of SWAP to detect the RGCs, to the best of our knowledge, we had no longitudinal visual function monitoring research via SWAP in NF1 OPG patients unexpectedly. Several studies proved that no significant difference was

observed between SAP, SWAP and FDT using different statistical methods.

## Radiotherapy or Chemotherapy for NF1 Patients Associated With OPGs

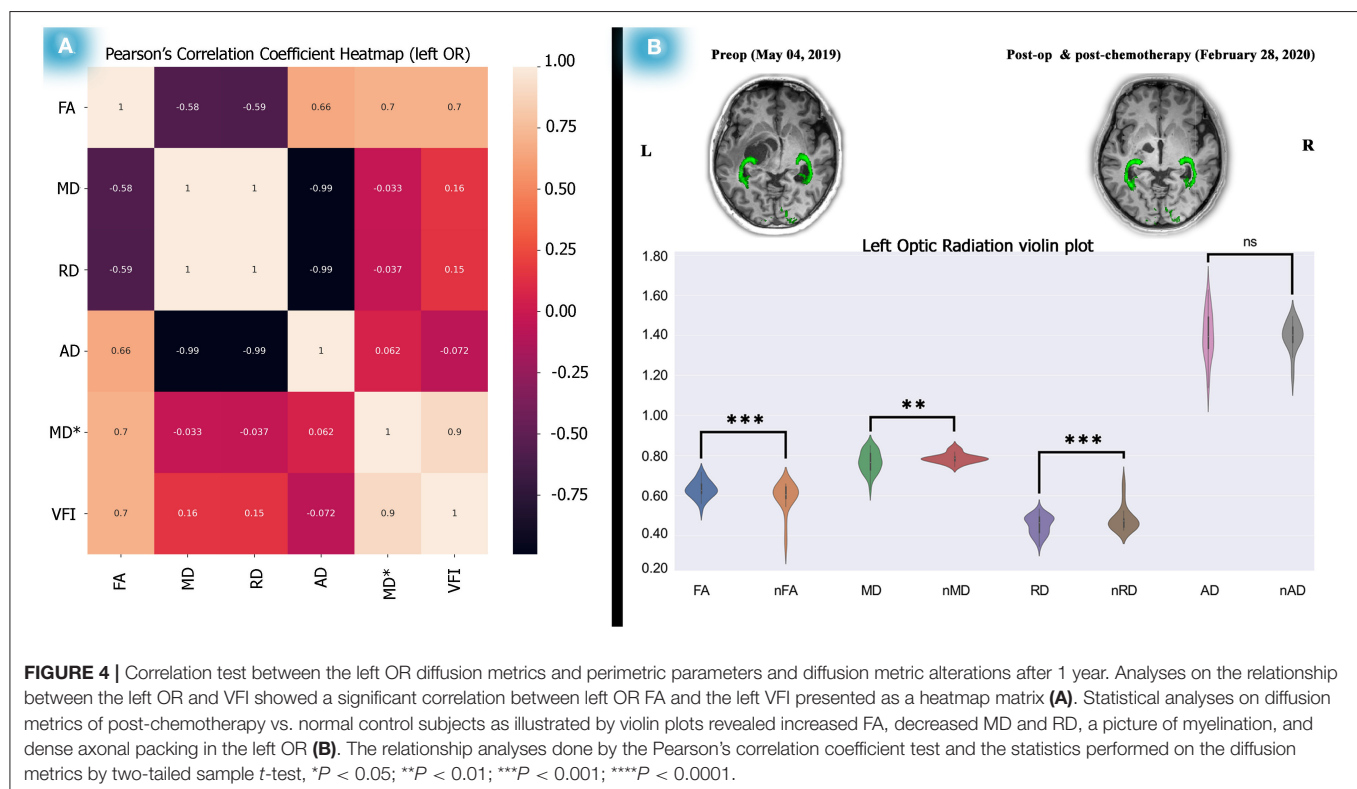
A previous multi-center investigation (Guillamo et al., 2002) of 104 NF1 patients with OP tumors reported that among 28 patients who underwent radiotherapy, 13 (46%) experienced growth hormone shortcomings. Another nine patients (32%) experienced radiation-related ischaemic strokes, and six patients (21%) underwent no radiotherapy.

According to this investigation, chemotherapy is a suitable alternative to radiotherapy. However, a few published papers (Listernick et al., 1999) suggest that NF1 patients with tumors that cause neurological symptoms may require surgical resection or chemotherapy (Gutmann et al., 2017).

More recently, treatments have become more focused on vision maintenance. This was initiated from a multi-center study, wherein carboplatin and vincristine as chemotherapeutic agents were applied instead of radiation on OPGs for initial therapy (Packer et al., 1997).

Procarbazine, lomustine, and vincristine increase survival in LGGs, but they correlate with major hematologic, hepatic, neurologic, and cutaneous toxicity (Jutras et al., 2018).

Following our study and previous investigations, radiation therapy is not useful for OPGs, particularly for NF1 tumor patients. NF1 patients commonly have PA as an LGG tumor, and radiotherapy could increase the risk of vasculopathy



complications and incidental malignancies (Grill et al., 1999; Sharif et al., 2006).

Single-agent TMZ and multi-agent PCV are both listed as equally appropriate options (Ziu et al., 2015), and TMZ and PCV provide equivalent objective response rates (45–62%) with a toxicity profile favoring TMZ in terms of better tolerability. Nevertheless, we used TMZ for chemotherapy in our case—the outcome was satisfactory.

Curiously, the authors of one previous study concluded that radiation therapy is an effective treatment for optic LGG and that older children without NF-1 have a low risk of late toxicity (Tsang et al., 2017).

Our analyses, considered alongside previous findings, suggest that chemotherapy is the best post-operation therapy technique for low-grade OPGs. It must be considered that our investigation is a longitudinal clinical case study of a single NF1-OPG patient, and, thus, the power of generalization is limited.

## Longitudinal Diffusion MRI Adjoining Differential Statistics

After reviewing the literature (and according to the association between white matter optic PA tumors and NF1 patients), we decided to focus on the ROI-based differential tractography analyses. Doing this enabled us to trace the connectivity changes of the OPs over time.

In addition to the statistical analyses, a feasible association picture of dMRI and perimetric parameters were obtained. Significant Pearson's correlation between left OR's FA and the left VFI ( $R^2 = 0.7011$ ,  $P$ -Value = 0.0025), illustrated as a heatmap matrix (see **Figure 4A**). The Spearman's correlation (see **Supplementary Table 2**) also showed the signification ( $r_s = 0.976$ ,  $P$  (2-tailed) < 0.001).

However, the Spearman's and Pearson's correlation analyses failed to detect a significant association between dMRI and perimetric parameters of the right side OR and VFI by methods (see **Supplementary Table 2**; **Supplementary Figure 5**). Likewise, our statistical analyses of mean deviation and diffusion alterations utilizing the mentioned statistical analysis methods showed no significant association (see **Supplementary Table 3**).

Several investigations on OPGs using dMRI revealed relationships between the dMRI and perimetric parameters (Ciccarelli et al., 2005; de Blank et al., 2013, 2018; Kolbe et al., 2016), thus supporting our results. The association between FA and visual acuity parameters is commonly observed in these papers, further supporting our findings.

However, some investigations utilizing dMRI were done previously on NF1-OPGs. However, to the best of our knowledge, the longitudinal ROI-based differential tractography method has not been investigated. Therefore, this approach was applied in this study to analyze diffusion changes of the ORs over time.

In an investigation using diffusion MRI (Hales et al., 2018), fractional anisotropy (FA) and apparent diffusion coefficient (ADC) found that the values of OPs were correlated with visual acuity in 26 patients. However, no longitudinal analyses were performed, and only FA and ADC values were extracted for

analyses. Interestingly, according to their results, lower FA was associated with poorer vision, which is in line with our study results (see **Figure 4A**; **Supplementary Table 3**). In addition, based on our findings, increased FA ( $t = 4.43$ ,  $P < 0.0001$ ) and decreased MD ( $t = -3.81$ ,  $P < 0.001$ ) and RD ( $t = -4.56$ ,  $P < 0.0001$ ) showed possible myelination and dense axonal packing in the left OR (see **Figure 4B**; **Supplementary Table 4E**) after 1 year.

Similar results were also reported in a previous investigation (de Blank et al., 2013). Specifically, the initial FA of ORs was associated with visual acuity in a 1-year follow-up. In contrast, in our study, diffusion MRI was assessed four times every 3 months alongside SWAP examinations. However, this study was done on 50 children with NF1-associated OPGs, and our study involved one young adult NF1-OPG case.

Another study that employed tract-based spatial statistics (Smith et al., 2006) on 40 children with NF1 claimed that reduced FA values were correlated with multiple WM regions (Zamboni et al., 2007; Karlsgodt et al., 2012; de Blank et al., 2020). The study's main limitation was that it is done on developing brains, whereas our investigation was longitudinal on a rare young adult woman with NF1-OPG.

In our study, the dMRI assessment after chemotherapy in the 1-year follow-up showed increased FA and decreased MD and RD values in the left OR (see **Figure 4**, **Supplementary Table 4E**). However, in the mentioned study (de Blank et al., 2020), decreased FA and increased MD and RD values were reported in nearly all WM regions.

However, these results were reported in terms of WM maturation, which is in contrast to the previous studies regarding the relationships between diffusion metrics and brain pathology (Feldman et al., 2010; Alexander et al., 2011); these demonstrated these changes as a form of axonal degeneration, which would be more reliable for NF1 properties.

As illustrated in **Figure 4**, post-chemotherapy, compared with normal subjects, revealed significant FA increases and MD and AD reductions (see **Supplementary Table 4E**) related to axonal packing and myelination. This supports the hypothesis that NF1 associated with OPGs does not require radiation therapy, as such therapy could induce cognitive problems, cerebrovascular complications, and OPs injury.

## LIMITATIONS OF THE STUDY

The present study is based on a dataset collected from a single participant, and thus, its generalizability is limited. Moreover, to reach a purpose-based criterion for glioma precision therapy, managing genetic, cellular, and behavior imaging in associated-NF1 patients with OPGs is a crucial step toward precision tailored treatment.

Also, deterministic tractography used in every step of treatment fits the WM pathway step by step, using diffusion directions in seed voxels to determine the next voxel in the tract and rely on minimum FA and maximum turning angle to reduce inaccurate tract directions. However, these procedures might increase the FA, which could be a disadvantage of applying this technique. However, differential tractography would be a relevant



approach for evaluating visual acuity over time. It could also be a useful complement to longitudinal perimetric tests.

## CONCLUSIONS

We decided to examine an old hypothesis that insists that chemotherapy is an effective treatment for NF1 patients associated with OPGs via the longitudinal differential tractography approach and SWAP tests, adjoining differential statistical analyses. This approach allowed us to trace the ORs' diffusion changes over time and check the possible association between diffusion and SWAP parameters (see **Figure 4A**; **Supplementary Tables 2–4**).

We also used whole-brain differential tractography to determine other altered WM tracts anisotropy over time. Doing this gave us a more detailed picture of the treatment efficacy. Interestingly, the connectivity between the body and genu of the corpus callosum increased by 10–30% over 1 year (see **Supplementary Figure 6**). This extends our previous study on glioma invasion, which revealed that the corpus callosum body played a role in this procedure (Sharifi et al., 2019).

Future works should design algorithms from field theory, anatomical modeling, and population genetics. Such algorithms could detect a genetic continuum wherein the brain structure is heavily genetically determined in some parts but not others (Thompson et al., 2001, 2002; Winkler et al., 2010; van der Lee et al., 2019). Thus, future investigations should focus on genetic-based imaging with a large sample size in conjunction with robust, distinctive statistical analyses.

Furthermore, neuroimaging meta-analyses would be suitable for investigators who wish to obtain an appropriate FOV for this specific problem. There is plenty of meta- and mega-analyses (Hoogman et al., 2017; Mufford et al., 2017; Thompson et al., 2017; Rinker et al., 2018; Schmaal et al., 2020; Tozzi et al., 2020) that have been utilized as a prototype to evaluate a new design to enhance precision tailored therapy. Meta- and mega-analyses could provide a proper FOV for pathological genomic imaging (Thompson et al., 2010) and basic science investigators in the future.

## DATA AVAILABILITY STATEMENT

The original contributions presented in the study are included in the article/**Supplementary Material**, further inquiries can be directed to the corresponding author/s.

## ETHICS STATEMENT

Written informed consent was obtained from the individual(s), and minor(s)' legal guardian/next of kin, for the publication of any potentially identifiable images, or data included in this article.

## AUTHOR CONTRIBUTIONS

AP designed the study, acquired, analyzed, and explained the data, wrote the manuscript, and revised it. GS and MS

are the main neurosurgeons of the case. AA is the main neuro-oncologist of the study. FB-Z and AP performed IHC analyses. SN and TM revised the manuscript. All authors contributed to the article and approved the submitted version.

## FUNDING

Skull Base Research Center supported the current clinical case study, Department of Neurosurgery, Lohman-e Hakim Hospital, Shahid Beheshti University of Medical Sciences, Tehran, Iran (Grant No. 133362-5445).

## ACKNOWLEDGMENTS

We would like to thank the Iranian National Brain Mapping Laboratory (NBML), Tehran, Iran, for providing data acquisition service for this research. We would also like to appreciate the Clinical Research Development Unit (CRDU) of Lohman Hakim Hospital, Shahid Beheshti University of Medical Sciences, Tehran, Iran, for their support, collaboration, and assistance throughout the study (Grant No. 133362-5445).

## SUPPLEMENTARY MATERIAL

The Supplementary Material for this article can be found online at: <https://www.frontiersin.org/articles/10.3389/fnhum.2021.620439/full#supplementary-material>

**Supplementary Figure 1 |** The Clinical manifestations of the NF1 young adult woman. Café au lait spots and neurofibromas on her front and back body (**A,B**). Freckling in the axillary regions (**C**). An OP glioma on the left geniculate WM. NF1, neurofibromatosis type 1; OP, optic pathway; WM, white matter.

**Supplementary Figure 2 |** Differential tractography according to the FDR protocol (Yeh et al., 2019). Three baseline scans were used to differentiate the pre-operation, pre-chemotherapy, and post-chemotherapy vs. SHAM scan wherein the ORs are displayed by red color. FDR, false discovery rate; OR, optic radiation.

**Supplementary Figure 3 |** Differential tractography approach and statistical analyses to discover the ORs connectivity and diffusion metric alterations. Increased connectivity of the left OR in 3 months post-operation vs. pre-operation. Statistical analyses revealed FA reduction, increased MD, RD, and AD relative to nFA, nMD, nRD, and nAD, respectively (**A**). The method utilized for post-chemotherapy vs. post-operation and presented increased connectivity of the left OR. The violin plots of diffusion metrics showed no significant pathological reflection (**B**). Statistics performed on the diffusion metrics by two-tailed sample *t*-test, \**P* < 0.05; \*\**P* < 0.01; \*\*\**P* < 0.001; \*\*\*\**P* < 0.0001. OR, optic radiation; FA, fractional anisotropy; MD, mean diffusivity; RD, radial diffusivity; AD, axial diffusivity; nFA, normal FA; nMD, normal MD; nRD, normal RD; nAD, normal AD.

**Supplementary Figure 4 |** The IHC analyses recognized the OP tumor as PA. Bright red, corkscrew-shaped Rosenthal fibers (RFs) are often found in compact regions (**A**). PAs are mostly biphasic with alternating compact and loose/microcytic growth patterns (**B**). Mulberry-shaped eosinophilic granular bodies (EGBs) are most common in the loose component (**C**). IHC, Immunohistochemistry; OP, optic pathway; PA, pilocytic astrocytoma.

**Supplementary Figure 5 |** Correlation analyses performed between the right OR diffusion metrics and perimetric parameters. Diffusion metrics of the right OR and perimetric parameters (VFI and MD) were extracted. The correlation analyses were performed by Pearson's correlation coefficient test and illustrated as a matrix

heatmap. OR, optic radiation; VFI, visual field index; MD, mean deviation.

**Supplementary Figure 6 |** Whole-brain differential tractography performed to identify the other WM tracts connectivity alteration over time. QA changes traced with utilizing three different thresholds (+10%, +20%, and +30%) to make connectivity comparisons between time points. Genu and body of the CC and left, and right cingulum showed increased connectivity over time. WM, white matter; QA, quantitative anisotropy; CC, corpus callosum.

**Supplementary Table 1 |** The FDR correction protocol was done five times to differentiate 3 months post-operation vs. pre-operation, post-chemotherapy relative to 3 months post-operation, pre-operation vs. pre-chemotherapy, post-chemotherapy vs. pre-chemotherapy, and post-chemotherapy relative to pre-operation. The FDR = (total number of differential tracks count from sham scans) / (total number of differential tracks count from the follow-up scans), \* $P < 0.05$ . FDR, false discovery rate.

**Supplementary Table 2 |** Spearman's correlation coefficient test performed between diffusion metrics and VFI. The correlation analyses were performed

between each dMRI metric and VFI at each time point. A significant association between left OR FA and the left VFI was found over time, \*\*\* $P < 0.001$ . VFI, visual field index; dMRI, diffusion magnetic resonance imaging; OR, optic radiation; FA, fractional anisotropy.

**Supplementary Table 3 |** Spearman's correlation coefficient test performed between diffusion metrics and MD. The correlation analyses were performed between each dMRI metric and MD at each time point. No significant association between each side of OR diffusion metrics and the MD was found over time. MD, mean deviation; dMRI, diffusion magnetic resonance imaging; OR, optic radiation.

**Supplementary Table 4 |** Statistical analyses between patient and normal ORs dMRI metrics performed in five stages including 3 months post-operation vs. pre-operation (A), post-chemotherapy relative to 3 months post-operation (B), pre-operation vs. pre-chemotherapy (C), post-chemotherapy vs. pre-chemotherapy (D), and post-chemotherapy relative to pre-operation (E). Statistics performed by two-tailed sample  $t$ -test, \* $P < 0.05$ ; \*\* $P < 0.01$ ; \*\*\* $P < 0.001$ ; \*\*\*\* $P < 0.0001$ . OR, optic radiation; dMRI, diffusion magnetic resonance imaging.

## REFERENCES

- Abdollahimzadeh, B., Piraino, D. C., Albanese, G., Cruciani, F., and Rahimi, S. (2016). Neurofibromatosis: an update of ophthalmic characteristics and applications of optical coherence tomography. *Clin. Ophthalmol.* 10, 851–860. doi: 10.2147/OPHTH.S102830
- Albers, A. C., and Gutmann, D. H. (2009). Gliomas in patients with neurofibromatosis type 1. *Expert Rev. Neurother.* 9, 535–539. doi: 10.1586/ern.09.4
- Alexander, A. L., Hurley, S. A., Samsonov, A. A., Adluru, N., Hosseinbor, A. P., Mossahebi, P., et al. (2011). Characterization of cerebral white matter properties using quantitative magnetic resonance imaging stains. *Brain Connect.* 1, 423–446. doi: 10.1089/brain.2011.0071
- Anderson, D. R., and Patella, V. M. (1999). *Automated Static Perimetry*. 2nd Edn. St. Louis, MO, 147–159. Available online: <https://zenodo.org/record/3747737>. X-SnXthKhPY (accessed on 13 September 2020).
- Bedre, R. (2020). *Bioinformatics Data Analysis and Visualization Toolkit*. Zenodo.
- Bouffet, E., Jakacki, R., Goldman, S., Hargrave, D., Hawkins, C., Shroff, M., et al. (2012). Phase II study of weekly vinblastine in recurrent or refractory pediatric low-grade glioma. *J. Clin. Oncol.* 30, 1358–1363. doi: 10.1200/JCO.2011.34.5843
- Campen, C. J., and Gutmann, D. H. (2018). Optic pathway gliomas in neurofibromatosis type 1. *J. Child Neurol.* 33, 73–81. doi: 10.1177/0883073817739509
- Cappellano, A. M., Petrilli, A. S., da Silva, N. S., Silva, F. A., Paiva, P. M., Cavalheiro, S., et al. (2015). Single agent vinorelbine in pediatric patients with progressive optic pathway glioma. *J. Neurooncol.* 121, 405–412. doi: 10.1007/s11060-014-1652-6
- Ciccarelli, O., Toosy, A. T., Hickman, S. J., Parker, G. J., Wheeler-Kingshott, C. A., Miller, D. H., et al. (2005). Optic radiation changes after optic neuritis detected by tractography-based group mapping. *Hum. Brain Mapp.* 25, 308–316. doi: 10.1002/hbm.20101
- Collins, V. P., Jones, D. T., and Giannini, C. (2015). Pilocytic astrocytoma: pathology, molecular mechanisms and markers. *Acta Neuropathol.* 129, 775–788. doi: 10.1007/s00401-015-1410-7
- Compton, A. (1994). The Neurofibromatoses. A pathogenetic and clinical overview. *J. Neurol. Neurosurg. Psychiatry* 57:1301. doi: 10.1136/jnnp.57.10.1301
- Dalla Via, P., Opocher, E., Pinello, M. L., Calderone, M., Viscardi, E., Clementi, M., et al. (2007). Visual outcome of a cohort of children with neurofibromatosis type 1 and optic pathway glioma followed by a pediatric neuro-oncology program. *Neuro Oncol.* 9, 430–437. doi: 10.1215/15228517-2007-031
- D'Angelo, F., Ceccarelli, M., Tala, G., Garofano L., Zhang, J., Frattini, V., Capelle, de Groot, J., DiMeco, F., et al. (2019). The molecular landscape of glioma in patients with Neurofibromatosis 1. *Nat. Med.* 25, 176–187. doi: 10.1038/s41591-018-0263-8
- de Blank, P., Berman, J. I., Prelack, M., Sollee, J. R., Lane, A., Waldman, A. T., et al. (2020). Effect of age and neurofibromatosis type 1 status on white matter integrity in the optic radiations. *Neurooncol. Adv.* 2(Suppl 1), i150–i158. doi: 10.1093/noajnl/vdaa037
- de Blank, P., Fisher, M. J., Gittleman, H., Barnholtz-Sloan, J. S., Badve, C., and Berman, J. I. (2018). Validation of an automated tractography method for the optic radiations as a biomarker of visual acuity in neurofibromatosis-associated optic pathway glioma. *Exp. Neurol.* 299, 308–316. doi: 10.1016/j.expneurol.2017.06.004
- de Blank, P. M., Berman, J. I., Liu, G. T., Roberts, T. P., and Fisher, M. J. (2013). Fractional anisotropy of the optic radiations is associated with visual acuity loss in optic pathway gliomas of neurofibromatosis type 1. *Neuro Oncol.* 15, 1088–1095. doi: 10.1093/neuonc/not068
- Drance, S. M., Lakowski, R., Schulzer, M., and Douglas, G. R. (1981). Acquired color vision changes in glaucoma. Use of 100-hue test and Pickford anomaloscope as predictors of glaucomatous field change. *Arch. Ophthalmol.* 99, 829–831. doi: 10.1001/archoph.1981.03930010829007
- Feldman, H. M., Yeatman, J. D., Lee, E. S., Barde, L. H., and Gaman-Bean, S. (2010). Diffusion tensor imaging: a review for pediatric researchers and clinicians. *J. Dev. Behav. Pediatr.* 31, 346–356. doi: 10.1097/DBP.0b013e3181dca8b
- Flammer, J., and Drance, S. M. (1984). Correlation between color vision scores and quantitative perimetry in suspected glaucoma. *Arch. Ophthalmol.* 102, 38–39. doi: 10.1001/archoph.1984.01040030022026
- Grill, J., Couanet, D., Cappelli, C., Habrand, J. L., Rodriguez, D., Sainte-Rose, C., et al. (1999). Radiation-induced cerebral vasculopathy in children with neurofibromatosis and optic pathway glioma. *Ann. Neurol.* 45, 393–396. doi: 10.1002/1531-8249(199903)45:3<393::AID-ANA17>3.0.CO;2-B
- Gu, S., Glaug, N., Cnaan, A., Packer, R. J., and Avery, R. A. (2014). Ganglion cell layer-inner plexiform layer thickness and vision loss in young children with optic pathway gliomas. *Invest. Ophthalmol. Vis. Sci.* 55, 1402–1408. doi: 10.1167/iovs.13-13119
- Guillamo, J. S., Créange, A., Kalifa, C., Grill, J., Rodriguez, D., Doz, F., et al. (2002). Prognostic factors of CNS tumours in Neurofibromatosis 1 (NF1): a retrospective study of 104 patients. *Brain* 126, 152–160. doi: 10.1093/brain/awg016
- Gutmann (1988). Neurofibromatosis. Conference statement. National Institutes of Health Consensus Development Conference. *Arch. Neurol.* 45, 575–578. doi: 10.1001/archneur.1988.00520290115023
- Gutmann, D. H., Aylsworth, A., Carey, J. C., Korf, B., Marks, J., Pyeritz, R. E., et al. (1997). The diagnostic evaluation and multidisciplinary management of neurofibromatosis 1 and neurofibromatosis 2. *JAMA* 278, 51–57. doi: 10.1016/S0002-9394(14)70930-4
- Gutmann, D. H., Ferner, R. E., Listernick, R. H., Korf, B. R., Wolters, P. L., and Johnson, K. J. (2017). Neurofibromatosis type 1. *Nat. Rev. Dis. Primers* 3:17004. doi: 10.1038/nrdp.2017.4
- Hales, P. W., Smith, V., Dhanoa-Hayre, D., O'Hare, P. K., Mankad d'Arco, F., Cooper, J., et al. (2018). Delineation of the visual pathway in paediatric optic pathway glioma patients using probabilistic tractography, and correlations with visual acuity. *Neuroimage Clin.* 17, 541–548. doi: 10.1016/j.nicl.2017.10.010

- Helfferich, J., Nijmeijer, R., Brouwer, O. F., Boon, M., Fock, A., Hoving, E. W., et al. (2016). Neurofibromatosis type 1 associated low grade gliomas: a comparison with sporadic low grade gliomas. *Crit. Rev. Oncol. Hematol.* 104, 30–41. doi: 10.1016/j.critrevonc.2016.05.008
- Hoogman, M., Bralten, J., Hibar, D. P., Mennes, M., Zwiers, M. P., Schwenen, L. S. J., et al. (2017). Subcortical brain volume differences in participants with attention deficit hyperactivity disorder in children and adults: a cross-sectional mega-analysis. *Lancet Psychiatry* 4, 310–319. doi: 10.1016/S2215-0366(17)30107-4
- Hu, R., Wang, C., Gu, Y., and Racette, L. (2016). Comparison of standard automated perimetry, short-wavelength automated perimetry, and frequency-doubling technology perimetry to monitor glaucoma progression. *Medicine* 95:e2618. doi: 10.1097/MD.00000000000002618
- Hughes, R. (1999). Neurofibromatosis type 1 from genotype to phenotype: Upadhyaya M, N D. Cooper BIOS Scientific Publishers (230 pages), ISBN 1-859-961 91-6, £67.50, Hardback. *Human Genetics* 104:438. doi: 10.1007/s004390050982
- Huson, S. M., Harper, P. S., and Compston, D. A. (1988). Von Recklinghausen neurofibromatosis. A clinical and population study in south-east Wales. *Brain* 111, 1355–1381. doi: 10.1093/brain/111.6.1355
- Jenkinson, M., Beckmann, C. F., Behrens, T. E., Woolrich, M. W., and Smith, S. M. (2012). Fsl. *Neuroimage* 62, 782–790. doi: 10.1016/j.neuroimage.2011.09.015
- Johnson, C. A., Cioffi, G. A., and Van Buskirk, M. E. (1999). Frequency doubling technology perimetry using a 24–2 stimulus presentation pattern. *Optom. Vis. Sci.* 76, 571–581. doi: 10.1097/00006324-199908000-00026
- Jutras, G., Belanger, K., Letarte, N., Adam, J. P., Roberge, D., Lemieux, B., et al. (2018). Procarbazine, lomustine and vincristine toxicity in low-grade gliomas. *Curr. Oncol.* 25, e33–e39. doi: 10.3747/co.25.3680
- Kalin-Hajdu, E., Decarie, J. C., Marzouki, M., Carret, A. S., and Ospina, L. H. (2014). Visual acuity of children treated with chemotherapy for optic pathway gliomas. *Pediatr. Blood Cancer* 61, 223–227. doi: 10.1002/pbc.24726
- Karlsgodt, K. H., Rosser, T., Lutkenhoff, E. S., Cannon, T. D., Silva, A., and Bearden, C. E. (2012). Alterations in white matter microstructure in neurofibromatosis-1. *PLoS ONE* 7:e47854. doi: 10.1371/journal.pone.0047854
- Kolbe, S. C., van der Walt, A., Butzkueven, H., Klistorner, A., Egan, G. F., and Kilpatrick, T. J. (2016). Serial diffusion tensor imaging of the optic radiations after acute optic neuritis. *J. Ophthalmol.* 2016:2764538. doi: 10.1155/2016/2764538
- Korf, B. R. (2000). Malignancy in neurofibromatosis type 1. *Oncologist* 5, 477–485. doi: 10.1634/theoncologist.5-6-477
- Lewis, R. A., Gerson, L. P., Axelson, K. A., Riccardi, V. M., and Whitford, R. P. (1984). von Recklinghausen neurofibromatosis. II. Incidence of optic gliomata. *Ophthalmology* 91, 929–935. doi: 10.1016/S0161-6420(84)34217-8
- Listernick, R., and Charrow, J. (1990). Neurofibromatosis type 1 in childhood. *J. Pediatr.* 116, 845–853. doi: 10.1016/S0022-3476(05)80639-0
- Listernick, R., Charrow, J., Tomita, T., and Goldman, S. (1999). Carboplatin therapy for optic pathway tumors in children with neurofibromatosis type-1. *J. Neurooncol.* 45, 185–190. doi: 10.1023/A:1006338322266
- Listernick, R., Ferner, R. E., Liu, G. T., and Gutmann, D. H. (2007). Optic pathway gliomas in neurofibromatosis-1: controversies and recommendations. *Ann. Neurol.* 61, 189–198. doi: 10.1002/ana.21107
- Liu, S., Yu, M., Weinreb, R. N., Lai, G., Lam, D. S., and Leung, C. K. (2014). Frequency doubling technology perimetry for detection of visual field progression in glaucoma: a pointwise linear regression analysis. *Invest. Ophthalmol. Vis. Sci.* 55, 2862–2869. doi: 10.1167/iovs.13-13225
- Margaret, R. W. (2000). Neurofibromatosis: phenotype, natural history, and pathogenesis. *Am. J. Hum. Genetics* 67:264. doi: 10.1086/302983
- Merchant, T. E., Kun, L. E., Wu, S., Xiong, X., Sanford, R. A., and Boop, F. A. (2009). Phase II trial of conformal radiation therapy for pediatric low-grade glioma. *J. Clin. Oncol.* 27, 3598–3604. doi: 10.1200/JCO.2008.20.9494
- Mufford, M. S., Stein, D. J., Dalvie, S., Groenewold, N. A., Thompson, P. M., and Jahanshad, N. (2017). Neuroimaging genomics in psychiatry—a translational approach. *Genome Med.* 9:102. doi: 10.1186/s13073-017-0496-z
- Nebbio, M., Moramarco, A., Lambiasi, A., Giustini, S., Marenco, M., Miraglia, E., et al. (2020). Neurofibromatosis type 1: ocular electrophysiological and perimetric anomalies. *Eye Brain* 12, 119–127. doi: 10.2147/EB.S255184
- Ostertagová, E. (2012). Modelling using polynomial regression. *Proc. Eng.* 48, 500–506. doi: 10.1016/j.proeng.2012.09.545
- Packer, R. J., Ater, J., Allen, J., Phillips, P., Geyer, R., Nicholson, H. S., et al. (1997). Carboplatin and vincristine chemotherapy for children with newly diagnosed progressive low-grade gliomas. *J. Neurosurg.* 86, 747–754. doi: 10.3171/jns.1997.86.5.0747
- Perry, A., and Wesseling, P. (2016). “Histologic classification of gliomas. *Handb. Clin. Neurol.* 134, 71–95. doi: 10.1016/B978-0-12-802997-8.00005-0
- Quinn, J. A., Reardon, D. A., Friedman, A. H., Rich, J. N., Sampson, J. H., Provenzale, J. M., et al. (2003). Phase II trial of temozolomide in patients with progressive low-grade glioma. *J. Clin. Oncol.* 21, 646–651. doi: 10.1200/JCO.2003.01.009
- Rinker, D. A., Jahanshad, N., Hibar, D. P., Faskowitz, J., McMahon, K. L., de Zubicaray, G. I., et al. (2018). Chapter Two - Genetic Connectivity–Correlated Genetic Control of Cortical Thickness, Brain Volume, White Matter. *Imaging Genetics*. Dalca AV, Batmanghelich NK, Shen L, Sabuncu MR. Academic Press, 25–43. doi: 10.1016/B978-0-12-813968-4.00002-X
- Rodriguez, F. J., Perry, A., Gutmann, D. H., O'Neill, B. P., Leonard, J., Bryant, S., et al. (2008). Gliomas in neurofibromatosis type 1: a clinicopathologic study of 100 patients. *J. Neuropathol. Exp. Neurol.* 67, 240–249. doi: 10.1097/NEN.0b013e318165eb75
- Sample, P. A. (2000). Short-wavelength automated perimetry: its role in the clinic and for understanding ganglion cell function. *Prog. Retin Eye Res.* 19, 369–383. doi: 10.1016/S1350-9462(00)00001-X
- Schmaal, L., Ching, C. R. K., McMahon, A. B., Jahanshad, N., and Thompson, P. M. (2020). Chapter 41 - Neuroimaging, Genetics, and Personalized Psychiatry: Developments and Opportunities From the ENIGMA Consortium. *Personalized Psychiatry*. B. T. Baune. San Diego, CA: Academic Press, 483–497. doi: 10.1016/B978-0-12-813176-3.00041-9
- Sharif, S., Ferner, R., Birch, J. M., Gillespie, J. E., Gattamaneni, H. R., Baser, M. E., et al. (2006). Second primary tumors in neurofibromatosis 1 patients treated for optic glioma: substantial risks after radiotherapy. *J. Clin. Oncol.* 24, 2570–2575. doi: 10.1200/JCO.2005.03.8349
- Sharifi, G., Pajavand, A. M., Nateghinia, S., Meybodi, T. E., and Hasooni, H. (2019). Glioma migration through the corpus callosum and the brainstem detected by diffusion and magnetic resonance imaging: initial findings. *Front. Hum. Neurosci.* 13:472. doi: 10.3389/fnhum.2019.00472
- Sievert, A. J., Lang, S. S., Boucher, K. L., Madsen, P. J., Slaunwhite, E., Choudhari, N., et al. (2013). Paradoxical activation and RAF inhibitor resistance of BRAF protein kinase fusions characterizing pediatric astrocytomas. *Proc. Natl. Acad. Sci. U.S.A.* 110, 5957–5962. doi: 10.1073/pnas.1219232110
- Smith, S. M., Jenkinson, M., Johansen-Berg, H., Rueckert, D., Nichols, T. E., Mackay, C. E., et al. (2006). Tract-based spatial statistics: voxelwise analysis of multi-subject diffusion data. *Neuroimage* 31, 1487–1505. doi: 10.1016/j.neuroimage.2006.02.024
- Soffietti, R., Baumert, B. G., L., Bello, von Deimling, A., Duffau, H., Frenay, M., et al. (2010). Guidelines on management of low-grade gliomas: report of an EFNS-EANO Task Force. *Eur. J. Neurol.* 17, 1124–1133. doi: 10.1111/j.1468-1331.2010.03151.x
- Szudek, J., Birch, P., Riccardi, V. M., Evans, D. G., and Friedman, J. M. (2000). Associations of clinical features in neurofibromatosis 1 (NF1). *Genetic Epidemiol.* 19, 429–439. doi: 10.1002/1098-2272(200012)19:4<429::AID-GEPI13>3.0.CO;2-N
- Tafreshi, A., Sample, P. A., Liebmann, J. M., Girkin, C. A., Zangwill, L. M., Weinreb, R. N., et al. (2009). Visual function-specific perimetry to identify glaucomatous visual loss using three different definitions of visual field abnormality. *Invest. Ophthalmol. Vis. Sci.* 50, 1234–1240. doi: 10.1167/iovs.08-2535
- Thompson, P., Cannon, T. D., and Toga, A. W. (2002). Mapping genetic influences on human brain structure. *Ann. Med.* 34, 523–536. doi: 10.1080/078538902321117733
- Thompson, P. M., Andreassen, O. A., Arias-Vasquez, A., Bearden, C. E., Boedhoe, P. S., Brouwer, R. M., et al. (2017). ENIGMA and the individual: predicting factors that affect the brain in 35 countries worldwide. *Neuroimage* 145, 389–408. doi: 10.1016/j.neuroimage.2015.11.057
- Thompson, P. M., Cannon, T. D., Narr, K. L., van Erp, T., Poutanen, V. P., Huttunen, M., et al. (2001). Genetic influences on brain structure. *Nat. Neurosci.* 4, 1253–1258. doi: 10.1038/nn758

- Thompson, P. M., Martin, N. G., and Wright, M. J. (2010). Imaging genomics. *Curr. Opin. Neurol.* 23, 368–373. doi: 10.1097/WCO.0b013e32833b764c
- Tozzi, L., Garczarek, L., Janowitz, D., Stein, D. J., Wittfeld, K., Dobrowolny, H., et al. (2020). Interactive impact of childhood maltreatment, depression, and age on cortical brain structure: mega-analytic findings from a large multi-site cohort. *Psychol. Med.* 50, 1020–1031. doi: 10.1017/S003329171900093X
- Tsang, D. S., Murphy, E. S., and Merchant, T. E. (2017). Radiation therapy for optic pathway and hypothalamic low-grade gliomas in children. *Int. J. Radiat. Oncol. Biol. Phys.* 99, 642–651. doi: 10.1016/j.ijrobp.2017.07.023
- Ullrich, N. J., Robertson, R., Kinnamon, D. D., Scott, R. M., Kieran, M. W., Turner, C. D., et al. (2007). Moyamoya following cranial irradiation for primary brain tumors in children. *Neurology* 68, 932–938. doi: 10.1212/01.wnl.0000257095.33125.48
- van der Lee, S. J., Knol, M. J., Chauhan, G., Satizabal, C. L., Smith, A. V., Hofer, E., et al. (2019). A genome-wide association study identifies genetic loci associated with specific lobar brain volumes. *Commun. Biol.* 2:285. doi: 10.1038/s42003-019-0537-9
- Van Rossum, G., and Drake, F. L. Jr. (2014). *The Python Language Reference*. Python Software Foundation.
- Vrabec, J. P., and Levin, L. A. (2007). The neurobiology of cell death in glaucoma. *Eye* 21(Suppl. 1), S11–S14. doi: 10.1038/sj.eye.6702880
- Winkler, A. M., Kochunov, P., Blangero, J., Almasy, L., Zilles, K., Fox, P. T., et al. (2010). Cortical thickness or grey matter volume? The importance of selecting the phenotype for imaging genetics studies. *Neuroimage* 53, 1135–1146. doi: 10.1016/j.neuroimage.2009.12.028
- Woolrich, M. W., Jbabdi, S., Patenaude, B., Chappell, M., Makni, S., Behrens, T., et al. (2009). Bayesian analysis of neuroimaging data in FSL. *Neuroimage* 45(1 Suppl), S173–S186. doi: 10.1016/j.neuroimage.2008.10.055
- Yeh, F. C., Tang, P. F., and Tseng, W. Y. (2013). Diffusion MRI connectometry automatically reveals affected fiber pathways in individuals with chronic stroke. *Neuroimage Clin.* 2, 912–921. doi: 10.1016/j.nicl.2013.06.014
- Yeh, F. C., and Tseng, W. Y. (2011). NTU-90: a high angular resolution brain atlas constructed by q-space diffeomorphic reconstruction. *Neuroimage* 58, 91–99. doi: 10.1016/j.neuroimage.2011.06.021
- Yeh, F. C., Zaydan, I. M., Suski, V. R., Lacomis, D., Richardson, R. M., Maroon, J. C., et al. (2019). Differential tractography as a track-based biomarker for neuronal injury. *Neuroimage* 202:116131. doi: 10.1016/j.neuroimage.2019.116131
- Zamboni, S. L., Loenneker, T., Boltshauser, E., Martin, E., and Il'yasov, K. A. (2007). Contribution of diffusion tensor MR imaging in detecting cerebral microstructural changes in adults with neurofibromatosis type 1. *AJNR Am. J. Neuroradiol.* 28, 773–776.
- Ziu, M., Kalkanis, S. N., Gilbert, M., Ryken, T. C., and Olson, J. J. (2015). The role of initial chemotherapy for the treatment of adults with diffuse low grade glioma: a systematic review and evidence-based clinical practice guideline. *J. Neurooncol.* 125, 585–607. doi: 10.1007/s11060-015-1931-x

**Conflict of Interest:** The authors declare that the research was conducted in the absence of any commercial or financial relationships that could be construed as a potential conflict of interest.

Copyright © 2021 Pajavand, Sharifi, Anvari, Bidari-Zerehpooosh, Shamsi, Nateghinia and Meybodi. This is an open-access article distributed under the terms of the Creative Commons Attribution License (CC BY). The use, distribution or reproduction in other forums is permitted, provided the original author(s) and the copyright owner(s) are credited and that the original publication in this journal is cited, in accordance with accepted academic practice. No use, distribution or reproduction is permitted which does not comply with these terms.





# Advancing Risk Analysis of COVID-19 Clinical Predictors: The Case of Fasting Blood Glucose

Hamad Ali<sup>1,2\*</sup>, Abdullah A. Al-Shammari<sup>2,3</sup>, Barrak Alahmad<sup>4</sup> and Fahd Al-Mulla<sup>2</sup>

<sup>1</sup> Department of Medical Laboratory Sciences, Faculty of Allied Health Sciences, Health Sciences Center, Kuwait University, Kuwait City, Kuwait, <sup>2</sup> Department of Genetics and Bioinformatics, Dasman Diabetes Institute (DDI), Kuwait City, Kuwait, <sup>3</sup> Department of Mathematics, Faculty of Sciences, Kuwait University, Kuwait City, Kuwait, <sup>4</sup> Department of Environmental Health, Harvard T.H. Chan School of Public Health, Harvard University, Boston, MA, United States

**Keywords:** COVID-19, risk analysis, nonlinearity, glucose, clinical outcomes, diabetes, glycolysis, inflammation

## OPEN ACCESS

### Edited by:

Reza Lashgari,  
Institute for Research in Fundamental  
Sciences, Iran

### Reviewed by:

Soroush Arabshahi,  
Columbia University, United States  
Erfan Zabeih,  
Columbia University, United States

### \*Correspondence:

Hamad Ali  
hamad.ali@ku.edu.kw;  
hamad.ali@dasmaninstitute.org

### Specialty section:

This article was submitted to  
Infectious Diseases - Surveillance,  
Prevention and Treatment,  
a section of the journal  
Frontiers in Medicine

**Received:** 30 November 2020

**Accepted:** 17 March 2021

**Published:** 09 April 2021

### Citation:

Ali H, Al-Shammari AA, Alahmad B  
and Al-Mulla F (2021) Advancing Risk  
Analysis of COVID-19 Clinical  
Predictors: The Case of Fasting Blood  
Glucose. *Front. Med.* 8:636065.  
doi: 10.3389/fmed.2021.636065

## HIGHLIGHTS

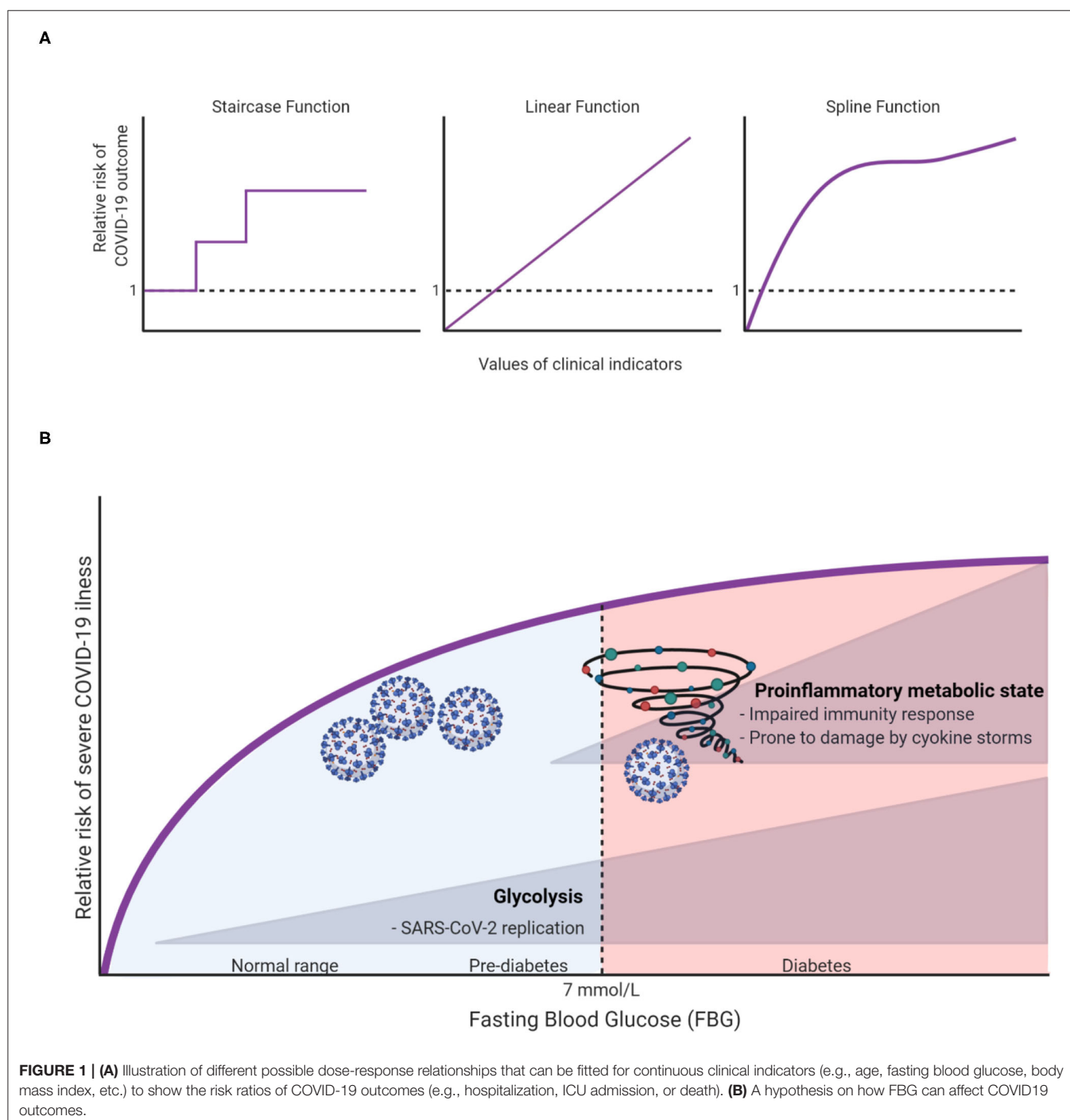
- Many of the clinical predictors of COVID-19 are naturally continuous.
- Such continuity may imply that a complex predictor-risk relationship is underplay.
- Risk analyses that allow continuous predictors to take a restriction-free shape can provide a better understanding of the clinical course of the disease. This refined approach can help generate hypotheses characterizing the mechanisms of disease progression.

To understand or predict the effects of serum glucose on COVID-19 outcomes such as hospitalization, intensive care unit (ICU) admission or death, one could try to use conventional regression techniques with glucose as the independent variable and one of these outcomes as the dependent variable. But how should the glucose variable be included in such models? One may try applying clinical threshold values to fit the regression model. For example, in the context of diabetes diagnosis, we can use the threshold values of hemoglobin A1c (A1C); A1C <5.7%, A1C between 5.7 and 6.4%, and A1C ≥6.5% to characterize patients as normal, prediabetic, or diabetic, respectively (1). Alternatively, we can use two categories instead of three: diabetics vs. non-diabetics. These threshold or categorical approaches, albeit commonly useful for identifying high risk groups, have underlying limitations. First, they assume complete homogeneity within each group, hence patients with A1C values of 6.5 and 10% are to be considered clinically identical. Put another way, these approaches assume that patients with A1C of 5.69% are entirely different from those with A1C of 5.70%. Secondly, the dose-response relationship is a step or staircase function, which is rarely a realistic description of real-life patient risks (2, 3).

To capture the natural trends of a continuous exposure variable, one may surprisingly benefit from allowing the dose-response relationship to take whatever natural shape the data describe, rather than forcing it to fit idealized relationships such as linear (straight line) and categorical (staircase) functions (Figure 1A). The risk analyses based on such natural relationships are only made possible with modern computational algorithms. Take penalized splines as an example. These are smoothing non-parametric functions that, unlike forcing steps and lines, allow significant flexibility in estimating the dose-response curve. The only thing that governs these specific types of splines is, in fact, the goodness-of-fit. In other words, this smoothing of the relationship comes without idealized assumptions and prevents under- or over-fitting the data (4).

To illustrate, let us take fasting blood glucose (FBG) as an indicator for in-hospital complications among COVID-19 patients. Creating a three diagnostic categories of FBG [ $<6.1$  mmol/L (reference), 6.1–6.9 mmol/L and  $\geq 7.0$  mmol/L] demonstrated that the odds ratios (OR) of developing 28-day in-hospital complications for the higher categories were 3.99 and 2.61, respectively (5). However, it remains unclear how much risk is associated with increasing FBG within the range of

each group, and whether the patients within each group have a sufficiently homogeneous risk. Applying splines for the glucose variable suggested that even small changes in FBG within normal ranges can significantly increase the risk of severe illness (6). Surely this cannot be overlooked clinically, hence warranting recommendations for strict monitoring of FBG upon admission. Unexpectedly, this “unconventional” type of risk analysis has also brought to light an important and uncharted scientific



question: why and how glucose can influence the outcome of COVID-19 even within normal ranges? At this stage we can only speculate as to what the answer might be, but we hope to inspire further research into this subject. In this spirit, we argue that there are potentially two independent mechanisms in which glucose can influence COVID-19 outcomes. First, at high levels of glucose (in the diabetic ranges), low-grade chronic inflammation state disturbs the homeostatic glucose regulation and insulin sensitivity. This could also in turn disrupt normal immune response by weakening T-cell function and add to the risk of hyperinflammation and cytokine storm syndrome which is associated with worse COVID-19 outcome (7). On the other hand, increases of FBG, even within normal ranges could affect COVID-19 outcomes through enhancing aerobic glycolysis in the infected monocytes with SARS-CoV2 which in turn enhance and facilitate viral replication and infection resulting in more severe outcome (8). The inflammation and glycolysis mechanisms are likely to be affected by different levels of FBG with the latter being sensitive to lower levels (Figure 1B).

The novelty presented here is the application of well-known tools that are not being applied much in the COVID-19 epidemiology, because in many cases, researchers opt to conventional and clinically straightforward approaches such as linear, dichotomous and categorical modeling. While this was acceptable for some time because of the computational complexity of the smoothing applications, they can be easily implemented in modern time computers and statistical softwares. We argue that they ought to be used.

Although utilizing smoothing functions, in our case, sounds reasonable, we must always exercise caution with smaller sample sizes. In addition, relying on cross-validation to determine penalty terms for penalized splines is computationally extensive. For example, the leave-one-out validation will leave one observation out at a time; fit the model on the remaining training

data; test on the held-out data point and so on. An alternative approach to specify penalized splines is using Restricted Maximum Likelihood, which is a Likelihood based approach. Furthermore, interpretation of coefficients is not straightforward. Improving the fit of the dose-response relationship comes at the expense of easy interpretation.

What we are advocating for in this opinion piece is the mere attention to the nature of the dose-response relationship which is usually overlooked by simplifying assumptions such as forcing a straight line or forcing a staircase shape. In fact, with the pandemic hitting us harder, we need to leverage all the tools we have in the toolbox in order to get a better understanding of the complex pathophysiology of clinical predictors (like FBG) during the state of infection.

Bottom line, non-linearities, steep slopes, plateaus, or any other shape should always be considered for continuous variables such as serum blood glucose or A1C, perhaps even age, body mass index, and so on. In the age of big data, electronic health records, and artificial intelligence the conventional practices maybe too archaic. Once we correctly characterize these complex relationships, we can better capture the clinical course of the disease.

## AUTHOR CONTRIBUTIONS

All authors listed have made a substantial, direct and intellectual contribution to the work, and approved it for publication.

## ACKNOWLEDGMENTS

This work was supported by the Coronavirus Emergency Resilience Program initiated by the Kuwait Foundation for the Advancement of Sciences.

## REFERENCES

1. American Diabetes Association. 2. Classification and diagnosis of diabetes: standards of medical care in diabetes-2020. *Diabetes Care*. (2020) 43:S14–31. doi: 10.2337/dc20-S002
2. Yoshimura, I. The effect of measurement error on the dose-response curve. *Environ. Health Perspect.* (1990) 87:173–8.
3. National Research Council. Chapter 12: Issues in the Assessment of Dose Response. In: *Assessing the Human Health Risks of Trichloroethylene: Key Scientific Issues*. Washington, DC: National Academies Press (2007).
4. Wood SN, Pya N, Säfken B. Smoothing parameter and model selection for general smooth models. *J Am Stat Assoc.* (2016) 111:1548–63. doi: 10.1080/01621459.2016.1180986
5. Wang S, Ma P, Zhang S, Song S, Wang Z, Ma Y, et al. Fasting blood glucose at admission is an independent predictor for 28-day mortality in patients with COVID-19 without previous diagnosis of diabetes: a multi-centre retrospective study. *Diabetologia*. (2020) 63:2102–11. doi: 10.1007/s00125-020-05209-1
6. Alahmad B, Al-Shammari AA, Bennakhi A, Al-Mulla F, Ali H. Fasting blood glucose and COVID-19 severity: nonlinearity matters. *Diabetes Care*. (2020) 43:3113–6. doi: 10.2337/dc20-1941

7. Apicella, M, Campopiano MC, Mantuano M, Mazoni L, Coppelli A, Del Prato S. COVID-19 in people with diabetes: understanding the reasons for worse outcomes. *Lancet Diabetes Endocrinol.* (2020) 8:782–92. doi: 10.1016/S2213-8587(20)30238-2
8. Codo AC, Davanzo GG, de Brito Monteiro L, de Souza GF, Muraro P, Virgilio-da-Silva JV, et al. Elevated glucose levels favor Sars-Cov-2 infection and monocyte response through a Hif-1 $\alpha$ /Glycolysis dependent axis. *Cell Metab.* (2020) 3:437–46. doi: 10.1016/j.cmet.2020.07.007

**Conflict of Interest:** The authors declare that the research was conducted in the absence of any commercial or financial relationships that could be construed as a potential conflict of interest.

Copyright © 2021 Ali, Al-Shammari, Alahmad and Al-Mulla. This is an open-access article distributed under the terms of the Creative Commons Attribution License (CC BY). The use, distribution or reproduction in other forums is permitted, provided the original author(s) and the copyright owner(s) are credited and that the original publication in this journal is cited, in accordance with accepted academic practice. No use, distribution or reproduction is permitted which does not comply with these terms.



# Frequency and Risk Factors for Spontaneous Pneumomediastinum in COVID-19 Patients

Tania Guadalupe Rodriguez-Arciniega<sup>1</sup>, Erick Sierra-Diaz<sup>2,3\*</sup>, Jesus Armando Flores-Martinez<sup>4</sup>, Maria Elena Alvizo-Perez<sup>5</sup>, Irlanda Nataly Lopez-Leal<sup>6</sup>, Ana Luisa Corona-Nakamura<sup>7</sup>, Hermes Ernesto Castellanos-Garcia<sup>4</sup> and Alejandro Bravo-Cuellar<sup>8</sup>

<sup>1</sup> Department of Internal Medicine, Western National Medical Center (IMSS), Guadalajara, Mexico, <sup>2</sup> Department of Public Health, University of Guadalajara, Guadalajara, Mexico, <sup>3</sup> Department of Urology, Western National Medical Center (IMSS), Guadalajara, Mexico, <sup>4</sup> Department of Radiology, Western National Medical Center (IMSS), Guadalajara, Mexico, <sup>5</sup> Department of Anesthesiology, Western National Medical Center (IMSS), Guadalajara, Mexico, <sup>6</sup> Department of Endocrinology, Western National Medical Center (IMSS), Guadalajara, Mexico, <sup>7</sup> Department of Infectious Diseases, Western National Medical Center (IMSS), Guadalajara, Mexico, <sup>8</sup> Department of Immunology, Western National Biomedical Center (IMSS), Guadalajara, Mexico

## OPEN ACCESS

### Edited by:

Atefeh Abedini,  
Shahid Beheshti University of Medical  
Sciences, Iran

### Reviewed by:

Mohammad Varahram,  
National Research Institute of  
Tuberculosis and Lung Diseases  
(NRIITLD), Iran  
Yoshihiko Raita,  
Massachusetts General Hospital and  
Harvard Medical School,  
United States

### \*Correspondence:

Erick Sierra-Diaz  
erksland@hotmail.com

### Specialty section:

This article was submitted to  
Pulmonary Medicine,  
a section of the journal  
Frontiers in Medicine

Received: 01 February 2021

Accepted: 12 March 2021

Published: 09 April 2021

### Citation:

Rodriguez-Arciniega TG, Sierra-Diaz E,  
Flores-Martinez JA, Alvizo-Perez ME,  
Lopez-Leal IN, Corona-Nakamura AL,  
Castellanos-Garcia HE and  
Bravo-Cuellar A (2021) Frequency and  
Risk Factors for Spontaneous  
Pneumomediastinum in COVID-19  
Patients. *Front. Med.* 8:662358.  
doi: 10.3389/fmed.2021.662358

**Background:** Spontaneous pneumomediastinum (SPM) is an uncommon condition in COVID-19 patients. No information about outcome or risk factors is available at the time. The aim of this research is to report on the frequency and risk factors of spontaneous pneumomediastinum in COVID-19 patients.

**Materials and Methods:** An unmatched case-control study was carried out in a tertiary health-care facility for patients with COVID-19. Electronic files were reviewed to identify patients with confirmed COVID-19 infection by RT-PCR. Univariate analysis was used to describe demographic data. Mean differences were calculated using the Mann-Whitney test. Frequency and odds ratios were calculated by standard operations.

**Results:** A total of 271 patients were included in the study. Nine patients showed spontaneous pneumomediastinum and four of them presented associated spontaneous pneumothorax. The most common risk factors associated with poor outcomes in COVID-19 patients were not considered as risk factors for spontaneous pneumomediastinum development.

**Conclusion:** Spontaneous pneumomediastinum is an uncommon clinical feature in COVID-19 patients. More research is necessary to formulate statements regarding prevalence, risk factors, and outcome.

**Keywords:** spontaneous pneumomediastinum, spontaneous pneumothorax, SARS-CoV-2, complications, risk factors, case-control study

## INTRODUCTION

Based on a report from the World Health Organization (WHO) from March 10, 2021, the number of confirmed COVID-19 cases worldwide were 117,332,262 and 2,605,356 deaths (1). Mexico is one of the countries with the highest number of cases. In the beginning of March, the number of confirmed cases was 2,130,477 with a total of 190,923 deaths (1). To date, the problem is of major concern for public health around the world.



Although a definitive diagnosis of COVID-19 infection is made by using a reverse transcription polymerase chain reaction (RT-PCR) assay (2), several authors reported on the role and utility of chest CT scan as a recommended tool for clinical practice for COVID-19 patients (3–5). In April 2020, the Dutch Radiological Society developed CO-RADS to assess the suspicion of pulmonary involvement of COVID-19. The scale is from 1 to 5, from very low to very high involvement (6). Nowadays, the CO-RADS scale is used widely in our medical facility as a complementary tool to measure the extent of compromised pulmonary parenchyma in COVID-19 patients.

Radiological features such as spontaneous pneumothorax have been described in 1% of COVID-19 patients (7, 8). Spontaneous pneumomediastinum (SPM), unrelated to assisted ventilation, is another radiological feature reported in literature as a frequent complication and is related to a poor outcome (9). In general terms, SPM has a reported frequency in non-COVID-19 patients of 1 in 25,000 and is more common in children (10). To date, there is no reliable data on the frequency of SPM in COVID-19 patients, however, some clinical cases are available in international literature (11–15).

Based on the previous information, the aim of this work is to report on the frequency of spontaneous pneumomediastinum and the related risk factors in a tertiary health-care facility that was converted for the caring of COVID-19 patients.

## MATERIALS AND METHODS

An unmatched case-control study was carried out at the Western National Medical Center in a 2-month period (July and August 2020). This research was performed under permission from the

ethics committee, Number 14 CEI 20190123/ COFEPRIS 17 CI 14 039 114. Electronic files from COVID-19 patients were reviewed (chest CT scans and laboratory results) that looked for clinical features related to spontaneous pneumomediastinum. Suspicious cases were reviewed by six physicians (including 2 radiologists) in order to validate the diagnosis. Selected files were reviewed in order to obtain anthropometric data, clinical features, inflammatory biomarkers, comorbidities, and outcomes. Inclusion criteria for cases and controls were complete electronic files (medical notes, laboratory results, and digital chest CT scan images) from both genders older than 18 years and COVID-19 diagnosis by RT-PCR. Selected patients were managed at the Western National Medical Center COVID-19 units by at least one of the authors of this report. A data analysis report used percentages, absolute frequencies, means, standard deviations, and a 95% confidence interval. Statistical significance was evaluated by means of the Mann-Whitney *U*-test ( $p < 0.05$ ). The frequency and Odds Ratio (OR) were calculated using standard methods. All data were processed using Excel® (Microsoft, Redmond, WA, USA) Open Epi (Open-Source Epidemiologic Statistics for Public Health, Bill and Melinda Gates Foundation, Emory University, Atlanta, GA, USA) and EpiInfo version 7.2.4 (Centers for Disease Control and Prevention, Atlanta, GA, USA).

## RESULTS

A total of 319 electronic files from COVID-19 patients confirmed by RT-PCR assay SARS-CoV-2 were reviewed. Those files without chest CT scans or complete laboratory reports were excluded ( $n = 48$ ). The files included in the study were 271,

**TABLE 1 |** Demographic data from SARS-CoV-2 patients.

| Variable            | Female ( $n = 99$ ) Mean (SD: 95%CI) | Male ( $n = 172$ ) Mean (SD: 95%CI) | <i>P</i> * |
|---------------------|--------------------------------------|-------------------------------------|------------|
| Age (years)         | 59.1 (15.9: 55.9–62.33)              | 59.5 (15.0: 57.23–61.76)            | >0.05      |
| Weight (Kg)         | 77.7 (19.5: 73.8–81.5)               | 85.0 (18.5: 82.21–87.78)            | <0.01      |
| Height (meters)     | 1.6 (0.07: 1.58–1.61)                | 1.7 (0.06: 1.69–1.70)               | <0.01      |
| BMI                 | 30.0 (7.3: 28.54–31.45)              | 29.0 (5.7: 28.14–29.85)             | >0.05      |
| Hospitalized (days) | 11 (6.1: 9.78–12.21)                 | 12.9 (7.5: 11.73–14.06)             | <0.05      |

\*Mann-Whitney *U*-test. BMI, Body Mass Index; Kg, kilograms; SD, standard deviation.

**TABLE 2 |** Comorbidities measured in the general population with COVID-19 diagnosis ( $n = 271$ ).

| Comorbidity            | Female ( $n = 99$ ) <i>n</i> (%) | Male ( $n = 172$ ) <i>n</i> (%) | <i>P</i> Fisher's exact test |
|------------------------|----------------------------------|---------------------------------|------------------------------|
| Tobacco smoking        | 9 (9.09)                         | 28 (16.3)                       | >0.05                        |
| *COPD/Asthma           | 5 (5.05)                         | 12 (6.9)                        | >0.05                        |
| Diabetes Mellitus      | 46 (46.4)                        | 67 (39)                         | >0.05                        |
| Hypertension           | 62 (62.6)                        | 97 (56.4)                       | >0.05                        |
| Chronic kidney disease | 11 (11.1)                        | 19 (11)                         | >0.05                        |
| Pneumothorax           | 0 (0)                            | 4 (2.3)                         | >0.05                        |
| Pneumomediastinum      | 2 (2.02)                         | 7 (4)                           | >0.05                        |

\*Chronic obstructive pulmonary disease.

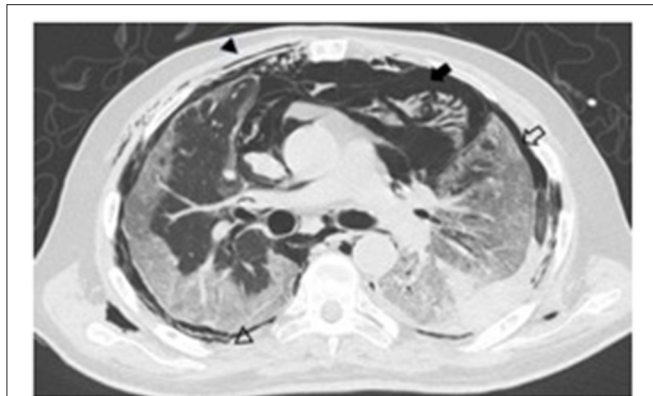


**FIGURE 1** | A 68-year-old male axial non-enhanced chest CT image showing subcutaneous emphysema (arrow heads), pneumomediastinum (black arrow), and pneumothorax (empty arrow).

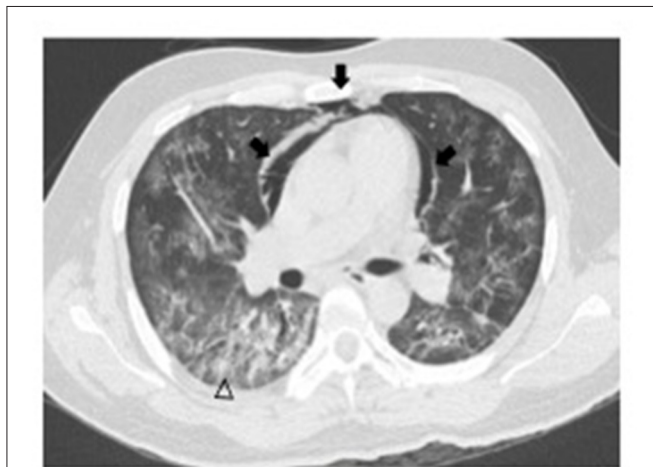


**FIGURE 2** | A 43-year-old male non-enhanced chest CT image showing pneumomediastinum (arrows) and ground glass opacity pattern over peripheral subpleural areas (arrowhead).

including cases and controls. From the patient cohorts, 36.5% were women and 63.5% were males. Demographic data is shown in **Table 1**.

The percentage of deceased patients from the entire cohort was 36.5 ( $n = 99/271$ ), corresponding to 23.9% for males and 12.6% for females. Comorbidities from the total sample were obtained from files. Details related to such are shown in **Table 2**.

Based on the results, a total of 9 COVID-19 hospitalized patients developed spontaneous pneumomediastinum (3.3%), and 4 cases of spontaneous pneumothorax were detected (1.47%). All patients underwent a non-enhanced chest CT scan immediately after hospital admission, upon which SPM was identified by a COVID-19 physician team (**Figures 1, 2**). None of them received invasive mechanical ventilation at the time they were admitted. The principal characteristics of patients who developed SPM are described in **Table 3**.

**TABLE 3** | Features from COVID-19 patients who developed spontaneous pneumomediastinum.

| Variable               | Cases ( $n = 9$ )<br>Mean (SD: 95%CI) | Controls ( $n = 262$ )<br>Mean (SD: 95%CI) | $P^*$   |
|------------------------|---------------------------------------|--|---------|
| Age (years)            | Mean 57 (15.26: 42.8–71.11)           | 59.5 (15.4: 58.02–61.77)                   | $>0.05$ |
| Weight (Kg)            | Mean 78.4 (17.8: 64.71–92.08)         | 82.5 (19.3: 80.15–84.84)                   | $>0.05$ |
| Height (meters)        | Mean 1.67 (0.09: 1.60–1.73)           | 1.66 (0.09: 1.64–1.67)                     | $>0.05$ |
| BMI                    | 27.2 (5.2: 23.20–31.19)               | 28.8 (6.5: 28–29.59)                       | $>0.05$ |
| Hospitalization (days) | 16.8 (13.9: 6.11–27.48)               | 12.06 (6.7: 11.24–12.87)                   | $>0.05$ |

\*Mann-Whitney U-test. BMI, Body Mass Index; Kg, kilograms; SD, standard deviation.

**TABLE 4** | Frequency of comorbidities in cases and controls.

| Comorbidity       | Cases $n$ (%) | Controls $n$ (%) |
|-------------------|---------------|------------------|
| COPD*/Asthma      | 0             | 19 (7.3)         |
| Diabetes mellitus | 3 (33)        | 110 (42)         |
| Hypertension      | 5 (56)        | 154 (59)         |
| Tobacco smoking   | 1 (11)        | 36 (14)          |
| Deaths            | 3 (33)        | 96 (36)          |

\*Chronic obstructive pulmonary disease.

No significant differences were observed with regard to inflammatory biomarkers ( $p > 0.05$ ). The main differences between non-spontaneous pneumomediastinum and SPM are shown in **Tables 4, 5**.

In order to calculate the Odds Ratio (OR), some independent variables (age and BMI) were adapted using a dichotomic approach that was used in the contingency tables. Age was considered as a risk factor if younger than 60-years old, and BMI was dichotomized in  $<25$  and 25 or higher. Regarding gender, being male was considered as a risk factor. The ORs were calculated individually for each risk factor. Results obtained from the ORs are described in **Table 6**.

## DISCUSSION

The results obtained in the present study clearly show that SPM is not always a pathologic feature related to invasive mechanical ventilation in COVID-19 patients. Indeed, main risk factors for SPM such as young age, tobacco smoking, asthma, and gender (10) did not show a significant statistical association. Other risk factors which are associated with poor outcomes in COVID-19 patients like hypertension and obesity were not statistically related to SPM either ( $p > 0.05$ ). International research reported a frequency of 1 in 25,000 (10), however, our results showed an increased frequency of SPM in COVID-19 patients (9 in 271). The difference between proportions is remarkable ( $p < 0.01$ ).

Spontaneous pneumomediastinum in COVID-19 patients has been reported as single cases in international literature (11–14). Other authors had reported some case series of SPM. Eperjesiova et al. reported 20 cases of air leak in a cohort of 976 COVID-19

**TABLE 5 |** Inflammatory biomarkers from cases and controls.

|                    |        | CRP mg/L | FER ng/mL | LDH U/L | LYMP × 10 <sup>9</sup> /L | WBC × 10 <sup>9</sup> /L | PLA × 10 <sup>9</sup> /L | D-d ng/mL      | PCT ng/mL   |
|--------------------|--------|----------|-----------|---------|---------------------------|--------------------------|--------------------------|----------------|-------------|
| Cases (n = 9)      | Mean   | 119.8    | 1440.2    | 558.5   | 0.9                       | 14.7                     | 277.7                    | 5441.1         | 0.5         |
|                    | SD     | 88       | 852.7     | 272.5   | 0.3                       | 8.3                      | 107.2                    | 7686.4         | 0.9         |
|                    | 95% CI | 52–187   | 784–2,095 | 349–767 | 0.6–1.1                   | 8.3–21                   | 195–360                  | –467 to 11,349 | –0.1 to 1.1 |
| Controls (n = 262) | Mean   | 156.3    | 1084.6    | 484.3   | 0.9                       | 11                       | 266                      | 2350.2         | 2.1         |
|                    | SD     | 107.3    | 741.9     | 265.6   | 0.5                       | 5.7                      | 111.8                    | 6780.9         | 8.6         |
|                    | 95%CI  | 143–169  | 994–1,174 | 451–516 | 0.8–0.9                   | 10.3–11.6                | 252–279                  | 1,525–3,175    | 1.0–3.1     |
| p*                 |        | >0.05    | >0.05     | >0.05   | >0.05                     | >0.05                    | >0.05                    | >0.05          | >0.05       |

CRP, C-reactive protein; FER, Ferritin; LDH, lactate dehydrogenase; LYMP, lymphocytes; WBC, white blood cells; PLA, platelets; D-d, D-dimer; PCT, procalcitonin. \*Mann-Whitney U-test.

**TABLE 6 |** Odds ratios obtained from contingency tables (case-control).

| Risk              | Cases | Controls | OR (95%CI)      | P Fisher's Exact test |
|-------------------|-------|----------|-----------------|-----------------------|
| Gender            |       |          | 2.05 (0.4–10.1) | >0.05                 |
| Male*             | 7     | 165      |                 |                       |
| Female            | 2     | 97       |                 |                       |
| Age (years)       |       |          | 1.2 (0.3–4.9)   | >0.05                 |
| <60*              | 5     | 129      |                 |                       |
| ≥60               | 4     | 133      |                 |                       |
| Tobacco smoking   |       |          | 0.7 (0.09–6.4)  | >0.05                 |
| Positive          | 1     | 36       |                 |                       |
| Negative          | 8     | 226      |                 |                       |
| Diabetes mellitus |       |          | 0.6 (0.16–2.8)  | >0.05                 |
| Positive          | 3     | 110      |                 |                       |
| Negative          | 6     | 152      |                 |                       |
| Hypertension      |       |          | 0.8 (0.2–3.3)   | >0.05                 |
| Positive          | 5     | 154      |                 |                       |
| Negative          | 4     | 108      |                 |                       |
| BMI               |       |          | 3.3 (0.85–12.7) | >0.05                 |
| <25*              | 4     | 51       |                 |                       |
| ≥25               | 5     | 211      |                 |                       |
| Mortality         |       |          | 0.8 (0.2–3.5)   | >0.05                 |
| Yes               | 3     | 96       |                 |                       |
| No                | 6     | 166      |                 |                       |

The \* means the risk factor for Spontaneous Pneumomediastinum. To be a male, younger than 60 years old and Body mass index < 25 are risk factors for spontaneous pneumomediastinum.

patients. Five cases were SPM and were unrelated to mechanical ventilation. Two patients developed spontaneous pneumothorax, and the rest (n = 13) were air leak cases that were associated with medical procedures (15). However, the manuscript does not describe the relationship between SPM and risk factors.

During the peak of the SARS-CoV-2 pandemics in Spain, Gorospe et al. reported four cases of SPM that were unrelated to mechanical ventilation. None of the patients had a previous history of tobacco consumption or predisposing risk factors. One patient died after an infection of *Pseudomonas aeruginosa* (8). No statistical analysis of risk factors was performed for the study.

Recently, Jones et al. reported an observational study in England that included 83 critically ill COVID-19 patients. The authors divided the group into barotrauma and non-barotrauma groups. The barotrauma group included a total of

8 patients. One hundred percent of them had subcutaneous emphysema, seven revealed pneumomediastinum, and four had pneumothorax (bilateral n = 2). The seven patients that developed pneumomediastinum received ventilatory support through CPAP or non-invasive mechanical ventilation (NIV). The study reported significant mean differences between some variables, and a 9.6% of barotrauma as a complication in the cohort of patients. They assumed that barotrauma in COVID-19 patients is related to longer management prior to critical care admission and the use of CPAP or NIV. However, the manuscript does not specify if the chest CT scans were performed before or after CPAP management, NIV, and invasive mechanical ventilation (16).

The inflammatory process induced by the SARS-CoV-2 infection in the respiratory tract is characterized by an increase in intrathoracic pressure. Differential pressure inside the pulmonary parenchyma is the main cause of alveolar rupture that causes air leak through interstitial and bronchovascular tissues including the pneumomediastinum (17). The abnormal increase in pressure in the mediastinum causes air to dissect in between the mediastinal structures. The effect of dissection, which is secondary to air leak, extends from the soft tissue structure in the anterior mediastinum up to the subcutaneous tissue over the upper abdomen and neck (10). Symptoms are characterized by retrosternal chest pain, neck pain and swelling, dyspnea, dysphagia, and facial swelling (18).

In general terms, our results reveal that SPM is an uncommon condition resulting from an inflammation of the respiratory tract in COVID-19 patients. No specific data on the incidence of SPM is available at the moment, however, based on the local number of cases, the frequency was calculated in 3.3% of hospitalized COVID-19 patients. It is important to mention that the development of SPM does not increase the risk of death, nor the length of hospital stay.

From the total number of cases of SPM (n = 9), two of them showed a bilateral pneumothorax. One of these patients required invasive mechanical ventilation and died 3 days later. The other patient recovered successfully. Another two patients with SPM required invasive mechanical ventilation after diagnosis and died 3 and 5 days later, respectively. The other 6 patients recovered without mechanical invasive ventilation and were discharged around 16 days after admission.

## CONCLUSION

Development of SPM in COVID-19 patients is becoming an interesting topic nowadays. Information and data from international literature is still not enough to draw conclusions about specific causes, pathology, and outcome. More research and epidemiological data are necessary to make statements regarding this uncommon condition in patients affected by the novel SARS-CoV-2 virus.

## DATA AVAILABILITY STATEMENT

The raw data supporting the conclusions of this article will be made available by the authors, without undue reservation.

## ETHICS STATEMENT

The studies involving human participants were reviewed and approved by this research was performed under permission from the ethics committee, Number 14 CEI 20190123/ COFEPRIS 17 CI 14 039 114. Instituto Mexicano del Seguro Social (IMSS). Written informed consent for participation was not required for

this study in accordance with the national legislation and the institutional requirements.

## AUTHOR CONTRIBUTIONS

All authors: participated directly in the care of COVID-19 patients. TR-A and ES-D: conceptualization, methodology, and writing-original draft preparation. ES-D: data analysis. TR-A, ES-D, JF-M, MA-P, IL-L, AC-N, and HC-G: investigation, formal analysis, validation, and sampling. TR-A, ES-D, JF-M, MA-P, IL-L, and HC-G: chest CT scan analysis. AC-N, TR-A, HC-G, and AB-C: writing-review and editing. AC-N, AB-C, and ES-D: project administration. All authors: have read and agreed to the published version of the manuscript.

## ACKNOWLEDGMENTS

The authors greatly appreciate the efforts made by the healthcare personnel that worked tirelessly in saving several lives. Special thanks to our patients and their families. It was a pleasure to attend to them.

## REFERENCES

1. WHO Coronavirus Disease (COVID-19) Dashboard. World Health Organization. Available online at: <https://covid19.who.int> (accessed March 10, 2021).
2. Li Y, Yao L, Li J, Chen L, Song Y, Cai Z, et al. Stability issues of RT-PCR testing of SARS-CoV-2 for hospitalized patients clinically diagnosed with COVID-19. *J Med Virol.* (2020) 92:903–8. doi: 10.1002/jmv.25786
3. Li Y, Xia L. Coronavirus disease 2019 (COVID-19): role of chest CT in diagnosis and management. *AJR Am J Roentgenol.* (2020) 214:1280–6. doi: 10.2214/AJR.20.22954
4. Tenda ED, Yulianti M, Asaf MM, Yunus RE, Septiyanti W, Wulani V, et al. The importance of chest CT scan in COVID-19. *Acta Med Indones.* (2020) 52:68–73.
5. Bernheim A, Mei X, Huang M, Yang Y, Fayad ZA, Zhang N, et al. Chest CT findings in coronavirus disease-19 (COVID-19): relationship to duration of infection. *Radiology.* (2020) 295:200463. doi: 10.1148/radiol.20200463
6. Prokop M, van Everdingen W, van Rees Vellinga T, Quarles van Ufford H, Stöger L, Beenen L, et al. CO-RADS: a categorical CT assessment scheme for patients suspected of having COVID-19-definition and evaluation. *Radiology.* (2020) 296:E97–104. doi: 10.1148/radiol.202001473
7. Yang Q, Liu Q, Xu H, Lu H, Liu S, Li H. Imaging of coronavirus disease 2019: a Chinese expert consensus statement. *Eur J Radiol.* (2020) 127:109008. doi: 10.1016/j.ejrad.2020.109008
8. Gorospe L, Ayala-Carbonero A, Ureña-Vacas A, Fra Fernández S, Muñoz-Molina GM, Arrieta P, et al. Spontaneous pneumomediastinum in patients with COVID-19: a case series of four patients. *Arch Bronconeumol.* (2020) 56:754–6. doi: 10.1016/j.arbres.2020.06.008
9. Chu CM, Leung YY, Hui JY, Hung IF, Chan VL, Leung WS, et al. Spontaneous pneumomediastinum in patients with severe acute respiratory syndrome. *Eur Respir J.* (2004) 23:802–4. doi: 10.1183/09031936.04.00096404
10. Kouritis VK, Papagiannopoulos K, Lazaridis G, Baka S, Mpoukovinas I, Karavasilis V, et al. Pneumomediastinum. *J Thorac Dis.* (2015) 7(Suppl. 1):S44–9. doi: 10.3978/j.issn.2072-1439.2015.01.11
11. Quincho-Lopez A, Quincho-Lopez DL, Hurtado-Medina FD. Case report: pneumothorax and pneumomediastinum as uncommon complications of COVID-19 pneumonia-literature review. *Am J Trop Med Hyg.* (2020) 103:1170–6. doi: 10.4269/ajtmh.20-0815
12. Kolani S, Houari N, Haloua M, Alaoui Lamrani Y, Boubbou M, Serraj M, et al. Spontaneous pneumomediastinum occurring in the SARS-COV-2 infection. *IDCases.* (2020) 21:e00806. doi: 10.1016/j.idcr.2020.e00806
13. Janssen J, Kamps MJA, Joosten TMB, Barten DG. Spontaneous pneumomediastinum in a male adult with COVID-19 pneumonia. *Am J Emerg Med.* (2020) 40: 228.e3–e5. doi: 10.1016/j.ajem.2020.07.066
14. Sun R, Liu H, Wang X. Mediastinal emphysema, giant bulla, and pneumothorax developed during the course of COVID-19 pneumonia. *Korean J Radiol.* (2020) 21:541–4. doi: 10.3348/kjr.2020.0180
15. Eperjesiova B, Hart E, Shokr M, Sinha P, Ferguson GT. Eperjesiova B, Hart E, Shokr M, Sinha P, Ferguson GT. Spontaneous pneumomediastinum/pneumothorax in patients with COVID-19. *Cureus.* (2020) 12:e8996. doi: 10.7759/cureus.8996
16. Jones E, Gould A, Pillay TD, Khorasane R, Sykes R, Bazo-Alvarez JC, et al. Subcutaneous emphysema, pneumomediastinum, and pneumothorax in critically ill patients with coronavirus disease 2019: a retrospective cohort study. *Crit Care Explorations.* (2020) 2:e0210. doi: 10.1097/CCE.0000000000000210
17. Varela-Patiño M, Torres-Blanco B. Pneumomediastinum and subcutaneous emphysema in relation with SARS-CoV-2 pandemic. *Med Gem Fam.* (2020) 9:162–4. doi: 10.24038/mgyf.2020.026
18. Mohamed W, Exley C, Sutcliffe IM, Dwarakanath A. Spontaneous pneumomediastinum (Hamman's syndrome): presenting as acute severe asthma. *J R Coll Physicians Edinb.* (2019) 49:31–3. doi: 10.4997/JRCPE.2019.106

**Conflict of Interest:** The authors declare that the research was conducted in the absence of any commercial or financial relationships that could be construed as a potential conflict of interest.

Copyright © 2021 Rodríguez-Arciniega, Sierra-Díaz, Flores-Martínez, Alvizo-Pérez, López-Leal, Corona-Nakamura, Castellanos-García and Bravo-Cuellar. This is an open-access article distributed under the terms of the Creative Commons Attribution License (CC BY). The use, distribution or reproduction in other forums is permitted, provided the original author(s) and the copyright owner(s) are credited and that the original publication in this journal is cited, in accordance with accepted academic practice. No use, distribution or reproduction is permitted which does not comply with these terms.





# Contact Tracing in Healthcare Settings During the COVID-19 Pandemic Using Bluetooth Low Energy and Artificial Intelligence—A Viewpoint

Guanglin Tang\*, Kenneth Westover and Steve Jiang

Medical Artificial Intelligence and Automation (MAIA) Laboratory, Department of Radiation Oncology, University of Texas Southwestern Medical Center, Dallas, TX, United States

## OPEN ACCESS

### Edited by:

Reza Lashgari,  
Institute for Research in Fundamental  
Sciences, Iran

### Reviewed by:

Lily Tang,  
Liyfe, United States  
Shima Moein,  
Institute for Research in Fundamental  
Sciences (IPM), Iran

### \*Correspondence:

Guanglin Tang  
Guanglin.Tang@utsouthwestern.edu

### Specialty section:

This article was submitted to  
Medicine and Public Health,  
a section of the journal  
Frontiers in Artificial Intelligence

**Received:** 10 February 2021

**Accepted:** 26 March 2021

**Published:** 23 April 2021

### Citation:

Tang G, Westover K and Jiang S  
(2021) Contact Tracing in Healthcare  
Settings During the COVID-19  
Pandemic Using Bluetooth Low  
Energy and Artificial Intelligence—A  
Viewpoint.  
Front. Artif. Intell. 4:666599.  
doi: 10.3389/frai.2021.666599

The COVID-19 pandemic has inflicted great damage with effects that will likely linger for a long time. This crisis has highlighted the importance of contact tracing in healthcare settings because hospitalized patients are among the high risk for complications and death. Moreover, effective contact tracing schemes are not yet available in healthcare settings. A good contact tracing technology in healthcare settings should be equipped with six features: promptness, simplicity, high precision, integration, minimized privacy concerns, and social fairness. One potential solution that addresses all of these elements leverages an indoor real-time location system based on Bluetooth Low Energy and artificial intelligence.

**Keywords:** COVID-19, deep learning, artificial intelligence, real-time location system, bluetooth, contact tracing, healthcare

## BACKGROUND

As of March, 2021, the COVID-19 pandemic has infected over 115 million people and led to more than 2.5 million deaths worldwide<sup>1</sup>. Presymptomatic and asymptomatic transmission via airborne respiratory droplets and aerosol allows COVID-19 to spread rapidly, leading to deaths and significant economic damage (Huff and Singh, 2020; Pollock and Lancaster, 2020).

Despite extensive measures to control the spread of COVID-19, many researchers believe that it will linger for many years (Kissler et al., 2020). There is no effective treatment for COVID-19 so far, and we may not have one in the near future. Although a few vaccines (Baden et al., 2020; Polack et al., 2020) have been developed recently and obtained emergency use authorization from U.S. Food and Drug Administration (FDA), their availability is currently limited and the deployment to the majority of people may take quite a few months or years. There are also many outstanding questions regarding when herd immunity through natural infection might occur, making it difficult to estimate the cost of such an approach. One prediction based on current death toll data estimates the cost to be ~2.5 deaths per thousand people to achieve herd immunity (Hernandez-Suarez et al., 2020). Emerging COVID variants also make it difficult to predict when COVID-19 will resolve. Worse yet, lack of compliance with social distancing and mask wearing contributed to the deadly winter outbreak of COVID-19 in the US. These factors together suggest that the COVID-19

<sup>1</sup>John Hopkins Corona Virus Resource Center. Available online at: <https://coronavirus.jhu.edu/map.html> (accessed March 2, 2021).

pandemic will remain a threat to the world in a long run and that the main methods of control will be timely testing and self-quarantining of infected individuals.

## PROBLEM AND EXISTING SOLUTIONS

Healthcare settings are a special concern for COVID-19 spread because these areas simultaneously house a high concentration of COVID-19 infected patients and other populations that are at high risk of death should they contract COVID-19. Although the transmission rate of COVID-19 in healthcare settings has not yet been fully characterized, current estimates suggest that 20% of patient infections and 89% of healthcare worker infections have occurred in hospitals (Evans et al., 2020). The U.S. estimates that healthcare workers constitute 5% of the its population but have accounted for 16% of its COVID-19 infections (CDC COVID-19 Response Team, 2020). Healthcare worker infections have a compounding effect because quarantining these workers decreases the healthcare system's capacity. The high rate of asymptomatic infections and the long period of viral shedding create difficult challenges for contact tracing, especially among healthcare providers (Long et al., 2020).

Current manual contact tracing approaches are problematic because of their low precision and long latency in reacting to exposures. In cases of suspected exposures, it takes time, if feasible at all, to contact potentially exposed patients and ask about their activities in healthcare facilities within the last 2 weeks. Moreover, memory is susceptible to failure given these parameters. Manual contact tracing also raises privacy concerns, as some patients may be unwilling to share personal information about their activities. The tracing process is also tedious and slow. Digital approaches based on underlying communications between smartphones via Bluetooth are more attractive than manual approaches because they are simpler, more precise, and more prompt than manual contact tracing. Such approaches can quickly inform people who may have been exposed with automatic messages. These can also provide instructions for follow-up testing and quarantining if a close contact tests positive. To address these problems, a number of smartphone apps have been deployed (Colizza et al., 2021; Rodríguez et al., 2021). However, these approaches have not translated well to healthcare settings and suffer from several drawbacks. In particular, despite efforts to protect privacy, privacy concerns remain regarding use of smartphones for contact tracing, preventing general deployment of this approach. For example, Singapore used such an approach for contact tracing, but it was met with a privacy backlash (Cho et al., 2020). Additionally, this approach relies on personal smartphones. This is problematic given that those at highest are typically older or lower income. Not only does this raise concerns for feasibility, it also raises concerns related to social inequality.

## SOLUTION FRAMEWORK

To effectively deal with these challenges, we propose that healthcare contact tracing approaches should have the following

features: (1) *Promptness*. This aspect is critical for reducing the number of exposures originating from a specific infected patient or healthcare worker. Automation and a streamlined response process are essential to achieving promptness. (2) *Simplicity*. Effortless use and management of the system will reduce human errors and costs, and increase the willingness of patients and healthcare workers to adopt it. Key components of simplicity include well-developed user interfaces and unobstructed communication. (3) *High precision*. Common sense and our current understanding of the data suggest that distance and time are the two factors that influence the viral transmission of COVID-19. For an automated contact tracing solution to give actionable data, it must accurately measure these parameters for interactions between individuals. By their nature, these systems also have the potential to evaluate whether subjects have donned facial masks or shields, which may further refine estimates of transmission probability. (4) *Integrable*. A good contact tracing system should be integrated with electronic healthcare record systems. Healthcare systems are unique in this regard, since they will typically have access to such data. (5) *Private*. Privacy concerns can be major barriers to the adoption of contact tracing techniques, since they lower patients' willingness to get involved. A good contact tracing system in healthcare settings should protect patient or staff privacy and alleviate their concerns about privacy. Possible approaches may include limiting tracing activities to within the hospitals and making system-generated data available to users, without sacrificing privacy. (6) *Fair*. It is socially unfair to exclude some patients because they lack access to certain digital technologies. For example, many older and low-income patients may not have access to smartphones.

## BLUETOOTH LOW ENERGY TECHNOLOGY AND ARTIFICIAL INTELLIGENCE

Although it will be challenging to develop and implement COVID-19 contact tracing systems for healthcare settings that include all of the above features, the current state of technology can provide elegant solutions. A real-time location system (RTLS) based on Bluetooth Low Energy (BLE) and artificial intelligence (Tang et al., 2020) is a good candidate. In this approach, sensors are installed in an array throughout the hospital to measure signals transmitted from small BLE tags worn by patients, visitors, and healthcare workers. With the assistance of a deep learning algorithm, this system can automatically determine interpersonal distance and duration of contacts with great accuracy. Specifically, the trained AI algorithm can compare signals measured by all sensors (so-called fingerprint) of two tags to determine their distance. Considering the temporal dependence of distance (e.g., distance cannot change suddenly because of limited speed), a recurrent neural network (RNN), specifically the Long Short-Term Memory (LSTM) network, which has proved effective in accurately localizing tags in RTLS, is capable of distance tracking. This system also has the potential for integration with the electronic healthcare record and hospital surveillance systems to gather

additional information about patients' demographic and medical information and facial mask/shield wearing compliance to more precisely estimate the infection risk and potential severity of a contact. Concerns about privacy can be alleviated by limiting the technology's use to specific hospital locations and to certain individuals, namely patients, visitors, and healthcare workers. It can be offered to every patient and visitor, whether they own a smartphone or not. It can be highly recommended to all healthcare workers and visitors to maximize effectiveness. Such a technology could be a highly precise, prompt, simple, and socially fair approach to contact tracing in healthcare settings that would have minimal privacy concerns.

In addition to BLE, other technologies have been used for indoor RTLS such as passive RFID (Radio-frequency identification), UWB (Ultra-Wideband), IR (infrared radiation) and Ultrasound. While these technologies also have potential for contact tracing, their shortcomings may prevent their wide clinic applications. For example, UTB and Ultrasound has a low cost-efficiency, and passive RFID and IR has limited range. Comparing to these technologies, BLE is very cost-efficient and has basically no blind spots in clinic settings. On the other hand, BLE also has shortcoming, e.g., relatively low accuracy. However, this has been recently solved by increasing number of sensors and employing deep learning technologies. In the 3-storage radiation oncology building at University of Texas Southwestern Medical Center, a BLE sensor network consisting of 142 sensors each costing ~\$50 with a deep learning algorithm based on LSTM achieved 100% of zone-localization accuracy. The total cost of such a system including hardware, construction, and software development was ~\$10,000 for a 63,000-square-foot facility (Tang et al., 2020).

## REFERENCES

- Baden, L. R., El Sahly, H. M., Essink, B., Kotloff, K., Frey, S., Novak, R., et al. (2020). Efficacy and safety of the mRNA-1273 SARS-CoV-2 vaccine. *N. Engl. J. Med.* 384, 403–416. doi: 10.1056/NEJMoa2035389
- CDC COVID-19 Response Team, (2020). Characteristics of health care personnel with COVID-19 — United States, February 12–April 9, 2020. *MMWR Morb. Mortal. Wkly. Rep.* 69, 477–481. doi: 10.15585/mmwr.mm6915e6
- Cho, H., Ippolito, D., and Yu, Y. W. (2020). Contact tracing mobile Apps for COVID-19: privacy considerations and related trade-offs. *arXiv:2003.11511*.
- Colizza, V., Grill, E., Mikolajczyk, R., Cattuto, C., Kucharski, A., Riley, S., et al. (2021). Time to evaluate COVID-19 contact-tracing apps. *Nat. Med.* 27, 361–362. doi: 10.1038/s41591-021-01236-6
- Evans, S., Agnew, E., Vynnycky, E., and Robotham, J. V. (2020). The impact of testing and infection prevention and control strategies on within-hospital transmission dynamics of COVID-19 in English hospitals. *medRxiv [Preprint]*. doi: 10.1101/2020.05.12.20095562
- Hernandez-Suarez, C., Murillo-Zamora, E., and Espinoza-Gomez, F. (2020). COVID-19 pandemics: how far are we from herd immunity? *medRxiv [Preprint]*. doi: 10.1101/2020.12.19.20248571
- Huff, H. V., and Singh, A. (2020). Asymptomatic transmission during the coronavirus disease 2019 pandemic and implications for public health strategies. *Clin. Infect. Dis.* 71, 2752–2756. doi: 10.1093/cid/ciaa654
- Kissler, S. M., Tedijanto, C., Lipsitch, M., and Grad, Y. (2020). Social distancing strategies for curbing the COVID-19 epidemic. *medRxiv [Preprint]*. doi: 10.1101/2020.03.22.20041079

## CONCLUSION

The COVID-19 pandemic has continued for over a year, infecting and killing millions of people. Many individuals are still at risk, and reinfection is known to happen, so it is likely that the pandemic will linger. Effective contact tracing technologies are urgently needed for healthcare settings that contain a high concentration of older adults and people with underlying conditions that increase the risks of COVID-19 infection. However, existing or currently proposed contract tracking technologies suffer from major challenges such as privacy concerns and limited access to the economically disadvantaged. A good contact tracing technology for healthcare settings should satisfy six requirements: promptness, simplicity, high precision, integrable, private, and fair.

Based on the success of using BLE and deep learning for accurate localization by RTLS, this technology can readily be adapted to contact tracing in healthcare settings. Such a system would meet the six requirements we propose as part of a good contact tracing technology in healthcare settings. We believe that such technology will not only be useful in controlling COVID-19, it is generally applicable to other infectious diseases.

## DATA AVAILABILITY STATEMENT

The original contributions presented in the study are included in the article/supplementary material, further inquiries can be directed to the corresponding author/s.

## AUTHOR CONTRIBUTIONS

All authors listed have made a substantial, direct and intellectual contribution to the work, and approved it for publication.

- Long, Q.-X., Tang, X.-J., Shi, Q.-L., Li, Q., Deng, H.-J., Yuan, J., et al. (2020). Clinical and immunological assessment of asymptomatic SARS-CoV-2 infections. *Nat. Med.* 26, 1200–1204. doi: 10.1038/s41591-020-0965-6
- Polack, F. P., Thomas, S. J., Kitchin, N., Absalon, J., Gurtman, A., Lockhart, S., et al. (2020). Safety and efficacy of the BNT162b2 mRNA Covid-19 vaccine. *N. Engl. J. Med.* 383, 2603–2615. doi: 10.1056/NEJMoa2034577
- Pollock, A. M., and Lancaster, J. (2020). Asymptomatic transmission of covid-19. *BMJ* 371:m4851. doi: 10.1136/bmj.m4851
- Rodríguez, P., Graña, S., Alvarez-León, E. E., Battaglini, M., Darias, F. J., Hernán, M. A., et al. (2021). A population-based controlled experiment assessing the epidemiological impact of digital contact tracing. *Nat. Commun.* 12:587. doi: 10.1038/s41467-020-20817-6
- Tang, G., Yan, Y., Shen, C., Jia, X., Zinn, M., Trivedi, Z., et al. (2020). Development of a real-time indoor location system using bluetooth low energy technology and deep learning to facilitate clinical applications. *Med. Phys.* 48, 3277–3285. doi: 10.1002/mp.14198

**Conflict of Interest:** The authors declare that the research was conducted in the absence of any commercial or financial relationships that could be construed as a potential conflict of interest.

Copyright © 2021 Tang, Westover and Jiang. This is an open-access article distributed under the terms of the Creative Commons Attribution License (CC BY). The use, distribution or reproduction in other forums is permitted, provided the original author(s) and the copyright owner(s) are credited and that the original publication in this journal is cited, in accordance with accepted academic practice. No use, distribution or reproduction is permitted which does not comply with these terms.



# How Genetics Might Explain the Unusual Link Between Malaria and COVID-19

Marta Rusmini<sup>1,2†</sup>, Paolo Uva<sup>1,2†</sup>, Antonio Amoroso<sup>3</sup>, Manlio Tolomeo<sup>4</sup> and Andrea Cavalli<sup>1,5\*</sup>

<sup>1</sup> Computational and Chemical Biology, Italian Institute of Technology, Genova, Italy, <sup>2</sup> Istituto di Ricovero e Cura a Carattere Scientifico (IRCCS) G. Gaslini, Genova, Italy, <sup>3</sup> Department of Medical Sciences, University of Turin, Turin, Italy, <sup>4</sup> Department of Health Promotion Sciences, Azienda Ospedaliera Universitaria Policlinico Paolo Giaccone, Palermo, Italy, <sup>5</sup> Department of Pharmacy and Biotechnology, University of Bologna, Bologna, Italy

## OPEN ACCESS

### Edited by:

Reza Lashgari,  
Institute for Research in Fundamental  
Sciences, Iran

### Reviewed by:

Filippo Biscarini,  
National Research Council (CNR), Italy  
Simone Furini,  
University of Siena, Italy

### \*Correspondence:

Andrea Cavalli  
andrea.cavalli@iit.it

<sup>†</sup>These authors have contributed  
equally to this work

### Specialty section:

This article was submitted to  
Infectious Diseases - Surveillance,  
Prevention and Treatment,  
a section of the journal  
Frontiers in Medicine

**Received:** 06 January 2021

**Accepted:** 24 March 2021

**Published:** 26 April 2021

### Citation:

Rusmini M, Uva P, Amoroso A,  
Tolomeo M and Cavalli A (2021) How  
Genetics Might Explain the Unusual  
Link Between Malaria and COVID-19.  
Front. Med. 8:650231.  
doi: 10.3389/fmed.2021.650231

Severe acute respiratory syndrome coronavirus 2 (SARS-CoV-2)-associated coronavirus disease 2019 (COVID-19) pandemic has been the subject of a large number of studies in recent times. Here, starting from the evidence that in Italy, the areas with the lowest number of COVID-19 cases were those with the highest incidence of malaria in the early 1900's, we explore possible inverse relationships between malaria and COVID-19. Indeed, some genetic variants, which have been demonstrated to give an advantage against malaria, can also play a role in the incidence and severity of SARS-CoV-2 infections (e.g., the ACE2 receptor). To verify this scientific hypothesis, we here use public data from whole-genome sequencing (WGS) experiments to extrapolate the genetic information of 46 world populations with matched COVID-19 data. In particular, we focus on 47 genes, including ACE2 and genes which have previously been reported to play a role in malaria. Only common variants (>5%) in at least 30% of the selected populations were considered, and, for this subset, we correlate the intra-population allele frequency with the COVID-19 data (cases/million inhabitants), eventually pinpointing meaningful variants in 6 genes. This study allows us to distinguish between positive and negative correlations, i.e., variants whose frequency significantly increases with increasing or decreasing COVID-19 cases. Finally, we discuss the possible molecular mechanisms associated with these variants and advance potential therapeutic options, which may help fight and/or prevent COVID-19.

**Keywords:** malaria, COVID-19, genomics, whole-genome sequencing analysis, epidemiology

## INTRODUCTION

Severe acute respiratory syndrome coronavirus 2 (SARS-CoV-2)-associated coronavirus disease 2019 (COVID-19) has gripped the world in a pandemic, challenging its healthcare infrastructure, economy, and culture. In the last months, the epidemic moved from Europe to other parts of the World, growing very rapidly in Latin America, USA, and India. In Africa, the impact of COVID-19 is worrying the whole world due to the precariousness of the healthcare system with limited financial resources and scarcity of solid infrastructures and trained health workers (1). Additionally, COVID-19 immune-response and symptoms, including fever, fatigue, headache, gastrointestinal issues, etc., are very similar to those of malaria and other infections, which are endemic in many sub-Saharan areas. This may lead to a delayed diagnosis and make the access to health facilities



more difficult. However, despite the fear and the alert about sub-Saharan countries, SARS-CoV-2 has not hit malaria-endemic regions so strongly as everyone would have expected (2). These observations prompted us to analyze from the epidemiological and genetic standpoints possible links between malaria and COVID-19.

Previous studies have shown an inverse relationship between the number of COVID-19 cases and cases of malaria (3–6). Three of the African countries most affected by COVID-19 on June 4, 2020 are South Africa (37,525 cases and 792 deaths), Algeria (9,733 cases and 673 deaths) and Egypt (28,615 cases and 1,088 deaths), which belong to the countries historically less affected by malaria (7). This has been reported to be due to prophylaxis with chloroquine and hydroxychloroquine, which however have shown limited efficacy in COVID-19 (8). Furthermore, a recent publication confirmed a lower risk of COVID-19 in malaria-endemic areas and, albeit with an underlying mechanism that has yet to be investigated, they identified shared immunodominant epitopes between SARS-CoV-2 and *P. falciparum* antigens (9). Against this scenario, here we aim to investigate this inverse relationship, from a genetic point of view.

Humans have been infected by and co-evolved with malaria for over 50,000 years (since the estimated date for the out-of-Africa migration) (10). Different human polymorphisms have been associated with this natural selection process (11). For example, hypertension confers an evolutionary advantage and protection for populations chronically exposed to malaria infections. Epidemiological data indicate that people with African background have a higher prevalence of hypertension compared to whites coming from malaria-free areas (12, 13). Hypertension could actually protect people from developing cerebral malaria, and angiotensin II is the key molecular effector in the hypertension-malaria relationship (14). Angiotensin II levels tend to be higher in populations living in malaria-endemic areas, and preclinical studies have shown that angiotensin II could inhibit the plasmodium growth and erythrocyte invasion (12). The angiotensin-converting enzyme 2 (ACE2) degrades angiotensin II to generate angiotensin 1-7, which acts as a vasodilator. Therefore, low levels of ACE2 cause an increase in angiotensin II and hypertension, and a natural selection process may have produced the association between ACE2 polymorphisms and protection from severe malaria (15).

The ACE2 gene is located on the X chromosome and several single-nucleotide polymorphisms (SNPs) within the ACE2 gene have been reported. For instance, the ACE2 rs2106809 T allele in intron 1 has been associated with reduced expression of the ACE2 enzyme (16). A recent finding has shown that the “D” allele of ACE I/D polymorphism, responsible for increased angiotensin II production, has a significant association with mild malaria, and the ACE2 rs2106809 T allele has gender specific effect with reduced expression of ACE2 in presence of “T” allele in women. This leads to increased level of angiotensin II and hence protection against severe, cerebral malaria (15). Remarkably, it has clearly been demonstrated that ACE2 is the major host cell receptor responsible for introducing SARS-CoV-2 into the human body (17).

The observations on ACE2 polymorphism suggest that a genetic predisposition could be worth to be investigated with the final objective to discover other common variations in the genome that could explain the low incidence of COVID-19 in areas where malaria is endemic. Indeed, while SARS-CoV-2 has infected humanity for only less than a year, for tens of thousands of years humans have been confronted with the pathogens responsible for malaria, and therefore natural selection has promoted the genetic variants of greater resistance to the disease.

Based on these preliminary observations, here we first evaluate whether the spread of SARS-CoV-2 infection in the Italian regions is actually different in relation to the historical presence of malaria. Then, we investigate a list of genes linked to positive/negative responses to malaria, using whole genome sequencing (WGS) data from different populations scattered around the world. Only variants with allele frequency (AF) > 5% in at least 30% of the selected populations were considered. For this subset, we subsequently correlate the intra-population allele frequency with the COVID-19 data (cases/million inhabitants) in the first wave (from the beginning of the pandemic to 13th July 2020). In this way, we could identify positive and negative correlations, i.e., variants whose frequency significantly increases with increasing or decreasing COVID-19 cases, hence discovering putative genetic links between malaria and COVID-19. These genetic variants led subsequently us to investigate novel mechanisms, which may help more in-depth understanding the physiopathology and the complexity of COVID-19. Studying these molecular mechanisms, we eventually propose potential novel therapeutic options to combat and/or prevent the spread of SARS-CoV-2 infections.

## METHODS

### Datasets

The incidence of malaria at the beginning of 20th century in Italy was reported as the number of deaths for malaria per million inhabitants in 1910, based on the Italian National Report on Causes of deaths (18) and the Italian Historical Statistical Repository (19). In particular, we considered deaths for malaria the total number of deaths for “malarial fever” and “marsh cachexia.” COVID-19 cases for the Italian provinces were obtained from the COVID-19 Italian Data Repository, maintained by the Italian Civil Protection Department (20).

Whole-genome genotyping data of 969 worldwide healthy people from 54 diverse human populations were obtained from the Human Genome Diversity (HGDP) project as VCF files (21). COVID-19 data reported on July 13th, 2020 from the COVID-19 Data Repository at the John Hopkins University (12) were analyzed. Populations with genotyping data were mapped to COVID-19 data according to geographic coordinates available at the HGDP website (22) and at the COVID-19 Data Repository and manually refined as follows: populations with similar coordinates in both repositories were matched. In cases where two populations were geographically very close, the COVID-19 or genetic data were aggregated in order to guarantee a geographical correspondence as reliable as possible. The final set, used for downstream analysis consists of 46 populations for

**TABLE 1** | Overview of the 46 HGDP populations selected for the study.

| Population       | Number of individuals | Population      | Number of individuals |
|------------------|-----------------------|-----------------|-----------------------|
| Adygei           | 16                    | Mbuti           | 13                    |
| Balochi          | 24                    | Miao            | 10                    |
| BantuSouthAfrica | 8                     | Mongolian       | 9                     |
| Basque           | 22                    | Mozabite        | 27                    |
| Bedouin          | 46                    | Naxi            | 8                     |
| Bergamoltalian   | 11                    | NorthernHan     | 10                    |
| Biaka            | 22                    | Orcadian        | 15                    |
| Bougainville     | 11                    | Oroqen          | 9                     |
| Brahui           | 25                    | Palestinian     | 46                    |
| Cambodian        | 7                     | PapuanHighlands | 9                     |
| Colombian        | 7                     | PapuanSepik     | 8                     |
| Dai              | 9                     | Pathan          | 24                    |
| Daur             | 9                     | Pima            | 13                    |
| Druze            | 42                    | Russian         | 25                    |
| French           | 28                    | San             | 6                     |
| Han              | 33                    | Sardinian       | 28                    |
| Hazara           | 19                    | She             | 10                    |
| Hezhen           | 9                     | Surui           | 8                     |
| Japanese         | 27                    | Tu              | 10                    |
| Karitiana        | 12                    | Tujia           | 9                     |
| Lahu             | 8                     | Tuscan          | 8                     |
| Mandenka         | 22                    | Yi              | 10                    |
| Maya             | 21                    | Yoruba          | 22                    |

The number of whole genome sequences available for each population is shown. These populations geographically reside in areas for which the number of COVID-19 cases is available.

which both data were available for a total of 786 individuals as reported in **Table 1**.

## Time Frame for Selection of COVID-19 Cases

The analysis of Italian provinces and worldwide populations started with COVID-19 data collected in the so-called “first wave,” i.e., from the beginning of the pandemic until mid-July 2020. In order to confirm the results obtained from the “first wave,” COVID-19 cases between 1st November 2020 and 15th February 2021, known as “second wave,” were also considered.

## Genes and Variants Selection

Forty-seven genes were considered in the present study. In particular, in addition to the ACE2 gene we selected (i) all the genes reported in Online Mendelian Inheritance in Man (OMIM) database (23) as related to the susceptibility/resistance to malaria; (ii) genes in known malaria resistance loci (24); (iii) genes with a role in the inflammatory pathway activated by malaria (25) (**Table 2**). Starting from 67.3 million single-nucleotide polymorphisms from the Whole Genome Sequencing data (21), the selected 47 genes from 46 populations were considered, thus reducing the number of variants to 42,978. Variants were annotated with VEP and custom scripts. The annotation includes the allele frequency of the variants in each of the 46 populations, the allele frequencies in healthy individuals (Gnomad v2.1), the effect of the variants on proteins and the

expression Quantitative Trait Loci (eQTLs) data reported on the Genotype-Tissue Expression portal (GTEx Analysis Release V8), showing the effect of each variant in the context of gene expression across different tissues, and the estimates of the effect size (slope coefficient). To pinpoint variants that regulate the transcription of genes, also according to the clinical aspects of COVID-19, only variants with extreme slope coefficients (i.e., outside the interquartile range) in at least four tissues, including lung, were considered at the end.

## Statistical Analysis

The Spearman's correlation has been used to compute the correlation between COVID-19 cases/10<sup>6</sup> inhabitants and (i) malaria prevalence in Italy (i.e., number of deaths for malaria/10<sup>6</sup> inhabitants), (ii) AF of the variants in each population (i.e., fraction of all the alleles in the population that carry the variant). This test assesses the monotonic relationship (whether linear or not) between two variables and is less sensitive to the presence of outliers.

To correct for multiple testing, FDR adjusted *p*-values were obtained using the Benjamini & Hochberg method implemented in *p.adjust* R function. All the analyses were performed in R.

## Linkage Disequilibrium Analysis

Haploview (26) was used to identify variants in Linkage Disequilibrium (LD). First, variants in VCF format were converted by vcftools (27) in the input format required

**TABLE 2 |** List of the genes included in the study.

| Gene    | Chr   | Start     | End       | OMIM entry | Phenotype (OMIM)                                   | Reference |
|---------|-------|-----------|-----------|------------|--|-----------|
| ABO     | chr9  | 133255602 | 133275214 | 110300     | Blood group, ABO system                            | (24)      |
| ACKR1   | chr1  | 159203307 | 159206498 | 613665     | Blood group, Duffy system                          | (24)      |
| ADORA2B | chr17 | 15944917  | 15975746  | 612446     |  | (24)      |
| ATP2B4  | chr1  | 203626561 | 203744081 | 613665     | Protection against malaria vivax                   | (24)      |
| C6      | chr5  | 41142234  | 41261438  | 217050     |  | (24)      |
| CD36    | chr7  | 80369575  | 80674409  | 173510     | Susceptibility to/reduced risk of cerebral malaria | (24)      |
| CD40LG  | chrX  | 136648193 | 136660390 | 308230     |  | (24, 25)  |
| CISH    | chr3  | 50606522  | 50611831  | 602441     | Susceptibility to malaria                          |           |
| CR1     | chr1  | 207496268 | 207639409 | 120620     | Resistance to severe malaria                       | (24, 25)  |
| FCGR2A  | chr1  | 161505430 | 161518558 | 146790     | Susceptibility to severe malaria                   |           |
| FCGR2B  | chr1  | 161663161 | 161678654 | 604590     | Resistance to malaria                              |           |
| FUT9    | chr6  | 96015974  | 96215612  | 606865     | Susceptibility to placental malarial infection     |           |
| G6PD    | chrX  | 154532000 | 154547572 | 305900     | Resistance to malaria due to G6PD deficiency       | (24)      |
| GNAS    | chr20 | 58841622  | 58909188  |            |  | (24)      |
| GYPA    | chr4  | 144109304 | 144140751 | 617922     | Resistance to malaria                              |           |
| GYPB    | chr4  | 143996106 | 144019339 | 617923     | Resistance to malaria                              |           |
| GYPC    | chr2  | 126656158 | 126696667 | 110750     | Resistance to malaria                              |           |
| HBB     | chr11 | 5225464   | 5227197   | 141900     | Resistance to malaria                              | (24)      |
| HMOX1   | chr22 | 35381096  | 35394207  |            |  | (25)      |
| ICAM1   | chr19 | 10271120  | 10286615  | 147840     | Susceptibility to cerebral malaria                 | (24)      |
| IFNA17  | chr9  | 21227243  | 21228222  |            |  | (25)      |
| IFNAR1  | chr21 | 33324970  | 33359864  |            |  | (25)      |
| IFNB1   | chr9  | 21077104  | 21077942  |            |  | (25)      |
| IFNG    | chr12 | 68154768  | 68159740  |            |  | (25)      |
| IL10    | chr1  | 206767602 | 206772494 |            |  | (24)      |
| IL13    | chr5  | 132658173 | 132661110 |            |  | (24)      |
| IL1A    | chr2  | 112773915 | 112784590 |            |  | (24)      |
| IL1B    | chr2  | 112829751 | 112836779 |            |  | (24)      |
| IL22    | chr12 | 68248242  | 68253604  |            |  | (24)      |
| IL4     | chr5  | 132673989 | 132682678 |            |  | (24, 25)  |
| IRF1    | chr5  | 132481609 | 132490773 |            |  | (24, 25)  |
| LTA     | chr6  | 31572054  | 31574324  |            |  | (24)      |
| NCR3    | chr6  | 31588895  | 31593006  | 611550     | Susceptibility to mild malaria                     |           |
| NOS2A   | chr17 | 27756766  | 27800529  | 163730     | Resistance to malaria                              | (25)      |
| PECAM1  | chr17 | 64319415  | 64390860  |            |  | (25)      |
| RNASE3  | chr14 | 20891399  | 20892348  |            |  | (25)      |
| SLC4A1  | chr17 | 44248390  | 44268135  | 109270     | Resistance to malaria                              |           |
| SPTB    | chr14 | 64746283  | 64879907  |            |  | (24)      |
| TGFB2   | chr1  | 218345284 | 218444619 |            |  | (25)      |
| TIRAP   | chr11 | 126283087 | 126294933 | 606252     | Protection against malaria                         |           |
| TLR1    | chr4  | 38796255  | 38804791  |            |  | (24, 25)  |
| TLR4    | chr9  | 117704403 | 117724735 |            |  | (24, 25)  |
| TLR5    | chr1  | 223109404 | 223143248 |            |  | (25)      |
| TLR6    | chr4  | 38823715  | 38856817  |            |  | (24)      |
| TLR9    | chr3  | 52221080  | 52226163  |            |  | (24, 25)  |
| TNF     | chr6  | 31575565  | 31578336  | 191160     | Susceptibility to cerebral malaria                 | (24, 25)  |
| ACE2    | chrX  | 15561033  | 15602069  |            |  |           |

Genes are reported with gene symbol, chromosome, start and end genomic position (hg38 coordinates). The MIM number is reported for all the genes associated with malaria in OMIM, and the corresponding phenotype if present. Two other publications were investigated to complete the list, as reported in the last column ("Reference").

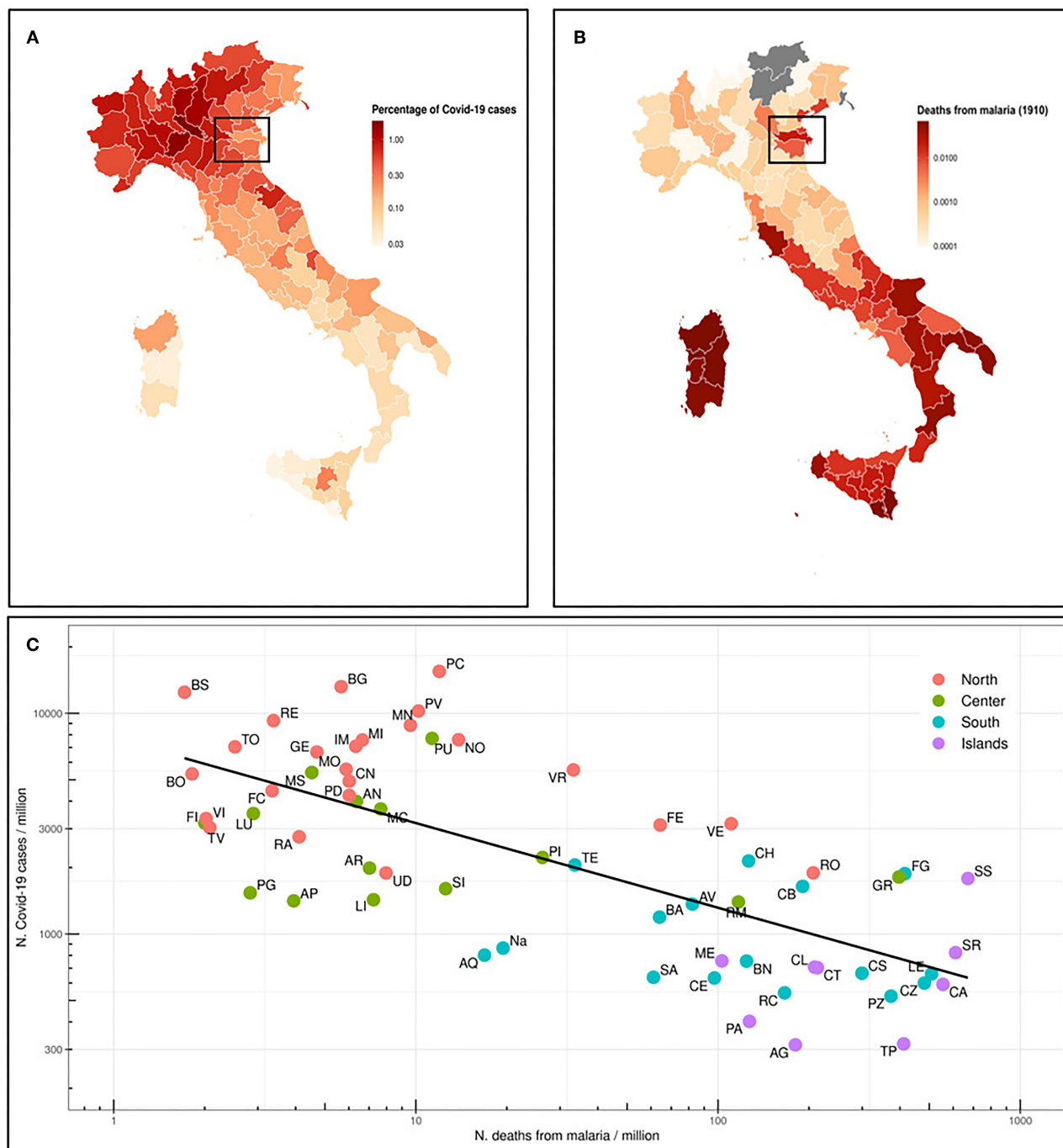


**FIGURE 1 | (A)** Map of the Italian provinces and representation as colorimetric scale of the percentage of deaths for malaria in 1910 (data not available for those provinces that were not included in the Italian Kingdom). The box highlights Ferrara and Rovigo provinces. **(B)** Map of the Italian provinces and the relative percentage of COVID-19 cases as n. COVID-19 cases/10<sup>6</sup> inhabitants in the province (situation on July 13th, 2020). **(C)** Prevalence of COVID-19 cases (n. cases/10<sup>6</sup> inhabitants) in Italian provinces (July 13th, 2020) vs. number of deaths from malaria in 1910. The regression line of log10 transformed values is shown. Spearman  $\rho = -0.69$  and  $p$ -value  $5.4 \times 10^{-10}$ .

by Haploview (26). Only common variants, significantly correlated with COVID19 cases, selected as described above and considered divided for chromosomes, were retained for Haploview analysis, using default parameters. Furthermore,

an application of Haploview, named Tagger (28), has been used on all the single nucleotide variants (SNVs) to identify tag SNVs, i.e. SNVs which are representative of a group of SNVs in LD.



## RESULTS

### The Italian Case: The Inverse Correlation Between Malaria and COVID-19

We first analyzed the situation in Italy, where malaria was endemic until the late 1950's, and therefore prophylaxis strategies have been abandoned several years ago. The Italian regions most affected by malaria were Sardinia, Sicily and other regions in Southern Italy, South Lazio, and the river Po delta (29). In **Figure 1A**, we represent the percentage of deaths from malaria in 1910 (18) in the current Italian provinces. We also map the percentage of COVID-19 cases as of July 13th, 2020, for the same provinces (**Figure 1B**) and we correlate both data in **Figure 1C**. A quite strong inverse correlation (Spearman  $\rho = -0.69$ ,  $p = 5.4E-10$ ) has been found. Indeed, COVID-19 distribution is clear, with Northern Italy far more affected than Southern Italy. Sicily and Sardinia, along with other regions in Southern Italy, have the lowest number of registered cases, whereas most of Northern Italy is greatly affected by SARS-CoV-2. Interestingly enough, the percentage of COVID-19 cases in Ferrara and Rovigo is much lower than in the rest of the North, and these areas were historically marshy, with a high incidence of malaria (box in **Figures 1A,B**).

### Genes and Variants Selected

42,978 variants at the 47 genes selected (see **Table 2**) were used for the analysis. Since the purpose of the study was to identify common susceptibility genetic elements that could help to understand the inverse correlation thus identified, rare variants were discarded. In particular, only 1,411 Single Nucleotide Variants (SNVs) with an allele frequency  $> 5\%$  in at least 30% of the populations in this study, were considered. Among these, 81 variants strongly correlated ( $FDR < 0.01$ ) with COVID-19 prevalence (n. cases/ $10^6$  inhabitants) were further investigated and classified based on their positive or negative correlation with COVID-19 cases.

Given the similar allele frequency of many variants throughout the populations, we performed a linkage disequilibrium (LD) analysis to identify blocks of variants in LD and we selected the tag SNVs in LD that could capture the other alleles, leading to a final number of 25 and 16 representative SNVs for positive and negative correlations, respectively (**Tables 3A,B**). All the genes reported are described in **Table 4**.

To focus on SNVs with a potential effect of gene expression, the GTEx database was interrogated to filter variants which were eQTLs. **Table 5** lists the 21 variants in five malaria genes and two variants in the ACE2 gene, that were finally selected: these are common variants, with an allele frequency in the studied population significantly correlated to COVID-19 cases (positively or negatively) and eQTLs in at least four tissues including lung.

Excepted for the two variants in ACE2, all the other variants in the same gene were in LD and could be, therefore, considered together (**Table 5**). Only one missense variant was identified, named rs7683365 in the GYPB gene. All the others are intronic variants. The last three columns of **Table 5** report the genes which are modulated by the variants and the effect on their expression

in lung and whole blood. A concordance of the expression change between the two tissues has been noticed for all the variants except for rs8081547 in ADORA2B gene that increases the expression of the CENPV in lung but has an opposite effect in whole blood.

Among the variants whose frequency positively correlates with COVID-19 cases, we identified (i) two variants at FCGR2A gene which may potentially decrease the expression of FCGR2C and HSPA7, (ii) one variant in IRF1 gene which may upregulate SLC22A, (iii) a variant in ADORA2B which increases the mRNA expression of CENPV gene in lung, and (iv) 9 variants in GYPB (see below).

Variants with inverse correlation with COVID-19 cases include a variant in ABO which increases the expression of its transcript, and the two unrelated variants in ACE2 which may potentially increase the expression of PIR mRNA in both lung and blood.

Particular attention must be paid to the variants of GYPB. Actually, some of these variants positively correlate with COVID-19 cases and increase the expression of GYPE. Others that negatively correlate with COVID-19 determine a reduction in the transcripts of FREM and GYPE. This contradiction can be interpreted by assuming that variants positively correlated with the cases of disease induce an increase in protein expression, exerting their putative risk effect for COVID-19. Conversely, the negatively correlated, and therefore protective variants, exert their effect by decreasing FREM expression, rather than decreasing GYPE.

SNVs in SPTB gene were not considered, since they resulted associated both positively and negatively with COVID-19 cases, all with eQTL with positive slopes. Variants thus selected are reported in **Figure 2**.

### Comparison With COVID-19 Cases From the Second Wave

The analysis of the correlation between Italian COVID-19 cases and deaths for malaria was also performed with the COVID-19 cases in the second wave (1st November 2020–15th February 2021), and we confirmed the correlation already observed (Spearman  $\rho = -0.53$ ,  $p$ -value  $1.2E-5$ ). Similarly, the significant trend between allele frequencies and COVID-19 cases worldwide observed for the 8 SNVs in the first wave was corroborated by the data from the second wave (Spearman  $FDR$  ranges from  $1.6E-04$  to  $3.3E-09$ ).

## DISCUSSION

In this study, we show that in the Italian population, the spread of SARS-CoV-2 in the first wave (until mid-July 2020) was more limited in the provinces where malaria was endemic at the beginning of the 20th century. Indeed, a highly significant inverse correlation emerged between COVID-19 cases and malaria mortality in 1910. A possible confounding factor could derive from the fact that the spread of SARS-CoV-2 is slightly greater in the northern Italian regions, while the malaria was endemic especially in the coasts of central and southern Italy. However, it

**TABLE 3** | List of variants with (A) positive and (B) negative correlation (FDR < 0.01).

| rs ID      | Location              | Allele | Consequence | Gene symbol | FDR (Spearman) | Captured alleles (Tagger)  |
|------------|-----------------------|--------|-------------|-------------|----------------|--|
| <b>A</b>   |                       |        |             |             |                |  |
| rs3027012  | 1:159204333-159204333 | T      | 5' UTR      | ACKR1       | 0.000119       | rs3027008, rs6676002   |
| rs72717040 | 1:161517662-161517662 | C      | Intronic    | FCGR2A      | 0.004313       | rs17400517   |
| rs7683365  | 4:143999443-143999443 | A      | Missense    | GYPB        | 0.000161       | rs7662277, rs7666297, rs7666296, rs12499907, rs12499906, rs10002395, rs10025455, rs7661933 |
| rs17622656 | 5:132485305-132485305 | A      | Intronic    | IRF1        | 0.002085       |  |
| rs2770146  | 9:117711060-117711060 | C      | Intronic    | TLR4        | 0.000303       | rs5030728  |
| rs2285002  | 14:64816958-64816958  | A      | Intronic    | SPTB        | 0.005651       |  |
| rs12587471 | 14:64825597-64825597  | G      | Intronic    | SPTB        | 0.004638       | rs11158561, rs4899147  |
| rs7149121  | 14:64864227-64864227  | C      | Intronic    | SPTB        | 0.000360       |  |
| rs28370916 | 14:64879376-64879376  | G      | Intronic    | SPTB        | 0.008414       |  |
| rs8081235  | 17:15964787-15964787  | T      | Intronic    | ADORA2B     | 0.001541       |  |
| rs8081547  | 17:15965007-15965007  | T      | Intronic    | ADORA2B     | 0.000487       |  |
| <b>B</b>   |                       |        |             |             |                |  |
| rs6840234  | 4:143996657-143996657 | C      | intronic    | GYPB        | 0.000468       | rs6857129, rs4835127, rs1473055, rs6537238, rs4835126, rs6816184                           |
| rs8176725  | 9:133257230-133257230 | A      | intronic    | ABO         | 0.009139       |  |
| rs74056021 | 14:64802733-64802733  | C      | intronic    | SPTB        | 0.001538       | rs74056022, rs45617438   |
| rs1535450  | 14:64840590-64840590  | T      | intronic    | SPTB        | 0.003294       | rs1475101  |
| rs28998799 | 17:27799104-27799105  | -      | intronic    | NOS2        | 0.000173       |  |
| rs4646120  | X:15599613-15599613   | A      | intronic    | ACE2        | 0.006377       |  |
| rs1978124  | X:15599940-15599940   | C      | intronic    | ACE2        | 0.001095       |  |

The first column "rsID" indicates the tag SNVs. "Location" column indicates chromosome and position in the Human Reference Genome Hg38; "Allele" column is the variant allele, "Consequence" column represents the impact of the variant (rsID) on the protein, and the "Gene symbol" is the gene where the variant is located. In "FDR (Spearman)" the FDR value for each SNVs has been reported (data from the first wave). The last column "Captured alleles (Tagger)" displays the rs number of all the SNVs in linkage disequilibrium with the tag SNV, according to Tagger analysis.

is interesting to note that in some areas, such as in the provinces of Ferrara and Rovigo, located in the Po river delta and areas of malarial endemic, the spread of SARS-CoV-2 is much lower than in the neighboring provinces. These data have led to the hypothesis that some genetic variants, positively selected because of advantage against malaria, could also confer greater resistance to SARS-CoV-2 infection and thus explain the lower spread of the virus in the malarial areas.

A bioinformatic analysis of public worldwide WGS data led to the final identification of variants in 6 malaria related genes, whose frequency is significantly associated to the incidence of COVID-19 cases. Indeed, some of these genes have already been identified by case control studies as associated with COVID-19, while for the others a direct evidence for a role in SARS-CoV-2 infections or in the progression/severity of COVID-19 has never been reported in the literature.

We are aware that several factors could affect our observations. First, given the lack of genomic data from COVID-19 cases in malarial regions, we leveraged allele frequencies from healthy populations worldwide to highlight significant trends between MAF of variants in malarial genes and the prevalence of SARS-COV-2. In particular, variants from

whole genome sequencing come from the Human Genome Diversity Project (HGDP) where, for each population, the approximate geographical place of origin was indicated by its latitude and longitude. Similarly, COVID-19 cases downloaded from the John Hopkins repository were annotated with latitude and longitude. We matched populations with similar coordinates in both datasets and, in cases where two populations were geographically very close, the COVID-19 or genetic data were aggregated in order to guarantee a geographical correspondence as reliable as possible. The final set used for downstream analysis consists of 46 populations for which both data were available. This approach does not take into account differences within countries (except for Italy and malaria) but we aimed at discovering global trends across populations worldwide. Although this is an indirect approach, several promising variants have emerged. Second, some of the subpopulations had a small sample size. Although they contribute to the estimate of the global genetic variability, the AF may not be representative of the population they belong to. The availability of multiple populations, and the use of a robust correlation, which is less sensitive to outliers, should mitigate this issue. Finally, in this study, we focused on the time frame corresponding to the

**TABLE 4 |** List of genes with variants significantly (FDR < 0.01) correlated (positively or negatively) to COVID-19 cases.

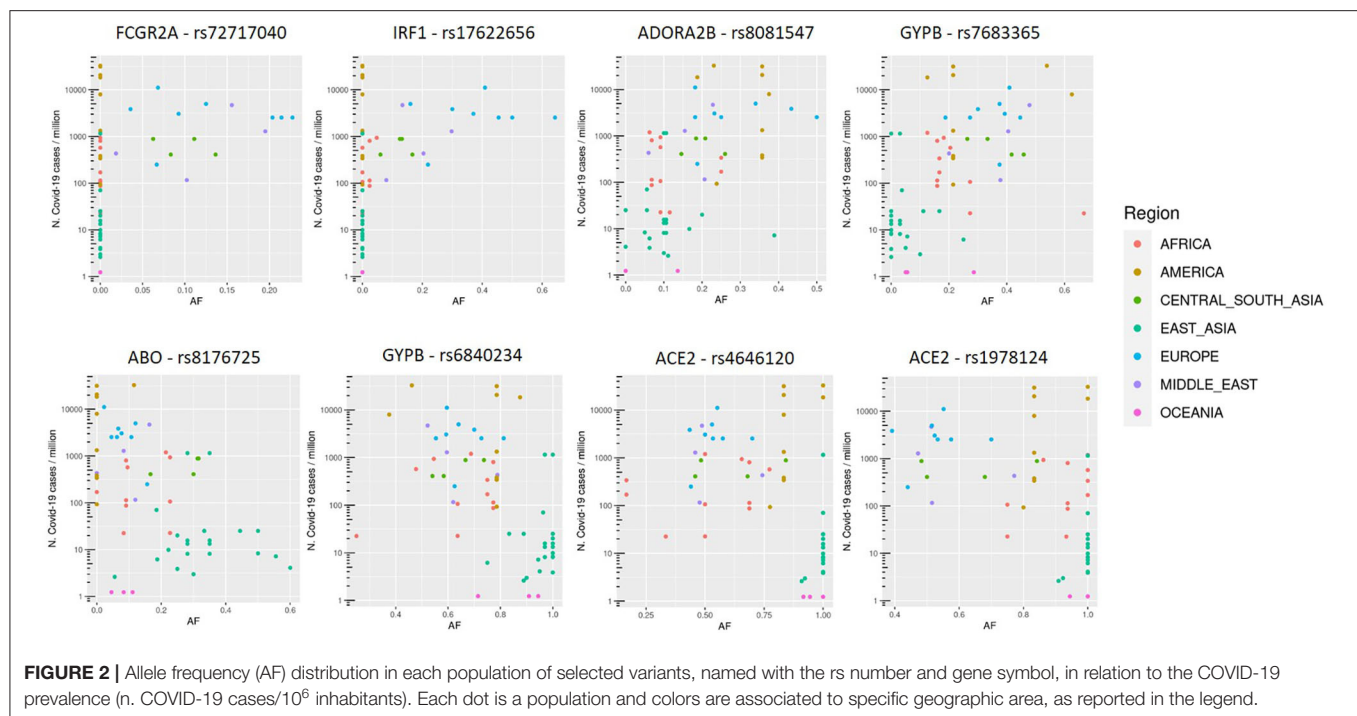
| Gene symbol | Gene name  | Protein function (Gene Cards)  |
|-------------|--|--|
| ABO         | ABO, alpha 1-3-N-acetylgalactosaminyltransferase and alpha 1-3-galactosyltransferase | This gene encodes proteins related to the first discovered blood group system, ABO.  |
| ACE2        | Angiotensin I converting enzyme 2  | The protein encoded by this gene belongs to the angiotensin-converting enzyme family of dipeptidyl carboxypeptidases   |
| ACKR1       | Atypical chemokine receptor 1 (Duffy blood group)                                    | The encoded protein is the receptor for the human malarial parasites <i>Plasmodium vivax</i> and <i>Plasmodium knowlesi</i> . Polymorphisms in this gene are the basis of the Duffy blood group system   |
| ADORA2B     | Adenosine A2b receptor   | This gene encodes an adenosine receptor that is a member of the G protein-coupled receptor superfamily. This integral membrane protein stimulates adenylate cyclase activity in the presence of adenosine.   |
| FCGR2A      | Fc fragment of IgG receptor IIa  | This gene encodes one member of a family of immunoglobulin Fc receptor genes found on the surface of many immune response cells. The protein encoded by this gene is a cell surface receptor found on phagocytic cells such as macrophages and neutrophils, and is involved in the process of phagocytosis and clearing of immune complexes                              |
| GYPB        | Glycophorin B (MNS blood group)  | Glycophorins A (GYPA) and B (GYPB) are major sialoglycoproteins of the human erythrocyte membrane which bear the antigenic determinants for the MN and Ss blood groups   |
| IRF1        | Interferon regulatory factor 1   | The encoded protein activates the transcription of genes involved in the body's response to viruses and bacteria, playing a role in cell proliferation, apoptosis, the immune response, and DNA damage response.   |
| NOS2        | Nitric oxide synthase 2  | This gene encodes a nitric oxide synthase which is expressed in liver and is inducible by a combination of lipopolysaccharide and certain cytokines.   |
| SPTB        | Spectrin beta, erythrocytic  | The protein encoded by this locus functions in stability of erythrocyte membranes  |
| TLR4        | Toll like receptor 4   | The protein encoded by this gene is a member of the Toll-like receptor (TLR) family which plays a fundamental role in pathogen recognition and activation of innate immunity. TLRs recognize pathogen-associated molecular patterns that are expressed on infectious agents, and mediate the production of cytokines necessary for the development of effective immunity |

Gene symbol, full gene name and its function are reported for the 10 genes listed in **Table 3**.

**TABLE 5 |** List of variants finally selected.

|                      | rs ID      | Consequence | Gene symbol (input) | Spearman $\rho$ | Spearman FDR | Captured alleles (Tagger)  | eQTL genes associated | eQTLs slope lung | eQTL slope whole blood |
|----------------------|------------|-------------|---------------------|-----------------|--------------|--|-----------------------|------------------|------------------------|
| Positive correlation | rs72717040 | Intronic    | FCGR2A              | 0.48806         | 0.00431      | rs17400517   | FCGR2C, HSPA7         | –                | –                      |
|                      | rs17622656 | Intronic    | IRF1                | 0.51287         | 0.00208      |  | SLC22A5               | –                | –                      |
|                      | rs8081547  | Intronic    | ADORA2B             | 0.55595         | 0.00049      |  | CENPV                 | –                | –                      |
|                      | rs7683365  | Missense    | GYPB                | 0.58510         | 0.00016      | rs7662277, rs7666297, rs7666296, rs12499907, rs12499906, rs10002395, rs10025455, rs7661933 | GYPE                  | –                | –                      |
| Negative correlation | rs8176725  | Intronic    | ABO                 | –0.45895        | 0.00914      |  | ABO                   | +                | +                      |
|                      | rs6840234  | Intronic    | GYPB                | –0.55690        | 0.00047      | rs6857129, rs4835127, rs1473055, rs6537238, rs4835126, rs6816184                           | GYPE, FREM3           | –                | –                      |
|                      | rs4646120  | Intronic    | ACE2                | –0.47397        | 0.00638      |  | PIR                   | +                | +                      |
|                      | rs1978124  | Intronic    | ACE2                | –0.53219        | 0.00109      |  | PIR                   | +                | +                      |

The list of SNVs positively and negatively correlated with COVID-19 is reported in the upper and lower part of the table, respectively. These variants are strongly associated to COVID-19 (FDR < 0.01), are associated to eQTL in at least four tissues, including lung, and are driver-variants of other alleles. The first three columns represent the rsID, the consequence of the SNV on the gene, and the name of the malaria-associated gene where the variant is located. Spearman  $\rho$  and FDR are reported for each tag SNP. All the variants captured by the tag SNP are listed in "Captured alleles (Tagger)" column. The last three columns indicate the eQTL genes associated and the slope of the eQTL for lung and whole blood (+, positive; –, negative).



first wave of pandemic (until mid-July 2020), however, the selected significant correlations were corroborated by the data from the second wave (Nov 2020-Feb 2021). Despite these issues, several variants passed all the filtering steps and were eventually selected.

In the following, we report on a possible link with SARS-CoV-2 infections, also in terms of molecular mechanisms and potential therapeutic options.

## ABO Blood Group

Several epidemiological analyses revealed that blood group O is associated with a lower risk of SARS-CoV infection (30). Using a cellular model of adhesion to investigate whether natural antibodies of the ABO system could block the S protein and ACE2 interaction, Guillon et al. have reported that the S protein/ACE2-dependent adhesion was specifically inhibited by either a monoclonal or human natural anti-A antibodies, indicating that these antibodies may block the interaction between the virus and its receptor, thereby providing protection. To fully appreciate the potential effect of the ABO polymorphism on the epidemiology of SARS-CoV, a mathematical model of the virus transmission dynamics that takes into account the protective effect of ABO natural antibodies was built. The model indicated that the ABO polymorphism could contribute to substantially reduce the virus transmission, affecting both the number of infected individuals and the kinetics of the epidemic (31).

These results gathered for SARS-CoV are consistent with recent observations with SARS-CoV-2. Li et al. have recently published “Association between ABO blood groups and risk of SARS-CoV-2 pneumonia” (32), an observation already reported

by Zhao et al., and which have had a certain impact in the press (33). In both studies, the ABO blood groups distribution of patients with COVID-19 were compared to that of controls from the local populations. These studies show that blood group A is associated with an increased risk of infection, whereas group O is associated with a decreased risk. Recently, a genome-wide association study (GWAS) has confirmed a higher risk among persons with blood group A relative to those with other blood groups and a clear protective role for blood group O (34).

Histo-blood group ABO system transferase is an enzyme with glycosyltransferase activity, which is encoded by the ABO gene in humans. ABO determines the ABO blood group of an individual by modifying the oligosaccharides on cell surface glycoproteins. In our study, we observed that the intron variant rs8176725 of ABO determined an increase in histo-blood group ABO system transferase expression and correlated negatively with COVID-19 cases. This is consistent with the previous reported observations revealing that blood group O was associated with a low risk of SARS-CoV and SARS-CoV-2 infections and that ABO natural antibodies can block the interaction between S protein and ACE2.

Of interest, similar results were obtained for malaria infection. A meta-analysis study showed an increased odds of severe *P. Falciparum* infection among individuals with blood group A, B, AB, or non-O compared with blood group O. However, the difference in the level of *P. Falciparum* parasitaemia was not significant among individuals with blood group A or non-O compared with blood group O. Blood group A likely promotes increased severity of disease through mechanisms dependent on rosetting and cytoadhesion (35).



## Glycophorin B

Glycophorin A, B, and E (GYPA, GYPB, and GYPE) represent a small gene family localized on chromosome 4q28-q31 that encodes the major red cell membrane glycoproteins, GPA and GPB, and GPE. Glycophorins play an important role in the invasion of red blood cells (RBCs) by malaria parasite. The glycophorin gene cluster has a complex pattern of gene conversion and structural variation, and selective pressure due to pathogens, including malaria, has contributed to induce diversity in this region (36). However, at present no data indicating a correlation between the GYPB rs6840234 variant and resistance to malaria are available. This intron-variant is characterized by a reduction in GYPE and FREM3 transcription. This finding is rather intriguing as the FREM3/GYPE is one of the most prominent examples of putative ancient balancing selection in a genome-wide analysis of haplotype sharing between humans and chimpanzees.

FREM3 (FRAS1-related extracellular matrix protein 3) is a gene located near GYPE and encodes an extracellular matrix protein that is required for maintaining the integrity of the skin epithelium and the differentiated state of renal epithelia. Although FREM3 apparently is not correlated with malaria and COVID-19, a recent study has demonstrated a link between a variant of FREM3 (rs186873296) and malaria (37). People carrying one copy of FREM3 rs186873296 allele have a reduced risk of severe malaria by about 40% (38). Moreover, the associations between sickle-cell trait and homozygosity for rs186873296 in FREM3 determines a phenotype with high hemoglobin concentration. The most likely reason for the high hemoglobin concentrations in cases with both these genotypes is that such children are protected from all forms of clinical malaria that result cumulatively in higher levels of anemia in children without these protective polymorphisms. Furthermore, rs186873296 FREM3 polymorphism correlates closely with the polymorphism that is specific to Dantu a hybrid gene comprising GYPA and GYPB, which encodes a blood antigen known as Dantu (Red blood cell tension protects against severe malaria in the Dantu blood group) (39). People with Dantu produce a hybrid molecule that consists of the extracellular domain of GYPB and the transmembrane plus intracellular domains of GYPA. The blood group variant Dantu provides 74% protection against all forms of severe malaria in homozygous individuals. This protection is due to a higher average tension in RBCs surface membrane which make them resistant to the parasite invasion.

If the role of GYPB as a protective factor against malarial infection, either directly or through FREM3, is sufficiently clarified, there are no data in the literature in relation to SARS-CoV-2 infection. GYPB rs6840234 decreases the expression of both glycophorin B and FREM3, and how this effect can protect against virus infection remains to be elucidated.

## Angiotensin Converting Enzyme 2

We observed two intron-variants of ACE2 gene that were negatively correlated with COVID-19 cases. These variants (rs4646120 and rs1978124) were able to increase the mRNA expression of PIR, a gene encoding the enzyme quercetin 2,3-dioxygenase, which is involved in the degradation of quercetin by

a dioxygenase reaction. ACE2 and PIR are two genes located on X-chromosome and are co-regulated by “double elite” enhancers. The co-regulation of ACE2 and PIR represents an important step during SARS-CoV-2 infections. Actually, after interaction between SARS-CoV-2 and the ACE2 receptor, this complex is internalized with a marked ACE2 depletion in cell surface. ACE2 is an essential protein under feedback regulation to restore protein expression. Thus, ACE2 depletion is followed by an upregulation of ACE2 gene transcription. ACE2 gene lies in a co-regulated cluster with PIR and VEGFD, sharing “double-elite” enhancers, implying homeostatic host responses (40). ACE2 gene is sited on human X-chromosome between CLTRN and PIR genes, which is adjacent to VEGF-D. These genes share enhancers and other regulatory elements with ACE2. Thus, homeostatic responses attempting to restore expression of cell surface ACE2, during SARS-CoV-2 infections, can induce the upregulation of these genes. In particular, two enhancers of ACE2, GH0XJ015596 and GH0XJ015579, have double-elite interaction with the promoter of PIR and the promoter of VEGF-D (41). Thus, ACE2 upregulation is associated with increased expression of PIR and VEGF-D.

Quercetin 2,3-dioxygenase encoded by PIR converts the “antioxidant” quercetin to quinone, with a semiquinone radical intermediate, which reacts with oxygen to generate reactive oxygen species (ROS) superoxide O<sub>2</sub><sup>-</sup> and H<sub>2</sub>O<sub>2</sub> (42). This causes a “ROS storm” which would account for a catastrophic deterioration in COVID-19 patients who are unable to suppress viral replication rapidly. Of interest, evidences indicate that quercetin is effective both for prophylaxis in high-risk populations and for the treatment of SARS-CoV-2 infections (43). The intron-variants rs4646120 and rs1978124 are characterized by high expression of PIR. Like to the ACE2 regulation during SARS-CoV-2 infection, overexpression of PIR may activate a negative feedback with reduction of the enhancers that co-regulate PIR and ACE2. The reduced expression of ACE2 would make people with these intronic variants less susceptible to SARS-CoV-2 infections.

## Interferon Regulatory Factor 1

We identified an intron variant in IRF1 gene (rs17622656) that positively correlated with COVID-19. Interferon regulatory factor 1 (IRF1) was the first member of the interferon regulatory transcription factor family identified. IRF1 regulates expression of target genes by binding to an interferon stimulated response element (ISRE) in their promoters. Several reports suggest that IFN- $\alpha$  and IFN- $\gamma$  can co-operatively inhibit some virus replication including SARS-CoV, and IRF-1 plays a key role in this process (44). Conversely, the intron variant IRF-1 rs17622656 positively correlated with COVID-19 cases. This variant is characterized by a reduced expression of SLC22A5 (OCTN2) gene. This gene encodes a protein involved in the active cellular uptake of carnitine.

The observation that leukocytes, including monocytes and lymphocytes, are enriched in carnitines first suggested that carnitine may regulate the immune response (45). A reduced pool of carnitines has been demonstrated in either serum or tissues, or both, from patients with unregulated and/or impaired

immune responses. Carnitine deficiency in peripheral blood lymphocytes and monocytes is common among HIV patients, and this is linked to a wide spectrum of mechanisms ranging from malabsorption to defective synthesis (46). Clinical studies have demonstrated that in HIV patients carnitine therapy in combination with standard antiretroviral treatment could have a greater improvement in CD4 counts (47). Therefore, the positive correlation between COVID-19 cases and the intron variant IRF1 rs17622656 could lead to a reduced uptake of carnitine and to an impaired immune response against SARS-CoV-2.

Recently, particular attention has been focused on IFN genes and those that regulate them. It is unknown whether rs17622656 negatively regulates IRF1, which in turn would act downstream on the IRF genes. If this effect was demonstrated, the positive correlation with COVID-19 cases would be explainable. In line with this hypothesis, there are findings demonstrating the presence of mutations in type I IFN-related genes in patients with life-threatening COVID-19 pneumonia (48).

## Adenosine A2b Receptor

ADORA2B encodes for an adenosine receptor. We found 2 introns variants (rs4646120 and rs1978124) of ADORA2B which correlated with COVID-19. These variants decrease protein expression in the lung. The activity of this adenosine receptor is mediated by G proteins which activate adenylyl cyclase. Adenosine is an endogenous ligand for four different adenosine receptor subtypes (AdoRA1, AdoRA2A, AdoRA2B, and AdoRA3). Increased concentrations of adenosine were found in ascites of MethA sarcoma or in culture medium of 3LL Lewis lung carcinoma growing under hypoxic conditions. Adenosine and its analogs efficiently inhibited the cytotoxic activity of LAK cells. In fact, intratumor adenosine impairs the ability of lymphokine-activated killer (LAK) cells to kill tumor cells. It is possible to hypothesize that a decrease in ADORA2B may decrease the NK response toward cells infected with SARS-CoV-2, although there are no experimental studies that can confirm this hypothesis (49).

Alternatively, ADORA2B could directly affect lung function. In fact, there are many instances where acute lung injury (ALI) resolves spontaneously through endogenous pathways that help to control excessive lung inflammation. Previous studies have implicated the extracellular signaling molecule adenosine and signaling events through the A2B adenosine receptor in lung protection. In this context, alveolar epithelial A2B adenosine receptor signaling contributes to lung protection. Thus, variants that induce a decrease in ADORA2B in the lung may be risk factors for the evolution of SARS-CoV-2 infection (50).

## Fc Fragment of IgG Receptor IIa

We found that the frequency of intron variants rs72717040 and rs17400517 of FCGR2A correlated with the frequency of COVID-19. This gene encodes one member of a family of immunoglobulin Fc receptor genes found on the surface of many immune response cells. The protein encoded by this gene is a cell surface receptor found on phagocytic cells such as macrophages and neutrophils and is involved in the process of phagocytosis

and clearing of immune complexes. It has also been associated with severe malaria in Gambia and in Kenya (51, 52).

The polymorphisms of FCGR2A exert a downregulation effect for both the FCGR2C and HSPA7 genes. The protein encoded by the first gene is again a receptor for the Fc region of complexed immunoglobulins gamma and is involved in a variety of effector and regulatory functions such as phagocytosis of immune complexes and modulation of antibody production by B-cells. HSPA7 is a pseudogene, member of Heat Shock Protein Family A (Hsp70). It is unclear how a decrease in FCGR2C can affect SARS-CoV-2 infection, and there is no association data between this gene and COVID-19. It is possible to hypothesize that its decrease in the lung and in phagocytic cells could reduce the effectiveness of the immune response to the virus.

It is also interesting to note that other polymorphisms in FCGR2A have been associated with Kawasaki disease (53, 54). This disease has been addressed in more than 200 studies published in the last 6 months: an unusually high incidence of Kawasaki disease in children was reported and in many of them IgG antibodies for SARS-CoV-2 were detected, suggesting an association between the SARS-CoV-2 and this syndrome in children. Although Kawasaki disease-like syndromes have previously been linked to other viral infections, these patients showed higher levels of pro-inflammatory markers than other cohorts, which may reflect a particularly strong immunological reaction to SARS-CoV-2 (55, 56). In brief, notwithstanding a direct link between FCGR2A and COVID-19 has not been identified yet, it appears quite intriguing that this gene has previously been associated to Kawasaki disease, which in turn has been associated to COVID-19.

## CONCLUSIONS

The present study demonstrates that some genetic variants selected to be protective against malaria may also play a role in the severity of SARS-CoV-2 infections. After identifying the genes known to be associated with malaria, we focused on those variants related to the frequency of COVID-19, both directly and inversely. After further skimming, we pinpointed six genes, representing a possible link between malaria and COVID-19. Indeed, for some of these, there is already direct evidence of implication with SARS-CoV-2 infection or with the evolution of COVID-19, such as ABO (blood groups) and ACE2 (a key human receptor for SARS-CoV-2). For other genes, there are interesting hypotheses for their role on COVID-19, as in IRF1 and ADORA2B. Finally, for the genes GYPB and FCGR2A, further investigations are needed to confirm an association with COVID-19 along with molecular studies to shed light on the mechanisms responsible for higher/lower incidence of SARS-CoV-2 infections.

Among the genetic outcomes, the one related to the uptake of carnitine particularly attracted our attention. Carnitine is actually responsible for maintaining a high level of the immune response, and a lower level of this amino acid can negatively impact lymphocytes and monocytes. Therefore, we point to L-carnitine (or its prodrug acetyl-L-carnitine) as a possible

dietary supplement to improve the immune response and combat/prevent COVID-19. A clinical trial to study the role of carnitine in addition to the standard of care has recently been launched.

We want to conclude that the COVID-19 pandemic was rather brutal, particularly in the initial steps, forcing the health systems to concentrate all energy on the hospitals' emergency. This hampered the possibility to plan the collection of biological samples from COVID-19 patients for subsequent genomics and/or other analyses. Furthermore, to carry out a malaria-COVID-19 correlation study, one would have needed to find biological samples from malarial areas, along with clinical information on the malarial patient's history. All these steps are currently planned and will represent the subject matter of subsequent studies in the field (which are currently ongoing), where the present genetic variants will be confirmed. New ones will likely be disclosed to shed further light on the biological and genetic mechanisms of this complex infection, responsible for the current worldwide pandemic. Finally, possible links may emerge among variants in the human and viral genome, as intensive programs of high throughput sequencing are currently ongoing worldwide.

## SUMMARY

Despite being rather different, malaria and COVID-19 may show some commonalities, mainly related to genetic variants present in populations living in malaria-endemic regions. In particular, starting from the evidence that in Italy, the areas with the lowest number of COVID-19 cases were those with the highest incidence of malaria, we here analyze genomic data from a May 2020 database. We filter the database for ACE2 and variants that are connected to malaria, pointing eventually to 47 genes. Further focusing only on those variants statistically relevant, we ultimately identify 6 genes that could be responsible for major susceptibility (or major resistance) to malaria. Surprisingly enough, these variants are also statistically related to higher/lower

incidence/severity of SARS-CoV-2 infections. Among others, we identified genetic variants connected to blood group O, to a reduced expression of the ACE2 receptor (the entry point of SARS-CoV-2 into the human body), and to a decreased uptake of carnitine, an amino acid that plays a key role in the immune system response to infections. In conclusion, this study sheds further light on the genetic and molecular mechanisms responsible for the high/low impact of COVID-19. It points to a possible dietary supplement (L-carnitine) as a therapeutic adjuvant in treating SARS-CoV-2 infections.

## DATA AVAILABILITY STATEMENT

Publicly available datasets were analyzed in this study. These data can be found at: <ftp://ngs.sanger.ac.uk/production/hgdp> (WGS data) and [https://github.com/CSSEGISandData/COVID-19/tree/master/csse\\_covid\\_19\\_data/csse\\_covid\\_19\\_daily\\_reports](https://github.com/CSSEGISandData/COVID-19/tree/master/csse_covid_19_data/csse_covid_19_daily_reports) (COVID-19 data).

## AUTHOR CONTRIBUTIONS

MR drafted the manuscript, performed the analysis, and analyzed the results. PU designed the pipeline, performed the bioinformatic analysis, and analyzed the results. AA and MT analyzed the results. AC conceived the study, analyzed the results, and wrote the manuscript. All authors contributed to manuscript revision, read, and approved the submitted version.

## ACKNOWLEDGMENTS

We thank the Italian Institute of Technology and Department of Medical Sciences (Excellence Grant 2018–2022 funded by the Italian Ministry of Education) of the University of Turin for financial support. The authors thank Adriana Zelli for the precious help in consultation of the archives of the Italian Historical Statistical Repository.

## REFERENCES

- Di Gennaro F, Marotta C, Locantore P, Pizzol D, Putoto G. Malaria and COVID-19: common and different findings. *Trop Med Infect Dis.* (2020) 5:141. doi: 10.3390/tropicalmed5030141
- WHO Coronavirus Disease (COVID-19) Dashboard. (2020). Available online at: <https://covid19.who.int> (accessed September 21, 2020).
- Napoli PE, Nioi M. Global spread of coronavirus disease 2019 and malaria: an epidemiological paradox in the early stage of a pandemic. *J Clin Med.* (2020) 9:1138. doi: 10.3390/jcm9041138
- Hajizadeh R, Behnemoon M. Is the new coronavirus disease (COVID-19) pandemic halted by malaria epidemics? *Arch Bone Jt Surg.* (2020) 8(Suppl. 1):319–20. doi: 10.22038/abjs.2020.47662.2336
- Panda AK, Tripathy R, Das BK. Plasmodium falciparum infection may protect a population from severe acute respiratory syndrome coronavirus 2 infection. *J Infect Dis.* (2020) 222:1570–1. doi: 10.1093/infdis/jiaa455
- Osama El-Gendy A, Saeed H, Ali AMA, Zawbaa HM, Gomaa D, Harb HS, et al. Bacillus Calmette-Guérin vaccine, antimalarial, age and gender relation to COVID-19 spread and mortality. *Vaccine.* (2020) 38:5564–8. doi: 10.1016/j.vaccine.2020.06.083
- WHO. World malaria report 2019. (2019). Available online at: <https://www.who.int/malaria/publications/world-malaria-report-2019/en/> (accessed July 13, 2020).
- Maraolo AE, Grossi A. Safety of hydroxychloroquine for treatment or prevention of SARS-CoV-2 infection: A rapid systematic review and meta-analysis of randomized clinical trials. *Immun Inflamm Dis.* (2020) 9:31–6. doi: 10.1002/iid3.374
- Iesa M a. M, Osman MEM, Hassan MA, Dirar AIA, Abuzeid N, Mancuso JJ, et al. SARS-CoV-2 and Plasmodium falciparum common immunodominant regions may explain low COVID-19 incidence in the malaria-endemic belt. *New Microbes New Infect.* (2020) 38:100817. doi: 10.1016/j.nmni.2020.100817
- Tanabe K, Mita T, Jombart T, Eriksson A, Horibe S, Palacpac N, et al. Plasmodium falciparum accompanied the human expansion out of Africa. *Curr Biol.* (2010) 20:1283–9. doi: 10.1016/j.cub.2010.05.053
- Gelabert P, Olalde I, de-Dios T, Civit S, Lalueza-Fox C. Malaria was a weak selective force in ancient Europeans. *Sci Rep.* (2017) 7:1377. doi: 10.1038/s41598-017-01534-5
- Sampson UKA, Edwards TL, Jahangir E, Munro H, Wariboko M, Wassef MG, et al. Factors associated with the prevalence of hypertension in the southeastern United States: insights from 69,211 blacks and whites in the



- Southern Community Cohort Study. *Circ Cardiovasc Qual Outcomes*. (2014) 7:33–54. doi: 10.1161/CIRCOUTCOMES.113.000155
13. Cappuccio FP. Ethnicity and cardiovascular risk: variations in people of African ancestry and South Asian origin. *J Hum Hypertens*. (1997) 11:571–6. doi: 10.1038/sj.jhh.1000516
  14. Gallego-Delgado J, Walther T, Rodriguez A. The high blood pressure-malaria protection hypothesis. *Circ Res*. (2016) 119:1071–5. doi: 10.1161/CIRCRESAHA.116.309602
  15. Dhangadamajhi G, Mohapatra BN, Kar SK, Ranjit M. Gene polymorphisms in angiotensin I converting enzyme (ACE I/D) and angiotensin II converting enzyme (ACE2 C→T) protect against cerebral malaria in Indian adults. *Infect Genet Evol*. (2010) 10:337–41. doi: 10.1016/j.meegid.2010.01.009
  16. Fan X, Wang Y, Sun K, Zhang W, Yang X, Wang S, et al. Polymorphisms of ACE2 gene are associated with essential hypertension and antihypertensive effects of Captopril in women. *Clin Pharmacol Ther*. (2007) 82:187–96. doi: 10.1038/sj.cpt.6100214
  17. Hoffmann M, Kleine-Weber H, Schroeder S, Krüger N, Herrler T, Erichsen S, et al. SARS-CoV-2 cell entry depends on ACE2 and TMPRSS2 and is blocked by a clinically proven protease inhibitor. *Cell*. (2020) 181:271–80.e8. doi: 10.1016/j.cell.2020.02.052
  18. ebiblio.istat. Available online at: <https://ebiblio.istat.it/digibib/Cause%20di%20morte/TO00195805StatCausemorte1910.pdf>
  19. Italian Historical Statistical Repository. (1914). Available online at: <https://ebiblio.istat.it/digibib/Censimenti%20popolazione/censpop1911/rav312263CP11vol2rilegato-OCR-ottim.pdf> (accessed June 15, 2020).
  20. COVID-19\_Italian data. Available online at: <https://github.com/pcm-dpc/COVID-19>
  21. Bergström A, McCarthy SA, Hui R, Almarri MA, Ayub Q, Danecek P, et al. Insights into human genetic variation and population history from 929 diverse genomes. *Science*. (2020) 367:6484. doi: 10.1126/science.aay5012
  22. cephb [Internet]. Available online at: [http://www.cephb.fr/en/hgdp\\_panel.php](http://www.cephb.fr/en/hgdp_panel.php)
  23. OMIM - Online Mendelian Inheritance in Man. (2021). Available online at: <https://www.omim.org/> (accessed March 3, 2021).
  24. Malaria Genomic Epidemiology Network, Malaria Genomic Epidemiology Network. Reappraisal of known malaria resistance loci in a large multicenter study. *Nat Genet*. (2014) 46:1197–204. doi: 10.1038/ng.3107
  25. Penha-Gonçalves C. Genetics of malaria inflammatory responses: a pathogenesis perspective. *Front Immunol*. (2019) 10:1771. doi: 10.3389/fimmu.2019.01771
  26. Barrett JC, Fry B, Maller J, Daly MJ. Haploview: analysis and visualization of LD and haplotype maps. *Bioinformatics*. (2005) 21:263–5. doi: 10.1093/bioinformatics/bth457
  27. Danecek P, Auton A, Abecasis G, Albers CA, Banks E, DePristo MA, et al. The variant call format and VCFtools. *Bioinformatics*. (2011) 27:2156–8. doi: 10.1093/bioinformatics/btr330
  28. de Bakker PIW, Yelensky R, Pe'er I, Gabriel SB, Daly MJ, Altshuler D. Efficiency and power in genetic association studies. *Nat Genet*. (2005) 37:1217–23. doi: 10.1038/ng1669
  29. Majori G. Short history of malaria and its eradication in Italy with short notes on the fight against the infection in the mediterranean basin. *Mediterr J Hematol Infect Dis*. (2012) 4:e2012016. doi: 10.4084/mjhid.2012.016
  30. Cheng Y, Cheng Y, Cheng G, Chui CH, Lau FY, Chan PKS, et al. ABO blood group and susceptibility to severe acute respiratory syndrome. *JAMA*. (2005) 293:1450–1. doi: 10.1001/jama.293.12.1450-c
  31. Guillon P, Clément M, Sébille V, Rivain J-G, Chou C-F, Ruvoën-Clouet N, et al. Inhibition of the interaction between the SARS-CoV spike protein and its cellular receptor by anti-histo-blood group antibodies. *Glycobiology*. (2008) 18:1085–93. doi: 10.1093/glycob/cwn093
  32. Li J, Wang X, Chen J, Cai Y, Deng A, Yang M. Association between ABO blood groups and risk of SARS-CoV-2 pneumonia. *Br J Haematol*. (2020) 190:24–7. doi: 10.1111/bjh.16797
  33. Zhao J, Yang Y, Huang H, Li D, Gu D, Lu X, et al. Relationship between the ABO blood group and the COVID-19 susceptibility. *Clin Infect Dis*. (2020) 4:ciaa1150. doi: 10.1093/cid/ciaa1150
  34. Ellinghaus D, Degenhardt F, Bujanda L, Buti M, Alballos A, Invernizzi P, et al. Genomewide association study of severe Covid-19 with respiratory failure. *N Engl J Med*. (2020) 383:1522–34. doi: 10.1056/NEJMoa2020283
  35. Degarege A, Gebregzi MT, Beck-Sague CM, Wahlgren M, de Mattos LC, Madhivanan P. Effect of ABO blood group on asymptomatic, uncomplicated and placental *Plasmodium falciparum* infection: systematic review and meta-analysis. *BMC Infect Dis*. (2019) 19:86. doi: 10.1186/s12879-019-3730-z
  36. Wang H-Y, Tang H, Shen C-KJ, Wu C-I. Rapidly evolving genes in human. I. The glycophorins and their possible role in evading malaria parasites. *Mol Biol Evol*. (2003) 20:1795–804. doi: 10.1093/molbev/msg185
  37. Ndila CM, Uyoga S, Macharia AW, Nyutu G, Peshu N, Ojal J, et al. Human candidate gene polymorphisms and risk of severe malaria in children in Kilifi, Kenya: a case-control association study. *Lancet Haematol*. (2018) 5:e333–45. doi: 10.1016/S2352-3026(18)30107-8
  38. Malaria Genomic Epidemiology Network, Band G, Rockett KA, Spencer CCA, Kwiatkowski DP. A novel locus of resistance to severe malaria in a region of ancient balancing selection. *Nature*. (2015) 526:253–7. doi: 10.1038/nature15390
  39. Kariuki SN, Marin-Menendez A, Introini V, Ravenhill BJ, Lin Y-C, Macharia A, et al. Red blood cell tension protects against severe malaria in the Dantu blood group. *Nature*. (2020) 585:579–83. doi: 10.1038/s41586-020-2726-6
  40. Shovlin CL, Vizcaychipi MP. Vascular inflammation and endothelial injury in SARS-CoV-2 infection: The overlooked regulatory cascades implicated by the ACE2 gene cluster. *QJM*. (2020) 10:hcaa241. doi: 10.1093/qjmed/hcaa241
  41. Lonsdale J, Thomas J, Salvatore M, Phillips R, Lo E, Shad S, et al. The genotype-tissue expression (GTEx) project. *Nat Genet*. (2013) 45:580–85. doi: 10.1038/ng.2653
  42. Murakami A, Ashida H, Terao J. Multitargeted cancer prevention by quercetin. *Cancer Lett*. (2008) 269:315–25. doi: 10.1016/j.canlet.2008.03.046
  43. Colunga Biancatelli RML, Berrill M, Catravas JD, Marik PE. Quercetin and vitamin C: an experimental, synergistic therapy for the prevention and treatment of SARS-CoV-2 related disease (COVID-19). *Front Immunol*. (2020) 11:1451. doi: 10.3389/fimmu.2020.01451
  44. Zhang X-N, Liu J-X, Hu Y-W, Chen H, Yuan Z-H. Hyper-activated IRF-1 and STAT1 contribute to enhanced interferon stimulated gene (ISG) expression by interferon alpha and gamma co-treatment in human hepatoma cells. *Biochim Biophys Acta*. (2006) 1759:417–25. doi: 10.1016/j.bbexp.2006.08.003
  45. Pons R, De Vivo DC. Primary and secondary carnitine deficiency syndromes. *J Child Neurol*. (1995) 10(suppl. 2):S8–24. doi: 10.1177/0883073895010002S03
  46. Famularo G, Moretti S, Marcellini S, Trinchieri V, Tzantzoglou S, Santini G, et al. Acetyl-carnitine deficiency in AIDS patients with neurotoxicity on treatment with antiretroviral nucleoside analogues. *AIDS*. (1997) 11:185–90. doi: 10.1097/00002030-199702000-00008
  47. De Simone C, Tzantzoglou S, Famularo G, Moretti S, Paoletti F, Vullo V, et al. High dose L-carnitine improves immunologic and metabolic parameters in AIDS patients. *Immunopharmacol Immunotoxicol*. (1993) 15:1–12. doi: 10.3109/08923979309066930
  48. Zhang Q, Bastard P, Liu Z, Le Pen J, Moncada-Velez M, Chen J, et al. Inborn errors of type I IFN immunity in patients with life-threatening COVID-19. *Science*. (2020) 370:eabd4570. doi: 10.1126/science.abd4570
  49. Raskovalova T, Huang X, Sitkovsky M, Zacharia LC, Jackson EK, Gorelik E. Gs protein-coupled adenosine receptor signaling and lytic function of activated NK cells. *J Immunol*. (2005) 175:4383–91. doi: 10.4049/jimmunol.175.7.4383
  50. Hoegl S, Brodsky KS, Blackburn MR, Karmouty-Quintana H, Zwissler B, Eltzschig HK. Alveolar epithelial A2B adenosine receptors in pulmonary protection during acute lung injury. *J Immunol*. (2015) 195:1815–24. doi: 10.4049/jimmunol.1401957
  51. Faik I, van Tong H, Lell B, Meyer CG, Kremsner PG, Velavan TP. Pyruvate Kinase and Fcy receptor gene copy numbers associated with malaria phenotypes. *J Infect Dis*. (2017) 216:276–82. doi: 10.1093/infdis/jix284
  52. Munde EO, Okeyo WA, Raballah E, Anyona SB, Were T, Ong'echa JM, et al. Association between Fcy receptor IIA, IIIA, and IIIB genetic polymorphisms and susceptibility to severe malaria anemia in children in western Kenya. *BMC Infect Dis*. (2017) 17:289. doi: 10.1186/s12879-017-2390-0
  53. Ferdosian F, Dastgheib SA, Hosseini-Jangjou SH, Nafei Z, Lookzadeh MH, Noorishadkam M, et al. Association of TNF- $\alpha$  rs1800629, CASP3 rs72689236 and FCGR2A rs1801274 polymorphisms with susceptibility to kawasaki disease: a comprehensive meta-analysis. *Fetal Pediatr Pathol*. (2019) 30:1–17. doi: 10.1080/15513815.2019.1707917
  54. Nagelkerke SQ, Tacke CE, Breunis WB, Tanck MWT, Geissler J, Png E, et al. Extensive ethnic variation and linkage disequilibrium at the FCGR2/3 locus:



- different genetic associations revealed in Kawasaki disease. *Front Immunol.* (2019) 10:185. doi: 10.3389/fimmu.2019.00185
55. Toubiana J, Poirault C, Corsia A, Bajolle F, Fourgeaud J, Angoulvant F, et al. Kawasaki-like multisystem inflammatory syndrome in children during the covid-19 pandemic in Paris, France: prospective observational study. *BMJ.* (2020) 369:m2094. doi: 10.1136/bmj.m2094
  56. Verdoni L, Mazza A, Gervasoni A, Martelli L, Ruggeri M, Ciuffreda M, et al. An outbreak of severe Kawasaki-like disease at the Italian epicentre of the SARS-CoV-2 epidemic: an observational cohort study. *Lancet.* (2020) 395:1771–8. doi: 10.1016/S0140-6736(20)31103-X

**Conflict of Interest:** The authors declare that the research was conducted in the absence of any commercial or financial relationships that could be construed as a potential conflict of interest.

Copyright © 2021 Rusmini, Uva, Amoroso, Tolomeo and Cavalli. This is an open-access article distributed under the terms of the Creative Commons Attribution License (CC BY). The use, distribution or reproduction in other forums is permitted, provided the original author(s) and the copyright owner(s) are credited and that the original publication in this journal is cited, in accordance with accepted academic practice. No use, distribution or reproduction is permitted which does not comply with these terms.



# False Negative Mitigation in Group Testing for COVID-19 Screening

Amir Reza Alizad-Rahvar<sup>1\*</sup>, Safar Vafadar<sup>2</sup>, Mehdi Totonchi<sup>3</sup> and Mehdi Sadeghi<sup>4\*</sup>

<sup>1</sup> School of Biological Sciences, Institute for Research in Fundamental Sciences (IPM), Tehran, Iran, <sup>2</sup> Laboratory of Biological Complex Systems and Bioinformatics (CBB), Institute of Biochemistry and Biophysics, University of Tehran, Tehran, Iran,

<sup>3</sup> Department of Genetics, Royan Institute for Reproductive Biomedicine, The Academic Center for Education, Culture, and Research (ACECR), Tehran, Iran, <sup>4</sup> Department of Medical Genetics, National Institute for Genetic Engineering and Biotechnology, Tehran, Iran

## OPEN ACCESS

### Edited by:

Atefeh Abedini,  
Shahid Beheshti University of Medical  
Sciences, Iran

### Reviewed by:

Hossein Peyvandi,  
University of Surrey, United Kingdom  
Pegah Khosravi,  
Cornell University, United States

### \*Correspondence:

Amir Reza Alizad-Rahvar  
alizad@ipm.ir  
Mehdi Sadeghi  
sadeghi@nigeb.ac.ir

### Specialty section:

This article was submitted to  
Infectious Diseases – Surveillance,  
Prevention and Treatment,  
a section of the journal  
Frontiers in Medicine

**Received:** 30 January 2021

**Accepted:** 06 April 2021

**Published:** 10 May 2021

### Citation:

Alizad-Rahvar AR, Vafadar S,  
Totonchi M and Sadeghi M (2021)  
False Negative Mitigation in Group  
Testing for COVID-19 Screening.  
Front. Med. 8:661277.  
doi: 10.3389/fmed.2021.661277

After lifting the COVID-19 lockdown restrictions and opening businesses, screening is essential to prevent the spread of the virus. Group testing could be a promising candidate for screening to save time and resources. However, due to the high false-negative rate (FNR) of the RT-PCR diagnostic test, we should be cautious about using group testing because a group's false-negative result identifies all the individuals in a group as uninfected. Repeating the test is the best solution to reduce the FNR, and repeats should be integrated with the group-testing method to increase the sensitivity of the test. The simplest way is to replicate the test twice for each group (the 2Rgt method). In this paper, we present a new method for group testing (the groupMix method), which integrates two repeats in the test. Then we introduce the 2-stage sequential version of both the groupMix and the 2Rgt methods. We compare these methods analytically regarding the sensitivity and the average number of tests. The tradeoff between the sensitivity and the average number of tests should be considered when choosing the best method for the screening strategy. We applied the groupMix method to screening 263 people and identified 2 infected individuals by performing 98 tests. This method achieved a 63% saving in the number of tests compared to individual testing. Our experimental results show that in COVID-19 screening, the viral load can be low, and the group size should not be more than 6; otherwise, the FNR increases significantly. A web interface of the groupMix method is publicly available for laboratories to implement this method.

**Keywords:** COVID-19 screening, false-negative mitigation, groupMix, group testing, pool testing, RT-PCR, SARS-CoV-2, sensitivity

## 1. INTRODUCTION

In the post-COVID-19 era, most countries are trying to lift their lockdown restrictions. However, an infected person can remain completely asymptomatic and spread the virus. Hence, it is essential to increase screening tests to identify and quarantine the infected person and identify any other person who has been exposed to that individual. Unfortunately, the testing capacity of many countries is not sufficient, and they have to save their capacity for the second or even the third wave of the coronavirus outbreak.

In this situation, the group testing (or pool testing) technique can immediately and dramatically increase worldwide testing capacity by decreasing the required number of individual tests in a population. In this technique, separate samples are mixed together to create a sample pool. After a single diagnostic test has been performed on each group of samples, a negative result indicates that

everyone in the group is uninfected; otherwise, at least one of the samples in the group is infected. Then, in conventional group testing (1, 2), an individual test on each sample in the infected group is performed to identify the infected samples. With this method, the number of tests is decreased by not testing the individual samples in an uninfected group.

Although different types of reverse-transcription polymerase chain reaction (RT-PCR) tests are the predominant diagnostic methods for detecting SARS-CoV-2, the accuracy of these methods for COVID-19 is still unknown (3). False positives are rare for RT-PCR testing when primers and probes are designed appropriately. There are many reports of specificity of 100% for SARS-CoV-2 RT-PCR assays, based on the *in vitro* cross-reactivity assessment (4–6). However, the clinical specificity, which is affected by the contamination of laboratory equipment and reagents or human error, could be less than 100%. Overall, the false positive rate (FPR) of SARS-CoV-2 RT-PCR diagnosis, without human error and contamination, can be considered to be zero.

The major problem in COVID-19 diagnosis with RT-PCR is false negatives. A false-negative rate (FNR) of up to 50% has been reported for RT-PCR-based SARS-CoV-2 diagnostic testing (4), but an FNR of 10–20% is more frequent in the reports (6, 7). An unsuitable type of sample [e.g., a throat swab rather than a nasal swab (8)] and inadequate or inappropriate specimen collection, storage, and transport are responsible for a large portion of this high FNR. Moreover, the FNR of SARS-CoV-2 RT-PCR diagnosis is affected by the number of days that have elapsed since an individual first became infected. Indeed, the FNR is about 67 and 38% on day 4 and on the day of symptom onset (day 5), respectively. Three days after symptom onset (day 8), the FNR decreases to 20%, and then, it gradually increases again to 66% on day 21 (9).

A false-negative result puts the whole society at risk by falsely indicating that an infected person does not have an infection. Hence, this person, might move around the community and infect others. False negatives in group testing are much riskier than in individual testing. If a group of specimens is infected, each sample in the group can potentially be infected. Consequently, if the test result of this infected pool is a false negative, this result indicates that every person with a specimen in the pool is infection-free. Also, the mixing of specimens in group testing makes an infected specimen become diluted by the uninfected samples. Therefore, if the group size is not determined wisely, the infected specimen becomes undetectable, and the sensitivity of the test is reduced, resulting in false negatives (the dilution effect). Hence, the group testing methods must be made resistant to false-negative results. Unfortunately, the main focus of most of the studies in the field of group testing is only on reducing the average number of tests. Hence, more studies are needed to mitigate the effect of false negatives and increase the sensitivity of the test in group testing. This paper aims to address this need.

In this work, we propose a new method of group testing, called the groupMix method, for mitigating the false negatives. We propose 1-stage and 2-stage sequential versions of this method. In (10), the authors propose a method for false-negative mitigation of SARS-CoV-2 group testing. We propose a 2-stage version of

this method and compare the sensitivity and the average number of tests of 1-stage and 2-stage versions of this method with those of the groupMix method. Then we present our experimental test results for COVID-19 screening by using the groupMix method. Finally, we introduce our web interface, which will help laboratories to implement the groupMix method.

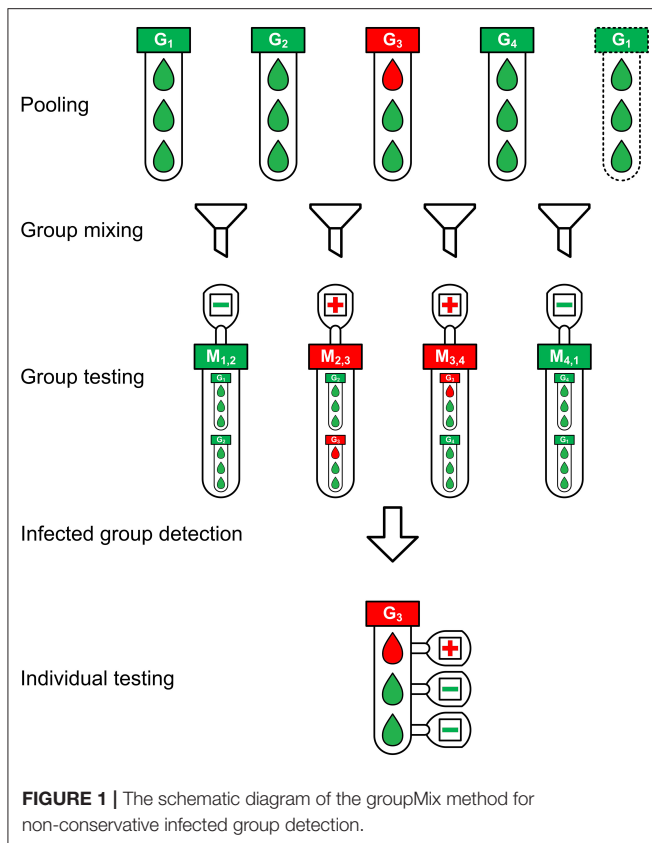
## 2. GROUP TESTING METHODS

In the case of individual testing, the best practice to mitigate the effect of false negatives is to repeat the test (11). If the false-positive results are ignored, a person can be diagnosed as positive if either test is positive. Assume that there is no human error and contamination resulting in false positive, and the FNR of the RT-PCR test is 20% and the test errors are independent. In this case, if we repeat the test for an individual twice independently by getting two samples, the chance of obtaining two false-negative results drops to 4%. Consequently, the sensitivity of the test increases from 80% (for a single test) to 96% (for two tests). Inspired by this easy method of false-negative mitigation for individual testing, this test repetition could be integrated into the group-testing procedure to mitigate the effect of false negatives in the detection of infected groups. For instance, an adaptive screening procedure is introduced in (12) so that the negative groups of each stage are re-tested. If both tests of a group are negative, this group is considered as a negative group. Recently, a group testing method has been proposed for SARS-CoV-2 in (10) for false-negative mitigation. Here, we call this method 2-replicate group testing, denoted by 2Rgt. We introduce this method in the next section, and then, we propose a 2-stage sequential version of it to reduce its required number of tests. We will compare the results of our proposed method, groupMix, with 2Rgt's results.

### 2.1. Model and Notation

Assume that the prevalence (prior probability) of the disease in the population is  $p$ . We want to test  $N$  independent specimens by using group testing. The group size, i.e., the number of specimens in each pool, is  $n$ . The optimum group size,  $n_{opt}$ , minimizes the average number of tests,  $\bar{T}$ . The FNR of the diagnostic method for a single test is denoted by  $f_N$ , and the FPR is negligible. It is assumed that testing the pooled sample does not change  $f_N$ . In other words, the group size  $n$  is determined wisely to prevent the dilution effect and a drop in the sensitivity.

Denoting a group of samples by  $G$ ,  $G = 0$  means that all samples in  $G$  are uninfected. In contrast,  $G = 1$  implies that  $G$  is a positive group; i.e., it has at least one infected specimen. By observing the results of group tests in different methods, we identify a group as infected or uninfected, denoted by  $\hat{G} = 1$  and  $\hat{G} = 0$ , respectively. Here, we define two types of sensitivity. The *sample-level sensitivity*,  $S_s$ , refers to the probability of detecting an infected sample as positive. On the other hand, the *group-level sensitivity*,  $S_g$ , refers to the probability of positive detection of an infected group; i.e.,  $P(\hat{G} = 1 | G = 1)$ . To be able to detect an infected sample, its corresponding pool should be diagnosed positive first, and then, its individual test should also be positive. Therefore,  $S_s = S_g(1 - f_N)$ . In comparing different methods of



group testing, we compare  $S_g$  values to measure the accuracy of the methods.

## 2.2. GroupMix Method

The schematic diagram of the groupMix method is depicted in **Figure 1**. This method has the following steps.

- 1) Pooling:** We make groups of samples with the group size of  $n$ . Therefore, we have  $m = \lceil N/n \rceil$  groups. We label each group as  $G_i$  where  $1 \leq i \leq m$ , and we call them *primary groups*.
- 2) Group mixing:** Each primary group  $G_i$  ( $2 \leq i \leq m-1$ ) is mixed with  $G_{i-1}$  and  $G_{i+1}$  separately, giving the mixed groups  $M_{i-1,i}$  and  $M_{i,i+1}$ , respectively, a group size of  $2n$ . In the case of the first ( $G_1$ ) and last ( $G_m$ ) groups, we mix them together and make  $M_{m,1}$ . With this form of mixing, each group exists in two mixed groups. Hence, each group will be tested twice by testing the mixed groups.
- 3) Group testing:** Each mixed group will be tested to identify the infected mixed groups. This form of group mixing results in  $m$  mixed groups, which equals the number of the primary groups  $G_i$ . Therefore, in this step, we need  $m$  tests.
- 4) Infected group detection:** In this step, we detect the infected primary groups from the test results of the mixed groups. Different approaches can be applied for this purpose, based on the level of compromising the false negatives and the tradeoff between sensitivity and the number of tests. Assume that we want to detect the infected group in **Figure 1**. Here,  $M_{2,3}$  and  $M_{3,4}$  are

positive. We can have the following detection approaches.

● **Conservative group detection:** In a conservative approach,  $M_{2,3} = 1$  indicates that both  $\hat{G}_2$  and  $\hat{G}_3$  should be considered as infected because both can cause a positive result for  $M_{2,3}$ . However,  $\hat{G}_2 = 1$  should also make the test result for  $M_{1,2}$  positive. Here, we assume pessimistically that the observed value of  $M_{1,2} = 0$  is a false-negative result. Similarly,  $M_{3,4} = 1$  results in  $\hat{G}_3 = 1$  and  $\hat{G}_4 = 1$ . Hence, with this approach, the primary groups  $\hat{G}_2$ ,  $\hat{G}_3$ , and  $\hat{G}_4$  should be detected as positive in **Figure 1**. Here,  $\hat{G}_2 = 1$  and  $\hat{G}_4 = 1$  are false positives due to our detection algorithm. Consequently, this method makes algorithmic false positives, increasing the number of tests. However, this approach results in  $S_g = 1 - f_N^2$ . In summary, in conservative group detection, we consider  $\hat{G}_i = 1$  and  $\hat{G}_{i+1} = 1$  provided that  $M_{i,i+1} = 1$ .

● **Non-conservative group detection:** To reduce the number of algorithmic false positives, and consequently, to decrease the number of tests in conservative group detection, we should be tolerant of false negatives. To achieve this goal, we can detect only more probable infected groups, with the cost of less sensitivity. In this way, both  $M_{2,3}$  and  $M_{3,4}$  in **Figure 1** are positive, most likely because  $G_3 = 1$ . Although these positive results can also occur if  $G_2 = 1$  and  $G_4 = 1$ , the lack of  $M_{1,2} = 1$  and  $M_{4,1} = 1$  makes it unlikely that  $G_2$  and  $G_4$  will both equal 1. In this approach, if, for example,  $G_2$  is truly positive and  $M_{1,2} = 0$  is a false-negative result, we will miss  $\hat{G}_2 = 1$ , resulting in less sensitivity. We will propose a 2-stage sequential version of this method to resolve this problem and increase the sensitivity.

If there is not any false-negative result, we should always see a pair of positive mixed groups for an infected group  $G_i$ , i.e.,  $M_{i-1,i}$  and  $M_{i,i+1}$ . Therefore, provided that we observe only a single positive mixed group, i.e.,  $M_{i-1,i} = 0$ ,  $M_{i,i+1} = 1$ , and  $M_{i+1,i+2} = 0$ , then the other mixed group of the pair is not diagnosed positive because of the false-negative result. Hence, a single positive mixed group  $M_{i,i+1}$  indicates that both  $G_i$  and  $G_{i+1}$  can potentially be infected. Consequently, we consider both groups positive to test all of their specimens individually in the next step.

In summary, we have the following rules in non-conservative group detection.

1. Provided that the test result of both  $M_{i-1,i}$  and  $M_{i,i+1}$  are positive,  $\hat{G}_i$  is considered as a positive group; otherwise, it is negative.
2. If we have a single positive mixed group, e.g.,  $M_{i,i+1}$ , both  $\hat{G}_i$  and  $\hat{G}_{i+1}$  are considered as infected.

**5) Individual testing:** The specimens of all primary groups that are detected positive ( $\hat{G}_i = 1$ ) are tested individually.

In **Figure 1**, there are  $N = 12$  samples with one infected sample. The pooling of samples is performed with a group size of  $n = 3$ . Hence, there are  $m = 4$  primary groups in which  $G_3$  is infected. **Figure 1** depicts the non-conservative group detection. We need 4 tests in the group-testing step and 3 individual tests in the last step, or a total of 7 tests. Using the conservative group detection, we need 4 tests in the group-testing step and 9 more individual tests, or a total of 13 tests. We can see the



effect of the algorithmic false positives in increasing the number of tests.

### 2.3. Sequential groupMix Method

We propose a 2-stage sequential version of the non-conservative groupMix method, denoted by 2S-groupMix, to increase its sensitivity. As explained in section 2.2, some cases are undetected by the non-conservative group detection. For instance, assume that  $G_1 = 0$ ,  $G_2 = 1$ ,  $G_3 = 0$ , and  $G_4 = 1$ . In this case, if we observe  $M_{1,2} = 0$  (a false negative),  $M_{2,3} = 1$ ,  $M_{3,4} = 1$ , and  $M_{4,1} = 1$ , the non-conservative method detects  $\hat{G}_3 = 1$  and  $\hat{G}_4 = 1$ . Here,  $\hat{G}_2 = 1$  is not detected because of the false-negative result. Since  $\hat{G}_3 = 1$  is an algorithmic false positive, the individual test of its specimens will not show any infected sample. This observation indicates that  $M_{2,3} = 1$  could be due to  $G_2 = 1$ , and implicitly shows that  $M_{1,2} = 0$  is a false negative. Therefore, in the second stage,  $\hat{G}_2$  is considered infected, and its specimens are tested individually. In this way, the sensitivity of the non-conservative groupMix method is increased by performing the second stage. In summary, the 2S-groupMix method is as follows.

1. Perform the groupMix method by using the non-conservative group detection.
2. Assume that the test of a mixed group is positive in the previous stage (e.g.,  $M_{i,i+1} = 1$ ), and that only one of its primary groups is detected as a positive group (for example,  $\hat{G}_i = 0$  and  $\hat{G}_{i+1} = 1$ ). Provided that the individual tests on the samples of the detected group (i.e.,  $G_{i+1}$ ) are all negative, perform the individual test on the specimens of the other undetected primary group (i.e.,  $G_i$ ).

Since this approach is a sequential method, we need to spend more time to increase the sensitivity of the test. In other words, there is a tradeoff between the test time and the sensitivity.

### 2.4. 2-Replicate Group Test

In 2-replicate group test (2Rgt) method, each group is tested twice. Provided that the result of at least one of the tests is positive, this group is diagnosed as a positive group. In this case,  $S_g = 1 - f_N^2$ . Note that the 2Rgt method has no algorithmic false positive.

In the case of **Figure 1**, we need 11 tests if we use the 2Rgt method, while 7 and 13 tests are required if we use the non-conservative and the conservative groupMix method, respectively.

### 2.5. Sequential 2-Replicate Group Test

Here, we present a 2-stage sequential version of the 2Rgt method, denoted by 2S-2Rgt, to reduce the number of tests, while the sensitivity of the test, i.e.,  $S_g = 1 - f_N^2$ , remains the same. The drawback of the 2Rgt method is that it uses two tests for each group and increases the required number of tests. Since observing only one positive result out of two tests is enough to consider a group as infected, we can separate these two tests on each group and avoid the second test for positive groups of the first stage. The summary of this method is as follows.

1. Test all groups once and identify the positive groups as infected.
2. Perform the second test only on the negative groups of the first stage and identify the positive groups.
3. Individually test the specimens of the positive groups of stages 1 and 2.

In this way, we reduce the number of tests by saving the second test of the infected groups identified in the first stage.

## 3. ANALYTICAL RESULTS

In this section, we present the results of the analytical analysis of the different group-testing methods regarding  $S_g$ , and the average number of tests per sample,  $\bar{T}/N$ . The proof for the analyses is available in Appendix A (**Supplementary Material**). All analytical results are verified by simulation. In the following results, it is assumed that the FNR of the diagnostic test is 10%.

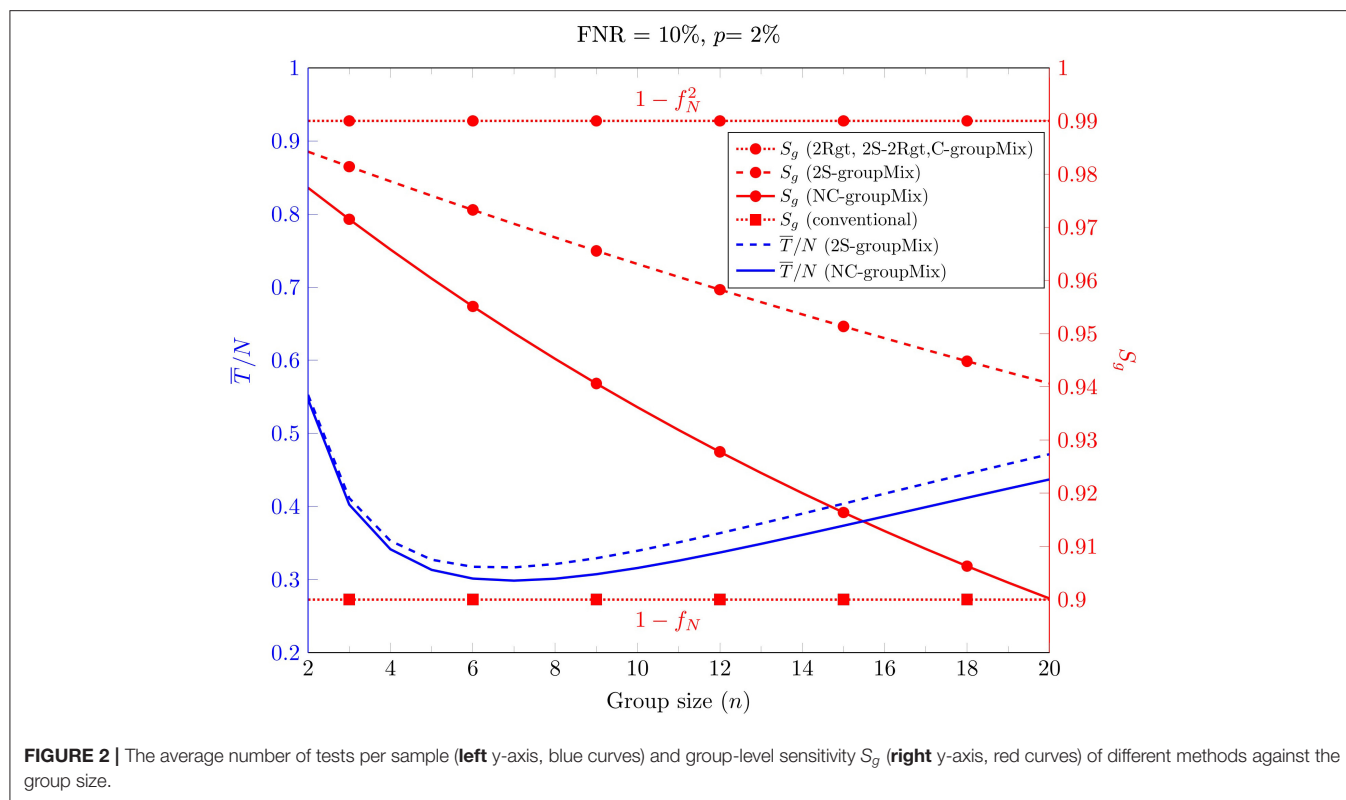
### 3.1. The Effect of Group Size on $\bar{T}$ and $S_g$

First, we consider the effect of the group size on  $\bar{T}/N$  and  $S_g$  in **Figure 2** for FNR = 10% and  $p = 2\%$ . This figure has two different y-axes. The right axis shows  $S_g$  for the non-conservative (NC), conservative (C), and 2-stage sequential (2S) groupMix methods, the 2Rgt and 2S-2Rgt methods, and the conventional method. The left axis shows  $\bar{T}/N$  for the NC-groupMix and the 2S-groupMix methods. This figure indicates that for these specific values of FNR and prevalence,  $n_{opt}$ , which minimizes the average number of tests, is 7.

Moreover, **Figure 2** shows that  $S_g$  of both the C-groupMix and 2Rgt methods is independent of  $n$ , equal to  $S_g = 1 - f_N^2$ , which is 0.99 for  $f_N = 0.1$ . Similarly, the conventional group-test method has the fixed group-level sensitivity  $S_g = 1 - f_N$  over  $n$ . However,  $S_g$  in NC- and 2S-groupMix methods varies with  $n$ . In other words, with smaller value of  $n$ , a larger value of  $S_g$  is achieved. In this figure, it is obvious that there is a tradeoff between  $S_g$  and  $\bar{T}/N$  for  $n \leq 7$ .

If the primary concern in group testing is only to reduce the average number of tests  $\bar{T}$ , then the group size should minimize  $\bar{T}$ . However, in practice, using the optimum value of  $n$  may not be possible in the presence of problems like the dilution effect. For example, the study in (13) shows that for detecting SARS-CoV-2 with the standard kits and protocols, a single infected sample can be detected in pools of up to 32 samples, with an estimated FNR of 10%. This finding could be valid for the specimen of an active symptomatic patient. However, in COVID-19 screening, we usually deal with asymptotically-infected or pre-symptomatic individuals or people with very mild or atypical symptoms. These cases may not have a high viral load and detectable amounts of the virus in their specimen.

Consequently, in the screening scenario, the maximum group size could be much less than 32. Our experiments show that a group size of 6 is a good choice for group testing in COVID-19 screening; otherwise, the viral load in the pool becomes very low, and the FNR increases dramatically. A thorough investigation is required to determine the maximum group size for COVID-19



screening rather than for diagnostic testing for detecting active symptomatic patients.

### 3.2. Optimum Group Size

**Figure 3A** depicts  $n_{opt}$  against the prevalence percentage  $p$  for  $FNR = 10\%$ . In the case of the groupMix methods,  $n_{opt}$  refers to the optimum group size of the primary group, i.e.,  $G_i$ . Hence, the optimum size of the mixed group tested by the diagnostic method is  $2n_{opt}$ . Theoretically, the smaller values of  $p$  allow us to have larger groups of specimens. However, as we discussed above, the use of larger groups can reduce the sensitivity of the test.

### 3.3. Group-Level Sensitivity

**Figure 3B** shows  $S_g$  vs.  $p$  for  $FNR = 10\%$ . Overall,  $S_g$  of the C-groupMix, 2Rgt, and 2S-2Rgt methods does not vary with  $p$  and has the fixed value of  $S_g = 1 - f_N^2$ . Similarly, the conventional group-test method has the  $p$ -independent sensitivity of  $S_g = 1 - f_N$ . However, when we utilize the non-conservative infected group detection in the groupMix method, i.e., the NC- and 2S-groupMix methods,  $S_g$  is a decreasing function of  $p$ . In non-conservative group detection, the sensitivity is compromised by accepting more false negatives to reduce the number of algorithmic false positives. The undetected cases in the non-conservative method occur more in higher values of  $p$ , resulting in less sensitivity. Even after a specific value of  $p$ , e.g.,  $p > 0.13$  for the NC-groupMix method and the FNR of 10%,  $S_g$  becomes less than that of the conventional method. Therefore, the usage of the NC-groupMix method is acceptable for small values of

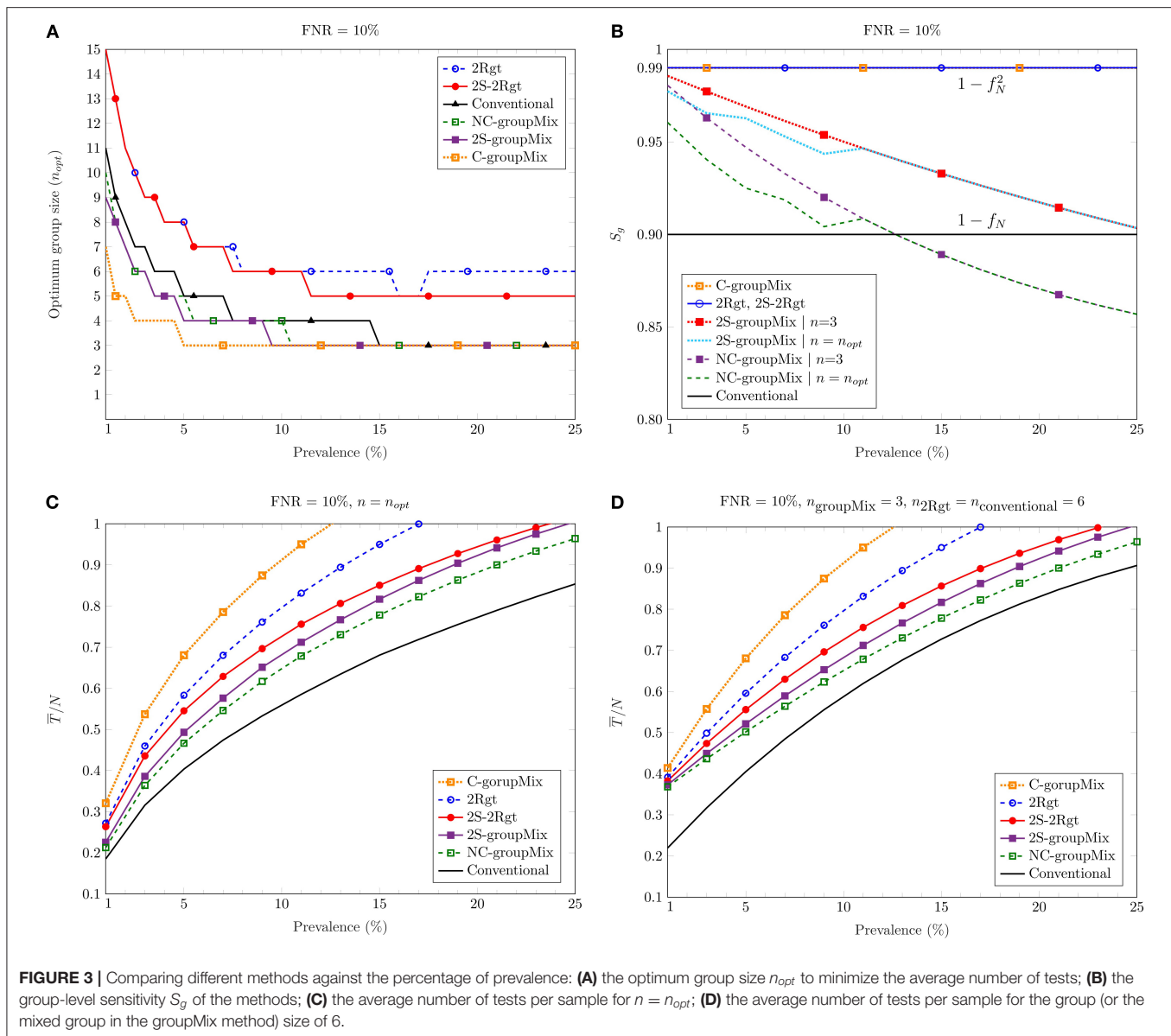
$p$ , say, less than 5%. Moreover, **Figure 3B** depicts that the 2S-groupMix method improves  $S_g$  significantly compared to the NC-groupMix method.

As we saw in **Figure 2**,  $S_g$  of the C-groupMix, the 2Rgt, and the conventional methods does not vary with  $n$ . On the contrary,  $S_g$  of the NC-groupMix and the 2S-groupMix methods depends on  $n$ . For these two methods, we see  $S_g$  in **Figure 3B** for two cases of  $n = 3$  (i.e., a mixed group size of 6) and  $n = n_{opt}$ . For  $FNR = 10\%$ ,  $n_{opt}$  equals 3 for  $p$  greater than about 10%, resulting in the same  $S_g$  for two different cases of group size. For smaller values of prevalence,  $n_{opt} > 3$ . Since  $S_g$  of the NC-groupMix and the 2S-groupMix methods is a decreasing function of  $n$  (**Figure 2**), the group testing with  $n = n_{opt}$  is less sensitive than  $n = 3$  for  $p < 10\%$ .

### 3.4. Average Number of Tests

**Figure 3C** depicts the average number of tests per sample,  $\bar{T}/N$ , against the prevalence percentage  $p$  for  $n = n_{opt}$ . As discussed earlier, in a COVID-19 screening scenario, the group size should not be more than 6 to prevent the dilution effect. Hence, **Figure 3D** shows  $\bar{T}/N$  of different methods vs.  $p$  for  $n_{groupMix} = 3$  (the size of the mixed group is 6),  $n_{2Rgt} = 6$ , and  $n_{conventional} = 6$ . As these figures show, all methods proposed for false-negative mitigation require more tests compared to the conventional method.

Among the 1-stage methods, the NC-groupMix method needs the least average number of tests. However, as mentioned before, its sensitivity reduces with  $p$ , and after a specific value of  $p$ , its sensitivity becomes even worse than that of the conventional



group test method. Therefore, it is reasonable to use the NC-groupMix method for small values of  $p$ , say  $p < 5\%$ , to have both high sensitivity and less number of tests. In a comparison between the 1-stage C-groupMix and the 1-stage 2Rgt methods, which both have the same sensitivity of  $S_g = 1 - f_N^2$ , the C-groupMix method needs more tests due to algorithmic false positives. Therefore, if the goal is to reach  $S_g = 1 - f_N^2$  by using a 1-stage method, the 2Rgt method is preferred.

In the case of the 2-stage sequential methods, the average number of tests in the 2S-2Rgt method is less than that of the 2Rgt method. This reduction in the number of tests occurs because, in the 2S-2Rgt method, we perform the second test only for the negative groups in the first stage, rather than using two tests for each group in 2Rgt. In contrast, in groupMix methods using the non-conservative infected group

detection, the 2S-groupMix needs more tests compared to the 1-stage NC-groupMix method. This increase in the number of tests occurs because the sequential version performs the full NC-groupMix test in the first stage, followed by the second stage.

In a comparison between the 2S-groupMix and the 2S-2Rgt methods, the former needs fewer tests than the latter. However, the sensitivity of the 2S-groupMix method is less than that of the 2S-2Rgt, and reduces with an increase of  $p$ . Therefore, there is a tradeoff between  $S_g$  and  $\bar{T}$  in decisions about choosing a 2-stage sequential group-test method for false-negative mitigation.

Considering the maximum group size (or the size of the mixed group in the groupMix method) of 6, compared to individual testing at 1% prevalence, we save 60% at the FNR of 10% for all proposed methods to mitigate the false negatives. For the

optimum group size, this saving is between 70 and 80% at 1% prevalence, but it may result in less sensitive tests.

Overall, in choosing the best group-testing method to mitigate the false-negative results, we should determine the desired level of sensitivity and the amount of saving in the number of the tests. Moreover, the expected time of the test determines whether the sequential method should be used.

## 4. EXPERIMENTAL METHODS

We performed COVID-19 screening in the Institute for Research in Fundamental Sciences (IPM), Tehran, Iran. A total of 263 individuals participated in the screening on 5 different days. These groups consisted of 78, 30, 31, 66, and 58 individuals, respectively. Swabs from the throat were collected and sent to the Clinical Genetic Laboratory at the Royan Institute, Tehran, Iran. Samples were collected between June 15 and 30, 2020.

The samples were pooled into the primary groups with a size of 3 prior to RNA extraction. Then, the primary groups were mixed according to the groupMix method's procedure, resulting in mixed groups of size 6.

A volume of 200  $\mu\text{L}$  of the sample was mixed with 600  $\mu\text{L}$  Lysis buffer, and RNA was extracted by using the Norgen Cell-Free RNA Purification Kit (Cat. No: 56300). 50  $\mu\text{L}$  of Elution buffer was used in the extraction procedure.

The Novel Coronavirus (2019-nCoV) Real-Time Multiplex kit (Liferiver, Cat. No: ZJ0009) was utilized for real-time RT-PCR diagnosis. This kit detects the presence of SARS-CoV-2 RNA by detecting the three genes N, OFR1ab, and E. Reactions were heated to 45°C for 10 min (1 cycle) for reverse transcription and denatured in 95°C for 90 s (1 cycle). Then, 45 cycles of amplification were carried out in 95°C for 15 s and 58°C for 30 s. Fluorescence was measured at 58°C. The 1-stage NC-groupMix method was performed to detect the infected specimens.

This study was approved by the ethical committee of the Royan institute with a waiver of informed consent due to de-identified nature of the data.

## 5. EXPERIMENTAL RESULTS

On the second, fourth, and fifth days, all groups with 30, 66, and 58 individuals were negative. For these days, we performed 10, 22, and 20 tests, respectively. Therefore, we saved 67, 67, and 66% in the number of tests, compared to individual testing.

In the first group, consisting of 78 individuals, we had 26 primary and mixed groups. With the NC-groupMix method, only the mixed group  $M_{20,21}$  was positive. Since we should always have a pair of positive mixed groups, this result indicates that one mixed group is a false negative. Therefore, both primary groups  $G_{20}$  and  $G_{21}$  were candidates to be infected. Ultimately, by performing the individual test on these primary groups, one specimen in  $G_{20}$  was identified as infected. Consequently, we performed 32 tests to detect one infected sample out of 78 samples. Indeed, we had a 59% saving in the number of tests, compared to individual testing.

Regarding the third group consisting of 31 individuals, the mixed groups  $M_{4,5}$  and  $M_{5,6}$  were positive. Hence,  $G_5$  was detected as the infected group. The individual test on  $G_5$  revealed the presence of one infected sample in this group. Hence, we detected this infected sample by using 14 tests (i.e., a 55% saving).

In conclusion, 2 positive samples were successfully identified out of 263 by using 98 tests, i.e., a 63% saving in the number of tests compared to individual testing. Since the average prevalence in this population was about 0.8%, the average group-level sensitivity  $S_g$  of this screening was very close to  $1 - f_N^2$ .

## 6. DISCUSSION AND CONCLUSION

In this paper, we investigated false-negative mitigation in group testing, focusing on massive testing for COVID-19 screening. Group testing is receiving attention as a strategy that can save time or resources for COVID-19 testing. Indeed, group testing is reasonable for screening since the percentage of infected people is very low, resulting in substantial savings. However, the high rate of false-negative results in RT-PCR-based COVID-19 diagnostic tests has been widely addressed recently as an important public health-related problem. This problem needs more attention in group testing because a false-negative result for a group of potentially infected individuals does not lead to isolating them, and they can quickly spread the virus in their community.

To mitigate the false-negative results and to increase the sensitivity of the group testing, we studied different strategies for repeating the test. By implementing  $r$  replicates in the test design, we can achieve the maximum group-level sensitivity of  $S_g = 1 - f_N^r$ , but there is a tradeoff between the sensitivity and the average number of tests; hence, we can reduce the average number of tests by compromising the false negatives. However, this compromising is negligible for the very low percentage of infected samples that usually occurs in screening.

Typically, in group-testing studies, researchers propose different methods for pooling and identifying the infected groups. Then, they find the optimum group size to minimize the average number of tests. However, we explained that in COVID-19 screening, the high viral load might not be available because we are dealing with asymptomatic, pre-symptomatic, or mild-symptomatic people. This fact is crucial in group testing because the dilution effect in the pooling of specimens can cause more false-negative cases. Therefore, the theoretical optimum group size of different methods may yield a severe dilution effect and high FNR in the screening scenario. Our experimental studies showed that the maximum group size in COVID-19 screening should be 6. However, systematic studies are still required to determine the maximum group size for COVID-19 screening. Moreover, by filtering out symptomatic individuals and testing them individually, we can increase the performance and sensitivity of the test. For further studies, we can pool specimens based on the age and medical background of individuals and investigate the effect of these factors on the performance of the group-testing method.



## 7. GROUPMIX WEB INTERFACE

A web interface is developed to help laboratories implement the NC-groupMix method. This website is freely accessible at <http://groupmix.ipm.ir>. This web interface will be elaborated in Appendix B (**Supplementary Material**).

## DATA AVAILABILITY STATEMENT

The original contributions presented in the study are included in the article/**Supplementary Material**, further inquiries can be directed to the corresponding author/s.

## ETHICS STATEMENT

The studies involving human participants were reviewed and approved by The Ethical Committee of the Royan Institute. The

patients/participants provided their written informed consent to participate in this study.

## AUTHOR CONTRIBUTIONS

AA-R developed, analyzed, and simulated the methods, wrote the manuscript, and tested the web interface functionality. SV developed the web interface. MT performed the laboratory tests and provided the laboratory methods for writing the manuscript. MS conceived the study and guided its method development. All authors read and approved the final manuscript.

## SUPPLEMENTARY MATERIAL

The Supplementary Material for this article can be found online at: <https://www.frontiersin.org/articles/10.3389/fmed.2021.661277/full#supplementary-material>

## REFERENCES

1. Dorfman R. The detection of defective members of large populations. *Ann Math Statist.* (1943) 14:436–40. doi: 10.1214/aoms/1177731363
2. Cahoon-Young B, Chandler A, Livermore T, Gaudino J, Benjamin R. Sensitivity and specificity of pooled versus individual sera in a human immunodeficiency virus antibody prevalence study. *J Clin Microbiol.* (1989) 27:1893–95. doi: 10.1128/JCM.27.8.1893-1895.1989
3. Bachelet VC. Do we know the diagnostic properties of the tests used in COVID-19? A rapid review of recently published literature. *Medwave.* (2020) 20:e7890. doi: 10.5867/medwave.2020.03.7891
4. Cohen AN, Kessel B. False positives in reverse transcription PCR testing for SARS-CoV-2. *medRxiv [Preprint].* (2020). doi: 10.1101/2020.04.26.20080911
5. Corman VM, Landt O, Kaiser M, Molenkamp R, Meijer A, Chu DK, et al. Detection of 2019 novel coronavirus (2019-nCoV) by real-time RT-PCR. *Euro Surveill.* (2020) 25:23–30. doi: 10.2807/1560-7917.ES.2020.25.3.2000045
6. Broughton JP, Deng X, Yu G, Fasching CL, Servellita V, Singh J, et al. CRISPR-Cas12-based detection of SARS-CoV-2. *Nat Biotechnol.* (2020) 38:870–4. doi: 10.1038/s41587-020-0513-4
7. Li D, Wang D, Dong J, Wang N, Huang H, Xu H, et al. False-negative results of real-time reverse-transcriptase polymerase chain reaction for severe acute respiratory syndrome coronavirus 2: role of deep-learning-based CT diagnosis and insights from two cases. *Korean J Radiol.* (2020) 21:505–8. doi: 10.3348/kjr.2020.0146
8. Yang Y, Yang M, Shen C, Wang F, Yuan J, Li J, et al. Evaluating the accuracy of different respiratory specimens in the laboratory diagnosis and monitoring the viral shedding of 2019-nCoV infections. *medRxiv [Preprint].* (2020). doi: 10.1101/2020.02.11.20021493
9. Kucirka LM, Lauer SA, Laeyendecker O, Boon D, Lessler J. Variation in false-negative rate of reverse transcriptase polymerase chain reaction-based SARS-CoV-2 tests by time since exposure. *Ann Intern Med.* (2020) 173:262–7. doi: 10.7326/M20-1495
10. Hanel R, Thurner S. Boosting test-efficiency by pooled testing for SARS-CoV-2-formula for optimal pool size. *PLoS ONE.* (2020) 15:e0240652. doi: 10.1371/journal.pone.0240652
11. Ramdas K, Darzi A, Jain S. 'Test, re-test, re-test': using inaccurate tests to greatly increase the accuracy of COVID-19 testing. *Nat Med.* (2020). doi: 10.1038/s41591-020-0891-7. [Epub ahead of print].
12. Litvak E, Tu XM, Pagano M. Screening for the presence of a disease by pooling sera samples. *J Am Stat Assoc.* (1994) 89:424–34. doi: 10.1080/01621459.1994.10476764
13. Yelin I, Aharony N, Tamar ES, Argoetti A, Messer E, Berenbaum D, et al. Evaluation of COVID-19 RT-qPCR test in multi sample pools. *Clin Infect Dis.* (2020) 71:2073–8. doi: 10.1093/cid/ciaa531

**Conflict of Interest:** The authors declare that the research was conducted in the absence of any commercial or financial relationships that could be construed as a potential conflict of interest.

Copyright © 2021 Alizad-Rahvar, Vafadar, Totonchi and Sadeghi. This is an open-access article distributed under the terms of the Creative Commons Attribution License (CC BY). The use, distribution or reproduction in other forums is permitted, provided the original author(s) and the copyright owner(s) are credited and that the original publication in this journal is cited, in accordance with accepted academic practice. No use, distribution or reproduction is permitted which does not comply with these terms.



# Clinical and Laboratory Findings of COVID-19 in High-Altitude Inhabitants of Saudi Arabia

Mostafa Abdelsalam<sup>1,2</sup>, Raad M. M. Althaqafi<sup>3</sup>, Sara A. Assiri<sup>3</sup>, Taghreed M. Althagafi<sup>4</sup>, Saleh M. Althagafi<sup>5</sup>, Ahmed Y. Fouda<sup>1,6</sup>, Ahmed Ramadan<sup>1,7</sup>, Mohammed Rabah<sup>1,7</sup>, Reham M. Ahmed<sup>1,8</sup>, Zein S. Ibrahim<sup>9</sup>, Dalal M. Nemenqani<sup>3</sup>, Ahmed N. Alghamdi<sup>3</sup>, Daifullah Al Aboud<sup>3</sup>, Ahmed S. Abdel-Moneim<sup>3\*</sup> and Adnan A. Alsulaimani<sup>1</sup>

<sup>1</sup> Alameen Hospital, Taif, Saudi Arabia, <sup>2</sup> Mansoura Nephrology and Dialysis Unit, Internal Medicine Department, College of Medicine, Mansoura University, Mansoura, Egypt, <sup>3</sup> College of Medicine, Taif University, Taif, Saudi Arabia, <sup>4</sup> Internal Medicine Department, King Abdulaziz Hospital, Jeddah, Saudi Arabia, <sup>5</sup> General Department of Medical Services, Security Forces Hospital, Mecca, Saudi Arabia, <sup>6</sup> Anesthesiology Department, Faculty of Medicine, Ain Shams University, Cairo, Egypt, <sup>7</sup> Radiology Department, Faculty of Medicine, Cairo University, Giza, Egypt, <sup>8</sup> Albbassia Chest Hospital, Cairo, Egypt, <sup>9</sup> Department of Physiology, Faculty of Veterinary Medicine, Kafrelsheikh University, Kafrelsheikh, Egypt

## OPEN ACCESS

### Edited by:

Reza Lashgari,  
Institute for Research in Fundamental  
Sciences, Iran

### Reviewed by:

Jawhar Gharbi,  
King Faisal University, Saudi Arabia  
Majid Marjani,  
National Research Institute of  
Tuberculosis and Lung Diseases  
(NRITLD), Iran

### \*Correspondence:

Ahmed S. Abdel-Moneim  
asa@tu.edu.sa

### Specialty section:

This article was submitted to  
Pulmonary Medicine,  
a section of the journal  
Frontiers in Medicine

**Received:** 20 February 2021

**Accepted:** 23 March 2021

**Published:** 12 May 2021

### Citation:

Abdelsalam M, Althaqafi RMM, Assiri SA, Althagafi TM, Althagafi SM, Fouda AY, Ramadan A, Rabah M, Ahmed RM, Ibrahim ZS, Nemenqani DM, Alghamdi AN, Al Aboud D, Abdel-Moneim AS and Alsulaimani AA (2021) Clinical and Laboratory Findings of COVID-19 in High-Altitude Inhabitants of Saudi Arabia. *Front. Med.* 8:670195. doi: 10.3389/fmed.2021.670195

**Background:** SARS-CoV-2, the causative agent of COVID-19, continues to cause a worldwide pandemic, with more than 147 million being affected globally as of this writing. People's responses to COVID-19 range from asymptomatic to severe, and the disease is sometimes fatal. Its severity is affected by different factors and comorbidities of the infected patients. Living at a high altitude could be another factor that affects the severity of the disease in infected patients.

**Methods:** In the present study, we have analyzed the clinical, laboratory, and radiological findings of COVID-19-infected patients in Taif, a high-altitude region of Saudi Arabia. In addition, we compared matched diseased subjects to those living at sea level. We hypothesized that people living in high-altitude locations are prone to develop a more severe form of COVID-19 than those living at sea level.

**Results:** Age and a high Charlson comorbidity score were associated with increased numbers of intensive care unit (ICU) admissions and mortality among COVID-19 patients. These ICU admissions and fatalities were found mainly in patients with comorbidities. Rates of leukocytosis, neutrophilia, higher D-dimer, ferritin, and highly sensitive C-reactive protein (CRP) were significantly higher in ICU patients. CRP was the most independent of the laboratory biomarkers found to be potential predictors of death. COVID-19 patients who live at higher altitude developed a less severe form of the disease and had a lower mortality rate, in comparison to matched subjects living at sea level.

**Conclusion:** CRP and Charlson comorbidity scores can be considered predictive of disease severity. People living at higher altitudes developed less severe forms of COVID-19 disease than those living at sea level, due to a not-yet-known mechanism.

**Keywords:** COVID-19, SARS-CoV-2, high-altitude, crp, CO-RADS classification, d-dimer

## INTRODUCTION

Humans worldwide have been besieged by the relentless spread of the SARS-CoV-2 pandemic. As of this writing, SARS-CoV-2 laboratory-confirmed cases have exceeded 147 million globally. Patients infected with this newly discovered coronavirus can be affected by either asymptomatic or symptomatic forms of the disease. The latter includes fever, sore throat, cough, shortness of breath, and a loss of smell and taste sensation. Some patients develop severe pneumonia and acute respiratory

distress syndrome with fatal consequences (1). Older people and those with other health problems such as diabetes, cancer, lung diseases, and heart disease are the most vulnerable groups afflicted by the severe form of COVID-19. Early diagnosis and treatment of infected patients are important to avoid a complicated form of the disease and to prevent further spread of the virus to uninfected subjects (2).

Lymphopenia, elevated inflammatory markers such as high C-reactive protein (CRP), ferritin, and elevated D-dimer, in association with abnormal radiological findings in both chest

**TABLE 1 |** Clinical and demographic criteria of the studied groups of patients.

| Parameters   | Total patients (760) | Recovered without ICU (695) (91.5%) | Recovered after ICU (1) (6.8%) | Passed away 13 (1.7%)   | <i>p</i> |
|--|----------------------|-------------------------------------|--------------------------------|-------------------------|----------|
| <b>Age</b> mean (SEM) years                            | 41.4 (0.53)          | 40.3 (0.6) <sup>ab</sup>            | 52 (2.3) <sup>a</sup>          | 57.3 (5.6) <sup>b</sup> | 0.0001   |
| <b>Gender</b>  |                      |                                     |                                |                         |          |
| Male <i>n</i> (%)                                      | 578 (76.1)           | 530 (76.3)                          | 40 (76.9)                      | 8 (61.5)                | 0.468    |
| Female <i>n</i> (%)                                    | 182 (23.9)           | 165 (23.7)                          | 12 (23.1)                      | 5 (38.5)                |          |
| <b>Nationality</b>                                     | 283 (37.2)           | 254 (36.5)                          | 25 (48.1)                      | 4 (30.8)                | 0.225    |
| Saudi <i>n</i> (%)                                     |                      |                                     |                                |                         |          |
| Others <i>n</i> (%)                                    | 477 (62.8)           | 441 (63.5)                          | 27 (51.9)                      | 9 (69.2)                |          |
| <b>Clinical presentation</b>                           | 644 (84.7)           | 590 (84.9)                          | 42 (80.8)                      | 12 (92.3)               | 0.58     |
| Fever <i>n</i> (%)                                     |                      |                                     |                                |                         |          |
| Cough <i>n</i> (%)                                     | 442 (58.2)           | 401 (57.7)                          | 33 (63.5)                      | 8 (61.5)                | 0.735    |
| Shortness of breath <i>n</i> (%)                       | 344 (45.3)           | 312 (44.9)                          | 24 (46.2)                      | 8 (61.5)                | 0.492    |
| GI symptoms <i>n</i> (%)                               | 193 (25.4)           | 182 (26.2)                          | 8 (15.4)                       | 3 (23.1)                | 0.227    |
| Chronic diseases <i>n</i> (%)                          | 197 (25.9)           | 155 (28.3)                          | 31 (59.6)                      | 11 (84.6)               | 0.0001   |
| History of contact <i>n</i> (%)                        | 178 (23.4)           | 171 (24.6)                          | 6 (11.5)                       | 1 (7.7)                 | 0.041    |
| Health care workers <i>n</i> (%)                       | 49 (6.4)             | 47 (6.8)                            | 1 (1.9)                        | 1 (7.7)                 | 0.354    |
| Sore throat <i>n</i> (%)                               | 82 (10.8)            | 79 (11.4)                           | 1 (1.9)                        | 2 (15.4)                | 0.046    |
| Loss of smell sensation <i>n</i> (%)                   | 159 (20.9)           | 153 (21)                            | 5 (9.6)                        | 1 (7.7)                 | 0.046    |
| Loss of taste sensation <i>n</i> (%)                   | 119 (15.7)           | 116 (16.7)                          | 3 (5.8)                        | 0                       | 0.033    |
| <b>Associated co-morbidities and chronic diseases:</b> | 91 (14)              | 64 (9.2)                            | 20 (38.5)                      | 7 (53.8)                | 0.0001   |
| Hypertension <i>n</i> (%)                              |                      |                                     |                                |                         |          |
| DM <i>n</i> (%)  | 123 (16.2)           | 93 (13.4)                           | 21 (40.4)                      | 9 (69.2)                | 0.0001   |
| CKD <i>n</i> (%)                                       | 20 (2.6)             | 11 (1.6)                            | 5 (9.6)                        | 4 (30.8)                | 0.0001   |
| CLD <i>n</i> (%)                                       | 7 (0.9)              | 5 (0.7)                             | 1 (1.9)                        | 1 (7.7)                 | 0.052    |
| CHF <i>n</i> (%)                                       | 11 (1.4)             | 8 (1.2)                             | 3 (5.8)                        | 0                       | 0.067    |
| CVA <i>n</i> (%)                                       | 10 (1.3)             | 7 (2)                               | 3 (5.8)                        | 0                       | 0.052    |
| Peripheral vascular disease <i>n</i> (%)               | 20 (2.6)             | 10 (1.4)                            | 7 (13.5)                       | 3 (23.1)                | 0.0001   |
| COPD <i>n</i> (%)                                      | 23 (4)               | 17 (2.4)                            | 5 (9.6)                        | 1 (7.7)                 | 0.015    |
| CAD <i>n</i> (%)                                       | 14 (1.8)             | 8 (1.2)                             | 3 (5.8)                        | 3 (23.1)                | 0.0001   |
| Dementia <i>n</i> (%)                                  | 7 (0.9)              | 5 (0.7)                             | 2 (3.8)                        | 0                       | 0.114    |
| Rheumatological diseases <i>n</i> (%)                  | 6 (0.8)              | 6 (0.9)                             | 0                              | 0                       | 1        |
| Peptic ulcers <i>n</i> (%)                             | 23 (4)               | 21 (3%)                             | 2 (3.8)                        | 0                       | 0.78     |
| Malignancy <i>n</i> (%)                                | 4 (0.5)              | 2 (0.3)                             | 0                              | 2 (15.4)                | 0.004    |
| PE <i>n</i> (%)  | 29 (3.8)             | 7 (2)                               | 12 (23.1)                      | 10 (76.9)               | 0.0001   |
| DVT <i>n</i> (%)                                       | 4 (0.5)              | 3 (0.4)                             | 1 (1.9)                        | 0                       | 0.301    |
| <b>Duration of admission (Days) (mean ± SE)</b>        | 6.9 ± 0.23           | 6.2 ± 0.2 <sup>ab</sup>             | 11.4 ± 1.6 <sup>a</sup>        | 13.2 ± 2.1 <sup>b</sup> | 0.0001   |
| <b>Charlson comorbidity score (mean ± SE)</b>          | 1 ± 0.05             | 0.57 ± 0.05 <sup>ab</sup>           | 1.7 ± 0.3 <sup>a</sup>         | 3.9 ± 0.9 <sup>b</sup>  | 0.0001   |

Means followed by the same superscript is not statistically significant.

**TABLE 2 |** Laboratory characteristic of the studied groups of patients.

| Item                                     | Total patients | Recovered without ICU     | Recovered after ICU        | Passed Away               | p      |
|--|----------------|---------------------------|----------------------------|---------------------------|--------|
| Number                                   | 760            | 695 (91.5%)               | 52 (6.8%)                  | 13 (1.7%)                 |        |
| O <sub>2</sub> saturation mean (%) (SEM) | 94.6 (0.13)    | 94.8 (0.14) <sup>ab</sup> | 90.6 (0.43) <sup>ac</sup>  | 85.2 (2.4) <sup>bc</sup>  | 0.0001 |
| Total WBCs count mean (SEM)/ $\mu$ l     | 7.1 (0.13)     | 6.8 (0.11) <sup>ab</sup>  | 8.3 (0.6) <sup>ac</sup>    | 12.8 (1.6) <sup>bc</sup>  | 0.0001 |
| Neutrophil count mean (SEM)/ $\mu$ l     | 4.9 (0.11)     | 4.65 (0.1)                | 6.1 (0.5)                  | 9.9 (1.4)                 | 0.0001 |
| Lymphocyte count mean (SEM)/ $\mu$ l     | 1.7 (0.04)     | 1.7 (0.04)                | 1.5 (0.1)                  | 1.75 (0.3)                | 0.186  |
| Hb mean (SEM)gm/dl                       | 14.2 (0.23)    | 14.4 (0.3)                | 13.8 (0.5)                 | 13.5 (0.5)                | 0.137  |
| PLT mean (SEM) $\mu$ l                   | 278.2 (10.4)   | 284.9 (13.5)              | 270.8 (17.6)               | 246.5 (27.3)              | 0.671  |
| INR mean (SEM)                           | 1.04 (0.01)    | 1.05 (0.01)               | 0.97 (0.02)                | 1.1 (0.05)                | 0.283  |
| PT mean (SEM)/sec.                       | 13.6 (0.12)    | 13.7 (0.13)               | 13.1 (0.19)                | 14.45 (0.6)               | 0.563  |
| PTT mean (SEM)/sec.                      | 35.6 (0.7)     | 35.5 (0.6)                | 35.2 (1.03)                | 36.6 (5.5)                | 0.903  |
| D-Dimer CRP mean (SEM) mcg/mL            | 0.7 (0.1)      | 0.48 (0.06) <sup>ab</sup> | 0.34 (0.05) <sup>ac</sup>  | 2.5 (0.88) <sup>bc</sup>  | 0.0001 |
| High CRP mean (SEM) mg/L                 | 23.6 (3.8)     | 10.7 (2.1) <sup>ab</sup>  | 48.3 (13.1) <sup>a</sup>   | 65.7 (14.9) <sup>b</sup>  | 0.0001 |
| Ferritin mean (SEM) ng/ml                | 540 (47.7)     | 416 (44.7) <sup>ab</sup>  | 745.9 (117.4) <sup>a</sup> | 1003 (197.4) <sup>b</sup> | 0.0001 |
| ALT mean (SEM) IU/L                      | 39 (5.4)       | 30.4 (2.7)                | 64.8 (25.5)                | 44.2 (7.9)                | 0.08   |
| AST mean (SEM) IU/L                      | 39 (5.1)       | 29.2 (1.8)                | 58.4 (23.2)                | 67.8 (15.9)               | 0.0001 |
| Creatinine mean (SEM) $\mu$ mol/L        | 78.2 (3.6)     | 78.4 (4.1)                | 102.75 (17.8)              | 70 (8.3)                  | 0.258  |

Means followed by the same superscript is not statistically significant.

X-rays and CT scans, are suggestive of COVID-19 (3). The COVID-19 Reporting and Data System (CO-RADS) is used as an indicator of the pulmonary engagement of COVID-19 (4). However, nucleic acid testing on respiratory tract specimens is the only laboratory confirmation of SARS-CoV-2. The angiotensin-converting enzyme 2 (ACE2) receptor has been recognized as the binding site of SARS-CoV-2 in the target cells (5). ACE2 plays a major role in patients with hypertension, CVD, obesity, and type 2 diabetes by opposing the harmful effects of the renin-angiotensin-aldosterone system (RAAS); therefore, the ACE/ACE2 ratio could be a good indicator of SARS-CoV-2 disease progression. There is a direct proportional relationship between COVID-19 infectivity and virulence that depends on the level of ACE2 expression on target cells (6, 7).

High-altitude-linked hypoxia has been reported to cause systemic inflammation associated with hypercoagulability and promotes venous thromboembolism development (8–10). Exposure to high altitudes has been reported to predispose patients to a series of thromboembolic events, due to increased blood hypercoagulability (11, 12). Platelet counts have been observed to rise within 1 week of exposure to high altitudes (13). Moreover, exposure to high altitudes for 1 year has been shown to increase plasma fibrinogen concentration by as much as 61% (14). In addition, a recent study showed that the mean platelet count is higher among high-altitude dwellers compared to low-altitude dwellers in Saudi Arabia, predisposing them for hypercoagulability (15).

The development of coagulation test abnormalities seen in COVID-19-infected patients is most likely a result of the profound inflammatory response caused by the virus and its associated coagulopathy (16). Based on these data, the combined causes of hypoxia and increased platelet counts in high-altitude dwellers may leave these people prone to more severe attacks of

disseminated intravascular coagulation if they develop a COVID-19 infection. However, a recent study has reported less severe manifestations of the disease in people living in high-altitude regions (17).

The current study aimed to analyze the clinical characteristics, laboratory findings, risk factors, associated comorbidities, radiological findings, and outcomes in patients admitted to the hospital with a confirmed COVID-19 infection in Taif, Saudi Arabia. In addition, we also aimed to investigate the effect of high altitude on the severity of the disease, based on the clinical outcomes and disease severity in the hospitalized COVID-19 patients from one high-altitude city, Taif, and a sea-level city, Jeddah.

## METHODS

### Patients and Time Frame

An observational retrospective study was conducted on a total of 760 COVID-19 laboratory-confirmed cases between April and September 2020 in Taif, Saudi Arabia. All patients were at least 18 years old and had confirmed positive polymerase chain reaction (PCR) results for COVID-19. Data from subjects were collected from the Alameen and King Faisal Hospitals, in Taif. An additional 208 subjects were recruited from Jeddah (which is at sea level), from patients at King Abdulaziz Hospital. The Jeddah data ( $n = 208$ ) were compared to matched patients from Taif ( $n = 272/760$ ). Matching patients' data from Taif were selected from the original 760 subjects based on patients' ages and comorbidities.

### Clinical and Laboratory Investigations

Initial investigations included complete blood count, highly sensitive CRP, and chest X-rays. CT chest scans were used as



**TABLE 3 |** Logistic regression analysis for independent predictors of ICU admission.

| Variable                   | Sig.  | Exp (B) | 95% C.I. for EXP(B) |        |
|----------------------------|-------|---------|---------------------|--------|
|                            |       |         | Lower               | Upper  |
| Age                        | 0.059 | 1.046   | 0.998               | 1.095  |
| DM                         | 0.663 | 0.806   | 0.305               | 2.129  |
| HTN                        | 0.646 | 0.666   | 0.117               | 3.781  |
| CKD                        | 0.855 | 1.196   | 0.176               | 8.139  |
| CAD                        | 0.597 | 0.325   | 0.005               | 20.944 |
| Charlson comorbidity index | 0.316 | 1.356   | 0.747               | 2.460  |
| WBCS                       | 0.714 | 1.105   | 0.649               | 1.880  |
| Neutrophil                 | 0.618 | 1.162   | 0.643               | 2.101  |
| CRP                        | 0.003 | 1.027   | 1.010               | 1.045  |
| D-dimer                    | 0.285 | 1.265   | 0.822               | 1.949  |
| Ferritin                   | 0.518 | 1.000   | 0.999               | 1.002  |
| Constant                   | 0.000 | 0.002   |                     |        |

a routine investigation for most of the Taif patients during the early months of the epidemic. X-rays were performed on all patients, while the CT chest scans were only applied to 722/760 (95%) of the patients. Other investigations, such as D-dimer, ferritin, alanine aminotransferase, aspartate aminotransferase (AST), creatinine, international normalized ratio, prothrombin time, and partial thromboplastin time were also conducted. Supplemental oxygen therapy was used if patients' oxygen levels were <90%, to keep these levels between 92 and 96%. Patients who were admitted to an intensive care unit (ICU) were closely monitored for adequate hemodynamic support and fluid therapy, depending on both dynamic and static parameters. Patients who required supplemental oxygen were also given dexamethasone (6 mg daily), either orally or via intravenous injection.

### The Charlson Comorbidity Index

The relationships among the severity of COVID-19, ICU admission, disease outcome, and associated comorbidities were assessed in patients from Taif. Twenty-nine points were assigned to different comorbidities: a history of myocardial infarction (one point), congestive heart failure (one point), peripheral vascular disease (one point), dementia (one point), chronic pulmonary disease (one point), rheumatologic disease (one point), peptic ulcer disease (one point), liver disease (three points), diabetes (two points), hemiplegia or paraplegia (two points), renal disease (two points), malignancy (six points), and HIV/AIDS (six points). The Charlson comorbidity index was used as previously described (18–20).

### CO-RADS Classification

CO-RADS classification was used to classify patients from Taif according to their CT results (4). Those in the CO-RADS 1 group had a normal CT or showed non-infectious radiological changes, while those in CO-RADS 2 had a CT that showed changes relevant to non-COVID-19 infectious diseases. Those described as CO-RADS 3 showed an intermediate suspension

of COVID-19, including widespread bronchopneumonia, lobar pneumonia, and ground-glass opacities (GGO) or septic emboli. Patients in CO-RADS 4 were cases in which COVID-19 was highly suspected. Unilateral GGO and multifocal consolidations without any other typical findings may be present in these patients' CT scans. A CO-RADS 5 classification is highly indicative for COVID-19, with CT showing multifocal GGO and consolidation. CO-RADS 6 was used to describe patients with a positive PCR with bilateral GGO.

### Statistical Analysis

Data are reported as means and standard error of mean (SEM) or counts and percentages, as appropriate. Comparisons among groups were made using *t* tests, the Mann–Whitney *U* test, chi-square, or Fisher exact tests, as dictated by data type and distribution. A multiple regression analysis using independent variables determined the predictors of ICU admission. One-way analysis of variance (ANOVA) was used to test differences among more than two groups. Pearson's or Spearman's correlations were used to test the correlations among variables. A  $p < 0.05$  was considered significant for all statistical analyses in this study. All analyses were performed using the Statistical Package for the Social Sciences (SPSS) version 24 for Windows (SPSS, Inc., Chicago, IL, USA).

## RESULTS

### Demographic Data of Patients From Taif

Healthcare workers accounted for 6.4% of all patients. The detected comorbidities included diabetes (16.2%), hypertension (12%), chronic obstructive pulmonary disease (3%), chronic kidney disease (2.6%), peripheral vascular disease (2.6%), coronary artery disease (1.8%), congestive heart failure (1.4%), and pulmonary embolism (PE) (3.8%). The symptoms included fever (84.7%), cough (58.2%), shortness of breath (45.3%), GIT symptoms (25.4%), sore throat (10.8%), anosmia (20.9%), and loss of taste sensation (15.7%). Sixty-four (8.5%) patients were admitted to the ICU, and 13 (1.7%) patients died. Patients were classified into three groups: (i) recovered patients without ICU admission, 695 (91.5%); (ii) recovered patients after ICU admission 52 (6.8%) patients; and (iii) deceased patients, 13 (1.7%) patients (**Table 1**).

Age is a major factor in the severity of COVID-19, as greater ages were associated with increased ICU admission and mortality rates, with  $p < 0.0001$ . We found no significant differences between the patient subgroups for gender and nationality. Patients who were admitted to the ICU and/or who died showed significant histories of hypertension, diabetes, chronic kidney disease, peripheral vascular disease, and coronary artery disease, with a  $p$  value of 0.0001 for all. We observed no significant differences in most of the initial clinical presentations among the patient subgroups, though patients with a history of ICU admission had a longer duration of hospital length of stay, with a  $p$  value of <0.0001. Charlson's comorbidity scores were significantly higher in patients admitted to the ICU and/or who died, with a  $p < 0.0001$  (**Table 1**).

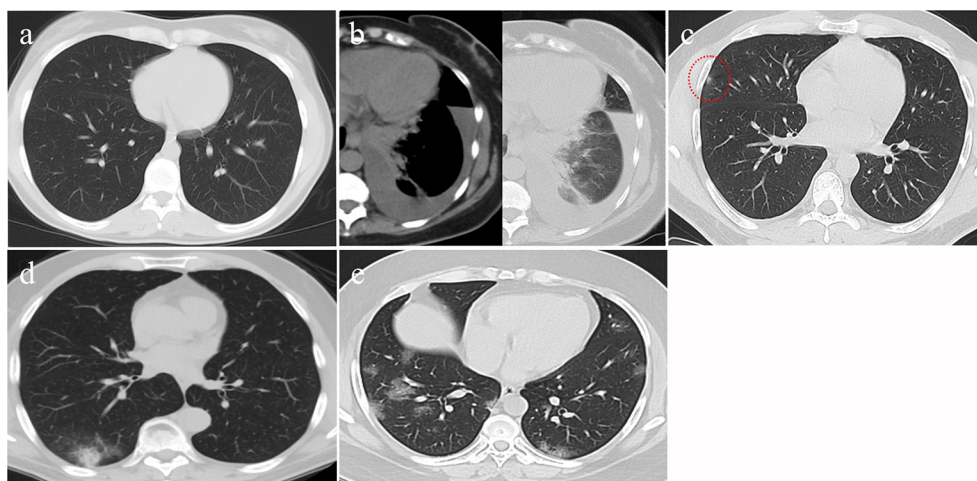


**FIGURE 1 |** CT findings of different CO-RAD stages. **(a)** Normal CT findings, in keeping with CO-RAD1. **(b)** CT showed a left lower lobar patchy area of consolidation associated with moderate pleural effusion. This picture is suggestive of bacterial pneumonia (in keeping with CO-RAD2). Note that pleural effusion is very unlikely to occur with COVID-19 pneumonia. **(c)** A very tiny right middle lobar patchy area of faint ground glass opacity (red dashed circle), in keeping with CO-RAD3. **(d)** CT chest showed right lower lobar patchy area of ground glass veiling, mounting to consolidation, in keeping with CO-RADS 4. **(e)** Bilateral, mainly peripheral and lower lobar, small patchy areas of ground glass opacity, in keeping with CO-RADS 5.

**TABLE 4 |** Radiological characteristics of the studied groups of patients.

| Item                      | Total patients | Recovered without ICU | Recovered after ICU | Passed Away | <i>p</i> |
|---------------------------|----------------|-----------------------|---------------------|-------------|----------|
| Number (%)                | 760 (100%)     | 695 (91.5%)           | 52 (6.8%)           | 13 (1.7%)   |          |
| <b>X-ray findings</b>     |                |                       |                     |             |          |
| Positive <i>n</i> (%)     | 566 (74.5)     | 504 (72.5)            | 49 (94.2)           | 13 (100)    | 0.0001   |
| <b>CT findings</b>        |                |                       |                     |             |          |
| CO-RADS 1 <i>n</i> (%)    | 138 (18.2)     | 129 (18.6)            | 9 (17.3)            | 0           | 0.03     |
| CO-RADS 2 <i>n</i> (%)    | 29 (3.8)       | 29 (4.2)              | 0                   | 0           |          |
| CO-RADS 3 <i>n</i> (%)    | 12 (1.6)       | 12 (1.7)              | 0                   | 0           |          |
| CO-RADS 4 <i>n</i> (%)    | 22 (2.9)       | 20 (2.9)              | 1 (1.9)             | 1 (7.7)     |          |
| CO-RADS 5 <i>n</i> (%)    | 521 (68.6)     | 468 (67.3)            | 51 (98.1)           | 12 (92.3)   |          |
| Un-available <i>n</i> (%) | 38 (6)         | 37 (5.3)              | 1 (1.9)             | 0           |          |

Patients' mean oxygen saturation percentage at the time of admission was 94.6%, and 45.1% of our patients showed absolute lymphocytopenia. The mean level of high-sensitivity CRP was 23.6 (3.8) mg/L, the mean ferritin level was 540 (47.7) ng/ml, and the mean D-dimer level was 0.7 (0.1) mcg/ml. Patients with a history of ICU admission and/or death showed significant hypoxia, with a  $p < 0.001$ . Leukocytosis and neutrophilia were found to be significant among patients admitted to the ICU and/or who died, in addition to significantly higher D-dimer, ferritin, and highly sensitive CRP levels, with a  $p < 0.0001$  for all patients (Table 2).

A logistic regression analysis for patients admitted to an ICU showed that the level of highly sensitive CRP was the most independent predictor for death, with a  $p$  value of 0.003 (Table 3). Radiological investigations of our confirmed cases showed that 74.5% had positive results in a chest x-ray. By contrast, 95% of our patients had CT chest affections and were classified according to the CO-RADS classification system (Figure 1); 18.2% were

CO-RADS 1, 3.8% were CO-RADS 2, 1.6% were CO-RADS 3, 2.9% were CO-RADS 4, and 68.6% were CO-RADS 5. There was a significant difference among patient subgroups regarding the chest CT and chest X-ray results, with  $p$ -values of 0.03 and 0.0001, respectively (Table 4).

Pearson's correlation was conducted between the different parameters with disease severity and radiological findings. Items that only showed significant correlation was presented in Table 5. Age, AST, D-dimer, ferritin, and CRP showed highly significant correlation ( $P > 0.01$ ) with both disease severity and radiological findings.

## Comparison of Matched Patients in High Altitude and Sea Level

Upon comparing the clinical data of matched patients from Taif and Jeddah, we noted that SARS-CoV-2 infection rates were found to be significantly higher in males than in females, and among subjects between the ages of 21–40 years and 41–60 years

**TABLE 5 |** Correlation between clinical, laboratory, disease severity and CT findings.

| Item             |          | Disease severity | CT results |
|------------------|----------|------------------|------------|
| Age              | <i>r</i> | 0.249**          | 0.164**    |
|                  | Sig.     | 0.000            | 0.000      |
| Disease severity | <i>r</i> | 1                | 0.080*     |
|                  | Sig.     |                  | 0.031      |
| O <sub>2</sub>   | <i>r</i> | −0.197-*         | −0.039-    |
|                  | Sig.     | 0.000            | 0.294      |
| RBCs             | <i>r</i> | −0.105-*         | −0.069-    |
|                  | Sig.     | 0.012            | 0.108      |
| ESR              | <i>r</i> | 0.334**          | 0.016      |
|                  | Sig.     | 0.000            | 0.763      |
| HCT              | <i>r</i> | −0.102-*         | −0.066-    |
|                  | Sig.     | 0.016            | 0.128      |
| MCV              | <i>r</i> | 0.110**          | 0.026      |
|                  | Sig.     | 0.009            | 0.553      |
| WBCs             | <i>r</i> | 0.275**          | 0.000      |
|                  | Sig.     | 0.000            | 0.995      |
| Neutrophils      | <i>r</i> | 0.319**          | 0.041      |
|                  | Sig.     | 0.000            | 0.337      |
| Lymphocyte       | <i>r</i> | −0.047-          | −0.091-*   |
|                  | Sig.     | 0.252            | 0.031      |
| ALT              | <i>r</i> | 0.110**          | 0.084*     |
|                  | Sig.     | 0.005            | 0.035      |
| AST              | <i>r</i> | 0.221**          | 0.122**    |
|                  | Sig.     | 0.000            | 0.002      |
| Urea             | <i>r</i> | 0.118*           | −0.103-*   |
|                  | Sig.     | 0.013            | 0.033      |
| D-dimer          | <i>r</i> | 0.225**          | −0.005-    |
|                  | Sig.     | 0.000            | 0.921      |
| Ferritin         | <i>r</i> | 0.292**          | 0.163**    |
|                  | Sig.     | 0.000            | 0.001      |
| CRP              | <i>r</i> | 0.348**          | 0.221**    |
|                  | Sig.     | 0.000            | 0.000      |

\*Correlation is significant at the 0.05 level.

\*\*Correlation is significant at the 0.01 level.

in both the high-altitude (Taif) and sea-level (Jeddah) regions (**Table 6**).

Interestingly, we detected a significantly higher percentage of recovery in the high-altitude region, in comparison with those living at sea level. Importantly, the death rate in the sea level region was nearly threefold that reported in the high-altitude region (**Table 7**).

Contrary to the above results, significantly higher rates of deep vein thrombosis, PE, MI, and acute large vessel occlusion were reported in the high-altitude region, compared to the sea-level region. However, the incidence of fever, cough, shortness of breath, and acute respiratory distress syndrome (ARDS) during the course of the disease were higher in Jeddah than in Taif. Importantly, the incidence of comorbidities such as diabetes mellitus, hypertension, asthma, ischemic stroke, and coronary

**TABLE 6 |** Demographic data of Jeddah and Taif COVID-19 patients.

| Demographic factors | Categories | Jeddah |       | Taif |       |
|---------------------|------------|--------|-------|------|-------|
|                     |            | No.    | %     | No.  | %     |
| Gender              | Male       | 136    | 65.40 | 183  | 67.30 |
|                     | Female     | 72     | 34.60 | 89   | 32.70 |
|                     | Total      | 208    | 100.0 | 272  | 100.0 |
| Age (year)          | 18–20      | 11     | 5.3   | 19   | 7.0   |
|                     | 21–40      | 104    | 50.0  | 132  | 48.5  |
|                     | 41–60      | 75     | 36.1  | 94   | 34.6  |
|                     | 61–80      | 14     | 6.7   | 25   | 9.2   |
|                     | 81+        | 4      | 1.9   | 2    | 0.7   |
| Healthcare worker   |            | 16     | 7.69  | 20   | 7.35  |

disease showed no significant differences between the high-altitude and sea-level regions (**Table 7**).

## DISCUSSION

In our study, as reported in other studies, patient age was a critical risk factor for ICU admission, with elderly patients being the most frequently admitted. In addition, comorbidities such as hypertension, diabetes mellitus, chronic kidney disease, ischemic heart disease, peripheral vascular disease, and malignancies were found to correlate with an increased probability of ICU admission and fatal consequences. Our findings also agree with previously available studies in this respect (21–25).

Patients who were admitted to the ICU and those who died showed significantly higher Charlson comorbidity scores than other patients did. These results were similar to previously published data from Denmark (26). Our results indicated that the Charlson comorbidity index is a valid indicator for COVID-19 patients with poor outcomes, in concordance with previous studies (27, 28).

In this study, we found no significant relationship between the presence of fever, cough, shortness of breath, GIT symptoms, and being a healthcare worker or with ICU admission or mortality. Our results did not match other studies (29, 30) that found a high fever to be associated with COVID-19 progression; we attribute this distance to differences in the studies' designs.

In contrast to the above, sore throat and a loss of smell and taste sensation were associated with a good prognosis among confirmed cases of COVID-19. Our results agree with a previous study that reported a correlation between smell loss and decreased hospitalization, intubation, and acute respiratory distress syndrome (31). In addition, another study also found that patients with a sore throat had better outcomes than others (32). However, there is no available explanation for these correlations.

Our study showed that low oxygen saturation at the time of admission was associated with poor outcomes. Hypoxia was found to be a powerful independent predictor of mortality in COVID-19 patients (33). Previous studies showed a strong relationship between hypoxia and both increasing the inflammatory response (34) and induction of viral replication

**TABLE 7 |** Clinical, laboratory and deaths among COVID-19 ICU patients in Jeddah and Taif.

| Variable                      |     | Jeddah (n = 208) |       | Taif (n = 272) |       | $\chi^2$ | P-value |
|-------------------------------|-----|------------------|-------|----------------|-------|----------|---------|
|                               |     | No.              | %     | No.            | %     |          |         |
| Fever                         | No  | 87               | 41.83 | 154            | 56.62 | 10.31    | 0.00**  |
|                               | Yes | 121              | 58.17 | 118            | 43.38 |          |         |
| Cough                         | No  | 98               | 47.12 | 163            | 59.93 | 7.79     | 0.00**  |
|                               | Yes | 110              | 52.88 | 109            | 40.07 |          |         |
| Shortness of breath           | No  | 115              | 55.29 | 192            | 70.59 | 11.96    | 0.00**  |
|                               | Yes | 93               | 44.71 | 80             | 29.41 |          |         |
| Headache and sore throat      | No  | 184              | 88.46 | 243            | 89.34 | 0.09     | 0.76    |
|                               | Yes | 24               | 11.54 | 29             | 10.66 |          |         |
| Smell                         | No  | 197              | 94.70 | 252            | 92.60 | 0.83     | 0.36    |
|                               | Yes | 11               | 5.30  | 20             | 7.40  |          |         |
| Loss of Taste                 | No  | 203              | 97.60 | 271            | 99.63 | 3.96     | 0.04*   |
|                               | Yes | 5                | 2.40  | 1              | 0.37  |          |         |
| GIT symptoms                  | No  | 181              | 87.02 | 233            | 85.7  | 0.183    | 0.669   |
|                               | Yes | 27               | 12.98 | 39             | 14.3  |          |         |
| Chronic diseases              | No  | 175              | 84.13 | 238            | 87.5  | 1.11     | 0.29    |
|                               | Yes | 33               | 15.87 | 34             | 12.5  |          |         |
| Diabetes mellites             | No  | 162              | 77.88 | 219            | 80.5  | 0.498    | 0.48    |
|                               | Yes | 46               | 22.12 | 53             | 19.5  |          |         |
| Hypertension                  | No  | 169              | 81.20 | 225            | 82.70 | 0.17     | 0.67    |
|                               | Yes | 39               | 18.80 | 47             | 17.30 |          |         |
| Asthma                        | No  | 194              | 93.30 | 251            | 92.30 | 0.17     | 0.67    |
|                               | Yes | 14               | 6.70  | 21             | 7.70  |          |         |
| DVT                           | No  | 205              | 98.60 | 256            | 94.10 | 6.11     | 0.01 *  |
|                               | Yes | 3                | 1.40  | 16             | 5.90  |          |         |
| PE                            | No  | 205              | 98.60 | 244            | 89.70 | 15.28    | 0.00**  |
|                               | Yes | 3                | 1.40  | 28             | 10.30 |          |         |
| MI                            | No  | 206              | 99.00 | 259            | 95.20 | 5.67     | 0.01*   |
|                               | Yes | 2                | 1.00  | 13             | 4.80  |          |         |
| Ischemic stroke               | No  | 202              | 97.10 | 259            | 95.20 | 1.11     | 0.29    |
|                               | Yes | 6                | 2.90  | 13             | 4.80  |          |         |
| ARDS                          | No  | 186              | 89.42 | 258            | 94.85 | 5        | 0.02*   |
|                               | Yes | 22               | 10.58 | 14             | 5.15  |          |         |
| Acute large vessels occlusion | No  | 207              | 99.52 | 259            | 95.22 | 7.69     | 0.00**  |
|                               | Yes | 1                | 0.48  | 13             | 4.78  |          |         |
| Coronary disease              | No  | 203              | 97.60 | 260            | 95.59 | 1.39     | 0.23    |
|                               | Yes | 5                | 2.40  | 12             | 4.41  |          |         |
| Tumor                         | No  | 205              | 98.56 | 272            | 205   | 3.94     | 0.04*   |
|                               | Yes | 3                | 1.44  | 0              | 0     |          |         |
| CKD                           | No  | 203              | 97.60 | 270            | 99.26 | 2.28     | 0.13    |
|                               | Yes | 5                | 2.40  | 2              | 0.74  |          |         |
| Death                         | No  | 30               | 14.42 | 13             | 4.78  | 11.37    | 0.00**  |
|                               | Yes | 178              | 85.58 | 259            | 95.22 |          |         |

\*P-value refers to statistically significant result. \*\*P-value refers to statistically highly significant result.

(35, 36). It might also play a role in the pathogenesis of hypercoagulation (37).

In our study, we found that the presence of leukocytosis, neutrophilia, high levels of highly sensitive CRP, ferritin, D-dimer, and AST at the time of admission were associated with patients' deterioration, ICU admission, and death. Additionally, a significant correlation was found between

such parameters and both the disease severity. These results were in line with previous studies that reported a significant association between disease progression and poor outcomes, with increased levels of inflammatory biomarkers and leukocytosis (38–40).

Logistic regression analysis showed that highly sensitive CRP was the most significant independent predictor of death among



COVID-19 patients who were admitted to an ICU. This finding corresponds with previous reports that confirmed that CRP is the major determinant of disease severity in COVID-19 patients (41, 42). It may also highlight the role of secondary infection in the deterioration of patients' health status. Interestingly, the use of steroids was reported to be associated with secondary infection (43, 44).

In all, 18.2% of our patients showed normal chest CT appearance. Chest CTs were conducted early for most of our patients, and it is well-known that chest CTs continue to be normal in the first 4–5 days of infection (45). Meanwhile, among those who were admitted to the ICU and who later died, the chest CT results were significantly positive. At present, chest CT is not routinely ordered, and its use is limited to specific cases, especially in patients with false negative PCR (46, 47). However, we found a significant correlation of the radiological findings and the severity of the disease. This finding was also in accordance with recent findings that found similar correlation (48, 49).

We observed a lower mortality rate among people living at a high altitude, in comparison to those living at sea level. Another study has suggested a reduced severity of SARS-CoV-2 in high-altitude-dwelling patients (17); however, there are no current data explaining the mechanism involved in such an effect. The number of ACE2 receptors in target cells affects the susceptibility of such cells to SARS-CoV-2 infection. One speculation is the assumption that high-altitude inhabitants possess hypoxia-induced downregulation of ACE2. The RAAS is the expression of both ACE1 and ACE2 in negative feedback manner. During hypoxia, ACE2 is downregulated in the concomitant upregulation of ACE1 (50). Accordingly, decreased expressions of ACE2 in the pulmonary endothelial lining among high-altitude inhabitants is assumed to reduce the amplitude of virus replication (17). This speculation was argued strongly by Pun et al. (51), who presented conflicting results regarding ACE2. Their argument was augmented by many previous studies that reported the upregulation of ACE2 via hypoxia (52–54). Furthermore, deciphering hypoxia as a potential factor that alters the ACE2 expression is still obscure and needs further investigation. It is possible that some other, still-unknown mechanism renders high-altitude inhabitants more resistant to the severe

consequences of COVID-19, compared to their sea-level-dwelling contemporaries.

## CONCLUSION

Fever, cough, and shortness of breath are the main clinical presentations in COVID-19 patients. Age, multiple comorbidities, a high Charlson comorbidity score, leukocytosis, neutrophilia, higher levels of highly sensitive CRP, ferritin, D-dimer, and AST are associated with poor outcomes among COVID-19 patients. High-altitude inhabitants showed reduced disease severity, in comparison with sea-level-dwelling patients.

## DATA AVAILABILITY STATEMENT

The original contributions presented in the study are included in the article/supplementary material, further inquiries can be directed to the corresponding author/s.

## ETHICS STATEMENT

The studies involving human participants were reviewed and approved by Research and Studies Department, Directorate of Health Affairs, Taif, Saudi Arabia (NO. 397 on 23/07/2020). The patients/participants provided their written informed consent to participate in this study.

## AUTHOR CONTRIBUTIONS

AF, AR, MR, RMMA, and AAA collected and analyzed the data from Alamin hospital. RMA, SAA, TA, and SMA collected and analyzed data from Jeddah. MA, ZI, DN, ANA, and DA analyzed the data and prepared the initial draft. DN, DA, ASA-M and AAA conceived the study protocol and critically revised the manuscript. All authors shared in data analysis and discussing and approved the final form of the manuscript.

## ACKNOWLEDGMENTS

The researchers gratefully acknowledge the Taif University Researchers Supporting Program (TURSP-2020/233) of Taif University, Taif, Saudi Arabia.

## REFERENCES

- McIntosh K, Hirsch M, Bloom A. *Coronavirus Disease 2019 (COVID-19). Up-to-Date.* (2020). Available online at: <https://www.uptodate.com/contents/middle-east-respiratory-syndrome-coronavirus-treatment-and-preventionUpdatedFebruary24,2020>. (accessed February 22, 2020).
- Carlos WG, Dela Cruz CS, Cao B, Pasnick S, Jamil S. Novel Wuhan (2019-nCoV) coronavirus. *Am J Respir Crit Care Med.* (2020) 201:P7–P8. doi: 10.1164/rccm.2014P7
- Guan W-J, Ni Z-Y, Hu Y, Liang W-H, Ou C-Q, He J-X, et al. Clinical characteristics of coronavirus disease 2019 in China. *N Engl J Med.* (2020) 382:1708–20. doi: 10.1056/NEJMoa2002032
- Prokop M, Van Everdingen W, Van Rees Vellinga T, Quarles Van Ufford H, Stöger L, Beenen L, et al. CO-RADS: a categorical CT assessment scheme for patients suspected of having COVID-19-definition and evaluation. *Radiology.* (2020) 296:E97–104. doi: 10.1148/radiol.2020201473
- Wan Y, Shang J, Graham R, Baric RS, Li F. Receptor recognition by the novel coronavirus from Wuhan: an analysis based on decade-long structural studies of SARS coronavirus. *J Virol.* (2020) 94:e00127–20. doi: 10.1128/JVI.00127-20
- Ferreira AJ, Shenoy V, Qi Y, Fraga-Silva RA, Santos RA, Katovich MJ, et al. Angiotensin-converting enzyme 2 activation protects against hypertension-induced cardiac fibrosis involving extracellular signal-regulated kinases. *Exp Physiol.* (2011) 96:287–94. doi: 10.1113/expphysiol.2010.055277
- Patel VB, Zhong JC, Grant MB, Oudit GY. Role of the ACE2/angiotensin 1-7 axis of the renin-angiotensin system in heart failure. *Circ Res.* (2016) 118:1313–26. doi: 10.1161/CIRCRESAHA.116.307708

8. Van Veen JJ, Makris M. Altitude and coagulation activation: does going high provoke thrombosis? *Acta Haematol.* (2008) 119:156–57. doi: 10.1159/000128045
9. Sabit R, Thomas P, Shale DJ, Collins P, Linnane SJ. The effects of hypoxia on markers of coagulation and systemic inflammation in patients with COPD. *Chest.* (2010) 138:47–51. doi: 10.1378/chest.09-2764
10. Brill A, Suidan GL, Wagner DD. Hypoxia, such as encountered at high altitude, promotes deep vein thrombosis in mice. *J Thromb Haemost.* (2013) 11:1773–75. doi: 10.1111/jth.12310
11. Schreijer AJ, Cannegieter SC, Rosendaal FR, Helmerhorst FM. A case of thrombosis at high altitude. *Thromb Haem.* (2005) 94:1104–5. doi: 10.1160/TH05-05-1104
12. Gupta N, Ashraf MZ. Exposure to high altitude: a risk factor for venous thromboembolism? *Semin Thromb Hemost.* (2012) 38:156–63. doi: 10.1055/s-0032-1301413
13. Hudson JG, Bowen AL, Navia P, Rios-Dalenz J, Pollard AJ, Williams D, et al. The effect of high altitude on platelet counts, thrombopoietin and erythropoietin levels in young Bolivian airmen visiting the Andes. *Int J Biometeorol.* (1999) 43:85–90. doi: 10.1007/s004840050120
14. Vij AG. Effect of prolonged stay at high altitude on platelet aggregation and fibrinogen levels. *Platelets.* (2009) 20:421–7. doi: 10.1080/09537100903116516
15. Algahtani FH, Alqahtany FS, Al-Shehri A, Abdelgader AM. Features and incidence of thromboembolic disease: a comparative study between high and low altitude dwellers in Saudi Arabia. *Saudi J Biol Sci.* (2020) 27:1632–6. doi: 10.1016/j.sjbs.2020.03.004
16. Connors JM, Levy JH. COVID-19 and its implications for thrombosis and anticoagulation. *Blood.* (2020) 135:2033–40. doi: 10.1182/blood.2020006000
17. Arias-Reyes C, Zubietta-Deurioste N, Poma-Machicao L, Aliaga-Raduan F, Carvajal-Rodriguez F, Dutschmann M, et al. Does the pathogenesis of SARS-CoV-2 virus decrease at high-altitude? *Respir Physiol Neurobiol.* (2020) 277:103443. doi: 10.1016/j.resp.2020.103443
18. Charlson ME, Pompei P, Ales KL, Mackenzie CR. A new method of classifying prognostic comorbidity in longitudinal studies: development and validation. *J Chronic Dis.* (1987) 40:373–83. doi: 10.1016/0021-9681(87)90171-8
19. Charlson M, Szatrowski TP, Peterson J, Gold J. Validation of a combined comorbidity index. *J Clin Epidemiol.* (1994) 47:1245–51. doi: 10.1016/0895-4356(94)90129-5
20. Quan H, Li B, Couris CM, Fushimi K, Graham P, Hider P, et al. Updating and validating the Charlson comorbidity index and score for risk adjustment in hospital discharge abstracts using data from 6 countries. *Am J Epidemiol.* (2011) 173:676–682. doi: 10.1093/aje/kwq433
21. Zheng Z, Peng F, Xu B, Zhao J, Liu H, Peng J, et al. Risk factors of critical & mortal COVID-19 cases: A systematic literature review and meta-analysis. *J Infect* 81, e16–e25. doi: 10.1016/j.jinf.2020.04.021
22. Huang C, Wang Y, Li X, Ren L, Zhao J, Hu Y, et al. Clinical features of patients infected with 2019 novel coronavirus in Wuhan, China. *Lancet.* (2020) 395:497–506. doi: 10.1016/S0140-6736(20)30183-5
23. Liu W, Tao ZW, Wang L, Yuan ML, Liu K, Zhou L, et al. Analysis of factors associated with disease outcomes in hospitalized patients with 2019 novel coronavirus disease. *Chin Med J (Engl).* (2020) 133:1032–8. doi: 10.1097/CM9.0000000000000775
24. Wang D, Hu B, Hu C, Zhu F, Liu X, Zhang J, et al. Clinical Characteristics of 138 Hospitalized Patients With 2019 Novel Coronavirus-Infected Pneumonia in Wuhan, China. *Jama* 323, 1061–1069. doi: 10.1001/jama.2020.1585
25. Zhou F, Yu T, Du R, Fan G, Liu Y, Liu Z, et al. Clinical course and risk factors for mortality of adult inpatients with COVID-19 in Wuhan, China: a retrospective cohort study. *Lancet* 395, 1054–1062. doi: 10.1016/S0140-6736(20)30566-3
26. Christensen DM, Strange JE, Gislason G, Torp-Pedersen C, Gerds T, Fosbøl E, et al. Charlson comorbidity index score and risk of severe outcome and death in danish COVID-19 patients. *J Gen Intern Med* 35, 2801–2803. doi: 10.1007/s11606-020-05991-z
27. Tuty Kuswardhani RA, Henrina J, Pranata R, Anthonius Lim M, Lawrensia S, Suastika K. Charlson comorbidity index and a composite of poor outcomes in COVID-19 patients: A systematic review and meta-analysis. *Diabetes Metab Syndr* 14, 2103–2109. doi: 10.1016/j.dsx.2020.10.022
28. Zhou W, Qin X, Hu X, Lu Y, Pan J. Prognosis models for severe and critical COVID-19 based on the Charlson and Elixhauser comorbidity indices. *Int J Med Sci* 17, 2257–2263. doi: 10.7150/ijms.50007
29. Chang MC, Park YK, Kim BO, Park D. Risk factors for disease progression in COVID-19 patients. *BMC Infect Dis.* (2020) 20:445. doi: 10.1186/s12879-020-05144-x
30. Rod JE, Oviedo-Trespalacios O, Cortes-Ramirez J. A brief-review of the risk factors for covid-19 severity. *Rev Saude Publica.* (2020) 54:60. doi: 10.11606/s1518-8787.2020054002481
31. Foster KJ, Jauregui E, Tajudeen B, Bishehsari F, Mahdavinia M. Smell loss is a prognostic factor for lower severity of coronavirus disease 2019. *Ann Allergy Asthma Immunol.* (2020) 125:481–3. doi: 10.1016/j.anai.2020.07.023
32. Kim SR, Nam SH, Kim YR. Risk factors on the progression to clinical outcomes of COVID-19 patients in south korea: using national data. *Int J Environ Res Public Health.* (2020) 17:1723884. doi: 10.3390/ijerph17238847
33. Somers VK, Kara T, Xie J. Progressive hypoxia: A pivotal pathophysiologic mechanism of COVID-19 pneumonia. *Mayo Clin Proc* 95, 2339–2342. doi: 10.1016/j.mayocp.2020.09.015
34. Eltzschig HK, Carmeliet P. Hypoxia and inflammation. *N Engl J Med.* (2011) 364:656–65. doi: 10.1056/NEJMra0910283
35. Vassilaki N, Kalliampakou KI, Kotta-Loizou I, Befani C, Liakos P, Simos G, et al. Low oxygen tension enhances hepatitis C virus replication. *J Virol.* (2013) 87:2935–48. doi: 10.1128/JVI.02534-12
36. López-Rodríguez DM, Kirillov V, Krug LT, Mesri EA, Andreansky S. A role of hypoxia-inducible factor 1 alpha in Murine Gammaherpesvirus 68 (MHV68) lytic replication and reactivation from latency. *PLoS Pathog.* (2019) 15:e1008192. doi: 10.1371/journal.ppat.1008192
37. Pilli VS, Datta A, Afreen S, Catalano D, Szabo G, Majumder R. Hypoxia downregulates protein S expression. *Blood.* (2018) 132:452–5. doi: 10.1182/blood-2018-04-841585
38. Cao G, Li P, Chen Y, Fang K, Chen B, Wang S, et al. A risk prediction model for evaluating the disease progression of COVID-19 pneumonia. *Front Med (Lausanne).* (2020) 7:556886. doi: 10.3389/fmed.2020.556886
39. Liu F, Li L, Xu M, Wu J, Luo D, Zhu Y, et al. Prognostic value of interleukin-6, C-reactive protein, and procalcitonin in patients with COVID-19. *J Clin Virol.* (2020) 127:104370. doi: 10.1016/j.jcv.2020.104370
40. Tan C, Huang Y, Shi F, Tan K, Ma Q, Chen Y, et al. C-reactive protein correlates with computed tomographic findings and predicts severe COVID-19 early. *J Med Virol.* (2020) 92:856–62. doi: 10.1002/jmv.25871
41. Malik P, Patel U, Mehta D, Patel N, Kelkar R, Akrmah M, et al. Biomarkers and outcomes of COVID-19 hospitalisations: systematic review and meta-analysis. *BMJ Evid Based Med.* (2020) bmjebm-2020-111536. doi: 10.1136/bmjebm-2020-111536
42. Sharifpour M, Rangaraju S, Liu M, Alabyad D, Nahab FB, Creel-Bulos CM, et al. C-Reactive protein as a prognostic indicator in hospitalized patients with COVID-19. *PLoS One.* (2020) 15:e0242400. doi: 10.1371/journal.pone.0242400
43. Obata R, Maeda T, Do DR, Kuno T. Increased secondary infection in COVID-19 patients treated with steroids in New York City. *Jpn J Infect Dis.* (2020). doi: 10.7883/yoken.JJID.2020.884
44. Ripa M, Galli L, Poli A, Oltolini C, Spagnuolo V, Mastrangelo A, et al. Secondary infections in patients hospitalized with COVID-19: incidence and predictive factors. *Clin Microbiol Infect.* (2020) 27:451–7. doi: 10.1016/j.cmi.2020.10.021
45. Adams HJA, Kwee TC, Yakar D, Hope MD, Kwee RM. Chest CT imaging signature of coronavirus disease 2019 infection: in pursuit of the scientific evidence. *Chest.* (2020) 158, 1885–95. doi: 10.1016/j.chest.2020.06.025
46. Pan F, Ye T, Sun P, Gui S, Liang B, Li L, et al. Time course of lung changes at chest ct during recovery from coronavirus disease 2019 (COVID-19). *Radiology.* (2020) 295:715–21. doi: 10.1148/radiol.2020200370
47. Rubin GD, Ryerson CJ, Haramati LB, Sverzellati N, Kanne JP, Raoof S, et al. The role of chest imaging in patient management during the COVID-19 pandemic: a multinational consensus statement from the fleischner society. *Chest.* (2020) 158:106–16. doi: 10.1016/j.chest.2020.04.003
48. Francome M, Iafrate F, Masci GM, Coco S, Cilia F, Manganaro L, et al. Chest CT score in COVID-19 patients: correlation with disease severity and short-term prognosis. *Eur Radiol.* (2020) 30:6808–17. doi: 10.1007/s00330-020-07033-y

49. Al-Smadi AS, Bhatnagar A, Ali R, Lewis N, Johnson S. Correlation of chest radiography findings with the severity and progression of COVID-19 pneumonia. *Clin Imag.* (2021) 71:17–23. doi: 10.1016/j.clinimag.2020.11.004
50. Zhang R, Wu Y, Zhao M, Liu C, Zhou L, Shen S, et al. Role of HIF-1 $\alpha$  in the regulation ACE and ACE2 expression in hypoxic human pulmonary artery smooth muscle cells. *Am J Physiol Lung Cell Mol Physiol.* (2009) 297:L631–40. doi: 10.1152/ajplung.90415.2008
51. Pun M, Turner R, Strapazzon G, Brugger H, Swenson ER. Lower incidence of COVID-19 at high altitude: facts and confounders. *High Alt Med Biol.* (2020) 21:217–22. doi: 10.1089/ham.2020.0114
52. Hampl V, Herget J, Bíbová J, Banasová A, Husková Z, Vanourková Z, et al. Intrapulmonary activation of the angiotensin-converting enzyme type 2/angiotensin 1-7/G-protein-coupled Mas receptor axis attenuates pulmonary hypertension in Ren-2 transgenic rats exposed to chronic hypoxia. *Physiol Res.* (2015) 64:25–38. doi: 10.33549/physiolres.932861
53. Oarhe CI, Dang V, Dang M, Nguyen H, Gopallawa I, Gewolb IH, et al. (2015). Hyperoxia downregulates angiotensin-converting enzyme-2 in human fetal lung fibroblasts. *Pediatric Res.* (2015) 77:656–62. doi: 10.1038/pr.2015.27
54. Joshi S, Wollenzien H, Leclerc E, Jarajapu YP. Hypoxic regulation of angiotensin-converting enzyme 2 and Mas receptor in human CD34(+) cells. *J Cell Physiol.* (2019) 234:20420–31. doi: 10.1002/jcp.28643

**Conflict of Interest:** The authors declare that the research was conducted in the absence of any commercial or financial relationships that could be construed as a potential conflict of interest.

Copyright © 2021 Abdelsalam, Althaqafi, Assiri, Althagafi, Althagafi, Fouda, Ramadan, Rabah, Ahmed, Ibrahim, Nemenqani, Alghamdi, Al Aboud, Abdel-Moneim and Alsulaimani. This is an open-access article distributed under the terms of the Creative Commons Attribution License (CC BY). The use, distribution or reproduction in other forums is permitted, provided the original author(s) and the copyright owner(s) are credited and that the original publication in this journal is cited, in accordance with accepted academic practice. No use, distribution or reproduction is permitted which does not comply with these terms.



# Unknown Disease Outbreaks Detection: A Pilot Study on Feature-Based Knowledge Representation and Reasoning Model

Rui Feng<sup>1</sup>, Qiping Hu<sup>1\*</sup> and Yingan Jiang<sup>2</sup>

<sup>1</sup> School of Computer Science, Wuhan University, Wuhan, China, <sup>2</sup> Department of Infectious Diseases, Renmin Hospital of Wuhan University, Wuhan, China

## OPEN ACCESS

### Edited by:

Reza Lashgari,  
Institute for Research in Fundamental  
Sciences, Iran

### Reviewed by:

Salem Y. Mohamed,  
Ministry of Defence, Brazil  
Rachid Ait Addi,  
Cadi Ayyad University, Morocco

### \*Correspondence:

Qiping Hu  
huqp@whu.edu.cn

### Specialty section:

This article was submitted to  
Infectious Diseases-Surveillance,  
Prevention and Treatment,  
a section of the journal  
Frontiers in Public Health

**Received:** 22 March 2021

**Accepted:** 14 April 2021

**Published:** 13 May 2021

### Citation:

Feng R, Hu Q and Jiang Y (2021)  
Unknown Disease Outbreaks  
Detection: A Pilot Study on  
Feature-Based Knowledge  
Representation and Reasoning Model.  
Front. Public Health 9:683855.  
doi: 10.3389/fpubh.2021.683855

**Background:** The outbreak of COVID-19 in 2019 has rapidly swept the world, causing irreparable loss to human beings. The pandemic has shown that there is still a delay in the early response to disease outbreaks and needs a method for unknown disease outbreak detection. The study's objective is to establish a new medical knowledge representation and reasoning model, and use the model to explore the feasibility of unknown disease outbreak detection.

**Methods:** The study defined abnormal values with diagnostic significances from clinical data as the Features, and defined the Features as the antecedents of inference rules to match with knowledge bases, achieved in detecting known or emerging infectious disease outbreaks. Meanwhile, the study built a syndromic surveillance base to capture the target cases' Features to improve the reliability and fault-tolerant ability of the system.

**Results:** The study combined the method with Severe Acute Respiratory Syndrome (SARS), Middle East Respiratory Syndrome (MERS), and early COVID-19 outbreaks as empirical studies. The results showed that with suitable surveillance guidelines, the method proposed in this study was capable to detect outbreaks of SARS, MERS, and early COVID-19 pandemics. The quick matching accuracies of confirmed infection cases were 89.1, 26.3–98%, and 82%, and the syndromic surveillance base would capture the Features of the remaining cases to ensure the overall detection accuracies. Based on the early COVID-19 data in Wuhan, this study estimated that the median time of the early COVID-19 cases from illness onset to local authorities' responses could be reduced to 7.0–10.0 days.

**Conclusions:** This study offers a new solution to transfer traditional medical knowledge into structured data and form diagnosis rules, enables the representation of doctors' logistic thinking and the knowledge transmission among different users. The results of empirical studies demonstrate that by constantly inputting medical knowledge into the system, the proposed method will be capable to detect unknown diseases from existing ones and perform an early response to the initial outbreaks.

**Keywords:** knowledge representation, reasoning model, medical diagnosis, medical expert systems, surveillance, unknown disease outbreaks



## INTRODUCTION

In December 2019, a series of pneumonia cases with unknown etiologies appeared in Wuhan, Hubei province, China. The clinical manifestations were similar to those of viral pneumonia (1). After sequencing and analyzing, researchers found a novel coronavirus and named it SARS-COV-2 (2). By April 28, 2021, the number of people infected with COVID-19 globally had exceeded 148 million, and the number of deaths had exceeded over 3.1 million (3). The outbreak has highlighted the inadequate global capacity to prevent, screen, and respond to unknown disease outbreaks, and the fight against infectious diseases remains one of the essential tasks of the 21st century.

A disease outbreak may start with a single infectious case that has not been presented for an extended period or caused by unknown agents (e.g., bacterium or virus) in the community or region, or the presence of a previously unknown disease (4). Most countries are now using syndromic surveillance as a method to identify potential public health threats. Syndromic surveillance collects data based primarily on non-specific health indicators and non-clinical indicators (5), and analyzes the time-space distortion of these data to achieve early detection and rapid response ability of public health events (6). However, the current syndromic surveillance systems belong to the passive surveillance mode and rely heavily on the reporters' identification of reportable diseases (7). Moreover, the surveillance objects are relatively single, unable to detect newly emerging outbreaks with previously unseen patterns of symptoms or other unexpected events of relevance to public health (8). Many medical staff members lack corresponding training and motivation toward emerging public health events in many regions, especially at the grassroots level (9). Therefore, relying only on syndromic surveillance is unable to detect unknown disease outbreaks, leading to the lag of response toward public health events (10).

Recently, researchers are focusing on using machine learning for pre-syndromic surveillance to identify relevant clusters of disease cases without pre-classification into syndromes. Lall et al. (11) and Walsh et al. (12) introduced a data-driven method to monitor the sudden increases in word frequency in the emergency department's chief complaint data to determine whether the text patterns in these data require further epidemiology investigation and continuous surveillance. Maurya et al. (13) proposed a Spatially Compact Semantic Scan (SCSS) method based on the Latent Dirichlet Allocation (LDA) model to identify spatially compact and temporally emerging topics in real-world text streams. Wu et al. (14) developed a deep learning framework to predict epidemiology profiles in the time series by using Recurrent Neural Network (RNNs) to obtain the long-term correlation in the data and Convolution Neural Networks (CNNs) to fuse information from data of different sources. Wang et al. (15) established a two-branch neural network structure to take both within-season and between-season observations as features. The framework enables detailed forecasting when high-resolution surveillance data is not available. Nobles et al. (16) developed a multidimensional semantic scanning method to study disease categories from data and monitor pre-syndromic diseases from the free-text

emergency department chief complaints. However, machine learning has its unique challenges, such as data sparsity, lack of positive training samples (8), and ensemble prediction optimization (17). More importantly, a system needs to increase users' experience, make it closer to the medical staff members' preferences (18). The analysis and training process of machine learning is a "black box" to doctors, who can only get the accuracy of results, neglecting the importance of diagnostic thinking and medical knowledge transmission.

Therefore, instead of focusing on machine learning, this paper offered a new way to transform medical knowledge into structured data and form diagnostic rules, and use the method to explore unknown disease outbreaks detection.

## MATERIALS AND METHODS

### Knowledge Collection and Organization

The modern medical model comprises three factors: biology, psychology, and society (19). Therefore, medical diagnostic knowledge collection should include clinical and non-clinical data, such as chief complaints, laboratory tests, auxiliary examinations, psychological states, working and living states, and epidemiological analysis of infectious diseases. This study collects diagnostic knowledge in the form of "concepts." The concepts contain the names, the fields, and consist of simple concepts and compound concepts. The compound concepts are composed of simple concepts, while simple concepts refer to those basic concepts, which cannot be further subdivided. For example, "syndrome" is a compound concept formed by the combination of multiple "symptoms." After establishing the diagnostic knowledge concepts, define the types and categories of concepts. According to the field attributes, classify concepts into numeric types, text types, sound and image types, and genetic types. Concepts belong to different categories: Combinations of fields define simple conceptual object categories; Combinations of simple conceptual categories define compound conceptual object categories.

### Define Concepts as the "Features"

Define the "Feature": The Feature value represents the medical data's abnormal value with diagnostic significance for diseases. The diagnostic data contains chief complaints, laboratory findings, auxiliary examination results, biological detections, and psychological states. According to the medical definitions, the data has normal and abnormal values. By combining abnormal values with other factors, such as working and living states, doctors can conduct a comprehensive analysis and differential to give final diagnostic conclusions. The abnormal value can be either a value or a range of values. Through medical knowledge collections and organizations, classify and identify concepts belonging to the same category in disease diagnosis, according to the International Classification of Diseases Codes-10 (ICD-10) (20). The conditions that satisfy the classification are the Feature values of the concept. For example:

- The ICD-10 code: R91 – "Abnormal findings on diagnostic imaging of lung," according to the "abnormal findings," can

be divided into different characteristics, such as unilateral involvement and bilateral involvement. Thus, the classification of its Feature value consists of the classification conditions (abnormal findings) and mathematical operators: Abnormal findings = Unilateral involvement OR Abnormal findings = Bilateral involvement;

- The ICD-10 code: *R50.9 – “Fever, unspecified,”* according to the “body temperature,” can be classified into low grade fever, moderate grade fever, high grade fever, and hyperpyrexia. The classification of its Feature value consists of the classification condition (body temperature,  $T$ ) and mathematical operators: Low grade fever =  $37.3^{\circ}\text{C} \leq T \leq 38^{\circ}\text{C}$ , Moderate grade fever =  $38^{\circ}\text{C} < T \leq 39^{\circ}\text{C}$ , High grade fever =  $39^{\circ}\text{C} < T \leq 41^{\circ}\text{C}$ , and Hyperpyrexia =  $41^{\circ}\text{C} < T$ ;
- The ICD-10 code: *D70 – “Leukopenia”* consists of combinations of multiple classification conditions (age, white blood cells (WBC) count) and mathematical operators: Adult leukopenia = Age  $\geq 18$  AND WBC count  $< 4 \times 10^9$  per L;
- It can also consist of the specified machine learning classification algorithms through Big Data training and algorithmic classification results.

For presentation, define the Feature value as  $F_{(x)}$ , where  $x$  is the object,  $F$  means that  $x$  satisfies the classification condition specified by  $F$ .  $F$  can be either a simple condition or a compound condition combined by connectives “AND” and “OR,” such as  $F = F_1 \text{ AND } F_2, \dots, \text{ AND } F_n$ , or  $F = F_1 \text{ OR } (F_2 \text{ AND } F_3)$ . When  $F = F_1 \text{ AND } F_2, \dots, \text{ AND } F_n$ ,  $F_{(x)} = F_{1(x)} \text{ AND } F_{2(x)}, \dots, \text{ AND } F_{n(x)}$ .

On the concept category  $A$ , define a series of Feature values of  $A$  as  $F_1, F_2, \dots, F_n$ . Denote the set of all concepts on  $A$  as  $O$ , and define the object set that satisfies the Feature  $f$  as  $O_f$ , as shown in [1]:

$$O_f = \{ o \mid \forall o \in O, F_{(o)} \} \quad (1)$$

If  $O = \bigcup_1^n O_{F_i}$ , then  $F_1, F_2, \dots, F_n$  is a complete classification. Otherwise, it is an incomplete classification.

And for any  $i, j = 1, \dots, n, i \neq j$ , if  $O_{F_i} \cap O_{F_j} = \emptyset$ , then  $F_1, F_2, \dots, F_n$  is a mutual exclusion Feature. Otherwise, it is a compatible Feature.

For concept category  $A$ , the Features set is the set of all Features  $F_1, F_2, \dots, F_n$  defined on  $A$ . For presentation, define the Features set as FeatureSet ( $A$ ), where  $A$  is the concept category, and FeatureSet ( $A$ ) represents the set of all Feature values defined on the concept category  $A$ .

For the compatible Features, specify the matching methods as priority match and full match:

- Priority match refers to matching according to the sequence and return as a unique Feature;
- Full match refers to returning with all Features that successfully matched.

## Define Inference Rules Based on the Features

Define the Features as the premises ( $P$ ) of inference rules, the conclusions (or actions) of inference rules is  $Q$ . Hence, the new inference rule can be expressed as [2]:

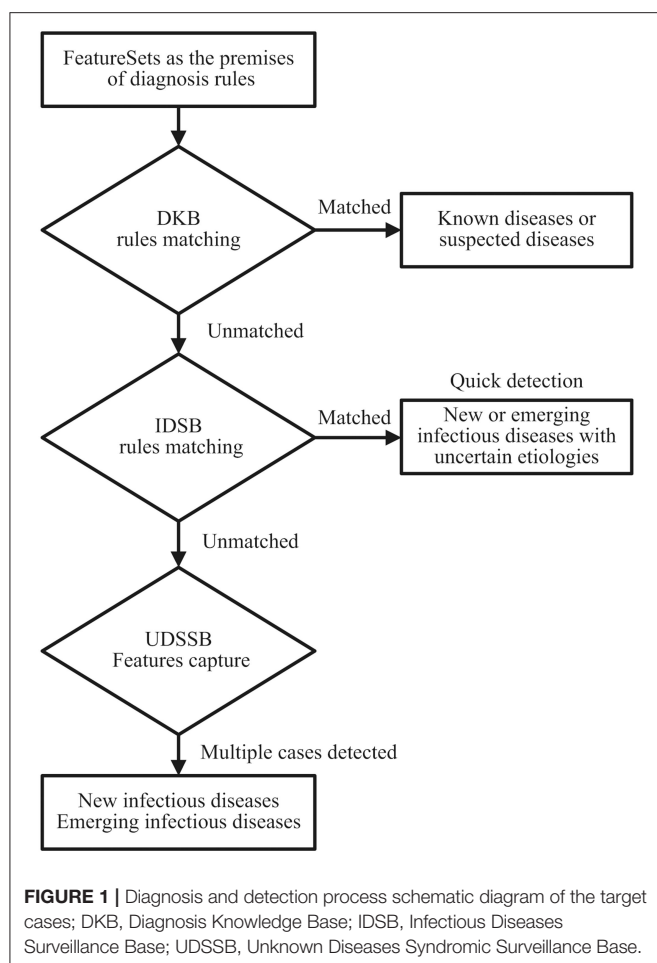
$$P: F_{1(x_1)} \bigwedge F_{2(x_2)} \bigwedge \dots \bigwedge F_{n(x_n)} \rightarrow Q \quad (2)$$

Where  $F_{1(x_1)}, F_{2(x_2)}, \dots, F_{n(x_n)}$  are the Features. The Features have truth and false values. The truth-value represents that the Feature meets conditions. If  $F_{1(x_1)}, F_{2(x_2)}, \dots, F_{n(x_n)}$  are all true, then obtain the corresponding conclusion  $Q$ . When defined the Feature  $F_{(x)}$ , it is known that  $F_{(x)}$  can be either a simple Feature or a compound Feature, which consists of multiple simple Features combined by “AND” or “OR.” Therefore, any Feature  $F_{n(x_n)}$  in inference rules can also be a compound Feature.

## Build Knowledge Bases to Store Inference Rules

As shown in **Figure 1**, define the diagnostic data of the target case as the FeatureSets, such as chief complaints, radiography findings, laboratory findings, and treatment outcomes. Use the FeatureSets as the antecedents (or premises) of inference rules and carry out the following processes:

1. Build a Diagnosis Knowledge Base (DKB) with the diagnostic knowledge collected and organized by professional medical teams, to form inference rules composed of the FeatureSets and consequents (diseases). Use the target case's Feature values as the antecedent and match with the rules stored in the DKB: If the match succeeds, it indicates that the target case is diagnosed as a known disease. If certain antecedent nodes are missing, for example, an absence of laboratory findings, the consequent of its relevant rule can be defined as a suspected disease. When the antecedent failed to match in the DKB, perform step 2;
2. Build an Infectious Diseases Surveillance Base (IDSB) to store surveillance guidelines, which consist of quick detection rules of new or emerging infectious diseases (EID) with different syndrome groups. Match the antecedent with the rules stored in the IDSB: If the match succeeds, it indicates that the target case may a new or emerging infectious disease, the etiology remains uncertain. The system will send a notification to the local centers for disease control and prevention (CDC) automatically, and staff members from the local CDC can carry out epidemiological surveys in response. If the system detects multiple cases within a short period, it indicates that these cases are possibly the aggregation of a certain infectious disease. When the antecedent again failed to match in the IDSB, perform step 3;
3. Build an Unknown Diseases Syndromic Surveillance Base (UDSSB) to capture the diagnostic FeatureSets of the target case and conduct statistical analysis: This situation indicates that the target case may be an unknown disease (non-infectious) or an EID, or the knowledge of the DKB and IDSB is insufficient and needs a supplement. In the UDSSB, if the system detects a sudden cluster of certain FeatureSets within



a short period, it indicates that these cases are possibly the aggregation of infectious disease, the system will send different levels of alerts according to the statistical results. If the system does not detect abnormal clusters, store the captured Features in the UDSSB with continuous surveillance. Simultaneously, the researchers can conduct an early epidemiological survey of the target case to collect data.

## RESULTS

Over the past decade, many countries and regions have established surveillance guidelines for EID, e.g., the Global Disease Detection International Emerging Infections Program (21). These surveillance guidelines cover different syndrome groups, such as respiratory, gastrointestinal, acute jaundice, and infectious neurological diseases. With the help of these guidelines, countries can perform quick responses to infectious disease threats (22).

This study used the surveillance guideline for pneumonia with uncertain etiologies in China to evaluate the feasibility of the proposed method. In 2007, the Chinese Ministry of Health established the “National Program for Surveillance, Screening,

and Management, for the cases of Pneumonia with Uncertain Etiologies (PUE) (23),” which stipulates that:

1. The case of PUE refers to the following four criteria, and cannot be diagnosed as other known diseases:
  - a) Fever (axillary temperature  $\geq 38^{\circ}\text{C}$ );
  - b) Diagnostic imaging of lung has pneumonia or ARDS characteristics;
  - c) In the early stage of the disease, the total number of WBC decreased or remained normal, or the classified count of lymphocytes decreased;
  - d) After standard treatment with antibiotics for 3–5 days, there was little improvement or revealed progressive disease exacerbation.
2. Aggregation of PUE cases: two or more cases with epidemiological correlations occurred within 2 weeks.

This study suggested that the guideline to some extent can be used to detect certain infectious disease outbreaks, mainly with respiratory syndromes, such as Severe Acute Respiratory Syndrome (SARS), Middle East Respiratory Syndrome (MERS), and COVID-19.

## Define the Features and Surveillance Rules

For adult patients, to meet the criteria of the guideline, the clinical characteristics should include:

1. Fever (the most common symptom, oral temperature  $\geq 37.3^{\circ}\text{C}$ );
2. Abnormalities on diagnostic imaging of lung with unilateral or bilateral involvement;
3. The WBC count remains normal or decreased, or the lymphocyte count decreased;
4. Resistance to antibiotic treatments;
5. Cannot be diagnosed as other known diseases.

By defining criteria 1–4 according to the ICD-10 codes (20), obtain the Features (sets) of PUE cases, as shown in **Table 1**. Define the surveillance rule of the PUE case based on the defined Features (sets) and store it in the IDSB, as shown in rule [3]:

$$F_{(R50.9)} \wedge F_{(R91)} \wedge F = F_{(D70)} \text{ OR } F_{(D72.8)} \wedge F_{(U83.9)} \rightarrow \text{PUE case (3)}$$

Where  $F_{(R50.9)} \wedge F_{(R91)} \wedge F = F_{(D70)} \text{ OR } F_{(D72.8)} \wedge F_{(U83.9)}$  is the antecedent (or premise) of the surveillance rule, “PUE case” is the consequent (or conclusion).

## SARS Outbreak Detection

Liu et al. (24) reviewed medical records for a total number of 36 patients with probable SARS from April 27 to May 24, 2003, in Taiwan, as shown in **Table 2**. According to the research, all patients presented fever (36/36, 100%) on admission, the mean temperature was  $38.8^{\circ}\text{C}$  ( $38.0\text{--}40.1^{\circ}\text{C}$ ). Other common symptoms include chills (75%), non-productive cough (44.4%), diarrhea (41.7%), myalgia (38.7%), and productive cough (19.4%). During hospitalization, the chest radiographs showed unifocal or multifocal infiltration in 35 (97.2%) patients, the

**TABLE 1 |** Feature definitions of pneumonia with uncertain etiologies cases according to the concept categories and the International Classification of Diseases codes-10.

| Categories                 | ICD-10 codes and definitions                         | Features (sets)  |
|----------------------------|--|--|
| Symptoms                   | R50.9: Fever, unspecified                            | Low grade fever = $37.3^{\circ}\text{C} \leq T \leq 38^{\circ}\text{C}$<br>Moderate grade fever = $38^{\circ}\text{C} < T \leq 39^{\circ}\text{C}$<br>High grade fever = $39^{\circ}\text{C} < T \leq 41^{\circ}\text{C}$<br>Hyperpyrexia = $41^{\circ}\text{C} < T$ |
| Chest radiography findings | R91: Abnormal findings on diagnostic imaging of lung | Abnormal findings = Unilateral involvement OR Bilateral involvement  |
| Laboratory findings        | D70: Leukopenia                                      | Adult leukopenia* = Age $\geq 18$ AND WBC count $< 4.0 \times 10^9$ per L  |
|                            | D72.8: Lymphopenia                                   | Adult lymphopenia* = Age $\geq 18$ AND lymphocyte count $< 1.0 \times 10^9$ per L  |
| Treatment outcomes         | U83.9: Resistance to unspecified antibiotic          | Antibiotic resistance = No significant effects OR Progressively exacerbated  |

ICD-10 = International Classification of Diseases codes-10; T = Oral temperature; WBC = White Blood Cells.

\*Varies based on the different definition criteria.

**TABLE 2 |** Characteristics summary of probable Severe Acute Respiratory Syndrome (SARS) patients according to the surveillance guideline for pneumonia with uncertain etiologies, from April 27 to May 24, 2003, in Taiwan (24).

| Characteristics   | Proportion, n/N* (%) |
|---|----------------------|
| Symptoms:   | —                    |
| Fever   | 36/36 (100%)         |
| Chest radiography findings:                             | —                    |
| Unifocal infiltration                                   | 13/36 (36.1%)        |
| Multifocal infiltration                                 | 22/36 (97.2%)        |
| Laboratory findings:                                    | —                    |
| Leukopenia: WBC count $< 3.5 \times 10^9$ per L         | 17/36 (47.2%)        |
| Lymphopenia: Lymphocyte count $< 1.0 \times 10^9$ per L | 33/36 (91.7%)        |
| Treatments:   | —                    |
| Macrolide and Fluoroquinolone                           | 36/36 (100%)         |

WBC = White Blood Cells.

\*N is the total number of patients with available data.

laboratory findings showed leukopenia in 17 (47.2%) patients and lymphopenia in 33 (91.7%) patients. All patients received antibiotic therapy (macrolide and fluoroquinolone) and no specific antibiotic appeared to be independently effective.

The detection process starts with data input. Doctors input the patient's chief complaints, laboratory findings, radiography findings, treatments, and outcomes data according to the system's prompts, forms the FeatureSets of the target case. For SARS cases, the system selected the FeatureSet  $F_{(R50.9)}$  of the most common symptom fever as the root node, radiographic abnormalities  $F_{(R91)}$ , hematological abnormalities lymphopenia  $F_{(D72.8)}$ , and antibiotic therapy outcomes  $F_{(U83.9)}$  as the children nodes 2-4 to set up the premise [P (SARS)] of the diagnosis rule, as shown in premise [4]:

$$P(\text{SARS}) = F_{(R50.9)} \bigwedge F_{(R91)} \bigwedge F_{(D72.8)} \bigwedge F_{(U83.9)} \quad (4)$$

The system carried out rule matching in the DKB based on premise [4], and could not match it with any stored rules, thus

concluded "Unmatched in the DKB" after searching, as shown in [5]:

$$P(\text{SARS}) : F_{(R50.9)} \bigwedge F_{(R91)} \bigwedge F_{(D72.8)} \bigwedge F_{(U83.9)} \rightarrow \text{Unmatched in the DKB} \quad (5)$$

Where  $F_{(R50.9)} \bigwedge F_{(R91)} \bigwedge F_{(D72.8)} \bigwedge F_{(U83.9)}$  is the premise, the matching result is "Unmatched." It indicated that the diagnostic knowledge in the DKB could not diagnose the target cases as any known diseases. Therefore, input the target cases into the IDSB to carry out rule matching. As shown in rule [6], the system searched in the IDSB and detected that premise [4] matched with the premise of rule [3], thus concluded: The disease of the patients was a kind of PUE, the cause of pneumonia remained uncertain.

$$P(\text{SARS}) : F_{(R50.9)} \bigwedge F_{(R91)} \bigwedge F_{(D72.8)} \bigwedge F_{(U83.9)} \rightarrow \text{PUE case} \quad (6)$$

Where  $F_{(R50.9)} \bigwedge F_{(R91)} \bigwedge F_{(D72.8)} \bigwedge F_{(U83.9)}$  is the premise, "PUE case" is the conclusion. The system reported to the local CDC automatically. The matching accuracy of the IDSB was calculated by the proportions of each inference node and the result was 89.1% ( $100 \times 97.2 \times 91.7 \times 100\%$ ). When the system detected multiple PUE cases within 2 weeks, the local CDC would notice that the target cases were possibly an aggregation of PUE cases. For the rest 10.9% of target cases that failed to match in the IDSB, the system captured the FeatureSets of the target cases, including other common symptoms into the UDSSB, and carried out similar case searches. If the system found similar cases that occurred in a region within 2 weeks, the system would send a notification to the local CDC, indicating that these cases were possibly the aggregation of an unknown or emerging infectious disease, thus the local CDC would respond by carrying out an early epidemiological investigation. If the system did not find similar cases, store the captured FeatureSets in the UDSSB with continuous surveillance.



**TABLE 3 |** Characteristics summary of Middle East Respiratory Syndrome (MERS) patients according to the surveillance guideline for pneumonia with uncertain etiologies, from September 1, 2012, to December 2018, in Saudi Arabia (25–27).

| Characteristics                       | Proportion, n/N* (%) |
|---------------------------------------|----------------------|
| Symptoms                              | –                    |
| Fever                                 | 85.7–98%             |
| Chest radiography findings            | –                    |
| Abnormalities with pneumonia evidence | 90.2–100%            |
| Laboratory findings                   | –                    |
| Leukopenia                            | 5–42.9%              |
| Lymphopenia                           | 34–100%              |
| Treatments                            | –                    |
| Antibiotic therapy                    | 100%                 |

\*N is the total number of patients with available data.

## MERS Outbreak Detection

This study reviewed the clinical and outcomes characteristics of confirmed cases of MERS from the prior studies (25–27). After statistically integrated their findings, this study summarized the clinical and outcomes data of MERS patients according to the surveillance guideline for the PUE, as shown in **Table 3**. The number of patients was 105 in total and the admission data was from September 1, 2012, to December 2018. The most common symptoms on admission included fever (85.7–98%, the median temperature was 37.5°C), fever with chills or rigors (87%), cough (83–100%), shortness of breath (57.1–72.5%), myalgia (14.3–32%), diarrhea (13.7–26%), and sore throat (13.7–21%). The chest radiographs showed abnormalities with pneumonia evidence among 90–100% of patients. The laboratory findings showed 14–42.9% of patients presented leukopenia, and 34–100% of patients presented lymphopenia. The patients received various antibiotics for treatments, including Azithromycin, Piperacillin/Tazobactam (Tazocin), Ceftriaxone, and Vancomycin, the effects were not obvious.

For MERS detection, the system set up the premise [P (MERS)] of the diagnosis rule. After matching in the DKB and IDSB, the system could not diagnose the target cases as any specific known diseases, but the P (MERS) met the criteria for PUE cases, as shown in rule [7]. Therefore, the system reported to the local CDC automatically.

$$P(MERS) : F_{(R50.9)} \bigwedge F_{(R91)} \bigwedge F_{(D72.8)} \bigwedge F_{(U83.9)} \rightarrow \text{PUE case} \quad (7)$$

The matching accuracy of the IDSB varied between 26.3% and 98%. When the system detected multiple cases within 2 weeks, the local CDC would notice that the target cases were possibly the aggregation of PUE cases. Simultaneously, for the rest 2–73.7% of target cases that failed to match in the IDSB, the system captured the FeatureSets of the target cases, including other common symptoms into the UDSSB, and carried out similar case searches. If the system found similar cases that occurred in a region within 2 weeks, the local CDC would carry out an early epidemiological

**TABLE 4 |** Characteristics summary of early COVID-19 patients according to the surveillance guideline for pneumonia with uncertain etiologies, from December 16, 2019, to January 2, 2020, in Wuhan (1).

| Characteristics   | Statistical results |             |
|---|---------------------|-------------|
| Symptoms  | n/N* (%)            |             |
| Fever   | 40/41 (98%)         |             |
| Highest temperature, °C                                     | –                   |             |
| 37.3–38.0   | 8/41 (20%)          |             |
| 38.1–39.0   | 18/41 (44%)         |             |
| >39.0   | 14/41 (34%)         |             |
| Chest radiography findings                                  | n/N (%)             |             |
| Bilateral involvement                                       | 40/41 (98%)         |             |
| Laboratory findings   | n/N (%)             |             |
| Leukopenia: WBC count < 4.0 × 10 <sup>9</sup> per L         | 10/40 (25%)         | 35/41 (85%) |
| Lymphopenia: Lymphocyte count < 1.0 × 10 <sup>9</sup> per L | 26/41 (63%)         |             |
| Treatments  | n/N (%)             |             |
| Antibiotic therapy  | 41/41 (100%)        |             |
| Time course   | Days, Median        |             |
| Time from onset of symptoms                                 | –                   |             |
| To first hospital admission                                 | 7.0 (4.0–8.0)       |             |
| To ARDS   | 9.0 (8.0–14.0),     |             |
| To mechanical ventilation                                   | 10.5 (7.0–14.0)     |             |
| To ICU admission  | 10.5 (8.0–17.0)     |             |

WBC = White Blood Cells; ARDS = Acute Respiratory Distress Syndrome; ICU = Intensive Care Unit.

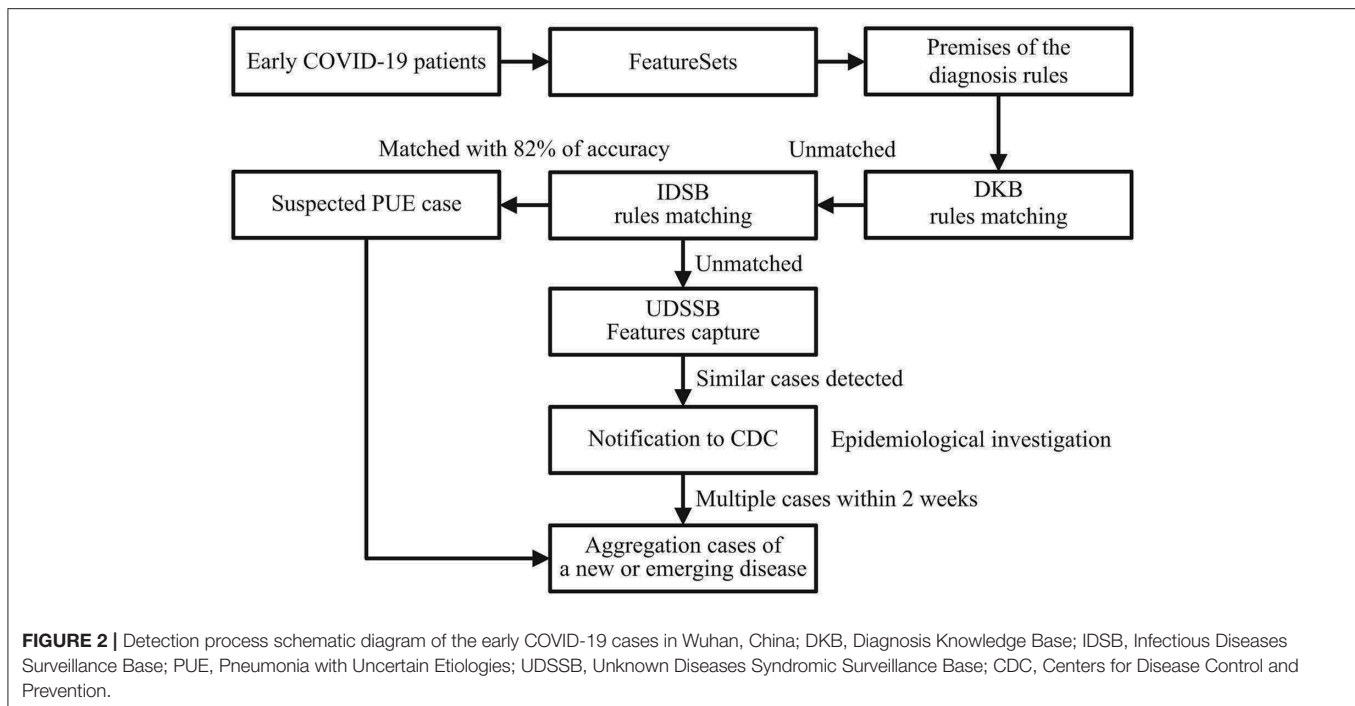
\*N is the total number of patients with available data.

investigation. If the system did not find similar cases, store the captured FeatureSets in the UDSSB with continuous surveillance.

## Early COVID-19 Outbreak Detection

Huang et al. (1) reviewed clinical charts, nursing records, laboratory findings, and chest x-rays for early patients with laboratory-confirmed COVID-19 infection in Wuhan, China. The number of the patients was 41 and the admission data was from December 16, 2019, to January 2, 2020. As shown in **Table 4**, 40/41 patients (98%) presented fever (highest temperature ≥ 37.3°C) on admission, abnormalities on chest radiography were detected among all patients (bilateral involvement, 98%). The laboratory findings showed 10/40 (25%) patients presented leukopenia (WBC count < 4.0 × 10<sup>9</sup> per L) and 26/41 (63%) patients presented lymphopenia (lymphocyte count < 1.0 × 10<sup>9</sup> per L). The total number of patients presented leukopenia or lymphopenia was 35/41 (85%). All patients (41/41, 100%) were given antibiotic treatments and no specific therapy showed independent effectiveness.

As shown in **Figure 2**, doctors first input the chief complaints, radiography findings, laboratory findings, and treatment outcomes of the patients to the system, formed the FeatureSets of the target cases. The system selected  $F_{(R50.9)}$  as the root node,  $F_{(R91)}$ ,  $F = F_{(D70)}$  OR  $F_{(D72.8)}$ , and  $F_{(U83.9)}$  as the children nodes to set up the premise [P (COVID-19)] of the diagnosis rule, as



shown in premise [8]:

$$P(\text{COVID} - 19) : F_{(R50.9)} \bigwedge F_{(R91)} \bigwedge F = F_{(D70)} \text{OR} F_{(D72.8)} \bigwedge F_{(U83.9)} \quad (8)$$

Through matching  $P(\text{COVID}-19)$  [8] with the rules in the DKB and IDSB, the system could not diagnose the patients as any known diseases, whereas  $P(\text{COVID}-19)$  [8] matched with the premise of rule [3], as shown in rule [9]. Therefore, the patients met the criteria for the PUE cases, the system reported to the local CDC automatically.

$$P(\text{COVID} - 19) : F_{(R50.9)} \bigwedge F_{(R91)} \bigwedge F = F_{(D70)} \text{OR} F_{(D72.8)} \bigwedge F_{(U83.9)} \rightarrow \text{PUE case} \quad (9)$$

The matching accuracy of the IDSB was 82% ( $98 \times 98 \times 85 \times 100\%$ ). Additionally, 27/41 (66%) patients had direct exposure to the Wuhan Huanan seafood market, and their date of illness onset was from December 10 to 31, 2019 (1). When the system detected multiple cases within 2 weeks, the system would send several notifications to the local CDC, thus the staff members would consider these cases as the aggregation of PUE and perform an early epidemiological survey in response. The early COVID-19 patients' data showed that except for the fever, the patients had other common symptoms at the onset of illness, such as cough (76%), dyspnea (55%), myalgia or fatigue (44%), and sputum production (28%) (1). For the rest 18% of patients that failed to match in the IDSB, the system would capture the FeatureSets of their clinical characteristics into the UDSSB and conduct similar case searches. When the system detected multiple cases that occurred in Wuhan within 2 weeks, the

local CDC would receive notifications and carry out an early epidemiological survey in response.

## DISCUSSION AND CONCLUSIONS

According to the early COVID-19 data in Wuhan, the median time from onset of symptoms to first hospital admission of 41 patients was 7.0 days (4.0–8.0), to acute respiratory distress syndrome (ARDS) was 9.0 days (8.0–14.0), to mechanical ventilation was 10.5 days (7.0–14.0), and to intensive care unit (ICU) admission was 10.5 days (8.0–17.0) (1). The data of 41 patients represented the real situation and response speed of local citizens when an unknown disease outbreak occurred in Wuhan, December 2019, and from hospital admission to local CDC responses, the whole process could be easily disturbed by human factors. Although the method proposed by this study cannot reduce the timeliness of patients from onset of symptoms to hospital admission, it can assist doctors in differential diagnosis after inputting the clinical characteristics data of patients, hence shortening the ambiguous process of diseases from unknown to known and providing early clues to CDC for carrying out epidemiological investigations. Once doctors input the patients' diagnostic data, the system will start to match the target case with the knowledge bases, some of the data may need a day or two to collect, such as radiography findings and treatment outcomes. After detecting two or more cases in the IDSB and UDSSB, the system will report to CDC automatically. Therefore, based on the early COVID-19 data in Wuhan, 2019, this study estimates that with the system's help, the detection and notification timeliness of the early COVID-19 pandemic can be reduced to 7.0–10.0

days, and the detection process can avoid being disturbed by human factors.

Since the outbreak of the COVID-19 pandemic in 2019, various studies have focused on collecting and delineating the demographic, clinical, and outcomes data on confirmed cases, some of the patients' numbers are over thousands (28, 29). However, the data from subsequent studies were obtained based on the increasing number of new scientific findings, as well as increasing awareness of the pandemic by hospitals, CDCs, and governments, which resulted in the strengthened prevention and control measurements of the pandemic. For example, for the confirmed cases recruited after January 1, 2020, in China, 31.3% of cases had recently been to Wuhan, 71.8% of cases had contact with people from Wuhan (28), hence other detection methods, such as cluster screening, molecular tests, diagnostic imaging, and biochemical detections can be more effective after the initial outbreak (30, 31). Moreover, the appearance of asymptomatic infections since 2020 has reduced the strength of using clinical characteristics for detection (29, 32, 33). Therefore, this study suggests that the data of the initial 41 patients with laboratory-confirmed COVID-19 infection in Wuhan is more suitable for evaluating our method.

The matching accuracy of the IDSB represents the system's ability to quickly detect suspected PUE cases according to the surveillance guideline stored in the IDSB, and it was calculated based on the proportions of each data presented in the prior studies. The surveillance rule of the PUE cases has four inference nodes, the proportion on each node represents the accuracy of the system to successfully match the node with patients. Multiply the proportions of each inference node, the final results represent the accuracy of the system to match the target cases with the surveillance rule of PUE cases in the IDSB. The empirical study of the MERS pandemic showed a higher matching accuracy fluctuation (26.3–98%) of the IDSB, this is due to the surveillance guideline we used has limited the detection scale of MERS cases, as well as the high fluctuation of patients' lymphopenia data (34–100%) (25–27). However, the UDSSB was designed to capture the FeatureSets of the remaining patients and ensure the overall detection accuracy of the system. After detecting multiple similar cases within a short period in the UDSSB, the system would send notifications to CDC, indicating the suspected aggregation of an unknown or emerging infectious disease. On the other hand, this study suggests that the matching accuracy is not the key factor for evaluating the feasibility of the method. The matching accuracy is not equal to the detection accuracy, which can be affected by several problems, such as the system's ability to detect an unknown disease, which may present similar presentations of a known disease, and the ability to diagnose a known disease, which may present nonstandard presentations. In this study, the system used medical knowledge in the DKB to solve such problems. To increase the detection accuracy of the system, we need to increase the width and depth of the system's DKB. The width of the knowledge base represents the system's ability to diagnose different types of diseases, the depth represents the system's ability to diagnose complex cases. Therefore, to improve the feasibility of the method, medical

knowledge should be constantly added to the knowledge base through daily diagnostic activities.

Our study has the following novelties. First, this is the first attempt to use a new Feature-based knowledge representation and reasoning approach to organize medical knowledge and detect unknown disease outbreaks. Unlike the other artificial intelligence methods that facing unique challenges such as data sparsity and lack of training data sets, our method will enable medical experts to continually input their professional knowledge into the system and form diagnostic rules with different criteria, hence adapt the system in response to the potential public threats under the global scenario. More importantly, for most doctors, especially those from remote and underdeveloped areas, this method can extend their expertise and experience, improve their abilities in clinical thinking and differential diagnosis. Second, by matching with diagnosis rules in the DKB, the system can assist doctors in their daily diagnosis and distinguish emerging diseases from common diseases, thus the surveillance mode can change from passive to active. Additionally, the method combined two knowledge bases with an additional syndromic surveillance base to ensure the overall detection accuracy and reduce the misdiagnosis rate.

The most noticeable limitation of this study is the lack of clinical characteristics and treatment outcomes data on the initial patients, who were the earliest patients confirmed infected by SARS and MERS coronavirus. An empirical study with initial infected patients' data can better evaluate the feasibility of our method for unknown disease outbreak detection. Secondly, as a pilot study, it has not yet compared the empirical results with other Artificial Intelligence approaches. We put more emphasis on the description of the Features' construction, and limitations may occur in data integrity, consistency, and validity. Thirdly, to improve the feasibility of the method, medical knowledge shall be constantly added to the DKB through daily diagnostic activities. Besides, the surveillance guideline our study used was established by the Chinese government in 2007, the definitions of the PUE case had limited the selection of outbreaks based on different epidemiological, demographic, and clinical characteristics in the empirical study, and need further supplements.

Future research work includes increasing the number of patients, adding comparisons between different syndrome groups, regions, and populations. Additionally, we are currently developing a new reasoning method combined with the Feature-based knowledge representation. The reasoning method will focus on several issues, including distinguishing different diseases from similar combinations of phenomena, getting multiple possible results from a group of phenomena, sorting the results according to certain rules, and screening the results based on the information input by doctors. The reasoning method will be designed with an empirical study to test the feasibility of unknown or complex disease detection in different circumstances.

In conclusion, this study proposed a new Feature-based knowledge representation and reasoning model under the main background of the COVID-19 pandemic in 2019 and used the model to explore the detection of unknown disease outbreaks.

By defining the abnormal diagnostic data as the Features, the medical knowledge can transform into structured data and use the Features as antecedents of the inference rules, which can then match with the system's knowledge bases to detect unknown or emerging disease outbreaks. The results of the empirical study demonstrate that by combining with suitable surveillance guidelines, the method proposed in this study is capable to detect outbreaks of SARS, MERS, and COVID-19 pandemics. Furthermore, the method will enable medical experts to input their professional knowledge into the system's knowledge bases, and by continuously accumulating the diagnostic knowledge and surveillance guidelines, the system's detection accuracy and scale will be improved. More importantly, the knowledge representation approach can activate the sharing and transmission process of medical knowledge, thus accelerate the accumulation speed of doctors' knowledge and experience, minimize the time of training an outstanding medical expert.

## DATA AVAILABILITY STATEMENT

The original contributions presented in the study are included in the article/supplementary material, further inquiries can be directed to the corresponding author/s.

## REFERENCES

- Huang C, Wang Y, Li X, Ren L, Zhao J, Hu Y, et al. Clinical features of patients infected with 2019 novel coronavirus in Wuhan, China. *Lancet*. (2020) 395:497–506. doi: 10.1016/S0140-6736(20)30183-5
- Gorbalenya AE, Baker SC, Baric RS, de Groot Raoul J, Drosten C, Gulyaeva AA, et al. The species severe acute respiratory syndrome-related coronavirus: classifying 2019-nCoV and naming it SARS-CoV-2. *Nat Microbiol*. (2020) 5:536–44. doi: 10.1038/s41564-020-0695-z
- Johns Hopkins University. *COVID-19 Dashboard by the Center for Systems Science and Engineering (CSSE)*. (2021). Available online at: <https://coronavirus.jhu.edu/map.html> (accessed April 28, 2021).
- WHO. *Topics: Disease Outbreaks*. (2017). Available online at: [https://www.who.int/topics/disease\\_outbreaks/zh/](https://www.who.int/topics/disease_outbreaks/zh/) (accessed Jul 2, 2020).
- Dupuy C, Bronner A, Watson E, Wuyckhuise-Sjouke L, Reist M, Fouillet A, et al. Inventory of veterinary syndromic surveillance initiatives in Europe (Triple-S project): current situation and perspectives. *Prev Vet Med*. (2013) 111:220–9. doi: 10.1016/j.prevetmed.2013.06.005
- Sosin DM. Draft framework for evaluating syndromic surveillance systems. *J Urban Health*. (2003) 80(2 Suppl. 1):8–13. doi: 10.1007/pl00022309
- Black J, Hulkower R, Suarez W, Suarez W, Patel S, Elliott B. Public health surveillance: electronic reporting as a point of reference. *J Law Med Ethics*. (2019) 47:19–22. doi: 10.1177/1073110519857309
- Zeng D, Cao Z, Neill DB. Artificial intelligence-enabled public health surveillance—from local detection to global epidemic monitoring and control. In: Lei X, Maryellen LG, James KM, editor. *Artificial Intelligence in Medicine Technical Basis and Clinical Applications*. New York, NY: Academic Press (2020). p. 437–53.
- Wang L, Wang Y, Jin S, Wu Z, Chin DP, Koplan JP, et al. Health system reform in China 2: emergence and control of infectious diseases in China. *Lancet*. (2008) 372:1598–1605. doi: 10.1016/S0140-6736(08)61365-3
- Mao RJ, Moa A, Chughtai A. The epidemiology of unknown disease outbreak reports globally. *GlobBioSecur*. (2020) 2. doi: 10.31646/gbio.62
- Lall R, Levin-Rector A, Mathes R, Weiss D. Detecting unanticipated increases in emergency department chief complaint keywords. *Online J Public Health Inform*. (2014) 6:e93. doi: 10.5210/ojphi.v6i1.5069

## ETHICS STATEMENT

Ethical review and approval was not required for the study on human participants in accordance with the local legislation and institutional requirements. Written informed consent for participation was not required for this study in accordance with the national legislation and the institutional requirements.

## AUTHOR CONTRIBUTIONS

RF, QH, and YJ shared research design and overall supervision of the process. RF took responsibility for putting together the final manuscript, all authors gave feedback on this process. RF and QH were responsible for the methods design and empirical study of the study. YJ provided additional support with data analysis. All authors contributed to the article and approved the submitted version.

## ACKNOWLEDGMENTS

We acknowledge Prof. Huang's research team for sharing their valuable COVID-19 data to help us complete our study.

- Walsh A, Hamby T, Lowery St. John T. Identifying clusters of rare and novel words in emergency department chief complaints. *Online J Public Health Inform*. (2014) 6:e146. doi: 10.5210/ojphi.v6i1.5111
- Maurya A, Murray K, Liu Y, Dyer C, Cohen WW, Neill DB. Semantic scan: detecting subtle, spatially localized events in text streams. *arXiv [Preprint]*. (2016).
- Wu Y, Yang Y, Nishiura H, Saitoh M. Deep learning for epidemiological predictions. In: *SIGIR' 18: The 41st International ACM SIGIR Conference on Research and Development in Information Retrieval*. Ann Arbor, MI; New York, NY: ACM (2018). p. 1085–8.
- Wang L, Chen J, Marathe M. DEFSI: deep learning based epidemic forecasting with synthetic information. In: *Proceedings of the AAAI Conference on Artificial Intelligence*. Honolulu, HI (2019). p. 9607–12. doi: 10.1609/aaai.v33i01.33019607
- Nobles M, Lall R, Mathes R, Neill DB. Multidimensional semantic scan for pre-syndromic disease surveillance. *Online J Public Health Inform*. (2019) 11:e255. doi: 10.5210/ojphi.v11i1.9764
- Viboud C, Vespignani A. The future of influenza forecasts. *Proc Natl Acad Sci USA*. (2019) 116:2802–4. doi: 10.1073/pnas.1822167116
- Caserio-Schoenemann C, Meynard JB. Ten years experience of syndromic surveillance for civil and military public health, France, 2004–2014. *Euro Surveill*. (2015) 20:35–8. doi: 10.2807/1560-7917.ES2015.20.19.21126
- Engel GL. The need for a new medical model: a challenge for biomedicine. *Science*. (1977) 196:129–36. doi: 10.1126/science.847460
- WHO. *ICD-10 Version: 2010*. (2019). Available online at: <https://icd.who.int/browse10/2019/en> (accessed Aug 3, 2020).
- Breiman RF, Van Beneden CA, Farnon EC. Surveillance for respiratory infections in low- and middle-income countries: experience from the centers for disease control and prevention's global disease detection international emerging infections program. *J Infect Dis*. (2013) 208(Suppl. 3):S167–72. doi: 10.1093/infdis/jit462
- Centers for Disease Control and Prevention (CDC). *Global Disease Detection (GDD) Program: 2004–2018 History and Accomplishments*. (2020). Available online at: <https://www.cdc.gov/globalhealth/healthprotection/gdd/gdd-accomplishments.html> (accessed Mar 27, 2021).
- China: National Health Commission. *General Office: Notice of the Ministry of Health on the issuance of the National Program for Surveillance, Screening,*



- and Management, for the cases of Pneumonia with Uncertain Etiologies. (2007). Available online at: <http://www.nhc.gov.cn/bgt/pw10708/200708/4455f46a2f5e4908a8561c079ecbcf0e.shtml> (accessed August 2, 2020).
24. Liu CY, Huang LJ, Lai CH, Chen HP, Chen TL, Fung CP, et al. Clinical characteristics, management and prognostic factors in patients with probable Severe Acute Respiratory Syndrome (SARS) in a SARS center in Taiwan. *J Chin Med Assoc.* (2005) 68:110–7. doi: 10.1016/S1726-4901(09)70231-X
  25. Assiri A, Al-Tawfiq JA, Al-Rabeeh AA, Al-Rabiah FA, Al-Hajjar S, Al-Barrak A, et al. Epidemiological, demographic, and clinical characteristics of 47 cases of Middle East respiratory syndrome coronavirus disease from Saudi Arabia: a descriptive study. *Lancet Infect Dis.* (2013) 13:752–61. doi: 10.1016/S1473-3099(13)70204-4
  26. Ajlan AM, Ahyad RA, Jamjoom LG, Alharthy A, Madani TA. Middle East Respiratory Syndrome Coronavirus (MERS-CoV) infection: chest CT findings. *Am J Roentgenol.* (2014) 203:782–7. doi: 10.2214/AJR.14.13021
  27. Al-Sulayyim HJ, Khorshid SM, Al-Moummar SH. Demographic, clinical, and outcomes of confirmed cases of Middle East Respiratory Syndrome coronavirus (MERS-CoV) in Najran, Kingdom of Saudi Arabia (KSA); A retrospective record based study. *J Infect Public Health.* (2020) 13:1342–6. doi: 10.1016/j.jiph.2020.04.007
  28. Guan W, Ni Z, Hu Y, Liang W, Ou C, He J, et al. Clinical characteristics of 2019 novel coronavirus infection in China. *N Engl J Med.* (2020) 382:1708–20. doi: 10.1056/NEJMoa2002032
  29. Israfil H, Sarker MR, Rashid RT, Talukder AA, Kawsar KA, Khan F, et al. Clinical characteristics and diagnostic challenges of COVID–19: an update from the global perspective. *Front Public Health.* (2021) 8:955. doi: 10.3389/fpubh.2020.567395
  30. Zou L, Ruan F, Huang M, Liang L, Huang H, Hong Z, et al. SARS-CoV-2 viral load in upper respiratory specimens of infected patients. *N Engl J Med.* (2020) 382:1177–9. doi: 10.1056/NEJMc2001737
  31. Nascimento JJAC, Santos AM, Oliveira AMS, Guimarães AG, Quintans-Júnior LJ, Coutinho HDM, et al. Trends in MERS-CoV, SARS-CoV, and SARS-CoV-2 (COVID-19) diagnosis strategies: a patent review. *Front Public Health.* (2020) 8:663. doi: 10.3389/fpubh.2020.563095
  32. Singhal T. A review of coronavirus disease-2019 (COVID-19). *Indian J Pediatr.* (2020) 87:281–6. doi: 10.1007/s12098-020-03263-6
  33. Day M. Covid-19: four fifths of cases are asymptomatic, China figures indicate. *BMJ.* (2020) 369:m1375. doi: 10.1136/bmj.m1375

**Conflict of Interest:** The authors declare that the research was conducted in the absence of any commercial or financial relationships that could be construed as a potential conflict of interest.

Copyright © 2021 Feng, Hu and Jiang. This is an open-access article distributed under the terms of the Creative Commons Attribution License (CC BY). The use, distribution or reproduction in other forums is permitted, provided the original author(s) and the copyright owner(s) are credited and that the original publication in this journal is cited, in accordance with accepted academic practice. No use, distribution or reproduction is permitted which does not comply with these terms.



# Data-Driven and Machine-Learning Methods to Project Coronavirus Disease 2019 Pandemic Trend in Eastern Mediterranean

Wenbo Huang<sup>1,2†</sup>, Shuang Ao<sup>1†</sup>, Dan Han<sup>3†</sup>, Yuming Liu<sup>4</sup>, Shuang Liu<sup>1,4</sup> and Yaojiang Huang<sup>1,5\*</sup>

<sup>1</sup> Beijing Engineering Research Center of Food Environment and Public Health, Minzu University of China, Beijing, China,

<sup>2</sup> Department of Software and Information, Beijing Information Technology College, Beijing, China, <sup>3</sup> College of Medicine, Minzu University of China, Beijing, China, <sup>4</sup> College of Life and Environmental Sciences, Minzu University of China, Beijing, China, <sup>5</sup> Harvard T.H. Chan School of Public Health, Boston, MA, United States

## OPEN ACCESS

### Edited by:

Babak A. Ardekani,  
Nathan Kline Institute for Psychiatric  
Research, United States

### Reviewed by:

Hamid Reza Pourghasemi,  
Shiraz University, Iran  
Abdulrahman Almazrou,  
Sulaiman Al Rajhi University,  
Saudi Arabia

### \*Correspondence:

Yaojiang Huang  
yaojiang@muc.edu.cn;  
yaojiangh@hsph.harvard.edu  
orcid.org/0000-0001-5409-5605

†These authors have contributed  
equally to this work

### Specialty section:

This article was submitted to  
Infectious Diseases - Surveillance,  
Prevention and Treatment,  
a section of the journal  
Frontiers in Public Health

Received: 24 November 2020

Accepted: 25 March 2021

Published: 13 May 2021

### Citation:

Huang W, Ao S, Han D, Liu Y, Liu S  
and Huang Y (2021) Data-Driven and  
Machine-Learning Methods to Project  
Coronavirus Disease 2019 Pandemic  
Trend in Eastern Mediterranean.  
Front. Public Health 9:602353.  
doi: 10.3389/fpubh.2021.602353

**Background:** The coronavirus disease 2019 (COVID-19) pandemic has become a major public health crisis worldwide, and the Eastern Mediterranean is one of the most affected areas.

**Materials and Methods:** We use a data-driven approach to assess the characteristics, situation, prevalence, and current intervention actions of the COVID-19 pandemic. We establish a spatial model of the spread of the COVID-19 pandemic to project the trend and time distribution of the total confirmed cases and growth rate of daily confirmed cases based on the current intervention actions.

**Results:** The results show that the number of daily confirmed cases, number of active cases, or growth rate of daily confirmed cases of COVID-19 are exhibiting a significant downward trend in Qatar, Egypt, Pakistan, and Saudi Arabia under the current interventions, although the total number of confirmed cases and deaths is still increasing. However, it is predicted that the number of total confirmed cases and active cases in Iran and Iraq may continue to increase.

**Conclusion:** The COVID-19 pandemic in Qatar, Egypt, Pakistan, and Saudi Arabia will be largely contained if interventions are maintained or tightened. The future is not optimistic, and the intervention response must be further strengthened in Iran and Iraq. The aim of this study is to contribute to the prevention and control of the COVID-19 pandemic.

**Keywords:** COVID-19, data-driven, machine learning, assessment, projection

## INTRODUCTION

Half a year has passed since the WHO announced the coronavirus disease 2019 (COVID-19) pandemic, which has not disappeared because of climate and other factors. Instead, the epidemic has spread to every corner of the world and is worsening. Obviously, the COVID-19 pandemic has no chance of ending before the end of 2020 (1–3). Countries around the world have successively implemented pharmaceutical and non-pharmaceutical intervention measures to

control the COVID-19 pandemic, but there are no special and specific drugs available for treatment. The intervention measures focus on isolation of suspected and confirmed cases, movement restrictions and social distancing, contact tracing, public health measures, and lockdowns (4–6), but the COVID-19 pandemic continues to spread in most countries.

In recent years, a large amount of theoretical and applied research evidence has shown that mathematical projection and modeling play a key role in understanding disease dynamics and transmission and finding the best intervention strategies for infectious diseases (7–15). The COVID-19 pandemic has become a major public health crisis worldwide, and it has severely affected the economies, employment, and livelihoods of all countries. The Eastern Mediterranean is one of the regions most affected by COVID-19 (2, 3, 16, 17). In the Eastern Mediterranean, oil exports have dropped significantly and income has fallen sharply this year, public health resources are relatively scarce, the population is large, and the economy is relatively underdeveloped (18). At the same time, in some countries, COVID-19 epidemiological data are inaccurate; or difficulty in identifying cases, underreporting, and misdiagnosis are problems. This poses a huge challenge to the prevention and control of COVID-19 in these countries (9, 12, 19–25). Therefore, it is especially important to use data-driven modeling to evaluate the current situation and the effectiveness of intervention measures in the uncertain stage of the COVID-19 epidemic and to use artificial intelligence to predict the trend of the pandemic in Eastern Mediterranean countries.

Data-driven methods were used in this study for evaluation, and machine-learning methods were used to predict the COVID-19 pandemic for the six countries with the largest number of COVID-19 confirmed cases in the Eastern Mediterranean. The purpose was to evaluate the *status quo* to conduct a model of COVID-19 spread, as well as to project the trend and time distribution of the total confirmed cases and the single-day confirmed cases of COVID-19 in those countries. The purpose of this work is to promote further applications and thereby help prevent and control the COVID-19 pandemic.

## MATERIALS AND METHODS

This study was conducted through data download, status assessment, the non-pharmaceutical intervention actions and epidemic trend prediction, etc. The flowchart of the method is shown in **Supplementary Figure 1**.

### Data Sources

Data from August 20, 2020, in six countries with the highest number of confirmed COVID-19 cases in the Eastern Mediterranean were studied. The data were downloaded from Johns Hopkins CSSE ([https://github.com/CSSEGISandData/COVID-19/tree/master/csse\\_covid\\_19\\_data](https://github.com/CSSEGISandData/COVID-19/tree/master/csse_covid_19_data)), COVID-19

Government Measures Dataset (5), and Oxford COVID-19 Government Response Tracker (OxCGRT).

### Evaluation of the Coronavirus Disease 2019 Pandemic in Eastern Mediterranean

The current status of the COVID-19 epidemic includes the total number of confirmed cases, deaths, active cases, overall growth rate, total number of confirmed cases per million people, and number of daily changes in each country. These were evaluated using the R (26) package COVID19. Analytics and EpiModel based on the current intervention actions.

### Non-pharmaceutical Intervention Actions

The R was used to analyze the OxCGRT intervention action data (**Supplementary Material 1**), which provide a composite of nine measures: school closures, stay-at-home requirements, workplace closures, restrictions on public gatherings, public information campaigns, closures of public transport, restrictions on internal movements, cancellation of public events, and international travel controls. The score of the nine measures was between 0 and 100 on any given day. This index indicates the strict government and societal response.

### Forecasting the Trend of the Coronavirus Disease 2019 Pandemic in Eastern Mediterranean

The trend of the total confirmed COVID-19 cases was forecast based on existing intervention actions, and a 180-day-ahead forecast was performed with a 95% prediction interval (PI) using machine learning with Python Prophet Module (27) in Iran, Saudi Arabia, Pakistan, Iraq, Qatar, and Egypt. The machine-learning forecast model was utilized with additional regression elements and no tweaking of season-related parameters. Machine-learning methods with Python Prophet module (27, 28) were used to project the daily growth rate in each country and generate a 180-day-ahead forecast with a 95% PI. The calculation formula and algorithm is as follows:

$$y(t) = g(t) + s(t) + h(t) + \epsilon_t$$

A basic model was established with additional regression elements. Machine learning with the Python Prophet module assigns a predicted value for each day in the future, named *Yhat\_lower*, *Yhat*, and *Yhat\_upper*, which are, respectively, the predicted *Yhat* and the lower and upper *Yhat* of the projection with a 95% PI.

## RESULTS

### Evaluation of the Coronavirus Disease 2019 Pandemic Status Quo of the Coronavirus Disease 2019 Pandemic

As of February 14, 2021, the six countries with the highest number of COVID-19 cases in the Eastern Mediterranean were Iran, Saudi Arabia, Pakistan, Iraq, Qatar, and Egypt. Iran had 1.518263 *M* confirmed cases, 1.298032 *M* recovered, 58.945 *k*

**Abbreviations:** COVID-19, coronavirus disease 2019; WHO, The World Health Organization; OxCGRT, Oxford; COVID-19, Government Response Tracker; PI, 95% prediction interval; *Yhat*, each day in a future predicted value.

deaths, and 161.295 *k* active cases with the rising curve of the wave (**Figures 1A–C** and **Supplementary Figure 2a**). The numbers of confirmed cases, recovered patients, deaths, and active cases were 564.077, 525.997, 12.333, and 25.747 *k* in Pakistan, with the number of active cases showing a wave decreasing trend. In Saudi Arabia, 372.732 *k* confirmed cases, 363.585 *k* recovered, 2,714 deaths, and 6,433 active cases with downward trends were reported. There were 643.852 *k* confirmed cases, 607.059 *k* recovered, 13.179 *k* deaths, and 23.614 *k* active cases that developed in waves in Iraq (**Figure 1** and **Supplementary Figure 2d**). Egypt had 173.813 *k* confirmed cases, 134.96 *k* recovered, 9.994 *k* deaths, and 28.859 *k* active cases that developed in waves and rose after November 2020. In Qatar, 157.244 *k* confirmed cases, 148.314 *k* recovered, 255 deaths, and 8,675 active cases with decreasing trend were confirmed (**Figures 1A–C** and **Supplementary Figure 2**).

The total number of confirmed cases per million people in the ongoing COVID-19 pandemic was estimated. Qatar had the highest number of confirmed cases per million people, followed by Saudi Arabia, Iraq, Pakistan, Iraq, Qatar, and Egypt, which was the lowest (**Figure 1D**). The overall growth rates and the total number of cases were evaluated with a confidence band

based on the moving average for different countries. The number of cases as a function of time was used to generate different fits to match the data in a linear-scale and log-scale plot for the given locations and types. If the overall growth rate is close to 1, it indicates that the spread of the virus has reached its logical asymptote. In other cases, as in the six countries in the Eastern Mediterranean on the date used in this study, it is still higher than 1, indicating that the total number of confirmed cases continues to grow (lm-exp GR: 1.02–1.03, glm-Poisson GR: 1.01, and **Supplementary Figures 3a–f**).

## Daily Changes in the Coronavirus Disease 2019 Pandemic

Daily changes in confirmed cases were evaluated by plotting two scatter plots in log scale (right vertical axis) and linear scale (left vertical axis) with the number of changes, and a mosaic-type layout heatmap comparing daily changes in confirmed cases in six countries was plotted (**Figure 2G**). As of February 14, 2021, the daily number of confirmed cases in Iran showed multiple peaks with an overall upward trend, whereas the daily change in Iraq continued to rise (**Figures 2A,D,G**). Saudi Arabia, Pakistan, Qatar, and Egypt had multiple peaks in the

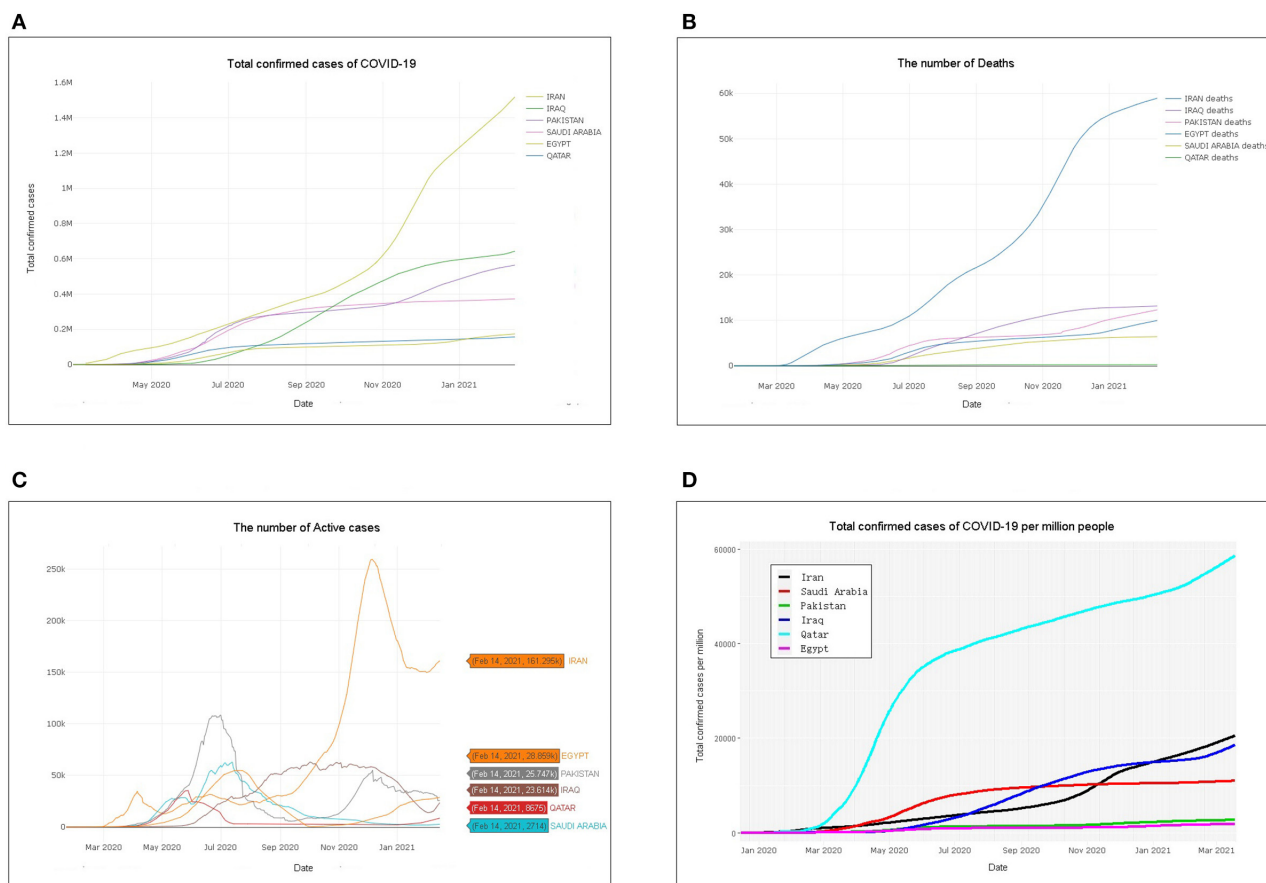
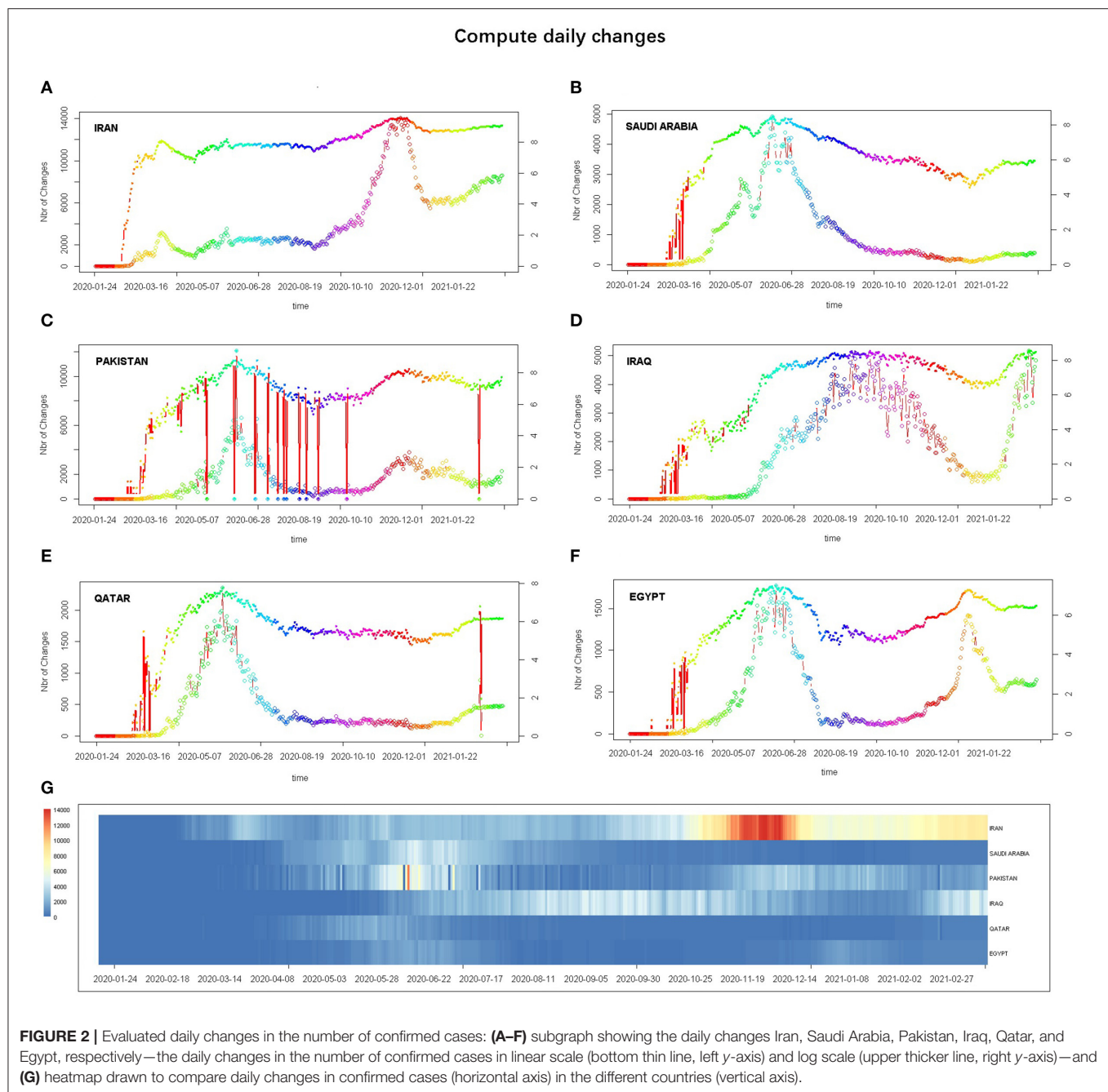


**FIGURE 1 |** Total confirmed cases, deaths, active cases, and total confirmed cases per million people: **(A)** number of total confirmed coronavirus disease 2019 (COVID-19) cases, **(B)** number of deaths in six Eastern Mediterranean countries, **(C)** number of active cases in six Eastern Mediterranean countries, and **(D)** total confirmed cases per million people.





number of daily confirmed cases and showed a downward trend (Figures 2B,C,E–G).

### Non-pharmaceutical Intervention Actions

The OxCGRT government intervention index data were analyzed to evaluate the level of government and social response using the R tidycovid19 package. The higher the score of the index, the stricter the government and societal response. Six countries began implementing strict intervention measures at approximately the same time. Since late March, Iran's intervention index has been approximately 50, while other countries have relatively high levels of intervention

(Figures 3A,B). The mean of intervention measures score since January shows that Iraq has the highest, followed by Qatar, Saudi Arabia, Pakistan, and Egypt, and Iran has the lowest (Figures 3B,C). Although Iran's regulatory index rose to first place around November 2020, the total number of confirmed cases was the highest (Figure 3C).

### Forecasting the Trend of the Coronavirus Disease 2019 Pandemic in Eastern Mediterranean

The total confirmed cases and daily growth rate of the COVID-19 pandemic were projected using machine learning with

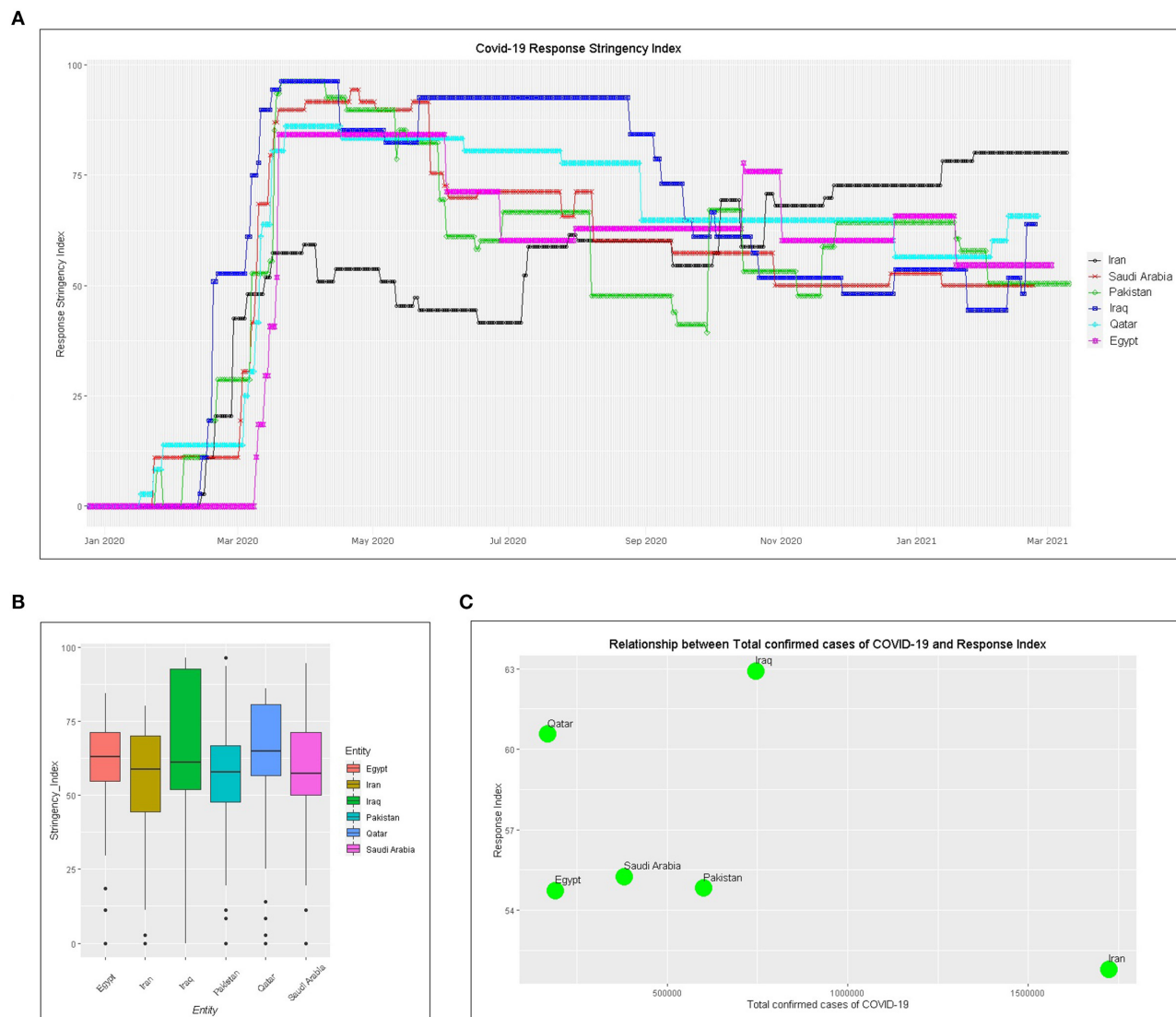


**FIGURE 3 |** Government intervention index and its relationship to confirmed cases: **(A)** government or societal intervention index, **(B)** bar plot of intervention score since January 2020, and **(C)** relationship between government response index and the number of confirmed cases.

additional regression elements and no tweaking of season-related parameters. A forecast value was assigned for each day in the future, namely,  $Y_{hat\_upper}$ ,  $Y_{hat}$ , and  $Y_{hat\_lower}$ . In terms of the growth trend of the total number of confirmed cases of COVID-19, as of August 13, 2021, Iran's  $Y_{hat}$ ,  $Y_{hat\_lower}$ , and  $Y_{hat\_upper}$  values are predicted to be 2,693.448, 1,799.289, and 3,630.919  $k$ , respectively. The predicted  $Y_{hat}$  value for Egypt is 324.325  $k$ , and  $Y_{hat\_upper}$  and  $Y_{hat\_lower}$  are 448.601 and 196.262  $k$ , respectively, in the total number of confirmed cases of COVID-19. Iraq's  $Y_{hat}$ ,  $Y_{hat\_lower}$ , and  $Y_{hat\_upper}$  values are predicted to be 867.794, 616.828, and 1,125.184  $k$ , respectively (**Figure 4** and **Supplementary Table 1**). Under existing intervention actions (**Figure 3**), machine-learning projections show that Saudi Arabia ( $Y_{hat}$ : 410.981  $k$ , PI: 59.156–763.790  $k$ ), Pakistan

( $Y_{hat}$ : 901.943  $k$ , PI: 344.972–1,415.126  $k$ ), and Qatar ( $Y_{hat}$ : 207.910  $k$ , PI: 73.118–339.932  $k$ ) will be flat in the total number of confirmed cases of COVID-19, while it does not seem to be slowing down in Iran and Egypt (**Figure 4** and **Supplementary Table 1**).

Under the circumstance that the severity of the existing interventions remains unchanged, Saudi Arabia, Pakistan, Iraq, and Egypt all showed a downward trend in the growth rate of daily confirmed cases, whereas Iran and Qatar showed no significant downward trend in the growth rate of daily confirmed cases (**Figures 5A–E**). The growth rate of the daily confirmed cases in Iraq is going to be  $<1$  around March 2021, that in Pakistan is going to be  $<1$  around January 2021, and that in Saudi Arabia and Egypt is going to be  $<1$  around February 2021 (**Figures 5B–D,F**).

### The trend of COVID-19 pandemic in the total confirmed casses

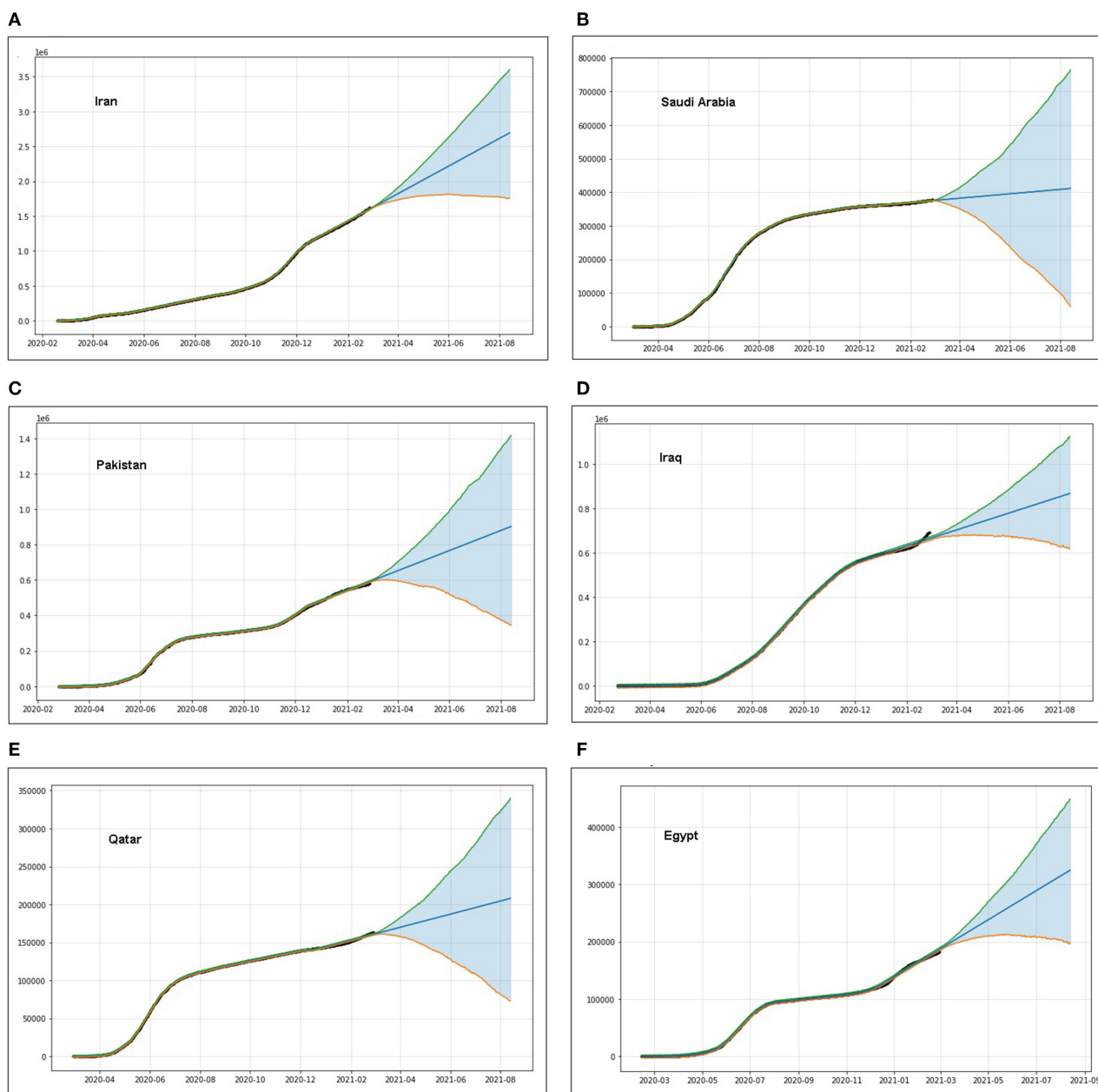
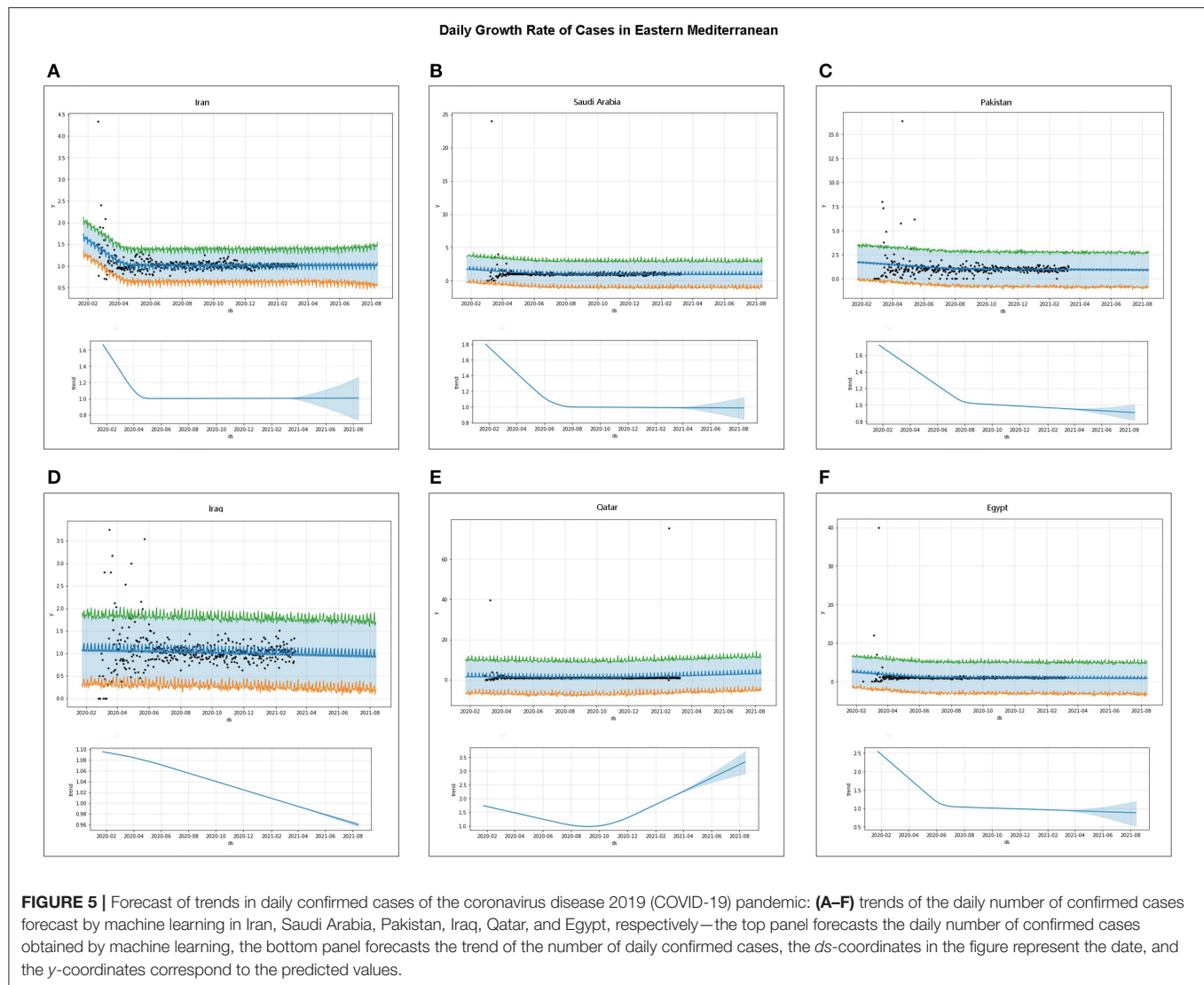


**FIGURE 4 |** Forecast of overall trends in the coronavirus disease 2019 (COVID-19) pandemic: **(A–F)** trends of the number of total COVID-19 confirmed cases forecast by machine-learning methods in Iran, Saudi Arabia, Pakistan, Iraq, Qatar, and Egypt, respectively.

## DISCUSSION

The current status of the COVID-19 pandemic was evaluated. Iran has the highest total number of COVID-19 confirmed cases, while Qatar has the highest number of confirmed cases of COVID-19 per million people (**Figures 1A,D**). The number of active cases in Pakistan peaked at 108,642 on July 1. In Qatar, it is also declining with a small active case stock, which indicates

that the epidemic is largely under control in both countries. The number of active cases in both Saudi Arabia is on a downward trend, suggesting that the epidemic should improve. The active cases in Iran, Iraq, and Egypt show a small rise in waves with a large stock, which is not optimistic (**Figure 1C**). Saudi Arabia, Pakistan, and Qatar have all peaked and show a downward trend in the daily number of confirmed cases, while Iran, Iraq, and Egypt show a wave (**Figures 2A,D,F**). It is worth noting that



the number of active cases and daily changes in all countries showed a slight upward trend toward the end of 2020 or the beginning of 2021 (**Figures 1C, 2**), which may be related to the reduction of non-pharmaceutical intervention actions in these countries starting in September 2020 (**Figure 3**). Although Iran's intervention index in November 2020 had risen to first place among the six countries, because its mean response index has been the lowest since the COVID-19 outbreak and the index score has been  $\sim 50$ , the total number of confirmed cases is the highest in the six countries (**Figures 3A–C**). Therefore, early government and societal intervention is important to control the COVID-19 pandemic.

The total confirmed cases and daily growth rate of the COVID-19 pandemic were projected using machine learning under current intervention actions. Saudi Arabia, Pakistan, and Qatar will be flat in total confirmed cases and show a downward trend in the daily growth rate, while Iran will continue to rise in total confirmed cases and show no significant downward trend

in the daily growth rate (**Figures 5A–F**). The daily confirmed case growth rates in Egypt, Pakistan, and Saudi Arabia are going to be  $<1$  before March 2021. These projections show that although the total number of cases is still increasing, the number of daily confirmed cases or the daily confirmed case growth rate of COVID-19 in Saudi Arabia, Pakistan, Qatar, and Egypt shows a significant downward trend (**Figures 2, 4, 5**), indicating that these countries may significantly reduce daily confirmed cases and the COVID-19 pandemic will be controlled if current interventions are maintained or tightened; the cases in these countries still have the potential to rise if they are not properly controlled and intervened. However, the situation is still severe and needs to be strengthened further in Iran and Iraq.

This research has obtained some appropriate results, but the study has several limitations. First, this project or evaluation is based on the current intervention actions, but the current situation is not static because the government and societal intervention measures and control levels, such as whether to



require masks, social distancing, and lockdowns, may change, and society also needs to resume work and gradual reopening (5, 6). It is also very important to note that the degree of societal compliance with these measures and regulations will determine the ultimate effectiveness of these interventions, but we did not analyze these because data on the extent of compliance with non-pharmaceutical measures are lacking and not comprehensive, which may have made the projection not very accurate. Therefore, the forecast results will also change as these interventions or societal compliance degree change. Even if the daily growth rate of some countries shows a downward trend, it is possible that the epidemic will re-erupt unless existing strict measures are strengthened and maintained at a high degree of compliance. Second, the total number of confirmed cases is not the actual number of infections daily and in total because it is impossible for all infected people to be reported or tested, especially in Eastern Mediterranean countries that do not trace contact and practice isolation of suspected and confirmed cases, so the confirmed cases in total and daily may be far below the true number (29–31). Finally, the projection and interpretation of the COVID-19 pandemic are challenging and should be carefully based on the situation of the COVID-19 pandemic and the above limitations (32). Unlike some studies that have predicted trends in COVID-19 (12, 14, 33), our study focused on changes and growth rate in the number of daily confirmed cases. However, it is believed that the evaluation and projection results are highly reliable because they are based not only on the number of cases but also on the shape of the pandemic curve to make predictions by machine learning (7, 9–11). These projections are useful in assessing the epidemic situation and taking appropriate intervention measures.

## CONCLUSION

The COVID-19 pandemic was evaluated and projected for six Eastern Mediterranean countries. The findings suggest that the number of active cases, daily confirmed cases, or daily confirmed-case growth rate of the COVID-19 pandemic in Egypt, Pakistan, Saudi Arabia, and Qatar showed a significant downward trend, which indicates that the COVID-19 pandemic will be basically under control in these countries, and the growth rate of daily confirmed cases may significantly reduce if current interventions are maintained or tightened, although these countries have the potential to rise if they are poorly controlled or intervened. Iran and Iraq may continue to rise in active cases and total confirmed cases with no significant downward trend in the daily

growth rate, which indicates that one cannot be optimistic and the response must be further strengthened. It is hoped that these assessments and projections will contribute to a better response to the COVID-19 pandemic.

## DATA AVAILABILITY STATEMENT

Publicly available datasets were analyzed in this study. This data can be found here: [https://github.com/CSSEGISandData/COVID-19/tree/master/csse\\_covid\\_19\\_data](https://github.com/CSSEGISandData/COVID-19/tree/master/csse_covid_19_data).

## AUTHOR CONTRIBUTIONS

YH proposed the idea and design of the study and had full access to all data in the study. WH, SA, and DH contributed to the raw data acquisition and writing of the manuscript. SA, WH, and YH contributed to important revisions of the manuscript. WH, SA, DH, SL, and YH contributed to the statistical analysis. All authors participated in data acquisition, data analysis, or data interpretation and reviewed and approved the final version.

## FUNDING

This study was supported by The Double Top University Plan from China Ministry of Education and by grant 2018MDTD25C from the Minzu University 985 Academic Team-building Fund and Beijing Municipal Science and Technology Commission.

## SUPPLEMENTARY MATERIAL

The Supplementary Material for this article can be found online at: <https://www.frontiersin.org/articles/10.3389/fpubh.2021.602353/full#supplementary-material>

**Supplementary Figure 1** | Flowchart for methodology.

**Supplementary Figure 2** | Overall situation of the COVID-19 pandemic in Eastern Mediterranean countries: (a–f) overall situation of the COVID-19 pandemic in Iran, Saudi Arabia, Pakistan, Iraq, Qatar, and Egypt, respectively.

**Supplementary Figure 3** | Overall growth rates in total number of confirmed cases: (a–f) subgraph showing Iran, Saudi Arabia, Pakistan, Iraq, Qatar, and Egypt — exp model, a linear fit to an exponential law in log scale; glm-Poisson, a general linear regression Poisson model; GLM-gamma, a general linear regression gamma model method.

**Supplementary Table 1** | Machine-learning methods to forecast the trend of COVID-19.

**Supplementary Material 1** | R code for non-pharmaceutical intervention actions.

## REFERENCES

1. WHO. WHO Director-General's Opening Remarks at the Mission Briefing on COVID-19 (2020). Available online at: <https://www.who.int/dg/speeches/detail/who-director-general-s-opening-remarks-at-the-mission-briefing-on-covid-19> (accessed March 12, 2020).
2. WHO. Coronavirus Disease (COVID-19) Weekly Epidemiological Update 2 (2020). Available online at: [https://www.who.int/docs/default-source/coronaviruse/situation-reports/20200824-weekly-epi-update.pdf?sfvrsn=806986d1\\_4](https://www.who.int/docs/default-source/coronaviruse/situation-reports/20200824-weekly-epi-update.pdf?sfvrsn=806986d1_4) (accessed August 26, 2020).
3. JHU. COVID-19 Map - Johns Hopkins Coronavirus Resource Center (2020). Available online at: <https://coronavirus.jhu.edu/map.html> (accessed August 26, 2020).
4. Abd El-Aziz TM, Stockand JD. Recent progress and challenges in drug development against COVID-19 coronavirus (SARS-CoV-2)-an update on the status. *Infect Genet Evolut.* (2020) 83:104327. doi: 10.1016/j.meegid.2020.104327
5. ACAPS. ACAPS COVID-19 Government Measures Dataset Geneva: (ACAPS) (2020).

6. Oxford. *Oxford COVID-19 Government Response Tracker (OxCGRT)* (2020). Available online at: <https://covidtracker.bsg.ox.ac.uk/> (accessed August 26, 2020).
7. Wu JT, Leung K, Leung GM. Nowcasting and forecasting the potential domestic and international spread of the 2019-nCoV outbreak originating in Wuhan, China: a modelling study. *Lancet*. (2020) 395:689–97. doi: 10.1016/S0140-6736(20)30260-9
8. Salathe M, Bengtsson L, Bodnar TJ, Brewer DD, Brownstein JS, Buckee C, et al. Digital epidemiology. *PLoS Comput Biol*. (2012) 8:e1002616. doi: 10.1371/journal.pcbi.1002616
9. Dil S, Dil N, Maken ZH. COVID-19 trends and forecast in the eastern mediterranean region with a particular focus on Pakistan. *Cureus*. (2020) 12:e8582. doi: 10.7759/cureus.8582
10. Jewell NP, Lewnard JA, Jewell BL. Predictive mathematical models of the COVID-19 pandemic: underlying principles and value of projections. *JAMA*. (2020) 323:1893–4. doi: 10.1001/jama.2020.6585
11. Li Q, Guan X, Wu P, Wang X, Zhou L, Tong Y, et al. Early transmission dynamics in Wuhan, China, of novel coronavirus-infected pneumonia. *N Engl J Med*. (2020) 382:1199–207. doi: 10.1056/NEJMoa2001316
12. Salameh P. COVID-19 in the Eastern Mediterranean Region: testing frequency, cumulative cases and mortality analysis. *East Mediter Health J*. (2020) 26:1005–10. doi: 10.26719/emhj.20.110
13. Alimadadi A, Aryal S, Manandhar I, Munroe PB, Joe B, Cheng X. Artificial intelligence and machine learning to fight COVID-19. *Physiol Genom*. (2020) 52:200–2. doi: 10.1152/physiolgenomics.00029.2020
14. Lalmuanawma S, Hussain J, Chhakchhuak L. Applications of machine learning and artificial intelligence for Covid-19 (SARS-CoV-2) pandemic: a review. *Chaos Solitons Fractals*. (2020) 139:110059. doi: 10.1016/j.chaos.2020.110059
15. Pinter G, Felde I, Mosavi A, Ghamisi P, Gloaguen R. COVID-19 pandemic prediction for Hungary; a hybrid machine learning approach. *Mathematics*. (2020) 8:890. doi: 10.3390/math8060890
16. Decerf B, Ferreira FH, Mahler DG, Sterck O. (2020) *Lives and Livelihoods: Estimates of the Global Mortality and Poverty Effects of the Covid-19 Pandemic*. Washington, DC: The World Bank.
17. Cash R, Patel V. Has COVID-19 subverted global health? *Lancet*. (2020) 395:1687–8. doi: 10.1016/S0140-6736(20)31089-8
18. EMRO. WHO: Eastern Mediterranean Regional Office (2021). Available online at: <http://www.emro.who.int/entity/about-us/index.html> (accessed August 26, 2020).
19. Zaki AM, Van Boheemen S, Bestebroer TM, Osterhaus AD, Fouchier RA. Isolation of a novel coronavirus from a man with pneumonia in Saudi Arabia. *N Engl J Med*. (2012) 367:1814–20. doi: 10.1056/NEJMoa1211721
20. EMRO. Eastern Mediterranean Regional Office COVID-19 Dashboard (2021). Available online at: <https://app.powerbi.com/view?r=eyJrIjojN2ExNWl3ZGQtZDk3My00YzE2LWFjYmQtNGMwZjk0OWQ1MjFhIiwidCI6ImY2MTBjMG13LWJkMjQ0NGl3OS04MTBiLTNkYzI4MGFmYjU5MCIslmMiOj9> (accessed August 26, 2020).
21. EMRO. *Update on COVID-19 in the Eastern Mediterranean Region* (2021). Available online at: <http://www.emro.who.int/media/news/update-on-covid-19-in-the-eastern-mediterranean-region.html> (accessed August 26, 2020).
22. Din M, Asghar M, Ali M. COVID-19 and dengue coepidemics: a double trouble for overburdened health systems in developing countries. *J Med Virol*. (2020) 93:601–2. doi: 10.1002/jmv.26348
23. Al-Tawfiq JA, Memish ZA. COVID-19 in the Eastern Mediterranean Region and Saudi Arabia: prevention and therapeutic strategies. *Int J Antimicrob Agents*. (2020) 55:105968. doi: 10.1016/j.ijantimicag.2020.105968
24. Alandijany TA, Faizo AA, Azhar EI. Coronavirus disease of 2019 (COVID-19) in the Gulf Cooperation Council (GCC) countries: current status and management practices. *J Infect Public Health*. (2020) 13:839–42. doi: 10.1016/j.jiph.2020.05.020
25. Baloch Z, Ma Z, Ji Y, Ghanbari M, Pan Q, Aljabr W. Unique challenges to control the spread of COVID-19 in the Middle East. *J Infect Public Health*. (2020) 13:1247–50. doi: 10.1016/j.jiph.2020.06.034
26. RStudio. *RStudio: Integrated Development for R.* Version 1.3.959 ed. Boston, MA RStudio, PBC (2020).
27. Python. *Python 3 Reference Manual.* Python 3.8 ed. Scotts Valley, CA: CreateSpace (2020).
28. Taylor SJ, Letham B. Forecasting at scale. *Am Statist*. (2018) 72:37–45. doi: 10.1080/00031305.2017.1380080
29. Favalli EG, Ingegnoli F, Cimaz R, Caporali R. What is the true incidence of COVID-19 in patients with rheumatic diseases? *Ann Rheum Dis*. (2020) 80:e18. doi: 10.1136/annrheumdis-2020-217615
30. Meyerowitz-Katz G, Merone L. (2020) A systematic review and meta-analysis of published research data on COVID-19 infection-fatality rates. *Int J Infect Dis*. 101:138–48. doi: 10.1016/j.ijid.2020.09.1464
31. Wilson L. SARS-CoV-2, COVID-19, Infection Fatality Rate (IFR) Implied by the Serology, Antibody, Testing in New York City. Rochester: SSRN (2020).
32. Wolkewitz M, Puljak L. (2020) *Methodological Challenges of Analysing COVID-19 Data During the Pandemic*. London: Springer.
33. Ardabili SF, Mosavi A, Ghamisi P, Ferdinand F, Varkonyi-Koczy AR, Reuter U, et al. COVID-19 outbreak prediction with machine learning. *Algorithms*. (2020) 13:249. doi: 10.3390/a13100249

**Conflict of Interest:** The authors declare that the research was conducted in the absence of any commercial or financial relationships that could be construed as a potential conflict of interest.

Copyright © 2021 Huang, Ao, Han, Liu, Liu and Huang. This is an open-access article distributed under the terms of the Creative Commons Attribution License (CC BY). The use, distribution or reproduction in other forums is permitted, provided the original author(s) and the copyright owner(s) are credited and that the original publication in this journal is cited, in accordance with accepted academic practice. No use, distribution or reproduction is permitted which does not comply with these terms.



# Investigation of Knowledge, Attitude and Practice of Personal Protection Among Different Types of Workers Returning to Work Under COVID-19 Epidemic

## OPEN ACCESS

### Edited by:

Atefeh Abedini,  
Shahid Beheshti University of Medical  
Sciences, Iran

### Reviewed by:

Majid Taati Moghadam,  
Iran University of Medical  
Sciences, Iran  
Hossein Ameri,  
Shahid Sadoughi University of Medical  
Sciences and Health Services, Iran  
Waqar Ahsan,  
Jazan University, Saudi Arabia

### \*Correspondence:

Fan Zhang  
epicqmu@163.com  
Yong Zhao  
zhaoyong@cqmu.edu.cn

### Specialty section:

This article was submitted to  
Infectious Diseases - Surveillance,  
Prevention and Treatment,  
a section of the journal  
Frontiers in Public Health

**Received:** 12 March 2021

**Accepted:** 19 April 2021

**Published:** 17 May 2021

### Citation:

Fan ZY, Mou YL, Cheng R, Zhao Y  
and Zhang F (2021) Investigation of  
Knowledge, Attitude and Practice of  
Personal Protection Among Different  
Types of Workers Returning to Work  
Under COVID-19 Epidemic.  
Front. Public Health 9:679699.  
doi: 10.3389/fpubh.2021.679699

**Zhaoya Fan, Yuanlin Mou, Rui Cheng, Yong Zhao\* and Fan Zhang\***

School of Public Health and Management, Research Center for Medicine and Social Development, Collaborative Innovation  
Center of Social Risks Governance in Health, Chongqing Medical University, Chongqing, China

**Background:** Since the outbreak of the coronavirus disease 2019 (COVID-19) world pandemic, it has had a significant negative impact on the economy and employment. The orderly resumption of work and production is an important factor in reducing the impact of the COVID-19 and an important guarantee of social and economic stability. The study aimed to investigate the knowledge, attitudes, and practice (KAP) of people returning to work about personal protection under the COVID-19 world pandemic.

**Methods:** During March 2020, based on WeChat, QQ and other internet platforms, online questionnaire survey was conducted by the convenience sampling method. SPSS version 20.0 (SPSS, Inc., Chicago, IL, USA) was used for statistics analysis. Descriptive statistics and multiple linear regression analyses were conducted to analyze the data.

**Results:** A total of 302 valid questionnaires was collected, and the valid response rate was 86.7%. About knowledge, people who return to work had the highest awareness rate of safe communication distance and the lowest awareness rate of exposure risk levels in different workplaces. The average scores of respondents in different occupations were higher than 95 in terms of personal protective attitude. In terms of practice, the average scores of respondents in different occupations were higher than 90 points. Multiple linear regression results showed that education and place of residence were the influencing factors of knowledge, while gender was the influencing factor of practice.

**Conclusion:** The awareness of prevention and control among the 302 participants was good. There were differences in personal protection knowledge among different occupational groups, but there were no differences in attitude and practice. Our findings were of great significance to improve the pertinence of COVID-19 prevention programs.

**Keywords:** COVID-19, knowledge, attitudes, practices, personal protection

## INTRODUCTION

Since the end of December 2019, coronavirus disease (COVID-19) has spread rapidly in various regions of the world, and has become an issue of concern (1, 2). On January 30, 2020, the World Health Organization (WHO) announced that the world pandemic was listed as a public health emergency of international concern and called on all countries to fight against the epidemic (3, 4). The disease has high infectiousness, and its main clinical symptoms include fever, dry cough, fatigue, muscle pain and dyspnea (2). As of April 13, 2021, 221 countries around the world have reported 137,265,460 confirmed cases and 2,958,863 confirmed deaths from COVID-19 (5). The world pandemic has disrupted the daily work and life of the public, and the global economy has been severely damaged. It is clear that COVID-19 has become a global public health issue. In order to reduce the impact of COVID-19 outbreak, China has actively adopted medical measures and social evacuation. For example, all staff except necessary occupations should stop working before February 9, 2020 to avoid population gathering due to work (6). This measure greatly curbed the spread of the virus (7). Studies have shown that, in the environment outside the hospital, the workplace may be the best breeding ground for the virus (8). Preventive measures in the workplace can have a significant impact on the spread of a pandemic disease (9). However, studies predicted that the best time to resume work in China would be in early April. If the restrictions were lifted earlier might lead to an earlier and higher second peak (10). Therefore, in the face of the severity of the world pandemic, it is important to take relevant protective measures for those who return to work in February and March. On March 5, news.cn/worldpro/ issued a series of guidelines related to returning to work: indoor ventilation and disinfection should be done well in the workplace; employers should establish health records of employees and do not discriminate against employees confirmed or suspected of being infected with COVID-19; employees should insist on wearing masks and keeping a safe distance from colleagues, etc. (11). Specifically, farmers can carry out agricultural activities on a staggered peak and time sharing to avoid unnecessary gathering and contact. For the general staff, try not to take public transport when going out, consciously accept temperature monitoring when entering the unit, and keep the office clean and hygienic. If conditions permit, the company can allow employees to telecommute from home to avoid the risks brought by commuting, and at the same time pay close attention to their daily physical conditions. It is more important for high-risk medical workers to do a good job of self-protection. At ordinary times, it is necessary to strengthen the disinfection of the environment, prevent nosocomial infection, establish a strict ward management system, control the entry and exit of irrelevant personnel, reduce the frequency and time of family visits, wear protective clothing, goggles and gloves correctly during work (12, 13). In addition, special attention should be paid to the adjustment of negative emotions. Studies have shown that medical workers are more likely to have psychological problems (14, 15).

So far, the global epidemic prevention and control is still in a critical period, and some areas have been in a state of resumption of work. It is worth noting that during the period of resuming work and increasing production, the effect of prevention and control of pneumonia is greatly affected by the knowledge, attitudes and practices (KAP) of the people returning to work. The level of knowledge of a disease can affect people's attitudes and practices, on the other hand, negative attitudes and practices can increase the risk of death from disease (16, 17). Therefore, the purpose of this study is to assess the KAP status quo and explore the possible influencing factors of different occupational groups, so as to provide valuable information for countries and regions that have returned to work or are ready to return to work.

## MATERIALS AND METHODS

### Study Design and Sampling

This cross-sectional study was conducted on a professional questionnaire survey platform (<https://www.wenjuan.com>) from March 23 to April 8, 2020. Convenience sampling method was used to select participants. According to the Kendall sample estimation method for multivariate analysis, the sample size was required to be 5–10 times the number of variables (18). In our survey, a total of 6 basic information items and 41 questionnaire dimensions were covered, therefore the minimum sample size of this survey was 235–470. Those returning to work who can understand the contents of the questionnaire and can access to the internet were eligible to participate. Finally, 348 people completed the online questionnaire, 302 of which were valid. We also performed *post hoc* power analysis using G-power 3.1.9.7 (Kiel University, Kiel, Germany) software to test the power of our study. The power (1- $\beta$ ) was determined to be 0.996, based on an error probability (significance level) of 0.05, and total sample size of 302.

### Measures and Analysis Instrument

The questionnaire was designed on the basis of guidelines for COVID-19 prevention and control issued by the WHO (19), the National Health Commission of the People's Republic of China (20), the Chinese Center for Disease Control and Prevention (21). The relevant experts were invited to discuss the questionnaire to make the questions and options as accurate and comprehensive as possible. Cronbach's alpha for the questionnaire total was 0.951 which indicated that the internal consistency of the questionnaire was good. The questionnaire was a voluntary and anonymous survey. No private information and sensitive language. The questionnaire consisted of four sections: demographic variables, knowledge, attitudes and practices with respect to COVID-19.

Demographic variables (six items): age, gender, education, occupation, etc. For occupations, it involved more than a dozen industries. In order to avoid too few people in each category, we divided the occupations into four groups: (1) white-collar workers (including officials, public servants, managers, office clerks, etc.); (2) professionals (including doctors, nurses, teachers, reporters, lawyers, etc.); (3) blue-collar workers (including mill workers, waiters, salespeople, etc.); (4)



**TABLE 1** | Demographic characteristics of respondents.

|                                  | White-collar workers (%) | Professionals (%) | Blue-collar workers (%) | Self-employments (%) | Total (%)   |
|----------------------------------|--------------------------|-------------------|-------------------------|----------------------|-------------|
| <b>Gender</b>                    |                          |                   |                         |                      |             |
| Male                             | 36 (43.9)                | 28 (24.8)         | 26 (56.5)               | 27 (44.3)            | 117 (38.7)  |
| Female                           | 46 (56.1)                | 85 (75.2)         | 20 (43.5)               | 34 (55.7)            | 185 (61.3)  |
| <b>Age (years)</b>               |                          |                   |                         |                      |             |
| 15-30                            | 25 (30.5)                | 41 (36.3)         | 17 (37)                 | 42 (68.9)            | 125 (41.4)  |
| 31-45                            | 29 (35.4)                | 43 (38.1)         | 14 (30.4)               | 10 (16.4)            | 96 (31.8)   |
| 46-60                            | 28 (34.1)                | 29 (25.7)         | 15 (32.6)               | 9 (14.8)             | 81 (26.8)   |
| <b>Education</b>                 |                          |                   |                         |                      |             |
| Senior high school and below     | 12 (14.6)                | 7 (6.2)           | 34 (73.9)               | 18 (29.5)            | 71 (23.5)   |
| Undergraduate and junior college | 61 (74.4)                | 88 (77.9)         | 12 (26.1)               | 42 (68.9)            | 203 (67.2)  |
| Master degree or above           | 9 (11)                   | 18 (15.9)         | 0 (0)                   | 1 (1.6)              | 28 (9.3)    |
| <b>Place of residence</b>        |                          |                   |                         |                      |             |
| Urban                            | 80 (97.6)                | 103 (91.2)        | 29 (63)                 | 37 (60.7)            | 249 (82.5)  |
| Rural                            | 2 (2.4)                  | 10 (8.8)          | 17 (37)                 | 24 (39.3)            | 53 (17.5)   |
| Total                            | 82 (27.2)                | 113 (37.4)        | 46 (15.2)               | 61 (20.2)            | 302 (100.0) |

self-employments (including contractors, freelancers, farmers, herdsmen, fishermen, etc.). As for the self-filled occupation questionnaires, we classified them into the above four categories according to the Code of Occupational Classification of the People's Republic of China (2015 Edition).

Knowledge of personal protection (10 items): infectious disease classification, measures to inactivate the virus, the source of infection, the main route of transmission, susceptible population, daily protection knowledge, safe communication distance, risk of infection in different workplaces, mask selection, anti-virus measures after going home. There were three options for each item, one point was given for a correct answer. The higher the score, the better the knowledge.

Attitude of personal protection (seven items): actively guard against virus, attitude toward confirmed cases around them, cooperate with the protective measures of the work unit, etc. Each item used the Likert scale to assess the degree of agreement with the statement, with options ranging from 1 (strongly disagree) to 5 (strongly agree). The total score was converted into a percentage system, the higher the score, the more positive attitude.

Practice of personal protection (24 items): pay attention to world pandemic information, wear masks, avoid crowds gathering, keep the indoor ventilation, etc. It involved the protective practice in four aspects: at home, commuting, working and dining behavior. Each item used the Likert scale to assess the degree of agreement with the statement, with options ranging from 1 (strongly disagree) to 5 (strongly agree). The total score was converted into a percentage system, with higher scores indicating better practice.

## Data Analysis

We described the characteristics of participants based on four groups according to their occupations, the results were presented as frequencies and percentages. The KAP scores of different occupational groups were presented as means and

interquartile rage. Mann-Whitney U test and Kruskal-Wallis *H* test were used to analyze the differences of KAP among different occupational groups. A multiple linear regression model was used to identify factors associated with KAP.  $P < 0.05$  (two-tailed) was considered statistically significant. All statistics analyses were performed with SPSS version 20.0 (SPSS, Inc., Chicago, IL, USA).

## RESULTS

### Basic Characteristics of the Respondents

Table 1 presented the basic characteristics in the whole sample. A total of 348 questionnaires was collected in this survey. After excluding duplicate and invalid questionnaires, 302 were enrolled, and the effective response rate was 86.7%. Most of the respondents were female (56.1%), urban residents (97.6%), with an educational level of undergraduate or junior college (74.4%). Among those who returned to work in different occupations, white-collar workers, professionals, blue-collar workers and self-employments were 82 (27.2%), 113 (37.4%), 46 (15.2%), and 61 (20.2%), respectively.

### COVID-19 Knowledge

Table 2 showed the options and responses for each question, of the 302 respondents, measures to inactivate the virus (96.4%), susceptible population (90.1%), and anti-virus measures after going home (94.7%) had a higher scoring rate. However, the scoring rates of infectious disease classification (45.0%), route of transmission (56.3%), and mask selection (47.0%) were lower. The highest (safe communication distance) and lowest (risk of infection in different workplaces) item scoring rates were 99.0 and 10.9%, respectively. Among those who answered correctly, the chi-square test was used to compare what aspects of knowledge were different among people returning to work in different occupations, and the results showed that there were statistical differences in infectious disease classification

**TABLE 2 |** Responses to knowledge of COVID-19 among people returning to work in different occupations.

| Item  | Response, n (%) |
|---|-----------------|
| <b>K1: What is the classification of infectious diseases in COVID-19?</b>   |                 |
| A. Class A infectious disease   | 163 (54.0)      |
| B. Class B infectious disease   | 136 (45.0)      |
| C. Class C infectious disease   | 3 (1.0)         |
| <b>K2: Which of the following measures can effectively inactivate novel coronavirus?</b>  |                 |
| A. Chlorine disinfectants, peracetic acid, etc.   | 291 (96.4)      |
| B. Smoked vinegar   | 4 (1.3)         |
| C. Gargle with salt water   | 7 (2.3)         |
| <b>K3: Which of the following is wrong about the possible source of infection of novel coronavirus?</b>   |                 |
| A. Asymptomatic infected  | 43 (14.2)       |
| B. COVID-19 patients  | 16 (5.3)        |
| C. Recovered from COVID-19  | 243 (80.5)      |
| <b>K4: Which of the following is not the main route of transmission of the novel coronavirus?</b>   |                 |
| A. Droplet and contact transmission   | 35 (11.6)       |
| B. High concentration aerosol transmission  | 97 (32.1)       |
| C. Fecal-oral transmission  | 170 (56.3)      |
| <b>K5: Which of the following is true about the susceptibility of the novel coronavirus?</b>  |                 |
| A. People are generally susceptible   | 272 (90.1)      |
| B. Old people and children are susceptible  | 15 (5.0)        |
| C. People with underlying diseases are susceptible  | 15 (5.0)        |
| <b>K6: Which of the following can enhance the protection against novel coronavirus?</b>   |                 |
| A. Wear a multi-layer mask  | 59 (19.5)       |
| B. Drink liquor   | 4 (1.3)         |
| C. Wash hands and disinfect in time   | 239 (79.1)      |
| <b>K7: Which of the following is true to contact with others in public during an outbreak?</b>  |                 |
| A. Normal communication   | 2 (0.7)         |
| B. Wear a mask and keep a distance of more than one meter   | 299 (99.0)      |
| C. Wear a mask  | 1 (0.3)         |
| <b>K8: What is the risk level of infection for staff in crowded place during the epidemic?</b>  |                 |
| A. High risk exposure   | 266 (88.1)      |
| B. Medium risk exposure   | 33 (10.9)       |
| C. Low risk exposure  | 3 (1.0)         |
| <b>K9: What kind of mask should be chosen when there is only particulate matter (such as dust, smoke) in the workplace during the epidemic?</b> |                 |
| A. Disposable mask  | 67 (22.2)       |
| B. Surgical mask  | 93 (30.8)       |
| C. Anti-particulate mask  | 142 (47.0)      |
| <b>K10: What are the correct anti-virus measures should be taken when going home during the epidemic?</b>                                       |                 |
| A. Replace clothes, wash hands and disinfect in time  | 286 (94.7)      |
| B. Place mask and clothes at will   | 10 (3.3)        |
| C. Clean the mask and use it again  | 6 (2.0)         |

( $\chi^2 = 53.658$ ,  $P < 0.001$ ), the source of infection ( $\chi^2 = 23.883$ ,  $P < 0.001$ ), the route of transmission ( $\chi^2 = 14.282$ ,  $P = 0.003$ ), the risk level of the workplace ( $\chi^2 = 8.986$ ,  $P = 0.029$ ) and the choice of masks ( $\chi^2 = 12.405$ ,  $P = 0.006$ ). More details were shown in Table 3.

## COVID-19 Attitude and Practice

The attitude scores of different occupational groups were all higher than 95, and practice scores were all higher than 90. For people of different occupations, the influencing factors of KAP were different. Education level was the influencing factor of white-collar workers practice, residence was the influencing factor of blue-collar attitude, and gender was the influencing factor of professional attitude and practice. The results of Kruskal-Wallis  $H$  test showed that there were differences in knowledge among people of different occupations, but not in attitudes and practices. More details were shown in Table 4.

## Multiple Linear Regression Analysis of the Factors Influencing KAP

Knowledge score was taken as the dependent variable, gender (male = 1, female = 2), age (15–30 years old = 1, 31–45 years old = 2, 46–60 years old = 3), education (senior high school and below = 1, undergraduate and junior college = 2, master degree or above = 3), place of residence (urban = 1, rural = 2), occupation (white-collar workers = 1, professionals = 2, blue-collar workers = 3, self-employments = 4), were the five independent variables. Multiple linear regression was conducted by the forced entry method to quantify the independent contributions of the above variables to knowledge. The same two models were built using the scores of attitude and practice as dependent variables. After adjusting for demographic variables, we found that the factors influencing knowledge were the level of education and place of residence, specifically reflected in living in the urban, the higher the level of education, the higher the level of knowledge. Gender was a predictor for practice, and females might have a better personal protective practice than males. More details were shown in Table 5.

## DISCUSSION

Since the discovery of novel coronavirus, COVID-19 has had a destructive impact on the world. Health departments must formulate effective strategies to educate and manage the public. It is particularly important to timely grasp the current status and influencing factors of workers' KAP on epidemic prevention and control in the process of resuming work and production. Therefore, the purpose of this study was to compare the KAP regarding to COVID-19 among people returning to work in different occupations in China, which provides a theoretical reference for strengthening society-wide efforts to prevent and control the world pandemic. In this study, there were great differences in knowledge scoring rates in different aspects. Some professional issues such as risk of infection in different workplaces (K8:10.9%), infectious disease classification (K1: 45%) and mask selection in different places (K9: 47%) had low scores, suggesting these are the weak areas to be

**TABLE 3 |** Comparison of knowledge level of people returning to work in different occupations regarding COVID-19.

|  | White-collar<br>workers (%) | Professionals<br>(%) | Blue-collar<br>workers (%) | Self-<br>employments(%) | Total (%)  | $\chi^2$ | P         |
|--|-----------------------------|----------------------|----------------------------|-------------------------|------------|----------|-----------|
| K1: What is the classification of infectious diseases in COVID-19?   | 27 (32.9)                   | 80 (70.8)            | 7 (15.2)                   | 22 (36.1)               | 136 (45.0) | 53.658   | <0.001*** |
| K2: Which of the following measures can effectively inactivate novel coronavirus?  | 79 (96.3)                   | 110 (97.3)           | 43 (93.5)                  | 59 (96.7)               | 291 (96.4) | 1.639    | 0.700     |
| K3: Which of the following is wrong about the possible source of infection of novel coronavirus?   | 67 (81.7)                   | 102 (90.3)           | 26 (56.5)                  | 48 (78.7)               | 243 (80.5) | 23.883   | <0.001*** |
| K4: Which of the following is not the main route of transmission of the novel coronavirus?   | 51 (62.2)                   | 74 (65.5)            | 21 (45.7)                  | 24 (39.3)               | 170 (56.3) | 14.282   | 0.003**   |
| K5: Which of the following is true about the susceptibility of the novel coronavirus?  | 78 (95.1)                   | 101 (89.4)           | 38 (82.6)                  | 55 (90.2)               | 272 (90.1) | 5.248    | 0.144     |
| K6: Which of the following can enhance the protection against novel coronavirus?   | 61 (74.4)                   | 95 (84.1)            | 32 (69.6)                  | 51 (83.6)               | 239 (79.1) | 6.076    | 0.108     |
| K7: Which of the following is true to contact with others in public during an outbreak?  | 80 (97.6)                   | 113 (100)            | 45 (97.8)                  | 61 (100.0)              | 299 (99.0) | 3.774    | 0.174     |
| K8: What is the risk level of infection for staff in crowded place during the epidemic?  | 7 (8.5)                     | 20 (17.7)            | 3 (6.5)                    | 3 (4.9)                 | 33 (10.9)  | 8.986    | 0.029*    |
| K9: What kind of mask should be chosen when there is only particulate matter (such as dust, smoke) in the workplace during the epidemic? | 36 (43.9)                   | 66 (58.4)            | 21 (45.7)                  | 19 (31.1)               | 142 (47.0) | 12.405   | 0.006**   |
| K10: What are the correct anti-virus measures should be taken when going home during the epidemic?                                       | 77 (93.9)                   | 109 (96.5)           | 44 (95.7)                  | 56 (91.8)               | 286 (94.7) | 2.000    | 0.583     |

\* $P < 0.05$ , \*\* $P < 0.01$ , \*\*\* $P < 0.001$ .

strengthened. This was different from the results of Zhong et al. (the overall correct rate of the knowledge questionnaire was 90%) (22). The reason might be that Zhong's survey area was mainly Wuhan city (where the first confirmed case was found in China), and most of the people surveyed were well-educated people (82.4% held an associate's degree or higher, and 56.2% engaged in mental labor). For the attitudes and practices about prevention and control of COVID-19 of the returning workers, with COVID-19 spread rapidly from a single city to the whole country, the vast of majority of respondents showed a high degree of compliance. The scores of attitude and practice were all higher than 95 and 90 respectively. According to the WHO, social distancing/self-isolation and lockdown were two crucial nationwide social measures during a public health crisis (23). After COVID-19 broke out across the country, the Chinese government took unprecedented measures to control the world pandemic, including quarantine and isolation, strict management of working and living spaces and the Examine and Approve Policy on the resumption of work. All occupations expressed high support for the measures taken by the government, health institutions and communities prevent and control the world pandemic.

Our study found that individual demographic characteristics had an impact on their KAP, which is consistent with previous studies (24–26). Educational level and place of residence were the influencing factors of respondents' knowledge, which was also in line with the law of low educational level in rural areas. The results suggested that people living in rural areas with a

low level of education also had a lower level of knowledge. This may be due to residents in rural areas have limited availability to the internet and online health information resources and they are more likely to have poor knowledge about COVID-19. Less educated residents may be more likely to receive visual media rather than textual official documents. We suggest that more targeted health education should be carried out. For villages and towns to increase broadcasting and other more acceptable publicity methods, for people with low educational level to use more easy-to-understand popular science means such as simple cartoons. For people of different occupations, the knowledge score of professional personnel was generally higher than that of other types of workers, probably because they have received more training, have stronger learning ability, and easier to master COVID-19's prevention and control knowledge. We also found that gender was a factor affecting practice. Females showed better protective practice, consistent with the results of a study in Vietnam (27), which may be related to the fact that males were more likely to engage in risk-taking behavior (28). Knowledge is the basis for establishing correct attitudes to change practice, while the attitude is the driving force of practice change. People's practice is influenced by their own knowledge and attitude (29). The KAP theoretical model is helpful for public health policy makers and health workers to identify the target population of COVID-19's prevention and health education.

During the outbreak of infectious diseases, timely understand the public's KAP of the epidemic and the needs of health education, and carry out effective risk communication with the

**TABLE 4 |** Univariate analysis of factors associated with KAP.

|           |                                  | White-collar workers    | Statistic                | Professionals           | Statistic                   | Blue-collar workers     | Statistic                  | Self-employment         | Statistic                   |
|-----------|----------------------------------|-------------------------|--------------------------|-------------------------|-----------------------------|-------------------------|----------------------------|-------------------------|-----------------------------|
| Knowledge | Gender                           |                         | 743.50 <sup>a</sup>      |                         | 1024.00 <sup>a</sup>        |                         | 222.50 <sup>a</sup>        |                         | 389.00 <sup>a</sup>         |
|           | Male                             | 7.00 (6.00, 8.00)       |                          | 8.00 (7.00, 8.00)       |                             | 6.00 (4.75, 7.00)       |                            | 7.00 (6.00, 8.00)       |                             |
|           | Female                           | 7.00 (6.00, 8.00)       |                          | 8.00 (7.00, 9.00)       |                             | 6.00 (6.00, 7.00)       |                            | 6.00 (6.00, 7.00)       |                             |
|           | Age (years)                      |                         | 1.69 <sup>b</sup>        |                         | 1.54 <sup>b</sup>           |                         | 5.55 <sup>b</sup>          |                         | 2.82 <sup>b</sup>           |
|           | 15–30                            | 7.00 (5.00, 8.00)       |                          | 8.00 (7.00, 8.50)       |                             | 5.00 (4.50, 6.50)       |                            | 6.00 (6.00, 7.00)       |                             |
|           | 31–45                            | 7.00 (6.50, 8.00)       |                          | 8.00 (7.00, 9.00)       |                             | 7.00 (6.00, 8.00)       |                            | 7.00 (6.75, 8.00)       |                             |
|           | 46–60                            | 7.00 (6.00, 7.75)       |                          | 8.00 (7.00, 9.00)       |                             | 6.00 (5.00, 7.00)       |                            | 6.00 (6.00, 7.50)       |                             |
|           | Education                        |                         | <b>6.50<sup>b*</sup></b> |                         | 5.33 <sup>b</sup>           |                         | 147.50 <sup>a</sup>        |                         | 0.74 <sup>b</sup>           |
|           | Senior high school and below     | 6.00 (4.00, 7.00)       |                          | 7.00 (3.00, 7.00)       |                             | 6.00 (5.00, 7.00)       |                            | 6.50 (5.75, 7.00)       |                             |
|           | Undergraduate and junior college | 7.00 (6.00, 8.00)       |                          | 8.00 (7.00, 9.00)       |                             | 5.50 (4.25, 6.75)       |                            | 7.00 (6.00, 7.25)       |                             |
|           | Master degree or above           | 7.00 (7.00, 8.50)       |                          | 8.00 (7.00, 9.00)       |                             | NA                      |                            | 6.00 (6.00, 6.00)       |                             |
|           | Place of residence               |                         | 38.50 <sup>a</sup>       |                         | 370.50 <sup>a</sup>         |                         | 195.00 <sup>a</sup>        |                         | 363.50 <sup>a</sup>         |
|           | Urban                            | 7.00 (6.00, 8.00)       |                          | 8.00 (7.00, 9.00)       |                             | 6.00 (5.00, 7.50)       |                            | 7.00 (6.00, 7.00)       |                             |
|           | Rural                            | 5.00 (3.00, NA)         |                          | 7.50 (6.25, 8.00)       |                             | 6.00 (4.50, 7.00)       |                            | 6.00 (5.00, 7.00)       |                             |
|           | Total                            | 7.00 (6.00, 8.00)       |                          | 8.00 (7.00, 9.00)       |                             | 6.00 (5.00, 7.00)       |                            | 7.00 (6.00, 7.00)       | <b>56.73<sup>b***</sup></b> |
| Attitude  | Gender                           |                         | 822.50 <sup>a</sup>      |                         | <b>944.50<sup>a*</sup></b>  |                         | 259.50 <sup>a</sup>        |                         | 441.00 <sup>a</sup>         |
|           | Male                             | 100.00 (97.14, 100.00)  |                          | 100.00 (89.29, 100.00)  |                             | 100.00 (99.29, 100.00)  |                            | 100.00 (94.29, 100.00)  |                             |
|           | Female                           | 100.00 (96.43, 100.00)  |                          | 100.00 (100.00, 100.00) |                             | 100.00 (97.86, 100.00)  |                            | 100.00 (93.58, 100.00)  |                             |
|           | Age (years)                      |                         | 1.10 <sup>b</sup>        |                         | 4.36 <sup>b</sup>           |                         | 1.37 <sup>b</sup>          |                         | 1.40 <sup>b</sup>           |
|           | 15–30                            | 100.00 (97.14, 100.00)  |                          | 100.00 (97.14, 100.00)  |                             | 100.00 (100.00, 100.00) |                            | 100.00 (88.57, 100.00)  |                             |
|           | 31–45                            | 100.00 (98.57, 100.00)  |                          | 100.00 (100.00, 100.00) |                             | 100.00 (98.57, 100.00)  |                            | 100.00 (99.29, 100.00)  |                             |
|           | 46–60                            | 100.00 (95.00, 100.00)  |                          | 100.00 (100.00, 100.00) |                             | 100.00 (97.14, 100.00)  |                            | 100.00 (95.72, 100.00)  |                             |
|           | Education                        |                         | 0.29 <sup>b</sup>        |                         | 3.56 <sup>b</sup>           |                         | 203.50 <sup>a</sup>        |                         | 0.77 <sup>b</sup>           |
|           | Senior high school and below     | 100.00 (85.72, 100.00)  |                          | 100.00 (91.43, 100.00)  |                             | 100.00 (99.29, 100.00)  |                            | 100.00 (94.29, 100.00)  |                             |
|           | Undergraduate and junior college | 100.00 (97.14, 100.00)  |                          | 100.00 (100.00, 100.00) |                             | 100.00 (97.86, 100.00)  |                            | 100.00 (90.72, 100.00)  |                             |
|           | Master degree or above           | 100.00 (97.14, 100.00)  |                          | 100.00 (98.57, 100.00)  |                             | NA                      |                            | 100.00 (100.00, 100.00) |                             |
|           | Place of residence               |                         | 54.00 <sup>a</sup>       |                         | 451.00 <sup>a</sup>         |                         | <b>172.50<sup>a*</sup></b> |                         | 437.50 <sup>a</sup>         |
|           | Urban                            | 100.00 (97.14, 100.00)  |                          | 100.00 (100.00, 100.00) |                             | 100.00 (95.72, 100.00)  |                            | 100.00 (94.29, 100.00)  |                             |
|           | Rural                            | 100.00 (100.00, 100.00) |                          | 100.00 (93.58, 100.00)  |                             | 100.00 (100.00, 100.00) |                            | 100.00 (90.00, 100.00)  |                             |
|           | Total                            | 100.00 (97.14, 100.00)  |                          | 100.00 (100.00, 100.00) |                             | 100.00 (98.29, 100.00)  |                            | 100.00 (94.29, 100.00)  | 5.84 <sup>b</sup>           |
| Practice  | Gender                           |                         | 805.50 <sup>a</sup>      |                         | <b>762.50<sup>a**</sup></b> |                         | 219.00 <sup>a</sup>        |                         | 403.50 <sup>a</sup>         |
|           | Male                             | 99.59 (89.17, 100.00)   |                          | 98.33 (84.37, 100.00)   |                             | 99.59 (94.17, 100.00)   |                            | 100.00 (85.83, 100.00)  |                             |
|           | Female                           | 99.17 (87.92, 100.00)   |                          | 100.00 (98.33, 100.00)  |                             | 97.09 (89.17, 100.00)   |                            | 100.00 (96.46, 100.00)  |                             |
|           | Age (years)                      |                         | 0.14 <sup>b</sup>        |                         | 0.35 <sup>b</sup>           |                         | 1.04 <sup>b</sup>          |                         | 5.05 <sup>b</sup>           |
|           | 15–30                            | 100.00 (86.25, 100.00)  |                          | 100.00 (97.50, 100.00)  |                             | 99.17 (95.84, 100.00)   |                            | 99.17 (88.12, 100.00)   |                             |
|           | 31–45                            | 99.17 (90.00, 100.00)   |                          | 100.00 (98.33, 100.00)  |                             | 96.67 (89.58, 100.00)   |                            | 100.00 (99.79, 100.00)  |                             |
|           | 46–60                            | 96.67 (91.67, 100.00)   |                          | 100.00 (96.25, 100.00)  |                             | 100.00 (86.67, 100.00)  |                            | 100.00 (84.17, 100.00)  |                             |
|           | Education                        |                         | <b>7.75<sup>b*</sup></b> |                         | 2.76 <sup>b</sup>           |                         | 191.50 <sup>a</sup>        |                         | 0.80 <sup>b</sup>           |
|           | Senior high school and below     | 96.25 (82.92, 99.79)    |                          | 100.00 (97.50, 100.00)  |                             | 99.17 (89.79, 100.00)   |                            | 100.00 (85.83, 100.00)  |                             |
|           | Undergraduate and junior college | 100.00 (92.92, 100.00)  |                          | 100.00 (98.33, 100.00)  |                             | 99.17 (96.04, 100.00)   |                            | 99.59 (92.50, 100.00)   |                             |
|           | Master degree or above           | 91.67 (84.17, 95.00)    |                          | 98.75 (91.87, 100.00)   |                             | NA                      |                            | 100.00 (100.00, 100.00) |                             |
|           | Place of residence               |                         | 36.00 <sup>a</sup>       |                         | 465.50 <sup>a</sup>         |                         | 208.50 <sup>a</sup>        |                         | 413.50 <sup>a</sup>         |
|           | Urban                            | 99.17 (88.33, 100.00)   |                          | 100.00 (97.50, 100.00)  |                             | 99.17 (89.59, 100.00)   |                            | 100.00 (89.17, 100.00)  |                             |
|           | Rural                            | 100.00 (100.00, 100.00) |                          | 100.00 (98.12, 100.00)  |                             | 100.00 (93.75, 100.00)  |                            | 100.00 (93.54, 100.00)  |                             |
|           | Total                            | 99.17 (88.33, 100.00)   |                          | 100.00 (97.50, 100.00)  |                             | 99.17 (91.67, 100.00)   |                            | 100.00 (91.67, 100.00)  | 7.10 <sup>b</sup>           |

<sup>a</sup>outcomes of Mann-Whitney U test, <sup>b</sup>outcomes of Kruskal-Wallis H test.\* $P < 0.05$ , \*\* $P < 0.01$ , \*\*\* $P < 0.001$ .**Bold indicates that the results are statistically significant.**



**TABLE 5 |** Multiple linear regression analysis of the factors influencing KAP.

|                    | Unstandardized Coefficient |                | Standardized Coefficient | <i>t</i> | 95% CI           | <i>P</i>  |
|--------------------|----------------------------|----------------|--------------------------|----------|------------------|-----------|
|                    | B                          | Standard Error | β                        |          |                  |           |
| <b>Knowledge</b>   |                            |                |                          |          |                  |           |
| Gender             | 0.337                      | 0.176          | 0.104                    | 1.918    | (−0.009, 0.683)  | 0.056     |
| Age                | 0.182                      | 0.112          | 0.094                    | 1.625    | (−0.038, 0.403)  | 0.105     |
| Education          | 0.745                      | 0.166          | 0.261                    | 4.479    | (0.418, 1.072)   | <0.001*** |
| Place of residence | −0.739                     | 0.251          | −0.177                   | −2.946   | (−1.232, −0.245) | 0.003**   |
| Occupation         | 0.002                      | 0.090          | 0.002                    | 0.025    | (−0.176, 0.18)   | 0.980     |
| <b>Attitude</b>    |                            |                |                          |          |                  |           |
| Gender             | 1.381                      | 1.236          | 0.065                    | 1.117    | (−1.052, 3.814)  | 0.265     |
| Age                | 0.475                      | 0.788          | 0.037                    | 0.602    | (−1.076, 2.025)  | 0.547     |
| Education          | 1.405                      | 1.170          | 0.075                    | 1.201    | (−0.897, 3.707)  | 0.231     |
| Place of residence | 1.547                      | 1.763          | 0.057                    | 0.877    | (−1.923, 5.016)  | 0.381     |
| Occupation         | 0.500                      | 0.636          | 0.052                    | 0.786    | (−0.752, 1.752)  | 0.433     |
| <b>Practice</b>    |                            |                |                          |          |                  |           |
| Gender             | 2.603                      | 1.299          | 0.116                    | 2.005    | (0.047, 5.159)   | 0.046*    |
| Age                | 0.951                      | 0.828          | 0.071                    | 1.148    | (−0.678, 2.58)   | 0.252     |
| Education          | 0.603                      | 1.229          | 0.031                    | 0.491    | (−1.815, 3.021)  | 0.624     |
| Place of residence | 1.520                      | 1.852          | 0.053                    | 0.821    | (−2.125, 5.165)  | 0.412     |
| Occupation         | 0.267                      | 0.668          | 0.026                    | 0.400    | (−1.048, 1.583)  | 0.689     |

\**P* < 0.05, \*\**P* < 0.01, \*\*\**P* < 0.001.

public, so as to take health education measures and strategies for different groups of people. So as to control the spread of virus in the population in a timely manner. This can effectively reduce the negative psychological reaction caused by the outbreak of the world pandemic, eliminate public panic, prevent the spread of virus, which is conducive to the prevention and control of the epidemic (30). This study conducted a rapid evaluation of public KAP in the rising phase of COVID-19, which can provide a basis for the government to formulate targeted health education and behavior intervention strategies.

This study also has some limitations. Although we have designed the questionnaire according to the official guidance manual and the latest literature, the depth of the survey may be limited. Second, this study is a web-based survey, which will result in the loss of some respondents (those who do not know how to use the internet or cannot use the internet or smart phones due to restrictions), and overestimate the KAP level of those who return to work to a certain extent. Third, there may be a recall bias because the data are collected through participants' self-reports.

## CONCLUSION

This study preliminarily explored the KAP and influencing factors of people returning to work in different occupations on the prevention and control of COVID-19. Overall, these workers in our survey showed positive attitude and appropriate practice toward COVID-19 during the world pandemic, which

are significant factors to limit the spread of the virus. The results of this survey can provide a reference for the subsequent improvement of COVID-19's prevention publicity and health education. Due to the sample limitation, more extensive studies are needed in the future to support our conclusions.

## DATA AVAILABILITY STATEMENT

The raw data supporting the conclusions of this article will be made available by the authors, without undue reservation.

## AUTHOR CONTRIBUTIONS

The manuscript writing for the original draft and data analysis were completed by ZYF. YLM collaborated in data extraction and gave the paper revision and format adjustment work. FZ and YZ gave the entire process technical and paper writing guidance support. All authors read and approved the final manuscript.

## FUNDING

This research was funded by Chongqing Medical University School of Public Health and Management, Research Center for Medicine and Social Development, COVID-19 Prevention, and Control Emergency Research (Management) Project.

## REFERENCES

- Li Q, Guan X, Wu P, Wang X, Zhou L, Tong Y, et al. Early transmission dynamics in wuhan, china, of novel coronavirus-infected pneumonia. *New Engl J Med*. (2020) 382:1199–207. doi: 10.1056/NEJMoa2001316
- Huang C, Wang Y, Li X, Ren L, Zhao J, Hu Y, et al. Clinical features of patients infected with 2019 novel coronavirus in Wuhan, China. *Lancet*. (2020) 395:497–506. doi: 10.1016/S0140-6736(20)30183-5
- World Health Organization (WHO). *WHO Director-General's statement on IHR Emergency Committee on Novel Coronavirus (2019-nCoV)*. (2021). Available online at: <https://www.who.int/director-general/speeches/detail/who-director-general-s-statement-on-ihf-emergency-committee-on-novel-coronavirus-2019-ncov> (accessed March 12, 2021).
- Dousari AS, Moghadam MT, Satarzadeh N. COVID-19 (Coronavirus Disease 2019): a new coronavirus disease. *Infect Drug Resist*. (2020) 13:2819–28. doi: 10.2147/IDR.S259279
- Worldmeter. *COVID-19 Update (Live)*. (2020). Available online at: <https://www.worldometers.info/coronavirus/> (accessed March 12, 2021).
- Fong MW, Gao H, Wong JY, Xiao J, Shiu EYC, Ryu S, et al. Nonpharmaceutical measures for pandemic influenza in nonhealthcare settings-social distancing measures. *Emerg Infect Dis*. (2020) 26:976–84. doi: 10.3201/eid2605.190995
- Ahmed F, Zviedrite N, Uzicanin A. Effectiveness of workplace social distancing measures in reducing influenza transmission: a systematic review. *BMC Public Health*. (2018) 18:518. doi: 10.1186/s12889-018-5446-1
- Tan W, Hao F, McIntyre RS, Jiang L, Jiang X, Zhang L, et al. Is returning to work during the COVID-19 pandemic stressful? A study on immediate mental health status and psychoneuroimmunity prevention measures of Chinese workforce. *Brain Behav Immun*. (2020) 87:84–92. doi: 10.1016/j.bbi.2020.04.055
- Ferguson NM, Cummings DAT, Fraser C, Cajka JC, Cooley PC, Burke DS. Strategies for mitigating an influenza pandemic. *Nature*. (2006) 442:448–52. doi: 10.1038/nature04795
- Prem K, Liu Y, Russell TW, Kucharski AJ, Eggo RM, Davies N. The effect of control strategies to reduce social mixing on outcomes of the COVID-19 epidemic in Wuhan, China: a modelling study. *Lancet Public Health*. (2020) 5:e261–70. doi: 10.1016/S2468-2667(20)30073-6
- Xinhua. *State Council's tips on workplace COVID-19 prevention, control*. (2020). Available online at: [http://www.china.org.cn/china/2020-03/05/content\\_75776272.htm](http://www.china.org.cn/china/2020-03/05/content_75776272.htm) (accessed March 12, 2021).
- The State Council. *Notice on prevention and control measures of resuming work and production*. (2020). Available online at: [http://www.gov.cn/zhengce/content/2020-02/22/content\\_5482025.htm](http://www.gov.cn/zhengce/content/2020-02/22/content_5482025.htm) (accessed April 10, 2021).
- Qu J, Lv X. The Response Measures to the Coronavirus Disease 2019 Outbreak in China. *Open Forum Infect Dis*. (2021) 8:ofab14. doi: 10.1093/ofid/ofab014
- Liang Y, Wu K, Zhou Y, Huang X, Zhou Y, Liu Z. Mental health in frontline medical workers during the 2019 novel coronavirus disease epidemic in china: a comparison with the general population. *Int J Environ Res Public Health*. (2020) 17:6550. doi: 10.3390/ijerph17186550
- Moghadam MT, Taati B, Ardakani SMP, Suzuki K. Ramadan fasting during the COVID-19 pandemic; observance of health, nutrition and exercise criteria for improving the immune system. *Front Nutr*. (2021) 7:570235. doi: 10.3389/fnut.2020.570235
- Saadatjoo S, Miri M, Hassanipour S, Ameri H, Arab-Zozani M. Knowledge, attitudes, and practices of the general population about Coronavirus disease 2019 (COVID-19): a systematic review and meta-analysis with policy recommendations [published online ahead of print]. *Public Health*. (2021). doi: 10.1016/j.puhe.2021.03.005
- Moghadam MT, Babakhani S, Rajabi S, Baravati FB, Raeisi M, Dousari AS. Does stress and anxiety contribute to COVID-19? *Iran J Psychiatry Behav Sci*. (2020) 15:e106041. doi: 10.5812/ijpbs.106041
- Chen B. Sample size methodology for multivariate analysis—synthetic estimate method for sample size in multivariate analysis. *Injury Med (Electronic Edition)*. (2012) 1:58–60. doi: 10.3868/j.issn.2095-1566.2012.04.012
- World Health Organization (WHO). *Q&As on COVID-19 and related health topics*. Available online at: <https://www.who.int/emergencies/diseases/novel-coronavirus-2019/question-and-answers-hub> (accessed March 12, 2021).
- National Health Commission of the People's Republic China (NHC). *Knowledge on prevention and control of COVID-19*. (2020). Available online at: [http://www.nhc.gov.cn/xcs/kpzs/list\\_gzbd.shtml](http://www.nhc.gov.cn/xcs/kpzs/list_gzbd.shtml) (accessed March 12, 2021).
- Chinese Center for Disease Control and Prevention (CDC). *Knowledge world*. (2020). Available online at: [http://www.chinacdc.cn/jkzt/crb/zl/szkb\\_11803/jzsl\\_2275/](http://www.chinacdc.cn/jkzt/crb/zl/szkb_11803/jzsl_2275/) (accessed March 12, 2021).
- Zhong B, Luo W, Li H, Zhang Q, Liu X, Li W, et al. Knowledge, attitudes, and practices towards COVID-19 among Chinese residents during the rapid rise period of the COVID-19 outbreak: a quick online cross-sectional survey. *Int J Biol Sci*. (2020) 16:1745–52. doi: 10.7150/ijbs.45221
- World Health Organization (WHO). *WHO Director-General's opening remarks at the media briefing on COVID-19—March 11, 2020*. (2020). Available online at: <https://www.who.int/director-general/speeches/detail/who-director-general-s-opening-remarks-at-the-media-briefing-on-covid-19--11-march-2020> (accessed March 12, 2021).
- Gao H, Hu R, Yin L, Yuan X, Tang H, Luo L, et al. Knowledge, attitudes and practices of the Chinese public with respect to coronavirus disease (COVID-19): an online cross-sectional survey. *BMC Public Health*. (2020) 20:1816. doi: 10.1186/s12889-020-09961-2
- Chen Y, Zhou R, Chen B, Chen H, Li Y, Chen Z, et al. Knowledge, perceived beliefs, and preventive behaviors related to COVID-19 among chinese older adults: cross-sectional web-based survey. *J Med Internet Res*. (2020) 22:e23729. doi: 10.2196/23729
- Lau LL, Hung N, Go DJ, Ferma J, Choi M, Dodd W, et al. Knowledge, attitudes and practices of COVID-19 among income-poor households in the Philippines: a cross-sectional study. *J Glob Health*. (2020) 10:11007. doi: 10.7189/jogh.10.011007
- Van Nhu H, Tuyet-Hanh TT, Van NTA, Linh TNQ, Tien TQ. Knowledge, attitudes, and practices of the vietnamese as key factors in controlling COVID-19. *J Community Health*. (2020) 45:1263–69. doi: 10.1007/s10900-020-00919-4
- Yang K, Liu H, Li H, Wang S, Tian Y, Zhang F, et al. Knowledge, attitude and practice of residents in the prevention and control of COVID-19: an online questionnaire survey. *J Adv Nurs*. (2020) 77:1839–55. doi: 10.1111/jan.14718
- Huang JT. *Health Education*. Beijing: Science Press (2000).
- The Lancet. Emerging understandings of 2019-nCoV. *Lancet*. (2020) 395:311. doi: 10.1016/S0140-6736(20)30186-0

**Conflict of Interest:** The authors declare that the research was conducted in the absence of any commercial or financial relationships that could be construed as a potential conflict of interest.

Copyright © 2021 Fan, Mou, Cheng, Zhao and Zhang. This is an open-access article distributed under the terms of the Creative Commons Attribution License (CC BY). The use, distribution or reproduction in other forums is permitted, provided the original author(s) and the copyright owner(s) are credited and that the original publication in this journal is cited, in accordance with accepted academic practice. No use, distribution or reproduction is permitted which does not comply with these terms.



# High Infection Fatality Rate Among Elderly and Risk Factors Associated With Infection Fatality Rate and Asymptomatic Infections of COVID-19 Cases in Hong Kong

Jun Tao<sup>1†</sup>, Xiaoyu Zhang<sup>1†</sup>, Saliu S. Musa<sup>2</sup>, Lin Yang<sup>3</sup> and Daihai He<sup>2\*</sup>

<sup>1</sup> School of Public Health, Li Ka Shing Faculty of Medicine, The University of Hong Kong, Hong Kong, China, <sup>2</sup> Department of Applied Mathematics, Hong Kong Polytechnic University, Hong Kong, China, <sup>3</sup> School of Nursing, Hong Kong Polytechnic University, Hong Kong, China

## OPEN ACCESS

### Edited by:

Arda Kiani,  
Shahid Beheshti University of Medical  
Sciences, Iran

### Reviewed by:

Zhiwei Xu,  
The University of  
Queensland, Australia  
Chun-Quan Ou,  
Southern Medical University, China

### \*Correspondence:

Daihai He  
daihai.he@polyu.edu.hk

<sup>†</sup>These authors have contributed  
equally to this work

### Specialty section:

This article was submitted to  
Infectious Diseases – Surveillance,  
Prevention and Treatment,  
a section of the journal  
Frontiers in Medicine

Received: 09 March 2021

Accepted: 03 May 2021

Published: 24 May 2021

### Citation:

Tao J, Zhang X, Musa SS, Yang L and  
He D (2021) High Infection Fatality  
Rate Among Elderly and Risk Factors  
Associated With Infection Fatality Rate  
and Asymptomatic Infections of  
COVID-19 Cases in Hong Kong.  
Front. Med. 8:678347.  
doi: 10.3389/fmed.2021.678347

**Background:** Since the emergence in December 2019, the COVID-19 pandemic has become one of the greatest global public health threats in history. However, asymptomatic infections have increased the challenges of providing accurate estimates for the infection fatality rate (IFR) of COVID-19.

**Methods:** We calculated the asymptomatic case ratios based on the reported COVID-19 cases in Hong Kong where intensive testing has been conducted in close contacts and high-risk populations. We estimated the IFR using both symptomatic and asymptomatic cases as denominator. The boosted regression tree (BRT) and multivariable logistic regression models were used to identify relative contribution and effect size of the risk factors associated with the asymptomatic cases and IFRs.

**Results:** The ratio of the asymptomatic patients in Hong Kong was higher than many other regions over the world. Imported cases had a higher asymptomatic proportion than local cases. Older age and male were associated with a higher IFR than younger age and females.

**Conclusion:** Policymakers should consider the potential risk factors for the asymptomatic infections and IFRs by the Hong Kong surveillance data to mitigate the diseases and reduce the case mortality of COVID-19.

**Keywords:** asymptomatic COVID-19 cases, Hong Kong, boosted regression tree, elderly, infection fatality rate

## INTRODUCTION

Since its emergence in December 2019, the COVID-19 pandemic has become one of the greatest global public health threats in history. As of 8 March 2021, more than 116 million cases have been confirmed, with more than 2.59 million deaths attributed to COVID-19 (1). As the pandemic spread, it has been found that some cases did not manifest any clinical symptoms, which could have been missed by the surveillance system based on healthcare settings, rendering serious underestimation of disease burden (2). Recent studies have reported that 13.1–27.4% of COVID-19 cases were asymptomatic, depending on geographical regions, case

definitions and the length of follow-up period (3–6). The lack of reliable data on asymptomatic cases in different age groups hinders accurate estimation of age-specific infection fatality rates (IFRs) for COVID-19, an important indicator for disease burden of the pandemic.

The infection fatality ratio is a critical estimation for the disease burden of the COVID-19 pandemic globally. It is of great policy value to have accurate and up-to-date estimates in different population stratifications so that appropriate prevention measures could be in place to mitigate risk. It is important to note that the infection fatality ratio is not constant among different populations because it depends on the age distribution in the population and the infection rates in each age group, the asymptomatic case ratios, and many other risk factors. There are mainly two approaches to estimate the IFRs, including the seroprevalence and the comprehensive tracing studies (7). Some research adopted the result of serological tests to estimate the cumulative infections among populations considering the limited testing capacity and asymptomatic cases, but the accuracy of serological tests also depends on the humoral immune response, the waning speed of antibodies in the circulation and testing sensitivity (8). Besides, some seroprevalence studies are based on “convenience samples” collected for other purposes and the sampling frame cannot represent the general population (7).

There are two approaches to estimate the IFRs, including the seroprevalence studies testing the antibody to SARS-CoV-2 or comprehensive case tracing by extensive live virus testing (7). The accuracy of IFRs estimated by case tracing is influenced by the extent to which infected individuals are identified, especially the asymptomatic cases (7). The IFRs could vary greatly across the world and depend crucially on the age groups infected in the specific region, with the elderly of significantly higher IFRs (7). Around the globe, Hong Kong is unique in its geographical proximity to mainland China and its preparedness to emerging infectious diseases based on the lessons learnt during SARS and avian influenza epidemics. In addition, the persistent efforts for contact tracing and testing among the local residents have contributed to the relatively robust surveillance system.

The city has experienced four waves of the COVID-19 outbreaks in communities and opened the access to deidentified data of individual COVID-19 cases. The Hong Kong surveillance data can provide good resources to estimate the asymptomatic ratios and IFRs by age group. Herein, the asymptomatic ratios and IFRs were estimated together with their corresponding risk factors to provide critical information for health policymaking.

## METHODS

The study used the Hong Kong COVID-19 surveillance data, which is publicly available from the Centre for Health Protection (CHP) in Hong Kong (9). By 27th January 2021, Hong Kong has recorded 10,283 confirmed cases of COVID-19. Among these cases, 2913 were asymptomatic and 174 were fatal cases. The average age of patients was  $45.0 \pm 19.9$  years, ranging from 14 days to 100 years. About half (48.4%) of them were men and over 80% were local residents. The 1,041 cases reported in the first

and second wave were combined together for analysis due to the similarity in control measures and the relatively small sample size (95 cases) in the first wave.

The demographic characteristics included age and gender, and the classification variables included the waves of COVID-19 outbreak which individual case was identified in, and classification of local and imported cases. We defined the first wave as the period of January 23rd 2020–February 29th 2020, the second wave as March 1st 2020–May 6th 2020, the third wave as May 7th 2020–November 22nd 2020, and the fourth wave as November 23rd 2020–January 27th 2021 (10). Six categories of cases were identified in the original data, including local/imported case, possibly local case, epidemiologically linked with local/imported case, epidemiologically linked with possibly local case. We classified local, possibly local, epidemiologically linked with possibly local case as local cases and the other three as imported cases. The proportion of asymptomatic cases and case fatality were set as the outcome variables. The distribution of each explanatory variable was firstly examined using Chi-square test for categorical variables and one-way analysis of variance (ANOVA) for continuous variables.

To quantify the relative contributions of these characteristics to the asymptomatic ratios and IFRs, the boosted regression tree (BRT) model was applied using package “gbm Version 2.1.5” in R Version 3.6.2. Three important model parameters were considered in the BRT model, including number of trees, learning rate and tree complexity. We tested values of tree complexity from 1 to 8 in the BRT model, and selected optimal value when further adding one level would not increase the cross-validated area under curve (AUC). The values of 2 and 4 were selected with AUC of 0.711 and 0.934 for outcome 1 and outcome 2, respectively. Learning rate, known as shrinkage, is set as 0.005. A bagging factor of 0.5 was set for boosting in the BRT model, as applied in the previous analysis (11). The multivariable logistic regression model was used to estimate the effect sizes of explanatory variables on each outcome. The adjusted odds ratio (AOR) and their 95% confidence intervals (95% CI) were then presented in the forest plot. The age and gender are reported to be potential influencing factors for asymptomatic COVID-19 infection and its infection fatality rate (12). We also included the case classification in the model since a previous study reported that the proportion of asymptomatic cases was relatively higher in the imported travelers than in local cases (13). This correlation is reasonable because imported cases are selected samples who have gone through temperature testing before travel. Aside from the age, gender and case classification, the dummy variables of four waves were also included in the regression to adjust for temporal change in local healthcare capacity and the dominant viral strains.

The asymptomatic ratio (the number of asymptomatic cases divided by the total cases) was plotted in combination with the case classification and the infection fatality rate (IFR: the number of fatal cases divided by the total cases) was plotted by age, in **Figures 3, 4**, respectively. **Figure 3** shows the proportion of asymptomatic COVID-19 patients plotted in red dots with a 95% confidence interval indicated by the vertical red lines. The serial trend was simulated in the smooth black curve. The classification



was shown in the bars, with the gray representing the local cases and the white representing imported cases. In **Figure 4**, the trends of IFR against age in Hong Kong and a previous report which included a global estimate from ten representative serological studies (14). IFRs by age in Hong Kong are shown in black dots and IFRs in other countries are shown in red squares. The rates were plotted in dots with 95% confidence interval indicated by the vertical lines. We used local cases only for calculation of infection fatality rate in Hong Kong since there are few cases were imported (4 out of 174).

The time series plot of daily confirmed cases was plotted in **Figure 5**. The number of all daily cases was plotted in black dots, and local cases were indicated in red triangles. The number of confirmed cases identified from the universal testing was plotted from September 4th to September 14th, shown in blue dots. The whole universal testing was lasting for 14 days since September 1st, with 42 confirmed cases identified from the testing directly or indirectly, over about 1.78 million participants.

## RESULTS

**Table 1** shows the proportion of asymptomatic cases was higher in patients aged 20 years or younger, in imported cases and the third and fourth wave. Meanwhile, the prevalence of deceased cases was higher in men than women, in patients with older ages, and local cases. Among the several waves in Hong Kong, more deceased cases were reported in the third wave.

**Figure 1A** shows the relative influence of each independent variable on the asymptomatic cases. Classification of imported or local cases contributed to over half of the relative importance (56.89%). The waves and patients' age had relative contributions of 31.81 and 11.01%, respectively. Gender only accounted for 0.29% of the importance of the BRT model.

**Figure 1B** shows the relative influence of each independent variable on the IFRs. Age was the dominating attributive factor for dead issues, contributing 83.09% of the BRT model's importance, followed by the wave dummy variables of COVID-19 (10.24%) and patients' gender (5.96%). Case classification contributed little to the deceased cases (0.71%).

**Figure 2A** shows that imported cases were more likely to be asymptomatic than local cases (OR:11.78, 95% CI: 10.24–13.54). Compared with cases in the first and second wave, the odds of asymptomatic cases were 7.29 times higher in the third wave (7.29, 5.95–8.92) and 10.14 times in the fourth wave (10.14, 8.18–12.56). We classified the age into three groups: <20 year, 20–65 years and >65 years to better explain the association between age and proportions of asymptomatic cases, since the odds ratio of asymptomatic cases for continuous variable of age was close to null, in spite of  $P$ -value < 0.05. The results showed that patients aged <20 or >65 years were more likely to be asymptomatic cases than patients aged 20–65 years, after adjusting for other explanatory variables with an OR (95% CIs) of 1.67 (1.44–1.94) for under-20-year-old cases and 1.15 (1.01–1.31) for over-65-year-old cases. No significant association was reported between gender and the proportion of asymptomatic cases in the logistic regression.

**TABLE 1** | Potential explanatory variables of cases according to interested outcomes.

|                                       | Cases without interested outcomes | Cases with interested outcomes | $P$ -value <sup>a</sup> |
|---------------------------------------|-----------------------------------|--------------------------------|-------------------------|
| <b>Outcome1: Asymptomatic</b>         |                                   |                                |                         |
| <b>Age</b>                            | 46.5 (19.6)                       | 41.3 (20.4)                    | <0.001                  |
| <20 years                             | 607 (58.1)                        | 437 (41.9)                     | <0.001                  |
| 20–65 years                           | 5,500 (72.6)                      | 2,075 (27.4)                   |                         |
| >65 years                             | 1,263 (75.9)                      | 401 (24.1)                     |                         |
| <b>Gender</b>                         |                                   |                                | 0.12                    |
| Female                                | 3,842 (72.4)                      | 1,468 (27.6)                   |                         |
| Male                                  | 3,528 (70.9)                      | 1,445 (29.1)                   |                         |
| <b>Wave</b>                           |                                   |                                | <0.001                  |
| 1st and 2nd wave                      | 845 (81.2)                        | 196 (18.8)                     |                         |
| 3rd wave                              | 3,191 (69.6)                      | 1,397 (30.4)                   |                         |
| 4th wave                              | 3,334 (71.6)                      | 1,320 (28.4)                   |                         |
| <b>Case classification</b>            |                                   |                                | <0.001                  |
| Local                                 | 6,583 (79)                        | 1,754 (21)                     |                         |
| Imported                              | 787 (40.4)                        | 1,159 (59.6)                   |                         |
| <b>Outcome2: Deceased<sup>b</sup></b> |                                   |                                |                         |
| <b>Age</b>                            | 44.4 (19.5)                       | 78.8 (11.2)                    | <0.001                  |
| <20 years                             | 1,035 (100)                       | 0 (0)                          | <0.001                  |
| 20–65 years                           | 7,514 (99.7)                      | 21 (0.3)                       |                         |
| >65 years                             | 1,500 (90.7)                      | 153 (9.3)                      |                         |
| <b>Gender</b>                         |                                   |                                | 0.02                    |
| Female                                | 5,206 (98.6)                      | 74 (1.4)                       |                         |
| Male                                  | 4,843 (98)                        | 100 (2)                        |                         |
| <b>Wave</b>                           |                                   |                                | <0.001                  |
| 1st and 2nd wave                      | 1,036 (99.5)                      | 5 (0.5)                        |                         |
| 3rd wave                              | 4,483 (97.7)                      | 105 (2.3)                      |                         |
| 4th wave                              | 4,530 (98.6)                      | 64 (1.4)                       |                         |
| <b>Case classification</b>            |                                   |                                | <0.001                  |
| Local                                 | 8,110 (97.9)                      | 170 (2.1)                      |                         |
| Imported                              | 1,939 (99.8)                      | 4 (0.2)                        |                         |

<sup>a</sup> $P$ -values were obtained by using one-way analysis of variance (ANOVA) for continuous variable (age), and chi-square test for other categorical variables.

<sup>b</sup>The total number used for the analysis of outcome 2 is 10,223 instead of 10,283 due to the 1-day lag in reporting.

**Figure 2B** also shows that people with higher age were at higher fatality risk with an OR (95% CI) of 1.14 (1.12–1.16). Besides, male patients had 1.77 times the odds of being deceased cases compared with females (OR: 1.77, 95% CI: 1.26–2.48). We also analyzed the association in the logistic regression by treating the variable as a continuous variable and found a significant association between the wave and IFR (AOR:0.69, 95% CI: 0.51–0.92). The results indicate that the IFR decreases in more recent waves probably due to the increased testing capability and healthcare capacity. No significant association was found between case classification and the proportion of deceased cases.

**Figure 3** visualizes the time serial distribution of weekly confirmation and asymptomatic ratio stratified by case

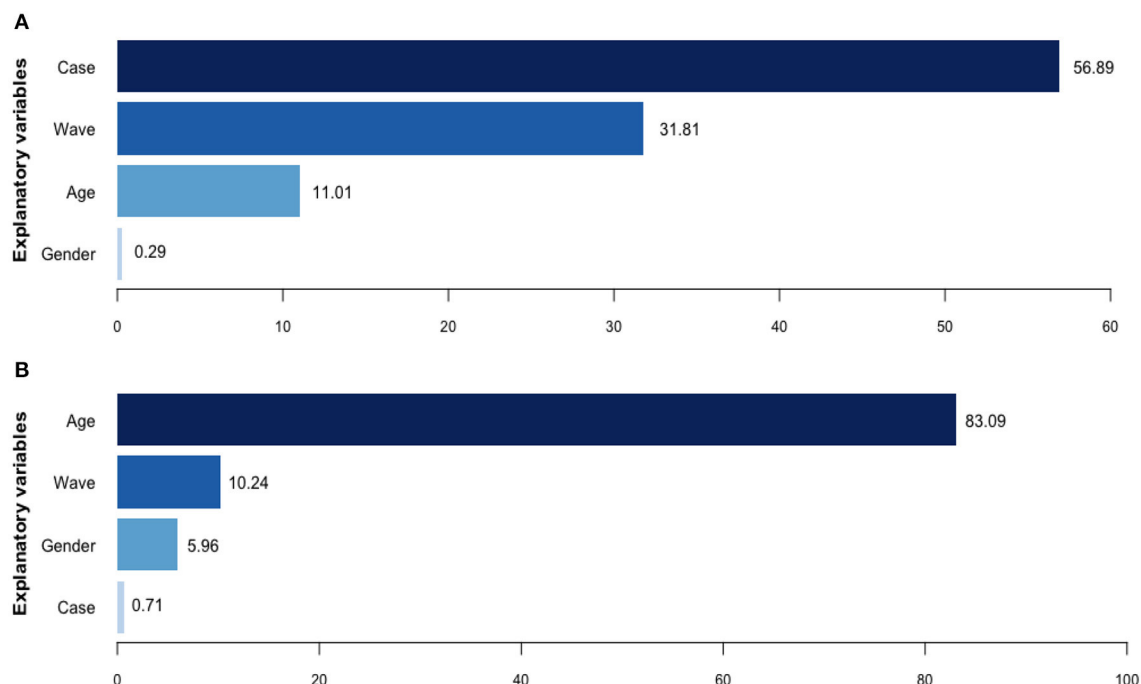


**FIGURE 1** | Relative contributions of potential explanatory variables for asymptomatic ratios and infection fatality ratios, by boosted regression tree model. **(A)** Relative contributions (%) for asymptomatic cases. **(B)** Relative contributions (%) for deceased cases.

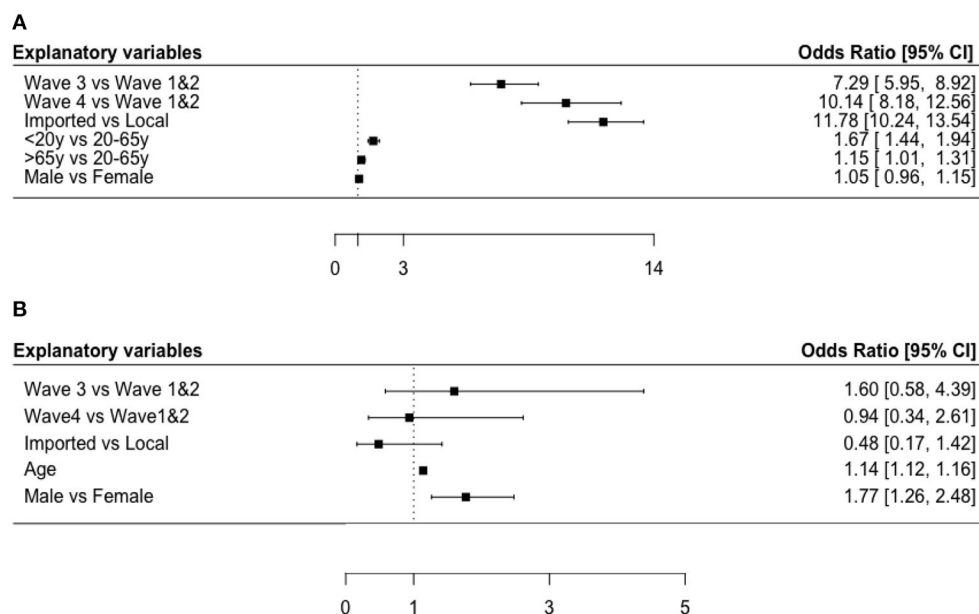


**FIGURE 2** | Forest plots of risk factors for asymptomatic cases and infection fatality ratios. **(A)** Odds ratio [95% CI] for asymptomatic cases in Hong Kong. **(B)** Odds ratio [95% CI] for deceased cases in Hong Kong.

classification and waves of COVID-19, the two most important explanatory variables for the asymptomatic cases. Imported cases were observed at the initial stage, while local cases dominated the latter two waves in Hong Kong. The proportion of asymptomatic

cases fluctuated over time, always reaching the peak during remission periods.

**Figure 4** compared the IFR by age in Hong Kong and other regions. The IFR increased dramatically after 60 years

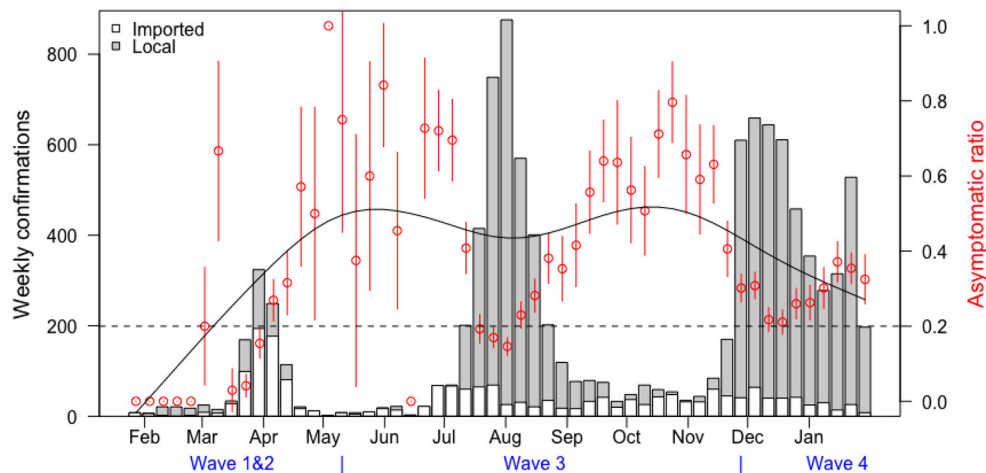


**FIGURE 3 |** The time serial distribution of weekly confirmation and asymptomatic ratio.

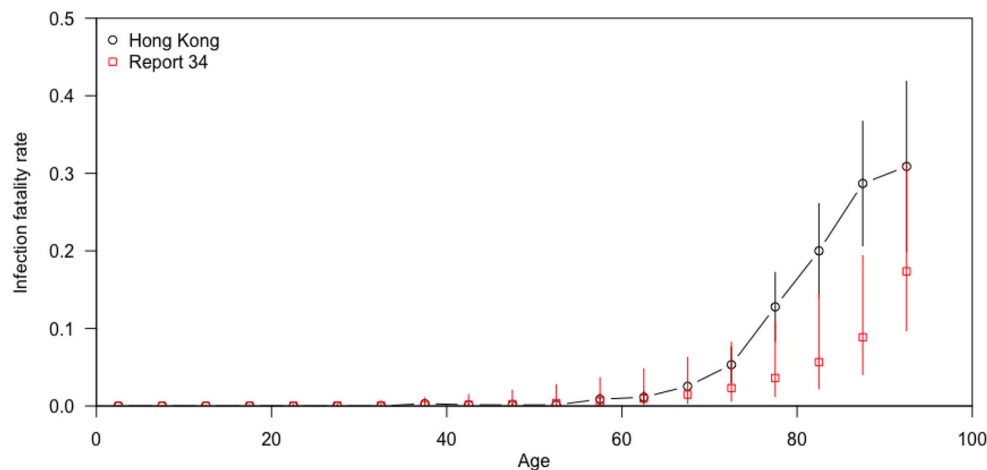


**FIGURE 4 |** Infection fatality rates by age in Hong Kong and in other countries (14).

old, and such trend was more obvious in Hong Kong than in other regions. **Figure 5** showed the waves of local COVID-19 transmission, which indicated the serial change of cases in Hong Kong.

## DISCUSSION

This study is based on the number of the COVID-19 cases and the death cases collected in Hong Kong since the outbreak of the COVID-19 in early 2020. As of January 26th, 2021, the accumulated confirmed cases in Hong Kong was 10,223 (1,360/100,000,000) with a leading virus testing coverage of 901,940/100,000,000 around the world. With the non-pharmaceutical interventions (including border restrictions, social distancing, quarantine and isolation) in place (15), the COVID-19 local outbreaks in Hong Kong overall have not much

overwhelmed the healthcare system and testing capability. This is crucial to ensure a reliable estimate of the asymptomatic case ratios and infection fatality rate compared with many other regions worldwide. According to previous reports, asymptomatic SARS-CoV-2 infection were more common in young people, and fatal cases were more common in older adults (16), which indicated the possible link between asymptomatic case ratio and IFRs. The estimated asymptomatic case ratios and IFRs should be able to represent the infection status among local residents in the latest two waves in Hong Kong given the testing capacity including the Universal Community Testing Programme launched in early September, 2020 which covered over 1.78 million residents in Hong Kong (9).

In our analysis, older age and male were significant risk factors for IFRs, which is consistent with previous studies (12, 17). A study combining age-specific mortality data from 45 countries with 22 seroprevalence surveys found that IFR was

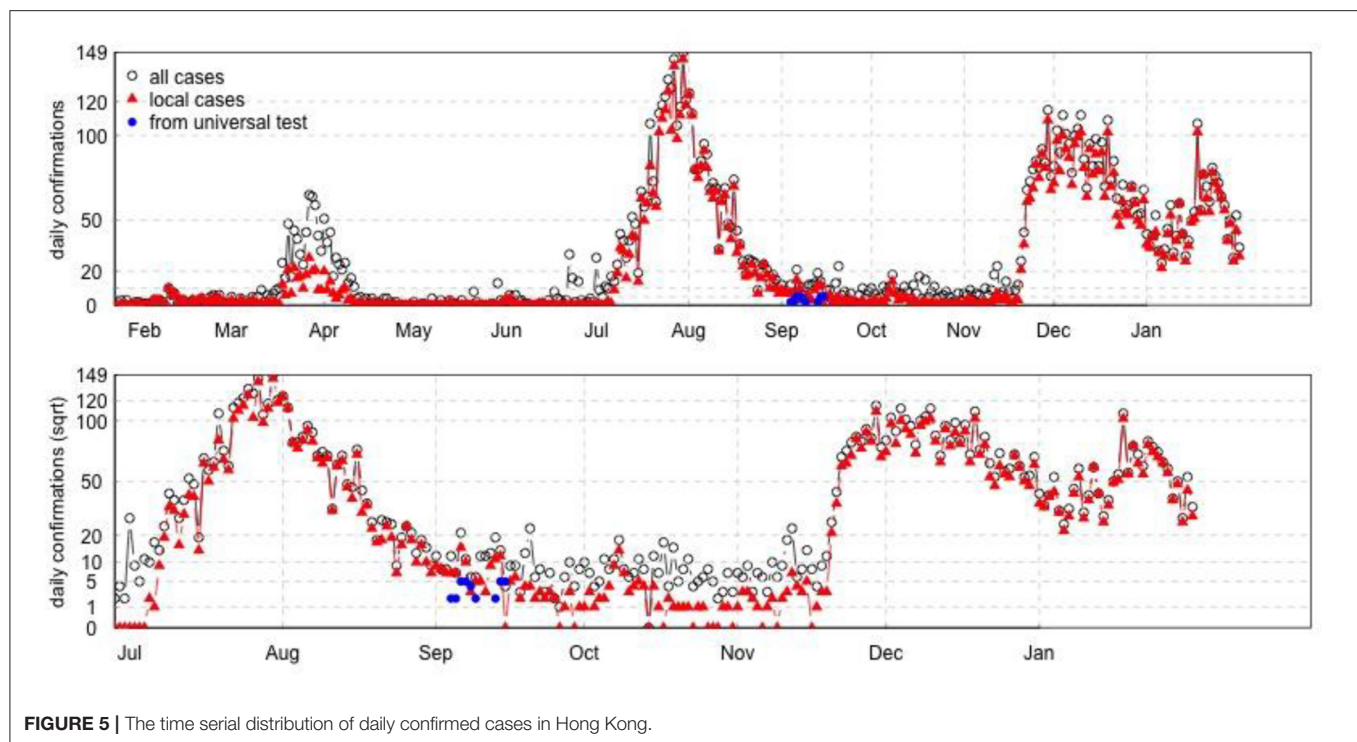


**FIGURE 5 |** The time serial distribution of daily confirmed cases in Hong Kong.

significantly higher in males than in females, and that IFR was positively associated with age among individuals aged 30 years or older (12). A meta-analysis of 27 studies showed an exponential relationship between age and IFR, starting with a very low rate in young adults and progressively increasing in the middle age (7). Consistently, the Imperial College COVID-19 response team in the UK identified 10 surveys from different countries (14) and showed a consistent pattern of age-specific IFR. Our study further compared the pattern with that reported by the Imperial College COVID-19 response team (14) and found the IFR for COVID-19 in Hong Kong was significantly higher, compared with other regions in the report, particularly in the elderly aged 65 years and older. The previous study has shown that the pattern of IFR by age is consistent across the globe among people aged below 65, while the pattern seemed to be more heterogeneous across settings in the elderly over 65 (12). Though we try to estimate the IFR as precisely as possible, it is also important to know that the overall IFR for COVID-19 might not be a fixed parameter because it depends on the age composition of the community and the extent to which the vulnerable population were exposed to SARS-CoV-2 (7).

Our study found the proportion of asymptomatic cases were higher in the third and fourth wave, possibly indicating an increase of test capacities in the latter waves. The higher proportion of asymptomatic among imported cases was reasonable because they should be “screened” before boarding and after arrival through taking temperature and the imported cases might have a higher social-economic status in general. In addition, the asymptomatic case ratios were higher during the interval of the local outbreaks and the government initiated

a universal community testing campaign, shown in **Figure 3**, which might contribute to more precise IFR estimation, since the results from comprehensive tracing programs depend on the accuracy of the number of infected individuals, especially those asymptomatic cases (18).

Our study has several limitations. First, although the BRT model considered several factors, there were other potential factors that remained unadjusted. For example, the mortalities of COVID-19 patients with diabetes, cardiovascular diseases and hypertension were much higher than the general population (19). Unfortunately, individual data of pre-existing conditions were not available to us. Nevertheless, in this study we developed a modeling strategy which can be easily applied to the other regions/countries to assess a wider range of influencing factors. Second, although Hong Kong had a relatively higher testing rate compared to most of the other regions/countries, the possibility of underestimating the asymptomatic ratios cannot be ruled out. In the universal community testing campaign in Hong Kong, 1.78 million local residents (around 23.7% of the total local residents in Hong Kong) were tested, of whom only 42 were positive without any symptoms (9). Hence, we believe that the asymptomatic cases could have accounted for a very small proportion in Hong Kong local residents and should not greatly affect our conclusions.

Hong Kong has taken border restrictions with 14-day quarantine since the early outbreak in Mainland China following by the COVID-19 pandemic. The length of quarantine has been extended to 21 days after the mutant virus strain is reported at the end of December, 2020. The local community outbreaks have not yet overwhelmed the local capability of



case track and record, which makes the COVID-19 cases recorded in this city among the most precise and representative over the world. In the regions suffering from high burden of COVID-19 cases, it is difficult to achieve such accurate estimation on case fatality. While in regions such as Singapore where the COVID-19 is under control with sporadic imported cases (20), it is hard to observe transmission in the local community which indicates that the case fatality might be not as representative as that in Hong Kong. With the non-pharmaceutical interventions in place, the sufficient testing capabilities and complete case recording infrastructure, the highly international city with 7.5 million residents has provided us with a unique data resource for understanding the disease profile amid the COVID-19 pandemic.

Although considerable investigation has been carried out to estimate the IFRs of COVID-19 in different settings, some have been challenged due to the non-representative samples such as the outbreak in the Diamond Princess Cruise, inappropriate statistical inference including falsely defaulting herd immunity in Brazil or duplicate use of data in meta-analysis (21). On the contrary, the estimates of asymptomatic ratio and case (infection)-fatality-rate in Hong Kong, China can be regarded as accurate given that (1) There are wide community transmission, thus local infections/cases are representative of the whole population; (2) There is extensive testing (under-reporting is less severe) so that the outbreak is under control; (3) The

health system has not yet broken down. Considering few places elsewhere could satisfy these three conditions, the estimation of IFRs using surveillance data of COVID-19 in Hong Kong can be established as a standard among the comprehensive COVID-19 case tracing studies.

## DATA AVAILABILITY STATEMENT

Publicly available datasets were analyzed in this study. This data can be found at: [https://www.chp.gov.hk/files/pdf/local\\_situation\\_covid19\\_en.pdf](https://www.chp.gov.hk/files/pdf/local_situation_covid19_en.pdf).

## AUTHOR CONTRIBUTIONS

JT and DH designed the study, carried out the statistical analysis, and wrote the manuscript. XZ, SM, and LY participated in data analysis and critically revised the manuscript. All authors contributed to the article and approved the submitted version.

## FUNDING

DH was supported by an Alibaba (China) Co. Ltd Collaborative Research Project. The funders had no role in study design, data collection and analysis, decision to publish, or preparation of the manuscript.

## REFERENCES

1. Johns Hopkins University. *COVID-19 Dashboard by the Center for Systems Science and Engineering (CSSE) at Johns Hopkins University (JHU)* (2021). Available online at: <https://gisanddata.maps.arcgis.com/apps/opsdashboard/index.html#/bda7594740fd40299423467b48e9ecf6> (accessed 8 March 2021).
2. Wilder-Smith A, Chiew CJ, Lee VJ. Can we contain the COVID-19 outbreak with the same measures as for SARS? *Lancet Infect Dis.* (2020) 20:E102–7. doi: 10.1016/S1473-3099(20)30129-8
3. Pollock AM, Lancaster J. Asymptomatic transmission of covid-19. *BMJ-Brit Med J.* (2020) 371:m4851. doi: 10.1136/bmj.m4851
4. Mizumoto K, Kagaya K, Zarebski A, Chowell G. Estimating the asymptomatic proportion of coronavirus disease 2019 (COVID-19) cases on board the diamond princess cruise ship, Yokohama, Japan, 2020. *Euro Surveill.* (2020) 25:2000180. doi: 10.2807/1560-7917.ES.2020.25.10.2000180
5. Wells PM, Doores KJ, Couvreur S, Nunez RM, Seow J, Graham C, et al. Estimates of the rate of infection and asymptomatic COVID-19 disease in a population sample from SE England. *J Infect.* (2020) 81:931–6. doi: 10.1016/j.jinf.2020.10.011
6. Xiao C, Huang Z, Wang J, Zhao S, Wong MCS, Chong MKC, et al. *The Rate of Asymptomatic COVID-19 Infection: A Systematic Review and Meta-Analysis Including 12,713 Infections From 136 Studies*. Modelling COVID-19 epidemics (2020).
7. Levin AT, Hanage WP, Owusu-Boaitey N, Cochran KB, Walsh SP, Meyerowitz-Katz G. Assessing the age specificity of infection fatality rates for COVID-19: systematic review, meta-analysis, and public policy implications. *Eur J Epidemiol.* (2020) 35:1123–38. doi: 10.1007/s10654-020-00698-1
8. Havers FP, Reed C, Lim T, Montgomery JM, Klena JD, Hall AJ, et al. Seroprevalence of Antibodies to SARS-CoV-2 in 10 sites in the United States, March 23–May 12, 2020. *JAMA Intern Med.* (2020). doi: 10.1101/2020.06.25.20140384
9. The Government of the Hong Kong Special Administrative region (2021). Available online at: <https://www.info.gov.hk/gia/general/202009/15/P2020091500931.htm> (accessed March 8, 2021).
10. OT&P Healthcare. *A Timeline of COVID-19 and OT&P Updates* (2021). <https://www.otandp.com/covid-19-timeline> (accessed March 8, 2021).
11. Tao J, Zhang X, Zhang X, Zhao S, Yang L, He D, et al. The time serial distribution and influencing factors of asymptomatic COVID-19 cases in Hong Kong. *One Health.* (2020) 10:100166. doi: 10.1016/j.onehlt.2020.100166
12. O'Driscoll M, Ribeiro Dos Santos G, Wang L, Cummings DAT, Azman AS, Paireau J, et al. Age-specific mortality and immunity patterns of SARS-CoV-2. *Nature.* (2020) 590:140–5. doi: 10.1038/s41586-020-2918-0
13. Wong J, Abdul Aziz ABZ, Chaw L, Mahamud A, Griffith MM, Lo YR, et al. High proportion of asymptomatic and presymptomatic COVID-19 infections in air passengers to Brunei. *J Travel Med.* (2020) 27:taaa066. doi: 10.1093/jtm/taaa066
14. Brazeau NF, Verity R, Jenks S, Fu H, Whittaker C, Winskill P, et al. *COVID-19 Infection Fatality Ratio: Estimates from Seroprevalence*. London: Imperial College London (2020).
15. Cowling BJ, Ali ST, Ng TWY, Tsang TK, Li JCM, Fong MW, et al. Impact assessment of non-pharmaceutical interventions against coronavirus disease 2019 and influenza in Hong Kong: an observational study. *Lancet Public Health.* (2020) 5:e279–88. doi: 10.1016/S2468-2667(20)30090-6
16. Ren R, Zhang Y, Li Q, McGoogan JM, Feng Z, Gao GF, et al. Asymptomatic SARS-CoV-2 infections among persons entering China from April 16 to October 12, 2020. *JAMA.* (2021) 325:489–92. doi: 10.1001/jama.2020.23942
17. Mallapaty S. The coronavirus is most deadly if you are old and male. *Nature.* (2020) 585:16–17. doi: 10.1038/d41586-020-02483-2
18. Vermund SH, Pitzer VE. Asymptomatic transmission and the infection fatality risk for COVID-19: implications for school reopening. *Clin Infect Dis.* (2020) 72:1493–6. doi: 10.1093/cid/ciaa855
19. Riddle MC, Buse JB, Franks PW, Knowler WC, Ratner RE, Selvin E. COVID-19 in people with diabetes: urgently needed lessons from early reports. *Diabetes Care.* (2020) 43:1378–81. doi: 10.2337/dci20-0024

20. Ngiam JN, Chew N, Tham SM, Beh DL, Lim ZY, Li TYW, et al. Demographic shift in COVID-19 patients in Singapore from an aged, at-risk population to young migrant workers with reduced risk of severe disease. *Int J Infect Dis.* (2020) 103:329–35. doi: 10.1016/j.ijid.2020.11.157
21. Shen C, VanGennep D, Siegenfeld AF, Bar-Yam Y. Unraveling the flaws of estimates of the infection fatality rate for COVID-19. *J Travel Med.* (2021) 28:taaa239. doi: 10.1093/jtm/taaa239

**Conflict of Interest:** DH was supported by an Alibaba (China)-Co. Ltd Collaborative Research Project.

The remaining authors declare that the research was conducted in the absence of any commercial or financial relationships that could be construed as a potential conflict of interest.

Copyright © 2021 Tao, Zhang, Musa, Yang and He. This is an open-access article distributed under the terms of the Creative Commons Attribution License (CC BY). The use, distribution or reproduction in other forums is permitted, provided the original author(s) and the copyright owner(s) are credited and that the original publication in this journal is cited, in accordance with accepted academic practice. No use, distribution or reproduction is permitted which does not comply with these terms.



# Noninvasive Ventilation in Patients With COVID-19-Related Acute Hypoxemic Respiratory Failure: A Retrospective Cohort Study

## OPEN ACCESS

### Edited by:

Reza Lashgari,  
Institute for Research in Fundamental  
Sciences, Iran

### Reviewed by:

Eduardo Luis De Vito,  
University of Buenos Aires, Argentina  
Shima Moein,  
Institute for Research in Fundamental  
Sciences (IPM), Iran

### \*Correspondence:

Lei Liu  
liulei3322@aliyun.com  
Rongchang Chen  
chenrc@vip.163.com  
Chen Qiu  
qiuchen@email.jnu.edu.cn

†These authors have contributed  
equally to this work and share first  
authorship

### Specialty section:

This article was submitted to  
Pulmonary Medicine,  
a section of the journal  
Frontiers in Medicine

Received: 05 December 2020

Accepted: 28 April 2021

Published: 24 May 2021

### Citation:

Fu Y, Guan L, Wu W, Yuan J, Zha S,  
Wen J, Lin Z, Qiu C, Chen R and Liu L  
(2021) Noninvasive Ventilation in  
Patients With COVID-19-Related  
Acute Hypoxemic Respiratory Failure:  
A Retrospective Cohort Study.  
Front. Med. 8:638201.  
doi: 10.3389/fmed.2021.638201

Yingyun Fu<sup>1†</sup>, Lili Guan<sup>1†</sup>, Weibo Wu<sup>2†</sup>, Jing Yuan<sup>2†</sup>, Shanshan Zha<sup>1†</sup>, Junmin Wen<sup>3</sup>,  
Zhenghao Lin<sup>2</sup>, Chen Qiu<sup>1\*</sup>, Rongchang Chen<sup>1\*</sup> and Lei Liu<sup>2\*</sup>

<sup>1</sup> Shenzhen Institute of Respiratory Diseases, Shenzhen People's Hospital (The Second Clinical Medical College, Jinan University; The First Affiliated Hospital, South University of Science and Technology), Shenzhen, China, <sup>2</sup> National Clinical Research Center for Infectious Disease, The Third People's Hospital of Shenzhen, The Second Affiliated Hospital of Southern University of Science and Technology, Shenzhen, China, <sup>3</sup> Fuwai Hospital Chinese Academy of Medical Sciences, Shenzhen, China

**Introduction:** Noninvasive ventilation (NIV) has been used to alleviate hypoxemia and dyspnea, but there is no consensus on the application of NIV in patients with coronavirus disease 2019 (COVID-19). Some staff use NIV as the rescue therapy which might lead to the adverse outcomes. This study was to identify early factors associated with intubation to help the medical staff select appropriate patients for receiving NIV treatment.

**Methods:** Patients with laboratory-confirmed COVID-19 who were treated with NIV in emergency department or ICU of the Third People's Hospital (the only designated hospital for treating COVID-19 in Shenzhen) between January 1 and August 31, 2020, were retrospectively analyzed.

**Results:** Thirty-nine patients with COVID-19 treated with NIV were included; of them, 16 (41%) received endotracheal intubation and 3 (8%) died. Significant differences were observed between intubated and non-intubated patients in PaO<sub>2</sub>/FiO<sub>2</sub> before NIV initiation, hospitalization duration, NIV as the rescue therapy, and PaO<sub>2</sub>/FiO<sub>2</sub> of ≤200 mmHg after 1–2 h of NIV initiation. Notably, 1–2 h after NIV initiation, a PaO<sub>2</sub>/FiO<sub>2</sub> of ≤200 mmHg (odds ratio [OR], 9.35; 95% confidence interval [CI], 1.84–47.62; *P* = 0.007) and NIV as the rescue therapy (OR, 5.43; 95% CI, 1.09–27.12; *P* = 0.039) were the risk factors for intubation.

**Conclusions:** In patients with COVID-19-related acute hypoxemic respiratory failure receiving NIV, close attention should be paid to PaO<sub>2</sub>/FiO<sub>2</sub> after 1–2 h of NIV initiation. Also, using NIV as rescue therapy should draw our awareness that it might delay escalation of respiratory support and lead to adverse outcomes.

**Keywords:** coronavirus disease 2019, noninvasive ventilation, rescue therapy, delayed intubation, acute hypoxemic respiratory failure

## INTRODUCTION

Since the identification of an initial cluster of patients in December 2019, the coronavirus disease 2019 (COVID-19) pandemic has continued to wreak global havoc. So far, ~20% of patients have been categorized as severely or critically ill, presenting with acute hypoxemic respiratory failure (AHRF) (1). Medical resources have been in short supply owing to the vast number of patients. Moreover, early intubation has inevitably led to some complications in these patients (2).

Using noninvasive respiratory support to treat patients without intubation can save medical resources and reduce the incidence of pain and complications (3–5). Noninvasive ventilation (NIV) has been used to alleviate hypoxemia and dyspnea in patients with COVID-19 during the pandemic (6). However, using NIV to treat AHRF remains showing some discrepancies, probably due to the patient selection and NIV parameter settings (7, 8). For now, there is no unified consensus on the application of NIV in patients with COVID-19-related AHRF; most of the consensus are based on previous experience in the treatment of viral pneumonia (9, 10). Medical staff tend to base their choice on personal preference or experience because there is no evidence-based recommendation for the NIV selection (6, 11). In addition, some staff tend to use NIV as the rescue therapy after conventional oxygen therapy or high-flow nasal oxygen therapy (HFNO) had failed, which might delay the escalation of respiratory support and lead to the adverse outcomes.

Therefore, in this retrospective cohort study, we aimed to identify early factors associated with intubation to help the medical staff select appropriate patients for receiving NIV treatment and avoid delayed intubation.

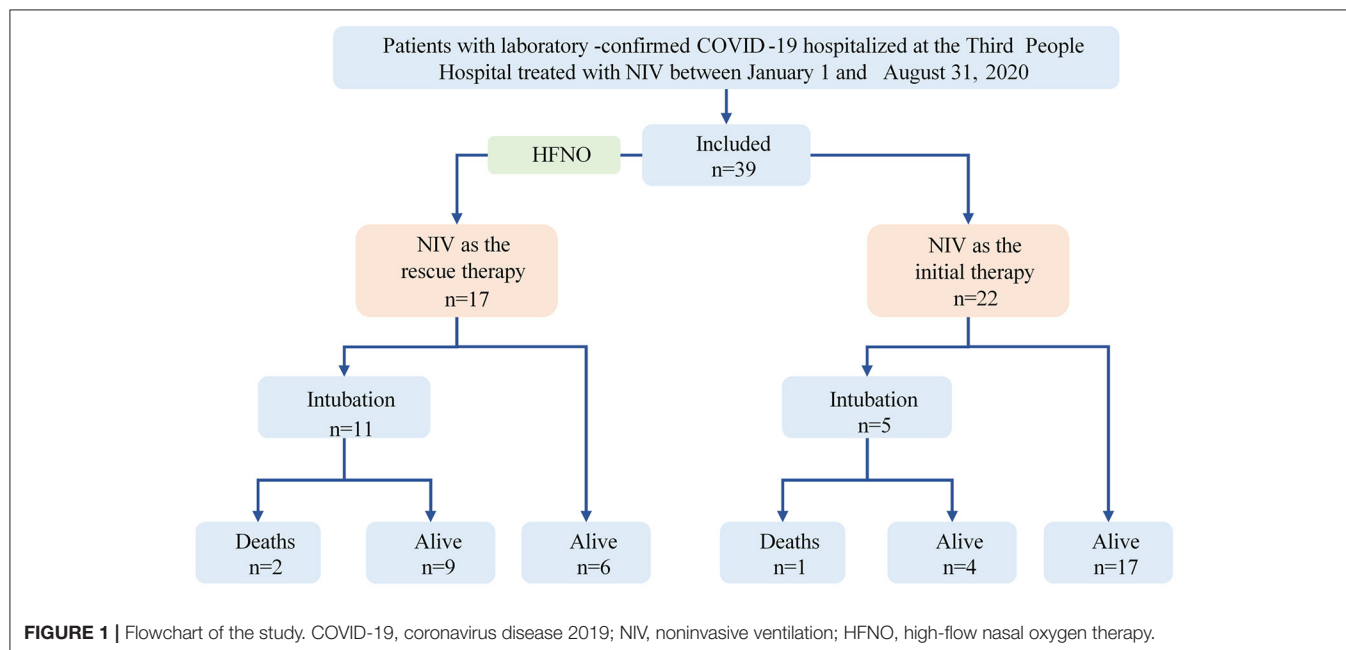
## METHODS

In this retrospective cohort study, patients with laboratory-confirmed COVID-19 in the emergency department or ICU of the Third People's Hospital which is the only designated hospital for treating COVID-19 in Shenzhen, a megacity with a population of more than 10 million, between January 1 and August 31, 2020, were included (**Figure 1**). All patients who were treated with NIV during their hospital stay and were identified from electronic medical records, were included. The treatment regimen was in accordance with the Chinese COVID-2019 treatment guidelines (12), and all patients have already been discharged from the hospital, except three deaths.

Demographic and clinical data and information on ventilatory settings and arterial blood gas samples were collected before and 1–2 h after NIV initiation. Two clinicians independently gathered demographic and clinical data from electronic medical records using standardized data collection forms; any variances or discrepancies were discussed, and a third clinician moderated and adjudicated the validity of disputed data.

NIV as the initial treatment was defined as using NIV as the first choice to correct hypoxemia after using conventional oxygen therapy. NIV as the rescue therapy was defined as using NIV to treat patients with AHRF in whom treatment with HFNO had failed. The criteria for intubation included the signs of persisting or worsening respiratory failure, hemodynamic instability, or consciousness deterioration (12). The primary outcome of the study was to identify early factors associated with intubation, whereas secondary outcomes included hospitalization duration and all-cause mortality during hospitalization.

SPSS version 19.0 (IBM SPSS Statistics, Armonk, NY, USA) was used for data analysis. Data were presented as median (interquartile range [IQR]), or number (percentage).





as appropriate. For continuous variables, comparisons were performed using Student's *t*-test for normally distributed data and nonparametric test for non-normally distributed data. For categorical variables, Pearson's chi-square test or Fisher's exact test was used. Factors associated with intubation were assessed via backward multivariate logistic regression analyses. The Kaplan–Meier method was used to evaluate the 28th day intubation rate from hospital admission and symptom onset, and between-group differences were estimated using the log-rank test. A two-tailed *P*

< 0.05 was considered significant. The ethics committee of the Third People's Hospital approved this study, and the trial was registered with www.chictr.org.cn (ChiCTR2000039567).

## RESULTS

In total, among 423 hospitalized patients with COVID-19 in Shenzhen, 39 patients with COVID-19 (9%) who were treated

**TABLE 1 |** Comparison of baseline clinical characteristics, NIV therapy, and clinical outcomes in patients who required intubation or not intubation.

|   | Intubation ( <i>n</i> = 16) | Nonintubation ( <i>n</i> = 23) | Unadjusted <i>p</i> -value | OR (95% CI)       | Adjusted <i>p</i> -value |
|---|-----------------------------|--------------------------------|----------------------------|-------------------|--------------------------|
| <b>Baseline clinical characteristics</b>  |                             |                                |                            |                   |                          |
| Age, years  | 65.0 (58.5–69.0)            | 62.0 (59.5–65.0)               | 0.343                      |                   |                          |
| Male, <i>n</i> (%)  | 11 (68.8)                   | 15 (65.2)                      | 0.818                      |                   |                          |
| BMI, kg/m <sup>2</sup>  | 24.6 (21.7–26.2)            | 25.4 (22.8–27.1)               | 0.394                      |                   |                          |
| White blood cell count, × 10 <sup>9</sup> /L  | 5.5 (4.1–6.9)               | 4.3 (3.5–5.1)                  | 0.112                      |                   |                          |
| Lymphocyte count, × 10 <sup>9</sup> /L  | 1.0 (0.9–1.3)               | 1.1 (0.8–1.4)                  | 0.746                      |                   |                          |
| Procalcitonin, ng/ml  | 0.08 (0.06–0.11)            | 0.07 (0.05–0.10)               | 0.563                      |                   |                          |
| D-dimer, μg/ml  | 0.7 (0.5–1.2)               | 0.6 (0.4–0.8)                  | 0.107                      |                   |                          |
| <b>Comorbidities</b>  |                             |                                |                            |                   |                          |
| Chronic respiratory disease, <i>n</i> (%)   | 2 (12.5)                    | 1 (4.3)                        | 0.557                      |                   |                          |
| Hypertension, <i>n</i> (%)  | 7 (43.8)                    | 7 (30.4)                       | 0.503                      |                   |                          |
| Chronic cardiovascular disease, <i>n</i> (%)  | 3 (3.3)                     | 5 (4.7)                        | 0.820                      |                   |                          |
| Chronic kidney disease, <i>n</i> (%)  | 0 (0)                       | 1 (4.3)                        | 0.398                      |                   |                          |
| Chronic hepatic disease, <i>n</i> (%)   | 1 (6.3)                     | 1 (4.3)                        | 0.791                      |                   |                          |
| Diabetes, <i>n</i> (%)  | 3 (18.8)                    | 4 (17.4)                       | 0.913                      |                   |                          |
| Cancer, <i>n</i> (%)  | 1 (6.3)                     | 1 (4.3)                        | 0.791                      |                   |                          |
| <b>Clinical data before NIV therapy</b>   |                             |                                |                            |                   |                          |
| Respiratory rate, breaths/min   | 25.0 (24.8–26.5)            | 23.0 (22.0–28.5)               | 0.159                      |                   |                          |
| Heart rate, breaths/min   | 83.0 (77.0–88.0)            | 81.0 (74.0–89.0)               | 0.938                      |                   |                          |
| pH  | 7.46 (7.45–7.48)            | 7.45 (7.43–7.47)               | 0.534                      |                   |                          |
| PaO <sub>2</sub> , mmHg   | 72.1 (64.6–78.8)            | 72.2 (63.5–80.5)               | 0.855                      |                   |                          |
| PaO <sub>2</sub> /FIO <sub>2</sub> , mmHg   | 144.1 (126.0–169.5)         | 180.0 (151.4–226.5)            | 0.016                      |                   |                          |
| The time interval from symptom onset to initiating NIV, days                                | 10.5 (5.8–13.5)             | 11.0 (9.0–13.5)                | 0.489                      |                   |                          |
| NIV as the rescue therapy, <i>n</i> (%)   | 11 (68.8)                   | 6 (26.1)                       | 0.011                      | 5.43 (1.09–27.12) | 0.039                    |
| APACHE II   | 12.0 (10.8–13.5)            | 10.0 (8.5–12.0)                | 0.094                      |                   |                          |
| <b>Clinical data after 1–2 h NIV therapy</b>  |                             |                                |                            |                   |                          |
| Respiratory rate, breaths/min   | 24.0 (21.5–28.5)            | 22.0 (20.0–23.5)               | 0.143                      |                   |                          |
| Heart rate, breaths/min   | 78.0 (73.5–85.5)            | 78.0 (71.0–86.0)               | 0.935                      |                   |                          |
| Pressure support, cmH <sub>2</sub> O  | 6.0 (6.0–6.3)               | 7.0 (6.0–7.0)                  | 0.046                      |                   |                          |
| EPAP, cmH <sub>2</sub> O  | 6.0 (6.0–6.3)               | 6.0 (6.0–7.0)                  | 0.703                      |                   |                          |
| PaO <sub>2</sub> , mmHg   | 87.2 (77.6–92.8)            | 110.0 (99.5–125.6)             | <0.001                     |                   |                          |
| PaO <sub>2</sub> /FIO <sub>2</sub> , mmHg   | 181.3 (155.2–204.7)         | 265.0 (215.2–306.7)            | <0.001                     |                   |                          |
| PaO <sub>2</sub> /FIO <sub>2</sub> of ≤200 mmHg after 1–2 h of NIV initiation, <i>n</i> (%) | 11 (68.8)                   | 4 (17.4)                       | 0.002                      | 9.35 (1.84–47.62) | 0.007                    |
| <b>Clinical outcomes</b>  |                             |                                |                            |                   |                          |
| Hospitalization duration, days  | 46.0 (35.0–52.5)            | 34.0 (28.0–40.0)               | 0.007                      |                   |                          |
| In-hospital mortality, <i>n</i> (%)   | 3 (18.8)                    | 0 (0)                          | 0.061                      |                   |                          |

Data represent as median (interquartile range) or *n* (%).

NIV, noninvasive ventilation; OR, odds ratio; CI, confidence interval; PaO<sub>2</sub>, arterial oxygen partial pressure; FIO<sub>2</sub>, fractional inspired oxygen; APACHE, acute physiology and chronic health evaluation; EPAP, expiratory positive airway pressure.

Variables entered in the model of logistic regression were: using NIV as the rescue therapy, APACHE II, pressure support, PaO<sub>2</sub>/FIO<sub>2</sub> of ≤200 mmHg after 1–2 h of NIV initiation.

with NIV were included in the study; of them, 16 (41%) received endotracheal intubation, and 3 (8%) died. All patients received bilevel ventilation. The median initial inspiratory positive airway pressure and expiratory positive airway pressure were 13.0 (IQR, 12.0–14.0) cmH<sub>2</sub>O and 6.0 (IQR, 6.0–6.5) cmH<sub>2</sub>O, respectively, with a median fractional inspired oxygen (FiO<sub>2</sub>) of 0.5 (IQR, 0.4–0.5).

There is no significant difference between intubated and non-intubated patients in the baseline demographic, comorbidities, severity blood markers (white blood cell count, lymphocyte count, procalcitonin, d-dimer) and severity scores (APACHE II score) (Table 1). Patients who required intubation had lower arterial oxygen partial pressure (PaO<sub>2</sub>) to FiO<sub>2</sub> ratio (PaO<sub>2</sub>/FiO<sub>2</sub>) before receiving NIV, higher proportion of using NIV as the rescue therapy, and longer hospitalization duration (Table 1). Significant differences were observed between intubated and non-intubated patients in PaO<sub>2</sub>/FiO<sub>2</sub> before NIV initiation (144.1 [IQR, 126.0–169.5] mmHg vs. 180.0 [IQR, 151.4–226.5] mmHg;  $P = 0.016$ ), hospitalization duration (46.0 [IQR, 35.0–52.5] days vs. 34.0 [IQR, 28.0–40.0] days;  $P = 0.007$ ), NIV as the rescue therapy (68.8 vs. 26.1%;  $P = 0.011$ ), PaO<sub>2</sub>/FiO<sub>2</sub> of  $\leq 200$  mmHg after 1–2 h of NIV initiation (68.8 vs. 17.4%;  $P = 0.002$ ), and the pressure support level (6.0 [IQR, 6.0–6.3] cmH<sub>2</sub>O vs. 7.0 [IQR, 6.0–7.0] cmH<sub>2</sub>O;  $P = 0.046$ ). Furthermore, a trend of higher in-hospital mortality was observed in the intubated patients (18.8 vs. 0%;  $P = 0.061$ ). Multivariate logistic regression analysis showed that 1–2 h after NIV initiation, a PaO<sub>2</sub>/FiO<sub>2</sub> of  $\leq 200$  mmHg (odds ratio [OR], 9.35; 95% confidence interval [CI], 1.84–47.62;  $P = 0.007$ ) and NIV as the rescue therapy (OR, 5.43; 95% CI, 1.09–27.12;  $P = 0.039$ ) were the risk factors for intubation (Table 1).

In the subgroup analysis of NIV as the rescue therapy, the medium time of using HFNO before NIV was 2 (IQR, 0.4–3.0) days, and the intubation rate at day 28 from hospital admission was much higher when comparing with NIV as the initial therapy (64.7 vs. 22.7%;  $P = 0.007$ ; Figure 2), as well as the intubation rate from symptom onset ( $P = 0.005$ ; Table 2). Furthermore, hospitalization duration was longer when NIV was used as the rescue therapy (42.0 [IQR, 31.5–52.5] days vs. 34.5 [IQR, 26.6–42.4] days;  $P = 0.005$ ). There was no difference in clinical characteristics before initiating noninvasive respiratory support

(HFNO or NIV), the time interval from symptom onset to initiating noninvasive respiratory support (initial therapy: 10.0 [IQR, 8.3–13.0] days vs. rescue therapy: 10.0 [IQR, 5.0–11.0] days,  $P = 0.307$ ) and the in-hospital mortality (initial therapy: 4.5% vs. rescue therapy: 11.8%,  $P = 0.570$ ) between patients who received NIV as initial therapy and those who received NIV as rescue therapy; however, PaO<sub>2</sub>/FiO<sub>2</sub> was observed to be lower before initiating NIV in the latter (144.2 [IQR, 119.6–175.5] mmHg vs. 174.4 [IQR, 158.0–208.7] mmHg;  $P = 0.034$ ) (Table 2).

## DISCUSSION

Our findings indicate that in patients with COVID-19-related AHRF receiving NIV, a PaO<sub>2</sub>/FiO<sub>2</sub> of  $\leq 200$  mmHg after 1–2 h of NIV initiation and using NIV as the rescue therapy are associated with a higher risk of intubation.

Recently, Franco et al. (13) performed a multicentered, retrospective study to analyze the feasibility and efficacy of using noninvasive respiratory support in patients with COVID-19-related AHRF outside ICU. All patients only used one form of noninvasive respiratory support (NIV/CPAP or HFNO) during the hospitalization. The results found that the 30-day mortality, intubation rate and length of hospitalization were similar among different noninvasive respiratory support methods, but HFNO was usually used for patients with mild COVID-19 in their clinical practice. Similar to Franco's study, we also tended to use HFNO in mild patients, but patients in our study would receive NIV as the rescue therapy when HFNO failed to improve the clinical status of patients. Actually, some medical staff in China and some consensus tended to choose HFNO as the first choice, especially during the early pandemic, because it is easy to use and has good tolerance (14). In cases where severe respiratory distress or hypoxemia could not be relieved via HFNO, NIV was used as the rescue therapy. Subsequently, the treatment failure may be related to the delayed use of NIV when using it as the rescue therapy, leading to a low PaO<sub>2</sub>/FiO<sub>2</sub> before NIV initiation (Table 2). The rate of NIV treatment failure in our study population was comparable to those reported in two previous observational studies (41.0 vs. 44.6 vs. 49.3%) (13, 15). However, on excluding the patients using NIV as the rescue therapy in our study, the failure rate would be much lower (rescue therapy: 64.7% vs. initial therapy: 22.7%). It might imply that when using HFNO as the initial treatment for mild COVID-19 patients, patients should be closely monitored in order to avoid the delayed escalation of respiratory support. In addition, our team proposed that when considering treatment rationale, adjustable pressure, oxygen consumption, and tolerance, NIV should be considered as the first-line therapy to treat patients with mild acute respiratory distress syndrome (ARDS) (6).

Furthermore, in line with Frat's findings that 1 h after NIV initiation, a PaO<sub>2</sub>/FiO<sub>2</sub> of  $\leq 200$  mmHg and a tidal volume of  $>9$  mL/kg of predicted body weight are the independent predictors of intubation among patients with AHRF, we found that after initiating NIV therapy, a PaO<sub>2</sub>/FiO<sub>2</sub> of  $\leq 200$  mmHg is an essential predictor of intubation in patients (16). We could not record the expired tidal volume because of the

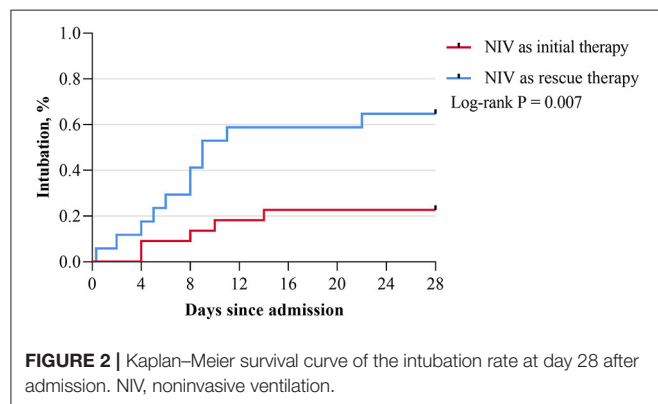


**TABLE 2 |** Comparison of baseline clinical characteristics and outcomes in patients who used NIV as initial or rescue therapy.

|  | NIV as initial therapy<br>(n = 22) | NIV as rescue therapy<br>(n = 17) | p-value                                  |
|--|------------------------------------|-----------------------------------|--|
| Age, years   | 62.5 (59.3–69.0)                   | 62.0 (59.0–66.0)                  | 0.944                                    |
| Male, n (%)  | 12 (54.5)                          | 14 (82.4)                         | 0.093                                    |
| BMI, kg/m <sup>2</sup>   | 24.8 (22.0–27.4)                   | 24.8 (22.9–26.6)                  | 0.726                                    |
| The time interval from symptom onset to initiating noninvasive respiratory support, days | 10.0 (8.3–13.0)                    | 10.0 (5.0–11.0)                   | 0.307                                    |
| The time interval from initiating HFNO to using NIV therapy, days                        | –                                  | 2 (0.4–3.0)                       | N.A.                                     |
| <b>Comorbidities</b>   |                                    |                                   |  |
| Chronic respiratory disease, n (%)   | 0 (0)                              | 3 (17.6)                          | 0.074                                    |
| Hypertension, n (%)  | 7 (31.8)                           | 7 (41.2)                          | 0.738                                    |
| Chronic cardiovascular disease, n (%)  | 4 (18.2)                           | 4 (23.5)                          | 0.709                                    |
| Chronic kidney disease, n (%)  | 0 (0)                              | 1 (5.9)                           | 0.436                                    |
| Chronic hepatic disease, n (%)   | 1 (4.5)                            | 1 (5.9)                           | 0.851                                    |
| Diabetes, n (%)  | 4 (18.2)                           | 3 (17.6)                          | 0.966                                    |
| Cancer, n (%)  | 1 (4.5)                            | 1 (5.9)                           | 0.851                                    |
| <b>Clinical data before noninvasive respiratory support*</b>                             |                                    |                                   |  |
| Respiratory rate, breaths/min  | 24.5 (23.0–27.5)                   | 22.0 (20.0–25.0)                  | 0.076                                    |
| Heart rate, breaths/min  | 85.0 (75.3–88.8)                   | 82.0 (80.0–89.0)                  | 0.893                                    |
| pH   | 7.46 (7.43–7.48)                   | 7.46 (7.45–7.47)                  | 0.928                                    |
| PaO <sub>2</sub> , mmHg  | 72.3 (61.1–79.2)                   | 73.0 (61.5–73.8)                  | 0.872                                    |
| PaO <sub>2</sub> /FiO <sub>2</sub> , mmHg  | 174.4 (158.0–208.7)                | 179.27 (165.9–224.1)              | 0.468                                    |
| <b>Clinical data before NIV therapy</b>  |                                    |                                   |  |
| Respiratory rate, breaths/min  | 24.5 (23.0–27.5)                   | 25.0 (23.0–29.0)                  | 0.410                                    |
| Heart rate, breaths/min  | 85.0 (75.3–88.8)                   | 78.0 (74.0–87.0)                  | 0.319                                    |
| pH   | 7.46 (7.43–7.48)                   | 7.45 (7.43–7.47)                  | 0.317                                    |
| PaO <sub>2</sub> , mmHg  | 72.3 (61.1–79.2)                   | 72.0 (65.3–81.0)                  | 0.664                                    |
| PaO <sub>2</sub> /FiO <sub>2</sub> , mmHg  | 174.4 (158.0–208.7)                | 144.2 (119.6–175.5)               | 0.034                                    |
| <b>Clinical outcomes</b>   |                                    |                                   |  |
| Intubation, n (%)  | 5 (22.7)                           | 11 (64.7)                         | 0.007 <sup>+</sup><br>0.005 <sup>#</sup> |
| Hospitalization duration, days   | 35.0 (29.0–41.0)                   | 42.0 (33.0–52.0)                  | 0.005                                    |
| In-hospital mortality, n (%)   | 1 (4.5)                            | 2 (11.8)                          | 0.570                                    |

Data represent as median (interquartile range) or n (%); HFNO, high-flow nasal oxygen therapy; NIV, noninvasive ventilation; PaO<sub>2</sub>, arterial oxygen partial pressure; FiO<sub>2</sub>, fractional inspired oxygen; N.A., Not applicable.

\*Noninvasive respiratory support refers to the HFNO or NIV; <sup>+</sup>intubation rate from hospital admission; <sup>#</sup>intubation rate from symptom onset.

emergency situation during the pandemic and the retrospective nature of the study. However, studies have pointed that the pathophysiological characteristics of some patients with COVID-19 who are diagnosed with ARDS according to the Berlin definition are not entirely consistent with those of patients with typical ARDS, presenting with the mismatch of severe hypoxia and relatively good respiratory compliance (17). Therefore, whether the targeted tidal volume of patients with COVID-19-related early ARDS receiving NIV may be higher, especially among those with hypercapnia, would need more evidence in further studies (18).

Whether NIV treatment would increase the risk of viral transmission among medical staff has always been a matter of concern and debate over the past few years (19). Previous studies have shown that the maximum distance of exhaled air dissemination will be increased when using

noninvasive respiratory support (20). However, there is no direct evidence indicating an increased risk of infection among medical workers while using NIV, and none of the medical staff was infected during NIV procedures performed under adequate protection in our study (20, 21). In future studies, further exploration will be needed regarding (1) the relationship between the use of NIV and the amount of virus dissemination and (2) the relationship between viral pathogenicity and the dilution effect of the increased ventilation volume.

The prone position could improve oxygenation by recruiting the collapsed region of the dorsal lung and promoting drainage of airway secretions in AHRF patients (22, 23). Recently, researchers applied prone position NIV in patients with COVID-19-related AHRF and found that it could reduce respiratory rate, improve oxygenation and comfort of patients (24). More evidence on

the benefits of the prone position NIV should be investigated by comparing with standard NIV and selecting the appropriate patients are needed in the future.

Obviously, our study has some limitations. First, some clinical variables or ventilator parameters could not be analyzed due to the retrospective study design. Moreover, this was a single center study with a small sample size, which could not get adequate power to draw definitive conclusions. However, this study included all patients with COVID-19-related AHRF receiving NIV in the city of Shenzhen (with 423 laboratory-confirmed cases on August 31, 2020), and these results could provide some help for the medical staff to select appropriate patients receiving NIV treatment. In future, large-scale prospective randomized control studies are warranted to give us more evidence for the use of NIV and further studies should also explore the treatment effect of different NIV modalities or interface in patients with COVID-19-related AHRF.

In conclusion, close attention should be paid to  $\text{PaO}_2/\text{FiO}_2$  after 1–2 h of NIV initiation in patients with COVID-19-related AHRF receiving NIV. In addition, using NIV as rescue therapy should draw our awareness that it might delay escalation of respiratory support and lead to adverse outcomes.

## REFERENCES

- Wang D, Hu B, Hu C, Zhu F, Liu X, Zhang J, et al. Clinical characteristics of 138 hospitalized patients with 2019 novel coronavirus-infected pneumonia in Wuhan, China. *Jama*. (2020) 323:1061–9. doi: 10.1001/jama.2020.1585
- Tobin MJ, Laghi F, Jubran A. Caution about early intubation and mechanical ventilation in COVID-19. *Ann Intensive Care*. (2020) 10:78. doi: 10.1186/s13613-020-00692-6
- Crummey F, Naughton MT. Non-invasive positive pressure ventilation for acute respiratory failure: justified or just hot air? *Intern Med J*. (2007) 37:112–8. doi: 10.1111/j.1445-5994.2007.01268.x
- Nicolini A, Stieglitz S, Bou-Khalil P, Esquinas A. Cost-utility of non-invasive mechanical ventilation: analysis and implications in acute respiratory failure. A brief narrative review. *Respir Investig*. (2018) 56:207–13. doi: 10.1016/j.resinv.2017.12.011
- Jahagirdar D, Picheca L. Heated Humidified High Flow Oxygen for Respiratory Support: A Review of Clinical Effectiveness, Cost-Effectiveness, and Guidelines. CADTH Rapid Response Reports, Ottawa, ON (2019).
- Guan L, Zhou L, Le Grange JM, Zheng Z, Chen R. Non-invasive ventilation in the treatment of early hypoxemic respiratory failure caused by COVID-19: considering nasal CPAP as the first choice. *Crit Care*. (2020) 24:333. doi: 10.1186/s13054-020-03054-7
- Ferreiro BL, Angriman F, Munshi L, Del Sorbo L, Ferguson ND, Rochweg B, et al. Association of noninvasive oxygenation strategies with all-cause mortality in adults with acute hypoxemic respiratory failure: a systematic review and meta-analysis. *JAMA*. (2020) 324:57–67. doi: 10.1001/jama.2020.9524
- Ni YN, Luo J, Yu H, Liu D, Ni Z, Cheng J, et al. Can high-flow nasal cannula reduce the rate of endotracheal intubation in adult patients with acute respiratory failure compared with conventional oxygen therapy and noninvasive positive pressure ventilation?: a systematic review and meta-analysis. *Chest*. (2017) 151:764–75. doi: 10.1016/j.chest.2017.01.004
- Raof S, Nava S, Carpati C, Hill NS. High-flow, noninvasive ventilation and awake (nonintubation) proning in patients with coronavirus disease 2019 with respiratory failure. *Chest*. (2020) 158:1992–2002. doi: 10.1016/j.chest.2020.07.013

## DATA AVAILABILITY STATEMENT

The raw data supporting the conclusions of this article will be made available by the authors, without undue reservation.

## ETHICS STATEMENT

The studies involving human participants were reviewed and approved by the ethics committee of the Third People's Hospital. Written informed consent for participation was not required for this study in accordance with the national legislation and the institutional requirements.

## AUTHOR CONTRIBUTIONS

LL, CQ, and RC contributed to determining the outline and content of the study. YF, LG, WW, and SZ contributed to retrieving literature and writing a draft of this manuscript. JY, JW, ZL, and SZ contributed to the data acquisition, the interpretation of outcomes, and data analysis. All authors contributed to revising the draft critically for important intellectual content, providing final confirmation of the revised version, and being responsible for all aspects of the work.

- Winck JC, Ambrosino N. COVID-19 pandemic and non invasive respiratory management: every Goliath needs a David. An evidence based evaluation of problems. *Pulmonology*. (2020) 26:213–20. doi: 10.1016/j.pulmoe.2020.04.013
- Rochweg B, Brochard L, Elliott MW, Hess D, Hill NS, Nava S, et al. Official ERS/ATS clinical practice guidelines: noninvasive ventilation for acute respiratory failure. *Eur Respir J*. (2017) 50:1602426. doi: 10.1183/13993003.02426-2016
- National Health Commission of the People's Republic of China. *Diagnosis and Treatment Guideline of COVID-2019*, 8th edn. Available online at: <http://www.nhc.gov.cn/yzygj/s7653p/202008/0a7bdf12bd4b46e5bd28ca7f9a7f5e5a.shtml> (accessed November 10, 2020).
- Franco C, Facciolo N, Tonelli R, Dongilli R, Vianello A, Pisani L, et al. Feasibility and clinical impact of out-of-ICU noninvasive respiratory support in patients with COVID-19-related pneumonia. *Eur Respir J*. (2020) 56:2002130. doi: 10.1183/13993003.02130-2020
- Frat JP, Coudroy R, Thille AW. Non-invasive ventilation or high-flow oxygen therapy: when to choose one over the other? *Respirology*. (2019) 24:724–31. doi: 10.1111/resp.13435
- Aliberti S, Radovanovic D, Billi F, Sotgiu G, Costanzo M, Pilone T, et al. Helmet CPAP treatment in patients with COVID-19 pneumonia: a multicentre cohort study. *Eur Respir J*. (2020) 56:2001935. doi: 10.1183/13993003.01935-2020
- Frat JP, Ragot S, Coudroy R, Constantin JM, Girault C, Prat G, et al. Predictors of intubation in patients with acute hypoxemic respiratory failure treated with a noninvasive oxygenation strategy. *Crit Care Med*. (2018) 46:208–15. doi: 10.1097/CCM.0000000000002818
- Chiumello D, Busana M, Coppola S, Romitti F, Formenti P, Bonifazi M, et al. Physiological and quantitative CT-scan characterization of COVID-19 and typical ARDS: a matched cohort study. *Intensive Care Med*. (2020) 46:2187–96. doi: 10.1007/s00134-020-06281-2
- Gattinoni L, Chiumello D, Caironi P, Busana M, Romitti F, Brazzi L, et al. COVID-19 pneumonia: different respiratory treatments for different phenotypes? *Intensive Care Med*. (2020) 46:1099–102. doi: 10.1007/s00134-020-06033-2
- Guan L, Zhou L, Zhang J, Peng W, Chen R. More awareness is needed for severe acute respiratory syndrome coronavirus 2019 transmission through



- exhaled air during non-invasive respiratory support: experience from China. *Eur Respir J.* (2020) 55:2000352. doi: 10.1183/13993003.00352-2020
20. Ferioli M, Cisternino C, Leo V, Pisani L, Palange P, Nava S. Protecting healthcare workers from SARS-CoV-2 infection: practical indications. *Eur Respir Rev.* (2020) 29:200068. doi: 10.1183/16000617.0068-2020
  21. Esquinas AM, Egbert Pravinkumar S, Scala R, Gay P, Soroksky A, Girault C, et al. Noninvasive mechanical ventilation in high-risk pulmonary infections: a clinical review. *Eur Respir Rev.* (2014) 23:427–38. doi: 10.1183/09059180.00009413
  22. Guerin C, Reignier J, Richard JC, Beuret P, Gacouin A, Boulain T, et al. Prone positioning in severe acute respiratory distress syndrome. *N Engl J Med.* (2013) 368:2159–68. doi: 10.1056/NEJMoa1214103
  23. Coppo A, Bellani G, Winterton D, Di Pierro M, Soria A, Faverio P, et al. Feasibility and physiological effects of prone positioning in non-intubated patients with acute respiratory failure due to COVID-19 (PRON-COVID): a prospective cohort study. *Lancet Respir Med.* (2020) 8:765–74. doi: 10.1016/S2213-2600(20)30268-X
  24. Sartini C, Tresoldi M, Scarpellini P, Tettamanti A, Carco F, Landoni G, et al. Respiratory parameters in patients with COVID-19 after using noninvasive ventilation in the prone position outside the intensive care unit. *JAMA.* (2020) 323:2338–40. doi: 10.1001/jama.2020.7861

**Conflict of Interest:** The authors declare that the research was conducted in the absence of any commercial or financial relationships that could be construed as a potential conflict of interest.

Copyright © 2021 Fu, Guan, Wu, Yuan, Zha, Wen, Lin, Qiu, Chen and Liu. This is an open-access article distributed under the terms of the Creative Commons Attribution License (CC BY). The use, distribution or reproduction in other forums is permitted, provided the original author(s) and the copyright owner(s) are credited and that the original publication in this journal is cited, in accordance with accepted academic practice. No use, distribution or reproduction is permitted which does not comply with these terms.



# Follow-Up SARS-CoV-2 PCR Testing Outcomes From a Large Reference Lab in the US

Adam Sullivan\*, David Alfego, Brian Poirier, Jonathan Williams, Dorothy Adcock and Stan Letovsky

Labcorp® Holdings of America, Inc., Burlington, NC, United States

## OPEN ACCESS

### Edited by:

Babak A. Ardekani,  
Nathan Kline Institute for Psychiatric  
Research, United States

### Reviewed by:

Timothy O'leary,  
Veterans Health Administration (VHA),  
United States  
Ozren Polašek,  
University of Split, Croatia

### \*Correspondence:

Adam Sullivan  
sullia6@labcorp.com

### Specialty section:

This article was submitted to  
Infectious Diseases – Surveillance,  
Prevention and Treatment,  
a section of the journal  
Frontiers in Public Health

**Received:** 10 March 2021

**Accepted:** 27 April 2021

**Published:** 31 May 2021

### Citation:

Sullivan A, Alfego D, Poirier B,  
Williams J, Adcock D and Letovsky S  
(2021) Follow-Up SARS-CoV-2 PCR  
Testing Outcomes From a Large  
Reference Lab in the US.  
Front. Public Health 9:679012.  
doi: 10.3389/fpubh.2021.679012

By analyzing COVID-19 sequential COVID-19 test results of patients across the United States, we herein attempt to quantify some of the observations we've made around long-term infection (and false-positive rates), as well as provide observations on the uncertainty of sampling variability and other dynamics of COVID-19 infection in the United States. Retrospective cohort study of a registry of RT-PCR testing results for all patients tested at any of the reference labs operated by Labcorp® including both positive, negative, and inconclusive results, from March 1, 2020 to January 28, 2021, including patients from all 50 states and outlying US territories. The study included 22 million patients with RT-PCR qualitative test results for SARS-CoV-2, of which 3.9 million had more than one test at Labcorp. We observed a minuscule <0.1% basal positive rate for follow up tests >115 days, which could account for false positives, long-haulers, and/or reinfection but is indistinguishable in the data. In observing repeat-testing, for patients who have a second test after a first RT-PCR, 30% across the cohort tested negative on the second test. For patients who test positive first and subsequently negative within 96 h (40% of positive test results), 18% of tests will subsequently test positive within another 96-h span. For those who first test negative and then positive within 96 h (2.3% of negative tests), 56% will test negative after a third and subsequent 96-h period. The sudden changes in RT-PCR test results for SARS-CoV-2 from this large cohort study suggest that negative test results during active infection or exposure can change rapidly within just days or hours. We also demonstrate that there does not appear to be a basal false positive rate among patients who test positive >115 days after their first RT-PCR positive test while failing to observe any evidence of widespread reinfection.

**Keywords:** COVID-19, laboratory, repeat infection, PCR, real world data

## INTRODUCTION

Examining the repeat-testing results of reverse transcription polymerase chain reaction (RT-PCR) testing for COVID-19 via nasal, nasopharyngeal, or oropharyngeal swab can help to derive population-level testing sensitivity and specificity levels as well as search for evidence of various logistical or operational false positives and negatives that could be systemic in nature (1). Despite strict guidelines for EUA approval of various RT-PCR testing platforms, population-level and epidemiological-level analysis shows that RT-PCR can have varying degrees of population-level sensitivity and specificity (2–5). For example, in looking at the sensitivity and specificity of PCR

testing in the literature survey, a study out of Singapore showed that the combination of RT-PCR and chest tomography (CT) has higher sensitivity (91.9%, 79/86) than RT-PCR alone (78.2%, 68/87), CT alone (66.7%, 54 of 81) or combination of two RT-PCR tests (86.2%, 75/87) (6). It is reported that population-level false negative rates can be as low as 3% and as high as 33% (7).

In this study, we use repeat-testing outcomes to attempt to quantify some of the population-level false positive and false negative rates for various time points. To use repeat-testing outcomes to infer single test sensitivity/specificity, we examined published literature on repeat testing outcomes. In one study examining repeat testing of head/neck injury surgeries in acute care settings, 43 of 52 patients required two or more preoperative PCR tests. Four (9.3%) had discrepant results (positive/negative) (8). In the case of an 81-year-old female who underwent urgent coronary artery bypass grafting and was readmitted following discharge to a nursing facility with a cluster of COVID-19 cases, despite symptomatology and imaging concerns for COVID-19, her two initial RT-PCR tests were negative, but a third test was positive (9).

Related to looking at negative PCR tests, a retrospective analysis was performed early in the pandemic by the French government, who decided to repatriate the 337 French nationals living in Wuhan and place them in quarantine in their home country (not a Labcorp tested site). They were all tested for SARS-CoV-2 twice and all tests at day 0 and day 5 were negative for RT-PCR testing (10). In another study, it was reported that 610 hospitalized patients clinically diagnosed with SARS-CoV-2 suffered from false negatives and multiple testing outcomes for repeat testing of the same patient (11). In a preprint systematic review of five studies involving 957 patients (“under suspicion of Covid-19” or with “confirmed cases”), false negatives ranged from 2 to 29%, although the researchers raise concerns of the lack of blinding to index-test results, failure to report key RT-PCR characteristics, among others (12).

Not specific to Labcorp’s testing, there are also various investigations into the methods by which false positives and false negatives can occur. Various studies of optimal methods have demonstrated the nasopharyngeal (NP) swab to capture up to twice as many positive tests as the oropharyngeal (OP) swab, as confirmed in Tang et al. (13). Additionally, it was reported there are various operational false positives that are possible, including swab cross-contamination, contamination of reagents, or cross-reactions, where the operational false-positive rate was estimated to be 0.8 and 4% (14).

Using Labcorp’s COVID-19 registry (2) allowed us to investigate follow-up PCR testing at a participating laboratory after an initial NP, at-home nasal collection specimens, or OP swab with the goal of identifying rates of positivity over time on a population-level analysis. The studies above are from patients often from non-US countries with unknown EUA operational guidelines, and test manufacturers outside the United States. An additional aim of this study is to shed light on the basal false positive rates in testing in the United States as well as understand the dynamics of a negative result in the context of an epidemiological study.

## MATERIALS AND METHODS

The registry maintained by Labcorp includes 29.8 million (and counting) SARS-CoV-2 PCR tests conducted through multiple channels, including physician ordered, drive-through testing sites, employer/government contracts, and Pixel by Labcorp (Labcorp’s at-home PCR test offering). Patients include a wide representation of the United States and specimen collections during the entire pandemic duration. Tests used in this analysis reflect all those who had repeat testing from March 1, 2020 to January 28, 2021 and reflect those who had at least one PCR test following an initial test, considered the patient’s index. Analysis was conducted using Python™ 3.6.

## RESULTS

We first consider that every PCR test can have multiple outcomes: positive, negative, or other (where other can include collection issues, contamination, damage, mislabeling, or other logistical issues with sample collection). Every PCR positive patient is labeled with an index date of when they received their first positive PCR test. **Figure 1** shows that for patients who receive their first positive PCR test with Labcorp and have a subsequent PCR test collected *the next day*, 25% of those PCR tests are now negative for the cohort.

The size of the cohort was 22.3 million unique patients, which the unique combinations can be observed in **Table 1**. We examined multiple scenarios of interest including patients with more than 1 test, patients with more than 2 tests, patients with

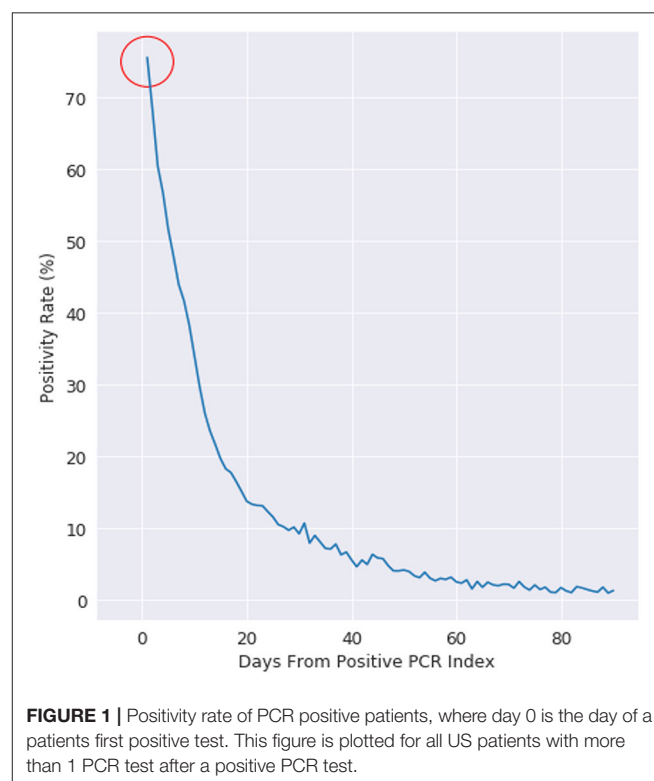


**TABLE 1** | General demographics of testing results for SARS-CoV-2 RT-PCR testing.

|                              | All patients | Patients >1 test | Patients >2 tests | Two tests within 24 h | First test pos, second test neg, third test pos | First test neg, second test pos, third test neg | >115 days after first positive |
|------------------------------|--------------|------------------|-------------------|-----------------------|---|---|--------------------------------|
| Unique patients              | 22,203,544   | 3,867,016        | 1,199,458         | 93,735                | 2,366   | 37,590  | 33,443                         |
| Positive tests               | 2,740,271    | 840,808          | 302,815           | 23,669                | 5,138   | 38,081  | 434                            |
| Negative tests               | 27,110,144   | 10,705,867       | 5,928,884         | 226,899               | 5,175   | 92,146  | 64,324                         |
| First test positive patients | 2,272,133    | 372,670          | 88,037            | 10,107                | 2,366   | –   | –                              |
| Any test positive patients   | 2,604,847    | 705,384          | 220,514           | 9,751                 | 2,327   | 37,421  | 408                            |
| Mean age (Female/Male)       | 42.7/45.5    | 44.3/47.6        | 47.7/53.2         | 39.4/42.5             | 48.4/55.4                                       | 42.0/44.6                                       | 51.1/45.3                      |
| Female                       | 55%          | 57%              | 59%               | 52%                   | 53%   | 58%   | 59.7%                          |

two tests within 24 h, patients with a test sequence that was positive  $\geq$  negative  $\geq$  positive, patients with a test sequence that was negative  $\geq$  positive  $\geq$  negative, and patients with >115 days where they are still positive.

We examine positivity rate decay in **Figure 1** with a negative exponential function, which is evidenced by the positivity rate expressed on the logarithmic scale on the right. At day 10, the positivity rate is about 30%. The decay rate starts at 75% (not 100%), as there is an intrinsic state change in up to 25% of the cohort population.

This retrospective analysis used North Carolina as a reference baseline, as Labcorp has a traditionally high coverage rate of diagnostic testing in the state. The 24 h re-test negativity rate (rate of negativity 24 h after Labcorp's first positive PCR test) is 15% in North Carolina, compared to 25% on the national cohort. The decay for both the NC baseline and the national cohort follows a well-defined negative exponential decay rate, which is what is typically expected for this type of viral infection status (15). The uncertainty at >60 days post first-PCR positive test is related to the decreasing number of people getting PCR tested >60 days between follow-up PCR tests.

## False Positive Rates Across US and Within a Control State

This study is an epidemiological study, so the evidence here is not related to any of the quantitative results from PCR testing such as cycle threshold (Ct) values. Manufacturers of testing assays have strict standards for how sensitivity and specificity rates are measured. However, the rates of positivity and negativity in repeat testing can be used to infer various false positive and false negative rates.

In **Figure 2**, we examine the rate of positive and negative PCR tests from 60 to 350 days after a patient's first positive PCR. The first observation is that we see miniscule rates of positive tests at 100 days and continuing outward. Given these are patients who were once PCR positive at day 0, we observe most who are repeat tested are now negative. The dwindling slope observed is that of less of the population being tested the further observed out from day 0.

The observations from **Figures 1 and 2** (as well as information in the **Supplemental Material**) demonstrate that while infection is active, PCR testing may result in sudden state changes (for example positive–negative–positive) during the active duration. However, for patients who have known to have a positive PCR test on day 0, the rate of positive re-tests is under 1% for any given day 100+ days past the infection. We would expect to see a significant positivity rate for these patients if PCR testing had a significant false positive rate.

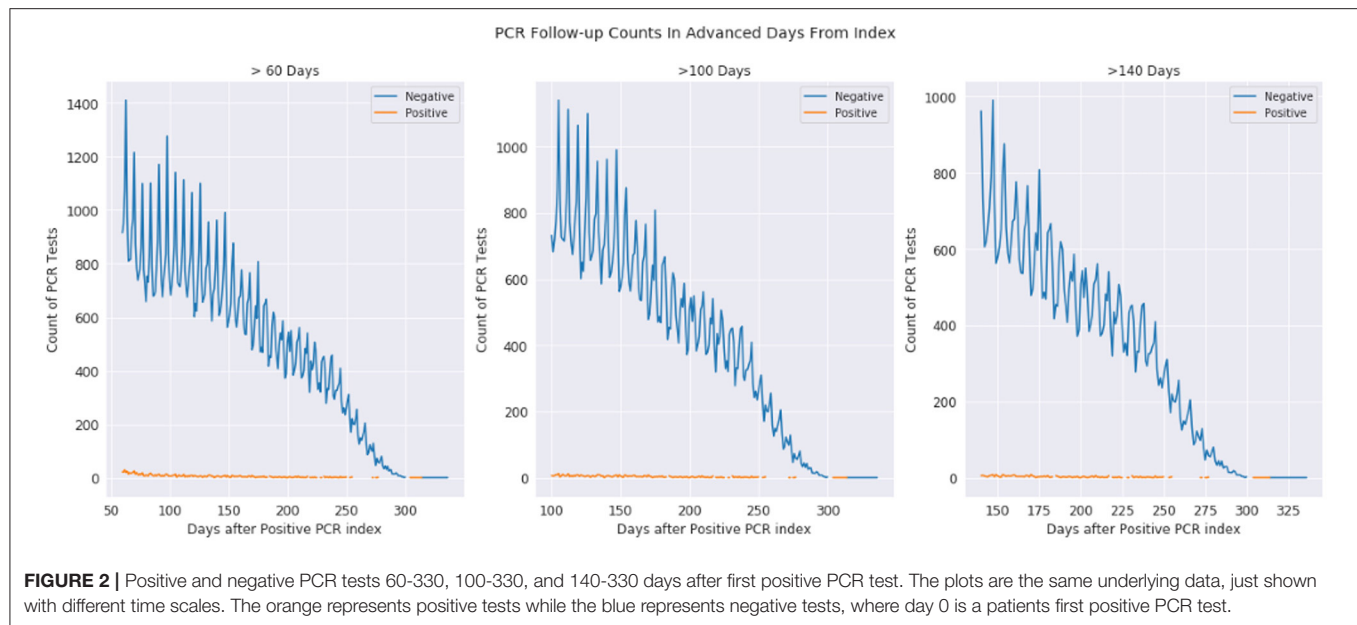
## Repeat PCR Testing Within 96 h

There is a sufficient number of patients (3.8 million patients with >1 test) who get repeat testing to draw inferences on effectiveness of testing and uncertainty within repeat testing. We cataloged a series of scenarios where patients take at least three tests, all within a given timeframe. There are three potential outcomes: positive, negative, and “other,” where other can represent various issues from collection to specimen quality.

We first restrict the PCR testing lifecycle to within 96 h between tests. This means that repeat testing can be at most 8 days, but as soon as 2 days for all three tests. The conditional probabilities of transitioning from one test outcome to the next is represented in the **Supplementary Material**. For example, for a randomly chosen sample in the cohort, there is 9.2% probability that the first PCR test will be positive. Given that a patient test is positive, we then examine the patient trajectory within the next 96 h. We observe that 40.2% of patients will test negative given that their first test was positive within a 96 h period. Similarly, when a patient test is negative, 96% of the time they do not test positive if get tested again within 96 h. Furthermore, we observe that when the first two tests are negative, the third test is positive 2.4% of the time. When a patient has tested positive followed by a negative test, 17.7% of the time the third test will come back positive within the 96 h time span.

Finally, when a patient has “other” as a test result two times in a row, 85.6% of the third test results will continue to come back as “other”. Similarly, we observe that 2.8% of tests will be positive after two “other” tests. A positive test follows two negative tests for 2.4% of patients.





## DISCUSSION

### False Positive Rates and Long-Term Infections

There is discussion of cycle times related to PCR testing affecting the outcomes of positive PCR tests (as referenced in the introduction) and leading to potential false positives. In our analysis, we were able to index positively infected patients (at day 0) and examine their trajectories at 100+ days after infection. These are patients who technically had two outcomes: either a false positive or a true positive. If the false positive rate is uniformly distributed among all tests, we would expect to see one of three outcomes at 100+ days after infection: the patient is still shedding viral load, the patient is reinfected, or we are observing the natural false positive rate. The rates of positive tests at >115 days is 0.015% (408 patients). There is no evidence of widespread false-positive rates for known positively tested patients at 115+ days.

The long-term infection rate of individuals is not well known because of how many tests are needed to make statistical inferences and the lack of evidence. In our analysis, we rarely see positives at >115 days. While it is possible that a patient could become infected at >180 days, we observe just 4 patients with PCR tests positive >115 days. It is impossible to conclude, but these could be reinfections, long-hauler shedders, or false positives. If we assumed the worst-case scenario that they are reinfections, the positivity rate <0.02% for >115 days would account for the combination of those 3 scenarios.

### Repeat Testing Within 96 h

We used the outcomes of repeat testing results to compare uncertainty in epidemiological characteristics of the Labcorp-tested population. It's important to remember that large reference laboratories like Labcorp likely test a wide range of circumstances, from routine drive-thru testing, at-home testing

to critical care settings. Some patients who are tested may be exceptionally symptomatic while others may be "exposed" with no symptoms and are getting a test at the direction of public health officials or to return to work or school. We are surprised to observe that a patient's first Labcorp-documented PCR test for a patient will be followed by a negative PCR test roughly 25% of the time (although the state of North Carolina, where LabCorp has a large market share, is just 15%).

Most likely the main difference is that people simply have true patho-physiological differences of viral load in respiratory mucosa, whereby results can sometimes be negative or positive (or even so close to the line of detection that a patient can test positive and negative within a 24 h period).

It's unlikely the case that the first test was a false positive, based on the evidence presented in the long-term positivity rates for repeat testers and the previous research presented in the introduction, as well as the published EUA approval metrics for positive test detection. We see miniscule rates of positive tests for patients who we know have tested positive for SARS-CoV-2 up to 100 days prior (it's worth noting that it may be possible that the patient was on the tail-end of infection or had a small viral load).

We also considered the case when a patient goes positive, then negative, and then positive again. Given that a patient is positive and then negative within the first 96 h, 17.6% of those patients will test positive on a third test. In some relaxing of COVID-19 protocols, there are some that say that the first subsequent negative test is a pass back into society. The middle test could be a false negative, or it could be a physiological response the body makes in response to complicated dynamics of the immune response. There is evidence of people becoming symptomatic, starting to recover, and then diverging quickly into a state of serious symptoms (16). A negative test after infection carries with it a 17.6% burden that a patient will subsequently test positive, albeit the mechanism of a secondary positive is unknown. We believe there are many other interesting observations from

viewing the conditional probability figure and invite the reader to make their own observations.

## Limitations

With this analysis, there are a few caveats that need to be considered. First, this does not account for people who received rapid tests, nor those that may have been tested at an internal lab in an acute care setting. Further, it is important to note that Labcorp has contracts with various government and industrial partners to conduct repeated surveillance of targeted populations (to reiterate, we are using repeat testing as a method to examine uncertainty in the overall population, and are not looking to specifically make inferences about repeat-testing outcomes). Additionally, Labcorp has a self-administered at-home testing kit that was Emergency Use Authorization (EUA) approved for the duration of this cohort study [Pixel by LabCorp™ (17, 18)]. Secondary analysis showed that the number of patients who tested positive using a Pixel test within 96 h of a non-Pixel positive PCR test did not differ significantly from those who tested positive in non-Pixel follow-up tests (Fisher exact,  $p = 0.200$ ). Method of collection was not available in this de-identified dataset, but we do suggest that a good follow-up investigation would be to repeat the analysis to look at changes when sample type is changed between OP and NP. Patients could have been tested through various channels through different locations or facilities.

The biggest caveat remains that it is impossible for us to know in this data where a patient has tested with regards to onset of symptoms. It is possible that a patient's first PCR test was not performed by Labcorp, and thus we would have missing data because their first PCR test was not recorded in the cohort. If this is a significant number of tests, we must be cautious of the metrics reported around second test positivity. We conducted the North Carolina baseline test to get a closer approximation to onset of symptoms at day 0. It's also possible people may be symptomatic and may not get tested for extended periods, which would not be detectable in this analysis. Disagreement between kits is certainly possible and must be mentioned as a potential, albeit slight, possibility.

## CONCLUSION

Repeat testing of PCR patients presents difficult decisions for clinicians and practitioners. There is little to no evidence of widespread continued infection or reinfection in our testing

populations after 115+ days from a patient's first PCR test. Given that a patient test is positive and then negative within 4 days, 17.6% of patients will test positive again if tested within the next 4 days. Further, 25% of patients nationwide (15% within the state of North Carolina) will test negative *just the next day* after testing positive. Even given the sudden change in dynamics of the virus as it takes its course, there is little evidence of a significant false positive rate because of our observations of patients who we know to be PCR positive.

## DATA AVAILABILITY STATEMENT

The datasets generated for this article are not readily available because this data, while de-identified, was generated from a PHI dataset and under HIPAA cannot be publicly posted. Requests to access the datasets should be directed to [sullia6@labcorp.com](mailto:sullia6@labcorp.com).

## ETHICS STATEMENT

Use of the data within Labcorp's COVID-19 registry was approved with waiver of authorization for the use and disclosure of protected health information by Western IRB on March 26, 2020.

## AUTHOR CONTRIBUTIONS

AS and DA did the analysis, wrote the draft, and created the hypotheses. DAd, JW, BP, and SL contributed to design, interpretation, discussion, and conclusions. All authors contributed to the article and approved the submitted version.

## SUPPLEMENTARY MATERIAL

The Supplementary Material for this article can be found online at: <https://www.frontiersin.org/articles/10.3389/fpubh.2021.679012/full#supplementary-material>

**Supplementary Figure 1 |** Conditional Probabilities of repeat PCR testing and have a caption/description of Conditional probabilities of positive (+), negative (−) and other (specimen issues, broken collection containers, etc.). There were 19,719 patients used to construct this cohort analysis. This conditional probability tree allows you to traverse the state changes of testing results from a patients' first, second, and third test.

## REFERENCES

- McNaughton CD, Adams NM, Johnson CH, Ward MJ, Lasko TA. Diurnal variation in SARS-CoV-2 PCR test results: test accuracy may vary by time of day. *medRxiv*. (2021). doi: 10.1101/2021.03.12.21253015
- Harvey RA, Rassen JA, Kabelac CA, Turenne W, Leonard S, Klesh R, et al. Association of SARS-CoV-2 seropositive antibody test with risk of future infection. *JAMA Intern Med*. (2021) 181:672–9. doi: 10.1001/jamainternmed.2021.0366
- Gupta-Wright A, MacLeod CK, Barrett J, Filson SA, Corrah T, Parris V, et al. False-negative RT-PCR for COVID-19 and a diagnostic risk score: a retrospective cohort study among patients admitted to hospital. *BMJ Open*. (2021) 11:e047110. doi: 10.1136/bmjopen-2020-047110
- Garg A, Ghoshal U, Patel SS, Singh DV, Arya AK, Vasanth S, et al. Evaluation of seven commercial RT-PCR kits for COVID-19 testing in pooled clinical specimens. *J Med Virol*. (2021) 93:2281–6. doi: 10.1002/jmv.26691
- Feng H, Liu Y, Lv M, Zhong J. A case report of COVID-19 with false negative RT-PCR test: necessity of chest CT. *Jpn J Radiol*. (2020) 38:409–10. doi: 10.1007/s11604-020-00967-9
- Ren X, Liu Y, Chen H, Liu W, Guo Z, Zhang Y, et al. Application and optimization of RT-PCR in diagnosis of SARS-CoV-2 infection. *SSRN Electron J*. (2020). doi: 10.2139/ssrn.3546086. [Epub ahead of print].

7. Arevalo-Rodriguez I, Buitrago-Garcia D, Simancas-Racines D, Zambrano-Achig P, Campo R Del, Ciapponi A, et al. False-negative results of initial RT-PCR assays for COVID-19: a systematic review. *PLoS ONE*. (2020) 15:e0242958. doi: 10.1371/journal.pone.0242958
8. Katz AP, Civantos FJ, Sargi Z, Leibowitz JM, Nicolli EA, Weed D, et al. False-positive reverse transcriptase polymerase chain reaction screening for SARS-CoV-2 in the setting of urgent head and neck surgery and otolaryngologic emergencies during the pandemic: clinical implications. *Head Neck*. (2020) 42:1621–8. doi: 10.1002/hed.26317
9. Fisher B, Seese L, Sultan I, Kilic A. The importance of repeat testing in detecting coronavirus disease 2019 (COVID-19) in a coronary artery bypass grafting patient. *J Card Surg*. (2020) 35:1342–4. doi: 10.1111/jocs.14604
10. Lagier JC, Colson P, Tissot Dupont H, Salomon J, Doudier B, Aubry C, et al. Testing the repatriated for SARS-Cov2: should laboratory-based quarantine replace traditional quarantine? *Travel Med Infect Dis*. (2020) 34:101624. doi: 10.1016/j.tmaid.2020.101624
11. Li Y, Yao L, Li J, Chen L, Song Y, Cai Z, et al. Stability issues of RT-PCR testing of SARS-CoV-2 for hospitalized patients clinically diagnosed with COVID-19. *J Med Virol*. (2020) 92:903–8. doi: 10.1002/jmv.25786
12. Woloshin S, Patel N, Kesselheim AS. False negative tests for SARS-CoV-2 infection — challenges and implications. *N Engl J Med*. (2020) 383:e38. doi: 10.1056/NEJMp2015897
13. Tang YW, Schmitz JE, Persing DH, Stratton CW. Laboratory diagnosis of COVID-19: current issues and challenges. *J Clin Microbiol*. (2020) 58:e00512–20. doi: 10.1128/JCM.00512-20
14. Surkova E, Nikolayevskyy V, Drobniewski F. False-positive COVID-19 results: hidden problems and costs. *Lancet Respir Med*. (2020) 8:1167–8. doi: 10.1016/S2213-2600(20)30453-7
15. Smith AM, Adler FR, Perelson AS. An accurate two-phase approximate solution to an acute viral infection model. *J Math Biol*. (2010) 60:711–26. doi: 10.1007/s00285-009-0281-8
16. Berlin DA, Gulick RM, Martinez FJ. Severe Covid-19. *N Engl J Med*. (2020) 383:2451–60. doi: 10.1056/NEJMc2009575
17. *LabCorp Receives FDA Authorization to Make At-Home COVID-19 Collection Kits Available Through Retail*. Burlington, NC (2020). Available online at: <https://www.labcorp.com/coronavirus-disease-covid-19/news/labcorp-receives-fda-authorization-make-home-covid-19-collection-kits-available-through-retail> (accessed December 16, 2020).
18. FDA. *FAQ's on Testing for SARS-CoV-2*. Available online at: <https://www.fda.gov/medical-devices/coronavirus-covid-19-and-medical-devices/faqs-testing-sars-cov-2>

**Conflict of Interest:** The authors declare that the research was conducted in the absence of any commercial or financial relationships that could be construed as a potential conflict of interest.

All authors are employees of Labcorp.

Copyright © 2021 Sullivan, Alfego, Poirier, Williams, Adcock and Letovsky. This is an open-access article distributed under the terms of the Creative Commons Attribution License (CC BY). The use, distribution or reproduction in other forums is permitted, provided the original author(s) and the copyright owner(s) are credited and that the original publication in this journal is cited, in accordance with accepted academic practice. No use, distribution or reproduction is permitted which does not comply with these terms.



# SARS-CoV-2 Gastrointestinal Infection Prolongs the Time to Recover From COVID-19

Zhijie Xu<sup>1,2,3,†</sup>, Meiwen Tang<sup>2,3,4†</sup>, Ping Chen<sup>1†</sup>, Hongyu Cai<sup>1†</sup> and Fei Xiao<sup>1,2,3\*</sup>

<sup>1</sup> Department of Infectious Diseases, The Fifth Affiliated Hospital of Sun Yat-Sen University, Zhuhai, China, <sup>2</sup> Guangdong Provincial key Laboratory of Biomedical Imaging, The Fifth Affiliated Hospital of Sun Yat-Sen University, Zhuhai, China, <sup>3</sup> Guangdong Provincial Engineering Research Center of Molecular Imaging, The Fifth Affiliated Hospital of Sun Yat-Sen University, Zhuhai, China, <sup>4</sup> Department of Hematology, The Fifth Affiliated Hospital of Sun Yat-Sen University, Zhuhai, China

**Objectives:** We previously reported that SARS-CoV-2 infects the gastrointestinal (GI) epithelium. In this study, we aimed to explore the impact of SARS-CoV-2 GI infection on clinical outcomes of COVID-19.

**Materials and Methods:** For this retrospective cohort study, 104 patients with COVID-19 were classified into a SARS-CoV-2 GI infection group and a non-infection group. The primary endpoint was the time of negative conversion of SARS-CoV-2 RNA in respiratory tract samples. The secondary outcome was the time of hospitalization for COVID-19.

**Results:** Patients with SARS-CoV-2 GI infection had a longer duration of positive SARS-CoV-2 RNA in respiratory tract samples (median 12.0 days [95% CI: 10.0–13.2] vs. 9.0 days [95% CI: 7.5–10.5]; HR 0.575 [95% CI: 0.386–0.857];  $P = 0.003$ ) and hospitalization (median 28.0 days [95% CI: 23.2–32.8] vs. 15.0 days [95% CI: 13.6–16.4]; HR 0.149 [95% CI: 0.087–0.252];  $P < 0.001$ ) than patients without SARS-CoV-2 GI infection. Subgroup analyses for sex, age, epidemiological history, clinical classification and antiviral treatment showed consistent results.

**Conclusion:** Our study indicates that SARS-CoV-2 GI infection prolongs the duration of SARS-CoV-2 shedding and hospitalization in the patients with COVID-19. More attention should be paid to SARS-CoV-2 GI infection of COVID-19 and fecal SARS-CoV-2 RNA test should be completed in time.

**Keywords:** SARS-CoV-2, gastrointestinal infection, adverse effect, stool viral load, alimentary tract

## INTRODUCTION

COVID-19, which is caused by SARS-CoV-2, is a global pandemic resulting in millions of deaths (1). The virus is mainly transmitted via respiratory droplets and usually causes a variety of respiratory symptoms. Various lines of evidence indicate that SARS-CoV-2 also infects the gastrointestinal (GI) system and causes corresponding GI symptoms (2). We previously reported that SARS-CoV-2 infects the GI epithelium by detecting positive staining for SARS-CoV-2 in the GI epithelium of patients positive for fecal SARS-CoV-2 RNA (3). Several laboratories around the world have also detected the virus in fecal samples, in GI biopsies and at autopsy (4–6). Subsequently, more attention is being given to the GI manifestations of SARS-CoV-2. The most common GI symptoms of COVID-19 are anorexia, diarrhea, nausea and abdominal pain (5, 7, 8).

## OPEN ACCESS

### Edited by:

Seyed Alireza Nadji,  
Shahid Beheshti University of Medical  
Sciences, Iran

### Reviewed by:

Mohammad Shehab,  
Mubarak Al Kabeer Hospital, Kuwait  
Alireza Shafiei,  
Tehran University of Medical  
Sciences, Iran

### \*Correspondence:

Fei Xiao  
xiaof35@mail.sysu.edu.cn

<sup>†</sup>These authors have contributed  
equally to this work

### Specialty section:

This article was submitted to  
Infectious Diseases – Surveillance,  
Prevention and Treatment,  
a section of the journal  
Frontiers in Medicine

**Received:** 21 March 2021

**Accepted:** 20 April 2021

**Published:** 04 June 2021

### Citation:

Xu Z, Tang M, Chen P, Cai H and  
Xiao F (2021) SARS-CoV-2  
Gastrointestinal Infection Prolongs the  
Time to Recover From COVID-19.  
Front. Med. 8:683551.  
doi: 10.3389/fmed.2021.683551



Several studies have investigated the relationship between GI symptoms and mortality of COVID-19 (9–11), however, no studies have described associations between SARS-CoV-2 GI infection and the clinical outcomes of COVID-19. Thus, to further explore the clinical characteristics of SARS-CoV-2 GI infection in patients with COVID-19, we aimed to explore its impact on clinical COVID-19 outcomes in a retrospective cohort study.

## METHODS

### Patients

This retrospective cohort study was conducted from 18 January to 24 August 2020 at the Fifth Affiliated Hospital of Sun Yat-Sen University (SYSU5) in Zhuhai, China. We recruited 105 patients who were hospitalized in the COVID-19 medical center of SYSU5. The diagnosis of COVID-19 was based on epidemiological history, symptoms, lung imaging manifestations and the presence of SARS-CoV-2 RNA in respiratory tract samples using the China CDC-standardized real-time reverse transcriptase polymerase chain reaction (rRT-PCR). The copy numbers of SARS-CoV-2 RNA were indicated by rRT-PCR cycle threshold (CT) values, with lower CT values corresponding to higher viral copy numbers. A CT value  $<40$  was defined as positive, as reported (12). GI infection of SARS-CoV-2 was defined as simultaneously positivity for SARS-CoV-2 RNA in a fecal sample. After excluding one patient for whom the fecal SARS-CoV-2 RNA test was not completed, 104 patients were included and divided into two groups according to whether SARS-CoV-2 GI infection was present (infection group;  $n = 54$ ) or absent (non-infection group;  $n = 50$ ).

This study was approved by the Ethics Committee of SYSU5 [No. ZDWY [2020] Lunzi No. (K22-1)]. All experiments in this study were performed according to the principles of the Declaration of Helsinki and Good Clinical Practice. All patients or their legal guardians provided written informed consent.

### Data Collection and Measurement

Information about sex, age, ethnicity, smoking, alcohol consumption, epidemiological history, medical history, clinical classification, and antiviral treatment was obtained from the hospital information system of SYSU5. Epidemiological history was recorded as local or overseas cases according to the possible location of infection with SARS-CoV-2. In the present study, local cases had travel history to Wuhan or contact with patients with COVID-19 or other person with fever or respiratory symptoms from Wuhan, and no overseas travel history within 14 days before illness onset. Overseas cases had overseas travel or residence history and tested positive for SARS-CoV-2 RNA in respiratory tract samples when they entered China. The identification of hypertension and diabetes was based on previous relevant medical history or diagnoses during hospitalization. Clinical classification was classified as mild (mild clinical symptoms and absent of pneumonia manifestations on imaging), moderate (obvious symptoms and present of pneumonia manifestations on imaging), severe (respiratory rate

$\geq 30$  breaths/min; oxygen saturation  $\leq 93\%$  at a resting state; arterial partial pressure of oxygen/oxygen concentration  $\leq 300$  mmHg) and critical (occurrence of respiratory failure requiring mechanical ventilation; presence of chock; other organ failure that requires monitoring and treatment in the ICU) according to the severity of clinical symptoms, imaging manifestations and hypoxia.

Venous blood sampling was performed immediately upon hospitalization, and the white blood cell count (WBC), neutrophil count (NEU), lymphocyte count (LYM), and procalcitonin (PCT) and C-reactive protein (CRP) levels were determined using standard laboratory methods. Consistent laboratory methods were adopted.

### Clinical Outcome Ascertainment

The primary endpoint was the conversion time from the first positive of SARS-CoV-2 RNA test to negative in respiratory tract samples. Negative conversion of SARS-CoV-2 RNA was defined as undetectable viral RNA for two consecutive respiratory tract or fecal samples (sampling interval more than 24 h). The secondary outcome was the time of hospitalization for COVID-19. Discharge standards were defined as follows: (1) body temperature remaining normal (axilla temperature  $\leq 36.6^{\circ}\text{C}$  or oral temperature  $\leq 37.2^{\circ}\text{C}$  or rectal temperature  $\leq 37.8^{\circ}\text{C}$ ) for at least 3 days; (2) respiratory symptoms improved,  $\text{SpO}_2 > 93\%$  without assisted oxygen inhalation; (3) lung imaging showing obvious improvement in lesions, CT improvement defined as that exudation or consolidation of the lesion are absorbed, the lesion area was gradually narrowed, and there may be residual linear fibrosis, which are independently judged by two radiologist until they reached the same conclusion; (4) negative conversion of SARS-CoV-2 RNA in respiratory tract and fecal samples; (5) disease course at least 14 days from onset; and (6) discharge approved by multi-disciplinary medical team.

### Statistical Analysis

Statistical analyses were performed using SPSS Statistics version 25.0. Basic characteristics of the study subjects are presented as the median (range) for continuous variables and as numbers with percentages for categorical variables. Independent  $t$ -tests or the Mann–Whitney U tests were performed for comparison of means of continuous variables depending on the normality of the distribution of groups. Paired-samples  $t$ -test was adopted to compare means of paired samples. For venous blood results, values beyond the defined lower limit of detection were set to the lower limit. The Pearson  $\chi^2$  test was used to assess differences in categorical variables between groups. The log-rank test and Kaplan–Meier curve analyses were performed to compare the duration of SARS-CoV-2 shedding and hospitalization between groups. A Cox proportional hazard model was applied to estimate the HRs and corresponding 95% CIs. Subgroup analysis including sex, age, epidemiological history, clinical classification and antiviral treatment was carried out to adjust for potential imbalance in baseline characteristics. For all comparative analyses,  $P < 0.05$  was considered to indicate statistical significance.

**TABLE 1** | Characteristics of the study population.

|                           | All patients<br>(n = 104) | Infection<br>(n = 54) | Non-infection<br>(n = 50) | P-value |
|---------------------------|---------------------------|-----------------------|---------------------------|---------|
| Sex                       |                           |                       |                           | 0.002   |
| Male, %                   | 50, 48.1                  | 34, 63.0              | 16, 32.0                  |         |
| Female, %                 | 54, 51.9                  | 20, 37.0              | 34, 68.0                  |         |
| Age group                 |                           |                       |                           | 0.637   |
| >65, %                    | 12, 11.5                  | 7, 13.0               | 5, 10.0                   |         |
| ≤65, %                    | 92, 88.5                  | 47, 87.0              | 45, 90.0                  |         |
| Ethnicity                 |                           |                       |                           | 0.389   |
| Asian, %                  | 102, 98.2                 | 52, 96.4              | 50, 100.0                 |         |
| Caucasian, %              | 1, 0.9                    | 1, 1.8                | 0, 0.0                    |         |
| Black, %                  | 1, 0.9                    | 1, 1.8                | 0, 0.0                    |         |
| Smoking, %                | 6, 5.8                    | 3, 5.6                | 3, 6.0                    | 0.923   |
| Drinking, %               | 2, 1.9                    | 1, 1.9                | 1, 2.0                    | 0.956   |
| Epidemiological history   |                           |                       |                           | 0.020   |
| Local cases, %            | 95, 91.3                  | 46, 85.2              | 49, 98.0                  |         |
| Overseas cases, %         | 9, 8.7                    | 8, 14.8               | 1, 2.0                    |         |
| Medical history           |                           |                       |                           |         |
| Hypertension, %           | 18, 17.3                  | 8, 14.8               | 10, 20.0                  | 0.485   |
| Diabetes, %               | 7, 6.7                    | 2, 3.7                | 5, 10.0                   | 0.200   |
| Clinical classification   |                           |                       |                           | 0.129   |
| Mild, %                   | 14, 13.4                  | 10, 18.5              | 4, 8.0                    |         |
| Moderate, %               | 66, 63.5                  | 29, 53.7              | 37, 74.0                  |         |
| Severe, %                 | 19, 18.3                  | 11, 20.4              | 8, 16.0                   |         |
| Critical, %               | 5, 4.8                    | 4, 7.4                | 1, 2.0                    |         |
| Antiviral treatment, %    | 93, 89.4                  | 48, 88.9              | 45, 90.0                  | 0.854   |
| WBC (10 <sup>9</sup> /L)* | 4.92<br>(0.19–24.72)      | 4.97<br>(0.19–14.95)  | 4.75<br>(2.62–24.72)      | 0.689   |
| NEU (10 <sup>9</sup> /L)* | 2.82<br>(0.46–10.63)      | 2.94<br>(0.46–10.63)  | 2.81<br>(0.95–7.43)       | 0.930   |
| LYM (10 <sup>9</sup> /L)* | 1.52<br>(0.21–9.02)       | 1.55<br>(0.21–9.02)   | 1.51<br>(0.58–4.19)       | 0.738   |
| CRP (mg/L)*               | 3.67<br>(0.01–115.14)     | 2.39<br>(0.01–74.11)  | 5.35<br>(0.03–115.14)     | 0.224   |
| PCT (ng/mL)*              | 0.10<br>(0.10–5.75)       | 0.10<br>(0.10–5.75)   | 0.10<br>(0.10–0.30)       | 0.056   |

WBC, white blood cell count; NEU, neutrophil count; LYM, lymphocyte count; CRP, C-reactive protein; PCT, procalcitonin. \*median (range).

## RESULTS

### Characteristics of the Study Population

This study included a total of 104 patients with COVID-19, with 54 (51.9%) in the infection group and 50 (48.1%) in the non-infection group. The characteristics of the study population are listed in **Table 1**. A significant difference in the sex was found between the groups ( $P = 0.002$ ). There were 34 male patients (63.0%) in the infection group and 16 male patients (32%) in the non-infection group. Compared with patients without SARS-CoV-2 GI infection, a significantly higher likelihood of GI infection was found for overseas cases (8 (14.8%) vs. 1 (2.0%);  $P = 0.020$ ). Among these overseas cases with GI infection, 5

patients were from the UK, 2 patients from Hong Kong, and 1 patient from Macau. In contrast, age, ethnicity, smoking, drinking, medical history, and clinical classification were not significantly different between the groups. We also observed no differences in the WBC, NEU, LYM, CRP and PCT levels between the two groups (**Table 1**).

### Clinical Outcome of Patients With SARS-CoV-2 GI Infection

In analyses of the full study population, patients with SARS-CoV-2 GI infection exhibited a longer duration of SARS-CoV-2 RNA positivity in respiratory tract samples than patients without SARS-CoV-2 GI infection (median 12.0 days [95% CI: 10.0–13.2] vs. 9.0 days [95% CI: 7.5–10.5]; HR 0.575 [95% CI: 0.386–0.857];  $P = 0.003$ ) (**Figure 1A**). We also found that patients with SARS-CoV-2 GI infection had a longer time of hospitalization than the patients without SARS-CoV-2 GI infection (median 28.0 days [95% CI: 23.2–32.8] vs. 15.0 days [95% CI: 13.6–16.4]; HR 0.149 [95% CI: 0.087–0.252];  $P < 0.001$ ) (**Figure 2A**). To adjust for potential imbalance in the baseline characteristics of the two groups, which is inevitable in a retrospective study, subgroup analyses of sex, age, epidemiological history, clinical classification and antiviral treatment were performed. Combined SARS-CoV-2 GI and respiratory infection had an adverse effect on the time to negative conversion of viral RNA in respiratory tract samples as well as hospitalization time in all strata (**Figures 1B, 2B**). Nonetheless, the effect was not statistically significant in some subgroups because of the small sample size.

### Evaluation of the Clinical Characteristics of Patients With Persistently Positive SARS-CoV-2 RNA in Feces

Among the GI infection group, we specially evaluated the viral load of 16 patients who remained persistently positive fecal SARS-CoV-2 RNA over nearly 2 weeks or more. Among the 16 patients, SARS-CoV-2 RNA in feces was detected 1–21 days (median: 6 days; mean: 8.44 days) after detection of viral RNA in nasopharyngeal swabs. The mean duration of positive fecal SARS-CoV-2 RNA was significantly longer than that of positive nasopharyngeal SARS-CoV-2 RNA (25.81 days vs. 9.88 days; difference in mean 15.94 [95% CI: 11.93–19.95];  $P < 0.001$ ) (**Table 2**).

We monitored CT value of fecal sample from 16 patients during their hospitalization. As shown in **Figure 3**, CT values of the fecal sample ranged from 11 to 40. The mean of the initial and the final CT values is 23.59 and 36.22, respectively (difference in mean  $-12.62$  [95% CI:  $-18.67$  to  $-6.579$ ];  $P < 0.001$ ). Except for Patient 11, 13, and 16, the CT values of the other 13 patients increased slowly over time during their hospitalization. The CT values of Patient 1 and 6 increased  $<1$  over 25 and 29 days.

Among 3 patients (Patient 5, Patient 11, and Patient 15) undergoing upper GI endoscopy, SARS-CoV-2 nucleocapsid was detected in the cytoplasm of gastric glandular epithelial cells in 2 patients (Patient 11 and 15), who remained positive for fecal SARS-CoV-2 RNA after negative conversion of viral RNA from pharyngeal swabs (**Table 2**).

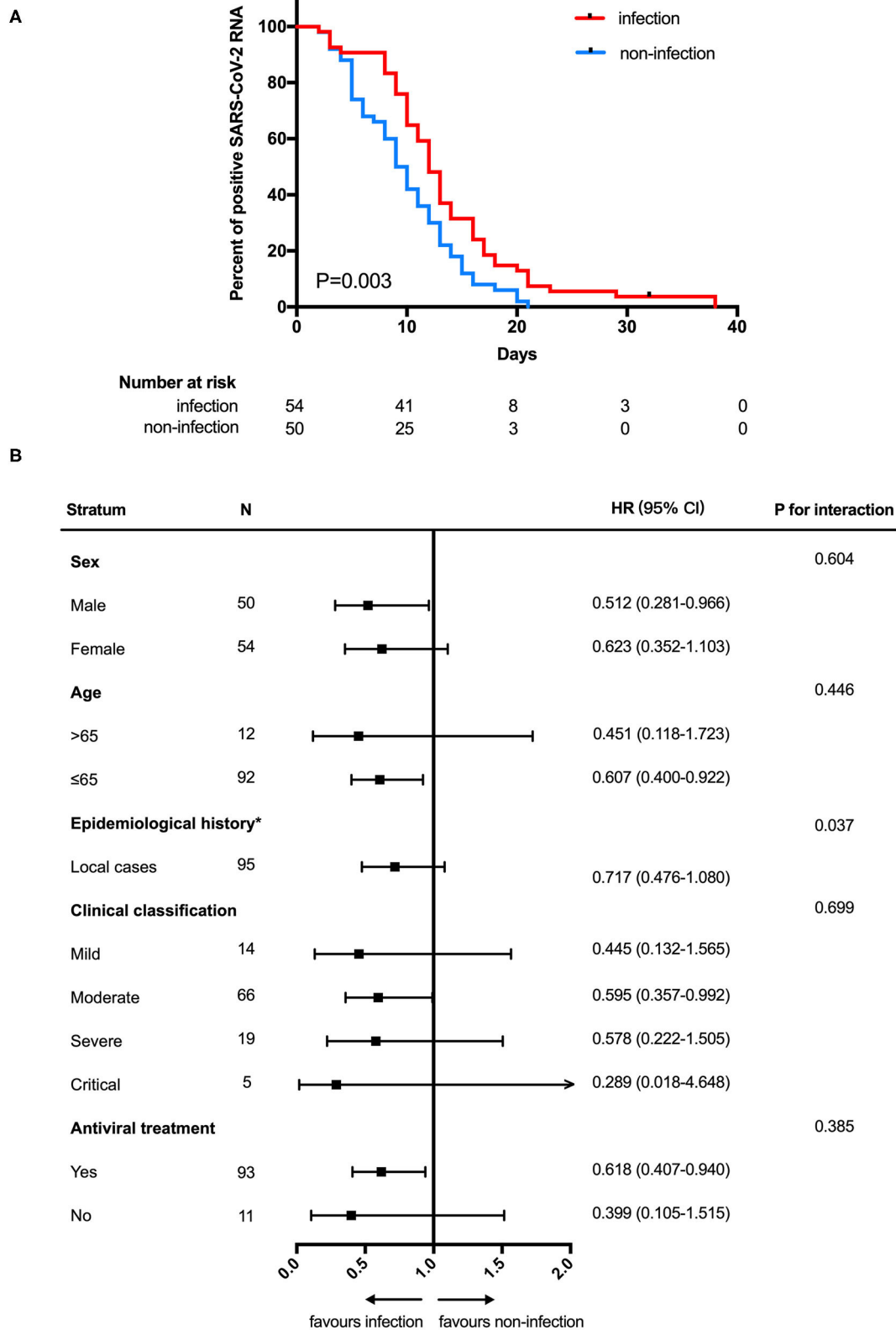


**FIGURE 1 |** Negative conversion time **(A)** Kaplan-Meier curve for the duration of SARS-CoV-2 RNA in respiratory tract samples between SARS-CoV-2 gastrointestinal infection and non-infection groups. **(B)** Subgroup analysis. NCT, negative conversion time; HR, hazard ratio. \*The number of patients in the overseas case subgroup was too few for comparison.

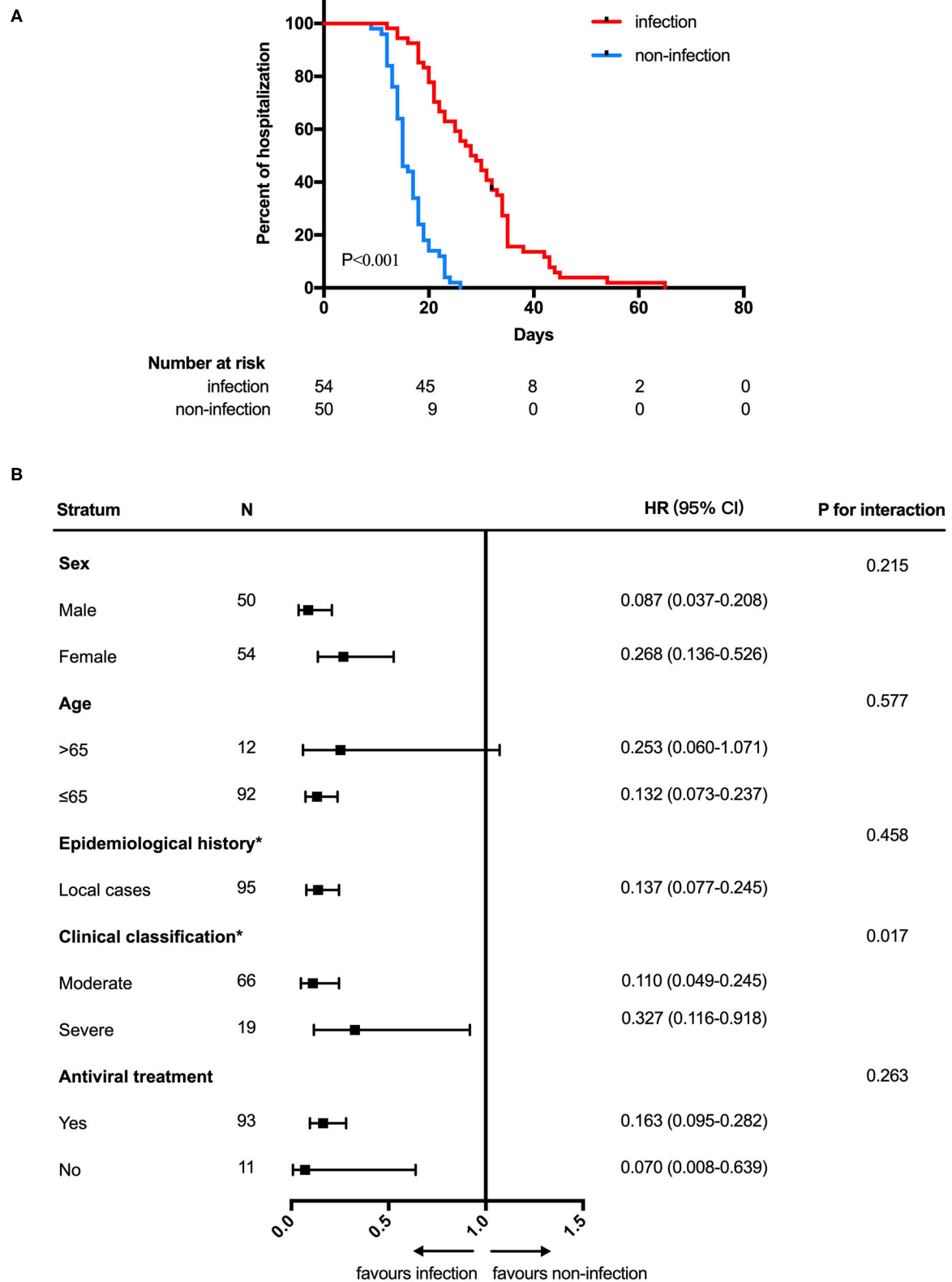


**FIGURE 2 |** Hospitalization time **(A)** Kaplan-Meier curve for hospitalization time between SARS-CoV-2 gastrointestinal infection and non-infection groups. **(B)**

Subgroup analysis. HOD, hospitalization days; HR, hazard ratio. \*The number of patients in the overseas case subgroup as well as the mild and critical subgroups were too few for comparison.



**TABLE 2 |** Clinical characteristics of patients with persistently positive SARS-CoV-2 RNA in feces.

| Patient    | Sex | Age (years) | Interval between initial detection of positive N and F (days) | Duration of positive N (days) | Duration of positive F (days) | SARS-CoV-2 nucleocapsid protein in gastric epithelial cells |
|------------|-----|-------------|---|-------------------------------|-------------------------------|---|
| patient 1  | M   | 29          | 6   | 7                             | 26                            | /   |
| patient 2  | M   | 35          | 16  | 13                            | 12                            | /   |
| patient 3  | M   | 1.4         | 9   | 6                             | 29                            | /   |
| patient 4  | F   | 29          | 6   | 10                            | 29                            | /   |
| patient 5  | F   | 34          | 6   | 15                            | 28                            | Negative  |
| patient 6  | M   | 32          | 8   | 10                            | 26                            | /   |
| patient 7  | M   | 44          | 5   | 15                            | 27                            | /   |
| patient 8  | M   | 42          | 6   | 3                             | 27                            | /   |
| patient 9  | F   | 53          | 4   | 10                            | 25                            | /   |
| patient 10 | M   | 45          | 1   | 1                             | 29                            | /   |
| patient 11 | M   | 65          | 14  | 18                            | 28                            | Positive  |
| patient 12 | F   | 0.9         | 5   | 8                             | 28                            | /   |
| patient 13 | M   | 38          | 21  | 7                             | 28                            | /   |
| patient 14 | F   | 63          | 21  | 14                            | 17                            | /   |
| patient 15 | M   | 64          | 6   | 13                            | 27                            | Positive  |
| patient 16 | M   | 64          | 1   | 8                             | 27                            | /   |
| Median     | NA  | 40          | 6   | 10                            | 27                            | /   |
| Mean       | NA  | 39.96       | 8.44  | 9.88                          | 25.81                         | /   |
| Max        | NA  | 65          | 21  | 18                            | 29                            | /   |
| Min        | NA  | 0.9         | 1   | 1                             | 12                            | /   |

N, nasopharyngeal swab; F, feces/no data; NA, not applicable.

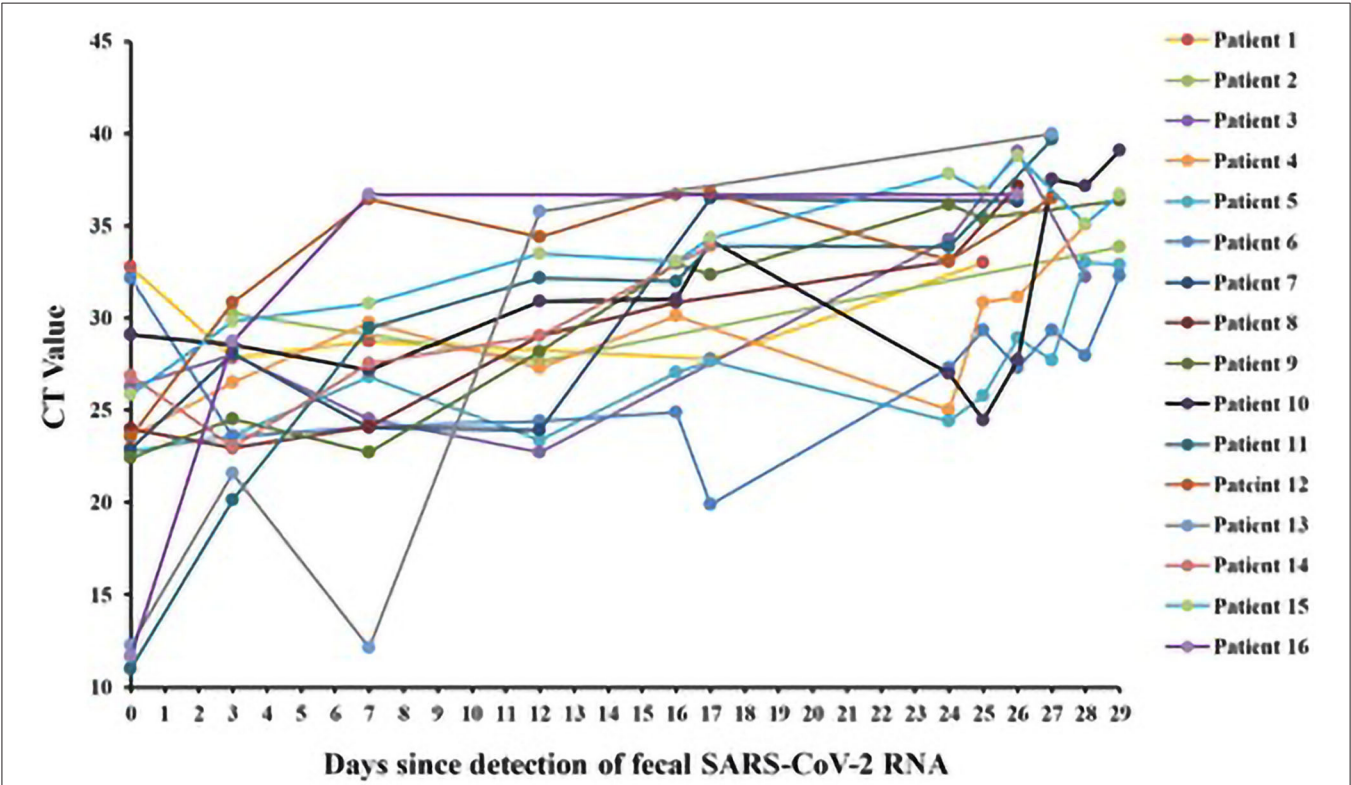


**FIGURE 3 |** CT values of fecal SARS-CoV-2 RNA in patients with persistently positive SARS-CoV-2 RNA in feces (n = 16).

## DISCUSSION

SARS-CoV-2 binds to angiotensin-converting enzyme 2 (ACE2) to enter host cells via its surface spike glycoprotein. ACE2 is highly expressed in GI epithelial cells and mediates SARS-CoV-2 entry, leading to GI infection and corresponding GI symptoms (13–15).

Although GI infection has received attention, there is still a lack of in-depth and comprehensive understanding of the clinical characteristics of SARS-CoV-2 GI infection. In the present study, we explored the impact of GI infection with SARS-CoV-2 on the clinical outcomes of COVID-19 and found that it prolongs the duration of SARS-CoV-2 shedding and hospitalization in patients with COVID-19.

51.9 percentage of patients with COVID-19 (54/104) had GI infection of SARS-CoV-2 in our study, and these patients tended to be male. Previous studies on COVID-19 also found that males might be more susceptible to SARS-CoV-2, with more serious medical conditions and higher mortality (16–19). This might be because of the robust T cell response in female patients (20) and protection against the virus by female hormones (21, 22). This finding also provides a possible explanation for the observed sex biases in the SARS-CoV-2 GI infection. Additionally, a significant difference in epidemiological history between the infection and non-infection groups was observed in our study. A previous study subdivided the global SARS-CoV-2 population into six well-defined subtypes by focusing on widely shared polymorphisms in non-structural cistrons and structural and accessory genes (23). Indeed, cases from different regions may be infected with different subtypes of the virus, which suggests that patients with COVID-19 in some regions may have higher morbidity of GI infection. However, this phenomenon needs to be confirmed, and its mechanism should be further explored.

We explored the relationship between clinical outcomes of COVID-19 and GI SARS-CoV-2 infection which defined as simultaneously positivity for SARS-CoV-2 RNA in a fecal sample. Several studies have evaluated the relationship between GI manifestations and clinical outcomes of COVID-19 and found that the presence of GI manifestations does not appear to affect mortality of COVID-19 (9–11). GI symptoms are common in viral infections and no specificity, which is not equal to GI infection. In this study, we found that SARS-CoV-2 GI infection led to a longer duration of SARS-CoV-2 RNA presence in respiratory tract samples and longer hospitalization time, which will result in more medical and financial investments. Because of the imbalance in the baseline characteristics of the two groups in this study, subgroup analyses of sex, age, epidemiological history, clinical classification and antiviral treatment were performed and we found that the adverse effect of SARS-CoV-2 GI infection on the duration of SARS-CoV-2 RNA in respiratory tract samples and hospitalization time to be consistent across subgroups. Evaluation of viral load for persistently SARS-CoV-2 GI infection suggested that the initial viral load of GI infection was high and decreased slowly. Nevertheless, detection of SARS-CoV-2 nucleocapsids in gastric glandular epithelial cells in 2 patients with positive feces and negative nasopharyngeal swabs indicated

that SARS-CoV-2 GI infection persisted. The GI system is an appropriate intrusion portal and is a potential virus pool, which may prolong the clinical course and influence the clinical outcomes of COVID-19. Regardless, due to the small sample of this study, larger-sample, multicenter and prospective studies should be undertaken to determine the effect.

The present study has several limitations. First, this was a small-sample, single-center, retrospective observational study, and the included population lacked satisfactory representation, even though it covered all age and ethnicity groups. Second, the discharge standards were based on handbook of COVID-19 prevention and treatment (in Chinese), which contained some subjective items and may interfere with the evaluation of the importance of SARS-CoV-2 GI infection in clinical outcomes of COVID-19. In the present study, discharge approved by fixed medical team, which minimized the influence of personal subjective factors on the results as much as possible. Moreover, it is not completely accurate to determine GI infection by detecting SARS-CoV-2 RNA in a fecal sample using rRT-PCR, and some patients with SARS-CoV-2 GI infection may have a negative rRT-PCR and be excluded from the study; thus, further study with more accurate testing methods and diagnostic criteria should be undertaken.

In conclusion, this study explored the impact of SARS-CoV-2 GI infection on clinical outcomes of COVID-19. About half of patients with COVID-19 have GI infection of SARS-CoV-2, and male patients and overseas cases may be more susceptible to GI infection. GI infection with SARS-CoV-2 had a high viral load and prolonged the duration of SARS-CoV-2 shedding as well as hospitalization in patients with COVID-19, which will cause more medical and financial investments. Therefore, it is necessary to pay more attention to SARS-CoV-2 GI infection and fecal SARS-CoV-2 RNA test should be completed in time.

## DATA AVAILABILITY STATEMENT

The original contributions presented in the study are included in the article/supplementary material, further inquiries can be directed to the corresponding author/s.

## AUTHOR CONTRIBUTIONS

All authors listed have made a substantial, direct and intellectual contribution to the work, and approved it for publication.

## FUNDING

This work was supported by Zhuhai Science and Technology Project ZH22036302200028PWC.

## ACKNOWLEDGMENTS

The authors of the present survey would like to thank all the participants enrolled in this study.

## REFERENCES

- Wu F, Zhao S, Yu B, Chen YM, Wang W, Song ZG, et al. A new coronavirus associated with human respiratory disease in China. *Nature*. (2020) 579:265–9. doi: 10.1038/s41586-020-2008-3
- Lee IC, Huo TI, Huang YH. Gastrointestinal and liver manifestations in patients with COVID-19. *J Chin Med Assoc.* (2020) 83:521–3. doi: 10.1097/JCMA.0000000000000319
- Xiao F, Tang M, Zheng X, Liu Y, Li X, Shan H. Evidence for gastrointestinal infection of SARS-CoV-2. *Gastroenterology*. (2020) 158:1831–3.e3. doi: 10.1053/j.gastro.2020.02.055
- Holshue ML, DeBolt C, Lindquist S, Lofy KH, Wiesman J, Bruce H, et al. First case of 2019 novel coronavirus in the United States. *N Engl J Med.* (2020) 382:929–36. doi: 10.1056/NEJMoa2001191
- Lin L, Jiang X, Zhang Z, Huang S, Zhang Z, Fang Z, et al. Gastrointestinal symptoms of 95 cases with SARS-CoV-2 infection. *Gut.* (2020) 69:997–1001. doi: 10.1136/gutjnl-2020-321013
- Zhang W, Du RH, Li B, Zheng XS, Yang XL, Hu B, et al. Molecular and serological investigation of 2019-nCoV infected patients: implication of multiple shedding routes. *Emerg Microbes Infect.* (2020) 9:386–9. doi: 10.1080/22221751.2020.1729071
- Pan L, Mu M, Yang P, Sun Y, Wang R, Yan J, et al. Clinical characteristics of COVID-19 patients with digestive symptoms in Hubei, China: a descriptive, cross-sectional, multicenter study. *Am J Gastroenterol.* (2020) 115:766–73. doi: 10.14309/ajg.0000000000000620
- Ong J, Young BE, Ong S. COVID-19 in gastroenterology: a clinical perspective. *Gut.* (2020) 69:1144–5. doi: 10.1136/gutjnl-2020-321051
- Jin X, Lian JS, Hu JH, Gao J, Zheng L, Zhang YM, et al. Epidemiological, clinical and virological characteristics of 74 cases of coronavirus-infected disease 2019 (COVID-19) with gastrointestinal symptoms. *Gut.* (2020) 69:1002–9. doi: 10.1136/gutjnl-2020-320926
- Shehab M, Alrashed F, Shuaibi S, Alajmi D, Barkun A. Gastroenterological and hepatic manifestations of patients with COVID-19, prevalence, mortality by country, and intensive care admission rate: systematic review and meta-analysis. *BMJ Open Gastroenterol.* (2021) 8:e000571. doi: 10.1136/bmjgast-2020-000571
- Tariq R, Saha S, Furqan F, Hassett L, Pardi D, Khanna S. Prevalence and mortality of COVID-19 patients with gastrointestinal symptoms: a systematic review and meta-analysis. *Mayo Clin Proc.* (2020) 95:1632–48. doi: 10.1016/j.mayocp.2020.06.003
- Wang W, Xu Y, Gao R, Lu R, Han K, Wu G, et al. Detection of SARS-CoV-2 in different types of clinical specimens. *JAMA.* (2020) 323:1843–4. doi: 10.1001/jama.2020.3786
- Mönkemüller K, Fry L, Rickes S. COVID-19, coronavirus, SARS-CoV-2 and the small bowel. *Rev Esp Enferm Dig.* (2020) 112:383–8. doi: 10.17235/reed.2020.7137/2020
- Liang W, Feng Z, Rao S, Xiao C, Xue X, Lin Z, et al. Diarrhoea may be underestimated: a missing link in 2019 novel coronavirus. *Gut.* (2020) 69:1141–3. doi: 10.1136/gutjnl-2020-320832
- Chen Y, Guo Y, Pan Y, Zhao ZJ. Structure analysis of the receptor binding of 2019-nCoV. *Biochem Biophys Res Commun.* (2020) 525:135–40. doi: 10.1016/j.bbrc.2020.02.071
- Guan WJ, Ni ZY, Hu Y, Liang WH, Ou CQ, He JX, et al. Clinical characteristics of coronavirus disease 2019 in China. *N Engl J Med.* (2020) 382:1708–20. doi: 10.1056/NEJMoa2002032
- Gebhard C, Regitz-Zagrosek V, Neuhauser HK, Morgan R, Klein SL. Impact of sex and gender on COVID-19 outcomes in Europe. *Biol Sex Differ.* (2020) 11:29. doi: 10.1186/s13293-020-00304-9
- Palaiodimos L, Kokkinidis DG, Li W, Karamanis D, Ognibene J, Arora S, et al. Severe obesity, increasing age and male sex are independently associated with worse in-hospital outcomes, and higher in-hospital mortality, in a cohort of patients with COVID-19 in the Bronx, New York. *Metabolism.* (2020) 108:154262. doi: 10.1016/j.metabol.2020.154262
- Meng Y, Wu P, Lu W, Liu K, Ma K, Huang L, et al. Sex-specific clinical characteristics and prognosis of coronavirus disease-19 infection in Wuhan, China: a retrospective study of 168 severe patients. *PLoS Pathog.* (2020) 16:e1008520. doi: 10.1371/journal.ppat.1008520
- Takahashi T, Ellingson MK, Wong P, Israelow B, Lucas C, Klein J, et al. Sex differences in immune responses that underlie COVID-19 disease outcomes. *Nature.* (2020) 588:315–20. doi: 10.1038/s41586-020-2700-3
- Mauvais-Jarvis F, Klein SL, Levin ER. Estradiol, progesterone, immunomodulation, and COVID-19 outcomes. *Endocrinology.* (2020) 161:bqaa127. doi: 10.1210/endo/bqaa127
- Al-Lami RA, Urban RJ, Volpi E, Algburi AMA, Baillargeon J. Sex hormones and novel corona virus infectious disease (COVID-19). *Mayo Clin Proc.* (2020) 95:1710–4. doi: 10.1016/j.mayocp.2020.05.013
- Morais IJ, Polveiro RC, Souza GM, Bortolin DI, Sasaki FT, Lima ATM. The global population of SARS-CoV-2 is composed of six major subtypes. *Sci Rep.* (2020) 10:18289. doi: 10.1038/s41598-020-74050-8

**Conflict of Interest:** The authors declare that the research was conducted in the absence of any commercial or financial relationships that could be construed as a potential conflict of interest.

Copyright © 2021 Xu, Tang, Chen, Cai and Xiao. This is an open-access article distributed under the terms of the Creative Commons Attribution License (CC BY). The use, distribution or reproduction in other forums is permitted, provided the original author(s) and the copyright owner(s) are credited and that the original publication in this journal is cited, in accordance with accepted academic practice. No use, distribution or reproduction is permitted which does not comply with these terms.



# A Coronavirus Outbreak Linked to a Funeral Among a Romani Community in Central Italy

Giancarlo Ripabelli<sup>1\*</sup>, Michela Lucia Sammarco<sup>1</sup>, Fabio Cannizzaro<sup>1</sup>, Carmen Montanaro<sup>2</sup>, Guido Vincenzo Ponzio<sup>2</sup> and Manuela Tamburro<sup>1</sup>

<sup>1</sup> Department of Medicine and Health Sciences "Vincenzo Tiberio", University of Molise, Campobasso, Italy, <sup>2</sup> Department of Prevention, Molise Regional Health Authority, Campobasso, Italy

## OPEN ACCESS

### Edited by:

Marc Jean Struelens,  
Université libre de Bruxelles, Belgium

### Reviewed by:

Chao Zhuo,  
Independent Researcher, Guangzhou,  
China

Saeed Shoar,  
ScientificWriting Corporation,  
United States

### \*Correspondence:

Giancarlo Ripabelli  
ripab@unimol.it

### Specialty section:

This article was submitted to  
Infectious Diseases - Surveillance,  
Prevention and Treatment,  
a section of the journal  
Frontiers in Medicine

**Received:** 14 October 2020

**Accepted:** 12 April 2021

**Published:** 04 June 2021

### Citation:

Ripabelli G, Sammarco ML,  
Cannizzaro F, Montanaro C,  
Ponzio GV and Tamburro M (2021) A  
Coronavirus Outbreak Linked to a  
Funeral Among a Romani Community  
in Central Italy. *Front. Med.* 8:617264.  
doi: 10.3389/fmed.2021.617264

**Background:** The epidemic dynamics of COVID-19 in the Molise region, central Italy, has dramatically changed from the beginning of May 2020, which was when infections were reported amongst Romani people. The aims of this study were to describe the characteristics of an outbreak that occurred in the Romani community and the interventions implemented for control.

**Methods:** A retrospective analysis of outbreak data was performed to describe the SARS-CoV-2 transmission dynamics.

**Results:** A young Romani woman was the first case reported and epidemiological investigation established a possible link with the funeral of a deceased member of this community. In total, 150 close contacts within 34 family groups in two cities were traced, and 109 (72.7%) Romani individuals were found to be infected by COVID-19. The patient's median age was 31 years, 58% were female, and the highest (20.2%) incidence occurred in the 0–9 years age group. A total of 26 (23.8%) patients developed typical SARS-CoV-2 symptoms, 15 (57.8%) were hospitalized, and 21 (22.1%) had comorbidities [most commonly hypertension (28.6%) and/or coronary heart diseases (23.8%)]. The outbreak was effectively controlled through compulsory quarantine and enhanced active surveillance.

**Conclusions:** This is the first study providing insight into COVID-19 transmission dynamics among a Romani population living in Italy. These findings support general conclusions about the role of crowded social gatherings in SARS-CoV-2 spread, the high communicability among close contacts and household settings, and the impact of asymptomatic carriers. These features are of relevance to certain Romani customs where family gatherings are a fundamental pillar of their lives. Although difficulties emerged in interacting with Romani people related to cultural drivers, beliefs, and lifestyle, the outbreak management was effective and should be considered as a valuable model applicable to similar incidents occurring in minority populations.

**Keywords:** COVID-19, epidemiological surveillance, ethnic groups, outbreak, SARS-CoV-2



## INTRODUCTION

As a consequence of a rapid and sudden increase in the number of COVID-19 infections in the Lombardy region (1), the Italian health authorities implemented strict containment measures, including quarantine “red zones” in northern Italy in February 2020 (2). On March 10, 2020, due to the rapid escalation of the epidemic in all Italian regions, lockdown measures were extended to the entire nation (3), which were effective until May 3, 2020 (4).

Molise is a small Italian region of ~300,000 inhabitants, located in central Italy. By May 6, 2020, the regional epidemiological trend of COVID-19 infections with typical symptoms (5) was characterized by a low incidence (99.5 cases/100,000), 7.2% case-fatality rate, 2.9% hospitalization rate, and 22 deaths. The epidemic curve showed a gradual increase of cases except for three major peaks (Table 1), which have been readily responded to the local healthcare infrastructure. On May 7, 2020, 22 new cases were reported by the regional health authority, of which 21 belonged to a Romani community living in Campobasso, the regional capital.

The Romani (also spelled Romany), colloquially known as Roma, are an Indo-Aryan ethnic group who mostly live in Europe, originating from northern India, and they have a traditional nomadic itinerant lifestyle.

A local epidemiological investigation was rapidly undertaken, establishing a possible causal link with the funeral of a member of this community, which took place April 30, 2020. Up to this date, COVID-19 cases had not been reported amongst members of the regional Romani community (Table 1), thus supporting a causal link between the funeral and the outbreak. In Italy, attendance at funerals was prohibited from March 8, 2020 (3), but arrangements were relaxed April 26, and then allowed for a maximum of 15 relatives to attend as long as face coverings were worn and social distancing of at least 1m was observed (6).

This study describes the characteristics of an outbreak among the Romani community in the Molise region, the interventions implemented to interrupt the transmission, as well as public health considerations based on their socio-cultural behaviors. To our knowledge, this is the first report of a COVID-19 outbreak in this ethnic group. The effective management and features of this outbreak may be of use as a general model for outbreaks amongst minority communities.

## METHODS

This study was a retrospective analysis of the confirmed cases attributable to the outbreak; the data described were anonymously encoded and provided by the department of prevention of the regional health service, which carried out the epidemiological investigation, the contact tracing, the monitoring of molecular testing, and follow up of the cases by a telephone interview.

The COVID-19 case definition was derived from the official documents of the Italian Government (DPCM – Decree of the President of the Council of the Ministers), according to the recommendation of the Italian National Health Institute

(ISS), European Centre for Disease Control (ECDC), Centers for Disease Control and Prevention (CDC), and the World Health Organization (WHO), and comprised the detection of the SARS-CoV-2 by reverse transcription (RT) PCR in a nasopharyngeal swab (7). The outbreak was defined as occurring in the Romani population, or linked with this ethnic group, in the Molise region from May 7 to May 26, 2020; the definition included both primary cases (until 14 days from the initial case detected), as well as secondary cases likely due to the household transmission.

No interventions were performed amongst the individuals included in the present study, above that for the public health controls applied throughout the Molise region by local authorities, and approval by an Ethics Committee was not required. A signed consent form was not obtained because no personal/specific and/or medical information about any identifiable living individuals was reported. For children and adolescents, the local health service acquired information from their parents.

All the individuals identified as cases or close contacts were registered, traced, and followed up by telephone interview by the local health authority according to the guidelines for SARS-CoV-2 contact tracing provided by the Italian Minister of Health. Information was collected on age, gender, general health status regarding previous or concurrent comorbidities, and, where relevant, date of onset of symptoms at diagnosis, severity of symptoms, and outcome. Data were analyzed by IBM Statistical Package for Social Science (SPSS) software version 26.0. Descriptive statistics were used, including means and standard deviation, median, and range for quantitative variables, while counts and percentages were calculated for the qualitative characteristics.

## RESULTS

### Outbreak Description

On the April 30, 2020, ~30 Romani people attended a crowded social gathering devoted to a deceased male belonging to this community who had severe comorbidities: the COVID-19 status of the deceased was unknown, and no pre- or post-mortem swabbing for the virus was performed. A crowded social gathering was likely to have occurred in the house of the deceased in the days preceding death, despite visits were forbidden in the lockdown period. The funeral participation was allowed up to a maximum of 15 relatives observing personal individual protection measures, while a crowded social gathering was reported at the religious ceremony that took place at the cemetery in Campobasso city.

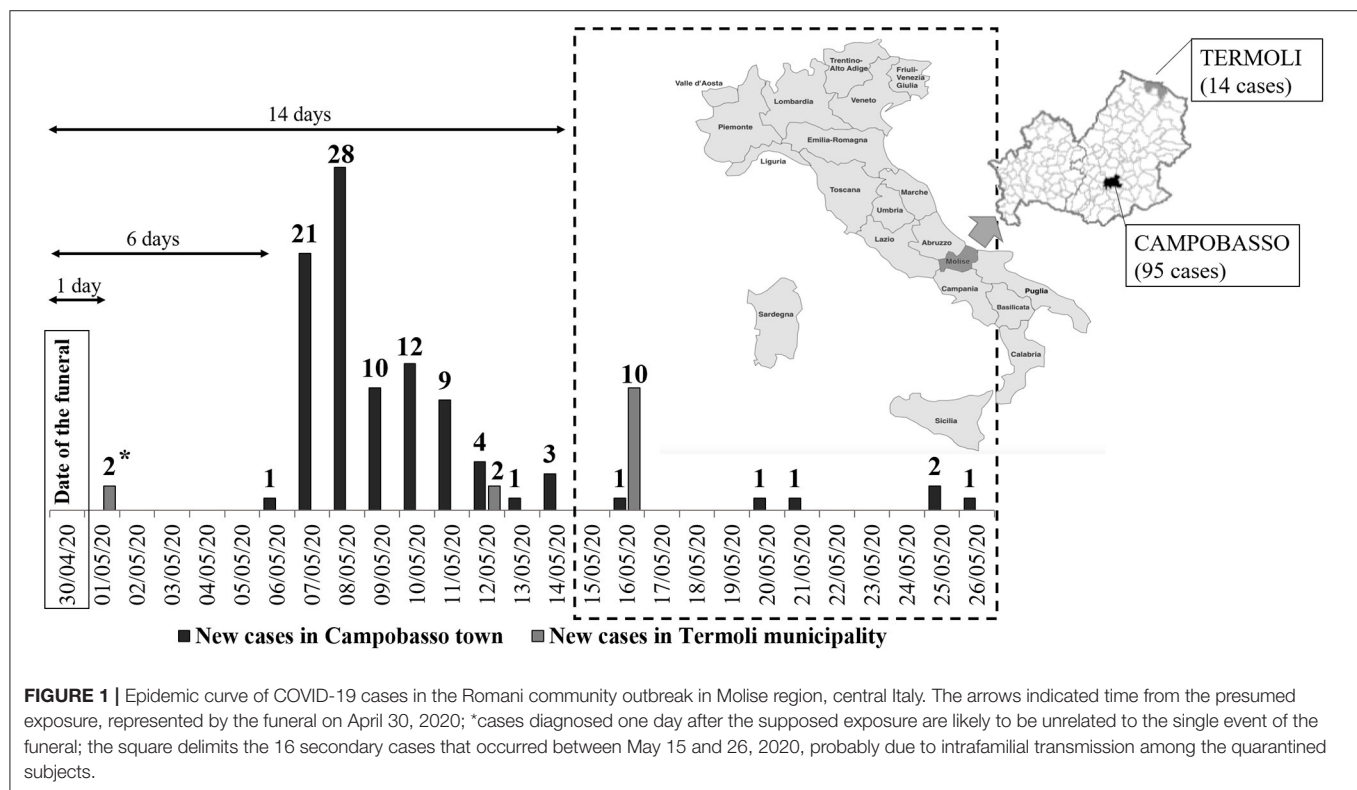
After the funeral, a sudden rise in the incidence of SARS-CoV-2 infections among the local Romani population was detected, and swab testing was soon performed on the members of the local Romani community as well as among people living in the same building as the deceased individual.

A total of 109 COVID-19 cases occurred in this outbreak, representing 24% of 445 total cases detected in Molise region between March 3 and July 8, 2020. All except 1 of the 109 cases belonged to the Romani community, who were residents in either

**TABLE 1** | Results of local COVID-19 surveillance from March to May 2020 in Molise, Italy.

| Date                                     | COVID-19 cases | Swabs tested  | Clusters identified in the period                      | Cases (% on the total cases) identified within the Romani community | Regional incidence per 100,000 inhabitants |
|--|----------------|---------------|--|---|--|
| 03/03/20                                 | 3              | 13            | None   | 0 (0)   | 0.99                                       |
| 04/03/20-30/04/20* (27 days)             | 295            | 6,433         | Private hospital<br>Nursing home A<br>Nursing home B # | 0 (0)   | 96.66                                      |
| 01/05/20-05/05/20 <sup>§</sup> (5 days)  | 3              | 1,082         | None   | 2 (66.7)  | 0.99                                       |
| 06/05/20-27/05/20 <sup>§</sup> (22 days) | 133            | 6,101         | Romani community                                       | 107 (80.5)  | 44.00                                      |
| <b>Total</b>                             | <b>434</b>     | <b>13,629</b> |  | <b>109 (25.1)</b>   | <b>143.58</b>                              |

\*The lockdown period started on March 9, 2020 in Italy until May 3; <sup>§</sup>The reopening phase commenced from May 4, although inter-regional travel was not yet allowed before June 4; #According to Decree of the President of the Council of Ministers on March 8, 2020, the access for relatives and visitors in hospitals and nursing homes or long-term facilities was prohibited since March 9, and only limited to the cases indicated by the Directive of the healthcare structure, strictly required to adopt all the measures needed to prevent any possible transmission and spread of infection; in bold, total number of COVID-19 cases, total swabs tested, total number of cases (%) identified among Romani people, and incidence per 100,000 in Molise region until May 27, 2020.



the main town of Campobasso (95 cases) or in Termoli (14 cases) (Figure 1), a municipality on the coast.

The Romani community living in the Campobasso and Termoli towns consists of ~300 people; therefore, one-third of all the community was involved in the outbreak. In total, 26 (23.8%) individuals developed typical COVID-19 symptoms (5), 15 (57.8%) were hospitalized in the Infectious Diseases ward at the COVID-19 hospital in Campobasso town, and none were admitted to the intensive care. The remaining 83 (76.1%) individuals were asymptomatic. None of the infected patients died.

The first case detected was a Romani person aged between 20–29 years living in Campobasso and who likely attended the burial on the April 30. On the May 5, the patient was admitted to the COVID-19 hospital of Campobasso suffering from symptoms of dyspnea, chest tightness, headache, ageusia, anosmia, and fever. SARS-CoV-2 was detected in a nasopharyngeal swab on May 6, 2020. The epidemic curve included 88 additional COVID-19 cases who were residents in Campobasso town, and were diagnosed within 8 days (up to May 14) from the first case (Figure 1). Cases were also detected in the Romani community in Termoli town with the virus detected in two nasopharyngeal

swabs on May 1, which was 1 day after the funeral. In Termoli, 2 and 10 cases were further diagnosed on May 12 and 16 (**Figure 1**), respectively. There was no information available about familial relationship with the deceased, or whether they had visited the deceased patient in the days preceding death or had attended the funeral. Between May 14 and 26, six cases were further diagnosed in Campobasso.

## Epidemiological Investigation of the Outbreak and Contact Tracing

Following the identification of the first case, contact tracing activities were rapidly implemented by the department of prevention of the regional health authority: 132 and 18 close contacts were identified in Campobasso and Termoli, respectively, among those within the wider family of the first case or those who lived in the same building as the deceased or had likely attended the funeral. Between May 6 and 26, SARS-CoV-2 was detected in 94 (71.2%) contacts in Campobasso and 12 (66.7%) in Termoli. After the first case on May 6, 75% ( $n = 71$ ) of the Romani individuals in Campobasso were identified as being infected with COVID-19 between May 7 and 10, while cases in Termoli mostly occurred between the May 12 and 16. A mandatory quarantine of 14 days was imposed for all traced contacts, including individuals in whom SARS-CoV-2 was not detected.

Analysis of the case contacts allowed identification of 32 Romani familial groups in Campobasso and 2 in Termoli, where one or more family members were identified as being infected with SARS-CoV-2 in 28 (87.5%) family groups in Campobasso town, while three and nine subjects were infected in the 2 groups in Termoli. Within these groups, on average, 82.0% of the family members became infected, with a range varying between 14.3 and 100%. Furthermore, six infected subjects (two family groups) lived in the same building as the deceased in Campobasso, five of which were of the Romani community and one was non-Romani.

## Demographic Characteristics and Underlining Disorders of COVID-19 Patients Within the Outbreak

All except 1 of the 109 cases in the outbreak belonged to the Romani community. The non-Romani adult patient lived in the same building as the deceased individual, but no information on participation in the funeral was available. In total, 57.8% ( $n = 63$ ) of the infected patients were female, and this distribution was observed both for the Campobasso and the Termoli cluster (**Table 2**). Furthermore, the highest incidence ( $n = 22$ , 20.2%) of COVID-19 cases occurred in the 0-to-9 years age group (**Table 3**). Comorbidities or other underlining conditions were self-reported by 19.3% of the COVID 19 cases in Campobasso: the most frequently reported disorder was hypertension in 28.6% (median age: 48 years) of individuals, followed by 23.8% coronary heart diseases (median age: 69 years; **Table 2**). Symptomatic individuals were male ( $n = 17/26$ , 65.4%) aged 40–49 years old (median age: 44 years; range: 1–88 years). Of these, 15 (88.2%) aged 50–59 years old were hospitalized. As of July 8, 2020,

there were six (5.5%) subjects still infected within the Romani community, and all were asymptomatic.

## Intervention Measures

The regional health authority required the reinforcement of local surveillance around the Romani community's residences in agreement with the police, to assure full compliance for control. Furthermore, on May 9, 2020, both the Mayors of Campobasso and Termoli issued ordinances to enhance the control activities to specific areas to allow the enforcement of isolation at home. During the period between May 6 and May 26 (dates from the first case being detected to the last case diagnosed within the regional Romani community), swab testing significantly increased to a total of 13,452 with a daily average of  $282.1 \pm 156.3$ . Soon after the rapid increase in cases, quarantine was established for 14 days after close contact with cases and was maintained until a virological negative result was obtained. Additionally, for outbreak management, timely effective risk communication was a specific task of the department of prevention of the regional health authority with a "culturally adapted" and context-specific strategy focusing on restrictions to minimize crowded social gatherings (which occur frequently in this particular ethnic group), as improving stay-at-home policies and hygiene measures in the household setting. The risk communication was carried out based on explanation and reiteration by telephone to both the householders and heads of the Romani community about the rules to be respected. Furthermore, the local authorities talked to them constantly about these issues and guaranteed all the needs to support them (i.e., foods and medicine). Between March 4 (the day after the first three SARS-CoV-2 cases detected in our region) and April 30, 2020 (date of the funeral of Romani subject), no SARS-CoV-2 cases were identified among the Romani population out of a total of 6,433 swab tests performed at the regional level (**Table 1**) including those performed on residents/workers in nursing homes or hospitals and in the general population. During this period, SARS-CoV-2 clusters occurred in nursing homes, hospitals, or long-term facilities, where, as of March 9, according to the Decree of the President of the Council of the Ministers, the access for relatives and visitors was prohibited and limited only to the cases indicated by the Directive of the healthcare structure, who was strictly required to adopt all the measures needed to prevent any possible transmission and spread of infection.

## DISCUSSION

The Romani community has its own lifestyle and rules that may not coincide with those of non-Romani citizens (9). Their society has a horizontal organization, with a central role of the family; contacts are extremely frequent between members, and great support is offered at the end of the life (10) since death is considered an important event reinforcing family and community bonds (11). Empathy for someone who is dying is one of the strongest drivers of their culture, as described for a female Romani leader in Catalonia who died accompanied by more than 200 people (11).

**TABLE 2 |** Characteristics of COVID-19 cases within the Romani outbreak.

|  | Overall outbreak<br>109 cases | Campobasso cluster<br>95 cases | Termoli cluster<br>14 cases |
|--|-------------------------------|--------------------------------|-----------------------------|
| <b>Ethnic group</b>                            |                               |                                |                             |
| Romani   | 108 (99.1%)                   | 94 (98.9%)                     | 14 (100%)                   |
| Non-Romani                                     | 1 (0.9%)                      | 1 (1.1%)                       | –                           |
| <b>Gender</b>                                  |                               |                                |                             |
| Female   | 63 (57.8%)                    | 54 (56.8%)                     | 9 (64.3%)                   |
| Male   | 46 (42.2%)                    | 41 (43.2%)                     | 5 (35.7%)                   |
| <b>Age</b>                                     |                               |                                |                             |
| Mean $\pm$ standard deviation                  | 32.1 $\pm$ 21.6 years         | 32.8 $\pm$ 21.5 years          | 30.3 $\pm$ 23.1 years       |
| Median   | 31 years                      | 33 years                       | 25.5 years                  |
| Range  | 1–88 years                    | 1–88 years                     | 1–83 years                  |
| <b>Comorbidities or underlining conditions</b> |                               |                                |                             |
| Hypertension                                   | 6 (5.5%)                      | 6 (6.3%)                       | –                           |
| Coronary heart diseases                        | 5 (4.6%)                      | 5 (5.3%)                       | –                           |
| Breast cancer                                  | 1 (0.9%)                      | 1 (1.1%)                       | –                           |
| Frail elderly with multiple pathologies        | 1 (0.9%)                      | 1 (1.1%)                       | –                           |
| Hepatitis B                                    | 1 (0.9%)                      | 1 (1.1%)                       | –                           |
| Microcytic anemia                              | 1 (0.9%)                      | 1 (1.1%)                       | –                           |
| Hiatal hernia                                  | 1 (0.9%)                      | 1 (1.1%)                       | –                           |
| Aphonia/dysphonia                              | 1 (0.9%)                      | 1 (1.1%)                       | –                           |
| Psoriasis                                      | 1 (0.9%)                      | 1 (1.1%)                       | –                           |
| Celiac disease                                 | 1 (0.9%)                      | 1 (1.1%)                       | –                           |
| Neurofibromatosis                              | 1 (0.9%)                      | 1 (1.1%)                       | –                           |
| Chronic colitis                                | 1 (0.9%)                      | 1 (1.1%)                       | –                           |

**TABLE 3 |** Age-based frequency of COVID-19 cases before, during, and after the Romani outbreak compared to the whole regional and national data.

| Age group | Cases ( <i>n</i> = 296) in Molise<br>before Romani outbreak<br>(Period 3 <sup>rd</sup> March–28 <sup>th</sup><br>April) (28) | Cases ( <i>n</i> = 109) within<br>the Romani outbreak<br>(Period 6 <sup>th</sup> –26 <sup>th</sup> May) | Cases ( <i>n</i> = 422) in Molise<br>after Romani outbreak<br>(Period 3 <sup>rd</sup> March–20 <sup>th</sup><br>May) (25) | Cases ( <i>n</i> = 199,470) in<br>Italy (Period 20 <sup>th</sup><br>February–28 <sup>th</sup> April) (28) |
|-----------|--|---|---|---|
| 0–9 years | 1.4%   | 20.2%   | 5.5% $\uparrow$   | 0.7%  |
| 10–19     | 4.7%   | 9.2%  | 6.2% $\uparrow$   | 1.3%  |
| 20–29     | 4.4%   | 15.6%   | 8.8% $\uparrow$   | 5.2%  |
| 30–39     | 10.5%  | 19.2%   | 12.6% $\uparrow$  | 7.5%  |
| 40–49     | 11.8%  | 13.8%   | 12.3% $\uparrow$  | 12.9%   |
| 50–59     | 25.0%  | 9.2%  | 21.6% $\downarrow$  | 18.0%   |
| 60–69     | 17.9%  | 7.3%  | 14.0% $\downarrow$  | 14.0%   |
| 70–79     | 8.8%   | 2.7%  | 6.9% $\downarrow$   | 15.1%   |
| 80–89     | 10.1%  | 2.7%  | 8.3% $\downarrow$   | 17.7%   |
| $\geq 90$ | 5.4%   | 0.0%  | 4.0% $\downarrow$   | 7.6%  |

The arrows ( $\uparrow$  and  $\downarrow$ ) indicated the increase or decrease of the frequency in the stratified age groups as consequences of the Romani outbreak.

The outbreak described in this study received nationwide attention and generated great concerns. Further cases linked to this outbreak occurred in the Romani communities in some neighboring regions, as individuals came to Molise to pay tribute to the prominent person who passed away. Before April 30, no cases within the Romani community were reported by the Molise health service. The outbreak caused prejudice toward Romani people although they have a good level of integration in the local

society, mainly because the stringent national rules on lockdown were still in force but were disregarded at the time of the funeral.

Development of a clear case definition is critical conducting an effective investigation of an outbreak that should be defined as more cases of the disease in time or place than expected, and when two or more cases have the same laboratory diagnosis of the etiologic agent. Hence, criteria for person, place, time, and clinical features should be included in a case definition



and should be specific. In the outbreak described here, the cases were identified as resulting from the contact tracing activities carried out by the department of prevention of the regional health service, representing an effective public health measure for the control of COVID-19, enabling prompt identification and management of the contacts of cases, and identifying secondary cases after transmission from the primary cases. Hence, considering contact tracing steps, persons who may have been exposed to SARS-CoV-2 as a result of being in contact with an infected person were identified; these contacts were traced, and information about suitable infection control measures, symptom monitoring, and other precautionary measures was provided.

Contact tracing remains of fundamental importance to delimitate clusters of infection, although the interactions with Romani people were difficult due to their social and behavioral rules.

The epidemiological investigation allowed identifying the outbreak, which was likely to have been linked to the participation and crowded social gathering of people together at the funeral or attending the body of the deceased before leaving home to be buried. However, the outbreak could not only be associated with participation in these ceremonies as well as to the presence of an initial infection “super spreader,” because it should be also considered the likelihood that many individuals visited the moribund in the days preceding death, with the funeral possibly amplifying a pre-existing viral circulation within the community.

Indeed, if the exposure was the funeral on April 30, this should exclude the two cases in Termoli town who tested positive on May 1 (**Figure 1**), which were counted as related to the outbreak by the local health authority since they were within the Romani community. These subjects denied having attended the funeral, and no information was available about familial relationship with the deceased, or whether they had gone to the home of the deceased in the days preceding death. We hypothesize that these two cases could reflect the virus circulating within the Romani community prior to the funeral but could also represent “patient zero” as well as an alternative source of disease transmission for the cases diagnosed on May 12 in the Termoli cluster (**Figure 1**). As reported by the regional health authority, the first case was diagnosed on May 6, a total of 5 days after the two cases reported in Termoli and 6 days after the funeral, in line with the estimated median incubation period of 5–6 days (12–14). Following the major peak on May 8 (**Figure 1**), 16 cases were diagnosed after May 14, which are likely to represent intrafamilial transmission amongst quarantined individuals in Campobasso: the secondary transmission rate was estimated as of 16.8%.

For an in-depth investigation of the outbreak, it is important to report the geographic distribution of the identified cases. Based on the available information, the regional Romani community resides in Campobasso (the capital city), as well as in the towns of Isernia and Termoli. Anyway, the outbreak described was composed only of two clusters of infections, diagnosed in Campobasso and Termoli.

This outbreak demonstrated the high communicability of COVID-19, which was evidenced by the secondary cases

identified among household contacts and is in agreement with the available reports for COVID-19 (12, 15, 16). It has been estimated that the basic reproduction number ( $R_0$ ) for COVID-19 ranged between 2 and 3.5 (17). Certainly, the transmission rate can be much higher in closed and crowded social gatherings (18), such as funerals that have been linked to the spread of other diseases (19). Furthermore, COVID-19 community transmission decreased over time, while household transmission increased under stay-at-home policies, leading to a secondary attack rate of 16.3% in the household context (20).

The outbreak described here confirms that household transmission is of high concern, underlining the need to implement appropriate management strategies. To control the outbreak, local authorities suggested transferring Romani people to locations different from their houses but disregarded this option. In the COVID-19 transmission, isolation at home is significant, especially for this population where overcrowding is common, and this is a well-recognized risk factor associated with various health problems, including respiratory infections (21).

In comparison to available Italian national data where 54.2% of COVID-19 cases were identified amongst females (22), this outbreak showed a higher incidence of 57.8% among females, which may reflect differences in social and behavioral habits amongst the Romani community (23). Globally, the ongoing COVID-19 pandemic is affecting the whole population, although different susceptibilities have been reported (24), considering males, old age, and those with comorbidities (mainly hypertension, diabetes, and cardiovascular disease) as the most important risk factors for severe symptoms and outcome (13, 25).

An additional key epidemiological feature of the Romani outbreak concerned the younger age of infected individuals (median age 31 years) compared to the total regional (median age 52 years) and national cases (median age 62 years) (26). This finding may be explained by the lower age of Romani people compared to the general population (21); the poor perception of younger people of COVID-19 risks as compared to older people (27), and because swab testing was extended to detect cases in this particular ethnic group, which is generally younger than the regional population, consisting of 25% of individuals aged  $\geq 65$  years. Estimates of the relative COVID-19 illness ratio revealed age-related increases in Spain and Italy, while higher ratios among middle or younger age groups were reported in China and Korea (28), probably due to more extensive swab testing.

The age-related frequency of COVID-19 cases in the Molise region underwent marked changes due to the outbreak described here, especially for the 0-to-9-year age group, accounting for 1.4% and 5.5% of cases before and after the outbreak (8, 26), respectively, being 20.2% in the infected Romani population. Hence, children were the most frequently infected group, in contrast to national data where only 0.9% cases occurred in the 0-to-9-year age group (**Table 3**).

In Italy, 34.3% of COVID-19 cases occurred in subjects with at least one co-existing/underlining pathologies, including cardiovascular, respiratory, metabolic, cancer, or other chronic diseases (29). Based on the data available, 19% of Romani cases living in Campobasso town declared pre-existing pathologies, and heart diseases were common together with other chronic

diseases, according to previous reports on this population group (30). However, the health status of this group remains largely unknown as does the distribution of disease-associated predisposing factors (31). The cases that occurred in Termoli did not report any underlining condition, and this finding is in agreement with previous evidence indicating that Romani people self-report better individual health status than the rest of the population due to the lower age, different health perceptions, and difficulties in accessing and receiving proper healthcare (32).

In conclusion, about a quarter of COVID-19 cases registered until May 2020 in the Molise region of Italy were related to the outbreak described here, which highlights the major role of crowded social gatherings in the spread of COVID-19 and the importance of transmission through asymptomatic individuals, including children. This is in line with data obtained through the national seroprevalence survey, which indicated that SARS-CoV-2 IgG positive individuals six times more than the total number of officially diagnosed cases through viral RNA detection (33).

The Romani population represents the largest ethnic minority group in Europe for which an increased vulnerability to COVID-19 pandemic faces a combination of health risks, leading the Council of Europe to issue a statement on the need for governments to ensure equal protection and care for this community (34). Difficulties related to socio-cultural barriers were encountered when trying to make contact with and acquire information from the Romani people involved in this outbreak. In such situations, facilitators and interventions to increase active participation in public health strategies should be identified and tailored for this population, as well as for “hard to reach” minority groups (35). Taking into account these difficulties, the response to the outbreak was effective in limiting further transmission and containing the cases. Hence, outbreak management can be considered as a general model for similar events amongst specific ethnic groups, particularly where there are health inequalities.

This study has some limitations, including the total number of Romani attending the funeral that could not be accurately ascertained, which might have over-estimated transmission level linked to this specific event. In addition, although the surveillance and contact tracing were rigorously implemented, some cases that occurred outside the Romani community could have been missed. Nonetheless, the study has noteworthy strengths. To our knowledge, no other study reported COVID-19 infections amongst ethnic Romani groups either nationally or internationally. Hence, this is the first report that provides insights into COVID-19 epidemiology, transmission dynamics, and control measures of crowded intrafamilial gatherings while continuing to deal with the pandemic. This study has great relevance to epidemiological findings and surveillance features: first, the younger age of the infected people involved in the outbreak as compared to the regional and national cases reported, and considering lifestyles, traditions, and viewpoint on health status, which significantly differ in Romani communities compared to the general population. Moreover, the peculiarity of this study relies on a well-defined ethnic population, with their own behavior and familial practices, providing an example for an adequate response, which can differ from normal management

procedures due to their cultural and social characteristics.

The outbreak had important implications also at the regional level even in the non-Romani population, because it occurred in the reopening phase following the national lockdown, generating serious concerns among the general population. To stop the propagation of the outbreak, it was necessary to reinforce the surveillance, which had an impact on the whole regional territory. Similarly, the enhanced communication about prevention measures to contain the transmission of the outbreak among Romani people, mainly avoiding crowded social gatherings, especially between families, had a huge influence on the general population as well.

This outbreak led to particular public health considerations, which could have been further investigated by phylogenetic analysis of the viral strains involved in this outbreak for comparison with those circulating locally within Molise region, as well as nationally and internationally.

## DATA AVAILABILITY STATEMENT

The datasets presented in this article are not readily available because, all data are already described in the study. Requests to access the datasets should be directed to [ripab@unimol.it](mailto:ripab@unimol.it).

## ETHICS STATEMENT

Ethical review and approval for the study on human participants was not required in accordance with the local legislation and institutional requirements. A signed consent form was not obtained because no personal/specific and/or medical information about any identifiable living individuals was reported, and the study was based on a retrospective analysis of outbreak data. For children and adolescents, the local health service acquired information from their parents.

## AUTHOR CONTRIBUTIONS

GR designed the study and contributed to data interpretation and critically editing the report. MS and FC performed the literature search, data organization, and result interpretation. CM and GVP contributed to data collection and encoding. MT led the principal analysis of the available data and wrote the draft and edited the manuscript. All authors read and approved the final report.

## ACKNOWLEDGMENTS

The authors acknowledge Dr. Donato Toma, President of the Regional Council of the Molise region for the endorsement of the study; Dr. Felice Di Donato and Dr. Nicandro Buccieri of the technical-scientific committee for COVID-19 in the Molise region for outbreak data discussion, which improved the manuscript; Dr. Jim McLauchlin, Public Health England, London, Colindale, UK, and Dr. Gianni Rezza, Italian National Institute of Health, Roma, Italy, for the helpful comments provided to this work; and Dr. Francesco Papalia for the support provided to data encoding and organization.

## REFERENCES

- Grasselli G, Pesenti, A, Cecconi M. Critical care utilization for the COVID-19 outbreak in Lombardy, Italy: early experience and forecast during an emergency response. *JAMA*. (2020) 323:1545–1546. doi: 10.1001/jama.2020.4031
- Bandirali M, Sconfienza LM, Serra R, Brembilla R, Albano D, Pregliasco FE, et al. Chest radiograph findings in asymptomatic and minimally symptomatic quarantined patients in Codogno, Italy during COVID-19 pandemic. *Radiology*. (2020) 295:E7. doi: 10.1148/radiol.2020201102
- Decreto del Presidente del Consiglio dei Ministri 8 marzo 2020. *Ulteriori Disposizioni Attuative del Decreto-legge 23 Febbraio 2020, n. 6, Recante Misure Urgenti in Materia di Contenimento e Gestione Dell'emergenza Epidemiologica da COVID-19*. (20A01522) (*GU Serie Generale n.59 del 08-03-2020*). (2020). Available online at: <https://www.gazzettaufficiale.it/eli/id/2020/03/08/20A01522/sg> (accessed June 30, 2020).
- Italian Government. Presidency of the Council of Ministers. *Provvedimenti Attualmente Vigenti, Approvati dal Governo in Seguito All'emergenza Sanitaria Internazionale*. Coronavirus, le misure adottate dal Governo (2020). Available online at: <http://www.governo.it/it/coronavirus-misure-del-governo> (accessed June 30, 2020).
- Borges do Nascimento IJ, Cacic N, Abdulazeem HM, Abdulazeem HM, Henderson C, Jayarajah U, et al. Novel Coronavirus infection (COVID-19) in humans: a scoping review and meta-analysis. *J Clin Med*. (2020) 9:941. doi: 10.2139/ssrn.3550028
- Decreto del Presidente del Consiglio dei Ministri 26 aprile 2020. *Ulteriori Disposizioni Attuative del Decreto-legge 23 Febbraio 2020, n. 6, Recante Misure Urgenti in Materia di Contenimento e Gestione Dell'emergenza Epidemiologica da COVID-19, Applicabili Sull'intero Territorio Nazionale (20A02352) (GU Serie Generale n. 108 del 27-04-2020)*. (2020). Available online at: <https://www.gazzettaufficiale.it/eli/id/2020/04/27/20A02352/sg> (accessed June 30, 2020).
- Italian National Health Ministry. *Circolare Ministero della Salute. Pandemia di COVID-19 - Aggiornamento delle Indicazioni sui test Diagnostici e sui Criteri da Adottare nella Determinazione Delle Priorità*. Aggiornamento delle indicazioni relative alla diagnosi di laboratorio (2020). Available online at: <http://www.salute.gov.it/portale/malattieInfettive/dettaglioNotizieMalattieInfettive.jsp?lingua=italiano&id=4397> (accessed July 5, 2020).
- Integrated surveillance of COVID-19 in Italy. *COVID-19 Epidemic. National Update April 30, 2020. Appendix With Regional Detail*. (2020). Available online at: [https://www.epicentro.iss.it/coronavirus/bollettino/Bollettino-sorveglianza-integrata-COVID-19\\_28-aprile-2020\\_appendix.pdf](https://www.epicentro.iss.it/coronavirus/bollettino/Bollettino-sorveglianza-integrata-COVID-19_28-aprile-2020_appendix.pdf) (accessed July 8, 2020).
- van Hout MC, Staniewicz T. Roma and Irish traveler housing and health: a public concern. *Crit Public Health*. (2012) 22:193–207. doi: 10.1080/09581596.2011.594872
- Roman G, Gramma R, Enache A, Pârnu A, Ioan B, Moisa SM, et al. Dying and death in some Roma communities: ethical challenges. *J Immigr Minor Health*. (2014) 16:290–300. doi: 10.1007/s10903-012-9738-8
- Garcia-Espinel T, Aso L, Redondo-Sama G, Flecha A. Roma never die alone. *Qual Health Res*. (2017) 27:2189–200. doi: 10.1177/1049732317729138
- Bi Q, Wu Y, Mei S, Ye C, Zou X, Zhang Z, et al. Epidemiology and transmission of COVID-19 in 391 cases and 1286 of their close contacts in Shenzhen, China: a retrospective cohort study. *Lancet Infect Dis*. (2020) 20:911–9. doi: 10.1016/S1473-3099(20)30287-5
- Huang C, Wang Y, Li X, Ren L, Zhao J, Hu Y, et al. Clinical features of patients infected with 2019 novel coronavirus in Wuhan, China. *Lancet*. (2020) 395:497–506. doi: 10.1016/S0140-6736(20)30183-5
- Lauer SA, Grantz KH, Bi Q, Jones FK, Zheng Q, Meredith HR, et al. The incubation period of Coronavirus disease 2019 (COVID-19) from publicly reported confirmed cases: estimation and application. *Ann Intern Med*. (2020) 172:577–82. doi: 10.7326/M20-0504
- Jiang X-L, Zhang X-L, Zhao X-N, Li C-B, Lei J, Kou Z-Q, et al. Transmission potential of asymptomatic and paucisymptomatic SARS-CoV-2 infections: a three-family cluster study in China. *J Infect Dis*. (2020) 221:1948–1952. doi: 10.1093/infdis/jiaa206
- Braubach M, Jacobs DE, Ormandy D. *World Health Organization. Environmental burden of disease associated with inadequate housing. A method guide to the quantification of health effects of selected housing risks in the WHO European Region. Summary report*. WHO Regional Office for Europe? (2011). Available online at: <https://apps.who.int/iris/handle/10665/108587> (accessed July 5, 2020).
- Li Q, Guan X, Wu P, Wang X, Zhou L, Tong Y, et al. Early transmission dynamics in Wuhan, China, of novel coronavirus-Infected pneumonia. *N Engl J Med*. (2020) 382:1199–207. doi: 10.1056/NEJMoa2001316
- Yusef D, Hayajneh W, Awad S, Momany S, Khassawneh B, Samrah S, et al. Large outbreak of Coronavirus disease among wedding attendees, Jordan. *Emerg Infect Dis*. (2020) 20:26. doi: 10.3201/eid2609.201469
- Curran KG, Gibson JJ, Marke D, Caulker V, Bomeh J, Redd JT, et al. Cluster of Ebola virus disease linked to a single funeral - Moyamba District, Sierra Leone, 2014. *MMWR Morb Mortal Wkly Rep*. (2016) 65:202–205. doi: 10.15585/mmwr.mm6508a2
- Li W, Zhang B, Lu J, Chang Z, Pen C g, Liu X, et al. The characteristics of household transmission of COVID-19. *Clin Infect Dis*. (2020) 71:1943–46. doi: 10.1093/cid/ciaa450
- Molinuevo D, Koomen M, Fóti K. *Living Conditions of the Roma: Substandard Housing and Health*. European foundation for the improvement of living and working conditions. Eurofound (2012). Available online at: <https://www.eurofound.europa.eu/publications/report/2012/quality-of-life-social-policies/living-conditions-of-the-roma-substandard-housing-and-health> (accessed July 5, 2020).
- Integrated surveillance of COVID-19 in Italy. *COVID-19 Epidemic. National Update June 23, 2020. Appendix with Regional Detail*. (2020). Available online at: [https://www.epicentro.iss.it/coronavirus/bollettino/Bollettino-sorveglianza-integrata-COVID-19\\_23-giugno-2020.pdf](https://www.epicentro.iss.it/coronavirus/bollettino/Bollettino-sorveglianza-integrata-COVID-19_23-giugno-2020.pdf) (accessed July 6, 2020).
- Gil-Lacruz M, Gil-Lacruz AI. Health perception and health care access: sex differences in behaviors and attitudes. *Am J Econ Sociol*. (2010) 69:783–801. doi: 10.1111/j.1536-7150.2010.00723.x
- Scully EP, Haverfield J, Ursin RL, Tannenbaum C, Klein SL. Considering how biological sex impacts immune responses and COVID-19 outcomes. *Nat Rev Immunol*. (2020) 20:442–7. doi: 10.1038/s41577-020-0348-8
- Wu C, Chen X, Cai Y, Xia J, Zhou X, Xu S, et al. Risk factors associated with acute respiratory distress syndrome and death in patients with coronavirus disease 2019 considering how biological sex impacts immune responses and COVID-19 outcomes pneumonia in Wuhan, China. *JAMA Intern Med*. (2020) 180:1–11. doi: 10.1001/jamainternmed.2020.0994
- Integrated surveillance of COVID-19 in Italy. *COVID-19 Epidemic. National Update May 20, 2020. Appendix With Regional Detail*. (2020). Available online at: [https://www.epicentro.iss.it/coronavirus/bollettino/Bollettino-sorveglianza-integrata-COVID-19\\_20-maggio-2020.pdf](https://www.epicentro.iss.it/coronavirus/bollettino/Bollettino-sorveglianza-integrata-COVID-19_20-maggio-2020.pdf) (accessed July 7, 2020).
- Kang SJ, Jung SI. Age related morbidity and mortality among patients with COVID-19. *Infect Chemother*. (2020) 52:154–64. doi: 10.3947/ic.2020.52.2.154
- Natale A, Ghio D, Tarchi D, Goujon A, Conte A. *COVID-19 Cases and Case Fatality Rate by Age. Knowledge for Policy*. (2020). Available online at: [https://ec.europa.eu/knowledge4policy/publication/covid-19-cases-case-fatality-rate-age\\_en](https://ec.europa.eu/knowledge4policy/publication/covid-19-cases-case-fatality-rate-age_en) (accessed July 8, 2020).
- Goumenou M, Sarigiannis D, Tsatsakis A, Anesti O, Docea AO, Petrakis D, et al. COVID-19 in Northern Italy: an integrative overview of factors possibly influencing the sharp increase of the outbreak. *Mol Med Rep*. (2020) 22:20–32. doi: 10.3892/mmr.2020.11079
- Vincze F, Földvári A, Pálkás A, Sipos V, Janka EA, Ádány R, et al. Prevalence of chronic diseases and activity-limiting disability among Roma and Non-Roma people: a cross-sectional, census-based investigation. *Int J Environ Res Public Health*. (2019) 16:3620. doi: 10.3390/ijerph16193620
- Papon C, Delarche N, Le Borgne C, Bauduer F. Assessment of cardiovascular risk factors in a Roma community from Southwestern France. *Am J Hum Biol*. (2017) 29:e22895. doi: 10.1002/ajhb.22895
- Masseria C, Mladovsky P, Hernández-Quevedo C. The socio-economic determinants of the health status of Roma in comparison with non-Roma in Bulgaria, Hungary and Romania. *Eur J Public Health*. (2010) 20:549–554. doi: 10.1093/eurpub/ckq102

33. Istituto Nazionale di Statistica. *Primi Risultati Dell'indagine di Sieroprevalenza sul SARS-Cov-2*. (2020). Available online at: <https://www.istat.it/it/files//2020/08/ReportPrimiRisultatiIndagineSiero.pdf> (accessed July 8, 2020).
34. Council of Europe. *Governments Must Ensure Equal Protection and Care for Roma and Travellers During the COVID-19 Crisis*. Strasbourg 07/04/2020 (2020). Available online at: <https://www.coe.int/en/web/commissioner/-/governments-must-ensure-equal-protection-and-care-for-roma-and-travellers-during-the-covid-19-crisis> (accessed July 8, 2020).
35. Slobodin O, Cohen O. A culturally-competent approach to emergency management: what lessons can we learn from the COVID-19? *Psychol Trauma*. (2020) 12:470–3. doi: 10.1037/tra0000790

**Conflict of Interest:** The authors declare that the research was conducted in the absence of any commercial or financial relationships that could be construed as a potential conflict of interest.

Copyright © 2021 Ripabelli, Sammarco, Cannizzaro, Montanaro, Ponzio and Tamburro. This is an open-access article distributed under the terms of the Creative Commons Attribution License (CC BY). The use, distribution or reproduction in other forums is permitted, provided the original author(s) and the copyright owner(s) are credited and that the original publication in this journal is cited, in accordance with accepted academic practice. No use, distribution or reproduction is permitted which does not comply with these terms.





# Monitoring Coronavirus Disease 2019: A Review of Available Diagnostic Tools

Shanshan Liu<sup>1</sup>, Qiuyue Li<sup>1</sup>, Xuntao Chu<sup>2</sup>, Minxia Zeng<sup>2</sup>, Mingbin Liu<sup>1,3</sup>, Xiaomeng He<sup>1</sup>, Heng Zou<sup>1</sup>, Jianghua Zheng<sup>4</sup>, Christopher Corpe<sup>5</sup>, Xiaoyan Zhang<sup>1</sup>, Jianqing Xu<sup>1</sup> and Jin Wang<sup>1\*</sup>

<sup>1</sup> Shanghai Public Health Clinical Center, Fudan University, Shanghai, China, <sup>2</sup> Zhuohai Livzon Diagnostics Inc., Guangdong, China, <sup>3</sup> School of Pharmacy, Gannan Medical University, Jiangxi, China, <sup>4</sup> Department of Laboratory Medicine, Zhoupu Hospital Affiliated to Shanghai University of Medicine and Health Sciences, Shanghai, China, <sup>5</sup> Nutritional Science Department, King's College London, London, United Kingdom

## OPEN ACCESS

### Edited by:

Reza Lashgari,  
Institute for Research in Fundamental  
Sciences, Iran

### Reviewed by:

Xianding Deng,  
University of California, San Francisco,  
United States  
Kundlik Gadhave,  
Johns Hopkins University,  
United States  
Dubravka Drabek,  
Erasmus Medical Center, Netherlands

### \*Correspondence:

Jin Wang  
wjincityu@yahoo.com

### Specialty section:

This article was submitted to  
Infectious Diseases – Surveillance,  
Prevention and Treatment,  
a section of the journal  
Frontiers in Public Health

**Received:** 25 February 2021

**Accepted:** 23 April 2021

**Published:** 07 June 2021

### Citation:

Liu S, Li Q, Chu X, Zeng M, Liu M,  
He X, Zou H, Zheng J, Corpe C,  
Zhang X, Xu J and Wang J (2021)  
Monitoring Coronavirus Disease 2019:  
A Review of Available Diagnostic  
Tools. *Front. Public Health* 9:672215.  
doi: 10.3389/fpubh.2021.672215

Coronavirus disease 2019 (COVID-19) pneumonia is caused by the virus severe acute respiratory syndrome coronavirus 2 (SARS-CoV-2) and has rapidly become a global public health concern. As the new type of *betacoronavirus*, SARS-CoV-2 can spread across species and between populations and has a greater risk of transmission than other coronaviruses. To control the spread of SARS-CoV-2, it is vital to have a rapid and effective means of diagnosing asymptomatic SARS-CoV-2-positive individuals and patients with COVID-19, an early isolation protocol for infected individuals, and effective treatments for patients with COVID-19 pneumonia. In this review, we will summarize the novel diagnostic tools that are currently available for coronavirus, including imaging examinations and laboratory medicine by next-generation sequencing (NGS), real-time reverse transcriptase–polymerase chain reaction (rRT-PCR) analysis, immunoassay for COVID-19, cytokine and T cell immunoassays, biochemistry and microbiology laboratory parameters in the blood of the patients with COVID-19, and a field-effect transistor-based biosensor of COVID-19. Specifically, we will discuss the effective detection rate and assay time for the rRT-PCR analysis of SARS-CoV-2 and the sensitivity and specificity of different antibody detection methods, such as colloidal gold and ELISA using specimen sources obtained from the respiratory tract, peripheral serum or plasma, and other bodily fluids. Such diagnostics will help scientists and clinicians develop appropriate strategies to combat COVID-19.

**Keywords:** COVID-19, SARS-CoV-2, rRT-PCR, immunoassay, coronavirus

## INTRODUCTION

Coronavirus (CoV) infections in humans primarily involve the upper respiratory and gastrointestinal tracts. Infections can result in a mild self-limiting disease similar to influenza or can become more severe life-threatening bronchitis and pneumonia with kidney involvement (1). The first human coronavirus (HCoV) was isolated from the mucus of a patient with influenza in 1965 and was known as B814 (2). Coronaviruses are enveloped viruses with a single-stranded, positive-sense RNA genome and have the largest known RNA virus genome of ~26–32 kb (3). Open reading frame 1a (ORF1a) mainly encodes non-structural proteins, such as enzymes

related to viral replication and transcription, and  $\sim 1/4$  of the genes at the 3' end mainly encode surface spike (S) protein, membrane (M) protein, small envelope membrane (E) protein, and nucleocapsid (N) protein (4). Six coronaviruses are known to cause human diseases, including two members of the genus *Alphacoronavirus* HCoV-229E and HCoV-OC43 and four members of the genus *Betacoronavirus* HCoV-NL63, HCoV-HKU1, severe acute respiratory syndrome coronavirus (SARS-CoV), and Middle East respiratory syndrome coronavirus (MERS-CoV) (5). MERS-CoV is the pathogen that led to the outbreak of severe respiratory diseases in the Middle East in 2012 (6), and SARS-CoV is the cause of SARS in Guangdong Province of China in 2002 and 2003 (7–9).

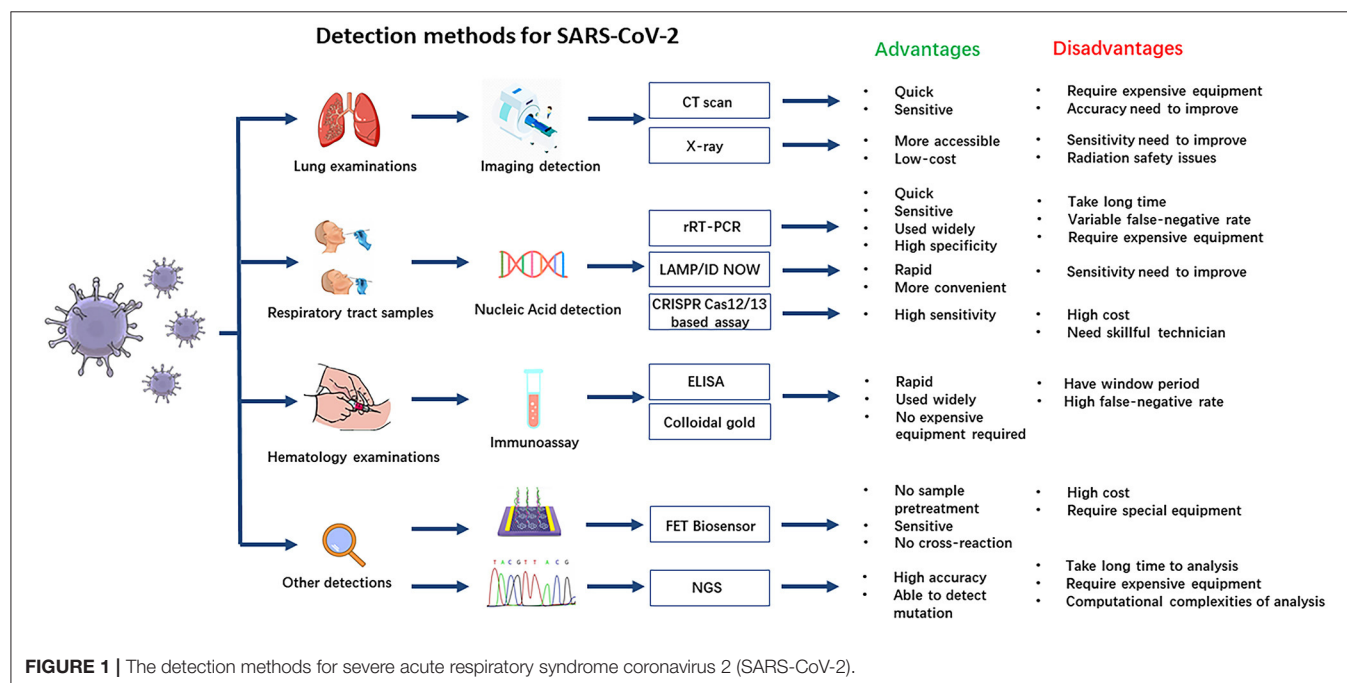
A novel *Betacoronavirus*, SARS-CoV-2, that causes coronavirus disease 2019 (COVID-19) was first identified amid an outbreak of respiratory illness in Wuhan and named by the World Health Organization (WHO) on February 11, 2020 (10). Chan et al. (11) analyzed a family cluster of six people who returned to their homes in Shenzhen with infections after traveling to Wuhan, China. The incubation periods, clinical manifestations, and laboratory and radiological information of these patients with COVID-19 and the possible infection route of SARS-CoV-2 have been analyzed (12). Most patients presented with fever, dry cough, dyspnea, and computed tomography (CT) chest scans that revealed bilateral ground-glass opacities (GGOs). However, the characteristics of SARS-CoV-2 infection have few similarities to those of SARS-CoV and MERS-CoV infections (13, 14). Along with MERS-CoV and SARS-CoV, as the seventh member of the coronavirus family that infects humans, SARS-CoV-2 is more closely related to bat-SL-CoVZC45 and bat-SL-CoVZXC21 (15). At the cellular level, angiotensin-converting enzyme II (ACE2) is the receptor used by SARS-CoV-2 (16). Similar to SARS-CoV infection, SARS-CoV-2

enters cells through the receptor ACE2 and activates its spike protein through TMPRSS2 (17, 18). However, SARS-CoV-2 infections may be combined with a superspreader event under certain circumstances and transmitted on a large scale (19); this poses a high risk at the population level and will cause disruptions to the global public health system and economic losses (19). Thus, better methods for the early detection of this novel coronavirus are urgently needed.

In clinical analysis laboratories around the world, real-time reverse transcriptase–polymerase chain reaction (rRT-PCR) is commonly used as an early detection method of the SARS-CoV-2 virus. rRT-PCR has several advantages, including reliability and high specificity, although analysis can take a long time, require expensive equipment, and produce quite variable false-negative rates (20). Immunoassays are a rapid bioanalytical method to detect an antigen–antibody that are widely used and take only about 20 min to give results, but immunoassays are not as specific as the tests recognizing viral RNA sequences, and during the early stages of infection may produce false-negative results (21). All the currently available diagnostic methods with their advantages and disadvantages are shown in **Figure 1**. Imaging examination is also a quick and sensitive diagnosis for COVID-19 in the early period, but it should be combined with other laboratory tests to improve its accuracy.

## IMAGING EXAMINATIONS FOR THE EARLY SCREENING OF CORONAVIRUS DISEASE 2019

The imaging manifestations of COVID-19 on CT are similar to those of many other viral pneumonias, such as influenza, respiratory syncytial virus, and adenovirus infection, which make



a differential diagnosis for COVID-19 difficult. For example, CT images in patients with SARS may show extensive disease and airspace consolidation (22), and MERS pneumonia appears on CT images as subpleural and basal airspace lesions with extensive GGOs and consolidation (23). Although the CT manifestations of COVID-19 have some similarities with those of MERS and SARS, CT is more sensitive for early stages of diseases (22), which still has a certain practicality when used for the early screening of COVID-19. The most common patterns of COVID-19 on thin-section CT images are pure GGOs that were defined as a hazy increase in lung attenuation with no obscuration of the underlying vessels and included reticular and/or interlobular thickened GGOs that are clearly distributed in the posterior and periphery of the lung (24). Among 21 patients with COVID-19 in China, GGOs were observed in 12 patients (57%), and consolidation was observed in six patients (29%) (25). COVID-19 is most likely to affect more than two lung lobes with bilateral involvement, with rapid evolution from focal, unilateral to diffuse, bilateral GGOs that progress to or coexist with consolidations within 1–3 weeks (26). CT is not specific for newborns, especially premature babies (27), and requires further scrutiny in case of diagnostic error. Although positive nucleic acid testing is the diagnostic gold standard, patients with fever and/or cough and prominent GGO lesions in the peripheral and posterior parts of the lungs on CT images, combined with normal or decreased white blood cells and a history of confirmed exposure, should be highly suspected of having COVID-19 (24). As a promising prognostic indicator for the clinical management of COVID-19, CT quantification of pneumonia lesions using artificial intelligence algorithms can predict the progression of serious diseases (28). A multicenter cohort study in 625 COVID-19 patients demonstrated that the consolidation in the upper lungs on initial CT was a risk factor associated with an adverse clinical outcome (29). The changes in CT images can help evaluate the treatment response of patients with COVID-19 (30). CT may also assist in the early detection of coronavirus cases. Chest radiography may also be considered to be a useful diagnostic tool for monitoring the rapid progression of lung abnormalities in COVID-19, particularly in the intensive care unit (ICU) (31). The sensitivity and specificity of chest CT were 85 and 50%, respectively, and sensitivity was significantly higher than that of X-ray (56%) (32). Compared to CT, chest radiography is cheaper and more accessible, which can minimize the risk of cross-infection (33). However, chest radiographs may provide a limited diagnosis because they may be normal in early or mild disease (34). Overall, imaging must be combined with other laboratory tests to establish the cause of the pneumonia observed by the CT scan. However, it still has certain limitations in terms of early diagnosis and differential diagnosis or correct diagnosis, and it cannot replace pathogen detection.

## NEXT-GENERATION SEQUENCING OF SEVERE ACUTE RESPIRATORY SYNDROME CORONAVIRUS 2

In the early stages of the pandemic, the first method used to detect the pathogen was next-generation sequencing (NGS) technology

(35). This technique produces genome-wide coverage in a single experiment and measures each nucleotide position repeatedly (4, 36). Analyses of MERS-CoV genetics have been performed using capture-based NGS approach or deep genome sequencing for complete genome analysis (37, 38). Considering the high genetic diversity of bat coronavirus (39), NGS can ensure unbiased sequencing and quickly determine the nucleic acid sequence of this novel coronavirus. *De novo* SARS-CoV-2 genome sequences of clinical specimens (bronchoalveolar lavage fluid) and human airway epithelial virus isolates were obtained by Illumina and Nanopore sequencing (35). The viral genome sequence was released for immediate public health support *via* the community online resource virological.org on January 10, 2020 (Wuhan-Hu-1, GenBank accession number MN908947) (40), followed by four other genomes that were deposited on January 12 in the viral sequence database curated by the Global Initiative on Sharing All Influenza Data (GISAID) (41). However, unbiased NGS is an expensive method, and because of the high background level of non-viral sequences present in field monitoring samples, it is easy to miss low-abundance coronavirus sequences (38). With the emergence of the pandemic, a variety of COVID-19 detection kits have been rapidly developed worldwide, and as a result of the discovery of specific nucleic acid detection technology, the diagnostic value of NGS has decreased because of its high cost (42). In addition, the limitations of NGS include the long sample-to-result turnaround time (>2 days), limitations in the knowledge of how to interpret novel or rare mutations, and limited ability to detect structural gene variation and copy number variation (43).

## REAL-TIME REVERSE TRANSCRIPTASE-POLYMERASE CHAIN REACTION ANALYSIS

rRT-PCR is more sensitive than conventional RT-PCR and has become the method of choice for the diagnosis of human coronaviruses (44). Sensitive rRT-PCR assays are essential for the rapid diagnosis of SARS-CoV in the early stages of the disease; multiple rRT-PCR assays have been developed to detect all four respiratory tract HCoV that can be further adapted for the new CoV (45). SARS-CoV can be quickly detected by rRT-PCR analysis, which is based on multiple primers and probe sets located in different regions of the SARS-CoV genome and can distinguish SARS-CoV from other human and animal coronaviruses with a potential detection limit of <10 genomic copies per reaction. Clinical rRT-PCR testing has been shown to be suitable for the detection of SARS-CoV in clinical specimens and is valuable for the diagnosis of SARS-CoV infection. However, the effectiveness of rRT-PCR for the detection of SARS-CoV in clinical specimens is greatly affected by the number, type, and timing of specimen collection (46). False-negative results may also be caused by mutations in the primer and probe target regions in the SARS-CoV genome. rRT-PCR also remains the gold standard to confirm MERS-CoV. Upstream of the E gene (upE), ORF1a, ORF1b, and N genes are common targets for RT-PCR analysis of MERS-CoV (Table 1), while RNA-dependent RNA polymerase (RdRp), ORF1b, and

N genes are targets for sequencing. The TaqMan probe-based one-step PCR assays allow for the rapid and sensitive internal diagnostic detection of MERS-CoV by detecting upE and ORF1b. In traditional RT-PCRs, step 1 is reverse transcription (RT) of RNA into cDNA, and step 2 is real-time PCR. The TaqMan probe-based one-step PCR kits use synthetic DNA templates and include the reverse transcriptase and DNA polymerase, which are premixed in a single reaction. The one-step method is reliable, specific, and reproducible (52). Compared to traditional RT-PCR, the one-step method combines two steps into one step, thus increasing the lower limits of sensitivity of the measurement; for example, <10 and ≤50 copies of RNA template per reaction are required for upE and ORF1b in MERS-CoV, respectively (52). ORF1ab/N gene nucleic acid assays are currently used for the detection of SARS-CoV-2. The expected amplicon sizes of the ORF1b and N gene assays for SARS-CoV-2 are 132 and 110 bp, respectively (53).

rRT-PCR analysis of SARS-CoV-2 in the respiratory tract, urine, stool, and blood specimens has been developed by several companies internationally. Since the RNA is susceptible to hydrolysis, cold chain transportation must be used during sample delivery. Specimens that can be delivered promptly to the laboratory can be stored and shipped at 2–8°C (54). When there is likely to be a delay in specimens reaching the laboratory, specimens may be frozen to –20°C or ideally –80°C and shipped on dry ice if further delays are expected (54). After freezing and thawing more than four times, specimens will be damaged. A positive test for SARS-CoV-2 by rRT-PCR or gene sequencing revealing high homology to the SARS-CoV-2 gene can be used as a diagnostic criterion for suspected clinical cases (47). In clinical samples that have tested positive, the N gene assay is ~10 times more sensitive than the ORF1b gene assay in detecting positive clinical specimens (53). In the process of infection, subgenomic mRNA is necessary for virus replication. It contains multiple translation initiation sites and can encode structural proteins of the virus (55). It is possible that these clinical samples contain infected cells expressing subgenomic mRNA (56), resulting in more N gene copies in the samples. As these samples can only be qualitatively tested by these assays at the test site, the exact copy number in these samples cannot be determined (53). To confirm that a case is positive in the laboratory, the cycle threshold value in the rRT-PCR is the basis for judgment (a cycle threshold value ≤ 37 cycles is confirmed as positive in most labs) (57). According to the SARS-CoV-2 isolate Wuhan-Hu-1 (GenBank: MN908947.3), the conserved and specific regions are ORF1a (266–13468 nt), ORF1b (13469–21555 nt), and the N gene (28274–29533 nt) (58). The molecular detection primers and probes used for the rRT-PCR detection of SARS-CoV-2, SARS-CoV, and MERS-CoV are shown in **Table 1**. For SARS-CoV-2, nucleic acid extraction is performed by the one-step method or the use of magnetic beads. The one-step method requires no RNA extraction, and viral lysis, reverse transcription, amplification, and detection are achieved in a single-tube homogeneous reaction (59). The magnetic bead method utilizes nanotechnology to prepare superparamagnetic silicon oxide nanomagnetic beads, which can specifically identify and efficiently bind to nucleic acid molecules at the microscopic

**TABLE 1 |** Molecular detection primers and probes used for the real-time quantitative RT-PCR detection of coronaviruses.

| Coronavirus | Target  | Forward primer (F)       | Reverse primer (R)         | Fluorescent probe (P)                       | Quencher probe (Q)            | References |
|-------------|---------|--------------------------|----------------------------|---|-------------------------------|------------|
| SARS-CoV-2  | ORF1ab  | CCCTGTGGGTTTACACTTAA     | ACGATTGTGCATCAGCTGA        | 5'-FAM-CCGTCTGGGGTATGTGGAAGGTTATGG-BHQ1-3'  | -                             | (47)       |
|             | N genes | GGGGAACCTCTCTGCTAGAAT    | CAGACATTTGCTCTCAGCTG       | 5'-FAM-TTGGTCTGCTTGACAGATT-TAMRA-3'         | -                             | (47)       |
| SARS-CoV    | -       | ACGGCTCTTCAGGAGTTGCTAA   | TTGCTACTACATTC TTGTGCTTACA | 5'-FAM-TGGATCCAAATTATGATGAGCCGACGA-3'       | GCTCATCAATAAATTGGATCCA-Dabcyl | (48)       |
|             | ORF1b   | CAGAAGCGTGTAGCTTCAAAATCT | TCAGAACCTGTGATGATCAACAG    | 5'-FAM-TCTGGGTAGGCAATCC-NFQ-3'              | -                             | (49)       |
|             | N genes | ACCAGATTGGAGGAGCGCAATG   | GCTGTGAACCAAGACGACGATATTAT | 5'-FAM-ACCCCAAGGTTTACCC-NFQ-3'              | -                             | (49)       |
| MERS-CoV    | S genes | TCGATCTTACCTACGAGATGTTGT | CAGCACAGTATGAAGAGACGC      | 5'-FAM-CCGTGGTACATTTGGCTTGGTTTCA-TAMRA-3'   | -                             | (50)       |
|             | ORF1a   | CCACTACTCCCATTTTCGTCAG   | CAGTATGTGTAGTGGCATATAGCA   | 5'-FAM-TTGCATAATTGGCTTGCCCCCACT-TAMRA-3'    | -                             | (51)       |
|             | upE     | GCAACGGCGGATTGAGTT       | GCCTCTACACGGGACCCATA       | 5'-FAM-CTCTTTCACATAATGCCGCCGAGCTCG-TAMRA-3' | -                             | (51)       |

FAM, 6-carboxyfluorescein; NFQ, nonfluorescent quencher; TAMRA, tetramethylrhodamine; SARS-CoV, severe acute respiratory syndrome coronavirus; MERS-CoV, Middle East respiratory syndrome coronavirus.



**TABLE 2 |** Detection of SARS-CoV-2 nucleic acid by molecular technology methods.

| Company                                 | Assay<br>(nucleic acid<br>extraction) | Amplification<br>method | Specimen source  | Target             | Detection<br>time (min) | PPA<br>(%) (no.) | NPA<br>(%) (no.) | DR<br>(%) | Eligibility                    | References |
|---|---------------------------------------|-------------------------|--|--------------------|-------------------------|------------------|------------------|-----------|--------------------------------|------------|
| Applied Bio-Tech                        | Magnetic beads                        | Standard PCR            | Respiratory tract  | ORF1ab/N/E         | 90                      | 100.0 (-)        | 100.0 (-)        | 100.0     | NMPA/WHO                       | (57)       |
| Bioperfectus<br>Technologies            | Magnetic beads                        | Standard PCR            | Respiratory tract/Stool  | ORF1ab/N/E         | 90                      | 97.2 (970)       | 100.0 (970)      | 100.0     | NMPA/WHO/US<br>FDA EUA<br>/TGA | (57, 61)   |
| DAAN Gene                               | Magnetic beads                        | Standard PCR            | Respiratory<br>tract/Serum/Urine/Stool                           | ORF1ab/N           | 110                     | 100.0 (-)        | 100.0 (-)        | 83.3      | NMPA/WHO/TGA                   | (57, 61)   |
| Zybio                                   | Magnetic beads                        | Standard PCR            | Respiratory<br>tract/Serum/Urine/Stool                           | ORF1ab/N           | 60                      | 100.0 (-)        | 100.0 (-)        | 100.0     | NMPA                           | (57)       |
| BGI Genomics                            | Magnetic beads                        | Standard PCR            | Respiratory<br>tract/Serum/Urine/Stool                           | ORF1ab             | -                       | 88.1 (126)       | 99.6 (258)       | 97.0      | NMPA/US FDA<br>EUA             | (54)       |
| Maccura Biotechnology                   | Magnetic beads                        | Standard PCR            | Oropharyngeal<br>swabs/nasopharyngeal<br>swabs/nasal swabs       | ORF1ab/N/E         | -                       | 100.0 (20)       | 96.7 (30)        | -         | US FDA EUA                     | (54)       |
| Thermo Fisher                           | Magnetic beads                        | Standard PCR            | Respiratory<br>tract/Serum/Urine/Stool                           | ORF1ab/N/S         | 60                      | 100.0 (-)        | 100.0 (-)        | 100.0     | US FDA EUA                     | (54)       |
| ZJ Bio-Tech                             | Magnetic beads                        | Standard PCR            | Respiratory tract/Stool  | ORF1ab/N/E         | 120                     | 100.0 (252)      | 100.0 (252)      | 100.0     | NMPA/WHO                       | (62)       |
| Coyote Bioscience                       | One-step                              | Standard PCR            | Respiratory tract  | ORF1ab/N           | 30                      | -                | -                | 66.6      | NMPA/TGA                       | (57)       |
| Easydiagnosis<br>Biomedicine            | One-step                              | Standard PCR            | Respiratory tract  | ORF1ab/N           | 75                      | 95.9 (750)       | 94.1 (750)       | 94.8      | NMPA/TGA                       | (63)       |
| Orient Gene Biotech                     | One-step                              | Standard PCR            | Respiratory tract  | ORF1ab/N           | 30                      | -                | -                | 97.0      | NMPA                           | (64)       |
| Promega                                 | One-step                              |                         | Respiratory tract  | N                  | -                       | 100.0 (13)       | 100.0 (104)      | 100.0     | -                              | (65)       |
| SANSURE Bio-Tech                        | One-<br>step/Magnetic<br>beads        | Standard PCR            | Respiratory<br>tract/Serum/Urine/Stool                           | ORF1ab/N           | 30                      | 100.0 (-)        | 100.0 (-)        | 100.0     | NMPA/US FDA<br>EUA/TGA         | (57, 66)   |
| Mammoth Biosciences                     | CRISPR-based<br>DETECTR               |                         | Oropharyngeal<br>swabs/Nasopharyngeal<br>swabs                   | N/E                | 40                      | 95.0 (30)        | 100.0 (30)       | -         | US FDA EUA                     | (67)       |
| -                                       | Cas13-based<br>SHERLOCK               | Isothermal              | Nasopharyngeal and throat<br>swab                                | ORF1ab/N/S         | -                       | 100.0 (154)      | 87.95 (154)      | -         | -                              | (68)       |
| Biofire                                 | -                                     | Standard PCR            | Nasopharyngeal Swab  | ORF1ab/ORF8        | -                       | 100.0 (33)       | 100.0 (66)       | 100.0     | US FDA EUA                     | (54)       |
| Rutgers Clinical<br>Genomics Laboratory | -                                     | Standard PCR            | Saliva   | ORF1ab/N/S         | -                       | 100.0 (30)       | 100.0 (30)       | -         | -                              | (54)       |
| Abbott ID Now                           | -                                     | Isothermal              | Nasal, nasopharyngeal and<br>throat swabs                        | RdRp               | 13                      | 94.0 (96)        | 100.0 (30)       | -         | US FDA<br>EUA/TGA              | (54)       |
| Cepheid                                 | -                                     | Standard PCR            | Nasopharyngeal Swab  | N <sub>2</sub> / E | 30                      | 97.9 (240)       | 100.0 (240)      | -         | WHO/US FDA<br>EUA/TGA          | (54)       |
| Diasorin Molecular                      | -                                     | Standard PCR            | Nasopharyngeal<br>swabs/nasal<br>swabs/bronchoalveolar<br>lavage | ORF1ab/S           | -                       | 100.0 (-)        | 100.0 (-)        | 100.0     | WHO/US FDA<br>EUA/TGA          | (54)       |

(Continued)

TABLE 2 | Continued

| Company           | Assay (nucleic acid extraction) | Amplification method | Specimen source   | Target   | Detection time (min) | PPA (%) (no.) | NPA (%) (no.) | DR (%)     | Eligibility    | References |
|-------------------|---------------------------------|----------------------|---|----------|----------------------|---------------|---------------|------------|----------------|------------|
| PerkinElmer       | -                               | Standard PCR         | Oropharyngeal swabs/Nasopharyngeal swabs/Anterior nasal swabs | ORF1ab/N | -                    | 100.0 (-)     | 100.0 (-)     | 95.0–100.0 | WHO/US FDA EUA | (54)       |
| Roche Diagnostics | -                               | Standard PCR         | Nasopharyngeal and nasal swabs                                | ORF1ab   | 20                   | 100.0 (-)     | 100.0 (-)     | -          | WHO/US FDA EUA | (54)       |

*Respiratory tract samples include throat swabs, sputum, and alveolar lavage fluid; one-step means no RNA extraction; NO, is number of samples tested; NPA, negative percent agreement; PPA, positive percent agreement; DR, detection rate; "-" is missing data; NMPPA, National Medical Products Administration of China; US FDA EUA, Food and Drug Administration (FDA) and Emergency Use Authorization (EUA) of the United States; TGA, Therapeutic Goods Administration; SARS-CoV, severe acute respiratory syndrome coronavirus.*

interface for RNA extraction (60). In **Table 2**, information is collected on several biotechnology companies undertaking the molecular diagnosis of COVID-19, including specimen source, methods of nucleic acid extraction, gene targeting, detection time, negative/positive percent agreement (NPA/PPA), and detection rate (DR). The analysis can be performed in as fast as 30 min with kits from Zhejiang Orient Gene Biotech Co., Ltd., Coyote Bioscience Co., Ltd. (57), and Hunan SANSURE BIOTECH INC. (57, 66). There are four companies (Cepheid, Diasorin Molecular, PerkinElmer, and Roche Diagnostics) on the list of SARS-CoV-2 diagnostic test kits by rRT-PCR analysis, which are updated on the Global Fund (GF) resources website based on eligibility criteria of WHO and US Food and Drug Administration (FDA) and Emergency Use Authorization (EUA) (69) and are shown in **Table 2**.

Compared with conventional RT-PCR, the loop-mediated isothermal amplification (LAMP) is 100-fold-greater sensitivity for detection of SARS-CoV, with a detection limit of 0.01 PFU (70). By doing the LAMP assay, the virus is quickly extracted and amplified at constant temperature without the expensive reagents and equipment (71), but LAMP may be of lower sensitivity or comparable to SARS-CoV-2 detection by RT-PCR. Rödel et al. (72) demonstrated that the isolated RNA variplex RT-LAMP for SARS-CoV-2 had a sensitivity of 75% compared to LightMix E gene RT-PCR. On the other hand, the ID NOW COVID-19 assay performed on the ID NOW Instrument is a rapid (5–13 min) *in vitro* molecular diagnostic test, which utilizes isothermal nucleic acid amplification technology and amplification of the unique region of RdRP segment and nicking and extension amplification reaction (NEAC) where each primer consists of binding region and nicking enzyme recognition site. The newly synthesized short-sequence single-stranded chain is combined with the fluorescently labeled molecular probes to provide a real-time readout (54). The sensitivity and NPA of ID NOW can reach 87.58 and 96.99%, respectively. The saliva test has also demonstrated a high sensitivity and comparable performance to the current standard of nasopharyngeal and throat swabs and can significantly minimize the likelihood of exposing health care workers to SARS-CoV-2 while sampling (54, 73).

In addition to RT-PCR and isothermal amplification, clustered regularly interspaced short palindromic repeats (CRISPR)-based technologies have also been developed to detect the nucleic acids of SARS-CoV-2 in <40 min (67). This assay performs simultaneous reverse transcription and isothermal amplification, followed by Cas12 detection of SARS-CoV-2 sequences, after which cleavage of a reporter molecule confirms the detection of the virus. The kit provides a visual and faster method of detection, which showed 95% PPA and 100% NPA (67). It is a portable assay that enables point of care (POC) outside of the clinical diagnostic laboratory and replaces regular RT-PCR. Additionally, the specific high-sensitivity enzymatic reporter unlocking (SHERLOCK) assay using the enzyme Cas13a was developed for the detection of SARS-CoV-2, and the PPA of this assay is as high as 100% (68).

Specifically, some novel mutations of SARS-CoV-2 have already been identified as B.1.1.7, B.1.351, P.1, N501Y, and HV69-70del (74, 75). A one-step reverse transcription and real-time

PCR (RT-qPCR) test is developed for screening Spike N501Y and HV69-70del mutations in 40 min. The specificity of this RT-qPCR assay relative to the sequencing-based technologies is 100% and can screen for SARS-CoV-2 efficiently (75).

## IMMUNOASSAY FOR CORONAVIRUS DISEASE 2019

False-negative results are often obtained in the rRT-PCR analyses of coronavirus because nucleic acid assays can be affected by low virus copies or efficiency during amplification. For the detection of SARS-CoV antigens, a chemiluminescence enzyme-linked immunosorbent assay (CLEIA) can sensitively detect the target protein below 2 pg/ml at different stages of infection. The CLEIA shows no cross-reactivities to recombinant nucleocapsid (N) proteins of coronaviruses such as 229E, OC43, and NL63, and the specificity and sensitivity of this assay are both 100% (76). In addition, double-antibody sandwich enzyme-linked immunosorbent assays (ELISAs) based on specific monoclonal antibodies are used to detect the N proteins of HCoV-NL63 and HCoV-229E (77) and the SARS-CoV S protein of SARS-CoV (78). For the detection of MERS-CoV, an ELISA capture assay is developed to detect the N protein antigen of MERS-CoV virus in nasopharyngeal samples with high specificity (almost 100%) and sensitivity (<1 ng/ml) (79). Under an EUA, the Sofia 2 SARS Antigen Fluorescent Immunoassay (FIA) can be the practice of qualitative detection of N protein from SARS-CoV-2 in 15 min by immunofluorescence-based lateral flow technology for testing of patients suspected of COVID-19 (54).

Compared with rRT-PCR assays of upper respiratory tract samples, immunoassays are used to detect antibodies against SARS-CoV-2 from blood samples of patients suspected to have the active disease or to have had the disease in the past and thus are not used to detect the virus directly. The time window is also important for virus-specific antibody detection (80). Serology is the practice of detecting antibodies and can increase the sensitivity and specificity of SARS-CoV detection and is suitable for rapid laboratory diagnosis. SARS-CoV-2 proteins are used as the coated antigens to identify virus-specific IgM/IgG antibodies in blood samples of patients with COVID-19. The study showed that (81) IgM and IgG antibodies against SARS-CoV-2 were detected as early as the fourth day after the onset of symptoms and that IgG increased sharply by the 12th day. At 28 days, the seropositivity of IgG decreased, which were detected by ELISA kits from Livzon Diagnostics Inc. The sensitivity, specificity, and positive predictive value (PPV) of IgM antibodies were 77.3% (51/66), 100%, and 100%, respectively (81). The specificity and PPV of IgG–IgM combined detection assays are higher than those of individual IgG or IgM antibody assays (82). We also classify and describe the specimen sources, detection methods, detected antibodies, virus targets, detection times, and specificities and sensitivities of SARS-CoV-2 antibody detection kits according to the manufacturers' protocols (Table 3). The detection time of the colloidal gold method is short (15 min), and the virus targets are mainly S or N protein. The assay methods from Cellex using colloidal gold showed sensitivity and specificity

to be more than 90%. The kit from Mount Sinai Laboratory also showed outstanding high sensitivity (92%) and specificity (100%). There are five companies (Advaita, Biocan Diagnostics, Biohit Healthcare, Biotest Biotech, and Laihe Biotech) on the list of diagnostic test kits using colloidal gold, which are updated on the GF resources website based on eligibility criteria of US FDA and EUA (69) and shown in Table 3. The ELISA from Beijing WANTAI BioPharm Co., Ltd., can simultaneously detect total antibodies (IgG/IgM/IgA). Moreover, the sensitivity and specificity of WANTAI BioPharm Co., Ltd., reach ~100% (83). The Chembio Dual Path Platform (DPP) COVID-19 IgM/IgG System is a single-use rapid immunochromatographic test for the qualitative detection of antibodies to SARS-CoV-2. The device employed Chembio's patented DPP technology that uses antibody capture to detect SARS-CoV-2 (54). If the sample contains SARS-CoV-2 antibodies, the conjugate binds to the antibodies captured in the test areas with more than 90% sensitivity and specificity. Rapid tests have great potential benefits for the prompt screening of COVID-19 infections. Thus, serological diagnostic approaches will aid in the diagnosis and treatment of novel coronavirus pneumonia and will also test the effectiveness of the vaccines and the selection of individuals who might act as plasma donors. However, rRT-PCR is widely adopted as the standard diagnostic method for SARS-CoV-2. Specifically, combining IgM and IgG detection methods with rRT-PCR assay results for the detection of the virus will greatly increase the accuracy of establishing the time of infection and predicting the progress of the disease (Table 4). Although the relationship between IgG levels in COVID-19 patients and protective immunity to SARS-CoV-2 virus has not been fully established (84), a positive result indicates an immune response to SARS-CoV-2 in COVID-19 patients. However, the patient is infected but has not yet produced IgG/IgM antibodies at detectable levels, resulting in false negatives (85). Also, cross-reactivity occurs when antibodies bind with an antigen, which is similar to the SARS-CoV-2 antigen, leading to a false-positive result. Thus, cross-reactivity is the biggest issue in the serological test.

## EFFECT OF CYTOKINES AND T CELLS ON CORONAVIRUS DISEASE 2019

SARS-CoV-2 can act as a factor for the development of a rapid autoimmune response that underlines COVID-19 outcomes. It is an important cause of acute respiratory distress syndrome and multiorgan illness that lasted for months in people with "long COVID" (86, 87). More than 10% of 987 patients with severe COVID-19 had antibodies that attacked and blocked the action of type 1 interferon, which could help to bolster the immune response against the virus (88) and played a key role in the pathophysiology of COVID-19 (89). After a novel coronavirus infection, pathogenic T cells are rapidly activated, and a large number of plasma cytokines and chemokines are produced, which causes a cytokine storm leading to severe immune damage to multiple organs (12, 90). Autoantibodies are more

**TABLE 3 |** Immunoassays for COVID-19.

| Company                    | Assay (detection method) | Specimen source               | SARS CoV-2 targets | Antibody detected | Time (min) | Sensitivity (%) (no.) | Specificity (%) (no.) | Eligibility         | References |
|----------------------------|--------------------------|-------------------------------|--------------------|-------------------|------------|-----------------------|-----------------------|---------------------|------------|
| Wandfo                     | Colloidal gold           | Peripheral blood/Serum/Plasma | S                  | IgG/IgM           | 15         | 86.4 (596)            | 99.6 (596)            | NMPA                | a          |
| Innovita                   | Colloidal gold           | Peripheral blood/Serum/Plasma | N                  | IgG/IgM           | 15         | 87.3 (126)            | 100.0 (126)           | NMPA/US FDA EUA/TGA | b          |
| Autobio Diagnostics        | Colloidal gold           | Serum/Plasma                  | S                  | IgG/IgM           | 15         | 88.2 (405)            | 99.0 (312)            | NMPA                | c          |
| Cellex                     | Colloidal gold           | Peripheral blood/Serum/Plasma | -                  | IgG/IgM           | 15         | 93.8 (128)            | 96.0 (250)            | US FDA EUA/TGA      | c          |
| Mount Sinai Laboratory     | ELISA                    | Serum/Plasma                  | S                  | IgG               | -          | 92.0 (40)             | 100.0 (74)            | -                   | c          |
| Ortho Clinical Diagnostics | ELISA                    | Serum/Plasma                  | S                  | IgG/IgM           | 48         | 83.3 (36)             | 100.0 (400)           | US FDA EUA          | c          |
| WANTAI BioPharm            | ELISA                    | Serum/Plasma                  | S                  | IgG/IgM/IgA       | 120        | 100.0 (28)            | 98.0 (84)             | NMPA/US FDA EUA/TGA | d          |
| Chembio Diagnostic System  | DPP                      | Peripheral blood/Serum/Plasma | N                  | IgG/IgM           | 15         | 93.5 (31)             | 90.2 (41)             | -                   | c          |
| Quidel                     | ELISA                    | Nasopharyngeal and nasal swab | N                  | -                 | 15         | 80.0 (48)             | 100.0 (48)            | US FDA EUA/TGA      | c          |
| Advaite                    | Colloidal gold           | Peripheral blood              | -                  | IgG               | 20         | 90.0 (30)             | 95.2 (104)            | US FDA EUA          | c          |
| Biocan Diagnostics         | Colloidal gold           | Serum/Plasma                  | N/S                | IgG/IgM           | -          | 93.3(-)               | 96.2 (-)              | US FDA EUA          | c          |
| Biohit Healthcare          | Colloidal gold           | Serum/Plasma                  | N                  | IgG/IgM           | 20         | 96.7 (30)             | 95.0 (80)             | US FDA EUA          | c          |
| Biotest Biotech            | Colloidal gold           | Serum/Plasma                  | S                  | IgG/IgM           | 20         | 100.0 (30)            | 100.0 (30)            | US FDA EUA          | c          |
| Laihe Biotech              | Colloidal gold           | Serum/Plasma                  | S                  | IgG/IgM           | 30         | 100.0 (30)            | 98.8 (80)             | US FDA EUA          | c          |

NO. is the number of samples tested; NMPA, National Medical Products Administration of China; US FDA EUA, Food and Drug Administration (FDA) and Emergency Use Authorization (EUA) of the United State; TGA, Therapeutic Goods Administration; DPP, dual path platform; COVID-19, coronavirus disease 2019; SARS-CoV, severe acute respiratory syndrome coronavirus. (a) Guangzhou Wandfo Co., Ltd. ([http://tech.gmw.cn/2020-02/24/content\\_33583856.htm](http://tech.gmw.cn/2020-02/24/content_33583856.htm)); (b) INNOVITA Co., Ltd. (<http://www.innovita.com.cn/html/cn/>); (c) US Food & Drug administration (<https://www.fda.gov/medical-devices/emergency-situations-medical-devices/emergency-use-authorizations>); (d) Shenzhen Third People's Hospital in conjunction with Xiamen University and Beijing WANTAI BioPharm Co., Ltd. (<https://www.medrxiv.org/content/10.1101/2020.04.09.20056325v1>).



**TABLE 4 |** Clinical significance of SARS-CoV-2 detection in COVID-19 patients.

| SARS-CoV-2<br>nucleic acid assay | Immunoassay |     | Clinical significance |                             |   |
|----------------------------------|-------------|-----|-----------------------|-----------------------------|---|
|                                  | IgM         | IgG | Infection period*     | Immune response<br>(Yes/No) | Other remarks   |
| +                                | +           | +   | Middle/Late           | Yes                         | /   |
| +                                | +           | -   | Early                 | Yes                         | /   |
| +                                | -           | +   | Middle/Late           | Yes                         | /   |
| +                                | -           | -   | /                     | No                          | "Window period" for 2 weeks   |
| -                                | +           | +   | /                     | Yes                         | Recovery/false-negative nucleic acid test   |
| -                                | +           | -   | Early                 | Yes                         | <a href="http://www.baidu.com/link?url=0kXBuXmzX8-U029eB-yK4emFTye783LAu2tVaOpN8Am0q9DplOpEzaFkTwUwFGcoK2rybVT1QQbEduUJEy4ar-mKBgVCPwhOQ91QYDlJmReview">http://www.baidu.com/link?url=0kXBuXmzX8-U029eB-yK4emFTye783LAu2tVaOpN8Am0q9DplOpEzaFkTwUwFGcoK2rybVT1QQbEduUJEy4ar-mKBgVCPwhOQ91QYDlJmReview</a> for nucleic acid test |
| -                                | +/-         | -   | Early                 | No                          | Review after 1 week   |
| -                                | -           | +   | /                     | Yes                         | Past exposure to SARS-CoV-2   |
| -                                | -           | -   | /                     | /                           | Health/latent period (0–14 days)  |

\*Infection process is divided into early (0–7 days), middle (8–14 days), and late (after 14 days) periods for the onset of symptoms; "+" is positive and "-" is negative in detection analysis. COVID-19, coronavirus disease 2019; SARS-CoV, severe acute respiratory syndrome coronavirus.

common in men than in women, and a poor T cell response negatively correlated with patients' age and was associated with worse disease outcome in male patients, which provides a possible explanation as to why COVID hits men harder (91). Cytokine storm refers to a phenomenon in which a large number of cytokines are rapidly released into bodily fluids after the patient is infected with microorganisms. Among T lymphocyte subpopulations in patients with COVID-19, both CD4<sup>+</sup> and CD8<sup>+</sup> T cell counts decreased, and the reduction in CD4<sup>+</sup> T cells was more pronounced (42). However, in children, leukocyte counts and absolute lymphocyte counts were mostly normal (92). It was reported that interleukin (IL)-6 was elevated in more than half (52%) of patients with COVID-19 (90). In the early stage, initial plasma IL-1B, IL-1RA, IL-7, IL-8, IL-9, IL-10, basic fibroblast growth factor (FGF), granulocyte colony-stimulating factor (GCSF), granulocyte/macrophage colony-stimulating factor (GM-CSF), interferon (IFN) $\gamma$ , IFN $\gamma$ -inducible protein (IP)10, monocyte chemotactic protein (MCP)1, macrophage inflammatory protein 1-alpha (MIP1A), MIP1B, platelet-derived growth factor (PDGF), tumor necrosis factor (TNF) $\alpha$ , and vascular endothelial growth factor (VEGF) concentrations were higher in all patients than those in healthy adults (12). The binding of COVID-19 to the Toll-like receptor (TLR) led to the release of pre-IL-1 $\beta$ , which was cleaved by caspase-1, followed by the activation of the inflammasome and the production of active mature IL-1 $\beta$ , which is a mediator of lung inflammation (62). Compared to those in non-ICU patients, IL-2, IL-7, IL-10, GCSF, IP10, MCP1, MIP1A, and TNF $\alpha$  levels were higher in ICU patients, suggesting that the cytokine storm was associated with disease severity (12). It was also found that the inflammatory factors IL-2R, IL-6, and C-reactive protein (CRP) were elevated in COVID-19 patients, and IL-2R and IL-6 had certain advantages in predicting the severity of the disease compared with traditional indicators (lymphocyte count and CRP) (93).

## BLOOD, BIOCHEMISTRY, AND MICROBIOLOGY LABORATORY PARAMETERS OF CORONAVIRUS DISEASE 2019

In the early stage of COVID-19, the total number of white blood cells was generally reduced or normal, the lymphocyte count was decreased, and monocyte counts were increased or normal. If the absolute value of lymphocytes was  $<0.8 \times 10^9/L$ , the general recommendation was to review routine blood changes after 3 days. Leukopenia was observed in approximately 33.7% of the overall COVID-19 patient population. Among these patients, 82.1% had lymphopenia and 36.2% had thrombocytopenia. Moreover, lymphocytopenia, leukopenia, and thrombocytopenia were significant in severe cases of COVID-19 (94). The examination of peripheral blood cell morphology could show abnormal lymphocytes, and Dohle bodies could be found in the cytoplasm of some neutrophils (92).

In 99 cases of COVID-19 in Wuhan, most patients had common inflammation-like biochemical indicators on admission. Seventy-three patients were tested for CRP, of whom 63 (86%) patients had increased levels of CRP. Forty-three of 99 patients had differing degrees of liver damage, as shown by abnormal levels of alanine aminotransferase (ALT) or aspartate aminotransferase (AST). A large number of patients, ~98%, had decreased serum albumin levels. In addition, there was an increase in serum ferritin (FER) in 62 (63%) patients, an increase in erythrocyte sedimentation rate (ESR) in 84 (85%) patients, and an increase in the levels of blood glucose in 51 (52%) patients (90). In another report on COVID-19 (12), levels of lactate dehydrogenase (LDH) were elevated above 245 U/L in 29 of 40 (73%) patients, including 12 of 13 (92%) patients requiring ICU care and 17 of 27 (63%) of non-ICU patients. Of the 40 patients, five (12%) patients had levels of hypersensitive troponin I (hs-cTnI) above 28 pg/ml, which was due to virus-related cardiac

injury, including 4 of 13 (31%) patients in the ICU. Procalcitonin (PCT) is a protein used to determine whether there is a bacterial infection in the lungs (95). On admission, the levels of PCT were in the normal range (PCT <0.1 ng/ml) for 27 (69%) of 39 patients. PCT levels were increased above 0.5 ng/ml in only three (8%) of the 39 patients. Among the 39 patients, there were four ICU patients who developed secondary infections. Three of the four patients with secondary infections had PCT levels >0.5 ng/ml. The arterial oxygen saturation (SpO<sub>2</sub>) and oxygen partial pressure decreased and carbon dioxide partial pressure increased in some severe cases of COVID-19, and those with metabolic acidosis occasionally had decreased pH (92).

COVID-19 is very different from other known viral pneumonia, such as influenza virus, adenovirus, respiratory syncytial virus, and mycoplasma pneumonia infections. Routinely detected influenza antigens are the A, B, and H7N subtypes (42). Due to the rapid detection method, the sampling of throat swabs can help to screen for influenza early in the clinical course, but the false-negative rate of the method is high (42). Therefore, the diagnosis of COVID-19 should be combined with nucleic acid, antibody, and antigen detection technology to improve the DR.

## **RAPID DETECTION OF CORONAVIRUS DISEASE 2019 SEVERE ACUTE RESPIRATORY SYNDROME CORONAVIRUS 2 USING A FIELD-EFFECT TRANSISTOR-BASED BIOSENSOR**

A field-effect transistor (FET)-based biosensing device has been invented recently for detecting SARS-CoV-2 in clinical samples. FET-based biosensors are considered to be potentially useful in clinical diagnosis, POC testing, and on-site detection (96). The sensor is fabricated by coating graphene sheets of the FET with a specific antibody against SARS-CoV-2 spike protein. The sensor is able to detect the SARS-CoV-2 spike protein at concentrations of 1 fg/ml in phosphate-buffered saline and 100 fg/ml clinical transport medium, which makes it a highly sensitive immunoassay for COVID-19. Additionally, the biosensor can avoid cross-reaction with MERS-CoV antigen, indicating that the FET sensor is sensitive and specific enough for the SARS-CoV-2 spike protein. This method does not require sample pretreatment and labeling, and the biosensor does not cross-react with SARS-CoV and MERS-CoV antigens due to high specificity to SARS-CoV-2 spike protein by the selected antibody (96).

## **SUMMARY AND PROSPECTS FOR THE DETECTION OF SEVERE ACUTE RESPIRATORY SYNDROME CORONAVIRUS 2 IN CORONAVIRUS DISEASE 2019**

Coronavirus-related diseases have become an urgent global public health problem, and the detection of coronavirus is particularly important in the diagnosis of coronavirus diseases.

RT-PCR has been widely used in diagnostic virology, and skilled diagnostic laboratories can rely on this powerful technique to internally establish new diagnostic assays during public health emergencies. In the face of a sudden outbreak, rapid and accurate detection and triage, with the isolation or treatment of suspected and confirmed cases, are the most powerful measures to prevent further spread of disease. Therefore, the SARS-CoV-2 nucleic acid assay is an important medical test for prevention, control, and medical treatment during an epidemic.

For suspected cases of COVID-19, rapid antigen and multiple PCR nucleic acid detection methods should be adopted as widely as possible. The detection of nucleic acids is the leading advance in the current clinical diagnostic technology for pathogenic microorganisms and is guiding the direction of lung infection diagnostic technology. Most commonly, the DR of this method is over 90%, and NPA and PPA are close to 100%, and this method is widely used in the clinical diagnosis and detection of various respiratory pathogens. However, with the widespread use of SARS-CoV-2 nucleic acid assays, an increasing number of problems are becoming apparent. The major issue is a high number of false-negative results in virus nucleic acid detection.

For rRT-PCR analysis, the results of the nucleic acid assay are affected by factors such as the disease development process, specimen collection, specimen preservation and transportation, nucleic acid extraction, amplification system, detection operating environment, and personnel operations. The concentration of SARS-CoV-2 in the alveolar lavage fluid of COVID-19 patients is the highest, but the procedure of collecting alveolar lavage fluid is complicated, it is only recommended for critically ill patients on ventilators. However, the most common and simplest sampling method remains a throat swab. Moreover, the correct handling of specimens during transportation is essential. Specimens for virus detection should be kept cold and stored at  $-70^{\circ}\text{C}$  if the testing is to be delayed for a long time. Most of the (RNA) vaccines also require logistics for storage at very low temperatures. Previously, it was stated by Shanghai ZJ Bio-Tech Co., Ltd., that because their kit requires a storage environment of  $-20^{\circ}\text{C}$ , only a few logistics companies with cold chain capabilities could supply the kit. Carelessness during transportation may affect the final test results of the assays. On the other hand, many sampling solutions cannot lyse the virus and cannot guarantee the stability of the viral nucleic acid, which is one of the factors that affects detection sensitivity.

Testing SARS-CoV-2-specific antibodies in patient blood is a good choice for rapid, simple, and highly sensitive diagnosis of COVID-19, which can also meet the urgent needs of a large number of patients. Hence, immunoassays are an excellent supplementary approach in clinical applications. Moreover, monoclonal antibodies have been developed against SARS-CoV-2 antigen proteins, which can target a single specific epitope and are highly specific compared to polyclonal antibodies. Overall, compared with polyclonal antibodies, monoclonal antibodies have been indicated to be efficient reagents in terms of specificity for clinical diagnostic tests, which is greatly valuable for clinical detection. Some of the antibodies do not react with the new emerging mutant variants of the virus. Therefore, the diagnosis of COVID-19 needs to be further improved to reduce the

misdiagnosis rate and to adapt to new mutated versions of SARS-CoV-2. Therefore, the diagnosis of COVID-19 needs to be further improved to reduce the misdiagnosis rate. Multiple detection methods can be used together to improve the correct diagnosis rate.

With the increase in the prevalence of SARS-CoV-2 variants containing spike mutations, a one-step rRT-qPCR test needs be developed that will rapidly detect mutations with low cost. When the evolution of the pandemic causes the number of asymptomatic SARS-CoV-2-positive individuals and patients with COVID-19 to grow exponentially, fully automated immunoassays and PCRs, capable of executing thousands of tests per day, have gained importance. New technologies, such as the POC diagnosis device, provide a portable, fast, and low-cost assay system for the diagnosis of COVID-19 that can be used not only in the doctor's offices but also in homes, airports, and remote locations. The integration of smartphones with COVID-19 detection technologies should be considered a promising testing platform in the future. Additionally, the development of a novel assay for coronavirus pneumonia still has a long way to

go, but it will greatly contribute to the clinical diagnosis of COVID-19.

## AUTHOR CONTRIBUTIONS

JW conceived and designed the study. SL, MZ, XH, HZ, and ML collected the literature. SL drafted the paper. JW, CC, and QL revised the manuscript with input from all coauthors. JW, XZ, and JX provided funding support. XC and JZ were the principal investigators for the detection of SARS-CoV-2. All authors read, contributed to, and approved the final manuscript.

## FUNDING

This research was supported by a grant from the Science and Technology Commission of Shanghai (20Y11900700), a grant from the Special Research Fund of Youan Medical Alliance for the Liver and Infectious Diseases (LM202020), a grant from the National Special Research Program of China for Important Infectious Diseases (2018ZX10302103-003), and a grant from the National Natural Science Foundation of China (81672383).

## REFERENCES

- Wevers BA, van der Hoek L. Recently discovered human coronaviruses. *Clin Lab Med.* (2009) 29:715–24. doi: 10.1016/j.cll.2009.07.007
- Tyrrell DAJ, Bynoe ML. Cultivation of a novel type of common-cold virus in organ cultures. *Br Med J.* (1965) 1:1467–70. doi: 10.1136/bmj.1.5448.1467
- Weiss SR, Navas Martin S. Coronavirus pathogenesis and the emerging pathogen severe acute respiratory syndrome coronavirus. *Microbiol Mol Biol Rev.* (2005) 69:635. doi: 10.1128/MMBR.69.4.635-664.2005
- van Boheemen S, de Graaf M, Lauber C, Bestebroer TM, Raj VS, Zaki AM, et al. Genomic characterization of a newly discovered coronavirus associated with acute respiratory distress syndrome in humans. *mBio.* (2012) 3:e00473–12. doi: 10.1128/mBio.00473-12
- Kin N, Miszczak F, Lin W, Gouilh M, Vabret A, Consortium E. Genomic analysis of 15 human coronaviruses OC43 (HCoV-OC43s) circulating in France from 2001 to 2013 reveals a high intra-specific diversity with new recombinant genotypes. *Viruses.* (2015) 7:2358–77. doi: 10.3390/v7052358
- Zaki AM, van Boheemen S, Bestebroer TM, Osterhaus ADME, Fouchier RAM. Isolation of a novel coronavirus from a man with pneumonia in Saudi Arabia. *N Engl J Med.* (2012) 367:1814–20. doi: 10.1056/NEJMoa1211721
- Zhong NS, Zheng BJ, Li YM, Poon, Xie ZH, Chan KH, et al. Epidemiology and cause of severe acute respiratory syndrome (SARS) in Guangdong, People's Republic of China, in February, 2003. *Lancet.* (2003) 362:1353–8. doi: 10.1016/S0140-6736(03)14630-2
- Ksiazek TG, Erdman D, Goldsmith CS, Zaki SR, Peret T, Emery S, et al. A novel coronavirus associated with severe acute respiratory syndrome. *N Engl J Med.* (2003) 348:1953–66. doi: 10.1056/NEJMoa030781
- Drosten C, Günther S, Preiser W, van der Werf S, Brodt HR, Becker S, et al. Identification of a novel coronavirus in patients with severe acute respiratory syndrome. *N Engl J Med.* (2003) 348:1967–76. doi: 10.1056/NEJMoa030747
- Shi Y, Wang G, Cai XP, Deng JW, Zheng L, Zhu HH, et al. An overview of COVID-19. *J Zhejiang Univ Sci B.* (2020) 21:343–60. doi: 10.1631/jzus.B2000083
- Chan JF-W, Yuan S, Kok K-H, To KK-W, Chu H, Yang J, et al. A familial cluster of pneumonia associated with the 2019 novel coronavirus indicating person-to-person transmission: a study of a family cluster. *Lancet.* (2020) 395:S0140-6736(20)30154-9. doi: 10.1016/S0140-6736(20)30154-9
- Huang C, Wang Y, Li X, Ren L, Zhao J, Hu Y, et al. Clinical features of patients infected with 2019 novel coronavirus in Wuhan, China. *Lancet.* (2020) 395:497–506. doi: 10.1016/S0140-6736(20)30183-5
- Assiri A, Al-Tawfiq JA, Al-Rabiee AA, Al-Rabiah FA, Al-Hajjar S, Al-Barrak A, et al. Epidemiological, demographic, and clinical characteristics of 47 cases of Middle East respiratory syndrome coronavirus disease from Saudi Arabia: a descriptive study. *Lancet Infect Dis.* (2013) 13:752–61. doi: 10.1016/S1473-3099(13)70204-4
- Lee N, Hui D, Wu A, Chan P, Cameron P, Joynt GM, et al. A major outbreak of severe acute respiratory syndrome in Hong Kong. *N Engl J Med.* (2003) 348:1986–94. doi: 10.1056/NEJMoa030685
- Dong N, Yang X, Ye L, Chen K, Wai-Chi Chan E, Yang M, et al. Genomic and protein structure modelling analysis depicts the origin and infectivity of 2019-nCoV, a new coronavirus which caused a pneumonia outbreak in Wuhan, China. *BioRxiv.* (2020). doi: 10.1101/2020.01.20.913368
- Li MY, Li L, Zhang Y, Wang XS. Expression of the SARS-CoV-2 cell receptor gene ACE2 in a wide variety of human tissues. *Infect Dis Poverty.* (2020) 9:45. doi: 10.1186/s40249-020-00662-x
- Glowacka I, Bertram S, Müller MA, Allen P, Soilleux E, Pfefferle S, et al. Evidence that TMPRSS2 activates the severe acute respiratory syndrome coronavirus spike protein for membrane fusion and reduces viral control by the humoral immune response. *J Virol.* (2011) 85:4122–34. doi: 10.1128/JVI.02232-10
- Kuhn JH, Li W, Choe H, Farzan M. Angiotensin-converting enzyme 2: a functional receptor for SARS coronavirus. *Cell Mol Life Sci.* (2004) 61:2738–43. doi: 10.1007/s00018-004-4242-5
- Munster VJ, Koopmans M, van Doremalen N, van Riel D, de Wit E. A novel coronavirus emerging in China - key questions for impact assessment. *N Engl J Med.* (2020) 382:692–4. doi: 10.1056/NEJMp2000929
- Pérez-López B, Mir M. Commercialized diagnostic technologies to combat SARS-CoV2: advantages and disadvantages. *Talanta.* (2021) 225:121898. doi: 10.1016/j.talanta.2020.121898
- Giri B, Pandey S, Shrestha R, Pokharel K, Ligler FS, Neupane BB. Review of analytical performance of COVID-19 detection methods. *Anal Bioanal Chem.* (2021) 413:35–48. doi: 10.1007/s00216-020-02889-x
- Paul NS, Roberts H, Butany J, Chung T, Gold W, Mehta S, et al. Radiologic pattern of disease in patients with severe acute respiratory syndrome: the Toronto experience. *Radiographics.* (2004) 24:553–63. doi: 10.1148/rg.242035193



23. Ajlan AM, Ahlyad RA, Jamjoom LG, Alharthy A, Madani TA. Middle East respiratory syndrome coronavirus (MERS-CoV) infection: chest CT findings. *AJR Am J Roentgenol.* (2014) 203:782–7. doi: 10.2214/AJR.14.13021
24. Song F, Shi N, Shan F, Zhang Z, Shen J, Lu H, et al. Emerging coronavirus 2019-nCoV pneumonia. *Radiology.* (2020) 295:200274. doi: 10.1148/radiol.2020020274
25. Chung M, Bernheim A, Mei X, Zhang N, Huang M, Zeng X, et al. CT imaging features of 2019 novel coronavirus (2019-nCoV). *Radiology.* (2020) 295:200230. doi: 10.1148/radiol.2020020230
26. Shi H, Han X, Jiang N, Cao Y, Alwalid O, Gu J, et al. Radiological findings from 81 patients with COVID-19 pneumonia in Wuhan, China: a descriptive study. *Lancet Infect Dis.* (2020) 20:425–34. doi: 10.1016/S1473-3099(20)30086-4
27. Ogimi C, Englund JA, Bradford MC, Qin X, Boeckh M, Waghmare A. Characteristics and outcomes of coronavirus infection in children: the role of viral factors and an immunocompromised state. *J Pediatr Infect Dis Soc.* (2019) 8:21–8. doi: 10.1093/jpids/pix093
28. Liu F, Zhang Q, Huang C, Shi C, Wang L, Shi N, et al. CT quantification of pneumonia lesions in early days predicts progression to severe illness in a cohort of COVID-19 patients. *Theranostics.* (2020) 10:5613–22. doi: 10.7150/tno.45985
29. Yu Q, Wang Y, Huang S, Liu S, Zhou Z, Zhang S, et al. Multicenter cohort study demonstrates more consolidation in upper lungs on initial CT increases the risk of adverse clinical outcome in COVID-19 patients. *Theranostics.* (2020) 10:5641–8. doi: 10.7150/tno.46465
30. Zhao W, Zhong Z, Xie X, Yu Q, Liu J. CT scans of patients with 2019 novel coronavirus (COVID-19) pneumonia. *Theranostics.* (2020) 10:4606–13. doi: 10.7150/tno.45016
31. Borghesi A, Maroldi R. COVID-19 outbreak in Italy: experimental chest X-ray scoring system for quantifying and monitoring disease progression. *Radiol Med.* (2020) 125:509–13. doi: 10.1007/s11547-020-01200-3
32. Borakati A, Perera A, Johnson J, Sood T. Diagnostic accuracy of X-ray versus CT in COVID-19: a propensity-matched database study. *BMJ Open.* (2020) 10:e042946. doi: 10.1136/bmjopen-2020-042946
33. Jacobi A, Chung M, Bernheim A, Eber C. Portable chest X-ray in coronavirus disease-19 (COVID-19): a pictorial review. *Clin Imaging.* (2020) 64:35–42. doi: 10.1016/j.clinimag.2020.04.001
34. Wong HYF, Lam HYS, Fong AH, Leung ST, Chin TW, Lo CSY, et al. Frequency and distribution of chest radiographic findings in patients positive for COVID-19. *Radiology.* (2020) 296:E72–8. doi: 10.1148/radiol.202001160
35. Zhu N, Zhang D, Wang W, Li X, Yang B, Song J, et al. A novel coronavirus from patients with pneumonia in China, 2019. *N Engl J Med.* (2020) 382:727–33. doi: 10.1056/NEJMoa2001017
36. Raj VS, Farag EA, Reusken CB, Lamers MM, Pas SD, Voermans J, et al. Isolation of MERS coronavirus from a dromedary camel, Qatar, 2014. *Emerg Infect Dis.* (2014) 20:1339–42. doi: 10.3201/eid2008.140663
37. Cotten M, Lam TT, Watson SJ, Palser AL, Petrova V, Grant P, et al. Full-genome deep sequencing and phylogenetic analysis of novel human betacoronavirus. *Emerg Infect Dis.* (2013) 19:736–42B. doi: 10.3201/eid1905.130057
38. Li B, Si HR, Zhu Y, Yang XL, Anderson DE, Shi ZL, et al. Discovery of bat coronaviruses through surveillance and probe capture-based next-generation sequencing. *mSphere.* (2020) 5:e00807–19. doi: 10.1128/mSphere.00807-19
39. Carroll D, Daszak P, Wolfe ND, Gao GF, Morel CM, Morzaria S, et al. The global virome project. *Science.* (2018) 359:872–4. doi: 10.1126/science.aap7463
40. Novel 2019 Coronavirus Genome. *Virological.* Available online at: <http://virological.org/t/novel-2019-coronavirus-genome/319> (accessed May 22, 2021).
41. Global Initiative on Sharing All Influenza Data. Available online at: <https://www.gisaid.org/> (accessed May 22, 2021).
42. Jin YH, Cai L, Cheng ZS, Cheng H, Deng T, Fan YP, et al. A rapid advice guideline for the diagnosis and treatment of 2019 novel coronavirus (2019-nCoV) infected pneumonia (standard version). *Mil Med Res.* (2020) 7:4. doi: 10.1186/s40779-020-0233-6
43. Yohe S, Thyagarajan B. Review of clinical next-generation sequencing. *Arch Pathol Lab Med.* (2017) 141:1544–57. doi: 10.5858/arpa.2016-0501-RA
44. Wang W, Xu Y, Gao R, Lu R, Han K, Wu G, et al. Detection of SARS-CoV-2 in different types of clinical specimens. *JAMA.* (2020) 323:1843–4. doi: 10.1001/jama.2020.3786
45. Emery SL, Erdman DD, Bowen MD, Newton BR, Winchell JM, Meyer RF, et al. Real-time reverse transcription-polymerase chain reaction assay for SARS-associated coronavirus. *Emerg Infect Dis.* (2004) 10:311–6. doi: 10.3201/eid1002.030759
46. Peiris JS, Chu CM, Cheng VC, Chan KS, Hung IF, Poon LL, et al. Clinical progression and viral load in a community outbreak of coronavirus-associated SARS pneumonia: a prospective study. *Lancet.* (2003) 361:1767–72. doi: 10.1016/S0140-6736(03)13412-5
47. General Office of National Health Commission of China. *Technical Guide for Laboratory Testing of Pneumonia in a Novel Coronavirus Infection.* General Office of National Health Commission of China (2020).
48. SuHong CZM, Jian H, Yu D, Xiao-Chen B, ShengQi W. Development of real time RT-PCR assay for the quantitation of SARS-associated coronavirus. *Prog Biochem Biophys.* (2004) 31:249–54.
49. Poon LL, Chan KH, Wong OK, Cheung TK, Ng I, Zheng B, et al. Detection of SARS coronavirus in patients with severe acute respiratory syndrome by conventional and real-time quantitative reverse transcription-PCR assays. *Clin Chem.* (2004) 50:67–72. doi: 10.1373/clinchem.2003.023663
50. Hang CZX, Weiwei G, Chong W, Hualei W, Na F, Tiecheng W, et al. Development of a real-time PCR assay to detect Middle East respiratory syndrome coronavirus. *J Pathogen Biol.* (2014) 9:673–7. doi: 10.13350/j.cjpb.140801
51. Corman VM, Ölschläger S, Wendtner CM, Drexler JF, Hess M, Drosten C. Performance and clinical validation of the RealStar MERS-CoV Kit for detection of Middle East respiratory syndrome coronavirus RNA. *J Clin Virol.* (2014) 60:168–71. doi: 10.1016/j.jcv.2014.03.012
52. Hashemzadeh MS, Rasouli R, Zahraei B, Izadi M, Tat M, Saadat SH, et al. Development of dual taqman based one-step rRT-PCR assay panel for rapid and accurate diagnostic test of MERS-CoV: a novel human coronavirus, ahead of Hajj Pilgrimage. *Iran Red Crescent Med J.* (2016) 18:e23874. doi: 10.5812/ircmj.23874
53. Chu DKW, Pan Y, Cheng SMS, Hui KPY, Krishnan P, Liu Y, et al. Molecular diagnosis of a novel coronavirus (2019-nCoV) causing an outbreak of pneumonia. *Clin Chem.* (2020) 66:549–55. doi: 10.1093/clinchem/hvaa029
54. FDA. *Emergency Use Authorizations.* Available online at: <https://www.fda.gov/emergency-preparedness-and-response/mcm-legal-regulatory-and-policy-framework/emergency-use-authorization> (accessed May 22, 2021).
55. Rüménapf T, Strauss EG, Strauss JH. Subgenomic mRNA of Aura alphavirus is packaged into virions. *J Virol.* (1994) 68:56–62. doi: 10.1128/JVI.68.1.56-62.1994
56. Simons FA, Vennema H, Rofina JE, Pol JM, Horzinek MC, Rottier PJM, et al. A mRNA PCR for the diagnosis of feline infectious peritonitis. *J Virol Methods.* (2005) 124:111–6. doi: 10.1016/j.jviromet.2004.11.012
57. Guo Y, Wang K, Zhang Y, Zhang W, Wang L, Liao P. Comparison and analysis of detection performance of six domestic new coronavirus nucleic acid detection reagents. *Chongqing Med.* (2020) 49:2435–9. doi: 10.3969/j.issn.1671-8348.2020.15.004
58. Ahn DG, Shin HJ, Kim MH, Lee S, Kim HS, Myoung J, et al. Current status of epidemiology, diagnosis, therapeutics, and vaccines for novel coronavirus disease 2019 (COVID-19). *J Microbiol Biotechnol.* (2020) 30:313–24. doi: 10.4014/jmb.2003.03011
59. Wee SK, Sivalingam SP, Yap EPH. Rapid direct nucleic acid amplification test without RNA extraction for SARS-CoV-2 using a portable PCR thermocycler. *Genes.* (2020) 11:664. doi: 10.3390/genes11060664
60. Pham XH, Baek A, Kim TH, Lee SH, Rho WY, Chung WJ, et al. Graphene oxide conjugated magnetic beads for RNA extraction. *Chem Asian J.* (2017) 12:1883–8. doi: 10.1002/asia.201700554
61. Jingbo Zou YZ, Jie Qiao, Xia Li, Jing Zhou, Tingyan Sun, Yiheng Ouyang, Zongyu Zhou, Xiaoyu Wei, Wenguang Tian, Mei Han. Case report on new type coronavirus positive in 2019 in the feces of treated “new crown” patients in Chongqing. *Chin J Virol.* (2020) 36:165–8. doi: 10.13242/j.cnki.bingduxuebao.003653
62. Conti P, Ronconi G, Caraffa A, Gallenga CE, Ross R, Frydas I, et al. Induction of pro-inflammatory cytokines (IL-1 and IL-6) and lung inflammation by Coronavirus-19 (COVI-19 or SARS-CoV-2): anti-inflammatory strategies. *J Biol Regul Homeost Agents.* (2020) 34:327–31. doi: 10.23812/CONTI-E
63. Wuhan Easy diagnosis Biomedicine Co., Ltd. Available online at: <http://www.mdeasydiagnosis.com/> (accessed May 22, 2021).



64. Zhejiang Orient Gene Biotech Co., Ltd. Available online at: <http://zjdfjyswzp.yixie8.com/> (accessed May 22, 2021).
65. Promega. Available online at: <https://www.promega.com.cn/products/> (accessed May 22, 2021).
66. Shaorui Shi BN, Guo Y, Luo L, Zhang L, Li W, Xian G, et al. Viral nucleic acid test results of multiple biological samples from new coronavirus pneumonia cases. *West China Med J.* (2020) 35:132–6. doi: 10.7507/1002-0179.202002063
67. Broughton JP, Deng X, Yu G, Fasching CL, Servellita V, Singh J, et al. CRISPR-Cas12-based detection of SARS-CoV-2. *Nat Biotechnol.* (2020) 38:870–4. doi: 10.1038/s41587-020-0513-4
68. Patchsung M, Jantarug K, Pattama A, Aphicho K, Suraritdechchai S, Meesawat P, et al. Clinical validation of a Cas13-based assay for the detection of SARS-CoV-2 RNA. *Nat Biomed Eng.* (2020) 4:1140–9. doi: 10.1038/s41551-020-00603-x
69. The Global Fund. *Diagnostic Test Kits and Equipments Eligible for Procurement According to Board Decision on Additional Support for Country Responses to COVID-19.* Available online at: [https://www.theglobalfund.org/media/9629/covid19\\_diagnosticproducts\\_list\\_en.pdf/](https://www.theglobalfund.org/media/9629/covid19_diagnosticproducts_list_en.pdf/) (accessed May 22, 2021).
70. Hong TC, Mai QL, Cuong DV, Parida M, Minekawa H, Notomi T, et al. Development and evaluation of a novel loop-mediated isothermal amplification method for rapid detection of severe acute respiratory syndrome coronavirus. *J Clin Microbiol.* (2004) 42:1956–61. doi: 10.1128/JCM.42.5.1956-1961.2004
71. Kashir J, Yaqinuddin A. Loop mediated isothermal amplification (LAMP) assays as a rapid diagnostic for COVID-19. *Med Hypotheses.* (2020) 141:109786. doi: 10.1016/j.mehy.2020.109786
72. Rödel J, Egerer R, Suleyman A, Sommer-Schmid B, Baier M, Henke A, et al. Use of the variplex<sup>TM</sup> SARS-CoV-2 RT-LAMP as a rapid molecular assay to complement RT-PCR for COVID-19 diagnosis. *J Clin Virol.* (2020) 132:104616. doi: 10.1016/j.jcv.2020.104616
73. Tworek JA, Khan F, Sekedat MD, Scheidel C, Malani AN. The utility of rapid nucleic acid amplification testing to triage symptomatic patients and to screen asymptomatic preprocedure patients for SARS-CoV-2. *Open Forum Infect Dis.* (2021) 8:ofaa607. doi: 10.1093/ofid/ofaa607
74. Lopez-Rincon A, Perez-Romero CA, Tonda A, Mendoza-Maldonado L, Claassen E, Garssen J, et al. Design of specific primer sets for the detection of B.1.1.7, B.1.351 and P.1 SARS-CoV-2 variants using deep learning. *BioRxiv.* (2021). doi: 10.1101/2020.12.29.424715
75. Korukluoglu G, Kolukirik M, Bayraktar F, Ozgumus GG, Altas AB, Cosgun Y, et al. 40 minutes RT-qPCR assay for screening spike N501Y and HV69-70del mutations. *BioRxiv.* (2021). doi: 10.1101/2021.01.26.428302
76. Fujimoto K, Chan KH, Takeda K, Lo KF, Leung RH, Okamoto T. Sensitive and specific enzyme-linked immunosorbent assay using chemiluminescence for detection of severe acute respiratory syndrome viral infection. *J Clin Microbiol.* (2008) 46:302–10. doi: 10.1128/JCM.01006-07
77. Sastre P, Dijkman R, Camunas A, Ruiz T, Jebbink MF, van der Hoek L, et al. Differentiation between human coronaviruses NL63 and 229E using a novel double-antibody sandwich enzyme-linked immunosorbent assay based on specific monoclonal antibodies. *Clin Vaccine Immunol.* (2011) 18:113–8. doi: 10.1128/0014-2935.110.00355-10
78. Sunwoo HH, Palaniyappan A, Ganguly A, Bhatnagar PK, Das D, El-Kadi AO, et al. Quantitative and sensitive detection of the SARS-CoV spike protein using bispecific monoclonal antibody-based enzyme-linked immunoassay. *J Virol Methods.* (2013) 187:72–8. doi: 10.1016/j.jviromet.2012.09.006
79. Chen Y, Chan KH, Kang Y, Chen H, Luk HK, Poon RW, et al. A sensitive and specific antigen detection assay for Middle East respiratory syndrome coronavirus. *Emerg Microbes Infect.* (2015) 4:e26. doi: 10.1038/emi.2015.26
80. Chao He HJ, Yi Xie, Jie Chen, Binwu Ying, Xiaojun Lu, Xingbo Song, Minjin Wang, Yong He, Mei Kang. Discussion on laboratory test path of diagnosis and treatment of new coronavirus pneumonia. *Chin J Respir Crit Care Med.* (2020) 19:125–7. doi: 10.7507/1671-6205.202002053
81. Xiang F, Wang X, He X, Peng Z, Yang B, Zhang J, et al. Antibody detection and dynamic characteristics in patients with coronavirus disease 2019. *Clin Infect Dis.* (2020) 71:1930–4. doi: 10.1093/cid/ciaa461
82. Li Z, Yi Y, Luo X, Xiong N, Liu Y, Li S, et al. Development and clinical application of a rapid IgM-IgG combined antibody test for SARS-CoV-2 infection diagnosis. *J Med Virol.* (2020) 92:1518–24. doi: 10.1002/jmv.25727
83. Lassaunière R, Frische A, Harboe ZB, Nielsen ACY, Fomsgaard A, Krogfelt KA, et al. Evaluation of nine commercial SARS-CoV-2 immunoassays. *medRxiv.* (2020). doi: 10.1101/2020.04.09.20056325
84. Garcia-Beltran WF, Lam EC, Astudillo MG, Yang D, Miller TE, Feldman J, et al. COVID-19-neutralizing antibodies predict disease severity and survival. *Cell.* (2021) 184:476–88.e11. doi: 10.1016/j.cell.2020.12.015
85. Yüce M, Filiztekin E, Özkaya KG. COVID-19 diagnosis - a review of current methods. *Biosens Bioelectron.* (2021) 172:112752. doi: 10.1016/j.bios.2020.112752
86. Ehrenfeld M, Tincani A, Andreoli L, Cattalini M, Greenbaum A, Kanduc D, et al. Covid-19 and autoimmunity. *Autoimmun Rev.* (2020) 19:102597. doi: 10.1016/j.autrev.2020.102597
87. Khamis R. Rogue antibodies could be driving severe COVID-19. *Nature.* (2021) 590:29–31. doi: 10.1038/d41586-021-00149-1
88. Bastard P, Rosen LB, Zhang Q, Michailidis E, Hoffmann HH, Zhang Y, et al. Autoantibodies against type I IFNs in patients with life-threatening COVID-19. *Science.* (2020) 370:eabd4585. doi: 10.1126/science.abd4585
89. Jamilloux Y, Henry T, Belot A, Viel S, Fauter M, El Jammal T, et al. Should we stimulate or suppress immune responses in COVID-19? Cytokine and anti-cytokine interventions. *Autoimmun Rev.* (2020) 19:102567. doi: 10.1016/j.autrev.2020.102567
90. Chen N, Zhou M, Dong X, Qu J, Gong F, Han Y, et al. Epidemiological and clinical characteristics of 99 cases of 2019 novel coronavirus pneumonia in Wuhan, China: a descriptive study. *Lancet.* (2020) 395:507–13. doi: 10.1016/S0140-6736(20)30211-7
91. Takahashi T, Ellingson MK, Wong P, Israelow B, Lucas C, Klein J, et al. Sex differences in immune responses that underlie COVID-19 disease outcomes. *Nature.* (2020) 588:315–20. doi: 10.1038/s41586-020-2700-3
92. Mingchao Zhu YZ. Laboratory examination of new coronavirus pneumonia and management of clinical laboratory. *J Trop Med.* (2020) 20:294–6.
93. *Cytokine Storm Detection Scheme in COVID-19.* Available online at: <https://wiki.antpedia.com/xinxingguanzhuangbingdufeiyanyixibaoyinzifengbaojiancefanganllaimple-2374441-news> (accessed May 22, 2021).
94. Guan WJ, Ni ZY, Hu Y, Liang WH, Ou CQ, He JX, et al. Clinical characteristics of coronavirus disease 2019 in China. *N Engl J Med.* (2020) 382:1708–20. doi: 10.1056/NEJMoa2002032
95. Karzai W, Oberhoffer M, Meier-Hellmann A, Reinhart K. Procalcitonin—a new indicator of the systemic response to severe infections. *Infection.* (1997) 25:329–34. doi: 10.1007/BF01740811
96. Seo G, Lee G, Kim MJ, Baek SH, Choi M, Ku KB, et al. Rapid detection of COVID-19 causative virus (SARS-CoV-2) in human nasopharyngeal swab specimens using field-effect transistor-based biosensor. *ACS Nano.* (2020) 14:5135–42. doi: 10.1021/acsnano.0c02823

**Conflict of Interest:** XC and MZ were employed by the company Zhuhai Livzon Diagnostics Inc.

The remaining authors declare that the research was conducted in the absence of any commercial or financial relationships that could be construed as a potential conflict of interest.

Copyright © 2021 Liu, Li, Chu, Zeng, Liu, He, Zou, Zheng, Corpe, Zhang, Xu and Wang. This is an open-access article distributed under the terms of the Creative Commons Attribution License (CC BY). The use, distribution or reproduction in other forums is permitted, provided the original author(s) and the copyright owner(s) are credited and that the original publication in this journal is cited, in accordance with accepted academic practice. No use, distribution or reproduction is permitted which does not comply with these terms.

## GLOSSARY

ACE2, angiotensin-converting enzyme II; ALT, alanine aminotransferase; AST, aspartate aminotransferase; CLEIA, chemiluminescence enzyme-linked immunosorbent assay; CoV, coronavirus; COVID-19, coronavirus disease 2019; CRP, C-reactive protein; CT, computed tomography; DPP, dual path platform; DR, detection rate; ELISA, enzyme-linked immunosorbent assay; ESR, erythrocyte sedimentation rate; FET, field-effect transistor; FER, ferritin; GISAIID, Global Initiative on Sharing All Influenza Data; GGOs, ground-glass opacities; HCoV, human coronavirus; hs-cTnI, hypersensitive troponin I; LAMP, loop-mediated

isothermal amplification; LDH, lactate dehydrogenase; MERS-CoV, Middle East respiratory syndrome coronavirus; NGS, next-generation sequencing; NPA, negative percent agreement; N protein, nucleocapsid protein; ORF1ab, open reading frame 1ab; POC, point of care; PCT, procalcitonin; PPA positive percent agreement; PPV, positive predictive value; PGV, ground-glass opacity volume; RdRp, RNA-dependent RNA polymerase; rRT-PCR, real-time reverse transcription polymerase chain reaction; SARS-CoV-1, severe acute respiratory syndrome coronavirus 1; S protein, spike protein; SpO<sub>2</sub>, oxygen saturation; TLR, Toll-like receptor; upE, upstream of the E protein; VL, viral load; WHO, World Health Organization.



# Can Clinical Symptoms and Laboratory Results Predict CT Abnormality? Initial Findings Using Novel Machine Learning Techniques in Children With COVID-19 Infections

## OPEN ACCESS

### Edited by:

Reza Lashgari,  
Institute for Research in Fundamental  
Sciences, Iran

### Reviewed by:

Chengjin Yu,  
Zhejiang University, China  
Lin Gu,  
RIKEN Yokohama, Japan

### \*Correspondence:

Jianbo Shao  
drshaojb@sina.com  
Jun Xia  
xiajun@email.szu.edu.cn  
Guang Yang  
g.yang@imperial.ac.uk

†These authors have contributed  
equally to this work

### Specialty section:

This article was submitted to  
Infectious Diseases - Surveillance,  
Prevention and Treatment,  
a section of the journal  
Frontiers in Medicine

Received: 24 April 2021

Accepted: 17 May 2021

Published: 14 June 2021

### Citation:

Ma H, Ye Q, Ding W, Jiang Y, Wang M,  
Niu Z, Zhou X, Gao Y, Wang C,  
Menpes-Smith W, Fang EF, Shao J,  
Xia J and Yang G (2021) Can Clinical  
Symptoms and Laboratory Results  
Predict CT Abnormality? Initial  
Findings Using Novel Machine  
Learning Techniques in Children With  
COVID-19 Infections.  
Front. Med. 8:699984.  
doi: 10.3389/fmed.2021.699984

Huijing Ma<sup>1†</sup>, Qinghao Ye<sup>2,3†</sup>, Weiping Ding<sup>4†</sup>, Yinghui Jiang<sup>2,3</sup>, Minhao Wang<sup>2,3</sup>,  
Zhangming Niu<sup>3</sup>, Xi Zhou<sup>5</sup>, Yuan Gao<sup>6,7</sup>, Chengjia Wang<sup>8</sup>, Wade Menpes-Smith<sup>7</sup>,  
Evandro Fei Fang<sup>9</sup>, Jianbo Shao<sup>10\*</sup>, Jun Xia<sup>6\*</sup> and Guang Yang<sup>11,12\*</sup>

<sup>1</sup> Imaging Center, Tongji Medical College, Wuhan Children's Hospital (Wuhan Maternal and Child Healthcare Hospital),  
Huazhong University of Science & Technology, Wuhan, China, <sup>2</sup> Hangzhou Ocean's Smart Boya Co., Ltd, Hangzhou, China,  
<sup>3</sup> Mind Rank Ltd, Hong Kong, China, <sup>4</sup> School of Information Science and Technology, Nantong University, Nantong, China,  
<sup>5</sup> Institute of Biomedical Engineering, University of Oxford, Oxford, United Kingdom, <sup>6</sup> Department of Radiology, Shenzhen  
Second People's Hospital, The First Affiliated Hospital of Shenzhen University Health Science Center, Shenzhen, China,  
<sup>7</sup> Aladdin Healthcare Technologies Ltd, London, United Kingdom, <sup>8</sup> British Heart Foundation (BHF) Centre for Cardiovascular  
Science, University of Edinburgh, Edinburgh, United Kingdom, <sup>9</sup> Department of Clinical Molecular Biology, University of Oslo,  
Oslo, Norway, <sup>10</sup> COVID-19 Specialist Team, Wuhan Children's Hospital, Tongji Medical College, Huazhong University of  
Science & Technology, Wuhan, China, <sup>11</sup> Cardiovascular Research Centre, Royal Brompton Hospital, London,  
United Kingdom, <sup>12</sup> National Heart and Lung Institute, Imperial College London, London, United Kingdom

The rapid spread of coronavirus 2019 disease (COVID-19) has manifested a global public health crisis, and chest CT has been proven to be a powerful tool for screening, triage, evaluation and prognosis in COVID-19 patients. However, CT is not only costly but also associated with an increased incidence of cancer, in particular for children. This study will question whether clinical symptoms and laboratory results can predict the CT outcomes for the pediatric patients with positive RT-PCR testing results in order to determine the necessity of CT for such a vulnerable group. Clinical data were collected from 244 consecutive pediatric patients (16 years of age and under) treated at Wuhan Children's Hospital with positive RT-PCR testing, and the chest CT were performed within 3 days of clinical data collection, from January 21 to March 8, 2020. This study was approved by the local ethics committee of Wuhan Children's Hospital. Advanced decision tree based machine learning models were developed for the prediction of CT outcomes. Results have shown that age, lymphocyte, neutrophils, ferritin and C-reactive protein are the most related clinical indicators for predicting CT outcomes for pediatric patients with positive RT-PCR testing. Our decision support system has managed to achieve an AUC of 0.84 with 0.82 accuracy and 0.84 sensitivity for predicting CT outcomes. Our model can effectively predict CT outcomes, and our findings have indicated that the use of CT should be reconsidered for pediatric patients, as it may not be indispensable.

**Keywords:** COVID-19, decision trees, machine learning, RT-PCR—polymerase chain reaction with reverse transcription, artificial intelligence, pediatric

## INTRODUCTION

Since December 2019, the worldwide spread of coronavirus 2019 disease (COVID-19) has had a significant impact on public health and the global economy. Although most people with COVID-19 manifest mild symptoms, ~20% of patients go through several clinical stages ending in diffuse lung injury, i.e., severe acute respiratory syndrome coronavirus 2 (SARS-CoV-2).

COVID-19 is highly contagious, and severe cases can lead to acute failure of the lungs, multiple organs and ultimately death. The diagnosis of COVID-19 can be confirmed by a laboratory test, i.e., the reverse transcription-polymerase chain reaction (RT-PCR) test; however, the test has high false-negative rates and low sensitivity, which leads to late diagnosis and treatment. Delays in the diagnosis of COVID-19 indicate that patients will amplify the hazard of patient-to-patient COVID-19 transmission within the hospital.

Chest imaging techniques, e.g., chest computed tomography (CT), provides valuable diagnostic and monitoring information that can be used as an important complementary indicator in COVID-19 screening due to high sensitivity (1–4). This is mainly due to most COVID-19 infected patients having chest imaging abnormalities, e.g., bilateral patchy shadows and ground glass opacity (GGO), which are manifested in chest CT scans (5). Meanwhile, subsequent chest CT imaging every 3–5 days are recommended to evaluate the disease progression for fast therapeutic response. Hence, chest CT imaging has become a viable method for early COVID-19 diagnosis and tracking the progression of the disease with high sensitivity. In addition, the WHO Guidelines on Imaging and COVID-19 suggest the diagnostic use of chest imaging for symptomatic patients suspected of having COVID-19 if: (1) RT-PCR testing is not available; (2) RT-PCR testing is available but results are delayed and (3) initial RT-PCR testing is negative but there remains a high clinical suspicion of COVID-19. From a global perspective, imaging techniques are important due to the fact that imaging infrastructures are more advanced in many countries compared to the COVID-19 RT-PCR diagnostic laboratories.

Although chest CT imaging can provide important and complementary diagnostic and prognostic information for COVID-19 patients, some studies believe that the results of CT scans are not highly specific and are not suitable for screening for COVID-19 (6–9). Moreover, multiple chest CT scans have potential carcinogenic effects, which have more prominent risk for vulnerable pediatric patients (10). Besides, for pediatric patients with positive RT-PCR testing results, it is well-known that they can have milder symptoms compared to adults patients (11–13). Despite the fact that chest CT examinations can help us understand the condition of the lungs in pediatric patients (14–16), 35% children with positive RT-PCR testing results can still have negative CT examinations (13, 15), and therefore these patients suffer from unnecessary ionizing radiation (17, 18). Currently, there is no decision support system that can help clinicians to determine whether these pediatric patients with positive RT-PCR testing results need further chest CT examinations.

In this study, we study the relationship between the results of the chest CT examinations and clinical symptoms, laboratory tests and other clinical factors for RT-PCR positive pediatric cases, retrospectively. Using our developed advanced machine learning methods, we establish a systematic decision support system to predict the chest CT results for RT-PCR positive pediatric patients. Our approach will help vulnerable pediatric patients to avoid receiving unnecessary radiation from chest CT scans. At the same time, early predictions of the chest CT results for the pediatric patients using our decision support system can provide better patient classification, clinical decision-making, and more efficient hospital resource allocation.

## METHODS

### Datasets

The pediatric patient datasets were collected from Wuhan Children's Hospital. The tabular data contained information for 244 pediatric cases, in which 3 cases had critical COVID-19 symptoms (**Table 1**). For the feature columns of the tabular data, we collected 32 clinical symptoms for diagnosis (e.g., cough, running nose, sneeze etc.). Following the standard experimental practice, we employed the 5-fold cross-validation for model selection and evaluation. In particular, we split the datasets into five disjoint folds with the same number of samples. Then, we held out each fold for evaluation and the rest 4-folds were used for training our machine learning models. The final result was calculated by averaging over the results of the five experiments. This study was approved by the local Ethics Committee of Wuhan Children's Hospital (Wuhan Maternal and Child Health Care Hospital #WHCH2020005). Written informed parental/guardian consent and child assent (where appropriate) were obtained prior to enrollment in the study.

### Proposed Methods

It is essential to explore the relationship between the clinical characteristics of children and the COVID-19 RT-PCR testing results. Therefore, an explainable model is required not only to find the implicit relations but can also yield reasonable explanations. Meanwhile, given tabulated data of children who were tested COVID-19 positive or negative, the proposed model should accurately predict the corresponding testing results. We denoted children who were infected by COVID-19 virus (RT-PCR positive) as class 1 and children who were COVID-19 negative (RT-PCR negative) as class 0.

Before building the model, the tabulated data were pre-processed to explore the mean and standard variance of each feature, which provided extra information for mining the relationship. Meanwhile, we also divided the discrete features (e.g., age, leukocyte etc.) into several disjoint intervals which could reduce the complexity of the model.

Besides, feature encoding was also applied due to the fact that some features were not inner correlated. Gender, for instance, was sequentially numbered instead of recorded separately. Therefore, we adopted the one-hot encoding to handle such problems. After pre-processing, we further explored the mutual relationship within the encoded features. We then used the



**TABLE 1** | Baseline characteristics of children with COVID-19.

|   | CT normal<br>(n = 102) | CT abnormal<br>(n = 142) | All patients<br>(n = 244) |
|---|------------------------|--------------------------|---------------------------|
| <b>Fundamental state</b>                              |                        |                          |                           |
| Age [Mean (SD)]                                       | 7.9 (4.5)              | 5.6 (4.8)                | 6.6 (4.8)                 |
| Sex (Male/Female)                                     | 54/48                  | 85/56                    | 139/104                   |
| Contact history                                       | 92                     | 126                      | 218                       |
| <b>Symptoms</b>                                       |                        |                          |                           |
| Fever   | 23                     | 70                       | 93                        |
| Cough   | 23                     | 70                       | 93                        |
| Vomit   | 3                      | 13                       | 16                        |
| Diarrhea  | 2                      | 9                        | 11                        |
| Poor spirit   | 0                      | 7                        | 7                         |
| Running nose  | 4                      | 11                       | 15                        |
| <b>Laboratory examination [median (Range, Q1–Q3)]</b> |                        |                          |                           |
| LDH(U/L)  | 221 (189–260)          | 246 (213–326.5)          | 238 (201–294)             |
| Ferritin (ng/mL)                                      | 58.1 (36.8–86.6)       | 61.6 (40.2–95.3)         | 58.9 (39.9–90.2)          |
| CK-MB (U/L)   | 20 (16–32)             | 24 (18–35)               | 23 (17–34)                |
| Leukocyte (10 <sup>9</sup> /L)                        | 7 (6–8.9)              | 6.9 (5.4–8.6)            | 6.9 (5.6–8.7)             |
| Neutrophils (10 <sup>9</sup> /L)                      | 3.6 (2.5–4.6)          | 2.4 (1.7–3.8)            | 3 (1.9–4.2)               |
| Lymphocyte (10 <sup>9</sup> /L)                       | 2.8 (2.3–3.5)          | 2.9 (2–4.5)              | 2.9 (2.1–4)               |
| C-Reactive protein (mg/L)                             | 1 (0.8–4)              | 3 (1–5.9)                | 1.2 (0.8–5)               |
| Neutrophil lymphocyte ratio (NLR)                     | 1.3 (0.9–1.9)          | 0.9 (0.5–1.5)            | 1 (0.6–1.7)               |

LDH, Lactic Dehydrogenase; CK-MB, Creatine Kinase-MB.

random walk to quantify the strength of the pairwise relations for different features. For example, we found that age had a strong correlation with the contents of the C-reactive protein (CRP).

Furthermore, since the contributions of each feature varied, we quantified the importance of features. Features were ranked by measurement generated from algorithms, and we adopted the features with high importance scores to train our model. The ultimate goal of our decision support system is to determine whether CT is required if the RT-PCR test is positive. This is a classification problem with prerequisites; therefore, the interpretability of the model is also very important. Our proposed decision support system (**Figure 1**) contains the two major modules as follows.

## An Explainable Feature Extractor Module

### TF-IDF Embedding

TF-IDF, which stands for Term Frequency–Inverse Document Frequency, is a numerical statistic that can reflect how important a word is to a document in a collection or corpus. A word with higher TF-IDF value is thought to be more important and representative for a document. In this study, for each patient, we extract all the feature values and combines them into a single document. These documents form the whole corpus collection. Then we use TfidfVectorizer from scikit-learn library to find the most important and influential features.

### Frequency Encoding/Count Encoding

Frequency Encoding/Count Encoding: Both frequency encoding and count encoding are methods to utilize counts of the

categories. Since these two methods mainly focus on the frequency and count of each category, they are less affected by the feature values. For example, if two features have similar frequency distribution, we can keep one feature and leave out the other. Although we may miss some information from the discarded features, our model is less likely to overfit as it has less features. In our current study, we develop frequency encoding and apply it to find connections and relationships between features.

### Target Encoding

Target encoding is a process of replacing a categorical value with the mean of the target variable.

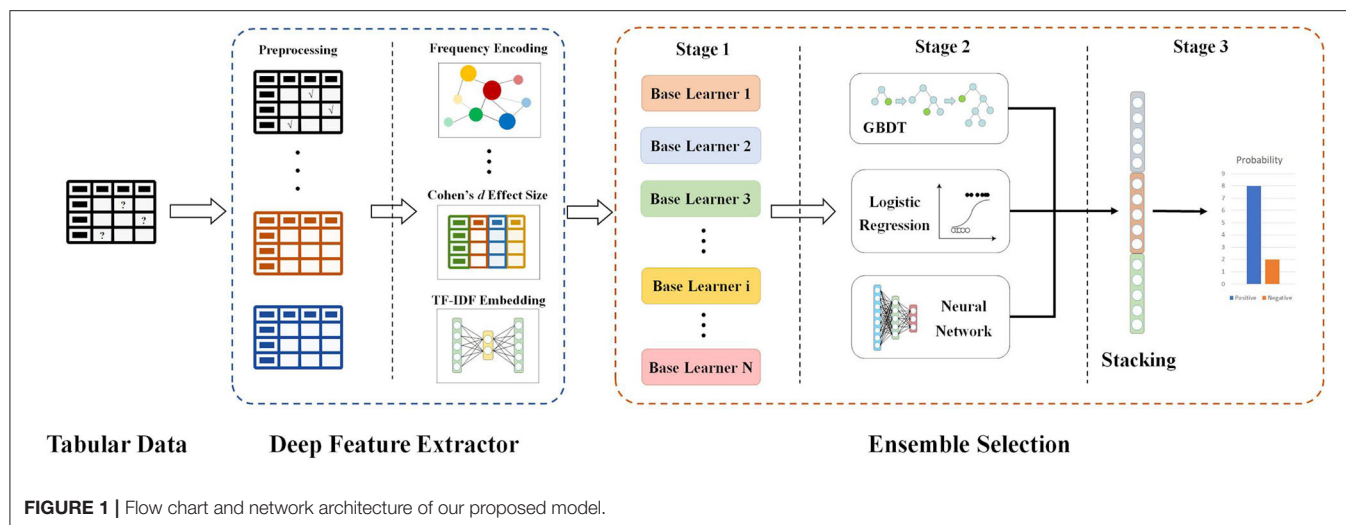
### Cohen Effect Size

Cohen's *d* is an appropriate effect size for the comparison between two means. To calculate the standardized mean difference *d* between two groups, subtract the mean of one group from the other and divide the result by the standard deviation *s* of the population from which the groups were sampled.

## An Explainable Classification Module

### GBDT

Gradient Boosting is a machine learning technique for regression and classification problems, which produces a prediction model in the form of an ensemble of weak prediction models, typically decision trees. It can be fitted to current residuals with gradients of the loss function, in a forward stepwise manner. The GBDT requires no feature normalization and it has an inherently feature

**TABLE 2 |** Odds ratio for features.

| Feature                            | OR value | 95% CI        | p-value |
|------------------------------------|----------|---------------|---------|
| Ferritin                           | 10.36    | [1.28, 83.69] | 0.0196  |
| Lymphocyte                         | 3.11     | [1.57, 6.15]  | 0.0014  |
| C-reactive protein                 | 2.40     | [1.42, 4.05]  | 0.0014  |
| LDH                                | 2.30     | [1.12, 4.72]  | 0.0322  |
| CK-MB                              | 1.67     | [0.5, 5.59]   | 0.5815  |
| Leukocyte                          | 0.47     | [0.26, 0.85]  | 0.0199  |
| Age                                | 0.41     | [0.24, 0.69]  | 0.0011  |
| Neutrophils                        | 0.41     | [0.24, 0.7]   | 0.0016  |
| Neutrophils lymphocyte ratio (NLR) | 0.37     | [0.15, 0.87]  | 0.0322  |

selection during the learning process. Besides, it is easy to specify different loss functions for the GBDT.

### Bayesian Optimization

Bayesian optimization is a sequential design strategy for global optimization for black-box functions that does not assume any functional forms.

Because of the imbalanced nature of the dataset, the traditional training process would lead to unstable performance. In order to tackle unstable training, we divide our dataset into 5-folds and apply the stratified sampling method to ensure each fold's ratio of the positive patients to the negative ones is close to the overall ratio. Furthermore, we adopt the idea of focal loss (19) in our Bayesian optimization process to minimize the influence of the imbalance.

We used the odds ratio (OR value) to quantify the impact of the individual feature against the output value of our model and the results are reported in **Table 2**. The OR value in our work referred to the ratio of the exposed patient to the unexposed patient in the positive group divided by the ratio of the exposed patient to the unexposed patient in the negative group. For each feature, if its OR value was  $>1$ , it indicated that the factor, which

patients were exposed to, was a risk factor that would increase the possibility of being positive. If the OR value was  $<1$ , the factor was one protective factor that decreased the chance to be positive. Besides, if the OR value equaled 1 or the confidence interval contained 1, the factor could be considered as irrelevant from a statistical perspective. For example, for feature age, we set the threshold to 7 so the factor is  $\text{age} \geq 7$ . As the OR value was  $<1$  and the confidence interval did not contain 1, so children exposed to this factor, in other words, children who were older than 7 years old were less likely to be positive in CT abnormality than those unexposed, who were under 7 years old.

We also used Spearman's correlation to find features most related to our target and screened out highly correlated features to minimize input feature numbers. We use a heat map in **Figure 2** to present our results. Then we set the threshold value to 0.4 and selected five features out of all the features, which were age, C-reactive protein, Neutrophils, lymphocyte, and ferritin.

However, when we used single-feature models, we could only obtain a relatively fair performance in predicting CT's abnormality. To improve the performance and generalization of our model, the combination of features was necessary. After grouping and aggregating all the patients by their ages and their CT results, we found three significant bounds in ages, which were 4, 7, and 14. We then divided patients into four age groups [0, 4], [4, 7], [7, 14], [14, 16] and calculated the ratio of positive ones to negative ones inside. So, we chose the age as our base feature and combined other features with it.

## RESULTS

As **Table 3** shows, compared to conventional and state-of-the-art models, our model has performed significantly better. For instance, our model achieves a higher AUC score of 0.8412, and it is performed better than compared methods by at least 0.8464 for the F1 score. This can be attributed to our effective feature extraction. Compared to our model, TabNet (20), AutoML (21), and DeepFM (22) can only extract the

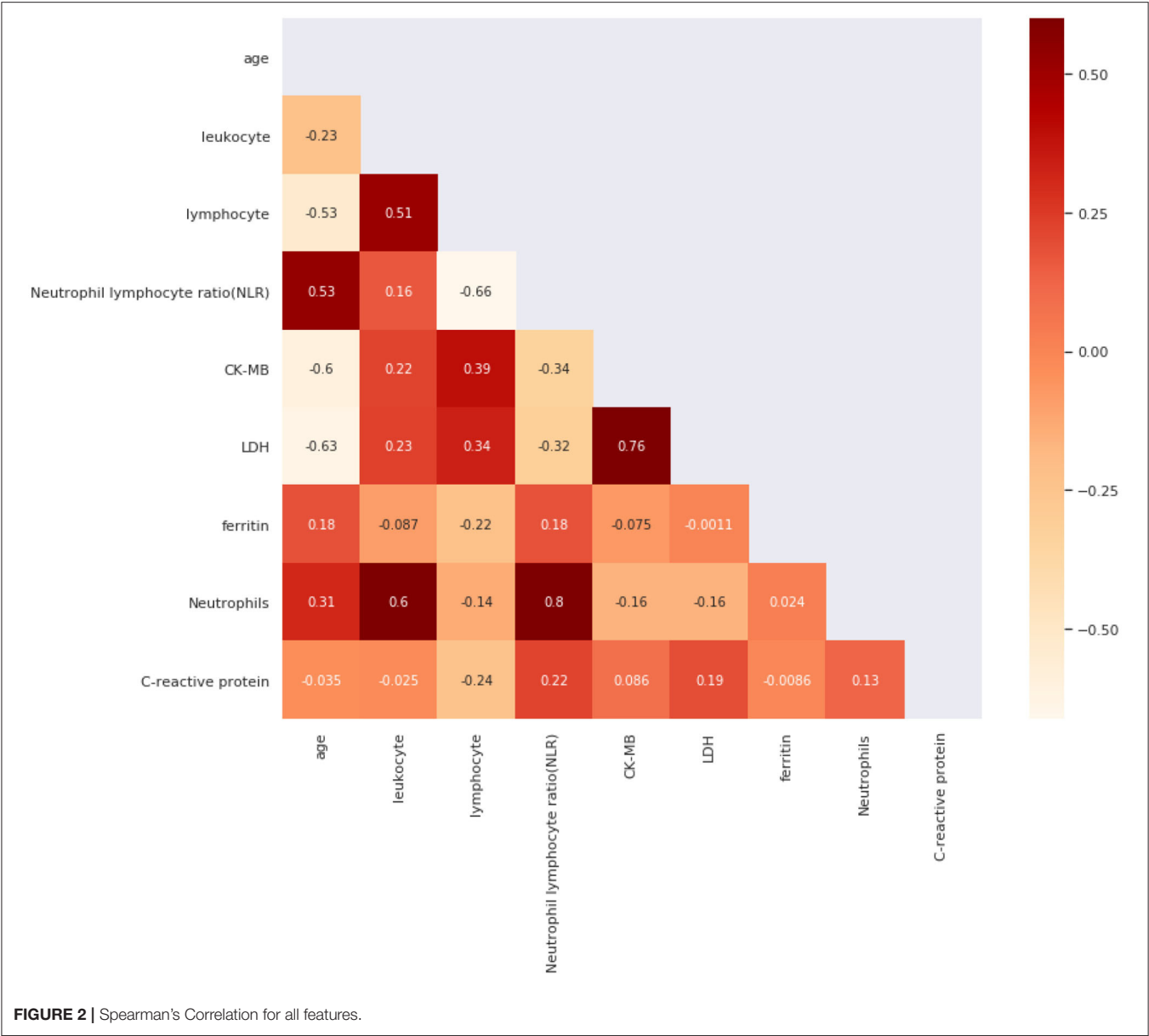


**TABLE 3 |** Comparison of general models.

| Method       | AUC           | Accuracy      | Recall        | Precision     | F1 score      |
|--------------|---------------|---------------|---------------|---------------|---------------|
| TabNet (20)  | 0.7891        | 0.7755        | 0.7727        | 0.7391        | 0.7559        |
| AutoML (21)  | 0.7453        | 0.7368        | 0.7143        | 0.7895        | 0.7519        |
| DeepFM (22)  | 0.6941        | 0.6818        | 0.7273        | 0.6667        | 0.6970        |
| XGBoost (23) | 0.7131        | 0.7097        | 0.6429        | 0.6923        | 0.6676        |
| Our Model    | <b>0.8412</b> | <b>0.8191</b> | <b>0.8597</b> | <b>0.8389</b> | <b>0.8464</b> |

For all the comparison methods please refer to the opensource implementations at TabNet: <https://github.com/dreamquark-ai/tabnet>, AutoML: <https://github.com/google/automl>, DeepFM: <https://github.com/ChenglongChen/tensorflow-DeepFM>, XGBoost: <https://github.com/dmlc/xgboost>. Bold values indicate the best performed method.

representation of the whole tabular while ignoring representation of the feature itself, which is also important for mining tabular

data. Meanwhile, compared with XGBoost (23), we project the feature into higher dimensions with embedding leading to better representation of features. Besides, this leads to an intuitive interpretation, for instance, C-reactive protein may not only indicate the body is healthy or not but can also share a correlation with other indicators (e.g., lymphocyte). Therefore, better feature representation can also lead to better capability of model generalization.

To examine the influence of each component and module in our model, we conducted ablation studies, and the results are summarized in **Table 4**. It can be seen from **Table 4** that with the equipment of the encoding procedure, our model can find strong connections between indicators thus has resulted in better performance than the model with GBDT only. Moreover, embedding the features in tabular data and projecting them into higher dimensional space can enrich the representation

**TABLE 4 |** Result of all cases where each proposed method can be applied.

| Model | GBDT | Encoding | Embedding | AUC           | Accuracy      | Recall        | Precision     | F1 score      |
|-------|------|----------|-----------|---------------|---------------|---------------|---------------|---------------|
| 1     | ✓    |          |           | 0.7081        | 0.6957        | 0.7297        | 0.7105        | 0.7201        |
| 2     | ✓    | ✓        |           | 0.7635        | 0.7581        | 0.7941        | 0.7714        | 0.7828        |
| 3     | ✓    |          | ✓         | 0.7812        | 0.7761        | 0.8158        | 0.7949        | 0.8053        |
| 4     | ✓    | ✓        | ✓         | <b>0.8412</b> | <b>0.8191</b> | <b>0.8597</b> | <b>0.8389</b> | <b>0.8464</b> |

Bold values indicate the best performed method.

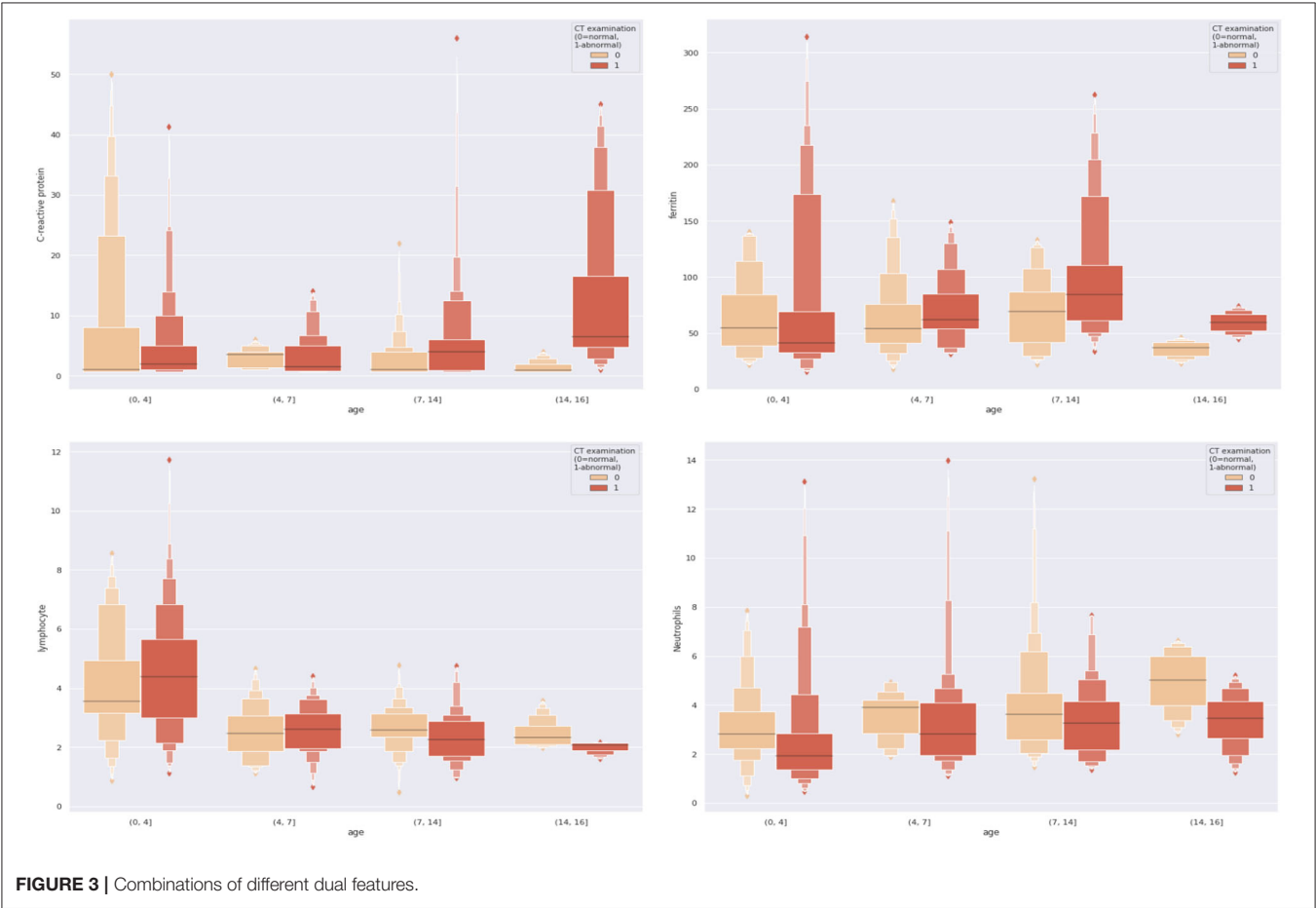


**FIGURE 3 |** Combinations of different dual features.

**TABLE 5 |** Results of single feature models.

| Feature            | AUC score       | Accuracy        | Sensitivity     | Specificity     | F1 score        |
|--------------------|-----------------|-----------------|-----------------|-----------------|-----------------|
| Age                | 0.6683 (0.0806) | 0.6477 (0.0561) | 0.8015 (0.1786) | 0.4371 (0.2707) | 0.7172 (0.0684) |
| C-reactive protein | 0.5981 (0.0864) | 0.6102 (0.0462) | 0.7387 (0.2140) | 0.4352 (0.3635) | 0.6771 (0.0536) |
| Ferritin           | 0.5327 (0.1163) | 0.6355 (0.0453) | 0.8613 (0.1161) | 0.3195 (0.2679) | 0.7322 (0.0103) |
| Lymphocyte         | 0.6194 (0.1047) | 0.6355 (0.0659) | 0.8500 (0.1225) | 0.3424 (0.2990) | 0.7302 (0.0266) |
| Neutrophils        | 0.6726 (0.0813) | 0.6513 (0.0523) | 0.8313 (0.1239) | 0.4048 (0.2651) | 0.7325 (0.0276) |

of features, which improves the model performance on all metrics when Model 1 and Model 3 are compared (Table 4). By incorporating the above two components, our model can achieve a significant improvement by at least 4% on the AUC and 2% on the accuracy.

To make our work more explicable and understandable, we visualized all the dual combinations. For each patient, we divide patients into different age groups and make them as the x-axis and the combined feature values as the y-axis. The results are demonstrated in Figure 3. We can see significant

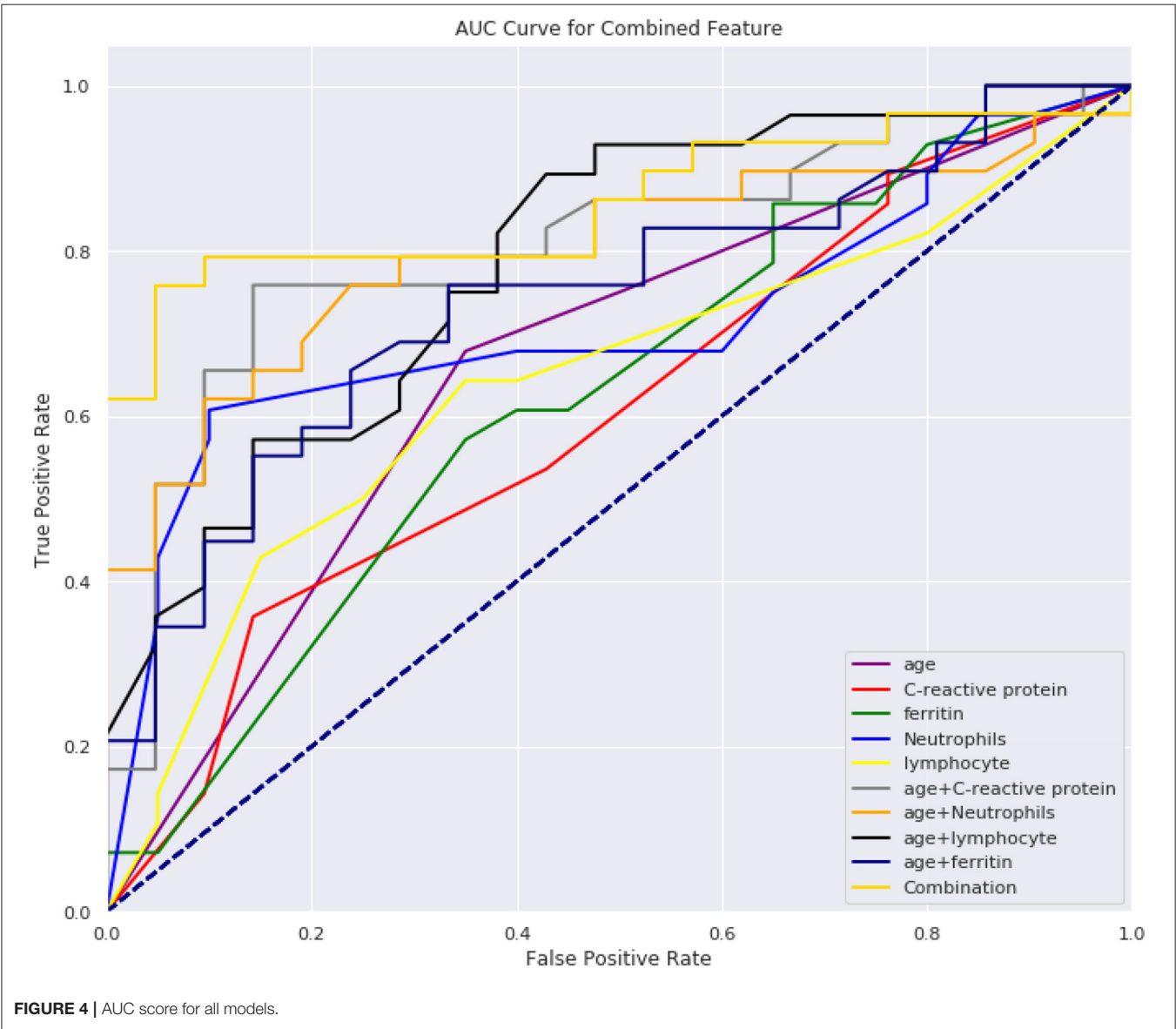


differences between negative and positive patients when features were combined. For example, with the combination of age and C-reactive protein, we found that for those pediatric patients older than 14 years old, if their C-reactive protein was relatively high, they were more likely to present positive results on CT scans.

From **Tables 5, 6**, we can see the performance of our combined-feature models have outperformed single feature models (**Figure 4**). With all features combined, we managed to get a model achieving AUC score over 0.84 and an accuracy of 0.82. Besides, this model has reached relatively high sensitivity of

**TABLE 6 |** Results of combined feature models.

| Feature                | AUC score       | Accuracy        | Sensitivity     | Specificity     | F1 score        |
|------------------------|-----------------|-----------------|-----------------|-----------------|-----------------|
| Age-C-reactive protein | 0.8163 (0.1311) | 0.7288 (0.0759) | 0.8589 (0.0854) | 0.5490 (0.2774) | 0.7883 (0.0334) |
| Age-Neutrophils        | 0.7915 (0.0326) | 0.7129 (0.0355) | 0.8512 (0.0255) | 0.5243 (0.1097) | 0.7748 (0.0182) |
| Age-Ferritin           | 0.7551 (0.0437) | 0.7214 (0.0375) | 0.7803 (0.0465) | 0.6410 (0.0660) | 0.7637 (0.0329) |
| Age-Lymphocyte         | 0.7956 (0.0775) | 0.7332 (0.0452) | 0.7724 (0.0873) | 0.6805 (0.0622) | 0.7679 (0.0472) |
| Combination            | 0.8412 (0.0982) | 0.8191 (0.0590) | 0.8597 (0.0407) | 0.7767 (0.1853) | 0.8464 (0.0348) |



0.86, which has indicated that our model is accurate at detecting positive patients, which is quite important for clinical usage.

## DISCUSSION

In this study, we have developed a decision support system which uses five laboratory indicators as inputs and predicts CT scan results of the pediatric patients who have positive RT-PCR testing results.

We found that the combination of five laboratory indicators, i.e., age, C-reactive protein, neutrophils, lymphocyte, and ferritin, can effectively predict whether the CT findings of COVID-19 children are positive or not. The ratio of CT positive to negative is  $>2$  for patients under the age of 4. Between the ages of 4 and 7, the ratio is between 1 and 2; The ratio between 7 and 14 is between 0.7 and 1;  $>14$ , the ratio is  $<0.7$ . Therefore, we used 4, 7, and 14 years as the cut-off points for predicting CT abnormalities in children, which was proved to be reasonable in our subsequent validation model (Figure 4). We speculate this may be related to the immune system of children. Children under 4 years of age have an immature immune system and weak resistance to the virus (6), which is likely to cause inflammatory changes in the lungs. Therefore, they are more likely to have lung CT abnormalities. Children over the age of 14 have a relatively mature immune system, and at the same time, they have been exposed to places where bacterial or other viral infections are more common, such as nurseries or schools, which allow them to have better-trained immunity, immune fitness and cross-protection (7). It is believed that previous exposure to milder respiratory pathogens can train the immune system of the hosts against the coronavirus (8). Children are less likely to develop severe symptoms of illness as they grow with age, perhaps because the immune system adapts to environmental influences, giving it greater stability (10). Therefore, they are less likely to have lung CT abnormalities.

Neutrophils and lymphocytes, as important components of the innate immune system, have vital functions in the development and recovery of influenza (11). The neutrophil count reflects mostly innate immune cell function, indicating systemic oxidative stress, inflammation, and tissue damage (12). Lymphopenia is very common in patients with influenza virus infection and bacterial infection (13, 14). Ferritin is an acute reactant that is highly expressed in infection and inflammation. Elevated ferritin levels are associated with pro-inflammatory cytokines (15). Ferritin may be a key marker and pathogenic factor in inflammatory pathology, and its signaling pathway is part of innate immune response and regulates lymphocyte function (16).

CRP has been used as a predictor in several previous studies of COVID-19 prediction models (17, 18, 24), and disease progression in MERS, influenza-infected and community-acquired pneumonia patients (25–27). CRP is a marker and indicator of inflammation and plays an important role in host resistance to invasive pathogens and inflammation (28).

CRP is elevated in response to inflammation (29) and the level can reflect a persistent state of inflammation which is not affected by factors such as age and gender, detected CRP levels in COVID-19 patients is of great value in assessing the severity of the disease (24, 30, 31). Moreover, CRP was correlated to the acute lung injury in COVID-19 patients (32).

From Figure 3, we can see that the combination of CRP, neutrophils, and ferritin with age is better than these indicators alone. This empirically proves the efficacy of the combination. At the same time, we can also see from Figure 3 that according to the age node we divided before, after combining age with CRP, neutrophils, and ferritin, there are indeed differences among different age groups, which also proves the rationality of our age node division. Finally, we combined age, C-reactive protein, neutrophils, and ferritin, which produced high clinical predictive value. It can be seen that the combined effect is better than the previous pairwise combination (Table 4), and the AUC value can reach to 0.83, which means that through the four indicators of the patient's, we can predict whether the CT appearance of children with COVID-19 is abnormal or not.

In conclusion, in this work, we focus on the explainable features and manage to find some hidden connections between different medical indicators. This is one major advantage of our prediction model compared most current deep learning based black-box models on CT images although different Explainable Artificial Intelligence (XAI) models are currently under development (33–35). The most important contribution of our work is to find five specific indicators out of 32 clinical indicators to predict CT abnormality results. These five indicators, i.e., age, C-reactive protein, Neutrophils, lymphocyte and ferritin, are all easy and quick to obtain under real clinical environment. Thus, pediatric patients with positive RT-PCR testing results may not need to take further CT scans. Besides, we introduced some deep learning methods to the traditional machine learning process. This innovative approach incorporated into our decision support system is a key factor of the success of our model. It is of note that in a recent study (36) it has shown that RT-PCR could yield false negative results at first. To prevent misdiagnosis, the study recommended to isolate patients with normal CT findings but unfavorable RT-PCR outcomes and repeating the RT-PCR. In our current study, we have relied on a single RT-PCR results for model construction and prediction, and we will consider repeating RT-PCR as our future strategy to prevent misdiagnosis and construct more robust gold standard for training the prediction model.

Although our model has outperformed other models for most of the evaluation metrics, there are limitations on the specificity, which means our models may perform less well on predicting negative samples. Moreover, our pediatric patients are all Asian populations, it needs further evaluation to validate if our model could perform well in other human races. These limitations can be eliminated by performing multi-institutional and multi-national studies.

## DATA AVAILABILITY STATEMENT

The datasets presented in this article are not readily available because the paediatric data is under embargo. Requests to access the datasets should be directed to xiajun@email.szu.edu.cn.

## ETHICS STATEMENT

This study was approved by the Local Ethics Committee of Wuhan Children's Hospital. Written informed consent to participate in this study was provided by the participants' legal guardian/next of kin.

## AUTHOR CONTRIBUTIONS

HM, YJ, JX, and GY conceived and designed the study. XZ, YG, CW, WD, ZN, CW, WM-S, EF, and JS contributed to the literature search. HM, JS, and JX contributed to data collection. QY, WD, YJ, MW, JX, and GY contributed to data analysis. HM, QY, MW, XZ, JX, and GY contributed to data interpretation. HM, YJ, MW, XZ, JX, and GY contributed to the tables and figures. HM, YJ, MW, ZN, XZ, JX, and GY contributed to writing of the

report. All the authors have read and approved the publication of this work.

## FUNDING

This work was supported in part by the Natural Science Foundation of Guangdong Province [2020A1515010918], in part by the Project of Shenzhen International Cooperation Foundation [GJHZ20180926165402083], in part by the Project of Shenzhen Basic Development Project [JCYJ20190806164409040], in part by the Hangzhou Economic and Technological Development Area Strategic Grant [Imperial Institute of Advanced Technology], in part by the European Research Council Innovative Medicines Initiative on Development of Therapeutics and Diagnostics Combatting Coronavirus Infections Award DRAGON: rapiD and secuRe AI imaging based diaGnosis, stratification, follow-up, and preparedness for coronavirus panDemics [H2020-JTI-IMI2 101005122], and in part by the AI for Health Imaging Award CHAIMELEON: Accelerating the Lab to Market Transition of AI Tools for Cancer Management [H2020-SC1-FA-DTS-2019-1 952172].

## REFERENCES

- Hu S, Gao Y, Niu Z, Jiang Y, Li L, Xiao X, et al. Weakly supervised deep learning for COVID-19 infection detection and classification from CT images. *IEEE Access*. (2020) 8:118869–83. doi: 10.1109/ACCESS.2020.3005510
- Li Y, Xia L. Coronavirus Disease 2019 (COVID-19): role of chest CT in diagnosis and management. *AJR Am J Roentgenol*. (2020) 214:1280–6. doi: 10.2214/AJR.20.22954
- Qin L, Yang Y, Cao Q, Cheng Z, Wang X, Sun Q, et al. A predictive model and scoring system combining clinical and CT characteristics for the diagnosis of COVID-19. *Eur Radiol*. (2020) 30:6797–807. doi: 10.1007/s00330-020-07022-1
- Dai WC, Zhang HW, Yu J, Xu HJ, Chen H, Luo SP, et al. CT imaging and differential diagnosis of COVID-19. *Can Assoc Radiol J*. (2020) 71:195–200. doi: 10.1177/0846537120913033
- Roberts M, Driggs D, Thorpe M, Gilbey J, Yeung M, Ursprung S, et al. Common pitfalls and recommendations for using machine learning to detect and prognosticate for COVID-19 using chest radiographs and CT scans. *Nat Mach Intell*. (2021) 3:199–217. doi: 10.1038/s42256-021-00307-0
- Li K, Fang Y, Li W, Pan C, Qin P, Zhong Y, et al. CT image visual quantitative evaluation and clinical classification of coronavirus disease (COVID-19). *Eur Radiol*. (2020) 30:4407–16. doi: 10.1007/s00330-020-06817-6
- Merkus P, Klein WM. The value of chest CT as a COVID-19 screening tool in children. *Eur Respir J*. (2020) 55:2001241. doi: 10.1183/13993003.01241-2020
- Shelmerdine SC, Lovrenski J, Caro-Dominguez P, Toso S. Coronavirus disease 2019 (COVID-19) in children: a systematic review of imaging findings. *Pediatr Radiol*. (2020) 50:1217–30. doi: 10.1007/s00247-020-04726-w
- Driggs D, Selby I, Roberts M, Effrossyni GK, Rudd JHF, Yang G, et al. Machine learning for COVID-19 diagnosis and prognostication: lessons for amplifying the signal while reducing the noise. *Radiol Artif Intell*. (2021) e210011. doi: 10.1148/ryai.2021210011
- Hong JY, Han K, Jung JH, Kim JS. Association of exposure to diagnostic low-dose ionizing radiation with risk of cancer among youths in South Korea. *JAMA Netw Open*. (2019) 2:e1910584. doi: 10.1001/jamanetworkopen.2019.10584
- Qiu H, Wu J, Hong L, Luo Y, Song Q, Chen D. Clinical and epidemiological features of 36 children with coronavirus disease 2019 (COVID-19) in Zhejiang, China: an observational cohort study. *Lancet Infect Dis*. (2020) 20:689–96. doi: 10.1016/S1473-3099(20)30198-5
- Bi Q, Wu Y, Mei S, Ye C, Zou X, Zhang Z, et al. Epidemiology and transmission of COVID-19 in 391 cases and 1286 of their close contacts in Shenzhen, China: a retrospective cohort study. *Lancet Infect Dis*. (2020) 20:911–9. doi: 10.1016/S1473-3099(20)30287-5
- Lu X, Zhang L, Du H, Zhang J, Li YY, Qu J, et al. SARS-CoV-2 infection in children. *N Engl J Med*. (2020) 382:1663–5. doi: 10.1056/NEJMc2005073
- Lu Y, Wen H, Rong D, Zhou Z, Liu H. Clinical characteristics and radiological features of children infected with the 2019 novel coronavirus. *Clin Radiol*. (2020) 75:520–5. doi: 10.1016/j.crad.2020.04.010
- Liguoro I, Pilotto C, Bonanni M, Ferrari ME, Pusiol A, Nocerino A, et al. SARS-COV-2 infection in children and newborns: a systematic review. *Eur J Pediatr*. (2020) 179:1029–46. doi: 10.1007/s00431-020-03684-7
- Li W, Fang Y, Liao J, Yu W, Yao L, Cui H, et al. Clinical and CT features of the COVID-19 infection: comparison among four different age groups. *Eur Geriatr Med*. (2020) 11:843–50. doi: 10.1007/s41999-020-00356-5
- Ma H, Hu J, Tian J, Zhou X, Li H, Laws MT, et al. A single-center, retrospective study of COVID-19 features in children: a descriptive investigation. *BMC Med*. (2020) 18:123. doi: 10.1186/s12916-020-01596-9
- Sun D, Zhu F, Wang C, Wu J, Liu J, Chen X, et al. Children infected with SARS-CoV-2 from family clusters. *Front Pediatr*. (2020) 8:386. doi: 10.3389/fped.2020.00386
- Lin TY, Goyal P, Girshick R, He K, Dollar P. Focal loss for dense object detection. *IEEE Trans Pattern Anal Mach Intell*. (2020) 42:318–27. doi: 10.1109/TPAMI.2018.2858826
- Arik SO, Pfister T. TabNet: attentive interpretable tabular learning. *arXiv [Preprint]*. (2019) arXiv:1908.07442.
- Gijsbers P, LeDell E, Thomas J, Poirier S, Bischl B, Vanschoren J. An open source AutoML benchmark. *arXiv [Preprint]*. (2019) arXiv:1907.00909.
- Guo H, Tang R, Ye Y, Li Z, He X. DeepFM: a factorization-machine based neural network for CTR Prediction. *arXiv*. (2017). doi: 10.24963/ijcai.2017/239
- Chen T, Guestrin C. *XGBoost: A Scalable Tree Boosting System*. San Francisco, CA: ACM. (2016).
- Chen Z, Tong L, Zhou Y, Hua C, Wang W, Fu J, et al. Childhood COVID-19: a multicentre retrospective study. *Clin Microbiol Infect*. (2020) 26:1260.e1–4. doi: 10.1016/j.cmi.2020.06.015

25. Xu H, Liu E, Xie J, Smyth RL, Zhou Q, Zhao R, et al. A follow-up study of children infected with SARS-CoV-2 from western China. *Ann Transl Med.* (2020) 8:623. doi: 10.21037/atm-20-3192
26. Korkmaz MF, Ture E, Dorum BA, Kilic ZB. The epidemiological and clinical characteristics of 81 children with COVID-19 in a pandemic hospital in Turkey: an observational cohort study. *J Korean Med Sci.* (2020) 35:e236. doi: 10.3346/jkms.2020.35.e236
27. Tan C, Huang Y, Shi F, Tan K, Ma Q, Chen Y, et al. C-reactive protein correlates with computed tomographic findings and predicts severe COVID-19 early. *J Med Virol.* (2020) 92:856–862. doi: 10.1002/jmv.25871
28. Wang L. C-reactive protein levels in the early stage of COVID-19. *Med Mal Infect.* (2020) 50:332–4. doi: 10.1016/j.medmal.2020.03.007
29. Xu Z, Shi L, Wang Y, Zhang J, Huang L, Zhang C, et al. Pathological findings of COVID-19 associated with acute respiratory distress syndrome. *Lancet Respir Med.* (2020) 8:420–2. doi: 10.1016/S2213-2600(20)30076-X
30. Weiskopf D, Schmitz KS, Raadsen MP, Grifoni A, Okba N, Endeman H, et al. Phenotype and kinetics of SARS-CoV-2-specific T cells in COVID-19 patients with acute respiratory distress syndrome. *Sci Immunol.* (2020) 5:1–10. doi: 10.1101/2020.04.11.20062349
31. Bilgir O, Bilgir F, Calan M, Calan OG, Yuksel A. Comparison of pre- and post-levothyroxine high-sensitivity c-reactive protein and fetuin-a levels in subclinical hypothyroidism. *Clinics.* (2015) 70:97–101. doi: 10.6061/clinics/2015(02)05
32. Fan L, Li D, Xue H, Zhang L, Liu Z, Zhang B, et al. Progress and prospect on imaging diagnosis of COVID-19. *Chin J Acad Radiol.* (2020) 3:4–13. doi: 10.1007/s42058-020-00031-5
33. Barredo Arrieta A, Díaz-Rodríguez N, Del Ser J, Bennetot A, Tabik S, Barbado A, et al. Explainable Artificial Intelligence (XAI) : concepts, taxonomies, opportunities and challenges toward responsible AI. *Inform Fusion.* (2020) 58:82–115. doi: 10.1016/j.inffus.2019.12.012
34. Yang G, Ye Q, Xia J. Unbox the BLack-box for the medical explainable AI via multi-modal and multi-centre data fusion: a mini-review, two showcases and beyond. *arXiv [Preprint].* (2021) arXiv:2102.01998.
35. Ye Q, Xia J, Yang G. Explainable AI for COVID-19 CT classifiers: an initial comparison study. *arXiv.* (2021).
36. Long C, Xu H, Shen Q, Zhang X, Fan B, Wang C, et al. Diagnosis of the Coronavirus disease (COVID-19): rRT-PCR or CT? *Eur J Radiol.* (2020) 126:108961. doi: 10.1016/j.ejrad.2020.108961

**Conflict of Interest:** ZN and WM-S are employed by Aladdin Healthcare Technologies Ltd. QY, YJ, and MW are employed by Hangzhou Ocean's Smart Boya Co., Ltd., China and Mind Rank Ltd., China.

The remaining authors declare that the research was conducted in the absence of any commercial or financial relationships that could be construed as a potential conflict of interest.

Copyright © 2021 Ma, Ye, Ding, Jiang, Wang, Niu, Zhou, Gao, Wang, Menpes-Smith, Fang, Shao, Xia and Yang. This is an open-access article distributed under the terms of the Creative Commons Attribution License (CC BY). The use, distribution or reproduction in other forums is permitted, provided the original author(s) and the copyright owner(s) are credited and that the original publication in this journal is cited, in accordance with accepted academic practice. No use, distribution or reproduction is permitted which does not comply with these terms.





# Radiomics Is Effective for Distinguishing Coronavirus Disease 2019 Pneumonia From Influenza Virus Pneumonia

Liaoyi Lin<sup>1</sup>, Jinjin Liu<sup>1</sup>, Qingshan Deng<sup>1</sup>, Na Li<sup>1</sup>, Jingye Pan<sup>2</sup>, Houzhang Sun<sup>1\*</sup> and Shichao Quan<sup>3\*</sup>

<sup>1</sup> Department of Radiology, First Affiliated Hospital of Wenzhou Medical University, Wenzhou, China, <sup>2</sup> Department of Intensive Care Unit, First Affiliated Hospital of Wenzhou Medical University, Wenzhou, China, <sup>3</sup> Department of General Medicine, First Affiliated Hospital of Wenzhou Medical University, Wenzhou, China

## OPEN ACCESS

### Edited by:

Reza Lashgari,  
Institute for Research in Fundamental  
Sciences, Iran

### Reviewed by:

Pei Pei Pang,  
GE Healthcare, China  
Amirmasoud Ahmadi,  
Max Planck Institute of  
Ornithology, Germany

### \*Correspondence:

Houzhang Sun  
shzlxm@163.com  
Shichao Quan  
generalpractice@qq.com

### Specialty section:

This article was submitted to  
Infectious Diseases – Surveillance,  
Prevention and Treatment,  
a section of the journal  
Frontiers in Public Health

**Received:** 04 February 2021

**Accepted:** 06 May 2021

**Published:** 15 June 2021

### Citation:

Lin L, Liu J, Deng Q, Li N, Pan J,  
Sun H and Quan S (2021) Radiomics  
Is Effective for Distinguishing  
Coronavirus Disease 2019 Pneumonia  
From Influenza Virus Pneumonia.  
Front. Public Health 9:663965.  
doi: 10.3389/fpubh.2021.663965

**Objectives:** To develop and validate a radiomics model for distinguishing coronavirus disease 2019 (COVID-19) pneumonia from influenza virus pneumonia.

**Materials and Methods:** A radiomics model was developed on the basis of 56 patients with COVID-19 pneumonia and 90 patients with influenza virus pneumonia in this retrospective study. Radiomics features were extracted from CT images. The radiomics features were reduced by the Max-Relevance and Min-Redundancy algorithm and the least absolute shrinkage and selection operator method. The radiomics model was built using the multivariate backward stepwise logistic regression. A nomogram of the radiomics model was established, and the decision curve showed the clinical usefulness of the radiomics nomogram.

**Results:** The radiomics features, consisting of nine selected features, were significantly different between COVID-19 pneumonia and influenza virus pneumonia in both training and validation data sets. The receiver operator characteristic curve of the radiomics model showed good discrimination in the training sample [area under the receiver operating characteristic curve (AUC), 0.909; 95% confidence interval (CI), 0.859–0.958] and in the validation sample (AUC, 0.911; 95% CI, 0.753–1.000). The nomogram was established and had good calibration. Decision curve analysis showed that the radiomics nomogram was clinically useful.

**Conclusions:** The radiomics model has good performance for distinguishing COVID-19 pneumonia from influenza virus pneumonia and may aid in the diagnosis of COVID-19 pneumonia.

**Keywords:** COVID-19, influenza, nomogram, radiomics, computed tomography

## INTRODUCTION

Nowadays, the coronavirus disease 2019 (COVID-19) is a serious global health problem. COVID-19 is caused by the novel coronavirus named severe acute respiratory syndrome coronavirus 2 (SARS-CoV-2), which can be transmitted through the respiratory tract and by contact and has evidence of human-to-human transmission. This episode shows the need for rapid

and accurate detection and identification methods that can be used in local hospitals for the diagnosis of COVID-19. The golden diagnosis methods are the nucleic acid amplification test of the respiratory tract and the reverse transcription real-time fluorescence polymerase chain reaction of the blood specimen (1). However, the detection rate is low when the viral load is low, which may lead to false-negative results (2). The computed tomography (CT) examination has been proved to be an essential auxiliary diagnostic tool; typical CT features of COVID-19 include multifocal bilateral GGO and patchy consolidations and prominent peripherally subpleural distribution (3, 4). However, few studies focus on distinguishing COVID-19 pneumonia from other viral pneumonia.

Influenza is a significant and highly contagious disease, and the majority of viral pneumonias were caused by influenza virus types A and B in immunocompetent adults (5). Influenza A virus can cause a rapidly progressive symptom, such as acute respiratory distress syndrome, like COVID-19. The most frequent CT findings of influenza virus pneumonia were poorly defined nodules, patchy areas of peribronchial ground-glass opacity, and airspace consolidation (5, 6), which were similar to those of COVID-19 pneumonia. As we know, there are differences as well as similarities in the CT features of COVID-19 pneumonia compared with those of other viral pneumonia, and CT is still limited to differentially diagnose viral pneumonia (7).

Radiomics is a quantitative analytic method by extracting specific features from medical images (8). This novel method exhibited potential applications in assessing pulmonary nodules or masses in chest imaging study, evaluating treatment response, and predicting survival outcomes of lung cancer (9–11). Some studies demonstrated the potential of radiomics features from CT in predicting a COVID-19 patient's prognostic outcome and identification of disease severity (12, 13); however, whether CT radiomics features can be used to differentiate pneumonia caused by COVID-19 or influenza remains unclear.

We hypothesized that radiomics might provide a non-invasive method for distinguishing COVID-19 pneumonia from influenza virus pneumonia and could assist radiologists in performing an exact diagnosis. Hence, the main objective of this study was to develop and validate a radiomics model for predicting COVID-19 pneumonia in order to help clinicians in quickly and accurately eliminating the influenza virus pneumonia.

## MATERIALS AND METHODS

### Patients and Ethical Approval

This study was approved by our institutional review board, and written informed consent was waived. The patients' data were collected from the First Affiliated Hospital of Wenzhou Medical University. During the period between January 25, 2020 and March 10, 2020, COVID-19 patients were included if they met the following criteria: (1) exhibiting positive results of SARS-CoV-2 nucleic acids and (2) having clear chest CT scan data and with pneumonia lesion during the initial diagnosis. The influenza virus pneumonia (type A or B) patients were confirmed by nucleic acid test from February 20, 2018 to February 9, 2020. Also, they all have clear chest CT scan data during the

initial diagnosis. Those with other obvious lung abnormalities (such as lung cancer, tuberculosis, silicosis, severe emphysema) or had pneumonia caused by other common bacterial or viral pathogens were excluded. Baseline clinical features were derived from medical records, including gender, age, and the symptom. COVID-19 is clinically divided into four types: mild, common, severe, and critically severe (13).

### Scanning

CT was performed for all patients using Phillips Brilliance 16, Siemens Somatom Scope 16, or GE LightSpeed VCT 64 with the following parameters: tube voltage of 120 kV, tube current-exposure time product of 50–150 mA s, scan thickness of 5 mm, and reconstruction thickness of 1.25–3 mm. The scanning range at least covered the area from the level of the apex of the lung to the costophrenic angle.

### Region-of-Interest Segmentation and Feature Extraction

The radiomics workflow began with image segmentation and feature extraction. All images were manually segmented on the AVIEW software package (Coreline Soft Co., Ltd., Korea, version 1.0.34.26). In consideration of the fact that pneumonia may have a wide range of lesions in the lung, the largest pneumonia lesion area was used in the analysis; the largest pneumonia lesion area was defined as having the largest range of lesions in a transverse section on one side of the lung, and consolidation took precedence over ground-glass opacity. The pneumonia always had larger lesion, and the lesion boundary is not clear. It is not appropriate to search a boundary for demarcation by manual operation; it may not actually get very accurate results. Therefore, we chose the lung contour to draw a cutting line that is clearer than the pneumonia lesion boundary. On the two-dimensional image, an experienced radiologist who was blind to the actual viral pneumonia results selected the transverse section of the largest pneumonia lesion area on one side of the lung and then manually delineated the region of interest (ROI) of the lung images using the system's own tools. The ROI included the transverse section of the unilateral lung tissue, which demarcated along the lung contour margin. Another radiologist checked the segmentation. Any difference in opinions was resolved through negotiation. The software automatically recognized and extracted the radiomics features. A total of 131 features were extracted, including fractal features, shape features, and texture features. The radiomics feature parameters are presented in **Supplementary Data Sheet 1**. After feature extraction, all the patients' image data were randomly divided into training and validation sets with a ratio of 9:1.

### Feature Selection and Predictive Model Construction

Feature selection was performed in two steps. First, for radiomics features, the Max-Relevance and Min-Redundancy (mRMR) algorithm was performed to eliminate the redundant and irrelevant features. The corresponding features were ranked according to their relevance-redundancy indexes, and 10 features in the top were retained. Second, the least absolute shrinkage and

selection operator (LASSO) was conducted to further choose the optimized features for improving the final model accuracy. To demonstrate the association between the selected features and the actual COVID-19 pneumonia, we constructed a radiomics score (Radscore) as the radiomics model in the training group using multivariate backward stepwise logistic regression. The aim of multivariate logistic regression was to derive the best-fitting and most parsimonious (smallest or most efficient) model to describe the relationship between an outcome and a set of predictors. The outcome variable (dependent variables) is dichotomous (e.g., COVID-19 or not COVID-19). The independent variables are called covariates. In multivariate logistic regression, the predictor variables may be of any data level, such as categorical, ordinal, or continuous data. Put the independent and dependent variables into the calculation formula to examine a series of predictor variables and determine those that best predict COVID-19. In our study, the most predictive features were chosen, and the corresponding coefficients were evaluated. The radiomics score was calculated by summing the selected features weighted by their coefficients to reflect the COVID-19 pneumonia probability. The discriminative capability was measured using receiver operating characteristic (ROC) curve analysis. The performance of the radiomics model was evaluated in both the training set and the validation set. The area under the curve (AUC), accuracy, sensitivity, and specificity were obtained. To avoid prediction errors, we further tested the proposed model using a 1,000-iteration bootstrap analysis in both the training and validation groups.

## Development and Validation of Nomogram

The nomogram was based on a multivariable logistic regression analysis using multiple medical indicators or biological attributes and then using line segments with high or low scores for the purpose of predicting clinical outcomes or the probability of an event. In our study, the nomogram was generated according to the proposed radiomics model using the R software. The calibration of the nomogram was detected by using the calibration curves accompanied by the Hosmer–Lemeshow test (14). The Hosmer–Lemeshow test accessed the goodness-of-fit of the nomogram models, and the calibration curves measured the consistency between the predicted COVID-19 pneumonia probability and the actual COVID-19 pneumonia probability. The clinical utility of the models was measured by the decision curve analysis. Decision curves are a useful tool to evaluate the population impact of adopting a risk prediction instrument into clinical practice. Given one risk model that predicts the probability of a binary outcome, it can display estimates of the standardized net benefit by categorizing observations as “high risk.” A larger area under the decision curve suggested a better clinical utility.

## Statistical Analysis

All statistical analyses were performed using SPSS Software (Version 24, IBM, Chicago, IL) and R software (version 3.6.1; www.R-project.org). Mann–Whitney *U*-test or independent *t*-test was used for continuous variables with abnormal distributions and normal distributions, respectively. For

**TABLE 1 |** Baseline characteristics of patients.

|                  | COVID-19 pneumonia<br>( <i>n</i> = 56) | Influenza virus<br>pneumonia ( <i>n</i> = 90) | <i>P</i> -value |
|------------------|--|---|-----------------|
| Sex              |  |   | 0.277           |
| Male             | 35                                     | 48  |                 |
| Female           | 21                                     | 42  |                 |
| Age (year)       | 55.91 ± 14.91                          | 53.31 ± 17.33                                 | 0.355           |
| Symptoms         |  |   | 0.022           |
| Fever            | 25                                     | 19  |                 |
| Fever with cough | 20                                     | 40  |                 |
| Cough            | 8                                      | 22  |                 |
| Other            | 3                                      | 9   |                 |

categorical variables, chi-square test or Fisher's exact test was used. Values of *P* < 0.05 were considered to be statistically significant.

## RESULTS

### Clinical Characteristics

In this study, 56 patients were diagnosed with COVID-19 pneumonia and 90 patients were diagnosed with influenza virus pneumonia. There were 83 male and 63 female patients, and the mean age was 54.31 ± 16.45 years. In the COVID-19 pneumonia patients, there were 35 males and 21 females, and the main age was 55.91 ± 14.92 years. In the influenza virus pneumonia patients, there were 48 males and 42 females, and the main age was 53.31 ± 17.34 years. In 56 COVID-19 patients, 30.4% was of the common type, 60.7% was of the severe type, and 8.9% was of the critically severe type.

There were no statistically significant differences in gender (*P* = 0.277) and age (*P* = 0.355) between the two groups. The most common symptoms were fever, fever with cough, and cough. In COVID-19 pneumonia patients, only two had other symptoms such as headache or weakness, and one patient had no symptom. In the influenza virus pneumonia patients, other symptoms such as sore throat, headache, and weakness were present in only one, one, and four, respectively, and three patients had no symptom. There was statistical difference in symptoms (*P* = 0.022). Patient characteristics are shown in **Table 1**.

### Radiomics Analysis

The prediction model was developed using a training set (**Figure 1**) that consisted of COVID-19 pneumonia and influenza virus pneumonia CT images. The mRMR was performed to get the top 10 redundant and irrelevant features, and then they were further reduced to 9 by using LASSO. Nine radiomics features were selected using mRMR and LASSO regularization methods, and these selected radiomics features were significantly associated with COVID-19 pneumonia. Finally, the coefficients of radiomics features were constructed, and the radiomics score

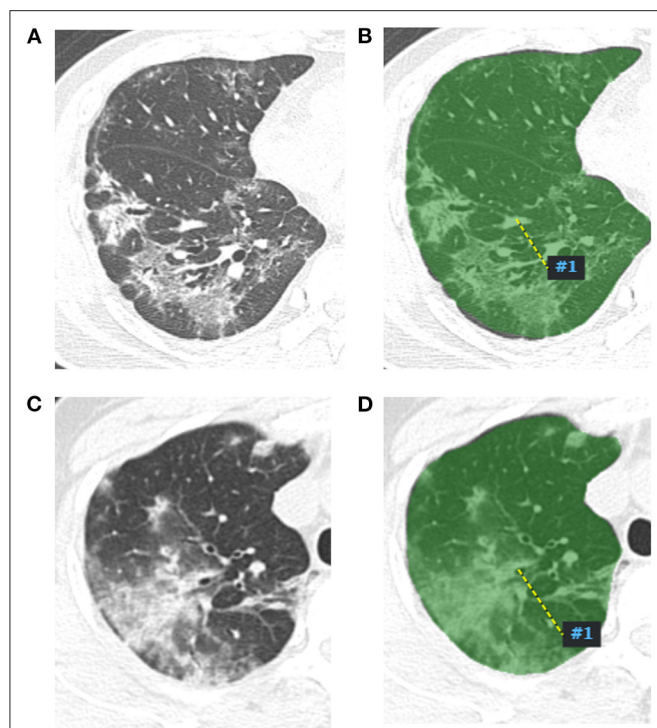


**FIGURE 1 |** Radiomics features extract map of pneumonia lesion. A two-dimensional image of the largest pneumonia lesion area of a COVID-19 patient in the right lung (A), the lesion presented as blurred patchy ground glass opacity with little consolidation. The region of interest of the largest pneumonia lesion area was manually delineated in the right lung image, which is displayed as the green area (B), and artificial intelligence software automatically extracted the radiomics features and output from a computer. A two-dimensional image of the largest pneumonia lesion area of an influenza viral pneumonia patient in the right lung (C), the lesion presented as ground glass opacity with some consolidation; the CT manifestation was similar with the COVID-19 pneumonia; we used the same method to extract radiomics features from the image (D).

was calculated as follows.

$$\begin{aligned} \text{Radscore} = & -1.119 - 0.214 * \text{Texture\_Histo\_Min} - 0.457 \\ & * \text{Texture\_GLCM\_MCC} + 0.888 * \text{Shape2D\_} \\ & \text{Perimeter} - 0.351 * \text{Texture\_GLRLM\_LRHGE} \\ & + 0.961 * \text{Texture\_GLCM\_DiffVariance} - 0.551 \\ & * \text{Texture\_NGTDM\_Strength} - 0.553 \\ & * \text{Texture\_GLCM\_IMC2} + 0.054 * \text{Shape2D\_} \\ & \text{Roundness} + 2.221 * \text{Texture\_FirstOrder\_Min} \end{aligned}$$

## Performance of Radiomics Model

The radiomics model yielded AUCs of 0.909 [95% confidence interval (CI), 0.859–0.958] and 0.911 (95% CI, 0.753–1.000) in the training and validation samples, respectively (Figure 2). These values were consistent with the AUC values calculated by using the 1,000 times bootstrap analysis in both the training and validation groups (mean  $\pm$  standard deviation;

the training group:  $0.909 \pm 0.014$ ; the validation group:  $0.910 \pm 0.045$ ). The distributions of AUCs from the bootstrap method for the radiomics model were provided as histograms in **Supplementary Data Sheet 2**. The accuracy, sensitivity, and specificity of the training sample were 84.8, 87.7, and 80.4%, respectively, and those of the validation sample were 85.7, 88.9, and 80.0%, respectively.

## Prediction Model

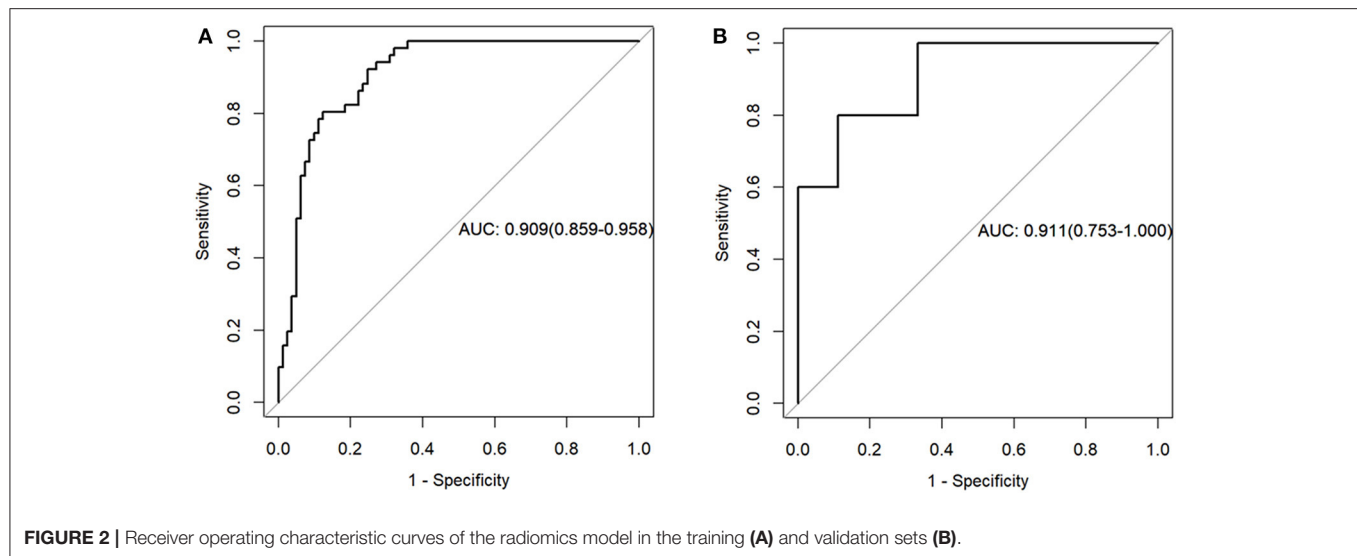
A prediction model was developed and presented as a nomogram based on the radiomics score. It was a graph that consists of four lines: points, radscore, total points, and risk; the lines were marked off to scale and arranged in sequence. The calibration curve of the nomogram demonstrated good agreement between predicted and observed COVID-19 pneumonia in the training and validation sets. For the training group, a non-significant statistic ( $P = 0.5758$ ) of the Hosmer–Lemeshow test suggested no significant deviation from an ideal fitting. For the validation group, the Hosmer–Lemeshow test also was a non-significant statistic ( $P = 0.3758$ ). The calibration curve showed that the predicted curve and the actual observation curve were close, which indicated that the result was reliable. The decision curves with a larger area under the curve indicated the nomogram's clinical usefulness. The decision curve analysis showed that using the radiomics nomogram to predict COVID-19 pneumonia added more benefit than the treat-all-patients as COVID-19 pneumonia scheme or the treat-all-patients as influenza viral pneumonia scheme. All of these are shown in **Figure 3**.

## DISCUSSION

In this study, we developed and validated a radiomics-based model for a non-invasive, individualized method to distinguish COVID-19 pneumonia from influenza virus pneumonia. The radiomics model demonstrated favorable discrimination in both the training set (AUC, 0.909) and the validation set (AUC, 0.911) cohorts and good calibration; DCA indicated the clinical usefulness of the radiomics model. And the influenza viral pneumonia patients more likely have fever with cough or cough than COVID-19 pneumonia patients.

Chest CT could be used to diagnosis and assess the COVID-19 patients (15). Traditional imaging methods use CT manifestations of the images for differential diagnosis. We can judge the disease by the lesion on the CT image, but the results may be subjective and inaccurate. Liu et al. found that there were differences in the CT manifestations of patients with COVID-19 and influenza. The rounded opacities and interlobular septal thickening were more commonly seen in COVID-19 compared with the influenza, and COVID-19 usually with the typical peripheral distribution (16). In a comparative study, radiologists blinded to the patient information reviewed 424 chest CT scans to differentiate COVID-19 from viral pneumonia. The accuracy of the three radiologists in differentiating COVID-19 from non-COVID-19 viral pneumonia was 83% (350 of 424), 80% (338 of 424), and 60% (255 of 424), with sensitivities of 72, 72, and 94% and specificities of 94, 88, and 24%, respectively (17). These studies showed that the CT manifestations might help us





differentiate COVID-19 from influenza, but the accuracy was based on the radiologist's experience, and the results of sensitivity and specificity were not always maintained on a high level at the same time. In the clinical setting, a more comprehensive and deeper understanding of the differential diagnosis of pneumonia is needed. Radiomics is theoretically a feasible method to give rise to a deeper understanding of COVID-19 pneumonia lesions.

There is much interest in the use of radiomics for assessing COVID-19 pneumonia image data. The pixel features and spatial parameters of the image are used to quantitatively extract the pathophysiological features of the lesions that cannot be recognized by the naked eye and to reveal the special manifestations between tissues (18). Wei et al. explored the value of CT texture analysis for determining COVID-19 severity, and their prediction model of textural features showed high predictive accuracy; the Spearman correlation analysis showed that most textural features had above-moderate correlations with disease severity (13). Wu et al. aimed to develop a non-invasive and easy-to-use prognostic signature by radiomics analysis of chest CT, and they used this method to individually predict poor outcome in patients with COVID-19. Their study suggested that the chest CT radiomics signature of COVID-19 was more effective and useful, and the Radscore can successfully stratify COVID-19 patients with different survival time of poor outcome (12). Fang et al. developed a radiomics nomogram to predict COVID-19 pneumonia and help clinical decision-making, and their result showed that the radiomics model has good performance (19). In our study, the largest pneumonia lesion area was used in the analysis, since the largest lesions reflected the CT manifestations of the pneumonia lesions and had enough features to characterize the pneumonia. We only focused on COVID-19 and influenza virus pneumonia (type A or B), and we found that nine radiomics features in COVID-19 pneumonia were significantly different from those in influenza virus pneumonia. Some previous studies have used radiomics to help radiologists discriminate COVID-19 and other viral pneumonia, and the radiomics features made the image information digitalized;

however, these studies mixed different types of viral pneumonia. Huang et al. included influenza A virus, influenza B virus, respiratory syncytial virus, parainfluenza virus, adenovirus, SARS coronavirus, Epstein-Barr virus, measles virus, or other viruses from nasopharyngeal swabs or bronchoalveolar lavage fluid (20). Chen et al. included influenza virus-induced, adenovirus-induced, syncytial virus-induced, and cytomegalovirus-induced pneumonias (21). Although their studies showed that the radiomics model was an effective predictive tool to distinguish COVID-19 from other viral pneumonias (with AUC 0.807–0.888), the different types of viral pneumonia had different CT findings, which is a potential confounding factor for further comparison. Our study limited the scope of viral pneumonia only for influenza virus types A and B in the comparison group. The influenza virus types A and B are among the main pathogens of community-acquired pneumonia, and they are usually required to identify with COVID-19. Our radiomics model achieved good prediction performance in both the training set (AUC, 0.909) and the validation set (AUC, 0.911). The result showed that radiomics was a valuable tool to help radiologists distinguish COVID-19 from influenza virus pneumonia. The nomogram had been widely applied to predict clinical diseases, such as the differentiation of benign and malignant cancers, cancer recurrence, and lymph node metastasis (22–24), and it was also commonly used in COVID-19 pneumonia diagnosis (20, 21). In our research, the radiomics nomogram was also developed to predict COVID-19 pneumonia and aimed to illustrate the relationship between Radscore and the risk of COVID-19 pneumonia graphically. In other words, the nomogram can quickly, intuitively, and accurately show the complex radiomics model in a graphic way, and this intuitive and convenient radiomics nomogram can be beneficial to clinical applications in distinguishing COVID-19 pneumonia from influenza viral pneumonia. Moreover, there was good calibration in both the training and validation samples for the nomogram by the Hosmer–Lemeshow test. DCA is a good tool to estimate the predicted net benefit of the model across all possible risk

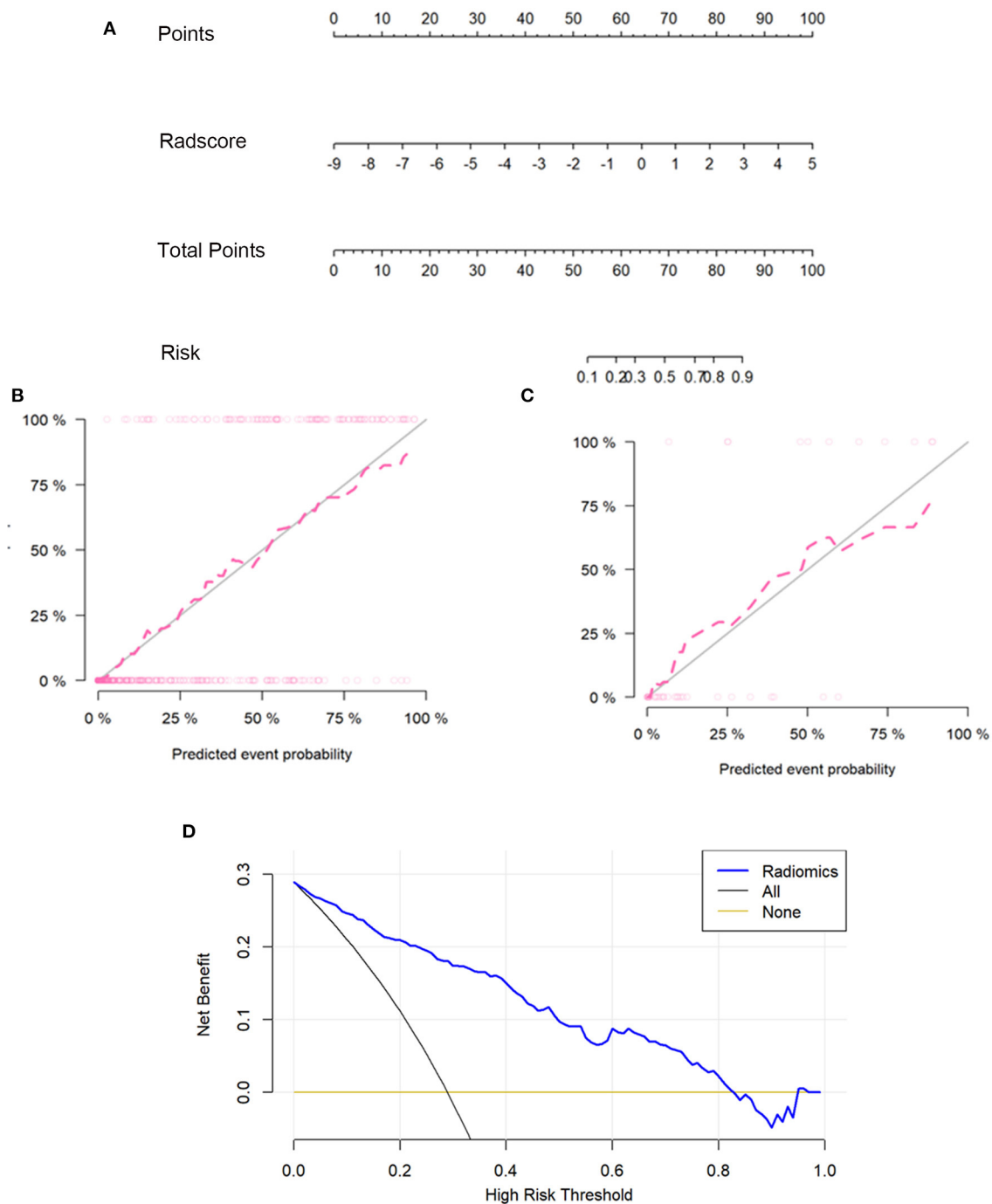


**FIGURE 3 |** The radiomics nomogram, the calibration curves, and the decision curves. A radiomics nomogram was developed in the training set according to the radiomics score (A). In the nomogram, radscore corresponded to a point due to it being a graph of a single factor; the point was the same as the total point, and the total point corresponded to the risk of COVID-19. Calibration curves of the radiomics nomogram in the training (B) and validation sets (C). The horizontal axis of the figure was the predicted event probability, which was the probability of occurrence of the events forecasted by the prediction model, and the vertical axis was the actual event probability, which was the actual event rate of patients. The red line was the fit line and represents the actual value corresponding to the predicted value. The gray line was the reference line. The decision curve (D) for the radiomics score. The vertical axis was the net benefit; the horizontal axis was the high-risk threshold probability at a range of 0.0–1.0. The black line represented the hypothesis that all patients had COVID-19 pneumonia. The brown line represented the hypothesis that all patients had influenza viral pneumonia. The blue line represented the DCA of the radiomics nomogram. The decision curves showed that using the radiomics nomogram in the current study to predict COVID-19 pneumonia had more benefits.

thresholds (25, 26). The DCA of the nomogram using the radiomics model in the current study to diagnose COVID-19 pneumonia has real utility; the treat-all-patients as COVID-19 pneumonia scheme or the treat-all-patients as influenza viral pneumonia scheme compared to the radiomics nomogram methods was significantly inferior. The calibration curve and the decision curve showed that the stability and availability of our prediction model were good; this result proved the practicability of radiomics.

Our study had several limitations. First, it was a retrospective study. Second, the radiomics features were extracted from two-dimensional images. Third, some clinical features of COVID-19 pneumonia and influenza viral pneumonia were not included to develop a model, such as the symptoms of the patients. A multicenter validation with a larger sample size is still needed in the future.

In conclusion, our study proposed a non-invasive and quantitative radiomics model for diagnosing COVID-19 based on CT imaging. Taking the ROC of the radiomics model into account, our study suggested that the CT radiomics features were more effective and ideal to distinguishing COVID-19 pneumonia from influenza viral pneumonia.

## DATA AVAILABILITY STATEMENT

The raw data supporting the conclusions of this article will be made available by the authors, without undue reservation.

## REFERENCES

- Corman VM, Landt O, Kaiser M, Molenkamp R, Meijer A, Chu DK, et al. Detection of 2019 novel coronavirus (2019-nCoV) by real-time RT-PCR. *Euro Surveill.* (2020) 25:2000045. doi: 10.2807/1560-7917.ES.2020.25.3.2000045
- Ai T, Yang Z, Hou H, Zhan C, Chen C, Lv W, et al. Correlation of chest CT and RT-PCR testing for coronavirus disease 2019 (COVID-19) in China: a report of 1014 cases. *Radiology.* (2020) 296:E32-40. doi: 10.1148/radiol.2020200642
- Kanne JP. Chest CT findings in 2019 novel coronavirus (2019-nCoV) infections from Wuhan, China: key points for the radiologist. *Radiology.* (2020) 295:16-7. doi: 10.1148/radiol.2020200241
- Wu J, Wu X, Zeng W, Guo D, Fang Z, Chen L, et al. Chest CT findings in patients with coronavirus disease 2019 and its relationship with clinical features. *Invest Radiol.* (2020) 55:257-61. doi: 10.1097/RLI.0000000000000670
- Kim EA, Lee KS, Primack SL, Yoon HK, Byun HS, Kim TS, et al. Viral pneumonias in adults: radiologic and pathologic findings. *Radiographics.* (2002) 22:S137-49. doi: 10.1148/radiographics.22.suppl\_1.g02oc15s137
- Oikonomou A, Müller NL, Nantel S. Radiographic and high-resolution CT findings of influenza virus pneumonia in patients with hematologic malignancies. *AJR Am J Roentgenol.* (2003) 181:507-11. doi: 10.2214/ajr.181.2.1810507
- Li Y, Xia L. Coronavirus disease 2019 (COVID-19): role of chest CT in diagnosis and management. *AJR Am J Roentgenol.* (2020) 214:1280-6. doi: 10.2214/AJR.20.22954
- Lambin P, Rios-Velazquez E, Leijenaar R, Carvalho S, van Stiphout RG, Granton P, et al. Radiomics: extracting more information from medical images using advanced feature analysis. *Eur J Cancer.* (2012) 48:441-6. doi: 10.1016/j.ejca.2011.11.036
- Trebeschi S, Drago SG, Birkbak NJ, Kurilova I, Călin AM, Delli Pizzi A, et al. Predicting response to cancer immunotherapy using noninvasive radiomic biomarkers. *Ann Oncol.* (2019) 30:998-1004. doi: 10.1093/annonc/mdz108

## ETHICS STATEMENT

The studies involving human participants were reviewed and approved by Medical ethics committee of The First Affiliated Hospital of Wenzhou Medical University. Written informed consent from the participants' legal guardian/next of kin was not required to participate in this study in accordance with the national legislation and the institutional requirements.

## AUTHOR CONTRIBUTIONS

LL, QD, and NL: data analysis and visualization. LL and JL: writing original draft. JP, HS, and SQ: review and editing. All authors contributed to the article and approved the submitted version.

## FUNDING

This work was supported by Wenzhou Key Technology Breakthrough Program on Prevention and Treatment for COVID-19 Epidemic, No. ZG2020012.

## SUPPLEMENTARY MATERIAL

The Supplementary Material for this article can be found online at: <https://www.frontiersin.org/articles/10.3389/fpubh.2021.663965/full#supplementary-material>

- Wu W, Pierce LA, Zhang Y, Pipavath SNJ, Randolph TW, Lastwika KJ, et al. Comparison of prediction models with radiological semantic features and radiomics in lung cancer diagnosis of the pulmonary nodules: a case-control study. *Eur Radiol.* (2019) 29:6100-8. doi: 10.1007/s00330-019-06213-9
- Wu G, Woodruff HC, Shen J, Refaee T, Sanduleanu S, Ibrahim A, et al. Diagnosis of invasive lung adenocarcinoma based on chest CT radiomic features of part-solid pulmonary nodules: a multicenter study. *Radiology.* (2020) 297:451-8. doi: 10.1148/radiol.2020192431
- Wu Q, Wang S, Li L, Wu Q, Qian W, Hu Y, et al. Radiomics analysis of computed tomography helps predict poor prognostic outcome in COVID-19. *Theranostics.* (2020) 10:7231-44. doi: 10.7150/thno.46428
- Wei W, Hu XW, Cheng Q, Zhao YM, Ge YQ. Identification of common and severe COVID-19: the value of CT texture analysis and correlation with clinical characteristics. *Eur Radiol.* (2020) 30:1-9. doi: 10.1007/s00330-020-07012-3
- Kramer AA, Zimmerman JE. Assessing the calibration of mortality benchmarks in critical care: the Hosmer-Lemeshow test revisited. *Crit Care Med.* (2007) 35:2052-6. doi: 10.1097/01.CCM.0000275267.64078.B0
- Wang Y, Dong C, Hu Y, Li C, Ren Q, Zhang X, et al. Temporal changes of CT findings in 90 patients with COVID-19 pneumonia: a longitudinal study. *Radiology.* (2020) 296:E55-64. doi: 10.1148/radiol.2020200843
- Liu M, Zeng W, Wen Y, Zheng Y, Lv F, Xiao K. COVID-19 pneumonia: CT findings of 122 patients and differentiation from influenza pneumonia. *Eur Radiol.* (2020) 30:5463-9. doi: 10.1007/s00330-020-06928-0
- Bai HX, Hsieh B, Xiong Z, Halsey K, Choi JW, Tran TML, et al. Performance of radiologists in differentiating COVID-19 from Non-COVID-19 viral pneumonia at chest CT. *Radiology.* (2020) 296:E46-54. doi: 10.1148/radiol.2020200823
- Gillies RJ, Kinahan PE, Hricak H. Radiomics: images are more than pictures, they are data. *Radiology.* (2016) 278:563-77. doi: 10.1148/radiol.2015151169

19. Fang X, Li X, Bian Y, Ji X, Lu J. Radiomics nomogram for the prediction of 2019 novel coronavirus pneumonia caused by SARS-CoV-2. *Eur Radiol.* (2020) 30:6888–901. doi: 10.1007/s00330-020-07032-z
20. Huang Y, Zhang Z, Liu S, Li X, Yang Y, Ma J, et al. CT-based radiomics combined with signs: a valuable tool to help radiologist discriminate COVID-19 and influenza pneumonia. *BMC Med Imaging.* (2021) 21:31. doi: 10.1186/s12880-021-00564-w
21. Chen Z, Li X, Li J, Zhang S, Zhou P, Yu X, et al. A COVID-19 risk score combining chest CT radiomics and clinical characteristics to differentiate COVID-19 pneumonia from other viral pneumonias. *Aging.* (2021) 13:9186–224. doi: 10.18632/aging.202735
22. Zhang H, Wang H, Hao D, Ge Y, Wan G, Zhang J, et al. An MRI-based radiomic nomogram for discrimination between malignant and benign sinonasal tumors. *J Magn Reson Imaging.* (2021) 53:141–51. doi: 10.1002/jmri.27298
23. Tang TY, Li X, Zhang Q, Guo CX, Zhang XZ, Lao MY, et al. Development of a novel multiparametric MRI radiomic nomogram for preoperative evaluation of early recurrence in resectable pancreatic cancer. *J Magn Reson Imaging.* (2020) 52:231–45. doi: 10.1002/jmri.27024
24. Dong D, Fang MJ, Tang L, Shan XH, Gao JB, Giganti F, et al. Deep learning radiomic nomogram can predict the number of lymph node metastasis in locally advanced gastric cancer: an international multicenter study. *Ann Oncol.* (2020) 31:912–20. doi: 10.1016/j.annonc.2020.04.003
25. Vickers AJ, Elkin EB. Decision curve analysis: a novel method for evaluating prediction models. *Med Decis Making.* (2006) 26:565–74. doi: 10.1177/0272989X06295361
26. Vickers AJ, Cronin AM, Elkin EB, Gonen M. Extensions to decision curve analysis, a novel method for evaluating diagnostic tests, prediction models and molecular markers. *BMC Med Inform Decis Mak.* (2008) 8:53. doi: 10.1186/1472-6947-8-53

**Conflict of Interest:** The authors declare that the research was conducted in the absence of any commercial or financial relationships that could be construed as a potential conflict of interest.

Copyright © 2021 Lin, Liu, Deng, Li, Pan, Sun and Quan. This is an open-access article distributed under the terms of the Creative Commons Attribution License (CC BY). The use, distribution or reproduction in other forums is permitted, provided the original author(s) and the copyright owner(s) are credited and that the original publication in this journal is cited, in accordance with accepted academic practice. No use, distribution or reproduction is permitted which does not comply with these terms.





# Differential Diagnosis of COVID-19 Pneumonia From Influenza A (H1N1) Pneumonia Using a Model Based on Clinicoradiologic Features

## OPEN ACCESS

### Edited by:

Reza Lashgari,  
Institute for Research in Fundamental  
Sciences, Iran

### Reviewed by:

Zhichao Feng,  
Central South University, China  
Marcelo Brandao,  
State University of Campinas, Brazil

### \*Correspondence:

Fei Shan  
shanfei@shphc.org.cn  
Nian Xiong  
nianxiong@hust.edu.cn

†These authors have contributed  
equally to this work

### Specialty section:

This article was submitted to  
Pulmonary Medicine,  
a section of the journal  
Frontiers in Medicine

Received: 10 January 2021

Accepted: 26 April 2021

Published: 15 June 2021

### Citation:

Shi W-Y, Hu S-P, Zhang H-L, Liu T-F,  
Zhou S, Tang Y-H, Zhang X-L, Shi Y-X,  
Zhang Z-Y, Xiong N and Shan F (2021)  
Differential Diagnosis of COVID-19  
Pneumonia From Influenza A (H1N1)  
Pneumonia Using a Model Based on  
Clinicoradiologic Features.  
Front. Med. 8:651556.  
doi: 10.3389/fmed.2021.651556

Wei-Ya Shi<sup>1†</sup>, Shao-Ping Hu<sup>2†</sup>, Hao-Ling Zhang<sup>3</sup>, Tie-Fu Liu<sup>4</sup>, Su Zhou<sup>5</sup>, Yu-Hong Tang<sup>6</sup>,  
Xin-Lei Zhang<sup>1</sup>, Yu-Xin Shi<sup>1</sup>, Zhi-Yong Zhang<sup>1</sup>, Nian Xiong<sup>2\*</sup> and Fei Shan<sup>1\*</sup>

<sup>1</sup> Department of Radiology, Shanghai Public Health Clinical Center, Fudan University, Shanghai, China, <sup>2</sup> Department of Radiology, Wuhan Union Red Cross Hospital, Wuhan, China, <sup>3</sup> Department of Radiology, Zhongshan Hospital, Fudan University, Shanghai, China, <sup>4</sup> Department of Scientific Research, Shanghai Public Health Clinical Center, Fudan University, Shanghai, China, <sup>5</sup> Department of Interventional Radiology, Shanghai Public Health Clinical Center, Fudan University, Shanghai, China, <sup>6</sup> Department of Research and Development, Winning Health Technology Group Co., Ltd., Shanghai, China

**Objectives:** Both coronavirus disease 2019 (COVID-19) pneumonia and influenza A (H1N1) pneumonia are highly contagious diseases. We aimed to characterize initial computed tomography (CT) and clinical features and to develop a model for differentiating COVID-19 pneumonia from H1N1 pneumonia.

**Methods:** In total, we enrolled 291 patients with COVID-19 pneumonia from January 20 to February 13, 2020, and 97 patients with H1N1 pneumonia from May 24, 2009, to January 29, 2010 from two hospitals. Patients were randomly grouped into a primary cohort and a validation cohort using a seven-to-three ratio, and their clinicoradiologic data on admission were compared. The clinicoradiologic features were optimized by the least absolute shrinkage and selection operator (LASSO) logistic regression analysis to generate a model for differential diagnosis. Receiver operating characteristic (ROC) curves were plotted for assessing the performance of the model in the primary and validation cohorts.

**Results:** The COVID-19 pneumonia mainly presented a peripheral distribution pattern (262/291, 90.0%); in contrast, H1N1 pneumonia most commonly presented a peribronchovascular distribution pattern (52/97, 53.6%). In LASSO logistic regression, peripheral distribution patterns, older age, low-grade fever, and slightly elevated aspartate aminotransferase (AST) were associated with COVID-19 pneumonia, whereas, a peribronchovascular distribution pattern, centrilobular nodule or tree-in-bud sign, consolidation, bronchial wall thickening or bronchiectasis, younger age, hyperpyrexia, and a higher level of AST were associated with H1N1 pneumonia. For the primary and validation cohorts, the LASSO model containing above eight clinicoradiologic features

yielded an area under curve (AUC) of 0.963 and 0.943, with sensitivity of 89.7 and 86.2%, specificity of 89.7 and 89.7%, and accuracy of 89.7 and 87.1%, respectively.

**Conclusions:** Combination of distribution pattern and category of pulmonary opacity on chest CT with clinical features facilitates the differentiation of COVID-19 pneumonia from H1N1 pneumonia.

**Keywords:** coronavirus disease 2019, influenza A (H1N1), computed tomography, multivariate analysis, differential diagnosis

## INTRODUCTION

Coronavirus disease 2019 (COVID-19), caused by the novel severe acute respiratory syndrome coronavirus 2 (SARS-CoV-2, previously known as 2019-nCoV), has become a global health concern that threaten human life and public health security. As of 3 January, 2021, more than 83 million cases and more than 1.8 million deaths have been reported worldwide according to World Health Organization (WHO) statistics (1). When assessing COVID-19, it is noteworthy that influenza viruses occur in the same season. Influenza A (H1N1) is the most common influenza, and it caused a worldwide pandemic in 2009–2010 with more than 18,449 deaths (2) and has now become an annual seasonal influenza, leading to a large number of hospitalizations and deaths (3, 4). Because of the differences in therapy, prognosis, and protective measure between COVID-19 and H1N1, it is important for clinicians and radiologists to identify these two respiroviral infections.

Both COVID-19 and H1N1 pneumonias share similar clinical manifestations, such as mild to moderate flulike syndromes, and are often cured by symptomatic treatments (5, 6). But a few patients develop severe or even lethal acute respiratory distress syndrome (ARDS), particularly in patients with comorbidities (7–11), and their laboratory exams often display lymphopenia, abnormalities in liver function, and myocardial zymogram (7, 8, 10–14).

Significantly, the typical findings on computed tomography (CT) seem different in both pneumonias: bilateral, multifocal ground-glass opacities (GGOs) with or without consolidations or intralobular lines, in a predominant peripheral distribution usually present in COVID-19 pneumonia (15–17); nodules and bud signs (18, 19), bronchiectasis (18, 20), and pleural effusion (20) are common in H1N1 pneumonia but rare in COVID-19 pneumonia (16). Unlike the predominant peripheral distribution in COVID-19 pneumonia, H1N1 pneumonia presents as a predominant peribronchovascular (18, 21) or peripheral (18, 21) or mixed distribution (18, 19). The differences in CT findings in category and the distribution patterns of pulmonary opacity suggest their significance in terms of a differential diagnosis of both pneumonias.

Although it is easy to identify these typical lesions, CT manifestations of COVID-19 and H1N1 pneumonia are very diverse. To date, knowledge regarding the comprehensive identification of both pneumonias still remains limited and cannot meet the urgent clinical needs. Therefore, this retrospective study aimed to assess initial CT and clinical

features of the two diseases and further establish a model based on clinicoradiologic features so as to provide some guidance for their early identification.

## METHODS

### Study Population

A search of the medical records in two hospitals' information system was conducted, and 303 COVID-19 patients from January 20 to February 13, 2020, and 224 patients with H1N1 pneumonia from May 24, 2009, to January 29, 2010, were identified. All patients were diagnosed according to the diagnostic criteria of the National Health Commission of China (22, 23) and were confirmed by real-time Polymerase Chain Reaction (RT-PCR) detection of virus nuclear acid. Our exclusion criteria were (a) patients without CT scans; (b) patients with normal CT imaging; and (c) COVID-19 patients with positive influenza A nuclear acid tests. Finally, 291 patients with COVID-19 pneumonia and 97 patients with H1N1 pneumonia were enrolled. All patients were randomly grouped in seven-to-three ratio into a primary cohort ( $n = 272$ ) and a validation cohort ( $n = 116$ ), respectively, by using computer-generated random numbers. The flow chart of patient selection, grouping, and disease subtypes is shown in **Figure 1**.

### Ethics Statement

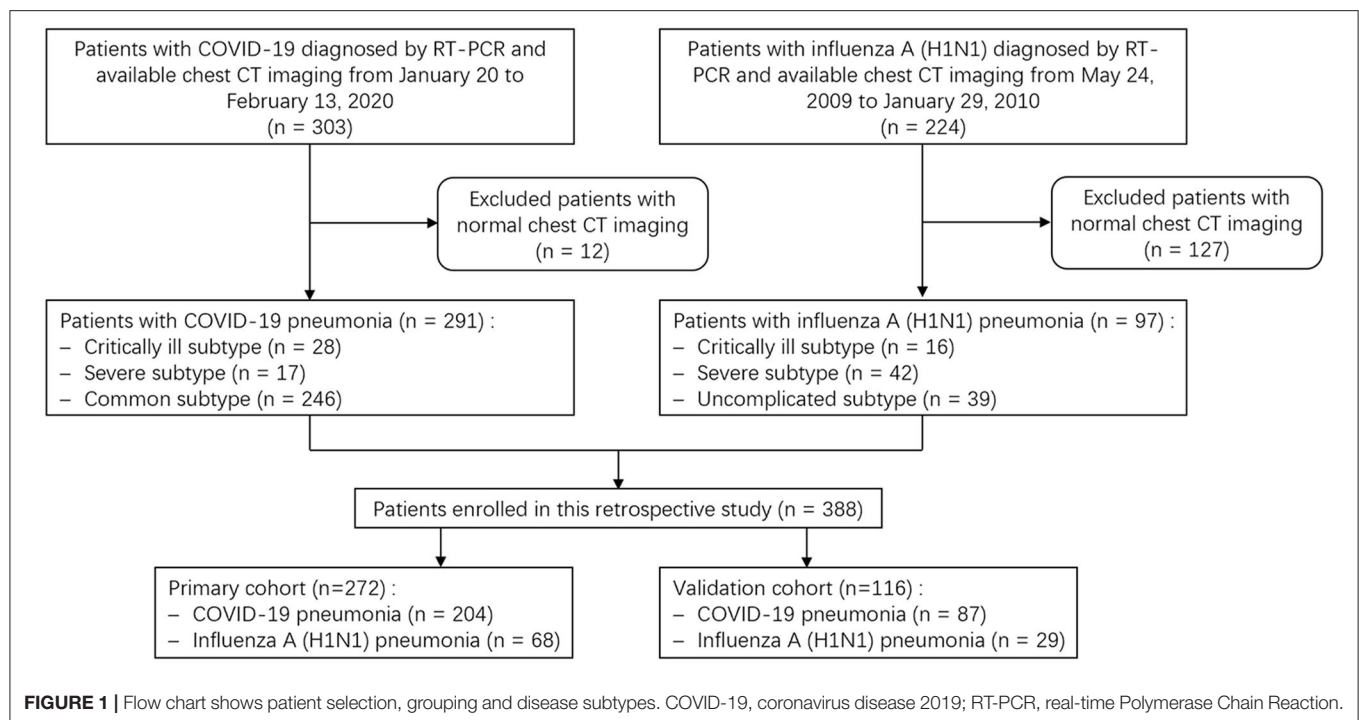
This work was approved by the Ethics Committee of Shanghai Public Health Clinical Center, China, and Wuhan Union Red Cross Hospital, China, and informed consent for this retrospective study was waived (YJ-2020-S035-01).

### Clinical Data Collection

The clinical data on admission were retrospectively collected. Particular attention was paid to the demographics, comorbidities, coinfection, symptoms, and laboratory findings. The comorbidities or underlying medical conditions mainly included chronic pulmonary, cardiac, renal and hepatic diseases, diabetes, cerebrovascular disease, hyperlipemia, malignancy, and immunosuppression.

### Imaging Acquiring

All patients underwent CT examinations at full inspiration from the thoracic inlet to the costophrenic angle level. CT scans were performed with one of two scanners (Hitachi Scenaria 64, Hitachi Medical Systems, Tokyo, Japan; or Siemens Sensation 16, Siemens Medical Systems, Forchheim, Germany) using automatic exposure control with the following parameters: tube



voltage, 120 or 140 kV; tube current, 150–250 mA; detector width,  $64 \times 0.625$  mm or  $16 \times 0.75$  mm; pitch, 1.57 or 1; rotation time, 0.35 or 0.5 s; field of view (FOV), 350 mm; and matrix,  $512 \times 512$ . The reconstruction kernel used was lung smooth with a thickness of 1 mm and an interval of 0.8 mm. The following windows were used: a mediastinal window with a window width of 350 Hounsfield unit (Hu) and a window level of 40 Hu, and a lung window with a width of 1,200 Hu and a level of  $-600$  Hu.

## Image Interpretation

CT images were assessed for the presence and distribution of pulmonary opacities, including pure GGOs, which manifested as a hazy opacity without obscuring the underlying vessels; GGO with interlobular septal thickening or reticulation, which was defined as a crazy-paving sign; GGOs with consolidation, which was defined as an area of opacification obscuring the underlying vessels in GGO; consolidation; centrilobular nodule or tree-in-bud sign, which was regarded present when centrilobular nodules or nodular branching structures resembled a budding tree.

The distribution pattern of pulmonary opacities was assessed as being in a predominant peripheral (outer third of the lungs), peribronchovascular, both of peripheral and peribronchovascular, or diffuse distribution, or lacking a specific distribution (**Figure 2**). The laterality (unilateral and bilateral) and predominant involved pulmonary lobes (upper, middle/lingula, lower, or diffuse) were also assessed.

Bronchial wall thickening or bronchiectasis, focal pulmonary fibrosis (including reticulation and liner opacity), pleural effusion, and mediastinal lymphadenopathy ( $>1$  cm in short-axis diameter) were noted. The number of pulmonary segments involved was counted. All the terms were defined according to the

Fleischner Society (24). The images were analyzed independently by two radiologists (Weiya Shi and Fei Shan, with 12 and 19 years of experience in chest radiology, respectively). In cases of disagreement, the results were determined by consensus.

## Statistical Analysis

The continuous data are expressed as the median and interquartile range (IQR, 25th and 75th percentiles), because a majority of them did not follow a normal distribution. The Fisher exact test and the chi-square test were used for categorical variables, and the Wilcoxon rank sum test was used for continuous variables when comparing the clinicoradiologic features of COVID-19 pneumonia with those of H1N1 pneumonia.

In order to evaluate the interobserver agreement (IA) between the two radiologists, the Cohen's Kappa test was used for categorical variables and the intraclass correlation coefficient (ICC) for continuous variables. The kappa coefficient ( $k$ ) between 0.00 and 0.20; 0.21 and 0.40; 0.41 and 0.60; 0.61 and 0.80; and 0.81 and 1.00 indicated slight, fair, moderate, substantial, and almost perfect agreement, respectively. The ICC values between 0.00 and 0.25; 0.26 and 0.40; 0.41 and 0.60; 0.61 and 0.75; 0.75 and 1.00, indicated poor, low, fair, good, and excellent agreement, respectively.

The clinicoradiologic characteristics found to be significant in univariate analysis were inputted into the least absolute shrinkage and selection operator (LASSO) logistic regression analysis to identify the optimal subset of clinicoradiologic features in order to develop a model for identification. Receiver operating characteristic (ROC) curves were plotted for assessing the performance of the model in the primary and validation



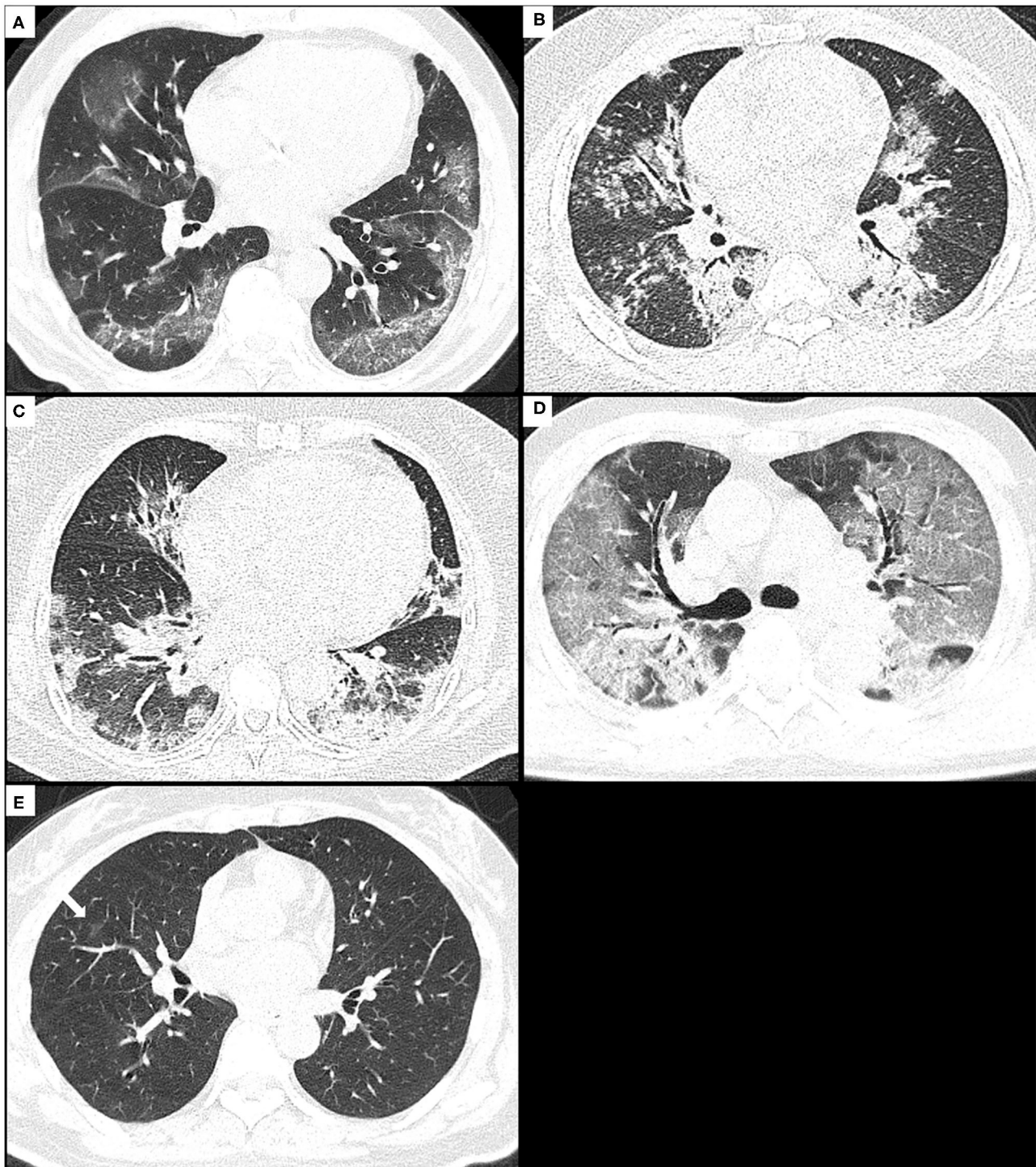


**FIGURE 2 |** The distribution patterns of pneumonia due to COVID-19 or H1N1. **(A)** A 74-year-old male with COVID-19 pneumonia presents the onset symptom of fever ( $37.5^{\circ}\text{C}$ ), and the CT shows GGO with consolidation and crazy-paving sign mainly along subpleural lungs, namely, as a peripheral distribution pattern. **(B)** A 29-year-old male with H1N1 pneumonia presents the onset symptoms of fever ( $39.5^{\circ}\text{C}$ ), cough, and shortness of breath, and the CT shows consolidation and small centrilobular nodules mainly along bronchovascular bundles, namely, as a peribronchovascular distribution pattern. **(C)** A 59-year-old female with H1N1 pneumonia presents the onset symptoms of fever ( $38.5^{\circ}\text{C}$ ), cough, and shortness of breath, and the CT shows consolidation with GGO along bronchovascular bundles and subpleural lungs, namely, as a distribution pattern of both peripheral and peribronchovascular. **(D)** A 71-year-old male with COVID-19 pneumonia presents the onset symptoms of fever ( $38^{\circ}\text{C}$ ) and dyspnea, and CT shows diffuse GGO with consolidation and crazy-paving sign in both lungs, namely, as a diffuse distribution pattern. **(E)** A 50-year-old female with COVID-19 pneumonia presents the onset symptoms of fever ( $39^{\circ}\text{C}$ ) and cough, and CT shows very small non-rounded GGO located in the middle lobe of the right lung lacking a specific distribution. COVID-19, coronavirus disease 2019; GGOs, ground-glass opacities.



**TABLE 1** | Baseline clinical and laboratory characteristics of the patients with COVID-19 pneumonia vs. those with H1N1 pneumonia.

| Characteristics   | COVID-19 (n = 291)  | H1N1 (n = 97)       | P-value |
|---|---------------------|---------------------|---------|
| Age, years  | 51.0 (37.0–64.0)    | 31.0 (23.0–45.0)    | <0.001* |
| <b>Sex</b>  |                     |                     |         |
| Male  | 156 (53.6%)         | 66 (68.0%)          | 0.013*  |
| Female  | 135 (46.4%)         | 31 (32.0%)          |         |
| Fever   | 239 (82.1%)         | 93 (95.9%)          | 0.001*  |
| Body temperature, °C  | 38.0 (37.5–38.5)    | 38.8 (38.0–39.5)    | <0.001* |
| Onset symptom to hospital admission, d  | 5.0 (3.0–8.0)       | 5.0 (2.0–7.0)       | 0.788   |
| <b>Comorbidities</b>  | 95 (32.6%)          | 30 (30.9%)          | 0.754   |
| Chronic pulmonary disease   | 7 (2.4%)            | 2 (2.1%)            | 0.601   |
| Coinfection   | 13 (4.5%)           | 16 (16.5%)          | <0.001* |
| White blood cell count, $\times 10^9/L$ ; normal range: 3.5–9.5                 | 4.7 (3.9–5.9)       | 4.3 (3.2–6.1)       | 0.082   |
| Lymphocyte count, $\times 10^9/L$ ; normal range: 1.1–3.2                       | 1.1 (0.8–1.5)       | 1.1 (0.8–1.6)       | 0.544   |
| Alanine aminotransferase, U/L; normal range: 7–40                               | 22.0 (15.0–33.5)    | 31.0 (21.0–56.0)    | <0.001* |
| AST, U/L; normal range: 13–35   | 24.0 (19.0–33.0)    | 41.0 (27.0–65.0)    | <0.001* |
| Lactate dehydrogenase, U/L; normal range: 120–250                               | 232.0 (199.0–293.0) | 263.5 (191.0–445.0) | 0.032*  |
| Total bilirubin, $\mu\text{mol/L}$ ; normal range: 3.4–20.5                     | 8.1 (6.5–10.5)      | 9.0 (7.3–12.0)      | 0.011*  |
| Albumin, g/L; normal range: 40.0–55.0   | 40.8 (37.9–43.1)    | 40.0 (35.2–45.4)    | 0.341   |
| Blood urea nitrogen, mmol/L; normal range: 2.6–7.5                              | 4.4 (3.6–5.5)       | 3.9 (3.1–5.1)       | 0.017*  |
| Serum creatinine, $\mu\text{mol/L}$ ; normal range: Male, 53–106; Female, 44–97 |                     |                     |         |
| Increased   | 21 (7.2%)           | 1 (1.0%)            | 0.023*  |
| C-reactive protein, mg/L; normal range: <3.0                                    | 14.8 (5.1–33.0)     | 22.7 (11.2–51.6)    | 0.001*  |
| CD4 <sup>+</sup> T counts, cell/ $\mu\text{L}$ ; normal range: 410–1,590        | 417.0 (291.0–618.0) | 365.0 (230.0–535.0) | 0.010*  |

Continuous variables are presented as median (interquartile range), and dichotomous variables are presented as numbers of patients, with percentages in parentheses. \* $P < 0.05$ ; P-values are from Fisher's exact test or Wilcoxon rank-sum test when comparing characteristics of COVID-19 pneumonia with those of H1N1 pneumonia; COVID-19, coronavirus disease 2019; AST, aspartate aminotransferase.

cohorts. The cut-off values were defined based on the maximal Youden index.

Statistical analysis was performed with R version 3.6.1 (R Project for Statistical Computing, Vienna, Austria). A two-tailed  $\alpha < 0.05$  was considered statistically significant.

## RESULTS

### Clinical and Laboratory Features

The baseline clinical and laboratory characteristics of the 388 cases were shown in **Table 1**. Compared with H1N1 pneumonia (97 patients), patients with COVID-19 pneumonia (291 patients) were older (51.0 vs. 31.0 years,  $p < 0.001$ ) and had a lower proportion of men (156/291, 53.6% vs. 66/97, 68.0%,  $p = 0.013$ ). They had lower fever incidence (239/291, 82.1% vs. 93/97, 95.9%,  $p = 0.001$ ) and lower body temperatures (38.0 vs. 38.8°C,  $p < 0.001$ ). H1N1 patients were more likely to have coinfection than COVID-19 patients (16/97, 16.5% vs. 13/291, 4.5%,  $p < 0.001$ ). Among them, all were bacterial infections except for 2 H1N1 cases with bacterial and fungal coinfections.

The laboratory exams displayed lower serum levels of alanine aminotransferase, aspartate aminotransferase (AST), lactate dehydrogenase, total bilirubin, and c-reactive protein, higher level of CD4<sup>+</sup> T counts and blood urea nitrogen, as well as more frequency of increased serum creatinine in COVID-19 pneumonia in contrast to those in H1N1 pneumonia ( $p <$

0.001,  $p < 0.001$ ,  $p = 0.032$ , 0.011, 0.001, 0.010, 0.017, and 0.023, respectively).

### CT Characteristics

The IA between the two radiologists was almost perfect for all CT findings except the tree-in-bud sign, for which it was substantial ( $k = 0.789$ ).

The baseline CT characteristics of the 388 cases were shown in **Table 2**. In terms of lesions' distribution pattern, 90.0% (262/291) of COVID-19 pneumonia had a peripheral distribution pattern in contrast to only 20.6% (20/97) in H1N1 pneumonia ( $p < 0.001$ ). In the H1N1 pneumonia, a peribronchovascular distribution pattern (52/97, 53.6%) was the most common, though this is rare in COVID-19 pneumonia (9/291, 3.1%,  $p < 0.001$ ). The H1N1 pneumonia was more likely to exist in a distribution pattern of both peripheral and peribronchovascular (17/97, 17.5% vs. 14/291, 4.8%,  $p < 0.001$ ) or be lacking a specific distribution (6/97, 6.2% vs. 3/291, 1.0%,  $p = 0.003$ ). The incidence of diffuse distribution pattern was 1.0% (3/291) and 2.1% (2/97) in COVID-19 pneumonia and H1N1 pneumonia, respectively, and had no significant difference.

With respect to other CT characteristics, the COVID-19 pneumonia was more likely to present a crazy-paving sign (206/291, 70.8% vs. 39/97, 40.2%,  $p < 0.001$ ), GGO with consolidation (216/291, 74.2% vs. 49/97, 50.5%,  $p < 0.001$ ), bilateral involvement (241/291, 82.8% vs. 71/97, 73.2%,

**TABLE 2 |** Baseline CT characteristics of the patients with COVID-19 pneumonia vs. those with H1N1 pneumonia.

| Characteristics                             | COVID-19 (n = 291) | H1N1 (n = 97) | P-value | Agreement (k or ICC; 95% CI) |
|---|--------------------|---------------|---------|------------------------------|
| <b>Main pulmonary opacities</b>             |                    |               |         |                              |
| pGGO  | 118 (40.5%)        | 37 (38.1%)    | 0.675   | 0.941 (0.903–0.973)          |
| Crazy-paving sign                           | 206 (70.8%)        | 39 (40.2%)    | <0.001* | 0.884 (0.835–0.931)          |
| GGO with consolidation                      | 216 (74.2%)        | 49 (50.5%)    | <0.001* | 0.915 (0.865–0.956)          |
| Consolidation                               | 91 (31.3%)         | 79 (81.4%)    | <0.001* | 0.912 (0.870–0.948)          |
| Centrilobular nodule or tree-in-bud sign    | 3 (1.0%)           | 43 (44.3%)    | <0.001* | 0.789 (0.687–0.891)          |
| NO. of pulmonary segments involved          | 9 (4–15)           | 12 (3–17)     | 0.183   | 0.998 (0.997–0.998)          |
| <b>Laterality</b>                           |                    |               |         |                              |
| Bilateral involvement                       | 241 (82.8%)        | 71 (73.2%)    | 0.039*  | 1.000 (1.000–1.000)          |
| <b>Involved pulmonary lobes</b>             |                    |               |         |                              |
| Upper                                       | 29 (10.0%)         | 10 (10.3%)    | 0.922   | 0.948 (0.916–0.972)          |
| Middle/lingula                              | 12 (4.1%)          | 12 (12.4%)    | 0.003*  |                              |
| Lower                                       | 172 (59.1%)        | 52 (53.6%)    | 0.342   |                              |
| Diffuse                                     | 78 (26.8%)         | 23 (23.7%)    | 0.548   |                              |
| <b>Distribution pattern</b>                 |                    |               |         |                              |
| Peripheral                                  | 262 (90.0%)        | 20 (20.6%)    | <0.001* | 0.877 (0.827–0.925)          |
| Peribronchovascular                         | 9 (3.1%)           | 52 (53.6%)    | <0.001* |                              |
| Peripheral + Peribronchovascular            | 14 (4.8%)          | 17 (17.5%)    | <0.001* |                              |
| Diffuse                                     | 3 (1.0%)           | 2 (2.1%)      | 0.436   |                              |
| Lacking a specific distribution             | 3 (1.0%)           | 6 (6.2%)      | 0.003*  |                              |
| <b>Other signs</b>                          |                    |               |         |                              |
| Bronchial wall thickening or bronchiectasis | 18 (6.2%)          | 28 (28.9%)    | <0.001* | 0.805 (0.692–0.891)          |
| Focal pulmonary fibrosis                    | 103 (35.4%)        | 21 (21.6%)    | 0.012*  | 0.928 (0.886–0.965)          |
| Pleural effusion                            | 14 (4.8%)          | 27 (27.8%)    | <0.001* | 1.000 (1.000–1.000)          |
| Mediastinal lymphadenopathy                 | 4 (1.4%)           | 1 (1.0%)      | 0.795   | 1.000 (1.000–1.000)          |

Continuous variables are presented as median (interquartile range), and dichotomous variables are presented as numbers of patients, with percentages in parentheses. \* $P < 0.05$ ; P-values are from Fisher's exact test or Wilcoxon rank-sum test when comparing characteristics of COVID-19 pneumonia with those of H1N1 pneumonia. For categorical variables and continuous variables, the interobserver agreement is assessed with the kappa coefficient (k) and the intraclass correlation coefficient (ICC), respectively. The k and ICC values are reported with 95% confidence intervals (95% CI). COVID-19, coronavirus disease 2019; GGOs, ground-glass opacities.

$p = 0.039$ ), and focal pulmonary fibrosis (103/291, 35.4% vs. 21/97, 21.6%,  $p = 0.012$ ); H1N1 pneumonia, however, was more likely to present consolidation (79/97, 81.4% vs. 91/291, 31.3%,  $p < 0.001$ ), centrilobular nodule or tree-in-bud sign (43/97, 44.3% vs. 3/291, 1.0%,  $p < 0.001$ ), predominant middle/lingula involvement (12/97, 12.4% vs. 12/291, 4.1%,  $p = 0.003$ ), bronchial wall thickening or bronchiectasis (28/97, 28.9% vs. 18/291, 6.2%,  $p < 0.001$ ), and pleural effusion (27/97, 27.8% vs. 14/291, 4.8%,  $p < 0.001$ ).

and a peribronchovascular distribution pattern were inversely associated with COVID-19 pneumonia.

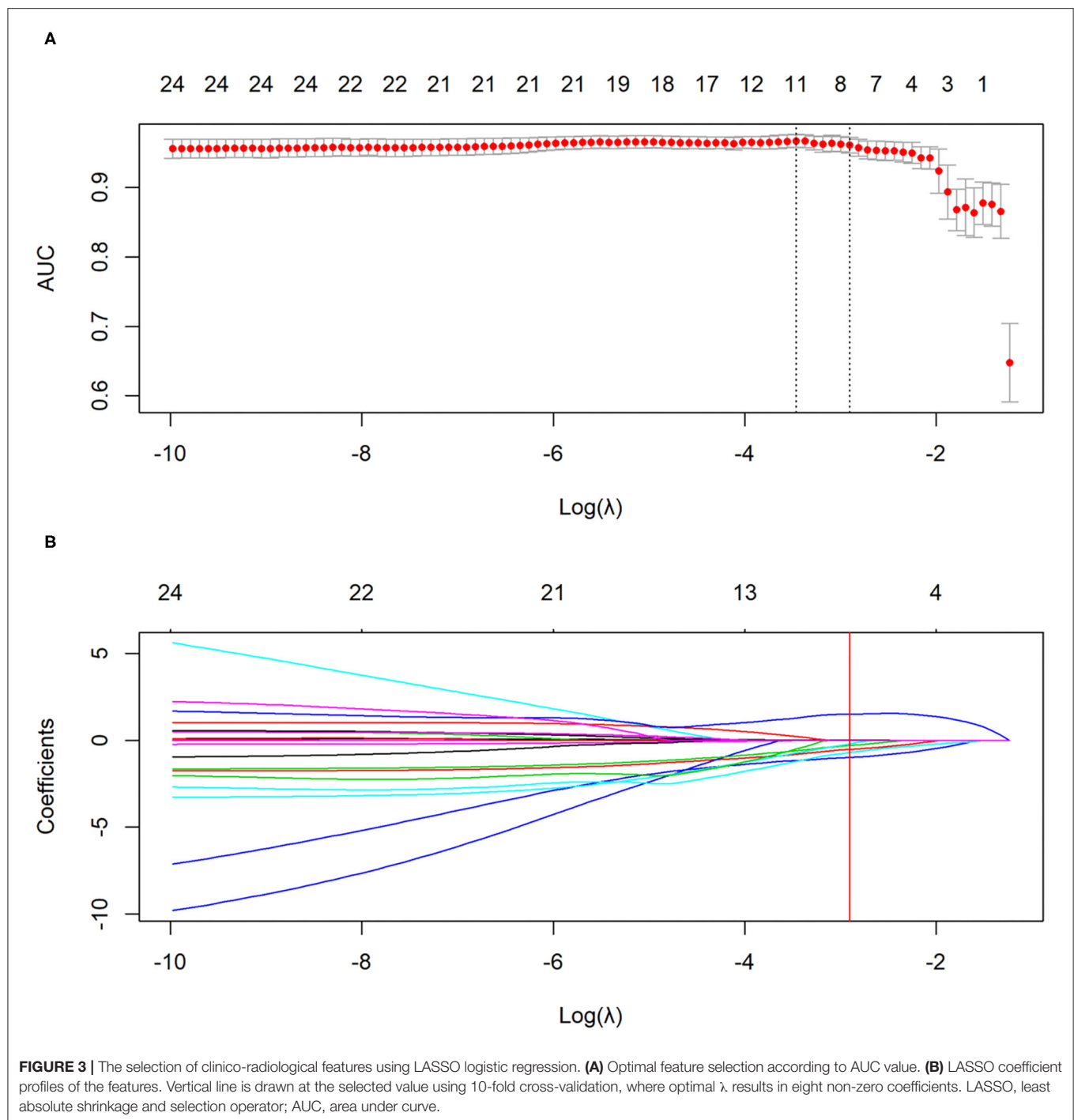
For the primary and validation cohorts, the LASSO model containing above eight features yielded an area under curve (AUC) of 0.963 (95% CI: 0.942–0.984) and 0.943 (95% CI: 0.900–0.986), with sensitivity of 89.7 and 86.2%, specificity of 89.7 and 89.7%, accuracy of 89.7 and 87.1%, positive predictive value of 96.3 and 96.1%, and negative predictive value of 74.4 and 68.4%, respectively (Table 4 and Figure 4).

## Performance of the Model for Differential Diagnosis

LASSO logistic regression analysis was applied to identify the most valuable clinico-radiological features for differentiating COVID-19 pneumonia from H1N1 pneumonia when the optimal value of log ( $\lambda$ ) was  $-2.906$  according to 10-fold cross-validation (Figure 3). The optimal features subset and their coefficient values were shown in Table 3. LASSO-based feature selection revealed that age and peripheral distribution patterns were positively associated with COVID-19 pneumonia, and body temperature, AST, consolidation, centrilobular nodule or tree-in-bud sign, bronchial wall thickening or bronchiectasis,

## DISCUSSION

RT-PCR detection of viral nuclear acid is widely used for diagnosis and conformation of COVID-19; however, its sensitivity is largely affected by the disease phase, viral loading, and sampling (25). Thus, the routine chest CT is a more sensitive and rapid method (25), and the expert consensus of the Radiological Society of North America (RSNA) has provided guidance to report CT findings attributable to COVID-19 pneumonia (16); however, the reported specificities of CT are low so far, ranging from 25 to 53% (16). Because of the distinct treatments and prognoses between COVID-19 and H1N1, we



aimed to accurately identify these two diseases. In our study, CT manifestations of consolidation, centrilobular nodule or tree-in-bud sign, bronchial wall thickening or bronchiectasis, peripheral distribution pattern and peribronchovascular distribution pattern, together with the clinical features such as age, body temperature and AST were identified the optimal features subset for differentiating COVID-19 pneumonia from H1N1 pneumonia. Our model had high diagnostic efficiency

(AUC, 0.943; sensitivity, 86.2%; specificity, 89.7%; accuracy, 87.1%) in the validation cohort, which provides guidance for clinical diagnosis.

Several previous studies have found that COVID-19 typically presents GGO with or without consolidation in a peripheral distribution (15–17), which was endorsed by the Society of Thoracic Radiology, the American College of Radiology, and RSNA (16) as guidance for COVID-19 diagnosis. Our study was

consistent with previous reports that the COVID-19 pneumonia mainly presented a peripheral distribution pattern (262/291, 90.0%); in contrast, H1N1 pneumonia most commonly presented a peribronchovascular distribution pattern (52/97, 53.6%). The differences in CT imaging between these two pneumonias may result from their distinct pathological changes in lungs. The pathological findings of COVID-19 pneumonia include exudative diffuse alveolar damage with alveolar and interstitial edema, alveolar fibrinous exudate with hyaline membranes, and reactive pneumocytes (26), whereas H1N1 pneumonia, in addition to diffuse alveolar damage, is usually accompanied by necrotizing bronchiolitis and alveolar hemorrhage (27). These pathologic lesion-dependent distribution patterns, which are very conspicuous at the first glance of the images, are valuable indicators for differentiating COVID-19 pneumonia from H1N1 pneumonia.

The bronchiolitis causes central lobular nodules or tree-bud signs, and bronchial wall thickening or bronchiectasis; therefore, it is quite understandable that these two signs were more common in H1N1 pneumonia than in COVID-19 pneumonia (both  $p < 0.001$ ), consisting with other studies (16, 18, 21). We also found that consolidation was more frequent in H1N1 pneumonia (79/97, 81.4%) than in COVID-19 pneumonia (91/291, 31.3%), which is consistent with previous studies and is possibly associated with pathologic basis (8), disease progression or more severe disease (28), bacterial coinfection (29). The latter phenomenon was also found in our study, that

is, coinfection (mainly bacterial infection) was more frequent in H1N1 pneumonia (16/97, 16.5%) than in COVID-19 pneumonia (13/291, 4.5%).

Besides radiological features, clinical features such as age, body temperature, and AST should be also taken into consideration for differentiation. Our cohort showed an older median age of the COVID-19 patients; however, it should be viewed cautiously, the statistics were based on the early stage of the outbreak in Shanghai and Hubei province, China. With the global spread, it has been found that the youth are also a susceptible population (30).

Although the model had high diagnostic efficiency, it should be noted that it had a negative predictive value of 68.4% in the validation cohort due to the misdiagnosis of 12 cases of COVID-19 pneumonia as H1N1 pneumonia. The misdiagnosed patients were relatively young (median, 38.5 years; IQR, 32.5–58.5), with high fever (median, 39.0°C; IQR, 38.3–39.7) and moderately elevated AST (median, 30.0 U/L; IQR, 22.5–48.0), and 75.0% (9/12) of them presented consolidation and 58.3% (7/12) a non-peripheral distribution pattern (two cases with a peribronchovascular distribution pattern, four cases with a distribution pattern of both peripheral and peribronchovascular, and one case with a diffuse distribution pattern). Radiologists should pay more attention to these atypical clinicoradiologic manifestations of COVID-19 in young individuals so as to avoid misdiagnosis.

However, our study had limitations. Firstly, there was an imbalance between the sample sizes of COVID-19 pneumonia and H1N1 pneumonia, and the proportion of severe and critically ill H1N1 patients was greater than those of the COVID-19 cohort, which may have led to statistical disequilibrium. Secondly, there is a bias in the laboratory tests because there were several laboratory changes in COVID-19 patients compared to H1N1 patients, using only the tests common to both groups. Thirdly, patients comorbid with chronic pulmonary disease were not excluded, which may lead to a bias in this study, although the proportion of these patients was very low and there was no statistically significant difference between both groups. Fourthly, coinfection is common in patients of both groups, especially in patients with H1N1. Due to the complex nature of the clinical situation, we believe that differential diagnosis is also necessary for these patients to obtain effective subsequent treatment. Therefore, we did not exclude these patients when constructing our analysis model, but this may lead to a bias.

**TABLE 3 |** The coefficients of the elected features by LASSO logistic regression analysis.

| Feature selected   | Coefficient |
|--|-------------|
| Age, years   | 0.013       |
| Body temperature, °C                                     | −0.523      |
| AST, U/L   | −2.998e-03  |
| Consolidation (yes vs. no)                               | −0.300      |
| Centrilobular nodule or tree-in-bud sign (yes vs. no)    | −0.984      |
| Bronchial wall thickening or bronchiectasis (yes vs. no) | −0.207      |
| Peripheral distribution pattern (yes vs. no)             | 1.505       |
| Peribronchovascular distribution pattern (yes vs. no)    | −0.712      |

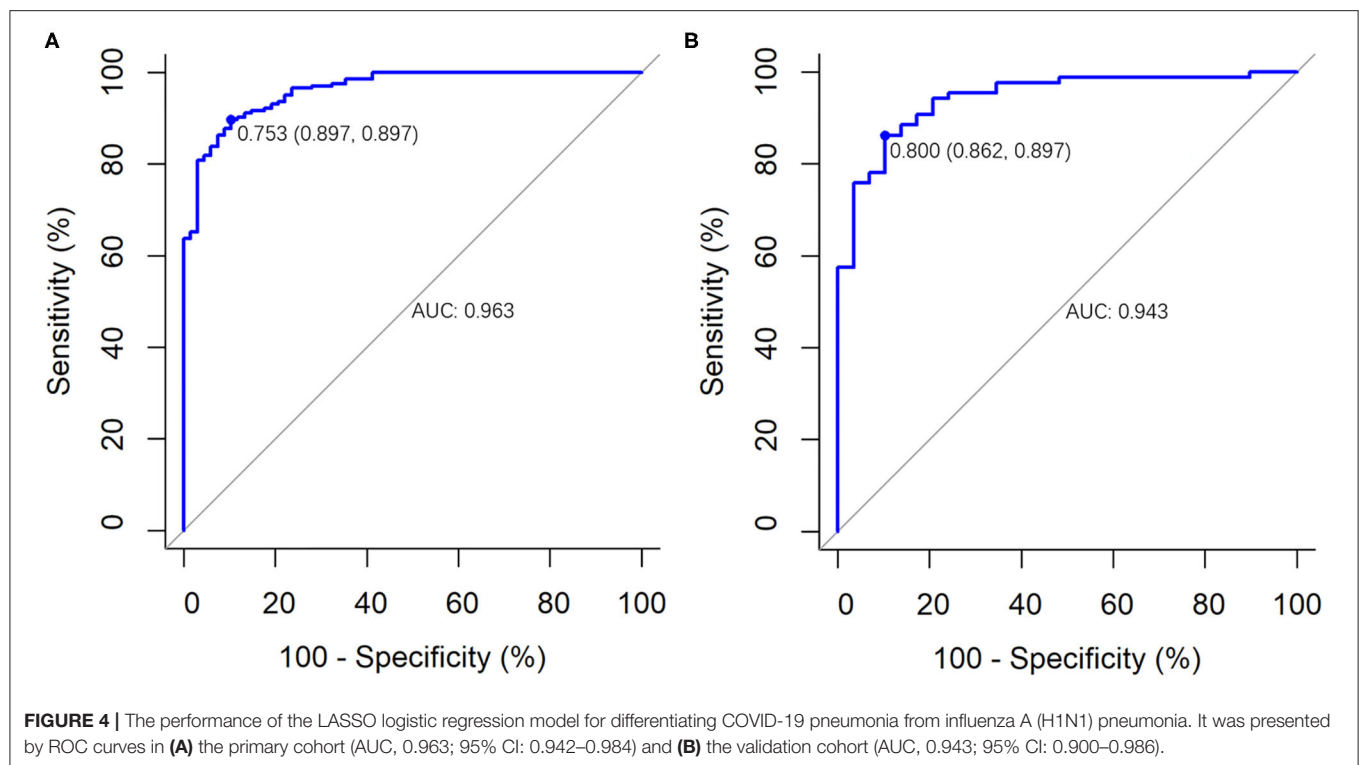
LASSO, least absolute shrinkage and selection operator; AST, aspartate aminotransferase.

**TABLE 4 |** AUC values of the LASSO regression model for differentiating COVID-19 pneumonia from H1N1 pneumonia in the primary and validation cohorts.

| LASSO regression model | AUC value (95% CI)     | Sensitivity (%) | Specificity (%) | Accuracy (%) | PPV (%) | NPV (%) |
|------------------------|------------------------|-----------------|-----------------|--------------|---------|---------|
| Primary cohort         | 0.963<br>(0.942–0.984) | 89.7            | 89.7            | 89.7         | 96.3    | 74.4    |
| Validation cohort      | 0.943<br>(0.900–0.986) | 86.2            | 89.7            | 87.1         | 96.1    | 68.4    |

COVID-19, coronavirus disease 2019; AUC, area under curve; LASSO, least absolute shrinkage and selection operator; PPV, positive predictive value; NPV, negative predictive value; 95% CI, 95% confidence intervals.





In conclusion, CT characteristics, including the distribution pattern and category of pulmonary opacity, combined with clinical features, can help the early differentiation of COVID-19 pneumonia from H1N1 pneumonia. CT manifestations of peripheral distribution patterns, together with older age, low-grade fever, and slightly elevated AST, indicate COVID-19 pneumonia; however, CT presentations of peribronchovascular distribution patterns, centrilobular nodule or tree-in-bud sign, consolidation, and bronchial wall thickening or bronchiectasis, together with younger age, hyperpyrexia and higher level of AST, suggest H1N1 pneumonia.

## DATA AVAILABILITY STATEMENT

The original contributions presented in the study are included in the article/supplementary material, further inquiries can be directed to the corresponding author/s.

## ETHICS STATEMENT

The studies involving human participants were reviewed and approved by the Ethics Committee of Shanghai Public Health Clinical Center, China, and Wuhan Union Red Cross Hospital, China, and informed consent for this retrospective study was waived (YJ-2020-S035-01). Written informed consent from the participants' legal guardian/next of kin was not required

to participate in this study in accordance with the national legislation and the institutional requirements.

## AUTHOR CONTRIBUTIONS

W-YS and FS participated in the study design and conceptualization. W-YS, X-LZ, H-LZ, SZ, and S-PH participated in the acquisition of data. W-YS, FS, and Y-HT participated in analysis and interpretation of data. W-YS and Y-HT participated in drafting of the manuscript and participated in the statistical analysis. FS and T-FL participated in critical revision of the manuscript for important intellectual content. Z-YZ, Y-XS, and NX participated in administrative, technical, material support, and participated in study supervision. All authors contributed to the article and approved the submitted version.

## FUNDING

This research was funded by the Novel Coronavirus Special Research Foundation of the Shanghai Municipal Science and Technology Commission (Grant Number: 20441900600).

## ACKNOWLEDGMENTS

We thank all the doctors, nurses, disease control workers, and researchers who have fought bravely and ceaseless against the virus on the frontline during the COVID-19 epidemic.

## REFERENCES

1. WHO. *Weekly Epidemiological Update - 5 January 2021*. (2021). Available online at: <https://www.who.int/publications/m/item/weekly-epidemiological-update---5-january-2021> (accessed January 7, 2021).
2. WHO. *Pandemic (H1N1) 2009 - Update 112*. (2010). Available online at: [https://www.who.int/csr/don/2010\\_08\\_06/en/](https://www.who.int/csr/don/2010_08_06/en/) (accessed March 9, 2020).
3. Dawood FS, Chung JR, Kim SS, Zimmerman RK, Nowalk MP, Jackson ML, et al. Interim estimates of 2019-20 seasonal influenza vaccine effectiveness - United States, February 2020. *MMWR Morb Mortal Wkly Rep*. (2020) 69:177-82. doi: 10.15585/mmwr.mm6907a1
4. Livingston E, Bucher K, Rekito A. Coronavirus disease 2019 and influenza 2019-2020. *JAMA*. (2020) 323:1122. doi: 10.1001/jama.2020.2633
5. Adhikari SP, Meng S, Wu YJ, Mao YP, Ye RX, Wang QZ, et al. Epidemiology, causes, clinical manifestation and diagnosis, prevention and control of coronavirus disease (COVID-19) during the early outbreak period: a scoping review. *Infect Dis Poverty*. (2020) 9:29. doi: 10.1186/s40249-020-00646-x
6. Writing Committee of the WHO CoCAoPi, Bautista E, Chotpitayasunondh T, Gao Z, Harper SA, Shaw M, et al. Clinical aspects of pandemic 2009 influenza A (H1N1) virus infection. *N Engl J Med*. (2010) 362:1708-19. doi: 10.1056/NEJMra1000449
7. Wang D, Hu B, Hu C, Zhu F, Liu X, Zhang J, et al. Clinical characteristics of 138 hospitalized patients with 2019 novel coronavirus-infected pneumonia in Wuhan, China. *JAMA*. (2020) 323:1061-9. doi: 10.1001/jama.2020.1585
8. Tang X, Du RH, Wang R, Cao TZ, Guan LL, Yang CQ, et al. Comparison of hospitalized patients with ARDS caused by COVID-19 and H1N1. *Chest*. (2020) 158:195-205. doi: 10.1016/j.chest.2020.03.032
9. Jain S, Kamimoto L, Bramley AM, Schmitz AM, Benoit SR, Louie J, et al. Hospitalized patients with 2009 H1N1 influenza in the United States, April-June 2009. *N Engl J Med*. (2009) 361:1935-44. doi: 10.1056/NEJMoa0906695
10. Huang C, Wang Y, Li X, Ren L, Zhao J, Hu Y, et al. Clinical features of patients infected with 2019 novel coronavirus in Wuhan, China. *Lancet*. (2020) 395:497-506. doi: 10.1016/S0140-6736(20)30183-5
11. Chen N, Zhou M, Dong X, Qu J, Gong F, Han Y, et al. Epidemiological and clinical characteristics of 99 cases of 2019 novel coronavirus pneumonia in Wuhan, China: a descriptive study. *Lancet*. (2020) 395:507-13. doi: 10.1016/S0140-6736(20)30211-7
12. Dominguez-Cherit G, Lapinsky SE, Macias AE, Pinto R, Espinosa-Perez L, de la Torre A, et al. Critically ill patients with 2009 influenza A(H1N1) in Mexico. *JAMA*. (2009) 302:1880-7. doi: 10.1001/jama.2009.1536
13. Kumar A, Zarychanski R, Pinto R, Cook DJ, Marshall J, Lacroix J, et al. Critically ill patients with 2009 influenza A(H1N1) infection in Canada. *JAMA*. (2009) 302:1872-9. doi: 10.1001/jama.2009.1496
14. Perez-Padilla R, de la Rosa-Zamboni D, Ponce de Leon S, Hernandez M, Quinones-Falconi F, Bautista E, et al. Pneumonia and respiratory failure from swine-origin influenza A (H1N1) in Mexico. *N Engl J Med*. (2009) 361:680-9. doi: 10.1056/NEJMoa0904252
15. Shi H, Han X, Jiang N, Cao Y, Alwalid O, Gu J, et al. Radiological findings from 81 patients with COVID-19 pneumonia in Wuhan, China: a descriptive study. *Lancet Infect Dis*. (2020) 20:425-34. doi: 10.1016/S1473-3099(20)30086-4
16. Simpson S, Kay FU, Abbara S, Bhalla S, Chung JH, Chung M, et al. Radiological society of North America expert consensus statement on reporting chest CT findings related to COVID-19. Endorsed by the Society of Thoracic Radiology, the American College of Radiology, and RSNA - secondary publication. *J Thorac Imaging*. (2020) 35:219-27. doi: 10.1097/RTI.0000000000000524
17. Song F, Shi N, Shan F, Zhang Z, Shen J, Lu H, et al. Emerging 2019 novel coronavirus (2019-nCoV) pneumonia. *Radiology*. (2020) 295:210-7. doi: 10.1148/radiol.2020200274
18. Kang H, Lee KS, Jeong YJ, Lee HY, Kim KI, Nam KJ. Computed tomography findings of influenza A (H1N1) pneumonia in adults: pattern analysis and prognostic comparisons. *J Comput Assist Tomogr*. (2012) 36:285-90. doi: 10.1097/RCT.0b013e31825588e6
19. Liu M, Zeng W, Wen Y, Zheng Y, Lv F, Xiao K. COVID-19 pneumonia: CT findings of 122 patients and differentiation from influenza pneumonia. *Eur Radiol*. (2020) 30:5463-9. doi: 10.1007/s00330-020-06928-0
20. Yin Z, Kang Z, Yang D, Ding S, Luo H, Xiao E. A comparison of clinical and chest CT findings in patients with influenza A (H1N1) virus infection and coronavirus disease (COVID-19). *AJR Am J Roentgenol*. (2020) 215:1065-71. doi: 10.2214/AJR.20.23214
21. Li P, Su DJ, Zhang JF, Xia XD, Sui H, Zhao DH. Pneumonia in novel swine-origin influenza A (H1N1) virus infection: high-resolution CT findings. *Eur J Radiol*. (2011) 80:e146-52. doi: 10.1016/j.ejrad.2010.05.029
22. China National Health Commission. *Diagnosis and Treatment of Pneumonitis Caused by New Coronavirus (Trial Version 7)*. Beijing: China National Health Commission (2020). Available online at: <http://www.nhc.gov.cn/yzygj/s7653p/202003/46c9294a7dfe4cef80dc7f5912eb1989.shtml> (accessed March 9, 2020).
23. China National Health Commission. *Diagnosis and Treatment of Influenza A (H1N1) (Version 3)*. Beijing: China National Health Commission (2009). Available online at: <http://www.nhc.gov.cn/yzygj/s3593g/201306/5fc4b2d158d7475fa0da32e959f9a7ac.shtml> (accessed March 9, 2020).
24. Hansell DM, Bankier AA, MacMahon H, McLoud TC, Muller NL, Remy J. Fleischner society: glossary of terms for thoracic imaging. *Radiology*. (2008) 246:697-722. doi: 10.1148/radiol.2462070712
25. Fang Y, Zhang H, Xie J, Lin M, Ying L, Pang P, et al. Sensitivity of chest CT for COVID-19: comparison to RT-PCR. *Radiology*. (2020) 296:E115-7. doi: 10.1148/radiol.2020200432
26. Xu Z, Shi L, Wang Y, Zhang J, Huang L, Zhang C, et al. Pathological findings of COVID-19 associated with acute respiratory distress syndrome. *Lancet Respir Med*. (2020) 8:420-2. doi: 10.1016/S2213-2600(20)30076-X
27. Nakajima N, Sato Y, Katano H, Hasegawa H, Kumasaka T, Hata S, et al. Histopathological and immunohistochemical findings of 20 autopsy cases with 2009 H1N1 virus infection. *Mod Pathol*. (2012) 25:1-13. doi: 10.1038/modpathol.2011.125
28. Marchiori E, Zanetti G, Fontes CA, Santos ML, Valiante PM, Mano CM, et al. Influenza A (H1N1) virus-associated pneumonia: high-resolution computed tomography-pathologic correlation. *Eur J Radiol*. (2011) 80:e500-4. doi: 10.1016/j.ejrad.2010.10.003
29. Coppola M, Porto A, De Santo D, De Fronzo S, Grassi R, Rotondo A. Influenza A virus: radiological and clinical findings of patients hospitalised for pandemic H1N1 influenza. *Radiol Med*. (2011) 116:706-19. doi: 10.1007/s11547-011-0622-0
30. Xinhua. *WHO Europe Head Warns Young People as COVID-19 Infection Rates Soar*. (2020). Available online at: <http://en.people.cn/n3/2020/0821/c90000-9737171.html> (accessed November 12, 2020).

**Conflict of Interest:** Y-HT was employed by Winning Health Technology Group Co., Ltd., Shanghai, China.

The remaining authors declare that the research was conducted in the absence of any commercial or financial relationships that could be construed as a potential conflict of interest.

Copyright © 2021 Shi, Hu, Zhang, Liu, Zhou, Tang, Zhang, Shi, Zhang, Xiong and Shan. This is an open-access article distributed under the terms of the Creative Commons Attribution License (CC BY). The use, distribution or reproduction in other forums is permitted, provided the original author(s) and the copyright owner(s) are credited and that the original publication in this journal is cited, in accordance with accepted academic practice. No use, distribution or reproduction is permitted which does not comply with these terms.



# CT Quantification of COVID-19 Pneumonia at Admission Can Predict Progression to Critical Illness: A Retrospective Multicenter Cohort Study

## OPEN ACCESS

### Edited by:

Reza Lashgari,  
Institute for Research in Fundamental  
Sciences, Iran

### Reviewed by:

Gisella Guido,  
Sapienza University of Rome, Italy  
Michaela Cellina,  
ASST Fatebenefratelli Sacco, Italy

### \*Correspondence:

Qingsi Zeng  
zengqingsi@gzhu.edu.cn  
Yumei Liu  
lymhankouyy@163.com  
Min Jiang  
jiang04511@163.com  
Qingling Zhang  
qingling@gird.cn

<sup>†</sup>These authors have contributed  
equally to this work

### Specialty section:

This article was submitted to  
Infectious Diseases - Surveillance,  
Prevention and Treatment,  
a section of the journal  
Frontiers in Medicine

Received: 01 April 2021

Accepted: 10 May 2021

Published: 17 June 2021

### Citation:

Pang B, Li H, Liu Q, Wu P, Xia T,  
Zhang X, Le W, Li J, Lai L, Ou C,  
Ma J, Liu S, Zhou F, Wang X, Xie J,  
Zhang Q, Jiang M, Liu Y and Zeng Q  
(2021) CT Quantification of COVID-19  
Pneumonia at Admission Can Predict  
Progression to Critical Illness: A  
Retrospective Multicenter Cohort  
Study. *Front. Med.* 8:689568.  
doi: 10.3389/fmed.2021.689568

Baoguo Pang<sup>1†</sup>, Haijun Li<sup>2†</sup>, Qin Liu<sup>3†</sup>, Penghui Wu<sup>4†</sup>, Tingting Xia<sup>3</sup>, Xiaoxian Zhang<sup>4</sup>,  
Wenjun Le<sup>5</sup>, Jianyu Li<sup>3</sup>, Lihua Lai<sup>3</sup>, Changxing Ou<sup>4</sup>, Jianjuan Ma<sup>6</sup>, Shuai Liu<sup>7</sup>,  
Fuling Zhou<sup>8</sup>, Xinlu Wang<sup>9</sup>, Jiaxing Xie<sup>10</sup>, Qingling Zhang<sup>4\*</sup>, Min Jiang<sup>11\*</sup>, Yumei Liu<sup>12\*</sup> and  
Qingsi Zeng<sup>3\*</sup>

<sup>1</sup> Department of Radiology, Huangpi District Hospital of Traditional Chinese Medicine, Wuhan, China, <sup>2</sup> Department of Radiology, Han Kou Hospital of Wuhan, Wuhan, China, <sup>3</sup> Department of Radiology, The First Affiliated Hospital of Guangzhou Medical University, Guangzhou, China, <sup>4</sup> Pulmonary and Critical Care Medicine, National Clinical Research Center for Respiratory Disease, National Center for Respiratory Medicine, State Key Laboratory of Respiratory Diseases, Guangzhou Institute of Respiratory Health, The First Affiliated Hospital of Guangzhou Medical University, Guangzhou, China, <sup>5</sup> Department of Respiratory, First Affiliated Hospital of Guangxi University of Science and Technology, Liuzhou, China, <sup>6</sup> Department of Pediatric Hematology, Affiliated Hospital of Guizhou Medical University, Guiyang, China, <sup>7</sup> Department of Hematology, Dawu County People's Hospital, Wuhan, China, <sup>8</sup> Department of Hematology, Zhongnan Hospital of Wuhan University, Wuhan, China, <sup>9</sup> Department of Nuclear Medicine, The First Affiliated Hospital of Guangzhou Medical University, Guangzhou, China, <sup>10</sup> National Clinical Research Center for Respiratory Disease, State Key Laboratory of Respiratory Diseases, Department of Allergy and Clinical Immunology, Guangzhou Institute of Respiratory Health, The First Affiliated Hospital of Guangzhou Medical University, Guangzhou, China, <sup>11</sup> Department of Pediatrics, The First Affiliated Hospital of Guangxi Medical University, Nanning, China, <sup>12</sup> Department of Respiratory, Hankou Hospital of Wuhan, Wuhan, China

**Objective:** Early identification of coronavirus disease 2019 (COVID-19) patients with worse outcomes may benefit clinical management of patients. We aimed to quantify pneumonia findings on CT at admission to predict progression to critical illness in COVID-19 patients.

**Methods:** This retrospective study included laboratory-confirmed adult patients with COVID-19. All patients underwent a thin-section chest computed tomography (CT) scans showing evidence of pneumonia. CT images with severe moving artifacts were excluded from analysis. Patients' clinical and laboratory data were collected from medical records. Three quantitative CT features of pneumonia lesions were automatically calculated using a care.ai Intelligent Multi-disciplinary Imaging Diagnosis Platform Intelligent Evaluation System of Chest CT for COVID-19, denoting the percentage of pneumonia volume (PPV), ground-glass opacity volume (PGV), and consolidation volume (PCV). According to Chinese COVID-19 guidelines (trial version 7), patients were divided into noncritical and critical groups. Critical illness was defined as a composite of admission to the intensive care unit, respiratory failure requiring mechanical ventilation, shock, or death. The performance of PPV, PGV, and PCV in discrimination of critical illness was assessed. The correlations between PPV and laboratory variables were assessed by Pearson correlation analysis.

**Results:** A total of 140 patients were included, with mean age of 58.6 years, and 85 (60.7%) were male. Thirty-two (22.9%) patients were critical. Using a cutoff value of 22.6%, the PPV had the highest performance in predicting critical illness, with an area under the curve of 0.868, sensitivity of 81.3%, and specificity of 80.6%. The PPV had moderately positive correlation with neutrophil (%) ( $r = 0.535$ ,  $p < 0.001$ ), erythrocyte sedimentation rate ( $r = 0.567$ ,  $p < 0.001$ ), d-Dimer ( $r = 0.444$ ,  $p < 0.001$ ), high-sensitivity C-reactive protein ( $r = 0.495$ ,  $p < 0.001$ ), aspartate aminotransferase ( $r = 0.410$ ,  $p < 0.001$ ), lactate dehydrogenase ( $r = 0.644$ ,  $p < 0.001$ ), and urea nitrogen ( $r = 0.439$ ,  $p < 0.001$ ), whereas the PPV had moderately negative correlation with lymphocyte (%) ( $r = -0.535$ ,  $p < 0.001$ ).

**Conclusions:** Pneumonia volume quantified on initial CT can non-invasively predict the progression to critical illness in advance, which serve as a prognostic marker of COVID-19.

**Keywords:** COVID-19, pneumonia, critical illness, chest CT, quantification

## INTRODUCTION

The rapid spread of coronavirus disease 2019 (COVID-19) has been a global pandemic and a major and urgent threat to the health care system worldwide (1). More than 100 million cases have been reported globally (2). Most COVID-19 patients had mild symptoms of respiratory infection, such as fever and dry cough, but some patients could rapidly develop fatal complications, including respiratory failure requiring mechanical ventilation, septic shock, or even death (3). Until now, no specific treatment strategies have been used in dealing with COVID-19 (4); thus, it is of great importance to predict COVID-19 with worse outcomes, which would enable the introduction of timely treatment and reduce the mortality of patients.

Chest computed tomography (CT) can play a valuable role in screening, diagnosis, and follow-up of COVID-19 patients (5). However, chest CT images are usually interpreted by radiologists, which is subjective with large interobserver and intraobserver variability and thus unable to accurately and quantitatively evaluate the disease severity and is also time-consuming and inefficient (6). Recently, radiomics use a variety of mathematical methods to convert chest CT images into a huge number of minable high-dimensional handcrafted features for predicting prognosis or outcome of COVID-19 patients (7–17). Radiomic features can be used as surrogate biomarkers for biological disease traits such as morphology and heterogeneity. The combination of clinical characteristics and radiomic features from CT could achieve better accuracy in prediction (18, 19). Some studies also apply deep learning to automatically learn features from CT images or in combination with clinical data and radiomics for risk assessment of COVID-19 (20–34). Deep learning and radiomics can be a more objective, quantitative, and stable system for the assessment of the COVID-19 disease course.

The interpretation of quantitative CT features is of great importance for understanding their potential biological meaning. Several biomarkers identified from laboratory features have been used to assess the probability of progressing to severe state in

COVID-19 patients (35–38). Therefore, we aimed to investigate the prognostic value of quantitative CT features in predicting the occurrence of critical illness in patients with COVID-19 and the correlation with laboratory features.

## MATERIALS AND METHODS

### Patient Cohort

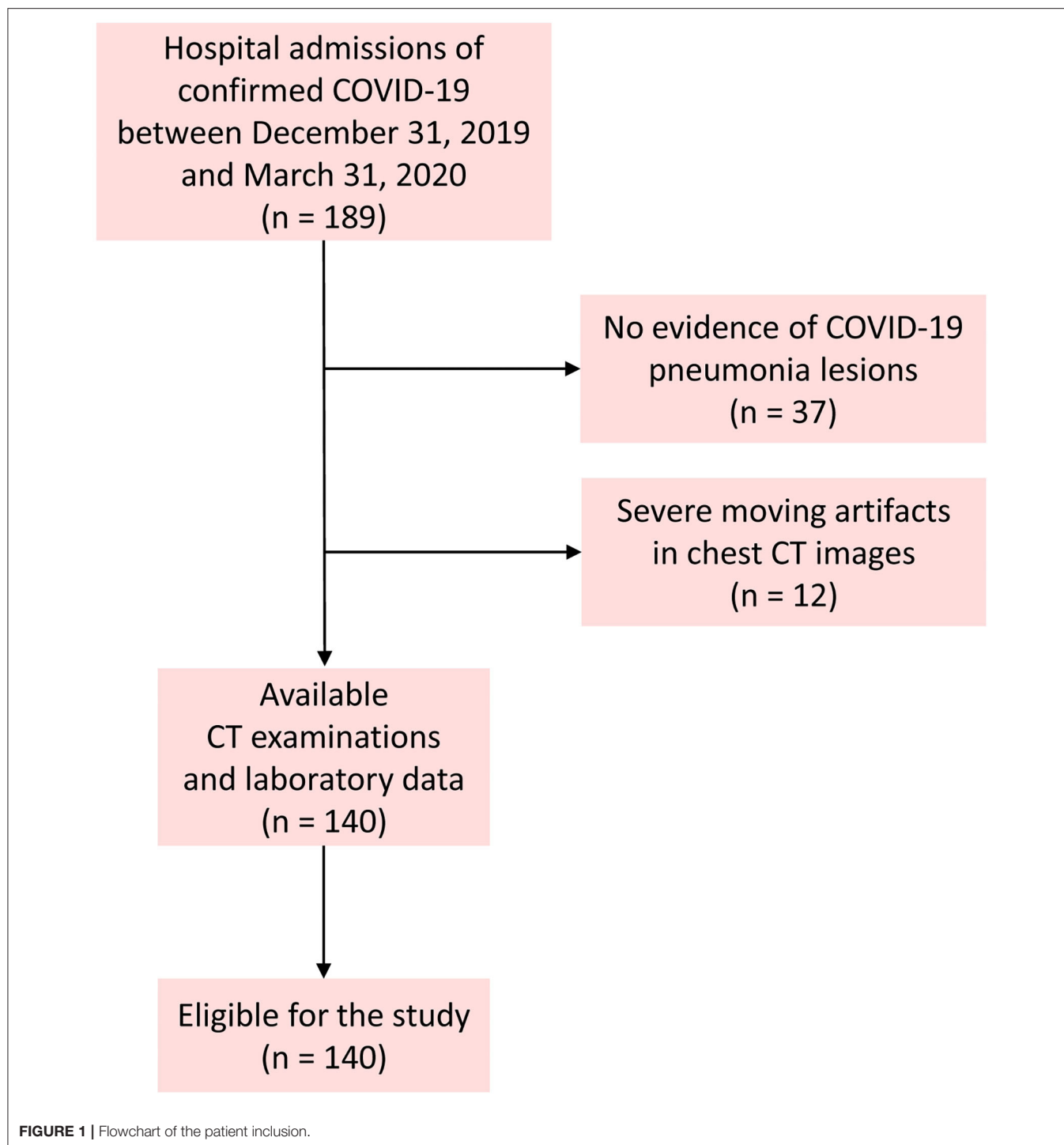
This retrospective study was approved by the ethics committee of our hospitals, and the requirement for informed consent was waived. We included COVID-19 patients who admitted to three designated hospitals from December 31, 2019, to March 31, 2020.

The inclusion criteria were as follows: (1) adult patients; (2) positive real-time reverse transcription polymerase chain reaction testing for COVID-19 on throat swabs; (3) a thin-slice chest CT scan showing any evidence of pneumonia; and (4) patients admitted for antiviral treatment. Patients with mechanical ventilation in the course were excluded because of the severe moving artifacts in chest CT images. **Figure 1** shows the pathway of patient inclusion. After admission, clinical data including demographics, comorbidities, and symptoms of patients and laboratory tests were collected. The data in source documents were confirmed independently by at least two researchers.

### CT Image Acquisition

Subjects were referred to the radiology department based on the algorithm suggested by evidence presented by the World Health Organization (39). All patients underwent chest CT scans by a 64-slice CT scanner (Siemens Definition AS + 128, Forchheim, Germany). All patients were scanned in the supine position from the lung apex to the diaphragm during end-inspiration. To reduce breathing artifacts, patients were instructed on breath-holding. No contrast agent was administered. CT acquisition was executed as follows: tube voltage, 120 kV; tube current, auto mAs; pitch, 1.2; rotation time, 0.5 s; field of view, 330 × 330 mm. Lung images were reconstructed at a slice thickness of 1.0 or





1.25 mm using I50 medium sharp algorithm. Lung window level and window width were set as  $-530$  to  $430$  Hounsfield units (HU) and  $1,400$ – $1,600$  HU, respectively.

### Quantitative CT Analysis

The quantification analysis of CT images was performed by a care.ai Intelligent Multi-disciplinary Imaging Diagnosis Platform

Intelligent Evaluation System of Chest CT for COVID-19 (YT-CT-Lung, YITU Healthcare Technology Co., Ltd., China). This system was constructed using a combination of U-net and fully convolutional networks (40, 41), which consists of three different network components: (1) 12 convolutional segments, which included convolutional layer (Conv2d), batch normalization layer, and an activation layer; (2) three max-pooling layers for

down-sampling; and (3) three transpose convolutional layer for up-sampling (**Figure 2**). The development of the COVID-Lesion Net has been described in a previous study (42).

Subsequently, by thresholding on CT values in the pneumonia lesions using two-dimensional neural network for classification, two quantitative features were generated, that is, ground-glass opacities (GGOs) with value ranges of  $-600$  to  $-500$  HU

and consolidation with density ranges of  $-250$  to  $60$  HU (43). A quantitative analysis of pneumonia lesions, GGO, and consolidation was performed based on the segmentation results, including the percentage of pneumonia volume (PPV), GGO volume (PGV), and consolidation volume (PCV) in both lungs, left lung, right lung, and five lobes (**Figure 3**). It took about 10 s to calculate the various CT parameters. All the image segmentations

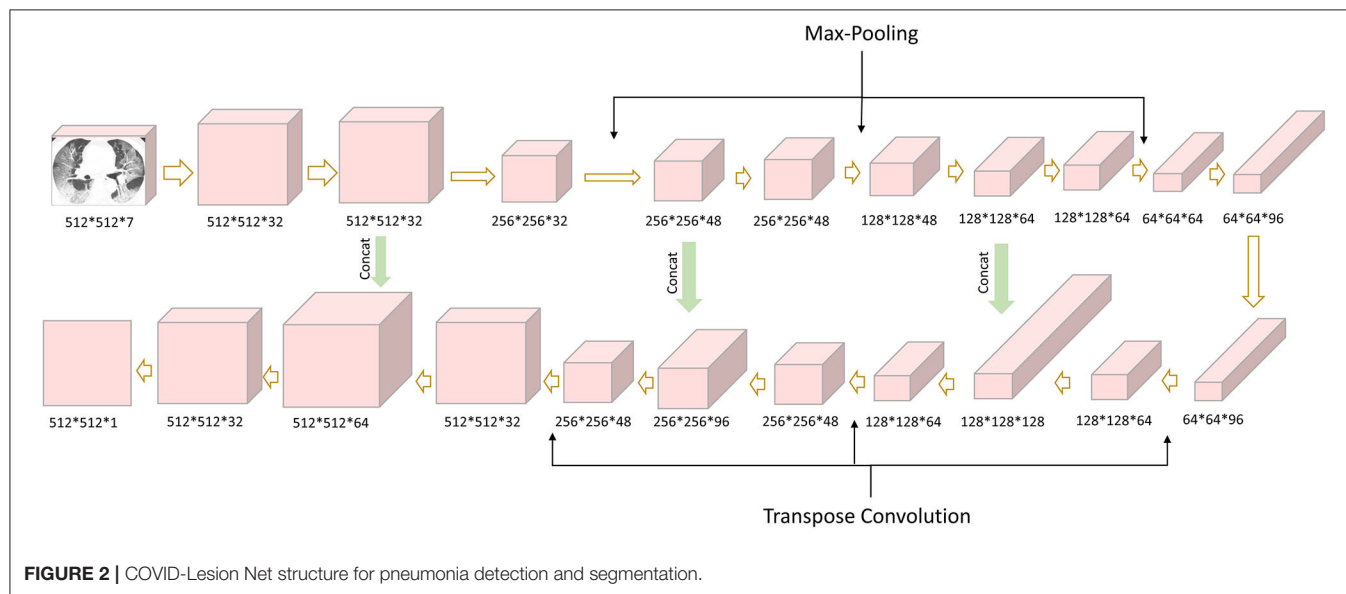


**FIGURE 2 |** COVID-Lesion Net structure for pneumonia detection and segmentation.



**FIGURE 3 |** CT image quantization and analysis with artificial intelligence system.

were reviewed independently and assessed by two radiologists (with 10 and 20 years of experience in thoracic imaging), and discrepancies were resolved by consensus.

## Definition of Endpoint

We defined the severity of COVID-19 according to the newest COVID-19 guidelines released by the National Health Commission of China (44). We defined critical illness as a composite of admission to intensive care unit, respiratory failure requiring mechanical ventilation, shock, or death.

## Statistical Analysis

Categorical variables were expressed as counts and percentages, whereas continuous variables are shown as median and interquartile range. Continuous variables were compared using *t*-test or Mann–Whitney *U*-test, and categorical variables were compared using  $\chi^2$ -test or Fisher exact test. CT features were compared using *t*-test or Mann–Whitney *U*-test. The optimal cutoff value for discriminating critical and non-critical COVID-19 patients was determined by using receiver operating characteristic analysis and maximizing the Youden index. The correlations between total pneumonia volume and laboratory variables were assessed by Pearson correlation analysis.  $P < 0.05$  was considered significant. All statistical analyses were conducted by IBM SPSS version 22.0 (Chicago, IL, USA).

## RESULTS

### Clinical Characteristics of Patients

This study finally included 140 patients, excluding 37 patients without evidence of COVID-19 lesions, and 12 had severe moving artifacts in chest CT images. **Table 1** demonstrates the clinical characteristics of patients. Among the 140 patients with COVID-19, 68 (48.6%) were moderate, 40 (28.6%) were severe, and 32 (22.9%) were critical (including 12 deaths). The mean age of all patients was  $58.6 \pm 13.8$  years (range, 25–86 years), and 85 patients (60.7%) were male. Fever (81.4%) was the most common symptom, followed by dry cough (76.4%), shortness of breath (55.0%), and fatigue (47.1%). Sixty-one patients (43.6%) had at least one comorbidity, with hypertension (30.0%) being the most common, followed by diabetes (16.4%) and cardiovascular disease (11.4%).

### CT Features and Laboratory Variables in the Critical and Non-Critical Groups

**Table 2** shows the difference of clinical and laboratory variables between the non-critical and critical groups. There were a total of 28 laboratory variables for the two groups. The median time from symptom onset to CT examination among the moderately, severely, and critically ill groups was 11, 10, and 10 days, respectively ( $p = 0.250$ ). Comparison of quantitative CT features between the non-critical and critical groups is depicted in **Table 3**. There were 24 CT features for the two groups. The PPV, PGV, and PCV in the left lung, right lung, both lungs, and five lobes were significantly higher in the critical group than the non-critical group (all  $p < 0.001$ ). **Figure 4** shows temporal changes

**TABLE 1 |** Clinical characteristics of patients.

| Characteristics                |                   |
|--------------------------------|-------------------|
| <b>Age (years)</b>             | $58.6 \pm 13.7$   |
| <b>Sex</b>                     |                   |
| Male                           | 85 (60.7)         |
| Female                         | 55 (39.3)         |
| <b>Comorbidities</b>           |                   |
| COPD                           | 6 (4.3)           |
| Cardiovascular disease         | 16 (11.4)         |
| Hypertension                   | 42 (30.0)         |
| Diabetes                       | 23 (16.4)         |
| <b>Symptoms</b>                |                   |
| Fever                          | 114 (81.4)        |
| Dry cough                      | 107 (76.4)        |
| Shortness of breath            | 77 (55.0)         |
| Diarrhea                       | 9 (6.4)           |
| Anorexia                       | 32 (22.9)         |
| Fatigue                        | 66 (47.1)         |
| <b>Disease severity</b>        |                   |
| Moderate                       | 68                |
| Severe                         | 40                |
| Critical                       | 32                |
| <b>Laboratory findings</b>     |                   |
| WBCs ( $\times 10^9/L$ )       | $6.3 \pm 3.7$     |
| Neutrophil ( $\times 10^9/L$ ) | $4.9 \pm 3.7$     |
| Neutrophil (%)                 | $69.8 \pm 15.0$   |
| Lymphocyte ( $\times 10^9/L$ ) | $1.2 \pm 0.6$     |
| Lymphocyte (%)                 | $21.6 \pm 11.6$   |
| Eosinophil ( $\times 10^9/L$ ) | $0.08 \pm 0.08$   |
| Eosinophil (%)                 | $1.4 \pm 1.5$     |
| Monocyte ( $\times 10^9/L$ )   | $0.4 \pm 0.2$     |
| Monocyte (%)                   | $7.2 \pm 3.1$     |
| Hemoglobin (g/L)               | $124.2 \pm 22.3$  |
| Platelet (g/L)                 | $220.1 \pm 75.7$  |
| Fibrinogen (g/L)               | $4.0 \pm 2.2$     |
| d-Dimer ( $\mu g/mL$ )         | $0.8 \pm 1.4$     |
| hs-CRP (mg/L)                  | $19.1 \pm 26.1$   |
| ALT (U/L)                      | $38.3 \pm 49.0$   |
| AST (U/L)                      | $31.6 \pm 28.4$   |
| TBIL ( $\mu mol/L$ )           | $12.5 \pm 9.1$    |
| DBIL ( $\mu mol/L$ )           | $5.5 \pm 18.3$    |
| ALP (U/L)                      | $63.8 \pm 26.8$   |
| Myohemoglobin ( $\mu g/L$ )    | $45.3 \pm 37.5$   |
| CK (ng/mL)                     | $75.7 \pm 91.9$   |
| LDH (U/L)                      | $260.7 \pm 121.0$ |
| PLT (ng/mL)                    | $0.3 \pm 1.6$     |
| ESR (s)                        | $38.4 \pm 30.1$   |
| NT-proBNP (pg/mL)              | $318.9 \pm 435.6$ |
| Scr ( $\mu mol/L$ )            | $71.8 \pm 18.4$   |
| BUN (mmol/L)                   | $5.3 \pm 2.8$     |
| NLR                            | $5.8 \pm 8.8$     |

Data were mean  $\pm$  standard deviation (SD) or number.

COPD, chronic obstructive pulmonary disease; WBC, white blood cells; hs-CRP, high-sensitivity C-reactive protein; ALT, alanine transaminase; AST, aspartate aminotransferase; TBIL, total bilirubin; DBIL, direct bilirubin; ALP, alkaline phosphatase; LDH, lactate dehydrogenase; CK, creatine kinase; PLT, procalcitonin; ESR, erythrocyte sedimentation rate; NT-proBNP, N-terminal brain natriuretic peptide precursor; Scr, serum creatinine; BUN, urea nitrogen; NLR, neutrophil-to-lymphocyte ratio.

**TABLE 2 |** Comparison of clinical and laboratory variables between the non-critical and critical groups.

| Characteristics                | Non-critical<br>(n = 108) | Critical<br>(n = 32) | P-value          |
|--------------------------------|---------------------------|----------------------|------------------|
| <b>Age (years)</b>             | 57.6 ± 14.3               | 61.9 ± 11.5          | 0.093            |
| <b>Sex</b>                     |                           |                      |                  |
| Male                           | 61 (56.5)                 | 24 (75.0)            | 0.060            |
| Female                         | 47 (43.5)                 | 8 (25.0)             |                  |
| <b>Comorbidities</b>           |                           |                      |                  |
| COPD                           | 6 (5.6)                   | 0                    | 0.336            |
| Cardiovascular disease         | 14 (13.0)                 | 2 (6.3)              | 0.364            |
| Hypertension                   | 30 (27.8)                 | 12 (37.5)            | 0.292            |
| Diabetes                       | 16 (14.8)                 | 7 (21.9)             | 0.344            |
| <b>Symptoms</b>                |                           |                      |                  |
| Fever                          | 82 (75.9)                 | 32 (100)             | <b>0.002</b>     |
| Dry cough                      | 76 (70.4)                 | 31 (96.9)            | <b>0.002</b>     |
| Shortness of breath            | 46 (42.6)                 | 31 (96.9)            | <b>&lt;0.001</b> |
| Diarrhea                       | 6 (5.6)                   | 3 (9.4)              | 0.427            |
| Anorexia                       | 28 (25.9)                 | 4 (12.5)             | 0.112            |
| Fatigue                        | 47 (43.5)                 | 19 (59.4)            | 0.115            |
| <b>Laboratory findings</b>     |                           |                      |                  |
| WBCs ( $\times 10^9/L$ )       | 5.7 ± 2.9                 | 8.4 ± 5.6            | <b>0.010</b>     |
| Neutrophil ( $\times 10^9/L$ ) | 4.2 ± 2.8                 | 7.4 ± 5.1            | <b>&lt;0.001</b> |
| Neutrophil (%)                 | 66.6 ± 14.7               | 81.2 ± 9.7           | <b>&lt;0.001</b> |
| Lymphocyte ( $\times 10^9/L$ ) | 1.3 ± 0.6                 | 0.9 ± 0.5            | <b>0.001</b>     |
| Lymphocyte (%)                 | 24.4 ± 11.1               | 11.7 ± 6.5           | <b>&lt;0.001</b> |
| Eosinophil ( $\times 10^9/L$ ) | 0.08 ± 0.07               | 0.06 ± 0.09          | 0.061            |
| Eosinophil (%)                 | 1.5 ± 1.5                 | 0.7 ± 1.1            | <b>0.002</b>     |
| Monocyte ( $\times 10^9/L$ )   | 0.4 ± 0.2                 | 0.5 ± 0.3            | 0.183            |
| Monocyte (%)                   | 7.4 ± 3.1                 | 6.1 ± 2.8            | 0.083            |
| Hemoglobin (g/L)               | 124.9 ± 20.4              | 121.7 ± 28.8         | 0.694            |
| Platelet (g/L)                 | 225.5 ± 74.2              | 200.3 ± 79.4         | 0.090            |
| Fibrinogen (g/L)               | 3.8 ± 2.2                 | 5.0 ± 1.5            | <b>0.001</b>     |
| d-Dimer ( $\mu g/mL$ )         | 0.6 ± 0.9                 | 1.6 ± 2.4            | 0.055            |
| hs-CRP (mg/L)                  | 14.9 ± 18.0               | 46.0 ± 47.5          | <b>&lt;0.001</b> |
| ALT (U/L)                      | 33.9 ± 45.4               | 56.6 ± 59.5          | <b>0.004</b>     |
| AST (U/L)                      | 26.9 ± 23.8               | 53.2 ± 37.4          | <b>&lt;0.001</b> |
| TBIL ( $\mu mol/L$ )           | 12.5 ± 9.8                | 12.6 ± 5.8           | 0.435            |
| DBIL ( $\mu mol/L$ )           | 5.7 ± 20.3                | 4.6 ± 2.5            | 0.054            |
| ALP (U/L)                      | 63.5 ± 26.2               | 65.7 ± 31.4          | 0.719            |
| Myohemoglobin ( $\mu g/L$ )    | 35.2 ± 25.9               | 79.5 ± 62.7          | 0.059            |
| CK (ng/mL)                     | 66.3 ± 91.7               | 107.4 ± 92.8         | 0.053            |
| LDH (U/L)                      | 225.7 ± 112.3             | 378.8 ± 147.3        | <b>&lt;0.001</b> |
| PLT (ng/mL)                    | 0.3 ± 1.8                 | 0.2 ± 0.3            | 0.270            |
| ESR (s)                        | 35.1 ± 31.9               | 49.4 ± 23.1          | 0.423            |
| NT-proBNP (pg/mL)              | 315.5 ± 418.0             | 330.5 ± 491.7        | 0.850            |
| Scr ( $\mu mol/L$ )            | 69.2 ± 16.5               | 81.2 ± 22.1          | <b>0.012</b>     |
| BUN (mmol/L)                   | 4.6 ± 1.6                 | 7.7 ± 4.5            | <b>&lt;0.001</b> |
| NLR                            | 4.8 ± 8.7                 | 9.3 ± 8.3            | <b>&lt;0.001</b> |

Data were mean ± SD or number (percentage). P-values were calculated by t-test, Mann–Whitney U-test,  $\chi^2$ -test, or Fisher exact test, as appropriate.

COPD, chronic obstructive pulmonary disease; WBCs, white blood cells; hs-CRP, high-sensitivity C-reactive protein; ALT, alanine transaminase; AST, aspartate aminotransferase; TBIL, total bilirubin; DBIL, direct bilirubin; ALP, alkaline phosphatase; LDH, lactate dehydrogenase; CK, creatine kinase; PLT, procalcitonin; ESR, erythrocyte sedimentation rate; NT-proBNP, N-terminal brain natriuretic peptide precursor; Scr, serum creatinine; BUN, urea nitrogen; NLR, neutrophil-to-lymphocyte ratio. Bold values indicate  $P < 0.05$ .

**TABLE 3 |** Comparison of quantitative CT features between non-critical and critically ill groups.

| CT features                          | Non-critical<br>(n = 108) | Critically ill<br>(n = 32) | P-value          |
|--------------------------------------|---------------------------|----------------------------|------------------|
| <b>PPV</b>                           |                           |                            |                  |
| PPV in both lungs                    | 12.4 (41.8)               | 41.8 (20.9)                | <b>&lt;0.001</b> |
| PPV in the left lung                 | 11.7 (14.4)               | 39.2 (22.1)                | <b>&lt;0.001</b> |
| PPV in the upper lobe of left lung   | 8.8 (13.1)                | 34.7 (21.7)                | <b>&lt;0.001</b> |
| PPV in the lower lobe of left lung   | 16.4 (20.0)               | 46.0 (24.9)                | <b>&lt;0.001</b> |
| PPV in the right lung                | 13.2 (15.8)               | 44.1 (21.9)                | <b>&lt;0.001</b> |
| PPV in the upper lobe of right lung  | 11.1 (15.8)               | 41.9 (24.0)                | <b>&lt;0.001</b> |
| PPV in the middle lobe of right lung | 7.5 (13.1)                | 31.4 (22.6)                | <b>&lt;0.001</b> |
| PPV in the lower lobe of right lung  | 18.2 (21.6)               | 51.4 (25.0)                | <b>&lt;0.001</b> |
| <b>PGV</b>                           |                           |                            |                  |
| PGV in both lungs                    | 10.0 (11.4)               | 32.4 (16.4)                | <b>&lt;0.001</b> |
| PGV in the left lung                 | 9.5 (11.7)                | 30.1 (16.8)                | <b>&lt;0.001</b> |
| PGV in the upper lobe of left lung   | 7.6 (11.2)                | 27.9 (16.8)                | <b>&lt;0.001</b> |
| PGV in the lower lobe of left lung   | 12.5 (15.2)               | 33.2 (18.4)                | <b>&lt;0.001</b> |
| PGV in the right lung                | 10.7 (12.8)               | 34.3 (17.5)                | <b>&lt;0.001</b> |
| PGV in the upper lobe of right lung  | 9.5 (13.4)                | 33.7 (20.1)                | <b>&lt;0.001</b> |
| PGV in the middle lobe of right lung | 6.7 (11.6)                | 28.0 (20.3)                | <b>&lt;0.001</b> |
| PGV in the lower lobe of right lung  | 13.8 (16.1)               | 37.5 (18.1)                | <b>&lt;0.001</b> |
| <b>PCV</b>                           |                           |                            |                  |
| PCV in both lungs                    | 2.4 (3.3)                 | 9.4 (7.8)                  | <b>&lt;0.001</b> |
| PCV in the left lung                 | 2.3 (3.4)                 | 9.2 (9.0)                  | <b>&lt;0.001</b> |
| PCV in the upper lobe of left lung   | 1.3 (2.7)                 | 6.8 (7.7)                  | <b>&lt;0.001</b> |
| PCV in the lower lobe of left lung   | 3.9 (5.9)                 | 12.8 (11.9)                | <b>&lt;0.001</b> |
| PCV in the right lung                | 2.5 (3.7)                 | 9.8 (7.8)                  | <b>&lt;0.001</b> |
| PCV in the upper lobe of right lung  | 1.6 (3.0)                 | 8.2 (7.6)                  | <b>&lt;0.001</b> |
| PCV in the middle lobe of right lung | 0.8 (1.8)                 | 3.4 (2.9)                  | <b>&lt;0.001</b> |
| PCV in the lower lobe of right lung  | 4.4 (7.0)                 | 13.9 (11.2)                | <b>&lt;0.001</b> |

PPV, percentage of pneumonia volume; PGV, percentage of ground-glass opacity volume; PCV, percentage of consolidation volume. Bold values indicate  $P < 0.05$ .

in lung lesions in two representative cases with COVID-19 pneumonia.

## Associations of CT Features With Critical Illness

The optimal cutoff value of PPV in both lungs was 22.6%, yielding an area under the curve (AUC) of 0.868 [95% confidence interval (CI) = 0.791–0.946], sensitivity of 81.3% (95% CI = 63.6–92.8%), and specificity of 80.6% (95% CI = 71.8–87.5%) in predicting the occurrence of critical illness of COVID-19 patients (**Figure 5A**). The optimal cutoff value of PGV in both lungs was 21.3%, obtaining an AUC of 0.858 (95% CI = 0.778–0.938), sensitivity of 78.1% (95% CI = 60.0–90.7%), and specificity of 85.2% (95% CI = 77.1–91.3%) in predicting the occurrence of critical illness of COVID-19 patients (**Figure 5B**). The optimal cutoff value of PCV in both lungs was 1.8%, achieving an AUC of 0.838 (95% CI = 0.764–0.912), sensitivity of 90.6% (95% CI = 75.0–98.0%), and specificity of 63.9% (95% CI = 54.1–72.9%) in predicting the occurrence of critical illness of COVID-19 patients (**Figure 5C**).



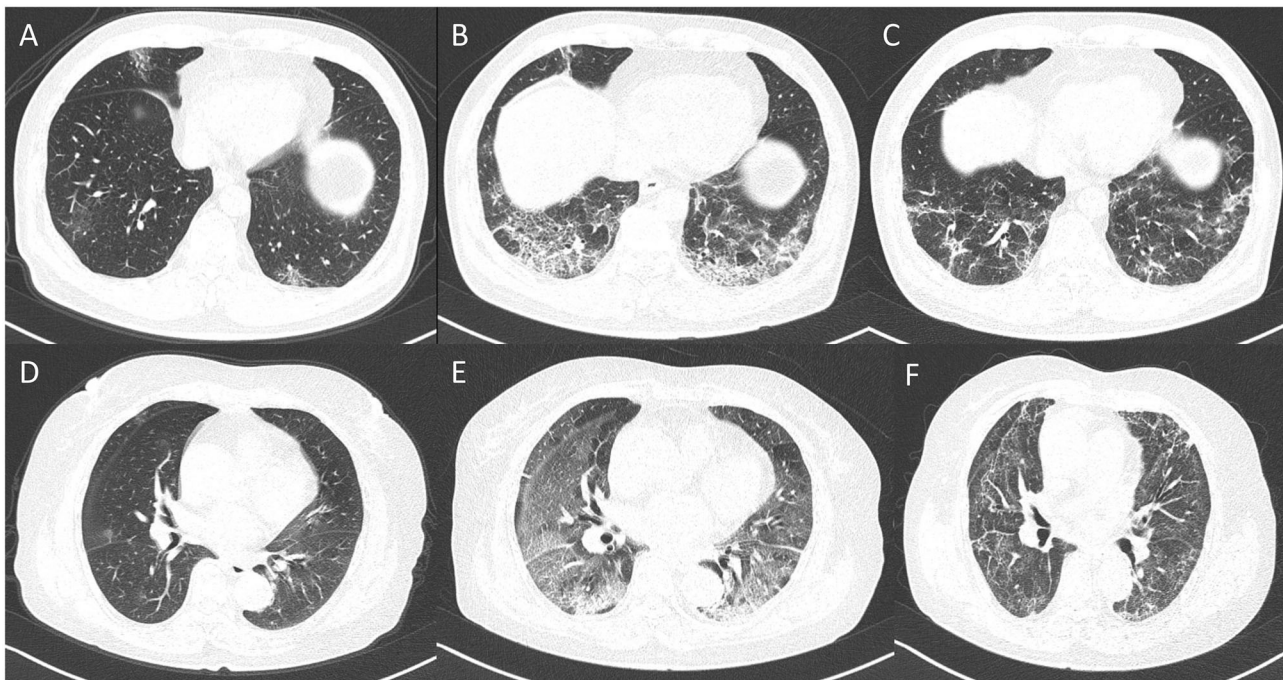


**FIGURE 4 |** Dynamic changes in lung lesions in two representative cases with COVID-19 pneumonia. A 65-year-old man: **(A)** scan obtained on day 2; multiple patchy GGOs were shown in the middle lobe and both lower lobes; the PPV, PGV, and PCV were 1.14, 1.07, and 0.07%, respectively. **(B)** Scan obtained on day 7 showed extensive GGOs with consolidation and crazy-paving pattern in the both lower lobes; the PPV, PGV, and PCV increased to 14.24, 11.38, and 2.86%, respectively. **(C)** Scan obtained on day 21 showed obvious absorption of abnormalities with fibrotic-like appearances; the PPV, PGV, and PCV were 7.73, 7.12, and 0.61%, respectively. A 67-year-old woman: **(D)** Scan obtained on day 2, small nodule of GGO was shown in the right lung; the PPV, PGV, and PCV were 0.19, 0.16, and 0.03%, respectively. **(E)** Scan obtained on day 10 showed extensive GGOs in both lungs with consolidation in the lower lobes; the PPV, PGV, and PCV increased to 48.67, 38.23, and 10.44, respectively. **(F)** Scan obtained on day 56 showed obvious absorption of GGOs and consolidation with fibrotic-like appearances; the PPV, PGV, and PCV were 39.47, 33.77, and 5.70%, respectively.

## Correlations Between Total Pneumonia Volume and Laboratory Variables

The PPV was positively correlated with white blood cell (WBC) count ( $r = 0.379$ ,  $p < 0.001$ ), neutrophil percentage ( $r = 0.535$ ,  $p < 0.001$ ), monocyte count ( $r = 0.244$ ,  $p = 0.010$ ), neutrophil-to-lymphocyte ratio (NLR) ( $r = 0.318$ ,  $p < 0.001$ ), erythrocyte sedimentation rate (ESR) ( $r = 0.567$ ,  $p < 0.001$ ), fibrinogen ( $r = 0.324$ ,  $p = 0.003$ ), D-Dimer ( $r = 0.444$ ,  $p < 0.001$ ), high-sensitivity C-reactive protein (hs-CRP) ( $r = 0.495$ ,  $p < 0.001$ ), alanine transaminase ( $r = 0.231$ ,  $p = 0.012$ ), aspartate aminotransferase ( $r = 0.410$ ,  $p < 0.001$ ), lactic dehydrogenase (LDH) ( $r = 0.644$ ,  $p < 0.001$ ), and blood urea nitrogen ( $r = 0.439$ ,  $p < 0.001$ ), whereas the PPV was negatively correlated with lymphocyte count ( $r = -0.323$ ,  $p < 0.001$ ), lymphocyte percentage ( $r = -0.523$ ,  $p < 0.001$ ), and eosinophil percentage ( $r = -0.285$ ,  $p = 0.001$ ) (Figure 6).

## DISCUSSION

This current study showed that artificial intelligence (AI)-derived quantitative CT features could predict the deterioration to critical illness in patients with COVID-19, in particular, the pneumonia volume percentage. Also, these CT features

were correlated with laboratory variables reflecting systemic inflammation, immune state, and multiple organ functions.

Lung CT can provide useful additional information in the detection, diagnosis, and follow-up of COVID-19 pneumonia (5). However, CT images are usually visually interpreted by radiologists with diverse levels of experience, which is subjective with large variability that is unable to quantitatively assess the disease severity and is also time-consuming and labor-intensive. Previous studies have shown that quantitative CT is comparable or superior to visual CT score in assessment of the severity of COVID-19 (28, 45, 46). Recently, several studies have used quantitative CT to predict clinical outcomes via AI software in patients with COVID-19 (43, 47, 48). Liu et al. found that quantitative CT features on days 0 and 4 as well as changes from days 0 to 4 could predict the progression to severe illness in COVID-19 patients, which outperformed the acute physiology and chronic health evaluation II score, NLR, and D-Dimer (43). Homayounieh et al. found that despite a high frequency of motion artifacts, quantitative features of pulmonary opacities from chest CT can help stratify patients with favorable and adverse outcomes (47). Salvatore et al. demonstrated that quantification of the consolidation, emphysema, and residual healthy lung parenchyma on chest CT images were independent predictors of outcome in patients

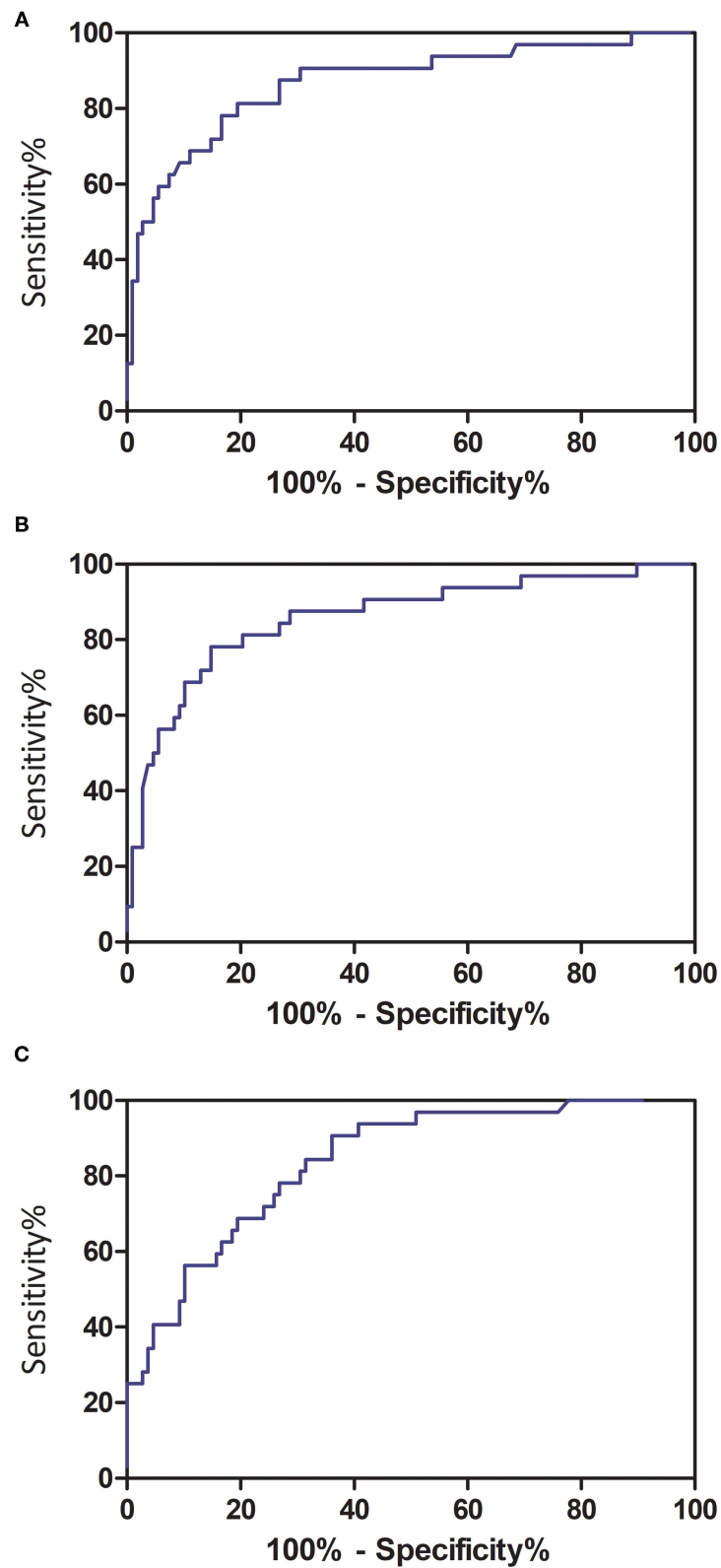


**FIGURE 5 |** Receiver operating characteristic curve analyses of quantitative CT features in predicting critical illness among COVID-19 patients. **(A)** Total pneumonia volume in both lungs; **(B)** ground-glass opacity volume in both lungs; and **(C)** consolidation volume in both lungs.

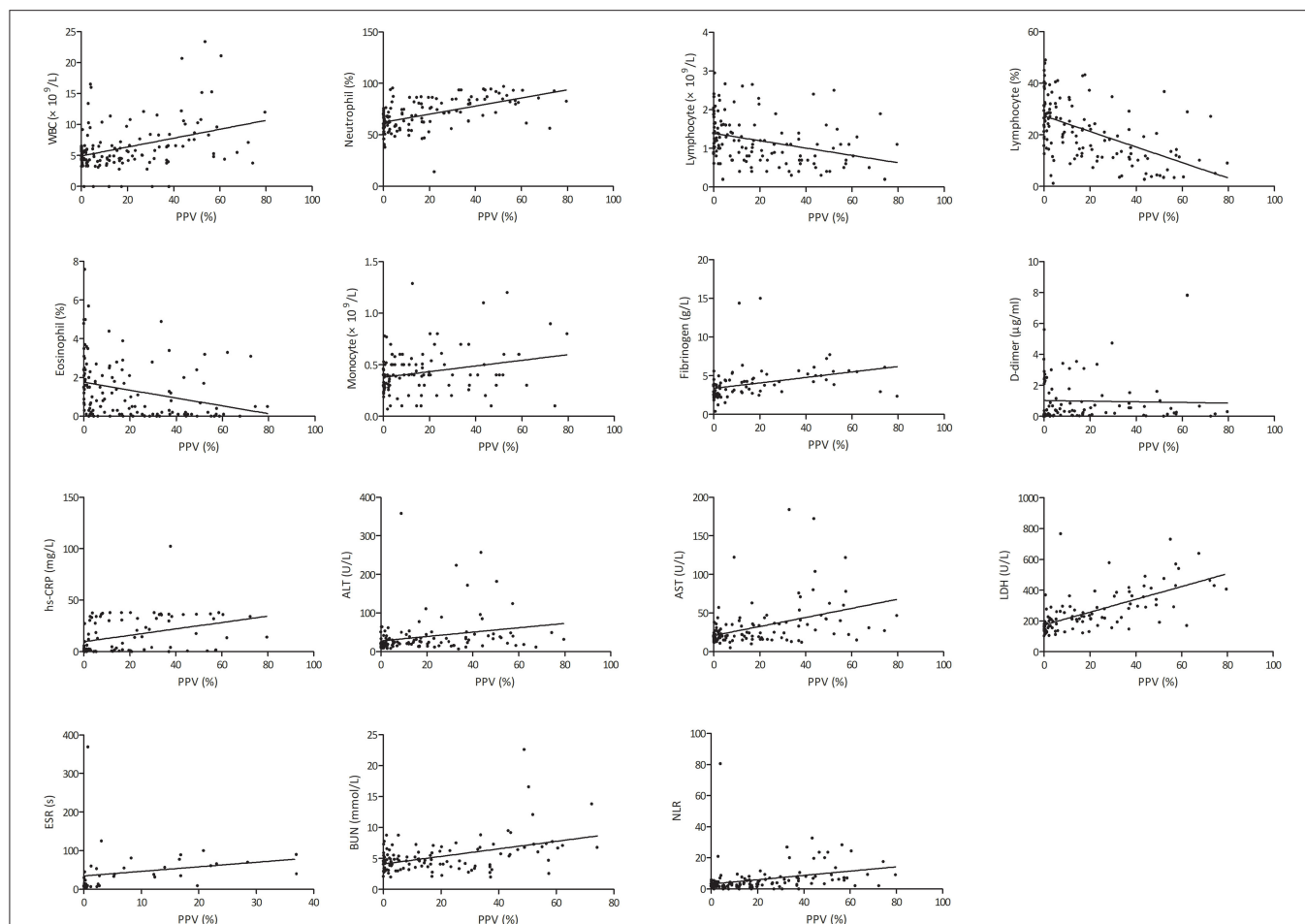


**FIGURE 6 |** Correlation of total pneumonia volume with different clinical parameters. hs-CRP, high-sensitivity C-reactive protein; ALT, alanine transaminase; AST, aspartate aminotransferase; LDH, lactic dehydrogenase; NLR, neutrophil-to-lymphocyte ratio; PPV, percentage of pneumonia volume.

with COVID-19 pneumonia (48). Our study demonstrated that quantitative CT measurements at admission could accurately predict adverse outcomes in COVID-19 patients. The total lesion volume had the best performance of assessing the severity of COVID-19, which was in agreement with a previous study (49). With the advance of image data-mining tools, radiomics and deep learning play a crucial role in the prediction of severity, prognosis, or outcome of patients with COVID-19 (7–34). The COVID-19 lesion images contained high-level features that can effectively represent morphological appearances and heterogeneous information. The handcrafted and learning features derived from CT images can be integrated into clinical and laboratory variables to form a combined model with more favorable performance. These models provided physicians with an important tool for improving the clinical care of patients with the worse disease outcomes.

The extent of GGO and consolidation can evaluate the disease severity of COVID-19 (50). As viruses spread *via* the respiratory mucosa and also infect other cells, they induce a cytokine storm and a series of immune responses that cause changes in peripheral blood and immune cells (51).

Coronaviruses invade the lungs, as well as the blood system, digestive system, and circulatory system (52). Therefore, the disease severity assessed by chest CT may correlate with laboratory inflammatory and immune biomarkers (53). The severity of lymphopenia and infection correlated with the severity of COVID-19 (54). Zhang et al. found that CT score had positive associations with inflammatory mediators, including WBC count, neutrophil count, prothrombin time, D-Dimer, CRP, ESR, procalcitonin, serum ferritin, IL-6, and IL-10, but a negative association with lymphocyte count (51). Another study revealed dynamic correlation between CT score and laboratory parameters, which showed that CT score at an early stage was correlated with neutrophil count, whereas CT score at progressive stage was correlated with neutrophil count, WBC count, hs-CRP, procalcitonin, and LDH (55). The correlation between laboratory, clinical data, and CT quantitative features has also been shown in several studies (49, 56). Kang et al. observed that histogram features were significantly correlated with National Early Warning Score, neutrophil percentage, procalcitonin, acute respiratory distress syndrome, and extracorporeal membrane oxygenation

and negatively correlated with lymphocyte percentage and lymphocyte count (56). Sun et al. demonstrated that CT quantitative parameters were significantly correlated with inflammatory markers, including neutrophil percentage, lymphocyte count, lymphocyte percentage, hs-CRP, and procalcitonin (49). These findings may prove the reliability of quantitative CT in assessment of disease severity at the level of biology.

This study has some limitations. First is the retrospective nature of this study with small sample size. Therefore, a large cohort is needed to validate the role of AI-derived CT features in assessment of prognosis of COVID-19 patients. Second, the effect of anti-COVID-19 treatment on prognosis was not considered because no specific strategies have been used in the treatment of COVID-19 except for supportive care until now. Third, CT-based radiomics or deep learning and follow-up CT scan may provide more prognostic information.

Our study illustrated that AI-derived CT features were correlated with laboratory variables reflecting systemic inflammation, immune state, and multiple organ functions (e.g., coagulation, liver, and renal functions). Thus, CT quantitative analysis might be an effective and important method for assessing the severity of COVID-19 and may provide additional guidance for planning clinical treatment strategies. This technique can be

used in routine practice. Large-scale prospective studies in the future are warranted to confirm the CT features in predicting the occurrence of critical illness in COVID-19 patients.

## DATA AVAILABILITY STATEMENT

The original contributions presented in the study are included in the article/supplementary material, further inquiries can be directed to the corresponding author/s.

## ETHICS STATEMENT

The studies involving human participants were reviewed and approved by First Affiliated Hospital of Guangzhou Medical University. The ethics committee waived the requirement of written informed consent for participation.

## AUTHOR CONTRIBUTIONS

BP, HL, QL, and PW: literature search. BP, HL, QL, XZ, PW, and TX: study design. BP, HL, QL, and XZ: data collection. TX, PW, WL, JL, LL, CO, JM, and SL: data analysis. FZ, XW, and JX: data interpretation. BP, HL, QL, PW, and XZ: writing. All authors manuscript review and approval.

## REFERENCES

- Pan A, Liu L, Wang C, Guo H, Hao X, Wang Q, et al. Association of public health interventions with the epidemiology of the COVID-19 outbreak in Wuhan, China. *JAMA*. (2020) 2020:6130. doi: 10.1001/jama.2020.6130
- World Health Organization. *Coronavirus Disease 2019 (COVID-19) Situation Report*. Available online at: <https://www.who.int/emergencies/diseases/novel-coronavirus-2019/situation-reports> (accessed March 1, 2021).
- Wu Z, McGoogan JM. Characteristics of and important lessons from the coronavirus disease 2019 (COVID-19) outbreak in China: summary of a report of 72,314 cases from the Chinese Center for Disease Control and Prevention. *JAMA*. (2020) 2020:2648. doi: 10.1001/jama.2020.2648
- Chen N, Zhou M, Dong X, Qu J, Gong F, Han Y, et al. Epidemiological and clinical characteristics of 99 cases of 2019 novel coronavirus pneumonia in Wuhan, China: a descriptive study. *Lancet*. (2020) 395:507–13. doi: 10.1016/S0140-6736(20)30211-7
- Liu J, Yu H, Zhang S. The indispensable role of chest CT in the detection of coronavirus disease 2019 (COVID-19). *Eur J Nucl Med Mol Imaging*. (2020) 47:1638–9. doi: 10.1007/s00259-020-04795-x
- Zhang HT, Zhang JS, Zhang HH, Nan YD, Zhao Y, Fu EQ, et al. Automated detection and quantification of COVID-19 pneumonia: CT imaging analysis by a deep learning-based software. *Eur J Nucl Med Mol Imaging*. (2020) 20:4953. doi: 10.1007/s00259-020-04953-1
- Wang S, Dong D, Li L, Li H, Bai Y, Hu Y, et al. A deep learning radiomics model to identify poor outcome in COVID-19 patients with underlying health conditions: a multicenter study. *IEEE J Biomed Health Inform*. (2021) 2021:3076086. doi: 10.1109/JBHI.2021.3076086
- Zhang B, Ni-Jia-Ti MY, Yan R, An N, Chen L, Liu S, et al. CT-based radiomics for predicting the rapid progression of coronavirus disease 2019 (COVID-19) pneumonia lesions. *Br J Radiol*. (2021) 2021:bjr.20201007. doi: 10.1259/bjr.20201007
- Xiao F, Sun R, Sun W, Xu D, Lan L, Li H, et al. Radiomics analysis of chest CT to predict the overall survival for the severe patients of COVID-19 pneumonia. *Phys Med Biol*. (2021) 6560:abf717. doi: 10.1088/1361-6560/abf717
- Li L, Wang L, Zeng F, Peng G, Ke Z, Liu H, et al. Development and multicenter validation of a CT-based radiomics signature for predicting severe COVID-19 pneumonia. *Eur Radiol*. (2021) 21:7727. doi: 10.1007/s00330-021-07727-x
- Shiri I, Sorouri M, Geramifar P, Nazari M, Abdollahi M, Salimi Y, et al. Machine learning-based prognostic modeling using clinical data and quantitative radiomic features from chest CT images in COVID-19 patients. *Comput Biol Med*. (2021) 132:104304. doi: 10.1016/j.compbiomed.2021.104304
- Ke Z, Li L, Wang L, Liu H, Lu X, Zeng F, et al. Radiomics analysis enables fatal outcome prediction for hospitalized patients with coronavirus disease 2019 (COVID-19). *Acta Radiol*. (2021). doi: 10.1177/0284185121994695. [Epub ahead of print].
- Chen H, Zeng M, Wang X, Su L, Xia Y, Yang Q, et al. A CT-based radiomics nomogram for predicting prognosis of coronavirus disease 2019 (COVID-19) radiomics nomogram predicting COVID-19. *Br J Radiol*. (2021) 94:20200634. doi: 10.1259/bjr.20200634
- Li C, Dong D, Li L, Gong W, Li X, Bai Y, et al. Classification of severe and critical covid-19 using deep learning and radiomics. *IEEE J Biomed Health Inform*. (2020) 24:3585–94. doi: 10.1109/JBHI.2020.3036722
- Tang Z, Zhao W, Xie X, Zhong Z, Shi F, Ma T, et al. Severity assessment of COVID-19 using CT image features and laboratory indices. *Phys Med Biol*. (2021) 66:035015. doi: 10.1088/1361-6560/abfb9e
- Homayounieh F, Babaei R, Karimi Mobin H, Arru CD, Sharifian M, Mohseni I, et al. Computed tomography radiomics can predict disease severity and outcome in coronavirus disease 2019 pneumonia. *J Comput Assist Tomogr*. (2020) 44:640–6. doi: 10.1097/RCT.0000000000001094
- Wu Q, Wang S, Li L, Wu Q, Qian W, Hu Y, et al. Radiomics analysis of computed tomography helps predict poor prognostic outcome in COVID-19. *Theranostics*. (2020) 10:7231–44. doi: 10.7150/thno.46428
- Homayounieh F, Ebrahimian S, Babaei R, Mobin HK, Zhang E, Bizzo BC, et al. CT radiomics, radiologists, and clinical information in predicting outcome of patients with COVID-19 pneumonia. *Radiol Cardiothorac Imaging*. (2020) 2:e200322. doi: 10.1148/ryct.2020200322
- Feng Z, Shen H, Gao K, Su J, Yao S, Liu Q, et al. Machine learning based on clinical characteristics and chest CT quantitative measurements for prediction



- of adverse clinical outcomes in hospitalized patients with COVID-19. *Eur Radiol.* (2021) 21:7957. doi: 10.1007/s00330-021-07957-z
20. Gong K, Wu D, Arru CD, Homayounieh F, Neumark N, Guan J, et al. A multi-center study of COVID-19 patient prognosis using deep learning-based CT image analysis and electronic health records. *Eur J Radiol.* (2021) 2021:109583. doi: 10.1016/j.ejrad.2021.109583
  21. He L, Zhang Q, Li Z, Shen L, Zhang J, Wang P, et al. Incorporation of urinary neutrophil gelatinase-associated lipocalin and computed tomography quantification to predict acute kidney injury and in-hospital death in COVID-19 patients. *Kidney Dis.* (2021) 7:120–30. doi: 10.1159/000511403
  22. Kohli A, Jha T, Pazhayattil AB. The value of AI based CT severity scoring system in triage of patients with Covid-19 pneumonia as regards oxygen requirement and place of admission. *Indian J Radiol Imaging.* (2021) 31:S61–9. doi: 10.4103/ijri.IJRI\_965\_20
  23. Chatzitofis A, Cancian P, Gkitsas V, Carlucci A, Stalidis P, Albanis G, et al. Volume-of-interest aware deep neural networks for rapid chest CT-based COVID-19 patient risk assessment. *Int J Environ Res Public Health.* (2021) 8:2842. doi: 10.3390/ijerph18062842
  24. Purkayastha S, Xiao Y, Jiao Z, Thepumnoysuk R, Halsey K, Wu J, et al. Machine learning-based prediction of COVID-19 severity and progression to critical illness using CT imaging and clinical data. *Korean J Radiol.* (2021) 2020:1104. doi: 10.3348/kjr.2020.1104
  25. Shi W, Peng X, Liu T, Cheng Z, Lu H, ang S, et al. A deep learning-based quantitative computed tomography model for predicting the severity of COVID-19: a retrospective study of 196 patients. *Ann Transl Med.* (2021) 9:216. doi: 10.21037/atm-20-2464
  26. Lee EH, Zheng J, Colak E, Mohammadzadeh M, Houshmand G, Bevins N, et al. Deep COVID DeteCT: an international experience on COVID-19 lung detection and prognosis using chest CT. *NPJ Digit Med.* (2021) 4:11. doi: 10.1038/s41746-020-00369-1
  27. Lassau N, Ammari S, Chouzenoux E, Gortais H, Herent P, Devilder M, et al. Integrating deep learning CT-scan model, biological and clinical variables to predict severity of COVID-19 patients. *Nat Commun.* (2021) 12:634. doi: 10.1038/s41467-020-20657-4
  28. Fang X, Kruger U, Homayounieh F, Chao H, Zhang J, Digumarthy SR, et al. Association of AI quantified COVID-19 chest CT and patient outcome. *Int J Comput Assist Radiol Surg.* (2021) 16:435–45. doi: 10.1007/s11548-020-02299-5
  29. Ho TT, Park J, Kim T, Park B, Lee J, Kim JY, et al. Deep learning models for predicting severe progression in COVID-19-infected patients: retrospective study. *JMIR Med Inform.* (2021) 9:e24973. doi: 10.2196/24973
  30. Shan F, Gao Y, Wang J, Shi W, Shi N, Han M, et al. Abnormal lung quantification in chest CT images of COVID-19 patients with deep learning and its application to severity prediction. *Med Phys.* (2021) 48:1633–45. doi: 10.1002/mp.14609
  31. Xiao LS, Li P, Sun F, Zhang Y, Xu C, Zhu H, et al. Development and validation of a deep learning-based model using computed tomography imaging for predicting disease severity of coronavirus disease 2019. *Front Bioeng Biotechnol.* (2020) 8:898. doi: 10.3389/fbioe.2020.00898
  32. Pu J, Leader JK, Bandos A, Ke S, Wang J, Shi J, et al. Automated quantification of COVID-19 severity and progression using chest CT images. *Eur Radiol.* (2021) 31:436–46. doi: 10.1007/s00330-020-07156-2
  33. Yu Z, Li X, Sun H, Wang J, Zhao T, Chen H, et al. Rapid identification of COVID-19 severity in CT scans through classification of deep features. *Biomed Eng Online.* (2020) 19:63. doi: 10.1186/s12938-020-00807-x
  34. Zhang K, Liu X, Shen J, Li Z, Sang Y, Wu X, et al. Clinically applicable ai system for accurate diagnosis, quantitative measurements, and prognosis of COVID-19 pneumonia using computed tomography. *Cell.* (2020) 181:1423–33.e11. doi: 10.1016/j.cell.2020.04.045
  35. Liang W, Liang H, Ou L, Chen B, Chen A, Li C, et al. Development and validation of a clinical risk score to predict the occurrence of critical illness in hospitalized patients with COVID-19. *JAMA Intern Med.* (2020) 2020:2033. doi: 10.1001/jamainternmed.2020.2033
  36. Yang X, Yu Y, Xu J, Shu H, Xia J, Liu H, et al. Clinical course and outcomes of critically ill patients with SARS-CoV-2 pneumonia in Wuhan, China: a single-centered, retrospective, observational study. *Lancet Respir Med.* (2020) 8:475–81. doi: 10.1016/S2213-2600(20)30079-5
  37. Petrilli CM, Jones SA, Yang J, Rajagopalan H, O'Donnell L, Chernyak Y, et al. Factors associated with hospital admission and critical illness among 5,279 people with coronavirus disease 2019 in New York City: prospective cohort study. *BMJ.* (2020) 369:m1966. doi: 10.1136/bmj.m1966
  38. Xu L, Mao Y, Chen G. Risk factors for 2019 novel coronavirus disease (COVID-19) patients progressing to critical illness: a systematic review and meta-analysis. *Aging.* (2020) 12:12410–21. doi: 10.18632/aging.103383
  39. World Health Organization. *Clinical Management of Severe Acute Respiratory Infection When Novel Coronavirus (nCoV) Infection Is Suspected: Interim Guidance, 25 January 2020.* *Iris.* (2020). Available online at: <https://apps.who.int/iris/handle/10665/330854> (accessed March 1, 2021).
  40. Ronneberger O, Fischer P, Brox T. U-net: convolutional networks for biomedical image segmentation. In: *International Conference on Medical Image Computing and Computer-Assisted Intervention.* Shanghai: Springer. (2015). p. 234–41.
  41. Wang S, Zhou M, Liu Z, Liu Z, Gu D, Zang Y, et al. Central focused convolutional neural networks: developing a data-driven model for lung nodule segmentation. *Med Image Anal.* (2017) 40:172–83. doi: 10.1016/j.media.2017.06.014
  42. Pan F, Li L, Liu B, Ye T, Li L, Liu D, et al. A novel deep learning-based quantification of serial chest computed tomography in Coronavirus Disease 2019 (COVID-19). *Sci Rep.* (2021) 11:417. doi: 10.1038/s41598-020-80261-w
  43. Liu F, Zhang Q, Huang C, Shi C, Wang L, Shi N, et al. CT quantification of pneumonia lesions in early days predicts progression to severe illness in a cohort of COVID-19 patients. *Theranostics.* (2020) 10:5613–22. doi: 10.7150/thno.45985
  44. National Health Commission of the People's Republic of China. *Guidelines for the Diagnosis and Treatment of Novel Coronavirus (2019-nCoV) Infection (Trial Version 7) (in Chinese).* Shanghai: National Health Commission of the People's Republic of China. (2020).
  45. Yin X, Min X, Nan Y, Feng Z, Li B, Cai W, et al. Assessment of the severity of coronavirus disease: quantitative computed tomography parameters versus semiquantitative visual score. *Korean J Radiol.* (2020) 2020:423. doi: 10.3348/kjr.2020.0423
  46. Shen C, Yu N, Cai S, Zhou J, Sheng J, Liu K, et al. Quantitative computed tomography analysis for stratifying the severity of Coronavirus Disease 2019. *J Pharm Anal.* (2020) 10:123–9. doi: 10.1016/j.jpah.2020.03.004
  47. Homayounieh F, Bezerra Cavalcanti Rockenbach MA, Ebrahimi S, Doda Khera R, Bizzo BC, Buch V, et al. Multicenter assessment of CT pneumonia analysis prototype for predicting disease severity and patient outcome. *J Digit Imaging.* (2021) 430:9. doi: 10.1007/s10278-021-00430-9
  48. Salvatore C, Roberta F, Angela L, Cesare P, Alfredo C, Giuliano G, et al. Clinical and laboratory data, radiological structured report findings and quantitative evaluation of lung involvement on baseline chest CT in COVID-19 patients to predict prognosis. *Radiol Med.* (2021) 126:29–39. doi: 10.1007/s11547-020-01293-w
  49. Sun D, Li X, Guo D, Wu L, Chen T, Fang Z, et al. CT quantitative analysis and its relationship with clinical features for assessing the severity of patients with COVID-19. *Korean J Radiol.* (2020) 21:859–68. doi: 10.3348/kjr.2020.0293
  50. Wu D, Gong K, Arru CD, Homayounieh F, Bizzo B, Buch V, et al. Severity and consolidation quantification of COVID-19 from CT images using deep learning based on hybrid weak labels. *IEEE J Biomed Health Inform.* (2020) 24:3529–38. doi: 10.1109/JBHI.2020.3030224
  51. Zhang J, Meng G, Li W, Shi B, Dong H, Su Z, et al. Relationship of chest CT score with clinical characteristics of 108 patients hospitalized with COVID-19 in Wuhan, China. *Respir Res.* (2020) 21:180. doi: 10.1186/s12931-020-01440-x
  52. Synowiec A, Szczepański A, Barreto-Duran E, Lie LK, Pyrc K. Severe acute respiratory syndrome coronavirus 2 (SARS-CoV-2): a systemic infection. *Clin Microbiol Rev.* (2021) 133:20. doi: 10.1128/CMR.00133-20
  53. Yilmaz A, Sabirli R, Seyit M, Ozen M, Oskay A, Cakmak V, et al. Association between laboratory parameters and CT severity in patients infected with Covid-19: a retrospective, observational study. *Am J Emerg Med.* (2021) 42:110–4. doi: 10.1016/j.ajem.2021.01.040
  54. Gallo Marin B, Aghagholi G, Lavine K, Yang L, Siff EJ, Chiang SS, et al. Predictors of COVID-19 severity: a literature review. *Rev Med Virol.* (2021) 31:1–10. doi: 10.1002/rmv.2146
  55. Zhang B, Zhang J, Chen H, Chen L, Chen Q, Li M, et al. Novel coronavirus disease 2019 (COVID-19): relationship between chest CT scores and laboratory parameters. *Eur J Nucl Med Mol Imaging.* (2020) 47:2083–9. doi: 10.1007/s00259-020-04854-3

56. Kang M, Hong KS, Chikontwe P, Luna M, Jang JG, Park J, et al. Quantitative assessment of chest CT patterns in COVID-19 and bacterial pneumonia patients: a deep learning perspective. *J Korean Med Sci.* (2021) 36:e46. doi: 10.3346/jkms.2021.36.e46

**Conflict of Interest:** The authors declare that the research was conducted in the absence of any commercial or financial relationships that could be construed as a potential conflict of interest.

Copyright © 2021 Pang, Li, Liu, Wu, Xia, Zhang, Le, Li, Lai, Ou, Ma, Liu, Zhou, Wang, Xie, Zhang, Jiang, Liu and Zeng. This is an open-access article distributed under the terms of the Creative Commons Attribution License (CC BY). The use, distribution or reproduction in other forums is permitted, provided the original author(s) and the copyright owner(s) are credited and that the original publication in this journal is cited, in accordance with accepted academic practice. No use, distribution or reproduction is permitted which does not comply with these terms.



# Identification of Variable Importance for Predictions of Mortality From COVID-19 Using AI Models for Ontario, Canada

Brett Snider<sup>1\*</sup>, Edward A. McBean<sup>1</sup>, John Yawney<sup>2</sup>, S. Andrew Gadsden<sup>1</sup> and Bhumi Patel<sup>1</sup>

<sup>1</sup> School of Engineering, University of Guelph, Guelph, ON, Canada, <sup>2</sup> Adastra Corporation, Toronto, ON, Canada

## OPEN ACCESS

### Edited by:

Babak A. Ardekani,  
Nathan Kline Institute for Psychiatric  
Research, United States

### Reviewed by:

Dejan Baskic,  
University of Kragujevac, Serbia  
Na Hong,  
Digital China Health Technologies Co.  
Ltd., China

### \*Correspondence:

Brett Snider  
bsnide01@uoguelph.ca

### Specialty section:

This article was submitted to  
Infectious Diseases - Surveillance,  
Prevention and Treatment,  
a section of the journal  
Frontiers in Public Health

**Received:** 03 March 2021

**Accepted:** 24 May 2021

**Published:** 21 June 2021

### Citation:

Snider B, McBean EA, Yawney J,  
Gadsden SA and Patel B (2021)  
Identification of Variable Importance  
for Predictions of Mortality From  
COVID-19 Using AI Models for  
Ontario, Canada.  
Front. Public Health 9:675766.  
doi: 10.3389/fpubh.2021.675766

The Severe Acute Respiratory Syndrome Coronavirus 2 pandemic has challenged medical systems to the brink of collapse around the globe. In this paper, logistic regression and three other artificial intelligence models (XGBoost, Artificial Neural Network and Random Forest) are described and used to predict mortality risk of individual patients. The database is based on census data for the designated area and co-morbidities obtained using data from the Ontario Health Data Platform. The dataset consisted of more than 280,000 COVID-19 cases in Ontario for a wide-range of age groups; 0–9, 10–19, 20–29, 30–39, 40–49, 50–59, 60–69, 70–79, 80–89, and 90+. Findings resulting from using logistic regression, XGBoost, Artificial Neural Network and Random Forest, all demonstrate excellent discrimination (area under the curve for all models exceeded 0.948 with the best performance being 0.956 for an XGBoost model). Based on SHapley Additive exPlanations values, the importance of 24 variables are identified, and the findings indicated the highest importance variables are, in order of importance, age, date of test, sex, and presence/absence of chronic dementia. The findings from this study allow the identification of out-patients who are likely to deteriorate into severe cases, allowing medical professionals to make decisions on timely treatments. Furthermore, the methodology and results may be extended to other public health regions.

**Keywords:** artificial intelligence, XGBoost, SHapley, COVID-19, mortality

## INTRODUCTION

Since the outbreak of severe acute respiratory syndrome coronavirus 2 (SARS-CoV-2), also known as COVID-19, in Wuhan, China in December 2019, the virus has caused chaos, extreme and widespread illness and mortalities, and shutdowns of country-wide economies around the globe. As a measure of the sheer magnitude of the impacts, more than 11.9% of the US population have tested positive for the virus, as of January 25, 2021 (1). In Ontario, COVID-19 has infected 282,511 people and resulted in 6,614 deaths as of February 13, 2021 (2).

In response to the day-to-day challenges of managing the COVID-19 pandemic, massive efforts continue to be made to protect the integrity of hospital systems to allow both treatment of COVID-19 cases as needed, as well as to avoid having to delay elective surgeries. However, the growth in caseloads continues to be an ongoing major concern, needing improved predictions to use for capacity planning. To better understand and assess the capacity of health care systems to respond to the medical needs arising from COVID-19, enormous efforts are being expended involving the use of epidemiological and machine learning modeling, to understand the projection of caseloads of the virus. An example is an artificial neural network (ANN) model developed by Abdulaal et al. to predict a patient-specific, point-of-admission mortality risk to inform clinical management decisions (3). Their modeling analyzed patient features including demographics, co-morbidities, smoking history, and presenting symptoms of 398 patients and achieved an area under the curve (AUC) of 86% (3). However, while epidemiological modeling has significant value for certain questions, the parameters of these models are typically resolved through some estimation procedure and future case counts through different classes are identified. As an example, the SEIR model approach assigned individuals to the susceptible (S), exposed (E), infected (I), and recovered (R) classes (1, 2, 4). However, the potential to predict how positive tests for COVID-19 at health centers will translate to ICU cases and mortality are limited. This information will be critical as health systems in North America are rapidly approaching capacity.

With issues of the second wave of the pandemic ongoing at the time of submission of this paper, interest continues to grow in obtaining more comprehensive caseload and patient data and predictions. Given there are now more accurate data available from the first and second waves, inclusion of these data has considerable merit. Until now, data security and privacy issues have to-date limited the accessibility of alternate and detailed data sources. Through obtaining detailed COVID-19 pandemic-related data, more powerful artificial intelligence (AI) techniques can be feasibly applied, offering the ability to uncover and understand the value of alternative interpretation procedures.

This paper describes results arising from use of AI models based on data from Ontario Health Data Platform (22 February 2020–20 October 2020) with the aim to improve prediction of caseloads and mortality risks in patients throughout the province of Ontario, with a population of more than 14 million. The dataset includes extensive information from the first wave and the beginning of the second wave of COVID-19 cases including Canadian census information by designated area. The census location information is based on a size of approximately three blocks and hence is able to capture representation of ethnicity, income level, and other social differences, and can therefore be considered robust. The results from this paper may be extended further to other public health regions throughout the world. The paper is organized as follows: related works are discussed in section Related Works. Section Materials and Methods describes the materials and methods. Results and discussion are found in section Results and Discussion and then the paper is concluded in section Conclusions.

## RELATED WORKS

AI models can be employed in the prediction of patient-specific, point-of-admission mortality risks helping to inform clinical management decisions. Thus, using AI models, healthcare practitioners have ways to accurately predict the potential for an individual ending up in the Intensive Care Unit (ICU). As well, due to the very high AUC, AI models have the capability to consider a broad range of patient data, including demographics, co-morbidities, and much more, to predict patient-specific mortality risk following their hospital admission.

The emergence of “big data” in the early 2000s has proven very beneficial for public health investigations. The capabilities of AI modeling have been able to accurately predict numerous public health trends such as in-hospital mortality and detection of emerging epidemics (4–6). With the emergence of the COVID-19 global epidemic, big data and machine learning models have enormous potential to understand who, and where, people are most at risk.

Since March 2020, COVID-19 has spread around the globe, affecting every country and causing more than 2.1 million deaths worldwide (7). As a result, researchers have focused on COVID-19, to understand individuals most at risk as well as how to best distribute scarce resources. Identification of co-morbidities and creation of models to predict COVID-19 mortality using big data has significant potential.

Predictive analytics for assessing the in-hospital risk of patients and patient mortality have traditionally been limited to clinical decision rules (rules to reduce uncertainties in medical decision-making), but these approaches are not easily updated with new developments or data. Additionally, clinical decision rules may take years to identify and test and have been criticized for their lack of generally applicability to entire populations (4, 5). Hence, in the current situation, with the rapid spread of COVID-19, clinical decision support systems are still being developed for this particular virus (8).

Both Hernesneimi et al. and Taylor et al. note that one of the biggest challenges in developing models to predict mortality is assembling quality data (4, 5). However, this is outweighed by the benefits of a machine learning model, which provides improved performance and ability to be generalized to entire populations, or readily adapted to new populations (9). As well, AI models are updateable over time to recognize changing trends in medical care, all of which are attainable dimensions, if provided the large datasets (4, 5).

Rodriguez-Nava et al. used a random forest algorithm that predicted ICU admissions with an AUC of 0.82 and mortality with an AUC of 0.70 (10). Similarly, Jimenez-Solemm et al. used a random forest machine learning model using a Danish dataset with 3,944 COVID-19 patients that predicted ICU admissions with an AUC of 0.820, mortality with an AUC of 0.902, hospital admission with an AUC of 0.820 and ventilator treatment with an AUC of 0.815 (11). They found age and BMI the most important features for predicting hospital admission and ventilator treatment (11). Among all models, the parameters



that were determined to have the highest severity of COVID-19 were heightened if male, had hypertension, and presence of dementia (11).

A study by Schöning et al. aiming to distinguish between severe and non-severe COVID-19 also found hypertension, along with diabetes mellitus (Type 2) and renal impairment to be prognostic of severe disease (12). Schöning et al. used a variety of machine learning models which were trained using data from the first wave in Switzerland and externally validated using data from the second wave (confirming findings to be generalizable) and achieved an accuracy of AUC values ranging from 0.86 (decision tree induction) to 0.96 (support vector machine) (12).

Kim et al. used Korean National Health Insurance data to identify co-morbidities and factors that increase mortality using multivariate logistic regression analysis with a confidence interval of 95% (13). A total of 9,148 COVID-19 patients, including 130 fatalities, were linked to their national health insurance record data, considering 298 medical conditions as co-morbidities (13). Williamson et al. performed a similar analysis on behalf of NHS England, with a sample size of 10,926 COVID-19 related deaths (14). Using a multivariable Cox model, Williamson et al. were able to estimate hazard ratios for characteristics such as smoking status, obesity, sex, age, deprivation, heart disease, etc. with a 95% confidence interval (14). Both studies identified age, deprivation, diabetes, bronchitis and severe asthma as top risk factors for COVID-19 (12, 13). Additionally, Kim et al. found that dental disorders were associated with high co-morbidity risk (13).

Machine learning has been found to predict mortality more accurately than non-machine learning models (4, 5). For example, mortality due to acute coronary syndrome is reliably predicted using the GRACE score, based on patients' variables in admission to the hospital. A machine learning model developed by Hernesneimi et al. achieved greatly improved results compared to traditional GRACE score (4). The machine learning model was developed using XGBoost and included phenotype data about the patient as well as hospital admission variables (4). The machine learning model outdid the traditional GRACE score method with an AUC of 0.904 compared to an AUC of 0.802 for GRACE score (4). Another example is a machine learning model developed by Taylor et al. to predict in-hospital mortality of patients with sepsis (5). This model considered 500 clinical variables including demographic information such as age, sex, insurance and employment status as well as health status and medical test results. Random Forest was reported to be a relatively interpretable option and produced the best results when compared with XGBoost, logistic regression or CART models (5).

A similar study from Zheng et al. used machine learning models to evaluate patients and predict rapid deterioration of in-hospital COVID-19 patients to determine triage priority (15). The model developed by Zheng et al. used the results of blood tests from 601 COVID-19 patients to predict deterioration up to 12 days before death occurred and reported that decreased lymphocyte count and increased lactate dehydrogenase levels, c-reactive protein levels and neutrophil counts, all corresponded with an increased likelihood for rapid deterioration (15). The best results were found using XGBoost and achieved an AUC of

0.953 for a small dataset (15). In addition, the illness trajectory (moderate, severe, critical – states as defined by Israeli Ministry of Health) of COVID-19 patients was predicted by Roimi et al. with an AUC of 0.88 using only patients' age, sex and day-by-day clinical state using a multistate Cox regression-based model (16).

Estiri et al. used nested generalized linear models to predict mortality using electronic health records (EHRs) of 16,709 COVID-19 age-separated cohorts from Mass General Brigham (a Boston-based non-profit hospital) (17). The data included were from the beginning of the EHR up to 14 days prior to the positive polymerase chain reaction (PCR) test to ensure COVID-related medications were not included in the model as risk factors (17). The model which included patients under the age of 45 had an AUC of 0.898, 0.789 in the 45–65 cohort and 0.753 in the 65–85 cohort, thus able to provide relatively high accuracy by relying only on data already stored in EHRs (17).

A prognostic machine learning model created by researchers from the Department of Decision Medicine at the University of Maastricht in The Netherlands reported the severity of COVID-19 in a patient (8). The model is based on the data from 299 patients' blood-test data and age and is readily available as an application (8). A similar application developed by ClosedLoop.ai determines a “vulnerability score” for an individual's susceptibility to severe COVID-19 illness (18).

Machine learning models have also been trained to predict rapid deterioration due to COVID-19 and even detect COVID-19 from lung X-Rays (19, 20). Zhu et al. used deep transfer learning to determine COVID-19 severity from X-rays and Elgendi et al. used deep neural networks to differentiate COVID-19 patient X-rays from other types of pneumonias (19, 20). Both methods used convolutional neural networks to a high degree of accuracy, reducing the need for radiologists (who may be in short supply in low-resource clinics) to read x-rays (19).

Mehta et al. used caseload and mortality data from early in the COVID-19 pandemic (March 2020), to determine the vulnerability of a county in the US to a large COVID-19 outbreak with high mortality (21). Mehta et al. used XGBoost to train a model that would predict which counties in the US were most at-risk using county-level population statistics such as age, gender, and density as well as CDC data for the health within a county (21). They reported that population size of a county was by far the most important variable, with population density, longitude, hypertension prevalence, chronic respiratory mortality rate, cancer crude rate, and diabetes prevalence, also playing large roles (21). While Mehta et al. do not state which counties are found to be the most at-risk, COVID-19 has reached virtually all parts of the U.S., including both rural and urban areas (21, 22).

As widely apparent from the numerous information venues, the magnitude of the impacts to people and the economies around the world are staggering. Hence, there is enormous interest in using available data, and in the development of models, that can combine available information in any manner to improve predictions of caseloads, supporting alternative strategies for predicting patient-specific mortality risk.

**TABLE 1** | Characteristics of 57,390 Ontario residents with COVID-19.

| Variable                     | Description  | Range of values       |
|------------------------------|--|-----------------------|
| Age                          | Age in years, as of Jan 1, 2020  | 0–105                 |
| Test date                    | Test date  | Feb 22–Oct 20         |
| Sex                          | Indicator Variable for sex   | 26,861 (M = 1, F = 0) |
| Hypertension                 | Chronic hypertension, as of Jan 1, 2020  | 15,778 (0, 1)         |
| LTC resident                 | LTC resident, as of Jan 1, 2020  | 5,179 (0, 1)          |
| Chronic_dementia             | Chronic dementia diagnosed, as of Jan 1, 2020  | 4,746 (0, 1)          |
| Chronic_odd                  | Chronic diabetes diagnosed as of Jan 1, 2020   | 9,002 (0, 1)          |
| Ethnic concentration quint.  | Calculated from ontario marginalization index, based on census designation. Refers to Visible minorities and/or recent immigrants (0–5 ranging from least diverse to most diverse) | (0–5)                 |
| Commuter concentration quint | % of people that commute within Census designated area - converted to quintiles (5 being the highest, 0 referring to missing DA info).   | (0–5)                 |
| Median income quint.         | Median income within census-designated area - converted to quintiles (0–5 ranging from Lowest income to highest income, 0 referring to missing DA info).                           | (0–5)                 |
| Charl                        | Charlson co-morbidity index. Only 2,059 patients with charl above 0.   | (0–10)                |
| Household size quint.        | Avg. household size within Census-designated area - converted to quintiles (5 being the Highest, 0 = missing DA info).   | (0–5)                 |
| CKD                          | Chronic kidney disease.  | 2,523 (0, 1)          |
| Cancer                       | Cancer index   | 2,995 (0–1)           |
| Chronic_copd                 | Chronic obstructive pulmonary disease  | 4,030 (0–1)           |
| Chronic_asthma               | Asthma   | 9,100 (0–1)           |
| Chronic_chf                  | Congestive heart failure   | 2,257 (0–1)           |
| Stroke                       | If patient suffered a stroke previous to Jan 1, 2020   | 1,016 (0–1)           |
| Cardiac ISCH                 | Cardiac ischemia   | 1,916 (0–1)           |
| Rural                        | Indicator if a patient lives in a rural residence  | 1,746 (0–1)           |
| Chronic_ra                   | Rheumatoid arthritis   | 567 (0–1)             |
| Tia                          | Transient Ischemic Attack  | 722 (0–1)             |
| Immuno_comp                  | Immuno-compromised   | 237 (0–1)             |
| Thala                        | History of Thalassemia   | 36 (0–1)              |
| Cases recovered              |  | 54,568                |
| Cases died                   |  | 2,822                 |

## MATERIALS AND METHODS

### Dataset Description

For this research, to ensure adherence to strict security protocols, extensive data for 57,390 individual cases from Ontario Health Data Platform where data related to positive COVID-19 tests were collected between 22 February and 20 October 2020 were obtained for use in machine learning modeling. The dataset contained epidemiological and demographic information, recovery/mortality outcome information and co-morbidities of individuals residing in Ontario at census level. The attributes which proved most useful in the machine learning and statistical models are indicated in **Table 1**. Co-morbidities and age were collected from patient health records as of January 1, 2020; hence diagnoses of other medical conditions after this date were excluded. Of the 57,390 cases included in the dataset, 2,822 patients died of COVID-19 and the remaining 54,568 either recovered from COVID-19 or are still hospitalized.

Several input variables were derived using 2016 census data for the designated area of the individual patients. Census

data in Canada are collected at postal code level and hence, represent approximately at three city block intervals. Census data relied upon included: ethnic concentration (of residential area), commuter concentration, median income and household size (these values are unlikely to change significantly between date of census and start of pandemic). These values were converted into quintiles (division of the population into 5 equal groups according to the distribution of input variables) with “1” being the lowest quintile, and “5” being the highest. Long-term care residents (LTC) did not include census-designated area information and therefore were represented with a zero value in the AI modeling. As well, for case-specific data for which substantial data were not available, those cases were removed from the modeling prior to undertaking the modeling (decreasing the 280,000 data to 57,390 cases actually used in the modeling) since the remaining cases represented a very substantial dataset for analyses. Individuals with missing data were not included in the analyses, however, for LTC residents’ variables derived based on postal code, such as income, ethnic concentration, household size, and commuter percentage, were

coded as zero since postal code information was not available for these individuals.

## Model Development

This study compared three machine learning models and one statistical model. The following models were employed: artificial neural network (ANN), Random Forest (RF), extreme gradient boosting decision tree (XGBoost) all of which are tree structure machine learning models, and logistic regression (23–25). These models were adopted due to their high accuracy in binary classification problems as well as their prevalence/adoption in previous literature. The hardware used for developing the models included: a virtual server from OHDP specifically to run the code, 8 virtual CPUs and 128 GB of RAM, all running on Centos 7 Operating System. The software used included: R for coding and Rstudio as the integrated development environment (IDE).

## Data Processing

Prior to model calibration, the dataset was randomly split into two segments, namely an 80% training dataset as an operational characterization and a 20% testing dataset where each model was calibrated using the training dataset and assessed for accuracy using the testing dataset. A grid search approach was used to adjust the hyperparameters of the models using a 10-fold cross-validation technique, repeated three times per model and optimized to produce the maximum area under the receiver operating characteristic curve (Area Under Curve, or AUC).

The logistic regression's input variables were chosen by a stepwise Akaike Information Criterion (AIC) function (23). The computer programming language R was used to develop and analyze all models (26). The final predicted outcome, recovered or died, was determined by the probability of mortality for each recorded case outcome generated by the models, based on a 50% threshold value ensuring highest total accuracy.

## RESULTS AND DISCUSSION

As a measure of accuracy, the Receiver Operating Characteristic curve (ROC) was calculated for each model. The Area Under the ROC curve was used to provide the basis of comparison between each model. Since an AUC value approaching “1” indicates high model accuracy while a value of 0.5 represents a model that is no better than random change, **Table 2** demonstrates that all models utilized show strong predictive values.

**TABLE 2** | Comparison of models employed in the base case analyses.

| Model          | AUC          |
|----------------|--------------|
| Logit          | 0.9518       |
| <b>XGboost</b> | <b>0.956</b> |
| Random forest  | 0.948        |
| Neural net     | 0.9475       |

*The bold values represent the accuracy for the model (i.e., XGBoost) which is used primarily in this paper to explore the importance of variables.*

All models developed have very high AUC values ( $>0.94$ ). The most accurate model is XGBoost which has an AUC of 0.956. To the best of the authors' knowledge, this is the highest accuracy reported for COVID-19 mortality prediction models published to-date using Canadian data.

Although the AUC is a useful metric in understanding the overall accuracy of a binary prediction model, that metric does not provide specific accuracy for each class (accuracy in predicting survival vs. accuracy in predicting mortality). To highlight the accuracy of both predictions, a confusion matrix was developed. The confusion matrix as developed and highlighted in **Table 3**, compares the prediction accuracy of the XGBoost model with the reference (or actual outcome) of COVID-19 patients within the test dataset, assuming any patient with a predicted risk score below 0.5 will survive.

The confusion matrix indicates the model is extremely accurate in predicting which patients will survive, with 97% of the alive predictions actually surviving. The mortality prediction accuracy is substantially lower, with 49% of predicted deaths actually occurring. Even at 49%, the mortality prediction still provides a strong indicator on whether a COVID-19 patient will die and is helpful in strategic planning of possible medical caseloads, in terms of potential overload of the medical system.

It is noted that the mortality prediction accuracy of the modeling could be improved by increasing the risk score threshold, but this would also increase false negative predictions. Various methods have been created in an attempt to quantify the variable impact but many of them are flawed when using tree structure machine learning models (which includes XGBoost, Random Forests, decision trees, etc.). While the values could be adjusted to make a new set point, the models are quite accurate and are best represented by the AUC, meaning it is a good indicator of the actual risk of mortality. Overall, the results indicate the risk score predicted by the XGBoost model provides very strong insights regarding the outcome for Ontario COVID-19 patients, including the ability to plan for possible medical caseloads.

## Variable Importance

Since the XGBoost model is the most accurate mortality prediction model developed for COVID-19 patients in Ontario, there is strong merit in investigating which variables are the most important and quantify how these variables contribute to the final predictions. To explore the impact of each variable on the final prediction, SHapley Additive exPlanations (SHAP) values have been used.

SHAP values determine the importance of a feature by comparing a model prediction with, and without, the feature for

**TABLE 3** | Confusion matrix and statistics.

| Prediction | Alive  | Dead |
|------------|--------|------|
| Alive      | 10,710 | 353  |
| Dead       | 203    | 211  |

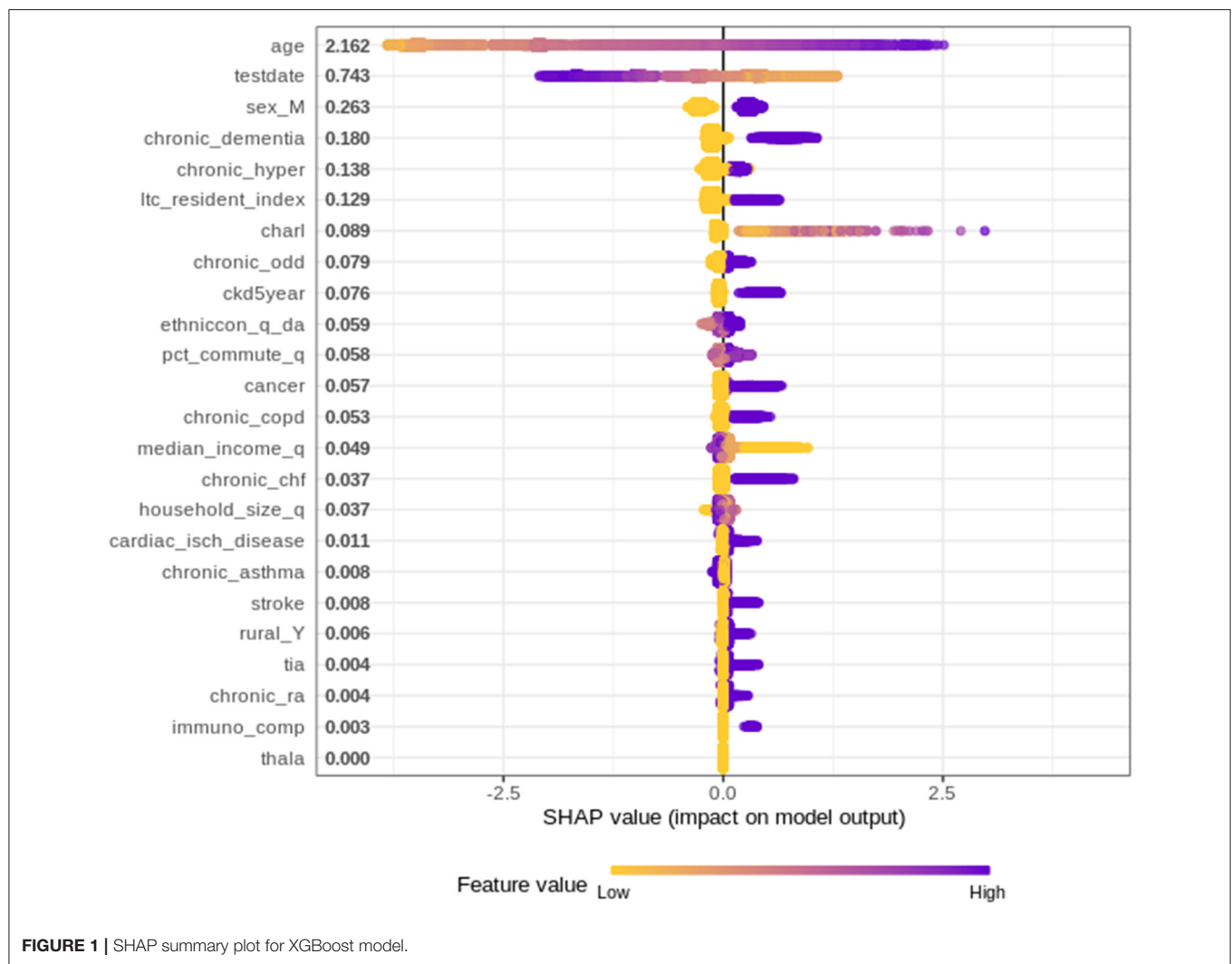


**FIGURE 1** | SHAP summary plot for XGBoost model.

each observation within the training data. The SHAP values are calculated using SHAPforXGBoost R package and present the variable contribution on a log-odds scale (logarithm of the ratio of high mortality risk to low mortality risk) (27).

**Figure 1** plots the SHAP value for each individual patient within the training dataset by input variable. The input variables, as listed on the y-axis, are ranked from most important (at the top) to least important (at the bottom) with their mean absolute SHAP value indicated next to the name. The X axis represents the SHAP value associated with each variable and patient within the training dataset (i.e., there is a plotted point for each case based on the influence that variable has on the prediction of that case). The color indicates whether the individual patients' input variable value was high (purple) or low (yellow). For example, in **Figure 1** a "high" age has a high and "positive" impact on predicting mortality. The "high" comes from the purple color and the "positive" impact is shown in the X axis. Note, a range of SHAP values can exist per input variable value based on the SHAP values calculated for each observation and how they independently contribute to the machine learning model's predictions.

Overall, 24 variables were identified/ranked, with age as being unquestionably the most important variable for the XGBoost model. As a patient's age increases (approaches purple) the SHAP value impact increases, with a very high age being associated with an additional 2.5 increase in log-odds. The date of when someone tested positive for COVID-19 also demonstrated a strong impact on overall mortality risk, indicating as the positive test date increases (i.e., later in the pandemic) the risk of mortality decreases. The importance of the date when someone tested positive is very likely due to improved understanding of treatment options by the medical systems. Since the start of the pandemic in March 2020, health care workers and researchers worked fast to try to find the most effective ways to treat and prevent COVID-19 (e.g., including the use of antivirals and immune modulators, such as remdesivir, hydroxychloroquine, and dexamethasone) (28, 29). This finding described herein is supported by the European Medicines Agency indicated in June 2020 that it was discussing 132 potential treatments with developers, showing the rapid speed with which drugs and therapies against the virus are being developed (29, 30).



Other variables of high importance in terms of predicting the outcomes included “sex,” and chronic dementia, etc. on through the list of 24 variables, as depicted in **Figure 1**.

## CONCLUSIONS

The impact of COVID-19 has been felt throughout populations around the world. In Ontario, COVID-19 has infected over 280,000 people with over 6,000 deaths (2). As the people of Ontario experience the second wave of the pandemic, the number of deaths associated with the pandemic will continue to increase. Understanding which Ontarians are most at risk will be important in determining how the medical system can most effectively deal with the pandemic, implement effective intervention strategies, and refine vaccination priorities.

This paper described a model with an accurate mortality prediction that can be used to assist Ontario’s medical system in combating this pandemic and further highlight the risks faced by individual patients. By including patient demographics, co-morbidities, geographic, and census-based attributes, the XGBoost model developed surpassed all other Ontario mortality predictions published to date, with an AUC of 0.956; all four modeling approaches provided high AUCs where findings resulting from using logistic regression, XGBoost, ANN and RF, all demonstrate excellent discrimination (area under the curve for all four modeling approaches exceeded 0.948).

Findings related to the importance of 24 variables in characterizing mortality based on SHAP values, the importance of the variables found the most important parameters in order of importance were age, date of test, sex and chronic dementia, providing guidance to the medical professionals to identify the highest risks for out-patients who are likely to deteriorate into severe cases with the features indicating the risk of mortality.

## DATA AVAILABILITY STATEMENT

The data analyzed in this study is subject to the following licenses/restrictions: the dataset obtained from the Ontario Health Data Platform limits access to these data sets to trustworthy researchers, who are bound by law, ethics, the terms of their employment, and their research grants to protect the privacy and confidentiality of the data they work with. Requests to access these datasets should be directed to <https://ohdp.ca/pre-application-form/>.

## AUTHOR CONTRIBUTIONS

EAM, BS, JY, and SAG: conceptualization. BS: methodology and software. BS, EAM, JY, SAG, and BP: validation. BS, EAM, JY, SAG, and BP: formal analysis. EM: investigation. BS and EAM: data curation. BS, EAM, and BP: writing—original draft preparation. BS, EAM, JY, SAG, and BP: writing—review and editing. EAM: supervision, project administration, and funding acquisition. All authors have read and agreed to the published version of the manuscript.

## FUNDING

This work was supported by Natural Sciences and Engineering Research Council of Canada Alliance (Grant Number 401636) and University of Guelph Research Leadership Chair Professor funding.

## ACKNOWLEDGMENTS

This study was supported by ICES, which is funded by an annual grant from the Ontario Ministry of Health (MOH) and the Ministry of Long-Term Care (MLTC). This study was supported by the Ontario Health Data Platform (OHDP), a Province of Ontario initiative to support Ontario’s ongoing response to COVID-19 and its related impacts. The analyses, opinions, results, and conclusions reported in this paper are those of the authors and are independent from the funding sources. No endorsement by ICES, the OHDP, its partners, or the Province of Ontario is intended or should be inferred. Parts of this material are based on data and/or information compiled and provided by CIHI. However, the analyses, conclusions, opinions, and statements expressed in the material are those of the author(s), and not necessarily those of CIHI.

These datasets were linked using unique encoded identifiers and analyzed at ICES.

REB: The use of the data in this project is authorized under section 45 of Ontario’s Personal Health Information Protection Act (PHIPA) and does not require review by a Research Ethics Board.

Access to datasets: The dataset from this study is held securely in coded form at ICES. While legal data sharing agreements between ICES and data providers (e.g., healthcare organizations and government) prohibit ICES from making the dataset publicly available, access may be granted to those who meet pre-specified criteria for confidential access, available at [www.ices.on.ca/DAS](http://www.ices.on.ca/DAS) (email: [das@ices.on.ca](mailto:das@ices.on.ca)). The full dataset creation plan and underlying analytic code are available from the authors upon request, understanding that the computer programs may rely upon coding templates or macros that are unique to ICES and are therefore either inaccessible or may require modification.

OCR: Parts of this material are based on data and information provided by Cancer Care Ontario (CCO). The opinions, results, view, and conclusions reported in this paper are those of the authors and do not necessarily reflect those of CCO. No endorsement by CCO is intended or should be inferred.

ODB: We thank IQVIA Solutions Canada Inc. for use of their Drug Information Database.

Ontario Community Health Profiles Partnership (OCHPP): OCHPP created Ontario Marginalization Index (ON-Marg) which is a source for this paper as ON-Marg is used to understand inequalities in health and other social problems related to health among either population groups or geographic areas across Ontario.

Statistics Canada: Postal Code Conversion File and census data were adapted from Statistics Canada. This does not constitute an endorsement by Statistics Canada of this product.

## REFERENCES

- Centres for Disease Control and Prevention. *COVID Data Tracker Weekly Review*. CDC (2020). Available online at: <https://www.cdc.gov/coronavirus/2019-ncov/covid-data/covidview/index.html> (accessed January 25, 2021).
- Ontario Agency for Health Protection and Promotion (Public Health Ontario). *Epidemiologic Summary: COVID-19 in Ontario – January 15, 2020 to February 15, 2021*. Toronto, ON: Queen's Printer for Ontario (2021).
- Abdulaal A, Patel A, Charani E, Denny S, Mughal N, Moore L. Prognostic modeling of COVID-19 using artificial intelligence in the United Kingdom: model development and validation. *J Med Internet Res*. (2020) 22:e20259. doi: 10.2196/20259
- Scheele BC, Pasmans F, Skerratt LF, Berger L, Martel AN, Beukema W, et al. Extensive phenotype data and machine learning in prediction of mortality in acute coronary syndrome—the MADDEC study. *Ann Med*. (2019) 51:156–63. doi: 10.1080/07853890.2019.1596302
- Taylor RA, Pare JR, Venkatesh AK, Mowafi H, Melnick ER, Fleischman W, et al. Prediction of in-hospital mortality in emergency department patients with sepsis: a local big data–driven, machine learning approach. *Acad Emerg Med*. (2016) 23:269–78. doi: 10.1111/acem.12876
- Poirier C, Lavenu A, Bertaud V, Campillo-Gimenez B, Chazard E, Cuggia M, et al. Real time influenza monitoring using hospital big data in combination with machine learning methods: comparison study. *JMIL Public Health Surveill*. (2018) 4:e11361. doi: 10.2196/11361
- Johns Hopkins University and Medicine. *COVID-19 Dashboard by the Center for Systems Science and Engineering (CSSE) at Johns Hopkins University (JHU)*. Johns Hopkins University and Medicine (2020). Available online at: <https://coronavirus.jhu.edu/map.html> (accessed February 10, 2021).
- Department of Precision Medicine. COVID-19 Risk. Department of Precision Medicine (2020). Available online at: <https://covid19risk.ai/> (accessed November 18, 2020).
- Tuite AR, Fisman DN, Greer AL. Mathematical modelling of COVID-19 transmission and mitigation strategies in the population of Ontario, Canada. *CMAJ Open*. (2020) 192:E497–505. doi: 10.1503/cmaj.200476
- Rodriguez-Nava G, Trelles-Garcia DP, Yanez-Bello MA, Chung CW, Chaudry S, Khan A, et al. Using machine learning for prediction of poor clinical outcomes in adult patients hospitalized with COVID-19. *Open Forum Infect Dis*. (2020) 7:S162–3. doi: 10.1093/ofid/ofaa439.371
- Jimenez-Solem E, Petersen TS, Hansen C, Hansen C, Lioma C, Igel C, et al. Developing and validating COVID-19 adverse outcome risk prediction models from a bi-national European cohort of 5594 patients. *Sci Rep*. (2021) 11:1–12. doi: 10.1038/s41598-021-81844-x
- Schöning V, Liakoni E, Baumgartner K, Exadaktylos AK, Hautz WE, Atkinson A, et al. Development and validation of a prognostic COVID-19 severity assessment (COSA) score and machine learning models for patient triage at a tertiary hospital. *J Transl Med*. (2021) 19:1–11. doi: 10.1186/s12967-021-02720-w
- Kim DW, Byeon KH, Kim J, Cho KD, Lee N. The correlation of comorbidities on the mortality in patients with COVID-19: an observational study based on the Korean National Health Insurance Big Data. *J Korean Med Sci*. (2020) 35:e243. doi: 10.3346/jkms.2020.35.e243
- Williamson EJ, Walker AJ, Bhaskaran K, Bacon S, Bates C, Morton CE, et al. Factors associated with COVID-19-related death using OpenSAFELY. *Nature*. (2020) 584:430–36. doi: 10.1038/s41586-020-2521-4
- Zheng Y, Zhu Y, Ji M, Wang R, Liu X, Zhang M, et al. A learning-based model to evaluate hospitalization priority in COVID-19 pandemics. *Patterns*. (2020) 1:100092. doi: 10.1016/j.patter.2020.100173
- Roimi M, Gutman R, Somer J, Arie AB, Calman I, Bar-Lavie Y, et al. Development and validation of a machine learning model predicting illness trajectory and hospital utilization of COVID-19 patients—a nationwide study. *JAMIA Open*. (2021) ocab005. doi: 10.1093/jamia/ocab005
- Estiri H, Strasser ZH, Klann JG, Naseri P, Waghlikar KB, Murphy SN. Predicting COVID-19 mortality with electronic medical records. *NPJ Digit Med*. (2021) 4:15. doi: 10.1038/s41746-021-00383-x
- ClosedLoop. *C-19 Index*. (2020). Available online at: <https://closedloop.ai/c19index/> (accessed November 18, 2020)
- Zhu J, Shen B, Abbasi A, Hoshmand-Kochi M, Li H, Duong TQ. Deep transfer learning artificial intelligence accurately stages COVID-19 lung disease severity on portable chest radiographs. *PLoS ONE*. (2020) 15:e0236621. doi: 10.1371/journal.pone.0236621
- Elgendi M, Nasir MU, Tang Q, Fletcher RR, Howard N, Menon C, et al. The performance of deep neural networks in differentiating chest x-Rays of COVID-19 patients from other bacterial and viral pneumonias. *Front Med*. (2020) 7:550. doi: 10.3389/fmed.2020.00550
- Mehta M, Julaiti J, Griffin P, Kumara S. Early stage machine learning–based prediction of US county vulnerability to the COVID-19 pandemic: machine learning approach. *JMIR Public Health Surveill*. (2020) 6:e19446. doi: 10.2196/19446
- John Hopkins University & Medicine. *COVID-19 United States Cases by County*. John Hopkins University & Medicine (2020). Available online at: <https://coronavirus.jhu.edu/us-map> (accessed November 17, 2020).
- Venables W Riple B. *Modern Applied Statistics with S*. 4th ed. New York, NY: Springer (2002).
- Wiens J, Shenoy ES. Machine learning for healthcare: on the verge of a major shift in healthcare epidemiology. *Clin Infect Dis*. (2018) 66:149–53. doi: 10.1093/cid/cix731
- Chen T, He T, Benesty M, Khotilovich V, Tang Y, Cho H, et al. *xgboost: Extreme gradient boosting Version 1.0.0.2*. (2021). Available online at: <https://CRAN.R-project.org/package=xgboost> (accessed January 26, 2021).
- R Core Team. *R: A Language and Environment for Statistical Computing*. Vienna: R Core Team (2018).
- Liu Y, Just A. *SHAPforxgboost: SHAP Plots for 'XGBoost'*. R Package Version 0.1.0. (2020). Available online at: <https://github.com/liuyanguu/SHAPforxgboost/> (accessed January 26, 2021)
- Greshko M. These promising coronavirus treatments are saving lives. *Natl Geogr Res*. (2020). Available online at: <https://www.nationalgeographic.com/science/article/these-promising-coronavirus-treatments-are-saving-lives-cvdNatl> (accessed April 28, 2021).
- Robinson J. Everything you need to know about the COVID-19 therapy trials. *Pharm J*. (2021). Available online at: <https://pharmaceutical-journal.com/article/feature/everything-you-need-to-know-about-the-covid-19-therapy-trials> (accessed April 28, 2021).
- Treatments and Vaccines for COVID-19*. European Medicines Agency (2020). <https://www.ema.europa.eu/en/human-regulatory/overview/public-health-threats/coronavirus-disease-covid-19/treatments-vaccines-covid-19> (accessed April 28, 2021).

**Conflict of Interest:** JY is employed by the company Adastra Corporation however Adastra has no financial or other conflicts of interest in this work.

The remaining authors declare that the research was conducted in the absence of any commercial or financial relationships that could be construed as a potential conflict of interest.

**Publisher's Note:** All claims expressed in this article are solely those of the authors and do not necessarily represent those of their affiliated organizations, or those of the publisher, the editors and the reviewers. Any product that may be evaluated in this article, or claim that may be made by its manufacturer, is not guaranteed or endorsed by the publisher.

Copyright © 2021 Snider, McBean, Yawney, Gadsden and Patel. This is an open-access article distributed under the terms of the Creative Commons Attribution License (CC BY). The use, distribution or reproduction in other forums is permitted, provided the original author(s) and the copyright owner(s) are credited and that the original publication in this journal is cited, in accordance with accepted academic practice. No use, distribution or reproduction is permitted which does not comply with these terms.



# Corrigendum: Identification of Variable Importance for Predictions of Mortality From COVID-19 Using AI Models for Ontario, Canada

Brett Snider<sup>1\*</sup>, Edward A. McBean<sup>1</sup>, John Yawney<sup>2</sup>, S. Andrew Gadsden<sup>1</sup> and Bhumi Patel<sup>1</sup>

<sup>1</sup> School of Engineering, University of Guelph, Guelph, ON, Canada, <sup>2</sup> Adastra Corporation, Toronto, ON, Canada

**Keywords:** artificial intelligence, XGBoost, SHapley, COVID-19, mortality

## A Corrigendum on

### Identification of Variable Importance for Predictions of Mortality From COVID-19 Using AI Models for Ontario, Canada

by Snider, B., McBean, E. A., Yawney, J., Gadsden, S. A., and Patel, B. (2021). *Front. Public Health* 9:675766. doi: 10.3389/fpubh.2021.675766

## OPEN ACCESS

### Approved by:

Frontiers Editorial Office,  
Frontiers Media SA, Switzerland

### \*Correspondence:

Brett Snider  
bsnide01@uoguelph.ca

### Specialty section:

This article was submitted to  
Infectious Diseases—Surveillance,  
Prevention and Treatment,  
a section of the journal  
Frontiers in Public Health

**Received:** 15 August 2021

**Accepted:** 16 August 2021

**Published:** 23 September 2021

### Citation:

Snider B, McBean EA, Yawney J,  
Gadsden SA and Patel B (2021)  
Corrigendum: Identification of Variable  
Importance for Predictions of Mortality  
From COVID-19 Using AI Models for  
Ontario, Canada.  
*Front. Public Health* 9:759014.  
doi: 10.3389/fpubh.2021.759014

In the original article, there was an error in the **Acknowledgments**, the dataset we analyzed requires very specific language regarding **Acknowledgments**.

The original statement read: “The authors gratefully acknowledge support from the Ontario Ministry of Health, Canada who supplied critical medical data for this study as well as the assistance of Ontario Health Data Platform for handling the security protocols pertinent to protecting the privacy of the data.”

However, it should read:

“This study was supported by ICES, which is funded by an annual grant from the Ontario Ministry of Health (MOH) and the Ministry of Long-Term Care (MLTC). This study was supported by the Ontario Health Data Platform (OHDP), a Province of Ontario initiative to support Ontario’s ongoing response to COVID-19 and its related impacts. The analyses, opinions, results, and conclusions reported in this paper are those of the authors and are independent from the funding sources. No endorsement by ICES, the OHDP, its partners, or the Province of Ontario is intended or should be inferred. Parts of this material are based on data and/or information compiled and provided by CIHI. However, the analyses, conclusions, opinions, and statements expressed in the material are those of the author(s), and not necessarily those of CIHI.

These datasets were linked using unique encoded identifiers and analyzed at ICES.

REB: The use of the data in this project is authorized under section 45 of Ontario’s Personal Health Information Protection Act (PHIPA) and does not require review by a Research Ethics Board.

Access to datasets: The dataset from this study is held securely in coded form at ICES. While legal data sharing agreements between ICES and data providers (e.g., healthcare organizations and government) prohibit ICES from making the dataset publicly available, access may be granted to those who meet pre-specified criteria for confidential access, available at [www.ices.on.ca/DAS](http://www.ices.on.ca/DAS) (email: [das@ices.on.ca](mailto:das@ices.on.ca)). The full dataset creation plan and underlying analytic code are available from the authors upon request, understanding that the computer programs may rely upon coding

templates or macros that are unique to ICES and are therefore either inaccessible or may require modification.

OCR: Parts of this material are based on data and information provided by Cancer Care Ontario (CCO). The opinions, results, view, and conclusions reported in this paper are those of the authors and do not necessarily reflect those of CCO. No endorsement by CCO is intended or should be inferred.

ODB: We thank IQVIA Solutions Canada Inc. for use of their Drug Information Database.

Ontario Community Health Profiles Partnership (OCHPP): OCHPP created Ontario Marginalization Index (ON-Marg) which is a source for this paper as ON-Marg is used to understand inequalities in health and other social problems related to health among either population groups or geographic areas across Ontario.

Statistics Canada: Postal Code Conversion File and census data were adapted from Statistics Canada. This

does not constitute an endorsement by Statistics Canada of this product.”

The authors apologize for this error and state that this does not change the scientific conclusions of the article in any way. The original article has been updated.

**Publisher's Note:** All claims expressed in this article are solely those of the authors and do not necessarily represent those of their affiliated organizations, or those of the publisher, the editors and the reviewers. Any product that may be evaluated in this article, or claim that may be made by its manufacturer, is not guaranteed or endorsed by the publisher.

*Copyright © 2021 Snider, McBean, Yawney, Gadsden and Patel. This is an open-access article distributed under the terms of the Creative Commons Attribution License (CC BY). The use, distribution or reproduction in other forums is permitted, provided the original author(s) and the copyright owner(s) are credited and that the original publication in this journal is cited, in accordance with accepted academic practice. No use, distribution or reproduction is permitted which does not comply with these terms.*





# Sero-Prevalence and Sero-Incidence of Antibodies to SARS-CoV-2 in Health Care Workers in Israel, Prior to Mass COVID-19 Vaccination

Khitam Muhsen<sup>1\*</sup>, Mitchell J. Schwaber<sup>2,3</sup>, Jihad Bishara<sup>3,4</sup>, Elias Kassem<sup>5</sup>, Alaa Atamna<sup>3,4</sup>, Wasef Na'amni<sup>1</sup>, Sophy Goren<sup>1</sup>, Anya Bialik<sup>1</sup>, Jameel Mohsen<sup>6</sup>, Yona Zaide<sup>7</sup>, Nimrod Hazan<sup>7</sup>, Ortal Ariel-Cohen<sup>1</sup>, Regev Cohen<sup>8</sup>, Pnina Shitrit<sup>3,9</sup>, Dror Marchaim<sup>3,10</sup>, Shmuel Benenson<sup>11</sup>, Debby Ben-David<sup>3,12</sup>, Bina Rubinovitch<sup>13</sup>, Tamar Gotessman<sup>14</sup>, Amir Nutman<sup>2,3</sup>, Yonit Wiener-Well<sup>15</sup>, Yasmin Maor<sup>3,12,16</sup>, Yehuda Carmeli<sup>2,3</sup> and Dani Cohen<sup>1</sup>

## OPEN ACCESS

### Edited by:

Reza Lashgari,  
Institute for Research in Fundamental  
Sciences, Iran

### Reviewed by:

Elizabeth Miller,  
University of London, United Kingdom  
Jonathan Zenilman,  
Johns Hopkins University,  
United States

### \*Correspondence:

Khitam Muhsen  
kmuhsen@tauex.tau.ac.il

### Specialty section:

This article was submitted to  
Infectious Diseases - Surveillance,  
Prevention and Treatment,  
a section of the journal  
Frontiers in Medicine

Received: 01 April 2021

Accepted: 13 May 2021

Published: 24 June 2021

### Citation:

Muhsen K, Schwaber MJ, Bishara J, Kassem E, Atamna A, Na'amni W, Goren S, Bialik A, Mohsen J, Zaide Y, Hazan N, Ariel-Cohen O, Cohen R, Shitrit P, Marchaim D, Benenson S, Ben-David D, Rubinovitch B, Gotessman T, Nutman A, Wiener-Well Y, Maor Y, Carmeli Y and Cohen D (2021) Sero-Prevalence and Sero-Incidence of Antibodies to SARS-CoV-2 in Health Care Workers in Israel, Prior to Mass COVID-19 Vaccination. *Front. Med.* 8:689994. doi: 10.3389/fmed.2021.689994

<sup>1</sup> Department of Epidemiology and Preventive Medicine, School of Public Health, Sackler Faculty of Medicine, Tel Aviv University, Tel Aviv, Israel, <sup>2</sup> National Institute for Antibiotic Resistance and Infection Control, Israel Ministry of Health, Tel Aviv, Israel, <sup>3</sup> Sackler Faculty of Medicine, Tel Aviv University, Tel Aviv, Israel, <sup>4</sup> Infectious Diseases Unit, Rabin Medical Centre, Beilinson Hospital, Petah-Tiqva, Israel, <sup>5</sup> Department of Pediatrics, Hillel Yaffe Medical Centre, Hadera, Israel, <sup>6</sup> Department of Cardiology, Hillel Yaffe Medical Centre, Hadera, Israel, <sup>7</sup> American Medical Laboratories, Herzliya, Israel, <sup>8</sup> Infection Control Unit, Sanz Medical Centre, Netanya, Israel, <sup>9</sup> Infection Control Unit, Meir Medical Centre, Kfar Saba, Israel, <sup>10</sup> Infection Control Unit, Shamir (Assaf Harofeh) Medical Centre, Be'er Ya'akov, Israel, <sup>11</sup> Department of Clinical Microbiology and Infectious Diseases, Hadassah Hebrew University Medical Centre, Jerusalem, Israel, <sup>12</sup> Infection Control Unit, Wolfson Medical Centre, Wolfson, Israel, <sup>13</sup> Infection Control Unit, Beilinson Hospital, Rabin Medical Centre, Petah-Tiqva, Israel, <sup>14</sup> Infectious Disease and Infection Control Service, Hasharon Hospital, Rabin Medical Centre, Petah-Tiqva, Israel, <sup>15</sup> Infectious Disease Unit, Shaare Zedek Medical Centre, Jerusalem, Israel, <sup>16</sup> Infectious Disease Unit, Wolfson Medical Centre, Wolfson, Israel

**Objectives:** This study aims to examine the prevalence and risk factors of severe acute respiratory syndrome coronavirus 2 (SARS-CoV-2) sero-positivity in health care workers (HCWs), a main risk group, and assess the sero-incidence of SARS-CoV-2 infection between the first and second waves of coronavirus disease 2019 (COVID-19) in Israel.

**Methods:** A longitudinal study was conducted among 874 HCWs from nine hospitals. Demographics, health information, and blood samples were obtained at baseline (first wave—April–May 2020) and at follow-up ( $n = 373$ ) (second wave—September–November 2020). Sero-positivity was determined based on the detection of total antibodies to the nucleocapsid antigen of SARS-CoV-2, using electro-chemiluminescence immunoassay (Elecys® Anti-SARS-CoV-2, Roche Diagnostics, Rotkreuz, Switzerland).

**Results:** The sero-prevalence of SARS-CoV-2 antibodies was 1.1% [95% confidence intervals (CI) 0.6–2.1] at baseline and 8.3% (95% CI 5.9–11.6) at follow-up. The sero-conversion of SARS-CoV-2 serum antibody was 6.9% (95% CI 4.7–9.9) during the study period. The increase in SARS-CoV-2 sero-prevalence paralleled the rise in PCR-confirmed SARS-CoV-2 infections among the HCWs across the country. The likelihood of SARS-CoV-2 sero-prevalence was higher in males vs. females [odds ratio (OR) 2.52 (95% CI 1.05–6.06)] and in nurses vs. physicians [OR 4.26 (95% CI 1.08–16.77)] and

was associated with being quarantined due to exposure to COVID-19 patients [OR 3.54 (95% CI 1.58–7.89)] and having a positive PCR result [OR 109.5 (95% CI 23.88–502.12)].

**Conclusions:** A significant increase in the risk of SARS-CoV-2 infection was found among HCWs between the first and second waves of COVID-19 in Israel. Nonetheless, the sero-prevalence of SARS-CoV-2 antibodies remains low, similar to the general population. Our findings reinforce the rigorous infection control policy, including quarantine, and utilization of personal protective equipment that should be continued together with COVID-19 immunization in HCWs and the general population.

**Keywords:** health care workers, sero-epidemiology, SARS-CoV-2, nucleocapsid antigen, risk factors, longitudinal study, occupational risk

## INTRODUCTION

The coronavirus disease 2019 (COVID-19) pandemic, caused by severe acute respiratory syndrome coronavirus 2 (SARS-CoV-2) (1), poses a huge health and societal burden globally. SARS-CoV-2 is easily transmitted from person to person (2) via droplets from the respiratory tract of infected people, including asymptomatic individuals (2, 3). COVID-19 may be severe and result in death, particularly among the elderly and persons with chronic diseases (4–6).

Health care workers (HCWs) comprise a main occupational risk group for SARS-CoV-2 infection (6, 7). Accordingly, special attention should be given to this group to maintain functional healthcare systems, including preventive measures, ensuring the availability of personal protective equipment, assessment of exposure, and prioritization in vaccination with COVID-19 vaccines. A survey conducted toward the end of the first COVID-19 wave (April–May 2020) in Israel showed a low prevalence (0.2%) of asymptomatic SARS-CoV-2 infection among HCWs (8) as confirmed by PCR. A second wave of COVID-19 occurred in Israel with a peak in mid-September 2020; this resulted in a second lockdown during September–October 2020. A third wave of COVID-19 during December 2020–January 2021 resulted in a third lockdown, coinciding with a mass vaccination campaign targeting the adult population and HCWs, using the BNT162b2 mRNA COVID-19 vaccine (9, 10).

Sero-epidemiological studies can provide a more sensitive tool for the assessment of exposure to SARS-CoV-2 than molecular assays that identify only current infection. Sero-epidemiological studies in HCWs have shown variable seropositivity for SARS-CoV-2 serum antibodies, with low estimates between 1.3 and 4.0% in Greece, Germany, and Denmark (11–13) and higher estimates ranging from 10 to 31.6% in the United Kingdom, Spain, Sweden, and some regions in the United States (14–16). Within-country variation in SARS-CoV-2 antibody sero-prevalence among HCWs was also reported (16). For example, a multicenter study in the United States showed point estimates ranging from 0.8 to 31.6% (16), with generally higher sero-prevalence found in HCWs from communities with higher incidence rates of COVID-19 (16). Most studies on the prevalence of SARS-CoV-2 antibodies in HCWs were cross-sectional and typically captured the initial

months of COVID-19 surge (11, 13). Moreover, evidence on the risk factors for SARS-CoV-2 sero-prevalence among HCWs remains elusive and conflicting (11, 12, 15). For example, some studies showed higher SARS-CoV-2 antibody sero-positivity in HCWs of hospitals or departments designated for the treatment of COVID-19 patients compared to HCWs who worked in non-COVID-19 hospitals/departments (12, 13). Other studies, however, found no significant differences in SARS-CoV-2 serum antibodies between HCWs of COVID-19 units, or those who were involved in COVID-19 treatment, than those who were not (11, 15). Another conflicting issue is whether the risk of SARS-CoV-2 differs according to profession of HCWs (e.g., nurses, physicians, and technicians) (15–17). Such evidence is highly important for the enhancement of preventive measures to mitigate COVID-19 risk among HCWs. Accordingly, the aim of the current study was to examine the prevalence of and risk factors for SARS-CoV-2 sero-positivity in HCWs and to assess the sero-incidence between the first and second waves of COVID-19 in Israel. We also described the incidence of PCR-confirmed SARS-CoV-2 infection in HCWs in Israel.

## MATERIALS AND METHODS

### Study Design and Population

Baseline sero-epidemiological studies were undertaken during April–May 2020 (the end of the first wave of COVID-19 in Israel) among HCWs [physicians, nurses, and others (technicians and administrative staff)], employees of nine general medical centers in Israel: Shamir (Assaf Harofe), Beilinson, HaSharon, Meir, Wolfson, Hadassah Ein Kerem, Sha'arei Zedek, Laniado, and Hillel Yaffe medical centers. Demographic and health information were collected using self-administered questionnaire, and a blood sample was obtained. A follow-up assessment was performed in a sub-sample of the participants, employees of five out of the nine medical centers, during September–November 2020 (the second COVID-19 wave).

Publicly available aggregated data on the number of HCWs, employees of hospitals, who had PCR-confirmed SARS-CoV-2 infection was obtained. This information is reported to the Ministry of Health by the general hospitals, public and private, in Israel.

## Study Variables

The main dependent variables are the prevalence of serum antibodies against SARS-CoV-2 at baseline and at the follow-up assessments, which provides a picture of change over time and cumulative infection burden. Sero-conversion (sero-incidence) was defined as positive serological results at the follow-up assessment among HCWs who tested negative at the baseline assessment, which measures the rate at which new infections occurred. Laboratory-confirmed COVID-19 was defined as a positive PCR test result for SARS-CoV-2 RNA, based on the participant's report.

The main independent variables were defined based on self-reports of the participants in the study questionnaire. The independent variables included the following: (i) demographics (age and sex); (ii) occupational characteristics [profession (physician, nurse, or other (e.g., administrative staff and nursing assistants)), years working in the profession, and working in a coronavirus department]; and (iii) types of COVID-19-related exposures, which were defined based on multiple questions. Participants were asked whether they were exposed to COVID-19 patients in the past 3 months and whether they were requested to be in quarantine due to exposure to COVID-19 patients in the past 3 months. The rationale to ask about these two levels of exposure was that HCWs were given an exemption from quarantine if the exposure to a COVID-19 patient occurred while adequately using personal protective equipment (i.e., while being at work in the hospital). Exposures of HCWs to COVID-19 patients might occur outside work, while being at work, but not adequately using personal protective equipment, or unprotected exposure to infected co-workers (e.g., during breaks); under these circumstances, HCWs were asked to be in quarantine. Information was also obtained on quarantine of family members due to exposure to COVID-19 patient in the past 3 months. Participants were also asked whether they performed PCR test for the detection SARS-CoV-2 and for the results of the test.

Information was also obtained on clinical symptoms of COVID-19 among HCWs.

## Laboratory Methods

Blood specimens were collected and transferred in cooled conditions immediately after collection to the study laboratory at Tel Aviv University. The samples were centrifuged and aliquots of the serum were frozen at  $-80^{\circ}\text{C}$  until testing. At baseline assessment, the levels of serum immunoglobulin G (IgG) antibody against the spike (S) protein of SARS-CoV-2 were measured by an enzyme-linked immunosorbent assay (ELISA), using a validated commercial kit (EUROIMMUN AG, Luebeck, Germany), according to the manufacturer's instructions. The reported sensitivity of this assay ranged between 93.8 and 100%, 2–3 weeks after symptom onset, and its specificity ranged between 95.6 and 99.3% (18–20). All specimens with positive and borderline results and a randomly selected subset with negative results (total 69 samples) were retested using an electrochemiluminescence immunoassay (ECLIA) (Elecsys® Anti-SARS-CoV-2, Roche Diagnostics, Rotkreuz, Switzerland) for the detection of total antibodies (including IgG) to SARS-CoV-2 nucleocapsid (N) antigen. The tests were run

on the Cobas 6000 e601 analyzer in collaboration with American Medical Laboratories, Herzliya, Israel. The sensitivity and specificity of the assay were reported at 89 and 100% (21), respectively. Sero-positive participants at baseline were classified based on positive results in both the Roche and EUROIMMUN kits; otherwise, participants were classified as sero-negative. This strategy was used to lower the potential of false positive results. At follow-up, only the Elecsys® Roche kit was used, and samples were classified as positive or negative using this kit. The laboratory tests were performed in a blinded manner to the background characteristics of the participants.

## Statistical Methods

Characteristics of participants were described using means and standard deviations (SD) for continuous variables and counts and percentages for categorical variables. Both at baseline and follow-up, the proportion [and 95% confidence intervals (CI)] of participants with SARS-CoV-2 serum antibodies (sero-prevalence) was calculated as the number of participants with positive results out of all tested participants. The sero-incidence rate was calculated as the proportion of participants who tested positive for SARS-CoV-2 serum antibodies, among participants who tested sero-negative at baseline.

Differences between participants with and without SARS-CoV-2 serum antibodies in demographic and occupational characteristics and possible exposures to the SARS-CoV-2 were examined using the chi-square test for categorical variables and Student's *t*-test for continuous variables. For each independent variable, odds ratio (OR) and 95% CI were calculated using logistic regression models. Adjusted associations were obtained by multivariable logistic regression models. The selection of independent variables to be included in the multivariable models was based on prior evidence of possible association between the variable and the risk of SARS-CoV-2 infection and our hypotheses of possible association between variables of interest and SARS-CoV-2 antibody sero-positivity (e.g., sex, profession, and being in quarantine due to exposure to a confirmed COVID-19 patient). Variables associated with SARS-CoV-2 sero-prevalence with  $P < 0.2$  in the bivariate analysis were assessed in the multivariable models. In case of highly correlated variables, only one was included in the model. For example, since the variables “ever worked in a coronavirus department” and “working in a coronavirus department in the last 3 months” were highly correlated (phi correlation coefficient 0.82,  $P < 0.001$ ), we assessed only one of these variables in the multivariable models. Since our sample of sero-positive individuals was modest, our aim was to include four–five variables in the multivariable model (22). Since it is expected that HCWs who had a positive PCR test results will be most likely sero-positive for SARS-CoV-2 antibodies, we conducted two models, one with and one without the variable “positive SARS-Cov-2 PCR test results.” This approach was followed to enable the identification of risk factors for SARS-CoV-2 transmission among HWCs.

$P < 0.05$  was considered statistically significant. Data were analyzed using SPSS version 27 (Armonk, NY: IBM Corp).

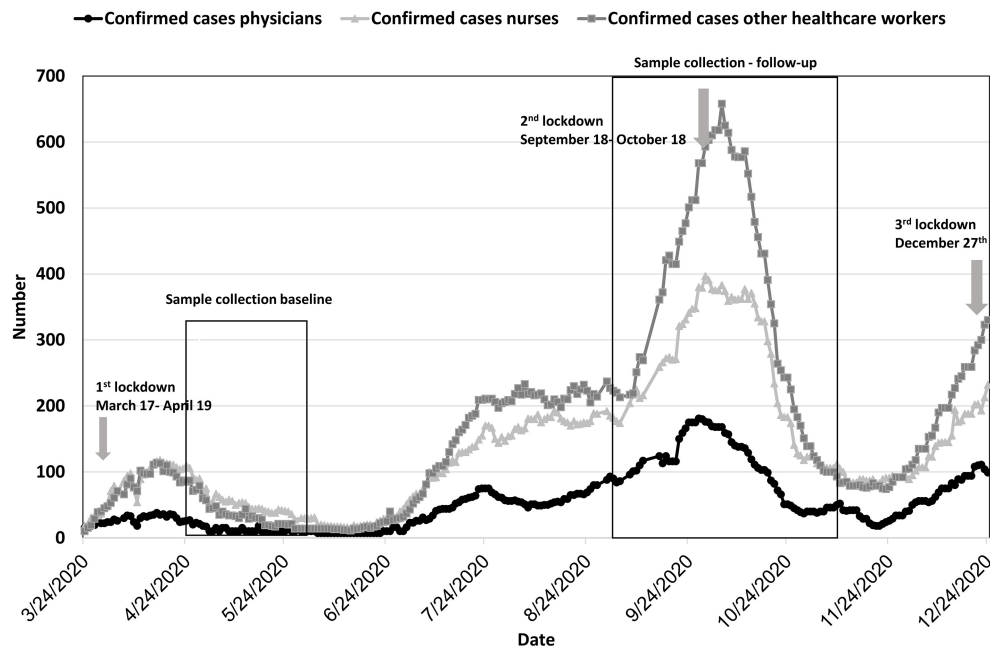


**FIGURE 1 |** PCR-confirmed cases of SARS-CoV-2 in health care workers in general hospitals in Israel ( $N = 95,405$ ). Black line—physicians; light gray line with triangles—nurses; dark gray line with squares—other.

## RESULTS

### Incidence of SARS-CoV-2 Infection in HCWs

The daily number of HCW employees of all general hospitals who had PCR-confirmed SARS-CoV-2 infection is presented in **Figure 1**. There were two peaks of SARS-CoV2 infection in HCWs, the first in mid-April 2020 and the second in mid-September 2020. Since December 2020, an increase in the number of cases has been observed. The incidence in HCWs corresponded to the incidence of COVID-19 in the general population in Israel.

### Sero-Epidemiological Studies

The participants' mean age was 39.6 years (SD 11.0), and 37.5% of them were males. The demographic and professional characteristics of participants in the follow-up assessment were comparable to that of the entire cohort (**Table 1**).

At baseline, 48.9% of the participants reported ever having worked in a coronavirus department vs. 55.2% at the follow-up assessment. Exposure to a confirmed COVID-19 patient outside the hospital was reported in 23.6% of the baseline participants and in 59.2% at the follow-up assessment. Performing a SARS-CoV-2 PCR test increased between baseline and follow-up, as well as the proportion of those who tested positive (**Supplementary Table 1**).

At baseline, 10 out of 874 participants tested positive for SARS-CoV-2 antibodies by both Roche and EUROIMMUN assays, yielding a prevalence of 1.1% (95% CI 0.6–2.1). Only three of these sero-positive participants had PCR-confirmed

SARS-CoV-2 infection, one was asymptomatic and two had symptoms of fever, cough, fatigue, and sore throat.

At follow-up, 31 out of 372 HCW with usable samples tested positive for SARS-CoV-2 serum antibodies, yielding a seroprevalence of 8.3% (95% CI 5.9–11.6). Among 369 participants with paired sera, four tested positive at both assessments, and 25 sero-converted; thus, the sero-incidence was estimated at 25/365 [6.9% (95% CI 4.7–9.9)].

Among 27 sero-positive participants who were tested by PCR in the past, 21 (77.8%) reported a positive result and reported symptoms of fever ( $n = 7$ ), cough ( $n = 7$ ), fatigue ( $n = 9$ ), muscle pain ( $n = 9$ ), and loss of taste/smell ( $n = 8$ ).

### Factors Associated With the Prevalence of SARS-CoV-2 Serum Antibodies

A higher proportion of males was found in sero-positive than in sero-negative participants, as well as a higher proportion of nurses compared to physicians, but these differences were not statistically significant. The proportion of participants who reported ever working in a coronavirus department was higher in the sero-positive vs. sero-negative group ( $P = 0.056$ ). A similar but not statistically significant ( $P = 0.098$ ) trend was found for working in a coronavirus department in the past 3 month preceding the interview. No significant association was found between reports on exposure to a confirmed COVID-19 patient and SARS-CoV-2 sero-positivity ( $P = 0.166$ ). However, the proportion of those who had been quarantined due to exposure to a confirmed COVID-19 case was higher among sero-positive vs. sero-negative personnel ( $P < 0.001$ ). A similar result was found for having a family member who had been quarantined



**TABLE 1** | Characteristics of the participants at baseline and follow-up assessments.

|                                | Baseline April–May<br>2020 <i>N</i> (%) | Follow-up<br>September–<br>November 2020 <i>N</i><br>(%) |
|--------------------------------|---|--|
| <b>Total</b>                   | 874 (100.0%)                            | 373 (100.0%)   |
| <b>Medical center</b>          |   |  |
| Shamir (Assaf Harofe)          | 61 (7.0%)                               | –  |
| Bilenson                       | 166 (19.0%)                             | 108 (29.0%)  |
| HaSharon                       | 41 (4.7%)                               | –  |
| Hadassah Ein Kerem             | 66 (7.6%)                               | –  |
| Wolfson                        | 63 (7.2%)                               | 30 (8.0%)  |
| Laniado                        | 68 (7.8%)                               | 43 (11.5%)   |
| Meir                           | 66 (7.6%)                               | –  |
| Shaare Zedek                   | 121 (13.8%)                             | 83 (22.3%)   |
| Hillel Yaffe                   | 222 (25.4%)                             | 109 (29.2%)  |
| <b>Sex</b>                     |   |  |
| Males                          | 328 (37.5%)                             | 130 (34.9%)  |
| Females                        | 546 (62.5%)                             | 243 (65.1%)  |
| <b>Mean age (SD), years</b>    | 39.6 (11.0)                             | 40.9 (11.3)  |
| Missing                        | 12 (1.3%)                               | 5 (1.3%)   |
| <b>Profession</b>              |   |  |
| Physician                      | 341 (39.0%)                             | 149 (39.9%)  |
| Nurse                          | 334 (38.2%)                             | 128 (34.3%)  |
| Other                          | 188 (21.5%)                             | 93 (24.9%)   |
| Missing                        | 11 (1.3%)                               | 3 (0.8%)   |
| <b>Years in the profession</b> |   |  |
| 0–3 years                      | 253 (28.9%)                             | 94 (25.2%)   |
| 4–10 years                     | 196 (22.4%)                             | 77 (20.6%)   |
| > 10 years                     | 363 (41.5%)                             | 180 (48.3%)  |
| Missing                        | 62 (7.1%)                               | 22 (5.9%)  |

SD, standard deviation.

due to exposure to a confirmed COVID-19 patient ( $P = 0.003$ ). Having a positive PCR result for the detection of SARS-CoV-2 was more common in the sero-positive vs. the sero-negative group ( $P < 0.001$ ) (Table 2).

A multivariable model showed that males had higher odds to be sero-positive than females. Being asked to be in quarantine due to exposure to a confirmed COVID-19 patient was related to increased likelihood for SARS-CoV-2 sero-prevalence. A trend of a positive but non-statistically significant association was found between reporting a quarantine of a family member and SARS-CoV-2 antibody sero-positivity ( $P = 0.069$ ). These models also showed that nurses were more likely than physicians to be sero-positive for SARS-CoV-2 antibodies ( $P = 0.076$ ). The Nagelkerke  $R$  square (pseudo  $R$  square measure) for this model was 0.147.

Another model that included the same variables, in addition to SARS-CoV-2 PCR test result, showed a strong association between having a positive PCR result and SARS-CoV-2 sero-prevalence, and nurses had 4.26 higher odds to be sero-positive

than physicians ( $P = 0.038$ ). The Nagelkerke  $R$  square for this model was 0.555 (Table 3).

## DISCUSSION

We showed a substantial increase in the risk of SARS-CoV-2 infection among HCWs between the first and second waves of COVID-19 in Israel. This was reflected in a 7-fold increase in the prevalence of SARS-CoV-2 serum antibodies between baseline and follow-up, from 1.1 to 8.3% during a 4–7 month period.

The estimated 1.1% prevalence of SARS-CoV-2 serum antibodies during the first wave of the epidemic is comparable to the reported estimates in HCWs in Germany, Greece, and Saudi Arabia (11, 12, 23). A massive increase in COVID-19 incidence occurred in Israel in parallel to the lifting of the first lockdown and especially with family vacations with crowding and the schools re-opening in September 2020. This change in the incidence in COVID-19 in the general population also affected HCWs, as shown in our study. These findings are particularly alarming, illustrating the risk of SARS-CoV-2 infection in vital workforces in times they are needed most, as during a second morbidity surge. This noteworthy finding reinforces the need to continually strengthen infection control and preventive measures among HCWs.

Despite the substantial increase in the prevalence of SARS-CoV-2 antibodies among HCWs in the second wave, the sero-prevalence remained relatively low (8.3%), being similar to a weighted sero-prevalence of 5.5% reported in a large sample of the general population during June–September (24). Our estimate is lower than the reported estimates of SARS-CoV-2 sero-prevalence in HCWs in the United Kingdom (14, 17), New York City (25), Spain (15), and Sweden (26, 27). Some of this dissimilarity might be the result of variation in study design and population, serological assays used in the study, and the circulation of SARS-CoV-2 in the community. Importantly, adherence to stringent infection control measures and high availability and utilization of personal protective equipment in medical facilities, as it is the case in Israel, seem to be critical in reducing the risk of SARS-CoV-2 infection in HCWs (11, 16). The increased incidence of seroconversion even with personal protective equipment might suggest that some of the new infections might have been acquired outside work. This also points to the need for continued vigilance and continuous quality management focusing on protection induced by adequate use of personal protective equipment to prevent transmission of the virus during patient–worker encounters.

We identified several risk factors for SARS-CoV-2 sero-prevalence. Interestingly, nurses compared to physicians were more likely to be sero-positive for SARS-CoV-2 antibodies. Common with our finding, others reported that nurses and nursing assistants were at increased risk for SARS-CoV-2 compared with physicians and other health professionals (27, 28). Under equitable and universal access to personal protective equipment, we assume that the increased risk for SARS-CoV-2 infection in nurses vs. physicians might be attributed to

**TABLE 2 |** Factors associated with the prevalence of SARS-CoV-2 serum antibodies at follow-up.

|  | Positive for<br>SARS-CoV-2<br>antibodies ( <i>n</i> = 31) | Negative for<br>SARS-CoV-2<br>antibodies ( <i>n</i> = 341) | <i>P</i> -value <sup>a</sup> | Unadjusted OR<br>(95% CI) <sup>b</sup> | <i>P</i> -value <sup>b</sup> |
|--|---|--|------------------------------|--|------------------------------|
| <b>Sex</b>   |   |  | 0.101                        |  | 0.105                        |
| Males  | 15 (48.4%)  | 115 (33.7%)  |                              | 1.84 (0.88–3.86)                       |                              |
| Females  | 16 (51.6%)  | 226 (66.3%)  |                              | Reference                              |                              |
| <b>Mean age (SD), years</b>  | 40.7 (12.0)   | 40.9 (11.2)  | 0.900                        | 0.99 (0.97–1.03)                       | 0.893                        |
| <b>Profession</b>  |   |  | 0.246                        |  | 0.100                        |
| Physician  | 10 (32.3%)  | 139 (41.1%)  |                              | Reference                              |                              |
| Nurse  | 15 (48.4%)  | 113 (33.4%)  |                              | 1.88 (0.81–4.33)                       | 0.141                        |
| Other  | 6 (19.4%)   | 86 (25.4%)   |                              | 0.98 (0.35–2.81)                       | 0.982                        |
| <b>Years in the profession</b>   |   |  | 0.561                        |  | 0.553                        |
| 0–3 years  | 10 (32.3%)  | 84 (26.3%)   |                              | Reference                              |                              |
| 4–10 years   | 8 (25.8%)   | 69 (21.6%)   |                              | 0.95 (0.35–2.54)                       | 0.920                        |
| > 10 years   | 13 (41.9%)  | 166 (52.0%)  |                              | 0.64 (0.27–1.53)                       | 0.316                        |
| <b>Ever worked in a coronavirus department</b>                                     |   |  | 0.056                        |  | 0.061                        |
| Yes  | 22 (73.3%)  | 184 (55.3%)  |                              | 2.23 (0.96–5.14)                       |                              |
| No   | 8 (26.7%)   | 149 (44.7%)  |                              | Reference                              |                              |
| <b>Worked in a coronavirus department in the past 3 months</b>                     |   |  | 0.098                        |  | 0.102                        |
| Yes  | 19 (63.3%)  | 170 (52.5%)  |                              | 1.91 (0.88–4.13)                       |                              |
| No   | 11 (36.7%)  | 154 (47.5%)  |                              | Reference                              |                              |
| <b>Exposure to a confirmed COVID-19 patient in the past 3 months</b>               |   |  | 0.166                        |  | 0.171                        |
| Yes  | 22 (73.3%)  | 199 (60.5%)  |                              | 1.79 (0.78–4.16)                       |                              |
| No   | 8 (26.7%)   | 130 (39.5%)  |                              | Reference                              |                              |
| <b>Requested to be quarantined due to exposure to a confirmed COVID-19 patient</b> |   |  | <0.001                       |  | <0.001                       |
| Yes  | 16 (53.3%)  | 75 (22.7%)   |                              | 3.90 (1.82–8.60)                       |                              |
| No   | 14 (46.7%)  | 256 (77.3%)  |                              | Reference                              |                              |
| <b>A quarantined family member due to exposure to a COVID-19 patient</b>           |   |  | 0.003                        |  | 0.004                        |
| Yes  | 16 (51.6%)  | 87 (26.3%)   |                              | 2.99 (1.42–6.31)                       |                              |
| No   | 15 (48.4%)  | 244 (73.7%)  |                              | Reference                              |                              |
| <b>SARS-CoV-2 test by PCR</b>  |   |  | 0.057                        |  | 0.067                        |
| Yes  | 27 (87.1%)  | 237 (71.2%)  |                              | 2.73 (0.93–8.02)                       |                              |
| No   | 4 (12.9%)   | 96 (28.8%)   |                              | Reference                              |                              |
| <b>Result of SARS-CoV-2 PCR test</b>   |   |  | <0.001                       |  | <0.001                       |
| Positive   | 16 (61.5%)  | 4 (1.7%)   |                              | 93.2<br>(26.29–330.33)                 |                              |
| Negative   | 10 (38.5%)  | 233 (98.3%)  |                              | Reference                              |                              |

<sup>a</sup>*P*-value was obtained by the chi-square test; <sup>b</sup>*P*-value was obtained by bivariate logistic regression; OR, odds ratio; CI, confidence intervals. Some participants did not answer all questions, therefore totals might differ (**Supplementary Table 2**).

occupational characteristics, such as prolonged direct contact between nurses and patients, while such direct encounters between physicians and patients might be less frequent. A policy implemented during periods of increased volume of COVID-19 patients in hospitals is expanding the nurses' shifts up to 12 h, which might decrease the risk of exposure in the community and potential for cross-infection between HCWs. Hence, it is essential to assess the influence of such a policy on SARS-CoV-2 risk in HCWs. Collectively, our and others' findings (11, 15,

27, 28) reveal a differential risk for SARS-CoV-2 infection in various health professions, which should dictate locally tailored interventions to mitigate the risk of SARS-CoV-2 infection.

It has been shown that exposure to COVID-19 patients increases the risk for SARS-CoV-2 infection (27), especially if the contact occurred without using personal protective equipment (11, 16). In Israel, HCWs exposed to COVID-19 patients while using adequate personal equipment are exempted from quarantine, based on the protection afforded by use of

**TABLE 3 |** Multivariable logistic regression model of factors associated with the prevalence of SARS-CoV-2 serum antibodies at follow-up.

|  | Model 1 <sup>a</sup> | P-value | Model 2 <sup>b</sup> | P-value |
|--|----------------------|---------|----------------------|---------|
|  | Adjusted OR (95% CI) |         | Adjusted OR (95% CI) |         |
| <b>Sex</b>   |                      |         |                      |         |
| Males  | 2.52 (1.05–6.06)     | 0.039   | 4.77 (1.26–18.05)    | 0.021   |
| Females  | Reference            |         |                      |         |
| <b>Profession</b>  |                      | 0.164   |                      | 0.087   |
| Physician  | Reference            |         | Reference            |         |
| Nurse  | 2.38 (0.92–6.17)     | 0.076   | 4.26 (1.08–16.77)    | 0.038   |
| Other  | 1.24 (0.37–4.16)     | 0.730   | 1.34 (0.22–7.99)     | 0.751   |
| <b>Requested to be quarantined due to exposure to a confirmed COVID-19 patient</b> |                      |         |                      |         |
| Yes  | 3.54 (1.58–7.89)     | 0.002   | 1.97 (0.59–6.59)     | 0.259   |
| No   | Reference            |         | Reference            |         |
| <b>A quarantined family member due to exposure to a COVID-19 patient</b>           |                      |         |                      |         |
| Yes  | 2.09 (0.94–4.65)     | 0.069   | 2.17 (0.67–6.99)     | 0.196   |
| No   | Reference            |         |                      |         |
| <b>Result of SARS-CoV-2 PCR test</b>   |                      |         |                      | <0.001  |
| Positive   | Not included         |         | 109.5 (23.88–502.12) |         |
| Negative   |                      |         | Reference            |         |

<sup>a</sup>P value = 0.672 by the Hosmer & Lemeshow test. Model summary Nagelkerke R square = 0.147.

<sup>b</sup>P value = 0.553 by the Hosmer & Lemeshow test. Model summary Nagelkerke R square = 0.555. OR, odds ratio; CI, confidence intervals.

this equipment; otherwise, the workers are requested to be quarantined for 10–14 days. This means that if exposure to a confirmed COVID-19 patient occurred outside the hospital, or while being at work, but not using personal protective equipment, HCWs were thus requested to be in quarantine. Indeed, we found no significant difference between HCWs who reported that they were exposed to COVID-19 patients and those who were not in terms of risk of SARS-CoV-2 sero-prevalence, likely since such exposure occurred while adequately using personal protective equipment. An intriguing finding is that HCWs who were requested to be in quarantine due to exposure to COVID-19 patients had a significant 3.5-fold higher likelihood to be sero-positive compared to those who were not in quarantine. Quarantine of HCWs is usually implemented if there is a tangible concern for SARS-CoV-2 infection that might be due to exposure to COVID-19 patients under improper use of personal protective equipment, or exposures that occurred in the community, which increase the risk for SARS-CoV-2 infection. Hence, our findings reinforce the so-far implemented policy of prevention and control of SARS-CoV-2 infections in HCWs in Israel, including quarantine when needed.

SARS-CoV-2-PCR positivity was reported by 7.6% of the participants at the follow-up assessment, which is lower than the identified 8.3% sero-prevalence. This finding supports the addition of sero-monitoring tools in the risk assessment of SARS-CoV-2 in HCWs and in other populations at risk especially when PCR testing is not performed systematically. Not surprisingly, having a positive PCR result for SARS-CoV-2 was strongly associated with sero-prevalence of SARS-CoV-2 antibodies. Previous sero-epidemiological studies mostly lacked information on SARS-CoV-2 PCR results. Hence, this

finding supports previous reports on positive associations between the existence of prior symptoms consistent with COVID-19 and SARS-CoV-2 antibody sero-prevalence (13, 17, 25).

Our study has limitations. Mainly, we relied on a convenience sample of HCWs who were willing to take part in the study. We also focused on HCWs who work in hospitals that might not represent well HCWs in community clinics. Also, four of the nine hospitals elected not to participate in the follow-up assessment, and this resulted in a smaller sample size ( $N = 373$ ) at the follow-up compared to baseline ( $N = 874$ ). Nonetheless, the demographic and occupational profile of the participants at the follow-up assessment were similar to the baseline cohort, and we were able to identify several risk factors for SARS-CoV-2 antibody sero-positivity.

Our study has several strengths. First, the longitudinal design enabled the assessment of the change in sero-positivity between the first and second waves of COVID-19 in Israel. Second, it included HCWs from multiple centers, various regions, and tertiary and non-tertiary care hospitals. Third, it included HCWs who worked in dedicated coronavirus and non-coronavirus wards, as well as low-risk employees such as administrative staff. These elements increase the generalizability of our findings. Fourth, it provides a comprehensive assessment of potential exposures to SARS-CoV-2 infection that enabled the identification of risk factors with sufficient granularity to support policy-making. Fifth, in the classification of sero-positive individuals, we relied on a highly specific approach to reduce to the possibility of false positive findings.

In conclusion, in this longitudinal study of HCWs, we demonstrated a 7-fold increase in the sero-prevalence of

SARS-CoV-2 antibodies among HCWs between the first and second waves of COVID-19 in Israel, which paralleled a substantial rise in the number of PCR-confirmed SARS-CoV-2 infections among HCWs across the country and in the general population. Despite this increase, the cumulative exposure to SARS-CoV-2 among HCWs in Israel remains relatively low, which reinforces the current rigorous policy of infection control, proper utilization of personal protective equipment, and quarantine. Interventions to reduce the risk of SARS-CoV-2 in HCWs should prioritize nurses and focus on decreasing direct unprotected contact with SARS-CoV-2 patients that leads to exposure and a need for quarantine. These measures should be continued in parallel to the roll-out of COVID-19 vaccines in HCWs and the general population.

## DATA AVAILABILITY STATEMENT

The datasets presented in this article are not readily available because legal restrictions apply. Requests to access the datasets should be directed to kmuhsen@tauex.tau.ac.il.

## ETHICS STATEMENT

The study protocol was approved by Institutional Review Boards of participating hospitals and by the Ethics Committee of Tel Aviv University. All participants volunteered for the survey and consented in writing.

## AUTHOR CONTRIBUTIONS

KM, JB, AA, YC, DC, and EK conceived and designed the study. MS, JB, EK, and WN made significant contributions in the

coordination of the study. MS, JB, AA, EK, WN, JM, RC, PS, DM, SB, DB-D, BR, TG, AN, YW-W, and YM performed the studies, including enrollment and sample and data collection. AB, YZ, NH, and OA-C performed the laboratory experiments. SG, DC, and KM analyzed the data. KM and DC drafted the manuscript. All authors critically revised the manuscript for important intellectual content, gave final approval for the version to be published, and agreed to be accountable for all aspects of the work in ensuring that questions related to the accuracy or integrity of any part of the work are appropriately investigated and resolved.

## FUNDING

Partial funding was received from the Millner Foundation support to COVID-19 applied research at the Tel Aviv University School of Public Health.

## ACKNOWLEDGMENTS

The authors thank Dr. Elizabeth Temkin for her support in the study design and data analysis, Mr. Yonatan Amir and Mrs. Saritte Perlman for their support in logistics. Thanks are due to Gamidor Diagnostics for the donation of Roche kits used in the sero-survey.

## SUPPLEMENTARY MATERIAL

The Supplementary Material for this article can be found online at: <https://www.frontiersin.org/articles/10.3389/fmed.2021.689994/full#supplementary-material>

## REFERENCES

1. WHO. *Coronavirus Disease (COVID-19) Pandemic* (2020). Available online at: <https://www.who.int/emergencies/diseases/novel-coronavirus-2019> (accessed January 17, 2021).
2. Li Q, Guan X, Wu P, Wang X, Zhou L, Tong Y, et al. Early transmission dynamics in Wuhan, China, of novel coronavirus-infected pneumonia. *N Engl J Med*. (2020) 382:1199–207. doi: 10.1056/NEJMoa2001316
3. Yu P, Zhu J, Zhang Z, Han Y, Huang L. A familial cluster of infection associated with the 2019 novel coronavirus indicating potential person-to-person transmission during the incubation period. *J Infect Dis*. (2020) 221:1757–61. doi: 10.1093/infdis/jiaa077
4. Wu C, Chen X, Cai Y, Xia J, Zhou X, Xu S, et al. Risk factors associated with acute respiratory distress syndrome and death in patients with coronavirus disease 2019. Pneumonia in Wuhan, China. *JAMA Intern Med*. (2020) 180:934–43. doi: 10.1001/jamainternmed.2020.0994
5. Yanover C, Mizrahi B, Kalkstein N, Marcus K, Akiva P, Barer Y, et al. What factors increase the risk of complications in SARS-CoV-2-infected patients? A cohort study in a nationwide Israeli health organization. *Jmir Public Health Sur*. (2020) 6:349–59. doi: 10.2196/preprints.20872
6. Working Group for the Surveillance and Control of COVID-19 in Spain; Members of the Working Group for the Surveillance and Control of COVID-19 in Spain. The first wave of the COVID-19 pandemic in Spain: characterisation of cases and risk factors for severe outcomes, as at 27 April, 2020. *Euro Surveill*. (2020) 25:2001431. doi: 10.2807/1560-7917.ES.2020.25.50.2001431
7. Lastrucci V, Lorini C, Del Riccio M, Gori E, Chiesi F, Sartor G, et al. SARS-CoV-2 seroprevalence survey in people involved in different essential activities during the general lock-down phase in the Province of Prato (Tuscany, Italy). *Vaccines*. (2020) 8:778. doi: 10.3390/vaccines8040778
8. Temkin E, Healthcare Worker COVID-19 Surveillance Working Group. Extremely low prevalence of asymptomatic COVID-19 among healthcare workers caring for COVID-19 patients in Israeli hospitals: a cross-sectional study. *Clin Microbiol Infect*. (2021) 27:130 e1–4. doi: 10.1016/j.cmi.2020.09.040
9. Polack FP, Thomas SJ, Kitchin N, Absalon J, Gurtman A, Lockhart S, et al. Safety and efficacy of the BNT162b2 mRNA Covid-19 vaccine. *N Engl J Med*. (2020) 383:2603–15. doi: 10.1056/NEJMoa2034577
10. Rudberg AS, Havervall S, Månberg A, Jernbom Falk A, Aguilera K, Ng H, et al. *Coronavirus Daily Report*. Israel Ministry of Health (2021).
11. Brehm TT, Schwinge D, Lampalzer S, Schlicker V, Küchen J, Thompson M, et al. Seroprevalence of SARS-CoV-2 antibodies among hospital workers in a German tertiary care center: a sequential follow-up study. *Int J Hyg Environ Health*. (2020) 232:113671. doi: 10.1016/j.ijheh.2020.113671
12. Psychogiou M, Karabinis A, Pavlopoulou ID, Basoulis D, Petsios K, Roussos S, et al. Antibodies against SARS-CoV-2 among health care workers in a country with low burden of COVID-19. *PLoS ONE*. (2020) 15:e0243025. doi: 10.1371/journal.pone.0243025
13. Iversen K, Bundgaard H, Hasselbalch RB, Kristensen JH, Nielsen PB, Pries-Heje M, et al. Risk of COVID-19 in health-care workers in Denmark: an observational cohort study. *Lancet Infect Dis*. (2020) 20:1401–8. doi: 10.1016/S1473-3099(20)30589-2



14. Pallett SJC, Rayment M, Patel A, Fitzgerald-Smith SAM, Denny SJ, Charani E, et al. Point-of-care serological assays for delayed SARS-CoV-2 case identification among health-care workers in the UK: a prospective multicentre cohort study. *Lancet Respir Med.* (2020) 8:885–94. doi: 10.1016/S2213-2600(20)30315-5
15. Moncunill G, Mayor A, Santano R, Jiménez A, Vidal M, Tortajada M, et al. SARS-CoV-2 seroprevalence and antibody kinetics among health care workers in a Spanish hospital after 3 months of follow-up. *J Infect Dis.* (2021) 223:62–71. doi: 10.1101/2020.08.23.20180125
16. Self WH, Tenforde MW, Stubblefield WB, Feldstein LR, Steingrub JS, Shapiro NI, et al. Seroprevalence of SARS-CoV-2 among frontline health care personnel in a multistate hospital network - 13 academic medical centers, April–June, 2020. *MMWR Morb Mortal Wkly Rep.* (2020) 69:1221–6. doi: 10.15585/mmwr.mm6935e2
17. Shields A, Faustini SE, Perez-Toledo M, Jossi S, Aldera E, Allen JD, et al. SARS-CoV-2 seroprevalence and asymptomatic viral carriage in healthcare workers: a cross-sectional study. *Thorax.* (2020) 75:1089–94. doi: 10.1136/thoraxjnl-2020-215414
18. Nicol T, Lefeuve C, Serri O, Pivert A, Joubaud F, Dubée V, et al. Assessment of SARS-CoV-2 serological tests for the diagnosis of COVID-19 through the evaluation of three immunoassays: two automated immunoassays (Euroimmun and Abbott) and one rapid lateral flow immunoassay (NG Biotech). *J Clin Virol.* (2020) 129:104511. doi: 10.1016/j.jcv.2020.104511
19. Pflüger LS, Bannasch JH, Brehm TT, Pfeifferle S, Hoffmann A, Nörz D, et al. Clinical evaluation of five different automated SARS-CoV-2 serology assays in a cohort of hospitalized COVID-19 patients. *J Clin Virol.* (2020) 130:104549. doi: 10.1016/j.jcv.2020.104549
20. GeurtsvanKessel CH, Okba NMA, Igloi Z, Bogers S, Embregts CWE, Laksono BM, et al. An evaluation of COVID-19 serological assays informs future diagnostics and exposure assessment. *Nat Commun.* (2020) 11:3436. doi: 10.1038/s41467-020-17317-y
21. Oved K, Olmer L, Shemer-Avni Y, Wolf T, Supino-Rosin L, Prajgrod G, et al. Multi-center nationwide comparison of seven serology assays reveals a SARS-CoV-2 non-responding seronegative subpopulation. *EClinicalMedicine.* (2020) 29:100651. doi: 10.1016/j.eclinm.2020.100651
22. Vittinghoff E, McCulloch CE. Relaxing the rule of ten events per variable in logistic and Cox regression. *Am J Epidemiol.* (2007) 165:710–8. doi: 10.1093/aje/kwk052
23. Alserehi HA, Alqunaibet AM, Al-Tawfiq JA, Alharbi NK, Alshukairi AN, Alanazi KH, et al. Seroprevalence of SARS-CoV-2 (COVID-19) among healthcare workers in Saudi Arabia: comparing case and control hospitals. *Diagn Microbiol Infect Dis.* (2020) 99:115273. doi: 10.1016/j.diagmicrobio.2020.115273
24. Results of the National Seroosurvey for SARS-CoV-2 (2020). Available online at: <https://www.gov.il/he/departments/news/08102020-01> (accessed February 3, 2021).
25. Venugopal U, Jilani N, Rabah S, Shariff MA, Jawed M, Mendez Batres A, et al. SARS-CoV-2 seroprevalence among health care workers in a New York City hospital: a cross-sectional analysis during the COVID-19 pandemic. *Int J Infect Dis.* (2021) 102:63–9. doi: 10.1016/j.ijid.2020.10.036
26. Rashid-Abdi M, Krifors A, Salleber A, Eriksson J, Mansson E. Low rate of COVID-19 seroconversion in health-care workers at a Department of Infectious Diseases in Sweden during the later phase of the first wave; a prospective longitudinal seroepidemiological study. *Infect Dis.* (2020) 53:169–75. doi: 10.1080/23744235.2020.1849787
27. Rudberg AS, Havervall S, Manberg A, Falk AJ, Aguilera K, Ng H, et al. SARS-CoV-2 exposure, symptoms and seroprevalence in healthcare workers in Sweden. *Nat Commun.* (2020) 11:5064. doi: 10.1038/s41467-020-18848-0
28. Plebani M, Padoan A, Fedeli U, Schievano E, Vecchiato E, Lippi G, et al. SARS-CoV-2 serosurvey in health care workers of the Veneto Region. *Clin Chem Lab Med.* (2020) 58:2107–11. doi: 10.1515/cclm-2020-1236

**Conflict of Interest:** The authors declare that the research was conducted in the absence of any commercial or financial relationships that could be construed as a potential conflict of interest.

Copyright © 2021 Muhsen, Schwaber, Bishara, Kassem, Atamna, Na'amnih, Goren, Bialik, Mohsen, Zaide, Hazan, Ariel-Cohen, Cohen, Shitrit, Marchaim, Benenson, Ben-David, Rubinovitch, Gotesman, Nutman, Wiener-Well, Maor, Carmeli and Cohen. This is an open-access article distributed under the terms of the Creative Commons Attribution License (CC BY). The use, distribution or reproduction in other forums is permitted, provided the original author(s) and the copyright owner(s) are credited and that the original publication in this journal is cited, in accordance with accepted academic practice. No use, distribution or reproduction is permitted which does not comply with these terms.



# Comparison of Residual Pulmonary Abnormalities 3 Months After Discharge in Patients Who Recovered From COVID-19 of Different Severity

## OPEN ACCESS

### Edited by:

Arda Kiani,

Shahid Beheshti University of Medical Sciences, Iran

### Reviewed by:

Chih-Hsin Lee,

Taipei Medical University, Taiwan

Huan Ma,

University of Science and Technology of China, China

Reza Lashgari,

Shahid Beheshti University, Iran

### \*Correspondence:

Yang Jin

whuhjy@126.com

<sup>†</sup>These authors have contributed equally to this work

### Specialty section:

This article was submitted to Pulmonary Medicine, a section of the journal *Frontiers in Medicine*

**Received:** 17 March 2021

**Accepted:** 02 June 2021

**Published:** 25 June 2021

### Citation:

Zhou M, Xu J, Liao T, Yin Z, Yang F, Wang K, Wang Z, Yang D, Wang S, Peng Y, Peng S, Wu F, Chen L and Jin Y (2021) Comparison of Residual Pulmonary Abnormalities 3 Months After Discharge in Patients Who Recovered From COVID-19 of Different Severity. *Front. Med.* 8:682087. doi: 10.3389/fmed.2021.682087

Mei Zhou<sup>1†</sup>, Juanjuan Xu<sup>1†</sup>, Tingting Liao<sup>1†</sup>, Zhengrong Yin<sup>1†</sup>, Fan Yang<sup>2†</sup>, Kai Wang<sup>3†</sup>, Zhen Wang<sup>1</sup>, Dan Yang<sup>1</sup>, Sufei Wang<sup>1</sup>, Yi Peng<sup>1</sup>, Shuyi Peng<sup>2</sup>, Feihong Wu<sup>2</sup>, Leqing Chen<sup>2</sup> and Yang Jin<sup>1\*</sup>

<sup>1</sup> NHC Key Laboratory of Pulmonary Diseases, Department of Respiratory and Critical Care Medicine, Union Hospital, Tongji Medical College, Huazhong University of Science and Technology, Wuhan, China, <sup>2</sup> Department of Radiology, Union Hospital, Tongji Medical College, Huazhong University of Science and Technology, Wuhan, China, <sup>3</sup> Key Laboratory for Environmental and Health, Department of Epidemiology and Biostatistics, School of Public Health, Tongji Medical College, Huazhong University of Science and Technology, Wuhan, China

**Background and Objectives:** To investigate whether coronavirus disease 2019 (COVID-19) survivors who had different disease severities have different levels of pulmonary sequelae at 3 months post-discharge.

**Methods:** COVID-19 patients discharged from four hospitals 3 months previously, recovered asymptomatic patients from an isolation hotel, and uninfected healthy controls (HCs) from the community were prospectively recruited. Participants were recruited at Wuhan Union Hospital and underwent examinations, including quality-of-life evaluation (St. George Respiratory Questionnaire [SGRQ]), laboratory examination, chest computed tomography (CT) imaging, and pulmonary function tests.

**Results:** A total of 216 participants were recruited, including 95 patients who had recovered from severe/critical COVID-19 (SPs), 51 who had recovered from mild/moderate disease (MPs), 28 who had recovered from asymptomatic disease (APs), and 42 HCs. In total, 154 out of 174 (88.5%) recovered COVID-19 patients tested positive for serum SARS-COV-2 IgG, but only 19 (10.9%) were still positive for IgM. The SGRQ scores were highest in the SPs, while APs had slightly higher SGRQ scores than those of HCs; 85.1% of SPs and 68.0% of MPs still had residual CT abnormalities, mainly ground-glass opacity (GGO) followed by strip-like fibrosis at 3 months after discharge, but the pneumonic lesions were largely absorbed in the recovered SPs or MPs relative to findings in the acute phase. Pulmonary function showed that the frequency of lung diffusion capacity for carbon monoxide abnormalities were comparable in SPs and MPs (47.1 vs. 41.7%), while abnormal total lung capacity (TLC) and residual volume (RV) were more frequent in SPs than in MPs (TLC, 18.8 vs. 8.3%; RV, 11.8 vs. 0%).

**Conclusions:** Pulmonary abnormalities remained after recovery from COVID-19 and were more frequent and conspicuous in SPs at 3 months after discharge.

**Keywords:** recovered COVID-19 patients, health-related quality of life, pulmonary function, chest computerized tomography, laboratory findings

## INTRODUCTION

The outbreak of coronavirus disease 2019 (COVID-19), which is caused by the severe acute respiratory syndrome coronavirus 2 (SARS-CoV-2), has posed an unprecedented threat to global public health. As of March 1, 2021, the pandemic has infected more than 113 million people and caused 2,527,891 deaths worldwide (1). SARS-CoV-2 mainly attacks the respiratory tract epithelium *via* the ACE2 receptor and causes varying degrees of pneumonia from symptomless to acute respiratory distress syndrome or septic shock (2). Currently, increasing numbers of infected people recover and are discharged. Understanding the pulmonary sequelae of SARS-CoV-2 infection is of great significance for management and rehabilitation training.

According to previous studies, ~20 and 60% of survivors of the global SARS outbreak caused by SARS-CoV and the Middle East respiratory syndrome coronavirus (MERS-CoV) had persistent physiological impairment and abnormal radiological findings consistent with pulmonary fibrosis, respectively (3–5). In fact, several studies (6–8) have shown that some discharged COVID-19 survivors developed undesirable sequelae, such as ground-glass opacity (GGO) and pulmonary fibrosis on computed tomography (CT), irrespective of whether the acute illness was mild, moderate, or severe. Preliminary evidence (6, 9) revealed abnormal pulmonary function (i.e., restrictive abnormalities, reduced diffusion capacity, and small airway obstruction) in patients who had COVID-19 at discharge and 2 weeks after discharge, and the abnormalities were associated with disease severity. However, follow-up studies that comprehensively evaluated pulmonary function, CT findings, and health-related quality of life (HRQoL) and explored the correlation between them in COVID-19 survivors were scarce, especially among survivors with asymptomatic infection.

In this study, we enrolled recovered patients (RPs) with different severities of previous illness 3 months after discharge, RPs with asymptomatic disease, and healthy controls (HCs). Our purpose was to understand COVID-19-associated pulmonary sequelae at earlier stages to allow early medical intervention, with an attempt to prevent this situation or improve its prognosis.

## METHODS

### Study Design and Participants

We conducted a prospective cohort study including COVID-19 RPs who were discharged 3 months previously from four hospitals (Wuhan Union Hospital, Wuhan Pulmonary Hospital, Wuhan Central Hospital, and Fangcang Hospital) between March 5th and March 31st, 2020 in Wuhan. All patients met the standard discharge criteria (normal body temperature for more than 3 days; significantly improved respiratory

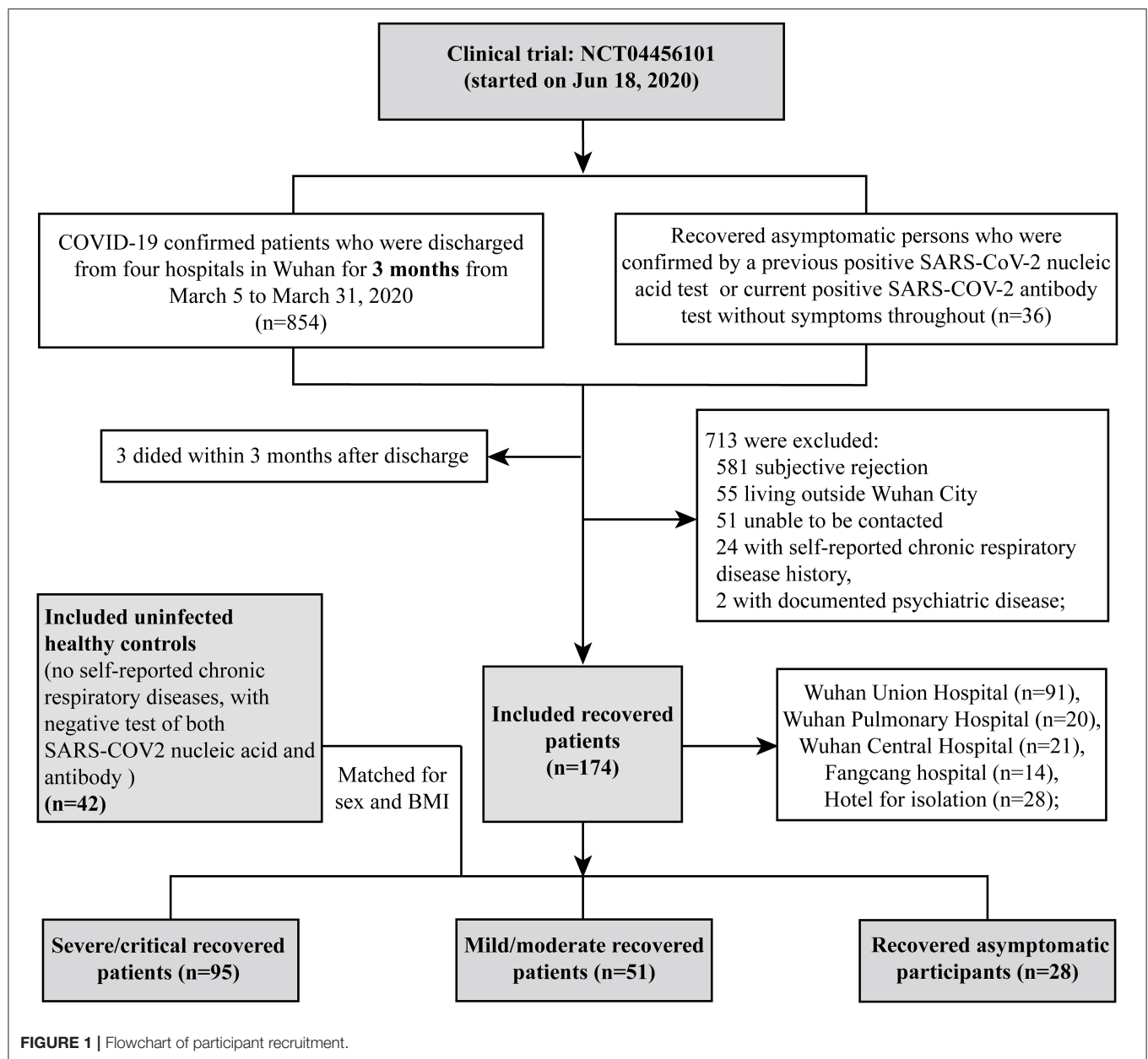
symptoms; negative results on two consecutive SARS-CoV-2 RNA tests at least 24 h apart). Volunteers who recovered from asymptomatic COVID-19 from an isolation hotel and uninfected healthy controls from the community were also recruited as controls. Recruitment and testing were carried out in the outpatient clinic of Wuhan Union Hospital *via* telephone at 3 months after discharge by trained medical staff. All patients were contacted in order of their discharge date, as documented in their medical records. The exclusion criteria were chronic respiratory or psychotic disease, death before follow-up, declining participation, or an inability to participate for reasons such as living outside Wuhan city or inability to be contacted (see the flowchart in **Figure 1**). COVID-19 RPs were categorized as having had severe/critical and mild/moderate disease according to the World Health Organization guidelines (10). Recovered asymptomatic patients (APs) were confirmed based on a previous positive SARS-CoV-2 nucleic acid test or current positive SARS-CoV-2 antibody test who had no symptoms. HCs were confirmed by having both negative SARS-CoV-2 nucleic acid and antibody tests (**Figure 1**). All participants underwent nucleic acid tests and antibody detection for SARS-CoV-2 and completed the St. George's Respiratory Questionnaire (SGRQ), which was designed and conducted as previously reported (11, 12) (see details in the **Supplementary Method**). They were also subjected to a physical checkup, pulmonary function test, and chest CT scan. Routine blood test, biochemical tests (liver and renal function), CRP, LDH, and coagulation tests were completed at the same time.

### Serum Antibody Test for SARS-CoV-2

Vazyme 2019-nCoV IgG/IgM Detection Kit (Colloidal Gold-Based), a rapid, cost-effective, and clinically easy-to-use method, was used for the serum antibody detection. The assay was carried out in accordance with the manufacturer's instructions. In short, the test kit was warmed to room temperature, removed from the foil bag, and placed horizontally on a flat and dry surface. Using the dropper provided, add 1 drop (~20  $\mu$ l) of serum and 3 drops (~60  $\mu$ l) of dilution buffer to the sample loading position. The test results were then read after 10 min.

### CT Scan and Artificial Intelligence-Based Quantitative Analysis of CT Images

All CT scans were obtained with patients in the supine position to maintain the same position as the previous CT scans performed during acute COVID-19. The standard scanning protocol has been previously reported (13). The CT images were quantitatively evaluated using the Quantitative Evaluation System of CT for COVID-19 (YT-CT-Lung, YITU Healthcare Technology Co., Ltd., China) (14) under the supervision of two senior radiologists. Two AI-derived CT features corresponding to ground glass



opacity (GGO) and solid components (SC) were obtained and outlined (see details in the **Supplementary Method**), and the proportion of lesions to lung volume were also calculated (total%, GGO%, SC%) and analyzed longitudinally. Another three common CT features, such as traction bronchiectasis, pleural adhesion, and hypertrophy, were also included in the analysis. Importantly, all images were interpreted independently by three senior radiologists experienced in chest radiology, who were blinded to the clinical and laboratory findings during the analysis, to ensure the accuracy of the AI results. Any discrepancies were resolved by comparing the notes and discussion with a senior radiologist. In addition, previous CT images in the acute phase of disease were compared to accurately identify the lesions caused by COVID-19.

## Pulmonary Function Test

Pulmonary function tests (PFTs) were performed on the Master screen pneumotachograph system (CareFusion, Hochberg, Germany) by two experienced technicians following the ERS/ATS criteria (15, 16). Static and dynamic lung volumes were determined using the repeated breath helium dilution technique. The lung diffusion capacity for carbon monoxide (DLCO) and per-unit alveolar volume (DLCO/VA) were measured using the single-breath method. For each subject, the measured values of pulmonary function parameters were expressed as a percentage of the predicted value (e.g., FEV1% pred, TLC% pred, FVC% pred, RV% pred, DLCO% pred, etc.), which were calculated based on the ethnicity, age, sex, and height of each subject with reference to the Global Lung Function 2012 equations (17).



Fractional exhaled nitric oxide (FeNO) and alveolar nitric oxide (CaNO) were determined using a SUNVOU-P100 Expiratory Analyzer (SUNVOU, Wuxi, China) in accordance with the ERS/ATS guidelines (18).

## Statistical Analysis

Categorical variables are presented as count (%) and continuous variables are expressed as median (interquartile range [IQR]). To compare the differences in demographics, underlying diseases, laboratory findings, SGRQ scores, pulmonary function, and CT abnormalities among the four groups (recovered severe/critical patients [SPs], recovered mild/moderate patients [MPs], recovered asymptomatic patients [APs], and HCs), we used the Kruskal–Wallis test for continuous variables and the chi-squared test or Fisher's exact test for categorical variables to obtain the overall *p*-value. The Bonferroni correction method was used to correct for multiple comparisons (significance threshold was  $p < 0.05/n$ , where,  $n$  = the number of comparisons). For variables with an overall *p*-value less than the Bonferroni-corrected significance threshold, we performed pairwise subgroup comparisons (SPs vs. HCs, MPs vs. HCs, and APs vs. HCs). The Mann–Whitney *U*-test and chi-squared test or Fisher's exact test were used for continuous variables and categorical variables, respectively. Bonferroni correction was also conducted for the multiple subgroup comparison, and the corrected significance threshold was  $p < 0.017$  (0.05/3). A linear mixed model (LMM), which was adjusted for age, sex, and body mass index (BMI), was used for the analysis of longitudinal data (temporal changes in laboratory data and CT images). Associations between PFT results and laboratory findings, SGRQ scores, and CT quantitative data in COVID-19 RPs were examined using Spearman correlation analysis and visualized with corresponding correlation matrix plots.

All tests were two-sided, and a *p*-value <0.05 or below the Bonferroni-corrected threshold was statistically significant. All statistical analyses were performed using R software (version 4.0.2, R Foundation) and SPSS (Statistics 26).

## Ethics Approval

This project was registered on the Clinical Trials website (No. NCT04456101). The protocol used in this project was reviewed and approved by the institutional review board of the Medical Ethics Committee of Wuhan Union Hospital (No. 0271-01). All participants or their surrogates provided informed consent.

## RESULTS

### Clinical Characteristics of Study Population

In our study, a total of 216 participants were recruited, including 95 severe/critical RPs, 51 mild/moderate RPs, 28 asymptomatic RPs, and 42 HCs (median age of 63 vs. 56 vs. 46 vs. 46.5 years, respectively) (Table 1). The median time from illness onset to this follow up was ~4 months (128.5 vs. 125.0 days for severe/critical and mild/moderate RPs, respectively). All 95 severe/critical COVID-19 RPs who had signs of severe pneumonia received nasal catheter oxygen therapy. Among

them, 10 (10.5%) patients received mechanical ventilation, of whom six (6.3%) received non-invasive ventilation for 9–17 days and four (4.2%) received intubation for 12–20 days; 39 (41.1%) patients received high-flow nasal oxygen therapy. In addition, 22 (23.2%) patients received steroids during the hospital stay. The differences in SGRQ scores, CT findings, and pulmonary function at the 3-month follow-up of severe/critical COVID-19 patients receiving different oxygen therapies and steroids during hospitalization are shown in **Supplementary Tables 1, 2**, respectively. Among 51 mild/moderate patients, 14 mild patients had no viral pneumonia or hypoxia during hospitalization, and 37 moderate patients had signs of pneumonia (fever, cough, dyspnea, tachypnea) but no signs of severe pneumonia; none of them received oxygen therapy (**Supplementary Result 1**). Twenty-eight recovered asymptomatic patients came from isolation hotels (see the recruitment details in **Figure 1**). During follow-up, all participants tested negative for SARS-COV-2 nucleic acids. Of the COVID-19 RPs with severe/critical disease, 96.7% were positive for serum SARS-COV-2 IgG 3 months after discharge, and the rate was significantly higher than that in RPs with mild/moderate disease (86%) and asymptomatic infection (85.2%). Similarly, the rate of positive serum IgM was also higher in severe/critical COVID-19 RPs than in mild/moderate RPs and asymptomatic RPs (15.4 vs. 6.0 vs. 7.4%,  $p = 0.017$ ) (Table 1).

As shown in **Table 1**, comorbidities were more common in severe/critical RPs than in the other three groups (SPs = 66.7% vs. MPs = 59.6% vs. APs = 37.0% vs. HCs = 19.0%) with hypertension alone, showing a statistically significant difference. Health-related quality of life (HRQoL) was measured using the SGRQ, and 202 (93.5%) out of 216 participants completed the questionnaire. The total score and three sub-aspect scores were all significantly different between the COVID-19 RPs and HCs (all  $p < 0.0001$ ). Furthermore, all scores increased with the severity of disease, while no significant differences were found between severe/critical RPs requiring mechanical ventilation or high-flow nasal oxygen therapy and those not receiving these two types of oxygen therapy (**Supplementary Table 1**). Also, all scores at the 3-month follow-up had no significant differences between SPs who received steroids and those who did not receive the steroids during the hospitalization (**Supplementary Table 2**).

The laboratory findings of COVID-19 RPs with different disease severities are listed in **Supplementary Table 3**. Most indicators returned to the normal level and were comparable to those of the HCs, while the levels of cystatin C (Cys-C), lactic dehydrogenase (LDH), C-reactive protein (CRP), and thrombin time (TT) still showed significant differences between the four groups, and the value also varied with the severity of the disease (all  $p < 0.001$ ) (Table 1). The longitudinal changes in laboratory markers in 78 severe/critical RPs and 10 mild/moderate RPs at four time points are given in **Supplementary Results 2, 3** and **Supplementary Figure 1**. As can be seen, all laboratory markers improved from values at admission to 3 months after discharge, except creatinine, uric acid (UA), Cys-C, and LDH, which remained unchanged or increased 3 months after discharge.

**TABLE 1 |** Clinical characteristics and St. George respiratory questionnaire in COVID-19 recovered patients at 3-month post-discharge.

| Characteristics                                | Group (N = 216)                     |                                  |                                |                                | Overall p-value |
|--|-------------------------------------|----------------------------------|--------------------------------|--------------------------------|-----------------|
|  | Severe/critical RPs (SPs, n = 95)   | Mild/moderate RPs (MPs, n = 51)  | Asymptomatic RPs (APs, n = 28) | Healthy controls (HCs, n = 42) |                 |
| Age, median (IQR), years                       | 63.00 (56.00–69.00) <sup>a</sup>    | 56.00 (47.50–63.00) <sup>b</sup> | 46.00 (39.50–57.00)            | 46.50 (35.50–56.75)            | <0.0001*        |
| Male, n (%)                                    | 47 (49.5%)                          | 16 (31.4%)                       | 12 (42.9%)                     | 20 (47.6%)                     | 0.20            |
| BMI, median (IQR), kg/m <sup>2</sup>           | 24.52 (22.46–26.71)                 | 23.99 (22.12–25.50)              | 23.44 (22.54–25.42)            | 23.41 (21.20–25.11)            | 0.095           |
| Smoking history                                |                                     |                                  |                                |                                |                 |
| Past/current smokers, n (%)                    | 19 (20.0%)                          | 3 (5.9%)                         | 8 (28.6%)                      | 5 (11.9%)                      | 0.033           |
| Second-hand smokers, n (%)                     | 42 (44.2%)                          | 21 (41.2%)                       | 14 (50.0%)                     | 19 (45.2%)                     | 0.90            |
| Comorbidities, n/N (%)                         | 62/93 (66.7%) <sup>a</sup>          | 28/47 (59.6%) <sup>b</sup>       | 10/27 (37.0%)                  | 8/42 (19.0%)                   | <0.0001*        |
| Hypertension                                   | 38 (40.9%) <sup>a</sup>             | 13 (27.7%) <sup>b</sup>          | 6 (22.2%)                      | 3 (7.1%)                       | 0.0008*         |
| Hyperlipidemia                                 | 17 (18.3%)                          | 8 (17%)                          | 2 (7.4%)                       | 2 (4.8%)                       | 0.13            |
| Diabetes                                       | 23 (24.7%)                          | 7 (14.9%)                        | 3 (11.1%)                      | 2 (4.8%)                       | 0.024           |
| Heart disease                                  | 11 (11.8%)                          | 4 (8.5%)                         | 3 (11.1%)                      | 1 (2.4%)                       | 0.34            |
| Cerebrovascular disease                        | 2 (2.2%)                            | 0 (0.0%)                         | 0 (0.0%)                       | 0 (0.0%)                       | 0.80            |
| Liver disease                                  | 11 (11.8%)                          | 3 (6.4%)                         | 3 (11.1%)                      | 1 (2.4%)                       | 0.28            |
| Kidney disease                                 | 3 (3.2%)                            | 1 (2.1%)                         | 0 (0.0%)                       | 0 (0.0%)                       | 0.89            |
| Solid tumor                                    | 2 (2.2%)                            | 2 (4.3%)                         | 0 (0.0%)                       | 0 (0.0%)                       | 0.54            |
| Hospital stays, days                           | 40.0 (35.0–48.75)                   | 22.0 (16.5–27.5)                 | -                              | -                              | <0.0001*        |
| Duration from illness onset to follow-up, days | 128.50 (125.75–133.25)              | 125.0 (118.50–134.75)            | -                              | -                              | 0.066           |
| SGRQ scores (n = 202/216), median (IQR)        |                                     |                                  |                                |                                |                 |
| Total score                                    | 24.31 (14.05–34.77) <sup>a</sup>    | 18.70 (12.88–32.41) <sup>b</sup> | 9.33 (4.70–24.58) <sup>c</sup> | 3.91 (1.59–7.50)               | <0.0001*        |
| Impact score                                   | 15.08 (6.15–27.98) <sup>a</sup>     | 13.20 (4.70–27.54) <sup>b</sup>  | 6.08 (0.00–18.38) <sup>c</sup> | 0.00 (0.00–3.86)               | <0.0001*        |
| Symptom score                                  | 31.37 (14.86–45.85) <sup>a</sup>    | 31.56 (23.12–46.16) <sup>b</sup> | 20.19 (12.87–36.34)            | 12.16 (6.32–19.74)             | <0.0001*        |
| Activity score                                 | 29.82 (12.51–48.84) <sup>a</sup>    | 20.88 (5.97–36.68) <sup>b</sup>  | 9.23 (0.00–25.62)              | 5.93 (0.00–12.02)              | <0.0001*        |
| Serum antibody (n = 210/216)                   |                                     |                                  |                                |                                |                 |
| IgM positive, n/N (%)                          | 14/91 (15.4%)                       | 3/50 (6.0%)                      | 2/27 (7.4%)                    | 0/42 (0.0%)                    | 0.017           |
| IgG positive, n/N (%)                          | 88/91 (96.7%) <sup>a</sup>          | 43/50 (86.0%) <sup>b</sup>       | 23/27 (85.2%) <sup>c</sup>     | 0/42 (0.0%)                    | <0.0001*        |
| Significant laboratory findings                |                                     |                                  |                                |                                |                 |
| Cys-C, mg/L                                    | 1.06 (0.94–1.29) <sup>a</sup>       | 0.95 (0.86–1.11)                 | 0.90 (0.82–0.99)               | 0.92 (0.86–1.10)               | <0.0001*        |
| LDH, U/L                                       | 235.00 (204.50–269.00) <sup>a</sup> | 208.00 (187.00–237.50)           | 205.50 (184.00–234.00)         | 197.00 (181.25–217.00)         | 0.0002*         |
| CRP, median (IQR), mg/L                        | 1.23 (0.50–2.08) <sup>a</sup>       | 0.98 (0.32–2.50) <sup>b</sup>    | 0.90 (0.56–1.54) <sup>c</sup>  | 0.39 (0.11–0.89)               | 0.0005*         |
| TT, s  | 16.70 (16.40–17.80) <sup>a</sup>    | 16.70 (16.20–17.20)              | 16.30 (15.83–16.90)            | 16.30 (15.83–16.78)            | 0.0008*         |

Data were presented as median (IQR) for continuous variables and n (%) for category variables. Kruskal-Wallis (K-W) test was used for analysis of continuous variables and chi-square test or Fisher's exact test for analysis of all category variables among the four groups. The Bonferroni-corrected significance threshold for overall p-value is 0.0021 (0.05/25). For variables with overall p-value <0.002, we performed pairwise subgroup comparisons (recovered SPs vs. HCs, MPs vs. HCs, and APs vs. HCs). Mann-Whitney U-test and Chi-square test or Fisher's exact test was used for continuous variables and categorical variables, respectively. Bonferroni correction was also conducted for subgroup comparison, and the corrected significance threshold of subgroup p-value is 0.017 (0.05/3). RPs, recovered patients; SPs, Severe/Critical patients; MPs, Mild/Moderate patients; APs, Asymptomatic patients; HCs, Healthy controls; IQR, interquartile range; BMI, body mass index; SGRQ, St. George questionnaire; Cys-C, cystatin C; LDH, lactate dehydrogenase; CRP, C-reactive protein; TT, thrombin time.

\*overall p < 0.002.

<sup>a</sup>p < 0.017: recovered SPs vs. HCs.

<sup>b</sup>p < 0.017: recovered MPs vs. HCs.

<sup>c</sup>p < 0.017: recovered APs vs. HCs.

## Residual CT Abnormalities and Temporal Changes in COVID-19 Recovered Survivors

As shown in Table 2, there were still apparent residual lesions on chest CT scans. In the severe/critical recovered group, 85.1% of subjects showed CT abnormalities, and the rate was significantly higher than that in the other three groups. Moreover, patients requiring mechanical ventilation or high-flow nasal oxygen therapy showed more significant residual CT

abnormalities, while no significant differences were found in SPs who received steroids previously (Supplementary Tables 1, 2). In terms of lesion type on CT images, GGO, the most frequent image feature in acute COVID-19, was still significantly more frequent in recovered severe/critical patients (79.3%) than in mild/moderate RPs (60%) and asymptomatic RPs (22.2%). Evidence of fibrosis, such as stripe-like fibrosis but not reticular opacity, was found more frequently in RPs with severe/critical

**TABLE 2 |** Artificial intelligence (AI) assisted manual identification of CT features in patients recovered from COVID-19 at 3 months post-discharge.

| Characteristics                                  | Group (n = 194)                   |                                 |                                |                                | p-value  |
|--|-----------------------------------|---------------------------------|--------------------------------|--------------------------------|----------|
|  | Severe/critical RPs (SPs, n = 87) | Mild/moderate RPs (MPs, n = 50) | Asymptomatic RPs (APs, n = 27) | Healthy controls (HCs, n = 30) |          |
| Age, median (IQR), years                         | 62.00 (56.00–68.00) <sup>a</sup>  | 56.00 (48.50–63.00)             | 46.00 (41.50–57.00)            | 47.50 (38.25–58.50)            | <0.0001* |
| Sex  |                                   |                                 |                                |                                |          |
| Male, n (%)                                      | 41 (47.1%)                        | 15 (30.0%)                      | 12 (44.4%)                     | 15 (50.0%)                     | 0.20     |
| BMI, median (IQR), kg/m <sup>2</sup>             | 24.24 (22.43–26.49)               | 23.99 (22.27–25.43)             | 23.44 (22.67–25.45)            | 23.58 (21.20–25.29)            | 0.45     |
| CT residual lesion, n (%)                        | 74 (85.1%) <sup>a</sup>           | 34 (68.0%) <sup>b</sup>         | 6 (22.2%)                      | 3 (10.0%)                      | <0.0001* |
| Lesion ratio of bilateral lungs, median (IQR), % | 0.12 (0.02–1.47) <sup>a</sup>     | 0.02 (0.00–0.19) <sup>b</sup>   | 0.00 (0.00–0.01)               | 0.00 (0.00–0.01)               | <0.0001* |
| Lesion ratio of left lung, median (IQR), %       | 0.06 (0.00–0.78) <sup>a</sup>     | 0.01 (0.00–0.15)                | 0.00 (0.00–0.00)               | 0.01 (0.00–0.01)               | <0.0001* |
| Lesion ratio of right lung, median (IQR), %      | 0.16 (0.02–1.57) <sup>a</sup>     | 0.02 (0.00–0.16) <sup>b</sup>   | 0.00 (0.00–0.01)               | 0.00 (0.00–0.01)               | <0.0001* |
| GGO lesion, n (%)                                | 69 (79.3%) <sup>a</sup>           | 30 (60.0%) <sup>b</sup>         | 6 (22.2%)                      | 3 (10.0%)                      | <0.0001* |
| GGO ratio of bilateral lungs, median (IQR), %    | 0.12 (0.01–1.40) <sup>a</sup>     | 0.02 (0.00–0.16) <sup>b</sup>   | 0.00 (0.00–0.00)               | 0.00 (0.00–0.01)               | <0.0001* |
| GGO ratio of left lung, median (IQR), %          | 0.05 (0.00–0.69) <sup>a</sup>     | 0.01 (0.00–0.14)                | 0.00 (0.00–0.00)               | 0.00 (0.00–0.02)               | <0.0001* |
| GGO ratio of right lung, median (IQR), %         | 0.15 (0.01–1.30) <sup>a</sup>     | 0.02 (0.00–0.16) <sup>b</sup>   | 0.00 (0.00–0.01)               | 0.00 (0.00–0.00)               | <0.0001* |
| Solid components (SC), n (%)                     | 61 (70.1%) <sup>a</sup>           | 18 (36.0%) <sup>b</sup>         | 3 (11.1%)                      | 0 (0.0%)                       | <0.0001* |
| SC ratio of bilateral lungs, median (IQR), %     | 0.01 (0.00–0.04) <sup>a</sup>     | 0.00 (0.00–0.02)                | 0.00 (0.00–0.00)               | 0.00 (0.00–0.00)               | <0.0001* |
| SC ratio of left lung, median (IQR), %           | 0.01 (0.00–0.02) <sup>a</sup>     | 0.00 (0.00–0.01)                | 0.00 (0.00–0.00)               | 0.00 (0.00–0.00)               | <0.0001* |
| SC ratio of right lung, median (IQR), %          | 0.01 (0.00–0.06) <sup>a</sup>     | 0.00 (0.00–0.02)                | 0.00 (0.00–0.00)               | 0.00 (0.00–0.00)               | <0.0001* |
| Strip-like fibrosis, n (%)                       | 57 (65.5%) <sup>a</sup>           | 16 (32.0%) <sup>b</sup>         | 3 (11.1%)                      | 0 (0.0%)                       | <0.0001* |
| Reticular opacity, n (%)                         | 10 (11.5%)                        | 8 (16.0%)                       | 0 (0.0%)                       | 0 (0.0%)                       | 0.019    |
| Traction bronchiectasis, n (%)                   | 4 (4.6%)                          | 0 (0.0%)                        | 0 (0.0%)                       | 0 (0.0%)                       | 0.32     |
| Pleural adhesion and hypertrophy, n (%)          | 20 (23.0%)                        | 9 (18.0%)                       | 3 (11.1%)                      | 0 (0.0%)                       | 0.011    |

All the ratio refers to the volume ratio. Data were presented as median (interquartile range, IQR) for continuous variables and n (%) for category variables. Kruskal-Wallis (K-W) test was used for analysis of continuous variables and chi-square test or Fisher's exact test for analysis of all category variables among the four groups. The Bonferroni-corrected significance threshold for overall p-value is 0.0026 (0.05/19), and  $p < 0.0026$  is considered statistically significant. For variables with overall p-value  $< 0.0026$ , we performed pairwise subgroup comparisons (recovered SPs vs. HCs, MPs vs. HCs, and APs vs. HCs). Mann-Whitney U test and Chi-square test or Fisher's exact test was used for continuous variables and categorical variables, respectively. Bonferroni correction was also conducted for subgroup comparison, and the corrected significance threshold of subgroup p-value is 0.017 (0.05/3). RP, recovered patients; SPs, Severe/Critical patients; MPs, Mild/Moderate patients; APs, Asymptomatic patients; HCs, Healthy controls; IQR, interquartile range; BMI, body mass index; GGO, ground-glass opacity; SC, solid components.

\* $p < 0.0026$ .

<sup>a</sup> $p < 0.017$ : recovered SPs vs. HCs.

<sup>b</sup> $p < 0.017$ : recovered MPs vs. HCs.

No variable with a p value  $< 0.017$  in recovered APs vs. HCs.

disease than in the mild/moderate recovered group; however, in general, these changes were not more common than GGO (Table 2). Importantly, the GGO ratio of the whole lungs was obviously much larger than that of solid components among severe/critical RPs (0.12% [IQR: 0.01–1.40%] vs. 0.01% [IQR: 0.0–0.04%]). However, all residual lesions on CT were very small.

The temporal change in CT findings in 56 severe/critical RPs and 23 mild/moderate RPs at three time points (peak lesion during hospitalization, at discharge, and 3 months after discharge) are shown in Figure 2. The percentage of normal CT images gradually increased in both groups but was higher in the mild/moderate group. The predominant abnormality in the severe/critical group was a mixed pattern, with the percentage of patients dropping from 94.6% during hospitalization to 60.8% at 3 months after discharge, while the mixed pattern in the mild/moderate group sharply declined and the predominant pattern of abnormality was GGO at 3 months after discharge (Figure 2A). In addition, the lesions in patients with mild/moderate illness, regardless of the total lesion, GGO, or solid components, were smaller than those in the severe/critical

group for all three timepoints. Importantly, the ratio of total and sub-type lesions in whole lungs was sharply reduced or even completely absorbed from hospitalization to 3 months after discharge; however, the GGO lesions were larger than the solid component throughout the course of COVID-19 (Figure 2B). Two cases with serial CT scans are shown in Figure 2C, and the AI-based segmentation of lesions is shown in Figure 2D.

## Pulmonary Function of COVID-19 Survivors 3 Months After Discharge

Spirometry, lung volume, and diffusion capacity tests were completed in 200 (92.6%) participants. In addition, 193 (89.4%) subjects completed exhaled nitric oxide tests, which indicated airway inflammation. The measured and predicted values of PFT variables were displayed in Supplementary Table 4. Anomalies were mainly noted in lung volume and diffusion capacity (Table 3), as revealed by the significantly reduced TLC%, RV%, and DLCO% values in the COVID-19 recovered groups (all  $p < 0.0001$ ). The decrease in these variables was associated

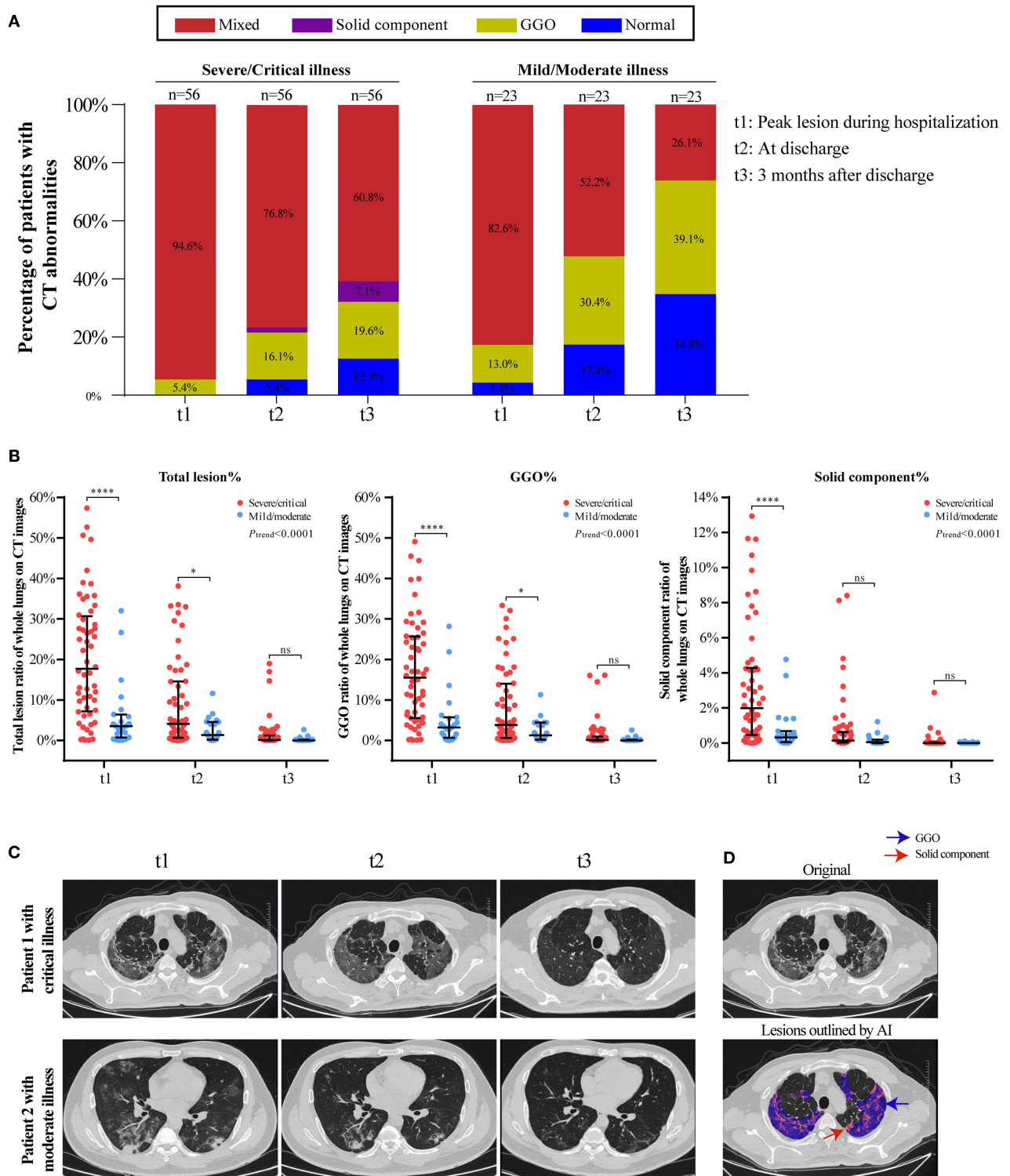


**FIGURE 2 |** Temporal changes of CT findings in 56 severe/critical RPs and 23 mild/moderate RPs from hospitalization to 3 months after discharge. **(A)** The distribution of the main patterns of chest CT abnormalities at three time points (t1: peak lesion during hospitalization, t2: at discharge, t3: 3 months after discharge) among severe/critical and mild/moderate RPs. Stacked-bar graphs show the proportion of patients with GGO/solid component/mixed lesions on CT images. **(B)** The ratio of total lesion, GGO and solid components in the whole lungs at three time points. Linear mixed model (LMM) was applied for comparing the change trend of lesion ratio between severe/critical RPs and mild/moderate RPs, and the statistical difference was indicated by P<sub>trend</sub>. The comparison of lesion ratio between two (Continued)



**FIGURE 2** | groups at three different time point is also displayed, respectively, and expressed as \*\*\*\* $P < 0.0001$ ; \* $P < 0.05$ ; ns: not statistically significant. **(C)** Series CT scans of a representative critical patient and a moderate patient. The upper row showed a 72-year-old man with critical COVID-19 pneumonia and the lower row was a 36-year old man with moderate COVID-19 pneumonia. The lesions on CT images of both patients dramatically decreased from t1 to t3. **(D)** Schematic diagram of lesions outlined by AI on CT images. The upper image is the original CT slice and the lower one is the AI-based lesion outline. The outlined blue area represents lesions of GGO, and the red area represents lesions of solid component.

with the severity of the disease; among the severe/critical RPs, patients requiring mechanical ventilation, or high-flow nasal oxygen therapy had significantly lower TLC%, FVC%, RV%, and DLCO% values than those who did not receive these two types of oxygen therapy (**Supplementary Table 1**). However, there is no significant difference in most lung function variables between patients receiving steroids and those who did not receive the steroids during the hospital stay, except that the RV% pred value and the incidence of TLC abnormalities were significantly different between these two groups (**Supplementary Table 2**). As shown in **Table 3**, 16 (18.8%) out of 85 individuals in the recovered severe/critical group had an aberrant TLC%, while the abnormality existed only in 8.3% of the recovered mild/moderate group and 7.4% of the asymptomatic RPs. However, RV% anomaly was only observed in the severe/critical COVID-19 RPs (11.8%, [10/85]). In terms of diffusion capacity, subjects with reduced DLCO% accounted for 47.1% of the recovered severe/critical group, 41.7% of the recovered mild/moderate group, and 11.1% of the recovered asymptomatic individuals ( $p < 0.0001$ ). However, there was no significant difference among the discharged survivors who had had different COVID-19 severities in terms of obstructive ventilatory defects (e.g., FEV1%, FEV1/FVC) and airway inflammation (FeNO, CaNO).

### Correlation Between Pulmonary Function, Chest CT, and SGRQ in Recovered Severe/Critical and Mild/Moderate COVID-19 Patients at the 3-Month Follow-Up

As shown in **Figure 3**, there was a significant negative correlation between the extent of CT abnormalities and TLC% and RV% at the 3-month follow-up, but a weaker correlation with DLCO% (all  $p < 0.05$ ). The correlation coefficient ( $r$ ) of the total lesion ratio on CT images and TLC% was  $-0.33$  and  $-0.47$  for RV%, respectively (all  $p < 0.001$ ). However, it was only  $-0.18$  for DLCO% ( $p < 0.05$ ), which was of smaller magnitude than those for TLC% and RV%. Moreover, the association between residual CT abnormalities and obstructive ventilatory function (such as FEV1%, FEV1/FVC, MMEF%, and MEF50%), and airway inflammation (FeNO, CaNO) were not significant ( $p > 0.05$ ) (**Figure 3A**). Regarding SGRQ scores (**Figure 3B**), we found significant negative correlations ( $p < 0.05$ ,  $r < -0.3$ ) between all SGRQ scores (except SGRQ symptom score) and lung obstructive ventilatory function variables (FEV1/FVC, FEV1%, MEF75%, MEF50%, MMEF%). Nevertheless, no significant correlations were found in SGRQ scores and almost all lesion statistics on CT images 3 months after discharge (all  $p > 0.05$ ) (**Figure 3C**).

## DISCUSSION

To date, reports on the aftermath of COVID-19 during the recovery stage are limited, and few studies have focused on the evaluation of discharged COVID-19 survivors who had different disease severities. In this study, we found that at 3 months after discharge, COVID-19 RPs had an abnormal health status relative to HCs. Aberrant pulmonary function and radiological abnormalities were observed in COVID-19 patients, and the recovery status of the patients varied with disease severity.

In this study, we found that most patients (88.5%) were positive for SARS-COV-2 IgG antibodies, with no more than a quarter (10.9%) of them being positive for IgM. In addition, the positive rate was higher in COVID-19 RPs who had severe or critical illness (IgG-positive, 96.7%; IgM positive, 15.4%) than in those who had suffered from mild/moderate illness (86.0 and 6.0%, respectively) or who were asymptomatic (85.2 and 7.4%, respectively), indicating that the more serious the condition, the longer the antibodies might linger in RPs.

Previous questionnaire studies indicated that the health status of SARS survivors remained impaired at 3 months to 2 years after illness onset (3, 19, 20). In our study, the SGRQ results showed that COVID-19 RPs had significantly higher SGRQ sub-scores and total scores than those of HCs. Moreover, the trend of increasing SGRQ scores in COVID-19 RPs who had different disease severities indicates that HRQoL impairment was more severe in severe/critical RPs than in mild/moderate and asymptomatic RPs. However, in the recovered severe/critical group, patients requiring mechanical ventilation or high-flow nasal oxygen did not present higher scores than those who did not, as were patients who received steroid therapy. In addition, SGRQ sub-scores and total scores showed only a modest negative correlation with obstruction of airway ventilation (FEV1/FVC, FEV1%, MEF50%, MMEF%), but had no correlation with lung volume or diffusion capacity, which was consistent with previous studies regarding other chronic progressive pulmonary diseases, for example, chronic obstructive pulmonary disease (11) and idiopathic pulmonary fibrosis (12).

In the present study, we found that the main anomalies with regard to pulmonary function were impaired diffusion capacity (as indicated by the significantly reduced DLCO%) and restrictive ventilatory dysfunction (as revealed by the significantly reduced TLC%, RV%). These findings were consistent with the results of Mo et al. (9) and similar to residual pulmonary dysfunction in SARS, MERS, and H1N1 survivors (3, 19–22). Moreover, the impairment of the aforementioned three indicators was associated with the degree of severity of COVID-19; severe/critical patients had the lowest values for restrictive ventilation and diffusion capacity, and those who received mechanical ventilation or high-flow oxygen therapy had even

**TABLE 3 |** Pulmonary function test of patients recovered from COVID-19 at 3 months post-discharge.

| Characteristics                               | Group (n = 200/216)               |                                  |                                |                                | p-value  |
|---|-----------------------------------|----------------------------------|--------------------------------|--------------------------------|----------|
|   | Severe/critical RPs (SPs, n = 85) | Mild/moderate RPs (MPs, n = 48)  | Asymptomatic RPs (APs, n = 27) | Healthy controls (HCs, n = 40) |          |
| Age, median (IQR), years                      | 62.00 (56.00–68.00) <sup>a</sup>  | 56.00 (49.50–63.00) <sup>b</sup> | 46.00 (41.50–57.00)            | 48.50 (37.75–57.25)            | <0.0001* |
| Sex   |                                   |                                  |                                |                                |          |
| Male, n (%)                                   | 41 (47.7%)                        | 15 (31.2%)                       | 12 (44.4%)                     | 20 (50.0%)                     | 0.24     |
| BMI, median (IQR), kg/m <sup>2</sup>          | 24.57 (22.58–26.66)               | 23.91 (22.19–25.46)              | 23.44 (22.67–25.45)            | 23.48 (21.22–25.13)            | 0.14     |
| Spirometry, median (IQR)                      |                                   |                                  |                                |                                |          |
| FEV1/FVC, %                                   | 77.46 (72.76–81.11)               | 75.61 (71.88–79.07)              | 73.66 (69.66–77.16)            | 77.15 (73.15–81.57)            | 0.089    |
| <70%, n/N (%)                                 | 16/85 (18.8%)                     | 9/48 (18.8%)                     | 8/27 (29.6%)                   | 6/40 (15.0%)                   | 0.52     |
| FEV1 (L) % pred                               | 96.40 (88.70–109.90)              | 99.40 (92.10–113.67)             | 94.10 (86.10–101.85)           | 100.80 (93.47–110.10)          | 0.11     |
| <80%, n/N (%)                                 | 6/85 (7.1%)                       | 3/48 (6.3%)                      | 3/27 (11.1%)                   | 2/40 (5%)                      | 0.80     |
| FVC (L) % pred                                | 106.70 (96.10–115.10)             | 111.20 (102.62–123.62)           | 104.80 (97.65–114.85)          | 105.80 (99.12–122.15)          | 0.20     |
| <80%, n/N (%)                                 | 3/85 (3.5%)                       | 0 (0.0%)                         | 0 (0.0%)                       | 0 (0.0%)                       | 0.55     |
| Lung volume, median (IQR)                     |                                   |                                  |                                |                                |          |
| TLC (L) % pred                                | 89.10 (81.80–96.90) <sup>a</sup>  | 95.60 (87.05–103.52)             | 95.30 (90.80–101.35)           | 98.40 (91.67–105.32)           | <0.0001* |
| <80%, n/N (%)                                 | 16/85 (18.8%) <sup>a</sup>        | 4/48 (8.3%)                      | 2/27 (7.4%)                    | 1/40 (2.5%)                    | 0.040    |
| RV (L) % pred                                 | 84.70 (75.50–96.30) <sup>a</sup>  | 93.55 (86.28–104.28)             | 97.10 (89.60–104.05)           | 100.05 (91.15–109.05)          | <0.0001* |
| <65%, n/N (%)                                 | 10/85 (11.8%)                     | 0 (0.0%)                         | 0 (0.0%)                       | 0 (0.0%)                       | 0.003    |
| RV/TLC, %                                     | 36.93 (32.66–39.81)               | 35.76 (31.36–40.13)              | 33.21 (30.74–36.78)            | 33.88 (30.24–37.92)            | 0.096    |
| Diffusion capacity, median (IQR)              |                                   |                                  |                                |                                |          |
| DLCO (mmol/min/kPa) % pred                    | 80.20 (71.80–91.00) <sup>a</sup>  | 82.75 (75.68–93.22) <sup>b</sup> | 88.20 (84.00–95.25)            | 94.05 (85.70–99.65)            | 0.0001*  |
| <80%, n/N (%)                                 | 40/85 (47.1%) <sup>a</sup>        | 20/48 (41.7%) <sup>b</sup>       | 3/27 (11.1%)                   | 4/40 (10%)                     | <0.0001* |
| DLCO/VA % pred                                | 97.30 (85.10–106.20)              | 89.80 (83.30–102.70)             | 100.40 (88.70–105.40)          | 96.90 (85.65–110.55)           | 0.13     |
| <80%, n/N (%)                                 | 14/85 (16.5%)                     | 8/48 (16.7%)                     | 2/27 (7.4%)                    | 4/40 (10%)                     | 0.54     |
| Fractional exhaled nitric oxide, median (IQR) |                                   |                                  |                                |                                |          |
| FeNO, ppb                                     | 21.00 (15.00–26.50)               | 18.00 (14.25–26.75)              | 20.00 (16.00–25.00)            | 18.00 (14.00–23.50)            | 0.61     |
| CaNO, ppb                                     | 4.90 (2.60–7.85)                  | 4.85 (3.40–6.30)                 | 5.10 (3.00–7.60)               | 4.60 (3.15–6.95)               | 0.93     |

Data were presented as median (interquartile range, IQR) for continuous variables and n (%) for category variables. Kruskal-Wallis (K-W) test was used for analysis of continuous variables and chi-square test or Fisher's exact test for analysis of all category variables among the four groups. The Bonferroni-corrected significance threshold for overall p-value is 0.0025 (0.05/20), and  $p < 0.0025$  is considered statistically significant. For variables with overall p-value  $< 0.0025$ , we performed pairwise subgroup comparisons (recovered SPs vs. HCs, MPs vs. HCs, and APs vs. HCs). Mann-Whitney U-test and Chi-square test or Fisher's exact test was used for continuous variables and categorical variables, respectively. Bonferroni correction was conducted for subgroup comparison, and the corrected significance threshold of subgroup p-value is 0.017 (0.05/3). RPs, recovered patients; SPs, Severe/Critical patients; MPs, Mild/Moderate patients; APs, Asymptomatic patients; HCs, Healthy controls; IQR, interquartile range; BMI, body mass index; FEV1, forced expiratory volume in 1 s; FVC, forced vital capacity; TLC, total lung capacity; RV, residual volume; DLCO, diffusing capacity of the lung for carbon monoxide; VA, alveolar ventilation; FeNO, fractional exhaled nitric oxide; CaNO, the exhaled alveolar fraction of nitric oxide.

\* $p < 0.0025$ .

<sup>a</sup> $p < 0.017$ : recovered SPs vs. HCs.

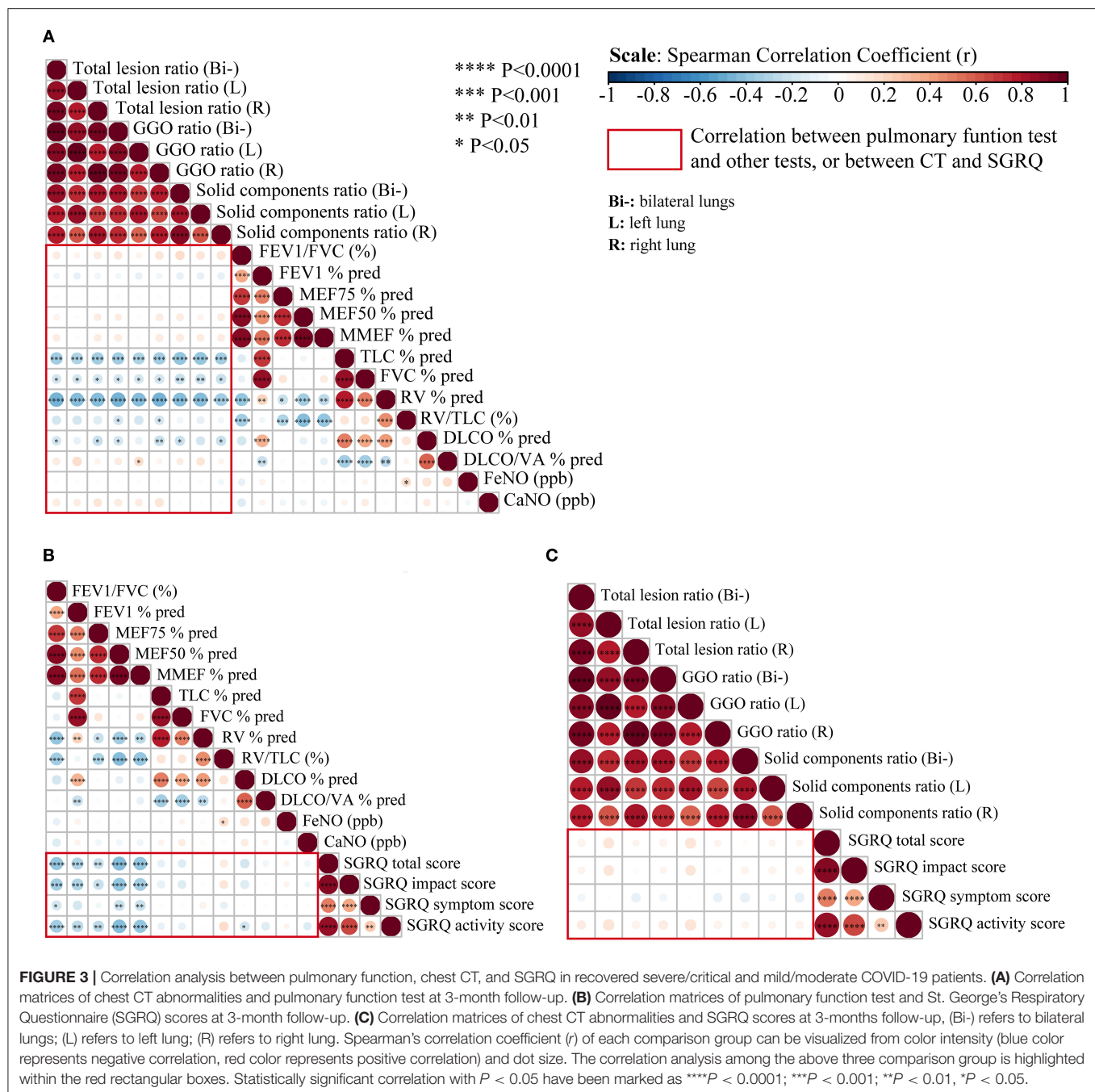
<sup>b</sup> $p < 0.017$ : recovered MPs vs. HCs.

No variable with a p value  $< 0.017$  in recovered APs vs. HCs.

worse values, which is in line with a recent study (9). Obstructive ventilatory disorder, such as that reflected by FEV1% and FEV1/FVC was observed in some RPs; however, no significant differences were found between them and HCs. Diffuse alveolar damage, severe endothelial injury, widespread thrombosis with microangiopathy, alveolar septal fibrous proliferation, and pulmonary consolidation could be observed in the lungs of deceased COVID-19 patients (23, 24), which might account for the remaining impairment of diffusion capacity (decreased DLCO%) in the COVID-19 RPs. Importantly, abnormalities of TLC% and RV% were almost only found in rehabilitated severe/critical patients (18.8 and 11.8%, respectively), which suggests that some severely ill patients with COVID-19 may

have sequelae of decreased lung elasticity. In contrast, the incidence of DLCO% abnormalities was comparable (47.1 vs. 41.7%) between recovered severe/critical and mild/moderate patients, which indicates that diffuse pulmonary dysfunction is a common and high-incidence pulmonary sequelae, regardless of disease severity.

A preliminary follow-up study revealed that 83.3% of RPs still had residual CT abnormalities after discharge (6). We found that more than half of RPs (85.1% of severe/critical RPs, 68% of mild/moderate RPs) still had chest CT abnormalities 3 months after discharge, and up to 90% of the severe/critical patients who previously received mechanical ventilation or high-flow nasal oxygen therapy had residual lung lesions



on CT images. GGO was the most common abnormality, followed by stripe-like fibrosis that newly emerged during the recovery period, which is in line with a previous study conducted in SARS-CoV infection survivors (25). Moreover, patients with more severe disease during the acute stage tended to have more residual opacities 3 months after discharge. The lesion ratio of GGO in whole lungs was much larger than that of solid components in RPs, especially in severe/critical cases. However, the extent of residual lesions

at 3 months after discharge was sharply reduced or even completely absorbed compared to the peak lesion size during hospitalization, regardless of the severity of the lesions. In general, the pneumonic lesion gradually disappeared and was well-absorbed; however, fibrotic lesions in the recovery period began to appear, and the proportion of recovered severe/critical patients with fibrotic lesions (solid component) was similar to the proportion of patients with residual GGO lesions (70.1 vs. 79.3%).

In addition, it would be necessary to compare the structural and functional changes in the lungs in COVID-19 RPs. The correlation analysis between pulmonary function and high-resolution CT scans in survivors of SARS during the early recovery phase (i.e., 25 days to 6 months after hospital discharge) found that FEV1%, TLC%, RV%, and DLCO% negatively correlated with HRCT scores (3, 26). In our study, almost all lesion statistics on CT images significantly negatively correlated with restrictive abnormalities of pulmonary function (TLC%, RV%) and DLCO%, but exhibited no significant correlations with obstructive ventilatory function. However, all significant correlations were modest ( $p < 0.05$ ,  $|r| < 0.5$ ), and the correlation for DLCO% was smaller than that for TLC% and RV%. The main pulmonary function abnormalities were lowered diffusion capacity and reduced lung volume (i.e., restrictive ventilatory dysfunction). The lung lesion statistics on CT images also significantly negatively correlated with lung volume and diffusion capacity but not with the obstructive ventilatory function of airways. This indicates that lesions on CT were consistently linked with abnormalities in pulmonary function. However, SGRQ scores for the evaluation of quality of life showed no significant correlations with residual CT abnormalities, which may be ascribed to the fact that pronounced symptoms require more extensive parenchymal involvement.

This study has several limitations. First, the sample size was limited. Second, we cannot guarantee the same number of subjects in the four groups, because not all discharged patients could be enrolled as scheduled. Third, this is a cross-sectional study and focused only on intermediate-term (3 months after discharge) follow-up findings. Fourth, although, we excluded participants with self-reported underlying lung diseases, we were unable to exclude those with abnormal pulmonary function before SARS-COV-2 infection. Fifth, questionnaires regarding psychological and mental conditions were not included in this study. Sixth, only static lung function tests were performed; however, exercise testing and the 6-minute walk test were not performed. Finally, no baseline lung function tests or SGRQ scores were available in this study.

In conclusion, we found that COVID-19 survivors in Wuhan, China still have reduced quality of life, decreased diffusion capacity, impaired restrictive ventilation, and residual CT abnormalities 3 months after discharge, and these changes were more frequent and conspicuous in severe/critical RPs than in mild/moderate and asymptomatic RPs. Meanwhile, previous lesions on CT images showed good absorption, but the strip-like fibrosis that newly emerged during the convalescent phase occurred frequently among recovered severe/critical RPs.

## DATA AVAILABILITY STATEMENT

The original contributions presented in the study are included in the article/**Supplementary Material**, further inquiries can be directed to the corresponding author/s.

## ETHICS STATEMENT

The studies involving human participants were reviewed and approved by this project was registered on the Clinical Trials website (No. NCT04456101). The protocol used in this project has been reviewed and approved by the institutional review boards of Medical Ethics Committee of Wuhan Union Hospital (No. 0271-01). All participants or their surrogates provided their written informed consent to participate in this study.

## AUTHOR CONTRIBUTIONS

YJ designed the study and took responsibility for the integrity of the work as a whole, from inception to published article. MZ, JX, TL, ZY, and SW collected the clinical data and information based on the follow-up protocols. MZ and ZY carried out the questionnaire survey. ZW and YP performed the pulmonary function test. FY, SP, FW, and LC evaluated and analyzed the CT images. DY and SW collected the peripheral blood samples. MZ, JX, ZY, and TL summarized and checked all data. MZ, KW, and ZY conducted the statistical analysis and draw all article figures. The manuscript was drafted by MZ, TL, and ZY. YJ and MZ critically revised the manuscript and all authors approved the final submission.

## FUNDING

This study was supported in part by the National Natural Science Special Foundation of China (82041018), Ministry of Science and Technology of the People's Republic of China (2020YFC0844300), and the Fundamental Research Funds for the Central Universities (HUST: 2020kfyXGYJ011). The research sponsors did not participate in the study design; data collection, analysis, and interpretation; not involved in the writing of the manuscript and the decision to submit the manuscript for publication.

## ACKNOWLEDGMENTS

We are indebted to the medical staff members and volunteers who are on the front line of caring for patients, and all the citizens in Hubei, especially those in Wuhan, who have sacrificed so much to fight against the COVID-19 epidemic. Also, we thank all the technicians of the Shanghai Key Laboratory of Artificial Intelligence for Medical Image and Knowledge Graph for their kind help in the AI interpretation and process.

## SUPPLEMENTARY MATERIAL

The Supplementary Material for this article can be found online at: <https://www.frontiersin.org/articles/10.3389/fmed.2021.682087/full#supplementary-material>



## REFERENCES

1. WHO. *Coronavirus Disease (COVID-19) Dashboard*. (2021). Available online at: <https://covid19.who.int> (accessed March 1, 2021).
2. Hou YJ, Okuda K, Edwards CE, Martinez DR, Asakura T, Dinnon KH, et al. SARS-CoV-2 reverse genetics reveals a variable infection gradient in the respiratory tract. *Cell*. (2020) 182:429–46.e14. doi: 10.1016/j.cell.2020.05.042
3. Hui DS, Joynt GM, Wong KT, Gomersall CD, Li TS, Antonio G, et al. Impact of severe acute respiratory syndrome (SARS) on pulmonary function, functional capacity and quality of life in a cohort of survivors. *Thorax*. (2005) 60:401–9. doi: 10.1136/thx.2004.030205
4. Antonio GE, Wong KT, Hui DS, Wu A, Lee N, Yuen EH, et al. Thin-section CT in patients with severe acute respiratory syndrome following hospital discharge: preliminary experience. *Radiology*. (2003) 228:810–5. doi: 10.1148/radiol.2283030726
5. Das KM, Lee EY, Singh R, Enani MA, Al Dossari K, Gorkom KV, et al. Follow-up chest radiographic findings in patients with MERS-CoV after recovery. *Indian J Radiol Imaging*. (2017) 27:342–9. doi: 10.4103/ijri.IJRI\_469\_16
6. You J, Zhang L, Ni-Jia-Ti MY, Zhang J, Hu F, Chen L, et al. Abnormal pulmonary function and residual CT abnormalities in rehabilitating COVID-19 patients after discharge. *J Infect*. (2020) 81:e150–2. doi: 10.1016/j.jinf.2020.06.003
7. Yu M, Liu Y, Xu D, Zhang R, Lan L, Xu H. Prediction of the development of pulmonary fibrosis using serial thin-section ct and clinical features in patients discharged after treatment for COVID-19 pneumonia. *Korean J Radiol*. (2020) 21:746–55. doi: 10.3348/kjr.2020.0215
8. Wang Y, Dong C, Hu Y, Li C, Ren Q, Zhang X, et al. Temporal changes of CT findings in 90 patients with COVID-19 pneumonia: a longitudinal study. *Radiology*. (2020) 296:E55–64. doi: 10.1148/radiol.2020200843
9. Mo X, Jian W, Su Z, Chen M, Peng H, Peng P, et al. Abnormal pulmonary function in COVID-19 patients at time of hospital discharge. *Eur Respir J*. (2020) 55:2001217. doi: 10.1183/13993003.01217-2020
10. WHO. *Clinical Management of Severe Acute Respiratory Infection When COVID-19 is Suspected*. Available online at: [https://www.who.int/publications/i/item/clinical-management-of-severe-acute-respiratory-infection-when-novel-coronavirus-\(ncov\)-infection-is-suspected](https://www.who.int/publications/i/item/clinical-management-of-severe-acute-respiratory-infection-when-novel-coronavirus-(ncov)-infection-is-suspected). Clinical management of COVID-19 (accessed May 27, 2020).
11. Jones PW, Quirk FH, Baveystock CM, Littlejohns P. A self-complete measure of health status for chronic airflow limitation. The St. George's respiratory questionnaire. *Am Rev Respir Dis*. (1992) 145:1321–7. doi: 10.1164/ajrccm/145.6.1321
12. Swigris JJ, Esser D, Wilson H, Conoscenti CS, Schmidt H, Stansen W, et al. Psychometric properties of the St George's respiratory questionnaire in patients with idiopathic pulmonary fibrosis. *Eur Respir J*. (2017) 49:1601788. doi: 10.1183/13993003.01788-2016
13. Shi H, Han X, Jiang N, Cao Y, Alwalid O, Gu J, et al. Radiological findings from 81 patients with COVID-19 pneumonia in Wuhan, China: a descriptive study. *Lancet Infect Dis*. (2020) 20:425–34. doi: 10.1016/S1473-3099(20)30086-4
14. Liu F, Zhang Q, Huang C, Shi C, Wang L, Shi N, et al. CT quantification of pneumonia lesions in early days predicts progression to severe illness in a cohort of COVID-19 patients. *Theranostics*. (2020) 10:5613–22. doi: 10.7150/thno.45985
15. Graham BL, Steenbruggen I, Miller MR, Barjaktarevic IZ, Cooper BG, Hall GL, et al. Standardization of spirometry 2019 update. An official American Thoracic Society and European Respiratory Society technical statement. *Am J Respir Crit Care Med*. (2019) 200:e70–88. doi: 10.1164/rccm.201908-1590ST
16. Culver BH, Graham BL, Coates AL, Wanger J, Berry CE, Clarke PK, et al. Recommendations for a standardized pulmonary function report. An official American Thoracic Society technical statement. *Am J Respir Crit Care Med*. (2017) 196:1463–72. doi: 10.1164/rccm.201710-1981ST
17. Quanjer PH, Stanojevic S, Cole TJ, Baur X, Hall GL, Culver BH, et al. Multi-ethnic reference values for spirometry for the 3–95-yr age range: the global lung function 2012 equations. *Eur Respir J*. (2012) 40:1324–43. doi: 10.1183/09031936.00080312
18. American Thoracic Society, European Respiratory Society. ATS/ERS recommendations for standardized procedures for the online and offline measurement of exhaled lower respiratory nitric oxide and nasal nitric oxide, 2005. *Am J Respir Crit Care Med*. (2005) 171:912–30. doi: 10.1164/rccm.200406-710ST
19. Hui DS, Wong KT, Ko FW, Tam LS, Chan DP, Woo J, et al. The 1-year impact of severe acute respiratory syndrome on pulmonary function, exercise capacity, and quality of life in a cohort of survivors. *Chest*. (2005) 128:2247–61. doi: 10.1378/chest.128.4.2247
20. Ngai JC, Ko FW, Ng SS, To KW, Tong M, Hui DS. The long-term impact of severe acute respiratory syndrome on pulmonary function, exercise capacity and health status. *Respirology*. (2010) 15:543–50. doi: 10.1111/j.1440-1843.2010.01720.x
21. Park WB, Jun KI, Kim G, Choi JP, Rhee JY, Cheon S, et al. Correlation between pneumonia severity and pulmonary complications in middle east respiratory syndrome. *J Korean Med Sci*. (2018) 33:e169. doi: 10.3346/jkms.2018.33.e169
22. Luyt CE, Combes A, Becquemin MH, Beigelman-Aubry C, Hatem S, Brun AL, et al. Long-term outcomes of pandemic 2009 influenza A(H1N1)-associated severe ARDS. *Chest*. (2012) 142:583–92. doi: 10.1378/chest.11-2196
23. Ackermann M, Verleden SE, Kuehnel M, Haverich A, Welte T, Laenger F, et al. Pulmonary vascular endothelialitis, thrombosis, and angiogenesis in Covid-19. *N Engl J Med*. (2020) 383:120–8. doi: 10.1056/NEJMoa2015432
24. Xu Z, Shi L, Wang Y, Zhang J, Huang L, Zhang C, et al. Pathological findings of COVID-19 associated with acute respiratory distress syndrome. *Lancet Respir Med*. (2020) 8:420–422. doi: 10.1016/S2213-2600(20)30076-X
25. Wong KT, Antonio GE, Hui DS, Ho C, Chan PN, Ng WH, et al. Severe acute respiratory syndrome: thin-section computed tomography features, temporal changes, and clinoradiologic correlation during the convalescent period. *J Comput Assist Tomogr*. (2004) 28:790–5. doi: 10.1097/00004728-200411000-00010
26. Hsu HH, Tzao C, Wu CP, Chang WC, Tsai CL, Tung HJ, et al. Correlation of high-resolution CT, symptoms, and pulmonary function in patients during recovery from severe acute respiratory syndrome. *Chest*. (2004) 126:149–58. doi: 10.1378/chest.126.1.149

**Conflict of Interest:** The authors declare that the research was conducted in the absence of any commercial or financial relationships that could be construed as a potential conflict of interest.

Copyright © 2021 Zhou, Xu, Liao, Yin, Yang, Wang, Wang, Yang, Wang, Peng, Peng, Wu, Chen and Jin. This is an open-access article distributed under the terms of the Creative Commons Attribution License (CC BY). The use, distribution or reproduction in other forums is permitted, provided the original author(s) and the copyright owner(s) are credited and that the original publication in this journal is cited, in accordance with accepted academic practice. No use, distribution or reproduction is permitted which does not comply with these terms.



# Clinical Outcomes of Severe COVID-19 Patients Admitted to an Intermediate Respiratory Care Unit

Guillermo Suarez-Cuartin<sup>1\*</sup>, Merce Gasa<sup>1</sup>, Guadalupe Bermudo<sup>1</sup>, Yolanda Ruiz<sup>1</sup>, Marta Hernandez-Argudo<sup>1</sup>, Alfredo Marin<sup>1</sup>, Pere Trias-Sabria<sup>1</sup>, Ana Cordoba<sup>1</sup>, Ester Cuevas<sup>1</sup>, Mikel Sarasate<sup>1</sup>, Albert Ariza<sup>2</sup>, Joan Sabater<sup>3</sup>, Nuria Romero<sup>1</sup>, Cristina Subirana<sup>1</sup>, Maria Molina-Molina<sup>1</sup> and Salud Santos<sup>1</sup>

<sup>1</sup> Respiratory Department, Bellvitge University Hospital, Bellvitge Biomedical Research Institute (IDIBELL), L'Hospitalet de Llobregat, Spain, <sup>2</sup> Cardiology Department, Bellvitge University Hospital, Bellvitge Biomedical Research Institute (IDIBELL), L'Hospitalet de Llobregat, Spain, <sup>3</sup> Critical Care Department, Bellvitge University Hospital, Bellvitge Biomedical Research Institute (IDIBELL), L'Hospitalet de Llobregat, Spain

## OPEN ACCESS

### Edited by:

Atefeh Abedini,  
Shahid Beheshti University of Medical  
Sciences, Iran

### Reviewed by:

Alessandro Tomelleri,  
San Raffaele Hospital (IRCCS), Italy  
Chuanhao Jiang,  
Central South University, China

### \*Correspondence:

Guillermo Suarez-Cuartin  
gsuarezc@bellvitgehospital.cat

### Specialty section:

This article was submitted to  
Pulmonary Medicine,  
a section of the journal  
Frontiers in Medicine

**Received:** 17 May 2021

**Accepted:** 09 June 2021

**Published:** 01 July 2021

### Citation:

Suarez-Cuartin G, Gasa M,  
Bermudo G, Ruiz Y,  
Hernandez-Argudo M, Marin A,  
Trias-Sabria P, Cordoba A, Cuevas E,  
Sarasate M, Ariza A, Sabater J,  
Romero N, Subirana C,  
Molina-Molina M and Santos S (2021)  
Clinical Outcomes of Severe  
COVID-19 Patients Admitted to an  
Intermediate Respiratory Care Unit.  
Front. Med. 8:711027.  
doi: 10.3389/fmed.2021.711027

**Introduction:** Many severe COVID-19 patients require respiratory support and monitoring. An intermediate respiratory care unit (IMCU) may be a valuable element for optimizing patient care and limited health-care resources management. We aim to assess the clinical outcomes of severe COVID-19 patients admitted to an IMCU.

**Methods:** Observational, retrospective study including patients admitted to the IMCU due to COVID-19 pneumonia during the months of March and April 2020. Patients were stratified based on their requirement of transfer to the intensive care unit (ICU) and on survival status at the end of follow-up. A multivariable Cox proportional hazards method was used to assess risk factors associated with mortality.

**Results:** A total of 253 patients were included. Of them, 68% were male and median age was 65 years (IQR 18 years). Ninety-two patients (36.4%) required ICU transfer. Patients transferred to the ICU had a higher mortality rate (44.6 vs. 24.2%;  $p < 0.001$ ). Multivariable proportional hazards model showed that age  $\geq 65$  years (HR 4.14; 95%CI 2.31–7.42;  $p < 0.001$ ); chronic respiratory conditions (HR 2.34; 95%CI 1.38–3.99;  $p = 0.002$ ) and chronic kidney disease (HR 2.96; 95%CI 1.61–5.43;  $p < 0.001$ ) were independently associated with mortality. High-dose systemic corticosteroids followed by progressive dose tapering showed a lower risk of death (HR 0.15; 95%CI 0.06–0.40;  $p < 0.001$ ).

**Conclusions:** IMCU may be a useful tool for the multidisciplinary management of severe COVID-19 patients requiring respiratory support and non-invasive monitoring, therefore reducing ICU burden. Older age and chronic respiratory or renal conditions are associated with worse clinical outcomes, while treatment with systemic corticosteroids may have a protective effect on mortality.

**Keywords:** COVID-19, pneumonia, mortality, IMCU, ICU, non-invasive ventilation, high-flow nasal cannula, intermediate care unit

## INTRODUCTION

Coronavirus disease 2019 (COVID-19) is a respiratory condition caused by severe acute respiratory syndrome-coronavirus-2 (SARS-CoV-2) (1). Patients with COVID-19 may become severely ill and require hospital admission, with estimated hospitalization rates of 1 to 18%, increasing with older age (2). Current recommendations state that patients with COVID-19 related acute respiratory failure should be monitored, and support with high-flow nasal cannula (HFNC) oxygen therapy or non-invasive ventilation (NIV) should be considered when conventional oxygen therapy fails (3). In this regard, during the months of March and April of 2020, the COVID-19 pandemic conditioned a significant increase in healthcare burden across Europe, as 17 to 32% of admitted patients required critical care management (4–7). The intensive care unit (ICU) beds and invasive mechanical ventilators achieved their limits of occupation, hence non-invasive supportive care was a valuable option for maintaining respiratory conditions. Therefore, a proper healthcare resource management was necessary to warrant an adequate patient care.

Intermediate respiratory care units (IMCU) are a useful resource for the management of complex patients that do not require admission to the ICU, invasive mechanical ventilation or invasive monitoring (8). IMCU can function as a space for management escalation and de-escalation between the general ward and the ICU, especially when patient monitoring is needed and/or when respiratory support with HFNC or NIV is required (8–10). Benefits of IMCU include reducing ICU admission time and increasing ICU bed capacity, as well as lowering mortality and health care costs (8, 10, 11). Although the role of the ICU is well-known, there is scarce data regarding the outcomes of severe COVID-19 patients managed in an IMCU during the pandemic.

To this date, there have been more than 158 million reported cases worldwide, with over 3 million deaths (12). Mortality is variable among hospitalized patients with COVID-19 pneumonia. Studies from Chinese cohorts estimate a hospital mortality of 4 to 28% (4, 5, 13). Furthermore, a recent study from the United Kingdom showed an overall mortality of 26% in admitted patients (7). Most of these deaths were related to sepsis, respiratory failure, acute respiratory distress syndrome (ARDS) and heart failure (4). Moreover, mortality rates of patients in critical care are higher, ranging from 26 to 32% (7, 14), including ICU and IMCU. Nevertheless, the specific mortality of COVID-19 patients admitted to an IMCU has not been widely studied.

We aim to evaluate the outcomes of severely ill COVID-19 patients requiring monitoring and/or non-invasive respiratory support admitted to an IMCU, and to identify clinical factors that may have led to these results.

## METHODS

### Study Design

An observational and retrospective study was performed on consecutive patients admitted to the IMCU of a tertiary care hospital in Barcelona (Spain) throughout the months of March and April 2020. The final date of follow-up was June

28, 2020. Study protocol was approved by the local ethics committee (No. PR260/20). Inclusion criterion was admission to IMCU due to respiratory failure related to COVID-19 pneumonia requiring non-invasive monitoring and/or non-invasive respiratory support. Patients were diagnosed with a positive polymerase chain reaction for SARS-CoV2 from nasopharyngeal swab and the presence of pulmonary opacities on chest X-ray. According to local protocol, IMCU admission was limited to subjects with an oxygen saturation (SpO<sub>2</sub>) to inspired oxygen fraction (FiO<sub>2</sub>) ratio lower than 200 but not expected to require immediate support with invasive mechanical ventilation. Subjects were admitted directly from the emergency department or transferred from a regional hospital or general wards due to clinical impairment. Exclusion criteria were: recent admission to the ICU, as these patients had already shown clinical improvement, subjects with COVID-19 pneumonia not requiring oxygen support through HFNC or NIV, and respiratory failure due to any etiology other than COVID-19. **Figure 1** shows the algorithm of multidisciplinary patient management including specialists in respiratory medicine, critical care and internal medicine.

### Data Collection and Analysis

Demographic, clinical, radiological and laboratory data were collected from electronic medical records for all patients at the time of IMCU admission. All participants were treated according to hospital protocols. Systemic corticosteroid therapy was divided into four categories depending on dose and administration route, as patients were treated before preliminary results from the RECOVERY trial (15): (a) no corticosteroid treatment, (b) and (c) intravenous (IV) bolus of 1–2 mg/Kg/day methylprednisolone or its equivalent dexamethasone dose for 3 days, followed or not by oral prednisone starting from 0.5 mg/Kg/day, tapering the dose over 7 to 10 days; and (d) only oral prednisolone in doses lower than 0.5 mg/Kg/day for 7 to 10 days. Treatment schemes were chosen depending on clinical and radiological severity, where more severe individuals received longer treatments and higher doses. Patients were categorized depending on survival status and ICU transfer requirement during hospitalization. ICU admission criteria included cardiopulmonary arrest, sudden fall in level of consciousness, invasive ventilation requirement and shock requiring support with vasoactive drugs. The decision of whether or not to transfer a patient to the ICU was always made by a multidisciplinary team including pulmonologists and intensive care physicians. For the survival analysis, clinical and laboratory features were studied using criteria for ARDS (16) and cut-off values identified in severe cases from previous studies (4, 5, 17–19).

### Statistical Analysis

Frequency and percentages were used to present categorical data, and chi-squared test or Fisher's exact test were used to evaluate their differences. Continuous variables are expressed as mean and standard deviation (SD) for normally distributed variables or median and interquartile range (IQR) otherwise. ANOVA and Student's *t* test or their corresponding non-parametrical tests (Kruskal–Wallis and Mann–Whitney *U* tests, respectively)

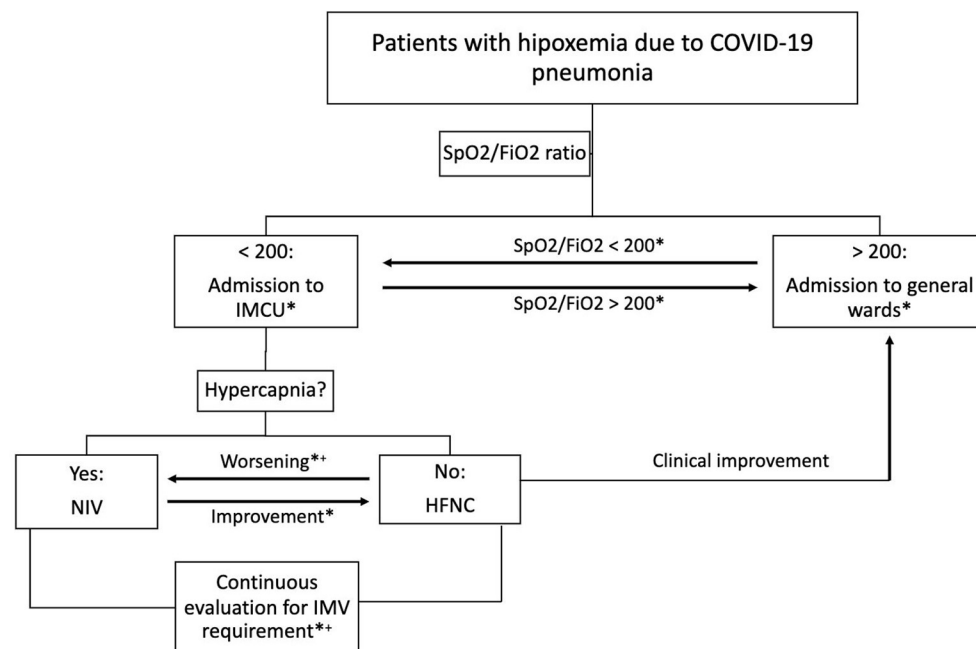


**FIGURE 1 |** Algorithm of multidisciplinary patient management. Clinical worsening is defined as  $\text{SpO}_2/\text{FiO}_2 < 100$  and/or tachypnea  $> 30$  breaths per minute. Clinical improvement is defined as  $\text{SpO}_2/\text{FiO}_2 > 200$  and respiratory rate  $< 30$  breaths per minute. \*Daily multidisciplinary team assessment; +Transfer to ICU if IMV and/or vasoactive drugs are required. COVID-19, coronavirus disease-2019;  $\text{SpO}_2/\text{FiO}_2$ , oxygen saturation to fraction of inspired oxygen ratio; IMCU, intermediate respiratory care unit; ICU, intensive care unit; NIV, non-invasive ventilation; HFNC, high-flow nasal cannula; IMV, invasive mechanical ventilation.

were used to evaluate their differences, when required. Kaplan–Meier curves were used for the survival analysis. In order to identify factors associated with mortality, a multivariable Cox proportional hazards analysis was performed including significant variables from univariate analysis. A  $p$ -value  $< 0.05$  was considered statistically significant. Data were analyzed using R (software version 3.6.2).

## RESULTS

### Patient Description

A total of 291 patients were admitted to the IMCU during the months of March and April of 2020 due to COVID-19 pneumonia. After excluding 38 patients that were previously treated in the ICU, 253 patients were finally included. Of them, 68% were male and median age was 65 years (IQR 18 years). The most frequent comorbidities were hypertension (50.2%), dyslipidemia (47.8%) and diabetes mellitus (29.6%). Demographic and clinical characteristics of included patients at admission to IMCU are described in **Table 1**.

### Clinical Outcomes

Ninety-two patients (36.4%) required transfer to the ICU. There were no significant differences in age, gender or comorbidities between ICU and non-ICU groups. However, patients requiring ICU management had higher systemic inflammatory markers and a significant lower  $\text{SpO}_2/\text{FiO}_2$  ratio on admission. A

comparison of patient characteristics between those that were admitted to the ICU and those who did not, is shown in **Table 1**.

A higher proportion of patients received home discharge in the IMCU group compared to those that required transfer to ICU (50.3 vs. 22.8%, respectively;  $p < 0.001$ ). However, a similar proportion of subjects needed admission to socio-health centers or transfer to their regional hospital for convalescence. Six patients of the ICU group were still hospitalized, while none of the IMCU subjects were in the hospital at the end of follow-up. A comparison of clinical outcomes between groups is presented in **Table 2**.

### Mortality

Eighty patients (31.6%) died during hospitalization. Main causes of death were ARDS and septic shock. Patients requiring transfer to the ICU had a higher mortality rate (44.6 vs. 24.2%;  $p < 0.001$ ). When comparing survivors and non-survivors, a significant difference was observed regarding age (median 61 years, IQR 17 vs. median 72 years, IQR 10.3, respectively;  $p < 0.001$ ). Non-survivors had a higher proportion of comorbidities such as dyslipidemia, chronic respiratory diseases and chronic kidney disease. Furthermore, these patients had higher blood leukocyte counts, serum lactate dehydrogenase (LDH), C-reactive protein and D-dimer, and lower blood lymphocyte counts on admission to the IMCU (**Table 3**).

We compared groups of deceased patients. Subjects who died at the IMCU were significantly older (median 76 years, IQR 4.5 vs. median 66 years, IQR 12;  $p < 0.001$ ). Nevertheless, similar



**TABLE 1** | Characteristics of all patients admitted to the respiratory intermediate care unit, and according to requirement of transfer to the ICU.

|   | <b>Total<br/>(N = 253)</b> | <b>No ICU admission<br/>(N = 161)</b> | <b>ICU admission<br/>(N = 92)</b> | <b>P-value</b> |
|---|----------------------------|---------------------------------------|-----------------------------------|----------------|
| Male, n (%)   | 172 (67.9%)                | 104 (64.6%)                           | 68 (73.9%)                        | 0.165          |
| Age in years, median (IQR)                                  | 65 (18)                    | 66 (19)                               | 63 (15.3)                         | 0.072          |
| <b>Comorbidities</b>  |                            |                                       |                                   |                |
| Hypertension, n (%)   | 127 (50.2%)                | 85 (52.8%)                            | 42 (45.7%)                        | 0.336          |
| Diabetes, n (%)   | 75 (29.6%)                 | 44 (27.3%)                            | 31 (33.7%)                        | 0.356          |
| Dyslipidemia, n (%)   | 121 (47.8%)                | 75 (46.6%)                            | 46 (50%)                          | 0.695          |
| Obesity, n (%)  | 63 (24.9%)                 | 40 (24.9%)                            | 23 (25%)                          | >0.999         |
| Cardiovascular disease, n (%)                               | 27 (10.7%)                 | 19 (11.8%)                            | 8 (8.7%)                          | 0.577          |
| <b>Chronic respiratory disease, n (%)</b>                   |                            |                                       |                                   |                |
| Asthma  | 14 (5.5%)                  | 8 (4.9%)                              | 6 (6.5%)                          | 0.789          |
| COPD  | 17 (6.7%)                  | 13 (8.1%)                             | 4 (4.3%)                          |                |
| Interstitial lung disease                                   | 6 (2.4%)                   | 3 (1.9%)                              | 3 (3.3%)                          |                |
| Bronchiectasis  | 1 (0.4%)                   | 1 (0.6%)                              | 0                                 |                |
| OSAS  | 15 (5.9%)                  | 9 (5.6%)                              | 6 (6.5%)                          |                |
| History of malignancy, n (%)                                | 37 (14.6%)                 | 24 (14.9%)                            | 13 (14.1%)                        | >0.999         |
| Chronic liver disease, n (%)                                | 22 (8.7%)                  | 18 (11.2%)                            | 4 (4.4%)                          | 0.105          |
| Chronic kidney disease, n (%)                               | 27 (10.7%)                 | 19 (11.8%)                            | 8 (8.7%)                          | 0.577          |
| Immunosuppression, n (%)                                    | 13 (5.1%)                  | 10 (6.2%)                             | 3 (3.3%)                          | 0.386          |
| <b>Symptoms</b>   |                            |                                       |                                   |                |
| Dyspnea, n (%)  | 149 (58.9%)                | 86 (53.4%)                            | 63 (68.5%)                        | 0.027*         |
| Cough, n (%)  | 189 (74.7%)                | 117 (72.7%)                           | 72 (78.3%)                        | 0.405          |
| Fever, n (%)  | 211 (83.4%)                | 131 (81.4%)                           | 80 (86.9%)                        | 0.330          |
| Myalgias, n (%)   | 71 (28.1%)                 | 49 (30.4%)                            | 22 (23.9%)                        | 0.334          |
| Diarrhea, n (%)   | 64 (25.3%)                 | 38 (23.6%)                            | 26 (28.3%)                        | 0.503          |
| Nausea, n (%)   | 22 (8.7%)                  | 12 (7.5%)                             | 10 (10.9%)                        | 0.487          |
| Days from symptom onset to hospital admission, median (IQR) | 8 (5)                      | 8 (5)                                 | 8 (5)                             | 0.821          |
| Days from symptom onset to IMCU admission, median (IQR)     | 10 (7)                     | 10 (7)                                | 9 (7.3)                           | 0.176          |
| <b>Chest X-ray on admission</b>                             |                            |                                       |                                   |                |
| Bilateral opacities, n (%)                                  | 149 (58.9%)                | 143 (90.5%)                           | 89 (96.7%)                        | 0.113          |
| Peripheral distribution of opacities, n (%)                 | 189 (74.7%)                | 96 (60.8%)                            | 48 (52.2%)                        | 0.233          |
| <b>Laboratory blood tests</b>                               |                            |                                       |                                   |                |
| Leukocyte count ( $\times 10^9/L$ ), median (IQR)           | 8.60 (5.6)                 | 7.80 (4.8)                            | 10.15 (6.5)                       | <0.001*        |
| Lymphocyte count ( $\times 10^9/L$ ), median (IQR)          | 0.68 (0.6)                 | 0.73 (0.6)                            | 0.64 (0.6)                        | 0.039*         |
| Lactate dehydrogenase (U/L), median (IQR)                   | 418 (221)                  | 398 (220.5)                           | 446 (237)                         | 0.005*         |
| C-Reactive protein (mg/L), median (IQR)                     | 137 (177)                  | 108 (148)                             | 179.50 (188)                      | <0.001*        |
| Ferritin ( $\mu g/L$ ), median (IQR)                        | 1,443 (1,337)              | 1,479 (1,426)                         | 1,410 (1,242.8)                   | 0.829          |
| D-dimer ( $\mu g/L$ ), median (IQR)                         | 531 (814.3)                | 506.50 (821.3)                        | 599.50 (757.5)                    | 0.446          |
| <b>Treatment</b>  |                            |                                       |                                   |                |
| Lopinavir/Ritonavir, n (%)                                  | 202 (79.8%)                | 126 (78.3%)                           | 76 (82.6%)                        | 0.505          |
| Remdesivir, n (%)   | 11 (4.4%)                  | 2 (1.2%)                              | 9 (9.8%)                          | 0.004*         |
| Hydroxychloroquine, n (%)                                   | 243 (96.1%)                | 151 (93.8%)                           | 92 (100%)                         | 0.035*         |
| Tocilizumab, n (%)  | 124 (49%)                  | 73 (45.3%)                            | 51 (55.4%)                        | 0.157          |
| <b>Systemic corticosteroids, n (%)</b>                      |                            |                                       |                                   |                |
| Intravenous bolus   | 114 (45.1%)                | 67 (41.6%)                            | 47 (51.1%)                        | 0.022*         |
| Intravenous bolus + oral tapering regimen                   | 52 (20.6%)                 | 28 (17.4%)                            | 24 (26.1%)                        |                |
| Oral tapering regimen                                       | 4 (1.6%)                   | 3 (1.9%)                              | 1 (1.1%)                          |                |
| SpO <sub>2</sub> /FiO <sub>2</sub> ratio, median (IQR)      | 132.90 (52.5)              | 137.10 (74.3)                         | 118.80 (37.1)                     | <0.001*        |
| <b>Respiratory support</b>                                  |                            |                                       |                                   |                |
| High-flow oxygen, n (%)                                     | 165 (65.2%)                | 88 (54.7%)                            | 77 (83.7%)                        | <0.001*        |
| Non-invasive ventilation, n (%)                             | 133 (52.6%)                | 58 (36%)                              | 75 (81.5%)                        | <0.001*        |
| Invasive mechanical ventilation, n (%)                      | 82 (32.4%)                 | 0                                     | 82 (89.1%)                        | <0.001*        |

ICU, intensive care unit; IQR, interquartile range; COPD, chronic obstructive pulmonary disease; OSAS, obstructive sleep apnea syndrome; SpO<sub>2</sub>, oxygen saturation; FiO<sub>2</sub>, fraction of inspired oxygen; IMCU, Intermediate care unit.

\*Indicates significant p-value < 0.05.

**TABLE 2 |** Clinical outcomes of all patients admitted to the respiratory intermediate care unit, and according to requirement of transfer to the ICU.

|   | Total<br>(N = 253) | No ICU admission<br>(N = 161) | ICU admission<br>(N = 92) | P-value |
|---|--------------------|-------------------------------|---------------------------|---------|
| Home discharge, n (%)                         | 103 (40.7%)        | 81 (50.3%)                    | 22 (23.9%)                | <0.001* |
| Socio-health center transfer, n (%)           | 70 (27.7%)         | 41 (25.5%)                    | 29 (31.5%)                | >0.999  |
| Deaths during admission, n (%)                | 80 (31.6%)         | 39 (24.2%)                    | 41 (44.6%)                | 0.001*  |
| Length of IMCU stay in days, median (IQR)     | 6 (7)              | 7 (6.3)                       | 4 (5.3)                   | <0.001* |
| Length of hospital stay in days, median (IQR) | 16 (19)            | 13 (10.3)                     | 31 (31)                   | <0.001* |

IQR, interquartile range; ICU, intensive care unit; IMCU, intermediate care unit.

\*Indicates significant p-value < 0.05.

proportions of gender, comorbidities and laboratory findings on admission were observed between groups.

## Survival Analysis

Kaplan-Meier survival analysis identified a significant higher mortality in patients of 65 years of age or older (**Figure 2**). Also, significant differences in survival time were observed regarding chronic respiratory and renal conditions and corticosteroid treatment during hospitalization (**Figure 3**).

Variables that independently increased risk of death in the multivariable Cox proportional hazards analysis included: age equal or older than 65 years [hazard ratio (HR) 4.14; 95% confidence interval (CI) 2.31–7.42;  $p < 0.001$ ]; chronic respiratory conditions (HR 2.34; 95% CI 1.38–3.99;  $p = 0.002$ ) and chronic kidney disease (HR 2.96; 95% CI 1.61–5.43;  $p < 0.001$ ). Patients receiving high dose systemic corticosteroids followed by or progressive dose tapering showed a significant lower risk of death (HR 0.15; 95% CI 0.06–0.40;  $p < 0.001$ ). Regarding laboratory findings on admission, blood leukocyte counts higher than  $10 \times 10^9/L$  and lymphocyte counts lower than  $0.4 \times 10^9/L$  were associated with higher risk of death (HR 2.19; 95% CI 1.30–3.71;  $p = 0.003$  and HR 2.05; 95% CI 1.19–3.53;  $p = 0.010$ ). Furthermore, serum LDH higher than 445 U/L was also independently associated with mortality (HR 1.83; 95% CI 1.04–3.21;  $p = 0.035$ ). **Figure 4** shows the results for the multivariable Cox proportional hazards model.

## DISCUSSION

This is one of the first and largest studies to assess the clinical outcomes of severe COVID-19 patients admitted to an IMCU during the first wave of the pandemic. The IMCU allows a secure environment for providing non-invasive respiratory support and patient monitoring, potentially improving healthcare resource management. Our patient model management, including continuous assessment by specialists of respiratory medicine, critical care and internal medicine showed relatively low mortality rates and positive clinical outcomes compared to results from other critical care cohorts. Factors associated with higher mortality in these patients were older age, chronic pulmonary or kidney diseases, while treatment with systemic corticosteroid treatment was protective.

Patient characteristics and clinical presentation of the disease were similar to what has been described in previous studies

(7, 18–20). Our cohort includes a large number of patients with severe respiratory failure, determined by a median SpO<sub>2</sub>/FiO<sub>2</sub> ratio of 132.90. These patients may have required admission to ICU in hospitals without IMCU, possibly leading to further ICU collapse. To this date, there is limited data addressing the specific role of IMCU as a way of reducing the ICU transfer rate of severe COVID-19 patients. A study by Lagi et al. showed that improving nurse/patient ratio to 1:6 and using HFNC on regular wards resulted in a 12% reduction of ICU transfer (21). In this regard, our hospital rapidly increased the number of IMCU beds due to the pandemic situation, maintaining a nurse/patient ratio of 1:4 and non-invasive monitoring. In our cohort, only 36% of patients admitted to an IMCU required upscaling management to the ICU. This resulted in a reduction of ICU burden and allowed for more response time to face the rapid increase of severe cases. A previous study by Heili-Frades et al. showed that IMCU may avoid ~500.000 euros per year of hospital costs, especially in high complexity patients requiring HFNC oxygen therapy or NIV (8). Although the specific admission costs of COVID-19 patients have not been estimated, the IMCU not only could help to improve ICU bed availability, but also to lower overall healthcare costs.

All-cause mortality in our cohort was 31.6%, similar to what has been observed in other cohorts. A recent study by Li et al. showed that mortality in severe cases was 32.5% during the 32 days follow-up period, regardless of respiratory support requirement (18). Also, two cohorts of patients admitted to critical care (ICU or IMCU), one from UK and the other from Italy, reported a similar mortality rate (14). A multicenter European cohort study demonstrated that the availability of IMCU significantly reduced adjusted hospital mortality for adults admitted to the ICU (11). However, data is scarce regarding the mortality of severe COVID-19 patients specifically in an IMCU. In this regard, Franco et al. observed that the implementation of non-invasive respiratory support outside the ICU had favorable results, with an overall mortality rate of 26.9% (22). Similarly, we observed that mortality in IMCU patients who did not require ICU admission was 24.2%, significantly lower than in the ICU group. This may be expected, as most of the patients in the ICU group were more severely ill and required invasive mechanical ventilation. A large proportion of deceased patients received respiratory support with NIV, as this was the escalation support for those patients that continued to show clinical worsening with HFNC, unless otherwise decided by the patient and/or the multidisciplinary medical team. Although we cannot rule out the

**TABLE 3 |** Patient characteristics regarding in-hospital mortality.

|   | <b>Survivors<br/>(N = 173)</b> | <b>Non-survivors<br/>(N = 80)</b> | <b>P-value</b> |
|---|--------------------------------|-----------------------------------|----------------|
| Male, n (%)   | 121 (69.9%)                    | 51 (63.8%)                        | 0.403          |
| Age, median (IQR)   | 61 (17)                        | 72 (10.3)                         | <0.001*        |
| <b>Comorbidities</b>  |                                |                                   |                |
| Hypertension, n (%)   | 83 (47.9%)                     | 44 (55%)                          | 0.366          |
| Diabetes, n (%)   | 49 (28.3%)                     | 26 (32.5%)                        | 0.597          |
| Dyslipidemia, n (%)   | 73 (42.2%)                     | 48 (60%)                          | 0.012*         |
| Obesity, n (%)  | 46 (26.6%)                     | 17 (21.3%)                        | 0.449          |
| Cardiovascular disease, n (%)                               | 16 (9.3%)                      | 11 (13.8%)                        | 0.390          |
| <b>Chronic respiratory disease, n (%)</b>                   |                                |                                   |                |
| Asthma  | 8 (4.6%)                       | 6 (7.5%)                          | 0.008*         |
| COPD  | 8 (4.6%)                       | 9 (11.3%)                         |                |
| Interstitial lung disease                                   | 1 (0.6%)                       | 5 (6.3%)                          |                |
| Bronchiectasis  | 1 (0.6%)                       | 0                                 |                |
| OSAS  | 9 (5.2%)                       | 6 (7.5%)                          |                |
| History of malignancy, n (%)                                | 20 (11.6%)                     | 17 (21.3%)                        | 0.066          |
| Hepatopathy, n (%)  | 19 (10.9%)                     | 3 (3.8%)                          | 0.097          |
| Chronic kidney disease, n (%)                               | 11 (6.4%)                      | 16 (20%)                          | 0.002*         |
| Immunosuppression, n (%)                                    | 6 (3.5%)                       | 7 (8.8%)                          | 0.121          |
| <b>Symptoms</b>   |                                |                                   |                |
| Dyspnea, n (%)  | 103 (59.5%)                    | 46 (57.5%)                        | 0.866          |
| Cough, n (%)  | 134 (77.5%)                    | 55 (68.8%)                        | 0.185          |
| Fever, n (%)  | 149 (86.1%)                    | 62 (77.5%)                        | 0.125          |
| Myalgias, n (%)   | 53 (30.6%)                     | 18 (22.5%)                        | 0.235          |
| Diarrhea, n (%)   | 45 (26%)                       | 19 (23.8%)                        | 0.819          |
| Nausea, n (%)   | 14 (8.1%)                      | 8 (10%)                           | 0.794          |
| Days from symptom onset to hospital admission, median (IQR) | 8 (5)                          | 8 (4.8)                           | 0.457          |
| Days from symptom onset to IMCU admission, median (IQR)     | 10 (7)                         | 10 (7)                            | 0.745          |
| <b>Chest X-ray on admission</b>                             |                                |                                   |                |
| Bilateral opacities, n (%)                                  | 158 (92.9%)                    | 74 (92.5%)                        | >0.999         |
| Peripheral distribution, n (%)                              | 105 (61.8%)                    | 39 (48.8%)                        | 0.071          |
| <b>Laboratory blood tests</b>                               |                                |                                   |                |
| Leukocyte count ( $\times 10^9/L$ ), median (IQR)           | 8.20 (5.2)                     | 10.20 (5.7)                       | <0.001*        |
| Lymphocyte count ( $\times 10^9/L$ ), median (IQR)          | 0.75 (0.6)                     | 0.52 (0.5)                        | <0.001*        |
| Lactate dehydrogenase (U/L), median (IQR)                   | 395 (184.3)                    | 476 (251)                         | <0.001*        |
| C-Reactive protein (mg/L), median (IQR)                     | 108 (167)                      | 169 (196.5)                       | <0.001*        |
| Ferritin ( $\mu g/L$ ), median (IQR)                        | 1,369 (1,213.5)                | 1,792 (1,444)                     | 0.128          |
| D-dimer ( $\mu g/L$ ), median (IQR)                         | 432 (784)                      | 701 (1,756)                       | <0.001*        |
| <b>Treatment</b>  |                                |                                   |                |
| Lopinavir/Ritonavir, n (%)                                  | 134 (77.5%)                    | 68 (85%)                          | 0.222          |
| Remdesivir, n (%)   | 9 (5.2%)                       | 2 (2.5%)                          | 0.510          |
| Hydroxychloroquine, n (%)                                   | 164 (94.8%)                    | 79 (98.8%)                        | 0.177          |
| Tocilizumab, n (%)  | 83 (47.9%)                     | 41 (51.3%)                        | 0.727          |
| <b>Systemic corticosteroids, n (%)</b>                      |                                |                                   |                |
| Intravenous bolus   | 70 (40.5%)                     | 44 (55%)                          | 0.002*         |
| Intravenous bolus + oral tapering regimen                   | 46 (26.6%)                     | 6 (7.5%)                          |                |
| Oral tapering regimen                                       | 3 (1.7%)                       | 1 (1.3%)                          |                |
| <b>SpO2/FiO2 ratio, median (IQR)</b>                        | 137.10 (82.2)                  | 123.39 (37.4)                     | <0.001*        |
| <b>Respiratory support</b>                                  |                                |                                   |                |
| High-flow oxygen, n (%)                                     | 110 (63.6%)                    | 55 (68.8%)                        | 0.509          |
| Non-invasive ventilation, n (%)                             | 64 (36.9%)                     | 69 (86.3%)                        | <0.001*        |
| Invasive mechanical ventilation, n (%)                      | 42 (24.3%)                     | 40 (50%)                          | <0.001*        |
| Tracheostomy, n (%)   | 18 (10.4%)                     | 11 (13.8%)                        | 0.572          |
| <b>Transfer to ICU, n (%)</b>                               | 51 (29.5%)                     | 41 (51.3%)                        | 0.001*         |
| <b>Length of IMCU stay in days, median (IQR)</b>            | 6 (8)                          | 4 (5)                             | <0.001*        |
| <b>Length of hospital stay in days, median (IQR)</b>        | 18 (22)                        | 12 (15)                           | <0.001*        |

IQR, interquartile range; COPD, chronic obstructive pulmonary disease; OSAS, obstructive sleep apnea syndrome; SpO2, oxygen saturation; FiO2, fraction of inspired oxygen; IMCU, intermediate care unit; ICU, intensive care unit.

\*Indicates significant p-value < 0.05.

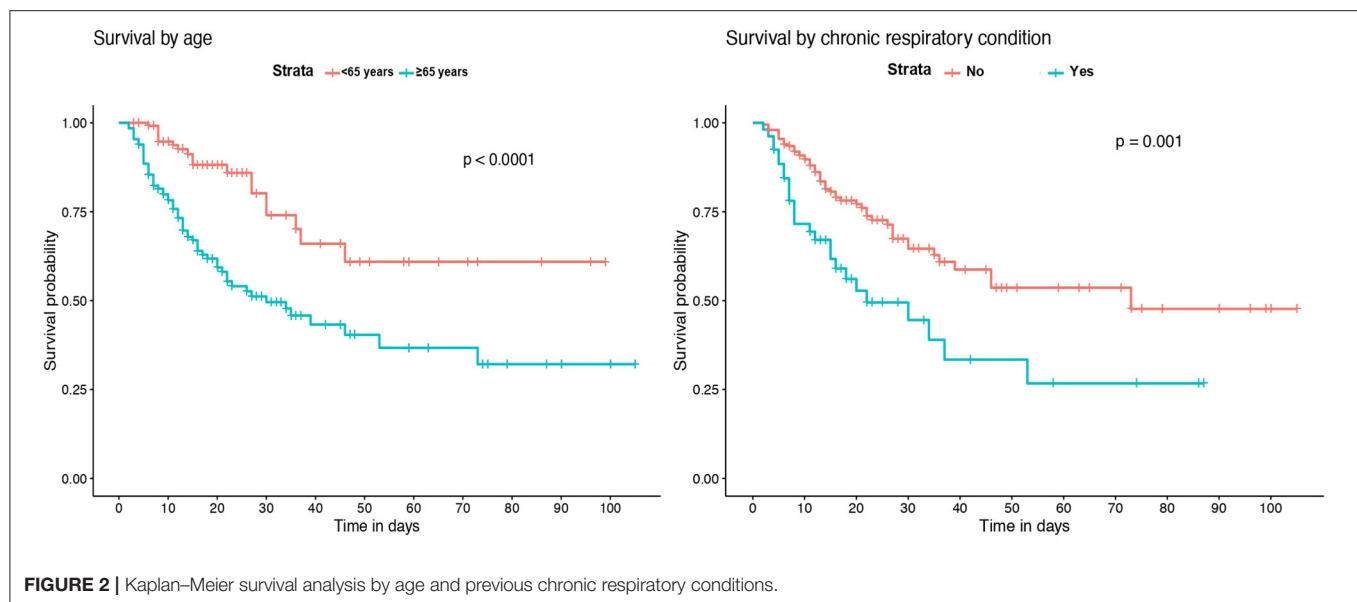


**FIGURE 2 |** Kaplan–Meier survival analysis by age and previous chronic respiratory conditions.

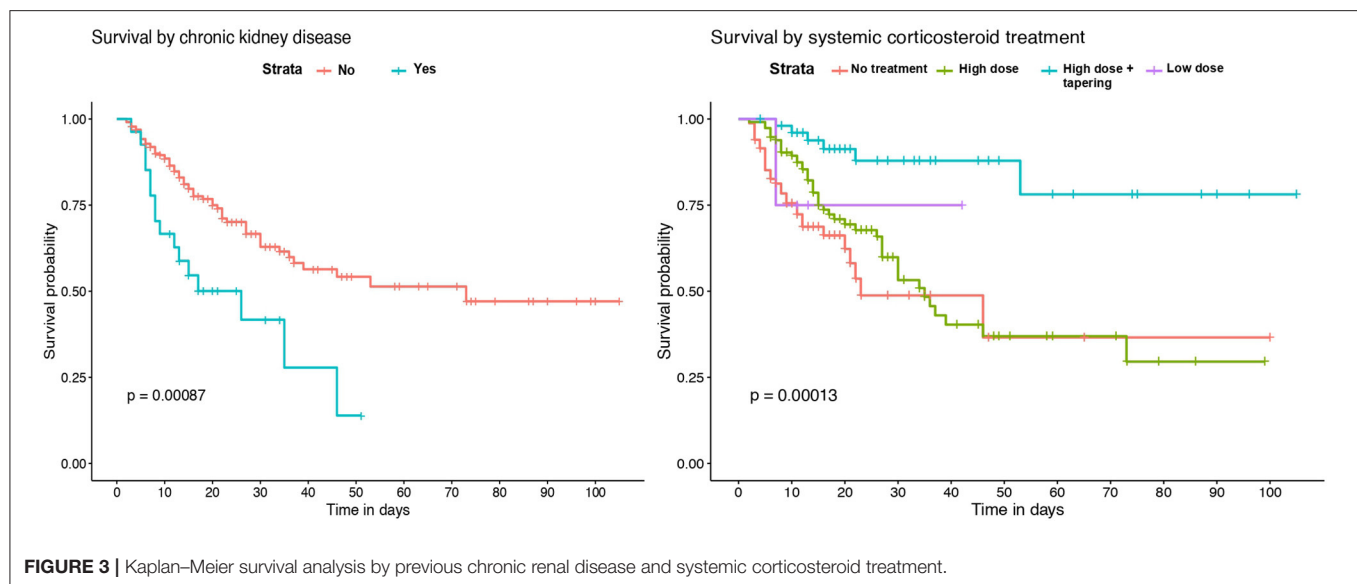


**FIGURE 3 |** Kaplan–Meier survival analysis by previous chronic renal disease and systemic corticosteroid treatment.

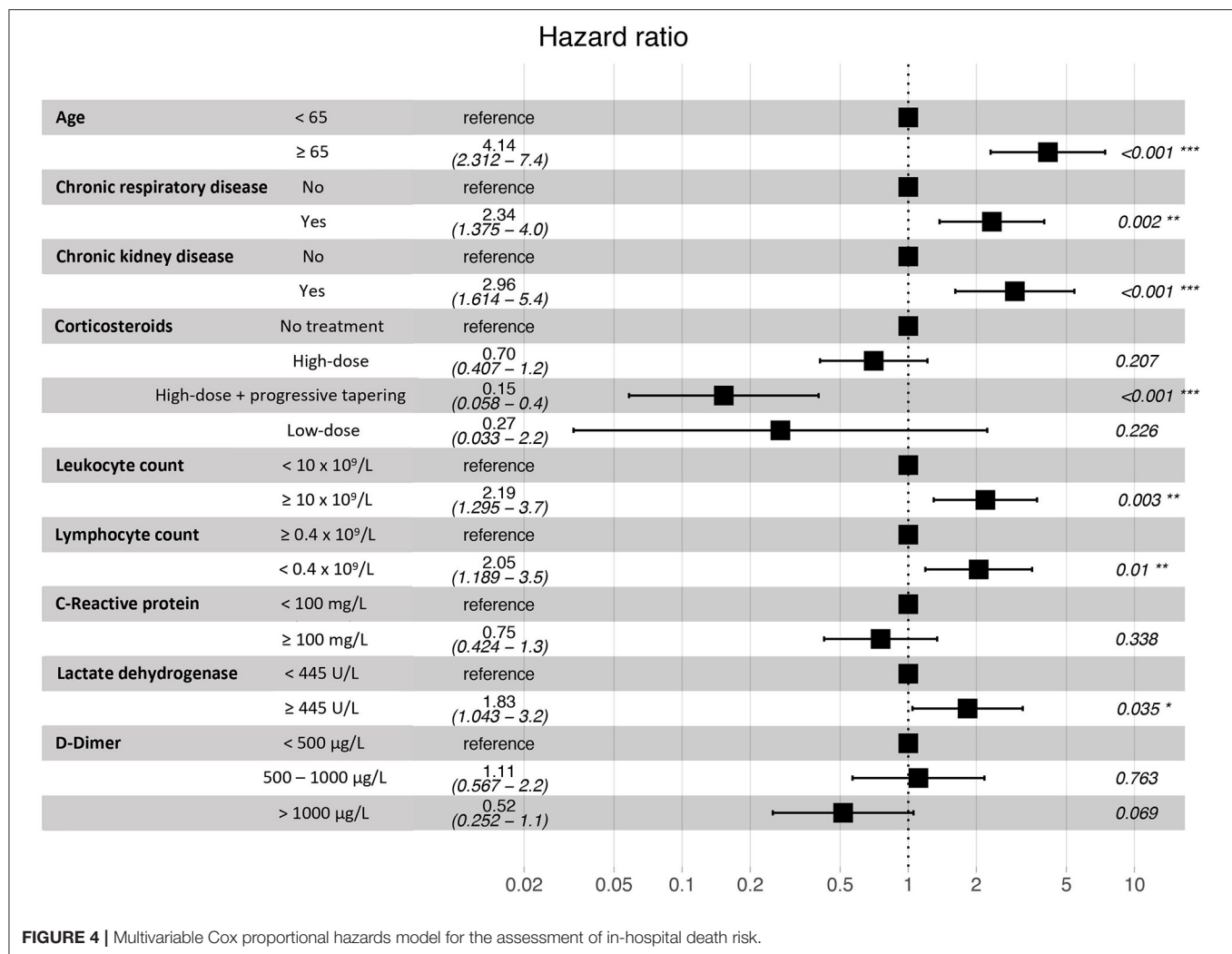
possible effect of delayed intubation on these results, all patients with NIV were assessed continuously by pulmonologists and intensive care physicians to determine whether intubation and IMV were required or not.

Survival analysis showed significant differences between patients of 65 years of age or older, and in those with chronic renal and respiratory diseases. These conditions were identified as independent risk factors for in-hospital mortality. Older age has been associated with an increase in the risk of death in several previous studies (18–20, 23). However, few of the published multivariable models for mortality risk in COVID-19 patients include chronic respiratory and renal diseases. Our results are in agreement with recent observations showing that patients with chronic obstructive pulmonary disease, interstitial lung diseases

or chronic kidney disease that require hospitalization because of COVID-19 have higher risk of death (7, 20, 24). While the overall in-hospital mortality rate of interstitial lung disease (ILD) patients was 49% in the ISARIC4C study (24), the mortality rate of those ILD patients in our IMCU cohort was 83.3%, which suggests that the requirement of high-flux or non-invasive mechanical ventilation in ILD patients with severe COVID-19 associates a poor prognosis. Regarding laboratory findings, our model results show similarities with observations from prior cohorts, where patients with leukocytosis, lymphopenia and elevated serum LDH on admission have a higher mortality risk (4, 18, 19, 23).

Concerning patient treatment, only systemic corticosteroids were independently associated with a reduction of mortality





in our cohort. Subjects receiving 3 days of high-dose methylprednisolone or dexamethasone followed by 7 days of oral dose tapering had a lower risk of death than those who received shorter treatments or were not treated. The positive effect of systemic corticosteroids has been described in recent studies. In a cohort from Wuhan, patients treated with methylprednisolone had a lower mortality rate (23). Also, a preliminary report of the RECOVERY trial showed that patients receiving dexamethasone for up to 10 days resulted in lower all-cause mortality (15). Furthermore, a recent meta-analysis by the World Health Organization Rapid Evidence Appraisal for COVID-19 Therapies (REACT) Working Group concluded that the administration of systemic corticosteroids in critically-ill COVID-19 patients was associated with a lower 28-day mortality, compared to usual care or placebo (25). Nevertheless, though the beneficial effect is clear in severe cases, the optimal dose and dose-reduction should be better evaluated for avoiding adverse events at the same time than achieving a proper lung recovery.

This study has several limitations, mainly related to the retrospective design of the analysis including a single center.

The lack of a control group (non-IMCU hospital) does not allow to directly quantify the impact of IMCU in COVID-19 mortality or health-care burden. Also, our cohort included only severe patients, as we focused on the role of IMCU in patient management. This may limit the generalization of our results to less severe cases. Furthermore, local treatment protocols changed during the inclusion period due to the pandemic situation and the scarce data on COVID-19, which may have influenced the clinical outcomes of our study. However, the number of participants is higher than most previous studies, and our results agree with observations from different cohorts.

## CONCLUSIONS

Our study shows that IMCU may be useful tools for the multidisciplinary management of severe COVID-19 patients requiring non-invasive respiratory support and monitoring, therefore helping to reduce ICU burden. Older age and chronic respiratory or renal conditions are associated with worse clinical outcomes while treatment with systemic corticosteroids

may have a protective effect on mortality. These results may help to further validate the feasibility of IMCU during the COVID-19 pandemic.

## DATA AVAILABILITY STATEMENT

The raw data supporting the conclusions of this article will be made available by the authors, without undue reservation.

## ETHICS STATEMENT

The studies involving human participants were reviewed and approved by Bellvitge University Hospital Ethics Committee. Study reference No. PR260/20. Written informed consent for participation was not required for this study in accordance with the national legislation and the institutional requirements.

## AUTHOR CONTRIBUTIONS

GS-C and MG participated in study design, acquisition, analysis, and interpretation of data, and in the elaboration of the manuscript. GB participated in data acquisition and

in the elaboration of the manuscript. YR participated in data acquisition, analysis, and interpretation of data. MH-A, AM, PT-S, AC, EC, MS, AA, NR, and CS participated in data acquisition and analysis. JS participated in data acquisition, analysis, and interpretation of the results. MM-M participated in study design, interpretation of data, and in the elaboration of the manuscript. SS participated in study design, interpretation of data, and in the elaboration of the manuscript. All authors read and approved the final manuscript.

## FUNDING

This study received funding from Linde Healthcare and Menarini. Funding bodies did not participate in the design of the study or in the collection, analysis, and interpretation of data.

## ACKNOWLEDGMENTS

The authors acknowledge all health-care workers involved in patient management for their hard work and dedication and also thank CERCA Programme/Generalitat de Catalunya for institutional support.

## REFERENCES

- Zhu N, Zhang D, Wang W, Li X, Yang B, Song J, et al. A novel coronavirus from patients with pneumonia in China, 2019. *N Engl J Med.* (2020) 382:727–33. doi: 10.1056/NEJMoa2001017
- Verity R, Okell LC, Dorigatti I, Winskill P, Whittaker C, Imai N, et al. Estimates of the severity of coronavirus disease 2019: a model-based analysis. *Lancet Infect Dis.* (2020) 20:669–77. doi: 10.1016/S1473-3099(20)30243-7
- Cinesi Gómez C, Peñuelas Rodríguez Ó, Luján Torné M, Egea Santaolalla C, Masa Jiménez JF, García Fernández J, et al. Clinical consensus recommendations regarding non-invasive respiratory support in the adult patient with acute respiratory failure secondary to SARS-CoV-2 infection. *Arch Bronconeumol.* (2020) 56 (Suppl 2):11–8. doi: 10.1016/j.redare.2020.05.001
- Zhou F, Yu T, Du R, Fan G, Liu Y, Liu Z, et al. Clinical course and risk factors for mortality of adult inpatients with COVID-19 in Wuhan, China: a retrospective cohort study. *Lancet.* (2020) 395:1054–62. doi: 10.1016/S0140-6736(20)30566-3
- Wang D, Hu B, Hu C, Zhu F, Liu X, Zhang J, et al. Clinical characteristics of 138 hospitalized patients with 2019 novel coronavirus-infected pneumonia in Wuhan, China. *JAMA.* (2020) 323:1061–9. doi: 10.1001/jama.2020.1585
- Huang C, Wang Y, Li X, Ren L, Zhao J, Hu Y, et al. Clinical features of patients infected with 2019 novel coronavirus in Wuhan, China. *Lancet.* (2020) 395:497–506. doi: 10.1016/S0140-6736(20)30183-5
- Docherty AB, Harrison EM, Green CA, Hardwick HE, Pius R, Norman L, et al. Features of 20 133 UK patients in hospital with covid-19 using the ISARIC WHO Clinical Characterisation Protocol: prospective observational cohort study. *BMJ.* (2020) 369:m1985. doi: 10.1136/bmj.m1985
- Heili Frades S, Carballosa de Miguel M del P, Naya Prieto A, Galdeano Lozano M, Mate García X, Mahillo Fernández I, et al. Cost and mortality analysis of an intermediate respiratory care unit. is it really efficient and safe? *Arch Bronconeumol.* (2019) 55:634–41. doi: 10.1016/j.arbr.2019.06.008
- Prin M, Wunsch H. The role of stepdown beds in hospital care. *Am J Respir Crit Care Med.* (2014) 190:1210–6. doi: 10.1164/rccm.201406-1117PP
- Plate JDJ, Leenen LPH, Houwert M, Hietbrink F. Utilisation of intermediate care units: a systematic review. *Crit Care Res Pract.* (2017) 2017:8038460. doi: 10.1155/2017/8038460
- Capuzzo M, Volta CA, Tassinati T, Moreno RP, Valentin A, Guidet B, et al. Hospital mortality of adults admitted to intensive care units in hospitals with and without intermediate care units: a multicentre European cohort study. *Crit Care.* (2014) 18:551. doi: 10.1186/s13054-014-0551-8
- European Centre for Disease Prevention and Control. *COVID-19 situation update worldwide, as of May 12, 2021.* Available online at: <https://www.ecdc.europa.eu/en/geographical-distribution-2019-ncov-cases> (accessed May 17, 2021).
- Chen N, Zhou M, Dong X, Qu J, Gong F, Han Y, et al. Epidemiological and clinical characteristics of 99 cases of 2019 novel coronavirus pneumonia in Wuhan, China: a descriptive study. *Lancet.* (2020) 395:507–13. doi: 10.1016/S0140-6736(20)30211-7
- Grasselli G, Zangrillo A, Zanella A, Antonelli M, Cabrini L, Castelli A, et al. Baseline Characteristics and Outcomes of 1,591 Patients Infected with SARS-CoV-2 Admitted to ICUs of the Lombardy Region, Italy. *JAMA.* (2020) 323:1574–81. doi: 10.1001/jama.2020.5394
- The RECOVERY Collaborative Group. Dexamethasone in hospitalized patients with covid-19—preliminary report. *N Engl J Med.* (2020) 384:693–704. doi: 10.1056/NEJMoa2021436
- Rice TW, Wheeler AP, Bernard GR, Hayden DL, Schoenfeld DA, Ware LB. Comparison of the SpO<sub>2</sub>/FIO<sub>2</sub> ratio and the PaO<sub>2</sub>/FIO<sub>2</sub> ratio in patients with acute lung injury or ARDS. *Chest.* (2007) 132:410–7. doi: 10.1378/chest.07-0617
- Guan W, Ni Z, Hu YY, Liang W, Ou C, He J, et al. Clinical characteristics of coronavirus disease 2019 in China. *N Engl J Med.* (2020) 382:1708–20. doi: 10.1056/NEJMoa2002032
- Li X, Xu S, Yu M, Wang K, Tao Y, Zhou Y, et al. Risk factors for severity and mortality in adult COVID-19 inpatients in Wuhan. *J Allergy Clin Immunol.* (2020) 146:110–8. doi: 10.1016/j.jaci.2020.04.006
- Du RH, Liang LR, Yang CQ, Wang W, Cao TZ, Li M, et al. Predictors of mortality for patients with COVID-19 pneumonia caused by SARS-CoV-2: a prospective cohort study. *Eur Respir J.* (2020) 55:2000524. doi: 10.1183/13993003.00524-2020
- Imam Z, Odish F, Gill I, O'Connor D, Armstrong J, Vanood A, et al. Older age and comorbidity are independent mortality predictors in a large cohort of 1,305 COVID-19 patients in Michigan, United States. *J Intern Med.* (2020) 288:469–76. doi: 10.1111/joim.13119
- Lagi F, Piccica M, Graziani L, Vellere I, Botta A, Tilli M, et al. Early experience of an infectious and tropical diseases

- unit during the coronavirus disease (COVID-19) pandemic, Florence, Italy, February to March 2020. *Eurosurveillance*. (2020) 25:2000556. doi: 10.2807/1560-7917.ES.2020.25.17.2000556
22. Franco C, Facciolo N, Tonelli R, Dongilli R, Vianello A, Pisani L, et al. Feasibility and clinical impact of out-of-ICU non-invasive respiratory support in patients with COVID-19 related pneumonia. *Eur Respir J*. (2020) 56:2002130. doi: 10.1183/13993003.02130-2020
  23. Wu C, Chen X, Cai Y, Xia J, Zhou X, Xu S, et al. Risk factors associated with acute respiratory distress syndrome and death in patients with coronavirus disease 2019 pneumonia in Wuhan, China. *JAMA Intern Med*. (2020) 180:934–3. doi: 10.1001/jamainternmed.2020.0994
  24. Drake TM, Docherty AB, Harrison EM, Quint JK, Adamali H, Agnew S, et al. Outcome of hospitalization for covid-19 in patients with interstitial lung disease: an international multicenter study. *Am J Respir Crit Care Med*. (2020) 202:1656–65. doi: 10.1164/rccm.202007-2794OC
  25. WHO Rapid Evidence Appraisal for COVID-19 Therapies (REACT) Working Group, Sterne JAC, Murthy S, Diaz JV, Slutsky AS, Villar J, Angus DC, et al. Association between administration of systemic corticosteroids and mortality among critically ill patients with covid-19: a meta-analysis. *JAMA*. (2020) 324:1330–41. doi: 10.1001/jama.2020.17023
- Conflict of Interest:** GS-C reports grants from Grifols. MM-M reports grants from Boehringer Ingelheim, Roche, Glaxo-Smith-Kline, Esteve-Teijin, Almirall, and Chiesi outside the submitted work.
- The remaining authors declare that the research was conducted in the absence of any commercial or financial relationships that could be construed as a potential conflict of interest.
- Copyright © 2021 Suarez-Cuartin, Gasa, Bermudo, Ruiz, Hernandez-Argudo, Marin, Trias-Sabria, Cordoba, Cuevas, Sarasate, Ariza, Sabater, Romero, Subirana, Molina-Molina and Santos. This is an open-access article distributed under the terms of the Creative Commons Attribution License (CC BY). The use, distribution or reproduction in other forums is permitted, provided the original author(s) and the copyright owner(s) are credited and that the original publication in this journal is cited, in accordance with accepted academic practice. No use, distribution or reproduction is permitted which does not comply with these terms.



# Comparison of the Filtration Efficiency of Different Face Masks Against Aerosols

Connor Stahl<sup>1</sup>, Kevin Frederick<sup>2</sup>, Sachin Chaudhary<sup>3</sup>, Christopher J. Morton<sup>4</sup>, Douglas Loy<sup>2</sup>, Krishna Muralidharan<sup>2</sup>, Armin Sorooshian<sup>1,5</sup> and Sairam Parthasarathy<sup>3,4\*</sup>

<sup>1</sup> Department of Chemical and Environmental Engineering, University of Arizona, Tucson, AZ, United States, <sup>2</sup> Department of Materials Science and Engineering, University of Arizona, Tucson, AZ, United States, <sup>3</sup> Division of Pulmonary, Allergy, Critical Care and Sleep Medicine, University of Arizona, Tucson, AZ, United States, <sup>4</sup> University of Arizona Health Sciences Center for Sleep and Circadian Sciences, University of Arizona, Tucson, AZ, United States, <sup>5</sup> Department of Hydrology and Atmospheric Sciences, University of Arizona, Tucson, AZ, United States

## OPEN ACCESS

### Edited by:

Reza Lashgari,  
Shahid Beheshti University, Iran

### Reviewed by:

Manel Luján,  
Instituto de Investigación e Innovación  
Parc Taulí (I3PT), Spain  
Yevgen Nazarenko,  
McGill University, Canada

### \*Correspondence:

Sairam Parthasarathy  
sparthasarathy@  
deptofmed.arizona.edu

### Specialty section:

This article was submitted to  
Pulmonary Medicine,  
a section of the journal  
Frontiers in Medicine

Received: 15 January 2021

Accepted: 31 May 2021

Published: 02 July 2021

### Citation:

Stahl C, Frederick K, Chaudhary S,  
Morton CJ, Loy D, Muralidharan K,  
Sorooshian A and Parthasarathy S  
(2021) Comparison of the Filtration  
Efficiency of Different Face Masks  
Against Aerosols.  
Front. Med. 8:654317.  
doi: 10.3389/fmed.2021.654317

**Background:** The severe acute respiratory syndrome coronavirus 2 (SARS-CoV-2) pandemic can spread through virus-containing aerosols ( $\leq 5 \mu\text{m}$ ) and larger airborne droplets. Quantifying filtration efficiency of different kinds of masks and linings for aerosols that fall within the most penetrating particle size (80–400 nm) is critical to limiting viral transmission. The objective of our experiment was to compare the “real-world” filtering efficiency of different face masks for fine aerosols (350 nm) in laboratory simulations.

**Methods:** We performed a simulated bench test that measured the filtering efficiency of N95 vs. N99 masks with elastomeric lining in relation to baseline (“background”) aerosol generation. A mannequin head was placed within a chamber and was attached to an artificial lung simulator. Particles of known size ( $350 \pm 6 \text{ nm}$  aerodynamic diameter) were aerosolized into the chamber while simulating breathing at physiological settings of tidal volume, respiratory rate, and airflow. Particle counts were measured between the mannequin head and the lung simulator at the tracheal airway location.

**Results:** Baseline particle counts without a filter (background) were  $2,935 \pm 555$  (SD)  $\text{cm}^{-3}$ , while the N95 ( $1348 \pm 92 \text{ cm}^{-3}$ ) and N99 mask with elastomeric lining ( $279 \pm 164 \text{ cm}^{-3}$ ;  $p < 0.0001$ ) exhibit lower counts due to filtration.

**Conclusion:** The filtration efficiency of the N95 (54.1%) and N99 (90.5%) masks were lower than the filtration efficiency rating. N99 masks with elastomeric lining exhibit greater filtration efficiency than N95 masks without elastomeric lining and may be preferred to contain the spread of SARS-CoV-2 infection.

**Keywords:** COVID-19, mask, aerosol, SARS-CoV-2, viral transmission

## INTRODUCTION

The severe acute respiratory syndrome coronavirus 2 (SARS-CoV-2) pandemic continues to spread worldwide and has caused almost 2.6 million deaths as of March 11, 2021 (1). Research suggests that such spread is mediated by airborne transmission and that face masks are more effective in limiting the spread of SARS-CoV-2 infection compared to social distancing (2). Considering that there are various mask types, inter-disciplinary research comparing mask filtration efficacy are needed (2). Large airborne particles ( $> 5 \mu\text{m}$ ) are more likely to deposit in the head airways,



whereas smaller particles are likely to deposit in the conducting airways of the lungs. Fine aerosols ( $0.01\text{--}1\text{ }\mu\text{m}$ ) in single breath assessments are associated with least deposition ( $\sim 10\%$ ), but under multiple breath conditions they can continue to be retained within the lung and deposit to a greater degree through gravitational forces (3, 4). Therefore, prolonged exposure to  $100\text{--}500\text{ nm}$  particles can lead to progressively greater cumulative deposition of virus inoculum if the exposure time is sufficiently long. Interestingly, such a particle size corresponds to the  $300\text{ nm}$  particulate size threshold used for grading the filtration efficiency of masks (5) and the most penetrating particle size of single-filter masks (6). Moreover, in field tests, investigators have reported poor performance of N95 masks (7). A key reason for such a finding may have been poor mask seal afforded by N95 masks which could be prevented by elastomeric linings. Accordingly, the overarching objective of our experiment was to compare the “real-world” filtration efficiency of different face masks for fine aerosols over multiple breaths and to study the effect of elastomeric lining in laboratory simulations.

## METHODS

We performed a bench test of a N95 filtering-facepiece respirator (N95 respirator, N95;1860S; 3M Company, St. Paul, MN) and a 3D printed full face mask with elastomeric lining with a N99 filter, or no mask (baseline) using an artificial lung simulator (ASL-5000; IngMar Medical, Inc. Pittsburgh, PA; **Figures 1, 2**) (8). The masks were applied to a mannequin head placed inside a chamber into which aerosol could be introduced. The N95 mask and N99 mask were fitted as well as possible by ensuring the nasal bridge wire was contoured to the face and that the straps were tight to provide adequate pressure to the face to provide the best fit possible (**Figures 1, 2**). The mannequin head was connected through an artificial passageway (mimicking the tracheal airway) to the artificial lung simulator. A constant-rate atomizer with controllable liquid supply flow rate and an in-line desiccant dryer (all stainless-steel construction) (Brechtel Manufacturing Inc. Model 9200) were used for aerosol generation. Polystyrene latex sphere (PSL; Thermo Scientific 3000 Series Nanosphere) aerosols were generated at a fixed diameter of  $350 \pm 6\text{ nm}$ . The generated aerosol sample was transported to a sealed chamber ( $93.4\text{ L}$ ) containing the mannequin head and allowed to equilibrate prior to data collection. Particle number concentration was measured within the tracheal airway at  $1\text{ Hz}$  resolution using a butanol-based mixing-type condensation particle counter (Brechtel Manufacturing Inc. Model 1710). Measurements were collected using the instrument manufacturer’s MCPC\_Recording\_V2.1 software. Proximal to the artificial lung simulator, measurements of flow (heated pneumotachograph, Fleisch, Lausanne, Switzerland) and airway pressure (Validyne, Northridge, CA) were made and stored in a laptop for subsequent review and analysis (**Figure 1**).

Fine aerosol particles with a diameter of  $350 \pm 6\text{ nm}$  were assessed because such aerosols are capable of spreading the virus at short to medium distances (several meters or entire room) as they remain suspended in the air (9, 10). We chose to affix

the masks on mannequin heads to more closely mimic real-life scenarios rather than merely test the filters to address the potential for leakage or penetration of the interface between the mask and the face. The N95 mask has built in metal strips that allow affixing the mask on the face of the mannequin whereas the N99 mask was 3-D printed with an elastomeric lining that can afford a better fit to the mannequin face. Three runs of  $15\text{ min}$  each were performed for each of the two masks and at baseline without a mask and the particle counts were measured over the last  $3\text{-min}$  period when there were stable particle concentrations. Particles were measured in  $3\text{-min}$  blocks at  $1\text{ s}$  time resolution after particle generation and the chamber equilibrated for each mask test. This gave sufficient data for each respective mask ( $180$  points per mask or  $540$  points per group) allowing for robust comparison of the masks as well as the variation from inhalation and exhalation through the masks. The respiratory rate ( $12$  breaths per minute), tidal volume ( $500\text{ ml}$ ), peak inspiratory flow rate ( $60\text{ L/min}$ ) and simulator effort were kept constant when testing each mask against the baseline (background) condition without any mask. The tidal volume, respiratory rate, minute ventilation, and baseline relative humidity inside the chamber (and outside the PPE) were the same across all conditions ( $p > 0.9$ ). Statistical analysis was performed using Generalized Linear Mixed Models (IBM SPSS v25, Armonk, NY).

## RESULTS

Representative raw tracings of particle concentration are shown in **Figure 2** for the baseline condition without a mask and for the N95 and N99 masks. Baseline particle counts were  $2,935 \pm 555$  (mean  $\pm$  standard deviation)  $\text{cm}^{-3}$ , and much higher than that for the N95 mask ( $1,348 \pm 92\text{ cm}^{-3}$ ) and N99 mask with elastomeric lining ( $279 \pm 164\text{ cm}^{-3}$ ;  $p < 0.0001$ ; **Figure 2**). The filtering efficiency was  $54.1$  and  $90.5\%$  for the N95 and N99 masks, respectively.

## DISCUSSION

We found that for fine aerosols with diameters of  $350 \pm 6\text{ nm}$ , the N99 mask with elastomer lining had superior filtration efficiency than the N95 respirator and they both performed lower than their ratings. In general, the total efficiency for filtration by a single-fiber filter includes the summative effects of various mechanisms such as diffusion (for particles smaller than  $100\text{ nm}$ ); interception ( $> 50\text{ nm}$ ), impaction ( $> 100\text{ nm}$ ), and settling ( $> 1,000\text{ nm}$ ) (6). However, there is a *most penetration* for particles between  $80$  and  $400\text{ nm}$  in diameter (6). Interestingly, such a particle size range is remarkably similar to the particle size of fine aerosols that are most likely to be retained within the respiratory tract ( $30\%$  retention) and achieve modest deposition in the lower respiratory tract  $\sim 10\%$  deposition ( $100\text{--}500\text{ nm}$ ). However, these very same particle sizes that correspond to the most penetration particle sizes are more likely to remain suspended in a room as an aerosol and eventually penetrate the mask filter and then be retained in the lung with gradual deposition over multiple breaths. We recognize that

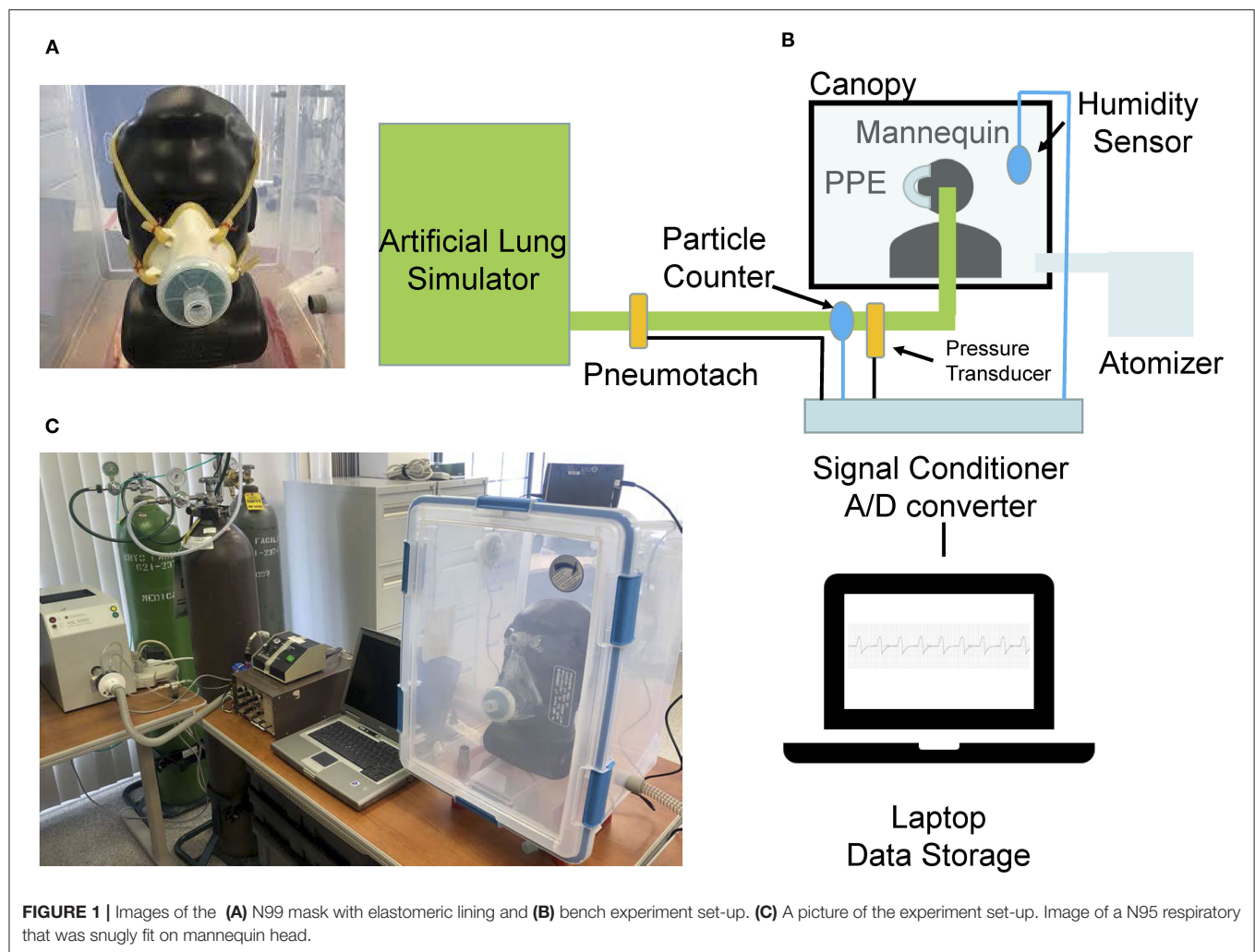


**FIGURE 1 |** Images of the (A) N99 mask with elastomeric lining and (B) bench experiment set-up. (C) A picture of the experiment set-up. Image of a N95 respiratory that was snugly fit on mannequin head.

there was some variability in the particle count. Sources of concentration variability include perturbations in the system's air flow induced by the lung simulator's respiratory cycles, imperfect mixing, potential variability in particle generation at fixed concentration, and potential particle losses to surfaces. Also, we recognize that while these filtration mechanisms do work on their own, often they work in conjunction with one or more other mechanisms depending on particle size and velocity. For instance, large particles with low velocities are filtered more efficiently *via* interception and gravity, particles  $>1\ \mu\text{m}$  will filter out with impaction and interception at high velocities, particles between  $0.2$  and  $0.3\ \mu\text{m}$  will filter out with impaction, interception, and diffusion at high velocities, and lastly particles between  $0.1$  and  $1\ \mu\text{m}$  will filter out with diffusion and interception with decreasing velocity as particle size increases.

Others have reported poor field performance of N95 masks, which may be due to gaps between the N95 mask and the mannequin face that could be prevented by elastomeric linings (7). There are two important aspects of the mask that can be manipulated to improve filtration efficiency. The filter rating and the mask lining. We chose to compare N95 masks without

elastomeric lining to N99 mask with elastomeric lining because these are generally the types of mask plus lining combinations that were available at the beginning of the pandemic. The N99 mask with elastomeric lining in our study was made by combining readily available air-filters (N99 filter rating) into 3D printed masks with elastomeric linings [that could also be replaced by continuous positive airway pressure (CPAP) masks for sleep apnea treatment (11)] to yield the N99 rating mask with elastomeric lining that was tested in our study. There are over 7 million patients with sleep apnea in the U.S. alone who use continuous positive airway pressure (CPAP) machines and N99 filters used in our study were more readily available than N95 masks at the start of the pandemic (11). Such an issue can again arise in future pandemics when supply chains are disrupted. We recognize that "laboratory-based" filtration efficiency measurements is ideally not a combination of leakage around the mask and the filter efficiency, but when simulating real-world conditions in the laboratory, we found lower than anticipated levels of filtration efficiency due to mask filter leakage and additional mask leakage.

Another explanation for the poor performance of the N95 mask observed in our study could be the cumulative

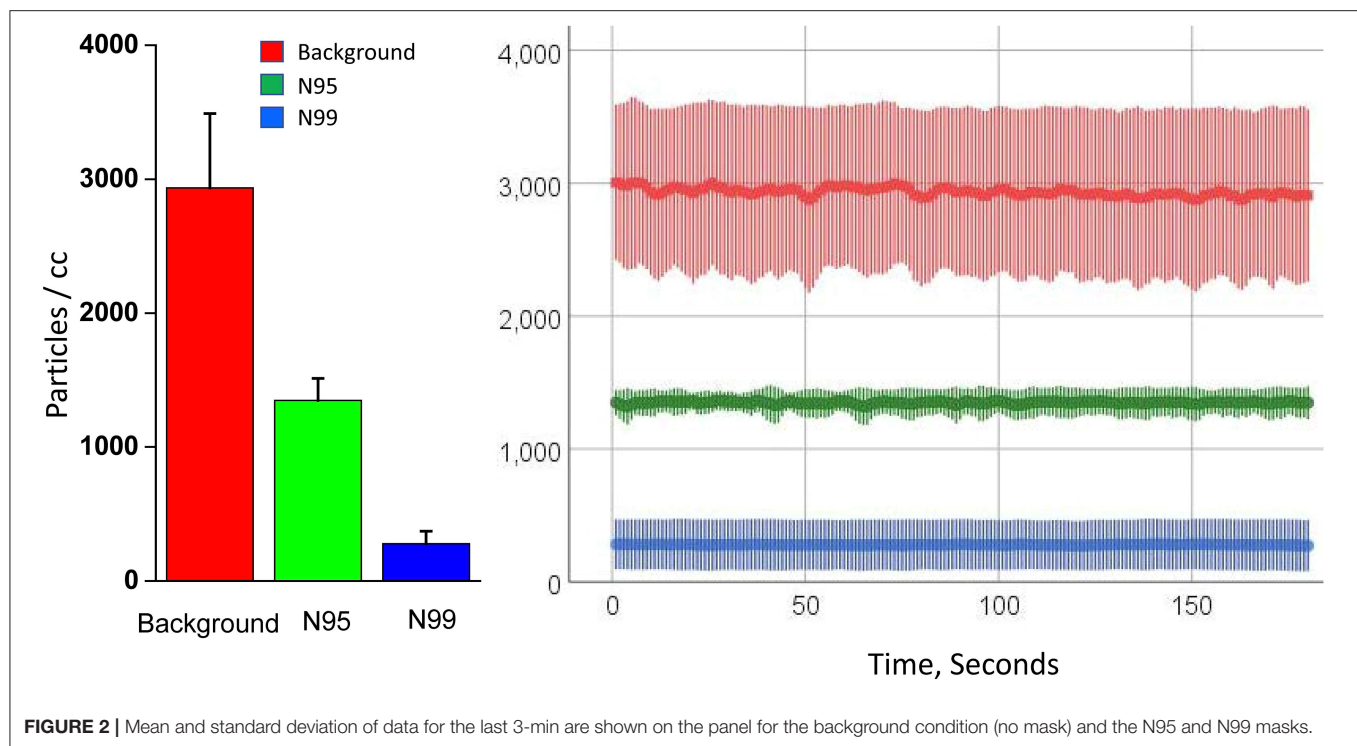


**FIGURE 2 |** Mean and standard deviation of data for the last 3-min are shown on the panel for the background condition (no mask) and the N95 and N99 masks.

accumulation of retained particles that had penetrated through the filter over the course of each breathing run. Such multiple breath simulation is relevant considering that healthcare workers may be within a patient room for >3 min and accumulate and deposit aerosols in their lungs over multiple breaths that can spread the virus several meters or even the entire room (12). In conclusion, we believe that public health recommendations should encourage masks with greater filtration efficiency with elastomeric linings during respiratory viral outbreaks until inoculation is deemed sufficient.

## DATA AVAILABILITY STATEMENT

The raw data supporting the conclusions of this article will be made available by the authors, without undue reservation.

## REFERENCES

1. Our World in Data: Coronavirus (COVID-19) Deaths. Available online at: <https://ourworldindata.org/covid-deaths> (accessed January 15, 2021).
2. Zhang R, Li Y, Zhang AL, Wang Y, Molina MJ. Identifying airborne transmission as the dominant route for the spread of COVID-19. *Proc Natl Acad Sci USA*. (2020) 117:14857–63. doi: 10.1073/pnas.2009637117
3. Park SS, Wexler AS. Size-dependent deposition of particles in the human lung at steady-state breathing. *Aerosol Sci*. (2008) 39:266–76. doi: 10.1016/j.jaerosci.2007.11.006
4. Haber S, Yitzhak D, Tsuda A. Gravitational deposition in a rhythmically expanding and contracting alveolus. *J Appl Physiol* (1985). (2003) 95:657–71. doi: 10.1152/japplphysiol.00770.2002
5. Qian Y, Willeke K, Grinshpun SA, Donnelly J, Coffey CC. Performance of N95 respirators: filtration efficiency for airborne microbial and inert particles. *Am Ind Hyg Assoc J*. (1998) 59:128–32. doi: 10.1080/15428119891010389
6. Hinds WC. *Aerosol Technology*. 2nd ed., New York, NY: John Wiley & Sons. (1999).
7. Adhikari A, Mitra A, Rashidi A, Ekpo I, Schwartz J, Doehling J. Field Evaluation of N95 filtering facepiece respirators on construction jobsites for protection against airborne ultrafine particles. *Int J Environ Res Public Health*. (2018) 15:1958. doi: 10.3390/ijerph15091958
8. Collier D, Stanley D, Parthasarathy S. Effect of air leak on the performance of auto-PAP devices: a bench study. *Sleep Breath*. (2005) 9:167–75. doi: 10.1007/s11325-005-0032-z
9. Morawska L, Milton DK. It is time to address airborne transmission of COVID-19. *Clin Infect Dis*. (2020) 71:2311–3. doi: 10.1093/cid/ciaa939
10. Dhand R, Li J. Coughs and sneezes: their role in transmission of respiratory viral infections, including SARS-CoV-2. *Am J Respir Crit Care Med*. (2020) 202:651–9. doi: 10.1164/rccm.202004-1263PP

## AUTHOR CONTRIBUTIONS

AS, KM, DL, and SP: conception, funding, study design, analysis, drafting the manuscript, and reviewing and editing the manuscript critically. CS, SC, and CM: study design, analysis, conducting experiment, and reviewing and editing the manuscript critically. All authors contributed to the article and approved the submitted version.

## FUNDING

SP was supported by National Institutes of Health Grants (OT2HL156812, HL126140, AG059202, OD028307, HL151254, HL138377) and PCORI (DI-2018C2-13161, PPRND-1507-31666, PCS-1504-30430) during writing of this manuscript. Arizona Board of Regents - RIF grant.

11. Antonescu-Turcu A, Parthasarathy S. CPAP and bi-level PAP therapy: new and established roles. *Respir Care*. (2010) 55:1216-29. Available online at: <http://rc.rcjournal.com/content/55/9/1216.short>
12. Center for Disease Control and Prevention. *Public Health Guidance for Community-Related Exposure*. (2020). Available online at: <https://www.cdc.gov/coronavirus/2019-ncov/php/public-health-recommendations.html> (accessed January 15, 2021).

**Disclaimer:** The statements in this manuscript are solely the responsibility of the authors and do not necessarily represent the views of Patient Centered Outcomes Research Institute (PCORI), its Board of Governors or Methodology Committee.

**Conflict of Interest:** The authors declare that the research was conducted in the absence of any commercial or financial relationships that could be construed as a potential conflict of interest.

Copyright © 2021 Stahl, Frederick, Chaudhary, Morton, Loy, Muralidharan, Sorooshian and Parthasarathy. This is an open-access article distributed under the terms of the Creative Commons Attribution License (CC BY). The use, distribution or reproduction in other forums is permitted, provided the original author(s) and the copyright owner(s) are credited and that the original publication in this journal is cited, in accordance with accepted academic practice. No use, distribution or reproduction is permitted which does not comply with these terms.





# Using Proper Mean Generation Intervals in Modeling of COVID-19

Xiujuan Tang<sup>1</sup>, Salihu S. Musa<sup>2,3</sup>, Shi Zhao<sup>4,5</sup>, Shujiang Mei<sup>1</sup> and Daihai He<sup>2\*</sup>

<sup>1</sup> Shenzhen Center for Disease Control and Prevention, Shenzhen, China, <sup>2</sup> Department of Applied Mathematics, The Hong Kong Polytechnic University, Hong Kong, China, <sup>3</sup> Department of Mathematics, Kano University of Science and Technology, Wudil, Nigeria, <sup>4</sup> The Jockey Club School of Public Health and Primary Care, Chinese University of Hong Kong, Hong Kong, China, <sup>5</sup> Shenzhen Research Institute of Chinese University of Hong Kong, Shenzhen, China

## OPEN ACCESS

### Edited by:

Reza Lashgari,  
Institute for Research in Fundamental  
Sciences, Iran

### Reviewed by:

Hamid Reza Marateb,  
Universitat Politècnica de  
Catalunya, Spain  
Antonella Agodi,  
University of Catania, Italy

### \*Correspondence:

Daihai He  
daihai.he@polyu.edu.hk

### Specialty section:

This article was submitted to  
Infectious Diseases – Surveillance,  
Prevention and Treatment,  
a section of the journal  
Frontiers in Public Health

**Received:** 06 April 2021

**Accepted:** 19 May 2021

**Published:** 05 July 2021

### Citation:

Tang X, Musa SS, Zhao S, Mei S and  
He D (2021) Using Proper Mean  
Generation Intervals in Modeling of  
COVID-19.  
Front. Public Health 9:691262.  
doi: 10.3389/fpubh.2021.691262

In susceptible–exposed–infectious–recovered (SEIR) epidemic models, with the exponentially distributed duration of exposed/infectious statuses, the mean generation interval (GI, time lag between infections of a primary case and its secondary case) equals the mean latent period (LP) plus the mean infectious period (IP). It was widely reported that the GI for COVID-19 is as short as 5 days. However, many works in top journals used longer LP or IP with the sum (i.e., GI), e.g., >7 days. This discrepancy will lead to overestimated basic reproductive number and exaggerated expectation of infection attack rate (AR) and control efficacy. We argue that it is important to use suitable epidemiological parameter values for proper estimation/prediction. Furthermore, we propose an epidemic model to assess the transmission dynamics of COVID-19 for Belgium, Israel, and the United Arab Emirates (UAE). We estimated a time-varying reproductive number [ $R_0(t)$ ] based on the COVID-19 deaths data and we found that Belgium has the highest AR followed by Israel and the UAE.

**Keywords:** COVID-19, reproduction number, generation interval, latent period, infectious period

## INTRODUCTION

Emerging and re-emerging infectious diseases pathogens remain an enormous issue for public health and socio-economic growth because they can spread rapidly worldwide. The coronavirus disease 2019 (COVID-19) is a respiratory disease caused by the severe acute respiratory syndrome coronavirus 2 (SARS-CoV-2) (1, 2), and has become a tremendous public health problem affecting every corner of the world (2). Since its appearance in late 2019, about 124 million people contracted and over 2.7 million died worldwide as of March 25, 2021 (2). Until recently, many clinical features and underlying etiology of the SARS-CoV-2 remain unclear. Timely treatment and effective non-pharmaceutical interventions (NPIs) measures against disease are important for effective mitigation (2).

Generation interval (GI), also referred to as the generation time, is the time lag between infection incidents in an infector–infectee pair (3). It is a proxy of serial interval (SI) of infectious disease, which represent the time lag between onsets of the symptoms in an infector–infectee pair (4). The SI and GI are vital biological quantities (epidemic parameters) used for estimating the basic reproductive number (denoted by  $R_0$ ), which is defined as the number of secondary cases that one infected person will generate on average over the course of his/her infectious period (IP) in a population that is completely susceptible (1, 5), as well as effective reproduction number,  $R_0(t)$ ,

which determines the average number of secondary cases per infectious case in a population made up of both susceptible and non-susceptible hosts (4). Moreover, the importance of GI is also reflected in the renewal equation  $R_0(t) = \frac{I_t}{\sum I_{t-k} w_k}$ , where  $w_k$  represents the GI distribution,  $I_t$  denotes daily infections, and  $R_0(t)$  represents the daily instantaneous reproductive number (in this case), which reflects transmission dynamics at a time,  $t$  (6). Recently, many works have been done to understand and/or estimate the GI, and its proxy, i.e., SI, associated with infectious diseases, including the SARS-CoV and the SARS-CoV-2 (3, 4, 7–13).

Previous reports highlighted that when the SI is larger, the uncertainty and overestimation would be higher (4, 14). The SI (which depends hugely on the incubation period of infectious disease) can be a negative value if the start of symptoms in the infectee happens earlier than the start of the symptoms in the infector (person who transmit the disease) (15–20). The SI can also be a negative value when the incubation period has a relatively wide range than the latent period (LP), which could result in pre-asymptomatic transmission as reported in recent COVID-19 studies (4, 7). However, unlike SI, the GI is solely non-negative according to its definition (10, 21).

The incubation period is the time between infection and the onset of symptoms (21). Although the time of exposure for an individual who transmits the disease (infector) is usually indistinguishable, the time of exposure of an individual who gets the infection (infectee) can be determined by the contact tracing history of the “infector–infectee” pair. This subsequently indicates that for “infector–infectee” pairs, there is a single infector that relates to the infectee epidemiologically. Hence, the incubation periods of infectees can be identifiable. However, the LP differs from the incubation period; it is defined as the time lag between the infection in exposure and onset (beginning) of infectiousness of a typical case (21). Since the beginning of infectiousness is indistinguishable, the LP is unidentifiable. Thus, we noticed that in many diseases (mostly infectious), the mean LP is less than or equal to the mean incubation period (such as COVID-19) (4), whereas some diseases have a long LP, e.g., Ebola virus disease. Note that people infected with Ebola are not infectious until the symptoms started (the incubation period of Ebola varies between 2 and 21 days).

Moreover, the LP is the time interval when an infected individual is unable to transmit the disease, while the time interval during which an infected individual can transmit the disease is called the IP. Both are random variables and are considered independent; thus, the LP and IP are not generally traceable. However, SI is identifiable and well-studied and reported by epidemic models (8, 9). We observed that some studies in the literature did not use the LP and IP appropriately, as the sum of their mean equals the mean GI in susceptible–exposed–infectious–recovered (SEIR)-based models; that is, mean GI = mean LP + mean IP. Using the same notation as in Svensson (3), we have the expectation of the random GI given by  $E(T) = E(X) + E(Y)$ , where  $T$  is the random variable representing the GI of the infection, and  $X$  and  $Y$  represent the random latent time and random infectious time, respectively. Details

on this relation an SEIR-based model can be found in Svensson (3).

Furthermore, it is vital to forecast the size of the outbreak, including infection attack rate (AR), the need for ventilators and hospital beds, the expected severe cases and deaths, the herd immunity threshold, and the vaccine supply needed. All of these are associated with estimate of effective reproductive number,  $R_0(t)$ . Given the important role of  $R_0(t)$ , it is imperative to obtain their estimation more accurately. Therefore, it is crucial to use the proper value for the mean LP and mean IP in SEIR compartmental models.

In the current study, we highlight that using longer IP or LP leads to an overestimation of the reproductive number and other key epidemiological parameters, which, in the initial phase, leads to overestimation of herd immunity threshold and exaggerated control effectiveness. To demonstrate the impact of the GI on  $R_0(t)$  and to provide more qualitative insights into the use of the GI for controlling infectious disease outbreaks, we fitted a simple model using COVID-19 confirmed death data for Belgium, Israel, and the United Arab Emirates (UAE), by employing a more appropriate LP/IP to reveal and shed light and understanding on the transmission dynamics of COVID-19 in each of these countries. We noticed that Belgium was hit badly by two waves and have high AR than the other two countries. Israel and the UAE have started large-scale vaccination programs.

## METHODS

This study adopts a SEIHRD model which is widely used in modeling of COVID-19 with minor modification that hospitalization be interpreted as symptomatic cases. We focus on daily reported COVID-19 deaths data retrieved from the official website of the World Health Organization (WHO) public surveillance reports for Belgium, Israel, and the UAE available from <https://covid19.who.int/> (2). The time-series distribution of weekly confirmations of COVID-19 cases and deaths in Belgium, Israel, and the UAE is depicted in **Figure 1**, which shows the patterns of the COVID-19 epidemics in these three countries. The cases and deaths for COVID-19 are represented by black and red dotted curves, respectively. We observed that Israel and the UAE show similar epidemic curve patterns, while Belgium was hit harder with the two waves of COVID-19 outbreaks. The population data for the three countries were obtained from the worldometer, available from <https://www.worldometers.info/population/> (22).

Thus, we formulate the following simple epidemic model.

$$\begin{aligned}\dot{S} &= -\frac{\beta SI}{N}, \\ \dot{E} &= \frac{\beta SI}{N} - \sigma E, \\ \dot{I} &= \sigma E - \gamma I, \\ \dot{H} &= \theta \gamma I - \kappa H, \\ \dot{D} &= \theta \kappa H, \\ \dot{R} &= (1 - \theta) \gamma I + (1 - \theta) \kappa H.\end{aligned}$$

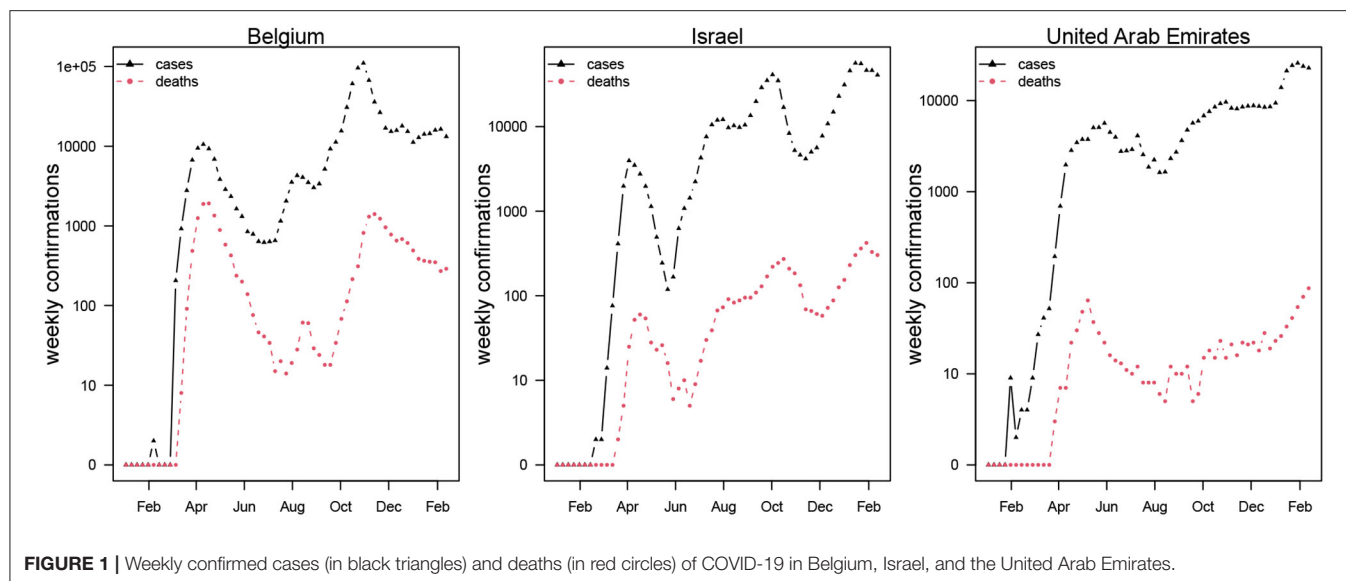


**FIGURE 1 |** Weekly confirmed cases (in black triangles) and deaths (in red circles) of COVID-19 in Belgium, Israel, and the United Arab Emirates.

Here,  $S$ ,  $E$ ,  $I$ ,  $R$ ,  $H$ , and  $D$  represent susceptible, exposed, infection, recovered, hospitalized, and death classes. The parameters  $\beta$ ,  $\sigma$ ,  $\gamma$ , and  $\kappa$  are transmission rate, progression rate from  $E$  to  $I$ , recovery rate (for fitting simplicity, we assumed the recovery rate and hospitalization rate to be the same), and the proportion of individuals moving from  $H$  to  $D$ , respectively.  $\theta$  represents both proportions of hospitalization among infection and the proportion of death among hospitalization. Here, we assumed that hospitalization can be interpreted as symptomatic cases. The infection fatality rate equals  $\theta^2$ . We fit the daily integrated  $D$  to the reported deaths in each country. We assume a negative nominal measurement noise in reporting with an over-dispersion parameter  $\tau$ . We assume a time-varying  $\beta$ , which is an exponential cubic spline function with the number of nodes as 7, which was evenly distributed over the study period from March 1, 2020, to February 18, 2021. The effective reproductive number is given by  $R_0(t) \approx \beta(t)/\gamma$ .

The model fitting package, POMP, has been widely used in previous studies (23–25). The POMP utilized iterated filtering algorithm, which is based on sequential Monte Carlo (SMC). The method has been extensively validated and used in previous studies. Some recent examples include the work of Stone et al. (26) and He et al. (27). The detailed model-fitting method can be found in many previous studies (23–25).

In the classic susceptible–exposed–recovered-based models, the mean GI of an infectious disease equals the sum of the mean LP and the mean IP (3). The duration of individuals in an exposed/infectious class follows exponential distributions. Due to the discrete time in the simulation of the model, the realized (or simulated) mean LP and mean IP according to He et al. (28) are  $LP = \frac{\delta}{1-e^{-\delta\sigma}}$ ,  $IP = \frac{\delta}{1-e^{-\delta\gamma}}$ , where  $\delta$  designates the time discretization step. Thus,  $\sigma^{-1}$  and  $\gamma^{-1}$  are theoretical mean LP and mean IP. The simulated periods were slightly larger than theoretical values due to the time discretization. The discrepancy diminishes when the time step size approaches zero. Hence, the

sum of the mean LP and mean IP is estimated at 6.07 days with a 1-day time step size and theoretical 2 days LP and 3 days IP. The mean GI equals 5 days when the time step size approaches zero. Besides  $\sigma^{-1}$  at 2 days and  $\gamma^{-1}$  at 3 days, we set  $\kappa^{-1} = 14$  days and  $\theta^2$  in the range of 0.5–1% (29). All these parameter values are biologically reasonable.

Therefore, using iterated filtering methods, we fitted a SEIHRD model with an additional death class to reported COVID-19 deaths in the three countries (i.e., Belgium, Israel, and the UAE) to examine the influence of the mean LP and the mean IP for the estimation of reproduction number. We fitted the model to COVID-19 deaths data since COVID-19 mortality data seem less affected by testing policy compared to other diseases.

## RESULTS AND DISCUSSION

Based on recently published studies on GI and SI, we observed that the SI (and/or GI) of COVID-19 varies between 5 and 6 days (30). In particular, Ferretti et al. (31) reported the mean GI as 5.0 days, Ganyani et al. (16) used the data for Singapore and Tianjin, China, and found that the mean GI is estimated at 5.20 (3.78–6.78) days and 3.95 (3.01–4.91) days, respectively. In 40 research papers reviewed by Griffin et al. (30) on the GI and SI, about three studies provided an estimate for the mean GI, which varies roughly between 3.95 and 5.20 days. One paper provided an estimate for the median of the GI as 5.0 days (1, 30, 32, 33). Furthermore, Zhang et al. (12) reported that the incubation period of COVID-19 was estimated at 5.2 (95% CI: 1.8–12.4), and the mean IP was estimated at 4.4 (95% CI: 0.0–14.0) from December 24 to January 27, 2020, and 2.6 (95% CI: 0.0–9.0) from January 28 to February 17, 2020.

However, several studies reported the period of disease progression before the infectiousness stage as the LP in an SEIR epidemic model. For example, Yin et al. (34) conducted a modeling study to assess the effectiveness of NPI measures

**TABLE 1 |** Mean latent period and mean infectious period of COVID-19.

| Mean LP (days)/mean IP (days)  | Equivalent mean GI (days)   | References |
|--|---|------------|
| None   | 5.0   | (31)       |
| None   | 5.20 (3.78–6.78) for Singapore<br>3.95 (3.01–4.91) for Tianjin, China | (16)       |
| 5.2 (95% CI: 1.8–12.4) (incubation period)/4.4 (95% CI: 0.0–14.0) from December 24 to January 27, 2020, and 2.6 (95% CI: 0.0–9.0) from January 28 to February 17, 2020 | >5.2  | (12)       |
| 4.6/9.5  | 14.1  | (34)       |
| 4.6/5  | 9.6   | (35)       |
| 4.3/(5 + 2.1 + 2.9 = 10)   | 10  | (36)       |
| 5.1 (incubation period) 12 (95% CI: 2–14)  | >12   | (37)       |

(including contact tracing, facemask wearing, and rapid testing) to curtail the spread of COVID-19 in China. They reported that asymptomatic patients lasted 4.6 days in LP and 9.5 days in IP until removal. See **Table 1** for more details. Many studies did not follow the rule that mean GI = mean LP + mean IP < 6 days. Therefore, we emphasized that appropriate use of the GI in an epidemiological study is essential to effectively control the COVID-19 outbreaks, because it provides a more accurate estimate on reproduction number for the epidemics, and is crucial for pandemic mitigation planning and forecasting.

For demonstration purposes, we compared epidemiological dynamics of COVID-19 for some randomly selected countries (Belgium, Israel, and the UAE) while varying LP and IP from 2 and 3 days to 3 and 6 days. We employed the model to the COVID-19 mortality data and obtained the time-series fitting results using the COVID-19 data for Belgium, Israel, and the UAE to quantify the effects of longer GI for the estimation of (time-varying) reproduction numbers. In particular, **Figures 2, 3** present the time-series fitting results of the daily confirmed COVID-19 deaths (red circled) with different LP and IP (2 and 3 days to 3 and 6 days) in (a) Belgium, (b) Israel, and (c) the UAE, respectively. The median of the simulation is represented by the black curve, and the time-varying effective reproduction number is denoted by the blue dashed curve. The 95% range of the simulation is shown by the shaded gray region. Based on our results obtained from **Figures 2, 3**, we discovered that using longer mean LP and mean IP would significantly increase an estimate of reproduction number. Thus, the magnitude of reduction in the initial reproduction number would be much higher in the latter cases (3 and 6 days for LP and IP) than in the proper former cases (2 and 3 days for LP and IP). Besides, a higher initial reproduction number would imply a much higher expected infection AR and herd immunity threshold.

Furthermore, a summary of the results of the COVID-19 infection ARs for Belgium, Israel, and the UAE is presented

**TABLE 2 |** Summary results of the estimated infection attack rates (AR) in Belgium, Israel, and the UAE by February 18, 2021.

| Country | Population | Death  | AR    |
|---------|------------|--------|-------|
| Belgium | 11,589,623 | 21,041 | 0.182 |
| Israel  | 8,655,535  | 4,634  | 0.059 |
| UAE     | 9,890,402  | 819    | 0.009 |

in **Table 2** with reasonable LP and IP values. The choice of LP and IP had an important influence on the estimate of AR, likely due to the choice of the flexible transmission rate in our model and the assumption of the infection fatality rate, which varies between 0.5 and 1%. **Appendix Table 1** presents the results of the estimated parameter values including the log likelihood (which is the performance index) for Belgium, Israel, and the UAE. We observed that Belgium has the lowest log likelihood values, indicating that Belgium has hit harder than the other two countries. Also, a summary of the results of the estimated values for the time-varying transmission rate with a fixed number of nodes (denoted by  $n_m$ ) is given in **Appendix Table 2**. The initial values for the state variables used for the model are given in **Appendix Table 3**. Therefore, based on the results obtained and the comparison of the epidemic dynamics of COVID-19 for Belgium, Israel, and the UAE with varying LP and IP, we hypothesize that appropriate LP and IP should be used in epidemiological modeling study to effectively mitigate the spread of disease and to provide suitable suggestions of control strategies for public health implementation and policymaking.

In summary, this study showed that using longer IP or LP leads to overestimation of reproductive number and some other key biological quantities, which, in the initial phase, leads to overestimation of herd immunity threshold and exaggerated control effectiveness. We also quantified the impact of the GI on  $R_0(t)$  to provide insights into the proper use of GI for controlling infectious disease outbreaks by employing COVID-19 mortality data for Belgium, Israel, and the UAE. We noticed that Belgium was hit badly by two waves and have high AR of 0.182 followed by Israel with AR of 0.059 and the UAE with AR of 0.009, whereas Israel and the UAE have started large-scale vaccination programs. Our proposed epidemic model of the COVID-19 presented in this work is similar to previous models discussed in various studies (3, 8, 23, 25, 27, 38–41), with the assumption that hospitalization is considered as symptomatic cases. We employed COVID-19 mortality data for Belgium, Israel, and the UAE in the model to demonstrate the impact of the GI on the reproductive number, and to provide more qualitative insights into the use of the LP/IP for modeling infectious diseases. For future work, we plan to extend our paper by designing a technique that would be used to test the reliability and efficiency of proper validation and performance indices in relation to our fitting results as well as to adapt our existing technique for the design and analysis of the complex scenario. Furthermore, we plan to integrate the existing technique for system implementation modeling and to come up with a model protocol to check and test the reliability of the model and its futures on disease dynamics for timely and effectual control and prevention.



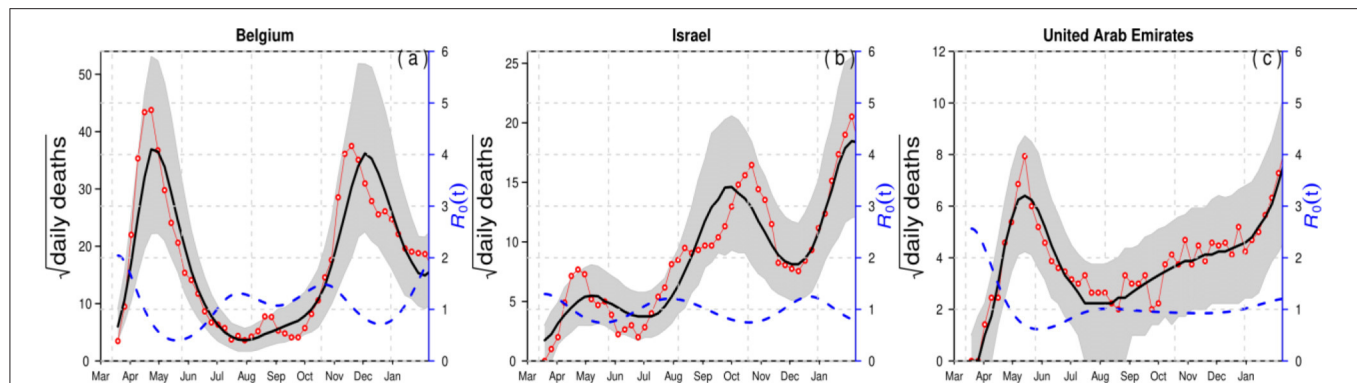


**FIGURE 2 |** Time-series fitting results of daily confirmed COVID-19 deaths (in red circled) in (a) Belgium, (b) Israel, and (c) the United Arab Emirates represented, respectively. The medium of the simulation is represented by the black curve, and the time-varying effective reproduction number  $[R_0(t)]$  is denoted in the blue dashed curve. The 95% confidence interval of the simulation is shown by the shaded (gray) region. The mean LP = 2 and the mean IP = 3.

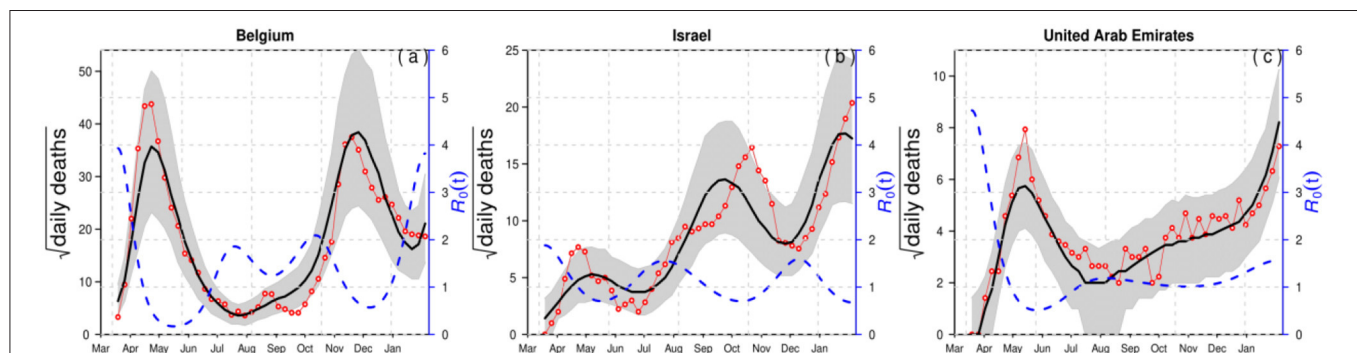


**FIGURE 3 |** Time-series fitting results of daily confirmed COVID-19 deaths (in red circled) in (a) Belgium, (b) Israel, and (c) the United Arab Emirates represented, respectively. The medium of the simulation is represented by the black curve, and the time-varying effective reproduction number  $[R_0(t)]$  is denoted in the blue dashed curve. The 95% confidence interval of the simulation is shown by the shaded (gray) region. The mean LP = 3 days and the mean IP = 6 days.

## CONCLUSIONS

Mean LP, IP, and GI are essential quantities in epidemiological modeling studies that are used for estimation of reproductive number of an infectious disease. For COVID-19, current knowledge showed that the mean GI (mean LP + mean IP) varies between 5 and 6 days, which implies that the mean LP and IP in SEIR models should be around 2–3 days, respectively. We emphasized that this estimate should be used to provide a more reasonable estimation of reproductive number ( $R_0$ ) and other key epidemic quantities, which helps in providing suggestion to policymakers to curtail the spread of an infectious disease. We showed that the estimated  $R_0(t)$  for Belgium, Israel, and the UAE are elevated substantially when longer LP and IP are used. Since now vaccination programs are ongoing in these countries, all modeling fitting is timely to lay the groundwork for the efficacy evaluation of the vaccination programs in these countries.

## DATA AVAILABILITY STATEMENT

The original contributions presented in the study are included in the article/Supplementary Material, further inquiries can be directed to the corresponding author/s.

## AUTHOR CONTRIBUTIONS

All authors listed have equally contributed to the work and approved it for publication.

## FUNDING

DH was supported by an Alibaba China Co. Ltd. Collaborative Research grant (ZG9Z). SM was supported by Shenzhen KeyMedical Discipline Construction Fund (No. SZXK064), Sanming Project of Medicine in Shenzhen (No. SZSM202011008), the National Science Projects Foundation of China (No. 41771441), and the Science and Technology plan project of Shenzhen (No. JSGG20200225152848007). The funder had no role in study design, data collection and analysis, decision to publish, or preparation of the manuscript.

## SUPPLEMENTARY MATERIAL

The Supplementary Material for this article can be found online at: <https://www.frontiersin.org/articles/10.3389/fpubh.2021.691262/full#supplementary-material>

## REFERENCES

- Li Q, Guan X, Wu P, Wang X, Zhou L, Tong Y, et al. Early transmission dynamics in Wuhan, China, of novel coronavirus-infected pneumonia. *New Engl J Med*. (2020) 382:1199–207. doi: 10.1056/NEJMoa2001316
- World Health Organization. *Coronavirus Disease (COVID-19) Dashboard* (2021). Available online at: <https://covid19.who.int/> (accessed January 1, 2021).
- Svensson Å. A note on generation times in epidemic models. *Math Biosci*. (2007) 208:300–11. doi: 10.1016/j.mbs.2006.10.010
- Ali ST, Wang L, Lau EH, Xu X-K, Du Z, Wu Y, et al. Serial interval of SARS-CoV-2 was shortened over time by nonpharmaceutical interventions. *Science*. (2020) 369:1106–9. doi: 10.1126/science.abc9004
- Musa SS, Zhao S, Wang MH, Habib AG, Mustapha UT, He D. Estimation of exponential growth rate and basic reproduction number of the coronavirus disease 2019 (COVID-19) in Africa. *Infect Dis Poverty*. (2020) 9:1–6. doi: 10.1186/s40249-020-00718-y
- Park SW, Sun K, Viboud C, Grenfell BT, Dushoff J. Potential role of social distancing in mitigating spread of coronavirus disease, South Korea. *Emerg Infect Dis*. (2020) 26:2697. doi: 10.3201/eid2611.201099
- He X, Lau EH, Wu P, Deng X, Wang J, Hao X, et al. Temporal dynamics in viral shedding and transmissibility of COVID-19. *Nat Med*. (2020) 26:672–5. doi: 10.1038/s41591-020-0869-5
- Lipsitch M, Cohen T, Cooper B, Robins JM, Ma S, James L, et al. Transmission dynamics and control of severe acute respiratory syndrome. *Science*. (2003) 300:1966–70. doi: 10.1126/science.1086616
- Nishiura H, Linton NM, Akhmetzhanov AR. Serial interval of novel coronavirus (COVID-19) infections. *Int J Infect Dis*. (2020) 93:284–6. doi: 10.1016/j.ijid.2020.02.060
- Wallinga J, Lipsitch M. How generation intervals shape the relationship between growth rates and reproductive numbers. *Proc R Soc B Biol Sci*. (2007) 274:599–604. doi: 10.1098/rspb.2006.3754
- Wang X, Pasco RF, Du Z, Petty M, Fox SJ, Galvani AP, et al. Impact of social distancing measures on coronavirus disease healthcare demand, central Texas, USA. *Emerg Infect Dis*. (2020) 26:2361. doi: 10.3201/eid2610.201702
- Zhang J, Litvinova M, Wang W, Wang Y, Deng X, Chen X, et al. Evolving epidemiology and transmission dynamics of coronavirus disease 2019 outside Hubei province, China: a descriptive and modelling study. *Lancet Infect Dis*. (2020) 20:793–802. doi: 10.1016/S1473-3099(20)30230-9
- Zhao S, Gao D, Zhuang Z, Chong MK, Cai Y, Ran J, et al. Estimating the serial interval of the novel coronavirus disease (COVID-19): a statistical analysis using the public data in Hong Kong from January 16 to February 15, 2020. *Front Phys*. (2020) 8:347. doi: 10.21203/rs.3.rs-18805/v2
- Zhao S, Cao P, Gao D, Zhuang Z, Cai Y, Ran J, et al. Serial interval in determining the estimation of reproduction number of the novel coronavirus disease (COVID-19) during the early outbreak. *J Travel Med*. (2020) 27:taaa033. doi: 10.1093/jtm/taaa033
- Du Z, Xu X, Wu Y, Wang L, Cowling BJ, Meyers LA. Serial interval of COVID-19 among publicly reported confirmed cases. *Emerg Infect Dis*. (2020) 26:1341–3. doi: 10.3201/eid2606.200357
- Ganyani T, Kremer C, Chen D, Torneri A, Faes C, Wallinga J, et al. Estimating the generation interval for coronavirus disease (COVID-19) based on symptom onset data, March 2020. *Euro Surveill*. (2020) 25:2000257. doi: 10.2807/1560-7917.ES.2020.25.17.2000257
- Kong D, Zheng Y, Wu H, Pan H, Wagner AL, Zheng Y, et al. Pre-symptomatic transmission of novel coronavirus in community settings. *Influenza Other Respir Viruses*. (2020) 14:610–4. doi: 10.1111/irv.12773
- Ren X, Li Y, Yang X, Li Z, Cui J, Zhu A, et al. Evidence for pre-symptomatic transmission of coronavirus disease 2019 (COVID-19) in China. *Influenza Other Respir Viruses*. (2020) 15:19–26. doi: 10.1111/irv.12787
- Tindale LC, Stockdale JE, Coombe M, Garlock ES, Lau WYV, Saraswat M, et al. Evidence for transmission of COVID-19 prior to symptom onset. *Elife*. (2020) 9:e57149. doi: 10.7554/eLife.57149
- Zhao S. Estimating the time interval between transmission generations when negative values occur in the serial interval data: using COVID-19 as an example. *Math Biosci Eng*. (2020) 17:3512–9. doi: 10.3934/mbe.2020198
- Yan P. Separate roles of the latent and infectious periods in shaping the relation between the basic reproduction number and the intrinsic growth rate of infectious disease outbreaks. *J Theoretical Biol*. (2008) 251:238–52. doi: 10.1016/j.jtbi.2007.11.027
- Worldometer. *COVID-19 Coronavirus Pandemic 2020* (2021). Available online at: <https://www.worldometers.info/coronavirus/#countries> (accessed January 1, 2021).
- He D, Zhao S, Lin Q, Musa SS, Stone L. New estimates of the Zika virus epidemic attack rate in Northeastern Brazil from 2015 to 2016: A modelling analysis based on Guillain-Barré Syndrome (GBS) surveillance data. *PLoS Neglect Trop Dis*. (2020) 14:e0007502. doi: 10.1371/journal.pntd.0007502
- Musa SS, Zhao S, Gao D, Lin Q, Chowell G, He D. Mechanistic modelling of the large-scale Lassa fever epidemics in Nigeria from 2016 to 2019. *J Theoretical Biol*. (2020) 493:110209. doi: 10.1016/j.jtbi.2020.110209
- Zhao S, Stone L, Gao D, He D. Modelling the large-scale yellow fever outbreak in Luanda, Angola, and the impact of vaccination. *PLoS Neglect Trop Dis*. (2018) 12:e0006158. doi: 10.1371/journal.pntd.0006158
- Stone L, He D, Lehnstaedt S, Artzy-Randrup Y. Extraordinary curtailment of massive typhus epidemic in the Warsaw Ghetto. *Sci Adv*. (2020) 6:eabc0927. doi: 10.1126/sciadv.abc0927
- He D, Artzy-Randrup Y, Musa SS, Stone L. The unexpected dynamics of COVID-19 in Manaus, Brazil: herd immunity versus interventions. *medRxiv [Preprint]*. (2021). doi: 10.1101/2021.02.18.21251809
- He D, Ionides EL, King AA. Plug-and-play inference for disease dynamics: measles in large and small populations as a case study. *J R Soc Interface*. (2010) 7:271–83. doi: 10.1098/rsif.2009.0151
- Mellan TA, Hoeltgebaum HH, Mishra S, Whittaker C, Schnekenberg RP, Gandy A, et al. Subnational analysis of the COVID-19 epidemic in Brazil. *medRxiv [Preprint]*. (2020). doi: 10.1101/2020.05.09.20096701
- Griffin J, Casey M, Collins A, Hunt K, McEvoy D, Byrne A, et al. Rapid review of available evidence on the serial interval and generation time of COVID-19. *BMJ Open*. (2020) 10:e040263. doi: 10.1136/bmjopen-2020-040263
- Ferretti L, Wymant C, Kendall M, Zhao L, Nurtay A, Abeler-Dörner L, et al. Quantifying SARS-CoV-2 transmission suggests epidemic control with digital contact tracing. *Science*. (2020) 368:eabb6936. doi: 10.1101/2020.03.08.20032946
- Backer JA, Klinkenberg D, Wallinga J. Incubation period of 2019 novel coronavirus (2019-nCoV) infections among travellers from Wuhan, China, 20–28 January 2020. *Eurosurveillance*. (2020) 25:2000062. doi: 10.2807/1560-7917.ES.2020.25.5.2000062
- Ferguson N, Laydon D, Nedjati Gilani G, Imai N, Ainslie K, Baguelin M, et al. *Report 9: Impact of Non-pharmaceutical Interventions (NPIs) to Reduce COVID19 Mortality and Healthcare Demand*. London: Imperial College London (2020). p. 1–20.
- Yin L, Zhang H, Li Y, Liu K, Chen T, Luo W, et al. Effectiveness of contact tracing, mask wearing and prompt testing on suppressing COVID-19 resurgences in megacities: an individual-based modelling study. *SSRN Electron J*. (2021). doi: 10.2139/ssrn.3765491
- Kissler SM, Tedijanto C, Goldstein E, Grad YH, Lipsitch M. Projecting the transmission dynamics of SARS-CoV-2 through the postpandemic period. *Science*. (2020) 368:860–8. doi: 10.1126/science.ab5793
- Emery JC, Russel TW, Liu Y, Hellewell J, Pearson CA, Knight GM, et al. The contribution of asymptomatic SARS-CoV-2 infections to transmission: a model-based analysis of the Diamond Princess outbreak. *medRxiv [Preprint]*. (2020). doi: 10.1101/2020.05.07.20093849
- Lauer SA, Grantz KH, Bi Q, Jones FK, Zheng Q, Meredith HR, et al. The incubation period of coronavirus disease 2019 (COVID-19) from publicly reported confirmed cases: estimation and application. *Ann Intern Med*. (2020) 172:577–82. doi: 10.7326/M20-0504

38. Ahmad MD, Usman M, Khan A, Imran M. Optimal control analysis of Ebola disease with control strategies of quarantine and vaccination. *Infect Dis Poverty*. (2016) 5:1–12. doi: 10.1186/s40249-016-0161-6
39. Britton T, Ball F, Trapman P. A mathematical model reveals the influence of population heterogeneity on herd immunity to SARS-CoV-2. *Science*. (2020) 369:846–9. doi: 10.1126/science.abc6810
40. Buss LF, Prete CA, Abraham CM, Mendrone A, Salomon T, de Almeida-Neto C, et al. Three-quarters attack rate of SARS-CoV-2 in the Brazilian Amazon during a largely unmitigated epidemic. *Science*. (2021) 371:288–92. doi: 10.1126/science.abe9728
41. Chowell G, Viboud C, Simonsen L, Moghadas SM. Characterizing the reproduction number of epidemics with early subexponential growth dynamics. *J R Soc Interface*. (2016) 13:20160659. doi: 10.1098/rsif.2016.0659

**Conflict of Interest:** DH was supported by an Alibaba China Co. Ltd. Collaborative Research grant (ZG9Z).

The remaining authors declare that the research was conducted in the absence of any commercial or financial relationships that could be construed as a potential conflict of interest.

Copyright © 2021 Tang, Musa, Zhao, Mei and He. This is an open-access article distributed under the terms of the Creative Commons Attribution License (CC BY). The use, distribution or reproduction in other forums is permitted, provided the original author(s) and the copyright owner(s) are credited and that the original publication in this journal is cited, in accordance with accepted academic practice. No use, distribution or reproduction is permitted which does not comply with these terms.



# Original Hosts, Clinical Features, Transmission Routes, and Vaccine Development for Coronavirus Disease (COVID-19)

Ting Wu<sup>1,2,3†</sup>, Shuntong Kang<sup>1,3,4†</sup>, Wenyao Peng<sup>1,4</sup>, Chenzhe Zuo<sup>1,4</sup>, Yuhao Zhu<sup>1,4</sup>, Liangyu Pan<sup>1</sup>, Keyun Fu<sup>1,4</sup>, Yaxian You<sup>1</sup>, Xinyuan Yang<sup>1,4</sup>, Xuan Luo<sup>1,5</sup>, Liping Jiang<sup>4</sup> and Meichun Deng<sup>1,3,4\*</sup>

<sup>1</sup> Department of Biochemistry and Molecular Biology, Hunan Province Key Laboratory of Basic and Applied Hematology, School of Life Sciences, Central South University, Changsha, China, <sup>2</sup> Department of Cardiovascular Medicine, The Third Xiangya Hospital, Central South University, Changsha, China, <sup>3</sup> Hunan Key Laboratory of Animal Models for Human Diseases, Hunan Key Laboratory of Medical Genetics, School of Life Sciences, Central South University, Changsha, China, <sup>4</sup> Xiangya School of Medicine, Central South University, Changsha, China, <sup>5</sup> Hunan Yuanpin Cell Biotechnology Co., Ltd, Changsha, China

## OPEN ACCESS

### Edited by:

Arda Kiani,  
Shahid Beheshti University of Medical  
Sciences, Iran

### Reviewed by:

Daxi Wang,  
Beijing Genomics Institute (BGI), China  
Kewal Krishan,  
Panjab University, India

### \*Correspondence:

Meichun Deng  
dengmch@csu.edu.cn

<sup>†</sup>These authors have contributed  
equally to this work

### Specialty section:

This article was submitted to  
Infectious Diseases - Surveillance,  
Prevention and Treatment,  
a section of the journal  
Frontiers in Medicine

Received: 29 April 2021

Accepted: 31 May 2021

Published: 06 July 2021

### Citation:

Wu T, Kang S, Peng W, Zuo C, Zhu Y,  
Pan L, Fu K, You Y, Yang X, Luo X,  
Jiang L and Deng M (2021) Original  
Hosts, Clinical Features, Transmission  
Routes, and Vaccine Development for  
Coronavirus Disease (COVID-19).  
Front. Med. 8:702066.  
doi: 10.3389/fmed.2021.702066

The pandemic of coronavirus disease 2019 (COVID-19), which is caused by severe acute respiratory syndrome coronavirus 2 (SARS-CoV-2), has led to public concern worldwide. Although a variety of hypotheses about the hosts of SARS-CoV-2 have been proposed, an exact conclusion has not yet been reached. Initial clinical manifestations associated with COVID-19 are similar to those of other acute respiratory infections, leading to misdiagnoses and resulting in the outbreak at the early stage. SARS-CoV-2 is predominantly spread by droplet transmission and close contact; the possibilities of fecal-oral, vertical, and aerosol transmission have not yet been fully confirmed or rejected. Besides, COVID-19 cases have been reported within communities, households, and nosocomial settings through contact with confirmed COVID-19 patients or asymptomatic individuals. Environmental contamination is also a major driver for the COVID-19 pandemic. Considering the absence of specific treatment for COVID-19, it is urgent to decrease the risk of transmission and take preventive measures to control the spread of the virus. In this review, we summarize the latest available data on the potential hosts, entry receptors, clinical features, and risk factors of COVID-19 and transmission routes of SARS-CoV-2, and we present the data about development of vaccines.

**Keywords: SARS-CoV-2, COVID-19, original host, transmission modes, vaccine development**

## INTRODUCTION

In late December 2019, a novel coronavirus associated with pneumonia spread rampantly. The World Health Organization (WHO) named the infectious condition coronavirus disease 2019 (COVID-19), and the virus was classified as severe acute respiratory syndrome coronavirus 2 (SARS-CoV-2). Compared to SARS-CoV-1, SARS-CoV-2 has a higher basic reproduction number and higher transmissibility. The origin of SARS-CoV-2 remains unknown and within a short period, COVID-19 has become a serious threat to the global economy and human health. The clinical symptoms generally include fever, fatigue, cough, vomit, diarrhea, and dyspnea in humans



(1). However, patients in the incubation period and asymptomatic patients do not show these symptoms, and are hence easily misdiagnosed, which leads to an increased risk of SARS-CoV-2 transmission. It has been reported that each patient with COVID-19 infects ~2.2 close contacts (2, 3). Currently, there is no specific treatment for COVID-19, so the best strategy to control the number of COVID-19 cases is to limit the spread of the virus. To predict the epidemic trend and guide control measures, reliable information is urgently needed. In this review, we summarize the recent data on potential SARS-CoV-2 hosts, the clinical features of COVID-19, the risk factors of severe COVID-19, and the different modes of viral transmission. Finally, we summarized the safety and efficacy of some vaccines.

## POTENTIAL HOSTS OF SARS-COV-2

Virus hosts are divided into natural, intermediate, and final hosts according to the viral transmission routes and the progenitor viruses existing in the natural host cannot effectively use human susceptible cell receptors and fail to invade directly, which is the main factor that limits the direct transmission of progenitor viruses to humans (4). Despite the international research effort conducted, a natural host, either direct or intermediate, has not yet been identified (**Figure 1**). It is currently thought that SARS-CoV-2 has a zoonotic origin and has secondarily acquired human-to-human spreading capacity (5).

The discovery of diverse bat coronaviruses closely related to SARS-CoV-2 suggests that bats are possible reservoirs of SARS-CoV-2 (6). Bats are critical natural hosts of alpha- and beta-coronavirus. So far, the virus closest to SARS-CoV-2 is a bat coronavirus named RaTG13 found in *Rhinolophus affinis* in Yunnan Province, China, whose full-length genome sequence is 96.2% matching the total length of SARS-CoV-2 (7) and phylogenetic analysis verified that SARS-CoV-2 is tightly combined with RaTG13 (8). Another novel bat virus RmYN02 noted more recently in a *Rhinolophus malayanus* bat found in Yunnan is 93.3% identical to SARS-CoV-2 across the genome, which exhibits 97.2% identity to SARS-CoV-2, which is even higher than for RaTG13 in the long lab gene (9). Moreover, bat related coronaviruses ZC45 and ZXC21, which are previously detected in *Rhinolophus pusillus* bats in eastern China, also belong to the SARS-CoV-2 lineage of the sarbecovirus subgenus by phylogenetic analysis (10).

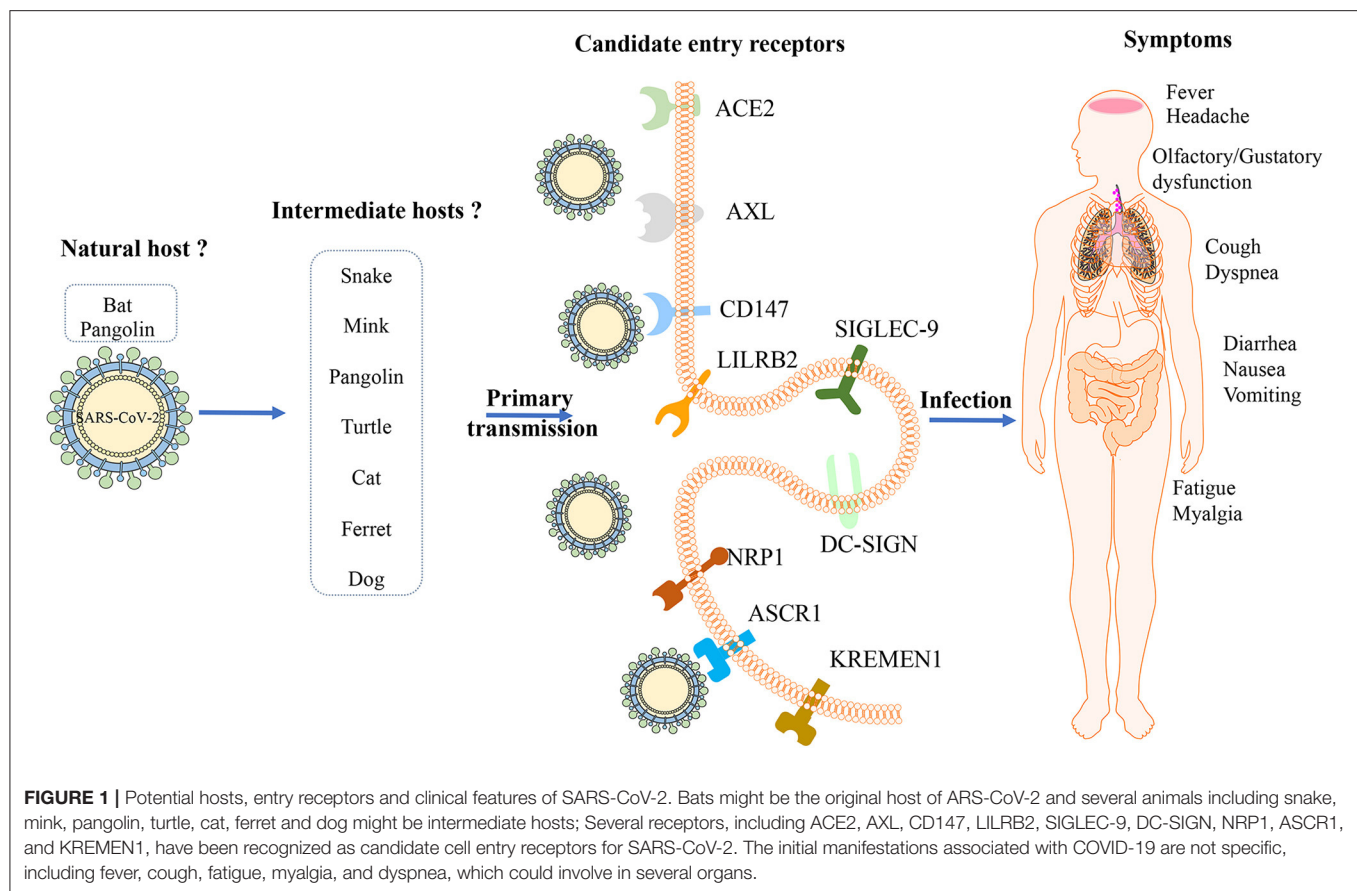
From 2017 to 2019, a variety of SARS-CoV-2 related viruses have been identified in *Malayan pangolin* tissues smuggled from Southeast Asia to China. Some independent studies suggested the pangolin as SARS-CoV-2 host (11–13), while other studies proposed that the pangolin may be a natural host rather than an intermediate host (14, 15). The latest study revealed the receptor-binding domain (RBD) of the S protein of Guangdong pangolin coronaviruses is similar to SARS-CoV-2 with one difference in a non-critical amino acid, remaining all five critical residues identical for receptor binding (12). Compared with the Guangdong strains, the pangolin coronaviruses reported in Guangxi is similar to SARS-CoV-2 with only 85.5% genome sequence identity (11). The results indicate that pangolins have

the potential to act as intermediate hosts for SARS-CoV-2, but the genome identity of pangolin coronaviruses known to date with SARS-CoV-2 does not exceed 92% (16). Existing data are insufficient to be the evidence explaining that pangolins directly participated in the emergence of SARS-CoV-2.

Additionally, comprehensive sequence analysis and comparison with respect to relative synonymous codon usage (RSCU) suggested that SARS-CoV-2 has a codon usage bias similar to that in snakes (17). However, it's argued that the data based on RSCU were not sufficient to regard snakes as an immediate host of SARS-CoV-2, as the relation between coronaviruses and vertebrates has never been reported (14). By predicting the interaction between the RBD of coronavirus spike protein and the host receptor, angiotensin-converting enzyme 2 (ACE2) with systematic comparison and analysis, turtles (*Chrysemys picta bellii*, *Chelonia mydas*, and *Pelodiscus sinensis*) should also be considered as potential intermediate hosts that can transmit SARS-CoV-2 to humans (18).

Besides wildlife, a virus–host prediction analysis with a deep learning algorithm showed that the infectivity pattern of potential hosts by mink viruses resembles that of SARS-CoV-2 (19), which is subsequently confirmed by a report on the outbreak of SARS-CoV-2 infection in farmed mink documenting the susceptibility of mink in Netherlands (20). Although most infected minks have mild symptoms, some develop severe respiratory distress and die of interstitial pneumonia. But the latest test of mink farm related staff showed 68% had evidence of SARS-CoV-2 infection with an animal sequence signature, which proved the two-way transmission on mink farms (21). A serological investigation evaluated the infection of cats by SARS-CoV-2 by detecting specific neutralizing serum antibodies (22), and it demonstrated that SARS-CoV-2 could infect cat populations. But cats will recover quickly after being infected with SARS-CoV-2, and their infectiousness will not last too long, so cats will not pose a threat to human health in the long run and the potential for the spread of SARS-CoV-2 from cats to humans can't be ignored. Meanwhile, 2 out of 15 dogs from households with confirmed human cases of COVID-19 in Hong Kong were found SARS-CoV-2 positive and remained asymptomatic during quarantine (23). An experimental study showed that SARS-CoV-2 effectively replicates in the upper respiratory tract of cats and ferrets, while dogs, pigs, chickens and ducks are not sensitive to SARS-CoV-2 (24). So far, studies based on RBD domain analysis have ruled out the possibility of mice, rats and rabbits participating in the SARS-CoV-2 cycle (25). These results suggest that people with COVID-19 should limit contact with their pets to avoid potential transmission.

It is worth noting that investigations and researches deny that SARS-CoV-2 emerged through laboratory manipulation of any linked SARS-CoV-like coronavirus and for the RBD of SARS-CoV-2 is optimized and can be combined with human ACE2 through an effective solution different from the previously predicted solution (5). In addition, if genetic manipulations have been performed, one of several reverse gene systems available for beta-coronavirus may have been used, the genetic data irrefutably demonstrate that SARS-CoV-2 is not derived from any previously used virus backbone (26). But on the



basis of other analyses, an artificial origin of SARS-CoV-2 is not a baseless conspiracy theory that is to be condemned (27, 28). They presume that SARS-CoV-2 may be a chimera, most of its sequence is closest to bat coronavirus RaTG13, and its RBD is almost the same as pangolin MP789-like CoV, and the furin cleavage site in the SARS-CoV-2 spike protein which gives the virus the ability to cross species and tissue barriers was previously not seen in other SARS-like CoVs, thus human intervention cannot be ruled out. However, this hypothesis was immediately rejected in the view that SARS-CoV-2 origin doesn't require recombination. The RBD of SARS-CoV-2 represent a non-recombinant variant of the ancestor and the hypothesis of artificial creation does not agree with a number of findings based on genetic analysis of SARS-CoV-2 and its relatives (29). The origin of SARS-CoV-2 is the subject of many hypotheses, most arguments have greatly weakened the hypothesis of the laboratory origin, and the hypothesis of natural origin is consistent with all available genetic and experimental data.

The source of SARS-CoV-2 remains increasingly obscure, but it is crucial to determine where exactly it first appeared and how it initially spread through the population to clarify the viral transmission routes and to eliminate secondary transmission. Hence, it is necessary to strengthen cooperation between countries to treat patients

and conduct COVID-19-related research to overcome the novel coronavirus pandemic.

## ENTRY RECEPTOR FOR SARS-COV-2

Attachment of the viruses to the cell surface receptor is the first step in infection and most viruses have evolved to recognize receptors, which are glycans on cell surface glycoproteins or glycolipids (30). After the SARS-CoV outbreak in 2003, ACE2 was confirmed as a receptor that enters lung epithelial cells (Figure 1) (31). It seems that both SARS-CoV-2 and SARS-CoV use a similar host cell entry mechanism and work by binding to the host ACE2, which is located on the surface of the host cell and is abundantly present (32). ACE2 is a type I transmembrane protein, which is mainly involved in the regulation of blood pressure, humoral balance and cell proliferation. It consists of a highly glycosylated N-terminal domain located outside the cell and a shorter C-terminal domain located in the cell. The N-terminal domain contains the binding site of the virus S protein. ACE2 is mainly distributed in alveolar epithelial cells, intestinal epithelial cells and bronchial epithelial cells. Some studies have shown that it is also expressed in vascular endothelial cells, heart, kidney and other organs, but the expression is low in spleen, thymus, lymph nodes, bone marrow and immune cells (33). The results of pathological study also showed that the pathological

damage caused by SARS-CoV-2 was mainly concentrated in the lung, and the digestive organs and kidneys were also damaged to varying degrees (34). It's worth noting that the affinity between ACE2 and a SARS-CoV-2 S ectodomain is ~10–20-fold higher than ACE2 and SARS-CoV S (35). To fulfill its entry, the SARS-CoV-2 spike binds to its receptor human ACE2 (hACE2) through its RBD and is activated by human proteases proteolytically. It shows although SARS-CoV-2 RBD albeits more potent, its exposure is less than SARS-CoV RBD. And SARS-CoV-2 is preactivated by the proprotein convertase furin, thereby reducing its dependence on the entry of target cell proteases, which is different from SRAR-CoV (36).

Relying on ACE2 receptor alone does not seem to be enough to explain the strong infectivity and transmission of SARS-CoV-2. Although the role of ACE2 as a SARS-CoV-2 receptor is clear, studies have shown that the expression of ACE2 in various human tissues, especially in the respiratory tract, is extremely low. Combining proteomics, bioinformatics and computational biology methods, researchers found that the tyrosine-protein kinase receptor UFO (AXL) interacts with the N-terminal domain of SARS-CoV-2 S specifically and there is a strong co-localization on the cell membrane. In the bronchoalveolar lavage fluid cells of COVID-19 patients, the expression level of AXL is highly correlated with the level of SARS-CoV-2 S and AXL is highly expressed in almost all types of respiratory system cells including lung type I/II epithelial cells, basal cells, and fibroblasts. So AXL is a candidate receptor for SARS-CoV-2 (37). Additionally, CD147 is a transmembrane glycoprotein, a member of the immunoglobulin superfamily, involved in tumorigenesis and development, malaria parasite invasion and influenza virus infection. CD147 exists in a variety of cells in the lungs and is highly expressed in type II alveolar cells and macrophages in patients with pulmonary fibrosis (38). CD147 can also interact directly with the RBD domain of SARS-CoV-2 S protein because humanized anti-CD147 antibody can competitively inhibit the binding of S protein and CD147 and inhibit virus infection in host cells, suggesting that CD147 may also be one of the receptors mediating SARS-CoV-2 infection (39). This finding has been recognized by other research groups, and through determination that the binding affinity of CD147 to SARS-CoV-2 S protein is 0.185  $\mu$ M, which is 15 nM lower than the affinity of ACE2 to S protein (40).

Also, Type II transmembrane glycoprotein C-type lectin dendritic cells specifically bind to non-integrated molecules (Dendritic cell-specific ICAM-3 grabbing non-integrin, DC-SIGN) and liver/lymphocytes specifically bind to non-integrated molecules (Liver/lymph cell-specific ICAM-3 grabbing non-integrin, L-SIGN) are reported to interact with SARS-CoV S protein to mediate virus invasion, but its mediated infection efficiency is much lower than that of ACE2. L-SIGN is a potential receptor for SARS-CoV, similar to Ebola virus and Sindbis virus. In addition, L-SIGN can also internalize viruses and promote virus degradation in a proteasome-dependent manner (41). The three potential receptors of the SARS-CoV-2, ACE-2, DC-SIGN, and L-SIGN, have higher expression levels in the lungs of smokers and the elderly, and higher expression levels in whites than Asians. However, this study is only based on

gene expression databases, and more experiments are needed for verification (42).

Studies have confirmed that SARS-CoV-2 S protein can bind to neuropilin-1(NRP-1) on the surface of host cells through the CendR domain of the S1 protein subunit. The interaction of S1 CendR-Neuropilin-1 may promote the invasion and infection of SARS-CoV-2 (43, 44). Additionally, ASGR1 is an endocytic recycling receptor, which plays a key role in serum glycoprotein homeostasis and is reported to promote the invasion of hepatitis C virus (45, 46). Wnt/ $\beta$ -catenin signal transduction is essential for taste bud cell renewal and behavioral taste perception, and KREMEN1 is a negative regulator of this pathway, which can antagonize classic WNT signal transduction, and is also an invasion receptor for most enteroviruses. Odor and taste loss is often observed in COVID-19 patients, which suggests that SARS-CoV-2 may act through these receptors, thereby affecting Wnt/ $\beta$ -catenin signaling and causing loss of taste (47, 48). ASGR1 and KREMEN1 are speculated to be the co-receptors of SARS-CoV-2. Studies show that the susceptibility to viruses in airway epithelial cilia, secretory cells and immune macrophages are highly correlated with the expression of ACE2, KREMEN1 and ASGR1, respectively, and ACE2/ASGR1/KREMEN1 (ASK) together show a greater correlation than any single one (49). The interaction between the virus and the host receptor can induce cytokine secretion, apoptosis and stimulate immune response. Both LILRB2 and SIGLEC-9 are mainly expressed in myeloid cells, and COVID-19 is related to the excessive activation of myeloid cells. Therefore, these receptors may be involved in the activation of pro-inflammatory monocyte-derived macrophages, which in turn causes local inflammation (**Figure 1**) (49, 50).

In addition to the receptor, the host protease acting on the S protein can also promote viral infection. After the S1 subunit of the coronavirus S protein recognizes and binds the cell receptor, some proteases on the surface of the target cell will cut the S protein into S1 and S2 subunits, and then the S2 subunit will induce the fusion of the virus membrane and the cell membrane. If there are no these proteases on the cell surface, the virus will enter the host cell through endocytosis, and then the S protein will be cut into S1 and S2 subunits by cathepsin in endosome or lysosome, and then membrane fusion will occur to complete the invasion of the virus (51). Furin protease is a member of the precursor protein invertase (Proproteinconvertase, PACE) family, which mainly recognizes arginine-rich protein sites, can cleave secretory protein precursors into active proteins, and plays an important role in membrane receptor maturation, tumor metastasis, processing and activation of viral coat proteins and bacterial exotoxins. The existence of Furin protease cleavage site in SARS-CoV-2 S protein makes its infection mechanism different from that of most coronaviruses such as SARS-CoV, but more similar to that of HIV, Ebola virus and some avian influenza viruses, which may be one of the reasons why its transmission ability is higher than that of SARS virus CoV (52). Transmembrane prostease serine 2 (TMPRSS2) belongs to type II transmembrane protein, which is mainly located on the surface of cell membrane. It is highly expressed on the surface of respiratory epithelial cells and participates in the activation of many respiratory viruses. It can cleave the S proteins



of coronavirus SARS-CoV, MERS-CoV, HCoV229 and SARS-CoV-2, and promote the fusion between virus and target cells. TMPRSS2 forms a receptor proteasome complex with ACE2, and cut the extracellular domain of receptor ACE2 to improve the efficiency of direct invasion of SARS CoV on the cell surface (53, 54). Transmembrane protease serine 11a (TMPRSS11a), Human airway trypsin-like protease (HAT), Trypsin, Thermolysin and Elastase can induce the fusion of SARS-CoV and cell membrane on the cell surface and promote virus infection, so it is speculated that they may have similar functions for SARS-CoV-2 (55). Cathepsins include cysteine, serine, and aspartyl proteases with endopeptidase and exopeptidase activities. They are widely distributed in the endosomes and lysosomes in the acidic environment of cells, and play a role in degrading proteins and processing antigens (56). Studies have proved that Cathepsin L (CatL) inhibitors is possibly safer and more effective therapy to block coronavirus host cell entry and intracellular replication, without compromising the immune system (57). In the SARS-CoV related study, some other factors are also involved in the process of virus entry. Interferon-induced transmembrane protein (IFITM) can inhibit the virus from entering the cell through the endocytic pathway (58) and Phosphatidylinositol-4-kinase III $\beta$  (PI4KB) can produce the lipid microenvironment needed to promote the virus to enter the cell when the S protein invades the cell (59).

In summary, host cell receptors are a key determinant of virus tropism and pathogenesis. In addition to ACE2, SARS-CoV-2 can also interact with multiple receptors to invade the human body. These receptors are likely to interact with SARS-CoV-2 under different environmental or physiological conditions, trigger different signals, and ultimately lead to virus infection and host immune response, thereby promoting the pathogenic process of the virus. In view of the fact that SARS-CoV-2 has a stronger spreading power than SARS-CoV and is more harmful, scientists around the world are conducting research on SARS-CoV-2 and more specific mechanisms of SARS-CoV-2 invading cells will be clarified.

## CLINICAL FEATURES OF COVID-19

SARS-CoV-2 targets the respiratory tract, but the initial manifestations associated with COVID-19 are not specific (**Figure 1**), so it is difficult to distinguish between COVID-19 and other coronavirus infections, including SARS and Middle East respiratory syndrome (MERS) (60–62). When patients present with acute respiratory infection signs, including fever, cough, and headache, at the beginning of the illness, it is easily misdiagnosed, indicating clinicians should pay much attention to the underlying causes.

COVID-19 can be asymptomatic, and it can lead to mild or severe disease, or even death. The incubation period for COVID-19 is generally <14 days, and the mean incubation period is ~5 days (63). However, Wang et al. collected clinical data of 2015 laboratory-confirmed COVID-19 patients, and found that the incubation period varied from 0 to 33 days, and the incubation period of 11.6% of the patients was longer than 14 days (64).

Individuals at any age can be infected with SARS-CoV-2, and the average age of patients with COVID-19 is 49.8 years. The most predominant symptoms in mild COVID-19 patients are fever, cough, fatigue, myalgia, and dyspnea (65, 66). Gastrointestinal symptoms, including diarrhea, nausea, and vomiting, have also been reported, but were less common (63). However, the digestive symptoms could be preceding the onset of respiratory symptoms in mild COVID-19 patients (67). Interestingly, it was reported that sudden and complete loss of olfactory function is also a main symptom in patients with COVID-19 (68). A multicenter study revealed that olfactory and gustatory dysfunction, which are less common in Asia, could be significant symptoms in European patients with mild-to-moderate COVID-19 (69, 70). The significantly different manifestations in different regions remind us to highlight the complexity of COVID-19. In patients recovering from COVID-19, the hallmark of COVID-19 is the presence of ground-glass opacities (GGOs) in CT images of the lungs at the early stage after symptom onset (71). In the progressive stage (5–8 days after symptom onset), patients present with more GGOs, extending to multiple pulmonary lobes and with a crazier paving appearance. The CT score and the number of lung zones involved aggravate rapidly, peaking at ~10 days after symptom onset. At this stage, consolidation and diffused GGOs are predominant findings. After 2 weeks, lesions are gradually absorbed, with a decreased GGO ratio (72, 73). Patients with severe COVID-19 are more likely to experience severe complications, including acute cardiac injury, arrhythmia, acute kidney injury, and shock (70). In terms of laboratory findings, an increased erythrocyte sedimentation rate (ESR) and elevated levels of C-reactive protein (CRP), lactate dehydrogenase (LDH), ferritin, interleukin 6 (IL-6), and tumor necrosis factor- $\alpha$  (TNF- $\alpha$ ) are commonly observed in patients with COVID-19. The lymphocyte count is generally below normal values (74). Recently, high rate of thromboembolism has also been defined as an important feature of patients with COVID-19 (75, 76). Compared with mild patients, higher levels of plasma cytokines were observed among severe patients, suggesting an immunopathological process caused by a cytokine storm (77, 78). Fortunately, most patients recovered enough to be discharged in 2 weeks.

## RISK FACTORS FOR SEVERE DISEASE AND DEATH

Patients older than 80 years old have a substantially higher CFR than younger patients (79). Severe infection was found to be associated with older age and male gender (80). It was reported that race could be identified as an independent factor for severity and death in COVID-19 patients. Black and other minority races were associated with higher risk of hospitalization as well as severity and mortality (81, 82). Patients having any medical comorbidities (e.g., obesity, diabetes, tumor, or heart, lung, or kidney diseases) have a greater risk of developing severe COVID-19 and higher mortality rates (70, 83). The ESR and levels of CPR, IL-6, LDH, high-sensitivity cardiac troponin I, N-terminal prob-type natriuretic peptide, creatine kinase,

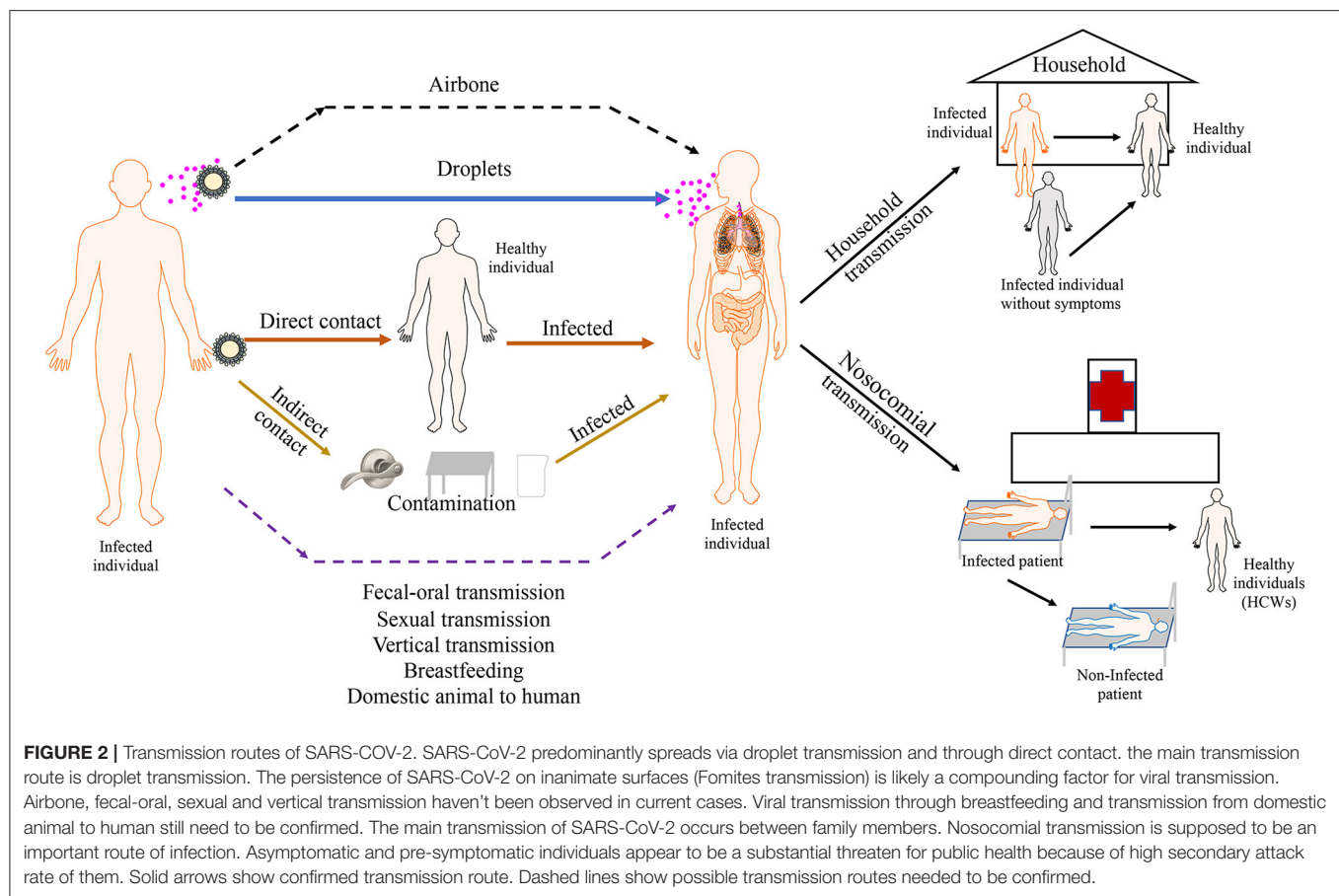


D-dimer, ferritin, creatinine, liver enzymes, and procalcitonin are commonly high in severe COVID-19 cases. Smoking, lymphopenia, low serum albumin levels, longer prothrombin time, and oxygen saturation <88% are also associated with the severity of COVID-19 (84, 85). Pregnancy was also a risk factor for severe infection and death caused by SARS-CoV-2 (86). The data revealed a higher viral load of nasopharyngeal swabs at the time of admission and a longer virus shedding period in patients with severe COVID-19 than in patients with non-severe COVID-19 (87). However, this relationship was not observed in posterior oropharyngeal and throat swab samples in different studies (88). However, the patient with the longest duration of virus shedding (49 days) had mild infection and a favorable outcome (89). Thus, the association between virus dynamics and severity of COVID-19 require further study. Although neutralizing antibodies were detected in all patients, the antibody titer showed no close correlation with the clinical course (90). Blood group A is associated with a higher risk of COVID-19 mortality compared with non-A groups, with an OR of 1.482 (95% CI, 1.113–1.972). Conversely, group O individuals had a lower risk of death (91). Compared with Rh+ blood type, Rh- was protective against SARS-CoV-2 infection and was associated with lower risk of severe COVID-19 illness or death (92). Environment is another important factor affecting COVID-19 mortality; COVID-19-induced death is positively associated with the diurnal temperature range and negatively with temperature and humidity (93). Recently, SARS-CoV-2 variant of concern B.1.1.7 (VOC) has been identified in United Kingdom (UK). Infection with VOC was associated with higher rate of death (94). Hu et al. performed genome-wide association study and eight genetic variants were identified to significantly increase the risk of COVID-19 mortality (95), suggesting the genetic basis of heterogeneous susceptibility.

## TRANSMISSION MODELS

SARS-CoV-2 RNA is commonly detected in clinical specimens from different sites of COVID-19 patients, including bronchoalveolar lavage fluid, lung tissue, endotracheal aspirates, blood, serum, sputum, feces, rectum and anal swabs, and oral and throat swabs (96, 97). It is sometimes identified in urine samples (96). SARS-CoV-2 predominantly spreads via the respiratory tract and through close contact (2, 98), and the main transmission route is droplet transmission (99) (**Figure 2**). When infected patients cough, sneeze, or talk, viruses are released from the respiratory tract, which are able to infect people within 2 m proximity by directly infecting the mucous membranes. Until now, evidences for possible airborne transmission of SARS-CoV-2 are still accumulating. It was reported that SARS-CoV-2 was detected in air samples from newly built hospital with a concentration up to 42 copies/m<sup>3</sup> (100). Airborne transmission has not yet been reported. A case of nosocomial transmission from two patients to healthcare workers (HCWs) is reported and the result addresses that a majority transmission of SARS-CoV-2 is close contact, rather than airborne route (101). However, SARS-CoV-2 is detectable in aerosols for up to 3 h, providing

the possibility of aerosol transmission for SARS-CoV-2 in confined spaces or under specific circumstances (102). In addition, SARS-CoV-2 is stable on copper, cardboard, plastic, and stainless steel for several hours to days, suggesting that people can be infected if they touch their nose, mouth, or eyes after contacting contaminated objects (102). Although SARS-CoV-2 RNA could be detected in the conjunctival swab samples of COVID-19 patients and some COVID-19 patients had ocular manifestations, such as conjunctivitis, transmission through the conjunctival route does not seem probable because of the limited number of clinical cases (103). Nevertheless, it is necessary for HCWs to protect their eyes. Recently, SARS-CoV-2 RNA was detected in gastrointestinal tissues, and the successful isolation of SARS-CoV-2 from stool samples demonstrated the possibility of fecal–oral transmission, although there is a lack of direct evidence and no clinical cases have been reported (96, 104). Some studies report that semen samples, testicular tissues, and the vaginal environment of COVID-19 patients are negative for SARS-CoV-2 RNA, supporting the notion that SARS-CoV-2 is not sexually transmitted (105). However, recent study finds that SARS-CoV-2 is detectable in semen samples of COVID-19 patients (6 of 38 patients) and 2 of these patients have achieved clinical recovery (106). The result provides the possibility that SARS-CoV-2 can be transmitted sexually, although no clinical evidence supported sexual transmission. A study finds that SARS-CoV-2 RNA can be detected in placental and fetal membrane sample, however, none of infants tested positive for SARS-CoV-2 in the first 5 days of life (107). In another study, seven neonates are tested within the first 24–36 h of life and only one has positive result (108). Although a neonate was diagnosed with COVID-19 36 h after birth, SARS-CoV-2 RNA was not detected in the placenta and cord blood (109). Similarly, a newborn with COVID-19 was successfully delivered, although SARS-CoV-2 RNA was not detected by PCR in the amniotic fluid, throat swabs, and rectal swabs at birth and neonatal blood was negative for antibodies (IgM and IgG) against SARS-CoV-2 (110). However, elevated levels of antibodies (IgM and IgG) against SARS-CoV-2 were observed in another neonate 2 h after birth. Interestingly, multiple PCR results on nasopharyngeal swabs taken between 2 h and 16 days after birth were negative. Unfortunately, PCR analysis of the amniotic fluid or the placenta was not performed (110). Based on these clinical cases, we cannot determine whether COVID-19 can spread vertically. In addition, low risk of intrapartum SARS-CoV-2 transmission to the newborn is possible during vaginal delivery (111). Another major concern about pregnant COVID-19 patients is the safety of breastfeeding after childbirth. In several studies, the detection of SARS-CoV-2 RNA in breastmilk was negative (110). Recently, SARS-CoV-2 is detectable in one patient's breastmilk. Additionally, even after delivery for 2 and 3 days, the results remain positive (112), which highlights the concern of SARS-CoV-2 infection risk through breastfeeding. Several studies have indicated that SARS-CoV-2 can infect domestic animals, including cats and dogs (23, 24). It is reported the virus is transmissible between cats and ferrets (113, 114). Although no cases of transmission from domestic animals to humans were confirmed, animal to human transmission can't



be ignore. Munnink et al. provided evidence of mink to human transmission of SARS-CoV-2 within mink farms (21). The full picture of transmission routes is not yet complete (Figure 2), so additional studies are necessary before including or ruling out certain routes.

## RISK FACTORS FOR HUMAN-TO-HUMAN TRANSMISSION

Human-to-human transmission has been reported within community, household, and nosocomial settings. According to current clinical data, individuals of all ages are susceptible to SARS-CoV-2 infection. However, people in close contact with confirmed COVID-19 patients are at a higher risk of infection. A recent study included 4,950 persons having close contact with confirmed COVID-19 patients. After 14 days of isolation or after symptom onset, throat swabs were collected for PCR analysis. Older age was significantly associated with an increased risk of infection ( $P = 0.0016$ ). However, this association was not observed in another study (115). Hence, it remains unknown whether age is a risk factor of infection for people in close contact with confirmed COVID-19 patients. Household contact (including sharing a room, apartment, or other sleeping arrangements) (OR, 6.3; 95% CI, 1.5–26.3) is more likely to pass the infection (115, 116). Patients with severe infection have

a higher risk of spreading the virus to close contacts (116). Another study showed that sharing a bedroom and being spoken to by an index case for 30 min or longer were identified as risk factors of viral transmission among household contacts (117). HCWs working at the forefront to fight COVID-19 run the greatest risk of getting infected. HCWs in the respiratory department, infection department, intensive care unit (ICU), and surgical department are particularly vulnerable to SARS-CoV-2 infection. HCWs work long hours and have suboptimal hand hygiene after contacting COVID-19 patients, and they are therefore at a high risk of SARS-CoV-2 infection (118). If the number of encounters and the time of interaction between HCWs and COVID-19 patients increase, the chance of HCWs getting infected also increases. A crowded workplace likewise increases the risk to HCWs of infection by SARS-CoV-2. Personal protective equipment (PPE) significantly decreases the infection risk for HCWs (119). High-risk occupations also include drivers, transport workers, and sales workers (120). The potential risk of COVID-19 transmission among hospitalized psychotic patients should not be ignored, especially those without insight (121). In addition, Zhao et al. analyzed the association of ABO blood type and the susceptibility to COVID-19 in 1,775 patients infected by SARS-CoV-2; they found the population with blood group A had a significantly higher risk of SARS-CoV-2 infection (OR, 1.279; 95% CI, 1.136–1.440). The population with blood group O had a significantly lower risk of SARS-CoV-2 infection (OR, 0.680;

95% CI, 0.599–0.771) (91). The environment is also a major factor influencing the incidence of SARS-CoV-2 infection. Inactivation of SARS-CoV-2 on surfaces will be accelerated by increasing temperature and relative humidity (122). These identified risk factors allow managers to take effective measures to prevent and control the transmission of SARS-CoV-2 in the early stage.

## HOUSEHOLD TRANSMISSION

The main transmission of SARS-CoV-2 occurs between family members, including relatives and their friends, who may intimately contact carriers or patients (**Figure 2**). On January 10, 2020, Chan et al. enrolled a family of six patients, all infected with SARS-CoV-2 (123). Five of them, aged between 36 and 66 years, presented with fever and upper or lower respiratory disease symptoms. Another child, aged 10 years, was asymptomatic with radiological pulmonary GGOs. They found that patients aged >60 years had more systemic symptoms, such as extensive radiological pulmonary ground-glass changes and lymphopenia, compared with the child. On February 4, 2020, Ye et al. reported a person who was infected with SARS-CoV-2, and her family members were admitted to the hospital the next day (124). In this family-clustered SARS-CoV-2 infection case, the first patient who got pneumonia had only had contact with her four family members, and the day when she attended the family reunion dinner, she did not have any SARS-CoV-2 symptoms. Li et al. reported a patient who was infected with SARS-CoV-2 and had lived together with other families for 4 days when he did not have any symptoms (125). However, several days later, one of his relatives who had lived with him previously was diagnosed with SARS-CoV-2 infection. The next day, as the closest contact of that relative, he was confirmed to have SARS-CoV-2 infection by PCR of his swab samples. These observations indicate SARS-CoV-2 is highly infectious and might be transmitted by asymptomatic carriers during the incubation period. The infectivity during this incubation period in the household is a big challenge for disease control. Recently, the characteristic of household transmission is assessed. Wang et al. enrolled 85 patients and their household members, and all close contacts received RT-PCR analysis. They found the rate of secondary transmission among household contacts of COVID-19 patients was 30% (126). In another study, 27,101 households with 29,578 primary cases and 57,581 household contacts were enrolled. The estimated secondary attack rate within households was 15.6% and older individuals were more susceptible to SARS-CoV-2 infection (127). Reukers et al. enrolled a total of 55 households with 187 household contacts in Dutch. Estimated secondary attack rate was high and ranged from 35% in children and 51% in adults (128). These data reinforced the role of households as a major of transmission route of SARS-CoV-2 infection.

## NOSOCOMIAL TRANSMISSION

Given the high infectivity of SARS-CoV-2, hospital-related transmission is supposed to be an important route of infection

(**Figure 2**). Wang et al. reported hospital cases of COVID-19 (74). Of the 138 patients in their report, 57 (41.3%) were presumed to be infected with SARS-CoV-2 in the hospital, including 17 patients (12.3%) who were hospitalized previously for other reasons and 40 HCWs (29%). One patient who had SARS-CoV-2 and presented with abdominal symptoms was soon admitted to the surgical department, and more than 10 HCWs who worked in the surgical department were presumed to be infected by this patient. This report also revealed that patient-to-patient transmission seems to occur. At least four hospitalized patients in the same ward as an infected patient were infected; those infected patients all presented with atypical abdominal symptoms, and soon one of the four patients was diagnosed with COVID-19 during his hospitalization. Characteristics of HCWs who underwent SARS-CoV-2 testing in Italy were described. There were 139 positive result among 1,573 HCWs. Among infected HCWs, 122 patients were symptomatic and 17 patients were asymptomatic. The highest frequency of infection was occurred in physicians, while clerical workers and technicians were the groups with the lowest infection rates. The key symptoms for symptomatic HCWs to guide diagnosis were taste and smell disorders. A median of 27 days is necessary from first positive test to a negative test (129). Fortunately, there wasn't significant association between nosocomial COVID-19 and increased mortality (130). Notably, various studies have proposed that there are multiple possible routes of in-hospital transmission. A retrospective study including 66 hospital-acquired cases demonstrated that evidence of transmission through close contact was found in 55% cases. Cross-infection may have occurred in 14% cases through using shared facilities and equipment. However, no sources were identified for the remaining cases (131). Goldberg et al. firstly reported 6 HCWs were infected from 1 family despite using PPE and keeping physical distance, providing possible evidence for airborne transmission of SARS-CoV-2 (132). Therefore, comprehensive infection prevention and control measures should be performed in hospital.

## SARS-COV-2 TRANSMISSION WITHOUT SYMPTOMS

Asymptomatic patients include those with positive nucleic acid test yet without clinical symptoms, whereas pre-symptomatic individuals develop symptoms later in the course of infection. When some experts believe that because patients without symptoms have no cough, sneeze, or other clinical symptoms, the chance of transmission caused by pathogenic discharge from the body is smaller than that of confirmed cases, while some think that risk of transmission rates of asymptomatic or pre-symptomatic patients should not be underestimated (**Figure 2**). Since the viral load in the respiratory tract samples of asymptomatic patients is not significantly different from that of confirmed cases (133). Another report suggested that patients were infectious 1–3 days before any symptoms appeared (134). Moreover, a typical cluster spreading event was reported where an asymptomatic person went to a public bath center



and transmitted SARS-CoV-2 to eight other individuals (135). Transmission among family clusters was also observed in a hospital in Beijing after the nephew of index patients was found to be SARS-CoV-2-positive by PCR assay (136). This study also showed that asymptomatic individuals can transmit SARS-CoV-2. In China, a large SARS-CoV-2 outbreak caused by a single asymptomatic individual was reported in Heilongjiang Province and a total of 71 positive cases had been identified (137). Wu et al. enrolled 185 asymptomatic cases with 1,078 close contacts. They found the secondary attack rate among close contacts of asymptomatic cases was 1.1%, which was lower than that of symptomatic cases (4.1%). More than one third of the infections occurred from exposure to symptomatic cases was attributed to pre-symptomatic transmission. In addition, infected contacts of asymptomatic cases were less likely to be severe (138). Compared with asymptomatic transmission, pre-symptomatic transmission was more likely to have a higher secondary attack rates (139). Although asymptomatic transmission posed a lower transmission risk, they still appeared to be a substantial threaten for public health. For pre-symptomatic transmission, it was confirmed that viral shedding is higher before symptoms begin. Therefore, it was critical to ensure individuals exposed to confirmed patients stay home.

## SARS-COV-2 VIRAL LOAD AND TRANSMISSION

The viral loads detected in asymptomatic patients are similar to those detected in symptomatic patients, indicating the transmission potential of asymptomatic and mild patients are similar (133). Rapid viral proliferation was detected 0–5 days before symptom onset and highest viral load in throat swabs was observed at the time of symptom development (140, 141). In addition, 44% of secondary cases were infected due to pre-symptomatic transmission, indicating there was a positive association between viral load and transmissibility of SARS-CoV-2 (141). Compared with onco-index patients, viral load at the initial sample collection was higher in the index patients (142). Mark et al. identified 314 COVID-19 patients with 753 contacts in total. They found the secondary attack rate when the index cases had a viral load lower than  $1 \times 10^6$  copies per mL was 12%. However, when the viral load of the index cases was higher than  $1 \times 10^{10}$  copies per mL, the secondary attack rate was 24% (143). Goyal et al. identified the secondary attack rate was very low when the viral load of infected person was lower than  $1 \times 10^4$  copies per mL. On the other hand, transmission was much more likely (39%) when the infected person was shedding  $> 1 \times 10^7$  copies per mL, and 75% when the viral load was higher than  $1 \times 10^8$  copies per mL. Furthermore, Massive super-spreading events always occurred at viral loads exceeding  $1 \times 10^7$  copies per mL (144). These data demonstrated that the viral load of index cases was a strong drive of SARS-CoV-2 transmission.

## FOMITES TRANSMISSION AND SARS-COV-2

Various studies suggested persistence of SARS-CoV-2 on inanimate surfaces for days, with potential implications for

viral transmission. In one study, the distribution of SARS-CoV-2 in hospital wards was examined by testing air and surface samples. The results revealed that contamination in ICUs was more widespread than in general wards. Viruses were widely distributed on garbage cans, computer mice, floors, and sickbed handrails, and were detected in air ~4m away from patients (145). Extensive environmental contamination has been detected, and toilet bowl and sink samples of SARS-CoV-2-infected patients were tested positive (146). Liu et al. measured viral RNA in aerosols in different areas in two hospitals. They found that the concentration of SARS-CoV-2 RNA in aerosols was higher in the toilet areas used by the patients. Airborne SARS-CoV-2 was detectable in two crowd areas, while levels of airborne SARS-CoV-2 couldn't be detected in the most public areas. High concentration of viral RNA also could be detected in some medical staff areas (100). Of the 182 isolation ward samples, SARS-CoV-2 RNA was detectable in 9 samples. These positive samples were collected from a facemask, the floor, mobile phones and the air in the patient room and bathroom (147). Therefore, fomite transmission may occur indirectly through touching infected surfaces or objects. Xie et al. reported an evidence of indirect transmission of SARS-CoV-2 (148). They found individual could be infected through touching an elevator button contaminated by index patients (148). Although the fomite transmission is difficult to prove definitively, we also need to take some measure to prevent it. Hand hygiene is a barrier to fomite transmission and is closely associated with lower risk of infection (149).

## MUTANT STRAINS OF SARS-COV-2 AND TRANSMISSION

Recently, several novel variants strains of the SARS-CoV-2 virus have emerged carrying multiple mutation during the COVID-19 pandemic. SARS-CoV-2 B.1.1.7 was first identified in September 2020 in England, while B.1.351 was detected in late 2020 in South Africa (150). In addition, B.1.1.28.1 (P.1) variant and CAL.20C (B.1.427/B.1.429) were first detected in Brazil and California, respectively (151, 152). A major concern about these mutation strains is whether any of these variants have the ability to alter viral features, such as the transmission mode or rate. These variants share a special point mutation, named D614G. D614G, a non-synonymous mutation, results in a replacement of aspartic acid with glycine at position 614 of the virus's spike protein (153). Using multiple human cell lines, Daniloski et al. found that D614G variant was more effective at entering cells (154). Hou et al. generated SARS-CoV-2 variant harboring mutation D614G and explored the effects of D614G on SARS-CoV-2 infectivity, spread and transmission (155). Compared with D614 virus, G614 virus have higher efficiency to enter cell lines and D614G substitution enhances SARS-CoV-2 replication fitness in the primary cells. Importantly, G614 virus transmitted faster between hamsters than the D614 virus, suggesting D614G variant may confer increased transmissibility (155). Similar results were observed in Zhou's study. They found D614G substitution enhanced the ability to bind to ACE2 and also increased replication in primary human epithelial cells and



hACE2 knock-in mice model. Notably, increased transmissibility of D614G substitution was also observed in ferret models of SARS-CoV-2 infection (156). Zhao et al. analyzed that a per 0.01 increase in the prevalence of D614G substitution was associated with a 0.49% increase in time-varying reproduction number, indicating a significant positive association between COVID-19 transmissibility and the D614G substitution (157). In addition to the mutation caused the D614G substitution, these new mutation strains also contain other different mutations in the spike gene, including N501Y substitution, E484K substitution, K417N substitution, L452R substitution and deletion mutations ( $\Delta$ H69/ $\Delta$ V70 and  $\Delta$ Y144) (158). Therefore, there is a growing concern that new variants could alter the transmission model and rate of the virus. Using a variety of statistical and dynamic modeling approaches, Davies et al. estimated that B.1.1.7 variants has a 43–90% higher reproduction number than original variants and will result in large resurgences of COVID-19 cases. Concerningly, B.1.1.7 has emerged globally and shows an increased transmission rate in many countries (159). By sequencing and analyzing B.1.1.7 SARS-CoV-2 genomes, Washington et al. found that growth rate of B.1.1.7 was at least 35–45% increased and doubling every week and a half in USA (160). Using globally available data, Pearson et al. assessed the B.1.351 variant for increased transmissibility and estimated that B.1.351 was 1.50 times as transmissible as previous variants (161). B.1.427/B.1.429 variants emerged around May 2020 and dramatically increased from September 2020 to January 2021, demonstrating an 18.6–24% increase in transmissibility compared with original strain (162). Faria et al. integrated available data by employing two-category dynamical model and estimated that P.1 may be 1.4–2.2 times more transmissible than non-P.1 lineages (163). Notably, B.1.617 (double mutant) has been reportedly in India and caused a rapidly increased COVID-19 cases in the country. Three primary mutations have been detected in spike glycoprotein in B.1.617 lineage, including P681R, E484Q, and L452R—the latter two mutations were mutation of concern (164). Therefore, many people also have referred to the variant as the “double mutant.” In fact, the two mutations have been found in other variants separately. L452R has been spotted in B.1.427/B.1.429 variants, while E484Q was similar to the E484K detected in the B.1.351 and B.1.1.28.1. It was the first time that these two mutations were reported to coexist together, which was an indication of higher transmissibility. Compared with wild type, E484Q and L452R mutants in B.1.617 lineage demonstrated an increased hydrogen bond interaction with hACE2. In addition, B.1.617 mediated an enhanced entry into the human lung and intestine-derived cell lines Calu-3 and Caco-2, respectively, suggesting a higher transmissibility (165, 166). Compared with B.1 (D614G) variant, the increased severity of B.1.617 infection in hamsters was evident by the higher viral load and body weight reduction, and more severe lung lesions (167). L452R was previously demonstrated to be resistant to some neutralizing antibodies (168). E484K mutation also conferred antibody resistance (169). It was found B.1.617 evaded antibodies induced by infection and vaccination, although with moderate efficiency, which might contribute to increased transmission dynamics (166, 170).

## SARS-COV-2 VACCINE

A safe and effective vaccine against SARS-CoV-2 will be an important tool to control the global COVID-19 pandemic. BNT162b2, a nucleoside-modified RNA vaccine, encodes the SARS-CoV-2 full-length spike and is modified by two proline mutations to lock it in the prefusion conformation (35). The findings from the phase 2/3 part of a global phase 1/2/3 trial revealed that BNT162b2 conferred 95% protection against COVID-19 infection in persons 16 years of age or older from 7 days after the second dose (30 ug/dose, given 21 days apart). There wasn't significant difference in incidence of serious adverse events between placebo and vaccine group (171). In addition, BNT162b2 also was 51% efficient in preventing SARS-CoV-2 infection 13–24 days after the first dose (172). A real-world evidence confirmed that viral load was significantly decreased for infections occurring 12–27 days after the first dose, suggesting a lower infectiousness (173). Antibody responses induced by the first dose of BNT162b2 in individuals with prior infection were similar to those seen after a two-dose vaccination in individuals without prior infection, suggesting a single dose of BNT162b2 is sufficient for previously infected individuals. After the first dose, symptomatology was more prominent for individuals with prior infection. Post-vaccine symptoms were similar between groups after second dose (174). Recently, several variants of SARS-CoV-2 have emerged and it was unclear whether these new strains could be neutralized efficiently by BNT162b2. For B.1.1.7 lineage, Slight reduction of the immune sera was observed. However, the overall largely preserved neutralization of B.1.1.7 lineage by BNT162b2-immune sera made it unlikely to escape from BNT162b2-mediated protection (175). Sasone et al. analyzed the evaluated the effectiveness of BNT162b2 in Brescia country, where the B.1.1.7 variant was highly prevalent (70–97%). They found the vaccine was effective in reducing infection rate among vaccinated HCWs (176). The estimated effectiveness of the BNT162b2 against infection with B.1.1.7 variant and B.1.351 variant was 89.5 and 75%, respectively. BNT162b2 against severe, critical or fatal infection with B.1.1.7 or B.1.351 variant was 97.4%. Although vaccine effectiveness against B.1.351 variant was 20% lower than the effectiveness against original virus, it was still highly effective against severe and critical cases (177). Similar results were observed in another studies (178, 179). In addition, Xie et al. found neutralization geometric mean titers of human sera elicited by BNT162b2 against N501Y, 69/70-deletion+N501Y+D614G and E484K+N501Y+D614G mutant virus were 0.81–1.46-folds of the geometric mean titers against wild-type strain, indicating small effects of these mutations on neutralization by BNT162b2 vaccine-elicited sera (180). A phase 3 trial reported that mRNA-1273 vaccine was 94.1% efficient in preventing COVID-19 illness from 14 days after the second dose and no safety concerns were identified (181). Similarly, B.1.1.7 variant escapes a subset of monoclonal antibodies but remains susceptible to neutralizing antibodies elicited by mRNA-1273 vaccine (182). The protective humoral immunity induced by mRNA-1273 vaccine was still retained against B.1.351 variant (183) and B.1.429 variant (184). One of the candidate vaccines Ad26.COV2.S, a recombinant adenovirus serotype 26 vector

encodes the spike glycoprotein (185). On April 13, 2021, FDA had recommended a pause in the use of Ad26.COV2.S vaccine due to the reports of a rare and severe type of blood clot (186). CoronaVac, an inactivated vaccine candidate against SARS-CoV-2, developed by Sinovac Life Science (Beijing, China). The phase 3 clinical trial confirmed that CoronaVac was 50.7% efficient in preventing SARS-CoV-2 infection, 83.7% efficient in preventing moderate cases and 100% efficient in preventing severe cases. In addition, B.1.128, P.1 and P.2 variants were susceptible to neutralizing antibodies elicited by CoronaVac vaccine (187). BBIBP-CorV, another inactivated vaccine, was safe and well-tolerated. Immune responses could be induced rapidly and against SARS-CoV-2 (188). 501Y.V2 variant can't escape the immunity induced by BBIBP-CorV vaccine (189). In the context of the current, SARS-CoV-2 vaccine can contribute to reducing the infection rate and the devastating loss of health and life, together with other public health measures. Although slight reduction of the immune sera was observed, the overall largely preserved neutralization of SARS-CoV-2 variants made them unlikely to escape from vaccine-mediated protection. Furthermore, we still need to get more evidence in the real world.

## RECOMMENDATIONS

The cumulative number of confirmed cases of COVID-19 around the world is still increasing. The epidemic situation in some countries has reversed, virus mutations have occurred frequently, and the pressure on foreign defense imports has increased. In order to further guide the prevention and control of new coronavirus pneumonia in various regions, we give the following suggestions. (1) Everyone should maintain social distance, minimize indoor activities or control the number of participants. In principle, we need to ensure that the distance between people is more than 1 m, and all participants should strictly take personal protective measures, wear masks, and strictly conduct hand disinfection. (2) At present, the rapid detection technology of viral nucleic acid and serum has matured, and countries should strengthen the monitoring of people, objects and the environment, such as imported cold chain foods and items, and timely detect and report the epidemic situation. (3) Pay attention to pathogen monitoring, dynamically monitor virus mutations, and understand the impact of virus mutations on pathogen detection and vaccine protection. (4) Strengthen the management of quarantine medical observation for entry personnel and close contacts, and two nasopharyngeal swab samples should be collected at the same time when the quarantine is released, and different nucleic acid detection reagents should be used for testing. (5) Nucleic acid tests should be carried out on the 2nd and 7th days after the quarantine is lifted and health monitoring should be carried out to reduce mobility during the period. Individuals should maintain self-protection when going out and no gathering activities are allowed. (6) Once symptoms such as fever and cough occur, patients should wear a disposable medical surgical mask and try to walk or go to the hospital by private car. In the hospital, the corresponding

treatment strategy is adopted according to the classification of the disease. (7) Improve the vaccination work for high-risk groups, and further improve the vaccination strategy based on the progress of vaccine research and development and clinical trial results. (8) Countries all over the world should introduce measures to prohibit the hunting, trading, and consumption of wild animals. This is for the sake of protecting human health and maintaining ecological harmony. (9) In view of the objective situation of relatively weak epidemic prevention and control capabilities in economically underdeveloped areas, the state and the government should focus on providing guidance and support for the epidemiological investigation, isolation medical observation, nucleic acid testing and disinfection. (10) According to the current situation of epidemic prevention and control, we need to conduct training on prevention, control, diagnosis and treatment plans for medical institutions. Improve the ability of medical and health personnel to ensure that the hospital finds suspicious cases and conducts isolation treatment as soon as possible, so as to effectively control the current epidemic situation in time.

## CONCLUSION

As an ongoing public health risk, SARS-CoV-2 has received much attention. Many studies support the idea that bats are the original host of SARS-CoV-2, and some animals, including minks, pangolins, snakes, and turtles, might be intermediate hosts, facilitating the primary transmission of SARS-CoV-2. To limit transmission to animals or humans, we must elucidate the evolutionary path from the original host to cross-species transmission. Respiratory infection signs are the predominant manifestations among COVID-19 patients, and extrapulmonary symptoms preceding the onset of respiratory symptoms should not be ignored. Clinicians should evaluate COVID-19 patients according to risk factors that are closely associated with the severity of COVID-19 for prioritized and aggressive treatment. Since there is no specific treatment, it is still a top priority to (i) control the spread of the virus, (ii) study the transmission routes, and (iii) identify factors that stimulate viral spread. (iv) get vaccination against SARS-CoV-2. Considering the threat posed by COVID-19, it remains a priority to strengthen international collaborative relationships to advance our knowledge of SARS-CoV-2.

## AUTHOR CONTRIBUTIONS

TW, SK, WP, CZ, YZ, LP, KF, YY, XY, XL, LJ, and MD contribute to the material collection and manuscript writing. All authors read and approved the final manuscript.

## FUNDING

This work was supported by the National Natural Science Foundation of China under contract (Nos. 82071250 and 31672290), National Undergraduate Innovation Training Program of Central South University (Nos. S2020105330717,

S2020105330440, and S2020105330947), Innovation and entrepreneurship education reform research project of Central South University (2019CG052), Postgraduate education

and teaching reform project of Central South University (2021JGB105), and Biochemistry Maker Space of Central South University (2015CK009).

## REFERENCES

- Huang C, Wang Y, Li X, Ren L, Zhao J, Hu Y, et al. Clinical features of patients infected with 2019 novel coronavirus in Wuhan, China. *Lancet*. (2020) 395:497–506. doi: 10.1016/S0140-6736(20)30183-5
- Li Q, Guan X, Wu P, Wang X, Zhou L, Tong Y, et al. Early transmission dynamics in Wuhan, China, of novel coronavirus-infected pneumonia. *N Engl J Med*. (2020) 382:1199–207. doi: 10.1056/NEJMoa2001316
- Pan X, Chen D, Xia Y, Wu X, Li T, Ou X, et al. Asymptomatic cases in a family cluster with SARS-CoV-2 infection. *Lancet Infect Dis*. (2020) 20:410–1. doi: 10.1016/S1473-3099(20)30114-6
- Li W, Shi Z, Yu M, Ren W, Smith C, Epstein JH, et al. Bats are natural reservoirs of SARS-like coronaviruses. *Science*. (2005) 310:676–9. doi: 10.1126/science.1118391
- Andersen KG, Rambaut A, Lipkin WI, Holmes EC, Garry RF. The proximal origin of SARS-CoV-2. *Nat Med*. (2020) 26:450–2. doi: 10.1038/s41591-020-0820-9
- Lau SKP, Luk HKH, Wong ACP, Li KSM, Zhu L, He Z, et al. Possible bat origin of severe acute respiratory syndrome coronavirus 2. *Emerg Infect Dis*. (2020) 26:1542–7. doi: 10.3201/eid2607.200092
- Zhou P, Yang XL, Wang XG, Hu B, Zhang L, Zhang W, et al. A pneumonia outbreak associated with a new coronavirus of probable bat origin. *Nature*. (2020) 579:270–3. doi: 10.1038/s41586-020-2951-z
- Hu B, Guo H, Zhou P, Shi ZL. Characteristics of SARS-CoV-2 and COVID-19. *Nat Rev Microbiol*. (2021) 19:141–54. doi: 10.1038/s41579-020-00459-7
- Zhou H, Chen X, Hu T, Li J, Song H, Liu Y, et al. A novel bat coronavirus closely related to SARS-CoV-2 contains natural insertions at the S1/S2 cleavage site of the spike protein. *Curr Biol*. (2020) 30:2196–203.e3. doi: 10.1016/j.cub.2020.05.023
- Hu D, Zhu C, Ai L, He T, Wang Y, Ye F, et al. Genomic characterization and infectivity of a novel SARS-like coronavirus in Chinese bats. *Emerg Microbes Infect*. (2018) 7:154. doi: 10.1038/s41426-018-0155-5
- Lam TT, Jia N, Zhang YW, Shum MH, Jiang JF, Zhu HC, et al. Identifying SARS-CoV-2-related coronaviruses in Malayan pangolins. *Nature*. (2020) 583:282–5. doi: 10.1038/s41586-020-2169-0
- Xiao K, Zhai J, Feng Y, Zhou N, Zhang X, Zou JJ, et al. Isolation of SARS-CoV-2-related coronavirus from Malayan pangolins. *Nature*. (2020) 583:286–9. doi: 10.1038/s41586-020-2313-x
- Lopes LR, de Mattos Cardillo G, Paiva PB. Molecular evolution and phylogenetic analysis of SARS-CoV-2 and hosts ACE2 protein suggest Malayan pangolin as intermediary host. *Braz J Microbiol*. (2020) 51:1593–9. doi: 10.1007/s42770-020-00321-1
- Zhang C, Zheng W, Huang X, Bell EW, Zhou X, Zhang Y. Protein structure and sequence reanalysis of 2019-nCoV genome refutes snakes as its intermediate host and the unique similarity between its spike protein insertions and HIV-1. *J Proteome Res*. (2020) 19:1351–60. doi: 10.1021/acs.jproteome.0c01029
- Dong R, Pei S, Yin C, He RL, Yau SS. Analysis of the hosts and transmission paths of SARS-CoV-2 in the COVID-19 outbreak. *Genes*. (2020) 11:60637. doi: 10.3390/genes11060637
- Zhang T, Wu Q, Zhang Z. Probable pangolin origin of SARS-CoV-2 associated with the COVID-19 outbreak. *Curr Biol*. (2020) 30:1346–51.e2. doi: 10.1016/j.cub.2020.03.022
- Ji W, Wang W, Zhao X, Zai J, Li X. Cross-species transmission of the newly identified coronavirus 2019-nCoV. *J Med Virol*. (2020) 92:433–40. doi: 10.1002/jmv.25682
- Liu Z, Xiao X, Wei X, Li J, Yang J, Tan H, et al. Composition and divergence of coronavirus spike proteins and host ACE2 receptors predict potential intermediate hosts of SARS-CoV-2. *J Med Virol*. (2020) 92:595–601. doi: 10.1002/jmv.25726
- Guo Q, Li M, Wang C, Wang P, Fang Z, Tan J, et al. Host and infectivity prediction of Wuhan 2019 novel coronavirus using deep learning algorithm. *bioRxiv [Preprint]*. doi: 10.1101/2020.01.21.914044
- Oreshkova N, Molenaar RJ, Vreman S, Harders F, Oude Munnink BB, Hakze-van der Honing RW, et al. SARS-CoV-2 infection in farmed minks, the Netherlands, April and May (2020). *Euro Surveill*. (2020) 25:1005. doi: 10.2807/1560-7917.ES.2020.25.23.2001005
- Oude Munnink BB, Sikkema RS, Nieuwenhuijse DF, Molenaar RJ, Munger E, Molenkamp R, et al. Transmission of SARS-CoV-2 on mink farms between humans and mink and back to humans. *Science*. (2021) 371:172–7. doi: 10.1126/science.abe5901
- Zhang Q, Zhang H, Huang K, Yang Y, Hui X, Gao J, et al. A serological survey of SARS-CoV-2 in cat in Wuhan. *Emerg Microbes Infect*. (2020) 9: 2013–9. doi: 10.1080/22221751.2020.1817796
- Sit THC, Brackman CJ, Ip SM, Tam KWS, Law PYT, To EMW, et al. Infection of dogs with SARS-CoV-2. *Nature*. (2020) 586:776–8. doi: 10.1038/s41586-020-2334-5
- Shi J, Wen Z, Zhong G, Yang H, Wang C, Huang B, et al. Susceptibility of ferrets, cats, dogs, and other domesticated animals to SARS-coronavirus 2. *Science*. (2020) 368:1016–20. doi: 10.1126/science.abb7015
- Lutz C, Maher L, Lee C, Kang W. COVID-19 preclinical models: human angiotensin-converting enzyme 2 transgenic mice. *Hum Genomics*. (2020) 14:20. doi: 10.1186/s40246-020-00272-6
- Cui J, Li F, Shi ZL. Origin and evolution of pathogenic coronaviruses. *Nat Rev Microbiol*. (2019) 17:181–92. doi: 10.1038/s41579-018-0118-9
- Cyranoski D. The biggest mystery: what it will take to trace the coronavirus source. *Nature*. (2020). doi: 10.1038/d41586-020-01541-z
- Segreto R, Deigin Y. The genetic structure of SARS-CoV-2 does not rule out a laboratory origin: SARS-COV-2 chimeric structure and furin cleavage site might be the result of genetic manipulation. *Bioessays*. (2021) 43:e2000240. doi: 10.1002/bies.202000240
- Tyshkovskiy A, Panchin AY. There is no evidence of SARS-CoV-2 laboratory origin: response to segreto and deigin. *Bioessays*. (2021) 2021:e2000325. doi: 10.1002/bies.202000325
- Thompson AJ, de Vries RP, Paulson JC. Virus recognition of glycan receptors. *Curr Opin Virol*. (2019) 34:117–29. doi: 10.1016/j.coviro.2019.01.004
- Kuhn JH, Li W, Choe H, Farzan M. Angiotensin-converting enzyme 2: a functional receptor for SARS coronavirus. *Cell Mol Life Sci*. (2004) 61:2738–43. doi: 10.1007/s00018-004-4242-5
- Lan J, Ge J, Yu J, Shan S, Zhou H, Fan S, et al. Structure of the SARS-CoV-2 spike receptor-binding domain bound to the ACE2 receptor. *Nature*. (2020) 581:215–20. doi: 10.1038/s41586-020-2180-5
- Gheblawi M, Wang K, Viveiros A, Nguyen Q, Zhong JC, Turner AJ, et al. Angiotensin-converting enzyme 2: SARS-CoV-2 receptor and regulator of the renin-angiotensin system: celebrating the 20th anniversary of the discovery of ACE2. *Circ Res*. (2020) 126:1456–74. doi: 10.1161/CIRCRESAHA.120.317015
- Liu Q, Wang RS, Qu GQ, Wang YY, Liu P, Zhu YZ, et al. Gross examination report of a COVID-19 death autopsy. *Fa Yi Xue Za Zhi*. (2020) 36:21–3. doi: 10.12116/j.issn.1004-5619.2020.01.005
- Wrapp D, Wang N, Corbett KS, Goldsmith JA, Hsieh CL, Abiona O, et al. Cryo-EM structure of the 2019-nCoV spike in the prefusion conformation. *Science*. (2020) 367:1260–3. doi: 10.1126/science.abb2507
- Shang J, Wan Y, Luo C, Ye G, Geng Q, Auerbach A, et al. Cell entry mechanisms of SARS-CoV-2. *Proc Natl Acad Sci USA*. (2020) 117:11727–34. doi: 10.1073/pnas.2003138117
- Wang S, Qiu Z, Hou Y, Deng X, Xu W, Zheng T, et al. AXL is a candidate receptor for SARS-CoV-2 that promotes infection of pulmonary and bronchial epithelial cells. *Cell Res*. (2021) 31:126–40. doi: 10.1038/s41422-020-00460-y



38. Guillot S, Delaval P, Brinchault G, Caulet-Maugendre S, Depince A, Lena H, et al. Increased extracellular matrix metalloproteinase inducer (EMMPRIN) expression in pulmonary fibrosis. *Exp Lung Res.* (2006) 32:81–97. doi: 10.1080/01902140600710512
39. Wang K, Chen W, Zhang Z, Deng Y, Lian JQ, Du P, et al. CD147-spike protein is a novel route for SARS-CoV-2 infection to host cells. *Signal Transduct Target Ther.* (2020) 5:283. doi: 10.1038/s41392-020-00426-x
40. Muus C, Lueken MD, Eraslan G, Sikkema L, Waghay A, Heimberg G, et al., Single-cell meta-analysis of SARS-CoV-2 entry genes across tissues and demographics. *Nat Med.* (2021) 27:546–59. doi: 10.1038/s41591-020-01227-z
41. Jeffers SA, Tusell SM, Gillim-Ross L, Hemmila EM, Achenbach JE, Babcock GJ, et al. CD209L (L-SIGN) is a receptor for severe acute respiratory syndrome coronavirus. *Proc Natl Acad Sci USA.* (2004) 101:15748–53. doi: 10.1073/pnas.0403812101
42. Cai G, Cui X, Zhu X, Zhou J. A hint on the COVID-19 risk: population disparities in gene expression of three receptors of SARS-CoV. *Preprints.* (2020). doi: 10.20944/preprints202002.0408.v1
43. Daly JL, Simonetti B, Klein K, Chen KE, Williamson MK, Antón-Plágaro C, et al. Neuropilin-1 is a host factor for SARS-CoV-2 infection. *Science.* (2020) 370:861–5. doi: 10.1126/science.abd3072
44. Cantuti-Castelvetri L, Ojha R, Pedro LD, Djannatian M, Franz J, Kuivanen S, et al. Neuropilin-1 facilitates SARS-CoV-2 cell entry and infectivity. *Science.* (2020) 370:856–60. doi: 10.1126/science.abd2985
45. Seidah NG, Chrétien M, Mbikay M. The ever-expanding saga of the proprotein convertases and their roles in body homeostasis: emphasis on novel proprotein convertase subtilisin kexin number 9 functions and regulation. *Curr Opin Lipidol.* (2018) 29:144–50. doi: 10.1097/MOL.0000000000000484
46. Saunier B, Triyatni M, Ulianich L, Maruvada P, Yen P, Kohn LD. Role of the asialoglycoprotein receptor in binding and entry of hepatitis C virus structural proteins in cultured human hepatocytes. *J Virol.* (2003) 77:546–59. doi: 10.1128/JVI.77.1.546-559.2003
47. Mao B, Wu W, Davidson G, Marhold J, Li M, Mechler BM, et al. Kremen proteins are Dickkopf receptors that regulate Wnt/beta-catenin signalling. *Nature.* (2002) 417:664–7. doi: 10.1038/nature756
48. Liu F, Thirumangalathu S, Gallant NM, Yang SH, Stoick-Cooper CL, Reddy ST, et al. Wnt-beta-catenin signaling initiates taste papilla development. *Nat Genet.* (2007) 39:106–12. doi: 10.1038/ng1932
49. Gu Y, Cao J, Zhang X, Gao H, Wang Y, Wang J, et al. Interaction network of SARS-CoV-2 with host receptome through spike protein. *bioRxiv [Preprint].* (2020). doi: 10.1101/2020.09.09.287508
50. Liao M, Liu Y, Yuan J, Wen Y, Xu G, Zhao J, et al. Single-cell landscape of bronchoalveolar immune cells in patients with COVID-19. *Nat Med.* (2020) 26:842–4. doi: 10.1038/s41591-020-0901-9
51. Tang T, Bidon M, Jaimes JA, Whittaker GR, Daniel S. Coronavirus membrane fusion mechanism offers a potential target for antiviral development. *Antiviral Res.* (2020) 178:104792. doi: 10.1016/j.antiviral.2020.104792
52. Coutard B, Valle C, de Lamballerie X, Canard B, Seidah NG, Decroly E. The spike glycoprotein of the new coronavirus 2019-nCoV contains a furin-like cleavage site absent in CoV of the same clade. *Antiviral Res.* (2020) 176:104742. doi: 10.1016/j.antiviral.2020.104742
53. Hoffmann M, Kleine-Weber H, Schroeder S, Krüger N, Herrler T, Erichsen S, et al. SARS-CoV-2 cell entry depends on ACE2 and TMPRSS2 and is blocked by a clinically proven protease inhibitor. *Cell.* (2020) 181:271–80.e8. doi: 10.1016/j.cell.2020.02.052
54. Lukassen S, Chua RL, Trefzer T, Kahn NC, Schneider MA, Muley T, et al. SARS-CoV-2 receptor ACE2 and TMPRSS2 are primarily expressed in bronchial transient secretory cells. *Embo J.* (2020) 39:e105114. doi: 10.15252/embj.20105114
55. Matsuyama S, Ujiike M, Morikawa S, Tashiro M, Taguchi F. Protease-mediated enhancement of severe acute respiratory syndrome coronavirus infection. *Proc Natl Acad Sci USA.* (2005) 102:12543–7. doi: 10.1073/pnas.0503203102
56. Millet JK and Whittaker GR. Host cell proteases: Critical determinants of coronavirus tropism and pathogenesis. *Virus Res.* (2015) 202:120–34. doi: 10.1016/j.virusres.2014.11.021
57. Liu T, Luo S, Libby P, and Shi GP. Cathepsin L-selective inhibitors: a potentially promising treatment for COVID-19 patients. *Pharmacol Ther.* (2020) 213:107587. doi: 10.1016/j.pharmthera.2020.107587
58. Huang IC, Bailey CC, Weyer JL, Radoshitzky SR, Becker MM, Chiang JJ, et al. Distinct patterns of IFITM-mediated restriction of filoviruses, SARS coronavirus, and influenza A virus. *PLoS Pathog.* (2011) 7:e1001258. doi: 10.1371/journal.ppat.1001258
59. Yang N, Ma P, Lang J, Zhang Y, Deng J, Ju X, et al. Phosphatidylinositol 4-kinase IIIβ is required for severe acute respiratory syndrome coronavirus spike-mediated cell entry. *J Biol Chem.* (2012) 287:8457–67. doi: 10.1074/jbc.M111.312561
60. Hu Y, Sun J, Dai Z, Deng H, Li X, Huang Q, et al. Prevalence and severity of corona virus disease 2019. COVID-19: A systematic review and meta-analysis. *J Clin Virol.* (2020) 127:104371. doi: 10.1016/j.jcv.2020.104371
61. Booth CM, Matukas LM, Tomlinson GA, Rachlis AR, Rose DB, Dwosh HA, et al. Clinical features and short-term outcomes of 144 patients with SARS in the greater Toronto area. *JAMA.* (2003) 289:2801–9. doi: 10.1001/jama.289.21.JOC30885
62. Choi WS, Kang CI, Kim Y, Choi JP, Joh JS, Shin HS, et al. Clinical presentation and outcomes of middle east respiratory syndrome in the Republic of Korea. *Infect Chemother.* (2016) 48:118–26. doi: 10.3947/ic.2016.48.2.118
63. Guan W-j, Ni Z-y, Hu Y, Liang W-h, Ou C-q, He J-x, et al. Clinical characteristics of coronavirus disease 2019 in China. *N Engl J Med.* (2020) 382:1708–20. doi: 10.1056/NEJMoa2002032
64. Jiang X, Niu Y, Li X, Li L, Cai W, Chen Y, et al. Is a 14-day quarantine period optimal for effectively controlling coronavirus disease 2019 (COVID-19)? *medRxiv.* (2020). doi: 10.1101/2020.03.15.20036533
65. Li K, Wu J, Wu F, Guo D, Chen L, Fang Z, et al. The clinical and chest CT features associated with severe and critical COVID-19 pneumonia. *Invest Radiol.* (2020) 55:327–31. doi: 10.1097/RLI.0000000000000672
66. Zhou F, Yu T, Du R, Fan G, Liu Y, Liu Z, et al. Clinical course and risk factors for mortality of adult inpatients with COVID-19 in Wuhan, China: a retrospective cohort study. *Lancet.* (2020) 395:1054–62. doi: 10.1016/S0140-6736(20)30566-3
67. Han C, Duan C, Zhang S, Spiegel B, Shi H, Wang W, et al. Digestive symptoms in COVID-19 patients with mild disease severity: clinical presentation, stool viral RNA testing, and outcomes. *Am J Gastroenterol.* (2020) 115:916–23. doi: 10.14309/ajg.0000000000000664
68. Eliezer M, Hautefort C, Hamel AL, Verillaud B, Herman P, Houdart E, et al. Sudden and complete olfactory loss of function as a possible symptom of COVID-19. *JAMA Otolaryngol Head Neck Surg.* (2020) 146:674–5. doi: 10.1001/jamaoto.2020.0832
69. Lechien JR, Chiesa-Estomba CM, De Siati DR, Horoi M, Le Bon SD, Rodriguez A, et al. Olfactory and gustatory dysfunctions as a clinical presentation of mild-to-moderate forms of the coronavirus disease (COVID-19): a multicenter European study. *Eur Arch Otorhinolaryngol.* (2020) 277:2251–61. doi: 10.1007/s00405-020-05965-1
70. Wu T, Zuo Z, Kang S, Jiang L, Luo X, Xia Z, et al. Multi-organ dysfunction in patients with COVID-19: a systematic review and meta-analysis. *Aging Dis.* (2020) 11:874–94. doi: 10.14336/AD.2020.0520
71. Bernheim A, Mei X, Huang M, Yang Y, Fayad ZA, Zhang N, et al. Chest CT findings in coronavirus disease-19 (COVID-19): relationship to duration of infection. *Radiology.* (2020) 295:200463. doi: 10.1148/radiol.202000463
72. Wang Y, Dong C, Hu Y, Li C, Ren Q, Zhang X, et al. Temporal changes of CT findings in 90 patients with COVID-19 pneumonia: a longitudinal study. *Radiology.* (2020) 296:E55–64. doi: 10.1148/radiol.2020020843
73. Pan F, Ye T, Sun P, Gui S, Liang B, Li L, et al. Time course of lung changes at chest CT during recovery from coronavirus disease 2019 (COVID-19). *Radiology.* (2020) 295:715–21. doi: 10.1148/radiol.2020020370
74. Wang D, Hu B, Hu C, Zhu F, Liu X, Zhang J, et al. Clinical characteristics of 138 hospitalized patients with 2019. Novel coronavirus-infected pneumonia in Wuhan, China. *JAMA.* (2020) 323:1061–9. doi: 10.1001/jama.2020.1585
75. Trigoni RA, Holt DB, Yuan R, Siddiqui AA, Craft MK, Khan BA, et al. Incidence of venous thromboembolism in critically ill coronavirus disease 2019. Patients receiving prophylactic anticoagulation. *Crit Care Med.* (2020) 48:e805–8. doi: 10.1097/CCM.00000000000004472



76. Wu T, Zuo Z, Yang D, Luo X, Jiang L, Xia Z, et al. Venous thromboembolic events in patients with COVID-19: a systematic review and meta-analysis. *Age Ageing*. (2021) 50:284–93. doi: 10.1093/ageing/afaa259
77. Zuo Z, Wu T, Pan L, Zuo C, Hu Y, Luo X, et al. Modalities and mechanisms of treatment for coronavirus disease 2019. *Front Pharmacol*. (2020) 11:583914. doi: 10.3389/fphar.2020.583914
78. Yang X, Yu Y, Xu J, Shu H, Xia J, Liu H, et al. Clinical course and outcomes of critically ill patients with SARS-CoV-2 pneumonia in Wuhan, China: a single-centered, retrospective, observational study. *Lancet Respir Med*. (2020) 8:475–81. doi: 10.1016/S2213-2600(20)30079-5
79. Wu Z, McGoogan JM. Characteristics of and important lessons from the coronavirus disease 2019 (COVID-19) outbreak in China: summary of a report of 72,314 cases from the Chinese center for disease control and prevention. *JAMA*. (2020) 323:1239–42. doi: 10.1001/jama.2020.2648
80. Zhang JJ, Cao YY, Tan G, Dong X, Wang BC, Lin J, et al. Clinical, radiological, and laboratory characteristics and risk factors for severity and mortality of 289 hospitalized COVID-19 patients. *Allergy*. (2021) 76:533–50. doi: 10.1111/all.14496
81. Williamson EJ, Walker AJ, Bhaskaran K, Bacon S, Bates C, Morton CE, et al. Factors associated with COVID-19-related death using OpenSAFELY. *Nature*. (2020) 584:430–6. doi: 10.1038/s41586-020-2521-4
82. Lassale C, Gaye B, Hamer M, Gale CR, Batty GD. Ethnic disparities in hospitalisation for COVID-19 in England: The role of socioeconomic factors, mental health, and inflammatory and pro-inflammatory factors in a community-based cohort study. *Brain Behav Immun*. (2020) 88:44–9. doi: 10.1016/j.bbi.2020.05.074
83. Liang W, Guan W, Chen R, Wang W, Li J, Xu K, et al. Cancer patients in SARS-CoV-2 infection: a nationwide analysis in China. *Lancet Oncol*. (2020) 21:335–7. doi: 10.1016/S1470-2045(20)30096-6
84. Wu C, Chen X, Cai Y, Xia J, Zhou X, Xu S, et al. Risk factors associated with acute respiratory distress syndrome and death in patients with coronavirus disease 2019 pneumonia in Wuhan, China. *JAMA Intern Med*. (2020) 180:934–43. doi: 10.1001/jamainternmed.2020.0994
85. Liu W, Tao ZW, Wang L, Yuan ML, Liu K, Zhou L, et al. Analysis of factors associated with disease outcomes in hospitalized patients with 2019 novel coronavirus disease. *Chin Med J*. (2020) 133:1032–8. doi: 10.1097/CM9.0000000000000775
86. Martinez-Portilla RJ, Sotiriadis A, Chatzakis C, Torres-Torres J, Espino YSS, Sandoval-Mandujano K, et al. Pregnant women with SARS-CoV-2 infection are at higher risk of death and pneumonia: propensity score matched analysis of a nationwide prospective cohort (COV19Mx). *Ultrasound Obstet Gynecol*. (2021) 57:224–31. doi: 10.1002/uog.23575
87. Liu Y, Yan LM, Wan L, Xiang TX, Le A, Liu JM, et al. Viral dynamics in mild and severe cases of COVID-19. *Lancet Infect Dis*. (2020) 20:656–7. doi: 10.1016/S1473-3099(20)30232-2
88. To KK, Tsang OT, Leung WS, Tam AR, Wu TC, Lung DC, et al. Temporal profiles of viral load in posterior oropharyngeal saliva samples and serum antibody responses during infection by SARS-CoV-2: an observational cohort study. *Lancet Infect Dis*. (2020) 20:565–74. doi: 10.1016/S1473-3099(20)30196-1
89. Tan L, Kang X, Zhang B, Zheng S, Liu B, Yu T, et al. A special case of COVID-19 with long duration of viral shedding for 49 days. *medRxiv [Preprint]*. (2020). doi: 10.1101/2020.03.22.20040071
90. Wölfel R, Corman VM, Guggemos W, Seilmaier M, Zange S, Müller MA, et al. Virological assessment of hospitalized patients with COVID-2019. *Nature*. (2020) 581:465–9. doi: 10.1038/s41586-020-2196-x
91. Muñoz-Díaz E, Llopis J, Parra R, Roig I, Ferrer G, Grifols J, et al. Relationship between the ABO blood group and COVID-19 susceptibility, severity and mortality in two cohorts of patients. *Blood Transfus*. (2021) 19:54–63. doi: 10.2450/2020.0256-20
92. Ray JG, Schull MJ, Vermeulen MJ, Park AL. Association between ABO and Rh blood groups and SARS-CoV-2 infection or severe COVID-19 illness: a population-based cohort study. *Ann Intern Med*. (2021) 174:308–15. doi: 10.7326/M20-4511
93. Ma Y, Zhao Y, Liu J, He X, Wang B, Fu S, et al. Effects of temperature variation and humidity on the death of COVID-19 in Wuhan, China. *Sci Total Environ*. (2020) 724:138226. doi: 10.1016/j.scitotenv.2020.138226
94. Grint DJ, Wing K, Williamson E, McDonald HI, Bhaskaran K, Evans D, et al. Case fatality risk of the SARS-CoV-2 variant of concern B.1.1.7 in England, 16 November to 5 February. *Euro Surveill*. (2021) 26:256. doi: 10.2807/1560-7917.ES.2021.26.11.2100256
95. Hu J, Li C, Wang S, Li T, Zhang H. Genetic variants are identified to increase risk of COVID-19 related mortality from UK Biobank data. *Hum Genomics*. (2021) 15:10. doi: 10.1186/s40246-021-00306-7
96. Wang W, Xu Y, Gao R, Lu R, Han K, Wu G, et al. Detection of SARS-CoV-2 in different types of clinical specimens. *JAMA*. (2020) 323:1843–4. doi: 10.1001/jama.2020.3786
97. Pan Y, Zhang D, Yang P, Poon LLM, Wang Q. Viral load of SARS-CoV-2 in clinical samples. *Lancet Infect Dis*. (2020) 20:411–2. doi: 10.1016/S1473-3099(20)30113-4
98. Ghinai I, McPherson TD, Hunter JC, Kirking HL, Christiansen D, Joshi K, et al. First known person-to-person transmission of severe acute respiratory syndrome coronavirus 2 (SARS-CoV-2) in the USA. *Lancet*. (2020) 395:1137–44. doi: 10.1016/S0140-6736(20)30607-3
99. Han Q, Lin Q, Ni Z, You L. Uncertainties about the transmission routes of 2019 novel coronavirus. *Influenza Other Respir Viruses*. (2020) 14:470–1. doi: 10.1111/irv.12735
100. Liu Y, Ning Z, Chen Y, Guo M, Liu Y, Gali NK, et al. Aerodynamic analysis of SARS-CoV-2 in two Wuhan hospitals. *Nature*. (2020) 582:557–60. doi: 10.1038/s41586-020-2271-3
101. Bays DJ, Nguyen MH, Cohen SH, Waldman S, Martin CS, Thompson GR, et al. Investigation of nosocomial SARS-CoV-2 transmission from two patients to health care workers identifies close contact but not airborne transmission events. *Infect Control Hosp Epidemiol*. (2020) 2020:1–22. doi: 10.1017/ice.2020.321
102. van Doremalen N, Bushmaker T, Morris DH, Holbrook MG, Gamble A, Williamson BN, et al. Aerosol and surface stability of SARS-CoV-2 as compared with SARS-CoV-1. *N Engl J Med*. (2020) 382:1564–7. doi: 10.1056/NEJMc2004973
103. Wu P, Duan F, Luo C, Liu Q, Qu X, Liang L, et al. Characteristics of ocular findings of patients with coronavirus disease 2019 (COVID-19) in Hubei Province, China. *JAMA Ophthalmol*. (2020) 138:575–8. doi: 10.1001/jamaophthalmol.2020.1291
104. Xiao F, Tang M, Zheng X, Liu Y, Li X, Shan H. Evidence for gastrointestinal infection of SARS-CoV-2. *Gastroenterology*. (2020) 158:1831–3.e3. doi: 10.1053/j.gastro.2020.02.055
105. Song C, Wang Y, Li W, Hu B, Chen G, Xia P, et al. Detection of 2019 novel coronavirus in semen and testicular biopsy specimen of COVID-19 patients. *medRxiv [Preprint]*. (2020). doi: 10.1101/2020.03.31.20042333
106. Li D, Jin M, Bao P, Zhao W, Zhang S. Clinical characteristics and results of semen tests among men with coronavirus disease 2019. *JAMA Netw Open*. (2020) 3:e208292. doi: 10.1001/jamanetworkopen.2020.8292
107. Penfield CA, Brubaker SG, Limaye MA, Lighter J, Ratner AJ, Thomas KM, et al. Detection of severe acute respiratory syndrome coronavirus 2 in placental and fetal membrane samples. *Am J Obstet Gynecol MFM*. (2020) 2:100133. doi: 10.1016/j.ajogmf.2020.100133
108. Hu X, Gao J, Luo X, Feng L, Liu W, Chen J, et al. Severe acute respiratory syndrome coronavirus 2 (SARS-CoV-2) vertical transmission in neonates born to mothers with coronavirus disease 2019 (COVID-19) pneumonia. *Obstet Gynecol*. (2020) 136:65–7. doi: 10.1097/AOG.0000000000003926
109. Wang S, Guo L, Chen L, Liu W, Cao Y, Zhang J, et al. A case report of neonatal 2019 coronavirus disease in China. *Clin Infect Dis*. (2020) 71:853–7. doi: 10.1093/cid/ciaa225
110. Dong L, Tian J, He S, Zhu C, Wang J, Liu C, et al. Possible vertical transmission of SARS-CoV-2 from an infected mother to Her Newborn. *JAMA*. (2020) 323:1846–8. doi: 10.1001/jama.2020.4621
111. Ferrazzi E, Frigerio L, Savasi V, Vergani P, Prefumo F, Barresi S, et al. Vaginal delivery in SARS-CoV-2-infected pregnant women in Northern Italy: a retrospective analysis. *Bjog*. (2020) 127:1116–21. doi: 10.1111/1471-0528.16278
112. Zhu C, Liu W, Su H, Li S, Shereen MA, Lv Z, et al. Breastfeeding risk from detectable severe acute respiratory syndrome coronavirus 2 in breastmilk. *J Infect*. (2020) 81:452–82. doi: 10.1016/j.jinf.2020.06.001

113. Richard M, Kok A, de Meulder D, Bestebroer TM, Lamers MM, Okba NMA, et al. SARS-CoV-2 is transmitted via contact and via the air between ferrets. *Nat Commun.* (2020) 11:3496. doi: 10.1038/s41467-020-17367-2
114. Halfmann PJ, Hatta M, Chiba S, Maemura T, Fan S, Takeda M, et al. Transmission of SARS-CoV-2 in domestic cats. *N Engl J Med.* (2020) 383:592–4. doi: 10.1056/NEJMc2013400
115. Bi Q, Wu Y, Mei S, Ye C, Zou X, Zhang Z, et al. Epidemiology and transmission of COVID-19 in 391 cases and 1286 of their close contacts in Shenzhen, China: a retrospective cohort study. *Lancet Infect Dis.* (2020) 20:911–919. doi: 10.1016/S1473-3099(20)30287-5
116. Luo L, Liu D, Liao X-L, Wu X-b, Jing Q-l, Zheng J-z, et al. Modes of contact and risk of transmission in COVID-19 among close contacts. *medRxiv [Preprint].* (2020). doi: 10.1101/2020.03.24.20042606
117. Ng OT, Marimuthu K, Koh V, Pang J, Linn KZ, Sun J, et al. SARS-CoV-2 seroprevalence and transmission risk factors among high-risk close contacts: a retrospective cohort study. *Lancet Infect Dis.* (2021) 21:333–43. doi: 10.1016/S1473-3099(20)30833-1
118. Ran L, Chen X, Wang Y, Wu W, Zhang L, Tan X. Risk factors of healthcare workers with coronavirus disease 2019: a retrospective cohort study in a designated hospital of Wuhan in China. *Clin Infect Dis.* (2020) 71:2218–21. doi: 10.1093/cid/ciaa287
119. Wang X, Pan Z, Cheng Z. Association between 2019-nCoV transmission and N95 respirator use. *J Hosp Infect.* (2020) 105:104–5. doi: 10.1016/j.jhin.2020.02.021
120. Lan FY, Wei CF, Hsu YT, Christiani DC, Kales SN. Work-related COVID-19 transmission in six Asian countries/areas: A follow-up study. *PLoS ONE.* (2020) 15:e0233588. doi: 10.1371/journal.pone.0233588
121. Zhu Y, Chen L, Ji H, Xi M, Fang Y, Li Y. The risk and prevention of novel coronavirus pneumonia infections among inpatients in psychiatric hospitals. *Neurosci Bull.* (2020) 36:299–302. doi: 10.1007/s12264-020-00476-9
122. Biryukov J, Boydston JA, Dunning RA, Yeager JJ, Wood S, Reese AL, et al. Increasing temperature and relative humidity accelerates inactivation of SARS-CoV-2 on surfaces. *mSphere.* (2020) 5:441. doi: 10.1128/mSphere.00441-20
123. Chan JF, Yuan S, Kok KH, To KK, Chu H, Yang J, et al. A familial cluster of pneumonia associated with the 2019 novel coronavirus indicating person-to-person transmission: a study of a family cluster. *Lancet.* (2020) 395:514–23. doi: 10.1016/S0140-6736(20)30154-9
124. Ye F, Xu S, Rong Z, Xu R, Liu X, Deng P, et al. Delivery of infection from asymptomatic carriers of COVID-19 in a familial cluster. *Int J Infect Dis.* (2020) 94:133–8. doi: 10.1016/j.ijid.2020.03.042
125. Li P, Fu JB, Li KF, Liu JN, Wang HL, Liu LJ, et al. Transmission of COVID-19 in the terminal stages of the incubation period: A familial cluster. *Int J Infect Dis.* (2020) 96:452–3. doi: 10.1016/j.ijid.2020.03.027
126. Wang Z, Ma W, Zheng X, Wu G, Zhang R. Household transmission of SARS-CoV-2. *J Infect.* (2020) 81:179–82. doi: 10.1016/j.jinf.2020.03.040
127. Li F, Li YY, Liu MJ, Fang LQ, Dean NE, Wong GWK, et al. Household transmission of SARS-CoV-2 and risk factors for susceptibility and infectivity in Wuhan: a retrospective observational study. *Lancet Infect Dis.* (2021) 21:617–28. doi: 10.1016/S1473-3099(20)30981-6
128. Reukers DFM, van Boven M, Meijer A, Rots N, Reusken C, Roof I, et al. High infection secondary attack rates of SARS-CoV-2 in Dutch households revealed by dense sampling. *Clin Infect Dis.* (2021). doi: 10.1093/cid/ciab237
129. Lombardi A, Consonni D, Carugno M, Bozzi G, Mangioni D, Muscatello A, et al. Characteristics of 1573 healthcare workers who underwent nasopharyngeal swab testing for SARS-CoV-2 in Milan, Lombardy, Italy. *Clin Microbiol Infect.* (2020) 26:1413.e9–1413.e13. doi: 10.1016/j.cmi.2020.06.013
130. Khan KS, Reed-Embleton H, Lewis J, Saldanha J, Mahmud S. Does nosocomial COVID-19 result in increased 30-day mortality? A multi-centre observational study to identify risk factors for worse outcomes in patients with COVID-19. *J Hosp Infect.* (2021) 107:91–4. doi: 10.1016/j.jhin.2020.09.017
131. Rickman HM, Rampling T, Shaw K, Martinez-Garcia G, Hail L, Coen P, et al. Nosocomial transmission of coronavirus disease 2019: a retrospective study of 66 hospital-acquired cases in a London teaching hospital. *Clin Infect Dis.* (2021) 72:690–3. doi: 10.1093/cid/ciaa816
132. Goldberg L, Levinsky Y, Marcus N, Hoffer V, Gafner M, Hadas S, et al. SARS-CoV-2 infection among health care workers despite the use of surgical masks and physical distancing—the role of airborne transmission. *Open Forum Infect Dis.* (2021) 8:ofab036. doi: 10.1093/ofid/ofab036
133. Zou L, Ruan F, Huang M, Liang L, Huang H, Hong Z, et al. SARS-CoV-2 viral load in upper respiratory specimens of infected patients. *N Engl J Med.* (2020) 382:1177–9. doi: 10.1056/NEJMc2001737
134. Wei WE, Li Z, Chiew CJ, Yong SE, Toh MP, Lee VJ. Presymptomatic transmission of SARS-CoV-2 - Singapore, January 23-March 16, 2020. *MMWR Morb Mortal Wkly Rep.* (2020) 69:411–5. doi: 10.15585/mmwr.mm6914e1
135. Luo C, Yao L, Zhang L, Yao M, Chen X, Wang Q, et al. Possible transmission of severe acute respiratory syndrome coronavirus 2 (SARS-CoV-2) in a public bath center in Huai'an, Jiangsu Province, China. *JAMA Netw Open.* (2020) 3:e204583. doi: 10.1001/jamanetworkopen.2020.4583
136. Zhang J, Tian S, Lou J, Chen Y. Familial cluster of COVID-19 infection from an asymptomatic. *Crit Care.* (2020) 24:119. doi: 10.1186/s13054-020-2817-7
137. Liu J, Huang J, Xiang D. Large SARS-CoV-2 outbreak caused by asymptomatic traveler, China. *Emerg Infect Dis.* (2020) 26:2260–3. doi: 10.3201/eid2609.201798
138. Wu P, Liu F, Chang Z, Lin Y, Ren M, Zheng C, et al. Assessing asymptomatic, pre-symptomatic and symptomatic transmission risk of SARS-CoV-2. *Clin Infect Dis.* (2021) 27:ciab271. doi: 10.1093/cid/ciab271
139. Chun JY, Baek G, Kim Y. Transmission onset distribution of COVID-19. *Int J Infect Dis.* (2020) 99:403–7. doi: 10.1016/j.ijid.2020.07.075
140. Jang S, Rhee JY, Wi YM, Jung BK. Viral kinetics of SARS-CoV-2 over the preclinical, clinical, and post-clinical period. *Int J Infect Dis.* (2021) 102:561–5. doi: 10.1016/j.ijid.2020.10.099
141. He X, Lau EHY, Wu P, Deng X, Wang J, Hao X, et al. Temporal dynamics in viral shedding and transmissibility of COVID-19. *Nat Med.* (2020) 26:672–5. doi: 10.1038/s41591-020-0869-5
142. Kawasuji H, Takegoshi Y, Kaneda M, Ueno A, Miyajima Y, Kawago K, et al. Transmissibility of COVID-19 depends on the viral load around onset in adult and symptomatic patients. *PLoS ONE.* (2020) 15:e0243597. doi: 10.1371/journal.pone.0243597
143. Marks M, Millat-Martinez P, Ouchi D, Roberts CH, Alemany A, Corbacho-Monné M, et al. Transmission of COVID-19 in 282 clusters in Catalonia, Spain: a cohort study. *Lancet Infect Dis.* (2021) 21:629–36. doi: 10.1016/S1473-3099(20)30985-3
144. Goyal A, Reeves DB, Cardozo-Ojeda EF, Schiffer JT, Mayer BT. Viral load and contact heterogeneity predict SARS-CoV-2 transmission and super-spreading events. *Elife.* (2021) 10:63537. doi: 10.7554/eLife.63537
145. Guo ZD, Wang ZY, Zhang SF, Li X, Li L, Li C, et al. Aerosol and surface distribution of severe acute respiratory syndrome coronavirus 2 in hospital wards, Wuhan, China, 2020. *Emerg Infect Dis.* (2020) 26:1583–91. doi: 10.3201/eid2607.200885
146. Ong SWX, Tan YK, Chia PY, Lee TH, Ng OT, Wong MSY, et al. Air, surface environmental, and personal protective equipment contamination by severe acute respiratory syndrome coronavirus 2 (SARS-CoV-2) from a symptomatic patient. *JAMA.* (2020) 323:1610–2. doi: 10.1001/jama.2020.3227
147. Lei H, Ye F, Liu X, Huang Z, Ling S, Jiang Z, et al. SARS-CoV-2 environmental contamination associated with persistently infected COVID-19 patients. *Influenza Other Respir Viruses.* (2020) 14:688–99. doi: 10.1111/irv.12783
148. Xie C, Zhao H, Li K, Zhang Z, Lu X, Peng H, et al. The evidence of indirect transmission of SARS-CoV-2 reported in Guangzhou, China. *BMC Public Health.* (2020) 20:1202. doi: 10.1186/s12889-020-09296-y
149. Doung-Ngern P, Suphanchaimat R, Panjangampatthana A, Janekrongtham C, Ruampoom D, Daochaeng N, et al. Case-control study of use of personal protective measures and risk for SARS-CoV 2 infection, Thailand. *Emerg Infect Dis.* (2020) 26:2607–16. doi: 10.3201/eid2611.203003
150. Tegally H, Wilkinson E, Giovanetti M, Iranzadeh A, Fonseca V, Giandhari J, et al. Emergence and rapid spread of a new severe acute respiratory syndrome-related coronavirus 2 (SARS-CoV-2) lineage with multiple spike mutations in South Africa. *medRxiv [Preprint].* (2020). doi: 10.1101/2020.12.21.20248640

151. Zhang W, Davis BD, Chen SS, Sincuir Martinez JM, Plummer JT, Vail E. Emergence of a novel SARS-CoV-2 Variant in Southern California. *JAMA*. (2021) 325:1324–6. doi: 10.1001/jama.2021.1612
152. Mwenda M, Saasa N, Sinyange N, Busby G, Chipimo PJ, Hendry J, et al. Detection of B.1.351 SARS-CoV-2 variant strain - Zambia, December (2020). *MMWR Morb Mortal Wkly Rep*. (2021) 70:280–2. doi: 10.15585/mmwr.mm7008e2
153. Korber B, Fischer WM, Gnanakaran S, Yoon H, Theiler J, Abfalterer W, et al. Tracking changes in SARS-CoV-2 spike: evidence that D614G increases infectivity of the COVID-19 virus. *Cell*. (2020) 182:812–27.e19. doi: 10.1016/j.cell.2020.06.043
154. Daniloski Z, Jordan TX, Ilmain JK, Guo X, Bhabha G, tenOever BR, et al. The Spike D614G mutation increases SARS-CoV-2 infection of multiple human cell types. *Elife*. (2021) 10:65365. doi: 10.7554/eLife.65365.sa2
155. Hou YJ, Chiba S, Halfmann P, Ehre C, Kuroda M, Dinno KH, et al. SARS-CoV-2 D614G variant exhibits efficient replication *ex vivo* and transmission *in vivo*. *Science*. (2020) 370:1464–8. doi: 10.1126/science.abe8499
156. Zhou B, Thao TTN, Hoffmann D, Taddeo A, Ebert N, Labrousse A, et al. *Nature*. (2021) 592:122–7. doi: 10.1038/s41586-021-03361-1
157. Zhao S, Lou J, Cao L, Zheng H, Chong MKC, Chen Z, et al. Modelling the association between COVID-19 transmissibility and D614G substitution in SARS-CoV-2 spike protein: using the surveillance data in California as an example. *Theor Biol Med Model*. (2021) 18:10. doi: 10.1186/s12976-021-00140-3
158. Wang P, Nair MS, Liu L, Iketani S, Luo Y, Guo Y, et al. Antibody resistance of SARS-CoV-2 variants B.1.351 and B.1.1.7. *Nature*. (2021) 593:130–5. doi: 10.1038/s41586-021-03398-2
159. Davies NG, Abbott S, Barnard RC, Jarvis CI, Kucharski AJ, Munday JD, et al. Estimated transmissibility and impact of SARS-CoV-2 lineage B.1.1.7 in England. *Science*. (2021) 372:abg3055. doi: 10.1126/science.abg3055
160. Washington NL, Gangavarapu K, Zeller M, Bolze A, Cirulli ET, Schiabor Barrett KM, et al. Genomic epidemiology identifies emergence and rapid transmission of SARS-CoV-2 B.1.1.7 in the United States. *medRxiv [Preprint]*. (2021). doi: 10.1101/2021.02.06.21251159
161. Carl AB, Pearson TWR, Nicholas D, Kucharski AJ. *Estimates of Severity and Transmissibility of Novel SARS-CoV-2 Variant 501Y.V2 in South Africa*. (2021). Available online at: <https://cmmid.github.io/topics/covid19/sa-novel-variant.html>
162. Deng X, Garcia-Knight MA, Khalid MM, Servellita V, Wang C, Morris MK, et al. *Cell*. (2021). doi: 10.1016/j.cell.2021.04.025
163. Faria NR, Mellan TA, Whittaker C, Claro IM, Candido DDS, Mishra S, et al. Genomics and epidemiology of the P.1 SARS-CoV-2 lineage in Manaus, Brazil. *Science*. (2021) 372:815–21. doi: 10.1126/science.abh2644
164. Mallapaty S. India's massive COVID surge puzzles scientists. *Nature*. (2021) 592:667–8. doi: 10.1038/d41586-021-01059-y
165. Kumar V, Singh J, Hasnain SE, Sundar D. Possible link between higher transmissibility of B.1.617 and B.1.1.7 variants of SARS-CoV-2 and increased structural stability of its spike protein and hACE2 affinity. *bioRxiv [Preprint]*. (2021). doi: 10.1101/2021.04.29.441933
166. Hoffmann M, Hofmann-Winkler H, Krüger N, Kempf A, Nehlmeier I, Graichen L, et al. SARS-CoV-2 variant B.1.617 is resistant to Bamlanivimab and evades antibodies induced by infection and vaccination. *bioRxiv [Preprint]*. (2021). doi: 10.1101/2021.05.04.442663
167. Yadav PD, Mohandas S, Shete AM, Nyayanit DA, Gupta N, Patil DY, et al. SARS CoV-2 variant B.1.617.1 is highly pathogenic in hamsters than B.1 variant. *bioRxiv [Preprint]*. (2021). doi: 10.1101/2021.05.05.442760
168. Li Q, Wu J, Nie J, Zhang L, Hao H, Liu S, et al. The impact of mutations in SARS-CoV-2 Spike on viral infectivity and antigenicity. *Cell*. (2020) 182:1284–94.e9. doi: 10.1016/j.cell.2020.07.012
169. Li Q, Nie J, Wu J, Zhang L, Ding R, Wang H, et al. SARS-CoV-2 501Y.V2 variants lack higher infectivity but do have immune escape. *Cell*. (2021) 184:2362–71.e9. doi: 10.1016/j.cell.2021.02.042
170. Zhang L, Huynh T, Luan B. *In silico* assessment of antibody drug resistance to bamlanivimab of SARS-CoV-2 variant B.1.617. *bioRxiv [Preprint]*. (2021). doi: 10.1101/2021.05.12.443826
171. Skowronski DM and De Serres G. Safety and Efficacy of the BNT162b2 mRNA Covid-19 Vaccine. *N Engl J Med*. (2021) 384:2036242. doi: 10.1056/NEJMc2036242
172. Chodick G, Tene L, Patalon T, Gazit S, Tov AB, Cohen D, et al. Assessment of effectiveness of 1 dose of BNT162b2 vaccine for SARS-CoV-2 infection 13 to 24 days after immunization. *JAMA Netw Open*. (2021) 4:e2115985. doi: 10.1001/jamanetworkopen.2021.15985
173. Levine-Tiefenbrun M, Yelin I, Katz R, Herzl E, Golan Z, Schreiber L, et al. Initial report of decreased SARS-CoV-2 viral load after inoculation with the BNT162b2 vaccine. *Nat Med*. (2021) 27:790–2. doi: 10.1038/s41591-021-01316-7
174. Ebinger JE, Fert-Bober J, Printsev I, Wu M, Sun N, Prostko JC, et al. Antibody responses to the BNT162b2 mRNA vaccine in individuals previously infected with SARS-CoV-2. *Nat Med*. (2021). doi: 10.1038/s41591-021-01325-6
175. Muik A, Wallisch AK, Sängler B, Swanson KA, Mühl J, Chen W, et al. Neutralization of SARS-CoV-2 lineage B.1.1.7 pseudovirus by BNT162b2 vaccine-elicited human sera. *Science*. (2021) 371:1152–3. doi: 10.1126/science.abg6105
176. Sansone E, Tiraboschi M, Sala E, Albini E, Lombardo M, Castelli F, et al. Effectiveness of BNT162b2 vaccine against the B.1.1.7 variant of SARS-CoV-2 among healthcare workers in Brescia, Italy. *J Infect*. (2021). doi: 10.1016/j.jinf.2021.04.038
177. Abu-Raddad LJ, Chemaitelly H, Butt AA. Effectiveness of the BNT162b2 Covid-19 Vaccine against the B.1.1.7 and B.1.351 Variants. *N Engl J Med*. (2021) 5:NEJMc2104974. doi: 10.1056/NEJMc2104974
178. Haas EJ, Angulo FJ, McLaughlin JM, Anis E, Singer SR, Khan F, et al. Impact and effectiveness of mRNA BNT162b2 vaccine against SARS-CoV-2 infections and COVID-19 cases, hospitalisations, and deaths following a nationwide vaccination campaign in Israel: an observational study using national surveillance data. *Lancet*. (2021) 397:1819–29. doi: 10.1016/S0140-6736(21)00947-8
179. Hall VJ, Foulkes S, Saei A, Andrews N, Oguti B, Charlett A, et al. COVID-19 vaccine coverage in health-care workers in England and effectiveness of BNT162b2 mRNA vaccine against infection (SIREN): a prospective, multicentre, cohort study. *Lancet*. (2021) 397:1725–35. doi: 10.1016/S0140-6736(21)00790-X
180. Xie X, Liu Y, Liu J, Zhang X, Zou J, Fontes-Garfias CR, et al. Neutralization of SARS-CoV-2 spike 69/70 deletion, E484K and N501Y variants by BNT162b2 vaccine-elicited sera. *Nat Med*. (2021) 27:620–1. doi: 10.1038/s41591-021-01270-4
181. Baden LR, El Sahly HM, Essink B, Kotloff K, Frey S, Novak R, et al. Efficacy and safety of the mRNA-1273 SARS-CoV-2 vaccine. *N Engl J Med*. (2021) 384:403–16. doi: 10.1056/NEJMoa2035389
182. Shen X, Tang H, McDaniel C, Wagh K, Fischer W, Theiler J, et al. SARS-CoV-2 variant B.1.1.7 is susceptible to neutralizing antibodies elicited by ancestral spike vaccines. *Cell Host Microbe*. (2021) 29:529–39.e3. doi: 10.1016/j.chom.2021.03.002
183. Edara VV, Norwood C, Floyd K, Lai L, Davis-Gardner ME, Hudson WH, et al. Infection- and vaccine-induced antibody binding and neutralization of the B.1.351 SARS-CoV-2 variant. *Cell Host Microbe*. (2021) 29:516–21.e3. doi: 10.1016/j.chom.2021.03.009
184. Shen X, Tang H, Pajon R, Smith G, Glenn GM, Shi W, et al. Neutralization of SARS-CoV-2 Variants B.1.429 and B.1.351. *N Engl J Med*. (2021) 7:NEJMc2103740. doi: 10.1056/NEJMc2103740
185. Bos R, Rutten L, van der Lubbe JEM, Bakkers MJG, Hardenberg G, Wegmann F, et al. Ad26 vector-based COVID-19 vaccine encoding a prefusion-stabilized SARS-CoV-2 Spike immunogen induces potent humoral and cellular immune responses. *NPJ Vaccines*. (2020) 5:91. doi: 10.1038/s41541-020-00243-x
186. Muir KL, Kallam A, Koepsell SA, Gundabolu K. Thrombotic thrombocytopenia after Ad26.COV2.S vaccination. *N Engl J Med*. (2021) 384:1964–5. doi: 10.1056/NEJMc2105869
187. Ricardo P, Batista AP. Efficacy and safety of a COVID-19 inactivated vaccine in healthcare 2 professionals in Brazil: The PROFISCOV study. *Preprint*. (2021). doi: 10.2139/ssrn.3822780
188. Xia S, Zhang Y, Wang Y, Wang H, Yang Y, Gao GF, et al. Safety and immunogenicity of an inactivated SARS-CoV-2 vaccine, BBIBP-

- CorV: a randomised, double-blind, placebo-controlled, phase 1/2 trial. *Lancet Infect Dis.* (2021) 21:39–51. doi: 10.1016/S1473-3099(20)30831-8
189. Huang B, Dai L, Wang H, Hu Z, Yang X, Tan W, et al. Neutralization of SARS-CoV-2 VOC 501Y.V2 by human antisera elicited by both inactivated BBIBP-CorV and recombinant dimeric RBD ZF2001 vaccines. *bioRxiv [Preprint]*. (2021). doi: 10.1101/2021.02.01.429069

**Conflict of Interest:** XL was employed by Hunan Yuanpin Cell Biotechnology Co., Ltd.

The remaining authors declare that the research was conducted in the absence of any commercial or financial relationships that could be construed as a potential conflict of interest.

Copyright © 2021 Wu, Kang, Peng, Zuo, Zhu, Pan, Fu, You, Yang, Luo, Jiang and Deng. This is an open-access article distributed under the terms of the Creative Commons Attribution License (CC BY). The use, distribution or reproduction in other forums is permitted, provided the original author(s) and the copyright owner(s) are credited and that the original publication in this journal is cited, in accordance with accepted academic practice. No use, distribution or reproduction is permitted which does not comply with these terms.





# Digital Technology-Based Telemedicine for the COVID-19 Pandemic

Yu-Ting Shen<sup>1</sup>, Liang Chen<sup>2</sup>, Wen-Wen Yue<sup>1\*</sup> and Hui-Xiong Xu<sup>1</sup>

<sup>1</sup> Department of Medical Ultrasound, Shanghai Tenth People's Hospital, Ultrasound Research and Education Institute, Tongji University Cancer Center, Shanghai Engineering Research Center of Ultrasound Diagnosis and Treatment, Tongji University School of Medicine, Shanghai, China, <sup>2</sup> Department of Gastroenterology, Shanghai Tenth People's Hospital, Shanghai, China

## OPEN ACCESS

### Edited by:

Reza Lashgari,  
Shahid Beheshti University, Iran

### Reviewed by:

Anthony Bokolo Jr.,  
Norwegian University of Science and  
Technology, Norway  
Saeed Hamood Alsamhi,  
Ibb University, Yemen  
Francesco Di Carlo,  
University of Studies G. d'Annunzio  
Chieti and Pescara, Italy

### \*Correspondence:

Wen-Wen Yue  
yuewen0902@163.com

### Specialty section:

This article was submitted to  
Infectious Diseases - Surveillance,  
Prevention and Treatment,  
a section of the journal  
Frontiers in Medicine

**Received:** 27 December 2020

**Accepted:** 31 May 2021

**Published:** 06 July 2021

### Citation:

Shen Y-T, Chen L, Yue W-W and  
Xu H-X (2021) Digital  
Technology-Based Telemedicine for  
the COVID-19 Pandemic.  
Front. Med. 8:646506.  
doi: 10.3389/fmed.2021.646506

In the year 2020, the coronavirus disease 2019 (COVID-19) crisis intersected with the development and maturation of several digital technologies including the internet of things (IoT) with next-generation 5G networks, artificial intelligence (AI) that uses deep learning, big data analytics, and blockchain and robotic technology, which has resulted in an unprecedented opportunity for the progress of telemedicine. Digital technology-based telemedicine platform has currently been established in many countries, incorporated into clinical workflow with four modes, including “many to one” mode, “one to many” mode, “consultation” mode, and “practical operation” mode, and has shown to be feasible, effective, and efficient in sharing epidemiological data, enabling direct interactions among healthcare providers or patients across distance, minimizing the risk of disease infection, improving the quality of patient care, and preserving healthcare resources. In this state-of-the-art review, we gain insight into the potential benefits of demonstrating telemedicine in the context of a huge health crisis by summarizing the literature related to the use of digital technologies in telemedicine applications. We also outline several new strategies for supporting the use of telemedicine at scale.

**Keywords:** COVID-19, SARS-CoV-2, telemedicine, respiratory diseases, infectious diseases

## INTRODUCTION

During the year 2020, the whole world is suffering from a serious health crisis associated with the outbreak of coronavirus disease 2019 (COVID-19), a novel respiratory infectious disease caused by severe acute respiratory syndrome coronavirus 2 (SARS-CoV-2) (1, 2). And as of December 26, 2020, COVID-19 had spread to more than 200 countries worldwide and has affected over 80 million individuals, with nearly 1.7 million known deaths (<https://www.worldometers.info/coronavirus/>). With the rapid spread of this pandemic, the global healthcare system has been experiencing a severe scarcity of necessary equipment, consumables, and staff. Therefore, hospitals should make efforts to determine the best way to provide timely and high-quality patient care and simultaneously protect providers who are already at the highest risk for contracting this disease (3). Significantly, although tackling the direct impact from COVID-19 is important, in many healthcare settings, it is also vital to maintain the core and critical clinical service. However, in the context of the current situation, the initial reaction of healthcare facilities in a great number of countries is to reduce or even cease many clinical services, such as closure of clinics and postponement of elective surgeries

or medical appointments. Actually, such strategies cannot be sustained indefinitely in case this pandemic extends over 6 months, or it must be fully considered if this pandemic even worsens. Therefore, all the healthcare organizations have been continuously striking a balance in their own ways, recognizing that constraints in certain resources can sometimes be limiting, while always placing the safety and care of all the potential patients as their top priority.

As the saying goes, “a crisis provides an opportunity”; the crisis of 2020 would provide an unprecedented opportunity for the progress of telemedicine. During the COVID-19 pandemic, because of the containment efforts such as social distancing, quarantine, and cordon sanitaire, if indicated, medical professionals are confronted with great challenges in delivering healthcare. For such a situation, telemedicine has currently been catapulted into the core role of essential services for patients to help reduce the burden of COVID-19 and preserve some valuable equipment and supplies. Although few kinds of telemedicine services were available during the epidemic of SARS in 2003, since then, they have become more available following the popularization of internet services, the emergence of smartphones, and the fourth-/fifth-generation (4G/5G) transmission technology, making it ideal for addressing some unique challenges posed by this global infectious disease outbreak. For example, implementing telemedicine platforms can mitigate overcrowding in the emergency departments, providing the guidance that patients are seeking while addressing disease exposure concerns of low-acuity patients. Telemedicine can also help to deal with the ongoing healthcare needs from chronic illnesses patients while reducing in-person clinic visits. Besides, telemedicine can deliver specialty care to patients at distant regions where scarce intensivists are available, ensuring that high-quality medical supplies are reserved for those who are in need while reducing human exposures (among both healthcare providers and patients) to this highly contagious disease.

The year 2020 should be the beginning of an exciting decade for telemedicine, particularly when combined with the development and maturation of several emerging technologies, including the internet of things (IoT), 5G networks (4, 5), artificial intelligence (AI) (6, 7), big data analytics (8), and robot and blockchain technology (9), which can be synthetically applied to tackle certain major clinical problems or diseases, such as COVID-19. The emergence of SARS-CoV-2 and its subsequent spread has surpassed those of its predecessors (e.g., SARS), causing an evolving global health crisis. Fortunately, telemedicine networks have currently been established in many countries, incorporated into clinical workflow during this outbreak and shown to be feasible, effective, and efficient in sharing epidemiological data, enabling direct interactions among healthcare providers or patients across distance, minimizing the risk of SARS-CoV-2 infection, and improving access to patient care. Although several reviews have examined the historical use and effects of telemedicine (10–12), however, to our knowledge, the current status of telemedicine approaches based on the ever-emerging technologies, particularly associated with the COVID-19 pandemic, has not been timely summarized yet.

Given the excellent performance and growing awareness in digital technology-based telemedicine during the COVID-19 outbreak, the time seems optimal to present a systematic review on telemedicine associated with COVID-19 for healthcare providers and certain biomedical researchers that involves a general understanding of telemedicine systems and the related advanced digital technologies, as well as their applications during the COVID-19 outbreak, aiming to provide structure and guidance for practitioners and certain policymakers to understand various key aspects of this rapidly advancing field and extensively accelerate the application of telemedicine technique in this pandemic, eventually improving the quality of patient care while simultaneously protecting the personal health of medical staffs and saving public resources.

In this review, first, we will provide a general understanding of telemedicine as well as several associated technologies. We then review the growing applications of telemedicine within the context of the COVID-19 outbreak by covering teleconsulting, telemonitoring, telecare, and teleeducation (**Figure 1**). The COVID-19 pandemic can make a good paradigm for presenting the potential benefits of telemedicine nowadays, owing to the emergence of various technological platforms. Finally, we offer our perspective on the potential opportunities and challenges for telemedicine systems in the clinical world, as well as outline several new strategies for supporting the use of telemedicine at scale.

## TELEMEDICINE

Rather than a very specific term, telemedicine can be broadly defined as “the use of communication and information technologies to provide healthcare services without barriers of time and space” (13). As a communication system, telemedicine proposes a brand new model for the production, transmission, and control of medical data and services. And telemedicine has already constituted an organizational innovation, continuously changing the form of diagnostic process, consultation, supervision, and education and training. The use of telemedicine can be traced to as early as the year 1877, when the first telephone exchange system was built in adjoining areas by 21 doctors to allow easier communication with the local drugstore (12). After that, although numerous attempts were made to advance information-based technologies to augment healthcare delivery, the number of clinical telemedicine application practice was still relatively small and restricted, rather than deployed nationwide for quite a long time, mainly due to the clinical, financial, or technical barriers.

Nowadays, telemedicine is widely used across various medical specialties including psychiatry (14, 15), ophthalmology (16), dermatology (17), and neurology (18) and has the potential to impel a transformational change in the way healthcare is delivered via altering the interactive process between patient and provider. Fortunately, it has already undergone five of the nine steps of transformational change presented by Tipton



(19) (Figure 2) and is moving beyond the tolerance stage toward the acceptance stage by most healthcare organizations. Once this technology has passed the tolerance stage, it would be difficult to get back to the original way of care, restricting to some episodic in-person visits. We believe that this COVID-19 global outbreak will inevitably accelerate this process and anticipate rapid movement toward the stage of agreement and ultimately expect advocacy to be spread worldwide (20–23).

## TELEMEDICINE-RELATED TECHNOLOGIES AND THEIR CRITICAL ROLES DURING THE COVID-19 OUTBREAK

Advancements in modern technologies such as IoT, AI, blockchain, and big data have revolutionized the medicine practice to its current state. Especially, 5G-based cloud servers could offer more stable and faster data transmission (up to

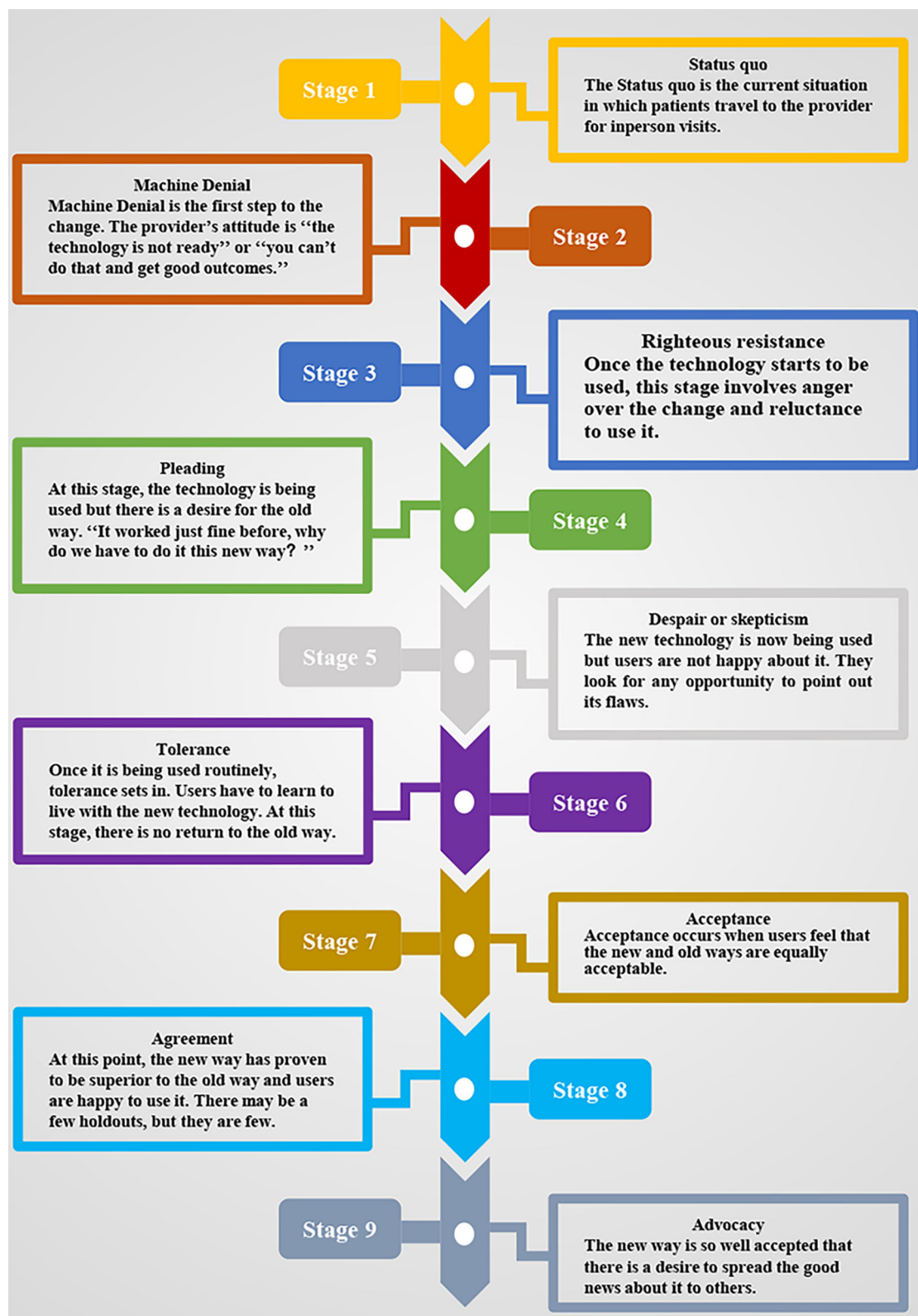


**FIGURE 2 |** The nine stages of transformational change of telemedicine (19).



100-fold than predecessors) while reducing the latency to 1 ms, enabling them to rapidly and reliably disseminate great amounts of interactive data, from or to anywhere in the world (24–26). Utilizing these ever-growing technologies for telemedicine can provide an entirely immersive experience for those healthcare providers around the world and simultaneously eliminate the perception of distance, marking an optimal transformation from an in-person clinical visit to a synchronized/unsynchronized virtual reality. Some of these technologies and their critical role during the COVID-19 outbreak can be briefly explained as follows.

## Internet of Things

The term IoT can be defined as a worldwide network of the interconnected objects, which are uniquely addressable by standard communication protocols (27), in that all the physical devices, such as smart appliances, autonomous transportation systems, and personal health monitors, which are embedded in the digital technologies, can be networked together to allow these devices to interact with each other via communicating data (27, 28). During the COVID-19 outbreak, the value and function of IoT can be reflected in providing a data platform that could allow public health agencies access to continuously monitor the status of the pandemic. For example, the “Worldometer” presents a real-time update on the exact number of people infected with COVID-19 worldwide, including the daily new cases and severity of disease, as well as disease distribution by countries (<https://www.worldometers.info/coronavirus/>). Also, Johns Hopkins University has developed a real-time tracking map for following up the COVID-19 patients around the world, by collecting data from the World Health Organization (WHO) and the U.S., European, and Chinese Centers for Disease Control and Prevention (<https://gisanddata.maps.arcgis.com/apps/opsdashboard/index.html#/bda7594740fd40299423467b48e9ecf6>).

## Artificial Intelligence

AI is a field of computer science that aims to mimic the human perception process to independently represent and interpret complex datasets. This term was first put forward in 1956 as “the conjecture that every aspect of learning or any other feature of intelligence can in principle be so precisely described that a machine can be made to simulate it” (29). Although it was once believed that algorithmic decision making could surpass the accuracy of human judgment, AI was dismissed in 1987 by the *New England Journal of Medicine* due to “the field of medicine is so broad and complex that it is difficult, if not impossible, to capture the relevant information in rules” (30). Since early 2010s, it experienced a resurgence mainly because of the improvements in computing power, development of AI algorithms, and the increasing number and quality of datasets (31). Nowadays, AI is dramatically reshaping the landscape of our lives, ranging from facial recognition and search engines to self-driving cars and natural language processing. AI is rapidly evolving and also plays an important role in this pandemic to improve the detection and diagnosis of COVID-19. For example, based on the large datasets of COVID-19-positive cases from

China (<https://www.wired.com/story/chinese-hospitals-deploy-ai-help-diagnose-covid-19/>), some AI algorithms have been developed and used as an initial tool for screening suspected cases (i.e., exposure to confirmed cases and travel history to China, South Korea, or Iran); thus, patients at high risk could be isolated or further confirmed with laboratory-based tests. In addition, an AI-based triage system, online medical “chat bot,” (32) has been implemented in context of this outbreak to help people recognize early symptoms and the importance of hand hygiene, potentially alleviating the workload of physicians.

## Big Data

Digital phenotyping can yield large datasets that are amenable to the big data analytics. Big data is a term defined by Google that refers to extremely large datasets that can be analyzed computationally to uncover the patterns, trends, and associations, particularly those associated with human interactions and behavior (33). In the field of healthcare, initial forays into the big data have been restricted primarily to analyses of genomics, biomarkers, and clinical information. In the context of this pandemic, big data provides great opportunities for carrying out modeling studies of the viral activity and guiding medical policy organization to enhance the preparation for this outbreak. Based on three global databases from Official Aviation Guide, Location Services of Tencent (Shenzhen, China), and Municipal Transportation Management Bureau of Wuhan, Wu and coworkers conducted a modeled study on “nowcasting” to forecast the COVID-19 disease activity inside and outside China, which could also be used by authorities for public health control worldwide (34). Similarly, utilizing WHO International Health Regulations, Joint External Evaluation reports and the Infectious Disease Vulnerability Index, and State Parties Self-Assessment Annual Reporting Tool, Gilbert et al. (35) evaluated the vulnerability and preparedness of African countries in coping with COVID-19, which would help to raise awareness in the health authorities to better prepare for this viral outbreak in Africa (Figure 3A). Concurrently, it has already been increasingly clear that big data analytics would be quite necessary to detect and further understand the complex genetic sequence and biological mechanisms of SARS-CoV-2 (38).

## Blockchain

Blockchain was first conceptualized and gained recognition in 2009 due to Bitcoin, the first digital cryptocurrency (39). Even if it was at first regarded as a public, decentralized collection of several technologies to allow for storing data permanently while being immune to fraud without the need of a central or reliable authority like a bank, this concept has currently been not confined to the exchange of payments. With numerous investments from venture capital and large multinational technology companies, the use of blockchain technology is growing in markets beyond finance, such as the healthcare industries (40–42). At the hospital level, blockchain is one of the widely used technologies for electronic medical records (EMRs) in the modern hospital ecosystems. And at the patient level, blockchain is increasingly used for sharing health data between patients and providers. Also, blockchain-based

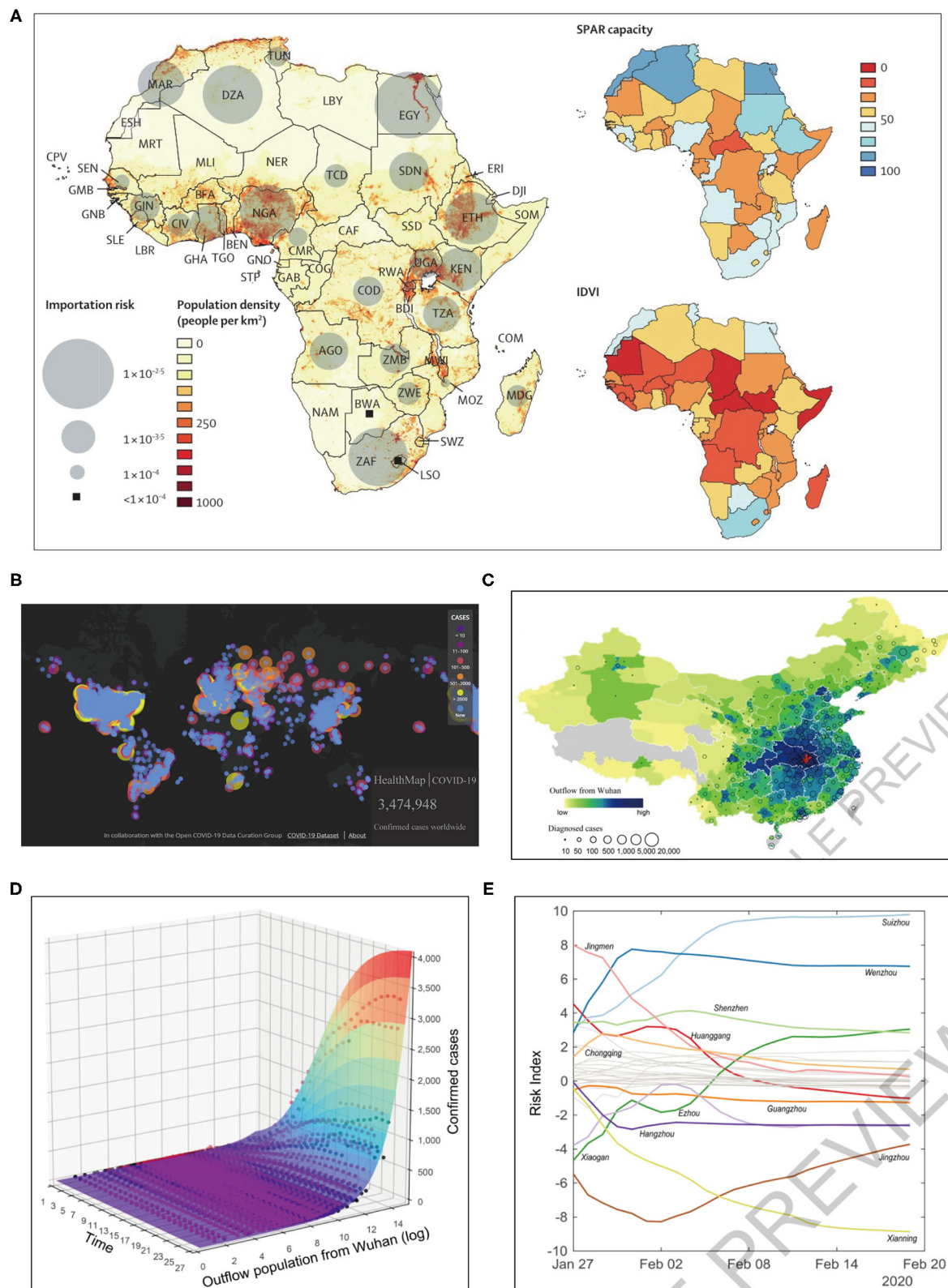


**FIGURE 3 |** Telemedicine based on artificial intelligence and big data technologies for the surveillance of COVID-19 pandemic. **(A)** Big data based modeling study: preparedness and vulnerability of African countries against importations of COVID-19 (35). **(B)** Online contagious COVID-19 surveillance mapping provided by (Continued)

**FIGURE 3 |** HealthMap (36). **(C)** Geographic distribution of population outflow from Wuhan through January 24, 2020 (in red) and the confirmed COVID-19 cases in other Chinese prefectures as of February 19, 2020 (37). **(D,E)** Predictive model supported by the population outflow data from Wuhan: **(D)** the surface displays the fitted performance of this epidemiological model, with dots representing actual number of confirmed cases, and **(E)** the risk scores over time present a dynamic picture of the shifting transmission risks in different prefectures (37). SPAR, State Party Self-Assessment Annual Reporting; IDVI, Infectious Disease Vulnerability Index.

telemedicine interventions are enabling remotely monitor patient via biosensors, bridging access gaps regarding patient-level health services (43). Blockchain technology might have a role in addressing two challenges associated with the internet: trust and identity (44). It is capable of digitizing reliable records in a way that is independent of a single database, which would allow the validation of certain clinical credentials across different care providers, providing great opportunity for supporting adoption of a new digital environment for improving healthcare (45). In addition, utilizing blockchain technology in research might have potential for acquiring more public records of database that could help to address the reproducibility challenge via creating links across related communities. Besides, there are also attempts to use blockchain to battle with this COVID-19 outbreak. For example, many hospitals of China—or in some other countries—are collaborating with blockchain pharmacies and companies to deliver the medication to patients' doorsteps, thus allowing hospitals to deliver medications timely and also with accurate tracking (32).

Actually, the above technologies are highly interrelated and ultimately facilitate the running of telemedicine. That is to say, the proliferation of IoT (e.g., instruments and devices) in hospitals and clinics could contribute to the establishment of a greatly interrelated digital ecosystem, enabling real-time large-scale data collection, which can then be used by the AI, especially deep learning system, to fully understand the healthcare trends and the model risk associations and to predict outcomes. This should be enhanced by the blockchain technique, a network of computers distributed in different organizations and a back-linked database with some pre-designated cryptographic protocols, integrating the peer-to-peer networks to allow data to be copied in various physical locations, with certain modified algorithms to ensure the data are not only secured but also traceable (9). The good cooperation between these technologies, together with 5G-based cloud servers, can offer network platforms as well as act as a dependable resource for the currently unprecedented development of telemedicine.

## OVERVIEW OF THE APPLICATION OF TELEMEDICINE BASED ON MODERN TECHNOLOGIES DURING THE COVID-19 OUTBREAK

In this article, we have used PubMed or Web of Science databases to summarize the literature based on the keywords “fifth generation (5G) networks” OR “Internet of things” OR “artificial intelligence” OR “block-chain” OR “big data” and “robotics” AND “telemedicine” in the period since the COVID-19 pandemic to the present to augment the performance of

traditional public health strategies used in tackling the COVID-19 outbreak, including the (1) surveillance, screening and triage, diagnosis, treatment and monitoring of COVID-19, and (2) mitigation of the impact to healthcare system indirectly related to COVID-19 including management of common and chronic conditions, tele-surgery, tele-psychology, tele-education, and tele-conferencing (Table 1).

## SURVEILLANCE, SCREENING AND TRIAGE, DIAGNOSIS, TREATMENT, AND MONITORING OF COVID-19

### Surveillance and Sharing Data of the COVID-19 Pandemic

Controlling epidemics requires effective and extensive surveillance and timely sharing of epidemiological data (65). During this COVID-19 pandemic, one notable example is Iran (66): as of February 23, 2020, it confirmed its first 43 cases with a fatality rate of 19%, while the reporting transmission modeling prompts that the actual number of infected cases was in the thousands. The rapid global spread of the COVID-19 outbreak has been catalyzed by the insufficient communication and underreporting (67). Healthcare facilities, from the local hospital to WHO, require tools that could improve the speed of communication to better manage the spread of infectious diseases. Telemedicine system based on modern technologies can be implemented for this purpose, as it possesses connectivity, computational power, and hardware to facilitate the electronic reporting and epidemiological databasing. AI and big data can help address the unprecedented amounts of data derived from public health surveillance and real-time epidemic outbreak monitoring (68). For example, the online surveillance mapping tools, including the HealthMap (36) (Figure 3B) and Surveillance Outbreak Response Management and Analysis System (SORMAS) (46), have already been used for surveilling COVID-19, with great potential to improve early detection of the infectious diseases compared with traditional epidemiological tools (69). Sun et al. (70) testified to the strength of monitoring COVID-19 epidemiological information from news media and social networks to help reconstruct the progression of an outbreak and to provide detailed patient-level data during a health emergency. Similarly, Qin et al. (47) exploited the big data technique to predict the number of new infected patients, either suspected or confirmed. Besides, Blue Dot, a Canadian company, has developed an AI-based surveillance system to reveal news of the pandemic, which is widely regarded as the first organization to detect the epidemic outbreak in late December 2019, well ahead of Chinese authorities and any other international institutions and agencies (71, 72). Zhang et al. (49) described a real-time system for sentiment prediction of COVID-19

**TABLE 1** | Digital technology based telemedicine and their impact on public-health strategies during the COVID-19 pandemic.

| Digital technology | Study                    | Country   | Intervention   | Patient location  | Telemedicine Modality                  | Findings   |
|--------------------|--------------------------|---|--|-------------------|--|--|
| IoT, Big data      | Worldometer              | –   | –  | At home/In clinic | Surveillance the status of pandemic    | Presents a real time update on the exact number of people infected with COVID-19 worldwide, including the daily new cases and severity of disease, as well as disease distribution by countries  |
| IoT, Big data      | Johns Hopkins University | The United States   | Develop a real time tracking map for following the COVID-19 patients                     | At home/In clinic | Surveillance the status of pandemic    | Following the COVID-19 patients around the world   |
| Big data           | Wu et al. (34)           | China   | Conduct a modeled study on “nowcasting” based on global databases                        | At home/In clinic | Surveillance the status of pandemic    | Forecast the COVID-19 disease activity inside and outside China, which could also be used by authorities for public health control worldwide   |
| Big data           | Gilbert et al. (35)      | Belgium; France; the United States; Côte d'Ivoire; United Kingdom | Evaluate the vulnerability and preparedness of African countries in coping with COVID-19 | At home/In clinic | Surveillance the status of pandemic    | Countries with the highest importation risk (i.e., Egypt, Algeria, and South Africa) have moderate to high capacity to respond to outbreaks. Countries at moderate risk (i.e., Nigeria, Ethiopia, Sudan, Angola, Tanzania, Ghana, and Kenya) have variable capacity and high vulnerability. Three clusters of countries that share the same exposure to the risk originating from the provinces of Guangdong, Fujian, and the city of Beijing, respectively. |
| Big data           | HealthMap (46)           | The United States   | Develop an online surveillance-mapping tool  | At home/In clinic | Surveillance the status of pandemic    | Surveilling COVID-19 pandemic  |
| Big data           | SORMAS (46)              | Germany   | Develop an online surveillance-mapping tool  | At home/In clinic | Surveillance of the COVID-19 pandemic  | Surveilling COVID-20 pandemic  |
| Big data           | Qin et al. (47)          | China   | Exploite the big data technique  | At home/In clinic | Surveillance the COVID-19 pandemic     | By employing techniques such as subset selection method, new COVID-19 suspected and confirmed cases could be detected 6-9 and 10 days in advance, respectively.  |
| Big data, AI       | Yang et al. (48)         | China   | Establish a modified SEIR model  | At home/In clinic | Surveillance the COVID-20 pandemic     | A 5-day delay in the adoption of stringent public health measures by the Chinese authorities would have led to a COVID-19 epidemic size increased by up to three times. Also, loosening or lifting the lock-down intervention in the Hubei province would cause a second peak by mid-March until late April.   |
| Big data, AI       | Blue Dot                 | Canada  | Develop an AI-based surveillance system  | At home/In clinic | Surveillance the COVID-19 pandemic     | Reveal news of the pandemic, which is widely regarded as the first organization to detect the epidemic outbreak in late December, 2019, well ahead of any other international institution and agency.  |
| Big data, AI       | Zhang et al. (49)        | –   | Develop an AI-based surveillance and prediction system                                   | At home/In clinic | Surveillance the COVID-19 pandemic     | A real-time system to surveilling and sentiment prediction COVID-19 pandemic.  |
| AI                 | Zivkovic et al. (50)     | –   | Improve the current time-series prediction algorithms system                             | At home/In clinic | Surveillance the COVID-19 pandemic     | Achieved good predictive efficacy of COVID-19 pandemic by using a hybrid algorithmic approach that combines machine learning, an enhanced beetle tentacle search population intelligent metaheuristic algorithm.   |
| AI                 | Yan et al. (51)          | China   | Develop an “online self-assessment tool” supported by AI                                 | At home           | Screening and Triage COVID-19 patients | Help individuals self-evaluate the risk of COVID-19.   |

(Continued)



**TABLE 1 |** Continued

| Digital technology | Study   | Country           | Intervention  | Patient location  | Telemedicine Modality  | Findings  |
|--------------------|---|-------------------|---|-------------------|--|---|
| AI                 | Srinivasa Rao et al. (52)<br>Zahedi et al. (53) | the United States | Provided a framework based on AI algorithm that could enable quick identification of COVID-19 cases | At home           | Screening and Triage COVID-19 patients                                       | Depending on these replies, this algorithm could send alerts to the respondent, as well as clinics or the mobile health units, for further health visits and case confirmation. |
| AI                 | D'Angelo et al. (54)                            | Italy             | Establish a convolutional deep neural network-based human activity classifier                       | At home/In clinic | Screening and Triage COVID-19 patients                                       | Improve the performance of the new COVID-19 patient tracking application by using a human activity classifier based on convolutional neural networks and multichannel images.   |
| Robot              | Global Health Security (55, 56)                 | China             | Develop robots to treat and test Covid-19 patients  | At home/In clinic | Screening and Triage COVID-19 patients                                       | Develop robots to treat and test Covid-19 patients in a bid to protect health workers.  |
| Blockchain         | Ting et al. (32)                                | Singapore         | Hospitals collaborating with blockchain pharmacies and companies                                    | In clinic         | Treatment of COVID-19 patients   | Deliver the medication of patients to their doorsteps, thus allowing hospitals deliver medications timely also with accurate tracking.  |
| 5G, Blockchain     | Hong et al. (57)                                | China             | Conduct CT scanning   | In clinic         | Diagnosis of COVID-19 patients   | The first reported case of remote CT scanning during the COVID-19 pandemic.   |
| AI, Big data       | Zhang et al. (58)                               | China             | Reported an AI-powered CT diagnostic system   | In clinic         | Diagnosis of COVID-19 patients   | Diagnose COVID-19 with an accuracy of 92.49%, and had been made available globally to assist the clinicians to combat COVID-19.   |
| 5G, Blockchain     | Li et al. (59)<br>Lv et al. (60)                | China             | 5G-based teleultrasound network   | In clinic         | Diagnosis and treatment of COVID-19 patients                                 | Facilitate "on-line" imaging data transmission, and the further "real-time" diagnosis or operation guidance for COVID-19 patients, especially those in ICUs.                    |
| 5G, Robot          | Li et al. (59)                                  | China             | 5G remote robotic ultrasound diagnostic" system   | In clinic         | Diagnosis of COVID-19 patients   | Enable real-time remote control for ultrasound scanning, thus eliminating exposure to COVID-19 to the greatest extent.  |
| AI                 | Li et al. (61)                                  | China             | AI diagnostic model based on chest CT   | In clinic         | Diagnosis of COVID-19 patients   | Distinguishes COVID-19 from community acquired pneumonia with the sensitivity and specificity of 90% and 96%, with an AUC of 0.96   |
| AI, Big data       | CLEW (62)                                       | Israeli           | AI-powered tele-ICU system  | In clinic         | Monitoring status of COVID-19 patients                                       | Support monitoring COVID-19 patients status with certain respiratory deterioration prediction models, which was later installed in two Israeli hospitals.                       |
| 5G, Robot          | Tian et al. (63)                                | China             | 5G based tele-robotic spinal surgery  | In clinic         | Mitigation of the impact to healthcare system indirectly related to COVID-19 | All the 12 patients treated with this technology had substantial relief from their symptoms, while without any intraoperative adverse event.                                    |
| AI                 | Wang (64)                                       | China             | Tree Holes Rescue (a kind of AI psychological programme)  | At home           | Mitigation of the impact to healthcare system indirectly related to COVID-20 | Recognized individuals at risk of suicide by monitoring and analyzing the messages posted on Weibo, and further alerting the designated volunteers to take action accordingly.  |

5G, fifth generation; AI, artificial intelligence; IoT, internet of things; CT, computed tomography; US, ultrasound; COVID-19, coronavirus disease 2019; WHO, World Health Organization; ICU, intensive care unit; SEIR, Susceptible-Exposed-Infectious-Removed.

epidemiological information based on Twitter data. And by evaluation, it was found that predictive analysis with a random forest classifier has the best performance. Zivkovic et al. (50) achieved good predictive efficacy by using a hybrid algorithmic approach that combines machine learning, an enhanced beetle tentacle search population intelligent metaheuristic algorithm, and an adaptive neuro-fuzzy inference system to predict new COVID-19 patient cases.

Considering that sudden large-scale human migration could amplify the localized outbreak into widespread epidemic (73, 74). rapidly and accurately tracking the aggregate population flows can be epidemiologically informative. Jia et al. (37) based on the mobile phone datasets of 11,478,484 people egressing or transiting through the COVID-19 epidemic epicenter, Wuhan of Hubei Province, developed a spatio-temporal "risk source" model (Figures 3C–E) to forecast confirmed cases and also

to identify the highly transmission-risk locations at an early stage, which can help the local authorities to make better risk assessment and further to plan allocation of the limited resources before ongoing outbreaks. Similarly, supported by population migration data, Yang et al. (48) established a “Susceptible-Exposed-Infectious-Removed” (SEIR) model, which, combined with an AI approach, is able to predict the pandemic curve, and the authors presented that a 5-day delay in the adoption of stringent public health measures by the Chinese authorities would have led to a COVID-19 epidemic size increased by up to three times. Also, loosening or lifting the lockdown intervention in Hubei Province would cause a second epidemic peak by mid-March until late April. Colubri et al. (75) used AI technique to harmonize several datasets from the Ebola epidemic to offer informed access to the evidence-based guidelines. And then these guidelines were incorporated into an app of the Ebola Care Guidelines (75). Many of these lessons can be re-applied for COVID-19. The app has the potential of including real-time updates of the evidence-based guidelines to inform both the general population and the healthcare providers. Integrating real-time updates into the EMRs could also serve as a reliable resource for guiding clinical practice. Telemedicine platform can be paired with the accessible information technologies to provide real-time, shareable, epidemic information during outbreaks like COVID-19, which empowers individuals, clinicians, and national and global healthcare agencies to adopt coordinated control strategies.

## Screening and Triage of COVID-19 Patients

A central strategy for healthcare pandemic control is “forward triage,” sorting patients before they arrive in the clinical departments. Direct-to-consumer telemedicine system, an approach to forward triage, could allow patients to be timely and efficiently screened; thus, it is patient-centered and simultaneously conducive to the self-quarantine, protecting providers, patients, and the community from disease exposure. Health institutions in many countries are offering free triage telemedicine assessments for COVID-19 by providing patients with access to certain websites or mobile apps that involve a short survey regarding the age, symptoms, and travel history of patient. Based on these results, respondents will be offered with tips, to visit a nearby COVID-19 testing site, or be connected digitally with physicians. In addition, health-focused chat bots, such as Lark Health (76) and Buoy Health (77), can also be used to interpret symptoms of individuals and further present appropriate advices. And Yan et al. (51) provided an “online self-assessment tool” supported by AI technologies to help individuals self-evaluate the risk of COVID-19, thus relieving pressure on the healthcare staff and alleviating the anxiety of patients.

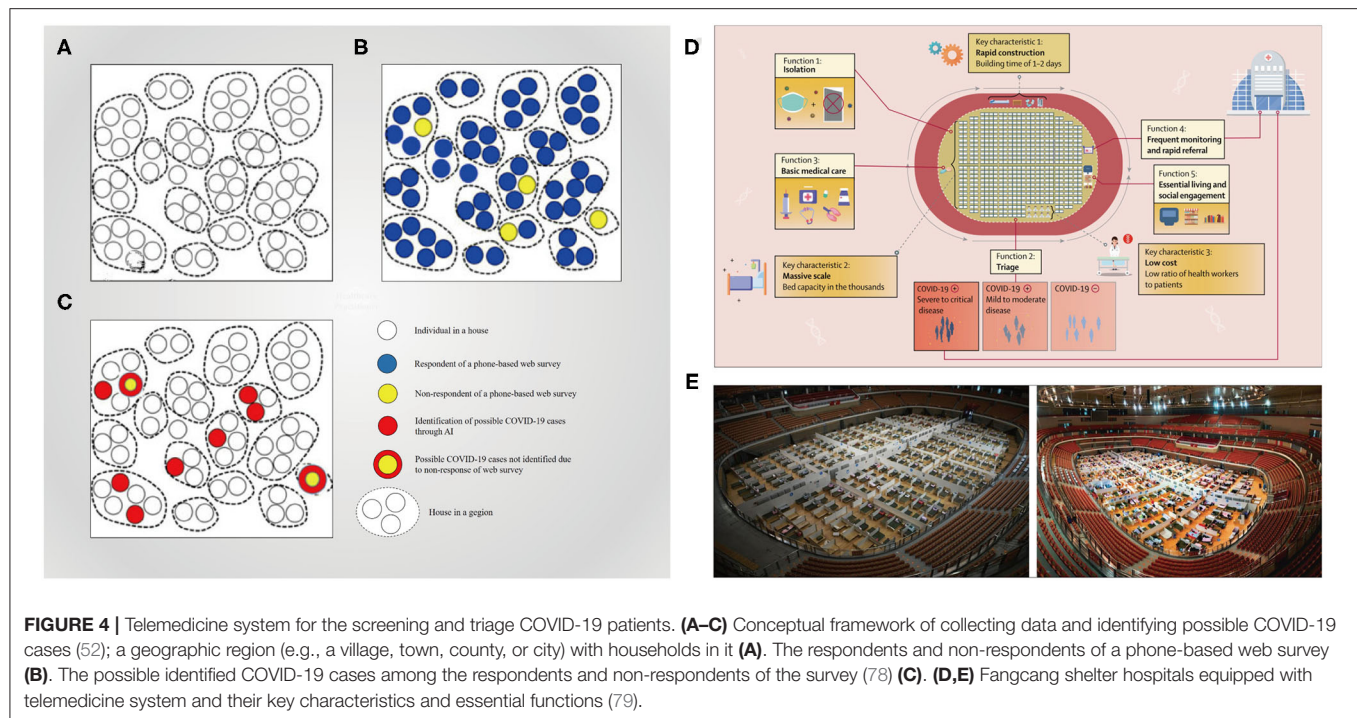
In response to this pandemic, many countries have devoted to virtual medical care development, which could allow patients and providers to communicate through smartphones or webcam-enabled computers. Community residents with respiratory symptoms, which might be early signs of COVID-19, could consult using the online clinic consultation services. Srinivasa Rao et al. (52) and Zahedi et al. (53) provided frameworks

(Figures 4A–C) based on AI algorithm and IoT that could enable quick identification of COVID-19 cases, by performing risk assessment on the symptoms and signs associated with this novel coronavirus through web- and mobile-based survey, respectively. And, depending on the replies, this algorithm could send alerts to the respondent, as well as to clinics or the mobile health units, for further health visits and case confirmation. Automated screening algorithm can be integrated into the tele-consultation process, and the local epidemiologic information can also be utilized to standardize the screening and practice patterns between healthcare providers. More than 50 U.S. health agencies already have such programs. Kaiser Permanente, Jefferson Health, Mount Sinai, and Cleveland Clinic, for example, all leverage telemedicine platform to allow clinicians to screen potential patients who are at home (67). The D’Angelo team (54) utilized a human activity classifier based on convolutional neural networks and multichannel images to improve the performance of the new COVID-19 patient tracking application.

During this pandemic, Fangcang shelter hospitals (Figures 4D,E), which are a novel public health concept built by converting the existing public venues (e.g., stadiums and exhibition centers) into healthcare facilities, were first implemented in China to tackle the COVID-19 outbreak (79). In Wuhan of Hubei Province, they served to isolate patients experiencing mild-to-moderate symptoms of COVID-19 from their families, and importantly, digital technology-based telemedicine was integrated into the workflow of Fangcang shelter hospitals to support medical care; that is, health workers had access to the electronic information systems, which were connected with higher-level hospitals and based on cloud platforms, for record keeping, data transfer, and remote monitoring (80), thus offering high-quality medical care and fulfilling an important triage function. Fangcang shelter hospitals could be powerful components of the national response to COVID-19 and was even considered a major reason for the successful pandemic control in China (79). In addition, the safety of healthcare workers is greatly protected by the use of a remote-controlled robot with pharyngeal swab detection and a robotic arm for SARS-CoV-2 detection to screen suspected patients (55, 56).

## Diagnosis and Treatment of COVID-19 Patients

In context of the COVID-19 outbreak, the telemedicine system can provide a good platform for enhancing communication among healthcare providers, could increase diagnostic accuracy of some difficult cases, and improve the treatment results of severe or critical COVID-19 patients in areas with limited medical resource. In China, in efforts to cope with this epidemic, an “Anti-epidemic Expert Group” was launched to formulate quarantine, diagnosis, treatment, and reporting protocols (81). Also, this expert group comprehensively utilized the available professional platforms, including telemedicine system to connect the patients, experts, and information for better managing of the COVID-19 patients not only in China but also around the globe. Additionally, at the time that the WHO declared



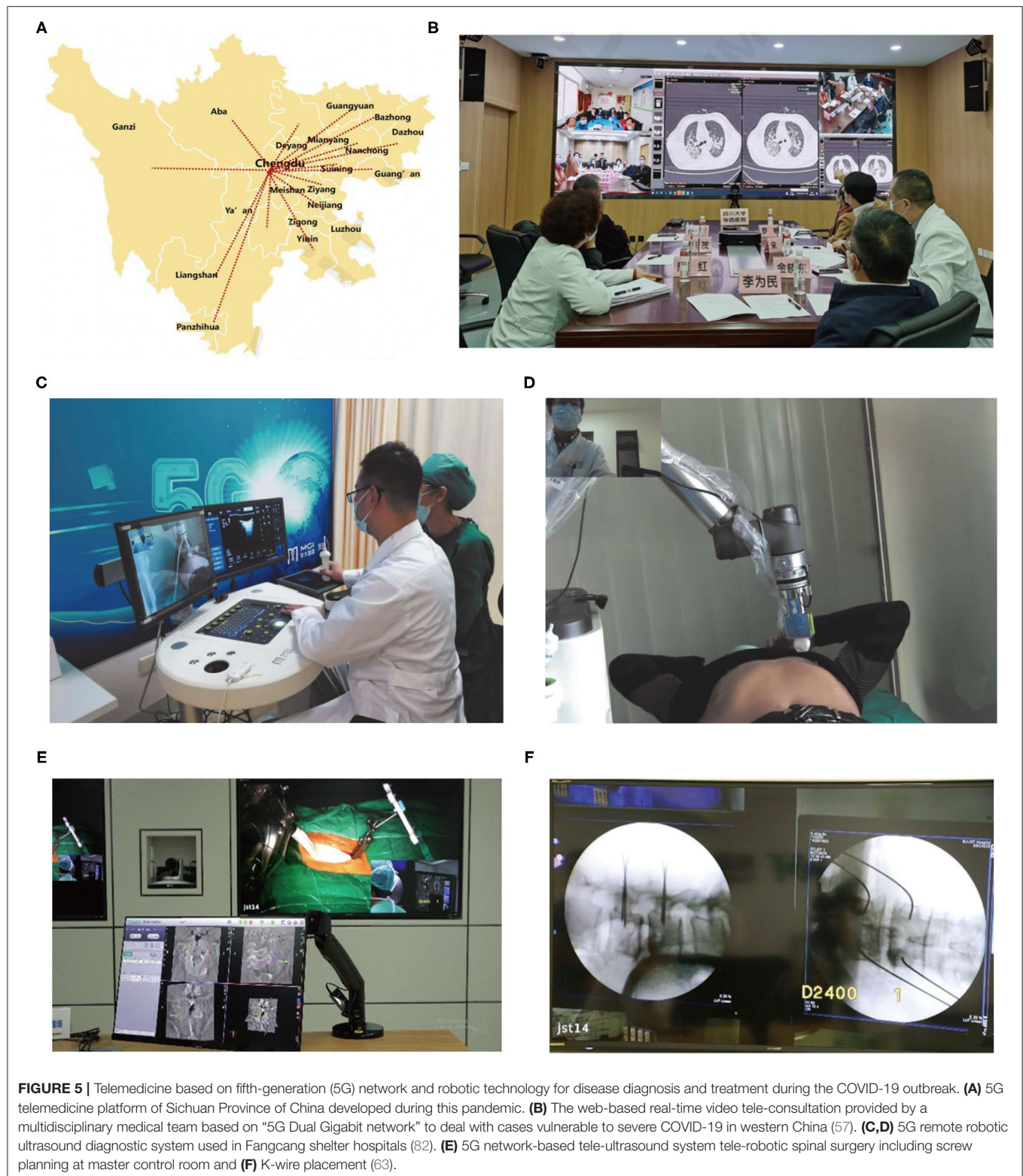
COVID-19 a pandemic, this expert group invited many Chinese topic experts to use the “Cloud Intensive Care Unit (ICU)” telemedicine platform to share personal experiences in managing critical COVID-19 patients to help mitigate global burden of COVID-19 (81). Simultaneously, based on a “5G Dual Gigabit network,” the West China Hospital of Sichuan University (WCHSU) established a multidisciplinary medical team to deal with cases vulnerable to severe COVID-19, such as the elderly, children, pregnant women, and patients with certain chronic health problems (57) (**Figures 5A,B**). From January 26 to March 12, 2020, a total of 424 consultations were performed for confirmation of COVID-19 diagnosis (15%), adjustment of antiviral therapy (75%) or respiratory therapy (55%), and management of complications (68%) via this new telemedicine system for severe or critical COVID-19 patients, which has been highly praised by the WHO owing to the increased diagnostic accuracy and improved treatment outcomes for a large rural population in western China. This system can help explain why the case fatality rate (CFR) of COVID-19 cases is only 0.55% in the Sichuan Province of China, much lower than that in Hubei Province (4.64%) and the world averages so far (57).

Driven by the COVID-19 pandemic, various types of medical imaging platforms have been launched worldwide to address the diagnosis problems for COVID-19 patients. Considering that computed tomography (CT) imaging is currently being used for confirming cases of COVID-19 (83, 84), radiologists at WCHSU utilized “5G Dual Gigabit network” to remotely conduct CT scanning on COVID-19 patients, which, to our knowledge, is the first reported case of remote CT scanning during the COVID-19 pandemic (57). Experts at WCHSU were also able to view the CT imaging dataset just as the local clinicians. So far, 152

patients with the aid of telemedicine platform have undergone CT scanning that is remotely guided by WCHSU physicians (57). Also, supported by the telemedicine system and imaging cloud services, radiological medical experts from the Wuhan Union Hospital of China communicated with their Kenyan counterparts regarding the CT imaging diagnosis of COVID-19 and also shared their initial diagnostic criteria for COVID-19 as a way to assist Kenya and other African countries in quickly mastering diagnosis and treatment methods of this disease. And as of March 23, 2020, it reported that 37 counties in Kenya had adopted China’s high-end medical imaging equipment, cloud services, and their clinical application training and other one-stop solutions, which were quite helpful for fighting against the epidemic (85). Also, researchers developed AI models that could accurately detect COVID-19 disease and differentiate it from other forms of pneumonia, (61) which can be used remotely by physicians beyond the epidemic areas. As one example, Zhang et al. (58) recently reported their AI-powered CT diagnostic system (**Figure 6A**) in *Cell*, which could diagnose COVID-19 with an accuracy of 92.49% and had been made available globally to assist the clinicians to combat COVID-19. Abdel-Basset et al. (86) utilized an intelligent framework incorporating emerging technologies (e.g., AI, IoT, big data, autonomous robotics, and 5G) to help make rapid decisions to treat COVID-19 patients while ensuring patient and healthcare team safety.

Additionally, Xu’s group (59, 60) launched a “5G-based teleultrasound network” for fighting against this pandemic in China, which incorporated several advanced information technologies including cloud services, AI and robot techniques, greatly facilitating “online” imaging data transmission, and the

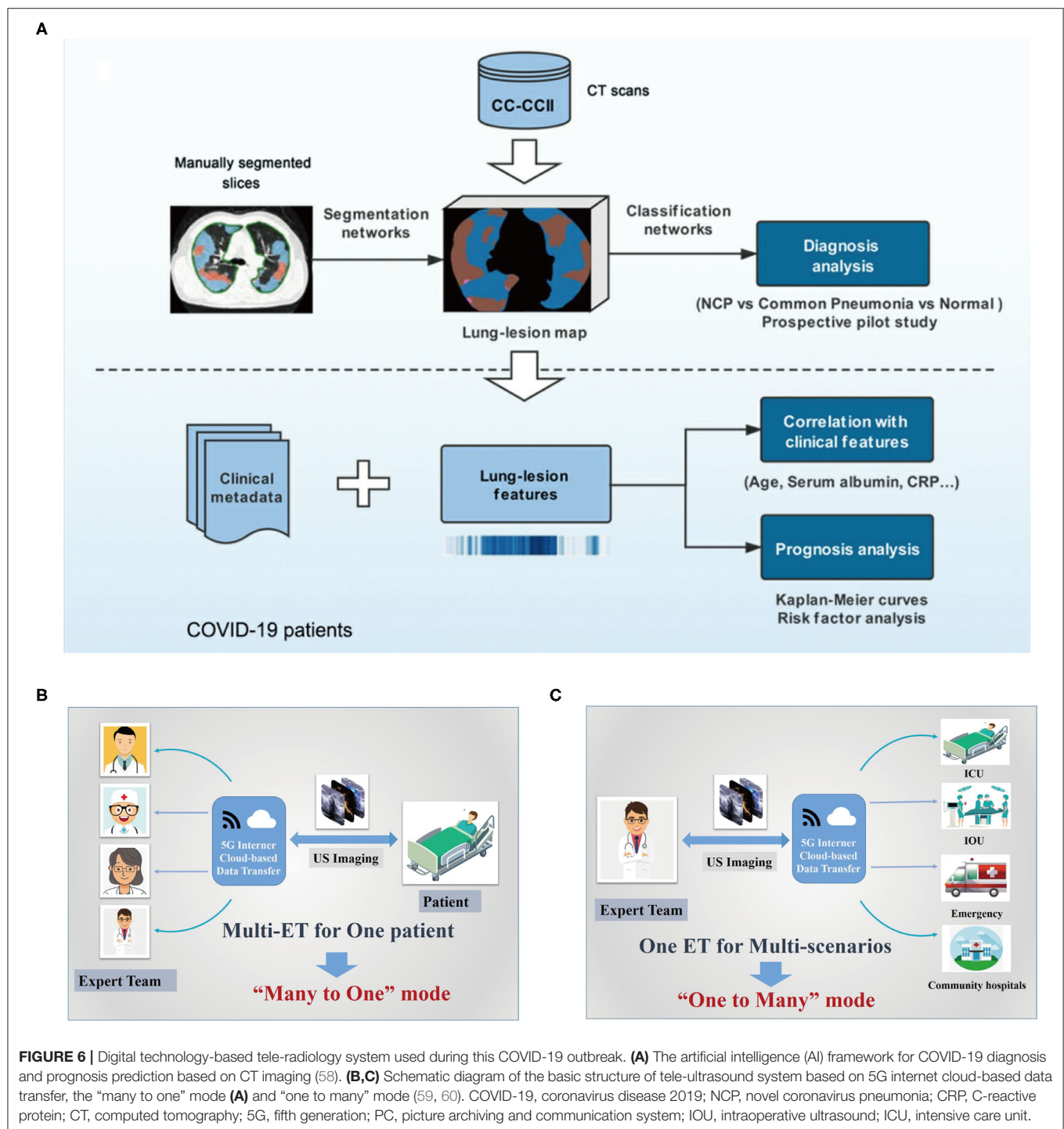




further “real-time” diagnosis or operation guidance for COVID-19 patients, especially those in ICUs, which also greatly pushes the further development of “many to one” and “one to many”

remote clinical patterns (**Figures 6B,C**). “Many to one” implies that several experts or medical teams synergistically deal with a single clinical scenario, which can integrate expert knowledge





from different professional backgrounds, thus facilitating the management of certain critical patients, for example, those in the ICU. Similarly, “one to many” is that one expert or medical team deals with multiple clinical scenarios, which can make better use of the limited expert resources to provide high-quality healthcare for patients, particularly in some extreme environments such as the current pandemic. Importantly, the cloud-based data could

further serve as a “Digital Imaging and Communications in Medicine data bank,” providing large-scale shared datasets for the wireless ultrasound (US) imaging analysis, which provides a great opportunity for AI technology development. Synchronously, the “5G remote robotic US diagnostic” system can enable real-time remote control for US scanning, thus eliminating exposure to COVID-19 to the greatest extent. Notably, in Fangcang

shelter hospitals, where CT scanning cannot be performed and simultaneously there is a lack of qualified US physicians, it has already been successfully utilized to timely and accurately assess cardiopulmonary function of COVID-19 patients (82) (**Figures 5C,D**). Together with the reported “remote conduct CT scanning” system, it marks a significant transition of telemedicine from traditional “consultation” mode to a new “practical operation” mode, ensuring excellent US/CT performance even in areas with limited experts or qualified technicians.

The global fight against this pandemic is bound to trigger a great leap in science and technology and thus push for industrial upgrade. One notable example is the rush construction of Huoshenshan Hospital and Leishenshan Hospital in Wuhan, Hubei Province, where in a short span of 2 weeks is equipped with full 5G coverage and several other advanced technologies such as AI, robot, and cloud services. And importantly, the two “smart hospitals” can provide good examples showing the power of digital technology-based telemedicine system in the battle against the novel coronavirus outbreak. For example, an audio and video real-time interconnection system supported by 5G technique has been installed in the two hospitals to facilitate share case information among medical workers within isolation wards. With this system, staff in non-isolation areas and the administrative centers could also see the real-time situation in the isolation area through a large screen at any time and could ensure direct and effective communication at multiple places. In addition, the system can be connected via 5G hot spots, so as to allow multidisciplinary resources from other major cities such as Shanghai, Beijing, and Guangzhou to help remotely diagnose and treat critically ill patients at Leishenshan or Huoshenshan Hospital. This tele-platform runs 24 h a day, so clinicians at the two hospitals could seek help online whenever they have difficulties in case diagnosis or treatment, thus greatly improving treatment levels. Also, robot systems with delivery and disinfection services, as well as remote CT scanning platform, have been adopted in the two hospitals to minimize the potential risk of cross-infection. It reported that, supported by these cutting-edge equipment, during the first 2 months of operation, a total of 2,011 COVID-19 patients were received by the makeshift hospitals and the overall mortality rate was 2.3%, and none of medical personnel contracted this highly contagious disease (87). The two “smart hospitals,” together with Fangcang shelter hospitals, had played an “irreplaceable role” in the battle against COVID-19 in Wuhan of Hubei Province, and China’s efficient use of modern technologies has helped the country gain the upper hand in its virus fight, which is a good model for other countries to follow in their fight against this disease.

## Monitoring Status of COVID-19 Patients

During the COVID-19 pandemic, telemedicine services can be applied as a remote-monitoring tool to better understand the evolution of COVID-19 disease, as well as status of high-risk patient populations. At patient level, the evaluation data can be derived from self-reporting system or wearable sensing equipment. An extensive body of literature exist regarding the use of telemedicine system in remote monitoring of some chronic diseases just in this way (88, 89). Indeed, the same concept

can also be used for monitoring of infectious diseases such as COVID-19. South Korea, which can be touted as a good global example of effective pandemic response, implemented early a novel “Community Treatment Center” outside hospitals to treat mild COVID-19 patients (90). To minimize the exposure of healthcare providers, patients in the center were asked to self-report their daily temperatures via a phone-based app (inPHR<sup>®</sup>, SoftNet, Seoul, Korea) for clinicians to remotely monitor their disease status, and the adherence rate reached greater than 80%, 2.3% of which were eventually transferred to inpatient units and 31% had been discharged at home (90). Synchronously, considering the importance of reducing the amount of community spread of COVID-19 by keeping people at home, Cleveland Clinic, to our knowledge, is the first reported to implement a home-based intervention program that incorporates a patient-engagement app and monitors symptoms for the early intervention, ultimately promoting a holistic view of healthcare (91). Interestingly, following the widespread interest in remote monitoring for COVID-19 patients, Annis et al. (92) conducted a study to evaluate the outcomes, acceptability, and lessons regarding the remote-monitoring program implementation. An existing third-party application, which previously had been used for enhancing recovery after surgery was introduced for monitoring COVID-19 cases, and 300 patients responded to the satisfaction questions regarding application, of which 74% had been extremely grateful about their experience using this tool, which demonstrated what could be accomplished through shared effective and imperative partnerships between industry and healthcare delivery (92).

Apart from the aforementioned self-reported remote-monitoring systems, robots equipped with devices such as thermometer, cameras, and radar, which could move in isolation areas while controlled remotely by clinicians via mobile phones, have already been used in wards of Fangcang shelter hospitals of Wuhan, Hubei Province, to help protect medical staff members from infection and save protective resources. Also, the automatic infrared thermal imaging temperature detection and warning systems have been adopted in Huoshenshan and Leishenshan hospitals of Wuhan to enable real-time and continuous monitoring of the changes in body temperature and automatically alert the febrile individuals, which could contribute to better management COVID-19 cases via early detection and simultaneously avoid cross-infection. Dong et al. (93) and Alsamhi et al. (94) also summarized the active role of IoT and blockchain during the COVID-19 epidemic, covering the diagnosis of COVID-19 symptoms, quarantine monitoring, and real-time tracking to combat the epidemic. It also revealed the meaningful role of digital technology during the epidemic.

As COVID-19 is an extremely contagious pneumonia that can quickly develop into severe form of respiratory failure, there is a great possibility of overwhelming available ICU resources. The management of critical care patients especially those in ICU has become a topic of great concern. Telemedicine in the ICU provides 24/7 specialist care for critically ill patients combined with remote patient monitoring, which is increasingly touted as a nursing mode to improve efficiencies and quality of care (95). To reduce the contact between healthcare personnel and

infected patients, the electronic ICU monitoring and surveillance program such as services offered by Sutter Health, Mercy Virtual Care Center, and Sentara Healthcare enables nurses and clinicians to remotely monitor the status of patients in the ICU (95). At the HIMSS 2020, CLEW, a company focused on intelligent healthcare, demonstrated its AI-powered tele-ICU system to support monitoring of COVID-19 patients' status with certain respiratory deterioration prediction models, which was later installed in two Israeli hospitals (62). Real-time risk stratification will enable timely interventions and thus improve clinical outcomes for critically ill patients.

## MITIGATION OF THE IMPACT TO HEALTHCARE SYSTEM INDIRECTLY RELATED TO COVID-19

### Telemedicine for Management of Common and Chronic Conditions

Hospitals are potential areas of high COVID-19 cross-infection; thus, to reduce the people accumulation in outpatient centers during this pandemic, online medical consultations, website-based prescription, and delivery services for patients with certain common and chronic diseases have been developed by hospital agencies in many countries. In China, these telemedicine services can be acquired through the websites of hospitals, WeChat accounts, and several widely used apps, for example, "Huayitong" (57). It reported that by March 23, 2020, 31,905 patients had benefited from this service for prescriptions or medicines, greatly reducing the number of patient visits, easing the overcrowding in outpatient clinics, and allaying worry for patients with chronic disease (57).

Actually, telemedicine system is not a new mode for delivering healthcare for common and chronic disease patients, as it has already been used for ongoing management of long-distance clinical care, health administration, and education over the last few years, though several common modalities, such as live-video tele-conferencing, store-and-forward technologies, home monitoring programs, and mobile health applications (96, 97). Despite the great potential of telemedicine system to improve access to healthcare, its uptake is limited in scale due to interstate licensing barriers, inadequate reimbursement, and to some extent the resistance to change and lack of infrastructure (98). The COVID-19 outbreak, particularly together with modern technologies, has, in the short term, accelerated the ever-growing development of telemedicine platform as a distancing measure to cope with this current public health crisis. Integrating the advanced digital technologies into the telemedicine platform makes it rapidly move to be the frontline clinical practice for chronic disease management, due to the demand for prevention and mitigation strategies; it has also been encouraged and facilitated by changes in payer-driven reimbursement policies, as well as government rules and regulations (18). Currently, a variety of telemedicine tools, many of which are free or of low cost, such as Skype, Facebook Messenger video chat, Apple FaceTime, and Google Hangouts video, can be used for

consulting specific care (99), and this technology has been re-despoiled and used across various medical specialties including pediatrics, neurology, dermatology, ophthalmology, psychiatry, and oncology (99). For example, Serper et al. (100) in the context of COVID-19 crisis, launched a "telehepatology tertiary-care team" (telemedicine for advanced liver disease) via a VidoConnect™ between tertiary care site and referring site, to guide the community-based gastroenterology practice. Net Promoter Score (NPS), a gold standard customer satisfaction tool, was calculated by the authors to help evaluate patient likelihood of recommending the telehepatology service to surroundings, and a mean NPS of 92 (range from -100 to 100) was acquired from the respondents, indicating they had undergone a highly satisfied and excellent experience, well above the levels typically seen in healthcare settings, and thus telehepatology was proved to be a feasible, acceptable, efficient way to provide care to these patients with complex liver diseases while not compromising clinical care (100). Additionally, Grossman et al. (18) presented their tele-neurology platform in response to the COVID-19 pandemic by using synchronous audio and video connections between provider and patient, also integrated with an EMR, and showed that it is clinically meaningful mode for virtual services. Similarly, Garg et al. (101) provided a continuous glucose monitoring system by utilizing the commercially available software (i.e., Dexcom, Clarity, and Glooko) to manage type 1 diabetes virtually. Indeed, type 1 diabetes is particularly suited to such a kind of remote care, as most of the visits are built around reviewing data and consulting therapies.

With the WHO declaring this pandemic, there is an inevitable impact on cancer patients; however, due to the limited data, currently, there are no available international guidelines to enable the management of these patients in times of crisis. In an effort to minimize the interruption of cancer treatment, telemedicine has been recommended as a practical approach by an international collaborative group including eight countries, (102) to support cancer patient management during such an infectious pandemic. Also, Prasad et al. (103), drawing upon their experience, compiled a set of guidelines and a valuable patient handout for head and neck cancer patients to optimize telemedicine visit during the era of COVID-19. Synchronously, Quek's group (104) developed a telemedicine platform (video conferencing) between interventional radiologists and nuclear medicine physicians during this crisis to ensure continuity of care for cancer patients requiring yttrium-90 radioembolization; and at the time of writing their article, three cases including two cases of hepatocellular carcinoma and a metastatic hepatic carcinoma had been successfully treated without complications via this technology. Taiwo et al. (105) also proposed a remote smart home healthcare support system (ShHeS) that can be used by patients who need regular health checkups to receive consultations and doctor's prescriptions at home. Considering the importance of telemedicine system, the European Association of Nuclear Medicine (EANM) and the Society of Nuclear Medicine and Molecular Imaging (SNMMI) promulgated guidelines for the tele-nuclear medicine in remotely interpreting routine nuclear medicine studies, as well as in interpreting emergency studies in

on-call settings (106). This outbreak can enable a wider adoption of tele-nuclear medicine during the post COVID-19 era—not only in patient diagnosis and therapy but also in clinician education for certain developing countries with limited access to the formal training in nuclear medicine.

## Tele-Surgery

With the evolution of the COVID-19 outbreak during March 2020, increasing concerns on conserving healthcare resources led to wide calls for delaying or canceling non-urgent services. As such, the Centers for Medicare & Medicaid Services (CMS), on March 18, 2020, announced that all the elective surgeries and non-essential surgical procedures should be delayed. This announcement from CMS came as a specific problem for clinicians, as accurately interpreting the meaning of “elective” and well balancing this definition with patient health can sometimes become a major challenge even for the most experienced surgeons (107). In this context, tele-surgery such as remotely guiding the surgical procedure or robot-assisted remote surgery can be the best option for both doctors and patients.

Remote surgery that is based on the mutual telecommunication information, such as image, video, and audio, digitally transmitting via wireless or cable networks, enables surgeons to manipulate surgical robots to perform operations across distance (108, 109). The instability of network and system delay should be the main obstacles of robot-assisted real-time tele-surgery. Fortunately, the recent revolution of 5G network with spectacular performances in high speed and low latency (78) has facilitated the clinical practice of remote surgery. Tian et al. (63) in collaboration of 5G network and orthopedic robot technology performed 12 cases of tele-robotic spinal surgery (**Figures 5E,F**). All the patients had substantial relief from their symptoms, while without any intraoperative adverse event. Actually, robot-assisted spinal tele-surgery has been regarded as a popular and reliable surgical technique in the past few years (110–112). Roser et al. (113) reported an accuracy of up to 99% for pedicle screw placement by the robot-assisted spinal surgery. Similarly, Lonjon et al. (114) presented that the accuracy of the pedicle screw placement was 97.3% by using ROSA robot system, higher than that of freehand method (92%). Nowadays, the breakthrough in 5G network system and robot technology, particularly sparked by this health crisis, makes the fast-paced practice of tele-robotic surgery. Huddy et al. (115) reported a simultaneous installation of the da Vinci Si and Versius robotic system, which provided an emergency surgical strategy during a COVID outbreak with excellent outcomes and high patient satisfaction.

## Tele-Psychology

Deep emotional traumas in society overwhelmed by huge human disasters, such as global pandemic diseases, man-made tragedies, natural disasters, social crises, and war conflicts, can cause plenty of stress-related disorders (116). Following this broader context, although treating of COVID-19 patients, virus containment, and vaccine development are the critically urgent issues that should be addressed, it is mandatory to start focusing on the long-term effects on the mental health of the global societies.

Even the WHO technical guidance note warned that “the main psychological impact to date is elevated rates of stress or anxiety,” due to the public health crisis and destabilized economic reasons. In the United States, Hamel et al. (117) launched a coronavirus poll and showed that 32% of the adults feel stress and worry associated with coronavirus, which had negative effects on their mental health, with a “major” impact rate of 14%. Also, in China, a COVID-19 poll of 2,091 inhabitants presented that the prevalence of psychological symptoms in mainland China 1 month after the outbreak was 4.6%, while this rate in provinces with higher number of infected cases was 18.4% (118). These scientific papers are important in enabling global health authorities to allocate available health resources and undertake timely actions to minimize the psychosocial impact of this pandemic on the world population. Limited resources of psychosocial services in many countries around the world have been illustrated, which should be further stretched by increasing demand during the global COVID-19 pandemic. Comprehensive approaches based on telepsychiatry is proposed to cope with the lack of access to mental health services, which includes AI, as well as an array of advanced technologies, like internet-based psychological tools and services. For example, online psychological counseling services (for example, WeChat-based resources) currently have been widely developed by mental health professionals from medical institutions or academic societies throughout 31 provinces in mainland China (119). Also, online mental health self-help intervention systems, such as online cognitive behavioral therapies for anxiety, depression, and insomnia, have been established (120). Additionally, several AI programs have already been put into use as interventions for certain psychological crises during this epidemic. For instance, individuals at risk of suicide can be recognized by Tree Holes Rescue (a kind of AI program) (64), by monitoring and analyzing the messages posted on Weibo and further alerting the designated volunteers to take action accordingly. In addition, Di Carlo et al. (121) summarized the important role that technologies such as telepsychiatry played in the management of mental health assistance during the COVID-19 outbreak. The technology offers a promising approach to tele-mental health services.

This COVID-19 outbreak has brought serious psychological impact on societies, while leading to proposals of lots of technology-assisted psychological intervention models based on the internet-based technologies, AI technique, particularly the popularization of 5G mobile networks and smartphones, enabling individuals to acquire telepsychiatry services during this COVID-19 outbreak. All the available tools should be fully utilized as an important part of the whole package of measures to mitigate negative health effects of this current global coronavirus pandemic.

## Tele-Education and Tele-Conferencing

The impact of this rapidly evolving crisis has pervaded nearly the whole society and is now threatening the medical education and conferences. Due to restrictions declared by the Centers for Disease Control and Prevention and other public health organizations, in-person medical education and academic conferences should be suspended to help address the rapid spread



of virus, which is a huge challenge for students, the education sector, and medical staffs. Telemedicine platform can provide tele-education and tele-conferencing services, which allow a great deal of flexibility and have been proposed and adopted widely as an effective alternative model. Although this method cannot completely replace the traditional face-to-face form, telemedicine may prove to be an appropriate way to solve the current cancellation of courses and medical activities.

Chick et al. (122) implemented a tele-conference format for their weekday academic conferences by using a commercial online software (GoToMeeting; LogMeIn Inc., Boston, MA, USA), which is free to the users with the paid institutional accounts. For the most part, it is logged in via computers, while this program can also be accessed through tablets or smartphones, thus allowing learner engagement from any place. Similar capabilities are currently accessible from a variety of platforms, such as Skype (Skype Technologies, Palo Alto, CA, USA), WebX WebEx (Cisco Webex, Milpitas, CA, USA), and Zoom (Zoom Video Communications, San Jose, CA, USA). As this strategy is widely successful, the authors call on collaboration between nearby institutions, particularly in a form of educational tele-conference, to ensure trainees have access to high-quality education during difficult times (122). Synchronously, due to the suspended face-to-face teaching in the context of coronavirus, Imperial College London is now using EdTech, an education technology, to keep delivering its mission (123). Also, as an alternative to the clinical placements, Imperial students are being given access to the online recordings of patients, and Imperial clinicians are performing tele-teaching through computers on the hospital sites, which have displayed excellent student interaction. Additionally, some medical schools are now turning to remotely conduct assessments, in order to ensure that graduating students have already met the required competencies just before they begin clinical practice (124).

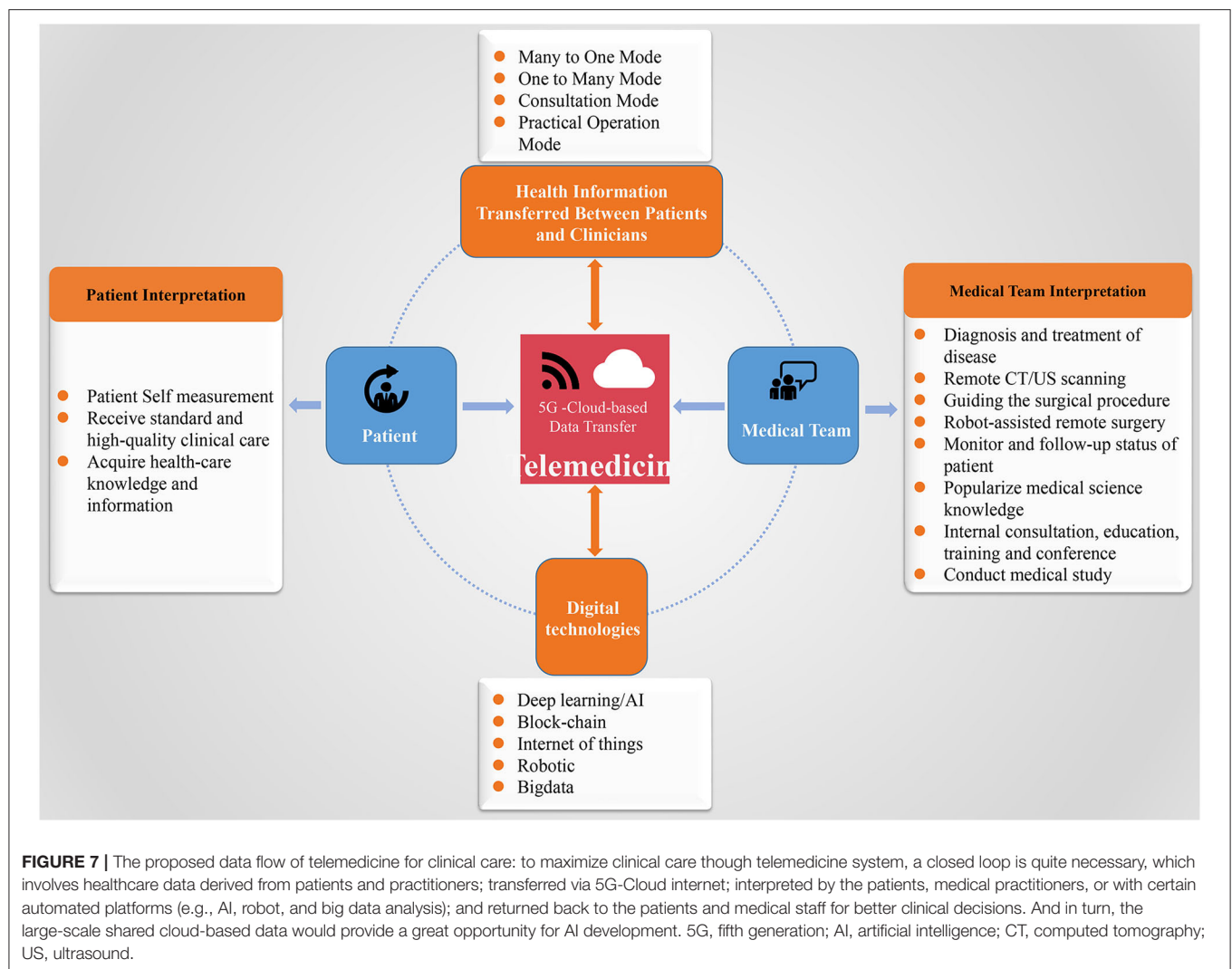
After a meeting in Massachusetts was related to a number of suspected cases, global medical conferences have been canceled or postponed (125). Many important meetings and symposiums should be held in a virtual way for academic exchange or special case sharing and analysis, which might be the only solution at present. In the United States, Academic Life in Emergency Medicine (ALiEM) launched an ALiEM Connect to demonstrate live stream videos and fully discuss with others in an effort to meet the requirements of weekly conferences (126). Also, in the University of Miami, Miller School of Medicine in collaboration with the Clinical Good Hope in Peru and Universidad Peruana Union developed a video conferencing program to expand epidemic knowledge by introducing different clinical cases for the invited physicians to analyze and diagnose, playing a potentially important role in this pandemic (127).

As health systems are set to be further stretched due to the increasing burden of the COVID-19 pandemic, disruptions in medical education and conference are inevitable across the whole world. However, in the year 2020, there is an ecosystem of universities, healthcare agencies, and associations, as well as charities and education platforms, which can understand the trend toward the tele-technology enhanced learning and academic communication, which might be highly beneficial. Such

approaches not only can be utilized for effectively tackling the medical dilemma during this crisis but also will serve to lay the foundation for teaching and academic exchange during future disasters and beyond, which may imply a fast unexpected shift from one form of academic activities and education to another, with wide long-term effects to everyone involved.

## OPPORTUNITIES AND CHALLENGES

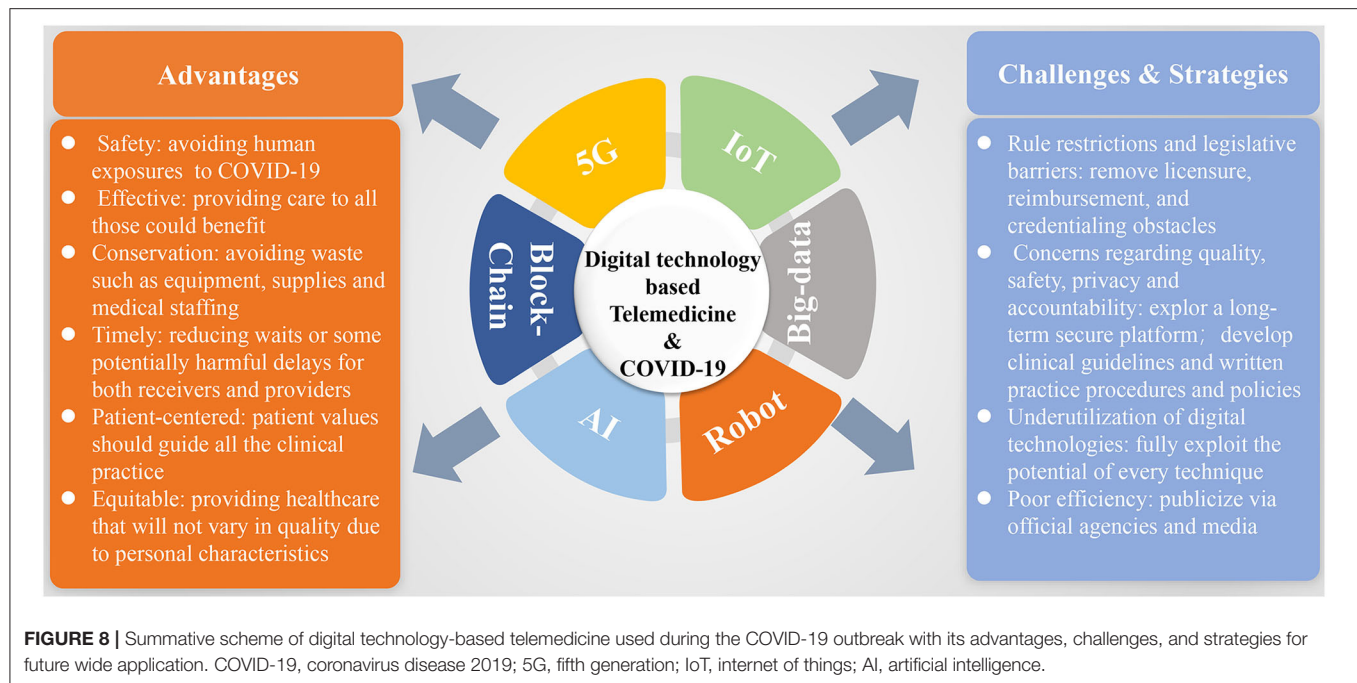
In the context of the COVID-19 outbreak, the rapidly growing modern technologies have brought powerful potential for many applications, which will globally transform the way in which we work, learn, and live. Among them, healthcare is such a specific industry that is experiencing an interesting transformation by integrating these telecommunications technologies. Indeed, to maximize clinical care though the telemedicine system, a closed loop is quite necessary, which involves patient- or practitioner-derived healthcare data and internet (e.g., 5G-Cloud)-based data transfer interpreted by the patients, medical practitioners, or certain automated platforms (e.g., AI, robot, and big data analysis) and returned back to the patients and medical staffs for better clinical decisions. And in turn, the large-scale shared cloud-based data would provide a great opportunity for AI development (Figure 7). Increasingly, great amounts of real-world experience regarding digital technology-based telemedicine system have already been developed and can be conducted in four modes (i.e., many to one mode, one to many mode, consultation mode, and practical operation mode) (Figure 7), which increase the medical staffs' capacity to offer high-quality care to more patients while protecting the personal health of medical staffs and saving public resources, by increasing the efficiencies and methods in which expert evaluation could be provided beyond geographic restriction. Importantly, telemedicine system has been demonstrated to be quite useful in handling critically ill patients, as well as the stable outpatients without barriers of time and distance. These are all good examples of ways in which telemedicine based on several digital technologies can currently address these unique challenges posed by an infectious disease outbreak such as COVID-19. Optimizing the application of telemedicine in this pandemic uniquely brings six domains of healthcare quality: as follows (Figure 8): (a) safety: avoiding human exposures (healthcare providers, patients, and exposed community) to COVID-19 and reducing the risk of SARS-CoV-2 infection; (b) effective: providing care to all those who could benefit, for not only critically ill patients acquiring expert services but also people with mild illnesses getting the supportive care to avoid the consequences of delayed diagnosis, as well as reducing their stress and anxiety; (c) conservation: avoiding waste of equipment, supplies, and medical staffs; (d) timely: reducing wait time or some potentially harmful delays for both receivers and providers; (e) patient-centered: providing healthcare that relies on individual patient needs and preferences and ensuring that patient values should guide all the clinical practice; and (f) equitable: providing healthcare that will not vary in quality due to personal characteristics including sex,



ethnicity, socioeconomic status, and geographic location, as well as the physician engagement levels. Despite the great potential of telemedicine in clinical application, we should note that its uptake has been variable, mainly due to interstate licensing barriers, inadequate reimbursement and concerns associated with the technical and clinical quality, safety, privacy, and accountability (such as who should be prosecuted if something goes wrong) (98, 128). In this context, several strategies should be adopted to facilitate telemedicine to be globally used and integrated into the public health response to COVID-19 and future outbreaks.

First, the lawmakers and regulatory agencies should promulgate some measures that could facilitate the widespread adoption of telemedicine. The key challenges in wide adoption of telemedicine can be the rule restrictions and legislative barriers. For example, the state licensing restrictions in the United States hamper the providers' ability to deliver healthcare, as they limit the patients' ability to access it. Thus, a national clinical training standard should be set by Committee on

Medical Education and be adhered by medical licensing for physicians. Licensure board exams should be national but state-specific. Also, hospital organizations could develop and accept universal credentialing by certain proxy procedures to accelerate the growth of telemedicine delivery, and if possible, an international standard might be developed by the WHO for better transnational cooperation on some difficult public health issues such as COVID-19, because medicine is a special science without boundary. In addition, the full realization of comprehensive implementation of telemedicine requires federal governments and the public and private payers to develop policies that could allow reimbursement of telemedicine services to be equal to that of traditional care to reduce costs. Fortunately, CMS and some private payers have modified the payment policies in response to COVID-19. And Health and Human Services (HHS) waived enforcement of the Health Insurance Portability and Accountability Act (HIPAA) regulation to allow the use of video and audio communication for telemedicine visits (129). This pandemic now serves as a call to action for these



groups to work closely with medical experts to remove these licensure, reimbursement, and credentialing obstacles, allowing telemedicine to be fully integrated into our healthcare system.

Second, we should invest time and effort in exploring a long-term secure platform if none is being used now, to define telemedicine frameworks and to develop clinical guidelines and written practice procedures and policies using case scenarios if necessary, for any outbreak at local, national, or global scales. The critical aspect that makes deployment of telemedicine services imperfect and inefficient during the COVID-19 outbreak in some countries such as Italy can be the scarcity of a standard workflow management system or a formal input on telemedicine given by health authorities, which is suitable for integration of telemedicine into clinical practice. Often, a standardized telemedicine protocol and monitoring system technology proposal should exist that are developed by the healthcare facility collaborating with the community site and need to be repeatedly tuned and optimized to ensure that telemedicine system can be operated immediately, safely, and effectively, when suitable.

Third, in times full of danger and uncertainty, we should gather all the resources to help patients and ourselves manage this crisis. The ever-growing technologies including 5G, IoT, AI, blockchain, big data, and robotic technology have markedly affected the progression of telemedicine, and they can be mustered and put into action to strengthen the construction and management of the telemedicine system. In an encouraging sign, all the technologies have already been applied in many respects associated with telemedicine in context of the COVID-19 outbreak and have been proved to be of great practical importance, for example, the “big data” resource in case identification, AI in tele-consultations, standardize screening,

and tele-psychology. However, the property of these techniques has not been utilized to the most extent. Take the blockchain technique, for example; it can be fully integrated into the infectious disease reporting systems, enabling data to be automatically and directly reported to the final authority and be avoided passing through intermediary processing, which would greatly improve the efficiency of data transmission regarding the infectious disease outbreaks. Importantly, as any arbitrary editing for the data can be impossible, this blockchain technology will make circumstances of the outbreak be transparent to the public without manipulation (130). In addition, the drone technique, which, to our knowledge has not been used in this epidemic, can be applied as a delivery method to ensure timely diagnosis and patient confidentiality. In the future, we can fully exploit the potential of every technique to help improve performance of telemedicine application.

Finally, given that the lack of certain practical recommendations or a common repository over telemedicine for patients or even some medical staffs can be responsible for the current poor efficiency of care delivered via telemedicine, we should publicize and demonstrate the operation methods of telemedicine through the official agencies and media software, to ensure that both the providers and patients develop a routine way of thinking while performing clinical practice. Also, we can incorporate telemedicine into education and training process to increase routine use of telemedicine services. The preparative work should ensure that the people, equipment, administrative, and systems are all in place to respond immediately and effectively. Such preparedness is of vital important for response. Systems that are not used on a daily basis can rarely work well during disasters; telemedicine is no exception. All stakeholders are encouraged to collaborate to promote the evidence-based

use of the telemedicine services during this pandemic and future outbreaks.

## CONCLUSIONS

In conclusion, although the world continues to adopt some classic public health measures to cope with the COVID-19 pandemic, there are now various ever-emerging technologies that can be used to facilitate the application of telemedicine system to augment and enhance the traditional public health strategies. The COVID-19 pandemic can make a good “case study” for presenting the potential benefits of telemedicine in real-world clinical practice owing to those advanced technologies. Telemedicine provides a great opportunity to fully take advantage of modern technologies and simultaneously leverage the progressive push toward value and efficiency. Although there is a longer-term goal, the good performance of telemedicine to tackle this enormous, global public health challenge in the year 2020 will undoubtedly create great opportunities to increase the governmental and public acceptance of such a technique in the field of healthcare in the future, as well as to inspire lawmakers and relevant regulatory agencies to promulgate certain measures that will gain more widespread

adoption of the telemedicine technology. And so, as predicted by Wootton (131), in the coming years, the term telemedicine will probably lose the “tele-” prefix and become “medicine” with all the telemedicine work regarded as part of routine medical practice.

## AUTHOR CONTRIBUTIONS

W-WY and H-XX conceived this project. W-WY, H-XX, and LC designed and supervised the project and commented on the project. W-WY, Y-TS, and LC wrote the manuscript. All the authors contributed to the discussion during the whole project.

## FUNDING

This work was supported in part by the National Natural Science Foundation of China (Grants 81601502, 81671695, 81900491, and 81927801), Fundamental Research Funds for the Central Universities (Grants 22120190213, 22120190021, and 22120190137), Shanghai Municipal Health Commission (Grants 2019LJ21 and SHSLCZDZK 03502), and the Science and Technology Commission of Shanghai Municipality (Grants 19441903200 and 19DZ2251100).

## REFERENCES

- Huang C, Wang Y, Li X, Ren L, Zhao J, Hu Y, et al. Clinical features of patients infected with 2019 novel coronavirus in Wuhan, China. *Lancet*. (2020) 395:497–506. doi: 10.1016/s0140-6736(20)30183-5
- Zhu N, Zhang D, Wang W, Li X, Yang B, Song J, et al. A novel coronavirus from patients with pneumonia in China, 2019. *N Engl J Med*. (2020) 382:727–33. doi: 10.1056/NEJMoa2001017
- Wang D, Hu B, Hu C, Zhu F, Liu X, Zhang J, et al. Clinical characteristics of 138 hospitalized patients with 2019 novel coronavirus-infected pneumonia in Wuhan, China. *JAMA*. (2020) 323:1061–9. doi: 10.1001/jama.2020.1585
- Parker JM. The internet of things comes to the lab. *Nature*. (2017) 542:125–6. doi: 10.1038/542125a
- Ting DSW, Lin H, Ruamviboonsuk P, Wong TY, Sim DA. Artificial intelligence, the internet of things, and virtual clinics: ophthalmology at the digital translation forefront Comment. *Lancet Digit Health*. (2020) 2:E8–9. doi: 10.1016/s2589-7500(19)30217-1
- LeCun Y, Bengio Y, Hinton G. Deep learning. *Nature*. (2015) 521:436–44. doi: 10.1038/nature14539
- Ting DSW, Liu Y, Burlina P, Xu X, Bressler NM, Wong TY. AI for medical imaging goes deep. *Nat Med*. (2018) 24:539–40. doi: 10.1038/s41591-018-0029-3
- Shilo S, Rossman H, Segal E. Axes of a revolution: challenges and promises of big data in healthcare. *Nat Med*. (2020) 26:29–38. doi: 10.1038/s41591-019-0727-5
- Heaven D. Bitcoin for the biological literature. *Nature*. (2019) 566:141–2. doi: 10.1038/d41586-019-00447-9
- Matusitz J, Breen G-M. Telemedicine: its effects on health communication. *Health Commun*. (2007) 21:73–83. doi: 10.1080/10410230701283439
- Kvedar J, Coye MJ, Everett W. Connected health: a review of technologies and strategies to improve patient care with telemedicine and telehealth. *Health Affairs*. (2014) 33:194–9. doi: 10.1377/hlthaff.2013.0992
- Mun SK, Turner JW. Telemedicine: Emerging e-medicine. *Annu Rev Biomed Eng*. (1999) 1:589–610. doi: 10.1146/annurev.biomed.1.1.589
- Santiago I. Trends and innovations in biosensors for COVID-19 mass testing. *Chembiochem*. (2020) 21:2880–9. doi: 10.1002/cbic.202000250
- Andersson G. Using the Internet to provide cognitive behaviour therapy. *Behav Res Ther*. (2009) 47:175–80. doi: 10.1016/j.brat.2009.01.010
- Fortney JC, Pyne JM, Kimbrell TA, Hudson TJ, Robinson DE, Schneider R, et al. Telemedicine-based collaborative care for posttraumatic stress disorder a randomized clinical trial. *JAMA Psychiatry*. (2015) 72:58–67. doi: 10.1001/jamapsychiatry.2014.1575
- Kern C, Fu DJ, Kortuem K, Huemer J, Barker D, Davis A, et al. Implementation of a cloud-based referral platform in ophthalmology: making telemedicine services a reality in eye care. *Br J Ophthalmol*. (2020) 104:312–7. doi: 10.1136/bjophthalmol-2019-314161
- Wolf JA, Moreau JF, Akilov O, Patton T, English JC III, Ho J, et al. Diagnostic inaccuracy of smartphone applications for melanoma detection. *JAMA Dermatol*. (2013) 149:422–6. doi: 10.1001/jamadermatol.2013.2382
- Grossman SN, Han SC, Balcer LJ, Kurzweil A, Weinberg H, Galetta SL, et al. Rapid implementation of virtual neurology in response to the COVID-19 pandemic. *Neurology*. (2020) 94:1077–87. doi: 10.1212/wnl.00000000000009677
- B. T. *Nine Stages of Transformational Change*. Denver, CO: RS Tipton, PBC (2019). Available online at: <https://teamtpton.com/nine-stages-of-transformationalchange/> (accessed November 14, 2019).
- Bokolo Anthony J. Use of telemedicine and virtual care for remote treatment in response to COVID-19 pandemic. *J Med Syst*. (2020) 44:132. doi: 10.1007/s10916-020-01596-5
- Bokolo AJ. Exploring the adoption of telemedicine and virtual software for care of outpatients during and after COVID-19 pandemic. *Ir J Med Sci*. (2021) 190:1–10. doi: 10.1007/s11845-020-02299-z
- Whitelaw S, Mamas MA, Topol E, Van Spall HGC. Applications of digital technology in COVID-19 pandemic planning and response. *Lancet Digit Health*. (2020) 2:e435–40. doi: 10.1016/S2589-7500(20)30142-4
- Anthony B Jr. Integrating telemedicine to support digital health care for the management of COVID-19 pandemic. *Int J Healthc Manage*. (2021) 14:280–9. doi: 10.1080/20479700.2020.1870354
- Agiwal M, Roy A, Saxena N. Next generation 5g wireless networks: a comprehensive survey. *IEEE Commun Surv Tutor*. (2016) 18:1617–55. doi: 10.1109/comst.2016.2532458



25. Hsieh J-C, Li A-H, Yang C-C. Mobile, cloud, and big data computing: contributions, challenges, and new directions in telecardiology. *Int J Environ Res Public Health*. (2013) 10:6131–53. doi: 10.3390/ijerph10116131
26. Stefano GB, Kream RM. The micro-hospital: 5G telemedicine-based care. *Med Sci Monit Basic Res*. (2018) 24:103–4. doi: 10.12659/msmbr.911436
27. Hittinger E, Jaramillo P. Internet of things: energy boon or bane? *Science*. (2019) 364:326–8. doi: 10.1126/science.aau8825
28. Sim I. Mobile devices and health. *N Engl J Med*. (2019) 381:956–68. doi: 10.1056/NEJMr1806949
29. Jim HSL, Hoogland AI, Brownstein NC, Barata A, Dicker AP, Knoop H, et al. Innovations in research and clinical care using patient-generated health data. *Cancer J Clin*. (2020) 70:182–99. doi: 10.3322/caac.21608
30. Schwartz WB, Patil RS, Szolovits P. Artificial-intelligence in medicine-where do we stand. *N Engl J Med*. (1987) 316:685–8. doi: 10.1056/nejm198703123161109
31. Angermueller C, Parnamaa T, Parts L, Stegle O. Deep learning for computational biology. *Mol Syst Biol*. (2016) 12:878. doi: 10.15252/msb.20156651
32. Ting DSW, Carin L, Dzau V, Wong TY. Digital technology and COVID-19. *Nat Med*. (2020) 26:459–61. doi: 10.1038/s41591-020-0824-5
33. Google. *Big Data*. Available online at: [google.com/search?client=safari&rls=en&q=big+data+definition&ie=UTF-8&oe=UTF-8](https://www.google.com/search?client=safari&rls=en&q=big+data+definition&ie=UTF-8&oe=UTF-8) (accessed January 2, 2020).
34. Wu JT, Leung K, Leung GM. Nowcasting and forecasting the potential domestic and international spread of the 2019-nCoV outbreak originating in Wuhan, China: a modelling study. *Lancet*. (2020) 395:689–97. doi: 10.1016/s0140-6736(20)30260-9
35. Gilbert M, Pullano G, Pinotti F, Valdano E, Poletto C, Boelle P-Y, et al. Preparedness and vulnerability of African countries against importations of COVID-19: a modelling study. *Lancet*. (2020) 395:871–7. doi: 10.1016/s0140-6736(20)30411-6
36. Contagious Disease Surveillance. *Healthmap*. Available online at: <https://healthmap.org/en/> (accessed March 30, 2020).
37. Jia JS, Lu X, Yuan Y, Xu G, Jia J, Christakis NA. Population flow drives spatio-temporal distribution of COVID-19 in China. *Nature*. (2020) 582:389–94. doi: 10.1038/s41586-020-2284-y
38. Holshue ML, DeBolt C, Lindquist S, Lofy KH, Wiesman J, Bruce H, et al. First case of 2019 novel coronavirus in the United States. *N Engl J Med*. (2020) 382:929–36. doi: 10.1056/NEJMoa2001191
39. *Bitcoin: A Peer-to-Peer Electronic Cash System*. (2008). Available online at: <https://bitcoin.org/en/bitcoin-paper> (accessed May 1, 2019).
40. Mettler M. Blockchain technology in healthcare the revolution starts here [Conference presentation]. In: *2016 IEEE 18th International Conference on e-Health Networking, Applications and Services (Healthcom)*. Munich: IEEE (2016).
41. Gammon K. Experimenting with blockchain Can one technology boost both data integrity and patients' pocketbooks? *Nat Med*. (2018) 24:378–81. doi: 10.1038/nm0418-378
42. Mertz L. (Block)Chain reaction. *IEEE Pulse*. (2018) 9:4–7. doi: 10.1109/mpul.2018.2814879
43. Saravanan M, Shubha R, Marks AM, Iyer V. SMEAD: a secured mobile enabled assisting device for diabetics monitoring [Conference presentation]. In: *IEEE International Conference on Advanced Networks and Telecommunications Systems (ANTS)*. Odisha: C V Raman Coll Engn (2017).
44. Leeming G, Ainsworth J, Clifton DA. Blockchain in health care: hype, trust, and digital health. *Lancet*. (2019) 393:2476–7. doi: 10.1016/s0140-6736(19)30948-1
45. Gietl D, Brody P, Champion de Crespigny AAB. *Blockchain in Health: How Distributed Ledgers Can Improve Provider Data Management and Support Interoperability*. (2016). Available online at: <https://www.hyperledger.org/wp-content/uploads/2016/10/ey-blockchain-in-healthpdf> (accessed May 1, 2019).
46. *SORMAS the Surveillance, Outbreak Response Management and Analysis System*. (2020). Available online at: <https://sormasorg.helmholtz-hzi.de/> (accessed March 28, 2020).
47. Qin L, Sun Q, Wang Y, Wu K-F, Chen M, Shia B-C, et al. Prediction of number of cases of 2019 novel coronavirus (COVID-19) using social media search index. *Int J Environ Res Public Health*. (2020) 17:2365. doi: 10.3390/ijerph17072365
48. Yang Z, Zeng Z, Wang K, Wong S-S, Liang W, Zanin M, et al. Modified SEIR and AI prediction of the epidemics trend of COVID-19 in China under public health interventions. *J Thorac Dis*. (2020) 12:165–74. doi: 10.21037/jtd.2020.02.64
49. Zhang X, Saleh H, Younis EMG, Sahal R, Ali AA, Khalil AM. Predicting coronavirus pandemic in real-time using machine learning and big data streaming system. *Complexity*. (2020) 2020:1–10. doi: 10.1155/2020/6688912
50. Zivkovic M, Bacanin N, Venkatachalam K, Nayyar A, Djordjevic A, Strumberger I, et al. COVID-19 cases prediction by using hybrid machine learning and beetle antennae search approach. *Sustain Cities Soc*. (2021) 66:102669. doi: 10.1016/j.scs.2020.102669
51. Yan A, Zou Y, Mirchandani DA. How hospitals in mainland China responded to the outbreak of COVID-19 using IT-enabled services: an analysis of hospital news webpages. *JAMA*. (2020) 27:991–9. doi: 10.1093/jamia/ocaa064
52. Srinivasa Rao ASR, Vazquez JA. Identification of COVID-19 can be quicker through artificial intelligence framework using a mobile phone-based survey when cities and towns are under quarantine. *Infect Control Hosp Epidemiol*. (2020) 41:826–30. doi: 10.1017/ice.2020.61
53. Zahedi A, Salehi-Amiri A, Smith NR, Hajiaghahi-Keshteli M. Utilizing IoT to design a relief supply chain network for the SARS-COV-2 pandemic. *Appl Soft Comput*. (2021) 104:107210. doi: 10.1016/j.asoc.2021.107210
54. D'Angelo G, Palmieri F. Enhancing COVID-19 tracking apps with human activity recognition using a deep convolutional neural network and HAR-images. *Neural Comput Appl*. (2021) 30:1–17. doi: 10.1007/s00521-021-05913-y
55. *Engineers Develop Robots to Treat and Test Covid-19 Patients in a Bid to Protect Health Workers*. (2020). Available online at: <https://www.telegraph.co.uk/global-health/science-and-disease/engineers-develop-robots-treat-test-covid-19-patients-bid-protect/> (accessed May 10, 2020).
56. *Robots Help to Make Drive-Through Virus Testing Safer*. (2020). Available online at: [https://drivesncontrols.com/news/fullstory.php/aid/6334/Robots\\_help\\_to\\_make\\_drive-through\\_virus\\_testing\\_safer.html](https://drivesncontrols.com/news/fullstory.php/aid/6334/Robots_help_to_make_drive-through_virus_testing_safer.html) (accessed May 10, 2020).
57. Hong Z, Li N, Li D, Li J, Li B, Xiong W, et al. Telemedicine during the COVID-19 pandemic: experiences from Western China. *J Med Intern Res*. (2020) 22:e19577. doi: 10.2196/19577
58. Zhang K, Liu X, Shen J, Li Z, Sang Y, Wu X, et al. Clinically applicable AI system for accurate diagnosis, quantitative measurements, and prognosis of COVID-19 pneumonia using computed tomography. *Cell*. (2020) 182:1360. doi: 10.1016/j.cell.2020.04.045
59. Li XL, Guo LH, Sun LP, Yue WW. Teleultrasound for the COVID-19 pandemic: a statement from China. *Adv Ultrasound Diagn Ther*. (2020) 4:27–111. doi: 10.37015/AUDT.2020.200036
60. Lv F, Wang J, Yu X, Yang A, Liu J-B, Qian L, et al. Chinese Expert Consensus on critical care ultrasound applications at COVID-19 pandemic. *Adv Ultrasound Diagn Ther*. (2020) 2:27–42. doi: 10.37015/AUDT.2020.200022
61. Li L, Qin L, Xu Z, Yin Y, Wang X, Kong B, et al. Artificial intelligence distinguishes COVID-19 from community acquired pneumonia on chest CT. *Radiology*. (2020) 296:E65–71. doi: 10.1148/radiol.2020200905
62. *Two Israeli Hospitals Launch AI-Based Tele-ICU to Support COVID-19 Patients*. (2020). Available online at: <https://www.healthcareitnews.com/news/europe/two-israeli-hospitals-launch-ai-based-tele-icu-support-covid-19-patients> (accessed March 27, 2020).
63. Tian W, Fan M, Zeng C, Liu Y, He D, Zhang Q. Telerobotic spinal surgery based on 5G network: the first 12 cases. *Neurospine*. (2020) 17:114–20. doi: 10.14245/ns.1938454.227
64. Wang Y. *The Chinese Suicides Prevented by AI From Afar*. BBC World Service (2019). Available online at: <https://www.bbc.com/news/technology-50314819> (accessed November 9, 2019).
65. Ohannessian R, Tu Anh D, Odone A. Global telemedicine implementation and integration within health systems to fight the COVID-19 pandemic: a call to action. *JMIR Public Health Surveill*. (2020) 6:121–5. doi: 10.2196/18810
66. Tuite AR, Bogoch II, Sherbo R, Watts A, Fisman D, Khan K. Estimation of coronavirus disease 2019 (COVID-19) burden and potential for

- international dissemination of infection from Iran. *Ann Intern Med.* (2020) 172:699–701. doi: 10.7326/m20-0696
67. Udagama B, Kadhiresan P, Kozłowski HN, Malekjahani A, Osborne M, Li VYC, et al. Diagnosing COVID-19: the disease and tools for detection. *ACS Nano.* (2020) 14:3822–35. doi: 10.1021/acsnano.0c02624
  68. Wong ZSY, Zhou J, Zhang Q. Artificial Intelligence for infectious disease big data analytics. *Infect Dis Health.* (2019) 24:44–8. doi: 10.1016/j.idh.2018.10.002
  69. Bempong N-E, De Castaneda RR, Schutte S, Bolon I, Keiser O, Escher G, et al. Precision global health - The case of Ebola: a scoping review. *J Global Health.* (2019) 9:010404. doi: 10.7189/jogh.09.010404
  70. Sun K, Chen J, Viboud C. Early epidemiological analysis of the coronavirus disease 2019 outbreak based on crowdsourced data: a population-level observational study. *Lancet Digit Health.* (2020) 2:E201–8. doi: 10.1016/s2589-7500(20)30026-1
  71. Bogoch II, Watts A, Thomas-Bachli A, Huber C, Kraemer MUG, Khan K. Potential for global spread of a novel coronavirus from China. *J Travel Med.* (2020) 27:taaa011. doi: 10.1093/jtm/taaa011
  72. McCall B. COVID-19 and artificial intelligence: protecting health-care workers and curbing the spread. *Lancet Digit Health.* (2020) 2:E166–7. doi: 10.1016/s2589-7500(20)30054-6
  73. Colizza V, Barrat A, Barthelemy M, Vespignani A. The role of the airline transportation network in the prediction and predictability of global epidemics. *Proc Natl Acad Sci USA.* (2006) 103:2015–20. doi: 10.1073/pnas.0510525103
  74. Halloran ME, Vespignani A, Bharti N, Feldstein LR, Alexander KA, Ferrari M, et al. Ebola: mobility data. *Science.* (2014) 346:433. doi: 10.1126/science.346.6208.433-a
  75. Colubri A, Hartley M-A, Siakor M, Wolfman V, Felix A, Sesay T, et al. Machine-learning Prognostic Models from the 2014-16 Ebola outbreak: data-harmonization challenges, validation strategies, and mhealth applications. *EClinicalMedicine.* (2019) 11:54–64. doi: 10.1016/j.eclinm.2019.06.003
  76. *Digital Disease Management & Prevention Platform.* Lark Health (2020). Available online at: <https://lark.com/> (accessed March 30, 2020).
  77. *Symptom Checker, Check Your Symptoms in Real Time.* Buoyhealth.com (2020). Available online at: <https://www.buoyhealth.com/symptom-checker/> (accessed March 30, 2020).
  78. Akpakwu GA, Silva BJ, Hancke GP, Abu-Mahfouz AM. A survey on 5G networks for the internet of things: communication technologies and challenges. *IEEE Access.* (2018) 6:3619–47. doi: 10.1109/access.2017.2779844
  79. Chen S, Zhang Z, Yang J, Wang J, Zhai X, Barnighausen T, et al. Fangcang shelter hospitals: a novel concept for responding to public health emergencies. *Lancet.* (2020) 395:1305–14. doi: 10.1016/s0140-6736(20)30744-3
  80. Yao G, Zhang X, Wang H, Li J, Tian JLW. Practice and thinking of the informationized cabin hospitals during the novel coronavirus pneumonia period (in Chinese). *Chin J Hosp Admin.* (2020) 36:334–6. doi: 10.3760/cma.j.cn112225-20200218-00200
  81. Song X, Liu X, Wang C. The role of telemedicine during the COVID-19 epidemic in China-experience from Shandong province. *Crit Care.* (2020) 24:178. doi: 10.1186/s13054-020-02884-9
  82. Wu S, Li K, Peng C, Ye R, Li Y, Lv F. 5G-based robotic teleultrasound assessment of pulmonary and cardiac function on a novel coronavirus pneumonia patient in isolation ward of mobile hospital: a case report. *J Clin Ultrasound Med.* (2020) 22:228–32. doi: 10.16245/j.cnki.issn1008-6978.2020.03.026
  83. Wu J, Pan J, Teng D, Xu X, Feng J, Chen Y-C. Interpretation of CT signs of 2019 novel coronavirus (COVID-19) pneumonia. *Eur Radiol.* (2020) 30:5455–62. doi: 10.1007/s00330-020-06915-5
  84. Yang W, Yan F. Patients with RT-PCR-confirmed COVID-19 and Normal Chest CT. *Radiology.* (2020) 295:E3. doi: 10.1148/radiol.20200702
  85. *Wuhan Medics Share COVID-19 Information With Kenyan Medical Teams.* (2020). Available online at: <https://www.chinadaily.com.cn/a/202003/23/WS5e78b4cda3101282172815b6.html> (accessed May 23, 2020).
  86. Abdel-Basset M, Chang V, Nabeeh NA. An intelligent framework using disruptive technologies for COVID-19 analysis. *Technol Forecast Soc Change.* (2021) 163:120431. doi: 10.1016/j.techfore.2020.120431
  87. Chinadaily. *Medical Leader Calls Makeshift Hospitals a Success.* (2020). Available online at: <https://www.chinadaily.com.cn/a/202005/04/WS5eb00605a310a8b2411535f4.html>
  88. Reed ME, Parikh R, Wargon C. Real-time patient-provider video telemedicine integrated with clinical care. *N Engl J Med.* (2018) 379:1478–9. doi: 10.1056/NEJMc1805746
  89. de Jong MJ, van der Meulen-de Jong AE, Romberg-Camps MJ, Becx MC, Maljaars JP, Cilissen M, et al. Telemedicine for management of inflammatory bowel disease (myIBDcoach): a pragmatic, multicentre, randomised controlled trial. *Lancet.* (2017) 390:959–68. doi: 10.1016/s0140-6736(17)31327-2
  90. Park PG, Kim CH, Heo Y, Kim TS, Park CW, Kim C-H. Out-of-hospital cohort treatment of coronavirus disease 2019 patients with mild symptoms in Korea: an experience from a single community treatment center. *J Korean Med Sci.* (2020) 35:e140. doi: 10.3346/jkms.2020.35.e140
  91. Medina M, Babiuch C, Card M, Gavrilescu R, Zafrau W, Boose E, et al. Home monitoring for COVID-19. *Cleveland Clin J Med.* (2020) 8:6. doi: 10.3949/ccjm.87a.ccc028
  92. Annis T, Pleasants S, Hultman G, Lindemann E, Thompson JA, Billecke S, et al. Rapid implementation of a COVID-19 remote patient monitoring program. *J Am Med Inform Assoc.* (2020) 27:1326–30. doi: 10.1093/jamia/ocaa097
  93. Dong Y, Yao Y-D. IoT platform for COVID-19 prevention and control: a survey. *IEEE Access.* (2021) 9:49929–41. doi: 10.1109/access.2021.3068276
  94. Alsamhi SH, Lee B, Guizani M, Kumar N, Qiao Y, Liu X. Blockchain for decentralized multi-drone to combat COVID-19 and future pandemics: framework and proposed solutions. *Trans Emerg Telecommun Technol.* (2021) 32:e4255. doi: 10.1002/ett.4255
  95. Hollander JE, Carr BG. Virtually Perfect? Telemedicine for Covid-19. *New Engl J Med.* (2020) 382:1679–81. doi: 10.1056/NEJMp2003539
  96. Harrington RA, Califf RM, Balamurugan A, Brown N, Benjamin RM, Braund WE, et al. Call to action: rural health: a presidential advisory from the American Heart Association and American Stroke Association. *Circulation.* (2020) 141:E615–44. doi: 10.1161/cir.0000000000000753
  97. Kuehn BM. Telemedicine helps cardiologists extend their reach. *Circulation.* (2016) 134:1189–91. doi: 10.1161/circulationaha.116.025282
  98. Serper M, Volk ML. Current and future applications of telemedicine to optimize the delivery of care in chronic liver disease. *Clin Gastroenterol Hepatol.* (2018) 16:157–61. doi: 10.1016/j.cgh.2017.10.004
  99. Calton B, Abedini N, Fratkan M. Telemedicine in the time of coronavirus. *J Pain Symp Manage.* (2020) 60:e12–4. doi: 10.1016/j.jpainsymman.2020.03.019
  100. Serper M, Cubell AW, Deleener ME, Casher TK, Rosenberg DJ, Whitebloom D, et al. Telemedicine in liver disease and beyond: can the COVID-19 crisis lead to action? *Hepatology.* (2020) 72:723–8. doi: 10.1002/hep.31276
  101. Garg SK, Rodbard D, Hirsch IB, Forlenza GP. Managing new-onset type 1 diabetes during the COVID-19 Pandemic: challenges and opportunities. *Diabetes Technol Ther.* (2020) 22:431–9. doi: 10.1089/dia.2020.0161
  102. Al-Shamsi HO, Alhazzani W, Alhuraiji A, Coomes EA, Chemaly RF, Almuhamma M, et al. A practical approach to the management of cancer patients during the novel coronavirus disease 2019 (COVID-19) pandemic: an international collaborative group. *Oncologist.* (2020) 25:e936–45. doi: 10.1634/theoncologist.2020-0213
  103. Prasad A, Brewster R, Newman JG, Rajasekaran K. Optimizing your telemedicine visit during the COVID-19 pandemic: practice guidelines for patients with head and neck cancer. *Head Neck J Sci Spec Head Neck.* (2020) 42:1317–21. doi: 10.1002/hed.26197
  104. Quek LHH, Kannivelu A, Pua U. Yttrium-90 Radioembolization: telemedicine during COVID-19 outbreak, opportunity for prime time. *J Nuclear Med.* (2020) 61:780. doi: 10.2967/jnumed.120.246389
  105. Taiwo O, Ezugwu AE. Smart healthcare support for remote patient monitoring during covid-19 quarantine. *Inform Med Unlocked.* (2020) 20:100428. doi: 10.1016/j.imu.2020.100428

106. Parker JA, Christian P, Jadvar H, Sattler B, Wallis JW. The SNMMI and EANM practice guideline for tele-nuclear medicine 2.0. *J Nuclear Med Technol.* (2014) 42:15–9. doi: 10.2967/jnmt.113.133231
107. Diaz A, Sarac BA, Schoenbrunner AR, Janis JE, Pawlik TM. Elective surgery in the time of COVID-19. *Am J Surg.* (2020) 219:900–2. doi: 10.1016/j.amjsurg.2020.04.014
108. Pattichis CS, Kyriacou E, Voskarides S, Pattichis MS, Istepanian R, Schizas CN. Wireless telemedicine systems: an overview. *IEEE Antennas Propag Magaz.* (2002) 44:143–53. doi: 10.1109/map.2002.1003651
109. Marescaux J, Leroy J, Gagner M, Rubino F, Mutter D, Vix M, et al. Transatlantic robot-assisted telesurgery. *Nature.* (2001) 413:379–80. doi: 10.1038/35096636
110. Chen AF, Kazarian GS, Jessop GW, Makhdom A. Robotic technology in orthopaedic surgery. *J Bone Joint Surg Am.* (2018) 100:1984–92. doi: 10.2106/jbjs.17.01397
111. Tian W, Wang H, Liu Y-J. Robot-assisted anterior odontoid screw fixation: a case report. *Orthop Surg.* (2016) 8:400–4. doi: 10.1111/os.12266
112. Joseph JR, Smith BW, Liu X, Park P. Current applications of robotics in spine surgery: a systematic review of the literature. *Neurosurg Focus.* (2017) 42:E2. doi: 10.3171/2017.2.Focus16544
113. Roser F, Tatagiba M, Maier G. Spinal robotics: current applications and future perspectives. *Neurosurgery.* (2013) 72:A12–8. doi: 10.1227/NEU.0b013e318270d02c
114. Lonjon N, Chan-Seng E, Costalat V, Bonnafoux B, Vassal M, Boetto J. Robot-assisted spine surgery: feasibility study through a prospective case-matched analysis. *Eur Spine J.* (2016) 25:947–55. doi: 10.1007/s00586-015-3758-8
115. Huddy JR, Crockett M, Nizar AS, Smith R, Malki M, Barber N, et al. Experiences of a “COVID protected” robotic surgical centre for colorectal and urological cancer in the COVID-19 pandemic. *J Robot Surg.* (2021) 11:1–6. doi: 10.1007/s11701-021-01199-3
116. Cosic K, Popovic S, Sarlija M, Kesedzic I. Impact of human disasters and COVID-19 pandemic on mental health: potential of digital psychiatry. *Psychiatr Danubina.* (2020) 32:25–31. doi: 10.24869/psychd.2020.25
117. Hamel L, Lopes L, Muñana C, Kates J, Michaud J, Brodie M. *KFF coronavirus poll: March 2020.* (2020). Available online at: <https://www.kff.org/global-health-policy/poll-finding/kffcoronavirus-poll-march-2020/> (accessed March 17, 2020).
118. Sun L, Sun Z, Wu L, Zhu Z, Zhang FZS. Prevalence and risk factors of acute posttraumatic stress symptoms during the COVID-19 outbreak in Wuhan, China. *medRxiv* (2020) 283:123–9. doi: 10.1016/j.jad.2021.01.050
119. Li JB, Yang A, Dou K, RY C. Self-control moderates the association between perceived severity of the coronavirus disease 2019 (COVID-19) and mental health problems among the Chinese public. *Int J Environ Res Public Health.* (2020) 17:4820. doi: 10.3390/ijerph17134820
120. Liu S, Yang L, Zhang C, Xiang Y-T, Liu Z, Hu S, et al. Online mental health services in China during the COVID-19 outbreak. *Lancet Psychiatry.* (2020) 7:E17–8. doi: 10.1016/s2215-0366(20)30077-8
121. Di Carlo F, Sociali A, Picutti E, Pettorruso M, Vellante F, Verrastro V, et al. Telepsychiatry and other cutting-edge technologies in COVID-19 pandemic: bridging the distance in mental health assistance. *Int J Clin Pract.* (2021) 75:e13716. doi: 10.1111/ijcp.13716
122. Chick RC, Clifton GT, Peace KM, Propper BW, Hale DF, Alseidi AA, et al. Using technology to maintain the education of residents during the COVID-19 pandemic. *J Surg Educ.* (2020) 77:729–32. doi: 10.1016/j.jsurg.2020.03.018
123. M. M. COVID-19 Response: EdTech Expertise Strengthening Remote Learning Transition. Imperial College London 2020 (2020). Available online at: <https://www.imperial.ac.uk/news/196253/covid-19-response-edtech-expertise-strengtheningremote/> (accessed March 27, 2020).
124. Mian A, Khan S. Medical education during pandemics: a UK perspective. *BMC Med.* (2020) 18:100. doi: 10.1186/s12916-020-01577-y
125. Rimmer A. Covid-19: Medical conferences around the world are cancelled after US cases are linked to Massachusetts meeting. *BMJ Br Med J.* (2020) 368:m1054. doi: 10.1136/bmj.m1054
126. Rose C, Mott S, Alvarez A, Lin M. Physically distant, educationally connected: interactive conferencing in the era of COVID-19. *Med Educ.* (2020) 54:758–9. doi: 10.1111/medu.14192
127. Gonzales-Zamora JA, Alave J, De Lima-Corvino DF, Fernandez A. Videoconferences of Infectious Diseases: an educational tool that transcends borders. A useful tool also for the current COVID-19 pandemic. *Le Infezioni Med.* (2020) 28:135–8.
128. Greenhalgh T, Wherton J, Shaw S, Morrison C. Video consultations for covid-19. *BMJ Br Med J.* (2020) 368:m998. doi: 10.1136/bmj.m998
129. United States Department of Health & Human Services. *Notification of Enforcement Discretion for Telehealth Remote Communications During the COVID-19 Nationwide Public Health Emergency.* (2020). Available online at: <https://www.hhs.gov/hipaa/for-professionals/specialtopics/emergency-preparedness/notification-enforcement-discretiontelehealth/index.html> (accessed March 28, 2020).
130. Chang MC, Park D. How can blockchain help people in the event of pandemics such as the COVID-19? *J Med Syst.* (2020) 44:102. doi: 10.1007/s10916-020-01577-8
131. Wootton R, Bonnardot L. Telemedicine in low-resource settings. *Front Public Health.* (2015) 3:3. doi: 10.3389/fpubh.2015.00003

**Conflict of Interest:** The authors declare that the research was conducted in the absence of any commercial or financial relationships that could be construed as a potential conflict of interest.

Copyright © 2021 Shen, Chen, Yue and Xu. This is an open-access article distributed under the terms of the Creative Commons Attribution License (CC BY). The use, distribution or reproduction in other forums is permitted, provided the original author(s) and the copyright owner(s) are credited and that the original publication in this journal is cited, in accordance with accepted academic practice. No use, distribution or reproduction is permitted which does not comply with these terms.



# Traditional Chinese Medicine Enema Therapy in a Patient With a Confirmed Negative SARS-CoV-2 Test in the Respiratory Tract but Positive in the Intestinal Tract: A Case Report

## OPEN ACCESS

### Edited by:

Seyed Alireza Nadji,  
Shahid Beheshti University of Medical  
Sciences, Iran

### Reviewed by:

Hao Chen,  
Guangzhou Medical University, China  
Seetha Harilal,  
Kerala University of Health  
Sciences, India

### \*Correspondence:

Jun Cheng  
cj1171967@163.com  
Xiaoxiao Jiang  
1003014364@qq.com

†These authors have contributed  
equally to this work

### Specialty section:

This article was submitted to  
Infectious Diseases - Surveillance,  
Prevention and Treatment,  
a section of the journal  
Frontiers in Public Health

**Received:** 29 March 2021

**Accepted:** 19 May 2021

**Published:** 09 July 2021

### Citation:

Dai Y, Zhao Z, Zhou H, Huang D,  
Luo J, Zhang C, Chen Q, Chen X,  
Yao Y, Jiang X and Cheng J (2021)  
Traditional Chinese Medicine Enema  
Therapy in a Patient With a Confirmed  
Negative SARS-CoV-2 Test in the  
Respiratory Tract but Positive in the  
Intestinal Tract: A Case Report.  
*Front. Public Health* 9:687283.  
doi: 10.3389/fpubh.2021.687283

Yuzhu Dai<sup>1†</sup>, Zhiyou Zhao<sup>2†</sup>, Huajun Zhou<sup>1†</sup>, Dedong Huang<sup>3</sup>, Jianjun Luo<sup>4</sup>,  
Cunhai Zhang<sup>4</sup>, Qingyong Chen<sup>5</sup>, Xingcan Chen<sup>6</sup>, Yuan Yao<sup>7</sup>, Xiaoxiao Jiang<sup>5\*</sup> and  
Jun Cheng<sup>1\*</sup>

<sup>1</sup> Department of Clinical Laboratory, West Lake Hospital Affiliated to Hangzhou Medical College, Hangzhou, China,

<sup>2</sup> Department of Traditional Chinese Medicine, West Lake Hospital Affiliated to Hangzhou Medical College, Hangzhou, China,

<sup>3</sup> Department of Infection, West Lake Hospital Affiliated to Hangzhou Medical College, Hangzhou, China, <sup>4</sup> Department of  
Critical Care Medicine, West Lake Hospital Affiliated to Hangzhou Medical College, Hangzhou, China, <sup>5</sup> Department of  
Respiratory and Digestive Medicine, West Lake Hospital Affiliated to Hangzhou Medical College, Hangzhou, China,

<sup>6</sup> Department of Radiology, West Lake Hospital Affiliated to Hangzhou Medical College, Hangzhou, China, <sup>7</sup> West Lake  
Hospital Affiliated to Hangzhou Medical College, Hangzhou, China

We report the case of a 43-year-old man who was infected with SARS-CoV-2 in February 2020 and actively cooperated with treatment in the hospital. During the course of treatment, we found that the respiratory SARS-CoV-2 nucleic acid became negative, but remained positive in the intestinal tract. As a result, we adjusted the treatment plan to include traditional Chinese medicine enema treatment. The patient had negative intestinal SARS-CoV-2 nucleic acid test within 4 days, and the subsequent repeated review of intestinal SARS-CoV-2 nucleic acid was negative, and the virus was undetectable. It is suggested that traditional Chinese medicine enema treatment may be helpful to remove the SARS-CoV-2 in the intestines of patients with COVID-19 infection, and may support the treatment of patients with respiratory SARS-CoV-2 nucleic acid negative and positive in the intestinal tract.

**Keywords:** SARS-CoV-2 infection, traditional Chinese medicine enema therapy, discharge standard, nucleic acid test of SARS-CoV-2, fecal-oral transmission

## INTRODUCTION

In December 2019, an unknown viral pneumonia was first reported in Wuhan, China, and subsequently reported worldwide (1–4). The virus was later identified as a novel coronavirus (SARS-CoV-2) belonging to the genus Betacoronavirus, which is ~80% similar to the severe acute respiratory syndrome coronavirus (SARS-CoV) reported in 2003 (4, 5). In response to the emerging threat posed by this virus, the World Health Organization (WHO) announced a public health emergency of international concern on January 30, 2020, and further declared a pandemic on March 11, 2020. The new virus was named SARS-CoV-2 by the Coronavirus Study Group of the



International Committee for the Taxonomy of Viruses, while the resulting disease was termed coronavirus disease (COVID-19) by the WHO. As of February 24, 2021, the available WHO data show that almost all countries have reported continuous cases of SARS-CoV-2 infection.

SARS-CoV-2 is a positive-sense, single-stranded RNA virus with strong genetic similarity to bat-borne coronavirus (88%), but the intermediate host has not yet been identified. SARS-CoV-2 is the seventh coronavirus that is known to infect humans (1); among which, 229E, NL63, OC43, and HKU1 only cause symptoms of the common cold and upper respiratory tract infections (6, 7). In contrast, SARS coronavirus (SARS-CoV) in 2003, Middle East Respiratory Syndrome coronavirus (MERS-CoV) in 2012, and novel coronavirus (SARS-CoV-2) in 2019 can all be cross-infected by human-to-human transmission, thus causing large-scale atypical pneumonia (8), which leads to severe lower respiratory tract infection with acute respiratory distress syndrome (ARDS) and extra-pulmonary manifestations (9–11). The responding CD4<sup>+</sup> cells access the small intestine through the intestinal lung shaft after the infection of lung cells by SARS-CoV-2 binding to the angiotensin converting enzyme 2 (ACE2) receptor, which leads to intestinal immune damage and diarrhea. In addition, since SARS-CoV-2 can combine with ACE2 in the intestinal mucosa, gastrointestinal symptoms may occur as a result of destruction of the intestinal mucosal barrier and release of inflammatory cytokines. Gastrointestinal symptoms are the most common complications and can cause liver damage; indeed, if not treated, they may also cause coma and circulatory failure (11, 12). Therefore, treatment regimens should be adjusted in a timely manner when patients with COVID-19 develop gastrointestinal symptoms.

The guidelines for COVID-19 issued by the National Health Council (13), and the army's support for the Hubei medical team COVID-19 diagnosis and treatment plan (14) did not require the results of SARS-CoV-2 nucleic acid in the stool as a discharge standard. However, in the consensus reached by experts on the comprehensive treatment of COVID-19 issued by Shanghai (15), it is clear that patients with COVID-19 can only be discharged after their fecal nucleic acid becomes negative. In particular, it is unclear whether negative SARS-CoV-2 nucleic acid in the respiratory tract and positive SARS-CoV-2 nucleic acid in the stool meets the discharge criteria. Here we report a patient with COVID-19 who presented with SARS-CoV-2 negative nucleic acid in the respiratory tract twice (meeting the discharge standard) and persistent positive stool after receiving emergency treatment. In this case, we used traditional Chinese medicine (TCM) enema for further treatment of this patient, which may be providing a novel way to accelerate intestinal virus cleaning. In addition, we describe the clinical characteristics of the patient before and after treatment. The details are provided below.

## CASE DESCRIPTION

### Case Report

On February 3, 2020, a 43-year-old man developed a fever without a clear cause, and his body temperature was 38°C with no other obvious symptoms. After taking Lianhua Qingwen Capsule

himself, his body temperature returned to normal. On February 5, 2020, the patient experienced fever again, with a normal body temperature after measurement, a slight cough, a small amount of white sputum, and reported being more sleepy than usual. On February 6, the patient visited the Fever Clinic of West Lake Hospital, affiliated with Hangzhou Medical College. The patient's past medical history involved generally good health, with no history of high blood pressure, diabetes or heart disease, and no travel to Wuhan, Wenzhou, or other key COVID-19 outbreak areas or exposure history. However, the patient described that he had gone to Lanxi County, Zhejiang Province, where COVID-19 had been confirmed and reported before January 22, and his sister, who lived with him at home, had cough, low fever, diarrhea, and other clinical symptoms before February 3 (later confirmed as COVID-19 by Xixi Hospital in Hangzhou). According to the above description, the patient was immediately requested to undergo chest computed tomography (CT). The CT scans showed multiple lamellar ground glass, nodular, slightly high-density shadows in both lungs, and prominent sculptural shadows. Viral pneumonia was also considered (Figure 1A). As a result, the patient was admitted to the hospital on February 7 with suspected COVID-19 (16).

Physical examination on admission showed (Figure 1B) the following: body temperature, 37.6°C; blood pressure, 129/77 mmHg; respiratory rate, 18 times/min; pulse, 82 times/min; and blood oxygen saturation, 98%. After admission, the patient's vital signs were stable, with a few coughs, a small amount of white sputum, mild congestion of the eyelid conjunctiva, pharynx redness, and no obvious tonsil enlargement. Blood tests showed a decrease in lymphocyte percentage (16.8%, normal: 20–50%) and a lymphocyte count of  $1.26 \times 10^9/L$  (normal:  $0.8\text{--}4 \times 10^9/L$ ). The proportion of neutrophils was increased (76.6%, normal: 40–75%), the absolute value of neutrophils was normal (5.74, normal:  $1.40\text{--}7.13 \times 10^9/L$ ), and the hypersensitive C-reactive protein (CRP) was increased (10.77 mg/L, normal < 8 mg/L). The test results for influenza A and B, parainfluenza, respiratory syncytial virus, rhinovirus, adenovirus, and mycoplasma pneumoniae antigen were negative. The test results of two specimens (nasopharyngeal swabs and sputum) of SARS-CoV-2 were positive, and the preliminary diagnosis was COVID-19 (common type).

On February 7, the patient was treated with moxifloxacin hydrochloride tablets (400 mg, once daily, oral administration) to prevent infection. Abidol hydrochloride granule (0.2 g, three times daily, oral administration), ribavirin injection (0.5 g, twice daily, intravenous injection), recombinant human interferon  $\alpha 2b$  injection (6 million U, twice daily, aerosol inhalation), Lianhua Qingwen capsule (1.4 g, three times daily, oral administration) was used to clear away heat and detoxify, and human immunoglobulin (PH4) was injected intravenously (20 g, once daily) to enhance immunity. In addition, patients were treated with antipyretic and fluid supplements according to their symptoms (Figure 1C).

On February 7–9, the patient's vital physical signs were stable, with intermittent fever and blood oxygen saturation fluctuating between 93 and 99%. The patient complained of cough with white mucous sputum, poor gastric uptake,

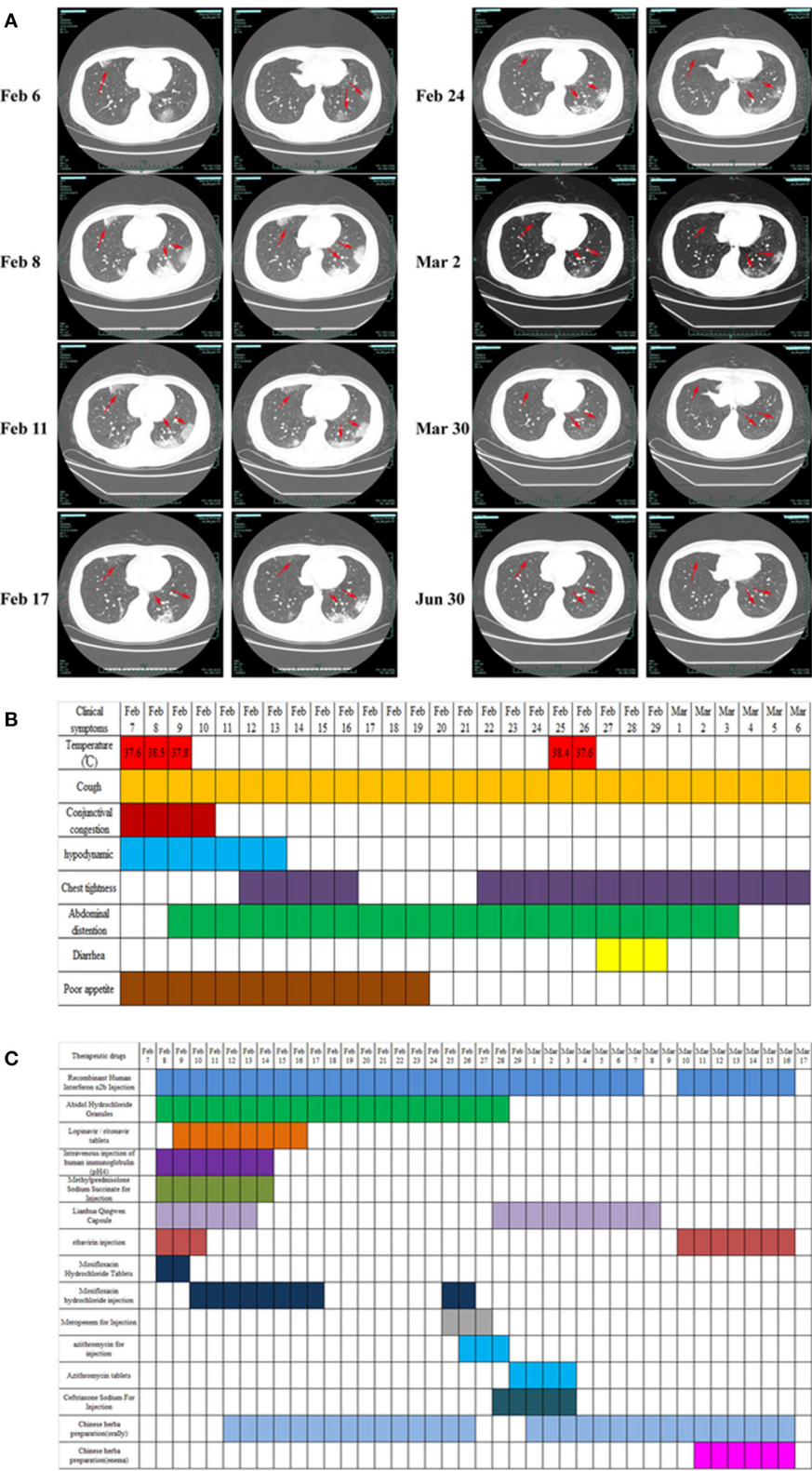


**FIGURE 1 |** Clinical imaging, symptoms, and drug treatment data of patients with COVID-19. **(A)** CT image changes of patients with COVID-19 from first visit to discharge. **(B)** Changes in clinical symptoms in patients with COVID-19 during treatment after admission. **(C)** Medication information for patients with COVID-19 (Continued)

**FIGURE 1 |** during hospitalization. Drug dosage: Recombinant human interferon  $\alpha 2b$  injection (6 million U, twice daily, aerosol inhalation); abidol hydrochloride granule (0.2 g, 3 times daily, oral administration); lopinavir/ritonavir (2 capsules, twice daily, oral administration); intravenous injection of human immunoglobulin (pH 4) (20 g, once daily, intravenous injection); methylprednisolone sodium succinate for injection (40 mg, once daily, subcutaneous injection); Lianhua Qingwen capsule (1.4 g, 3 times daily, oral administration); ribavirin injection (0.5 g, twice daily, intravenous injection); moxifloxacin hydrochloride tablets (400 mg, once daily, oral administration); moxifloxacin hydrochloride injection (0.4 g, once daily, intravenous injection); meropenem for injection (1 g, once per 8 h, intravenous injection); azithromycin for injection (0.5 g, once daily, intravenous injection); azithromycin tablets (0.5 g, once daily, oral administration); ceftriaxone sodium for injection (2 g, once daily, intravenous injection).

fatigue, loss of appetite, abdominal distension, and occasional retching. Re-examination chest CT showed that the lesion of the bilateral lung infection was larger and thicker than before, and the image showed significant progress compared to before (**Figure 1A**). On the same day, the ongoing drugs were switched to moxifloxacin hydrochloride injection (0.4 g, once daily, intravenous injection) for anti-infection, the use of lopinavir/ritonavir was increased (2 capsules, twice daily, oral administration), and methylprednisolone sodium succinate was injected (40 mg, once daily, subcutaneous injection) to reduce pulmonary interstitial edema and control the progression of the disease. The patient's third chest CT re-examination on February 11 showed no enlargement of the lesion, and the progress of the disease was basically under control (**Figure 1A**). Oral Chinese medicine decoction treatment was started on February 12 (the Chinese medicine prescription is shown in **Table 1**), and Chinese medicine diagnosed "loemia" (damp toxin epidemic). The patient's fourth chest CT on February 14 showed scattered small nodules in the right lung and some absorption of the left lung lesions (**Figure 1A**). The patient's respiratory symptoms improved, and his body temperature remained normal. The nucleic acid test of SARS-CoV-2 on nasopharyngeal swabs was negative, the sputum specimen was still positive, and as such, the antiviral treatment regimen was maintained.

On February 17 and February 24, the fifth and sixth chest CT scans showed that the scope of the lung lesions narrowed and gradually absorbed. The white blood cell (WBC) count, lymphocyte count, and high-sensitivity CRP (hs-CRP) levels were normal. In the evening of February 25, the patient had a fever with a body temperature of 38.2°C. The sputum and feces of SARS-CoV-2 nucleic acids were all positive. The blood routine examination showed that the WBCs were elevated ( $9.82 \times 10^9/L$ , normal,  $4.0\text{--}10.0 \times 10^9/L$ ), the neutrophils were increased ( $9.05 \times 10^9/L$ , normal:  $1.40\text{--}7.13 \times 10^9/L$ ), the lymphocyte count was decreased ( $0.50 \times 10^9/L$ , normal:  $0.8\text{--}4 \times 10^9/L$ ), and the erythrocyte sedimentation rate was increased by 55 mm/h (normal: 0–15 mm/h). According to the results of laboratory examination, considering bacterial infection, meropenem (1 g, once per 8 h, intravenous injection), azithromycin for injection (0.5 g, once daily, intravenous injection) combined with anti-infection, and abidol hydrochloride granules (0.2 g, three times daily, oral administration), recombinant human interferon- $\alpha 2B$  injection (6 million U, twice daily, aerosol inhalation) were added to continue the antiviral treatment. On February 27, the patient's temperature returned to normal. On February 29, SARS-CoV-2 nucleic acid (nasopharyngeal swab, sputum, urine, blood) was negative, but diarrhea symptoms appeared (from February 27–29, stopping TCM decoction), and

chest tightness was more obvious than before. Azithromycin was discontinued considering the side effects. Azithromycin tablets (0.5 g, once daily, oral administration) and ceftriaxone sodium for injection (2 g, once daily, intravenous injection) were used for anti-infection, and Huangqi Shengmai drink (10 mL, three times daily, oral administration) was added for the treatment of chest tightness. On March 3, diarrhea and chest tightness were better than before. The patient's seventh chest CT re-examination showed that the focus of pulmonary infection was further absorbed than on February 24, and the scope of the focus continued to narrow. Symptomatic treatment and TCM adjuvant treatment were continued. On March 9, the sputum SARS-CoV-2 nucleic acid was recovered, the stool nucleic acid was positive, and other specimens (urine, blood, and throat swabs) were negative. The antiviral regimens were continued, and Chinese medicine enema was used to promote the elimination of SARS-CoV-2 and promote the negative conversion of SARS-CoV-2 nucleic acid in the gut. The detailed medication plans are shown in **Table 1** and **Figure 1C**. On March 17, three consecutive re-examinations of the respiratory tract and feces showed SARS-CoV-2 nucleic acid as being negative. The patient's body temperature remained normal for more than 3 days, and re-examination of chest CT showed improvement in absorption. According to the latest version of the Diagnosis and Treatment Protocol for Novel Coronavirus Pneumonia of China, patients who meet the following criteria can be discharged (<http://www.nhc.gov.cn/xcs/fkdt/202002/54e1ad5c2aac45c19eb541799bf637e9.shtml>), and the patient was discharged into the isolation point for follow-up observation.

## Imaging Examination

From the first chest CT examination on February 6, 2020, to the re-examination after discharge, the patient underwent a total of eight chest CT scans. In the early stage of the disease (February 6–8), CT showed that the lung lesions had imaging manifestations of continuous progress. From February 11, CT showed that the lesions gradually shrunk. On March 30, the re-examination CT showed that the lung images had returned to normal (**Figure 1A**).

## Laboratory Examination

Clinical samples, nasopharyngeal swabs, feces, urine, whole blood, serum, and sputum were collected. Routine tests were carried out on the day of admission, including blood; sputum; throat swab culture (fungi and bacteria); blood routine (cell count and proportion); liver function [albumin (ALB), alanine aminotransferase (ALT), gamma glutamyl transpeptidase (GGT)]; renal function; inflammatory indexes [hs-CRP, lipopolysaccharide (LPS), procalcitonin (PCT)]; and coagulation



**TABLE 1 |** Traditional Chinese medicine prescriptions from February 12 to March 13, 2020.

| Date        | Herb prescription   |
|-------------|---|
| February 12 | <i>Radix Bupleuri</i> 10 g, <i>Bamboo Sap Pinellia</i> 10 g, <i>Radix Scutellariae</i> 10 g, <i>Radix Codonopsis</i> 10 g, <i>Pericarpium Citri Reticulatae</i> 10 g, <i>Rehmannia Dried Rhizome</i> 10 g, <i>Radix Aucklandiae</i> 10 g, <i>Amomum villosum</i> 6 g, <i>stir-baked Fructus Setariae Germinatus</i> 15 g, <i>stir-baked Fructus Hordei Germinatus</i> 15 g, <i>prepared Radix Glycyrrhizae</i> 6 g; take 7 doses, once daily, oral administration.  |
| February 19 | <i>Broil Dwarf Yellow Daylily</i> 15 g, <i>Radix Codonopsis</i> 15 g, <i>Radix Glehniae</i> 15 g, <i>Ophiopogonis Tuber</i> 15 g, <i>prepared Rhizome of Rehmannia</i> 15 g, <i>prepared Radix Scutellariae</i> 10 g, <i>Armeniacae Semen</i> 10 g, <i>Pericarpium Trichosanthis</i> 15 g, <i>Lignum Santali Album</i> 5 g, <i>Salvia Miltiorrhiza</i> 15 g, <i>Chinese Magnoliavine Fruit</i> 6 g, <i>Radix Scutellariae</i> 10 g, <i>Heartleaf Houltuynia Herb</i> 15 g, <i>Fasciculus Vascularis Luffae</i> 15 g, <i>Radix Glycyrrhizae</i> 10 g; take 7 doses, once daily, oral administration. |
| February 27 | <i>Honeysuckle</i> 15 g, <i>Forsythia</i> 10 g, <i>Lophatherum Gracile</i> 10 g, <i>Achene of Great Burdock</i> 10 g, <i>Schizonepeta</i> 10 g, <i>Rhizoma Phragmitis</i> 10 g, <i>Coptis Chinensis</i> 10 g, <i>Radix Paoniae Rubra</i> the Root of Common Peony 10 g, <i>Coix Seed</i> 60 g, <i>Polyporus Umbellatus</i> 15 g, <i>Rhizoma Atractylodis Macrocephalae</i> 20 g, <i>seed of Asiatic Plantain</i> 15 g, <i>prepared rhubarb</i> 10 g, <i>Radix Glycyrrhizae</i> 10 g; take 7 doses, once daily, oral administration.   |
| March 6     | <i>Radix Codonopsis</i> 15 g, <i>Radix Pseudostellariae</i> 15 g, <i>Astragalus Membranaceus</i> 20 g, <i>Radix Aucklandiae</i> 10 g, <i>Amomum Villosum</i> 6 g, <i>Poria Cocos</i> 20 g, <i>Coptis Chinensis</i> 10 g, <i>parched white Atractylodes Rhizome</i> 15 g, <i>Pinellia Ternata</i> 10 g, <i>Pericarpium Citri Reticulatae</i> 10 g, <i>Semen Ziziphi Spinosae</i> 30 g, <i>stir-fried green beans</i> 15 g, <i>honey-fried Radix Glycyrrhizae</i> 6 g, <i>stir-fried Coix Seed</i> 30 g; take 7 doses, once daily, oral administration.   |
| March 10    | <i>Rhubarb</i> 10 g, <i>Mangnolia Officinalis</i> 20 g, <i>Radix Scutellariae</i> 15 g, <i>Coptis Chinensis</i> 10 g, <i>Radix Glycyrrhizae</i> 10 g, <i>fruit of Citron or Trifoliate Orange</i> 20 g; take 3 doses, once daily, enema therapy.  |
| March 13    | <i>Radix Codonopsis</i> 20 g, <i>Astragalus Membranaceus</i> 30 g, <i>Radix Pseudostellariae</i> 10 g, <i>Amomum Villosum</i> 6 g, <i>Bighead Atractylodes Rhizome</i> 15 g, <i>Poria Cocos</i> 15 g, <i>stir-fried green beans</i> 15 g, <i>Coix Seed</i> 30 g, <i>Salvia Miltiorrhiza</i> 30 g, <i>Agastache rugosa</i> 10 g, <i>Eupatorium</i> 10 g, <i>Pinellia Ternata</i> 10 g, <i>Pericarpium Citri Reticulatae</i> 10 g, <i>prepared Radix Glycyrrhizae</i> 10 g; take 7 doses, once daily, oral administration.  |
| March 13    | <i>Rhubarb</i> 15 g, <i>Mangnolia Officinalis</i> 20 g, <i>Fruit of Citron or Trifoliate Orange</i> 15 g, <i>Coptis Chinensis</i> 15 g, <i>Radix Scutellariae</i> 15 g, <i>Radix Glycyrrhizae</i> 6 g; take 3 doses, once daily, enema therapy.   |

function (D-dimer). In addition, common acute respiratory pathogens (influenza A virus, influenza B virus, adenovirus, parainfluenza, and syncytial virus), coronavirus (MERS, SARS, 229E, NL63, OC43, and HKU1), and SARS-CoV-2 nucleic acids were detected. Following identification of the pathogen of infection, serum SARS-CoV-2 antibody, cellular immunity, and humoral immunity were detected. Disease progression was observed by continuous sample collection (Figures 2, 3).

## DISCUSSION

The outbreak of SARS-CoV-2 from December 2019 to the present has been catastrophic, has seriously damaged the global public health system, and continues to pose a serious threat to the health of humans worldwide (17–19). With the deepening of the research on the clinical characteristics and mechanism of

SARS-CoV-2 infection, many studies have confirmed that SARS-CoV-2 and SARS-CoV have similar infection mechanisms (20, 21), mainly through the ACE2 receptor to infect target cells. Moreover, the main symptoms after infection are respiratory system reactions, while gastrointestinal symptoms are also very common. Patients with COVID-19 accompanied by gastrointestinal symptoms are more likely to experience ARDS and liver damage with an inadequate prognosis (10, 22). Although there is no direct evidence to prove the fecal oral transmission of SARS-CoV-2, existing studies have shown that SARS-CoV-2 can be detected in the respiratory tract and fecal samples of most patients with COVID-19 RNA (22–24). In addition, it has been proven that SARS-CoV-2 can be isolated from the feces of patients with COVID-19 (25, 26), which further reflects the risk of fecal oral transmission of SARS-CoV-2 (27), and may pose new challenges to the control and prevention of COVID-19. Here we report a case of COVID-19 with negative conversion of SARS-CoV-2 nucleic acid in the respiratory tract and persistent positivity in the intestinal tract. In order to speed up the clearance of SARS-CoV-2 in the intestinal tract and reduce the risk of fecal oral transmission, we used a TCM enema for treatment and achieved good results.

In this study, we report that patients with COVID-19 developed rapidly in the early stage of the disease (Figure 1A). We added methylprednisolone sodium succinate (40 mg, once daily, subcutaneous injection) in the clinic, which effectively controlled the disease progression, indicating the effectiveness of appropriate glucocorticoid treatment in the early stage (28). In addition, the laboratory results (Figures 2F–H) also indicate that the humoral and cellular immunity of patients is active, and each index is at a high level in the early stage of infection. This may be related to immune disorders caused by the early progression of the disease and induction of cellular immune factors, which is consistent with previous reports (29, 30). With improvement of the disease, each index of the immune system shows a decline. In particular, the high level of IgE (Figure 2H) indicates that there is a certain degree of type I allergy in COVID-19 (31). Indeed, anti-SARS-CoV-2 IgM antibody can be detected as early as 1 week after the onset of the disease, and anti-SARS-CoV-2 IgG antibody is produced relatively rapidly. Anti-SARS-CoV-2 IgM and anti-SARS-CoV-2 IgG reached their peak 3 weeks after infection, and, as of December 2020, the anti-SARS-CoV-2 IgG antibody in patients was weakly positive (Figure 2J), which was consistent with that reported in the literature (24). During treatment, the patient developed fever again, and the laboratory results (Figures 2A–E) showed an increase in inflammatory indices (Hs-CRP, D-dimer, WBC count, PCT), which indicated that the patient had a secondary pulmonary infection. At the same time, the secondary infection induced positive conversion of SARS-CoV-2 RNA in sputum samples (Figure 3A; February 26). In view of this phenomenon, combined antiviral and anti-infection treatments should be considered (Figure 1C). Therefore, in the process of treatment and nursing, secondary infection of the lung must be prevented and controlled. In the current case, the patient's sputum samples were negative for SARS-CoV-2 nucleic acid on February 27 and 28 (Figure 3A; February 27 and 28). At this time, antiviral drugs were stopped, and only inhaled interferon was maintained. On March 9, the patient



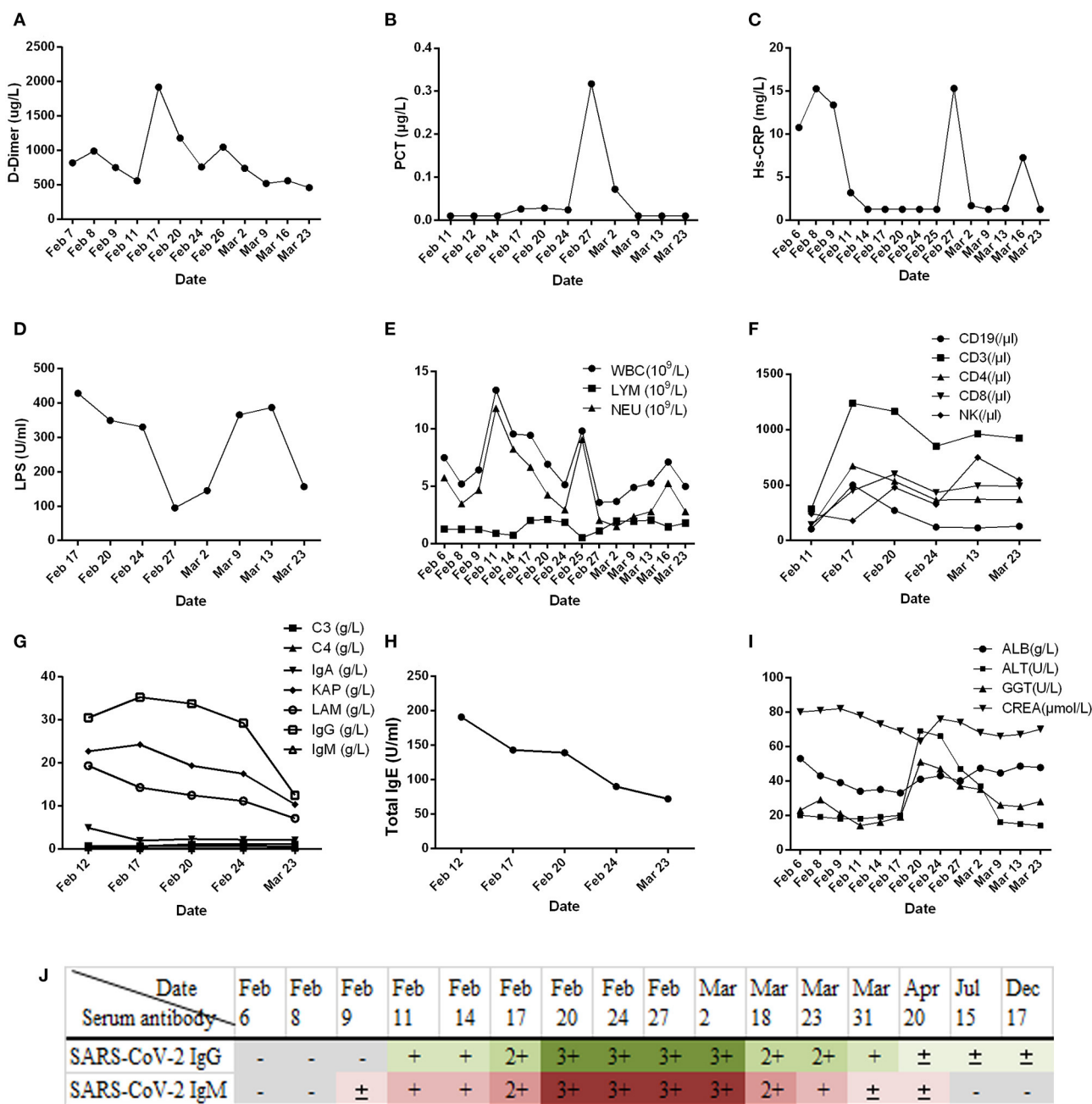


**FIGURE 2 |** Results of routine laboratory examination of patients with COVID-19 during admission. **(A)** Plasma D-dimer; **(B)** serum procalcitonin (PCT); **(C)** high-sensitivity C-reactive protein (Hs-CRP); **(D)** lipopolysaccharide (LPS); **(E)** white blood cell count; **(F)** classification count of lymphocyte subsets; **(G)** complement (C3, C4), immunoglobulin (IgA, IgG, IgM), and light chain (KAP, LAM: Immunoglobulin light chain kappa and lambda); **(H)** immunoglobulin E (IgE); **(I)** liver (ALB, albumin; ALT, alanine aminotransferase; GGT, gamma glutamyl transpeptidase) and kidney function (CREA, creatinine); **(J)** results of serum SARS-CoV-2 IgG/IgM detection in patients with COVID-19. The SARS-CoV-2 serum antibody (IgG/IgM) test kit (colloidal gold method) was provided by Zhuhai Lizhu Reagent Co., Ltd.; “-” represents negative, “±” represents weak positive, and “+”, “2+”, “3+” represents positive, and it was enhanced step by step.

again tested positive for SARS-CoV-2 nucleic acid in the sputum and remained positive for SARS-CoV-2 nucleic acid in the stool (Figure 3A, from February 19 to March 9). According to the analysis of previous literature, the apparent re-emergence of SARS-CoV-2 nucleic acid in the sputum may be related to the

persistent positive SARS-CoV-2 in the feces (32). Therefore, we adjusted the treatment plan again, and TCM enema treatment was added. After treatment with the TCM enema, the threshold cycle value (Ct-value) of the virus gradually increased to > 40 cycles (Figure 3B), and patients with COVID-19 who met the

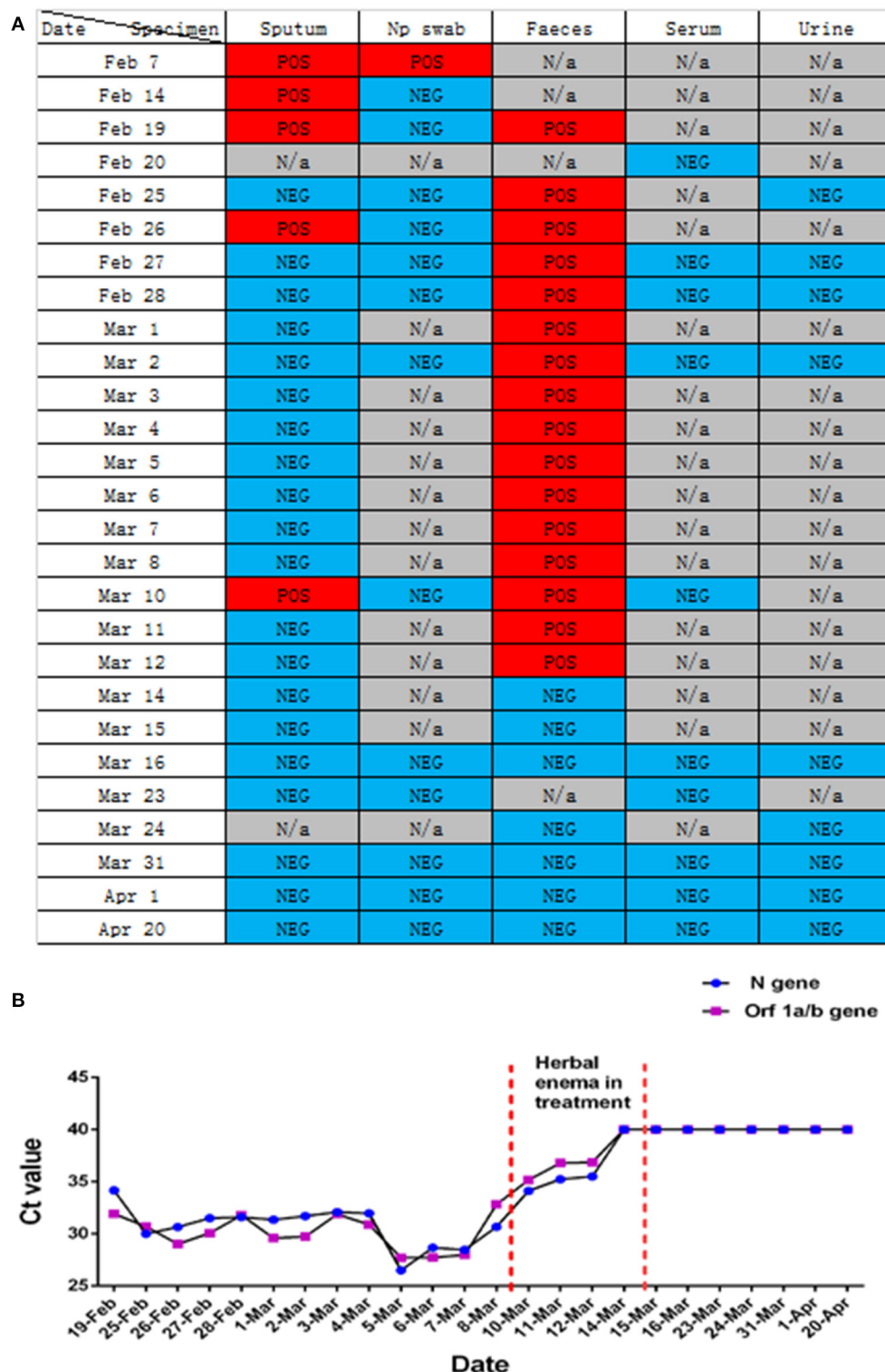


**FIGURE 3 |** Changes in nucleic acid detection in various patients with COVID-19. **(A)** Detection of SARS-CoV-2 nucleic acids in different samples of patients with COVID-19 during hospitalization. POS, Test result was positive; NEG, Test result was negative; N/a, No relevant tests were carried out. **(B)** Detection of SARS-CoV-2 nucleic acid in the feces of patients with COVID-19 pneumonia during hospitalization. Before February 25, 2020, the New Coronavirus 2019-nCoV nucleic acid detection kit (real-time fluorescent PCR method) provided by Shanghai Berger Biotechnology Co., Ltd. was used, and the New Coronavirus 2019-nCoV nucleic acid detection kit (real-time fluorescence PCR method) provided by Da'an gene Limited by Share Ltd. of Zhongshan University was used after February 25, 2020.

discharge criteria were discharged from the hospital (33). After repeated re-examination, SARS-CoV-2 RNA in feces, sputum, urine, and blood samples was negative.

With the outbreak of SARS-CoV-2, medical experts worldwide have a new understanding of the role of TCM in the treatment of infectious diseases. Multiple studies have reported the efficacy of TCM enema in other diseases, such as epidemic encephalitis B (34), hand foot mouth disease (35), and viral hepatitis (36, 37). We focused on the clinical manifestations of this patient: aversion to cold, fever, sore throat, white phlegm, chest tightness, dry stool, white, and greasy tongue coating. Based on the dialectical system of viscera in TCM, the lung and large intestine interact with each other, and the residual toxin of lung heat moves down to the large intestine. The syndrome types in the patients were dampness heat stagnation of the lung and heat stagnation of the large intestine. TCM *Coptis Chinensis* and *Radix Scutellariae* can clear heat and dampness, relieve fire, and detoxify; *rhubarb* can break accumulation and remove heat between intestines; and *fruit of citrus or trifoliate orange* and *Magnoliae Officinalis* can disperse dampness and remove distension. The corresponding enema scheme was formulated to allow the medicine to directly reach the disease center (Table 1). After 4 days of TCM enema treatment, the intestinal stool SARS-CoV-2 was negative. Many studies have reported variations in the time of SARS-CoV-2 turning negative in the feces of patients with COVID-19 (38, 39), which is related to different treatment schemes and different immune responses to the virus. However, it is clear that the nucleic acid in the feces of most patients with COVID-19 lasts longer than that in the respiratory tract. According to the laboratory nucleic acid test results (Figures 3A,B). On March 10, the nucleic acid of sputum samples returned to positive, indicating that the infection process of the patient was still repeated, and then the patient received TCM enema treatment. The viral intestinal nucleic acid showed an obvious downward trend (Ct value suddenly increased) during the treatment. It indirectly reflects that SARS-CoV-2 may be effectively removed from the intestine with the use of drugs, was effectively removed from the intestine, which may effectively shortened the intestinal clearance time of the virus. However, this study only used TCM enema for one patient with COVID-19, and did not set up a control case. Therefore, regardless of TCM enema is effective for different patients with COVID-19, and the mechanism of TCM enema accelerating intestinal virus clearance need to be further studied.

## REFERENCES

- Zhu N, Zhang D, Wang W, Li X, Yang B, Song J, et al. China novel coronavirus investigating and research team. A novel coronavirus from patients with pneumonia in China, 2019. *N Engl J Med.* (2020) 382:727–33. doi: 10.1056/NEJMoa2001017
- Holshue ML, DeBolt C, Lindquist S, Lofy KH, Wiesman J, Bruce H, et al. First case of 2019 novel coronavirus in the United States. *N Engl J Med.* (2020) 382:929–36. doi: 10.1056/NEJMoa2001191
- Wang C, Horby PW, Hayden FG, Gao GF. A novel coronavirus outbreak of global health concern. *Lancet.* (2020) 395:470–3. doi: 10.1016/S0140-6736(20)30185-9
- Guo YR, Cao QD, Hong ZS, Tan YY, Chen SD, Jin HJ, et al. The origin, transmission and clinical therapies on coronavirus disease 2019 (COVID-19) outbreak—an update on the status. *Mil Med Res.* (2020) 7:11. doi: 10.1186/s40779-020-00240-0
- Chan JF, Kok KH, Zhu Z, Chu H, To KK, Yuan S, et al. Genomic characterization of the 2019 novel human-pathogenic coronavirus isolated from a patient with atypical pneumonia after visiting Wuhan. *Emerg Microbes Infect.* (2020) 9:221–36. doi: 10.1080/22221751.2020.1719902
- Cui J, Li F, Shi ZL. Origin and evolution of pathogenic coronaviruses. *Nat Rev Microbiol.* (2019) 17:181–92. doi: 10.1038/s41579-018-0118-9
- Su S, Wong G, Shi W, Liu J, Lai ACK, Zhou J, et al. Epidemiology, genetic recombination, and pathogenesis of coronaviruses.

In summary, although some vaccines against SARS-CoV-2 have been used clinically, including inactivated SARS-CoV-2, mRNA, and recombinant adenovirus vaccines (40, 41), due to the long development cycle of vaccines and other new drugs, it is still an effective method to cut off the source of infection. TCM enema therapy has been shown may accelerate the clearance of SARS-CoV-2 in the intestines of patients with COVID-19, shorten the positive time, and realize the negative effect of feces during hospitalization. The negative fecal nucleic acid can be further used as the discharge standard for patients with COVID-19 after hospitalization to prevent fecal oral transmission.

## DATA AVAILABILITY STATEMENT

The original contributions presented in the study are included in the article/supplementary material, further inquiries can be directed to the corresponding authors.

## ETHICS STATEMENT

Written informed consent was obtained from the individual(s) for the publication of any potentially identifiable images or data included in this article.

## AUTHOR CONTRIBUTIONS

YD and JC conceived the study, participated in its design, drafted and revised the manuscript for content including medical writing for content, analysis, and interpretation of data. ZZ, HZ, DH, JL, CZ, QC, XC, and YY conceived the study, participated in its design managed microbiology laboratory assays, revised the manuscript, and collected TCM treatment prescription. XJ was responsible for the collection and collation of clinical data. All authors read and approved the final manuscript.

## FUNDING

This work was supported by the Natural Science Foundation of Zhejiang Province (No. LGF20H200009).

## ACKNOWLEDGMENTS

We thank the patient for providing informed consent for this publication.

- Trends Microbiol.* (2016) 24:490–502. doi: 10.1016/j.tim.2016.03.003
8. Zhou P, Yang XL, Wang XG, Hu B, Zhang L, Zhang W, et al. A pneumonia outbreak associated with a new coronavirus of probable bat origin. *Nature*. (2020) 579:270–3. doi: 10.1038/s41586-020-2012-7
  9. Shah VK, Fimal P, Alam A, Ganguly D, Chattopadhyay S. Overview of immune response during SARS-CoV-2 infection: lessons from the past. *Front Immunol.* (2020) 11:1949. doi: 10.3389/fimmu.2020.01949
  10. Ye Q, Wang B, Zhang T, Xu J, Shang S. The mechanism and treatment of gastrointestinal symptoms in patients with COVID-19. *Am J Physiol Gastrointest Liver Physiol.* (2020) 319:G245–52. doi: 10.1152/ajpgi.00148.2020
  11. Zhong P, Xu J, Yang D, Shen Y, Wang L, Feng Y, et al. COVID-19-associated gastrointestinal and liver injury: clinical features and potential mechanisms. *Signal Transduct Target Ther.* (2020) 5:256. doi: 10.1038/s41392-020-00373-7
  12. Cha MH, Regueiro M, Sandhu DS. Gastrointestinal and hepatic manifestations of COVID-19: a comprehensive review. *World J Gastroenterol.* (2020) 26:2323–32. doi: 10.3748/wjg.v26.i19.2323
  13. National Health commission of the People's Republic of China. *The New Coronavirus-Infected Pneumonia Diagnosis and Treatment Plan (Trial version 8)*. Available online at: <http://www.nhc.gov.cn/xcs/zhengcwj/202008/0a7bdf12bd4b46e5bd28ca7f9a7f5e5a.shtml> (accessed August 19, 2020).
  14. Military Medical Expert Group on the Front-line Diagnosis and treatment of disease 2019 novel coronavirus infection suitable for Military support Hubei medical team. *Zhonghua Jie He He Hu Xi Za Zhi.* (2020) 43:285–7. doi: 10.3760/cma.j.cn112147-20200224-00172
  15. Zhang WH, Lu HZ. Shanghai New coronary virus disease clinical treatment expert group. Shanghai 2019 coronary virus disease treatment expert consensus. *Chin J Infect Dis.* (2020) 20:134–8. doi: 10.3760/cma.k.issn.1000-6680.2020.03.002
  16. National Health commission of the People's Republic of China. *The New Coronavirus-Infected Pneumonia Diagnosis and Treatment Plan (Trial version 5)*. Available online at: <http://www.nhc.gov.cn/zyzyj/s7653p/202002/3b09b894ac9b4204a79db58912d4440.shtml> (accessed February 5, 2020).
  17. Vellingiri B, Jayaramayya K, Iyer M, Narayanasamy A, Govindasamy V, Giridharan B, et al. COVID-19: a promising cure for the global panic. *Sci Total Environ.* (2020) 725:138277. doi: 10.1016/j.scitotenv.2020.138277
  18. KamelBoulos MN, Geraghty EM. Geographical tracking and mapping of coronavirus disease COVID-19/severe acute respiratory syndrome coronavirus 2 (SARS-CoV-2) epidemic and associated events around the world: how 21st century GIS technologies are supporting the global fight against outbreaks and epidemics. *Int J Health Geogr.* (2020) 19:8. doi: 10.1186/s12942-020-00202-8
  19. Anderson RM, Heesterbeek H, Klinkenberg D, Hollingsworth TD. How will country-based mitigation measures influence the course of the COVID-19 epidemic? *Lancet.* (2020) 395:931–4. doi: 10.1016/S0140-6736(20)30567-5
  20. Xu J, Zhao S, Teng T, Abdalla AE, Zhu W, Xie L, et al. Systematic comparison of two animal-to-human transmitted human coronaviruses: SARS-CoV-2 and SARS-CoV. *Viruses.* (2020) 12:244. doi: 10.3390/v12020244
  21. Chu H, Chan JF, Wang Y, Yuen TT, Chai Y, Hou Y, et al. Comparative replication and immune activation profiles of SARS-CoV-2 and SARS-CoV in human lungs: an *ex vivo* study with implications for the pathogenesis of COVID-19. *Clin Infect Dis.* (2020) 71:1400–9. doi: 10.1093/cid/ciaa410
  22. Mao R, Qiu Y, He JS, Tan JY, Li XH, Liang J, et al. Manifestations and prognosis of gastrointestinal and liver involvement in patients with COVID-19: a systematic review and meta-analysis. *Lancet Gastroenterol Hepatol.* (2020) 5:667–78. doi: 10.1016/S2468-1253(20)30126-6
  23. Wölfel R, Corman VM, Guggemos W, Seilmaier M, Zange S, Müller MA, et al. Virological assessment of hospitalized patients with COVID-2019. *Nature.* (2020) 581:465–9. doi: 10.1038/s41586-020-2196-x
  24. Zhang W, Du RH, Li B, Zheng XS, Yang XL, Hu B, et al. Molecular and serological investigation of 2019-nCoV infected patients: implication of multiple shedding routes. *Emerg Microbes Infect.* (2020) 9:386–9. doi: 10.1080/22221751.2020.1729071
  25. Zhang Y, Chen C, Zhu S, Shu C, Wang D, Song J, et al. Isolation of the 2019-nCoV from a stool specimen of a laboratory-confirmed case of the coronavirus disease 2019 (COVID-19). *China CDC Wkly.* (2020) 2:123–4. doi: 10.46234/ccdcw2020.033
  26. Zhang Y, Chen C, Song Y, Zhu S, Wang D, Zhang H, et al. Excretion of SARS-CoV-2 through faecal specimens. *Emerg Microbes Infect.* (2020) 9:2501–8. doi: 10.1080/22221751.2020.1844551
  27. Kang M, Wei J, Yuan J, Guo J, Zhang Y, Hang J, et al. Probable evidence of fecal aerosol transmission of SARS-CoV-2 in a high-rise building. *Ann Intern Med.* (2020) 173:974–80. doi: 10.7326/M20-0928
  28. Mattos-Silva P, Felix NS, Silva PL, Robba C, Battaglini D, Pelosi P, et al. Pros and cons of corticosteroid therapy for COVID-19 patients. *Respir Physiol Neurobiol.* (2020) 280:103492. doi: 10.1016/j.resp.2020.103492
  29. Chang FY, Chen HC, Chen PJ, Ho MS, Hsieh SL, Lin JC, et al. Immunologic aspects of characteristics, diagnosis, and treatment of coronavirus disease 2019 (COVID-19). *J Biomed Sci.* (2020) 27:72. doi: 10.1186/s12929-020-00663-w
  30. Chen G, Wu D, Guo W, Cao Y, Huang D, Wang H, et al. Clinical and immunological features of severe and moderate coronavirus disease 2019. *J Clin Invest.* (2020) 130:2620–9. doi: 10.1172/JCI137244
  31. Song Y, Zhong H, Li L, Yin M, Yin Y, Guo X, et al. Dynamic monitoring of immune function indexes in COVID-19 patients. *Aging (Albany, NY).* (2020) 12:24596–603. doi: 10.18632/aging.202362
  32. Li Y, Hu Y, Yu Y, Zhang X, Li B, Wu J, et al. Positive result of Sars-Cov-2 in faeces and sputum from discharged patients with COVID-19 in Yiwu, China. *J Med Virol.* (2020) 92:1938–47. doi: 10.1002/jmv.25905
  33. National Health commission of the People's Republic of China. *The New Coronavirus-Infected Pneumonia Diagnosis and Treatment Plan (Trial version 6)*. Available online at: [http://www.gov.cn/zhengce/zhengceku/2020-02/19/content\\_5480948.htm](http://www.gov.cn/zhengce/zhengceku/2020-02/19/content_5480948.htm) (accessed February 18, 2020).
  34. Liu Y, Guo JC, Wan H, Lv TF, Lou GQ. Clinical analysis of epidemic encephalitis B with Chinese medicine mainly in herb enema. *Chin Arch Trad Chin Med.* (2011) 29:1248–9. doi: 10.13193/j.archtcm.2011.06.58.liuy.013
  35. Li X, Zhang X, Ding J, Xu Y, Wei D, Tian Y, et al. Comparison between Chinese herbal medicines and conventional therapy in the treatment of severe hand, foot, and mouth disease: a randomized controlled trial. *Evid Based Complement Alternat Med.* (2014) 2014:140764. doi: 10.1155/2014/140764
  36. Liang X, Wen L, Wu Y, Hao Y, Wang S, Hu X. Retention enema with traditional Chinese medicine for hepatic encephalopathy: a protocol for a systematic review and meta-analysis. *Med (Baltim).* (2020) 99:e22517. doi: 10.1097/MD.00000000000022517
  37. Li Y, Wang L, Su C, Sun HN. Clinical observation on the treatment of chronic severe hepatitis B by retention enema with Huchang Jiedu Decoction. *Chin J Integr Med.* (2010) 16:348–52. doi: 10.1007/s11655-010-0519-8
  38. Cheung KS, Hung IFN, Chan PPY, Lung KC, Tso E, Liu R, et al. Gastrointestinal manifestations of SARS-CoV-2 infection and virus load in fecal samples from a Hong Kong cohort: systematic review and meta-analysis. *Gastroenterology.* (2020) 159:81–95. doi: 10.1053/j.gastro.2020.03.065
  39. Tian Y, Rong L, Nian W, He Y. Review article: gastrointestinal features in COVID-19 and the possibility of faecal transmission. *Aliment Pharmacol Ther.* (2020) 51:843–51. doi: 10.1111/apt.15731
  40. Loch C. Vaccines against COVID-19. *Anaesth Crit Care Pain Med.* (2020) 39:703–5. doi: 10.1016/j.accpm.2020.10.006
  41. Forni G, Mantovani A. COVID-19 commission of accademia nazionale dei lincei, Rome; COVID-19 commission of accademia nazionale dei lincei, rome. COVID-19 vaccines: where we stand and challenges ahead. *Cell Death Differ.* (2021) 28:626–39. doi: 10.1038/s41418-020-00720-9

**Conflict of Interest:** The authors declare that the research was conducted in the absence of any commercial or financial relationships that could be construed as a potential conflict of interest.

Copyright © 2021 Dai, Zhao, Zhou, Huang, Luo, Zhang, Chen, Chen, Yao, Jiang and Cheng. This is an open-access article distributed under the terms of the Creative Commons Attribution License (CC BY). The use, distribution or reproduction in other forums is permitted, provided the original author(s) and the copyright owner(s) are credited and that the original publication in this journal is cited, in accordance with accepted academic practice. No use, distribution or reproduction is permitted which does not comply with these terms.





# The Prognostic Accuracy of National Early Warning Score 2 on Predicting Clinical Deterioration for Patients With COVID-19: A Systematic Review and Meta-Analysis

Kai Zhang<sup>1†</sup>, Xing Zhang<sup>1,2†</sup>, Wenyun Ding<sup>3†</sup>, Nanxia Xuan<sup>1</sup>, Baoping Tian<sup>1</sup>, Tiancha Huang<sup>1</sup>, Zhaocai Zhang<sup>1</sup>, Wei Cui<sup>1</sup>, Huaqiong Huang<sup>3\*</sup> and Gensheng Zhang<sup>1\*</sup>

<sup>1</sup> Department of Critical Care Medicine, Second Affiliated Hospital, Zhejiang University School of Medicine, Hangzhou, China, <sup>2</sup> Medical Security Bureau of Yinzhou District, Ningbo, China, <sup>3</sup> Department of Respiration and Critical Care Medicine, Second Affiliated Hospital, Zhejiang University School of Medicine, Hangzhou, China

## OPEN ACCESS

### Edited by:

Reza Lashgari,  
Shahid Beheshti University, Iran

### Reviewed by:

Yanfei Shen,  
Zhejiang Hospital, China  
Zsolt Szakács,  
University of Pécs, Hungary

### \*Correspondence:

Gensheng Zhang  
genshengzhang@zju.edu.cn  
Huaqiong Huang  
zr\_hhq@zju.edu.cn

†These authors have contributed  
equally to this work

### Specialty section:

This article was submitted to  
Infectious Diseases - Surveillance,  
Prevention and Treatment,  
a section of the journal  
Frontiers in Medicine

Received: 24 April 2021

Accepted: 07 June 2021

Published: 09 July 2021

### Citation:

Zhang K, Zhang X, Ding W, Xuan N,  
Tian B, Huang T, Zhang Z, Cui W,  
Huang H and Zhang G (2021) The  
Prognostic Accuracy of National Early  
Warning Score 2 on Predicting Clinical  
Deterioration for Patients With  
COVID-19: A Systematic Review and  
Meta-Analysis. *Front. Med.* 8:699880.  
doi: 10.3389/fmed.2021.699880

**Background:** During the coronavirus disease 2019 (COVID-19) pandemic, the National Early Warning Score 2 (NEWS2) is recommended for the risk stratification of COVID-19 patients, but little is known about its ability to detect severe cases. Therefore, our purpose is to assess the prognostic accuracy of NEWS2 on predicting clinical deterioration for patients with COVID-19.

**Methods:** We searched PubMed, Embase, Scopus, and the Cochrane Library from December 2019 to March 2021. Clinical deterioration was defined as the need for intensive respiratory support, admission to the intensive care unit, or in-hospital death. Sensitivity, specificity, and likelihood ratios were pooled by using the bivariate random-effects model. Overall prognostic performance was summarized by using the area under the curve (AUC). We performed subgroup analyses to assess the prognostic accuracy of NEWS2 in different conditions.

**Results:** Eighteen studies with 6,922 participants were included. The NEWS2 of five or more was commonly used for predicting clinical deterioration. The pooled sensitivity, specificity, and AUC were 0.82, 0.67, and 0.82, respectively. Benefitting from adding a new SpO<sub>2</sub> scoring scale for patients with hypercapnic respiratory failure, the NEWS2 showed better sensitivity (0.82 vs. 0.75) and discrimination (0.82 vs. 0.76) than the original NEWS. In addition, the NEWS2 was a sensitive method (sensitivity: 0.88) for predicting short-term deterioration within 72 h.

**Conclusions:** The NEWS2 had moderate sensitivity and specificity in predicting the deterioration of patients with COVID-19. Our results support the use of NEWS2 monitoring as a sensitive method to initially assess COVID-19 patients at hospital admission, although it has a relatively high false-trigger rate. Our findings indicated that the development of enhanced or modified NEWS may be necessary.

**Keywords:** NEWS2, COVID-19, systematic review, meta-analysis, prediction

## INTRODUCTION

The recent outbreak of coronavirus disease 2019 (COVID-19), caused by severe acute respiratory syndrome coronavirus 2 (SARS-CoV-2), has challenged healthcare systems worldwide (1). As of March 26, 2021, SARS-CoV-2 has resulted in more than 12.5 million confirmed cases, with more than 2.7 million deaths (2). Although the majority of patients infected with COVID-19 are symptomless or oligosymptomatic, about one-fifth of patients may develop severe COVID-19 with a high risk of mortality (3, 4). Thus, for patients with COVID-19, early identification of the deteriorating patients is of importance because it could direct finite resources toward those patients in greatest clinical need. However, risk stratification and early identification of patients with high risk of clinical deterioration at admission remain as major challenges. Frontline health workers constantly meet the challenges of determining the severity and prognosis of COVID-19 cases in order to provide high-quality care and effectively allocate resources (5). Therefore, there is a need for an easy-to-use and effective risk-predictive tool to assess the possibility of deterioration of patients with COVID-19.

The National Early Warning Score (NEWS), first introduced in 2012 and updated in 2017 (NEWS2), has received a formal

endorsement from the National Health Service to become the early warning system for deterioration of acutely ill patients in the United Kingdom (UK) (6, 7). The NEWS/NEWS2 is a scoring system based on routine physiological parameters, which can be obtained easily and rapidly at the bedside. Each indicator is given a score, where 0 is considered normal, and simple addition allows a total score from 0 to 23. A score of 5 or more represents the key threshold for urgent response, and patients with a score of 7 or more would be deemed to have a high clinical risk and trigger a high-level clinical alert (**Table 1**) (6, 7). Since some components (e.g., temperature, oxygen saturation, and supplemental oxygen dependency) were proved to be associated with the progression of COVID-19 (8, 9), guidelines from the Royal College of Physicians (10) and the Swiss Society of Intensive Care Medicine (11) advocate the use of the NEWS2 for initial assessment in patients with COVID-19. However, these recommendations were only based on expert opinions, and there have been no published meta-analyses to evaluate the predictive performance of the NEWS2.

Therefore, the aim of the present study was to evaluate the prognostic accuracy of the NEWS2 on predicting clinical deterioration for patients with COVID-19. In addition, we performed a comparison of the NEWS2 with the original NEWS.

## METHODS

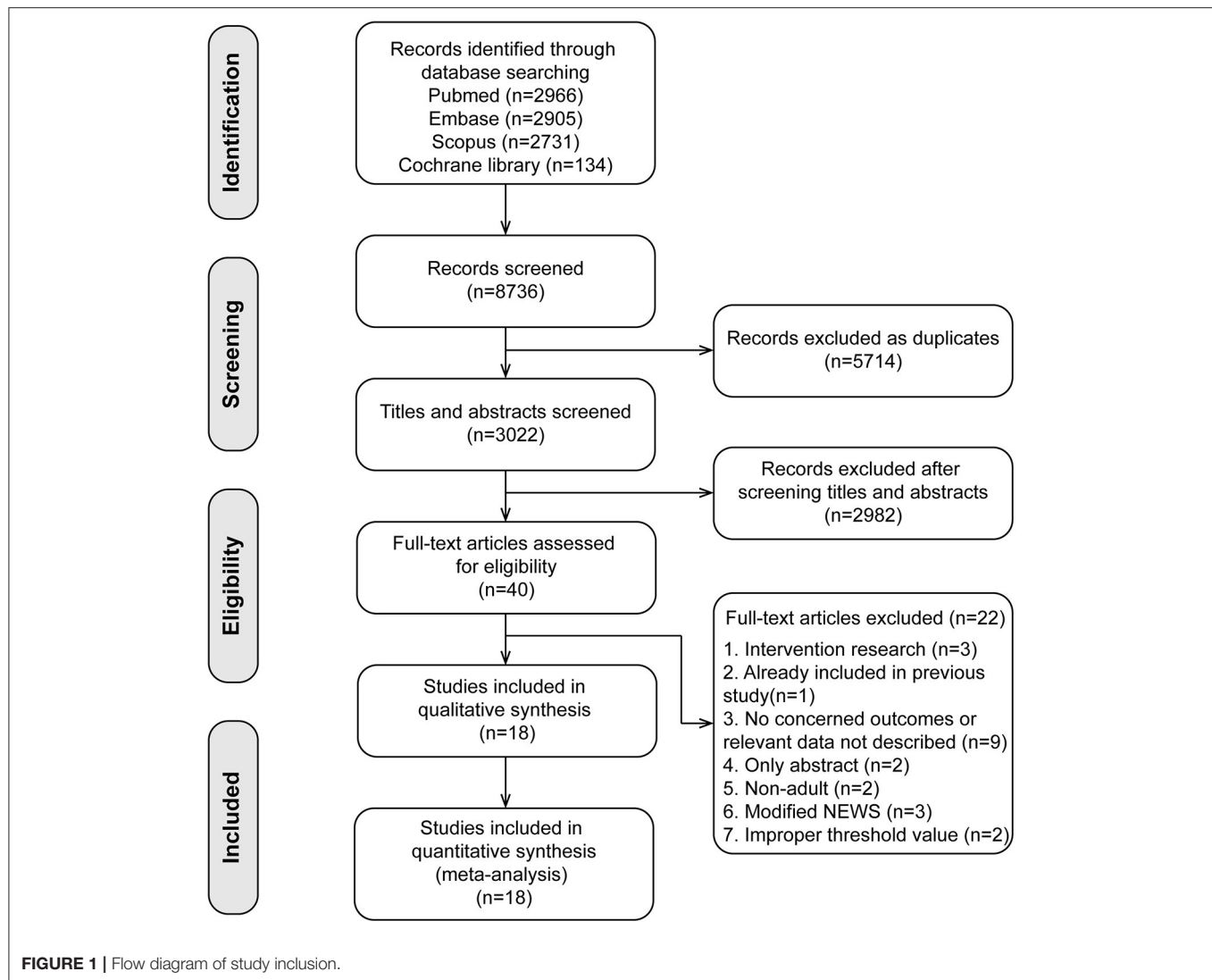
### Study Selection

We followed the PRISMA statement (12) to structure the meta-analysis (**Supplementary Material 1**). A predefined protocol has been registered in PROSPERO (CRD42021243845,

**Abbreviations:** COVID-19, coronavirus disease 2019; SARS-CoV-2, severe acute respiratory syndrome coronavirus 2; UK, United Kingdom; ICU, intensive care unit; ED, emergency department; qSOFA, quick Sequential Organ Failure Assessment; AUC, area under the curve; NEWS, National Early Warning Score; CI, confidence interval; PLR, positive likelihood ratio; NLR, negative likelihood ratio; DOR, diagnostic odds ratio; HSROC, hierarchical summary receiver operating characteristic.

**TABLE 1 |** The NEWS scoring system, thresholds, and triggers.

|  | 3                    | 2      | 1         | 0                                 | 1               | 2               | 3             |
|--|----------------------|--------|-----------|-----------------------------------|-----------------|-----------------|---------------|
| <b>NEWS</b>                            |                      |        |           |                                   |                 |                 |               |
| Respiration rate                       | ≤8                   |        | 9–11      | 12–20                             |                 | 21–24           | ≥25           |
| Oxygen saturations                     | ≤91                  | 92–93  | 94–95     | ≥96                               |                 |                 |               |
| Any supplemental oxygen                |                      | Yes    |           | No                                |                 |                 |               |
| Temperature                            | ≤35.0                |        | 35.1–36.0 | 36.1–38.0                         | 38.1–39.0       | ≥39.1           |               |
| % Systolic blood pressure              | ≤90                  | 91–100 | 101–110   | 111–219                           |                 |                 | ≥220          |
| Heart rate                             | ≤40                  |        | 41–50     | 51–90                             | 91–110          | 111–130         | ≥131          |
| Level of Consciousness                 |                      |        |           | Alert                             |                 |                 | V, P, or U    |
| <b>NEWS2</b>                           |                      |        |           |                                   |                 |                 |               |
| Respiration rate                       | ≤8                   |        | 9–11      | 12–20                             |                 | 21–24           | ≥25           |
| SpO <sub>2</sub> scale 1               | ≤91                  | 92–93  | 94–95     | ≥96                               |                 |                 |               |
| SpO <sub>2</sub> scale 2               | ≤83                  | 84–85  | 86–87     | 88–92 ≥93 on air                  | 93–94 on oxygen | 95–96 on oxygen | ≥97 on oxygen |
| Air or oxygen?                         |                      | Oxygen |           | Air                               |                 |                 |               |
| Systolic blood pressure                | ≤90                  | 91–100 | 101–110   | 111–219                           |                 |                 |               |
| Pulse                                  | ≤40                  |        | 41–50     | 51–90                             | 91–110          | 111–130         | ≥131          |
| Consciousness                          |                      |        |           | Alert                             |                 |                 | CVPU          |
| Temperature                            | ≤35.0                |        | 35.1–36.0 | 36.1–38.0                         | 38.1–39.0       | ≥39.1           |               |
|  |                      |        |           |                                   |                 |                 |               |
| <b>Score</b>                           | <b>Clinical risk</b> |        |           | <b>Response</b>                   |                 |                 |               |
| Aggregate score 0–4                    | Low                  |        |           | Ward-based response               |                 |                 |               |
| Score of 3 in any individual parameter | Low–medium           |        |           | Urgent ward-based response        |                 |                 |               |
| Aggregate score 5–6                    | Medium               |        |           | Key threshold for urgent response |                 |                 |               |
| Aggregate score 7 or more              | High                 |        |           | Urgent or emergency response      |                 |                 |               |



**Supplementary Material 2).** We searched the PubMed, Embase, Scopus, and the Cochrane Library from December 2019 to March 2021 for relevant articles.

The basic inclusive criteria are as follows: (1) recruited adult patients with confirmed cases of SARS-CoV-2 infection, (2) applied the NEWS2 or the NEWS to predict clinical deterioration (including the need for intensive respiratory support, admission to the ICU, or in-hospital death), and (3) provided sufficient data to estimate the prognostic accuracy. There was no language restriction. The detailed searching strategies and inclusion and exclusion criteria are recorded in **Supplementary Material 3**.

## Data Extraction

Two authors independently retrieved and extracted studies according to the inclusion criteria. We recorded the true positive, false positive, false negative, and true negative from the articles directly or through a recalculation according to the sensitivity and specificity. Any disagreement in the process was resolved by a discussion.

## Quality Assessment

Two authors employed the PROBAST to assess the risk of bias and applicability concerns of the included studies (13). The detailed quality assessment standard is recorded in **Supplementary Material 3**.

## Statistical Synthesis and Analysis

We used a bivariate random-effects regression model (14) to pool the sensitivity, specificity, positive likelihood ratio (PLR), negative likelihood ratio (NLR), and area under the curve (AUC) as point estimates with 95% confidence interval (CI). We also constructed the hierarchical summary receiver operating characteristic (HSROC) curve to present the summary point estimates of sensitivity and specificity.  $I^2$  statistics were calculated to assess the statistical heterogeneity between the included studies, where  $I^2 > 50\%$  indicated a substantial level of heterogeneity (15).

We performed subgroup analyses to evaluate the performance of the NEWS2 in different conditions. Studies were stratified

**TABLE 2 |** Characteristics of the included studies.

| References                   | Sample size | Design        | Participants  | Score                              | Outcome                                       | Time of calculating scores                           |
|------------------------------|-------------|---------------|---|------------------------------------|---|--|
| Aliberti et al. (17)         | 1,428       | Prospective   | Age: 66 (59, 74); male: 58%; 30-day mortality: 37%      | NEWS $\geq 6$                      | 30-day mortality, 60-day mortality            | At admission   |
| Baker et al. (18)            | 296         | Retrospective | Age: 75 (62, 84); male: 55%; in-hospital mortality: 26% | NEWS2 $\geq 5$<br>qSOFA $\geq 2$   | Serious events with 24 h                      | Daily from admission until the occurrence of outcome |
| Bradley et al. (19)          | 830         | Retrospective | Age: 70 (58, 80); male: 61%; 30-day mortality: 36%      | NEWS2 $\geq 5$<br>qSOFA $\geq 2$   | 72-h mortality, 30-day mortality              | Earliest measurement recorded after admission        |
| Covino et al. (20)           | 334         | Retrospective | Age: 66 (54, 78); male: 64%; 7-day mortality: 8%        | NEWS $\geq 5$<br>NEWS2 $\geq 5$    | ICU admission within 48 h, and 7 days         | At ED arrival  |
| De Socio et al. (32)         | 121         | Retrospective | Age: 65 $\pm$ 13; male: 65%; mortality: NR              | NEWS2 $\geq 4$                     | ICU admission, invasive ventilation, or death | At admission   |
| Fan et al. (21)              | 654         | Retrospective | Age: NR; male: NR; in-hospital mortality: 20%           | NEWS2 $\geq 5$                     | In-hospital mortality                         | At admission   |
| Gidari et al. (22)           | 68          | Retrospective | Age: 64 (31, 93); male: 66%; mortality: NR              | NEWS2 $\geq 5$                     | ICU admission                                 | At admission   |
| Holten et al. (23)           | 169         | Prospective   | Age: 59; male: 58%; 14-day mortality: 7%                | NEWS2 $\geq 5$<br>qSOFA $\geq 2$   | Death or admission to ICU within 14 days      | At ED arrival  |
| Ihle-Hansen et al. (24)      | 42          | Retrospective | Age: 73; male: 67%; in-hospital mortality: 47%          | NEWS2 $\geq 5$ ,<br>qSOFA $\geq 2$ | Death or admission to ICU                     | First examination after admission                    |
| Jang et al. (25)             | 110         | Retrospective | Age: 57 $\pm$ 17; male: 44%; 28-day mortality: 6%       | NEWS2 $\geq 5$                     | Death or admission to ICU                     | NR   |
| Liu et al. (26)              | 673         | Retrospective | Age: 61 (50, 69); male: 51%; in-hospital mortality: 18% | NEWS $\geq 5$<br>NEWS2 $\geq 5$    | In-hospital mortality                         | At admission   |
| Maguire et al. (27)          | 224         | Retrospective | Age: NR; male: 55%; 30-day mortality: 23%               | NEWS $\geq 5$                      | 30-day mortality                              | At admission   |
| Martin-Rodriguez et al. (33) | 261         | Retrospective | Age: 80 (69, 88); male: 46%; 2-day mortality: 12%       | NEWS2 $\geq 8$                     | Death within 2 days                           | At admission   |
| Myrstad et al. (28)          | 66          | Prospective   | Age: 72; male: 58%; in-hospital mortality: 20%          | NEWS2 $\geq 5$<br>qSOFA $\geq 2$   | Death or admission to ICU                     | At ED admission                                      |
| Pokeerbux et al. (29)        | 202         | Retrospective | Age: 65 (52, 78); male: 61%; in-hospital mortality: 11% | NEWS $\geq 5$                      | Death or admission to ICU                     | At admission   |
| Prower et al. (34)           | 708         | Retrospective | Age: 62 $\pm$ 18; male: 58%; in-hospital mortality: 12% | NEWS2 $\geq 5$                     | Death or admission to ICU                     | At admission   |
| Richardson et al. (30)       | 620         | Retrospective | Age: 73; male: 55%; in-hospital mortality: 32%          | NEWS $\geq 5$<br>NEWS2 $\geq 5$    | 24-h mortality, in-hospital mortality         | With 24 h of admission                               |
| Su et al. (31)               | 116         | Retrospective | Age: 63 (51, 72); male: 48%; in-hospital mortality: 8%  | NEWS $\geq 6$<br>qSOFA $\geq 2$    | Need intensive respiratory support            | At admission   |

NEWS, National Early Warning Score; NEWS2, National Early Warning Score 2; qSOFA, quick Sequential Organ Failure Assessment; ICU, intensive care unit; ED, emergency department.

according to the time of outcome measurement (within 72 h vs. in-hospital) and disease severity (mortality rate  $<10$  vs.  $\geq 10\%$ ). Sensitivity analyses were conducted by repeating the analyses within studies that calculated the NEWS2 at hospital admission. Publication bias was evaluated by using the Deek's test for funnel plot asymmetry (16), with  $p$ -value  $< 0.1$  indicating publication bias. All analyses were performed using Stata 14.0 (StataCorp LP, College Station, TX, USA) and Review Manager 5.3 (The Cochrane Collaboration).

## RESULTS

### Study Selection and Characteristics

A total of 8,746 published studies were initially identified. After removing the duplicate articles and screening the abstracts, we

identified 40 studies, and 22 studies were excluded with reasons in the full-text assessments (the list of excluded studies with reasons is shown in **Supplementary Material 4**). Finally, we included 18 studies (17–34) in our meta-analyses (**Figure 1**).

**Table 2** shows the basic information and characteristics of the included studies. A total of 6,922 participants were included in the analysis, with the mortality rate in each study ranging from 6 to 47%. Three studies (22, 24, 28) were relatively small in sample size ( $<100$ ), and six studies (17, 19, 21, 26, 30, 34) enrolled more than 400 patients. Fifteen studies (17–19, 21, 22, 24–27, 29–34) investigated general ward patients, and three (20, 23, 28) investigated only the emergency department (ED) population. Fourteen studies (18–26, 28, 30, 32–34) used the NEWS2, while another four (17, 27, 29, 31) studies only used the original NEWS. Moreover, in six studies (18, 19, 23, 24, 28, 31), the investigators



**TABLE 3 |** PROBAST results.

| Study            | ROB          |            |         |          | Applicability |            |         | Overall |               |
|------------------|--------------|------------|---------|----------|---------------|------------|---------|---------|---------------|
|                  | Participants | Predictors | Outcome | Analysis | Participants  | Predictors | Outcome | ROB     | Applicability |
| Aliberti         | –            | +          | +       | ?        | +             | –          | +       | –       | –             |
| Baker            | +            | +          | –       | –        | +             | +          | +       | –       | +             |
| Bradley          | +            | +          | ?       | –        | +             | +          | ?       | –       | ?             |
| Covino           | +            | +          | +       | –        | +             | +          | +       | –       | +             |
| De Socio         | +            | +          | +       | –        | +             | +          | +       | –       | +             |
| Fan              | ?            | +          | +       | –        | +             | +          | +       | –       | +             |
| Gidari           | +            | +          | +       | –        | +             | +          | +       | –       | +             |
| Holten           | +            | +          | +       | ?        | +             | +          | +       | ?       | +             |
| Ihle-Hansen      | +            | +          | ?       | –        | +             | +          | +       | –       | +             |
| Jang             | +            | +          | ?       | ?        | +             | +          | ?       | ?       | ?             |
| Liu              | +            | +          | +       | +        | +             | +          | +       | +       | +             |
| Maguire          | +            | +          | +       | –        | +             | +          | +       | –       | +             |
| Martin-Rodriguez | +            | +          | +       | +        | +             | +          | +       | +       | +             |
| Mystad           | +            | +          | +       | –        | +             | +          | +       | –       | +             |
| Pokeerbux        | +            | +          | +       | ?        | +             | +          | +       | ?       | +             |
| Prower           | +            | +          | +       | ?        | +             | +          | +       | ?       | +             |
| Richardson       | +            | +          | +       | –        | +             | +          | +       | –       | +             |
| Su               | +            | +          | +       | ?        | +             | –          | +       | –       | –             |

PROBAST, Prediction model Risk Of Bias ASsessment Tool; ROB, risk of bias.

“+” indicates low ROB/low concern regarding applicability; “–” indicates high ROB/high concern regarding applicability; and “?” indicates unclear ROB/unclear concern regarding applicability.

employed a positive quick Sequential Organ Failure Assessment qSOFA ( $\geq 2$ ) to predict clinical deterioration.

## Quality Assessment

**Table 3** shows the summary results of the quality assessments by using PROBAST. Overall, 16 studies had a high or unclear risk of bias, mainly because of the inappropriate handling method of missing data (11 studies excluded participants with missing values from the analyses, and five studies did not explicitly state the handling method of the missing data). Four studies had a high or unclear concern regarding applicability since the threshold value of the NEWS or the time interval between the evaluation of predictor and the determination of the outcome were not consistent with other studies. The details of the quality assessment are reported in **Supplementary Material 5**.

In addition, the Deek's funnel plot indicated that there was a potential publication bias among the included studies (Deek's test:  $P < 0.10$ , **Supplementary Material 6**).

## Results of the Synthesis

Eleven studies used the NEWS2 to predict clinical deterioration for patients with COVID-19. **Figure 2** shows the forest plot of sensitivity and specificity for the NEWS2; the pooled sensitivity and specificity of the NEWS2 were 0.82 (95% CI: 0.75, 0.87) and 0.67 (95% CI: 0.58, 0.75). The pooled PLR and NLR of the NEWS2 were 2.50 (95% CI: 1.96, 3.20) and 0.27 (95% CI: 0.20, 0.37). In seven studies reporting the prognostic accuracy of the NEWS (**Figure 3**), the pooled sensitivity and specificity were 0.75 (95% CI: 0.63, 0.84) and 0.65 (95% CI: 0.52, 0.76). **Figure 4** shows

the HSROC curves for the NEWS2 (**Figure 4A**) and the NEWS (**Figure 4B**); the AUC was 0.82 (95% CI: 0.79, 0.85) and 0.76 (95% CI: 0.72, 0.79), respectively. Considerable heterogeneity existed across the studies.

In six studies, the researchers employed the qSOFA to predict clinical deterioration. The pooled sensitivity, specificity, and AUC of qSOFA were 0.26 (95% CI: 0.20, 0.33), 0.94 (95% CI: 0.86, 0.97), and 0.64 (95% CI: 0.60, 0.80), respectively (**Table 4**).

## Subgroup and Sensitivity Analyses

There was evidence that the prognostic performance of the NEWS2 varied across different subgroups (**Table 4**). The performance of the NEWS2 for predicting clinical deterioration within 72 h was better than that during hospitalization (AUC: 0.86 vs. 0.80). In addition, the NEWS2 had more moderate sensitivity and specificity and better discrimination in patients with a less severe disease (mortality rate,  $<10\%$ ).

In sensitivity analyses, we restricted the analyses to studies that evaluated the NEWS2 at hospital admission or studies that used the threshold of  $\geq 5$ ; the pooled sensitivity, specificity, PLR, NLR, and AUC were largely consistent with the primary results (**Table 4**).

## DISCUSSION

It is vital to determine as quickly as possible which patients with COVID-19 infection are at a high risk of deterioration, especially in poor healthcare resource settings, so as to make proper use of all available resources. To the best of our knowledge, this

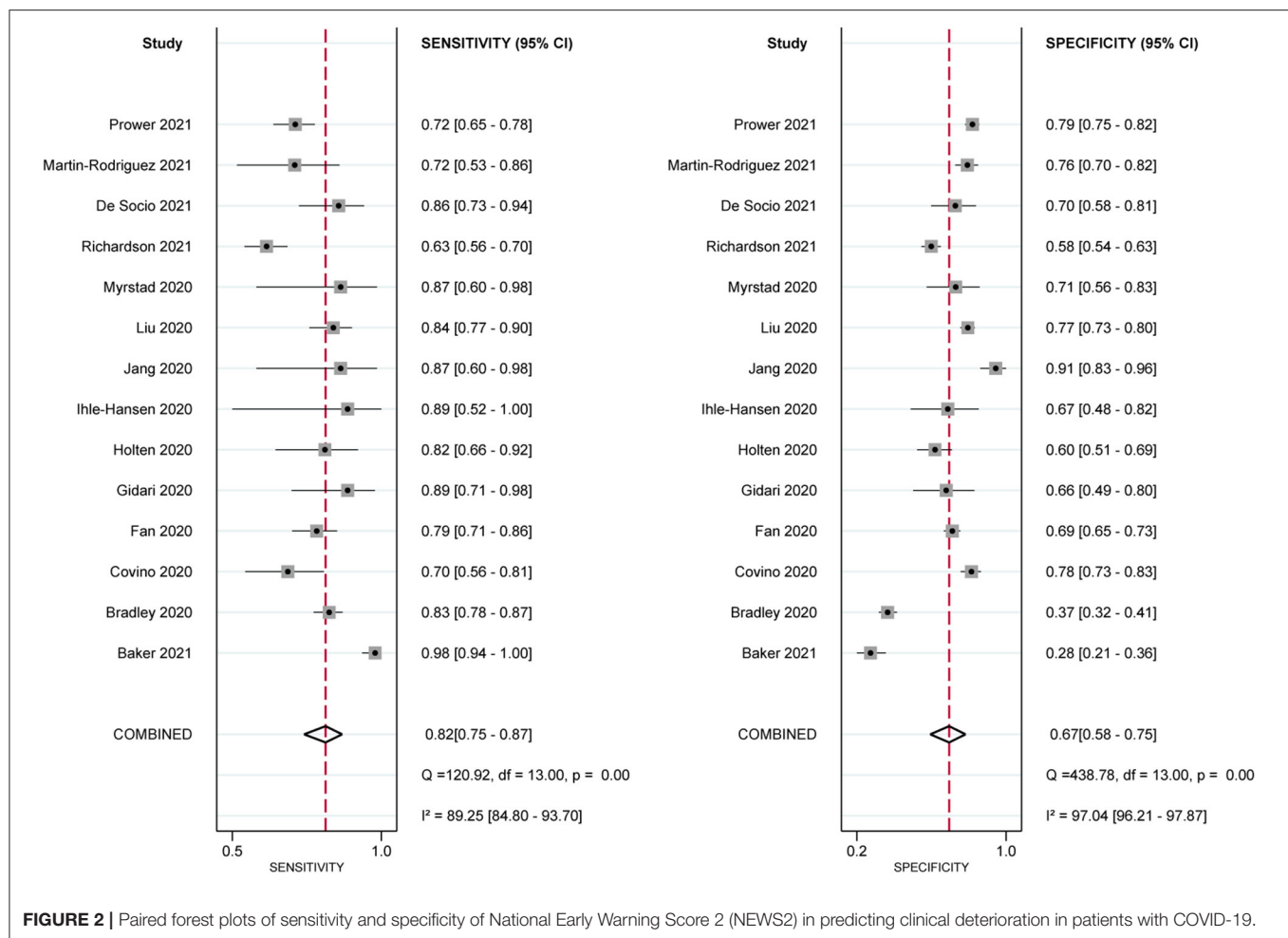


**FIGURE 2 |** Paired forest plots of sensitivity and specificity of National Early Warning Score 2 (NEWS2) in predicting clinical deterioration in patients with COVID-19.

is the first meta-analysis to evaluate the prognostic accuracy of the NEWS2 on predicting clinical deterioration for patients with COVID-19. In general, the NEWS2 has good discrimination in predicting the combined outcome of the need for intensive respiratory support, admission to the ICU, or in-hospital death. The high sensitivity ensured that the NEWS2 could be used as a sensitive method to initially assess COVID-19 patients at hospital admission. In addition, our results showed that using a threshold of 5 results in high sensitivity (0.83), moderate specificity (0.65), and good discrimination (0.82). It means that early interventions should be implemented for COVID-19 patients with more than five NEWS2 points as soon as possible because the clinical situation of those patients is expected to rapidly deteriorate.

The estimates of the pooled results showed a considerable heterogeneity between studies. Investigating the source of heterogeneity and the prognostic performance of the NEWS2 in different conditions are important objectives in our study. First of all, the NEWS2, an updated version of the NEWS, differs from that of the original NEWS by the inclusion of a new SpO<sub>2</sub> scoring scale for use in patients with hypercapnic respiratory failure. Oxygen supplementation has been proven to be an independent risk factor for novel coronavirus

pneumonia progressing to a critical condition (35). Liu et al. (26) demonstrated that the oxygen saturation level had a good prognostic performance for predicting death in patients with COVID-19 infection. Thus, benefitting from adding a specific scale for patients with hypercapnic respiratory failure, the NEWS2 showed better sensitivity and discrimination than the original NEWS. Second, the time window between score calculation and outcome measurement could also account for heterogeneity. Since predictive accuracy can be improved because the score is calculated close to the occurrence of the outcome, the NEWS2 has a high sensitivity in predicting clinical deterioration within 72 h for patients with COVID-19. The result supports the use of NEWS2 monitoring as a sensitive method to conduct an initial assessment of COVID-19 patients at hospital admission. Third, the severity of a disease might affect the prognostic accuracy as well. For patients with higher mortality rates ( $\geq 10\%$ ), the NEWS has a high sensitivity but a relatively low specificity, indicating a relatively high false-trigger rate. However, the sensitivity and specificity of the NEWS2 are more moderate in patients with lower mortality ( $< 10\%$ , mostly in the ED). The result supports using the NEWS2 as an adjunct to the process of triage and disposition of newly admitted patients

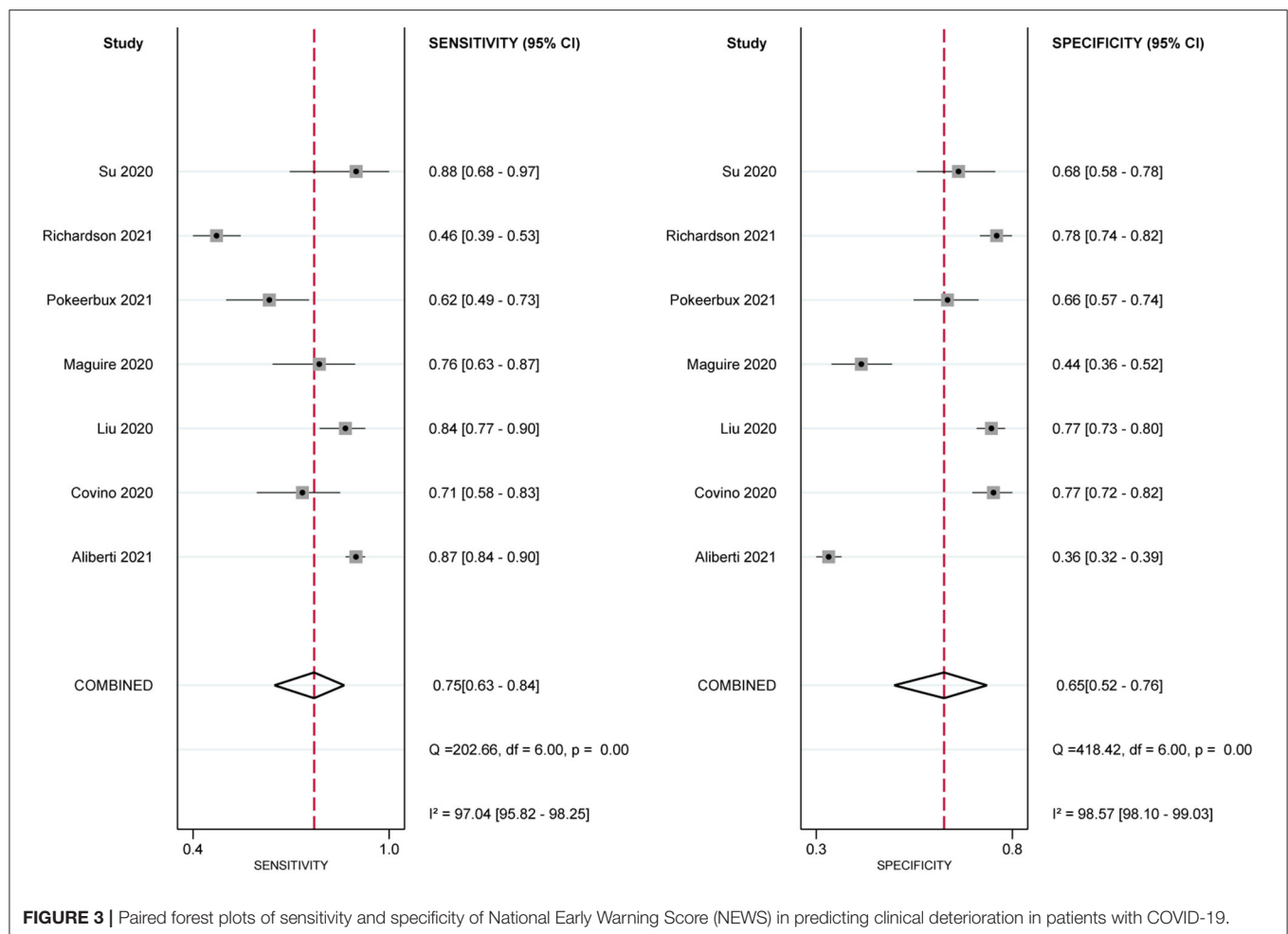


**FIGURE 3 |** Paired forest plots of sensitivity and specificity of National Early Warning Score (NEWS) in predicting clinical deterioration in patients with COVID-19.

with COVID-19, especially in overcrowded emergency rooms (20). Moreover, study location might be a source of heterogeneity because differences in the healthcare systems of each country could affect clinical outcomes. Specifically, early warning score systems have been introduced and linked to effective clinical responses in many UK hospitals (36). It might introduce the treatment paradox, where some deteriorating patients were likely to receive rapid medical interventions after triggering the alert. Hence, the actual deteriorating rate tends to be lower than predicted and biases our estimate of accuracy. In addition, the primary outcome consists of the need for intensive respiratory support, admission to the ICU, and in-hospital mortality. The indications for the use of intensive respiratory support and the standards of ICU admission were varied among the included studies, which might affect the occurrence of positive results and become a source of heterogeneity.

The NEWS2 is a summary score derived from six physiological parameters; some parameters relate to the degree of respiratory failure, such as oxygen saturation and oxygen supplementation. Since COVID-19 is often characterized by solitary respiratory failure (37, 38), an advantage of NEWS2 compared to other scoring systems is that both hypoxemia and

supportive oxygen treatment are included as scoring parameters. It could explain its relatively better performance compared to other scoring systems. In our study, compared with qSOFA, the NEWS had better discrimination and moderate sensitivity and specificity.

Although our research suggests that the NEWS2 has good prognostic performance, it is worth highlighting some potential pitfalls in clinical practice. For instance, in patients with COVID-19, the oxygen requirement might increase rapidly if their respiratory function continued to worsen, but the increased oxygen requirement does not directly cause an increase in the NEWS2 since oxygen supplementation is only a binary variable (yes or no) in the NEWS2 scoring system. Therefore, clinically, we suggest that any increase in oxygen requirement for patients with COVID-19 should arouse the attention of clinicians. Furthermore, given that older patients with COVID-19 have a higher proportion of severe cases and fatality ratio (39, 40), the pandemic has prompted the need to pay particular attention to the health of older persons. Evidence also showed that increased age was independently associated with poor prognosis in COVID-19 patients (8). A Chinese group put forward a modified version of the NEWS2 with the addition of

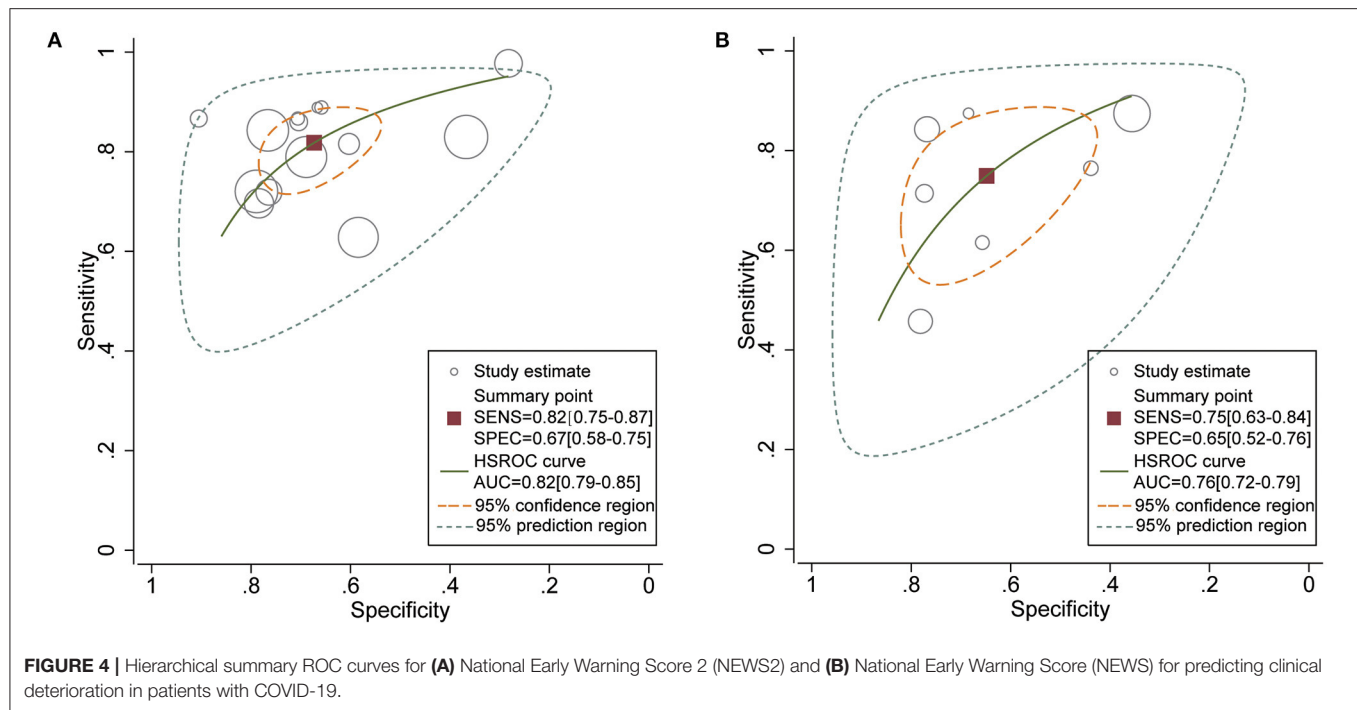


**TABLE 4 |** Results of the meta-analysis.

| Results                            | N  | Sensitivity (95% CI) | Specificity (95% CI) | PLR (95% CI)      | NLR (95% CI)      | AUC (95% CI)      |
|------------------------------------|----|----------------------|----------------------|-------------------|-------------------|-------------------|
| NEWS2                              | 14 | 0.82 (0.75, 0.87)    | 0.67 (0.58, 0.75)    | 2.50 (1.96, 3.20) | 0.27 (0.20, 0.37) | 0.82 (0.79, 0.85) |
| NEWS                               | 7  | 0.75 (0.63, 0.84)    | 0.65 (0.52, 0.76)    | 2.13 (1.58, 2.87) | 0.39 (0.27, 0.56) | 0.76 (0.72, 0.79) |
| qSOFA                              | 6  | 0.26 (0.20, 0.33)    | 0.94 (0.86, 0.97)    | 4.13 (1.88, 9.08) | 0.79 (0.73, 0.86) | 0.64 (0.78, 0.84) |
| <b>SUBGROUP ANALYSIS</b>           |    |                      |                      |                   |                   |                   |
| <b>Time of outcome measurement</b> |    |                      |                      |                   |                   |                   |
| Within 72 h                        | 5  | 0.88 (0.74, 0.95)    | 0.56 (0.36, 0.74)    | 2.01 (1.39, 2.91) | 0.21 (0.12, 0.37) | 0.82 (0.79, 0.85) |
| In-hospital                        | 12 | 0.79 (0.74, 0.84)    | 0.70 (0.61, 0.77)    | 2.62 (2.01, 3.42) | 0.30 (0.23, 0.39) | 0.82 (0.79, 0.85) |
| <b>Disease severity</b>            |    |                      |                      |                   |                   |                   |
| Light (mortality rate <10%)        | 4  | 0.79 (0.67, 0.87)    | 0.76 (0.62, 0.86)    | 3.27 (2.01, 5.32) | 0.28 (0.18, 0.45) | 0.83 (0.79, 0.86) |
| Severe (mortality rate ≥10%)       | 9  | 0.82 (0.72, 0.89)    | 0.63 (0.51, 0.47)    | 2.22 (1.69, 2.92) | 0.29 (0.19, 0.43) | 0.80 (0.76, 0.83) |
| <b>Sensitivity analysis</b>        |    |                      |                      |                   |                   |                   |
| NEWS2 ≥ 5                          | 12 | 0.82 (0.74, 0.88)    | 0.66 (0.55, 0.76)    | 2.44 (1.84, 3.22) | 0.27 (0.19, 0.38) | 0.82 (0.79, 0.85) |
| Calculating score at admission     | 12 | 0.78 (0.72, 0.83)    | 0.70 (0.61, 0.77)    | 2.56 (1.98, 3.32) | 0.32 (0.25, 0.41) | 0.81 (0.77, 0.84) |

NEWS, National Early Warning Score; NEWS2, National Early Warning Score 2; qSOFA, quick Sequential Organ Failure Assessment; N, number of studies; CI, confidence interval; PLR, positive likelihood ratio; NLR, negative likelihood ratio; AUC, area under the curve.

age >65 years as an independent component, termed NEWS-C (41). An external validation study found that the NEWS-C has the best predictive accuracy among common scoring systems for predicting the deterioration of respiratory function in patients with COVID-19 (31). Therefore, it is possible that the prognostic accuracy of the NEWS2 could be improved by modifying the score.

Notably, the NEWS2 is not an alternative to the clinical judgment by experienced clinicians; it should be utilized to help in clinical decision-making by providing objective data. According to the guidelines of the Royal College of Physicians (10), patients with the NEWS2 <5 should also receive strict

monitoring because a considerable proportion may still rapidly progress to severe respiratory failure. Finally, in addition to the initial assessment of illness severity, the NEWS was originally designed as a track-and-trigger tool to identify acute clinical deterioration and guide the clinical response for patients. By recording the score on a regular basis, the trends in the clinical response of a patient can be tracked, providing an early warning of clinical deterioration and the need for more intensive treatment (6). Baker et al. found an increasing trend of the NEWS2 beginning many hours prior to the occurrence of a serious clinical deterioration event (18). Therefore, the score should be calculated not only at the admission of patients but also



throughout their hospital stay to evaluate a possible deterioration in their clinical situation.

## Strength and Limitations

The strengths of this meta-analysis include, first, a standard protocol and comprehensive search strategies across multiple databases. Thus, we believe that we did not miss any relevant studies. Second, a statistically robust hierarchical model was employed to estimate pooled results and to construct HSROC plots. This approach allows for both between-study variability in sensitivity and specificity and flexibility in the estimation of summary statistics (42). Our findings can contribute to a better understanding of the NEWS2 in patients with COVID-19, which could be useful for implementing the NEWS2 in clinical practice.

Meanwhile, there are some important limitations in the meta-analysis. First, previous research suggest that heterogeneities are widely observed in the systematic reviews of diagnostic test accuracy (43, 44). We also identified significant heterogeneity among the included studies, which might affect the credibility of the pooled estimates. Second, most of the included studies were single-center studies with a relatively small sample size, which may limit the generalizability and certainty of our analysis. Furthermore, the NEWS2 was not designed as a single-time-point predictive tool. Since existing research only show the prognostic accuracy of the NEWS2 in predicting clinical deterioration at a single time point (mostly at the time of admission), we could not evaluate the NEWS2 in any other context. On the other hand, the timings of the NEWS2 measurement were not entirely consistent in the included studies. We assume that the accuracy might be improved if multiple time points were considered, and the changed trend of NEWS2 with time has a potential application value of predicting mortality, just like the delta SOFA (45).

## CONCLUSION

We perform the first meta-analysis to examine the prognostic accuracy of the NEWS2 on predicting clinical deterioration for patients with COVID-19. The NEWS2 has moderate sensitivity and specificity in predicting the deterioration of patients with COVID-19, and the threshold of 5 is an optimal trigger threshold for activating a rapid response. Our results support

the recommendations for use of NEWS2 monitoring as a sensitive method to initially assess COVID-19 patients at hospital admission, although it has a relatively high false-trigger rate. However, the discriminative power of the NEWS2 is far from excellent. Further improvements of the NEWS2 by modifying the score or combining more important predictors is still necessary. In addition, the value of a single assessment is limited. Further research should focus on the utility of longitudinal NEWS2 monitoring to identify deteriorating patients and guide clinical response, not solely for initial assessment at hospital admission.

## DATA AVAILABILITY STATEMENT

The original contributions presented in the study are included in the article/**Supplementary Material**, further inquiries can be directed to the corresponding author/s.

## AUTHOR CONTRIBUTIONS

KZ conceived the idea, performed the analysis, and drafted the manuscript. XZ and WD contributed to the study design, data acquisition, and interpretation. NX, BT, and TH helped in the statistical analysis. ZZ and WC critically revised the manuscript for important intellectual content. GZ and HH helped to frame the idea of the study and provided technical support. All authors have read and approved the submitted version.

## FUNDING

This work was supported in part by grants from the National Natural Science Foundation of China (No. 81971871, GZ) and the Medical and Health Research Program of Zhejiang Province (No. 2021KY174, GZ). The sponsors of this study had no role in study design, data collection, data analysis, data interpretation, or writing of the report.

## SUPPLEMENTARY MATERIAL

The Supplementary Material for this article can be found online at: <https://www.frontiersin.org/articles/10.3389/fmed.2021.699880/full#supplementary-material>

## REFERENCES

- Wang C, Horby PW, Hayden FG, Gao GF. A novel coronavirus outbreak of global health concern. *Lancet*. (2020) 395:470–3. doi: 10.1016/S0140-6736(20)30185-9
- WHO Coronavirus (COVID-19) Dashboard. Available online at: <https://covid19.who.int/> (accessed March 26, 2021).
- Clark A, Jit M, Warren-Gash C, Guthrie B, Wang HHX, Mercer SW, Sanderson C, et al. Global, regional, and national estimates of the population at increased risk of severe COVID-19 due to underlying health conditions in 2020: a modelling study. *Lancet Glob Health*. (2020) 8:e1003–17. doi: 10.1016/S2214-109X(20)30264-3
- Wu Z, McGoogan JM. Characteristics of and important lessons from the coronavirus disease 2019 (COVID-19) outbreak in China: summary of a report of 72,314 cases from the Chinese Center for Disease Control and Prevention. *JAMA*. (2020) 323:1239–42. doi: 10.1001/jama.2020.2648
- Farrell TW, Ferrante LE, Brown T, Francis L, Widera E, Rhodes R, et al. AGS position statement: resource allocation strategies and age-related considerations in the COVID-19 era and beyond. *J Am Geriatr Soc*. (2020) 68:1136–42. doi: 10.1111/jgs.16537
- National Early Warning Score (NEWS). *Standardising the Assessment of Acute-Illness Severity in the NHS*. Report of a working party. London: RCP: Royal College of Physicians (2012).
- National Early Warning Score (NEWS) 2. *Standardising the Assessment of Acute-Illness Severity in the NHS*. Updated report of a working party. London: Royal College of Physicians: RCP (2017).

8. Zheng Z, Peng F, Xu B, Zhao J, Liu H, Peng J, et al. Risk factors of critical & mortal COVID-19 cases: a systematic literature review and meta-analysis. *J Infect.* (2020) 81:e16–25. doi: 10.1016/j.jinf.2020.04.021
9. Zhou F, Yu T, Du R, Fan G, Liu Y, Liu Z, et al. Clinical course and risk factors for mortality of adult inpatients with COVID-19 in Wuhan, China: a retrospective cohort study. *Lancet.* (2020) 395:1054–62. doi: 10.1016/S0140-6736(20)30566-3
10. NEWS2 and Deterioration in COVID-19. Available online at: <https://www.rcplondon.ac.uk/news/news2-and-deterioration-covid-19> (accessed March 26, 2021).
11. Swiss Society Of Intensive Care M. Recommendations for the admission of patients with COVID-19 to intensive care and intermediate care units (ICUs and IMCUs). *Swiss Med Wkly.* (2020) 150:w20227. doi: 10.4414/smw.2020.20227
12. Liberati A, Altman DG, Tetzlaff J, Mulrow C, Gøtzsche PC, Ioannidis JP, et al. The PRISMA statement for reporting systematic reviews and meta-analyses of studies that evaluate healthcare interventions: explanation and elaboration. *BMJ.* (2009) 339:b2700. doi: 10.1136/bmj.b2700
13. Wolff RF, Moons KGM, Riley RD, Whiting PF, Westwood M, Collins GS, et al. PROBAST: a tool to assess the risk of bias and applicability of prediction model studies. *Ann Intern Med.* (2019) 170:51–8. doi: 10.7326/M18-1376
14. Reitsma JB, Glas AS, Rutjes AW, Scholten RJ, Bossuyt PM, Zwinderman AH. Bivariate analysis of sensitivity and specificity produces informative summary measures in diagnostic reviews. *J Clin Epidemiol.* (2005) 58:982–90. doi: 10.1016/j.jclinepi.2005.02.022
15. Higgins JP, Thompson SG. Quantifying heterogeneity in a meta-analysis. *Stat Med.* (2002) 21:1539–58. doi: 10.1002/sim.1186
16. Deeks JJ, Macaskill P, Irwig L. The performance of tests of publication bias and other sample size effects in systematic reviews of diagnostic test accuracy was assessed. *J Clin Epidemiol.* (2005) 58:882–93. doi: 10.1016/j.jclinepi.2005.01.016
17. Aliberti MJR, Covinsky KE, Garcez FB, Smith AK, Curiati PK, Lee SJ, et al. A fuller picture of COVID-19 prognosis: the added value of vulnerability measures to predict mortality in hospitalised older adults. *Age Ageing.* (2021) 50:32–9. doi: 10.1093/ageing/afaa240
18. Baker KF, Hanrath AT, van der Loeff IS, Kay LJ, Back J, Duncan CJ. National early warning score 2 (NEWS2) to identify inpatient COVID-19 deterioration: a retrospective analysis. *Clin Med (Lond).* (2021) 21:84–9. doi: 10.7861/clinmed.2020-0688
19. Bradley P, Frost F, Tharmaratnam K, Wootton DG. Utility of established prognostic scores in COVID-19 hospital admissions: multicentre prospective evaluation of CURB-65, NEWS2 and qSOFA. *BMJ Open Respir Res.* (2020) 7:e000729. doi: 10.1136/bmjresp-2020-000729
20. Covino M, Sandroni C, Santoro M, Sabia L, Simeoni B, Bocci MG, et al. Predicting intensive care unit admission and death for COVID-19 patients in the emergency department using early warning scores. *Resuscitation.* (2020) 156:84–91. doi: 10.1016/j.resuscitation.2020.08.124
21. Fan G, Tu C, Zhou F, Liu Z, Wang Y, Song B, et al. Comparison of severity scores for COVID-19 patients with pneumonia: a retrospective study. *Eur Respir J.* (2020) 56:2002113. doi: 10.1183/13993003.02113-2020
22. Gidari A, De Socio GV, Sabbatini S, Francisci D. Predictive value of national early warning score 2 (NEWS2) for intensive care unit admission in patients with SARS-CoV-2 infection. *Infect Dis (Lond).* (2020) 52:698–704. doi: 10.1080/23744235.2020.1784457
23. Holten AR, Nore KG, Tveiten C, Olasveengen TM, Tonby K. Predicting severe COVID-19 in the emergency department. *Resusc Plus.* (2020) 4:100042. doi: 10.1016/j.resplu.2020.100042
24. Ihle-Hansen H, Berge T, Tveita A, Rønning EJ, Ernø PE, Andersen EL, et al. COVID-19: symptoms, course of illness and use of clinical scoring systems for the first 42 patients admitted to a Norwegian local hospital. *Tidsskr Nor Lægeforen.* (2020) 140. doi: 10.4045/tidsskr.20.0301
25. Jang JG, Hur J, Hong KS, Lee W, Ahn JH. Prognostic accuracy of the SIRS, qSOFA, and NEWS for early detection of clinical deterioration in SARS-CoV-2 infected patients. *J Korean Med Sci.* (2020) 35:e234. doi: 10.3346/jkms.2020.35.e234
26. Liu FY, Sun XL, Zhang Y, Ge L, Wang J, Liang X, et al. Evaluation of the risk prediction tools for patients with coronavirus disease 2019 in Wuhan, China: a single-centered, retrospective, observational study. *Crit Care Med.* (2020) 48:e1004–11. doi: 10.1097/CCM.0000000000004549
27. Maguire D, Woods M, Richards C, Dolan R, Veitch JW, Sim WMJ, et al. Prognostic factors in patients admitted to an urban teaching hospital with COVID-19 infection. *J Transl Med.* (2020) 18:354. doi: 10.1186/s12967-020-02524-4
28. Myrstad M, Ihle-Hansen H, Tveita AA, Andersen EL, Nygård S, Tveit A, et al. National early warning score 2 (NEWS2) on admission predicts severe disease and in-hospital mortality from Covid-19 - a prospective cohort study. *Scand J Trauma Resusc Emerg Med.* (2020) 28:66. doi: 10.1186/s13049-020-00764-3
29. Pockerbux MR, Yelnik CM, Faure E, Drumez E, Bruandet A, Labreuche J, et al. National early warning score to predict intensive care unit transfer and mortality in COVID-19 in a French cohort. *Int J Clin Pract.* (2021) 75:e14121. doi: 10.1111/ijcp.14121
30. Richardson D, Faisal M, Fiori M, Beatson K, Mohammed M. Use of the first National Early Warning Score recorded within 24 hours of admission to estimate the risk of in-hospital mortality in unplanned COVID-19 patients: a retrospective cohort study. *BMJ Open.* (2021) 11:e043721. doi: 10.1136/bmjopen-2020-043721
31. Su Y, Ju MJ, Xie RC, Yu SJ, Zheng JL, Ma GG, et al. Prognostic accuracy of early warning scores for clinical deterioration in patients with COVID-19. *Front Med (Lausanne).* (2021) 7:624255. doi: 10.3389/fmed.2020.624255
32. De Socio GV, Gidari A, Sicari F, Palumbo M, Francisci D. National early warning score 2 (NEWS2) better predicts critical coronavirus disease 2019 (COVID-19) illness than COVID-GRAM, a multi-centre study. *Infection.* (2021) 1–6. doi: 10.1007/s15010-021-01620-x
33. Martín-Rodríguez F, Martín-Conty JL, Sanz-García A, Rodríguez VC, Rabbione GO, Cebrian Ruiz I, et al. Early warning scores in patients with suspected COVID-19 infection in emergency departments. *J Pers Med.* (2021) 11:170. doi: 10.3390/jpm11030170
34. Prower E, Grant D, Bisquera A, Breen CP, Camporota L, Gavrilovski M, et al. The ROX index has greater predictive validity than NEWS2 for deterioration in Covid-19. *E Clin Med.* (2021) 35:100828. doi: 10.1016/j.eclinm.2021.100828
35. Sun Q, Qiu H, Huang M, Yang Y. Lower mortality of COVID-19 by early recognition and intervention: experience from Jiangsu Province. *Ann Intensive Care.* (2020) 10:33. doi: 10.1186/s13613-020-00650-2
36. Scott LJ, Redmond NM, Garrett J, Whiting P, Northstone K, Pullyblank A. Distributions of the national early warning score (NEWS) across a healthcare system following a large-scale roll-out. *Emerg Med J.* (2019) 36:287–92. doi: 10.1136/emered-2018-208140
37. Richardson S, Hirsch JS, Narasimhan M, Crawford JM, McGinn T, Davidson KW, et al. Presenting characteristics, comorbidities, and outcomes among 5700 patients hospitalized with COVID-19 in the New York City Area. *JAMA.* (2020) 323:2052–9. doi: 10.1001/jama.2020.6775
38. Wu C, Chen X, Cai Y, Xia J, Zhou X, Xu S, et al. Risk factors associated with acute respiratory distress syndrome and death in patients with coronavirus disease 2019 pneumonia in Wuhan, China. *JAMA Intern Med.* (2020) 180:934–43. doi: 10.1001/jamainternmed.2020.0994
39. Guan WJ, Ni ZY, Hu Y, Liang WH, Ou CQ, He JX, et al. Clinical characteristics of coronavirus disease 2019 in China. *N Engl J Med.* (2020) 382:1708–20. doi: 10.1056/NEJMoa2002032
40. Grasselli G, Zangrillo A, Zanella A, Antonelli M, Cabrini L, Castelli A, et al. Baseline characteristics and outcomes of 1591 patients infected with SARS-CoV-2 admitted to ICUs of the Lombardy Region, Italy. *JAMA.* (2020) 323:1574–81. doi: 10.1001/jama.2020.5394
41. Liao X, Wang B, Kang Y. Novel coronavirus infection during the 2019-2020 epidemic: preparing intensive care units-the experience in Sichuan Province, China. *Intensive Care Med.* (2020) 46:357–60. doi: 10.1007/s00134-020-05954-2
42. Rutter CM, Gatsonis CA. A hierarchical regression approach to meta-analysis of diagnostic test accuracy evaluations. *Stat Med.* (2001) 20:2865–84. doi: 10.1002/sim.942
43. Dinnes J, Deeks J, Kirby J, Roderick P. A methodological review of how heterogeneity has been examined in systematic reviews of diagnostic

- test accuracy. *Health Technol Assess.* (2005) 9:1–113, iii. doi: 10.3310/hta9120
44. Song JU, Sin CK, Park HK, Shim SR, Lee J. Performance of the quick sequential (sepsis-related) organ failure assessment score as a prognostic tool in infected patients outside the intensive care unit: a systematic review and meta-analysis. *Critical Care (London, England)*. (2018) 22:28. doi: 10.1186/s13054-018-1952-x
45. de Grooth HJ, Geenen IL, Girbes AR, Vincent JL, Parienti JJ, Oudemans-van et al. SOFA and mortality endpoints in randomized controlled trials: a systematic review and meta-regression analysis. *Crit Care (London, England)*. (2017) 21:38. doi: 10.1186/s13054-017-1609-1

**Conflict of Interest:** The authors declare that the research was conducted in the absence of any commercial or financial relationships that could be construed as a potential conflict of interest.

Copyright © 2021 Zhang, Zhang, Ding, Xuan, Tian, Huang, Zhang, Cui, Huang and Zhang. This is an open-access article distributed under the terms of the Creative Commons Attribution License (CC BY). The use, distribution or reproduction in other forums is permitted, provided the original author(s) and the copyright owner(s) are credited and that the original publication in this journal is cited, in accordance with accepted academic practice. No use, distribution or reproduction is permitted which does not comply with these terms.



# Probable Causes and Risk Factors for Positive SARS-CoV-2 Testing in Recovered Patients: Evidence From Guangzhou, China

## OPEN ACCESS

### Edited by:

Seyed Alireza Nadji,  
Shahid Beheshti University of Medical  
Sciences, Iran

### Reviewed by:

Donato Amodio,  
IRCCS, Italy  
Hao Chen,  
Guangzhou Medical University, China  
Reza Lashgari,  
Shahid Beheshti University, Iran

### \*Correspondence:

Hui Wang  
gzcdc\_wangh@gz.gov.cn  
Chen Mao  
maochen9@smu.edu.cn

†These authors have contributed  
equally to this work

### Specialty section:

This article was submitted to  
Infectious Diseases - Surveillance,  
Prevention and Treatment,  
a section of the journal  
Frontiers in Medicine

Received: 22 March 2021

Accepted: 15 June 2021

Published: 12 July 2021

### Citation:

Luo L, Liu D, Zhang Z, Li Z, Xie C,  
Wang Z, Chen Z, Zhang P, Zhang X,  
Zhang Y, Zhong W, Zhang W, Yang P,  
Huang Q, Song W, Wang H and  
Mao C (2021) Probable Causes and  
Risk Factors for Positive SARS-CoV-2  
Testing in Recovered Patients:  
Evidence From Guangzhou, China.  
Front. Med. 8:684101.  
doi: 10.3389/fmed.2021.684101

Lei Luo <sup>1†</sup>, Dan Liu <sup>2†</sup>, Zhoubin Zhang <sup>1</sup>, Zhihao Li <sup>2</sup>, Chaojun Xie <sup>1</sup>, Zhenghe Wang <sup>2</sup>,  
Zongqiu Chen <sup>1</sup>, Peidong Zhang <sup>2</sup>, Xiru Zhang <sup>2</sup>, Yujie Zhang <sup>2</sup>, Wenfang Zhong <sup>2</sup>,  
Wenting Zhang <sup>2</sup>, Pei Yang <sup>2</sup>, Qingmei Huang <sup>2</sup>, Weiqi Song <sup>2</sup>, Hui Wang <sup>1\*</sup> and Chen Mao <sup>2\*</sup>

<sup>1</sup> Guangzhou Center for Disease Control and Prevention, Guangzhou, China, <sup>2</sup> Department of Epidemiology, School of Public Health, Southern Medical University, Guangzhou, China

Some patients retested positive for SARS-CoV-2 following negative testing results and discharge. However, the potential risk factors associated with redetectable positive testing results in a large sample of patients who recovered from COVID-19 have not been well-estimated. A total of 745 discharged patients were enrolled between January 30, 2020, and September 9, 2020, in Guangzhou, China. Data on the clinical characteristics, comorbidities, drug therapy, RT-PCR testing, and contact modes to close contacts were collected. Patients who tested positive for SARS-CoV-2 after discharge were confirmed by guidelines issued by China. The repositive rate in different settings was calculated. Among 745 discharged patients, 157 (21.1%; 95% CI, 18.2–24.0%) tested repositive and the repositive rate was 16.8% (95% CI, 14.1–24.0%) for nasopharyngeal swabs and 9.7% (95% CI, 7.0–12.5%) for anal swabs. Among them, 55 (35.0%) were asymptomatic, 15 (9.6%) had mild symptoms, 83 (52.9%) had moderate symptoms, and 4 (2.6%) had severe symptoms at the first admission. The days from discharge to repositivity was 8.0 (IQR, 8.0–14.0). Most repositive patients were without clinical symptoms, and lymphocyte cell counts were higher than before being discharged. The likelihood of repositive testing for SARS-CoV-2 RNA was significantly higher among patients who were of younger age (OR, 3.88; 95% CI, 1.74–8.66, 0–17 years old), had asymptomatic severity (OR, 4.36; 95% CI, 1.47–12.95), and did not have clinical symptoms (OR, 1.89; 95% CI, 1.32–2.70, without fever). No other positive patients emerged within the families or close contacts of repositive patients. Our findings support prolonged but intermittent viral shedding as the probable cause for this phenomenon; we need to familiarize with the possibility that the virus will remain endemic.

**Keywords:** risk factors, COVID-19, discharged patients, cohort study, repositive



## INTRODUCTION

Since the outbreak in December 2019, coronavirus disease 2019 (COVID-19), caused by severe acute respiratory syndrome coronavirus 2 (SARS-CoV-2), has given rise to a worldwide pandemic (1). As of April 4, 2021, 145 million COVID-19 patients and 3.1 million deaths have been reported globally (2). At the same time, tens of millions of patients with COVID-19 have recovered and been discharged from the hospital. However, some patients affected by COVID-19 who fully met the criteria for discontinuation of quarantine and subsequently report positive real-time reverse transcriptase-polymerase chain reaction (RT-PCR) again (hereafter referred as “repositive”) at a follow-up visit (3–8), which increases the complexity of disease control and has attracted widespread concern.

Several studies, mainly case reports, have been performed to investigate the clinical characteristics and virologic course of discharged patients (3–8). However, to date, many questions about repositive patients have not been answered; these questions include the overall prognosis of patients with COVID-19 after meeting the criteria for hospital discharge, the potential risk factors associated with redetectable positive test results, and whether the persistent presence of virus fragments means that the discharged patient is still contagious. As the number of discharged patients increases, effective management becomes critical to successfully reducing the spread of SARS-CoV-2. To promote the comprehensive rehabilitation of COVID-19 patients, China has implemented a series of measures for discharged COVID-19 patients, including management of quarantine, regular follow-up, health monitoring, and rehabilitation therapy, which provide empirical information and evidence support for the management of patients with COVID-19 (9).

Up till September 9, 2020, Guangzhou, China, recorded a total of 745 COVID-19 patients, of whom all have been discharged. We conducted a retrospective cohort study of all discharged patients to examine those who are repositive, describe their clinical and epidemiological outcomes, and analyze the predictors of repositive status.

## MATERIALS AND METHODS

### Patients and Study Design

Between January 30, 2020, and September 9, 2020, a total of 745 patients who officially recovered from COVID-19 were discharged from the hospital and enrolled in this study in Guangzhou, China. Only COVID-19 patients who met all the following criteria of China (10) could be discharged from the hospital: (1) body temperature returns to normal for more than three consecutive days; (2) significant improvement in any symptoms, such as fever, dry cough, and expectoration; (3) substantial improvement in acute exudative lesions on chest computed tomography (CT) images; and (4) negative RT-PCR testing for SARS-CoV-2 RNA of nasopharyngeal swabs, anal swabs, and other respiratory specimens for two consecutive times (at least 24 h apart).

All discharged patients were required to undergo 14 days of quarantine in designated healthcare facilities and 28 days of community follow-up to observe their clinical symptoms and RT-PCR testing results. The repositive patients were re-admitted to the hospital for therapy and their close contacts were traced. The remaining discharged patients who continued to have negative RT-PCR testing results were closely followed up in their communities. **Figure 1** shows the flowchart of the management of discharged patients.

These data were collected as part of a continuing public health response required by the National Health Commission of China and hence was determined not to be human subjects research and therefore was considered exempt from institutional review board approval after consultation with GZCDC. Patients were informed about the surveillance before providing written consent, and data were collected and anonymized for analysis. All analyses of personally identifiable data took place onsite at the GZCDC.

### Definition of Repositive Patients

Based on open reading frame 1ab (ORF 1ab) and nucleocapsid (N) protein genes in the SARS-CoV-2 genome, RT-PCR was performed to assess the results (11, 12). If the cycle threshold (Ct) value of RT-PCR is  $<37$ , the sample is positive; if the Ct value ranges between 37 and 40, and if the amplification curve has an obvious peak, then the sample is considered positive. Otherwise, the sample is considered as negative.

The following three conditions are considered positive. First, the two targets, ORF 1ab and N protein, are both positive. Second, in case of the result showing positivity for one target, samples shall be recollected for another test. If it is still positive for a single target, the result should be considered positive. Third, if two types of specimens show one single target as positive at the same time or if one target is positive in two samples of the same type, then the result should be considered positive.

### Management for Discharged Patients

After discharge from the hospital, patients were put under centralized quarantine and health monitoring for 14 days at designated healthcare facilities. During the quarantine period, the discharged patients lived in a well-ventilated single room, dined separately, and practiced hand hygiene. For children 14 years and younger, household management with medical observation can be used under the guidance of community health workers and family members can be with the child using personal protection and maintaining interpersonal distance. People with underlying medical conditions and elderly individuals cannot be with children who are discharged patients. Nasopharyngeal and anal specimens collected on the 1st, 7th, and 14th days or more frequently were sent to the laboratory for RT-PCR testing. The discharged patients were recorded for body temperature and respiratory or digestive tract symptoms (such as fever, dry cough, and diarrhea) every day. If the RT-PCR testing result was consecutively negative and no symptoms or CT images progressed (one or more times without fixed scanning time), these patients could return to normal life and be regularly followed up by the community. If they had a positive RT-PCR

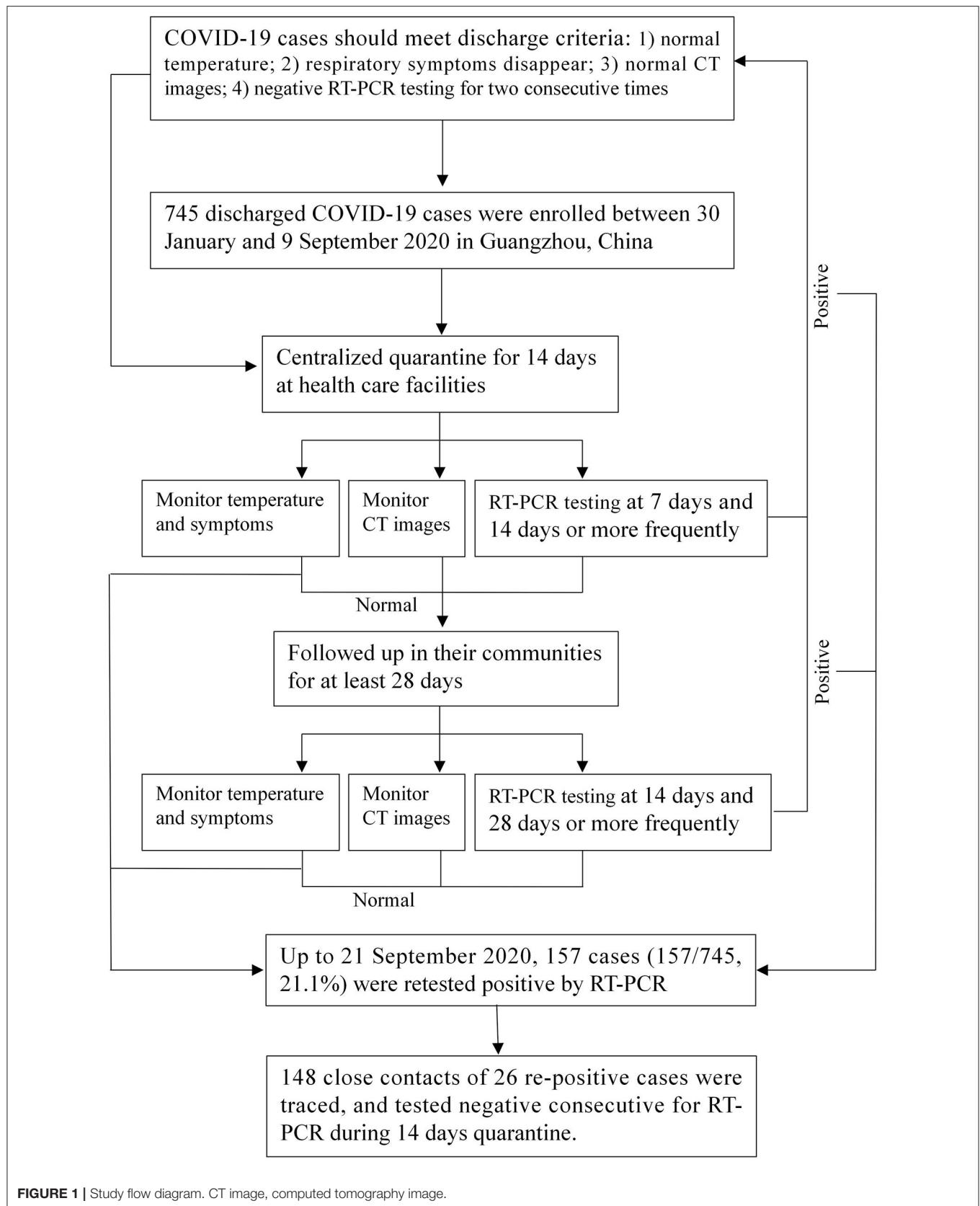


**FIGURE 1** | Study flow diagram. CT image, computed tomography image.

testing result, diagnosis and treatment should be conducted strictly in accordance with Chinese clinical guidance for COVID-19 (10).

After discharged patients completed 14 days of quarantine, it is recommended for these patients to be followed up in their communities for at least 28 days. GZCDC follows the health management plan for discharged patients released by the National Health Commission of China (9), and RT-PCR testing

was performed on the 14th and 28th days after quarantine or more frequently.

## Close Contact Tracing of Repositive Patients

If the discharged patient was tested positive again, close contacts should be traced and followed up (13). The quarantine period should last until 14 days after the last contact without effective

**TABLE 1** | Characteristic of 157 repesitive and 588 non-repositive patients with COVID-19.

| Characteristic                                | All patients (n = 745) | Non-repositive (n = 588) | Repositive (n = 157) | P-value |
|---|------------------------|--------------------------|----------------------|---------|
| Total repesitive rate, % (95% CI)             | –                      | –                        | 21.1 (18.2–24.0)     | –       |
| <b>Repositive rate by type of specimen</b>    |                        |                          |                      |         |
| From nasopharyngeal swab (n = 119)            | –                      | –                        | 16.8 (14.1–24.0)     | –       |
| From anal swab (n = 43)                       | –                      | –                        | 9.7 (7.0–12.5)       | –       |
| <b>Repositive rate by days from discharge</b> |                        |                          |                      |         |
| 1 day (n = 1)                                 | –                      | –                        | 0.1 (0.0–0.4)        | –       |
| 2–7 days (n = 37)                             | –                      | –                        | 5.0 (3.4–6.5)        | –       |
| 8–14 days (n = 84)                            | –                      | –                        | 11.3 (9.0–13.6)      | –       |
| > 14 days (n = 35)                            | –                      | –                        | 4.7 (3.2–6.2)        | –       |
| Median age, years (range)                     | 37.0 (0.25, 90.0)      | 38.0 (0.33, 90.0)        | 33.0 (0.25, 82.0)    | 0.001   |
| <b>Gender, n (%)</b>                          |                        |                          |                      | 0.080   |
| Male  | 424 (56.9)             | 325 (55.3)               | 99 (63.1)            |         |
| Female  | 321 (43.1)             | 263 (44.7)               | 58 (36.9)            |         |
| <b>Severity, n (%)*</b>                       |                        |                          |                      | <0.001  |
| Asymptomatic                                  | 159 (21.3)             | 104 (17.7)               | 55 (35.0)            |         |
| Mild  | 81 (10.9)              | 66 (11.2)                | 15 (9.6)             |         |
| Moderate                                      | 468 (62.8)             | 385 (65.5)               | 83 (52.9)            |         |
| Severe  | 37 (5.0)               | 33 (5.6)                 | 4 (2.6)              |         |
| <b>Comorbidities, n (%)</b>                   |                        |                          |                      |         |
| Hypertension                                  | 77 (10.3)              | 65 (11.1)                | 12 (7.6)             | 0.212   |
| Diabetes                                      | 32 (4.3)               | 29 (4.9)                 | 3 (1.9)              | 0.097   |
| Lung diseases                                 | 22 (3.0)               | 18 (3.1)                 | 4 (2.6)              | 0.736   |
| Cardiovascular disease                        | 30 (4.0)               | 29 (4.9)                 | 1 (0.6)              | 0.015   |
| Other chronic diseases                        | 59 (7.9)               | 55 (9.4)                 | 4 (2.6)              | 0.005   |
| <b>Drug therapy, n (%)</b>                    |                        |                          |                      |         |
| Anti-infectious drugs                         | 366 (49.1)             | 308 (52.4)               | 58 (36.9)            | 0.001   |
| Hormone therapy drugs                         | 22 (3.0)               | 21 (3.6)                 | 1 (0.6)              | 0.054   |
| Antivirals                                    | 38 (5.1)               | 29 (4.9)                 | 9 (5.7)              | 0.686   |
| Chloroquine phosphate                         | 10 (1.3)               | 7 (1.2)                  | 3 (1.9)              | 0.486   |
| Traditional Chinese medicine                  | 96 (12.9)              | 76 (12.9)                | 20 (12.7)            | 0.951   |
| <b>ICU, n (%)</b>                             |                        |                          |                      | 0.068   |
| No  | 704 (94.5)             | 551 (93.7)               | 153 (97.5)           |         |
| Yes   | 41 (5.5)               | 37 (6.3)                 | 4 (2.6)              |         |
| <b>Median days, days (IQR)</b>                |                        |                          |                      |         |
| From onset to admission                       | 2.8 (1.0, 6.0)         | 2.0 (1.0, 6.0)           | 3.7 (1.8, 6.4)       | 0.065   |
| From admission to discharge                   | 12.2 (7.0, 20.0)       | 13.0 (8.0, 20.0)         | 11.2 (5.5, 16.4)     | 0.005   |
| From discharge to repositivity                | –                      | –                        | 8.0 (8.0, 14.0)      | –       |
| <b>Median no. of RT-PCR testing, n (IQR)</b>  |                        |                          |                      |         |
| Nasopharyngeal swab                           | 2.0 (2.0, 2.0)         | 2.0 (2.0, 2.0)           | 3.0 (2.0, 4.0)       | <0.001  |
| Anal swab                                     | 2.0 (0.0, 2.0)         | 2.0 (0.0, 2.0)           | 2.0 (0.0, 3.0)       | 0.000   |
| Any of above                                  | 4.0 (2.0, 4.0)         | 4.0 (2.0, 4.0)           | 4.0 (3.0, 6.0)       | <0.001  |

\*All patients were updated by progression of illness at their first admission, and the most severe condition was their final severity designation.

protection with a positive retest patient. Samples including nasopharyngeal and anal swabs were all collected for RT-PCR diagnosis. Monitoring and evaluating close contacts were documented in a previous study (14).

## Data Collection

The information collected for COVID-19 patients included demographic characteristics (age, sex, and continent), comorbidities (hypertension, diabetes, etc.), drug therapy, severity, clinical symptoms (fever, dry cough, myalgia, etc.), radiological examinations (CT), and blood examinations (white blood cell count, lymphocyte cell count, and lymphocyte cell percentage) at the first admission. The second admission information of positive retest patients was also collected. The information collected for close contacts included demographic characteristics, quarantine site (healthcare facilities and home), frequency of contact (often, moderate, and occasional), and contact modes (household, public transportation, healthcare settings, workplaces, and entertainment places).

COVID-19 severity includes five categories (10): asymptomatic, mild, moderate, severe, and critical. Asymptomatic infected persons were those with etiological detection of SARA-CoV-2 in respiratory specimens or specific IgM detected in serum. Mild cases were those who had mild symptoms and no sign of pneumonia on chest imaging. Moderate cases are those who had fever and respiratory symptoms and signs of pneumonia. Severe cases were those who meet any of the falling criteria: (1) shortness of breath, RR  $\geq 30$  times/min; (2) oxygen saturation  $\leq 93\%$  at rest; and (3) alveolar oxygen partial pressure/fraction of inspiration  $O_2$  (PaO<sub>2</sub>/FiO<sub>2</sub>)  $\leq 300$  mmHg. Critical cases are those who meet any of the falling conditions: (1) respiratory failure requiring mechanical ventilation; (2) shock; and (3) patients combined with other organ failure needed ICU monitoring and treatment. In this study, we combined severe and critical cases into the severe group.

## Statistical Analysis

The repositive rate of SARS-CoV-2 was estimated by dividing the number of repositive patients by the number of COVID-19 patients. Categorical variables are described as absolute numbers and percentages (%). Skewed and normally distributed continuous variables are described as the median [interquartile range (IQR) or range] and mean [standard deviation (SD)], respectively. Chi-square tests and *t*-tests were used to compare characteristics between repositive patients or not.

Univariate and multivariable logistic regression models (15) were performed to estimate odds ratios (ORs) and 95% confidence intervals (95% CIs) for predictors of repositive status. Age (0–17, 18–44, 45–59, or  $\geq 60$  years), sex (male or female), continent (Asia, Africa, or others), severity (asymptomatic, mild, moderate, or severe), and clinical symptoms (fever, dry cough, expectoration, myalgia, diarrhea, or shortness of breath) at the first admission were included in the multivariable model.

Analyses were all performed with SAS software (version 9.4 for Windows, SAS Institute, Inc., Cary, NC, USA). Statistical tests were two-sided, and *p*-values of  $<0.05$  were considered to indicate statistical significance.

## RESULTS

### Clinical Characteristics of Repositive Patients

Among 745 patients, 157 of them (21.1%; 95% CI, 18.2–24.0) retested positive by RT-PCR. The re-positive rate by types of specimen was 16.8% (95% CI, 14.1–24.0%) for nasopharyngeal swabs and 9.7% (95% CI, 7.0–12.5%) for anal swabs. The re-positive rate by days from discharge was 0.1% (95% CI, 0.0–0.4%) for 1 day, 5.0% (95% CI, 3.4–6.5%) for 2–7 days, 11.3% (95% CI, 9.0–13.6%) for 8–14 days, and 4.7% (95% CI, 3.2–6.2%) for  $>14$  days (Table 1). The re-positive rate at different stages of the epidemic of COVID-19 was 17.0% (13.1–20.9%) for domestic case stage, 22.4% (14.5–30.3%) for imported case stage, and 25.8% (20.7–30.9%) for imported case associated local epidemic stage (Supplementary Figure 1). The characteristics at the first admission of the 157 repositive patients are shown in Table 1. Repositive results were observed in patients in all age groups (age ranging from 3 months to 82.0 years, with a median age of 33.0 years), which was significantly younger than that of negative retest patients (median age of 38.0 years) ( $p = 0.001$ ). The days from first admission to discharge of repositive patients were significantly shorter than those of negative retest patients (11.2 vs. 13.0 days). One in three (35.0%) repositive patients were asymptomatic compared with one in six (17.7%) negative retest patients ( $p < 0.001$ ). The repositive patients had fewer comorbidities [such as cardiovascular disease, 1 (0.6%) vs. 29 (4.9%)] and were less likely to be treated with anti-infective drugs [58 (36.9%) vs. 308 (52.4%)] and in the ICU [4 (2.6%)

**TABLE 2 |** Characteristic of 157 repositive patients at first and second admission.

| Characteristic  | First admission   | Second admission  | <i>P</i> -value |
|---|-------------------|-------------------|-----------------|
| <b>Clinical symptoms, <i>n</i> (%)</b>                  |                   |                   |                 |
| Fever   | 65 (41.4)         | 0 (0.0)           | –               |
| Dry cough   | 61 (38.9)         | 4 (2.6)           | $<0.001$        |
| Expectoration   | 25 (15.9)         | 10 (6.4)          | 0.004           |
| Sore throat   | 28 (17.8)         | 2 (1.3)           | $<0.001$        |
| Fatigue   | 19 (12.1)         | 2 (1.3)           | $<0.001$        |
| Headache  | 17 (10.8)         | 0 (0.0)           | –               |
| Chill   | 5 (3.2)           | 0 (0.0)           | –               |
| Myalgia   | 12 (7.6)          | 0 (0.0)           | –               |
| Diarrhea  | 6 (3.8)           | 0 (0.0)           | –               |
| Shortness of breath                                     | 9 (5.7)           | 0 (0.0)           | –               |
| CT lung abnormalities, <i>n</i> (%) <sup>*</sup>        | 96 (82.1)         | 104 (81.3)        | 0.248           |
| <b>Median blood biochemical index (IQR)<sup>†</sup></b> |                   |                   |                 |
| WBC (10 <sup>9</sup> /L)                                | 5.6 (4.5, 6.7)    | 5.5 (4.8, 6.6)    | 0.430           |
| Ly (10 <sup>9</sup> /L)                                 | 1.4 (1.1, 2.0)    | 2.0 (1.6, 2.3)    | $<0.001$        |
| Ly%   | 29.2 (22.0, 38.0) | 32.5 (28.7, 41.8) | 0.014           |

CT, computed tomography; WBC, white blood cell count; Ly, lymphocyte cell count; Ly%, lymphocyte cell percentage.

<sup>\*</sup>Missing values: 40 at first admission, 29 at second admission.

<sup>†</sup>Missing values: 46 of WBC, 50 of lymphocyte, 57 of lymphocyte percentage at first admission; 32 of the three at second admission.



vs. 37 (6.3%)]]. Sampling and RT-PCR testing were performed with median number of 4.0 times (IQR, 3.0–6.0 times) for repositive patients, which was significantly greater than that of negative retest patients ( $p < 0.001$ ). The days for discharged patients retested positive was 8.0 (IQR, 8.0–14.0 days) (Table 1 and Supplementary Figure 2).

Characteristics of 157 repositive cases at first and second admission are shown in Table 2. At second admission, 4 (2.6%) patients had dry cough, 10 (6.4%) had expectoration and 2 (1.3%) had sore throat, which was lower than that of the first admission. No one presented gastrointestinal symptoms at second admission. Among the 127 patients who underwent

CT examination, 104 (81.3%) patients had abnormal but obvious absorption. Lymphocyte cell counts and lymphocyte cell percentages were increased compared with those before ( $p < 0.001$ ).

## Risk Factors Associated With Repositive Status

We compared repositive rates in Table 3. A higher repositivity rate of males than females [23.4% (95% CI, 19.3–27.4) vs. 18.1% (13.9–22.3)] was observed, but this difference was not statistically significant. The highest repositive rate was observed in patients aged 0–17 years old (42.9%; 95% CI, 27.9–57.8%) with OR of

**TABLE 3 |** Risk factors associated with re-positivity among COVID-19 patients ( $n = 157$ ).

| Characteristic           | Repositive patients (n) | Repositive rate % (95% CI) | Crude odds ratio (95% CI) | Adjusted odds ratio (95% CI) |
|--------------------------|-------------------------|----------------------------|---------------------------|------------------------------|
| <b>Age group*</b>        |                         |                            |                           |                              |
| 0–17 years               | 18                      | 42.9 (27.9–57.8)           | 3.88 (1.74–8.66)          | 2.58 (1.05–6.32)             |
| 18–44 years              | 95                      | 22.0 (18.1–25.9)           | 1.46 (0.83–2.57)          | 0.96 (0.50–1.81)             |
| 45–59 years              | 27                      | 16.3 (10.7–21.9)           | 1.01 (0.52–1.95)          | 0.79 (0.40–1.57)             |
| ≥60 years                | 17                      | 16.2 (9.1–23.2)            | 1.00 (ref)                | 1.00 (ref)                   |
| <b>Sex</b>               |                         |                            |                           |                              |
| Male                     | 99                      | 23.4 (19.3–27.4)           | 1.38 (0.96–1.99)          | 1.45 (0.98–2.15)             |
| Female                   | 58                      | 18.1 (13.9–22.3)           | 1.00 (ref)                | 1.00 (ref)                   |
| <b>Continent</b>         |                         |                            |                           |                              |
| Asia                     | 125                     | 20.0 (16.9–23.1)           | 1.00 (ref)                | 1.00 (ref)                   |
| Africa                   | 29                      | 27.6 (19.1–36.2)           | 1.53 (0.95–2.44)          | 0.73 (0.39–1.35)             |
| Others                   | 3                       | 20.0 (0.0–40.2)            | 1.00 (0.28–3.60)          | 0.60 (0.15–2.37)             |
| <b>Severity†‡</b>        |                         |                            |                           |                              |
| Asymptomatic             | 55                      | 34.6 (27.2–42.0)           | 4.36 (1.47–12.95)         | 3.83 (1.07–13.71)            |
| Mild                     | 15                      | 18.5 (10.1–27.0)           | 1.88 (0.58–6.10)          | 1.27 (0.34–4.72)             |
| Moderate                 | 83                      | 17.7 (14.3–21.2)           | 1.78 (0.61–5.16)          | 1.63 (0.52–5.11)             |
| Severe or critical       | 4                       | 10.8 (0.8–20.8)            | 1.00 (ref)                | 1.00 (ref)                   |
| <b>Clinical symptoms</b> |                         |                            |                           |                              |
| Fever                    |                         |                            |                           |                              |
| No                       | 92                      | 26.7 (22.1–31.4)           | 1.89 (1.32–2.70)          | 1.51 (1.00–2.28)             |
| Yes                      | 65                      | 16.2 (12.6–19.8)           | 1.00 (ref)                | 1.00 (ref)                   |
| Dry cough                |                         |                            |                           |                              |
| No                       | 96                      | 23.7 (19.6–27.9)           | 1.42 (0.99–2.04)          | 0.90 (0.57–1.42)             |
| Yes                      | 61                      | 17.9 (13.9–22.0)           | 1.00 (ref)                | 1.00 (ref)                   |
| Expectoration            |                         |                            |                           |                              |
| No                       | 132                     | 22.4 (19.0–25.8)           | 1.51 (0.95–2.42)          | 1.05 (0.61–1.81)             |
| Yes                      | 25                      | 16.0 (10.3–21.8)           | 1.00 (ref)                | 1.00 (ref)                   |
| Myalgia                  |                         |                            |                           |                              |
| No                       | 145                     | 22.0 (18.8–25.2)           | 1.74 (0.92–3.29)          | 1.11 (0.56–2.20)             |
| Yes                      | 12                      | 14.0 (6.6–21.3)            | 1.00 (ref)                | 1.00 (ref)                   |
| Diarrhea                 |                         |                            |                           |                              |
| No                       | 151                     | 21.4 (18.4–24.5)           | 1.54 (0.64–3.74)          | 1.28 (0.50–3.26)             |
| Yes                      | 6                       | 15.0 (3.9–26.1)            | 1.00 (ref)                | 1.00 (ref)                   |
| Shortness of breath      |                         |                            |                           |                              |
| No                       | 148                     | 21.7 (18.6–24.8)           | 1.63 (0.79–3.38)          | 0.91 (0.41–2.04)             |
| Yes                      | 9                       | 14.5 (5.8–23.3)            | 1.00 (ref)                | 1.00 (ref)                   |

\* $p$  for trend = 0.002.

†All patients were updated by progression of illness at their first admission, and the most severe condition was their final severity designation.

‡ $p$  for trend <0.001.

3.88 (95% CI, 1.74–8.66) compared with patients aged 60 years or over ( $p$  for trend = 0.0023). The asymptomatic patients also had a higher repositive rate (34.6%; 95% CI, 27.2–42.0%) with OR of 4.36 (95% CI, 1.47–12.95) compared with severe patients. In addition, the repositive cases were found in younger age groups among four severity of disease (**Supplementary Table 1**). Patients without symptoms, such as without fever (OR = 1.89; 95% CI, 1.32–2.70), was associated with an increased risk of repositivity (**Table 3**). In addition, comorbidities, CT lung abnormalities, and some clinical symptoms (such as fatigue, chills, and sore throat) were not separately assessed due to multicollinearity with age, severity, and other clinical symptoms, and the repositive rate of COVID-19 by these variables is shown in **Supplementary Table 2**.

We performed strata analysis according to the types of specimen, and the repositive rate of nasopharyngeal and anal swabs is shown in **Supplementary Table 3**. Generally, the overall repositive rate of anal swabs was lower than that of nasopharyngeal swabs except for the group of 0–17 years old [39.3% (95% CI, 21.2–57.4%) vs. 22.6% (95% CI, 7.9–37.3%)], mild severity [13.6% (95% CI, 3.5–23.8%) vs. 12.0% (95% CI, 4.7–19.4%)], and symptoms of diarrhea [10.0% (95% CI, 0.0–20.7%) vs. 8.1% (95% CI, 0.0–16.9%)].

## Infection in Close Contacts of Repositive Patients

Because all the discharged patients were put under centralized quarantine for 14 days at healthcare facilities, only 26 positive retest patients had close contacts, and 148 close contacts were traced. **Table 4** presents the characteristics of repositive patients and close contacts. A total of 137 (92.6%) close contacts were quarantined at healthcare facilities, and 11 (7.4%) close contacts quarantined at home. After quarantine for 12.0 days (IQR, 6.0–14.0) at a healthcare facility or at home and 4.5 times (IQR, 3.0–10.0) of RT-PCR testing, 148 close contacts tested negative for SARS-CoV-2 RNA, and no suspicious clinical symptoms were reported.

## DISCUSSION

We found that the repositive rate of SARS-CoV-2 was 21.1% among discharged patients at a follow-up visit after at least 6 weeks. They reported positive RT-PCR testing results with 8.0 days after discharge. Over 4 in 10 children were found to be positive again; in contrast, the repositive rate of SARS-CoV-2 in middle-aged and elderly individuals was 16%. Moreover, patients with more clinically severe disease were less likely to have repositive testing results than those who were asymptomatic. Manifestation of certain symptoms at first admission, such as fever, was also associated with a lower risk for repositivity. Based on the Chinese guidelines for discharged patients (9), repositive patients were required to quarantine for a second time. No other positive patients emerged within their families and close contacts.

Several studies have been performed to investigate the percentage of repositivity of discharged patients (3, 16, 17). Previous studies reported that the repositive rate ranged from

**TABLE 4 |** Characteristic of repositive patients and the close contacts.

| Characteristic                             | Repositive patients (n = 26) | Close contacts (n = 148) |
|--|------------------------------|--------------------------|
| <b>Age group, n (%)</b>                    |                              |                          |
| 0–17 years                                 | 3 (11.5)                     | 15 (10.1)                |
| 18–44 years                                | 13 (50.0)                    | 92 (62.2)                |
| 45–59 years                                | 4 (15.4)                     | 34 (23.0)                |
| ≥60 years                                  | 6 (23.1)                     | 7 (4.7)                  |
| <b>Sex, n (%)</b>                          |                              |                          |
| Male                                       | 17 (65.4)                    | 89 (60.1)                |
| Female                                     | 9 (34.6)                     | 59 (39.9)                |
| <b>Quarantine site, n (%)</b>              |                              |                          |
| Healthcare facilities                      | 26 (100.0)                   | 137 (92.6)               |
| Home                                       | 0 (0.0)                      | 11 (7.4)                 |
| <b>Frequency of contact, n (%)</b>         |                              |                          |
| Often                                      | 11 (26.8)                    | 27 (18.2)                |
| Moderate                                   | 10 (24.4)                    | 24 (16.2)                |
| Occasional                                 | 20 (48.8)                    | 97 (65.5)                |
| <b>Contact modes, n (%)</b>                |                              |                          |
| Household                                  | 14 (29.8)                    | 42 (28.4)                |
| Public transportation                      | 18 (38.3)                    | 61 (41.2)                |
| Healthcare settings                        | 2 (4.3)                      | 2 (1.4)                  |
| Workplaces                                 | 6 (12.8)                     | 12 (8.1)                 |
| Entertainment places                       | 7 (14.9)                     | 31 (21.0)                |
| <b>Severity of patients, n (%)*</b>        |                              |                          |
| Asymptomatic                               | 3 (11.5)                     | 40 (27.0)                |
| Mild                                       | 3 (11.5)                     | 8 (5.4)                  |
| Moderate                                   | 18 (69.2)                    | 96 (64.9)                |
| Severe                                     | 2 (7.7)                      | 4 (2.7)                  |
| <b>Days from discharge to repositivity</b> |                              |                          |
| 3–13                                       | 18                           | –                        |
| ≥14  | 8                            | –                        |
| Median days of quarantine, days (IQR)      | –                            | 12.0 (6.0, 14.0)         |
| Median no. of RT-PCR testing, n (IQR)      | –                            | 4.5 (3.0, 10.0)          |
| Infected close contacts, n (%)             | –                            | 0 (0.0)                  |

\*Severity of patients means that the progression of illness at first admission of repositive patients, and the severity of close contacts is not the symptoms of close contacts, but the symptoms of patients who have contact the close contacts.

6.9% to 69.0% for discharged patients (16–19). However, the studies were limited to a small number of patients with mild or moderate infection. In our study, we evaluated the overall prognosis of patients with COVID-19 after meeting the criteria for discharge in Guangzhou, China. Our study has lasted more than 7 months since the start of the outbreak, which was far longer than other studies (most lasted for 1 or 2 months) (7, 17, 20, 21) and to some extent represented the overall prognosis of the disease. After screening 745 discharged patients, the repositive rate was over 20% (157/745), which was higher than that in other countries, such as Brunei Darussalam (21/106, 19.8%) (19) and Italy (22/131, 16.7%) (18), and this may be due to the longer follow-up time, more stringent monitoring, and higher frequency of RT-PCR testing in China. In our study, one patient tested repositive on the first day (**Table 1**),

which may be attributed to the false negative of last time. The repositive rate at different stages of the epidemic of COVID-19 was increased (**Supplementary Figure 1**), which may be related to improvements of testing reagents and changes of discharge standards (22, 23).

Some reports suggested reinfection as a possible cause (24); our findings do not support this. According to the Chinese clinical guidance for COVID-19 (10), all repositive patients should test negative for nasopharyngeal and anal swabs for two successive tests before discharge. Then, all discharged patients were continuously quarantined in designated healthcare facilities with strict interventions on disease transmission. Thus, the identification of another positive SARS-CoV-2 test during the quarantine period likely excludes the possibility that positive retest patients are caused by secondary viral infection. A recent study also experimentally confirmed that the virus was not a secondary infection (8).

Abnormal CT and lymphopenia are common and correlate with poor clinical outcomes in patients with COVID-19 (25). In our study, most positive retest patients at the second admission showed increased lymphocyte cell counts, and CT examination showed abnormal but obvious improvements, suggesting that repositive patients have no obvious disease progression and reactivation is also unlikely. In addition, current evidence to date showed that the probable causes of repositivity with false-negative or false-positive results of qPCR are the most frequent. However, in our study, sampling and RT-PCR testing were performed with 4.0 times for all discharged patients, and samples including nasopharyngeal and anal swabs were all collected for RT-PCR diagnosis in an attempt to reduce the chance of false negatives caused by differences in primer specificity and sensitivity.

At present, virological studies have reported prolonged viral shedding in SARS-CoV-2-positive patients, which took 2 to 3 weeks or longer (26–30). Genetic studies on SARS suggested that host responses might result in undetectable levels of nasopharyngeal virus shedding at certain times (31). Our findings support prolonged but intermittent viral shedding as the most plausible explanation. In our study, the days of first hospitalization were shorter in repositive patients than in negative retest patients, and the observation of repositive patients was not random and was mainly observed in young patients without severe clinical symptoms, suggesting that the SARS-CoV-2 virus may not be completely eliminated due to the lighter symptoms and the faster attainment of the discharge standard.

Whether discharged patients have infectivity is an issue of concern around the world at present. However, positive testing induced by viral RNA shedding of SARS-CoV-2 may not necessarily imply an ability to transmit infection, unless there is proof that the virus can be isolated and cultured from the particular samples. While we did not culture the samples in our study, other studies reported that no infectious strain could be obtained by culture, and no full-length viral genomes could be sequenced using samples of positive retest patients (20). Among positive retest patients in our study, no families or close contacts of positive retest patients tested positive, which was consistent with current studies (20, 32).

## LIMITATIONS

Our study has some limitations. First, as our data were based on the public health response to COVID-19, sample collection did not follow a stringent study design. Therefore, some of the patients, especially in the early stage, had missing fecal samples. However, patients who retest positive from anal swab are not recommended to follow-up since no evidence of fecal–oral transmission have been described for SARS-CoV2 so far (33, 34). Second, nasopharyngeal swab samples cannot differentiate whether the virus comes from the nasopharynx or from secretions from the lower respiratory tract; thus, virus elimination in the lower respiratory tract cannot be confirmed. In contrast, the positive rate of RT-PCR testing through alveolar lavage fluid may be higher. However, this method is invasive and cannot be widely performed in clinical practice. In our opinion, both qualities of respiratory samples and the variability of technique sensitivity can be attributed to the influencing factors of repositivity. Third, as the discharge patients were usually placed under centralized quarantine and medical observation, the infectivity of the positive retest patients might be underestimated. Fourth, we could not provide the serological status in terms of IgG against the Spike protein and/or N protein in these discharged patients during the follow-up and we did not perform any infectivity test *in vitro* to validate the contagiousity of repositive patients.

## CONCLUSIONS

We found that the repositive rate of discharged patients was higher (21.1%) than commonly reported. The observation of positive retest patients was not random and was mainly observed in young patients without severe clinical symptoms. No other positive patients emerged within the families or close contacts of patients who resulted “repositive.” Our findings support prolonged but intermittent viral shedding as the probable cause for this phenomenon; we need to familiarize with the possibility that the virus will remain endemic.

## DATA AVAILABILITY STATEMENT

The raw data supporting the conclusions of this article will be made available by the authors, without undue reservation.

## AUTHOR CONTRIBUTIONS

DL contributed to the statistical analyses and drafted the manuscript. CM, LL, DL, ZL, ZW, PZ, XZ, YZ, WZho, and WS revised the final manuscript. ZZ, CX, ZC, WZha, PY, and QH collected the epidemiological and clinical data. HW and DL are responsible for summarizing all epidemiological and clinical data, and contributed to data cleaning. All authors critically reviewed the manuscript for important intellectual content.

## FUNDING

This work was supported by the Guangdong Province Higher Vocational Colleges and Schools Pearl River Scholar Funded Scheme (2019), the Construction of High-level University of Guangdong (G820332010, G618339167, and G618339164), the Young Elite Scientists Sponsorship Program by CAST (2019QNRC001), the National Natural Science Foundation of China (82041030), the Zhejiang University Special Scientific Research Fund for COVID-19 prevention and control (K920330111), the Key Project of Medicine Discipline of Guangzhou (No. 2021–2023-11), and the Basic Research Project of Key Laboratory of Guangzhou (No. 202102100001).

## REFERENCES

- Li Q, Guan X, Wu P, Wang X, Zhou L, Tong Y, et al. Early transmission dynamics in Wuhan, China, of novel coronavirus-infected pneumonia. *N Engl J Med.* (2020) 382:1199–207. doi: 10.1056/NEJMoa2001316
- WHO. Coronavirus disease 2019 (COVID-19) situation report. Available online at: [https://www.who.int/docs/default-source/coronaviruse/situation-reports/20210420-weekly-epi-update\\_36.pdf?sfvrsn=ab75add5\\_7&download=true](https://www.who.int/docs/default-source/coronaviruse/situation-reports/20210420-weekly-epi-update_36.pdf?sfvrsn=ab75add5_7&download=true); <https://covid19.who.int/> (accessed 25 April, 2021).
- Lan L, Xu D, Ye G, Xia C, Wang S, Li Y, et al. Positive RT-PCR test results in patients recovered from COVID-19. *JAMA.* (2020) 323:1502–3. doi: 10.1001/jama.2020.2783
- Su Y, Zhu L-S, Gao Y, Li Y, Xiong Z, Hu B, et al. Clinical characteristics of Covid-19 patients with re-positive test results: an observational study. *medRxiv.* (2020) 1–16. doi: 10.1101/2020.06.23.20138149
- An J, Liao X, Xiao T, Qian S, Yuan J, Ye H, et al. Clinical characteristics of the recovered COVID-19 patients with re-detectable positive RNA test. *Ann Transl Med.* (2020) 8:1084. doi: 10.1101/2020.03.26.20044222
- Mei Q, Li J, Du R, Yuan X, Li M, Li J. Assessment of patients who tested positive for COVID-19 after recovery. *Lancet Infect Dis.* (2020) 20:1004–5. doi: 10.1016/S1473-3099(20)30433-3
- Zheng J, Zhou R, Chen F, Tang G, Wu K, Li F, et al. Incidence, clinical course and risk factor for recurrent PCR positivity in discharged COVID-19 patients in Guangzhou, China: a prospective cohort study. *PLoS Negl Trop Dis.* (2020) 14:e0008648. doi: 10.1371/journal.pntd.0008648
- Hu F, Chen F, Ou Z, Fan Q, Tan X, Wang Y, et al. A compromised specific humoral immune response against the SARS-CoV-2 receptor-binding domain is related to viral persistence and periodic shedding in the gastrointestinal tract. *Cell Mol Immunol.* (2020) 17:1119–25. doi: 10.1038/s41423-020-00550-2
- National Health Commission of China. *Health Management Plan for COVID-19 discharged Patients (Trial)*. (2020). Available online at: [http://www.gov.cn/zhengce/zhengceku/2020-03/15/content\\_5491535.htm](http://www.gov.cn/zhengce/zhengceku/2020-03/15/content_5491535.htm) (accessed July 6, 2020).
- National Health Commission of China. *Chinese Clinical Guidance for COVID-19 Pneumonia Diagnosis and Treatment* (Edition 7). Available online at: <http://kjfy.meetingchina.org/msite/news/show/cn/3337.html> (accessed July 6, 2020).
- Corman VM, Landt O, Kaiser M, Molenkamp R, Meijer A, Chu DK, et al. Detection of 2019 novel coronavirus (2019-nCoV) by real-time RT-PCR. *Euro Surveill.* (2020) 25:2000045. doi: 10.2807/1560-7917.ES.2020.25.3.2000045
- Luo L, Liu D, Zhang H, Li Z, Zhen R, Zhang X, et al. Air and surface contamination in non-health care settings among 641 environmental specimens of 39 COVID-19 cases. *PLoS Negl Trop Dis.* (2020) 14:e0008570. doi: 10.1371/journal.pntd.0008570
- Chinese CDC. *Guidelines for Investigation and Management of Close Contacts of COVID-19 Cases*. (2020). Available online at: <http://weekly.chinacdc.cn/en/article/doi/10.46234/ccdcw2020.084> (accessed April 20, 2020).
- Luo L, Liu D, Liao X, Wu X, Jing Q, Zheng J, et al. Contact settings and risk for transmission in 3410 close contacts of patients with COVID-19

## ACKNOWLEDGMENTS

We acknowledge all staffs involved in the prevention and control of COVID-19 at the Guangzhou Centers for Disease Control and Prevention. We thank all patients involved in the study.

## SUPPLEMENTARY MATERIAL

The Supplementary Material for this article can be found online at: <https://www.frontiersin.org/articles/10.3389/fmed.2021.684101/full#supplementary-material>

- in Guangzhou, China: a prospective cohort study. *Ann Intern Med.* (2020) 173:879–87. doi: 10.7326/M20-2671
- Tripepi G, Jager KJ, Dekker FW, Zoccali C. Linear and logistic regression analysis. *Kidney Int.* (2008) 73:806–10. doi: 10.1038/sj.ki.5002787
- Habibzadeh P, Sajadi MM, Emami A, Karimi MH, Yadollahie M, Kucheki M, et al. Rate of re-positive RT-PCR test among patients recovered from COVID-19. *Biochem Med.* (2020) 30:030401. doi: 10.11613/BM.2020.030401
- Tao W, Wang X, Zhang G, Guo M, Ma H, Zhao D, et al. Re-detectable positive SARS-CoV-2 RNA tests in patients who recovered from COVID-19 with intestinal infection. *Protein Cell.* (2020) 12:1–6. doi: 10.1007/s13238-020-00778-8
- Landi F, Carli A, Benvenuto F, Brandi V, Ciciarello F, Lo Monaco MR, et al. Predictive factors for a new positive nasopharyngeal swab among patients recovered from COVID-19. *Am J Prevent Med.* (2020) 60:13–9. doi: 10.1016/j.amepre.2020.08.014
- Wong J, Koh WC, Momin RN, Alikhan MF, Fadillah N, Naing L. Probable causes and risk factors for positive SARS-CoV-2 test in recovered patients: Evidence from Brunei Darussalam. *J Med Virol.* (2020) 92:2847–51. doi: 10.1002/jmv.26199
- Lu J, Peng J, Xiong Q, Liu Z, Lin H, Tan X, et al. Clinical, immunological and virological characterization of COVID-19 patients that test re-positive for SARS-CoV-2 by RT-PCR. *EBioMedicine.* (2020) 59:102960. doi: 10.1016/j.ebiom.2020.102960
- Yuan B, Liu HQ, Yang ZR, Chen YX, Liu ZY, Zhang K, et al. Recurrence of positive SARS-CoV-2 viral RNA in recovered COVID-19 patients during medical isolation observation. *Sci Rep.* (2020) 10:11887. doi: 10.1038/s41598-020-68782-w
- Li C, Ren L. Recent progress on the diagnosis of 2019 Novel Coronavirus. *Transbound Emerg Dis.* (2020) 67:1485–91. doi: 10.1111/tbed.13620
- Chan JF, Yip CC, To KK, Tang TH, Wong SC, Leung KH, et al. Improved molecular diagnosis of COVID-19 by the novel, highly sensitive and specific COVID-19-RdRp/Hel real-time reverse transcription-PCR assay validated in vitro and with clinical specimens. *J Clin Microbiol.* (2020) 58:e00310–20. doi: 10.1128/JCM.00310-20
- Babiker A, Marvil C, Waggoner JJ, Collins M, Piantadosi A. The importance and challenges of identifying SARS-CoV-2 reinfections. *J Clin Microbiol.* (2021) 59:e02769–20. doi: 10.1128/JCM.02769-20
- Cheng LL, Guan WJ, Duan CY, Zhang NF, Lei CL, Hu Y, et al. Effect of recombinant human granulocyte colony-stimulating factor for patients with coronavirus disease 2019 (COVID-19) and lymphopenia: a randomized clinical trial. *JAMA Intern Med.* (2020) 181:71–8. doi: 10.1001/jamainternmed.2020.5503
- To KK-W, Tsang OT-Y, Leung W-S, Tam AR, Wu T-C, Lung DC, et al. Temporal profiles of viral load in posterior oropharyngeal saliva samples and serum antibody responses during infection by SARS-CoV-2: an observational cohort study. *Lancet Infect Dis.* (2020) 20:565–74. doi: 10.1016/S1473-3099(20)30196-1



27. Hu X, Xing Y, Jia J, Ni W, Liang J, Zhao D, et al. Factors associated with negative conversion of viral RNA in patients hospitalized with COVID-19. *Sci Total Environ.* (2020) 728:138812. doi: 10.1016/j.scitotenv.2020.138812
28. Hung IF, Cheng VC, Li X, Tam AR, Hung DL, Chiu KH, et al. SARS-CoV-2 shedding and seroconversion among passengers quarantined after disembarking a cruise ship: a case series. *Lancet Infect Dis.* (2020) 20:1051–60. doi: 10.1016/S1473-3099(20)30364-9
29. Zou L, Ruan F, Huang M, Liang L, Huang H, Hong Z, et al. SARS-CoV-2 Viral Load in Upper Respiratory Specimens of Infected Patients. *N Engl J Med.* (2020) 382:1177–9. doi: 10.1056/NEJMc2001737
30. Wu Y, Guo C, Tang L, Hong Z, Zhou J, Dong X, et al. Prolonged presence of SARS-CoV-2 viral RNA in faecal samples. *Lancet Gastroenterol Hepatol.* (2020) 5:434–5. doi: 10.1016/S2468-1253(20)30083-2
31. Chen WJ, Yang JY, Lin JH, Fann CS, Osyetrov V, King CC, et al. Nasopharyngeal shedding of severe acute respiratory syndrome-associated coronavirus is associated with genetic polymorphisms. *Clin Infect Dis.* (2006) 42:1561–9. doi: 10.1086/503843
32. Chandrashekar A, Liu J, Martinot AJ, McMahan K, Mercado NB, Peter L, et al. SARS-CoV-2 infection protects against rechallenge in rhesus macaques. *Science.* (2020) 369:812–7. doi: 10.1126/science.abc4776
33. Zang R, Gomez Castro MF, McCune BT, Zeng Q, Rothlauf PW, Sonnek NM, et al. TMPRSS2 and TMPRSS4 promote SARS-CoV-2 infection of human small intestinal enterocytes. *Sci Immunol.* (2020) 5:eabc3582. doi: 10.1101/2020.04.21.054015
34. Shi J, Sun J, Hu Y. Enteric involvement of SARS-CoV-2: Implications for the COVID-19 management, transmission, and infection control. *Virulence.* (2020) 11:941–4. doi: 10.1080/21505594.2020.1794410

**Conflict of Interest:** The authors declare that the research was conducted in the absence of any commercial or financial relationships that could be construed as a potential conflict of interest.

Copyright © 2021 Luo, Liu, Zhang, Li, Xie, Wang, Chen, Zhang, Zhang, Zhang, Zhong, Zhang, Yang, Huang, Song, Wang and Mao. This is an open-access article distributed under the terms of the Creative Commons Attribution License (CC BY). The use, distribution or reproduction in other forums is permitted, provided the original author(s) and the copyright owner(s) are credited and that the original publication in this journal is cited, in accordance with accepted academic practice. No use, distribution or reproduction is permitted which does not comply with these terms.



# Exploring the Clinical Characteristics of COVID-19 Clusters Identified Using Factor Analysis of Mixed Data-Based Cluster Analysis

Liang Han<sup>1</sup>, Pan Shen<sup>1</sup>, Jiahui Yan<sup>1</sup>, Yao Huang<sup>1</sup>, Xin Ba<sup>1</sup>, Weiji Lin<sup>1</sup>, Hui Wang<sup>2</sup>, Ying Huang<sup>1</sup>, Kai Qin<sup>1</sup>, Yu Wang<sup>1</sup>, Zhe Chen<sup>1\*</sup> and Shenghao Tu<sup>1\*</sup>

## OPEN ACCESS

### Edited by:

Babak A. Ardekani,  
Nathan Kline Institute for Psychiatric  
Research, United States

### Reviewed by:

Carl-Magnus Svensson,  
Leibniz Institute for Natural Product  
Research and Infection  
Biology, Germany  
Wondwossen Amogne Degu,  
Addis Ababa University, Ethiopia  
Antonio Lalueza,  
Hospital Universitario 12 de  
Octubre, Spain

### \*Correspondence:

Shenghao Tu  
shtu@tjh.tjmu.edu.cn  
Zhe Chen  
zhepi2006@163.com

<sup>†</sup>These authors have contributed  
equally to this work and share last  
authorship

### Specialty section:

This article was submitted to  
Infectious Diseases – Surveillance,  
Prevention and Treatment,  
a section of the journal  
Frontiers in Medicine

Received: 21 December 2020

Accepted: 23 June 2021

Published: 16 July 2021

### Citation:

Han L, Shen P, Yan J, Huang Y, Ba X,  
Lin W, Wang H, Huang Y, Qin K,  
Wang Y, Chen Z and Tu S (2021)  
Exploring the Clinical Characteristics  
of COVID-19 Clusters Identified Using  
Factor Analysis of Mixed Data-Based  
Cluster Analysis.  
Front. Med. 8:644724.  
doi: 10.3389/fmed.2021.644724

<sup>1</sup> Department of Integrated Chinese Traditional and Western Medicine, Tongji Hospital, Tongji Medical College of Huazhong University of Science and Technology, Wuhan, China, <sup>2</sup> Rehabilitation & Sports Medicine Research Institute of Zhejiang Province, Zhejiang Provincial People's Hospital, People's Hospital of Hangzhou Medical College, Hangzhou, China

The COVID-19 outbreak has brought great challenges to healthcare resources around the world. Patients with COVID-19 exhibit a broad spectrum of clinical characteristics. In this study, the Factor Analysis of Mixed Data (FAMD)-based cluster analysis was applied to demographic information, laboratory indicators at the time of admission, and symptoms presented before admission. Three COVID-19 clusters with distinct clinical features were identified by FAMD-based cluster analysis. The FAMD-based cluster analysis results indicated that the symptoms of COVID-19 were roughly consistent with the laboratory findings of COVID-19 patients. Furthermore, symptoms for mild patients were atypical. Different hospital stay durations and survival differences among the three clusters were also found, and the more severe the clinical characteristics were, the worse the prognosis. Our aims were to describe COVID-19 clusters with different clinical characteristics, and a classifier model according to the results of FAMD-based cluster analysis was constructed to help provide better individualized treatments for numerous COVID-19 patients in the future.

**Keywords: COVID-19, cluster analysis, factor analysis of mixed data, symptoms, laboratory findings, support vector machine**

## INTRODUCTION

Over the last year, severe acute respiratory syndrome coronavirus 2 (SARS-CoV-2) has spread all over the world, and it has been concluded that long-term coexistence of humans and the virus is inevitable in the future (1). As a respiratory tract infection disease, coronavirus disease 2019 (COVID-19) usually presents with common symptoms, such as fever, tiredness, headache, cough, and sore throat (2). However, the clinical presentations and disease severity of COVID-19 patients may vary widely. For example, some individuals are asymptomatic, whereas others may develop to life-threatening acute respiratory failure. Although mainly spread via droplets and aerosols, a few SARS-CoV-2-infected individuals show digestive tract symptoms including diarrhea, abdominal pain, nausea, and vomiting, which could be caused by SARS-CoV-2 infection of the digestive tract system or triggered by therapeutic drugs, liver function injury and mental factors (3–6). In addition to specific symptoms, many publications have revealed that the disease severity and prognosis can be predicted by lymphocytes, D-dimer, C-reactive protein (CRP), and other laboratory indicators (7–10).

Previously, the clinical classifications of COVID-19 were mainly based on clinical indexes and radiological manifestations (11, 12). However, the potential relationship among disease severity, syndromes and laboratory tests was barely considered in those classifications. Therefore, it is necessary and meaningful to consider those relationships comprehensively and identify the subtypes of COVID-19.

Our study aimed to identify the subtypes of COVID-19 by using an unsupervised classifier. Factor analysis of mixed data (FAMD)-based cluster analysis was used to identify COVID-19 subtypes based on clinical symptoms, laboratory tests and demographic characteristics (13). Three COVID-19 subtypes were identified in our study, and the differences among the COVID-19 subtypes would contribute to our understanding of COVID-19 clinical characteristics. Moreover, subtypes with different clinical characteristics in this study showed different prognoses. Given this, a support vector machine (SVM)-based classifier was trained to recognize different COVID-19 subgroups. We believe that this classifier model could assist clinicians in rapidly identifying individuals with more severe and worse prognoses according to their symptoms and laboratory findings.

## MATERIALS AND METHODS

### Participants

Inpatient COVID-19 patients from January 21, 2020 to March 9, 2020 were initially recruited, and their medical history and laboratory findings were collected from Tongji Hospital of Tongji Medical College of Huazhong University of Science and Technology. Ethics approval was obtained by the ethics committee of Tongji Hospital of Tongji Medical College of Huazhong University of Science and Technology, and the approval reference number is TJ-IRB20200365. An exemption was granted obtaining written informed consent from the subjects. The present study design is depicted in **Figure 1**.

### Data Extraction

We selected the above mentioned 1,413 COVID-19 patients with positive COVID-19 nucleic acid or antibodies for this study, which were tested either before admission or during admission. Patients with incomplete medical records were excluded, and the remaining individuals' admission records were analyzed and collected by two clinicians independently to determine their age, sex, and symptoms because of the unstructured nature of the medical records. Simultaneously, laboratory data within 48 h after admission, including routine blood tests, blood biochemistry, coagulation function and other laboratory indicators, were also screened. However, laboratory tests performed at the time of patient admission to the hospital are not always the same but depend on the severity of each patient condition. Nevertheless, some tests such as routine blood tests, were analyzed for almost all patients within 48 h, but other tests such as interleukin tests, were performed only for severely ill patients. Consequently, we balanced the selection of patients and laboratory indicators to ensure that as many patients and indicators were included in the study as possible. For

this purpose, we examined the missing rate of each laboratory indicator (**Supplementary Figures 1, 2**). Finally, only tests with more than 90% completeness rates were selected for further analysis, and COVID-19 patient with missing laboratory were also excluded. Symptoms, laboratory indicators, age, sex, were finally collected and analyzed in our study (**Tables 1–3**). Total hospital days and outcomes were also collected to compare in-hospital survival rate, which was also the endpoint of this study (**Table 1**).

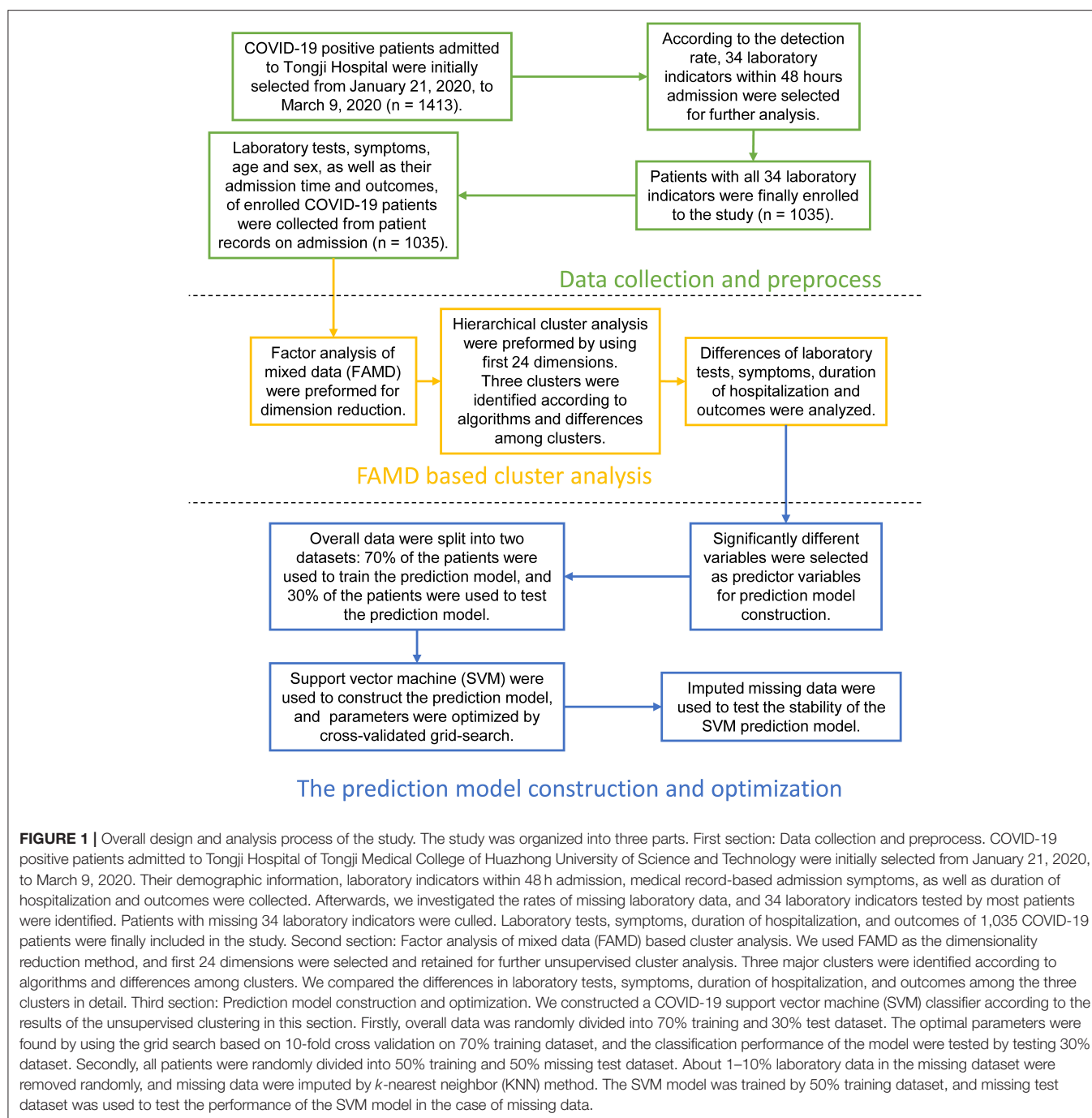
### Identification of COVID-19 Clusters

Both many studies and clinical experience indicate potential links between different laboratory indicators and symptoms among COVID-19 patients. There are also correlations between some laboratory tests, for example, lymphocyte count, and percentage of lymphocytes. Thus, factor analysis of mixed data (FAMD), a principal component method dedicated to analyzing a data set containing both quantitative and qualitative variables, was used to deconstruct the original complex data into fewer relevant factors. FAMD was performed using the R package FactoMineR (<https://cran.r-project.org/package=FactoMineR>), and the factoextra package (<https://cran.r-project.org/package=factoextra>) was used to extract the FAMD results. The first 24 dimensions were selected and retained for further cluster analysis, as these explained >80% of the total variance.

Cluster analysis is one of the most popular unsupervised learning methods to identify subgroups sharing similar characteristics, with no predefined information necessary. Agglomerative hierarchical cluster analysis of COVID-19 patients based on the FAMD-transformed matrix was performed according to the Ward criterion, which could minimize the total intracluster variance. Function `dist()` and function `hclust()` from the R package `base` were used for the cluster analysis. The R packages `ggtree` (<https://cran.r-project.org/package=ggtree>) and `ape` (<https://cran.r-project.org/package=ape>) were used to visualize the cluster analysis result, and the last several steps of cluster analysis were shown as a dendrogram, which was constructed by the R packages `ggraph` (<https://cran.r-project.org/package=ggraph>) and `tidygraph` (<https://cran.r-project.org/package=tidygraph>) (14–16). The R package `NbClust` was used to evaluate the range of the number of COVID-19 patients (17).

### Difference in Prognosis Among COVID-19 Clusters

Considering significantly different characteristics in different COVID-19 clusters, we assume that they have distinct prognoses. Thus, the prognoses of COVID-19 patients were recorded as the hospitalization days and outcomes. Patient outcomes were followed up until discharge from the hospital or death. Total hospital days were compared, survival analysis was performed using the R package `survival` (<https://cran.r-project.org/package=survival>), and Kaplan-Meier survival curves were plotted by the R package `survminer` (<https://cran.r-project.org/package=survminer>) (18).



## Statistical Analysis

Statistical analyses were conducted in R (R version 3.6.0). Continuous data are expressed as medians (interquartile range), and the rate is expressed as counts (percentages). Normal distribution and homogeneous variance were tested for all data. Normal distribution test was performed by Shapiro–Wilk test via function `shapiro.test()` in R, and homogeneity of variance test was performed by Bartlett’s Test via function `bartlett.test()` in R. Differences in characteristics between

the clusters were assessed using analysis of variance for continuous normally distributed and homogeneous variance values, and the nonparametric Kruskal–Wallis test with Dunn’s posttest for continuous nonnormally distributed and/or inhomogeneous variances values using the R package FSA (<https://cran.r-project.org/package=FSA>). The difference between rates was tested by  $\chi^2$  test or Fisher’s exact test for categorical variables. Survival curves were compared by log-rank analysis. The Benjamini–Hochberg procedure was



**TABLE 1 |** Demographic characteristics, hospitalization days, and outcomes of 1,035 COVID-19 patients.

| Characteristics             | Median (IQR)        |
|-----------------------------|---------------------|
| Age (years)                 | 63.20 (52.00–70.33) |
| Sex                         |                     |
| Female                      | 525 (50.72%)        |
| Male                        | 510 (49.28%)        |
| Hospitalization days (days) | 21.00 (14.00–31.00) |
| Outcomes                    |                     |
| Dead                        | 61 (5.89%)          |
| Alive                       | 974 (94.1%)         |

Continuous variables are presented as median (interquartile ranges), while categorical variables as counts and percentages (%).

used for multiple comparison correlation. A  $p < 0.05$  was considered statistically significant. Box plots and radar charts were compiled using the R packages ggpubr (<https://cran.r-project.org/package=ggpubr>) and fmsb (<https://cran.r-project.org/package=fmsb>), respectively.

## Construction of the Classifier Model to Forecast COVID-19 Clusters

SVM is a popular supervised learning method that constructs hyperplanes in a high-dimensional space to separate training data into different classes and is often used for classification. In our study, an SVM classifier model of COVID-19 clusters were constructed by the R package e1071 (<https://cran.r-project.org/package=e1071>). Indicators of the COVID-19 patients on admission, including their clinical symptoms and laboratory tests, with statistically significant differences among the three clusters, were chosen as the predictor variables, and the response variable was the FAMD-based clustering results.

All 1,035 patients were randomly divided into 70% training and 30% test datasets. We implemented a grid search and 10-fold cross validation for tuning and validating the prediction model on the training dataset. Then the model with optimal parameters were tested on the test dataset. Kappa statistic was calculated using the R package caret (<https://CRAN.R-project.org/package=caret>) and used to evaluate the performance of SVM model with different kernel and parameters. A receiver operating characteristic (ROC) curve was constructed, and the ROC areas under the curve (AUCs) were calculated using the R package pROC (<https://cran.r-project.org/package=pROC>) (19).

To test the performance of model in the case of missing data, all patients were divided into 50% training and 50% missing test dataset. About 1–10% laboratory data in the missing dataset was removed randomly using the R package simFrame (<https://cran.r-project.org/package=simFrame>) (20), and missing data were imputed by k-nearest neighbor (KNN) method using the R package DMwR2 (<https://cran.r-project.org/package=DMwR2>). The SVM model was firstly trained on the 50% training dataset and then tested on the 50% missing dataset. Tests were repeated 50 times with the same missing rate.

**TABLE 2 |** Laboratory findings within 48 h after admission of 1,035 COVID-19 patients.

| Laboratory tests                     | Median (IQR)           | Reference intervals |
|--------------------------------------|------------------------|---------------------|
| ALT (U/L)                            | 23.00 (15.00–40.00)    | ≤41                 |
| AST (U/L)                            | 24.00 (18.00–36.00)    | ≤40                 |
| γ-GT (U/L)                           | 29.00 (18.00–52.00)    | 10–71               |
| Albumin (g/L)                        | 36.10 (32.40–39.90)    | 35–52               |
| Globulin (g/L)                       | 31.80 (28.50–35.60)    | 20–35               |
| Total protein (g/L)                  | 68.30 (64.90–72.00)    | 64–83               |
| Creatinine (μmol/L)                  | 68.00 (57.00–83.00)    | 59–104              |
| Urea (mmol/L)                        | 4.40 (3.50–5.70)       | 3.1–8.0             |
| Uric acid (μmol/L)                   | 262.10 (208.00–324.40) | 202.3–416.5         |
| Total cholesterol (mmol/L)           | 3.82 (3.23–4.48)       | <5.18               |
| Blood glucose (mmol/L)               | 5.80 (5.11–7.31)       | 4.11–6.05           |
| LDH (U/L)                            | 249.00 (200.00–316.00) | 135–225             |
| ALP (U/L)                            | 67.00 (55.00–81.00)    | 40–130              |
| WBC count ( $\times 10^9/L$ )        | 5.78 (4.63–7.26)       | 3.50–9.50           |
| RBC count ( $\times 10^{12}/L$ )     | 4.09 (3.69–4.47)       | 4.30–5.80           |
| Lymphocyte rate (%)                  | 22.40 (14.60–30.50)    | 20–50               |
| Lymphocyte count ( $\times 10^9/L$ ) | 1.24 (0.85–1.65)       | 1.10–3.20           |
| Monocyte rate (%)                    | 8.50 (6.80–10.30)      | 3.0–10.0            |
| Monocyte count ( $\times 10^9/L$ )   | 0.49 (0.37–0.64)       | 0.10–0.60           |
| Neutrophil rate (%)                  | 66.30 (57.30–75.70)    | 40.0–75.0           |
| Neutrophil count ( $\times 10^9/L$ ) | 3.72 (2.74–5.23)       | 1.80–6.30           |
| Eosinophil rate (%)                  | 1.00 (0.20–2.00)       | 0.4–0.8             |
| Eosinophil count ( $\times 10^9/L$ ) | 0.06 (0.01–0.12)       | 0.02–0.52           |
| Basophil rate (%)                    | 0.20 (0.10–0.40)       | 0.0–1.0             |
| Basophil count ( $\times 10^9/L$ )   | 0.01 (0.01–0.03)       | 0.00–0.10           |
| Hematocrit (%)                       | 36.60 (33.30–39.40)    | 40.0–50.0           |
| Hemoglobin (g/L)                     | 126.00 (115.00–136.00) | 130.0–175.0         |
| Platelet ( $\times 10^9/L$ )         | 237.00 (180.00–309.50) | 125.0–350.0         |
| D-dimer (μg/ml FEU)                  | 0.67 (0.34–1.48)       | <0.5                |
| PTA (%)                              | 93.00 (86.00–101.00)   | 75.0–125.0          |
| PT (s)                               | 13.70 (13.10–14.20)    | 11.5–14.5           |
| INR                                  | 1.05 (0.99–1.10)       | 0.80–1.20           |
| CRP (mg/L)                           | 10.20 (1.90–49.50)     | <1                  |
| eGFR (ml/min/1.73 m <sup>2</sup> )   | 92.60 (78.80–102.50)   | >90                 |

ALT, alanine transaminase; AST, aspartate transaminase; γ-GT, gamma-glutamyl transferase; LDH, lactic dehydrogenase; ALP, alkaline phosphatase; WBC, white blood cell; RBC, red blood cell; PTA, prothrombin time activity; PT, prothrombin time; INR, international normalized ratio; CRP, C-reactive protein; eGFR, estimated glomerular filtration rate. The reference intervals of laboratory tests were aligned with those used by the laboratory of Tongji Hospital. Continuous variables are presented as median (interquartile ranges).

## RESULTS

### Demographic, Clinical, and Laboratory Characteristics of 1,035 COVID-19 Patients

A total of 1,413 COVID-19 positive patients were primarily enrolled to the study. The heat map of missing laboratory tests analysis was illustrated in **Supplementary Figure 1**, and the completeness rates of laboratory tests were illustrated in **Supplementary Figure 2**. Only the laboratory tests with more than 90% completeness were kept for the next analysis. In

**TABLE 3 |** Frequencies of symptoms before admission of 1,035 COVID-19 patients.

| Symptoms                        | <i>n</i> = 1,035 (%) |
|---------------------------------|----------------------|
| Fever                           | 797 (77.00%)         |
| Chills                          | 196 (18.94%)         |
| Inappetence                     | 301 (29.08%)         |
| Fatigue                         | 334 (32.27%)         |
| Myalgia                         | 171 (16.52%)         |
| Headache                        | 79 (7.63%)           |
| Palpitations                    | 47 (4.54%)           |
| Night sweat                     | 40 (3.86%)           |
| Dizziness                       | 50 (4.83%)           |
| Cough                           | 774 (74.78%)         |
| Nasal obstruction or runny nose | 28 (2.70%)           |
| Sore throat                     | 63 (6.09%)           |
| Dyspnea                         | 361 (34.88%)         |
| Diarrhea                        | 245 (23.67%)         |
| Abdominal pain                  | 20 (1.93%)           |
| Nausea                          | 108 (10.43%)         |
| Vomiting                        | 56 (5.41%)           |

Categorical variables are presented as counts and percentages (%).

addition, to ensure the accuracy of the study, only patients with all more than 90% completeness laboratory tests were retained. After the screening process, 1,035 patients and 34 laboratory indicators remained. Then we collected age, sex, syndromes, and laboratory findings from 1,035 COVID-19 patients. Women made up 50.72%, and the median age of the group was 63.20 (52.00–70.33). The most common clinical symptom was fever (77.00%), followed by cough (74.78%), dyspnea (34.88%), fatigue (32.27%), and inappetence (29.08%). Lactate dehydrogenase (LDH), albumin, blood glucose, red blood cell (RBC) count, lymphocyte count, percentage of lymphocytes, percentage of eosinophils, hemoglobin, hematocrit, estimated glomerular filtration rate (eGFR), CRP, and D-dimer were clearly abnormal in all 1,035 individuals.

### FAMD-Based Cluster Analysis

FAMD was applied to the original matrix, which consisted of age, sex, 17 symptoms and 34 laboratory indicators of the 1,035 COVID-19 patients, and 53 dimensions were obtained (**Supplementary Table 1**). Variances of 53 dimensions decreased gradually, and variances of the top 24 dimensions accounted for more than 80% of the total variance. Thus, the top 24 dimensions were retained for further analysis. Subsequently, unsupervised hierarchical cluster analysis was performed with the matrix made with the top 24 dimensions values of 1,035 individuals. A dendrogram (**Figure 2A**) showed the last five steps of cluster analysis.

Agglomerative hierarchical cluster analysis had a bottom-up approach, and all subjects were clustered into a single cluster at last, so it had to decide when to stop clustering. If the number of clusters was too small, the clinical features of COVID-19 patients would be more homogeneous, and it could not well-reveal

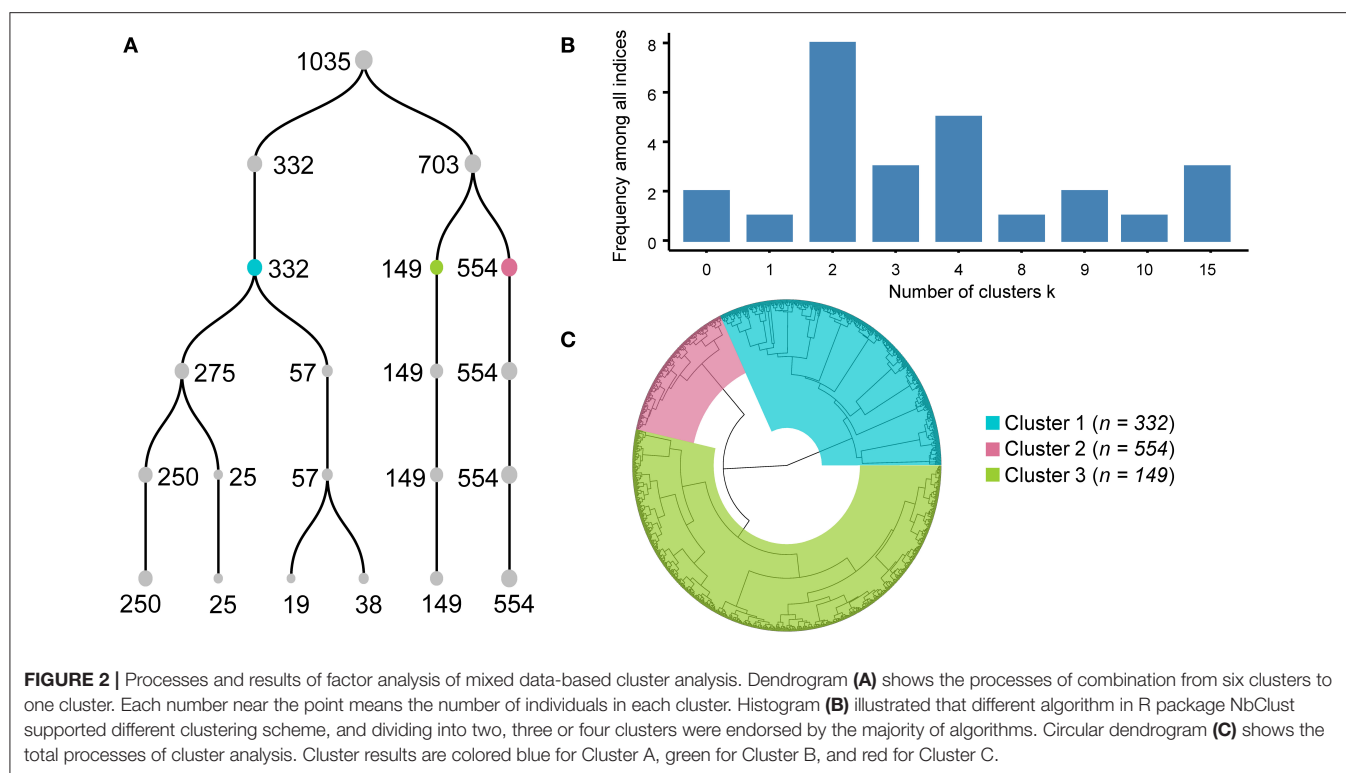
the clinical pattern of COVID-19. Conversely, the COVID-19 patterns represented by multiple clusters were unintelligible and difficult to understand. Therefore, it was crucial to determine how many clusters to use. We first evaluated the range of the number of clusters by the R package NbClust using 26 algorithms. Six, four, and six algorithms supposed that the best cluster numbers were 2, 3, and 4, respectively (**Figure 2B**), which indicated that the range of best cluster number was 2–4.

Then, we examined the differences in laboratory tests among different clusters under the conditions of dividing them into 2, 3, and 4 clusters separately. All laboratory test values under the conditions of dividing them into 2, 3, and 4 clusters did not meet normal distribution and homogeneity of variance, so the nonparametric Kruskal–Wallis test with Dunn's posttest was used for multiple comparison analysis (**Supplementary Tables 2–5**). We found that when the individuals were divided into two clusters, it was not hard to observe that almost all indexes of patients in Cluster A were more severe than those in patients of Cluster B (**Supplementary Figure 3**). When the COVID-19 individuals were divided into four clusters, the levels of CRP, D-dimer, PT, and the percentage of lymphocytes, which have been reported as crucial disease severity indexes, had no differences between Cluster D and the other three clusters (**Supplementary Figure 4**). In contrast, the above crucial indicators can be distinguished well when divided into three clusters (**Figures 3, 4**). Thus, it is natural to suppose that the severity of COVID-19 patients in Cluster D had no significant difference, which indicated that this clustering scheme might just be in accordance with the characteristics of the data itself instead of the clinical phenotypes of COVID-19. Accordingly, we thought that dividing into three clusters was the best clustering scheme, and the 1,035 COVID-19 patients were divided into three clusters in the following analysis (**Figure 2C**).

### Demographic, Symptoms, and Laboratory Characteristics in Different COVID-19 Clusters

The demographic characteristics of the three clusters are presented in **Table 4**. Surprisingly, there was no difference in age or sex among the clusters. The laboratory indicators and syndrome characteristics of the three clusters are shown in **Tables 5, 6**. Most laboratory findings and syndromes differed among the clusters, and the differences in laboratory indicators and syndromes among the three clusters can be seen intuitively from box plots (**Figures 3, 4**) and radar charts (**Figure 5**). Overall, the patients in Cluster A presented with the most severe conditions at the time of admission, and patients in Cluster C were the mildest. In contrast, the conditions of individuals in Cluster B were in between these two.

A total of 332 patients were included in Cluster A. Almost all laboratory indicators and symptoms were worst in Cluster A. In terms of blood biochemistry tests, patients in Cluster A presented the highest levels of alanine transaminase (ALT), aspartate transaminase (AST), gamma-glutamyl transferase ( $\gamma$ -GT), LDH, alkaline phosphatase (ALP), total cholesterol, blood glucose, and albumin and the lowest level of globin. Additionally, their median



eGFR was abnormally low and the level of creatinine was high in Cluster A. In routine blood tests, Cluster A showed higher white blood cell (WBC) counts, neutrophil counts, percentage of neutrophils, and lower levels of lymphocyte counts and percentage of lymphocytes than the other two clusters. Moreover, the levels of eosinophil and basophils were also lowest in Cluster A individuals. Regarding coagulation function, Cluster A patients exhibited higher levels of D-dimer, prothrombin time (PT), and international normalized ratio (INR) and lower levels of prothrombin time activity (PTA). Finally, the highest level of CRP was also observed in Cluster A, and the median CRP was up to 18.05 mg/L.

The frequencies of many systemic and neurological symptoms in Cluster A patients, including fever, chills, fatigue, myalgia, headache, palpitation, night sweat, and dizziness, were highest among the three clusters. For respiratory symptoms and digestive tract symptoms, the frequencies of nasal obstruction or runny nose, sore throat, dyspnea, diarrhea, abdominal pain, nasal obstruction or runny nose, vomiting and anorexia were also at the top level among the three clusters. Although the frequency of cough was the second highest among the clusters, three-quarters of individuals in Cluster A had cough before their hospitalization. Therefore, Cluster A could also be designated as a severe cluster.

Cluster B was the largest cluster in this study, and almost all of their laboratory indicators and frequencies of symptoms seem to be intermediate between Clusters A and C; however, the frequency of cough was an exception. The most prominent symptom in Cluster B was a cough, which was reported in almost all individuals in Cluster B. In addition to a cough, patients in Cluster B showed moderate frequencies of fever, fatigue,

myalgia, headache and nausea. The frequencies of chills, dyspnea and diarrhea in Cluster B were as high as those in Cluster A; however, the frequencies of palpitation, night sweat, dizziness, nasal obstruction or runny nose, sore throat, abdominal pain, vomiting, and anorexia in Cluster B were uniformly low relative to those in Cluster C. Notably, the frequencies of palpitation, night sweat, dizziness, nasal obstruction or runny nose, sore throat, abdominal pain, nausea, and vomiting in Clusters B and C were very close to 0%.

Cluster C, with 149 individuals, had the lowest number of COVID-19 patients and the lowest levels of almost all indicators, including CRP and symptoms, among the three clusters. It is worth mentioning that the conditions of individuals in Cluster C were rather mild, not only because of those better indicators but also because of their close to 0% frequencies of palpitations, night sweats, dizziness, nasal obstruction or runny nose, sore throat, abdominal pain, nausea and vomiting, and even coughing. In contrast, the frequencies of fever (65.77%), dyspnea (24.16%), anorexia (22.15%), fatigue (18.79%), diarrhea (12.75%), and chills (11.40%) in Cluster C were relatively high, but they were still not higher than those in Cluster B.

There were statistically significant differences between the two clusters in most laboratory indicators. However, statistically significant differences were observed between two arbitrary clusters only for AST, LDH, albumin, D-dimer and CRP, which implied that only those indicators could well-distinguish the three clusters. Few laboratory indicators, including hemoglobin, hematocrit, platelet count, and monocyte count, did not differ between any two clusters, and those indicators without any differences are not presented in Figures 3, 4.

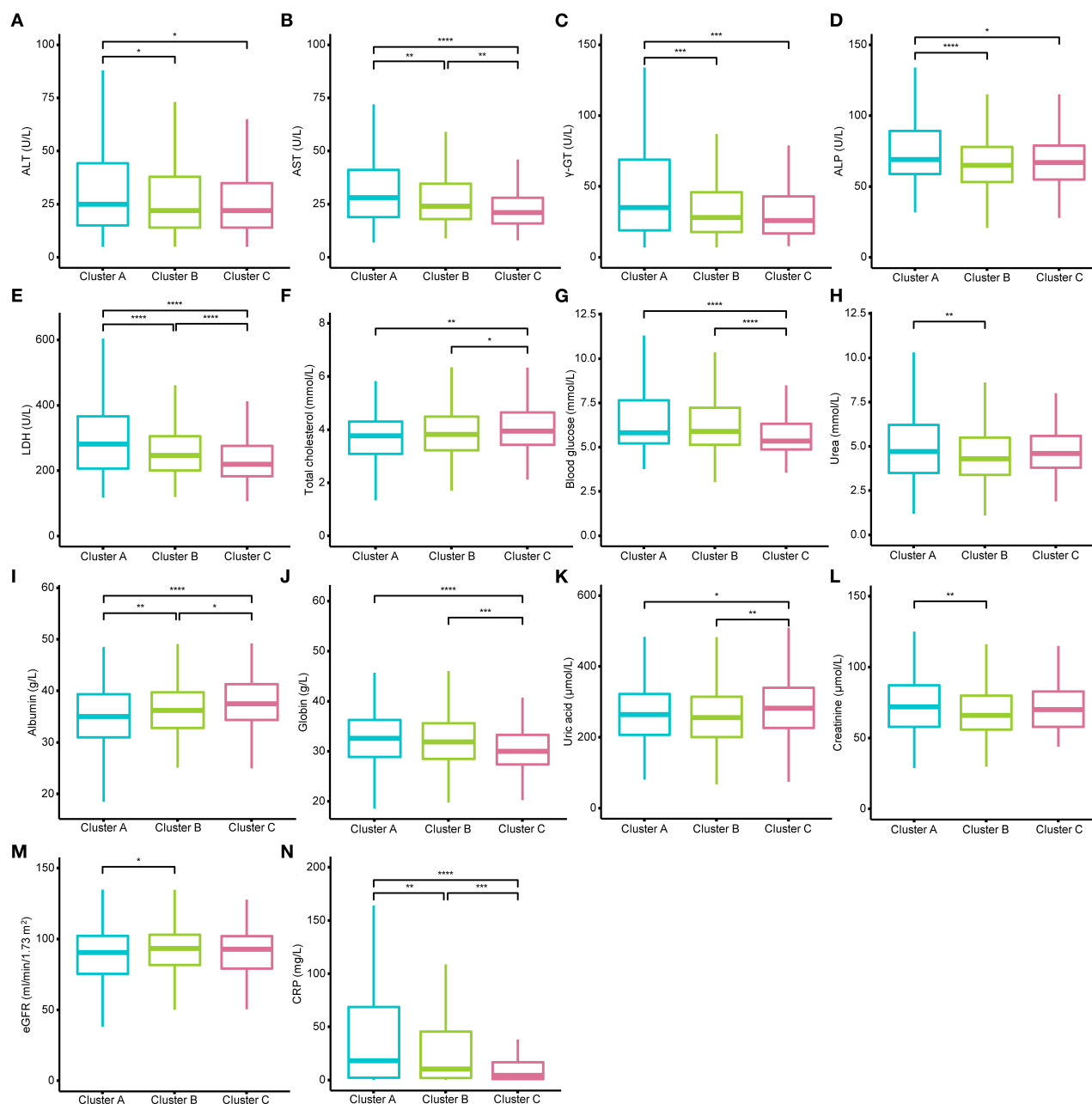


**FIGURE 3 |** Different levels of blood biochemistry tests among the three clusters. (A–N) show the different levels of alanine transaminase (ALT), aspartate transaminase (AST), gamma-glutamyl transferase (γ-GT), alkaline phosphatase (ALP), lactic dehydrogenase (LDH), total cholesterol, blood glucose, urea, albumin, globulin, uric acid, creatinine, estimated glomerular filtration rate (eGFR), and C-reactive protein (CRP) among the three clusters. AST, LDH, CRP, and albumin could well-distinguish the three clusters. The Kruskal–Wallis tests with Dunn's post-test was performed, and the *p*-value were adjusted by the Benjamini–Hochberg procedure. \**p* < 0.05; \*\**p* < 0.01; \*\*\**p* < 0.001; \*\*\*\**p* < 0.0001.

## Clinical Prognosis of Different COVID-19 Clusters

To evaluate outcomes of patients in different clusters, we first compared the length of hospitalization among the three cluster first. We found that the length of hospitalization in Cluster C was lower than that in Clusters A and B (Figure 6A).

Subsequently, Kaplan–Meier survival analysis of three clusters classified by FAMD-based hierarchical clustering was performed. The mortalities of the three clusters were 9.94, 4.51, and 2.01%, respectively. Survival rates were statistically assessed by the log-rank test. The results indicated that there were significant differences between Clusters A and B and between Clusters A and



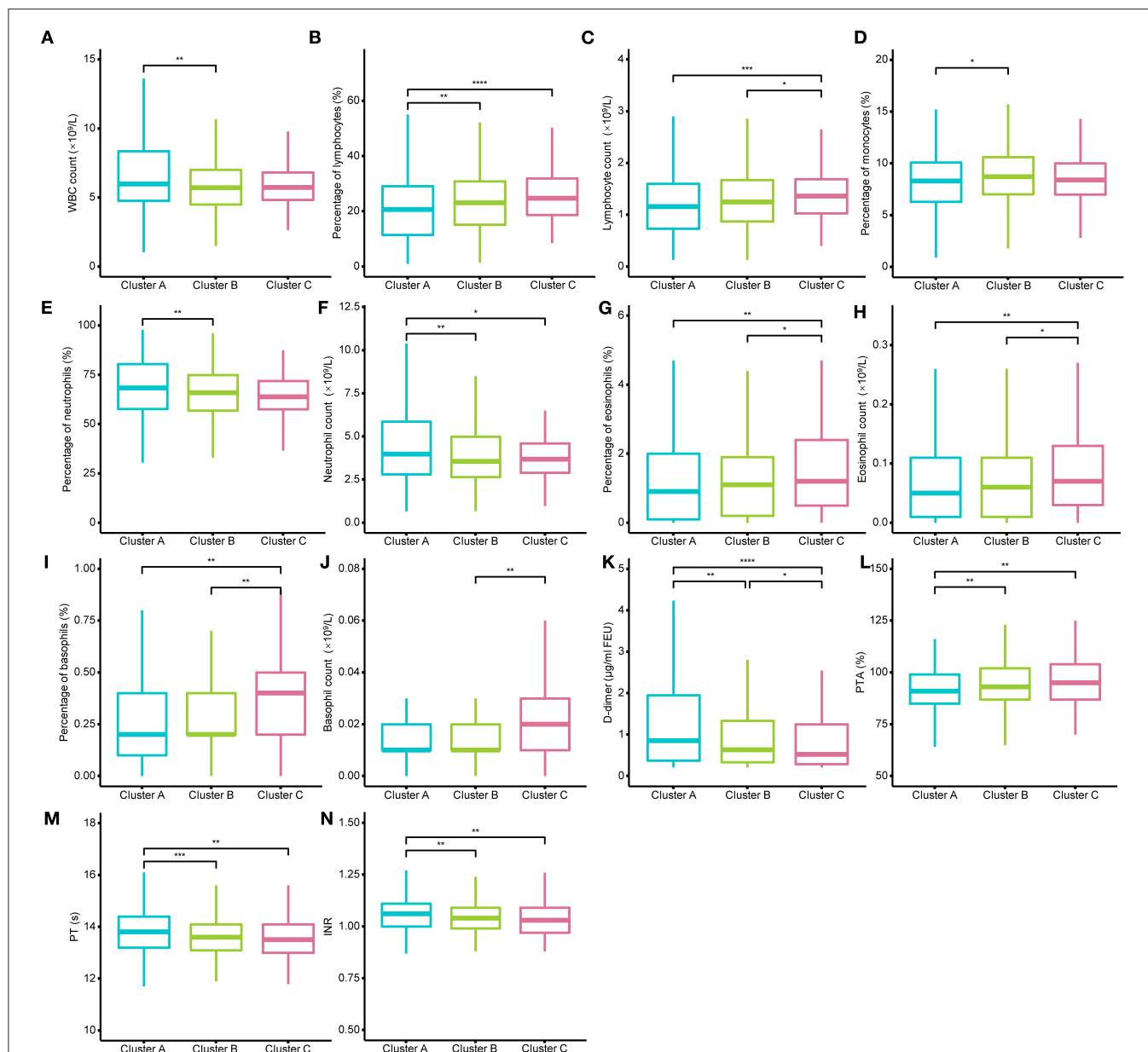


**FIGURE 4 |** Different levels of routine blood tests and coagulation function among the three clusters. (A–N) show the different levels of white blood cell (WBC) count, percentage of lymphocytes, lymphocyte count, percentage of monocytes, percentage of neutrophils, neutrophil count, percentage of eosinophils, eosinophil count, percentage of basophils, basophil count, D-dimer, prothrombin time activity (PTA), and prothrombin time (PT), international normalized ratio (INR). D-dimer could well distinguish the three clusters. The Kruskal–Wallis tests with Dunn’s posttest was performed, and  $p$ -values were adjusted by the Benjamini–Hochberg procedure. \* $p < 0.05$ ; \*\* $p < 0.01$ ; \*\*\* $p < 0.001$ ; \*\*\*\* $p < 0.0001$ .

C (Figure 6B). As with the length of hospitalization, no difference was observed between Clusters B and C (Figure 6B).

## SVM Classifier Model Construction and Parameter Optimization

Using the results of the unsupervised hierarchical clustering, we trained an SVM classifier model to aid clinical judgement. We chose all symptoms and AST, albumin, LDH, lymphocyte count, percentage of lymphocytes,

neutrophil count, percentage of eosinophils, eosinophil count, basophil count, D-dimer, PTA, INR, and CRP as predictor variables in the model. Laboratory indicators in the prediction model could well-distinguish three clusters according to the above the nonparametric Kruskal–Wallis test with Dunn’s posttest, so they were chosen for the predictor variables.

A grid-search on 10-fold cross validation for parameters was performed to find the best model, and parameters producing

**TABLE 4 |** Demographic characteristics of three COVID-19 clusters identified by Factor Analysis of Mixed Data-based cluster analysis.

| Characteristics             |        | Cluster A (n = 332) | Cluster B (n = 554) | Cluster C (n = 149) | p-value  |
|-----------------------------|--------|---------------------|---------------------|---------------------|----------|
| Age (years)                 |        | 63.28 (51.95–71.15) | 63.23 (51.62–69.67) | 62.86 (54.18–70.98) | 0.81651  |
| Sex                         | Female | 165                 | 289                 | 71                  | 0.55872  |
|                             | Male   | 167                 | 265                 | 78                  |          |
| Hospitalization days (days) |        | 23.00 (14.00–35.25) | 22.00 (14.00–32.00) | 19.00 (11.00–24.00) | <0.00001 |
| Outcomes                    | Dead   | 33                  | 25                  | 3                   | 0.00052  |
|                             | Alive  | 299                 | 529                 | 146                 |          |

Continuous variables are presented as median (interquartile ranges), and Kruskal–Wallis test was applied for continuous variables. Categorical variables are expressed as counts and percentages (%), and the  $\chi^2$  test or Fisher's exact test were applied for categorical variables.

the best result were chosen (Supplementary Figure 5). The highest mean total kappa statistic on the training dataset was 0.847, which was predicted by the radial basis function (RBF) kernel (Supplementary Figure 5B). The confusion matrix for the classifier model on the test dataset was shown in Figure 7A, and kappa statistic of the model on the test dataset was 0.848, which suggested that the model was not over-fitted. So the RBF kernel (gamma = 0.01 and cost = 100) was chosen for the final construction of the classifier model. Three ROC curves represented the prediction performances of the three clusters respectively. The AUCs were 0.9704 (95% CI: 0.9483–0.9926), 0.9686 (95% CI: 0.9463–0.9909), and 0.9832 (95% CI: 0.9642–1), respectively (Figures 7B–D). ROC curves and AUCs also indicated the excellent predictive power of FAMD-based cluster analysis results.

Subsequently, we tested the performance of the SVM model in the case of missing data. Mean kappa statistics remained consistently >0.8, and the result indicated that the model could well-cope with up to 10% missing laboratory data imputed by KNN method (Supplementary Figure 6). Data with more than 10% missing rate could not be imputed well by KNN method, so we did not test it with higher missing rate.

There were 17 laboratory tests in the classifier model, which were not hard to get according to reviewing medical records or directly asking patients at their admission. Other thirteen predictor variables were laboratory tests, and six of them (lymphocyte count, percentage of lymphocytes, neutrophil count, eosinophil count, percentage of eosinophils, and basophil count) were belonged to routine blood tests, which is a common and cheap clinical test and easily to get. Additionally, C-reactive protein (CRP), aspartate transaminase (AST), lactic dehydrogenase (LDH), albumin, as well as D-dimer, prothrombin time activity (PTA), and international normalized ratio (INR) were commonly used to evaluate the disease progression. Even though medical institutions could not test part of them, data imputation could well-cope with this point. In short, the model has a broad range of clinical applications, and lots of predictor variables would not restrain it from application. Our classifier model is open-sourced and available at <https://github.com/Spider-Rom/Support-Vector-Machine-Based-Classifer-Model-of-COVID-19-patients>.

## DISCUSSION

Over the past year, a wave of COVID-19 has hit people around the world. In response, a number of correlated studies have been carried out, and our knowledge of COVID-19 has grown rapidly. It has been reported that COVID-19 has a wide spectrum of clinical manifestations, ranging from asymptomatic carrier infection to life-threatening complications (2, 21, 22). The diversity of clinical manifestations of COVID-19 means two different things. On the one hand, the same patient could present mild symptoms shortly after infection, and the clinical manifestations could worsen as the disease progresses. On the other hand, some patients are always in asymptomatic states, but other patients might present with severe conditions. Heterogeneous clinical manifestations of COVID-19 make its diagnosis and a determination of their prognosis challenging. Moreover, a broad spectrum of COVID-19 clinical manifestations and clinical course pose difficulty in the systematic analysis of COVID-19 clinical features. Additionally, it is difficult for clinicians to give comprehensive consideration to the vast amount of information on multiple symptoms and laboratory findings, especially when patients have a less severe condition. Furthermore, the classifications of COVID-19 in past studies were often based on a few key laboratory findings or on whether complications or adverse events happened rather than based on the clinical manifestations, which would be unfavorable to systematic and comprehensive research on COVID-19.

On account of these points, FAMD-based clustering hierarchical analysis, an unsupervised machine learning method, was performed on the clinical information at the time of admission of 1,035 COVID-19 patients. The cluster analysis results in the identification of three distinct clusters: Cluster A, most severe syndromes and laboratory findings, longest hospital stays; Cluster B, intermediate severe syndromes and laboratory findings, equally long length of hospital stay with Cluster A; Cluster C, mildest clinical syndromes and laboratory findings, shortest length of hospital stays among the three clusters. Survival analysis showed that the worst survival of COVID-19 patients in Cluster A. There were no contradictions in the three clusters among laboratory findings, symptoms, and prognosis, which was also consistent with our experience in clinical practice. It is easy to see that Cluster B had the greatest number of individuals, and Cluster C had the smallest number

**TABLE 5 |** Laboratory findings of three COVID-19 clusters identified by Factor Analysis of Mixed Data-based cluster analysis.

| Laboratory tests                     | Cluster A (n = 332)    | Cluster B (n = 554)    | Cluster C (n = 149)    | p-value  |
|--------------------------------------|------------------------|------------------------|------------------------|----------|
| ALT (U/L)                            | 25.00 (15.00–44.25)    | 22.00 (14.00–38.00)    | 22.00 (14.00–35.00)    | 0.00294  |
| AST (U/L)                            | 28.00 (19.00–41.25)    | 24.00 (18.00–34.75)    | 21.00 (16.00–28.00)    | <0.00001 |
| $\gamma$ -GT (U/L)                   | 35.00 (19.00–69.00)    | 28.00 (18.00–46.00)    | 26.00 (17.00–43.00)    | 0.00002  |
| Albumin (g/L)                        | 35.05 (31.00–39.40)    | 36.20 (32.83–39.78)    | 37.50 (34.40–41.30)    | 0.00010  |
| Globulin (g/L)                       | 32.60 (28.90–36.30)    | 31.90 (28.53–35.65)    | 30.00 (27.40–33.30)    | 0.00006  |
| Total protein (g/L)                  | 67.90 (64.85–71.73)    | 68.70 (64.90–72.30)    | 68.50 (64.90–71.50)    | 0.44564  |
| Creatinine ( $\mu$ mol/L)            | 72.00 (58.00–87.25)    | 66.00 (56.00–80.00)    | 70.00 (58.00–83.00)    | 0.00361  |
| Urea (mmol/L)                        | 4.70 (3.50–6.23)       | 4.30 (3.40–5.50)       | 4.60 (3.80–5.60)       | 0.01137  |
| Uric acid ( $\mu$ mol/L)             | 264.20 (207.53–322.53) | 255.65 (200.95–315.00) | 282.00 (226.70–340.00) | 0.00556  |
| Total cholesterol (mmol/L)           | 3.77 (3.09–4.31)       | 3.82 (3.23–4.50)       | 3.94 (3.44–4.65)       | 0.00162  |
| Blood glucose (mmol/L)               | 5.81 (5.22–7.65)       | 5.89 (5.14–7.24)       | 5.34 (4.88–6.33)       | 0.00011  |
| LDH (U/L)                            | 281.00 (207.00–366.25) | 247.00 (201.25–305.75) | 220.00 (183.00–276.00) | <0.00001 |
| ALP (U/L)                            | 69.00 (59.00–89.25)    | 65.00 (53.25–78.00)    | 67.00 (55.00–79.00)    | 0.00017  |
| WBC count ( $\times 10^9$ /L)        | 5.98 (4.77–8.35)       | 5.71 (4.49–7.02)       | 5.72 (4.83–6.81)       | 0.00722  |
| RBC count ( $\times 10^{12}$ /L)     | 4.11 (3.64–4.47)       | 4.07 (3.70–4.46)       | 4.11 (3.73–4.47)       | 0.86039  |
| Lymphocyte rate (%)                  | 20.65 (11.48–29.10)    | 23.05 (15.20–30.90)    | 24.70 (18.70–31.90)    | 0.00023  |
| Lymphocyte count ( $\times 10^9$ /L) | 1.16 (0.73–1.60)       | 1.25 (0.87–1.67)       | 1.36 (1.03–1.69)       | 0.00316  |
| Monocyte rate (%)                    | 8.30 (6.30–10.10)      | 8.70 (7.03–10.60)      | 8.40 (7.00–10.00)      | 0.03766  |
| Monocyte count ( $\times 10^9$ /L)   | 0.49 (0.37–0.65)       | 0.48 (0.37–0.64)       | 0.50 (0.38–0.60)       | 0.80982  |
| Neutrophil rate (%)                  | 68.40 (57.68–80.53)    | 65.95 (56.83–74.90)    | 63.80 (57.60–71.90)    | 0.00332  |
| Neutrophil count ( $\times 10^9$ /L) | 3.98 (2.80–5.87)       | 3.55 (2.65–4.99)       | 3.68 (2.90–4.60)       | 0.00318  |
| Eosinophil rate (%)                  | 0.90 (0.10–2.00)       | 1.10 (0.20–1.90)       | 1.20 (0.50–2.40)       | 0.03027  |
| Eosinophil count ( $\times 10^9$ /L) | 0.05 (0.01–0.11)       | 0.06 (0.01–0.11)       | 0.07 (0.03–0.13)       | 0.05311  |
| Basophil rate (%)                    | 0.20 (0.10–0.40)       | 0.20 (0.20–0.40)       | 0.40 (0.20–0.50)       | 0.00175  |
| Basophil count ( $\times 10^9$ /L)   | 0.01 (0.01–0.02)       | 0.01 (0.01–0.02)       | 0.02 (0.01–0.03)       | 0.01233  |
| Hematocrit (%)                       | 36.60 (32.60–39.43)    | 36.45 (33.40–39.30)    | 36.90 (33.60–39.30)    | 0.61877  |
| Hemoglobin (g/L)                     | 126.00 (113.00–136.00) | 125.00 (115.00–136.00) | 127.00 (115.00–137.00) | 0.89523  |
| Platelet ( $\times 10^9$ /L)         | 239.50 (179.00–301.00) | 235.00 (180.25–314.00) | 235.00 (182.00–304.00) | 0.94041  |
| D-dimer ( $\mu$ g/ml FEU)            | 0.86 (0.37–1.95)       | 0.63 (0.33–1.33)       | 0.52 (0.29–1.25)       | 0.00008  |
| PTA (%)                              | 91.00 (85.00–99.00)    | 93.00 (87.00–102.00)   | 95.00 (87.00–104.00)   | 0.00179  |
| PT (s)                               | 13.80 (13.20–14.40)    | 13.60 (13.10–14.10)    | 13.50 (13.00–14.10)    | 0.00096  |
| INR                                  | 1.06 (1.00–1.11)       | 1.04 (0.99–1.09)       | 1.03 (0.97–1.09)       | 0.00133  |
| CRP (mg/L)                           | 18.05 (2.28–68.88)     | 10.25 (2.10–45.70)     | 4.30 (1.00–16.90)      | <0.00001 |
| eGFR (ml/min/1.73 m <sup>2</sup> )   | 90.4 (75.45–102.20)    | 93.35 (81.83–103.05)   | 92.60 (79.20–102.00)   | 0.04890  |

ALT, alanine transaminase; AST, aspartate transaminase;  $\gamma$ -GT, gamma-glutamyl transferase; LDH, lactic dehydrogenase; ALP, alkaline phosphatase; WBC, white blood cell; RBC, red blood cell; PTA, prothrombin time activity; PT, prothrombin time; INR, international normalized ratio; CRP, C-reactive protein; eGFR, estimated glomerular filtration rate. Laboratory tests are presented as median (interquartile ranges). Comparisons were performed using the Kruskal–Wallis test.

of individuals. However, the proportion of people in each cluster could not well-reflect the proportion of each cluster within all COVID-19 patients and partly because not all infected peoples would visit hospitals.

It is not easy to follow detailed clinical features of each cluster because of too many laboratory findings and symptoms were analyzed. Overall, Cluster A had the most severe symptoms and laboratory findings among the three clusters, so Cluster A should be characterized as the “severe” cluster. Patients in Cluster B had higher levels of CRP, D-dimer, AST, and LDH, indicating more severe clinical phenotypes. However, it is interesting that Clusters B and C had significantly different frequencies of respiratory symptoms and digestive symptoms. There were higher frequencies of respiratory symptom such as

cough, in Cluster B than those in Cluster C. In contrast, Cluster C almost had no respiratory symptoms. Patients in Cluster C mainly had systemic and digestive symptoms, including fever, fatigue, diarrhea, and inappetence. Remarkably, the clinical manifestations of COVID-19 patients in Cluster C were not typical due to their low frequencies of fever and cough symptoms, which may increase the difficulty of diagnosis (23).

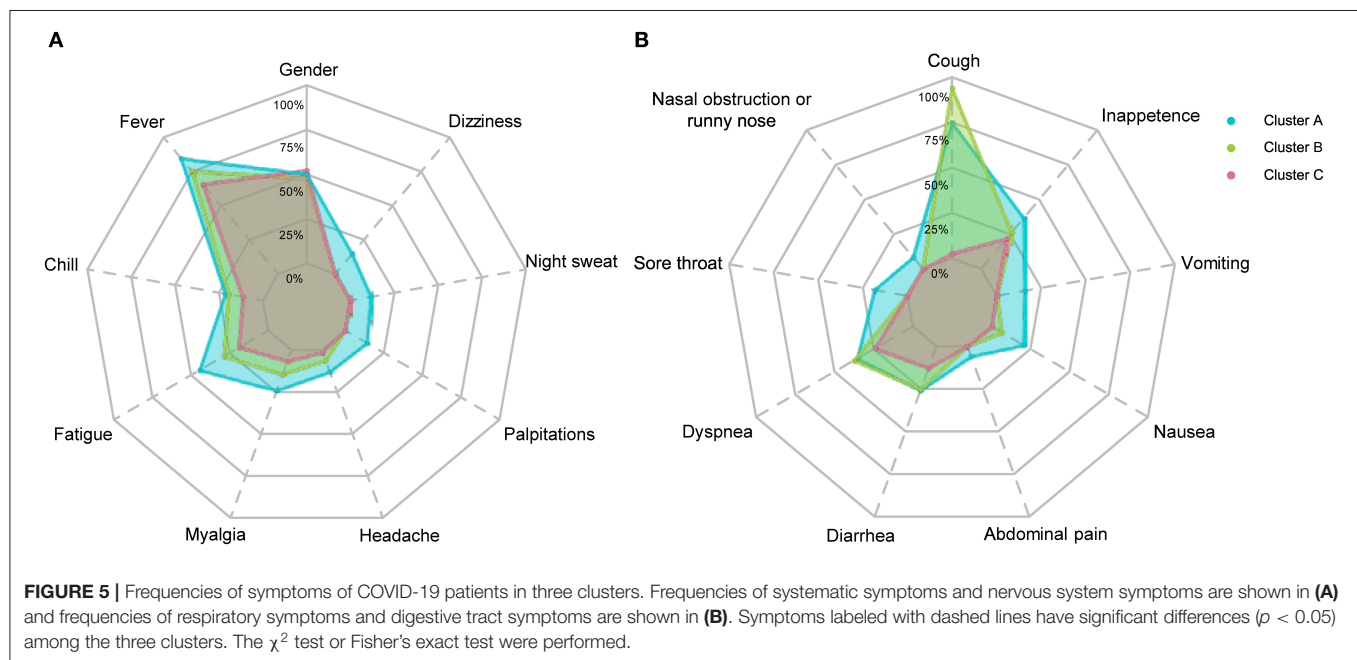
Taken together, Clusters B and C not only represented different severity of COVID-19, but also represented different clinical disease patterns. That is, the Cluster B could be characterized as the “classical” COVID-19 cluster, and Cluster C could be characterized as the “atypical” COVID-19 cluster.

Different laboratory indicators showed different abilities to identify three clusters. LDH, an intracellular enzyme, is present

**TABLE 6** | Frequencies of symptoms of three COVID-19 clusters identified by Factor Analysis of Mixed Data-based cluster analysis.

| Symptoms                        | Cluster A (%) (n = 332) | Cluster B (%) (n = 554) | Cluster C (%) (n = 149) | p-value  |
|---------------------------------|-------------------------|-------------------------|-------------------------|----------|
| Fever                           | 281 (84.64%)            | 418 (75.45%)            | 98 (65.77%)             | 0.00001  |
| Chills                          | 71 (21.39%)             | 108 (19.49%)            | 17 (11.40%)             | 0.02649  |
| Inappetence                     | 122 (36.75%)            | 146 (26.35%)            | 33 (22.15%)             | 0.00067  |
| Fatigue                         | 147 (44.28%)            | 159 (28.70%)            | 28 (18.79%)             | <0.00001 |
| Myalgia                         | 80 (24.10%)             | 81 (14.62%)             | 10 (6.71%)              | <0.00001 |
| Headache                        | 43 (12.95%)             | 34 (6.14%)              | 2 (1.34%)               | <0.00001 |
| Palpitations                    | 47 (14.16%)             | 0 (0.00%)               | 0 (0.00%)               | <0.00001 |
| Night sweat                     | 39 (11.75%)             | 1 (0.18%)               | 0 (0.00%)               | <0.00001 |
| Dizziness                       | 49 (14.76%)             | 1 (0.18%)               | 0 (0.00%)               | <0.00001 |
| Cough                           | 249 (75.00%)            | 521 (94.04%)            | 4 (2.68%)               | <0.00001 |
| Nasal obstruction or runny nose | 28 (8.43%)              | 0 (0.00%)               | 0 (0.00%)               | <0.00001 |
| Sore throat                     | 61 (18.37%)             | 2 (0.36%)               | 0 (0.00%)               | <0.00001 |
| Dyspnea                         | 117 (35.24%)            | 208 (37.55%)            | 36 (24.16%)             | 0.00832  |
| Diarrhea                        | 86 (25.90%)             | 140 (25.27%)            | 19 (12.75%)             | 0.00188  |
| Abdominal pain                  | 20 (6.02%)              | 0 (0.00%)               | 0 (0.00%)               | <0.00001 |
| Nausea                          | 69 (20.78%)             | 38 (6.86%)              | 1 (0.67%)               | <0.00001 |
| Vomiting                        | 53 (15.96%)             | 3 (5.42%)               | 0 (0.00%)               | <0.00001 |

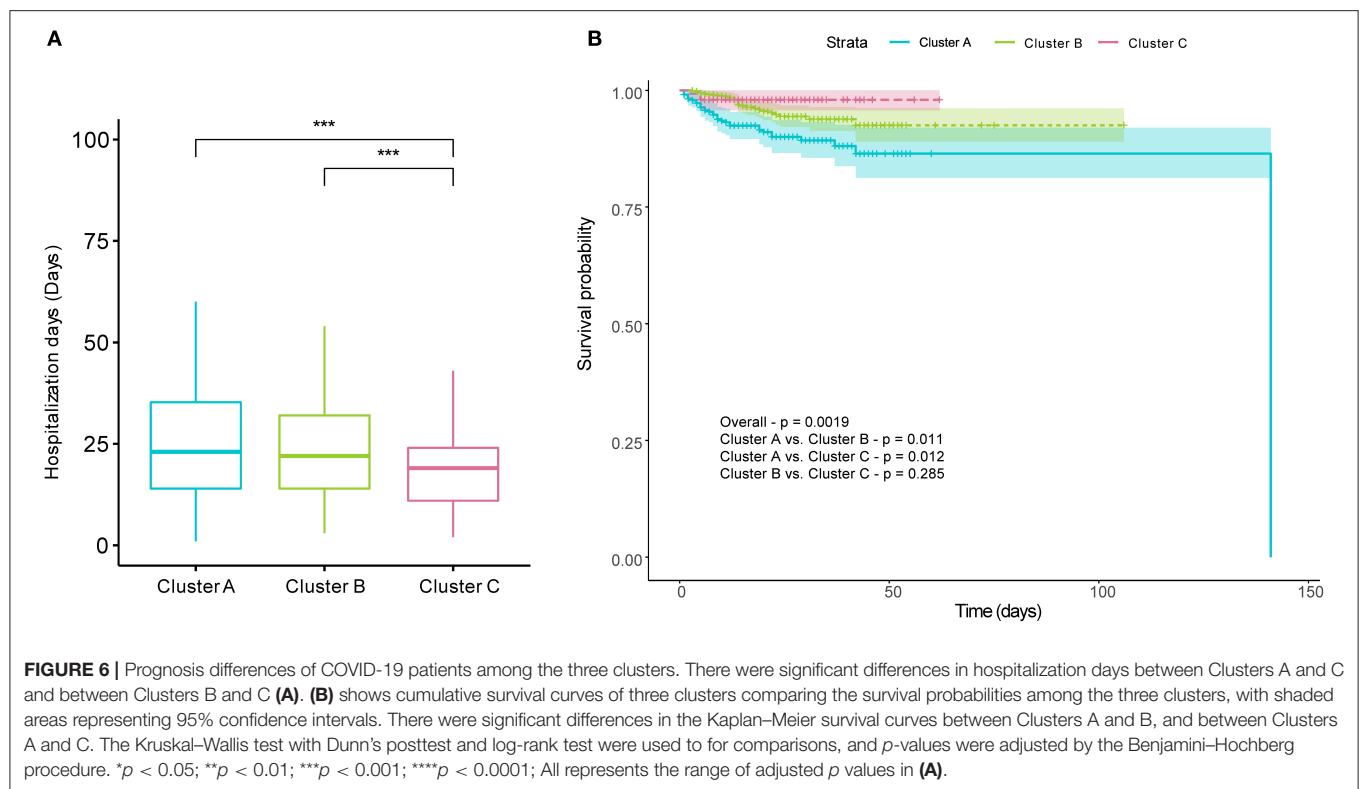
Symptoms are presented as counts and percentages (%). Comparisons were performed using the  $\chi^2$  test or Fisher's exact test.



in almost all human cells, and it is released to the extracellular space due to severe infections. Thus, a high level of LDH is associated with injury to the heart, lung, kidney, and other organs (24). Studies have indicated that elevated LDH levels indicate worse outcomes in COVID-19 patients (25). CRP, a well-known marker of inflammation, reflects systemic inflammation and tissue damage. Increased CRP levels are also associated with worse symptoms and worse organ injury among COVID-19 patients (26, 27). Furthermore, AST and D-dimer reflect the level of liver injury and coagulation dysfunction, respectively.

These two indicators are also closely relevant to the severity of COVID-19 patients (9, 28, 29). In our study, differences were present in CRP, AST, LDH, and D-dimer between any two clusters, so these four indicators were better to distinguishing the three clusters. Clinicians should pay more attention to these indicators considering their relationship between the indicators and the disease prognosis. In addition to these four indicators, hemocyte-relevant indicators, such as lymphocytes, neutrophils, eosinophils and basophils, are linked to the severity of COVID-19 (7, 30–32). Differences in hemocyte-relevant indicators were also





found among the three clusters in our study, although the ability to identify the three clusters of indicators was not as powerful as LDH and CRP. Nevertheless, abnormal hemocyte-relevant indicators of the COVID-19 patients also deserve attention.

Different frequencies of symptoms among the three clusters were also interesting, but difficult to understand. Some symptoms, such as dyspnea and diarrhea, had lower frequencies only in Cluster C; however, some other symptoms, such as sore throat, nasal obstruction or runny nose, vomiting and chills, had higher frequencies only in Cluster A. Elusive differences mean we have insufficient understanding of the disease. From the point of symptoms alone, Cluster B was closer to Cluster C than Cluster A. Contradictorily, almost all individuals in Cluster B had experienced different degrees of cough symptoms, but coughing in Cluster C was rare. Moreover, patients in Cluster C did not present cough symptoms before they were admitted to the hospital, which may indicate that patients in different clusters exhibited distinct immune response patterns when facing SARS-CoV-2 infection. It is worth noting that the three clusters did not differ in age. Therefore, we speculated that there were differences in aspects of viral loads during infection, patients’ basal diseases and immune defense abilities and whether patients rested appropriately after infection. Atypical symptoms mean better outcomes; however, they are also barriers to seeking medical attention because it is difficult for the patients themselves to realize they have a viral infection. Thus, it is necessary to regularly screen high-risk individuals by pathogenic tests.

In our study, Cluster C showed the shortest hospitalization time with a median duration of 19 days. The median

hospitalization days of patients in Clusters A and B was increased by 3–4 days, which means that those patients found it more difficult to recover. However, hospitalization days in our study are longer than other studies (33). Even if in Cluster C, COVID-19 patients exhibited 19 days of median length of a hospital stay. That might be associated with insufficient medical resources and inexperienced clinicians during the early COVID-19 epidemic in Wuhan.

Interestingly, there was no statistically significant difference in age or sex among the three clusters. Many studies have identified advanced age as a risk factor for adverse outcomes in COVID-19 patients (34, 35). However, three clusters divided by FAMD-based cluster analysis in our study showed significant differences in laboratory findings, symptoms, and outcomes but no significant difference in age. This might be interpreted as different disease patterns upon hospital admission may depend on the time elapsed from symptoms onset. However, the onset time of most COVID-19 patients in our study was not available. Our study only collected hospitalization days of COVID-19 patients and the time before admission was not included. Thus, it is hard to reveal the relationship between different disease patterns and the time elapsed from symptom onsets. Different lifestyles caused by gender differences may affect COVID-19-related mortality, but no difference was observed in sex among the three clusters (36). This could also be interpreted as minor discrepancy causing weak discriminative power.

We are able to view the clinical characteristics of COVID-19 from a novel perspective with the help of unsupervised learning methods. As previously mentioned, the clinical manifestation of

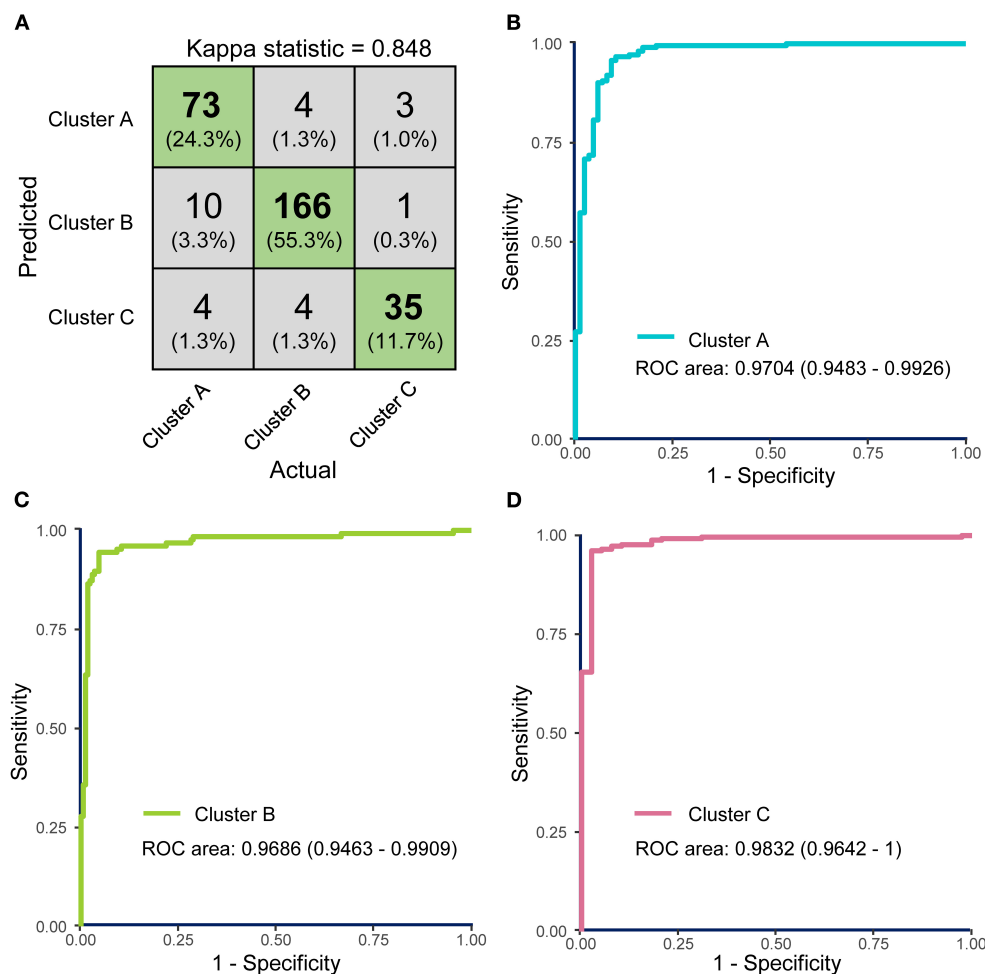


**FIGURE 7 |** The performance of the support vector machine (SVM)-based classifier model was evaluated by receiver operating characteristics (ROC) curves. **(A)** Confusion matrix showed that most COVID-19 samples in test dataset were classified precisely. **(B–D)** ROC curves for the SVM classifier represent the predictive powers of Clusters A, B, and C, respectively. The areas under the curves (AUCs) of the three ROC curves were 0.9926 (95% CI: 0.9872–0.9981), 0.9906 (95% CI: 0.9859–0.9960), and 0.9979 (95% CI: 0.9957–1.000).

COVID-19 is highly heterogeneous, and it is not appropriate to divide patients into several groups according to a few clinical indexes when exploring clinical characteristics of COVID-19. To obtain comprehensive and meaningful conclusions, we examined the data to ensure that patients enrolled in this study showed different condition severities. FAMD transformation was applied before cluster analysis because FAMD is a dimensionality reduction method similar to principal component analysis (PCA), which is able to handle categorical and continual variables simultaneously. Using FAMD, the dimensionality of the medical information matrix was decreased, and multicollinearity among independent variables, could make cluster analysis more effective (37). Because of the clinical diversity of samples in our study, clusters divided by FAMD-based cluster analysis have important implications for clinical practice. However, the differences among clusters were so complex and elusive that it was difficult to manually annotate the dataset. Given this, we finally constructed

an SVM-based classifier model to help with cluster division. Clinicians could easily determine the severity of the illness in COVID-19 patients and propose rough prognoses with the help of the model so that the treatment schemes could be adjusted in a timely manner, especially at the time of disease outbreaks.

However, there were some unavoidable shortcomings of our study. First, some symptoms of COVID-19 patients, such as loss of taste or smell, were not included because they were hardly mentioned in the primary medical records. Second, pulmonary imaging features of COVID-19 patients were also not collected in our study. In addition, some meaningful indexes such as oxygenation index ( $\text{PaO}_2/\text{FiO}_2$ ), blood gas test, and intensive care unit (ICU) length of stay, were not included in the study due to hard data collection. Furthermore, although asymptomatic infected individuals and mild cases individuals were enrolled, the frequencies of moderate and severely ill patients were higher than those in all COVID-19 patients in this single-center study

because of selection bias considering that Tongji Hospital is not primary medical institution. Last but not least, the symptoms may not be reliable enough because of unstructured nature of the clinical records, even though we excluded parsimonious and unspecific records before analysis.

In conclusion, FAMD-based cluster analysis, an exploratory unsuspended classification method, was first applied to the clinical information at the time of admission of COVID-19 patients, and three COVID-19 clusters with different symptoms, different laboratory findings and different prognoses were identified. Our study further reveals the relationship among the symptoms, laboratory findings, and prognosis of COVID-19 from a novel perspective. Results from unsupervised hierarchical clustering also have a lot of potential to help clinicians. First, some laboratory indicators such as CRP, LDH, and AST, are crucial indexes to indicate the illness severity. It has been widely reported by other studies and our study also confirmed that. Secondly, our study demonstrated that some symptoms such as fever, dizziness, palpitations, fatigue as well as nausea and vomiting, are also important to indicating the disease severity and prognosis, which has been infrequently explored in other studies. In addition, clinicians were regularly faced with dozens of indexes including laboratory findings and symptoms. Thus, the SVM-based classifier model was constructed to aid clinical assessment, which could help with developing individualized and specific treatments for COVID-19 patients in the background of continuously increasing numbers of infected people. The prediction model can not only be used for newly admitted patients, and it also works with COVID-19 patients who were under medical treatment and need to reassess their conditions.

## CONCLUSIONS

In our study, COVID-19 patients were divided into three clusters with different clinical characteristics and prognoses using FAMD-based cluster analysis, which was the first attempt at exploratory analysis of the spectrum of COVID-19 clinical characteristics, and the relationship between clinical characteristics and outcomes of COVID-19 patients was revealed from a novel perspective. An SVM-based classifier model was constructed according to the FAMD-based cluster analysis results so that this classification based on a few key laboratory findings and symptoms of COVID-19 patients can be used conveniently in clinical practice.

## DATA AVAILABILITY STATEMENT

The raw data supporting the conclusions of this article will be made available by the authors, without undue reservation.

## ETHICS STATEMENT

The studies involving human participants were reviewed and approved by the ethics committee of Tongji Hospital of Tongji Medical College of Huazhong University of Science and Technology. Written informed consent from the participants'

legal guardian/next of kin was not required to participate in this study in accordance with the national legislation and the institutional requirements.

## AUTHOR CONTRIBUTIONS

ST, ZC, and LH contributed to conception and design of the study. ZC collected the original clinical data. LH and JY processed the data. LH performed the statistical analysis. LH constructed and optimized the SVM model. ZC, JY, YaH, YiH, HW, YW, and ST interpreted the results. LH wrote the first draft of the manuscript. ZC, PS, XB, WL, and KQ revised the manuscript. PS and LH revised the manuscript according to the reviewer's suggestion. ZC and ST dominated and guided the revision of the manuscript. All authors have approved the submitted manuscript.

## FUNDING

This work was supported by the National Natural Science Foundation of China (81874383).

## ACKNOWLEDGMENTS

We are grateful to all COVID-19 patients enrolled in our study, as well as the hardworking and dedicated nurses and doctors in Tongji Hospital. In addition, all healthcare workers and researchers who fight against COVID-19 are gratefully acknowledged.

## SUPPLEMENTARY MATERIAL

The Supplementary Material for this article can be found online at: <https://www.frontiersin.org/articles/10.3389/fmed.2021.644724/full#supplementary-material>

**Supplementary Figure 1** | Distribution of missing laboratory tests in 1413 COVID-19 patients. Heatmap showed distribution of missing laboratory tests in 1413 COVID-19 patients (presence: blue; absence: white).

**Supplementary Figure 2** | Completeness rates of laboratory tests in 1413 COVID-19 patients. Histograms indicated the completeness rates of different laboratory tests. Only laboratory tests with above 90% completeness were kept for the next steps.

**Supplementary Figure 3** | Different levels of blood biochemistry tests between two clusters. (A) to (K) show the different levels of alanine transaminase (ALT), aspartate transaminase (AST), gamma-glutamyl transferase ( $\gamma$ -GT), alkaline phosphatase (ALP), lactic dehydrogenase (LDH), total cholesterol, urea, albumin, globin, creatinine, and estimated glomerular filtration rate (eGFR) between two clusters, respectively. (L) to (X) show the different levels of white blood cell (WBC) count, neutrophil count, lymphocyte count, eosinophil count, percentage of neutrophil, percentage of lymphocyte, percentage of eosinophil, percentage of basophil, D-dimer, prothrombin time (PT), international normalized ratio (INR), prothrombin time activity (PTA), C-reactive protein (CRP) between two clusters, respectively. The Kruskal-Wallis tests with Dunn's posttest were performed, and  $p$  value were adjusted by the Benjamini-Hochberg procedure. \*,  $p < 0.05$ ; \*\*,  $p < 0.01$ ; \*\*\*,  $p < 0.001$ ; \*\*\*\*,  $p < 0.0001$ .

**Supplementary Figure 4** | Different levels of blood biochemistry tests among four clusters. (A) to (L) show the different levels of alanine transaminase (ALT), aspartate transaminase (AST), gamma-glutamyl transferase ( $\gamma$ -GT), albumin, globin, creatinine, urea, uric acid, total cholesterol (TC), blood glucose, lactic

dehydrogenase (LDH) and alkaline phosphatase (ALP) among four clusters, respectively. **(M)** to **(Z)** show the different levels of white blood cell (WBC) count, percentage of lymphocyte, lymphocyte count, percentage of neutrophil, neutrophil count, percentage of eosinophil, eosinophil count, percentage of basophil, basophil count, D-dimer, prothrombin time activity (PTA), prothrombin time (PT), international normalized ratio (INR), C-reactive protein (CRP) among four clusters, respectively. The Kruskal-Wallis tests with Dunn's posttest were performed, and  $p$  value were adjusted by the Benjamini-Hochberg procedure. \*,  $p < 0.05$ ; \*\*,  $p < 0.01$ ; \*\*\*,  $p < 0.001$ ; \*\*\*\*,  $p < 0.0001$ .

**Supplementary Figure 5** | Parameter optimization of prediction model using the cross validated grid search. Overall dataset was randomly divided into 70% training and 30% tests datasets, and the optimal parameters were found by using grid search based on 10-fold cross-validation on 70% training dataset. **(A)** Kappa statistics of the linear kernel support vector machine (SVM) with different cost value. The blue dashed line indicated the change trend of mean kappa statistics with different cost value. Grey crosses indicated different kappa statistics obtained in each ten-fold cross validation, and grey area represented the range of kappa statistics. **(B)** Heat map of mean kappa statistics of a radial basis function (RBF) kernel SVM in different cost and gamma value. **(C)** Heat map of mean kappa statistics of a polynomial kernel SVM in different degree, cost and gamma value. **(D)** Heat map of mean kappa statistics of a sigmoid kernel SVM in different cost and gamma value.

## REFERENCES

- Furuse Y, Oshitani H. Viruses that can and cannot coexist with humans and the future of SARS-CoV-2. *Front Microbiol.* (2020) 11:583252. doi: 10.3389/fmicb.2020.583252
- Baj J, Karakula-Juchnowicz H, Teresiński G, Buszewicz G, Ciesielka M, Sitarz E, et al. COVID-19: specific and non-specific clinical manifestations and symptoms: the current state of knowledge. *J Clin Med.* (2020) 9:1753. doi: 10.3390/jcm9061753
- Cholankeril G, Podboy A, Aivaliotis VI, Tarlow B, Pham EA, Spencer SP, et al. High prevalence of concurrent gastrointestinal manifestations in patients with severe acute respiratory syndrome coronavirus 2: early experience from California. *Gastroenterology.* (2020) 159:775–7. doi: 10.1053/j.gastro.2020.04.008
- Pan L, Mu M, Yang P, Sun Y, Wang R, Yan J, et al. Clinical characteristics of COVID-19 patients with digestive symptoms in Hubei, China: a descriptive, cross-sectional, multicenter study. *Am J Gastroenterol.* (2020) 115:766–73. doi: 10.14309/ajg.0000000000000620
- Zhang X, Tang C, Tian D, Hou X, Yang Y. Management of digestive disorders and procedures associated with COVID-19. *Am J Gastroenterol.* (2020) 115:1153–5. doi: 10.14309/ajg.0000000000000728
- Tian Y, Rong L, Nian W, He Y. Review article: gastrointestinal features in COVID-19 and the possibility of faecal transmission. *Aliment Pharmacol Ther.* (2020) 51:843–51. doi: 10.1111/apt.15731
- Tan L, Wang Q, Zhang D, Ding J, Huang Q, Tang YQ, et al. Lymphopenia predicts disease severity of COVID-19: a descriptive and predictive study. *Signal Transduct Target Ther.* (2020) 5:33. doi: 10.1038/s41392-020-0159-1
- Potempa LA, Rajab IM, Hart PC, Bordon J, Fernandez-Botran R. Insights into the use of C-reactive protein as a diagnostic index of disease severity in COVID-19 infections. *Am J Trop Med Hyg.* (2020) 103:561–3. doi: 10.4269/ajtmh.20-0473
- Yao Y, Cao J, Wang Q, Shi Q, Liu K, Luo Z, et al. D-dimer as a biomarker for disease severity and mortality in COVID-19 patients: a case control study. *J Intensive Care.* (2020) 8:49. doi: 10.1186/s40560-020-00466-z
- Long H, Nie L, Xiang X, Li H, Zhang X, Fu X, et al. D-dimer and prothrombin time are the significant indicators of severe COVID-19 and poor prognosis. *Biomed Res Int.* (2020) 2020:6159720. doi: 10.1155/2020/6159720
- Liao D, Zhou F, Luo L, Xu M, Wang H, Xia J, et al. Haematological characteristics and risk factors in the classification and prognosis evaluation of COVID-19: a retrospective cohort study. *Lancet Haematol.* (2020) 7:e671–e8. doi: 10.1016/S2352-3026(20)30217-9
- Öztürk S, Özkaya U, Barstugan M. Classification of Coronavirus (COVID-19) from X-ray and CT images using shrunken features. *Int J Imaging Syst Technol.* (2020) 31:5–15. doi: 10.1002/ima.22469
- Page J. Analyse factorielle de donnees mixtes: principe et exemple d'application. *Rev Stat Appl.* (2004) 52:93–111. Available online at: <https://link.springer.com/article/10.1186/s13570-020-00170-5>
- Yu G. Using ggtree to visualize data on tree-like structures. *Curr Protoc Bioinf.* (2020) 69:e96. doi: 10.1002/cpbi.96
- Paradis E, Schliep K. ape 5.0: an environment for modern phylogenetics and evolutionary analyses in R. *Bioinformatics.* (2019) 35:526–8. doi: 10.1093/bioinformatics/bty633
- Csardi G, Nepusz T. The igraph software package for complex network research. *Interj Complex Syst.* (2006) 1695:1–9. Available online at: <https://link.springer.com/article/10.1007/s10764-021-00227-1>
- Charrad M, Ghazzali N, Boiteau V, Niknafs A. Nbclust: an R package for determining the relevant number of clusters in a data set. *J Stat Softw.* (2014) 61:1–36. doi: 10.18637/jss.v061.i06
- Lin H, Zelterman D. Modeling survival data: extending the Cox model. *Technometrics.* (2002) 44:85–6. doi: 10.1198/tech.2002.s656
- Robin X, Turck N, Hainard A, Tiberti N, Lisacek F, Sanchez JC, et al. pROC: an open-source package for R and S+ to analyze and compare ROC curves. *BMC Bioinf.* (2011) 12:77. doi: 10.1186/1471-2105-12-77
- Alfons A, Templ M, Filzmoser P. An object-oriented framework for statistical simulation: the R package simFrame. *J Stat Softw.* (2010) 37:1–36. doi: 10.18637/jss.v037.i03
- Yu C, Zhou M, Liu Y, Guo T, Ou C, Yang L, et al. Characteristics of asymptomatic COVID-19 infection and progression: a multicenter, retrospective study. *Virulence.* (2020) 11:1006–14. doi: 10.1080/21505594.2020.1802194
- Hu Z, Song C, Xu C, Jin G, Chen Y, Xu X, et al. Clinical characteristics of 24 asymptomatic infections with COVID-19 screened among close contacts in Nanjing, China. *Sci China Life Sci.* (2020) 63:706–11. doi: 10.1007/s11427-020-1661-4
- Li Z, Yi Y, Luo X, Xiong N, Liu Y, Li S, et al. Development and clinical application of a rapid IgM-IgG combined antibody test for SARS-CoV-2 infection diagnosis. *J Med Virol.* (2020) 92:1518–24. doi: 10.1002/jmv.25727
- Henry BM, Aggarwal G, Wong J, Benoit S, Vikse J, Plebani M, et al. Lactate dehydrogenase levels predict coronavirus disease 2019 (COVID-19) severity and mortality: a pooled analysis. *Am J Emerg Med.* (2020) 38:1722–6. doi: 10.1016/j.ajem.2020.05.073
- Wu MY, Yao L, Wang Y, Zhu XY, Wang XF, Tang PJ, et al. Clinical evaluation of potential usefulness of serum lactate dehydrogenase (LDH)



- in 2019 novel coronavirus (COVID-19) pneumonia. *Respir Res.* (2020) 21:171. doi: 10.1186/s12931-020-01427-8
26. Ali N. Elevated level of C-reactive protein may be an early marker to predict risk for severity of COVID-19. *J Med Virol.* (2020) 92:2409–11. doi: 10.1002/jmv.26097
  27. Tan C, Huang Y, Shi F, Tan K, Ma Q, Chen Y, et al. C-reactive protein correlates with computed tomographic findings and predicts severe COVID-19 early. *J Med Virol.* (2020) 92:856–62. doi: 10.1002/jmv.25871
  28. Lei F, Liu YM, Zhou F, Qin JJ, Zhang P, Zhu L, et al. Longitudinal association between markers of liver injury and mortality in COVID-19 in China. *Hepatology.* (2020) 72:389–98. doi: 10.1002/hep.31301
  29. Bertolini A, van de Peppel IP, Bodewes F, Moshage H, Fantin A, Farinati F, et al. Abnormal liver function tests in patients with COVID-19: relevance and potential pathogenesis. *Hepatology.* (2020) 72:1864–72. doi: 10.1002/hep.31480
  30. Qin C, Zhou L, Hu Z, Zhang S, Yang S, Tao Y, et al. Dysregulation of immune response in patients with coronavirus 2019 (COVID-19) in Wuhan, China. *Clin Infect Dis.* (2020) 71:762–8. doi: 10.1093/cid/cia248
  31. Xie G, Ding F, Han L, Yin D, Lu H, Zhang M. The role of peripheral blood eosinophil counts in COVID-19 patients. *Allergy.* (2020) 76:471–82. doi: 10.1111/all.14465
  32. Tabachnikova A, Chen ST. Roles for eosinophils and basophils in COVID-19? *Nat Rev Immunol.* (2020) 20:461. doi: 10.1038/s41577-020-0379-1
  33. Rees EM, Nightingale ES, Jafari Y, Waterlow NR, Clifford S, Pearson CAB, et al. COVID-19 length of hospital stay: a systematic review and data synthesis. *BMC Med.* (2020) 18:22. doi: 10.1186/s12916-020-01726-3
  34. Palmieri L, Vanacore N, Donfrancesco C, Lo Noce C, Canevelli M, Punzo O, et al. Clinical characteristics of hospitalized individuals dying with COVID-19 by age group in Italy. *J Gerontol A Biol Sci Med Sci.* (2020) 75:1796–800. doi: 10.1093/gerona/glaa146
  35. Klaiber P, Wen JH, DeLongis, A, Sin NL. The ups and downs of daily life during COVID-19: Age differences in affect, stress, and positive events. *J Gerontol B Psychol Sci Soc Sci.* (2020) 76:E30–7. doi: 10.1093/geronb/gbaa096
  36. Wenham C, Smith J, Morgan R. COVID-19: the gendered impacts of the outbreak. *Lancet.* (2020) 395:846–8. doi: 10.1016/S0140-6736(20)30526-2
  37. Ben-Hur A, Guyon I. Detecting stable clusters using principal component analysis. *Methods Mol Biol.* (2003) 224:159–82. doi: 10.1385/1-59259-364-X:159

**Conflict of Interest:** The authors declare that the research was conducted in the absence of any commercial or financial relationships that could be construed as a potential conflict of interest.

Copyright © 2021 Han, Shen, Yan, Huang, Ba, Lin, Wang, Huang, Qin, Wang, Chen and Tu. This is an open-access article distributed under the terms of the Creative Commons Attribution License (CC BY). The use, distribution or reproduction in other forums is permitted, provided the original author(s) and the copyright owner(s) are credited and that the original publication in this journal is cited, in accordance with accepted academic practice. No use, distribution or reproduction is permitted which does not comply with these terms.



# Network Analysis of Outpatients to Identify Predictive Symptoms and Combinations of Symptoms Associated With Positive/Negative SARS-CoV-2 Nasopharyngeal Swabs

Hervé Spechbach<sup>1\*</sup>, Frédérique Jacquerioz<sup>1,2,3</sup>, Virginie Prendki<sup>4,5</sup>, Laurent Kaiser<sup>3,4,6,7</sup>, Mikaela Smit<sup>7,8</sup>, Alexandra Calmy<sup>7,8</sup>, François Chappuis<sup>2,7</sup>, Idris Guessous<sup>1,7</sup>, Julien Salamun<sup>1</sup> and Stéphanie Baggio<sup>9,10</sup>

## OPEN ACCESS

### Edited by:

Seyed Alireza Nadji,  
Shahid Beheshti University of Medical  
Sciences, Iran

### Reviewed by:

Elmira Esmailzadeh,  
Brigham and Women's Hospital and  
Harvard Medical School,  
United States  
Tim Kacprowski,  
Technische Universität  
Braunschweig, Germany

### \*Correspondence:

Hervé Spechbach  
herve.spechbach@hcuge.ch

### Specialty section:

This article was submitted to  
Infectious Diseases—Surveillance,  
Prevention and Treatment,  
a section of the journal  
Frontiers in Medicine

**Received:** 24 March 2021

**Accepted:** 23 June 2021

**Published:** 20 July 2021

### Citation:

Spechbach H, Jacquerioz F,  
Prendki V, Kaiser L, Smit M, Calmy A,  
Chappuis F, Guessous I, Salamun J  
and Baggio S (2021) Network Analysis  
of Outpatients to Identify Predictive  
Symptoms and Combinations of  
Symptoms Associated With  
Positive/Negative SARS-CoV-2  
Nasopharyngeal Swabs.  
Front. Med. 8:685124.  
doi: 10.3389/fmed.2021.685124

<sup>1</sup> Division of Primary Care Medicine, Geneva University Hospitals, Geneva, Switzerland, <sup>2</sup> Division of Tropical and Humanitarian Medicine, Geneva University Hospitals, Geneva, Switzerland, <sup>3</sup> Geneva Center for Emerging Viral Diseases, Geneva University Hospitals, Geneva, Switzerland, <sup>4</sup> Division of Infectious Diseases, Geneva University Hospitals, Geneva, Switzerland, <sup>5</sup> Division of Internal Medicine for the Aged, Geneva University Hospitals, Geneva, Switzerland, <sup>6</sup> Laboratory of Virology, Geneva University Hospitals, Geneva, Switzerland, <sup>7</sup> Faculty of Medicine, University of Geneva, Geneva, Switzerland, <sup>8</sup> HIV/AIDS Unit, Department of Infectious Diseases, Geneva University Hospitals, Geneva, Switzerland, <sup>9</sup> Division of Prison Health, Geneva University Hospitals, Geneva, Switzerland, <sup>10</sup> Office of Corrections, Department of Justice and Home Affairs of the Canton of Zurich, Zurich, Switzerland

**Background:** Limited data exist on early predictive clinical symptoms or combinations of symptoms that could be included in the case definition of coronavirus disease 2019 (COVID-19), particularly for mild-to-moderate disease in an outpatient setting.

**Methods:** A cohort study of individuals presenting with clinical symptoms to one of the largest dedicated networks of COVID-19 test centers in Geneva, Switzerland, between March 2 and April 23, 2020. Individuals completed a symptom questionnaire, received a nurse-led check-up, and nasopharyngeal swabs were obtained. An analysis of clinical features predicting the positivity and negativity of the SARS-CoV-2 RT-PCR test was performed to determine the relationship between symptoms and their combinations.

**Results:** Of 3,248 patients included (mean age, 42.2 years; 1,504 [46.3%] male), 713 (22%) had a positive RT-PCR; 1,351 (41.6%) consulted within 3 days of symptom onset. The strongest predictor of a positive SARS-CoV-2 RT-PCR was anosmia, particularly in early disease, followed by fever, myalgia, and cough. Symptoms predictive of a negative test were breathing difficulties, abdominal symptoms, thoracic pain and runny nose. Three distinct networks of symptoms were identified, but did not occur together: respiratory symptoms; systemic symptoms related to fever; and other systemic symptoms related to anosmia.

**Conclusions:** Symptoms and networks of symptoms associated with a positive/negative SARS-CoV-2 RT-PCR are emerging and may help to guide targeted testing. Identification of early COVID-19-related symptoms alone or in combination can

contribute to establish a clinical case definition and provide a basis for clinicians and public health authorities to distinguish it from other respiratory viruses early in the course of the disease, particularly in the outpatient setting.

**Keywords: SARS-CoV-2, COVID-19, outpatient, diagnosis, predictive symptoms, clinical features, combination of symptoms**

## INTRODUCTION

On January 12, 2020, several severe pneumonia cases were identified in Hubei Province, China, and later related to coronavirus disease 2019 (COVID-19) caused by the novel severe acute respiratory syndrome coronavirus 2 (SARS-CoV-2) (1). On March 11, 2020, the World Health Organization (WHO) declared the outbreak a pandemic (2). At present, the number of confirmed cases exceeds 100 million worldwide, with more than 2.2 million deaths (3).

The clinical manifestations of COVID-19 comprise a wide range of symptoms (4, 5), with most infected individuals experiencing only mild or subclinical illness, particularly in the early phase. To date, the focus has primarily been on describing clinical symptoms among hospitalized patients, which mainly include respiratory symptoms (e.g., cough, shortness of breath) and fever associated with myalgia and fatigue, similar to early case reports from China (6–9). The set of symptoms outlined by WHO for the COVID-19 case definition (10) has changed over time to reflect the spectrum of reported symptoms, including non-respiratory manifestations, such as loss of smell/taste (11), neurological symptoms (12), ocular manifestations (13), and dermatological signs (14). Some studies have also described asymptomatic presentations (15) or the presence of milder respiratory symptoms (4).

Studies analyzing the early clinical symptoms as risk factors for testing positive for SARS-CoV-2 in an outpatient setting are sparse (16) and often focus on specific populations, such as veterans (17) or healthcare workers (18), rather than the general population. In the absence of proven prophylactic candidates and at the beginning of widespread vaccination on an unprecedented scale, the containment of SARS-CoV-2 currently focuses on the interruption of transmission, notably through rapid and targeted testing, prompt isolation and contact tracing. However, the clinical definition of COVID-19 remains to be fully established, particularly among paucisymptomatic patients (19, 20). Importantly, this would facilitate targeted testing at the early stage of the disease and be particularly valuable in resource-limited settings or in a situation of SARS-CoV-2 high incidence where costly laboratory tests are restricted.

Efforts have been made to identify more specific symptoms or combinations of symptoms to discriminate between COVID-19 and other respiratory tract infections. Some authors showed that COVID-19 infection had a similar onset to other types of pneumonia (21), whereas, others reported that it initiates with fever, as for other coronavirus-related diseases, but unlike influenza that starts with cough (22). New approaches, including network analysis, a graph, theory-based methodology, have allowed to visualize and identify the relationship between several

symptoms and their combinations associated with a disease. For example, network analysis has been used in oncology (23) and for neuropsychiatric symptoms associated with COVID-19 since the beginning of the pandemic by establishing three symptom categories (24).

In the present study, we aimed to identify early clinical symptoms predictive of a positive or negative SARS CoV-2 test in nasopharyngeal swab material based on reverse-transcription polymerase chain reaction (RT-PCR) among a large cohort of outpatients presenting with mild-to-moderate symptoms. We also established how symptoms combine together to form three distinct categories.

## METHODS

### Study Design and Setting

The study was approved by the regional ethics committee (no. 2020-00813).

Geneva University Hospitals (HUG) is the largest of the five university hospitals in Switzerland and one of the largest hospitals in Europe. It serves the region of Geneva and its surrounding population (approximately 800,000 persons) and operates across several sites, including eight hospitals, two clinics and 30 outpatient care centers. We included all individuals aged 16 years old and over consulting for a suspicion of SARS-CoV-2 infection at any of the dedicated outpatient test centers within the HUG network. Patients who refused the use of their personal data for research purposes were excluded.

At the beginning of March 2020, four dedicated test centers were set up within the existing HUG outpatient facilities. In each center, a standardized triage oriented patients with severe symptoms to the emergency room, while other patients were evaluated and tested on site. Patients were screened according to the Swiss Federal Office of Public Health definition of suspected cases based on WHO recommendations. Data for all eligible patients presenting to the centers were collected from March 2, 2020, to April 23, 2020, during the first wave of the pandemic. Data collected during the week of March 18, 2020, to March 26, 2020, were excluded as only patients with fever and cough were tested due to a lack of logistic testing possibilities.

### Variables and Data Sources

All outpatients completed a questionnaire upon admission with the support of a nurse, a trained medical student or a physician. The questionnaire collated structured information on sociodemographic and medical factors including age, gender, social determinants, clinical symptoms, and onset, comorbidities, and risk factors for more severe illness. The Treatment section

was unstructured and completed by the patients in the free-text comments. Vital signs were only noted if the patient presented comorbidities. In the present analysis, we focused on clinical symptoms. Our questionnaire was adapted throughout the study period in accordance with best evidence on the evolution of the disease and its symptoms. Specifically, symptoms initially included runny nose, sore throat, cough (dry and with sputum), fever, muscle pain, and chills. Anosmia and headache were added on March 24, 2020. Breathing difficulties, abdominal symptoms, fatigue and thoracic pain were added on April 1, 2020. The above-mentioned additional symptoms were reported as free text in the section “other symptoms” in early versions of the questionnaire and were subsequently recoded. Participants who did not report any symptoms were considered asymptomatic. Risk factors for severe illness or complications included hypertension, chronic respiratory diseases, diabetes, heart diseases, and immunosuppression.

### Outcome Variable: RT-PCR SARS-CoV-2

The main outcome was a positive SARS-CoV-2 RT-PCR test performed on a nasopharyngeal swab. All swabs were processed at the HUG virology laboratory, which is also the Swiss national reference laboratory for SARS-CoV-2. RT-PCR was performed according to manufacturers' instructions on various platforms, including initially an in-house method using eMAG (bioMérieux, Marcy l'Etoile, France) and the Charité/Berlin RT-PCR protocol, followed by the BD SARS-CoV-2 reagent kit for BD Max system (Becton Dickinson & Co, Franklin Lakes, NJ, USA) and Cobas 6800 SARS CoV2 RT-PCR (Roche Diagnostics, Rotkreuz, Switzerland).

### Statistical Analyses

We computed descriptive statistics for demographics using percentages, means, and standard deviations, according to the distribution of variables. We then computed the prevalence rate of infected cases, together with 95% confidence intervals (CI). Third, we computed descriptive statistics (percentages) for symptoms in the whole sample and then among participants infected, not infected, and not tested. Predictive clinical symptoms for positive or negative SARS-CoV-2 RT-PCR tests were evaluated using multiple logistic regression, which included all symptoms as potential predictors of a SARS-CoV-2 positive test. A clinical symptom was considered to be predictive if it had a  $p$ -value  $< 0.05$ .

To investigate further COVID-19 symptomatology, we then used network analysis, a recent data-driven method that tests the direct relationships of a constellation of symptoms and identifies how symptoms relate to each other and how they combine together (25, 26). Networks were estimated using the IsingFit model designed for binary variables (27) and a penalty parameter to shrink small coefficients to zero using the graphical LASSO algorithm (28). We tested whether symptoms were combined together using the Spinglass algorithm, a modularity-community detection algorithm (29). Usual model accuracy checks were performed, including edge-weight accuracy and centrality stability (30).

Finally, four sensitivity analyses were conducted. As analyses were performed at the visit level, meaning that we did not consider whether visits were nested within participants, we first used mixed-effect logistic regression to test whether results were similar when taking into account the network of symptoms. As only a small subset (2.5%) of participants came more than once to the test center, the main results were presented at the visit level. Second, results of the logistic regressions were controlled for age and gender. We also performed a logistic regression controlled for the number of risk factors. Fourth, an analysis limited to a sub-sample of outpatients who completed the last version of the questionnaire was performed, which included all symptoms (no recoding needed). Findings were similar to those already observed in the previous analyses. Descriptive statistics and logistic regressions were performed using Stata 15. The network analysis was computed using R 3.6.2 and the packages IsingFit 0.3.1 (network estimation and visualization, using default parameters), igraph 1.2.5 (community detection analysis) and bootnet 1.3 (model accuracy).

## RESULTS

### Patient Demographics and Clinical Characteristics

Among the 6,018 visits to the test centers during the study period, 2,744 (45.6%) were excluded as they corresponded to the widespread test strategy targeting asymptomatic healthcare workers. Of the remaining 3,274 visits, 20 (0.6%) were excluded as patients did not consent to the use of their data; six additional patients were excluded as they were probable SARS-CoV-2 cases with a non-detected RT-PCR. A total of 3,248 visits were included in the final analysis. Among these, 3,166 (97.5%) individuals came only once, 81 (2.5%) came twice, and one participant came three times (mean [SD] age 42.2 [14.8] years; 46.3% male). Detailed demographics are reported in **Table 1**. Evaluation of symptoms among patients presenting for testing are shown in **Table 2**. Most presented with cough (65.9%), runny nose (45.6%) or muscle pain (45.6%) and visits generally occurred in the first 3 days after symptom onset (**Table 2**).

### Infection Rate

Among the 3,248 tests performed, 712 (21.9%) were positive (95% CI, 20.5–23.4). Of these, 98.3% ( $n = 707$ ) had a first positive test result and 0.7% ( $n = 5$ ) had a second positive test (individuals previously diagnosed positive). A total of 2467 (76.0%; 95% CI, 74.5–77.4) patients tested negative; 69 (2.1%; 95% CI, 1.7–2.7) were not tested as they did not present with symptoms that made them eligible according to national recommendations at that time.

### Symptoms Associated With SARS-CoV-2 Infection

The multivariate analysis suggested that predictive symptoms for a positive SARS-CoV-2 test were anosmia (odds ratio [OR], 5.85 [95% CI, 4.62–7.40];  $p < 0.001$ ), followed by fever (OR, 1.96 [95% CI, 1.62–2.37];  $p < 0.001$ ), muscle pain (OR, 1.71 [95% CI, 1.41–2.07];  $p < 0.001$ ), and cough (OR, 1.53 [95% CI, 1.25–1.88];  $p <$



**TABLE 1 |** Demographics and sample characteristics.

|                                       | Overall          | SARS-CoV-2 test |                  |               |
|---------------------------------------|------------------|-----------------|------------------|---------------|
|                                       |                  | Positive        | Negative         | No test       |
|                                       | <i>n</i> = 3,248 | <i>n</i> = 712  | <i>n</i> = 2,467 | <i>n</i> = 69 |
| <b>No. of patients (% , <i>n</i>)</b> |                  |                 |                  |               |
| 1 visit                               | 97.5 (3,166)     | 97.8 (696)      | 97.4 (2,402)     | 98.6 (68)     |
| 2 visits                              | 2.5 (81)         | 2.2 (16)        | 2.6 (64)         | 1.4 (1)       |
| 3 visits                              | 0.0 (1)          | -               | 0.0 (1)          | -             |
| <b>Age (mean, SD)</b>                 |                  |                 |                  |               |
|                                       | 42.17 (14.78)    | 42.71 (14.00)   | 42.11 (14.93)    | 38.88 (17.19) |
| <b>Gender (% , <i>n</i>)</b>          |                  |                 |                  |               |
| Female                                | 53.7 (1,744)     | 49.7 (354)      | 55.0 (1,358)     | 46.4 (32)     |
| Male                                  | 46.3 (1,504)     | 50.3 (358)      | 45.0 (1,109)     | 53.6 (37)     |
| <b>Risk factors (% , <i>n</i>)</b>    |                  |                 |                  |               |
| Hypertension                          | 10.9 (353)       | 10.3 (73)       | 11.3 (278)       | 3.0 (2)       |
| Chronic respiratory diseases          | 13.2 (427)       | 10.1 (72)       | 14.2 (349)       | 8.7 (6)       |
| Diabetes                              | 4.6 (149)        | 4.9 (35)        | 4.5 (112)        | 2.9 (2)       |
| Heart diseases                        | 4.7 (152)        | 3.8 (27)        | 5.0 (123)        | 3.0 (2)       |
| Immunosuppression                     | 6.5 (210)        | 4.9 (35)        | 7.0 (173)        | 2.9 (2)       |
| No. of risk factors (mean, SD)        | 0.49 (0.72)      | 0.34 (0.70)     | 0.42 (0.73)      | 0.21 (0.48)   |

SD, standard deviation.

0.001). Symptoms predicting a negative SARS-CoV-2 test were difficulty in breathing (OR, 0.53 [95% CI, 0.41–0.68];  $p < 0.001$ ), sore throat (OR, 0.63 [95% CI, 0.52–0.76];  $p < 0.001$ ), abdominal symptoms (OR, 0.69 [95% CI, 0.54–0.88];  $p < 0.002$ ), thoracic pain (OR, 0.70 [95% CI, 0.53–0.92];  $p < 0.012$ ), and runny nose (OR, 0.76 [95% CI, 0.63–0.92];  $p < 0.004$ ) (Table 3).

Figure 1 presents the results of the network analysis of symptoms associated with a positive SARS-Cov-2 test. Symptoms were found to gather into three distinct symptom combinations with one or more symptoms predictive for a positive SARS-CoV-2 test within each combination: systemic symptoms including chills, fever, and muscle pain (systemic 1); respiratory symptoms including cough, difficulty breathing, and thoracic pain; and a further, systemic (systemic 2) combination of symptoms including abdominal pain, anosmia, headache, fatigue. Runny nose and sore throat were not related to other symptoms and were not part of any combination (i.e., no edge with any other symptom). Some combinations of symptoms were not related (e.g., systemic 1 and respiratory symptoms), meaning that these symptoms were not likely to occur together. Of note, anosmia did not occur simultaneously with other predictive symptoms or respiratory symptoms.

## DISCUSSION

This cohort study analyzed data from the general population presenting to one of the major test centers in Switzerland during the first COVID-19 wave to establish early predictive clinical symptoms for a positive and negative SARS-CoV-2 test. Based on 712 (21.9%) positive cases among a population of 3,248 patients, a multivariate analysis found that the best predictors

for a positive SARS-CoV-2 test results were anosmia, fever, muscle pain, and cough. These results suggest that the clinical definition for mild-to-moderate COVID-19 in the early stage should include these symptoms. By contrast, difficulty breathing, sore throat, abdominal pain, thoracic pain, and runny nose were all associated with negative test results.

Our findings regarding symptoms predictive of a positive test are consistent with those identified by other studies focused on specific populations (16, 17), as well as a recent (16 December, 2020) WHO statement that patients with anosmia may represent a probable case of SARS-CoV-2 infection. Of note, our results regarding symptoms predictive of a negative test result were not consistent with other studies on specific populations, such as US veterans or healthcare workers, who found that diarrhea and difficulty breathing were predictive for a positive test (16, 17). One reason could be that as our patient cohort tended to present for testing early in the course of the disease, difficulty in breathing and diarrhea tended to appear later, as reported by the authors of these studies. Another reason for this inconsistency may be that breathing difficulties in our study were self-reported. The recent WHO definition also suggests that headache should be considered as a suspicion of SARS-CoV2 infection. This was not confirmed in our multivariate analysis.

Our findings should feed into ongoing discussions regarding future public health approaches to containing further COVID-19 outbreaks. Viral loads tend to be elevated at the beginning of COVID-19 infection. It is therefore crucial to define positive and negative clinical predictors during the early stage of the disease to facilitate early diagnosis, isolation, contact tracing, and consequently, interruption of transmission. As our understanding of this novel disease evolves, establishing a clear case definition will help patients, healthcare providers and public

**TABLE 2 |** Description of symptoms.

|  | Overall          | SARS-CoV-2 test |                  |               |
|--|------------------|-----------------|------------------|---------------|
|  |                  | Positive        | Negative         | No test       |
| <b>Number of patients</b>                      | <i>n</i> = 3,248 | <i>n</i> = 712  | <i>n</i> = 2,467 | <i>n</i> = 69 |
| <b>Symptoms (% , <i>n</i>)</b>                 |                  |                 |                  |               |
| Runny nose                                     | 45.6 (1,481)     | 43.0 (306)      | 46.9 (1,156)     | 27.5 (19)     |
| Sore throat                                    | 41.8 (1,356)     | 34.7 (247)      | 44.3 (1,093)     | 23.2 (16)     |
| Muscle pain                                    | 45.6 (1,481)     | 58.4 (416)      | 42.6 (1,050)     | 21.7 (15)     |
| Chills   | 34.2 (1,111)     | 40.3 (287)      | 32.9 (812)       | 17.4 (12)     |
| Fever  | 32.8 (1,066)     | 47.6 (339)      | 28.9 (713)       | 20.3 (14)     |
| Headache                                       | 44.8 (1,456)     | 50.0 (356)      | 43.9 (1,084)     | 23.2 (16)     |
| Anosmia  | 13.7 (444)       | 31.7 (226)      | 8.8 (217)        | 1.5 (1)       |
| Abdominal symptoms                             | 23.2 (751)       | 20.1 (143)      | 24.3 (600)       | 11.6 (8)      |
| Fatigue  | 31.7 (1,030)     | 28.8 (205)      | 33.1 (817)       | 11.6 (8)      |
| Cough  | 65.9 (2,139)     | 71.1 (506)      | 65.2 (1,609)     | 34.8 (24)     |
| Difficulty breathing                           | 23.9 (777)       | 16.7 (119)      | 26.5 (653)       | 7.3 (5)       |
| Thoracic pain                                  | 17.6 (571)       | 12.9 (92)       | 19.1 (472)       | 10.1 (7)      |
| No symptom                                     | 3.0 (96)         | 1.0 (7)         | 2.9 (71)         | 26.1 (71)     |
| Total no. of symptoms (mean, SD)               | 4.35 (2.25)      | 4.67 (2.13)     | 4.32 (2.26)      | 2.17 (1.95)   |
| <b>Time since symptom onset (% , <i>n</i>)</b> |                  |                 |                  |               |
| 0–3 days                                       | 41.6 (1,351)     | 41.7 (297)      | 41.7 (1,029)     | 36.2 (25)     |
| 4–7 days                                       | 26.5 (862)       | 31.6 (225)      | 25.3 (625)       | 17.4 (12)     |
| 8 days or more                                 | 24.1 (783)       | 22.5 (160)      | 24.9 (613)       | 14.5 (10)     |
| Missing <sup>a</sup>                           | 7.8 (252)        | 4.2 (30)        | 8.1 (200)        | 31.9 (22)     |

<sup>a</sup>Including asymptomatic visits (*n* = 88).

SD, standard deviation. Combination of symptoms highlighted by color: light gray = systemic 1 ("flu-like" syndrome); orange = respiratory symptoms; and white = systemic 2. Dark-gray symptoms were not included in any community.

health authorities to make informed decisions regarding early diagnosis and isolation measures with a positive impact on the epidemiological spread.

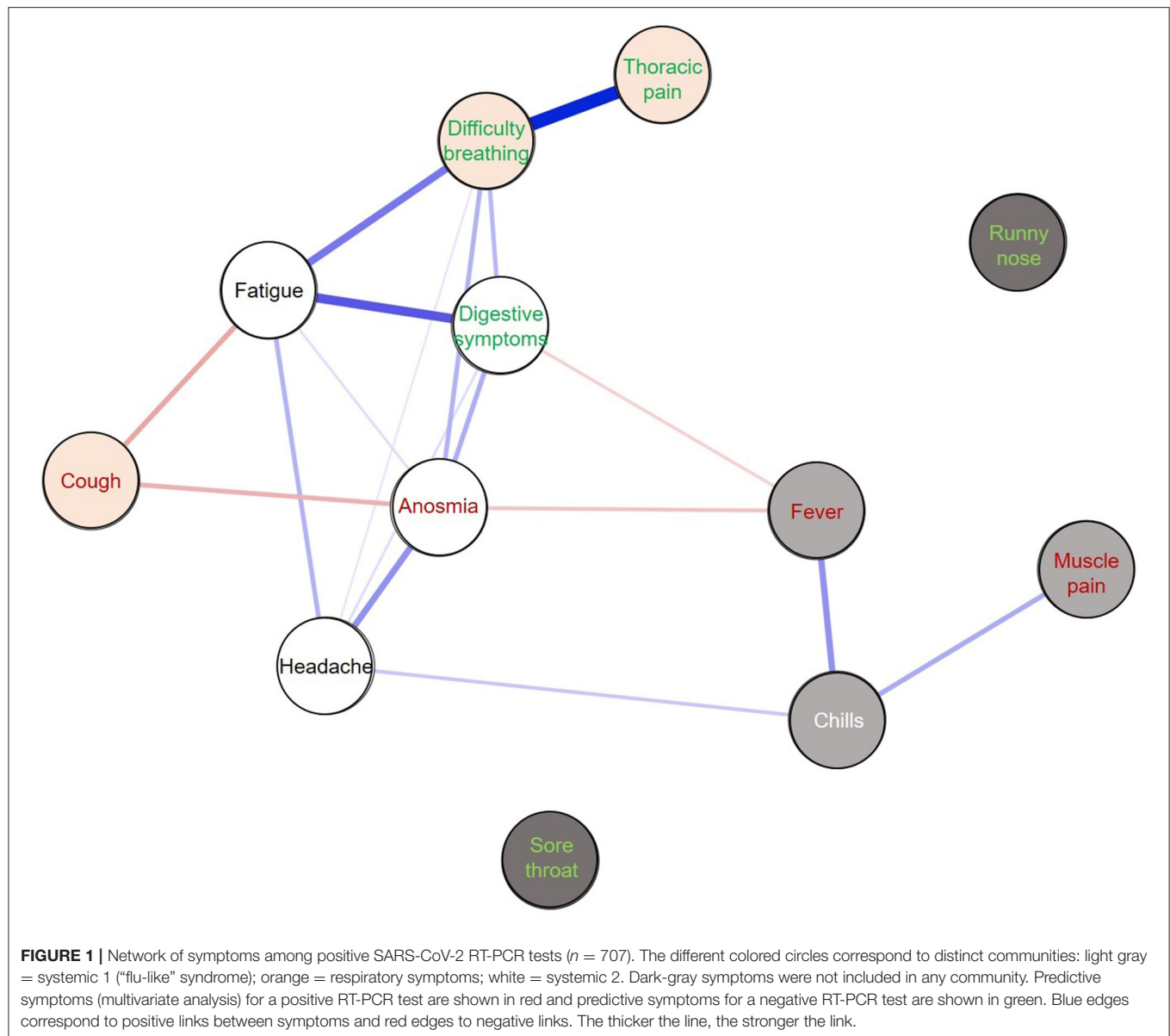
Beyond the impact on public health and onward transmission, a clear case definition will also provide a powerful decision tool for resource-limited settings or situations. During the second wave in autumn 2020, many European settings, including the Geneva region, had to face unprecedented pressure. The high and rising caseloads of positive and suspected cases generated a bottleneck in the provision of molecular testing due to the large patient volume and limited laboratory capacity, resulting in a delay in testing of several days. Similar to the first wave, key decisions had to be made regarding limiting the provision of tests for a given period to those considered most at risk in order to preserve precious resources and prevent test centers and laboratories from being completely overwhelmed. The availability of data such as presented here is vital to make evidence-based decisions regarding such restrictive measures, while ensuring a robust and strong public health response. It goes without saying that large-scale testing remains an important public health intervention to control the epidemic, but only when resources - both human and laboratory-based - allow for this.

In addition to identifying predictive and non-predictive symptoms, this study also provides critical information on the clinical forms of SARS-CoV-2 infection. The network analysis identified three distinct combinations of symptoms that were

**TABLE 3 |** Multiple logistic regression with all symptoms predicting the SARS-CoV-2 RT-PCR result (*n* = 3,179).

| Symptoms             | Odds ratio        | <i>p</i> -value |
|----------------------|-------------------|-----------------|
| Runny nose           | 0.76 (0.63; 0.92) | 0.004           |
| Sore throat          | 0.63 (0.52; 0.76) | <0.001          |
| Muscle pain          | 1.71 (1.41; 2.07) | <0.001          |
| Chills               | 0.98 (0.80; 1.19) | 0.832           |
| Cough                | 1.53 (1.25; 1.88) | <0.001          |
| Fever                | 1.96 (1.62; 2.37) | <0.001          |
| Headache             | 1.12 (0.92; 1.37) | 0.245           |
| Anosmia              | 5.85 (4.62; 7.40) | <0.001          |
| Abdominal symptoms   | 0.69 (0.54; 0.88) | 0.002           |
| Fatigue              | 0.83 (0.66; 1.03) | 0.089           |
| Difficulty breathing | 0.53 (0.41; 0.68) | <0.001          |
| Thoracic pain        | 0.70 (0.53; 0.92) | 0.012           |

not likely to occur together and confirmed that COVID-19 can have very different clinical presentations. Each combination of symptoms has one or more predictive symptoms for a positive test. For example, the network of "systemic 1" symptoms, which corresponds to a flu-like syndrome (muscle pain, chills, and fever), was not associated with respiratory symptoms. Anosmia, which seems specific and the strongest predictor for



test positivity, was associated with non-specific symptoms such as digestive symptoms, fatigue, and headache. Results related to cough should be carefully considered because it was not positively related to other symptoms of the same combination but was rather inversely related to other symptoms such as anosmia. Indeed, the presence of negative edges may increase the probability of being in a combination of symptoms (here "respiratory") and weaken the influence of positive edges (31).

This study analyzed a large cohort of outpatients in one of the largest networks of dedicated test centers in Switzerland, a country hard hit by COVID-19. Detailed questionnaires allowed to collect data on a large number of symptoms and evaluate a large range of clinical features, whereas, previous studies mostly focused on positive cases or hospitalized patients. Hence, this cohort provided an opportunity to establish predictive early clinical symptoms for both positive and negative tests in

outpatients who were representative of the general population. It provided also an original analysis of how symptoms are combined.

Our study has some limitations. First, test centers used different versions of the questionnaire over time as these were updated as new data on clinical symptoms became available. Although, symptoms not specifically listed in the earlier versions of the questionnaires could be reported as free text, this may have resulted in the underreporting of some symptoms in the early phase of the study. However, we do not believe that this had a major impact on results. We were able to compute robust statistics in the multivariate regression for all symptoms of interest and our sensitivity analysis (limited to patients who completed the last versions of the questionnaire) showed similar results to the main analysis. Second, the results may suffer from severity bias, with some RT-PCR results showing false negatives,

although, it should be noted that we used the current gold standard diagnostic test. Unfortunately, we did not perform any follow-up of patients to confirm the RT-PCR test results by serology testing, but this could be a good focus for future studies. Some symptoms appeared as being non-specific, such as difficulty in breathing, sore throat, abdominal symptoms, thoracic pain, and runny nose. We interpreted “difficulty in breathing” as a subjective symptom linked to anxiety when assessed as a self-reported symptom. Concerning “thoracic pain,” we made a clinical choice to use a generic term permitting to include most types of pain of the thoracic region, including cardiac, respiratory, digestive, and back pain. Regarding the physical examination findings and treatment, we observed a substantial amount of missing data and we decided to exclude these elements from the analysis. Therefore, some severe cases may have been missed as we referred these immediately to the emergency department. Third, the interpretation and generalizability of the results are limited by the sample size and geographical range (one single canton). It would be useful to perform similar analyses of symptoms and how they are combined in other settings by using data from subsequent outbreaks to confirm the proposed case definition across regions and time. The same analysis could be done with SARS-CoV-2 variants. Finally, the analyses relied on self-reported symptoms, which may have resulted in some degree of bias. For example, it is likely that anxiety may have acted as a confounder for self-reported breathing difficulty, or that some patients reported non-existing symptoms or a more severe level of symptoms in order to gain access to a test.

## CONCLUSIONS

This study identified four early clinical signs associated with a positive SARS-CoV-2 RT-PCR result in an outpatient setting as well as three combinations of symptoms. The results of this study add crucial information concerning the mild-to-moderate stage of COVID-19 by using the innovative network analysis and including a large cohort of outpatients. In the current context of recurrent epidemic waves, this study contributes important data to inform public health approaches, including a rapid identification of outpatients

infected with SARS-CoV-2, as well as raising the awareness of early symptoms that are predictive or non-predictive of a positive RT-PCR.

## DATA AVAILABILITY STATEMENT

The data analyzed in this study is subject to the following licenses/restrictions: on demand we could add the anonymised data. Requests to access these datasets should be directed to herve.spechbach@hcuge.ch.

## ETHICS STATEMENT

The studies involving human participants were reviewed and approved by The study was reviewed and approved by the Geneva regional ethics committee. Written informed consent for participation was not required for this study in accordance with the national legislation and the institutional requirements.

## AUTHOR CONTRIBUTIONS

The study was conceived by HS, FJ, JS, and SB and supervised by FJ, JS, and SB. Data were collected, analyzed, and interpreted by HS, FJ, JS and SB with statistical analyses performed by SB. HS drafted the first version of the manuscript, FJ, VP, LK, MS, AC, FC, IG, JS, and SB provided critical revision of the manuscript. All authors contributed to the redrafting and finalization of the manuscript.

## ACKNOWLEDGMENTS

We thank Rosemary Sudan for editorial assistance.

## SUPPLEMENTARY MATERIAL

The Supplementary Material for this article can be found online at: <https://www.frontiersin.org/articles/10.3389/fmed.2021.685124/full#supplementary-material>

## REFERENCES

1. Zhou P, Yang X-L, Wang X-G, Hu B, Zhang L, Zhang W, et al. A pneumonia outbreak associated with a new coronavirus of probable bat origin. *Nature*. (2020) 579:270–3. doi: 10.1038/s41586-020-2012-7
2. World Health Organization. *WHO Director-General's Opening Remarks at the Media Briefing on COVID-19 - 11 March 2020*. (2020). Available online at: <https://www.who.int/director-general/speeches/detail/who-director-general-s-opening-remarks-at-the-media-briefing-on-covid-19-11-march-2020> (accessed December 9, 2020).
3. World Health Organization. *Weekly Epidemiological Update-8 December 2020*. (2020). Available online at: <https://www.who.int/publications/m/item/weekly-epidemiological-update-8-december-2020> (accessed December 9, 2020).
4. Vetter P, Vu DL, L'Huillier AG, Schibler M, Kaiser L, Jacquerioz F. Clinical features of covid-19. *BMJ*. (2020) 369:m1470. doi: 10.1136/bmj.m1470
5. Rodriguez-Morales AJ, Cardona-Ospina JA, Gutiérrez-Ocampo E, Villamizar-Peña R, Holguin-Rivera Y, Escalera-Antezana JP, et al. Clinical, laboratory and imaging features of COVID-19: a systematic review and meta-analysis. *Travel Med Infect Dis*. (2020) 34:101623. doi: 10.1016/j.tmaid.2020.101623
6. Huang C, Wang Y, Li X, Ren L, Zhao J, Hu Y, et al. Clinical features of patients infected with 2019 novel coronavirus in Wuhan, China. *Lancet*. (2020) 395:497–506. doi: 10.1016/S0140-6736(20)30183-5
7. Chen N, Zhou M, Dong X, Qu J, Gong F, Han Y, et al. Epidemiological and clinical characteristics of 99 cases of 2019 novel coronavirus pneumonia in Wuhan, China: a descriptive study. *Lancet*. (2020) 395:507–13. doi: 10.1016/S0140-6736(20)30211-7
8. Wang D, Hu B, Hu C, Zhu F, Liu X, Zhang J, et al. Clinical characteristics of 138 hospitalized patients with 2019 novel coronavirus-infected pneumonia in Wuhan, China. *JAMA*. (2020) 323:1061–9. doi: 10.1001/jama.2020.1585



9. Guan W, Ni Z, Hu Y, Liang W, Ou C, He J, et al. Clinical characteristics of coronavirus disease 2019 in China. *N Engl J Med.* (2020) 382:1708–20. doi: 10.1056/NEJMoa2002032
10. World Health Organization. *Global Surveillance for COVID-19 Caused by Human Infection with COVID-19 Virus: Interim Guidance, 20 March 2020.* (2020). Available online at: <https://apps.who.int/iris/handle/10665/331506> (accessed December 9, 2020).
11. Kaye R, Chang CWD, Kazahaya K, Brereton J, Denny JC. COVID-19 anosmia reporting tool: initial findings. *Otolaryngol Head Neck Surg.* (2020) 163:132–4. doi: 10.1177/0194599820922992
12. Mao L, Jin H, Wang M, Hu Y, Chen S, He Q, et al. Neurologic manifestations of hospitalized patients with coronavirus disease 2019 in Wuhan, China. *JAMA Neurol.* (2020) 77:683–90. doi: 10.1001/jamaneurol.2020.1127
13. Wu P, Duan F, Luo C, Liu Q, Qu X, Liang L, et al. Characteristics of ocular findings of patients with coronavirus disease 2019 (COVID-19) in Hubei Province, China. *JAMA Ophthalmol.* (2020) 138:575–8. doi: 10.1001/jamaophthalmol.2020.1291
14. Sachdeva M, Gianotti R, Shah M, Bradanini L, Tosi D, Veraldi S, et al. Cutaneous manifestations of COVID-19: report of three cases and a review of literature. *J Dermatol Sci.* (2020) 98:75–81. doi: 10.1016/j.jdermsci.2020.04.011
15. Hu Z, Song C, Xu C, Jin G, Chen Y, Xu X, et al. Clinical characteristics of 24 asymptomatic infections with COVID-19 screened among close contacts in Nanjing, China. *Sci China Life Sci.* (2020) 63:706–11. doi: 10.1007/s11427-020-1661-4
16. Wagner T, Shweta F, Murugadosh K, Awasthi S, Venkatakrishnan A, Bade S, et al. Augmented curation of clinical notes from a massive EHR system reveals symptoms of impending COVID-19 diagnosis. *Elife.* (2020) 9:e58227. doi: 10.7554/eLife.58227
17. Fan VS, Dominitz JA, Eastment MC, Locke E, Green P, Berry K, et al. Risk factors for testing positive for SARS-CoV-2 in a national US healthcare system. *Clin Infect Dis.* (2020). doi: 10.1093/cid/ciaa1624. [Epub ahead of print].
18. Lan F-Y, Filler R, Mathew S, Buley J, Iliaki E, Bruno-Murtha LA, et al. COVID-19 symptoms predictive of healthcare workers' SARS-CoV-2 PCR results. *PLoS ONE.* (2020) 15:e0235460. doi: 10.1371/journal.pone.0235460
19. Wu Z, McGoogan JM. Characteristics of and important lessons from the coronavirus disease 2019 (COVID-19) outbreak in china: summary of a report of 72 314 cases from the chinese center for disease control and prevention. *JAMA.* (2020) 323:1239–42. doi: 10.1001/jama.2020.2648
20. Bi Q, Wu Y, Mei S, Ye C, Zou X, Zhang Z, et al. Epidemiology and transmission of COVID-19 in 391 cases and 1286 of their close contacts in Shenzhen, China: a retrospective cohort study. *Lancet Infect Dis.* (2020) 20:911–9. doi: 10.1016/S1473-3099(20)30287-5
21. Zhao D, Yao F, Wang L, Zheng L, Gao Y, Ye J, et al. A comparative study on the clinical features of coronavirus 2019 (COVID-19) pneumonia with other pneumonias. *Clin Infect Dis.* (2020) 71:756–61. doi: 10.1093/cid/ciaa247
22. Larsen JR, Martin MR, Martin JD, Kuhn P, Hicks JB. Modeling the onset of symptoms of COVID-19. *Front Public Health.* (2020) 8:473. doi: 10.3389/fpubh.2020.00473
23. Papachristou N, Barnaghi P, Cooper B, Kober KM, Maguire R, Paul SM, et al. Network analysis of the multidimensional symptom experience of oncology. *Sci Rep.* (2019) 9:2258. doi: 10.1038/s41598-018-36973-1
24. Mirfazeli FS, Sarabi-Jamab A, Jahanbakhshi A, Kordi A, Javadnia P, Shariat SV, et al. Neuropsychiatric manifestations of COVID-19 can be clustered in three distinct symptom categories. *Sci Rep.* (2020) 10:20957. doi: 10.1038/s41598-020-78050-6
25. Fried EI, van Borkulo CD, Cramer AOJ, Boschloo L, Schoevers RA, Borsboom D. Mental disorders as networks of problems: a review of recent insights. *Soc Psychiatry Psychiatr Epidemiol.* (2017) 52:1–10. doi: 10.1007/s00127-016-1319-z
26. Cramer AOJ, Waldorp LJ, van der Maas HLJ, Borsboom D. Comorbidity: a network perspective. *Behav Brain Sci.* (2010) 33:137–50; discussion 150–93. doi: 10.1017/S0140525X09991567
27. van Borkulo CD, Borsboom D, Epskamp S, Blanken TF, Boschloo L, Schoevers RA, et al. A new method for constructing networks from binary data. *Sci Rep.* (2014) 4:5918. doi: 10.1038/srep05918
28. Friedman J, Hastie T, Tibshirani R. Sparse inverse covariance estimation with the graphical lasso. *Biostatistics.* (2008) 9:432–41. doi: 10.1093/biostatistics/kxm045
29. Traag VA, Bruggeman J. Community detection in networks with positive and negative links. *Phys Rev E Stat Nonlin Soft Matter Phys.* (2009) 80:036115. doi: 10.1103/PhysRevE.80.036115
30. Epskamp S, Borsboom D, Fried EI. Estimating psychological networks and their accuracy: a tutorial paper. *Behav Res.* (2018) 50:195–212. doi: 10.3758/s13428-017-0862-1
31. Esmailian P, Jalili M. Community detection in signed networks: the role of negative ties in different scales. *Sci Rep.* (2015) 5:14339. doi: 10.1038/srep14339

**Conflict of Interest:** The authors declare that the research was conducted in the absence of any commercial or financial relationships that could be construed as a potential conflict of interest.

Copyright © 2021 Spechbach, Jacqueroiz, Prendki, Kaiser, Smit, Calmy, Chappuis, Guessous, Salamun and Baggio. This is an open-access article distributed under the terms of the Creative Commons Attribution License (CC BY). The use, distribution or reproduction in other forums is permitted, provided the original author(s) and the copyright owner(s) are credited and that the original publication in this journal is cited, in accordance with accepted academic practice. No use, distribution or reproduction is permitted which does not comply with these terms.



# Prolonged Active Prone Positioning in Spontaneously Breathing Non-intubated Patients With COVID-19-Associated Hypoxemic Acute Respiratory Failure With $\text{PaO}_2/\text{FiO}_2 > 150$

Paola Pierucci<sup>1\*</sup>, Nicolino Ambrosino<sup>2</sup>, Valentina Di Lecce<sup>1</sup>, Michela Dimitri<sup>1</sup>, Stefano Battaglia<sup>3</sup>, Esterina Boniello<sup>1</sup>, Andrea Portacci<sup>1</sup>, Onofrio Resta<sup>1</sup> and Giovanna Elisiana Carpagnano<sup>1</sup>

## OPEN ACCESS

### Edited by:

Reza Lashgari,  
Shahid Beheshti University, Iran

### Reviewed by:

Eduardo Luis De Vito,  
University of Buenos Aires, Argentina  
Pedro David Wendel Garcia,  
University Hospital Zürich, Switzerland

### \*Correspondence:

Paola Pierucci  
paola.pierucci@policlinico.ba.it

### Specialty section:

This article was submitted to  
Pulmonary Medicine,  
a section of the journal  
Frontiers in Medicine

Received: 05 November 2020

Accepted: 09 June 2021

Published: 21 July 2021

### Citation:

Pierucci P, Ambrosino N, Di Lecce V,  
Dimitri M, Battaglia S, Boniello E,  
Portacci A, Resta O and  
Carpagnano GE (2021) Prolonged  
Active Prone Positioning in  
Spontaneously Breathing  
Non-intubated Patients With  
COVID-19-Associated Hypoxemic  
Acute Respiratory Failure With  
 $\text{PaO}_2/\text{FiO}_2 > 150$ .  
Front. Med. 8:626321.  
doi: 10.3389/fmed.2021.626321

<sup>1</sup> A. Cardiothoracic Department, Respiratory and Critical Care Unit Bari Policlinic University Hospital, B. Section of Respiratory Diseases, Department of Basic Medical Science Neuroscience and Sense Organs, University of Bari 'Aldo Moro', Bari, Italy, University of Bari, Bari, Italy, <sup>2</sup> Istituti Clinici Scientifici Maugeri Istituto di Ricovero e Cura a Carattere Scientifico Pneumologia Riabilitativa, Istituto di Montescano, Montescano, Italy, <sup>3</sup> Department of Emergency and Organ Transplantation, University of Bari, Bari, Italy

**Background:** The COVID-19 pandemic has led to new approaches to manage patients outside the ICU, including prone positioning in non-intubated patients.

**Objectives:** To report the use of prolonged active prone positioning in spontaneously breathing patients with COVID-19-associated acute respiratory failure. Spontaneously breathing vs non-invasive respiratory support for COVID19 associated acute respiratory failure.

**Methods:** Patients with  $\text{PaO}_2/\text{FiO}_2 > 150$ , with lung posterior consolidations as assessed by means of lung ultrasound, and chest x-ray were studied. Under continuous pulse oximetry ( $\text{SpO}_2$ ) monitoring, patients maintained active prone position. A  $\text{PaO}_2/\text{FiO}_2 < 150$  was considered as treatment failure and patients had to be switched to non-invasive respiratory support. Retrospectively, data of 16 patients undergoing who refused proning and underwent non-invasive respiratory support were used as controls. The primary outcome was the proportion of patients maintaining prolonged prone position and discharged home. Secondary outcomes included improvement in oxygenation, hospital length of stay, and 6-month survival.

**Results:** Three out of 16 (18.7%) patients did not tolerate the procedure. Three more patients showed a worsening in  $\text{PaO}_2/\text{FiO}_2$  to  $< 150$  and required non-invasive support, two of whom finally needing endotracheal intubation. After 72 h, 10 out of 16 (62.5%) patients improved oxygenation [ $\text{PaO}_2/\text{FiO}_2$ : from 194.6 (42.1) to 304.7 (79.3.2) ( $p < 0.001$ )] and were discharged home. In the control group, three out of 16 failed, required invasive ventilatory support, and died within 1 month in ICU. Thirteen were successful and discharged home.

**Conclusion:** In non-intubated spontaneously breathing COVID-19 patients with  $\text{PaO}_2/\text{FiO}_2 > 150$ , active prolonged prone positioning was feasible and tolerated with significant improvement in oxygenation.

**Keywords:** COVID-19, prone position, non-intubated, spontaneously breathing, hypoxic respiratory failure

## INTRODUCTION

The Coronavirus disease 19 (COVID-19) pandemic has led to more than 1 million casualties worldwide (1). COVID-19 severely hit Italy with an increasingly number of patients admitted to hospitals with hypoxemic acute respiratory failure (ARF) needing intensive care unit (ICU) admission, often exceeding the availability of ICU beds. Due to ICU bed and ventilator shortage, critical care resources were saved to care for patients with ARF also outside the ICU (2, 3).

Mechanical ventilation in the prone position (PP) is a validated strategy in the treatment of acute respiratory distress syndrome (ARDS) (4) with several beneficial effects on pulmonary physiology. In supine position, pulmonary edema accumulates in basal regions, leading to increased air volume delivered to apical and anterior lung units, which are also the regions receiving less pulmonary circulation. Prone positioning leads to more homogeneous distribution of ventilation, thus decreasing the shunt fraction and improving matching of ventilation and perfusion (4). Recently, studies have reported improvement in oxygenation during PP in non-intubated awake patients with COVID-19 during spontaneous and non-invasively assisted breathing (5–8, 8–11). However, those were mainly physiologic studies of active PP for a few daily hours. We aimed to report the feasibility and the tolerability of prolonged active PP in non-intubated, spontaneously breathing patients with arterial oxygen tension to inspiratory oxygen fraction ratio ( $\text{PaO}_2/\text{FiO}_2$ )  $> 150$  in a respiratory intensive care unit (RICU). Secondary outcomes were  $\text{PaO}_2/\text{FiO}_2$  before and after the trial and during PP, the length of stay (LoS) in hospital, and 1- and 6-month survival rates.

## METHODS

This observational, prospective, single-center study was approved by the Bari Policlinico ethic committee (study number 6363), and written or verbal informed consent was obtained from all patients.

### Patients

From March 11, to April 30, 2020, all consecutive patients with confirmed COVID-19 without indication for immediate non-invasive respiratory support (NRS) were considered eligible if they had (1)  $\text{PaO}_2/\text{FiO}_2 > 150$  and (2) lung ultrasound (LUS) and chest x-ray signs of basal and posterior consolidations. Under continuous pulse oximetry ( $\text{SpO}_2$ ) and EKG monitoring and oxygen supplementation to maintain  $\text{SpO}_2 > 96\%$ , spontaneously breathing patients were asked to actively maintain

PP (Study Group). Active PP had to be maintained as longest as possible with intervals for meals and other personal care.

Patients who refused to undergo PP were initiated to NRS either with high-flow nasal cannula (HFNC), continuous positive airway pressure (CPAP), or non-invasive ventilation (NIV). These patients with the same clinical and physiological characteristics as the study group were retrospectively considered as controls.

One or more of the following drugs were administered: hydroxy-chloroquine, macrolides, steroids, anticoagulants, tocilizumab, N-acetyl-cysteine, vitamin D, and vitamin C (12), and the rest of patients' comorbidities treatment.

### Measurements

Demographics, clinical characteristics, comorbidities, the sequential organ failure assessment (SOFA), and 1- and 6-month survival were recorded. Chest x-ray and LUS were assessed at admission and at discharge. The CT chest was not promptly available in the same location; therefore, considering the severity of the hypoxic ARF, it was not performed in all patients.

The study group underwent arterial blood gas analysis at the 6th, 24th, 48th, and 72nd hour during PP and in supine position before and after the trial. Controls underwent arterial blood gas analysis at the start of the NRS and at discharge from the RICU.

In patients of the study group, the ventilatory ratio (VR), an index of respiratory effort, was calculated according to Morales-Quinteros et al. (13).

Worsening in  $\text{PaO}_2/\text{FiO}_2$  to  $< 150$  was considered as treatment failure. Patients in the PP group who dropped out or who were failing treatment were switched to NRS. Control patients failing NRS were transferred to the ICU for invasive ventilator support.

### Procedure

The nurse-to-patient ratio in the RICU was 1:4 to 1:5. Patients enrolled maintained PP with the Venturi Oxygen mask under non-invasive monitoring of EKG,  $\text{SpO}_2$ , and arterial blood pressure. During PP, EKG patches were moved from the front to the back of the patients' chest. All healthcare providers wore personal protective equipment, whereas all patients were wearing a surgical mask on top of the Venturi mask (14, 15) (Figure 1).

Control patients continuously performed NRS in semi-recumbent supine position, with only short intervals for eating and personal care. Patients on HFNC were wearing a surgical mask on top of nasal cannula, whereas those on CPAP and NIV used masks closed without expiratory holes and an antiviral filter was inserted between the mask and the circuit to filter all patients' exhaled air.

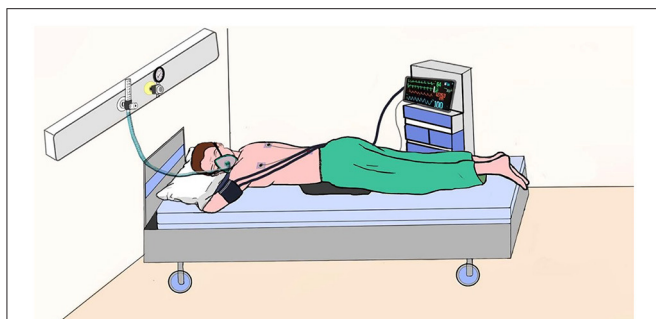


**FIGURE 1** | Cartoon demonstrating continuous prone positioning with oxygen supplementation only via Venturi Mask demonstrated under continuous monitoring.

## Statistical Analysis

Statistical analysis was performed using the R statistical environment (16). For each variable, Shapiro–Wilk test and graphical evaluations (Q–Q plots) were applied to assess the correspondence with the normal distribution. Descriptive statistics are shown as mean  $\pm$  standard deviation (SD) and/or median and interquartile range [IQR] for normally distributed and non-normally distributed continuous variables, respectively, whereas categorical variables were indicated with absolute frequency (%). Student's *t*-test and Mann–Whitney *U*-test were performed to assess between group comparisons, as appropriate. In particular, to evaluate differences between PaO<sub>2</sub>/FiO<sub>2</sub> at admission and discharge, a paired *t*-test was used. Differences for categorical variables between groups were assessed by a Pearson  $\chi^2$  test and or Fisher's exact test. Then, multivariate ANOVA and ANCOVA analyses were performed to compare PaO<sub>2</sub>/FiO<sub>2</sub> at discharge between the two experimental groups, namely, PaO<sub>2</sub>/FiO<sub>2</sub> at admission as a covariate. *p*-values lower than 0.05 were regarded as significant. Plots and graphs were realized using the Excel graph tool.

## RESULTS

Sixteen patients showed eligible criteria and agreed to be enrolled in the study. The other 16 patients were controls. The flow diagram of the study is shown in **Figure 2**. The demographic, anthropometric, and clinical characteristics of patients at admission are shown in **Table 1**. The baseline characteristics were similar between the two groups, with the exception of age, CRP, and PaCO<sub>2</sub>, with the controls being older, being more hypercapnic, and having a higher CRP.

Three out of 16 (18.7%) patients did not tolerate PP for chronic osteoarticular pain related to knee and spine degeneration; therefore, they received oxygen therapy in supine position. However, within 24 h from the discontinuation of PP, they all experienced worsening of their gas exchange. In more detail, one of them was supported *via* HFNC with FiO<sub>2</sub> 0.75 and two were supported *via* helmet CPAP with FiO<sub>2</sub> 0.70. None of them required intubation (**Figure 2**). Three more patients showed worsening in PaO<sub>2</sub>/FiO<sub>2</sub> to <150 and underwent NIV;

two of them finally needed endotracheal intubation. Ten out of 16 patients of the study group showed a significant improvement in oxygenation [PaO<sub>2</sub>/FiO<sub>2</sub> from 194.6 (42.1) before to 304.7 (79.32) after 72 h of PP *via* ANCOVA test (*p* < 0.001)]. **Figure 3** shows the individual and mean PaO<sub>2</sub>/FiO<sub>2</sub> values during the trial in the successful patients of study group. The mean PaO<sub>2</sub>/FiO<sub>2</sub> before discharge from the RICU was 330  $\pm$  89.1.

As shown in **Table 2**, the baseline clinical characteristics of successful patients were not significantly different between groups with the exception of the PaCO<sub>2</sub> being higher in controls. However, only two patients were affected by chronic respiratory failure in the control group before admission.

The baseline VR was not different between the two groups. The LUS scores of the 10 successful patients changed from 13.0 [IQR 6.0–16.5] before, to 5.0 [IQR 2.5–12.0] at the end of PP (*p* = 0.0364), indicating a significant improvement in lung consolidations. All 10 patients were discharged home after a mean LoS of 21.0 (7.0) days (**Figure 2**). Patients undergoing active PP <12 days from hospital admission had a significantly shorter LoS as compared to the others [17.0 (5.0) vs. 25.0 (6.0) days, *p* = 0.04]. No patient who had undergone PP had died at 1- and 6-month follow-up.

As also shown in **Figures 2, 4** out of 16 controls showed a worsening in PaO<sub>2</sub>/FiO<sub>2</sub> to <150, requiring admission to ICU and endotracheal intubation. All three patients died in ICU within 1 month. The 13 successful controls showed a significant improvement in oxygenation from admission to discharge [PaO<sub>2</sub>/FiO<sub>2</sub> from 181.2 (19.1) at the start to 290.5 (81.4) at discharge from RICU (*p* < 0.001)]. There was no significant difference in discharge to admission changes in PaO<sub>2</sub>/FiO<sub>2</sub> between the successful patients of the study group or control group (*p* = 0.3156).

**Figure 4A** shows the individual and mean PaO<sub>2</sub>/FiO<sub>2</sub> values at admission and discharge of all patients and controls while **Figure 4B** shows only successful patients including study group and controls.

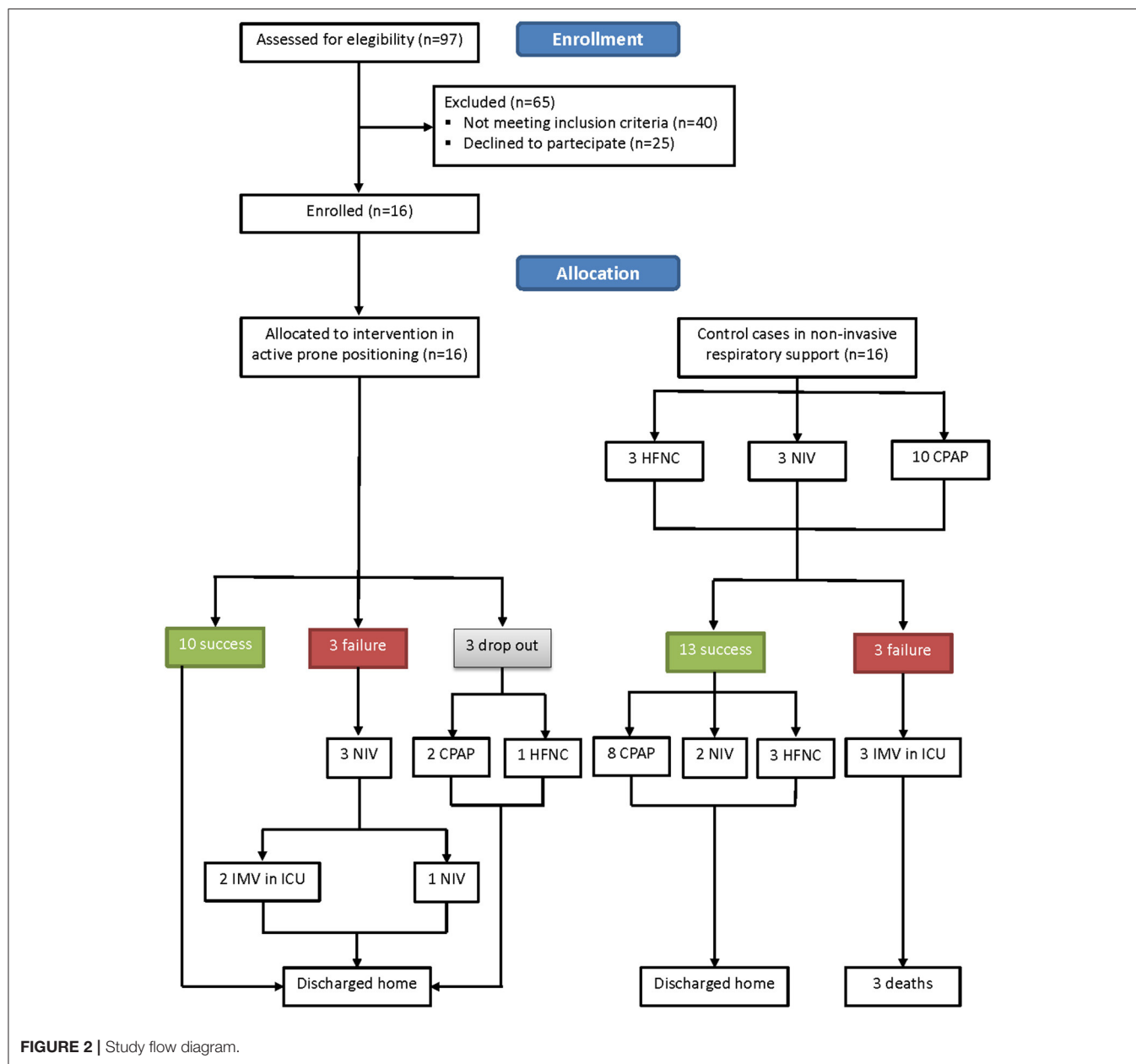
Only one healthcare provider suffered from COVID-19 infection during the study period.

## DISCUSSION

In this small single-center cohort study, we found that the use of PP in awake, spontaneously breathing patients with COVID-19-induced hypoxemic ARF with PaO<sub>2</sub>/FiO<sub>2</sub> > 150 was feasible, tolerated for a prolonged time (three consecutive days), with similar results to patients undergoing NRS. The PP was associated with improved oxygenation and lung consolidations. Patients did not require ventilatory support in 62.5% of cases with good 1- and 6-month outcome.

Before the COVID-19 pandemic, there was limited published research on PP in non-intubated patients. The COVID-19 pandemic has led to a dramatic increase in patients requiring critical care, pushing clinicians to use new approaches to save resources for mechanical ventilation, including awake proning. A few physiological and clinical studies have evaluated the effects of PP in non-intubated patients with COVID-19 under NRS or





spontaneously breathing (6–8, 8–10), and early helmet CPAP with moderate pressure and PP has been suggested (11).

This study enrolled unsupported breathing patients, and the active PP was tolerated all day long, with just short intervals for meals and personal care, for 3 consecutive days: to the best of our knowledge, this is the longest reported period: in literature, up to 8 daily hours of active PP are reported (9).

During the PP, the expansion of the anterior chest wall is limited, resulting in more homogeneous chest wall compliance and gravitational forces on lung parenchyma. This enables greater recruitment of the posterior zones, recruiting a larger proportion of alveoli clusters to participate in gas exchange. The diaphragm also greatly contributes to improve stress forces

during PP, which may help to reduce lung injury during spontaneous breathing (17, 18). Indeed, the PP enhances the inferior movement of the diaphragm, which relieves compression on posterior lung zones that are usually atelectatic during supine positioning, thus improving their recruitment (19, 20).

The Ventilatory ratio (VR) is considered an index of respiratory effort, and it has been found to be independently associated with mortality in non-COVID-19 ARDS patients (21). In our patients, the mean VR was similar to survivors of non-COVID ARDS (13). Further studies will be required to confirm the VR ranges within COVID-19 patients.

**TABLE 1** | Demographic, physiological, and clinical characteristics of patients at RICU admission.

| Variables                            | Study group | Control group | p-value |
|--------------------------------------|-------------|---------------|---------|
| Number                               | 16          | 16            |         |
| Age, years                           | 59 ± 11     | 70 ± 15       | 0.01    |
| Males, n (%)                         | 13 (81)     | 10 (62)       | 0.71    |
| Smokers, n (%)                       | 9 (56)      | 8 (50)        | 1       |
| Presence of comorbidities, n (%)     | 13 (81.2)   | 13 (81.2)     | 1       |
| Obesity, n (%)                       | 5 (27.8)    | 4 (25)        | 1       |
| Hypertension, n (%)                  | 5 (31.2)    | 11 (68.8)     | 0.07    |
| Diabetes, n (%)                      | 3 (18.8)    | 4 (25)        | 1       |
| Chronic cardiac failure, n (%)       | 0           | 3 (18.8)      | 0.22    |
| Ischemic cardiac disease, n (%)      | 2 (12.5)    | 2 (12.5)      | 1       |
| Chronic kidney disease, n (%)        | 5 (31.2)    | 6 (37.5)      | 1       |
| Respiratory disease, n (%)           | 0           | 2 (12.5)      | 0.48    |
| Autoimmune diseases, n (%)           | 2 (12.5)    | 0             | 0.48    |
| SOFA*                                | 2 [0.25]    | 2 [0]         | 0.61    |
| PaO <sub>2</sub>                     | 142 ± 62    | 127 ± 27      | 0.46    |
| FiO <sub>2</sub>                     | 57 ± 7      | 59 ± 13       | 0.31    |
| PaO <sub>2</sub> /FiO <sub>2</sub>   | 226 ± 74    | 179 ± 18      | 0.11    |
| PaCO <sub>2</sub> , mmHg             | 37 ± 4      | 43 ± 6        | 0.03    |
| CPR, mg/L                            | 78 ± 63     | 137 ± 80      | 0.03    |
| WBC, 10 <sup>3</sup> μl              | 6.8 ± 2.4   | 8.9 ± 4.9     | 0.83    |
| NLR                                  | 6.6±3.8     | 8.8 ± 6.5     | 0.13    |
| HR, bpm                              | 78 ± 10     | 80 ± 12       | 0.38    |
| RR, bpm                              | 20 ± 4      | 20 ± 3        | 0.32    |
| VR                                   | 1.6±0.5     | 1.5±0.8       | 0.46    |
| Time from ED to RICU admission, days | 11 ± 7      | 10 ± 10       | 0.47    |

Values are shown as mean ± SD, respectively, for normal distributed numeric variables or as median [IQR] for non-normal distributed numeric variables (\*), and with % for categorical ones. SOFA, sequential organ failure assessment; ED, emergency department; CPR, C-reactive protein; WBC, white blood cell; NLR, neutrophil-to-lymphocyte ratio; HR, heart rate; RR, respiratory rate; VR, ventilatory ratio; LUS, lung ultrasound; RICU, respiratory intensive care unit.

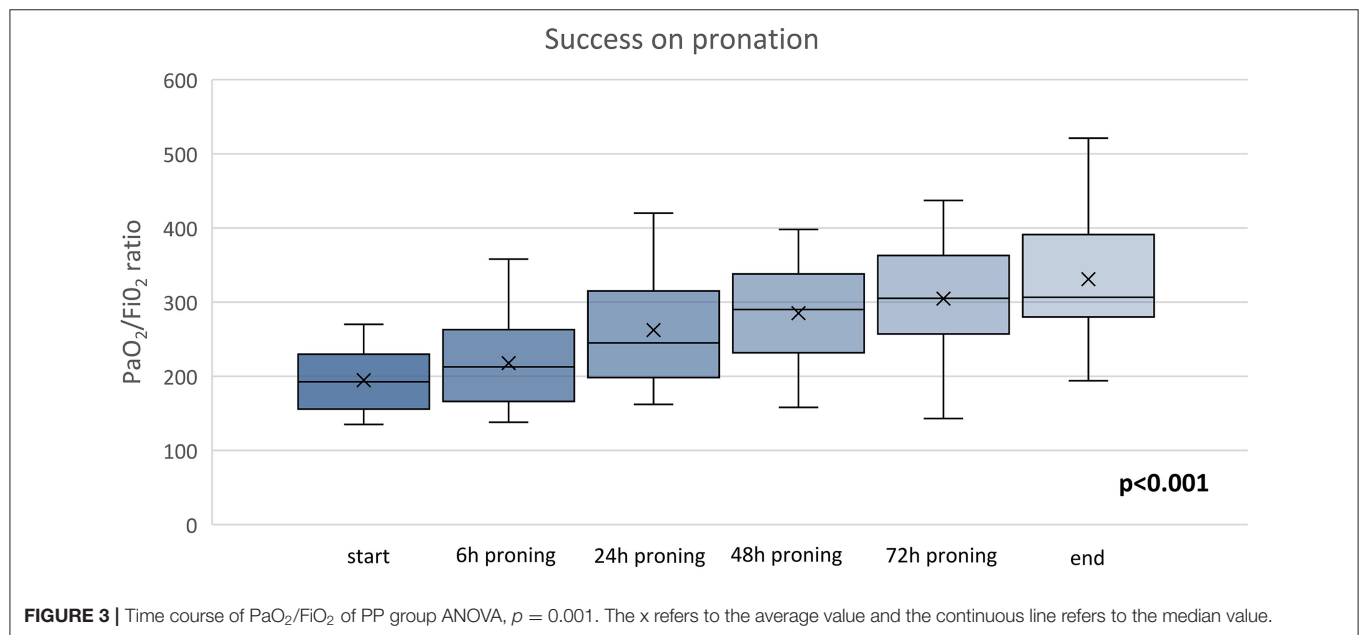
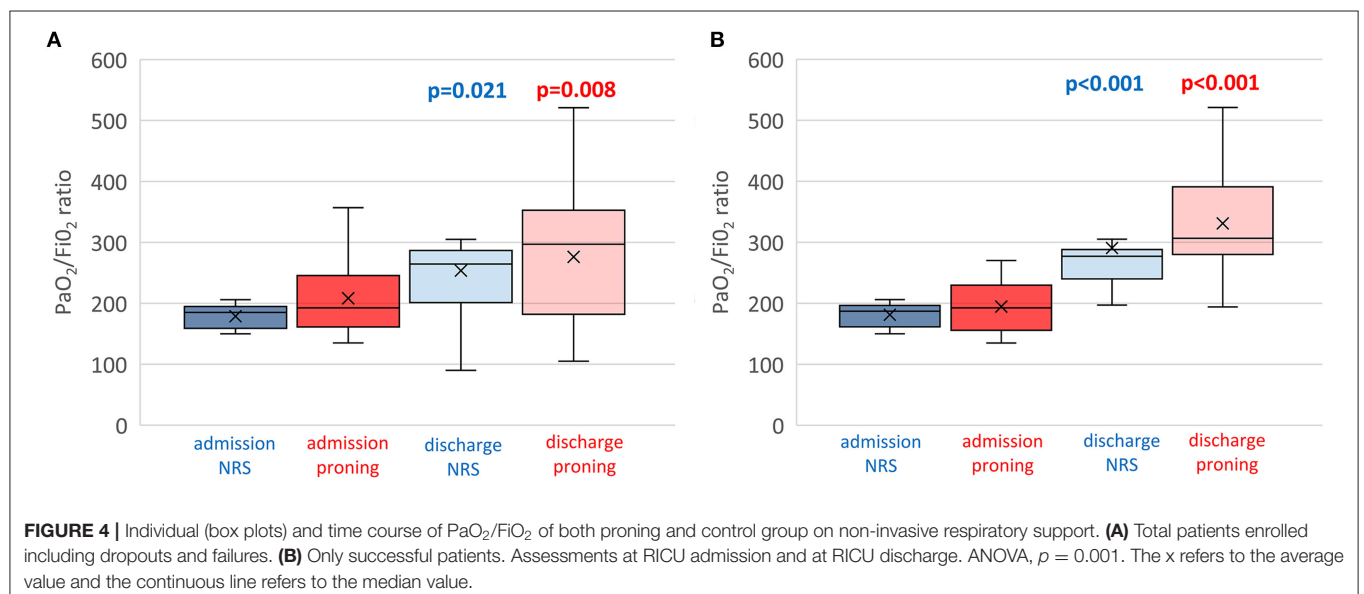


**TABLE 2 |** Demographic, physiological, and clinical characteristics of successful patients at admission.

| Variables                               | Study group   | Control group   | p-value |
|---|---------------|-----------------|---------|
|   | 10            | 13              |         |
| Age, years $\wedge$                     | 60 $\pm$ 9    | 69 $\pm$ 17     | 0.07    |
| Males, <i>n</i> (%)                     | 8 (80)        | 10 (80)         | 1       |
| Smokers, <i>n</i> (%)                   | 5 (50)        | 6 (46)          | 1       |
| Presence of comorbidities, <i>n</i> (%) | 7 (70)        | 10 (77)         | 0.1     |
| Obesity, <i>n</i> (%)                   | 4 (40)        | 4 (30.8)        | 0.68    |
| Hypertension, <i>n</i> (%)              | 4 (40)        | 8 (61.5)        | 0.41    |
| Diabetes, <i>n</i> (%)                  | 3 (30)        | 3 (23.1)        | 1       |
| Chronic cardiac failure, <i>n</i> (%)   | 0             | 3 (23.1)        | 0.23    |
| Ischemic cardiac disease, <i>n</i> (%)  | 1 (10)        | 2 (15.4)        | 1       |
| Chronic kidney disease, <i>n</i> (%)    | 3 (30)        | 5 (38.5)        | 1       |
| Respiratory disease, <i>n</i> (%)       | 0             | 2 (15.4)        | 0.48    |
| Autoimmune diseases, <i>n</i> (%)       | 1(10)         | 0               | 0.43    |
| SOFA*                                   | 2 [0.75]      | 2 [0]           | 0.12    |
| PaO <sub>2</sub>                        | 117 $\pm$ 25  | 117 $\pm$ 27    | 0.65    |
| FiO <sub>2</sub>                        | 60 $\pm$ 0    | 55.8 $\pm$ 10.6 | 0.42    |
| PaO <sub>2</sub> /FiO <sub>2</sub>      | 195 $\pm$ 42  | 181 $\pm$ 19    | 0.17    |
| PaCO <sub>2</sub> , mmHg                | 35 $\pm$ 3    | 42 $\pm$ 5      | 0.001   |
| CPR, mg/L                               | 84 $\pm$ 62   | 127 $\pm$ 70    | 0.09    |
| WBC, 10 <sup>3</sup> $\mu$ l            | 6.5 $\pm$ 2.6 | 8.7 $\pm$ 4.7   | 0.14    |
| NLR                                     | 6.8 $\pm$ 3.4 | 8.7 $\pm$ 6.1   | 0.25    |
| HR, bpm                                 | 76 $\pm$ 9    | 80 $\pm$ 12     | 0.29    |
| RR, bpm                                 | 20 $\pm$ 4    | 21 $\pm$ 3      | 0.33    |
| VR                                      | 1.5 $\pm$ 0.3 | 1.4 $\pm$ 0.4   | 0.43    |
| Time from ED to RICU admission, days    | 13 $\pm$ 4    | 10 $\pm$ 10     | 0.40    |

Values are shown as mean  $\pm$  SD, respectively, for normal distributed numeric variables or as median [IQR] for non-normal distributed numeric variables (\*), and with % for categorical ones. SOFA, sequential organ failure assessment; ED, emergency department; CPR, C-reactive protein; WBC, white blood cell count; NLR, neutrophil-to-lymphocyte ratio; HR, heart rate; RR, respiratory rate; VR, ventilatory ratio; LUS, lung ultrasound; RICU, respiratory intensive care unit.



Active PP may result in good physiological and clinical results, avoiding contacts and waste of human, economic, therapeutic resources and personal protective equipment (12, 14, 15). These patients were able to maintain active PP, and the only additional nursing workload was to move the EKG patches from the front to the back of the patients' chest.

The two groups of patients analyzed were similar but showed one significant difference in terms of age with the control group being older. Furthermore, the control group showed higher CRP and PaCO<sub>2</sub> compared to the other. This, on one hand, would potentially expose the control group to a better response to NRS; on the other hand, both the SOFA score and the P/F ratio did not differ between the two groups, showing a substantial similar prediction of mortality and grade of severity of hypoxic respiratory failure.

The setting of the study allows its repeatability in a clinical unit with patients under 24 h monitoring and adequate nurse support and supervision. Although promising, our case series should be interpreted with caution. In this selected group (PaO<sub>2</sub>/FiO<sub>2</sub> > 150), three patients did not tolerate the PP, and two patients required intubation. The RICU is the right location for these unstable patients where adequately trained personnel may promptly recognize the need for treatment escalation and switch to NIV or IMV, respectively (22). Although improved oxygenation with the PP is important, hypoxemia has not been a reliable surrogate biomarker for mortality in clinical trials of ARDS (23).

This study has limitations. The sample size of patients was small (16 patients vs. 16 controls), and the data of controls were retrospectively collected. The performance of a chest CT scan in all admitted patients with hypoxic ARF would have added important information on the status of the lung parenchyma. However, due to the large number of patients to manage at that time, this was not promptly available for all admitted patients.

A control population of consecutively admitted patients only on low flow oxygen not undergoing NRS would have been more suitable for adequate comparison; however, at the time of the study, patients with PaO<sub>2</sub>/FiO<sub>2</sub> > 150 used to be initiated to NRS.

The choice of SpO<sub>2</sub>/FiO<sub>2</sub> would have been useful as a surrogate evaluation of time points in the initial 24 h; however, this parameter, although monitored, was not recorded.

On the other hand, our study highlights the feasibility, tolerability, and effectiveness of prolonged PP. Indeed, the shorter LoS of patients undergoing earlier PP suggests greater effectiveness in early application. Within the 6-month follow-up, no deaths occurred in the group that underwent PP. Furthermore, in consideration of the high shortage of ICU beds, the PP may represent a first-line treatment outside the ICU.

Spontaneously breathing patients with hypoxemic ARF may generate relatively large tidal volumes with potential self-inflicted

lung injury (SILI) (24). Therefore, continuous monitoring of paradoxical breathing pattern and vital parameters should be warranted in these patients as they may deteriorate very fast. These concerns should be balanced with the lack of ICU bed availability and the risks of mechanical ventilation, including the need for prolonged sedation and the risk of ventilator-associated pneumonia.

## CONCLUSION

In conclusion, in the majority of the studied non-intubated spontaneously breathing series of patients with COVID-19-associated hypoxemic ARF with PaO<sub>2</sub>/FiO<sub>2</sub> ratio >150 prolonged active PP was feasible and well-tolerated and associated to improvement in PaO<sub>2</sub>/FiO<sub>2</sub>. This approach may be confirmed by larger randomized controlled studies.

## DATA AVAILABILITY STATEMENT

The raw data supporting the conclusions of this article will be made available by the authors, without undue reservation.

## ETHICS STATEMENT

The studies involving human participants were reviewed and approved by Bari Policlinico Ethic committee. Written informed consent was obtained from the individual(s) for the publication of any potentially identifiable images or data included in this article.

## AUTHOR CONTRIBUTIONS

PP, VD, and GC made substantial contribution to the conception and design of the work. MD, EB, and AP: data acquisition. SB, NA, and GC: analysis. NA and OR: interpretation. PP, VD, MD, SB, EB, and AP helped in drafting the article. NA, GC, and OR revised it critically for important intellectual content. All authors gave the final approval of the version to be published and agreed for the accuracy or integrity of any part of the work.

## ACKNOWLEDGMENTS

The authors would like to thank Mrs. Barione, Dr. Buonamico, Dr. Carrassi, Dr. Diaferia, Dr. Di Gioia, Dr. Labate, Dr. Majorano, Dr. Palumbo, Dr. Santomasi, Dr. Valerio, and all the RICU team for their contribution in the study. We also thank Dr. D Portacci for the **Figure 1** cartoon design.

## REFERENCES

1. Johns Hopkins University. *Covid-19 Dashboard by the Centre for Systems Science and Engineering (CSSE) at Johns Hopkins University*. Available online at: <https://coronavirus.jhu.edu/map.html> (accessed October 30, 2020).
2. Franco C, Facciolo N, Tonelli R, Dongilli R, Vianello A, Pisani L, et al. Feasibility and clinical impact of out-of-ICU non-invasive respiratory support in patients with COVID-19 related pneumonia. *Eur Respir J*. (2020) 3:2002130. doi: 10.1183/13993003.02130-2020



3. Di Lecce V, Carpagnano GE, Pierucci P, Quaranta VN, Barratta F, Zito A, et al. Baseline characteristics and outcomes of COVID-19 patients admitted to a Respiratory Intensive Care Unit (RICU) in Southern Italy. *Multidiscip Respir Med.* (2020) 15:704. doi: 10.4081/mrm.2020.704
4. Gattinoni L, Taccone P, Carlesso E, Marini JJ. Prone position in acute respiratory distress syndrome. Rationale, indications, and limits. *Am J Respir Crit Care Med.* (2013) 188:1286–93. doi: 10.1164/rccm.201308-1532CI
5. Ding L, Wang L, Ma W, He H. Efficacy and safety of early prone positioning combined with HFNC or NIV in moderate to severe ARDS: a multi-center prospective cohort study. *Critical Care.* (2020) 24:28. doi: 10.1186/s13054-020-2738-5
6. Elharrar X, Trigui Y, Dols A-M, Touchon F, Martinez S, Prud'homme E, et al. Use of prone positioning in nonintubated patients with COVID-19 and hypoxemic acute respiratory failure. *J Am Med Assoc.* (2020) 323:2336–8. doi: 10.1001/jama.2020.8255
7. Sartini C, Tresoldi M, Scarpellini P, Tettamanti A, Carcò F, Landoni G, et al. Respiratory parameters in patients with COVID-19 after using non-invasive ventilation in the prone position outside the intensive care unit. *J Am Med Assoc.* (2020) 323:2338–40. doi: 10.1001/jama.2020.7861
8. Paul V, Patel V, Royse M, Odish M, Malhotra A, Koenig S. Prone in non-intubated (PINI) in times of COVID-19: case series and a review. *J Intensive Care Med.* (2020) 35:818–24. doi: 10.1177/0885066620934801
9. Coppo A, Bellani G, Winterton D, DI Pierro M, Soria A, Faverio P, et al. Feasibility and physiological effects of prone positioning in non-intubated patients with acute respiratory failure due to COVID-19 (PRON-COVID): a prospective cohort study. *Lancet Respir Med.* (2020) 8:765–74. doi: 10.1016/S2213-2600(20)30268-X
10. Scaravilli V, Grasselli G, Castagna L, Zanella A, Isgro' S, Lucchini A, et al. Prone positioning improves oxygenation in spontaneously breathing non-intubated patients with hypoxemic acute respiratory failure: a retrospective study. *J Crit Care.* (2015) 30:1390–4. doi: 10.1016/j.jcrc.2015.07.008
11. Longhini F, Bruni A, Garofalo E, Navalesi P, Grasselli G, Cosentini R, et al. Helmet Continuous Positive Airway Pressure and prone positioning: a proposal for an early management of COVID-19 patients. *Pulmonology.* (2020) 26:186–91. doi: 10.1016/j.pulmoe.2020.04.014
12. World Health Organization. *Severe Acute Respiratory Infections Treatment Centre Practical Manual to Set Up and Manage a SARI Treatment Centre and a SARI Screening Facility in Health Care Facilities.* (2020).
13. Morales-Quinteros L, Schultz MJ, Bringué J, Calfee CS, Camprubí M, Cremer OL, et al. Estimated dead space fraction and the ventilatory ratio are associated with mortality in early ARDS. *Ann Intensive Care.* (2019) 9:128. doi: 10.1186/s13613-019-0601-0
14. Ippolito M, Vitale F, Accurso G, Ozzo P, Gregoretto C, Giarratano A, et al. Medical masks and respirators for the protection of healthcare workers from COVID-19 and other viruses. *Pulmonology.* (2020) 26:204–12. doi: 10.1016/j.pulmoe.2020.04.009
15. NIH. *Covid-19 Treatment Guidelines.* Available online at: <https://www.covid19treatmentguidelines.nih.gov/whats-new/> (accessed May 30, 2021).
16. RCore Team. *R: A Language and Environment for Statistical Computing.* Vienna: R Foundation for Statistical Computing (2020). Available online at: <https://www.r-project.org/> (accessed June 19, 2021).
17. Scholten EL, Beitler JR, Prisk GK, Malhotra A. Treatment of ARDS with prone positioning. *Chest.* (2017) 151:215–24. doi: 10.1016/j.chest.2016.06.032
18. Pappert D, Rossaint R, Slama K, Grüning T, Falkeet KJ. Influence of positioning on ventilation–perfusion relationships in severe adult respiratory distress syndrome. *Chest.* (1994) 106:1511–6. doi: 10.1378/chest.106.5.1511
19. Telias I, Katira BH, Brochard L. Is the prone position helpful during spontaneous breathing in patients with COVID-19? *J Am Med Assoc.* (2020) 323:2265–7. doi: 10.1001/jama.2020.8539
20. Slessarev M, Cheng J, Ondrejicka M, Arntfield R. Patient self-prone with high-flow nasal cannula improves oxygenation in COVID-19 pneumonia. *Can J Anaesth.* (2020) 67:1288–90. doi: 10.1007/s12630-020-01661-0
21. Sinha P, Calfee CS, Beitler JR, Soni N, Ho K, Matthay MA, et al. Physiologic analysis and clinical performance of the ventilatory ratio in acute respiratory distress syndrome. *Am J Respir Crit Care Med.* (2019) 199:333–41. doi: 10.1164/rccm.201804-0692OC
22. Karim HMR, Burns KEA, Ciobanu LD, El-Khatib M, Nicolini A, Vargas N, et al. Noninvasive ventilation: education and training. A narrative analysis and an international consensus document. *Adv Respir Med.* (2019) 87:36–45. doi: 10.5603/ARM.a2019.0006
23. Acute Respiratory Distress Syndrome Network, Brower RG, Matthay MA, Morris A, Schoenfeld D, Thompson BT, et al. Ventilation with lower tidal volumes as compared with traditional tidal volumes for acute lung injury and the acute respiratory distress syndrome. *N Engl J Med.* (2000) 342:1301–8. doi: 10.1056/NEJM200005043421801
24. Jardin F, Delorme G, Hardy A, Auvert B, Beauchet A, Bourdarieset JP. Reevaluation of hemodynamic consequences of positive pressure ventilation: emphasis on cyclic right ventricular after loading by mechanical lung inflation. *Anesthesiology.* (1990) 72:966. doi: 10.1097/0000542-199006000-00003

**Conflict of Interest:** The authors declare that the research was conducted in the absence of any commercial or financial relationships that could be construed as a potential conflict of interest.

Copyright © 2021 Pierucci, Ambrosino, Di Lecce, Dimitri, Battaglia, Boniello, Portacci, Resta and Carpagnano. This is an open-access article distributed under the terms of the Creative Commons Attribution License (CC BY). The use, distribution or reproduction in other forums is permitted, provided the original author(s) and the copyright owner(s) are credited and that the original publication in this journal is cited, in accordance with accepted academic practice. No use, distribution or reproduction is permitted which does not comply with these terms.



# COVID-19 as a Research Dynamic Transformer: Emerging Cross-Disciplinary and National Characteristics

Ryosuke L. Ohniwa<sup>1,2\*†</sup>, Joji Kijima<sup>3†</sup>, Mizuho Fukushima<sup>1</sup> and Osamu Ohneda<sup>1</sup>

<sup>1</sup>Faculty of Medicine, University of Tsukuba, Tsukuba, Japan, <sup>2</sup>Center for Biotechnology, National Taiwan University, Taipei, Taiwan, <sup>3</sup>Bureau of Global Initiatives, University of Tsukuba, Tsukuba, Japan

## OPEN ACCESS

### Edited by:

Reza Lashgari, ShahidBeheshti University, Iran

### Reviewed by:

Gregory R. Hart, Yale University, United States  
Sohrab Najafian, SUNY College of Optometry, United States  
Mahdi Mahdavi, ShahidBeheshti University of Medical Sciences, Iran

### \*Correspondence:

Ryosuke L. Ohniwa  
ohniwa@md.tsukuba.ac.jp

<sup>†</sup>These authors have contributed equally to this work

### Specialty section:

This article was submitted to Medicine and Public Health, a section of the journal Frontiers in Big Data

**Received:** 19 November 2020

**Accepted:** 21 June 2021

**Published:** 26 July 2021

### Citation:

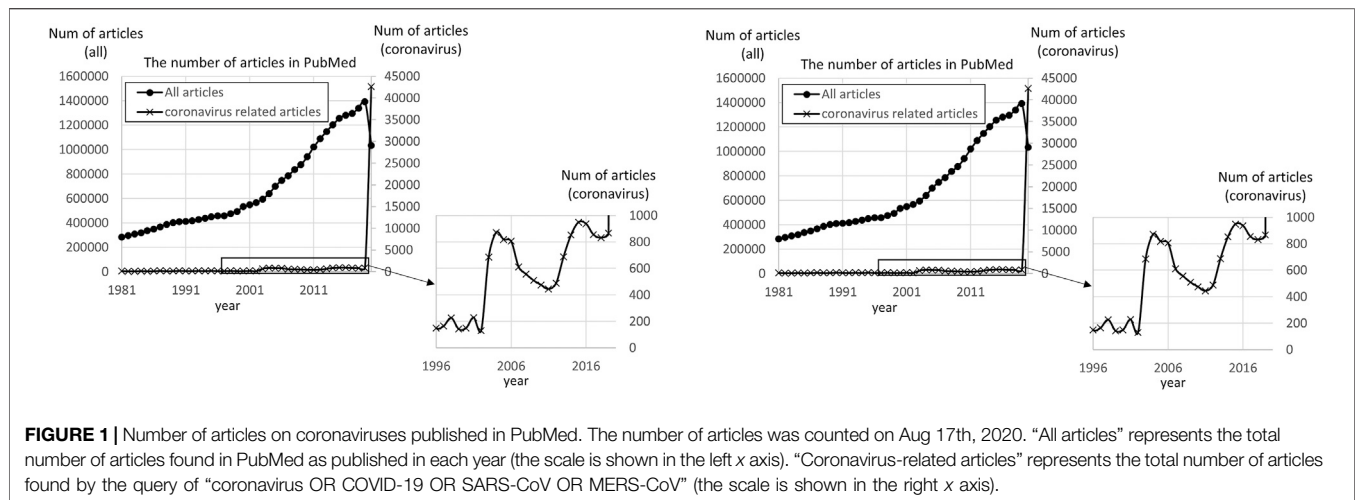
Ohniwa RL, Kijima J, Fukushima M and Ohneda O (2021) COVID-19 as a Research Dynamic Transformer: Emerging Cross-Disciplinary and National Characteristics. *Front. Big Data* 4:631073. doi: 10.3389/fdata.2021.631073

The outbreak of the COVID-19 pandemic has had an unprecedented impact on humanity as well as research activities in life sciences and medicine. Between January and August 2020, the number of coronavirus-related scientific articles was roughly 50 times more than that of articles published in the entire year of 2019 in PubMed. It is necessary to better understand the dynamics of research on COVID-19, an emerging topic, and suggest ways to understand and improve the quality of research. We analyze the dynamics of coronavirus research before and after the outbreaks of SARS, MERS, and COVID-19 by examining all the published articles from the past 25 years in PubMed. We delineate research networks on coronaviruses as we identify experts' background in terms of topics of previous research, affiliations, and international co-authorships. Two distinct dynamics of coronavirus research were found: 1) in the cases of regional pandemics, SARS and MERS, the scope of cross-disciplinary research remained between neighboring research areas; 2) in the case of the global pandemic, COVID-19, research activities have spread beyond neighboring disciplines with little transnational collaboration. Thus, COVID-19 has transformed the structure of research on coronaviruses as an emerging issue. Knowledge on COVID-19 is distributed across the widest range of disciplines, transforming research networks well beyond the field of medicine but within national boundaries. Given the unprecedented scale of COVID-19 and the nationalization of responses, the most likely way forward is to accumulate local knowledge with the awareness of transdisciplinary research dynamics.

**Keywords:** COVID-19, coronavirus research, researcher dynamics, PubMed, scientometrics

## INTRODUCTION

COVID-19 [SARS-CoV-2 (severe acute respiratory syndrome coronavirus 2)]—since first reported in Wuhan, China, in December 2019—has spread around the globe with more than 172 million confirmed cases and more than three million deaths from December 2019 to June 2021 (WHO 2021). Earlier in this century, the world was also plagued by the outbreaks of SARS [SARS-CoV (severe acute respiratory syndrome coronavirus)]—originating from Guangdong Province, China, in November 2002 (Rosling and Rosling, 2003; Xu et al., 2004)—and MERS [MERS-CoV (Middle East respiratory syndrome coronavirus)] that emerged in March 2012 (Hijawi et al., 2013; Cauchemez et al., 2014). In the 21st century, coronaviruses have become the root causes of emerging infectious diseases in the world (Guarner, 2020; Wang et al., 2020).



Meanwhile, the number of scientific research articles on coronaviruses in the fields of life sciences and medicine has increased dramatically (**Figure 1**). In the case of SARS-CoV, the number of publications increased fivefold by 2003—in just one year after the outbreak. In the case of MERS-CoV, the number increased steadily from the year after the outbreak in 2012 and doubled by 2015. In the case of SARS-CoV2, the number of research articles published between January 2020 and August 2020 was 50 times more than the number of scientific publications on coronaviruses in the entire year of 2019 (see Results). Indeed, coronaviruses have become an emerging research topic as a result (Rotolo et al., 2015).

It has been shown by bibliometric and sociological studies that researchers tend to publish articles on topics outside of their own area of expertise and begin diversifying their publications once certain topics—such as new technologies and concepts—are recognized as something scientifically valuable in the forthcoming future. That is how the corresponding topics become “emerging” (Van Merkerk and Van Lente, 2005; Borup et al., 2006; Gustafsson et al., 2015). At the same time, the rapid growth of publications makes these emerging topics the foci of cross-disciplinary studies (Rotolo et al., 2015). However, more studies are needed to adequately understand the relationship between emerging topics—such as infectious diseases—and the scope of cross-disciplinary research. This study aimed to fill part of that gap in the literature on the relationship between the emerging topics.

In this study, we analyze the Medical Subject Headings (MeSH) attached to PubMed (Medline) articles to identify the research topics and specialties of each researcher. PubMed (Medline), a literature database search engine run by the National Library of Medicine (NLM), contains approximately 10 million articles. MeSH is a popular keyword thesaurus developed by NLM, and it is typically used in PubMed to support literature searches (Lipscomb, 2000). It is attached to each article under the supervision of professional curators according to article contents (Lowe and Barnett, 1994). We have developed a method to identify emerging topics as clusters of emerging MeSH terms (Ohniwa et al., 2010; Ohniwa and Hibino, 2019). For the present study, we have modified this

method to identify the characteristics of research topics and areas of expertise by selecting unique MeSH terms instead of those emerging (see Materials and Methods).

We investigate all the articles in PubMed between 1996 and 2020 to elucidate the following: 1) trends in coronavirus research before and after the outbreaks of the novel coronavirus infectious diseases—namely, SARS, MERS, and COVID-19—in terms of their impact on the nature of research; 2) the dynamics of how researchers venture across disciplinary boundaries to tackle emerging topics in times of crises by identifying their areas of research prior to the outbreaks and their countries of origin; and 3) the relational mechanism between cross-disciplinary research and transnational collaboration on coronaviruses. The results indicate the current COVID-19 pandemic has transformed coronavirus research into a nationalized body of knowledge across a wider range of disciplines. Finally, we suggest the most likely way forward for coronavirus research and draw an implication from the transformation of research dynamics based on the concepts of “transdisciplinarity (Stenner, 2017)” and “event (Whitehead, 1925)”.

## MATERIALS AND METHODS

### Dataset

MeSH terms attached to articles published between 1996 and 2020 were collected through PubMed (<https://www.ncbi.nlm.nih.gov/pubmed/>) on August 17th, 2020. A total of 21,706,508 articles were included in the analysis.

MeSH terms attached on each article were identified from the XML data, and any overlaps in terms for each article were eliminated by our original Perl scripts as described in our previous articles (Ohniwa et al., 2010; Ohniwa and Hibino, 2019). Here, to identify the set of MeSH terms attached to each article, terms tagged as <DescriptorNameUI = @> and <NameOfSubstance UI = @> from the XML data (@ represents each UI) were extracted, and then overlaps in the terms for each article were eliminated by Perl with our original scripts. Then, to eliminate the terms not concerned with research

topics, all the MeSH terms under the following hierarchies were excluded: “Geographicals [Z],” “Publication Characteristics [V],” “Named Groups [M],” “Health Care [N],” “Information Services [L01.453],” “Communications Media [L01.178],” “Communication [L01.143],” “Information Centers [L01.346],” and “Publishing [L01.737]” according to the 2018 MeSH Tree Hierarchy (<https://meshb-prev.nlm.nih.gov/search>). These categories involve MeSH terms which represent the style or the background of articles rather than its research contents. A total of 1,776,759 kinds of terms with a total of 957,790,657 occurrences were obtained between 1996 and 2020 by this operation.

To identify the sets of authors and affiliations attached to each article, terms tagged as <AffiliationInfo>, <LastName>, and <Initials> within <Author ValidYN = @> (@ represents each “Y or N”) were extracted by our original Perl script. A total of 42,923,027 kinds of authors (with affiliation) with a total of 56,467,393 occurrences were obtained by this operation (in the case of only author name, a total of 7,395,577 kinds of authors with a total of 108,977,113 occurrences).

Coronavirus-related articles published between 1996 and 2020 were separately obtained by searching PubMed using the query terms of “coronavirus OR COVID-19 OR SARS-CoV OR MERS-CoV.” A total of 56,077 articles and 66,850 kinds of MeSH terms with a total of 1,739,841 occurrences were obtained between 1996 and 2020 by this operation. From these articles, a total of 252,292 kinds of authors (with affiliations) with a total of 273,759 occurrences were obtained (in the case of using only authors’ names, a total of 157,593 kinds of authors with a total of 337,946 occurrences).

## Countries of Origin

The number of articles having the following words in the affiliation was counted: “Argentina”, “Australia”, “Austria”, “Belgium”, “Brazil”, “Bulgaria”, “Canada”, “Chile”, “China (‘China’ or ‘People’s Republic of China’),” “Croatia”, “Czech Republic”, “Denmark”, “Egypt”, “Finland”, “France”, “Germany”, “Greece”, “HongKong”, “Hungary”, “India”, “Iran”, “Ireland”, “Israel”, “Italy”, “Japan”, “Korea”, “Malaysia”, “Mexico”, “Netherlands”, “New Zealand”, “Norway”, “Pakistan”, “Poland”, “Portugal”, “Romania”, “Russia”, “Saudi Arabia”, “Singapore”, “Slovakia”, “Slovenia”, “South Africa”, “Spain”, “Sweden”, “Switzerland”, “Taiwan (‘Taiwan’ or ‘Republic of China’),” “Thailand”, “Turkey”, “Ukraine”, “United Arab Emirates (‘UAE’ or ‘United Arab Emirates’),” “United Kingdom (‘England’, ‘U.K’, ‘UK’, ‘United Kingdom’, ‘Scotland’),” and “United States (‘USA’ or ‘United States’).”

## Unique Keywords

Among MeSH terms, we arbitrary defined unique keywords to coronavirus research as follows:

$$(A_{\alpha \text{ in } \beta} C / B_{\beta}) / (C_{\alpha \text{ in } \beta} / D_{\beta}) \geq 2,$$

where  $A_{\alpha \text{ in } \beta}$  is the number of appearances of the MeSH term  $\alpha$  in years  $\beta$  found in coronavirus-related articles,  $B_{\beta}$  is the total

number of the coronavirus-related articles in years  $\beta$ ,  $C_{\alpha \text{ in } \beta}$  is the number of appearances of the MeSH term  $\alpha$  in years  $\beta$  in PubMed, and  $D_{\beta}$  is the total number of articles counted in years  $\beta$  in PubMed. The terms whose rates were more than 2 were defined as unique keywords. A total of 13,125 kinds of MeSH terms as unique keywords with a total of 1,739,841 occurrences were collected between 1996 and 2020.

## Co-Word Analysis With Unique Keywords

Top 50 most frequently occurring unique keywords were collected for each period, and they were examined whether they coappeared in the same article. The coappearance was examined by using Perl with our original scripts. The coappearance of the keywords was visualized using Pajek software (Batagelj and Mrvar, 2002). To eliminate any weak relation among keywords, the threshold for making edges was set at 10% of the number of keywords (selecting smaller sized nodes) linked by the edges, according to the clusters appeared in the networks visualized by Pajek.

## RESULTS

The number of articles covering coronaviruses in the fields of life sciences and medicine rapidly increased in 2003 and decreased until 2011, and it increased again in 2015 and decreased until 2018 (**Figure 1**). From Jan 1st, 2020 to Aug 17th, 2020, the number reached 42,647, which is approximately 50 times more than the number, 831 articles, in 2019. This tendency coincided with the emergence of coronavirus infectious diseases such as the emergence of SARS in November 2002 (Xu et al., 2004), MERS in November 2012 (Hijawi et al., 2013; Cauchemez et al., 2014), and COVID-19 in 2019. Once the diseases emerged, research on coronaviruses was rapidly activated and sustained for a few years. In the case of COVID-19, compared with SARS and MERS, the increment rate of the related articles was huge. Coronavirus has become an emerging research topic as a result (Rotolo et al., 2015).

## By Topic: Cross-Disciplinary Consequences and the Scope of Impact

Regarding their impact on research contents, this study identified unique keywords which represented the characteristics of coronavirus research before and after the outbreaks of SARS, MERS, and COVID-19. Since the collection of frequently appeared MeSH terms by itself did not reveal the unique characteristics of the research contents owing to their generality of use in numerous articles (Ohniwa et al., 2010), unique keywords from coronavirus research in a particular year were selected. These unique keywords defined as MeSH terms in coronavirus-related articles had the appearance rate that was at least twice as high as their appearance rate in all articles of the year (see Materials and Methods). This operation helped identify representative terms such as “SARS Virus” between 2003 and 2006 and “Middle East Respiratory Syndrome Coronavirus” between 2013 and 2016 as top 25 frequently appeared unique



**TABLE 1 |** Top 25 unique keywords in coronavirus research articles.

|  | 1996–2002    | 2003–2006    | 2007–2012    | 2013–2016    | 2017–2019    | 2020 Jan–Aug |
|--|--------------|--------------|--------------|--------------|--------------|--------------|
| Number of articles                           | 1,189        | 3,180        | 3,083        | 3,427        | 2,551        | 42,647       |
| Viruses                                      | <i>1,113</i> | <i>2,646</i> | <i>2,631</i> | <i>2,705</i> | <i>1908</i>  | 15,166       |
| RNA viruses                                  | <i>1,100</i> | <i>2,611</i> | <i>2,547</i> | <i>2,596</i> | <i>1828</i>  | 15,154       |
| Nidovirales                                  | <i>1,058</i> | <i>2,533</i> | <i>2,349</i> | <i>2,422</i> | <i>1705</i>  | 15,129       |
| Coronaviridae                                | <i>1,051</i> | <i>2,529</i> | <i>2,337</i> | <i>2,408</i> | <i>1,697</i> | 15,129       |
| Coronavirus                                  | <i>1,046</i> | <i>2,508</i> | <i>2,311</i> | <i>2,336</i> | <i>1,682</i> | 15,126       |
| Proteins                                     | <i>706</i>   |              | <i>1742</i>  |              | <i>910</i>   |              |
| Infections                                   | <i>655</i>   | <i>2092</i>  | <i>1894</i>  | <i>2,383</i> | <i>1707</i>  | 17,959       |
| Virus diseases                               | <i>638</i>   | <i>2041</i>  | <i>1777</i>  | <i>2,259</i> | <i>1,630</i> | 17,939       |
| RNA virus infections                         | <i>602</i>   | <i>1960</i>  | <i>1,608</i> | <i>2,103</i> | <i>1,506</i> | 17,929       |
| Nidovirales infections                       | <i>567</i>   | <i>1901</i>  | <i>1,473</i> | <i>1972</i>  | <i>1,412</i> | 17,914       |
| Coronaviridae infections                     | <i>565</i>   | <i>1899</i>  | <i>1,463</i> | <i>1963</i>  | <i>1,410</i> | 17,914       |
| Coronavirus infections                       | <i>551</i>   | <i>1884</i>  | <i>1,436</i> | <i>1912</i>  | <i>1,406</i> | 17,912       |
| Cells  | <i>534</i>   |              | <i>1,039</i> |              |              |              |
| Genetic phenomena                            | <i>518</i>   |              | <i>1,214</i> |              | <i>708</i>   |              |
| Betacoronavirus                              | <i>506</i>   | <i>1963</i>  | <i>1,270</i> | <i>1,028</i> | <i>715</i>   | 14,995       |
| Rodentia                                     | <i>491</i>   |              |              |              |              |              |
| Muridae                                      | <i>490</i>   |              |              |              |              |              |
| Murinae                                      | <i>471</i>   |              |              |              |              |              |
| Mice   | <i>459</i>   |              | <i>550</i>   |              |              |              |
| Animal diseases                              | <i>446</i>   | <i>432</i>   | <i>838</i>   | <i>1,006</i> | <i>898</i>   |              |
| Hepatitis viruses                            | <i>414</i>   | <i>212</i>   | <i>301</i>   | <i>132</i>   | <i>59</i>    |              |
| Biochemical phenomena                        | <i>412</i>   |              | <i>1,035</i> |              |              |              |
| Murine hepatitis virus                       | <i>408</i>   | <i>191</i>   | <i>265</i>   | <i>103</i>   | <i>45</i>    | 6            |
| Cells, cultured                              | <i>379</i>   | <i>625</i>   | <i>784</i>   | <i>478</i>   | <i>423</i>   |              |
| Nucleic acids, nucleotides, and nucleosides  | <i>369</i>   | <i>704</i>   | <i>698</i>   | <i>494</i>   | <i>342</i>   |              |
| Genetic techniques                           | <i>352</i>   | <i>860</i>   | <i>939</i>   | <i>782</i>   | <i>513</i>   | 805          |
| Viral proteins                               | <i>343</i>   | <i>913</i>   | <i>1,064</i> | <i>705</i>   | <i>502</i>   | 507          |
| Genetic structures                           | <i>333</i>   | <i>624</i>   | <i>599</i>   | <i>442</i>   | <i>290</i>   |              |
| Nucleic acids                                | <i>327</i>   | <i>590</i>   | <i>595</i>   | <i>409</i>   | <i>298</i>   |              |
| Molecular structure                          | <i>322</i>   | <i>732</i>   | <i>737</i>   | <i>456</i>   | <i>258</i>   |              |
| Blood proteins                               | <i>290</i>   | <i>570</i>   | <i>497</i>   | <i>385</i>   | <i>309</i>   | 919          |
| Artiodactyla                                 | <i>280</i>   |              | <i>286</i>   | <i>601</i>   | <i>603</i>   |              |
| Microbiological phenomena                    | <i>264</i>   | <i>412</i>   | <i>680</i>   | <i>684</i>   | <i>534</i>   | 734          |
| Viral structural proteins                    | <i>258</i>   | <i>653</i>   | <i>673</i>   | <i>438</i>   | <i>343</i>   | 359          |
| Alphacoronavirus                             | <i>230</i>   | <i>196</i>   | <i>432</i>   | <i>525</i>   | <i>539</i>   | 49           |
| Virus physiological phenomena                | <i>189</i>   | <i>345</i>   | <i>534</i>   | <i>488</i>   | <i>354</i>   | 481          |
| Swine  | <i>160</i>   | <i>67</i>    | <i>174</i>   | <i>375</i>   | <i>459</i>   |              |
| Respiratory tract infections                 | <i>81</i>    | <i>1,591</i> | <i>866</i>   | <i>659</i>   | <i>322</i>   | 17,774       |
| Disease outbreaks                            | <i>39</i>    | <i>404</i>   | <i>199</i>   | <i>389</i>   | <i>277</i>   | 17,576       |
| Pneumonia                                    | <i>8</i>     | <i>53</i>    | <i>47</i>    | <i>74</i>    | <i>33</i>    | 17,732       |
| Pneumonia, viral                             | <i>4</i>     | <i>21</i>    | <i>24</i>    | <i>52</i>    | <i>22</i>    | 17,719       |
| SARS virus                                   | <i>1</i>     | <i>1743</i>  | <i>926</i>   | <i>301</i>   | <i>115</i>   | 576          |
| Severe acute respiratory syndrome            | <i>1</i>     | <i>1,465</i> | <i>569</i>   | <i>230</i>   | <i>77</i>    | 393          |
| Respiratory tract diseases                   |              | <i>1,617</i> | <i>911</i>   | <i>696</i>   | <i>346</i>   | 17,785       |
| Amino acids, peptides, and proteins          |              |              | <i>1756</i>  |              | <i>930</i>   |              |
| Biological phenomena                         |              |              | <i>542</i>   | <i>677</i>   | <i>521</i>   |              |
| Middle East respiratory syndrome coronavirus |              |              |              | <i>625</i>   | <i>500</i>   | 165          |
| Health care quality, access, and evaluation  |              |              |              |              | <i>587</i>   | 7,365        |
| Eukaryota                                    |              |              |              |              |              | 17,968       |
| Animals                                      |              |              |              |              |              | 17,967       |
| Vertebrates                                  |              |              |              |              |              | 17,947       |
| Chordata                                     |              |              |              |              |              | 17,947       |
| Mammals                                      |              |              |              |              |              | 17,939       |
| Eutheria                                     |              |              |              |              |              | 17,938       |
| Primates                                     |              |              |              |              |              | 17,845       |
| Haplorhini                                   |              |              |              |              |              | 17,843       |
| Catarrhini                                   |              |              |              |              |              | 17,842       |
| Hominidae                                    |              |              |              |              |              | 17,813       |
| Humans                                       |              |              |              |              |              | 17,812       |
| Environment and public health                |              |              |              |              |              | 17,778       |
| Public health                                |              |              |              |              |              | 17,773       |
| Lung diseases                                |              |              |              |              |              | 17,741       |

*Italic numbers represent the number of appearances of keywords ranked in top 25. We sorted the order based on the total number in "1996–2002."*

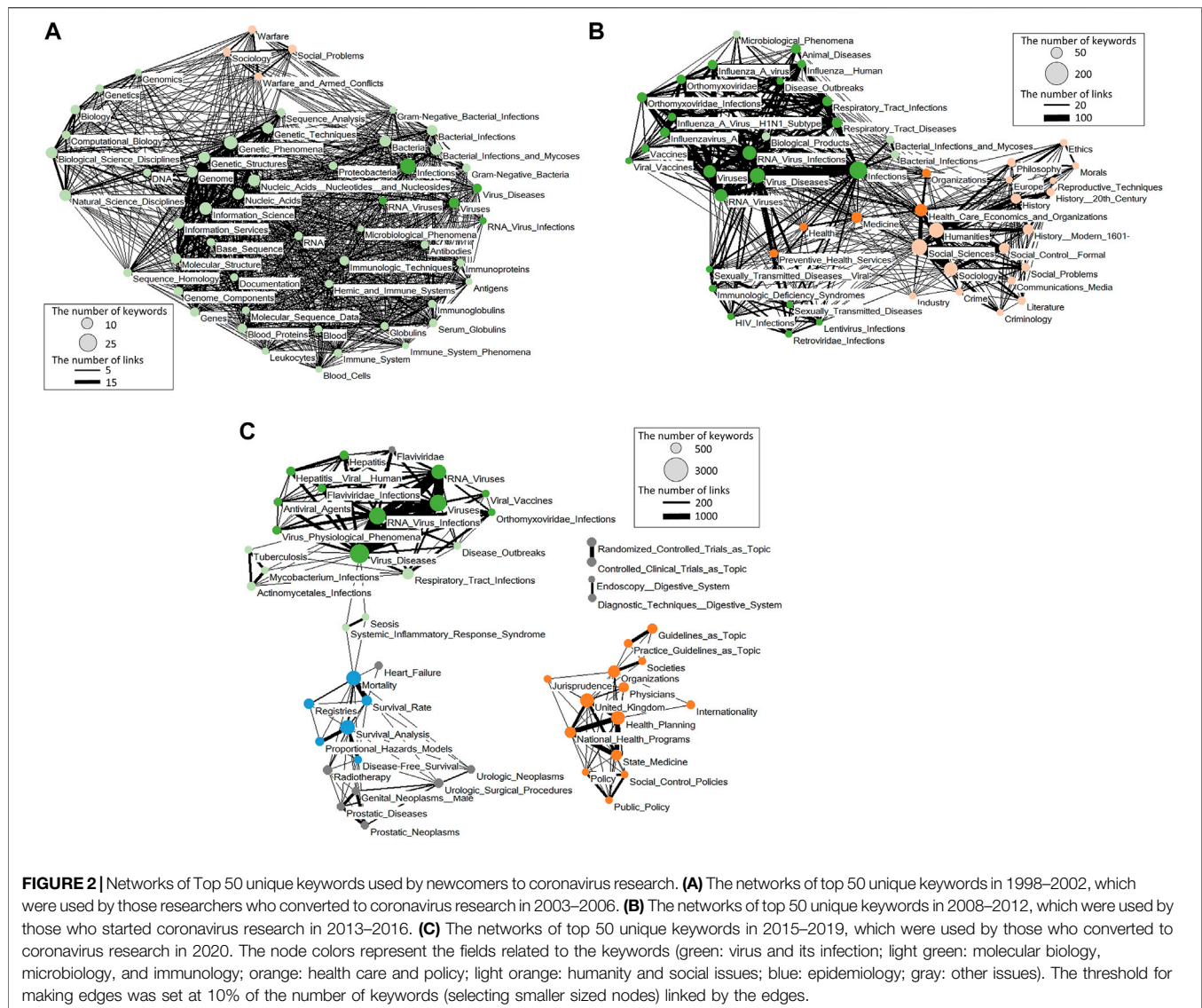
**TABLE 2 |** Top 25 unique keywords used by newly entered researchers in the past.

| MeSH   | 1998–2002<br>Author in<br>2003–2006 | 2008–2012<br>Author in<br>2013–2016 | 2015–2020<br>Author in<br>2020 | MeSH                                       | 1998–2002<br>Author in<br>2003–2006 | 2008–2012<br>Author in<br>2013–2016 | 2015–2020<br>Author in<br>2020 |
|--|-------------------------------------|-------------------------------------|--------------------------------|--|-------------------------------------|-------------------------------------|--------------------------------|
| Number of articles                             | 70                                  | 681                                 | 49,798                         | Number of articles                         | 70                                  | 681                                 | 49,798                         |
| Infections                                     | 28                                  | 176                                 |                                | History                                    | 5                                   | 69                                  |                                |
| Genetic phenomena                              | 25                                  |                                     |                                | Animal diseases                            | 5                                   | 46                                  |                                |
| Information science                            | 20                                  |                                     |                                | History, Modern 1601-                      | 4                                   | 58                                  |                                |
| Bacterial infections and<br>mycoses            | 16                                  | 44                                  |                                | Respiratory tract infections               | 3                                   | 50                                  | 963                            |
| Nucleic acids, nucleotides,<br>and nucleosides | 16                                  |                                     |                                | Orthomyxoviridae                           | 3                                   | 47                                  | 373                            |
| Genetic structures                             | 16                                  |                                     |                                | Influenza A virus                          | 3                                   | 47                                  | 321                            |
| Genetic techniques                             | 16                                  |                                     |                                | Influenza A virus                          | 3                                   | 47                                  | 319                            |
| Nucleic acids                                  | 16                                  |                                     |                                | Organizations                              | 3                                   | 41                                  | 1,145                          |
| Bacteria                                       | 15                                  |                                     |                                | Antiviral agents                           | 3                                   | 15                                  | 624                            |
| Genome   | 15                                  |                                     |                                | Orthomyxoviridae infections                | 2                                   | 50                                  | 427                            |
| Biological science<br>disciplines              | 15                                  |                                     |                                | Influenza, human                           | 2                                   | 42                                  | 355                            |
| Natural science disciplines                    | 15                                  |                                     |                                | United Kingdom                             | 2                                   |                                     | 1,265                          |
| Viruses  | 14                                  | 100                                 | 2079                           | Social sciences                            |                                     | 162                                 |                                |
| Bacterial infections                           | 14                                  | 42                                  |                                | Health care economics and<br>organizations |                                     | 96                                  |                                |
| Molecular structure                            | 13                                  |                                     |                                | Social control, formal                     |                                     | 70                                  |                                |
| Information services                           | 12                                  |                                     |                                | Respiratory tract diseases                 |                                     | 64                                  |                                |
| Virus diseases                                 | 11                                  | 126                                 | 2,903                          | Medicine                                   |                                     | 56                                  |                                |
| Immunologic techniques                         | 11                                  |                                     |                                | Philosophy                                 |                                     | 43                                  |                                |
| Genome components                              | 11                                  |                                     |                                | Communications media                       |                                     | 43                                  |                                |
| Biology  | 11                                  |                                     |                                | Physicians                                 |                                     | 18                                  | 756                            |
| Blood proteins                                 | 11                                  |                                     |                                | Flaviviridae infections                    |                                     | 7                                   | 625                            |
| Genes  | 10                                  |                                     |                                | Survival analysis                          |                                     |                                     | 1,658                          |
| Sociology                                      | 9                                   | 113                                 |                                | Mortality                                  |                                     |                                     | 1,522                          |
| Social problems                                | 9                                   | 41                                  |                                | Health planning                            |                                     |                                     | 1,436                          |
| Warfare and armed<br>conflicts                 | 9                                   | 3                                   |                                | National health programs                   |                                     |                                     | 912                            |
| Warfare  | 9                                   | 3                                   |                                | State medicine                             |                                     |                                     | 835                            |
| Molecular sequence data                        | 9                                   |                                     |                                | Survival rate                              |                                     |                                     | 774                            |
| Computational biology                          | 9                                   |                                     |                                | Urologic surgical<br>procedures            |                                     |                                     | 744                            |
| Hemic and immune<br>systems                    | 9                                   |                                     |                                | Guidelines as topic                        |                                     |                                     | 678                            |
| Proteobacteria                                 | 9                                   |                                     |                                | Controlled clinical trials as<br>topic     |                                     |                                     | 659                            |
| Gram-negative bacteria                         | 9                                   |                                     |                                | Randomized controlled<br>trials as topic   |                                     |                                     | 651                            |
| Documentation                                  | 9                                   |                                     |                                | Registries                                 |                                     |                                     | 647                            |
| Base sequence                                  | 9                                   |                                     |                                | Radiotherapy                               |                                     |                                     | 641                            |
| RNA viruses                                    | 8                                   | 88                                  | 1,571                          | Prostatic diseases                         |                                     |                                     | 594                            |
| RNA virus infections                           | 7                                   | 110                                 | 2,261                          | Practice guidelines as topic               |                                     |                                     | 589                            |
| Humanities                                     | 6                                   | 141                                 |                                | Proportional hazard models                 |                                     |                                     | 580                            |

*Italic numbers represent the number of appearances of keywords ranked in top 25. We sorted the order based on the total number in “1998–2002 author in 2003–2006.”*

keywords (**Table 1**). Keywords related to “biological classification of coronaviruses,” “infection matters of coronaviruses,” and “respiratory tract issues [respiratory tract is the target infection site for coronaviruses as well as the site where its major symptom appears (Channappanavar and Perlman, 2017; Singhal, 2020)]” were commonly used between 1996 and 2020—consistent with the collection of unique keywords from coronavirus-related articles in this study. Keywords related to “components of the virus” and “biological aspect” were found in all of the years except for 2020, while others such as “public health” and “human” began to appear in 2020. When the list was expanded to top 50

frequently appeared unique keywords, this tendency was even strengthened (**Supplementary Table S1**). In the meantime, conventional keywords such as “immunology” were still found in all of the years. In addition to the fact that these top 50 keywords frequently coappeared in the coronavirus-related articles (**Supplementary Figures S1–S6**), the results of this investigation suggest the following: 1) the regional outbreaks of SARS and MERS did not change the cross-disciplinary research trends that had existed before the outbreaks as keywords fell well within the scope of existing well-connected networks for coronavirus research focusing on the topics which



had been constantly studied regardless of the outbreaks; 2) the global outbreak of COVID-19, on the other hand, initially had a diversifying impact on the existing research trend as newly emerged keywords formed unconnected research networks across different disciplines, including areas of research such as jurisprudence and public policy.

### By Author: Identifying Converted Experts

The increase in the number of coronavirus-related articles after the outbreaks of SARS, MERS, and COVID-19 was largely due to the entry of new researchers (**Supplementary Table S2**). For example, between 2015 and 2019, a total of 24,745 authors with specific affiliations were identified in coronavirus-related articles. Their names with the same affiliations were found in only 369 out of 39,804 (0.9%) coronavirus-related articles in 2020. In the case of SARS, the authors of publications between 1998 and 2002 accounted for 23 out of 2,805 (0.8%) published articles on coronavirus between 2003 and 2006. In the case of

MERS, the authors from the years between 2008 and 2012 occupied 123 out of 3,052 (4.0%) coronavirus-related articles published between 2013 and 2016. As a reference, we also analyzed the case of “Influenza,” resulting in a higher rate of occupation [the authors from the years between 2014 and 2018 occupied 1,364 out of 5,542 influenza-related articles published in 2019 (24.6%)]. Here, because not all affiliations were attached to the authors in PubMed before 2014 (**Supplementary Table S3**), the authors regardless of their affiliations were counted in (**Supplementary Table S4**). The risk of counting different authors as the same authors had to be taken. In any case, the results of this investigation show that most of these converted experts were conducting their coronavirus research on a temporary basis as they did not continue publishing on coronaviruses after new outbreaks.

This study then examined unique keywords used by the newcomers to coronavirus research from the past 5 years (searched by their names with affiliations). Those listed as top 25

**TABLE 3 |** Top 10 countries for coronavirus articles in each period.

|                | 1996–2002 | 2003–2006 | 2007–2012 | 2013–2016 | 2017–2019 | 2020 Jan–Aug |
|----------------|-----------|-----------|-----------|-----------|-----------|--------------|
| United States  | 1         | 1         | 1         | 1         | 2         | 1            |
| Japan          | 2         | 8         | 4         | 7         | 6         |              |
| Canada         | 3         | 6         | 6         |           | 5         | 6            |
| Germany        | 4         | 5         | 7         | 3         | 4         | 7            |
| Spain          | 5         |           | 9         |           |           | 8            |
| France         | 6         | 10        |           | 4         | 7         | 5            |
| Italy          | 7         | 9         | 8         |           | 9         | 3            |
| Switzerland    | 8         |           |           |           |           |              |
| Singapore      | 9         | 7         |           |           |           |              |
| Australia      | 10        |           | 10        | 9         |           | 9            |
| Belgium        | 10        |           |           |           |           |              |
| United Kingdom | 10        |           |           |           |           | 10           |
| Korea          |           |           |           | 8         | 8         |              |
| Taiwan         |           | 4         | 5         | 10        |           |              |
| China          |           | 2         | 2         | 2         | 1         | 2            |
| Hong Kong      |           | 3         | 3         | 6         |           |              |
| India          |           |           |           |           |           | 4            |
| Saudi Arabia   |           |           |           | 5         | 3         |              |
| Egypt          |           |           |           |           | 10        |              |

The value in each column represents the ranking for the number of articles published from the corresponding country in each period. We sorted the order based on the total number in “1996–2002.”

frequently appeared unique keywords used by the newly entered researchers (Table 2) did not largely overlap with those of coronavirus research between 1996 and 2020 (Table 1) (11 out of 72 keywords). This tendency did not change when we compared them with top 50 frequently appeared unique keywords (Supplementary Tables S1, S5). Thus, it is likely that such new researchers came from different disciplines.

After the outbreak of SARS, experts on “infection of RNA viruses and bacteria especially in the fields of immunology, molecular biology, bioinformatics, and/or sociology” began to take part in coronavirus studies (Figure 2A). In the case of MERS, many RNA virus researchers handling “influenza virus infection” and “HIV infection” as well as experts on “health-care issues” joined in (Figure 2B). In the case of COVID-19, it attracted experts on the “hepatitis virus” and “*mycobacterium*” (Figure 2C).

Furthermore, for COVID-19, many converted experts had no background in the research on “RNA virus and infection.” They consequently formed a separate scientific network apart from those with their background in “RNA viruses and infections” in the beginning. They started from forming networks with those with their background in “urology and prostate,” “diagnosis of digestive system,” “clinical trial,” or “health care and guide line planning,” “jurisprudence,” “public policy,” and others. Such outside-in networking, due to the wide disciplinary base of the network, was one of the characteristics of COVID-19 research dynamics in the beginning.

## By Nationality: The Prioritization of National Contingencies as an International Trend

Once a novel infectious disease emerges in a certain country, scientific publications on the disease increase in the corresponding country (Table 3 and Supplementary Table S6). The United States and Germany have always been ranked among top 10 countries frequently publishing coronavirus

articles, regardless of contingencies involving novel coronaviruses—suggesting that these countries have been the leaders of coronavirus research over the past 25 years. China became the No. 2 country after the SARS outbreak in November 2002 in China. Taiwan, Hong Kong, Singapore, and Canada—the countries and regions that prevailed after being hit hard by SARS in 2003 (Chan-Yeung and Xu, 2003; Wallinga and Teunis, 2004)—were also in top 10 between 2003 and 2006. In the case of the MERS outbreak in November 2012, Saudi Arabia was ranked among top 10 as one of the major countries that overcame the epidemic. Korea was also ranked among top 10 countries between 2013 and 2016, quite possibly due to the outbreak of the MERS epidemic in Korea in 2015 (Chen et al., 2017). With regard to the case of COVID-19, the exponential increase in the number of scientific publications originating from all the countries examined in this article suggests its impact on a global scale. It was also found that many researchers converted to the field of coronavirus studies after the outbreaks of infectious diseases (Supplementary Table S7). Accordingly, the outbreaks of novel coronavirus diseases accelerate coronavirus research activities in the affected countries by attracting new researchers.

The proportion of internationally co-authored articles on coronaviruses to all the coronavirus-related articles among the countries listed in Supplementary Table S6 was 0.22–0.26 between 2016 and 2019 (Supplementary Table S8). This rate was higher than that of all the internationally co-authored articles during the same period (0.16–0.18). Thus, compared with the average collaboration ratio of articles, a higher rate of transnational collaboration was present for coronavirus research. In contrast, in 2020 after the outbreak of COVID-19, the rate of internationally co-authored coronavirus articles was 0.16. This was lower than the rate of all the international research articles published in the same year (0.19). In this way, transnational collaboration on coronavirus research as



indicated in the rate of international co-authorships has decreased since the outbreak of COVID-19.

## DISCUSSION

This study investigated the dynamics of research on COVID-19 (SARS-CoV-2) by comparing it to the previous cases of SARS (SARS-CoV) and MERS (MERS-CoV). Results show two different modes of research dynamics with regard to the scale of social impact as follows: 1) in the cases of two regional pandemics, SARS and MERS, the scope of cross-disciplinary research remained between neighboring research areas as experts on surrounding research areas joined the networks of coronavirus experts; 2) in the case of the global pandemic, COVID-19, with overwhelming global impact, cross-disciplinary activities have spread far beyond neighboring areas of research to form new research networks. These dynamics of cross-disciplinary research are national in character as newly converted researchers came from the countries seriously affected by the coronaviruses. However, the majority of these converted experts are likely to conduct their coronavirus research on a temporary basis, and they might change their research subjects once an outbreak is over. Such temporary participation of researchers in coronavirus research suggests that securing the source of funding could be one of the factors for sustaining transdisciplinary research on coronaviruses and lowering the fatality of future outbreaks.

Knowledge on COVID-19 is distributed across a wide range of disciplines forming research networks within national boundaries. More technically, while MeSH terms may not be sufficient to completely identify the background of authors with different roles, this research shows that MeSH terms are still useful to the extent that they help identify the scope of cross-disciplinarity regarding coronavirus research. It would also be valuable to examine the dynamics of research beyond those fields covered by PubMed to further unveil the impact of COVID-19 on an even wider range of research activities in the world.

In short, COVID-19 has transformed the structure of coronavirus research. The greater the scale of social impact is, the more cross-disciplinary research emerges. In the case of COVID-19, the national character of research has been reinforced by the finding that transnational collaboration in terms of international co-authorships has decreased since the outbreak of the global pandemic. Given the unprecedented scale of COVID-19 and the nationalization of responses, the most likely way forward for medical experts is to accumulate local knowledge with the awareness of transdisciplinary research dynamics. For a coordinated response to COVID-19, an implication here is to be aware of the perspective that the

global pandemic can be grasped into a bodily event for each medical and nonmedical expert to become an extension to a transdisciplinary solution to the health problem of the one and the many. An “event” or a “prehension” (apprehension which may or may not be cognitive) of things, here in this place such as a local response to the COVID-19 pandemic, has reference to other places since things gathered into the grasped unity of an event as a spatiotemporal unity here and now have essential reference to other places and other times (Whitehead, 1925). Events are previsions of things that constitute realities of nature given that nature is a structure of evolving “processes” and each single event within its own context has all the reality that is interlocked with the whole (Whitehead, 1925). Finally, while the present study—with its focus on the articles published by August 17, 2020—demonstrated the initial impact of COVID-19, continuous research is still necessary to grasp the further transformation of research dynamics in the long-term challenge against COVID-19.

## DATA AVAILABILITY STATEMENT

The original contributions presented in the study are included in the article/**Supplementary Material**; further inquiries can be directed to the corresponding author.

## AUTHOR CONTRIBUTIONS

All the authors contributed to this work and approved the final version for submission. RO and JK wrote the article. RO carried out the data collection and the analyses reported in this study. MF helped informing the discussion. OO supervised the study.

## FUNDING

This work has been funded by the Japan Society for the Promotion of Science as Grant-in-Aid for Scientific Research (C) to RO (20K00266), and by the University of Tsukuba as a research support program to tackle COVID-19-related emergency problems to RO, JK, MF, and OO.

## SUPPLEMENTARY MATERIAL

The Supplementary Material for this article can be found online at: <https://www.frontiersin.org/articles/10.3389/fdata.2021.631073/full#supplementary-material>

## REFERENCES

- Batagelj, V., and Mrvar, A. (2002). Pajek- Analysis and Visualization of Large Networks. *Graph Drawing* 2265, 477–478. doi:10.1007/3-540-45848-4\_54
- Borup, M., Brown, N., Konrad, K., and Van Lente, H. (2006). The Sociology of Expectations in Science and Technology. *Technol. Anal.Strateg.Manage.* 18, 285–298. doi:10.1080/09537320600777002
- Cauchemez, S., Fraser, C., Van Kerkhove, M. D., Donnelly, C. A., Riley, S., Rambaut, A., et al. (2014). Middle East Respiratory Syndrome Coronavirus: Quantification of the Extent of the Epidemic, Surveillance Biases, and Transmissibility. *Lancet Infect. Dis.* 14, 50–56. doi:10.1016/s1473-3099(13)70304-9
- Chan-Yeung, M., and Xu, R.-H. (2003). SARS: Epidemiology. *Respirology* 8 (Suppl. 1), S9–S14. doi:10.1046/j.1440-1843.2003.00518.x
- Channappanavar, R., and Perlman, S. (2017). Pathogenic Human Coronavirus Infections: Causes and Consequences of Cytokine Storm and

- Immunopathology. *Semin.Immunopathol*39, 529–539. doi:10.1007/s00281-017-0629-x
- Chen, X., Chughtai, A.A., Dyda, A., and Macintyre, C.R. (2017). Comparative Epidemiology of Middle East Respiratory Syndrome Coronavirus (MERS-CoV) in Saudi Arabia and South Korea. *Emerg. Microbes Infect.*6, e51. doi:10.1038/emi.2017.40
- Guarner, J. (2020). Three Emerging Coronaviruses in Two Decades. *Am. J.Clin.Pathol.*153, 420–421. doi:10.1093/ajcp/aqaa029
- Gustafsson, R., Kuusi, O., and Meyer, M. (2015). Examining Open-Endedness of Expectations in Emerging Technological fields: The Case of Cellulosic Ethanol. *Technol. Forecast.Soc. Change*91, 179–193. doi:10.1016/j.techfore.2014.02.008
- Hijawi, B., Abdallat, M., Sayaydeh, A., Alqasrawi, S., Haddadin, A., Jaarour, N., et al. (2013). Novel Coronavirus Infections in Jordan, April 2012: Epidemiological Findings from a Retrospective Investigation. *East.Mediterr. Health J.*19 (Suppl. 1), S12–S18. doi:10.26719/2013.19.supp1.s12
- Lipscomb, C. E. (2000). Medical Subject Headings (MeSH). *Bull Med. Libr. Assoc.* 88, 265–266.
- Lowe, H. J., and Barnett, G.O. (1994). Understanding and Using the Medical Subject Headings (MeSH) Vocabulary to Perform Literature Searches. *Jama-Journal Am. Med. Assoc.*271, 1103–1108. doi:10.1001/jama.271.14.1103
- Ohniwa, R. L., and Hibino, A. (2019). Generating Process of Emerging Topics in the Life Sciences. *Scientometrics*121, 1549–1561. doi:10.1007/s11192-019-03248-z
- Ohniwa, R. L., Hibino, A., and Takeyasu, K. (2010). Trends in Research Foci in Life Science fields over the Last 30 Years Monitored by Emerging Topics. *Scientometrics*85, 111–127. doi:10.1007/s11192-010-0252-2
- Rosling, L., and Rosling, M. (2003). Pneumonia Causes Panic in Guangdong Province. *BMJ*326, 416. doi:10.1136/bmj.326.7386.416
- Rotolo, D., Hicks, D., and Martin, B. R. (2015). What Is an Emerging Technology?. *Res.Pol.*44, 1827–1843. doi:10.1016/j.respol.2015.06.006
- Singhal, T. (2020). A Review of Coronavirus Disease-2019 (COVID-19). *Indian J.Pediatr.* 87, 281–286. doi:10.1007/s12098-020-03263-6
- Stenner, P. (2017). “*Liminality and Experience A Transdisciplinary Approach to the Psychosocial*, (London: Palgrave Macmillan UK Imprint). doi:10.1057/978-1-137-27211-9
- Van Merkerk, R. O., and Van Lente, H. (2005). Tracing Emerging Irreversibilities in Emerging Technologies: The Case of Nanotubes. *Technol. Forecast.Soc. Change*72, 1094–1111. doi:10.1016/j.techfore.2004.10.003
- Wallinga, J., and Teunis, P. (2004). Different Epidemic Curves for Severe Acute Respiratory Syndrome Reveal Similar Impacts of Control Measures. *Am. J.Epidemiol.*160, 509–516. doi:10.1093/aje/kwh255
- Wang, Y., Wang, Y., Chen, Y., and Qin, Q. (2020). Unique Epidemiological and Clinical Features of the Emerging 2019 Novel Coronavirus Pneumonia (COVID-19) Implicate Special Control Measures. *J. Med.Virol.*92, 568–576. doi:10.1002/jmv.25748
- Whitehead, A. N. (1925). *Science and the Modern World Lowell Lectures, 1925*. New York: The Macmillan company.
- Xu, R.-H., He, J.-F., Evans, M. R., Peng, G.-W., Field, H. E., Yu, D.-W., et al. (2004). Epidemiologic Clues to SARS Origin in China. *Emerg. Infect. Dis.*10, 1030–1037. doi:10.3201/eid1006.030852

**Conflict of Interest:** The authors declare that the research was conducted in the absence of any commercial or financial relationships that could be construed as a potential conflict of interest.

**Publisher's Note:** All claims expressed in this article are solely those of the authors and do not necessarily represent those of their affiliated organizations, or those of the publisher, the editors and the reviewers. Any product that may be evaluated in this article, or claim that may be made by its manufacturer, is not guaranteed or endorsed by the publisher.

Copyright © 2021 Ohniwa, Kijima, Fukushige and Ohneda. This is an open-access article distributed under the terms of the Creative Commons Attribution License (CC BY). The use, distribution or reproduction in other forums is permitted, provided the original author(s) and the copyright owner(s) are credited and that the original publication in this journal is cited, in accordance with accepted academic practice. No use, distribution or reproduction is permitted which does not comply with these terms.



# Laboratory Testing Implications of Risk-Stratification and Management of COVID-19 Patients

Caidong Liu<sup>1†</sup>, Ziyu Wang<sup>2†</sup>, Wei Wu<sup>2†</sup>, Changgang Xiang<sup>3†</sup>, Lingxiang Wu<sup>2</sup>, Jie Li<sup>2</sup>, Weiye Hou<sup>1</sup>, Huiling Sun<sup>4</sup>, Youli Wang<sup>1</sup>, Zhenling Nie<sup>1</sup>, Yingdong Gao<sup>1</sup>, Ruisheng Zhang<sup>1</sup>, Haixia Tang<sup>5</sup>, Qianhu Wang<sup>2,6,7</sup>, Kening Li<sup>2,6,7\*</sup>, Xinyi Xia<sup>8,9,10\*</sup>, Pengping Li<sup>2\*</sup> and Shukui Wang<sup>1\*</sup>

## OPEN ACCESS

### Edited by:

Reza Lashgari,  
Shahid Beheshti University, Iran

### Reviewed by:

Chunguang Yang,  
Huazhong University of Science and  
Technology, China  
Haoyu Wen,  
Wuhan University, China

### \*Correspondence:

Shukui Wang  
sk\_wang@njmu.edu.cn  
Pengping Li  
lipengping@njmu.edu.cn  
Xinyi Xia  
xiaxynju@163.com  
Kening Li  
likeninghappy@163.com

<sup>†</sup>These authors have contributed  
equally to this work

### Specialty section:

This article was submitted to  
Infectious Diseases – Surveillance,  
Prevention and Treatment,  
a section of the journal  
Frontiers in Medicine

Received: 24 April 2021

Accepted: 19 July 2021

Published: 13 August 2021

### Citation:

Liu C, Wang Z, Wu W, Xiang C, Wu L,  
Li J, Hou W, Sun H, Wang Y, Nie Z,  
Gao Y, Zhang R, Tang H, Wang Q,  
Li K, Xia X, Li P and Wang S (2021)  
Laboratory Testing Implications of  
Risk-Stratification and Management of  
COVID-19 Patients.  
Front. Med. 8:699706.  
doi: 10.3389/fmed.2021.699706

<sup>1</sup> Department of Laboratory Medicine, Nanjing First Hospital, Nanjing Medical University, Nanjing, China, <sup>2</sup> Department of Bioinformatics, Nanjing Medical University, Nanjing, China, <sup>3</sup> Department of Laboratory Medicine, First People's Hospital of Jiangxia District of Wuhan, Wuhan, China, <sup>4</sup> General Clinical Research Center, Nanjing First Hospital, Nanjing Medical University, Nanjing, China, <sup>5</sup> Department of Critical Care Medicine, Luan Hospital of Chinese Medicine, Lu'an, China, <sup>6</sup> Jiangsu Key Lab of Cancer Biomarkers, Prevention and Treatment, Collaborative Innovation Center for Personalized Cancer Medicine, Nanjing Medical University, Nanjing, China, <sup>7</sup> Collaborative Innovation Center for Cardiovascular Disease Translational Medicine, Nanjing, China, <sup>8</sup> COVID-19 Research Center, Institute of Laboratory Medicine, Jinling Hospital, Nanjing University School of Medicine, Nanjing, China, <sup>9</sup> Department of Laboratory Medicine and Blood Transfusion, Wuhan Huoshenshan Hospital, Wuhan, China, <sup>10</sup> Joint Expert Group for COVID-19, Wuhan Huoshenshan Hospital, Wuhan, China

**Objective:** To distinguish COVID-19 patients and non-COVID-19 viral pneumonia patients and classify COVID-19 patients into low-risk and high-risk at admission by laboratory indicators.

**Materials and methods:** In this retrospective cohort, a total of 3,563 COVID-19 patients and 118 non-COVID-19 pneumonia patients were included. There are two cohorts of COVID-19 patients, including 548 patients in the training dataset, and 3,015 patients in the testing dataset. Laboratory indicators were measured during hospitalization for all patients. Based on laboratory indicators, we used the support vector machine and joint random sampling to risk stratification for COVID-19 patients at admission. Based on laboratory indicators detected within the 1st week after admission, we used logistic regression and joint random sampling to develop the survival mode. The laboratory indicators of COVID-10 and non-COVID-19 were also compared.

**Results:** We first identified the significant laboratory indicators related to the severity of COVID-19 in the training dataset. Neutrophils percentage, lymphocytes percentage, creatinine, and blood urea nitrogen with AUC >0.7 were included in the model. These indicators were further used to build a support vector machine model to classify patients into low-risk and high-risk at admission in the testing dataset. Results showed that this model could stratify the patients in the testing dataset effectively (AUC = 0.89). Our model still has good performance at different times (Mean AUC: 0.71, 0.72, 0.72, respectively for 3, 5, and 7 days after admission). Moreover, laboratory indicators detected within the 1st week after admission were able to estimate the probability of death (AUC = 0.95). We identified six indicators with permutation  $p < 0.05$ , including eosinophil percentage ( $p = 0.007$ ), white blood cell count ( $p = 0.045$ ), albumin ( $p = 0.041$ ), aspartate transaminase ( $p = 0.043$ ), lactate dehydrogenase ( $p = 0.002$ ),

and hemoglobin ( $p = 0.031$ ). We could diagnose COVID-19 and differentiate it from other kinds of viral pneumonia based on these laboratory indicators.

**Conclusions:** Our risk-stratification model based on laboratory indicators could help to diagnose, monitor, and predict severity at an early stage of COVID-19. In addition, laboratory findings could be used to distinguish COVID-19 and non-COVID-19.

**Keywords:** COVID-19, laboratory testing, diagnosis, monitoring, prediction model

## INTRODUCTION

Coronavirus disease 2019 (COVID-19) has become a serious worldwide problem. It is caused by a novel coronavirus severe acute respiratory syndrome coronavirus (SARS-CoV-2). As of March 1, 2021, there have been 100,221,840 confirmed cases of COVID-19, including 114,040,659 deaths (<https://who.sprinklr.com/>). The global outbreak of COVID-19 highlights the importance of early and rapid diagnosis, monitoring, risk assessment, and medical resource management in the prevention and control of epidemics (1).

The death of COVID-19 patients is mainly caused by the progression from mild to critical illness (2). Therefore, there is an urgent need for effective methods to predict prognosis early. At present, nucleic acid detection and antibody detection are the main technical approaches for clinical diagnosis of COVID-19 patients, but both of them are affected by many factors, such as sample location, type, quality, and patient condition as well as sample storage, which causes a certain degree of false positives and false negatives (3). Most importantly, they all failed to help judge whether a patient will progress to severe illness (4–6). CT imaging is also a common method, but it lacks specificity and requires a large number of professional technicians, and thus easily exhausts resources when the epidemic is serious. The latest research shows that, based on artificial intelligence methods, CT can be used to diagnose or stratify COVID-19 quickly. However, the accuracy of using CT alone to predict patient severity is limited (7–9).

Previous studies have reported that in the early published 41 COVID-19 cases, five patients presented with varying degrees of myocardial injury, cardiovascular disease patients are more likely to develop into severe patients after COVID-19 infection, and the risk of death is higher (10). The abnormal of different laboratory indicators can represent damage to different organs. For example, NT-proBNP indicates cardiac dysfunction and Alkaline phosphatase (ALP) indicates liver dysfunction. In addition, other laboratory indicators are highly

correlated with the risk of disease progression, such as the lymphocyte, IL-6, etc. (11, 12). These findings suggested that laboratory indicators can be used to predict the severity of COVID-19 pneumonia patients. It is of significant importance to perform risk-stratification and management of epidemic disease, especially in countries with a shortage of medical resources, where using limited resources to a greater extent for more critically ill patients will help improve the utilization of medical resources. It is necessary to perform more rigorous testing and clinical observation for patients who tend to have a more severe reaction.

This study aims to identify the laboratory indicators that could predict severity as early as admission, and build a practical risk-stratification model for screening severe COVID-19 patients, as well as predicting the risk of death. This prognostic model based on laboratory indicators could provide important information for the diagnosis, stratification, and monitoring for COVID-19 patients as early as possible.

## METHODS

### Data Collection

From December 1, 2019, to February 13, 2020, a total of 548 cases of confirmed COVID-19 patients were collected from the First People's Hospital of Jiangxia District of Wuhan, including 474 moderate COVID-19 patients and 74 severe COVID-19 patients (FPHJ-548 dataset). Three hundred eighty-five COVID-19 patients who received blood tests at admission were included for the analysis. Eighteen non-COVID-19 viral pneumonia cases were also collected from December 1, 2019, to February 13, 2020, in the First People's Hospital of Jiangxia District of Wuhan. One-hundred patients with non-COVID-19 pneumonia were collected from October 1, 2019, to April 40, 2020, in the Nanjing First Hospital. These 118 non-COVID-19 viral pneumonia cases were designated as the nCVP-118 dataset, including 40 patients with parainfluenza virus, 20 patients with the respiratory syncytial virus, 13 patients with influenza A, 29 patients with influenza B, and 16 patients with adenovirus. One thousand four hundred fifty-two moderate and 1,563 severe COVID-19 patients were collected from Wuhan Huoshenshan Hospital as a validated dataset (HSSH-3015) from February 4, 2020, to April 10, 2020. The diagnosis of COVID-19 in these datasets is based on the "New Coronavirus Pneumonia Diagnosis and Treatment Plan (provisional Sixth Edition)" issued by the National Health and

**Abbreviations:** COVID-19, the coronavirus disease 2019; ALP, Alkaline phosphatase; FPHJ-548, data of 548 patients from First People's Hospital of Jiangxia District of Wuhan; HSSH-3015, data of 3015 patients from Wuhan Huoshenshan Hospital; nCVP, non-COVID-19 viral pneumonia; SVM, support vector machine; LR, logistic regression; PCT, procalcitonin; CRP, C-reactive protein; NEUT%, neutrophils percentage; LYMPH%, lymphocytes percentage; LDH, lactate dehydrogenase; t-SNE, t-distributed stochastic neighbor embedding; CREA, creatinine; BUN, urea nitrogen; ROC, receiver operating characteristic; AI, artificial intelligence; RSS, risk-stratification score; PED, pre-existing disease.



Health Commission. Written informed consent was obtained from each patient.

## SVM Approach for Risk-Stratification Based on Laboratory Indicators at Admission

Using the highest severity during hospitalization of each patient in training dataset (FPHJ-548) as labels, an SVM model was constructed to predict severity at admission based on blood test results. The steps of the SVM risk-stratification method are described as follows: (1) The laboratory indicators with AUC > 0.7 were selected. The indicators which had no detection data in the testing dataset (HSSH-3015) were excluded. Finally, four laboratory findings (LYMPH%, NEUT%, CREA, and BUN) were used to develop a risk-stratification model. (2) We normalized the original value of each indicator according to the normal range. A normalized value > 1 means they exceeded the maximum normal range. A normalized value of < 0 indicates that it is below the minimum normal range. A normalized value range from 0 to 1 indicates that it is within the normal range (Equation 1). (3) We predicted the severity of each patient using the SVM model. The basic principle of this method is to find a fractal hyperplane for the training set in the sample space, which will maximize the separation of categories. We defined the distance from the sample to the hyperplane as the risk-stratification score (RSS) (Equation 2).  $W$  represents the coefficient of laboratory indicators trained by SVM.  $X$  represents the vector of laboratory indicators. We used 5-fold cross-validation in the training dataset (FPHJ-548) to prove the feasibility of risk stratification based on the four indicators. Due to the emergency of the epidemic, only 200 patients in the training dataset without any missing value on laboratory indicators. Finally, we used 200 patients to develop the risk model. To include more patients in the external validation dataset and validate the stability of our model at different time points, we considered the status of laboratory indicators within 3, 5, and 7 days after admission. The total number of patients without any missing laboratory indicators was respectively 2,036, 2,427, and 2,617 within 3, 5, 7 after admission. To match the number of patients in the training dataset (FPHJ-548), we randomly selected 200 patients without replacement within 3, 5, and 7 days after admission from the testing dataset (HSSH-3015 dataset). We used the same method to evaluate the robustness of our model. The process was repeated 50 times. Patients were grouped based on age and sex to validate the model. The prediction performances of AUC were calculated using the predicted values estimated by the model with the combination of selected features as predictors and the status of progression as an outcome.

$$\text{normalized value} = \frac{\text{Detected value} - \min(\text{normal range})}{\max(\text{normal range}) - \min(\text{normal range})} \quad (1)$$

$$\text{RSS} = \sum_{i=1}^N W_i * X_i + B \quad (2)$$

## LR Approach for Survival Outcome Based on Laboratory Indicators Within 1 Week Since Admission

To monitor the risk of deaths of severe COVID-19 patients, we randomly split HSSH-3015 into a leave-in training set and a leave-out test set for data analysis at a ratio of ~50%:50% (using a random number generator). To predict the survival outcome early, we only selected laboratory findings within the 1st week after admission. For the training set, 724 survival samples, and 28 deaths were selected. For the matched leave-out test set, 724 survivors, and 27 dead samples were selected. For the training dataset, we randomly selected 28 survivors. We incorporated group sizes of 28 dead individuals and 28 deaths to develop the model by stepwise LR. This random process was repeated 100 times, leading to 100 different model-building. Indicators that were significant in over 10 out of 100 models were considered as potential risk-related factors. Thirteen indicators were involved for the next modeling, including Albumin/Globulin, DD dimer, leukocyte, monocytes, cystatin C, creatinine, lymphocyte, urea nitrogen, thrombin time, prothrombin time, lactate dehydrogenase, fibrinogen, percentage of neutrophils. Then, we trained the LR model by these indicators in the training dataset and validated it in the leave-out test set. RSS was calculated as above (Equation 2).  $W$  represents the coefficient of laboratory indicators trained by LR.

## Distinguishing COVID-19 From Non-COVID-19 Based on Laboratory Indicators

Laboratory findings at admission were used to distinguish COVID-19 from non-COVID-19 patients. Thirteen laboratory findings, shared between the FPHJ-548 and nCVP-118 datasets were included, in which six indicators showed a significant difference between COVID-19 and non-COVID-19 patients selected for further analysis (adjust  $p < 0.05$ ). To eliminate the influence of missing values, we only considered patients with no missing values in these indicators. We finally selected 212 patients from FPHJ-548, 99 patients from nCVP-118, and 2,828 patients from HSSH-3015. For FPHJ-548 and nCVP-118, we clustered based on the maximum distance and performed multidimensional scaling and validated by HSSH-3015 and nCVP-118.

## Statistical Analysis

Continuous and categorical variables were presented as median (IQR) and  $n$  (%), respectively. We used the Wilcoxon rank-sum test (for continuous quantitative variables) or Fisher's exact test (for categorical variables) to compare differences between moderate and severe patients where appropriate. In the bilateral test, the index of  $p < 0.05$  is considered statistically significant. ROC curves and their correspondent AUC of RSS were calculated by R package pROC. The permutation  $p$ -value was based on 1,000 iterations. In each iteration, we randomly sampled 20 COVID-19 and 20 non-COVID-19 patients and calculated the proportion that fit the trend. Analysis was carried out using the

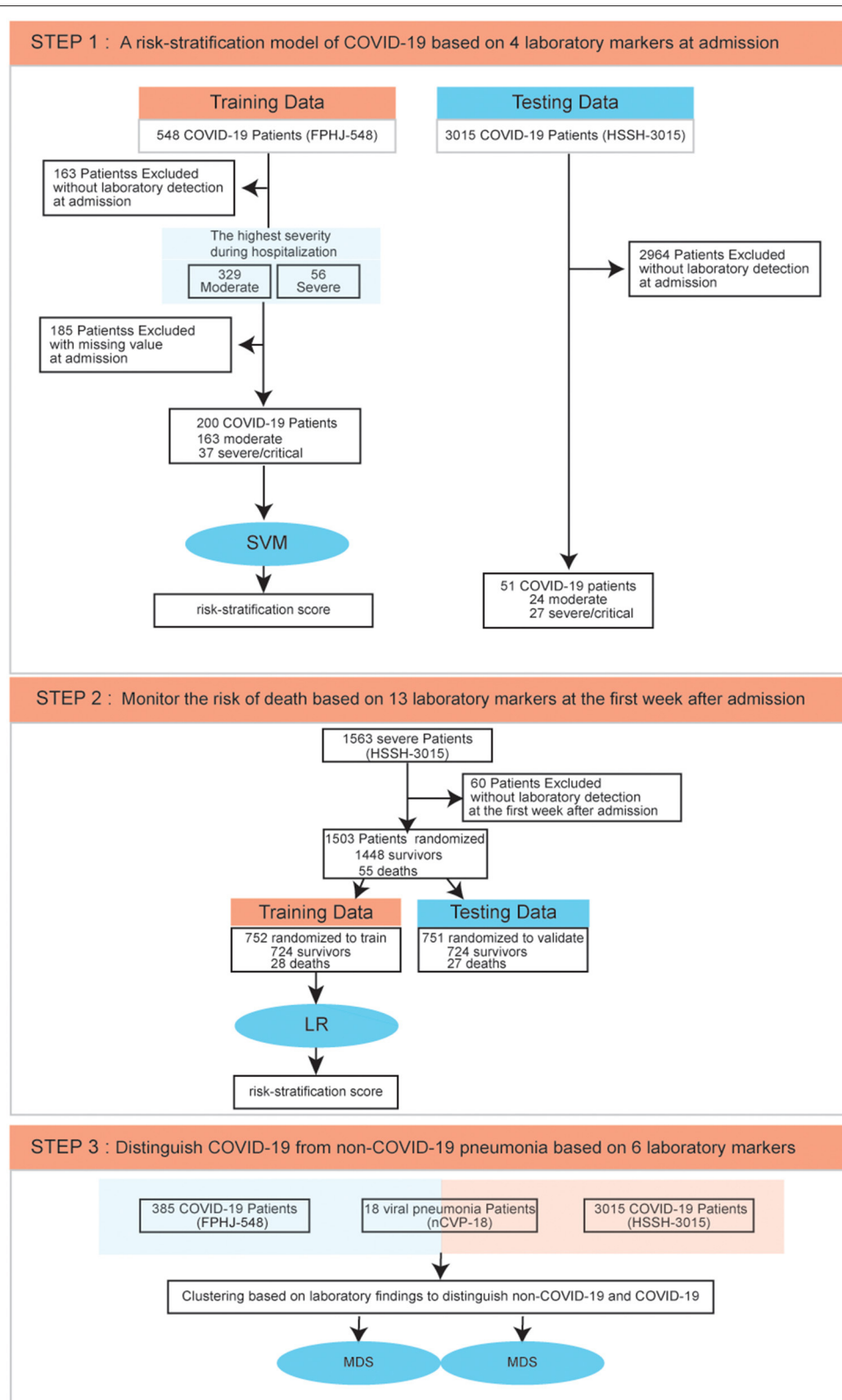


**FIGURE 1 |** Data process flowchart. SVM, Support Vector Machine; LR, Logistic Regression; MDS, Multidimensional Scaling.

**TABLE 1** | Comparing laboratory findings between moderate and severe COVID-19 patients.

|   | Total<br>( <i>N</i> = 385) | Moderate<br>( <i>N</i> = 329) | Severe<br>( <i>N</i> = 56) | <i>P</i> -value |
|---|----------------------------|-------------------------------|----------------------------|-----------------|
| <b>Laboratory findings</b>                |                            |                               |                            |                 |
| <b>Infection markers</b>                  |                            |                               |                            |                 |
| Procalcitonin, ng/ml                      | 0.07 (0.04–0.14) (157)     | 0.06 (0.04–0.11) (130)        | 0.225 (0.14–0.53) (27)     | <0.001          |
| C-reactive protein                        | 24 (12–52) (288)           | 21.8 (9.4–41) (190)           | 44.5 (25–120) (38)         | <0.001          |
| Lymphocyte percentage, %                  | 21.07 (14–29) (372)        | 22.4 (16–30) (318)            | 13.8 (7–21) (54)           | <0.001          |
| Monocyte percentage, %                    | 8.98 (6.7–12) (373)        | 9.6 (7–13) (319)              | 7.5 (5.4–9.1) (54)         | <0.001          |
| Neutrophil percentage, %                  | 67.92 (58–77) (372)        | 66.4 (57–75) (318)            | 78.8 (69–86) (54)          | <0.001          |
| <b>Liver injury markers</b>               |                            |                               |                            |                 |
| Albumin, g/L                              | 38.95 (36–42) (206)        | 39.2 (36–43) (167)            | 37.95 (33–42) (39)         | 0.039           |
| Creatine Kinase MB                        | 15 (12–19) (185)           | 14.5 (12–17) (148)            | 17.85 (18–21) (37)         | 0.018           |
| Uric acid, umol/L                         | 261 (200–360) (208)        | 250 (190–330) (169)           | 337 (270–430) (39)         | <0.001          |
| Cholinesterase                            | 6,903 (5,900–8,100) (198)  | 7,088 (6,000–8,300) (160)     | 6296.55 (4,600–7,400) (38) | 0.007           |
| <b>Heart injury markers</b>               |                            |                               |                            |                 |
| Lactate dehydrogenase, U/L                | 242.85 (200–330) (215)     | 235 (200–300) (173)           | 314 (240–500) (42)         | <0.001          |
| N terminal pro B type natriuretic peptide | 90.285 (49–410) (81)       | 80.34 (45–190) (55)           | 292.1 (78–11,000) (26)     | 0.0021          |
| High-sensitivity troponin T               | 0.009 (0.006–0.016) (179)  | 0.008 (0.006–0.013) (145)     | 0.016 (0.0095–0.04) (34)   | <0.001          |
| <b>Kidney injury markers</b>              |                            |                               |                            |                 |
| Creatinine                                | 66.45 (53–81) (208)        | 64.85 (51–78) (169)           | 81.5 (65–330) (39)         | <0.001          |
| Glomerular filtration rate                | 98.7 (80–110) (208)        | 100.7 (89–110) (169)          | 85.5 (14–100) (39)         | <0.001          |
| Homocysteine                              | 13.75 (11–17) (141)        | 13 (11–17) (111)              | 17 (14–27) (30)            | <0.001          |
| <b>Bloodexamination</b>                   |                            |                               |                            |                 |
| Hematocrit, %                             | 39.85 (36–43) (373)        | 40.1 (37–43) (319)            | 37.75 (34–42) (54)         | 0.002           |
| Hemoglobin, g/L                           | 135.25 (120–150) (373)     | 136 (120–150) (319)           | 129.5 (110–140) (54)       | 0.012           |
| Platelet count, 10 <sup>9</sup> /L        | 177 (140–230) (373)        | 179.5 (150–230) (319)         | 153 (120–210) (54)         | <0.001          |
| Red blood cell count                      | 4.37 (4–4.7) (373)         | 4.39 (4.1–4.7) (319)          | 4.23 (3.7–4.6) (54)        | <0.001          |
| White blood cell count, g/L               | 5.7 (4.6–7.4) (372)        | 5.7 (4.5–7.2) (318)           | 6.25 (4.9–9.5) (54)        | 0.01            |
| Platelet volume distribution width        | 13.4 (12–16) (372)         | 13.3 (12–16) (318)            | 15.2 (12–16) (54)          | 0.023           |
| CO2                                       | 21.7 (20–23) (208)         | 22.1 (20–24) (169)            | 19.85 (18–21) (39)         | <0.001          |
| γ-glutamyltranspeptidase, U/L             | 25 (17–51) (206)           | 24 (16–44) (166)              | 38.5 (24–64) (40)          | 0.0015          |
| MG  | 0.9 (0.85–0.96) (204)      | 0.9 (0.84–0.94) (164)         | 0.93 (0.89–1) (40)         | 0.0018          |
| Urea                                      | 4.6 (3.5–6) (208)          | 4.4 (3.4–5.6) (169)           | 6.45 (4.9–19) (39)         | <0.001          |
| Myoglobin                                 | 46.64 (24–99) (178)        | 40.25 (21–81) (144)           | 106.9 (54–200) (34)        | <0.001          |

statistical software R (version: 3.6.0). All figures were plotted by ggplot2 package.

## RESULTS

### Study Design

We collected the clinical data of 3,563 COVID-19 patients and 118 non-COVID-19 viral pneumonia (designated as non-COVID-19) to build and validate the risk-stratification model. Specifically, data of 548 patients from the First People's Hospital of Jiangxia District of Wuhan were used as a training dataset (FPHJ-548); data of 3,015 patients from Wuhan Huoshenshan Hospital were used as a testing dataset (HSSH-3015); data of 18 non-COVID-19 viral pneumonia patients from the First People's Hospital of the Jiangxia District of Wuhan and data of 100 non-COVID-19 viral pneumonia patients from Nanjing

First Hospital were used to differentiate COVID-19 from non-COVID-19 (nCVP-118).

The highest severity during the hospitalization of each patient was recorded, and the laboratory findings of their blood test at admission were used to predict the progression of these patients. In the FPHJ-548 dataset, the average age of these patients was 52.4 (SD: 14.2), and 49.8% were female. Notably, the median age of severe patients was significantly higher than that of moderate patients (Fisher's exact test,  $P < 0.01$ , **Supplementary Table 1**). The clinical information of 385 cases (including 329 moderate and 56 severe cases) that had detection data at admission were selected to do the following analysis. To predict the severity of COVID-19 patients at admission, we employed a risk-stratification model based on a support vector machine (SVM) by laboratory indicators in the FPHJ-548 dataset. This model was further

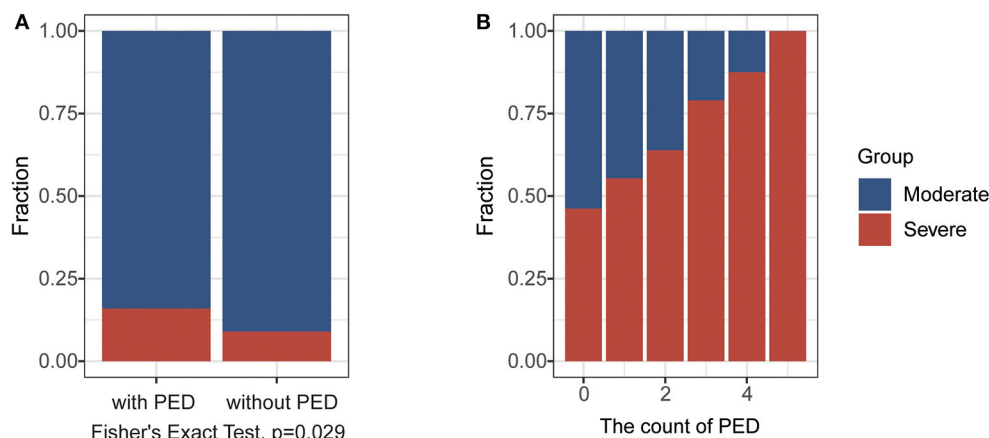


**FIGURE 2 |** The impact of the pre-existing disease (PED) on the progression of COVID-19. **(A)** The fraction of severe cases in patients with or without in PED in the FPHJ-548 dataset. The red represents the severe COVID-19 patients and the blue represents moderate COVID-19 patients. **(B)** The fraction of severe cases in patients with different numbers of PED in HSSH-3015 dataset. The red represents the severe COVID-19 patients and the blue represents moderate COVID-19 patients.

validated in an independent dataset (HSSH-3015) (Figure 1, details see Methods).

Then, to monitor the survival outcome of severe COVID-19 patients, we selected 1,448 survival patients and 55 deaths from the HSSH-3015 dataset. 60 patients without laboratory findings within the 1st week since admission were excluded. We randomly split the HSSH-3015 dataset into a leave-in training set and a leave-out test set for data analysis at a ratio of ~1:1. We assembled a logistic regression model (LR) based on laboratory findings in the training set and validated it in the testing set (Figure 1, details see Methods). To distinguish COVID-19 from non-COVID-19 viral pneumonia, we compared the laboratory difference between COVID-19 datasets (FPHJ-548 or HSSH-3015) and the non-COVID-19 dataset (nCVP-118) (Figure 1, details see Methods).

## A Risk-Stratification Model of COVID-19 Based on Four Laboratory Findings at Admission

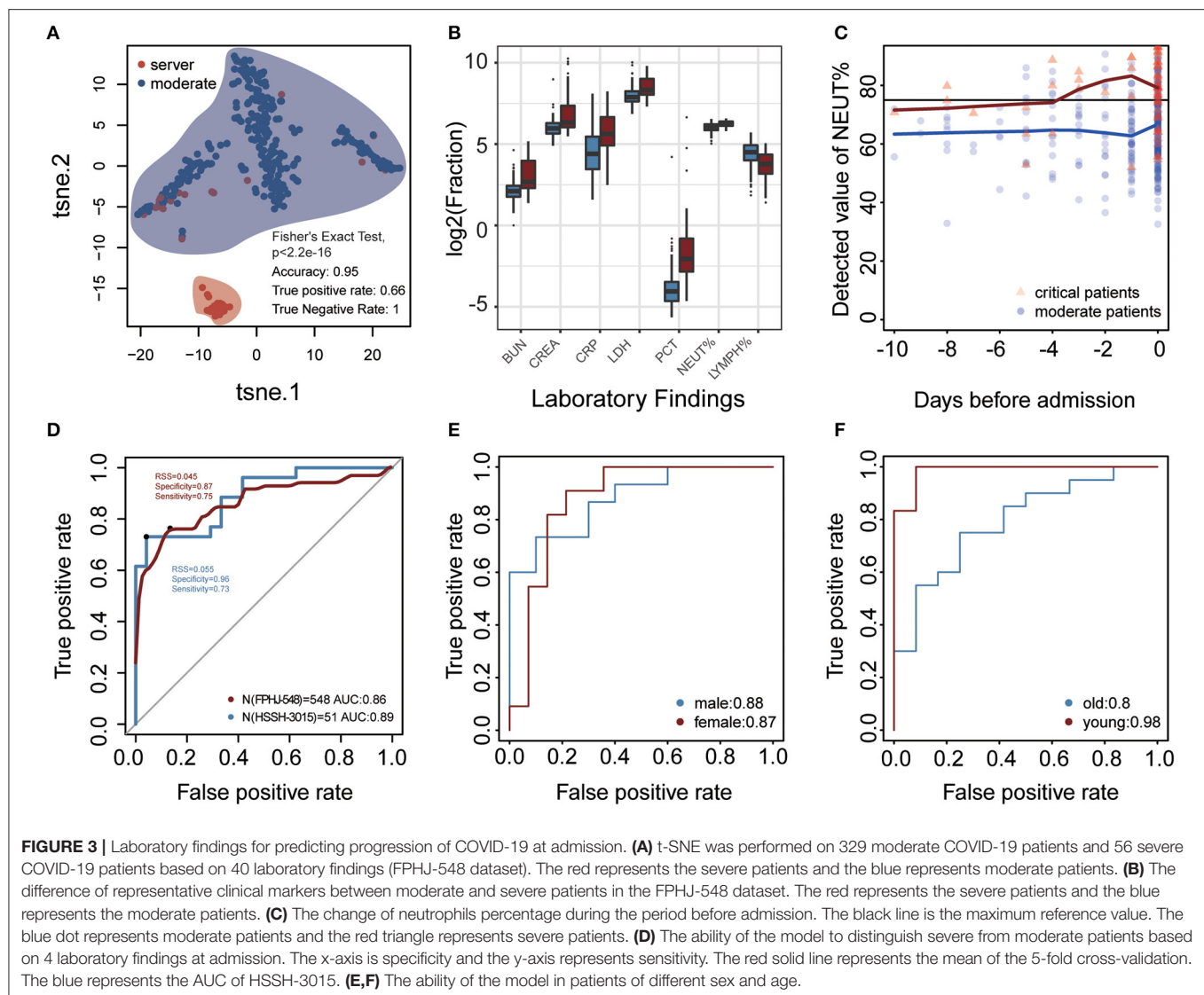
According to the highest severity of each patient during hospitalization, we explored the difference in laboratory findings between moderate and severe COVID-19 cases in the FPHJ-548 dataset. We found that high-risk factors related to the progression of COVID-19 included procalcitonin (PCT), C-reactive protein (CRP), neutrophils percentage (NEUT%), lymphocytes percentage (LYMPH%), lactate dehydrogenase (LDH) (Wilcoxon rank-sum test,  $P < 0.001$ , Table 1). We noted that most of the severe patients presented lymphopenia and elevated levels of inflammatory biomarkers. The levels of PCT in severe patients at the initial stage were higher than those in moderate patients (0.225 vs. 0.06, Wilcoxon rank-sum test,  $P < 0.001$ ), suggesting that serial procalcitonin measurement may play a role in predicting evolution toward a more critical condition (13). The CRP showed a similar trend to PCT, which became significantly higher in severe patients (44.5 vs. 21.8,

Wilcoxon rank-sum test,  $P < 0.001$ ). Lymphocyte percentage was significantly higher in the moderate COVID-19 patients than severe COVID-19 patients (22.4 vs. 13.8%, Wilcoxon rank-sum test,  $P < 0.001$ ). The percentage of neutrophils was elevated along with the severity of COVID-19 (77.8 vs. 66.4, Wilcoxon rank-sum test,  $P < 0.001$ ). The LDH (314 vs. 235, Wilcoxon rank-sum test,  $P < 0.001$ ) of severe patients was significantly higher than those of moderate patients. Considering that most of these differential indicators are related to organ damage, we next explored the impact of the pre-existing diseases on the progression of COVID-19. Based on the FPHJ-548 dataset, we found that only 9% of patients without pre-existing disease progressed to severe conditions. In contrast, 16% of severe patients were diagnosed with at least one kind of pre-existing disease (Fisher's Exact Test,  $P = 0.029$ , Figure 2A), suggesting that COVID-19 patients with a pre-existing disease were prone to develop severe illness. We found the same trend in the HSSH-3015 dataset. Patients with multiple pre-existing diseases were more inclined to progress to severe cases (Figure 2B).

The difference in laboratory indicators between severe and moderate patients prompted us to develop a model based on laboratory indicators to predict the state of patients (Figure 1, details see Methods). To validate that whether laboratory findings could predict the progression of COVID-19, we performed t-distributed stochastic neighbor embedding (t-SNE) based on the laboratory indicators in the FPHJ-548 dataset. The result showed that there was an essential difference in laboratory indicators between moderate and severe patients. 95% of the samples were correctly classified (true positive rate: 0.66, true negative rate: 1, Figure 3A).

For each indicator in FPHJ-548, the correspondent AUC was calculated using the detected value as predictor and the status of progression as an outcome. We selected features whose AUC is  $> 0.7$  and only kept indicators that have detection data at admission in both the FPHJ-548 dataset and HSSH-3015 dataset





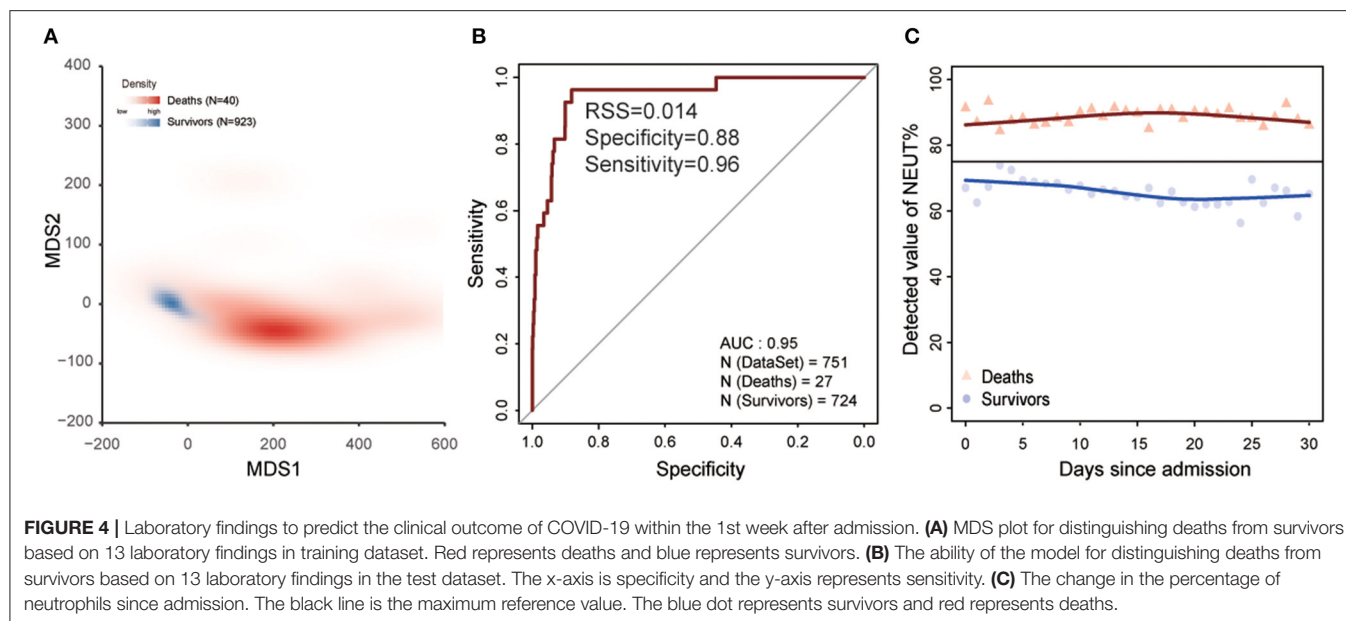
(Supplementary Figure 1). Finally, our model incorporated four indicators, including LYMPH%, NEUT%, creatinine (CREA), and urea nitrogen (BUN) (Figure 3B). The NEUT% between moderate and severe patients showed a noticeable increase at about 4 days before the admission in the FPHJ-548 dataset (Figure 3C). On the contrary, the neutrophil of moderate patients were stable, and between the range of normal reference.

We then applied these four indicators to develop a support vector machine model, followed by 5-fold cross-validations as internal validation. The average sensitivity and specificity of five cross-validations were 0.89 and 0.84, respectively. The average AUC of the five cross-validations was 0.86 (AUC 95% CI: 0.84–0.88). The representative receiver operating characteristic (ROC) curve for the external validation (HSSH-3015 dataset) is shown in Figure 3D. It still achieved satisfying results in the testing dataset (sensitivity and specificity, 0.73 and 0.96, respectively, AUC: 0.89). Lastly, to avoid the biases of age and sex, we divided patients into two groups by age or sex to test our model. The results showed

that our model still had good performance when considering age and sex (Figures 3E,F). To validate the stability of our model at different time points, we considered the status of laboratory indicators within 3, 5, and 7 days after admission. Although the AUC of the model was lower than at admission, our model still had good performance (Mean AUC: 0.71, 0.72, 0.72, respectively for 3, 5, and 7 days after admission, Supplementary Figure 2).

### Laboratory Findings Within the 1st Week After Admission Could Predict the Risk of Death of COVID-19

The progression of COVID-19 into severe illness increases the risk of death, so we predicted the survival outcome of severe patients in the HSSH-3015 dataset based on the laboratory findings within the 1st week after admission (Figure 1). Patients were randomly divided into a training group and validation group at the ratio of 1:1. To avoid the deviation caused by



the difference between the number of deaths and the number of survivors, we randomly selected the surviving patients so that the number of surviving patients equals the number of dead patients. We used stepwise logistic regression to identify the important laboratory indicators. This process was repeated 100 times (details see Methods). Thirteen indicators with statistically significant differences between survivors and deaths were identified. These were Albumin/Globulin, DD dimer, leukocyte, monocytes, cystatin C, creatinine, lymphocyte, urea nitrogen, thrombin time, prothrombin time, lactate dehydrogenase, fibrinogen, percentage of neutrophils. We performed multidimensional scaling in the training dataset based on these 13 markers. Results show that these indicators could distinguish deaths from survival (accuracy = 0.96, true positive rate: 0.82, true negative rate: 0.97, **Figure 4A**). Then, based on these 13 indicators, we developed a logistic model to predict the survival outcome in the training dataset. We found that the model predicts the survival outcome with high accuracy in the testing dataset (AUC = 0.95, **Figure 4B**). The average NEUT% of dead patients exceeded the maximum normal value during hospitalization. In contrast, the neutrophil of survivors was stable, and between the range of normal reference (**Figure 4C**).

### Distinguishing COVID-19 From Non-COVID-19 Viral Pneumonia Based on Laboratory Findings

Increasing studies have shown that the infection of viral pneumonia might be associated with organ dysfunction (14–17). Hence, we explored the change of organ function-related indicators between FPHJ-548 and nCVP-118. Interestingly, we found that some indicators related to organ dysfunction showing significant differences between the two groups (**Table 2**, Wilcoxon two-sided rank-sum test,  $P < 0.05$ ). Our studies showed that patients in the non-COVID-19 group had higher levels of WBC than those of the COVID-19 group (6.65L vs.

5.7,  $P = 0.002$ ). Besides, the level of LDH in the non-COVID-19 group was lower than that of COVID-19 patients (182 vs. 242.85,  $P < 0.001$ ). The level of aspartate transaminase (22 vs. 27.4,  $P < 0.001$ ) was higher in the COVID-19 group. To further confirm the reliability and stability of the above results, we randomly selected 20 COVID-19 patients and 20 non-COVID-19 patients to compare the difference in laboratory indicators. This process was repeated 100 times. The different indicators are consistent across 100 iterations (**Supplementary Figure 3**). We calculated the permutation  $p$ -value for each indicator to identify the significant indicators in most of the random sampling. Six indicators with significant differences permutation  $p$  values were selected (permutation  $p < 0.05$ ), including eosinophil percentage, white blood cell count, albumin, aspartate transaminase, lactate dehydrogenase, and hemoglobin. Hence, we used these laboratory findings to perform multidimensional scaling among FPHJ-548, nCVP-118, HSSH-3015, and nCVP-118 (**Figure 5A**, details see Methods). We found that these indicators can distinguish COVID-19 and non-COVID-19. For verification, we performed the same method on HSSH-3015 and nCVP-118 and found similar results (**Figure 5B**).

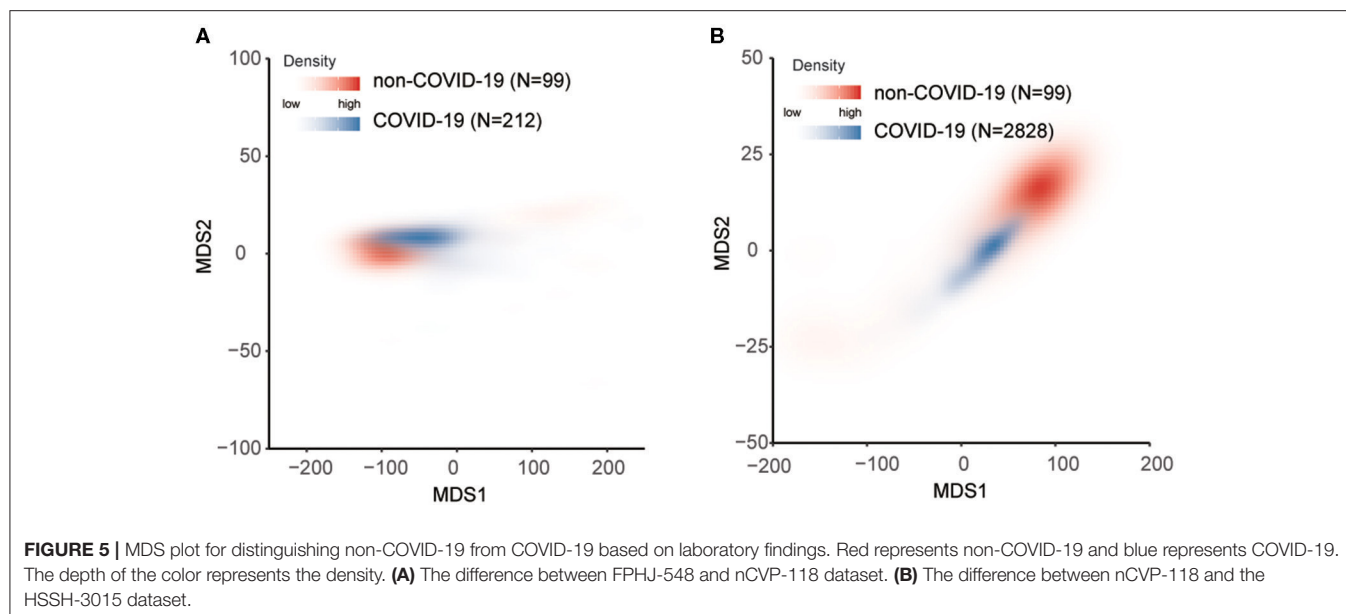
Considering that these indicators were related to liver disease and heart disease, we removed the patients with liver and heart disease in the HSSH-3015 dataset to exclude the impact of pre-existing disease. Results showed that these indicators could still differentiate COVID-19 from non-COVID-19 (**Supplementary Figure 4**). In summary, these findings demonstrated that laboratory findings can distinguish COVID-19 patients from non-COVID-19 patients.

## DISCUSSION

About 6.5% of COVID-19 patients experience a sudden progression to severe conditions, with a fatality rate of 49% in these patients (18). There is an urgent need for effective

**TABLE 2** | Comparing laboratory findings between COVID-19 and non-COVID-19 patients.

|  | Normal range | Total<br>(N = 403) | Non-COVID-19<br>(N = 118) | COVID-19<br>(N = 385) | P-value | Adjust<br>P-value |
|--|--------------|--------------------|---------------------------|-----------------------|---------|-------------------|
| <b>Laboratory findings</b>               |              |                    |                           |                       |         |                   |
| <b>Infection markers</b>                 |              |                    |                           |                       |         |                   |
| Eosinophil percentage, %                 | 0.4~8        | 0.64 (0.2–1.3)     | 1.1 (0.5–1.9)             | 0.5 (0.2–1.2)         | <0.001  | 0.007             |
| White blood cell count, g/L              | 3.5~9.5      | 5.9 (4.6–7.6)      | 6.65 (5.1–8.3)            | 5.7 (4.6–7.4)         | 0.002   | 0.045             |
| <b>Liver injury markers</b>              |              |                    |                           |                       |         |                   |
| Albumin, g/L                             | 35~55        | 38.4 (35–42)       | 36.8 (33–41)              | 38.95 (36–42)         | <0.001  | 0.041             |
| Alanine transaminase                     | 9~50         | 18.2 (12–29)       | 16.5 (11–23)              | 19 (12–29)            | 0.1     | 0.272             |
| Aspartate Transaminase                   | 13~35        | 25.8 (19–36)       | 22 (17–28)                | 27.4 (20–41)          | <0.001  | 0.043             |
| <b>Heart injury markers</b>              |              |                    |                           |                       |         |                   |
| Lactate Dehydrogenase, U/L               | 80~285       | 231<br>(180–320)   | 182 (150–300)             | 242.85<br>(200–330)   | <0.001  | 0.002             |
| N-terminal pro-brain natriuretic peptide | 0~125        | 76.8 (49–240)      | 65.25 (48–120)            | 90.285<br>(49–410)    | 0.067   | 0.086             |
| <b>Blood examination</b>                 |              |                    |                           |                       |         |                   |
| Activated partial thromboplastin time    | 24~36        | 30.3 (28–32)       | 31 (29–36)                | 30.1 (28–32)          | 0.0039  | 0.16              |
| Hematocrit, %                            | 40~50        | 39.6 (36–43)       | 38.4 (34–41)              | 39.85 (36–43)         | 0.001   | 0.113             |
| Hemoglobin, g/L                          | 130~175      | 134<br>(120–150)   | 127.5 (110–140)           | 135.25<br>(120–150)   | <0.001  | 0.031             |
| Calcium, mmol/L                          | 2.08~2.8     | 2.12 (2–2.2)       | 2.2 (2.1–2.3)             | 2.1 (2–2.2)           | <0.001  | 0.075             |
| Potassium, mmol/L                        | 3.5~5.3      | 4 (3.7–4.3)        | 3.9 (3.7–4.3)             | 4.02 (3.7–4.4)        | 0.25    | 0.299             |
| Sodium, mmol/L                           | 137~147      | 139<br>(136–141)   | 139 (138–140)             | 139<br>(136–141)      | 0.46    | 0.474             |



methods of predicting and monitoring the progression of COVID-19 patients from moderate to severe conditions. First, based on the FPHJ-548 dataset, we systematically explored the difference in laboratory findings between severe and moderate patients. We found that the high-risk factors related to the progression of COVID-19 included PCT, CRP, NT-proBNP, neutrophils percentage, LDH, and LYMPH%, etc. Most of these

laboratory indicators were reported to be associated with the progression of COVID-19 (19). The lymphocyte count was lower in non-survivors than survivors (11). Severe cases presented lower lymphocyte counts and higher neutrophil levels (11, 20). LDH was found to be a risk factor associated with disease progression in patients infected with COVID-19 (21). Many types of research have proven that elevated NT-proBNP was

significantly correlated with critical disease (22). Initial blood urea nitrogen and serum creatinine were related to increased mortality in COVID-19 (23, 24). In addition, we found that the proportion of severe conditions was positively associated with the increase in the number of pre-existing diseases diagnosed in the patients. Many studies demonstrated that these pre-existing diseases might promote the expression of ACE2 (25, 26), leading to a high-risk of COVID-19 infection. Based on a set of laboratory indicators (NEUT%, LYMPH%, CREA, and BUN), we finally constructed a risk-stratification model by using an SVM model, achieved the AUC of 0.89 in an independent dataset. Then, we based it on 13 laboratory findings ensemble a model to predict survival outcome with high accuracy. At last, we proved that laboratory findings could distinguish COVID-19 patients from non-COVID-19 patients. In the latest research, Zhang et.al. have developed an artificial intelligence (AI) tool, which could classify the severity and predict critical illness based on chest CT images and laboratory indicators (7). The deep learning survival Cox model was also developed to predict the clinical outcome of COVID-19 patients with high accuracy. This model uses ten clinical variables, including common demographic and clinical characteristics, as well as laboratory results (27). However, in the emergency of the pandemic, the requirements of professional devices and clinicians make these methods difficult to use rapidly. Our model used four laboratory indicators that are available at most hospitals and achieve comparable sensitivity and specificity. When the medical system is overloaded in a pandemic or rural area, this risk-stratification model can help screen patients who may develop severe illness accurately by easy detection and low-cost testing, as early as admission.

Our model has some limitations. First, because of the emergency of the epidemic, some patients did not take the blood tests at admission, which limited the power of prediction and validation. Second, further studies on different populations with larger patient cohorts are required to verify our findings, especially in distinguishing COVID-19 from non-COVID-19 viral pneumonia based on laboratory findings. As the tendency of organ dysfunction of COVID-19 and other pneumonia is controversial currently, more extensive comparison analysis is needed to validate the difference (28, 29). Our practical prognostic model, based on laboratory indicators, is a convenient and effective method of risk-stratification for COVID-19 at admission, providing a way of ensuring that severe patients receive treatment early, and enabling medical resources to be allocated effectively. Our study provides vital information for clinical practice in the diagnosis and monitoring of COVID-19 patients.

## DATA AVAILABILITY STATEMENT

The original contributions presented in the study are included in the article/Supplementary Material, further inquiries can be directed to the corresponding author/s.

## ETHICS STATEMENT

The studies involving human participants were reviewed and approved by the Medical Ethical Committee of the First People's Hospital of Jiangxia District of Wuhan (2020029), Wuhan Huoshenshan Hospital (HSSL011). The protocol of this study was approved by the Ethical Committee of Nanjing Medical University (2020-511). The patients/participants provided their written informed consent to participate in this study.

## AUTHOR CONTRIBUTIONS

SW, PL, XX, and KL had full access to all of the data in the study and all take responsibility for the integrity of the data analysis, and contributed to concept and design. CL, CX, WH, HS, YW, ZN, YG, and RZ undertook data collection. ZW, WW, LW, JL, QW, and HT undertook data analysis and interpretation. All authors contributed to the article and approved the submitted version.

## FUNDING

This study was supported by the National Natural Science Foundation of China (Grant Nos. 81572893, 81972358, and 91959113) and the Key Research and Development Program of Jiangsu Province (Grant No. BE2017733).

## SUPPLEMENTARY MATERIAL

The Supplementary Material for this article can be found online at: <https://www.frontiersin.org/articles/10.3389/fmed.2021.699706/full#supplementary-material>

**Supplementary Figure 1** | The receiver operating characteristic (ROC) curve of identified indicators to distinguish severe and moderate patients in the FPHJ-dataset.

**Supplementary Figure 2** | The receiver operating characteristic (ROC) curve of risk-stratification score to distinguish severe and moderate patients within 3, 5, 7 days after admission in the HSSH-3015 dataset. **(A)** The model performance within 3 days. **(B)** The model performance within 5 days. **(C)** The model performance within 7 days.

**Supplementary Figure 3** | The difference of laboratory findings between non-COVID-19 and COVID-19. 20 patients were randomly selected without replacement from the nCVP-118 dataset and FPHJ-548 dataset, respectively. This process was repeated 100 times. The y-axis represents the median value in each iteration. \*\* $P < 0.01$ .

**Supplementary Figure 4** | MDS plot for distinguishing non-COVID-19 from COVID-19 without liver or heart disease based on laboratory findings. Red represents non-COVID-19 and blue represents COVID-19. The depth of the color represents the density.

**Supplementary Table 1** | Clinical characteristics of patients in the FPHJ-458 dataset.



## REFERENCES

- Wu JT, Leung K, Leung GM. Nowcasting and forecasting the potential domestic and international spread of the 2019-nCoV outbreak originating in Wuhan, China: a modelling study. *Lancet*. (2020) 395:689–97. doi: 10.1016/S0140-6736(20)30260-9
- Baud D, Qi X, Nielsen-Saines K, Musso D, Pomar L, Favre G. Real estimates of mortality following COVID-19 infection. *Lancet Infect Dis*. (2020) 20:773. doi: 10.1016/S1473-3099(20)30195-X
- Li X, Geng M, Peng Y, Meng L, Lu S. Molecular immune pathogenesis and diagnosis of COVID-19. *J Pharm Anal*. (2020) 10:102–8. doi: 10.1016/j.jpha.2020.03.001
- Wang Y, Kang H, Liu X, Tong Z. Combination of RT-qPCR testing and clinical features for diagnosis of COVID-19 facilitates management of SARS-CoV-2 outbreak. *J Med Virol*. (2020) 92:538–9. doi: 10.1002/jmv.25721
- Fang Y, Zhang H, Xie J, Lin M, Ying L, Pang P, et al. Sensitivity of chest CT for COVID-19: comparison to RT-PCR. *Radiology*. (2020) 296:E115–7. doi: 10.1148/radiol.20200432
- Xiao AT, Tong YX, Zhang S. False-negative of RT-PCR and prolonged nucleic acid conversion in COVID-19: Rather than recurrence. *J Med Virol*. (2020) 92:1755–6. doi: 10.1002/jmv.25855
- Zhang K, Liu X, Shen J, Li Z, Sang Y, Wu X, et al. Clinically applicable ai system for accurate diagnosis, quantitative measurements, and prognosis of COVID-19 pneumonia using computed tomography. *Cell*. (2020) 181:1423–33.e11. doi: 10.1016/j.cell.2020.08.029
- Dadario AMV, Paiva JPQ, Chate RC, Machado BS, Szarf G. Regarding “artificial intelligence distinguishes COVID-19 from community acquired pneumonia on chest CT”. *Radiology*. (2020) 19:201178. doi: 10.1148/radiol.2020020905
- Bai HX, Wang R, Xiong Z, Hsieh B, Chang K, Halsey K, et al. AI augmentation of radiologist performance in distinguishing COVID-19 from pneumonia of other etiology on chest CT. *Radiology*. (2020) 299:E225. doi: 10.1148/radiol.2021219004
- Huang C, Wang Y, Li X, Ren L, Zhao J, Hu Y, et al. Clinical features of patients infected with 2019 novel coronavirus in Wuhan, China. *Lancet*. (2020) 395:497–506. doi: 10.1016/S0140-6736(20)30183-5
- Zhou F, Yu T, Du R, Fan G, Liu Y, Liu Z, et al. Clinical course and risk factors for mortality of adult inpatients with COVID-19 in Wuhan, China: a retrospective cohort study. *Lancet*. (2020) 395:1054–62. doi: 10.1016/S0140-6736(20)30566-3
- Gao Y, Li T, Han M, Li X, Wu D, Xu Y, et al. Diagnostic utility of clinical laboratory data determinations for patients with the severe COVID-19. *J Med Virol*. (2020) 92:791–6. doi: 10.1002/jmv.25770
- Lippi G, Plebani M. Procalcitonin in patients with severe coronavirus disease 2019 (COVID-19): A meta-analysis. *Clin Chim Acta*. (2020) 505:190–1. doi: 10.1016/j.cca.2020.03.004
- Ronco C, Reis T. Kidney involvement in COVID-19 and rationale for extracorporeal therapies. *Nat Rev Nephrol*. (2020) 16:308–10. doi: 10.1038/s41581-020-0284-7
- Liu PP, Blet A, Smyth D, Li H. The science underlying COVID-19: implications for the cardiovascular system. *Circulation*. (2020) 142:68–78. doi: 10.1161/CIRCULATIONAHA.120.047549
- Feng G, Zheng KI, Yan QQ, Rios RS, Targher G, Byrne CD, et al. COVID-19 and liver dysfunction: current insights and emergent therapeutic strategies. *J Clin Transl Hepatol*. (2020) 8:18–24. doi: 10.14218/JCTH.2020.00018
- Lechien JR, Chiesa-Estomba CM, De Siaty DR, Horoi M, Le Bon SD, Rodriguez A, et al. Olfactory and gustatory dysfunctions as a clinical presentation of mild-to-moderate forms of the coronavirus disease (COVID-19): a multicenter European study. *Eur Arch Oto-Rhino-L*. (2020) 277:2251–61. doi: 10.1007/s00405-020-05965-1
- Guan WJ, Ni ZY, Hu Y, Liang WH, Ou CQ, He JX, et al. Clinical characteristics of coronavirus disease 2019 in China. *N Engl J Med*. (2020) 382:1708–20. doi: 10.1056/NEJMoa2002032
- Meizlish ML, Pine AB, Bishai JD, Goshua G, Nadelmann ER, Simonov M, et al. A neutrophil activation signature predicts critical illness and mortality in COVID-19. *Blood Adv*. (2021) 5:1164–77. doi: 10.1182/bloodadvances.2020003568
- Kong M, Zhang HM, Cao XC, Mao XL, Lu ZX. Higher level of neutrophil-to-lymphocyte is associated with severe COVID-19. *Epidemiol Infect*. (2020) 148:1557. doi: 10.1017/S0950268820001557
- Lo IL, Lio CE, Cheong HH, Lei CI, Cheong TH, Zhong X, et al. Evaluation of SARS-CoV-2 RNA shedding in clinical specimens and clinical characteristics of 10 patients with COVID-19 in Macau. *Int J Biol Sci*. (2020) 16:1698–707. doi: 10.7150/ijbs.45357
- Chen C, Chen C, Yan JT, Zhou N, Zhao JB, Wang DW. [Analysis of myocardial injury in patients with COVID-19 and association between concomitant cardiovascular diseases and severity of COVID-19]. *Zhonghua Xin Xue Guan Bing Za Zhi*. (2020) 48:E008. doi: 10.3760/cma.j.cn112148-20200225-00123
- Cheng A, Hu L, Wang Y, Huang L, Zhao L, Zhang C, et al. Diagnostic performance of initial blood urea nitrogen combined with D-dimer levels for predicting in-hospital mortality in COVID-19 patients. *Int J Antimicrob Agents*. (2020) 56:106110. doi: 10.1016/j.ijantimicag.2020.106110
- Cheng YC, Luo R, Wang K, Zhang M, Wang ZX, Dong L, et al. Kidney disease is associated with in-hospital death of patients with COVID-19. *Kidney Int*. (2020) 97:829–38. doi: 10.1016/j.kint.2020.03.005
- Fang L, Karakioulakis G, Roth M. Are patients with hypertension and diabetes mellitus at increased risk for COVID-19 infection? *Lancet Resp Med*. (2020) 8:E21. doi: 10.1016/S2213-2600(20)30116-8
- Zheng YY, Ma YT, Zhang JY, Xie X. COVID-19 and the cardiovascular system. *Nat Rev Cardiol*. (2020) 17:259–60. doi: 10.1038/s41569-020-0360-5
- Liang W, Yao J, Chen A, Lv Q, Zanin M, Liu J, et al. Early triage of critically ill COVID-19 patients using deep learning. *Nat Commun*. (2020) 11:3543. doi: 10.1038/s41467-020-17280-8
- Zhao D, Yao F, Wang L, Zheng L, Gao Y, Ye J, et al. A comparative study on the clinical features of coronavirus 2019 (COVID-19) pneumonia with other pneumonias. *Clin Infect Dis*. (2020) 71:756–61. doi: 10.1093/cid/ciaa247
- Inamura N, Miyashita N, Hasegawa S, Kato A, Fukuda Y, Saitoh A, et al. Management of refractory Mycoplasma pneumoniae pneumonia: utility of measuring serum lactate dehydrogenase level. *J Infect Chemother*. (2014) 20:270–3. doi: 10.1016/j.jiac.2014.01.001

**Conflict of Interest:** The authors declare that the research was conducted in the absence of any commercial or financial relationships that could be construed as a potential conflict of interest.

**Publisher's Note:** All claims expressed in this article are solely those of the authors and do not necessarily represent those of their affiliated organizations, or those of the publisher, the editors and the reviewers. Any product that may be evaluated in this article, or claim that may be made by its manufacturer, is not guaranteed or endorsed by the publisher.

Copyright © 2021 Liu, Wang, Wu, Xiang, Wu, Li, Hou, Sun, Wang, Nie, Gao, Zhang, Tang, Wang, Li, Xia, Li and Wang. This is an open-access article distributed under the terms of the Creative Commons Attribution License (CC BY). The use, distribution or reproduction in other forums is permitted, provided the original author(s) and the copyright owner(s) are credited and that the original publication in this journal is cited, in accordance with accepted academic practice. No use, distribution or reproduction is permitted which does not comply with these terms.



# Containing the Transmission of COVID-19: A Modeling Study in 160 Countries

Yan Niu<sup>1†</sup>, Jia Rui<sup>2†</sup>, Qiupeng Wang<sup>2,3†</sup>, Wei Zhang<sup>2</sup>, Zhiwei Chen<sup>4</sup>, Fang Xie<sup>2</sup>, Zeyu Zhao<sup>2</sup>, Shengnan Lin<sup>2</sup>, Yuanzhao Zhu<sup>2</sup>, Yao Wang<sup>2</sup>, Jingwen Xu<sup>2</sup>, Xingchun Liu<sup>2</sup>, Meng Yang<sup>2</sup>, Wei Zheng<sup>2</sup>, Kaixin Chen<sup>2</sup>, Yilan Xia<sup>2</sup>, Lijuan Xu<sup>2</sup>, Shi Zhang<sup>2</sup>, Rongrong Ji<sup>4</sup>, Taisong Jin<sup>4</sup>, Yong Chen<sup>5</sup>, Benhua Zhao<sup>2</sup>, Yanhua Su<sup>2</sup>, Tie Song<sup>6</sup>, Tianmu Chen<sup>2\*</sup> and Guoqing Hu<sup>7\*</sup>

## OPEN ACCESS

### Edited by:

Reza Lashgari,  
Shahid Beheshti University, Iran

### Reviewed by:

Pankaj Bhardwaj,  
All India Institute of Medical Sciences,  
Jodhpur, India  
Abed Khorasani,  
Kerman Medical University, Iran  
Hadi Choubdar,  
Shahid Beheshti University of Medical  
Sciences, Iran

### \*Correspondence:

Guoqing Hu  
huguoqing009@gmail.com  
Tianmu Chen  
chentianmu@xmu.edu.cn;  
136986665@qq.com

<sup>†</sup>These authors have contributed  
equally to this work

### Specialty section:

This article was submitted to  
Infectious Diseases—Surveillance,  
Prevention and Treatment,  
a section of the journal  
Frontiers in Medicine

Received: 28 April 2021

Accepted: 20 July 2021

Published: 18 August 2021

### Citation:

Niu Y, Rui J, Wang Q, Zhang W,  
Chen Z, Xie F, Zhao Z, Lin S, Zhu Y,  
Wang Y, Xu J, Liu X, Yang M,  
Zheng W, Chen K, Xia Y, Xu L,  
Zhang S, Ji R, Jin T, Chen Y, Zhao B,  
Su Y, Song T, Chen T and Hu G (2021)  
Containing the Transmission of  
COVID-19: A Modeling Study in 160  
Countries. *Front. Med.* 8:701836.  
doi: 10.3389/fmed.2021.701836

<sup>1</sup> Chinese Center for Disease Control and Prevention, Beijing, China, <sup>2</sup> State Key Laboratory of Molecular Vaccinology and Molecular Diagnostics, School of Public Health, Xiamen University, Xiamen, China, <sup>3</sup> School of Journalism and Communication, Peking University, Beijing, China, <sup>4</sup> Media Analytics and Computing Lab, Department of Artificial Intelligence, School of Informatics, Xiamen University, Xiamen, China, <sup>5</sup> Department of Stomatology, School of Medicine, Xiamen University, Xiamen, China, <sup>6</sup> Guangdong Provincial Center for Disease Control and Prevention, Guangzhou, China, <sup>7</sup> Department of Epidemiology and Health Statistics, Xiangya School of Public Health, Central South University, Changsha, China

**Background:** It is much valuable to evaluate the comparative effectiveness of the coronavirus disease 2019 (COVID-19) prevention and control in the non-pharmacological intervention phase of the pandemic across countries and identify useful experiences that could be generalized worldwide.

**Methods:** In this study, we developed a susceptible–exposure–infectious–asymptomatic–removed (SEIAR) model to fit the daily reported COVID-19 cases in 160 countries. The time-varying reproduction number ( $R_t$ ) that was estimated through fitting the mathematical model was adopted to quantify the transmissibility. We defined a synthetic index ( $I_{AC}$ ) based on the value of  $R_t$  to reflect the national capability to control COVID-19.

**Results:** The goodness-of-fit tests showed that the SEIAR model fitted the data of the 160 countries well. At the beginning of the epidemic, the values of  $R_t$  of countries in the European region were generally higher than those in other regions. Among the 160 countries included in the study, all European countries had the ability to control the COVID-19 epidemic. The Western Pacific Region did best in continuous control of the epidemic, with a total of 73.76% of countries that can continuously control the COVID-19 epidemic, while only 43.63% of the countries in the European Region continuously controlled the epidemic, followed by the Region of Americas with 52.53% of countries, the Southeast Asian Region with 48% of countries, the African Region with 46.81% of countries, and the Eastern Mediterranean Region with 40.48% of countries.

**Conclusion:** Large variations in controlling the COVID-19 epidemic existed across countries. The world could benefit from the experience of some countries that demonstrated the highest containment capabilities.

**Keywords:** COVID-19, transmissibility, mathematical model, the effective reproduction number, epidemic

## INTRODUCTION

Coronavirus disease 2019 (COVID-19) is a novel infectious disease caused by severe acute respiratory syndrome coronavirus 2 virus (SARS-CoV-2) (1). On March 11, 2020, the World Health Organization (WHO) declared a global pandemic of COVID-19 (2). The COVID-19 pandemic has brought tremendous economic and medical burden, and has severely affected people's normal work and daily lives. In most countries, the health system faces collapse, and there are medical shortages of varying degrees (3). In countries affected by COVID-19, many factories and shops have been closed, and thus many people have lost their jobs and income. The International Labor Organization estimated that 25 million jobs were lost, which could lead to a loss of at least US\$220 billion in income in developing countries (4). In 2020, the World Travel and Tourism Council warned that up to 1.67% of the world's gross domestic product could be lost due to the reduction in flight travel (5). Therefore, it is very important for the world to evaluate the comparative effectiveness of COVID-19 prevention and control across countries.

Current research on COVID-19 mainly focuses on issues such as transmission mechanisms, pathogenic mechanisms, prevention and control measures, and infection control (6). Mathematical models of pandemics are useful for understanding the early transmission dynamics of infections, achieving pandemic prediction, and evaluating the effectiveness of control measures. They have been widely used in the prediction of the basic reproduction number ( $R_0$ ) of COVID-19, and reports of  $R_0$  for COVID-19 have ranged from 2.6 to 4.71 (6–12). One recent study suggested that the median  $R_0$  of COVID-19 may be up to 5.7 (13), which was much higher than the previously estimated maximum value of  $R_0$ . The reported  $R_0$  varied across countries. The extent each country to control the epidemic of COVID-19 in the early stage significantly affect the future development of the global pandemic. Several models, such as the stochastic transmission model (14), and ordinary differential equation model (11, 12, 15, 16), have been used in the research on COVID-19; however, research has yet to be conducted at the global level.

This study developed an innovative mathematical model to assess the transmissibility and control capability of COVID-19 epidemic of 160 countries in the initial phase of global pandemic (before August 22, 2020). Considering that COVID-19 can cause a lot asymptomatic infections (A), we added “A” to the SEIR model and formulated a susceptible–exposure–infectious–asymptomatic–removed (SEIAR) model, which better characterized the transmission of COVID-19 compared to the SEIR model. Reproduction number was used to reflect the transmissibility of COVID-19. We also evaluated the ability of 160 countries to control the COVID-19 epidemic.

## METHODS

### Study Design

The analysis process used in this study is shown in **Figure 1**. First, we collected COVID-19 data from each country in the six regions defined by the World Health Organization (WHO)

from January 22, 2020, to August 22, 2020, and excluded countries (11 countries) with poor data quality. Second, we fit the mathematical model for the remaining 172 countries and excluded countries (12 countries) due to the poor goodness of fit (the  $p$  values of goodness of fit was  $<0.05$ ). Finally, we calculated the transmissibility of COVID-19 and evaluated the prevention and control capacities of the remaining 160 countries.

The level of data monitoring varies across the six WHO regions. The African countries included in the study accounted for 74.47% of the total number of countries in the African region due to insufficient monitoring systems and economic backwardness (17). The remaining five regions were the Southeast Asian Region (100%), the Eastern Mediterranean Region (95.24%), the European Region (92.72%), the Region of Americas (88.57%), and the Western Pacific Region (86.67%). The three countries with the highest cumulative COVID-19 cases were the United States (5,667,112), Brazil (3,582,362), and India (3,044,940). Although some countries in the Western Pacific region, such as China and South Korea, were reported earlier among the countries with the highest cumulative total, the increase of number of cases slowed in the later period. The cumulative number of COVID-19 cases in the European region was between 50,000 and 1,000,000.

### Data Sources

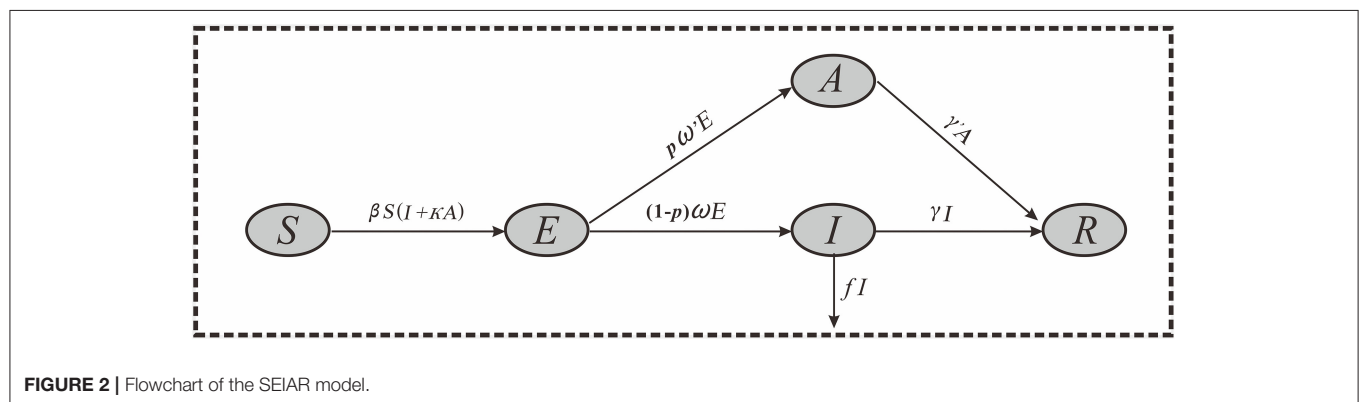
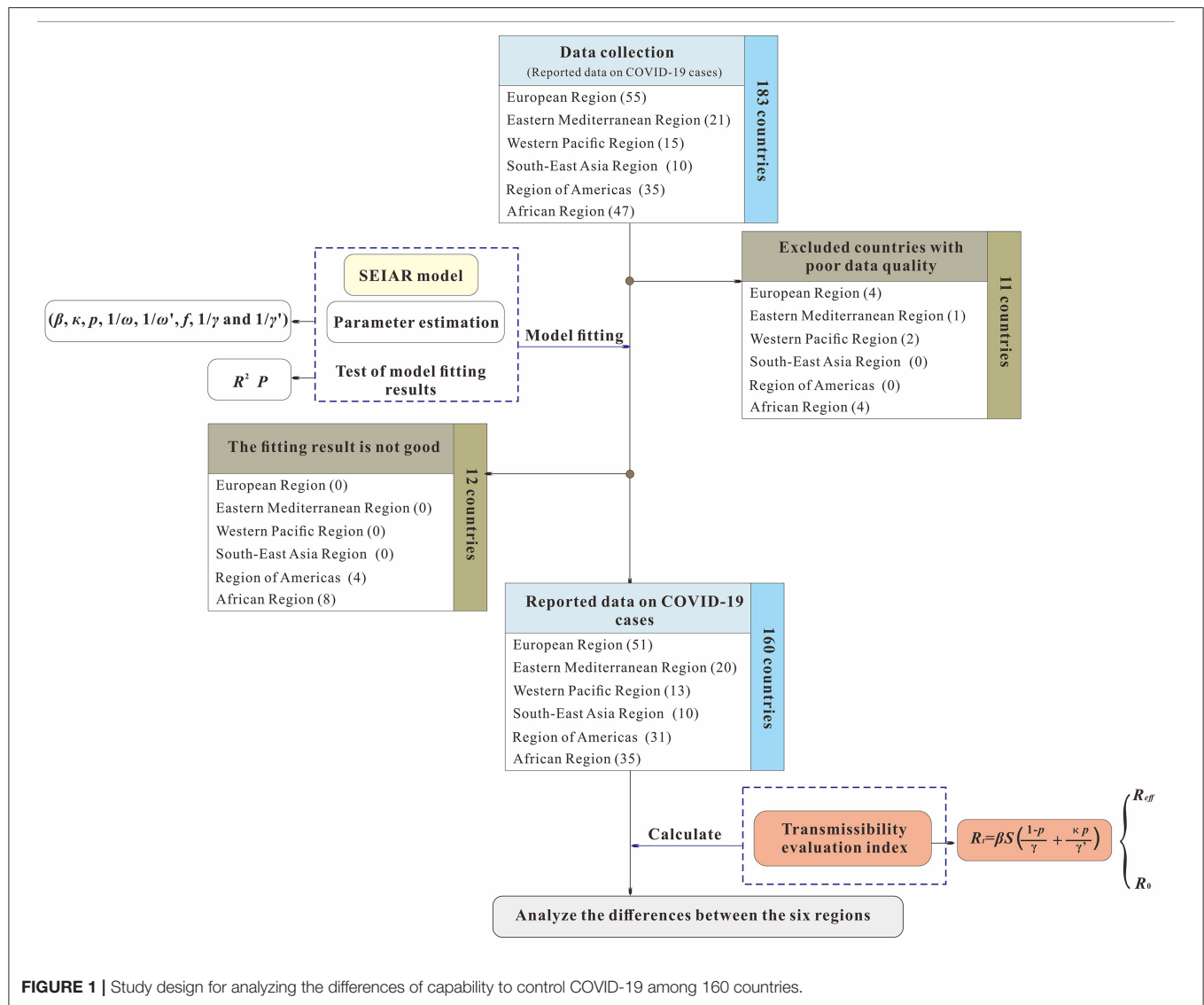
To determine the newly confirmed cases and cumulative deaths globally, we used data from the repository published by Johns Hopkins University Center for Systems Science and Engineering and the Esri Living Atlas team and Johns Hopkins University Applied Physics Lab. Then, we applied our codes to clean and process off-the-shelf data for model building. Our code repository will be published after the paper is accepted.

### The Model of COVID-19

Considering that COVID-19 can cause asymptomatic infections, we developed a SEIAR model based on our previous work (15, 18). The SEIAR model involves five group of populations: susceptible individuals (S), individuals in incubation period (E), symptomatic individuals (I), asymptomatic individuals (A), and recovered individuals (R). A SEIAR model was developed based on the reported data of COVID-19. The model framework is shown in **Figure 2**.

The model was based on the following assumptions:

- 1) Assuming that the infection rate coefficient after effective contact between S and I is  $\beta$ , and assuming that A is infectious, and the transmissibility is  $\kappa$  ( $0 < \kappa < 1$ ) times that of I, then at time  $t$ , the number of new infections is  $\beta S(I + \kappa A)$ .
- 2) Assuming that the proportion of asymptomatic infection is  $p$ , and the incubation period and latent period are  $1/\omega$  and  $1/\omega'$ , respectively. At time  $t$ , the number of people who change from E to A and I are  $p\omega'E$  and  $(1-p)\omega E$ , respectively.
- 3) Assuming that the time interval from the onset of the case I to the first diagnosis is  $1/\gamma$ , then at time  $t$ , the number of people who change from I to R is  $\gamma I$ . Because there are deaths in the reported data, we set  $f$  as the case fatality rate, and then the number of deaths at time  $t$  is  $fI$ .



- 4) Assuming that the infectious period of the recessive infected person  $A$  is  $1/\gamma'$ , then at time  $t$ , the number of people who change from  $A$  to  $R$  is  $\gamma' A$ .

Based on these assumptions, the equations of the SEIAR model are presented as follows:



**TABLE 1** | Parameter estimation.

| Parameter   | Description   | Value  | Range    | Source                    |
|-------------|---|--------|----------|---------------------------|
| $\beta$     | Transmission relative rate  | -      | $\geq 0$ | Curve fitting             |
| $\kappa$    | Relative transmissibility rate of asymptomatic to symptomatic individuals | 1      | 0–1      | (15)                      |
| $p$         | Proportion of the asymptomatic  | 0.2    | 0–1      | (11)                      |
| $1/\omega$  | Incubation of symptomatic   | 0.2    | 0–1      | (16, 17)                  |
| $1/\omega'$ | Incubation of asymptomatic  | 0.3333 | 0–1      | (16, 17)                  |
| $f$         | Fatality of the disease   | -      | 0–1      | Reported data calculation |
| $1/\gamma$  | Recovery rate of symptomatic  | 0.2    | 0–1      | (12)                      |
| $1/\gamma'$ | Recovery rate of asymptomatic   | 0.1    | 0–1      | (12)                      |

$$\frac{dS}{dt} = -\beta S(I + \kappa A)$$

$$\frac{dE}{dt} = \beta S(I + \kappa A) - p\omega'E - (1-p)\omega E$$

$$\frac{dI}{dt} = (1-p)\omega E - \gamma I - fI$$

$$\frac{dA}{dt} = p\omega'E - \gamma'A$$

$$\frac{dR}{dt} = \gamma I + \gamma'A$$

## Parameter Estimation

The values of the model parameters and their methods are listed in **Table 1**. There were 8 parameters in the model:  $\beta$ ,  $\kappa$ ,  $p$ ,  $1/\omega$ ,  $1/\omega'$ ,  $f$ ,  $1/\gamma$ , and  $1/\gamma'$ .

- 1) The collected data of reported COVID-19 cases were employed to fit the SEIAR model to calculate  $\beta$  in each region. In this study, the nodes were segmented according to the inflection point of the epidemic curve shown by the date of onset, and the models were fitted to estimate the  $\beta$  values at different time periods, namely,  $\beta_1, \beta_2, \dots, \beta_n$ .
- 2) We assumed that the transmissibility of asymptomatic infection was one times that of symptomatic infection ( $\kappa = 1$ ) from information in a previous study (19).
- 3) Because free-access data of asymptomatic infections were unavailable for each country, we determined the parameter  $p$  based on the published literatures. Studies showed that the values of  $p$  ranged from 16.1 to 50.6% (20, 21). In this study, we set a mean value of 0.2 in the model. We also performed a sensitivity analysis with the  $p$  value of 0.1, 0.2, ..., and 0.9, respectively, to assess the uncertainty of our results related to with the parameter  $p$ .
- 4) Based on previous studies (22, 23), we set the incubation period of COVID-19 to 5 days, and the latent period to 3 days in this study; therefore,  $1/\omega = 0.2$ ,  $1/\omega' = 0.3333$ .
- 5) Parameter  $f$  was the fatality rate of COVID-19 that was calculated using actual data.
- 6) Based on a previous study (12), we set the infectious period of symptomatic infection as 5 days and the infectious period of asymptomatic infection as 10 days; therefore,  $1/\gamma = 0.2$  and  $1/\gamma' = 0.1$ .

## Transmissibility Evaluation Index

In this study, the population was not completely susceptible and artificially adopted some prevention and control measures, so we chose the time-varying reproduction number ( $R_t$ ) to calculate transmissibility. The calculation formula was as follows:

$$R_t = \beta S \left( \frac{1-p}{\gamma} + \frac{\kappa p}{\gamma'} \right)$$

The  $R_t$  value at the beginning of the epidemic is defined as the basic reproduction number ( $R_0$ ), which was the initial  $R_t$  value of each country. When countries have adopted control measures for COVID-19,  $R_t$  was defined as the effective reproduction number ( $R_{eff}$ ).

A synthetic index ( $I_{AC}$ ) was constructed to evaluate the capability to control COVID-19 in each country. The calculation formula was as follows:

$$I_{AC} = I_{Tn} + I_{WNi} + I_{Cj}$$

In the equation,  $I_{Tn}$  was defined as the grade of time it took to make COVID-19 under control;  $n$  represented the level of the time required to control the COVID-19 epidemic. We divided the time into five grades ( $\leq 30$ , 31–60, 61–90, 91–120, 121–150, and 151–180 days) and gave a value of  $n = 1, 2, 3, 4, 5$ , and 6, respectively. The specific values are shown in **Table 2**.

$I_{WNi}$  is the grade of wave number of COVID-19;  $i$  represents the number of COVID-19 epidemic fluctuation in each country. When the number of fluctuation is 1,  $i = 1$ . When the number is 2, 3, and 4, the value of  $i$  is 2, 3, and 4 respectively. The specific values are shown in **Table 2**.

$I_{Cj}$  is the grade of countries where COVID-19 has been brought under control ( $R_{eff} < 1$ ) as of August 22;  $j$  represents whether the country under study has the ability to control the COVID-19 epidemic. The condition of whether it can be controlled is whether the country can reduce  $R_{eff}$  to below 1. When the country is able to control COVID-19,  $j = 1$ , and when it is unable to control it,  $j = 0$ . The specific values are shown in **Table 2**.

## Simulation Methods and Statistical Analysis

Berkeley Madonna 8.3.18 software (developed by Robert Macey and George Oster of the University of California, Berkeley at

Berkeley. Copyright©1993-2001 Robert I. Macey & George F. Oster) was used for the curve fitting. The fourth-order Runge–Kutta method, with tolerance set at 0.001, was used to perform the curve fitting. The coefficient of determination ( $R^2$ ) was used to assess the goodness of fit. SPSS 13.0 software (IBM Corp., Armonk, NY, USA) was used to calculate the  $R^2$ .

## RESULTS

### Epidemiological Characteristics of the COVID-19 Pandemic of 184 Countries

**TABLE 2** | The specific values of  $I_{Tn}$ ,  $I_{WNI}$ , and  $I_{Cj}$ .

|  | $N$ | $I_{Tn}$  |
|--|-----|-----------|
| The grade of time it will take to bring COVID-19 under control                       | 1   | 6         |
|  | 2   | 5         |
|  | 3   | 4         |
|  | 4   | 3         |
|  | 5   | 2         |
|  | 6   | 1         |
| The grade of wave number of COVID-19   | $i$ | $I_{WNI}$ |
|  | 1   | 4         |
|  | 2   | 3         |
|  | 3   | 2         |
|  | 4   | 1         |
| The grade of countries where COVID-19 has been brought under control as of August 22 | $j$ | $I_{Cj}$  |
|  | 0   | 0         |
|  | 1   | 5         |

**Figure 3** shows the spatial and temporal distribution of the cumulative incidence of COVID-19 in 184 countries since January 31, 2020. By 24:00 on January 31, 2020, the cumulative number of COVID-19 cases in China exceeded 10,000, and there were only a few confirmed cases in other countries. On February 29, the cumulative number of confirmed cases in China exceeded 70,000, and more than 10 cases occurred in some countries in the Western Pacific, Europe, and Canada in the Americas, of which the number of cases in Italy and South Korea exceeded 500 and 3,000, respectively. By March 11, the pandemic had spread globally. The cumulative number of confirmed cases in Italy, France, Spain, Germany, Iran, and other places exceeded 1,000, while the growing rate of China slowed down at this time. By March 31, the COVID-19 pandemic became very serious. The cumulative number of confirmed cases in the United States and Italy exceeded 100,000 cases. By April 21, the cumulative number of confirmed cases in the United States exceeded 800,000, and the cumulative number of newly confirmed cases in France, Spain, Germany, and the United Kingdom exceeded 100,000.

### Model Fitting

The goodness-of-fit tests showed that the SEIAR model fitted well for the COVID-19 data of most countries (**Figure 4**). The  $R^2$ , which is determined by the number of confirmed cases and the number of fitted new cases, was  $>0.5$  for 112 countries,  $p < 0.05$ . The  $R^2$  of the Southeast Asian Region, Eastern Mediterranean Region, and European Region were much higher than those of the other regions. However, the SEIAR model did not fit the data of 12

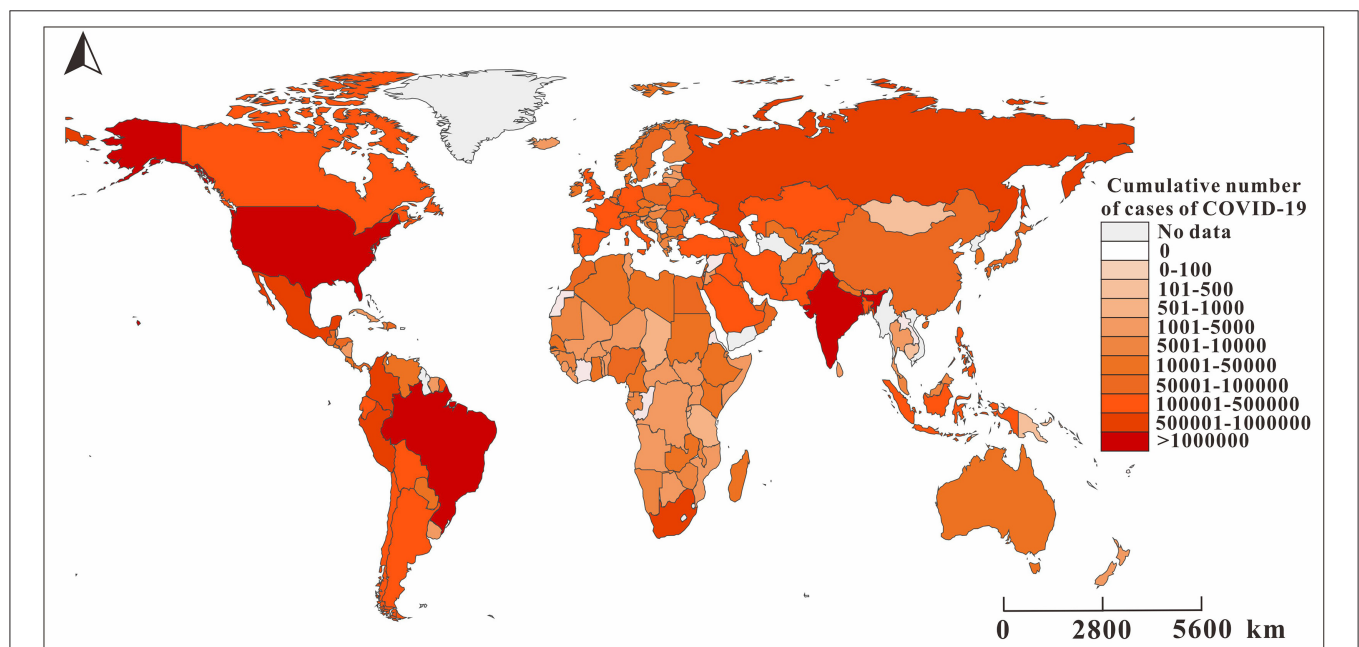


**FIGURE 3** | The reported cumulative number of cases of COVID-19 in 160 countries as of August 22, 2020. The map depicted in these figures were taken from Wikimedia Commons ([http://commons.wikimedia.org/wiki/Main\\_Page](http://commons.wikimedia.org/wiki/Main_Page)).

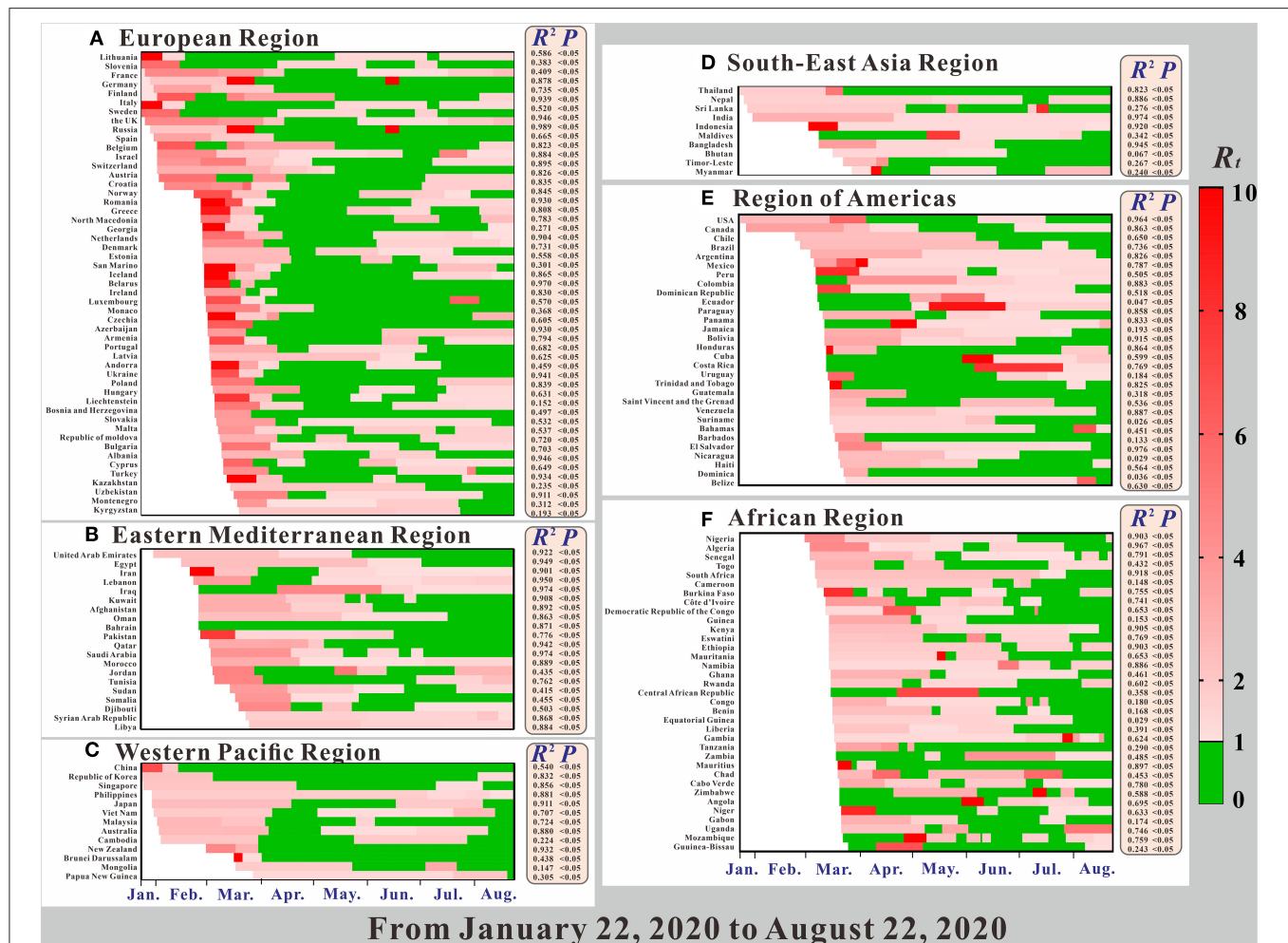


**FIGURE 4 |** The time-varying reproduction number ( $R_t$ ), the coefficient of determination ( $R^2$ ), and  $p$  of model fitting results.

countries. Thus, we excluded the 12 countries from further data analyses.

## Transmissibility of the COVID-19 Pandemic of 160 Countries

As shown in **Figure 5**, the  $R_0$  in the early stage of the pandemic was clearly higher than the  $R_{eff}$  value after the control was carried out in the later period, and the  $R_{eff}$  value in a few countries increased in the later period. As shown in **Figure 4A**, in the early stage of the pandemic, the European Region had the strongest transmissibility of COVID-19, where the  $R_0$  of many countries exceeds 10.

**Figure 4** shows a clear relationship between the reproduction number ( $R_t$ ),  $R^2$ , and  $p$  in 160 countries in the six regions. All regions, except for the African region, began to spread COVID-19 on January 22. Among them, the largest  $R_t$  range were in the Western Pacific Region and the Region of Americas, and for each, the maximum value was more than 20. Compared with other regions, the  $R_t$  value in the Region of Americas was larger. Secondly, the  $R_t$  ranges of the European Region and the African

Region were largest, followed by the Eastern Mediterranean Region. The region with the smallest  $R_t$  range was the Southeast Asian Region.

Overall, the  $R_t$  value of COVID-19 in most countries showed a trend from strong to weak (e.g., China in the Western Pacific Region), but there are also some countries for which the  $R_t$  value increased in the later period (e.g., France in the European Region). However, there are still some countries showing further upward trends, such as Sweden, which implemented the policy of “herd immunity”. Of all the regions, changes in the  $R_t$  of various countries in the African region are more complicated, and the changes in the  $R_t$  values of the other regions are obviously greater. In the Region of Americas, the majority of countries'  $R_t$  at the beginning of the pandemic were concentrated and were above 2.0. In terms of overall changes in  $R_t$  trends, prevention and control measures were not as effective in the two regions, compared with the other regions. In these two regions, COVID-19 was not effectively controlled in the early stage, making them epicenters of the COVID-19 pandemic today.

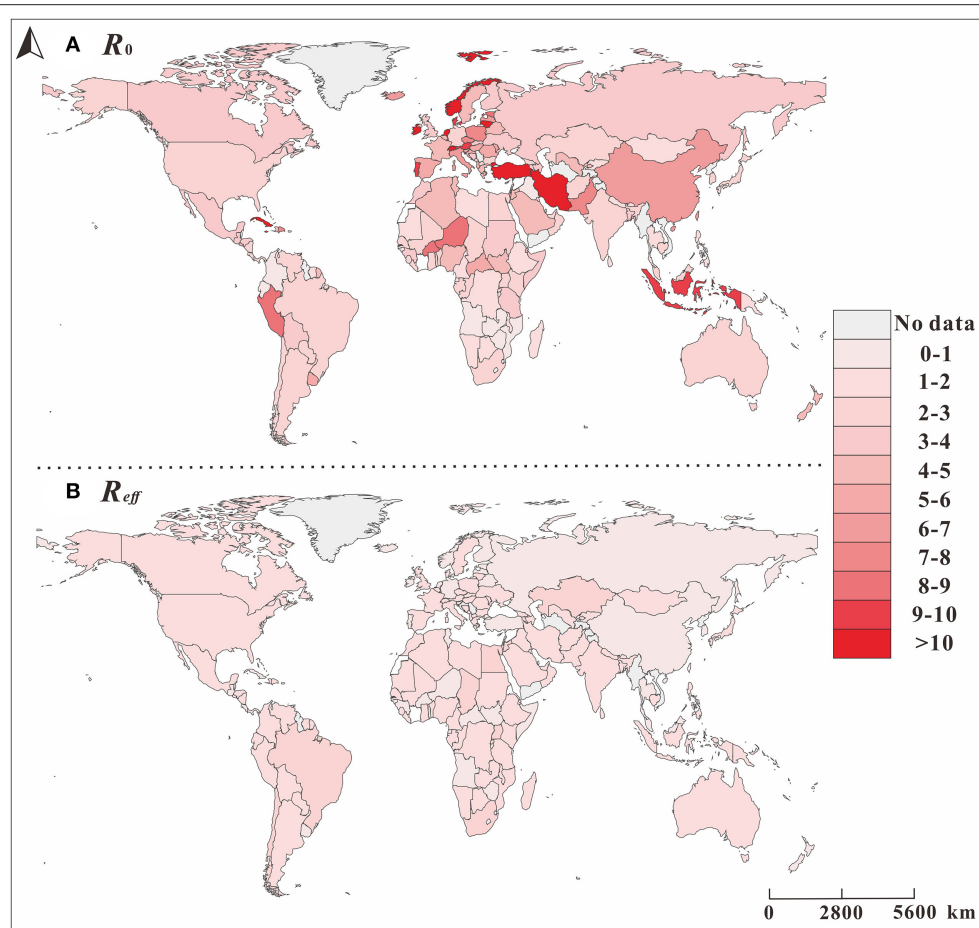


**FIGURE 5 |** The spatial distribution of basic reproduction number ( $R_0$ ) and the effective reproduction number ( $R_{eff}$ ) of COVID-19 in different countries. The map depicted in these figures were taken from Wikimedia Commons ([http://commons.wikimedia.org/wiki/Main\\_Page](http://commons.wikimedia.org/wiki/Main_Page)).

## Ability to Control COVID-19 Epidemic of 160 Countries

**Figure 6A** shows that from January 22, 2020, to August 11, 2020, there was great variation in the number of days in the period in which  $R_t$  of COVID-19 was  $<1$  among the 160 countries. Compared with **Figure 6B**, the longer the period in which  $R_t$  was 1, the shorter the time needed to control COVID-19. For example, in China in the Western Pacific region, where  $R_t$  was  $<1$  for more than 180 days, it took  $<20$  days to reduce  $R_0$  below 1. At the time of the study, many countries in the African Region were not under control, and it took a relatively long time to control COVID-19 in the Regions of Americas.

**Figure 7A** shows that among the 160 countries included in the study, those in the European Region had the strongest national control capability. All 51 European countries included in the study were able to control COVID-19, and the European Region had the highest rate of all the regions (100%), followed by the Region of Americas (85.71%), the Eastern Mediterranean Region (80.95%), the Western Pacific Region (80.87%), the Southeast Asian Region (80%), and the African Region (74.47%). Among all the countries in the European Region, 76.4% were able

to control COVID-19 within 60 days. However, in terms of continuous control, the Western Pacific Region did relatively better than the others: 73.76% of its countries on August 22, 2020, at the time of this study. This region was followed by the Region of Americas (52.53%), the Southeast Asian Region (48%), the African Region (46.81%), the European Region (43.63%), and the Eastern Mediterranean Region (40.48%). In countries where the COVID-19 epidemic was continuously controlled, the wave number ( $I_{WN}$ ) varied among the six regions. In the Western Pacific Region and the Region of Americas, the  $I_{WN}$  was up to 2. Control of COVID-19 was relatively stable. In the European Region, Eastern Mediterranean Region, Southeast Asian Region, and African region, the  $I_{WN}$  was frequently and relatively unstable.

We further evaluated the ability to control COVID-19 ( $I_{AC}$ ) in 160 countries. At the most powerful level ( $I_{AC} = 15$ ), six regions had countries with control of COVID-19. Although the European Region and the Western Pacific Region each had three countries, in terms of proportion, 5.88% of the European Region and 23.08% of the Western Pacific Region were able to control COVID-19. The Region of Americas had two countries, and the remaining three continents each had one country.



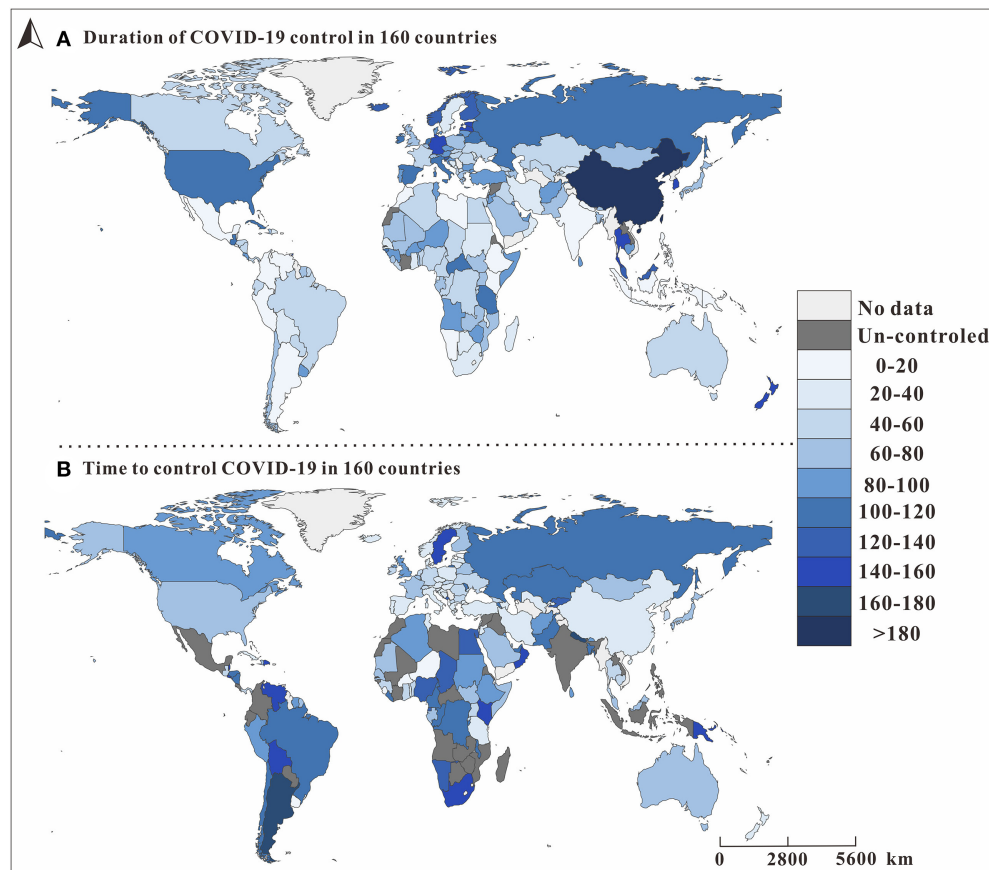


**FIGURE 6 |** The spatial distribution of  $I_{Tn}$  and  $I_{Cj}$  in 160 countries.  $I_{Tn}$  is defined as the grade of time it will take to bring COVID-19 under control, and  $n$  represents the level of the time required to control the COVID-19 epidemic.  $I_{Cj}$  is the grade of countries where COVID-19 has been brought under control ( $R_{eff} < 1$ ) as of August, 22, 2020;  $j$  represents whether the country under study has the ability to control the COVID-19 epidemic. The map depicted in these figures were taken from Wikimedia Commons ([http://commons.wikimedia.org/wiki/Main\\_Page](http://commons.wikimedia.org/wiki/Main_Page)).

Seven countries, including Morocco, Syrian Arab Republic, Libya, Philippines, India, Indonesia, and Mexico, had the worst epidemic control effect ( $I_{AC} = 0$ ), and the  $R_t$  was  $<1$  for all of these countries throughout the study. From **Figure 8**, we can see that the countries in the Western Pacific Region were mainly distributed in the front position. Although many countries in the European Region did better, some countries did worse. The Eastern Mediterranean Region and the Southeast Asian Region were relatively evenly distributed in each interval, the countries of the Region of Americas are concentrated at the middle level, and the countries of the African Region are concentrated at the lower level.

## Sensitivity Analysis

The six countries randomly selected (South Africa, USA, China, Iran, the UK, and India) located in six WHO regions, respectively. The results of the sensitivity analysis showed that  $p$  was significantly affected (see **Figure 9**). The results of sensitivity analysis of countries are consistent in six WHO regions, the larger the value of  $p$ , the smaller the value of  $R_t$ . We set the  $p$  value of each country to 0.2 for each country, which may result in a larger or smaller  $R_t$  value deviating from the actual situation. The range

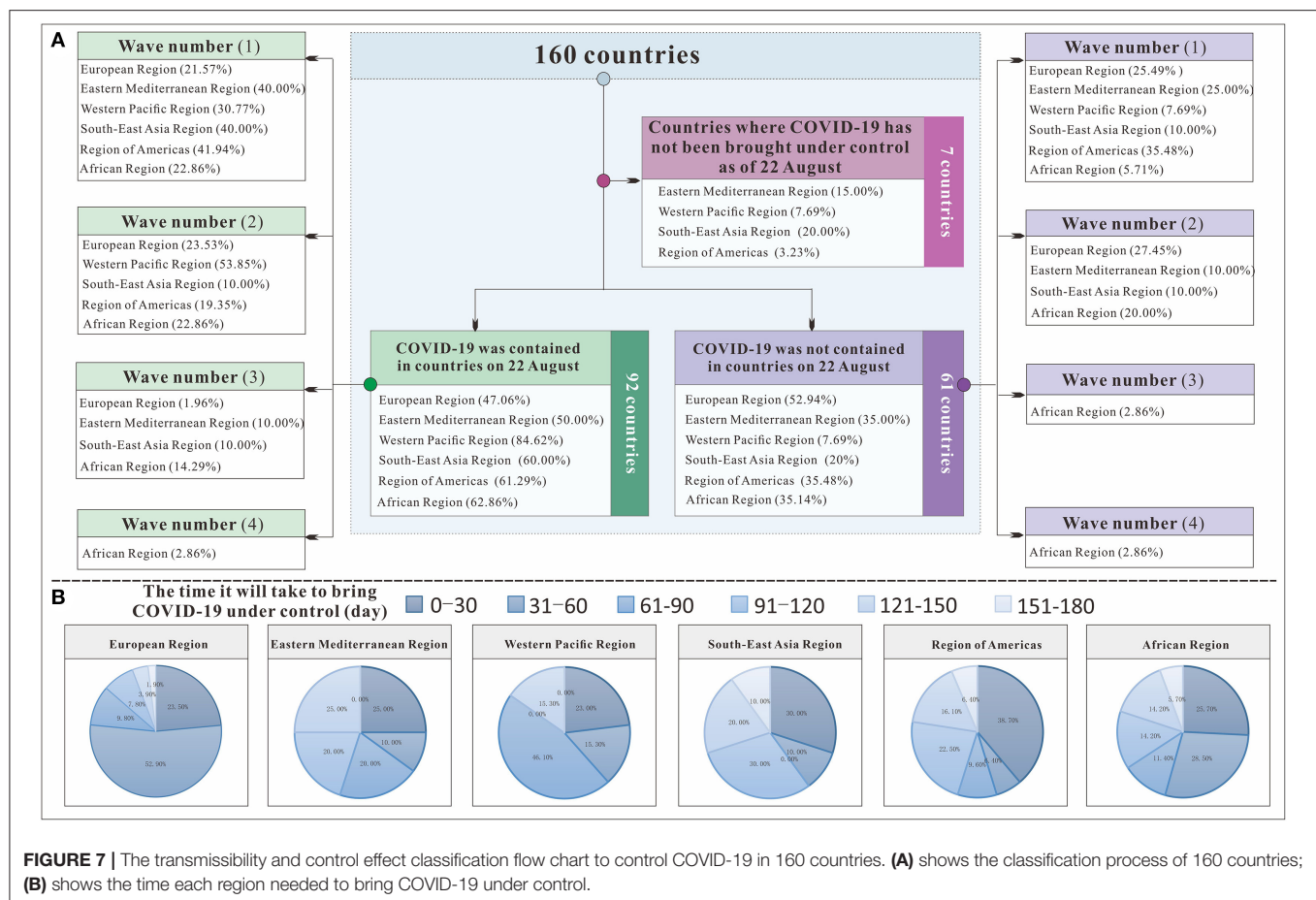
of  $R_t$  values corresponding to different  $p$  values in six countries was 1.12–3.45, 1.24–3.97, 4.27–8.78, 5.44–13.77, 4.52–12.19, and 0.99–3.29, respectively. We set the same  $p$  value in the SEIAR model for all countries to ensure the comparability of results across 160 countries.

## DISCUSSION

We constructed a theoretical epidemiological model, used  $R_t$  to reflect the transmissibility of COVID-19 in each country, and explained the differences in the cumulative incidence of COVID-19 across the six regions. Changes in  $R_t$  between January 22 and August 22 indicated a slight or moderate effect of local epidemic prevention and control measures. Based on the indicators above, we further constructed the  $I_{AC}$  to evaluate the comprehensive effectiveness of prevention and control measures in 160 countries.

## Model Fitting

From **Figure 4**, we can see that the model fitted the data of most countries, suggesting that the SEIAR model was useful. Therefore, the SEIAR model that we choose was applicable to



the data of these countries. The  $R^2$  of the Southeast Asian Region, the Eastern Mediterranean Region, and the European Region were much higher than those of other regions. This finding may be due to the early outbreak of COVID-19 in these areas, the large number of infected people, or the high detection rate. The reported data from these areas are more in line with the actual data, thus improving the model's fitness. Some countries with low incidences had lower  $R^2$  (e.g., Equatorial Guinea, Guinea, Cameroon, Mongolia, and Liechtenstein). This finding may be related to factors such as the economy of these countries, the level of testing, or the lack of public awareness. There were no obvious epidemiological characteristics in the reported data, which makes poor model fitting results.

## Effect of Prevention and Control Measures Among Six Regions

Coronavirus disease spread regionally in a natural transmission state. However, the estimates of  $R_t$  at the beginning of the pandemic may depend on numerous biological, socio-behavioral, and environmental factors (24). The duration and severity of each pandemic phase can vary depending on the characteristics of COVID-19 and the public health response. Italy and Iran

were the original hot spots outside China, from which new infections were disseminated to nearby countries. There have been higher magnitudes of COVID-19 infection in Europe and America than in Asia, whereas Europe and America show similar strengths of infection (25). The prevention and control measures adopted and implemented by local governments of various countries in the early stages helped to a certain extent (26, 27). Globally, the number of new cases per day tends to be flat. However, there were still some countries without any reduction in transmissibility after interventions, which suggests that prevention and control measures may not have played important roles in the early stages of the pandemic. Such containment is unlikely to be achievable in most countries around the world, although China succeeded in containing the spread of the pandemic for 2 months by carrying out timely and effective measures (28). Some of the literature has shown that without non-pharmaceutical interventions (including intensive case and contact tracking, isolation of moderately ill patients in containment centers, social distancing, and shutting down public life of a whole province and many major cities outside Hubei), the COVID-19 cases in China would likely have shown a 67-fold increase (interquartile range from 44 to 94) by February 29, 2020 (29). However, it is worth noting that the intervention effect

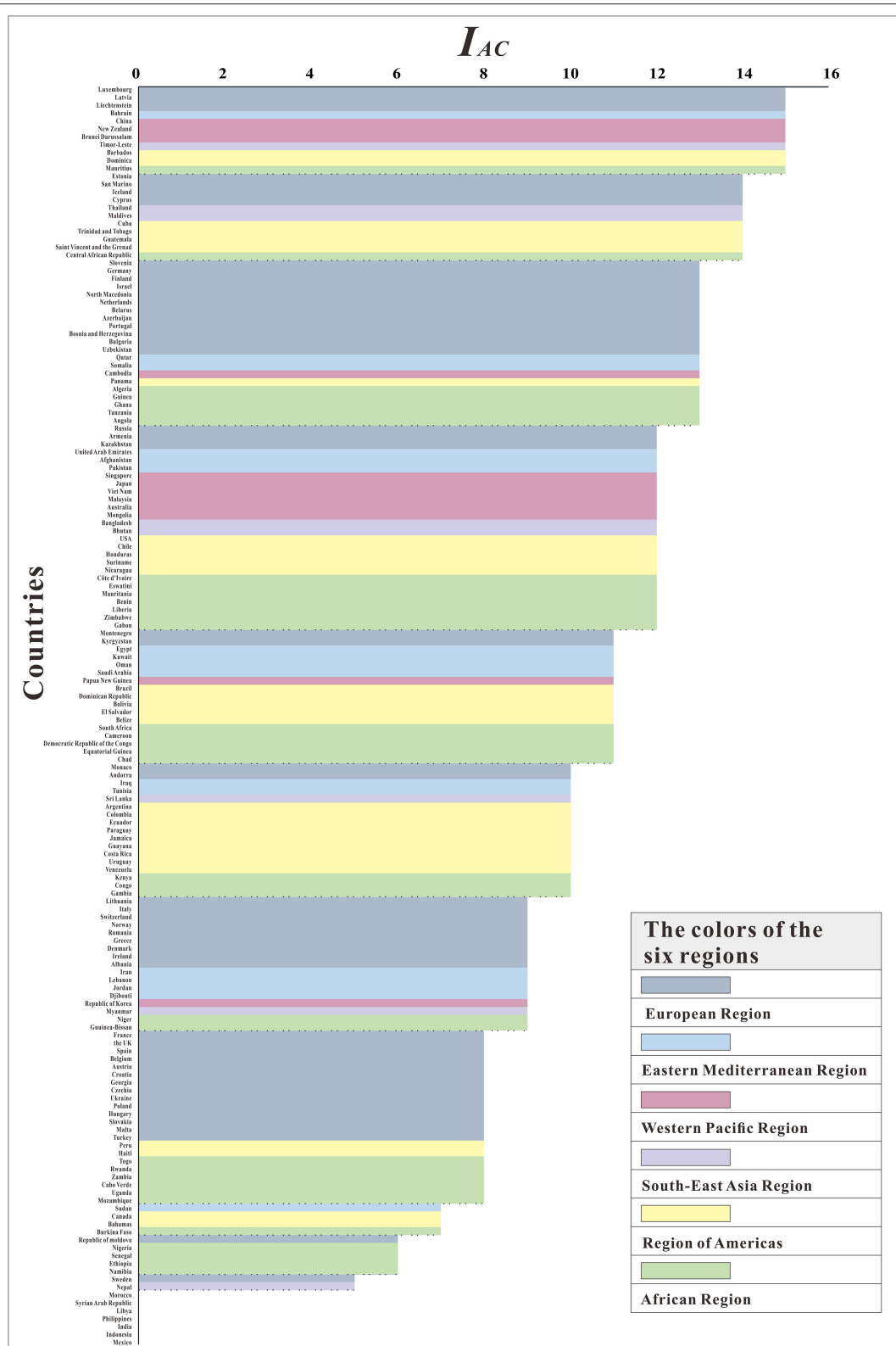


**FIGURE 8 |** The ranking of  $I_{AC}$  among 160 countries.

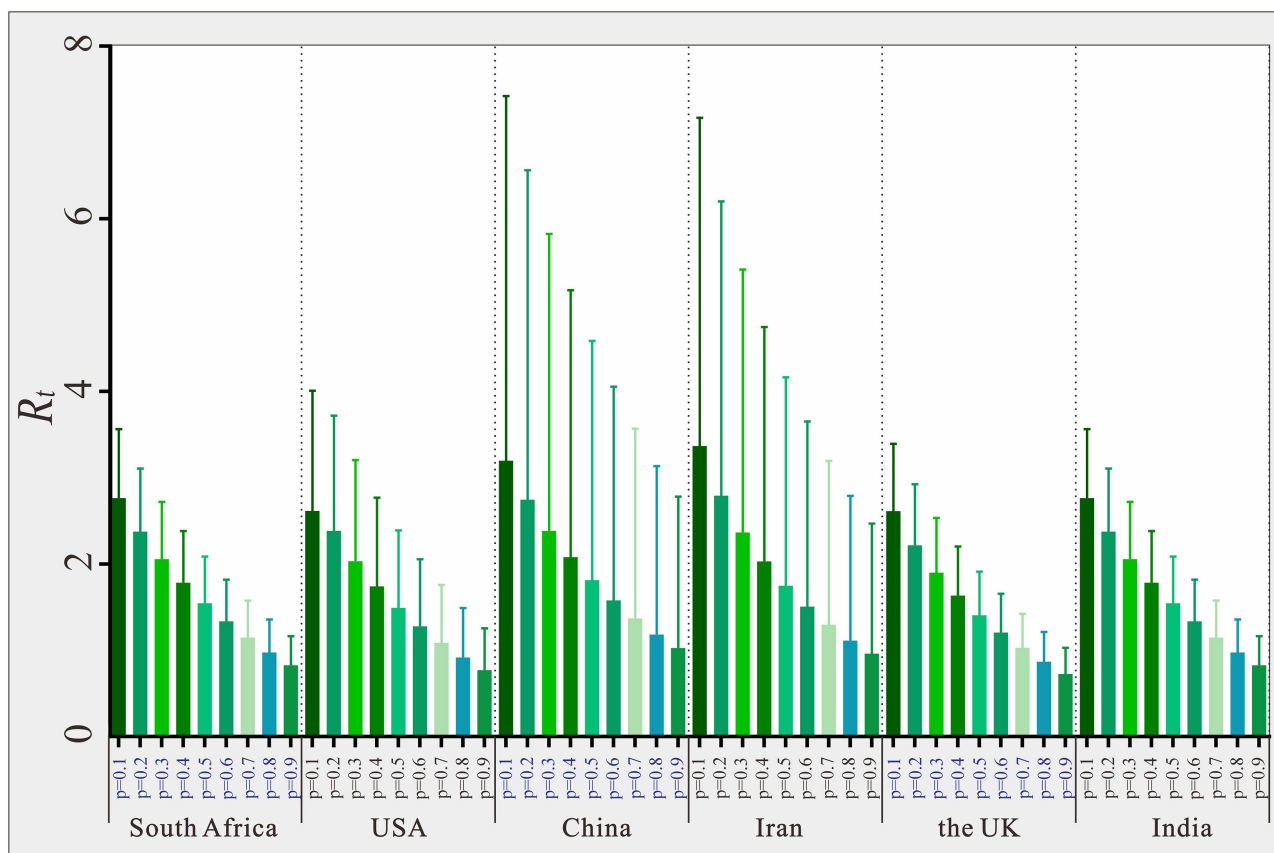


**FIGURE 9 |** Estimated  $R_t$  value based on different  $p$  in six selected countries in six WHO region.

of the African Region was not as good as that of other regions because of its weak healthcare system, which urgently needs to be improved.

The lack of effective interventions is a major driver of the pandemic. Moreover, the fact that the virus is an unknown, new mutant type may be a major factor for the current overwhelming increase in cases despite the preemptively implemented precautions and countermeasures taken by at-risk countries (6). In general, although countries in the Western Pacific region may not be able to control COVID-19 as well as those in the European Region, countries in the European Region have relatively weak continuous response and prevention and control, which is also one of the reasons for the repeated severe epidemics.

Of note, there are some limitations in our study, such as setting of  $p$  value as 0.2 in 160 countries, but we set the  $p$  value in the SEIAR model to the same value to ensure comparability among 160 countries. In practice, some asymptomatic patients may die because of the COVID-19 infection. This issue was not considered in our mathematical model and may probably affect the results slightly. However, it would not have a significant impact on our results considering that the mortality

of asymptomatic COVID-19 infection was much lower than that of symptomatic infection.

## DATA AVAILABILITY STATEMENT

The original contributions presented in the study are included in the article/**Supplementary Material**, further inquiries can be directed to the corresponding author/s.

## AUTHOR CONTRIBUTIONS

GH, TC, JR, and YN made substantial contributions to conception and design. QW, ZC, FX, WZha, ZZ, SL, and YW collected the data. JR, YN, YZ, MY, JX, XL, and WZhe conceived the experiments. JR, FX, QW, KC, YX, LX, SZ, TJ, BZ, YS, and TS conducted the experiments and analyzed the results. JR and QW wrote the manuscript. TC, GH, BZ, and YS revised it critically for important intellectual content. All authors approved the final manuscript and agreed to be accountable for all aspects of the work.



## FUNDING

This study was partly supported by the Bill & Melinda Gates Foundation (INV-005834). The funders had no role in the study design, data collection and analysis, and decision to publish.

## REFERENCES

- Li Q, Guan X, Wu P, Wang X, Zhou L, Tong Y, et al. Early transmission dynamics in Wuhan, China, of Novel Coronavirus-Infected Pneumonia. *N Engl J Med.* (2020) 1199–1207. doi: 10.1056/NEJMoa2001316
- Zhao S, Lin Q, Ran J, Musa SS, Yang G, Wang W, et al. Preliminary estimation of the basic reproduction number of novel coronavirus (2019-nCoV) in China, from 2019 to 2020: A data-driven analysis in the early phase of the outbreak. *Int J Infect Dis.* (2020) 92:214–7. doi: 10.1101/2020.01.23.916395
- Chattu VK, Yaya S, Emerging infectious diseases and outbreaks: implications for women's reproductive health and rights in resource-poor settings. *Reprod Health.* (2020) 17:43. doi: 10.1186/s12978-020-0899-y
- I.L. Organization. Almost 25 million jobs could be lost worldwide as a result of COVID-19, Says ILO. (2020). Available online at: [https://www.ilo.org/hanoi/Informationresources/Publicinformation/Pressreleases/WCMS\\_738992/lang--en/index.htm](https://www.ilo.org/hanoi/Informationresources/Publicinformation/Pressreleases/WCMS_738992/lang--en/index.htm)
- Iacus SM, Natale F, Santamaria C, Spyrtos S, Vespe M. Estimating and projecting air passenger traffic during the COVID-19 coronavirus outbreak and its socio-economic impact. *Safety Science.* (2020) 129:104791. doi: 10.1016/j.ssci.2020.104791
- Abduljalil JM, Abduljalil BM. Epidemiology, genome, and clinical features of the pandemic SARS-CoV-2: a recent view. *New Microbes New Infect.* (2020) 35:100672. doi: 10.1016/j.nmni.2020.100672
- C.A, Imai N, Dorigatti I, Baguelin M, Donnelly CA, Riley S, et al. Report 3: Transmissibility of 2019-nCoV. (2020). Available online at: <https://www.imperial.ac.uk/mrc-global-infection-disease-analysis/covid-19/report-3-transmissibility-of-covid-19/>
- Read JM, Bridgen JR, Cummings DA, Ho A, Jewell CP. Novel coronavirus 2019-nCoV: early estimation of epidemiological parameters and epidemic predictions. *Philos. Trans. R. Soc.* (2020) 365. doi: 10.1098/rstb.2020.0265
- Riou J, Althaus CL. Pattern of early human-to-human transmission of Wuhan 2019 novel coronavirus (2019-nCoV), December 2019 to January 2020. *Eurosurveillance.* (2020) 25:7–11. doi: 10.2807/1560-7917.ES.2020.25.4.2000058
- Shen M, Peng Z, Xiao Y, Zhang L. Modelling the epidemic trend of the 2019 novel coronavirus outbreak in China. *The Innovation.* (2020) 1:100048. doi: 10.1016/j.xinn.2020.100048
- Wu JT, Leung K, Leung GM. Nowcasting and forecasting the potential domestic and international spread of the 2019-nCoV outbreak originating in Wuhan, China: a modelling study. *Lancet.* (2020) 395:689–97. doi: 10.1016/S0140-6736(20)30260-9
- Luo L, Guo Z, Lei Z, Hu Q, Chen M, Chen F, et al. Epidemiology of tsutsugamushi disease and its relationship with meteorological factors in Xiamen city, China. *PLoS Negl Trop Dis.* (2020) 14:e0008772. doi: 10.1371/journal.pntd.0008772
- Sanche S, Lin YT, Xu C, Romero-Severson E, Hengartner N, Ke R. High contagiousness and rapid spread of severe acute respiratory syndrome coronavirus 2. *Emerg Infect Dis.* (2020) 26:1470–7. doi: 10.3201/eid2607.200282
- Kucharski AJ, Russell TW, Diamond C, Liu Y, Edmunds J, Funk S, et al. Early dynamics of transmission and control of COVID-19: a mathematical modelling study. *Lancet Infect Dis.* (2020) 20:553–8. doi: 10.1016/S1473-3099(20)30144-4
- Zhao ZY, Zhu YZ, Xu JW, Hu SX, Hu QQ, Lei Z, et al. A five-compartment model of age-specific transmissibility of SARS-CoV-2. *Infect Dis Poverty.* (2020) 9:117. doi: 10.1186/s40249-020-00735-x
- Lin SN, Rui J, Chen QP, Zhao B, Yu SS, Li ZY, et al. Effectiveness of potential antiviral treatments in COVID-19 transmission control: a modelling study. *Infect Dis Poverty.* (2021) 10:53. doi: 10.1186/s40249-021-00835-2
- U.N.D. PROGRAMME, Global Human Development Indicators. Available online at: <http://hdr.undp.org/en/2020-report>
- Chen TM, Rui J, Wang QP, Zhao ZY, Cui JA, Yin L. A mathematical model for simulating the phase-based transmissibility of a novel coronavirus. *Infect Dis Poverty.* (2020) 9:24. doi: 10.1186/s40249-020-00640-3
- Xuying Lao LL, Lei Z, Fang T, Chen Y, Liu Y, Ding K, et al. Epidemiological characteristics and the effectiveness of countermeasures to control coronavirus disease 2019 in Ningbo City, China. *Sci Rep.* (2021) 11:9545. doi: 10.1038/s41598-021-88473-4
- Mizumoto K, Kagaya K, Zarebski A, Chowell G. Estimating the asymptomatic proportion of coronavirus disease 2019 (COVID-19) cases on board the Diamond Princess cruise ship, Yokohama, Japan, 2020. *Eurosurveillance.* (2020) 25:2000180. doi: 10.2807/1560-7917.ES.2020.25.10.2000180
- Miura F, Matsuyama R, Nishiura H. Estimating the asymptomatic ratio of norovirus infection during foodborne outbreaks with laboratory testing in Japan. *J Epidemiol.* (2018) 28:382–7. doi: 10.2188/jea.JE20170040
- Lauer SA, Grantz KH, Bi Q, Jones FK, Zheng Q, Meredith HR, et al. The incubation period of coronavirus disease 2019 (COVID-19) from publicly reported confirmed cases: estimation and application. *Ann Intern Med.* (2020) 172:577–82. doi: 10.7326/M20-0504
- C.C.f.D.C.a. Prevention., Investigation and management guide for close contacts of novel coronavirus pneumonia case (Trial Version), 2020.
- Delamater PL, Street EL, Leslie TE, Yang YT, Jacobsen KH. Complexity of the Basic Reproduction Number (R0). *Emerg Infect Dis.* (2019) 25:1–4. doi: 10.3201/eid2501.171901
- Acter T, Uddin N, Das J, Akhter A, Choudhury TR, Kim S. Evolution of severe acute respiratory syndrome coronavirus 2 (SARS-CoV-2) as coronavirus disease 2019 (COVID-19) pandemic: A global health emergency. *Sci Total Environ.* (2020) 730:138996. doi: 10.1016/j.scitotenv.2020.138996
- Lai S, Ruktanonchai NW, Zhou L, Prosper O, Luo W, Floyd JR, et al. Tatem, Effect of non-pharmaceutical interventions to contain COVID-19 in China. *Nature.* (2020) 585:410–3. doi: 10.1038/s41586-020-2293-x
- Salzberger B, Gluck T, Ehrenstein B. Successful containment of COVID-19: the WHO-Report on the COVID-19 outbreak in China. *Infection.* (2020) 48:151–3. doi: 10.1007/s15010-020-01409-4
- Verity R, Okell LC, Dorigatti I, Winskill P, Whittaker C, Imai N, et al. Estimates of the severity of coronavirus disease 2019: a model-based analysis. *Lancet Infect Dis.* (2020). 20:669–77. doi: 10.1016/S1473-3099(20)30243-7
- Costs vs benefits of tackling COVID-19. *PharmacoEcon Outcomes News.* (2020) p. 852:1. doi: 10.1007/s40274-020-6760-2

**Conflict of Interest:** The authors declare that the research was conducted in the absence of any commercial or financial relationships that could be construed as a potential conflict of interest.

**Publisher's Note:** All claims expressed in this article are solely those of the authors and do not necessarily represent those of their affiliated organizations, or those of the publisher, the editors and the reviewers. Any product that may be evaluated in this article, or claim that may be made by its manufacturer, is not guaranteed or endorsed by the publisher.

Copyright © 2021 Niu, Rui, Wang, Zhang, Chen, Xie, Zhao, Lin, Zhu, Wang, Xu, Liu, Yang, Zheng, Chen, Xia, Xu, Zhang, Ji, Jin, Chen, Zhao, Su, Song, Chen and Hu. This is an open-access article distributed under the terms of the Creative Commons Attribution License (CC BY). The use, distribution or reproduction in other forums is permitted, provided the original author(s) and the copyright owner(s) are credited and that the original publication in this journal is cited, in accordance with accepted academic practice. No use, distribution or reproduction is permitted which does not comply with these terms.



# Development of an Early Warning Model for Predicting the Death Risk of Coronavirus Disease 2019 Based on Data Immediately Available on Admission

## OPEN ACCESS

### Edited by:

Reza Lashgari,  
Shahid Beheshti University, Iran

### Reviewed by:

Faris Hasan al Lami,  
University of Baghdad, Iraq  
Yuyong Jiang,  
Capital Medical University, China

### \*Correspondence:

Kai Qu  
joanne8601@163.com  
Chang Liu  
liuchangdoctor@163.com  
Jingyao Zhang  
you12ouy@163.com

<sup>†</sup>These authors have contributed  
equally to this work

### Specialty section:

This article was submitted to  
Infectious Diseases - Surveillance,  
Prevention and Treatment,  
a section of the journal  
Frontiers in Medicine

Received: 23 April 2021

Accepted: 16 July 2021

Published: 19 August 2021

### Citation:

Wang H, Ai H, Fu Y, Li Q, Cui R, Ma X,  
Ma Y-f, Wang Z, Liu T, Long Y, Qu K,  
Liu C and Zhang J (2021)  
Development of an Early Warning  
Model for Predicting the Death Risk of  
Coronavirus Disease 2019 Based on  
Data Immediately Available on  
Admission. *Front. Med.* 8:699243.  
doi: 10.3389/fmed.2021.699243

Hai Wang<sup>1†</sup>, Haibo Ai<sup>2†</sup>, Yunong Fu<sup>1</sup>, Qinglin Li<sup>1</sup>, Ruixia Cui<sup>1</sup>, Xiaohua Ma<sup>1</sup>, Yan-fen Ma<sup>3</sup>,  
Zi Wang<sup>1</sup>, Tong Liu<sup>1</sup>, Yunxiang Long<sup>1</sup>, Kai Qu<sup>1\*</sup>, Chang Liu<sup>1\*</sup> and Jingyao Zhang<sup>1,4\*</sup>

<sup>1</sup> Department of Hepatobiliary Surgery, The First Affiliated Hospital of Xi'an Jiaotong University, Xi'an, China, <sup>2</sup> Rehabilitation Medicine Department, The Third Hospital of Mianyang, Sichuan Mental Health Center, Mianyang, China, <sup>3</sup> Department of Clinical Laboratory, The First Affiliated Hospital of Xi'an Jiaotong University, Xi'an, China, <sup>4</sup> Department of Surgical ICU, The First Affiliated Hospital of Xi'an Jiaotong University, Xi'an, China

**Introduction:** COVID-19 has overloaded worldwide medical facilities, leaving some potentially high-risk patients trapped in outpatient clinics without sufficient treatment. However, there is still a lack of a simple and effective tool to identify these patients early.

**Methods:** A retrospective cohort study was conducted to develop an early warning model for predicting the death risk of COVID-19. Seventy-five percent of the cases were used to construct the prediction model, and the remaining 25% were used to verify the prediction model based on data immediately available on admission.

**Results:** From March 1, 2020, to April 16, 2020, a total of 4,711 COVID-19 patients were included in our study. The average age was  $63.37 \pm 16.70$  years, of which 1,148 (24.37%) died. Finally, age, SpO<sub>2</sub>, body temperature (T), and mean arterial pressure (MAP) were selected for constructing the model by univariate analysis, multivariate analysis, and a review of the literature. We used five common methods for constructing the model and finally found that the full model had the best specificity and higher accuracy. The area under the ROC curve (AUC), specificity, sensitivity, and accuracy of full model in train cohort were, respectively, 0.798 (0.779, 0.816), 0.804, 0.656, and 0.768, and in the validation cohort were, respectively, 0.783 (0.751, 0.815), 0.800, 0.616, and 0.755. Visualization tools of the prediction model included a nomogram and an online dynamic nomogram (<https://wanghai.shinyapps.io/dynnomapp/>).

**Conclusion:** We developed a prediction model that might aid in the early identification of COVID-19 patients with a high probability of mortality on admission. However, further research is required to determine whether this tool can be applied for outpatient or home-based COVID-19 patients.

**Keywords:** COVID-19, early warning, prediction model, death risk, visualization tools

## INTRODUCTION

Since the worldwide COVID-19 epidemic in 2019, up to now (2021/04/03), 129 million people had been infected, and 2.82 million people had died, and the number of confirmed patients with COVID-19 infection was continually growing by hundreds of thousands every day (1), leaving global medical institutions overburdened (2). Because of the substantial growth in COVID-19, several nations are experiencing serious shortages of regular hospital beds and ICU beds (3). As a result, a substantial proportion of COVID-19 patients were trapped in outpatient clinics or at home, unable to receive proper therapy (4); among these there were some patients with a potentially high risk of death. How to early and effectively identify a COVID-19 patient with a high risk of death is a major challenge we face. Although there are more than 100 prediction models about the prognosis of COVID-19 (5, 6), there are relatively few early warning models about the severity of COVID-19. Qing-Lei Gao built an early death risk prediction tool for COVID-19 through machine learning (7, 8). Although the model had high prediction accuracy, the modified model comprised 14 variables, the majority of which were laboratory indicators, making it hard to acquire useful indications immediately on admission. The effect of early warning (7) on admission could not be realized, and because this study did not provide a visual prediction tool, its operability was poor. Furthermore, several researchers investigated other scoring systems such as QSOFA, SOFA, early warning score (EWS), and national early warning Score 2 (NEWS 2) for early warning of the severity of patients with COVID-19. Among them, NEWS2 had a higher warning value for the severity of patients with COVID-19 (9–11). However, these studies about NEWS2 were with minimal sample size, and the score contains eight variables, which made it more difficult to use and affected its clinical application value.

To summarize, the current prediction model or prior illness severity scores were almost all that was required to get laboratory indicators and a large number of items. As a result, completing a COVID-19 severity evaluation and early warning in a timely manner is difficult. More importantly, no matter what prediction model or illness severity scores were used, they were all extremely inconvenient. Therefore, it is necessary to develop a more straightforward prediction tool for predicting the death risk of COVID-19.

## MATERIALS AND METHODS

### Study Design

A retrospective cohort study.

### Objective

To develop a simple and effective prediction model based on data immediately available on admission to early predict the death risk of COVID-19.

**Abbreviations:** COVID-19, Coronavirus disease 2019; T, body temperature; MAP, mean arterial pressure; AUC, area under the ROC curve; EWS, early warning score; COPD, chronic obstructive pulmonary disease; MFP model, multiple fractional multivariate models; stepwise model, stepwise selected model.

### Setting

Four hospitals in New York City.

### Data Source

The data in this study were shared by Altschul, David and stored in Dryad Database (<https://datadryad.org/stash/dataset/10.5061/dryad.7d7wm37sz>) (12–14).

### Diagnosis of COVID-19

SARS-CoV-2 RNA was detected by RT-PCR, and the positive patients were diagnosed as COVID-19 patients.

### Inclusion Criteria

- (a) Patients diagnosed as COVID-19 and older than 18 years old;
- (b) For patients admitted to hospital many times, only the last admission was included for analysis.

### Exclusion Criteria

- (a) Although the patient was evaluated in the emergency room, the patient was not admitted to the hospital;
- (b) Patients who died in the emergency room.

### Participants

From March 1, 2020, to April 16, 2020, patients infected with COVID-19 diagnosed by RT-PCR were collected. The follow-up ended on May 7, 2020, and the follow-up varied from 3 weeks to 80 days. Among them, a total of 4,711 cases confirmed by COVID-19 met the inclusion and exclusion criteria and were included in this study.

### Ethics Statement

New ethics approval was not applicable because the original author had obtained ethical approval when conducting this study. Permission to participate was also not appropriate because our review was a retrospective study of data reuse, and the message of the patients was anonymous.

### Data Immediately Available on Admission Included

- (a) Demographic data only include age and race, while other relevant data were not provided in the data set, so it could not be included in our study for further analysis;
- (b) Past medical history included myocardial infarction, congestive heart failure, cerebrovascular disease, diabetes, dementia, and chronic obstructive pulmonary disease (COPD);
- (c) The vital signs at admission include SpO<sub>2</sub>, mean arterial pressure (MAP), and body temperature (T). All the above variables were collected on admission.

### Collection of Outcome Indicators

Death-related data were collected through hospital death registration and deaths in the national death registry.

### Selection of Predictor Variables

The following three ways were used to select the variables for the model construction and then construct the corresponding models: (a) All variables that can be obtained immediately on admission were included in the construction and verification of

the prediction model; (b) All variables that could be obtained immediately on admission were included in multivariate analysis, and variables with  $P$ -value  $<0.05$  were included in the construction and verification of the model; (c) According to the literature review, we further constructed a more concise prediction model.

## Statistical Analysis

(a) Mean  $\pm$  S.D ( $\bar{x} \pm s$ ) was used for measurement data, while  $n$  (%) was used for counting data. (b) Seventy-five percent of the sample size was used to construct the prediction model, and the remaining 25% was used to verify the prediction model. (c) The following methods were used to construct and verify the prediction model, including multiple fractional multivariate models (MFP model), full model, stepwise selected model (stepwise model), bootstrap full (bootstrap resampling 500 times), and bootstrap stepwise (bootstrap resampling 500 Times). (d) The corresponding nomogram was constructed based on the best model described above, and then we used the “DynNom” package to construct a corresponding online dynamic nomogram (15). (e) The missing value of variables included in our study was very few, so there was no special handling of the missing values during model building. Statistical analysis was performed using Empower Stats version 2020 epidemiology software (www.empowerstats.com) and R software.

## RESULTS

### The Clinical Characteristics of Patients

This study comprised 4,711 verified COVID-19 patients who satisfied the inclusion and exclusion criteria. The patients' mean age of the patients was  $63.37 \pm 16.70$  years old, and the races of Black, White, Asian, and Latino were 1,743 (37.00%), 466 (9.89%), 121 (2.57%), and 1,753 (37.21%), respectively, and their SpO<sub>2</sub> was  $92.89 \pm 8.11\%$ , T was  $37.31 \pm 0.90^\circ\text{C}$ , in which those complicated with myocardial infarction, congestive heart failure, cerebrovascular disease, diabetes, dementia, and COPD were, respectively, 201 (4.27%), 541 (11.48%), 506 (10.74%), 686 (14.56%), 372 (7.90%), and 265 (5.63%), and death cases were 1,148 (24.37%) (See Table 1).

### Univariate Analysis Results

Univariate analysis was performed for the following variables: age, SpO<sub>2</sub>, MAP, T, black, Asian, White, Latino, myocardial infarction, congestive heart failure, cerebrovascular disease, diabetes, dementia, and COPD. Univariate analysis showed that age, SpO<sub>2</sub>, MAP, White and COPD were shown to be associated with patient prognosis, with OR values of 1.051 (1.045, 1.056), 0.946 (0.938, 0.954), 0.947 (0.943, 0.952), 1.286 (1.040, 1.591), and 1.368 (1.043, 1.794) (See Table 2).

### The Result of Multivariate Logistic Regression Analysis

Multivariate logistic regression analysis was performed for the following variables: age, SpO<sub>2</sub>, MAP, T, black, Asian, white, Latino, myocardial infarction, congestive heart failure, cerebrovascular disease, diabetes, dementia, and COPD. The

**TABLE 1 |** The clinical characteristics of patients.

| Patient characteristics            | Mean $\pm$ SD/N (%) |
|------------------------------------|---------------------|
| Age, year                          | 63.37 $\pm$ 16.70   |
| SpO <sub>2</sub> , %               | 92.89 $\pm$ 8.19    |
| Mean arterial pressure (MAP), mmHg | 85.79 $\pm$ 16.81   |
| Temperature, $^\circ\text{C}$      | 37.31 $\pm$ 0.90    |
| <b>Race</b>                        |                     |
| Black, $n$ (%)                     | 1,743 (37.00%)      |
| White, $n$ (%)                     | 466 (9.89%)         |
| Asian, $n$ (%)                     | 121 (2.57%)         |
| Latino, $n$ (%)                    | 1,753 (37.21%)      |
| Myocardial infarction, $n$ (%)     | 201 (4.27%)         |
| Congestive heart failure, $n$ (%)  | 541 (11.48%)        |
| Cerebrovascular disease, $n$ (%)   | 506 (10.74%)        |
| Diabetes, $n$ (%)                  | 686 (14.56%)        |
| Dementia, $n$ (%)                  | 372 (7.90%)         |
| COPD, $n$ (%)                      | 265 (5.63%)         |
| Death                              | 1,148 (24.37%)      |

multivariate logistic regression analysis revealed that age, SpO<sub>2</sub>, MAP, T, and Asian were associated with the prognosis of patients with COVID-19, and their OR values were, respectively, 1.052 (1.046, 1.058), 0.954 (0.945, 0.963), 0.952 (0.947, 0.957), 1.109 (1.015, 1.211), and 1.788 (1.109, 2.883) (See Table 2).

### The Construction and Verification of the Prediction Model

Seventy-five percent of the sample was used to construct the prediction model: (1) Firstly, age, SpO<sub>2</sub>, MAP, T, Black, Asian, White, Latino, myocardial infarction, congestive heart failure, cerebrovascular disease, diabetes, dementia, and COPD were all included for constructing the prediction model. The AUC of MFP model, full model, stepwise model, bootstrap full, and bootstrap stepwise were, respectively, 0.828 (0.8115, 0.845), 0.802 (0.784, 0.821), 0.802 (0.783, 0.820), 0.802 (0.784, 0.821), and 0.802 (0.783, 0.820). (2) Secondly, according to the results of multivariate logistic regression analysis, age, SpO<sub>2</sub>, MAP, T, and Asian were included for constructing the prediction model, and its AUC of MFP model, full model, stepwise model, bootstrap full, and bootstrap stepwise were, respectively, 0.827 (0.811, 0.844), 0.800 (0.782, 0.819), 0.800 (0.782, 0.819), 0.800 (0.782, 0.819), and 0.800 (0.782, 0.819). (3) Finally, age, SpO<sub>2</sub>, MAP, and T were included for constructing the prediction model, and the AUC of MFP model, full model, stepwise model, bootstrap full, and bootstrap stepwise were, respectively, 0.825 (0.808, 0.841), 0.798 (0.779, 0.816), 0.798 (0.779, 0.816), 0.798 (0.779, 0.816) and 0.798 (0.779, 0.816) (See Table 3; Figure 1).

The remaining 25% was used to verify the prediction model: (1) Firstly, age, SpO<sub>2</sub>, MAP, T, Black, Asian, White, Latino, myocardial infarction, congestive heart failure, cerebrovascular disease, diabetes, dementia, and COPD all were included for verifying the prediction model, and its AUC of MFP model, full model, stepwise model, bootstrap full, and bootstrap stepwise



**TABLE 2 |** The results of univariate analysis and multivariate logistic regression analysis.

| Exposure                                      | Univariate,<br>OR (95% CI), <i>P</i> | Multivariate,<br>OR (95% CI), <i>P</i> |
|---|--------------------------------------|--|
| Age, year                                     | 1.051 (1.045, 1.056), <0.001         | 1.052 (1.046, 1.058), <0.001           |
| SpO <sub>2</sub> , %                          | 0.946 (0.938, 0.954), <0.001         | 0.954 (0.945, 0.963), <0.001           |
| MAP, mmHg                                     | 0.947 (0.943, 0.952), <0.001         | 0.952 (0.947, 0.957), <0.001           |
| Temperature, °C                               | 1.039 (0.965, 1.120), 0.310          | 1.109 (1.015, 1.211), 0.022            |
| <b>Black, <i>n</i> (%)</b>                    |                                      |  |
| No  | Reference                            | Reference                              |
| Yes   | 0.920 (0.801, 1.057), 0.239          | 0.953 (0.765, 1.188), 0.671            |
| <b>White, <i>n</i> (%)</b>                    |                                      |  |
| No  | Reference                            | Reference                              |
| Yes   | 1.286 (1.040, 1.591), 0.020          | 0.849 (0.634, 1.137), 0.272            |
| <b>Asian, <i>n</i> (%)</b>                    |                                      |  |
| No  | Reference                            | Reference                              |
| Yes   | 1.435 (0.972, 2.120), 0.069          | 1.788 (1.109, 2.883), 0.017            |
| <b>Latino, <i>n</i> (%)</b>                   |                                      |  |
| No  | Reference                            | Reference                              |
| Yes   | 0.896 (0.780, 1.029), 0.120          | 0.848 (0.683, 1.054), 0.137            |
| <b>Myocardial infarction, <i>n</i> (%)</b>    |                                      |  |
| No  | Reference                            | Reference                              |
| Yes   | 1.117 (0.810, 1.540), 0.450          | 1.065 (0.674, 1.683), 0.786            |
| <b>Congestive heart failure, <i>n</i> (%)</b> |                                      |  |
| No  | Reference                            | Reference                              |
| Yes   | 1.219 (0.997, 1.491), 0.053          | 1.108 (0.844, 1.455), 0.458            |
| <b>Cerebrovascular disease, <i>n</i> (%)</b>  |                                      |  |
| No  | Reference                            | Reference                              |
| Yes   | 1.121 (0.908, 1.383), 0.288          | 0.881 (0.673, 1.152), 0.354            |
| <b>Diabetes, <i>n</i> (%)</b>                 |                                      |  |
| No  | Reference                            | Reference                              |
| Yes   | 1.008 (0.835, 1.217), 0.936          | 0.897 (0.684, 1.177), 0.432            |
| <b>Dementia, <i>n</i> (%)</b>                 |                                      |  |
| No  | Reference                            | Reference                              |
| Yes   | 1.207 (0.952, 1.531), 0.121          | 1.114 (0.832, 1.492), 0.469            |
| <b>COPD, <i>n</i> (%)</b>                     |                                      |  |
| No  | Reference                            | Reference                              |
| Yes   | 1.368 (1.043, 1.794), 0.024          | 1.154 (0.829, 1.605), 0.396            |

were, respectively, 0.804 (0.774, 0.835), 0.782 (0.750, 0.814), 0.780 (0.748, 0.812), 0.782 (0.750, 0.814), and 0.779 (0.747, 0.810). (2) Secondly, age, SpO<sub>2</sub>, MAP, T, and Asian were included for verifying the prediction model, and its AUC of MFP model, full model, stepwise model, bootstrap full, and bootstrap stepwise were, respectively, 0.806 (0.776, 0.837), 0.782 (0.751, 0.814), 0.782 (0.751, 0.814), 0.783 (0.751, 0.814), and 0.782 (0.750, 0.814). (3) Finally, age, SpO<sub>2</sub>, MAP, and T were included for verifying the prediction model, and the AUC of MFP model, full model, stepwise model, bootstrap full, and bootstrap stepwise were, respectively, 0.807 (0.776, 0.838), 0.783 (0.751, 0.815), 0.783 (0.751, 0.815), 0.783 (0.751, 0.815), and 0.783 (0.751, 0.815). The calibration curve of the full model for the training cohort and validation cohort showed that predicted probability > observed probability (See **Table 3**; **Figures 1, 2**).

**TABLE 3 |** The construction and validation of prediction model.

| Model                    | AUC                   | Specificity | Sensitivity | Accuracy |
|--------------------------|-----------------------|-------------|-------------|----------|
| <b>METHOD 1</b>          |                       |             |             |          |
| <b>Training cohort</b>   |                       |             |             |          |
| MFP model                | 0.828 (0.8115, 0.845) | 0.761       | 0.734       | 0.755    |
| Full model               | 0.802 (0.784, 0.821)  | 0.809       | 0.658       | 0.772    |
| Stepwise model           | 0.802 (0.783, 0.820)  | 0.789       | 0.677       | 0.762    |
| Bootstrap full           | 0.802 (0.784, 0.821)  | 0.813       | 0.652       | 0.774    |
| Bootstrap stepwise       | 0.802 (0.783, 0.820)  | 0.794       | 0.674       | 0.765    |
| <b>Validation cohort</b> |                       |             |             |          |
| MFP model                | 0.804 (0.774, 0.835)  | 0.721       | 0.736       | 0.724    |
| Full model               | 0.782 (0.750, 0.814)  | 0.815       | 0.590       | 0.760    |
| Stepwise model           | 0.780 (0.748, 0.812)  | 0.864       | 0.540       | 0.784    |
| Bootstrap full           | 0.782 (0.750, 0.814)  | 0.807       | 0.598       | 0.756    |
| Bootstrap stepwise       | 0.779 (0.747, 0.810)  | 0.815       | 0.580       | 0.757    |
| <b>METHOD 2</b>          |                       |             |             |          |
| <b>Training cohort</b>   |                       |             |             |          |
| MFP model                | 0.827 (0.811, 0.844)  | 0.760       | 0.733       | 0.753    |
| Full model               | 0.800 (0.782, 0.819)  | 0.790       | 0.673       | 0.762    |
| Stepwise model           | 0.800 (0.782, 0.819)  | 0.790       | 0.673       | 0.762    |
| Bootstrap full           | 0.800 (0.782, 0.819)  | 0.789       | 0.674       | 0.761    |
| Bootstrap stepwise       | 0.800 (0.782, 0.819)  | 0.796       | 0.668       | 0.765    |
| <b>Validation cohort</b> |                       |             |             |          |
| MFP model                | 0.806 (0.776, 0.837)  | 0.730       | 0.732       | 0.731    |
| Full model               | 0.782 (0.751, 0.814)  | 0.800       | 0.612       | 0.754    |
| Stepwise model           | 0.782 (0.751, 0.814)  | 0.800       | 0.612       | 0.754    |
| Bootstrap full           | 0.783 (0.751, 0.814)  | 0.792       | 0.620       | 0.749    |
| Bootstrap stepwise       | 0.782 (0.750, 0.814)  | 0.793       | 0.620       | 0.750    |
| <b>METHOD 3</b>          |                       |             |             |          |
| <b>Training cohort</b>   |                       |             |             |          |
| MFP model                | 0.825 (0.808, 0.841)  | 0.770       | 0.721       | 0.759    |
| Full model               | 0.798 (0.779, 0.816)  | 0.804       | 0.656       | 0.768    |
| Stepwise model           | 0.798 (0.779, 0.816)  | 0.804       | 0.656       | 0.768    |
| Bootstrap full           | 0.798 (0.779, 0.816)  | 0.797       | 0.663       | 0.765    |
| Bootstrap stepwise       | 0.798 (0.779, 0.816)  | 0.803       | 0.658       | 0.768    |
| <b>Validation cohort</b> |                       |             |             |          |
| MFP model                | 0.807 (0.776, 0.838)  | 0.743       | 0.728       | 0.740    |
| Full model               | 0.783 (0.751, 0.815)  | 0.800       | 0.616       | 0.755    |
| Stepwise model           | 0.783 (0.751, 0.815)  | 0.800       | 0.616       | 0.755    |
| Bootstrap full           | 0.783 (0.751, 0.815)  | 0.799       | 0.616       | 0.754    |
| Bootstrap stepwise       | 0.783 (0.751, 0.815)  | 0.799       | 0.616       | 0.754    |

*The variables of method 1: age, SpO<sub>2</sub>, MAP, temperature, Black, White, Asian, Latino, myocardial infarction, congestive heart failure, cerebrovascular disease, diabetes, dementia and COPD; the variables of method 2: age, SpO<sub>2</sub>, MAP, temperature and Asian; the variables of method 3: age, SpO<sub>2</sub>, MAP and temperature.*

## Visualization Tool Construction

We discovered that the prediction model constructed by age, SpO<sub>2</sub>, MAP, and T had a similar predictive value comparing with the prediction model constructed by other variables. Further, we found that the full model had the highest specificity and similar accuracy, as compared with MFP model, stepwise model, bootstrap full, and bootstrap

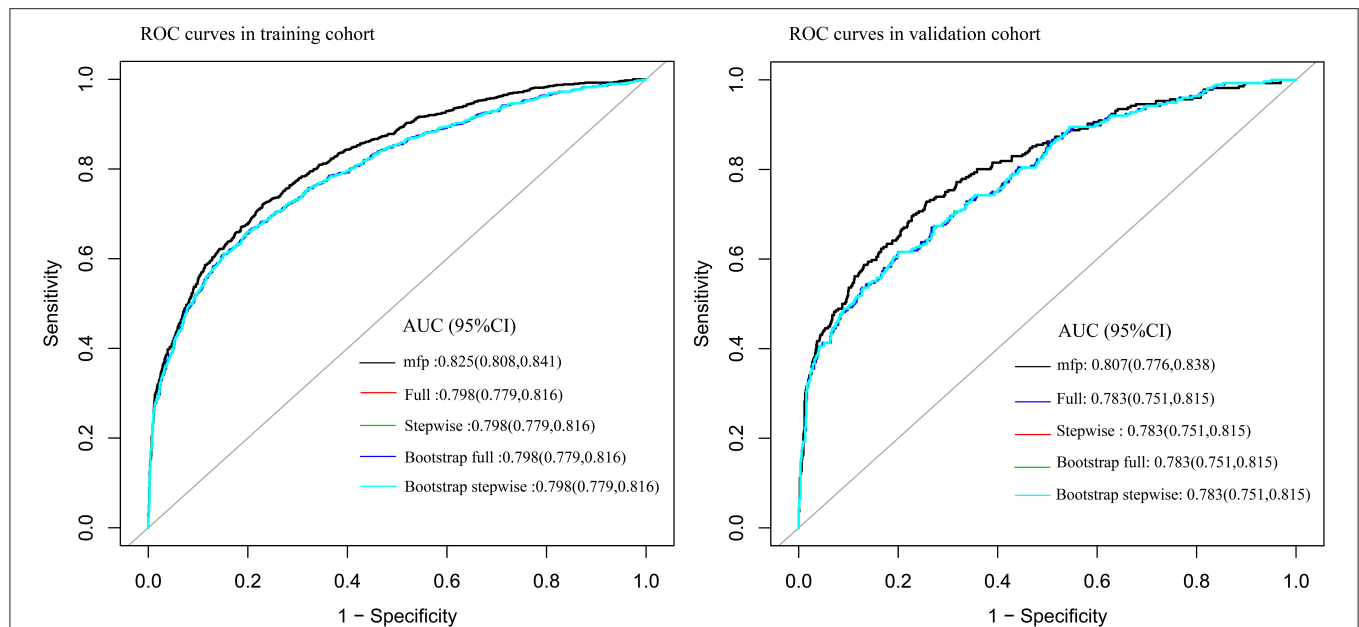


**FIGURE 1 |** The ROC curve of the predictive model in training cohort and validation cohort.

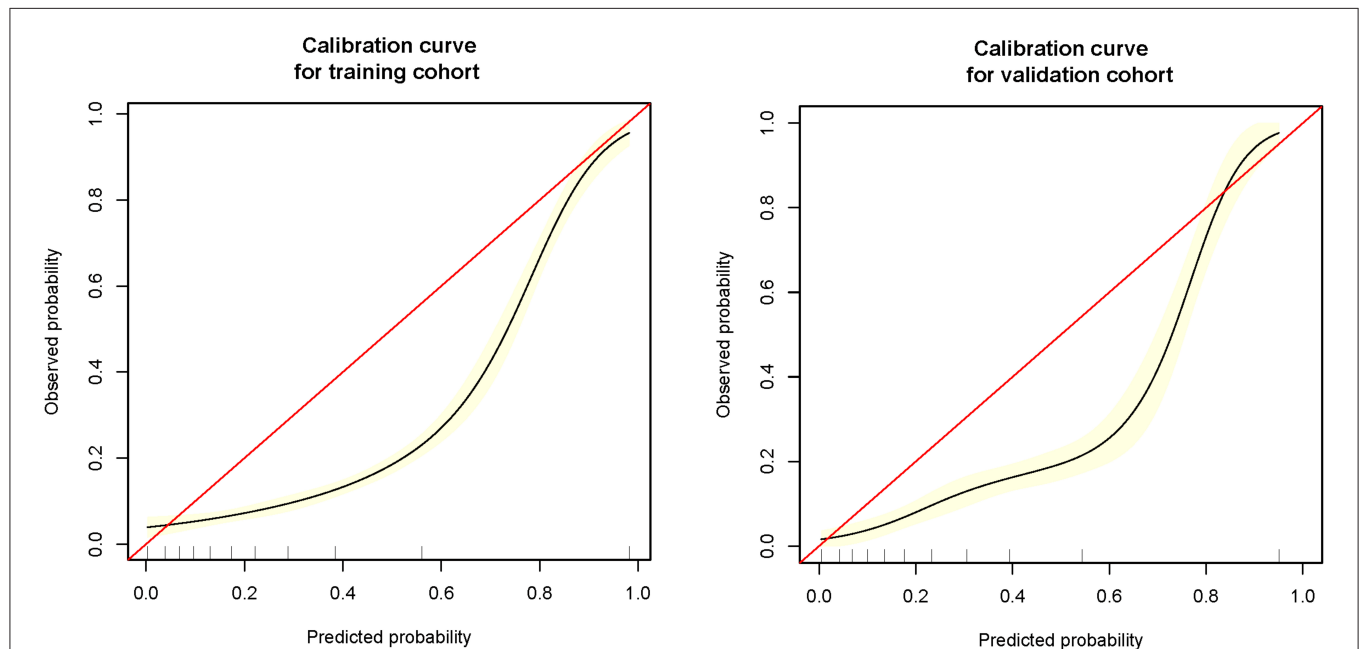


**FIGURE 2 |** The nomogram of the full model.

stepwise. As a result, we chose the Full model as our target prediction model. According to this model, the corresponding nomogram was constructed, and then we used the “DynNom” package to construct a corresponding online dynamic nomogram (<https://wanghai.shinyapps.io/dynnomapp/>) (See Table 3; Figure 3).

## DISCUSSION

We constructed a prediction model with high predictive value through age, SpO<sub>2</sub>, MAP, and T, and most important was that the model had high specificity and was simple and easy to be used. All the variables included in the prediction model: age, SpO<sub>2</sub>,

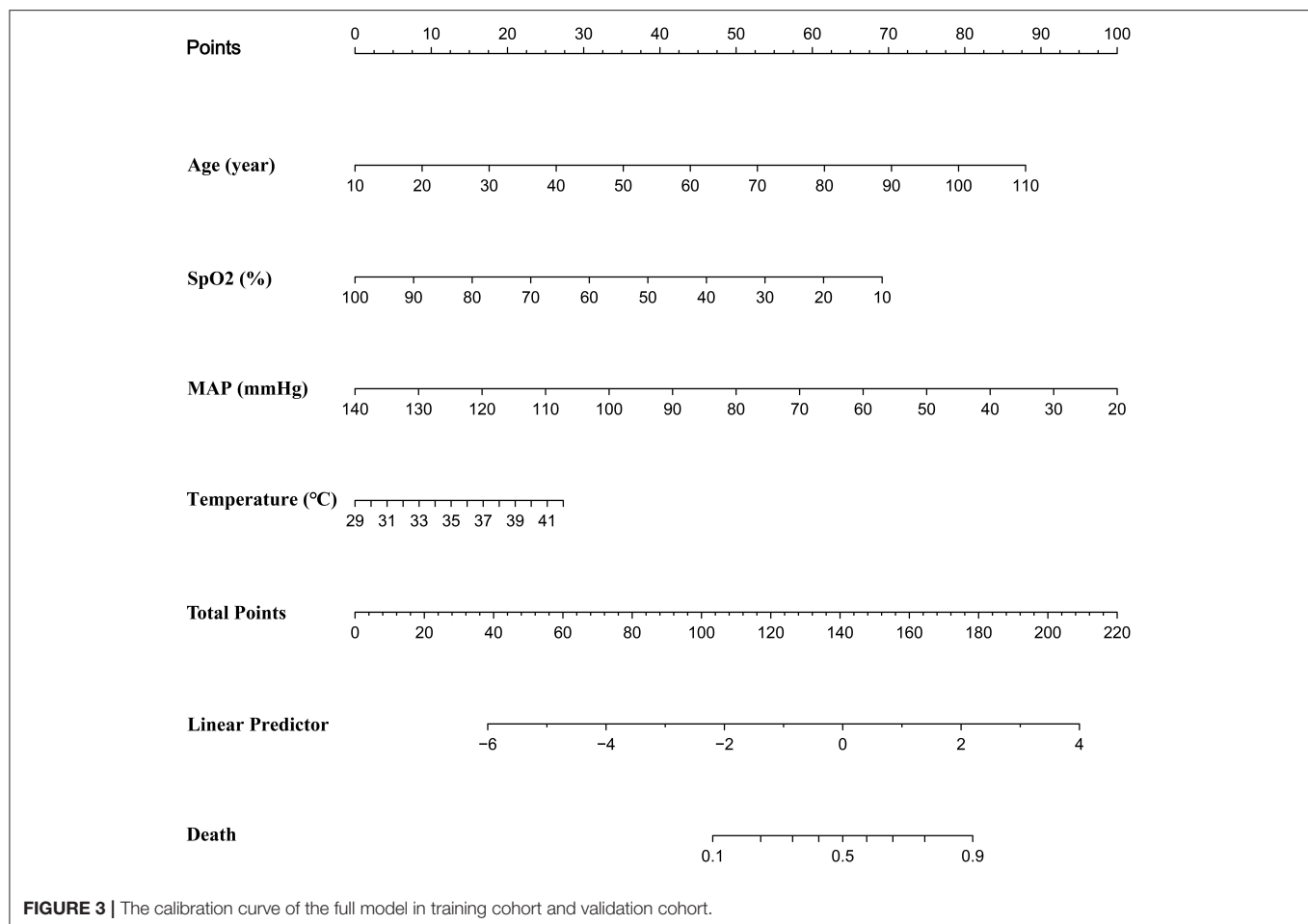


**FIGURE 3 |** The calibration curve of the full model in training cohort and validation cohort.

MAP, and T were confirmed to be closely related to the prognosis of COVID-19.

According to some researches, variations in COVID-19 mortality risks across various ethnic groups might be due to economic and cultural differences (16). However, because the data set lacked information on the economy and culture, it was difficult to modify the associated factors to establish whether Asians' death risks were indeed higher than those of other ethnic groups. Furthermore, research has indicated that Asians' death risk is not higher than that of other ethnic groups (17). For the reasons stated above, we did not include Asians as a variable in the prediction model's construction and validation.

A large number of studies had found that age was an independent risk for COVID-19 mortality. In Wuhan, a two-way cohort study involving 548 COVID-19 patients (including 269 severe cases) discovered that the older the patients, the higher the risk of COVID-19 severity and fatality (18). Another study, which included 221 COVID-19 infected individuals, systematically explored the relationship between age and clinical manifestations and prognosis of COVID-19. The study found that elderly patients were more likely to be complicated by bacterial infection, and that the severity of the disease was associated with lower serum albumin levels, higher urea nitrogen levels, higher lactate dehydrogenase levels, and higher inflammatory factors levels, as

well as the use of glucocorticoid and ventilator-assisted therapy (19). According to Massimo Volpe's research, the elderly patients had a higher Charlson comorbidity index and higher mortality (20). Wenru Su et al. discovered that SARS-CoV-2 susceptibility gene expression in circulating immune cells increased, as did immune system abnormalities in older individuals (21). To summarize, the elderly patients often had more complications, more likely to be complicated with bacterial infection and hypoproteinemia, immune disorders, and more severity and higher mortality. In this study, the higher the age, the higher the death of patients, consistent with the above studies.

COVID-19 mostly harmed the respiratory system, with acute respiratory distress syndrome being a deadly consequence (22, 23). Ruiguang Zhang et al. found that patients with hypoxemia ( $\text{SpO}_2 < 90\%$ ) had higher levels of IL-6, IL-10, LDH, and C-reactive protein and higher mortality. The above results were consistent with our study.

MAP was one of the indexes reflecting tissue perfusion. A large number of studies showed that MAP on admission was strongly connected to the prognosis of patients. The higher the MAP on admission, the lower the risk of mortality (13, 24).

One of the most prevalent signs of COVID-19 was fever. Dong Chen et al. discovered that around 36% of COVID-19-infected hospitalized patients had a fever, and the greater their

body temperature, the worse their prognosis (25). Furthermore, Yongxi Zhang et al. also found that patients with refractory COVID-19 had higher body temperature (26).

To sum up, the variables included in the early warning model: age, SpO<sub>2</sub>, MAP, and T had been widely confirmed to be closely related to the prognosis of COVID-19, which were also consistent with our research results, so it was reasonable to use the four variables to construct the prediction model.

When compared to previously published prediction models (such as EWS, NEWS2), our prediction model was with relatively low predictive value for the severity of patients with COVID-19. However, these prediction models were with more variables, and meanwhile these variables cannot be obtained in a short time, which made them more difficult to use (9–11). Therefore, these models were not suitable for early warning of COVID-19 severity. However, our model still couldn't instead of these models for subsequent prediction of COVID-19 patients' prognosis. In clinical applications, we might utilize our model for early warning while also combining it with other models to minimize further delays in identifying severely unwell patients.

## The Application Value of This Model

(a) Firstly, we constructed a straightforward prediction tool, besides the traditional nomogram, and we also built a web version of the prediction tool to help doctors or patients predict the death risk of COVID-19 anytime and anywhere. (b) The variables involved in the model of this study could be obtained in a few minutes, without waiting for the laboratory test results for a long time, and could achieve the death risk of COVID-19 at an early stage. (c) The prediction model of our study had high specificity and relatively low sensitivity, which was helpful for doctors to identify those patients with a high risk of death at an early stage, optimize the allocation of medical resources, and alleviate the current shortage of medical resources. (d) The calibration curve showed that the predicted probability was greater than the observed probability in the training cohort and validation cohort. Although our model overestimated the risk of disease (27), our model would be beneficial for physicians to prepare in advance for patients who were likely to develop into severe diseases, and finally improve patients' prognosis. (e) Dynamic Nomogram is a web-based application (28) that integrates measures of AGE, SpO<sub>2</sub>, T, and MAP. We may use the mouse to choose values of the above four variables and then click the Predict button to calculate the probability of mortality in COVID patients.

## REFERENCES

1. WHO Coronavirus (COVID-19) Dashboard WHO Coronavirus (COVID-19) Dashboard With Vaccination Data. (2021). Available online at: <https://covid19.who.int/> (accessed April 03, 2021).
2. Han E, Tan MM, Turk E, Sridhar D, Leung GM, Shibuya K, et al. Lessons learnt from easing COVID-19 restrictions: an analysis of countries and regions in asia pacific and Europe. *Lancet*. (2020) 396:1525–34. doi: 10.1016/S0140-6736(20)32007-9
3. An C, Lim H, Kim D-W, Chang JH, Choi YJ, Kim SW. Machine learning prediction for mortality of patients diagnosed with COVID-19: a nationwide Korean cohort study. *Sci Rep*. (2020) 10:18716. doi: 10.1038/s41598-020-75767-2

## Limitations of Research

(a) Since this study was a retrospective study, further prospective studies would be needed to verify the predictive value of our prediction model. (b) All the cases included in this study were hospitalized patients, which might lead to the limitation of its application population. (c) Our study lacked verification of external validity, the adaptive scope of the model in this study needed to be further verified. Meanwhile, the model in this study needed to be applied cautiously.

## CONCLUSION

We developed a prediction model that might aid in the early identification of COVID-19 patients with a high probability of mortality on admission. However, further research is required to determine whether this tool can be applied for outpatient or home-based COVID-19 patients.

## DATA AVAILABILITY STATEMENT

The datasets presented in this study can be found in online repositories. The names of the repository/repositories and accession number(s) can be found below: 10.5061/dryad.7d7wm37sz.

## AUTHOR CONTRIBUTIONS

HW conceived of the study and drafted the manuscript. HA, YF, QL, and RC participated in the statistical analysis. XM, Y-fM, ZW, TL, and YL participated the design of the study. KQ, CL, and JZ participated in its design and coordination and helped to draft the manuscript. All authors contributed to the article and approved the submitted version.

## FUNDING

Basic Research Program of Natural Science of Shaanxi Province Youth programs, funding number: 2020JQ-548.

## ACKNOWLEDGMENTS

Thank you for Altschul, David sharing the data in the dryad database.



- for COVID-19. *Nat Commun.* (2020) 11:5033. doi: 10.1038/s41467-020-18684-2
8. Bai Z, Gong Y, Tian X, Cao Y, Liu W, Li J. The rapid assessment and early warning models for COVID-19. *Viol Sin.* (2020) 35:272–9. doi: 10.1007/s12250-020-00219-0
  9. Su Y, Ju M-J, Xie R-C, Yu S-J, Zheng J-L, Ma G-G, et al. Prognostic accuracy of early warning scores for clinical deterioration in patients with COVID-19. *Front Med.* (2020) 7:624255. doi: 10.3389/fmed.2020.624255
  10. Covino M, Sandroni C, Santoro M, Sabia L, Simeoni B, Bocci MG, et al. Predicting intensive care unit admission and death for COVID-19 patients in the emergency department using early warning scores. *Resuscitation.* (2020) 156:84–91. doi: 10.1016/j.resuscitation.2020.08.124
  11. Myrstad M, Ihle-Hansen H, Tveita AA, Andersen EL, Nygård S, Tveit A, et al. National early warning score 2 (NEWS2) on admission predicts severe disease and in-hospital mortality from Covid-19 - a prospective cohort study. *Scand J Trauma Resusc Emerg Med.* (2020) 28:66. doi: 10.1186/s13049-020-00764-3
  12. Eskandar EN, Altschul DJ, de la Garza Ramos, Rafael, Cezayirli P, Unda SR, et al. Neurologic syndromes predict higher in-hospital mortality in COVID-19. *Neurology.* (2021) 96:e1527–38. doi: 10.1212/WNL.00000000000011356
  13. Altschul DJ, Unda SR, Benton J, de la Garza Ramos, Rafael, Cezayirli P, et al. A novel severity score to predict inpatient mortality in COVID-19 patients. *Sci Rep.* (2020) 10:16726. doi: 10.1038/s41598-020-73962-9
  14. Altschul, David. *Neurologic Complications of COVID-19, Dryad, Dataset.* (2021). Available online at: <https://doi.org/10.5061/dryad.7d7wm37sz> (accessed February 01, 2021).
  15. Ding Y, Jiang R, Chen Y, Jing J, Yang X, Wu X, et al. Comparing the characteristics and predicting the survival of patients with head and neck melanoma versus body melanoma: a population-based study. *BMC Cancer.* (2021) 21:420. doi: 10.1186/s12885-021-08105-y
  16. Townsend MJ, Kyle TK, Stanford FC. Outcomes of COVID-19: disparities in obesity and by ethnicity/race. *Int J Obes.* (2020) 44:1807–9. doi: 10.1038/s41366-020-0635-2
  17. Webb Hooper M, Nápoles AM, Pérez-Stable EJ. COVID-19 and racial/ethnic disparities. *JAMA.* (2020) 323:2466–7. doi: 10.1001/jama.2020.8598
  18. Li X, Xu S, Yu M, Wang K, Tao Y, Zhou Y, et al. Risk factors for severity and mortality in adult COVID-19 inpatients in Wuhan. *J Allergy Clin Immunol.* (2020) 146:110–8. doi: 10.1016/j.jaci.2020.04.006
  19. Liu Y, Mao B, Liang S, Yang J-W, Lu H-W, Chai Y-H, et al. Association between age and clinical characteristics and outcomes of COVID-19. *Eur Respir J.* (2020) 55:2001112. doi: 10.1183/13993003.01112-2020
  20. Iaccarino G, Grassi G, Borghi C, Ferri C, Salvetti M, Volpe M. Age and multimorbidity predict death among COVID-19 patients: results of the SARS-RAS study of the Italian society of hypertension. *Hypertension.* (2020) 76:366–72. doi: 10.1161/HYPERTENSIONAHA.120.15324
  21. Zheng Y, Liu X, Le W, Xie L, Li H, Wen W, et al. A human circulating immune cell landscape in aging and COVID-19. *Protein Cell.* (2020) 11:740–70. doi: 10.1007/s13238-020-00762-2
  22. Li X, Ma X. Acute respiratory failure in COVID-19: is it “typical” ARDS? *Crit Care.* (2020) 24:198. doi: 10.1186/s13054-020-02911-9
  23. Xie J, Covassin N, Fan Z, Singh P, Gao W, Li G, et al. Association between hypoxemia and mortality in patients with COVID-19. *Mayo Clin Proc.* (2020) 95:1138–47. doi: 10.1016/j.mayocp.2020.04.006
  24. Hajifathalian K, Sharaiha RZ, Kumar S, Krisko T, Skaf D, Ang B, et al. Development and external validation of a prediction risk model for short-term mortality among hospitalized U.S. COVID-19 patients: a proposal for the COVID-AID risk tool. *PLoS ONE.* (2020) 15:e0239536. doi: 10.1371/journal.pone.0239536
  25. Qiu H, Wu J, Hong L, Luo Y, Song Q, Chen D. Clinical and epidemiological features of 36 children with coronavirus disease 2019 (COVID-19) in Zhejiang, China: an observational cohort study. *Lancet Infect Dis.* (2020) 20:689–96. doi: 10.1016/S1473-3099(20)30198-5
  26. Chen T, Dai Z, Mo P, Li X, Ma Z, Song S, et al. Clinical characteristics and outcomes of older patients with coronavirus disease 2019 (COVID-19) in Wuhan, China: a single-centered, retrospective study. *J Gerontol A Biol Sci Med Sci.* (2020) 75:1788–95. doi: 10.1093/gerona/glaa089
  27. Alba AC, Agoritsas T, Walsh M, Hanna S, Iorio A, Devereaux PJ, et al. Discrimination and calibration of clinical prediction models: users’ guides to the medical literature. *JAMA.* (2017) 318:1377–84. doi: 10.1001/jama.2017.12126
  28. Chen S, Li X, Lv H, Wen X, Ding Q, Xue N, et al. Prognostic dynamic nomogram integrated with inflammation-based factors for non-small cell lung cancer patients with chronic hepatitis B viral infection. *Int J Biol Sci.* (2018) 14:1813–21. doi: 10.7150/ijbs.27260

**Conflict of Interest:** The authors declare that the research was conducted in the absence of any commercial or financial relationships that could be construed as a potential conflict of interest.

**Publisher’s Note:** All claims expressed in this article are solely those of the authors and do not necessarily represent those of their affiliated organizations, or those of the publisher, the editors and the reviewers. Any product that may be evaluated in this article, or claim that may be made by its manufacturer, is not guaranteed or endorsed by the publisher.

Copyright © 2021 Wang, Ai, Fu, Li, Cui, Ma, Ma, Wang, Liu, Long, Qu, Liu and Zhang. This is an open-access article distributed under the terms of the Creative Commons Attribution License (CC BY). The use, distribution or reproduction in other forums is permitted, provided the original author(s) and the copyright owner(s) are credited and that the original publication in this journal is cited, in accordance with accepted academic practice. No use, distribution or reproduction is permitted which does not comply with these terms.



# Mapping Trends and Hotspots Regarding Clinical Research on COVID-19: A Bibliometric Analysis of Global Research

Demeng Xia<sup>1,2†</sup>, Renqi Yao<sup>3,4†</sup>, Sheng Wang<sup>1†</sup>, Gaoqi Chen<sup>5</sup> and Yin Wang<sup>6\*</sup>

<sup>1</sup> Department of Emergency, Changhai Hospital, Naval Medical University, Shanghai, China, <sup>2</sup> Department of Orthopaedics, The Naval Hospital of Eastern Theater Command of People's Liberation Army of China (PLA), Zhoushan, China, <sup>3</sup> Translational Medicine Research Center, Fourth Medical Center and Medical Innovation Research Division of the Chinese PLA General Hospital, Beijing, China, <sup>4</sup> Department of Burn Surgery, Changhai Hospital, Second Military Medical University, Shanghai, China, <sup>5</sup> Department of Pancreatic Hepatobiliary Surgery, Changhai Hospital, Naval Medical University, Shanghai, China, <sup>6</sup> Department of Ultrasound, Shanghai Pulmonary Hospital, Tongji University School of Medicine, Shanghai, China

## OPEN ACCESS

### Edited by:

Reza Lashgari,  
Shahid Beheshti University, Iran

### Reviewed by:

Maria Helena De Aguiar Pereira E  
Pestana,  
University Institute of Lisbon, Portugal  
Xueqiang Wang,  
Shanghai University of Sport, China

### \*Correspondence:

Yin Wang  
lpbb1@aliyun.com

<sup>†</sup>These authors have contributed  
equally to this work

### Specialty section:

This article was submitted to  
Infectious Diseases – Surveillance,  
Prevention and Treatment,  
a section of the journal  
Frontiers in Public Health

**Received:** 25 May 2021

**Accepted:** 26 July 2021

**Published:** 23 August 2021

### Citation:

Xia D, Yao R, Wang S, Chen G and  
Wang Y (2021) Mapping Trends and  
Hotspots Regarding Clinical Research  
on COVID-19: A Bibliometric Analysis  
of Global Research.  
Front. Public Health 9:713487.  
doi: 10.3389/fpubh.2021.713487

**Purpose:** The coronavirus disease 2019 (COVID-19) outbreak, which began in December 2019, has not been completely controlled; therefore, COVID-19 has received much attention from countries around the world. Many related clinical studies, such as clinical trials, have been published, but to the knowledge of the authors, there has been no bibliometric analysis of these publications focusing on clinical research studies on COVID-19.

**Methods:** Global publications on COVID-19 from January 2020 to December 2020 were extracted from the Web of Science (WOS) collection database. The VOSviewer software and CiteSpace were employed to perform a bibliometric study. In addition, we obtained information on relevant clinical trials from the website <http://clinicaltrials.gov>.

**Results:** China published most of the articles in this field and had the highest number of citations and H-index. The *Journal of Medical Virology* published most of the articles related to COVID-19. In terms of institutions, Huazhong University of Science and Technology had the most publications, and Wang, JW received the highest number of citations.

**Conclusion:** The diagnosis, prevention, and prognosis of COVID-19 are still the focus of attention at present. The overall analysis of the disease were identified as the emerging topics from the perspectives of epidemiology and statistics. However, finding an effective treatment remains the focus of clinical trials.

**Keywords:** COVID-19, clinical research, publications, citation frequency, bibliometrics

## INTRODUCTION

At the end of December 2019, there was a serious outbreak caused by a type of coronavirus in Wuhan, China, which has been the third coronavirus epidemic since the new millennium, after severe acute respiratory syndrome (SARS) and Middle East respiratory syndrome (MERS). Currently, it is known that this outbreak was caused by a new type of coronavirus, severe

acute respiratory syndrome coronavirus 2 (SARS-CoV-2) (1, 2), which is highly pathogenic and infectious with unknown dynamics. Similar to SARS and MERS, SARS-CoV-2 can also cause severe clinical manifestations, ranging from mild symptoms (fever, dry cough, and shortness of breath) to fatal disease (e.g., sepsis and acute respiratory failure) (3). The seasonality of SARS-CoV-2 is unknown, and SARS-CoV-2 has an incubation period (normally 2–14 days) longer than that of SARS. In addition, some patients with coronavirus disease 2019 (COVID-19) have no signs of upper respiratory tract infection, abnormal laboratory findings, or early chest x-ray features, which makes it difficult to diagnose and treat COVID-19 in a timely manner (4, 5). Unfortunately, the number of confirmed cases and the number of deaths due to COVID-19 have progressively increased worldwide.

Coronavirus disease 2019 has undoubtedly become a global health threat, especially for people with underlying diseases, and has become the top priority and a great challenge in more than 200 countries (6). To address this global health threat, the scientific community (such as researchers and research institutions), Medical experts such as Nanshan Zhong and Wenliang Li, and institutions, such as Wuhan University School of Medicine and Huazhong University of Science and Technology, are constantly exploring this field. There are 100s of academic articles published every day that are closely related to various aspects of COVID-19, which include its epidemiology, pathology, drugs, and treatment. (7, 8). As a commonly used research method, clinical studies are of great significance in determining the prognosis of diseases, evaluating drugs, and selecting surgical procedures. Similarly, as an important part of clinical studies, clinical trials are defined as studies on specific drugs in patients or healthy volunteers that evaluate the clinical effects and adverse reactions of experimental drugs and, finally, ensure the effectiveness and safety of the experimental drugs. In the process of dealing with COVID-19, it is even more urgent to obtain effective drugs through clinical trials (9, 10). Therefore, these aspects should be given more attention. Of note, the number of scientific articles on COVID-19 doubles every 15 days since the onset of the epidemic; among them, there is a considerable number of clinical studies. Given that, a large amount of scientific output on COVID-19 makes it difficult to accurately locate information in PubMed, Web of Science (WOS), and Scopus databases by keywords.

To facilitate the search for scientific information related to COVID-19, academics have synthesized and simplified research results mainly through comprehensive reviews, bibliometric analyses, and the establishment of a COVID-19 database. Among them is bibliometrics, which refers to a statistical method that quantitatively analyses publications related to a certain subject *via* mathematical methods, with results providing descriptions and visual quantifications. Based on the bibliometric study of the literature and preprint articles on COVID-19, El Hawary et al. (11), and Kambhampati et al. (12), among others, comprehensively analyzed the subjects, authors, and nationalities of COVID-19-related articles published 3 months before the declaration of the pandemic. Similarly, Odone et al. (13) and Deng et al. (14), among others,

have been distinguishing the main branches, authors, journals, and collaborative links of COVID-19 articles since December 2019. However, to the knowledge of the authors, there is no bibliometric analysis specifically focusing on COVID-19 clinical studies. Since the COVID-19 pandemic has not been controlled and more knowledge on the clinical research study is needed, it is urgent to conduct a bibliometric analysis of COVID-19 clinical studies.

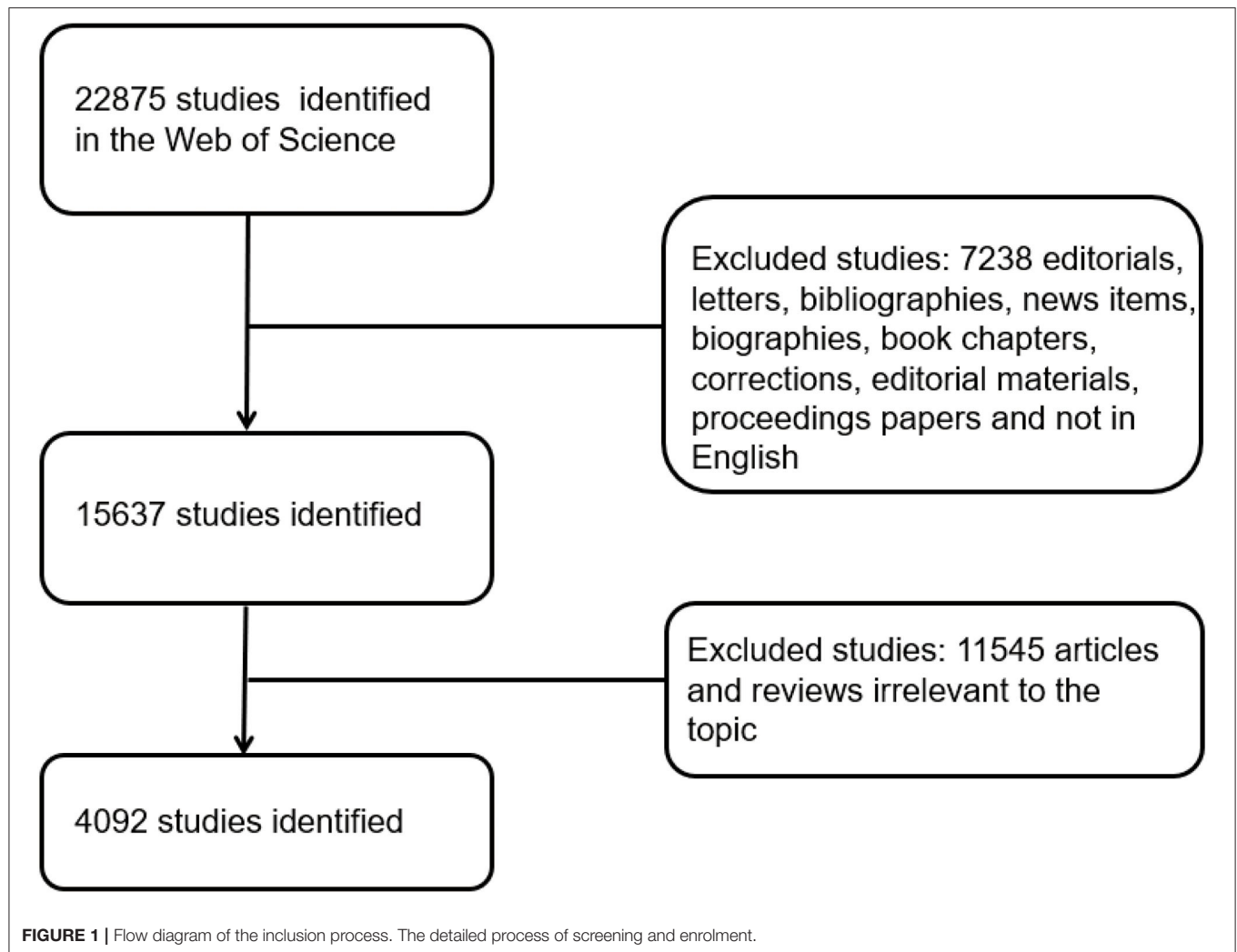
## MATERIALS AND METHODS

### Data Sources and Search Strategies

The WOS, one of the most appropriate databases for conducting bibliometric analyses, was used to perform comprehensive online searches on clinical studies relevant to COVID-19 from January 2020 to December 2020. As all the data were collected online and no human subjects were involved, ethical consent was not applicable. To avoid bias due to database renewal, we conducted all the searches on December 27, 2020. The search strategy was as follows: TS = (2019 Novel Coronavirus Disease or COVID-19 or coronavirus 2 or SARS-CoV-2 or Novel coronavirus pneumonia or NCP or Novel Coronavirus or 2019-nCoV or coronavirus disease 2019 or coronavirus disease-19) and (Clinical or Trial or Random\* or Characteristics or Features or Manifestations or Retrospective or Prospective or Epidemiology or Epidemiologic or Observational or Interventional or Cross-sectional or Case-control or Cohort or Real world or Descriptive). Only original articles and reviews were included in this analysis, and other types of studies were excluded. The search processes were carried out by two of the authors, and if there was a disagreement on inclusion, the final decision was made by the experienced corresponding author. In terms of details, we will first make a preliminary judgment on whether the articles are consistent with the research topic according to the abstract. For the articles that are not certain, we will download the full text and conduct a more detailed evaluation. For the not certain articles, we will download the full text and conduct a more detailed evaluation. If there are questions, experienced corresponding authors will review them. Detailed information on enrolment and selection is shown in **Figure 1**. ClinicalTrials.gov is a web-based resource that provides patients and their family members, healthcare professionals, researchers, and the public with easy access to information on publicly and privately supported clinical studies on a wide range of diseases and conditions. Regarding clinical trials, information was obtained from the website <http://clinicaltrials.gov>. On this website, the search process included the keyword “COVID-19,” and the limitations were “completed” and “clinical trials” (ongoing, stopped halfway, and non-clinical trials were excluded).

### Data Collection and Processing

All the data were extracted from the identified publications by three authors (XDM, YRQ, and WS). The extracted data included titles, keywords, authors, publication dates, countries and regions of origin, institutions, journals, numbers of citations, H-indexes, and other information on publications. Microsoft



Excel 2016 (Microsoft, Redmond, WA, United States), GraphPad Prism 8 (GraphPad Prism Software Inc., San Diego, CA, United States), VOSviewer version 1.6.12 (Leiden University, Leiden, the Netherlands), CiteSpace version 5.6.R5 64 bit (Drexel University, Philadelphia, PA, United States), and the Online Analysis Platform of Literature Metrology (<http://bibliometric.com/>) were applied for the presentation, analysis, and description of the data. Excel is one of the commonly used software for data processing, and it is used to perform a visual representation of histograms in this study. VOSviewer is a program developed for constructing and viewing bibliometric maps of authors or journals based on co-citation data or constructing maps of keywords based on co-occurrence, and it is applied for the analysis of countries, authors, and keywords in this study. While Citespace is a Java application for analyzing and visualizing co-citation networks, its primary goal is to facilitate the analysis of emerging trends in a knowledge domain, and it can be used for keyword clustering, which is helpful in summarizing the general research direction.

## Bibliometric Analysis

We selected the WOS of Thomson Reuters because it is a large collection of studies, especially those focused on biomedicine. The impact factor (IF) was obtained from the information provided by the journal citation reports (JCRs) published in 2020, and the relative research interest (RRI) was defined as the number of publications per year in a particular research field divided by the total number of publications across all fields. The H-index of articles serves as a tool to measure academic productivity, and it indicates that a researcher or a country has published at least H articles and that each article has been cited in other publications at least H times. It is widely accepted that the H-index plays an important role in evaluating the scientific research impact of a researcher or a country, especially in the medical field (15).

As practical statistical software, VOSviewer can use the links between nodes in the map to determine bibliometric characteristics, such as references, institutions, authors, and terms. Additionally, VOSviewer can analyse and predict potential trends in future research studies. The VOSviewer software



was also used to extract keywords. Compared with Vosviewer, Citespace can complement the aspects in clustering of more keywords and analyse the type of cited articles and articles citing others, which will be more conducive to our understanding of research focus and the field that is related to the research topic (16).

## RESULTS

### Contributions of Countries to Global Publications

In total, 4,092 articles (7,238 articles that did not meet the type requirements and 11,545 articles that were not related to the topic were excluded) published from January 2020 to December 2020 met the inclusion criteria. China ranked first in the number of publications with 1,413 articles (30.4%), which accounted for approximately one-third of the total publications, followed by the United States (USA) at 949 (20.4%) and Italy at 438 (9.42%) (Figure 2A). Figures 2B,C show that the top five countries in the field of COVID-19 with respect to the number of published articles are China, the USA, Italy, Britain, and Spain. As shown in Figure 2D, the regional correlation shows that almost all of the countries that published many articles are mainly from Europe, the USA, and Asia. China, with the largest number of publications, also ranked first globally in regard to institutions, and Chinese authors issued most of the articles.

### Citation and H-index Analysis

According to the JCRs from the WOS database, all clinical studies related to COVID-19 have been cited 150,402 times (141,101 times when self-citations were excluded), with an average citation frequency of 32.38 times per article. As the country with the largest number of publications, China accounted for 56.57% of the total citations (85,081 times [77,911 times when self-citations were excluded]) and had an H-index of 105. The number of citations from the USA was 21,203 (20,015 when self-citations were excluded), with an H-index of 60; thus, the USA ranked second among all the involved countries and districts (Figure 2A).

### Institutions With Clinical Research Publications on COVID-19

Institutions that had more than 10 publications and cited more than 20 times are included in Figure 3A. Huazhong University of Science and Technology had the most publications; the 376 articles from Huazhong University of Science and Technology have been cited 31,727 times, and we can get clear information about institutional contribution based on color (red represents more contributions, and green represents less contributions) from Figure 3B. Figure 2B shows that Huazhong University of Science and Technology, Wuhan University (213 articles), and Capital Medical University (80 articles) are the top three publishing institutions. On the list of the top 20 institutions, 11 were Chinese (mainland China and Taiwan district) institutions, 4 were institutions located in the USA, 2 were English institutions, and the other 3 institutions were in France, Iran, and Italy.

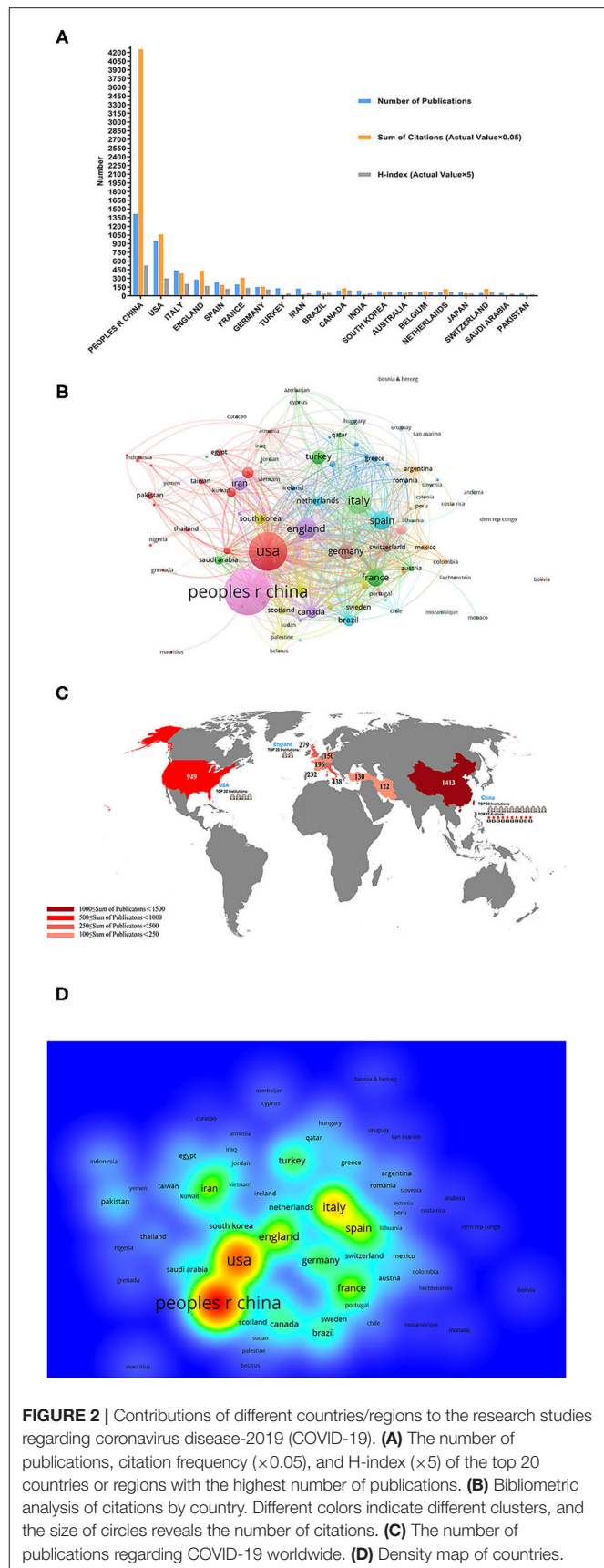


**FIGURE 2 |** Contributions of different countries/regions to the research studies regarding coronavirus disease-2019 (COVID-19). **(A)** The number of publications, citation frequency ( $\times 0.05$ ), and H-index ( $\times 5$ ) of the top 20 countries or regions with the highest number of publications. **(B)** Bibliometric analysis of citations by country. Different colors indicate different clusters, and the size of circles reveals the number of citations. **(C)** The number of publications regarding COVID-19 worldwide. **(D)** Density map of countries.

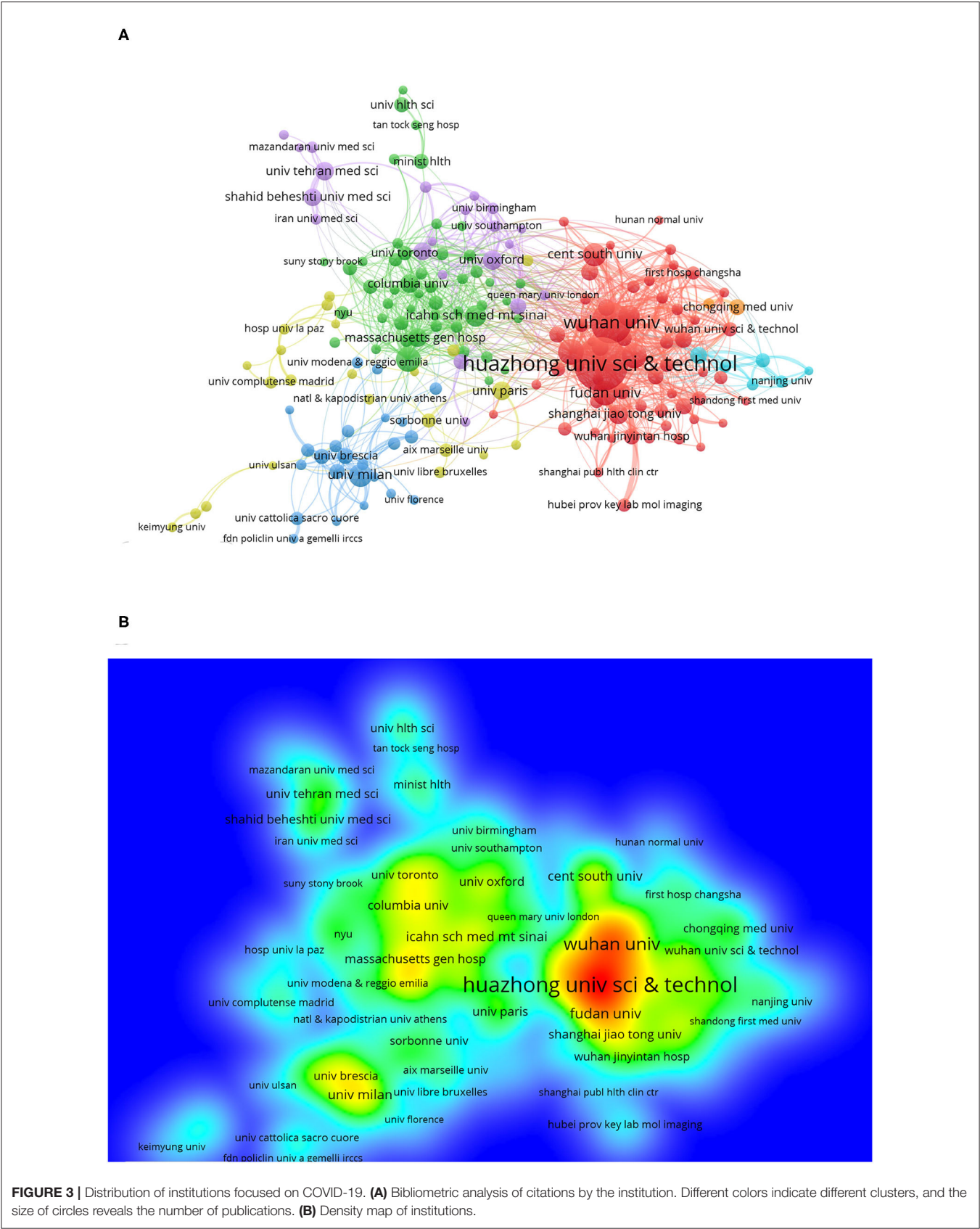


**FIGURE 3 |** Distribution of institutions focused on COVID-19. **(A)** Bibliometric analysis of citations by the institution. Different colors indicate different clusters, and the size of circles reveals the number of publications. **(B)** Density map of institutions.

**TABLE 1** | Top 10 most cited studies on coronavirus disease-2019 (COVID-19).

| Title  | Corresponding authors | Journal  | IF     | Publication year | Total citations | Article type  |
|--|-----------------------|--|--------|------------------|-----------------|---|
| Clinical features of patients infected with 2019 novel coronavirus in Wuhan, China   | Wang, JW              | LANCET   | 60.39  | 2020             | 9,702           | Descriptive study                                   |
| Clinical Characteristics of Coronavirus Disease 2019 in China  | Zhong, N              | NEW ENGLAND JOURNAL OF MEDICINE                  | 74.699 | 2020             | 5,933           | Descriptive study                                   |
| Clinical Characteristics of 138 Hospitalized Patients With 2019 Novel Coronavirus-Infected Pneumonia in Wuhan, China                                     | Peng, ZY              | JAMA-JOURNAL OF THE AMERICAN MEDICAL ASSOCIATION | 45.54  | 2020             | 5,494           | Descriptive study                                   |
| A Novel Coronavirus from Patients with Pneumonia in China, 2019  | Wu, GZ                | NEW ENGLAND JOURNAL OF MEDICINE                  | 74.699 | 2020             | 5,189           | Retrospective cohort study                          |
| Clinical course and risk factors for mortality of adult inpatients with COVID-19 in Wuhan, China: a retrospective cohort study                           | Chen, H               | LANCET   | 60.39  | 2020             | 5,046           | Retrospective cohort study                          |
| Epidemiological and clinical characteristics of 99 cases of 2019 novel coronavirus pneumonia in Wuhan, China: a descriptive study                        | Zhang, L              | LANCET   | 60.39  | 2020             | 4,934           | Descriptive study                                   |
| A familial cluster of pneumonia associated with the 2019 novel coronavirus indicating person-to-person transmission: a study of a family cluster         | Yuen, KY              | LANCET   | 60.39  | 2020             | 2,423           | Descriptive study                                   |
| Clinical course and outcomes of critically ill patients with SARS-CoV-2 pneumonia in Wuhan, China: a single-centered, retrospective, observational study | Shang, Y              | LANCET RESPIRATORY MEDICINE                      | 25.094 | 2020             | 1,964           | Single-centered, retrospective, observational study |
| Abnormal coagulation parameters are associated with poor prognosis in patients with novel coronavirus pneumonia  | Sun, ZY               | JOURNAL OF THROMBOSIS AND HAEMOSTASIS            | 4.157  | 2020             | 1,665           | Retrospective cohort study                          |
| Hydroxychloroquine and azithromycin as a treatment of COVID-19: results of an open-label non-randomized clinical trial                                   | Raoult, D             | INTERNATIONAL JOURNAL OF ANTIMICROBIAL AGENTS    | 4.621  | 2020             | 1,475           | non-randomized clinical trial                       |

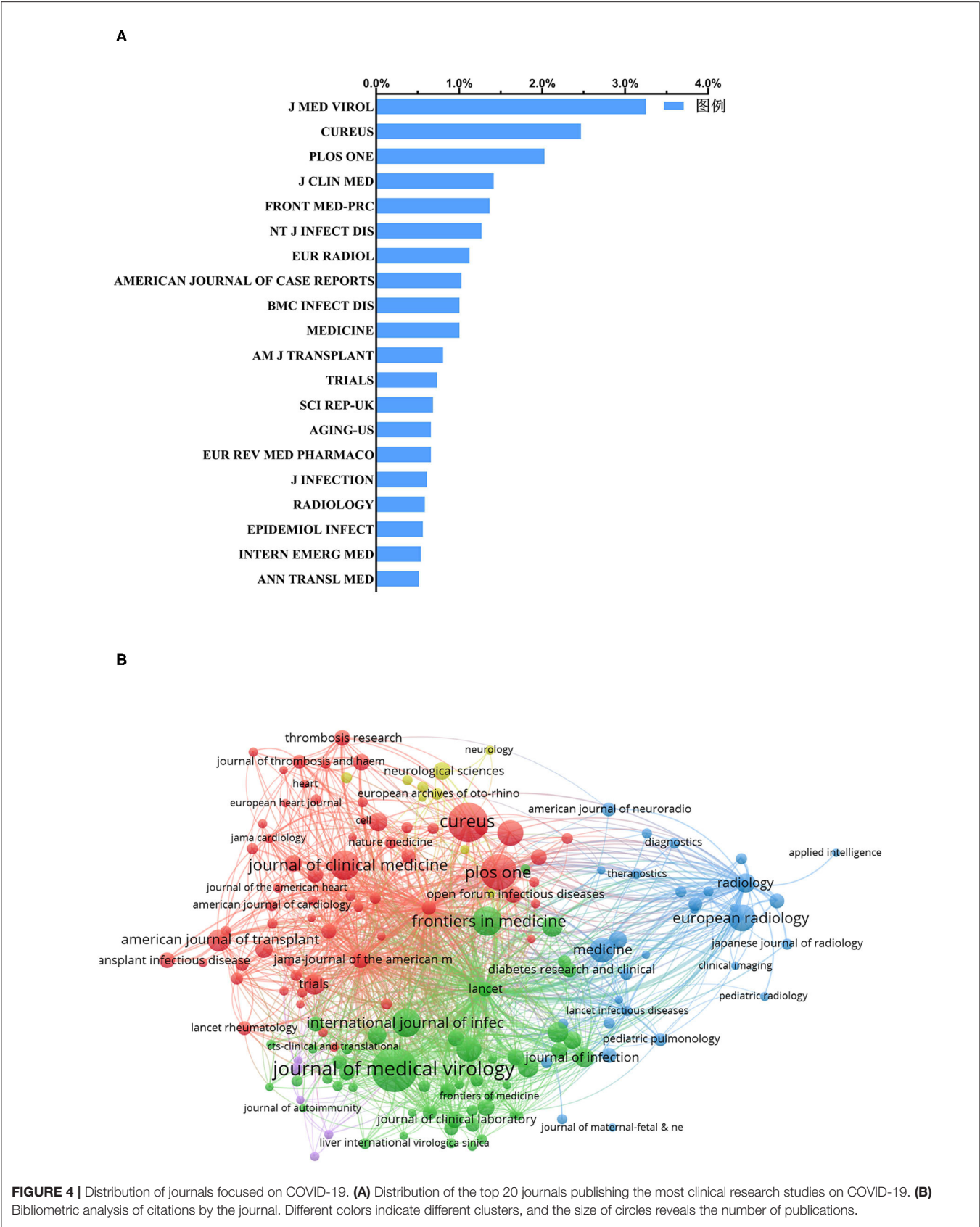
## Journals About Clinical Research Publications on COVID-19

Overall, the publications included in this analysis do not appear to be concentrated in a few journals. The total publications of the top 20 journals accounted for 22.3% of the total literature included in this analysis, while the publications of the top-ranked journal (*Journal of Medical Virology*) accounted for only 3.3% (**Figure 4A**). As shown in **Figure 3A**, the number of papers published in the *Journal of Medical Virology* (IF = 2.0218) was the highest, with 133 records, which were cited 2,787 times. Cureus

(no IF) ranked second, with 101 publications that were cited 101 times. Additionally, the journal with the highest IF was *Radiology* (IF = 7.931) and ranked 17th, with a total of 24 publications.

## Articles About Clinical Research Publications on COVID-19

The most cited article about the use of publications on COVID-19 worldwide was *Clinical features of patients infected with 2019 novel coronavirus in Wuhan, China*, which was published by Wang, JW in China, and this article was cited 9,702 times.





Unsurprisingly, among the top 10 most cited articles listed in this field, 9 came from China. It should be noted that 4 of the top 10 most cited articles were published in the special columns for COVID-19 of *The Lancet*, and 8 of them had an IF of over 20 (Table 1).

### Clinical Trials on COVID-19

The results showed that there were a total of 17 trials and that the 17 clinical trials were an independent part, which is different from the 4,092 articles extracted from WOS. Nearly 20 countries participated in the 17 trials, with 5 of the 17 included trials being from the USA. Although China is the country with the largest number of publications, it does not contribute in this regard at present. Of note, one of the trials was sponsored and conducted by more than 10 countries. With respect to research purposes, unsurprisingly, 10 of the 17 studies involved treatments. Similarly, 13 of the 17 trials mostly involved drug selection and use. Treatment-related clinical trials also covered a wide range of drugs, such as areplivir, favipiravir, povidone-iodine, and hydroxychloroquine. Of note, there are six trials in this field related to ivermectin (Supplementary Table 1).

### Analysis of Keywords About Clinical Research Publications on COVID-19

The keywords chosen by article authors when they submitted their manuscripts for publication were extracted with VOSviewer. We analyzed the keywords extracted from 4,092 publications. As shown in Figure 5A, 218 keywords, defined as terms that occurred more than 15 times within titles and abstracts in all articles during the analysis, are frequently mentioned, such as COVID-19 (2,367 times), SARS-CoV-2 (973 times), coronavirus (743 times), pneumonia (627 times), mortality (323 times), and Wuhan (261 times).

Detailed data on the co-occurrence of all included keywords are presented in Figure 5A. More graphical data are shown in Figure 5B. As shown in Figure 5C, VOSviewer color all keywords according to the average number of appearances of each word. In particular, the color blue indicates that the word appeared relatively early, while the color yellow indicates a more recent appearance. For example, symptoms, cytokine, comorbidities, hyperglycaemia, artificial intelligence, viral shedding, liver injury, and corticosteroids are eight of the earlier keywords that have been highlighted recently, and the two most recent keywords are pandemic and meta-analysis, which also reflects the change in the focus and the future research trend to a certain extent.

### Clustering Analysis of Types of Articles and Keywords

As shown in Figure 6A, cited journals are distributed across the fields of medicine and medical and clinical research, while cited references come from two major clusters, one of which includes molecular, biology, and genetics, and the other includes healthy, nursing, and medicine. In the co-cited analysis of keywords, the top five clusters were diabetes, CT, clinical characteristics, pulmonary embolism, and lymphocytes (Figure 6B), which reflected the focus of keywords in the field on the clinical features,

examination methods, test methods, and underlying diseases and complications of the disease.

## DISCUSSION

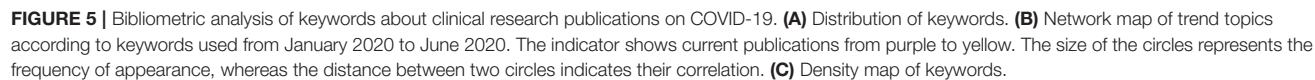
### Research Trends in Clinical Research Publications on COVID-19

In terms of the publication volume of all countries, China ranked first, followed by the USA and Italy (Figure 2A). Similarly, Asia, North America, and Europe were also the areas hardest hit by COVID-19 (Figure 2C). We speculate that the reason for this phenomenon is related to the timing of the virus outbreak and the number of people infected with the disease. China topped the list, because it was the first country to be affected. As early as December 2019, SARS-CoV-2 was identified as the cause of the onset of an outbreak of the respiratory disease in Wuhan, Hubei province, China (17). The fact that the USA and Italy were the areas most affected by COVID-19 may explain their high number of published articles. As of April 7, 2020, Italy had the second highest number of registered cases in Europe (135,586) (18). Additionally, as of early June 2020, SARS-CoV-2 has infected more than 6.3 million people worldwide, of whom more than 1.9 million were from the USA, which also had the highest number of infections and deaths from the outbreak (19).

At present, the articles that have mainly appeared in this field have not been published in a certain type of journal (Figure 4A). The top 20 journals according to the number of published articles covered epidemiology (20), virology (21), radiology (22), emergency medicine (23), and more. It is reasonable to believe that COVID-19 has attracted the attention of a wide range of medically relevant fields, not just one discipline, which is also an indication that the solution to the COVID-19 pandemic will require the communication of various disciplines.

In terms of institutions, the top two institutions were Huazhong University of Science and Technology and Wuhan University. As the city where the COVID-19 outbreak first occurred, Wuhan has had the first-hand clinical case and clinical treatment experience (17), so the number of published articles from this city is relatively high. Although COVID-19 is globally prevalent, the top 20 publishing agencies were all from Europe and North America except for China, which is related to the advanced level of research studies in Europe and North America in the medical field, especially when COVID-19 was combined with other diseases. For example, the guidelines for tracheal intubation for patients with COVID-19 were developed by the Canadian Pediatric Anesthesia Society (18), and the guidelines for oncology treatment for patients with COVID-19 were based on the oncology guidelines in the United Kingdom and the USA (24).

Table 1 shows the detailed information on COVID-19 and the 10 most frequently cited publications. The top three cited articles, published in *The Lancet*, *New England Journal of Medicine*, and *JAMA—Journal of the American Medical Association* (25), described clinical manifestations in patients with COVID-19, and 4 of the top 10 articles were related to COVID-19 clinical features. Similarly, among the top 10 articles, there were 3 related to the prognoses of patients. Therefore, we have a reason to believe



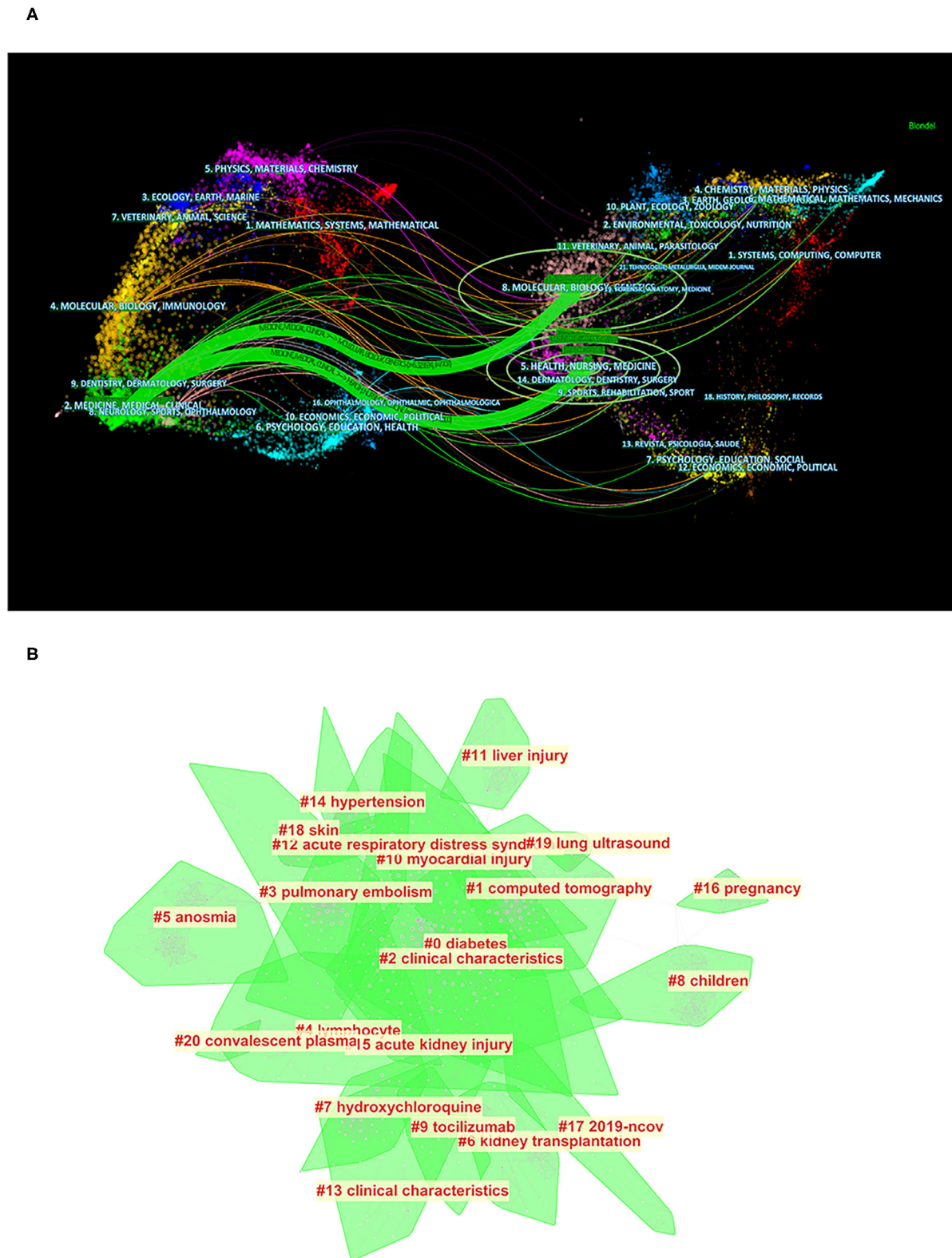


**FIGURE 6 |** Bibliometric analysis of the clustering of types of articles and keywords. **(A)** Clustering analysis of articles being cited and articles that cited literature (distribution of cited literature and journals on the left and articles that cited literature on the right). **(B)** Clustering analysis of keywords (the order is from 0 to 20; the smaller the number, the more keywords the cluster contains, and therefore the more attention it receives).



that the clinical manifestations, characteristics, treatments, and prognoses of COVID-19 patients are the key points of research study at present.

## Research Focused on Clinical Research Publications on COVID-19

**Figure 5** shows that almost all of the cited articles are from the fields of medicine and medical and clinical research. The articles being cited are mostly from the fields of health, nursing, and medicine, as well as molecular, biology, and genetics, which indicate that the ideal solution to the COVID-19 pandemic will require the joint efforts of researchers from multiple fields such as basic biology and genetics. In particular, molecular studies have speculated on the pathogenesis of COVID-19, and angiotensin-converting enzyme 2, expressed in human vascular endothelium, respiratory epithelium, and other cell types, is thought to be a primary mechanism of SARS-CoV-2 entry and infection (26). At the same time, in the cell biology field, macrophages, as key cells in response to viral infection, can lead to the aggravation of infection. While an adaptive immune response is essential for the elimination of SARS-CoV-2, in some cases, macrophages show significant production of IL-6, suggesting that they may cause excessive inflammation in COVID-19 (27). Together, these findings also suggest that the ideal solution to the COVID-19 pandemic will require the involvement of researchers in molecular science, cytology, and other basic medicine fields.

In terms of clustering analysis of keywords, the top five keyword clusters included diabetes, CT, clinical characteristics, pulmonary embolism, and lymphocytes, and the above five clusters represented the research studies on basic diseases, clinical manifestations, examinations, complications, and tests. A study has shown that diabetes predisposes patients to a particularly severe course, with COVID-19 doubling the risk of death because of lung and heart involvement (28). As an effective test index, a reduced peripheral blood absolute lymphocyte count with an elevated neutrophil count has been a consistent observation in hospitalized patients with COVID-19 and has certain significance in the diagnosis of the disease (29). Symptoms, such as fever, cough, and fatigue (17), also indicate the possibility of SARS-CoV-2 infection. At present, the findings from chest CT and reverse transcriptase-polymerase chain reaction (RT-PCR) can complement each other in the clinical diagnosis of COVID-19. Consolidation, a reticular pattern, and a crazy-paving pattern are typical CT manifestations of COVID-19 (30). The results of this study also suggest that the prevalence of pulmonary embolism in patients with COVID-19 is close to 5% in the whole population and that pulmonary embolism seems to be associated with more extensive lung damage (31). Through clustering analysis of keywords, we have a reason to believe that the diagnosis, prevention, and prognosis of the disease are still the focus of our attention at present.

A map of all the keywords and hotspots (**Figures 5A–C**) was obtained and analyzed. Among the 10 latest hotspots, 8 were closely related to symptoms, underlying diseases, complications, and treatment. Surprisingly, the two most recent hotspots were pandemics and meta-analyses. Pandemic is an epidemiological term that describes the severity of the spread of infectious diseases. The outbreak of COVID-19 in China was brought to

global attention and declared a pandemic by the WHO (32). The fact that the disease has crossed national boundaries in such a short period of time is sufficient to demonstrate that the problem needs to be addressed from an epidemiological perspective. Meta-analyses, with their statistical content, are important features of clinical trial evaluation because of their objectivity and systematic nature. Meta-analyses are of great significance for the integration and analysis of clinical research (33). In COVID-19 research, many studies in this area have come to the attention of the authors, especially those regarding the risk factors, treatment effects, and diagnosis of the disease (34). Meta-analyses have helped clinicians and researchers summarize problems in the field of COVID-19.

Clinical research studies address the diagnosis, treatment, prognostic prediction, and prevention of diseases, and the results of the research studies can be quickly converted to clinical applications. As a highly contagious epidemic, COVID-19 has received global attention, clinical research study is a key factor in addressing the pandemic in this field. Clinical trials can provide highly reliable evidence. We searched clinicaltrials.gov and obtained 17 documented clinical trials (**Supplementary Table 1**). The results from this field showed that most of the trials were related to treatment, especially the use of drugs. Thirteen of the studies were related to specific drugs. At present, antiviral drugs, such as areplivir and favipiravir, are being used in trials. The days from the onset of fever to defervescence were shown to be positively correlated with the duration from the onset of fever to the initiation of favipiravir treatment (35). However, no specific antiviral drugs have been approved for the treatment of COVID-19 (36). Therefore, more clinical trials are needed. Hydroxychloroquine, as a treatment for malaria, has also received widespread attention. Hydroxychloroquine has been shown to have a certain effect on the treatment of patients with mild disease; however, in patients with severe COVID-19, the use of hydroxychloroquine resulted in significant worsening of clinical status because of renal dysfunction and increased need for invasive mechanical ventilation (37). The clinical use of hydroxychloroquine still needs to be studied. In trials, ivermectin has attracted the most attention as an antiviral drug with potential effects, and the dose and mechanism of action of this drug are still the focus of our study (38, 39). Based on the findings, the objective of the current clinical trials is to find a more practical drug that can inhibit the transmission of SARS-CoV-2.

This study investigated publications from the WOS database and clinical trials, and we tried to obtain objective and reliable results. However, due to the limitation of the search to studies in English and the constant updating of the database, as well as the exclusion of non-research articles, the results may differ slightly from the actual results. For more comprehensive results, databases such as Medline, Scopus, or Google Scholar could be searched in further studies.

## CONCLUSIONS

China has published the most research studies on COVID-19. In terms of clinical trials, the USA has the largest number of studies, and the diagnosis, prevention, and prognosis of the disease are still the focus of our attention



at present. The overall analysis of the disease from the perspective of epidemiology and statistics will receive more attention. However, finding an effective treatment remains the focus of clinical trials. The ideal solution to the COVID-19 pandemic will require the joint efforts of all disciplines.

## DATA AVAILABILITY STATEMENT

The original contributions presented in the study are included in **Supplementary Material**.

## REFERENCES

- Wu Z, McGoogan JM. Characteristics of and important lessons from the coronavirus disease 2019 (COVID-19) outbreak in China: summary of a report of 72 314 cases from the chinese center for disease control and prevention. *JAMA*. (2020) 323:1239–42. doi: 10.1001/jama.2020.2648
- Zhou F, Yu T, Du R, Fan G, Liu Y, Liu Z, et al. Clinical course and risk factors for mortality of adult inpatients with COVID-19 in Wuhan, China: a retrospective cohort study. *Lancet*. (2020) 395:1054–62. doi: 10.1016/S0140-6736(20)30566-3
- Wiersinga WJ, Rhodes A, Cheng AC, Peacock SJ, Prescott HC. Pathophysiology, transmission, diagnosis, and treatment of coronavirus disease 2019 (COVID-19): a review. *JAMA*. (2020) 324:782–93. doi: 10.1001/jama.2020.12839
- Huang WH, Teng LC, Yeh TK, Chen YJ, Lo WJ, Wu MJ, et al. 2019 novel coronavirus disease (COVID-19) in Taiwan: reports of two cases from Wuhan, China. *J Microbiol Immunol Infect*. (2020) 53:481–4. doi: 10.1016/j.jmii.2020.02.009
- Burke RM, Midgley CM, Dratch A, Fenstersheib M, Haupt T, Holshue M, et al. Active monitoring of persons exposed to patients with confirmed COVID-19 - United States, January-February 2020. *MMWR Morb Mortal Wkly Rep*. (2020) 69:245–6. doi: 10.15585/mmwr.mm6909e1
- Ahmad I, Rathore FA. Neurological manifestations and complications of COVID-19: a literature review. *J Clin Neurosci*. (2020) 77:8–12. doi: 10.1016/j.jocn.2020.05.017
- Pascarella G, Strumia A, Pilego C, Bruno F, Del Buono R, Costa F, et al. COVID-19 diagnosis and management: a comprehensive review. *J Internal Med*. (2020) 288:192–206. doi: 10.1111/joim.13091
- Harapan H, Itoh N, Yufika A, Winardi W, Keam S, Te H, et al. Coronavirus disease 2019 (COVID-19): a Literature review. *J Infect Public Health*. (2020) 13:667–73. doi: 10.1016/j.jiph.2020.03.019
- Christie RV. Penicillin in subacute bacterial endocarditis; report to the Medical Research Council on 147 patients treated in 14 centres appointed by the Penicillin Clinical Trials Committee. *Br Med J*. (1946) 1:381–3.
- Choy DS. Clinical trials of a new plastic dressing for burns surgical wounds. *AMA Arch Surg*. (1954) 68:33–43. doi: 10.1001/archsurg.1954.01260050035005
- ElHawary H, Salimi A, Diab N, Smith L. Bibliometric analysis of early COVID-19 research: the top 50 cited papers. *Infect Dis*. (2020) 13:1178633720962935. doi: 10.1177/1178633720962935
- Kambhampati SBS, Vaishya R, Vaish A. Unprecedented surge in publications related to COVID-19 in the first three months of pandemic: a bibliometric analytic report. *J Clin Orthopaed Trauma*. (2020) 11:S304–6. doi: 10.1016/j.jcot.2020.04.030
- Odone A, Salvati S, Bellini L, Bucci D, Capraro M, Gaetti G, et al. The runaway science: a bibliometric analysis of the COVID-19 scientific literature. *Acta Biomed*. (2020) 91:34–9. doi: 10.23750/abm.v91i9-S.10121
- Deng Z, Chen J, Wang T. Bibliometric and visualization analysis of human coronaviruses: prospects and implications for COVID-19 research. *Front Cell Infect Microbiol*. (2020) 10:581404. doi: 10.3389/fcimb.2020.581404
- Rad AE, Brinjikji W, Cloft HJ, Kallmes DF. The H-index in academic radiology. *Acad Radiol*. (2010) 17:817–21. doi: 10.1016/j.acra.2010.03.011
- Eyre-Walker A, Stoletzki N. The assessment of science: the relative merits of post-publication review, the impact factor, and the number of citations. *PLoS Biol*. (2013) 11:e1001675. doi: 10.1371/journal.pbio.1001675
- Adhikari SP, Meng S, Wu YJ, Mao YP, Ye RX, Wang QZ, et al. Epidemiology, causes, clinical manifestation and diagnosis, prevention and control of coronavirus disease (COVID-19) during the early outbreak period: a scoping review. *Infect Dis Poverty*. (2020) 9:29. doi: 10.1186/s40249-020-00646-x
- Izzetti R, Nisi M, Gabriele M, Graziani F. COVID-19 transmission in dental practice: brief review of preventive measures in Italy. *J Dental Res*. (2020) 99:1030–38. doi: 10.1177/0022034520920580
- Wang ML, Behrman P, Dulin A, Baskin ML, Buscemi J, Alcaraz KI, et al. Addressing inequities in COVID-19 morbidity and mortality: research and policy recommendations. *Transl Behav Med*. (2020) 10:516–9. doi: 10.1093/tbm/ibaa055
- Ge H, Wang X, Yuan X, Xiao G, Wang C, Deng T, et al. The epidemiology and clinical information about COVID-19. *Europ J Clin Microbiol Infect Dis*. (2020) 39:1011–9. doi: 10.1007/s10096-020-03874-z
- Vellas C, Delobel P, de Souto Barreto P, Izopet J. COVID-19 J, virology and geroscience: a perspective. *J Nutr Health Aging*. (2020) 24:685–91. doi: 10.1007/s12603-020-1416-2
- Kooraki S, Hosseiny M, Myers L, Gholamrezaezhad A. Coronavirus (COVID-19) outbreak: what the department of radiology should know. *J Am Coll Radiol*. (2020) 17:447–51. doi: 10.1016/j.jacr.2020.02.008
- Thoma B, Woods R, Patocka C. Context: how COVID-19 exposed key factors of emergency medicine education. *CJEM*. (2020) 22:561–2. doi: 10.1017/cem.2020.447
- Burki TK. Cancer guidelines during the COVID-19 pandemic. *Lancet Oncol*. (2020) 21:629–30. doi: 10.1016/S1470-2045(20)30217-5
- Huang C, Wang Y, Li X, Ren L, Zhao J, Hu Y, et al. Clinical features of patients infected with 2019 novel coronavirus in Wuhan, China. *Lancet*. (2020) 395:497–506. doi: 10.1016/S0140-6736(20)30183-5
- Amraei R, Rahimi N. COVID-19 renin-angiotensin system and endothelial dysfunction. *Cells*. (2020) 9:1652. doi: 10.3390/cells9071652
- Paces J, Strizova Z, Smrz D, Cerny J. COVID-19 and the immune system. *Physiol Res*. (2020) 69:379–88. doi: 10.33549/physiolres.934492
- Peric S, Stulnig TM. Diabetes and COVID-19 : disease-management-people. *Wien Klin Wochenschr*. (2020) 132:356–61. doi: 10.1007/s00508-020-01672-3
- Huang W, Berube J, McNamara M, Saksena S, Hartman M, Arshad T, et al. Lymphocyte subset counts in COVID-19 patients: a meta-analysis. *Cytometry A*. (2020) 97:772–6. doi: 10.1002/cyto.a.24172
- Ye Z, Zhang Y, Wang Y, Huang Z, Song B. Chest CT manifestations of new coronavirus disease 2019 (COVID-19): a pictorial review. *Europ Radiol*. (2020) 30:4381–9. doi: 10.1007/s00330-020-06801-0
- Planquette B, Le Berre A, Khider L, Yannoutsos A, Gendron N, de Torcy M, et al. Prevalence and characteristics of pulmonary embolism in 1042 COVID-19 patients with respiratory symptoms: a nested case-control study. *Thromb Res*. (2021) 197:94–9. doi: 10.1016/j.thromres.2020.11.001

## AUTHOR CONTRIBUTIONS

DMX and RQY collected, analyzed the data, and wrote the manuscript. DMX, SW, GQC, and YW designed the study and revised the manuscript.

## SUPPLEMENTARY MATERIAL

The Supplementary Material for this article can be found online at: <https://www.frontiersin.org/articles/10.3389/fpubh.2021.713487/full#supplementary-material>

32. Jin Y, Yang H, Ji W, Wu W, Chen S, Zhang W, et al. Virology epidemiology, pathogenesis, and control of COVID-19. *Viruses*. (2020) 12:372. doi: 10.3390/v12040372
33. Barendregt JJ, Doi SA, Lee YY, Norman RE, Vos T. Meta-analysis of prevalence. *J Epidemiol Community Health*. (2013) 67:974–8. doi: 10.1136/jech-2013-203104
34. Zhang JJY, Lee KS, Ang LW, Leo YS, Young BE. Risk factors for severe disease and efficacy of treatment in patients infected with COVID-19: a systematic review, meta-analysis, meta-regression analysis. *Clin Infect Dis*. (2020) 71:2199–206. doi: 10.1093/cid/ciaa576
35. Fujii S, Ibe Y, Ishigo T, Inamura H, Kunimoto Y, Fujiya Y, et al. Early favipiravir treatment was associated with early defervescence in non-severe COVID-19 patients. *J Infect Chemother*. (2021) 27:1051–7. doi: 10.1016/j.jiac.2021.04.013
36. Du YX, Chen XP. Favipiravir: pharmacokinetics and concerns about clinical trials for 2019-nCoV infection. *Clin Pharmacol Ther*. (2020) 108:242–7. doi: 10.1002/cpt.1844
37. Réa-Neto Á, Bernardelli RS, Câmara BMD, Reese FB, Queiroga MVO, Oliveira MC. An open-label randomized controlled trial evaluating the efficacy of chloroquine/hydroxychloroquine in severe COVID-19 patients. *Sci Rep*. (2021) 11:9023. doi: 10.1038/s41598-021-88509-9
38. Schmith VD, Zhou JJ, Lohmer LRL. The approved dose of ivermectin alone is not the ideal dose for the treatment of COVID-19. *Clin Pharmacol Ther*. (2020) 108:762–5. doi: 10.1002/cpt.1889
39. Rizzo E. Ivermectin, antiviral properties and COVID-19: a possible new mechanism of action. *Naunyn Schmiedebergs Arch Pharmacol*. (2020) 393:1153–6. doi: 10.1007/s00210-020-01902-5

**Conflict of Interest:** The authors declare that the research was conducted in the absence of any commercial or financial relationships that could be construed as a potential conflict of interest.

**Publisher's Note:** All claims expressed in this article are solely those of the authors and do not necessarily represent those of their affiliated organizations, or those of the publisher, the editors and the reviewers. Any product that may be evaluated in this article, or claim that may be made by its manufacturer, is not guaranteed or endorsed by the publisher.

Copyright © 2021 Xia, Yao, Wang, Chen and Wang. This is an open-access article distributed under the terms of the Creative Commons Attribution License (CC BY). The use, distribution or reproduction in other forums is permitted, provided the original author(s) and the copyright owner(s) are credited and that the original publication in this journal is cited, in accordance with accepted academic practice. No use, distribution or reproduction is permitted which does not comply with these terms.



# Regional COVID-19 Dynamics: Surrogate Synchrony in Case Infection Rates

**Samantha Robinson\***

*Department of Mathematical Sciences, University of Arkansas, Fayetteville, AR, United States*

## OPEN ACCESS

### Edited by:

Reza Lashgari,  
Shahid Beheshti University, Iran

### Reviewed by:

Wolfgang Tschacher,  
University of Bern, Switzerland  
Ronan Lordan,  
University of Pennsylvania,  
United States

### \*Correspondence:

Samantha Robinson  
sewrob@uark.edu

### Specialty section:

This article was submitted to  
Infectious Diseases - Surveillance,  
Prevention and Treatment,  
a section of the journal  
Frontiers in Public Health

**Received:** 29 December 2020

**Accepted:** 02 August 2021

**Published:** 26 August 2021

### Citation:

Robinson S (2021) Regional  
COVID-19 Dynamics: Surrogate  
Synchrony in Case Infection Rates.  
Front. Public Health 9:647441.  
doi: 10.3389/fpubh.2021.647441

As many jurisdictions consider in-person learning strategies (including at Institutions of Higher Education, IHE), implementing travel restrictions or quarantines, and/or establishing interstate pacts to reduce COVID-19 spread, this study explores the degree to which COVID-19 case infection rates in a group of neighboring, Southern and Midwestern U.S. states (namely, Arkansas and its contiguous neighbors) are patterned in a non-random way known as synchrony. Utilizing surrogate synchrony (SUSY) to estimate the dyadic coupling between the COVID-19 case infection rate processes in this region from March to December 2020, results indicate that significant synchrony is present between Arkansas and three of its neighbors. The highest level of instantaneous synchrony occurs between Arkansas and Tennessee, with the next highest level occurring between Arkansas and Missouri. There is evidence of directionality in the synchrony, indicating that Arkansas case infection rates lead Mississippi while rates in Missouri and Tennessee lead Arkansas. The lagged cross-correlations suggest the greatest synchrony to occur between 3 and 6 days. To explore the effect of IHE reopening on COVID-19, synchrony is compared between pre- and post-reopening windows. Results suggested that, following reopening, there are gains in detectable synchrony and that COVID-19 is in-flowing to Arkansas from all of its neighboring states. Taken together, results suggest that there is spatiality to COVID-19 with neighboring states having case infection rates that are significantly synchronous at a lag time that would be expected based on symptom onset. This synchrony is potentially strengthened by the in-flow and cross-border movement of IHE students.

**Keywords:** COVID-19, dyadic processes, dynamic systems, synchrony, disease surveillance, disease prevention, regional dynamics

## INTRODUCTION

Severe Acute Respiratory Syndrome Coronavirus 2 (SARS-CoV-2), the virus that causes the Coronavirus Disease 2019 (COVID-19), was originally identified in the Chinese city of Wuhan, the capital city of the Hubei province, in December 2019. The Chinese government, in an effort to limit the spread of COVID-19, implemented large-scale social distancing measures, the strictest of which was the complete lockdown of Wuhan (1). Such measures were applauded by the World Health Organization (WHO) and models have demonstrated that tightly controlling the movement of people substantially reduces virus spread (1–3).

Despite Chinese lockdown measures and mitigation strategies, COVID-19 emerged all around the world and, by early 2020, was rapidly spreading throughout Europe and parts of the United States. By March the WHO had declared COVID-19 a pandemic (4). Additional lockdowns and stay-at-home orders of various forms were implemented across the world. California would be the first U.S. state to issue a mandatory stay-at-home order and, eventually, all but five U.S. states would issue some type of advisory order, shuttering businesses, and keeping schools closed to in-person instruction for the remainder of the spring (5).

By late April, attempts were already being made across the United States to strategically reopen (6). Many states drafted phased reopening plans with gating criteria while some states even participated in multi-state regional approaches, such as the Midwest Partnership, the Northeast Multi-State Council, and the Western States Pact (6). This regional approach to reopening is supported by preliminary evidence that COVID-19 disease transmission might have a spatiality that arises from local economic structures (7).

Van Pelt et al. noted that the pandemic forced Institutions of Higher Education (IHE) in the United States (i.e., institutions engaging in post-secondary, tertiary education) to transition to virtual instruction quickly during spring 2020, disrupting the operations of over 4,000 IHE and impacting the education of more than 25 million students (8). While much of the initial planning for reopening in April and May 2020 was focused on reopening specific sectors of the economy, primary and secondary schools as well as IHE also began to draft plans for fall instruction.

The College Crisis Initiative (C2i), an initiative of Davidson College, began surveying IHE to understand fall semester plans. Of approximately 3,000 IHE (including both public and private 2-year and 4-year institutions), only 10% committed to fully online instruction for the fall 2020 term (9). The remaining 90% of institutions, even if planning for fall instruction to be delivered primarily online, maintained that there would be some in-person coursework offered. With that promise of in-person, face-to-face instruction in IHE, cross-state movement of younger individuals would no longer be as tightly controlled as it had been during the spring and summer months. This increase in necessary cross-state movement of college students, a high proportion of which are likely to be asymptomatic (10, 11), had the potential to increase the spread of COVID-19. In fact, infections did spike and the virus death rate rose faster than the national average in counties across the United States where college students make up 10% or more of the population (12, 13).

The purpose of this study was to explore the regional dynamics of COVID-19 infections between a group of neighboring states in the Southern and Midwestern regions of the United States. Specifically, this study investigated the synchrony between Arkansas COVID-19 infections with that of its contiguous neighbors, while making particular note of any differences in synchrony observed before and after the August reopening of IHE in the region. Case infection rates of each state that are patterned or synchronized to a significant degree would suggest that the interacting processes driving COVID-19

in these neighboring states are or have become correlated at a level exceeding random chance (14). Detection of such synchrony could help inform higher education stakeholders, along with public health officials, about the case infection dynamics of a particular region and, thus, guide the development of recommendations for instructional plans at IHE during the pandemic.

## METHOD

### Regional Selection and Data Source

Arkansas has six contiguous neighbors: Louisiana, Mississippi, Missouri, Oklahoma, Tennessee, and Texas. While the state was one of only five U.S. states to never issue a stay-at-home order, many businesses and schools (including IHE) closed temporarily in the spring.

According to the most recent Rural Profile of Arkansas (15), Arkansas is a very rural state. When using the Office of Management and Budget Metropolitan Statistical Area county-based definition of rural, 41% of Arkansans live in rural counties as of 2017 compared to only 14% of the U.S. population as a whole. Despite the rural nature of the state, White House coronavirus task force reports leaked to the Center of Public Integrity reveal that Arkansas has been in the red zone since at least June in terms of cases and in the red zone for deaths since at least August (16–21). The virus spread is unyielding in Arkansas, which is currently (as of December 2020) in the red zone for cases, test positivity, deaths, and hospital admissions (21).

Arkansas has a number of IHE, a majority of which planned to reopen either in a hybrid or fully in-person manner for the fall 2020 term (9). Similar to the larger national picture of IHE fall instructional plans, approximately 10% of all 4-year IHE in the state planned to be fully online. However, that 10% represents only 0.57% of the 4-year IHE student enrollment in the state (9). At the largest IHE in the state, 46% of all enrolled students are from out of state and nearly 35% of all enrolled students come from contiguous neighbors of Arkansas (22).

Since one interest of the current study was to explore regional dynamics of COVID-19 infections with particular attention paid to cross-state travel following IHE reopening, Arkansas was selected given a unique combination of characteristics, namely,

- Arkansas has six contiguous neighbors, making it tied for the fifth most connected U.S. state.
- Two of six contiguous neighbors of Arkansas, Missouri and Tennessee, tie for having the most shared borders of any other states in the United States.
- Arkansas is a very rural state and, hypothetically, should have been shielded from virus transmission and spread in the early weeks and months of the pandemic.
- Following IHE reopening, Arkansas has continued to be listed in the red zone according to White House coronavirus task force reports and is in a critical stage with unyielding community transmission.
- More than 99% of students enrolled at 4-year IHE in the state were offered some in-person learning opportunities for fall 2020 and many of these students are from out of state.



Time series data of COVID-19 case infection rate 7-day moving averages were obtained on December 19, 2020, from the Centers for Disease Control and Prevention (CDC) COVID-19 Case Surveillance Public Use Data (23). According to the CDC, rates are calculated using U.S. Census Bureau, 2018, American Community Survey 1-year estimates and are shown as cases per 100,000 people, with the 7-day moving average of new cases calculated to smooth expected variability in daily counts. Time series used in the current study began on March 24 and ended on December 17, 2020. The start of each series was determined by selecting the first date on which each of all seven states had started reporting confirmed COVID-19 infections. The end of the series was selected to minimize the effect of an explainable December 18 outlier, as Texas began reporting probable cases on this day, resulting in a total of 184,758 cases reported in 1 day (23). It should be noted that all data used in this study is considered provisional according to the CDC (23).

All ethical standards of data collection were adhered to during this study. The COVID-19 Case Surveillance Public Use Data is publicly available and accessible through the CDC COVID Data Tracker (*c.f.* <https://covid.cdc.gov/covid-data-tracker>).

## Analytic Approach

All data pre-processing and analyses were performed in R (24).

Synchrony is roughly defined as the degree to which two interacting processes or systems are patterned or synchronized in timing and in the form in a non-random way (14, 25). Instantaneous synchrony would suggest that the systems are correlated beyond random chance with no lag time. However, synchrony can occur with a dynamic lag such that there is a direction of entrainment whereby one system entrains the other.

In order to detect synchrony that may not be instantaneous and to determine the direction of entrainment of the COVID-19 cases in these neighboring states, an algorithm based on time-lagged cross-correlations of bivariate time series was utilized in the current study, that is, the surrogate synchrony (SUSY, *c.f.* [www.embodiment.ch](http://www.embodiment.ch)) algorithm (26).

The bivariate time series is split into segments of a set size, with cross-correlations computed segment-wise at all time lags up to a selected maximum lag time. The lagged cross-correlations are transformed using Fisher's *Z* transformation to allow for aggregation, with a segment-wise synchrony represented by the average of all transformed, lagged cross-correlations within each segment. The segment synchronies are then aggregated with an overall synchrony determined by averaging over all segment-wise synchrony measures in the entire time period. Typically, absolute values of the lagged cross-correlations are utilized to detect "anti-phase" and "in-phase" synchrony, that is, consistently negative or positive associations. However, in order to differentiate between in-phase and anti-phase coupling, SUSY can be conducted without absolute lagged cross-correlation values.

Effect sizes and statistical significance can be assessed utilizing permutation. Randomized segment shuffling creates a permuted sampling distribution of the overall synchrony measure, which can then be utilized to determine effect sizes and statistical significance for synchrony measured with or without absolute values as well as for the direction of entrainment.

In the current study, the segment size for the dyadic time series was set to be 28 days with a maximum lag time of 7 days. Both absolute and non-absolute lagged cross-correlations were evaluated, and the direction of entrainment was of interest.

SUSY was implemented for the COVID-19 case infection rate 7-day moving averages between Arkansas and each of its contiguous neighbors for the entire time period from March to December as well as separately for each distinct pre- and post-IHE reopening time period.

## RESULTS

### Descriptive

Each state-level time series consisted of 269 days of provisional data on COVID-19 case and case infection rate 7-day moving averages. The pre- and post-IHE reopening time series consisted of ~130 and 139 days, respectively, from March to July and from August to December.

Despite an initial surge in Louisiana, driven mostly by cases in the New Orleans metro area where COVID-19 infection grew rapidly relative to other states in the early months of the pandemic (27), **Figure 1** reveals that the COVID-19 case rates in the region appear to be moving fairly synchronously.

Descriptive statistics for the 7-day moving average of cases and case infection rates is displayed in **Table 1** below for the entire period as well as for the pre- and post-reopening periods. Despite Texas experiencing more COVID-19 cases overall and during each of the two partitioned time periods, the case rate is actually highest in Tennessee and Arkansas overall. Additionally, the case infection rate increased from the pre- to post-reopening period for all states (see **Table 1**). In particular, Missouri and Oklahoma case infection rates increased at the steepest rate, with case infection rates increasing by over 400% from pre- to post-reopening while Arkansas and Tennessee both experienced nearly 250% increases in their average COVID-19 case infection rate from the early stages of the pandemic to the time period following IHE reopening (see **Table 1**).

These descriptive findings are in line with the recent surge of COVID-19 across the United States (regardless of fall IHE plans).

### Instantaneous Synchrony

Instantaneous synchrony was assessed using linear correlation between each pairwise, bivariate time series within the region from March to December at a time lag of 0 days. Results indicated that Arkansas COVID-19 case infection rates had the greatest instantaneous synchrony with Tennessee and Missouri, with linear correlation coefficients of 0.94–0.93, respectively. However, instantaneous synchrony with Arkansas COVID-19 case infection rates was significant for all neighboring states with linear correlation coefficients between 0.70 and 0.94.

Instantaneous synchrony with Arkansas during the pre-reopening period from March to July was significant for all neighboring states with linear correlation coefficients between 0.74 and 0.93. Instantaneous synchrony with Arkansas increased for three of the six neighboring states following IHE reopening: Louisiana, Missouri, and Tennessee.

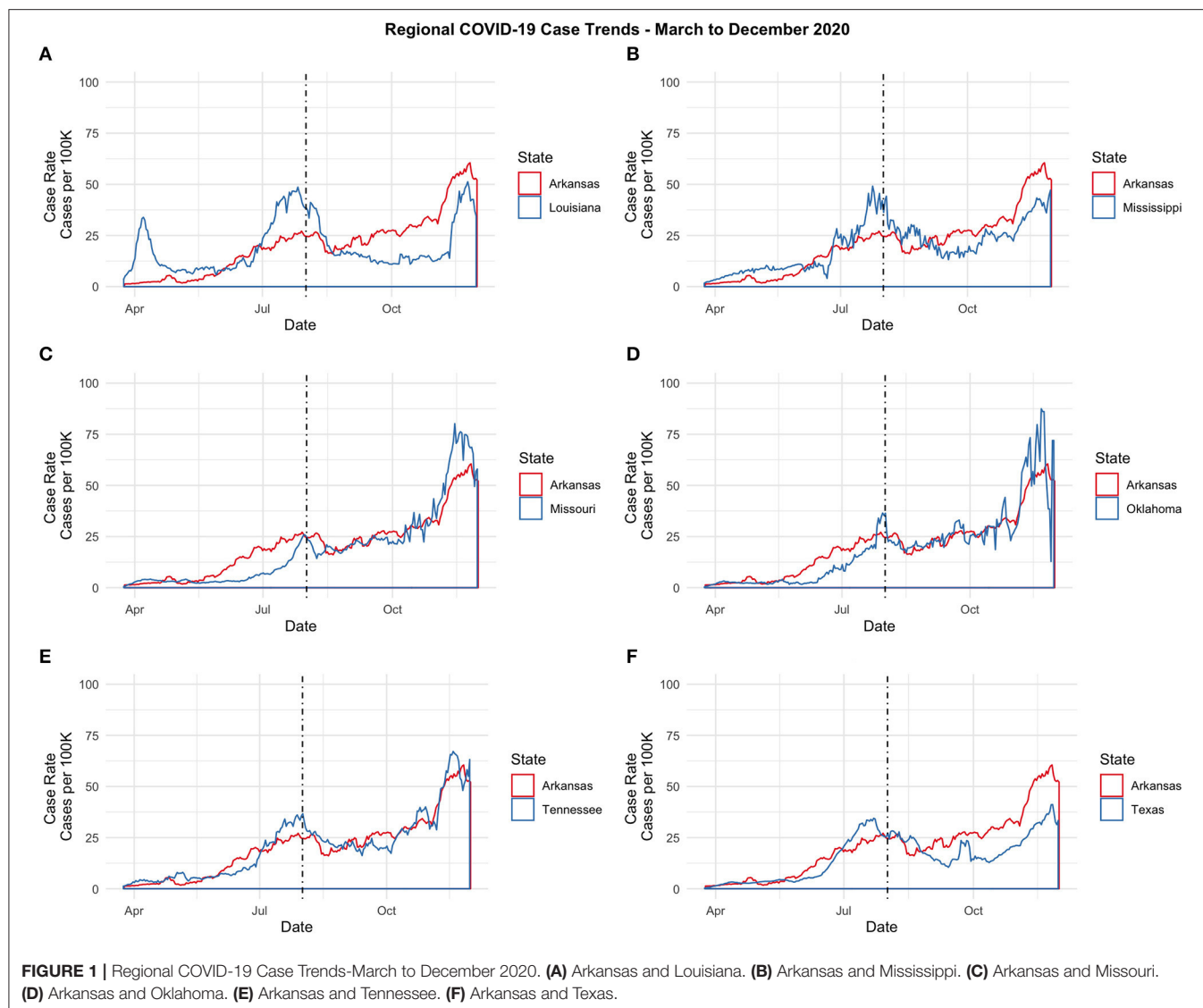


**TABLE 1 |** Means and standard deviations by state and time period for COVID-19 case and case rate 7-day moving averages.

| State       | Overall<br>(N = 269) |             | March-July<br>(N = 130) |             | August-December<br>(N = 139) |             |
|-------------|----------------------|-------------|-------------------------|-------------|------------------------------|-------------|
|             | Cases                | Case Rate   | Cases                   | Case Rate   | Cases                        | Case Rate   |
| Arkansas    | 698 (551)            | 23.2 (18.3) | 308 (258)               | 10.2 (8.6)  | 1,064 (499)                  | 35.3 (16.6) |
| Louisiana   | 1,003 (677)          | 21.5 (14.5) | 848 (618)               | 18.2 (13.3) | 1,149 (698)                  | 24.7 (15.0) |
| Mississippi | 682 (478)            | 22.8 (16.0) | 425 (347)               | 14.3 (11.6) | 922 (460)                    | 30.9 (15.4) |
| Missouri    | 1,294 (1,257)        | 21.1 (20.5) | 346 (324)               | 5.7 (5.3)   | 2,179 (1,155)                | 35.6 (18.9) |
| Oklahoma    | 903 (974)            | 22.9 (24.7) | 274 (317)               | 7.0 (8.0)   | 1,490 (1,015)                | 37.8 (25.7) |
| Tennessee   | 1,724 (1,605)        | 25.5 (23.7) | 755 (681)               | 11.2 (10.1) | 2,629 (1,692)                | 38.8 (25.0) |
| Texas       | 4,983 (3,450)        | 17.4 (12.0) | 3,046 (3,119)           | 10.6 (10.9) | 6,795 (2,679)                | 23.7 (9.3)  |

## Synchrony

While mean synchrony with Arkansas appeared to be highest for Texas, this synchrony appeared to be no more than random chance and the effect size was quite small (see **Table 2**). However, utilizing the surrogate synchrony algorithm to estimate the

dyadic coupling between the COVID-19 processes between Arkansas and its contiguous neighbors from March to December, results indicated that significant in-phase synchrony in case infection rates is present between Arkansas and three of its contiguous neighbors: Mississippi, Missouri, and Tennessee.

**TABLE 2 |** Overall synchrony with Arkansas ( $N = 269$ ).

| State       | $\bar{Z}_{Abs}$ | $ES_{Abs}$ | $p$ -Value | $ES_{NoAbs}$ | $ES_{Lead}$ |
|-------------|-----------------|------------|------------|--------------|-------------|
| Louisiana   | 0.415           | -0.064     | 0.7062     | 3.235        | -0.294      |
| Mississippi | 0.393           | 0.206      | 0.0402     | 0.223        | -0.281      |
| Missouri    | 0.442           | 0.292      | 0.0066     | 0.875        | 0.282       |
| Oklahoma    | 0.316           | -0.154     | 0.9047     | 0.951        | 0.334       |
| Tennessee   | 0.446           | 0.194      | 0.0498     | 1.092        | 0.396       |
| Texas       | 0.585           | 0.097      | 0.2048     | 0.633        | 0.165       |

$\bar{Z}_{Abs}$  indicates mean synchrony.

$ES_{Abs}$  indicates effect size of synchrony.

$ES_{NoAbs}$  indicates effect size of synchrony, with the ability to differentiate anti-phase and in-phase.

$ES_{Lead}$  indicates effect size for directionality of entrainment.

**TABLE 3 |** Comparison of March–July to August–December synchrony with Arkansas.

| State       | March–July ( $N = 130$ ) |             | August–December ( $N = 139$ ) |             |
|-------------|--------------------------|-------------|-------------------------------|-------------|
|             | $ES_{Abs}$               | $ES_{Lead}$ | $ES_{Abs}$                    | $ES_{Lead}$ |
| Louisiana   | -0.161                   | -0.131      | 0.132                         | 0.084       |
| Mississippi | 0.180                    | -0.580      | 0.190                         | 0.279       |
| Missouri    | 0.221                    | 0.690       | 0.344                         | 1.150       |
| Oklahoma    | -0.290                   | -0.111      | 0.333                         | 0.868       |
| Tennessee   | 0.252                    | 0.858       | 0.417                         | 0.499       |
| Texas       | 0.011                    | 0.222       | 0.241                         | 0.285       |

$ES_{Abs}$  indicates effect size of synchrony.

$ES_{Lead}$  indicates effect size for directionality of entrainment.

Missouri had the highest level of overall synchrony with Arkansas during the time period ( $\bar{Z}_{Abs} = 0.44$ ,  $ES_{Abs} = 0.29$ ,  $p < 0.01$ ). Positive effect sizes when no absolute cross-correlation values are utilized in SUSY, as indicated by  $ES_{NoAbs}$ , suggest in-phase synchrony. The highest levels of in-phase synchrony with Arkansas were detected in Louisiana, Tennessee, Oklahoma, and Missouri.

The effect size for the directionality of entrainment, as indicated by  $ES_{Lead}$ , suggests that COVID-19 case infection rates in Arkansas somehow entrain those in Louisiana and Mississippi, whereas the rates in the remaining neighbor states entrain the process in Arkansas.

Lagged cross-correlations for the entire bivariate time series were calculated, with the highest observed lagged correlations existing between Arkansas and Tennessee at a lag of 3–6 days.

## Pre- and Post-reopening Synchrony

To further explore the potential effect of IHE reopening on the regional synchrony of COVID-19, synchrony was examined for the shorter pre- and post-reopening windows.

During the early months of the pandemic, effect sizes indicate that the magnitude of synchrony with Arkansas was greatest for Tennessee and Missouri, with Arkansas being largely entrained by the COVID-19 infection rate trends in these states (see Table 3).

Following IHE reopening and subsequent cross-border travel, moderate gains in the magnitude of in-phase synchrony with Arkansas were observed for all neighbor states. While the magnitude of synchrony was still greatest between Arkansas and

two of its contiguous neighbors, Tennessee and Missouri, the directionality of entrainment effect sizes indicated that COVID-19 was predominantly in-flowing to Arkansas from all of its neighbors. The magnitude of observed entrainment for COVID-19 with Arkansas, while increasing in magnitude for all states except Tennessee, reversed direction for Oklahoma and was greatest for Missouri and Oklahoma following IHE reopening (see Table 3).

It appears that there is a spatiality to COVID-19, with certain neighboring states having case infection rates that are significantly synchronized in timing and in form with moderate-to-large effect sizes. This significant synchrony within the region is in stark contrast to the non-significant synchrony in case infection rates that was observed during the same time period between Arkansas and a non-neighboring region, such as New York city (see Supplementary Figure 1).

The synchrony of contiguous neighbors within a spatial region appears to be greatest at a lag time consistent with COVID-19 symptom onset. Using Google COVID-19 Community Mobility Reports, Arkansas movement from the pre- to post-reopening windows did increase, with a 19% increase in workplace mobility, a 26% increase in retail mobility, and a nearly 70% increase in transit mobility (28). Accordingly, this synchrony is potentially intensified as resultant cross-border movements and community mobility increase following IHE reopening.

## DISCUSSION

Despite immense adjustments to instruction at IHE, a *New York Times* survey of nearly 2,000 IHE revealed that as of December 11, 2020, nearly 400,000 cases and almost 100 deaths were linked to such institutions (29). As noted by Walke et al., young adults contributed to large regional COVID-19 surges in the Southern United States during the summer months and, with the reopening of IHE, the virus spread would not be limited to the campus community; IHE function within their surrounding communities and virus spread within IHE necessarily poses a risk for areas where they are located (30). Following IHE reopening, case infections and deaths did increase at rates above the national average in communities with student populations of ~10% or more (12, 13).

Facing financial consequences if some level of in-person instruction was not offered, IHE implemented a variety of strategies to mitigate and prevent the spread of COVID-19 on campus during fall 2020 (30). Despite these strategies, IHE became a potential source of community spread in many parts of the United States (12, 13, 29). While transmission among students, staff, faculty, and the greater community is complex, testing proved one possible strategy to effectively minimize the spread at IHE allowing for early detection, more effectual contact tracing, and the implementation of rapid isolation and quarantine. However, previous research suggests that testing strategies at IHE should involve repeated testing and, potentially, testing that occurs every 2 days (8, 31).

As noted by Bradley et al. and, especially given the financial constraints already placed on many IHE during this time, reopening plans that require testing every 2 days are simply not feasible for all campuses (32). However, a combination

of strategies and behavioral interventions could be nearly as effective. With financial consequences still more grave and an escalating winter surge of COVID-19 throughout the United States, additional planning for how IHEs might best approach instruction in 2021 to maintain financial viability while safeguarding public health of the broader community is essential.

IHE campus communities are unavoidably linked and intertwined with their surrounding communities, requiring close partnerships between the two (30). The results of the current study suggest that this inevitable interrelationship between campus communities and surrounding communities is potentially much broader in scope, with neighboring areas (e.g., contiguous states from which student populations are drawn) displaying significant COVID-19 synchrony with one another. Utilizing surrogate synchrony analysis, results suggest that a particular state could: (1) examine the synchrony over time of COVID-19 with particular neighbors, which need not be defined as contiguous states, (2) determine the directionality of entrainment, (3) analyze the impact of particular interventions and/or reopening, and (4) use such analyses to inform the development of IHE and public health policy measures to slow the spread of COVID-19. For instance, if synchrony is detected with the direction of entrainment in-flowing to a particular state or campus community, IHE testing resources could be targeted so that students first arriving on campus from particularly synchronous areas receive more repetitive testing compared to other students. Alternatively, detectable synchrony could guide decisions about the timing of IHE holiday/vacation breaks and/or whether or not to allow students to engage in cross-state or cross-region travel.

There are limitations to the current study. The CDC data are provisional in nature. Additionally, state reporting of data differed over the period from March to December. Some states reported confirmed cases and, then, began reporting both confirmed and probable cases while some states were still only reporting confirmed cases as late as December 17, 2020. Additionally, all reported data on COVID-19 cases were necessarily connected to testing availability, which may have differed between the U.S. states considered in this study at different time points during the study period. Different age groups and other individuals that might have presented as asymptomatic infections and, consequently, were less likely to be tested also suggested that the data used in this study actually underestimated the infection. Even if tested, testing in particular locations also had different turnaround times, resulting in different case reporting delays for the various states. Due to the variability of the COVID-19 cases reported daily, the data utilized in the study involved 7-day moving averages that could have inflated some cross-correlation calculations within the SUSY algorithm. Moreover, the number of observations in each time series, especially when looking at pre- and post-reopening series, are relatively short when attempting to analyze longer-term trends and synchronous properties between regional neighbors. The relatively short length of the series also limits the statistical power and restricts alteration of algorithm parameters, such as segment size or maximum time lag. Additionally, the SUSY algorithm is a measure of dyadic coupling and, thus, has

been utilized multiple times in the current study to explore all pairwise, bivariate synchrony between Arkansas and its six contiguous neighboring states. Future work would look to extend the surrogate synchrony approach to more than two time series.

However, beyond extending the SUSY algorithm, future work could also involve the use of synchrony algorithms for virus surveillance across space and time, exploring the synchrony of COVID-19 or other infectious diseases between major travel hubs, such as highly connected major airports (i.e., “neighbors” in a transportation network). Future work could also look at the dyadic coupling and synchronous behavior of COVID-19 with other potentially correlated time series (e.g., weather patterns, economic measures, and mobility data.).

Keeping IHE students on campus is known to limit the mutual exposure between the campus and surrounding communities (30, 32). While many schools that implemented basic mitigation strategies (i.e., distancing, masking, hand hygiene, ventilation, and staying home when symptomatic) were able to prevent large outbreaks during fall 2020 (33), limiting secondary transmission by retaining isolated cohorts further minimized the risk of transmission. However, the politicization of the pandemic now prevents basic yet effective mitigation strategies, such as wearing a mask at some IHE, including in Arkansas (34). Additionally, shared/congregate housing is common in IHE, for example, dormitories, making isolation of cohorts and contact tracing further complicated. Therefore, without firm travel restrictions on the movement of students both in the surrounding local community and in cross-border travel, individual mobility of students is unlikely to decline to a level that would prevent the influx of COVID-19 or prevent any potential external outbreaks connected to the IHE (3). Despite limitations, this study suggests that there is a spatiality to COVID-19 that is not simply patterned on the local economy but also likely connected to the flow patterns of the IHE students within and across regions (7). Moreover, this study demonstrates how SUSY can be utilized to detect regional COVID-19 synchrony, to determine the direction of entrainment, to evaluate intervention effects on regional synchrony, and to guide targeted IHE and public health policy.

## DATA AVAILABILITY STATEMENT

Publicly available datasets were analyzed in this study. This data can be found here: COVID-19 Case Surveillance Public Use Data is accessible through the CDC COVID Data Tracker: <https://covid.cdc.gov/covid-data-tracker>.

## AUTHOR CONTRIBUTIONS

The author confirms being the sole contributor of this work and has approved it for publication.

## SUPPLEMENTARY MATERIAL

The Supplementary Material for this article can be found online at: <https://www.frontiersin.org/articles/10.3389/fpubh.2021.647441/full#supplementary-material>



## REFERENCES

- Yuan Z, Xiao Y, Dai Z, Huang J, Zhang Z, Chen Y. Modelling the effects of Wuhan's lockdown during COVID-19, China. *Bull World Health Organ.* (2020) 98:484–94. doi: 10.2471/BLT.20.254045
- Kraemer MUG, Yang CH, Gutierrez B, Wu CH, Klein B, Pigott DM, et al. The effect of human mobility and control measures on the COVID-19 epidemic in China. *Science.* (2020) 368:493–7. doi: 10.1126/science.abb4218
- Vinceti M, Filippini T, Rothman KJ, Ferrari F, Goffi A, Maffei G, et al. Lockdown timing and efficacy in controlling COVID-19 using mobile phone tracking. *E Clin Med.* (2020) 25:100457. doi: 10.1016/j.eclinm.2020.100457
- World Health Organization (WHO). *Coronavirus disease 2019 (COVID-2019). Situation Report 51.* Geneva: World Health Organization (2020).
- Moreland A, Herlihy C, Tynan MA, Sunshine G, McCord RF, Hilton C, et al. Timing of state and territorial COVID-19 stay-at-home orders and changes in population movement – United States, March 1–May 31, 2020. *MMWR Morb Mortal Wkly Rep.* (2020) 69:1198–203. doi: 10.15585/mmwr.mm6935a2
- National Governor's Association (NGA). *Summary of Public Health Criteria in Reopening Plans.* Available online at: <https://www.nga.org/coronavirus-reopening-plans/> (accessed December 01, 2020).
- Ascani A, Faggian A, Montresor S. The geography of COVID-19 and the structure of local economies: The case of Italy. *J Reg Sci.* (2020) 61:407–41. doi: 10.1111/jors.12510
- Van Pelt A, Glick HA, Yang W, Rubin D, Feldman M, Kimmel SE. Evaluation of COVID-19 testing strategies for repopulating college and university campuses: a decision tree analysis. *J Adolesc Health.* (2021) 68:28–34. doi: 10.1016/j.jadohealth.2020.09.038
- The College Crisis Initiative (C2i) @ Davidson College. Available online at: <https://collegecrisis.org/> (accessed November 29, 2020).
- Ebell MH, Chupp C, Bentivegna M. A high proportion of SARS-CoV-2-infected university students are asymptomatic. *J Fam Pract.* (2020) 69:428–9. doi: 10.12788/jfp.0102
- Oran DP, Topol EJ. Prevalence of asymptomatic SARS-CoV-2 infection : a narrative review. *Ann Intern Med.* (2020) 173:362–7. doi: 10.7326/M20-3012
- Watson S, Hubler S, Ivory D, Gebeloff R. *A New Front in America's Pandemic: College Towns.* Available online at: <https://www.nytimes.com/2020/09/06/us/colleges-coronavirus-students.html> (accessed December 10, 2020).
- Ivory D, Gebeloff R, Mervosh S. *Young People Have Less Covid-19 Risk, but in College Towns, Deaths Rose Fast.* Available online at: [https://www.nytimes.com/2020/12/12/us/covid-colleges-nursing-homes.html?action=click&pgtype=Article&state=default&module=styl-n-coronavirus-schools-reopening&region=MAIN\\_CONTENT\\_3&context=storyline\\_keepup\\_recirc](https://www.nytimes.com/2020/12/12/us/covid-colleges-nursing-homes.html?action=click&pgtype=Article&state=default&module=styl-n-coronavirus-schools-reopening&region=MAIN_CONTENT_3&context=storyline_keepup_recirc) (accessed December 13, 2020).
- Moulder RG, Boker SM, Ramseyer F, Tschacher W. Determining synchrony between behavioral time series: an application of surrogate data generation for establishing falsifiable null-hypotheses. *Psychol Meth.* (2018) 23:757–73. doi: 10.1037/met0000172
- Miller W, Knapp T. *Rural Profile of Arkansas 2019: Social & Economic Trends Affecting Rural Arkansas.* Available online at: <https://www.uaex.edu/publications/pdf/MP551.pdf>. Published March 01, 2019 (accessed December 20, 2020).
- White House Coronavirus Task Force State Report 6.23.2020. Available online at: <https://assets.documentcloud.org/documents/7049057/50-States-06-23-20-Report.pdf> (accessed December 15, 2020).
- White House Coronavirus Task Force State Report 7.14.2020. Available online at: <https://assets.documentcloud.org/documents/6990125/Governor-s-Report-14-July-20.pdf> (accessed December 15, 2020).
- White House Coronavirus Task Force State Report 8.23.2020. Available online at: <https://assets.documentcloud.org/documents/7273581/50-States-08-23-20-Task-Force-Report.pdf> (accessed December 15, 2020).
- White House Coronavirus Task Force State Report 9.13.2020. Available online at: <https://assets.documentcloud.org/documents/7273583/50-States-09-13-20-Task-Force-Report.pdf> (accessed December 15, 2020).
- White House Coronavirus Task Force State Report 11.22.2020. Available online at: [https://assets.documentcloud.org/documents/20418114/50-states-11\\_22\\_20-report.pdf](https://assets.documentcloud.org/documents/20418114/50-states-11_22_20-report.pdf) (accessed December 15, 2020).
- White House Coronavirus Task Force State Report 12.13.2020. Available online at: [https://assets.documentcloud.org/documents/20433022/50\\_state\\_12\\_13\\_2020.pdf](https://assets.documentcloud.org/documents/20433022/50_state_12_13_2020.pdf) (accessed December 15, 2020).
- University of Arkansas (UA) Office of Institutional Research and Assessment (OIRA). *2019-2020 Mini Fact Book.* Available online at: <https://oir.uark.edu/quickfacts/factbook-2019-2020.pdf> (accessed December 20, 2020).
- Centers for Disease Control Prevention (CDC). *Department of Health and Human Services, Centers for Disease Control and Prevention.* Available online at: <https://covid.cdc.gov/covid-data-tracker> (accessed December 19, 2020).
- R Core Team. *R: A Language and Environment for Statistical Computing.* Vienna: R Foundation for Statistical Computing (2020).
- Bernieri FJ, Rosenthal R. Interpersonal coordination: behavior matching and interactional synchrony. In: Feldman RS, Rime B, editors. *Fundamentals of Nonverbal Behavior. Studies in Emotion & Social Interaction.* New York, NY: Cambridge University Press (1991). p. 401–32.
- Tschacher W, Haken H. *The Process of Psychotherapy – Causation and Chance.* Cham: Springer (2019).
- Governor's Office of Homeland Security & Emergency Management. *COVID-19 Louisiana Case Info.* (2020). Available online at: <https://gov.louisiana.gov/assets/docs/covid/govCV19Brief-2.pdf> (accessed December 15, 2020).
- Google LLC. *Arkansas google COVID-19 community mobility reports.* Available online at: <https://www.google.com/covid19/mobility> (accessed July 01, 2021).
- The New York Times. *Tracking the Coronavirus at U.S. Colleges and Universities.* Available online at: <https://www.nytimes.com/interactive/2020/us/covid-college-cases-tracker.html> (accessed December 12, 2020).
- Walke HT, Honein MA, Redfield RR. Preventing and responding to COVID-19 on college campuses. *JAMA.* (2020) 324:1727–8. doi: 10.1001/jama.2020.20027
- Paltiel AD, Zheng A, Walensky RP. Assessment of SARS-CoV-2 screening strategies to permit the safe reopening of college campuses in the United States. *JAMA Netw Open.* (2020) 3:e2016818. doi: 10.1001/jamanetworkopen.2020.16818
- Bradley EH, An M, Fox E. Reopening colleges during the coronavirus disease 2019 (COVID-19) pandemic—one size does not fit all. *JAMA Netw Open.* (2020) 3:e2017838. doi: 10.1001/jamanetworkopen.2020.17838
- Lordan R, FitzGerald GA, Grosser T. Reopening schools during covid-19. *Science.* (2020) 369:1146–6. doi: 10.1126/science.abe5765
- Acts - Arkansas state legislature. *Arkansas Act 1002.* Available online at: <https://www.arkleg.state.ar.us/Acts/> (accessed July 02, 2021).

**Conflict of Interest:** The author declares that the research was conducted in the absence of any commercial or financial relationships that could be construed as a potential conflict of interest.

**Publisher's Note:** All claims expressed in this article are solely those of the authors and do not necessarily represent those of their affiliated organizations, or those of the publisher, the editors and the reviewers. Any product that may be evaluated in this article, or claim that may be made by its manufacturer, is not guaranteed or endorsed by the publisher.

Copyright © 2021 Robinson. This is an open-access article distributed under the terms of the Creative Commons Attribution License (CC BY). The use, distribution or reproduction in other forums is permitted, provided the original author(s) and the copyright owner(s) are credited and that the original publication in this journal is cited, in accordance with accepted academic practice. No use, distribution or reproduction is permitted which does not comply with these terms.



# Follow-Ups on Persistent Symptoms and Pulmonary Function Among Post-Acute COVID-19 Patients: A Systematic Review and Meta-Analysis

Qiuyue Long<sup>1,2</sup>, Jiwei Li<sup>1,2</sup>, Xiaoyi Hu<sup>1,2</sup>, Yangyuyan Bai<sup>1,2</sup>, Yali Zheng<sup>1\*</sup> and Zhancheng Gao<sup>1,3\*</sup>

<sup>1</sup> Department of Respiratory, Critical Care and Sleep Medicine, Xiang'an Hospital of Xiamen University, Xiamen, China,

<sup>2</sup> School of Medicine, Xiamen University, Xiamen, China, <sup>3</sup> Department of Respiratory Medicine, Peking University People's Hospital, Beijing, China

## OPEN ACCESS

### Edited by:

Reza Lashgari,  
Shahid Beheshti University, Iran

### Reviewed by:

Konstantinos Samitas,  
Athens Chest Hospital Sotiria, Greece  
Francesco Poti,  
University of Parma, Italy

### \*Correspondence:

Yali Zheng  
zcgao@bjmu.edu.cn  
Zhancheng Gao  
yali\_zheng@126.com

### Specialty section:

This article was submitted to  
Pulmonary Medicine,  
a section of the journal  
Frontiers in Medicine

**Received:** 29 April 2021

**Accepted:** 16 July 2021

**Published:** 03 September 2021

### Citation:

Long Q, Li J, Hu X, Bai Y, Zheng Y and  
Gao Z (2021) Follow-Ups on  
Persistent Symptoms and Pulmonary  
Function Among Post-Acute  
COVID-19 Patients: A Systematic  
Review and Meta-Analysis.  
Front. Med. 8:702635.  
doi: 10.3389/fmed.2021.702635

**Objective:** As the number of recovering COVID-19 patients increases worldwide, the persistence of symptoms and signs through the post-acute phase indicates an urgent need for prolonged follow-up care. To explore existing data about post-acute COVID-19 syndrome, this meta-analysis assesses the prevalence of persistent manifestations in multiple systems and abnormalities in lung function, as well as their related risks in patients with various severities.

**Methods:** Articles about discharged COVID-19 patients (published from January 1, 2020 to February 23, 2021) were obtained by searching four databases. Cohort studies with follow-up periods >1 month post-discharge or >2 months post-admission were included.

**Results:** A total of 4,478 COVID-19 patients from 16 cohort studies were included in this meta-analysis. Fatigue or weakness (47%) were the most prevalent physical effects of post-acute COVID-19 syndrome, while psychosocial (28%) symptoms were the most common manifestations among several systems. Abnormalities in lung function of recovering patients, i.e., DLCO <80% (47%, 95% CI: 32–61%) persisted for long periods. Severe patients were more likely to present joint pain (OR 1.84, 95% CI: 1.11–3.04) and decreased lung functions compared with non-severe patients, with pooled ORs for abnormal TLC, FEV1, FVC, and DLCO of 3.05 (95% CI: 1.88–4.96), 2.72 (95% CI: 1.31–5.63), 2.52 (95% CI: 1.28–4.98), and 1.82 (95% CI: 1.32–2.50), respectively.

**Conclusions:** Our research indicates that patients recovering from COVID-19 manifest long-term, multi-system symptoms, and the adverse effects on psychosocial health and lung functions were the most extensive and persistent. These findings together may facilitate much needed in-depth study of clinical treatments for long-term, post-acute phase symptoms that affect a great number of recovering COVID-19 patients.

**Keywords:** SARS-CoV-2, post-acute COVID-19 syndrome, post-discharge, epidemiology, meta-analysis

## INTRODUCTION

Coronavirus disease 2019 (COVID-19) is a respiratory disease caused by a highly transmissible and pathogenic virus, the severe acute respiratory syndrome coronavirus 2 (SARS-CoV-2) (1). So far, more than 100 million people worldwide have contracted COVID-19. Recovery is gradual and it is estimated that most COVID-19 patients take an average of 2–6 weeks to recover. However, symptoms may persist for weeks or even months in a subset of patients even after their initial hospital discharge. In addition, some patients may even manifest medical complications or sequelae that adversely affect their long-term health (2, 3). This phenomenon has been described as “long COVID-19,” also known as “post-acute COVID-19 syndrome,” which is defined as persistent signs and symptoms that emerge during or after SARS-CoV-2 infection, usually lasting more than 4 weeks and with all other possible diagnoses excluded (4).

A clinical investigation (5) has found that COVID-19 survivors were more likely to develop medical sequelae than patients never infected with SARS-CoV-2, strongly suggesting that these signs and symptoms may indeed be adverse consequences of COVID-19. A recent study (6) reported that 32% of hospitalized COVID-19 patients presented with one to two symptoms at 2 months after disease onset, 55% presented three or more symptoms, while only 12.6% had no symptoms at all. In another study (7), more than 70% of patients still exhibited at least one symptom even at 6 months after onset. With the steady increase in patients recovering from COVID-19 globally, public focus has gradually shifted away from the rapid disease progression in the acute phase to the long-term health effects of COVID-19. In the meanwhile, there is an increasingly urgent need for clear guidelines regarding how to alleviate the burden of COVID-19 symptomatic aftershock.

Although lungs are the primary target of SARS-CoV-2 infection, evidence from the acute phase also has shown that extra-pulmonary manifestations of COVID-19 can occur in a surprisingly wide range of organs (8). The underlying pathophysiological mechanisms (9–11) include direct viral invasion, systemic inflammation, endothelial injury mediated by infection, as well as disorders of the immune system among others. Therefore, the adverse effects of post-acute COVID-19 may similarly involve multiple organ systems. Based on previous studies of Severe Acute Respiratory Syndrome (SARS) and Middle East Respiratory Syndrome (MERS) survivors (12, 13), several short-term and potential long-term outcomes have been proposed for SARS-CoV-2 (14). Specifically, the relevant adverse consequences mainly occur in the immune, respiratory, cardiovascular, neurological, and gastrointestinal systems as well as affecting mental health. Furthermore, a small proportion of patients with severe or critical diseases, especially those who have undergone ventilator support in an intensive care unit (ICU), were found to have a higher risk of developing organ-specific, functional, and cognitive disorders than those with less severe diseases (15). Currently, guidelines based on epidemiological evidence from other coronaviruses have been proposed for the rehabilitation of post-COVID-19 patients (16, 17). However, it is still necessary to further determine the indeed long-term adverse

symptoms and functional abnormalities of the post-COVID-19 syndrome and explore closely related risk factors to establish targeted and effective intervention measures.

To this end, we performed a meta-analysis of cohort studies that described the residual symptoms and pulmonary function tests (PFT) of discharged COVID-19 patients (including those discharged from ICU) to determine the adverse effects on multiple systems and differences between severe and non-severe patients in the post-acute phase. Our findings will provide clinicians and physicists with a summary of information relevant to the rehabilitation, treatment, and management of post-acute COVID-19 patients, thus facilitating better preparedness and management of the long-term consequences of the global pandemic.

## METHODS

This meta-analysis was conducted using the guidelines described in the Preferred Reporting Project of Systematic Review and Meta-Analysis (PRISMA) and registered in PROSPERO under study number CRD42021238955.

### Search Strategy and Selection Criteria

A systematic search was conducted on studies published in PubMed, Embase, Web of Science, and WHO COVID-19 Database from January 1, 2020 to February 23, 2021. Search terms including “COVID-19,” “SARS-CoV-2,” “2019-nCoV” and “novel coronavirus” were used to find articles related to the novel coronavirus pandemic. To obtain literature pertaining specifically to post-acute outcomes, the terms “long-term effect,” “post-acute,” “post-discharge,” “long-COVID,” and “chronic-COVID” were used to screen the hits obtained using the broader COVID-19 search terms. Only articles in English were considered for inclusion. To identify missing studies, we checked the bibliography of each selected paper. Records were managed by EndNote X9.0 software to exclude duplicates. Full-text screening was performed for publications describing systemic manifestations and pulmonary function of adult hospitalized COVID-19 patients. Only cohort studies were used for analysis. Studies were excluded for the following criteria: (a) they were reviews, preprints, comments, editorials, or case reports; (b) lacked data regarding primary outcomes; or (c) if they included outpatients or had insufficient follow-up exams (<1 month post-discharge or <2 months post-admission).

### Risk of Bias Assessment

The Newcastle-Ottawa scale (NOS) was used to assess the risk of bias in non-randomized cohort studies through eight criteria across three overall categories related to study rigor, including participant selection methodology, comparability with other studies, and evaluation of outcomes. Quality was assessed by scoring each publication with a star based on whether it used the most reliable reporting for each of eight criteria (with some criteria allowing multiple stars). The highest possible score was a full score of 9 stars. Cohort studies that received <6 stars, 6 to

7 stars, or more than 7 stars had a high, medium, or low risk of bias, respectively.

## Data Extraction and Definitions

The two reviewers (XH and YB) who performed the literature search also independently extracted the relevant data from the included studies. Disagreements were resolved with a third reviewer (QL) or by consensus. The following variables were extracted: study features (first author, year, country, study design), population characteristics (age, sex, sample sizes, follow-ups, severity groups), and outcomes (multi-system symptoms and lung functions). The diagnosis of COVID-19 was based on WHO guidelines and confirmed by reverse transcription-polymerase chain reaction (RT-PCR), next-generation sequencing, or chest imaging. Severe COVID-19 was self-defined by each of the included studies. For studies lacking a definition of disease severity, severe cases were defined as those with a WHO ordinal score of 5 (noninvasive ventilation or high flow oxygen therapy), 6 (intubation and mechanical ventilation), 7 (additional organic support), or patients admitted to the ICU. According to the included studies, symptoms other than fatigue or weakness were categorized as cardiopulmonary, neurological, gastrointestinal, musculoskeletal, psychosocial system, or other. Total lung capacity (TLC), diffusion capacity for carbon monoxide (DLCO), forced expiratory volume in the first second (FEV1) and forced vital capacity (FVC) <80% of the predicted value, as well as FEV1/FVC <70% were defined as abnormal lung functions.

## Data Analysis

Data were analyzed by Stata MP16.0 software (Stata Corp LP, College Station, Texas, USA). Symptoms and abnormal lung functions appeared in at least three studies that were included in the meta-analysis. The prevalence was calculated based on the occurrence of events, standard error (SE), and 95% confidence intervals (CI) in each study. Odds ratio (OR) was used to describe the risk of events in severe patients compared with non-severe patients. Heterogeneity was determined by Cochran's  $Q$ -test and  $I^2$  statistical analysis. A fixed-effect model was applied for studies with acceptable levels of heterogeneity ( $I^2 < 50\%$ ,  $P > 0.1$ ). Otherwise, a random-effects model was used to adjust for significant heterogeneity. Sensitivity analysis was used to evaluate the robustness of the comprehensive results by re-analyzing the data in aggregate, independently of individual studies.

## RESULTS

### Study Selection and Risk of Bias

The literature search yielded a total of 2,011 articles, 2,007 of which were obtained through database searches and the remaining four articles were identified through other search methods (Figure 1). Following de-duplication, 1,293 records were reviewed by screening titles and abstracts, of which 58 appeared to be eligible for this analysis. After full-text screening, 16 cohort studies (5, 7, 18–31) were found to meet the inclusion criteria, and were thus used in the meta-analysis. These studies

were mainly from Europe, China, and the United States. Of the 16 included studies, only 2 (12.5%) were rated as high quality ( $\geq 7$  stars) by NOS assessment, while the remaining studies were of moderate quality (ten studies with 6–7 stars; four studies with 5 stars), primarily due to poor comparability and/or outcome bias. Both post-acute symptoms and lung function indicators showed significant heterogeneity in our study. We therefore conducted sensitivity analysis and the results showed that no single publication affected the final pooled prevalence (see **Supplementary Figures**).

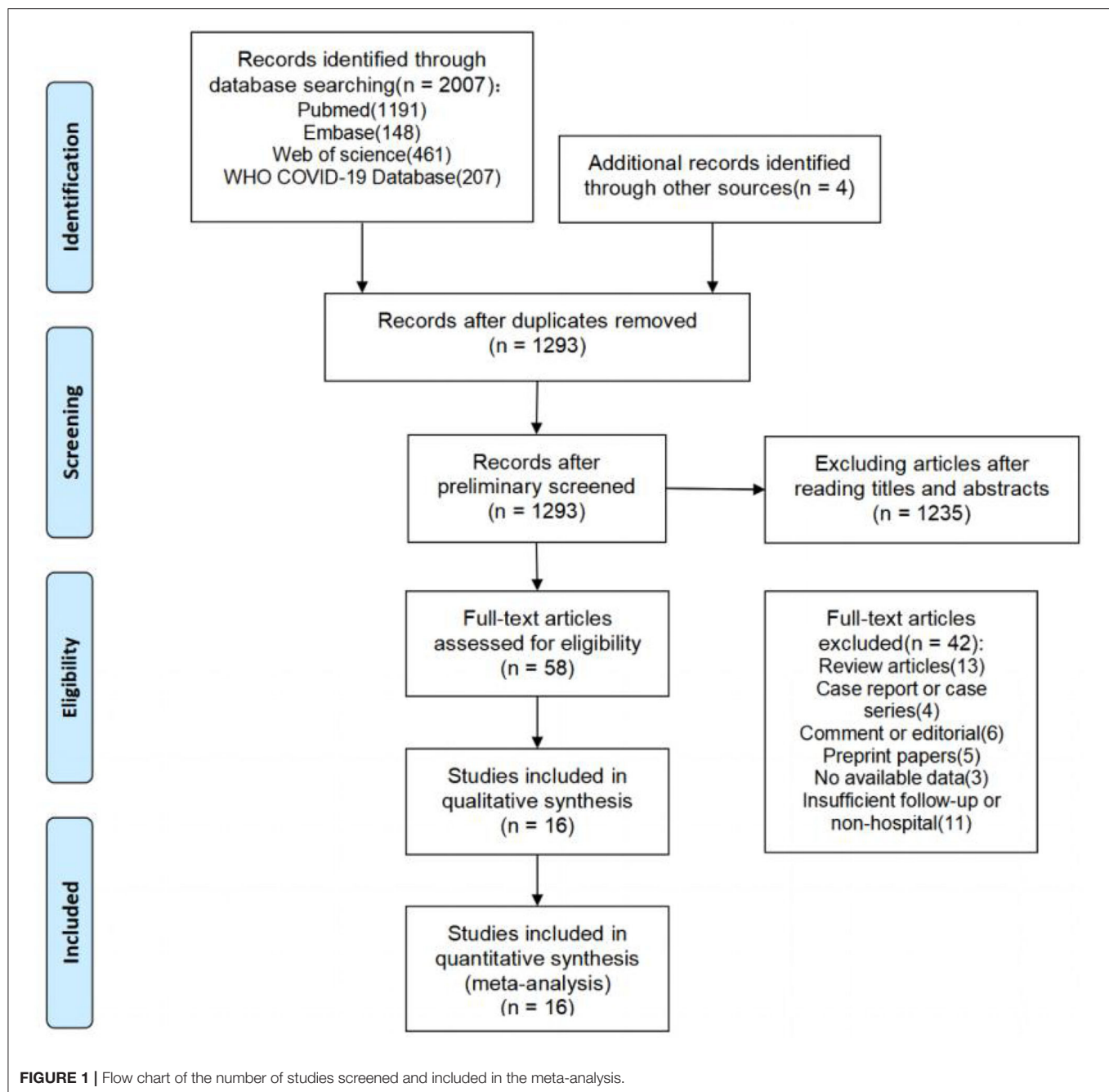
### Study Population Characteristics and Outcomes

The main characteristics of the included cohort studies are shown in **Table 1**. Most of the studies (10/12, 83.3%) included in this meta-analysis were prospective cohort studies. The combined total of 4,478 COVID-19 patients included in our analysis were diagnosed predominantly by RT-PCR, with sample sizes for each study ranging from 55 to 1,733 patients. Among them, 2,309 (51.56%) were men (median or mean ages generally between 50 and 60 years old). Study follow-ups lasted for 1–4 months post-discharge or 2–6 months post-admission. The manifestations of post-acute COVID-19 syndrome recorded in these studies included a wide range of multiple affected organs, involving the cardiopulmonary, neurological, musculoskeletal, gastrointestinal, and psychosocial systems (see **Supplementary Table 1**). The cardiopulmonary system had the widest spectrum of related symptoms, including chest pain, dyspnea, cough, sore throat, palpitation, and chest distress. Symptoms associated with the neurological system included memory impairment, cognitive impairment, headache, taste disorder, and smell disorder. Musculoskeletal symptoms included myalgia and joint pain. Gastrointestinal symptoms included diarrhea or vomiting, abdominal pain, and decreased appetite. Psychosocial manifestations included Post-Traumatic Stress Disorder (PTSD), anxiety or depression, attention deficit disorder, sleep difficulties, and hair loss. Fatigue or weakness, skin rash, fever, pain, discomfort, and dizziness, which were occasionally reported among discharged patients, were categorized into other symptoms. In addition, seven studies investigated abnormal lung function in post-acute patients. These studies included multiple parameters, such as DLCO for lung diffusion capacity, TLC for restrictive respiratory function, and FEV1 and FVC for obstructive respiratory function.

### Prevalence of Post-acute Manifestations in Multiple Organ Systems

As shown in **Table 2**, among several organ systems, psychosocial (28%, 95% CI 24–31%) manifestations were most common and the prevalence of its three symptoms including anxiety or depression, sleeping difficulty (27%, 95% CI 21–32%), and hair loss (24%, 95% CI 19–29%) was generally higher than most symptoms in other systems. Followed by cardiopulmonary (15%, 95% CI 13–17%) and neurological system (15%, 95% CI 12–19%), both had similar prevalence of overall symptoms. But the prevalence of their single symptom varied widely, especially





the cardiopulmonary, ranging from 5 to 33%. The next was the musculoskeletal system (13%, 95% CI 9–16%), including myalgia (13%, 95% CI 8–18%) and joint pain (12%, 95% CI 8–16%). In contrast, the gastrointestinal (7%, 95% CI 4–10%) had the lowest prevalence of symptoms. Other symptoms such as fever (2%, 95% CI 0–3%) and skin rash (3%, 95% CI 1–5%), were even rarer. In general, the most prevalent post-acute COVID-19 symptom was fatigue or weakness (47%, 95% CI 36–59%), then the memory impairment (35%, 95% CI 21–48%) and anxiety or depression (33%, 95% CI 23–43%), dyspnea (33%, 95% CI 22–43%) followed.

## Prevalence of Abnormal Lung Function

Pulmonary function tests (including spirometry, lung volume, and diffusion capacities) were reported for 894 subjects from seven studies (**Figure 2**). The overall prevalence of abnormalities in lung function was 20% (95% CI 13–17%), and included low diffusion capacity, reduced lung volume, or airflow obstruction. Impaired diffusion capacity (DLCO < 80%) was the most common abnormality, observed in six studies (47%, 95% CI 32–61%), followed by reduced lung volume measurements, including TLC < 80% (14%, 95% CI 9–18%), FVC < 80% (12%, 95% CI 1–23%), and FEV1 < 80% (7%, 95% CI 5–9%). Airflow

**TABLE 1 |** Main characteristics of included studies in the meta-analysis.

| Author                       | Country     | Study design               | COVID-19 diagnosis | Sample sizes | Age   | Sex (M %) | Follow-up time (days)  | Settings  | NOS assessment |
|------------------------------|-------------|----------------------------|--------------------|--------------|---|-----------|------------------------|---|----------------|
| Huang C                      | China       | Prospective cohort study   | RT-PCR             | 1,733        | Median 57.0 (IQR 47.0–65.0)                           | 52%       | PA:180                 | Scale 3 (439)<br>Scale 4 (1,172)<br>Scale 5–6 (122) | 8              |
| Qin W                        | China       | Prospective cohort study   | RT-PCR             | 647          | Mean 58.0 ( $\pm$ 15.0)                               | 44%       | PD:90                  | Severe (248)<br>Non-severe (399)                    | 8              |
| Sykes DL                     | UK          | Prospective cohort study   | RT-PCR             | 134          | Median 58.0 (range 25.0–89.0)                         | 65.7%     | PD:113 (range 46–167)  | Ward (107) ICU (27)                                 | 7              |
| Garrigues E                  | France      | Prospective cohort study   | RT-PCR CT          | 120          | Mean 63.2( $\pm$ 15.7)                                | 62.5%     | PA:110.9 ( $\pm$ 11.1) | Ward (96) ICU (24)                                  | 7              |
| van der Sar-van der Brugge S | Netherlands | Prospective cohort study   | RT-PCR             | 101          | Mean 66.4 ( $\pm$ 12.6)                               | 57.4%     | PD:42                  | Scale 3 (28) Scale 4 (73)                           | 7              |
| Jacobs LG                    | USA         | Prospective cohort study   | RT-PCR             | 183          | Median 57.0 (IQR 48.0–68.0)                           | 61.5%     | PD:35 ( $\pm$ 5)       | –   | 6              |
| Arnold DT                    | UK          | Prospective cohort study   | RT-PCR             | 110          | Median 60.0 (IQR 46.0–73.0)                           | 56%       | PD: 83 (IQR 74–88)     | Mild (27) Moderate (65) Severe (18)                 | 6              |
| Bellan M                     | Italy       | Prospective cohort study   | RT-PCR             | 238          | Median 61.0 (IQR 50.0–71.0)                           | 59.7%     | PD:120                 | –   | 6              |
| Halpin SJ                    | UK          | Prospective cohort study   | RT-PCR             | 100          | Median Ward 70.5 (range 20–93) ICU 58.5 (range 34–84) | 54%       | PD:48 ( $\pm$ 10.3)    | Ward (68) ICU (32)                                  | 6              |
| Suárez-Robles M              | France      | Prospective cohort study   | RT-PCR             | 134          | Mean 58.53 ( $\pm$ 18.53)                             | 46.3%     | PD:90                  | –   | 5              |
| Méndez R                     | Spain       | Prospective cohort study   | RT-PCR             | 179          | Median 57.0 (IQR 49–67)                               | 41.3%     | PD:60                  | –   | 5              |
| Raman B                      | UK          | Prospective cohort study   | RT-PCR             | 58           | Mean 55.4 ( $\pm$ 13.2)                               | 58.6%     | PA:60–90               | –   | 5              |
| Taboada M                    | Spain       | Prospective cohort study   | RT-PCR             | 91           | Mean 65.5( $\pm$ 10.4)                                | 64.8%     | PA:180                 | –   | 6              |
| Xiong Q                      | China       | Prospective cohort study   | RT-PCR             | 538          | Median 52.0 (IQR 41.0–62.0)                           | 45.5%     | PD: 97 (IQR 95–102)    | General (331)<br>Severe (180)<br>Critical (27)      | 7              |
| Zhao YM                      | China       | Retrospective cohort study | RT-PCR             | 55           | Mean 47.74 ( $\pm$ 15.49)                             | 58.18%    | PD:90                  | Mild (4) Moderate (47) Severe (4)                   | 5              |
| Huang Y                      | China       | Retrospective cohort study | RT-PCR NGS         | 57           | Mean 46.72 ( $\pm$ 13.78)                             | 45.6%     | PD:30                  | Severe (17)<br>Non-severe (4)                       | 6              |

CT, computed tomography; RT-PCR, reverse transcription polymerase chain reaction; NGS, next generation sequencing; IQR, interquartile range; PA, post admission; PD, post discharge; ICU, intensive care unit.

**TABLE 2 |** The prevalence of symptoms and manifestations in multiple systems.

| Outcomes            |                       | Studies | Effects             |                |                     |
|---------------------|-----------------------|---------|---------------------|----------------|---------------------|
|                     |                       |         | Prevalence (95% CI) | I <sup>2</sup> | p for heterogeneity |
| Fatigue or weakness |                       | 9       | 47% (36–59%)        | 97%            | < 0.01              |
| Cardiopulmonary     | Sputum                | 3       | 7% (1–13%)          | –              | –                   |
|                     | Chest pain            | 8       | 7% (5–10%)          | 95.29%         | < 0.01              |
|                     | Dyspnea               | 9       | 33% (22–43%)        | 97.83%         | < 0.01              |
|                     | Cough                 | 8       | 17% (11–22%)        | 95.01%         | < 0.01              |
|                     | Sore throat           | 4       | 5% (3–8%)           | 76.1%          | 0.01                |
|                     | Palpitation           | 4       | 11% (9–14%)         | 75.86%         | 0.01                |
|                     | Overall               |         | 15% (13–17%)        | 96.99%         | < 0.01              |
| Musculoskeletal     | Myalgia               | 6       | 13% (8–18%)         | 95.66%         | < 0.01              |
|                     | Joint pain            | 7       | 12% (8–16%)         | 88.46%         | < 0.01              |
|                     | Overall               |         | 13% (9–16%)         | 95.22          | < 0.01              |
| Neurological        | Memory impairment     | 4       | 35% (21–48%)        | 91.25%         | < 0.01              |
|                     | Headache              | 4       | 15% (3–26%)         | 95.56%         | < 0.01              |
|                     | Taste disorder        | 6       | 10% (6–13%)         | 77.03%         | < 0.01              |
|                     | Smell disorder        | 8       | 11% (8–14%)         | 80.59%         | < 0.01              |
|                     | Overall               |         | 15% (12–19%)        | 96.04%         | < 0.01              |
| Gastrointestinal    | Diarrhea or vomiting  | 5       | 3% (1–6%)           | 86.71%         | < 0.01              |
|                     | Decreased appetite    | 3       | 14% (5–23%)         | –              | –                   |
|                     | Overall               |         | 7% (4–10%)          | 93.6%          | < 0.01              |
| Psychosocial        | Anxiety or depression | 5       | 33% (23–43%)        | 92.18%         | < 0.01              |
|                     | Sleep difficulties    | 6       | 27% (21–32%)        | 83.83%         | < 0.01              |
|                     | Hair loss             | 3       | 24% (19–29%)        | –              | –                   |
|                     | Overall               |         | 28% (24–31%)        | 86.46%         | < 0.01              |
| Other               | Skin rash             | 3       | 3% (1–5%)           | –              | –                   |
|                     | Fever                 | 4       | 2% (0–3%)           | 82.87%         | < 0.01              |
|                     | Overall               |         | 2% (1–4%)           | 91.63%         | < 0.01              |

obstruction (FEV1/FVC < 70%) was relatively uncommon, and only reported in three studies (9%, 95% CI 0–18%).

### Risk of Post-acute Manifestations and Abnormal Lung Function in Severe Patients Compared to Non-severe Patients

We also compared the systemic symptoms and pulmonary functions between severe and non-severe COVID-19 patients. As shown in **Table 3** and **Figure 3**, severe patients were more likely to develop adverse manifestations of the musculoskeletal (OR 1.60, 95% CI 1.12–2.29), cardiopulmonary (OR 1.36, 95% CI 1.13–1.64), and psychosocial (OR 1.23, 95% CI 1.02–1.48) systems. More specifically, joint pain (OR 1.84, 95% CI 1.11–3.04), dyspnea (OR 1.52, 95% CI 1.12–2.06), palpitation (OR 1.57, 95% CI 1.07–2.30), and anxiety or depression (OR 1.42, 95% CI 1.03–1.97) were more prevalent among severe COVID-19 cases than in non-severe subjects. The occurrence of fatigue or weakness, the most common symptoms of post-acute COVID-19 syndrome, were not significantly different between the two groups.

In addition, severe COVID-19 patients were more likely to suffer from persistent abnormal pulmonary functions (OR 2.17,

95% CI 1.73–2.72). Lung volumes were significantly reduced in severe COVID-19 patients, including TLC < 80% (OR 3.05, 95% CI 1.88–4.96), FEV1 < 80% (OR 2.72, 95% CI 1.31–5.63), FVC < 80% (OR 2.52, 95% CI 1.28–4.98), and DLCO < 80% (OR 1.82, 95% CI 1.32–2.50). However, the PFT parameters FEV1/FVC < 70%, which indicated airway obstruction, showed no difference between groups.

### DISCUSSION

In the current study, we analyzed the data retrieved from 16 cohort studies with verified and hospitalized COVID-19 patients. Cumulatively, these studies reported a total of 29 multi-system symptoms associated with post-acute COVID-19, involving the cardiopulmonary (15%), neurological (15%), musculoskeletal (13%), gastrointestinal systems (7%), and psychosocial manifestations (28%). The most common symptoms were fatigue or weakness (47%), memory impairment (35%), anxiety or depression (33%), and dyspnea (33%), while DLCO < 80% (47%) was widely present among these post-acute phase patients. Patients who recovered from severe COVID-19 were more likely to develop joint pain (OR 1.84), dyspnea (OR 1.52), palpitation (OR 1.57), and anxiety or depression

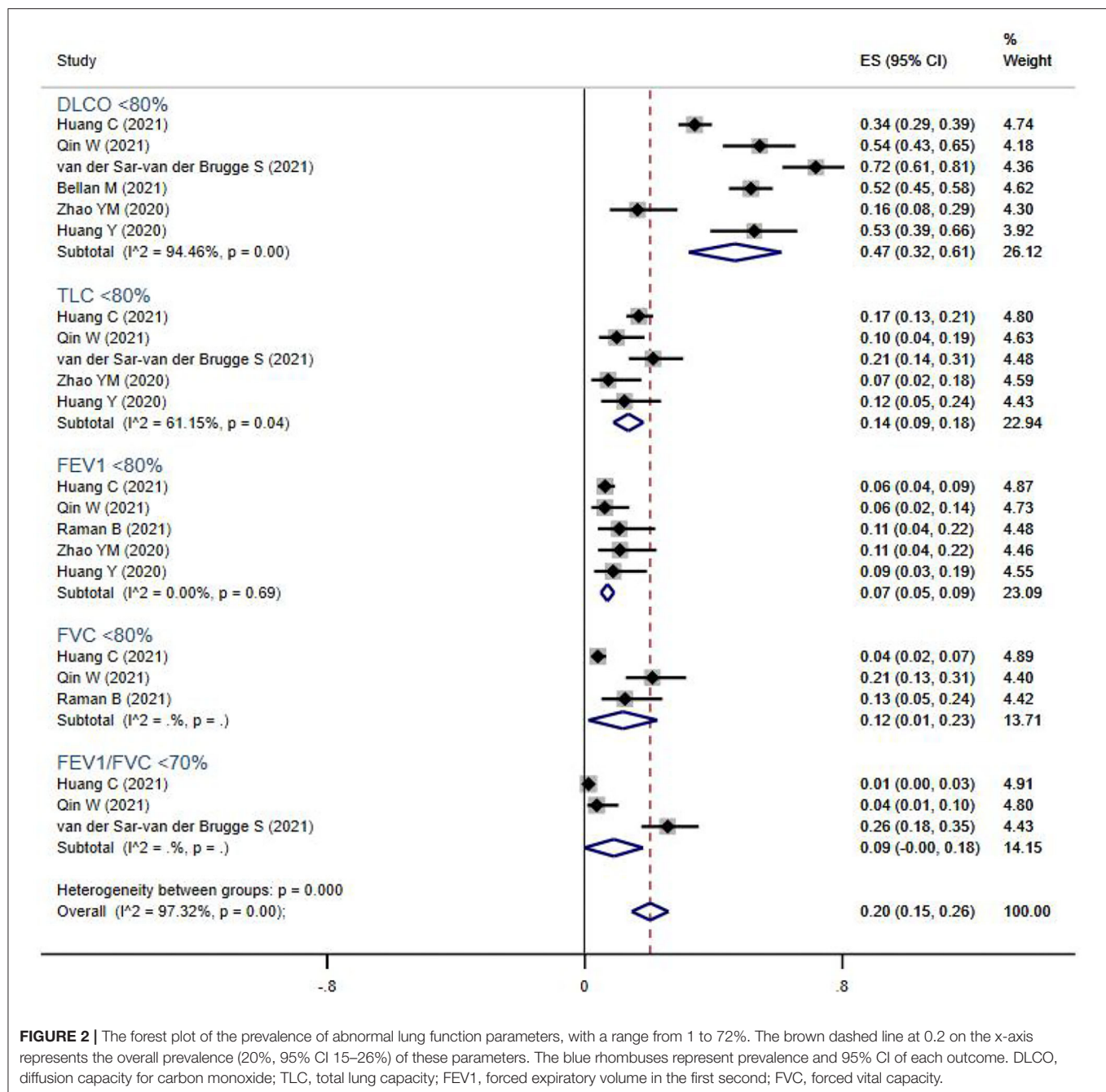


**FIGURE 2 |** The forest plot of the prevalence of abnormal lung function parameters, with a range from 1 to 72%. The brown dashed line at 0.2 on the x-axis represents the overall prevalence (20%, 95% CI 15–26%) of these parameters. The blue rhombuses represent prevalence and 95% CI of each outcome. DLCO, diffusion capacity for carbon monoxide; TLC, total lung capacity; FEV1, forced expiratory volume in the first second; FVC, forced vital capacity.

(OR 1.42). Moreover, PFT parameters were all significantly different between severity groups. Collectively, these residual multi-system manifestations illustrate that hospital discharge does not indicate complete recovery, and that these patients require prolonged care, ideally through multidisciplinary clinics capable of comprehensive rehabilitation strategies.

Lopez et al. (3) reported more than 50 long-term symptoms of post-COVID-19 syndrome, among which fatigue (58%) was the most common, in agreement with our findings of a high prevalence of fatigue or weakness (47%). Previous work by Perrin and co-workers suggested that a subset of COVID-19 patients

may develop chronic fatigue syndrome (CFS) similar to those reported to follow SARS and MERS (32). CFS is characterized by persistent or recurrent unexplained severe fatigue that is not improved by rest, and may be accompanied by manifestations such as myalgia, depression, and sleep disorder. Perrin and colleagues also recently proposed that CFS could be induced by SARS-CoV-2 invasion of olfactory neurons, which can result in congestion of the lymphatic duct and subsequent accumulation of toxic agents in the central nervous system (33), thus induction of lymphatic circulation might be an effective measure to alleviate CFS follow COVID-19.



**TABLE 3 |** The pooled OR of symptoms and manifestations in multiple systems between severe and non-severe patients.

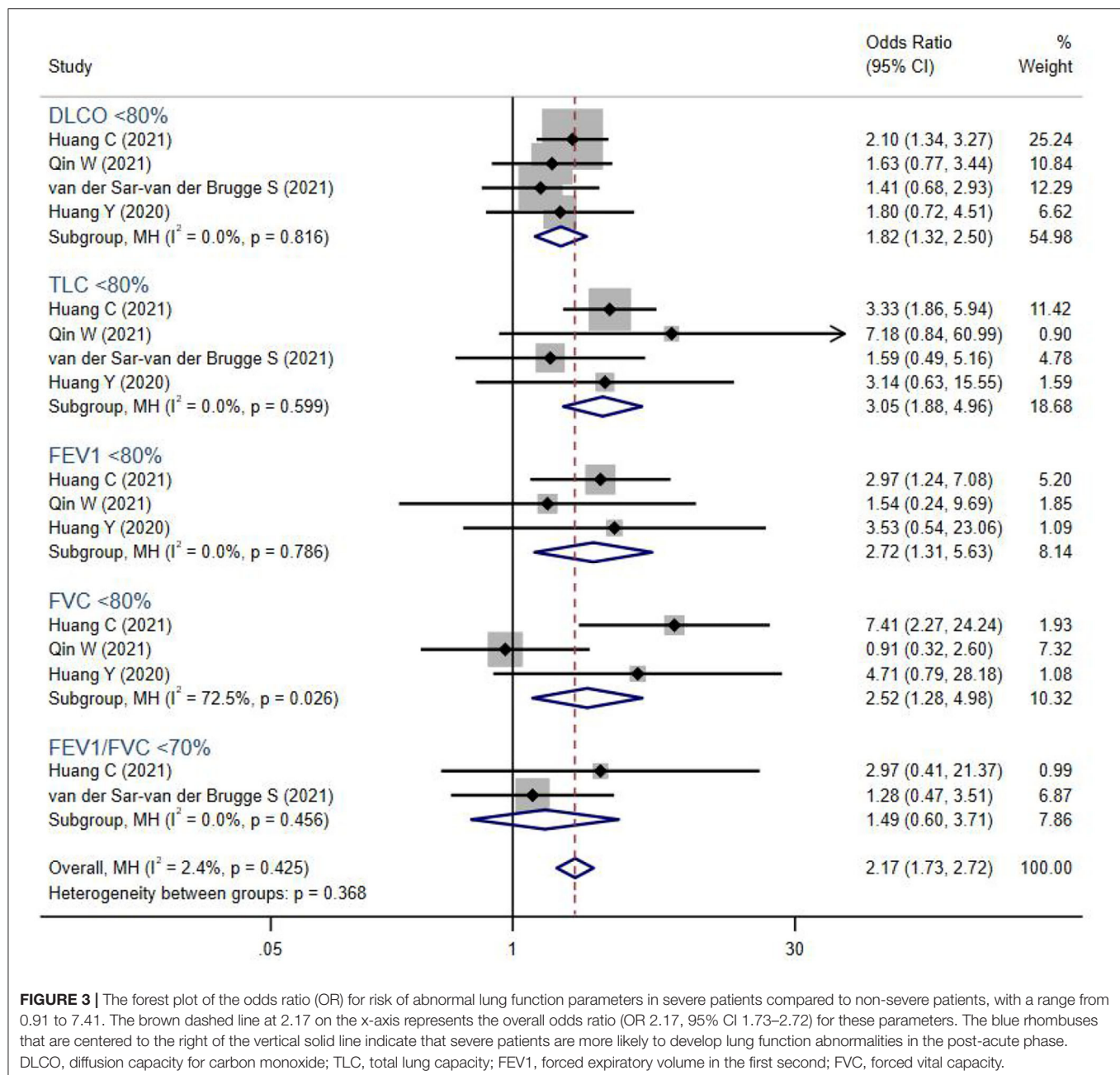
| Outcomes            |                            | Studies | Sample sizes |            | Effects           |                |                     |
|---------------------|----------------------------|---------|--------------|------------|-------------------|----------------|---------------------|
|                     |                            |         | Severe       | Non-severe | OR (95% CI)       | I <sup>2</sup> | p for heterogeneity |
| Fatigue or weakness |                            | 5       | 218          | 1,901      | 1.13 (0.91, 1.42) | 0.0%           | 0.884               |
| Cardiopulmonary     | Chest pain                 | 5       | 434          | 2,232      | 1.09 (0.64, 1.83) | 41.0%          | 0.148               |
|                     | Dyspnea                    | 5       | 349          | 762        | 1.52 (1.12, 2.06) | 0.0%           | 0.903               |
|                     | Cough                      | 4       | 317          | 694        | 1.04 (0.65, 1.64) | 38.2%          | 0.183               |
|                     | Sore throat                | 3       | 176          | 1,713      | 1.37 (0.73, 2.56) | 0.0%           | 0.661               |
|                     | Palpitation                | 2       | 365          | 1,937      | 1.57 (1.07, 2.30) | 16.4%          | 0.274               |
|                     | Overall                    |         |              |            | 1.36 (1.13, 1.64) | 0.0%           | 0.610               |
| Musculoskeletal     | Myalgia                    | 3       | 162          | 1,737      | 1.42 (0.85, 2.35) | 0.0%           | 0.716               |
|                     | Joint pain                 | 2       | 135          | 1,630      | 1.84 (1.11, 3.04) | 59.3%          | 0.117               |
|                     | Overall                    |         |              |            | 1.60 (1.12, 2.29) | 0.0%           | 0.465               |
| Neurological        | Memory impairment          | 3       | 83           | 271        | 0.70 (0.40, 1.24) | 0.0%           | 0.667               |
|                     | Taste disorder             | 3       | 168          | 1,741      | 0.96 (0.52, 1.74) | 0.0%           | 0.412               |
|                     | Smell disorder             | 3       | 159          | 1,726      | 1.14 (0.70, 1.87) | 0.0%           | 0.392               |
|                     | Overall                    |         |              | 111        | 0.93 (0.67, 1.28) | 0.0%           | 0.630               |
| Gastrointestinal    | Decreased appetite         | 2       | 149          | 1,606      | 1.06 (0.58, 1.94) | 0.0%           | 0.600               |
| Psychosocial        | Anxiety or depression      | 3       | 170          | 1,681      | 1.42 (1.03, 1.97) | 17.6%          | 0.297               |
|                     | Attention deficit disorder | 2       | 56           | 164        | 1.18 (0.60, 2.30) | 67.5%          | 0.080               |
|                     | Sleep difficulties         | 4       | 186          | 1,833      | 1.14 (0.83, 1.56) | 15.7%          | 0.313               |
|                     | Hair loss                  | 2       | 141          | 1,634      | 1.14 (0.77, 1.70) | 0.0%           | 0.749               |
|                     | Overall                    |         |              |            | 1.23 (1.02, 1.48) | 2.5%           | 0.418               |

Moreover, it was noteworthy that there was a significantly higher prevalence of psychosocial manifestations (28%) compared with the cardiopulmonary, neurological, musculoskeletal, and gastrointestinal systems. Patients previously infected with other coronaviruses also presented with serious depression, anxiety, and PTSD (13). This finding suggested that the COVID-19 pandemic may have caused more profound impacts on mental health than direct organ damage. For such psychosocial disorders, the effectiveness of a one-size-fits-all response can vary greatly between different groups (34). Thus, epidemiological studies are warranted to evaluate the long-term impacts on mental health and social function in overall and specific groups of COVID-19 patients (such as the elderly, children, patients with mental complications, patients with different income levels, etc.) (35).

In addition to the psychological effects, a large body of evidence indicates that the lung is the most severely affected organ in COVID-19 patients (36). The related histopathological findings include diffuse alveolar epithelial injury, capillary injury or hemorrhage, hyaline membrane formation, fibrous hyperplasia of the alveolar septum, and lung consolidation (37). These cumulative changes could generate markedly adverse impacts on respiratory capacity in COVID-19 patients, but it is not clear whether lung functions remain impaired throughout the post-acute phase. In a previous meta-analysis conducted by Torres et al. (38), DLCO (39%) impairment was the most commonly observed lung function abnormality in post-infection COVID-19 patients, which agreed with our results of 47% prevalence of DLCO <80%. The higher prevalence is potentially

due to our inclusion of only hospitalized patients who suffered relatively severe disease symptoms. More importantly, this result suggested the pulmonary diffusion capacity of recovering patients remained extensively affected through 1 month post-discharge or 2 months post-admission, and might largely explain the persistence of residual respiratory symptoms such as dyspnea (33%), since physical function tests are typically more reliable than self-reported symptoms in reflecting a patient's actual health status. The decrease in DLCO is often associated with pulmonary fibrosis, such as interstitial disease and systemic sclerosis (39, 40). Cases of pulmonary fibrosis have been reported in COVID-19 recovery patients (41), and thus long-term follow-ups are necessary to determine whether DLCO damage in post-acute patients indicates an increased risk of pulmonary fibrosis.

One cohort study (25) reported that ICU care was a risk factor for impaired lung function. Our results were consistent with this finding, and also showed differences in TLC, FEV1, FVC, and DLCO abnormalities between severe and non-severe post-acute COVID-19 patients, among which TLC < 80% (OR 3.05) was the most significant. Although we found no difference in FEV1/FVC < 70% between severity groups, its related parameters FEV1 and FVC were both lower and more likely to be abnormal in severe patients. This suggested the higher severity was associated with more seriously impaired diffusion capacity, as well as restrictive and obstructive dysfunction in post-acute patients. A previous study (42) in SARS implied that pulmonary function could be improved when viral pneumonia was effectively managed at the acute phase, whereas almost no substantial recovery was observed in the following 2 years after infection. Consequently, once the



infection is controlled, exercise programs should be undertaken as early as possible to strengthen lung function in severe patients. It is also important to note that this study did not include pre-existing respiratory diseases which contribute to abnormal lung function, possibly leading to an overestimation of the effects of COVID-19 alone.

Lastly, we also compared events of post-acute symptoms in discharged COVID-19 patients with severe and non-severe diseases COVID-19 patients. Generally, there was no significant difference in overall symptoms of multiple organs or systems between the two groups with different levels of severity, with only just slight differences in musculoskeletal (OR

1.60), cardiopulmonary (OR 1.36), and psychosocial (OR 1.23) manifestations. Among musculoskeletal symptoms, however, it was noteworthy that joint pain (OR 1.84) was more likely to appear in severe patients than the non-severe. In our previous follow-up study (42) in SARS patients, joint disorders persisting over 15 years were presumed to be closely related to high-dose steroid therapy and had little direct relation with the viral infection. As systemic glucocorticoids were recommended for use in hospitalized COVID-19 patients who require mechanical ventilation, regular assessments of joint function and prophylactically rehabilitative interventions of musculoskeletal systems should be advocated for these severe populations.

This meta-analysis also had limitations that should be addressed in future and ongoing studies. First, quality assessment of the included cohort studies revealed that most studies were of low to medium quality. Second, we observed high heterogeneity in the prevalence of both symptoms and lung function, possibly due to wide variation in follow-up duration (1–6 months), disease severity, and sample sizes (55–1,733 patients). The method of self-reporting symptoms through questionnaires could also lead to bias, so it is necessary to standardize investigational methods for post-acute COVID-19 syndrome, such as through the adoption of the “Post-COVID-19 Functional Status Scale” proposed by Klok et al. (43). Third, not all outcomes were examined through subgroup analysis because of an insufficient number of studies and too many outcome indicators. In particular, subgroup analysis based on treatment regimen during hospitalization was not possible based on a lack of information, though future studies exploring this point will likely reveal important differences in therapeutic approach that affect the long-term symptoms. The available treatment information for each study is provided in **Supplementary Table 2**. Given that COVID-19 is a newly-emerged epidemic, longer follow-up studies are recommended to explore the effects of age, pre-existing disease, duration, and certain interventions on post-acute COVID-19 syndrome, especially from the functional parameters of multiple systems.

## CONCLUSION

The evidence presented in this systematic review and meta-analysis supports the wide spectrum of multi-system manifestations associated with post-acute COVID-19. Fatigue or weakness, progressing to CFS, was the most prevalent physiological symptom, and although respiratory dysfunction

is widespread among discharged patients, especially diffusion disorders, pandemic-related psychosocial effects were more extensive in survivors than direct physical damage by SARS-CoV-2. In addition, we found that severe COVID-19 is a risk factor for abnormalities in almost all PFT parameters, and that exercise regimens adopted soon after the acute phase, with regular assessments of lung and joint function, could potentially alleviate long-term COVID-19 symptoms.

## DATA AVAILABILITY STATEMENT

The original contributions presented in the study are included in the article/**Supplementary Material**, further inquiries can be directed to the corresponding author/s.

## AUTHOR CONTRIBUTIONS

QL designed the analysis and wrote the first draft. XH and YB collected the data. JL analyzed the data. YZ and ZG supervised the work and edited the final version of the paper. All authors contributed to the article and approved the submitted version.

## FUNDING

The analysis was supported by the Novel Coronavirus Prevention and Treatment Emergency Scientific Research Project of Xiamen University under Grant numbers 20720200017 and 20720200032.

## SUPPLEMENTARY MATERIAL

The Supplementary Material for this article can be found online at: <https://www.frontiersin.org/articles/10.3389/fmed.2021.702635/full#supplementary-material>

## REFERENCES

- Chen N, Zhou M, Dong X, Qu J, Gong F, Han Y, et al. Epidemiological and clinical characteristics of 99 cases of 2019 novel coronavirus pneumonia in Wuhan, China: a descriptive study. *Lancet*. (2020) 395:507–13. doi: 10.1016/S0140-6736(20)30211-7
- Sigfrid L, Cevik M, Jesudason E, Lim WS, Rello J, Amuasi JH, et al. What is the recovery rate and risk of long-term consequences following a diagnosis of COVID-19? A harmonised, global longitudinal observational study. *BMJ Open*. (2021) 11:e043887. doi: 10.1101/2020.08.26.20180950
- Lopez-Leon S, Wegman-Ostrosky T, Perelman C, Sepulveda R, Rebolledo PA, Cuapio A, et al. More than 50 Long-term effects of COVID-19: a systematic review and meta-analysis. *medRxiv*. (2021). doi: 10.21203/rs.3.rs-266574/v1
- Nabavi N. Long covid: how to define it how to manage it. *BMJ*. (2020) 370:m3489. doi: 10.1136/bmj.m3489
- Xiong Q, Xu M, Li J, Liu Y, Zhang J, Xu Y, et al. Clinical sequelae of COVID-19 survivors in Wuhan, China: a single-centre longitudinal study. *Clin Microbiol Infect*. (2021) 27:89–95. doi: 10.1016/j.cmi.2020.09.023
- Carfì A, Bernabei R, Landi F. Persistent symptoms in patients after acute COVID-19. *JAMA*. (2020) 324:603–5. doi: 10.1001/jama.2020.12603
- Huang C, Huang L, Wang Y, Li X, Ren L, Gu X, et al. 6-month consequences of COVID-19 in patients discharged from hospital: a cohort study. *Lancet*. (2021) 397:220–32. doi: 10.1016/S0140-6736(20)32656-8
- Gupta A, Madhavan MV, Sehgal K, Nair N, Mahajan S, Sehrawat TS, et al. Extrapulmonary manifestations of COVID-19. *Nat Med*. (2020) 26:1017–32. doi: 10.1038/s41591-020-0968-3
- Qi F, Qian S, Zhang S, Zhang Z. Single cell RNA sequencing of 13 human tissues identify cell types and receptors of human coronaviruses. *Biochem Biophys Res Commun*. (2020) 526:135–40. doi: 10.1016/j.bbrc.2020.03.044
- Varga Z, Flammer AJ, Steiger P, Haberecker M, Andermatt R, Zinkernagel AS, et al. Endothelial cell infection and endotheliitis in COVID-19. *Lancet*. (2020) 395:1417–8. doi: 10.1016/S0140-6736(20)30937-5
- Synowiec A, Szczepański A, Barreto-Duran E, Lie LK, Pyrc K. Severe acute respiratory syndrome coronavirus 2 (SARS-CoV-2): a systemic infection. *Clin Microbiol Rev*. (2021) 34:e00133–20. doi: 10.1128/CMR.00133-20
- Ahmed H, Patel K, Greenwood DC, Halpin S, Lewthwaite P, Salawu A, et al. Long-term clinical outcomes in survivors of severe acute respiratory syndrome and middle east respiratory syndrome coronavirus outbreaks after hospitalisation or ICU admission: a systematic review and meta-analysis. *J Rehabil Med*. (2020) 52:jrm00063. doi: 10.2340/16501977-2694
- Rogers JP, Chesney E, Oliver D, Pollak TA, McGuire P, Fusar-Poli P, et al. Psychiatric and neuropsychiatric presentations associated with severe coronavirus infections: a systematic review and meta-analysis with comparison to the COVID-19 pandemic. *Lancet Psychiatry*. (2020) 7:611–27. doi: 10.1016/S2215-0366(20)30203-0
- Leung TYM, Chan AYL, Chan EW, Chan VKY, Chui CSL, Cowling BJ, et al. Short- and potential long-term adverse health outcomes

- of COVID-19: a rapid review. *Emerg Microbes Infect.* (2020) 9:2190–9. doi: 10.1080/22221751.2020.1825914
15. Stam HJ, Stucki G. Bickenbach Covid-19], and post intensive care syndrome: a call for action. *J Rehabil Med.* (2020) 52:jrm00044. doi: 10.2340/16501977-2677
  16. Barker-Davies RM, O'Sullivan O, Senaratne KPP, Baker P, Cranley M, Dharm-Datta S, et al. The stanford hall consensus statement for post-COVID-19 rehabilitation. *Br J Sports Med.* (2020) 54:949–59. doi: 10.1136/bjsports-2020-102596
  17. Greenhalgh T, Knight M, A'Court C, Buxton M, Husain L. Management of post-acute covid-19 in primary care. *Bmj.* (2020) 370:m3026. doi: 10.1136/bmj.m3026
  18. Arnold DT, Hamilton FW, Milne A, Morley AJ, Viner J, Attwood M, et al. Patient outcomes after hospitalisation with COVID-19 and implications for follow-up: results from a prospective UK cohort. *Thorax.* (2021) 76:399–401. doi: 10.1101/2020.08.12.20173526
  19. Garrigues E, Janvier P, Kherabi Y, Le Bot A, Hamon A, Gouze H, et al. Post-discharge persistent symptoms and health-related quality of life after hospitalization for COVID-19. *J Infect.* (2020) 81:e4–6. doi: 10.1016/j.jinf.2020.08.029
  20. Halpin SJ, McIvor C, Whyatt G, Adams A, Harvey O, McLean L, et al. Postdischarge symptoms rehabilitation needs in survivors of COVID-19 infection: A cross-sectional evaluation. *J Med Virol.* (2021) 93:1013–22. doi: 10.1002/jmv.26368
  21. Huang Y, Tan C, Wu J, Chen M, Wang Z, Luo L, et al. Impact of coronavirus disease 2019 on pulmonary function in early convalescence phase. *Respir Res.* (2020) 21:163. doi: 10.1186/s12931-020-01429-6
  22. Jacobs LG, Paleoudis EG, Bari DLD, Nyirenda T, Friedman T, Gupta A, et al. Persistence of symptoms and quality of life at 35 days after hospitalization for COVID-19 infection. *PLoS ONE.* (2020) 15:e0243882. doi: 10.1371/journal.pone.0243882
  23. Suárez-Robles M, Iguaran-Bermúdez MR, García-Klepiz JL, Lorenzo-Villalba N, Méndez-Bailón M. Ninety days post-hospitalization evaluation of residual covid-19 symptoms through a phone call check list. *Pan Afri Med J.* (2020) 37:1–4. doi: 10.11604/pamj.2020.37.289.27110
  24. Zhao YM, Shang YM, Song WB, Li QQ, Xie H, Xu QF, et al. Follow-up study of the pulmonary function and related physiological characteristics of COVID-19 survivors three months after recovery. *Eclin Med.* (2020) 25:100463. doi: 10.1016/j.eclinm.2020.100463
  25. Bellan M, Soddu D, Balbo PE, Baricich A, Zeppego P, Avanzi GC, et al. Respiratory and psychophysical sequelae among patients with COVID-19 four months after hospital discharge. *JAMA Netw Open.* (2021) 4:e2036142. doi: 10.1001/jamanetworkopen.2020.36142
  26. Méndez R, Balanzá-Martínez V, Luperdi SC, Estrada I, Latorre A, González-Jiménez P, et al. Short-term neuropsychiatric outcomes and quality of life in COVID-19 survivors. *J Intern Med.* (2021). doi: 10.1111/joim.13262. [Epub ahead of print].
  27. Qin W, Chen S, Zhang Y, Dong F, Zhang Z, Hu B, et al. Diffusion capacity abnormalities for carbon monoxide in patients with COVID-19 at three-month follow-up. *Eur Respir J.* (2021) 58:2003677. doi: 10.1183/13993003.03677-2020
  28. Raman B, Cassar MP, Tunnicliffe EM, Filippini N, Griffanti L, Alfaro-Almagro F, et al. Medium-term effects of SARS-CoV-2 infection on multiple vital organs, exercise capacity, cognition, quality of life and mental health, post-hospital discharge. *Eclin Med.* (2021) 31:100683. doi: 10.1016/j.eclinm.2020.100683
  29. Sykes DL, Holdsworth L, Jawad N, Gunasekera P, Morice AH, Crooks MG. Post-COVID-19 symptom burden: what is long-COVID and how should we manage it? *Lung.* (2021) 199:113–9. doi: 10.21203/rs.3.rs-164000/v1
  30. Taboada M, Moreno E, Cariñena A, Rey T, Pita-Romero R, Leal S, et al. Quality of life, functional status, and persistent symptoms after intensive care of COVID-19 patients. *Br J Anaesth.* (2021) 126:e110–13. doi: 10.1016/j.bja.2020.12.007
  31. van der Sar-van der Brugge S, Talman S, Boonman-de Winter L, de Mol M, Hoefman E, van Etten RW, et al. Pulmonary function and health-related quality of life after COVID-19 pneumonia. *Respir Med.* (2021) 176:106272. doi: 10.1016/j.rmed.2020.106272
  32. Perrin R, Riste L, Hann M, Walther A, Mukherjee A, Heald A. Into the looking glass: post-viral syndrome post COVID-19. *Med Hypoth.* (2020) 144:110055. doi: 10.1016/j.mehy.2020.110055
  33. Wostyn P. COVID-19 and chronic fatigue syndrome: Is the worst yet to come? *Med Hypoth.* (2021) 146:110469. doi: 10.1016/j.mehy.2020.110469
  34. Lee Y, Ragguett RM, Mansur RB, Boutilier JJ, Rosenblat JD, Trevizol A, et al. Applications of machine learning algorithms to predict therapeutic outcomes in depression: a meta-analysis and systematic review. *J Affect Disord.* (2018) 241:519–32. doi: 10.1016/j.jad.2018.08.073
  35. Holmes EA, Ghaderi A, Harmer CJ, Ramchandani PG, Cuijpers P, Morrison AP, et al. The lancet psychiatry commission on psychological treatments research in tomorrow's science. *Lancet Psychiatry.* (2018) 5:237–86. doi: 10.1016/S2215-0366(17)30513-8
  36. Shi H, Han X, Jiang N, Cao Y, Alwalid O, Gu J, et al. Radiological findings from 81 patients with COVID-19 pneumonia in Wuhan, China: a descriptive study. *Lancet Infect Dis.* (2020) 20:425–34. doi: 10.1016/S1473-3099(20)30086-4
  37. Xu Z, Shi L, Wang Y, Zhang J, Huang L, Zhang C, et al. Pathological findings of COVID-19 associated with acute respiratory distress syndrome. *Lancet Respir Med.* (2020) 8:420–2. doi: 10.1016/S2213-2600(20)30076-X
  38. Torres-Castro R, Vasconcello-Castillo L, Alsina-Restoy X, Solis-Navarro L, Burgos F, Puppo H, et al. Respiratory function in patients post-infection by COVID-19: a systematic review and meta-analysis. *Pulmonology.* (2021) 27:328–37. doi: 10.1016/j.pulmoe.2020.10.013
  39. Martinez FJ, Flaherty K. Pulmonary function testing in idiopathic interstitial pneumonias. *Proc Am Thorac Soc.* (2006) 3:315–21. doi: 10.1513/pats.200602-022TK
  40. Nihtyanova SI, Schreiber BE, Ong VH, Rosenberg D, Moinzadeh P, Coghlan JG, et al. Prediction of pulmonary complications and long-term survival in systemic sclerosis. *Arthritis Rheumatol.* (2014) 66:1625–35. doi: 10.1002/art.38390
  41. Ojo AS, Balogun SA, Williams OT, Ojo OS. Pulmonary fibrosis in COVID-19 survivors: predictive factors and risk reduction strategies. *Pulm Med.* (2020) 2020:6175964. doi: 10.1155/2020/6175964
  42. Zhang P, Li J, Liu H, Han N, Ju J, Kou Y, et al. Long-term bone and lung consequences associated with hospital-acquired severe acute respiratory syndrome: a 15-year follow-up from a prospective cohort study. *Bone Res.* (2020) 8:8. doi: 10.1038/s41413-020-0084-5
  43. Klok FA, Boon G, Barco S, Endres M, Geelhoed JJM, Knauss S, et al. The post-COVID-19 functional status scale: a tool to measure functional status over time after COVID-19. *Eur Respir J.* (2020) 56:2001494. doi: 10.1183/13993003.01494-2020

**Conflict of Interest:** The authors declare that the research was conducted in the absence of any commercial or financial relationships that could be construed as a potential conflict of interest.

**Publisher's Note:** All claims expressed in this article are solely those of the authors and do not necessarily represent those of their affiliated organizations, or those of the publisher, the editors and the reviewers. Any product that may be evaluated in this article, or claim that may be made by its manufacturer, is not guaranteed or endorsed by the publisher.

Copyright © 2021 Long, Li, Hu, Bai, Zheng and Gao. This is an open-access article distributed under the terms of the Creative Commons Attribution License (CC BY). The use, distribution or reproduction in other forums is permitted, provided the original author(s) and the copyright owner(s) are credited and that the original publication in this journal is cited, in accordance with accepted academic practice. No use, distribution or reproduction is permitted which does not comply with these terms.





# Longitudinal Characterization of Cytokine Overproduction: A Case Report in Critically Ill COVID-19 Patients With Hyperinflammation in Bronchoalveolar Lavage

## OPEN ACCESS

### Edited by:

Arda Kiani,  
Shahid Beheshti University of Medical  
Sciences, Iran

### Reviewed by:

Roopa Biswas,  
Uniformed Services University of the  
Health Sciences, United States  
Reza Lashgari,  
Shahid Beheshti University, Iran

### \*Correspondence:

Jianguo Wu  
jwu898@jnu.edu.cn  
Yuchen Xia  
yuchenxia@whu.edu.cn

<sup>†</sup> These authors have contributed  
equally to this work

### Specialty section:

This article was submitted to  
Infectious Diseases – Surveillance,  
Prevention and Treatment,  
a section of the journal  
Frontiers in Medicine

Received: 03 April 2021

Accepted: 11 August 2021

Published: 07 September 2021

### Citation:

Luo Z, Zhu C, Ruan Z, Cui X,  
Shereen MA, Pan P, Huang J, Wang F,  
Su H, Xia Y and Wu J (2021)  
Longitudinal Characterization of  
Cytokine Overproduction: A Case  
Report in Critically Ill COVID-19  
Patients With Hyperinflammation in  
Bronchoalveolar Lavage.  
Front. Med. 8:690523.  
doi: 10.3389/fmed.2021.690523

Zhen Luo<sup>1†</sup>, Chengliang Zhu<sup>2†</sup>, Zhihui Ruan<sup>1</sup>, Xianghua Cui<sup>2</sup>,  
Muhammad Adnan Shereen<sup>3</sup>, Pan Pan<sup>1</sup>, Jingtao Huang<sup>2</sup>, Fubing Wang<sup>4</sup>, Hanwen Su<sup>2</sup>,  
Yuchen Xia<sup>5\*</sup> and Jianguo Wu<sup>1,3\*</sup>

<sup>1</sup> Guangdong Provincial Key Laboratory of Virology, Institute of Medical Microbiology, Jinan University, Guangzhou, China,

<sup>2</sup> Department of Clinical Laboratory, Renmin Hospital of Wuhan University, Wuhan, China, <sup>3</sup> State Key Laboratory of Virology, College of Life Science, Wuhan University, Wuhan, China, <sup>4</sup> Department of Laboratory Medicine, Zhongnan Hospital of Wuhan University, Wuhan, China, <sup>5</sup> State Key Laboratory of Virology, School of Basic Medical Sciences, Wuhan University, Wuhan, China

**Objectives:** The longitudinal characterization and risk of poor outcomes related to cytokine overproduction in critical coronavirus disease 2019 (COVID-19) patients with hyperinflammation in bronchoalveolar lavage requires further investigation.

**Methods:** We enrolled two critically ill patients with comorbidities diagnosed with severe acute respiratory syndrome coronavirus 2 (SARS-CoV-2) detected by RT-PCR during hospitalization. Clinical characteristics, longitudinal immunological, and biochemical parameters of each critical COVID-19 case were collected.

**Main Results:** The clinical characteristics and laboratory results of each case demonstrated critical symptoms of COVID-19 with poor outcomes. Both nasopharyngeal swabs and bronchoalveolar lavage fluid (BALF) samples tested positive for SARS-CoV-2. Two patients received targeted treatments against pathogen infection and inflammation in addition to interventional therapies, except for Patient 2, who received an additional artificial liver system treatment. Hyperinflammation with a dominantly high level of IL-6 was observed in BALF samples from both critical cases with decreased T cell populations. High levels of cytokines and pathological parameters were successively maintained in Patient 1, but rapidly reduced at the late treatment stage in Patient 2. The outcome of Patient 1 is death, whereas the outcome of Patient 2 is recovery.

**Conclusions:** This case report suggests that a high risk of poor outcomes was related to a heavily hyperinflammatory milieu in both the blood and lungs of critical COVID-19 patients. The artificial liver intervention on cytokines overproduction might be beneficial

for the recovery of critical COVID-19 patients as a reliable therapy that can be coordinated with targeted treatments, which ought to be further tested in adequately designed and powered clinical trials.

**Keywords: SARS-CoV-2, COVID-19, poor outcomes, bronchoalveolar lavage fluid, hyperinflammation, cytokine overproduction**

## INTRODUCTION

Severe acute respiratory syndrome coronavirus 2 (SARS-CoV-2) led to the coronavirus disease 2019 (COVID-19) pandemic; it has a fatality rate of 0.5–1.0% and has led to significant increases in fatalities in those with preexisting comorbidities (1). Upon SARS-CoV-2 infection, the clinical manifestations of most COVID-19 patients are asymptomatic or mild, but some cases would develop acute respiratory distress syndrome (ARDS), multiple organ failure (MOF), and even sudden death (2). During the progression of COVID-19, overproduction of inflammatory cytokines and a dysregulated host immune response, eventually act as a cytokine storm, is considered to be the primary cause of ARDS and MOF in severe and critical patients, thereby contributing to the severity and poor prognosis of the illness (3).

SARS-CoV-2 infection generates a delayed but overactive production of cytokines resembling interleukin-1 $\beta$  (IL-1 $\beta$ ), IL-6, IL-8, IL-10, tumor necrosis factor- $\alpha$  (TNF- $\alpha$ ), and monocyte chemoattractant protein-1, inducing dysregulated innate immune responses (2, 4). In addition, SARS-CoV-2-mediated impairment of lymphoid organs is responsible for lymphopenia, resulting in an impaired adaptive immune response, especially in those with severe infection (5, 6). Since hyperinflammation is closely related to the exacerbation of symptoms in severe and critical COVID-19 patients (7), the relationship between SARS-CoV-2 presence and host hyperinflammation needs to be fully explored.

SARS-CoV-2 preferentially infects type II alveolar cells (AT2) in the lungs as the viral target organs (8, 9), and bronchoalveolar lavage (BAL) samples from COVID-19 patients serve as the optimal cytologic specimens. There is increasing evidence that exuberant plasmacytosis and transcriptional changes of inflammatory genes can be detected in the BAL specimens of COVID-19 patients (10–12), suggesting the presence of hyperinflammation upon SARS-CoV-2 infection in the lungs. Although bronchoalveolar inflammation in COVID-19 patients correlates with the clinical outcomes (13), the dynamic inflammatory response to severe forms of the illness in COVID-19 patients based on the detection of hyperinflammation in BAL specimens is still unclear. In this study, we present the clinical characteristics of two critical COVID-19 patients, as well as the high risk of poor outcomes related to cytokine overproduction during severe COVID-19 treatments with hyperinflammation detected from bronchoalveolar lavage fluid (BALF) samples.

## METHODS

### Study Design and Patients

The patients were clinically diagnosed with COVID-19 according to the “pneumonia diagnosis protocol for novel coronavirus

infection (trial version 7)” (Released by National Health Commission & State Administration of Traditional Chinese Medicine on March 3, 2020). They were subjected to tests including clinical examination, computed tomography (CT), and real-time reverse-transcription polymerase chain reaction (RT-PCR) for SARS-CoV-2 (Table 1). The patients were admitted to the Renmin Hospital of Wuhan University, Wuhan, China, from January 25 to April 8, 2020. Patient 1 was admitted on February 11, 2020 and transferred into intensive care unit (CCU) on February 18, 2020, while Patient 2 was admitted on February 6, 2020 and transferred into CCU on February 13, 2020 (Table 2).

The study was approved by the ethics committee and the institutional review board of the Renmin Hospital of Wuhan University (file no. WDRY2020-K066).

### Data Collection

Information including clinical symptoms, epidemiological survey, radiological and laboratory results, and clinical treatments were obtained from electronic medical records or via direct communication with the patients and their families. SARS-CoV-2 infection in patients was confirmed by a broad series of investigations including clinical examinations, laboratory tests, chest X-rays, and two independent RT-PCR tests for SARS-CoV-2 using a SARS-CoV-2 ORF1ab/N PCR detection kit (GeneDx Biotech, Shanghai, China) and a SARS-CoV-2 antibody detection kit (YHLO Biotech, Shenzhen, China). According to the standard procedure protocol, an RT-PCR test was performed for SARS-CoV-2 nucleic acids from nasopharyngeal swabs, BALF samples, feces, urine, whole blood, and sputum. IgM-IgG antibody tests were performed using serum.

Peripheral blood samples were longitudinally collected from two individually confirmed COVID-19 patients and examined for lymphocyte subsets (CD16<sup>+</sup>CD56<sup>+</sup>, CD19<sup>+</sup>, CD3<sup>+</sup>, CD4<sup>+</sup>, and CD8<sup>+</sup> T cells) by flow cytometry using a flow cytometer BNII (Becton Dickinson, Cockeysville, MD, USA) as previously described (5), the pathological parameter profiles using specific immunoassays, and cytokines using BD FACSCalibur flow cytometer (BD FACSCalibur, BD Bioscience, CA, USA) following manufactures' instructions. Longitudinal plots of parameter data were visualized using GraphPad Prism 7 software (GraphPad Software Inc., San Diego, CA, USA).

### BALF Preparation

The lung segment was locally anesthetized after injection with 2% lidocaine. A total of 150 mL fractions of room-temperature sterile saline were instilled through the bronchial lumen into the right middle or lower lobe of the lung. BALF was retrieved by gentle syringe suction and removed into sterile containers for further analysis.

**TABLE 1 |** Summary of clinical features and laboratory test results of critically ill patients with COVID-19.

|   | Patient 1   | Patient 2                                      |
|---|---|--|
| <b>Characteristics</b>  |   |  |
| Age (years)   | 69  | 42   |
| Gender  | Female  | Male   |
| Interval between admission to hospital and symptom onset (days)                 | 8   | 12   |
| Interval between confirmed test for SARS-CoV-2 and admission to hospital (days) | 2   | 8  |
| CT findings   | Blurred borders in both lungs with tuberculosis in upper lobe or apex of the lung | Scattered ground-glass opacities in both lungs |
| <b>Symptoms and signs</b>   |   |  |
| Fever   | –   | +  |
| Cough   | +   | +  |
| Nasal congestion  | –   | –  |
| Asthenia  | +   | +  |
| Rhinorrhoea   | –   | –  |
| Poor appetite   | –   | –  |
| Chest distress  | –   | –  |
| Dyspnea   | +   | +  |
| Diarrhea  | –   | –  |
| Body temperature (°C)   | 37.1  | 38.7   |
| <b>Clinical course</b>  |   |  |
| Duration of fever (days)  | 0   | 12   |
| Duration in CCU   | 22  | 55   |
| Duration of hospitalization (days)  | 29  | 62   |
| <b>Laboratory test</b>  |   |  |
| White blood cell count, $\times 10^9/L$ (Normal range: 3.5–9.5)                 | 11.37   | 7.12   |
| Neutrophil count, $\times 10^9/L$ (Normal range: 1.8–6.3)                       | 9.52  | 6.43   |
| Neutrophil ratio, % (Normal range: 40–75)                                       | 83.70   | 90.40  |
| Lymphocyte count, $\times 10^9/L$ (Normal range: 1.1–3.2)                       | 1.00  | 0.38   |
| Lymphocyte ratio, % (Normal range: 20–50)                                       | 8.80  | 5.30   |
| ATL, U/L (Normal range: 7–40)   | 36.00   | 77.00  |
| AST, U/L (Normal range: 13–35)  | 42.00   | 64.00  |
| PCR of nasopharyngeal swab  | + Ct = 39   | + Ct = 34.83                                   |
| PCR of whole blood  | –   | NA   |
| PCR of sputum   | NA  | +  |
| PCR of feces  | –   | +  |
| PCR of urine  | +   | –  |
| PCR of BALF   | + Ct=34.29  | + Ct=33.8                                      |
| SARS-CoV-2 IgG, AU/mL (Normal range: <10)                                       | 58.22   | 159.60   |
| SARS-CoV-2 IgM, AU/mL (Normal range: <10)                                       | 28.17   | 21.94  |
| ADV DNA   | –   | –  |
| Boca DNA  | –   | –  |
| H1N1 RNA  | –   | –  |
| H3N2 RNA  | –   | –  |
| HCoV RNA  | –   | –  |
| HMPV RNA  | –   | –  |
| HPIV RNA  | –   | –  |
| HRSV RNA  | –   | –  |
| HRV RNA   | –   | –  |
| LPN1 IgM  | –   | –  |
| CP IgM  | –   | –  |

(Continued)

TABLE 1 | Continued

|                        | Patient 1   | Patient 2  |
|------------------------|---|--|
| <b>Treatments</b>      |   |  |
| Comorbidities          | Primary hypertension (Grade III), coagulation disorders, hypokalemia                                | Secondary hypertension (Grade III), coagulation disorders, hypoalbuminemia   |
| Anti-viral             | Oseltamivir, Arbidol  | Arbidol, Interferon-alpha, Hydroxychloroquine  |
| Anti-bacterial         | Cefperazone-Sulbactam, Moxifloxacin, Piperacillin, Tazobactam, Vancomycin, Polymyxin B, Tigecycline | Cefperazone-Sulbactam, Meropenem, Teicoplanin, Imipenem, Tigecycline, Polymyxin B, Vancomycin, Daptomycin, Linezolid |
| Anti-fungal            | Voriconazole, Micafungin  | Voriconazole, Micafungin   |
| Anti-inflammatory      | Intravenous immune globulin, Methylprednisolone   | Intravenous immune globulin, Methylprednisolone  |
| Supplemental oxygen    | Invasive ventilation  | Invasive ventilation   |
| Interventional therapy | Bronchoscopy, bronchoalveolar lavage, Thoracic closed drainage                                      | Li's ALS, Bronchoscopy, bronchoalveolar lavage, Thoracic closed drainage   |
| Outcomes               | Died  | Survived   |

NA, not available; +, positive; -, negative; CT, Computed Tomography; CCU, Cardiovascular Intensive Care Unit; ALT, Alanine aminotransferase; AST, Aspartate aminotransferase; PCR, short for Real-time PCR against SARS-CoV-2 nucleic acid; Ct, Cycle threshold value of SARS-CoV-2 N gene; BALF, bronchoalveolar lavage fluid; ADV, Adenovirus; H1N1, Influenza virus A, H1N1; H3N2, Influenza virus A, H3N2; HCoV, Human seasonal coronavirus; HMPV, Human metapneumovirus; HPIV, Human parainfluenza virus; HRSV, Human respiratory syncytial virus; HRV, Human rhinovirus; LPN1, Legionella pneumophila serum type 1; CP, Chlamydia pneumoniae; Li's ALS, Li Lanjuan's artificial liver system (ALS).

## Treatments

Both patients received regular medical treatments involving a combination of antiviral, bacterial, and fungal drugs, anti-inflammatory agents, and high-flow oxygen supplements (Table 1). With preexisting comorbidities of hypertension and hematological disorders, both critical COVID-19 patients developed underlying pyemia and underwent interventional therapies including bronchoscopy, bronchoalveolar lavage (on days 29 and 39 post-onset for Patient 1 and Patient 2, respectively), and thoracic closed chest drainage (on days 36 and 48 post-onset for Patient 1 and Patient 2, respectively). In addition, Patient 2 received an artificial liver system treatment six times at 20, 21, 23, 26, 27, and 31 days after the onset of illness, respectively.

## RESULTS

### Clinical Manifestations and Laboratory Findings

Between January 25 and April 8, 2020, two critical COVID-19 patients admitted to the Renmin Hospital of Wuhan University, Wuhan, China, were retrospectively analyzed (Table 1). Both patients (69-year-old female and 43-year-old male) had pre-existing comorbidities of high-grade hypertension and hematological disorders. The main onset symptoms in both cases were cough, asthenia, and dyspnea, whereas one patient (Patient 2) had fever, which is consistent with the clinical signs previously described (2). The chest CT scan in two COVID-19 patients showed typical changes in viral pneumonia, including blurred borders and patchy, scattered ground-glass opacities.

After hospital admission, the patients were transferred to the CCU because of the severity of illness.

During the hospitalization period, both patients underwent laboratory tests with detailed information in the timeline (Figure 1A). The white blood cell (WBC) count was mildly increased in Patient 1 and normal in Patient 2. Both patients had low cell numbers and ratios of lymphocytes but high numbers of neutrophils (Table 1), which is in line with SARS-CoV-2-induced lymphopenia (6). Increased concentrations of alanine aminotransferase (ALT) and aspartate aminotransferase (AST) in Patient 2 indicated some level of liver dysfunction, as previously reported (14). None of the patients had co-infection with other common respiratory viruses or pathogens (Table 1).

Both nasopharyngeal swab and BALF samples from patients were tested for SARS-CoV-2 RT-PCR with positive results. In addition, the SARS-CoV-2 RT-PCR test results were positive in the urine from Patient 1, along with the sputum and feces from Patient 2, but negative in the whole blood and feces from Patient 1 and the urine from Patient 2. During follow-up, the serum samples from the two patients had noticeably elevated concentrations of SARS-CoV-2 IgM and IgG antibodies (Table 1).

### Treatments and Outcomes

During the period of illness, the two patients underwent medical treatments, including a combination of antiviral, bacterial, and fungal drugs, with anti-inflammatory agents, high-oxygen, and interventional (bronchoscopy, bronchoalveolar lavage, and thoracic closed chest drainage) therapies (Table 1). Importantly, Patient 2 received Li's artificial liver system treatment six



**TABLE 2 |** Timeline of physical examination and clinical intervention in critically ill patients with COVID-19.

| Date*     | Days of follow-up <sup>#</sup> | Patient 1   |                                      | Patient 2                                 |                                      |
|-----------|--------------------------------|---|--------------------------------------|---|--------------------------------------|
|           |                                | Examination   | Intervention                         | Examination                               | Intervention                         |
| 25-Jan-20 | 1                              |   |                                      | Illness onset                             |                                      |
| 26-Jan-20 | 2                              |   |                                      |   |                                      |
| 27-Jan-20 | 3                              |   |                                      |   |                                      |
| 28-Jan-20 | 4                              |   |                                      |   |                                      |
| 29-Jan-20 | 5                              |   |                                      | Confirmed test for SARS-CoV-2             |                                      |
| 30-Jan-20 | 6                              |   |                                      |   |                                      |
| 31-Jan-20 | 7                              |   |                                      |   |                                      |
| 1-Feb-20  | 8                              |   |                                      |   |                                      |
| 2-Feb-20  | 9                              |   |                                      |   |                                      |
| 3-Feb-20  | 10                             | Illness onset   |                                      |   |                                      |
| 4-Feb-20  | 11                             |   |                                      |   |                                      |
| 5-Feb-20  | 12                             |   |                                      |   |                                      |
| 6-Feb-20  | 13                             |   |                                      | Admission to hospital; Routine blood test |                                      |
| 7-Feb-20  | 14                             |   |                                      |   |                                      |
| 8-Feb-20  | 15                             |   |                                      |   |                                      |
| 9-Feb-20  | 16                             | Confirmed test for SARS-CoV-2                               |                                      |   |                                      |
| 10-Feb-20 | 17                             |   |                                      |   |                                      |
| 11-Feb-20 | 18                             | Admission to hospital; Routine blood test                   |                                      |   |                                      |
| 12-Feb-20 | 19                             |   |                                      |   |                                      |
| 13-Feb-20 | 20                             |   |                                      |   | Transferred into CCU                 |
| 14-Feb-20 | 21                             |   |                                      |   | Artificial liver system              |
| 15-Feb-20 | 22                             |   |                                      |   | Artificial liver system              |
| 16-Feb-20 | 23                             |   |                                      |   |                                      |
| 17-Feb-20 | 24                             |   |                                      |   | Artificial liver system              |
| 18-Feb-20 | 25                             |   | Transferred into CCU                 |   |                                      |
| 19-Feb-20 | 26                             |   |                                      |   |                                      |
| 20-Feb-20 | 27                             |   |                                      |   | Artificial liver system              |
| 21-Feb-20 | 28                             |   |                                      |   | Artificial liver system              |
| 22-Feb-20 | 29                             |   |                                      |   |                                      |
| 23-Feb-20 | 30                             |   |                                      |   |                                      |
| 24-Feb-20 | 31                             |   |                                      |   |                                      |
| 25-Feb-20 | 32                             |   |                                      |   | Artificial liver system              |
| 26-Feb-20 | 33                             |   |                                      |   |                                      |
| 27-Feb-20 | 34                             |   |                                      |   |                                      |
| 28-Feb-20 | 35                             |   |                                      |   |                                      |
| 29-Feb-20 | 36                             |   |                                      |   |                                      |
| 1-Mar-20  | 37                             | PCR of nasopharyngeal swab                                  |                                      | PCR of nasopharyngeal swab                |                                      |
| 2-Mar-20  | 38                             |   |                                      |   |                                      |
| 3-Mar-20  | 39                             | PCR of whole blood; PCR of BALF; PCR of urine; PCR of feces | Bronchoscopy, bronchoalveolar lavage |   |                                      |
| 4-Mar-20  | 40                             | Serological test  |                                      | PCR of BALF; PCR of urine                 | Bronchoscopy, bronchoalveolar lavage |
| 5-Mar-20  | 41                             |   |                                      |   |                                      |
| 6-Mar-20  | 42                             |   |                                      |   |                                      |
| 7-Mar-20  | 43                             |   |                                      |   |                                      |
| 8-Mar-20  | 44                             |   |                                      |   |                                      |

(Continued)

TABLE 2 | Continued

| Date*     | Days of follow-up <sup>#</sup> | Patient 1        |                                | Patient 2        |                                |
|-----------|--------------------------------|------------------|--------------------------------|------------------|--------------------------------|
|           |                                | Examination      | Intervention                   | Examination      | Intervention                   |
| 9-Mar-20  | 45                             |                  |                                |                  |                                |
| 10-Mar-20 | 46                             |                  | Thoracic closed chest drainage |                  |                                |
| 11-Mar-20 | 47                             | End of follow-up |                                |                  |                                |
| 12-Mar-20 | 48                             |                  |                                |                  |                                |
| 13-Mar-20 | 49                             |                  |                                |                  | Thoracic closed chest drainage |
| 14-Mar-20 | 50                             |                  |                                |                  |                                |
| 15-Mar-20 | 51                             |                  |                                |                  |                                |
| 16-Mar-20 | 52                             |                  |                                |                  |                                |
| 17-Mar-20 | 53                             |                  |                                |                  |                                |
| 18-Mar-20 | 54                             |                  |                                |                  |                                |
| 19-Mar-20 | 55                             |                  |                                |                  |                                |
| 20-Mar-20 | 56                             |                  |                                |                  |                                |
| 21-Mar-20 | 57                             |                  |                                |                  |                                |
| 22-Mar-20 | 58                             |                  |                                | PCR of sputum    |                                |
| 23-Mar-20 | 59                             |                  |                                |                  |                                |
| 24-Mar-20 | 60                             |                  |                                |                  |                                |
| 25-Mar-20 | 61                             |                  |                                |                  |                                |
| 26-Mar-20 | 62                             |                  |                                |                  |                                |
| 27-Mar-20 | 63                             |                  |                                | PCR of anal swab |                                |
| 28-Mar-20 | 64                             |                  |                                | PCR of feces     |                                |
| 29-Mar-20 | 65                             |                  |                                |                  |                                |
| 30-Mar-20 | 66                             |                  |                                |                  |                                |
| 31-Mar-20 | 67                             |                  |                                |                  |                                |
| 1-Apr-20  | 68                             |                  |                                |                  |                                |
| 2-Apr-20  | 69                             |                  |                                |                  |                                |
| 3-Apr-20  | 70                             |                  |                                |                  |                                |
| 4-Apr-20  | 71                             |                  |                                |                  |                                |
| 5-Apr-20  | 72                             |                  |                                |                  |                                |
| 6-Apr-20  | 73                             |                  |                                |                  |                                |
| 7-Apr-20  | 74                             |                  |                                |                  |                                |
| 8-Apr-20  | 75                             |                  |                                | End of follow-up |                                |

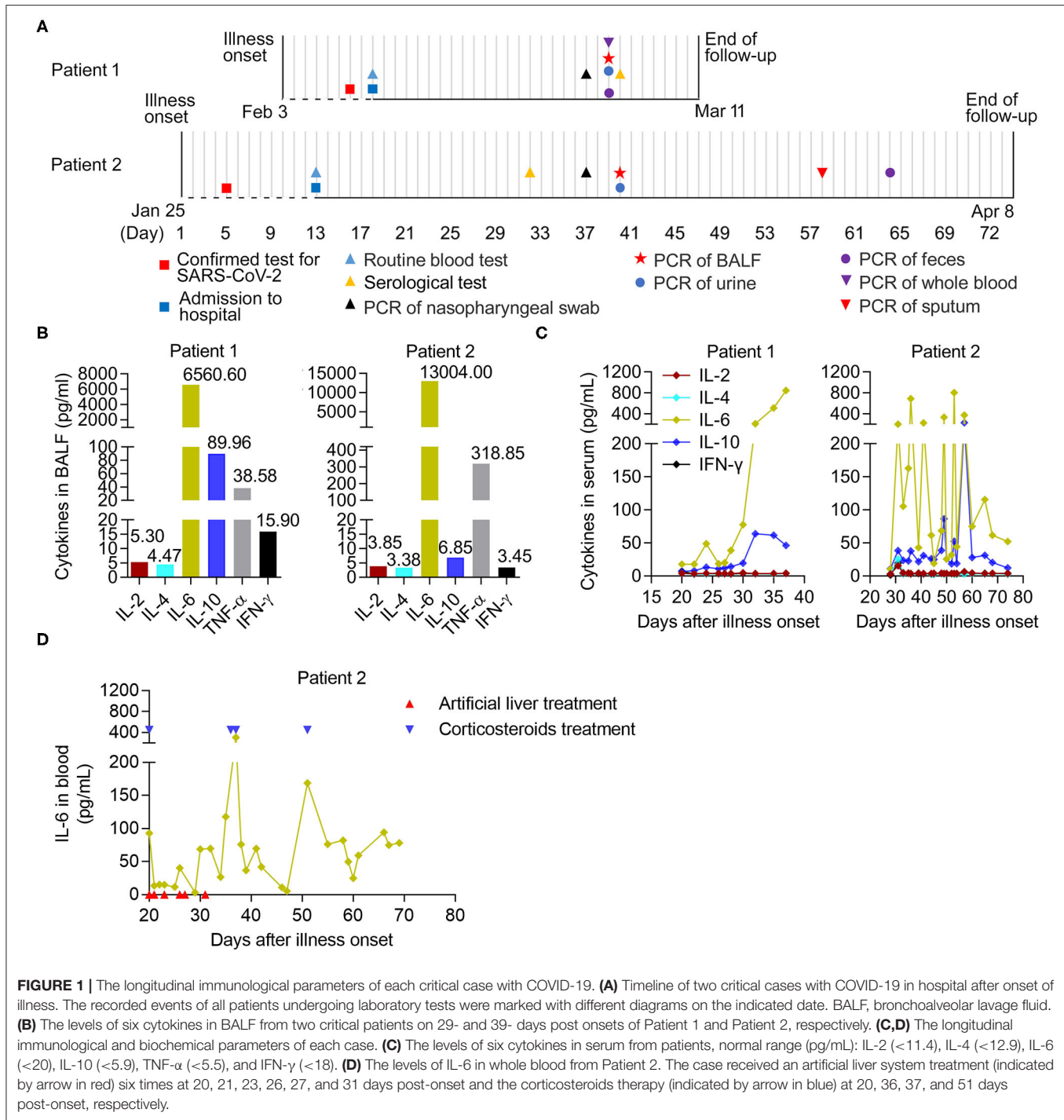
\*Data is expressed as day-month-year. <sup>#</sup>indicates the period of each event from the first record.

times in succession (20, 21, 23, 26, 27, and 31 days after onset of illness) (Table 2), aiming to reduce the potential lung injury resulting from the cytokine storm (15, 16). Later, the outcomes resulted in the death of Patient 1 and recovery of Patient 2, respectively.

### Analysis of Immunological and Biochemical Parameters in Critical COVID-19 Patients

We further analyzed the dynamic immunological and biochemical parameters of the two critical cases. To directly evaluate inflammation in the lungs, the levels of six cytokines (IL-2, IL-4, IL-6, IL-10, TNF- $\alpha$ , and IFN- $\gamma$ ) in BALF samples from two critical patients (29 and 39 days after onset for Patient 1 and Patient 2, respectively), were measured upon admission and during treatment. Among them, IL-6 and

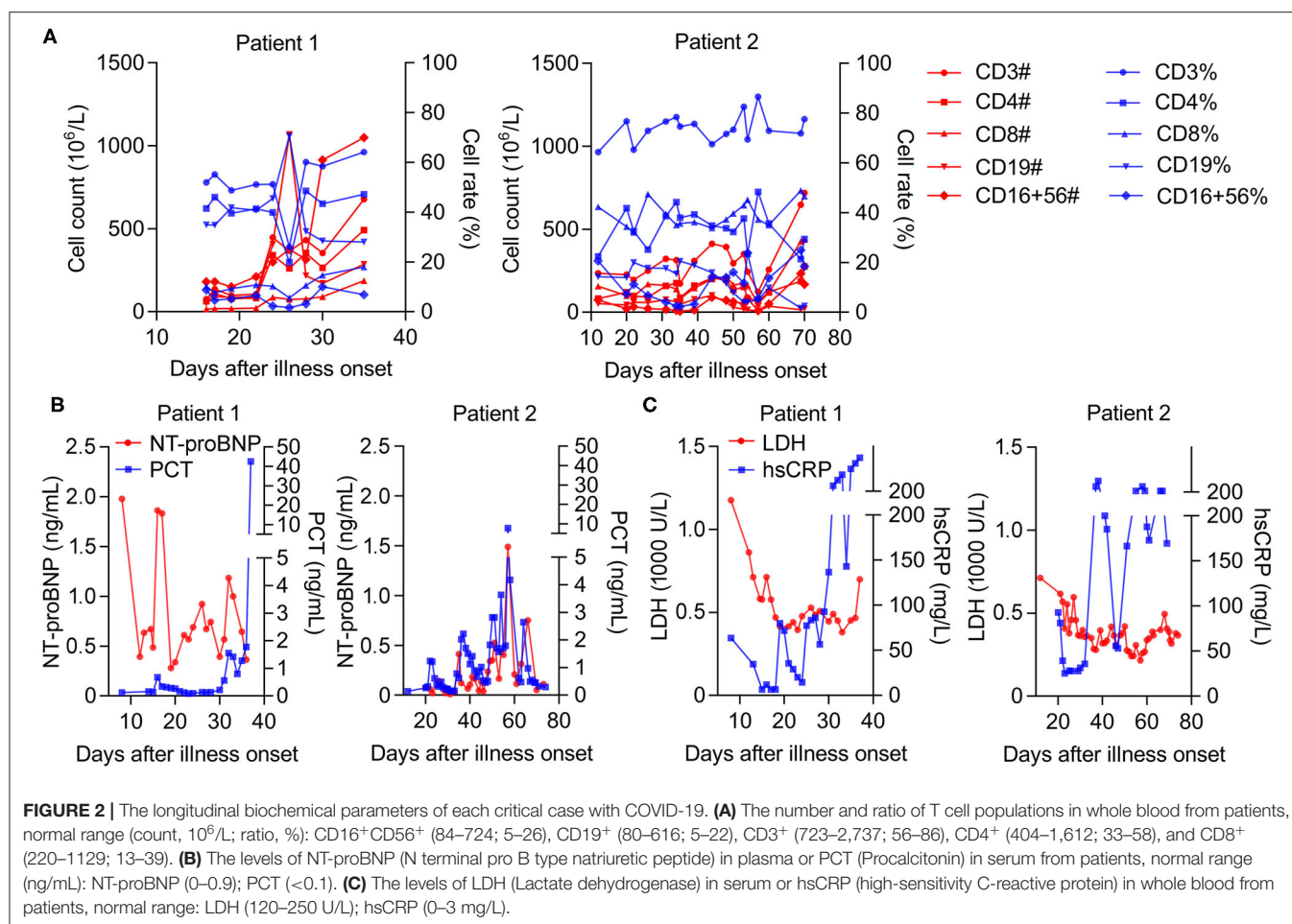
TNF- $\alpha$  showed significant increases compared to normal levels. Notably, increased secretion of the anti-inflammatory cytokine IL-10 was also observed (Figure 1B). Furthermore, we combined the longitudinal immunological and biochemical data of each case and plotted their fluctuation patterns against the time points post-onset. During treatment, the levels of IL-6 and IL-10 were continuously elevated in the serum of Patient 1. In the serum from Patient 2, these two cytokine levels dropped transiently due to the targeted treatment and remained high in the early stage; however, these sharply declined later on (after 57 days post-onset) (Figure 1C). Particularly, the levels of IL-6 in whole blood from Patient 2 transiently decreased during artificial liver treatment (21 to 31 days post-onset) and sharply declined after 37 days post-onset, indicating the beneficial effect from artificial liver treatment (Figure 1D).



## High Risk and Longitudinal Factors Associated With Cytokine Overproduction in Critical COVID-19 Patients

Considering that decreased T cell populations contribute to the severity of COVID-19 (6), a detailed analysis of lymphocytopenia subtypes revealed that the number rather than the ratio of CD16<sup>+</sup>CD56<sup>+</sup>, CD3<sup>+</sup>, and CD4<sup>+</sup> T cells decreased more

significantly than that of CD19<sup>+</sup> and CD8<sup>+</sup> T cells in both cases in the early stage. However, these were obviously restored later (after 30- and 57-days post-onset in Patients 1 and 2, respectively) (Figure 2A). Correspondingly, we observed a successively increased level of PCT (procalcitonin) in Patient 1; however, Patient 2's PCT levels were high in the early stage but sharply declined later (57 days post-onset) (Figure 2B),



suggesting a good prognosis from MOF in Patient 2 but not in Patient 1. We also noticed a decreased level of N-terminal pro-B-type natriuretic peptide levels in both cases (**Figure 2B**), indicating a certain relief from acute cardiovascular failure. More importantly, there was a successive increase in high-sensitivity C-reactive protein (hsCRP), with a high level of lactate dehydrogenase (LDH) in Patient 1. Meanwhile, these high factor levels rapidly reduced at the late treatment stage in Patient 2 (after 67 days post-onset) (**Figure 2C**), indicating the deterioration of Patient 1 and improvement of Patient 2 in terms of their COVID-19 progression.

## DISCUSSION

Our analysis of two typically treated patients with critical COVID-19 explores the further discovery of the high risk of poor outcomes related to cytokine overproduction in severe COVID-19 via the detection of hyperinflammation in BALF. Among multiple cytokines (including IL-2, IL-4, IL-6, IL-10, TNF- $\alpha$ , and IFN- $\gamma$ ) contributing to an excessive inflammatory response in lung injury (17), we observed a dominantly elevated level of IL-6 in BALF samples from both critical COVID-19 cases.

Although exuberant plasmacytosis and some transcriptional changes of inflammatory genes in the BAL specimens from COVID-19 patients suggest local hyperinflammation in the lungs (4, 10–12), these provides direct evidence that the overactive production of cytokines (especially IL-6) occurred upon SARS-CoV-2 infection in the lungs and led to the subsequent development of a cytokine storm in the blood, which might act as a prognostic indicator for the severity of COVID-19.

To extend the relationship between host immune response and hyperinflammation detected from BALF samples, the longitudinal characteristics of cytokine profiles, lymphocyte responses, and pathological parameters were further analyzed in the peripheral blood of critical COVID-19 patients. During treatment, the levels of IL-6 were continuously elevated in the serum of Patient 1 and remained high in the early stage. Notably, Patient 2 received targeted treatments and their IL-6 levels dropped transiently after six rounds of artificial liver treatment in the early stage (21–31 days post-onset), until they sharply declined after 37 days post-onset. This decline could be explained by the use of corticosteroids (18), which temporarily inhibits cytokine overproduction (especially IL-6)



and is further stably relieved with the application of Li's artificial liver system (16). We also noticed increased secretion of the anti-inflammatory cytokine IL-10, indicating divergence in the immunological lung injury, as previously observed (17). It could be recommended that the decreased levels of IL-6 and IL-10 in blood from COVID-19 patients act as the sign of the alleviating disease, which might be helpful for personal physical examination in the future clinical guidelines. Interestingly, a similar phenomenon was also observed in lymphocytopenia subtype population changes and PCT levels. Notably, the number of CD16<sup>+</sup>CD56<sup>+</sup>, CD3<sup>+</sup>, and CD4<sup>+</sup>T cells decreased more significantly than that of CD19<sup>+</sup> and CD8<sup>+</sup> T cells, which is in line with the findings of reduced T cell populations as well as lymphopenia leading to the severity of COVID-19 (5, 6, 19). Importantly, the changes in PCT levels in the two cases were correlated with the immune responses, reflecting the status of pyemia-related MOF in critical COVID-19 patients (20).

Emerging biomarkers have been identified as prognostic factors for severe COVID-19. In addition to lymphocytes, high levels of LDH, and hsCRP can predict interpretable mortality in COVID-19 patients (21). Based on this, the longitudinal levels of LDH and hsCRP in the peripheral blood of critical COVID-19 patients were also retrospectively analyzed. A sequentially increased level of hsCRP along with a high level of LDH in Patient 1 was reported, whereas these high levels were rapidly reduced in the late treatment stage in Patient 2. These changes demonstrated deterioration of Patient 1 and improvement in Patient 2 in terms of their COVID-19 progression resulting from a cytokine storm during treatment.

Until now, the common strategy for treating COVID-19 is a host-based treatment, including anti-infection, anti-inflammatory, or anti-cytokine overactivity therapies (22, 23). In our retrospective study, we summarized the treatments for two severe COVID-19 patients, such as the combination of antiviral, bacterial, and fungal drugs, along with anti-inflammatory agents and high-flow oxygen supplementation as previously described (24). Due to preexisting comorbidities of hypertension and hematological disorders, both critical COVID-19 patients developed underlying pyemia, which frequently reemerges in COVID-19 patients in ICUs (14). Both underwent interventional therapies including bronchoscopy, bronchoalveolar lavage, and thoracic closed chest drainage. In particular, Patient 2 received Li's artificial liver system treatment six times, ranging from 20 to 31 days after onset. Interestingly, we reviewed the levels of cytokines and pathological parameters in Patient 2 and found a visible restoration at the late stage of treatment (after 57 days post-onset), which may have resulted in the good outcome in Patient 2. Commonly, the time period of SARS virus-associated ARDS is 16.52 days post-onset (25), while the duration of other pulmonary and extrapulmonary ARDS is more than 60 days (26), however, during the treatment, the duration of COVID-19 ARDS is up to 90 days post-onset (27). It could be viewed as a normal period of treatment in this observational study. Consequently, except for targeted therapies against virus or other pathogen infections such as

organ function support, artificial liver systems and facilitating the removal of cytokines through blood purification technology (19, 28) may be beneficial for the recovery of critical COVID-19 patients.

The limitations of this study include its small sample size and retrospective design. Some considerations should be considered when interpreting the findings. First, the BALF samples from the enrolled patients were difficult to collect, and we could not determine the longitudinal presence of SARS-CoV-2 and the dynamic levels of cytokines, such as daily collected samples. Second, more evidence should be obtained in order to investigate the relationship between the host immune response and hyperinflammation (such as IL-6 production) detected in BALF. Third, to exclude the individual variation including age and gender, a larger sample size might statistically support the conclusion that the removal of cytokines through Li's artificial liver system was beneficial for the recovery of critical COVID-19 patients. Finally, the data of longitudinal cytokine levels in the early stage during artificial liver treatment were absent, leading to failure to directly access the decrease of cytokine levels after the immediate performance of treatment. Fortunately, we presented the longitudinal level of IL-6 in whole blood from Patient 2 transiently decreased during first five rounds of treatment (21–27 days post-onset), indicating the beneficial effect from artificial liver treatment. Nevertheless, we believe this report could provide an appropriate reference for artificial liver treatment in future large-scale clinical trials for critically ill COVID-19 patients.

Collectively, we reported that the clinical characteristics of two critically ill COVID-19 patients were similar to those reported previously. We also revealed the poor outcomes related to cytokine overproduction in critical COVID-19 patients with hyperinflammation detected in BALF and the potential effect on the decrease of cytokines through an artificial liver system is beneficial for the treatment of critical COVID-19 patients. In sum, this single uncontrolled clinical observation is compatible with a possible effect of the artificial liver intervention in reducing circulating cytokine levels, and suggests that the supportive intervention ought to be further tested in adequately designed and powered clinical trials.

## DATA AVAILABILITY STATEMENT

The original contributions presented in the study are included in the article/supplementary material, further inquiries can be directed to the corresponding author/s.

## ETHICS STATEMENT

The studies involving human participants were reviewed and approved by the Ethics Committee and the Institutional Review Board of the Renmin Hospital of Wuhan University (file no. WDRY2020-K066). The patients/participants provided their written informed consent to participate in this study. Written informed consent was obtained from the individual(s) for the

publication of any potentially identifiable images or data included in this article.

## AUTHOR CONTRIBUTIONS

ZL, CZ, YX, and JW: conceptualization and investigation. ZR, XC, MS, and PP: methodology and software. CZ, XC, JH, FW, and HS: resources and data curation. ZL and CZ: validation and writing. ZR, XC, MS, PP, JH, FW, and HS: formal analysis. ZL, CZ, and YX: funding acquisition. YX and JW: supervision and writing—review & editing. All authors have approved to submit manuscript of this study and took responsibility for the integrity of the data and the accuracy of the data analysis.

## REFERENCES

- Ioannidis JPA. Infection fatality rate of COVID-19 inferred from seroprevalence data. *Bull World Health Organ.* (2021) 99:19–33F. doi: 10.2471/BLT.20.265892
- Huang C, Wang Y, Li X, Ren L, Zhao J, Hu Y, et al. Clinical features of patients infected with 2019 novel coronavirus in Wuhan, China. *Lancet.* (2020) 395:497–506. doi: 10.1016/S0140-6736(20)30183-5
- Pain CE, Felsenstein S, Cleary G, Mayell S, Conrad K, Harave S, et al. Novel paediatric presentation of COVID-19 with ARDS and cytokine storm syndrome without respiratory symptoms. *Lancet Rheumatol.* (2020) 2:e376–9. doi: 10.1016/S2665-9913(20)30137-5
- Zeng HL, Chen D, Yan J, Yang Q, Han QQ, Li SS, et al. Proteomic characteristics of bronchoalveolar lavage fluid in critical COVID-19 patients. *FEBS J.* (2020). doi: 10.1111/febs.15609. [Epub ahead of print].
- Liu R, Wang Y, Li J, Han H, Xia Z, Liu F, et al. Decreased T cell populations contribute to the increased severity of COVID-19. *Clin Chim Acta.* (2020) 508:110–4. doi: 10.1016/j.cca.2020.05.019
- Zhang X, Tan Y, Ling Y, Lu G, Liu F, Yi Z, et al. Viral and host factors related to the clinical outcome of COVID-19. *Nature.* (2020) 583:437–40. doi: 10.1038/s41586-020-2355-0
- Andreaskos E, Tsiodras S. COVID-19: lambda interferon against viral load and hyperinflammation. *EMBO Mol Med.* (2020) 12:e12465. doi: 10.15252/emmm.202012465
- Hoffmann M, Kleine-Weber H, Schroeder S, Kruger N, Herrler T, Erichsen S, et al. SARS-CoV-2 cell entry depends on ace2 and tmprss2 and is blocked by a clinically proven protease inhibitor. *Cell.* (2020) 181:271–80.e8. doi: 10.1016/j.cell.2020.02.052
- Chen L, Liu W, Zhang Q, Xu K, Ye G, Wu W, et al. RNA based mNGS approach identifies a novel human coronavirus from two individual pneumonia cases in 2019 Wuhan outbreak. *Emerg Microbes Infect.* (2020) 9:313–9. doi: 10.1080/22221751.2020.1725399
- Giani M, Seminati D, Lucchini A, Foti G, Pagni F. Exuberant plasmocytosis in bronchoalveolar lavage specimen of the first patient requiring extracorporeal membrane oxygenation for SARS-CoV-2 in Europe. *J Thorac Oncol.* (2020) 15:e65–6. doi: 10.1016/j.jtho.2020.03.008
- Xiong Y, Liu Y, Cao L, Wang D, Guo M, Jiang A, et al. Transcriptomic characteristics of bronchoalveolar lavage fluid and peripheral blood mononuclear cells in COVID-19 patients. *Emerg Microbes Infect.* (2020) 9:761–70. doi: 10.1080/22221751.2020.1747363
- Zhou Z, Ren L, Zhang L, Zhong J, Xiao Y, Jia Z, et al. Heightened innate immune responses in the respiratory tract of COVID-19 patients. *Cell Host Microbe.* (2020) 27:883–90.e2. doi: 10.1016/j.chom.2020.04.017
- Pandolfi L, Fossali T, Frangipane V, Bozzini S, Morosini M, D'Amato M, et al. Broncho-alveolar inflammation in COVID-19 patients: a correlation with clinical outcome. *BMC Pulm Med.* (2020) 20:301. doi: 10.1186/s12890-020-01343-z
- Wang D, Hu B, Hu C, Zhu F, Liu X, Zhang J, et al. Clinical characteristics of 138 hospitalized patients with 2019 novel coronavirus-infected pneumonia in Wuhan, China. *JAMA.* (2020) 323:1061–9. doi: 10.1001/jama.2020.1585
- Zhou N, Li J, Zhang Y, Lu J, Chen E, Du W, et al. Efficacy of coupled low-volume plasma exchange with plasma filtration adsorption in treating pigs with acute liver failure: a randomised study. *J Hepatol.* (2015) 63:378–87. doi: 10.1016/j.jhep.2015.03.018
- Guo J, Xia H, Wang S, Yu L, Zhang H, Chen J, et al. The artificial-liver blood-purification system can effectively improve hypercytokinemia for COVID-19. *Front Immunol.* (2020) 11:586073. doi: 10.3389/fimmu.2020.586073
- Liu J, Li S, Liu J, Liang B, Wang X, Wang H, et al. Longitudinal characteristics of lymphocyte responses and cytokine profiles in the peripheral blood of SARS-CoV-2 infected patients. *EBioMedicine.* (2020) 55:102763. doi: 10.1016/j.ebiom.2020.102763
- Wu C, Chen X, Cai Y, Xia J, Zhou X, Xu S, et al. Risk factors associated with acute respiratory distress syndrome and death in patients with coronavirus disease 2019 pneumonia in Wuhan, China. *JAMA Intern Med.* (2020) 180:934–43. doi: 10.1001/jamainternmed.2020.0994
- Duijff PHG. Low baseline pulmonary levels of cytotoxic lymphocytes as a predisposing risk factor for severe COVID-19. *mSystems.* (2020) 5:e00741–20. doi: 10.1128/mSystems.00741-20
- Ke C, Wang Y, Zeng X, Yang C, Hu Z. 2019 Novel coronavirus disease (COVID-19) in hemodialysis patients: a report of two cases. *Clin Biochem.* (2020) 81:9–12. doi: 10.1016/j.clinbiochem.2020.04.008
- Yan L, Zhang H-T, Gonçalves J, Xiao Y, Wang M, Guo Y, et al. An interpretable mortality prediction model for COVID-19 patients. *Nat Mach Intell.* (2020) 2:283–8. doi: 10.1038/s42256-020-0180-7
- Zhou Y, Fu B, Zheng X, Wang D, Zhao C, Qi Y, et al. Pathogenic T cells and inflammatory monocytes incite inflammatory storm in severe COVID-19 patients. *Natl Sci Rev.* (2020) 7:998–1002. doi: 10.1093/nsr/nwaa041
- Yousefi B, Valizadeh S, Ghaffari H, Vahedi A, Karbalaee M, Eslami M. A global treatments for coronaviruses including COVID-19. *J Cell Physiol.* (2020) 235:9133–42. doi: 10.1002/jcp.29785
- Xu X, Han M, Li T, Sun W, Wang D, Fu B, et al. Effective treatment of severe COVID-19 patients with tocilizumab. *Proc Natl Acad Sci USA.* (2020) 117:10970–5. doi: 10.1073/pnas.2005615117
- Sah A, Fabian EJ, Remolina C. Ventilator-induced barotrauma in critically ill patients with COVID-19: a retrospective observational study. *J Community Hosp Intern Med Perspect.* (2021) 11:304–10. doi: 10.1080/20009666.2021.1896831
- Anan K, Kawamura K, Suga M, Ichikado K. Clinical differences between pulmonary and extrapulmonary acute respiratory distress syndrome: a retrospective cohort study of prospectively collected data in Japan. *J Thorac Dis.* (2018) 10:5796–803. doi: 10.21037/jtd.2018.09.73

## FUNDING

This study was supported by the National Natural Science Foundation of China (81971936 and 82041004 to YX, 81672079 to CZ, 31800147 and 32070148 to ZL) and the Guangdong Basic and Applied Basic Research Foundation (2019A1515011073 to ZL). The sponsors had no role in the design, execution, interpretation, or writing of the study.

## ACKNOWLEDGMENTS

We would like to thank Editage (www.editage.com) for English language editing.

27. Autschbach T, Hatam N, Durak K, Grottko O, Dreher M, Nubbemeyer K, et al. Outcomes of extracorporeal membrane oxygenation for acute respiratory distress syndrome in COVID-19 patients: a propensity-matched analysis. *J Clin Med.* (2021) 10:2547. doi: 10.3390/jcm10122547
28. Zhang C, Huang S, Zheng F, Dai Y. Controversial treatments: an updated understanding of the coronavirus disease 2019. *J Med Virol.* (2020) 92:1441–8. doi: 10.1002/jmv.25788

**Conflict of Interest:** The authors declare that the research was conducted in the absence of any commercial or financial relationships that could be construed as a potential conflict of interest.

**Publisher's Note:** All claims expressed in this article are solely those of the authors and do not necessarily represent those of their affiliated organizations, or those of the publisher, the editors and the reviewers. Any product that may be evaluated in this article, or claim that may be made by its manufacturer, is not guaranteed or endorsed by the publisher.

Copyright © 2021 Luo, Zhu, Ruan, Cui, Shereen, Pan, Huang, Wang, Su, Xia and Wu. This is an open-access article distributed under the terms of the Creative Commons Attribution License (CC BY). The use, distribution or reproduction in other forums is permitted, provided the original author(s) and the copyright owner(s) are credited and that the original publication in this journal is cited, in accordance with accepted academic practice. No use, distribution or reproduction is permitted which does not comply with these terms.



# The Association Between Risk Perception and COVID-19 Vaccine Hesitancy for Children Among Reproductive Women in China: An Online Survey

Min Du<sup>1</sup>, Liyuan Tao<sup>2</sup> and Jue Liu<sup>1,3,4\*</sup>

## OPEN ACCESS

### Edited by:

Atefeh Abedini,  
Shahid Beheshti University of Medical  
Sciences, Iran

### Reviewed by:

Ayokunle A. Olagoke,  
University of Illinois at Chicago,  
United States  
Bijaya Kumar Padhi,  
Post Graduate Institute of Medical  
Education and Research  
(PGIMER), India  
Khezar Hayat,  
University of Veterinary and Animal  
Sciences, Pakistan

### \*Correspondence:

Jue Liu  
jueliu@bjmu.edu.cn

### Specialty section:

This article was submitted to  
Infectious Diseases - Surveillance,  
Prevention and Treatment,  
a section of the journal  
Frontiers in Medicine

**Received:** 14 July 2021

**Accepted:** 11 August 2021

**Published:** 08 September 2021

### Citation:

Du M, Tao L and Liu J (2021) The  
Association Between Risk Perception  
and COVID-19 Vaccine Hesitancy for  
Children Among Reproductive Women  
in China: An Online Survey.  
Front. Med. 8:741298.  
doi: 10.3389/fmed.2021.741298

<sup>1</sup> Department of Epidemiology and Biostatistics, School of Public Health, Peking University, Beijing, China, <sup>2</sup> Research Center of Clinical Epidemiology, Peking University Third Hospital, Beijing, China, <sup>3</sup> Institute for Global Health and Development, Peking University, Beijing, China, <sup>4</sup> National Health Commission Key Laboratory of Reproductive Health, Peking University, Beijing, China

**Background:** This study aimed to explore the association between risk perception and coronavirus disease 2019 (COVID-19) vaccine hesitancy among reproductive women in China to supplement limited studies in this area.

**Methods:** From December 14, 2020, to January 31, 2021, an anonymous cross-sectional online survey was conducted on COVID-19 vaccine hesitancy for children among reproductive women in China. We assessed risk perception, including perceived susceptibility, severity, barriers, and benefits using the health belief model, and then classified each variable into three groups (low, moderate, and high) based on tertiles. Information on sociodemographic characteristics, health status, and knowledge of COVID-19 was also collected. The Pearson  $\chi^2$ -test was used to compare vaccine hesitancy among the above mentioned factors. Logistic regression models were used to calculate the adjusted odds ratio (aOR) of risk perception related to vaccine hesitancy after controlling for the above covariates.

**Results:** Among 3,011 reproductive women, 8.44% (95%CI: 7.44–9.43) had COVID-19 vaccine hesitancy. Vaccine hesitancy was observed more in women who lived in eastern China (11.63%), aged >45 years (12.00%), had a lower than high school education level (12.77%), and a low score on knowledge of COVID-19 (12.22%). Vaccine hesitancy was associated with lower perceived susceptibility (moderate: aOR = 1.72, 95%CI: 1.17–2.54,  $P$  = 0.0061; low: aOR = 2.44, 95%CI: 1.60–3.70,  $P$  < 0.0001), high perceived barriers (aOR = 2.86, 95%CI: 1.57–5.22,  $P$  < 0.0001), and lower perceived benefit (moderate: aOR = 3.29, 95%CI: 2.30–4.70,  $P$  < 0.0001; low: aOR = 4.59, 95%CI: 2.98–7.07,  $P$  < 0.0001), but not with perceived severity.

**Conclusions:** Although the proportion of COVID-19 vaccine hesitancy for children among Chinese reproductive women was <1 out of 10, to improve COVID-19 vaccine



hesitancy, our findings suggest that tailored public health measures are needed to increase perceived susceptibility and benefit, and decrease perceived barriers among reproductive women.

**Keywords:** vaccine hesitancy, COVID-19, Chinese, reproductive women, risk perception

## INTRODUCTION

As of July 2, 2021, coronavirus disease 2019 (COVID-19) is a major public health concern with more than one hundred million confirmed cases and three million deaths worldwide (1). Vaccination is considered the most economical and effective method for preventing infectious diseases. The World Health Organization (WHO) on June 30, 2021, reported that a total of 2,950,104,812 vaccine doses have been administered for COVID-19 (1). Although children with COVID-19 mainly have mild symptoms as compared to adults or are asymptomatic, some may be at risk for severe COVID-19, including a serious complication called multisystem inflammatory syndrome (2, 3). Therefore, COVID-19 vaccination is important for children. Currently, no COVID-19 vaccines are authorized for use among children aged <12 years, but the safety and efficacy of vaccines for children aged 6 months–17 years have been evaluated (4–6). The mRNA vaccine developed by Pfizer showed 100% efficacy and robust antibody responses among children aged 12–15 years (5). Han et al. reported that CoronaVac developed by Sinovac Life Sciences (Beijing, China) was well-tolerated and safe, and induced humoral response among healthy participants aged 3–17 years in China (7). Therefore, it is now essential to focus on the prospects of COVID-19 vaccination and the possible influencing factors in pediatric populations.

According to the WHO's Strategic Advisory Group of Experts, vaccine hesitancy is defined as the delay in acceptance or refusal to vaccinate oneself despite the availability of vaccination services (8). Vaccine hesitancy has been one of the ten threats to global health in 2019 (9). Children often rely on parental guidance and decision making, so reducing caregivers' vaccine hesitancy is a key point in achieving higher vaccination coverage among children in the future (10). Previous studies have investigated COVID-19 vaccine hesitancy in children. Skjefte et al. reported that only 69.2% of women indicated an intention to vaccinate their children across 16 countries (11). The percentage of parental COVID-19 vaccine hesitancy was 9.9% in Bologna, Italy (12), 10.9% in England (13), 20 and 27% in America (14, 15), 35% in British Columbia (16), 39.2 and 46.1% in Ankara (17, 18), and 49% in Germany (19). Investigations on COVID-19 vaccine hesitancy for children in lower middle income countries (LMICs) were limited. Skjefte et al. found that the proportion of COVID-19 vaccine hesitancy for children was below 15% in India and 30% in Philippine (11). Carcelen et al. reported that 8% of the caregivers had unwillingness of COVID-19 vaccination for their children in Zambia (20). Few researchers have investigated parental COVID-19 vaccine hesitancy in some provinces or

territories of China. The proportion of parental unwillingness to vaccinate their children against COVID-19 was 14.7 and 12.5% in Shanghai, China (21, 22), 27.3% in Shenzhen, China (23), and 40.7% in Wuxi, China (24). Numerous factors are independently associated with parental vaccine decision-making, including risk perception (14, 15, 25), lifestyle, knowledge of vaccines (19), parental education (25, 26), vaccines' country of origin (27), history of vaccination against influenza (16), and parental psychological distress (23). Risk perception is a subjective construction process comprising multiple dimensions, including judgments on the severity and controllability of risks (28). People may develop risk perception for potential or actual consequences and the controllability of the COVID-19 pandemic based on cognitive appraisal theory (29, 30). Some studies have explored the association between risk perception and COVID-19 vaccine hesitancy in children in the USA (14, 15, 25), but related studies are scarce in China. The unknown situation of COVID-19 vaccine hesitancy for children and possible influencing factors especially for risk perception, were crucial and urgent for formulating policies to promote vaccination among children.

In summary, the proportion of COVID-19 vaccine hesitancy among children in China still remains unclear. Additionally, to prepare for COVID-19 vaccination among children, the association of risk perception and vaccine hesitancy to children should be explored so that we can provide a reference for proposing relevant measures. We used a sample of reproductive Chinese women to estimate the proportion of COVID-19 vaccine hesitancy for children and examine the association between risk perception and vaccine hesitancy after controlling for sociodemographic characteristics, health status, and knowledge of COVID-19.

## MATERIALS AND METHODS

### Study Design, Participants, and Sampling

This anonymous cross-sectional survey was conducted from December 14, 2020, to January 31, 2021, in China using a stratified random sampling method via an online survey company established in 2006: Wen Juan Xing (Changsha Ranxing Information Technology Co., Ltd., Hunan, China). Wen (31), a specialized data science company with a database covers factual and well-characterized personal information (e.g., sex, region, and age) of over 2.6 million Chinese respondents. We can use the platform to conduct stratified random sampling, recruit target participants, and distribute questionnaires. Many researchers have used the recorded information in the database to obtain a representative sample and collect data from cross-sectional studies to investigate people's attitudes (32–34).

We recruited target participants for this study in China as the following inclusion criteria: (1) women aged 18–49 years; (2)

**Abbreviations:** COVID-19, coronavirus disease 2019; HBM, Health Belief Model; SD, standard deviation; cOR, crude odds ratio; aOR, adjusted odds ratios.

Chinese speakers; and (3) voluntary agreement to participate in the present study. Considering that the proportion of COVID-19 vaccine hesitancy for children was 12.5% (22), with the alpha set as 0.05 and the confidence interval width as 0.1p (0.0125), the sample size was 2,690 when using PASS for calculation. Besides, regarding the rate of uncompleted questionnaire was 10%, so we planned to recruit at least 3,000 participants using an online survey platform (Wen Juan Xing) in three stages. First, we divided target participants into three tiers by region (eastern, central, and western regions), and selected two provinces randomly from each region. Second, the sample size for each province was allocated in proportion to the population of each province according to the China Statistical Yearbook 2020 (35). Third, Wen Juan Xing randomly selected and recruited target participants according to the sample size requirements in the sample database via the Wen Juan Xing online platform. We used Wen Juan Xing to set up logical jumps and other checked steps between questions to reduce missed and wrong answers. At the same time, before the questionnaire was released, internal staff pre-answered the questionnaire to estimate the reasonable time for answering the questionnaire (3–10 min). The study was approved by the Ethical Committee of Peking University Third Hospital (IRB00006761-M2020528) and conducted in accordance with the Declaration of Helsinki. Informed consent was obtained from all participants.

## Assessment of Risk Perception

We estimated risk perception to COVID-19 vaccination using the survey tool which was commonly used in previous studies for vaccination intention based on Health Belief Model (HBM) with good internal consistency reliability (17, 36, 37). HBM is an appropriate theoretical framework for understanding vaccination intent and illustrating the factors influencing people's decision-making about vaccination which is important to improve health promotion and reduce the barriers to vaccination (17, 36–38). The HBM includes five dimensions (perceived susceptibility, perceived severity, perceived barriers, and perceived benefits, and cues to action) comprising nine questions. In the present study, we used seven questions of HBM which evaluated risk perception, including perceived susceptibility, severity, barriers, and benefits. Two questions evaluated perceived susceptibility of infection to themselves and their children (if they had any), one question evaluated perceived severity of infection, three questions evaluated perceived barriers (vaccine safety, effectiveness, and the possibility of infection after vaccination), and one question evaluated perceived benefits of vaccination (protective effects). Participants answered each question on a three-point Likert scale (“very concerned or agree”, “concerned or not sure,” and “not concerned or disagree”), which were assigned the scores of 3, 2, and 1, respectively. We classified the participants into three groups based on the summed score for each HBM dimension by tertiles, with the top 33.3% of the participants being assigned to the “high” group, bottom 33.3% assigned to the “low” group, and middle ones assigned to the “moderate” group. Questions related to the Health Belief Model dimensions in the questionnaire as shown in **Supplementary File 1**. We did a pilot testing using a convenience

sample of 20 participants and calculated Cronbach's alpha index for different dimensions of the health belief model. Cronbach's alpha index was 0.81 (perceived susceptibility), 0.88 (perceived severity), 0.76 (perceived barriers), and 0.87 (perceived benefits), respectively, showing an adequate internal consistency reliability.

## Measurement of Vaccine Hesitancy for Children

The primary outcome was the attitude toward COVID-19 vaccination for children. The question “If you have children under 18 years old, would you be willing to vaccinate them against COVID-19, when the vaccine becomes available?” was required to be answered by participants. People who answered “no” to this question were categorized into the hesitancy group.

## Covariates

In addition to HBM and attitudes toward COVID-19 vaccination, the following three aspects were investigated in the structured self-administered online questionnaire: (1) sociodemographic characteristics, (2) health status, and (3) knowledge of COVID-19.

Sociodemographic characteristics included age group, region, education, occupation, and monthly household income per capita (RMB). Health status included gravidity, parity, history of chronic disease, and history of influenza vaccination. Knowledge of COVID-19 comprised six aspects: source of infection, route of transmission, susceptible population, common symptoms, high-risk population for severe illness and death, and individual preventive measures for infection. For every correct response, the respondent received a score of one; otherwise, they received a score of zero. Then, we divided the total knowledge score into three groups (low, moderate, and high) by tertiles.

## Data Analysis

Mean (standard deviation; SD), frequencies and percentages were used to describe continuous and categorical variables, respectively. We compared the characteristics of participants with COVID-19 vaccine hesitancy using Pearson's  $\chi^2$ -test. The crude odds ratios (cORs) and adjusted odds ratios (aORs) of vaccine hesitancy in different risk perception groups were estimated using univariate and multivariate logistic regression models which were most frequently used statistical model for analyzing the relationship between outcomes and influencing factors (39, 40). We performed a sensitivity analysis by fitting different models to examine the robustness of the estimation. Model A was used as a univariate model. Sociodemographic characteristics—including age group, region, education, occupation, and monthly household income per capita, were adjusted in model B. Furthermore, all the covariates—including age group, region, education, occupation, monthly household income per capita, gravidity, parity, history of chronic disease, history of influenza vaccination, knowledge of COVID-19, and the other three risk perceptions—were adjusted in model C. Additionally, we supplemented model D which only adjusted the significant covariates and the other three risk perceptions based the Pearson's  $\chi^2$ -test.

**TABLE 1 |** Risk perception among 3,011 reproductive women in China during COVID-19 pandemic.

| Risk perception                 | N     | %     |
|---------------------------------|-------|-------|
| <b>Perceived susceptibility</b> |       |       |
| Low                             | 798   | 26.50 |
| Moderate                        | 1,485 | 49.32 |
| High                            | 728   | 24.18 |
| <b>Perceived severity</b>       |       |       |
| Low                             | 164   | 5.45  |
| Moderate                        | 899   | 29.86 |
| High                            | 1,948 | 64.70 |
| <b>Perceived barriers</b>       |       |       |
| Low                             | 323   | 10.73 |
| Moderate                        | 2,139 | 71.04 |
| High                            | 549   | 18.23 |
| <b>Perceived benefit</b>        |       |       |
| Low                             | 349   | 11.59 |
| Moderate                        | 1,417 | 47.06 |
| High                            | 1,245 | 41.35 |

We performed subgroup analyses on age group, region, education, occupation, monthly household income per capita, gravidity, parity, history of chronic disease, history of influenza vaccination, and knowledge of COVID-19 after adjusting for all the covariates. The heterogeneity test was used to examine differences between the groups. A  $P < 0.05$ , indicated statistical significance in this study. All analyses were conducted using SPSS 25.0, R 3.4.0, and Stata 16.0.

## RESULTS

### Participants' Characteristics

In total, 3,150 participants out of 3,213 recruited participants completed the questionnaire (rate of completed questionnaire was 98.04%). We excluded 139 participants who completed the questionnaire in a short time ( $<1$  min). Ultimately, our study included 3,011 eligible reproductive women. The average time for completing the survey was 8.93 min.

Of 3,011 women, 41.35% lived in central China, 61.04% were 30 years old or younger, and 94.92% had an education level of bachelor's degree or lower. The mean scores for perceived susceptibility, severity, barriers, and benefits were 4.14 (SD = 1.36), 2.59 (SD = 0.59), 5.22 (SD = 1.46), and 2.30 (SD = 0.66), respectively. Of the 3,011 reproductive women, 49.32, 64.70, 71.04, and 47.06% had moderate perceived susceptibility, high perceived severity, moderate perceived barriers, and moderate perceived benefit, respectively (Table 1).

The total proportion of COVID-19 vaccine hesitancy for children was 8.44% (95%CI: 7.44, 9.43) among 3,011 reproductive women. According to  $\chi^2$ -tests, there were no differences in COVID-19 vaccine hesitancy according to income, gravidity, parity, history of chronic disease, history of influenza vaccination, and perceived severity among groups. Vaccine hesitancy was observed more in women who lived in eastern

China (11.63%), aged  $>45$  years (12.00%), had a below high school level education (12.77%), with a low score of knowledge on COVID-19 (12.22%). Additionally, vaccine hesitancy was more likely to be observed in women with low perceived susceptibility (11.03%), perceived benefit (14.94%), and perceived barriers (16.05%) (Table 2).

### Association Between Risk Perception and COVID-19 Vaccine Hesitancy to Children

Models A, B, and C were established using logistic regression models, as shown in Table 3. In model A, without controlling for confounding factors, vaccine hesitancy for children was associated with lower perceived susceptibility (moderate: cOR = 1.71, 95%CI: 1.18–2.49,  $P = 0.0047$ ; low: cOR = 2.25, 95%CI: 1.52–3.34,  $P < 0.0001$ ; reference: high perceived susceptibility), low perceived severity (cOR = 1.68, 95%CI: 1.02–2.69,  $P = 0.0413$ ; reference: high perceived severity), high perceived barriers (cOR = 3.61, 95%CI: 2.04–6.37,  $P < 0.0001$ ; reference: low perceived barriers), and lower perceived benefit (moderate: cOR = 3.33, 95%CI: 2.36–4.70,  $P < 0.0001$ ; low: cOR = 5.22, 95%CI: 3.44–7.90,  $P < 0.0001$ ; reference: high perceived benefit). After controlling for sociodemographic characteristics in Model B, the above associations remained stable. After controlling for all covariates, vaccine hesitancy was associated with lower perceived susceptibility (moderate: aOR = 1.72, 95%CI: 1.17–2.54,  $P = 0.0061$ ; low: aOR = 2.44, 95%CI: 1.60–3.70,  $P < 0.0001$ ; reference: high perceived susceptibility), high perceived barriers (aOR = 2.86, 95%CI: 1.57–5.22,  $P < 0.0001$ ; reference: low perceived barriers), and lower perceived benefit (moderate: aOR = 3.29, 95%CI: 2.30–4.70,  $P < 0.0001$ ; low: aOR = 4.59, 95%CI: 2.98–7.07,  $P < 0.0001$ ; reference: high perceived benefit), but not with perceived severity. Model D also showed the similar results (Table 3).

Subgroup analysis showed no interactions in most subgroups (Supplementary Table 1). Regarding perceived severity, the vaccine hesitancy was more likely occurred among women with moderate perceived severity who had chronic diseases, as compared to those who had no chronic diseases ( $P$  for difference = 0.001, as shown in Figure 1), but vaccine hesitancy was not associated with moderate perceived severity in women with or without chronic diseases (Table 3).

## DISCUSSION

As of July 2, 2021, COVID-19 is still a pandemic worldwide, with more than one hundred million confirmed cases and three million deaths worldwide (1). As of June 30, 2021, a total of 2,950,104,812 vaccine doses have been administered globally (1). The National Health Commission of the People's Republic of China reported that as of July 3, 2021, more than one billion vaccine doses have been administered to adults (41). Children are a susceptible population, however, no COVID-19 vaccines have been authorized for use among children aged  $<12$  years (4–6). At the initial stage of COVID-19 vaccination in China, children were not a priority population for vaccination, with the completion of COVID-19 vaccination for adults, vaccination for children

**TABLE 2 |** COVID-19 vaccine hesitancy to children among 3,011 reproductive women in China by characteristics.

| Characteristics                                  | N     | COVID-19 vaccine hesitancy to children (%) | $\chi^2$ | P       |
|--|-------|--|----------|---------|
| <b>Total</b>                                     | 3,011 | 254 (8.44)                                 |          |         |
| <b>Sociodemographic characteristics</b>          |       |  |          |         |
| <b>Region</b>                                    |       |  | 18.582   | <0.0001 |
| Eastern  | 920   | 107 (11.63)                                |          |         |
| Central  | 1,245 | 94 (7.55)                                  |          |         |
| Western  | 846   | 53 (6.26)                                  |          |         |
| <b>Age group (years)</b>                         |       |  | 15.313   | 0.018   |
| ≤20  | 543   | 32 (5.89)                                  |          |         |
| 21–25  | 712   | 48 (6.74)                                  |          |         |
| 26–30  | 583   | 50 (8.58)                                  |          |         |
| 31–35  | 469   | 48 (10.23)                                 |          |         |
| 36–40  | 322   | 31 (9.63)                                  |          |         |
| 41–45  | 207   | 24 (11.59)                                 |          |         |
| >45  | 175   | 21 (12.00)                                 |          |         |
| <b>Education</b>                                 |       |  | 10.88    | 0.012   |
| Lower than high school                           | 321   | 41 (12.77)                                 |          |         |
| High school or some college                      | 886   | 77 (8.69)                                  |          |         |
| Bachelor's degree                                | 1,651 | 121 (7.33)                                 |          |         |
| Postgraduate degree                              | 153   | 15 (9.80)                                  |          |         |
| <b>Monthly household income per capita (RMB)</b> |       |  | 3.496    | 0.321   |
| ≤3,000   | 1,562 | 122 (7.81)                                 |          |         |
| 3,001–5,000                                      | 693   | 56 (8.08)                                  |          |         |
| 5,001–10,000                                     | 571   | 58 (10.16)                                 |          |         |
| >10,000  | 185   | 18 (9.73)                                  |          |         |
| <b>Health status</b>                             |       |  |          |         |
| <b>Gravidity</b>                                 |       |  | 5.419    | 0.067   |
| 0  | 1,607 | 118 (7.34)                                 |          |         |
| 1  | 624   | 62 (9.94)                                  |          |         |
| ≥2   | 780   | 74 (9.49)                                  |          |         |
| <b>Parity</b>                                    |       |  | 4.567    | 0.102   |
| 0  | 1,624 | 121 (7.45)                                 |          |         |
| 1  | 825   | 81 (9.82)                                  |          |         |
| ≥2   | 562   | 52 (9.25)                                  |          |         |
| <b>Chronic disease</b>                           |       |  | 0.07     | 0.791   |
| Yes  | 121   | 11 (9.09)                                  |          |         |
| No   | 2,890 | 243 (8.41)                                 |          |         |
| <b>History of influenza vaccination</b>          |       |  | 2.266    | 0.132   |
| Yes  | 833   | 60 (7.20)                                  |          |         |
| No   | 2,178 | 194 (8.91)                                 |          |         |
| <b>Score of knowledge</b>                        |       |  | 19.326   | <0.0001 |
| Low  | 769   | 94 (12.22)                                 |          |         |
| Moderate   | 1,337 | 93 (6.96)                                  |          |         |
| High   | 905   | 67 (7.40)                                  |          |         |
| <b>Risk perception</b>                           |       |  |          |         |
| <b>Perceived susceptibility</b>                  |       |  | 16.753   | <0.0001 |
| Low  | 798   | 88 (11.03)                                 |          |         |
| Moderate   | 1,485 | 128 (8.62)                                 |          |         |
| High   | 728   | 38 (5.22)                                  |          |         |

(Continued)



TABLE 2 | Continued

| Characteristics           | N     | COVID-19 vaccine hesitancy to children (%) | $\chi^2$ | P       |
|---------------------------|-------|--|----------|---------|
| <b>Perceived severity</b> |       |  | 5.771    | 0.056   |
| Low                       | 164   | 20 (12.20)                                 |          |         |
| Moderate                  | 899   | 85 (9.45)                                  |          |         |
| High                      | 1,948 | 149 (7.65)                                 |          |         |
| <b>Perceived barriers</b> |       |  | 39.372   | <0.0001 |
| Low                       | 323   | 15 (4.64)                                  |          |         |
| Moderate                  | 2,139 | 157 (7.34)                                 |          |         |
| High                      | 549   | 82 (14.94)                                 |          |         |
| <b>Perceived benefit</b>  |       |  | 75.746   | <0.0001 |
| Low                       | 349   | 56 (16.05)                                 |          |         |
| Moderate                  | 1,417 | 154 (10.87)                                |          |         |
| High                      | 1,245 | 44 (3.53)                                  |          |         |

TABLE 3 | The association between risk perception and the risk of COVID-19 vaccine hesitancy to children among 3,011 reproductive women in China.

|                                 | Model A             |         | Model B                      |         | Model C                      |         | Model D                      |         |
|---------------------------------|---------------------|---------|------------------------------|---------|------------------------------|---------|------------------------------|---------|
|                                 | Odds ratio (95% CI) | P-value | Adjusted odds ratio (95% CI) | P-value | Adjusted odds ratio (95% CI) | P-value | Adjusted odds ratio (95% CI) | P-value |
| <b>Perceived susceptibility</b> |                     |         |                              |         |                              |         |                              |         |
| Low                             | 2.25 (1.52, 3.34)   | <0.0001 | 2.32 (1.56, 3.46)            | <0.0001 | 2.44 (1.60, 3.70)            | <0.0001 | 2.37 (1.57, 3.58)            | <0.0001 |
| Moderate                        | 1.71 (1.18, 2.49)   | 0.0047  | 1.75 (1.20, 2.54)            | 0.0037  | 1.72 (1.17, 2.54)            | 0.0061  | 1.69 (1.15, 2.49)            | 0.0075  |
| High                            | Reference           |         | Reference                    |         | Reference                    |         | Reference                    |         |
| <b>Perceived severity</b>       |                     |         |                              |         |                              |         |                              |         |
| Low                             | 1.68 (1.02, 2.76)   | 0.0413  | 1.73 (1.04, 2.86)            | 0.0346  | 1.38 (0.81, 2.37)            | 0.2351  | 1.47 (0.87, 2.50)            | 0.1530  |
| Moderate                        | 1.26 (0.95, 1.67)   | 0.1035  | 1.25 (0.94, 1.66)            | 0.1175  | 1.06 (0.78, 1.42)            | 0.7251  | 1.10 (0.82, 1.48)            | 0.5333  |
| High                            | Reference           |         | Reference                    |         | Reference                    |         | Reference                    |         |
| <b>Perceived barriers</b>       |                     |         |                              |         |                              |         |                              |         |
| Low                             | Reference           |         | Reference                    |         | Reference                    |         | Reference                    |         |
| Moderate                        | 1.63 (0.94, 2.80)   | 0.0792  | 1.59 (0.92, 2.74)            | 0.0974  | 1.09 (0.62, 1.93)            | 0.7550  | 1.09 (0.62, 1.91)            | 0.7709  |
| High                            | 3.61 (2.04, 6.37)   | <0.0001 | 3.76 (2.12, 6.68)            | <0.0001 | 2.86 (1.57, 5.22)            | <0.0001 | 2.84 (1.56, 5.15)            | 0.0006  |
| <b>Perceived benefit</b>        |                     |         |                              |         |                              |         |                              |         |
| Low                             | 5.22 (3.44, 7.90)   | <0.0001 | 5.19 (3.41, 7.90)            | <0.0001 | 4.59 (2.98, 7.07)            | <0.0001 | 4.57 (2.97, 7.03)            | <0.0001 |
| Moderate                        | 3.33 (2.36, 4.70)   | <0.0001 | 3.36 (2.37, 4.75)            | <0.0001 | 3.29 (2.30, 4.70)            | <0.0001 | 3.21 (2.25, 4.57)            | <0.0001 |
| High                            | Reference           |         | Reference                    |         | Reference                    |         | Reference                    |         |

Model A is a univariate model. Sociodemographic characteristics were adjusted in Model B. All covariates were adjusted in Model C, including region, age group, education, occupation, monthly household income per capita, gravidity, parity, history of chronic disease, history of influenza vaccination, knowledge of COVID-19, and the other three risk perceptions. Model D only adjusted the significant covariates including region, age group, education and knowledge of COVID-19, and the other three risk perceptions based the Pearson's  $\chi^2$ -test.

had been considered. CoronaVac has a well-tolerated, safe, and induced humoral response in Chinese children, according to a double-blind, randomized, controlled, phase 1/2 clinical trial (7). Therefore, on June 11, 2021, the Joint Prevention and Control Mechanism of the State Council announced that Chinese authorities have approved CoronaVac for emergency use in children aged 3–17 years, and experts are discussing formulating specific policies for vaccination (42). On July 20, 2021, Beijing Center for Disease Prevention and Control announced that COVID-19 vaccination for children aged 12–17 years old had been started in Beijing, China (43). However, the willingness to vaccinate children is not yet known. Moreover, the possible

influencing factors, particularly, risk perception, were unclear. The unknown situation of the willingness to vaccinate children and possible influencing factors were crucial and urgent for formulating policies to promote vaccination among children. To our knowledge, this is the first online survey that investigated the proportion of COVID-19 vaccine hesitancy among children and examined its association with risk perception among reproductive women in six provinces of China.

We found that COVID-19 vaccine hesitancy to children associated with lower perceived susceptibility, high perceived barriers, and lower perceived benefit, but not with perceived severity. Some studies have reported that perceived higher risk

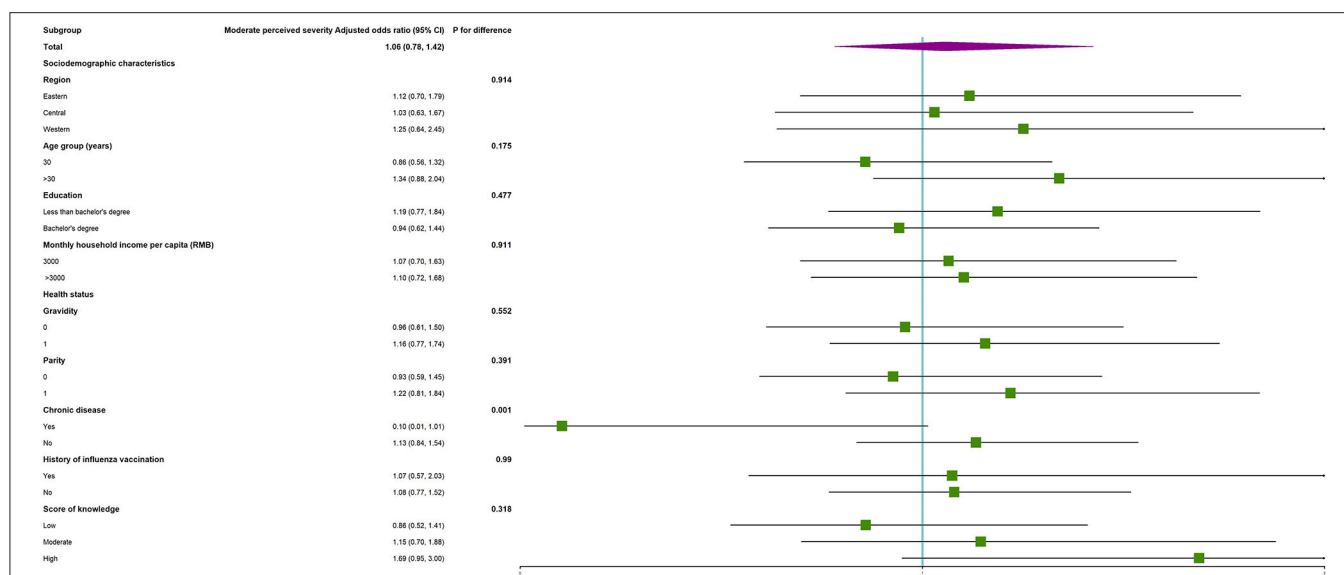


**FIGURE 1 |** The subgroup analysis on the association between risk perception and the risk of COVID-19 vaccine hesitancy to children among reproductive women with moderate perceived severity.

of infection (34, 44), and lower perceived benefits and higher perceived barriers (36) among adults were associated with a high vaccine hesitancy. Our study found that vaccine hesitancy in children was associated with lower perceived susceptibility, perceived barriers, and perceived benefits in China, which is in line with other similar studies in the United States (14, 15, 25). Viswanath et al. found that perceived susceptibility (OR = 2.26, 95% CI: 1.56–3.27) to COVID-19 was associated with vaccine uptake for vaccinating those under one's care in the United States (25). Compared to the low perceived threat group, willingness to get children vaccinated was higher among those with high perceived threat (perceived severity and perceived susceptibility) (OR = 1.82, 95% CI: 1.21–2.72) (15). Thunström et al. reported that a higher degree of infectivity of the coronavirus may influence vaccine intentions (14). Additionally, our study found that perceived severity was not associated with vaccine hesitancy among children. Unlike Viswanath et al.'s findings (25), Thunström et al. (14) reported no statistically significant effect on parental vaccine intentions based on the severity of COVID-19. A systematic review regarded the link between perceived severity of illness as tenuous (45). Therefore, more research is needed to confirm the association between the perceived severity and COVID-19 vaccine hesitancy. Taken together, our findings suggest that elevating perceived susceptibility to COVID-19 and benefit of receiving the COVID-19 vaccine, while decreasing perceived barriers of receiving the COVID-19 vaccine, is an effective way to prevent COVID-19 vaccine hesitancy in children in China.

In our study, 26.50, 18.23, and 11.59% still had low perceived susceptibility, high perceived barriers, and low perceived benefits based on the summed score for each HBM dimension by tertiles. Taking measures and establishing programmes to increase perceived susceptibility and benefit and decrease perceived

barriers is essential. Perceived barriers were evaluated by three questions including vaccine safety, effectiveness, and the possibility of infection after vaccination. Many studies also found that doubts regarding vaccine safety and efficacy were the main reasons for vaccine reluctance (11, 14, 18, 21, 22, 46, 47). Therefore, healthcare providers should use face-to-face education, autodialers, mail, and text messages to emphasize the COVID-19 pandemic situation, the benefits of vaccination, and the safety and efficacy of vaccines, to address parental concerns about vaccines. Moreover, training for healthcare providers, support from health authorities, and related media and social media channels should promote vaccinations (48, 49).

According to our investigation, the proportion of COVID-19 vaccine hesitancy among reproductive women in China was 8.44%, which was lower than that in some provinces or territories of China (21–24). For example, 87.5% would accept a vaccine with the most ideal attributes for their child, while with the least ideal attributes, these numbers dropped to 31.3% in Shanghai, China (22). Xu et al. reported that the proportion of COVID-19 vaccine hesitancy for their children was 27.3% in Shenzhen, China (23). Only 59.3% of parents reported willingness to avail COVID-19 vaccine for their children in Wuxi, China (24). The differences may be related to many factors, including the characteristics of the survey population, survey time, and region. Additionally, the results of this study showed that vaccine hesitancy was more likely to be observed in women who lived in eastern China, aged >45 years, had a high school or lower level of education, with a low score on knowledge of COVID-19. Montalti et al. and Khubchandani et al. also found that the highest vaccine hesitancy rates were detected in guardians with low educational levels (12, 50). Kelly et al. found that older individuals' willingness to vaccinate was higher (15). In addition, people with low knowledge scores on COVID-19 may be less

aware of the susceptibility to disease and the importance of vaccination. These findings suggest that there should be targeted interventions for older women with a low education level and score of knowledge on COVID-19 in eastern China to decrease the proportion of vaccine hesitancy to children.

Our study has some limitations. First, reproductive women responding to the survey did not completely represent caregivers' attitudes in China as some of them had no children. Additionally, although we recruited participants using stratified random sampling from an online platform in six provinces of China, the database of the online platform may use an opt-in recruitment strategy, then there was a possibility of selection bias and an under coverage of sample frame which means that the results were not nationally representative and may not be generalizable to all women in China. Second, risk perception which was estimated using HBM may not be comparable to the reported situation of risk perception from other studies that used other models. Finally, we could not control for the effect of public health measures on vaccine hesitancy in China. What's more, the age of children for those who have children was not investigated in our study, so the specific situation of vaccine hesitancy for different aged children was unclear.

## CONCLUSION

The proportion of COVID-19 vaccine hesitancy among Chinese reproductive women was <1 out of 10. Vaccine hesitancy was more likely to be observed in women who lived in eastern China, aged >45 years, had high school or lower level of education, with a low score of knowledge on COVID-19. Importantly, vaccine hesitancy in children was associated with lower perceived susceptibility, perceived barriers, and perceived benefits.

To improve COVID-19 vaccine hesitancy to children, our findings suggest that tailored public health measures are needed to increase perceived susceptibility and benefit, and decrease perceived barriers among reproductive women. Additionally, there should be target interventions for older women with a low education level and score of knowledge on COVID-19 in eastern China to decrease the proportion of vaccine hesitancy

to children. These findings have important implications for proposing strategies on COVID-19 vaccination for children in the future.

## DATA AVAILABILITY STATEMENT

The raw data supporting the conclusions of this article will be made available by the authors, without undue reservation.

## ETHICS STATEMENT

The studies involving human participants were reviewed and approved by Ethical Committee of Peking University Third Hospital (IRB00006761-M2020528). The patients/participants provided their written informed consent to participate in this study.

## AUTHOR CONTRIBUTIONS

JL conceptualized and designed the study. LT and JL did data acquisition and writing—reviewing and editing. MD did data curation, formal analysis, visualization, and writing—original draft. All authors contributed to the article and approved the submitted version.

## FUNDING

This study was funded by the National Natural Science Foundation of China, grant number 72122001, the National Science and Technology Key Projects on Prevention and Treatment of Major Infectious Disease of China, grant number 2020ZX10001002, and the National Key Research and Development Project of China, grant number 2020YFC0846300.

## SUPPLEMENTARY MATERIAL

The Supplementary Material for this article can be found online at: <https://www.frontiersin.org/articles/10.3389/fmed.2021.741298/full#supplementary-material>

## REFERENCES

- World Health Organization. *WHO Coronavirus Disease (COVID-19) Situation Dashboard*. (2020). Available online at: <https://covid19.who.int/> (accessed July 3, 2021).
- Ebina-Shibuya R, Namkoong H, Shibuya Y, Horita N. Multisystem Inflammatory Syndrome in Children (MIS-C) with COVID-19: insights from simultaneous familial Kawasaki Disease cases. *Int J Infect Dis*. (2020) 97:371–3. doi: 10.1016/j.ijid.2020.06.014
- Maltezou HC, Magaziotou I, Dedoukou X, Eleftheriou E, Raftopoulos V, Michos A, et al. Children and adolescents with SARS-CoV-2 infection: epidemiology, clinical course and viral loads. *Pediatr Infect Dis J*. (2020) 39:e388–92. doi: 10.1097/INF.0000000000002899
- National Institutes of Health. *Safety and Immunogenicity Study of Inactivated Vaccine for Prevention of COVID-19*. (2020). Available online at: <https://clinicaltrials.gov/ct2/show/NCT04551547?cond=NCT04551547&draw=2&rank=1> (accessed July 3, 2021).
- Pfizer. *Pfizer-Biontech Announce Positive Topline Results of Pivotal COVID-19 Vaccine Study in Adolescents*. Available online at: Pfizer-BioNTech Announce Positive Topline Results of Pivotal COVID-19 Vaccine Study in Adolescents | [pfizer.com](https://www.pfizer.com/news/press-release/press-release-content?contentID=2021-07-01-01) (accessed July 3, 2021).
- Cooper DM, Afghani B, Byington CL, Cunningham CK, Golub S, Lu KD, et al. SARS-CoV-2 vaccine testing and trials in the pediatric population: biologic, ethical, research, and implementation challenges. *Pediatr Res*. (2021). doi: 10.1038/s41390-021-01402-z. [Epub ahead of print].
- Han B, Song Y, Li C, Yang W, Ma Q, Jiang Z, et al. Safety, tolerability, and immunogenicity of an inactivated SARS-CoV-2 vaccine (CoronaVac) in healthy children and adolescents: a double-blind, randomised, controlled, phase 1/2 clinical trial. *Lancet Infect Dis*. (2021). doi: 10.1016/S1473-3099(21)00319-4. [Epub ahead of print].

8. MacDonald NE SAGE Working Group on Vaccine Hesitancy. Vaccine hesitancy: Definition, scope and determinants. *Vaccine*. (2015) 33:4161–4. doi: 10.1016/j.vaccine.2015.04.036
9. World Health Organization. *Vaccination: European Commission and World Health Organization Join Forces to Promote the Benefits of Vaccines*. Available online at: <https://www.who.int/news/item/12-09-2019-vaccination-european-commission-and-world-health-organization-join-forces-to-promote-the-benefits-of-vaccines> (accessed July 20, 2021)
10. Dosanjh A. Pediatric vaccine hesitancy and the utilization of antibody measurements: a novel strategy with implications for COVID 19. *J Asthma Allergy*. (2021) 14:427–31. doi: 10.2147/JAA.S303309
11. Skjefte M, Ngirbabul M, Akeju O, Escudero D, Hernandez-Diaz S, Wyszynski DF, et al. COVID-19 vaccine acceptance among pregnant women and mothers of young children: results of a survey in 16 countries. *Eur J Epidemiol*. (2021) 36:197–211. doi: 10.1007/s10654-021-00728-6
12. Montalti M, Rallo F, Guaraldi F, Bartoli L, Po G, Stillo M, et al. Would Parents get their children vaccinated against SARS-CoV-2? Rate and predictors of vaccine hesitancy according to a survey over 5000 families from Bologna, Italy. *Vaccines*. (2021) 9:366. doi: 10.3390/vaccines9040366
13. Bell S, Clarke R, Mounier-Jack S, Walker JL, Paterson P. Parents' and guardians' views on the acceptability of a future COVID-19 vaccine: a multi-methods study in England. *Vaccine*. (2020) 38:7789–98. doi: 10.1016/j.vaccine.2020.10.027
14. Thunström L, Ashworth M, Finnoff D, Newbold SC. Hesitancy toward a COVID-19 vaccine. *Ecohealth*. (2021) 18:44–60. doi: 10.1007/s10393-021-01524-0
15. Kelly BJ, Southwell BG, McCormack LA, Bann CM, MacDonald PDM, Frasier AM, et al. Predictors of willingness to get a COVID-19 vaccine in the U.S. *BMC Infect Dis*. (2021) 21:338. doi: 10.1186/s12879-021-06085-9
16. Goldman RD, Yan TD, Seiler M, Parra Cotanda C, Brown JC, Klein EJ, et al. Caregiver willingness to vaccinate their children against COVID-19: cross sectional survey. *Vaccine*. (2020) 38:7668–73. doi: 10.1016/j.vaccine.2020.09.084
17. Marquez RR, Gosnell ES, Thikkurissy S, Schwartz SB, Cully JL. Caregiver acceptance of an anticipated COVID-19 vaccination. *J Am Dent Assoc*. (2021). doi: 10.1016/j.adaj.2021.03.004. [Epub ahead of print].
18. Yigit M, Ozkaya-Parlakay A, Senel E. Evaluation of COVID-19 vaccine refusal in parents. *Pediatr Infect Dis J*. (2021) 40:e134–6. doi: 10.1097/INF.0000000000003042
19. Brandstetter S, Böhmer MM, Pawellek M, Seelbach-Göbel B, Melter M, Kabesch M, et al. Parents' intention to get vaccinated and to have their child vaccinated against COVID-19: cross-sectional analyses using data from the KUNO-Kids health. *Eur J Pediatr*. (2021). doi: 10.1007/s00431-021-04094-z. [Epub ahead of print].
20. Carcelen AC, Prosperi C, Mutembo S, Chongwe G, Mwansa FD, Ndubani P, et al. COVID-19 vaccine hesitancy in Zambia: a glimpse at the possible challenges ahead for COVID-19 vaccination rollout in sub-Saharan Africa. *Hum Vaccin Immunother*. (2021). doi: 10.1080/21645515.2021.1948784. [Epub ahead of print].
21. Zhou Y, Zhang J, Wu W, Liang M, Wu QS. Willingness to receive future COVID-19 vaccines following the COVID-19 epidemic in Shanghai, China. *BMC Public Health*. (2021) 21:1103. doi: 10.1186/s12889-021-11174-0
22. Lu J, Wen X, Guo Q, Ji M, Zhang F, Wagner AL, et al. Sensitivity to COVID-19 vaccine effectiveness and safety in Shanghai, China. *Vaccines*. (2021) 9:472. doi: 10.3390/vaccines9050472
23. Xu Y, Zhang R, Zhou Z, Fan J, Liang J, Cai L, et al. Parental psychological distress and attitudes towards COVID-19 vaccination: a cross-sectional survey in Shenzhen, China. *J Affect Disord*. (2021) 292:552–8. doi: 10.1016/j.jad.2021.06.003
24. Wang Q, Xiu S, Zhao S, Wang J, Han Y, Dong S, et al. Vaccine hesitancy: COVID-19 and influenza vaccine willingness among parents in Wuxi, China: A cross-sectional study. *Vaccines*. (2021) 9:342. doi: 10.3390/vaccines9040342
25. Viswanath K, Bekalu M, Dhawan D, Pinnamaneni R, Lang J, McLoud R. Individual and social determinants of COVID-19 vaccine uptake. *BMC Public Health*. (2021) 21:818. doi: 10.1186/s12889-021-10862-1
26. Rhodes ME, Sundstrom B, Ritter E, McKeever BW, McKeever R. Preparing for a COVID-19 vaccine: a mixed methods study of vaccine hesitant parents. *J Health Commun*. (2020) 25:831–7. doi: 10.1080/10810730.2021.1871986
27. Issanov A, Akhmetzhanova Z, Riethmacher D, Aljofan M. Knowledge, attitude, and practice toward COVID-19 vaccination in Kazakhstan: a cross-sectional study. *Hum Vaccin Immunother*. (2021). doi: 10.1080/21645515.2021.1925054. [Epub ahead of print].
28. Liu C, Huang N, Fu M, Zhang H, Feng XL, Guo J. Relationship between risk perception, social support, and mental health among general Chinese population during the COVID-19 pandemic. *Risk Manag Healthc Policy*. (2021) 14:1843–53. doi: 10.2147/RMHP.S302521
29. Folkman S, Lazarus RS, Dunkel-Schetter C, DeLongis A, Gruen RJ. Dynamics of a stressful encounter: cognitive appraisal, coping, and encounter outcomes. *J Pers Soc Psychol*. (1986) 50:992–1003. doi: 10.1037/0022-3514.50.5.992
30. Goldman RD, McGregor S, Marneni SR, Katsuta T, Griffiths MA, Hall JE, et al. Willingness to vaccinate children against influenza after the coronavirus disease 2019. *Pandemic J Pediatr*. (2021) 228:87–93.e2. doi: 10.1016/j.jpeds.2020.08.005
31. Wen JX. Available online at: <https://www.wxj.cn/> (accessed March 8, 2021).
32. Wang J, Jing R, Lai X, Zhang H, Lyu Y, Knoll MD, et al. Acceptance of COVID-19 vaccination during the COVID-19 Pandemic in China. *Vaccines*. (2020) 8:482. doi: 10.3390/vaccines8030482
33. Liu J, Liu M, Zhang S, Ma Q, Wang Q. Intent to have a second child among Chinese women of childbearing age following China's new universal two-child policy: a cross-sectional study. *BMJ Sex Reprod Health*. (2019) 46:59–66. doi: 10.1136/bmjsh-2018-200197
34. Wang J, Lu X, Lai X, Lyu Y, Zhang H, Fenghuang Y, et al. The changing acceptance of COVID-19 vaccination in different epidemic phases in China: a longitudinal study. *Vaccines*. (2021) 9:191. doi: 10.3390/vaccines9030191
35. National Bureau of Statistics. *China Statistical Yearbook*. (2020). Available online at: <http://www.stats.gov.cn/tjsj/ndsj/2020/indexch.htm> (accessed June 26, 2021).
36. Lin Y, Hu Z, Zhao Q, Alias H, Danaee M, Wong LP. Understanding COVID-19 vaccine demand and hesitancy: a nationwide online survey in China. *PLoS Negl Trop Dis*. (2020) 14:e0008961. doi: 10.1371/journal.pntd.0008961
37. Hu Y, Wang Y, Liang H, Chen Y. Seasonal influenza vaccine acceptance among pregnant women in Zhejiang Province, China: evidence based on health belief model. *Int J Environ Res Public Health*. (2017) 14:1551. doi: 10.3390/ijerph14121551
38. Tao L, Wang R, Liu J. Comparison of vaccine acceptance between COVID-19 and seasonal influenza among women in China: a national online survey based on health belief model. *Front Med*. (2021) 8:679520. doi: 10.3389/fmed.2021.679520
39. Jamaluddine Z, Irani A, Salti N, Abdulrahman S, Chaaban J, El-Asmar K, et al. Child deprivation among Palestinian refugees in Lebanon and Palestinian refugees from Syria living in Lebanon: a cross-sectional analysis of co-occurrence of deprivation indicators. *Lancet*. (2021) 398(Suppl. 1):S32. doi: 10.1016/S0140-6736(21)01518-X
40. Nick TG, Campbell KM. Logistic regression. *Methods Mol Biol*. (2007) 404:273–301. doi: 10.1007/978-1-59745-530-5\_14
41. National Health Commission of the People's Republic of China. *Novel Coronavirus Vaccine Inoculation*. Available online at: <http://www.nhc.gov.cn/> (accessed July 3, 2021).
42. Joint Prevention and Control Mechanism of the State Council. Available online at: [http://www.gov.cn/xinwen/2021-06/12/content\\_5617313.htm](http://www.gov.cn/xinwen/2021-06/12/content_5617313.htm) (accessed July 3, 2021).
43. Beijing Center for Disease Prevention and Control. Available online at: <https://mp.weixin.qq.com/s/aiyDNLzXtxCXBV4UwJD7sg> (accessed July 28, 2021).
44. İkışık H, Akif Sezerol M, Taşçı Y, Maral I. COVID-19 vaccine hesitancy: a community-based research in Turkey. *Int J Clin Pract*. (2021) 75:e14336. doi: 10.1111/ijcp.14336
45. Smith LE, Amlöt R, Weinman J, Yiend J, Rubin GJ. A systematic review of factors affecting vaccine uptake in young children. *Vaccine*. (2017) 35:6059–69. doi: 10.1016/j.vaccine.2017.09.046
46. Paul E, Steptoe A, Fancourt D. Attitudes towards vaccines and intention to vaccinate against COVID-19: implications for public health communications. *Lancet Reg Health Eur*. (2021) 1:100012. doi: 10.1016/j.lanpe.2020.100012



47. Panda DS, Giri RK, Nagarajappa AK, Basha S. Covid-19 vaccine, acceptance, and concern of safety from public perspective in the state of Odisha, India. *Hum Vaccin Immunother.* (2021). doi: 10.1080/21645515.2021.1924017. [Epub ahead of print].
48. Kara A, Ilbay S, Topaç O, Arabulan EA, Tezer H, Tavukçu N, et al. Alteration in vaccination rates and an evaluation of physicians' perceptions of the possible impact of the SARS-CoV-2 pandemic on childhood vaccinations in Ankara, Turkey. *Hum Vaccin Immunother.* (2021). doi: 10.1080/21645515.2021.1923345. [Epub ahead of print].
49. Fedele F, Aria M, Esposito V, Micillo M, Cecere G, Spano M, et al. COVID-19 vaccine hesitancy: a survey in a population highly compliant to common vaccinations. *Hum Vaccin Immunother.* (2021) 1–7. doi: 10.1080/21645515.2021.1928460
50. Khubchandani J, Sharma S, Price JH, Wiblishauser MJ, Sharma M, Webb FJ. COVID-19 vaccination hesitancy in the United States: a rapid national assessment. *J Community Health.* (2021) 46:270–7. doi: 10.1007/s10900-020-00958-x

**Conflict of Interest:** The authors declare that the research was conducted in the absence of any commercial or financial relationships that could be construed as a potential conflict of interest.

**Publisher's Note:** All claims expressed in this article are solely those of the authors and do not necessarily represent those of their affiliated organizations, or those of the publisher, the editors and the reviewers. Any product that may be evaluated in this article, or claim that may be made by its manufacturer, is not guaranteed or endorsed by the publisher.

Copyright © 2021 Du, Tao and Liu. This is an open-access article distributed under the terms of the Creative Commons Attribution License (CC BY). The use, distribution or reproduction in other forums is permitted, provided the original author(s) and the copyright owner(s) are credited and that the original publication in this journal is cited, in accordance with accepted academic practice. No use, distribution or reproduction is permitted which does not comply with these terms.



## OPEN ACCESS

## Edited by:

Seyed Alireza Nadji,  
Shahid Beheshti University of Medical  
Sciences, Iran

## Reviewed by:

Hayder Al-kuraishy,  
Al-Mustansiriya University, Iraq  
Majid Taati Moghadam,  
Iran University of Medical  
Sciences, Iran

## \*Correspondence:

Marco Di Carlo  
dica.marco@yahoo.it

## †ORCID:

Fausto Salaffi  
orcid.org/0000-0002-3794-6831  
Marina Carotti  
orcid.org/0000-0001-6562-180X  
Marco Di Carlo  
orcid.org/0000-0002-0906-4647  
Luca Ceccarelli  
orcid.org/0000-0002-0510-0970  
Massimo Galli  
orcid.org/0000-0001-8887-6215  
Piercarlo Sarzi-Puttini  
orcid.org/0000-0002-8673-5133  
Andrea Giovagnoni  
orcid.org/0000-0002-5264-652X

## Specialty section:

This article was submitted to  
Infectious Diseases-Surveillance,  
Prevention and Treatment,  
a section of the journal  
Frontiers in Medicine

Received: 14 April 2021

Accepted: 12 July 2021

Published: 08 September 2021

## Citation:

Salaffi F, Carotti M, Di Carlo M,  
Ceccarelli L, Galli M, Sarzi-Puttini P  
and Giovagnoni A (2021) Predicting  
Severe/Critical Outcomes in Patients  
With SARS-CoV2 Pneumonia:  
Development of the prediCtion  
severe/critical outcome in COVID-19  
(CRITIC) Model.  
Front. Med. 8:695195.  
doi: 10.3389/fmed.2021.695195

# Predicting Severe/Critical Outcomes in Patients With SARS-CoV2 Pneumonia: Development of the prediCtion severe/critical outcome in COVID-19 (CRITIC) Model

Fausto Salaffi<sup>1†</sup>, Marina Carotti<sup>2†</sup>, Marco Di Carlo<sup>1\*†</sup>, Luca Ceccarelli<sup>3†</sup>, Massimo Galli<sup>4†</sup>,  
Piercarlo Sarzi-Puttini<sup>5†</sup> and Andrea Giovagnoni<sup>2†</sup>

<sup>1</sup> Rheumatology Clinic, Dipartimento di Scienze Cliniche e Molecolari, Università Politecnica delle Marche, Jesi, Italy,

<sup>2</sup> Dipartimento di Scienze Radiologiche Struttura Organizzativa Dipartimentale Radiologia Pediatrica e Specialistica, Azienda Ospedaliera Universitaria, Ospedali Riuniti di Ancona, Ancona, Italy, <sup>3</sup> Unità Operativa di Radiologia – Ospedale degli Infermi, Azienda Unità Sanitaria Locale della Romagna, Faenza, Italy, <sup>4</sup> Divisione di Malattie Infettive, Dipartimento di Scienze Biomediche e Cliniche “Luigi Sacco,” Azienda Socio Sanitaria Territoriale Fatebenefratelli-Sacco, Milan University School of Medicine, Milan, Italy, <sup>5</sup> Divisione di Reumatologia, Dipartimento di Scienze Biomediche e Cliniche “Luigi Sacco,” Azienda Socio Sanitaria Territoriale Fatebenefratelli-Sacco, Milan University School of Medicine, Milan, Italy

**Objective:** To create a prediction model of the risk of severe/critical disease in patients with Coronavirus disease (COVID-19).

**Methods:** Clinical, laboratory, and lung computed tomography (CT) severity score were collected from patients admitted for COVID-19 pneumonia and considered as independent variables for the risk of severe/critical disease in a logistic regression analysis. The discriminative properties of the variables were analyzed through the area under the receiver operating characteristic curve analysis and included in a prediction model based on Fagan’s nomogram to calculate the post-test probability of severe/critical disease. All analyses were conducted using Medcalc (version 19.0, MedCalc Software, Ostend, Belgium).

**Results:** One hundred seventy-one patients with COVID-19 pneumonia, including 37 severe/critical cases (21.6%) and 134 mild/moderate cases were evaluated. Among all the analyzed variables, Charlson Comorbidity Index (CCI) was that with the highest relative importance ( $p = 0.0001$ ), followed by CT severity score ( $p = 0.0002$ ), and age ( $p = 0.0009$ ). The optimal cut-off points for the predictive variables resulted: 3 for CCI [sensitivity 83.8%, specificity 69.6%, positive likelihood ratio (+LR) 2.76], 69.9 for age (sensitivity 94.6%, specificity 68.1, +LR 2.97), and 53 for CT severity score (sensitivity 64.9%, specificity 84.4%, +LR 4.17).

**Conclusion:** The nomogram including CCI, age, and CT severity score, may be used to stratify patients with COVID-19 pneumonia.

**Keywords:** COVID-19, prediction model, Charlson Comorbidity Index, age, lung computed tomography

## INTRODUCTION

Coronavirus disease (COVID-19) is a highly life-threatening infectious disease. The pandemic of the novel severe acute respiratory syndrome coronavirus 2 (SARS-CoV-2) pandemic, which is still ongoing, has resulted in huge costs in terms of human lives, economic and social damage (1, 2). COVID-19 pneumonia can result in acute respiratory distress syndrome (ARDS) and multiple organ failure (3, 4). The severe/critical patients have a poor prognosis and a high mortality rate as compared to the mild/typical patients (5, 6). In patients admitted to hospitals have been identified certain factors related to increased severity (7, 8).

The use of imaging in the diagnosis and identification of risk factors for the development of COVID-19 pneumonia is important. Lung CT is the first-line imaging modality in cases where there is a deep suspicion (9). CT can accurately evaluate the type and extent of lung lesions (10). Recent studies showed that lung CT may enable the detection of the disease with higher sensitivity in comparison to reverse-transcription polymerase chain reaction (RT-PCR). A recent meta-analysis performed to determine the diagnostic accuracy of the initial lung CT scan compared to RT-PCR in COVID-19 patients, demonstrated that the sensitivity of CT, compared to RT-PCR, was 87% and that the specificity was 46%, with a positive predictive value of 69% and a negative predictive value of 89% (11). Although lung CT findings such as consolidation, linear opacities, crazy-paving pattern, bronchial wall thickening, and extrapulmonary lesions are features of severe/critical COVID-19 pneumonia (10), there is still limited information about the prognostic implication of CT findings in patients with COVID-19. Identifying admission CT predictors of adverse outcome in patients without underlying medical issues would help to identify the most vulnerable patients in this age range and, as a result, change their therapy. Several recent studies reported imaging CT findings of patients with adverse outcomes (12–15). However, data on the outcomes of consecutive patients, factors influencing hospital admission vs. outpatient management, and risk factors for COVID-19 adverse effects is still lacking in Italy. The significance of recognizing patients that are at risk of developing severe COVID-19 is mandatory for optimizing intra-hospital resources. Patients with serious illnesses often need a wide range of medical services. As a result, through patient prioritization, early identification of patients at high risk of developing severe COVID-19 will encourage appropriate supportive treatment and reduce mortality rates, as well as unnecessary or insufficient healthcare usage (16, 17).

As a method for rapid clinical management of hospitalized patients, the aim of this study is to build an individualized research model to identify the risk of severe/critical disease in patients with COVID-19 pneumonia.

## METHODS

### Study Design and Participants

The present study is an extension of the data collected in a previous study aimed at realizing a prognostic lung CT score

for worse outcomes in COVID-19 pneumonia (18). In that study, between February 20th, 2020 and April 15th, 2020, data concerning a cohort of patients diagnosed as having COVID-19 pneumonia were retrospectively collected from four hospitals in the Italian regions of Marche, Lombardy and Emilia-Romagna. The inclusion criteria were: an epidemiological history plausible of SARS-CoV2 infection, the identification of SARS-CoV-2 nucleic acid in throat swabs or the lower respiratory tract by real-time reverse transcription polymerase chain reaction, and at least one thin-section lung CT. On the basis of the clinical stages of COVID-19 proposed by WHO (19), patients were assigned to 1 of 2 categories: those with mild/moderate disease and those with severe/critical disease. Mild symptomatic patients meeting the case definition for COVID-19 without evidence of viral pneumonia or hypoxia. Moderate patients meeting clinical signs of pneumonia (fever, cough, dyspnea, and fast breathing) but no signs of severe pneumonia, including pulse oximeter oxygen saturation  $\geq 90\%$  on room air. Severe disease was defined as a respiratory rate of  $\geq 30$  beats per minute, or  $\leq 93\%$  resting oxygen saturation, or arterial oxygen partial pressure ( $\text{PaO}_2$ )/fraction of inspired oxygen ( $\text{FiO}_2$ )  $\leq 300$  mmHg (1 mm Hg = 0.133 kPa), or a  $\geq 50\%$  progression of lung CT findings of pneumonia (fever, cough, dyspnea, fast breathing) within 24–48 h (20). Critical disease was defined as admission to an ICU for mechanical ventilation or oxygenation impairment (mild ARDS:  $200 \text{ mmHg} < \text{PaO}_2/\text{FiO}_2 \leq 300 \text{ mmHg}$  [with positive end-respiratory pressure (PEEP) or continuous positive airway pressure  $\geq 5 \text{ cmH}_2\text{O}$ ]; moderate ARDS:  $100 \text{ mmHg} < \text{PaO}_2/\text{FiO}_2 \leq 200 \text{ mmHg}$  (with PEEP  $\geq 5 \text{ cmH}_2\text{O}$ ); severe ARDS:  $\text{PaO}_2/\text{FiO}_2 \leq 100 \text{ mmHg}$  (with PEEP  $\geq 5 \text{ cmH}_2\text{O}$ ) (21). The patients' recorded demographic and clinical characteristics included age and sex, the time since symptom onset to hospital admission, co-morbidities (systemic hypertension, diabetes mellitus, heart disease, and chronic obstructive pulmonary disease), symptoms, and clinical and laboratory signs.

### Predictors

Several variables were collected from the electronic health record: age at time of testing, sex, height, weight, dyspnea, days from illness onset, smoking history, and comorbidity burden.

Laboratory values were analyzed for the “worst” value occurring during the day of admission for inpatients. For the purposes of this study only C-reactive protein (CRP) was collected as laboratory variable.

All patients had lung CT scans, which were examined by two radiologists who had no access to the clinical or laboratory results. We selected these predictors based on previous published literature and our clinical experience of patients with COVID-19 (18, 22).

Dyspnea was assessed with the Borg Dyspnea Index (Borg score) (23). The Borg score evaluates the perceived dyspnea (breathing discomfort) with a numerical rating scale from 0 to 10 [0 = no breathlessness at all, 0.5 = very very slight (just noticeable), 1 = very slight, 2 = slight breathlessness, 3 = moderate, 4 = somewhat severe, 5 = severe breathlessness, 7 = very severe breathlessness, 9 = very, very severe (almost maximum) and 10 = maximum].

The Charlson Comorbidity Index (CCI) estimated the comorbidity burden (24). The CCI includes the following comorbid conditions: acute myocardial infarction, congestive heart failure, peripheral vascular disease, cerebrovascular disease, dementia, chronic obstructive pulmonary disease, rheumatoid arthritis, peptic ulcer disease, mild and moderate/severe liver disease, diabetes mellitus with and without complications, hemiplegia/paraplegia, renal disease, cancer (any malignancy) and metastatic solid tumor, AIDS/HIV. When computing the weighted CCI, each condition from the CCI is given a ranking, regardless of the coding system used. In particular, diabetes with complications, hemiplegia/paraplegia, renal disease, and malignancies are assigned a score of 2; moderate/severe liver disease is assigned a score of 3; metastatic solid tumor and AIDS/HIV are assigned a score of 6; the remaining comorbidities are assigned a score of 1. The total score in the CCI is derived by summing the assigned weights of all comorbid conditions. Higher scores indicate a more severe condition and consequently, a worse prognosis. While it was initially designed to predict mortality risk after hospitalization, it has been shown to predict adverse outcomes independently over a wide range of conditions (25).

## Lung Computed Tomography Analysis

Two CT scanners with helical acquisitions in end-inspiration were used for the lung CT examinations. The detailed protocol of CT image acquisition is described elsewhere (18).

Lung CT examinations were independently examined by two radiologists with 3 (LC) and 20 (MC) years of lung CT interpretation experience, respectively. The images were viewed on both lung (width, 1,500 HU; level, -700 HU) and mediastinal (width, 350 HU; level, 40 HU) settings. The two readers analyzed the axial CT images but were free to evaluate the multiplanar reformats. The CT scans were assessed for the presence of ground-glass opacities, consolidation, cavitation, centrilobular nodules, tree-in-bud pattern, septal thickening, peribular opacities, reticulation, architectural distortion, subpleural bands, traction bronchiectasis, bronchial wall thickening, intrathoracic lymph node enlargement, and pleural effusions. Ground-glass opacity (GGO) was defined as increased lung density with no obscuration of the underlying lung markings. Increased lung density with obscuration of the underlying lung markings was known as consolidation. Polygonal or curvilinear bands bordering the secondary pulmonary lobule were known as peribular opacities. Interlobular or intralobular irregular septal thickening was known as reticulation. Thin linear opacities peripheral and parallel to the pleura were known as subpleural bands. Traction bronchiectasis was defined as irregular or distorted dilated airways seen in areas of fibrosis.

The degree and type of abnormalities were measured to determine the severity of pulmonary parenchymal involvement using a semi-quantitative scoring (19). In this scoring system, each lung was evaluated on three levels: upper (above the carina), middle (below the carina up to the upper limit of the inferior pulmonary vein), and lower (below the inferior pulmonary vein). Each level's final score was determined by combining the results of the right and left lungs. The percentage of lung involvement

in each level was evaluated independently and categorized as follows: 0 as normal, 1 as <25% abnormality, 2 as 25–49% abnormality, 3 as 50–74% abnormality, and 4 as ≥75% of the pulmonary cross-section CT scan. Further, the scoring system included the nature of abnormalities on a 4-point scale for defining the pattern of CT lung abnormalities. The two scores (abnormality degree and nature) were then multiplied by each other. After adding the scores from all six levels (3 levels on each side), a final radiologic severity score for parenchymal involvement was measured for each patient, with values ranging from 0 to 96. The previous work recorded the inter-observer agreements between the two readers for the measurement of lung CT-severity scores were excellent, with an intraclass correlation coefficient (ICC) of 0.987 (95% CI. 0.982–0.991;  $p < 0.001$ ). The detailed description of the CT scoring system is provided in the first study in which the method is proposed (18).

## Statistical Analysis

All analyses were conducted using Medcalc (version 19.0, MedCalc Software, Ostend, Belgium). Kolmogorov-Smirnov test was used to evaluate the normality of quantitative data. Mean and standard deviation (SD) were used to describe normally distributed data, while median and interquartile range (IQR) was used to describe non-normally distributed data. Categorical variables were presented as numbers and percentages. Student's *t*-test, Mann-Whitney *U*-test, Pearson  $\chi^2$ -test, and Fisher's exact test were used to compare variables between mild/moderate disease vs. severe/critical disease.

Logistic regression analysis was used to assess the factors linked to the risk of severe/critical disease. Covariates considered in the model included: age, gender, BMI, days from illness onset, CRP, smoking history, Borg score, CCI, and lung CT severity score. The results were expressed as multivariate coefficients with standard errors and Wald statistic for the number of variables entered in the analysis. Significance was set at  $p < 0.05$ .

Then a predictive model was realized based on Bayes' theorem for determining severe/critical disease (post-test probability) using the pre-test probability of disease and the product of the positive likelihood ratio (+LR) from the predictive variables. The Fagan nomogram was used to graphically represent the model. The predictor variables included in the predictive model were those that demonstrated significance at logistic regression analysis. The predictive performance of each variable was estimated by the area under the receiver operating characteristic curve (AUC-ROC). Youden's index on the ROC curve analysis was used to determine the optimal cut-off point for the single predictive variables (26).

## RESULTS

### Patient Characteristics

The study involved 171 COVID-19 patients [136 men (79.5%) and 35 women (20.5%), mean age (SD) 61.9 (11.8) years, range 33–86 years]. Thirty-seven (21.6%) had severe/critical disease and 134 (78.4%) mild/typical disease. The mean time (SD) interval between the days from illness onset was 6.3 (4.9).



One hundred and fifty-one (88.3%) patients complained of fever, in the majority of the patients (120/171, 70.2%)  $>38^{\circ}\text{C}$ . Dry cough was also a common symptom at onset (108/171, 63.15%), followed by fatigue (102/171, 59.64%), myalgia (86/171, 50.29%), anosmia (67/171, 39.18%), and dyspnea (70/171, 40.9%). The mean (SD) Borg score was 2.61 (1.57).

Comorbidities were detected in 89 (52%) patients, of whom 49.4% (44/89) had only one comorbidity. The mean (SD) CCI was 3.37 (2.21). Of note, severe/critical group had a higher frequency of comorbidities, especially more than one comorbidity (all  $p < 0.001$ ), compared with mild/typical group). Compared with mild/typical group, patients in severe/critical group were older ( $p < 0.001$ ) and more frequently males ( $p < 0.05$ ). Ninety-four of these 171 (54.9%) patients were admitted to hospital of whom 57 (60.6%) were discharged alive without hospital care. Among the 37 patients admitted to hospital, with critical illness, 25 (67.6%) required mechanical ventilation, nine (24.3%) required intensive care without mechanical ventilation, and three patients (8.1%) died.

The most common pattern seen on lung CT was multiple lobe involvement (90.9%) with more extensive GGO (81.9%) than consolidation (71.3%). The patients with severe/critical disease had a higher prevalence of consolidation ( $p = 0.031$ ), interlobular septal thickening ( $p = 0.005$ ), a crazy-paving pattern ( $p = 0.023$ ), reticular opacities ( $p = 0.009$ ), and air bronchogram ( $p = 0.001$ ). The mean (SD) lung CT-severity score was 76.65 (6.93) in the group with severe/critical disease and 61.69 (13.21) in the group with mild/typical disease ( $p = 0.001$ ). **Table 1** summarizes the differences between mild/moderate group and severe/critical group.

## Variables Predicting a Severe/Critical Disease

In logistic regression model, only the variables found to be significant in the univariate analysis were considered in predicting a severe/critical disease. Among all the analyzed variables, CCI was found to have the highest relative importance with a Wald value of 15.99 ( $p < 0.0001$ ), followed by CT severity score (Wald 13.41;  $p = 0.0002$ ) and age (Wald 10.94;  $p = 0.0009$ ) (**Table 2**).

The predictive performance of a single variable was estimated by the area under the AUC-ROC curve analysis. Age showed an AUC of 0.838 ( $p = 0.0001$ ) (**Figure 1A**) and an optimal cut-off point of 69.9 (sensitivity 94.6%, specificity 68.1%, +LR 2.97) (**Supplementary Table 1**). The CCI demonstrated excellent discriminative ability, with an AUC of 0.854 ( $p = 0.0001$ ) (**Figure 1B**) and an optimal cut-off point of 3 (sensitivity 83.8%, specificity 69.6%, +LR 2.76) (**Supplementary Table 2**). The CT severity score revealed an AUC of 0.824 ( $p = 0.0001$ ) (**Figure 1C**) and an optimal cut-off point of 53 (sensitivity 64.9%, specificity 84.4%, +LR 4.17) (**Supplementary Table 3**).

The three predictive variables (age, CCI, CT severity score) can be applied to the Fagan nomogram to calculate the post-test probability of severe/critical disease risk (**Figure 2**). Calculation of the post-test probability is based on the pre-test probability (21.6% in the case series studied) and the product of the +LRs of the three predictor variables in the individual patient. This type of calculation is suitable to be performed through

smartphone apps. With the results of this study, a quick and user-friendly smartphone app based on these findings was created to calculate the post-test probability of severe/critical disease in COVID-19 pneumonia patients (CRITIC-App<sup>®</sup>, Fausto Salaffi, 2021, all rights reserved; the app is accessible for iOS/Android mobile platforms to interested researchers at website <http://www.faustosalaffi.it/app/covid/>).

## DISCUSSION

In this study it has been proposed a prediction model, calculated at hospital admission, to establish the subsequent presence of disease deterioration and the occurrence of severe/critical disease (serious clinical outcomes, such as ICU admission or death) in patients with COVID-19 pneumonia.

Consistent with previous studies, our study found that age, comorbidities and CT severity score are important and independent predictors of severe/critical or fatality risk of COVID-19 patients.

Age is a pivotal variable in predicting unfavorable outcomes in COVID-19 patients (27, 28). A study of 191 COVID-19 patients showed that older age was associated with a higher risk of in-hospital death, with an odds ratio (OR) of 1.10 for every year added (7). Similarly, Wu and coworkers discovered that older age was related to a higher risk of developing ARDS and dying as a result of it, which is possibly due to elderly patients' lower immune function (27). Older people were considered to be physically frail and more likely to have comorbidities, which placed them at a higher risk of negative consequences, including death (29). Data from the present study support that older age is a predictor for adverse outcomes. In particular, the cut-off point of  $\sim 70$  years seems to correlate with an augmented risk. Among the possible causes of an increased risk in the elderly population is also considered the treatment with angiotensin-converting enzyme (ACE) inhibitors or angiotensin II type-I receptor blockers (ARBs), drugs that would seem to increase the expression of the ACE-2 receptor, the gateway for the entry of the virus into the cells (30).

Coexisting comorbidities are similarly associated with an increased risk of COVID-19 severity. Huang and colleagues found that a known history of type 2 diabetes increased the likelihood of developing severe illness in COVID-19 patients by six times (31, 32). Another study found that 64.3% of patients had at least one comorbidity, with hypertension (30%) and diabetes (12.1%) being the most common, and that older men with comorbidities were more likely to be affected by COVID-19 (33). Several reports of COVID-19 related comorbidities, on the other hand, proposed that comorbidity should be considered further (32, 34, 35). A more comprehensive evaluation of the impact of various comorbidities on COVID-19 patients is needed and valuable in guiding proper inter-disciplinary management, especially for elderly patients. Patients with severe cardiovascular injury and underlying cardiac insufficiency, for example, are more likely to experience adverse events, according to recent reports (16, 36). For clinical prognosis, summary comorbidity scales such as the CCI are widely used (37, 38). The CCI was created to predict the probability of death within 1 year

**TABLE 1** | Demographic, clinical, laboratory findings of patients on admission.

|  | All           | Mild/moderate disease | Severe/critical disease | <i>p</i> |
|--|---------------|-----------------------|-------------------------|----------|
| Total sample, N° (%)                               | 171 (100%)    | 134 (78.47%)          | 37 (21.63%)             | —        |
| Age years, mean (SD)                               | 64.91 (13.59) | 61.69 (13.21)         | 76.65 (6.93)            | 0.001    |
| Male patients, N° (%)                              | 136 (79.53%)  | 102 (76.11%)          | 34 (91.89%)             | 0.021    |
| Smoking history, N° (%)                            | 39 (22.83%)   | 28 (20.89%)           | 11 (29.72%)             | 0.039    |
| Body Mass Index, kg/m <sup>2</sup> , mean (SD)     | 25.58 (3.85)  | 24.31 (3.97)          | 27.55 (3.21)            | 0.041    |
| Charlson Comorbidity Index, mean (SD)              | 3.37 (2.21)   | 2.72 (1.69)           | 5.72 (2.28)             | 0.001    |
| Signs and symptoms on admission                    |               |                       |                         |          |
| Days from first symptoms, mean (SD)                | 6.3 (4.92)    | 5.1 (3.92)            | 7.4 (3.22)              | 0.034    |
| Fever $\geq 38.8^{\circ}\text{C}$ , N° (%)         | 120 (70.21%)  | 93 (69.4%)            | 27 (74.41%)             | 0.176    |
| Dry cough, N° (%)                                  | 108 (63.15%)  | 85 (63.4%)            | 23 (62.21%)             | 0.784    |
| Fatigue, N° (%)                                    | 102 (59.64%)  | 79 (58.95%)           | 23 (62.16%)             | 0.482    |
| Myalgia, N° (%)                                    | 86 (50.29%)   | 66 (49.25%)           | 20 (54.05%)             | 0.091    |
| Anosmia, N° (%)                                    | 67 (39.18%)   | 51 (38.305%)          | 15 (40.54%)             | 0.599    |
| Dyspnea, N° (%)                                    | 63 (36.84%)   | 47 (35.07%)           | 16 (43.24%)             | 0.058    |
| Borg dyspnea index, mean (SD)                      | 2.61 (1.57)   | 2.07 (1.61)           | 3.25 (1.44)             | 0.025    |
| Laboratory findings                                |               |                       |                         |          |
| C-Reactive protein, mg/L, mean (SD)                | 11.28 (13.75) | 9.40 (13.65)          | 11.87 (14.26)           | 0.046    |
| Computed tomography findings                       |               |                       |                         |          |
| Ground-glass opacity, N° (%)                       | 140 (81.87%)  | 110 (82.15%)          | 30 (81.11%)             | 0.768    |
| Consolidation, N° (%)                              | 122 (71.34%)  | 93 (69.41%)           | 29 (78.42%)             | 0.031    |
| Interlobular septal thickening, N° (%)             | 78 (45.61%)   | 49 (36.56%)           | 29 (78.37%)             | 0.005    |
| Reticular opacity, N° (%)                          | 76 (44.44%)   | 50 (37.31%)           | 26 (70.27%)             | 0.009    |
| Air bronchogram, N° (%)                            | 69 (40.35%)   | 46 (34.32%)           | 23 (62.16%)             | 0.021    |
| Crazy-paving pattern, N° (%)                       | 35 (20.54%)   | 24 (17.91%)           | 11 (29.72%)             | 0.023    |
| Lymph node enlargement, N° (%)                     | 25 (14.61%)   | 20 (14.92%)           | 5 (13.51%)              | 0.679    |
| Pericardial effusion, N° (%)                       | 16 (9.35%)    | 11 (8.21%)            | 5 (13.51%)              | 0.066    |
| Pleural effusion, N° (%)                           | 14 (8.18%)    | 10 (7.46%)            | 4 (10.81%)              | 0.054    |
| Lung computed tomography severity score, mean (SD) | 64.91 (13.59) | 61.69 (13.21)         | 76.65 (6.93)            | 0.001    |

SD, standard deviation.

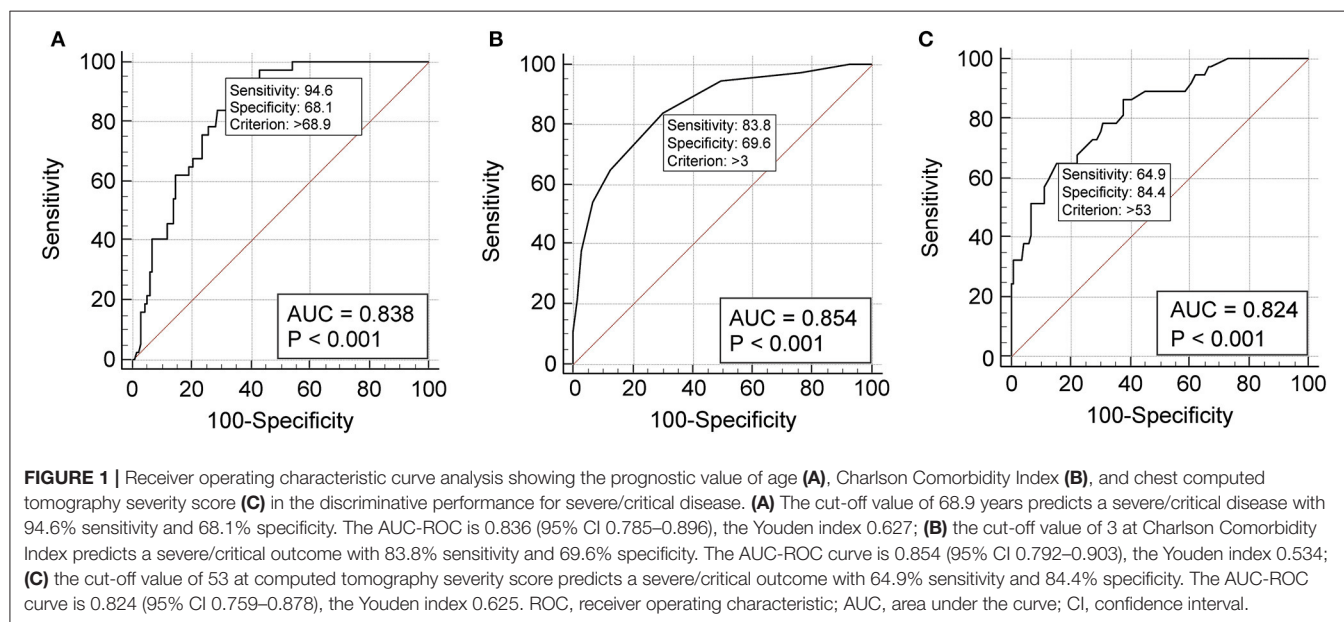
of being admitted to the hospital. The scores are based on a variety of comorbidities, each of which is assigned a weighted integer from one to six dependent on the severity of the condition (39). CCI is a well-validated and easy-to-use indicator for assessing patient's prognosis and survival. Age, gender, and the existence of comorbidities such as diabetes, cardiovascular, cerebrovascular, and respiratory disorders are frequently used to predict the severity and mortality of COVID-19 during the present pandemic (40–43). In a nationwide study of Danish COVID-19 patients it has been investigated if CCI score was associated with the risk of severe outcome and death (44). It has been found that the odds of severe COVID-19 were significantly increased in CCI score 1–2 (OR 1.7), CCI score 3–4 (OR 2.36), and CCI score  $>4$  (OR 2.67) compared to CCI score 0. In the present study it has been revealed that the CCI score of  $\geq 3$  was associated with an  $\sim 4$ -fold time increase in the risk of adverse outcomes. A systematic review and meta-analysis of CCI score and a composite of poor outcomes demonstrated that, compared to a CCI score of 0, a CCI score of 1–2 and CCI score of  $\geq 3$  was prognostically associated with mortality and associated

with a composite of poor outcomes. Per point increase of CCI score also increased mortality risk by 16%. Moreover, a higher mean CCI score is also significantly associated with mortality and disease severity. The CCI score, which adds together ages and summarizes comorbidity measures, predicts death in COVID-19 patients by an exponential increase in the odds ratio at each point in the score (45).

Lung CT scanning has a higher sensitivity than chest radiography, allowing abnormalities in the lungs to be identified sooner. CT identifies the processes underlying severe/critical conditions and improve clinical diagnosis and treatment by studying their clinical and imaging features. Consistently with several recent reports (46–48), it has been showed that predominant pattern observed was bilateral and peripheral GGO and consolidation (49–51). Despite the fact that pleural and/or pericardial effusion were more frequent in critically ill COVID-19 patients, a multivariable study found no connection between them and death or negative outcomes (10). Qualitative indicators by themselves could differentiate extreme/serious cases from mild/typical cases, but they were unsuccessful in separating

**TABLE 2 |** Logistic regression analysis of the dependent variables predicting the development of a severe/critical disease.

| Variable                                | Coefficient | Standard error | Wald    | p       |
|---|-------------|----------------|---------|---------|
| Constant                                | -19.76394   | 4.59177        | 18.5262 | <0.0001 |
| Age (years)                             | 0.14981     | 0.045292       | 10.9411 | 0.0009  |
| Gender                                  | -0.50030    | 0.94867        | 0.2781  | 0.5979  |
| Smoking history                         | 1.46950     | 0.85989        | 2.9205  | 0.0875  |
| Body Mass Index                         | 0.017179    | 0.10363        | 0.02748 | 0.8683  |
| Days from illness onset                 | -0.082411   | 0.045339       | 3.3039  | 0.0691  |
| C-reactive protein (mg/L)               | -0.013485   | 0.030438       | 0.1963  | 0.6577  |
| Borg score                              | 0.16300     | 0.21696        | 0.5645  | 0.4525  |
| Charlson Comorbidity Index              | 1.07359     | 0.26844        | 15.9954 | 0.0001  |
| Lung computed tomography severity score | 0.086068    | 0.023500       | 13.4143 | 0.0002  |



severe cases from critical cases. The use of a combination of qualitative and quantitative metrics to identify cases at various clinical stages (52) could assist in the rapid detection and management of critical cases, potentially lowering mortality (19). Previous studies used a semi-quantitative lung CT severity score to measure COVID-19 lung involvement, with the score being assigned based on the severity of all abnormal lung areas involved, similar to the CT severity score system applied to the present study (6, 10, 49, 53, 54). The ideal cut-off point for the CT score employed for study in the prediction of severe/critical disease is 53 (range of the score 0–96).

Conversely, some variables potentially expected to be suggestive of worse outcomes did not prove to be so. For example, cigarette smoking or CRP levels have not been shown to be associated with worse prognosis. High levels of CRP and erythrocyte sedimentation rate (ESR) have been previously reported in COVID-19 patients. Previous works have documented that CRP might play a role in predicting a higher severity of COVID-19 in the early stages, before the development of CT findings (55). A recent systematic review and meta-analysis confirmed that elevated CRP levels are predictors of a worse

prognosis in COVID-19 patients (56). Interestingly, a role on CRP values would also be determined by oral cavity health, these two variables being inversely correlated (57).

The main novelty of the present study consists in having applied a comprehensive model of the main variables conditioning outcomes in patients with COVID-19 pneumonia. The integration between the variables was possible through the Fagan nomogram that, calculated on the app, allows a rather rapid estimation of unfavorable prognosis at the patient's bedside. Some works have already proposed the application of algorithms in COVID-19. A retrospective study that assessed the risk of hospitalization in 4,536 COVID-19 patients documented how the variables influencing this risk are multiple, both clinical and demographic (29).

This study has several limitations. First, due to the retrospective nature of the study, there is a chance of knowledge bias. As a result, some information was lacking, and some information, such as the timing of symptom initiation and exposure history, was focused on patients' memories, which may be skewed by recall bias. At the same time, the presence of heterogeneity in some clinical data, such as ICU admission, was

## prediction severe/critical outcome In COVID-19 (CRITIC)

Pre-test probability % = 21.6  
(prevalence of patients with severe disease)

LR+ Age = 2.97

LR+ Charlson Comorbidity Index = 2.76

LR+ Computed tomography severity score = 4.17

Product of the three +LR :  $2.97 \times 2.76 \times 4.17 = 34.18$

Post-test probability % = 89%

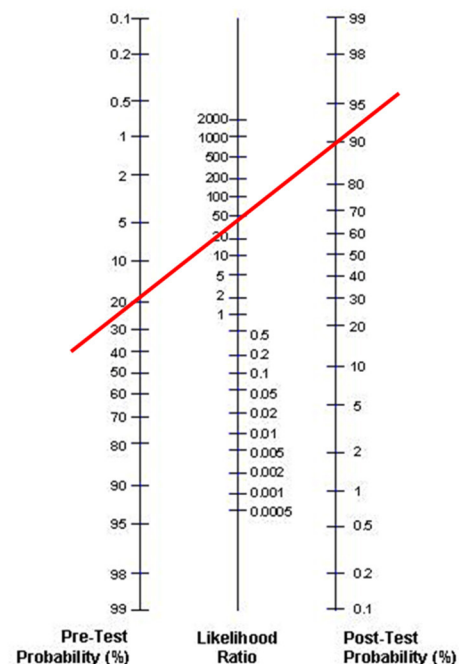


**FIGURE 2 |** Example of application of the nomogram in the calculation of the CRITIC post-test probability. In the nomogram left axis represents the pre-test probability (21.6% in this case study), middle axis represents positive likelihood ratio, and the right axis shows post-test probability. To calculate the actual risk (post-test probability, %) of severe/critical disease in a given patient with COVID-19 pneumonia, the positive likelihood ratio of each item in that patient have to be multiplied. The resulting positive likelihood ratio product represents the point intercepted on the middle axis.

unavoidable. Second, there were variations in care, and it was not taken into consideration how treatment influenced prognosis. Third, the data from the two groups were not matched, and the severe/critical group's sample size was limited. Fourth, our patients came from a single geographic area and were treated in a single health system; although our patient population is diverse, factors correlated with poor outcomes may vary elsewhere. Fifth, in this study, well-experienced thoracic radiologists scored the CT images in agreement, and CT scoring is time consuming and can be difficult to apply routinely.

In conclusion, the findings of the present study suggested that the main risk factors predicting a severe/critical outcome in COVID-19 pneumonia patients are older age, comorbidities, and lung CT severity. The prediction model proposed could be used as a quantitative risk predictor method at the time of admission, however it needs further validation in larger cohort studies due to small sample size.

## DATA AVAILABILITY STATEMENT

The raw data supporting the conclusions of this article will be made available by the authors, upon reasonable request to the corresponding author.

## ETHICS STATEMENT

The studies involving human participants were reviewed and approved by Review board of Luigi Sacco University Hospital.

Written informed consent for participation was not required for this study in accordance with the national legislation and the institutional requirements.

## AUTHOR CONTRIBUTIONS

FS, PS-P, and MG conceived and designed the study and the protocol. MC, LC, and AG performed the lung CT examinations and their relative interpretation and were involved in revising the paper for important intellectual content. FS and MD carried out data interpretation and analysis. FS, MD, and MC wrote the paper. MC, LC, PS-P, MG, and AG were involved in drafting the article or revising it critically for important intellectual content. All authors have read and approved the final manuscript.

## ACKNOWLEDGMENTS

The authors would like to express their appreciation for all of the emergency services, nurses, doctors, and other hospital staff for their efforts to combat the COVID-19 outbreak. We would like to thank APPYCOM ([www.appycom.it](http://www.appycom.it)) for developing the Mobile Web-app and providing technical assistance during the study.

## SUPPLEMENTARY MATERIAL

The Supplementary Material for this article can be found online at: <https://www.frontiersin.org/articles/10.3389/fmed.2021.695195/full#supplementary-material>



## REFERENCES

- Sadeghi Dousari A, Taati Moghadam M, Satarzadeh N. COVID-19 (coronavirus disease 2019): A new coronavirus disease. *Infect Drug Resist.* (2020) 12:2819–28. doi: 10.2147/IDR.S259279
- Moghadam MT, Taati B, Paydar Ardakani SM, Suzuki K. Ramadan fasting during the COVID-19 pandemic; observance of health, nutrition and exercise criteria for improving the immune system. *Front Nutr.* (2021) 7:570235. doi: 10.3389/fnut.2020.570235
- Zhu N, Zhang D, Wang W, Li X, Yang B, Song J, et al. A novel coronavirus from patients with pneumonia in China, 2019. *N Engl J Med.* (2020) 382:727–33. doi: 10.1056/NEJMoa2001017
- Huang C, Wang Y, Li X, Ren L, Zhao J, Hu Y, et al. Clinical features of patients infected with 2019 novel coronavirus in Wuhan, China. *Lancet.* (2020) 395:497–506. doi: 10.1016/S0140-6736(20)30183-5
- Wang C, Horby PW, Hayden FG, Gao GF. A novel coronavirus outbreak of global health concern. *Lancet.* (2020) 395:470–3. doi: 10.1016/S0140-6736(20)30185-9
- Bernheim A, Mei X, Huang M, Yang Y, Fayad ZA, Zhang N, et al. Chest CT findings in coronavirus disease-19 (COVID-19): relationship to duration of infection. *Radiology.* (2020) 295:200463. doi: 10.1148/radiol.20200463
- Zhou F, Yu T, Du R, Fan G, Liu Y, Liu Z. Clinical course and risk factors for mortality of adult inpatients with COVID-19 in Wuhan, China: a retrospective cohort study. *Lancet.* (2020) 395:1054–62. doi: 10.1016/S0140-6736(20)30566-3
- Guan WJ, Liang WH, Zhao Y, Liang HR, Chen ZS, Li YM, et al. Comorbidity and its impact on 1590 patients with COVID-19 in China: a nationwide analysis. *Eur Respir J.* (2020) 55:2000547. doi: 10.1183/13993003.01227-2020
- Zhao W, Zhong X, Xie X, Yu Q, Liu J. Relation between chest CT findings and clinical conditions of coronavirus disease (COVID-19) pneumonia: a multicenter study. *Am J Roentgenol.* (2020) 214:1072–7. doi: 10.2214/AJR.20.22976
- Li K, Wu J, Wu F, Guo D, Chen L, Fang Z, et al. The clinical and chest CT features associated with severe and critical COVID-19 pneumonia. *Invest Radiol.* (2020) 55:327–31. doi: 10.1097/RLI.0000000000000672
- Khatami F, Saatchi M, Zadeh SST, Aghamir ZS, Shabestari AN, Reis LO, et al. A meta-analysis of accuracy and sensitivity of chest CT and RT-PCR in COVID-19 diagnosis. *Sci Rep.* (2020) 10:22402. doi: 10.1038/s41598-020-80061-2
- Tabatabaei SMH, Rahimi H, Moghaddas F, Rajebi H. Predictive value of CT in the short-term mortality of Coronavirus Disease 2019 (COVID-19) pneumonia in non-elderly patients: a case-control study. *Eur J Radiol.* (2020) 132:109298. doi: 10.1016/j.ejrad.2020.109298
- Liu S, Nie C, Xu Q, Xie H, Wang M, Yu C, et al. Prognostic value of initial chest CT findings for clinical outcomes in patients with COVID-19. *Int J Med Sci.* (2021) 18:270–5. doi: 10.7150/ijms.48281
- Khosravi B, Aghaghazvini L, Sorouri M, Atashi SN, Abdollahi M, Mojtavavi H, et al. Predictive value of initial CT scan for various adverse outcomes in patients with COVID-19 pneumonia. *Heart Lung.* (2021) 50:13–20. doi: 10.1016/j.hrtlng.2020.10.005
- Eslami V, Abrishami A, Zarei E, Khalili N, Baharvand Z, Sanei-Taheri M. The association of CT-measured cardiac indices with lung involvement and clinical outcome in patients with COVID-19. *Acad Radiol.* (2021) 28:8–17. doi: 10.1016/j.acra.2020.09.012
- Du RH, Liang LR, Yang CQ, Wang W, Cao TZ, Li M, et al. Predictors of mortality for patients with COVID-19 pneumonia caused by SARS-CoV-2: a prospective cohort study. *Eur Respir J.* (2020) 55:2000524. doi: 10.1183/13993003.00524-2020
- Liang WH, Liang HR, Ou LM, Chen B, Chen A, Li C, et al. Development and validation of a clinical risk score to predict the occurrence of critical illness in hospitalized patients with COVID-19. *JAMA Intern Med.* (2020) 180:e202033. doi: 10.1001/jamainternmed.2020.2033
- Salaffi F, Carotti M, Tardella M, Borgheresi A, Agostini A, Minorati D, et al. The role of a chest computed tomography severity score in coronavirus disease 2019 pneumonia. *Medicine.* (2020) 99:e22433. doi: 10.1097/MD.00000000000022433
- World Health Organization. *Clinical Management of Severe Acute Respiratory Infection When Novel Coronavirus (nCoV) Infection Is Suspected: Interim Guidance.* (2020). Available online at: <https://www.who.int/publications/item/10665-332299> (accessed April 14, 2021).
- World Health Organization. *IMAI District Clinician Manual. Hospital Care for Adolescents and Adults.* (2011). Available online at: [https://apps.who.int/iris/bitstream/handle/10665/77751/~9789241548290\\_Vol2\\_eng.pdf?sequence=3](https://apps.who.int/iris/bitstream/handle/10665/77751/~9789241548290_Vol2_eng.pdf?sequence=3) (accessed April 14, 2021).
- ARDS Definition Task Force, Ranieri VM, Rubenfeld GD, Thompson BT, Ferguson ND, Caldwell E, et al. Acute respiratory distress syndrome: the Berlin Definition. *J Am Med Assoc.* (2012) 307:2526–33. doi: 10.1001/jama.2012.5669
- Sarzi-Puttini P, Marotto D, Caporali R, Montecucco C, Favalli EG, Franceschini F, et al. Prevalence of COVID infections in a population of rheumatic patients from Lombardy and Marche treated with biological drugs or small molecules: a multicentre retrospective study. *J Autoimmun.* (2021) 116:102545. doi: 10.1016/j.jaut.2020.102545
- Borg GA. Psychophysical bases of perceived exertion. *Med Sci Sports Exerc.* (1982) 14:377–81. doi: 10.1249/00005768-198205000-00012
- Charlson ME, Pompei P, Ales K, MacKenzie CR. A new method of classifying prognostic comorbidity in longitudinal studies: development and validation. *J Chronic Dis.* (1987) 40:373–83. doi: 10.1016/0021-9681(87)90171-8
- Reyes C, Estrada P, Nogués X, Orozco P, Cooper C, Díez-Pérez A, et al. The impact of common co-morbidities (as measured using the Charlson index) on hip fracture risk in elderly men: a population-based cohort study. *Osteoporos Int.* (2014) 25:1751–8. doi: 10.1007/s00198-014-2682-9
- Medina LS, Aguirre E, Zurakowski D. Introduction to evidence-based imaging. *Neuroimaging Clin N Am.* (2003) 13:157–65. doi: 10.1016/S1052-5149(03)00021-2
- Wu C, Chen X, Cai Y, Xia J, Zhou X, Xu S, et al. Risk factors associated with acute respiratory distress syndrome and death in patients with coronavirus disease 2019 pneumonia in Wuhan, China. *J Am Med Assoc Intern Med.* (2020) 180:934–43. doi: 10.1001/jamainternmed.2020.0994
- Fathi M, Vakili K, Sayehmiri F, Mohamadkhani A, Hajiesmaeili M, Rezaei-Tavirani M, et al. The prognostic value of comorbidity for the severity of COVID-19: a systematic review and meta-analysis study. *PLoS ONE.* (2021) 16:e0246190. doi: 10.1371/journal.pone.0246190
- Jehi L, Ji X, Milinovich A, Erzurum S, Merlino A, Gordon S, et al. Development and validation of a model for individualized prediction of hospitalization risk in 4,536 patients with COVID-19. *PLoS ONE.* (2020) 15:e0237419. doi: 10.1371/journal.pone.0237419
- Shahid Z, Kalayanamitra R, McClafferty B, Kepko D, Ramgobin D, Patel R, et al. COVID-19 and older adults: what we know. *J Am Geriatr Soc.* (2020) 68:926–9. doi: 10.1111/jgs.16472
- Huang R, Zhu L, Xue L, Liu L, Yan X, Wang J, et al. Clinical findings of patients with coronavirus disease 2019 in Jiangsu Province, China: a retrospective, multi-center study. *PLoS Negl Trop Dis.* (2020) 14:e0008280. doi: 10.1371/journal.pntd.0008280
- Wu Z, McGoogan JM. Characteristics of and important lessons from the coronavirus disease 2019 (COVID-19) outbreak in China: summary of a report of 72 314 cases from the Chinese Center for Disease Control and Prevention. *J Am Med Assoc.* (2020) 323:1239–42. doi: 10.1001/jama.2020.2648
- Zhang JJ, Dong X, Cao YY, Yuan YD, Yang YB, Yan YQ, et al. Clinical characteristics of 140 patients infected with SARS-CoV-2 in Wuhan, China. *Allergy.* (2020) 75:1730–41. doi: 10.1111/all.14238
- Li X, Xu S, Yu M, Wang K, Tao Y, Zhou Y, et al. Risk factors for severity and mortality in adult COVID-19 inpatients in Wuhan. *J Allergy Clin Immunol.* (2020) 146:110–8. doi: 10.1016/j.jaci.2020.04.006
- Chen N, Zhou M, Dong X, Qu J, Gong F, Han Y, et al. Epidemiological and clinical characteristics of 99 cases of 2019 novel coronavirus pneumonia in Wuhan, China: a descriptive study. *Lancet.* (2020) 395:507–13. doi: 10.1016/S0140-6736(20)30211-7
- Zheng YY, Ma YT, Zhang JY, Xie X. COVID-19 and the cardiovascular system. *Nat Rev Cardiol.* (2020) 17:259–60. doi: 10.1038/s41569-020-0360-5
- Harrison SL, Fazio-Eynullayeva E, Lane DA, Underhill P, Lip GYH. Comorbidities associated with mortality in 31,461 adults with COVID-19 in the United States: a federated electronic medical record analysis. *PLoS Med.* (2020) 17:e1003321. doi: 10.1371/journal.pmed.1003321
- Socolovitch RL, Fumis RRL, Tomazini BM, Pastore L, Galas FRBG, de Azevedo LCP, et al. Epidemiology, outcomes, and the use of intensive care unit resources of critically ill patients diagnosed with

- COVID-19 in São Paulo, Brazil: a cohort study. *PLoS ONE*. (2020) 15:e0243269. doi: 10.1371/journal.pone.0243269
39. Austin SR, Wong YN, Uzzo RG, Beck JR, Egleston BL. Why summary comorbidity measures such as the Charlson comorbidity index and Elixhauser score work. *Med Care*. (2015) 53:e65–72. doi: 10.1097/MLR.0b013e318297429c
  40. Pranata R, Huang I, Lim MA, Wahjoepramono EJ, July J. Impact of cerebrovascular and cardiovascular diseases on mortality and severity of COVID-19—systematic review, meta-analysis, and meta-regression. *J Stroke Cerebrovasc Dis*. (2020) 29:104949. doi: 10.1016/j.jstrokecerebrovasdis.2020.104949
  41. Yonas E, Alwi I, Pranata R, Huang I, Lim MA, Gutierrez EJ, et al. Effect of heart failure on the outcome of COVID-19—a meta-analysis and systematic review. *Am J Emerg Med*. (2020) 46:204–11. doi: 10.1016/j.ajem.2020.07.009
  42. Pranata R, Lim MA, Yonas E, Vania R, Lukito AA, Siswanto BB, et al. Body mass index and outcome in patients with COVID-19: a dose-response meta-analysis. *Diabetes Metab*. (2020) 47:101178. doi: 10.1016/j.diabet.2020.07.005
  43. Pranata R, Lim MA, Huang I, Raharjo SB, Lukito AA. Hypertension is associated with increased mortality and severity of disease in COVID-19 pneumonia: a systematic review, meta-analysis and meta-regression. *J Renin Angiotensin Aldosterone Syst*. (2020) 21:1470320320926899. doi: 10.1177/1470320320926899
  44. Christensen DM, Strange JE, Gislason G, Torp-Pedersen C, Gerds T, Fosbøl E, et al. Charlson comorbidity index score and risk of severe outcome and death in Danish COVID-19 patients. *J Gen Intern Med*. (2020) 35:2801–3. doi: 10.1007/s11606-020-05991-z
  45. Tuty Kuswardhani RA, Hennina J, Pranata R, Anthonius Lim M, Lawrensia S, Suastika K. Charlson comorbidity index and a composite of poor outcomes in COVID-19 patients: a systematic review and meta-analysis. *Diabetes Metab Syndr*. (2020) 14:2103–9. doi: 10.1016/j.dsx.2020.10.022
  46. Shi H, Han X, Zheng C. Evolution of CT manifestations in a patient recovered 2019 novel coronavirus (2019-nCoV) pneumonia in Wuhan, China. *Radiology*. (2020) 295:20. doi: 10.1148/radiol.2020200269
  47. Fang Y, Zhang H, Xu Y, Xie J, Pang P, Ji W, et al. Manifestations of two cases of 2019 novel coronavirus (2019-nCoV) pneumonia. *Radiology*. (2020) 295:208–9. doi: 10.1148/radiol.2020200280
  48. Yuan M, Yin W, Tao Z, Tan W, Hu Y. Association of radiologic findings with mortality of patients infected with 2019 novel coronavirus in Wuhan, China. *PLoS ONE*. (2020) 15:e0230548. doi: 10.1371/journal.pone.0230548
  49. Pan F, Ye T, Sun P, Gui S, Liang B, Li L, et al. Time course of lung changes at chest CT during recovery from coronavirus disease 2019 (COVID-19). *Radiology*. (2020) 295:715–21. doi: 10.1148/radiol.2020200370
  50. Xiong Y, Sun D, Liu Y, Fan Y, Zhao L, Li X, et al. Clinical and high-resolution CT features of the COVID-19 infection: comparison of the initial and follow-up changes. *Invest Radiol*. (2020) 55:332–9. doi: 10.1097/RLI.0000000000000674
  51. Shi H, Han X, Jiang N, Cao Y, Alwalid O, Gu J, et al. Radiological findings from 81 patients with COVID-19 pneumonia in Wuhan, China: a descriptive study. *Lancet Infect Dis*. (2020) 20:425–34. doi: 10.1016/S1473-3099(20)30086-4
  52. Salaffi F, Carotti M, Di Donato E, Di Carlo M, Ceccarelli L, Giuseppetti G. Computer-aided tomographic analysis of interstitial lung disease (ILD) in patients with systemic sclerosis (SSc). Correlation with pulmonary physiologic tests and patient-centred measures of perceived dyspnea and functional disability. *PLoS ONE*. (2016) 11:e0149240. doi: 10.1371/journal.pone.0149240
  53. Zheng Y, Xiong C, Liu Y, Qian X, Tang Y, Liu L, et al. Epidemiological and clinical characteristics analysis of COVID-19 in the surrounding areas of Wuhan, Hubei Province in 2020. *Pharmacol Res*. (2020) 157:104821. doi: 10.1016/j.phrs.2020.104821
  54. Wu J, Wu X, Zeng W, Guo D, Fang Z, Chen L. Chest CT findings in patients with coronavirus disease 2019 and its relationship with clinical features. *Invest Radiol*. (2020) 55:257–61. doi: 10.1097/RLI.0000000000000670
  55. Tan C, Huang Y, Shi F, Tan K, Ma Q, Chen Y, et al. C-reactive protein correlates with computed tomographic findings and predicts severe COVID-19 early. *J Med Virol*. (2020) 92:856–62. doi: 10.1002/jmv.25871
  56. Xie J, Wang Q, Xu Y, Zhang T, Chen L, Zuo X, et al. Clinical characteristics, laboratory abnormalities and CT findings of COVID-19 patients and risk factors of severe disease: a systematic review and meta-analysis. *Ann Palliat Med*. (2021) 10:1928–49. doi: 10.21037/apm-20-1863
  57. Kamel AHM, Basuoni A, Salem ZA, AbuBakr N. The impact of oral health status on COVID-19 severity, recovery period and C-reactive protein values. *Br Dent J*. (2021). doi: 10.1038/s41415-021-2656-1. [Epub ahead of print].

**Conflict of Interest:** The authors declare that the research was conducted in the absence of any commercial or financial relationships that could be construed as a potential conflict of interest.

**Publisher's Note:** All claims expressed in this article are solely those of the authors and do not necessarily represent those of their affiliated organizations, or those of the publisher, the editors and the reviewers. Any product that may be evaluated in this article, or claim that may be made by its manufacturer, is not guaranteed or endorsed by the publisher.

Copyright © 2021 Salaffi, Carotti, Di Carlo, Ceccarelli, Galli, Sarzi-Putini and Giovagnoni. This is an open-access article distributed under the terms of the Creative Commons Attribution License (CC BY). The use, distribution or reproduction in other forums is permitted, provided the original author(s) and the copyright owner(s) are credited and that the original publication in this journal is cited, in accordance with accepted academic practice. No use, distribution or reproduction is permitted which does not comply with these terms.



# Asthma Patients Benefit More Than Chronic Obstructive Pulmonary Disease Patients in the Coronavirus Disease 2019 Pandemic

Ruoyan Xiong<sup>1,2,3</sup>, Zhiqi Zhao<sup>1,2,3</sup>, Huanhuan Lu<sup>1,2,3</sup>, Yiming Ma<sup>1,2,3</sup>, Huihui Zeng<sup>1,2,3\*</sup> and Yan Chen<sup>1,2,3\*</sup>

<sup>1</sup> Department of Pulmonary and Critical Care Medicine, The Second Xiangya Hospital of Central South University, Changsha, China, <sup>2</sup> Research Unit of Respiratory Diseases, Central South University, Changsha, China, <sup>3</sup> Hunan Centre for Evidence-Based Medicine, Changsha, China

## OPEN ACCESS

### Edited by:

Reza Lashgari,  
Shahid Beheshti University, Iran

### Reviewed by:

Valerie G. Press,  
University of Chicago, United States  
David Joseph De La Zerda,  
University of Miami, United States

### \*Correspondence:

Huihui Zeng  
bonemarrow@csu.edu.cn  
Yan Chen  
chenyan99727@csu.edu.cn

### Specialty section:

This article was submitted to  
Pulmonary Medicine,  
a section of the journal  
Frontiers in Medicine

**Received:** 13 May 2021

**Accepted:** 23 July 2021

**Published:** 10 September 2021

### Citation:

Xiong R, Zhao Z, Lu H, Ma Y, Zeng H  
and Chen Y (2021) Asthma Patients  
Benefit More Than Chronic  
Obstructive Pulmonary Disease  
Patients in the Coronavirus Disease  
2019 Pandemic.  
Front. Med. 8:709006.  
doi: 10.3389/fmed.2021.709006

**Background:** Coronavirus disease 2019 (COVID-19) has raised many questions about the role of underlying chronic diseases on disease outcomes. However, there is limited information about the effects of COVID-19 on chronic airway diseases. Therefore, we conducted the present study to investigate the impact of COVID-19 on patients with asthma or chronic obstructive pulmonary disease (COPD) and ascertain risk factors for acute exacerbations (AEs).

**Methods:** This single-center observational study was conducted at the Second Xiangya Hospital of Central South University, involving asthma or COPD patients who had been treated with inhaled combination corticosteroids (ICSs), such as budesonide, and one long-acting beta-2-agonist (LABA), such as formoterol, for at least a year before the COVID-19 pandemic. We conducted telephone interviews to collect demographic information and clinical data between January 1, 2019, and December 31, 2020, focusing on respiratory and systemic symptoms, as well as times of exacerbations. Data for asthma and COPD were then compared, and the risk factors for AEs were identified using logistic regression analysis.

**Results:** A total of 251 patients were enrolled, comprising 162 (64.5%) who had asthma and 89 who had COPD, with none having COPD/asthma overlap. Frequency of AEs among asthma patients was significantly lower in 2020 than in 2019 ( $0.82 \pm 3.33$  vs.  $1.00 \pm 3.16$ ;  $P < 0.05$ ). Moreover, these patients visited the clinic less ( $0.37 \pm 0.93$  vs.  $0.49 \pm 0.94$ ;  $P < 0.05$ ) and used emergency drugs less ( $0.01 \pm 0.11$  vs.  $0.07 \pm 0.38$ ;  $P < 0.05$ ) during the COVID-19 pandemic. In contrast, among COPD patients, there were no significant differences in AE frequency, clinic visits, or emergency drug use. Furthermore, asthma patients visited clinics less frequently during the pandemic than those with COPD. Logistic regression analysis also showed that a history of at least one AE within the last 12 months was associated with increased AE odds for both asthma and COPD during the COVID-19 pandemic (odds ratio: 13.73, 95% CI: 7.04–26.77;  $P < 0.01$ ).

**Conclusion:** During the COVID-19 pandemic, patients with asthma showed better disease control than before, whereas patients with COPD may not have benefited from the pandemic. For both diseases, at least one AE within the previous 12 months was a risk factor for AEs during the pandemic. Particularly, among asthma patients, the risk factors for AE during the COVID-19 pandemic were urban environment, smoking, and lower asthma control test scores.

**Keywords:** COVID-19, pandemic, asthma, chronic obstructive pulmonary disease, management

## INTRODUCTION

Coronavirus disease 2019 (COVID-19) is an acute respiratory infectious disease caused by severe acute respiratory syndrome coronavirus 2 (SARS-CoV-2). By March 30, 2021, the ongoing pandemic was reported to have a global morbidity of more than 126 million and a global mortality of over 2.7 million deaths (1). Given that COVID-19 mainly spreads via respiratory droplets during close contact (2) and SARS-CoV-2 can infect both the upper and lower airways (3), the roles of existing chronic airway diseases on COVID-19 outcomes have received much attention (4–7). However, limited information is available about the impact of the COVID-19 pandemic on chronic airway disease patients.

Of these chronic airway diseases, asthma and chronic obstructive pulmonary disease (COPD) are the most common worldwide, reporting a global morbidity of more than 330 million in asthma and 251 million in COPD (8, 9). Asthma is defined as a non-communicable disease characterized by airway inflammation, airway hyper-responsiveness, variable airflow limitation, and airway remodeling (10). On the other hand, chronic obstructive pulmonary disease (COPD), which is known as the third leading cause of death globally (11), is a common chronic airway disease characterized by constant respiratory symptoms and airflow limitation (12). Although epidemiological studies have shown no increased risk of COVID-19 morbidity or severity in patients with asthma (13), COPD was found to seemingly increase the risk of death in COVID-19 patients (14, 15). Moreover, a cohort study including 8.3 million (16) people reported that COPD was an independent risk factor for hospital admission.

With the spread of the COVID-19 pandemic, strict protective measures, including social distancing, mask wearing, and home quarantine, have been implemented to reduce SARS-CoV-2 transmission. As asthma and COPD exacerbations can both be triggered by respiratory infections and air pollution, among others (12, 17), COVID-19 and its resulting social isolation measures may have had effects on chronic airway disease patients in several ways. Since previous studies have indicated that patients with asthma or COPD experienced improved disease control during the pandemic due to behavioral changes (18–21), we hypothesized that the COVID-19 pandemic would confer an impact on the conditions of chronic respiratory diseases patients. Therefore, the present study aimed to compare the differences in clinical characteristics before and during the pandemic between asthma and COPD patients to analyze their risk factors for acute

exacerbations (AEs) during the pandemic, and further to develop management strategies for chronic airway disease patients.

## PATIENTS AND METHODS

### Study Design

This study was a single-center observational survey performed at the Second Xiangya Hospital of Central South University and was approved by the Medical Research Ethics Committee of the Second Xiangya Hospital of Central South University. Patients were selected from the hospital records database, using the inclusion criteria as follows: (1) at least 2 years since COPD diagnosis according to the Global Initiative for Chronic Obstructive Lung Disease (GOLD) Report (22), or asthma diagnosis according to the Global Initiative for Asthma (GINA) Guidelines (10); and (2) history of using inhaled combination corticosteroids (ICSs), such as budesonide, and one long-acting beta-2-agonist (LABA), such as formoterol, for at least 1 year before January 1, 2020. Meanwhile, patients who refused to answer calls or co-operate with interviews were excluded from the study (Figure 1). All enrolled COPD patients were noted to have met the ICS/LABA indications, and informed written consent was signed by all participants. Afterwards, demographic and clinical data were collected from database records and routine follow-ups, and telephone interviews were conducted between January 5 and January 15, 2021 to collect clinical data between January 1, 2019, and December 31, 2020, focusing on respiratory and systemic symptoms, and times of exacerbations, among others. Collected data for asthma and COPD patients were then compared, and the risk factors for AEs were explored using logistic regression analysis.

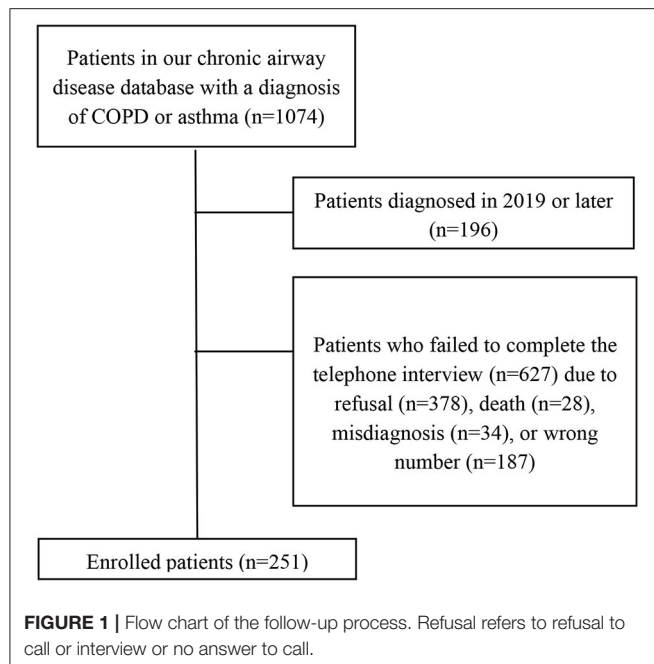
### Data Collection

Data were collected in telephone interviews between January 5 and January 15, 2021. Interviewers participating in this study were required to have undergone centralized training. After obtaining approval from the participants, the interviewers asked them questions from a designed case report form.

### Demographic Characteristics and Clinical Data

Demographic characteristics included age, sex, occupation, residence, smoking history, and history of dust exposure. Clinical data from 2019, prior to the COVID-19 pandemic, comprised history of COPD or asthma, number of AEs, emergency drug use due to AEs, and the number of online consultations or clinic





visits. In addition, the following clinical data were collected in 2020, during the COVID-19 pandemic, including number of AEs, emergency drug use due to COPD or asthma AEs, and the number of online consultations and clinic visits. Specifically, the modified Medical Research Council (mMRC) dyspnea scale (23) and the asthma control test (ACT) (24) were used to assess the symptoms of COPD and asthma, respectively. In these cases, AEs were referred to as AECOPDs in COPD patients, according to the GOLD Report, (22) or AEs of asthma, according to the GINA Guidelines (10).

## Statistical Analysis

Continuous variables were expressed as means  $\pm$  standard deviation or as medians (interquartile range [IQR]), whereas categorical variables were expressed as numbers (Irb%). The significance of differences were assessed by paired-sample or independent-sample *t* test for continuous variables and by the  $\chi^2$  test for categorical variables. Association between risk factors and asthma/COPD AEs was examined by multivariable logistic regression analyses. The SPSS software (version 23.0) was used for all analyses, and results were considered statistically significant at  $P < 0.05$ .

## RESULTS

Patients from our database who met the inclusion criteria were contacted by telephone. Of the 878 contacted patients, 627 were excluded due to refusal to call or interview, death, misdiagnosis, or wrong numbers, ultimately enrolling 251 patients. Of these, 162 (64.5%) had asthma, 89 had COPD, and none had a COPD and asthma overlap. No severe infections or COVID-19 cases were also observed among the included patients. Median age was noted to be 56 years (IQR: 47–63 years), and 55.0% of all patients

**TABLE 1 |** Demographic Characteristics of the included patients ( $N = 251$ ).

| Characteristic           | Category                       | Median or N (%) |
|--------------------------|--------------------------------|-----------------|
| Total                    |                                | 251             |
| Age (years, 18–81 years) |                                | 56 (47, 63)     |
| Sex                      | Male                           | 138 (55.0)      |
| Residence                | Urban                          | 154 (61.4)      |
| Dust exposure            | Former or current <sup>#</sup> | 25 (10.0)       |
| Smoking                  | Former or current              | 84 (33.5)       |
| Diagnosis                | Asthma                         | 162 (64.5)      |

Data are expressed as medians (interquartile range) or as N (%).

<sup>#</sup>, Patients who were firework factory workers, coal mine workers, welders, or builders. COPD, chronic obstructive pulmonary disease.

**TABLE 2 |** Comparisons of demographic characteristics between asthma and COPD patients.

| Variables                         | Asthma ( $n = 162$ ) | COPD ( $n = 89$ ) | <i>P</i> |
|-----------------------------------|----------------------|-------------------|----------|
| Age (years)                       | 51.60 $\pm$ 13.18    | 59.96 $\pm$ 9.78  | <0.01    |
| Sex (male)                        | 74 (45.7%)           | 64 (71.9%)        | <0.01    |
| Residence (rural)                 | 57 (35.2%)           | 40 (44.9%)        | 0.13     |
| Dust exposure (former or current) | 13 (8.0%)            | 12 (13.5%)        | 0.17     |
| Smoker (former or current)        | 14 (8.6%)            | 11 (12.4%)        | 0.35     |

Data expressed as *n* (%) or as means  $\pm$  standard deviation.

COPD, chronic obstructive pulmonary disease.

were male, comprising 74 of the 162 asthma patients (45.7%) and 64 of the 89 COPD patients (71.9%). Regarding risk factors for AEs, ~10% of all patients had a history of dust exposure, 33.5% (84) were former or current smokers, and ~60% of them lived in urban areas. Demographic characteristics are further detailed in **Tables 1, 2**.

The number of AEs was reported to be lower in 2020 than in 2019 ( $0.86 \pm 2.97$  vs.  $1.00 \pm 2.85$ ;  $P < 0.05$ ). Similarly, the number of clinic visits and emergency drug use also decreased, which persisted even when asthma patients were analyzed separately. Specifically, patients with asthma suffered fewer AEs ( $0.84 \pm 3.34$  vs.  $1.00 \pm 3.16$ ;  $P < 0.01$ ), visited the hospital less frequently ( $0.37 \pm 0.93$  vs.  $0.49 \pm 0.94$ ;  $P < 0.05$ ), and had a decreased frequency of emergency drug use in 2020 as compared to that of 2019 ( $0.30 \pm 1.42$  vs.  $2.05 \pm 6.36$ ;  $P < 0.05$ ). Additionally, asthma patients scored higher on the ACT in 2020 than that in 2019 ( $22.18 \pm 3.13$  vs.  $21.20 \pm 3.60$ ;  $P < 0.01$ ); however, no demographic differences in the clinical information of COPD patients were observed between 2020 and 2019 (**Table 3**). Given these findings, it seemed that the COVID-19 pandemic had a greater impact on patients with asthma than on those with COPD.

Differences in conditions between COPD and asthma patients were also studied. Regarding clinic visits, patients with asthma visited the clinic less frequently than those with COPD in 2020 ( $0.37 \pm 0.93$  vs.  $0.62 \pm 0.96$ ;  $P < 0.05$ ). Conversely, frequencies of AEs and emergency drug use were not significantly different in between COPD and asthma patients (**Table 3**). Furthermore,

**TABLE 3 |** Comparisons of patients' conditions between asthma and COPD.

| Variables                               | Total       |             |       | Asthma       |              |       | COPD        |             |      | P <sup>#</sup> |
|---|-------------|-------------|-------|--------------|--------------|-------|-------------|-------------|------|----------------|
|   | 2019        | 2020        | P     | 2019         | 2020         | P     | 2019        | 2020        | P    |                |
| Frequency of AEs (/year)                | 1.00 ± 2.85 | 0.86 ± 2.97 | 0.01  | 1.00 ± 3.16  | 0.84 ± 3.34  | <0.01 | 1.01 ± 2.19 | 0.93 ± 2.16 | 0.47 | 0.20           |
| Frequency of clinic visits (/year)      | 0.61 ± 1.17 | 0.46 ± 0.95 | <0.01 | 0.49 ± 0.94  | 0.37 ± 0.93  | <0.01 | 0.16 ± 0.51 | 0.62 ± 0.96 | 0.31 | 0.03           |
| Frequency of emergency drug use (/year) | 1.36 ± 5.15 | 0.23 ± 1.16 | <0.01 | 2.05 ± 6.36  | 0.30 ± 1.42  | <0.01 | 0.16 ± 0.51 | 0.12 ± 0.50 | 0.16 | 0.78           |
| ACT score                               |             |             |       | 21.20 ± 3.60 | 22.18 ± 3.13 | <0.01 |             |             |      |                |
| mMRC                                    |             |             |       |              |              |       | 1.44 ± 1.24 | 1.41 ± 1.22 | 0.44 |                |

Data are expressed as means ± standard deviation.

P<sup>#</sup>, Comparisons of patients' conditions in 2020 between asthma and COPD.

ACT, asthma control test; AE, acute exacerbation; COPD, chronic obstructive pulmonary disease.

**TABLE 4 |** Comparisons between AE and non-AE patients during the COVID-19 pandemic (2020).

| Variable                          | Total      |             |         | Asthma       |              |         | COPD        |             |         |
|-----------------------------------|------------|-------------|---------|--------------|--------------|---------|-------------|-------------|---------|
|                                   | AE         | Non-AE      | P-Value | AE           | Non-AE       | P-Value | AE          | Non-AE      | P-Value |
| N                                 | 70         | 181         |         | 42           | 120          |         | 28          | 61          | —       |
| Sex (male)                        | 46 (65.7%) | 92 (50.8%)  | 0.03    | 26 (61.9%)   | 48 (40%)     | 0.01    | 20 (71.4%)  | 44 (72.1%)  | 0.95    |
| Residence (rural)                 | 33 (47.1%) | 64 (35.4%)  | 0.09    | 21 (50.0%)   | 36 (30.0%)   | 0.02    | 12 (42.9%)  | 28 (45.9%)  | 0.79    |
| Age (>60)                         | 40 (57.1%) | 120 (66.3%) | 0.18    | 27 (64.3%)   | 91 (75.8%)   | 0.15    | 13 (46.4%)  | 29 (47.5%)  | 0.92    |
| Dust exposure (former or current) | 13 (18.6%) | 12 (6.6%)   | <0.01   | 14 (33.3%)   | 12 (10.0%)   | <0.01   | 6 (21.4%)   | 6 (9.8%)    | 0.14    |
| Smoker (former or current)        | 36 (51.4%) | 48 (26.5%)  | <0.01   | 20 (47.6%)   | 9 (7.5%)     | <0.01   | 12 (42.9%)  | 26 (42.6%)  | 0.98    |
| Diagnosis (asthma)                | 42 (60.0%) | 120 (65.7%) | 0.40    |              |              |         |             |             |         |
| AE in last 12 months              | 51 (72.9%) | 29 (16.0%)  | <0.01   | 29 (69.0%)   | 20 (16.7%)   | <0.01   | 22 (78.6%)  | 9 (14.8%)   | <0.01   |
| ACT                               |            |             |         | 20.15 ± 3.20 | 22.88 ± 2.75 | <0.01   |             |             |         |
| mMRC                              |            |             |         |              |              |         | 2.18 ± 1.19 | 1.05 ± 1.06 | <0.01   |

Data were expressed as n (%) or means ± standard deviation.

ACT, asthma control test; AE, acute exacerbation; COPD, chronic obstructive pulmonary disease; mMRC, modified Medical Research Council.

there were no significant differences between the patients living in urban areas and those living in rural areas, with regards to the frequency of AEs, clinic visits, and emergency drug use (**Supplementary Table**).

To determine the potential risk factors for AEs during the pandemic, the patients were divided into two groups: (1) an AE group, comprising patients who had at least one AE in 2020, and (2) a non-AE group, comprising patients who had no AEs in 2020. Comparisons of the proportions and correlation analyses were performed using the chi-squared test between these two groups. In the AE and non-AE groups, 65.7% and 50.8% of the patients were male, respectively ( $P < 0.05$ ). Moreover, the AE group had a greater proportion of patients with a history of dust exposure (18.6 vs. 6.6%;  $P < 0.01$ ), and 51.4% of the AE group patients were former or current smokers, which was markedly higher than in the non-AE group (26.5%). Additionally, the proportion of patients who had an AE in 2019 was higher in the AE group (72.9 vs. 16.0%;  $P < 0.01$ ), which persisted even when we analyzed asthma patients separately from those with COPD (**Table 4**). In addition to sex, dust exposure, smoking history, and AE in 2019, the residence distribution was also different between the two groups, wherein more rural residents in the AE group

were noted as compared to the non-AE group. Furthermore, the AE group had lower ACT scores than the non-AE group, and among the COPD patients, the AE group had higher mMRC scores than the non-AE group. These details are further listed in **Table 4**.

Binary logistic regression was used to assess possible risk factors, showing that the proportion or mean was significantly different between the AE and non-AE groups. Among all chronic airway disease patients, the final logistic model revealed two risk factors: dust exposure and AE in 2019. Specifically, patients with a history of dust exposure had a 2.91-fold higher risk of AE than those without, and a history of at least one AE in 2019 was also associated with increased odds of AE in this year (odds ratio [OR]: 13.73; 95% confidence interval [CI]: 7.04–26.77;  $P < 0.01$ ). Among patients with asthma, rural patients had a lower risk of AE than those living in urban areas (OR: 0.36, 95% CI: 0.14–0.94;  $P < 0.05$ ). In addition, smoking (OR: 3.34, 95% CI: 1.27–8.74;  $P < 0.05$ ), history of AE in 2019 (OR: 8.93, 95% CI: 3.56–22.39;  $P < 0.001$ ), and lower ACT scores (OR: 4.32, 95% CI: 1.56–12.01;  $P < 0.01$ ) were associated with increased odds of AE. On the other hand, in patients with COPD, only a history of AE in 2019 (OR: 18.22, 95% CI: 5.59–59.32;  $P < 0.01$ ) was associated with increased odds of AE. More

**TABLE 5 |** Logistic regression analysis of risk factors related to AE.

| Variable                          | Total              |         | Asthma            |         | COPD               |         |
|-----------------------------------|--------------------|---------|-------------------|---------|--------------------|---------|
|                                   | OR (95% CI)        | P-Value | OR (95% CI)       | P-Value | OR (95% CI)        | P-Value |
| Residence (rural)                 |                    |         | 0.36 (0.14–0.94)  | 0.04    |                    |         |
| Dust exposure (former or current) | 2.91 (1.05–8.09)   | 0.04    |                   |         |                    |         |
| Smoker (former or current)        |                    |         | 3.34 (1.27–8.74)  | 0.01    |                    |         |
| AE in last 12 months              | 13.73 (7.04–26.77) | <0.01   | 8.93 (3.56–22.39) | <0.01   | 18.22 (5.59–59.32) | <0.01   |
| ACT (<23)                         |                    |         | 4.32 (1.56–12.01) | <0.01   |                    |         |
| mMRC (>1)                         |                    |         |                   |         | 3.21 (0.99–10.43)  | 0.05    |

Variables that significantly differed in the univariate analysis (Table 4) were included in the logistic regression analysis.

ACT, asthma control test; AE, acute exacerbation; COPD, chronic obstructive pulmonary disease; mMRC, modified Medical Research Council; OR, odds ratio.

information on the logistic regression findings is provided in Table 5.

## DISCUSSION

To date and to the best of our knowledge, this was the first study to analyze the differences between asthma and COPD patients during the COVID-19 pandemic. It was found that there was a decrease in the frequency of AEs, clinic visits, and emergency drug use in 2020 among asthma patients; however, this was not observed in COPD patients. Moreover, patients with asthma went to the clinic less frequently than those with COPD in 2020. The population in the present study had used combined budesonide and formoterol since 2018, which were maintained before and during the pandemic, indicating that drug bias was likely low. Furthermore, no severe infections or COVID-19 cases were found, also indicating that ICS-induced infection incidence was low. Given that previous studies (25–27) have found variable AE frequencies of asthma and COPD in different seasons, the present study collected data from January 1, 2019, to December 31, 2020, avoiding season bias in our comprehensive observation and analysis of data across two entire years.

In the present survey, the patients' conditions before and during the COVID-19 pandemic were evaluated. During the pandemic, asthma patients showed better disease control, with fewer AEs, fewer medical visits, lower emergency drug use frequencies, and higher ACT scores in 2020 than in 2019. This finding may be attributed to their less exposure to outdoor air pollutants (28, 29), allergens (30), and respiratory viruses (31, 32) as they practiced social isolation measures, including home quarantine, social distancing, and public health initiatives (33). Moreover, one study reported a significant decline in the concentration of air pollutants caused by control measures to mitigate the spread of COVID-19 during the pandemic (34). As such, the improved air quality may have helped stabilize the condition of asthma patients and reduce the frequency of AE. This is also affirmed by one multinational cohort study involving 1,054 children with asthma, showing that the outcomes of childhood asthma improved during the pandemic (18). Furthermore, research in the US and UK has shown a marked reduction in emergency visits by asthma patients during

the pandemic (19, 35). However, it should be noted that past research has mainly focused on childhood asthma, whereas adults were mainly involved in the present study. Nevertheless, the aforementioned findings demonstrated that patients with asthma experienced improved conditions during the COVID-19 pandemic.

In patients with asthma, a history of at least one AE in the last 12 months was determined as a risk factor for AE during the COVID-19 pandemic, which is consistent with previous findings (36). Logistic regression analysis revealed that rural environments could be a protective factor in asthma patients, perhaps because there are lower concentrations of outdoor air pollutants in rural areas than in urban areas in China (37), given that outdoor air pollution, including particulate matter and gaseous pollutants, has already been associated with asthma prevalence and AEs (38, 39). The present results also supported the prior finding (40) that cigarette smoking and lower ACT scores were risk factors for AE.

Meanwhile, in patients with COPD, the frequency of AEs, medical visits, and emergency drug use before the pandemic did not differ significantly from those during. In contrast with our findings, Faria et al. (20) reported a 73.4% decrease in severe AECOPD events in the first half of 2020 as compared to the same timeline of previous years, whereas Tan et al. (21) found that AECOPD admissions decreased by more than 50% over a sustained 6-month period in 2020 as compared to previous years. These discrepancies may have arisen due to the different drugs used or these previous studies may have shown season bias due to insufficient observation. In the COPD patients from our study, only two variables were included in the final logistic model. Additionally, even though mMRC was included, no significant differences were found between the two groups ( $P = 0.05$ ). Although previous studies have shown that smoking was one of the most common reasons for COPD prevalence and exacerbations (12), it was not included in the final logistic model. However, it should also be noted that only 89 COPD patients were included in the present study, so the sample size seems limited for logistic regression analysis.

In the present study, COPD patients were found to be older than those with asthma, possibly due to the difference in disease onset (12, 17). In addition, the proportion of males

was higher among COPD patients, which was likely because the smoking rate was lower among females (41). There were also significant differences in the clinical data between asthma and COPD patients. Specifically, the frequencies of AE, clinic visits, and emergency drug use decreased in 2020 among patients with asthma, whereas no significant differences were observed in patients with COPD. These findings seemed to show that the outcomes in asthma patients improved during the COVID-19 pandemic, while those in COPD patients did not, which was perhaps due to the differences in the risk factors for the progression and exacerbation of the two diseases. Although social isolation measures were found to reduce exposure to respiratory viruses, which play an important role in both asthma and COPD AEs (31, 32), prolonged exposure to indoor air pollution during home quarantine may increase the risk of AE among COPD patients. In fact, studies have shown that excessive passive smoking and harmful fumes from kitchens during home quarantine are closely related to COPD prevalence and exacerbations (42–45). As nearly half of the COPD patients in the present study were rural residents, fuels may have adverse effects on disease control during the pandemic, given that coal and wood are still widely used for cooking in Chinese rural areas (46). The China Pulmonary Health [CPH] study reported an overall COPD prevalence of 8.6% in Chinese population and higher prevalence in rural residents than in urban residents (9.6 vs 7.4%;  $p = 0.047$ ) (47), but no significant difference in asthma prevalence was observed between rural and urban areas (4.9 vs 3.6%,  $p = 0.27$ ) (38). Furthermore, recent studies (39) and the logistic regression of the present study indicated that outdoor air pollution played a significant role in asthma exacerbations and that outdoor air pollution played a smaller role than smoking in COPD prevalence and exacerbations (48). Additionally, since the rate of rural residents was higher among asthma patients in this study, poorer access to health care facilities in rural areas might also explain the fewer frequency of clinical visits in 2020 in asthma patients than that in COPD patients. Nonetheless, asthma patients still showed significant benefits with fewer AEs and higher ACT scores. This may demonstrate that personal protection and social distance ensured a better disease control for asthma patients during the pandemic.

Taken together, patients with asthma may be more sensitive to outdoor air pollution and allergens than those with COPD, indicating that home quarantine and mask-wearing were sufficient for exacerbation prevention and control in these patients during the COVID-19 pandemic. Although there is a need to conduct multi-centers and larger-sample study, we speculate that there are different effects of indoor or outdoor air pollutions and various personal protections on asthma and COPD patients in future potential pandemics. On the other hand, the result of our study supported personal protection and social distance during pandemic not only for communicable disease, but also for the management of chronic airway diseases. Additionally, due to a worse control of COPD patients in our study, we suggest that physicians should pay more attention to COPD patients in future potential pandemics.

Despite these findings, we admit that there were certain limitations in our study. Firstly, the single and limited data source made the research less credible and reproducible as compared to a multi-center research study. However, with regard to telephone interviews, a single-center research will better avoid bias caused by the unevenness of the interviewer's level between different centers. Secondly, the patients' self-reported data may have affected the accuracy of the follow-up results due to subjective factors or memory bias. To mitigate this, we chose two internationally recognized symptom assessment scales, the modified Medical Research Council (mMRC) dyspnea scale and the asthma control test (ACT), to help us understand the symptoms and conditions of our patients. Interviewers participating in the study were also required to undergo centralized training. Thirdly, 627 patients were excluded due to refusal to call or interview, death, misdiagnosis, or wrong numbers, which may have led to follow-up bias to our results. This relatively high rate of loss to follow-up may have been caused by the people's increasing vigilance against phone scams and changing mobile phone numbers. Furthermore, since people who died before we conducted telephone interviews were excluded, we may have lost data from those with severe symptoms, which would have affected the representativeness and reliability of our research. Fourthly, only 89 COPD patients were enrolled in the present study, and this small sample size may have reduced the reliability of the data. Fifthly, since most of the patients were adults, our study lacked data on children and teenagers. Lastly, population in this study used only budesonide/formoterol, and thus outcomes may differ in patients who use other ICS/LABA regimens.

## CONCLUSION

During the COVID-19 pandemic, patients with asthma showed better disease control than before, whereas those with COPD did not. Among the population that used ICS/LABA, at least one AE within the previous 12 months was a risk factor for AE during the pandemic in both asthma and COPD patients. For patients with asthma, urban environment, smoking, and lower ACT scores were also risk factors for AE during the COVID-19 pandemic.

## DATA AVAILABILITY STATEMENT

The original contributions presented in the study are included in the article/**Supplementary Material**, further inquiries can be directed to the corresponding author.

## ETHICS STATEMENT

The studies involving human participants were reviewed and approved by Medical Research Ethics Committee of the Second Xiangya Hospital of Central South University. Written informed consent for participation was not required for this study in accordance with the national



legislation and the institutional requirements. Written informed consent was obtained from the minor(s)' legal guardian/next of kin for the publication of any potentially identifiable images or data included in this article.

## AUTHOR CONTRIBUTIONS

All authors contributed to data analysis, drafting and revising the article, gave final approval of the version to be published, and agree to be accountable for all aspects of the work.

## REFERENCES

1. WHO. *Weekly epidemiological update on COVID-19 - 30 March*. 2021. (2021). Available online at: <https://www.who.int/publications/m/item/weekly-epidemiological-update-on-covid-19-31-march-2021> (accessed may 10, 2021).
2. Wiersinga WJ, Rhodes A, Cheng AC, Peacock SJ, Prescott HC. Pathophysiology, Transmission, Diagnosis, and Treatment of Coronavirus Disease 2019. (COVID-19) A Review. *JAMA*. (2020) 324:782–93. doi: 10.1001/jama.2020.12839
3. Sungnak W, Huang N, Becavin C, Berg M, Queen R, Litvinukova M, et al. SARS-CoV-2 entry factors are highly expressed in nasal epithelial cells together with innate immune genes. *Nat Med*. (2020) 26:681–7. doi: 10.1038/s41591-020-0868-6
4. Chen N, Zhou M, Dong X, Qu J, Gong F, Han Y, et al. Epidemiological and clinical characteristics of 99 cases of 2019 novel coronavirus pneumonia in Wuhan, China: a descriptive study. *Lancet*. (2020) 395:507–13. doi: 10.1016/S0140-6736(20)30211-7
5. Schultze A, Walker AJ, MacKenna B, Morton CE, Bhaskaran K, Brown JP, et al. Risk of COVID-19-related death among patients with chronic obstructive pulmonary disease or asthma prescribed inhaled corticosteroids: an observational cohort study using the OpenSAFELY platform. *Lancet Respir Med*. (2020) 8:1106–20. doi: 10.1016/S2213-2600(20)30415-X
6. Garg S, Kim L, Whitaker M, O'Halloran A, Cummings C, Holstein R, et al. Hospitalization Rates and Characteristics of Patients Hospitalized with Laboratory-Confirmed Coronavirus Disease (2019) - COVID-NET, 14 States, March 1–30, (2020). *MMWR Morb Mortal Wkly Rep*. (2020) 69:458–64. doi: 10.15585/mmwr.mm6915e3
7. Song J, Zeng M, Wang H, Qin C, Hou HY, Sun ZY, et al. Distinct effects of asthma and COPD c s of asthma and COPD comorbidity on disease expression and outcome in patients with COVID-19. *Allergy*. (2021) 76:483–96. doi: 10.1111/all.14517
8. WHO. *Asthma*. Available online at: <https://www.who.int/news-room/fact-sheets/detail/asthma> (accessed may 10, 2021).
9. WHO. *Chronic Obstructive Pulmonary Disease (COPD)*. (2017). Available online at: [https://www.who.int/news-room/fact-sheets/detail/chronic-obstructive-pulmonary-disease-\(copd\)](https://www.who.int/news-room/fact-sheets/detail/chronic-obstructive-pulmonary-disease-(copd)) (accessed may 10, 2021).
10. Global Initiative for Asthma. *Global Strategy for Asthma Management and Prevention*. (2020). Available online at: [www.ginasthma.org](http://www.ginasthma.org) (accessed may 10, 2021).
11. WHO. *The top 10 causes of death*. (2020). Available online at: <https://www.who.int/news-room/fact-sheets/detail/the-top-10-causes-of-death> (accessed may 10, 2021).
12. Global Strategy for the Diagnosis. *Management and Prevention of Chronic Obstructive Pulmonary Disease, Global initiative for chronic obstructive lung disease (GOLD)*. (2021). Available online at: <http://www.goldcopd.org/> (accessed may 10, 2021).
13. Terry PD, Heidell RE, Dhand R. Asthma in Adult Patients with COVID-19. Prevalence and Risk of Severe Disease. *Am J Respir Crit Care Med*. (2021) 203:893–905. doi: 10.1164/rccm.202008-3266OC
14. Lippi G, Henry BM. Chronic obstructive pulmonary disease is associated with severe coronavirus disease (2019) (COVID-19). *Respir Med*. (2020) 167:105941. doi: 10.1016/j.rmed.2020.105941
15. Grasselli G, Greco M, Zanella A, Albano G, Antonelli M, Bellani G, et al. Risk Factors Associated With Mortality Among Patients With COVID-19 in Intensive Care Units in Lombardy, Italy. *JAMA Intern Med*. (2020) 180:1345–55. doi: 10.1001/jamainternmed.2020.3539
16. Hippisley-Cox J, Young D, Coupland C, Channon KM, Tan PS, Harrison DA, et al. Risk of severe COVID-19 disease with ACE inhibitors and angiotensin receptor blockers: cohort study including 8.3 million people. *Heart*. (2020) 106:1503–11. doi: 10.1136/heartjnl-2020-317393
17. Global Strategy for Asthma Management and Prevention, Global Initiative for Asthma (GINA) (2020). Available online at: [www.ginasthma.org](http://www.ginasthma.org) (accessed may 10, 2021).
18. Papadopoulos NG, Mathioudakis AG, Custovic A, Deschildre A, Phipatanakul W, Wong G, et al. Childhood asthma outcomes during the COVID-19 pandemic: Findings from the PeARL multinational cohort. *Allergy*. (2021) 76:1765–75. doi: 10.1101/2020.10.27.20219436
19. Gupta A, Bush A, Nagakumar P. Asthma in children during the COVID-19 pandemic: lessons from lockdown and future directions for management. *Lancet Respir Med*. (2020) 8:1070–71. doi: 10.1016/S2213-2600(20)30278-2
20. Faria N, Costa MI, Gomes J, Sucena M. Reduction of Severe Exacerbations of COPD during COVID-19 Pandemic in Portugal: A Protective Role of Face Masks?. *COPD*. (2021) 18:226–30. doi: 10.1080/15412555.2021.1904387
21. Tan JY, Conceicao EP, Wee LE, Sim JXY, Venkatachalam I. COVID-19 public health measures: a reduction in hospital admissions for COPD exacerbations. *Thorax*. (2020) 76:512–3. doi: 10.1136/thoraxjnl-2020-216083
22. Global Strategy for the Diagnosis. *Management and prevention of chronic obstructive pulmonary disease, Global initiative for chronic obstructive lung disease (GOLD)*. (2020). Available online at: <http://www.goldcopd.org/> (accessed may 10, 2021).
23. Bestall JC, Paul EA, Garrod R, Garnham R, Jones PW, Wedzicha JA. Usefulness of the Medical Research Council (MRC) dyspnoea scale as a measure of disability in patients with chronic obstructive pulmonary disease. *Thorax*. (1999) 54:581–6. doi: 10.1136/thx.54.7.581
24. Asthma Control Test (ACT). Available online at: <https://www.asthmacontroltest.com/> (accessed may 10, 2021).
25. Jenkins CR, Celli B, Anderson JA, Ferguson GT, Jones PW, Vestbo J, et al. Seasonality and determinants of moderate and severe COPD exacerbations in the TORCH study. *Eur Respir J*. (2012) 39:38–45. doi: 10.1183/09031936.00194610
26. Teach SJ, Gergen PJ, Szeffler SJ, Mitchell HE, Calatroni A, Wildfire J, et al. Seasonal risk factors for asthma exacerbations among inner-city children. *J Allergy Clin Immunol*. (2015) 135:1465–73 e5. doi: 10.1016/j.jaci.2014.12.1942
27. Bloomberg GR, Trinkaus KM, Fisher EB, Jr., Musick JR, Strunk RC. Hospital readmissions for childhood asthma: a 10-year metropolitan study. *Am J Respir Crit Care Med*. (2003) 167:1068–76. doi: 10.1164/rccm.2201015
28. Tanaka H, Nakatani E, Fukutomi Y, Sekiya K, Kaneda H, Iikura M, et al. Identification of patterns of factors preceding severe or life-threatening asthma exacerbations in a nationwide study. *Allergy*. (2018) 73:1110–18. doi: 10.1111/all.13374

## FUNDING

This work was supported by National Natural Science Foundation of China (No.81873410, No.82070049, and No.81400032), National Key R&D Program of China (2016YFC1304700).

## SUPPLEMENTARY MATERIAL

The Supplementary Material for this article can be found online at: <https://www.frontiersin.org/articles/10.3389/fmed.2021.709006/full#supplementary-material>

29. Perez L, Declercq C, Iniguez C, Aguilera I, Badaloni C, Ballester F, et al. Chronic burden of near-roadway traffic pollution in 10 European cities (APHEKOM network). *Eur Respir J*. (2013) 42:594–605. doi: 10.1183/09031936.00031112
30. Eguiluz-Gracia I, Mathioudakis AG, Bartel S, Vijverberg SJH, Fuertes E, Comberiat P, et al. The need for clean air: The way air pollution and climate change affect allergic rhinitis and asthma. *Allergy*. (2020) 75:2170–84. doi: 10.1111/all.14177
31. Taquechel K, Diwadkar AR, Sayed S, Dudley JW, Grundmeier RW, Kenyon CC, et al. Pediatric Asthma Health Care Utilization, Viral Testing, and Air Pollution Changes During the COVID-19 Pandemic. *J Allergy Clin Immunol Pract*. (2020) 8:3378–87 e11. doi: 10.1016/j.jaip.2020.07.057
32. Green RM, Custovic A, Sanderson G, Hunter J, Johnston SL, Woodcock A. Synergism between allergens and viruses and risk of hospital admission with asthma: case-control study. *BMJ*. (2002) 324:763. doi: 10.1136/bmj.324.7340.763
33. Niespodziana K, Borochova K, Pazderova P, Schleder T, Astafyeva N, Baranovskaya T, et al. Toward personalization of asthma treatment according to trigger factors. *J Allergy Clin Immunol*. (2020) 145:1529–34. doi: 10.1016/j.jaci.2020.02.001
34. Zhang X, Tang M, Guo F, Wei F, Yu Z, Gao K, et al. Associations between air pollution and COVID-19 epidemic during quarantine period in China. *Environ Pollut*. (2021) 268:115897. doi: 10.1016/j.envpol.2020.115897
35. Kenyon CC, Hill DA, Henrickson SE, Bryant-Stephens TC, Zorc JJ. Initial effects of the COVID-19 pandemic on pediatric asthma emergency department utilization. *J Allergy Clin Immunol Pract*. (2020) 8:2774–6 e1. doi: 10.1016/j.jaip.2020.05.045
36. Buelo A, McLean S, Julious S, Flores-Kim J, Bush A, Henderson J, et al. At-risk children with asthma (ARC): a systematic review. *Thorax*. (2018) 73:813–24. doi: 10.1136/thoraxjnl-2017-210939
37. Wang Y, Bao M, Zhang Y, Tan F, Zhao H, Zhang Q, et al. Polycyclic aromatic hydrocarbons in the atmosphere and soils of Dalian, China: Source, urban-rural gradient, air-soil exchange. *Chemosphere*. (2020) 244:125518. doi: 10.1016/j.chemosphere.2019.125518
38. Huang K, Yang T, Xu J, Yang L, Zhao J, Zhang X, et al. Prevalence, risk factors, and management of asthma in China: a national cross-sectional study. *Lancet*. (2019) 394:407–18. doi: 10.1016/S0140-6736(19)31147-X
39. Guarnieri M, and Balmes JR. Outdoor air pollution and asthma. *Lancet*. (2014) 383:1581–92. doi: 10.1016/S0140-6736(14)60617-6
40. Loymans RJB, Honkoop PJ, Termeer EH, Snoeck-Stroband JB, Assendelft WJJ, Schermer T.R. J., et al. Identifying patients at risk for severe exacerbations of asthma: development and external validation of a multivariable prediction model. *Thorax*. (2016) 71:838–46. doi: 10.1136/thoraxjnl-2015-208138
41. Chen Z, Peto R, Zhou M, Iona A, Smith M, Yang L, et al. Contrasting male and female trends in tobacco-attributed mortality in China: evidence from successive nationwide prospective cohort studies. *Lancet*. (2015) 386:1447–56. doi: 10.1016/S0140-6736(15)00340-2
42. Schultze A, Walker AJ, MacKenna B, Morton CE, Bhaskaran K, Brown JP, et al. Chronic obstructive pulmonary disease associated with biomass fuel use in women: a systematic review and meta-analysis. *BMJ Open Respir Res*. (2018) 5:e000246. doi: 10.1136/bmjresp-2017-000246
43. Zhou Y, Zou Y, Li X, Chen S, Zhao Z, He F, et al. Lung function and incidence of chronic obstructive pulmonary disease after improved cooking fuels and kitchen ventilation: a 9-year prospective cohort study. *PLoS Med*. (2014) 11:e1001621. doi: 10.1371/journal.pmed.1001621
44. Yin P, Jiang CQ, Cheng KK, Lam TH, Lam KH, Miller MR, et al. Passive smoking exposure and risk of COPD among adults in China: the Guangzhou Biobank Cohort Study. *Lancet*. (2007) 370:751–7. doi: 10.1016/S0140-6736(07)61378-6
45. Li J, Qin C, Lv J, Guo Y, Bian Z, Zhou W, et al. Solid Fuel Use and Incident COPD in Chinese Adults: Findings from the China Kadoorie Biobank. *Environ Health Perspect*. (2019) 127:57008. doi: 10.1289/EHP2856
46. Tang X, Liao H. Energy poverty and solid fuels use in rural China: Analysis based on national population census. *Ener Sustainable Dev*. (2014) 23:122–9. doi: 10.1016/j.esd.2014.08.006
47. Wang C, Xu J, Yang L, Xu Y, Zhang X, Bai C, et al. Prevalence and risk factors of chronic obstructive pulmonary disease in China (the China Pulmonary Health [CPH] study): a national cross-sectional study. *Lancet*. (2018) 391:1706–17. doi: 10.1016/S0140-6736(18)30841-9
48. Eisner MD, Anthonisen N, Coultas D, Kuenzli N, Perez-Padilla R, Postma D, et al. An official American Thoracic Society public policy statement: Novel risk factors and the global burden of chronic obstructive pulmonary disease. *Am J Respir Crit Care Med*. (2010) 182:693–718. doi: 10.1164/rccm.200811-1757ST

**Conflict of Interest:** The authors declare that the research was conducted in the absence of any commercial or financial relationships that could be construed as a potential conflict of interest.

**Publisher's Note:** All claims expressed in this article are solely those of the authors and do not necessarily represent those of their affiliated organizations, or those of the publisher, the editors and the reviewers. Any product that may be evaluated in this article, or claim that may be made by its manufacturer, is not guaranteed or endorsed by the publisher.

Copyright © 2021 Xiong, Zhao, Lu, Ma, Zeng and Chen. This is an open-access article distributed under the terms of the Creative Commons Attribution License (CC BY). The use, distribution or reproduction in other forums is permitted, provided the original author(s) and the copyright owner(s) are credited and that the original publication in this journal is cited, in accordance with accepted academic practice. No use, distribution or reproduction is permitted which does not comply with these terms.



# Elaboration of a Radiomics Strategy for the Prediction of the Re-positive Cases in the Discharged Patients With COVID-19

Xiao-Hui Wang<sup>1†</sup>, Xiaopan Xu<sup>2†</sup>, Zhi Ao<sup>1</sup>, Jun Duan<sup>1</sup>, Xiaoli Han<sup>1</sup>, Xing Tang<sup>3</sup>, Yu-Fei Fu<sup>3</sup>, Xu-Sha Wu<sup>3</sup>, Xue Wang<sup>1</sup>, Linxiao Zhu<sup>1</sup>, Wenbing Zeng<sup>4\*</sup> and Shuliang Guo<sup>1\*</sup>

## OPEN ACCESS

### Edited by:

Atefeh Abedini,  
Shahid Beheshti University of Medical  
Sciences, Iran

### Reviewed by:

Alireza Shafiei,  
Tehran University of Medical  
Sciences, Iran  
Zhongqing Xu,  
Shanghai Jiao Tong University School  
of Medicine, China

### \*Correspondence:

Shuliang Guo  
guosl999@sina.com  
orcid.org/0000-0003-3572-7421  
Wenbing Zeng  
422817593@qq.com

<sup>†</sup>These authors have contributed  
equally to this work

### Specialty section:

This article was submitted to  
Infectious Diseases - Surveillance,  
Prevention and Treatment,  
a section of the journal  
Frontiers in Medicine

Received: 28 June 2021

Accepted: 11 August 2021

Published: 16 September 2021

### Citation:

Wang X-H, Xu X, Ao Z, Duan J, Han X,  
Tang X, Fu Y-F, Wu X-S, Wang X,  
Zhu L, Zeng W and Guo S (2021)  
Elaboration of a Radiomics Strategy  
for the Prediction of the Re-positive  
Cases in the Discharged Patients With  
COVID-19. *Front. Med.* 8:730441.  
doi: 10.3389/fmed.2021.730441

<sup>1</sup> Department of Pulmonary and Critical Care Medicine, The First Affiliated Hospital of Chongqing Medical University, Chongqing, China, <sup>2</sup> School of Biomedical Engineering, Air Force Medical University, Xi'an, China, <sup>3</sup> Department of Radiology, Xijing Hospital, Air Force Medical University, Xi'an, China, <sup>4</sup> Department of Radiology, Chongqing University Three Gorges Hospital, Chongqing, China

**Objective:** A considerable part of COVID-19 patients were found to be re-positive in the SARS-CoV-2 RT-PCR test after discharge. Early prediction of re-positive COVID-19 cases is of critical importance in determining the isolation period and developing clinical protocols.

**Materials and Methods:** Ninety-one patients discharged from Wanzhou Three Gorges Central Hospital, Chongqing, China, from February 10, 2020 to March 3, 2020 were administered nasopharyngeal swab SARS-CoV-2 tests within 12–14 days, and 50 eligible patients (32 male and 18 female) with completed data were enrolled. Average age was  $48 \pm 11.5$  years. All patients underwent non-enhanced chest CT on admission. A total of 568 radiomics features were extracted from the CT images, and 17 clinical factors were collected based on the medical record. Student's *t*-test and support vector machine-based recursive feature elimination (SVM-RFE) method were used to determine an optimal subset of features for the discriminative model development.

**Results:** After Student's *t*-test, 62 radiomics features showed significant inter-group differences ( $p < 0.05$ ) between the re-positive and negative cases, and none of the clinical features showed significant differences. These significant features were further selected by SVM-RFE algorithm, and a more compact feature subset containing only two radiomics features was finally determined, achieving the best predictive performance with the accuracy and area under the curve of 72.6% and 0.773 for the identification of the re-positive case.

**Conclusion:** The proposed radiomics method has preliminarily shown potential in identifying the re-positive cases among the recovered COVID-19 patients after discharge. More strategies are to be integrated into the current pipeline to improve its precision, and a larger database with multi-clinical enrollment is required to extensively verify its performance.

**Keywords:** COVID-19, re-positive cases, computed tomography, radiomics, prediction

## INTRODUCTION

Since the outbreak of COVID-19 in December 2019, infection by severe acute respiratory syndrome coronavirus 2 (SARS-CoV-2) has led to an increasing number of confirmed patients and deaths all over the world, with an estimated mortality of 4.1% (<https://www.who.int/emergencies/diseases/novel-coronavirus-2019>). Many patients have recovered and were discharged to the designed place for isolation. In February 2020, Lan et al. first reported that four patients who met the criteria for hospital discharge had positive real-time reverse transcriptase-polymerase chain reaction (RT-PCR) of SARS-CoV-2 test (1). With the increasing number of recovered patients discharged from the hospital by regular follow-up, more and more patients with COVID-19 were found to have re-positive RT-PCR test after discharge (2–5). The proportion of re-positive cases among the discharged patients with COVID-19 varies from 10.6 to 21.4% (4, 6, 7). Reasons for re-positive COVID-19 patients after discharge from the hospital may include the biological characteristics of SARS-CoV-2, clinical status of patients, underlying medical conditions, impact of drug therapy and other treatments, sampling and detection, and re-infection (8). Since re-positive COVID-19 patients after discharge may cause serious consequences as a source of infection (9), early prediction of the re-positive COVID-19 cases among the discharged patients is critically significant to determine the isolation period and develop clinical protocols.

A study reported that there is no significant difference in age between re-positive patients and patients in the control group (6). However, another study reported that the risk of re-positive test after discharge is more than six times higher in persons aged  $\geq 60$  years (10). So, there is controversy about risk factors of re-positive patients. Although previous studies have tried to predict the re-positive cases using the clinical features like age, underlying disease,  $CD4^+$  T lymphocytes, inflammatory indicators, drugs, and duration of treatment (11, 12), the predictive effect is far less than satisfactory (13). Moreover, artificial intelligence and radiomics strategy have been used to fight against COVID-19, including classification of COVID-19 from non-COVID-19 or other pneumonia, severity assessment, and follow-up of COVID-19 (14–16). Until now, as far as we are concerned, no researches have investigated the feasibility and performance of the radiomics strategy for the discrimination of the re-positive cases among the recovered COVID-19 patients after discharge. The purpose of this study was to explore a CT-based radiomics strategy to predict the re-positive case in the test of recovered patients with COVID-19.

## MATERIALS AND METHODS

### Patients

A total of 91 patients discharged from Wanzhou Three Gorges Central Hospital, Chongqing, China, from February 10, 2020 to March 3, 2020, who followed strict self-isolation or designated isolation, were administered nasopharyngeal swab SARS-CoV-2 test 12–14 days after discharge, and 50 eligible patients with completed data were enrolled [Appendix Figure E1 (online)].

The patients with positive result were defined as “re-positive” group, and the others were “negative” group. All the recovered patients met the discharge criteria according to the *Diagnosis and Treatment of 2019-nCoV Pneumonia in China* (5th edition) (<http://www.nhc.gov.cn/>): (1) normal temperature for more than 3 days, (2) significant improvement of respiratory symptoms, (3) significant absorption of acute exudative lesions on chest radiograph, and (4) two consecutively negative results by RT-PCR assay of nasal and pharyngeal swabs with at least 1-day interval. The definition of severity of COVID-19 (severe vs. non-severe) at the time of admission is in accordance with the American Thoracic Society guidelines for community-acquired pneumonia (17). Ethical approval was obtained for this retrospective analysis, and informed consent was waived.

Among 91 recovered patients, all 50 recovered patients (32 male and 18 female) with completed detailed clinical features, laboratory findings, and chest CT images on admission were enrolled and underwent SARS-CoV-2 assay. Average age was  $48 \pm 11.5$  years. In total, 24 (48%) patients again have a positive SARS-CoV-2 RT-PCR test result of nasopharyngeal swab. Four patients were marked as severe cases, and the rest were non-severe cases. A total of 17 clinical factors were collected from the institutional medical records, including sex, age, severity level, location of the largest lesion, ratio of lesion area in the thoracic cavity, the slice ID of the CT image with the largest lesion, location of all the lesions on this slice, ratio of all the lesions area in the thoracic cavity on this slice, the number of all the lesions on this slice, leukocytes, neutrophils, lymphocytes, lymphocyte ratio,  $CD4^+$  T lymphocytes,  $CD8^+$  T lymphocytes, and  $CD4^+/CD8^+$  T lymphocytes, to verify their predictive capacity for the discrimination of the re-positive cases among all the discharged patients.

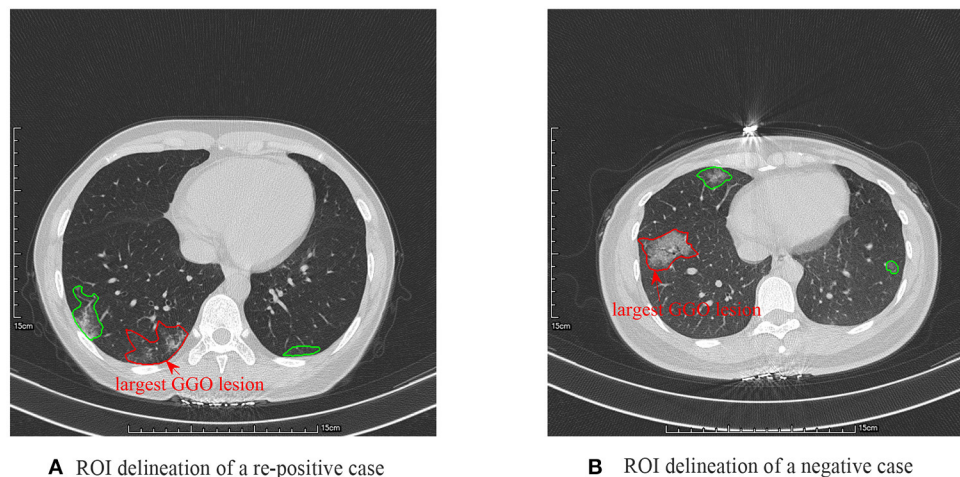
### Image Acquisition

All patients underwent non-enhanced chest CT with a 64-slice spiral CT scanner (SOMATOM Sensation scanner; Siemens Healthineers). The CT scan parameters were as follows: 120 kVp, 150 mA, 1.5 mm collimation, reconstruction matrix of  $512 \times 512$ , slice thickness of 1.0 mm, and high spatial resolution algorithm.

### Region of Interest Definition

Since the scanning thickness and spacing of the CT images were relatively large, the ground-glass opacity (GGO) lesion size changed dramatically between two neighboring image slices. Therefore, to alleviate the effect of slice thickness and spacing on the analysis, we only selected the CT image slice with the largest GGO lesion region for each patient. And then, the largest GGO lesion region of interest (ROI) was delineated by two radiologists in consensus with a custom-developed package, whose thoracic CT interpretation experience was both more than 9 years, as shown in Figure 1. After that, the other smaller lesions on this image slice were also delineated. The ROIs enclosed by the red curve were the largest GGO lesions of the two cases, respectively, and further used for the radiomics feature extraction, whereas the regions marked by the green curve were the other smaller lesions on this slice, which were used for the computation of some important clinical factors, like the location of all the lesions on





**A** ROI delineation of a re-positive case

**B** ROI delineation of a negative case

**FIGURE 1** | Region of interest delineation results of a re-positive case (A) and a negative case (B).

this slice, ratio of all the lesions area in the thoracic cavity on this slice, and the number of all the lesions on this slice.

## Radiomics Feature Extraction

After the GGO ROI definition, the next step was radiomics feature extraction. Two groups of radiomics features, including the morphological features and the texture features, were employed to fully describe the lesions on CT images. A total of eight morphological features were extracted from the lesion ROI, including the *major axis length*, *minor axis length*, *equivalent diameter*, *area*, *eccentricity*, *orientation*, *convex area*, and *solidity*. Five categories of texture features, including the histogram features, the second-order texture features like gray-level co-occurrence matrix (GLCM)-based features, the high-order texture features like gray-level run-length matrix (GLRLM)-based features, neighborhood gray-tone difference matrix (NGTDM)-based features, and the gray-level size zone matrix (GLSZM)-based features, were used to comprehensively illustrate the intensity distribution characteristics of the lesions. From each ROI, eight histogram features were extracted.

Considering that the construction of the GLCM, GLRLM, NGTDM, and GLSZM was closely related to the grayscale of the ROI, which would eventually affect the second- and high-order texture features computation, prior to the extraction of these features, a multi-grayscale standardization strategy was used to normalize the grayscale of each ROI into six grayscales widely used in the previous studies (18–20), including 8, 16, 32, 64, 128, and 256. Therefore, for each normalized grayscale, 39 GLCM-based features, 33 GLRLM-based features, 5 NGTDM-based features (21), and 15 GLSZM-based features (22) were calculated from each ROI, and a total of 552 features of these four categories were finally calculated.

After the radiomics feature extraction, eight morphological features and 560 texture features (8 histogram features and 552 second- and high-order texture features) constituted the entire radiomics feature set for the quantitatively describing

the geometrical appearance and the local, regional, and global intensity distribution characteristics of the lesion ROI. The detailed information of all these radiomics features is organized in **Appendix Table E1** (online).

## Feature Selection

To select the optimal features significantly reflecting the differences between the re-positive and negative cases, a two-step feature selection strategy was employed. First, all the clinical factors and the radiomics features were statistically analyzed using Student's *t*-test to select the features with significant differences ( $p < 0.05$ ) between the re-positive and negative cases. Then, the support vector machine (SVM)-based recursive feature elimination (RFE) algorithm was used for the determination of the optimal features. Detailed description on SVM-RFE has been summarized in Xu et al. (23, 24).

## Development and Validation of the Prediction Model

After feature selection, the prediction models were developed by using the optimal radiomics features, the optimal clinical factors, and both the optimal radiomics and clinical features, and their performance for the discrimination of the re-positive cases was then compared with the quantitative metrics of sensitivity, specificity, accuracy, and the area under the curve (AUC) of receiver operating characteristic. Prior to classification, each feature were normalized to  $[-1, 1]$ . Labels of the re-positive cases were set as “+1,” and that of negative cases were set as “-1.” Grid search method was performed in the model training process to select the optimal parameters for the classifier. Considering such a limited database only containing 50 subjects (24 of them were re-positive cases), randomly dividing the database into training and validation cohorts would induce insufficient training and performance validation. Therefore, a 3-fold cross-validation (CV) strategy was used to fully use each of the dataset for model

**TABLE 1** | Baseline demographics and clinical characteristics of the patients involved in this research.

| Characteristics  | Re-positive cases<br>( <i>n</i> = 24) | Negative cases<br>( <i>n</i> = 26) | <i>p</i> -value |
|--|---------------------------------------|------------------------------------|-----------------|
| <b>Age, years</b>  |                                       |                                    | 0.777           |
| Median (range)   | 47 (30, 79)                           | 47 (27, 68)                        |                 |
| <b>Sex, no. (%)</b>  |                                       |                                    | 0.333           |
| Male   | 17/24 (71%)                           | 15/26 (58%)                        |                 |
| Female   | 7/24 (29%)                            | 11/26 (42%)                        |                 |
| <b>Severity, no. (%)</b>   |                                       |                                    | 0.340           |
| Non-severe cases   | 21/24 (88%)                           | 25/26 (96%)                        |                 |
| Severe cases   | 3/24 (12%)                            | 1/26 (4%)                          |                 |
| <b>Blood routine</b>   |                                       |                                    |                 |
| Leukocytes ( $\times 10^9/L$ , normal range 3.5–9.5)                                     | 5 (2.7, 8.5)                          | 5.1 (2.1, 10.0)                    | 0.813           |
| Neutrophils ( $\times 10^9/L$ , normal range 1.8–6.3)                                    | 3.4 (1.3, 7.6)                        | 3.5 (1.1, 8.2)                     | 0.884           |
| Neutrophil ratio (% , normal range 40–75)  | 66.3 (38.5, 89.0)                     | 67.4 (37.7, 84.6)                  | 0.776           |
| Lymphocytes ( $\times 10^9/L$ , normal range 1.1–3.2)                                    | 1.2 (0.4, 2.3)                        | 1.1 (0.6, 2.0)                     | 0.880           |
| Lymphocyte ratio (% , normal range 20–50)  | 23.5 (7.4, 42.0)                      | 24.4 (10.6, 51.3)                  | 0.716           |
| <b>Lymphocyte classification</b>   |                                       |                                    |                 |
| CD4 <sup>+</sup> T lymphocytes (/μl, normal range 410–1,590)                             | 378 (132–862)                         | 403 (203–767)                      | 0.639           |
| CD8 <sup>+</sup> T lymphocytes (/μl, normal range 190–1,140)                             | 286 (74–621)                          | 269 (129–602)                      | 0.667           |
| CD4 <sup>+</sup> /CD8 <sup>+</sup> T lymphocytes (normal range 0.7–2.87)                 | 1.5 (0.59–3.71)                       | 1.6 (0.54–3.1)                     | 0.834           |
| <b>Location of the largest lesion on the cross-section, no. (%)</b>                      |                                       |                                    |                 |
| Upper left lobe  | 10/24 (42%)                           | 7/26 (27%)                         | 0.272           |
| Lower left lobe  | 15/24 (63%)                           | 15/26 (58%)                        | 0.729           |
| Upper right lobe   | 0/24 (0%)                             | 2/26 (8%)                          | 0.491           |
| Middle right lobe  | 7/24 (29%)                            | 6/26 (23%)                         | 0.435           |
| Lower right lobe   | 16/24 (62%)                           | 20/26 (77%)                        | 0.420           |
| <b>Area ratio of the largest lesion on the cross-section, %</b>                          |                                       |                                    |                 |
| Median (range)   | 4.61 (0.17, 67.40)                    | 6.93 (1.09, 33.67)                 | 0.764           |
| <b>Quantified distribution of all lesions on the same cross-sectional slice, no. (%)</b> |                                       |                                    |                 |
| Median (range)   | 8 (3,8)                               | 10.5 (1,27)                        | 0.779           |
| <b>Area ratio of all lesions on the same cross-sectional slice, %</b>                    |                                       |                                    |                 |
| Median (range)   | 8.47 (0.17, 100)                      | 9.85 (1.58, 63.22)                 | 0.819           |
| <b>Number of all lesions on the same cross-sectional slice, no.</b>                      |                                       |                                    |                 |
| Median (range)   | 2 (1,11)                              | 3 (1,8)                            | 0.638           |
| <b>Slice ID of the largest lesion area among the entire CT data</b>                      |                                       |                                    |                 |
| Median (range)   | 437 (60, 573)                         | 417 (32, 614)                      | 0.973           |

training and validation, and the average results after the 100-round classifications were obtained as the overall performance.

## Ethics Statement

This study was approved by the Medical Ethical Committee of the First Affiliated Hospital of Chongqing Medical University (approval number 20200601). Due to the special reasons of the epidemic, the patients' informed consent was not obtained.

## RESULTS

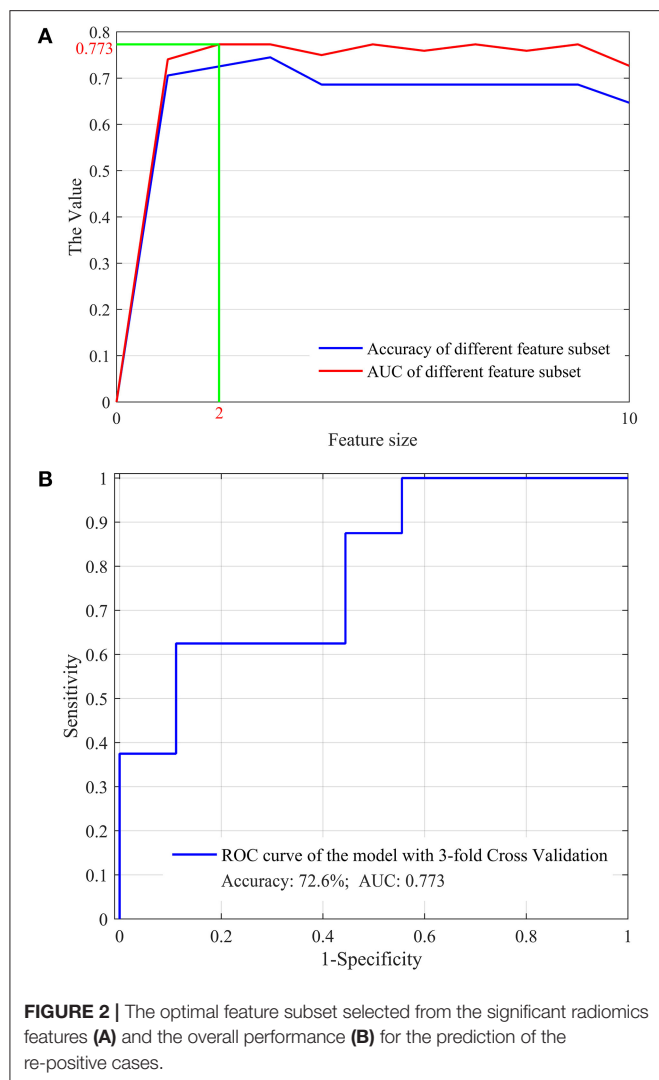
### Clinical Characteristics

Compared with the control group, the re-positive cases had no significant differences in age, gender, severity of disease, leukocytes, neutrophils, neutrophil ratio, lymphocytes, lymphocyte ratio, CD4<sup>+</sup> T lymphocytes, CD8<sup>+</sup> T lymphocytes,

CD4<sup>+</sup>/CD8<sup>+</sup>, location of the largest lesion on the cross-sectional slice of the thoracic cavity, area ratio of the largest lesion on the cross-sectional slice of the thoracic cavity, quantified distribution of all the lesions on this slice, area ratio of all the lesions on this slice, the amount of lesions on this slice, and the ID of this slice among the entire CT data. The strategy we adopted to quantify distribution of all the lesions on the same cross-sectional slice is described in the **Appendix** (online). The demographics and clinical factors of the patients are listed in **Table 1**.

### Results of the Optimal Features Selection

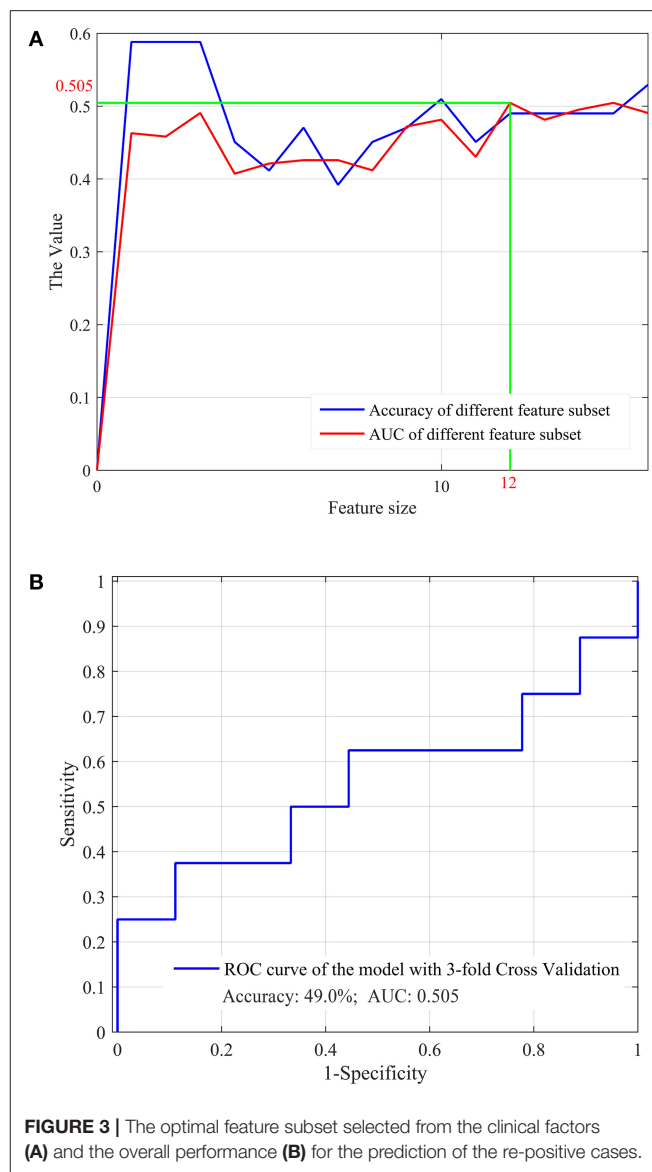
After Student's *t*-test, 62 radiomics features showed significant inter-group differences ( $p < 0.05$ ) between the re-positive cases and the negative cases, including one morphological feature (*eccentricity*), two histogram features (*entropy*, *uniformity*), and 59 of the second- and high-order texture



features. Detailed information of these features is listed in **Appendix Table E2** (online). Of the 17 clinical factors, none of them have shown significant inter-group differences between these two groups.

### Performance of the Optimal Features Selected From the 62 Significant Radiomics Features

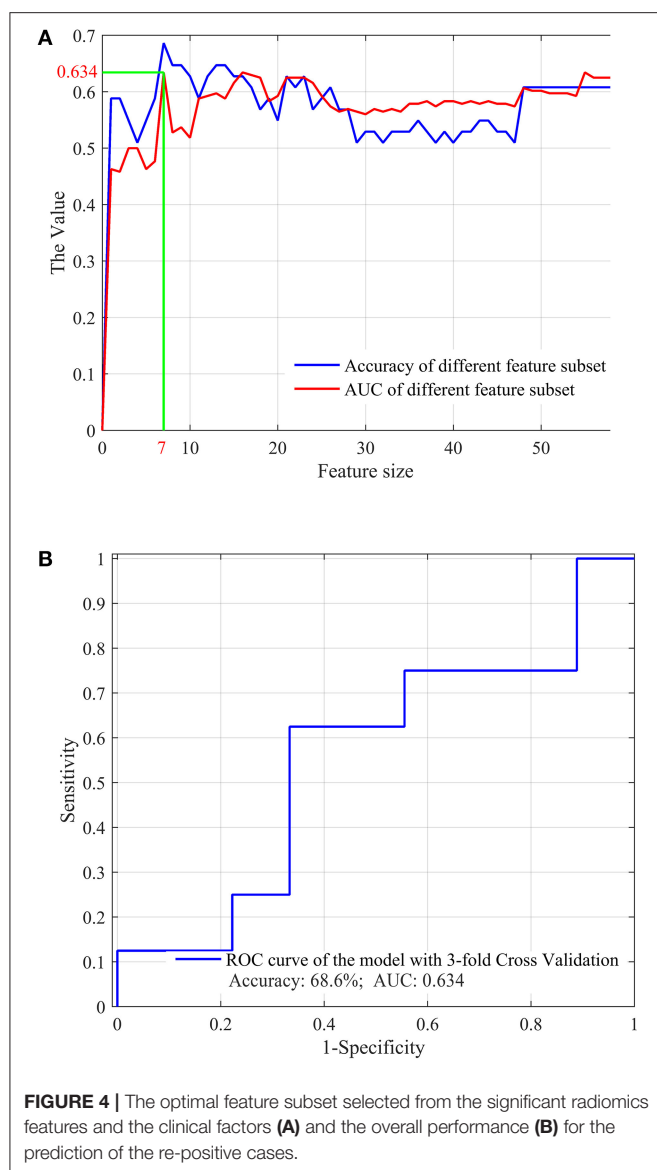
Using the 62 significant radiomics features with SVM-RFE method, we further obtained a more compact feature subset with only two radiomics features determined, which achieved the best performance for the prediction of the re-positive cases, as shown in **Figure 2A**. The two features were GLRLM-11-16GL and GLRLM-11-8GL, which represented the 11th feature of the GLRLM feature category, namely, the long run high gray-level emphasis (LRHGE), extracted from the ROIs with the intensity grayscale normalized to 16 and 8, respectively. The prediction model was then developed using these two features



and an SVM classifier, and its overall performance with 3-fold CV and 100-round classification was fair and acceptable, as shown in **Figure 2B**.

### Performance of the Optimal Features Selected From the 17 Clinical Factors

Although no clinical factor showed significant inter-group differences between the re-positive cases and the negative ones, these factors were still used for the optimal feature selection and prediction model development. The results showed that 12 factors were determined as the optimal factors, as shown in **Figure 3A**, and achieved the best prediction performance, with the accuracy and AUC of 49.0 and 0.505, respectively, as shown in **Figure 3B**.



## Performance of the Optimal Features Selected From the Radiomics Features and the Clinical Factors

We further selected the optimal features from the significant radiomics features and all the clinical factors, aiming to evaluate the performance of combining the radiomics features with the clinical factors for the prediction task. The optimal feature determination process is shown in **Figure 4A**, and the prediction performance using these optimal features and an SVM classifier is shown in **Figure 4B**.

**Table 2** shows the performance comparison of the prediction models developed by using the optimal radiomics features, the optimal clinical factors, and both the optimal radiomics and clinical features, and their performance for the discrimination of the re-positive cases was then compared, which indicates

the superiority of the radiomics features for the re-positive case prediction.

## DISCUSSION

Although previous studies have tried to predict the re-positive RT-PCR test of COVID-19 through clinical features, the predictive effect is not very satisfactory (13). It remains to be determined whether the clinical features are related to the re-positivity of COVID-19 after discharge. Yan et al. reported that older age and the lack of lopinavir/ritonavir treatment were independently associated with prolonged SARS-CoV-2 RNA shedding in patients with COVID-19 (25). In another study, it was also confirmed that the risk of re-positive test after discharge is more than six times higher in persons aged 60 years and above (10), whereas Xiao et al. reported that there is no significant difference in age between re-positive patients and patients in the control group (6). In this study, our data showed that clinical characteristics and laboratory indicators were not effective in predicting the possibility of re-positivity in patients with COVID-19, including age, sex, severity of disease, leukocytes, neutrophils, neutrophil ratio, lymphocytes, lymphocyte ratio, CD4<sup>+</sup> T lymphocytes, CD8<sup>+</sup> T lymphocytes, CD4<sup>+</sup>/CD8<sup>+</sup>, location of the largest lesion on the cross-sectional slice of the thoracic cavity, area ratio of the largest lesion on the cross-sectional slice of the thoracic cavity, quantified distribution of all the lesions on this slice, area ratio of all the lesions on this slice, the amount of lesions on this slice, and the ID of this slice among the entire CT data. This reflects the need to assess not only clinical symptoms but also radiological features and assessing whether a patient can be discharged from hospital.

Currently, the diagnosis, isolation, and discharge mainly depend on RT-PCR of SARS-CoV-2. Ai et al. reported that the sensitivity of chest CT based on positive RT-PCR results in detecting COVID-19 was 97% (26). In addition, chest CT findings can be more early and sensitive than RT-PCR in diagnosis of COVID-19. Fang et al. showed that the sensitivity of chest CT was greater than that of RT-PCR, namely the detection rate of initial chest CT and RT-PCR and reported a higher detection rate for initial CT (98%) than first RT-PCR (71%) patients ( $p < 0.001$ ) (27). In the research of Long et al., CT sensitivity was 97.2%, whereas the sensitivity of RT-PCR was only 83.3% at initial presentation (28). Ducray et al. reported that the accuracy, sensitivity, and specificity of positive chest CT results respectively reached 88.9, 90.2, and 88%, which are relative to the final RT-PCR test (29). Compared with chest CT, there are many factors affecting the detection process of RT-PCR, so it can be easily restricted by false-negative results.

Chest CT may be considered as a primary tool for the detection of COVID-19 because it is readily performed and obtained. Furthermore, CT can also assess the disease severity and differential diagnosis, and monitor the course of COVID-19 to guide clinical management (30, 31). The greatest severity of lung disease on CT is reported about 10 days and chest CT



**TABLE 2 |** Discriminative capability of different nomogram models in MI prediction.

| Prediction model                 | Feature size | Sensitivity (%) | Specificity (%) | Accuracy (%) | AUC   |
|----------------------------------|--------------|-----------------|-----------------|--------------|-------|
| Optimal clinical factors         | 12           | 41.7            | 55.6            | 49.0         | 0.505 |
| <b>Optimal radiomic features</b> | 2            | 70.8            | 74.1            | 72.6         | 0.773 |
| Combined                         | 7            | 58.3            | 77.8            | 68.6         | 0.634 |

signs of improvement began at  $\geq 14$  days after the onset of initial symptoms (32). As the development of artificial intelligence system, which may be a helpful tool for radiologists, it is possible to improve their work efficiency by identifying COVID-19 from other pneumonia with good accuracy and less time (33). Murphy et al. evaluated the performance of an AI system for detecting COVID-19 pneumonia on chest radiographs, and their results showed that the AI system correctly classified chest X-ray images as COVID-19 pneumonia with an AUC of 0.81 (34). Bai et al. established and evaluated an AI system for differentiating COVID-19 and other pneumonia on chest CT, which demonstrated that their model can improve radiologists' performance better than without it (90 vs. 85% accuracy, 88 vs. 79% sensitivity, 91 vs. 88% specificity) (35). In the current study, clinical characteristics were not effective in predicting the possibility of re-positivity in patients with COVID-19, while our models developed by using the optimal radiomics features showed predictive capability with an accuracy of 72.6%. These results have preliminarily shown potential in identifying the re-positive cases among the recovered COVID-19 patients after discharge.

However, the results of this study should be carefully interpreted due to the following limitations. First of all, the sample size of our study is relatively small and single centered, which might cause certain influence on the generalizability of the predictive model for multicenter applications. Second, a retrospective decision might have a potential impact on these findings. While there was no significant intergroup difference of 17 demographic and clinical characteristics between re-positive and negative patients, given such a limited sample set size, the findings in our study might underestimate the predictive capability of the clinical factors for predicting the re-positive cases. However, the baseline data showed no significant intergroup difference that may highlight the importance and reliability of the results predicted by radiomics features. Other limitations including insufficient non-viral pneumonia controls, without timely and sensitive diagnostic feedback criteria for COVID-19 infection, and imaging diagnosis are non-specific to identify COVID-19 from a variety of viral pneumonia. Multicenter data with subtle differences between scans from different countries, institutions, or CT instruments may better support the generalizability of the findings.

## DATA AVAILABILITY STATEMENT

The original contributions presented in the study are included in the article/**Supplementary Material**, further inquiries can be directed to the corresponding author/s.

## ETHICS STATEMENT

The studies involving human participants were reviewed and approved by Medical Ethical Committee of the First Affiliated Hospital of Chongqing Medical University. Written informed consent for participation was not required for this study in accordance with the national legislation and the institutional requirements.

## AUTHOR CONTRIBUTIONS

X-HW and SG made substantial contributions to the study concept and design. X-HW was in charge of the article draft. XX participated in drafting of the article and was in charge of image data analysis. XT, Y-FF, and X-SW participated in dealing with images. ZA, XW, WZ, and LZ collected and confirmed data accuracy and images. JD applied for the ethical approval. XH and SG were the clinical experts. WZ was the radiologist in charge of the treatment of the patients. All authors made substantial revisions to the article.

## FUNDING

This study was supported by: (1) National Natural Science Foundation of China under Grant No. 81901698; (2) Young Eagle Plan of High Ambition Project under grant No. 2020CYJHXXP; (3) Chongqing Education Board "COVID-19's Infection and Prevention" Emergency Scientific Research Project No. KYYJ202006; (4) Chongqing Science and Technology Bureau "COVID-19's Epidemic Emergency Science and Technology Special" the Fourth Batch of Projects No. cstc2020jscx-fyzzX0040; (5) Chongqing Technology Foresight and System Innovation Project No. ctsc2020jsyj-zzysbA0074.

## ACKNOWLEDGMENTS

The authors thank Dr. Longbiao Cui from the Chinese PLA General Hospital for his insightful comments and suggestions.

## REFERENCES

- Lan L, Xu D, Ye G, Xia C, Wang S, Li Y, et al. Positive RT-PCR test results in patients recovered from COVID-19. *JAMA*. (2020) 323:1502–3. doi: 10.1001/jama.2020.2783
- Cao H, Ruan L, Liu J, Liao W. The clinical characteristic of eight patients of COVID-19 with positive RT-PCR test after discharge. *J Med Virol*. (2020) 92:2159–64. doi: 10.1002/jmv.26017
- Cento V, Colagrossi L, Nava A, Lamberti A, Senatore S, Travi G, et al. Persistent positivity and fluctuations of SARS-CoV-2 RNA in clinically-recovered COVID-19 patients. *J Infect*. (2020) 81:e90–2. doi: 10.1016/j.jinf.2020.06.024
- Deng W, Guang TW, Yang M, Li JR, Jiang DP, Li CY, et al. Positive results for patients with COVID-19 discharged from hospital in Chongqing, China. *BMC Infect Dis*. (2020) 20:429. doi: 10.1186/s12879-020-05151-y
- Zou Y, Wang BR, Sun L, Xu S, Kong YG, Shen LJ, et al. The issue of recurrently positive patients who recovered from COVID-19 according to the current discharge criteria: investigation of patients from multiple medical institutions in Wuhan, China. *J Infect Dis*. (2020) 3:jiaa301. doi: 10.1093/infdis/jiaa301
- Xiao AT, Tong YX, Zhang S. False negative of RT-PCR and prolonged nucleic acid conversion in COVID-19: Rather than recurrence. *J Med Virol*. (2020) 92:1755–6. doi: 10.1002/jmv.25855
- Yuan J, Kou S, Liang Y, Zeng J, Pan Y, Liu L. PCR assays turned positive in 25 discharged COVID-19 patients. *Clin Infect Dis*. (2020) 71:2230–2. doi: 10.1093/cid/ciaa398
- Zhou L, Liu K, Liu HG. [Cause analysis and treatment strategies of “recurrence” with novel coronavirus pneumonia (COVID-19) patients after discharge from hospital]. *Zhonghua Jie He He Hu Xi Za Zhi*. (2020) 43:281–4. doi: 10.3760/cma.j.cn112147-20200229-00219
- Cao G, Tang S, Yang D, Shi W, Wang X, Wang H, et al. The potential transmission of SARS-CoV-2 from patients with negative RT-PCR swab tests to others: two related clusters of COVID-19 outbreak. *Jpn J Infect Dis*. (2020) 73:399–403. doi: 10.7883/yoken.JJID.2020.165
- Wong J, Koh WC, Momin RN, Alikhan MF, Fadillah N, Naing L. Probable causes and risk factors for positive SARS-CoV-2 test in recovered patients: evidence from brunei darussalam. *J Med Virol*. (2020) 92:26199. doi: 10.1002/jmv.26199
- Ling Y, Xu SB, Lin YX, Tian D, Zhu ZQ, Dai FH, et al. Persistence and clearance of viral RNA in 2019 novel coronavirus disease rehabilitation patients. *Chin Med J*. (2020) 133:1039–43. doi: 10.1097/CM9.0000000000000774
- Wu F, Zhang W, Zhang L, Wang D, Wan Y. Discontinuation of antiviral drugs may be the reason for recovered COVID-19 patients testing positive again. *Br J Hosp Med*. (2020) 81:1–2. doi: 10.12968/hmed.2020.0156
- Li C, Luo F, Xie L, Gao Y, Zhang N, Wu B. Chest CT study of fifteen COVID-19 patients with positive RT-PCR retest results after discharge. *Quant Imaging Med Surg*. (2020) 10:1318–24. doi: 10.21037/qims-20-530
- Albahri OS, Zaidan AA, Albahri AS, Zaidan BB, Abdulkareem KH, Al-Qaysi ZT, et al. Systematic review of artificial intelligence techniques in the detection and classification of COVID-19 medical images in terms of evaluation and benchmarking: Taxonomy analysis, challenges, future solutions and methodological aspects. *J Infect Public Health*. (2020) 13:1381–96. doi: 10.1016/j.jiph.2020.06.028
- Alimadadi A, Aryal S, Manandhar I, Munroe PB, Joe B, Cheng X. Artificial intelligence and machine learning to fight COVID-19. *Physiol Genomics*. (2020) 52:200–2. doi: 10.1152/physiolgenomics.00029.2020
- Shi F, Wang J, Shi J, Wu Z, Wang Q, Tang Z, et al. Review of artificial intelligence techniques in imaging data acquisition, segmentation and diagnosis for COVID-19. *IEEE Rev Biomed Eng*. (2020) 14:4–15. doi: 10.1109/RBME.2020.2987975
- Metlay JP, Waterer GW, Long AC, Anzueto A, Brozek J, Crothers K, et al. Diagnosis and treatment of adults with community-acquired pneumonia. An official clinical practice guideline of the american thoracic society and infectious diseases society of america. *Am J Respir Crit Care Med*. (2019) 200:e45–67. doi: 10.1164/rccm.201908-1581ST
- Li Q, Bai H, Chen Y, Sun Q, Liu L, Zhou S, et al. A fully-automatic multiparametric radiomics model: towards reproducible and prognostic imaging signature for prediction of overall survival in glioblastoma multiforme. *Sci Rep*. (2017) 7:14331. doi: 10.1038/s41598-017-14753-7
- Xu X, Liu Y, Zhang X, Tian Q, Wu Y, Zhang G, et al. Preoperative prediction of muscular invasiveness of bladder cancer with radiomic features on conventional MRI and its high-order derivative maps. *Abdom Radiol*. (2017) 42:1896–905. doi: 10.1007/s00261-017-1079-6
- Zhang X, Xu X, Tian Q, Li B, Wu Y, Yang Z, et al. Radiomics assessment of bladder cancer grade using texture features from diffusion-weighted imaging. *J Magn Reson Imaging*. (2017) 46:1281–1288. doi: 10.1002/jmri.25669
- Amadasun M, King R. Textural features corresponding to textural properties. *IEEE Transact Syst Man Cybernetics*. (1989) 19:1264–74. doi: 10.1109/21.44046
- Thibault G, Angulo J, Meyer F. Advanced statistical matrices for texture characterization: application to cell classification. *IEEE Transact Biomed Eng*. (2014) 61:630–7. doi: 10.1109/TBME.2013.2284600
- Xu X, Wang H, Du P, Zhang F, Li S, Zhang Z, et al. A predictive nomogram for individualized recurrence stratification of bladder cancer using multiparametric MRI and clinical risk factors. *J Magnet Resonance Imag*. (2019) 50:1893–904. doi: 10.1002/jmri.26749
- Xu X, Zhang X, Tian Q, Wang H, Cui L, B., et al. Quantitative identification of nonmuscle-invasive and muscle-invasive bladder carcinomas: a multiparametric MRI radiomics analysis. *J Magn Reson Imaging*. (2019) 49:1489–98. doi: 10.1002/jmri.26327
- Yan D, Liu XY, Zhu YN, Huang L, Dan BT, Zhang GJ, et al. Factors associated with prolonged viral shedding and impact of lopinavir/ritonavir treatment in hospitalised non-critically ill patients with SARS-CoV-2 infection. *Eur Respir J*. (2020) 56:799. doi: 10.1183/13993003.00799-2020
- Ai T, Yang Z, Hou H, Zhan C, Chen C, Lv W, et al. Correlation of chest CT and RT-PCR testing for coronavirus disease 2019 (COVID-19) in China: A report of 1014 cases. *Radiology*. (2020) 296:E32–40. doi: 10.1148/radiol.2020200642
- Fang Y, Zhang H, Xie J, Lin M, Ying L, Pang P, et al. Sensitivity of Chest CT for COVID-19: comparison to RT-PCR. *Radiology*. (2020) 296:E115–7. doi: 10.1148/radiol.2020200432
- Long C, Xu H, Shen Q, Zhang X, Fan B, Wang C, et al. Diagnosis of the coronavirus disease (COVID-19): rRT-PCR or CT? *Euro J Radiol*. (2020) 126:108961. doi: 10.1016/j.ejrad.2020.108961
- Ducray V, Vlachomitrou AS, Bouscambert-Duchamp M, Si-Mohamed S, Goutard S, Mansuy A, et al. Chest CT for rapid triage of patients in multiple emergency departments during COVID-19 epidemic: experience report from a large French university hospital. *Eur Radiol*. (2020) 31:795–803. doi: 10.1007/s00330-020-07154-4
- Dai WC, Zhang HW, Yu J, Xu HJ, Chen H, Luo SP, et al. CT imaging and differential diagnosis of COVID-19. *Canad Assoc Radiol J*. (2020) 71:195–200. doi: 10.1177/0846537120913033

## SUPPLEMENTARY MATERIAL

The Supplementary Material for this article can be found online at: <https://www.frontiersin.org/articles/10.3389/fmed.2021.730441/full#supplementary-material>

31. Zu ZY, Jiang MD, Xu PP, Chen W, Ni QQ, Lu GM, et al. Coronavirus disease 2019 (COVID-19): a perspective from China. *Radiology*. (2020) 296:E15–25. doi: 10.1148/radiol.202000490
32. Pan F, Ye T, Sun P, Gui S, Liang B, Li L, et al. Time course of lung changes at chest CT during recovery from coronavirus disease 2019 (COVID-19). *Radiology*. (2020) 295:715–721. doi: 10.1148/radiol.202000370
33. Li L, Qin L, Xu Z, Yin Y, Wang X, Kong B, et al. Using artificial intelligence to detect COVID-19 and community-acquired pneumonia based on pulmonary CT: evaluation of the diagnostic accuracy. *Radiology*. (2020) 296:E65–71. doi: 10.1148/radiol.202000905
34. Murphy K, Smits H, Knoop AJG, Korst M, Samson T, Scholten ET, et al. COVID-19 on chest radiographs: a multireader evaluation of an artificial intelligence system. *Radiology*. (2020) 296:E166–72. doi: 10.1148/radiol.202001874
35. Bai HX, Wang R, Xiong Z, Hsieh B, Chang K, Halsey K, et al. Artificial intelligence augmentation of radiologist performance in distinguishing COVID-19 from pneumonia of other origin at chest CT. *Radiology*. (2020) 296:E156–65. doi: 10.1148/radiol.202001491

**Conflict of Interest:** The authors declare that the research was conducted in the absence of any commercial or financial relationships that could be construed as a potential conflict of interest.

**Publisher's Note:** All claims expressed in this article are solely those of the authors and do not necessarily represent those of their affiliated organizations, or those of the publisher, the editors and the reviewers. Any product that may be evaluated in this article, or claim that may be made by its manufacturer, is not guaranteed or endorsed by the publisher.

Copyright © 2021 Wang, Xu, Ao, Duan, Han, Tang, Fu, Wu, Wang, Zhu, Zeng and Guo. This is an open-access article distributed under the terms of the Creative Commons Attribution License (CC BY). The use, distribution or reproduction in other forums is permitted, provided the original author(s) and the copyright owner(s) are credited and that the original publication in this journal is cited, in accordance with accepted academic practice. No use, distribution or reproduction is permitted which does not comply with these terms.



# The Similarities and Distances of Growth Rates Related to COVID-19 Between Different Countries Based on Spectral Analysis

Ray-Ming Chen\*

School of Mathematics and Statistics, Baise University, Baise, China

## OPEN ACCESS

### Edited by:

Reza Lashgari,  
Shahid Beheshti University, Iran

### Reviewed by:

Sohrab Najafian,  
SUNY College of Optometry,  
United States  
Mehdi Yousefzadeh,  
Institute for Research in Fundamental  
Sciences (IPM), Iran

### \*Correspondence:

Ray-Ming Chen  
raymingchen@bsuc.cn

### Specialty section:

This article was submitted to  
Infectious Diseases – Surveillance,  
Prevention and Treatment,  
a section of the journal  
Frontiers in Public Health

**Received:** 12 May 2021

**Accepted:** 16 July 2021

**Published:** 23 September 2021

### Citation:

Chen R-M (2021) The Similarities and  
Distances of Growth Rates Related to  
COVID-19 Between Different  
Countries Based on Spectral Analysis.  
Front. Public Health 9:695141.  
doi: 10.3389/fpubh.2021.695141

The COVID-19 pandemic has taken more than 1.78 million of lives across the globe. Identifying the underlying evolutive patterns between different countries would help us single out the mutated paths and behavior of this virus. I devise an orthonormal basis which would serve as the features to relate the evolution of one country's cases and deaths to others another's via coefficients from the inner product. Then I rank the coefficients measured by the inner product via the featured frequencies. The distances between these ranked vectors are evaluated by Manhattan metric. Afterwards, I associate each country with its nearest neighbor which shares the evolutive pattern via the distance matrix. Our research shows such patterns is are not random at all, i.e., the underlying pattern could be contributed to by some factors. In the end, I perform the typical cosine similarity on the time-series data. The comparison shows our mechanism differs from the typical one, but is also related to each it in some way. These findings reveal the underlying interaction between countries with respect to cases and deaths of COVID-19.

**Keywords:** growth rate, COVID-19, Manhattan metric, similarity measures, spectral analysis

## 1. INTRODUCTION

COVID-19 is in full, the COVID-19 pandemic is still ongoing and is spreading across all the continents (1, 2). The spread of this pandemic is has been studied by many researchers (3–6). There are many ways to look into the behaviors of the viruses or the pandemic itself (7, 8) for the sake of efficacy of travel bans or vaccines (9). Some researches have even have established the relations between cases and deaths of COVID-19 from demographic, economic, and social perspectives (10). In this article, I devise an orthonormal basis (11)  $\mathbb{B}_N$  which is motivated by Fourier analysis (12) and could thus take the underlying frequencies of data into consideration. I utilize the COVID-19 database (13) which records the weekly COVID-19 cases and deaths from Week 15 to 51 (37 weeks in total). By filtering out some non-essential data (countries), I obtain 90 countries as our research targets. By calculating the 36 (the number of intervals from Week 15 to 51) growth rates of the cases and deaths for the 90 countries, I have an input vector. By transforming this vector into a set of coefficients, which is the results of inner product via  $\mathbb{B}_{36}$ , I start to rank the coefficients by positive integers; from 1 to 36. The ranks indicate the strength (relation) between the input vector and the underlying frequencies. A larger coefficient will be assigned a larger positive integer. By doing so, I have a  $90 \times 36$  coefficient matrix, where 90 is the number of the sampled countries and 36 is the number of frequencies (or the length of the input vector). Then, I use Manhattan



metric (14) to measure the distances between all the ranked vectors and yield a  $90 \times 90$  distance matrix. Afterwards, I associate each country with its nearest neighbor via the minimal distance in the distance matrix. In the end, I rerun our data with another typical approach: cosine similarity, which could be calculated either from the original time-series data or the transformed frequency coefficients, i.e., both would produce the identical results by the property of an inner product. The interaction between these two approaches are also revealed via Jaccard Index (15). Our research shows that the patterned evolutive correlation between counties not random, i.e., there are some fundamental factors that contribute to such relation. The research also reveals that the correlated patterns for cases and deaths between countries bears no similarity at all. This also indicates that there is a strong discrepancy between evolution of cases and the one of deaths.

## 2. METHODOLOGY AND PROCEDURES

I devise a class of orthogonal bases, which are serve as our feature extractors. Then a complete set of procedures are is also described in this section.

### 2.1. Orthogonal Basis

Motivated by the Fourier series and Fourier transform, I devise an orthonormal basis which is easier and much more intuitive to adopt and interpret the analysis of, since it involves only the real numbers—not the complex numbers, which normally are harder to use to interpret the analyzed results.

Let  $\mathbb{N}$  denote the set of positive integers. Suppose  $\vec{v}$  is a vector whose elements are all non-negative integers.  $\vec{v}_i$  is used to denote its  $i$ 'th element in the vector and  $|\vec{v}|$  is used to denote its length. Let us assume  $|\vec{v}| = N + 1$ , where  $N$  stands for a natural number in this article. I use  $\Delta\vec{v}$  to denote its growth vector, i.e.,  $\Delta\vec{v} = (\frac{\vec{v}_2 - \vec{v}_1}{\vec{v}_1}, \frac{\vec{v}_3 - \vec{v}_2}{\vec{v}_2}, \dots, \frac{\vec{v}_{N+1} - \vec{v}_N}{\vec{v}_N})$ . Observe that  $|\Delta\vec{v}| = N$ . This growth vector is our main research target, since I study the (weekly) growth rates of cases and deaths regarding COVID-19. Later on, I would tweak the definition of growth vector slightly to fit our analytical purpose. For any two vectors  $\vec{v}$  and  $\vec{w}$ , I use  $\langle \vec{v}, \vec{w} \rangle$  to denote their inner product. Define real functions  $I(x) = \sqrt{\frac{1}{N}}$  and  $b_m(x) := \sqrt{\frac{2}{N}} \cdot \cos[(\frac{2\pi}{N} \cdot m) \cdot x]$  and  $\tilde{b}_m(x) := \sqrt{\frac{2}{N}} \cdot \sin[(\frac{2\pi}{N} \cdot m) \cdot x]$ , where  $x \in \{1, 2, \dots, N\}$ . Define

$$\mathbb{B}_N := \begin{cases} \{I, b_1, \tilde{b}_1, b_2, \tilde{b}_2, \dots, b_m, \tilde{b}_m, \dots, b_{\frac{N}{2}-1}, \tilde{b}_{\frac{N}{2}-1}, \sqrt{\frac{1}{2}} \cdot b_{\frac{N}{2}}\} & , \text{ if } N \text{ is even;} \\ \{I, b_1, \tilde{b}_1, b_2, \tilde{b}_2, \dots, b_m, \tilde{b}_m, \dots, b_{\frac{N-1}{2}}, \tilde{b}_{\frac{N-1}{2}}\} & , \text{ if } N \text{ is odd.} \end{cases}$$

By some manipulation of mathematical operations,  $\mathbb{B}_N$  is provend to be an orthogonal basis for all natural number  $N$ .

### 2.2. Procedures

In this section, I describe a procedure to analyze (in the form of a matrix)  $M \times (N + 1)$  time-series data, where  $M$  is the number of the sets and  $N + 1$ , which is the number of points of time. The purpose for adding 1 is to simplify our further analysis which utilizes its difference (or  $N$  intervals). The whole analytical steps go as follows:

1. Specify the  $M$  researched subjects (for example, countries) and  $N + 1$  points of times (for example, weeks). Then collect the sets of time-series data which could then be represented by  $\{\vec{v}^1, \vec{v}^2, \dots, \vec{v}^M\}$ , where each  $|\vec{v}^k| = N + 1$ .
2. Calculate the growth vector for growth rate of each  $\vec{v}^k$  by  $\Delta\vec{v}_i^k = \frac{\vec{v}_{i+1}^k - \vec{v}_i^k}{1 + \vec{v}_i^k}$ , where  $1 \leq i \leq N$  for all  $k \in \{1, 2, \dots, M\}$ . Here (for our analytical purpose) the denominator is deliberately added by 1 to avoid the divisor being 0.

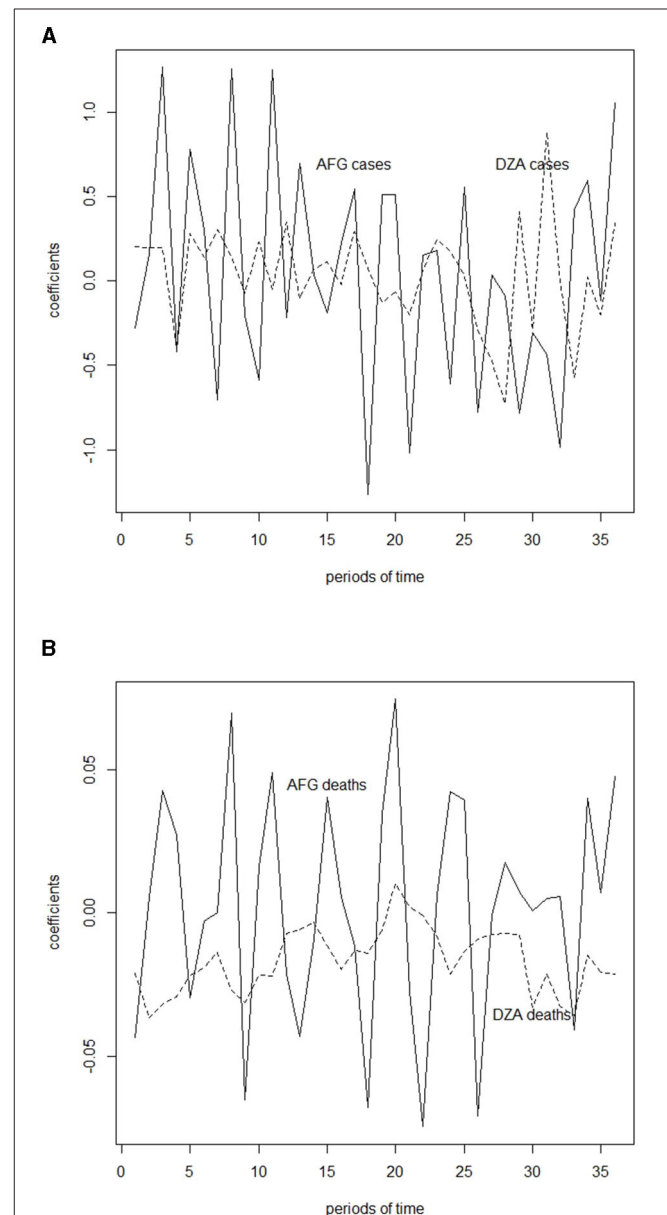


**FIGURE 1** | Inner product of case and death growth rates and featured frequencies, which is calculated in **Table 1** for Afghanistan (AFG) and Algeria (DZA). **(A)** Inner product of case growth rates and featured frequencies for Afghanistan (AFG) and Algeria (DZA). **(B)** Inner product of death growth rates and featured frequencies for Afghanistan (AFG) and Algeria (DZA).

**TABLE 1** | Numbers representing sampled countries.

| 1   | 2   | 3   | 4   | 5   | 6   | 7   | 8   | 9   | 10  |
|-----|-----|-----|-----|-----|-----|-----|-----|-----|-----|
| AFG | DZA | AGO | ARG | AUS | AZE | BGD | BEL | BEN | BOL |
| 11  | 12  | 13  | 14  | 15  | 16  | 17  | 18  | 19  | 20  |
| BRA | BFA | BDI | KHM | CMR | CAN | TCD | CHL | CHN | COL |
| 21  | 22  | 23  | 24  | 25  | 26  | 27  | 28  | 29  | 30  |
| CIV | CUB | CZE | COD | DOM | ECU | EGY | ETH | FRA | DEU |
| 31  | 32  | 33  | 34  | 35  | 36  | 37  | 38  | 39  | 40  |
| GHA | GRC | GTM | GIN | HTI | IND | IDN | IRN | IRQ | ITA |
| 41  | 42  | 43  | 44  | 45  | 46  | 47  | 48  | 49  | 50  |
| JPN | JOR | KAZ | KEN | MDG | MWI | MYS | MLI | MEX | MAR |
| 51  | 52  | 53  | 54  | 55  | 56  | 57  | 58  | 59  | 60  |
| MOZ | MMR | NPL | NLD | NER | NGA | PAK | PER | PHL | POL |
| 61  | 62  | 63  | 64  | 65  | 66  | 67  | 68  | 69  | 70  |
| PRT | ROU | RUS | RWA | SAU | SEN | SOM | ZAF | KOR | SSD |
| 71  | 72  | 73  | 74  | 75  | 76  | 77  | 78  | 79  | 80  |
| ESP | LKA | SDN | SWE | SYR | CNG | THA | TUN | TUR | UGA |
| 81  | 82  | 83  | 84  | 85  | 86  | 87  | 88  | 89  | 90  |
| UKR | GBR | TZA | USA | UZB | VEN | VNM | YEM | ZMB | ZWE |

3. Calculate the inner products or coefficient vector for each growth vector  $\Delta \vec{v}^k$  by  $\langle \Delta \vec{v}^k, \vec{b} \rangle$ , where  $\vec{b} \in \mathbb{B}_N$  for all  $k \in \{1, 2, \dots, M\}$ . Let  $\mathbb{B}_N(\Delta \vec{v}^k)$  denote the corresponding coefficient vector. These coefficients serve as the extracted features of the growth rates, as shown in **Figure 1**.
4. Rank  $\mathbb{B}_N(\Delta \vec{v}^k)$  via positive numbers in which the higher the value is among  $\mathbb{B}_N(\Delta \vec{v}^k)$ , the higher the positive integer assigned. Let us call this ranked vector  $R\mathbb{B}_N(\Delta \vec{v}^k)$ .
5. Calculate the distances between all the ranked vectors via Manhattan metric  $d$  among all the  $M$  subjects that would result in a distance matrix  $[d(R\mathbb{B}_N(\Delta \vec{v}^k), R\mathbb{B}_N(\Delta \vec{v}^h))]_{k,h=1}^M$ .
6. Find the minimal pairs (or nearest neighbors) for all the subjects with least distance via the above distance matrix.

### 3. RESULTS

In correspondence to section 2, I embark on data analysis and produce the results in this section. I download the historical weekly data (up to Week 51, 2020) of the reported COVID-19 cases and deaths worldwide. In order to avoid biased sampling, I filter the data according to the following criteria:

1. Among all the countries, only the populations with of more than 10 millions are included;
2. Only data from Week 15 to 51, Year 2020 are taken as samples.

First of all, the global weekly data regarding COVID-19 are read from its source file (13) and stored in a matrix  $DT$  whose size is 9,152 by 10. After filtering out the non-essential samples by the above criteria, I obtain 90 countries (with abbreviated country codes and corresponding labels) as shown in **Table 1**—each of which contains 37 weekly data (from Week 15 to 51). Furthermore, each country is represented by a 37 by 2 matrix, where 2 indicates the two columns chosen (cases weekly and

**TABLE 2** | Weekly (from Week 15 to 51) COVID-19 cases (c) and deaths (d) for Afghanistan, which is indicated by 1, and Algeria, which is indicated by 2.

| Week | 1c    | 2c    | 1d  | 2d  | Week | 1c    | 2c    | 1d  | 2d  |
|------|-------|-------|-----|-----|------|-------|-------|-----|-----|
| 15   | 308   | 594   | 11  | 141 | 34   | 403   | 2,877 | 12  | 65  |
| 16   | 389   | 715   | 15  | 82  | 35   | 163   | 2,686 | 15  | 66  |
| 17   | 535   | 753   | 24  | 50  | 36   | 236   | 2,218 | 10  | 55  |
| 18   | 1,173 | 1,092 | 28  | 38  | 37   | 318   | 1,890 | 8   | 56  |
| 19   | 1,698 | 1,249 | 35  | 39  | 38   | 328   | 1,572 | 21  | 60  |
| 20   | 2,262 | 1,296 | 49  | 46  | 39   | 183   | 1,241 | 12  | 42  |
| 21   | 3,918 | 1,287 | 49  | 52  | 40   | 114   | 1,069 | 9   | 46  |
| 22   | 4,623 | 1,088 | 39  | 53  | 41   | 458   | 936   | 15  | 41  |
| 23   | 5,137 | 760   | 100 | 54  | 42   | 401   | 1,330 | 15  | 55  |
| 24   | 4,424 | 765   | 114 | 60  | 43   | 633   | 1,741 | 22  | 58  |
| 25   | 4,067 | 852   | 110 | 78  | 44   | 800   | 2,129 | 27  | 59  |
| 26   | 2,134 | 1,502 | 140 | 52  | 45   | 606   | 3,779 | 24  | 75  |
| 27   | 1,984 | 2,668 | 143 | 55  | 46   | 1,164 | 5,628 | 61  | 106 |
| 28   | 1,500 | 3,254 | 146 | 59  | 47   | 1,368 | 7,183 | 69  | 121 |
| 29   | 1,024 | 3,889 | 171 | 67  | 48   | 1,073 | 7,359 | 68  | 135 |
| 30   | 788   | 4,273 | 88  | 77  | 49   | 1,672 | 6,031 | 137 | 106 |
| 31   | 447   | 4,108 | 15  | 76  | 50   | 1,757 | 3,850 | 71  | 80  |
| 32   | 344   | 3,749 | 28  | 71  | 51   | 740   | 3,101 | 111 | 70  |
| 33   | 542   | 3,369 | 63  | 68  |      |       |       |     |     |

deaths weekly) out of the original ten columns. An example of such matrices for Country AFG and DZA are listed in **Table 2**. Data for other countries are omitted here for limited space. In the table, “1c” denotes the cases of COVID-19 in AFG; “2c” denotes the cases of COVID-19 in DZA; “1d” denotes the deaths of COVID-19 in AFG and “2d” denotes the deaths of COVID-19 in DZA. Based on this table, I start to calculate the weekly growth rates for cases and deaths by the formula

$$\Delta_n = \frac{Week(n+1) - Week(n)}{1 + Week(n)},$$

where  $Week(n)$  denotes the growth rates for cases or deaths at Week  $n$ . Observe that 1 is added to the denominator to avoid the infinite growth rate. An example of cases and deaths regarding the growth rates for AFG and DZA are presented in **Table 3**.

Based on this table and the featured frequencies (vectors), i.e., orthonormal basis  $\mathbb{B}_N$  (or  $\mathbb{B}_{36}$  in our case), one could then calculate (an example for AFG and DZA) their coefficients (or inner product) as shown in **Table 4**, in which the meaning of  $b_j$  is explained in section 2.1.

Now I rank the coefficients. A higher positive integer is assigned, if a coefficient is higher. The assignment for each country (here I present only AFG and DZA) is shown in **Table 5**. The distances of ranked vectors between different countries could then be calculated by Manhattan metric. The results are shown in **Table 6**. Based on these distance matrices, one could associate each country with its nearest neighbor(s) with respect to cases and deaths. The results are presented in **Table 7**. In the table, “Cty” stands for Country. Since the death rate

**TABLE 3 |** Weekly growth rates of cases and deaths for COVID-19 from Week 15 to 50 for Afghanistan (AFG) and Algeria (DZA).

| Week                          | 15     | 16     | 17     | 18     | 19     | 20     |
|-------------------------------|--------|--------|--------|--------|--------|--------|
| Weekly growth rate: AFG case  | 0.262  | 0.374  | 1.19   | 0.447  | 0.332  | 0.732  |
| Weekly growth rate: DZA case  | 0.203  | 0.053  | 0.45   | 0.144  | 0.038  | −0.007 |
| Weekly growth rate: AFG death | 0.013  | 0.023  | 0.007  | 0.006  | 0.008  | 0      |
| Weekly growth rate: DZA death | −0.099 | −0.045 | −0.016 | 0.001  | 0.006  | 0.005  |
| <b>Week</b>                   | 21     | 22     | 23     | 24     | 25     | 26     |
| Weekly growth rate: AFG case  | 0.18   | 0.111  | −0.139 | −0.081 | −0.475 | −0.07  |
| Weekly growth rate: DZA case  | −0.155 | −0.301 | 0.007  | 0.114  | 0.762  | 0.776  |
| Weekly growth rate: AFG death | −0.003 | 0.013  | 0.003  | −0.001 | 0.007  | 0.001  |
| Weekly growth rate: DZA death | 0.001  | 0.001  | 0.008  | 0.023  | −0.03  | 0.002  |
| <b>Week</b>                   | 27     | 28     | 29     | 30     | 31     | 32     |
| Weekly growth rate: AFG case  | −0.244 | −0.317 | −0.23  | −0.432 | −0.23  | 0.574  |
| Weekly growth rate: DZA case  | 0.22   | 0.195  | 0.099  | −0.039 | −0.087 | −0.101 |
| Weekly growth rate: AFG death | 0.002  | 0.017  | −0.081 | −0.093 | 0.029  | 0.101  |
| Weekly growth rate: DZA death | 0.001  | 0.002  | 0.003  | 0      | −0.001 | −0.001 |
| <b>Week</b>                   | 33     | 34     | 35     | 36     | 37     | 38     |
| Weekly growth rate: AFG case  | −0.256 | −0.594 | 0.445  | 0.346  | 0.031  | −0.441 |
| Weekly growth rate: DZA case  | −0.146 | −0.066 | −0.174 | −0.148 | −0.168 | −0.21  |
| Weekly growth rate: AFG death | −0.094 | 0.007  | −0.030 | −0.008 | 0.041  | −0.027 |
| Weekly growth rate: DZA death | −0.001 | 0      | −0.004 | 0      | 0.002  | −0.011 |
| <b>Week</b>                   | 39     | 40     | 41     | 42     | 43     | 44     |
| Weekly growth rate: AFG case  | −0.375 | 2.991  | −0.124 | 0.577  | 0.263  | −0.242 |
| Weekly growth rate: DZA case  | −0.138 | −0.124 | 0.42   | 0.309  | 0.223  | 0.775  |
| Weekly growth rate: AFG death | −0.016 | 0.052  | 0      | 0.017  | 0.008  | −0.004 |
| Weekly growth rate: DZA death | 0.003  | −0.005 | 0.015  | 0.002  | 0.001  | 0.008  |
| <b>Week</b>                   | 45     | 46     | 47     | 48     | 49     | 50     |
| weekly growth rate: AFG case  | 0.919  | 0.175  | −0.215 | 0.558  | 0.051  | −0.578 |
| weekly growth rate: DZA case  | 0.489  | 0.276  | 0.024  | −0.18  | −0.362 | −0.194 |
| weekly growth rate: AFG death | 0.061  | 0.007  | −0.001 | 0.064  | −0.039 | 0.023  |
| weekly growth rate: DZA death | 0.008  | 0.003  | 0.002  | −0.004 | −0.004 | −0.003 |

for Country 14 is 0, the associated values are ignored when it is involved. Some countries might associate with more than one country.

## 4. DISCUSSION

### 4.1. Comparison

Here I utilize another typical approach, namely: cosine similarity, to compare our method with others. Though the cosine similarity is highly frequently used in many fields, it focuses less on the some internal structures. For example, if  $\vec{p} = (5, 4)$ ,  $\vec{q} = (-4, 5)$ ,  $\vec{r} = (1, -\frac{5}{4})$ . Then  $\cos(\vec{p}, \vec{q}) = \cos(\vec{p}, \vec{r}) = 0$ . But, with our ranked Manhattan metric (or  $d$ )  $d(\vec{p}, \vec{q}) = 2$  and  $d(\vec{p}, \vec{r}) = 0$ . Moreover, when the coefficients are ranked, they tend to reduce the noise of the data—in particular, the cases and deaths are affected by many factors. The results of the cosine similarities for the 90 countries (except the for country 14, which is ignored for the part of deaths, due to its death cases are being zero). The results are presented in **Table 8**. Again, by linking each country to its neighbor which has the maximal cosine similarities, one has **Table 9**.

### 4.2. Optimal Pairings

In this section, I list and compare the optimal minimal and maximal pairs from **Tables 7, 9**. The results are shown in **Table 10**. I could apply Jaccard Index  $J(A, B) = \frac{|A \cap B|}{|A \cup B|}$  to analyze their relation, where  $A, B$  are sets.

## 5. CONCLUSION AND FUTURE WORK

Based on our devised orthonormal basis, which is motivated by Fourier analysis, I perform spectral analysis on 90 representative 90 countries. The main purpose for such an analysis is to identify the patterns of evolution of COVID-19 across the globe. To this end, the coefficients which measure the relation between the growth rate of COVID-19 country and the given features in the spectrum are utilized. Then I rank the coefficients to reveal their internal structures and then apply the Manhattan metric to compute the distances between countries. This constructed distance matrix would reveal the relations between the countries regarding the evolution of COVID-19 cases and deaths. In addition, I also identify the nearest neighbor with respect to minimal distance via the

**TABLE 4 |** Coefficients, or inner product, for 36 frequencies (or features) with respect to weekly growth rates of cases and deaths for Afghanistan (AFG) and Algeria (DZA).

| Frequency  | $b_0$            | $b_1$    | $\tilde{b}_1$    | $b_2$    | $\tilde{b}_2$    | $b_3$    |
|------------|------------------|----------|------------------|----------|------------------|----------|
| AFG cases  | -0.276           | 0.162    | 1.269            | -0.422   | 0.782            | 0.306    |
| DZA cases  | 0.205            | 0.198    | 0.2              | -0.4     | 0.285            | 0.144    |
| AFG deaths | -0.043           | 0.006    | 0.043            | 0.027    | -0.03            | -0.003   |
| DZA deaths | -0.021           | -0.036   | -0.032           | -0.029   | -0.022           | -0.019   |
| Frequency  | $\tilde{b}_3$    | $b_4$    | $\tilde{b}_4$    | $b_5$    | $\tilde{b}_5$    | $b_6$    |
| AFG cases  | -0.707           | 1.259    | -0.204           | -0.588   | 1.255            | -0.217   |
| DZA cases  | 0.304            | 0.144    | -0.07            | 0.234    | -0.047           | 0.35     |
| AFG deaths | 0                | 0.07     | -0.065           | 0.016    | 0.049            | -0.021   |
| DZA deaths | -0.014           | -0.027   | -0.031           | -0.021   | -0.022           | -0.007   |
| Frequency  | $\tilde{b}_6$    | $b_7$    | $\tilde{b}_7$    | $b_8$    | $\tilde{b}_8$    | $b_9$    |
| AFG cases  | -0.438           | -0.983   | 0.422            | 0.598    | -0.116           | 1.057    |
| DZA cases  | 0.882            | -0.003   | -0.568           | 0.027    | -0.2             | 0.346    |
| AFG deaths | 0.005            | 0.006    | -0.041           | 0.04     | 0.007            | 0.048    |
| DZA deaths | -0.021           | -0.032   | -0.036           | -0.015   | -0.021           | -0.021   |
| Frequency  | $\tilde{b}_9$    | $b_{10}$ | $\tilde{b}_{10}$ | $b_{11}$ | $\tilde{b}_{11}$ | $b_{12}$ |
| AFG cases  | 0.696            | 0.033    | -0.191           | 0.229    | 0.545            | -1.269   |
| DZA cases  | -0.105           | 0.067    | 0.116            | -0.022   | 0.297            | 0.075    |
| AFG deaths | -0.043           | -0.009   | 0.04             | 0.006    | -0.011           | -0.068   |
| DZA deaths | -0.006           | -0.003   | -0.012           | -0.02    | -0.013           | -0.014   |
| Frequency  | $\tilde{b}_{12}$ | $b_{13}$ | $\tilde{b}_{13}$ | $b_{14}$ | $\tilde{b}_{14}$ | $b_{15}$ |
| AFG cases  | 0.513            | 0.513    | -1.018           | 0.152    | 0.18             | -0.607   |
| DZA cases  | -0.125           | -0.066   | -0.201           | 0.062    | 0.251            | 0.179    |
| AFG deaths | 0.035            | 0.075    | -0.027           | -0.075   | 0.006            | 0.042    |
| DZA deaths | -0.006           | 0.01     | 0.002            | -0.001   | -0.008           | -0.021   |
| Frequency  | $\tilde{b}_{15}$ | $b_{16}$ | $\tilde{b}_{16}$ | $b_{17}$ | $\tilde{b}_{17}$ | $b_{18}$ |
| AFG cases  | 0.557            | -0.778   | 0.038            | -0.085   | -0.786           | -0.308   |
| DZA cases  | 0.034            | -0.292   | -0.475           | -0.73    | 0.41             | -0.286   |
| AFG deaths | 0.039            | -0.071   | -0.001           | 0.017    | 0.007            | 0.001    |
| DZA deaths | -0.013           | -0.009   | -0.007           | -0.007   | -0.007           | -0.033   |

**TABLE 5 |** Ranking the coefficients calculated in **Table 4** for Afghanistan (AFG) and Algeria (DZA).

| Frequency  | $b_0$            | $b_1$    | $\tilde{b}_1$    | $b_2$    | $\tilde{b}_2$    | $b_3$    | $\tilde{b}_3$    | $b_4$    | $\tilde{b}_4$    | $b_5$    | $\tilde{b}_5$    | $b_6$    |
|------------|------------------|----------|------------------|----------|------------------|----------|------------------|----------|------------------|----------|------------------|----------|
| AFG cases  | 12               | 21       | 36               | 10       | 32               | 24       | 6                | 35       | 14               | 8        | 34               | 13       |
| DZA cases  | 27               | 25       | 26               | 4        | 30               | 23       | 32               | 22       | 11               | 28       | 13               | 34       |
| AFG deaths | 5                | 19       | 32               | 26       | 8                | 13       | 15               | 35       | 4                | 24       | 34               | 10       |
| DZA deaths | 15               | 1        | 5                | 7        | 10               | 18       | 21               | 8        | 6                | 11       | 9                | 29       |
| Frequency  | $\tilde{b}_6$    | $b_7$    | $\tilde{b}_7$    | $b_8$    | $\tilde{b}_8$    | $b_9$    | $\tilde{b}_9$    | $b_{10}$ | $\tilde{b}_{10}$ | $b_{11}$ | $\tilde{b}_{11}$ | $b_{12}$ |
| AFG cases  | 31               | 18       | 15               | 23       | 28               | 1        | 27               | 26       | 2                | 20       | 22               | 7        |
| DZA cases  | 10               | 19       | 21               | 14       | 31               | 20       | 9                | 12       | 7                | 18       | 29               | 24       |
| AFG deaths | 6                | 12       | 30               | 18       | 11               | 3        | 27               | 36       | 9                | 1        | 21               | 31       |
| DZA deaths | 32               | 33       | 24               | 17       | 23               | 20       | 31               | 36       | 35               | 34       | 26               | 13       |
| Frequency  | $\tilde{b}_{12}$ | $b_{13}$ | $\tilde{b}_{13}$ | $b_{14}$ | $\tilde{b}_{14}$ | $b_{15}$ | $\tilde{b}_{15}$ | $b_{16}$ | $\tilde{b}_{16}$ | $b_{17}$ | $\tilde{b}_{17}$ | $b_{18}$ |
| AFG cases  | 29               | 5        | 19               | 17       | 4                | 11       | 9                | 3        | 25               | 30       | 16               | 33       |
| DZA cases  | 17               | 5        | 3                | 1        | 35               | 6        | 36               | 15       | 2                | 16       | 8                | 33       |
| AFG deaths | 28               | 2        | 14               | 25       | 23               | 16       | 17               | 20       | 7                | 29       | 22               | 33       |
| DZA deaths | 22               | 25       | 27               | 30       | 28               | 3        | 12               | 4        | 2                | 19       | 16               | 14       |

The higher the coefficients are, the higher the ranks are. The higher ranks also indicate the main features of weekly growth rates of COVID-19 in terms of the chosen 36 frequencies.



**TABLE 6 |** Manhattan distance (or  $d(\vec{x}, \vec{y}) := \sum_{i=1}^n |\vec{x}_i - \vec{y}_i|$ ) matrix, which is calculated from table for 90 countries with respect to COVID-19 cases (top block) and COVID-19 deaths (bottom block).

| Countries | 1   | 2   | 3   | 4   | ... | 87  | 88  | 89  | 90  |
|-----------|-----|-----|-----|-----|-----|-----|-----|-----|-----|
| 1         | 0   | 428 | 444 | 416 | ... | 450 | 340 | 432 | 400 |
| 2         | 428 | 0   | 428 | 386 | ... | 390 | 350 | 400 | 402 |
| 3         | 444 | 428 | 0   | 316 | ... | 416 | 394 | 388 | 430 |
| 4         | 416 | 386 | 316 | 0   | ... | 370 | 462 | 400 | 422 |
| ⋮         | ⋮   | ⋮   | ⋮   | ⋮   | ⋮   | ⋮   | ⋮   | ⋮   | ⋮   |
| 87        | 450 | 390 | 416 | 370 | ... | 0   | 404 | 332 | 418 |
| 88        | 340 | 350 | 394 | 462 | ... | 404 | 0   | 408 | 462 |
| 89        | 432 | 400 | 388 | 400 | ... | 332 | 408 | 0   | 374 |
| 90        | 400 | 402 | 430 | 422 | ... | 418 | 462 | 374 | 0   |
| Countries | 1   | 2   | 3   | 4   | ... | 87  | 88  | 89  | 90  |
| 1         | 0   | 468 | 416 | 484 | ... | 424 | 494 | 412 | 426 |
| 2         | 468 | 0   | 410 | 470 | ... | 434 | 462 | 472 | 426 |
| 3         | 416 | 410 | 0   | 366 | ... | 444 | 468 | 406 | 396 |
| 4         | 484 | 470 | 366 | 0   | ... | 446 | 336 | 446 | 408 |
| ⋮         | ⋮   | ⋮   | ⋮   | ⋮   | ⋮   | ⋮   | ⋮   | ⋮   | ⋮   |
| 87        | 424 | 434 | 444 | 446 | ... | 0   | 486 | 426 | 402 |
| 88        | 494 | 462 | 468 | 336 | ... | 486 | 0   | 430 | 500 |
| 89        | 412 | 472 | 406 | 446 | ... | 426 | 430 | 0   | 438 |
| 90        | 426 | 426 | 396 | 408 | ... | 402 | 500 | 438 | 0   |

This distance is derived directly from **Table 5**.

**TABLE 7 |** Minimal pairs, in term of Manhattan distances from **Table 6**, for COVID-19 cases and deaths for the 90 countries.

| Cty    | 1   | 2     | 3  | 4     | 5         | 6     | 7  | 8  | 9  | 10 | 11 | 12    |
|--------|-----|-------|----|-------|-----------|-------|----|----|----|----|----|-------|
| Cases  | 72  | 84    | 37 | 86    | 43        | 44    | 57 | 54 | 89 | 20 | 88 | 23    |
| Deaths | 14  | 19    | 78 | 9     | 9, 10, 27 | 15    | 37 | 82 | 4  | 25 | 17 | 8     |
| Cty    | 13  | 14    | 15 | 16    | 17        | 18    | 19 | 20 | 21 | 22 | 23 | 24    |
| Cases  | 53  | 28    | 24 | 8     | 70        | 10    | 77 | 10 | 39 | 41 | 8  | 27    |
| Deaths | 19  | –     | 6  | 54    | 11        | 55    | 13 | 39 | –  | 83 | 84 | –     |
| Cty    | 25  | 26    | 27 | 28    | 29        | 30    | 31 | 32 | 33 | 34 | 35 | 36    |
| Cases  | 11  | 33,51 | 24 | 14    | 90        | 44,55 | 35 | 74 | 26 | 24 | 31 | 17,18 |
| Deaths | 10  | 53    | 5  | 35    | 76        | 54    | 72 | 41 | 86 | –  | 28 | 11    |
| Cty    | 37  | 38    | 39 | 40    | 41        | 42    | 43 | 44 | 45 | 46 | 47 | 48    |
| Cases  | 3,4 | 74    | 57 | 60    | 43        | 35    | 5  | 90 | 66 | 90 | 85 | 67    |
| Deaths | 7   | 47    | 20 | 54    | 30,79     | 52    | 31 | 17 | 67 | 48 | –  | 66    |
| Cty    | 49  | 50    | 51 | 52    | 53        | 54    | 55 | 56 | 57 | 58 | 59 | 60    |
| Cases  | 66  | 55    | 26 | 69    | 13        | 8     | 50 | 10 | 7  | 10 | 90 | 40    |
| Deaths | 70  | 80    | 16 | 42    | 26        | 30    | 89 | 17 | 11 | 80 | 76 | 62    |
| Cty    | 61  | 62    | 63 | 64    | 65        | 66    | 67 | 68 | 69 | 70 | 71 | 72    |
| Cases  | 40  | 60    | 70 | 69    | 57        | 7     | 48 | 88 | 64 | 17 | 8  | 1     |
| Deaths | 82  | 60    | 56 | –     | 73        | 48    | 45 | 49 | 52 | 49 | 36 | 31    |
| Cty    | 73  | 74    | 75 | 76    | 77        | 78    | 79 | 80 | 81 | 82 | 83 | 84    |
| Cases  | 7   | 81    | 4  | 78    | 19        | 55,76 | 76 | 65 | 74 | 19 | 78 | 2     |
| Deaths | 65  | 15    | 89 | 29    | 78        | 77    | 30 | 58 | 62 | 8  | 22 | 13    |
| Cty    | 85  | 86    | 87 | 88    | 89        | 90    |    |    |    |    |    |       |
| Cases  | 47  | 4     | 14 | 11,70 | 28        | 46    |    |    |    |    |    |       |
| Deaths | 61  | 90    | 10 | 20    | 55        | 86    |    |    |    |    |    |       |

**TABLE 8 |** Typical cosine similarities of COVID-19 cases (top block) and deaths (bottom block) for 90 countries (Cty).

| Cty | 1      | 2      | 3      | 4      | ... | 87     | 88     | 89     | 90     |
|-----|--------|--------|--------|--------|-----|--------|--------|--------|--------|
| 1   | 1      | 0.032  | 0.099  | 0.112  | ... | −0.081 | 0.3    | 0.014  | 0.082  |
| 2   | 0.032  | 1      | 0.134  | 0.089  | ... | 0.141  | 0.168  | 0.228  | 0.024  |
| 3   | 0.099  | 0.134  | 1      | 0.503  | ... | 0.05   | 0.202  | 0.146  | −0.057 |
| 4   | 0.112  | 0.089  | 0.503  | 1      | ... | 0.284  | 0.046  | 0.26   | 0.204  |
| ⋮   | ⋮      | ⋮      | ⋮      | ⋮      | ⋮   | ⋮      | ⋮      | ⋮      | ⋮      |
| 87  | −0.081 | 0.141  | 0.05   | 0.284  | ... | 1      | 0.079  | 0.342  | 0.061  |
| 88  | 0.3    | 0.168  | 0.202  | 0.046  | ... | 0.079  | 1      | 0.087  | 0      |
| 89  | 0.014  | 0.228  | 0.146  | 0.26   | ... | 0.342  | 0.087  | 1      | 0.176  |
| 90  | 0.082  | 0.024  | −0.057 | 0.204  | ... | 0.061  | 0      | 0.176  | 1      |
| Cty | 1      | 2      | 3      | 4      | ... | 87     | 88     | 89     | 90     |
| 1   | 1      | −0.078 | −0.009 | −0.173 | ... | 0.022  | −0.073 | 0.134  | −0.072 |
| 2   | −0.078 | 1      | 0.085  | 0.097  | ... | 0.005  | −0.07  | −0.043 | 0.696  |
| 3   | −0.009 | 0.085  | 1      | 0.225  | ... | −0.012 | 0.039  | 0.005  | 0.011  |
| 4   | −0.173 | 0.097  | 0.225  | 1      | ... | −0.001 | 0.245  | −0.079 | 0.243  |
| ⋮   | ⋮      | ⋮      | ⋮      | ⋮      | ⋮   | ⋮      | ⋮      | ⋮      | ⋮      |
| 87  | 0.022  | 0.005  | −0.012 | −0.001 | ... | 1      | −0.033 | −0.038 | 0.051  |
| 88  | −0.073 | −0.07  | 0.039  | 0.245  | ... | −0.033 | 1      | −0.034 | −0.081 |
| 89  | 0.134  | −0.043 | 0.005  | −0.079 | ... | −0.038 | −0.034 | 1      | −0.073 |
| 90  | −0.072 | 0.696  | 0.011  | 0.243  | ... | 0.051  | −0.081 | −0.073 | 1      |

**TABLE 9 |** Maximal pairs, in terms of typical similarities, of COVID-19 cases and deaths for the 90 countries (Cty).

| Cty    | 1  | 2  | 3  | 4  | 5  | 6  | 7  | 8  | 9  | 10 | 11 | 12 |
|--------|----|----|----|----|----|----|----|----|----|----|----|----|
| Cases  | 72 | 84 | 37 | 86 | 41 | 61 | 83 | 54 | 31 | 68 | 68 | 23 |
| Deaths | 58 | 86 | 78 | 9  | 10 | 13 | 15 | 82 | 4  | 87 | 56 | 8  |
| Cty    | 13 | 14 | 15 | 16 | 17 | 18 | 19 | 20 | 21 | 22 | 23 | 24 |
| Cases  | 90 | 28 | 57 | 82 | 70 | 11 | 77 | 10 | 39 | 32 | 8  | 27 |
| Deaths | 19 | –  | 19 | 51 | 44 | 55 | 13 | 39 | 12 | 83 | 83 | 57 |
| Cty    | 25 | 26 | 27 | 28 | 29 | 30 | 31 | 32 | 33 | 34 | 35 | 36 |
| Cases  | 68 | 13 | 24 | 14 | 71 | 40 | 35 | 22 | 51 | 24 | 31 | 11 |
| Deaths | 86 | 53 | 9  | 35 | 30 | 54 | 72 | 60 | 35 | 7  | 28 | 11 |
| Cty    | 37 | 38 | 39 | 40 | 41 | 42 | 43 | 44 | 45 | 46 | 47 | 48 |
| Cases  | 4  | 6  | 20 | 30 | 5  | 35 | 5  | 90 | 66 | 90 | 82 | 73 |
| Deaths | 7  | 23 | 20 | 82 | 30 | 52 | 31 | 17 | 67 | 90 | 10 | 66 |
| Cty    | 49 | 50 | 51 | 52 | 53 | 54 | 55 | 56 | 57 | 58 | 59 | 60 |
| Cases  | 73 | 81 | 33 | 81 | 7  | 8  | 50 | 7  | 73 | 10 | 90 | 40 |
| Deaths | 11 | 86 | 16 | 42 | 26 | 30 | 18 | 11 | 63 | 80 | 76 | 62 |
| Cty    | 61 | 62 | 63 | 64 | 65 | 66 | 67 | 68 | 69 | 70 | 71 | 72 |
| Cases  | 40 | 60 | 7  | 69 | 7  | 56 | 48 | 10 | 64 | 88 | 8  | 1  |
| Deaths | 82 | 76 | 56 | 21 | 73 | 48 | 45 | 57 | 52 | 49 | 76 | 86 |
| Cty    | 73 | 74 | 75 | 76 | 77 | 78 | 79 | 80 | 81 | 82 | 83 | 84 |
| Cases  | 7  | 60 | 33 | 78 | 19 | 76 | 76 | 9  | 63 | 54 | 7  | 2  |
| Deaths | 88 | 82 | 19 | 29 | 78 | 77 | 30 | 58 | 34 | 8  | 22 | 19 |
| Cty    | 85 | 86 | 87 | 88 | 89 | 90 |    |    |    |    |    |    |
| Cases  | 78 | 4  | 28 | 70 | 36 | 46 |    |    |    |    |    |    |
| Deaths | 53 | 90 | 10 | 17 | 28 | 86 |    |    |    |    |    |    |

**TABLE 10 |** Optimal pairings for the countries with respect to cases and deaths in terms of minimal and maximal values.

| Cases-min  |          |          |          |          |          |          |
|------------|----------|----------|----------|----------|----------|----------|
| {1, 72}    | {2, 84}  | {3, 37}  | {4, 86}  | {5, 43}  | {7, 57}  | {8, 54}  |
| {10, 20}   | {11, 88} | {13, 53} | {14, 28} | {17, 70} | {19, 77} | {24, 27} |
| {26, 33}   | {31, 35} | {40, 60} | {46, 90} | {47, 85} | {48, 67} | {50, 55} |
| {26, 51}   | {64, 69} | {74, 81} | {76, 78} |          |          |          |
| Deaths-min |          |          |          |          |          |          |
| {4, 9}     | {5, 27}  | {6, 15}  | {7, 37}  | {8, 82}  | {10, 25} | {11, 17} |
| {13, 19}   | {20, 39} | {22, 83} | {26, 53} | {28, 35} | {29, 76} | {30, 54} |
| {31, 72}   | {42, 52} | {45, 67} | {48, 66} | {49, 70} | {55, 89} | {58, 80} |
| {60, 62}   | {65, 73} | {77, 78} | {86, 90} |          |          |          |
| Cases-max  |          |          |          |          |          |          |
| {1, 72}    | {2, 84}  | {4, 86}  | {5, 41}  | {7, 83}  | {8, 54}  | {10, 68} |
| {14, 28}   | {19, 77} | {22, 32} | {24, 27} | {30, 40} | {31, 35} | {33, 51} |
| {46, 90}   | {64, 69} | {70, 88} | {76, 78} |          |          |          |
| Deaths-max |          |          |          |          |          |          |
| {4, 9}     | {8, 82}  | {10, 87} | {11, 56} | {13, 19} | {16, 51} | {17, 44} |
| {18, 55}   | {20, 39} | {22, 83} | {26, 53} | {28, 35} | {30, 54} | {42, 52} |
| {45, 67}   | {46, 90} | {48, 66} | {58, 80} | {77, 78} | {86, 90} |          |

**TABLE 11 |** Jaccard index (or  $J(A, B) = \frac{|A \cap B|}{|A \cup B|}$ ) for minimal and maximal pairings.

|            | Cases-min       | Deaths-min      | Cases-max       | Deaths-max      |
|------------|-----------------|-----------------|-----------------|-----------------|
| Cases-min  | 1               | 0               | $\frac{11}{32}$ | $\frac{1}{44}$  |
| Deaths-min | 0               | 1               | 0               | $\frac{14}{31}$ |
| Cases-max  | $\frac{11}{32}$ | 0               | 1               | $\frac{1}{37}$  |
| Deaths-max | $\frac{1}{44}$  | $\frac{14}{31}$ | $\frac{1}{37}$  | 1               |

distance matrix. By the end, I compare our mechanism with the usual cosine similarity analysis. The result shows these two approaches yield quite different results - this indicates our approach provides another aspect to look into the evolution of

COVID-19. The comparison also reveals some points: first of all, the evolutive pattern for cases and deaths are very different—which is concluded from **Table 11**; secondly, regardless of the cases or the deaths, our method and the typical one are highly related to each other; and thirdly, the relation between the paired countries—no matter which approach one adopts—is not random, since the ratios of pairs formed are very high. This indicates our research provides some insightful structure of the evolution of COVID-19 between countries. However, some of the results about causal relations in this study might not comply with other researches (10). This is reasonable, since the approach I adopt focuses more on feature detection, not solely on causal relation finding. For the future research, one could look into the pairs to identify the fundamental factors that contribute to such correlated patterns between countries. Furthermore, one could also delve into the shift of phrases of the frequencies by lifting the constraint on weekly growth rates. This might yield an even more dynamical pictures of the evolutions.

## DATA AVAILABILITY STATEMENT

The original contributions presented in the study are included in the article/supplementary material, further inquiries can be directed to the corresponding author/s.

## AUTHOR CONTRIBUTIONS

The author confirms being the sole contributor of this work and has approved it for publication.

## FUNDING

This work was supported by the Humanities and Social Science Research Planning Fund Project under the Ministry of Education of China (No. 20XJAGAT001).

## REFERENCES

- Mahase E. Covid-19: What have we learnt about the new variant in the UK? *BMJ*. (2020) 371:m4944. doi: 10.1136/bmj.m4944
- Allyson M Pollock. Asymptomatic transmission of COVID-19. *BMJ*. (2020) 371:m4851. doi: 10.1136/bmj.m4851
- Priyadarshini I, Mohanty P, Kumar R, Son LH, Chau HTM, Nhu VH, et al. Analysis of outbreak and global impacts of the COVID-19. *Healthcare*. (2020) 8:148. doi: 10.3390/healthcare8020148
- Asch DA, Sheils NE, Islam MN, Chen Y, Werner RM, Buresh J, et al. Variation in US hospital mortality rates for patients admitted with COVID-19 during the first 6 months of the pandemic. *JAMA Intern Med*. (2020) 181:471–8. doi: 10.1001/jamainternmed.2020.8193
- Boudourakis L, Uppal A. Decreased COVID-19 mortality—a cause for optimism. *JAMA Intern Med*. (2020) 181:478–9. doi: 10.1001/jamainternmed.2020.8438
- Chen R-M. Randomness for nucleotide sequences of SARS-CoV-2 and its related subfamilies. *Comput Math Methods Med*. (2020) 2020:8819942. doi: 10.1155/2020/8819942
- Chen R-M. Quantifying collective intelligence and behaviours of SARS-CoV-2 via environmental resources from virus-perspectives. *Environ Res*. (2021) 198:111278. doi: 10.1016/j.envres.2021.111278
- Chen R-M. Track the dynamical features for mutant variants of COVID-19 in the UK. *Math Biosci Eng*. (2021) 18:4572–85. doi: 10.3934/mbe.2021232
- Chen R-M. On COVID-19 country containment metrics: a new approach. *J Decis Syst*. (2021). doi: 10.1080/12460125.2021.1886625. [Epub ahead of print].
- Valev D. Relationships of total COVID-19 cases and deaths with ten demographic, economic and social indicators. *medRxiv* (2020). doi: 10.1101/2020.09.05.20188953
- Roman S. *Advanced Linear Algebra*. 3rd Edn. New York, NY Springer (2007).
- Schoenstadt AL. *An Introduction to Fourier Analysis*. (2020). Available online at: [https://www.math.bgu.ac.il/~leonid/ode\\_9171\\_files/Schoenstadt\\_Fourier\\_PDE.pdf](https://www.math.bgu.ac.il/~leonid/ode_9171_files/Schoenstadt_Fourier_PDE.pdf) (accessed December 29, 2020).
- European Centre for Disease Prevention and Control. Available online at: <https://www.ecdc.europa.eu/en/publications-data/download-todays-data-geographic-distribution-covid-19-cases-worldwide>
- Paul BE. *Manhattan Distance*. Dictionary of Algorithms and Data Structures (Retrieved December 29, 2020).

15. Chung N, Miasojedow B, Startek M, Gambin A. Jaccard/Tanimoto similarity test and estimation methods for biological presence-absence data. *BMC Bioinformatics*. (2019) 20:644. doi: 10.1186/s12859-019-3118-5

**Conflict of Interest:** The author declares that the research was conducted in the absence of any commercial or financial relationships that could be construed as a potential conflict of interest.

**Publisher's Note:** All claims expressed in this article are solely those of the authors and do not necessarily represent those of their affiliated organizations, or those of

the publisher, the editors and the reviewers. Any product that may be evaluated in this article, or claim that may be made by its manufacturer, is not guaranteed or endorsed by the publisher.

Copyright © 2021 Chen. This is an open-access article distributed under the terms of the Creative Commons Attribution License (CC BY). The use, distribution or reproduction in other forums is permitted, provided the original author(s) and the copyright owner(s) are credited and that the original publication in this journal is cited, in accordance with accepted academic practice. No use, distribution or reproduction is permitted which does not comply with these terms.





# Pneumonia Patients Caused by Co-infection With SARS-CoV-2 and Human Adenovirus in China

## OPEN ACCESS

### Edited by:

Atefeh Abedini,  
Shahid Beheshti University of Medical  
Sciences, Iran

### Reviewed by:

Man-Qing Liu,  
Wuhan Centre for Disease Prevention  
and Control, China  
Faris Hasan al Lami,  
University of Baghdad, Iraq

### \*Correspondence:

Zhifei Zhan  
zhazhifei74@163.com  
Hongbin Song  
hongbinsong@263.net  
Shixiong Hu  
379788967@qq.com

<sup>†</sup>These authors have contributed  
equally to this work

### Specialty section:

This article was submitted to  
Infectious Diseases - Surveillance,  
Prevention and Treatment,  
a section of the journal  
Frontiers in Medicine

Received: 03 July 2021

Accepted: 30 August 2021

Published: 28 September 2021

### Citation:

Qiu S, Zeng G, Li P, Li X, Liu H, Du X,  
Liu H, Zhang H, Xiang X, Wang H,  
Chen X, Yang G, Tian S, Wang L,  
Yang M, Yang C, Gao L, Hu S, Song H  
and Zhan Z (2021) Pneumonia  
Patients Caused by Co-infection With  
SARS-CoV-2 and Human Adenovirus  
in China. *Front. Med.* 8:735779.  
doi: 10.3389/fmed.2021.735779

Shaofu Qiu<sup>1†</sup>, Ge Zeng<sup>2†</sup>, Peihan Li<sup>1†</sup>, Xiaohui Li<sup>3†</sup>, Hongbo Liu<sup>1</sup>, Xinying Du<sup>1</sup>,  
Hongbo Liu<sup>1</sup>, Heng Zhang<sup>4</sup>, Xingyu Xiang<sup>2</sup>, Hui Wang<sup>1</sup>, Xiangbing Chen<sup>3</sup>,  
Guangyao Yang<sup>3</sup>, Sai Tian<sup>1</sup>, Ligui Wang<sup>1</sup>, Mingjuan Yang<sup>1</sup>, Chaojie Yang<sup>1</sup>, Lidong Gao<sup>2</sup>,  
Shixiong Hu<sup>2\*</sup>, Hongbin Song<sup>1\*</sup> and Zhifei Zhan<sup>2\*</sup>

<sup>1</sup> Chinese PLA Center for Disease Control and Prevention, Beijing, China, <sup>2</sup> Hunan Provincial Center for Disease Control and Prevention, Workstation for Emerging Infectious Disease Control and Prevention, Chinese Academy of Medical Sciences, Changsha, China, <sup>3</sup> Wangcheng Center for Disease Control and Prevention, Changsha, China, <sup>4</sup> Changsha Center for Disease Control and Prevention, Changsha, China

**Objectives:** To date, no patients with obvious epidemiological relationship co-infected with SARS-CoV-2 and other pathogens have been reported. Here, we investigated 10 patients caused by co-infection with SARS-CoV-2 and human adenovirus (HAdV), resulting in third-generation transmission.

**Materials and Methods:** From Jan 15, 2020, we enrolled 10 patients with pneumonia in Hunan Province, China. Epidemiological, clinical, and laboratory investigation results from these patients were analyzed. An epidemiological investigation was performed to assess whether patient infections were linked using conventional methods and metagenomic sequencing.

**Results:** The presence of co-infection with SARS-CoV-2 and HAdV was determined via RT-PCR and metagenomic sequencing. Phylogenetic analysis revealed that SARS-CoV-2 and HAdV genomes clustered together, with similar genetic relationships. The first patient likely became co-infected during meetings or travel in Wuhan. The patient transmitted the virus via dinners and meetings, which resulted in four second-generation cases. Then, a second-generation case transmitted the virus to her family members or relatives via presymptomatic transmission.

**Conclusions:** This study described an example of co-infection with SARS-CoV-2 and HAdV in pneumonia patients, which caused third-generation cases and inter-regional transmission via meetings, household interactions, and dinner parties. We also observed the persistent and presymptomatic transmission of co-infection, which has the potential to make the continued control of the COVID-19 pandemic challenging. Continuous surveillance is needed to monitor the prevalence, infectivity, transmissibility, and pathogenicity of SARS-CoV-2 co-infection with other pathogens to evaluate its real risk.

**Keywords:** SARS-CoV-2, HAdV, co-infection, metagenomic sequencing, presymptomatic transmission

## INTRODUCTION

The coronavirus disease 2019 (COVID-19) pandemic caused by severe acute respiratory syndrome coronavirus 2 (SARS-CoV-2) is ongoing (1, 2). As of July 2, 2021, data from the WHO have shown that a total of 182,319,261 confirmed cases of COVID-19 have been reported worldwide, including 3,954,324 deaths (<https://covid19.who.int/>). Thus, the virus continues to be a serious public health problem globally.

The COVID-19 outbreak was first reported in Wuhan, China on December 31, 2019, and was associated with the Huanan Seafood Wholesale Market (1, 2). It has been reported that 5 million people emigrated from Wuhan to other regions of China and other countries before the city was locked down, a situation that likely allowed for the spread of the virus (3, 4). SARS-CoV-2 infections among medical workers and family clusters have been identified, and human-to-human transmission of SARS-CoV-2 occurs largely in families in China (5–7). SARS-CoV-2 co-infection alongside other pathogens have been reported, including occasional co-infections involving human adenovirus (HAdV) and SARS-CoV-2. However, reports of co-infections are rare (8–12). Moreover, little is known regarding whether SARS-CoV-2 co-infections are transmitted between individuals at rates capable of causing clusters of acute respiratory infections. Here, using conventional and genomic epidemiological methods, we investigated a clustered pneumonia patients caused by co-infection with SARS-CoV-2 and HAdV, resulting in a large-scale transmission and even third-generation human-to-human transmission.

## MATERIALS AND METHODS

### Patients and Samples

In January of 2020, we enrolled 10 patients with fever, respiratory symptoms, and pulmonary infiltrates. Among them, three patients were admitted to a local hospital in Huaihua City, Hunan Province, China, and seven were admitted to another hospital in Shaoyang City, Hunan Province. Due to the serious outbreak of SARS-CoV-2 in Wuhan, a joint team comprising staff from provincial and municipal Centers for Disease Control and Prevention (CDC) conducted detailed field investigations of all suspected SARS-CoV-2 cases. Data were collected via standardized forms through interviews with infected persons, relatives, and close contacts. We recorded and analyzed the epidemiological, clinical, laboratory, and microbiological investigation results from the patients. Throat swab samples were collected from patients and their close contacts, and were stored in viral transport media for further identification. This study was approved by the institutional review board of the participating units, and written informed consent was obtained from all patients.

### Laboratory Identification of Patient Samples

Respiratory samples from patients with suspected infections and their contacts were initially detected for the presence of

SARS-CoV-2 at the local CDC facility, using real-time reverse-transcriptase PCR (RT-PCR) assays (Sansure Biotech, Changsha, Hunan, China). Samples positive for SARS-CoV-2 were sent to our laboratory for further identification. Nucleic acids were extracted using the TIANamp Virus DNA/RNA Kit (Tiangen, Beijing, China), and tested for the presence of SARS-CoV-2, HAdV, influenza A virus and influenza B virus via RT-PCR assays (Shanghai BioGerm Medical Biotechnology Co., Ltd., Shanghai, China).

### Whole-Genome Sequencing and Bioinformatics Analysis

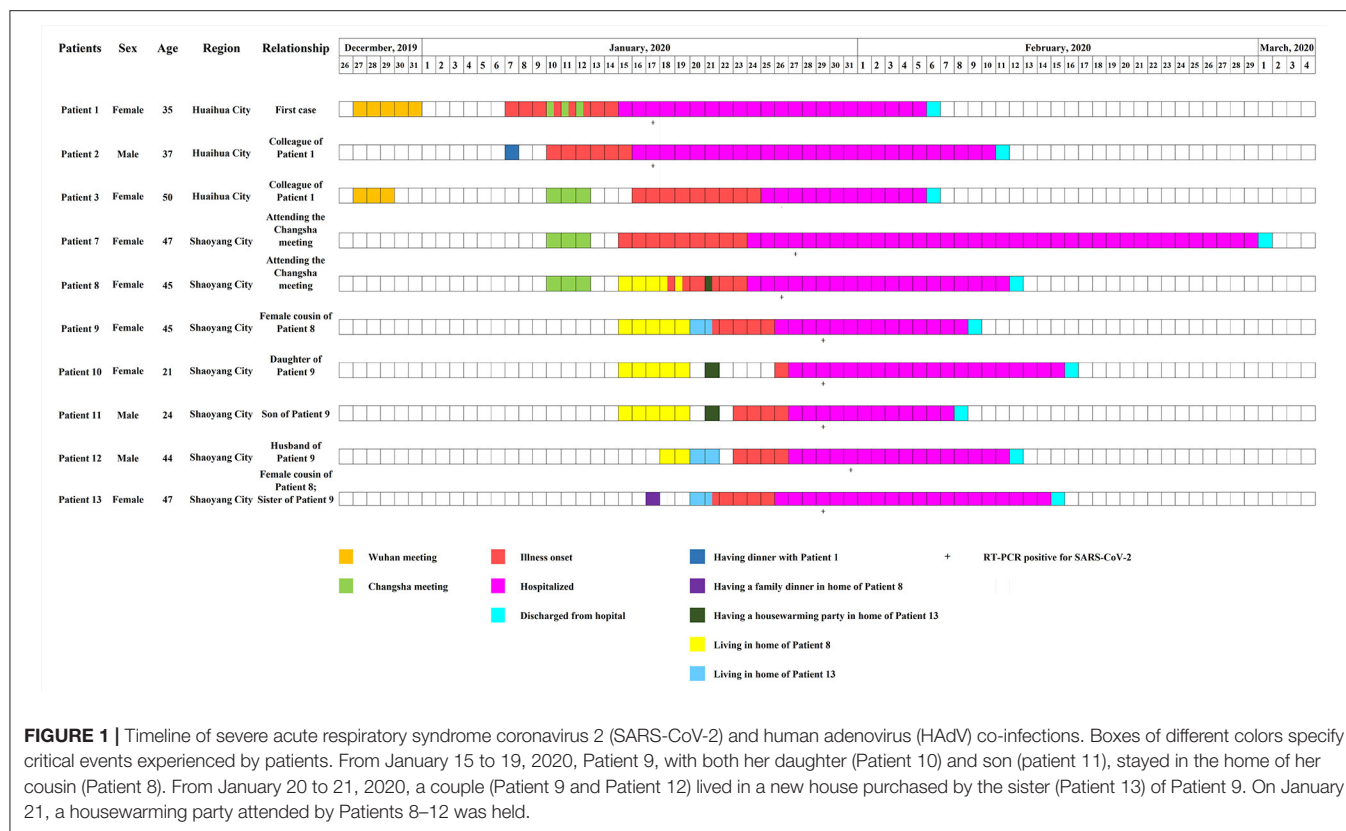
Metagenomic sequencing was performed directly on throat swab samples using the Illumina Novaseq platform, and de novo assembly was performed using SPAdes v3.13.0 (13). Sanger sequencing was used to close gaps and verify ambiguous sequences. Representative Betacoronavirus genomes, including that of SARS-CoV-2, and genomes of HAdV species B, including HAdV serotype 3 (HAdV-3), were retrieved from GenBank, and multiple sequence alignments were performed using Mafft 7.450 (14). Phylogenetic analysis was performed using Mega 7.0.21 (15), with the maximum likelihood method with 1,000 bootstrap replicates. Single nucleotide variants were analyzed using Bwa 0.7.17-r1188 (16) and Samtools 1.9 (17).

## RESULTS

### Epidemiological Investigation of the Patients

On January 15, 2020, the first patient (Patient 1) was enrolled. The patient presented to a hospital in Huaihua City, Hunan Province, China with respiratory symptoms and multiple small patchy shadows in bilateral lungs on chest computed tomography (CT) scan (**Supplementary Table 1**). This patient tested positive for SARS-CoV-2 by using RT-PCR at a local CDC on January 17, 2020. Epidemiological investigation showed that this patient and her colleague (Patient 3) both had a history of travel to Wuhan, China (**Figure 1**), and had attended an annual meeting held by a company in Wuhan between December 27 and 31, 2019. During the meeting, they had no history of contact with wild animals, or game food. Nor did they visit markets including the Huanan Seafood Wholesale Market. Her colleague (Patient 3) returned to Huaihua from Wuhan on December 29, and she returned on December 31, 2019. 7 days later (January 7, 2020), she felt uncomfortable, but kept dinner plans with a colleague (Patient 2) that evening. Her colleague (Patient 2) developed respiratory symptoms on January 10, 2020 (**Figure 1**), but her colleague (Patient 3) did not yet display symptoms.

Patient 1, with her colleague (Patient 3), attended another meeting in Changsha City, Hunan Province, China, between January 10 and January 12, 2020 (**Figures 1, 2**). During the meeting, 282 participants stayed in the same hotel, and gathered in a large conference room. After the meeting, on January 12,



2020, Patients 1 and 3 returned from Changsha to Huaihua and Patient 3 developed respiratory symptoms on January 16, 2020.

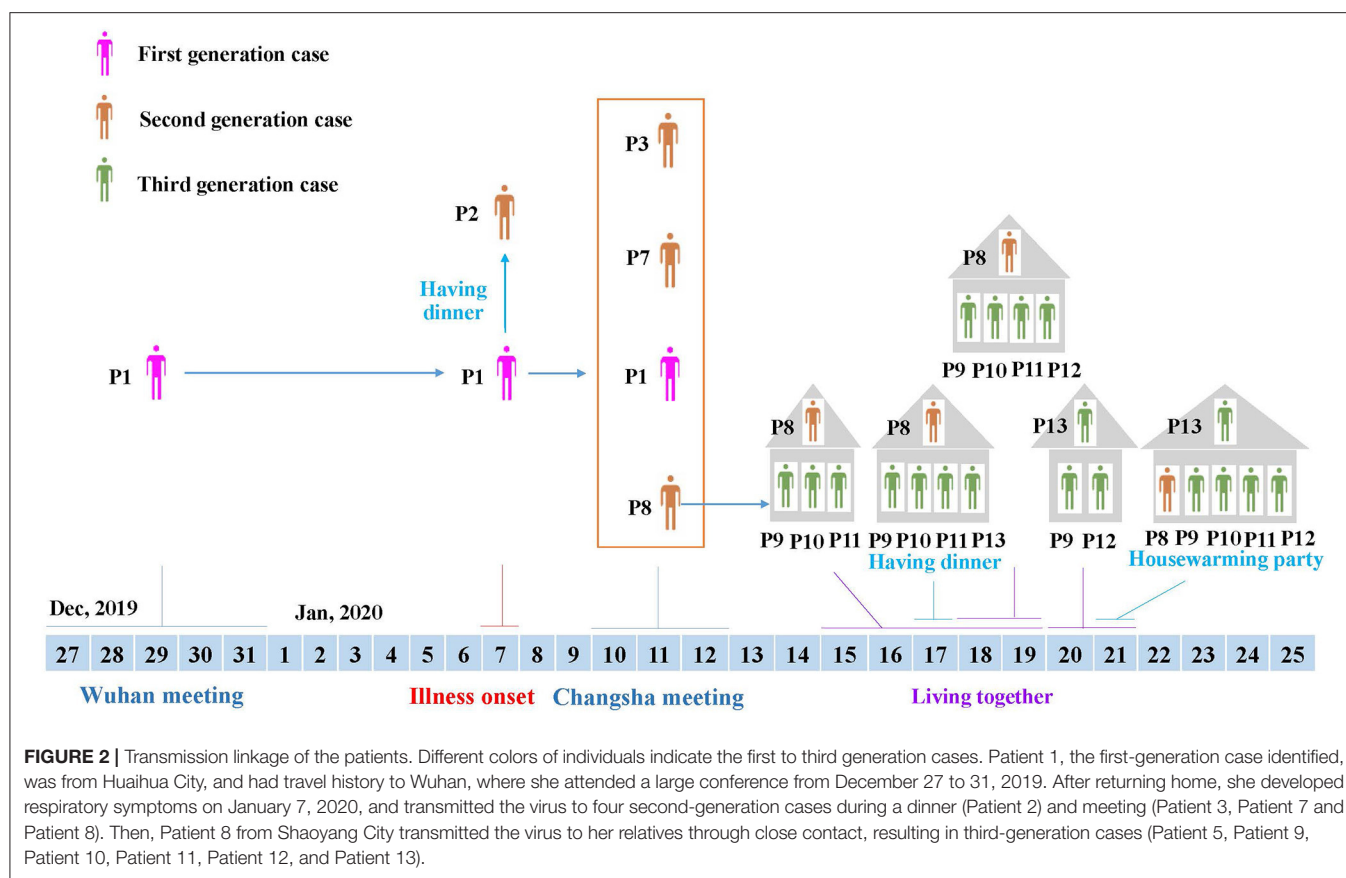
Meanwhile, after the Changsha meeting, another two participants (Patients 7 and 8) returned from Changsha to Shaoyang City on January 12, 2020, and showed respiratory illnesses on January 15 (Patient 7), and January 18 (Patient 8), 2020, respectively (**Figure 1**). Patient 8 was in close contact with relatives, including female cousins (Patients 9 and 13), and her cousins' family members. From January 15 to January 19, 2020, Patient 9 stayed in the house of Patient 8 with her daughter (Patient 10) and son (Patient 11) (**Figures 1, 2**). On January 17, Patient 13 (female cousin of Patient 8; sister of Patient 9) had a family dinner with Patients 8–11 in the home of Patient 8 (**Figure 2**). From January 18 to January 19, Patient 12 (husband of Patient 9) also stayed in the house of Patient 8 (**Figure 2**). In order to celebrate moving into a new house, Patient 13 invited her sister (Patient 9) and her sister's husband (Patient 12) to live in her new house from January 20 to January 21, 2020. On January 21, 2020 she invited her relatives including Patient 8 and her sister's family members (Patients 9, 10, 11, and 12) to a housewarming party (**Figures 1, 2**). Both Patients 9 and 13 showed respiratory symptoms on January 21, while Patients 11 and 12 showed symptoms on January 23, and Patient 10 became symptomatic on January 26, 2020 (**Figure 1**).

Among the 10 patients mentioned, three were male and seven were female, and their ages ranged between 21 and 50 years (**Supplementary Table 1**). The most common symptoms

observed were cough (100%), fever (90%), sputum production (70%), shortness of breath (70%), fatigue (40%), and sore throat (30%), followed by diarrhea (20%), chills (10%), rhinorrhea (10%), nasal congestion (10%), nausea (10%), and chest pain (10%). Four patients had chronic comorbidities, including hypertension, coronary disease, and nasosinusitis. All patients showed multiple patchy ground-glass opacities, and most were involved with bilateral lungs on chest CT scans. Blood tests revealed that most patients had normal level of white-cell count, but 60% had lymphopenia. According to the clinical and laboratory results, one was classified as a severe case, five as moderate and four as mild (**Supplementary Table 1**). All patients were treated with antiviral therapy with Ribavirin (500 mg per dose, 2–3 times daily) and Kaletra (lopinavir-ritonavir, 400/100 mg per dose, 2 times daily) and anti-infection therapy with moxifloxacin. All patients recovered and were discharged on March 1, 2020 (**Figure 1**). A total of 352 close contacts were traced, and no respiratory symptoms were observed during the medical observation period.

## Laboratory and Genomic Investigation of Patient Samples

Respiratory samples from the 10 patients were detected positive for SARS-CoV-2 via RT-PCR, and samples from 352 of their close contacts were negative for SARS-CoV-2. Sequences of SARS-CoV-2 were obtained directly from respiratory samples using metagenomic sequencing, and unexpectedly HAdV sequences



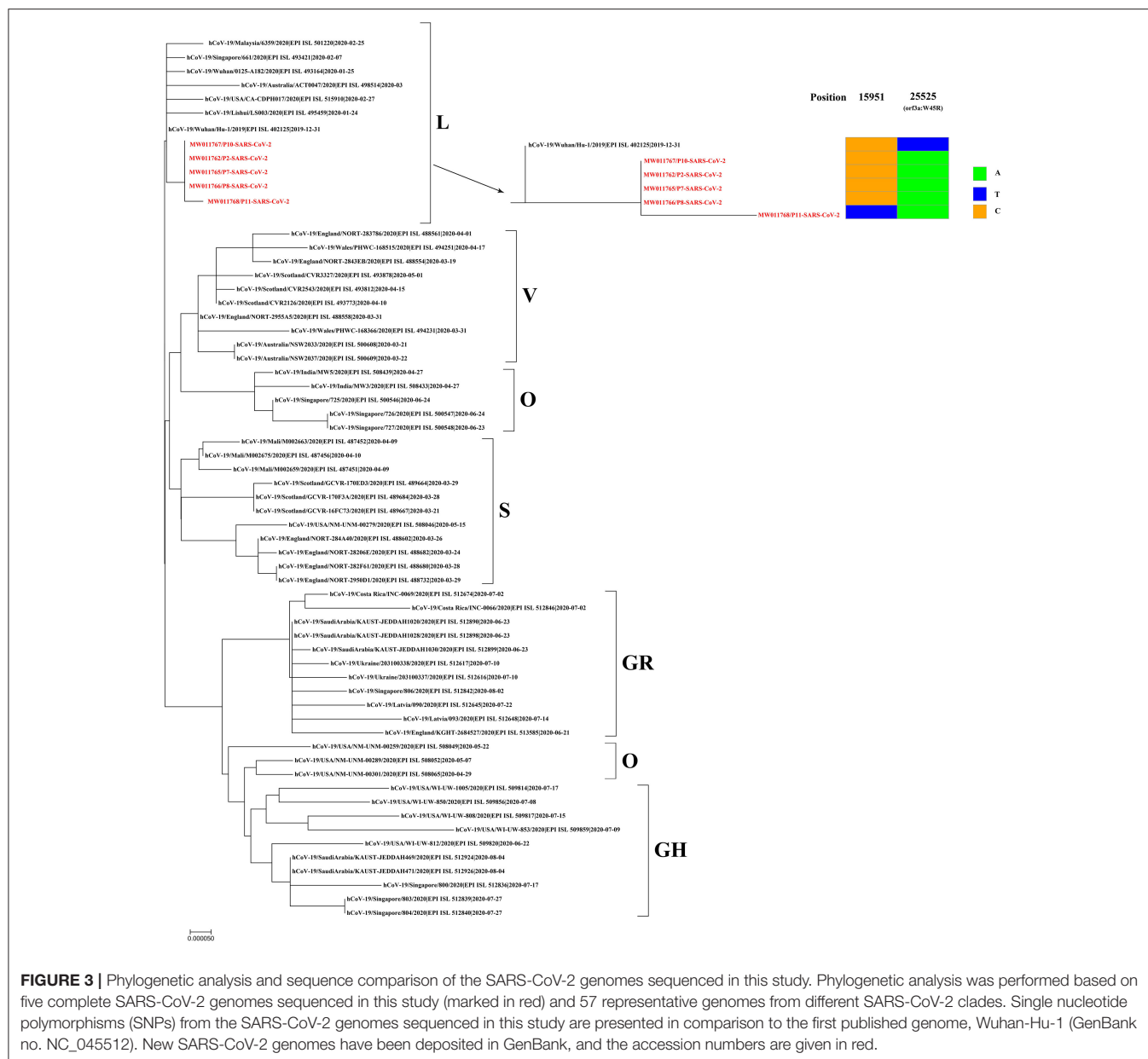
were also identified. RT-PCR assays confirmed that the samples were positive for SARS-CoV-2 and HAdV, but negative for influenza A and B viruses. Using combined whole-genome and Sanger sequencing, we obtained five complete genomes of SARS-CoV-2 and 10 genomes of HAdV. The SARS-CoV-2 and HAdV genomes have been deposited in GenBank under accession nos: MW011762, MW011765-MW011768 for SARS-CoV-2; MW013769-MW013771, MW013774-MW013780 for HAdV. Phylogenetic analysis revealed that the SARS-CoV-2 genomes sequenced in this study clustered together with the early identified SARS-CoV-2 sequences, including the first published SARS-CoV-2 genome, Wuhan-Hu-1 (GenBank no. NC\_045512) (Figure 3), which were located in the original lineage (clade L) of SARS-CoV-2 (18). Compared with the first published SARS-CoV-2 genome Wuhan-Hu-1 (GenBank no. NC\_045512), two single nucleotide polymorphisms (SNPs) were identified, including one nonsynonymous SNP (W45R) in the orf3a gene and one synonymous SNP in the orf1ab gene. The complete genomes of Patient 2, Patient 7, Patient 8, Patient 10, and Patient 11 all had the W45R mutation in the orf3a gene, and additionally the genome from Patient 11 had a synonymous mutation in the orf1ab gene (Figure 3; Supplementary Table 2). The HAdV genomes sequenced in this study were identified as genotype 3 (HAdV-3), and they clustered together to form a distinct subclade with other HAdV-3 genomes (Figure 4). The HAdV-3 genomes sequenced in this study were determined to

be closely related to a genome (GenBank no. KF268311) which was identified in Guangzhou City, China in 2007. Comparative genomic analysis showed that no SNPs were identified among the HAdV-3 genomes sequenced in this study (Figure 4). However, when compared with the reference genome KF268311, five SNPs were identified, including three non-synonymous SNPs (M1I, F4S, I135M) in the E3 gene, one non-synonymous SNP (M1392I) in the E2B gene, and one synonymous SNP in the E2B (Figure 4; Supplementary Table 2).

## DISCUSSION

The most important finding of the present study is that we described an example of co-infection with SARS-CoV-2 and HAdV among some pneumonia patients with obvious epidemiological relationship. Previous studies have reported sporadic cases caused by co-infections of SARS-CoV-2 with other pathogens, including influenza A virus, respiratory syncytial virus, metapneumovirus, rhinovirus, and HAdV (8–12). The detection of SARS-CoV-2 co-infection with other respiratory viruses is difficult. Metagenomic sequencing has shown great potential for the identification of co-infections. When samples positive for SARS-CoV-2 were sent to our laboratory, we performed metagenomic sequencing directly on throat swab samples. Unexpectedly, the sequences of SARS-CoV-2 and

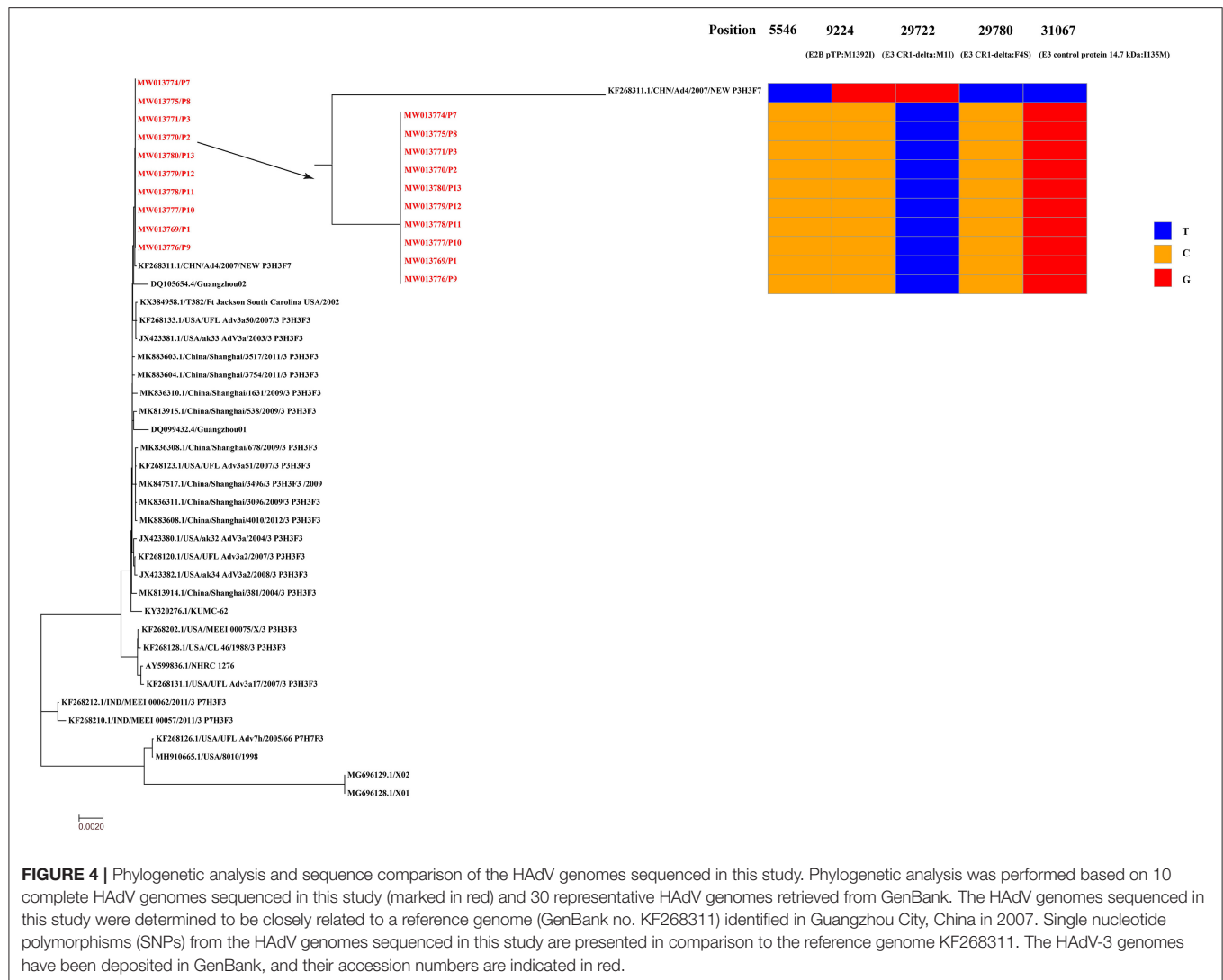




HAdV were identified directly from the respiratory samples, and the viral genomes detected within patients clustered together, displaying similar genetic characteristics. These results demonstrated that co-infection with SARS-CoV-2 and HAdV had occurred. Such infections have the potential to result in a cluster of pneumonia patients, and pose unique challenge in the control of the COVID-19 pandemic.

Also of importance are the complex transmission dynamics of co-infection with SARS-CoV-2 and HAdV that are revealed, which resulted in multiple waves of virus transmission through meetings, household interactions, and dinner parties. The first enrolled patient (Patient 1) had traveled from Huaihua City to Wuhan City with her colleague (Patient 3) to attend a conference. She returned to Huaihua City later, but developed

respiratory symptoms earlier than her colleague, within the estimated incubation period of SARS-CoV-2 (19). The HAdV-3 genome from Patient 1 was identical to those from other patients, and similar to the genome identified in 2007 in China. HAdV-3 is one of the most prevalent serotypes of HAdV globally, especially in Asia, and is commonly associated with epidemic infections among civilian and military populations (20). Moreover, the SARS-CoV-2 genome from Patient 1 was closely related to the first published genome Wuhan-Hu-1, and it was located in the original L clade (18), indicative of its likely Wuhan origin. Therefore, we believe that Patient 1 was the first to be infected among the patients considered, and probably acquired the infection while attending a meeting in Wuhan.



During her illness, Patient 1 had contact with her colleague (Patient 2) at a dinner, and attended the Changsha meeting with another colleague (Patient 3). Although Patients 1 and 3 all attended the Wuhan meeting and Changsha meeting, Patient 3 returned home from Wuhan earlier than Patient 1, and the timing of respiratory symptom onset was beyond the maximum incubation period of SARS-CoV-2 (6, 19). This suggested that Patient 3 acquired the infection during the Changsha, and not Wuhan meeting. Notably, two persons (Patients 7 and 8) from Shaoyang City also attended the Changsha meeting and lived in the same hotel as Patient 1. After returning home, they developed respiratory illness within the incubation period of SARS-CoV-2. These results suggested that Patient 1 was the first case, who acquired an infection during the Wuhan meeting or travel, and subsequently transmitted the virus to at least four second-generation cases (Patients 2, 3, 7, and 8) (Figure 2). Thereafter, Patient 8 who lived in Shaoyang City, transmitted the virus to family members via a family gathering, which resulted in third-generation cases (Figure 2). Since SARS-CoV-2 has emerged in

Wuhan, thousands of exported and resultant secondary cases have been reported in multiple countries, and many infection clusters have been identified, mostly among secondary cases (5, 7, 21–24). Our present study provides a clear example of the persistent transmission of co-infection with SARS-CoV-2 and HAdV, which can result in at least third-generation cases.

Symptom-based screening of suspected SARS-CoV-2 patients may fail to identify all SARS-CoV-2 infections. Currently, the asymptomatic and presymptomatic transmission of SARS-CoV-2 infections have been reported, which are challenges to effective disease control (21–27). In this study, we also observed the presymptomatic transmission of SARS-CoV-2 and HAdV co-infection. Patient 8 attended the Changsha meeting, and she developed respiratory symptoms 6 days later. During the virus incubation period, she was in close contact with four of her relatives (Patients 9–12) through family clustering. The family members developed illnesses 3, 5, and 8 days later. Patient 13 attended a family dinner with Patient 8 and her sister's family members (Patients 9–11) when they were all presymptomatic.

4 days later, Patient 13 was ill. Thus, attendees likely acquired infections from Patient 8, a presymptomatic case who was shedding the virus but not yet showing symptoms. The present study, in combination with previous studies, demonstrates that presymptomatic COVID-19 cases are infectious, and have resulted in presymptomatic transmission and clusters of patients (22, 24–26). Notably, a recent study by Zhu *et al.* showed that SARS-CoV-2 has a high rate of co-infection rate with other pathogens, which was observed in patients 4–10 days after symptom onset. This indicates that presymptomatic individuals have a great potential to transmit co-infection (8). Further, presymptomatic individuals are potentially contagious, highlighting the role of presymptomatic cases in mediating viral expansion. Especially in family clusters, family members should be closely monitored and carefully examined to rule out infection, even if they test negative for SARS-CoV-2 or are asymptomatic, to prevent and control the further transmission of the virus.

In this study, the patients identified showed clinical symptoms similar to those that have been described in previous reports (1, 6, 28). They had typical characteristics of SARS-CoV-2 infections, including lymphopenia and bilateral ground-glass opacity presence (1, 6). Most patients were defined as moderate or mild cases, and only one severe case was identified. Further, all patients recovered. HAdV species B is reported to be one of the primary causes of acute respiratory disease, and can cause severe illnesses, particularly in children and individuals with underlying health conditions. HAdV is also commonly associated with acute respiratory disease outbreaks, especially in military and hospital settings (20, 29, 30). The study by Zhu *et al.* reported that patients co-infected with SARS-CoV-2 and HAdV tended to be 15–65 years of age, with mild symptoms (8). Thus, co-infection seemingly did not aggravate disease (11). However, further studies and comprehensive surveillance are needed to determine the role of co-infection in the mediation of illness severity in patients with SARS-CoV-2.

This study has several limitations. Only 10 patients with co-infection of SARS-CoV-2 and HAdV were identified and included. All patients presented to the hospitals after symptom onset. The patients were distributed over two cities, and involved two Provinces of China. Detailed epidemiological data are difficult to obtain, and systematic sample collection early during the course of illness was limited. Thus, the limitations of this study are its flaws or shortcomings which could be the result of unavailability of resources, small sample size, flawed methodology, etc.

In summary, we identified some pneumonia patients with obvious epidemiological relationship, which were caused by co-infection with SARS-CoV-2 and HAdV. This study provides a clear example of the persistent transmission of SARS-CoV-2 and HAdV co-infection, which spread inter-regionally and

throughout third generations of patients. Our findings also indicate that co-infection with SARS-CoV-2 and HAdV can be latently spread, a characteristic that makes controlling the COVID-19 pandemic especially challenging. Therefore, continuous surveillance is needed to monitor the prevalence, infectivity, transmissibility, and pathogenicity of pathogen-SARS-CoV-2 co-infection to evaluate the precise risk associated with co-infections.

## DATA AVAILABILITY STATEMENT

The datasets presented in this study can be found in online repositories. The names of the repository/repositories and accession number(s) can be found at: GenBank under accession numbers: MW011762, MW011765–MW011768 for SARS-CoV-2; MW013769–MW013771, MW013774–MW013780 for HAdV.

## AUTHOR CONTRIBUTIONS

SQ, SH, HS, and ZZ contributed to the conception and design of the study. GZ, XL, HZ, XX, XC, GY, LG, SH, and ZZ carried out sample collection and data acquisition. SQ, GZ, HL (Seventh Author), XD, HL (Fifth Author), HZ, XX, HW, ST, MY, and LG performed the laboratory sample analysis. SQ, PL, and LW performed statistical analyses. SQ, PL, and ZZ wrote the first draft of the manuscript. HS and ZZ supervised this study. All authors approved the final manuscript as submitted, and agreed to be accountable for all aspects of the work.

## FUNDING

This work was supported in part by the National Science and Technology Major Project of China (2018ZX10101003 and 2018ZX10714002), Hunan Provincial Construction of Innovative Provinces Special Social Development Areas Key Research and Development Project (2020SK3012), and the Chinese Academy of Medical Sciences Coronavirus Disease 2019 Science and Technology Research Project in 2020 (2020HY320003).

## ACKNOWLEDGMENTS

The authors of the present study would like to thank all participants enrolled in this study.

## SUPPLEMENTARY MATERIAL

The Supplementary Material for this article can be found online at: <https://www.frontiersin.org/articles/10.3389/fmed.2021.735779/full#supplementary-material>

## REFERENCES

- Huang C, Wang Y, Li X, Ren L, Zhao J, Hu Y, et al. Clinical features of patients infected with 2019 novel coronavirus in Wuhan, China. *Lancet*. (2020) 395:497–506. doi: 10.1016/S0140-6736(20)30183-5
- Zhu N, Zhang D, Wang W, Li X, Yang B, Song J, et al. A novel coronavirus from patients with pneumonia in China, 2019. *N Engl J Med*. (2020) 382:727–33. doi: 10.1056/NEJMoa2001017
- Zeliang Chen, Qi Zhang, Yi Lu, Zhongmin Guo, Xi Zhang, Wenjun Zhang, et al. Distribution of the 2019-nCoV epidemic and correlation with population

- emigration from wuhan, China. *Chin Med J (Engl)*. (2020) 133:1044–50. doi: 10.1097/CM9.0000000000000782
4. Hoehl S, Rabenau H, Berger A, Kortenbusch M, Cinatl J, Bojkova D, et al. Evidence of SARS-CoV-2 infection in returning travelers from wuhan, China. *N Engl J Med*. (2020) 382:1278–80. doi: 10.1056/NEJMc2001899
  5. Chan JF, Yuan S, Kok KH, To KK, Chu H, Yang J, et al. A familial cluster of pneumonia associated with the 2019 novel coronavirus indicating person-to-person transmission: a study of a family cluster. *Lancet*. (2020) 395:514–23. doi: 10.1016/S0140-6736(20)30154-9
  6. Guan WJ, Ni ZY, Hu Y, Liang WH, Ou CQ, He JX, et al. Clinical characteristics of coronavirus disease 2019 in China. *N Engl J Med*. (2020) 382:1708–20. doi: 10.1056/NEJMoa2002032
  7. Yu P, Zhu J, Zhang Z, Han Y, Huang L. A familial cluster of infection associated with the 2019 novel coronavirus indicating potential person-to-person transmission during the incubation period. *J Infect Dis*. (2020) 221:1757–61. doi: 10.1093/infdis/jiaa077
  8. Xiaojuan Zhu, Yiyue Ge, Tao Wu, Kangchen Zhao, Yin Chen, Bin Wu, et al. Co-infection with respiratory pathogens among COVID-2019 cases. *Virus Res*. (2020) 285:198005. doi: 10.1016/j.virusres.2020.198005
  9. David Kim, James Quinn, Benjamin Pinsky, Nigam H Shah, Ian Brown. Rates of co-infection between SARS-CoV-2 and other respiratory pathogens. *JAMA*. (2020) 323:2085–6. doi: 10.1001/jama.2020.6266
  10. Danley K, Kent P. 4-month-old boy coinfecting with COVID-19 and adenovirus. *BMJ Case Rep*. (2020) 13:e236264. doi: 10.1136/bcr-2020-236264
  11. Ding Q, Lu P, Fan Y, Xia Y, Liu M. The clinical characteristics of pneumonia patients co-infected with 2019 novel coronavirus and influenza virus in Wuhan, China. *J Med Virol*. (2020) 92:1549–55. doi: 10.1002/jmv.25781
  12. Wu X, Cai Y, Huang X, Yu X, Zhao L, Wang F, et al. Co-infection with SARS-CoV-2 and Influenza A virus in patient with pneumonia, China. *Emerg Infect Dis*. (2020) 26:1324–6. doi: 10.3201/eid2606.200299
  13. Bankevich A, Nurk S, Antipov D, Gurevich AA, Dvorkin M, Kulikov AS, et al. SPAdes: a new genome assembly algorithm and its applications to single-cell sequencing. *J comput biol*. (2012) 19:455–77. doi: 10.1089/cmb.2012.0021
  14. Katoh K, Standley DM, MAFFT. Multiple sequence alignment software version 7: improvements in performance and usability. *Mol Biol Evol*. (2013) 30:772–80. doi: 10.1093/molbev/mst010
  15. Kumar S, Stecher G, Tamura K. MEGA7: molecular evolutionary genetics analysis version 7. 0 for bigger datasets. *Mol Biol Evol*. (2016) 33:1870–4. doi: 10.1093/molbev/msw054
  16. Li H, Durbin R. Fast and accurate long-read alignment with Burrows-Wheeler transform. *Bioinformatics*. (2010) 26:589–95. doi: 10.1093/bioinformatics/btp698
  17. Li H, Handsaker B, Wysoker A, Fennell T, Ruan J, Homer N, et al. The sequence alignment/map format and SAMtools. *Bioinformatics*. (2009) 25:2078–9. doi: 10.1093/bioinformatics/btp352
  18. Mercatelli D, Giorgi FM. Geographic and genomic distribution of SARS-CoV-2 mutations. *Front Microbiol*. (2020) 11:1800. doi: 10.3389/fmicb.2020.01800
  19. Li Q, Guan X, Wu P, Wang X, Zhou L, Tong Y, et al. Early transmission dynamics in wuhan, China, of novel coronavirus-infected pneumonia. *N Engl J Med*. (2020) 382:1199–07. doi: 10.1056/NEJMoa2001316
  20. James L, Vernon MO, Jones RC, Stewart A, Lu X, Zollar LM, et al. Outbreak of human adenovirus type 3 infection in a pediatric long-term care facility—Illinois, 2005. *Clin Infect Dis*. (2007) 45:416–20. doi: 10.1086/519938
  21. Bai Y, Yao L, Wei T, Tian F, Jin DY, Chen L, et al. Presumed asymptomatic carrier transmission of COVID-19. *JAMA*. (2020) 323:1406–7. doi: 10.1001/jama.2020.2565
  22. Huang R, Xia J, Chen Y, Shan C, Wu C. A family cluster of SARS-CoV-2 infection involving 11 patients in Nanjing, China. *Lancet Infect Dis*. (2020) 20:534–5. doi: 10.1016/S1473-3099(20)30147-X
  23. Pan X, Chen D, Xia Y, Wu X, Li T, Ou X, et al. Asymptomatic cases in a family cluster with SARS-CoV-2 infection. *Lancet Infect Dis*. (2020) 20:410–1. doi: 10.1016/S1473-3099(20)30114-6
  24. Tong ZD, Tang A, Li KF, Li P, Wang HL, Yi JP, et al. Potential presymptomatic transmission of SARS-CoV-2, Zhejiang Province, China, 2020. *Emerg Infect Dis*. (2020) 26:1052–4. doi: 10.3201/eid2605.200198
  25. Kimball A, Hatfield KM, Arons M, James A, Taylor J, Spicer K, et al. Asymptomatic and presymptomatic SARS-CoV-2 infections in residents of a long-term care skilled nursing facility - king county, Washington, March 2020. *MMWR Morb Mortal Wkly Rep*. (2020) 69:377–81. doi: 10.15585/mmwr.mm6913e1. Epub ahead of print.
  26. Qiu J. Covert coronavirus infections could be seeding new outbreaks. *Nature*. (2020). doi: 10.1038/d41586-020-00822-x
  27. Rothe C, Schunk M, Sothmann P, Bretzel G, Froeschl G, Wallrauch C, et al. Transmission of 2019-nCoV infection from an asymptomatic contact in Germany. *N Engl J Med*. (2020) 382:970–1. doi: 10.1056/NEJMc2001468
  28. Wang D, Hu B, Hu C, Zhu F, Liu X, Zhang J, et al. Clinical characteristics of 138 hospitalized patients with 2019 novel coronavirus-infected pneumonia in wuhan, China. *JAMA*. (2020) 323:1061–9. doi: 10.1001/jama.2020.1585
  29. Chang SY, Lee CN, Lin PH, Huang HH, Chang LY, Ko W, et al. A community-derived outbreak of adenovirus type 3 in children in Taiwan between 2004 and 2005. *J Med Virol*. (2008) 80:102–12. doi: 10.1002/jmv.21045
  30. Qiu S, Li P, Liu H, Wang Y, Liu N, Li C, et al. Whole-genome sequencing for tracing the transmission link between two ARD outbreaks caused by a novel HAdV serotype 7 variant, China. *Sci Rep*. (2015) 5:13617. doi: 10.1038/srep13617

**Conflict of Interest:** The authors declare that the research was conducted in the absence of any commercial or financial relationships that could be construed as a potential conflict of interest.

**Publisher's Note:** All claims expressed in this article are solely those of the authors and do not necessarily represent those of their affiliated organizations, or those of the publisher, the editors and the reviewers. Any product that may be evaluated in this article, or claim that may be made by its manufacturer, is not guaranteed or endorsed by the publisher.

Copyright © 2021 Qiu, Zeng, Li, Li, Liu, Du, Liu, Zhang, Xiang, Wang, Chen, Yang, Tian, Wang, Yang, Yang, Gao, Hu, Song and Zhan. This is an open-access article distributed under the terms of the Creative Commons Attribution License (CC BY). The use, distribution or reproduction in other forums is permitted, provided the original author(s) and the copyright owner(s) are credited and that the original publication in this journal is cited, in accordance with accepted academic practice. No use, distribution or reproduction is permitted which does not comply with these terms.





# Prevalence of Covid-19 Associated Symptoms, Their Onset and Duration, and Variations Among Different Groups of Patients in Bangladesh

**Md. Tanzilul Amin<sup>1</sup>, Mahmud Hasan<sup>2</sup> and N. M. Mahmudul Alam Bhuiya<sup>1\*</sup>**

<sup>1</sup> Department of Pharmacy, Jagannath University, Dhaka, Bangladesh, <sup>2</sup> Department of Radiology and Radiological Science, Johns Hopkins University, Baltimore, MD, United States

## OPEN ACCESS

### Edited by:

Reza Lashgari,  
Shahid Beheshti University, Iran

### Reviewed by:

Pritom Chowdhury,  
Tea Research Association, India  
Alireza Shafiei,  
Bahrami Children's Hospital, Tehran  
University of Medical Sciences, Iran

### \*Correspondence:

N. M. Mahmudul Alam Bhuiya  
mahmudul@pharm.jnu.ac.bd

### Specialty section:

This article was submitted to  
Infectious Diseases - Surveillance,  
Prevention and Treatment,  
a section of the journal  
Frontiers in Public Health

**Received:** 08 July 2021

**Accepted:** 30 August 2021

**Published:** 29 September 2021

### Citation:

Amin MT, Hasan M and  
Bhuiya NMMA (2021) Prevalence of  
Covid-19 Associated Symptoms,  
Their Onset and Duration, and  
Variations Among Different Groups of  
Patients in Bangladesh.  
Front. Public Health 9:738352.  
doi: 10.3389/fpubh.2021.738352

**Objective:** This study aimed to assess the prevalence, onset, and duration of COVID-19 associated symptoms, hospitalization, and recovery time from the infection in Bangladesh.

**Methods:** A retrospective study was designed adopting the snowball sampling technique ( $n = 439$ ). The association of gender, age, and comorbidity on COVID-19 associated complications was determined using chi-square and binary logistic regression analysis ( $p < 0.05$ ).

**Result:** Fever, exhaustion, cough, loss of taste, sore throat, body ache, and hair-loss were prevalent among more than 50% of the participants and developed within fourth days in above 90% of the patients. Shortness of breath was significantly higher in males ( $\chi^2 = 5.671$ ; OR 1.641). Significant comorbidity association on the shortness of breath ( $\chi^2 = 40.119$ ; OR 2.564), vomiting ( $\chi^2 = 4.422$ ; OR 1.018), and loss of speech ( $\chi^2 = 17.299$ ; OR 3.430) was observed. Patients ( $>40$  years) exerted higher association in shortness of breath ( $\chi^2 = 24.083$ ; OR 2.901). Age and comorbidity were significantly associated with COVID-19 associated hospitalization ( $\chi^2 = 16.890$  and  $\chi^2 = 23.638$ , respectively) and recovery time ( $\chi^2 = 12.870$  and  $\chi^2 = 26.924$ , respectively).

**Conclusion:** The study suggests that the hospitalization rate increased for older ( $>40$  years) and comorbid patients. Comorbid patients demonstrated higher susceptibility to have shortness of breath, vomiting, loss of speech, and confusion, whereas male patients showed significant increase in the prevalence of sore throat, loss of smell, and vomiting compared to female patients.

**Keywords:** COVID-19, SARS-CoV-2, COVID-19 symptoms, corona, flu, symptoms, fever, cold

## INTRODUCTION

In late December 2019, a small number of inexplicable respiratory infections were recorded in Wuhan, Hubei province, China. It has clinical similarities to viral pneumonia and Prevention Research Centers, Centers for Disease Control (CDC) experts determined that pneumonia was caused by a novel  $\beta$ -coronavirus (1, 2). Afterward, WHO relabeled the name of this virus as severe acute respiratory syndrome coronavirus-2 (SARS-CoV-2)

suggested by the Coronavirus Study Group of the International Committee on Taxonomy of Viruses (ICTV), and the disease was termed as coronavirus disease 2019 or simply COVID-19 (3). Although no animal source has been confirmed yet, due to the similarity in genomic features, it is postulated that bat or pangolin may work as a reservoir of SARS-CoV-2 (4). On Mar 11, 2020, WHO stated the COVID-19 outbreak as a global pandemic as reported cases reach 200,000 people, with over 8,000 people died due to the complications related to COVID-19 in over 160 countries (5, 6). The number of confirmed cases increases every day, exerting a wide variety of symptoms in the infected persons. SARS-CoV-2 has now spread to more than 213 countries worldwide.

Coronaviruses are a broad family of viruses that cause respiratory disorders, which diagnosis varies from the common cold to more severe disorders such as Middle East Respiratory Syndrome (MERS), Severe Acute Respiratory Syndrome (SARS), and COVID-19 (7). The symptoms of coronavirus infections include cough, fever, diarrhea, chest pain, fatigue, body ache, sore throat, rhinorrhea, tachypnea, dyspnea (7, 8). The presence of glycoprotein spikes on the envelope of this RNA virus gives it a classic crown-like look under an electron microscope (9). This group of viruses is zoonotic, meaning they can be transmitted between animals and people (10–12). Coronaviruses are classified into four genera, one of which is  $\alpha$ - $\beta$ - $\gamma$ - $\delta$ -coronavirus. The  $\alpha$ - and  $\beta$ -coronaviruses are both capable of infecting mammals, while  $\gamma$ - and  $\delta$ -coronaviruses are more commonly found in birds (13). Six coronaviruses had long been described as human-susceptible viruses. Among them,  $\alpha$ -coronavirus HCoV-229E and HCoV-NL63 bear low pathogenicity, and  $\beta$ -CoVs HCoV-HKU1 and HCoV-OC43 cause moderate respiratory symptoms, identical to a common cold. On the other hand, the other known  $\beta$ -CoVs, SARS-CoV and MERS-CoV could result in a severe and potentially fatal respiratory illness (14, 15). The disease is generally known to be transmitted between animals and humans through sneezing, coughing, touching or shaking hands, and contacting a surface or object and the incubation period ranges from 2 to 14 days (9, 14). The infection has been predicted by a loss of smell and taste in addition to other symptoms (16, 17). The prevalence of gastrointestinal symptoms before fever and difficulty in breathing was also reported in a previous study (18). COVID-19 has caused millions of people to be hospitalized around the world, with symptoms including fever, dry cough, exhaustion, diarrhea, breathing problem, headache, nausea, and vomiting (19). After 60 days, just 13% of people in Italy were completely free of COVID-19 symptoms, with 55% reporting three or more persistent symptoms and 32% reporting one or two residual symptoms (20). Similarly, COVID-19 patients who suffered from chronic symptoms exhibited a lower life expectancy after 2–3 weeks of infection in the United States (21).

COVID-19 associated symptoms and complications may vary from person to person. COVID-19 has a wide range of frequency and severity, which is believed to be influenced by various biological, cultural, and economic factors. Many of those who died had other advanced age, hypertension, diabetes, or cardiovascular disease that impaired their immune systems (14). According to previous clinical investigations, females are less

likely to be infected and have lower cytokine production than previous clinical investigations (22). African and Asian races have a higher chance of acquiring COVID-19 than Caucasian people; Asians may also have a higher chance of hospitalization and mortality (23).

In Bangladesh, the first documented incidence was reported on Mar 08, 2020 (24). Infection rates remained low until the end of March, following which a significant surge in infected cases occurred that persisted till June 2020 (25, 26). The number of new COVID-19 infection cases, COVID-19-related deaths, recovery from COVID-19, and the number of Real-Time Reverse Transcription Polymerase Chain Reaction (RT-PCR) tests conducted in Bangladesh is illustrated in **Figure 1**. There has been very limited information regarding the COVID-19 symptoms and associated consequences among the patient of Bangladesh. In this study, we were focused on assessing the prevalence, onset, and duration of the severity of the symptoms and recovery time in the study participants. We also tried to determine the impact of different factors such as gender, age, and comorbidity on hospitalization, recovery time as well as the prevalence of the COVID-19 associated symptoms.

## METHODS

### Study Design and Time

A cross-sectional study design using “Google Form” was adopted to assess the prevalence of COVID-19-related symptoms among the patients of Bangladesh during the outbreak of COVID-19. Data were collected from Sept 08, 2020, to Nov 08, 2020. At that time, it was not feasible to conduct community-based surveys due to the countrywide lockdown implemented by the government (27, 28). This self-reported retrospective study was conducted using a standardized questionnaire. Only those infected with coronavirus between Mar 08, 2020, and Aug 08, 2020, had their infection verified by RT-PCR test and then recovered from the condition- were included in the study.

### Sampling of the Study

The online link was circulated by the Exponential Non-Discriminative snowballing method (29, 30). An online-based advertisement campaign was designed to recruit participants for this online survey who suffered and eventually recovered from COVID-19 (31). Participants residing in Bangladesh were randomly selected, and none of them were related to any study. We covered the people who use social media platforms (e.g., Facebook and LinkedIn) to collect information for this study. People receiving the message were requested to participate in the survey and forward the link to their close contacts infected by this coronavirus. Participants whose age was 18 years old or above were allowed to participate in this study. A total of 453 complete responses were received in this survey who agreed to take part. Of these, six responses were also omitted due to incomplete data. In addition, answers from the participants having COVID-19 like symptoms but not performing the RT-PCR test- were also excluded. Finally, a total of 439 responses were considered for final data analysis.

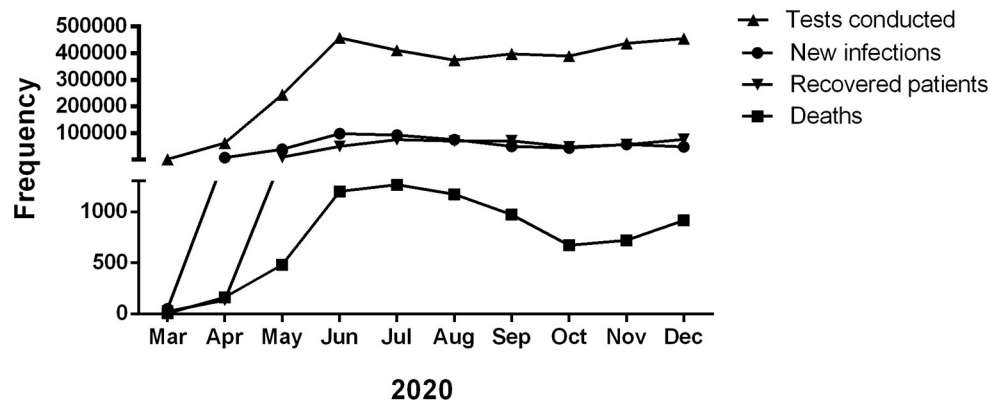


**FIGURE 1** | Month-wise total number of COVID-19 patients, death, recovered, and RT-PCR test conducted in Bangladesh in 2020 (Ref: DGHS, Bangladesh).

## Study Tool Preparation

The survey consisted of 23 questions. Except for two unstructured, open-ended questions, all of the questions were closed-ended. The questionnaire has four domains. The first one collected the demographic details of the participants. The second domain was constructed to contain participants' infection date, RT-PCR test information (to ascertain the infection and recovery from the disease), treatment, hospitalization and recovery time, and other comorbidity histories. The questions of the third and fourth domains were designed to measure the onset and duration of the symptoms, respectively. A set of nineteen symptoms was included in the questionnaire to check the symptoms' prevalence, onset, and duration. In addition, participants were allowed to report any other symptoms that were not mentioned in the questionnaire through an open-ended question. The history of other chronic diseases was also recorded. The questions were constructed in English to understand the scientific terminologies better, whereas a Bengali (most participants' mother tongue) translation was also provided. A forward-backward translation process was followed for the finalization of the questionnaire.

## Data Management

The data from the "Google Form" was initially extracted in .xlsx format. Participants who disagreed with using their information, those who did not complete an RT-PCR test to confirm infection, and incomplete responses were then deleted from this study. After that, the data was converted to .sav format for further statistical analysis. Descriptive statistics (frequency, percentages, and means) were used to examine the participants' responses and demographic distribution. Participants were divided into different groups for further analysis based on gender (male-female), age (aging  $\leq 40$  years old and aging  $> 40$  years old), and comorbidity (other chronic disease(s)-no other disease(s) during the infection) based on other relevant conditions (32, 33). The Pearson's chi-squared test followed by binary logistic regression analysis was applied to determine the association of different predictors in the prevalence of the symptoms. Statistical

significance was defined when  $p < 0.05$ . All statistical tests were performed using STATA 12.0 and IBM SPSS 23.0 version.

## Ethical Consideration

The current study was carried out following the Helsinki declaration changed in 2014 and the checklist for reporting internet e-surveys (CHERRIES) (34, 35). The study was reviewed and approved by The Jagannath University Research Cell, Dhaka, Bangladesh (File no.- JnURes-001/2020). The objectives, potential benefits, risks, and the confidentiality of given responses were communicated with participants before starting the online survey. Participants also received an option to provide their consent to use their provided information for further analysis in the study.

## RESULTS

### Demographics

The final analysis consisted of 439 respondents where 69% ( $n = 303$ ) were male, and 31% ( $n = 136$ ) were female (Table 1). The participants' ages ranged from 18 years to above 60 years. About 42% ( $n = 183$ ) participants aged from 18 to 30 years followed by 31% ( $n = 135$ ) people aged from 31 to 40 years. Although respondents were from all divisions of Bangladesh, the highest response rate was from Barishal Division (49%,  $n = 215$ ), whereas the lowest was from the Rangpur division (0.7%,  $n = 3$ ). The division wise participant information is illustrated in Supplementary Figure 1.

Out of all the participants, 44.5% were students, and most non-student participants had a baccalaureate degree. There was a larger response among those with higher secondary education and graduates. The majority of the respondents (more than 70%) work in the private sector, whereas some were government job holders (25.28%) healthcare professionals and mostly worked or did Private Job holder or business (39.86) in a crowded place, 19.81% were students, and 18 % of the respondents reported that a relative, colleagues or a neighbor had been diagnosed with COVID-19.

**TABLE 1** | Demographic distribution of the participants, Bangladesh, 2020.

| Variables                  | Total (%)   | Male (%)    | Female (%) |
|----------------------------|-------------|-------------|------------|
| Participants               | 439 (100%)  | 303 (69%)   | 136 (31%)  |
| <b>Age</b>                 |             |             |            |
| 16–30 Yrs                  | 183 (41.7%) | 112 (37%)   | 71 (52.2%) |
| 31–40 Yrs                  | 135 (30.8%) | 101 (33.3%) | 34 (25%)   |
| 41–50 Yrs                  | 66 (15%)    | 50 (16.5%)  | 16 (11.8%) |
| 51–60 Yr                   | 40 (9.1%)   | 31 (10.2%)  | 9 (6.6%)   |
| Above 60 Yrs               | 15 (3.4%)   | 9 (3%)      | 6 (4.4%)   |
| <b>Divisional location</b> |             |             |            |
| Barishal                   | 215 (49%)   | 146 (48.2%) | 69 (50.7%) |
| Chittagong                 | 17 (3.9%)   | 10 (3.3%)   | 7 (5.1%)   |
| Dhaka                      | 103 (23.5%) | 71 (23.4%)  | 32 (23.5%) |
| Khulna                     | 37 (8.4%)   | 22 (7.3%)   | 15 (11%)   |
| Mymensingh                 | 3 (0.7%)    | 2 (0.7%)    | 1 (0.7%)   |
| Rajshahi                   | 7 (1.6%)    | 4 (1.3%)    | 3 (2.2%)   |
| Rangpur                    | 3 (0.7%)    | 2 (0.7%)    | 1 (0.7%)   |
| Sylhet                     | 54 (12.3%)  | 46 (15.2%)  | 8 (5.9%)   |
| <b>Occupation</b>          |             |             |            |
| Govt. job                  | 111 (25.3%) | 89 (29.4%)  | 22 (16.2%) |
| Housewife                  | 58 (13.2%)  | 0 (0.0%)    | 50 (36.8%) |
| Private job                | 122 (27.8%) | 105 (34.7%) | 17 (12.5%) |
| Self-employed              | 53 (12.1%)  | 49 (16.2%)  | 4 (2.9%)   |
| Student                    | 87 (19.8%)  | 48 (15.8%)  | 39 (28.7%) |
| Unemployed                 | 8 (1.8%)    | 12 (3.9%)   | 4 (2.9%)   |
| <b>Monthly income</b>      |             |             |            |
| Undisclosed                | 12 (2.7%)   | 5 (1.7%)    | 7 (5.1%)   |
| <BDT 10,000                | 130 (29.6%) | 51 (16.9%)  | 77 (56.6%) |
| BDT 10,000–20,000          | 75 (17.1%)  | 63 (20.9%)  | 12 (8.8%)  |
| BDT 21,000–40,000          | 134 (30.5%) | 107 (35.5%) | 27 (19.8%) |
| BDT 41,000–60,000          | 53 (12.1%)  | 42 (13.9%)  | 11 (8%)    |
| More than BDT 60,000       | 35 (8%)     | 33 (11%)    | 2 (1.5%)   |
| <b>Month of infection</b>  |             |             |            |
| March–April, 2020          | 8 (1.8%)    | 6 (2%)      | 2 (1.5%)   |
| May–June, 2020             | 124 (28.2%) | 92 (30.4%)  | 32 (23.5%) |
| July–August, 2020          | 160 (36.4%) | 105 (34.7%) | 55 (40.4%) |
| September–October, 2020    | 147 (33.5%) | 100 (33%)   | 47 (34.5%) |

One-third (29.6%,  $n = 130$ ) of respondents' monthly income was below 10,000 BDT (117.81 USD), whereas another one-third (30.5%,  $n = 134$ ) of respondent's monthly income was between 21,000 BDT to 40,000 BDT (247.41 USD to 471.27 USD). The exchange rate was considered 1 USD = 84.8775 (average of day's lowest and day's highest, data obtained from [www.bb.org.bd/econdata/exchangerate.php](http://www.bb.org.bd/econdata/exchangerate.php) on June 25th, 2021). Monthly income of above 60,000 BDT (706.9 USD) consist of 8% ( $n = 35$ ), where 2.7% ( $n = 12$ ) did not disclose the information (Table 1).

## Comorbidity

The prevalence and severity of the COVID-19 associated symptoms tend to be impacted by comorbidities. Therefore,

participants were asked to report any chronic disease(s) they had been suffering from. Among 439 participants, 26.19% of participants (a total of 115 participants, among them 76 male and 39 female) reported that they had been suffering from different chronic diseases(s) or comorbidities (single or multiple chronic diseases) before being infected by the coronavirus, such as asthma, chronic obstructive pulmonary disease (COPD), diabetes, hypertension, stroke, heart attack, other heart diseases, kidney disease, allergy, arthritis, liver disease, and obesity. The self-reported comorbidities were later categorized as Lung disease (asthma, COPD, and other respiratory problems), diabetes, cardiac disease (hypertension, stroke, heart attack, and other heart diseases), and miscellaneous (kidney disease, allergy, rhinitis, liver disease, and obesity). 18.67% of total participants



**TABLE 2 |** Hospitalization due to COVID-19 associated complications, Bangladesh, 2020.

| Variable           | Group                     | Admitted into hospital | Home quarantined | $\chi^2$ (p-value) |
|--------------------|---------------------------|------------------------|------------------|--------------------|
| Total participants | <i>N</i> = 439            | 57 (12.99%)            | 382 (87.01%)     |                    |
| Gender             | Male ( <i>n</i> = 303)    | 45 (14.85%)            | 258 (85.15%)     | 3.019 (0.082)      |
|                    | Female ( <i>n</i> = 136)  | 12 (8.82%)             | 124 (91.18%)     |                    |
| Age                | ≤40 Yrs ( <i>n</i> = 318) | 30 (9.43%)             | 288 (90.57%)     | 12.870 (0.000)     |
|                    | >40 Yrs ( <i>n</i> = 121) | 27 (22.31%)            | 94 (77.69%)      |                    |
| Comorbidity        | Yes ( <i>n</i> = 115)     | 31 (26.95%)            | 84 (73.05%)      | 26.924 (0.000)     |
|                    | No ( <i>n</i> = 324)      | 26 (8.02%)             | 298 (91.98%)     |                    |

Values are expressed as frequency and % response of the final respondents. The percentage was calculated considering the samples in the individual groups. Pearson's chi-squared test was applied to observe the association of gender, age, and the previous history of comorbidity in the incidence of hospitalization.  $P < 0.05$  was considered statistically significant.

( $n = 82$ ) had cardiac disease, 6.83% ( $n = 30$ ) had diabetes, 5% ( $n = 22$ ) had lung disease, and the rest of the comorbid participants (2.96%,  $n = 13$ ) were suffering from miscellaneous chronic conditions.

## COVID-19 Complications Associated With Hospitalization

The obtained result found that COVID-19-related complications led to the admission of 13% of participants to the hospital (Table 2). Comorbid patients were more prone to be hospitalized due to COVID-19 associated complications. Significant association in gender ( $\chi^2 = 12.870$ ,  $p = 0.000$ ) and comorbidity ( $\chi^2 = 26.924$ ,  $p = 0.000$ ) was also found in hospitalization due to COVID-19 associated complications.

## Prevalence of COVID-19 Associated Symptoms

Table 3 shows the prevalence of COVID-19-related symptoms. Table 4 depicts how male gender, older age (>40 years), and comorbidity were associated (odds ratio) with the prevalence of these symptoms among the participants. Fever (93.60%), exhaustion (88.80%), and cough (70.80%) were the most prevalent symptoms reported by the participants. Loss of taste, sore throat, body ache, and hair loss were common among more than 50%. Nearly half of the respondents (49.70%) complained about the loss of smell due to the infection. Significant gender association was observed in sore throat ( $\chi^2 = 4.210$ ;  $p = 0.040$ ), loss of smell ( $\chi^2 = 5.671$ ;  $p = 0.017$ ), and vomiting ( $\chi^2 = 4.724$ ;  $p = 0.030$ ). The findings revealed that gender and comorbidities also had an impact on the characteristics of COVID-19-related symptoms. Older adults (>40 years) were significantly associated with shortness of breath ( $\chi^2 = 24.083$ ;  $p = 0.000$ ) and hair loss ( $\chi^2 = 38.887$ ;  $p = 0.000$ ). A significant difference was observed in the group based on comorbidity in shortness of breath ( $\chi^2 = 40.119$ ;  $p = 0.000$ ), vomiting ( $\chi^2 = 4.442$ ;  $p = 0.035$ ), confusion ( $\chi^2 = 15.558$ ;  $p = 0.000$ ), Loss of speech ( $\chi^2 = 17.299$ ;  $p = 0.000$ ) and hair loss ( $\chi^2 = 20.212$ ;  $p = 0.000$ ). Male patients showed 1.641 times higher odds (95% CI 1.090–2.472) of having the symptom of loss of smell than the female patients. Patients over 40 years old were significantly associated with shortness of breath

[OR = 2.901 (95% CI 1.881–4.476)]. According to the findings, comorbidity was also found to be substantially linked with the prevalence of shortness of breath [OR = 4.042; (95% CI 2.564–6.374)], vomiting [OR = 1.689; (95% CI 1.018–2.802)], loss of speech [OR = 3.430 (1.944–6.053)], and Confusion [OR = 2.746 (95% CI 1.686–4.476)].

## Onset and Duration of COVID-19 Associated Symptoms

The onset and duration of COVID-19 related symptoms are described in Table 5 and Table 6, respectively. In brief, the most common symptom in COVID-19 patients was fever (93.6%,  $n = 411$ ), which lasted for 1–4 days for most of the patients (77.4%,  $n = 340$ ). The second most common symptom was exhaustion, reported in 89.8% ( $n = 390$ ) patients and lasted for 11–14 days for 50% of the patients who have the symptom. Other accompanying symptoms were cough, body ache, loss of taste, loss of smell, lack of appetite, and headache, whereas more than 100 patients were affected by those symptoms. Out of all the symptoms we reported, exhaustion, sore throat, shortness of breath, body ache, vomiting, headache, digestive problems, lack of appetite, blistering, Confusion, and/or loss of speech were developed in some patients 14th days of infection. Interestingly, the onset of blistering was after 14th days for 20% of patients ( $n = 2$ ). However, all the symptoms persisted in some patients for more than 14 days, whereas 33% ( $n = 127$ ) exhibited exhaustion for more than 14 days. Similarly, Confusion occurred for more than 14 days in 27% of patients ( $n = 22$ ).

## Time Required for the Recovery From the COVID-19 Associated Symptoms

In various patients, the time it takes to get a coronavirus infection negative by RT-PCR test may differ from the time it takes to recover from all symptoms. The duration required to get rid of all the COVID-19 associated symptoms was also assessed in this study and illustrated in Table 7. More than 53% of patients were recovered from all COVID-19 related symptoms within 8 to 14 days. However, most patients older than 40 years (45.5%) required 15–21 days to recover from the symptoms. Significant differences in the groups of age ( $\chi^2 = 16.890$ ;  $p = 0.005$ ) and

**TABLE 3 |** Prevalence of the Covid-19 associated symptoms among the participants, Bangladesh, 2020.

| Response            | Total frequency (%) | Male frequency (%) | Female frequency (%) | $\chi^2$ (p-Value) | $\leq 40$ Yrs frequency (%) | $> 40$ Yrs frequency (%) | $\chi^2$ (p-Value) | No Comorbidity | Comorbidity | $\chi^2$ (p-Value) |
|---------------------|---------------------|--------------------|----------------------|--------------------|-----------------------------|--------------------------|--------------------|----------------|-------------|--------------------|
| Fever               | 411 (93.6%)         | 285 (94.1%)        | 126 (92.6%)          | 0.314 (0.576)      | 296 (93.2%)                 | 115 (95.0%)              | 0.564 (.453)       | 306 (94.2%)    | 105 (92.1%) | 0.593 (0.441)      |
| Runny Nose          | 95 (21.6%)          | 6 (19%)            | 35 (25.7%)           | 1.949 (0.163)      | 70 (22.0%)                  | 25 (20.7%)               | 0.094 (.759)       | 67 (20.6%)     | 28 (24.6%)  | 0.775 (0.379)      |
| Cough               | 311 (70.8%)         | 207 (68.3%)        | 104 (76.5%)          | 3.021 (0.082)      | 220 (69.2%)                 | 91 (75.2%)               | 1.540 (0.215)      | 224 (68.9%)    | 87 (76.3%)  | 2.233 (0.135)      |
| Sore throat         | 279 (63.6%)         | 183 (60.40%)       | 96 (70.6%)           | 4.21 (0.04)        | 208 (65.4%)                 | 71 (58.7%)               | 1.714 (0.190)      | 212 (65.2%)    | 67 (58.8%)  | 1.520 (0.218)      |
| Shortness of breath | 193 (44%)           | 128 (42.2%)        | 65 (47.8%)           | 1.174 (0.279)      | 117 (36.8%)                 | 76 (62.8%)               | 24.083 (.000)      | 114 (35.1%)    | 79 (69.3%)  | 40.119 (0.000)     |
| Body ache           | 275 (62.6%)         | 196 (64.7%)        | 79 (58.1%)           | 1.746 (0.186)      | 199 (62.6%)                 | 76 (62.8%)               | 0.002 (.964)       | 199 (61.2%)    | 76 (66.7%)  | 1.066 (0.302)      |
| Diarrhea            | 135 (30.8%)         | 95 (31.4%)         | 40 (29.40%)          | 0.166 (0.684)      | 93 (29.2%)                  | 42 (34.7%)               | 1.229 (0.268)      | 92 (28.3%)     | 43 (37.7%)  | 3.511 (0.061)      |
| Loss of taste       | 281 (64%)           | 201 (66.3%)        | 80 (58.8%)           | 2.3 (0.129)        | 204 (64.2%)                 | 77 (63.6%)               | 0.912 (.502)       | 208 (64.0%)    | 73 (64.0%)  | 0.000 (0.995)      |
| Loss of smell       | 218 (49.7%)         | 162 (53.5%)        | 56 (41.2%)           | 5.671 (0.017)      | 156 (49.1%)                 | 62 (51.2%)               | 0.167 (0.683)      | 162 (49.8%)    | 56 (49.1%)  | 0.018 (0.894)      |
| Vomiting            | 86 (19.6%)          | 51 (16.8%)         | 35 (25.7%)           | 4.724 (0.03)       | 60 (18.9%)                  | 26 (21.5%)               | 0.382 (0.537)      | 56 (17.2%)     | 30 (26.3%)  | 4.422 (0.035)      |
| Headache            | 154 (35.1%)         | 101 (33.3%)        | 53 (39%)             | 1.31 (0.252)       | 117 (36.8%)                 | 37 (30.6%)               | 1.486 (0.223)      | 112 (34.5%)    | 42 (36.8%)  | 0.210 (0.647)      |
| Digestive problem   | 65 (14.8%)          | 41 (13.5%)         | 24 (17.6%)           | 1.261 (0.262)      | 48 (15.1%)                  | 17 (14.0%)               | 0.076 (0.783)      | 47 (14.5%)     | 18 (15.8%)  | 0.118 (0.731)      |
| Lack of appetite    | 173 (39.4%)         | 114 (37.6%)        | 59 (43.4%)           | 1.304 (0.254)      | 120 (37.7%)                 | 53 (43.8%)               | 1.351 (0.245)      | 123 (37.8%)    | 50 (43.9%)  | 1.278 (0.258)      |
| Rashes              | 44 (10%)            | 31 (10.20%)        | 13 (9.60%)           | 0.047 (0.828)      | 33 (10.4%)                  | 11 (9.1%)                | 0.161 (0.688)      | 32 (9.8%)      | 12 (10.5%)  | 0.043 (0.835)      |
| Blistering          | 10 (2.3%)           | 7 (2.3%)           | 3 (2.2%)             | 0.005 (0.946)      | 7 (2.2%)                    | 3 (2.5%)                 | 0.030 (0.861)      | 5 (1.5%)       | 5 (4.4%)    | 3.074 (0.080)      |
| Confusion           | 90 (20.5%)          | 62 (20.50%)        | 28 (20.6%)           | 0.001 (0.976)      | 62 (19.5%)                  | 28 (23.1%)               | 0.714 (0.398)      | 52 (16.0%)     | 38 (33.3%)  | 15.558 (0.000)     |
| Loss of speech      | 58 (13.2%)          | 43 (14.2%)         | 15 (11%)             | 0.819 (0.366)      | 39 (12.3%)                  | 19 (15.7%)               | 0.904 (0.342)      | 30 (9.2%)      | 28 (24.6%)  | 17.299 (0.000)     |
| Exhaustion          | 390 (88.8%)         | 268 (88.4%)        | 122 (89.7%)          | 0.15 (0.699)       | 281 (88.4%)                 | 109 (90.1%)              | 0.261 (0.610)      | 286 (88.0%)    | 104 (91.2%) | 0.887 (0.346)      |
| Hair loss           | 222 (50.6%)         | 159 (52.5%)        | 63 (46.3%)           | 1.421 (0.233)      | 190 (59.7%)                 | 32 (26.4%)               | 38.887 (0.000)     | 185 (56.9%)    | 37 (32.5%)  | 20.212 (0.000)     |

Values are expressed as frequency and % response of the final respondents. Total participants  $n=439$ ; Male  $n=303$ , Female  $n=136$ ; Age  $\leq 40$  years old,  $n=318$ , Age  $> 40$  years old,  $n=121$ . The percentage was calculated within the group. Pearson's chi-squared test was applied to observe the association of gender (male and female), age ( $\leq 40$  years old and  $> 40$  years old patients), and comorbidity in the prevalence of Covid-19 associated symptoms.  $P < 0.05$  was considered statistically significant.

**TABLE 4 |** Odds Ratios of Covid-19 associated symptoms, Bangladesh, 2020.

| Symptom             | OR [CI] Male         | OR [CI] >40 years old  | OR [CI] Comorbidity    |
|---------------------|----------------------|------------------------|------------------------|
| Fever               | 1.257 [0.564–2.799]  | 1.425 [0.563–3.603]    | 0.734 [0.322–1.671]    |
| Runny Nose          | 0.713 [0.442–1.148]  | 0.923 [0.552–1.542]    | 1.318 [0.799–2.174]    |
| Cough               | 0.663 [0.417–1.055]  | 1.351 [0.839–2.176]    | 1.387 [0.853–2.257]    |
| Sore Throat         | 0.635 [0.411–0.982]* | 0.751 [0.489–1.154]    | 0.774 [0.501–1.199]    |
| Shortness of Breath | 0.799 [0.532–1.200]  | 2.901 [1.881–4.476]*** | 4.042 [2.564–6.374]*** |
| Body Ache           | 1.322 [0.873–2.000]  | 1.010 [0.655–1.557]    | 1.224 [0.783–1.912]    |
| Diarrhea            | 1.096 [0.705–1.705]  | 1.286 [0.824–2.008]    | 1.506 [0.962–2.358]    |
| Loss of Taste       | 1.379 [0.910–2.092]  | 0.978 [0.633–1.512]    | 0.969 [0.623–1.509]    |
| Loss of Smell       | 1.641 [1.090–2.472]* | 1.091 [0.718–1.659]    | 0.949 [0.620–1.453]    |
| Vomiting            | 0.584 [0.358–0.952]* | 1.177 [0.702–1.973]    | 1.689 [1.018–2.802]*   |
| Headache            | 0.783 [0.515–1.191]  | 0.757 [0.483–1.185]    | 1.146 [0.737–1.783]    |
| Digestive Problem   | 0.730 [0.421–1.266]  | 0.919 [0.506–1.671]    | 1.196 [0.668–2.142]    |
| Loss of appetite    | 0.787 [0.522–1.187]  | 1.286 [0.841–1.967]    | 1.257 [0.816–1.935]    |
| Rashes              | 1.078 [0.545–2.132]  | 0.864 [0.422–1.769]    | 1.063 [0.528–2.142]    |
| Blistering          | 1.048 [0.267–4.117]  | 1.130 [0.287–4.441]    | 2.900 [0.824–10.207]   |
| Loss of Speech      | 1.334 [0.713–2.495]  | 1.333 [0.736–2.412]    | 3.430 [1.944–6.053]*** |
| Confusion           | 0.992 [0.601–1.637]  | 1.243 [0.750–2.061]    | 2.746 [1.686–4.476]*** |
| Extreme Exhaustion  | 0.879 [0.456–1.693]  | 1.196 [0.601–2.379]    | 1.256 [0.619–2.549]    |
| Hair Loss           | 1.279 [0.853–1.919]  | 0.242 [0.153–0.384]*** | 0.375 [0.240–0.587]    |

OR = odds ratio; [CI] = 95% confidence interval. OR > 1 means greater odds of association with the exposure and outcome; OR = 1 means there is no association between exposure and outcome; OR < 1 means there is a lower odds of association between the exposure and outcome. Logistic binary regression analysis was applied to determine the correlation of gender (male), age (>40 years old) and comorbidity (previous history of other chronic diseases) on the prevalence of the Covid-19 associated symptoms. \* $p < 0.05$ , \*\*\* $p < 0.001$ .

comorbidity ( $\chi^2 = 23.638$ ;  $p = 0.040$ ) was observed in time required for the complete symptomatic recovery.

## DISCUSSION

In the last 20 years, several respiratory-related viral diseases such as SARS-CoV, H1N1 influenza, and MERS-CoV epidemics outbreak (36). Although previous coronaviruses, SARS-CoV and MERS-CoV, exhibited a high death rate, 9.6, and 35%, respectively, SARS-CoV-2 was declared as pandemic because of its high contagiousness and global spreading (36).

This study was conducted on 439 people in Bangladesh who recovered from COVID-19 at least 1 month before participating. Conforming to the first COVID-19 patient detection in Bangladesh, the survey includes the patients who got infected between March 2020 to September 2020. Our study found that most participants got infected from May–June, which matches the data obtained from the Directorate General of Health Services (DGHS) (Figure 1). Only 8 (1.8%) respondents got infected between March and April, suggesting that the virus took about 2 months to widespread. Most patients were between the ages above 40 years, and the male patient rate was 74.38%.

When we try to assess the relationship between hospitalization rate and predictors such as gender, age, or comorbidity, we found elderly patients had a significantly high hospitalization rate (22.31 vs. 9.43%), and 26.95% of patients with comorbidity were hospitalized compared to the patients (8.02%) who were hospitalized without any comorbid condition. The data

suggest that age and comorbid conditions play a significant role in the severity of COVID-19. A recent study also found that the elder patients group (median age 69) had a long time of illness onset to hospitalization compared to the younger patients group (median age 40) (37). The study conducted in rural US patients found that hospitalized patients had a higher comorbidity burden (38). However, one of the major drawbacks of this cross-sectional study is determining the disease conditions. Since most were treated at home, we excluded some symptoms such as pneumonia because of a complicated diagnosis. Another limitation could include the lack of mortality data since we did not include deceased patients.

Next, we conducted a chi-square test to study the role of gender, age, and comorbidity in the prevalence of the Covid-19 associated symptoms. Out of all the symptoms we have tested, we found gender is a risk factor for sore throat and loss of smell, whereas aging and comorbidity could be a risk factors for shortness of breath and hair loss. Furthermore, we found a difference in symptomatic prevalence for vomiting, confusion, and loss of speech between the comorbid patients and the patients without any second disease. Further, odd ratios were calculated to assess the high risk of certain groups in the gender, age, and comorbidity predictors. Male patients showed a high-risk factor for the loss of smell symptom, whereas elderly patients had higher risk factors in developing shortness of breath than  $\leq 40$  years of age. Four symptoms such as shortness of breath, vomiting,

**TABLE 5 |** Onset of COVID-19-associated symptoms in the patients, Bangladesh, 2020.

| Symptom             | Group                    | 1st–4th day        | 5th–10th day       | 11th–14th day    | After 14th day   |
|---------------------|--------------------------|--------------------|--------------------|------------------|------------------|
| Fever               | Male ( <i>n</i> = 285)   | 277 (97.2%)        | 8 (2.8%)           | 0 (0.0%)         | 0 (0.0%)         |
|                     | Female ( <i>n</i> = 126) | 118 (93.6%)        | 7 (5.6%)           | 1 (0.8%)         | 0 (0.0%)         |
|                     | <b>Total</b>             | <b>395 (96.1%)</b> | <b>15 (3.6%)</b>   | <b>1 (0.2%)</b>  | <b>0 (0.0%)</b>  |
| Exhaustion          | Male ( <i>n</i> = 268)   | 243 (90.7%)        | 18 (6.7%)          | 4 (1.5%)         | 3 (1.1%)         |
|                     | Female ( <i>n</i> = 122) | 104 (85.2%)        | 10 (8.2%)          | 5 (4.1%)         | 3 (2.5%)         |
|                     | <b>Total</b>             | <b>347 (89.0%)</b> | <b>28 (7.2%)</b>   | <b>9 (2.3%)</b>  | <b>6 (1.5%)</b>  |
| Runny nose          | Male ( <i>n</i> = 60)    | 49 (81.7%)         | 11 (18.3%)         | 0 (0.0%)         | 0 (0.0%)         |
|                     | Female ( <i>n</i> = 35)  | 28 (80.0%)         | 5 (14.3%)          | 2 (5.7%)         | 0 (0.0%)         |
|                     | <b>Total</b>             | <b>77 (81.0%)</b>  | <b>16 (16.8%)</b>  | <b>2 (2.1%)</b>  | <b>0 (0.0%)</b>  |
| Cough               | Male ( <i>n</i> = 207)   | 183 (88.4%)        | 20 (9.7%)          | 4 (1.9%)         | 0 (0.0%)         |
|                     | Female ( <i>n</i> = 104) | 91 (87.5%)         | 10 (9.6%)          | 3 (2.9%)         | 0 (0.0%)         |
|                     | <b>Total</b>             | <b>274 (88.1%)</b> | <b>30 (9.6%)</b>   | <b>7 (2.2%)</b>  | <b>0 (0.0%)</b>  |
| Sore throat         | Male ( <i>n</i> = 183)   | 165 (90.2%)        | 16 (8.7%)          | 1 (0.5%)         | 1 (0.5%)         |
|                     | Female ( <i>n</i> = 96)  | 86 (89.6%)         | 9 (9.4%)           | 0 (0.0%)         | 1 (1.0%)         |
|                     | <b>Total</b>             | <b>251 (90.0%)</b> | <b>25 (9.0%)</b>   | <b>1 (0.4%)</b>  | <b>2 (0.7%)</b>  |
| Shortness of breath | Male ( <i>n</i> = 128)   | 44 (34.4%)         | 78 (60.9%)         | 3 (2.3%)         | 3 (2.3%)         |
|                     | Female ( <i>n</i> = 65)  | 22 (33.8%)         | 37 (56.9%)         | 4 (6.1%)         | 2 (3.1%)         |
|                     | <b>Total</b>             | <b>66 (34.2%)</b>  | <b>115 (59.6%)</b> | <b>7 (3.6%)</b>  | <b>5 (2.6%)</b>  |
| Body ache           | Male ( <i>n</i> = 196)   | 180 (91.8%)        | 13 (6.6%)          | 1 (0.5%)         | 2 (1.0%)         |
|                     | Female ( <i>n</i> = 79)  | 73 (92.4%)         | 6 (7.6%)           | 0 (0.0%)         | 0 (0.0%)         |
|                     | <b>Total</b>             | <b>253 (92.0%)</b> | <b>19 (6.9%)</b>   | <b>1 (0.4%)</b>  | <b>2 (0.7%)</b>  |
| Diarrhea            | Male ( <i>n</i> = 95)    | 76 (80.0%)         | 15 (15.8%)         | 4 (4.2%)         | 0 (0.0%)         |
|                     | Female ( <i>n</i> = 40)  | 32 (80.0%)         | 6 (15.0%)          | 2 (5.0%)         | 0 (0.0%)         |
|                     | <b>Total</b>             | <b>108 (80.0%)</b> | <b>21 (15.6%)</b>  | <b>6 (4.4%)</b>  | <b>0 (0.0%)</b>  |
| Loss of taste       | Male ( <i>n</i> = 201)   | 71 (35.3%)         | 128 (63.7%)        | 2 (1.0%)         | 0 (0.0%)         |
|                     | Female ( <i>n</i> = 80)  | 34 (42.5%)         | 45 (56.2%)         | 1 (1.2%)         | 0 (0.0%)         |
|                     | <b>Total</b>             | <b>105 (37.4%)</b> | <b>173 (61.6%)</b> | <b>3 (1.1%)</b>  | <b>0 (0.0%)</b>  |
| Loss of smell       | Male ( <i>n</i> = 162)   | 67 (41.4%)         | 89 (54.9%)         | 6 (3.7%)         | 0 (0.0%)         |
|                     | Female ( <i>n</i> = 56)  | 18 (32.1%)         | 35 (62.5%)         | 3 (5.4%)         | 0 (0.0%)         |
|                     | <b>Total</b>             | <b>85 (39.0%)</b>  | <b>124 (56.9%)</b> | <b>9 (4.1%)</b>  | <b>0 (0.0%)</b>  |
| Vomiting            | Male ( <i>n</i> = 51)    | 35 (68.6%)         | 14 (27.4%)         | 1 (2.0%)         | 1 (2.0%)         |
|                     | Female ( <i>n</i> = 35)  | 27 (77.1%)         | 5 (14.3%)          | 1 (2.9%)         | 2 (5.7%)         |
|                     | <b>Total</b>             | <b>62 (72.1%)</b>  | <b>19 (22.1%)</b>  | <b>2 (2.3%)</b>  | <b>3 (3.5%)</b>  |
| Headache            | Male ( <i>n</i> = 101)   | 89 (88.1%)         | 11 (10.9%)         | 0 (0.0%)         | 1 (1.0%)         |
|                     | Female ( <i>n</i> = 53)  | 48 (90.6%)         | 3 (5.7%)           | 0 (0.0%)         | 2 (3.8%)         |
|                     | <b>Total</b>             | <b>137 (89.0%)</b> | <b>14 (9.1%)</b>   | <b>0 (0.0%)</b>  | <b>3 (1.9%)</b>  |
| Digestive problems  | Male ( <i>n</i> = 41)    | 26 (63.4%)         | 12 (29.3%)         | 1 (2.4%)         | 2 (4.9%)         |
|                     | Female ( <i>n</i> = 24)  | 16 (66.7%)         | 7 (29.2%)          | 1 (4.2%)         | 0 (0.0%)         |
|                     | <b>Total</b>             | <b>42 (64.6%)</b>  | <b>19 (29.2%)</b>  | <b>2 (3.1%)</b>  | <b>2 (3.1%)</b>  |
| Lack of appetite    | Male ( <i>n</i> = 114)   | 104 (91.2%)        | 9 (7.9%)           | 0 (0.0%)         | 1 (0.9%)         |
|                     | Female ( <i>n</i> = 59)  | 51 (86.4%)         | 6 (10.2%)          | 2 (3.4%)         | 0 (0.0%)         |
|                     | <b>Total</b>             | <b>155 (89.6%)</b> | <b>15 (8.7%)</b>   | <b>2 (1.2%)</b>  | <b>1 (0.6%)</b>  |
| Rashes              | Male ( <i>n</i> = 31)    | 17 (54.8%)         | 12 (38.7%)         | 2 (6.4%)         | 0 (0.0%)         |
|                     | Female ( <i>n</i> = 13)  | 9 (69.2%)          | 1 (7.7%)           | 3 (23.1%)        | 0 (0.0%)         |
|                     | <b>Total</b>             | <b>26 (59.1%)</b>  | <b>13 (29.5%)</b>  | <b>5 (11.4%)</b> | <b>0 (0.0%)</b>  |
| Blistering          | Male ( <i>n</i> = 7)     | 4 (57.1%)          | 1 (14.3%)          | 0 (0.0%)         | 2 (28.6%)        |
|                     | Female ( <i>n</i> = 3)   | 2 (66.7%)          | 1 (33.3%)          | 0 (0.0%)         | 0 (0.0%)         |
|                     | <b>Total</b>             | <b>6 (60.0%)</b>   | <b>2 (20.0%)</b>   | <b>0 (0.0%)</b>  | <b>2 (20.0%)</b> |

(Continued)



TABLE 5 | Continued

| Symptom        | Group           | 1st–4th day       | 5th–10th day      | 11th–14th day     | After 14th day  |
|----------------|-----------------|-------------------|-------------------|-------------------|-----------------|
| Confusion      | Male (n = 62)   | 23 (37.1%)        | 21 (33.9%)        | 15 (24.2%)        | 3 (4.8%)        |
|                | Female (n = 28) | 5 (17.9%)         | 10 (35.7%)        | 9 (32.1%)         | 4 (14.3%)       |
|                | <b>Total</b>    | <b>28 (31.1%)</b> | <b>31 (34.4%)</b> | <b>24 (26.7%)</b> | <b>7 (7.8%)</b> |
| Loss of speech | Male (n = 43)   | 18 (41.9%)        | 16 (37.2%)        | 8 (18.6%)         | 1 (2.3%)        |
|                | Female (n = 15) | 4 (26.7%)         | 1 (6.7%)          | 2 (13.3%)         | 8 (53.3%)       |
|                | <b>Total</b>    | <b>22 (37.9%)</b> | <b>24 (41.4%)</b> | <b>10 (17.2%)</b> | <b>2 (3.4%)</b> |

Values are expressed as frequency and % response of the final respondents. The percentage was calculated considering the samples in the individual groups.

loss of speech, confusion demonstrated high prevalence in comorbid patients.

One plausible reason for the gender differences could be due to hormonal differences. Female has shown higher incidence rate than male; however, female age between 20s and 70s exhibited lower incidence rate than similar age of male. The study suggests that estrogen may play a protective role with the other susceptible factors by inhibiting the entry of the SARS-CoV-2 virus into the host cells (39). Another important susceptible factor is age. A study conducted in 5,484 case contacts found that only 18.1% of participants developed symptoms below age 20, whereas 64.6% of participants demonstrated symptoms above age 80 (40). Chronic illnesses including hypertension, respiratory disease, kidney disease, diabetes, and cancer are considered underlying conditions that put people at greater risk with COVID-19. Hence we have included comorbid conditions (such as lung disease, cardiac disease, diabetes, and miscellaneous) to find their impacts on the symptoms. The study found that patients with comorbid disease/diseases had increased hospitalization rates and longer extended recovery periods. A retrospective study also described that aging and comorbid diseases possess higher severity and mortality in COVID-19 and SARS patients (41). Studies also found that patients with diabetes, heart disease, and other comorbidities had an increased risk of severity (42, 43). Similar to other studies, we also found comorbidity is a prime risk factor for COVID-19 patients in Bangladesh.

The most prevalent symptom in the COVID-19 patient was fever followed by exhaustion, cough, loss of taste, sore throat, and body ache. In general, all the symptoms showed up within 10 days of infection. However, 20% of patients who developed blistering demonstrated onset after 14th days of disease. While the incidence rate is low and the actual mechanism is still unknown, it is possible that angiotensin-converting enzyme-2 (ACE-2) available under the skin may play a role in the dermatological manifestation of SARS-CoV-2 virus can enter through ACE-2 receptors (44). Furthermore, some other neurological symptoms such as Confusion and loss of speech were also developed after the 14th day of infection. Neurological symptoms were found in 36.4% of patients in a previous study conducted in 214 patients (45). Another study conducted in France found that more than two-thirds of the cases demonstrated altered consciousness, including agitation and Confusion (46). Although SARS-CoV-2 can induce neurological

damage, the exact mechanism is yet to be discovered. It is postulated that the virus can disseminate through the cribriform plate and olfactory bulb; and damage the capillary endothelium to induce brain injury (45). A preclinical study showed that the SARS virus could cause neuronal loss through transneuronal spreading from the olfactory bulb in K18-hACE2 mice (47). Hence, several reasons such as viral encephalitis, metabolic perturbation, infectious, toxic encephalopathy, seizures with post-ictal Confusion, and stroke could be the underlying reason behind neurological symptoms (46).

While most symptoms persisted for 1 to 10 days, some symptoms such as extreme exhaustion (33%), loss of smell (11%), loss of speech, blistering (20%), and confusion (27%) persisted for more than 14 days. While it is not clear why the onset and duration of symptoms vary from patient to patient, studies suggest that low interferon response in some patients could be the possible underlying mechanism of severity (48, 49). Nevertheless, the onset and duration data also match the study conducted by Lauer et al., where they analyzed 181 cases from outside Hubei province, China, and found the onset of symptoms for SARS-CoV-2 is ~5 days, and 101 out of every 10,000 cases developed symptoms after 14 days of monitoring or quarantine (50).

## CONCLUSION

This study demonstrates the prevalent symptoms in COVID-19 patients affected from March 2020 to September 2020 in Bangladesh. To date, there are limited data available for the prevalence of symptoms in COVID-19 patients in Bangladesh. This study found that older (>40 years old) and comorbid patients required more hospitalization due to the COVID-19 associated complications, where comorbid patients were more susceptible to have shortness of breath, vomiting, loss of speech, and confusion. In regards of gender difference, the prevalence of sore throat, loss of smell, and vomiting were significantly higher in the male patient. Age and comorbidity also played a crucial role in the duration required to recover from all the COVID-19 associated symptoms. Since this study is highly relevant to the clinical outcomes of COVID-19, the data on different predictors such as age, gender, and comorbidity observed can provide valuable insight into the management of COVID-19 symptoms and can also lead to the understanding of disease progression.

**TABLE 6 |** Duration of the COVID-19-associated symptoms of the patients, Bangladesh, 2020.

| Symptoms            | Group        | 1–4 days           | 5–10 days          | 11–14 days         | > 14 days          |
|---------------------|--------------|--------------------|--------------------|--------------------|--------------------|
| Fever               | Male         | 241 (85.2%)        | 34 (12.0%)         | 3 (1.1%)           | 5 (1.8%)           |
|                     | Female       | 99 (79.8%)         | 23 (18.5%)         | 0 (0.0%)           | 2 (1.6%)           |
|                     | <b>Total</b> | <b>340 (83.5%)</b> | <b>57 (14.0%)</b>  | <b>3 (0.7%)</b>    | <b>7 (1.7%)</b>    |
| Exhaustion          | Male         | 17 (6.6%)          | 23 (8.9%)          | 125 (48.6%)        | 92 (35.8%)         |
|                     | Female       | 10 (8.4%)          | 11 (9.2%)          | 63 (52.9%)         | 35 (29.4%)         |
|                     | <b>Total</b> | <b>27 (7.2%)</b>   | <b>34 (9.0%)</b>   | <b>188 (50.0%)</b> | <b>127 (33.8%)</b> |
| Runny nose          | Male         | 49 (74.2%)         | 13 (19.7%)         | 2 (3.0%)           | 2 (3.0%)           |
|                     | Female       | 21 (63.6%)         | 5 (15.1%)          | 3 (9.1%)           | 4 (12.1%)          |
|                     | <b>Total</b> | <b>70 (70.7%)</b>  | <b>18 (18.2%)</b>  | <b>5 (5.0%)</b>    | <b>6 (6.1%)</b>    |
| Cough               | Male         | 141 (68.8%)        | 44 (21.5%)         | 11 (5.4%)          | 9 (4.4%)           |
|                     | Female       | 74 (74.0%)         | 12 (12.0%)         | 7 (7.0%)           | 7 (7.0%)           |
|                     | <b>Total</b> | <b>215 (70.5%)</b> | <b>56 (18.4%)</b>  | <b>18 (5.9%)</b>   | <b>16 (5.2%)</b>   |
| Sore throat         | Male         | 168 (92.8%)        | 9 (5.0%)           | 2 (1.1%)           | 2 (1.1%)           |
|                     | Female       | 84 (86.6%)         | 10 (10.3%)         | 1 (1.0%)           | 2 (2.1%)           |
|                     | <b>Total</b> | <b>252 (90.6%)</b> | <b>19 (6.8%)</b>   | <b>3 (1.1%)</b>    | <b>4 (1.4%)</b>    |
| Shortness of breath | Male         | 20 (17.5%)         | 39 (34.2%)         | 50 (43.9%)         | 11 (9.6%)          |
|                     | Female       | 14 (22.9%)         | 29 (47.5%)         | 12 (19.7%)         | 6 (9.8%)           |
|                     | <b>Total</b> | <b>34 (18.8%)</b>  | <b>68 (37.6%)</b>  | <b>62 (34.2%)</b>  | <b>17 (9.4%)</b>   |
| Body ache           | Male         | 105 (55.3%)        | 68 (35.8%)         | 10 (5.3%)          | 7 (3.7%)           |
|                     | Female       | 38 (49.35%)        | 28 (36.4%)         | 7 (9.1%)           | 4 (5.2%)           |
|                     | <b>Total</b> | <b>143 (53.6%)</b> | <b>96 (36.0%)</b>  | <b>17 (6.4%)</b>   | <b>11 (4.1%)</b>   |
| Diarrhea            | Male         | 81 (88.0%)         | 7 (7.6%)           | 3 (3.3%)           | 1 (1.1%)           |
|                     | Female       | 28 (80.0%)         | 4 (11.4%)          | 3 (8.6%)           | 0 (0.0%)           |
|                     | <b>Total</b> | <b>109 (85.8%)</b> | <b>11 (8.7%)</b>   | <b>6 (4.7%)</b>    | <b>1 (0.8%)</b>    |
| Loss of taste       | Male         | 12 (6.0%)          | 31 (15.4%)         | 140 (69.6%)        | 18 (9.0%)          |
|                     | Female       | 8 (10.3%)          | 23 (29.5%)         | 39 (50.0%)         | 8 (10.3%)          |
|                     | <b>Total</b> | <b>20 (7.2%)</b>   | <b>54 (19.3%)</b>  | <b>179 (64.2%)</b> | <b>26 (9.3%)</b>   |
| Loss of smell       | Male         | 15 (9.2%)          | 30 (18.6%)         | 99 (61.5%)         | 17 (10.6%)         |
|                     | Female       | 5 (8.93%)          | 21 (37.50%)        | 23 (41.1%)         | 7 (12.5%)          |
|                     | <b>Total</b> | <b>20 (9.2%)</b>   | <b>51 (23.5%)</b>  | <b>122 (56.2%)</b> | <b>24 (11.1%)</b>  |
| Vomiting            | Male         | 28 (54.9%)         | 21 (41.2%)         | 2 (3.9%)           | 0 (0.0%)           |
|                     | Female       | 16 (51.6%)         | 9 (29.0%)          | 3 (9.7%)           | 3 (9.7%)           |
|                     | <b>Total</b> | <b>44 (53.7%)</b>  | <b>30 (36.6%)</b>  | <b>5 (6.1%)</b>    | <b>3 (3.7%)</b>    |
| Headache            | Male         | 82 (71.9%)         | 16 (14.0%)         | 7 (6.1%)           | 9 (7.9%)           |
|                     | Female       | 40 (71.4%)         | 6 (10.7%)          | 7 (12.5%)          | 3 (5.4%)           |
|                     | <b>Total</b> | <b>122 (71.8%)</b> | <b>22 (13.0%)</b>  | <b>14 (8.2%)</b>   | <b>12 (7.1%)</b>   |
| Digestive problems  | Male         | 10 (27.8%)         | 22 (61.1%)         | 1 (2.8%)           | 3 (8.3%)           |
|                     | Female       | 10 (47.6%)         | 6 (28.6%)          | 2 (9.5%)           | 2 (9.5%)           |
|                     | <b>Total</b> | <b>20 (35.1%)</b>  | <b>28 (49.1%)</b>  | <b>4 (7.0%)</b>    | <b>5 (8.8%)</b>    |
| Lack of appetite    | Male         | 28 (25.2%)         | 73 (65.8%)         | 5 (4.5%)           | 5 (4.5%)           |
|                     | Female       | 15 (25.4%)         | 35 (59.3%)         | 7 (11.9%)          | 2 (3.4%)           |
|                     | <b>Total</b> | <b>43 (25.3%)</b>  | <b>108 (63.5%)</b> | <b>12 (7.1%)</b>   | <b>7 (4.1%)</b>    |
| Rashes              | Male         | 23 (74.2%)         | 7 (22.6%)          | 0 (0.0%)           | 1 (3.2%)           |
|                     | Female       | 9 (81.8%)          | 0 (0.0%)           | 0 (0.0%)           | 2 (18.2%)          |
|                     | <b>Total</b> | <b>32 (76.2%)</b>  | <b>7 (16.7%)</b>   | <b>0 (0.0%)</b>    | <b>3 (7.1%)</b>    |
| Blistering          | Male         | 5 (71.4%)          | 1 (14.3%)          | 0 (0.0%)           | 1 (33.3%)          |
|                     | Female       | 1 (33.3%)          | 1 (33.3%)          | 0 (0.0%)           | 1 (33.3%)          |
|                     | <b>Total</b> | <b>6 (60.0%)</b>   | <b>2 (20.0%)</b>   | <b>0 (0.0%)</b>    | <b>2 (20.0%)</b>   |

(Continued)

**TABLE 6 |** Continued

| Symptoms       | Group        | 1–4 days          | 5–10 days         | 11–14 days        | > 14 days         |
|----------------|--------------|-------------------|-------------------|-------------------|-------------------|
| Confusion      | Male         | 24 (42.1%)        | 14 (24.6%)        | 4 (7.0%)          | 15 (26.3%)        |
|                | Female       | 9 (36.0%)         | 3 (12.0%)         | 6 (24.0%)         | 7 (28.0%)         |
|                | <b>Total</b> | <b>33 (40.2%)</b> | <b>17 (20.7%)</b> | <b>10 (12.2%)</b> | <b>22 (26.8%)</b> |
| Loss of speech | Male         | 17 (41.5%)        | 12 (29.3%)        | 4 (9.8%)          | 8 (19.5%)         |
|                | Female       | 8 (50.0%)         | 3 (18.7%)         | 3 (18.7%)         | 2 (12.5%)         |
|                | <b>Total</b> | <b>25 (43.9%)</b> | <b>15 (26.3%)</b> | <b>7 (12.3%)</b>  | <b>10 (17.5%)</b> |

Values are expressed as frequency and % response of the final respondents). The percentage was calculated considering the samples in the individual groups.

**TABLE 7 |** Days required for symptomatic recovery in both male and female patients, Bangladesh, 2020.

| Variable    | Group             | 1–7 days  | 8–14 days   | 15–21 days  | 22–28 days | More than 28 days | $\chi^2$ (p-value) |
|-------------|-------------------|-----------|-------------|-------------|------------|-------------------|--------------------|
| Total       | N = 439           | 16 (3.6%) | 233 (53.1%) | 136 (31%)   | 7 (1.6%)   | 47 (10.7%)        | –                  |
| Gender      | Male (n = 303)    | 9 (3.0%)  | 152 (50.2%) | 106 (35.0%) | 3 (1.0%)   | 33 (10.9%)        | 10.157 (0.071)     |
|             | Female (n = 136)  | 7 (5.1%)  | 81 (59.6%)  | 30 (22.1%)  | 4 (2.9%)   | 14 (10.3%)        |                    |
| Age         | ≤40 Yrs (n = 318) | 12 (3.8%) | 183 (57.5%) | 81 (25.5%)  | 5 (1.6%)   | 37 (11.6%)        | 16.890 (0.005)     |
|             | >40 Yrs (n = 121) | 4 (3.3%)  | 50 (41.3%)  | 55 (45.5%)  | 2 (1.7%)   | 10 (8.3%)         |                    |
| Comorbidity | Yes (n = 115)     | 4 (3.5%)  | 41 (36.0%)  | 51 (44.7%)  | 4 (3.5%)   | 14 (12.3%)        | 23.638 (0.000)     |
|             | No (n = 324)      | 12 (3.7%) | 192 (59.1%) | 85 (26.2%)  | 3 (0.9%)   | 33 (10.2%)        |                    |

Values are expressed as frequency and % response of the final respondents. The percentage was calculated considering the samples in the individual groups. Pearson's chi-squared test was applied to observe the association of the gender, age, and comorbidity in the complete recovery of all COVID-19 associated symptoms.  $P < 0.05$  was considered statistically significant.

## DATA AVAILABILITY STATEMENT

The raw data supporting the conclusions of this article will be made available by the authors, without undue reservation.

## ETHICS STATEMENT

The studies involving human participants were reviewed and approved by Jagannath University Research Cell. The patients/participants provided their written informed consent to participate in this study.

## AUTHOR CONTRIBUTIONS

MA, MH, and TA conceptualized the study, analyzed the data, developed the methods and materials, and wrote the manuscript. MA and TA conducted the study. MH and TA edited the manuscript. All authors contributed to the article and approved the submitted version.

## SUPPLEMENTARY MATERIAL

The Supplementary Material for this article can be found online at: <https://www.frontiersin.org/articles/10.3389/fpubh.2021.738352/full#supplementary-material>

## REFERENCES

- Huang C, Wang Y, Li X, Ren L, Zhao J, Hu Y, et al. Clinical features of patients infected with 2019 novel coronavirus in Wuhan, China. *Lancet*. (2020) 395:497–506. doi: 10.1016/S0140-6736(20)30183-5
- McIntosh K, Hirsch MS, Bloom A. Coronavirus disease 2019 (COVID-19). *UpToDate Hirsch MS Bloom*. (2020) 5:1–1.
- WHO Announces Simple, Easy-to-Say Labels for SARS-CoV-2 Variants of Interest and Concern. Available online at: <https://www.who.int/news/item/31-05-2021-who-announces-simple-easy-to-say-labels-for-sars-cov-2-variants-of-interest-and-concern> (accessed October 07, 2021).
- Andersen KG, Rambaut A, Lipkin WI, Holmes EC, Garry RF. The proximal origin of SARS-CoV-2. *Nat Med*. (2020) 26:450–2. doi: 10.1038/s41591-020-0820-9
- Baloch S, Baloch MA, Zheng T, Pei X. The coronavirus disease 2019 (COVID-19) pandemic. *Tohoku J Exp Med*. (2020) 250:271–8. doi: 10.1620/tjem.250.271
- Spinelli A, Pellino G. COVID-19 pandemic: perspectives on an unfolding crisis. *J Br Surg*. (2020) 107:785–7. doi: 10.1002/bjs.11627
- Zhang S, Tuo J, Huang X, Zhu X, Zhang D, Zhou K, et al. Epidemiology characteristics of human coronaviruses in patients with respiratory infection symptoms and phylogenetic analysis of HCoV-OC43 during 2010–2015 in Guangzhou. *PLoS ONE*. (2018) 13:e0191789. doi: 10.1371/journal.pone.0191789
- Li J, Chen Z, Nie Y, Ma Y, Guo Q, Dai X. Identification of symptoms prognostic of COVID-19 severity: multivariate data analysis of a case series in Henan Province. *J Med Internet Res*. (2020) 22:e19636. doi: 10.2196/19636
- Di Gennaro F, Pizzol D, Marotta C, Antunes M, Racalbutto V, Veronese N, et al. Coronavirus diseases (COVID-19) current status and future perspectives: a narrative review. *Int J Environ Res Public Health*. (2020) 17:2690. doi: 10.3390/ijerph17082690
- Mackenzie JS, Smith DW. COVID-19: a novel zoonotic disease caused by a coronavirus from China: what we know and what we don't. *Microbiol Aust*. (2020) MA20013. doi: 10.1071/MA20013. [Epub ahead of print].

11. Hafeez A, Ahmad S, Siddiqui SA, Ahmad M, Mishra S. A review of COVID-19 (Coronavirus Disease-2019) diagnosis, treatments and prevention. *EJMO*. (2020) 4:116–25. doi: 10.14744/ejmo.2020.90853
12. Perlman S, Netland J. Coronaviruses post-SARS: update on replication and pathogenesis. *Nat Rev Microbiol*. (2009) 7:439–50. doi: 10.1038/nrmicro.2147
13. Hu H, Jung K, Wang Q, Saif LJ, Vlasova AN. Development of a one-step RT-PCR assay for detection of pancoronaviruses ( $\alpha$ -,  $\beta$ -,  $\gamma$ -, and  $\delta$ -coronaviruses) using newly designed degenerate primers for porcine and avian fecal samples. *J Virol Methods*. (2018) 256:116–22. doi: 10.1016/j.jviromet.2018.02.021
14. Budholiya P, Ali AW, Gunwan D, Sahil S, Tyagi CK, Sharma H. COVID-19: a global pandemic of 21st Century. *J Drug Deliv Ther*. (2020) 10(3-s):311–21. doi: 10.22270/jddt.v10i3-s.4088
15. He X, Lau EH, Wu P, Deng X, Wang J, Hao X, et al. Temporal dynamics in viral shedding and transmissibility of COVID-19. *Nat Med*. (2020) 26:672–5. doi: 10.1038/s41591-020-0869-5
16. Lechien JR, Chiesa-Estomba CM, Hans S, Barillari MR, Jouffe L, Saussez S. Loss of smell and taste in 2013 European patients with mild to moderate COVID-19. *Ann Intern Med*. (2020) 173:672–5. doi: 10.7326/M20-2428
17. Menni C, Valdes AM, Freidin MB, Sudre CH, Nguyen LH, Drew DA, et al. Real-time tracking of self-reported symptoms to predict potential COVID-19. *Nat Med*. (2020) 26:1037–40. doi: 10.1038/s41591-020-0916-2
18. Wang D, Hu B, Hu C, Zhu F, Liu X, Zhang J, et al. Clinical characteristics of 138 hospitalized patients with 2019 novel coronavirus-infected pneumonia in Wuhan, China. *JAMA*. (2020) 323:1061–9. doi: 10.1001/jama.2020.1585
19. Li L, Huang T, Wang Y, Wang Z, Liang Y, Huang T, et al. COVID-19 patients' clinical characteristics, discharge rate, and fatality rate of meta-analysis. *J Med Virol*. (2020) 92:577–83. doi: 10.1002/jmv.25757
20. Carfi A, Bernabei R, Landi F. Persistent symptoms in patients after acute COVID-19. *Jama*. (2020) 324:603–5. doi: 10.1001/jama.2020.12603
21. Tenforde MW, Kim SS, Lindsell CJ, Rose EB, Shapiro NI, Files DC, et al. Symptom duration and risk factors for delayed return to usual health among outpatients with COVID-19 in a multistate health care systems network—United States, March–June 2020. *Morb Mortal Wkly Rep*. (2020) 69:993. doi: 10.15585/mmwr.mm6930e1
22. Kopel J, Perisetti A, Roghani A, Aziz M, Gajendran M, Goyal H. Racial and gender-based differences in COVID-19. *Front Public Health*. (2020) 8:418. doi: 10.3389/fpubh.2020.00418
23. Sze S, Pan D, Nevill CR, Gray LJ, Martin CA, Nazareth J, et al. Ethnicity and clinical outcomes in COVID-19: a systematic review and meta-analysis. *EClin Med*. (2020) 29–30:100630. doi: 10.1016/j.eclinm.2020.100630
24. World Health O. *Novel Coronavirus (2019-nCoV): Situation Report, 11* (Geneva) (2020). Retrieved from: <https://apps.who.int/iris/handle/10665/330776>
25. Ferdous MZ, Islam MS, Sikder MT, Mosaddek ASM, Zegarar-Valdivia JA, Gozal D. Knowledge, attitude, and practice regarding COVID-19 outbreak in Bangladesh: an online-based cross-sectional study. *PLoS ONE*. (2020) 15:e0239254. doi: 10.1371/journal.pone.0239254
26. Islam MS, Potenza MN, van Os J. Posttraumatic stress disorder during the COVID-19 pandemic: upcoming challenges in Bangladesh and preventive strategies. *Int J Soc Psychiatry*. (2020) 67:205–6. doi: 10.1177/0020764020954469
27. Bhattacharjee A. Epidemiology and clinical course of asymptomatic COVID-19 infection. *Sch J App Med Sci*. (2021) 2:194–8. doi: 10.36347/sjams.2021.v09i02.004
28. Khan MAS, Debnath S, Islam MS, Zaman S, Ambia N-E, Barshan AD, et al. Mental health of young people amidst COVID-19 pandemic in Bangladesh. *Heliyon*. (2021) 7:e07173. doi: 10.1016/j.heliyon.2021.e07173
29. Biernacki P, Waldorf D. Snowball sampling: problems and techniques of chain referral sampling. *Soc Meth Res*. (1981) 10:141–63. doi: 10.1177/004912418101000205
30. Goodman LA. Snowball sampling. *Ann Math Stat*. (1961) 32:148–70. doi: 10.1214/aoms/1177705148
31. Hosen I, Pakpour AH, Sakib N, Hussain N, Al Mamun F, Mamun MA. Knowledge and preventive behaviors regarding COVID-19 in Bangladesh: a nationwide distribution. *PLoS ONE*. (2021) 16:e0251151. doi: 10.1371/journal.pone.0251151
32. Islam M, Islam US, Mosaddek ASM, Potenza MN, Pardhan S. Treatment, persistent symptoms, and depression in people infected with COVID-19 in Bangladesh. *Int J Environ Res Public Health*. (2021) 18:1453. doi: 10.3390/ijerph18041453
33. Wang Y, Di Y, Ye J, Wei W. Study on the public psychological states and its related factors during the outbreak of coronavirus disease 2019 (COVID-19) in some regions of China. *Psychol Health Med*. (2021) 26:13–22. doi: 10.1080/13548506.2020.1746817
34. Association GA of the WM. World medical association declaration of helsinki: ethical principles for medical research involving human subjects. *J Am Coll Dent*. (2014) 81:14–8.
35. Bryson GL, Turgeon AF, Choi PT. The science of opinion: survey methods in research. *Can J Anesth Can Anesth*. (2012) 59:736–42. doi: 10.1007/s12630-012-9727-3
36. Cascella M, Rajnik M, Aleem A, Dulebohn SC, Di Napoli R. Features, evaluation, and treatment of coronavirus (COVID-19). In: *StatPearls [Internet]*. Treasure Island, FL: StatPearls Publishing (2021).
37. Deng Y, Liu W, Liu K, Fang Y-Y, Shang J, Zhou L, et al. Clinical characteristics of fatal and recovered cases of coronavirus disease 2019 in Wuhan, China: a retrospective study. *Chin Med J*. (2020) 133:1261–7. doi: 10.1097/CM9.0000000000000824
38. Shah P, Owens J, Franklin J, Mehta A, Heymann W, Sewell W, et al. Demographics, comorbidities and outcomes in hospitalized Covid-19 patients in rural southwest Georgia. *Ann Med*. (2020) 52:354–60. doi: 10.1080/07853890.2020.1791356
39. O'Brien J, Du KY, Peng C. Incidence, clinical features, and outcomes of COVID-19 in Canada: impact of sex and age. *J Ovarian Res*. (2020) 13:1–12. doi: 10.1186/s13048-020-00734-4
40. Poletti P, Tirani M, Cereda D, Trentini F, Guzzetta G, Sabatino G, et al. Association of age with likelihood of developing symptoms and critical disease among close contacts exposed to patients with confirmed sars-cov-2 infection in Italy. *JAMA Netw Open*. (2021) 4:e211085. doi: 10.1001/jamanetworkopen.2021.1085
41. Jin J-M, Bai P, He W, Wu F, Liu X-F, Han D-M, et al. Gender differences in patients with COVID-19: focus on severity and mortality. *Front Public Health*. (2020) 8:152. doi: 10.3389/fpubh.2020.00152
42. Henry BM, de Oliveira MHS, Benoit J, Lippi G. Gastrointestinal symptoms associated with severity of coronavirus disease 2019 (COVID-19): a pooled analysis. *Intern Emerg Med*. (2020) 15:857–9. doi: 10.1007/s11739-020-02329-9
43. Sanyaolu A, Okorie C, Marinkovic A, Patidar R, Younis K, Desai P, et al. Comorbidity and its impact on patients with COVID-19. *SN Compr Clin Med*. (2020) 2:1–8. doi: 10.1007/s42399-020-00363-4
44. Gottlieb M, Long B. Dermatologic manifestations and complications of COVID-19. *Am J Emerg Med*. (2020) 38:1715–21. doi: 10.1016/j.ajem.2020.06.011
45. Montalvan V, Lee J, Bueso T, De Toledo J, Rivas K. Neurological manifestations of COVID-19 and other coronavirus infections: a systematic review. *Clin Neurol Neurosurg*. (2020) 194:105921. doi: 10.1016/j.clineuro.2020.105921
46. Lahiri D, Ardila A. COVID-19 pandemic: a neurological perspective. *Cureus*. (2020) 12:e7889. doi: 10.7759/cureus.7889
47. Netland J, Meyerholz DK, Moore S, Cassell M, Perlman S. Severe acute respiratory syndrome coronavirus infection causes neuronal death in the absence of encephalitis in mice transgenic for human ACE2. *J Virol*. (2008) 82:7264–75. doi: 10.1128/JVI.00737-08
48. Acharya D, Liu G, Gack MU. Dysregulation of type I interferon responses in COVID-19. *Nat Rev Immunol*. (2020) 20:397–8. doi: 10.1038/s41577-020-0346-x
49. Salman AA, Waheed MH, Ali-Abdulsahib AA, Atwan ZW. Low type I interferon response in COVID-19 patients: interferon response may be a potential treatment for COVID-19. *Biomed Rep*. (2021) 14:1–5. doi: 10.3892/br.2021.1419



50. Lauer SA, Grantz KH, Bi Q, Jones FK, Zheng Q, Meredith HR, et al. The incubation period of coronavirus disease 2019 (COVID-19) from publicly reported confirmed cases: estimation and application. *Ann Intern Med.* (2020) 172:577–82. doi: 10.7326/M20-0504

**Conflict of Interest:** The authors declare that the research was conducted in the absence of any commercial or financial relationships that could be construed as a potential conflict of interest.

**Publisher's Note:** All claims expressed in this article are solely those of the authors and do not necessarily represent those of their affiliated organizations, or those of

the publisher, the editors and the reviewers. Any product that may be evaluated in this article, or claim that may be made by its manufacturer, is not guaranteed or endorsed by the publisher.

Copyright © 2021 Amin, Hasan and Bhuiya. This is an open-access article distributed under the terms of the Creative Commons Attribution License (CC BY). The use, distribution or reproduction in other forums is permitted, provided the original author(s) and the copyright owner(s) are credited and that the original publication in this journal is cited, in accordance with accepted academic practice. No use, distribution or reproduction is permitted which does not comply with these terms.



# Artificial Intelligence for COVID-19: A Systematic Review

Lian Wang<sup>1†</sup>, Yonggang Zhang<sup>2,3\*†</sup>, Dongguang Wang<sup>1</sup>, Xiang Tong<sup>1</sup>, Tao Liu<sup>1</sup>, Shijie Zhang<sup>1</sup>, Jizhen Huang<sup>1</sup>, Li Zhang<sup>1</sup>, Lingmin Chen<sup>4</sup>, Hong Fan<sup>1\*</sup> and Mike Clarke<sup>5\*</sup>

<sup>1</sup> Department of Respiratory and Critical Care Medicine, West China Hospital/West China School of Medicine, Sichuan University, Chengdu, China, <sup>2</sup> Department of Periodical Press and National Clinical Research Center for Geriatrics, West China Hospital, Sichuan University, Chengdu, China, <sup>3</sup> Chinese Evidence-Based Medicine Center, West China Hospital, Sichuan University, Chengdu, China, <sup>4</sup> Department of Anesthesiology and National Clinical Research Center for Geriatrics, West China Hospital, Sichuan University and The Research Units of West China, Chinese Academy of Medical Sciences, Chengdu, China, <sup>5</sup> Northern Ireland Methodology Hub, Queen's University Belfast, Belfast, United Kingdom

## OPEN ACCESS

### Edited by:

Reza Lashgari,  
Shahid Beheshti University, Iran

### Reviewed by:

Saeid Gorgin,  
Iranian Research Organization for  
Science and Technology, Iran  
Seyed Mohammad Sadegh Movahed,  
Shahid Beheshti University, Iran  
Hadi Choubdar,  
Shahid Beheshti University of Medical  
Sciences, Iran

### \*Correspondence:

Hong Fan  
fanhongfan@qq.com  
Yonggang Zhang  
jebm\_zhang@yahoo.com  
Mike Clarke  
m.clarke@qub.ac.uk

<sup>†</sup>These authors have contributed  
equally to this work and share first  
authorship

### Specialty section:

This article was submitted to  
Infectious Diseases – Surveillance,  
Prevention and Treatment,  
a section of the journal  
Frontiers in Medicine

Received: 02 May 2021

Accepted: 09 August 2021

Published: 30 September 2021

### Citation:

Wang L, Zhang Y, Wang D, Tong X,  
Liu T, Zhang S, Huang J, Zhang L,  
Chen L, Fan H and Clarke M (2021)  
Artificial Intelligence for COVID-19: A  
Systematic Review.  
Front. Med. 8:704256.  
doi: 10.3389/fmed.2021.704256

**Background:** Recently, Coronavirus Disease 2019 (COVID-19), caused by severe acute respiratory syndrome virus 2 (SARS-CoV-2), has affected more than 200 countries and lead to enormous losses. This study systematically reviews the application of Artificial Intelligence (AI) techniques in COVID-19, especially for diagnosis, estimation of epidemic trends, prognosis, and exploration of effective and safe drugs and vaccines; and discusses the potential limitations.

**Methods:** We report this systematic review following the Preferred Reporting Items for Systematic Reviews and Meta-Analyses (PRISMA) guidelines. We searched PubMed, Embase and the Cochrane Library from inception to 19 September 2020 for published studies of AI applications in COVID-19. We used PROBAST (prediction model risk of bias assessment tool) to assess the quality of literature related to the diagnosis and prognosis of COVID-19. We registered the protocol (PROSPERO CRD42020211555).

**Results:** We included 78 studies: 46 articles discussed AI-assisted diagnosis for COVID-19 with total accuracy of 70.00 to 99.92%, sensitivity of 73.00 to 100.00%, specificity of 25 to 100.00%, and area under the curve of 0.732 to 1.000. Fourteen articles evaluated prognosis based on clinical characteristics at hospital admission, such as clinical, laboratory and radiological characteristics, reaching accuracy of 74.4 to 95.20%, sensitivity of 72.8 to 98.00%, specificity of 55 to 96.87% and AUC of 0.66 to 0.997 in predicting critical COVID-19. Nine articles used AI models to predict the epidemic of the COVID-19, such as epidemic peak, infection rate, number of infected cases, transmission laws, and development trend. Eight articles used AI to explore potential effective drugs, primarily through drug repurposing and drug development. Finally, 1 article predicted vaccine targets that have the potential to develop COVID-19 vaccines.

**Conclusions:** In this review, we have shown that AI achieved high performance in diagnosis, prognosis evaluation, epidemic prediction and drug discovery for COVID-19. AI has the potential to enhance significantly existing medical and healthcare system efficiency during the COVID-19 pandemic.

**Keywords:** artificial intelligence, COVID-19, diagnosis, prognosis evaluation, epidemic prediction, drug discovery 2

## INTRODUCTION

Coronavirus Disease 2019 (COVID-19), caused by severe acute respiratory syndrome virus 2 (SARS-CoV-2) was first detected in December 2019, and spread rapidly to most cities and countries around the world (1–3). During face-to-face contact, SARS-CoV-2 is mainly transmitted through respiratory droplets (4). The infection may cause mild symptoms of upper respiratory tract infections, as well as extremely severe sepsis and shock. It may lead to serious and lethal complications in vulnerable populations, especially in the elderly with comorbidities (4–6). As of 16 March 2021, SARS-CoV-2 has affected more than 200 countries and led to enormous losses, causing more than 120 million confirmed cases and 2.6 million identified deaths. The rising incidence and massive casualties caused by COVID-19 exert considerable pressure on limited healthcare resources. Effective tools are needed to streamline the diagnosis, treatment and surveillance of COVID-19 and increase the clinical efficiency of healthcare systems (7). Recent studies have shown that artificial intelligence is a promising technology as they can achieve better scale-up, accelerate processing power, and even outperform humans in specific healthcare tasks (8).

Artificial intelligence (AI) is a field of algorithm-based applications that enable machines to solve knowledge problems and use algorithms to simulate human decision-making, and continuously improves performance by applying inputted data to perform specific tasks (9–11). The advantages of AI are reflected in high sensitivity and specificity in identifying the object, the speed of reporting and consistency of results (9). In recent years, AI has made significant progress, especially in predictive machine learning models for medical care. Deep learning is a method of ML, based on the complex architectures of Artificial Neural Networks (ANN). Deep learning reveals significant discriminative performance after providing sufficient training data sets and is essential for making predictions (12). In medicine, technologies based on Artificial intelligence and machine learning (AI/ML) aim to improve the quality of medical care, increase diagnostic accuracy and reduce potential errors and predict outcomes by discovering new insights from the enormous amount of data produced by the experience of many patients (10).

Researchers have made significant contributions to the campaign against COVID-19, and new COVID-19-related AI models in the literature are rapidly increasing. Well-trained artificial intelligence models can ensure accurate and rapid diagnosis or assist doctors to streamline the diagnosis and reduce manual labor (13, 14). AI models could early detect the patients at higher risk and characterize the epidemiology of COVID-19 and model disease transmission by training data (15, 16). Artificial intelligence-based methods could assist in the discovery of novel drugs and vaccines, such as repurpose exist drugs, screen targets as vaccines based on the potential mutation model to SARS-CoV-2, as well as screen compounds as potential adjuvants for vaccines (3, 17). AI-powered chatbots have been used with success in clinical scenarios and can advise many more people than a manned call center and ease the stress placed on medical hotlines (18). AI could manage the pandemic by using

thermal imaging to scan public spaces for people potentially infected, and by enforcing social distancing and lockdown measures (3, 17).

Artificial intelligence has been widely used in COVID-19, including diagnosis, public health, clinical decision making, social control, therapeutics, vaccine development, surveillance, combination with big data, operation of other core clinical services, and management of patients with COVID-19 (3, 18, 19). In order to solve the significant pressure of the limited medical resources caused by the pandemic of COVID-19, rapid diagnosis, accurate prediction, enhanced monitoring, and effective treatments are the most important measures to control the spread of the pandemic. Many related review articles have been published. However, the results of these studies are inconsistent and there is little research systematically assessing the application of AI for COVID-19 in accordance with PRISMA, and most of them only discuss aspects such as diagnosis or treatment. Therefore, we conducted this review to assess the performance of AI for COVID-19 systematically, and to describe the main categories of AI use, the potential benefits and limitations and future directions for AI.

## METHODS

We registered the protocol for this review in advance (PROSPERO CRD42020211555, URL: <https://www.crd.york.ac.uk/prospero/>).

### Search Strategy and Eligibility Criteria

This systematic review is reported in accordance with the Preferred Reporting Items for Systematic Reviews and Meta-Analyses (PRISMA) guidelines (20) (**Supplementary Material 2**). We searched PubMed, Embase and the Cochrane Library for published studies from the inception of these resources to 19 September 2020 using the following terms related to artificial intelligence and COVID-19: “Artificial intelligence,” “Machine Intelligence,” “Machine learning,” “Deep learning,” “Predictive model,” “2019 novel coronavirus disease,” “COVID-19,” “2019 novel coronavirus infection,” “coronavirus disease-19,” and “2019-nCoV disease.” The details of the search strategy are in the **Supplementary Material 1**.

We included original studies fulfilling the following criteria: (I) research topic was focused on the application of AI for COVID-19, (II) participants had a confirmed diagnosis of COVID-19 by reverse transcription-polymerase chain reaction (RT-PCR) testing or other laboratory examination (where appropriate), and (III) article was published in English.

We excluded studies if: (I) insufficient data were available, (II) we were unable to access the full text or complete data, or (III) the report was a review, case-report or comment.

Two trained researchers (Lian Wang, Dongguang Wang) screened titles, abstracts and the full text of potentially eligible studies independently using Endnote X8.2 software, Thomson Reuters. Discrepancies were resolved through consultation with a third researcher (Xiang Tong, Tao Liu).

## Data Abstraction and Quality Assessment

We extracted data and recorded the following information for each study: basic information for the article (title, first author, date of publication), experimental design (algorithm, sample size) and primary outcome (sensitivity, accuracy and specificity of AI for diagnosis and prognosis evaluation; prediction of epidemic; drug repurposing and development). If a study used multiple models, we extracted the most discriminative one.

Three researchers (SZ, JH, LZ) used PROBAST (prediction model risk of bias assessment tool) to assess the risk of bias in the included studies (21). The PROBAST statement was divided into four domains: participants, predictors, outcome, and analysis. These domains contain a total of 20 signal questions to help structure judgment of risk of bias for prediction models, such as the range of included patients, whether the same predictors and results were defined for all participants, whether the clinical decision rule was determined prospectively, and whether a relevant measure of accuracy was reported (22). The details of PROBAST are in the **Supplementary Material 3**.

We divided the included studies into four categories: diagnosis, prognosis, epidemic prediction, and drug discovery. In the diagnosis and prognosis domains, we evaluated the classification performance using AUC, accuracy, sensitivity, and specificity. For epidemic trends and drugs and vaccines discovery, we listed the results only because there are no suitable evaluation indicators.

## Role of the Funding Source

This study was supported by National Key R&D Program of China (2017YFC1309703) and 1-3-5 project for disciplines of excellence—Clinical Research Incubation Project, West China Hospital, Sichuan University (2019HXFH008). The funders of this research did not contribute to the study design, data analysis, data interpretation or preparation of the manuscript.

## RESULTS

We retrieved a total of 870 records from PubMed, Embase and the Cochrane Library. Of these, 78 studies met our inclusion criteria. Details of the study selection process are shown in **Figure 1**. Among the 78 included studies (12, 14, 17, 23–97), 46 discussed AI-assisted diagnosis of COVID-19 (14, 23–67), 14 evaluated prognosis (12, 68–80), 9 estimated infected cases, infection rates and epidemic trends (81–89), 8 explored potential effective and safe drugs (90–97), primarily through drug repurposing and drug development and 1 article predicted vaccine targets that has the potential to develop COVID-19 vaccines (17).

We used PROBAST to evaluate the quality of the 60 articles related to diagnosis or prognosis for COVID-19 (**Table 1**) (12, 14, 23–80). According to the assessment with PROBAST, all models had a high risk of bias. In the absence of appropriate evaluation tools for the other 18 articles, the quality of these was not assessed (17, 81–97).

## AI-Assisted Diagnosis for COVID-19

We included 46 studies related to AI-assisted diagnosis through chest images for COVID-19 (14, 23–67). The findings of these studies ranged as follows, total accuracy: 70.00 to 99.92%, sensitivity: 73.00 to 100.00%, specificity: 25 to 100.00%, AUC: 0.732 to 1.000.

### Chest CT Images

Deep learning with a convolutional neural network (CNN) has gained increasing attention for its outstanding image recognition performance (98). Several of the studies ( $n = 18$ ) we identified had developed AI models based on CNN and these showed excellent ability to discriminate COVID-19 and non-COVID pneumonia by automatically detecting chest CT images with an accuracy of 70.00 to 99.87%, sensitivity of 73.00 to 100.00%, specificity of 25 to 100.00%, and AUC of 0.732 to 1.000 (**Table 2**) (14, 23, 24, 26, 27, 29–31, 33–40, 43, 44). Mei et al. (29) developed a joint CNN model that diagnoses COVID-19 patients rapidly by combining chest CT findings with clinical symptoms, exposure history, and laboratory tests. Moreover, Mishra et al. (30) proposed a decision-fusion approach, which combined the predictions of each Deep CNN model and achieved results above 86% for all the performance metrics under consideration. Three studies (14, 41, 42) found that AI models had higher test accuracy, sensitivity, specificity than radiologists, and with the assistance of AI, the radiologists made diagnosis with much faster speeds and achieved a higher diagnostic performance.

In addition, some studies reported applications distinguishing COVID-19 from non-COVID-19 or other pneumonia by using the AD3D-MIL model (25), Ensemble of Bagged Tree (28), AutoML Cloud Vision (32). All of these performed well.

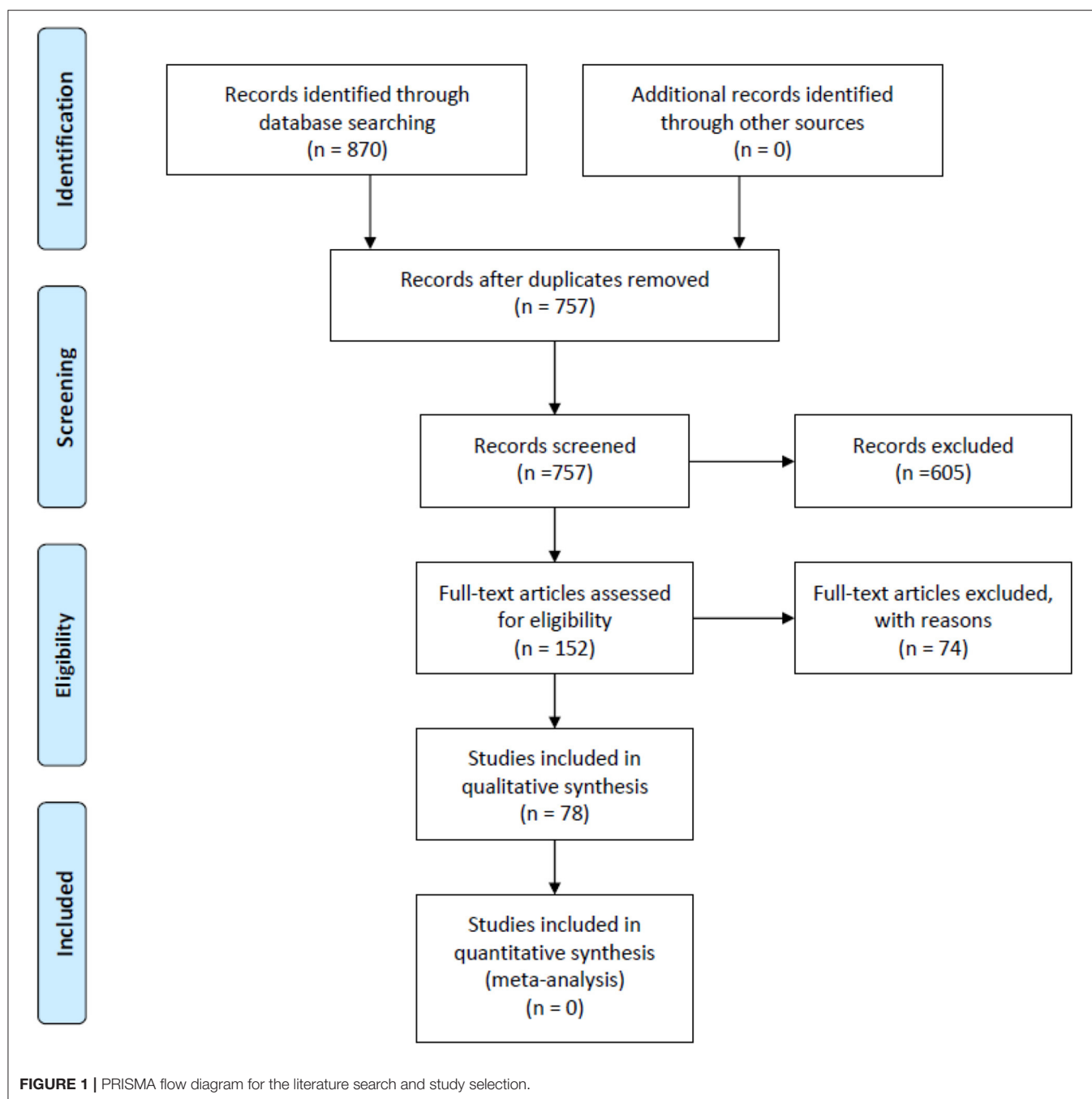
### Chest X-Ray Images

Although CT images have high sensitivity in detecting COVID-19, costs and radiation doses are relatively high. On the contrary, chest X-ray is a low-cost and rapid detection method, which might be used in initial screening of suspected cases of COVID-19 infection, supporting the timely application of quarantine measures in positive patients (45). Several studies have developed AI techniques to automatically detect and extract features from chest X-rays to assist in the diagnosis of COVID-19 with high accuracy (71.90 to 99.92%), sensitivity (75.00 to 99.44%), specificity (71.80 to 100.00%), and AUC (0.81 to 0.999) (45–67) (**Table 3**).

## Predicting the Prognosis of COVID-19

The ability to identify a patient's risk of deterioration during their hospitalization is critical for effective medical resource allocation and to ensure that patients receive appropriate management during the COVID-19 pandemic. We identified several AI models built on the chest CT images that accurately quantified lung abnormalities related to COVID-19 and evaluated the severity and prognosis of the disease (70, 76, 79, 80). Some studies showed that deep learning models could predict the risk of COVID-19 patients developing critical illness, based on clinical characteristics at hospital admission, such as clinical, laboratory and radiological characteristics (68, 71, 73–75, 77, 78).





Iwendi et al. (69) developed a model using the geographical, traveling, health, and demographic data of COVID-19 patients to predict the severity and the possible outcomes of the cases. In general, AI models reached accuracy of 74.4 to 95.20%, sensitivity of 72.8 to 98.00%, specificity of 55 to 96.87% and AUC of 0.66 to 0.997 in predicting critical COVID-19 (Table 4). Accurately determining the prognosis of COVID-19 patients as early as possible and starting early treatment may improve their prognosis and reduce mortality from COVID-19.

## Predicting the Epidemic Trend of COVID-19

COVID-19 has spread globally and had a substantial impact. It was defined as a pandemic by the World Health Organization (WHO) in March 2020. As the COVID-19 pandemic evolves, it is vital to focus on building prediction models to help policymakers and health managers to allocate healthcare resources and prevent or limit outbreaks (82). We identified 9 studies that sought to predict the epidemic trend of COVID-19 (81–89) (Table 5). Of these, 6 studies used long short-term memory (LSTM) models with or without other models to predict the

**TABLE 1 |** Risk of bias assessment (by PROBAST).

| References                       | Risk of bias |            |         |          |
|----------------------------------|--------------|------------|---------|----------|
|                                  | Participants | Predictors | Outcome | Analysis |
| <b>Diagnosis</b>                 |              |            |         |          |
| Abbasian Ardakani et al. (23)    | High         | Unclear    | Low     | High     |
| Bai et al. (14)                  | High         | Unclear    | Low     | High     |
| Ardakani et al. (24)             | High         | Unclear    | Low     | High     |
| Han et al. (25)                  | High         | Unclear    | Low     | High     |
| Ko et al. (26)                   | High         | High       | Low     | High     |
| Li et al. (27)                   | High         | Unclear    | Low     | High     |
| Liu et al. (28)                  | High         | Unclear    | Low     | High     |
| Mei et al. (29)                  | High         | Unclear    | Unclear | High     |
| Mishra et al. (30)               | High         | High       | High    | High     |
| Ouyang et al. (31)               | High         | Unclear    | Low     | High     |
| Sakagianni et al. (32)           | High         | High       | High    | High     |
| Sharma (33)                      | High         | High       | High    | High     |
| Wang et al. (34)                 | High         | High       | High    | High     |
| Wang et al. (35)                 | Low          | High       | Low     | High     |
| Wu et al. (36)                   | High         | Unclear    | High    | High     |
| Yan et al. (37)                  | High         | Unclear    | Low     | High     |
| Zhang et al. (38)                | Low          | High       | High    | High     |
| Harmon et al. (39)               | Low          | Unclear    | High    | High     |
| Jaiswal et al. (40)              | High         | High       | High    | High     |
| Ni et al. (41)                   | Low          | Unclear    | High    | High     |
| Song et al. (42)                 | Low          | High       | Low     | High     |
| Xu et al. (43)                   | Low          | High       | Low     | High     |
| Yang et al. (44)                 | Low          | Low        | Low     | High     |
| Apostolopoulos and Mpesiana (45) | High         | High       | High    | High     |
| Das et al. (47)                  | High         | High       | High    | High     |
| Khan et al. (49)                 | High         | High       | High    | High     |
| Mahmud et al. (50)               | High         | High       | High    | High     |
| Murphy et al. (51)               | High         | Unclear    | Low     | High     |
| Ouchicha et al. (52)             | High         | High       | High    | High     |
| Ozturk et al. (53)               | High         | High       | High    | High     |
| Togaçar et al. (54)              | High         | High       | High    | High     |
| Vaid et al. (55)                 | High         | High       | High    | High     |
| Elaziz et al. (48)               | Low          | Unclear    | Low     | High     |
| Bressem et al. (46)              | High         | High       | High    | High     |
| Altan and Karasu (56)            | High         | High       | High    | High     |
| Brunese et al. (57)              | High         | High       | High    | High     |
| Che Azemin et al. (58)           | High         | High       | High    | High     |
| Islam et al. (59)                | High         | High       | High    | High     |
| Jain et al. (60)                 | High         | High       | High    | High     |
| Nour et al. (61)                 | High         | High       | High    | High     |
| Rahaman et al. (62)              | High         | High       | High    | High     |
| Rahimzadeh and Attar (63)        | High         | High       | High    | High     |
| Rajaraman et al. (64)            | High         | High       | High    | High     |
| Toraman et al. (65)              | High         | High       | High    | High     |
| Ucar and Korkamz (66)            | High         | High       | High    | High     |
| Waheed et al. (67)               | High         | High       | High    | High     |
| <b>Prognosis</b>                 |              |            |         |          |
| Assaf et al. (68)                | High         | High       | High    | High     |

(Continued)

TABLE 1 | Continued

| References           | Risk of bias |            |         |          |
|----------------------|--------------|------------|---------|----------|
|                      | Participants | Predictors | Outcome | Analysis |
| Li et al. (70)       | High         | Unclear    | Low     | High     |
| Liang et al. (71)    | High         | High       | Low     | High     |
| Yao et al. (75)      | High         | High       | High    | High     |
| Yu et al. (76)       | High         | High       | High    | High     |
| Iwendi et al. (69)   | High         | High       | High    | High     |
| Abdulaal et al. (12) | High         | High       | Low     | High     |
| Ma et al. (72)       | High         | High       | Low     | High     |
| Mushtaq et al. (73)  | High         | High       | Low     | High     |
| Wu et al. (77)       | High         | High       | High    | High     |
| Cheng et al. (78)    | High         | Unclear    | Low     | High     |
| Fu et al. (79)       | High         | High       | High    | High     |
| Wu et al. (74)       | High         | Low        | Low     | High     |
| Xiao et al. (80)     | High         | Low        | Low     | High     |

PRISMA, the Preferred Reporting Items for Systematic Reviews and Meta-Analyses; PROBAST, prediction model risk of bias assessment tool.

incidence, confirmed cases, deaths and recoveries, development trend and possible stopping time of COVID-19 (82, 84–86, 88, 89). Alsayed et al. (81) used the Susceptible–Exposed–Infectious–Recovered (SEIR) model combined with machine learning to predict the epidemic's evolution or estimate the unreported number of infections. Mollalo et al. (83) tested the applicability of multi-layer perceptron (MLP) artificial neural networks in simulating cumulative incidence of COVID-19 at the county-level across the continental USA. Shahid et al. (84) proposed prediction models including support vector regression (SVR), autoregressive integrated moving average (ARIMA), long short-term memory (LSTM) and Bi-directional long short-term memory (Bi-LSTM) to predict confirmed cases, deaths and recoveries in ten major countries affected by COVID-19. Zheng et al. (85) proposed an improved susceptible–infected (ISI) model to estimate the variety of the infection rates and to analyze the transmission laws and development trend. Ribeiro et al. (88) used several machine learning models to forecast the cumulative confirmed cases of COVID-19 in the ten Brazilian states with a high daily incidence, and rank the models based on their accuracy. The results of these studies may bring broad benefits by helping to control and prevent COVID-19.

## Drug Discovery and Vaccine Development for COVID-19

With the spread of COVID-19 showing no signs of slowing and there are few proven effective therapeutics for COVID-19, thousands of people continue to die from the disease every day. It is essential to develop antiviral drugs and vaccines against SARS-CoV-2. It usually needs a long time to develop a drug or vaccine using traditional methods but to try to accelerate this process, several studies have applied AI techniques to identify potential drugs and develop effective and safe vaccines for COVID-19. We identified 9 studies that developed models to find potential drugs and vaccines for COVID-19 (17, 90–97) (Table 6).

## Drug Repurposing

Drug repurposing refers to the application of approved drugs to new therapeutic indications, which has become a successful drug development strategy for reducing development costs and increasing the simplicity of drug approval procedures (99). AI algorithms could be trained and then be used to screen existing drugs that may prove effective in the treatment of COVID-19. Ke et al. (91) used AI to identify 13 drugs with activities against feline infectious peritonitis (FIP) coronavirus, and further studies proved their activities against SARS-CoV-2 in clinical applications. In another study, Zeng et al. (92) identified 41 high-confidence repurposed drug candidates with a higher area under the receiver operating characteristic (AUROC) of 0.85. Gao et al. (90) developed a gradient-boosted decision trees (GBDT) model for screening 8,565 drugs in DrugBank, finally finding 20 FDA-approved drugs and 20 investigational or off-market drugs that might be effective against SARS-CoV-2. Stebbing et al. (93) used AI prediction to identify Baricitinib, which is used to treat rheumatoid arthritis and myelofibrosis, can be used for COVID-19 infection through proposed anti-cytokine effects and as an inhibitor of host cell viral propagation.

## Drug Development

Zhang et al. (94) built a protein 3D model of 3CLpro and used a deep learning method to identify protein-ligand interacting pairs, and finally provided potential compound and tripeptide lists for 3CLpro. Batra et al. (95) combined machine learning and high-fidelity ensemble docking to identify 75 FDA-approved and 100 other ligands from drug data sets as potential therapeutic agents against COVID-19. Joshi et al. (96) used deep-learning models to screen natural compounds and found that two compounds Palmatine and Sauchinone formed very stable complex with Mpro, which may be considered for therapeutic development against the SARS-CoV-2. Ton et al. (97) developed Deep Docking (DD) to screen 1.3 billion compounds from ZINC15

**TABLE 2 |** Application of AI in using chest CT images to diagnose COVID-19.

| References                    | Algorithm                        | Subjects                               | Objective  | Results  |
|-------------------------------|----------------------------------|--|--|--|
| Abbasian Ardakani et al. (23) | CAD                              | 612 patients (306 COVID-19)            | Identify COVID-19/non-COVID-19                             | Accuracy, 91.94%; Sensitivity, 93.54%; Specificity, 90.32%; AUC, 0.965   |
| Bai et al. (14)               | EfficientNet B4                  | 1,186 patients (521 COVID-19)          | Identify COVID-19/non-COVID-19                             | Accuracy, 96%; Sensitivity, 95%; Specificity, 96%; AUC, 0.95   |
| Ardakani et al. (24)          | ResNet-101                       | 194 patients (108 COVID-19)            | Identify COVID-19/non-COVID-19                             | Accuracy, 99.51%; Sensitivity, 100%; Specificity, 99.02%; AUC, 0.994   |
| Han et al. (25)               | AD3D-MIL                         | 460 chest CT images (230 COVID-19)     | Identify COVID-19/non-COVID-19                             | Accuracy, 97.9%; Sensitivity, 97.9%; AUC, 0.99; Precision, 97.9%; F1 score 97.9%   |
| Ko et al. (26)                | FCONet                           | 2,551 chest CT images (1,194 COVID-19) | Identify COVID-19/other pneumonia/non-pneumonia            | Accuracy, 99.87%; Sensitivity, 99.58%; Specificity, 100%; AUC, 1.00  |
| Li et al. (27)                | COVNet                           | 4,356 chest CT images (1,296 COVID-19) | Identify COVID-19/CAP/non-pneumonia                        | Sensitivity, 90%; Specificity, 96%; AUC, 0.96  |
| Liu et al. (28)               | EBT                              | 100 patients (73 COVID-19)             | Identify COVID-19/general pneumonia                        | Accuracy, 94.16%; Sensitivity, 88.62%; Specificity, 100%; AUC, 0.99  |
| Mei et al. (29)               | CNN                              | 905 patients (419 COVID-19)            | Identify COVID-19/non-COVID-19                             | Accuracy, 79.6%; Sensitivity, 83.6%; Specificity, 75.9%; AUC, 0.86   |
| Mishra et al. (30)            | DCNN                             | 727 chest CT images (360 COVID-19)     | Identify COVID-19/non-COVID-19                             | Accuracy, 88.34%; Sensitivity, 88.13%; Specificity, 90.51%; AUC, 0.883; F1 score 86.7%   |
| Ouyang et al. (31)            | Attention RN34 + DS (3D CNN)     | 4,982 chest CT images (3,389 COVID-19) | Identify COVID-19/CAP                                      | Accuracy, 87.5%; Sensitivity, 86.9%; Specificity, 90.1%; AUC, 0.944; F1 score 82%  |
| Sakagianni et al. (32)        | AutoML Cloud Vision              | 746 chest CT images (349 COVID-19)     | Identify COVID-19/non-COVID-19                             | Sensitivity, 88.31%; Precision, 88.31%   |
| Sharma (33)                   | ResNet                           | 2,200 chest CT images (800 COVID-19)   | Identify COVID-19/viral pneumonia                          | Accuracy, 91%; Sensitivity, 92.1%; Specificity, 90.29%   |
| Wang et al. (34)              | 3D-ResNet (DCNN)                 | 4,657 chest CT images (1,315 COVID-19) | Identify COVID-19/viral pneumonia                          | Accuracy, 93.3 ± 0.8%; Sensitivity, 87.6 ± 4.3%; Specificity, 95.5 ± 2.1%; AUC, 97.3 ± 1.1; Precision, 88.4 ± 4.1%; F1 score 87.8 ± 1.5%                       |
| Wang et al. (35)              | DenseNet121-FPN/COVID-19Net      | 1,266 chest CT images (924 COVID-19)   | Identify COVID-19/viral pneumonia /other pneumonia         | Accuracy, 80.12%; Sensitivity, 79.35%; Specificity, 81.16%; AUC, 0.88; F1 score 82.02%   |
| Wu et al. (36)                | ResNet50                         | 495 patients (368 COVID-19)            | Identify COVID-19 /other pneumonia                         | Accuracy, 70%; Sensitivity, 73%; Specificity, 61.5%; AUC, 0.732  |
| Yan et al. (37)               | MSCNN                            | 828 chest CT images (416 COVID-19)     | Identify COVID-19/common pneumonia                         | Accuracy, 97.7%; Sensitivity, 99.5%; Specificity, 95.6%; AUC, 0.962  |
| Zhang et al. (38)             | AI-based system                  | 260 patients (83 COVID-19)             | Identify COVID-19/common pneumonia/normal pneumonia/normal | Accuracy, 92.49%; Sensitivity, 94.93%; Specificity, 91.13%; AUC, 0.9813  |
| Harmon et al. (39)            | 3D models (based on Densnet-121) | 2,617 patients (922 COVID-19)          | Identify COVID-19/non-COVID-19                             | Accuracy, 90.8%; Sensitivity, 84%; Specificity, 93%; AUC, 0.949  |
| Jaiswal et al. (40)           | DTL with DenseNet201             | 2,492 CT scan images (1,262 COVID-19)  | Identify COVID-19/non-COVID-19                             | Accuracy, 96.25%; Sensitivity, 96.29%; Specificity, 96.21%; AUC, 0.97  |
| Ni et al. (41)                | Convolutional MVP-Net, 3D U-Net  | 14,435 patients (2,154 COVID-19)       | Identify COVID-19/non-COVID-19                             | For patient level, Accuracy, 94%; Sensitivity, 100%; Specificity, 25%; AUC, 0.86. For lobe level, Accuracy, 82%; Sensitivity, 96%; Specificity, 63%; AUC, 0.87 |
| Song et al. (42)              | BigBiGAN                         | 201 patients (98 COVID-19)             | Identify COVID-19/non-COVID-19                             | Sensitivity, 92%; Specificity, 91%   |
| Xu et al. (43)                | CNN                              | 509 patients (110 COVID-19)            | Identify COVID-19/IAPV/non-COVID-19                        | Accuracy, 86.7%; Sensitivity, 86.7%; Specificity, 81.2%; F1 score 83.9%  |
| Yang et al. (44)              | DenseNet                         | 295 patients (146 COVID-19)            | Identify COVID-19/normal                                   | Accuracy, 92%; Sensitivity, 97%; Specificity, 87%; AUC, 0.98; F1 score 93%   |

CNN, Convolutional Neural Network; DFCNN, Dense Fully Convolutional Neural Network; EBT, Ensemble of Bagged Tree; DCNN, Dense Convolutional Neural Network; MSCNN, Multi-Scale Convolutional Neural Network; DTL, Deep Transfer Learning; IAPV, Influenza-A Viral Pneumonia.



**TABLE 3 |** Application of AI in using chest x-ray images to diagnose COVID-19.

| References                       | Algorithm               | Subjects                                  | Objective  | Results  |
|----------------------------------|-------------------------|---|--|--|
| Apostolopoulos and Mpesiana (45) | MobileNet v2            | 1,442 chest x-ray images (224 COVID-19)   | Identify COVID-19/viral/bacterial/pneumonia/normal           | Accuracy, 96.78%; Sensitivity, 98.66%; Specificity, 96.46%   |
| Das et al. (47)                  | Truncated Inception Net | 6,845 chest x-ray images (162 COVID-19)   | Identify COVID-19/non-COVID-19                               | Accuracy, 99.92%; Sensitivity, 93%; Specificity, 100%; AUC, 0.99; Precision, 100%; F1 score 96%            |
| Khan et al. (49)                 | CoroNet                 | 3,084 chest x-ray images (290 COVID-19)   | Identify COVID-19/viral/bacterial/pneumonia/normal           | Accuracy, 89.60%; Sensitivity, 89.92%; Specificity, 96.4%; Precision, 90%; F1 score 89.8%                  |
| Mahmud et al. (50)               | CovXNet                 | 6,161 chest x-ray images (305 COVID-19)   | Identify COVID-19/viral/bacterial/pneumonia/normal           | Accuracy, 90.2%; Sensitivity, 89.9%; Specificity, 89.1%; AUC, 0.911; Precision, 90.8%; F1 score 90.4%      |
| Murphy et al. (51)               | CAD4COVID-XRay          | 24,678 chest x-ray images (730 COVID-19)  | Identify COVID-19/non-COVID-19                               | Sensitivity, 75%; Specificity, 78%; AUC, 0.81  |
| Ouchicha et al. (52)             | CVDNet                  | 2,905 chest x-ray images (219 COVID-19)   | Identify COVID-19/viral pneumonia/normal                     | Accuracy, 96.69%; Sensitivity, 96.84%; Precision 96.72%; F1 score 96.68%                                   |
| Ozturk et al. (53)               | DarkCovidNet            | 1,127 chest x-ray images (127 COVID-19)   | Identify COVID-19/pneumonia/normal                           | Accuracy, 98.08%; Sensitivity, 95.13%; Specificity, 95.30%; Precision, 98.03%; F1 score 96.51%             |
| Togaçar et al. (54)              | MobileNetV2, SqueezeNet | 458 chest x-ray images (295 COVID-19)     | Identify COVID-19/pneumonia/normal                           | Accuracy, 99.34%; Sensitivity, 99.32%; Specificity, 99.37%; AUC, 0.982; Precision, 99.66%; F1 score 99.49% |
| Vaid et al. (55)                 | CNN                     | 545 chest x-ray images (181 COVID-19)     | Identify COVID-19/ normal                                    | Accuracy>96.3%; Sensitivity, 97.1%; Precision 91.7%; F1 score 94.3%  |
| Elaziz et al. (48)               | FrMEMs                  | 1,891 chest x-ray images (216 COVID-19)   | Identify COVID-19/non-COVID-19                               | Accuracy, 96.09%; Sensitivity, 98.75%; Precision 98.75%  |
| Bressem et al. (46)              | DenseNet-121            | 46,754 chest x-ray images (196 COVID-19)  | Identify COVID-19/non-COVID-19/normal                        | Sensitivity, 93%; Specificity, 100%  |
| Altan and Karasu (56)            | EfficientNet-B0         | 2,905 chest x-ray images (219 COVID-19)   | Identify COVID-19/viral pneumonia/normal                     | Accuracy, 99.69%; Sensitivity, 99.44%; Specificity, 99.81%; Precision, 99.62%; F1 score 99.53%             |
| Brunese et al. (57)              | VGG16                   | 6,523 chest x-ray images (250 COVID-19)   | Identify COVID-19/pulmonary diseases                         | Accuracy, 98%; Sensitivity, 87%; Specificity, 94%; Precision, 89%  |
| Che Azemin et al. (58)           | ResNet-101              | 5,982 chest x-ray images (154 COVID-19)   | Identify COVID-19/non-COVID19                                | Accuracy, 71.9%; Sensitivity, 77.3%; Specificity, 71.8%; AUC, 0.82   |
| Islam et al. (59)                | CNN, LSTM               | 4,575 chest x-ray images (1,525 COVID-19) | Identify COVID-19/pneumonia/normal                           | Accuracy, 99.4%; Sensitivity, 99.3%; Specificity, 99.2%; AUC, 0.999; F1 score 98.9%                        |
| Jain et al. (60)                 | ResNet                  | 1,215 chest x-ray images (250 COVID-19)   | Identify COVID-19/viral pneumonia/bacterial pneumonia/normal | Accuracy, 97.77%; Sensitivity, 97.14%  |
| Nour et al. (61)                 | CNN, Machine leaning    | 2,905 chest x-ray images (219 COVID-19)   | Identify COVID-19/viral pneumonia/normal                     | Accuracy, 98.97%; Sensitivity, 89.39%; Specificity, 99.75%; F1 score 96.72%                                |
| Rahaman et al. (62)              | CNN                     | 860 chest x-ray images (260 COVID-19)     | Identify COVID-19/pneumonia/normal                           | Accuracy, 89.3%; Sensitivity, 89%; Precision, 90%; F1 score 90%  |
| Rahimzadeh et al. (63)           | Xception, ResNet50V2    | 15,085 chest x-ray images (180 COVID-19)  | Identify COVID-19/pneumonia/normal                           | Accuracy, 99.5%; Sensitivity, 80.53%   |
| Rajaraman et al. (64)            | CNN                     | 14,997 chest x-ray images (286 COVID-19)  | Identify COVID-19/viral pneumonia/bacterial pneumonia/normal | Accuracy, 99.01%; Sensitivity, 99.01%; AUC, 0.9972   |
| Toraman et al. (65)              | Convolutional CapsNet   | 2,331 chest x-ray images (231 COVID-19)   | Identify COVID-19/normal                                     | Accuracy, 97.24%; Sensitivity, 97.42%; Specificity, 97.04%; Precision, 97.06%; F1 score 97.24%             |
| Ucar and Korkamz (66)            | Deep Bayes-SqueezeNet   | 5,949 chest x-ray images (76 COVID-19)    | Identify COVID-19/pneumonia/normal                           | Accuracy, 98.26%; Sensitivity, 98.26%; Specificity, 99.13%; F1 score 98.25%                                |
| Waheed et al. (67)               | CovidGAN (ACGAN)        | 1,124 chest x-ray images (403 COVID-19)   | Identify COVID-19/normal                                     | Accuracy, 95%; Sensitivity, 90%; Specificity, 97%  |

CNN, Convolutional Neural Network; LSTM, Long Short-Term Memory; ACGAN, Auxiliary Classifier Generative Adversarial Network.

**TABLE 4 |** Application of AI in predicting prognosis of COVID-19.

| References           | Algorithm                        | Subjects                | Objective   | Results  |
|----------------------|----------------------------------|-------------------------|---|--|
| Assaf et al. (68)    | ANN, Random Forest and CRT       | 389 COVID-19 patients   | Predict severity of COVID-19                          | Accuracy, 92%; Sensitivity, 88%; Specificity, 92.7%                              |
| Li et al. (70)       | POI and iHU                      | 196 COVID-19 patients   | Predict severity of COVID-19                          | Sensitivity, 93.67%; Specificity, 88.05%; AUC, 0.97                              |
| Liang et al. (71)    | Deep learning survival cox model | 1,590 COVID-19 patients | Predict severity of COVID-19                          | Concordance index 0.894; AUC, 0.911  |
| Yao et al. (75)      | SVM                              | 137 COVID-19 patients   | Predict severity of COVID-19                          | Accuracy, 81.48%   |
| Yu et al. (76)       | DenseNet-201, SVM model          | 202 COVID-19 patients   | Predict severity of COVID-19                          | Accuracy, 95.2%; Sensitivity, 91.87%; Specificity, 96.87%; AUC, 0.99             |
| Iwendi et al. (69)   | Random forest                    | –                       | Predict severity of COVID-19                          | Accuracy, 94%; Sensitivity, 75%; F1 score 86%                                    |
| Abdulaal et al. (12) | ANN                              | 398 COVID-19 patients   | Predict mortality risk of COVID-19                    | Accuracy, 86.25%; Sensitivity, 87.50%; Specificity, 85.94%; AUC, 0.9012          |
| Ma et al. (72)       | Random Forest and XGboost        | 292 COVID-19 patients   | Predict mortality risk of COVID-19                    | AUC 0.9521   |
| Mushtaq et al. (73)  | CNN                              | 697 COVID-19 patients   | Predict severity and mortality risk for COVID-19      | For mortality, the AUCs were 0.66, for critical COVID-19, the AUCs were 0.77     |
| Wu et al. (77)       | LASSO logistic regression model  | 110 COVID-19 patients   | Predict mortality risk of COVID-19                    | Sensitivity, 98%; Specificity, 91%; AUC, 0.997                                   |
| Cheng et al. (78)    | Random Forest                    | 1,987 COVID-19 patients | Identify patients at risk of ICU transfer within 24 h | Accuracy, 76.2%; Sensitivity, 72.8%; Specificity, 76.3%; AUC, 0.799              |
| Fu et al. (79)       | LASSO, mRMR, SVM                 | 64 COVID-19 patients    | Identify the progression of COVID-19                  | Sensitivity, 80.95%; Specificity, 74.42%; AUC, 0.833                             |
| Wu et al. (74)       | ADASYN, Logistic Regression      | 426 COVID-19 patients   | Predict severity risk for COVID-19                    | Accuracy, 74.4–87.5%; Sensitivity, 75–96.9%; Specificity, 55–88%; AUC, 0.84–0.93 |
| Xiao et al. (80)     | MIL, ResNet34                    | 408 COVID-19 patients   | Predict severity risk for COVID-19                    | Accuracy, 81.9%; AUC, 0.892  |

ANN, Artificial Neural Network; RF, Random Forest; CRT, Classification and Regression Decision Tree; POI, portion of infection; iHU, average infection Hounsfield unit; SVM, Support Vector Machine; LASSO, Least Absolute Shrinkage and Selection Operator; mRMR, Minimum Redundancy Maximum Correlation; ADASYN, Adaptive Synthetic Sampling; MIL, Multiple Instance Learning.

library and identify top 1,000 potential ligands for SARS-CoV-2 Mpro protein.

## Vaccine Development

Without an existing effective medical therapy, the development of an effective and safe vaccine is an important method to deal with this highly infectious disease caused by the SARS-CoV-2 coronavirus. Ong et al. applied a ML tool to predict the S protein, nsp3, 3CL-pro, and nsp8-10 were crucial to the viral adhering and host invasion by investigating the entire proteome of SARS-CoV-2. SARS-CoV-2 S protein has the highest protective antigenicity score and was identified as the most favorable vaccine candidate, besides, the nsp3 protein was selected for further investigation (17). The predicted vaccine targets have the potential for COVID-19 vaccine developed, however, they need to be further evaluated in clinical studies.

## DISCUSSION

Our systematic review includes 78 articles on the application of AI for COVID-19. These spanned radiological diagnosis,

prediction of prognosis, estimation of epidemic trends and drugs and vaccines discovery for COVID-19.

The gold standard for diagnostic tests for COVID-19 is real-time reverse-transcriptase polymerase chain reaction (RT-PCR). However, RT-PCR does produce false negatives or fluctuating results (100). A study compared the diagnostic performance of chest computed tomography (CT) scan with RT-PCR and found that the chest CT is more sensitive than RT-PCR (98 vs. 71%, respectively,  $P < 0.001$ ) (101), suggesting that Chest CT could be a supplementary diagnostic measure to help physicians make faster and more accurate decisions. AI technique is used for identifying or classifying images, recognizing speech and processing natural language (102). It is well-suited to developing tools to assist with the use of chest CT to diagnose COVID-19 (103). Advanced AI-based algorithms can learn the typical CT image signs, such as bilateral and subpleural ground-glass opacities (GGO), vascular thickening, spider web, and even crazy-paving patterns (104). In addition, the algorithms can also learn some high-dimensional features that radiologists cannot handle, such as texture and wavelet information, thereby allowing pneumonia caused by SARS-CoV-2 to be distinguished from that caused by other pathogens, through advanced AI-based

**TABLE 5 |** Application of AI in predicting the epidemic trend of COVID-19.

| References              | Algorithm   | Country        | Objective  | Results   |
|-------------------------|---|----------------|--|---|
| Alsayed et al. (81)     | GA, SEIR, ANFIS   | Malaysia       | Estimate the infection rate, epidemic peak, and the number of infected cases | Infection rate is $0.228 \pm 0.013$ , NRMSE 0.041, MAPE 2.45%, R2 of 0.9964   |
| Ayyoubzadeh et al. (82) | LSTM, linear regression                                       | Iran           | Predict the incidence  | RMSE: LSTM, 27.187 (SD 20.705); Linear regression, 7.562 (SD 6.492)   |
| Mollalo et al. (83)     | MLP neural network  | The US         | Predict incidence rates  | RMSE, 0.722409; MAE. 0.355843; correlation coefficient 0.645481   |
| Shahid et al. (84)      | ARIMA, SVR, LSTM, Bi-LSTM                                     | Ten countries  | Predict confirmed cases, deaths, and recoveries                              | Bi-LSTM generates lowest MAE and RMSE values of 0.0070 and 0.0077 in China; r2_score 0.9997   |
| Zheng et al. (85)       | ISI, NLP, LSTM  | China          | Analyze the transmission laws and development trend                          | Obtain MAPEs with 0.52, 0.38, 0.05, and 0.86% for the next 6 days in Wuhan, Beijing, Shanghai, and countrywide, respectively  |
| Arora et al. (86)       | LSTM  | India          | Predict daily and weekly positive cases                                      | Daily predictions MAPE <3% and weekly predictions MAPE <8%  |
| Chimmula and Zhang (87) | LSTM  | Canada         | Predict the trends and possible stopping time of COVID-19                    | For short term predictions, RMSE, 4.83; accuracy, 93.4%. For long term predictions, RMSE, 45.70; accuracy, 92.67%   |
| Ribeiro et al. (88)     | SVR, stacking-ensemble learning, ARIMA, CUBIST, RIDGE, and RF | Brazil         | Forecast the cumulative confirmed cases                                      | sMAPE in a range of 0.87–3.51, 1.02–5.63, and 0.95–6.90% in 1, 3, and 6-days-ahead, respectively  |
| Shastri et al. (89)     | Variants of LSTM  | India, The USA | Forecast the confirmed cases and death cases                                 | Achieved accuracies of 97.82, 98, 96.66, and 97.50%, MAPE of 2.17, 2.00, 3.33, 2.50 for India confirmed cases, USA confirmed cases, India death cases and USA death cases, respectively |

GA, Genetic Algorithm; SEIR, Susceptible–Exposed–Infectious–Recovered; ANFIS, Adaptive Neuro-Fuzzy Inference System; LSTM, Linear regression and long short-term memory;  $R_0$ , Reproductive number; MLP, Multilayer perceptron; RMSE, Root-mean-square error; NRMSE, Normalized root mean square error; MAE, Mean absolute error; ISI, Improved susceptible–infected; PSO, Particle Swarm Optimization; MAPE, Mean Absolute Percentage Error; NLP, Natural Language Processing; ARIMA, Autoregressive Integrated Moving Average; CUBIST, Cubist Regression; RF, Random Forest; RIDGE, Ridge Regression; SVR, Support Vector Regression.

**TABLE 6 |** Application of AI in drug discovery of COVID-19.

| References           | Algorithm               | Objective        | Results  |
|----------------------|-------------------------|------------------|--|
| Ke et al. (91)       | DNN                     | Drug repurposing | Identified 80 marketed drugs with potential, there are 13 drugs with great potentials for further development toward treating COVID-19 |
| Zeng et al. (92)     | Deep-learning (CoV-KGE) | Drug repurposing | Identified 41 repurposable drugs (AUROC = 0.85)  |
| Gao et al. (90)      | GBDT model              | Drug repurposing | Identified 20 drugs with potential (Pearson correlation coefficient, 0.78; RMSE, 0.792)  |
| Stebbing et al. (93) | AI algorithms           | Drug repurposing | Baricitinib can be used for COVID-19 infection   |
| Zhang et al. (94)    | DFCNN                   | Drug development | Provided potential compound and tripeptide lists for 2019-nCoV_3Clike protease   |
| Batra et al. (95)    | Machine learning        | Drug development | Identified 75 FDA-approved and 100 other ligands, molecular fragments and molecular descriptors  |
| Joshi et al. (96)    | RNN                     | Drug development | Found two compounds Palmatine and Sauchinone formed very stable complex with Mpro  |
| Ton et al. (97)      | Deep learning           | Drug development | Screening 1.3 billion compounds from ZINC15 library to identify top 1,000 potential ligands for Mpro                                   |

GBDT, Gradient-boosted decision trees; DFCNN, Dense Fully Convolutional Neural Network; RNN, Recurrent Neural Networks; Mpro, Main Protease.

algorithms (36). Several studies have shown that deep learning can automatically differentiate COVID-19 from non-COVID-19 or other pneumonia diseases through extracting features from chest CT and X-rays images. As shown in **Tables 2, 3**, most of the studies achieved over 90% accuracy, sensitivity and specificity. The performance of AI-assisted diagnosis was comparable to radiologists with significant clinical experience and could assist and improve the performance of radiologists. This means that AI-assisted diagnosis is a useful screening tool, which might

shorten patient waiting time, simplify the workflow, reduce the workload of radiologists and allow them to respond more quickly and effectively in emergencies (38). AI techniques have recently shown great potential in the real-time diagnosis of COVID-19 by using images. However, the severity of disease, comorbidities, and the proportion of asymptomatic patients have an impact on the diagnostic sensitivity of chest CT (105). Chest CT have a relatively high sensitivity in symptomatic COVID-19 patients, but low specificity (106). The Italian Society of Medicine and

Interventional Radiology recommends that CT should be used as a screening tool only for symptomatic patients with specific indications (107). AI should be used to assist diagnosis, not an independent diagnostic tool. Second, the evaluation of patients based on a single data type may be biased, therefore, AI-assisted diagnosis needs to be used in combination with other laboratory tests and a multimodal AI framework was required to analyze different data types (108). Third, several studies used a relatively small amount of data to train the deep learning models, and the testing data set had the same sources as the training data set. This may cause the problem of overfitting of the models (108, 109). Fourth, there is little evidence to directly compare the performance of humans and machines or the performance of AI in actual clinical work. Only Bai, Song, Ni, and a latest research show that AI assistance improved radiologists' performance in identifying COVID-19 (13, 14, 41, 42). In addition, confounding factors can influence the internal validity of researches and the accuracy of AI-based radiological interpretation, such as the variation of respiratory effort, image contrast, technique, and resolution of radiological images (110).

In regard to the prognosis of patients with COVID-19, information available at hospital admission, typically 6 days (median) before the patient developed severe COVID-19, can be used by AI for early detection of patients at higher risk, allowing adjustments to their in-hospital allocation and management (68). AI can evaluate the prognosis of COVID-19 patients by clinical manifestations, laboratory and radiological characteristics and identify potential predictive biomarkers related to the disease's severity. The significantly elevated LDH levels reflects the severity of pneumonia, and increased serum CRP predicts the risk of death in patients with severe COVID-19 (72). Age and comorbidities may be risk factors for severe COVID-19 after hospitalization, such as diabetes, hypertension and cardiovascular diseases (74). As well as chest CT images being a powerful tool to assist clinical diagnosis because of its high sensitivity and the ability to quantify the COVID-19 associated lung abnormalities, they also help assess the severity and prognosis of the disease and monitor the development of the disease (70, 76, 80). Accurate risk prediction of patients with critical COVID-19 may help to optimize patient triage and in-hospital allocation, monitor disease progression and treatment response, prioritize medical resources and improve the overall management of the COVID-19 pandemic (68). However, several of the studies we identified were retrospective single-center studies, which reduces their external validity. Therefore, the results in this review may not be generalizable to other environment and healthcare systems, especially considering the high variability of COVID-19 in different countries and populations (68, 72). In addition, prospective studies with a larger number of patients from multiple locations are required to verify the predictive ability of a model (81).

Many statistical and numerical models have been used to predict the trend of the COVID-19 pandemic, such as the epidemic peak, transmission and development trend, the SEIR model is one of the most popular models (81). Alsayed et al. combined the SEIR model with machine learning to characterize the epidemic dynamics and to predict possible

contagion scenarios of COVID-19 in Malaysia (81). Long short-term memory (LSTM) is a recurrent neural network that is an effective model for the prediction of time series where data are sequential (82). Therefore, LSTM has been widely used to predict the confirmed cases, death and recovery, development trend of COVID-19 through time (82, 84–87, 89). Embed the NLP and LSTM into the Improved susceptible–infected (ISI) model is more accurate and reliable than the traditional epidemic model, providing a basis for estimating the law of virus transmission (85). In addition, AI models, such as SVR, stacking-ensemble learning, ARIMA, CUBIST, RIDGE, RF and MLP also play an important role in estimating the epidemic of COVID-19 (83, 88). AI techniques provide useful tools to help policy makers make decisions and take actions to prevent diffusion at the early stage of the epidemic and to minimize the subsequent impact of COVID-19. However, we cannot verify and validate the database, so it is difficult to compare and calibrate results with other studies.

Traditional drug repurposing design methods are based on repeated trials and there is no systematic way to screen the enormous drug-dose parameter space (111). AI is an effective approach to quickly detect potential drugs as antiviral therapeutics for COVID-19 (91). Deep learning, using the relationship between drug targets and diseases can be used as a helpful tool to assist drug repurposing and minimize the possibility of failure in clinical trials (92). Chymotrypsin-like protease is a major therapeutic target, and several studies used it to identify potential therapeutic drugs against COVID-19 by performing drug screening over protein–ligand or protein–peptide among existing drugs (90, 94, 112). In addition, using AI techniques to conduct virtual screening of biologically active compounds can support new drug discovery. However, all predicted drugs must be tested in randomized trials before being used in COVID-19 patients (92).

During the COVID-19 pandemic, an effective and safe vaccine is essential to prevent infection and reduce deaths. The development of vaccines was a complicated process with many difficulties, such as the complexity of the human immune system and the variability between different populations (113). Research organizations in many nations and multinational companies are developing various vaccines, including whole virus vaccine, subunit vaccine, nucleic acid vaccines. Researchers are trying to use AI techniques to explore the vaccine development. Ong et al. (17) predict 6 vaccine candidates, including S protein, nsp3, 3CL-pro, and nsp8-10, S protein was identified as the most favorable vaccine candidate. Nsp3 has a high antigen protection score and has not been used for vaccine development, therefore it was also selected for further investigation. Currently, S protein has been widely used in subunit vaccines, and other proteins are expected to be used in vaccine development. In addition, the latest research analyzed the entire SARS-CoV-2 proteome via AI and identified some of the epitope hotspots that can be used in vaccine formulations (114).

AI has the potential to be an important tool in the fight against COVID-19 and similar pandemics. However, there were many problems in using AI to predict and diagnose COVID-19, and rigorous clinical trials were required before drugs and vaccines developed by AI are approved, so the use of AI has so far been



rather limited. It requires continuous efforts by researchers. But recent studies have shown that AI tools such as computer vision and robots have the potential to be widely promoted and used in the short term, such as infrared thermal cameras have been paired with AI-powered facial recognition systems to determine if the individual are wearing masks, using camera images to observe whether social distancing rules are complied, AI-based dialogue chatbots can complete symptom screening and patient education (19). Robotics, AI, and digital technology have been implemented in sanitation for hospitals and public areas, delivery in hospitals and public spaces, patrolling, screening, health consulting, and virus tracking (115).

Our systematic review has several limitations that should be noted. First, although we conducted a systematic search, we only included articles published in English, introducing the possibility of publication bias. Second, in the included studies, the models in 60 studies were at high risk of bias according to assessment with PROBAST (Table 1), and the remaining 18 studies were not evaluated due to lack of suitable evaluation tools. Therefore, the predictive performance of these AI models when used in practice is probably lower than that reported, which means that the predictions of these models may be unreliable. Third, many studies had small sample sizes, and the testing data set had the same sources as the training data set, which leads to an increased risk of overfitting. Fourth, over one fifth of the studies were retrospective single-center studies, which might limit their applicability to the specific center or the same geographical region. This means that results may not be generalizable to other settings and places.

## CONCLUSIONS

Artificial intelligence has been widely explored in the medical field, especially for enhancing medical and healthcare capabilities. At present, many countries continue to struggle to contain the spread of COVID-19. Facing limited medical resource and increasing healthcare pressure, the use of AI techniques to assist

with diagnosis, treatment, prediction of prognosis, evaluation of epidemic trends, surveillance and public health decision-making may improve the efficiency and ability of humans to fight the COVID-19 pandemic.

## DATA AVAILABILITY STATEMENT

The original contributions presented in the study are included in the article/**Supplementary Material**, further inquiries can be directed to the corresponding author/s.

## AUTHOR CONTRIBUTIONS

YZ and LW conceived of the study. LW and DW screened the literature for relevancy and did the data extraction. SZ, JH, and LZ did the quality appraisal. XT and TL resolved any disagreements in study relevancy, extraction, and quality appraisal. LW and LC drafted and revised the manuscript. HF, YZ, and MC directed and revised the manuscript. All authors participated in data interpretation and revised the manuscript for intellectual content.

## FUNDING

This study was supported by National Key R&D Program of China (2017YFC1309703), 1·3·5 project for disciplines of excellence—Clinical Research Incubation Project, West China Hospital, Sichuan University (2019HXXFH008), and Science & Technology Department of Sichuan Province (2020YFS0186). The funders of this research did not contribute to the study design, data analysis, data interpretation or preparation of the manuscript.

## SUPPLEMENTARY MATERIAL

The Supplementary Material for this article can be found online at: <https://www.frontiersin.org/articles/10.3389/fmed.2021.704256/full#supplementary-material>

## REFERENCES

1. Zhou P, Yang XL, Wang XG, Hu B, Zhang L, Zhang W, et al. A pneumonia outbreak associated with a new coronavirus of probable bat origin. *Nature*. (2020) 579:270–3. doi: 10.1038/s41586-020-2012-7
2. Zhou T, Liu Q, Yang Z, Liao J, Yang K, Bai W, et al. Preliminary prediction of the basic reproduction number of the Wuhan novel coronavirus 2019-nCoV. *J Evid Based Med*. (2020) 13:3–7. doi: 10.1111/jebm.12376
3. Ma X, Wang Y, Gao T, He Q, He Y, Yue R, et al. Challenges and strategies to research ethics in conducting COVID-19 research. *J Evid Based Med*. (2020) 13:173–177. doi: 10.1111/jebm.12388
4. Wiersinga WJ, Rhodes A, Cheng AC, Peacock SJ, Prescott HC. Pathophysiology, transmission, diagnosis, and treatment of coronavirus disease 2019 (COVID-19): a review. *JAMA*. (2020) 324:782–93. doi: 10.1001/jama.2020.12839
5. Huang C, Wang Y, Li X, Ren L, Zhao J, Hu Y, et al. Clinical features of patients infected with 2019 novel coronavirus in Wuhan, China. *Lancet*. (2020) 395:497–506. doi: 10.1016/S0140-6736(20)30183-5
6. Wang D, Hu B, Hu C, Zhu F, Liu X, Zhang J, et al. clinical characteristics of 138 hospitalized patients with 2019 novel coronavirus-infected pneumonia in Wuhan, China. *JAMA*. (2020) 323:1061–9. doi: 10.1001/jama.2020.1585
7. Yassine HM, Shah Z. How could artificial intelligence aid in the fight against coronavirus? *Expert Rev Anti Infect Ther*. (2020) 18:493–7. doi: 10.1080/14787210.2020.1744275
8. Davenport T, Kalakota R. The potential for artificial intelligence in healthcare. *Fut Healthc J*. (2019) 6:94–8. doi: 10.7861/futurehosp.6-2-94
9. Shen J, Zhang CJP, Jiang B, Chen J, Song J, Liu Z, et al. Artificial intelligence versus clinicians in disease diagnosis: systematic review. *JMIR Med Informat*. (2019) 7:e10010. doi: 10.2196/10010
10. Hwang TJ, Kesselheim AS, Vokinger KN. Lifecycle regulation of artificial intelligence- and machine learning-based software devices in medicine. *JAMA*. (2019) 322:2285–6. doi: 10.1001/jama.2019.16842
11. Adamson AS, Smith A. Machine learning and health care disparities in dermatology. *JAMA Dermatol*. (2018) 154:1247–8. doi: 10.1001/jamadermatol.2018.2348

12. Abdulaal A, Patel A, Charani E, Denny S, Mughal N, Moore L. Prognostic modeling of COVID-19 using artificial intelligence in the united kingdom: model development and validation. *J Med Internet Res.* (2020) 22:e20259. doi: 10.2196/20259
13. Yousefzadeh M, Esfahanian P, Movahed SMS, Gorgin S, Rahmati D, Abedini A, et al. ai-corona: Radiologist-assistant deep learning framework for COVID-19 diagnosis in chest CT scans. *PLoS ONE.* (2021) 16:e0250952. doi: 10.1371/journal.pone.0250952
14. Bai HX, Wang R, Xiong Z, Hsieh B, Chang K, Halsey K, et al. Artificial intelligence augmentation of radiologist performance in distinguishing COVID-19 from pneumonia of other origin at chest CT. *Radiology.* (2020) 296:E156–65. doi: 10.1148/radiol.2020201491
15. Fang C, Bai S, Chen Q, Zhou Y, Xia L, Qin L, et al. Deep learning for predicting COVID-19 malignant progression. *Med Image Anal.* (2021) 72:102096. doi: 10.1016/j.media.2021.102096
16. Al-Qaness MAA, Saba AI, Elsheikh AH, Elaziz MA, Ibrahim RA, Lu S, et al. Efficient artificial intelligence forecasting models for COVID-19 outbreak in Russia and Brazil. *Process Saf Environ Prot.* (2021) 149:399–409. doi: 10.1016/j.psep.2020.11.007
17. Ong E, Wong MU, Huffman A, He Y. COVID-19 coronavirus vaccine design using reverse vaccinology and machine learning. *Front Immunol.* (2020) 11:1581. doi: 10.3389/fimmu.2020.01581
18. Naudé W. Artificial intelligence vs COVID-19: limitations, constraints and pitfalls. *AI Soc.* (2020) 35:761–65. doi: 10.1007/s00146-020-00978-0
19. Chen J, See KC. Artificial intelligence for COVID-19: rapid review. *J Med Internet Res.* (2020) 22:e21476. doi: 10.2196/21476
20. Moher D, Liberati A, Tetzlaff J, Altman DG. Preferred reporting items for systematic reviews and meta-analyses: the PRISMA statement. *PLoS Med.* (2009) 6:e1000097. doi: 10.1371/journal.pmed.1000097
21. Moons KGM, Wolff RF, Riley RD, Whiting PF, Westwood M, Collins GS, et al. PROBAST: a tool to assess risk of bias and applicability of prediction model studies: explanation and elaboration. *Ann Intern Med.* (2019) 170:W1–33. doi: 10.7326/M18-1377
22. Wolff RF, Moons KGM, Riley RD, Whiting PF, Westwood M, Collins GS, et al. PROBAST: a tool to assess the risk of bias and applicability of prediction model studies. *Ann Intern Med.* (2019) 170:51–8. doi: 10.7326/M18-1376
23. Abbasian Ardakani A, Acharya UR, Habibollahi S, Mohammadi A. COVIDiag: a clinical CAD system to diagnose COVID-19 pneumonia based on CT findings. *Eur Radiol.* (2020) 31:121–30. doi: 10.1007/s00330-020-07087-y
24. Ardakani AA, Kanafi AR, Acharya UR, Khadem N, Mohammadi A. Application of deep learning technique to manage COVID-19 in routine clinical practice using CT images: Results of 10 convolutional neural networks. *Comput Biol Med.* (2020) 121:103795. doi: 10.1016/j.combiomed.2020.103795
25. Han Z, Wei B, Hong Y, Li T, Cong J, Zhu X, et al. Accurate screening of COVID-19 using attention-based deep 3D multiple instance learning. *IEEE Trans Med Imaging.* (2020) 39:2584–94. doi: 10.1109/TMI.2020.2996256
26. Ko H, Chung H, Kang WS, Kim KW, Shin Y, Kang SJ, et al. COVID-19 pneumonia diagnosis using a simple 2d deep learning framework with a single chest CT image: model development and validation. *J Med Internet Res.* (2020) 22:e19569. doi: 10.2196/19569
27. Li L, Qin L, Xu Z, Yin Y, Wang X, Kong B, et al. Using artificial intelligence to detect COVID-19 and community-acquired pneumonia based on pulmonary CT: evaluation of the diagnostic accuracy. *Radiology.* (2020) 296:E65–71. doi: 10.1148/radiol.2020200905
28. Liu C, Wang X, Liu C, Sun Q, Peng W. Differentiating novel coronavirus pneumonia from general pneumonia based on machine learning. *Biomed Eng Online.* (2020) 19:66. doi: 10.1186/s12938-020-00809-9
29. Mei X, Lee HC, Diao KY, Huang M, Lin B, Liu C, et al. Artificial intelligence-enabled rapid diagnosis of patients with COVID-19. *Nat Med.* (2020) 26:1224–8. doi: 10.1038/s41591-020-0931-3
30. Mishra AK, Das SK, Roy P, Bandyopadhyay S. Identifying COVID19 from chest CT images: a deep convolutional neural networks based approach. *J Healthc Eng.* (2020) 2020:8843664. doi: 10.1155/2020/8843664
31. Ouyang X, Huo J, Xia L, Shan F, Liu J, Mo Z, et al. Dual-Sampling attention network for diagnosis of COVID-19 from community acquired pneumonia. *IEEE Trans Med Imaging.* (2020) 39:2595–605. doi: 10.1109/TMI.2020.2995508
32. Sakagianni A, Feretzakis G, Kalles D, Koufopoulou C, Kaldis V. Setting up an easy-to-use machine learning pipeline for medical decision support: a case study for COVID-19 diagnosis based on deep learning with CT scans. *Stud Health Technol Inform.* (2020) 272:13–6. doi: 10.3233/SHIT1200481
33. Sharma S. Drawing insights from COVID-19-infected patients using CT scan images and machine learning techniques: a study on 200 patients. *Environ Sci Pollut Res Int.* (2020) 27:37155–63. doi: 10.1007/s11356-020-10133-3
34. Wang J, Bao Y, Wen Y, Lu H, Luo H, Xiang Y, et al. Prior-Attention residual learning for more discriminative COVID-19 screening in CT images. *IEEE Trans Med Imaging.* (2020) 39:2572–83. doi: 10.1109/TMI.2020.2994908
35. Wang S, Zha Y, Li W, Wu Q, Li X, Niu M, et al. A fully automatic deep learning system for COVID-19 diagnostic and prognostic analysis. *Eur Respir J.* (2020) 56:2000775. doi: 10.1183/13993003.00775-2020
36. Wu X, Hui H, Niu M, Li L, Wang L, He B, et al. Deep learning-based multi-view fusion model for screening 2019 novel coronavirus pneumonia: a multicentre study. *Eur J Radiol.* (2020) 128:109041. doi: 10.1016/j.ejrad.2020.109041
37. Yan T, Wong PK, Ren H, Wang H, Wang J, Li Y. Automatic distinction between COVID-19 and common pneumonia using multi-scale convolutional neural network on chest CT scans. *Chaos Solitons Fractals.* (2020) 140:110153. doi: 10.1016/j.chaos.2020.110153
38. Zhang K, Liu X, Shen J, Li Z, Sang Y, Wu X, et al. Clinically applicable AI system for accurate diagnosis, quantitative measurements, and prognosis of COVID-19 pneumonia using computed tomography. *Cell.* (2020) 181:1423–33.e11. doi: 10.1016/j.cell.2020.04.045
39. Harmon SA, Sanford TH, Xu S, Turbey EB, Roth H, Xu Z, et al. Artificial intelligence for the detection of COVID-19 pneumonia on chest CT using multinational datasets. *Nat Commun.* (2020) 11:4080. doi: 10.1038/s41467-020-17971-2
40. Jaiswal A, Gianchandani N, Singh D, Kumar V, Kaur M. Classification of the COVID-19 infected patients using DenseNet201 based deep transfer learning. *J Biomol Struct Dyn.* (2020) 1–8. doi: 10.1080/07391102.2020.1788642
41. Ni Q, Sun ZY, Qi L, Chen W, Yang Y, Wang L, et al. A deep learning approach to characterize 2019 coronavirus disease (COVID-19) pneumonia in chest CT images. *Eur Radiol.* (2020) 30:6517–27. doi: 10.1007/s00330-020-07044-9
42. Song J, Wang H, Liu Y, Wu W, Dai G, Wu Z, et al. End-to-end automatic differentiation of the coronavirus disease 2019 (COVID-19) from viral pneumonia based on chest CT. *Eur J Nucl Med Mol Imaging.* (2020) 47:2516–24. doi: 10.1007/s00259-020-04929-1
43. Xu X, Jiang X, Ma C, Du P, Li X, Lv S, et al. a deep learning system to screen novel coronavirus disease 2019 pneumonia. *Engineering.* (2020) 6:1122–9. doi: 10.1016/j.eng.2020.04.010
44. Yang S, Jiang L, Cao Z, Wang L, Cao J, Feng R, et al. Deep learning for detecting corona virus disease 2019 (COVID-19) on high-resolution computed tomography: a pilot study. *Ann Transl Med.* (2020) 8:450. doi: 10.21037/atm.2020.03.132
45. Apostolopoulos ID, Mpesian TA. Covid-19: automatic detection from X-ray images utilizing transfer learning with convolutional neural networks. *Phys Eng Sci Med.* (2020) 43:635–40. doi: 10.1007/s13246-020-00865-4
46. Bressen KK, Adams LC, Erxleben C, Hamm B, Niehues SM, Vahldiek JL. Comparing different deep learning architectures for classification of chest radiographs. *Sci Rep.* (2020) 10:13590. doi: 10.1038/s41598-020-70479-z
47. Das D, Santosh KC, Pal U. Truncated inception net: COVID-19 outbreak screening using chest X-rays. *Phys Eng Sci Med.* (2020) 43:915–25. doi: 10.1007/s13246-020-00888-x
48. Elaziz MA, Hosny KM, Salah A, Darwish MM, Lu S, Sahlol AT. New machine learning method for image-based diagnosis of COVID-19. *PLoS ONE.* (2020) 15:e0235187. doi: 10.1371/journal.pone.0235187
49. Khan AI, Shah JL, Bhat MM. CoroNet: a deep neural network for detection and diagnosis of COVID-19 from chest x-ray images. *Comput Methods Programs Biomed.* (2020) 196:105581. doi: 10.1016/j.cmpb.2020.105581
50. Mahmud T, Rahman MA, Fattah SA. CovXNet: a multi-dilation convolutional neural network for automatic COVID-19 and other pneumonia detection from chest X-ray images with transferable

- multi-receptive feature optimization. *Comput Biol Med.* (2020) 122:103869. doi: 10.1016/j.combiomed.2020.103869
51. Murphy K, Smits H, Knoops AJG, Korst M, Samson T, Scholten ET, et al. COVID-19 on chest radiographs: a multireader evaluation of an artificial intelligence system. *Radiology.* (2020) 296:E166–72. doi: 10.1148/radiol.2020.201874
  52. Ouchicha C, Ammor O, Meknassi M. CVDNet: a novel deep learning architecture for detection of coronavirus (Covid-19) from chest x-ray images. *Chaos Solitons Fractals.* (2020) 140:110245. doi: 10.1016/j.chaos.2020.110245
  53. Ozturk T, Talo M, Yildirim EA, Baloglu UB, Yildirim O, Rajendra Acharya U. Automated detection of COVID-19 cases using deep neural networks with X-ray images. *Comput Biol Med.* (2020) 121:103792. doi: 10.1016/j.combiomed.2020.103792
  54. Togaçar M, Ergen B, Cömert Z. COVID-19 detection using deep learning models to exploit social mimic optimization and structured chest X-ray images using fuzzy color and stacking approaches. *Comput Biol Med.* (2020) 121:103805. doi: 10.1016/j.combiomed.2020.103805
  55. Vaid S, Kalantar R, Bhandari M. Deep learning COVID-19 detection bias: accuracy through artificial intelligence. *Int Orthop.* (2020) 44:1539–42. doi: 10.1007/s00264-020-04609-7
  56. Altan A, Karasu S. Recognition of COVID-19 disease from X-ray images by hybrid model consisting of 2D curvelet transform, chaotic salp swarm algorithm and deep learning technique. *Chaos Solitons Fractals.* (2020) 140:110071. doi: 10.1016/j.chaos.2020.110071
  57. Brunese L, Mercaldo F, Reginelli A, Santone A. Explainable deep learning for pulmonary disease and coronavirus COVID-19 detection from X-rays. *Comput Methods Programs Biomed.* (2020) 196:105608. doi: 10.1016/j.cmpb.2020.105608
  58. Che Azemin MZ, Hassan R, Mohd Tamrin MI, Md Ali MA. COVID-19 deep learning prediction model using publicly available radiologist-adjudicated chest X-Ray images as training data: preliminary findings. *Int J Biomed Imaging.* (2020) 2020:8828855. doi: 10.1155/2020/8828855
  59. Islam MZ, Islam MM, Asraf A. A combined deep CNN-LSTM network for the detection of novel coronavirus (COVID-19) using X-ray images. *Informat Med Unlock.* (2020) 20:100412. doi: 10.1016/j.imu.2020.100412
  60. Jain G, Mittal D, Thakur D, Mittal MK. A deep learning approach to detect Covid-19 coronavirus with X-Ray images. *Biocybernet Biomed Eng.* (2020) 40:1391–405. doi: 10.1016/j.bbe.2020.08.008
  61. Nour M, Cömert Z, Polat K. A novel medical diagnosis model for COVID-19 infection detection based on deep features and bayesian optimization. *Appl Soft Comput.* (2020) 97:106580. doi: 10.1016/j.asoc.2020.106580
  62. Rahaman MM, Li C, Yao Y, Kulwa F, Rahman MA, Wang Q, et al. Identification of COVID-19 samples from chest X-Ray images using deep learning: a comparison of transfer learning approaches. *J Xray Sci Technol.* (2020) 28:821–39. doi: 10.3233/XST-200715
  63. Rahimzadeh M, Attar A. A modified deep convolutional neural network for detecting COVID-19 and pneumonia from chest X-ray images based on the concatenation of Xception and ResNet50V2. *Informatics in medicine unlocked.* (2020) 19:100360. doi: 10.1016/j.imu.2020.100360
  64. Rajaraman S, Siegelman J, Alderson PO, Folio LS, Folio LR, Antani SK. Iteratively pruned deep learning ensembles for COVID-19 detection in chest X-rays. *IEEE Access Pract Innovat Open Solut.* (2020) 8:115041–50. doi: 10.1109/ACCESS.2020.3003810
  65. Toraman S, Alakus TB, Turkoglu I. Convolutional capsnet: a novel artificial neural network approach to detect COVID-19 disease from X-ray images using capsule networks. *Chaos Solitons Fractals.* (2020) 140:110122. doi: 10.1016/j.chaos.2020.110122
  66. Ucar F, Korkmaz D. COVIDiagnosis-Net: deep bayes-SqueezeNet based diagnosis of the coronavirus disease 2019 (COVID-19) from X-ray images. *Med Hypotheses.* (2020) 140:109761. doi: 10.1016/j.mehy.2020.109761
  67. Waheed A, Goyal M, Gupta D, Khanna A, Al-Turjman F, Pinheiro PR. CovidGAN: data augmentation using auxiliary classifier GAN for improved Covid-19 detection. *IEEE Access Pract Innovat Open Solut.* (2020) 8:91916–23. doi: 10.1109/ACCESS.2020.2994762
  68. Assaf D, Gutman Y, Neuman Y, Segal G, Amit S, Gefen-Halevi S, et al. Utilization of machine-learning models to accurately predict the risk for critical COVID-19. *Intern Emerg Med.* (2020) 15:1435–43. doi: 10.1007/s11739-020-02475-0
  69. Iwendi C, Bashir AK, Peshkar A, Sujatha R, Chatterjee JM, Pasupuleti S, et al. COVID-19 patient health prediction using boosted random forest algorithm. *Front Public Health.* (2020) 8:357. doi: 10.3389/fpubh.2020.00357
  70. Li Z, Zhong Z, Li Y, Zhang T, Gao L, Jin D, et al. From community-acquired pneumonia to COVID-19: a deep learning-based method for quantitative analysis of COVID-19 on thick-section CT scans. *Eur Radiol.* (2020) 30:6828–37. doi: 10.1101/2020.04.17.20070219
  71. Liang W, Yao J, Chen A, Lv Q, Zanin M, Liu J, et al. Early triage of critically ill COVID-19 patients using deep learning. *Nat Commun.* (2020) 11:3543. doi: 10.1038/s41467-020-17280-8
  72. Ma X, Ng M, Xu S, Xu Z, Qiu H, Liu Y, et al. Development and validation of prognosis model of mortality risk in patients with COVID-19. *Epidemiol Infect.* (2020) 148:e168. doi: 10.1017/S0950268820001727
  73. Mushtaq J, Pennella R, Lavallo S, Colarieti A, Steidler S, Martinenghi CMA, et al. Initial chest radiographs and artificial intelligence (AI) predict clinical outcomes in COVID-19 patients: analysis of 697 Italian patients. *Eur Radiol.* (2020) 31:1770–9. doi: 10.1007/s00330-020-07269-8
  74. Wu G, Yang P, Xie Y, Woodruff HC, Rao X, Guiot J, et al. Development of a clinical decision support system for severity risk prediction and triage of COVID-19 patients at hospital admission: an international multicentre study. *Eur Respir J.* (2020) 56:2001104. doi: 10.1183/13993003.01104-2020
  75. Yao H, Zhang N, Zhang R, Duan M, Xie T, Pan J, et al. Severity detection for the coronavirus disease 2019 (COVID-19) patients using a machine learning model based on the blood and urine tests. *Front Cell Dev Biol.* (2020) 8:683. doi: 10.3389/fcell.2020.00683
  76. Yu Z, Li X, Sun H, Wang J, Zhao T, Chen H, et al. Rapid identification of COVID-19 severity in CT scans through classification of deep features. *Biomed Eng Online.* (2020) 19:63. doi: 10.1186/s12938-020-00807-x
  77. Wu G, Zhou S, Wang Y, Lv W, Wang S, Wang T, et al. A prediction model of outcome of SARS-CoV-2 pneumonia based on laboratory findings. *Sci Rep.* (2020) 10:14042. doi: 10.1038/s41598-020-71114-7
  78. Cheng FY, Joshi H, Tandon P, Freeman R, Reich DL, Mazumdar M, et al. Using machine learning to predict ICU transfer in hospitalized COVID-19 patients. *J Clin Med.* (2020) 9:1668. doi: 10.3390/jcm9061668
  79. Fu L, Li Y, Cheng A, Pang P, Shu Z. A novel machine learning-derived radiomic signature of the whole lung differentiates stable from progressive COVID-19 infection: a retrospective cohort study. *J Thorac Imaging.* (2020) 35:361–8. doi: 10.1097/RTI.0000000000000544
  80. Xiao LS, Li P, Sun F, Zhang Y, Xu C, Zhu H, et al. Development and validation of a deep learning-based model using computed tomography imaging for predicting disease severity of coronavirus disease 2019. *Front Bioeng Biotechnol.* (2020) 8:898. doi: 10.3389/fbioe.2020.00898
  81. Alsayed A, Sadir H, Kamil R, Sari H. Prediction of epidemic peak and infected cases for COVID-19 disease in Malaysia, 2020. *Int J Environ Res Public Health.* (2020) 17:1–15. doi: 10.3390/ijerph1714076
  82. Ayyoubzadeh SM, Ayyoubzadeh SM, Zahedi H, Ahmadi M, S RNK. Predicting COVID-19 incidence through analysis of google trends data in iran: data mining and deep learning pilot study. *JMIR Public Health Surveill.* (2020) 6:e18828. doi: 10.2196/18828
  83. Mollalo A, Rivera KM, Vahedi B. Artificial neural network modeling of novel coronavirus (COVID-19) incidence rates across the continental United States. *Int J Environ Res Public Health.* (2020) 17:4204. doi: 10.3390/ijerph17124204
  84. Shahid F, Zameer A, Muneeb M. Predictions for COVID-19 with deep learning models of LSTM, GRU and Bi-LSTM. *Chaos Solitons Fractals.* (2020) 140:110212. doi: 10.1016/j.chaos.2020.110212
  85. Zheng N, Du S, Wang J, Zhang H, Cui W, Kang Z, et al. Predicting COVID-19 in China using hybrid AI model. *IEEE Trans Cybern.* (2020) 50:2891–904. doi: 10.1109/TCYB.2020.2990162
  86. Arora P, Kumar H, Panigrahi BK. Prediction and analysis of COVID-19 positive cases using deep learning models: a descriptive case study of India. *Chaos Solitons Fractals.* (2020) 139:110017. doi: 10.1016/j.chaos.2020.110017



87. Chimmula VKR, Zhang L. Time series forecasting of COVID-19 transmission in Canada using LSTM networks. *Chaos Solitons Fractals*. (2020) 135:109864. doi: 10.1016/j.chaos.2020.109864
88. Ribeiro M, da Silva RG, Mariani VC, Coelho LDS. Short-term forecasting COVID-19 cumulative confirmed cases: perspectives for Brazil. *Chaos Solitons Fractals*. (2020) 135:109853. doi: 10.1016/j.chaos.2020.109853
89. Shastri S, Singh K, Kumar S, Kour P, Mansotra V. Time series forecasting of Covid-19 using deep learning models: India-USA comparative case study. *Chaos Solitons Fractals*. (2020) 140:110227. doi: 10.1016/j.chaos.2020.110227
90. Gao K, Nguyen DD, Chen J, Wang R, Wei GW. Repositioning of 8565 existing drugs for COVID-19. *J Phys Chem Lett*. (2020) 11:5373–82. doi: 10.1021/acs.jpclett.0c01579
91. Ke YY, Peng TT, Yeh TK, Huang WZ, Chang SE, Wu SH, et al. Artificial intelligence approach fighting COVID-19 with repurposing drugs. *Biomed J*. (2020) 43:355–62. doi: 10.1016/j.bj.2020.05.001
92. Zeng X, Song X, Ma T, Pan X, Zhou Y, Hou Y, et al. Repurpose open data to discover therapeutics for COVID-19 using deep learning. *J Proteome Res*. (2020) 19:4624–36. doi: 10.1021/acs.jproteome.0c00316
93. Stebbing J, Krishnan V, de Bono S, Ottaviani S, Casalini G, Richardson PJ, et al. Mechanism of baricitinib supports artificial intelligence-predicted testing in COVID-19 patients. *EMBO Mol Med*. (2020) 12:e12697. doi: 10.15252/emmm.202012697
94. Zhang H, Saravanan KM, Yang Y, Hossain MT, Li J, Ren X, et al. Deep learning based drug screening for novel coronavirus 2019-nCoV. *Interdiscip Sci*. (2020) 12:368–76. doi: 10.1007/s12539-020-00376-6
95. Batra R, Chan H, Kamath G, Ramprasad R, Cherukara MJ, Sankaranarayanan S. Screening of therapeutic agents for COVID-19 using machine learning and ensemble docking studies. *J Phys Chem Lett*. (2020) 11:7058–65. doi: 10.1021/acs.jpclett.0c02278
96. Joshi T, Joshi T, Pundir H, Sharma P, Mathpal S, Chandra S. Predictive modeling by deep learning, virtual screening and molecular dynamics study of natural compounds against SARS-CoV-2 main protease. *J Biomol Struct Dyn*. (2020) 1–19. doi: 10.1080/07391102.2020.1802341
97. Ton AT, Gentile F, Hsing M, Ban F, Cherkasov A. Rapid identification of potential inhibitors of SARS-CoV-2 main protease by deep docking of 1.3 billion compounds. *Mol Inform*. (2020) 39:e2000028. doi: 10.1002/minf.202000028
98. Yasaka K, Akai H, Kunimatsu A, Kiryu S, Abe O. Deep learning with convolutional neural network in radiology. *Jpn J Radiol*. (2018) 36:257–72. doi: 10.1007/s11604-018-0726-3
99. Amelio I, Gostev M, Knight RA, Willis AE, Melino G, Antonov AV. DRUGSURV: a resource for repositioning of approved and experimental drugs in oncology based on patient survival information. *Cell Death Dis*. (2014) 5:e1051. doi: 10.1038/cddis.2014.9
100. Li Y, Yao L, Li J, Chen L, Song Y, Cai Z, et al. Stability issues of RT-PCR testing of SARS-CoV-2 for hospitalized patients clinically diagnosed with COVID-19. *J Med Virol*. (2020) 92:903–8. doi: 10.1002/jmv.25786
101. Fang Y, Zhang H, Xie J, Lin M, Ying L, Pang P, et al. Sensitivity of chest CT for COVID-19: comparison to RT-PCR. *Radiology*. (2020) 296:E115–7. doi: 10.1148/radiol.2020200432
102. LeCun Y, Bengio Y, Hinton G. Deep learning. *Nature*. (2015) 521:436–44. doi: 10.1038/nature14539
103. Miller DD, Brown EW. Artificial intelligence in medical practice: the question to the answer? *Am J Med*. (2018) 131:129–33. doi: 10.1016/j.amjmed.2017.10.035
104. Kanne JP. Chest CT findings in 2019 novel coronavirus (2019-nCoV) infections from Wuhan, China: key points for the radiologist. *Radiology*. (2020) 295:16–7. doi: 10.1148/radiol.2020200241
105. Kim H, Hong H, Yoon SH. Diagnostic performance of CT and reverse transcriptase polymerase chain reaction for coronavirus disease 2019: a meta-analysis. *Radiology*. (2020) 296:E145–55. doi: 10.1148/radiol.2020201343
106. Adams HJA, Kwee TC, Yakar D, Hope MD, Kwee RM. Systematic review and meta-analysis on the value of chest ct in the diagnosis of coronavirus disease (COVID-19): sol scientiae, illustra nos. *AJR Am J Roentgenol*. (2020) 215:1342–50. doi: 10.2214/AJR.20.23391
107. Neri E, Miele V, Coppola F, Grassi R. Use of CT and artificial intelligence in suspected or COVID-19 positive patients: statement of the Italian society of medical and interventional radiology. *Radiol Med*. (2020) 125:505–8. doi: 10.1007/s11547-020-01197-9
108. Santosh KC. AI-Driven tools for coronavirus outbreak: need of active learning and cross-population train/test models on multitudinal/multimodal data. *J Med Syst*. (2020) 44:93. doi: 10.1007/s10916-020-01562-1
109. Kim DW, Jang HY, Kim KW, Shin Y, Park SH. Design characteristics of studies reporting the performance of artificial intelligence algorithms for diagnostic analysis of medical images: results from recently published papers. *Korean J Radiol*. (2019) 20:405–10. doi: 10.3348/kjr.2019.0025
110. Chen J, See KC. Artificial intelligence for COVID-19: a rapid review. *J Med Internet Res*. (2020) 22:e21476. doi: 10.2196/preprints.21476
111. Abdulla A, Wang B, Qian F, Kee T, Blasiak A, Ong YH, et al. Project Identif.AI: harnessing artificial intelligence to rapidly optimize combination therapy development for infectious disease intervention. *Adv Ther*. (2020) 2000034. doi: 10.1002/adtp.202000034
112. Liu S, Zheng Q, Wang Z. Potential covalent drugs targeting the main protease of the SARS-CoV-2 coronavirus. *Bioinformatics*. (2020) 36:3295–8. doi: 10.1093/bioinformatics/btaa2294
113. Kaushal K, Sarma P, Rana SV, Medhi B, Naithani M. Emerging role of artificial intelligence in therapeutics for COVID-19: a systematic review. *J Biomol Struct Dyn*. (2020) 1–16. doi: 10.1080/07391102.2020.1855250
114. Malone B, Simovski B, Molin  C, Cheng J, Gheorghe M, Fontenelle H, et al. Artificial intelligence predicts the immunogenic landscape of SARS-CoV-2 leading to universal blueprints for vaccine designs. *Sci Rep*. (2020) 10:22375. doi: 10.1038/s41598-020-78758-5
115. Zhao Z, Ma Y, Mushtaq A, Rajper AMA, Shehab M, Heybourne A, et al. Applications of robotics, artificial intelligence, and digital technologies during COVID-19: a review. *Disaster Med Public Health Prep*. (2021) 1–11. doi: 10.1017/dmp.2021.9

**Conflict of Interest:** The authors declare that the research was conducted in the absence of any commercial or financial relationships that could be construed as a potential conflict of interest.

**Publisher's Note:** All claims expressed in this article are solely those of the authors and do not necessarily represent those of their affiliated organizations, or those of the publisher, the editors and the reviewers. Any product that may be evaluated in this article, or claim that may be made by its manufacturer, is not guaranteed or endorsed by the publisher.

Copyright   2021 Wang, Zhang, Wang, Tong, Liu, Zhang, Huang, Zhang, Chen, Fan and Clarke. This is an open-access article distributed under the terms of the Creative Commons Attribution License (CC BY). The use, distribution or reproduction in other forums is permitted, provided the original author(s) and the copyright owner(s) are credited and that the original publication in this journal is cited, in accordance with accepted academic practice. No use, distribution or reproduction is permitted which does not comply with these terms.





# A Novel Matrix Profile-Guided Attention LSTM Model for Forecasting COVID-19 Cases in USA

Qian Liu<sup>1,2,3†</sup>, Daryl L. X. Fung<sup>2†</sup>, Leann Lac<sup>3†</sup> and Pingzhao Hu<sup>1,2\*</sup>

<sup>1</sup> Department of Biochemistry and Medical Genetics, University of Manitoba, Winnipeg, MB, Canada, <sup>2</sup> Department of Computer Science, University of Manitoba, Winnipeg, MB, Canada, <sup>3</sup> Department of Statistics, University of Manitoba, Winnipeg, MB, Canada

## OPEN ACCESS

### Edited by:

Reza Lashgari,  
Shahid Beheshti University, Iran

### Reviewed by:

Tarek Mohamed Abd El-Aziz,  
The University of Texas Health Science  
Center at San Antonio, United States  
Arko Barman,  
Rice University, United States

### \*Correspondence:

Pingzhao Hu  
pingzhao.hu@umanitoba.ca

<sup>†</sup>These authors share first authorship

### Specialty section:

This article was submitted to  
Infectious Diseases - Surveillance,  
Prevention and Treatment,  
a section of the journal  
Frontiers in Public Health

**Received:** 26 July 2021

**Accepted:** 02 September 2021

**Published:** 07 October 2021

### Citation:

Liu Q, Fung DLX, Lac L and Hu P  
(2021) A Novel Matrix Profile-Guided  
Attention LSTM Model for Forecasting  
COVID-19 Cases in USA.  
Front. Public Health 9:741030.  
doi: 10.3389/fpubh.2021.741030

**Background:** The outbreak of the novel coronavirus disease 2019 (COVID-19) has been raging around the world for more than 1 year. Analysis of previous COVID-19 data is useful to explore its epidemic patterns. Utilizing data mining and machine learning methods for COVID-19 forecasting might provide a better insight into the trends of COVID-19 cases. This study aims to model the COVID-19 cases and perform forecasting of three important indicators of COVID-19 in the United States of America (USA), which are the adjusted percentage of daily admitted hospitalized COVID-19 cases (*hospital admission*), the number of daily confirmed COVID-19 cases (*confirmed cases*), and the number of daily death cases caused by COVID-19 (*death cases*).

**Materials and Methods:** The actual COVID-19 data from March 1, 2020 to August 5, 2021 were obtained from Carnegie Mellon University Delphi Research Group. A novel forecasting algorithm was proposed to model and predict the three indicators. This algorithm is a hybrid of an unsupervised time series anomaly detection technique called matrix profile and an attention-based long short-term memory (LSTM) model. Several classic statistical models and the baseline recurrent neural network (RNN) models were used as the baseline models. All models were evaluated using a repeated holdout training and test strategy.

**Results:** The proposed matrix profile-assisted attention-based LSTM model performed the best among all the compared models, which has the root mean square error (RMSE) = 1.23, 31612.81, 467.17, mean absolute error (MAE) = 0.95, 26259.55, 364.02, and mean absolute percentage error (MAPE) = 0.25, 1.06, 0.55, for *hospital admission*, *confirmed cases*, and *death cases*, respectively.

**Conclusion:** The proposed model is more powerful in forecasting COVID-19 cases. It can potentially aid policymakers in making prevention plans and guide health care managers to allocate health care resources reasonably.

**Keywords:** COVID-19 forecasting, LSTM models, matrix profile, attention mechanism, epidemiological indicators

## BACKGROUND

It has been more than 1 year since the first case of the novel coronavirus disease (COVID-19) came to light in December 2019 (1). According to the interactive COVID-19 dashboard created and maintained by Johns Hopkins Center for Systems Science and Engineering (JHU-CSSE), COVID-19 has spread to 191 countries and caused 4,370,447 global deaths out of more than 207 million diagnosed cases by August 16, 2021 (2). COVID-19 was confirmed to be caused by severe acute respiratory syndrome coronavirus 2 (SARS-CoV-2) as defined by the International Committee on Taxonomy of Viruses (ICTV) (3). SARS-CoV-2 coronavirus is a type of  $\beta$ -coronavirus with many potential hosts, leading to difficulties in prevention and treatment (4, 5).

As COVID-19 is rapidly spreading and putting the world under a very distressing situation, the WHO declared COVID-19 as a global pandemic in March 2020 (6). Since a whole year's data are now available, some epidemic patterns of COVID-19 have been observed. COVID-19 follows the dynamic transmission of an epidemic, with different magnitudes in terms of time, region, season, and weather, and exhibited as a non-linear relationship. Since new case prevention and healthcare resource management have become critical for every country, good time series forecasting tools for COVID-19 are extremely important and necessary for estimating the number of cases in the coming days.

There is a classic time series forecasting algorithm called autoregressive integrated moving average (ARIMA) (7), which is widely applied for infectious disease prediction in public health (8, 9). ARIMA has been applied to COVID-19 forecasting as early as February 2020 (10). Ceylan et al. used ARIMA to predict the prevalence of COVID-19 for confirmed and deceased cases in Italy, Spain, and France from February 21, 2020 to April 15, 2020 (11). Chintalapudi et al. have forecasted the number of registered and recovered cases after a 60-day lockdown in Italy by ARIMA with an accuracy rate of more than 80% (12). Researchers have also widely applied ARIMA in comparison with other approaches for COVID-19 forecasting (13–18). Since the trend of COVID-19 cases follows a seasonal pattern, and ARIMA is not able to capture seasonal patterns well, an improved variant of the ARIMA called Seasonal ARIMA (SARIMA) (19) was proposed to model the seasonality of time series data.

However, SARIMA is still considered to be too simple to recognize complex patterns in the data. In principle, more complex models, which could include other significant observed or hidden variables/factors in disease prevalence, could be considered when we design the forecasting framework. For example, unsupervised data-driven time series anomaly detection algorithms could find significant abnormal patterns within the time series data (20). If we could incorporate the anomaly information into the forecasting models, the performance may be increased. Matrix profile is one of such algorithms proposed by Keogh et al. (19). A matrix profile consists of two components: a distance vector and a profile index vector. The distance vector contains the minimum Euclidean distances among the patterns within the time series data. The indexes of the nearest neighbors are stored in the profile index vector. The idea is that if a part of the time series data is far different from its nearest neighbors,

then it is likely an anomaly. Keogh and his team further developed a series of algorithms to calculate the matrix profile to express the abnormal patterns within time-series data (21–25).

Some machine learning algorithms, such as echo state network (ESN) (26), gated recurrent unit (GRU) (27), and long short-term memory (LSTM) (28), have also been widely applied in time series forecasting. They all belong to a recurrent neural network (RNN), which is a family of neural network technologies with internal memory (state) to process sequences of inputs. With the memory mechanism in the RNN, the standard RNN can handle the time series data very well. However, if a time series is very long, it will be difficult to pass information from the earlier timesteps to the later ones. This problem is called the vanishing gradient problem (29). The ESN does not suffer from this vanishing gradient problem because the hidden neurons in an ESN are very sparsely connected to form a network reservoir. The weights of the reservoir are randomly assigned and not trainable. The information of the earlier time points is randomly passed to the last points. Due to the untrainable random hidden state, the ESN has high computational efficiency, but the untrainable random hidden state reduces the complexity of the model thus reduces the power (30). While the GRU and the LSTM reduce the vanishing gradient problem by making it easier to pass previous information throughout the state sequences. They all use gates to regulate the information flow (28). The difference is that the LSTM has three gates and a cell state while the GRU has only two gates. Therefore, the LSTM may have more flexible control of the information flow. Previous studies have tested the performance of GRU, LSTM, and several variants of LSTM models for predicting COVID-19 cases across different countries and confirmed their accuracy and robustness (31–34).

However, these models cannot detect which time point is the important one for future prediction. Recently, the attention mechanism in machine learning was developed to overcome this limitation (35). This is achieved by keeping the intermediate information from the LSTM units, training the model to pay selective attention to the inputs, and relating them to the items in the output time series (36). The attention mechanism increases the computational burden but results in a more targeted model with better performance. In addition, the model is also able to show how attention is paid to the input time series when predicting the output. It can increase the explainability of the LSTM model, which is an essential characteristic of gaining trust from end users.

Although great advancements have been made in the theories and applications of both the matrix profile and the LSTM, limited efforts have been made to investigate the combination of the two approaches and explore the applications of this combined approach to time series data forecasting (such as COVID-19 cases). In this study, we aim to propose a novel framework, which is a hybrid of the unsupervised matrix profile to detect a potential time series anomaly and an attention-based LSTM model, to model and forecast COVID-19 cases in the United States of America (USA). We aim to achieve a more accurate COVID-19 forecasting model to support decision-making and guide future advanced model building.

## MATERIALS AND METHODS

### Data Source

We considered the USA COVID-19 data from March 1, 2020 to August 5, 2021, which were obtained from the website of Carnegie Mellon University Delphi Research Group (37). We focused on three indicators: the adjusted percentage of daily admitted hospitalized COVID-19 cases (*hospital admission*), the number of daily confirmed COVID-19 cases (*confirmed cases*), and the number of daily death cases caused by COVID-19 (*death cases*). The *hospital admission* is the estimated percentage of new hospital admissions with COVID-19. It is based on insurance claims data from health system partners and smoothed using a Gaussian linear smoother.

### Methods

#### Data Pre-processing and Remapping

To improve model performance and consider the consistency in evaluating model performance between statistical and machine learning approaches, pre-processing raw data by normalization is necessary. We applied *z*-normalization or standardization to the data. The formulation to transform the observed raw data into *z*-score is  $Z_i = (Y_i - \bar{Y})/s$ , where  $\bar{Y}$  and  $s$  are the sample mean and standard deviation.  $Y_i$  is the observed raw data at time point  $i$ . After building a forecasting model and obtaining the predicted value  $Z_j$ , we remapped these values to the observed raw data scale by applying the formula:  $Y_j = s^*Z_j + \bar{Y}$ . Here,  $Y_j$  is the predicted data with raw data scale at time point  $j$ .

#### Matrix Profile for Time Series Data Analysis

Matrix profile compares snippets of the time series by computing the distance between each pair of snippets. A matrix profile consists of two components: a distance profile and a profile index vector. The distance profile contains the minimum Euclidean distances among the sub-snippets within the time series. If the minimum distance of a certain sub-snippet is very large, it is probably that this sub-snippet is an anomaly because it is very different from its nearest neighbor. The indexes of the nearest neighbors are stored in the profile index vector. Matrix profiles of the three COVID-19 indicators were calculated using the Python package “matrixprofile” (38). Several algorithms are provided by the package for computing the matrix profile, such as Scalable Time series Anytime Matrix Profile (STAMP) and Scalable Time series Ordered-search Matrix Profile (STOMP). We selected the STOMP function since it is faster. The window size was set as 7 (weekly anomaly). After the matrix profiles were calculated, top 10 discords (the top 10 sub-snippets with larger Euclidean distances with their nearest neighbors) were highlighted for the visualization. In addition to the distance profile, we also considered the index profile vector. The index profile vector stores the global index of the closest neighbor of each snippet. For instance, if the most similar snippet of the current snippet is at the 15th location, the global position of the current snippet will be 15. The relative position is the relative index of the closest neighbor of the current snippet. It can be calculated using the index profile vector. If the current snippet is at the 10th location and the nearest neighbor of the current snippet is at the 15th location, then the relative position will have a value of +5. In the

remaining parts of the report, we mainly focus on the distance profile and the relative position, which are passed together with the normalized observed raw data into the LSTM for forecasting the COVID-19 cases.

### Baseline Models

#### ARIMA Model for Seasonal Data (SARIMA)

Non-seasonal ARIMA is a generalized form of the autoregressive moving average (ARMA) model. The ARMA is a combination of the auto regression (AR) model of order  $p$ , and moving average (MA) model of order  $q$ .

Let  $y_t$  denote the  $d$ th difference of  $Y_t$ , and  $Y_t$  refer to the observation at time  $t$ , the general equation of the ARIMA ( $p, d, q$ ) model is as follows.

$$y_t = c + \phi_1 y_{t-1} + \phi_2 y_{t-2} + \dots + \phi_p y_{t-p} + \varepsilon_t - \theta_1 \varepsilon_{t-1} - \theta_2 \varepsilon_{t-2} - \dots - \theta_q \varepsilon_{t-q} \quad (1)$$

where  $\phi = [\phi_1, \phi_2, \dots, \phi_p]$  and  $\theta = [\theta_1, \theta_2, \dots, \theta_q]$  are coefficients of AR and MA parts of the model, respectively. Here,  $c$  is a constant and  $\varepsilon_t$  is the residual assumed to be uncorrelated in the final selected ARIMA model.

The ARIMA is not capable of modeling seasonal data. Therefore, the SARIMA model includes the additional seasonal term  $(p, d, q)_m$  where  $m$  is the number of observations per year. To estimate the coefficients in the SARIMA, the maximum likelihood estimation (MLE) and the least square estimation (LSE) were used (7). R function `auto.arima()` in the “forecast” package (39) was utilized to execute SARIMA.

#### Standard RNN Model

Vanilla RNN has backward-linking connections. It can be computed as follows:

$$y_t = \sigma(W_x \cdot x_t + W_y \cdot y_{t-1} + b_t), \quad (2)$$

which can also be described as: at a given timestep  $t$ , each recurrent layer receives the input  $x_t$  and the output from the previous timestep  $y_{t-1}$ , then outputs the non-linearly processed  $y_t$ . The non-linearity comes from the activation function  $\sigma$ .  $W_x$  and  $W_y$  are the input weights and output weights.  $b_t$  is the bias.

#### ESN Model

The simple ESN model can be computed as follows:

$$y_t = W_y \cdot \sigma(W_x \cdot x_t + W_r \cdot h_{t-1} + b_t), \quad (3)$$

Where  $x_t, h_t, y_t$  are the input, hidden state, and output at time point  $t$ , respectively.  $\sigma$  is the activation function.  $W_x$  and  $W_r$  weight matrices are randomly initialized and fixed in the training step, and only the output weight  $W_y$  is trainable.

#### GRU Model

The GRU model has a reset gate ( $r_t$ ), a cell state ( $h_t$ ), and an output gate ( $y_t$ ) to control the information flow.

$$y_t = \sigma(W_y \cdot [h_{t-1}, x_t] + b_o), \quad (4)$$

$$r_t = \sigma(W_r \cdot [h_{t-1}, x_t] + b_r), \quad (5)$$

$$h_t = (1 - y_t) * h_{t-1} + z_t * \tanh(W \cdot [r_t * h_{t-1}, x_t] + b_c), \quad (6)$$

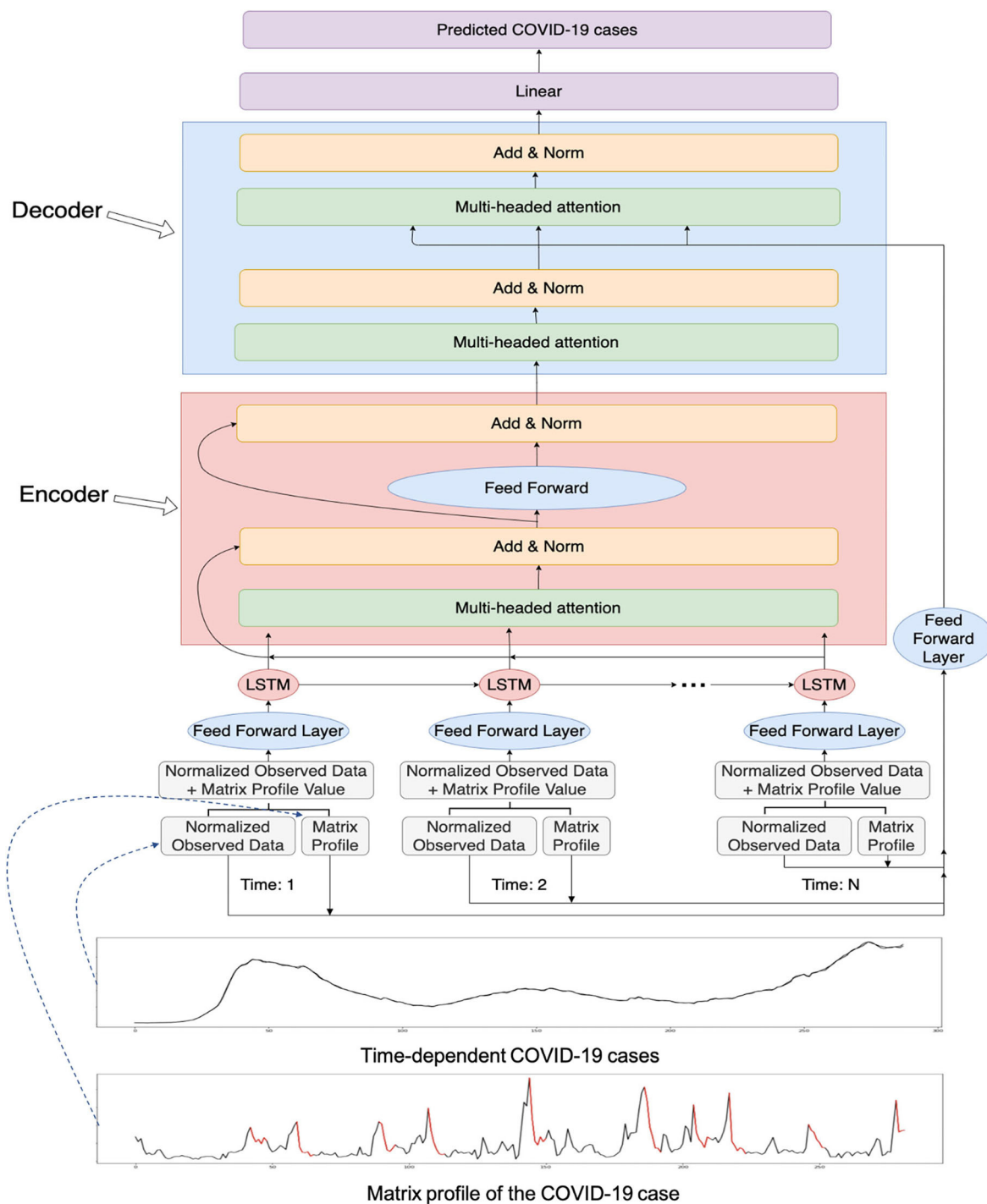


**FIGURE 1 |** The overall workflow of the proposed novel matrix profile-guided attention LSTM algorithm. Matrix profile feature could be the distance profile (the LSTM-MatAtt model) or the relative position profile (the LSTM-RelAtt). The matrix profile feature concatenated with the normalized observed data of the COVID-19 indicators are first input into the LSTM unit, then passed to the later steps of the encoder-decoder attention process. The final output is the predicted future values of the COVID-19 indicators.

where  $[h_{t-1}, x_t]$  is the concatenation between the hidden state of the previous timestep,  $h_{t-1}$ , and the input of the current timestep,  $x_t$ .  $b_o$ ,  $b_t$ ,  $b_c$  are the bias of each gate.

## Matrix Profile-Guided Attention LSTM Models

### LSTM Without Attention

The LSTM model contains a forget gate ( $f_t$ ), an input gate ( $i_t$ ), and an output gate ( $o_t$ ). The forget gate receives the hidden state



from the previous timestep ( $h_{t-1}$ ), and concatenates them with the input in the current timestep, then passes them into a linear layer with a sigmoid activation.

$$f_t = \sigma(W_f \cdot [h_{t-1}, x_t] + b_t), \quad (7)$$

$W_f$  is the weight of the forget gate.

The input gate controls how much new information will be passed into the current timestep, which can be formulated as follows:

$$i_t = \sigma(W_i \cdot [h_{t-1}, x_t] + b_t), \quad (8)$$

$$\tilde{C}_t = \tanh(W_C \cdot [h_{t-1}, x_t] + b_C), \quad (9)$$

$\tilde{C}$  is used to update the cell state ( $C_t$ ) of the current timestep.

$$C_t = f_t * C_{t-1} + i_t * \tilde{C}_t, \quad (10)$$

The output gate controls and filters the information from the cell state. The equation is:

$$y_t = \sigma(W_o \cdot [h_{t-1}, x_t] + b_o), \quad (11)$$

$$h_t = y_t * \tanh(C_t), \quad (12)$$

### Convolutional Neural Network LSTM

The convolutional neural network LSTM (CNN-LSTM) is a model that uses a combination of CNN (40) to extract the features of the input and pass the extracted features as an input to the LSTM model. A CNN extracts features from a group of inputs based on the kernel size. The equation for convolutional operations is:

$$\text{output}_{d,e} = \sum_i \sum_j^k w_{i,j}^l * I_{d+i,e+j}^{l-1} + b_{d,e}^l \quad (13)$$

Where  $w_{i,j}^l$  is the weights in layer  $l$  at row  $i$  and column  $j$  of the kernel,  $I^{l-1}$  is the output from the previous layer, and  $b^l$  is the bias in layer  $l$ . We kept the kernel size 2. With kernel size 2, the sequence length of the input will be reduced by 1 after every layer. In order to maintain the sequence length for the LSTM, we used a transposed CNN to expand the sequence length to the original length. The output of the CNN is fed as input to the LSTM.

### LSTM With Attention

We added an attention mechanism to our LSTM model. The proposed overall workflow can be found in **Figure 1**. As there are outliers in the forecasted values, the attention mechanism can help LSTM models to focus on important parts of the time series to prevent getting skewed values. We utilized multiheaded attention where there are several heads and each head contains a query, a key, and a value. Multiheaded attention has been shown to be beneficial with different learned linear projections (25). The equation for the attention is:

$$\text{Attention}(Q, K, V) = \text{softmax}\left(\frac{QK^T}{\sqrt{d_k}}\right)V, \quad (14)$$

where  $Q$  is the query,  $K$  is the key, and  $V$  is the value.  $d_k$  is the dimension of the current layer.  $Q = [Q_{t-p}, Q_{t-p+1}, \dots, Q_t]$ ,  $K = [K_{t-p}, K_{t-p+1}, \dots, K_t]$ ,  $V = [V_{t-p}, V_{t-p+1}, \dots, V_t]$ .  $p$  is the attention span. The attention span would look at the previous  $p$  timesteps, so the model attends to them.  $t$  is the current timestep. Each head contains the attention equation:

$$\text{head}_i = \text{Attention}(QW_i^Q, KW_i^K, VW_i^V), \quad (15)$$

$Q_t$ ,  $K_t$ ,  $V_t$  are obtained by passing the hidden outputs from the LSTM into a linear layer:

$$Q_t = h_t W^Q \quad (16)$$

$$K_t = h_t W^K \quad (17)$$

$$V_t = h_t W^V \quad (18)$$

The multiheaded attention concatenates the attentions of the heads and outputs the combination of the attentions of the head, which can be formulated as:

$$\begin{aligned} &\text{MultiHead}(Q, K, V) \\ &= \text{Concat}([head_1, head_2, \dots, head_k]) W^O \end{aligned} \quad (19)$$

Furthermore, we incorporate an encoder-decoder architecture for the LSTM with an attention model (**Figure 1**). The output of the LSTM is fed into the encoder. The attention architecture in the encoder undergoes multiheaded attention on its own input to determine which timestep the model should focus more on. It then passes its learned features to the decoder. The decoder

---

#### Algorithm 1: LSTM with attention

---

**Procedure** Training with LSTM Attention (D, MP, Y) // D = data, MP = matrix profile, Y = targets

X <- Concat([D, MP])

**For** all X, Y **do** // X = inputs, Y = targets

    // Pass inputs into LSTM to get LSTM output:

$O_L$  <- LSTM(X)

        // encoder part

$A_E$  <- MultiHeadAtt( $O_L$ )

$N_E$  <- LayerNorm( $O_L + A_E$ )

$A_O$  <- ReLU( $N_E W_{N_E} + B_{N_E}$ )

$E_O$  <- LayerNorm( $N_E + A_O$ )

    // pass encoderOutput into decoder

    // decoder part

$A_D$  <- MultiHeadAtt( $E_O$ )

$D_E$  <- LayerNorm( $A_D + E_O$ )

$D_A$  <- DecoderMultiHeadAtt( $D_E$ , MP) // MP = matrix profile value

$D_O$  <- LayerNorm( $D_E + D_A$ )

$\hat{Y}$  <- ReLU( $D_O W_{D_O} + B_{D_O}$ ) // Predicted output

    // update weights

    loss <- RMSELoss( $\hat{Y}$ , Y)

    backprop(loss)

**End For**

---

receives the input from the output of the encoder. To aid in more guidance for the attention stage in the decoder, the matrix profile input is fed into the attention stage in the decoder in addition to the hidden features of the decoder. The decoder outputs its learned features and passes them into a linear layer to output the predicted value. The overall procedure of the matrix profile-guided attention LSTM model is summarized in **Algorithm 1**.

Given the combination of the normalized observed raw data, matrix profiles, and the attention mechanism, we evaluated different LSTM models for each of the three COVID-19 indicators used in the study, which include the following LSTM-related models:

- 1) *LSTM*: using only the normalized observed raw data.
- 2) *CNN-LSTM*: using only the normalized observed raw data with convolutional LSTM network.
- 3) *LSTM-Att*: using only the normalized observed raw data with attention mechanism in LSTM.
- 4) *LSTM-MatAtt*: using the normalized observed raw data and the distance profile fed into the attention-based LSTM network.
- 5) *LSTM-RelAtt*: using the normalized observed raw data and the relative position matrix profile feature fed into the attention-based LSTM network.

## Hyperparameter Tuning

The number of reservoirs of ESN was tuned manually, ranging from 50 to 300, the best one was 200. GRU and simple RNN have one hidden unit, thus, there is no need to tune the number of hidden layers. The step size of the input time series was set as 12 for ESN, GRU, simple RNN, and all LSTM models with and without attention or matrix profile. Epochs were tuned separately for different models to achieve the best losses. The additional hyperparameters that we tuned for the LSTM networks, such as hidden dimensions, dropout, and feedforward dimensions, can be found in **Table 1**. These hyperparameters were tuned separately for different models with and without the addition of attention and the matrix profile to achieve the best convergence.

## Performance Evaluation

After building the models for each indicator, it is important to evaluate the prediction accuracy and compare the forecasting performance to other proposed models in forecasting the number of COVID-19 cases. Traditional K-fold cross-validation is designated for independent data. However, time-series data are considered as dependent data in which we use past events to forecast the future ones. Therefore, we consider a rep-holdout cross-validation method. In this method, we divided the time

**TABLE 1** | Parameters tuning of LSTM models.

|  |         |               |               |         |               |               |         |        |              |        |
|--|---------|---------------|---------------|---------|---------------|---------------|---------|--------|--------------|--------|
| <b>LSTM</b>                                |         |               |               |         |               |               |         |        |              |        |
| Runs                                       | 1       | 2             | 3             | 4       | 5             | 6             | 7       | 8      | 9            | 10     |
| Hidden dimension                           | 32      | 32            | 32            | 32      | 32            | 128           | 32      | 128    | 128          | 128    |
| Dropout                                    | 0.95    | 0.36          | 0.21          | 0.34    | 0.85          | 0.77          | 0.39    | 0.02   | 0.07         | 0.09   |
| Loss                                       | 404.74  | <b>229.33</b> | 316.65        | 188.39  | 293.42        | 297.75        | 242.4   | 258.1  | 287.42       | 309.82 |
| <b>CNN-LSTM</b>                            |         |               |               |         |               |               |         |        |              |        |
| Runs                                       | 1       | 2             | 3             | 4       | 5             | 6             | 7       | 8      | 9            | 10     |
| Hidden dimension                           | 32      | 32            | 32            | 32      | 32            | 128           | 32      | 128    | 128          | 128    |
| Dropout                                    | 0.95    | 0.36          | 0.21          | 0.34    | 0.85          | 0.77          | 0.39    | 0.02   | 0.07         | 0.09   |
| Loss                                       | 827.48  | 801.15        | 820.6         | 807.1   | 828.87        | 812.52        | 763.49  | 811.17 | <b>716.7</b> | 805.17 |
| <b>LSTM attention (LSTM-Att)</b>           |         |               |               |         |               |               |         |        |              |        |
| Runs                                       | 1       | 2             | 3             | 4       | 5             | 6             | 7       | 8      | 9            | 10     |
| Hidden dimension                           | 32      | 32            | 32            | 32      | 32            | 128           | 32      | 128    | 128          | 128    |
| Dropout                                    | 0.95    | 0.36          | 0.21          | 0.34    | 0.85          | 0.77          | 0.39    | 0.02   | 0.07         | 0.09   |
| ff_dim*                                    | 8       | 16            | 8             | 64      | 8             | 16            | 8       | 32     | 32           | 16     |
| Loss                                       | 421.18  | 505.58        | <b>265.48</b> | 444.86  | 534.89        | 435.63        | 530.28  | 506.72 | 571.58       | 461.99 |
| <b>LSTM matrix attention (LSTM-MatAtt)</b> |         |               |               |         |               |               |         |        |              |        |
| Runs                                       | 1       | 2             | 3             | 4       | 5             | 6             | 7       | 8      | 9            | 10     |
| Hidden dimension                           | 32      | 32            | 32            | 32      | 32            | 128           | 32      | 128    | 128          | 128    |
| Dropout                                    | 0.95    | 0.36          | 0.21          | 0.34    | 0.85          | 0.77          | 0.39    | 0.02   | 0.07         | 0.09   |
| ff_dim                                     | 8       | 16            | 8             | 64      | 8             | 16            | 8       | 32     | 32           | 16     |
| Loss                                       | 1377.05 | 1765.31       | 983.64        | 1618.63 | <b>677.07</b> | 1639.26       | 1194.62 | 887.21 | 1114.19      | 946.79 |
| <b>LSTM attention (LSTM-Att)</b>           |         |               |               |         |               |               |         |        |              |        |
| Runs                                       | 1       | 2             | 3             | 4       | 5             | 6             | 7       | 8      | 9            | 10     |
| Hidden dimension                           | 32      | 32            | 32            | 32      | 32            | 128           | 32      | 128    | 128          | 128    |
| Dropout                                    | 0.95    | 0.36          | 0.21          | 0.34    | 0.85          | 0.77          | 0.39    | 0.02   | 0.07         | 0.09   |
| ff_dim                                     | 8       | 16            | 8             | 64      | 8             | 16            | 8       | 32     | 32           | 16     |
| Loss                                       | 1542.63 | 516.51        | 1605.26       | 556.59  | 570.86        | <b>436.76</b> | 511.54  | 786.18 | 454.08       | 566.33 |

ff\_dim is the feedforward dimension layer after the attention module.

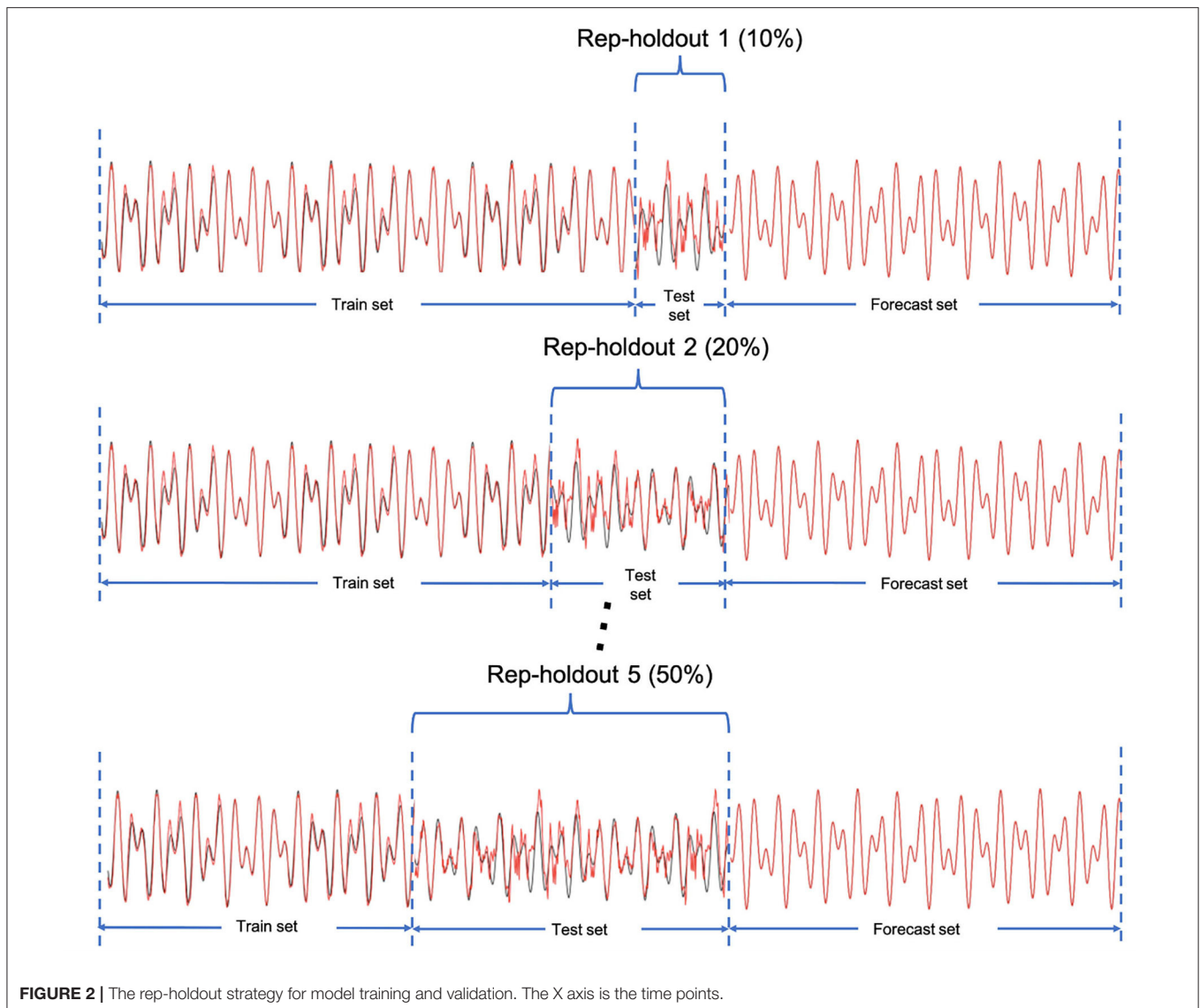


**FIGURE 2 |** The rep-holdout strategy for model training and validation. The X axis is the time points.

series data into training and testing sets by ascending time order. To conduct the model performance evaluation, we applied the rep-holdout strategy, in which the test sets are the last (most recent) 10, 20, 30, 40, and 50 percentage of all time points (Figure 2). We measured the forecasting accuracy by root mean square error (RMSE), mean absolute error (MAE), and mean absolute percentage error (MAPE) using the test set.

$$\text{RMSE} = \sqrt{\frac{\sum_{t=1}^n (y_t - y_t^{\text{predict}})^2}{n}}, \quad (20)$$

$$\text{MAE} = \frac{\sum_{t=1}^n |y_t - y_t^{\text{predict}}|}{n}, \quad (21)$$

$$\text{MAPE} = \frac{\sum_{t=1}^n \left| \frac{y_t - y_t^{\text{predict}}}{y_t} \right|}{n}, \quad (22)$$

where  $n$  is the sample size for each testing set,  $y_t$  is the actual data,  $y_t^{\text{predict}}$  is the predicted data.

## RESULTS

### Matrix Profiles

The observed signals of the three indicators and their matrix profiles can be found in Figure 3. The trends of the *hospital admission* and *death cases* showed two peaks in April 2020 and January 2021 (top panels of Figures 3A,C). In addition, some minor decreasing and increasing trends were also observed. Matrix profiles of these two indicators were able to detect these ups and downs (bottom panels of Figures 3A,C). It should be noted that the beginning of the *death cases* time series was also detected as an anomaly because the death cases were pretty low at the first few days. The *confirmed cases* time series was stable overall until around November 2020 (top panel of Figure 3B). The top 1 anomaly in its matrix profile was located

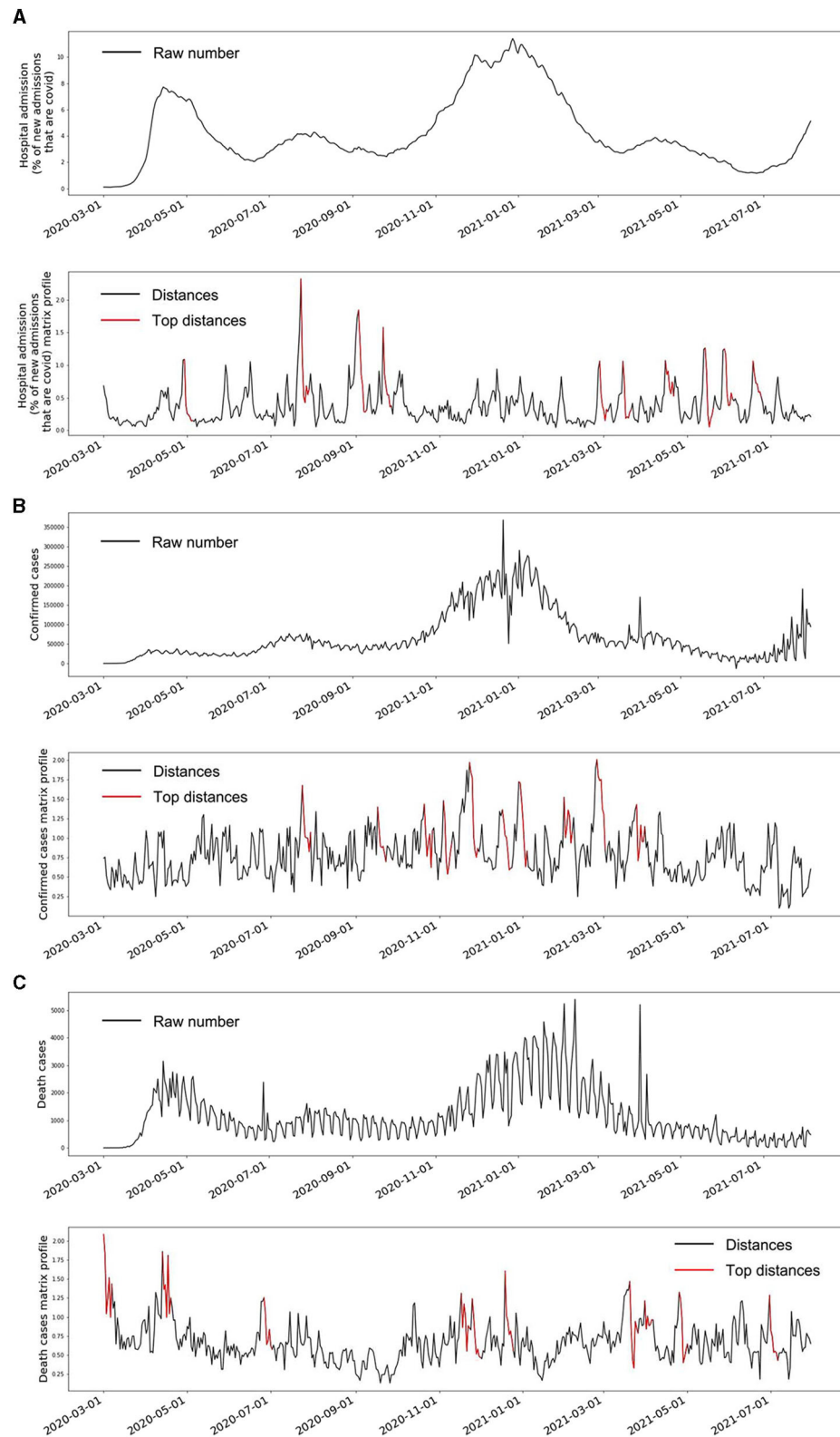


**FIGURE 3 |** The raw time series and the matrix profile of the three indicators. **(A)** is the time series of COVID-19 hospital admissions and its matrix profile. **(B)** is the time series of the daily confirmed COVID-19 cases and its matrix profile. **(C)** is the time series of the daily death cases caused by COVID-19 and its matrix profile. The red segments in the matrix profile plots indicate the corresponding weeks that have large Euclidean distances to their nearest neighbor compared to all the other weeks, which also means these weeks marked as red are the top anomalies within the whole time series.



**TABLE 2 |** Model performance.

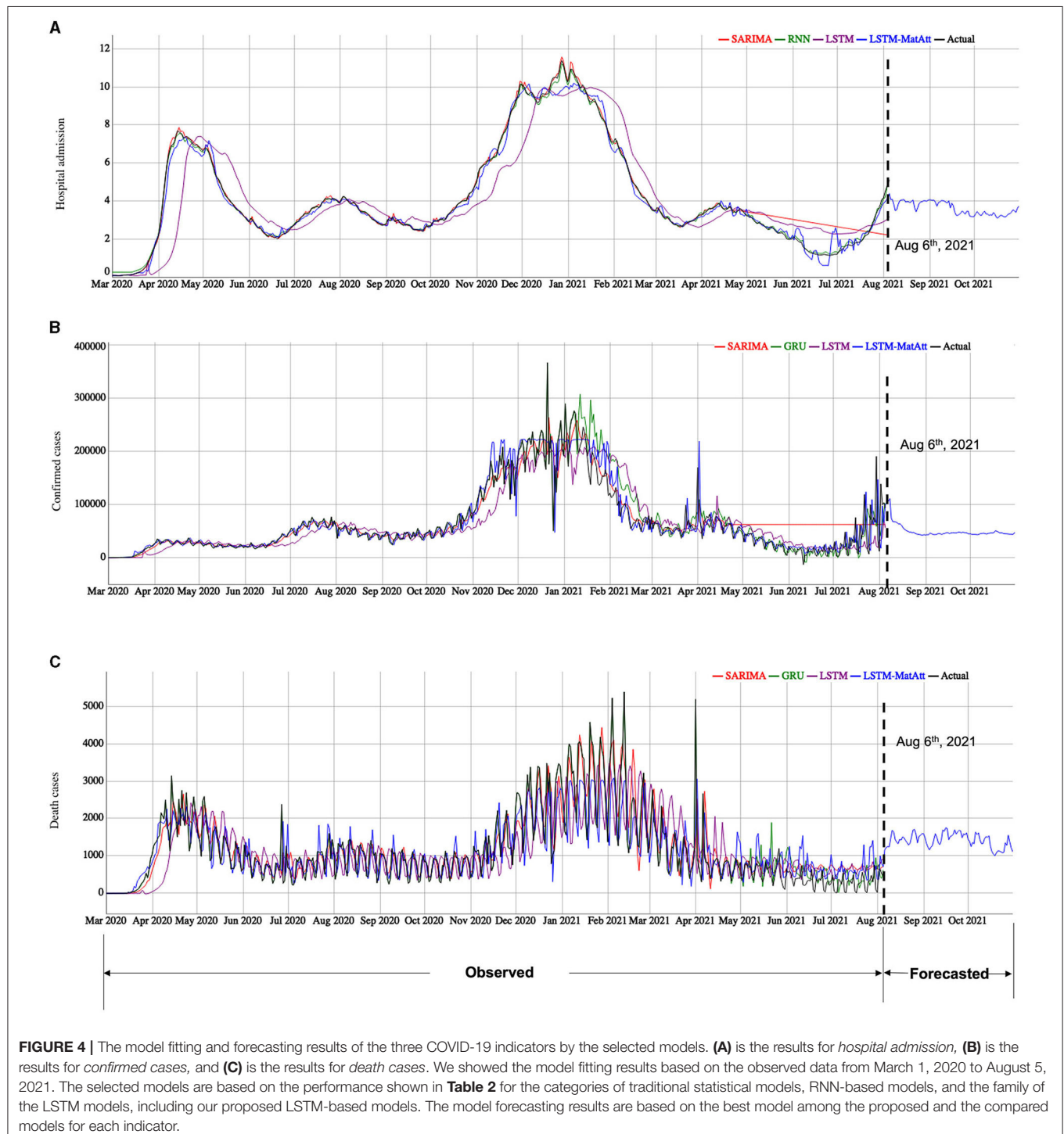
|  | Rep-hold                              | Admission |      |      |      |      |             | Confirmed |           |           |            |            |                  | Death  |        |          |          |          |               |
|--|---------------------------------------|-----------|------|------|------|------|-------------|-----------|-----------|-----------|------------|------------|------------------|--------|--------|----------|----------|----------|---------------|
|  |                                       | 1         | 2    | 3    | 4    | 5    | Average     | 1         | 2         | 3         | 4          | 5          | Average          | 1      | 2      | 3        | 4        | 5        | Average       |
| Seasonal autoregressive integrated moving average (SARIMA) | Root mean square error (rmse)         | 2.93      | 1.13 | 5.58 | 6    | 2.86 | 3.7         | 48,893.89 | 43,200.22 | 43,890.86 | 285,457.64 | 182,560.72 | 120,800.67       | 192.03 | 339.58 | 1,401.85 | 2,103.07 | 1,254.41 | 1,058.19      |
|  | mean absolute error (mae)             | 2.25      | 0.96 | 4.73 | 5.62 | 2.3  | 3.17        | 29,682.94 | 38,672.56 | 37,310.42 | 269,991.12 | 158,514.88 | 106,834.38       | 159.21 | 282.7  | 1,340.84 | 1,944.12 | 932.97   | 931.97        |
|  | Mean absolute percentage error (mape) | 0.89      | 0.53 | 2.2  | 2.42 | 0.67 | 1.34        | 0.76      | 3.65      | 3.05      | 14.88      | 8.7        | 6.21             | 2.51   | 3.15   | 7.94     | 9.55     | 2.49     | 5.13          |
| Echo state network (ESN)                                   | rmse                                  | 2.85      | 1.39 | 1.82 | 7.03 | 3.23 | 3.27        | 42,964.79 | 48,636.51 | 46,766.28 | 178,680.95 | 103,114.16 | 84,032.54        | 513.06 | 800.7  | 600.22   | 1,805.84 | 1,279.4  | 999.84        |
|  | mae                                   | 2.46      | 1.21 | 1.54 | 6.67 | 2.93 | 2.96        | 25,838.09 | 43,065.5  | 42,408.47 | 170,927.49 | 92,714.16  | 74,990.74        | 433.16 | 712.51 | 452.26   | 1,622.81 | 992.24   | 842.59        |
|  | mape                                  | 1.34      | 0.72 | 0.84 | 2.82 | 0.96 | 1.34        | 0.85      | 4.23      | 2.31      | 9.13       | 4.83       | 4.27             | 6.37   | 5.87   | 3.24     | 6.28     | 3.58     | 5.07          |
| Recurrent neural network (RNN)                             | rmse                                  | 1.50      | 1.14 | 1.04 | 1.24 | 1.25 | 1.25        | 36,301.76 | 48,930.03 | 48,582.78 | 44,627.97  | 46,251.33  | 44,938.77        | 618.95 | 516.87 | 697.39   | 924.08   | 1,033.18 | 758.09        |
|  | mae                                   | 1.24      | 0.86 | 0.76 | 0.96 | 0.98 | 0.96        | 27,413.55 | 30,122.34 | 28,976.36 | 28,576.04  | 30,771.02  | 29,171.86        | 458.87 | 354.16 | 463.03   | 594.38   | 681.61   | 510.41        |
|  | mape                                  | 0.48      | 0.34 | 0.27 | 0.26 | 0.23 | 0.32        | 2.64      | 2.04      | 1.66      | 1.15       | 0.76       | 1.65             | 5.78   | 3.28   | 2.69     | 1.72     | 1.64     | 3.02          |
| Gated recurrent unit (GRU)                                 | rmse                                  | 1.57      | 1.2  | 1.03 | 1.22 | 1.24 | 1.25        | 48,021.18 | 30,072.92 | 52,378.17 | 27,062.73  | 39,457.26  | 39,398.45        | 560.39 | 546.44 | 676.17   | 827.9    | 941.93   | 710.56        |
|  | mae                                   | 1.26      | 0.91 | 0.77 | 0.97 | 1.0  | 0.98        | 30,588.13 | 20,542.1  | 31,658.96 | 19,509.24  | 25,801     | 25,619.89        | 405.84 | 391.32 | 440.34   | 557.95   | 665.99   | 492.29        |
|  | mape                                  | 0.5       | 0.35 | 0.27 | 0.26 | 0.23 | 0.32        | 2.3       | 1.57      | 1.76      | 0.9        | 0.82       | 1.47             | 5.38   | 3.17   | 2.15     | 1.8      | 1.96     | 2.89          |
| Long short-term memory (LSTM)                              | rmse                                  | 0.99      | 0.58 | 0.50 | 2.27 | 3.18 | 1.50        | 40,777.76 | 8,524.12  | 6,615.82  | 54,148.58  | 76,302.02  | 37,273.66        | 199.09 | 387.76 | 709.34   | 1,191.08 | 588.35   | 615.12        |
|  | mae                                   | 0.65      | 0.58 | 0.50 | 1.80 | 2.55 | 1.22        | 26,680.90 | 6,745.04  | 6,524.89  | 37,704.15  | 58,703.45  | 27,271.69        | 162.23 | 372.73 | 576.72   | 874.00   | 543.57   | 505.85        |
|  | mape                                  | 0.23      | 0.17 | 0.14 | 0.60 | 0.44 | 0.31        | 1.03      | 0.13      | 0.11      | 0.74       | 0.59       | 0.52             | 1.88   | 0.54   | 0.52     | 0.61     | 0.32     | 0.77          |
| Convolutional neural network (CNN)-LSTM                    | rmse                                  | 1.37      | 0.96 | 0.92 | 2.08 | 2.80 | 1.62        | 40,404.43 | 16,663.18 | 13,230.96 | 45,052.20  | 74,871.81  | 38,044.51        | 837.00 | 535.74 | 589.30   | 1,175.13 | 458.34   | 719.10        |
|  | mae                                   | 1.27      | 0.77 | 0.92 | 1.49 | 2.34 | 1.36        | 28,413.84 | 15,329.70 | 11,412.55 | 28,374.41  | 55,020.34  | 27,710.17        | 813.65 | 519.59 | 354.60   | 800.40   | 396.15   | 576.88        |
|  | mape                                  | 0.78      | 0.29 | 0.26 | 0.46 | 0.38 | 0.43        | 1.37      | 0.29      | 0.20      | 0.70       | 0.53       | 0.62             | 2.64   | 0.75   | 0.45     | 0.55     | 0.22     | 0.92          |
| LSTM-Att   | rmse                                  | 1.03      | 0.92 | 0.84 | 2.34 | 2.82 | 1.59        | 40,190.04 | 15,190.05 | 12,312.38 | 54,340.17  | 76,099.67  | 39,626.46        | 196.35 | 452.30 | 682.91   | 1,190.51 | 492.40   | 602.89        |
|  | mae                                   | 0.69      | 0.92 | 0.80 | 1.96 | 2.54 | 1.38        | 27,157.88 | 13,731.57 | 10,316.78 | 40,776.23  | 58,692.52  | 30,135.00        | 156.49 | 390.36 | 537.24   | 907.07   | 434.72   | 485.18        |
|  | mape                                  | 0.25      | 0.26 | 0.23 | 0.55 | 0.38 | 0.34        | 0.71      | 0.26      | 0.18      | 0.70       | 0.53       | 0.48             | 0.79   | 0.71   | 0.46     | 0.55     | 0.25     | 0.55          |
| LSTM-MatAtt  | rmse                                  | 0.91      | 0.31 | 0.44 | 1.01 | 3.49 | <b>1.23</b> | 41,368.47 | 18,142.10 | 8,341.91  | 39,247.68  | 50,963.88  | <b>31,612.81</b> | 205.34 | 321.18 | 668.23   | 885.96   | 255.13   | <b>467.17</b> |
|  | mae                                   | 0.74      | 0.31 | 0.44 | 0.79 | 2.47 | <b>0.95</b> | 34,559.99 | 17,091.87 | 8,304.28  | 32,947.74  | 38,393.86  | <b>26,259.55</b> | 166.47 | 255.29 | 527.03   | 659.52   | 211.79   | <b>364.02</b> |
|  | mape                                  | 0.32      | 0.09 | 0.13 | 0.29 | 0.44 | <b>0.25</b> | 3.35      | 0.45      | 0.13      | 0.73       | 0.66       | <b>1.06</b>      | 0.69   | 0.83   | 0.45     | 0.60     | 0.17     | <b>0.55</b>   |
| LSTM-RelAtt  | rmse                                  | 0.71      | 0.63 | 0.78 | 2.17 | 3.23 | 1.50        | 33,139.11 | 24,263.36 | 683.29    | 51,316.31  | 70,101.06  | 35,900.62        | 194.75 | 229.07 | 698.72   | 1,180.69 | 197.48   | 500.14        |
|  | mae                                   | 0.58      | 0.63 | 0.75 | 1.66 | 2.49 | 1.22        | 24,412.11 | 23,770.01 | 505.07    | 36,789.93  | 50,511.32  | 27,197.69        | 155.75 | 191.42 | 688.39   | 782.20   | 195.39   | 402.63        |
|  | mape                                  | 0.27      | 0.18 | 0.23 | 0.58 | 0.48 | 0.35        | 1.34      | 0.61      | 0.01      | 0.68       | 0.61       | 0.65             | 0.81   | 1.38   | 0.37     | 0.56     | 0.17     | 0.66          |

in around November 2020, which is consistent with the visual observation (bottom panel of **Figure 3B**). Overall, the data-driven unsupervised matrix profile successfully detected the intrinsic anomalous data in the time series of the three indicators.

## Seasonal ARIMA

The performance of the SARIMA is summarized in **Table 2**. Overall, SARIMA had a decent average performance of

predicting the three indicators. Rep-holdout 1 (last 10% of time points as a testing set) did not always have best performance in predicting the three indicators among all other rep-holdout, and rep-holdout 5 (last 50% of time points as a testing set) was not the worst strategy, which indicates that the performance of the SARIMA model was not linearly related with the size of the training data. This is also applied to other models.



## RNN Models

The results of the simple RNN, ESN, and GRU models can be found in **Table 2**. The simple RNN and GRU achieved similar overall performance in predicting the three indicators, but their performances were better than that of the ESN model. The ESN performed slightly better than the SARIMA, while the simple RNN and GRU were much better than the SARIMA.

## LSTM Models

The LSTM model with attention mechanism and matrix profile (*Model: LSTM-MatAtt*) has achieved better-averaged performance in predicting the three indicators (**Table 2**). Furthermore, the *LSTM-MatAtt* model with rep-holdout 3 was the best model in predicting *hospital admission* (RMSE = 1.23, MAE = 0.95, MAPE = 0.25). This performance was far better than other models we tested, no matter if they were classic statistic models or any other RNN models (**Table 2**).

Overall, the LSTM models with attention mechanism fed together with the matrix profile outperformed the classic statistic models, the other RNN models, and the LSTM models without the attention mechanism as well as the matrix profile assistance in predicting the three indicators. Different models may need to be equipped with different rep-holdouts.

## COVID-19 Case Forecasting

After the performances of the models were evaluated and the hyperparameters were fine-tuned using the rep-holdout strategy, the final forecasting for the three indicators was performed based on the whole data (March 1, 2020 to August 5, 2021). We let the selected and well-trained models run freely to forecast the future data between August 6, 2021 and October 31, 2021 (**Figure 4**). Note: We can only access the data up to August 5, 2021 at the time we submit the report.

Using the best models show in **Table 2**, we forecasted the cases of *hospital admission*, *confirmed cases*, and *death cases* using the trained LSTM-MatAtt models for the period from August 6, 2021 to October 31, 2021 (**Figure 4**). The forecasting results of *hospital admission* show a significant rise between July 2021 and October 2021. The *confirmed cases* and *death cases* indicate a relatively stable trend in the next few months, but they have significantly decreased from the peaks in January–February in 2021.

## DISCUSSIONS AND CONCLUSIONS

Classic statistic time series forecasting models and the baseline RNN models, which are the benchmarks of this study, are able to achieve descent predictions of the three indicators of COVID-19. The proposed novel LSTM models combining matrix profile and attention mechanism achieved the overall best performance. A different number of time points was assigned to the training set according to the rep-holdout strategy. According to **Table 1**, the model performances were not associated with the size of the training sets, which means a larger training set may not guarantee a better performance. Careful selection of a proper training strategy could potentially increase the performance.

There are some limitations in this study. First, although the proposed models were selected through a five rep-holdout strategy, it was not validated in another totally independent dataset. Second, forecasting future cases is often not accurate while its uncertainty is seriously underestimated. One such example is the case of SARS, where the fear of becoming a pandemic was overblown, resulting in overspending and the application of restrictive measures to be taken that turned out to be unnecessary. Due to the uncertain measures taken, mathematical models overpredicted the number of cases. This calls us to fully take these potential uncertain factors into account when we build the forecasting models. In our modeling strategy, we used an indirect approach to first detect anomalies existing in the history data, which may be related to these uncertain measures. Despite the inaccuracies associated with the predictions, forecasting is still useful in allowing us to better understand the current situation and make plans.

In conclusion, a novel unsupervised matrix profile combined with an attention-based LSTM algorithm was proposed. Our experiments showed that the proposed algorithm has the best ability to forecast COVID-19 cases than the classical statistic methods and the baseline RNN models. The forecasted data may provide potentially useful information to help decision-makers to control the consequences of COVID-19.

## DATA AVAILABILITY STATEMENT

Publicly available datasets were analyzed in this study. This data can be found here: <https://cmu-delphi.github.io/delphi-epidata/>.

## AUTHOR CONTRIBUTIONS

QL and DF were responsible for the conceptualization, development of methodologies and writing, and editing the manuscript. LL performed data analysis and wrote the manuscript. PH provided advice on data analysis and critically reviewed the manuscript and was also involved in supervision and project administration. All authors had full access to all of the data in the study and can take responsibility for the integrity of the data and the accuracy of the data analysis.

## FUNDING

This work was supported in part by the Natural Sciences and Engineering Research Council of Canada and the University of Manitoba. PH is the holder of the Manitoba Medical Services Foundation (MMSF) Allen Rouse Basic Science Career Development Research Award.

## ACKNOWLEDGMENTS

Data were downloaded from the website of Carnegie Mellon University Delphi Research Group.

## REFERENCES

1. Disease outbreak news. WHO | Novel Coronavirus – China. WHO (2020). Available online at: <https://www.who.int/csr/don/12-january-2020-novel-coronavirus-china/en/> (accessed Sep 22, 2020).
2. Dong E, Du H, Gardner L. An interactive web-based dashboard to track COVID-19 in real time. *Lancet Infect Dis.* (2020) 20:533–4. doi: 10.1016/S1473-3099(20)30120-1
3. Gorbalenya AE, Baker SC, Baric RS, Groot RJ De, Gulyaeva AA, Haagmans BL, et al. The species Severe acute respiratory syndrome-related coronavirus: classifying 2019-nCoV and naming it SARS-CoV-2. *Nature microbiology* (2020) 536.
4. Vellingiri B, Jayaramayya K, Iyer M, Narayanasamy A, Govindasamy V, Giridharan B, et al. COVID-19: a promising cure for the global panic. *Sci Total Environ.* (2020) 725:138277. doi: 10.1016/j.scitotenv.2020.138277
5. Abd El-Aziz TM, Stockand JD. Recent progress and challenges in drug development against COVID-19 coronavirus (SARS-CoV-2) – an update on the status. *Infect Genet Evol.* (2020) 83:104327. doi: 10.1016/j.meegid.2020.104327
6. Cucinotta D, Vanelli M. WHO declares COVID-19 a pandemic. *Acta Biomed.* (2020) 91:157–160. doi: 10.23750/abm.v91i1.9397
7. Box GEP, Jenkins GM, Reinsel GC. Time series analysis: forecasting and control. *J Market Res.* (1977) 14:269. doi: 10.2307/3150485
8. Heisterkamp SH, Dekkers ALM, Heijne JCM. Automated detection of infectious disease outbreaks: hierarchical time series models. *Stat Med.* (2006) 25:4179–96. doi: 10.1002/sim.2674
9. Choi K, Thacker SB. An evaluation of influenza mortality surveillance, 1962–1979. *Am J Epidemiol.* (1981) 113:215–26. doi: 10.1093/oxfordjournals.aje.a113090
10. Benvenuto D, Giovanetti M, Vassallo L, Angeletti S, Ciccozzi M. Application of the ARIMA model on the COVID-2019 epidemic dataset. *Data Brief.* (2020) 29:105340. doi: 10.1016/j.dib.2020.105340
11. Ceylan Z. Estimation of COVID-19 prevalence in Italy, Spain, and France. *Sci Total Environ.* (2020) 729:138817. doi: 10.1016/j.scitotenv.2020.138817
12. Chintalapudi N, Battineni G, Amenta F. COVID-19 virus outbreak forecasting of registered and recovered cases after sixty day lockdown in Italy: a data driven model approach. *J Microbiol Immunol Infect.* (2020) 53:396–403. doi: 10.1016/j.jmii.2020.04.004
13. Alzahrani SI, Aljamaan IA, Al-Fakih EA. Forecasting the spread of the COVID-19 pandemic in Saudi Arabia using ARIMA prediction model under current public health interventions. *J Infect Public Health.* (2020) 13:914–9. doi: 10.1016/j.jiph.2020.06.001
14. Chaurasia V, Pal S. COVID-19 Pandemic: ARIMA and Regression Model-Based Worldwide Death Cases predictions. *SN Comput Sci.* (2020) 1:288. doi: 10.1007/s42979-020-00298-6
15. Chaurasia V, Pal S. Application of machine learning time series analysis for prediction COVID-19 pandemic. *Res Biomed Eng.* (2020) 24:1–13. doi: 10.1007/s42600-020-00105-4
16. Hernandez-Matamoros A, Fujita H, Hayashi T, Perez-Meana H. Forecasting of COVID19 per regions using ARIMA models and polynomial functions. *Appl Soft Comput J.* (2020) 96:106610. doi: 10.1016/j.asoc.2020.106610
17. Sahai AK, Rath N, Sood V, Singh MP. ARIMA modelling & forecasting of COVID-19 in top five affected countries. *Diabetes Metab Syndrome Clin Res Rev.* (2020) 14:1419–27. doi: 10.1016/j.dsx.2020.07.042
18. Wang Y, Xu C, Yao S, Zhao Y. Forecasting the epidemiological trends of COVID-19 prevalence and mortality using the advanced  $\alpha$ -Sutte Indicator. *Epidemiol Infect.* (2020) 148. doi: 10.1017/S095026882000237X
19. M. WB, A. HL. Modeling and forecasting vehicular traffic flow as a seasonal ARIMA process: theoretical basis and empirical results. *J Transport Eng.* (2003) 129:664–72. doi: 10.1061/(ASCE)0733-947X(2003)129:6(664)
20. Chandola V, Banerjee A, Kumar V. Anomaly detection: a survey. *ACM Comput Surveys.* (2009) 41:1–58. doi: 10.1145/1541880.1541882
21. Yeh C-CM, Zhu Y, Ulanova L, Begum N, Ding Y, Dau HA, et al. Matrix profile I: all pairs similarity joins for time series: a unifying view that includes motifs, discords and shapelets. In: *2016 IEEE 16th International Conference on Data Mining (ICDM)*. Barcelona: Institute of Electrical and Electronics Engineers (IEEE) (2016). p. 1317–22.
22. Zhu Y, Zimmerman Z, Senobari NS, Yeh C-CM, Funning G, Mueen A, et al. Matrix profile II: exploiting a novel algorithm and gpus to break the one hundred million barrier for time series motifs and joins. In: *2016 IEEE 16th International Conference on Data Mining (ICDM)*. Barcelona: Institute of Electrical and Electronics Engineers (IEEE) (2016), 739–48.
23. Yeh C-CM, Herle H Van, Keogh E. Matrix profile III: the matrix profile allows visualization of salient subsequences in massive time series. In: *2016 IEEE 16th International Conference on Data Mining (ICDM)*. Barcelona: Institute of Electrical and Electronics Engineers (IEEE). p. 579–88.
24. Yeh CCM, Zhu Y, Ulanova L, Begum N, Ding Y, Anh H, et al. Time series joins, motifs, discords and shapelets: a unifying view that exploits the matrix profile. *Data Mining Knowl Discov.* (2018) 32:83–123. doi: 10.1007/s10618-017-0519-9
25. Yeh CCM, Kavantzaz N, Keogh E. Matrix profile IV: using weakly labeled time series to predict outcomes. *Proc VLDB Endow.* (2017) 10:1802–12. doi: 10.14778/3137765.3137784
26. Jaeger H, Haas H. Harnessing nonlinearity: predicting chaotic systems and saving energy in wireless communication. *Science.* (2004) 304:78–80. doi: 10.1126/science.1091277
27. Cho K, Van Merriënboer B, Gulcehre C, Bahdanau D, Bougares F, Schwenk H, et al. Learning phrase representations using RNN encoder-decoder for statistical machine translation. In: *EMNLP 2014 - 2014 Conference on Empirical Methods in Natural Language Processing, Proceedings of the Conference*. Doha, Qatar, Association for Computational Linguistics (2014). p. 1724–34. doi: 10.3115/v1/D14-1179
28. Hochreiter S, Schmidhuber J. Long short-term memory. *Neural Comput.* (1997) 9:1735–80. doi: 10.1162/neco.1997.9.8.1735
29. Hochreiter S. The vanishing gradient problem during learning recurrent neural nets and problem solutions. *Int J Uncertain Fuzziness Knowl Based Syst.* (1998) 6:107–16. doi: 10.1142/S0218488598000094
30. Oztuik MC, Xu D, Principe JC. Analysis and design of echo state networks. *Neural Comput.* (2007) 19:111–38. doi: 10.1162/neco.2007.19.1.111
31. Shahid F, Zameer A, Muneeb M. Predictions for COVID-19 with deep learning models of LSTM, GRU and Bi-LSTM. *Chaos Solitons Fractals.* (2020) 140:110212. doi: 10.1016/j.chaos.2020.110212
32. Chimmula VKR, Zhang L. Time series forecasting of COVID-19 transmission in Canada using LSTM networks. *Chaos Solitons Fractals.* (2020) 135:109864. doi: 10.1016/j.chaos.2020.109864
33. Barman A. Time series analysis and forecasting of COVID-19 cases using LSTM and ARIMA models[J]. (2020). *arXiv [Preprint]*. arXiv 2006.13852
34. Shastri S, Singh K, Kumar S, Kour P, Mansotra V. Time series forecasting of Covid-19 using deep learning models: India-USA comparative case study. *Chaos Solitons Fractals.* (2020) 140:110227. doi: 10.1016/j.chaos.2020.110227
35. Wang Y, Huang M, Zhao L, Zhu X. Attention-based LSTM for aspect-level sentiment classification. In: *EMNLP 2016 - Conference on Empirical Methods in Natural Language Processing, Proceedings*. Austin, Texas, Association for Computational Linguistics (2016). p. 606–15. doi: 10.18653/v1/D16-1058
36. Xu J, Yao T, Zhang Y, Mei T. Learning multimodal attention LSTM networks for video captioning. In: *MM 2017 - Proceedings of the 2017 ACM Multimedia Conference*. New York, United States, Association for Computing Machinery (2017). p. 537–45. doi: 10.1145/3123266.3123448
37. Farrow DC, Brooks LC, Rumack A, Tibshirani RJ, Rosenfeld R. *Delphi Epidata API*. Delphi Research Group at Carnegie Mellon University, Available online at: [cmu-delphi.github.io/delphi-epidata/api/covidcast.html](https://cmu-delphi.github.io/delphi-epidata/api/covidcast.html) (2021).



38. Van Benschoten A, Ouyang A, Bischoff F, Marrs T. MPA: a novel cross-language API for time series analysis. *J Open Source Softw.* (2020) 5:2179. doi: 10.21105/joss.02179
39. Hyndman RJ, Khandakar Y. Automatic time series forecasting: the forecast package for R. *J Stat Softw.* (2008) 27:1–22. doi: 10.18637/jss.v027.i03
40. Petersen NC, Christoffer R, Rodrigues F, Pereira FC. Multi-output bus travel time prediction with convolutional LSTM neural network. *Expert Syst Applic.* (2019) 120:426–35. doi: 10.1016/j.eswa.2018.11.028

**Conflict of Interest:** The authors declare that the research was conducted in the absence of any commercial or financial relationships that could be construed as a potential conflict of interest.

**Publisher's Note:** All claims expressed in this article are solely those of the authors and do not necessarily represent those of their affiliated organizations, or those of the publisher, the editors and the reviewers. Any product that may be evaluated in this article, or claim that may be made by its manufacturer, is not guaranteed or endorsed by the publisher.

Copyright © 2021 Liu, Fung, Lac and Hu. This is an open-access article distributed under the terms of the Creative Commons Attribution License (CC BY). The use, distribution or reproduction in other forums is permitted, provided the original author(s) and the copyright owner(s) are credited and that the original publication in this journal is cited, in accordance with accepted academic practice. No use, distribution or reproduction is permitted which does not comply with these terms.



# BNT162b2 and ChAdOx1 SARS-CoV-2 Post-vaccination Side-Effects Among Saudi Vaccinees

Ahmed N. Alghamdi<sup>†</sup>, Mohammed I. Alotaibi<sup>†</sup>, Adel S. Alqahtani, Daifullah Al Aboud and Ahmed S. Abdel-Moneim<sup>\*</sup>

College of Medicine, Taif University, Taif, Saudi Arabia

## OPEN ACCESS

### Edited by:

Reza Lashgari,  
Shahid Beheshti University, Iran

### Reviewed by:

Shyh Poh Teo,  
Raja Isteri Pengiran Anak Saleha  
Hospital, Brunei  
Flor Pujol,  
Instituto Venezolano de  
Investigaciones Científicas  
(IVIC), Venezuela  
AbdulAzeez Adeyemi Anjorin,  
Lagos State University, Nigeria  
Andrew Clark,  
University of Texas Southwestern  
Medical Center, United States

### \*Correspondence:

Ahmed S. Abdel-Moneim  
asa@tu.edu.sa;  
asa@bsu.edu.eg

<sup>†</sup>These authors have contributed  
equally to this work

### Specialty section:

This article was submitted to  
Infectious Diseases - Surveillance,  
Prevention and Treatment,  
a section of the journal  
Frontiers in Medicine

**Received:** 17 August 2021

**Accepted:** 13 September 2021

**Published:** 08 October 2021

### Citation:

Alghamdi AN, Alotaibi MI,  
Alqahtani AS, Al Aboud D and  
Abdel-Moneim AS (2021) BNT162b2  
and ChAdOx1 SARS-CoV-2  
Post-vaccination Side-Effects Among  
Saudi Vaccinees.  
Front. Med. 8:760047.  
doi: 10.3389/fmed.2021.760047

**Background:** Vaccination against SARS-CoV-2 is important for reducing hospitalization and mortalities. Both Pfizer-BioNTech (BNT162b2) and the Oxford-AstraZeneca (ChAdOx1 nCoV-19) vaccines are used in Saudi Arabia and in many parts of the world. Post-vaccinal side effects were recorded, so we aimed to screen different complaints after vaccination among vaccinees in Saudi Arabia.

**Methods:** An online questionnaire was designed to screen the local, systemic, and allergic post vaccination reactions for vaccinees who received either one or two doses of the BNT162b2 vaccine or one dose of the ChAdOx1 vaccine. The number and percentage were recorded for each response and analyzed using cross-tab and Chi square tests. The degree of the severity of post vaccination reactions were analyzed using Roc curve. The cofactors that may affect the severity of post-vaccinal reactions including previous COVID-19 infection, age, sex, body mass index, and comorbidities were investigated.

**Results:** During our study, 4,170 individuals reported their responses: 2,601 received one dose of BNT162b2, of whom 456 completed the second dose, and 1,569 received a single dose of ChAdOx1. The side effects were reported in 85.6% of BNT162b2 vaccinees and 96.05% of ChAdOx1 vaccinees who voluntarily responded to a survey about post-vaccination side effects. The side effects were more severe in BNT162b2 than ChAdOx1. ChAdOx1 vaccinees reported mild, moderate, severe and critical side effects in 30.13, 28.62, 29.73, and 1.53%, respectively. In contrast, mild side effects were recorded among the majority of BNT162b2 vaccinees (63.92%) while moderate, severe, and critical side effects were 27.67, 7.68, and 0.72%, respectively. Both local and systemic side effects were recorded more frequently in ChAdOx1 in comparison to BNT162b2 vaccinees. Palpitation was among the new systemic side effects reported in the current study in high frequency. Abnormal menstrual cycle (delaying/increase hemorrhages or pain) was also reported in 0.98% (18/1846) of Pfizer-BioNTech and 0.68% (7/1028) of ChAdOx1 vaccinees, while deep vein thrombosis was only reported in a single case vaccinated with BNT162b2 vaccine.

**Conclusion:** Both vaccines induced post-vaccinal side effects; however, ChAdOx1 induces a higher frequency of post-vaccinal systemic side effects than BNT162b2.

**Keywords:** COVID-19, SARS-CoV-2, COVID vaccines, post vaccination side effects, ChAdOx1 nCoV-19 vaccine, BNT162b2 mRNA COVID-19 vaccine, palpitation, menstrual cycle disturbance

## BACKGROUND

The SARS-CoV-2 pandemic continues to spread worldwide, following its first emergence in December 2019. The virus induces coronavirus disease (COVID-19) that might be asymptomatic or mild in the majority of patients; however, 20% of infected patients are prone to develop severe to serious diseases with fatal consequences (1). Old age, gender, asthma, hypertension, and other cardiovascular diseases are among the risk factors of COVID-19 (2–4).

Vaccination is the most successful way to prevent the spread of many life-threatening infectious diseases. Thanks to vaccines, millions of lives are saved annually against more than 20 infectious diseases. Some countries have implemented local legislations for COVID-19 obligatory vaccination for access to private and governmental public sectors, making it mandatory for travelers prior to entry into such countries. Despite the significant number of vaccinated individuals worldwide, many people around the world are reluctant to get vaccinated against COVID-19. This fact could be due to the widespread rumors regarding the panic from the side effects that have led to a lack of trust in COVID-19 vaccines.

Starting from December 2020, many SARS-CoV-2 vaccines have been released for emergency use, including spike- gene RNA-vaccines encapsulated in lipid nanoparticles, such as BNT162b2 (Pfizer–BioNTech) and mRNA-1273 (Moderna); chimpanzee adenovirus vector vaccine harboring SARS-CoV-2 S gene (ChAdOx1- AstraZeneca), human adenovirus 26 (Ad26.COV2.S-Johnson & Johnson/Janssen), and inactivated SARS-CoV-2 vaccines (Sinopharm and Sinovac). Saudi Arabia approved BNT162b2 then ChAdOx1 for use in the vaccination protocol on 10 December 2020, and 18 February 2021, respectively. Both vaccines have proven to be safe and efficacious as evidenced by the results of clinical trials (5, 6). There is a need of up to 14 billion doses of COVID-19 vaccines to cover 70% of global coverage (7). This fact results in the recommendation of the WHO to temporary halt of giving the second dose of COVID-19 vaccine, with the aim of covering more unvaccinated people worldwide (8).

Pain, redness, swelling, fever, tiredness, headache, muscle pain, chills, and nausea are among the common side effects of the vaccines (9). Most of such side effects disappear within 2 days after vaccination (9). Other rare side effects, including vesiculous-bullous skin (10), herpes simplex or varicella zoster reactivation (11–13), nephrotic syndrome and acute kidney injury (14) were also reported. Meanwhile, serious post-vaccinal reactions, including intravascular thrombosis and thrombocytopenia are associated with both ChAdOx1 and the BNT162b2 vaccines; however, the frequency was 5-fold higher in ChAdOx1 than in BNT162b2 (15). It was found that the ChAdOx1 vaccine but not BNT162b2 enhances the production of anti-platelet factor 4 antibodies (15, 16). Accordingly, some countries in Europe suspended the use of the ChAdOx1 vaccine. However, KSA and other European countries decided to continue using the vaccine according to the WHO recommendation that benefits of using ChAdOx1 vaccine outweigh its risks (17).

On the other hand, anaphylaxis reaction has been reported among BNT162b2 vaccinees in an approximate rate of 1:200,000. Such reaction was most probably induced by the polyethylene glycol (PEG 2000 Da) (18). Interestingly ChAdOx1 vaccine contains polysorbate 80, a derivative of the PEG, which is used in a similar concentration in many vaccines including DTaP, HB vaccine, HPV, and influenza vaccines (19). The relatively lower molecular weight of the polysorbate 80 (1310 Da) in comparison to PEG (2000 Da) and the fact that polysorbate 80 is being used in many vaccines, monoclonal antibodies, and most of the injectable biological reagents for many decades alleviates its role as a possible trigger of anaphylaxis (18, 19).

SARS-CoV-2 vaccines are successful in reducing the severity of the disease, hospitalization, and mortality (20). The safety of SARS-CoV-2 vaccines has been successfully and carefully monitored prior to their authorization. However, the tracking of side effects that were not detected during clinical trials is still needed. The current study aimed to screen the incidence of local, systemic, and allergic reactions following SARS-CoV-2 vaccination. We also intended to screen possible factors that may affect the incidence and severity of post-vaccinal reactions, including previous COVID-19 infection, age, sex, and other immunocompromising conditions.

## METHODS

### Participants

Vaccination was an inclusion criterion for filling the questionnaire. The questions seek the following information: whether participants are suffering from any chronic diseases or immunosuppressive disorders, whether they suffered from a previous SARS-CoV-2 infection or not, and the type and number of doses of the vaccine. The questionnaire included a leading question asked about the presence of absence of the side effects following vaccination. In case they have symptoms, they were asked about the individual side effects they experienced after the first and the second doses of the vaccines in separate sets of questions. There were three main clusters of questions including those related to local, allergic, and systemic reactions in addition to other unlisted symptoms. A question about the intensity of reaction or the severity of side effects was included; it graded the severity into mild (minor reactions that extended for  $\leq 1$ –2 days), moderate (tolerable reactions extended to 2–3 days), severe (exacerbation of the post-vaccinal reactions in barely tolerable manner extended for  $\geq 3$  days but did not require hospitalization), and critical (adverse signs were severe enough to require hospitalization). We also asked about the duration of the post-vaccination side effects till the 7th day post vaccination and provided an option if the signs continued for more than 7 days. Also included was an open question so the respondent could write any other sign not listed in the questions. A link to the online questionnaire was distributed in different social media including Twitter, Snapchat, and WhatsApp.

### Statistical Analysis

The differences between the two vaccinated groups (BNT162b2 vs. those who received ChAdOx1) were compared using Chi

**TABLE 1** | Frequencies and characteristics of the subjects in the current study.

| Variable                                       | BNT162b2 n:2601 (55.22) | ChAdOx1 n:1569 (37.63) | Total n: 4170 | P-value |
|--|-------------------------|------------------------|---------------|---------|
| <b>Sex, n (%)</b>                              |                         |                        |               |         |
| Female   | 1,846 (70.97)           | 1,028 (65.52)          | 2,874 (68.92) | 0.001   |
| Male   | 755 (29.03)             | 541 (34.48)            | 1,296 (31.08) |         |
| <b>Age groups, n (%)</b>                       |                         |                        |               | 0.001   |
| < 20   | 476 (18.3)              | 195 (12.42)            | 671 (16.09)   |         |
| 20–30  | 1,152 (44.29)           | 813 (51.82)            | 1,965 (47.12) |         |
| 31–40  | 410 (15.76)             | 261 (16.63)            | 671 (16.09)   |         |
| 41–50  | 369 (14.19)             | 213 (13.57)            | 582 (13.96)   |         |
| 51–60  | 156 (5.99)              | 71 (4.53)              | 227 (5.44)    |         |
| > 60   | 38 (1.46)               | 16 (1.02)              | 54 (1.29)     |         |
| <b>Nationality, n (%)</b>                      |                         |                        |               |         |
| Saudi  | 2,484 (95.50)           | 1,416 (90.25)          | 3,900 (93.53) | 0.001   |
| Not Saudi                                      | 117 (4.50)              | 153 (9.75)             | 270 (6.47)    |         |
| <b>BMI, n (%)</b>                              |                         |                        |               |         |
| <18.5  | 287 (11.03)             | 149 (9.50)             | 436 (10.46)   | 0.041   |
| 18.5–24.9                                      | 1,066 (40.98)           | 655 (41.75)            | 1,721 (41.27) |         |
| 25–29.9  | 682 (26.22)             | 420 (26.77)            | 1,102 (26.43) |         |
| 30–34.9  | 356 (13.68)             | 217 (13.83)            | 573 (13.74)   |         |
| 35–39.9  | 156 (5.99)              | 75 (4.78)              | 231 (5.54)    |         |
| ≥40  | 54 (2.08)               | 53 (3.37)              | 107 (2.57)    |         |
| <b>Previous infection with COVID-19, n (%)</b> |                         |                        |               |         |
| No   | 2,283 (77.77)           | 1,390 (88.59)          | 3,673 (88.08) | 0.868   |
| Yes  | 318 (12.23)             | 179 (11.41)            | 497 (11.92)   |         |
| <b>The presence of chronic diseases, n (%)</b> |                         |                        |               |         |
| No   | 2,152 (82.73)           | 1,295 (82.54)          | 3,447 (82.66) | 0.43    |
| Yes  | 449 (17.26)             | 274 (17.47)            | 723 (17.34)   |         |
| DM   | 164 (36.53)             | 126 (45.98)            | 290 (40.11)   |         |
| Hypertension                                   | 176 (39.20)             | 110 (40.15)            | 286 (39.56)   |         |
| DM and HTN                                     | 27 (6.01)               | 2 (0.73)               | 29 (4.01)     |         |
| Asthma   | 24 (5.35)               | 13 (4.74)              | 37 (5.12)     |         |
| Cardiac diseases                               | 27 (6.01)               | 7 (2.55)               | 34 (4.7)      |         |
| Liver diseases                                 | 8 (1.78)                | 2 (0.73)               | 10 (1.38)     |         |
| Kidney diseases                                | 8 (1.78)                | 6 (2.19)               | 14 (1.94)     |         |
| Cancer   | 8 (1.78)                | 1 (0.36)               | 9 (1.24)      |         |
| Multiple sclerosis                             | 3 (0.67)                | 5 (1.82)               | 8 (1.11)      |         |
| Rheumatoid fever                               | 4 (0.89)                | 2 (0.73)               | 6 (0.83)      |         |

Data are showed as number (percentage). Chi-square test was used to calculate the p-value for the difference between the first dose of BNT162b2 and ChAdOx1 vaccines.

square and Mann Whitney tests. The differences between the severity of the post-vaccinal reaction after the first and second BNT162b2 vaccination doses were also compared. The percentage of vaccinees experiencing side effects after having received the vaccine were calculated. All vaccinees were included in the adverse effects' analysis, including those who received a single dose of BNT162b2 or ChAdOx1. The probability of having severe side effects following the first and second BNT162b2 doses were also compared. Roc curve and logistic regressions were used for each of the specified variables to investigate whether adverse effects varied among different groups, and whether the previous exposure to COVID-19 infection could alter the response. Area under the curve (AUC)  $\leq 0.5$  poor discrimination or not useful, 0.7–0.8 is considered a good or an acceptable value, while 0.8–0.9 is very good value, while  $\geq 0.9$  is an excellent (21, 22).

## RESULTS

### Demographic Characteristic of the Studied Subjects

The total number of users who reported vaccination with the BNT162b2 vaccine (2,601:1,846 females and 755 males) were higher than those who reported getting vaccinated with ChAdOx1 (1,569:1,028 females and 541 males). This included slightly younger individuals and they were more frequently female than users who reported receiving the ChAdOx1 inoculation (**Table 1**). A majority of respondents were 20–30 years old (44.29% (1152/2601), 51.8% (813/1569) for BNT162b2 and ChAdOx1, respectively). The study found a small number of respondents above 50 years old; 7.46% (194/2601) and 5.54% (87/1569), for BNT162b2 and ChAdOx1, respectively (**Table 1**).



**TABLE 2** | Correlation of the severity of the post-vaccinal reactions and different parameters.

| Variable                                       | Don't have side effect | Mild          | Moderate     | Severe      | Critical  | Significance and correlation |
|--|------------------------|---------------|--------------|-------------|-----------|------------------------------|
| <b>Sex, n (%)</b>                              |                        |               |              |             |           |                              |
| Female   | 227 (7.9)              | 1,262 (43.9)  | 887 (30.9)   | 471 (16.4)  | 27 (0.9)  | $P < 0.015$                  |
| Male   | 210 (16.2)             | 615 (47.5)    | 311 (24.0)   | 148 (11.4)  | 12 (0.9)  | $R = -0.133$                 |
| <b>Age groups, n (%)</b>                       |                        |               |              |             |           |                              |
| < 20   | 82 (12.2)              | 277 (41.3)    | 207 (30.8)   | 96 (14.3)   | 9 (1.3)   | $P < 0.016$                  |
| 20–30  | 158 (8.0)              | 874 (44.5)    | 604 (30.7)   | 314 (16.0)  | 15 (0.8)  | $R = -0.069$                 |
| 31–40  | 69 (10.3)              | 316 (47.1)    | 177 (26.4)   | 105 (15.6)  | 4 (0.6)   |                              |
| 41–50  | 69 (11.9)              | 283 (48.6)    | 143 (24.6)   | 79 (13.6)   | 8 (1.4)   |                              |
| 51–60  | 41 (18.1)              | 105 (46.3)    | 58 (25.6)    | 21 (9.3)    | 2 (0.9)   |                              |
| > 60   | 18 (33.3)              | 22 (40.7)     | 9 (16.7)     | 4 (7.4)     | 1 (1.9)   |                              |
| <b>Nationality, n (%)</b>                      |                        |               |              |             |           |                              |
| Saudi  | 410 (10.5)             | 1,776 (45.5)  | 1,113 (28.5) | 565 (14.5)  | 36 (0.9)  | $P < 0.016$                  |
| Non Saudi                                      | 27 (10.0)              | 101 (37.4)    | 85 (31.5)    | 54 (20.0)   | 3 (1.1)   | $R = 0.042$                  |
| <b>BMI, n (%)</b>                              |                        |               |              |             |           |                              |
| <18.5  | 42 (9.6)               | 197 (45.2)    | 125 (28.7)   | 68 (15.6)   | 4 (0.9)   | $P < 0.016$                  |
| 18.5–24.9                                      | 162 (9.4)              | 744 (43.2)    | 520 (30.2)   | 282 (16.4)  | 13 (0.8)  | $R = -0.040$                 |
| 25–29.9  | 133 (12.1)             | 500 (45.4)    | 317 (28.8)   | 140 (12.7)  | 12 (1.1)  |                              |
| 30–34.9  | 56 (9.8)               | 274 (47.8)    | 149 (26.0)   | 89 (15.5)   | 5 (0.9)   |                              |
| 35–39.9  | 29 (12.6)              | 121 (52.4)    | 55 (23.8)    | 24 (10.4)   | 2 (0.9)   |                              |
| ≥40  | 15 (14.0)              | 41 (38.3)     | 32 (29.9)    | 16 (15.0)   | 3 (2.8)   |                              |
| <b>Type of the vaccine</b>                     |                        |               |              |             |           |                              |
| BNT162b2 (n:2601)                              | 375 (14.42)            | 1,423 (54.71) | 616 (23.68)  | 171 (6.57)  | 16 (0.62) | $P < 0.01$                   |
| ChAdOx1 (n = 1,569)                            | 62 (3.95)              | 454 (28.93)   | 582 (37.09)  | 448 (28.55) | 23 (1.47) | $R = 0.381$                  |
| <b>Previous infection with COVID-19, n (%)</b> |                        |               |              |             |           |                              |
| No   | 385 (10.5)             | 1,681 (45.8)  | 1,040 (28.3) | 528 (14.4)  | 39 (1.1)  | $P < 0.016$                  |
| Yes  | 52 (10.5)              | 196 (39.4)    | 158 (31.8)   | 91 (18.3)   | 0 (0.0)   | $R = 0.035$                  |
| <b>The presence of chronic diseases, n (%)</b> |                        |               |              |             |           |                              |
| No   | 356 (10.3)             | 1564 (45.4)   | 1014 (29.4)  | 486 (14.1)  | 27 (0.8)  | $P < 0.016$                  |
| Yes  | 81 (11.2)              | 313 (43.3)    | 184 (25.4)   | 133 (18.4)  | 12 (1.7)  | $R = 0.20$                   |

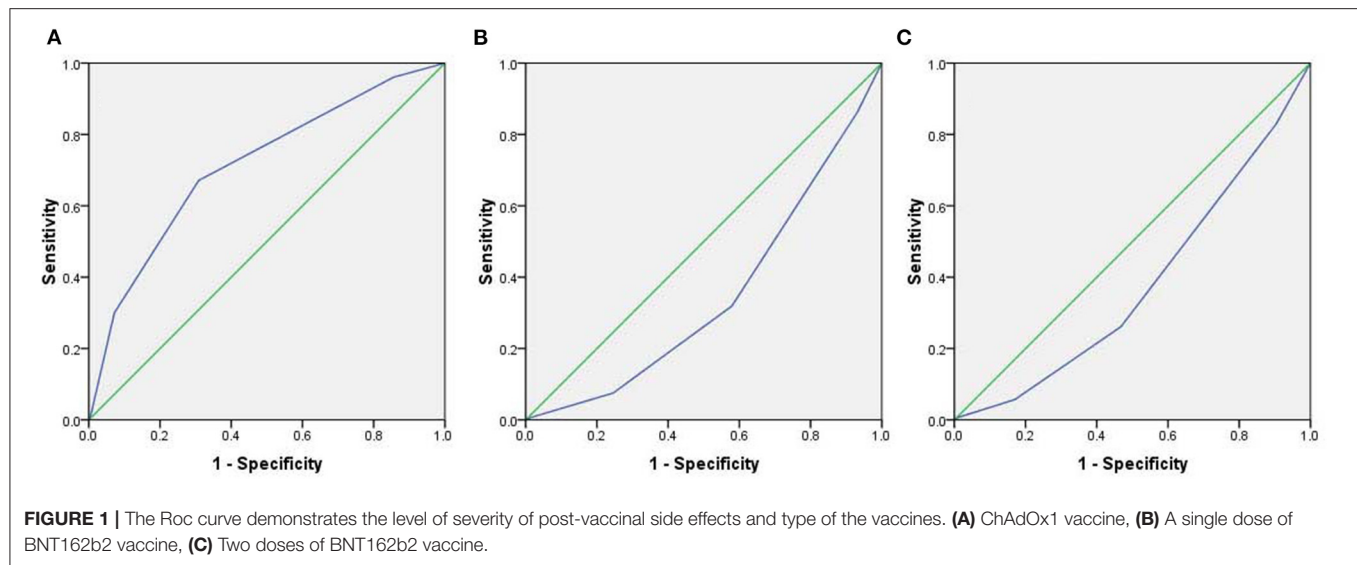
## Correlation Between the Severity of Post-vaccinal Reaction and Different Parameters

We studied the correlation between the severity of the post-vaccinal reactions and age, sex, nationality, body mass index, previous COVID-19 infection, and the presence of chronic diseases in the vaccinated subjected. The presence of chronic diseases was found to show significant correlation to the development of post-vaccinal adverse effects ( $P < 0.016$ ,  $R = 0.2$ ). The female gender was also associated with the development of moderate and severe post-vaccinal adverse effects ( $P < 0.015$ ,  $R = -0.133$ ) (Table 2). There is a significant correlation between the type of vaccine and the severity of the post-vaccinal reaction  $P > 0.01$ ,  $R = 0.381$ . The severe post vaccination side effects were found to be correlated with ChAdOx1 vaccine (Table 2). The Roc curve of the ChAdOx1 vaccine showed an acceptable good AUC value, 0.713, with the level of disease severity, 0.008 standard error and  $P < 0.001$ . While a single dose or two doses of BNT162b2 showed poor AUC of 0.347 and 0.378, respectively (Figure 1).

## Post-vaccinal Adverse Effects Following Administration of BNT162b2 or ChAdOx1

The severity of post-vaccinal side effects was found to be significantly higher in females in comparison to males (Table 3). ChAdOx1 vaccinees reported mild, moderate, severe, and critical side effects in 454/1569 (30.13%), 582/1569 (28.62%), 448/1569 (29.73%), and 23/1569 (1.53%), respectively. In contrast, mild side effects were recorded among the majority of BNT162b2 vaccinees 1423/2601 (63.92%) while moderate, severe, and critical side effects were 616/2601 (27.67%), 171/2601 (7.68%) and 16/2601 (0.72%), respectively (Table 4).

Most respondents to this survey about vaccine side effects suffered from one or more side effects while only 14.42% (375/2601) and 3.95% (62/1569) did not record any side effect for BNT162b2 and ChAdOx1, respectively. The most common side effect was localized pain after vaccine injection: 2,088 (80.27%), 1,347 (85.85%) for BNT162b2 and ChAdOx1, respectively. For ChAdOx1, fatigue 1,354 (86.30%), muscle pain 1,100 (70.11%), and headache were the common complaints. Meanwhile, for BNT162b2, fatigue 1,358 (52.21%), muscle pain 1,088 (41.83%), and headache were also the common systemic complaints but



were significantly lower than that detected for the ChAdOx1 vaccine. Insomnia 430 (27.40%), palpitation 269 (17.14%), chest pain 209 (13.32%), breathlessness 153 (9.75%), diarrhea 151 (9.62), and abdominal pain 149 (9.50) were recorded in respondents vaccinated with ChAdOx1, which was significantly higher than those reported for BNT162b2 (Table 4). The detected palpitation was not correlated to any of the reported chronic diseases related to cardiac diseases (Table 5). Fever, chills, palpitation, joint pain, and impaired concentration showed a highly significant variation among subjects vaccinated with ChAdOx1 (~2-fold or more of the percentage detected following BNT162b2 vaccination; Table 4). Other side effects, including allergies (itching, rashes, and swollen lips) were reported in both BNT162b2 and ChAdOx1 vaccinated subjects but there were no significant differences among the two groups. There were no significant differences between the vaccinees with regard to the allergic or local side effects. ChAdOx1 showed a higher percentage of local pain at the site of injection than BNT162b2. In contrast, subjects vaccinated with ChAdOx1 showed a highly significant increase in the duration of systemic reactions than those vaccinated with BNT162b2. About 11.96% (304/2601) and 13.7% (215/1569) showed side effects extended from 4–>7 days, while 72.9% (1897/2601) and 82.1% (1288/1569) showed side effects extended from 1–3 days for BNT162b2 and ChAdOx1, respectively (Table 4).

### Post-vaccinal Adverse Effects Following Administration of First and Second Doses of BNT162b2

Interestingly, subjects who received the second dose of BNT162b2 showed more moderate and severe reactions in a highly significant manner in comparison to the same subjects after the first dose of the vaccine ( $P < 0.001$ ). No significant variation in local pain or post-vaccinal allergic reactions or even the duration of side effects was detected among respondents got the first and second dose of BNT162b2. Significant systemic

reaction variations were more pronounced among subjects after getting the second dose in comparison to the same subjects after getting the first dose of the vaccine (Table 4). In contrast, the complaint of joint and muscle pain was more frequently detected after the first dose, as compared to the second dose. Diarrhea (308/456, 67.84%) and muscle pain (162/456, 70.11%) were very prominent complaints in a majority of the subjects who received the second dose in comparison to those got the first dose (19/456, 4.17%) (31/456, 6.83%), respectively (Table 4).

### Uncommon Post-vaccinal Adverse Effects Added by the Participants

The studied subjects reported uncommon post-vaccinal adverse effects, with a relatively considerable number of abnormal menstrual cycle, including increase in the time or increase in the pain or the bleeding, which was higher in BNT162b2 (18 cases) than in ChAdOx1 (7 cases). Other recorded signs included sore throat and/or dry mouth in 12 cases vaccinated with BNT162b2 and 3 cases vaccinated with ChAdOx1. Other rare signs were reported: anxiety, depression, sleepiness, mood disturbance, numbness of face, bruises in the leg, deep vein thrombosis, hypertension, pain in the testes, pain in the eyes, blurred vision, pain in the ear, and tinnitus (Table 6).

## DISCUSSION

In this study, the majority of respondents were 20–30 years old for both BNT162b2 and ChAdOx1. Considerable adverse side effects among respondents under 50 years of age, were reported. Previous studies support our findings as they showed that a higher rate of post-vaccinal side effects occurred among young subjects (23–25).

Subjects who suffered from chronic diseases are assumed to possess a weakened responsiveness to immunogens and hence are assumed to experience reduced side effects following vaccines (26, 27). In this study, chronic diseases were found to show significant correlation to the development of post-vaccinal

**TABLE 3 |** The post vaccine adverse effects after vaccination in male and female subjects.

|                              | Female         |      | Male           |      | P-value |
|------------------------------|----------------|------|----------------|------|---------|
|                              | Number (2,874) | %    | Number (1,296) | %    |         |
| Severity of the side effects |                |      |                |      |         |
| No side effects              | 227            | 7.9  | 210            | 16.2 | 0.001   |
| Mild                         | 1,262          | 43.9 | 615            | 47.5 |         |
| Moderate                     | 887            | 30.9 | 311            | 24.0 |         |
| Severe                       | 471            | 16.4 | 148            | 11.4 |         |
| Critical                     | 27             | 0.9  | 12             | 0.9  |         |
| Duration of the side effects |                |      |                |      |         |
| didn't have                  | 250            | 8.7  | 216            | 16.7 | 0.001   |
| 1 day                        | 699            | 24.3 | 425            | 32.8 |         |
| 2 days                       | 1,022          | 35.6 | 415            | 32.0 |         |
| 3 days                       | 492            | 17.1 | 132            | 10.2 |         |
| 4 days                       | 143            | 5.0  | 33             | 2.5  |         |
| 5 days                       | 84             | 2.9  | 22             | 1.7  |         |
| 6 days                       | 15             | 0.5  | 5              | 0.4  |         |
| 7 days                       | 57             | 2.0  | 10             | 0.8  |         |
| > 7 days                     | 112            | 3.9  | 38             | 2.9  |         |
| Local reactions, n (%)       |                |      |                |      |         |
| Pain                         | 2,490          | 86.6 | 945            | 72.9 | 0.001   |
| Swelling                     | 825            | 28.7 | 245            | 18.9 | 0.001   |
| Swollen lymph nodes          | 112            | 3.9  | 30             | 2.3  | 0.009   |
| Systemic reactions, n (%)    |                |      |                |      |         |
| Headache                     | 1,353          | 47.1 | 456            | 35.2 | 0.001   |
| Fever                        | 1,256          | 43.7 | 524            | 40.4 | 0.048   |
| Chill                        | 759            | 26.4 | 279            | 21.5 | 0.001   |
| Palpitation                  | 377            | 13.1 | 85             | 6.6  | 0.001   |
| Joint pain                   | 1,161          | 40.4 | 447            | 34.5 | 0.001   |
| Muscle pain                  | 1,590          | 55.3 | 598            | 46.1 | 0.001   |
| Fatigue                      | 1,971          | 68.6 | 741            | 57.2 | 0.001   |
| Impaired concentration       | 605            | 21.1 | 225            | 17.4 | 0.006   |
| Insomnia                     | 602            | 20.9 | 230            | 17.7 | 0.017   |
| Dizziness                    | 904            | 31.5 | 272            | 21.0 | 0.001   |
| Diarrhea                     | 238            | 8.3  | 77             | 5.9  | 0.008   |
| Abdominal pain               | 259            | 9.0  | 72             | 5.6  | 0.001   |
| Chest pain                   | 333            | 11.6 | 80             | 6.2  | 0.001   |
| Breathlessness               | 234            | 8.1  | 68             | 5.2  | 0.001   |
| Allergic reaction, n (%)     |                |      |                |      |         |
| Rash                         | 88             | 3.1  | 28             | 2.2  | 0.101   |
| Itching                      | 296            | 10.3 | 71             | 5.5  | 0.001   |
| Swollen lips                 | 64             | 2.2  | 16             | 1.2  | 0.031   |

Data are showed as number (percentage). Chi-square test was used to calculate the p-value for the difference between the male and female subjects after the first dose of either BNT162b2 or ChAdOx1.

adverse effects. However, no published information is available regarding these clusters of patients and their responsiveness or side effects following different COVID-19 vaccinations.

Subjects who previously experienced COVID-19 infection were reported to develop more severe side effects after vaccination (28). However, in our study, we did not find a considerable correlation between previous SARS-CoV-2 infection and the severity of post-vaccinal side effects.

In this study, the female gender was also associated with development of moderate and severe post-vaccinal adverse effects, showing a positive correlation of gender to the severity of the post-vaccinal side effects. This finding also agrees with other findings and confirms that the development of post-vaccinal side effects were significantly higher in females than in males (23, 24, 29). However, it disagrees with a recent study (30) that reported that males

**TABLE 4 |** Comparison between the post vaccine adverse effects after vaccination with BNT162b2 and ChAdOx1 as well as those after the first and the second doses of BNT162b2.

|                                     | First dose    |               |         | First and second doses of BNT162b2* |             |         |
|-------------------------------------|---------------|---------------|---------|-------------------------------------|-------------|---------|
|                                     | BNT162b2      | ChAdOx1       | P-value | 1st dose                            | 2nd dose    | P-value |
| Number                              | 2,601 (62.37) | 1569 (37.63)  | 0.001   | 456 (100)                           | 456 (100)   | 0.001   |
| <b>Severity of the side effects</b> |               |               |         |                                     |             |         |
| No side effects                     | 375 (14.42)   | 62 (3.95)     | 0.001   | 78 (17.11)                          | 63 (13.81)  | 0.149   |
| Presence of side effects            | 2,226 (85.58) | 1,507 (96.05) |         | 378 (82.89)                         | 392 (85.96) |         |
| Mild                                | 1,423 (63.92) | 454 (30.13)   | 0.001   | 258 (56.57)                         | 164 (35.96) | 0.001   |
| Moderate                            | 616 (27.67)   | 582 (38.62)   |         | 94 (20.6)                           | 135 (29.61) |         |
| Severe                              | 171 (7.68)    | 448 (29.73)   |         | 23 (5.04)                           | 86 (18.85)  |         |
| Critical                            | 16 (0.72)     | 23 (1.53)     |         | 3 (0.66)                            | 6 (1.32)    |         |
| <b>Duration of the side effects</b> |               |               |         |                                     |             |         |
| didn't have                         | 375 (14.42)   | 62 (3.95)     | 0.001   | 78 (17.11)                          | 63 (13.81)  | 0.246   |
| 1 day                               | 679 (30.50)   | 474 (31.45)   |         | 132 (34.92)                         | 126 (32.14) |         |
| 2 days                              | 877 (39.40)   | 560 (37.16)   |         | 156 (41.27)                         | 157 (40.05) |         |
| 3 days                              | 366 (16.44)   | 258 (17.12)   |         | 59 (15.61)                          | 61 (15.56)  |         |
| 4 days                              | 100 (4.49)    | 76 (5.04)     |         | 10 (2.64)                           | 18 (4.59)   |         |
| 5 days                              | 52 (2.34)     | 54 (3.58)     |         | 7 (1.85)                            | 4 (1.02)    |         |
| 6 days                              | 11 (0.49)     | 9 (0.60)      |         | 1 (0.26)                            | 3 (0.77)    |         |
| 7 days                              | 44 (1.98)     | 23 (1.52)     |         | 4 (1.06)                            | 8 (2.04)    |         |
| > 7 days                            | 97 (4.36)     | 53 (3.52)     |         | 9 (2.38)                            | 15 (3.83)   |         |
| <b>Local reactions, n (%)</b>       |               |               |         |                                     |             |         |
| Pain                                | 2,088 (80.27) | 1,347 (85.85) | 0.001   | 355 (77.85)                         | 334 (73.57) | 0.132   |
| Swelling                            | 677 (26.03)   | 393 (25.05)   | 0.482   | 132 (28.95)                         | 137 (30.18) | 0.658   |
| Swollen lymph nodes                 | 98 (3.77)     | 44 (2.80)     | 0.097   | 22 (4.82)                           | 34 (7.49)   | 0.094   |
| <b>Systemic reactions, n (%)</b>    |               |               |         |                                     |             |         |
| Headache                            | 861 (33.10)   | 948 (60.42)   | 0.001   | 143 (31.36)                         | 194 (42.73) | 0.001   |
| Fever                               | 617 (23.72)   | 1163 (51.75)  | 0.001   | 103 (22.59)                         | 236 (51.98) | 0.031   |
| Chill                               | 303 (11.65)   | 735 (46.85)   | 0.001   | 46 (10.09)                          | 131 (28.85) | 0.001   |
| Palpitation                         | 193 (7.42)    | 269 (17.14)   | 0.001   | 19 (4.17)                           | 60 (13.22)  | 0.001   |
| Joint pain                          | 735 (28.26)   | 873 (55.64)   | 0.001   | 28 (6.17)                           | 112 (24.56) | 0.001   |
| Muscle pain                         | 1,088 (41.83) | 1,100 (70.11) | 0.001   | 31 (6.83)                           | 162 (35.51) | 0.001   |
| Fatigue                             | 1,358 (52.21) | 1,354 (86.30) | 0.001   | 217 (47.59)                         | 198 (43.61) | 0.229   |
| Impaired concentration              | 367 (14.11)   | 463 (29.51)   | 0.001   | 46 (10.09)                          | 103 (22.69) | 0.001   |
| Insomnia                            | 402 (15.46)   | 430 (27.40)   | 0.001   | 54 (11.84)                          | 43 (9.47)   | 0.247   |
| Dizziness                           | 526 (20.2%)   | 650 (41.4%)   | 0.001   | 62 (13.6%)                          | 249 (54.8%) | 0.001   |
| Diarrhea                            | 164 (6.31)    | 151 (9.62)    | 0.001   | 19 (4.17)                           | 308 (67.84) | 0.001   |
| Abdominal pain                      | 182 (6.99)    | 149 (9.50)    | 0.004   | 14 (3.07)                           | 82 (18.06)  | 0.001   |
| Chest pain                          | 204 (7.84)    | 209 (13.32)   | 0.001   | 20 (4.39)                           | 33 (7.27)   | 0.063   |
| Breathlessness                      | 149 (5.73)    | 53 (9.75)     | 0.001   | 8 (1.75)                            | 18 (3.96)   | 0.045   |
| <b>Allergic reaction, n (%)</b>     |               |               |         |                                     |             |         |
| Rash                                | 75 (2.88)     | 41 (2.61)     | 0.067   | 9 (1.97)                            | 12 (2.64)   | 0.501   |
| Itching                             | 233 (8.96)    | 134 (8.54)    | 0.645   | 33 (7.24)                           | 42 (9.25)   | 0.269   |
| Swollen lips                        | 48 (1.85)     | 32 (2.04)     | 0.658   | 10 (2.19)                           | 8 (1.76)    | 0.654   |

Data are showed as number (percentage). Chi-square test was used to calculate the p-value for the difference between the first dose of BNT162b2 and ChAdOx1 or comparing the first dose of BNT162b2 with the second dose.

\*The people who got the second dose of the vaccine (n = 456) were extracted from the total number of Pfizer-BioNTech vaccinees (n = 2601).

developed more severe post-vaccinal reactions in comparison to females.

In general, ChAdOx1 showed a highly significant increase in the severity and duration of systemic post-vaccinal reactions than

BNT162b2. Meanwhile, the side effects of BNT162b2 after the second dose were more severe than that reported after the first dose of the vaccine. In this respect, our findings agree with other studies that reported similar findings (24, 31, 32).



**TABLE 5 |** Relationship between palpitation and the presence of hypertension, and cardiac disease in the tested subjects.

|                 |     | Palpitation |     | Significance and correlation |
|-----------------|-----|-------------|-----|------------------------------|
|                 |     | No          | Yes |                              |
| HTN             | No  | 3,443       | 441 | $P < 0.97$                   |
|                 | Yes | 265         | 21  | $R = 0.015$                  |
| Cardiac disease | No  | 3,678       | 458 | $P < 0.636$                  |
|                 | Yes | 30          | 4   | $R = 0.007$                  |
| HTN and DM      | No  | 4,220       | 461 | $P < 0.216$                  |
|                 | Yes | 28          | 1   | $R = 0.022$                  |

**TABLE 6 |** Uncommon post-vaccinal adverse effects reported by the participants.

|                          | BNT162b2       |                | ChAdOx1        |
|--------------------------|----------------|----------------|----------------|
|                          | 1st dose N (%) | 2nd dose N (%) | 1st dose N (%) |
| Abnormal menstrual cycle | 18 (0.69)      | 1 (0.22)       | 7 (0.45)       |
| Anxiety                  | 1 (0.04)       | 0 (0.00)       | 1 (0.06)       |
| Depression               | 2 (0.08)       | 0 (0.00)       | 1 (0.06)       |
| Mood disturbance         | 2 (0.08)       | 0 (0.00)       | 1 (0.06)       |
| Numbness of face         | 1 (0.04)       | 0 (0.00)       | 0 (0.00)       |
| Sore throat/dry mouth    | 12 (0.46)      | 3 (0.66)       | 3 (0.19)       |
| Bruises in the leg       | 2 (0.08)       | 0 (0.00)       | 1 (0.06)       |
| Deep venous thrombosis   | 1 (0.04)       | 0 (0.00)       | 0 (0.00)       |
| Hypertension             | 2 (0.08)       | 3 (0.66)       | 0 (0.00)       |
| Pain in testis           | 0 (0.00)       | 1 (0.22)       | 1 (0.06)       |
| Pain in eyes             | 4 (0.15)       | 0 (0.00)       | 2 (0.13)       |
| Blurred vision           | 1 (0.04)       | 0 (0.00)       | 1 (0.06)       |
| Pain in ear              | 1 (0.04)       | 1 (0.22)       | 1 (0.06)       |
| Tinnitus                 | 0 (0.00)       | 0 (0.00)       | 2 (0.13)       |

The most common side effect was local pain after vaccine injection: 80.27% and 85.85% for BNT162b2 and ChAdOx1, respectively. This finding agrees with the data of phase 2/3 clinical trial that reported 88% pain at the site of injection following vaccination with ChAdOx1 (25), in individuals 18–55 of age and it reached >80% in individuals ( $\geq 16$  years old) vaccinated with BNT162b2 (23). Similarly, the detected fatigue, muscle and joint pain following BNT162b2 and ChAdOx1 vaccinations matched what was reported previously (23, 25).

In the USA, many neurological side effects were reported (33, 34). In the current study, signs of transient central nervous system affections ranged from 14.1 to 29.5% of the reported side effects. They included impaired concentration, insomnia, and dizziness. These affections were reported in a significantly higher frequency in ChAdOx1 as compared to BNT162b2. Similarly, their frequencies were higher after the second dose of BNT162b2, in comparison to those after the first dose. Meanwhile, rare solitary neurological signs, including anxiety, depression, sleepiness, mood disturbance, numbness of face, pain in the ear, and tinnitus were also detected in the current study. Our finding agrees with previous reports of

rare reports of tremor, diplopia, dysphonia, seizures, tinnitus, herpes reactivation, facial palsy, transverse myelitis, and acute disseminated encephalomyelitis detected in the USA following COVID-19 vaccination (33, 34).

Palpitation was not previously reported among the side effects of COVID-19 vaccination; however, a case report of postural orthostatic tachycardia syndrome was recently reported following BNT162b2 vaccination (35). Interestingly, in the current study, palpitation was reported with high frequency after COVID-19 vaccination: 7.42% and 17.14% for BNT162b2 and ChAdOx1, respectively. Similarly, the signs were reported more frequently in vaccinees after the second dose (13.22%) in comparison to the first dose (4.17%) for BNT162b2. In addition, chest pain and breathlessness were also reported in this study with ChAdOx1 and to a lower frequency among BNT162b2 vaccinees. In April 2021, the Vaccine Adverse Event Reporting System (VAERS) detected more than 1,000 cases reporting myocarditis and pericarditis following mRNA vaccination (36). Palpitation was also reported in another study in Saudi Arabia in 7(0.4%) subjects following vaccination with ChAdOx1 (30) and in South Korea in 28.3% and 4.3% of ChAdOx1 and NT162b2 vaccinees, respectively (37).

Diarrhea and abdominal pain were recorded in respondents vaccinated with ChAdOx1. The percentages of such side effects were significantly higher than those reported for BNT162b2. The latter showed a higher frequency of complaints after the second dose in comparison to the first dose. A meta-analysis study reported similar side effects for both BNT162b2 and ChAdOx1 (38).

Menstrual disturbance, including excessive hemorrhage and irregular menstrual cycle were reported after the administration of BNT162b2 (643 cases) and ChAdOx1 (315 cases) (39). In contrast, in this study, irregular menstrual cycle was reported in 18 cases vaccinated with BNT162b2 (0.69%) and only 7 cases (0.45%) vaccinated with ChAdOx1. Thrombocytopenia and underlying platelets disorders, or possible hormonal disturbance may explain excessive menstrual bleeding. More investigations are needed to determine the link between COVID-19 vaccination and the menstrual irregularities (40, 41).

## CONCLUSION

In conclusion, both vaccines induce transient side effects that ranged from mild to severe. ChAdOx1 induced more severe side effects than BNT162b2. The latter vaccine induces more severe adverse effects after the second dose of the vaccine. High frequency of palpitation was reported following vaccination. All the reported side effects are tolerable. Women are more prone to developing more severe side effects and for longer durations. Palpitation is among the common systemic side effects that appear following vaccination of both vaccines.

## Limitation of the Study

The results of this questionnaire are self-reported from those receiving the vaccine and not clinically confirmed by physicians

as it may impact result reporting due to differences in interpretation and tolerance thresholds from patient to patient. The study is limited by possible information bias, including misclassification and the duration description of some important manifestations like palpitation and chest pain. The utilization of social media may bias the cohort toward age demographics most familiar with the technology (as evidenced by the high numbers of 20–30-year-olds and a lack of 50+ year old patients) and socioeconomic demographics with routine access to such platforms.

## DATA AVAILABILITY STATEMENT

The original contributions presented in the study are included in the article/supplementary material, further inquiries can be directed to the corresponding author/s.

## REFERENCES

1. Veiga VC, Prats JGG, Farias DLC, Rosa RG, Dourado LK, Zampieri FG, et al. Effect of tocilizumab on clinical outcomes at 15 days in patients with severe or critical coronavirus disease 2019: randomised controlled trial. *BMJ*. (2021) 372:n84–n84. doi: 10.1136/bmj.n84
2. Berlin DA, Gulick RM, Martinez FJ. Severe Covid-19. *N Engl J Med*. (2020) 383:2451–60. doi: 10.1056/NEJMcp2009575
3. Williamson EJ, Walker AJ, Bhaskaran K, Bacon S, Bates C, Morton CE, et al. Factors associated with COVID-19-related death using OpenSAFELY. *Nature*. (2020) 584:430–6. doi: 10.1038/s41586-020-2521-4
4. Wu C, Chen X, Cai Y, Xia J, Zhou X, Xu S, et al. Risk factors associated with acute respiratory distress syndrome and death in patients with coronavirus disease 2019 Pneumonia in Wuhan, China. *JAMA Intern Med*. (2020) 180:934–43. doi: 10.1001/jamainternmed.2020.0994
5. Folegatti PM, Ewer KJ, Aley PK, Angus B, Becker S, Belij-Rammerstorfer S, et al. Safety and immunogenicity of the ChAdOx1 nCoV-19 vaccine against SARS-CoV-2: a preliminary report of a phase 1/2, single-blind, randomised controlled trial. *Lancet*. (2020) 396:467–78. doi: 10.1016/S0140-6736(20)31604-4
6. Alley SJ, Stanton R, Browne M, To QG, Khalesi S, Williams SL, et al. As the pandemic progresses, how does willingness to vaccinate against COVID-19 evolve? *Int J Environ Res Public Health*. (2021) 18:797. doi: 10.3390/ijerph18020797
7. Kim J. COVID-19 vaccines: taking a shot beyond efficacy. In: Söderlund-Venermo M, Varma A, Pujol F, Venter M, Nevels MM, Kuhn R, et al. editors. *The First Meeting of the World Society for Virology | Tackling Global Viral Epidemics*. (2021).
8. WHO. Recommendation of temporary halt of giving the booster dose of COVID-19 vaccine. *Nature*. (2021) 596:317. doi: 10.1038/d41586-021-02219-w
9. CDC. Possible Side Effects After Getting a Covid-19 Vaccine. (2021). Available online at: <https://www.cdc.gov/coronavirus/2019-ncov/vaccines/expect/after.html> (accessed August 6, 2021).
10. Coto-Segura P, Fernández-Prada M, Mir-Bonafé M, García-García B, González-Iglesias I, Alonso-Penanes P, et al. Vesiculous-bullous skin reactions induced by COVID-19 mRNA vaccine: report of four cases and review of the literature. *Clin Exp Dermatol*. (2021). doi: 10.1111/ced.14835. [Epub ahead of print].
11. Catalá A, Muñoz-Santos C, Galván-Casas C, Roncero Riesco M, Revilla Nebreda D, Solá-Truyols A, et al. Cutaneous reactions after SARS-CoV-2 vaccination: A cross-sectional Spanish nationwide study of 405 cases. *Br J Dermatol*. (2021). doi: 10.1111/bjd.20639. [Epub ahead of print].
12. Marcantonio-Santa Cruz O, Vidal-Navarro A, Pesqué D, Giménez-Arnau AM, Pujol RM, Martín-Ezquerro G. Pityriasis rosea developing after COVID-19 vaccination. *J Eur Acad Dermatol Venereol*. (2021). doi: 10.1111/jdv.17498. [Epub ahead of print].
13. Psychogiou M, Samarkos M, Mikos N, Hatzakis A. Reactivation of varicella zoster virus after vaccination for SARS-CoV-2. *Vaccines*. (2021) 9:572. doi: 10.3390/vaccines9060572
14. Lebedev L, Sapojnikov M, Wechsler A, Varadi-Levi R, Zamir D, Tobar A, et al. Minimal change disease following the Pfizer-BioNTech COVID-19 vaccine. *Am J Kidney Dis*. (2021) 78:142–5. doi: 10.1053/j.ajkd.2021.03.010
15. Cari L, Fiore P, Naghavi Alhosseini M, Sava G, Nocentini G. Blood clots and bleeding events following BNT162b2 and ChAdOx1 nCoV-19 vaccine: An analysis of European data. *J Autoimmun*. (2021) 122:102685. doi: 10.1016/j.jaut.2021.102685
16. Greinacher A, Thiele T, Warkentin TE, Weisser K, Kyrle PA, Eichinger S. Thrombotic thrombocytopenia after ChAdOx1 nCov-19 vaccination. *N Engl J Med*. (2021) 384:2092–101. doi: 10.1056/NEJMoa2104840
17. WHO. WHO Statement on AstraZeneca COVID-19 Vaccine Safety Signals. (2021). Available online at: <https://www.who.int/news/item/17-03-2021-who-statement-on-astrazeneca-covid-19-vaccine-safety-signals> (accessed March 17, 2021).
18. Turner PJ, Ansotegui IJ, Campbell DE, Cardona V, Ebisawa M, El-Gamal Y, et al. COVID-19 vaccine-associated anaphylaxis: A statement of the World Allergy Organization Anaphylaxis Committee. *World Allergy Organ J*. (2021) 14:100517. doi: 10.1016/j.waojou.2021.100517
19. Banerji A, Wickner PG, Saff R, Stone CA, Robinson LB. mRNA vaccines to prevent COVID-19 disease and reported allergic reactions: current evidence and suggested approach. *J Allergy Clin Immunol Pract*. (2021) 9:1423–37. doi: 10.1016/j.jaip.2020.12.047
20. Swan DA, Bracis C, Janes H, Moore M, Matrajt L, Reeves DB, et al. COVID-19 vaccines that reduce symptoms but do not block infection need higher coverage and faster rollout to achieve population impact. *Sci Rep*. (2021) 11:15531. doi: 10.1038/s41598-021-94719-y
21. Šimundić AM. Measures of diagnostic accuracy: basic definitions. *EJIFCC*. (2009) 19:203–11.
22. Mandrekar JN. Receiver operating characteristic curve in diagnostic test assessment. *J Thorac Oncol*. (2010) 5:1315–6. doi: 10.1097/JTO.0b013e3181ec173d
23. Polack FP, Thomas SJ, Kitchin N, Absalon J, Gurtman A, Lockhart S, et al. Safety and efficacy of the BNT162b2 mRNA Covid-19 vaccine. *N Engl J Med*. (2020) 383:2603–15. doi: 10.1056/NEJMoa2034577
24. Menni C, Klaser K, May A, Polidori L, Capdevila J, Louca P, et al. Vaccine side-effects and SARS-CoV-2 infection after vaccination in users of the COVID

## ETHICS STATEMENT

The studies involving human participants were reviewed and approved by Taif University Ethical Committee with approval No. 42-169 on 3/05/2021.

## AUTHOR CONTRIBUTIONS

ASA, ANA, MA, and DA collected, curated, analyzed the data, and wrote the first draft of the manuscript. AA-M conceptualized the study, verified the results, and critically revise the manuscript. All authors reviewed and edited revisions of the manuscript.

## FUNDING

This work was funded by Taif University Deanship of Scientific Research (Project No. 1-441-41).

- symptom study app in the UK: a prospective observational study. *Lancet*. (2021) 21:939–49. doi: 10.1016/S1473-3099(21)00224-3
25. Ramasamy MN, Minassian AM, Ewer KJ, Flaxman AL, Folegatti PM, Owens DR, et al. Safety and immunogenicity of ChAdOx1 nCoV-19 vaccine administered in a prime-boost regimen in young and old adults (COV002): a single-blind, randomised, controlled, phase 2/3 trial. *Lancet*. (2021) 396:1979–93. doi: 10.1016/S0140-6736(20)32466-1
  26. O'Brien KL, Finlay DK. Immunometabolism and natural killer cell responses. *Nat Rev Immunol*. (2019) 19:282–90. doi: 10.1038/s41577-019-0139-2
  27. Berbudi A, Rahmadika N, Tjahjadi AI, Ruslami R. Type 2 diabetes and its impact on the immune system. *Curr Diabetes Rev*. (2020) 16:442–9. doi: 10.2174/1573399815666191024085838
  28. Tissot N, Brunel AS, Bozon F, Rosolen B, Chirouze C, Bouillier K. Patients with history of covid-19 had more side effects after the first dose of covid-19 vaccine. *Vaccine*. (2021) 39:5087–90. doi: 10.1016/j.vaccine.2021.07.047
  29. Izumo T, Kuse N, Awano N, Tone M, Sakamoto K, Takada K, et al. Side effects and antibody titer transition of the BNT162b2 messenger ribonucleic acid coronavirus disease 2019 vaccine in Japan. *Respir Investig*. (2021) 59:635–42. doi: 10.1016/j.resinv.2021.06.003
  30. Albahrani S, Albarra KA, Alghamdi OA, Abdullah Alghamdi M, Hakami FH, Abaadi AKA, et al. Safety and reactogenicity of the ChAdOx1 (AZD1222) COVID-19 vaccine in vaccinees in Saudi Arabia. *Int J Infect Dis*. (2021) 110:359–62. doi: 10.1016/j.ijid.2021.07.052
  31. Alhazmi A, Alamer E, Daws D, Hakami M, Darraj M, Abdelwahab S, et al. Evaluation of side effects associated with COVID-19 vaccines in Saudi Arabia. *Vaccines*. (2021) 9:674. doi: 10.3390/vaccines9060674
  32. Andrzejczak-Grzadko S, Czudy Z, Donderska M. Side effects after COVID-19 vaccinations among residents of Poland. *Eur Rev Med Pharmacol Sci*. (2021) 25:4418–21. doi: 10.26355/eurrev\_202106\_26153
  33. Gee J. First month of COVID-19 vaccine safety monitoring-United States, December 14, 2020-January 13, 2021. *MMWR Morb Mortal Wkly Rep*. (2021) 70:7008e3. doi: 10.15585/mmwr.mm7008e3
  34. Goss AL, Samudralwar RD, Das RR, Nath A. ANA investigates: neurological complications of COVID-19 vaccines. *Ann Neurol*. (2021) 89:856. doi: 10.1002/ana.26065
  35. Reddy S, Reddy S, Arora M. A case of postural orthostatic tachycardia syndrome secondary to the messenger RNA COVID-19 vaccine. *Cureus*. (2021) 13:e14837. doi: 10.7759/cureus.14837
  36. CDC. *Myocarditis and Pericarditis Following mRNA COVID-19 Vaccination*. (2021). Available online at: <https://www.cdc.gov/coronavirus/2019-ncov/vaccines/safety/myocarditis.html> (accessed September 8, 2021).
  37. Bae S, Lee YW, Lim SY, Lee JH, Lim JS, Lee S, et al. Adverse reactions following the first dose of ChAdOx1 nCoV-19 vaccine and BNT162b2 vaccine for healthcare workers in South Korea. *J Korean Med Sci*. (2021) 36:e115. doi: 10.3346/jkms.2021.36.e115
  38. Pormohammad A, Zarei M, Ghorbani S, Mohammadi M, Razizadeh MH, Turner DL, et al. Efficacy and safety of COVID-19 vaccines: a systematic review and meta-analysis of randomized clinical trials. *Vaccines*. (2021) 9:467. doi: 10.3390/vaccines9050467
  39. Merchant H. CoViD-19 post-vaccine menorrhagia, metrorrhagia or postmenopausal bleeding and potential risk of vaccine-induced thrombocytopenia in women. *BMJ*. (2021) 373:n958. doi: 10.1136/bmj.n958
  40. Akiyama H, Kakiuchi S, Rikitake J, Matsuba H, Sekinada D, Kozuki Y, et al. Immune thrombocytopenia associated with Pfizer-BioNTech's BNT162b2 mRNA COVID-19 vaccine. *IDCases*. (2021) 25:e01245. doi: 10.1016/j.idcr.2021.e01245
  41. Razzaq AK, Al-Jasim A. Oxford-AstraZeneca coronavirus disease-2019 vaccine-induced immune thrombocytopenia on day two. *Case Rep Hematol*. (2021) 2021:2580832. doi: 10.1155/2021/2580832

**Conflict of Interest:** The authors declare that the research was conducted in the absence of any commercial or financial relationships that could be construed as a potential conflict of interest.

**Publisher's Note:** All claims expressed in this article are solely those of the authors and do not necessarily represent those of their affiliated organizations, or those of the publisher, the editors and the reviewers. Any product that may be evaluated in this article, or claim that may be made by its manufacturer, is not guaranteed or endorsed by the publisher.

Copyright © 2021 Alghamdi, Alotaibi, Alqahtani, Al Aboud and Abdel-Moneim. This is an open-access article distributed under the terms of the Creative Commons Attribution License (CC BY). The use, distribution or reproduction in other forums is permitted, provided the original author(s) and the copyright owner(s) are credited and that the original publication in this journal is cited, in accordance with accepted academic practice. No use, distribution or reproduction is permitted which does not comply with these terms.



# Changes in Incidence of Notifiable Infectious Diseases in China Under the Prevention and Control Measures of COVID-19

Bizhen Chen<sup>1,2†</sup>, Meiling Wang<sup>1,3†</sup>, Xun Huang<sup>4</sup>, Maokun Xie<sup>1</sup>, Liting Pan<sup>3</sup>, Huiwen Liu<sup>3</sup>, Zhenguo Liu<sup>2\*</sup> and Pengcheng Zhou<sup>2,4\*</sup>

<sup>1</sup> Department of Healthcare-Associated Infection Management, The Second Affiliated Hospital of Fujian University of Traditional Chinese Medicine, Fuzhou, China, <sup>2</sup> Department of Infectious Diseases/Infection Control Center, The Third Xiangya Hospital of Central South University, Changsha, China, <sup>3</sup> School of Nursing, Fujian University of Traditional Chinese Medicine, Fuzhou, China, <sup>4</sup> Infection Control Center, Xiangya Hospital of Central South University, Changsha, China

## OPEN ACCESS

### Edited by:

Atefeh Abedini,  
Shahid Beheshti University of Medical  
Sciences, Iran

### Reviewed by:

Rano Mal Pirani,  
Liaquat University of Medical and  
Health Sciences, Pakistan  
Wen-Qiang He,  
University of New South  
Wales, Australia

### \*Correspondence:

Pengcheng Zhou  
xypcz@csu.edu.cn  
Zhenguo Liu  
liuzhenguo@csu.edu.cn

<sup>†</sup> These authors have contributed  
equally to this work and share first  
authorship

### Specialty section:

This article was submitted to  
Infectious Diseases – Surveillance,  
Prevention and Treatment,  
a section of the journal  
Frontiers in Public Health

**Received:** 22 June 2021

**Accepted:** 21 September 2021

**Published:** 15 October 2021

### Citation:

Chen B, Wang M, Huang X, Xie M,  
Pan L, Liu H, Liu Z and Zhou P (2021)  
Changes in Incidence of Notifiable  
Infectious Diseases in China Under the  
Prevention and Control Measures of  
COVID-19.  
Front. Public Health 9:728768.  
doi: 10.3389/fpubh.2021.728768

**Aim:** The aim of this study was to analyze the changes in incidence of notifiable infectious diseases in China under the prevention and control measures of COVID-19.

**Methods:** Using descriptive epidemiological methods, data were collected from the official website of the Health Commission of the People's Republic of China, and the prevalence characteristics of notifiable infectious diseases in the country in 2020 were analyzed and compared with the historical data in 2019. Monthly reporting data on influenza and tuberculosis from 2015 to 2019 were also collected.

**Results:** Except for COVID-19, the total number of notifiable infectious diseases cases in 2020 was 6,366,176, a decrease of 41.38% year-on-year compared with 2019. Category B and C notifiable infectious diseases decreased by 14.84 and 54.98% year-on-year, respectively ( $P < 0.01$ ). The top three incidence rates were influenza (87.63 cases/100,000), hepatitis B (81.36 cases/100,000) and other infectious diarrhea (76.33 cases/100,000). Three types of diseases with the largest decline were influenza (−2,280,502 cases), hand-foot-mouth disease (−1,174,588 cases), and other infectious diarrhea diseases (−275,746 cases). Compared with 2019, respiratory infectious diseases were reported to be in the largest decline in 2020, followed by intestinal infectious diseases, blood-borne and sexually transmitted diseases, natural foci, and insect-borne infectious diseases. The monthly reported incidences of influenza and tuberculosis in 2020 were lower than the average of the previous 5 years.

**Conclusion:** In 2020, the incidence of most notifiable infectious diseases in China showed a downward trend, non-pharmaceutical interventions (NPIs) such as the wearing of masks, frequent hand-washing, more ventilation, less gathering, etc, played a positive role in the prevention and control of respiratory and intestinal infectious diseases. The various public health intervention strategies and measures adopted by China to contain COVID-19 can provide a reference for the prevention and control of infectious diseases in other countries.

**Keywords:** COVID-19, notifiable infectious diseases, public health interventions, incidence, disease transmission



## INTRODUCTION

Since the end of 2019, the Coronavirus disease 2019 (COVID-19) epidemic has swept the world (1). Countries around the world have adopted different protective measures, and the situation and evolution of the epidemic differ from country to country (2). To contain COVID-19 in China, local governments responded quickly. Under various powerful prevention and control measures, the epidemic spread in China was basically controlled in just over 2 months. The prevention and control was a huge success (3). The white paper “Fighting COVID-19: China in Action (4)” divides China’s anti-COVID-19 process and measures into five stages, as shown in **Figure 1**. Under the ongoing prevention and control phase, the situation of COVID-19 in China is generally stable and controllable, with sporadic cases in some regions.

China has a vast territory and a large population. Except COVID-19, other major infectious diseases are among the top in the world. For example, there are more than 100 million hepatitis B and C virus infected people in China (5); the number of new cases of tuberculosis ranks the third in the world (6), which seriously affects public health, social and economic development and even national security. The spread of other infectious diseases cannot be ignored in the context of COVID-19. Studies have shown that these NPIs for COVID-19 may also reduce the incidence of respiratory infectious diseases such as influenza (7), as well as the number of other infectious diseases reported. Similar reports have been reported in the United States (8) and Germany (9). However, the long-term or short-term benefits of COVID-19 preventive and control interventions for other infectious diseases in China are still unclear, and there are still no studies based on national annual data.

Understanding the impact of the COVID-19 pandemic and related prevention and control measures on the incidence of other infectious diseases is of great significance for China’s public health and infectious disease supervision. Therefore, this study collected the reported incidence data of all notifiable infectious diseases in China before and after the COVID-19 epidemic, and discussed the incidence trends of other notifiable infectious diseases under the epidemic prevention and control measures, so as to provide reference basis for further infectious disease surveillance, prevention and control work.

## MATERIALS AND METHODS

### Data Collection

In this study, the incidence data of notifiable infectious diseases were obtained from the official website of the National Health Commission of the People’s Republic of China (<http://www.nhc.gov.cn/>). The notifiable infectious diseases refer to the infectious diseases reported in accordance with the law stipulated in the “Law of the People’s Republic of China on prevention and control of infectious diseases” (10), including a total of 40 infectious diseases in categories A, B, and C. In 2004, China established an infectious disease network reporting system, which realized the case, real-time, online reporting. This system covers in towns and townships and above all the medical and

health institutions, by clinical doctors to complete fill in the diagnosis of infectious diseases and infectious diseases reporting card, and then be transcribed and reported by a specialist from the Public Health Department or the Preventive Health Department. Statistics on the incidence and death of notifiable infectious diseases will be published on the website of the National Health Commission every month. The population data were obtained from China Statistical Yearbook 2020 (11). There are no ethical issues involved in this study, the data is publicly available and accessible in accordance with the law. We obtained the monthly reported incidence data of all notifiable infectious diseases in 2019 and 2020, and the incidence of influenza and tuberculosis monthly reported in 2015–2020.

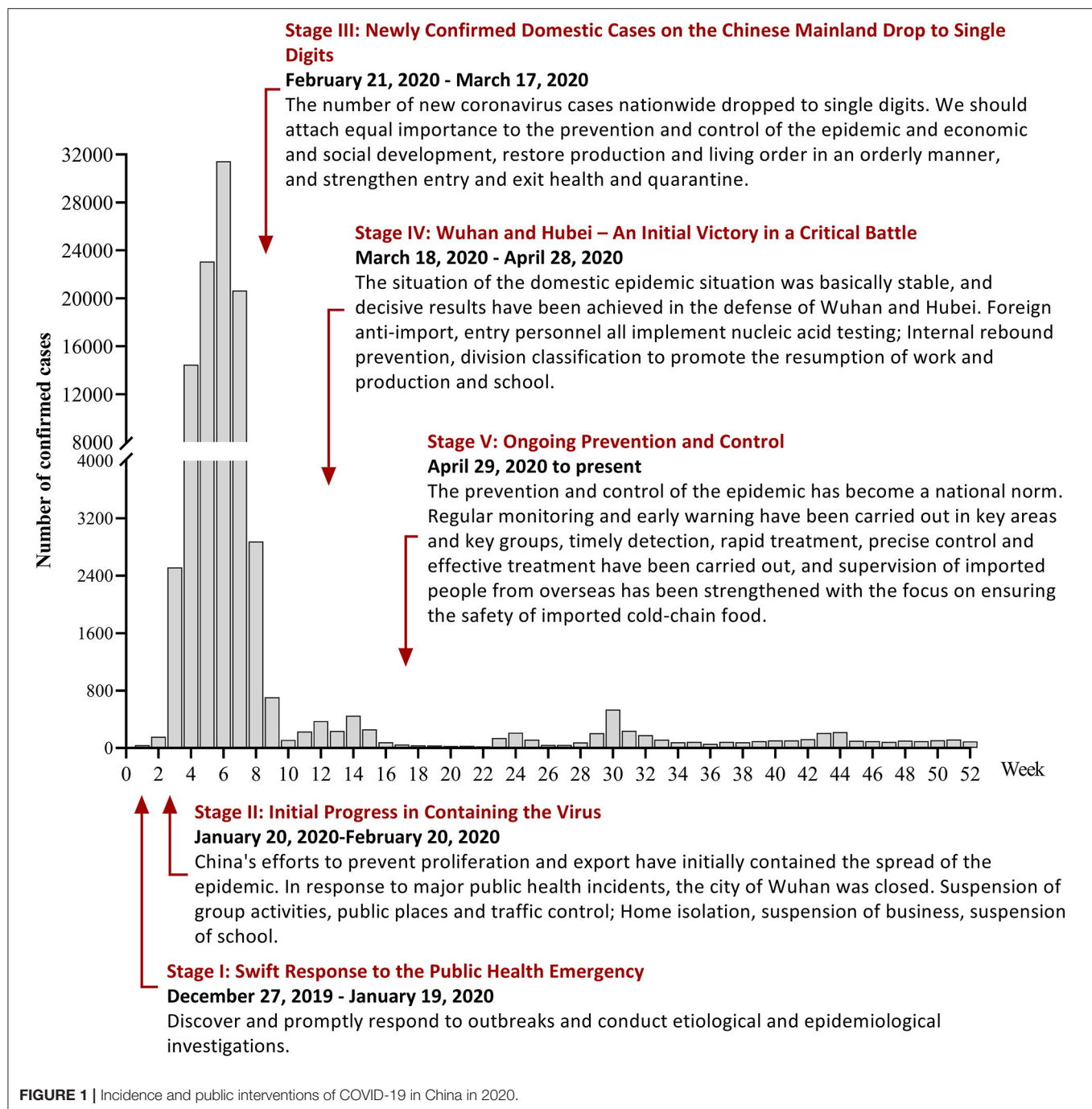
### Statistical Analysis

Excel 2016 was used for data summary processing, Graphpad Prism 9.0 was used for chart drawing, and SPSS 26.0 was used for data analysis. Using descriptive epidemiological survey method, the incidence (per 100,000) as the number of reported cases divided by the population size. The incidence differences of all notifiable infectious diseases in 2019 and 2020 were compared. The monthly reported data with normal distribution using the *t*-test, otherwise using the rank-sum test, and the annual total incidence and monthly increase rates and 95%CI were calculated. According to the transmission route, the notifiable infectious diseases were divided into respiratory infectious diseases, intestinal infectious diseases, blood and sexually transmitted diseases, natural foci and vector borne diseases, and several common ones in China were selected for specific analysis. Chi-squared test for trend was used to describe and judge the trend of diseases. The threshold for statistical significance was set at  $P < 0.05$ .

## RESULTS

### Overview of the Incidence of Notifiable Infectious Diseases in China in 2020

In addition to COVID-19, a total of 6,366,176 cases of notifiable infectious diseases were reported nationwide in 2020, the total incidence rate was 454.71 cases/100,000. The highest incidence infectious disease was influenza (87.63 cases/100,000), followed by hepatitis B (81.36 cases/100,000), and then other infectious diarrhea (76.33 cases/100,000). The three diseases accounted for 53.95% of all the diseases. Compared with the same period in 2019, except the brucellosis, leptospirosis and kala-azar, other notifiable infectious diseases in 2020 decreased to varying degrees, with a year-on-year decrease of 41.38% in total, and category B and category C infectious diseases decreased by 14.84 and 54.98%, respectively, with statistical significance ( $P < 0.01$ ). Dengue fever, rubella, and whooping cough experienced the greatest decrease in incidence. Influenza, hand-foot-mouth disease (HFMD) and other infectious diarrhea diseases had the largest decrease in reported cases (see attached **Table 1** for details).



## Incidence Trends of Common Notifiable Infectious Diseases

We found that there are differences in the incidence of infectious diseases in different transmission routes. Compared with the same period in 2019, the prevalence of respiratory infectious diseases in China has changed most obviously in 2020. As shown in **Figure 2**, except for the increase in influenza in January, the monthly reported incidence of other common respiratory infectious diseases was seen to decrease significantly, with the

largest decline from April to May. Although the overall growth of tuberculosis was negative, the decline was not significant compared with that of other respiratory infectious diseases.

As we can see in **Figure 3**, In 2020, the incidence of influenza peaked in early January, decreased sharply in February, reached the lowest level in April, and remained at a relatively low level; The monthly variation curve of tuberculosis epidemic is similar to that in previous years, the number of cases decreased significantly in February and gradually recovered from March

**TABLE 1 |** Incidence of notifiable infectious diseases nationwide in 2019 and 2020.

| Category   | Number of reported cases | Number of reported cases | Increase cases | Incidence rate (/ 100,000) | Incidence rate (/ 100,000) | Increase rate (95% CI)     | t/z-value | P      |
|--|--------------------------|--------------------------|----------------|----------------------------|----------------------------|----------------------------|-----------|--------|
|  | 2019                     | 2020                     |                | 2019                       | 2020                       |                            |           |        |
| Category A infectious diseases                         | 21                       | 15                       | /              | /                          | /                          | /                          | /         | /      |
| Plague   | 5                        | 4                        | /              | /                          | /                          | /                          | /         | /      |
| Cholera  | 16                       | 11                       | /              | /                          | /                          | /                          | /         | /      |
| Category B infectious diseases (Except COVID-19)       | 3,679,089                | 3,133,258                | -545,831       | 263.66                     | 223.80                     | -14.84% (-14.88 to -14.80) | -3.349*   | 0.001  |
| SARS   | 0                        | 0                        | /              | /                          | /                          | /                          | /         | /      |
| AIDS   | 72,630                   | 63,154                   | -9,476         | 5.21                       | 4.51                       | -13.05% (-13.30 to -12.81) | -1.559*   | 0.119  |
| HAV  | 20,005                   | 15,481                   | -4,524         | 1.43                       | 1.11                       | -22.61% (-23.19 to -22.04) | 3.901     | 0.001  |
| HBV  | 1,247,092                | 1,139,133                | -107,959       | 89.37                      | 81.36                      | -8.66% (-8.71 to -8.61)    | -1.963*   | 0.0496 |
| HCV  | 260,704                  | 229,204                  | -31,500        | 18.68                      | 16.37                      | -12.08% (-12.21 to -11.96) | -2.512*   | 0.012  |
| HDV  | 411                      | 217                      | -194           | 0.03                       | 0.02                       | -47.20% (-52.03 to -42.42) | 6.522     | 0.000  |
| HEV  | 29,126                   | 19,709                   | -9,417         | 2.09                       | 1.41                       | -32.33% (-32.87 to -31.80) | -4.157*   | 0.000  |
| Unclassified hepatitis                                 | 14,411                   | 9,382                    | -5,029         | 1.03                       | 0.67                       | -34.90% (-35.68 to -34.13) | -4.157*   | 0.000  |
| Poliomyelitis  | 0                        | 0                        | /              | /                          | /                          | /                          | /         | /      |
| Human infection with highly pathogenic avian influenza | 0                        | 0                        | /              | /                          | /                          | /                          | /         | /      |
| Measles  | 3,573                    | 1,234                    | -2,339         | 0.26                       | 0.09                       | -65.46% (-67.00 to -63.89) | -3.985*   | 0.000  |
| Epidemic hemorrhagic fever                             | 10,117                   | 8,546                    | -1,571         | 0.73                       | 0.61                       | -15.53% (-16.25 to -14.84) | -1.501*   | 0.133  |
| Rabies   | 312                      | 212                      | -100           | 0.02                       | 0.02                       | -32.05% (-37.42 to -27.12) | 3.334     | 0.003  |
| Japanese encephalitis                                  | 463                      | 312                      | -151           | 0.03                       | 0.02                       | -32.61% (-37.01 to -28.50) | -0.665*   | 0.506  |
| Dengue fever   | 22,317                   | 802                      | -21,515        | 1.60                       | 0.06                       | -96.41% (-96.65 to -96.16) | -3.465*   | 0.001  |
| Anthrax  | 320                      | 232                      | -88            | 0.02                       | 0.02                       | -27.50% (-32.64 to -22.90) | -1.070*   | 0.285  |
| Bacterial and amoebic dysentery                        | 81,781                   | 58,299                   | -23,482        | 5.86                       | 4.16                       | -28.71% (-29.02 to -28.40) | 1.900     | 0.071  |
| Tuberculosis   | 1,034,760                | 876,576                  | -158,184       | 74.16                      | 62.61                      | -15.29% (-15.36 to -15.22) | 2.827     | 0.010  |
| Typhoid and paratyphoid                                | 9,787                    | 7,321                    | -2,466         | 0.70                       | 0.52                       | -25.20% (-26.07 to -24.35) | 2.497     | 0.021  |
| Epidemic cerebrospinal meningitis                      | 124                      | 57                       | /              | /                          | /                          | /                          | /         | /      |
| Whooping cough   | 30,727                   | 4,994                    | -25,733        | 2.20                       | 0.36                       | -83.75% (-84.16 to -83.33) | -4.157*   | 0.000  |
| Diphtheria   | 0                        | 2                        | /              | /                          | /                          | /                          | /         | /      |
| Neonatal tetanus                                       | 67                       | 36                       | /              | /                          | /                          | /                          | /         | /      |
| Scarlet fever  | 83,028                   | 17,206                   | -65,822        | 5.95                       | 1.23                       | -79.28% (-79.55 to -79.00) | -3.695*   | 0.000  |
| Brucellosis  | 46,700                   | 50,115                   | 3,415          | 3.35                       | 3.58                       | 7.31% (7.08 to 7.55)       | -0.486    | 0.632  |
| Gonorrhea  | 120,146                  | 106,592                  | -13,554        | 8.61                       | 7.61                       | -11.28% (-11.46 to -11.10) | -0.346*   | 0.729  |
| Syphilis   | 587,402                  | 522,920                  | -64,482        | 42.10                      | 37.35                      | -10.98% (-11.06 to -10.90) | -2.656*   | 0.008  |
| Leptospirosis  | 226                      | 315                      | 89             | 0.02                       | 0.02                       | 39.38% (33.24 to 45.88)    | -0.145*   | 0.885  |
| Schistosomiasis  | 224                      | 67                       | /              | /                          | /                          | /                          | /         | /      |
| Malaria  | 2,635                    | 1,140                    | -1,495         | 0.19                       | 0.08                       | -56.74% (-58.62 to -54.84) | -3.465*   | 0.001  |
| Human infection with H7N9 bird flu                     | 1                        | 0                        | /              | /                          | /                          | /                          | /         | /      |

(Continued)

TABLE 1 | Continued

| Category                             | Number of reported cases | Number of reported cases | Increase cases | Incidence rate (/ 100,000) | Incidence rate (/ 100,000) | Increase rate (95% CI)     | t/z-value | P     |
|--------------------------------------|--------------------------|--------------------------|----------------|----------------------------|----------------------------|----------------------------|-----------|-------|
|                                      | 2019                     | 2020                     |                | 2019                       | 2020                       |                            |           |       |
| COVID-19                             | /                        | 86,746                   | /              | /                          | /                          | /                          | /         | /     |
| Category C infectious diseases       | 7,181,455                | 3,232,903                | -3,948,552     | 514.66                     | 230.91                     | -54.98% (-55.02 to -54.94) | -3.406*   | 0.001 |
| Influenza                            | 3,507,306                | 1,226,804                | -2,280,502     | 251.35                     | 87.63                      | -65.02% (-65.07 to -64.97) | -3.349*   | 0.001 |
| Mumps                                | 303,105                  | 130,911                  | -17,2194       | 21.72                      | 9.35                       | -56.81% (-56.99 to -56.63) | 5.968     | 0.000 |
| Rubella                              | 34,151                   | 2,839                    | -31,312        | 2.45                       | 0.20                       | -91.69% (-91.98 to -91.39) | -3.811*   | 0.000 |
| Acute hemorrhagic conjunctivitis     | 41,701                   | 28,633                   | -13,068        | 2.99                       | 2.05                       | -31.34% (-31.79 to -30.90) | 3.777     | 0.002 |
| Leprosy                              | 531                      | 449                      | -82            | 0.04                       | 0.03                       | -15.44% (-18.76 to -12.62) | 1.328     | 0.198 |
| Typhus                               | 1,201                    | 1,199                    | -2             | 0.09                       | 0.09                       | -0.17% (-0.61 to -0.05)    | 0.008     | 0.993 |
| Kala-azar                            | 178                      | 231                      | 53             | 0.01                       | 0.02                       | 29.78% (23.55 to 36.87)    | -1.876    | 0.074 |
| Echinococcosis                       | 4,850                    | 3,739                    | -1,111         | 0.35                       | 0.27                       | -22.91% (-24.11 to -21.75) | 2.836     | 0.010 |
| Filariasis                           | 0                        | 0                        | /              | /                          | /                          | /                          | /         | /     |
| Other infectious diarrhoeal diseases | 1,344,396                | 106,8650                 | -275,746       | 96.35                      | 76.33                      | -20.51% (-20.58 to -20.44) | 2.563     | 0.018 |
| HFMD                                 | 1,944,036                | 769,448                  | -1,174,588     | 139.32                     | 54.96                      | -60.42% (-60.49 to -60.35) | -2.367*   | 0.018 |
| Total (excluding COVID-19)           | 10,860,565               | 6,366,176                | -449,4389      | 778.32                     | 454.71                     | -41.38% (-41.41 to -41.35) | -3.522*   | 0.000 |

No comparison was made for diseases with reported numbers of  $\leq 100$  cases. The total number of reported cases is the sum of the monthly number of reported cases; \* is rank sum test, others are t-test (HFMD, Hand-Foot-Mouth Disease; HAV, Hepatitis A; HBV, Hepatitis B; HCV, Hepatitis C; HDV, Hepatitis D; HEV, Hepatitis E; SARS, Severe Acute Respiratory Syndrome; AIDS, Acquired Immune Deficiency Syndrome).

to April. The incidence trend of influenza and tuberculosis in 2020 were lower than the average from the last 5 years ( $P$  for trend  $< 0.000$ ).

In 2020, the incidence of four common intestinal infectious diseases, hepatitis A, hepatitis E, bacterial amoebic dysentery, and other infectious diarrhea diseases, decreased substantially. Although the decrease was not significant compared with several common respiratory infectious diseases, the incidence was still lower than that of the same period in 2019. The incidence of HFMD fluctuated the most, decreasing first and then increasing. The number of reported monthly incidences from March to June dropped by more than 95% year-on-year, and from October to December it was higher than the same period in 2019 (Figure 4).

Compared with 2019, the monthly incidence of several common blood-borne and sexually transmitted diseases in China in 2020 was still on a downward trend for the most part, with a relatively obvious decline in February 2020 and then a fluctuating recovery. Since June, the incidence of AIDS, gonorrhea and syphilis was even higher than that of the same period in 2019 (Figure 5).

Compared with the same period in 2019, the incidence rate of dengue fever and malaria decreased significantly in 2020. Dengue fever cases have dropped by more than 95% since April. The overall incidence of brucellosis was higher than that in

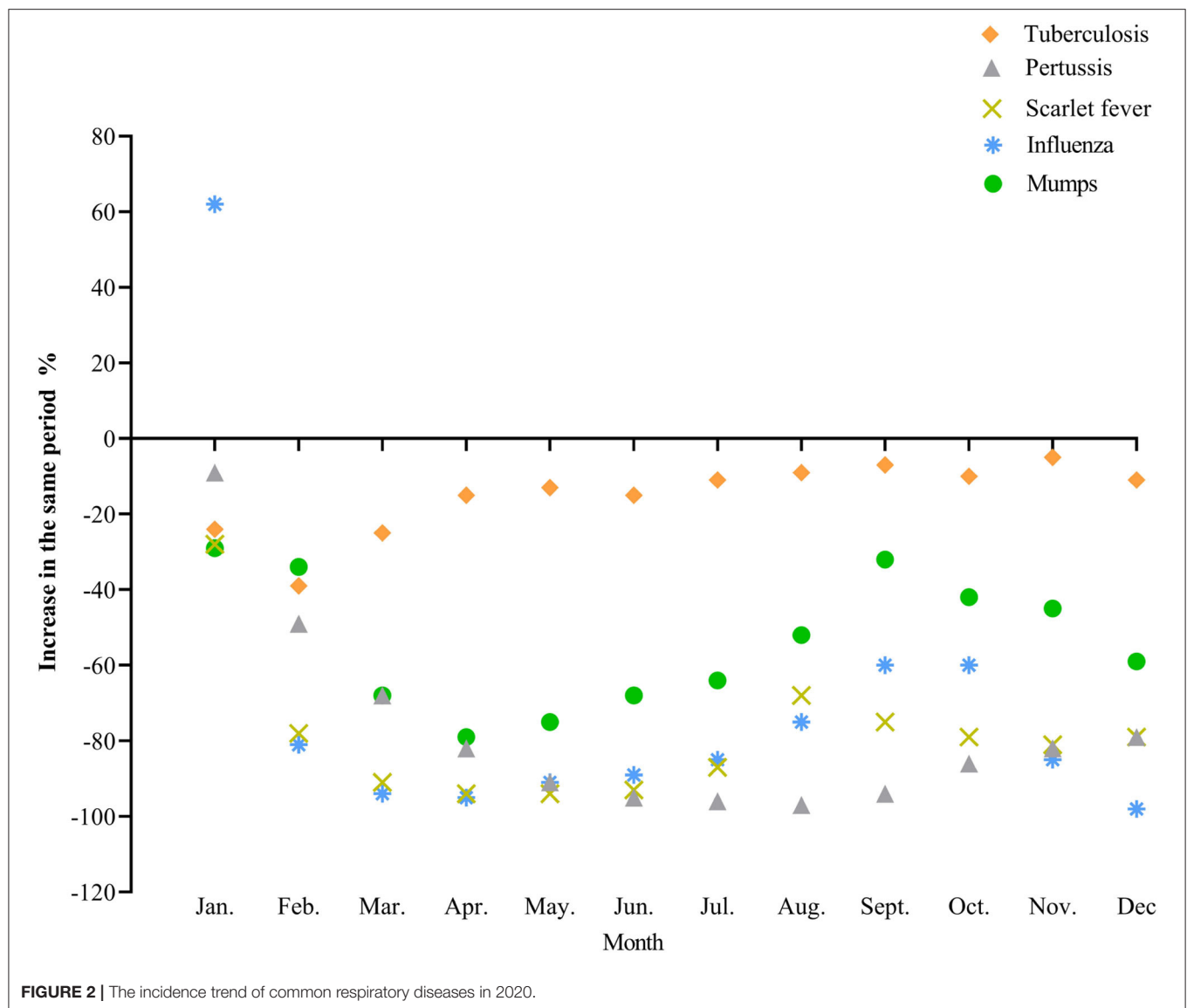
2019 (Figure 6). The incidence data of all the above diseases are detailed in the **Supplementary Materials**.

## DISCUSSION

In generally, compared with 2019 the total incidence of categories A, B, and C notifiable infectious diseases in China in 2020 showed a decreasing trend ( $P < 0.05$ ), suggesting that the COVID-19 prevention and control measures may have a good prevention effect on most other infectious diseases, and the risk of spread of infectious diseases is reduced.

Under COVID-19 prevention and control measures, the prevalence of respiratory infectious diseases in China has changed most obviously, and the decline incidence is closely related to the prevention and control measures at different stages. At the end of January 2020, China launched an emergency response to the epidemic and fully implemented prevention and control measures. Personal protective measures such as wearing masks, hand hygiene and social distancing have effectively prevented the spread of respiratory infections through droplets and aerosols. Measures such as school closures, home quarantine, transportation restrictions, and public place closures have significantly reduced population movement, reducing the probability of exposure to the virus and the risk of cross-infection among susceptible people (12, 13). The survey showed that

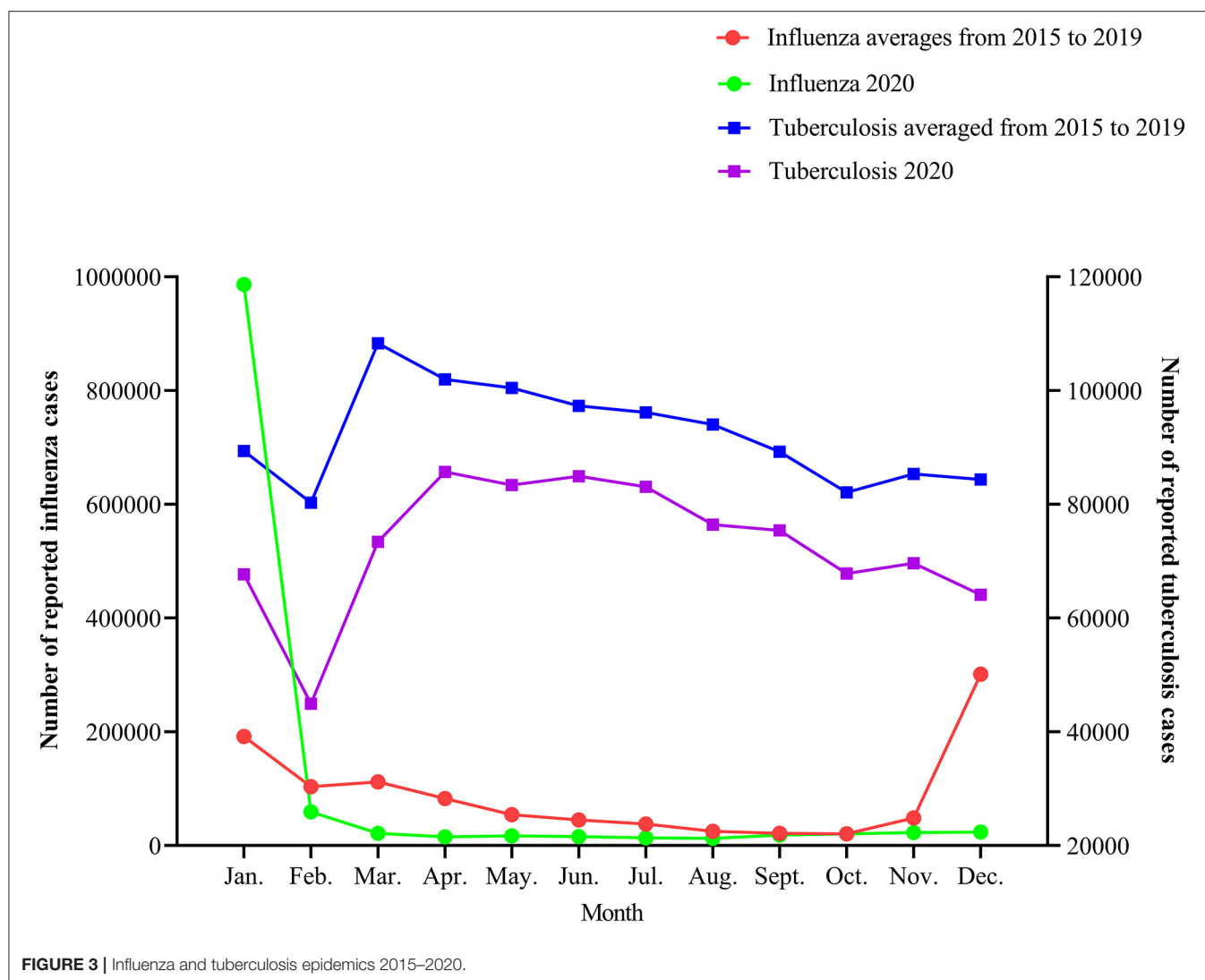




during the Spring Festival travel rush in 2020, the passenger flow of China's railways, highways, waterways, and aviation dropped by more than 50% year-on-year compared with 2018 and 2019 (14). At the same time, the closure of small and medium-sized medical institutions, public panic and heightened awareness of risk prevention may lead to a gradual decrease in the number of medical treatments, some mild patients were covered up (15), and the reporting rate of infectious diseases decreased. Every year, the period from March to May is the peak of pertussis, measles, and other respiratory infectious diseases. However, in 2020, this peak did not appear and the number of cases decreased, or even a trough period. At the end of April, the epidemic entered the stage of normal prevention and control. With the steady progress of the resumption of work, production, schools, and the resumption of normal production and living order, the incidence of common respiratory infectious diseases began to slowly and

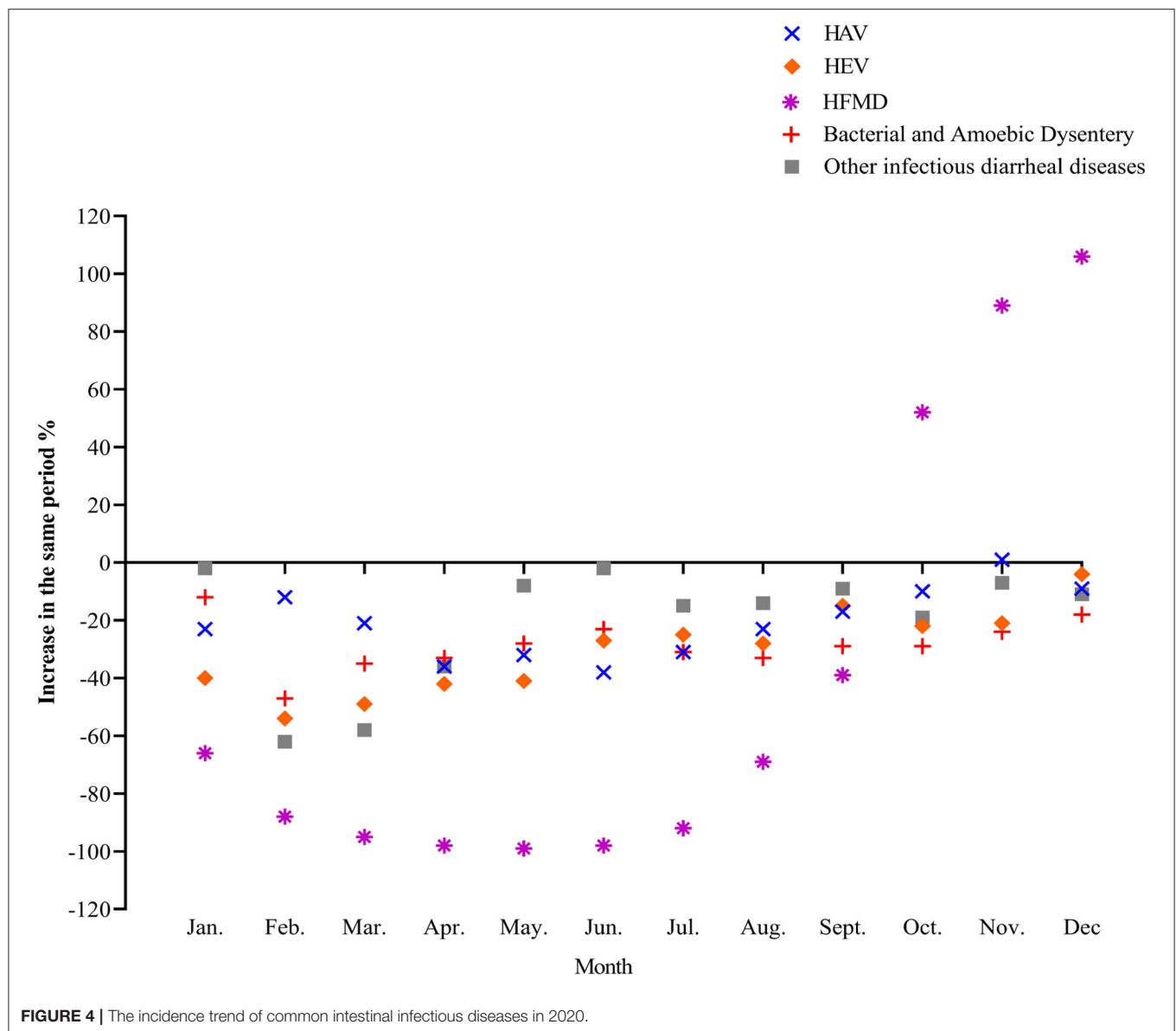
modestly recover, with the decline decreasing, but still lower than that of the same period in 2019.

The results of this study showed that the prevalence trends of influenza and tuberculosis in 2020 were significantly lower than the average of the previous 5 years ( $P < 0.05$ ). Influenza is the most common infectious disease in China. In recent 10 years, the incidence of seasonal influenza in China has been increasing year by year. In January 2020, the winter peak of influenza in China coincided with the outbreak of COVID-19. The large number of influenza reported in January may be the result of changes in its natural epidemic trend, while the sharp drop in February may be due to COVID-19 containment measures limiting the spread of influenza. Public data from the National Influenza Center of China shows that from the 5th week of 2020 (January 27, 2020 to February 02, 2020), the total testing number and the positive rate of influenza



decreased significantly. In the 7th week (from February 10, 2020 to February 16, 2020) the positive rate of influenza was significantly lower than that in 2016–2019 (16). The high-incidence period of influenza in China in 2020 ended ahead of schedule. We can see that even in the second half of the year, the COVID-19 epidemic has entered the normalized prevention and control stage, the reporting and testing of influenza have resumed and is even stricter than previously required, the incidence of influenza is still lower than that of the same period in the previous 5 years, indicating that the incidence of influenza has indeed declined. Although the response time and epidemic prevention measures of various countries and regions to COVID-19 were different, as well as slightly different epidemic trends of influenza, studies in Taiwan, Hong Kong, the United States, South Korea, and Europe have also obtained similar results. Overall, the seasonal duration of influenza was shortened under COVID-19 prevention and control, and the influenza positive rate declined rapidly within 7–12 weeks of 2020 (17–20).

Pulmonary tuberculosis has a delitescence onset and has no specificity the incubation period. The period is generally long, and the diseases can occur with in a few months to 1 year (or even over a longer time). People are generally susceptible to the disease. Compared with COVID-19, although it is also a respiratory disease, tuberculosis is mainly concentrated in close contacts in small areas, so the management of infection source is the key to controlling the spread of tuberculosis. As suggested in this study, a series of COVID-19 control measures might reduce the community transmission of tuberculosis. However, China has a large base of tuberculosis patients, high drug resistance rate, unsatisfactory therapeutic effect, and low cure rate (21). During the outbreak period, the closure of many medical institutions and emergency clinics, the suspension of admission of tuberculosis patients in some designated tuberculosis hospitals, the decrease in the number of tuberculosis screening patients, and the delay or interruption of treatment of tuberculosis patients may increase the risk of potential tuberculosis infection and the probability of chronic transmission. Therefore, the prevention

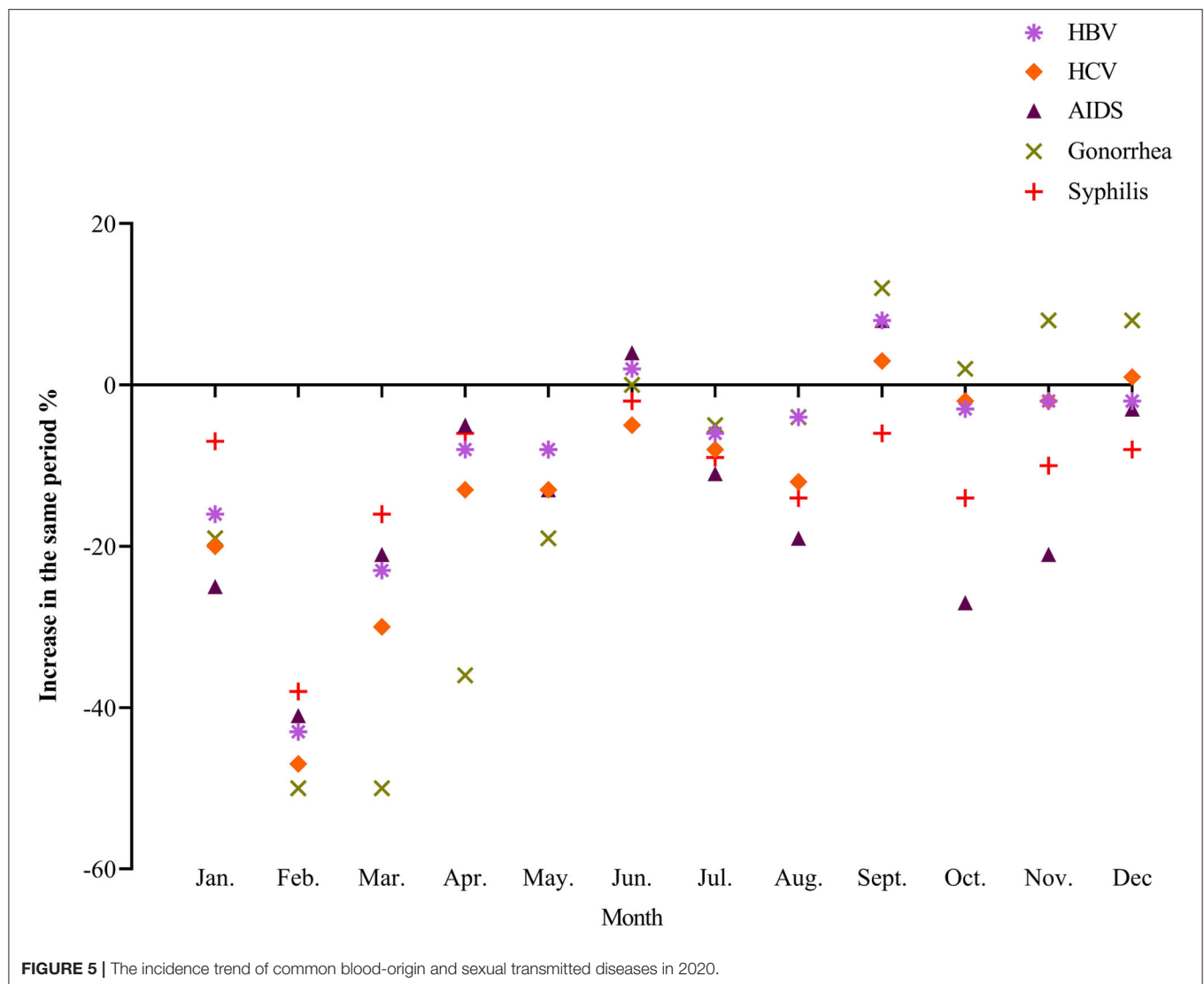


and control effect of the COVID-19 epidemic on tuberculosis and the epidemic trend still require more detailed long-term evaluations (22).

The results of this study showed that the incidence of common intestinal infectious diseases in China in 2020 were lower than that in the same period in 2019, among which there were statistically significant differences in the incidence of hepatitis A, hepatitis E, HFMD, and other infectious diarrhea ( $P < 0.05$ ). It shows that the NPIs for COVID-19, such as continuous monitoring of epidemic information, standardized operation of food and entertainment, national conscious epidemic prevention mechanism, related knowledge and health education, may played a certain role in the prevention and control of intestinal infectious diseases. The incidence of HFMD fluctuates greatly, the sharp drop in the number of cases in the first half of the year could

be related to protective measures such as post-ponement of school, home isolation and travel restrictions. At the same time, these measures can also conducive to preventing other children's susceptible diseases such as mumps (23). HFMD frequently occurs in autumn and winter, and the school starts in the second half of the year, the population was dense. Infants and children have low immunity, lack of ability to develop healthy behaviors, and poor implementation of hand hygiene and other protective measures, which can easily causes the spread of diseases and increase the incidence (24).

During the COVID-19 outbreak in February 2020, the incidence of blood-borne, and sexually transmitted diseases decreased rapidly. Some strict epidemic control measures like prohibiting gatherings and closing hotels, KTV, and other dangerous places resulted in a decrease in people's social

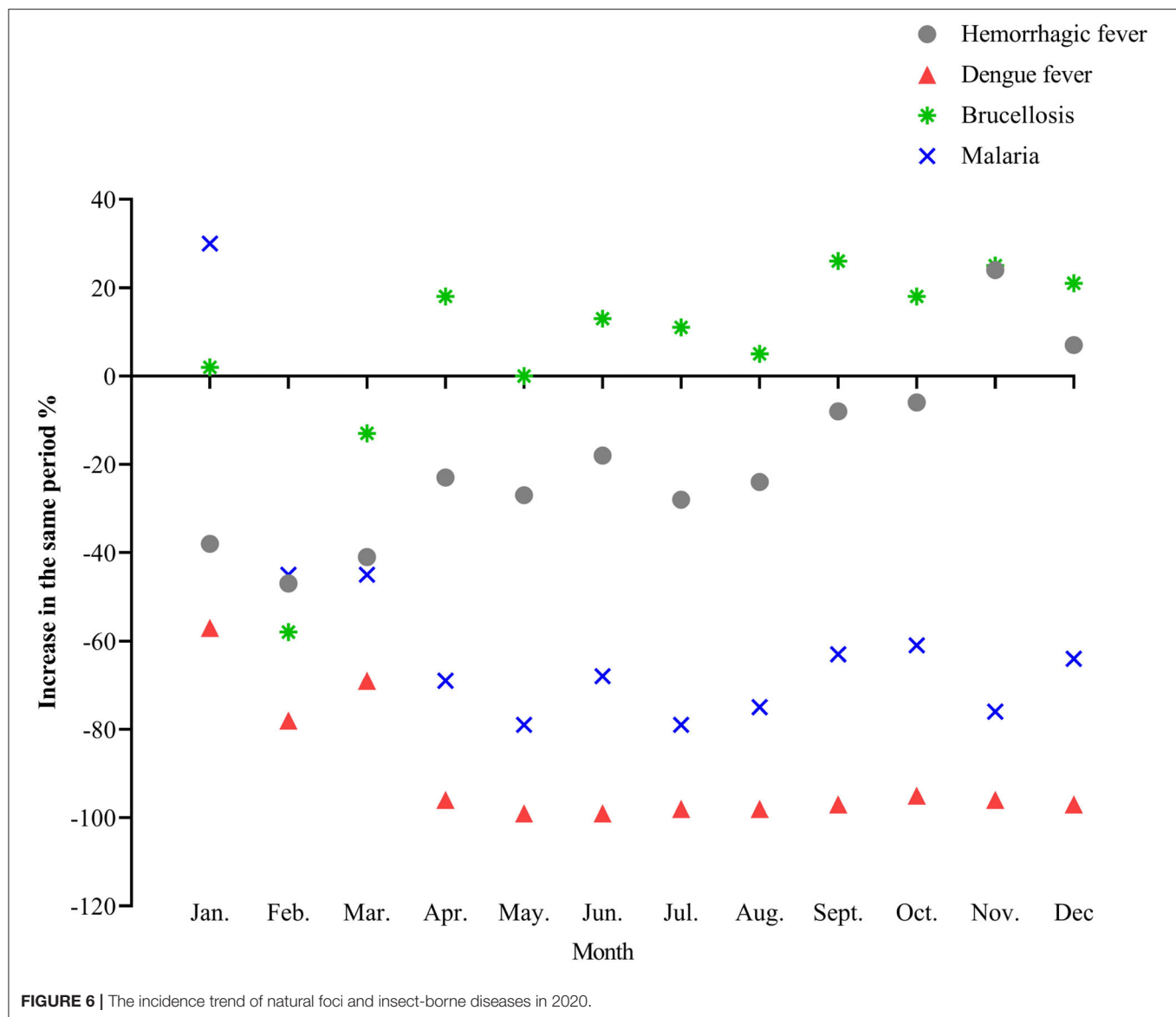


activities, and a significant decrease in high-risk groups such as whoring, men who have sex with men, migrant workers, drug users, and sexually transmitted diseases patients (25), which could directly affect the spread of related blood sources and sexually transmitted diseases. When entering the stage of normal prevention and control, the incidence of some blood-borne and sexually transmitted diseases, such as AIDS, syphilis, and gonorrhea, was even higher than the same period in 2019. At the same time, there was little change in the incidence of hepatitis B in the past 2 years ( $P > 0.05$ ), suggesting that the incidence of blood-borne and sexually transmitted diseases under the normal epidemic prevention and control has been impacted to some extent, although the change in its epidemic trend is not obvious (26, 27). In the future, it will still be necessary to strengthen the monitoring of key high-risk groups, restrict drug abuse, dangerous sex, and other high-risk activities, strengthen publicity and education, improve the public's self-protection

awareness, and further search for more effective prevention and control strategies.

The incidence of natural foci and insect-borne infectious diseases varies greatly with the different stages. In 2020, the incidence of dengue fever decreased significantly compared with the same period in 2019, and the monthly decrease since April was more than 95%, which may be related to the global outbreak of dengue fever in 2019 and the surge of dengue epidemic cases in many places in China (28). China has strengthened control over people living abroad following the COVID-19 outbreak, which also limited the spread of imported diseases such as dengue fever and malaria. At the same time, the country forbids the consumption of live wild animals, and people's awareness of protection is enhanced, which also reduces the possibility of cross-border transmission of infectious diseases to a certain extent (29). The year-on-year increase in the incidence of brucellosis was related to the "Lanzhou Event" in China in





2020, which led to the outbreak of brucellosis, the increase in detection quantity, and the increase in the number of reported cases (30). Other natural foci and insect-borne diseases have a relatively small number of people, are diverse and complex, and have a certain degree of occasionality. The current NPIs for COVID-19 have no clear impact on natural foci and insect-borne infectious diseases. In the future, we should pay more attention to the incidence trend of these diseases, early monitoring and early warning, adopt comprehensive prevention and control strategies, and take measures according to local conditions and time conditions to prevent and control its occurrence and development.

Scientific and reasonable epidemic prevention measures not only seem to reduce the incidence of infectious diseases and maintain public health, but also promote the recovery and

development of social economy to a certain extent. In the early days of the COVID-19 outbreak, social production was disrupted, and cities such as Wuhan were temporarily shut down. However, China's rapid response strategy has effectively controlled the spread of COVID-19 and reversed the trend of economic decline. In the post-epidemic period, China paid equal attention to the resumption of work and production and epidemic prevention and control, effectively balancing epidemic control and economic recovery (31, 32). Up to now, China has maintained a very low level of COVID-19 transmission. At the same time, China became the only major economy in the world with positive growth in 2020. It is suggested that taking such prevention and control measures to control infectious diseases is of great value for social and economic development. These experiences are worth learning from all over the world.

## LIMITATION

There are some limitations in this study. First, the epidemic of infectious disease is affected by multiple factors, it is difficult to obtain data on the interaction between vaccination and population immunity, seasonal and climate change, travel and human mobility, and virus variation. Second, the case data in this study came from passive monitoring reports of various places, which may lead to data bias due to missing reports, and the actual incidence may be underestimated. At present, it cannot be concluded that there is a direct causal relationship between the prevention and control measures of COVID-19 at different stages and the decrease of the incidence of related diseases. We cannot fully explain this by the monthly reported incidence data alone, and a decrease in the reported data, while revealing some issues, does not necessarily mean changes in the true prevalence and incidence. We can only interpret and analyze the possible influencing factors currently available. However, these strict non-pharmaceutical prevention and control measures may be a useful supplement to the prevention and control of related respiratory and intestinal infectious diseases. In the next steps, we will continue to strengthen surveillance and comprehensively assess the long-term impact of COVID-19 prevention and control measures on other notifiable infectious diseases.

## CONCLUSION

In conclusion, under the COVID-19 prevention and control measures, the changes in incidence of notifiable infectious diseases in China generally showed a downward trend, among which, respiratory infectious diseases showed the most obvious decline. Public health interventions such as frequent hand

washing, wearing masks, cough etiquette, and social distance provide certain references for the prevention and control of other infectious diseases in the future.

## DATA AVAILABILITY STATEMENT

The original contributions presented in the study are included in the article/**Supplementary Material**, further inquiries can be directed to the corresponding authors.

## AUTHOR CONTRIBUTIONS

BC, ZL, and PZ: design the study. MW, MX, LP, and HL: contribute to data acquisition. MW and LP: contribute to data analysis. BC and MW: write the manuscript. BC, MW, XH, and PZ: revise the manuscript. All authors contributed to manuscript revision, read, and approved the submitted version.

## FUNDING

This work was supported by the Science Popularization Project of Innovative Province Construction in Hunan (grant no: 2021ZK4198) and the Central South University COVID-19 Prevention and Control Emergency Project (grant no: 160260003).

## SUPPLEMENTARY MATERIAL

The Supplementary Material for this article can be found online at: <https://www.frontiersin.org/articles/10.3389/fpubh.2021.728768/full#supplementary-material>

## REFERENCES

- Mallah SI, Ghorab OK, Al-Salmi S, Abdellatif OS, Tharmaratnam T, Iskandar MA, et al. COVID-19: breaking down a global health crisis. *Ann Clin Microbiol Antimicrob.* (2021) 20:35. doi: 10.1186/s12941-021-00438-7
- Antunes BBP, Peres IT, Baião FA, Ranzani OT, Bastos LDSL, Silva AABD, et al. Progression of confirmed COVID-19 cases after the implementation of control measures. *Rev Bras Ter Intensiva.* (2020) 32:213–23. doi: 10.5935/0103-507X.20200028
- Liu W, Guan WJ, Zhong NS. Strategies and advances in combating COVID-19 in China. *Engineering (Beijing).* (2020) 6:1076–84. doi: 10.1016/j.eng.2020.10.003
- The State Council Information Office of the People's Republic of China. *China's Action Against COVID-19 Epidemic.* (2020). Available online at : [http://www.gov.cn/zhengce/2020-06/07/content\\_5517737.htm](http://www.gov.cn/zhengce/2020-06/07/content_5517737.htm) (accessed Jan 17, 2021).
- Zhang M, Wu R, Xu H, Uhanova J, Gish R, Wen X, et al. Changing incidence of reported viral hepatitis in China from 2004 to 2016: an observational study. *BMJ Open.* (2019) 9:e028248. doi: 10.1136/bmjopen-2018-028248
- Gao J, Liu Y. Key points of the 2019 WHO global tuberculosis report. *Int J Respir.* (2020) 40:161–6. doi: 10.3760/cma.j.issn.1673-436X.2020.03.001
- Dadras O, Alinaghi SAS, Karimi A, MohsseniPour M, Barzegary M, Vahedi F, et al. Effects of COVID-19 prevention procedures on other common infections: a systematic review. *Eur J Med Res.* (2021) 26:67. doi: 10.1186/s40001-021-00539-1
- Crane MA, Popovic A, Panaparambil R, Stolbach AI, Romley JA, Ghanem KG, et al. Reporting of infectious diseases in the united states during the COVID-19 pandemic. *Clin Infect Dis.* (2021) ciab529. <https://doi.org/10.1093/cid/ciab529>
- Ullrich A, Schranz M, Rexroth U, Hamouda O, Schaade L, Diercke M, et al. Impact of the COVID-19 pandemic and associated non-pharmaceutical interventions on other notifiable infectious diseases in Germany: an analysis of national surveillance data during week1-2016-week 32-2020. *Lancet Reg Health Eur.* (2021) 6:100103. doi: 10.1016/j.lanepe.2021.100103
- The National People's Congress of the People's Republic of China. *Law of the People's Republic of China on the Prevention and Treatment of Infectious Diseases.* (2020). Available online at: <http://www.npc.gov.cn/npc/c238/202001/099a493d03774811b058f0f0ece38078.shtml> (accessed Jan 17, 2021).
- National Bureau of Statistics. *China Statistical Yearbook-2020.* (2020). Available online at: <http://www.stats.gov.cn/tjsj/ndsj/2020/indexch.htm> (accessed Jan 17, 2021).
- Stefanoff P, Løvlie AL, Elstrøm P, Macdonald EA. Reporting of notifiable infectious diseases during the COVID-19 response. *Tidsskr Nor Lægeforen.* (2020) 140:9. doi: 10.4045/tidsskr.20.0334
- Steffen R, Lautenschlager S, Fehr J. Travel restrictions and lockdown during the COVID-19 pandemic-impact on notified infectious diseases in Switzerland. *J Travel Med.* (2020) 27:taaa180. doi: 10.1093/jtm/taaa180
- Ministry of Transport of the People's Republic of China. Available online at: [https://www.mot.gov.cn/zhuanti/2020chunyun\\_ZT/tupianbaodao](https://www.mot.gov.cn/zhuanti/2020chunyun_ZT/tupianbaodao) (accessed Sep 01, 2021).

15. Geng YM, Li G, Zhang LL. The Impact of COVID-19 interventions on influenza and mycobacterium tuberculosis infection. *Front Public Health*. (2021) 9:672568. doi: 10.3389/fpubh.2021.672568
16. Chinese National Influenza Center. *Influenza Weekly Report*. (2020). Available online at: <http://www.chinaivdc.cn/cnic/zyzx/lgzbl/>, 2020 (accessed Sep 01, 2021).
17. Chan CP, Wong NS, Leung CC, Lee SS. Positive impact of measures against COVID-19 on reducing influenza in the Northern Hemisphere. *J Travel Med*. (2020) 27:taaa087. doi: 10.1093/jtm/taaa087
18. Lee H, Lee H, Song KH, Kim ES, Park JS, Jung J, et al. Impact of public health interventions on seasonal influenza activity during the SARS-CoV-2 outbreak in Korea. *Clin Infect Dis*. (2020) 73:e132–40. doi: 10.1093/cid/ciaa672
19. Huang QS, Wood T, Jelley L, Jennings T, Jefferies S, Daniells K, et al. Impact of the COVID-19 non-pharmaceutical interventions on influenza and other respiratory viral infections in New Zealand. *Nat Commun*. (2021) 12:1001. doi: 10.1038/s41467-021-21157-9
20. Kim JH, Roh YH, Ahn JG, Kim MY, Huh K, Jung J, et al. Respiratory syncytial virus and influenza epidemics disappearance in Korea during the 2020–2021 season of COVID-19. *Int J Infect Dis*. (2021) 110:29–35. doi: 10.1016/j.ijid.2021.07.005
21. Jiang H, Liu M, Zhang Y, Yin J, Li Z, Zhu C, et al. Changes in incidence and epidemiological characteristics of pulmonary tuberculosis in Mainland China, 2005–2016. *JAMA Netw Open*. (2021) 4:e215302. doi: 10.1001/jamanetworkopen.2021.5302
22. Owolabi OA, Jallow AO, Jallow M, Sowe G, Jallow R, Genekah MD, et al. Delay in the diagnosis of pulmonary tuberculosis in the Gambia, West Africa: a cross-sectional study. *Int J Infect Dis*. (2020) 101:102–6. doi: 10.1016/j.ijid.2020.09.029
23. Viner RM, Russell SJ, Croker H, Packer J, Ward J, Stansfield C, et al. School closure and management practices during coronavirus outbreaks including COVID-19: a rapid systematic review. *Lancet Child Adolesc Health*. (2020) 4:397–404. doi: 10.1016/S2352-4642(20)30095-X
24. Niu Y, Luo L, Rui J, Yang S, Deng B, Zhao Z, et al. Control measures during the COVID-19 outbreak reduced the transmission of hand, foot, and mouth disease. *J Saf Sci Resilience*. (2021) 2:63–8. doi: 10.1016/j.jnlssr.2021.06.002
25. de Miguel Buckley R, Trigo E, de la Calle-Prieto F, Arsuaga M, Díaz-Menéndez M. Social distancing to combat COVID-19 led to a marked decrease in food-borne infections and sexually transmitted diseases in Spain. *J Travel Med*. (2020) 27:taaa134. doi: 10.1093/jtm/taaa134
26. Chen FF, Tang HL, Lu F. Research progress of the impact of COVID-19 outbreak on people living with HIV. *Chin J Epidemiol*. (2020) 41:1980–4. doi: 10.3760/cma.j.cn112338-20200603-00803
27. Chia C, Chao C, Lai C. Diagnoses of syphilis and HIV infection during the COVID-19 pandemic in Taiwan. *Sex Transm Infect*. (2021) 97:319. doi: 10.1136/sextrans-2020-054802
28. Yue Y, Liu X, Ren D, Wu H, Liu Q. Spatial dynamics of dengue fever in Mainland China, 2019. *Int J Environ Res Public Health*. (2021) 18:2855. doi: 10.3390/ijerph18062855
29. Zhu J, Zhang Q, Jia C, Xu S, Lei J, Chen J, et al. Challenges caused by imported cases abroad for the prevention and control of COVID-19 in China. *Front Med*. (2021) 8:573726. doi: 10.3389/fmed.2021.573726
30. Lanzhou Health Commission. *Lanzhou Actively Dealt With a Recessive Infection of Clustered Brucellosis*. (2019). Available online at: [http://wjw.lanzhou.gov.cn/art/2019/12/6/art\\_4476\\_833332.html](http://wjw.lanzhou.gov.cn/art/2019/12/6/art_4476_833332.html) (accessed Jan 17, 2021)
31. Wang Z, Jin Y, Jin X, Lu Y, Yu X, Li L, et al. Preliminary assessment of chinese strategy in controlling reemergent local outbreak of COVID-19. *Front Public Health*. (2021) 9:650672. doi: 10.3389/fpubh.2021.650672
32. Wang Q, Zhang F. What does the China's economic recovery after COVID-19 pandemic mean for the economic growth and energy consumption of other countries? *J Clean Prod*. (2021) 295:126265. doi: 10.1016/j.jclepro.2021.126265

**Conflict of Interest:** The authors declare that the research was conducted in the absence of any commercial or financial relationships that could be construed as a potential conflict of interest.

**Publisher's Note:** All claims expressed in this article are solely those of the authors and do not necessarily represent those of their affiliated organizations, or those of the publisher, the editors and the reviewers. Any product that may be evaluated in this article, or claim that may be made by its manufacturer, is not guaranteed or endorsed by the publisher.

Copyright © 2021 Chen, Wang, Huang, Xie, Pan, Liu, Liu and Zhou. This is an open-access article distributed under the terms of the Creative Commons Attribution License (CC BY). The use, distribution or reproduction in other forums is permitted, provided the original author(s) and the copyright owner(s) are credited and that the original publication in this journal is cited, in accordance with accepted academic practice. No use, distribution or reproduction is permitted which does not comply with these terms.



# Longer Prehospitalization and Preintubation Periods in Intubated Non-survivors and ECMO Patients With COVID-19: A Systematic Review and Meta-Analysis

Kenji Funakoshi<sup>1</sup>, Takayoshi Morita<sup>1\*</sup> and Atsushi Kumanogoh<sup>1,2,3,4</sup>

<sup>1</sup> Department of Respiratory Medicine and Clinical Immunology, Graduate School of Medicine, Osaka University, Suita, Japan,

<sup>2</sup> Department of Immunopathology, WPI, Immunology Frontier Research Center (IFReC), Osaka University, Suita, Japan,

<sup>3</sup> Integrated Frontier Research for Medical Science Division, Institute for Open and Transdisciplinary Research Initiatives (OTRI), Osaka University, Suita, Japan, <sup>4</sup> Center for Infectious Diseases for Education and Research (CiDER), Osaka University, Suita, Japan

## OPEN ACCESS

### Edited by:

Reza Lashgari,  
Shahid Beheshti University, Iran

### Reviewed by:

Shivank Singh,  
Southern Medical University, China  
Heidi J. Dalton,  
Inova Health System, United States

### \*Correspondence:

Takayoshi Morita  
t-morita@imed3.med.osaka-u.ac.jp

### Specialty section:

This article was submitted to  
Infectious Diseases - Surveillance,  
Prevention and Treatment,  
a section of the journal  
Frontiers in Medicine

**Received:** 18 June 2021

**Accepted:** 20 September 2021

**Published:** 15 October 2021

### Citation:

Funakoshi K, Morita T and  
Kumanogoh A (2021) Longer  
Prehospitalization and Preintubation  
Periods in Intubated Non-survivors  
and ECMO Patients With COVID-19:  
A Systematic Review and  
Meta-Analysis. *Front. Med.* 8:727101.  
doi: 10.3389/fmed.2021.727101

**Purpose:** There is no clear consensus on the clinical course of critical COVID-19 patients. We examined the clinical course among intubated survivors, non-survivors, and extracorporeal membrane oxygenation (ECMO) patients to reveal the standard clinical course and the difference among critical COVID-19 patients.

**Methods:** In this systematic review and meta-analysis, we searched PubMed, Web of Science, and Scopus for original studies published until December 11, 2020, including case accumulation and clinical course reporting. Pregnant patients and children were excluded. We followed PRISMA guidelines and registered them with PROSPERO (CRD42021235534).

**Results:** Of the 11,716 studies identified, 94 met the selection criteria, and 2,549 cases were included in this meta-analysis. The times from intubation to extubation and death were 12.07 days (95% confidence interval 9.80–14.33 days) and 10.14 days (8.18–12.10 days), respectively, and the ECMO duration was 14.72 days (10.57–18.87 days). The time from symptom onset to hospitalization (prehospitalization period) of intubated survivors, non-survivors, and ECMO patients was 6.15 (4.61–7.69 days), 6.45 (4.55–8.34 days), and 7.15 days (6.48–7.81 days), and that from symptom onset to intubation (preintubation period) was 8.58 (7.36–9.80 days), 9.14 (7.26–11.01 days), and 10.54 days (9.18–11.90 days), respectively. Sensitivity analysis showed that the time from intubation to extubation and death was longer in the US and Europe than in East Asia.

**Conclusion:** For COVID-19, we hypothesize that prehospitalization and preintubation periods are longer in intubated non-survivors and ECMO patients than in intubated survivors. These periods may serve as a predictor of disease severity or death and support therapeutic strategy determination.

**Keywords:** COVID-19, clinical course, invasive mechanical ventilation, extracorporeal membrane oxygenation, meta-analysis



## INTRODUCTION

Coronavirus disease 2019 (COVID-19) is a pandemic caused by severe acute respiratory syndrome coronavirus 2 (SARS-CoV-2) and was first reported in Wuhan, China, in December 2019 (1). As of August 2021, COVID-19 had spread to 223 countries, areas, or territories, and the global cumulative case numbers have reached 197 million. Over 4.2 million COVID-19 patients have died since the start of the pandemic (2), even though every government has taken aggressive preventive measures such as lockdown (3), universal masking (4), and social distancing (4). The hospitalization rate of COVID-19 is reportedly 14% (almost 10 times higher than influenza) (5–7). Moreover, up to 26.1% of hospitalized COVID-19 patients are admitted to the intensive care unit (ICU) (8). Therefore, COVID-19 has placed an unprecedented burden on the ICU, and in some regions, ICU capacity exceeds 100% with only COVID-19 patients because of the astonishing number, high rate of ICU admission, and long clinical course (9). Furthermore, 71–88% of COVID-19 patients in the ICU need intubation (2.45–4.01 times higher than influenza) (10–14), and 3–27.2% of intubated COVID-19 patients require ECMO (10, 15). Overall, the high occupancy rate of hospital beds and ICUs by COVID-19 patients is a serious problem worldwide.

The clinical course of patients with severe COVID-19 from symptom onset to clinical events is highly informative when considering prognosis, therapeutic strategy, ICU bed management, and medical economy. Nevertheless, comparing each patient's clinical course with the standard clinical course of COVID-19 is difficult because there is no consensus to date regarding the standard clinical course. For example, the duration of intubation has been reported to be 10–16 days (16, 17), yet both the patients' backgrounds and regions where the studies were conducted differed in these reports. Moreover, known risk factors for COVID-19 mortality include age (18), sex (19), comorbidities (19), and blood counts (absolute lymphocyte number and CRP) (20); however, few articles have assessed differences in the clinical course between intubated survivors, non-survivors, and ECMO patients.

In this study, we conducted a systematic review and meta-analysis of the clinical course, i.e., time (days) from symptom onset, hospitalization, intubation, and ECMO initiation to each

clinical event in critical COVID-19 patients. We also assessed the difference in the clinical course between intubated survivors, non-survivors, and ECMO patients with COVID-19 to reveal whether the clinical course is a prognostic factor. Finally, we conducted sensitivity analysis to assess factors (patient background and region) that may influence the time from intubation to extubation or death.

## METHODS

### Search Strategy and Selection Criteria

This meta-analysis was performed following the Preferred Reporting Items for Systematic Reviews and Meta-analyses (PRISMA) statement (**Supplementary Table 1**) (21). This study searched for articles documenting the clinical course in critical COVID-19 patients: the time (days) from symptom onset to hospitalization (prehospitalization period) to intubation (preintubation period) and to ECMO initiation (pre-ECMO period); the time from hospitalization to intubation (hospitalization-intubation period) and to ECMO initiation (hospitalization-ECMO period), discharge (hospitalization-discharge period), and death (hospitalization-death period); the time from hospitalization to death (hospitalization-death period); the time from intubation to extubation (intubation period), to ECMO (intubation-ECMO period), and to death (intubation-death period); and the time from ECMO initiation to decannulation (ECMO period) and to death (ECMO-death period). Three sources, namely, PubMed, Web of Science, and Scopus, were searched [(COVID-19) OR (SARS-CoV-2) AND (intensive care unit) OR (acute respiratory distress syndrome) OR (mechanical ventilation) OR (extracorporeal membrane oxygenation)], with no language restriction. The searches were performed to identify articles published until December 11th, 2020, when the SARS-CoV-2 vaccine was first approved in the world, including “online first” articles, published until December 11, 2020, when the SARS-CoV-2 vaccine was first approved. The last searches were performed on June 26, 2021.

The inclusion criteria were studies of human subjects, case accumulations, a title or abstract consisting of the clinical course of intubated survivors, non-survivors, and/or ECMO patients with COVID-19, and a link from the search site to the full text (PDF or website) of the article. In this study, “survivors” referred to extubated patients who had not died during the study period. This study excluded studies involving children (under 18 years old) and pregnant women and non-English articles; a case report was also excluded because properly calculating the average value and standard deviation (SD) was difficult. Redundancies between the search sites were eliminated, i.e., individual studies were counted only once in this analysis.

### Data Extraction and Quality Assessment

Data were extracted from all studies included in this analysis (author, year of publication, country where the study was conducted, number of patients, age, percentage of males, comorbidities, and treatment); the details are provided in **Table 1**. The average number of days and SD showing each clinical course or the median number of days and interquartile

**Abbreviations:** CIs, confidence intervals; COVID-19, Coronavirus disease 2019; ECMO, extracorporeal membrane oxygenation; ECMO-death period, duration from ECMO initiation to death; ECMO period, duration from ECMO initiation to decannulation; hospitalization-death period, duration from hospitalization to death; hospitalization-discharge period, duration from hospitalization to discharge; hospitalization-ECMO period, duration from hospitalization to ECMO initiation; hospitalization-intubation period, duration from hospitalization to intubation; ICU, intensive care unit; intubation-death period, duration from intubation to death; intubation-ECMO period, duration from intubation to ECMO initiation; intubation period, duration from intubation to extubation; IQR, interquartile range; preECMO period, duration from symptom onset to ECMO initiation; prehospitalization period, duration from symptom onset to hospitalization; preintubation period, duration from symptom onset to intubation; SARS-CoV-1, severe acute respiratory syndrome coronavirus 1; SARS-CoV-2, severe acute respiratory syndrome coronavirus 2; SD, standard deviation; symptom-death period, duration from symptom onset to death.

**TABLE 1 |** Background of critical COVID-19 patients.

| IMV/ECMO | Study                   | Sample size | Location of study | Age mean (SD) or Median (IQR) | Male  | HTN   | DM    | Reported treatment (%) |         |       |       |     |                       | Risk of bias |
|----------|-------------------------|-------------|-------------------|-------------------------------|-------|-------|-------|------------------------|---------|-------|-------|-----|-----------------------|--------------|
|          |                         |             |                   |                               |       |       |       | GC                     | TCZ/SAR | HCQ   | REM   | L/R | Others                |              |
| IMV      | Abe et al.              | 2           | Japan             | 64 (4)                        | 50    | 0     | 100   | ND                     | 100     | ND    | ND    | ND  | IVIg (100)            | 5            |
| IMV      | Argenziano et al.       | 152         | US                | ND                            | ND    | ND    | ND    | ND                     | ND      | ND    | ND    | ND  | ND                    | 8            |
| IMV      | Barrasa et al.          | 20          | Spain             | ND                            | ND    | ND    | ND    | ND                     | ND      | ND    | ND    | ND  | ND                    | 8            |
| IMV      | Beigmohammadi et al.    | 7           | Iran              | 66.67 (11.47)                 | 71.43 | 57.14 | 14.23 | ND                     | ND      | 100   | 14.29 | ND  | ND                    | 5            |
| IMV      | Bhatraju et al.         | 18          | US                | ND                            | ND    | ND    | ND    | ND                     | ND      | ND    | ND    | ND  | ND                    | 6            |
| IMV      | Cauchois et al.         | 5           | France            | ND                            | ND    | ND    | ND    | ND                     | ND      | ND    | ND    | ND  | Anakinra (40)         | 7            |
| IMV      | Chen et al.             | 2           | China             | 65 (2)                        | 100   | ND    | ND    | ND                     | ND      | ND    | ND    | ND  | ND                    | 6            |
| IMV      | Christie 3rd et al.     | 2           | US                | 75 (4.11)                     | 50    | 100   | 0     | ND                     | ND      | ND    | ND    | ND  | ND                    | 6            |
| IMV      | Cummings et al.         | 163         | US                | ND                            | ND    | ND    | ND    | ND                     | ND      | ND    | ND    | ND  | ND                    | 7            |
| IMV      | Dai et al.              | 5           | China             | ND                            | ND    | ND    | ND    | ND                     | ND      | ND    | ND    | ND  | ND                    | 8            |
| IMV      | Dastan et al.           | 6           | Iran              | ND                            | ND    | ND    | ND    | ND                     | ND      | ND    | ND    | ND  | ND                    | 9            |
| IMV      | De Luca et al.          | 3           | Italy             | ND                            | ND    | ND    | ND    | ND                     | ND      | ND    | ND    | ND  | GM-CSF blockade (100) | 9            |
| IMV      | Dogan et al.            | 4           | Turkey            | 45.25 (13.94)                 | 75    | 50    | 33.33 | ND                     | ND      | 100   | ND    | 25  | Plasmapheresis (100)  | 6            |
| IMV      | Elder et al.            | 3           | US                | 73.33 (3.77)                  | 66.67 | ND    | ND    | ND                     | ND      | ND    | ND    | ND  | ND                    | 5            |
| IMV      | Falces-Romero et al.    | 5           | Spain             | 66.6 (8.36)                   | 60    | 0     | 100   | 100                    | 20      | 100   | 0     | 20  | ND                    | 5            |
| IMV      | Flikweert et al.        | 7           | Netherlands       | 73 (7.48)                     | 71.43 | 28.57 | 14.23 | 57.14                  | ND      | 85.71 | ND    | ND  | Heparin (100)         | 5            |
| IMV      | Gavin et al.            | 53          | US                | ND                            | 67.92 | 73.58 | 45.28 | ND                     | ND      | ND    | ND    | ND  | ND                    | 8            |
| IMV      | Grasselli et al.        | 836         | Italy             | 68 (62–73)                    | 83.73 | 59.81 | 21.77 | ND                     | ND      | ND    | ND    | ND  | ND                    | 8            |
| IMV      | Grein et al.            | 19          | US                | ND                            | ND    | ND    | ND    | ND                     | ND      | ND    | 100   | ND  | ND                    | 7            |
| IMV      | Halvatsiotis et al.     | 26          | Greece            | 65 (53–70)                    | 80.77 | 46.15 | 30.77 | ND                     | ND      | ND    | ND    | ND  | ND                    | 8            |
| IMV      | Hernandez-Romieu et al. | 63          | US                | ND                            | ND    | ND    | ND    | ND                     | ND      | ND    | ND    | ND  | ND                    | 7            |
| IMV      | Kato et al.             | 7           | Japan             | ND                            | ND    | ND    | ND    | ND                     | ND      | ND    | ND    | ND  | ND                    | 7            |
| IMV      | Ketcham et al.          | 2           | US                | ND                            | ND    | ND    | ND    | ND                     | ND      | ND    | ND    | ND  | ND                    | 7            |
| IMV      | Kewan et al.            | 2           | US                | ND                            | ND    | ND    | ND    | ND                     | 0       | ND    | ND    | ND  | ND                    | 7            |
| IMV      | Khullar et al.          | 17          | US                | 57 (Range 25, 75)             | 64.71 | 47.06 | 41.18 | ND                     | ND      | ND    | ND    | ND  | ND                    | 8            |
| IMV      | Konopka et al.          | 3           | US                | 54 (16.5)                     | 66.67 | 33.33 | 100   | 33.33                  | 33.33   | 66.67 | ND    | ND  | ND                    | 7            |
| IMV      | Krishnan et al.         | 92          | US                | 71 (10)                       | 64.13 | 40.22 | 25    | 58.70                  | 11.96   | 93.48 | ND    | ND  | ND                    | 8            |
| IMV      | Kristinsson et al.      | 15          | Iceland           | ND                            | ND    | ND    | ND    | ND                     | ND      | ND    | ND    | ND  | ND                    | 7            |
| IMV      | Lê et al.               | 2           | France            | ND                            | ND    | ND    | ND    | ND                     | ND      | ND    | ND    | ND  | ND                    | 6            |
| IMV      | LeBrun et al.           | 3           | US                | 89 (3.74)                     | 66.67 | 100   | 66.67 | ND                     | ND      | ND    | ND    | ND  | ND                    | 7            |
| IMV      | Lechien et al.          | 15          | Italy             | 66.8 (11.97)                  | 93.33 | ND    | ND    | ND                     | ND      | ND    | ND    | ND  | ND                    | 8            |
| IMV      | Lee et al.              | 2           | Singapore         | 62.5 (8.5)                    | 100   | ND    | ND    | ND                     | ND      | ND    | ND    | ND  | ND                    | 7            |
| IMV      | Liu et al.              | 42          | China             | ND                            | ND    | ND    | ND    | ND                     | ND      | ND    | ND    | ND  | ND                    | 8            |

(Continued)

TABLE 1 | Continued

| IMV/ECMO | Study                                       | Sample size | Location of study | Age mean (SD) or Median (IQR) | Male  | HTN   | DM    | Reported treatment (%) |         |       |     |      |                                  | Risk of bias |
|----------|---|-------------|-------------------|-------------------------------|-------|-------|-------|------------------------|---------|-------|-----|------|----------------------------------|--------------|
|          |   |             |                   |                               |       |       |       | GC                     | TCZ/SAR | HCQ   | REM | L/R  | Others                           |              |
| IMV      | Lowe et al.                                 | 2           | US                | 59.5 (1.5)                    | 100   | 50    | 50    | ND                     | ND      | 100   | ND  | ND   | ND                               | 6            |
| IMV      | Maritati et al.                             | 2           | Italy             | 67.5 (4.5)                    | 50    | 100   | 0     | 100                    | 100     | 100   | ND  | 50   | ND                               | 5            |
| IMV      | Morassi et al.                              | 4           | Italy             | 63.25 (7.36)                  | 100   | 50    | 25    | ND                     | ND      | ND    | ND  | ND   | ND                               | 5            |
| IMV      | Morillas et al.                             | 3           | US                | 62.67 (10.96)                 | 33.33 | 66.67 | 33.33 | 66.67                  | 100     | 100   | ND  | 33.3 | ND                               | 7            |
| IMV      | Navarro-Millán et al.                       | 5           | US                | 61.4 (10.13)                  | 100   | 80    | 60    | 100                    | 20      | ND    | 0   | ND   | Anakinra (100)                   | 6            |
| IMV      | Novelli et al.                              | 3           | Italy             | ND                            | ND    | ND    | ND    | ND                     | ND      | ND    | ND  | ND   | ND                               | 8            |
| IMV      | Pan et al.                                  | 3           | China             | ND                            | ND    | ND    | ND    | ND                     | ND      | ND    | ND  | ND   | ND                               | 6            |
| IMV      | Peng et al.                                 | 7           | China             | 56.43 (11.15)                 | 42.86 | 28.57 | 14.29 | 100                    | ND      | ND    | ND  | 100  | ND                               | 6            |
| IMV      | Plotnikow et al.                            | 37          | Argentina         | ND                            | 81.8  | 32.43 | 29.73 | ND                     | ND      | ND    | ND  | ND   | ND                               | 8            |
| IMV      | Radnis et al.                               | 2           | US                | 38 (6)                        | 0     | 0     | 0     | ND                     | ND      | ND    | ND  | ND   | ND                               | 5            |
| IMV      | Riker et al.                                | 2           | US                | 72 (2)                        | 100   | 100   | 0     | ND                     | ND      | 50    | ND  | ND   | ND                               | 5            |
| IMV      | Rizo-Téllez et al.                          | 10          | Mexico            | ND                            | ND    | ND    | ND    | ND                     | ND      | ND    | ND  | ND   | ND                               | 7            |
| IMV      | Sakr et al.                                 | 2           | Germany           | 57.5 (8.5)                    | 100   | 50    | 50    | ND                     | ND      | ND    | ND  | ND   | Heparin (50),<br>Enoxaparin (50) | 5            |
| IMV      | Schaefer et al.                             | 5           | US                | 66 (8.80)                     | 60    | 80    | 80    | ND                     | ND      | 40    | 20  | ND   | ND                               | 5            |
| IMV      | Shen et al.                                 | 3           | China             | 50.67 (12.47)                 | 33.33 | 33.33 | 0     | 100                    | ND      | ND    | ND  | 100  | ND                               | 7            |
| IMV      | Singh et al.                                | 4           | US                | 52.25 (20.56)                 | 100   | ND    | ND    | ND                     | 100     | ND    | ND  | ND   | CAP-1002 (100)                   | 6            |
| IMV      | So et al.                                   | 7           | Japan             | 62.23 (12.48)                 | 57.14 | 42.86 | 42.86 | 100                    | ND      | ND    | ND  | ND   | Heparin (100)                    | 6            |
| IMV      | Søvik et al.                                | 4           | Norway            | 70 [Range<br>62–75]           | 100   | 25    | ND    | ND                     | ND      | ND    | ND  | ND   | ND                               | 7            |
| IMV      | Stony Brook COVID-19<br>Research Consortium | 87          | US                | ND                            | ND    | ND    | ND    | ND                     | ND      | ND    | ND  | ND   | ND                               | 7            |
| IMV      | Wali et al.                                 | 3           | France            | 63.33 (4.71)                  | 100   | 0     | 33.33 | ND                     | ND      | ND    | ND  | ND   | ND                               | 6            |
| IMV      | Wang et al.                                 | 97          | China             | 70 (62–77)                    | 76.29 | 71.13 | 30.93 | ND                     | ND      | ND    | ND  | ND   | ND                               | 7            |
| IMV      | Wang et al.                                 | 2           | China             | 66 (3)                        | 100   | ND    | ND    | ND                     | ND      | ND    | ND  | ND   | ND                               | 5            |
| IMV      | Weiskopf et al.                             | 5           | US                | 60.6 (3.01)                   | 60    | ND    | ND    | ND                     | ND      | 60    | ND  | 60   | ND                               | 6            |
| IMV      | Wilk et al.                                 | 2           | US                | 49 (15)                       | 100   | ND    | ND    | ND                     | ND      | ND    | ND  | ND   | ND                               | 7            |
| IMV      | Zhang et al.                                | 12          | China             | 71.33 (7.70)                  | 50    | 58.33 | 16.67 | ND                     | ND      | ND    | ND  | ND   | ND                               | 8            |
| IMV      | Ziehr et al.                                | 41          | US                | ND                            | ND    | ND    | ND    | ND                     | ND      | ND    | ND  | ND   | ND                               | 7            |
| ECMO     | Akhtar et al.                               | 18          | UK                | 47.3 (9.8)                    | 88.89 | 55.56 | 55.56 | ND                     | ND      | ND    | ND  | ND   | ND                               | 7            |
| ECMO     | Alnababteh et al.                           | 13          | US                | 44.54 (9.49)                  | 61.54 | 38.46 | 30.77 | 30.77                  | 69.23   | 76.92 | ND  | ND   | Anticoagulation<br>(92.31)       | 8            |
| ECMO     | Beyls et al.                                | 12          | France            | 62 (56–66)                    | 83.33 | ND    | ND    | ND                     | ND      | ND    | ND  | ND   | ND                               | 5            |
| ECMO     | Charlton et al.                             | 16          | UK                | 47.0 (8.4)                    | 75    | 12.5  | 6.25  | ND                     | ND      | ND    | ND  | ND   | ND                               | 7            |
| ECMO     | Dastan et al.                               | 3           | Iran              | ND                            | ND    | ND    | ND    | ND                     | ND      | ND    | ND  | ND   | ND                               | 9            |
| ECMO     | Falcoz et al.                               | 17          | France            | ND                            | 94.12 | 52.94 | 17.65 | 47.06                  | ND      | 47.06 | ND  | 94   | ND                               | 7            |

(Continued)

TABLE 1 | Continued

| IMV/ECMO | Study              | Sample size | Location of study | Age mean (SD) or Median (IQR) | Male  | HTN   | DM    | Reported treatment (%) |         |       |       |       |                             | Risk of bias |
|----------|--------------------|-------------|-------------------|-------------------------------|-------|-------|-------|------------------------|---------|-------|-------|-------|-----------------------------|--------------|
|          |                    |             |                   |                               |       |       |       | GC                     | TCZ/SAR | HCQ   | REM   | L/R   | Others                      |              |
| ECMO     | Goursaud et al.    | 2           | France            | 58.5 (5.5)                    | ND    | ND    | ND    | 100                    | ND      | ND    | ND    | ND    | ND                          | 5            |
| ECMO     | Grein et al.       | 5           | US                | ND                            | ND    | ND    | ND    | ND                     | ND      | ND    | 100   | ND    | ND                          | 7            |
| ECMO     | Guihaire et al.    | 24          | France            | ND                            | 83.33 | 20.83 | 20.83 | ND                     | ND      | ND    | ND    | ND    | ND                          | 6            |
| ECMO     | Guo et al.         | 7           | China             | 69.29 (6.98)                  | 85.71 | 57.14 | 28.57 | ND                     | ND      | ND    | ND    | ND    | ND                          | 5            |
| ECMO     | Heman-Ackah et al. | 2           | US                | 52 (6)                        | 50    | 50    | 50    | ND                     | ND      | ND    | ND    | ND    | ND                          | 5            |
| ECMO     | Huette et al.      | 12          | France            | ND                            | ND    | ND    | ND    | ND                     | ND      | ND    | ND    | ND    | ND                          | 6            |
| ECMO     | Jäckel et al.      | 15          | Germany           | 60.8 (54.1–67.0)              | 73.33 | 33.33 | 13.33 | ND                     | ND      | ND    | ND    | ND    | ND                          | 8            |
| ECMO     | Jacobs et al.      | 32          | US                | 52.41 (12.49)                 | 68.75 | ND    | 34.38 | 15.63                  | 18.75   | 3.13  | ND    | ND    | Anti-viral therapy (18.75)  | 8            |
| ECMO     | Kon et al.         | 27          | US                | 40 (30.5–47)                  | 85.19 | 18.52 | 14.81 | ND                     | ND      | ND    | ND    | ND    | ND                          | 7            |
| ECMO     | Le Breton et al.   | 13          | France            | 49.31 (7.45)                  | 76.9  | 30.77 | 23.08 | 92.03                  | 46.15   | 38.46 | ND    | ND    | ND                          | 6            |
| ECMO     | Li et al.          | 7           | China             | 69.86 (7.57)                  | 71.43 | 57.14 | 28.57 | ND                     | ND      | ND    | ND    | ND    | ND                          | 6            |
| ECMO     | Liu et al.         | 4           | China             | ND                            | ND    | ND    | ND    | ND                     | ND      | ND    | ND    | ND    | ND                          | 8            |
| ECMO     | Liu et al.         | 6           | China             | ND                            | ND    | ND    | ND    | 100                    | ND      | ND    | ND    | 100   | Arbidol (100)               | 8            |
| ECMO     | Loforte et al.     | 4           | Italy             | 49 (8.75)                     | 100   | ND    | ND    | ND                     | 100     | 100   | ND    | 66.67 | ND                          | 6            |
| ECMO     | Matsunaga et al.   | 31          | Japan             | ND                            | ND    | ND    | ND    | ND                     | ND      | ND    | ND    | ND    | ND                          | 7            |
| ECMO     | Miike et al.       | 3           | Japan             | ND                            | ND    | ND    | ND    | ND                     | ND      | ND    | ND    | ND    | ND                          | 6            |
| ECMO     | Mustafa et al.     | 40          | US                | 48.4 (1.5)                    | 75    | 57.5  | 25    | ND                     | ND      | ND    | ND    | ND    | ND                          | 6            |
| ECMO     | Osho et al.        | 6           | US                | 47 (43–53)                    | 83.33 | 50    | 66.67 | ND                     | 50      | 100   | 33.33 | 16.67 | ND                          | 7            |
| ECMO     | Ronit et al.       | 2           | Denmark           | 52.5 (12.5)                   | 50    | 0     | 0     | ND                     | ND      | ND    | ND    | ND    | ND                          | 5            |
| ECMO     | Schmidt et al.     | 83          | France            | 49 (41–56)                    | 73.49 | 38.55 | 31.33 | 14.46                  | 9.64    | 19.28 | 9.64  | 22.89 | ND                          | 8            |
| ECMO     | Shih et al.        | 37          | US                | 51 (40–59)                    | 72.97 | 67.57 | 51.35 | 70.27                  | 65.57   | 45.95 | 54.05 | ND    | Convalescent plasma (43.24) | 7            |
| ECMO     | Sultan et al.      | 10          | US                | ND                            | 70    | ND    | ND    | 40                     | 30      | 100   | 40    | ND    | ND                          | 6            |
| ECMO     | Usman et al.       | 10          | US                | 50.7 (47.5–58.8)              | 70    | 50    | ND    | 50                     | 60      | 90    | 20    | 0     | ND                          | 7            |
| ECMO     | Xu et al.          | 17          | China             | ND                            | ND    | ND    | ND    | ND                     | ND      | ND    | ND    | ND    | ND                          | 7            |
| ECMO     | Xuan et al.        | 5           | China             | 61.6 (9.18)                   | ND    | 80    | 60    | 80                     | ND      | ND    | ND    | ND    | IVIg (40)                   | 5            |
| ECMO     | Yang et al.        | 21          | China             | 58.50 (42.75–67.25)           | 57.14 | ND    | ND    | ND                     | ND      | ND    | ND    | ND    | ND                          | 8            |
| ECMO     | Zayat et al.       | 17          | Germany           | 57.0 (53.0, 62.0)             | 64.71 | 35.29 | 35.29 | ND                     | ND      | ND    | ND    | ND    | ND                          | 8            |
| ECMO     | Zeng et al.        | 12          | China             | 50.9 (13.5)                   | 91.67 | 8.33  | 8.33  | 83.33                  | ND      | ND    | ND    | ND    | Anti-viral therapy (100)    | 6            |
| ECMO     | Zeng et al.        | 2           | China             | 64.5 (1.5)                    | 100   | ND    | ND    | ND                     | ND      | ND    | ND    | ND    | ND                          | 8            |
| ECMO     | Zhang et al.       | 43          | UK                | 46 (35.5–52.5)                | 76.74 | 23.26 | 18.60 | ND                     | ND      | 4.65  | 9.30  | ND    | Anakinra (23.26)            | 8            |
| ECMO     | Zhang et al.       | 3           | US                | 55.67 (11.73)                 | ND    | ND    | ND    | ND                     | ND      | ND    | ND    | ND    | ND                          | 7            |
| ECMO     | Zheng et al.       | 11          | China             | ND                            | ND    | ND    | ND    | ND                     | ND      | ND    | ND    | ND    | ND                          | 8            |

The total score was calculated based on the study quality assessment tools from the NHLBI.

IMV, invasive mechanical ventilation; ECMO, extracorporeal membrane oxygenation; HTN, hypertension; DM, diabetes mellitus; GC, glucocorticoid; TCZ/SAR, tocilizumab/sarilumab; HCQ, hydroxychloroquine; REM, remdesivir; L/R, lopinavir-ritonavir; IVIG, intravenous immunoglobulin; NR, not reported.



range (IQR) and/or range were extracted. The average number of days and SD were calculated from the median and IQR or range data using the reported methods if only the median and IQR or range were given in the study (22).

Two authors (K.F. and T.M.) independently assessed and selected references. In cases of inconsistent results, a third author (A.K.) provided an opinion to resolve the issue. The quality of the selected studies was evaluated according to the study quality assessment tools (Quality Assessment Tool for Case Series Studies) from the National Heart, Lung, and Blood Institute (NHLBI) (23). The evidence level was assessed based on the Oxford Centre for Evidence-Based Medicine 2011 (24). Asymmetry in a funnel plot was employed to determine publication bias.

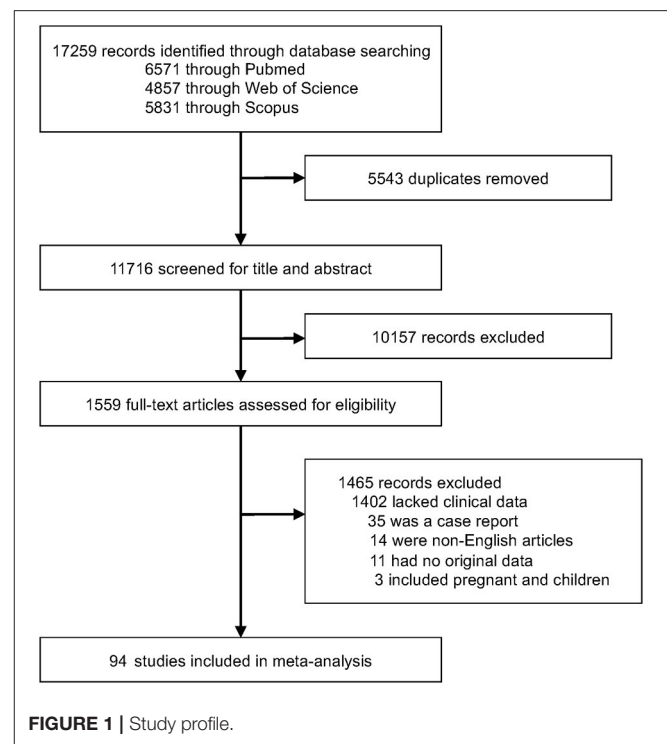
## Data Analysis

A meta-analysis was performed to estimate the clinical course of intubated survivors, non-survivors, and ECMO patients with COVID-19. Clinical data were analyzed using the metamean package. Outcomes are described as the mean number of days at each event, such as admission, intubation, or death from the onset of COVID-19 (baseline) and 95% confidence intervals (CIs) for each clinical course. For all outcomes, mean differences were calculated using the random-effects model (DerSimonian and Laird method) (25).  $I^2$  values of 25, 50, and 75% were defined as low, moderate, and high, respectively (26). All analyses were conducted using R version 4.0.3 (R Project for Statistical Computing) (27). Sensitivity analyses were carried out with regard to the intubation period and intubation-death period based on region (East Asia, the US, and Europe), age, sex, and comorbidities (hypertension and diabetes mellitus). Spearman's correlation coefficient was calculated in R version 4.0.3.  $P$  values  $\leq 0.05$  were considered statistically significant. This study was registered with PROSPERO (CRD42021235534).

## RESULTS

We identified 17,259 articles and excluded 5,543 due to duplication. We also screened 11,716 publications and identified 94 articles (15–17, 28–118), with 2,549 cases, from among 1,559 articles that underwent full-text assessment (Figure 1). Each article is summarized in **Supplementary Table 1**. The mean age ranged from 38 to 75 years, and the rate of male patients ranged from 0% to 100%. COVID-19 patients were reportedly treated with glucocorticoids, tocilizumab/sarilumab, remdesivir, and hydroxychloroquine; however, treatment was not described in more than 70% of the articles. There were 36 articles from the US, 19 from China, ten from France, seven from Italy, five from Japan, and a few from other countries. Despite several cohort studies, there were few intubated survivors and non-survivors, and most were case accumulations. Therefore, the risk of bias was calculated based on case accumulation. The risk of bias was more than 5 points, with 6.71 points as the average, i.e., moderate risk (**Supplementary Table 2**).

Moreover, we conducted a meta-analysis on the clinical course of intubated survivors, non-survivors, and ECMO patients



with COVID-19. First, we analyzed the intubation period and the intubation-death period of intubated survivors and non-survivors. Thirty-three reports with 325 survivors and 24 reports with 1,225 non-survivors were identified and analyzed (Figure 2). The average intubation period among intubated survivors was 12.07 days (95% CIs 9.80–14.33 days), and the average intubation-death period was 10.14 days (8.18–12.10 days). The prehospitalization periods for intubated survivors and non-survivors were 6.15 (4.61–7.69 days) and 6.45 (4.55–8.34 days) days, respectively, and the preintubation periods were 8.58 days (7.36–9.80 days) and 9.64 days (7.75–11.53 days), respectively. A symptom-death period of 17.86 days (13.02–22.69 days) was calculated (Figure 3). Additionally, the hospitalization-intubation period among intubated survivors and non-survivors was 2.62 days (1.66–3.58 days) and 3.28 days (2.15–4.41 days), respectively; the hospitalization-discharge and hospitalization-death periods were 24.48 days (12.54–36.41 days) and 12.47 days (10.56–14.39 days), respectively (Figure 4). Funnel plots are illustrated in **Supplementary Figure 1**.

Regarding the clinical course of those treated with ECMO, the ECMO period of both survivors and non-survivors and the ECMO-death period were 14.72 days (10.57–18.87 days) and 21.05 days (12.04–30.07 days), respectively (**Supplementary Figure 2**). For ECMO patients, the prehospitalization, preintubation, and pre-ECMO periods were 7.15 (6.48–7.81 days), 10.54 (9.18–11.90 days), and 14.80 (13.29–16.31 days) days, respectively, and the hospitalization-intubation, hospitalization-ECMO, and intubation-ECMO periods were 3.39 (2.08–4.69 days), 5.97 (3.91–8.02 days), and 4.57 (3.59–5.54 days) days, respectively (data not shown).

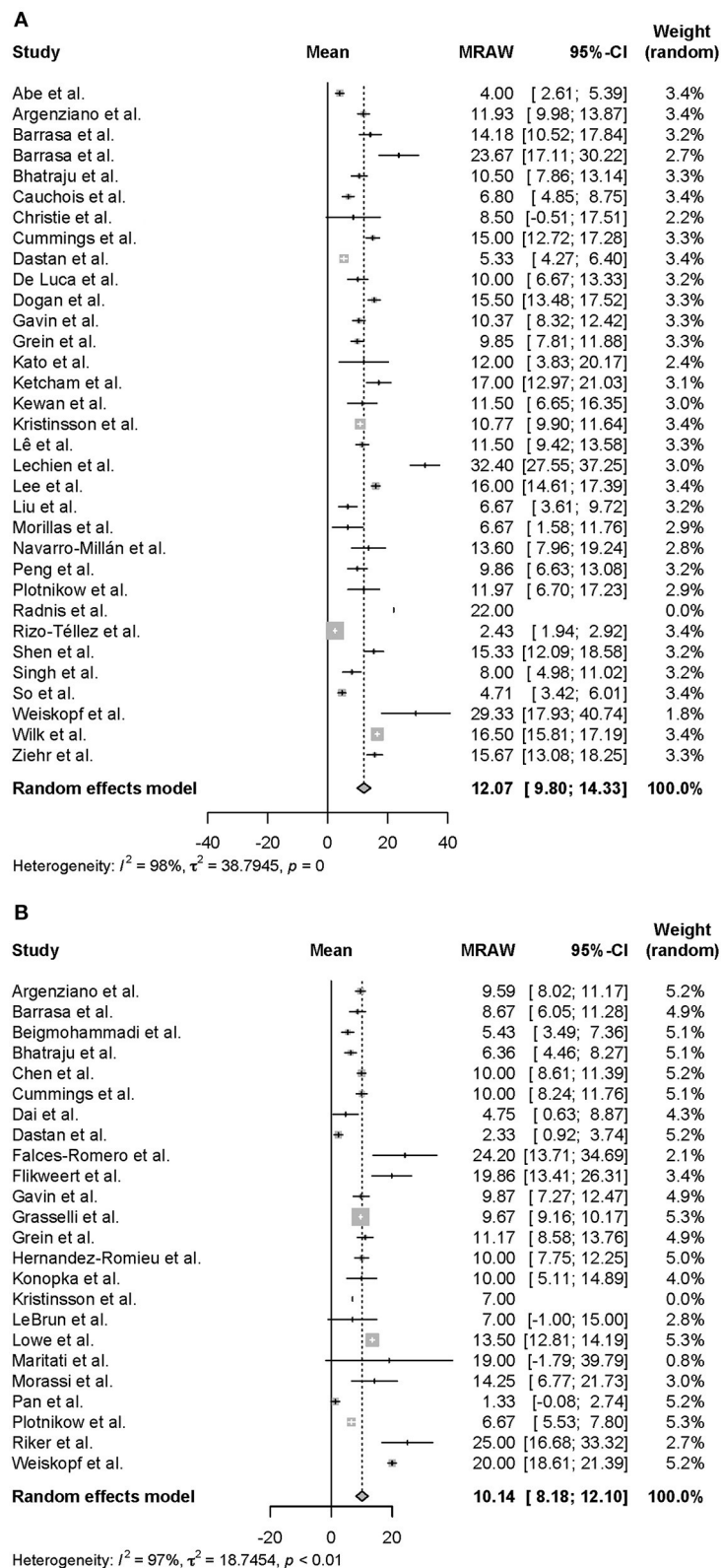


**FIGURE 2 |** Forrest plot: a meta-analysis of the intubation period and the intubation-death period. The intubation period of intubated COVID-19 survivors **(A)** and the intubation-death period of intubated COVID-19 non-survivors **(B)** were calculated using the random effects model. MRAW, the raw data of mean; 95% CI, 95% confidence interval.

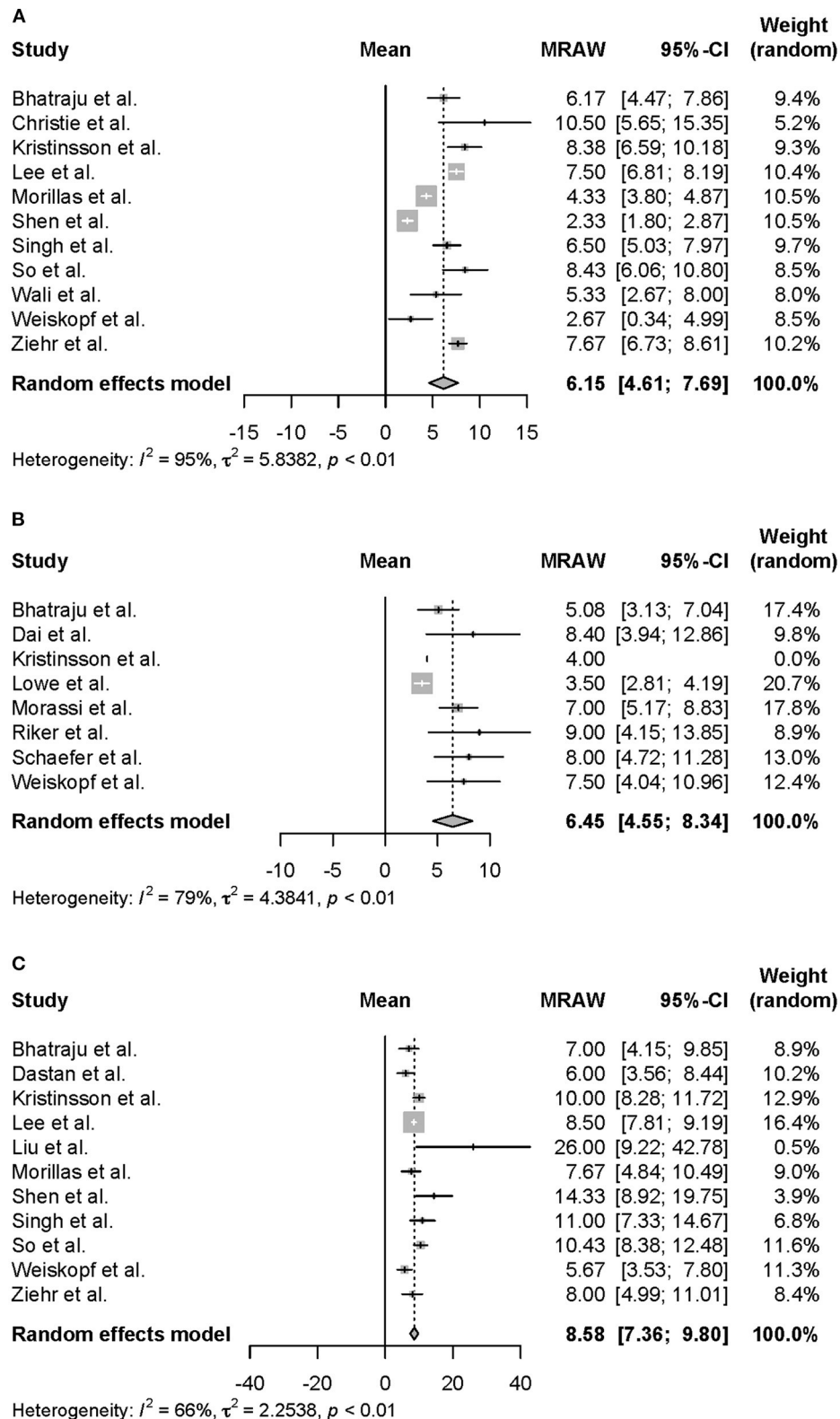
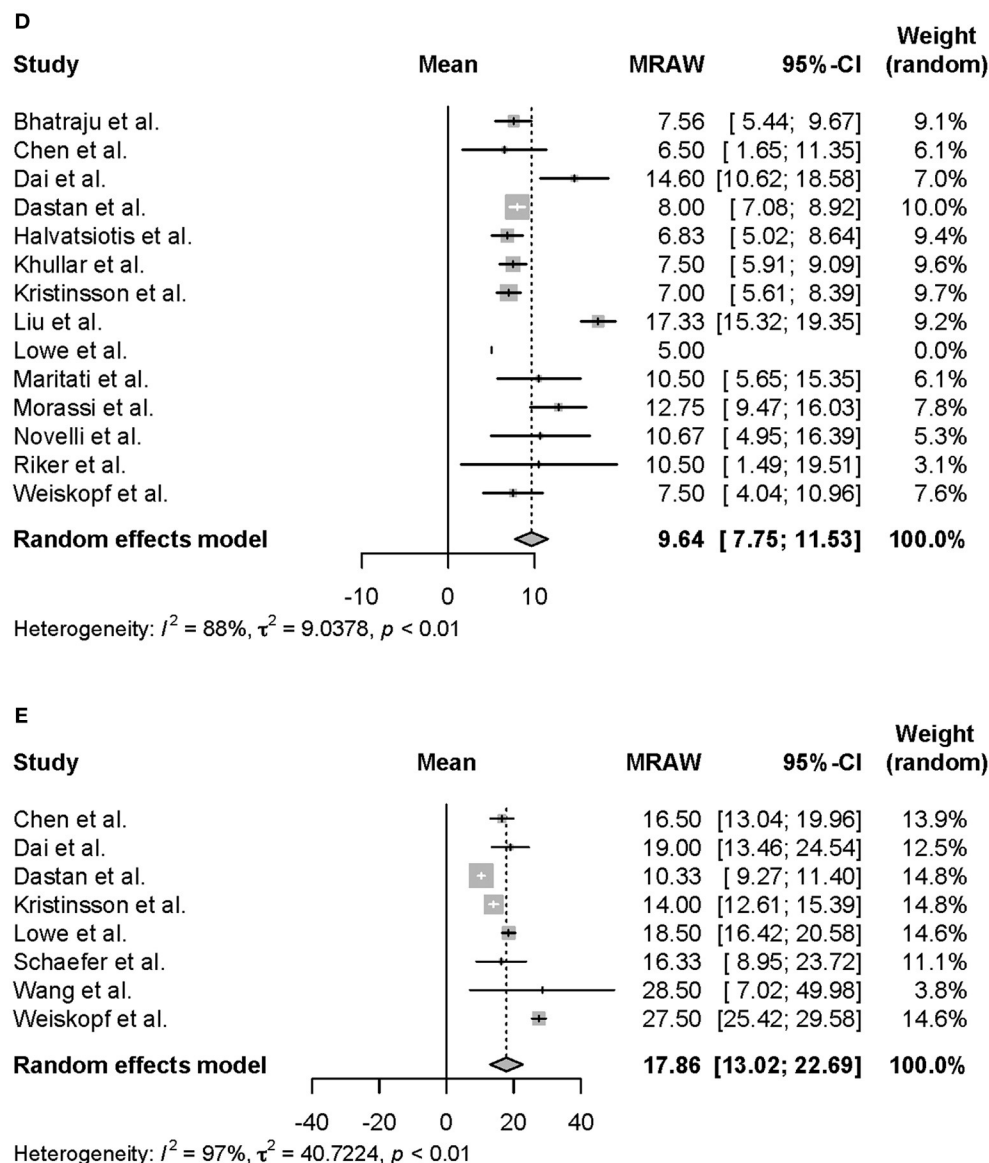


FIGURE 3 | Continued



**FIGURE 3 |** Forrest plot: a meta-analysis of the time from symptom onset to each clinical endpoint in intubated COVID-19 patients. The prehospitalization period of intubated survivors (A), the prehospitalization period of intubated non-survivors (B), the preintubation period of intubated survivors (C), the preintubation period of intubated non-survivors (D), and the symptom-death period (E) were calculated using the random effects model. MRAW, the raw data of mean; 95% CI, 95% confidence interval.

The results provided above are summarized in **Figure 5**. The prehospitalization and preintubation periods of intubated non-survivors and ECMO patients appeared to be longer than those of intubated survivors (no direct comparison).

Finally, sensitivity analysis focusing on regional differences and patient backgrounds was performed. The regions where the studies were conducted were classified into three groups: Europe, the US, and East Asia. The intubation period was 14.87 days (10.99–18.76 days), 12.61 days (10.50–14.72 days), and 9.66 days (5.07–14.25 days) in Europe, the US, and East Asia

(**Supplementary Figure 3**), and the intubation-death period was 13.05 days (9.53–16.58 days), 11.34 days (8.06–14.61 days), and 5.39 days (–1.14–11.91 days), respectively. Both the intubation period and intubation-death period tended to be longer in the US and Europe than in East Asia. Nevertheless, the mean age of intubated survivors did not differ much among Europe [64.85 (60.84–68.85)], the US [58.09 (49.32–66.87)], and Asia [61.64 (57.20–66.07)]; the mean age of intubated non-survivors was 67.86 (65.86–69.86) in Europe and 70.67 (61.88–79.46) in the US [one paper reported that the mean age of non-survivors in



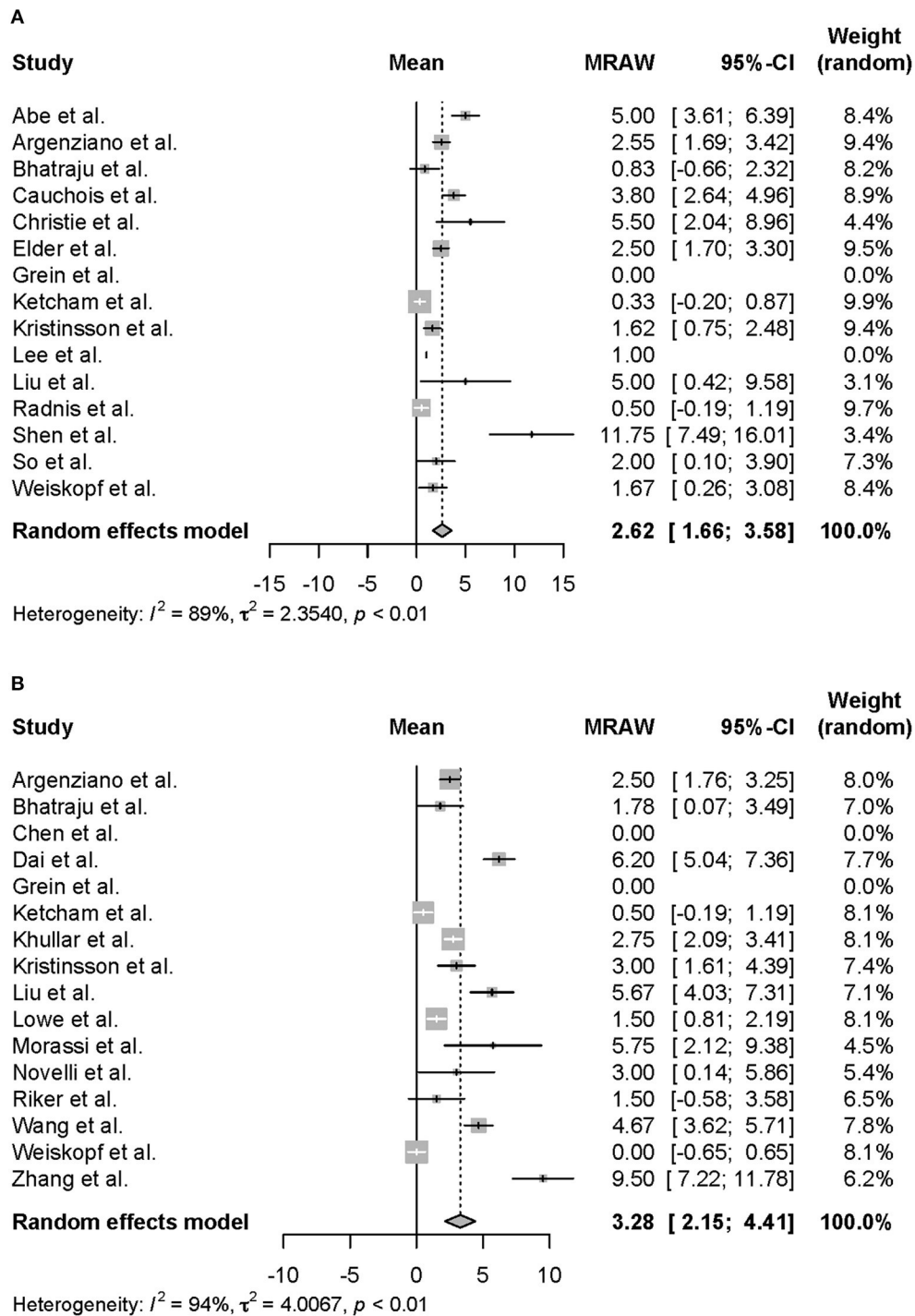
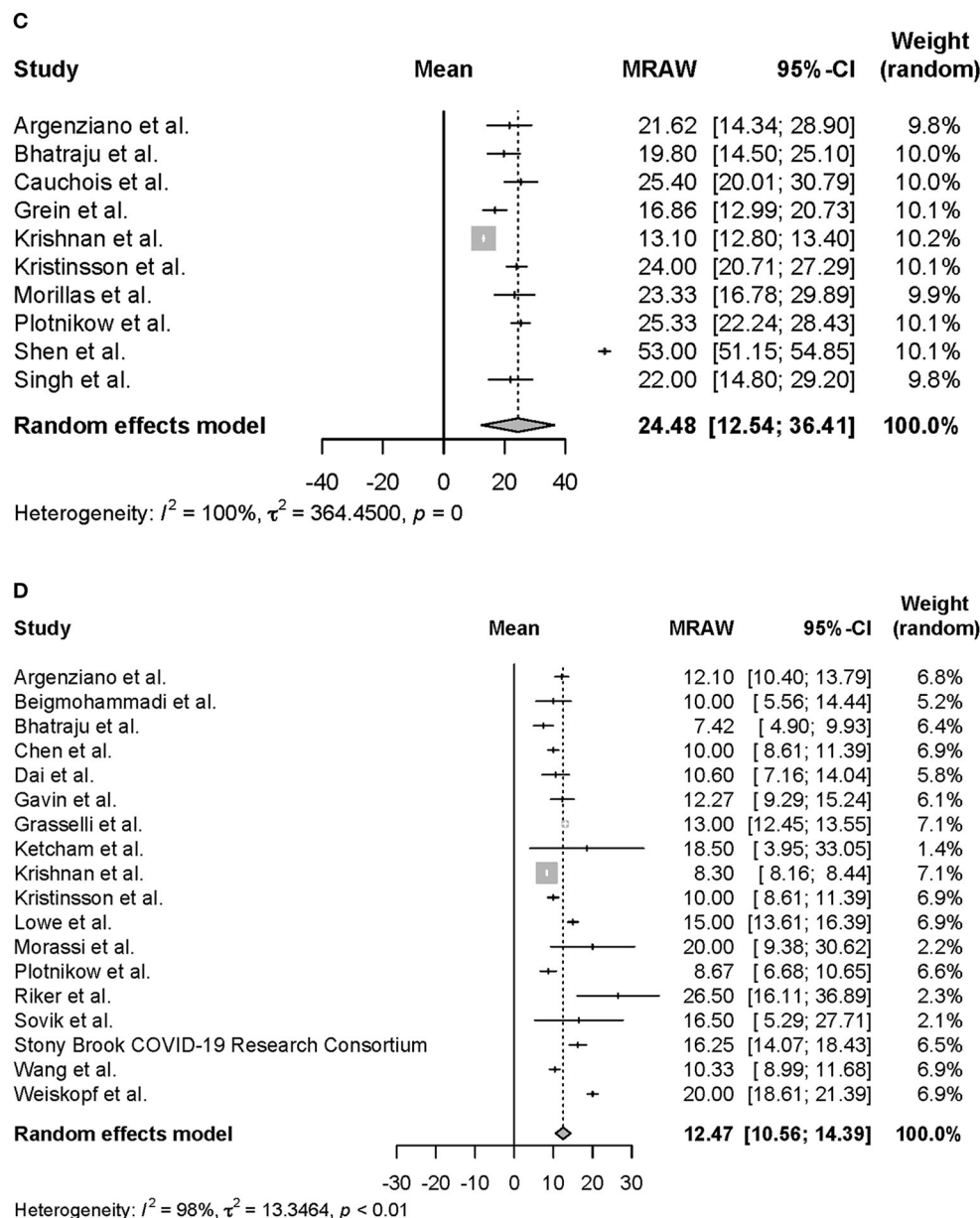


FIGURE 4 | Continued



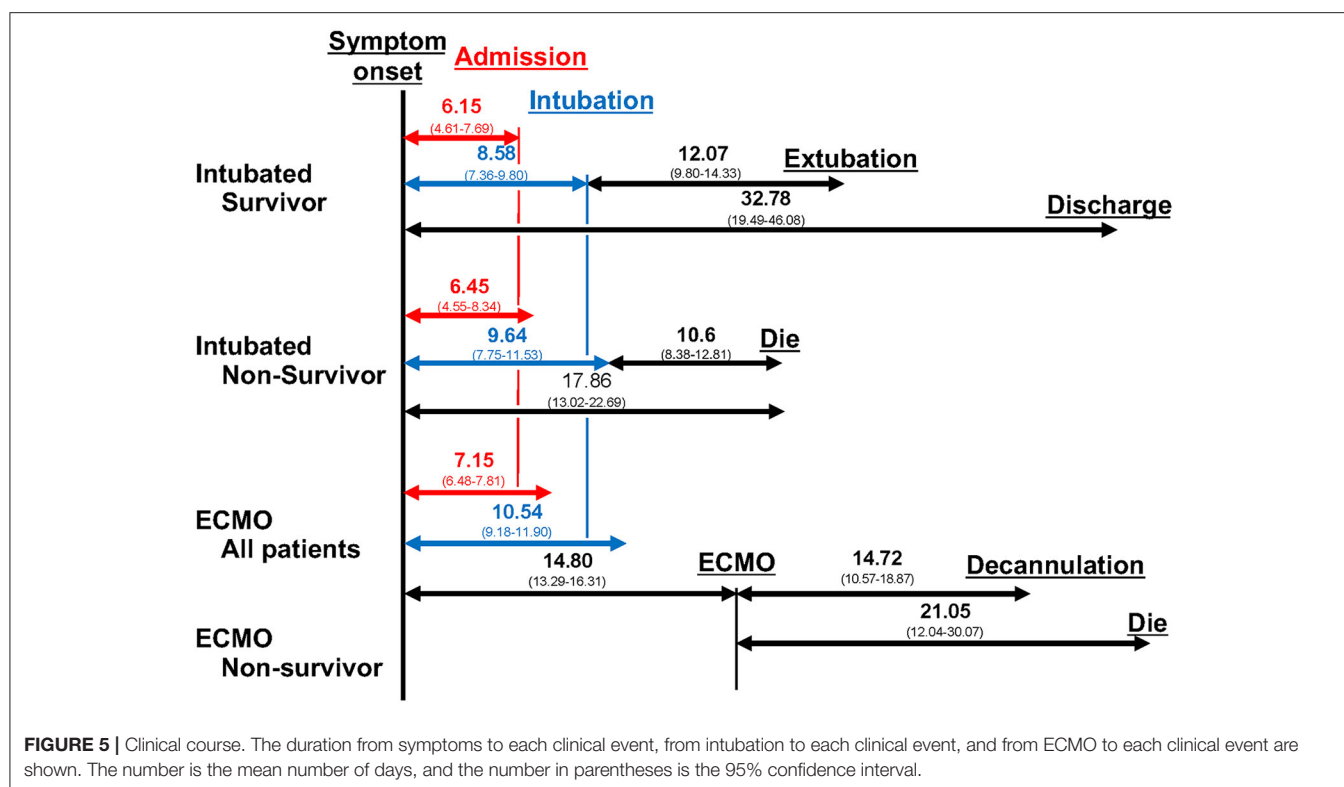
**FIGURE 4 |** Forrest plot: a meta-analysis of the time from hospitalization onset to each clinical endpoint in intubated COVID-19 patients. The hospitalization-intubation period of intubated survivors (A), the hospitalization-intubation period of intubated non-survivors (B), the hospitalization-discharge period of intubated survivors (C), and the hospitalization-death period of intubated non-survivors (D) were calculated using the random effects model. MRAW, the raw data of mean; 95% CI, 95% confidence interval.

China was  $65 (\pm 4)$ . We also analyzed age, sex, and comorbidities (diabetes mellitus and hypertension) but found no significant differences (data not shown).

## DISCUSSION

This study demonstrated the clinical course and differences among the clinical courses of intubated survivors, non-survivors,

and ECMO patients with COVID-19. In this meta-analysis, intubation, intubation-death, and ECMO periods were 12.07 days (9.80–14.33 days), 10.14 days (8.18–12.10 days), and 14.72 days (10.57–18.87 days), respectively. The prehospitalization periods of intubated survivors, non-survivors, and ECMO patients were 6.15 days (4.61–7.69 days), 6.45 days (4.55–8.34 days), and 7.15 days (6.48–7.81 days), respectively, and the preintubation periods were 8.58 days (7.36–9.80 days), 9.14 days (7.26–11.01 days), and 10.54 days (9.18–11.90 days),



respectively. According to sensitivity analysis, the intubation period in survivors and the intubation-death period were longer in the US and Europe than in East Asia.

For COVID-19, the intubation period in survivors and the intubation-death period appear to be more prolonged than those in patients intubated for other diseases or reasons. In addition, the intubation periods in survivors and non-survivors were 12.1 days and 10 days, respectively. In contrast, previously reported intubation periods in ICU patients, including postoperative patients, chronic obstructive pulmonary disease (COPD) patients, pneumocystis pneumonia survivors, acute respiratory distress syndrome (ARDS) patients, community-acquired pneumonia patients, and SARS-CoV-1 pneumonia survivors, were  $3.3 \pm 3$  days (mortality 24.3%) (119),  $6.8 \pm 4.9$  days (mortality 13%) (120),  $7.7 \pm 8.2$  days (121),  $8.8 (\pm 6)$  days (122), 10–11 days (123),  $12.1 \pm 6.1$  days (124), and 7.3–15 days (mean days are calculated from each original datum) (125–127), respectively. One study comparing COVID-19 with influenza found that the intubation period in COVID-19 patients was longer than that in influenza patients (16.2 vs. 7.3 days) (127). Thus, the intubation period in COVID-19 survivors is prolonged compared with that in patients intubated due to COPD, HIV-PCP, and influenza. However, approximately the same duration has been observed for patients intubated due to community-acquired pneumonia and SARS-CoV-1 or COVID-19.

Moreover, the ECMO period in COVID-19 patients was not longer than that in patients with ARDS for other reasons. Although ECMO is commonly used during cardiac surgery, severe ARDS patients (aPaO<sub>2</sub>:FiO<sub>2</sub> of <80 mmHg, a Murray

score >3.0 and pH<7.20) have been treated with ECMO, improving the survival rate to more than 50% (128, 129). Accordingly, critical COVID-19 patients also receive ECMO. In our meta-analysis, the ECMO period with COVID-19 was 10.3 days (10.57–18.87 days); in previous reports, the ECMO period in severe ARDS patients was  $10.3 \pm 7.5$  (mean days were calculated from the data) days (128) and  $15 \pm 13$  days (129), and that in severe ARDS patients with influenza was 10 days (130). These data indicate that the ECMO period in COVID-19 patients is not as long as we expected. We presume that time is needed to improve both ARDS caused by COVID-19 and ARDS caused by other reasons, as recovery in patients with critical ARDS is difficult.

In this study, the preintubation period was longer in intubated survivors than in intubated non-survivors or ECMO patients. This tendency was also observed when assessing data for the prehospitalization and hospitalization-intubation periods, despite no direct comparison. Indeed, the time from symptom onset to pneumonia was longer in COVID-19 patients with severe disease than in those without severe disease (131), the time from symptom onset to dyspnea and hospitalization in ICU COVID-19 patients was longer than that in non-ICU COVID-19 patients, and the time from symptom onset to ICU admission tended to be longer in COVID-19 non-survivors than in COVID-19 survivors (10).

There are two possibilities for these findings. First, hospitalization delay and lack of medical resources may contribute to the result. COVID-19 pandemic forces people to self-restraint, and it leads to hospitalization delay. Moreover, a

shortage of ventilators also leads to intubation delay and poor prognosis (132–134). In fact, the hospitalization-intubation period among non-survivors, and ECMO patients tended to be longer than that among intubated survivors; the hospitalization-intubation period among intubated survivors, non-survivors, and ECMO patients with COVID-19 was 2.62 days (1.66–3.58 days), 3.28 days (2.15–4.41 days), and 3.39 (2.08–4.69 days), respectively. Second, a critical condition itself leads to a long prehospitalization period. Although the mechanism has yet to be elucidated, some of the COVID-19 patients experience asymptomatic hypoxia, which is also called “silent hypoxia.” In COVID-19 patients, 28.1% of hospitalized patients are estimated to have “silent hypoxia;” 33% of hospitalized patients with “silent hypoxia” are admitted to the ICU, and 25.9% of hospitalized patients with “silent hypoxia” die (135). Hence, “silent hypoxia” itself is a critical condition that leads to a long prehospitalization period. In this situation, monitoring blood oxygen, early hospitalization with oxygen supplementation, and systemic management arguably lead to a better prognosis.

The reasons why the intubation period was shorter in East Asia than in the US and Europe may include selection bias, information bias, differences in treatment, ventilator and ICU bed availability, race, and genetics. We detected bias concerning the East Asia data, which showed minor variations in regions and faculties compared to those from the US and Europe because East Asia’s data were mainly from China, especially Wuhan. The shortage of ventilators and ICU beds has been highlighted in the US and Europe (132, 136), and it arguably contributed to a delay of intubation and a prolonged clinical course. Race and genetic background are also possible reasons for the observed clinical differences among regions. For example, data from the US show that Asians were hospitalized less but that Black and Hispanics were hospitalized more (137, 138). Sixteen percent of the genes were derived from Neanderthals, one of the prognostic factors maintained in Europe (almost 0% in East Asia) (139). GWASs have revealed that SNPs and blood type, the percentages of which differ among races and regions, are also prognostic factors. Thus, an international cohort study is needed to reveal the difference in clinical course between race and region.

## LIMITATIONS

There were also some limitations in this meta-analysis. Although many studies were included, more studies and patients are needed. Furthermore, heterogeneity was high because it was difficult to standardize the patients’ backgrounds. This study revealed the clinical course of survivors and non-survivors, but a direct comparison with survivors and non-survivors is still needed. Clinical information, for example, age, BMI, cardiac disease, kidney disease, and chronic obstructive disease, was not sufficiently described in the cases we included, and articles in some of the countries reporting were limited. Social information was also not described in the cases we included; however, whether social information, such as patient or national income level, affects the clinical course is of great interest. Moreover, differences in viral strain and treatment including

anti-inflammatory treatment, because of the study period. In general, comparing clinical data with our data will reveal more knowledge about COVID-19.

## CONCLUSIONS

Our data indicate that prehospitalization and intubation periods were longer in intubated non-survivors and ECMO patients than in intubated survivors with COVID-19. These periods might serve as predictors of disease severity or death and support therapeutic strategy determination. In the near future, viral strains and treatments should be taken into account when evaluating the clinical course of COVID-19.

## DATA AVAILABILITY STATEMENT

The original contributions presented in the study are included in the article/**Supplementary Material**, further inquiries can be directed to the corresponding author.

## AUTHOR CONTRIBUTIONS

KF and TM designed the study, carried out the literature search, independently acquired the data, screened the records, extracted the data, assessed the risk of bias, and performed the statistical analyses. All authors contributed to the article and approved the submitted version.

## FUNDING

This work was supported by research grants from the Center of Innovation program (COISTREAM) from the Ministry of Education, Culture, Sports, Science and Technology of Japan (MEXT) (to AK), the Japan Society for the Promotion of Science (JSPS) KAKENHI (JP18H05282 to AK), the Japan Agency for Medical Research and Development (AMED) (J200705023, J200705710, J200705049, JP18cm016335, JP18cm059042, and J210705582 to AK), a grant from the Kansai Economic Federation (KANKEIREN), and Grants from Mitsubishi Foundation (to AK). This work was also supported by the Japan Society for the Promotion of Science (JSPS) KAKENHI (JP21K16287 to TM).

## ACKNOWLEDGMENTS

We thank our colleagues from Osaka University Center of Medical Data Science and Advanced Clinical Epidemiology Investigator’s Research Project for their providing insight and expertise for our research.

## SUPPLEMENTARY MATERIAL

The Supplementary Material for this article can be found online at: <https://www.frontiersin.org/articles/10.3389/fmed.2021.727101/full#supplementary-material>



## REFERENCES

- Li Q, Guan X, Wu P, Wang X, Zhou L, Tong Y, et al. Early transmission dynamics in Wuhan, China, of novel coronavirus-infected pneumonia. *N Engl J Med*. (2020) 382:1199–207. doi: 10.1056/NEJMoa2001316
- Weekly Epidemiological Update on COVID-19. (2021). Available online at: <https://www.who.int/publications/m/item/weekly-epidemiological-update-on-covid-19-5-3-august-2021> (accessed August 5, 2021).
- Flaxman S, Mishra S, Gandy A, Unwin HJT, Mellan TA, Coupland H, et al. Estimating the effects of non-pharmaceutical interventions on COVID-19 in Europe. *Nature*. (2020) 584:257–61. doi: 10.1038/s41586-020-2405-7
- Chu DK, Akl EA, Duda S, Solo K, Yaacoub S, Schünemann HJ, et al. Physical distancing, face masks, and eye protection to prevent person-to-person transmission of SARS-CoV-2 and COVID-19: a systematic review and meta-analysis. *Lancet*. (2020) 395:1973–87. doi: 10.1016/S0140-6736(20)31142-9
- Wu Z, McGoogan JM. Characteristics of and important lessons from the coronavirus disease 2019 (COVID-19) outbreak in china: summary of a report of 72 314 cases from the chinese center for disease control and prevention. *JAMA*. (2020) 323:1239–42. doi: 10.1001/jama.2020.2648
- Stokes EK, Zambrano LD, Anderson KN, Marder EP, Raz KM, El Burai Felix S, et al. Coronavirus disease 2019 case surveillance - United States, January 22-May 30, 2020. *MMWR Morb Mortal Wkly Rep*. (2020) 69:759–65. doi: 10.15585/mmwr.mm6924e2
- CDC. Disease Burden of Influenza. (2020). Available online at: <https://www.cdc.gov/flu/about/burden/index.html> (accessed June 1, 2021).
- Wang D, Hu B, Hu C, Zhu F, Liu X, Zhang J, et al. Clinical characteristics of 138 hospitalized patients with 2019 novel coronavirus-infected pneumonia in Wuhan, China. *JAMA*. (2020) 323:1061–9. doi: 10.1001/jama.2020.1585
- Bravata DM, Perkins AJ, Myers LJ, Arling G, Zhang Y, Zillich AJ, et al. Association of intensive care unit patient load and demand with mortality rates in US department of veterans affairs hospitals during the COVID-19 pandemic. *JAMA Netw Open*. (2021) 4:e2034266. doi: 10.1001/jamanetworkopen.2020.34266
- Yang X, Yu Y, Xu J, Shu H, Xia J, Liu H, et al. Clinical course and outcomes of critically ill patients with SARS-CoV-2 pneumonia in Wuhan, China: a single-centered, retrospective, observational study. *Lancet Res Med*. (2020) 8:475–81. doi: 10.1016/S2213-2600(20)30079-5
- Arentz M, Yim E, Klaff L, Lokhandwala S, Riedo FX, Chong M, et al. Characteristics and outcomes of 21 critically ill patients with COVID-19 in Washington State. *JAMA*. (2020) 323:1612–4. doi: 10.1001/jama.2020.4326
- Grasselli G, Zangrillo G, Zanella A, Antonelli M, Cabrini L, Castelli A, et al. Baseline characteristics and outcomes of 1591 patients infected with sars-cov-2 admitted to ICUs of the lombardy region, Italy. *JAMA*. (2020) 323:1574–81. doi: 10.1001/jama.2020.5394
- Piroth L, Cottenet J, Mariet A-S, Bonniaud P, Blot M, Tubert-Bitter P, et al. Comparison of the characteristics, morbidity, and mortality of COVID-19 and seasonal influenza: a nationwide, population-based retrospective cohort study. *Lancet Respir Med*. (2021) 9:251–9. doi: 10.1016/S2213-2600(20)30527-0
- Xie Y, Bowe B, Maddukuri G, Al-Aly Z. Comparative evaluation of clinical manifestations and risk of death in patients admitted to hospital with covid-19 and seasonal influenza: cohort study. *BMJ*. (2020) 371:m4677. doi: 10.1136/bmj.m4677
- Cummings MJ, Baldwin MR, Abrams D, Jacobson SD, Meyer BJ, Balough EM, et al. Epidemiology, clinical course, and outcomes of critically ill adults with COVID-19 in New York City: a prospective cohort study. *Lancet*. (2020) 395:1763–70. doi: 10.1016/S0140-6736(20)31189-2
- Gavin W, Campbell E, Zaidi S-A, Gavin N, Dbeibo L, Beeler C, et al. Clinical characteristics, outcomes and prognosticators in adult patients hospitalized with COVID-19. *Am J Infect Control*. (2021) 49:158–65. doi: 10.1016/j.ajic.2020.07.005
- Ziehr DR, Alladina J, Petri CR, Maley JH, Moskowitz A, Medoff BD, et al. Respiratory pathophysiology of mechanically ventilated patients with COVID-19: a cohort study. *Am J Respir Crit Care Med*. (2020) 201:1560–4. doi: 10.1164/rccm.202004-1163LE
- Chen R, Liang W, Jiang M, Guan W, Zhan C, Wang T, et al. Risk factors of fatal outcome in hospitalized subjects with coronavirus disease 2019 from a nationwide analysis in China. *Chest*. (2020) 158:97–105. doi: 10.1016/j.chest.2020.04.010
- Chen T, Dai Z, Mo P, Li X, Ma Z, Song S, et al. Clinical characteristics and outcomes of older patients with coronavirus disease 2019 (COVID-19) in Wuhan, China: a single-centered, retrospective study. *J Gerontol A Biol Sci Med Sci*. (2020) 75:1788–95. doi: 10.1093/gerona/glaa089
- Wu S, Du Z, Shen S, Zhang B, Yang H, Li X, et al. Identification and validation of a novel clinical signature to predict the prognosis in confirmed coronavirus disease 2019 patients. *Clin Infect Dis*. (2020) 71:3154–62. doi: 10.1093/cid/ciaa793
- Moher D, Liberati A, Tetzlaff J, Altman DG, PRISMA Group. Preferred reporting items for systematic reviews and meta-analyses: the PRISMA statement. *PLoS Med*. (2009) 6:e1000097. doi: 10.1371/journal.pmed.1000097
- Wan X, Wang W, Liu J, Tong T. Estimating the sample mean and standard deviation from the sample size, median, range and/or interquartile range. *BMC Med Res Methodol*. (2014) 14:135. doi: 10.1186/1471-2288-14-135
- Study Quality Assessment Tools. Available online at: <https://www.nhlbi.nih.gov/health-topics/study-quality-assessment-tools> (accessed May 28, 2021).
- OCEBM Levels of Evidence (2020). Available online at: <https://www.cebm.ox.ac.uk/resources/levels-of-evidence/ocebm-levels-of-evidence> (Accessed March 28, 2021).
- DerSimonian R, Laird N. Meta-analysis in clinical trials. *Control Clin Trials*. (1986) 7:177–88. doi: 10.1016/0197-2456(86)90046-2
- Higgins JPT, Thompson SG, Deeks JJ, Altman DG. Measuring inconsistency in meta-analyses. *BMJ*. (2003) 327:557–60. doi: 10.1136/bmj.327.7414.557
- The R Project for Statistical Computing. Available online at: <https://www.r-project.org/> (accessed January 4, 2021).
- Abe T, Izumo T, Ueda A, Hayashi M, Ishibashi Y. Successful treatment of two Japanese ESRD cases with severe COVID-19 pneumonia. *CEN Case Rep*. (2021) 10:42–5. doi: 10.1007/s13730-020-00512-7
- Argenziano MG, Bruce SL, Slater CL, Tiao JR, Baldwin MR, Barr RG, et al. Characterization and clinical course of 1000 patients with coronavirus disease 2019 in New York: retrospective case series. *BMJ*. (2020) 369:m1996. doi: 10.1136/bmj.m1996
- Barrasa H, Rello J, Tejada S, Martín A, Balziskueta G, Vinuesa C, et al. SARS-CoV-2 in spanish intensive care units: early experience with 15-day survival in Vitoria. *Anaesth Crit Care Pain Med*. (2020) 39:553–61. doi: 10.1016/j.accpm.2020.04.001
- Beigomhamadi MT, Jahanbin B, Safaei M, Amoozadeh L, Khoshavi M, Mehrtrah V, et al. Pathological findings of postmortem biopsies from lung, heart, and liver of 7 deceased COVID-19 patients. *Int J Surg Pathol*. (2021) 29:135–45. doi: 10.1177/1066896920935195
- Bhatraju PK, Ghassemieh BJ, Nichols M, Kim R, Jerome KR, Nalla AK, et al. Covid-19 in critically ill patients in the seattle region - case series. *N Engl J Med*. (2020) 382:2012–22. doi: 10.1056/NEJMoa2004500
- Cauchois R, Koubi M, Delarbre D, Manet C, Carvelli J, Blasco VB, et al. Early IL-1 receptor blockade in severe inflammatory respiratory failure complicating COVID-19. *Proc Natl Acad Sci USA*. (2020) 117:18951–3. doi: 10.1073/pnas.2009017117
- Chen N, Zhou M, Dong X, Qu J, Gong F, Han Y, et al. Epidemiological and clinical characteristics of 99 cases of 2019 novel coronavirus pneumonia in Wuhan, China: a descriptive study. *Lancet*. (2020) 395:507–13. doi: 10.1016/S0140-6736(20)30211-7
- Christie DB 3rd, Nemec HM, Scott AM, Buchanan JT, Franklin CM, Ahmed A, et al. Early outcomes with utilization of tissue plasminogen activator in COVID-19-associated respiratory distress: a series of five cases. *J Trauma Acute Care Surg*. (2020) 89:448–52. doi: 10.1097/TA.0000000000002787
- Dai M, Liu D, Liu M, Zhou F, Li G, Chen Z, et al. Patients with cancer appear more vulnerable to SARS-CoV-2: a multicenter study during the COVID-19 outbreak. *Cancer Discov*. (2020) 10:783–91. doi: 10.1158/2159-8290.CD-20-0422
- Dastan F, Saffaei A, Haseli S, Marjani M, Moniri A, Abtahian Z, et al. Promising effects of tocilizumab in COVID-19: a non-controlled, prospective clinical trial. *Int Immunopharmacol*. (2020) 88:106869. doi: 10.1016/j.intimp.2020.106869
- De Luca G, Cavalli G, Campochiaro C, Della-Torre E, Angelillo P, Tomelleri A, et al. GM-CSF blockade with mavrilimumab in severe

- COVID-19 pneumonia and systemic hyperinflammation: a single-centre, prospective cohort study. *Lancet Rheumatol.* (2020) 2:e465–73. doi: 10.1016/S2665-9913(20)30170-3
39. Dogan L, Kaya D, Sarikaya T, Zengin R, Dincer A, Akinci IO, et al. Plasmapheresis treatment in COVID-19-related autoimmune meningoencephalitis: case series. *Brain Behav Immun.* (2020) 87:155–8. doi: 10.1016/j.bbi.2020.05.022
  40. Elder C, Bawa S, Anderson D, Atkinson S, Etzel J, Moritz T. Expectant management of pneumothorax in intubated COVID-19 positive patients: a case series. *J Cardiothorac Surg.* (2020) 15:263. doi: 10.1186/s13019-020-01297-7
  41. Falces-Romero I, Ruiz-Bastian M, Díaz-Pollán B, Maseda E, García-Rodríguez J, SARS-CoV-2 Working Group. Isolation of *Aspergillus* spp. in respiratory samples of patients with COVID-19 in a Spanish Tertiary Care Hospital. *Mycoses.* (2020) 63:1144–8. doi: 10.1111/myc.13155
  42. Flikweert AW, Grootenboers MJJH, Yick DCY, du Mée AWF, van der Meer NJM, Rettig TCD, et al. Late histopathologic characteristics of critically ill COVID-19 patients: different phenotypes without evidence of invasive aspergillosis, a case series. *J Crit Care.* (2020) 59:149–55. doi: 10.1016/j.jcrc.2020.07.002
  43. Grasselli G, Greco M, Zanella A, Albano G, Antonelli M, Bellani G, et al. Risk factors associated with mortality among patients with COVID-19 in intensive care units in lombardy, Italy. *JAMA Intern Med.* (2020) 180:1345–55. doi: 10.1001/jamainternmed.2020.3539
  44. Grein J, Ohmagari N, Shin D, Diaz G, Asperges E, Castagna A, et al. Compassionate use of remdesivir for patients with severe Covid-19. *N Engl J Med.* (2020) 382:2327–36. doi: 10.1056/NEJMoa2007016
  45. Halvatsiotis P, Kotanidou A, Tzannis K, Jahaj E, Magira E, Theodorakopoulou M, et al. Demographic and clinical features of critically ill patients with COVID-19 in Greece: the burden of diabetes and obesity. *Diabetes Res Clin Pract.* (2020) 166:108331. doi: 10.1016/j.diabres.2020.108331
  46. Hernandez-Romieu AC, Adelman MW, Hockstein MA, Robichaux CJ, Edwards JA, Fazio JC, et al. Timing of intubation and mortality among critically ill coronavirus disease 2019 patients: a single-center cohort study. *Crit Care Med.* (2020) 48:e1045–53. doi: 10.1097/CCM.0000000000004600
  47. Kato H, Shimizu H, Shibue Y, Hosoda T, Iwabuchi K, Nagamine K, et al. Clinical course of 2019 novel coronavirus disease (COVID-19) in individuals present during the outbreak on the Diamond Princess cruise ship. *J Infect Chemother.* (2020) 26:865–9. doi: 10.1016/j.jiac.2020.05.005
  48. Ketcham SW, Adie SK, Malliett A, Abdul-Aziz AA, Bitar A, Grafton G, et al. Coronavirus disease-2019 in heart transplant recipients in southeastern michigan: a case series. *J Card Fail.* (2020) 26:457–61. doi: 10.1016/j.cardfail.2020.05.008
  49. Kewan T, Covut F, Al-Jaghbeer MJ, Rose L, Gopalakrishna KV, Akbik B. Tocilizumab for treatment of patients with severe COVID-19: a retrospective cohort study. *EClin Med.* (2020) 24:100418. doi: 10.1016/j.eclinm.2020.100418
  50. Khullar R, Shah S, Singh G, Bae J, Gattu R, Jain S, et al. Effects of prone ventilation on oxygenation, inflammation, and lung infiltrates in COVID-19 related acute respiratory distress syndrome: a retrospective cohort study. *J Clin Med Res.* (2020) 9:4129. doi: 10.3390/jcm9124129
  51. Konopka KE, Nguyen T, Jentzen JM, Rayes O, Schmidt CJ, Wilson AM, et al. Diffuse alveolar damage (DAD) resulting from coronavirus disease 2019 infection is morphologically indistinguishable from other causes of DAD. *Histopathology.* (2020) 77:570–8. doi: 10.1111/his.14180
  52. Krishnan S, Patel K, Desai R, Sule A, Paik P, Miller A, et al. Clinical comorbidities, characteristics, and outcomes of mechanically ventilated patients in the State of Michigan with SARS-CoV-2 pneumonia. *J Clin Anesth.* (2020) 67:110005. doi: 10.1016/j.jclinane.2020.110005
  53. Kristinsson B, Kristinsdottir LB, Blondal AT, Thormar KM, Kristjansson M, Karason S, et al. Nationwide incidence and outcomes of patients with coronavirus disease 2019 requiring intensive care in Iceland. *Crit Care Med.* (2020) 48:e1102–5. doi: 10.1097/CCM.0000000000004582
  54. Lê MP, Jaquet P, Patrier J, Wicky P-H, Le Hingrat Q, Veyrier M, et al. Pharmacokinetics of lopinavir/ritonavir oral solution to treat COVID-19 in mechanically ventilated ICU patients. *J Antimicrob Chemother.* (2020) 75:2657–60. doi: 10.1093/jac/dkaa261
  55. LeBrun DG, Konnaris MA, Ghahramani GC, Premkumar A, DeFrancesco CJ, Gruskay JA, et al. Hip fracture outcomes during the COVID-19 pandemic: early results from New York. *J Orthop Trauma.* (2020) 34:403–10. doi: 10.1097/BOT.0000000000001849
  56. Lechien JR, Chiesa-Estomba CM, De Siaty DR, Horoi M, Le Bon SD, Rodriguez A, et al. Olfactory and gustatory dysfunctions as a clinical presentation of mild-to-moderate forms of the coronavirus disease (COVID-19): a multicenter European study. *Eur Arch Otorhinolaryngol.* (2020) 277:2251–61. doi: 10.1007/s00405-020-05965-1
  57. Lee AJY, Chung CLH, Young BE, Ling LM, Ho BCH, Puah SH, et al. Clinical course and physiotherapy intervention in 9 patients with COVID-19. *Physiotherapy.* (2020) 109:1–3. doi: 10.1016/j.physio.2020.06.002
  58. Liu J, Zhang S, Wu Z, Shang Y, Dong X, Li G, et al. Clinical outcomes of COVID-19 in Wuhan, China: a large cohort study. *Ann Intensive Care.* (2020) 10:99. doi: 10.1186/s13613-020-00706-3
  59. Lowe A, Chang DD, Creek G. Multiple fatalities in a family cluster of COVID-19 with acute respiratory distress syndrome. *Ochsner J.* (2020) 20:134–8. doi: 10.31486/toj.20.0056
  60. Maritati F, Cerutti E, Zuccatosta L, Fiorentini A, Finale C, Ficosecco M, et al. SARS-CoV-2 infection in kidney transplant recipients: experience of the italian marche region. *Transpl Infect Dis.* (2020) 22:e13377. doi: 10.1111/tid.13377
  61. Morassi M, Bagatto D, Cobelli M, D'Agostini S, Gigli GL, Bnà C, et al. Stroke in patients with SARS-CoV-2 infection: case series. *J Neurol.* (2020) 267:2185–92. doi: 10.1007/s00415-020-09885-2
  62. Morillas JA, Marco Canosa F, Srinivas P, Asadi T, Calabrese C, Rajendram P, et al. Tocilizumab therapy in 5 solid and composite tissue transplant recipients with early ARDS due to SARS-CoV-2. *Am J Transplant.* (2020) 20:3191–7. doi: 10.1111/ajt.16080
  63. Navarro-Millán I, Sattui SE, Lakhanpal A, Zisa D, Siegel CH, Crow MK. Use of anakinra to prevent mechanical ventilation in severe COVID-19: a case series. *Arthritis Rheumatol.* (2020) 72:1990–7. doi: 10.1002/art.41422
  64. Novelli L, Raimondi F, Ghirardi A, Pellegrini D, Capodanno D, Sotgiu G, et al. At the peak of COVID-19 age and disease severity but not comorbidities are predictors of mortality: COVID-19 burden in Bergamo, Italy. *Panminerva Med.* (2021) 63:51–61. doi: 10.23736/S0031-0808.20.04063-X
  65. Pan C, Chen L, Lu C, Zhang W, Xia J-A, Sklar MC, et al. Lung recruitability in COVID-19-associated acute respiratory distress syndrome: a single-center observational study. *Am J Respir Crit Care Med.* (2020) 201:1294–7. doi: 10.1164/rccm.202003-0527LE
  66. Peng M, Liu X, Li J, Ren D, Liu Y, Meng X, et al. Successful management of seven cases of critical COVID-19 with early noninvasive-invasive sequential ventilation algorithm and bundle pharmacotherapy. *Front Med.* (2020) 14:674–80. doi: 10.1007/s11684-020-0796-3
  67. Plotnikow GA, Matesa A, Nadur JM, Alonso M, Nuñez I I, Vergara G, et al. Characteristics and outcomes of patients infected with nCoV19 requiring invasive mechanical ventilation in Argentina. *Rev Bras Ter Intensiva.* (2020) 32:348–53. doi: 10.5935/0103-507X.20200062
  68. Radnis C, Qiu S, Jhaveri M, Da Silva I, Szwedka A, Koffman L. Radiographic and clinical neurologic manifestations of COVID-19 related hypoxemia. *J Neurol Sci.* (2020) 418:117119. doi: 10.1016/j.jns.2020.117119
  69. Riker RR, May TL, Fraser GL, Gagnon DJ, Bandara M, Zemrak WR, et al. Heparin-induced thrombocytopenia with thrombosis in COVID-19 adult respiratory distress syndrome. *Res Pract Thromb Haemost.* (2020) 4:936–41. doi: 10.1002/rth2.12390
  70. Rizo-Téllez SA, Méndez-García LA, Flores-Rebollo C, Alba-Flores F, Alcántara-Suárez R, Manjarrez-Reyna AN, et al. The neutrophil-to-monocyte ratio and lymphocyte-to-neutrophil ratio at admission predict in-hospital mortality in mexican patients with severe SARS-CoV-2 infection (Covid-19). *Microorganisms.* (2020) 8:1560. doi: 10.3390/microorganisms8101560
  71. Sakr Y, Giovini M, Leone M, Pizzilli G, Kortgen A, Bauer M, et al. The clinical spectrum of pulmonary thromboembolism in patients with coronavirus disease-2019 (COVID-19) pneumonia: a European case series. *J Crit Care.* (2021) 61:39–44. doi: 10.1016/j.jcrc.2020.09.021
  72. Schaefer I-M, Padera RF, Solomon IH, Kanjilal S, Hammer MM, Hornick JL, et al. In situ detection of SARS-CoV-2 in lungs and airways of patients with COVID-19. *Mod Pathol.* (2020) 33:2104–14. doi: 10.1038/s41379-020-0595-z

73. Shen C, Wang Z, Zhao F, Yang Y, Li J, Yuan J, et al. Treatment of 5 critically ill patients with COVID-19 with convalescent plasma. *JAMA*. (2020) 323:1582–9. doi: 10.1001/jama.2020.4783
74. Singh S, Chakravarty T, Chen P, Akhmerov A, Falk J, Friedman O, et al. Allogeneic cardiophere-derived cells (CAP-1002) in critically ill COVID-19 patients: compassionate-use case series. *Basic Res Cardiol*. (2020) 115:36. doi: 10.1007/s00395-020-0795-1
75. So C, Ro S, Murakami M, Imai R, Jinta T. High-dose, short-term corticosteroids for ARDS caused by COVID-19: a case series. *Respirol Case Rep*. (2020) 8:e00596. doi: 10.1002/rcr.2596
76. Søvik S, Bådstøløkken PM, Sørensen V, Myhre PL, Prebensen C, Omland T, et al. A single-centre, prospective cohort study of COVID-19 patients admitted to ICU for mechanical ventilatory support. *Acta Anaesthesiol Scand*. (2021) 65:351–9. doi: 10.1111/aas.13726
77. Stony Brook COVID-19 Research Consortium. Geospatial distribution and predictors of mortality in hospitalized patients with COVID-19: a cohort study. *Open Forum Infect Dis*. (2020) 7:ofaa436. doi: 10.1093/ofid/ofaa436
78. Wali A, Rizzo V, Bille A, Routledge T, Chambers AJ. Pneumomediastinum following intubation in COVID-19 patients: a case series. *Anaesthesia*. (2020) 75:1076–81. doi: 10.1111/anae.15113
79. Wang Y, Lu X, Li Y, Chen H, Chen T, Su N, et al. Clinical course and outcomes of 344 intensive care patients with COVID-19. *Am J Respir Crit Care Med*. (2020) 201:1430–4. doi: 10.1164/rccm.202003-0736LE
80. Wang X-H, Duan J, Han X, Liu X, Zhou J, Wang X, et al. High incidence and mortality of pneumothorax in critically ill patients with COVID-19. *Heart Lung*. (2021) 50:37–43. doi: 10.1016/j.hrtlng.2020.10.002
81. Weiskopf D, Schmitz KS, Raadsen MP, Grifoni A, Okba NMA, Endeman H, et al. Phenotype and kinetics of SARS-CoV-2-specific T cells in COVID-19 patients with acute respiratory distress syndrome. *Sci Immunol*. (2020) 5:eabd2071. doi: 10.1126/sciimmunol.abd2071
82. Wilk AJ, Rustagi A, Zhao NQ, Roque J, Martínez-Colón GJ, McKechnie JL, et al. A single-cell atlas of the peripheral immune response in patients with severe COVID-19. *Nat Med*. (2020) 26:1070–6. doi: 10.1038/s41591-020-0944-y
83. Zhang L, Li J, Zhou M, Chen Z. Summary of 20 tracheal intubation by anesthesiologists for patients with severe COVID-19 pneumonia: retrospective case series. *J Anesth*. (2020) 34:599–606. doi: 10.1007/s00540-020-02778-8
84. Akhtar W, Olusanya O, Baladia MM, Young H, Shah S. SARS-CoV-2 and ECMO: early results and experience. *Indian J Thorac Cardiovasc Surg*. (2020) 37:53–60. doi: 10.1007/s12055-020-01084-y
85. Alnababteh M, Hashmi MD, Vedantam K, Chopra R, Kohli A, Hayat F, et al. Extracorporeal membrane oxygenation for COVID-19 induced hypoxia: single-center study. *Perfusion*. (2021) 36:564–72. doi: 10.1177/0267659120963885
86. Beyls C, Huette P, Abou-Arab O, Berna P, Mahjoub Y. Extracorporeal membrane oxygenation for COVID-19-associated severe acute respiratory distress syndrome and risk of thrombosis. *Br J Anaesth*. (2020) 125:e260–2. doi: 10.1016/j.bja.2020.04.079
87. Charlton M, Dashey S, Stubbs A, Lai FY, Bird PW, Badhwar V, et al. Comparing SARS-CoV-2 and influenza A(H1N1)pdm09-infected patients requiring ECMO - a single-centre, retrospective observational cohort experience. *J Infect*. (2021) 82:84–123. doi: 10.1016/j.jinf.2020.11.003
88. Falcoz P-E, Monnier A, Puyraveau M, Perrier S, Ludes P-O, Olland A, et al. Extracorporeal membrane oxygenation for critically ill patients with COVID-19-related acute respiratory distress syndrome: worth the effort? *Am J Respir Crit Care Med*. (2020) 202:460–3. doi: 10.1164/rccm.202004-1370LE
89. Goursaud S, Descamps R, Daubin C, du Cheyron D, Valette X. Corticosteroid use in selected patients with severe acute respiratory distress syndrome related to COVID-19. *J Infect*. (2020) 81:e89–90. doi: 10.1016/j.jinf.2020.05.023
90. Guilhaire J, Owyang CG, Madhok J, Laverdure F, Gaillard M, Girault A, et al. Specific considerations for venovenous extracorporeal membrane oxygenation during coronavirus disease 2019 pandemic. *ASAIO J*. (2020) 66:1069–72. doi: 10.1097/MAT.0000000000001251
91. Guo Z, Sun L, Li B, Tian R, Zhang X, Zhang Z, et al. Anticoagulation management in severe coronavirus disease 2019 patients on extracorporeal membrane oxygenation. *J Cardiothorac Vasc Anesth*. (2021) 35:389–97. doi: 10.1053/j.jvca.2020.08.067
92. Heman-Ackah SM, Su YS, Spadola M, Petrov D, Chen HI, Schuster J, et al. Neurologically devastating intraparenchymal hemorrhage in COVID-19 patients on extracorporeal membrane oxygenation: a case series. *Neurosurgery*. (2020) 87:E147–51. doi: 10.1093/neuros/nyaa198
93. Huette P, Beyls C, Guilbart M, Coquet A, Berna P, Haye G, et al. Extracorporeal membrane oxygenation for respiratory failure in COVID-19 patients: outcome and time-course of clinical and biological parameters. *Can J Anaesth*. (2020) 67:1486–8. doi: 10.1007/s12630-020-01727-z
94. Jäckel M, Rillinger J, Lang CN, Zotzmann V, Kaier K, Stachon P, et al. Outcome of acute respiratory distress syndrome requiring extracorporeal membrane oxygenation in Covid-19 or influenza: a single-center registry study. *Artif Organs*. (2021) 45:593–601. doi: 10.1111/aor.13865
95. Jacobs JP, Stammers AH, St Louis J, Hayanga JWA, Firstenberg MS, Mongero LB, et al. Extracorporeal membrane oxygenation in the treatment of severe pulmonary and cardiac compromise in coronavirus disease 2019: experience with 32 patients. *ASAIO J*. (2020) 66:722–30. doi: 10.1097/MAT.0000000000001185
96. Kon ZN, Smith DE, Chang SH, Goldenberg RM, Angel LF, Carillo JA, et al. Extracorporeal membrane oxygenation support in severe COVID-19. *Ann Thorac Surg*. (2021) 111:537–43. doi: 10.1016/j.athoracsur.2020.07.002
97. Le Breton C, Besset S, Freitas-Ramos S, Amouretti M, Billiet PA, Dao M, et al. Extracorporeal membrane oxygenation for refractory COVID-19 acute respiratory distress syndrome. *J Crit Care*. (2020) 60:10–12. doi: 10.1016/j.jcrc.2020.07.013
98. Li X, Guo Z, Li B, Zhang X, Tian R, Wu W, et al. Extracorporeal membrane oxygenation for coronavirus disease 2019 in Shanghai, China. *ASAIO J*. (2020) 66:475–81. doi: 10.1097/MAT.0000000000001172
99. Liu J, Dong Y-Q, Yin J, He G, Wu X, Li J, et al. Critically ill patients with COVID-19 with ECMO and artificial liver plasma exchange: a retrospective study. *Medicine*. (2020) 99:e21012. doi: 10.1097/MD.00000000000021012
100. Loforte A, Dal Checco E, Gliozzi G, Benedetto M, Cavalli GG, Mariani C, et al. Veno-venous extracorporeal membrane oxygenation support in COVID-19 respiratory distress syndrome: initial experience. *ASAIO J*. (2020) 66:734–8. doi: 10.1097/MAT.0000000000001198
101. Matsunaga N, Hayakawa K, Terada M, Ohtsu H, Asai Y, Tsuzuki S, et al. Clinical epidemiology of hospitalized patients with COVID-19 in Japan: report of the COVID-19 REGISTRY JAPAN. *Clin Infect Dis*. (2020). doi: 10.1093/cid/ciaa1470
102. Miike S, Sakamoto N, Washino T, Kosaka A, Kuwahara Y, Ishida T, et al. Critically ill patients with COVID-19 in Tokyo, Japan: a single-center case series. *J Infect Chemother*. (2021) 27:291–5. doi: 10.1016/j.jiac.2020.10.019
103. Mustafa AK, Alexander PJ, Joshi DJ, Tabachnick DR, Cross CA, Pappas PS, et al. Extracorporeal membrane oxygenation for patients with COVID-19 in severe respiratory failure. *JAMA Surg*. (2020) 155:990–2. doi: 10.1001/jamasurg.2020.3950
104. Osho AA, Moonsamy P, Hibbert KA, Shelton KT, Trahanas JM, Attia RQ, et al. Veno-venous extracorporeal membrane oxygenation for respiratory failure in COVID-19 patients: early experience from a major academic medical center in North America. *Ann Surg*. (2020) 272:e75–8. doi: 10.1097/SLA.0000000000000484
105. Ronit A, Berg RMG, Bay JT, Haugaard AK, Ahlström MG, Burgdorf KS, et al. Compartmental immunophenotyping in COVID-19 ARDS: a case series. *J Allergy Clin Immunol*. (2021) 147:81–91. doi: 10.1016/j.jaci.2020.09.009
106. Schmidt M, Hajage D, Lebreton G, Monsel A, Voiriot G, Levy D, et al. Extracorporeal membrane oxygenation for severe acute respiratory distress syndrome associated with COVID-19: a retrospective cohort study. *Lancet Respir Med*. (2020) 8:1121–31. doi: 10.1016/S2213-2600(20)30328-3
107. Shih E, DiMaio JM, Squiers JJ, Banwait JK, Meyer DM, George TJ, et al. Venovenous extracorporeal membrane oxygenation for patients with refractory coronavirus disease 2019 (COVID-19): multicenter experience of referral hospitals in a large health care system. *J Thorac Cardiovasc Surg*. (2020) (inpress). doi: 10.1016/j.jtcvs.2020.11.073
108. Sultan I, Habertheuer A, Usman AA, Kilic A, Gnall E, Friscia ME, et al. The role of extracorporeal life support for patients with COVID-19: preliminary results from a statewide experience. *J Card Surg*. (2020) 35:1410–3. doi: 10.1111/jocs.14583



109. Usman AA, Han J, Acker A, Olia SE, Bermudez C, Cucchiara B, et al. A case series of devastating intracranial hemorrhage during venovenous extracorporeal membrane oxygenation for COVID-19. *J Cardiothorac Vasc Anesth.* (2020) 34:3006–12. doi: 10.1053/j.jvca.2020.07.063
110. Xuan W, Chen C, Jiang X, Zhang X, Zhu H, Zhang S, et al. Clinical characteristics and outcomes of five critical COVID-19 patients treated with extracorporeal membrane oxygenation in Leishenshan Hospital in Wuhan. *J Clin Anesth.* (2020) 67:110033. doi: 10.1016/j.jclinane.2020.110033
111. Xu J, Xie J, Du B, Tong Z, Qiu H, Bagshaw SM. Clinical characteristics and outcomes of patients with severe COVID-19 induced acute kidney injury. *J Intensive Care Med.* (2021) 36:319–26. doi: 10.1177/0885066620970858
112. Yang X, Cai S, Luo Y, Zhu F, Hu M, Zhao Y, et al. Extracorporeal membrane oxygenation for coronavirus disease 2019-induced acute respiratory distress syndrome: a multicenter descriptive study. *Crit Care Med.* (2020) 48:1289–95. doi: 10.1097/CCM.0000000000004447
113. Zayat R, Kalverkamp S, Grottko O, Durak K, Dreher M, Autschbach R, et al. Role of extracorporeal membrane oxygenation in critically ill COVID-19 patients and predictors of mortality. *Artif Organs.* (2021) 45:E158–70. doi: 10.1111/aor.13873
114. Zeng Y, Cai Z, Xianyu Y, Yang BX, Song T, Yan Q. Prognosis when using extracorporeal membrane oxygenation (ECMO) for critically ill COVID-19 patients in China: a retrospective case series. *Crit Care.* (2020) 24:148. doi: 10.1186/s13054-020-2840-8
115. Zeng J-H, Wu W-B, Qu J-X, Wang Y, Dong C-F, Luo Y-F, et al. Cardiac manifestations of COVID-19 in Shenzhen, China. *Infection.* (2020) 48:861–70. doi: 10.1007/s15010-020-01473-w
116. Zhang J, Merrick B, Correa GL, Camporota L, Retter A, Doyle A, et al. Venovenous extracorporeal membrane oxygenation in coronavirus disease 2019: a case series. *ERJ Open Res.* (2020) 6:00463. doi: 10.1183/23120541.00463-2020
117. Zhang Q, Shen J, Chen L, Li S, Zhang W, Jiang C, et al. Timing of invasive mechanic ventilation in critically ill patients with coronavirus disease 2019. *J Trauma Acute Care Surg.* (2020) 89:1092–8. doi: 10.1097/TA.0000000000002939
118. Zheng Y, Sun L-J, Xu M, Pan J, Zhang Y-T, Fang X-L, et al. Clinical characteristics of 34 COVID-19 patients admitted to intensive care unit in Hangzhou, China. *J Zhejiang Univ Sci B.* (2020) 21:378–87. doi: 10.1631/jzus.B2000174
119. Feng Y, Amoateng-Adjepong Y, Kaufman D, Gheorghe C, Manthous CA. Age, duration of mechanical ventilation, and outcomes of patients who are critically ill. *Chest.* (2009) 136:759–64. doi: 10.1378/chest.09-0515
120. Faisy C, Meziani F, Planquette B, Clavel M, Gacouin A, Bornstein C, et al. Effect of acetazolamide vs. placebo on duration of invasive mechanical ventilation among patients with chronic obstructive pulmonary disease: a randomized clinical trial. *JAMA.* (2016) 315:480–8. doi: 10.1001/jama.2016.0019
121. Barbier F, Coquet I, Legriel S, Pavie J, Darmon M, Mayaux J, et al. Etiologies and outcome of acute respiratory failure in HIV-infected patients. *Intensive Care Med.* (2009) 35:1678–86. doi: 10.1007/s00134-009-1559-4
122. Esteban A, Anzueto A, Frutos F, Alía I, Brochard L, Stewart TE, et al. Characteristics and outcomes in adult patients receiving mechanical ventilation: a 28-day international study. *JAMA.* (2002) 287:345–55. doi: 10.1001/jama.287.3.345
123. Shorr AF, Bodi M, Rodriguez A, Sole-Violan J, Garnacho-Montero J, Rello J, et al. Impact of antibiotic guideline compliance on duration of mechanical ventilation in critically ill patients with community-acquired pneumonia. *Chest.* (2006) 130:93–100. doi: 10.1016/S0012-3692(15)50958-6
124. Wang J-T, Sheng W-H, Fang C-T, Chen Y-C, Wang J-L, Yu C-J, et al. Clinical manifestations, laboratory findings, and treatment outcomes of SARS patients. *Emerg Infect Dis.* (2004) 10:818–24. doi: 10.3201/eid1005.030640
125. Tsai M-J, Yang K-Y, Chan M-C, Kao K-C, Wang H-C, Perng W-C, et al. Impact of corticosteroid treatment on clinical outcomes of influenza-associated ARDS: a nationwide multicenter study. *Ann Intensive Care.* (2020) 10:26. doi: 10.1186/s13613-020-0642-4
126. Kovacevic P, Matijasevic J, Dragic S, Zlojutro B, Gavrilovic S, Jandric M, et al. Characteristics and outcomes of critically ill patients with influenza A (H1N1) in the Western Balkans during the 2019 post-pandemic season. *Indian J Med Microbiol.* (2020) 38:415–20. doi: 10.4103/ijmm.IJMM\_20\_169
127. Ludwig M, Jacob J, Basedow F, Andersohn F, Walker J. Clinical outcomes and characteristics of patients hospitalized for Influenza or COVID-19 in Germany. *Int J Infect Dis.* (2021) 103:316–22. doi: 10.1016/j.ijid.2020.11.204
128. Peek GJ, Mugford M, Tiruvoipati R, Wilson A, Allen E, Thalanany MM, et al. Efficacy and economic assessment of conventional ventilatory support versus extracorporeal membrane oxygenation for severe adult respiratory failure (CESAR): a multicentre randomised controlled trial. *Lancet.* (2009) 374:1351–63. doi: 10.1016/S0140-6736(09)61069-2
129. Combes A, Hajage D, Capellier G, Demoule A, Lavoué S, Guervilly C, et al. Extracorporeal membrane oxygenation for severe acute respiratory distress syndrome. *N Engl J Med.* (2018) 378:1965–75. doi: 10.1056/NEJMoa1800385
130. Sukhal S, Sethi J, Ganesh M, Villablanca PA, Malhotra AK, Ramakrishna H. Extracorporeal membrane oxygenation in severe influenza infection with respiratory failure: a systematic review and meta-analysis. *Ann Card Anaesth.* (2017) 20:14–21. doi: 10.4103/0971-9784.197820
131. Guan W-J, Ni Z-Y, Hu Y, Liang W-H, Ou C-Q, He J-X, et al. Clinical characteristics of coronavirus disease 2019 in China. *N Engl J Med.* (2020) 382:1708–20. doi: 10.1056/NEJMoa2002032
132. Ranney ML, Griffith V, Jha AK. Critical supply shortages - the need for ventilators and personal protective equipment during the Covid-19 pandemic. *N Engl J Med.* (2020) 382:e41. doi: 10.1056/NEJMp2006141
133. Carrillo A, Gonzalez-Diaz G, Ferrer M, Martinez-Quintana ME, Lopez-Martinez A, Llamas N, et al. Non-invasive ventilation in community-acquired pneumonia and severe acute respiratory failure. *Intensive Care Med.* (2012) 38:458–66. doi: 10.1007/s00134-012-2475-6
134. Kang BJ, Koh Y, Lim C-M, Huh JW, Baek S, Han M, et al. Failure of high-flow nasal cannula therapy may delay intubation and increase mortality. *Intensive Care Med.* (2015) 41:623–32. doi: 10.1007/s00134-015-3693-5
135. Brouqui P, Amrane S, Million M, Cortaredona S, Parola P, Lagier J-C, et al. Asymptomatic hypoxia in COVID-19 is associated with poor outcome. *Int J Infect Dis.* (2021) 102:233–8. doi: 10.1016/j.ijid.2020.10.067
136. Ramachandran P, Swamy L, Kaul V, Agrawal A. A national strategy for ventilator and ICU resource allocation during the coronavirus disease 2019 pandemic. *Chest.* (2020) 158:887–9. doi: 10.1016/j.chest.2020.04.050
137. Cunningham JW, Vaduganathan M, Claggett BL, Jering KS, Bhatt AS, Rosenthal N, et al. Clinical outcomes in young US adults hospitalized with COVID-19. *JAMA Intern Med.* (2021) 181:379–81. doi: 10.1001/jamainternmed.2020.5313
138. Karaca-Mandic P, Georgiou A, Sen S. Assessment of COVID-19 hospitalizations by race/ethnicity in 12 States. *JAMA Intern Med.* (2021) 181:131–4. doi: 10.1001/jamainternmed.2020.3857
139. Zeberg H, Pääbo S. The major genetic risk factor for severe COVID-19 is inherited from Neanderthals. *Nature.* (2020) 587:610–2. doi: 10.1038/s41586-020-2818-3

**Conflict of Interest:** The authors declare that the research was conducted in the absence of any commercial or financial relationships that could be construed as a potential conflict of interest.

**Publisher's Note:** All claims expressed in this article are solely those of the authors and do not necessarily represent those of their affiliated organizations, or those of the publisher, the editors and the reviewers. Any product that may be evaluated in this article, or claim that may be made by its manufacturer, is not guaranteed or endorsed by the publisher.

Copyright © 2021 Funakoshi, Morita and Kumanogoh. This is an open-access article distributed under the terms of the Creative Commons Attribution License (CC BY). The use, distribution or reproduction in other forums is permitted, provided the original author(s) and the copyright owner(s) are credited and that the original publication in this journal is cited, in accordance with accepted academic practice. No use, distribution or reproduction is permitted which does not comply with these terms.





# Intermediate- vs. Standard-Dose Prophylactic Anticoagulation in Patients With COVID-19 Admitted in Medical Ward: A Propensity Score-Matched Cohort Study

David M. Smadja<sup>1,2,3\*</sup>, Guillaume Bonnet<sup>4,5</sup>, Nicolas Gendron<sup>1,2</sup>, Orianne Weizman<sup>4,6</sup>, Lina Khider<sup>7</sup>, Antonin Trimaille<sup>8</sup>, Tristan Mirault<sup>4,7</sup>, Charles Fauvel<sup>9</sup>, Jean-Luc Diehl<sup>1,10</sup>, Delphine Mika<sup>11</sup>, Aurelien Philippe<sup>1,2</sup>, Théo Pezel<sup>12</sup>, Guillaume Goudot<sup>4,7</sup>, Willy Sutter<sup>4,13</sup>, Benjamin Planquette<sup>1,3,14</sup>, Victor Waldmann<sup>4,15</sup>, Olivier Sanchez<sup>1,3,14</sup>, Ariel Cohen<sup>16</sup> and Richard Chocron<sup>4,17</sup> for the Critical COVID-19 France Investigators

## OPEN ACCESS

### Edited by:

Reza Lashgari,  
Shahid Beheshti University, Iran

### Reviewed by:

Lin Qi,  
Central South University, China  
Jung Hsu,  
Saint Mary's Hospital  
Luodong, Taiwan

### \*Correspondence:

David M. Smadja  
david.smadja@aphp.fr

### Specialty section:

This article was submitted to  
Infectious Diseases – Surveillance,  
Prevention and Treatment,  
a section of the journal  
Frontiers in Medicine

Received: 26 July 2021

Accepted: 08 September 2021

Published: 15 October 2021

### Citation:

Smadja DM, Bonnet G, Gendron N, Weizman O, Khider L, Trimaille A, Mirault T, Fauvel C, Diehl J-L, Mika D, Philippe A, Pezel T, Goudot G, Sutter W, Planquette B, Waldmann V, Sanchez O, Cohen A and Chocron R (2021) Intermediate- vs. Standard-Dose Prophylactic Anticoagulation in Patients With COVID-19 Admitted in Medical Ward: A Propensity Score-Matched Cohort Study. *Front. Med.* 8:747527. doi: 10.3389/fmed.2021.747527

<sup>1</sup> Innovative Therapies in Haemostasis, INSERM, Université de Paris, Paris, France, <sup>2</sup> Department of Hematology and Biosurgical Research Lab (Carpentier Foundation), AP-HP, Georges Pompidou European Hospital, Paris, France, <sup>3</sup> F-CRIN INNOVTE, Saint-Étienne, France, <sup>4</sup> Paris Cardiovascular Research Center (PARCC), INSERM, Université de Paris, Paris, France, <sup>5</sup> Center Hospitalier Universitaire de Bordeaux, Hôpital Cardiologique Haut-Lévêque, Unité Médico-Chirurgicale de Valvulopathies et Cardiomyopathies, Pessac, France, <sup>6</sup> Institut Lorrain du Cœur et des Vaisseaux, CHU de Nancy, Vandœuvre les Nancy, France, <sup>7</sup> Department of Vascular Medicine, AP-HP, Georges Pompidou European Hospital, Paris, France, <sup>8</sup> Nouvel Hôpital Civil, Center Hospitalier Régional Universitaire de Strasbourg, Strasbourg, France, <sup>9</sup> Rouen University Hospital, FHU REMOD-VHF, Rouen, France, <sup>10</sup> Medical Intensive Care Department and Biosurgical Research Lab (Carpentier Foundation), AP-HP, Georges Pompidou European Hospital, Paris, France, <sup>11</sup> INSERM, Université Paris-Saclay, Chatenay-Malabry, France, <sup>12</sup> Department of Cardiology, Lariboisière Hospital, AP-HP, University of Paris, Paris, France, <sup>13</sup> Department of Vascular Surgery, AP-HP, Georges Pompidou European Hospital, Paris, France, <sup>14</sup> Department of Pneumology and Intensive Care and Biosurgical Research Lab (Carpentier Foundation), AP-HP, Georges Pompidou European Hospital, Paris, France, <sup>15</sup> Department of Cardiology, AP-HP, Georges Pompidou European Hospital, Paris, France, <sup>16</sup> Department of Cardiology, AP-HP, Saint Antoine Hospital, Paris, France, <sup>17</sup> Department of Emergency, AP-HP, Georges Pompidou European Hospital, Paris, France

**Background:** Microthrombosis and large-vessel thrombosis are the main triggers of COVID-19 worsening. The optimal anticoagulant regimen in COVID-19 patients hospitalized in medical wards remains unknown.

**Objectives:** To evaluate the effects of intermediate-dose vs. standard-dose prophylactic anticoagulation (AC) among patients with COVID-19 hospitalized in medical wards.

**Methods and results:** We used a large French multicentric retrospective study enrolling 2,878 COVID-19 patients hospitalized in medical wards. After exclusion of patients who had an AC treatment before hospitalization, we generated a propensity-score-matched cohort of patients who were treated with intermediate-dose or standard-dose prophylactic AC between February 26 and April 20, 2020 (intermediate-dose,  $n = 261$ ; standard-dose prophylactic anticoagulation,  $n = 763$ ). The primary outcome of the study was in-hospital mortality; this occurred in 23 of 261 (8.8%) patients in the intermediate-dose group and 74 of 783 (9.4%) patients in the standard-dose prophylactic AC group ( $p = 0.85$ ); while time to death was also the same in both the treatment groups (11.5 and 11.6 days, respectively,  $p = 0.17$ ). We did not observe any difference regarding venous and arterial thrombotic events between the intermediate dose and standard

dose, respectively (venous thrombotic events: 2.3 vs. 2.4%,  $p=0.99$ ; arterial thrombotic events: 2.7 vs. 1.2%,  $p = 0.25$ ). The 30-day Kaplan–Meier curves for in-hospital mortality demonstrate no statistically significant difference in in-hospital mortality (HR: 0.99 (0.63–1.60);  $p = 0.99$ ). Moreover, we found that no particular subgroup was associated with a significant reduction in in-hospital mortality.

**Conclusion:** Among COVID-19 patients hospitalized in medical wards, intermediate-dose prophylactic AC compared with standard-dose prophylactic AC did not result in a significant difference in in-hospital mortality.

**Keywords:** SARS-CoV-2, anticoagulation, intermediate dose, prophylactic treatment, mortality, COVID-19, LMWH

## INTRODUCTION

More than respiratory disease, coronavirus disease 2019 (COVID-19) caused by severe acute respiratory syndrome coronavirus 2 (SARS-CoV-2) is a systemic acquired vascular disease associated with inflammation (1), endothelial injury (2), and high thrombosis prevalence, in particular pulmonary embolism (PE) (3–8). *In situ* microthrombosis has emerged as a key feature of COVID-19, in contrast to an embolus, commonly observed in deep vein thrombosis. Microthrombosis in COVID-19 has been observed in all postmortem lung examinations and could be explained, at least in part, by the large von Willebrand factor (VWF) released following endothelial activation (9). A massive release of plasma VWF is associated with an increase of the high-molecular-weight multimers, and a slight decrease in ADAMTS13 (a disintegrin and metalloprotease with thrombospondin type I repeats-13) levels or function, that is likely drive to the generation of microthrombosis in COVID-19 (10). More so than real thrombotic complication i.e., macrothrombosis, microthrombosis is probably an important trigger of pathophysiology and, in particular, hypoxemia. Thus, prophylactic anticoagulation (AC) is likely to be one of the best treatments to avoid the worsening of the disease. Empirically, higher prophylactic dosing of unfractionated heparin or low molecular weight heparin (LMWH) has become relatively common to limit the formation of microthrombi according to the second version of the International Society on Thrombosis and Haemostasis (11) and the French guidelines (12). Therapeutic AC should be administered only if a thrombotic event or PE is occurring. In a recent multicenter randomized trial (13), intermediate-dose in contrast to standard-dose prophylactic AC did not improve outcomes, including mortality in patients admitted in the intensive care units (ICU). The aim of our study was to investigate the effect on in-hospital mortality of intermediate- vs. standard-dose prophylactic AC in patients with COVID-19 admitted in medical wards using a propensity score-matched cohort study.

## METHODS

Data will be made available from the authors on reasonable request.

## Study Settings and Population

From February 26 to April 20, 2020, consecutive patients with a diagnosis of SARS-CoV-2 infection and initially hospitalized in medical wards were included (none of the patients were directly admitted to ICU). Patients were aged over 18 years and were included in a retrospective, multicenter (24 centers), observational cohort study, which was named the critical COVID-19 France (CCF) study, which initiated by the French Society of Cardiology. Following World Health Organization (WHO) criteria, SARS-CoV-2 infection was determined by a positive result from a real-time reverse transcriptase-polymerase chain reaction (RT-PCR) test of nasal or pharyngeal swabs, or lower respiratory tract aspirates (confirmed case), or by typical imaging characteristics on chest computed tomography (CT) when laboratory testing was inconclusive. The CCF study was declared to and authorized by the French data protection committee (authorization no. 2207326v0), and conducted in accordance with the ethical standards established in the Declaration of Helsinki and its later amendments (NCT04344327) (7, 14, 15).

## Data Collection and AC Regimen

All data were retrospectively collected by local investigators in an electronic case-report form *via* the REDCap® software (Research Electronic Data Capture®, Vanderbilt University, USA) hosted by a secured server from the French Institute of Health and Medical Research at the Paris Cardiovascular Research Center. Baseline information of the patient included demographic characteristics, coexisting medical conditions, cardiovascular comorbidities, and chronic medications. Clinical parameters and biological findings were recorded at admission. On the chest CT scan, the degree of pulmonary lesions with ground-glass opacities and areas of consolidation were categorized as low/moderate (<50% involvement) or severe ( $\geq 50\%$  involvement). Data on pharmacological therapies, mode of respiratory support, complications, and final vital status were also gathered throughout the hospitalization. Patients who had an AC treatment (whatever the regimen) before hospitalization were excluded from the analysis.

The AC regimens analyzed during hospitalization were categorized into two groups: standard-dose prophylactic (once daily LMWH; subcutaneous heparin injection or intravenous heparin infusions) or intermediate-dose prophylactic (twice

**TABLE 1 |** Baseline characteristics of the matched population between intermediate- vs. standard-dose prophylactic anticoagulation among patients with COVID-19 admitted in medical wards.

|  | Whole population (n = 1,044) | Prophylactic anticoagulation |                         |         |        |
|--|------------------------------|------------------------------|-------------------------|---------|--------|
|  |                              | Intermediate dose (n = 261)  | Standard dose (n = 783) | p-value | SMD    |
| Age, median [IQR]  | 63.7 [52.0–74.2]             | 63.0 [52.7–73.7]             | 63.9 [51.2–74.5]        | 0.78    | 0.016  |
| <b>Gender, n (%)</b>                                     |                              |                              |                         |         |        |
| Women  | 391 (37.5)                   | 100 (38.3)                   | 300 (38.3)              | 1.00    | 0.024  |
| Men  | 653 (62.5)                   | 161 (61.7)                   | 483 (61.7)              |         |        |
| Body Mass Index, median [IQR]                            | 28.6 [25.4–32.2]             | 28.6 [25.7–32.3]             | 28.7 [25.5–32.2]        | 0.77    | 0.043  |
| Time from illness onset to hospitalization, median [IQR] | 7.0 [4.0, 10.0]              | 7.0 [4.0, 9.0]               | 7.00 [4.0, 10.0]        | 0.29    | 0.076  |
| Lung extensive damage on CT scan >50%                    | 179 (17.1)                   | 85 (32.6)                    | 104 (13.3)              | <0.001  | 0.033  |
| <b>Coexisting conditions, n (%)</b>                      |                              |                              |                         |         |        |
| Hypertension   | 474 (45.4)                   | 120 (46.0)                   | 363 (46.4)              | 0.97    | 0.015  |
| Diabetes   | 291 (27.9)                   | 77 (29.5)                    | 224 (28.6)              | 0.84    | 0.037  |
| Hyperlipidemia   | 275 (26.3)                   | 69 (26.4)                    | 197 (25.2)              | 0.74    | 0.003  |
| Peripheral arterial disease                              | 42 (4.0)                     | 11 (4.2)                     | 25 (3.2)                | 0.56    | 0.013  |
| Ischemic stroke  | 57 (5.5)                     | 12 (4.6)                     | 36 (4.6)                | 1.00    | 0.052  |
| Kidney failure   | 113 (10.8)                   | 35 (13.4)                    | 75 (9.6)                | 0.10    | 0.107  |
| Cancer   |                              |                              |                         |         |        |
| No cancer  | 918 (87.9)                   | 228 (87.4)                   | 678 (86.6)              | 0.94    | 0.026  |
| Active cancer  | 52 (5.0)                     | 14 (5.4)                     | 43 (5.5)                |         |        |
| Cancer remission   | 74 (7.1)                     | 19 (7.3)                     | 62 (7.9)                |         |        |
| Current smoker   | 167 (16.0)                   | 40 (15.3)                    | 119 (15.2)              | 1.00    | 0.025  |
| Thromboembolic disease                                   |                              |                              |                         |         |        |
| None   | 998 (95.6)                   | 248 (95.0)                   | 746 (95.3)              | 0.36    | 0.087  |
| Arterial thrombosis                                      | 9 (0.9)                      | 4 (1.5)                      | 5 (0.6)                 |         |        |
| VTE  | 41 (4.0)                     | 9 (3.4)                      | 32 (4.1)                |         |        |
| Atrial fibrillation                                      | 39 (3.7)                     | 11 (4.2)                     | 21 (2.7)                | 0.30    | 0.007  |
| <b>Medication history, n (%)</b>                         |                              |                              |                         |         |        |
| Antiplatelet therapy                                     | 244 (23.4)                   | 62 (23.8)                    | 172 (22.0)              | 0.61    | 0.012  |
| Angiotensin-converting enzyme (ACE) inhibitors           | 176 (16.9)                   | 46 (17.6)                    | 129 (16.5)              | 0.74    | 0.027  |
| Renin-angiotensin-aldosterone system inhibitors          | 164 (15.7)                   | 41 (15.7)                    | 128 (16.3)              | 0.88    | <0.001 |
| <b>Laboratory values at baseline, median [IQR]</b>       |                              |                              |                         |         |        |
| Hemoglobin level, g/L                                    | 1,350 [123.8–146.2]          | 134.0 [120.0–145.0]          | 135.0 [123.0–147.0]     | 0.17    | 0.141  |
| Platelet count, x109/L                                   | 203 [157–266]                | 202 [157–263]                | 199 [155–265]           | 0.71    | 0.034  |
| White blood cell count, x109/L                           | 6.40 [4.8–8.7]               | 6.8 [4.9–9.0]                | 6.24 [4.7–8.2]          | 0.09    | 0.080  |
| Glomerular filtration rate by Cockcroft                  | 99.6 [67.1–134.2]            | 98.0 [66.4–131.0]            | 98.5 [67.1–132.2]       | 0.57    | 0.062  |
| C-reactive protein, mg/dL                                | 75.0 [38.0–134.1]            | 95.0 [50.0–152.0]            | 70.8 [32.7–127.0]       | <0.001  | 0.277  |
| <b>Acute respiratory support, n (%)</b>                  |                              |                              |                         |         |        |
| High flow nasal cannula                                  | 77 (7.4)                     | 43 (16.5)                    | 31 (4.0)                | <0.001  | 0.405  |
| Noninvasive positive pressure ventilation                | 34 (3.3)                     | 13 (5.0)                     | 22 (2.8)                | 0.14    | 0.120  |
| Endotracheal intubation                                  | 157 (15.0)                   | 82 (31.4)                    | 82 (10.5)               | <0.001  | 0.562  |
| <b>Outcomes, n (%)</b>                                   |                              |                              |                         |         |        |
| In-hospital mortality                                    | 93 (8.9)                     | 23 (8.8)                     | 74 (9.5)                | 0.85    | 0.004  |
| Time to death (median [IQR])                             | 11.2 [9.4–12.3]              | 11.3 [8.1–13.5]              | 11.6 [10.2–12.5]        | 0.17    | 0.107  |
| <b>Thrombotic events, n (%)</b>                          |                              |                              |                         |         |        |
| VTE  | 25 (2.4)                     | 6 (2.3)                      | 19 (2.4)                | 0.99    | 0.008  |
| PE   | 21 (2.1)                     | 5 (1.9)                      | 16 (2.0)                | 0.99    |        |
| DVT  | 9 (0.8)                      | 3 (1.1)                      | 6 (0.8)                 | 0.85    |        |
| Ischemic Thrombotic Events                               | 17 (1.6)                     | 7 (2.7)                      | 10 (1.2)                | 0.25    | 0.10   |
| Myocardial infarction                                    | 9 (0.8)                      | 4 (1.9)                      | 5 (0.6)                 | 0.34    |        |
| Cerebrovascular accident                                 | 5 (0.5)                      | 3 (1.1)                      | 2 (0.2)                 | 0.08    |        |
| Acute limb ischemia                                      | 3 (0.2)                      | 0 (0.0)                      | 3 (0.4)                 | 0.74    |        |

\*IQR, interquartile range; SMD, Standard Means Difference; VTE, venous thromboembolic event; PE, pulmonary embolism; DVT, deep venous thrombosis.

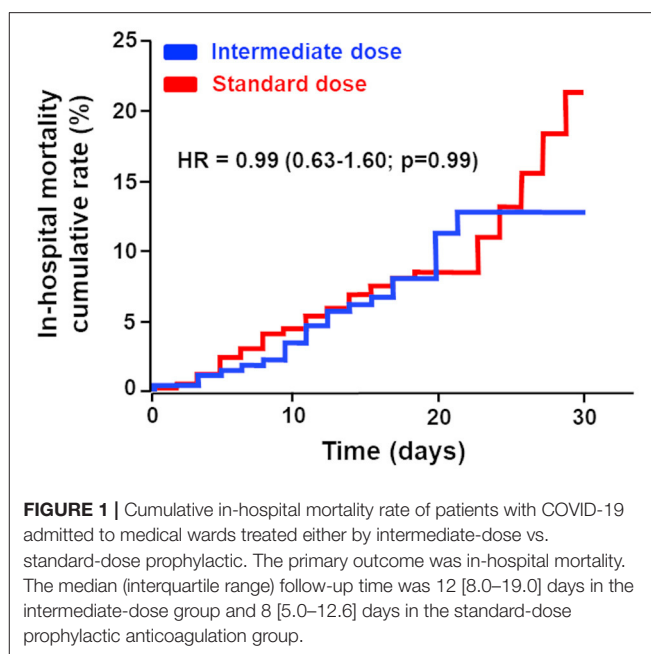
daily LMWH, subcutaneous heparin injection or intravenous heparin infusions). The exact dosing of AC was not reported in the database and was reported according to the treating clinician. During the study period, the dose of the AC regimen was based on the International Society on Thrombosis and Haemostasis (11) and the French guidelines (12). The time from hospitalization (Day 0) to death was used as an outcome. Symptomatic venous and ischemic thrombotic events and outcomes (in-hospital death) were assessed using electronic medical records.

## Statistical Analysis

To address confounding and other sources of bias arising from the use of observational data, we estimated a propensity-matched analysis for the likelihood of treatment with intermediate-dose prophylactic AC. We estimated the propensity score by running a logistic regression model where the outcome variable is a binary variable indicating treatment status (intermediate-dose or standard-dose prophylactic anticoagulation), including as covariates the following: age, sex, body mass index, high blood pressure, diabetes mellitus, dyslipidemia, current smoking status, and history of cancer. Then a 1:3 match was performed using Greedy matching techniques. All analyses were performed on matched populations. We used standardized mean difference (SMD), which is the most commonly used statistic to examine the balance of covariate distribution between the two groups (intermediate-dose or standard-dose prophylactic anticoagulation). Continuous data were expressed as median (interquartile range, IQR) and categorical data as  $n$  (%). Patients were compared according to the AC regimen during hospitalization (intermediate-dose or standard-dose prophylactic AC). In the multivariable analysis, we used conditional logistic regression to assess the association between the AC regimen and outcomes. The interactions between the AC regimen and specific subgroups were assessed *via* the Cochran–Mantel–Haenszel  $\chi^2$  test. For the survival analysis, the start of the study was triggered by the diagnosis of SARS-CoV-2 infection and hospitalization in a medical ward. The end of the study was defined either by the death of the patient during the hospitalization or by discharge alive from the hospital. We used the Cox proportional hazard (PH) model to investigate the relationships between AC regimen and outcomes. Missing data were handled using multiple random forest imputations using chained equations (10 sets of imputations). All analyses were two-sided and a  $p < 0.05$  was considered statistically significant. Statistical analysis was performed using R studio® software including R version 3.6.3 (R Development Core Team, 2019).

## RESULTS

During the study period, 2,878 consecutive patients were hospitalized for SARS-CoV-2 infection in medical wards and were included, as previously described (7, 14, 15). We excluded 382 patients from this analysis who had an AC treatment (whatever the regimen) before hospitalization. Among the study population, 261 (25%) patients started an



intermediate-dose of prophylactic AC during hospitalization. The propensity matching yielded 783 (75%) patients who received standard-dose and 261 (25%) patients who received intermediate-dose prophylactic AC during hospitalization, with balanced confounders between the groups.

As shown in **Table 1**, the study population had a median age of 63.7 (IQR 51.9–74.2) years, 391 (37.5%) patients were women, and the median body mass index was 28.6 (IQR 25.4–32.2). As expected according to international and French guidelines about the use of intermediate doses of prophylactic AC, fewer patients received the standard dose, and these had less lung extensive damage on CT scan, had decreased C-reactive protein (CRP) at admission, and received less high-flow nasal cannula or endotracheal intubation during follow-up, in contrast with patients who received an intermediate dose of prophylactic AC. In-hospital mortality occurred in 23 of 261 (8.8%) patients in the intermediate-dose group and 74 of 783 (9.4%) patients in the standard-dose prophylactic AC group ( $p = 0.85$ ); while time to death was also the same in both treatment groups (11.3 [8.1–13.5] and 11.6 [10.2–12.5] days, respectively,  $p = 0.17$ ). Moreover, the 30-day Kaplan–Meier curves for in-hospital mortality, shown in **Figure 1**, demonstrated no statistically significant differences in in-hospital mortality (hazard ratio: 0.99; confidence interval 0.63–1.60;  $p = 0.99$ ). Furthermore, we did not observe any difference regarding venous and arterial thrombotic events between intermediate dose and standard dose (respectively, venous thrombotic events: 2.3 vs. 2.4%,  $p = 0.99$ ; arterial thrombotic events: 2.7 vs. 1.2%,  $p = 0.25$ ). We finally performed a subgroup analysis and found that no particular subgroups were identified in which the use of any AC regimen was associated with a significant reduction in the primary outcome (**Table 2**). We did not observe any interaction between potential confounders and the AC regimen (**Table 2**).



**TABLE 2 |** Subgroup analysis for COVID-19 in-hospital mortality: the study of the interaction between the treatment group and each of the assessed variables for in-hospital mortality.

|   | Prophylactic anticoagulation |                     |  | Interaction term                   |
|---|------------------------------|---------------------|--|------------------------------------|
|   | Intermediate dose            | Standard dose       | Unadjusted OR (95%CI, <i>p</i> -value) |                                    |
| <b>No. of non-survivors/No. total (%)</b>       | <b>23/261 (8.8)</b>          | <b>74/783 (9.4)</b> |  |                                    |
| Age, years                                      |                              |                     |  |                                    |
| <65   | 6/133 (4.5)                  | 12/389 (3.1)        | -                                      |                                    |
| ≥65   | 17/128 (13.2)                | 62/394 (15.7)       | 4.99 (3.01–8.71, <i>p</i> <0.001)      | 2.11 (0.62–6.82, <i>p</i> =0.22)   |
| Gender  |                              |                     |  |                                    |
| Women   | 7/100 (7)                    | 27/300 (9.0)        | -                                      |                                    |
| Men   | 16/161 (9.9)                 | 47/483 (9.7)        | 1.17 (0.76–1.82, <i>p</i> = 0.49)      | 0.73 (0.24–2.05, <i>p</i> = 0.56)  |
| Body mass index, Kg/m <sup>2</sup>              |                              |                     |  |                                    |
| <25   | 10/51 (19.6)                 | 20/164 (12.2)       | -                                      |                                    |
| ≥25   | 13/210 (6.2)                 | 54/619 (8.7)        | 2.54 (2.35–2.87, <i>p</i> =0.009)      | 2.58 (0.90–7.32, <i>p</i> = 0.08)  |
| <b>Coexisting conditions, <i>n</i> (%)</b>      |                              |                     |  |                                    |
| Current smoker                                  | 3/40 (7.5)                   | 10/119 (8.4)        | 0.85 (0.44–1.51, <i>p</i> = 0.60)      | 1.32 (0.35–6.50, <i>p</i> = 0.70)  |
| Hypertension                                    | 18/120 (15.0)                | 47/363 (12.9)       | 2.57 (1.66–4.04, <i>p</i> <0.001)      | 0.70 (0.20–2.12, <i>p</i> = 0.55)  |
| Diabetes mellitus                               | 11/77 (14.3)                 | 29/224 (12.9)       | 1.84 (1.20–2.82, <i>p</i> =0.005)      | 0.58 (0.21–1.62, <i>p</i> = 0.30)  |
| Hyperlipidemia                                  | 10/69 (14.5)                 | 21/197 (10.7)       | 1.42 (0.90–2.22, <i>p</i> = 0.13)      | 0.65 (0.24–1.83, <i>p</i> = 0.41)  |
| Peripheral arterial disease                     | 1/11 (9.1)                   | 5/25 (20.0)         | 2.02 (0.74–4.65, <i>p</i> = 0.13)      | 2.49 (0.33–51.73, <i>p</i> = 0.44) |
| Ischemic stroke                                 | 2/12 (16.7)                  | 7/36 (19.4)         | 2.38 (1.05–4.87, <i>p</i> =0.03)       | 1.28 (0.25–9.79, <i>p</i> = 0.78)  |
| Kidney failure                                  | 6/35 (17.1)                  | 23/75 (30.7)        | 4.56 (2.76–7.40, <i>p</i> < 0.001)     | 1.78 (0.57–6.01, <i>p</i> = 0.33)  |
| Atrial fibrillation                             | 3/11 (27.2)                  | 4/21 (19.0)         | 1.06 (0.31–2.72, <i>p</i> = 0.91)      | 1.04 (0.21–6.06, <i>p</i> = 0.97)  |
| Cancer  |                              |                     |  |                                    |
| No cancer                                       | 19/228 (8.3)                 | 57/678 (8.4)        | -                                      |                                    |
| Active cancer                                   | 1/14 (7.1)                   | 5/43 (11.6)         | 2.48 (1.31–4.45, <i>p</i> = 0.003)     | 2.61 (0.36–53.73, <i>p</i> = 0.41) |
| Cancer in remission                             | 3/19 (15.8)                  | 12/62 (19.4)        | 1.28 (0.48–2.87, <i>p</i> = 0.58)      | 1.27 (0.30–6.69, <i>p</i> = 0.76)  |
| Thromboembolism disease                         |                              |                     |  |                                    |
| None  | 22/248 (8.8)                 | 70/746(9.4)         | -                                      |                                    |
| Arterial thrombosis                             | 0/4 (0.0)                    | 1/5 (20.0)          | 1.23 (0.07–6.79, <i>p</i> = 0.85)      | 0.97 (0.10–17.75, <i>p</i> = 0.98) |
| Venous thrombosis                               | 1/9 (11.1)                   | 3/32 (9.4)          | 1.06 (0.31–2.72, <i>p</i> = 0.91)      | 1.28 (0.07–7.48, <i>p</i> = 0.82)  |
| <b>Acute respiratory support, <i>n</i> (%)</b>  |                              |                     |  |                                    |
| High flow nasal cannula                         | 4/43 (9.3)                   | 5/34 (14.7)         | 1.07 (0.30–3.05, <i>p</i> = 0.90)      | 1.69 (0.37–8.01, <i>p</i> = 0.49)  |
| Non-invasive positive pressure ventilation      | 1/13 (7.7)                   | 2/21 (9.5)          | 0.86 (0.05–4.67, <i>p</i> = 0.88)      | 1.25 (0.10–29.63, <i>p</i> = 0.86) |
| Endotracheal intubation                         | 9/82 (10.9)                  | 13/75 (17.3)        | 1.45 (0.58–3.47, <i>p</i> = 0.41)      | 1.65 (0.55–5.01, <i>p</i> = 0.37)  |
| <b>Medication history, <i>n</i> (%)</b>         |                              |                     |  |                                    |
| Antiplatelet therapy                            | 10/62 (16.1)                 | 35/172 (20.4)       | 3.47 (2.25–5.33, <i>p</i> <0.001)      | 1.40 (0.51–3.92, <i>p</i> = 0.52)  |
| Angiotensin-converting enzyme inhibitors        | 5/46 (10.9)                  | 16/129 (12.4)       | 1.42 (0.83–2.34, <i>p</i> = 0.18)      | 1.17 (0.36–4.19, <i>p</i> = 0.80)  |
| Renin-angiotensin-aldosterone system inhibitors | 6/41 (14.6)                  | 13/128 (10.1)       | 1.29 (0.74–2.16, <i>p</i> = 0.34)      | 0.61 (0.19–2.09, <i>p</i> = 0.41)  |

\*95%CI, 95% confidence interval; OR, odds ratio.

## DISCUSSION

Establishing the appropriate AC prophylactic regimen in COVID-19 is an emergency according to the high rates of thrombotic complication and relevance of microthrombosis/lung obstruction observed in respiratory functional exploration (16) or autopsy studies (17). A prophylactic dose of heparin/LMWH has been used and was proposed very early in the COVID-19 outbreak after the description of their beneficial effects on mortality in the Chinese population (18). However, as thrombotic complications persisted even after a standard dose of prophylactic AC regimen, empirically, higher prophylactic dosing of heparin/LMWH has been proposed with either classic evidence-based medicine approaches or an evaluation of safety in

appropriate clinical trials. Our present study suggests the futility of an increased dose for prophylactic AC regimen in patients hospitalized for COVID-19 in medical wards, as previously described by Vaughn et al. (19). We used a propensity score-matched population to compare both AC regimens in this retrospective cohort study. However, it is obvious that our data need to be confirmed in a prospective, randomized, controlled study that will also take into consideration efficacy and safety, i.e., bleeding during hospitalization with both AC regimen strategies.

One potential explanation for the absence of efficacy of intermediate-dose AC may have been the lack of intensity to prevent micro- or macrothrombosis compared with the standard-dose prophylactic regimen. We can now affirm that this is not the case, since, in critically ill COVID-19

patients enrolled in three pivotal trials testing therapeutic-dose vs. standard prophylactic AC (ACTIV-4a, REMAP-CAP, and ATTACC), the authors reported the absence of efficacy, and an increase in the frequency of the bleeding event was demonstrated (20). Similar results have been observed in a recently published INSPIRATION prospective randomized study in critically ill COVID-19 patients after a 30-day evaluation (13). Furthermore, intermediate-dose compared with standard-dose prophylactic AC did not reduce either a composite outcome of death, treatment with extracorporeal membrane oxygenation, or venous or arterial thrombosis at the 90-day follow-up (21). Moreover, in patients hospitalized with COVID-19 and increased D-dimer levels, in-hospital therapeutic AC with rivaroxaban or enoxaparin followed by rivaroxaban on day 30 has been recently reported to have no impact on mortality, while increasing the risk of bleeding (22).

Even though AC has been shown to prevent macrothrombotic complications (23, 24), intermediate doses did not worsen or modify the mortality outcome in these studies likely because treatment was introduced too late into the course of the disease. Indeed, it is clear that microthrombosis/lung obstruction is pathognomonic of COVID-19 worsening and hypoxemia, in contrast to most other respiratory viral infections. We previously demonstrated that pre-hospital AC (vitamin K antagonist or direct oral anticoagulant) reduces endothelial lesions (25) and also prevents worsening of COVID-19 and in-hospital mortality (15). AC regimens are probably efficient in the early stages of the disease by preventing COVID-19-associated coagulopathy and endotheliopathy. Once microthrombosis and lung obstruction have occurred, COVID-19 inexorably worsens and the AC therapy is likely to lose its protective effect on outcomes. Early AC prior to hospitalization for COVID-19 could also directly block SARS-CoV-2 entry inside targeted cells. Indeed, transmembrane protease serine 2 (TMPRSS2) and also factor Xa and thrombin can directly cleave the SARS-CoV-2 spike, enhancing viral entry (26, 27). Thus, the AC strategy needs to be proposed as a treatment option very early and before hospitalization, at the time of being a contact case or of diagnosis by an RT-PCR test. This hypothesis needs to be tested in dedicated prospective clinical studies or in preclinical models of infection.

We acknowledge some limitations in the present study. Despite efforts to control confounders by using different analytical strategies such as propensity score matching,

some potential biases may have been disregarded such as the number of major bleeding events and the timing of AC therapy initiation after admission. All efforts were made to adjust the analyses for relevant variables, including cardio-vascular comorbidities, patient characteristics, and severity clinical features. We acknowledge that patients who received intermediate prophylactic dose had significantly more extensive lung damages, rates of endotracheal intubation, rates of high-flow nasal cannula use, and higher levels of CRP when compared with patients in the standard prophylactic group. Thus, it seems that intermediate prophylactic dose was started in more severe COVID-19 patients in medical wards. Moreover, in these patients, the higher prophylactic regimen of AC did not improve the outcomes.

All in all, our results highlight the futility of intermediate-dose prophylactic AC, for modification of in-hospital mortality, compared with standard-dose prophylactic AC, in patients admitted to medical wards. Our results confirm data recently published in critical patients with COVID-19. In the future, AC and its different regimens may be tested in ambulatory patients in a multicenter, randomized, controlled, open-label trial, stratified on the timing of the disease more than disease severity in already hospitalized patients.

## DATA AVAILABILITY STATEMENT

The raw data supporting the conclusions of this article will be made available by the authors, without undue reservation.

## ETHICS STATEMENT

The studies involving human participants were reviewed and approved by French Data Protection Committee. Written informed consent for participation was not required for this study in accordance with the national legislation and the institutional requirements.

## AUTHOR CONTRIBUTIONS

DS and RC designed the present study and wrote the manuscript. RC performed statistical analyses. AC and GB designed the trial. All authors reviewed the paper and have substantially contributed to the paper.

## REFERENCES

1. Debuc B, Smadja DM. Is COVID-19 a New hematologic disease? *Stem Cell Rev Rep.* (2021) 17:4–8. doi: 10.1007/s12015-020-09987-4
2. Smadja DM, Guerin CL, Chocron R, Yatim N, Boussier J, Gendron N, et al. Angiotensin-2 as a marker of endothelial activation is a good predictor factor for intensive care unit admission of COVID-19 patients. *Angiogenesis.* (2020) 23:611–20. doi: 10.1007/s10456-020-09730-0
3. Helms J, Severac F, Merdji H, Angles-Cano E, Meziani F. Prothrombotic phenotype in COVID-19 severe patients. *Intensive Care Med.* (2020) 46:1502–3. doi: 10.1007/s00134-020-06082-7
4. Bilaloglu S, Aphinyanaphongs Y, Jones S, Iturrate E, Hochman J, Berger JS. Thrombosis in hospitalized patients with COVID-19 in a New York City health system. *JAMA.* (2020) 324:799–801. doi: 10.1001/jama.2020.13372
5. Planquette B, Le Berre A, Khider L, Yannoutsos A, Gendron N, de Torcy M, et al. Prevalence and characteristics of pulmonary embolism in (1042). COVID-19 patients with respiratory symptoms: A nested case-control study. *Thromb Res.* (2021) 197:94–9. doi: 10.1016/j.thromres.2020.11.001
6. Jimenez D, Garcia-Sanchez A, Rali P, Muriel A, Bikdeli B, Ruiz-Artacho P, et al. Incidence of VTE and bleeding among hospitalized patients with Coronavirus Disease 2019: a systematic review and meta-analysis. *Chest.* (2021) 159:1182–96. doi: 10.1016/j.chest.2020.11.005

7. Fauvel C, Weizman O, Trimaille A, Mika D, Pommier T, Pace N, et al. Pulmonary embolism in COVID-19 patients: a French multicentre cohort study. *Eur Heart J*. (2020). doi: 10.1161/circ.142.suppl\_3.13478
8. Nopp S, Moik F, Jilma B, Pabinger I, Ay C. Risk of venous thromboembolism in patients with COVID-19: A systematic review and meta-analysis. *Res Pract Thromb Haemost*. (2020). doi: 10.1002/rth2.12439
9. Philippe A, Chocron R, Gendron N, Bory O, Beauvais A, Peron N, et al. Circulating Von Willebrand factor and high molecular weight multimers as markers of endothelial injury predict COVID-19 in-hospital mortality. *Angiogenesis*. (2021). doi: 10.1007/s10456-020-09762-6
10. Philippe A, Gendron N, Bory O, Beauvais A, Mirault T, Planquette B, et al. Von Willebrand factor collagen-binding capacity predicts in-hospital mortality in COVID-19 patients: insight from VWF/ADAMTS13 ratio imbalance. *Angiogenesis*. (2021). doi: 10.1007/s10456-021-09789-3
11. Thachil J, Juffermans NP, Ranucci M, Connors JM, Warkentin TE, Ortel TL, et al. ISTH DIC subcommittee communication on anticoagulation in COVID-19. *J Thromb Haemost*. (2020) 18:2138–44. doi: 10.1111/jth.15004
12. Susen S, Tacquard CA, Godon A, Mansour A, Garrigue D, Nguyen P, et al. Prevention of thrombotic risk in hospitalized patients with COVID-19 and hemostasis monitoring. *Crit Care*. (2020) 24:364. doi: 10.1186/s13054-020-03000-7
13. Investigators I, Sadeghipour P, Talasaz AH, Rashidi F, Sharif-Kashani B, Beigmohammadi MT, et al. Effect of intermediate-dose vs standard-dose prophylactic anticoagulation on thrombotic events, extracorporeal membrane oxygenation treatment, or mortality among patients with COVID-19 admitted to the intensive care unit: The INSPIRATION randomized clinical trial. *JAMA*. (2021) 325:1620–30. doi: 10.1001/jama.2021.4152
14. Chocron R, Duceau B, Gendron N, Ezzouhairi N, Khider L, Trimaille A, et al. D-dimer at hospital admission for COVID-19 are associated with in-hospital mortality, independent of venous thromboembolism: Insights from a French multicenter cohort study. *Arch Cardiovasc Dis*. (2021) 114:381–93. doi: 10.21203/rs.3.rs-62363/v1
15. Chocron R, Galand P, Cellier J, Gendron N, Pommier T, Bory O, et al. Anticoagulation prior to hospitalization is a potential protective factor for COVID-19: insight from a French multicenter cohort study. *J Am Heart Assoc*. (2021) 10:e018288. doi: 10.1161/JAHA.120.018624
16. Diehl JL, Peron N, Chocron R, Debuc B, Guerot E, Hauw-Berlemont C, et al. Respiratory mechanics and gas exchanges in the early course of COVID-19 ARDS: a hypothesis-generating study. *Ann Intensive Care*. (2020) 10:95. doi: 10.1186/s13613-020-00716-1
17. Ackermann M, Verleden SE, Kuehnel M, Haverich A, Welte T, Laenger F, et al. Pulmonary vascular endothelialitis, thrombosis, and angiogenesis in Covid-19. *N Engl J Med*. (2020) 383:120–8. doi: 10.1056/NEJMoa2015432
18. Tang N, Bai H, Chen X, Gong J, Li D, Sun Z. Anticoagulant treatment is associated with decreased mortality in severe coronavirus disease 2019 patients with coagulopathy. *J Thromb Haemost*. (2020) 18:1094–9. doi: 10.1111/jth.14817
19. Vaughn VM, Yost M, Abshire C, Flanders SA, Paje D, Grant P, et al. Trends in venous thromboembolism anticoagulation in patients hospitalized with COVID-19. *JAMA Network Open*. (2021) 4:e2111788. doi: 10.1001/jamanetworkopen.2021.11788
20. ATTACC. ACTIV-4a & REMAP-CAP multiplatform RCT. Results of interim analysis (2021). Available online at: <https://www.attacc.org/presentations> (accessed Feb 10, 2021).
21. Bikdeli B, Talasaz AH, Rashidi F, Bakhshandeh H, Rafiee F, Rezaeifar P, et al. Intermediate-dose versus standard-dose prophylactic anticoagulation in patients with COVID-19 admitted to the intensive care unit: 90-day results from the INSPIRATION randomized trial. *Thromb Haemost*. (2021).
22. Lopes RD, de Barros ESPGM, Furtado RHM, Macedo AVS, Bronhara B, Damiani LP, et al. Therapeutic versus prophylactic anticoagulation for patients admitted to hospital with COVID-19 and elevated D-dimer concentration (ACTION): an open-label, multicentre, randomised, controlled trial. *Lancet*. (2021) 397:2253–63. doi: 10.1016/S0140-6736(21)01203-4
23. Helms J, Severac F, Merdji H, Schenck M, Clere-Jehl R, Baldacini M, et al. Higher anticoagulation targets and risk of thrombotic events in severe COVID-19 patients: bi-center cohort study. *Ann Intensive Care*. (2021) 11:14. doi: 10.1186/s13613-021-00809-5
24. Tacquard C, Mansour A, Godon A, Godet J, Poissy J, Garrigue D, et al. Impact of high-dose prophylactic anticoagulation in critically ill patients with coronavirus disease 2019. *Pneumonia Chest*. (2021).
25. Khider L, Gendron N, Goudot G, Chocron R, Hauw-Berlemont C, Cheng C, et al. Curative anticoagulation prevents endothelial lesion in COVID-19 patients. *J Thromb Haemost*. (2020) 18:2391–9. doi: 10.1111/jth.14968
26. Hoffmann M, Kleine-Weber H, Schroeder S, Kruger N, Herrler T, Erichsen S, et al. SARS-CoV-2 cell entry depends on ACE2 and TMPRSS2 and is blocked by a clinically proven protease inhibitor. *Cell*. (2020) 181:271–80 e8. doi: 10.1016/j.cell.2020.02.052
27. Kastenhuber ER, Jaimes JA, Johnson JL, Mercadante M, Muecksch F, Weisblum Y, et al. Coagulation factors directly cleave SARS-CoV-2 spike and enhance viral entry. *bioRxiv*. (2021). doi: 10.1101/2021.03.31.437960

**Conflict of Interest:** DS, NG, OS, AC, and RC acknowledge the following without any relation with the current manuscript. DS received consultant, lecture fees, or travel awards from Aspen, Bayer, Carmat, Alliance BMS-Pfizer, LEO-Pharma, and Boehringer-Ingelheim. NG discloses consulting fees by Boehringer-Ingelheim, Bayer, Bristol-Myers Squibb/Pfizer, and LEO-Pharma. OS received grants, personal fees, or nonfinancial support from Bayer, Alliance BMS-Pfizer, Sanofi Aventis, Daiichi Sankyo, MSD, Boston Scientifics, and Chiesi. AC received a research grant from RESICARD (research nurses) and consultant and lecture fees from Amgen, AstraZeneca, Bayer Pharma, Alliance BMS-Pfizer, Novartis, and Sanofi-Aventis. RC received Consultant fees from Aspen.

The remaining authors declare that the research was conducted in the absence of any commercial or financial relationships that could be construed as a potential conflict of interest.

**Publisher's Note:** All claims expressed in this article are solely those of the authors and do not necessarily represent those of their affiliated organizations, or those of the publisher, the editors and the reviewers. Any product that may be evaluated in this article, or claim that may be made by its manufacturer, is not guaranteed or endorsed by the publisher.

Copyright © 2021 Smadja, Bonnet, Gendron, Weizman, Khider, Trimaille, Mirault, Fauvel, Diehl, Mika, Philippe, Pezel, Goudot, Sutter, Planquette, Waldmann, Sanchez, Cohen and Chocron. This is an open-access article distributed under the terms of the Creative Commons Attribution License (CC BY). The use, distribution or reproduction in other forums is permitted, provided the original author(s) and the copyright owner(s) are credited and that the original publication in this journal is cited, in accordance with accepted academic practice. No use, distribution or reproduction is permitted which does not comply with these terms.



# Investigating Fungi-Derived Bioactive Molecules as Inhibitor of the SARS Coronavirus Papain Like Protease: Computational Based Study

Aweke Mulu Belachew<sup>1\*</sup>, Asheber Feyisa<sup>2</sup>, Seid Belay Mohamed<sup>2</sup> and Jerusalem Fekadu W/Mariam<sup>3</sup>

<sup>1</sup> College of Applied Science, Addis Ababa Science and Technology University, Addis Ababa, Ethiopia, <sup>2</sup> College of Natural and Social Science, Addis Ababa Science and Technology University, Addis Ababa, Ethiopia, <sup>3</sup> College of Natural and Computational Science, Addis Ababa University, Addis Ababa, Ethiopia

## OPEN ACCESS

### Edited by:

Atefeh Abedini,  
Shahid Beheshti University of Medical  
Sciences, Iran

### Reviewed by:

Ibrahim Eissa,  
Al-Azhar University, Egypt  
Md Tabish Rehman,  
King Saud University, Saudi Arabia

### \*Correspondence:

Aweke Mulu Belachew  
aweke.mulu@aastu.edu.et

### Specialty section:

This article was submitted to  
Infectious Diseases – Surveillance,  
Prevention and Treatment,  
a section of the journal  
Frontiers in Medicine

**Received:** 02 August 2021

**Accepted:** 15 September 2021

**Published:** 21 October 2021

### Citation:

Belachew AM, Feyisa A, Mohamed SB  
and W/Mariam JF (2021) Investigating  
Fungi-Derived Bioactive Molecules as  
Inhibitor of the SARS Coronavirus  
Papain Like Protease: Computational  
Based Study. *Front. Med.* 8:752095.  
doi: 10.3389/fmed.2021.752095

Due to the rapid growth of the COVID-19 pandemic and its outcomes, developing a remedy to fight the predicament is critical. So far, it has infected more than 214,468,601 million people and caused the death of 4,470,969 million people according to the August 27, 2021, World Health Organization's (WHO) report. Several studies have been published on both computational and wet-lab approaches to develop antivirals for COVID-19, although there has been no success yet. However, the wet-lab approach is laborious, expensive, and time-consuming, and computational techniques have screened the activity of bioactive compounds from different sources with less effort and cost. For this investigation, we screened the binding affinity of fungi-derived bioactive molecules toward the SARS coronavirus papain-like protease (PLpro) by using computational approaches. Studies showed that protease inhibitors can be very effective in controlling virus-induced infections. Additionally, fungi represent a vast source of bioactive molecules, which could be potentially used for antiviral therapy. Fifty fungi-derived bioactive compounds were investigated concerning SARS-CoV-2 PLpro by using Auto Dock 4.2.1, Gromacs 2018. 2, ADMET, Swiss-ADME, FAF-Drugs 4.023, pKCSM, and UCLA-DOE server. From the list of the screened bioactive compounds, Dihydroaltersolanol C, Anthraquinone, Nigbeauvin A, and Catechin were selected with the Auto-Dock results of  $-8.68$ ,  $-7.52$ ,  $-10.46$ , and  $-10.58$  Kcal/mol, respectively, based on their binding affinity compared to the reference drug. We presented the drug likeliness, toxicity, carcinogenicity, and mutagenicity of all compounds using ADMET analysis. They interacted with the amino acid residues, Gly163, Trp106, Ser111, Asp164, and Cys270, through hydrogen bonds. The root-mean-square deviation (RMSD), root-mean-square fluctuations (RMSF), solvent-accessible surface area (SASA), and radius of gyration (Rg) values revealed a stable interaction. From the overall analyses, we can conclude that Dihydroaltersolanol C, Anthraquinone, Nigbeauvin A, and Catechin are classified as promising candidates for PLpro, thus potentially useful in developing a medicine for COVID-19.

**Keywords:** Gromacs, binding affinity, inhibitor, auto-dock, protease, COVID-19



## INTRODUCTION

The SARS-CoV-2 virus causes a lethal infection of the respiratory system. Most people infected with the virus showed mild to severe respiratory illness, while others were able to recover without demanding treatment (1). In contrast, older people and people with non-communicable diseases such as cardiovascular disease, diabetes, chronic respiratory disease, and cancer are more likely to develop severe illness and even death. Till now, the only best ways to prevent and slow the transmission of COVID-19 are to keep rooms well-ventilated, wash hands or use alcohol-based sanitizers frequently, cough into a bent elbow, practice social distancing, avoid crowds, and use face masks (2). Recently, SARS-CoV-2 mutated over time and developed new properties like vast and quick spread, disease severity, or inactive to vaccines and medicines, hence, there is a need for new diagnostic tools and other public health and social measures. Globally, several mutant viruses have already emerged and widely circulated among humans since the beginning of the pandemic. Until now, new SARS-CoV-2 variants of concern in the world including, Alpha (the United Kingdom, September 2020), Beta (South Africa, May 2020), Gamma (Brazil, November 2020), and Delta (India October 2020), Eta (Multiple countries, December 2020), Iota (the United States of America, November 2020), Kappa (India, October 2020), and Lambda (Peru, December 2020) have been reported (2–4). The COVID-19 pandemic has infected 216,867,420 million people, caused 4,507,837 million deaths, and 5,019,907,027 people have been vaccinated as of August 30, 2021 (2). In Ethiopia, from January 3, 2020, to August 31, 2021, there have been 306,810 confirmed cases of COVID-19 with 4,660 deaths and 2,434,041 people vaccinated, according to the report of WHO. Even though safe and effective vaccines are available to protect people from getting COVID-19, there is no effective inhibitor for the SARS-CoV-2 protease to prevent people from being seriously ill or dying (1, 2, 4). At present, computer-aided drug designs have been used as an efficient alternative for recognizing reliable candidates that can be repurposed drugs or/and phytochemicals to treat viral infection, including COVID-19 (5–7). Papain-like protease (PLpro) is an essential coronavirus protein required for the processing of viral polyproteins to generate functional protein for virus replication and enable viral spread; therefore, the inhibition of the PLpro is a feasible strategy to develop antiviral drugs and suppress the ongoing SARS-CoV-2 impacts (3–5). Furthermore, they are unique to the different viruses including COVID-19, thus offering the potential for specific treatments that produce minimal toxic side effects (5). Therefore, SARS-CoV-2 PLpro makes it an attractive antiviral drug target but, there is a limited study to address this area. Furthermore, studies revealed that PLpro and chymotrypsin-like protease (3CLpro), aka the main protease, are druggable targets (8, 9). Therefore, we screened the interaction of a library of fungi-derived bioactive molecules against PLpro as inhibitors with binding pocket residues.

For a long time, bioactive compounds isolated from microorganisms, plants, or animal sources have been utilized to treat infectious and non-infectious diseases (10–12). Several studies revealed that fungi provide different bioactive compounds

with diverse activities and are even developed into drugs such as Cyclosporine, Caspofungin, Lovastatin, and Fingolimod (13–15). Bioactive compounds with potent antiviral activity are presently under investigation, and the number of studies is continually increasing (14–16). Up until now, hundreds of fungi have been investigated for their metabolites, and most of them have been proven to be rich in bioactive compounds. Moreover, several novels and valuable bioactive compounds with antiviral, antimicrobial, insecticidal, cytotoxic, and anticancer activities have been reported from fungi (14, 15, 17–19). Previously, the potentials of fungal metabolites as anti-viral agents were explored and the success was promising. As far as antiviral therapy is concerned, the fungi metabolites helped treat viral infections, such as AIDS, influenza, and hepatitis, the leading causes of human death worldwide, and the metabolites belonged to the chemical class of Indole alkaloids, non-ribosomal peptides, polyketides, and terpenoids (14, 16, 19). With the urgent need for safe and effective drugs to treat COVID-19, we have explored bioactive molecules isolated from fungi that have been reported to possess an anti-HIV protease (13–16, 18–20). Conceptually, an identical work on fungi secondary metabolites, utilizing a similar method, was proposed by Fu et al. (7) targeting PLpro. With this rationale, the fungal metabolites were looked for in pursuing this research. Still, the negative role of the COVID-19 virus has increased, and new types of variants have emerged. Hence, the problem of the development of new antivirals has remained a big challenge. This makes it possible for candidates to develop more effective drugs from fungi, affecting different stages of virus reproduction and inhibiting the pathogenesis of the disease. The discovery and characterization of fungi metabolites due to their vast diversity, stereochemical properties, and preapproved biocompatibility having antiviral activities is an emerging field of research, and several compounds have been identified as promising candidates for new drug discovery (20–23). This study aims to investigate the binding affinity and stability of fungus-derived bioactive molecules and provide an insight into the therapeutics that might help treat COVID-19. In this study, 50 molecules were screened based on their binding energy and hydrogen bonds to PLpro via molecular docking, ADMET, and molecular dynamics study for 100 ns.

## MATERIALS AND METHODS

### The Platform for Molecular Modeling

A server computer with specifications processor (CPU) Intel® Xeon E5110 (Intel, Santa Clara, California, USA), graphics processing unit (GPU) Nvidia® GeForce GTX 780 (Nvidia, Santa Clara, California, USA), and 32GB Random Access Memory (RAM) DDR2 with Linux Ubuntu 20.04 LTS (Linux, San Francisco, California, USA) was used. Molecular dynamics (MD) simulations were performed by GROningen MAchine for Chemical Simulations (GROMACS 2018.2).

### Bioactive Compounds Preparation

After conducting a literature review, 50 bioactive compounds were collected from different fungi through PubMed, Pub-Chem,

and Google scholar platforms. Each compound was prepared to perform the molecular docking study. The statutory declaration form (SDF) of each structure was retrieved from the Pub-Chem database and presented in **Supplementary Table S1** (24). The bioactive compounds were uploaded into Avogadro (AV) followed by energy minimization and optimization by using the algorithm with the steepest descent for 2,000 steps (25). Finally, the 3D structure of all the bioactive molecules was generated by adding hydrogen atoms and was saved as a program database (PDB) file for further analysis.

## Protein Preparation

The crystal structure of the SARS CoV-2 PLpro in complex with the GRL0617 ligand (PDB ID: 7CJM) was retrieved from the Protein Data Bank (26). The protein structure was prepared by using Pymol (27) and Discovery Studio software (28) and then saved as a PDB file. The missing residues and 3D protonation were conceded on the PLpro via the Swiss-PDB viewer (Swiss Institute of Bioinformatics, Switzerland) and H++ server (Department of Computer Science, Virginia Tech, Blacksburg, VA, USA). During the preparation, the protein bond orders were assigned and hydrogen atoms were added as well. Water molecules and every heteroatom in the protein structure were removed. The cleaned crystal structure was then optimized, verified, and energy-minimized using the GROMOS 43B1 force field via the Swiss-PDB viewer (29). Finally, the modeled structure was validated using the UCLA-DOE server (<http://servicesn.mbi.ucla.edu/>) as discussed in our previous study (30). The modeled 3D structure was then confirmed by using the RAMPAGE, ERRAT, and Verify 3D online servers. After, validating the structure, we resolved the issue of the mismatched residues and missed structure across the models.

## DOCKING METHODOLOGY

The main focus of the experiments was to calculate the binding affinity with Auto-Dock 4.2 according to the previous study procedure (27). In this experiment, 50 bioactive molecules were screened for the binding affinity with PLpro binding sites. Before each docking experiment, the SARS CoV-2 PLpro structure was first prepared in Auto-Dock. First, the water molecules and the original inhibitor were removed from the PLpro structure. Then, any missing atoms were added. The optimization step was then employed to provide stable conformation before converting to PDBQT format for the docking analysis. All ligands and PLpro

structures were converted to PDBQT format to prepare them in an acceptable format for docking. To cover the whole protein, structure global docking was conducted with the spacing of 0.5 Å. The grid box was set to 126 × 108 × 114 points in an xyz-dimension that equated to a grid box spacing of 0.5 Å<sup>3</sup>, and the coordinate of the x, y, and z centers of the box was at 0.214, 15.986, and 14.518, respectively. All the docking parameters procedures were set to 250 genetic algorithm runs using the Lamarckian genetic algorithm conformational search, with the population size of 2,500,000 maximum numbers of energy evaluations, and 300 generations per run. Lastly, the best SARS CoV-2 PLpro-fungi derived bioactive complexes were selected according to the molecular docking results including binding energy, root mean square deviation, and type of favorable interactions and binding sites for further analysis.

## In silico Drug Likeness and Toxicity Assessment

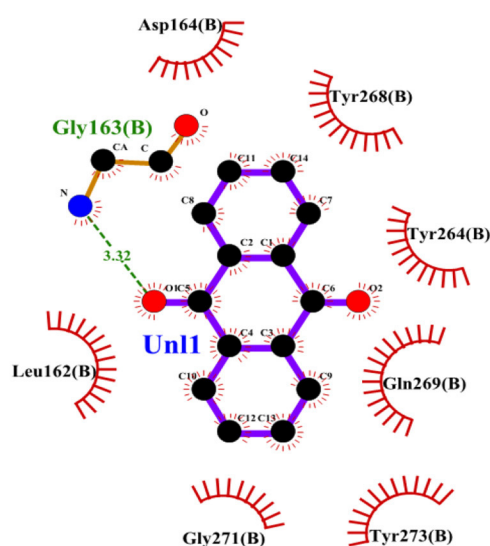
The structures of the compounds presented in the fungi-derived bioactive compounds (**Supplementary Table S1**) were obtained from the Pub-Chem database in the simplified molecular input line entry specification (SMILES) files and used for the web servers to generate, predicting their drug-likeness properties. Then toxicity assessment was made with online tools such as SwissADME (SIB Swiss Institute of Bioinformatics, 1015 Lausanne, Switzerland); FAF-Drugs 4.023 (MTi molecule Therapeutiques in silico, France) and pKCSM (Bio21 Institute University of Melbourne, 30 Flemington Rd - Parkville, Melbourne, VIC 3052, Australia) (31–33). Furthermore, the environmental toxicity assessments were also evaluated through admetSAR24 (32). The drug-likeness of the selected bioactive compounds was evaluated through the Lipinski Rule of Five to predict their pharmacokinetic properties using the Swiss ADME server (31).

## Molecular Dynamic Simulations

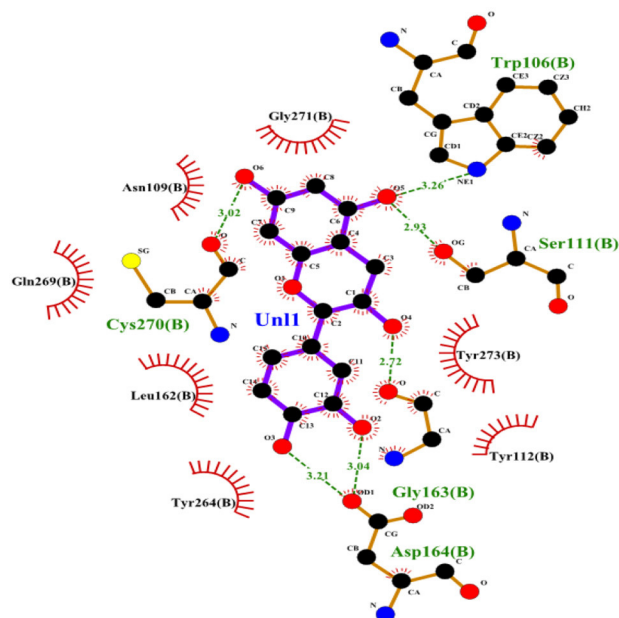
A molecular dynamic simulation of the top three docked complexes was run to see the structural stability by using a Gromacs package (2018.2) for 100 ns, in which the AMBER14 force field (34) was employed. A cubic simulation box was created and the PLpro-fungi-derived bioactive molecules complex was placed in with TIP3P water molecules. And then, the simulation environment was neutralized at a temperature of 299 K with sodium chloride (NaCl). The simulation box was extended at 1 Å more than the PLpro-fungi-derived bioactive molecules

**TABLE 1** | Shows the interaction between SARS-CoV-2 Papain-Like Protease (PLpro) and the top four Fungi-derived bioactive compounds.

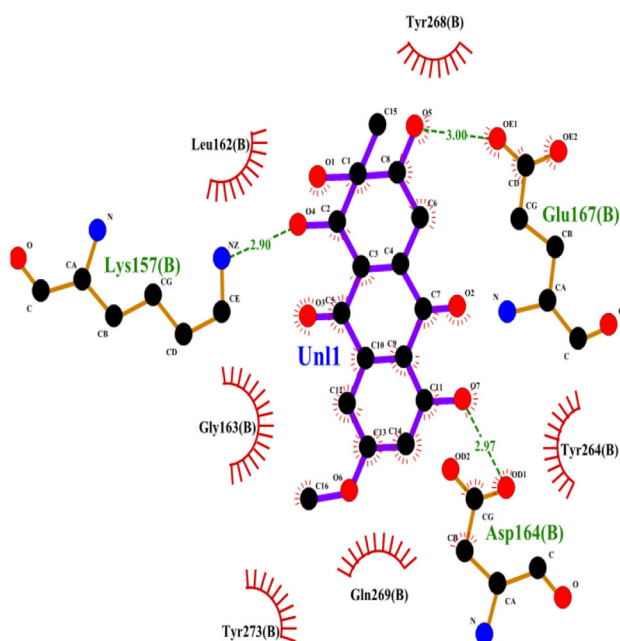
| Compounds             | Binding affinity | RMSD   | No. H-bonds | Amino acids involved in the interaction  |
|-----------------------|------------------|--------|-------------|--|
| Reference (GRL0617)   | −7.85            | 11.394 | 1           | Tyr268, Gln269, Ser111, His272, Asp286, Asp164, Pro247, Pro248, Gly163, and Asp164                 |
| Dihydroaltersolanol C | −8.68            | 11.309 | 3           | Tyr268, Glu167, Tyr264, Leu162, Lys157, Gly163, Tyr273, Gln269, and Asp164                         |
| Antraquinone          | −7.52            | 6.36   | 1           | Leu262, Gly163, Asp164, Tyr268, Tyr264, Gln269, Gly271, and Tyr273                                 |
| Catechin              | −10.58           | 14.709 | 6           | Asn109, Ser111, Gly271, Trp106, Tyr273, Tyr112, Gly163, Asp164, Tyr264, Leu162, Cys270, and Gln269 |
| Nigbeauvin A          | −10.46           | 15.564 | 1           | Pro248, Thr301, Tyr273, Tyr264, Gly163, Tyr112, Ser111, Asn109, Leu162, Gln269, Asp164, and Tyr268 |



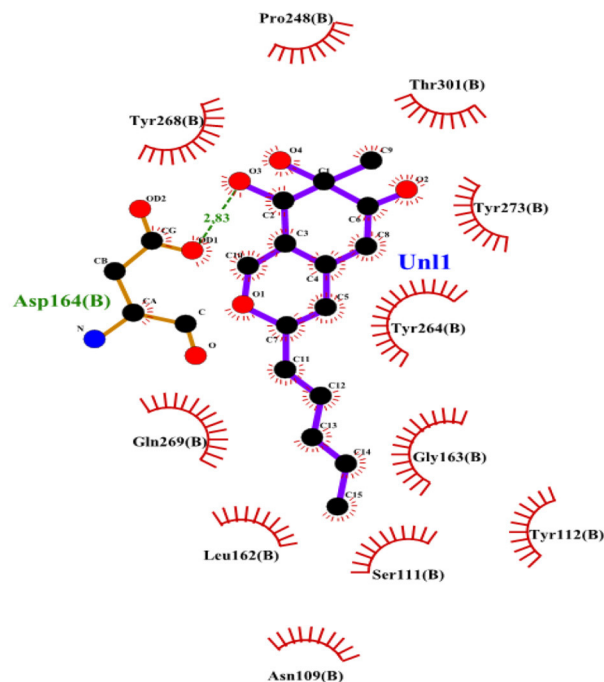
**Papain-Like Protease\_anthraquinone**



**Papain-Like Protease\_catechin**



**Papain-Like Protease\_DihydroaltersolanolC**



**Papain-Like Protease\_NigbeauvinaA**

**FIGURE 1 |** Interactions of the selected bioactive molecules and SARS-CoV-2 Papain-Like Protease (PLpro) binding pocket residues. For all the bioactive molecules, carbon atoms are shown in black, oxygen in red, and nitrogen in blue. Bonds in the Anthraquinone, Dihydroaltersolanol C, Catechin, and Nigbeauvina A.

complex, for them to be able to move freely. The long-range electrostatic interactions were calculated using Particle Mesh Ewald's algorithms by setting a cutoff radius of 3.5 Å (35). After these steps, the NVT [amount of substance (N), volume (V) and temperature (T) are conserved] stage was carried out to minimize the system structure and simultaneously, followed by the NPT [amount of substance (N), pressure (P) and temperature (T) are conserved] stage for the equilibration of the system structure by using 1,000 ps simulation time at the constant temperature of 298 K and pressure of 1 bar. The production part was carried out for 100 ns with the time step of 2 fs. Pymol and VMD 1.9.1 (36) were used to visualize the trajectory. Lastly, data analyses were performed for each complex

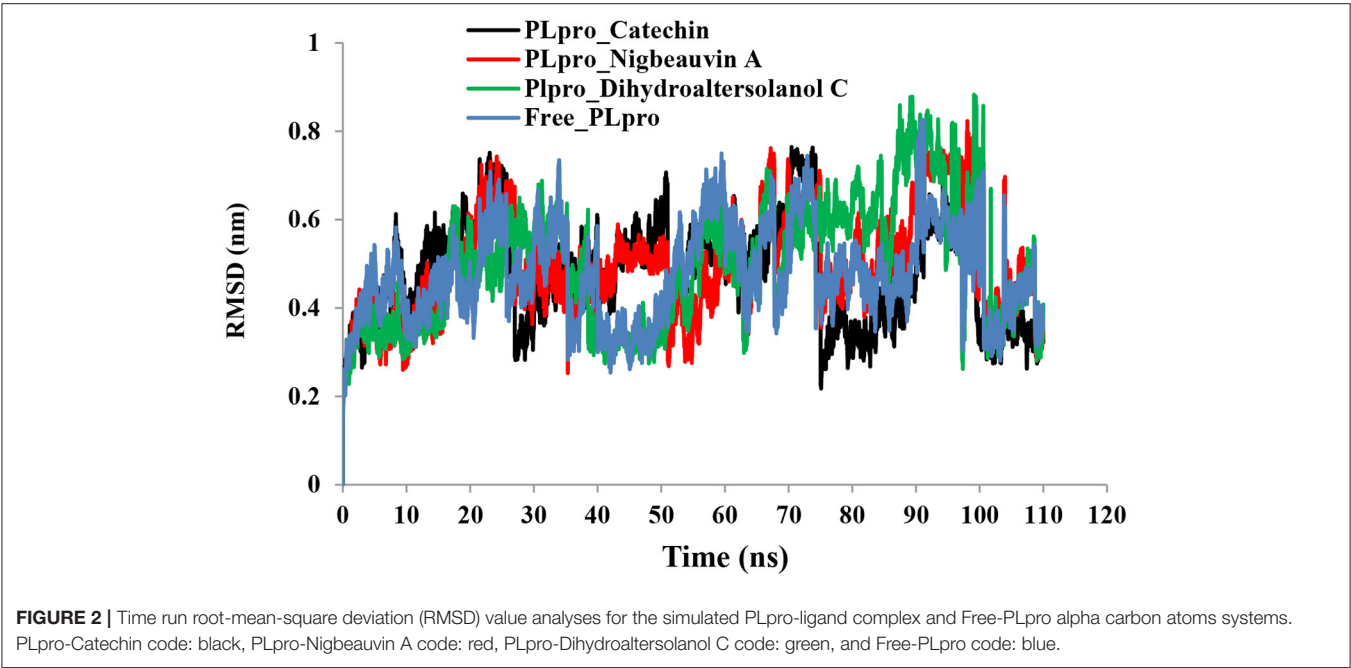
and free PLpro by using root-mean-square deviation (RMSD), root-mean-square fluctuation (RMSF), the radius of gyration (Rg), and solvent-accessible surface area (SASA).

DISCUSSION

To find a potential candidate for treating COVID-19 from bioactive fungus-derived molecules, first, we performed molecular docking studies on 50 molecules toward the binding pocket of the enzyme COVID-19 (PDB ID: 7CJM) (7). The minimized structure of the inhibitor, GRL0617, was re-docked into the original binding site of the PLpro. The results of the

TABLE 2 | Pharmacokinetic and Toxicity Properties for the top four bioactive fungi-derived molecules, which were derived from the SwissADME, admetSAR, and pKCSM web servers.

| Parameters                  | Dihydroaltersolanol C | Anthraquinone    | Nigbeauvin A     | Catechin         |
|-----------------------------|-----------------------|------------------|------------------|------------------|
| Molecular weight            | 322.31 g/mol          | 208.21 g/mol     | 262.30 g/mol     | 290.27 g/mol     |
| H-bond acceptor             | 7                     | 2                | 4                | 6                |
| H-bond donor                | 4                     | 0                | 2                | 5                |
| CYP2D6 substrate            | No                    | No               | No               | No               |
| CYP3A4 substrate            | No                    | No               | No               | No               |
| CYP1A2 inhibitor            | No                    | Yes              | No               | No               |
| CYP2C19 inhibitor           | No                    | Yes              | No               | No               |
| CYP2C9 inhibitor            | No                    | No               | No               | No               |
| CYP2D6 inhibitor            | No                    | No               | No               | No               |
| CYP3A4 inhibitor            | No                    | No               | No               | No               |
| Carcinogenicity             | Non-carcinogenic      | Non-carcinogenic | Non-carcinogenic | Non-carcinogenic |
| Hepatotoxicity              | No                    | No               | No               | No               |
| P-glycoprotein inhibitor    | No                    | No               | No               | No               |
| Human intestinal absorption | +0.9796               | +0.9956          | +0.9608          | +0.9887          |
| Ames mutagenesis            | −0.5000               | −0.7300          | −0.5900          | +0.6300          |
| Acute oral toxicity         | No                    | No               | No               | No               |
| Lipinski rule of five       | Yes                   | Yes              | Yes              | Yes              |





150 Genetic Algorithm runs of the re-docking were ranked and shown in **Table 1**. The best docking score of GRL0617 was  $-7.85$  kcal/mol. The superimposing of the re-docked PLpro-GRL0617 over the original X-ray structure indicated that GRL0617 was able to seek out the location of the binding site. For this study, the list of the bioactive fungus-derived molecules tested for the docking study is revealed in **Supplementary Table S1**. Out of the screened bioactive agents against the target, the PLpro enzyme was reported at the top four, based on their docked score. Accordingly, all the bioactive compounds reported here showed docking scores higher than  $-7.4$  kcal mol $^{-1}$  which are higher

than the reference drug (**Table 1**). The computational screening technique offered a reasonable screening result from an array of drugs and phytochemicals as a credible inhibitor for target molecules (5–7). But, the protein folding reactions took place at an ms level, which was at the limit of the accessible simulation times. It is still difficult to simulate the whole process of protein folding using the conventional MD method. Another limitation is that the study entirely focused on computational investigation. Based on our molecular docking results, four potent inhibitors targeting the SARS-CoV-2 PLpro were identified to exhibit significant binding affinities and interaction with the active site

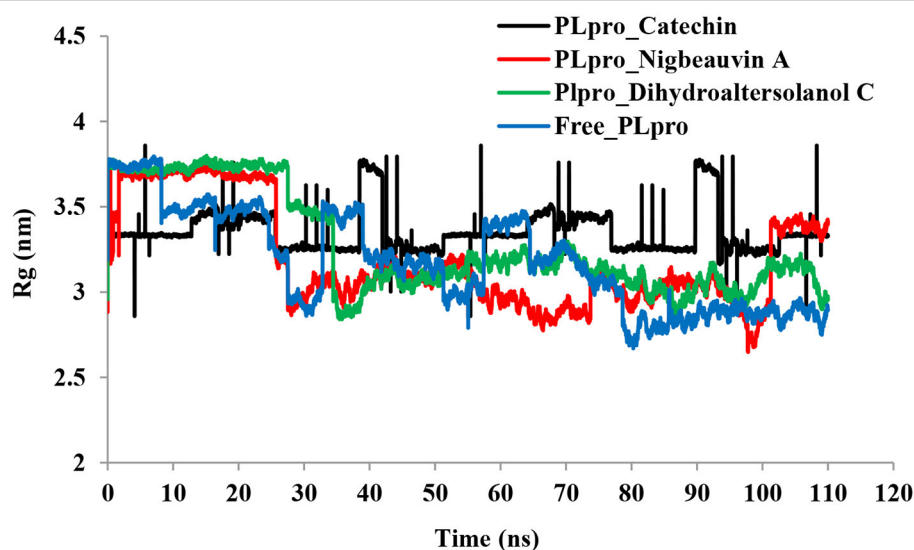


**FIGURE 3 |** Time series for the degree of rigidity and compactness analyses for the PLpro-ligand complex and Free-PLpro backbone of atoms simulated. PLpro-Catechin code: black, PLpro-Nigbeauvin A code: red, PLpro-Dihydroaltersolanol C code: green, and Free-PLpro code: blue.

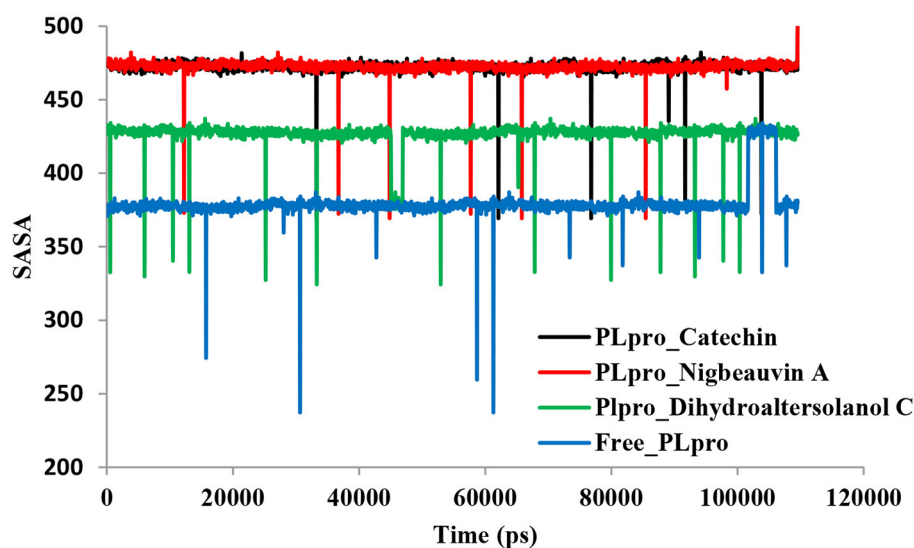


**FIGURE 4 |** Time series for the protein volume with expansion analyses for the PLpro-ligand complex and Free-PLpro alpha carbon atoms simulated systems. PLpro-Catechin code: black, PLpro-Nigbeauvin A code: red, PLpro-Dihydroaltersolanol C code: green, and Free-PLpro code: blue.

and pocket site, which are vital for inhibition as reported with the reference drug. Our first compound, Catechin found the docking result with a low RMSD value of 24.709 Å and a binding affinity score of  $-10.58 \text{ kcal/mol}^{-1}$  (Table 1). The second compound, Nigbeauvin A found the docking result with a low RMSD value of 25.564 Å and a binding affinity score of  $-10.46 \text{ kcal/mol}^{-1}$  (Table 1). The third compound, Dihydroaltersolanol C was found the docking result with a low RMSD value of 21.309 Å and a binding affinity score of  $-8.68 \text{ kcal/mol}^{-1}$  (Table 1). The fourth compound was found the docking result with a low RMSD value of 16.36 Å and a binding affinity score of  $-7.8 \text{ kcal/mol}^{-1}$  (Table 1). The Auto-Dock binding affinity results from the drugs through phytochemical and microbial studies were revealed to be within the range of  $-7.8$  to  $-6.5 \text{ kcal/mol}^{-1}$  (37–39). With the standard antiviruses repurposed drugs, the binding affinity ranges from  $-6.9$  to  $-7.3 \text{ Kcal/mol}^{-1}$  (7). Thus, Dihydroaltersolanol C, Anthraquinone, Nigbeauvin A, and Catechin showed better affinity toward PLpro and were selected for further analysis. Moreover, the 3CLpro complex formed six conventional hydrogen bonds with Ser111, Trp106, Cys270, Asp164 (2 times), and Gly163, which is consistent with the reference drug binding residues (7). In contrast, the PLpro-Nigbeauvin A complex and PLpro-Anthraquinone were stabilized by one hydrogen bond each at Asp164 and Gly163 positions, respectively, whereas Dihydroaltersolanol interacted with PLpro through three conventional hydrogen bonds at Glu167, Lys157, and Asp164 positions (Figure 1 and Table 1), which are consistent with the previous findings conducted by targeting the PLpro (7). These compounds formed numerous non-hydrogen-bonded interactions at the active site and pocket site *via* the Asn109, Ser111, Gly271, Trp106, Tyr268, Glu167, Tyr264, Leu162, Lys157, Gly163, Tyr273, Gln269, and Asp164 residues of PLpro, which are defined as binding pocket residues (7).

After the docking study, the top four selected bioactive molecules were screened for efficiency and safety in terms of various properties. As shown in Table 2, properties such as p-glycoprotein inhibition, carcinogenicity, hepatotoxicity, human intestinal absorption, and cytochrome P (CYP) inhibition, were predicted based on the web-based tools. Many studies showed that the toxicity and effectiveness of drugs mainly determine the success and failures of the candidate drugs in clinical trials (12, 30, 38). In the context of this study, the four top candidate bioactive molecules had no probability of toxicity, hepatotoxicity, CYP inhibition, oral toxicity, and carcinogenicity observed as shown in Table 2. To confirm the non-inhibitory effect of the selected compounds for cytochrome p450 as mentioned in the ADMET studies, we carried out docking studies against cytochrome p450 (PDB ID:6wr0), and the result revealed a high binding affinity between  $+6.28$  to  $+8.59$  as shown in Supplementary Table S1. The molecular weights (MWs) of the top four bioactive molecules were 322.31, 208.21, 262.30, and 290.27 g/mol for Dihydroaltersolanol C, Anthraquinone, Nigbeauvin A, and Catechin, respectively. Moreover, all the bioactive molecules were not violating Lipinski's rule of five. The numbers of the hydrogen bond donors for Dihydroaltersolanol C, Anthraquinone, Nigbeauvin A, and Catechin were reported as 4, 0, 2, and 5, respectively. The numbers of the hydrogen bond acceptors for Dihydroaltersolanol C, Anthraquinone, Nigbeauvin A, and Catechin were 7, 2, 4, and 6, respectively (Table 2).

An MD simulation study was performed to support the molecular docking assessment, and identify the binding stability. First, the RMSD of the backbone atoms from the simulation trajectories were assessed to understand the changes in the three ligands (Pub-Chem CID 9064, Pub-Chem CID 132562011, and Pub-Chem CID 146684151) with PLpro as shown in Figure 2. The PLpro-Catechin complex showed an average root mean SD of 0.23–0.74 nm (Figure 2), which is consistent

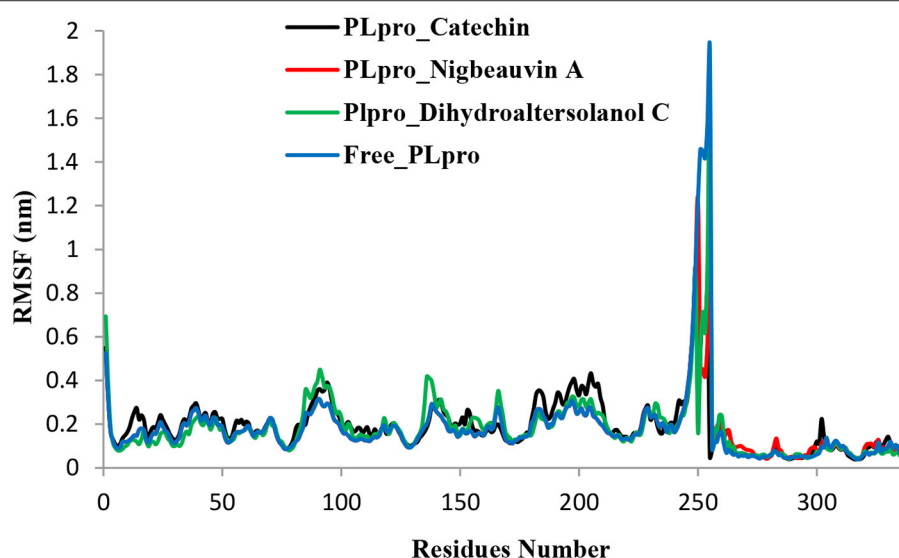
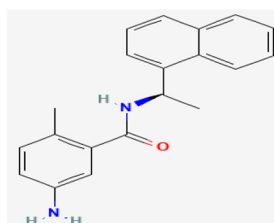
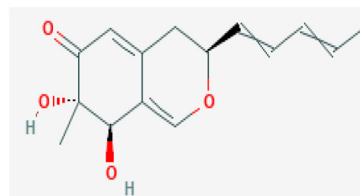


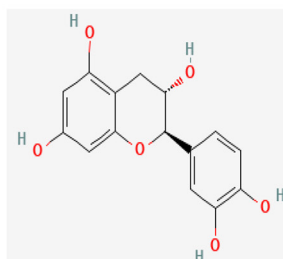
**FIGURE 5 |** Time series for the flexibility analysis of the amino acid residues for the PLpro-ligand complex and Free-PLpro alpha carbon atom simulated systems. PLpro-Catechin code: black, PLpro-Nigbeauvin A code: red, PLpro-Dihydroaltersolanol C code: green, and Free-PLpro code: blue.



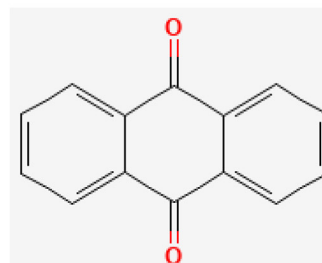
Reference compound (GRL0617)



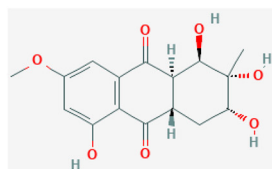
Nigbeauvin A (CID: 146684151)



Cianidanol (CID: 9064)



Anthraquinone (CID: 6780)



Dihydroaltersolanol C (CID: 132562011)

**FIGURE 6 |** The chemical structures of the reference compound (GRL0617) and the top four selected fungi-derived compounds retrieved from Pub-Chem (<https://pubchem.ncbi.nlm.nih.gov/>).

with the previous study (6, 16, 40). The RMSD value of the PLpro-Catechin complex revealed less stability between 20–30 ns, 40–50 ns, and 60–70 ns. This revealed that the PLpro-Catechin complex indicated maintenance of stability after 70 ns, with few fluctuations observed (**Figure 2**). Similarly, the other two complexes formed between PLpro-Dihydroaltersolanol C and PLpro-Nigbeauvin A shows an average root mean SD of 0.32–0.85, 0.26–0.88 nm, respectively, and both achieved stable RMSD profiles after 30 ns in the simulations. Even though, Free-PLpro exhibited a higher degree of deviation (0.24–0.88 nm) compared with PLpro-Dihydroaltersolanol C, PLpro-Nigbeauvin A, and PLpro-Catechin complex did not exceed its RMSD value more than 1 nm. The Rg values from the simulation trajectories were examined to understand the labile nature of the PLpro-Bioactive molecules as shown in **Figure 3**. The PLpro-Dihydroaltersolanol-C and PLpro-Nigbeauvin-A complexes decreased after 30 ns during the simulation. In contrast, PLpro-Catechin showed an increased rigidity of the simulated complexes (**Figure 3**). The average Rg value of the

Free-PLpro, PLpro-Catechin, PLpro-Dihydroaltersolanol C, and PLpro-Nigbeauvin A complexes were 2.75, 3.5, 2.75, and 2.75 Å, respectively. Here, the PLpro without ligand and in the complex was observed to be stable as no large fluctuations were observed; the protein is stable in the complex as well, which is consistent with another finding (41). The SASA of the simulation complexes was analyzed to determine the changes in the protein volume. The PLpro-catechin and PLpro-Nigbeauvin-A complex displayed an expanded surface area throughout the simulation, which was stably maintained within the simulation environment. A lower degree of change in the SASA profile was observed for PLpro-Dihydroaltersolanol-C compared with the other two compounds, but the deviations were not larger than Free-PLpro (**Figure 4**). The average of the SASA from Free-PLpro, PLpro-catechin, PLpro-Nigbeauvin-A, and PLpro-Dihydroaltersolanol-C complex were 475, 475, 425, and 325 Å<sup>2</sup>, respectively. The RMSF profiles of all three compounds were analyzed to understand the changes in the amino acid residues involved in the hydrogen bond formation as shown in **Figure 5**.

In this study, most of the residues had low RMSF values for all three complexes, except for amino acids whose value was close to 250. The binding interactions of the top three docked complexes were further evaluated after 100 ns in the simulation to understand their changes after the simulation (**Table 1**). The Catechin- PLpro complex formed six conventional hydrogen bonds at Ser111, Trp106, Cys270, and Asp164 (2 times), Gly163, and the RMSF values of the key residues around the active site were lower than those in the other regions of the protein, which implied that these residues had strong binding interactions with the inhibitors, similar to previous findings (7, 16, 41). The Dihydroaltersolanol interacted with PLpro through three conventional hydrogen bonds at Glu167, Lys157, and Asp164 position (**Figure 1** and **Table 1**). Based on these results we recommended laboratory assays targeting directly various steps along virus infection are needed to understand the mechanisms of action in detail. The free PLpro RMSF analysis shows the highest fluctuation ( $>1.5$  Å) in the regions of the amino acid at 237–265, comprising the binding site loop. The rest of the protein amino acids displayed low RMSF values highlighting their stability as well (**Figure 5**). The strengths of this study lie in the extensive virtual screening, molecular docking, and long molecular dynamics simulation. However, this study also suffers from some limitations such as the absence of any *in vitro* and/or *in vivo* experiments.

## CONCLUSIONS

There has been an increased recognition that more attention needs to be paid to COVID-19 drug discovery. In recent years, the natural products of bioactive molecules have revealed significant advances in the treatment of virus infection. However, previous studies are mainly limited to a subset of phytochemicals and repurpose of the drug. There is limited study on the antiviral mechanisms of fungal products on COVID-19 infection. To overcome the shortcomings of the previous studies outlined above, we proposed 50 fungi-derived bioactive compounds and investigates their binding affinity through a computational study. In this work, the molecular docking studies identified four potent inhibitors, namely, Catechin, Nigbeauvin-A, and

Dihydroaltersolanol-C out of the 50 that were identified. Moreover, the molecular simulation study of the three docked complexes supported the stable nature and rigid conformations formed by the docked complexes, as assessed by the simulation trajectories and based on multiple descriptor analyses. *In vitro* assays could be performed to confirm the precise targeting of these compounds against SARS-CoV-2. Thus, more detailed knowledge of the actual molecular targets is crucial to develop these molecules further to combat virus infections.

## DATA AVAILABILITY STATEMENT

The original contributions presented in the study are included in the article/**Supplementary Materials**, further inquiries can be directed to the corresponding author/s.

## AUTHOR CONTRIBUTIONS

The project approach was conceptually designed by AB, AB, AF, SM, and JF writing and original draft preparation. AB chemical structure drawing and run simulation. All authors have read and agreed to the published version of the manuscript.

## ACKNOWLEDGMENTS

Our deepest gratitude goes to my family, friends, the workers of the Minister of Innovation and Technology of Ethiopia, and the research participants for their unending support in making this work possible. Our sincere thanks to the Minister of Innovation and Technology of Ethiopia for offering a high-performance computational server (HPC). Last but not least, we acknowledge the Addis Ababa Science and Technology University for writing a letter of cooperation to the Minister of Innovation and Technology of Ethiopia.

## SUPPLEMENTARY MATERIAL

The Supplementary Material for this article can be found online at: <https://www.frontiersin.org/articles/10.3389/fmed.2021.752095/full#supplementary-material>

## REFERENCES

- Cao X. COVID-19: immunopathology and its implications for therapy. *Nat Rev Immunol.* (2020) 20:269–70. doi: 10.1038/s41577-020-0308-3
- World Health Organization. *Coronavirus Disease 2019 (COVID-19): Situation Report.* World Health Organization (2020).
- Zhou B, Thao TTN, Hoffmann D, Taddeo A, Ebert N, Labrousseau F, et al. SARS-CoV-2 spike D614G changes enhance replication and transmission. *Nature.* (2021) 592:122–7. doi: 10.1038/s41586-021-03361-1
- Volz E, Hill V, McCrone J, Price A, Jorgensen D, O'Toole A, et al. Evaluating the effects of SARS-CoV-2 spike mutation D614G on transmissibility and pathogenicity. *Cell.* (2021) 184:64–75.e11. doi: 10.1016/j.cell.2020.11.020
- Mulu A, Gajaa M, Woldekidan HB, W/mariam JF. The impact of curcumin derived polyphenols on the structure and flexibility COVID-19 main protease binding pocket: a molecular dynamics simulation study. *Peer J.* (2021) 9:e11590. doi: 10.7717/peerj.11590
- Rajpoot S, Alagumuthu M, Baig MS. Dual targeting of 3CLpro and PLpro of SARS-CoV-2: a novel structure-based design approach to treat COVID-19. *Curr Res Struct Biol.* (2021) 3:9–18. doi: 10.1016/j.crstbi.2020.12.001
- Fu Z, Huang B, Tang J, Liu S, Liu M, Ye Y, et al. The complex structure of GRL0617 and SARS-CoV-2 PLpro reveals a hot spot for antiviral drug discovery. *Nat Commun.* (2021) 12:488. doi: 10.1038/s41467-020-20718-8
- Sohraby F, Aryapour H. Unraveling the unbinding pathways of SARS-CoV-2 Papain-like proteinase known inhibitors by Supervised Molecular Dynamics simulation. *PLoS ONE.* (2021) 16:e0251910. doi: 10.1371/journal.pone.0251910
- Gupta S, Sarthi P, Satyaranjan B, Dipankar S, Malay Kumar R. Molecular mechanism of clinically oriented drug famotidine with the identified potential target of SARS-CoV-2. *ChemRxiv.* (2020) 1:1–15. doi: 10.26434/chemrxiv.12382265.v1
- Kim KJ, Liu X, Komabayashi T, Jeong SI, Selli S. Natural products for infectious diseases *Evid Compl Altern Med.* (2016) 2016:9459047. doi: 10.1155/2016/9459047



11. Kim JH, Kismali G, Gupta SC. Natural products for the prevention and treatment of chronic inflammatory diseases: integrating traditional medicine into modern chronic diseases care. *Evid Compl Altern Med*. (2018) 2018:9837863. doi: 10.1155/2018/9837863
12. Thorford NE, Senthilane DA, Rowe A, Munro D, Seele P, Maroyi A, et al. Natural products for drug discovery in the 21st century: innovations for novel drug discovery. *Int J Mol Sci*. (2018) 19:10. doi: 10.3390/ijms19061578
13. Saxena S, Chhibber M, Pal Singh I. Fungal bioactive compounds in pharmaceutical research and development. *Curr Bioactive Comp*. (2019) 15:1–18. doi: 10.2174/1573407214666180622104720
14. Biswajit GR. Potential of small-molecule fungal metabolites in antiviral chemotherapy. *Antiviral Chem Chemother*. (2017) 25:20–52. doi: 10.1177/2040206617705500
15. Linnakoski R, Reshamwala D, Veteli P, Cortina-Escribano M, Vanhanen H, Marjomäki V. Antiviral agents from fungi: diversity, mechanisms and potential applications. *Front Microbiol*. (2018) 9:2325. doi: 10.3389/fmicb.2018.02325
16. Suwannarach N, Kumla J, Sujarit K, Pattananandecha T, Saenjum C, Lumyong S. Natural bioactive compounds from fungi as potential candidates for protease inhibitors and immunomodulators to apply for coronaviruses. *Molecules*. (2020) 25:1800. doi: 10.3390/molecules25081800
17. Mayer AM, Rodriguez AD, Tagliatela-Scafati O, Fusetani N. Marine pharmacology in 2009–2011: marine compounds with antibacterial, antidiabetic, antifungal, anti-inflammatory, antiprotozoal, antituberculosis, and antiviral activities affecting the immune and nervous systems, and other miscellaneous mechanisms of action. *Mar Drugs*. (2013) 11:2510–73. doi: 10.3390/md11072510
18. Cheung RC, Wong JH, Pan WL, Chan YS, Yin CM, Dan XL, et al. Antifungal and antiviral products of marine organisms. *Appl Microbiol Biotechnol*. (2014) 98:3475–94. doi: 10.1007/s00253-014-5575-0
19. Moghadamtousi ZS, Nikzad S, Abdul Kadir H. Potential antiviral agents from marine fungi: an overview. *Mar Drugs*. (2015) 13:4520–38. doi: 10.3390/md13074520
20. Vlasenko V, Vlasenko A. Antiviral activity of fungi of the Novosibirsk Region: *Pleurotus ostreatus* and *P. pulmonarius* (Review). *Bio Web Conf*. (2018) 11:00044. doi: 10.1051/bioconf/20181100044
21. Butler MS. Natural products to drugs: natural product-derived compounds in clinical trials. *Nat Prod Rep*. (2008) 25:475–516. doi: 10.1039/b514294f
22. Newman DJ, Cragg GM. Natural products as sources of new drugs over the last 25 years. *J Nat Prod*. (2007) 70:461–77. doi: 10.1021/np068054v
23. Rosén J, Gottfries J, Muresan S. Novel chemical space exploration via natural products. *J Med Chem*. (2017) 52:1953–62. doi: 10.1021/jm801514w
24. Halgren TA. Performance of MMFF94. *J Comput Chem*. (1996) 17:490–519.
25. Kim S, Thiessen PA, Bolton EE, Chen J, Fu G, Gindulyte A, et al. Shoemaker BA. Pub-Chem substance and compound databases. *Nucleic Acids Res*. (2016) 44:D1202–13. doi: 10.1093/nar/gkv951
26. DeLano WL. *The PyMOL Molecular Graphics System, Version 1.1*. New York, NY: Schrödinger LLC (2002).
27. Kaplan W, Littlejohn TG. Software review Swiss-PDB viewer (Deep View). *Brief Bioinform*. (2001) 2:195–7. doi: 10.1093/bib/2.2.195
28. Daina A, Michielin O, Zoete V. SwissADME: a free web tool to evaluate pharmacokinetics, drug-likeness and medicinal chemistry friendliness of small molecules. *Sci Rep*. (2017) 7:427–17. doi: 10.1038/srep42717
29. Cheng F, Li W, Zhou Y, Shen J, Wu Z, Liu G, et al. AdmetSAR: a comprehensive source and free tool for assessment of chemical ADMET properties. *J Chem Inf Model*. (2012) 52:3099–105. doi: 10.1021/ci300367a
30. Pires DEV, Blundell TL, Ascher DB. pkCSM: predicting small-molecule pharmacokinetic and toxicity properties using graph-based signatures. *J Med Chem*. (2015) 58:4066–72. doi: 10.1021/acs.jmedchem.5b00104
31. Lagorce D, Sperandio O, Galons H, Miteva MA, Villoutreix BO. FAF-Drugs2: a free ADME/tox filtering tool to assist drug discovery and chemical biology projects. *BMC Bioinformatics*. (2008) 9:396. doi: 10.1186/1471-2105-9-396
32. Dickson CJ, Madej BD, Skjevik ÅA, Betz RM, Teigen K, Gould IR, et al. Lipid14: the amber lipid force field. *J Chem Theory Comput*. (2014) 10:865–79. doi: 10.1021/ct4010307
33. Krieger E, Nielsen JE, Spronk CM, Vriend G. Fast empirical pKa prediction by Ewald summation. *J Mol Graph Model*. (2006) 25:481–6. doi: 10.1016/j.jmgm.2006.02.009
34. Liu S, Zheng Q, Wang Z. Potential covalent drugs targeting the main protease of the SARS-CoV-2 coronavirus. *Bioinformatics*. (2020) 36:3295–8. doi: 10.1093/bioinformatics/btaa224
35. Rimanshee A, Amit D, Vishal P, et al. Potential inhibitors against papain-like protease of novel coronavirus (SARS-CoV-2) from FDA approved drugs. *ChemRxiv*. (2020) 2:1–8. doi: 10.26434/chemrxiv.11860011.v2
36. Allam AE, Amen Y, Ashour A, Assaf HK, Ali Hassan H, Abdel-Rahman IM, et al. *In silico* study of natural compounds from sesame against COVID-19 by targeting Mpro, PLpro and RdRp. *RSC Adv*. (2021) 11:22398–408. doi: 10.1039/D1RA03937G
37. Vuong W, Khan MB, Fischer C, Arutyunova E, Lamer T, Shields J, et al. Feline coronavirus drug inhibits the main protease of SARS-CoV-2 and blocks virus replication. *Nat Commun*. (2020) 11:4282. doi: 10.1038/s41467-020-18096-2
38. Ma C, Sacco MD, Hurst B, Townsend JA, Hu Y, Szeto T, et al. Boceprevir, GC-376, and calpain inhibitors II, XII inhibit SARS-CoV-2 viral replication by targeting the viral main protease. *Cell Res*. (2020) 30:678–92. doi: 10.1038/s41422-020-0356-z
39. Kouznetsova VL, Zhang A, Tatineni M, Miller MA, Tsigelny IF. Potential COVID-19 papain-like protease PLpro inhibitors: repurposing FDA-approved drugs. *Peer J*. (2020) 8:e9965. doi: 10.7717/peerj.9965
40. Pang J, Gao S, Sun Z, Yang G. Discovery of small molecule PLpro inhibitor against COVID-19 using structure-based virtual screening, molecular dynamics simulation, and molecular mechanics/Generalized Born surface area (MM/GBSA) calculation. *Struct Chem*. (2021) 32:879–86. doi: 10.1007/s11224-020-01665-y
41. Hosseini M, Chen W, Xiao D, Wang C. Computational molecular docking and virtual screening revealed promising SARS-CoV-2 drugs. *Prec Clin Med*. (2021) 4:1–16. doi: 10.1093/pcmedi/pbab001

**Conflict of Interest:** The authors declare that the research was conducted in the absence of any commercial or financial relationships that could be construed as a potential conflict of interest.

**Publisher's Note:** All claims expressed in this article are solely those of the authors and do not necessarily represent those of their affiliated organizations, or those of the publisher, the editors and the reviewers. Any product that may be evaluated in this article, or claim that may be made by its manufacturer, is not guaranteed or endorsed by the publisher.

Copyright © 2021 Belachew, Feyisa, Mohamed and W/Mariam. This is an open-access article distributed under the terms of the Creative Commons Attribution License (CC BY). The use, distribution or reproduction in other forums is permitted, provided the original author(s) and the copyright owner(s) are credited and that the original publication in this journal is cited, in accordance with accepted academic practice. No use, distribution or reproduction is permitted which does not comply with these terms.



# COVID-19 Risk Assessment for the Tokyo Olympic Games

Wenhui Zhu<sup>1</sup>, Jie Feng<sup>1</sup>, Cheng Li<sup>1</sup>, Huimin Wang<sup>1</sup>, Yang Zhong<sup>1</sup>, Lijun Zhou<sup>2</sup>, Xingyu Zhang<sup>3</sup> and Tao Zhang<sup>1\*</sup>

<sup>1</sup> Department of Epidemiology and Health Statistics, West China School of Public Health and West China Fourth Hospital, Sichuan University, Chengdu, China, <sup>2</sup> Sichuan Center for Disease Control and Prevention, Chengdu, China, <sup>3</sup> Thomas E. Starzl Transplantation Institute, University of Pittsburgh Medical Center, Pittsburgh, PA, United States

## OPEN ACCESS

### Edited by:

Reza Lashgari,  
Shahid Beheshti University, Iran

### Reviewed by:

Haijun Zhang,  
Harbin Institute of Technology, China  
Dr. Varun Tyagi,  
Eurofins Agrosience Services Pvt.  
Ltd., India  
Khondoker Nazmoon Nabi,  
Bangladesh University of Engineering  
and Technology, Bangladesh

### \*Correspondence:

Tao Zhang  
statzhangtao@scu.edu.cn

### Specialty section:

This article was submitted to  
Infectious Diseases - Surveillance,  
Prevention and Treatment,  
a section of the journal  
Frontiers in Public Health

**Received:** 25 June 2021

**Accepted:** 14 September 2021

**Published:** 25 October 2021

### Citation:

Zhu W, Feng J, Li C, Wang H,  
Zhong Y, Zhou L, Zhang X and  
Zhang T (2021) COVID-19 Risk  
Assessment for the Tokyo Olympic  
Games.  
Front. Public Health 9:730611.  
doi: 10.3389/fpubh.2021.730611

**Introduction:** As of June 7, 2021, the outbreak of Coronavirus Disease 2019 (COVID-19) has spread to more than 200 countries. The global number of reported cases is more than 172.9 million, with more than 3.7 million deaths, and the number of infected individuals is still growing rapidly. Consequently, events and activities around the world were canceled or postponed, and the preparation for sporting events were greatly challenged. Under such circumstances, about 11,000 athletes from ~206 countries are arriving in Tokyo for the 32nd Summer Olympic Games. Therefore, it is urgently necessary to assess the occurrence and spread risk of COVID-19 for the Games.

**Objectives:** To explore effective prevention and control measures for COVID-19 in large international events through simulations of different interventions according to risk assessment.

**Methods:** We used a random model to calculate the number of initial infected patients and used Poisson distribution to determine the number of initial infected patients based on the number of countries involved. Furthermore, to simulate the COVID-19 transmission, the susceptible-exposed-symptomatic-asymptomatic-recovered-hospitalized (SEIARH) model was established based on the susceptible-exposed-infectious-recovered (SEIR) mathematical model of epidemic diseases. According to risk assessment indicators produced by different scenarios of the simulated interventions, the risk of COVID-19 transmission in Tokyo Olympic Games was assessed.

**Results:** The current COVID-19 prevention measures proposed by the Japan Olympic Committee need to be enhanced. And large-scale vaccination will effectively control the spread of COVID-19. When the protective efficacy of vaccines is 78.1% or 89.8%, and if the vaccination rate of athletes reaches 80%, an epidemic prevention barrier can be established.

**Keywords:** COVID-19, SEIARH model, interventions, Tokyo Olympic Games, risk assessment

## INTRODUCTION

The 32nd Summer Olympic Games (Games of the XXII Olympiad) will be held from July 23 to August 8, 2021 in Tokyo, Japan (1). However, athletes and spectators of the Olympics Games are easily exposed to the Coronavirus Disease 2019 (COVID-19). As of June 7, 2021, the outbreak of COVID-19 has spread to more than 200 countries (2). The global epidemic situation remains grim,

with more than 172.9 million global cumulative reported cases and more than 3.7 million deaths (3), while the number of infected individuals is still growing rapidly. Consequently, numerous major events and activities around the world have been canceled or postponed, and preparations for all parts of upcoming sport events were greatly challenged. Under such circumstances, about 11,000 athletes from ~206 countries and regions are arriving in Tokyo for the 32nd Summer Olympic during the summer of 2021 (4), along with coaches, referees, and associated International Sport Organization officials, which will definitely increase the possibility of infectious disease outbreaks and transmissions. Although the International Olympic Committee (IOC) has stated that overseas audiences will not be allowed to enter Japan to view the Tokyo Olympic Games (5), it is far from enough to ensure the safety of the Olympic Games in terms of COVID-19. Therefore, it is urgently necessary to commence an evaluation for the risk of COVID-19 under different prevention measures.

So far the COVID-19 prevention measures proposed by the Japan Olympic Committee (JOC) include the following aspects (6, 7):

1. Keep a minimum of two meters from athletes at all times. Keep a minimum of one meter from others. All Games participants must minimize contact within one meter of Games participants who have already been in Japan for more than 14 days, and Japanese residents.
2. During your stay in Japan, you will be expected to limit your activities to what is required to carry out your role.
3. All participants are required to take two COVID-19 tests before their flight to Japan. All other Games participants will be tested daily for three days after their arrival. After the first 3 days and throughout their stay, they will be tested regularly, based on the operational nature of their role and level of contact with athletes.

Thomas Bach, the president of IOC, said that if a vaccine becomes available in time for the July 23–August 8 Games in 2021, the IOC would foot the bill (8). However, since vaccination is voluntary for athletes, different vaccine coverage may produce different effects on an outbreak in the Olympic Village. In light of how this has not been studied so far, we used different vaccine coverage statistics to simulate the transmission of COVID-19 in this study.

In this study, to assess the risk of COVID-19 during the Tokyo Olympic Games, a simulation study based on the transmission dynamic model was carried out. Firstly, we collected the number of athletes from different countries participating in the Tokyo Olympic Games, the current COVID-19 infection probability of each country, and the transmission parameters of the COVID-19 model. Secondly, utilizing the initial number of asymptomatic infections, the number of contacts and other aspects, the susceptible-exposed-symptomatic-asymptomatic-recovered-hospitalized (SEIARH) model was established. Thirdly, in order

to carry out risk assessments, the secondary infectors on the 17th day and peak hour of onset were calculated. Through realizing a comparison of the expected risks of COVID-19 under different prevention strategies, this study provided quantitative reference evidence regarding the formulation of COVID-19 prevention and control programs for the Tokyo Olympic Games. The specific process of analysis is shown in **Figure 1**.

## MATERIALS AND METHODS

The methods of this study consisted of three parts. Firstly, to determine the number of initial infected patients based on the number of countries coming to Japan, Poisson distribution was used. Secondly, based on the COVID-19 transmission mechanism, the SEIARH model was established to simulate COVID-19 transmission. And then we analyzed the robustness of the SEIARH model. Thirdly, according to the results of the SEIARH model, the risk assessment indicators (secondary infectors on the 17th day, peak hour of onset/d) were calculated.

### Data Collection and Preparation

National infection probability  $\pi_i (i = 1, 2, \dots, n)$  was approximated according to public data (3):

$$\pi_i = \frac{I_i}{N_{C_i}}, i = 1, 2, \dots, n \quad (1)$$

where  $I_i$  is the number of infections in country  $i$ ;  $N_{C_i}$  is the total population number of country  $i$ .

As the Olympic Games are held every 4 years, little change existed in the total number of the adjacent two sessions (9). Besides, the number of athletes was not available before the announcement of IOC, so we used the number of athletes announced in the last Olympic Games as a reference (10). Furthermore, we set the initial asymptomatic infected population  $A(0)$  as 10 because the previous imported asymptomatic infected cases did not exceed 10 at one time.

For the parameters of the SEIARH model, we referred to the published COVID-19 classic retrospective study (11–18).

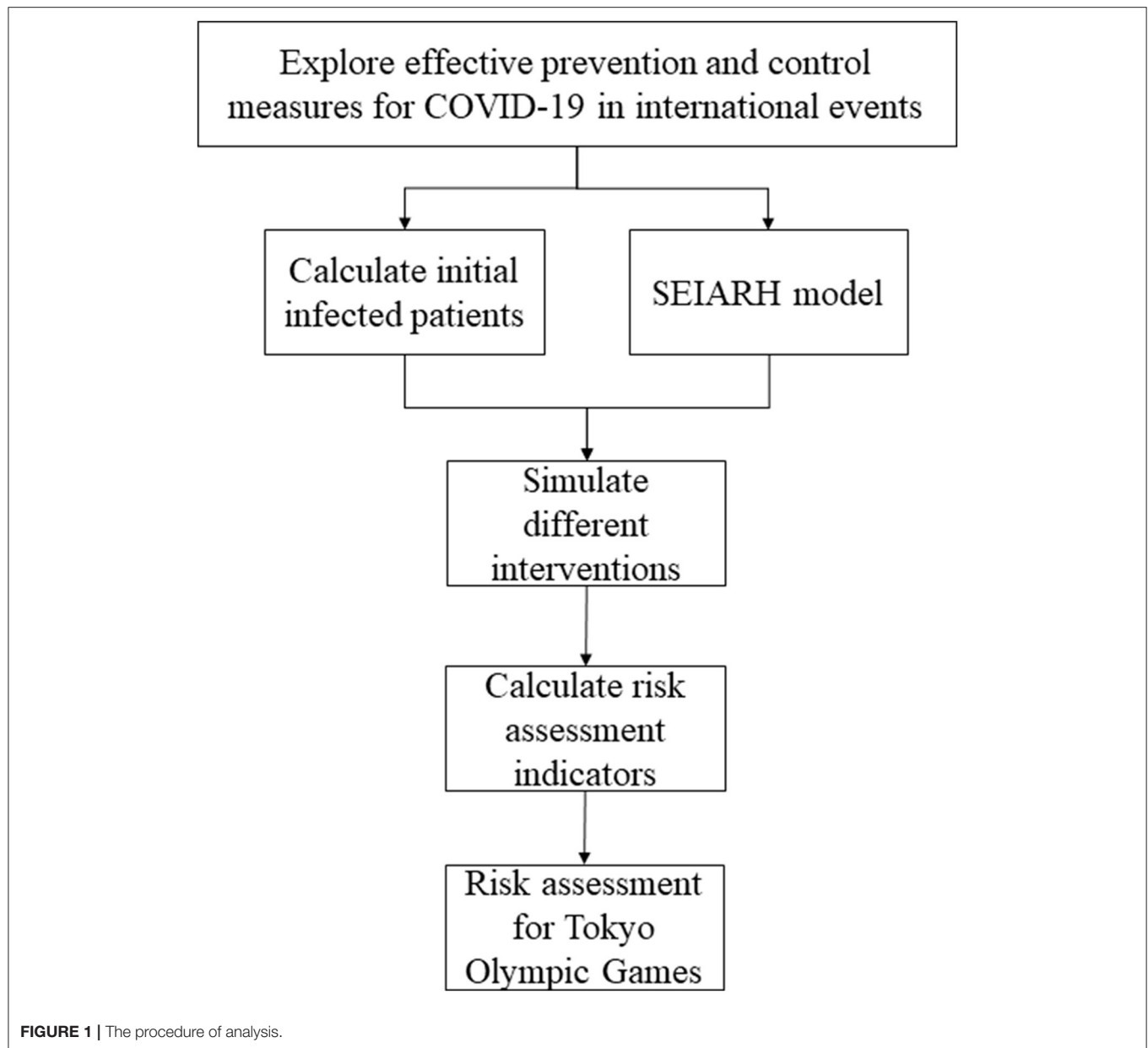
### Determining the Number of Initial Infected Patients

We assumed the presence of COVID-19 infectors at entry who were not identified by entry quarantine or health check-up. Here we leveraged the probability of infection  $\pi_i$  to approximate the number of overseas import infectors. Furthermore, since the number of participants and the spread of COVID-19 vary across different countries, the initial infected patients referred to unidentified infectors among athletes, coaches, referees, officials, and others who entered Japan for the Tokyo Olympics Games.

The number of infected patients assumed from different regions  $i (i = 1, 2, \dots, n)$  is  $X_i$ . It can be approximately seen that the Poisson distribution of compliance parameter  $\lambda_i = N_i \pi_i$ , which is in the form of:

$$P\{X_i = k\} = \frac{\lambda_i^k}{k!} e^{-\lambda_i}, i = 1, 2, \dots, n; k = 0, 1, \dots, \quad (2)$$

**Abbreviations:** COVID-19, coronavirus disease 2019; SEIARH, susceptible-exposed-symptomatic-asymptomatic-recovered-hospitalized; SEIR, susceptible-exposed-infectious-recovered; IOC, International Olympic Committee; JOC, Japan Olympic Committee.



where  $N_i$  is the number of athletes, coaches, referees, and officials from different regions;  $\pi_i$  is the infection probability of immigrants from different regions. The infected input probability  $P_{i\_imported}$  of a person from region  $i$  was:

$$P_{i\_imported} = 1 - P\{X_i = 0\}, i = 1, 2, \dots, n. \quad (3)$$

Furthermore, the total number of initial infected patients could be represented as:

$$I_{imported} = \sum_{i=1}^n N_i P_{i\_imported}. \quad (4)$$

## Simulating the Transmission of COVID-19 During the Tokyo Olympic Games

The mathematical models of infectious diseases can be classified into two types by the level of data unit, i.e., the micro-dynamic and macro-dynamic models. The former type of model includes scale-free networks, small-world networks, and so on (19, 20), aiming to show the transmission process of the disease based on the individual level. Thus, it requires a large amount of high-quality personal data. However, since the purpose of this study was to simulate the transmission of COVID-19 on the population level, it was unnecessary and inefficient to collect personal data for model building. Hence, this made the micro-dynamic model unsuitable for our simulation study. On the contrary, the macro-dynamic model provides us with tools for monitoring population



flow among different health statuses. For example, the traditional susceptible-exposed-infected-recovered (SEIR) model classifies the population into four categories by its name (21–24). However, for the specific purpose of simulating COVID-19 transmission in this study, neither the difference between asymptomatic and symptomatic patients nor the requirement of isolation treatment was reflected by the SEIR model. To this end, we added both the A (asymptomatic) and H (hospitalized) components to the SEIR model to establish the SEIARH model for the simulation of COVID-19 transmission. The transmission process is shown in **Figure 2**.

For the simulation study, the discrete-time stochastic compartment model for COVID-19 infection was constructed as:

$$\begin{cases} \frac{dS}{dt} = \frac{r_1(t)\beta_1(I+A)S}{N} - \frac{r_2(t)\beta_2ES}{N} \\ \frac{dE}{dt} = \frac{r_1(t)\beta_1(I+A)S}{N} - \alpha E + \frac{r_2(t)\beta_2ES}{N} \\ \frac{dI}{dt} = \alpha cE - \gamma_1 I - \delta_1 I \\ \frac{dA}{dt} = \alpha (1 - c) E - \gamma_2 A - \delta_2 A \\ \frac{dH}{dt} = \delta_1 I + \delta_2 A - \gamma_3 H \\ \frac{dR}{dt} = \gamma_1 I + \gamma_2 A + \gamma_3 H \end{cases} \quad (5)$$

The parameters are defined in **Table 1**. As the Japan authority has proposed that “During your stay in Japan, you will be expected to limit your activities to what is required to carry out your role” (6). Therefore, the range of activities of athletes outside the Olympic Village was not considered, and it was reasonable to set the total population number  $N = 11,000$ . Based on the historical data of Wuhan, China between January 11 and March 13, we used the Markov Chain Monte Carlo Method (MCMC) to estimate the recovery rate of symptomatic infected individuals. It turned out that the results of data-driven methods were consistent with the real-world results (25), where the 95% CI of  $\gamma_1$  and  $\gamma_2$  was (0.0085, 0.0085) and (0.0085, 0.0085), respectively. More details can be found in **Supplementary Material A**. In addition, we also initialized the other simulation parameters in **Table 1** through literature review (11–18).

Since the Tokyo Olympic Games lasted 17 days, a total of  $t = 1, 2, \dots, 17$  data points were simulated. **Figures 3–16** show the simulated results. The goal for this simulation was to investigate the transmission of COVID-19 during the Tokyo Olympic Games. According to the general principles of the simulation study design (26), we implemented our simulation study following the details as presented in **Table 2**.

The current regulations required all participants to take two COVID-19 tests before their flight to Japan, and the number of contacts should be strictly controlled after entry (7, 27, 28). To make the experiment more realistic, we defined the number of susceptible individuals exposed by infected [ $r_1(t)$ ] and exposed [ $r_2(t)$ ] as piecewise functions of time  $t$ , where  $t$  is the number of days after entry. The function forms were given as follows.

$$r_1(t) = \begin{cases} r_{10}, & 0 \leq t \leq 3 \\ r_{11}, & 3 \leq t \leq 14 \\ r_{12}, & 14 \leq t \leq 17 \\ r_{13}, & 17 \leq t \leq 21 \end{cases}, r_2(t) = \begin{cases} r_{20}, & 0 \leq t \leq 3 \\ r_{21}, & 3 \leq t \leq 14 \\ r_{22}, & 14 \leq t \leq 17 \\ r_{23}, & 17 \leq t \leq 21 \end{cases} \quad (6)$$

## Sensitivity Analysis

In order to verify the robustness of the SEIARH model, we analyzed the sensitivity of the model. The parameter  $\beta_1$  and  $\beta_2$  were increased or decreased by 5% at the same time. These two parameters directly affect the final number of infectors. The cumulative infectors and daily new infectors were observed to determine whether the model was effective.

## Assessing the Risks of COVID-19 Under Different Prevention Measures

Based on the results of the SEIARH model, we calculated the risk assessment index of COVID-19: peak hour of onset and secondary infectors on the 17th day. Since the Tokyo Olympic Games lasted for 17 days, secondary infectors on the 17th day were used as indicators. Secondary infectors on the 17th day refers to the number of daily new infectors at the end of the Tokyo Olympic Games; hour of onset is the time  $t$  corresponding to the maximum number of daily new infectors.

## RESULTS

### Transmission Simulation Without Intervention

In this case, we ignored the activities of athletes outside the Olympic Village, and then we used the parameters of the SEIARH model in **Table 1** to simulate the transmission within the Olympic Village in Japan without intervention, as shown in **Figure 3**. The number of daily new secondary infectors reached the peak on the 12th day, which was 1,683. The cumulative infectors were in an S-shaped curve.

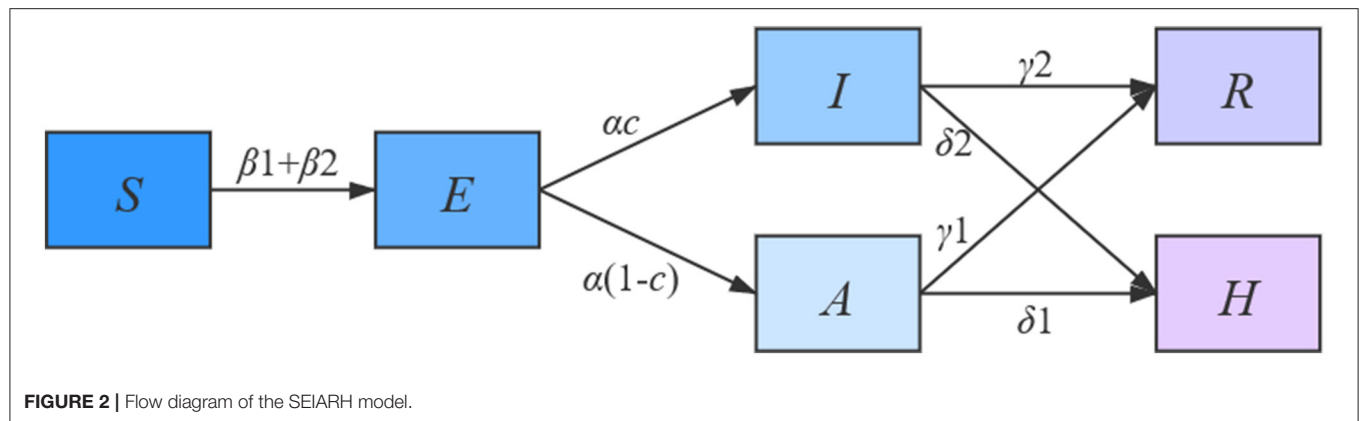
The red-shadowed region in **Figure 3** is the result of sensitivity analysis. We found that the cumulative infectors and daily new infectors changed little, indicating that the model was robust.

### Transmission Simulation Under Current Interventions of the Japan Olympic Committee (JOC)

According to the current prevention and control measures of JOC, the parameters of the average number of infected class contact with susceptible class ( $r_1$ ), average number of infected class contact with exposed class ( $r_2$ ), initial asymptomatic infected population [ $A(0)$ ] were adjusted, and the specific settings are shown in **Table 3**.

As can be seen from **Figure 4**, based on the measures currently proposed by JOC, it was assumed that the screening before take-off can reduce 20 and 40% of asymptomatic infectors, respectively, but the prevention and control effect was not ideal. The total number of secondary infectors still reached the level of no intervention measures, but the duration increased; the peak value of daily new secondary infectors decreased, reaching 1,159 on the 19th day and 1,141 on the 20th day, respectively. Secondary infectors on the 17th day reached 857.6 and 729.7, respectively. Compared with no intervention measures, the situation of current interventions of JOC improved.

The shadowed region in **Figure 4** is the result of sensitivity analysis. It can be seen that cumulative infectors and daily new

**TABLE 1 |** Parameter definition and estimation.

| Parameter  | Definition   | Value             | References |
|------------|--|-------------------|------------|
| $N$        | The total population number  | $1.1 \times 10^4$ | (4)        |
| $\beta_1$  | Probability of transmission from infected individuals to susceptible individuals       | 0.15747           | (11)       |
| $\beta_2$  | Probability of transmission from exposed individuals to susceptible individuals        | 0.78735           | (11)       |
| $r_1(t)$   | Average number of infected class contact with susceptible class                        | 2.20              | (12)       |
| $r_2(t)$   | Average number of infected class contact with exposed class                            | 2.22              | (13)       |
| $\alpha$   | Probability of susceptible individuals becoming infected individuals                   | 1/5.2             | (14)       |
| $\delta_1$ | Transition rate of symptomatic infected individuals to the quarantined infected class  | 0.6               | (15)       |
| $\delta_2$ | Transition rate of asymptomatic infected individuals to the quarantined infected class | 0.4               | (15)       |
| $\gamma_1$ | Recovery rate of symptomatic infected individuals                                      | 0.0085            | MCMC       |
| $\gamma_2$ | Recovery rate of asymptomatic infected individuals                                     | 0.0085            | MCMC       |
| $\gamma_3$ | Recovery rate of hospitalized individuals  | 0.15              | (17)       |
| $c$        | Probability of infected class have symptoms  | 0.4               | (18)       |
| $S(0)$     | Initial susceptible population   | $1.1 \times 10^4$ | (4)        |
| $E(0)$     | Initial exposed population   | 0                 |            |
| $A(0)$     | Initial asymptomatic infected population   | 10                |            |
| $I(0)$     | Initial symptomatic infected population  | 0                 | Assumed    |
| $R(0)$     | Initial recovered population   | 0                 |            |
| $H(0)$     | Initial quarantined infected population  | 0                 |            |

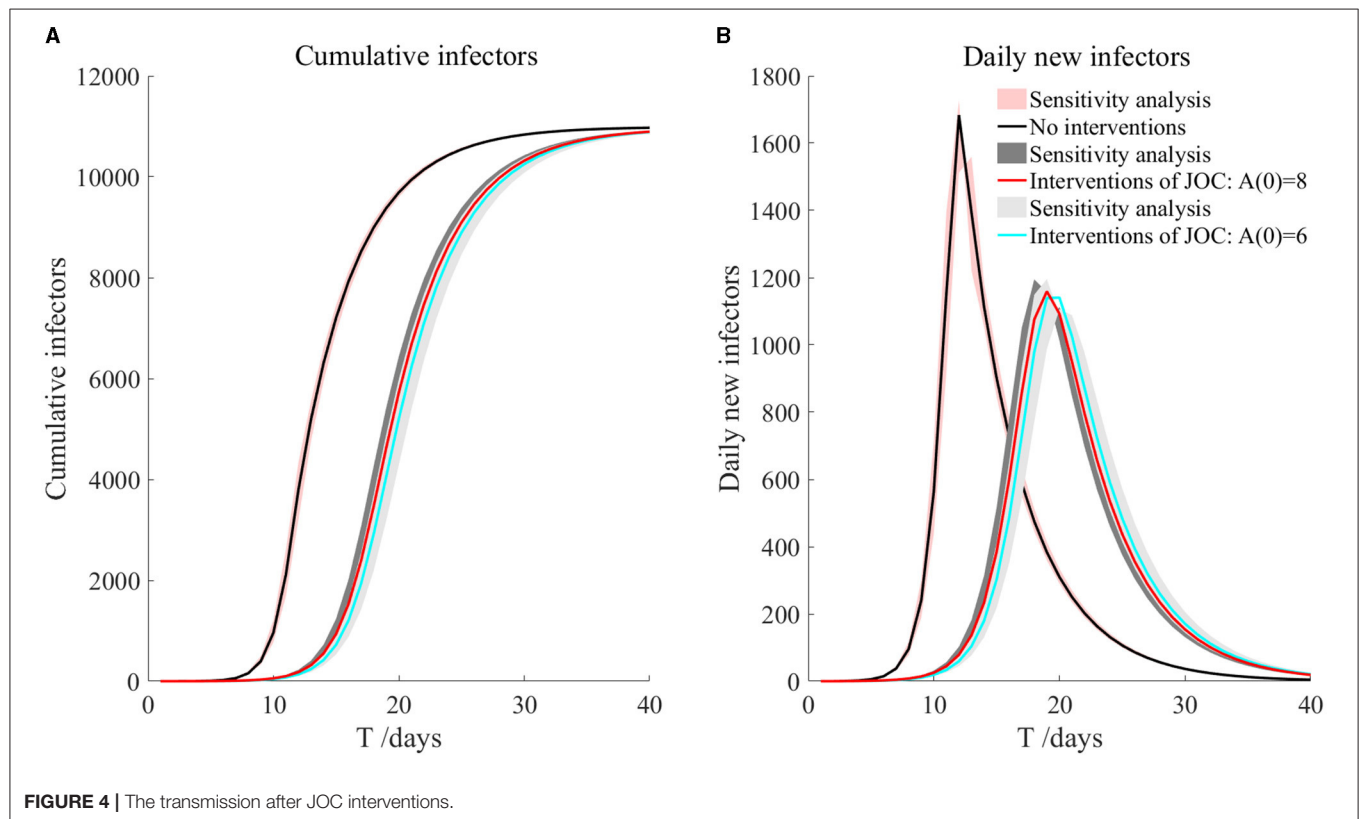
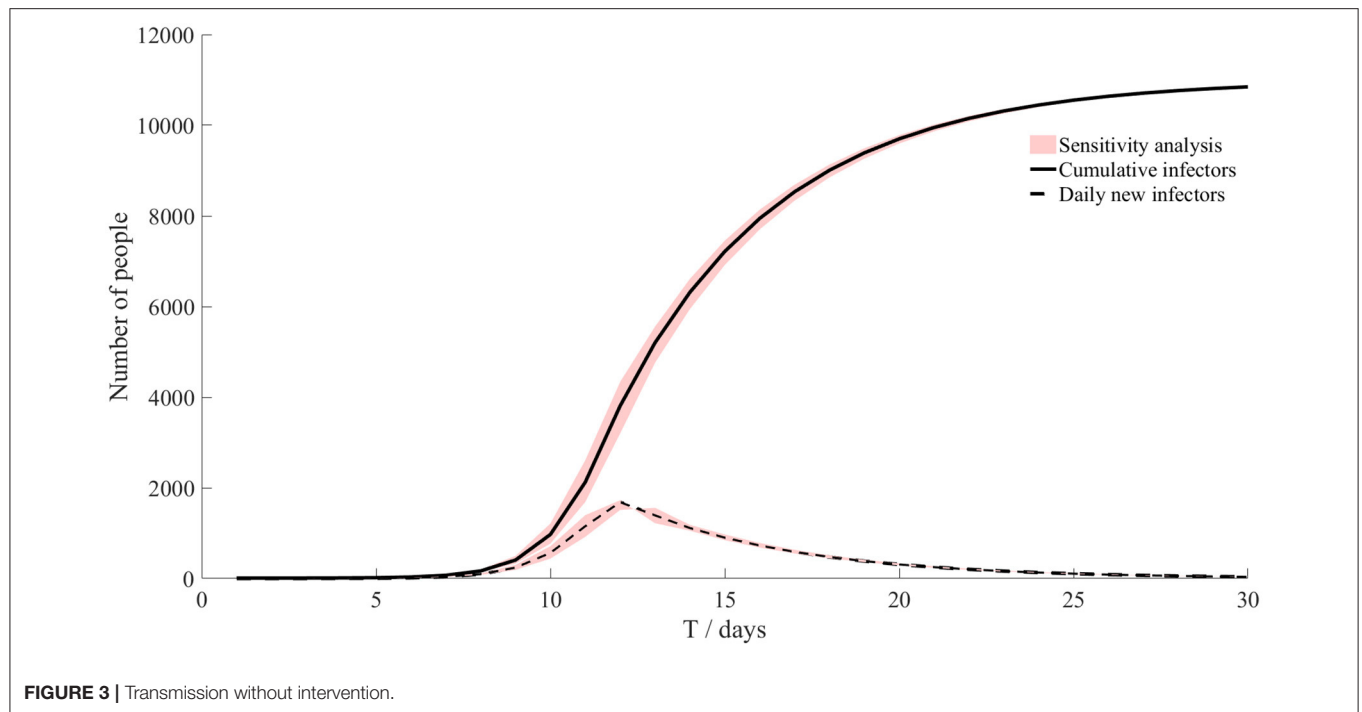
This study mainly considered the effect of different measures on the prevention and control of the Tokyo Olympic Games in the case of missed detection of asymptomatic infectors, so the initial asymptomatic infectors were 10, and the remaining initial values were 0.

infectors were almost unchanged, indicating that the model was robust. More importantly, through the simulations of the current prevention and control measures, it could be found that it was not enough to rely solely on the existing measures. Other measures (such as vaccination) must be supplemented to effectively reduce the risk of the epidemic during the Tokyo Olympic Games. We will discuss it further in the next section.

## Transmission Simulation Under Other Interventions

According to the simulation of intervention measures set in the above sections, we found that the current prevention and control effect was not ideal. But for various infectious diseases, vaccines are the most effective way to eradicate the transmission of infectious diseases. Therefore, based on the

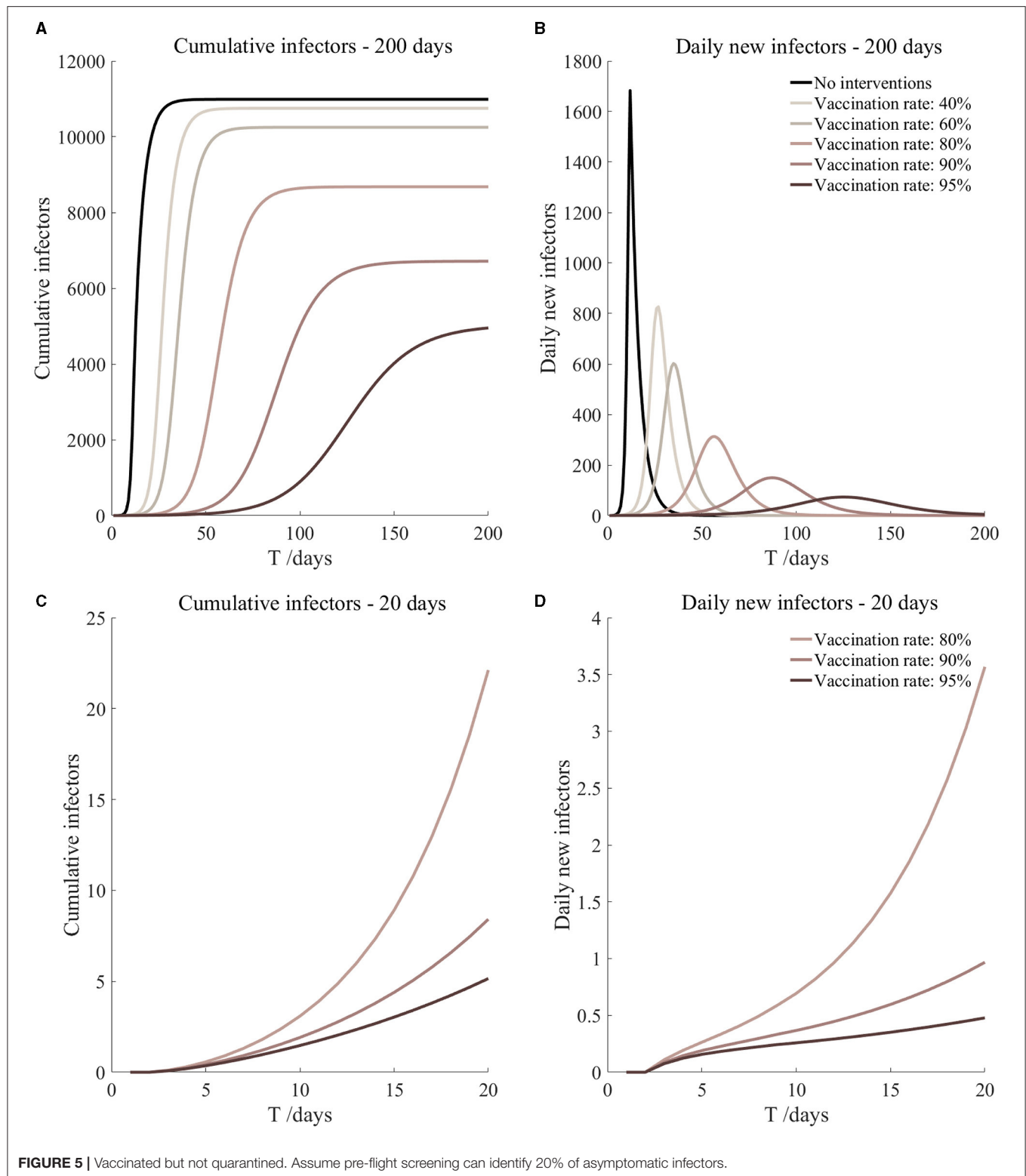
intervention measures proposed by JOC, we considered the transmission of athletes after vaccination. The transmission simulation was carried out by adding prevention and control scenarios such as “vaccinated but not quarantined,” “vaccination and 7-day compulsory quarantine,” and “vaccination and 14-day compulsory quarantine.” The protective efficacy of any vaccine cannot reach 100%, and the protective efficacy of the COVID-19 vaccine ranges from 50.7 to 95.0% (29–39), as shown in Table 4. Due to the limitations of clinical trials, vaccine development, and the fact that any vaccines have been used for <1 year, the protective efficacy of the COVID-19 vaccine is still under continuous observation. Therefore, we assumed that the protective efficacy of the vaccine is the median in Table 4, that was 78.1% (95% CI: 64.8–86.3%) (29). So the probability of transmission  $\beta_1$ ,  $\beta_2$  among athletes vaccinated fell by 21.9% (95% CI: 13.7–35.2%). Variants of COVID-19 can lead to a decrease in



neutralizing activity of the vaccine-induced antibodies, especially the mutant strain B.1.351, but the antibodies still possess a certain or high neutralizing ability to the mutant strain (33, 40–70). At present, there is not enough evidence that viral variation has a significant impact on the protection of the new coronavirus

vaccine. So, we did not consider the mutations of COVID-19 from different countries. The specific parameter adjustments are shown in **Table 5**.

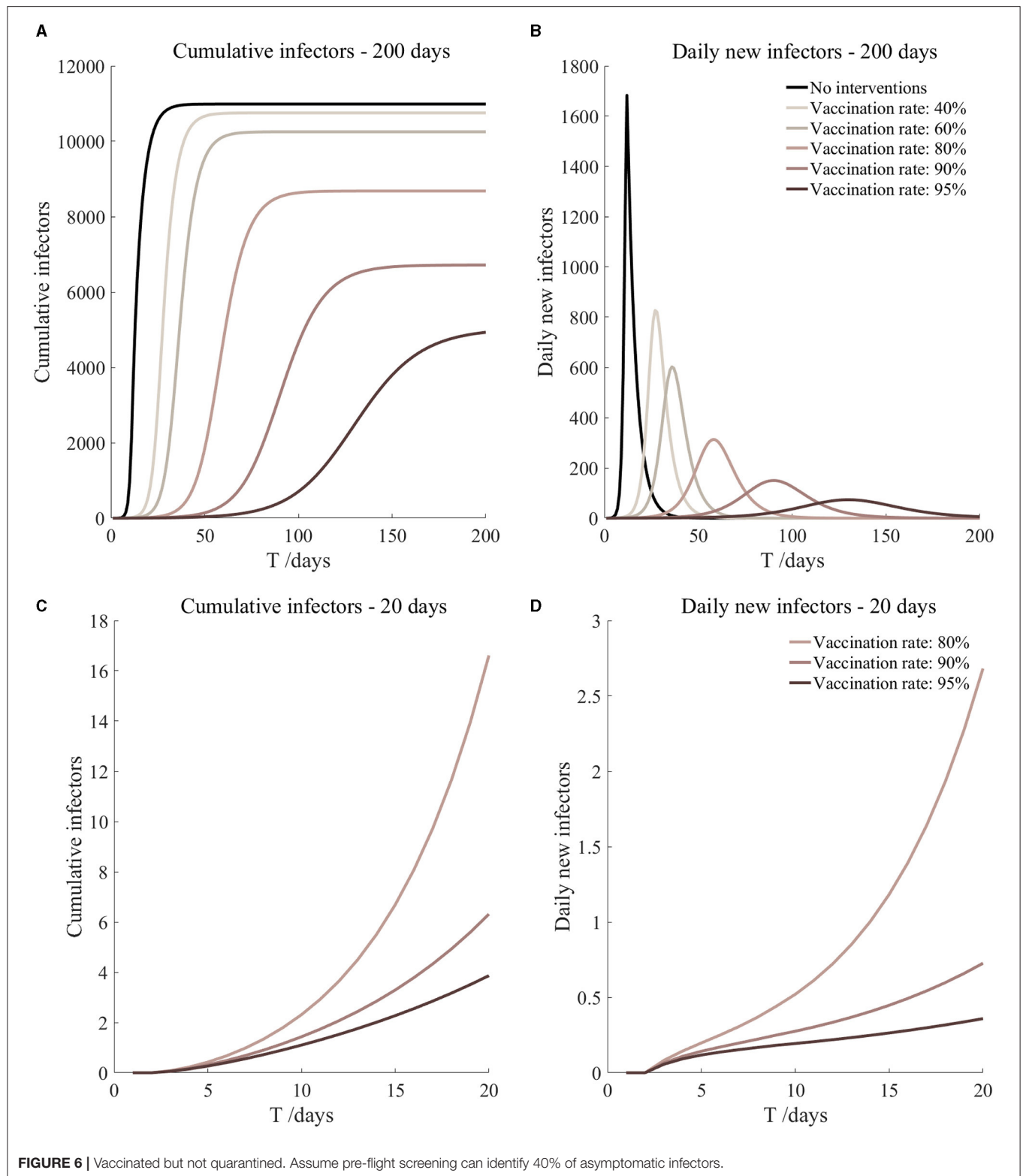
It can be found from **Figures 5–10** that the assumption of the protective efficacy of the vaccine was 78.1%. Whether



isolated or not, screening before take-off can identify 20% or 40% of asymptomatic infectors, which significantly reduced the number of secondary infectors on the 17th day and delayed

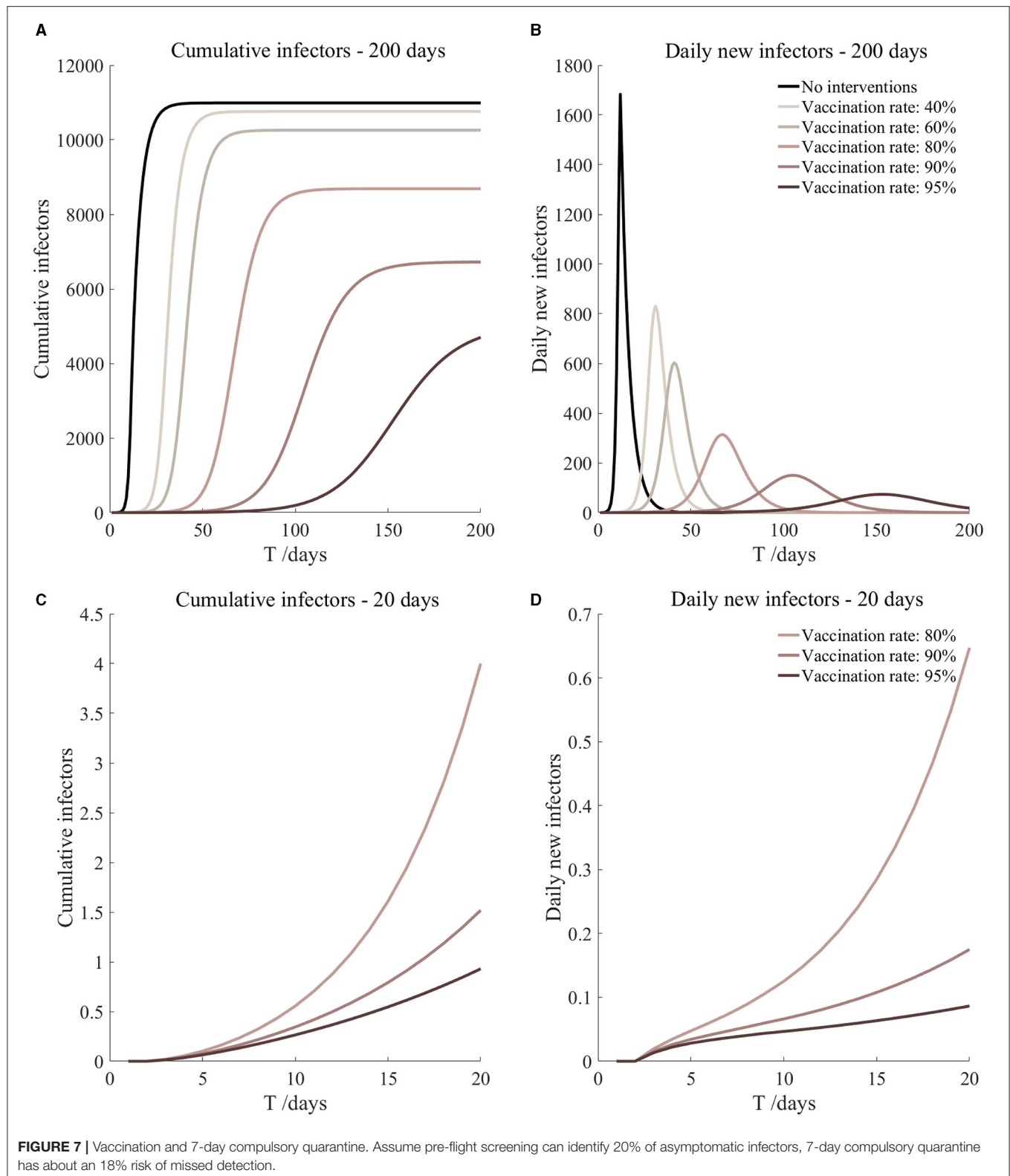
the peak hour of onset compared to no interventions and current interventions by the JOC. In the comparison of different vaccination rates of various measures, it can be found that

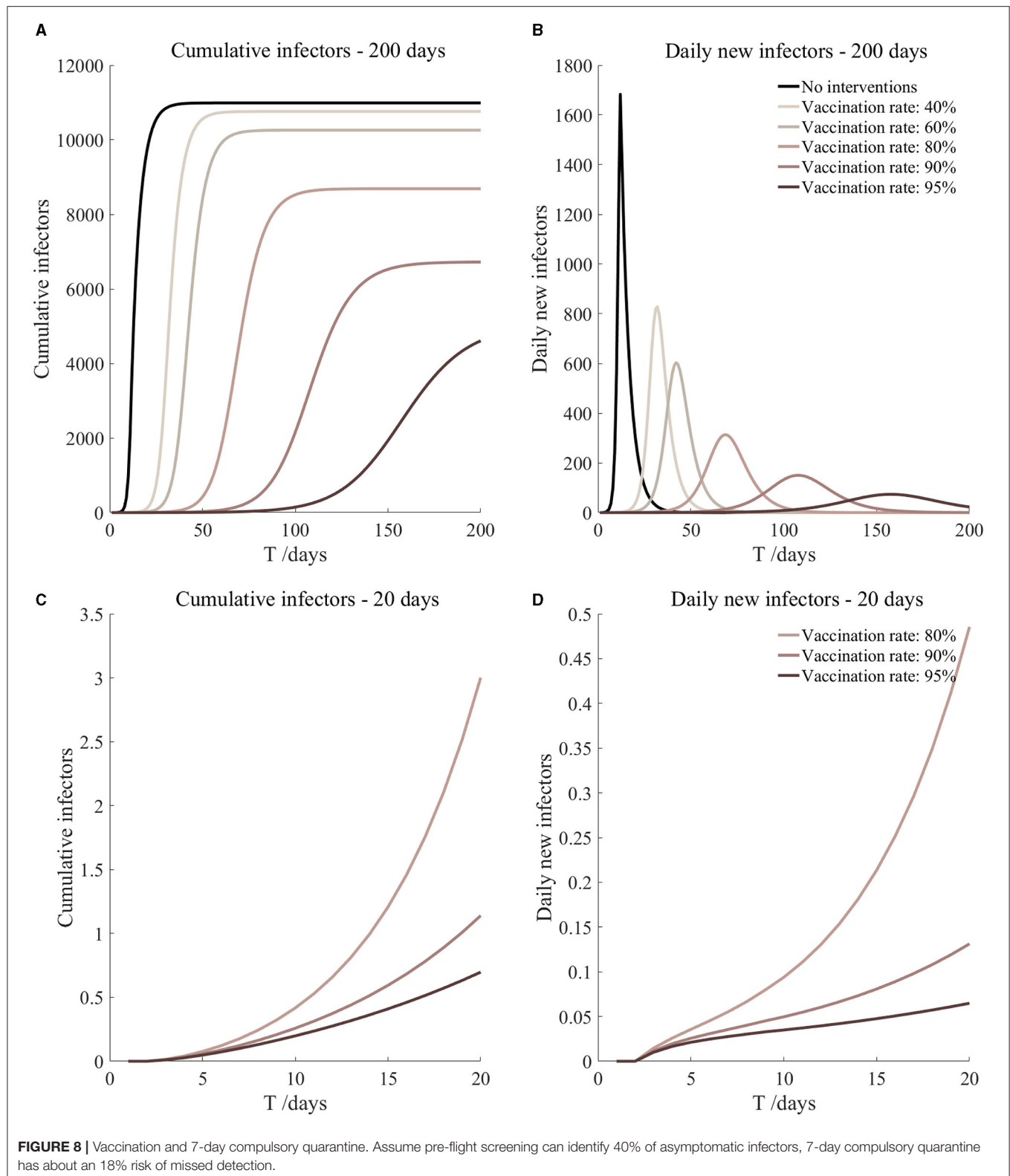


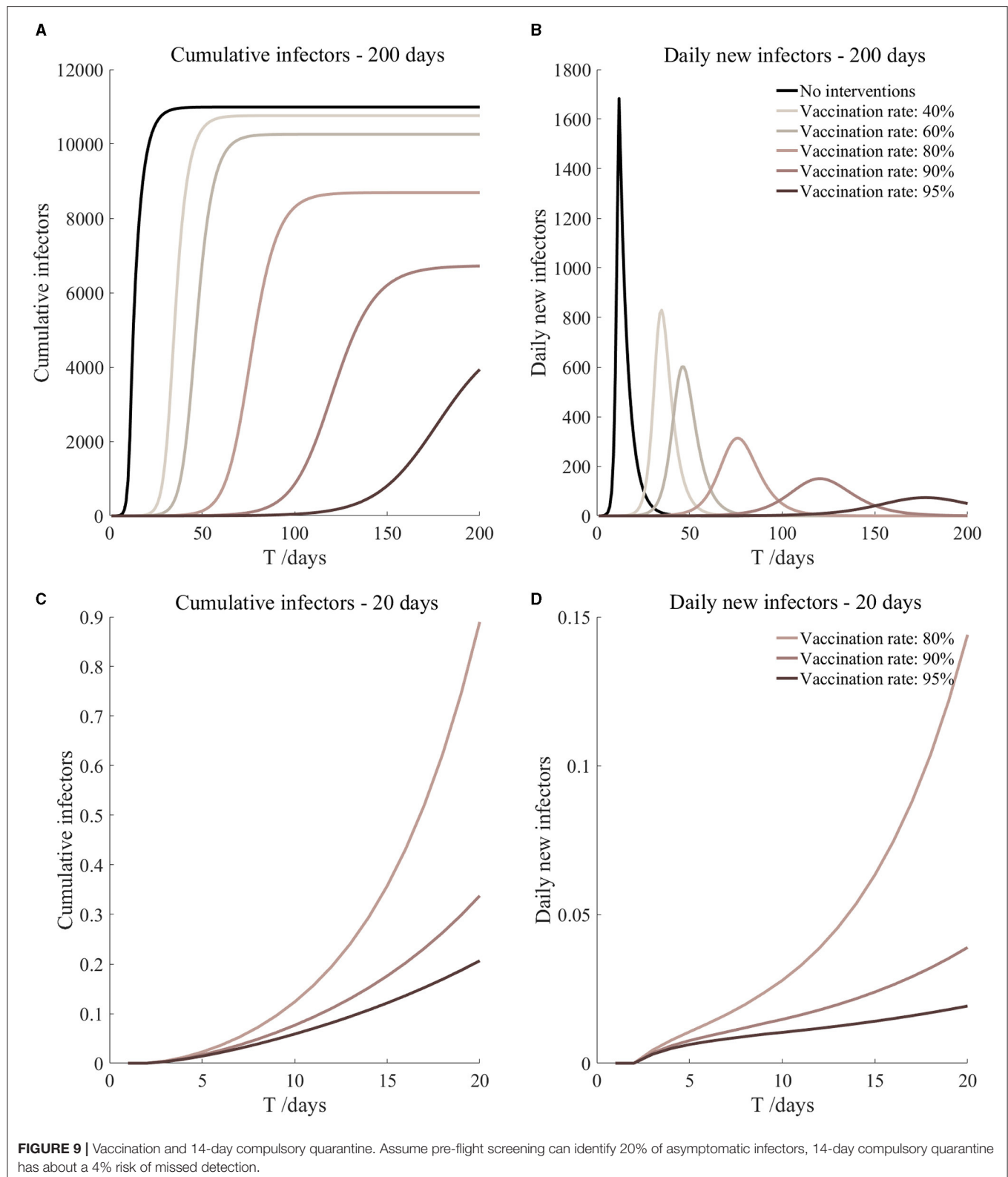


when the vaccination rate of athletes reached 80%, the number of secondary infectors on the 17th day decreased significantly. When vaccination rates were 80, 90, and 95%, cumulative infectors still reached a relatively high value at the end, but

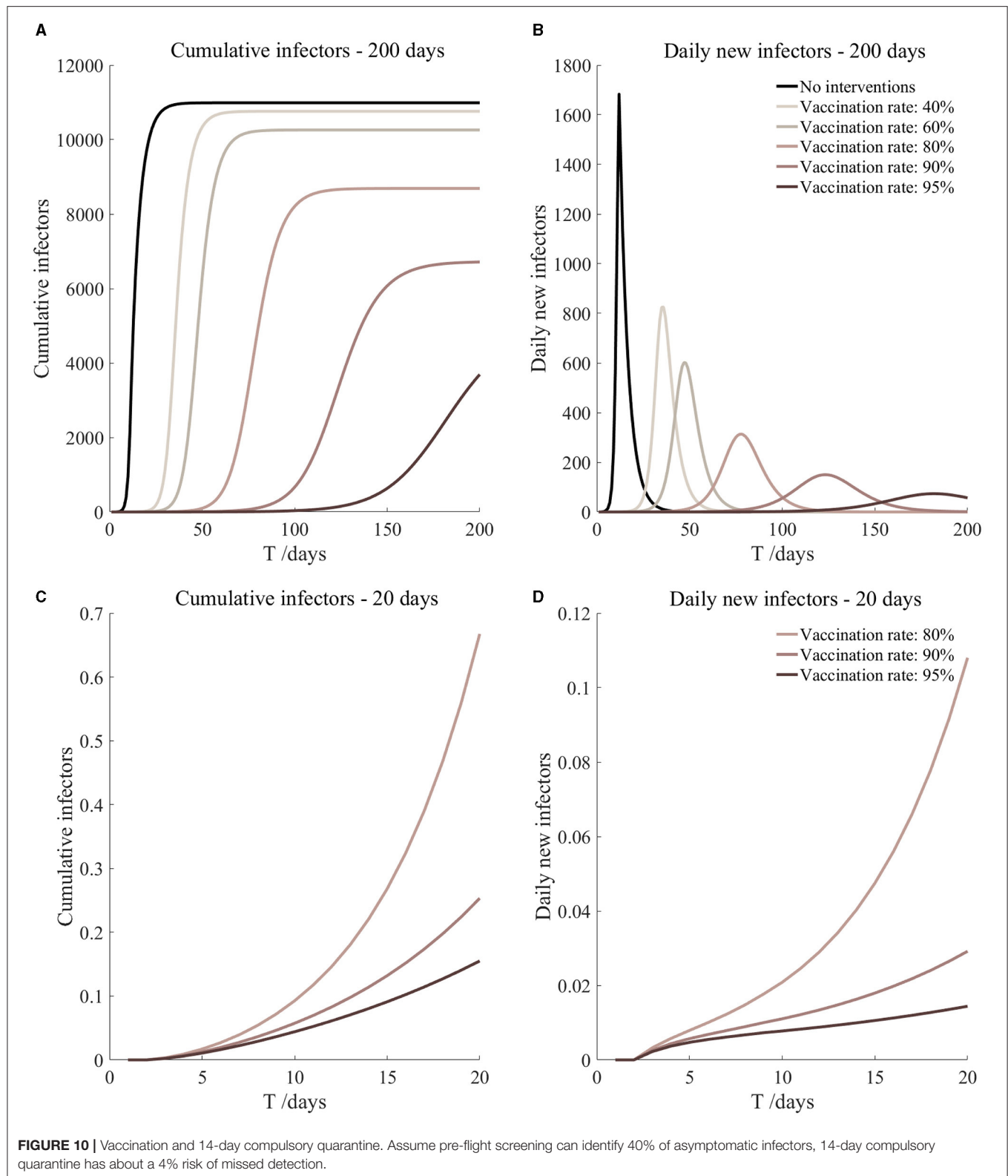
the first 17 days were very low. It showed that the vaccine was effective, and that extensive vaccination would be useful for the prevention and control of COVID-19 in the Tokyo Olympic Games.

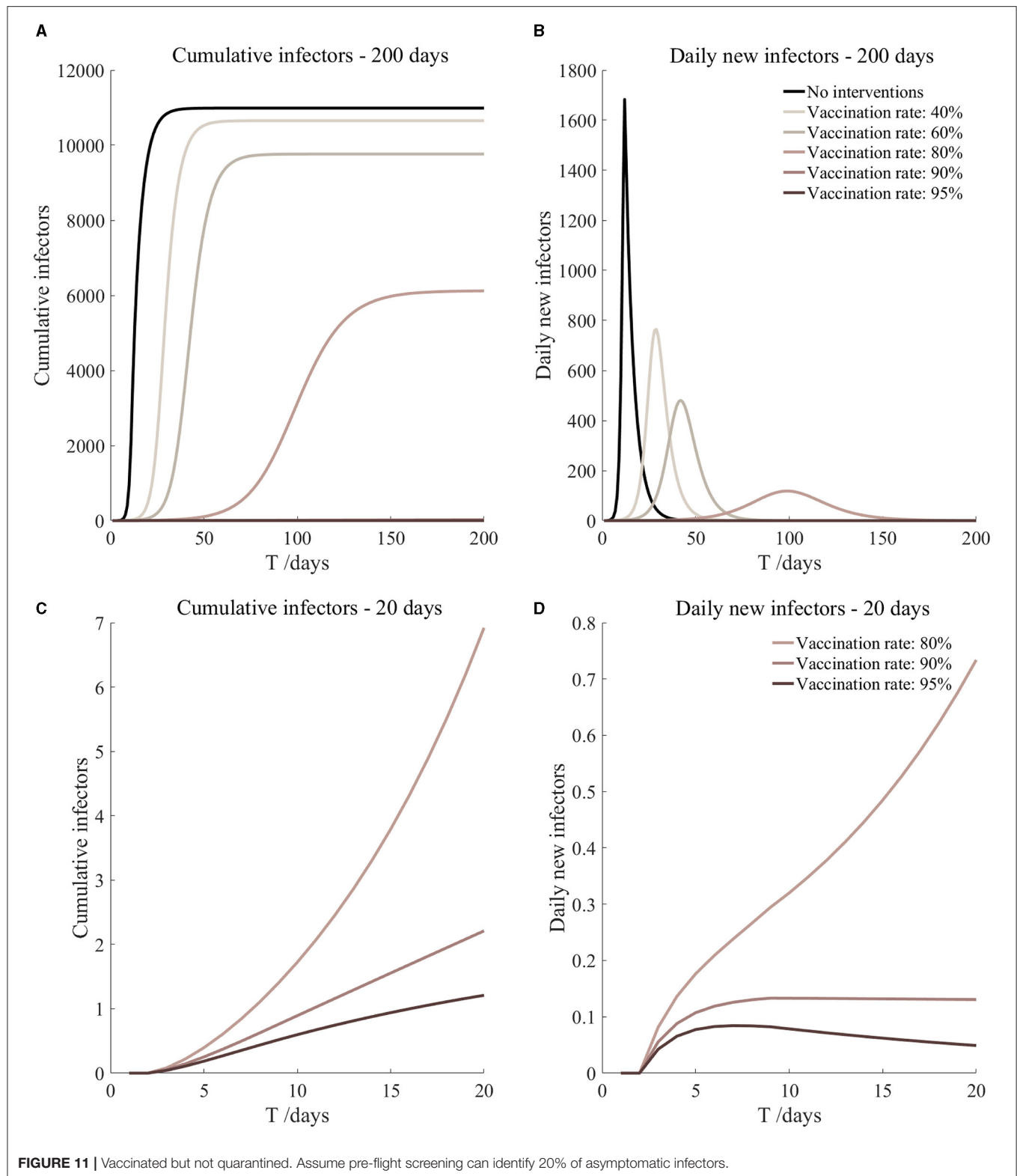


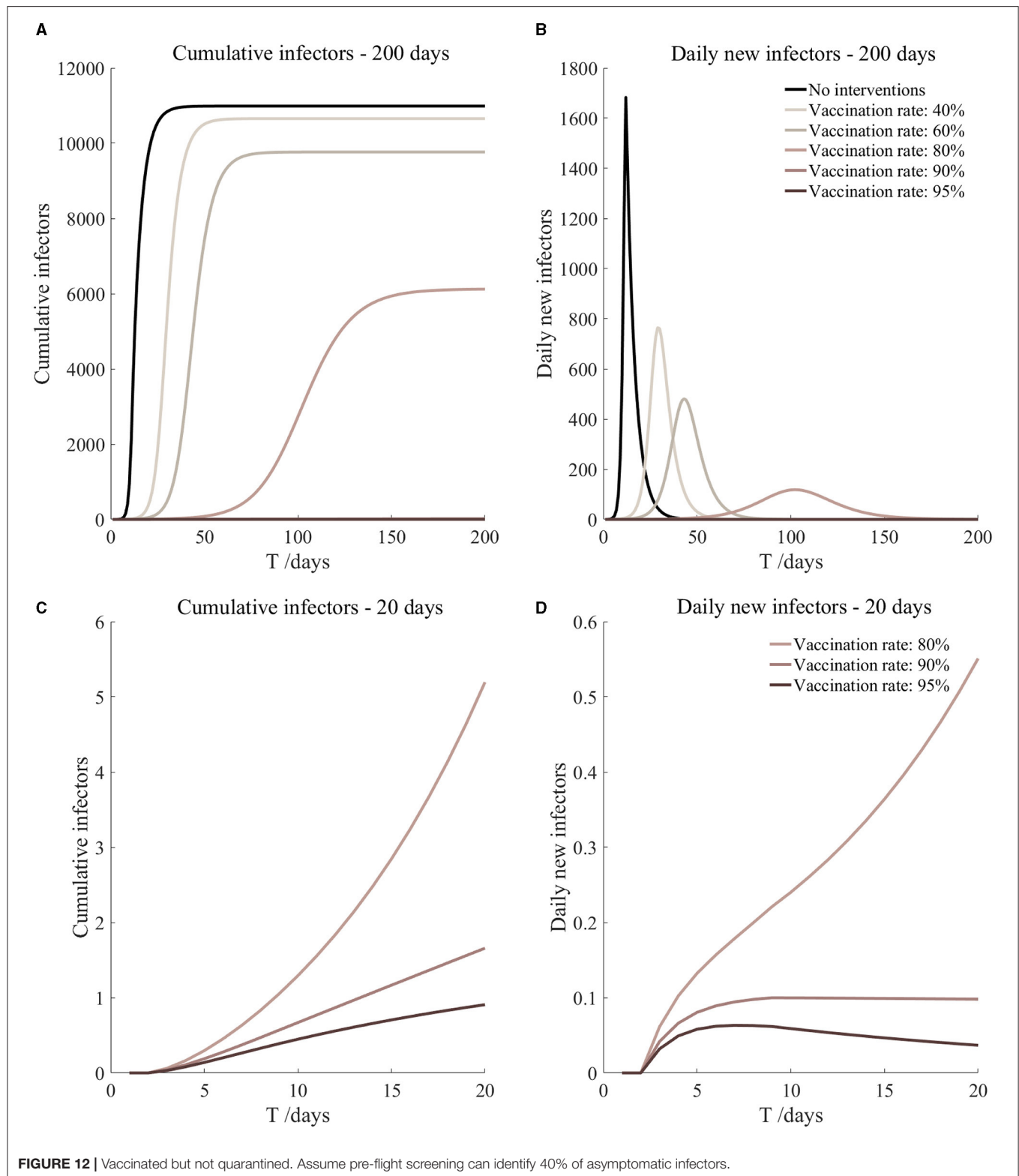


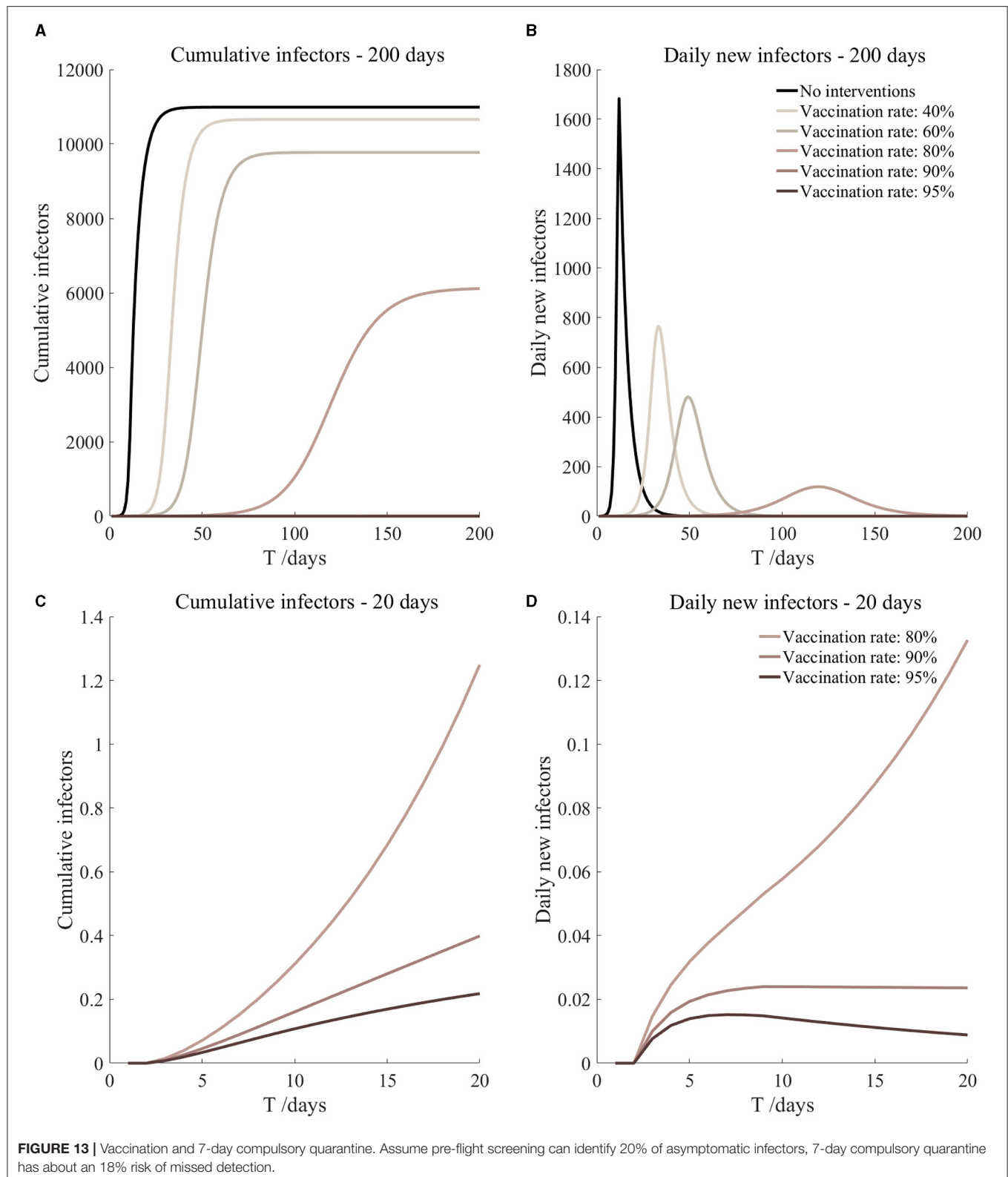




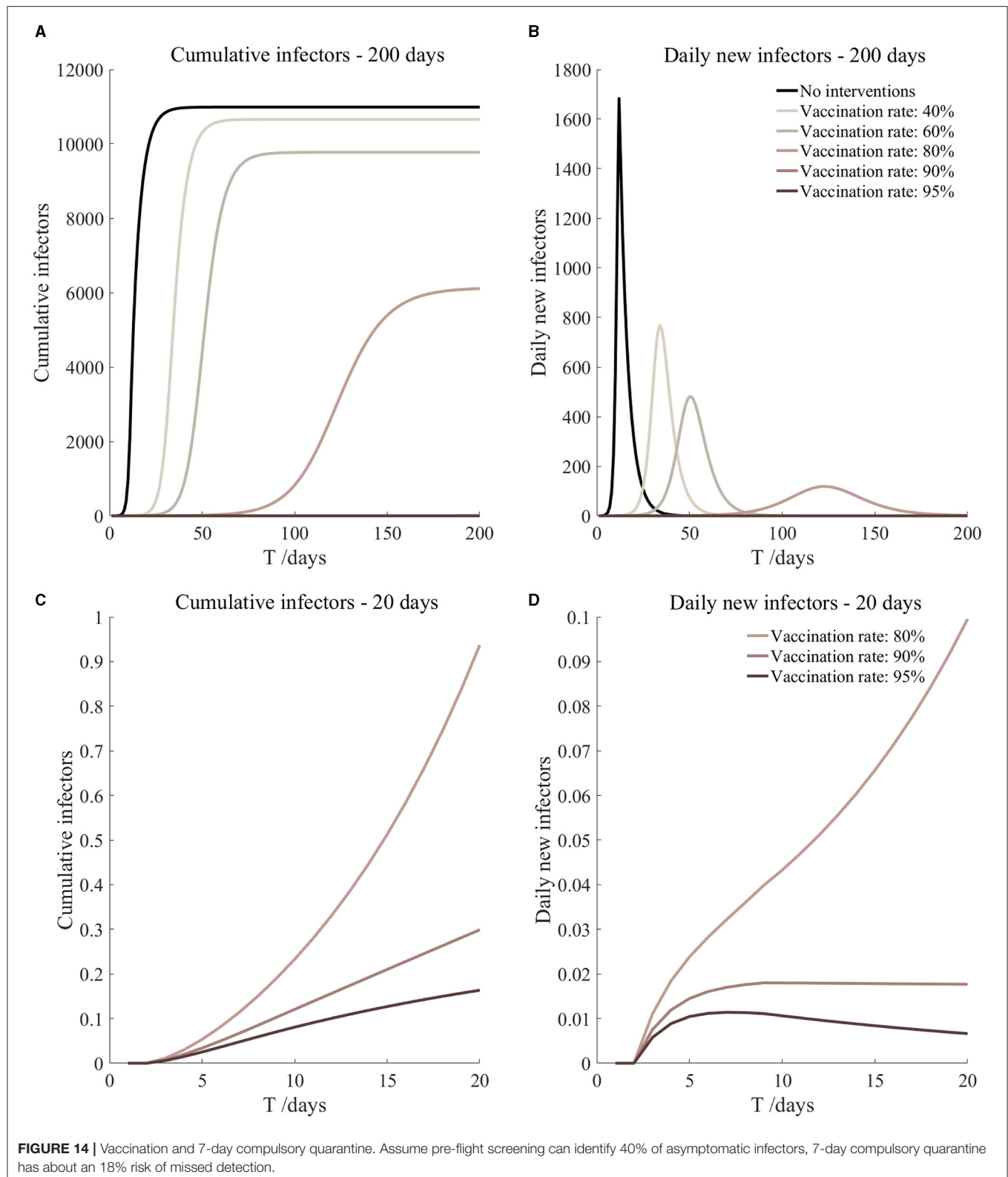


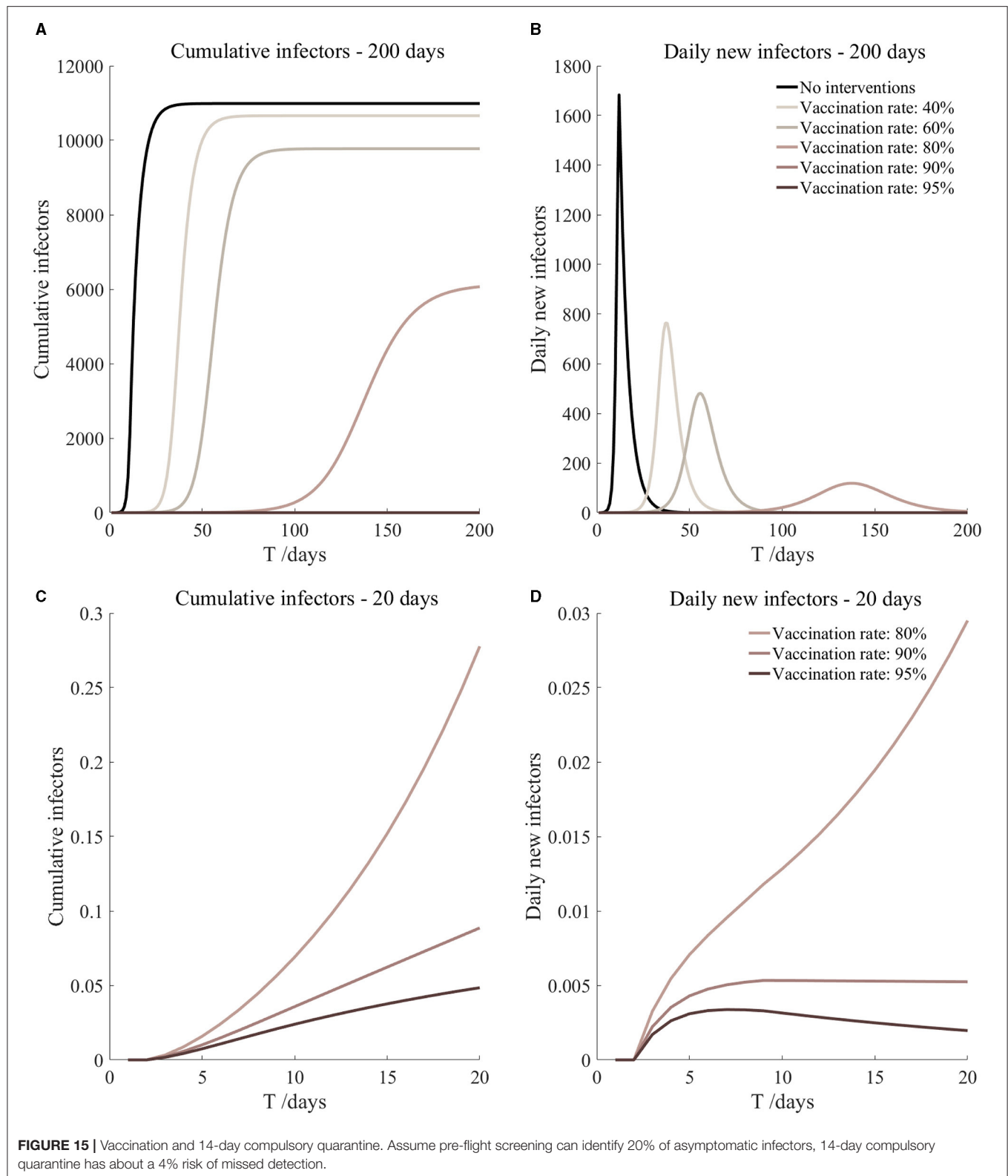












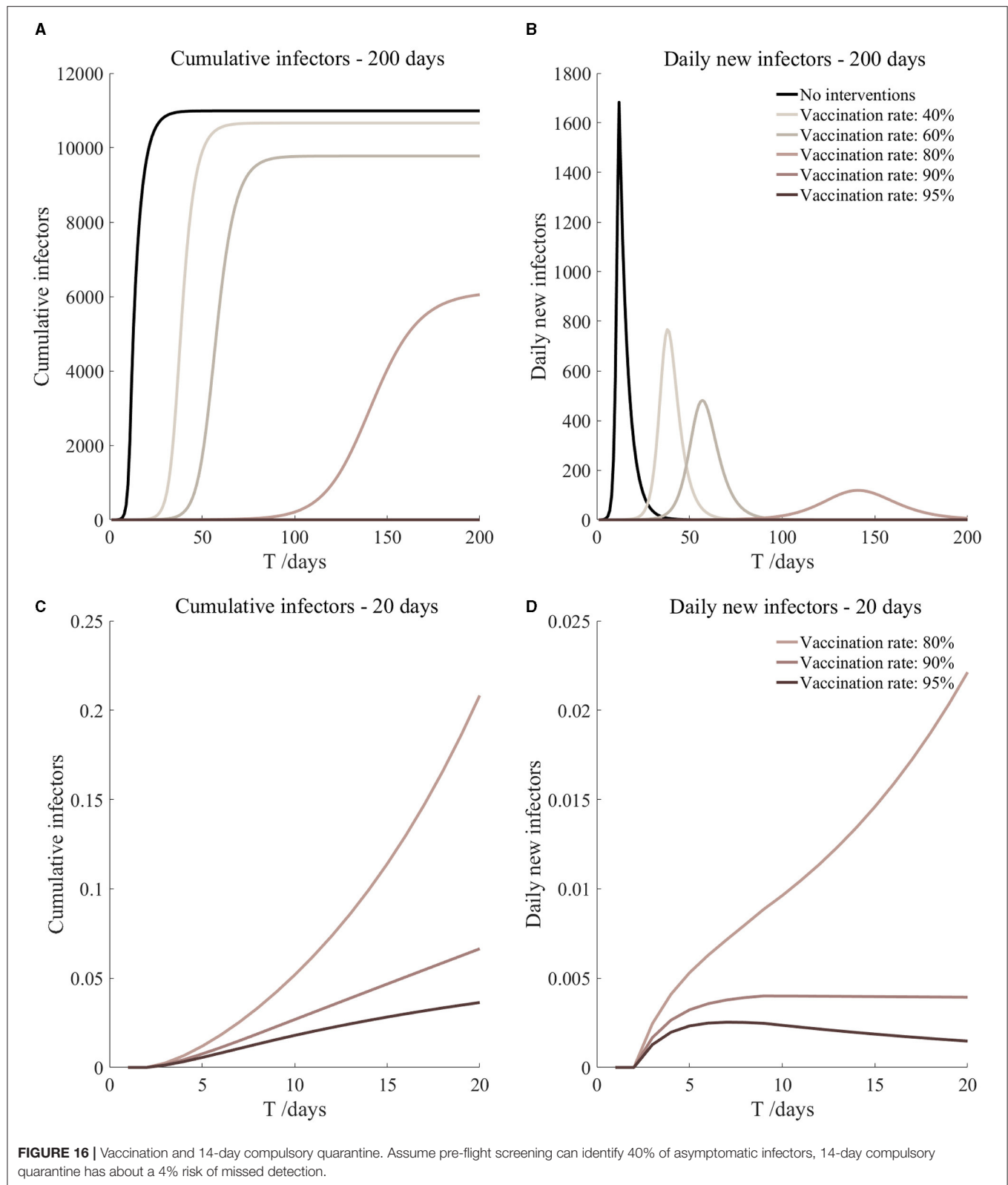


**TABLE 2 |** Key steps and results in the planning, coding, and analysis of this simulation study.

|   | Section |
|---|---------|
| <b>Planning</b>   | 2       |
| Aims  |         |
| • Simulate the transmission of COVID-19 during the Tokyo Olympic Games.   |         |
| Data-generating mechanisms  |         |
| • The parameters of the SEIARH model came from MCMC estimations based on real data or previous studies.   |         |
| Target of analysis  |         |
| • To explore effective prevention and control measures for COVID-19 in large international events.  |         |
| Methods   |         |
| • Used random model to calculate the number of initial infected patients and used Poisson distribution to determine the number of initial infected patients based on the number of countries involved.                                      |         |
| • Established the SEIARH model to simulate the transmission of COVID-19.  |         |
| • Estimated risk assessment indicators by different scenarios of the simulated interventions.   |         |
| Performance measures  |         |
| • Analyzed the robustness of the model by increasing or decreasing parameters $\beta_1$ and $\beta_2$ at the same time.   |         |
| <b>Coding and Execution</b>   | 2       |
| • More details can be found in <b>Supplementary Material B</b> .  |         |
| <b>Analysis</b>   | 3       |
| • The current COVID-19 prevention measures proposed by the Japan Olympic Committee need to be enhanced.   |         |
| • Large-scale vaccination will effectively control the spread of COVID-19. When the protective efficacy of vaccine is 78.1 or 89.8% and if the vaccination rate of athletes reaches 80%, an epidemic prevention barrier can be established. |         |

**TABLE 3 |** Parameter adjustment and transmission simulation.

| Prevention and control measures  | Parameter adjustment              | Setting basis  | Secondary infectors on the 17th day | Peak hour of onset/d |
|--|-----------------------------------|--|-------------------------------------|----------------------|
| No intervention ( <b>Figure 3</b> )  | –                                 | –  | 587.8                               | 12                   |
| Keep a minimum of two meters from athletes at all times. Keep a minimum of one meter from others. Take two COVID-19 tests before their flight to Japan ( <b>Figure 4</b> ) | $r_1 = 1.2, r_2 = 1.22, A(0) = 8$ | Assume pre-flight screening can identify 20% of asymptomatic infectors | 857.6                               | 19                   |
| The same as above ( <b>Figure 4</b> )  | $r_1 = 1.2, r_2 = 1.22, A(0) = 6$ | Assume pre-flight screening can identify 40% of asymptomatic infectors | 729.7                               | 21                   |

**TABLE 4 |** The protective efficacy of vaccines.

| Vaccine type              | Vaccine name                     | Protective efficacy (%) | 95% CI     |
|---------------------------|----------------------------------|-------------------------|------------|
| Inactivated vaccine       | SinoVac                          | 78.1                    | 64.8–86.3% |
|                           | CoronaVac                        | 50.7                    | 35.9–62.0% |
| Nucleic acid vaccine      | Pfizer mRNA vaccine (BNT162b2)   | 93.0                    | 78.0–98.0% |
|                           | Moderna mRNA vaccine (mRNA-1273) | 82.0                    | 20.0–96.0% |
| Adenovirus vector vaccine | Ad26.COV2.S                      | 66.9                    | 59.0–73.4% |
|                           | AstraZeneca                      | 70.4                    | 54.8–80.6% |
|                           | Gam-COVID-Vac                    | 87.6                    | 81.1–91.8% |

The protective efficacy in the table indicates the protective efficacy in preventing the occurrence of symptomatic COVID-19.

Comparing **Figure 5** and **Figure 6**, **Figure 7** and **Figure 8**, and **Figure 9** and **Figure 10**, it can be seen that under the intervention measures of “vaccinated but not quarantined,” “vaccination and 7-day compulsory quarantine,” and “vaccination and 14-day compulsory quarantine,” the proportion of asymptomatic

infected individuals identified by pre-flight screening had little effect on the number of secondarily infected individuals, and the outbreak time was basically the same under different vaccination proportions. However, for the intervention measures in **Figures 5–10**, as the vaccination rate increased, the secondary



**TABLE 5 |** Parameter adjustment and transmission after vaccination.

| Prevention and control measures   |  | Parameter adjustment   | Setting basis/vaccination rate (%) | Secondary infectors on the 17th day | Peak hour of onset/d |
|---|--|--|------------------------------------|-------------------------------------|----------------------|
| No intervention (Figure 3)  |  | –  | –                                  | 587.8                               | 12                   |
| Vaccinated but not quarantined. Assume pre-flight screening can identify 20% of asymptomatic infectors (Figure 5)   | $r_1 = 1.2,$<br>$r_2 = 1.22,$<br>$A(0) = 8$    | $\beta_1 = 0.1083$<br>(0.1031, 0.1167),<br>$\beta_2 = 0.5414$<br>(0.5156, 0.5833). | 40                                 | 79.54<br>(57.39, 131.72)            | 27                   |
|   |  | $\beta_1 = 0.0837$<br>(0.0759, 0.0962),<br>$\beta_2 = 0.4184$<br>(0.3797, 0.4812). | 60                                 | 15.17<br>(8.52, 36.50)              | 35                   |
|   |  | $\beta_1 = 0.0591$<br>(0.0488, 0.0758),<br>$\beta_2 = 0.2954$<br>(0.2438, 0.3792). | 80                                 | 2.19<br>(0.87, 8.45)                | 56                   |
|   |  | $\beta_1 = 0.0468$<br>(0.0352, 0.0656),<br>$\beta_2 = 0.2339$<br>(0.1758, 0.3282). | 90                                 | 0.72<br>(0.23, 3.78)                | 87                   |
|   |  | $\beta_1 = 0.0406$<br>(0.0284, 0.0605),<br>$\beta_2 = 0.2032$<br>(0.1418, 0.3027). | 95                                 | 0.40<br>(0.11, 2.47)                | 125                  |
| Vaccinated but not quarantined. Assume pre-flight screening can identify 40% of asymptomatic infectors (Figure 6)   | $r_1 = 1.2,$<br>$r_2 = 1.22,$<br>$A(0) = 6$    | $\beta_1 = 0.1083$<br>(0.1031, 0.1167),<br>$\beta_2 = 0.5414$<br>(0.5156, 0.5833). | 40                                 | 60.48<br>(43.50, 100.85)            | 27                   |
|   |  | $\beta_1 = 0.0837$<br>(0.0759, 0.0962),<br>$\beta_2 = 0.4184$<br>(0.3797, 0.4812). | 60                                 | 11.43<br>(6.41, 27.58)              | 36                   |
|   |  | $\beta_1 = 0.0591$<br>(0.0488, 0.0758),<br>$\beta_2 = 0.2954$<br>(0.2438, 0.3792). | 80                                 | 1.64<br>(0.65, 6.36)                | 58                   |
|   |  | $\beta_1 = 0.0468$<br>(0.0352, 0.0656),<br>$\beta_2 = 0.2339$<br>(0.1758, 0.3282). | 90                                 | 0.54<br>(0.17, 2.84)                | 90                   |
|   |  | $\beta_1 = 0.0406$<br>(0.0284, 0.0605),<br>$\beta_2 = 0.2032$<br>(0.1418, 0.3027). | 95                                 | 0.30<br>(0.08, 1.86)                | 130                  |
| Vaccination and 7-day compulsory quarantine. Assume pre-flight screening can identify 20% of asymptomatic infectors, 7-day compulsory quarantine has about an 18% risk of missed detection (Figure 7) | $r_1 = 1.2,$<br>$r_2 = 1.22,$<br>$A(0) = 1.44$ | $\beta_1 = 0.1083$<br>(0.1031, 0.1167),<br>$\beta_2 = 0.5414$<br>(0.5156, 0.5833). | 40                                 | 14.98<br>(10.70, 25.39)             | 31                   |
|   |  | $\beta_1 = 0.0837$<br>(0.0759, 0.0962),<br>$\beta_2 = 0.4184$<br>(0.3797, 0.4812). | 60                                 | 2.77<br>(1.55, 6.74)                | 41                   |
|   |  | $\beta_1 = 0.0591$<br>(0.0488, 0.0758),<br>$\beta_2 = 0.2954$<br>(0.2438, 0.3792). | 80                                 | 0.40<br>(0.16, 1.54)                | 67                   |
|   |  | $\beta_1 = 0.0468$<br>(0.0352, 0.0656),<br>$\beta_2 = 0.2339$<br>(0.1758, 0.3282). | 90                                 | 0.13<br>(0.04, 0.68)                | 105                  |

(Continued)

TABLE 5 | Continued

| Prevention and control measures  | Parameter adjustment                             | Setting basis/vaccination rate (%)   | Secondary infectors on the 17th day | Peak hour of onset/d |
|--|--|--|-------------------------------------|----------------------|
| Vaccination and 7-day compulsory quarantine. Assume pre-flight screening can identify 40% of asymptomatic infectors, 7-day compulsory quarantine has about an 18% risk of missed detection (Figure 8)  | $r_1 = 1.2$ ,<br>$r_2 = 1.22$ ,<br>$A(0) = 1.08$ | $\beta_1 = 0.0406$<br>(0.0284, 0.0605),<br>$\beta_2 = 0.2032$<br>(0.1418, 0.3027). | 95<br><br>(0.02, 0.45)              | 153                  |
|  |  | $\beta_1 = 0.1083$<br>(0.1031, 0.1167),<br>$\beta_2 = 0.5414$<br>(0.5156, 0.5833). | 40<br><br>(8.04, 19.11)             | 32                   |
|  |  | $\beta_1 = 0.0837$<br>(0.0759, 0.0962),<br>$\beta_2 = 0.4184$<br>(0.3797, 0.4812). | 60<br><br>(1.16, 5.06)              | 42                   |
|  |  | $\beta_1 = 0.0591$<br>(0.0488, 0.0758),<br>$\beta_2 = 0.2954$<br>(0.2438, 0.3792). | 80<br><br>(0.12, 1.15)              | 69                   |
|  |  | $\beta_1 = 0.0468$<br>(0.0352, 0.0656),<br>$\beta_2 = 0.2339$<br>(0.1758, 0.3282). | 90<br><br>(0.03, 0.51)              | 108                  |
|  |  | $\beta_1 = 0.0406$<br>(0.0284, 0.0605),<br>$\beta_2 = 0.2032$<br>(0.1418, 0.3027). | 95<br><br>(0.01, 0.34)              | 158                  |
| Vaccination and 14-day compulsory quarantine. Assume pre-flight screening can identify 20% of asymptomatic infectors, 14-day compulsory quarantine has about a 4% risk of missed detection (Figure 9)  | $r_1 = 1.2$ ,<br>$r_2 = 1.22$ ,<br>$A(0) = 0.32$ | $\beta_1 = 0.1083$<br>(0.1031, 0.1167),<br>$\beta_2 = 0.5414$<br>(0.5156, 0.5833). | 40<br><br>(2.39, 5.71)              | 35                   |
|  |  | $\beta_1 = 0.0837$<br>(0.0759, 0.0962),<br>$\beta_2 = 0.4184$<br>(0.3797, 0.4812). | 60<br><br>(0.34, 1.50)              | 46                   |
|  |  | $\beta_1 = 0.0591$<br>(0.0488, 0.0758),<br>$\beta_2 = 0.2954$<br>(0.2438, 0.3792). | 80<br><br>(0.04, 0.34)              | 76                   |
|  |  | $\beta_1 = 0.0468$<br>(0.0352, 0.0656),<br>$\beta_2 = 0.2339$<br>(0.1758, 0.3282). | 90<br><br>(0.01, 0.15)              | 120                  |
|  |  | $\beta_1 = 0.0406$<br>(0.0284, 0.0605),<br>$\beta_2 = 0.2032$<br>(0.1418, 0.3027). | 95<br><br>(0, 0.10)                 | 177                  |
|  |  | $\beta_1 = 0.1083$<br>(0.1031, 0.1167),<br>$\beta_2 = 0.5414$<br>(0.5156, 0.5833). | 40<br><br>(1.80, 4.29)              | 36                   |
| Vaccination and 14-day compulsory quarantine. Assume pre-flight screening can identify 40% of asymptomatic infectors, 14-day compulsory quarantine has about a 4% risk of missed detection (Figure 10) | $r_1 = 1.2$ ,<br>$r_2 = 1.22$ ,<br>$A(0) = 0.24$ | $\beta_1 = 0.0837$<br>(0.0759, 0.0962),<br>$\beta_2 = 0.4184$<br>(0.3797, 0.4812). | 60<br><br>(0.26, 1.13)              | 47                   |
|  |  | $\beta_1 = 0.0591$<br>(0.0488, 0.0758),<br>$\beta_2 = 0.2954$<br>(0.2438, 0.3792). | 80<br><br>(0.03, 0.26)              | 78                   |
|  |  |  |                                     |                      |
|  |  |  |                                     |                      |

(Continued)

TABLE 5 | Continued

| Prevention and control measures | Parameter adjustment   | Setting basis/vaccination rate (%) | Secondary infectors on the 17th day | Peak hour of onset/d |
|---------------------------------|--|------------------------------------|-------------------------------------|----------------------|
|                                 | $\beta_1 = 0.0468$<br>(0.0352, 0.0656),<br>$\beta_2 = 0.2339$<br>(0.1758, 0.3282). | 90                                 | 0.02<br>(0.01, 0.11)                | 123                  |
|                                 | $\beta_1 = 0.0406$<br>(0.0284, 0.0605),<br>$\beta_2 = 0.2032$<br>(0.1418, 0.3027). | 95                                 | 0.01<br>(0, 0.07)                   | 182                  |

Except "No intervention," all other situations considered "Keep a minimum of 2 m from athletes at all times. Keep a minimum of 1 m from others. Take two COVID-19 tests before their flight to Japan".

infectors on the 17th day and the peak hour of onset significantly decreased. When the vaccination rate of athletes reached 80%, the number of secondary infectors decreased significantly, and it was controlled within 1 when the vaccination rate of athletes reached 90%, indicating that the immune barrier could be established when the vaccination rate reached 80–90%.

Considering that athletes are generally physically fit, we took differences in population resistance into account. We assumed that the protective efficacy of the vaccine of athletes is 15% higher than the average person (78.1%), that is 89.8% (95% CI: 74.5–99.2%). Under this assumption, we developed new simulations. The optimal parameters are shown in Table 6.

From Figures 11–16, we know that when the vaccination rate of athletes reached 80%, the number of secondary infectors on the 17th day decreased significantly and was controlled within 1, indicating that the immune barrier could be established when the vaccination rate reached 80%.

## DISCUSSION

The strengths of our study were that the topic is timely, and we used an epidemic method to model the spread of COVID-19. We also discussed the sensitivity of parameters. And we discussed the relationship between vaccination services and spread of COVID-19, considering different protective efficacy of vaccines and vaccination rates. We took differences in population resistance into account as athletes are generally more physically fit. We tested the robustness of the SEIARH model and found that the model was stable. The model we constructed considered the time, environment, and behavior at the same time. The limitations were that we did not consider the transmission of COVID-19 from athletes to the audience, because the policy of JOC clearly limited the scope of activities of athletes and the distance from the audience (6, 7, 71). But we considered the latest results of protective efficacy of the vaccine to make the results more scientific and credible (28, 29). There was no specific number of participants from each country, so it was not possible to accurately estimate the initially infected individuals. The parameters of the model refer to other research based on real

data, which may be different from the real situation in Japan, but we set the interval of parameters to reduce bias.

Through the simulation of no intervention measures and various intervention measures, we found that the prevention and control effect of the measures currently proposed by JOC was not ideal. The total number of secondary infectors could still reach the level of no intervention measures, but with a longer duration. However, the prevention and control effect of the intervention measures proposed by us was significantly better than that of no intervention measures or the epidemic response measures proposed by JOC. The simulated number of secondary infectors without intervention measures on the 17th day was 587.8. As shown in Tables 3, 5, 6, we simulated no interventions and different levels of intervention. It showed that these measures can delay the outbreak of COVID-19 to some extent, but the number of infectors was not well-controlled. If the protective efficacy of the vaccine was 78.1% and the vaccination rate reached 90%, the number of secondary infectors under all intervention measures was <1; if the protective efficacy of vaccine was 89.8% and the vaccination rate reached 80%, the number of secondary infectors under all intervention measures was <1, indicating that the epidemic situation was effectively controlled, and vaccination can effectively prevent COVID-19. Comparing Table 5 and Table 6, it was found that under the same intervention circumstance, if the protective efficacy of vaccine was 89.8%, the number of secondary infectors decreased significantly. But the peak hour of onset for each control measure in Table 5 kept being postponed, while it was postponed first and then advanced in Table 6. This was because when the protective efficacy of vaccine was 89.8%, it could not trigger the transmission of COVID-19 and the transmission period was short. Vaccines gave a protection ability to COVID-19 infectors. Studies have found that vaccine uptake was the "main driver" of the decline in COVID-19 infectors rather than lockdown (72). Although there are variant strains of COVID-19, the vaccines still possessed a neutralizing ability to the mutant strain (33, 40–70). Both the Oxford AstraZeneca and Pfizer BioNTech COVID-19 vaccines were effective in reducing the risk of SARS-CoV-2 infection and COVID-19 hospitalization in people with the Delta Variant (55). Because people who participate in the Tokyo Olympic Games will have closed contact

**TABLE 6 |** Parameter adjustment (Consider differences in population resistance).

| Prevention and control measures  |  | Parameter adjustment   |  | Setting basis/vaccination rate (%) | Secondary infectors on the 17th day | Peak hour of onset/d |
|--|--|--|--|------------------------------------|-------------------------------------|----------------------|
| No intervention (Figure 3)   |  | –  |  | –                                  | 587.8                               | 12                   |
| Vaccinated but not quarantined. Assume pre-flight screening can identify 20% of asymptomatic infectors (Figure 11)   | $r_1 = 1.2,$<br>$r_2 = 1.22,$<br>$A(0) = 8$    | $\beta_1 = 0.1009$<br>(0.0950, 0.1105),<br>$\beta_2 = 0.5045$<br>(0.4749, 0.5527). |  | 40                                 | 49.71<br>(33.54, 91.36)             | 29                   |
|  |  | $\beta_1 = 0.0726$<br>(0.0637, 0.0871),<br>$\beta_2 = 0.3631$<br>(0.3187, 0.4354). |  | 60                                 | 6.60<br>(3.23, 19.38)               | 42                   |
|  |  | $\beta_1 = 0.0443$<br>(0.0325, 0.0636),<br>$\beta_2 = 0.2217$<br>(0.1625, 0.3181). |  | 80                                 | 0.57<br>(0.17, 3.20)                | 99                   |
|  |  | $\beta_1 = 0.0302$<br>(0.0169, 0.0519),<br>$\beta_2 = 0.1510$<br>(0.0844, 0.2594). |  | 90                                 | 0.13<br>(0.02, 1.16)                | 9                    |
|  |  | $\beta_1 = 0.0231$<br>(0.0091, 0.0460),<br>$\beta_2 = 0.1157$<br>(0.0454, 0.2301). |  | 95                                 | 0.06<br>(0.01, 0.67)                | 7                    |
| Vaccinated but not quarantined. Assume pre-flight screening can identify 40% of asymptomatic infectors (Figure 12)   | $r_1 = 1.2,$<br>$r_2 = 1.22,$<br>$A(0) = 6$    | $\beta_1 = 0.1009$<br>(0.0950, 0.1105),<br>$\beta_2 = 0.5045$<br>(0.4749, 0.5527). |  | 40                                 | 37.64<br>(25.34, 69.58)             | 29                   |
|  |  | $\beta_1 = 0.0726$<br>(0.0637, 0.0871),<br>$\beta_2 = 0.3631$<br>(0.3187, 0.4354). |  | 60                                 | 4.96<br>(2.43, 14.61)               | 43                   |
|  |  | $\beta_1 = 0.0443$<br>(0.0325, 0.0636),<br>$\beta_2 = 0.2217$<br>(0.1625, 0.3181). |  | 80                                 | 0.43<br>(0.13, 2.40)                | 102                  |
|  |  | $\beta_1 = 0.0302$<br>(0.0169, 0.0519),<br>$\beta_2 = 0.1510$<br>(0.0844, 0.2594). |  | 90                                 | 0.10<br>(0.02, 0.87)                | 9                    |
|  |  | $\beta_1 = 0.0231$<br>(0.0091, 0.0460),<br>$\beta_2 = 0.1157$<br>(0.0454, 0.2301). |  | 95                                 | 0.04<br>(0, 0.51)                   | 7                    |
| Vaccination and 7-day compulsory quarantine. Assume pre-flight screening can identify 20% of asymptomatic infectors, 7-day compulsory quarantine has about an 18% risk of missed detection (Figure 13) | $r_1 = 1.2,$<br>$r_2 = 1.22,$<br>$A(0) = 1.44$ | $\beta_1 = 0.1009$<br>(0.0950, 0.1105),<br>$\beta_2 = 0.5045$<br>(0.4749, 0.5527). |  | 40                                 | 9.24<br>(6.18, 17.30)               | 33                   |
|  |  | $\beta_1 = 0.0726$<br>(0.0637, 0.0871),<br>$\beta_2 = 0.3631$<br>(0.3187, 0.4354). |  | 60                                 | 1.20<br>(0.59, 3.55)                | 49                   |
|  |  | $\beta_1 = 0.0443$<br>(0.0325, 0.0636),<br>$\beta_2 = 0.2217$<br>(0.1625, 0.3181). |  | 80                                 | 0.10<br>(0.03, 0.58)                | 120                  |
|  |  | $\beta_1 = 0.0302$<br>(0.0169, 0.0519),<br>$\beta_2 = 0.1510$<br>(0.0844, 0.2594). |  | 90                                 | 0.02<br>(0, 0.21)                   | 9                    |

(Continued)

TABLE 6 | Continued

| Prevention and control measures  | Parameter adjustment                             | Setting basis/vaccination rate (%)   | Secondary infectors on the 17th day | Peak hour of onset/d |
|--|--|--|-------------------------------------|----------------------|
| Vaccination and 7-day compulsory quarantine. Assume pre-flight screening can identify 40% of asymptomatic infectors, 7-day compulsory quarantine has about an 18% risk of missed detection (Figure 14) | $r_1 = 1.2$ ,<br>$r_2 = 1.22$ ,<br>$A(0) = 1.08$ | $\beta_1 = 0.0231$<br>(0.0091, 0.0460),<br>$\beta_2 = 0.1157$<br>(0.0454, 0.2301). | 95<br>0.01<br>(0, 0.12)             | 7                    |
|  |  | $\beta_1 = 0.1009$<br>(0.0950, 0.1105),<br>$\beta_2 = 0.5045$<br>(0.4749, 0.5527). | 40<br>6.94<br>(4.64, 13.01)         | 34                   |
|  |  | $\beta_1 = 0.0726$<br>(0.0637, 0.0871),<br>$\beta_2 = 0.3631$<br>(0.3187, 0.4354). | 60<br>0.90<br>(0.44, 2.66)          | 50                   |
|  |  | $\beta_1 = 0.0443$<br>(0.0325, 0.0636),<br>$\beta_2 = 0.2217$<br>(0.1625, 0.3181). | 80<br>0.08<br>(0.02, 0.43)          | 123                  |
|  |  | $\beta_1 = 0.0302$<br>(0.0169, 0.0519),<br>$\beta_2 = 0.1510$<br>(0.0844, 0.2594). | 90<br>0.02<br>(0, 0.16)             | 9                    |
|  |  | $\beta_1 = 0.0231$<br>(0.0091, 0.0460),<br>$\beta_2 = 0.1157$<br>(0.0454, 0.2301). | 95<br><0.01<br>(0, 0.09)            | 7                    |
|  |  | $\beta_1 = 0.1009$<br>(0.0950, 0.1105),<br>$\beta_2 = 0.5045$<br>(0.4749, 0.5527). | 40<br>2.06<br>(1.38, 3.88)          | 37                   |
|  |  | $\beta_1 = 0.0726$<br>(0.0637, 0.0871),<br>$\beta_2 = 0.3631$<br>(0.3187, 0.4354). | 60<br>0.27<br>(0.13, 0.79)          | 56                   |
|  |  | $\beta_1 = 0.0443$<br>(0.0325, 0.0636),<br>$\beta_2 = 0.2217$<br>(0.1625, 0.3181). | 80<br>0.02<br>(0.01, 0.13)          | 137                  |
|  |  | $\beta_1 = 0.0302$ (0.0169, 0.0519),<br>$\beta_2 = 0.1510$<br>(0.0844, 0.2594).    | 90<br><0.01<br>(0, 0.05)            | 9                    |
| Vaccination and 14-day compulsory quarantine. Assume pre-flight screening can identify 20% of asymptomatic infectors, 14-day compulsory quarantine has about a 4% risk of missed detection (Figure 15) | $r_1 = 1.2$ ,<br>$r_2 = 1.22$ ,<br>$A(0) = 0.32$ | $\beta_1 = 0.0231$<br>(0.0091, 0.0460),<br>$\beta_2 = 0.1157$<br>(0.0454, 0.2301). | 95<br><0.01<br>(0, 0.03)            | 7                    |
|  |  | $\beta_1 = 0.1009$<br>(0.0950, 0.1105),<br>$\beta_2 = 0.5045$<br>(0.4749, 0.5527). | 40<br>1.55<br>(1.04, 2.91)          | 38                   |
|  |  | $\beta_1 = 0.0726$<br>(0.0637, 0.0871),<br>$\beta_2 = 0.3631$<br>(0.3187, 0.4354). | 60<br>0.20<br>(0.10, 0.59)          | 57                   |
|  |  | $\beta_1 = 0.0443$<br>(0.0325, 0.0636),<br>$\beta_2 = 0.2217$<br>(0.1625, 0.3181). | 80<br>0.02<br>(0, 0.10)             | 142                  |
|  |  | $\beta_1 = 0.0302$ (0.0169, 0.0519),<br>$\beta_2 = 0.1510$<br>(0.0844, 0.2594).    | 90<br><0.01<br>(0, 0.05)            | 9                    |
|  |  | $\beta_1 = 0.0231$<br>(0.0091, 0.0460),<br>$\beta_2 = 0.1157$<br>(0.0454, 0.2301). | 95<br><0.01<br>(0, 0.03)            | 7                    |
|  |  | $\beta_1 = 0.1009$<br>(0.0950, 0.1105),<br>$\beta_2 = 0.5045$<br>(0.4749, 0.5527). | 40<br>1.55<br>(1.04, 2.91)          | 38                   |
|  |  | $\beta_1 = 0.0726$<br>(0.0637, 0.0871),<br>$\beta_2 = 0.3631$<br>(0.3187, 0.4354). | 60<br>0.20<br>(0.10, 0.59)          | 57                   |
|  |  | $\beta_1 = 0.0443$<br>(0.0325, 0.0636),<br>$\beta_2 = 0.2217$<br>(0.1625, 0.3181). | 80<br>0.02<br>(0, 0.10)             | 142                  |
|  |  | $\beta_1 = 0.0302$ (0.0169, 0.0519),<br>$\beta_2 = 0.1510$<br>(0.0844, 0.2594).    | 90<br><0.01<br>(0, 0.05)            | 9                    |
| Vaccination and 14-day compulsory quarantine. Assume pre-flight screening can identify 40% of asymptomatic infectors, 14-day compulsory quarantine has about a 4% risk of missed detection (Figure 16) | $r_1 = 1.2$ ,<br>$r_2 = 1.22$ ,<br>$A(0) = 0.24$ | $\beta_1 = 0.0231$<br>(0.0091, 0.0460),<br>$\beta_2 = 0.1157$<br>(0.0454, 0.2301). | 95<br><0.01<br>(0, 0.03)            | 7                    |
|  |  | $\beta_1 = 0.1009$<br>(0.0950, 0.1105),<br>$\beta_2 = 0.5045$<br>(0.4749, 0.5527). | 40<br>1.55<br>(1.04, 2.91)          | 38                   |
|  |  | $\beta_1 = 0.0726$<br>(0.0637, 0.0871),<br>$\beta_2 = 0.3631$<br>(0.3187, 0.4354). | 60<br>0.20<br>(0.10, 0.59)          | 57                   |
|  |  | $\beta_1 = 0.0443$<br>(0.0325, 0.0636),<br>$\beta_2 = 0.2217$<br>(0.1625, 0.3181). | 80<br>0.02<br>(0, 0.10)             | 142                  |
|  |  | $\beta_1 = 0.0302$ (0.0169, 0.0519),<br>$\beta_2 = 0.1510$<br>(0.0844, 0.2594).    | 90<br><0.01<br>(0, 0.05)            | 9                    |
|  |  | $\beta_1 = 0.0231$<br>(0.0091, 0.0460),<br>$\beta_2 = 0.1157$<br>(0.0454, 0.2301). | 95<br><0.01<br>(0, 0.03)            | 7                    |
|  |  | $\beta_1 = 0.1009$<br>(0.0950, 0.1105),<br>$\beta_2 = 0.5045$<br>(0.4749, 0.5527). | 40<br>1.55<br>(1.04, 2.91)          | 38                   |
|  |  | $\beta_1 = 0.0726$<br>(0.0637, 0.0871),<br>$\beta_2 = 0.3631$<br>(0.3187, 0.4354). | 60<br>0.20<br>(0.10, 0.59)          | 57                   |
|  |  | $\beta_1 = 0.0443$<br>(0.0325, 0.0636),<br>$\beta_2 = 0.2217$<br>(0.1625, 0.3181). | 80<br>0.02<br>(0, 0.10)             | 142                  |
|  |  | $\beta_1 = 0.0302$ (0.0169, 0.0519),<br>$\beta_2 = 0.1510$<br>(0.0844, 0.2594).    | 90<br><0.01<br>(0, 0.05)            | 9                    |

(Continued)



TABLE 6 | Continued

| Prevention and control measures | Parameter adjustment   | Setting basis/vaccination rate (%) | Secondary infectors on the 17th day | Peak hour of onset/d |
|---------------------------------|--|------------------------------------|-------------------------------------|----------------------|
|                                 | $\beta_1 = 0.0302$<br>(0.0169, 0.0519),<br>$\beta_2 = 0.1510$<br>(0.0844, 0.2594). | 90                                 | <0.01<br>(0, 0.04)                  | 9                    |
|                                 | $\beta_1 = 0.0231$<br>(0.0091, 0.0460),<br>$\beta_2 = 0.1157$<br>(0.0454, 0.2301). | 95                                 | <0.01<br>(0, 0.02)                  | 7                    |

Except "No intervention," all other situations considered "Keep a minimum of 2 m from athletes at all times. Keep a minimum of 1 m from others. Take two COVID-19 tests before their flight to Japan".

(including athletes, staff, etc.), and the vaccine supply can also be guaranteed, we recommend that they should be vaccinated.

As of June 10, 2021, only 4.3% of Japan's population of about 126 million was fully vaccinated against COVID-19, and only 12.6% of the total population was partly vaccinated against COVID-19 (73). At the same time, the Japanese government is trying to complete the task of vaccinating one million times a day, so as to vaccinate all 36 million elderly people in the country before the Tokyo Olympic Games (74). So the prevention and control measures against COVID-19 in the Tokyo Olympic Games need to be further strengthened. In the face of infectious diseases such as COVID-19 with strong infectivity, in addition to the prevention and control measures listed in this study, the combination of multiple intervention measures will bring better results. For example, closed-loop management can be adopted during the Olympic Games, sites can be disinfected before the athletes arrive, and the staff can be trained on epidemic prevention and control.

Risk assessment includes risk identification, dose-response relationship, exposure assessment, etc. COVID-19 is mainly transmitted through direct transmission, aerosol transmission, and contact transmission. Therefore, we started from the potential risks, namely, intervening in the contact between people, then simulated the potential transmission risks, and finally formed a risk assessment for COVID-19. In this study, a simulation method of public health intervention prevention and control based on the dynamic model of COVID-19 was proposed, which can be extended to all kinds of large-scale activities or infectious disease prevention and control research. The intervention measures in this study were based on the epidemic prevention and control measures and ideas proposed by JOC and the IOC. At present, many countries can produce the COVID-19 vaccine, and IOC will also bear the cost of the vaccine, so it is feasible (8). Vaccination is not compulsory, so it does not involve human rights interventions, and it is a complex regulation. People who have been vaccinated still run the risk of infection, and there are variant strains, i.e., Alpha, Beta, Gamma, Delta, etc. (75). Therefore, we could consider reclassifying the population (e.g., adding vaccinated and unvaccinated, or/and according to COVID-19 virus subtype) and combining the latest data on the protective efficacy of vaccines in the future, with the

purpose of exploring effective prevention and control measures for COVID-19.

COVID-19 has an incubation period, and there were studies showing that the median incubation period was 4 days (interquartile range, 2–7) (76, 77). So athletes may be infectious after returning, and countries need to take relevant prevention and control measures for athletes, such as nucleic acid detection, isolation, etc.

## CONCLUSIONS

Based on the dynamic model, this paper simulated different prevention and control measures of the Tokyo Olympic Games, comparing the number of secondary infectors under different measures, and found that vaccination had the best prevention and control effect. When the protective efficacy of the vaccine was 78.1 or 89.8% and if the vaccination rate reached 90%, then the number of secondary infectors can be controlled within 1. Our study will contribute to the formulation of relevant measures by JOC and IOC. In summary, compared with the current public health interventions, mass vaccination will become a milestone in the control of COVID-19.

## DATA AVAILABILITY STATEMENT

The original contributions presented in the study are included in the article/**Supplementary Material**, further inquiries can be directed to the corresponding author/s.

## AUTHOR CONTRIBUTIONS

WZ consulted the literature, analyzed the data, wrote the programs, and was a major contributor in writing the manuscript. JF wrote part of the manuscript. CL collected the parameters of the model. HW made comments on the content of the article. YZ collected part of the data. LZ gave advice on setting parameters. XZ made constructive comments on the manuscript. TZ contributed significantly to analysis and manuscript preparation. All authors contributed to the article and approved the submitted version.

## FUNDING

This research work was funded by Sichuan Science and Technology Program (Grant nos. 2020YFS0015, 2020YFS0091, and 2021YFS0001-LH), Health Commission of Sichuan province (Grant no. 20PJ092), National Natural Science Foundation of China (Grant nos. 81602935 and 82041033), Chongqing Science and Technology Program (Grant no. cstc2020jscx-cylhX0003), Central government funding items (Grant no. 2021zc02), and Liangshan Yi Autonomous Prefecture Center for Disease Control and Prevention (Grant no. H210322). The funders played no role in the design of the study and collection, analysis, and interpretation of data and in writing the manuscript.

## REFERENCES

1. IOC, IPC. *Tokyo 2020 Organising Committee and Tokyo Metropolitan Government Announce New Dates for the Olympic and Paralympic Games Tokyo 2020*. (2020). Available online at: <https://www.olympic.org/news/ioc-ipc-tokyo-2020-organising-committee-and-tokyo-metropolitan-government-announce-new-dates-for-the-olympic-and-paralympic-games-tokyo-2020> (accessed March 30, 2020).
2. World Health Organization. *Coronavirus Disease (COVID-19) Weekly Epidemiological Update and Weekly Operational Update*. (2021). Available online at: <https://www.who.int/emergencies/diseases/novel-coronavirus-2019/situation-reports> (accessed April 10, 2020).
3. National Health Commission of the People's Republic of China. *Coronavirus Statistics Reports of the World*. (2021). Available online at: [https://voice.baidu.com/act/newpneumonia/newpneumonia/?from=osari\\_aladin\\_banner#tab4](https://voice.baidu.com/act/newpneumonia/newpneumonia/?from=osari_aladin_banner#tab4) (accessed March 30, 2021).
4. IOC. *What Goes Into Postponing the Olympic Games?* (2020). Available online at: <https://tokyo2020.org/en/news/what-goes-into-postponing-the-olympic-games> (accessed March 30, 2021).
5. IOC. *Statement on Overseas Spectators for the Olympic and Paralympic Games Tokyo 2020*. (2020). Available online at: <https://tokyo2020.org/en/news/statement-on-overseas-spectators-for-the-olympic-and-paralympic-games-tokyo-2020> (accessed March 30, 2021).
6. IOC. *First Playbook Published Outlining Measures to Deliver Safe and Successful Games*. (2020). Available online at: <https://tokyo2020.org/en/news/first-playbook-published-outlining-measures-to-deliver-safe-and-successful-games> (accessed March 30, 2021).
7. IOC, IPC. *Tokyo 2020, Tokyo Metropolitan Government and the Government of Japan*. (2020). Available online at: <https://olympics.com/tokyo-2020/en/news/joint-statement-by-the-ioc-ipc-tokyo-2020-tokyo-met-gov-and-the-gov-of-japan> (accessed June 8, 2021).
8. IOC. *Tokyo 2020 to Have 'Reasonable' Crowd Size, IOC President Bach Says*. (2020). Available online at: <https://tokyo2020.org/en/news/tokyo-2020-to-have-reasonable-crowd-size-ioc-president-bach-says> (accessed March 30, 2021).
9. Wikipedia. *Summer Olympic Games*. (2021). Available online at: [https://en.wikipedia.org/wiki/Summer\\_Olympic\\_Games#Popularity\\_of\\_Olympic\\_sports](https://en.wikipedia.org/wiki/Summer_Olympic_Games#Popularity_of_Olympic_sports) (accessed March 30, 2021).
10. Wikipedia. *2016 Summer Olympics wikipedia*. (2021). Available online at: [https://en.wikipedia.org/wiki/2016\\_Summer\\_Olympics#Number\\_of\\_athletes\\_by\\_National\\_Olympic\\_Committee](https://en.wikipedia.org/wiki/2016_Summer_Olympics#Number_of_athletes_by_National_Olympic_Committee) (accessed March 30, 2021).
11. Yang ZF, Zeng ZQ, Wang K, Wong SS, Liang WH, Zanin M, et al. Modified SEIR and AI prediction of the epidemics trend of COVID-19 in China under public health interventions. *J Thorac Dis*. (2020) 12:165–74. doi: 10.21037/jtd.2020.02.64
12. Peak CM, Kahn R, Grad YH, Childs LM, Li R, Lipsitch M, Buckee CO. Individual quarantine versus active monitoring of contacts for the

## ACKNOWLEDGMENTS

Many thanks are expressed to those who contributed to the prevention and control of COVID-19. The authors also want to thank Hongli Wan for the submission of the manuscript.

## SUPPLEMENTARY MATERIAL

The Supplementary Material for this article can be found online at: <https://www.frontiersin.org/articles/10.3389/fpubh.2021.730611/full#supplementary-material>

**Supplementary Material A** | Introduces a way to estimate parameters by data-driven methods.

**Supplementary Material B** | Shares our codes.

- mitigation of COVID-19: a modelling study. *Lancet Infect Dis*. (2020) 20:1025–33. doi: 10.1016/S1473-3099(20)30361-3
13. Song QQ, Zhao H, Fang LQ, Liu Y, Zheng C, Zhang Y. Study on assessing early epidemiological parameters of COVID-19 epidemic in China. *Chinese J Epidemiol*. (2020) 4:461–5. doi: 10.3760/cma.j.cn112338-20200205-00069
14. Wei YY, Lu ZZ, Du ZC, Zhang ZJ, Zhao Y, Sheng SP, et al. Fitting and forecasting the trend of COVID-19 by SEIR+CAQ dynamic model. *Chinese J Epidemiol*. (2020) 4:470–5. doi: 10.3760/cma.j.cn112338-20200216-00106
15. Kinoshita R, Anzai A, Jung SM, Linton NM, Miyama T, Kobayashi T, et al. Containment, contact tracing and asymptomatic transmission of novel coronavirus disease (COVID-19): a modelling study. *J Clin Med*. (2020) 9:3125. doi: 10.3390/jcm9103125
16. Wu JT, Leung K, Leung GM. Nowcasting and forecasting the potential domestic and international spread of the 2019-nCoV outbreak originating in Wuhan, China: a modelling study. *Lancet*. (2020) 395:689–97. doi: 10.1016/S0140-6736(20)30260-9
17. Tang B, Wang X, Li Q, Bragazzi NL, Tang SY, Xiao YN, et al. Estimation of the Transmission Risk of the COVID-19 and Its Implication for Public Health Interventions. *J Clin Med*. (2020) 9:462. doi: 10.2139/ssrn.3525558
18. Tang B, Xia F, Bragazzi NL, Wang X, He S, Sun XD, et al. Lessons drawn from China and South Korea for managing COVID-19 epidemic: insights from a comparative modeling study. *Bull World Health Organ*. (2020) 98:150. doi: 10.2471/BLT.20.257238
19. Lloyd AL, May RM. Epidemiology. How viruses spread among computers and people. *Science*. (2001) 292:1316–7. doi: 10.1126/science.1061076
20. Keeling MJ, Eames K. Networks and epidemic models[J]. *J R Soc Interface*. (2005) 2:295–307. doi: 10.1098/rsif.2005.0051
21. Hethcote HW. The mathematics of infectious diseases. *SIAM Rev*. (2000) 42:599–653. doi: 10.1137/S0036144500371907
22. Brauer F. Mathematical epidemiology: past, present, and future. *Infect Dis Model*. (2017) 2:113–27. doi: 10.1016/j.idm.2017.02.001
23. He SB, Peng YX, Sun KH. SEIR modeling of the COVID-19 and its dynamics. *Nonlinear Dyn*. (2020) 101:1667–80. doi: 10.1007/s11071-020-05743-y
24. Keeling MJ, Rohani P. *Modeling Infectious Diseases in Humans and Animals*. Princeton University Press (2008). doi: 10.1515/9781400841035
25. He S, Tang SY, Rong L. A discrete stochastic model of the COVID-19 outbreak: forecast and control. *Math Biosci Eng*. (2020) 17:2792–804. doi: 10.3934/mbe.2020153
26. Morris TP, White IR, Crowther MJ. Using simulation studies to evaluate statistical methods. *Stat Med*. (2019) 38:2074–102. doi: 10.1002/sim.8086
27. IOC. *Spectators, Athletes and Games Staff: Plans in Place to Ensure Successful Olympic and Paralympic Games Tokyo*. (2020). Available online at: <https://tokyo2020.org/en/news/plans-in-place-to-ensure-successful-tokyo-2020> (accessed March 30, 2021).
28. IOC. *Fifth Coordination Meeting for COVID-19 Countermeasures at the Olympic and Paralympic Games Tokyo 2020*. (2020). Available online at: <https://tokyo2020.org/en/news/fifth-coordination-meeting-for-covid-19-countermeasures-at-tokyo-2020> (accessed March 30, 2021).

29. Al KN, Zhang YT, Xia SL, Yang YK, Al QMM, Abdulrazzaq N, et al. Effect of 2 inactivated SARS-CoV-2 vaccines on symptomatic COVID-19 infection in adults: a randomized clinical trial. *JAMA*. (2021) 326:35–45. doi: 10.1001/jama.2021.8565
30. Palacios R, Batista AP, Albuquerque CSN, Patio EG, Santos JDP, Mnica TRPC, et al. Efficacy and safety of a COVID-19 inactivated vaccine in healthcare professionals in Brazil: the PROFISCOV Study. *Soc Sci Electron Publ*. (2021). doi: 10.2139/ssrn.3822780
31. Thompson MG, Burgess JL, Naleway AL, Tyner H, Yoon SK, Meece J, et al. Prevention and attenuation of Covid-19 with the BNT162b2 and mRNA-1273 vaccines. *N Engl J Med*. (2021) 385:320–9. doi: 10.1056/NEJMoa2107058
32. Chung H, He S, Nasreen S, Sundaram ME, Buchan SA, Wilson SE, et al. Effectiveness of BNT162b2 and mRNA-1273 COVID-19 vaccines against symptomatic SARS-CoV-2 infection and severe COVID-19 outcomes in Ontario, Canada. *BMJ*. (2021) 374:n1943. doi: 10.1136/bmj.n1943
33. Sadoff J, Gray G, Vandebosch A, Cárdenas V, Shukarev G, Grinsztejn B, et al. Safety and efficacy of single-dose Ad26.COV2.S vaccine against Covid-19. *N Engl J Med*. (2021) 384:2187–201. doi: 10.1056/NEJMoa2101544
34. Voysey M, Clemens SAC, Madhi SA, Weckx LY, Folegatti PM, Aley PK, et al. Safety and efficacy of the ChAdOx1 nCoV-19 vaccine (AZD1222) against SARS-CoV-2: an interim analysis of four randomised controlled trials in Brazil, South Africa, and the UK. *Lancet*. (2021) 397:99–111. doi: 10.1016/S0140-6736(20)32661-1
35. Logunov DY, Dolzhikova IV, Shcheblyakov DV, Tukhvatulin AI, Zubkova OV, Dzharullaeva AS, et al. Safety and efficacy of an rAd26 and rAd5 vector-based heterologous prime-boost COVID-19 vaccine: an interim analysis of a randomised controlled phase 3 trial in Russia. *Lancet*. (2021) 397:671–81. doi: 10.1016/S0140-6736(21)00234-8
36. Turner JS, Kim W, Kalaidina E, Goss CW, Rauseo AM, Schmitz AJ, et al. SARS-CoV-2 infection induces long-lived bone marrow plasma cells in humans. *Nature*. (2021) 595:421–5. doi: 10.1038/s41586-021-03647-4
37. Pušnik J, Richter E, Schulte B, Dolscheid-Pommerich R, Bode C, Putensen C, et al. Memory B cells targeting SARS-CoV-2 spike protein and their dependence on CD4+ T cell help. *Cell Rep*. (2021) 35:109320. doi: 10.1016/j.celrep.2021.109320
38. Doria-Rose N, Suthar MS, Makowski M, O'Connell S, McDermott AB, Flach B, et al. Antibody persistence through 6 months after the second dose of mRNA-1273 vaccine for Covid-19. *N Engl J Med*. (2021) 384:2259–61. doi: 10.1056/NEJMc2103916
39. Dan JM, Mateus J, Kato Y, Hastie KM, Yu ED, Faliti CE, et al. Immunological memory to SARS-CoV-2 assessed for up to 8 months after infection. *Science*. (2021) 371:6529. doi: 10.1126/science.abf4063
40. Muik A, Wallisch AK, Sängler B, Swanson KA, Mühl J, Chen W, et al. Neutralization of SARS-CoV-2 lineage B.1.1.7 pseudovirus by BNT162b2 vaccine-elicited human sera. *Science*. (2021) 371:1152–3. doi: 10.1126/science.abg6105
41. Gu H, Chen Q, Yang G, He L, Fan H, Deng YQ, et al. Adaptation of SARS-CoV-2 in BALB/c mice for testing vaccine efficacy. *Science*. (2020) 369:1603–7. doi: 10.1126/science.abc4730
42. Xie X, Zou J, Fontes-Garfias CR, Xia HJ, Swanson KA, Cutler M, et al. Neutralization of N501Y mutant SARS-CoV-2 by BNT162b2 vaccine-elicited sera. *bioRxiv [Preprint]*. (2021). doi: 10.1101/2021.01.07.425740
43. Garcia-beltran WF, Lam EC, Denis KS, Nitido AD, Garcia ZH, Hauser BM, et al. Multiple SARS-CoV-2 variants escape neutralization by vaccine-induced humoral immunity. *Cell*. (2021) 184:2372–83.e2379. doi: 10.1016/j.cell.2021.03.013
44. Supasa P, Zhou D, Dejnirattisai W, Liu C, Mentzer AJ, Ginn HM, et al. Reduced neutralization of SARS-CoV-2 B.1.1.7 variant by convalescent and vaccine sera. *Cell*. (2021) 184:2201–11.e2207. doi: 10.1016/j.cell.2021.02.033
45. Ho D, Wang PF, Liu LH, Iketani S, Luo Y, Guo YC, et al. Increased resistance of SARS-CoV-2 variants B.1.351 and B.1.1.7 to antibody neutralization. *Res Sq*. (2021) 372:1413–8. doi: 10.21203/rs.3.rs-155394/v1
46. Wall EC, Wu M, Harvey R, Kelly G, Warchal S, Sawyer C, et al. Neutralising antibody activity against SARS-CoV-2 VOCs B.1.617.2 and B.1.351 by BNT162b2 vaccination. *Lancet*. (2021) 397:2331–3. doi: 10.1016/S0140-6736(21)01290-3
47. Dejnirattisai W, Zhou D, Supasa P, Liu C, Mentzer AJ, Ginn HM, et al. Antibody evasion by the P.1 strain of SARS-CoV-2. *Cell*. (2021) 184:2939–54.e2939. doi: 10.1016/j.cell.2021.03.055
48. Anichini G, Terrosi C, Gori SG, Gandolfo C, Franchi F, Cusi MG, et al. Neutralizing antibody response of vaccinees to SARS-CoV-2 variants. *Vaccines*. (2021) 9:517. doi: 10.3390/vaccines9050517
49. Zhou D, Dejnirattisai W, Supasa P, Liu C, Mentzer AJ, Ginn HM, et al. Evidence of escape of SARS-CoV-2 variant B.1.351 from natural and vaccine-induced sera. *Cell*. (2021) 184:2348–61.e2346. doi: 10.1016/j.cell.2021.02.037
50. Wang P, Casner RG, Nair MS, Wang M, Yu J, Cerutti G, et al. Increased resistance of SARS-CoV-2 variant P.1 to antibody neutralization. *Cell Host Microbe*. (2021) 29:747–51. doi: 10.1016/j.chom.2021.04.007
51. Abu RLJ, Chemaitelly H, Butt AA. Effectiveness of the BNT162b2 Covid-19 vaccine against the B.1.1.7 and B.1.351 variants. *N Engl J Med*. (2021) 385:187–9. doi: 10.1056/NEJMc2104974
52. Bernal JL, Andrews N, Gower C, Gallagher E, Simmons R, Thelwall S, et al. Effectiveness of COVID-19 vaccines against the B.1.617.2 variant. *N Engl J Med*. (2021) 385:585–94. doi: 10.1056/NEJMoa2108891
53. Lopez BJ, Andrews N, Gower C, Robertson C, Stowe J, Tessier E, et al. Effectiveness of the Pfizer-BioNTech and Oxford-AstraZeneca vaccines on covid-19 related symptoms, hospital admissions, and mortality in older adults in England: test negative case-control study. *BMJ*. (2021) 373:n1088. doi: 10.1136/bmj.n1088
54. Vasileiou E, Simpson CR, Robertson C, Shi T, Kerr S, Agrawal U, et al. Effectiveness of first dose of COVID-19 vaccines against hospital admissions in Scotland: national prospective cohort study of 5.4 million people. *SSRN Electron J*. (2021). doi: 10.2139/ssrn.3789264
55. Sheikh A, Mcmenamin J, Taylor B, Robertson C, Public Health Scotland and the EAVE II Collaborators. SARS-CoV-2 Delta VOC in Scotland: demographics, risk of hospital admission, and vaccine effectiveness. *Lancet*. (2021) 397:2461–2. doi: 10.1016/S0140-6736(21)01358-1
56. Wu K, Werner AP, Moliva JJ, Koch M, Choi A, Stewart-Jones GBE, et al. mRNA-1273 vaccine induces neutralizing antibodies against spike mutants from global SARS-CoV-2 variants. *bioRxiv [Preprint]*. (2021). doi: 10.1101/2021.01.25.427948
57. Choi A, Koch M, Wu K, Dixon G, Oestreicher J, Legault H, et al. Serum neutralizing activity of mRNA-1273 against SARS-CoV-2 Variants. *bioRxiv [Preprint]*. (2021). doi: 10.1101/2021.06.28.449914
58. Emary KRW, Golubchik T, Aley PK, Ariani CV, Angus B, Bibi S, et al. Efficacy of ChAdOx1 nCoV-19 (AZD1222) vaccine against SARS-CoV-2 variant of concern 202012/01 (B.1.1.7): an exploratory analysis of a randomised controlled trial. *Lancet*. (2021) 397:1351–62.
59. Madhi SA, Baillie V, Cutland CL, Voysey M, Koen AL, Fairlie L, et al. Efficacy of the ChAdOx1 nCoV-19 Covid-19 vaccine against the B.1.351 variant. *N Engl J Med*. (2021) 384:1885–98. doi: 10.1056/NEJMoa2102214
60. Planas D, Vever D, Baidaliuka A, Staropoli I, Guivel-Benhassine F, Rajah MM, et al. Reduced sensitivity of infectious SARS-CoV-2 variant B.1.617.2 to monoclonal antibodies and sera from convalescent and vaccinated individuals. *bioRxiv [Preprint]*. (2021). doi: 10.1101/2021.05.26.445838
61. Katherine RWE, Tanya G, Parvinder KA, Cristina VA, Brian A, Sagida B, et al. Efficacy of ChAdOx1 nCoV-19 (AZD1222) vaccine against SARS-CoV-2 variant of concern 202012/01 (B.1.1.7): an exploratory analysis of a randomised controlled trial. *Lancet*. (2021) 397:1351–62. doi: 10.1016/S0140-6736(21)00628-0
62. Hossain MK, Hassanzadeganroudsari M, Apostolopoulos V. The emergence of new strains of SARS-CoV-2. What does it mean for COVID-19 vaccines? *Expert Rev Vaccines*. (2021) 20:635–8. doi: 10.1080/14760584.2021.1915140
63. Alter G, Yu J, Liu J, Chandrashekar A, Borducchi EN, Tostanoski LH, et al. Immunogenicity of Ad26.COV2.S vaccine against SARS-CoV-2 variants in humans. *Nature*. (2021) 596:268–72. doi: 10.1038/s41586-021-03681-2
64. Yu J, Tostanoski LH, Mercado NB, McMahan K, Liu J, Jacob-Dolan C, et al. Protective efficacy of Ad26.COV2.S against SARS-CoV-2 B.1.351 in macaques. *Nature*. (2021) 596:423–7. doi: 10.1038/s41586-021-03732-8
65. Abdool K SS, De OT. New SARS-CoV-2 variants - clinical, public health, and vaccine implications. *N Engl J Med*. (2021) 384:1866–8. doi: 10.1056/NEJMc2100362

66. Toback S, Heath PT, Galiza EP, Baxter DN, Boffito M, Smith K, et al. Efficacy of the NVX-CoV2373 Covid-19 vaccine against the B.1.1.7 Variant. *medRxiv [Preprint]*. (2021). doi: 10.1101/2021.05.13.21256639
67. Shinde V, Bhikha S, Hoosain Z, Archary M, Bhorat Q, Fairlie L, et al. Efficacy of NVX-CoV2373 Covid-19 vaccine against the B.1.351 variant. *N Engl J Med*. (2021) 384:1899–909. doi: 10.1056/NEJMoa2103055
68. Wang GL, Wang ZY, Duan LJ, Meng QC, Jiang MD, Cao J, et al. Susceptibility of circulating SARS-CoV-2 variants to neutralization. *N Engl J Med*. (2021) 384:2354–56. doi: 10.1056/NEJMc2103022
69. Huang BY, Dai LP, Wang H, Hu ZY, Yang XM, Tan WJ, et al. Neutralization of SARS-CoV-2 VOC 501Y.V2 by human antisera elicited by both inactivated BBIBP-CorV and recombinant dimeric RBD ZF2001 vaccines. *bioRxiv [Preprint]*. (2021). doi: 10.1101/2021.02.01.429069
70. Hitchings MDT, Ranzani OT, Torres MSS, de Oliveira SB, Almiron M, Said R, et al. Effectiveness of CoronaVac among healthcare workers in the setting of high SARS-CoV-2 Gamma variant transmission in Manaus, Brazil: a test-negative case-control study. *Lancet Reg Health Am*. (2021) 1:100025. doi: 10.1101/2021.04.07.21255081
71. IOC. *Safe and Secure Olympic and Paralympic Games Tokyo 2020: Version 2 of Tokyo 2020 Playbooks Released*. (2020). Available online at: <https://olympics.com/tokyo-2020/en/news/safe-and-secure-oly-and-para-games-tokyo-2020-v2-of-tokyo-2020-playbooks> (accessed June 6, 2021).
72. Haas EJ, Angulo FJ, McLaughlin JM, Anis E, Singer SR, Khan F, et al. Impact and effectiveness of mRNA BNT162b2 vaccine against SARS-CoV-2 infections and COVID-19 cases, hospitalisations, and deaths following a nationwide vaccination campaign in Israel: an observational study using national surveillance data. *Lancet*. (2021) 397:1819–29. doi: 10.1016/S0140-6736(21)00947-8
73. Mathieu E, Ritchie H, Ortiz-Ospina E, Roser M, Hasell J, Appel C, et al. A global database of COVID-19 vaccinations. *Nat Hum Behav*. (2021) 5:956–9. doi: 10.1101/2021.03.22.21254100
74. Netease times weekly. *No Tokyo Olympics? Kan Yiwei Said That If the Epidemic Is Serious, It Will Not Be "Forced"*. (2021). Available online at: [https://www.163.com/dy/article/GC82UVHV0519APGA.html?clickfrom=w\\_yw](https://www.163.com/dy/article/GC82UVHV0519APGA.html?clickfrom=w_yw) (accessed June 12, 2021).
75. World Health Organization. *WHO Announces Simple, Easy-To-Say Labels for SARS-CoV-2 Variants of Interest and Concern*. (2021). Available online at: <https://www.who.int/news/item/31-05-2021-who-announces-simple-easy-to-say-labels-for-sars-cov-2-variants-of-interest-and-concern> (accessed August 22, 2021).
76. Lauer SA, Grantz KH, Bi Q, Jones FK, Zheng Q, Meredith HR, et al. The incubation period of coronavirus disease 2019 (COVID-19) from publicly reported confirmed cases: estimation and application. *Ann Intern Med*. (2020) 172:577–82. doi: 10.7326/M20-0504
77. Guan WJ, Ni ZY, Hu Y, Liang WH, Ou CQ, He JX, et al. Clinical characteristics of coronavirus disease 2019 in China. *N Engl J Med*. (2020) 10:1708–20. doi: 10.1056/NEJMoa2002032

**Conflict of Interest:** The authors declare that the research was conducted in the absence of any commercial or financial relationships that could be construed as a potential conflict of interest.

**Publisher's Note:** All claims expressed in this article are solely those of the authors and do not necessarily represent those of their affiliated organizations, or those of the publisher, the editors and the reviewers. Any product that may be evaluated in this article, or claim that may be made by its manufacturer, is not guaranteed or endorsed by the publisher.

Copyright © 2021 Zhu, Feng, Li, Wang, Zhong, Zhou, Zhang and Zhang. This is an open-access article distributed under the terms of the Creative Commons Attribution License (CC BY). The use, distribution or reproduction in other forums is permitted, provided the original author(s) and the copyright owner(s) are credited and that the original publication in this journal is cited, in accordance with accepted academic practice. No use, distribution or reproduction is permitted which does not comply with these terms.





# Epidemiologic Characteristics of and Prognostic Factors for COVID-19 Among Hospitalized Patients: Updated Implications From Hubei Province, China

## OPEN ACCESS

### Edited by:

Reza Lashgari,  
Shahid Beheshti University, Iran

### Reviewed by:

Napoleon Bellua Sam,  
University for Development  
Studies, Ghana  
Parshal Bhandari,  
Lahore General Hospital, Pakistan  
Muhammed Elhadi,  
University of Tripoli, Libya

### \*Correspondence:

Qingyong Chen  
cqyong117@163.com  
Wenya Yu  
jsjyyuwenya@sina.cn

<sup>†</sup>These authors have contributed  
equally to this work and share first  
authorship

### Specialty section:

This article was submitted to  
Infectious Diseases - Surveillance,  
Prevention and Treatment,  
a section of the journal  
Frontiers in Public Health

**Received:** 17 June 2021

**Accepted:** 20 September 2021

**Published:** 27 October 2021

### Citation:

Liu X, Zhu L, Lu T, Liu X, Jiao D,  
Tang X, Chen J, Chen Y, Yu W and  
Chen Q (2021) Epidemiologic  
Characteristics of and Prognostic  
Factors for COVID-19 Among  
Hospitalized Patients: Updated  
Implications From Hubei Province,  
China. *Front. Public Health* 9:726491.  
doi: 10.3389/fpubh.2021.726491

Xiang Liu<sup>1†</sup>, Linzhi Zhu<sup>3†</sup>, Tingjuan Lu<sup>1,4†</sup>, Xibang Liu<sup>3</sup>, Demin Jiao<sup>1</sup>, Xiali Tang<sup>1</sup>,  
Jun Chen<sup>1</sup>, Yu Chen<sup>1</sup>, Wenya Yu<sup>2\*</sup> and Qingyong Chen<sup>1,3\*</sup>

<sup>1</sup> Department of Respiratory Disease, The 903rd Hospital of the People's Liberation Army, Hangzhou, China, <sup>2</sup> School of Public Health, Shanghai Jiao Tong University School of Medicine, Shanghai, China, <sup>3</sup> The First Affiliated Hospital of Wenzhou Medical University, Wenzhou, China, <sup>4</sup> The Optics Valley Branch of the Maternal and Child Hospital of Hubei Province, Wuhan, China

**Introduction:** The roles of some indicators in the prognosis of patients with coronavirus disease-19 (COVID-19) remain unclear and controversial. This study aimed to explore the epidemiologic characteristics of and prognostic factors for COVID-19 to provide updated recommendations for its prevention, diagnosis, and treatment.

**Methods:** For this retrospective study, demographic, epidemiologic, and clinical data were extracted from the medical records of patients admitted to the Maternal and Child Hospital of Hubei Province (Optical Valley) with COVID-19 between February 19, 2020, and March 19, 2020. The primary outcome was the prognosis that was determined at discharge as mentioned in the medical records. Descriptive statistics, univariate analyses, and stepwise logistic regression analysis were used for data analysis.

**Results:** Of the 1,765 patients included, 93.1% were cured and the mortality was 1.8%. Univariate analyses identified 63 factors significantly associated with COVID-19 prognosis. Logistic regression analysis revealed that a poorer prognosis was associated with undergoing resuscitation, complex disease manifestations, consultation with outside specialists, elevated basophil or lymphocyte counts, an albumin (ALB)/globulin (A/G) ratio > 2.4, and elevated levels of serum aspartate aminotransferase (AST) or creatinine. Patients had a better prognosis if the following conditions were met: dry cough reported as an initial symptom, fatigue as a clinical manifestation, and a diagnosis based on laboratory testing.

**Conclusion:** To prevent clinical deterioration, clinicians should provide special care to patients who underwent resuscitation, with a critical disease, or requiring consultation with outside specialists. Extra attention should be paid to patients with high basophil or lymphocyte counts, a high A/G ratio, and elevated AST or creatinine levels.

**Keywords:** COVID-19, indicator, pandemic, prognosis, prognostic factor



## INTRODUCTION

In early December 2019, several pneumonia cases of unknown origin emerged in Wuhan, China, later attributed to a novel coronavirus (1, 2). On February 11, 2020, the WHO officially named the disease coronavirus disease-19 (COVID-19) (3). Since then, COVID-19 has spread globally, and on March 11, 2020, the WHO declared COVID-19 a pandemic (3). By July 30, 2021, there had been 196,553,009 confirmed cases of COVID-19, of which 4,200,412 deaths were reported to the WHO, of which 102,553 confirmed cases and 5,635 deaths were from China (4). Although great progress has been achieved in epidemiological experience, clinical management, and vaccination, the pandemic continues to progress globally.

Because China was the first country to report the outbreak of COVID-19, Chinese clinicians and researchers have continued to explore and update the assessment of epidemic characteristics and COVID-19 prognostic factors, providing evidence for its prevention, diagnosis, and treatment. The prognostic factors include demographic characteristics (5), underlying diseases (6), laboratory parameters (7, 8), clinical manifestations (9, 10), radiological features (11), and treatment (12). In addition, vaccination becomes a positive prognostic factor recently, with more than 10 vaccines of different strategies being reported to reduce the severity of the disease (13–17). Similar findings regarding the aforementioned prognostic factors have been reported from various countries, namely, France (18), Saudi Arabia (19), Spain (20), Italy (21), and others (22).

Despite overall consistency in findings between different studies, data on several prognostic factors, such as sex (23, 24), clinical manifestations (25), and underlying diseases (25, 26), remain inconsistent or variable. For example, the African COVID-19 Critical Care Outcomes Study revealed that sex was not independently associated with outcome (24), while a study in Detroit revealed that male sex was significantly associated with mortality (23). Though having chronic diseases has been reported to be a risk factor for worse prognosis in some studies, other studies have found that they had no influence on prognosis (25–28). In addition, many studies had a small sample size, which may cause biases. Some prognostic factors, such as some laboratory test results, radiological features, and treatments, have not been explored owing to limited data availability.

Because there remains much about COVID-19 that is unknown or poorly understood and the disease continues to be prevalent and evolve as new variants emerge, it is important to understand demographic, epidemiologic characteristics, clinical features, laboratory test results, radiological features, and treatment, especially the controversial indicators or those not explored in previous studies. Therefore, to gain insight into

these inconsistencies and expand the understanding of additional indicators, this study aimed to explore the epidemiologic characteristics and factors influencing COVID-19 prognosis with a relatively large sample size. The findings of the potential prognostic indicators from this study will provide an updated assessment of their implications for the prevention, diagnosis, and treatment of COVID-19.

## METHODS

### Study Design and Participants

The study was a retrospective review of patients with COVID-19 hospitalized at the Optics Valley Branch of the Maternal and Child Hospital of Hubei Province (MCH-Optical Valley). During the first wave of the COVID-19 epidemic in Wuhan, MCH-Optical Valley was a designated hospital for the treatment of patients with COVID-19, starting on February 13, 2020. Eligible patients for this study included all inpatients admitted to MCH-Optical Valley with confirmed or suspected COVID-19 between February 19, 2020, and March 19, 2020. The prognosis was defined as the primary outcome at discharge as mentioned in medical records. All patients were discharged between February 19, 2020, and April 5, 2020.

### Data Collection

Medical records of patients at MCH-Optical Valley were obtained from the electronic medical record system. The inclusion criteria were (1) hospitalization owing to confirmed or suspected COVID-19; (2) hospitalization at MCH-Optical Valley between February 19, 2020, and March 19, 2020; and (3) complete medical records covering the seven dimensions mentioned below. The exclusion criteria were (1) outpatient consultation; (2) hospitalized during other time periods; and (3) in complete medical records. Finally, a total of 1,765 patients with detailed records were included in this study. Data in this medical record system could be divided into seven dimensions: (1) demographic characteristics, (2) epidemiological exposure history, (3) admission characteristics, (4) hospitalization and treatment characteristics, (5) imaging features, (6) laboratory findings, and (7) diagnosis and prognosis.

Demographic characteristics included sex, marital status, occupation, and age. Epidemiological exposure history referred to exposure history (contact with someone with confirmed or suspected COVID-19 during the 2 weeks preceding the onset of illness), the relationship between patients and people with COVID-19 to whom they were exposed, source of exposure, time period of exposure, and possible location of exposure. Admission characteristics included admission route, illness condition on admission, critical degree on admission, and vital signs on admission (body temperature, pulse rate, respiratory rate, systolic blood pressure [SBP], and diastolic blood pressure [DBP]). Hospitalization and treatment characteristics included whether patients underwent surgery, underwent resuscitation (life-threatening patients needing rescue), developed critical illness, required consultation, had complex cases, reported initial symptoms, current symptoms during hospitalization, clinical manifestations, previous medical history, self-reported

**Abbreviations:** AST, Aspartate aminotransferase; COVID-19, Coronavirus disease; CRP, C-reactive protein; CT, Computed tomography; D-Bil, Direct bilirubin; DBP, Diastolic blood pressure; GGO, Ground-glass opacity; MCH, Maternal and Child Hospital of Hubei; MCHC, Mean corpuscular hemoglobin concentration; PLT, Platelet; RBC, Red blood cell; RDW, Red blood cell distribution width; SBP, Systolic blood pressure; TP, Total protein; UN, Urea nitrogen; WBC, White blood cell; WHO, World Health Organization.

underlying diseases, smoking habits, treatment, and length of stay. Imaging features on CT or chest radiography included ground-glass opacity (GGO) characteristics, location, and other observations. Laboratory findings were classified into two categories (according to the sample), with a total of 44 indicators. The first category comprised the following indicators tested using whole blood: C-reactive protein (CRP), white blood cell (WBC) count, percentage of lymphocytes, percentage of eosinophils, neutrophil count, monocyte count, basophil count, hemoglobin level, mean corpuscular volume, mean corpuscular hemoglobin concentration (MCHC), platelet (PLT) count, percentage of neutrophils, percentage of monocytes, percentage of basophils, lymphocyte count, eosinophil count, red blood cell count, packed cell volume, mean corpuscular hemoglobin, red blood cell distribution width (RDW), and mean platelet volume. The second category comprised the following indicators tested using serum: blood glucose, albumin (ALB), ALB/globulin (A/G) ratio, direct bilirubin (D-BiL), alanine aminotransferase, alkaline phosphatase (ALP), total bile acid, sodium, calcium, serum magnesium, urea nitrogen (UN), uric acid, total protein (TP), globulin, total bilirubin, indirect bilirubin (I-BiL), aspartate aminotransferase (AST),  $\gamma$ -glutamyl transpeptidase, potassium, chlorine, phosphorus, total carbon dioxide, and creatinine. Diagnosis and prognosis considered outpatient and emergency diagnosis, admission diagnosis, discharge diagnosis, a subtype of COVID-19 at discharge (mild, normal, severe, critical, suspected, and clinical diagnosis subtypes), consistency between discharge and outpatient diagnoses, consistency between admission and discharge diagnoses, consistency between preoperative and postoperative diagnoses, consistency between clinical and pathological diagnoses, consistency between radiological and pathological diagnoses, the highest evidence of diagnosis (clinical diagnosis; radiography, CT, ultrasound, and endoscopy; biochemical and immunological test results; and cytological blood smear test), and the prognosis at discharge (dead, unhealed, improved, and cured).

## Data Analysis

Statistical analyses, such as descriptive statistics, univariate analyses, and multivariate analysis, were conducted using SAS 8.2 (SAS Institute Inc., Cary, NC, USA) and SPSS 18.0 (SPSS Inc., Chicago, IL, USA). First, descriptive statistics were used to describe the frequency and percentage of categorical variables. Continuous variables are presented as the median and interquartile ranges because all continuous variables had a skewed distribution. Second, univariate analyses were conducted to determine the association between prognosis and each variable. Specifically, the Wilcoxon rank test was used to test the relationship between prognosis and dichotomous variables (e.g., sex). The Kruskal-Wallis H test was used to test the relationship between prognosis and multivariate variables (e.g., marital status). The Spearman rank correlation test was used to test the relationship between prognosis and continuous variables (e.g., age). Third, because the prognosis (the dependent variable) was an ordinal multi-categorical variable, stepwise logistic regression analysis was used to explore the factors

influencing COVID-19 prognosis. Factors having a significant association with prognosis in the univariate analysis were included in the logistic model, with the significance level for entry set at 0.10 and the significance level for selection set at 0.15. To explain the results more explicitly, continuous variables were transformed into categorical variables according to their meanings and clinical reference ranges in the logistic regression analysis. All tests were two-sided, and  $P < 0.05$  were considered statistically significant.

## Ethical Approval and Patient Consent

This study was approved by the 903rd Hospital of PLA ethics committee (approval reference number: 20210224/02/01/002). The requirement for informed consent was waived by the ethics committee because of the retrospective nature of the study and the urgent nature of the pandemic.

## RESULTS

### Demographic and Epidemic Characteristics of Patients With COVID-19

As shown in **Table 1**, 58.4% of the 1,765 patients with COVID-19 were women, 89.6% were married, and 43.3% were retired. The average age was  $58.7 \pm 15.1$  years (**Supplementary Table 1**).

Of the total number of patients, 27.0% had an exposure history of contact with someone with suspected or confirmed COVID-19 during the 2 weeks preceding the onset of their illness. Most contacts (75.8%) were with people other than family members, colleagues, and people with social interactions and shared transportation. The most common source of exposure was through treatment and care. Of the patients, 74.8% had an uncertain time period of exposure and 53.5% were exposed in locations other than their home, workplace, dormitories, hospitals, or indoor public places (**Table 1**).

Most patients were admitted to the hospital through other routes (rather than through the emergency department, outpatient department, or referral from other hospitals); 98.1% had symptoms at the time of admission, and 92.2% had moderately severe disease on admission (**Table 1**). The vital signs on admission, such as body temperature, pulse rate, respiratory rate, SBP, and DBP, are shown in **Supplementary Table 1**.

The average length of stay was  $13.3 \pm 6.1$  days (**Supplementary Table 1**). During hospitalization, most did not undergo surgery (99.5%) or resuscitation (96.7%), did not develop critical illness (88.3%) or require consultation with outside specialists (68.2%), and did not have complex cases. The top three initial symptoms reported were fever, cough, and fatigue. Over 60% of the patients experienced cough (61.4%) and fever (60.0%) during hospitalization. The top three clinical manifestations were consistent with the reported initial symptoms. Most patients had no previous medical history of note. The top three self-reported underlying diseases were hypertension, diabetes, and coronary heart disease. Of the patients, 78.6% were non-smokers. Most received antiviral therapy during hospitalization. Chest CT or radiography showed that most had GGO, observed at multiple

**TABLE 1 |** Basic characteristics of patients with COVID-19.

| Characteristics   | N*           | %*         |
|---|--------------|------------|
| <b>Total</b>  | <b>1,765</b> | <b>1.0</b> |
| <b>Sex</b>  |              |            |
| Male  | 734          | 41.6       |
| Female  | 1,031        | 58.4       |
| <b>Marital status</b>   |              |            |
| Unmarried   | 67           | 3.8        |
| Married   | 1,582        | 89.6       |
| Widowed   | 90           | 5.1        |
| Divorced  | 26           | 1.5        |
| <b>Occupation</b>   |              |            |
| Worker  | 86           | 4.9        |
| Farmer  | 75           | 4.2        |
| Office worker   | 179          | 10.1       |
| Civil servant   | 44           | 2.5        |
| Professional and technological worker   | 48           | 2.7        |
| Self-employed person  | 44           | 2.5        |
| Freelancer  | 115          | 6.5        |
| Student   | 16           | 0.9        |
| Retiree   | 764          | 43.3       |
| Unemployed  | 197          | 11.2       |
| Others  | 197          | 11.2       |
| <b>Exposure history (contact with someone with confirmed or suspected COVID-19 during the 2 weeks preceding the onset of illness)</b> |              |            |
| No  | 998          | 56.5       |
| Yes   | 477          | 27.0       |
| Unknown   | 290          | 16.4       |
| <b>Relationship between patients and people with COVID-19 to whom they were exposed</b>   |              |            |
| Family members  | 330          | 18.7       |
| Colleagues  | 36           | 2.0        |
| Social interaction  | 50           | 2.8        |
| Shared transportation   | 12           | 0.7        |
| Others  | 1,337        | 75.8       |
| <b>Source of exposure</b>   |              |            |
| Eating together   | 125          | 7.1        |
| Staying in the same room  | 218          | 12.4       |
| Living in the same ward   | 17           | 1.0        |
| Sharing utensils with patients  | 5            | 0.3        |
| Contacting with patient secretions  | 4            | 0.2        |
| Treatment and care  | 828          | 46.9       |
| Visiting patient  | 5            | 0.3        |
| Others  | 563          | 31.9       |
| <b>Time period of exposure</b>  |              |            |
| Prolonged   | 345          | 19.5       |
| Brief   | 100          | 5.7        |
| Uncertain   | 1,320        | 74.8       |
| <b>Possible location of exposure</b>  |              |            |
| Home  | 307          | 17.4       |
| Workplace   | 40           | 2.3        |
| Dormitories   | 13           | 0.7        |
| Hospitals   | 31           | 1.8        |

(Continued)

**TABLE 1 |** Continued

| Characteristics   | N*    | %*   |
|---|-------|------|
| Indoor public places                                      | 40    | 2.3  |
| Others  | 945   | 53.5 |
| <b>Admission route</b>                                    |       |      |
| Emergency department                                      | 23    | 1.3  |
| Outpatient department                                     | 47    | 2.7  |
| Referral from other hospitals                             | 119   | 6.7  |
| Others  | 1,576 | 89.3 |
| <b>Illness condition on admission</b>                     |       |      |
| Without symptoms  | 10    | 0.6  |
| Unknown   | 3     | 0.2  |
| Clinically uncertain                                      | 20    | 1.1  |
| With symptoms   | 1,732 | 98.1 |
| <b>Critical degree on admission</b>                       |       |      |
| Dangerous   | 72    | 4.1  |
| Emergent  | 66    | 3.7  |
| Moderate  | 1,627 | 92.2 |
| <b>Undergoing surgery during hospitalization</b>          |       |      |
| No  | 1,757 | 99.5 |
| Yes   | 8     | 0.5  |
| <b>Undergoing resuscitation during hospitalization</b>    |       |      |
| No  | 1,707 | 96.7 |
| Yes   | 58    | 3.3  |
| <b>Developing critical illness during hospitalization</b> |       |      |
| No  | 1,559 | 88.3 |
| Yes   | 206   | 11.7 |
| <b>Requiring consultation during hospitalization</b>      |       |      |
| No  | 1,203 | 68.2 |
| In-hospital consultation                                  | 93    | 5.3  |
| Consultation with outside specialists                     | 469   | 26.6 |
| <b>Being complex cases during hospitalization</b>         |       |      |
| No  | 1,731 | 98.1 |
| Yes   | 34    | 1.9  |
| <b>Reported initial symptoms</b>                          |       |      |
| Fever   | 959   | 54.3 |
| Cough   | 787   | 44.6 |
| Expectoration   | 112   | 6.3  |
| Dry cough   | 159   | 9.0  |
| Stuffy nose and/or runny nose                             | 18    | 1.0  |
| Pant  | 162   | 9.2  |
| Shortness of breath                                       | 126   | 7.1  |
| Fatigue   | 537   | 30.4 |
| Chest distress and/or chest pain                          | 237   | 13.4 |
| Dizziness and/or headache                                 | 28    | 1.6  |
| Abdominal pain and/or diarrhea and/or bloating            | 38    | 2.2  |
| Sore throat   | 58    | 3.3  |
| Dyspnea   | 31    | 1.8  |
| Hemoptysis  | 2     | 0.1  |
| Palpitation   | 19    | 1.1  |
| Muscle pain   | 45    | 2.5  |
| Chest and/or back pain                                    | 7     | 0.4  |
| Nausea and/or vomit                                       | 21    | 1.2  |

(Continued)

TABLE 1 | Continued

| Characteristics                                | N*    | %*   |
|--|-------|------|
| Poor appetite                                  | 49    | 2.8  |
| Chill  | 25    | 1.4  |
| Disturbance of consciousness and apathy        | 10    | 0.6  |
| Viral pneumonia                                | 2     | 0.1  |
| Tuberculosis                                   | 1     | 0.1  |
| Unknown  | 18    | 1.0  |
| <b>Current symptoms during hospitalization</b> |       |      |
| Fever  | 1,059 | 60.0 |
| Cough  | 1,084 | 61.4 |
| Chest distress                                 | 390   | 22.1 |
| Dyspnea  | 77    | 4.4  |
| <b>Clinical manifestations</b>                 |       |      |
| Fever  | 732   | 41.5 |
| Cough  | 800   | 45.3 |
| Catarrh of the upper respiratory tract         | 196   | 11.1 |
| Chest distress                                 | 476   | 27.0 |
| Dyspnea  | 176   | 10.0 |
| Fatigue  | 658   | 37.3 |
| Diarrhea                                       | 74    | 4.2  |
| <b>Previous medical history</b>                |       |      |
| Without  | 1,263 | 71.6 |
| With   | 502   | 28.4 |
| <b>Self-reported underlying diseases</b>       |       |      |
| Hypertension                                   | 528   | 29.9 |
| Diabetes                                       | 226   | 12.8 |
| Coronary heart disease                         | 100   | 5.7  |
| Chronic bronchitis                             | 41    | 2.3  |
| COPD   | 9     | 0.5  |
| Hyperlipidemia                                 | 23    | 1.3  |
| Asthma   | 14    | 0.8  |
| Atrial fibrillation                            | 12    | 0.7  |
| Bronchiectasis                                 | 8     | 0.5  |
| Alzheimer's disease                            | 15    | 0.8  |
| Parkinson's disease                            | 6     | 0.3  |
| <b>Smoking habits</b>                          |       |      |
| No   | 1,387 | 78.6 |
| Yes  | 74    | 4.2  |
| Unknown  | 304   | 17.2 |
| <b>Treatment</b>                               |       |      |
| Oxygen therapy measures                        | 677   | 38.4 |
| Antiviral therapy                              | 1,255 | 71.1 |
| Mechanical Ventilation                         | 30    | 1.7  |
| ECMO   | 4     | 0.2  |
| Circulatory support                            | 2     | 0.1  |
| Renal failure and renal replacement therapy    | 2     | 0.1  |
| Blood purification therapy                     | 2     | 0.1  |
| Immunotherapy with tocilizumab                 | 20    | 1.1  |
| Severe or critical child cases                 | 9     | 0.5  |
| Pregnancy with severe or critical illness      | 1     | 0.1  |

(Continued)

TABLE 1 | Continued

| Characteristics   | N*    | %*   |
|---|-------|------|
| <b>Ground-glass opacity tested by CT or chest radiography</b> |       |      |
| No  | 231   | 13.1 |
| Yes   | 1,534 | 86.9 |
| <b>Location of ground-glass opacity</b>                       |       |      |
| Only right lung   | 135   | 7.6  |
| Only left lung  | 93    | 5.3  |
| Multiple points of both lungs                                 | 1,226 | 69.5 |
| Right and upper left lung                                     | 31    | 1.8  |
| Right and lower left lung                                     | 32    | 1.8  |
| Left and upper right lung                                     | 1     | 0.1  |
| Left and middle right lung                                    | 10    | 0.6  |
| Left and lower right lung                                     | 8     | 0.5  |
| Unknown   | 229   | 13   |
| <b>Other observations obtained from imaging</b>               |       |      |
| Bronchial vascular bundle thickening                          | 493   | 27.9 |
| Swollen lymph node  | 174   | 9.9  |
| Pleural effusion  | 91    | 5.2  |
| <b>Outpatient and emergency diagnosis</b>                     |       |      |
| Confirmed COVID-19 case                                       | 1,331 | 75.4 |
| Clinically diagnosed COVID-19 case                            | 266   | 15.1 |
| Suspected COVID-19 case                                       | 140   | 7.9  |
| Infected by novel coronavirus                                 | 14    | 0.8  |
| Viral pneumonia   | 13    | 0.7  |
| Hypertension  | 1     | 0.1  |
| <b>Admission diagnosis</b>                                    |       |      |
| Confirmed COVID-19 case                                       | 1,329 | 75.3 |
| Clinically diagnosed COVID-19 case                            | 289   | 16.4 |
| Suspected COVID-19 case                                       | 125   | 7.1  |
| Infected by novel coronavirus                                 | 14    | 0.8  |
| Viral pneumonia   | 5     | 0.3  |
| Hypertension  | 2     | 0.1  |
| Chronic bronchitis  | 1     | 0.1  |
| <b>Discharge diagnosis</b>                                    |       |      |
| Confirmed COVID-19 case                                       | 1,536 | 87.0 |
| Clinically diagnosed COVID-19 case                            | 200   | 11.3 |
| Suspected COVID-19 case                                       | 14    | 0.8  |
| Infected by novel coronavirus                                 | 14    | 0.8  |
| Pneumonia   | 1     | 0.1  |
| <b>Subtype of COVID-19 at discharge</b>                       |       |      |
| Mild  | 25    | 1.4  |
| Normal  | 928   | 52.6 |
| Severe  | 60    | 3.4  |
| Critical  | 26    | 1.5  |
| Suspected   | 7     | 0.4  |
| Clinical diagnosis  | 194   | 11.0 |
| Unknown   | 525   | 29.7 |
| <b>Consistency between discharge and outpatient diagnoses</b> |       |      |
| Consistent  | 1,730 | 98.0 |
| Uncertain   | 2     | 0.1  |

(Continued)

TABLE 1 | Continued

| Characteristics   | N*    | %*   |
|---|-------|------|
| Unknown   | 33    | 1.9  |
| <b>Consistency between admission and discharge diagnoses</b>        |       |      |
| Consistent  | 1,755 | 99.4 |
| Uncertain   | 2     | 0.1  |
| Unknown   | 8     | 0.5  |
| <b>Consistency between preoperative and postoperative diagnoses</b> |       |      |
| Inconsistent  | 14    | 0.8  |
| Consistent  | 125   | 7.1  |
| Uncertain   | 2     | 0.1  |
| Unknown   | 1,624 | 92.0 |
| <b>Consistency between clinical and pathological diagnoses</b>      |       |      |
| Inconsistent  | 14    | 0.8  |
| Consistent  | 13    | 0.7  |
| Uncertain   | 1     | 0.1  |
| Unknown   | 1,737 | 98.4 |
| <b>Consistency between radiological and pathological diagnoses</b>  |       |      |
| Inconsistent  | 14    | 0.8  |
| Consistent  | 23    | 1.3  |
| Uncertain   | 2     | 0.1  |
| Unknown   | 1,726 | 97.8 |
| <b>The highest evidence of diagnosis</b>                            |       |      |
| Clinical diagnosis  | 414   | 23.5 |
| Radiography, CT, ultrasound, endoscopy                              | 107   | 6.1  |
| Biochemical and immunological test results                          | 928   | 52.6 |
| Cytological blood smear test  | 21    | 1.2  |
| Unknown   | 295   | 16.7 |
| <b>Prognosis at discharge</b>                                       |       |      |
| Dead  | 32    | 1.8  |
| Unhealed  | 4     | 0.2  |
| Improved  | 85    | 4.8  |
| Cured   | 1,644 | 93.1 |

\*The frequency and percentage of these categorical variables were calculated by the descriptive statistics. COVID-19, coronavirus disease-19.

points in both lungs. In addition, 27.9% of the patients had bronchial vascular bundle thickening (Table 1). The results of laboratory tests that include the 44 indicators are shown in Supplementary Table 1.

Most patients were diagnosed with confirmed COVID-19 at the time of outpatient or emergency department consultation, admission, and discharge. Over 50% of the patients were diagnosed with a normal subtype of COVID-19 at discharge. For most patients, the discharge and outpatient diagnoses and the admission and discharge diagnoses were consistent. However, the preoperative and postoperative diagnoses, clinical and pathological diagnoses, and radiological and pathological diagnoses could not be compared because of insufficient data. In terms of the diagnoses mentioned above, 52.6% of patients were diagnosed based on the highest level of evidence of biochemical and immunological tests, indicating that most (93.1%) patients were cured at discharge and the case fatality rate was 1.8% (Table 1).

## Univariate Analysis of Factors Influencing COVID-19 Prognosis

Univariate analyses (Supplementary Tables 1, 2) suggested the following 63 factors significant to the prognosis: marital status; occupation; age; exposure history (contact with someone with confirmed or suspected COVID-19 during the 2 weeks preceding the onset of illness); source of exposure; time period of exposure; critical degree on admission; undergoing surgery; undergoing resuscitation; critical disease; need for consulting outside specialists; complex disease manifestations; reported initial symptom of dry cough, fatigue, dyspnea, disturbance of consciousness and apathy, and unknown; current symptom of dyspnea; clinical manifestation of fever, cough, and fatigue; medical history; self-reported underlying hypertension, diabetes, atrial fibrillation, and Alzheimer's disease; smoking habits; treatment method of oxygen therapy measures, mechanical ventilation, and immunotherapy with tocilizumab; imaging feature of pleural effusion; lymphocyte count; percentage of lymphocytes; percentage of eosinophils; neutrophil count; basophil count; MCHC; PLT count; percentage of neutrophils; percentage of monocytes; percentage of basophils; lymphocyte count; eosinophil count; RDW; blood glucose; ALB; A/G ratio; D-BiL; ALP; UN; TP; AST; chlorine; creatinine; CRP; outpatient and emergency diagnosis; admission diagnosis; discharge diagnosis; subtype of COVID-19 at discharge; consistency between discharge and outpatient diagnoses; consistency between admission and discharge diagnoses; consistency between preoperative and postoperative diagnoses; and the highest level of evidence of diagnosis.

## Logistic Regression Analysis of COVID-19 Prognosis

Logistic regression analysis (Table 2) revealed that the prognosis of patients with COVID-19 was influenced by the following factors: undergoing resuscitation, developing a critical illness, requiring outside specialist consultation, having dry cough as an initial symptom, the clinical manifestation of fatigue, the highest level of evidence of diagnosis, basophil count, lymphocyte count, A/G ratio, and AST and creatinine levels.

A poorer prognosis was associated with undergoing resuscitation (odds ratio [OR]: 0.067), developing critical illness during hospitalization (OR: 0.425), requiring consultation with outside specialists (OR: 0.077), basophil count  $> 0.06 \times 10^9$  cells/L (OR: 0.396), lymphocyte count  $> 3.2 \times 10^9$  cells/L (OR: 0.211), an A/G ratio  $> 2.4$  (OR: 0.038), AST level  $> 34$  U/L (OR: 0.375), male patients with creatinine level  $> 104 \mu\text{mol/L}$ , and female patients with a creatinine level  $> 90 \mu\text{mol/L}$  (OR: 0.347). A better prognosis was associated with initial symptoms of dry cough (OR: 6.17), the clinical manifestation of fatigue (OR: 1.96), and is diagnosed based on the highest level of evidence by means of biochemical and immunological tests (OR: 2.395).

## DISCUSSION

In this study, 93.1% of the 1,765 patients with COVID-19 were cured, 4.8% improved, 0.2% were unhealed, and 1.8% died.



**TABLE 2 |** Logistic regression analysis of the influencing factors of the prognosis of patients with COVID-19.

| Characteristic  |                                       | Estimate <sup>a</sup> | Wald Chi-Square <sup>a</sup> | P <sup>a</sup> | OR <sup>a</sup> | 95% Wald confidence limits <sup>a</sup> |          |
|---|---------------------------------------|-----------------------|------------------------------|----------------|-----------------|---|----------|
|   |                                       |                       |                              |                |                 | Lower                                   | Upper    |
| Critical degree on admission                            | Dangerous                             | Ref                   |                              |                |                 |   |          |
|   | Emergent                              | −0.727                | 2.458                        | 0.117          | 0.483           | 0.195                                   | 1.200    |
|   | Moderate                              | 0.410                 | 0.982                        | 0.322          | 1.507           | 0.670                                   | 3.393    |
| Undergoing resuscitation during hospitalization         | No                                    | Ref                   |                              |                |                 |   |          |
|   | Yes                                   | −2.700                | 48.307                       | <0.0001*       | 0.067           | 0.031                                   | 0.144    |
| Developing critical illness during hospitalization      | No                                    | Ref                   |                              |                |                 |   |          |
|   | Yes                                   | −0.856                | 6.441                        | 0.011*         | 0.425           | 0.219                                   | 0.823    |
| Requiring consultation during hospitalization           | No                                    | Ref                   |                              |                |                 |   |          |
|   | In-hospital consultation              | −0.650                | 3.146                        | 0.076          | 0.522           | 0.255                                   | 1.071    |
|   | Consultation with outside specialists | −2.559                | 14.310                       | 0.000*         | 0.077           | 0.021                                   | 0.291    |
| Having a dry cough as an initial symptom                | No                                    | Ref                   |                              |                |                 |   |          |
|   | Yes                                   | 1.820                 | 5.510                        | 0.019*         | 6.170           | 1.350                                   | 28.197   |
| Having an unknown initial symptom                       | No                                    | Ref                   |                              |                |                 |   |          |
|   | Yes                                   | −1.210                | 3.541                        | 0.060          | 0.298           | 0.085                                   | 1.052    |
| Clinical manifestation of fatigue                       | No                                    | Ref                   |                              |                |                 |   |          |
|   | Yes                                   | 0.673                 | 7.234                        | 0.007*         | 1.960           | 1.200                                   | 3.200    |
| The highest evidence of diagnosis                       | Clinical diagnosis                    | Ref                   |                              |                |                 |   |          |
|   | X-ray, CT, ultrasound, endoscopy      | −0.128                | 0.089                        | 0.766          | 0.880           | 0.378                                   | 2.046    |
|   | Biochemical and immunological test    | 0.873                 | 10.990                       | 0.001*         | 2.395           | 1.429                                   | 4.014    |
|   | Cytological blood smear               | −1.023                | 2.490                        | 0.115          | 0.359           | 0.101                                   | 1.281    |
|   | Unknown                               | 0.117                 | 0.135                        | 0.713          | 1.124           | 0.604                                   | 2.091    |
| Basophil count ( $\times 10^9/L$ ) <sup>b</sup>         | 0–0.06                                | Ref                   |                              |                |                 |   |          |
|   | >0.06                                 | −0.927                | 5.797                        | 0.016*         | 0.396           | 0.186                                   | 0.842    |
| Lymphocyte count ( $\times 10^9/L$ ) <sup>b</sup>       | 1.1–3.2                               | Ref                   |                              |                |                 |   |          |
|   | <1.1                                  | −0.098                | 0.123                        | 0.726          | 0.907           | 0.525                                   | 1.566    |
|   | >3.2                                  | −1.554                | 6.731                        | 0.010*         | 0.211           | 0.065                                   | 0.684    |
| Albumin (ALB) / globulin (GLB) (A/G) ratio <sup>b</sup> | 1–2.4                                 | Ref                   |                              |                |                 |   |          |
|   | <1                                    | 0.425                 | 1.831                        | 0.176          | 1.53            | 0.826                                   | 2.831    |
|   | >2.4                                  | −3.273                | 5.490                        | 0.019*         | 0.038           | 0.002                                   | 0.586    |
| Aspartate aminotransferase (AST) (U/L) <sup>b</sup>     | 5–34                                  | Ref                   |                              |                |                 |   |          |
|   | <5                                    | 9.257                 | 0.000                        | 0.987          | >999.999        | <0.001                                  | >999.999 |
|   | >34                                   | −0.982                | 10.587                       | 0.001*         | 0.375           | 0.207                                   | 0.677    |
| Creatinine ( $\mu\text{mol/L}$ ) <sup>b</sup>           | Male 64–104 Female 49–90              | Ref                   |                              |                |                 |   |          |
|   | Male <64 Female <49                   | −0.308                | 1.188                        | 0.276          | 0.735           | 0.422                                   | 1.279    |
|   | Male >104 Female >90                  | −1.058                | 7.968                        | 0.005*         | 0.347           | 0.167                                   | 0.724    |

\*Indicates statistically significant results ( $P < 0.05$ ).

<sup>a</sup>The stepwise logistic regression analysis was used to explore the factors influencing COVID-19 prognosis.

<sup>b</sup>To explain the results more explicitly, these continuous variables were transformed into categorical variables according to their meanings and clinical reference ranges in the logistic regression analysis.

COVID-19, coronavirus disease-19.

Univariate analyses identified 63 significant factors for COVID-19 prognosis, while logistic regression analysis identified factors related to the severity of illness, symptoms and manifestations, diagnosis, and laboratory findings as factors independently associated with COVID-19 prognosis.

Patients with more severe diseases had a poorer prognosis. Undergoing resuscitation, consultation with outside specialists, and critical disease during hospitalization were all associated with more severe diseases. More critical patients were at a higher risk of death, which was consistent with the findings of a previous

study, conducted in Wuhan, of 109 patients with COVID-19 who were serious enough to be admitted to the intensive care unit; all died owing to the rapid progress of the disease (29). Our finding was also indirectly supported by findings from a study from Detroit (23) and a study from Saudi Arabia (30) that emphasized admission to the intensive care unit would increase the incidence of death.

Patients who reported initial symptoms of dry cough and who had clinical manifestations of fatigue had a better prognosis. Our findings were consistent with those of other studies that

found that though fatigue and dry cough are common symptoms and clinical manifestations, especially at the onset of illness (1, 31), among patients with a fatal disease, the most common symptom was dyspnea, followed by fatigue (29). Therefore, it was understandable that patients with a dry cough had a 6-fold better survival than those without this symptom and that those with the clinical manifestation of fatigue had double the survival of those without fatigue. However, some other studies have found the opposite association with survival. A study of 47 patients with COVID-19 in Xinyu, China (32) and a systematic review of 207 studies (33) found that fatigue was associated with a poorer prognosis. We were unable to find any studies that assessed dry cough as a prognostic indicator, and only a few studies have mentioned cough when describing the clinical characteristics of patients with COVID-19 (2, 34, 35).

Those diagnosed based on the highest level of evidence of biochemical and immunological tests were more than twice as likely to have a favorable outcome than patients with a diagnosis based on clinical findings. Considering that the admission period of patients in this study was from February 19, 2020, to March 19, 2020, the diagnosis and treatment were based on the *Diagnosis and Treatment Plan for COVID-19, Version 6.0* (36) and *Version 7.0* (37). The diagnostic criteria indicated that clinical diagnoses, along with radiological examinations (i.e., radiography and CT), should be used to identify suspected cases, while biochemical and immunological tests should be used for confirmation. Patients with confirmed COVID-19 were more likely to receive appropriate treatment, which could explain the better prognosis among patients diagnosed with COVID-19 based on the highest level of evidence of biochemical and immunological tests.

In terms of laboratory parameters, basophil count, lymphocyte count, A/G ratio, AST, and creatinine levels were associated with prognosis. Several previous studies have found that lymphocyte count is one of the most significant factors for COVID-19 prognosis and is a predictor of death (38). Most results of previous studies conducted in China and other countries found that lymphopenia was associated with a poorer prognosis (33, 35, 39–42), and one study found that a lymphocyte count  $<0.8 \times 10^9$  cells/L was associated with an increased risk of severe COVID-19 (43). However, in our study, a lymphocyte count exceeding the upper limit of normal ( $>3.2 \times 10^9$  cells/L) was associated with a poorer prognosis. Similarly, a study from Saudi Arabia found that the lymphocyte count of patients with moderate disease was higher than that of patients with mild disease (19), which indicated that the severity of the disease might be a confounding factor. Therefore, more evidence from larger samples in other countries or other regions of China is needed to explore the contradictory results of the lymphocyte count.

Concerning AST, a study from Libya (42) reached a similar conclusion as that of our study. The increased level of AST would increase the possibility of death.

Creatinine was another sensitive prognostic laboratory indicator. A higher level of creatinine was associated with a higher probability of death or severe disease. This finding was consistent with a study on 113 patients in China with fatal disease (7), a study on 1,207 patients in Libya (42), and a systematic

review of 207 studies from multiple countries (33). Furthermore, to identify and care for patients with increasing creatinine levels, attention should be focused on male patients with creatinine levels  $>104 \mu\text{mol/L}$  and female patients with creatinine levels  $>90 \mu\text{mol/L}$ .

Regarding other laboratory indicators with significance in univariate analyses in our study for which there was supporting evidence from national and international studies, WBC count (30, 33, 39, 42–45), percentage of lymphocytes (8), PLT count (8, 33, 42, 46–48), CRP level (8, 33, 43, 46, 48, 49), neutrophil count (33, 42, 43, 48), ALB level (33, 43, 49), blood UN (9, 33), and blood glucose level (45) were also associated with prognosis. However, some significant laboratory parameters, such as lactate dehydrogenase (7, 8, 33, 44, 45), D-dimer (7, 8, 10, 33, 43), and procalcitonin (5, 33, 44, 50), were not investigated in our study owing to a lack of data.

Furthermore, our study found that basophil count and A/G ratio were associated with COVID-19 prognosis, though few other studies have investigated these parameters. Extra attention should be paid to patients with a basophil count  $>0.06 \times 10^9$  cells/L and A/G ratio  $>2.4$  to prevent disease progression. However, some controversial factors in previous studies were not significant to the prognosis in our study; these included sex and comorbidities (23, 24, 30).

There are some limitations to this study. First, it was a single-center study, which might have led to some biases. Further, the generalization of our findings is limited to some extent. Second, many patients were transferred from other hospitals and were not first diagnosed at MCH-Optical Valley; however, all laboratory indicators were tested on admission, implying that the laboratory findings of some patients were not their first test results—this might have introduced some biases. Third, data in this study were from February 19, 2020, to March 19, 2020, i.e., relatively old, though analyses were conducted on some inconsistent or previously unexplored indicators. Follow-up after discharge should be considered to compare the first wave with the following waves (e.g., the emergence of new variants) in future studies to provide further evidence for the prevention, diagnosis, and treatment of COVID-19. Fourth, some important factors (e.g., lactate dehydrogenase, D-dimer, and procalcitonin) investigated in other studies were not explored in this study owing to a lack of data. Fifth, this study had no control group, and the heterogeneity of the population might influence the generalization of the findings to other populations. Sixth, because some characteristics were self-reported, there existed some unreasonable classifications, such as viral pneumonia and tuberculosis in the reported initial symptoms. We did not make any corrections about these self-reported characteristics due to the lack of follow-up, which might bring some biases.

## CONCLUSIONS

The cure rate of 1,765 patients with COVID-19 in this study was 93.1%, and the mortality rate was 1.8%. To prevent the deterioration of the condition of the patient, clinicians should provide special care to patients developing critical illness

during hospitalization, undergoing resuscitation, or needing consultation with outside specialists. In addition, patients with a basophil count  $>0.06 \times 10^9$  cells/L, lymphocyte count  $> 3.2 \times 10^9$  cells/L, an A/G ratio  $> 2.4$ , AST level  $> 34$  U/L, and male sex with creatinine levels  $>104 \mu\text{mol/L}$ , or female sex with creatinine levels  $> 90 \mu\text{mol/L}$  were at a higher risk of having a poorer prognosis. Dry cough as an initial symptom, the clinical manifestation of fatigue, and being diagnosed with COVID-19 based on the highest level of evidence of biochemical and immunological tests were protective factors and was associated with a more favorable prognosis.

## DATA AVAILABILITY STATEMENT

The raw data supporting the conclusions of this article will be made available by the authors, without undue reservation.

## ETHICS STATEMENT

The studies involving human participants were reviewed and approved by the 903rd Hospital of PLA Ethics Committee. Written informed consent from the participants' legal guardian/next of kin was not required to participate in this study in accordance with the national legislation and the institutional requirements.

## REFERENCES

- Huang C, Wang Y, Li X, Ren L, Zhao J, Hu Y, et al. Clinical features of patients infected with 2019 novel coronavirus in Wuhan, China. *Lancet*. (2020) 395:497–506. doi: 10.1016/S0140-6736(20)30183-5
- Guan WJ, Ni ZY, Hu Y, Liang WH, Ou CQ, He JX, et al. Clinical characteristics of coronavirus disease 2019 in China. *N Engl J Med*. (2020) 382:1708–20. doi: 10.1056/NEJMoa2002032
- World Health Organization. *Timeline: WHO's COVID-19 Response*. Geneva: World Health Organization (2020). Available online at: <https://www.who.int/emergencies/diseases/novel-coronavirus-2019/interactive-timeline#/>
- World Health Organization. *WHO Coronavirus Disease (COVID-19) Dashboard*. Geneva: World Health Organization (2020). Available online at: <https://covid19.who.int>
- Chen R, Liang W, Jiang M, Guan W, Zhan C, Wang T, et al. Risk factors of fatal outcome in hospitalized subjects with coronavirus disease 2019 from a nationwide analysis in China. *Chest*. (2020) 158:97–105. doi: 10.1016/j.chest.2020.04.010
- Guan WJ, Liang WH, Zhao Y, Liang HR, Chen ZS, Li YM, et al. Comorbidity and its impact on 1590 patients with COVID-19 in China: a nationwide analysis. *Eur Respir J*. (2020) 55:2000547. doi: 10.1183/13993003.00547-2020
- Chen T, Wu D, Chen H, Yan W, Yang D, Chen G, et al. Clinical characteristics of 113 deceased patients with coronavirus disease 2019: retrospective study. *BMJ*. (2020) 368:m1091. doi: 10.1136/bmj.m1091
- Ma X, Wang H, Huang J, Geng Y, Jiang S, Zhou Q, et al. A nomogram model based on clinical and laboratory parameters at admission for predicting the survival of COVID-19 patients. *BMC Infect Dis*. (2020) 20:899. doi: 10.1186/s12879-020-05614-2
- Wang B, Zhong F, Zhang H, An W, Liao M, Cao Y. Risk factor analysis and nomogram construction for non-survivors among critical patients with COVID-19. *Jpn J Infect Dis*. (2020) 73:452–8. doi: 10.7883/yoken.JJID.2020.227
- Zhou F, Yu T, Du R, Fan G, Liu Y, Liu Z, et al. Clinical course and risk factors for mortality of adult inpatients with COVID-19 in Wuhan, China: a retrospective cohort study. *Lancet*. (2020) 395:1054–62. doi: 10.1016/S0140-6736(20)30566-3

## AUTHOR CONTRIBUTIONS

All the authors contributed to the conception and design of the study. Material preparation, data collection, and analysis were performed by XiaL, LZ, TL, XibL, WY, and QC. The first draft of the manuscript was written by XiaL. All the authors have commented on previous versions of the manuscript and read and approved the final manuscript.

## FUNDING

This study was supported by the Zhejiang Provincial Natural Science Foundation of China (Grant No: LQ21H100001), the Soft Science Project of Shanghai Science and Technology Innovation Action Plan (Grant No: 21692191300), and the National Natural Science Foundation of China (Grant Nos: 82101870 and 72104140).

## SUPPLEMENTARY MATERIAL

The Supplementary Material for this article can be found online at: <https://www.frontiersin.org/articles/10.3389/fpubh.2021.726491/full#supplementary-material>

- Zhang J, Wang M, Zhao M, Guo S, Xu Y, Ye J, et al. The clinical characteristics and prognosis factors of mild-moderate patients with COVID-19 in a mobile cabin hospital: a retrospective, single-center study. *Front Public Health*. (2020) 8:264. doi: 10.3389/fpubh.2020.00264
- Liu Z, Bai X, Han X, Jiang W, Qiu L, Chen S, et al. The association of diabetes and the prognosis of COVID-19 patients: a retrospective study. *Diabetes Res Clin Pract*. (2020) 169:108386. doi: 10.1016/j.diabres.2020.108386
- Zhu FC, Guan XH, Li YH, Huang JY, Jiang T, Hou LH, et al. Immunogenicity and safety of a recombinant adenovirus type-5-vectored COVID-19 vaccine in healthy adults aged 18 years or older: a randomised, double-blind, placebo-controlled, phase 2 trial. *Lancet*. (2020) 396:479–88. doi: 10.1016/S0140-6736(20)31605-6
- Xia S, Duan K, Zhang Y, Zhao D, Zhang H, Xie Z, et al. Effect of an inactivated vaccine against SARS-CoV-2 on safety and immunogenicity outcomes: interim analysis of 2 randomized clinical trials. *JAMA*. (2020) 324:951–60. doi: 10.1001/jama.2020.15543
- Polack FP, Thomas SJ, Kitchin N, Absalon J, Gurtman A, Lockhart S, et al. Safety and efficacy of the BNT162b2 mRNA Covid-19 vaccine. *N Engl J Med*. (2020) 383:2603–15. doi: 10.1056/NEJMoa2034577
- Baden LR, El Sahly HM, Essink B, Kotloff K, Frey S, Novak R, et al. Efficacy and safety of the mRNA-1273 SARS-CoV-2 vaccine. *N Engl J Med*. (2021) 384:403–16. doi: 10.1056/NEJMoa2035389
- Heath PT, Galiza EP, Baxter DN, Boffito M, Browne D, Burns F, et al. Safety and efficacy of NVX-CoV2373 Covid-19 vaccine. *N Engl J Med*. (2021) 385:1172–83. doi: 10.1056/NEJMoa2107659
- Louapre C, Collongues N, Stankoff B, Giannesini C, Papeix C, Bensa C, et al. Clinical characteristics and outcomes in patients with coronavirus disease 2019 and multiple sclerosis. *JAMA Neurol*. (2020) 77:1079–88. doi: 10.1001/jamaneurol.2020.2581
- Al Mutair A, Alhumaid S, Alhuqbani WN, Zaidi ARZ, Alkoraisi S, Al-Subaie MF, et al. Clinical, epidemiological, and laboratory characteristics of mild-to-moderate COVID-19 patients in Saudi Arabia: an observational cohort study. *Eur J Med Res*. (2020) 25:61. doi: 10.1186/s40001-020-00462-x
- Trigo J, García-Azorín D, Planchuelo-Gómez Á, Martínez-Pías E, Talavera B, Hernández-Pérez I, et al. Factors associated with the presence of headache

- in hospitalized COVID-19 patients and impact on prognosis: a retrospective cohort study. *J Headache Pain*. (2020) 21:94. doi: 10.1186/s10194-020-01165-8
21. Lanza E, Muglia R, Bolengo I, Santonocito OG, Lisi C, Angelotti G, et al. Quantitative chest CT analysis in COVID-19 to predict the need for oxygenation support and intubation. *Eur Radiol*. (2020) 30:6770–8. doi: 10.1007/s00330-020-07013-2
  22. Albitar O, Ballouze R, Ooi JP, Sheikh Ghadzi SM. Risk factors for mortality among COVID-19 patients. *Diabetes Res Clin Pract*. (2020) 166:108293. doi: 10.1016/j.diabres.2020.108293
  23. Suleyman G, Fadel RA, Malette KM, Hammond C, Abdulla H, Entz A, et al. Clinical characteristics and morbidity associated with coronavirus disease 2019 in a series of patients in metropolitan Detroit. *JAMA Netw Open*. (2020) 3:e2012270. doi: 10.1001/jamanetworkopen.2020.12270
  24. Patient care and clinical outcomes for patients with COVID-19 infection admitted to African high-care or intensive care units (ACCCOS): a multicentre, prospective, observational cohort study. *Lancet*. (2021) 397:1885–94. doi: 10.1016/S0140-6736(21)00441-4
  25. Woolford SJ, D'Angelo S, Curtis EM, Parsons CM, Ward KA, Dennison EM, et al. COVID-19 and associations with frailty and multimorbidity: a prospective analysis of UK Biobank participants. *Aging Clin Exp Res*. (2020) 32:1897–905. doi: 10.1007/s40520-020-01653-6
  26. Alyammahi SK, Abdin SM, Alhamad DW, Elgendy SM, Altell AT, Omar HA. The dynamic association between COVID-19 and chronic disorders: An updated insight into prevalence, mechanisms and therapeutic modalities. *Infect Genet Evol*. (2021) 87:104647. doi: 10.1016/j.meegid.2020.104647
  27. Tadic M, Cuspidi C, Sala C. COVID-19 and diabetes: is there enough evidence? *J Clin Hypertens*. (2020) 22:943–8. doi: 10.1111/jch.13912
  28. Drager LF, Pio-Abreu A, Lopes RD, Bortolotto LA. Is hypertension a real risk factor for poor prognosis in the COVID-19 pandemic? *Curr Hypertens Rep*. (2020) 22:43. doi: 10.1007/s11906-020-01057-x
  29. Du RH, Liu LM, Yin W, Wang W, Guan LL, Yuan ML, et al. Hospitalization and critical care of 109 decedents with COVID-19 pneumonia in Wuhan, China. *Ann Am Thorac Soc*. (2020) 17:839–46. doi: 10.1513/AnnalsATS.202003-225OC
  30. Ibrahim ME, Al-Aklabi OS, Abomughaid MM, Al-Ghamdi MA. Epidemiological, clinical, and laboratory findings for patients of different age groups with confirmed coronavirus disease 2019 (COVID-19) in a hospital in Saudi Arabia. *PLoS ONE*. (2021) 16:e0250955. doi: 10.1371/journal.pone.0250955
  31. Wang D, Hu B, Hu C, Zhu F, Liu X, Zhang J, et al. Clinical characteristics of 138 hospitalized patients with 2019 novel coronavirus-infected pneumonia in Wuhan, China. *JAMA*. (2020) 323:1061–9. doi: 10.1001/jama.2020.1585
  32. Lu J, Yin Q, Li Q, Fu G, Hu X, Huang J, et al. Clinical characteristics and factors affecting the duration of positive nucleic acid test for patients of COVID-19 in XinYu, China. *J Clin Lab Anal*. (2020) 34:e23534. doi: 10.1002/jcla.23534
  33. Izcovich A, Ragusa MA, Tortosa F, Lavena Marzio MA, Agnoletti C, Bengolea A, et al. Prognostic factors for severity and mortality in patients infected with COVID-19: a systematic review. *PLoS ONE*. (2020) 15:e0241955. doi: 10.1371/journal.pone.0241955
  34. Zhang SY, Lian JS, Hu JH, Zhang XL, Lu YF, Cai H, et al. Clinical characteristics of different subtypes and risk factors for the severity of illness in patients with COVID-19 in Zhejiang, China. *Infect Dis Poverty*. (2020) 9:85. doi: 10.1186/s40249-020-00710-6
  35. Xu Y, Xu Z, Liu X, Cai L, Zheng H, Huang Y, et al. Clinical findings of COVID-19 patients admitted to intensive care units in Guangdong Province, China: a multicenter, retrospective, observational study. *Front Med*. (2020) 7:576457. doi: 10.3389/fmed.2020.576457
  36. National Health Commission of PRC. *Diagnosis and Treatment Plan for COVID-19, Version 6.0*. Beijing: National Health Commission of PRC (2020).
  37. National Health Commission of PRC. *Diagnosis and Treatment Plan for COVID-19, Version 7.0*. Beijing: National Health Commission of PRC (2020).
  38. Mei J, Hu W, Chen Q, Li C, Chen Z, Fan Y, et al. Development and external validation of a COVID-19 mortality risk prediction algorithm: a multicentre retrospective cohort study. *BMJ Open*. (2020) 10:e044028. doi: 10.1136/bmjopen-2020-044028
  39. Sun H, Ning R, Tao Y, Yu C, Deng X, Zhao C, et al. Risk factors for mortality in 244 older adults with COVID-19 in Wuhan, China: a retrospective study. *J Am Geriatr Soc*. (2020) 68:E19–23. doi: 10.1111/jgs.16533
  40. Fu J, Kong J, Wang W, Wu M, Yao L, Wang Z, et al. The clinical implication of dynamic neutrophil to lymphocyte ratio and D-dimer in COVID-19: a retrospective study in Suzhou China. *Thromb Res*. (2020) 192:3–8. doi: 10.1016/j.thromres.2020.05.006
  41. Wang L, He W, Yu X, Hu D, Bao M, Liu H, et al. Coronavirus disease 2019 in elderly patients: characteristics and prognostic factors based on 4-week follow-up. *J Infect*. (2020) 80:639–45. doi: 10.1016/j.jinf.2020.03.019
  42. Elhadi M, Momen AA, Alsoufi A, Msherghi A, Zaid A, Ali Senussi Abdulhadi OM, et al. Epidemiological and clinical presentations of hospitalized COVID-19 patients in Libya: an initial report from Africa. *Travel Med Infect Dis*. (2021) 42:102064. doi: 10.1016/j.tmaid.2021.102064
  43. Yao Q, Wang P, Wang X, Qie G, Meng M, Tong X, et al. A retrospective study of risk factors for severe acute respiratory syndrome coronavirus 2 infections in hospitalized adult patients. *Pol Arch Intern Med*. (2020) 130:390–9. doi: 10.20452/pamw.15312
  44. Zhang JJY, Lee KS, Ang LW, Leo YS, Young BE. Risk factors for severe disease and efficacy of treatment in patients infected with COVID-19: a systematic review, meta-analysis, and meta-regression analysis. *Clin Infect Dis*. (2020) 71:2199–206. doi: 10.1093/cid/ciaa576
  45. Li X, Xu S, Yu M, Wang K, Tao Y, Zhou Y, et al. Risk factors for severity and mortality in adult COVID-19 inpatients in Wuhan. *J Allergy Clin Immunol*. (2020) 146:110–8. doi: 10.1016/j.jaci.2020.04.006
  46. Shang W, Dong J, Ren Y, Tian M, Li W, Hu J, et al. The value of clinical parameters in predicting the severity of COVID-19. *J Med Virol*. (2020) 92:2188–92. doi: 10.1002/jmv.26031
  47. Yang X, Yang Q, Wang Y, Wu Y, Xu J, Yu Y, et al. Thrombocytopenia and its association with mortality in patients with COVID-19. *J Thromb Haemost*. (2020) 18:1469–72. doi: 10.1111/jth.14848
  48. Elhadi M, Alsoufi A, Abusalama A, Alkaseek A, Abdeewi S, Yahya M, et al. Epidemiology, outcomes, and utilization of intensive care unit resources for critically ill COVID-19 patients in Libya: a prospective multi-center cohort study. *PLoS ONE*. (2021) 16:e0251085. doi: 10.1371/journal.pone.0251085
  49. Liu W, Tao ZW, Wang L, Yuan ML, Liu K, Zhou L, et al. Analysis of factors associated with disease outcomes in hospitalized patients with 2019 novel coronavirus disease. *Chin Med J*. (2020) 133:1032–8. doi: 10.1097/CM9.0000000000000775
  50. Lippi G, Plebani M. Procalcitonin in patients with severe coronavirus disease 2019 (COVID-19): a meta-analysis. *Clin Chim Acta*. (2020) 505:190–1. doi: 10.1016/j.cca.2020.03.004

**Conflict of Interest:** The authors declare that the research was conducted in the absence of any commercial or financial relationships that could be construed as a potential conflict of interest.

**Publisher's Note:** All claims expressed in this article are solely those of the authors and do not necessarily represent those of their affiliated organizations, or those of the publisher, the editors and the reviewers. Any product that may be evaluated in this article, or claim that may be made by its manufacturer, is not guaranteed or endorsed by the publisher.

Copyright © 2021 Liu, Zhu, Lu, Liu, Jiao, Tang, Chen, Chen, Yu and Chen. This is an open-access article distributed under the terms of the Creative Commons Attribution License (CC BY). The use, distribution or reproduction in other forums is permitted, provided the original author(s) and the copyright owner(s) are credited and that the original publication in this journal is cited, in accordance with accepted academic practice. No use, distribution or reproduction is permitted which does not comply with these terms.





# Adapting the Surveillance Platform for Enteric and Respiratory Infectious Organisms at United States Veterans Affairs Medical Centers (SUPERNOVA) for COVID-19 Among Hospitalized Adults: Surveillance Protocol

## OPEN ACCESS

### Edited by:

Reza Lashgari,  
Shahid Beheshti University, Iran

### Reviewed by:

Guangwen Cao,  
Second Military Medical  
University, China  
Berislav Žmuk,  
University of Zagreb, Croatia

### \*Correspondence:

Elissa Meites  
emeites@cdc.gov

### Specialty section:

This article was submitted to  
Infectious Diseases - Surveillance,  
Prevention and Treatment,  
a section of the journal  
Frontiers in Public Health

**Received:** 10 July 2021

**Accepted:** 05 October 2021

**Published:** 29 October 2021

### Citation:

Meites E, Bajema KL,  
Kambhampati A, Prill M, Marconi VC,  
Brown ST, Rodriguez-Barradas MC,  
Beenhouwer DO, Holodniy M,  
Lucero-Obusan C, Cardemil C,  
Cates J, Surie D and The  
SUPERNOVA COVID-19 Surveillance  
Group (2021) Adapting the  
Surveillance Platform for Enteric and  
Respiratory Infectious Organisms at  
United States Veterans Affairs Medical  
Centers (SUPERNOVA) for COVID-19  
Among Hospitalized Adults:  
Surveillance Protocol.  
Front. Public Health 9:739076.  
doi: 10.3389/fpubh.2021.739076

Elissa Meites<sup>1\*</sup>, Kristina L. Bajema<sup>1</sup>, Anita Kambhampati<sup>1</sup>, Mila Prill<sup>1</sup>,  
Vincent C. Marconi<sup>2,3,4</sup>, Sheldon T. Brown<sup>5,6</sup>, Maria C. Rodriguez-Barradas<sup>7,8</sup>,  
David O. Beenhouwer<sup>9,10</sup>, Mark Holodniy<sup>11,12,13</sup>, Cynthia Lucero-Obusan<sup>11,12</sup>,  
Cristina Cardemil<sup>1</sup>, Jordan Cates<sup>1</sup>, Diya Surie<sup>1</sup> and  
The SUPERNOVA COVID-19 Surveillance Group

<sup>1</sup> National Center for Immunization and Respiratory Diseases, Centers for Disease Control and Prevention, Atlanta, GA, United States, <sup>2</sup> Atlanta VA Medical Center, Atlanta, GA, United States, <sup>3</sup> Department of Medicine, Emory University School of Medicine, Atlanta, GA, United States, <sup>4</sup> Department of Global Health, Rollins School of Public Health, Emory University, Atlanta, GA, United States, <sup>5</sup> James J. Peters VA Medical Center, Bronx, NY, United States, <sup>6</sup> Department of Medicine, Icahn School of Medicine at Mount Sinai, New York, NY, United States, <sup>7</sup> Michael E. DeBakey VA Medical Center, Houston, TX, United States, <sup>8</sup> Department of Medicine, Baylor College of Medicine, Houston, TX, United States, <sup>9</sup> VA Greater Los Angeles Healthcare System, Los Angeles, CA, United States, <sup>10</sup> Department of Medicine, David Geffen School of Medicine at UCLA, Los Angeles, CA, United States, <sup>11</sup> VA Palo Alto Health Care System, Palo Alto, CA, United States, <sup>12</sup> Public Health Surveillance and Research, Department of Veterans Affairs, Washington, DC, United States, <sup>13</sup> Department of Medicine, Stanford University, Stanford, CA, United States

**Introduction:** Early in the COVID-19 pandemic, the Centers for Disease Control and Prevention (CDC) rapidly initiated COVID-19 surveillance by leveraging existing hospital networks to assess disease burden among hospitalized inpatients and inform prevention efforts.

**Materials and Methods:** The Surveillance Platform for Enteric and Respiratory Infectious Organisms at Veterans Affairs Medical Centers (SUPERNOVA) is a network of five United States Veterans Affairs Medical Centers which serves nearly 400,000 Veterans annually and conducts laboratory-based passive and active monitoring for pathogens associated with acute gastroenteritis and acute respiratory illness among hospitalized Veterans. This paper presents surveillance methods for adapting the SUPERNOVA surveillance platform to prospectively evaluate COVID-19 epidemiology during a public health emergency, including detecting, characterizing, and monitoring patients with and without COVID-19 beginning in March 2020. To allow for case-control analyses, patients with COVID-19 and patients with non-COVID-19 acute respiratory illness were included.

**Results:** SUPERNOVA included 1,235 participants with COVID-19 and 707 participants with other acute respiratory illnesses hospitalized during February through December 2020. Most participants were male (93.1%), with a median age of 70 years, and 45.8% non-Hispanic Black and 32.6% non-Hispanic White. Among those with COVID-19,



28.2% were transferred to an intensive care unit, 9.4% received invasive mechanical ventilation, and 13.9% died. Compared with controls, after adjusting for age, sex, and race/ethnicity, COVID-19 case-patients had significantly higher risk of mortality, respiratory failure, and invasive mechanical ventilation, and longer hospital stays.

**Discussion:** Strengths of the SUPERNOVA platform for COVID-19 surveillance include the ability to collect and integrate multiple types of data, including clinical and illness outcome information, and SARS-CoV-2 laboratory test results from respiratory and serum specimens. Analysis of data from this platform also enables formal comparisons of participants with and without COVID-19. Surveillance data collected during a public health emergency from this key U.S. population of Veterans will be useful for epidemiologic investigations of COVID-19 spectrum of disease, underlying medical conditions, virus variants, and vaccine effectiveness, according to public health priorities and needs.

**Keywords:** surveillance, public health, COVID-19, Veterans health, epidemiology, research methods

## INTRODUCTION

In response to the emergence of a novel coronavirus, severe acute respiratory syndrome coronavirus 2 (SARS-CoV-2), the Centers for Disease Control and Prevention (CDC) activated its Emergency Operations Center on January 21, 2020, to offer operational support and public health expertise (1). By February 2020, CDC had initiated COVID-19 surveillance by leveraging existing systems, including the Surveillance Platform for Enteric and Respiratory Infectious Organisms at the VA (SUPERNOVA). SUPERNOVA is a network of VA Medical Centers (VAMC) conducting laboratory-based passive and active monitoring for pathogens associated with acute gastroenteritis and acute respiratory illness among hospitalized adult Veterans in the United States.

Over 9 million Veterans—people who have served as military, naval, air, and other uniformed service members in the United States—currently receive health care from the Veterans Health Administration of the Department of Veterans Affairs (VA), an integrated health care delivery network providing comprehensive health services to eligible Veterans through medical centers and community-based outpatient clinics across the United States (2, 3). Within the VA network, sites use a comprehensive electronic health record system, Veterans Health Information Systems and Technology Architecture (VistA), and Computerized Patient Record System (CPRS), with existing functionalities that support data collection for clinical and research purposes (4). Patients served by the VA are predominantly male (88%), older, and with a higher illness burden compared to civilians (5, 6). Veterans who are of Black/African-American race or Hispanic ethnicity may seek care within the VA system more commonly than Veterans of other racial/ethnic groups (7).

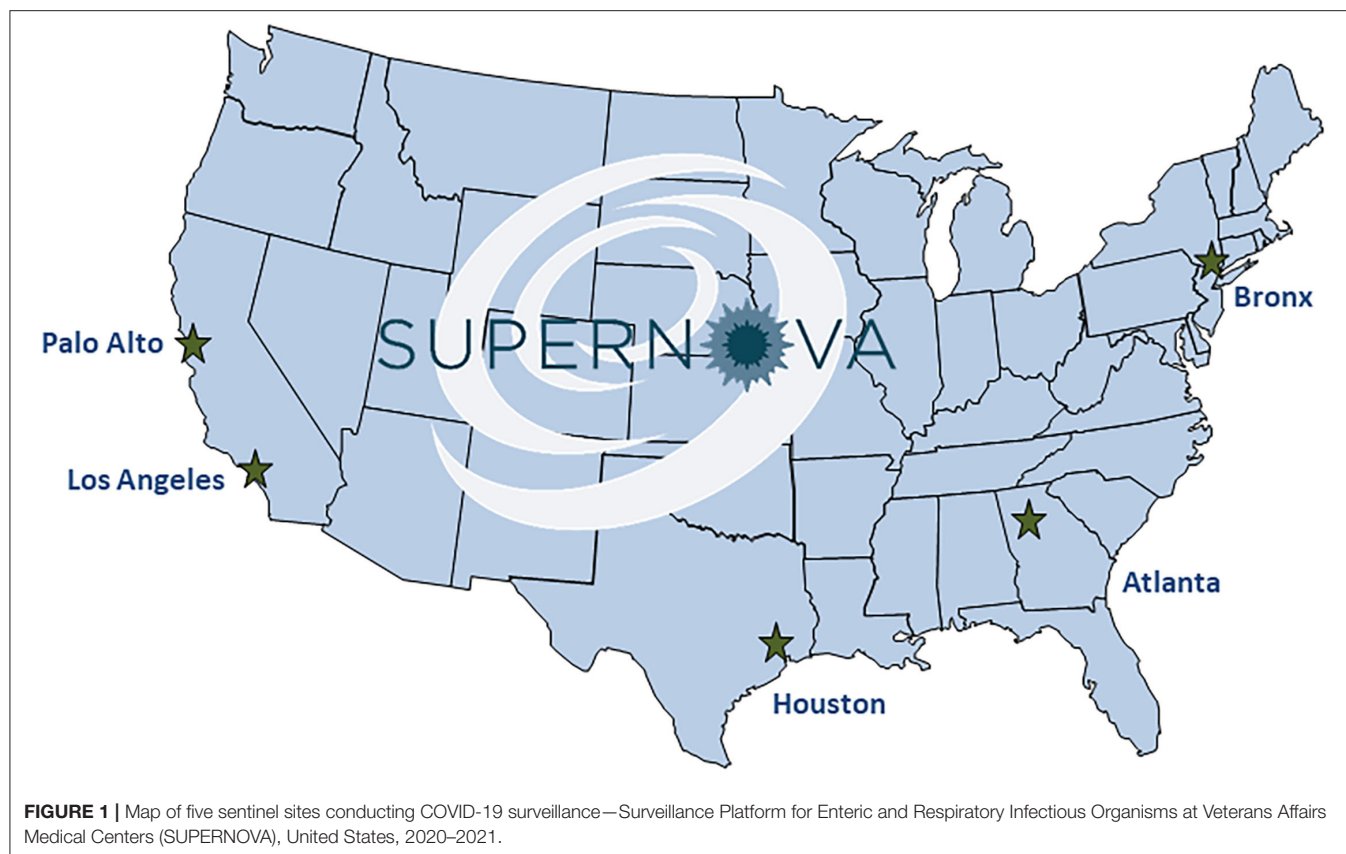
Data from Veterans can provide key insights into the impact of COVID-19 in the United States. During the COVID-19 pandemic, people who are male, aged >65 years, or of Black

race were identified as being disproportionately affected by severe illness caused by SARS-CoV-2 infection, (8, 9) supporting the importance of studying this novel disease among VA patients. In addition, certain underlying medical conditions common among Veterans such as chronic lung diseases, diabetes, and heart conditions (5), are known to increase the risk of severe COVID-19 illness (10). Early COVID-19 research using large national datasets from hospitalized U.S. Veterans have noted increased risk for in-hospital complications with COVID-19 compared to influenza (11); identified associations between excess burden of COVID-19 and race/ethnicity (12); evaluated risk factors for hospitalization, mechanical ventilation, or death (13); assessed critical care strain (14); and described readmissions and deaths within 60 days after initial hospital discharge (15).

Although disease dynamics among VA patients are not necessarily comparable to those among members of the general U.S. population, examination of populations at increased risk for severe disease is relevant to understanding the full range of COVID-19 effects. Prospective surveillance at sentinel sites, as in SUPERNOVA, while not nationally representative, allows for collection of granular data, such as results of laboratory testing on clinical specimens, that can be challenging to capture in larger analyses of administrative data. In this paper, we present surveillance methods for adapting the SUPERNOVA surveillance platform to prospectively evaluate COVID-19 epidemiology during a public health emergency, including detecting, characterizing, and monitoring patients with and without COVID-19.

## MATERIALS AND METHODS

SUPERNOVA is a sentinel network of five participating VAMCs located in four U.S. states (**Figure 1**), collectively serving an estimated patient population of 400,000 Veterans



annually (Table 1). Surveillance is conducted among Veterans aged  $\geq 18$  years who seek care at a participating VAMC.

### Surveillance for Acute Gastroenteritis and Acute Respiratory Illness

Before 2020, primary objectives for the SUPERNOVA network included surveillance to estimate the incidence of norovirus and other causes of acute gastroenteritis in inpatient and outpatient settings, and active and passive surveillance to determine the inpatient burden of adult respiratory syncytial virus, influenza viruses, and other viruses that cause acute respiratory illness (Figure 2). Acute gastroenteritis surveillance using stool specimens ordered for clinician-directed diagnostic testing began at four sites in 2011, and expanded in 2015 to include medical chart review and collection of saliva and serum specimens, with a fifth site (Palo Alto) added in 2017 (16, 17). Acute respiratory illness surveillance with laboratory confirmation began as a pilot at one site (Houston) in 2016, with a second site (Los Angeles) added in 2017. Acute respiratory illness surveillance included: (1) identification of patients who had been admitted with a diagnosis consistent with acute respiratory illness and/or had received clinician-ordered viral respiratory diagnostic testing; (2) medical record reviews and chart abstractions to obtain demographic and clinical information including clinical course; and (3) collection of residual respiratory and serum specimens (18). By 2019–2020, surveillance for acute gastroenteritis and acute respiratory illness was including  $\sim 900$  and  $\sim 1,600$  patients, respectively.

### Adaptation for COVID-19 Surveillance

Beginning in March 2020, SUPERNOVA shifted focus to expand acute respiratory illness surveillance to prospective inpatient surveillance with a focus on COVID-19 at all five participating VAMC sites, while pausing surveillance for acute gastroenteritis. Objectives included understanding characteristics of patients with COVID-19 and the spectrum of disease severity, COVID-19 hospitalization rates, underlying medical conditions that increase risk of severe outcomes, virus variants, immune responses, multisystem inflammatory syndrome in adults, and health care use among patients with COVID-19. Additionally, given inclusion of case and control groups, this surveillance platform was positioned to assess COVID-19 vaccine effectiveness among hospitalized Veterans.

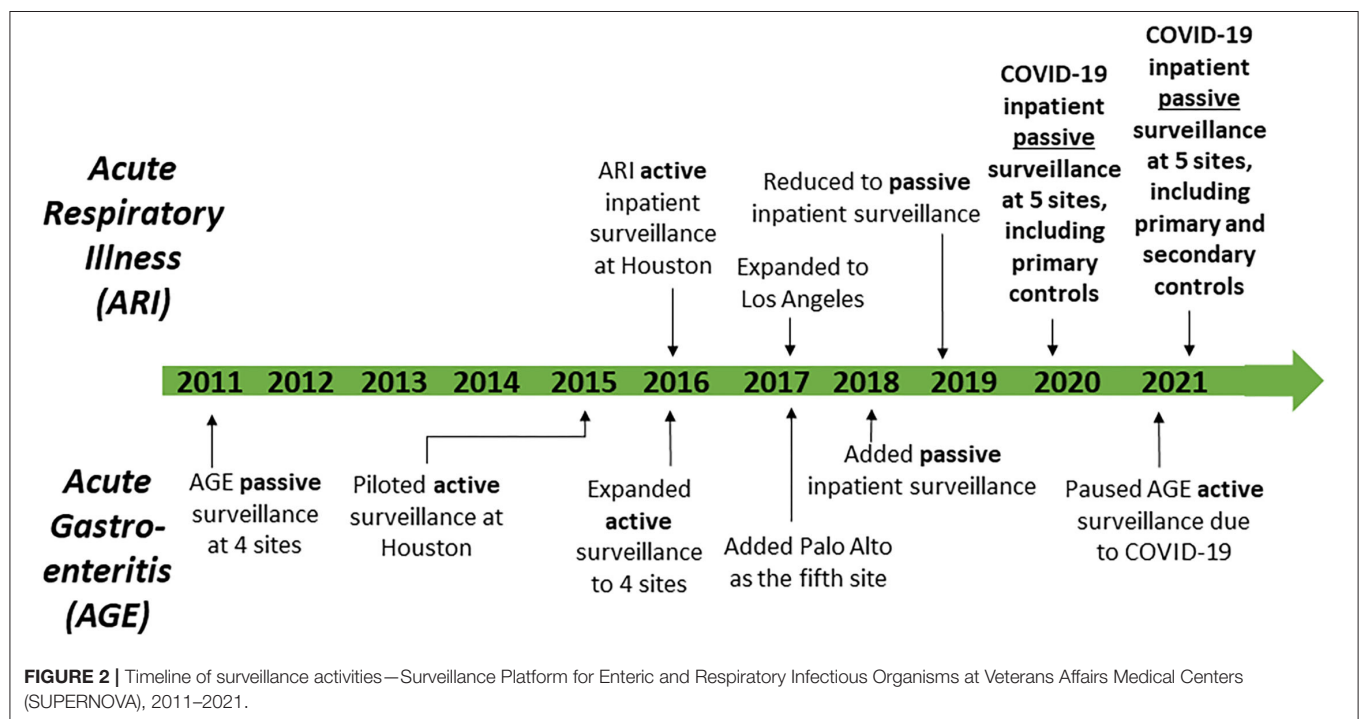
### Identification of Patients With and Without COVID-19

Beginning in February 2020, clinician-directed testing and then universal inpatient screening at hospital admission for SARS-CoV-2 were implemented at the five VAMC sites. Patients with COVID-19 (i.e., cases) were eligible for inclusion in SUPERNOVA if they had a positive molecular SARS-CoV-2 test result within the first 72 hours of hospitalization (Figure 3). Cases were considered symptomatic if they had  $\geq 1$  COVID-19-like signs or symptoms documented in their medical records (e.g., admission

**TABLE 1** | Selected characteristics of participating sentinel sites—Surveillance Platform for Enteric and Respiratory Infectious Organisms at Veterans Affairs Medical Centers (SUPERNOVA).

| Site name and location   | Size     | Description   | Estimated population served annually                                      |
|--|----------|---|---|
| Atlanta VA Medical Center,<br><b>Atlanta, GA, USA</b>                | 405 beds | Tertiary care facility (teaching hospital) with 273 hospital beds, CLC with 120 beds, Psychosocial Rehabilitation Treatment Program with 12 beds; seven CBOCs | 120,000 Veterans in northeastern Georgia (GA)                             |
| James J. Peters VA Medical Center,<br><b>Bronx, NY, USA</b>          | 431 beds | Tertiary care facility (teaching hospital) with 311 hospital beds, CLC with 120 beds; three CBOCs   | 24,000 Veterans in the New York City metropolitan region in New York (NY) |
| Michael E. DeBakey VA Medical Center,<br><b>Houston, TX, USA</b>     | 531 beds | Tertiary care facility (teaching hospital) with 350 acute care beds, Spinal Cord Injury Center with 40 beds, CLC with 141 beds; 10 CBOCs                      | 113,000 Veterans in southeastern Texas (TX)                               |
| VA Greater Los Angeles Health System,<br><b>Los Angeles, CA, USA</b> | 945 beds | Tertiary care facility (teaching hospital), CLC, community care center for homeless Veterans; eight CBOCs   | 82,000 Veterans in southern California (CA)                               |
| VA Palo Alto Health Care System,<br><b>Palo Alto, CA, USA</b>        | 800 beds | Three tertiary care facilities (teaching hospital), homeless domiciliary with 100 beds, three CLCs; seven CBOCs   | 67,000 Veterans in northern California (CA)                               |

Community Living Centers (CLCs) provide extended care rehabilitation and general long-term care; Community-Based Outpatient Clinics (CBOCs) include outpatient primary care.

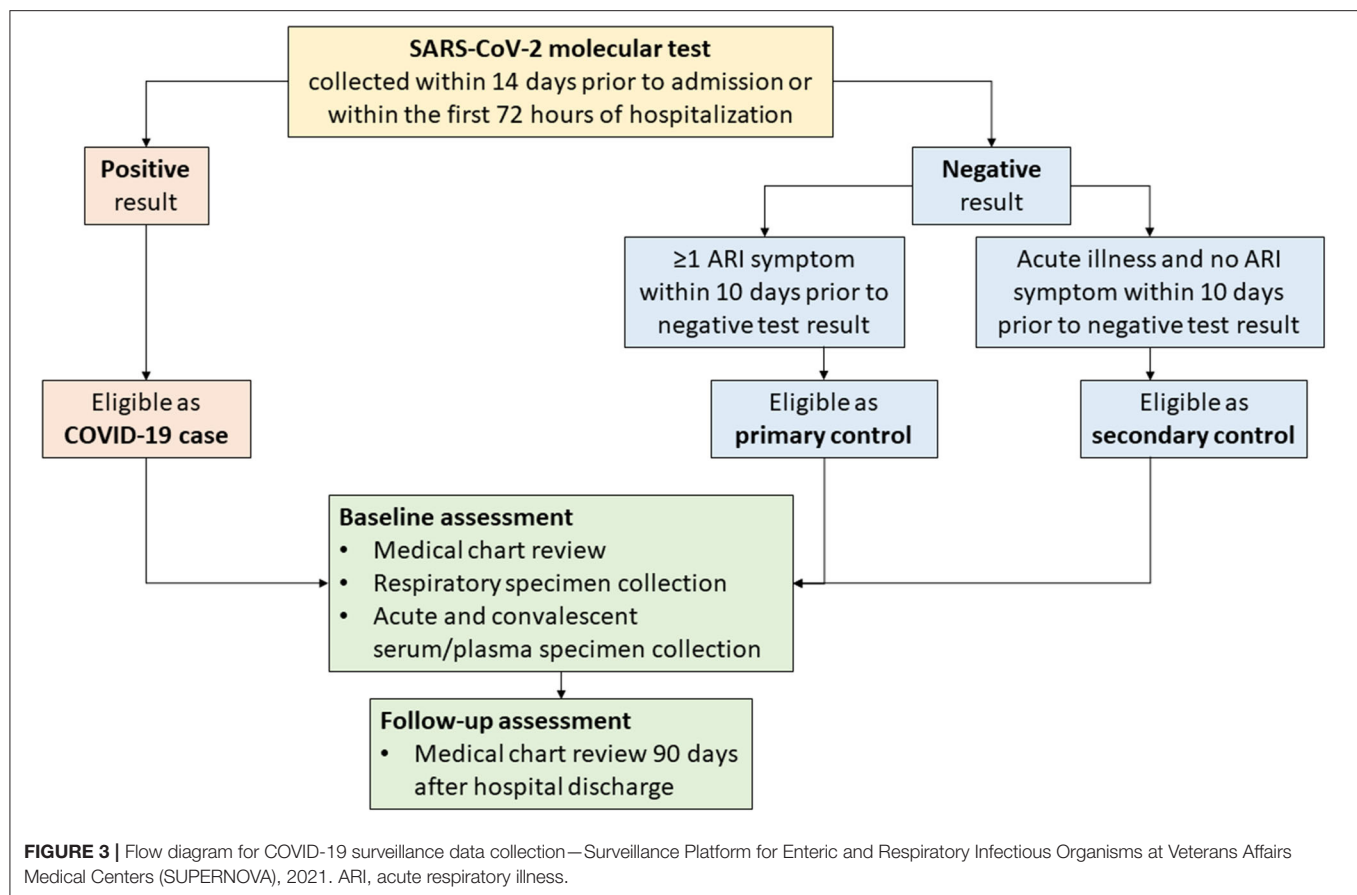


history and physical examination, or emergency department note)<sup>1</sup>.

To allow for case-control analyses, for each case, 1–2 inpatients without COVID-19 (i.e., controls) were targeted

<sup>1</sup>COVID-19-like signs or symptoms included fever, new or worsened cough, new or worsened shortness of breath, loss of taste or smell, increased sputum production, SpO<sub>2</sub> on room air <94%, invasive or non-invasive ventilation requirement, and pulmonary findings on chest imaging consistent with pneumonia.

for inclusion in SUPERNOVA (Figure 3). In keeping with existing surveillance procedures for acute respiratory illness within SUPERNOVA, controls were identified from among other patients with respiratory symptoms. Patients were eligible for inclusion as a non-COVID-19 control if they had both a negative SARS-CoV-2 molecular test result (reverse transcription-polymerase chain reaction [RT-PCR] or isothermal nucleic acid amplification test [NAAT]) within 14 days prior to admission or within the first 72 hours of hospitalization,



and, if they presented with  $\geq 1$  respiratory symptom<sup>2</sup> (primary controls) at admission. An additional set of controls without respiratory symptoms was included beginning in early 2021. Secondary controls, defined as persons admitted for a non-respiratory acute illness (e.g., chest pain, hypotension) with a negative test result for SARS-CoV-2 and without respiratory symptoms, were also included. Primary or secondary controls who later had a positive SARS-CoV-2 antigen or molecular test result during hospitalization would become ineligible as controls; however, controls could have a positive test result for a different pathogen (e.g., influenza). To ensure similar participation dates, controls were identified daily according to hospital admission dates falling within 1–14 days of COVID-19 case admission dates.

## Medical Record Review

VAMC electronic health records (EHR) of participants with and without COVID-19 were reviewed. Using standardized case report forms, information was collected on patient demographic and clinical characteristics, including SARS-CoV-2 and other viral pathogen test results; history of vaccination against COVID-19 (including state immunization registry data, where available), influenza, and pneumococcal disease; history of present illness and clinical presentation with vital

signs and laboratory values upon admission; past medical history including underlying medical conditions; imaging and interventions including intensive care unit admission and mechanical ventilation; treatments provided during hospitalization (e.g., anti-inflammatory agents, anticoagulants, antivirals, vasopressors, hemodialysis, and other therapies); hospital complications and discharge diagnoses using ICD-10 codes; advance directive code status, and disposition (including deaths). Medical records of both cases and controls were reviewed again 90 days after hospital discharge to assess outcomes including clinical and functional status, and additional health care use.

## Clinical Specimens

Residual clinical respiratory swab specimens and serum or plasma specimens were collected from both COVID-19 case-patients and controls where possible. Residual respiratory specimens were stored at  $-70^{\circ}\text{C}$  before shipment to CDC for testing using CDC's 2019-Novel Coronavirus Real-Time RT-PCR Diagnostic Panel (19). Residual serum or plasma specimens (1–2 mL) were retrieved after clinically indicated testing was completed, divided into aliquots (minimum 250 microliters each) and frozen at  $<-20^{\circ}\text{C}$  for further testing. Available laboratory testing at CDC included testing for SARS-CoV-2 antibodies, molecular diagnostics for select respiratory pathogens, or SARS-CoV-2 whole genome sequencing of respiratory specimens with

<sup>2</sup>Symptoms of acute respiratory illness included fever, chills, cough, shortness of breath, sinus congestion/runny nose, or sore throat.



qualifying cycle threshold values. Specimens with a Ct value <33 were submitted for sequencing, and those with genome coverage >90% had a confirmed lineage reported. Results of research-use only laboratory tests were not expected to be provided to VAMC patients or their clinicians.

## Institutional Review and Consent

Modified protocols were reviewed and approved by the VAMC Research and Development Committee and institutional review boards for each of the five sites; in addition, the activity was reviewed by CDC and conducted consistent with applicable federal law and policy<sup>3</sup>. Sites tailored a generic consent form to provide their site-specific information and include necessary authorizations for release of medical records, for clinical specimen collection, and for potential future testing.

## Data Management

Standardized case report forms and data dictionaries were developed and used across all participating sites. Data were entered into a standardized surveillance database in REDCap, a secure web application for building and managing online surveys and databases designed to comply with Health Insurance Portability and Accountability Act (HIPAA) regulations (20, 21). Original participant medical records located at the participating sites were linked to surveillance data solely through sequentially assigned participant identification numbers. Local data were stored behind secure institutional firewalls. Following federal data handling requirements, data were transferred to CDC using participant identification numbers; personally identifiable information, such as patient name or medical record number, was not shared with CDC or other sites.

## Data Analysis

In addition to simple descriptive analyses of data from COVID-19 cases, including median and interquartile range (IQR), formal statistical comparisons of data from cases and controls may be performed to estimate pathogen-specific relative risk of disease progression and mortality. For example, to estimate the effects of underlying medical conditions on adverse clinical outcomes including mortality, respiratory failure, mechanical ventilation, intensive care unit (ICU) admission, and length of hospital stay, we calculated adjusted risk ratios (aRR) and 95% confidence intervals (CI) for these outcomes among participants with and without COVID-19 hospitalized from February 23–October 31, 2020.

## RESULTS

Initial results from the adapted SUPERNOVA platform have been useful to demonstrate characteristics of adults hospitalized with COVID-19 and the spectrum of disease severity, clarify COVID-19 hospitalization rates among Veterans, and understand underlying medical conditions that increase

**TABLE 2 |** Characteristics of Veterans hospitalized with and without COVID-19—Surveillance Platform for Enteric and Respiratory Infectious Organisms at Veterans Affairs Medical Centers (SUPERNOVA), February–December 2020.

|                                  | Veterans<br>hospitalized with<br>COVID-19<br>(cases)<br><i>n</i> (%) | Veterans<br>hospitalized without<br>COVID-19<br>(primary controls)*<br><i>n</i> (%) |
|----------------------------------|--|---|
| <b>Total</b>                     | 1,235  | 707   |
| <b>City</b>                      |  |   |
| Atlanta, GA, USA                 | 296 (24.0)   | 179 (25.3)  |
| Bronx, NY, USA                   | 220 (17.8)   | 101 (14.3)  |
| Houston, TX, USA                 | 285 (23.1)   | 194 (27.4)  |
| Los Angeles, CA, USA             | 377 (30.5)   | 171 (24.2)  |
| Palo Alto, CA, USA               | 57 (4.6)   | 62 (8.8)  |
| <b>Median age</b> in years (IQR) | 70 (59, 76)  | 69 (61, 75)   |
| <b>Sex</b>                       |  |   |
| Male                             | 1,153 (93.4)   | 656 (92.8)  |
| Female                           | 82 (6.6)   | 51 (7.2)  |
| <b>Race/ethnicity</b>            |  |   |
| Non-Hispanic Black               | 585 (47.4)   | 304 (43.0)  |
| Non-Hispanic White               | 359 (29.1)   | 275 (38.9)  |
| Hispanic or Latino               | 200 (16.2)   | 75 (10.6)   |
| Asian                            | 16 (1.3)   | 5 (0.7)   |
| Native Hawaiian/Pacific Islander | 10 (0.8)   | 7 (1.0)   |
| American Indian/Alaskan Native   | 8 (0.7)  | 3 (0.4)   |
| All other races**                | 57 (4.6)   | 38 (5.4)  |

IQR, interquartile range.

\*Primary controls had both a negative SARS-CoV-2 molecular test result and ≥1 acute respiratory infection (ARI) symptom.

\*\*Includes multiple races (*n* = 3) and unknown race and/or ethnicity (*n* = 54).

risk of severe outcomes from COVID-19. As of March 4, 2021, SUPERNOVA included 1,235 patients with COVID-19 (COVID-19 cases) and 707 patients with other acute respiratory illnesses (primary controls) admitted to one of the five participating VAMC sites from February 23 through December 31, 2020. Overall, SUPERNOVA participants were predominantly male (93.1%), of non-Hispanic Black (45.8%) or non-Hispanic White (32.6%) race/ethnicity, and older, with a median age of 70 years (Table 2). Among 1,177 COVID-19 cases with available information about their hospitalization, many were severely ill: 332/1,177 (28.2%) were transferred to an intensive care unit (ICU); 107/1,137 (9.4%) received invasive mechanical ventilation; and 158/1,134 (13.9%) died while hospitalized.

To assess disparities in COVID-19 hospitalization rates by race/ethnicity, case data from SUPERNOVA were analyzed rapidly early in the pandemic. Among the first 621 laboratory-confirmed, hospitalized COVID-19 cases participating in SUPERNOVA, hospitalization rates were highest among Veterans aged ≥85 years (430 per 100,000), of Hispanic or Latino ethnicity (317 per 100,000), and of non-Hispanic Black race (298 per 100,000). Additionally, Veterans aged ≥65 years had a 4.5-fold increased risk of death compared with younger

<sup>3</sup>See e.g., 45 C.F.R. part 46.102(l) (2), 21 C.F.R. part 56; 42 U.S.C. §241(d); 5 U.S.C. §552a; 44 U.S.C. §3501 et seq.



Veterans (95% confidence interval: 2.4–8.6). A short report on these findings highlighted the need for targeted prevention and timely treatment of COVID-19, particularly for older adults (22).

To enhance the evidence base for underlying medical conditions including those with limited evidence to date, we conducted an interim analysis of SUPERNOVA data on comorbidities among COVID-19 cases and controls for outcomes indicating more severe COVID-19 illness. Among 1,254 symptomatic participants through October 2020, including 786 with COVID-19 and 468 without COVID-19, a high prevalence of underlying medical conditions was documented among all participants; median number of underlying medical conditions was four (IQR 2–6) and five (IQR 3–7) among participants with and without COVID-19, respectively. The most common underlying medical conditions among all participants were hypertension (71.4%), cardiovascular disease (53.7%), diabetes mellitus (45.3%), and chronic non-asthmatic lung disease (41.0%). Compared with controls, after adjusting for age, sex, and race/ethnicity, COVID-19 case-patients had significantly higher risk of mortality, respiratory failure, and invasive mechanical ventilation, and longer hospital stays; 11 categories of underlying medical conditions increased risk for at least one of these outcomes: cancer, recent chemotherapy, cerebrovascular disease, chronic kidney disease, chronic non-asthmatic lung disease, cardiovascular disease, smoking, and diabetes mellitus (data not shown). Risk of death was more than three times higher among participants with COVID-19 (18.1%) compared to those without COVID-19 (6.8%) (aRR 3.07 [95% CI: 2.13, 4.41]).

## DISCUSSION

Data from the SUPERNOVA platform enhance COVID-19 surveillance among hospitalized Veterans and are useful to describe the burden and natural history of COVID-19 in this key population. The SUPERNOVA population includes many males, older adults, racial and ethnic minority groups, and people with chronic diseases and other underlying medical conditions, who thus may be disproportionately affected by severe COVID-19 disease outcomes. Strengths of the SUPERNOVA platform for COVID-19 surveillance include the ability to collect and integrate multiple types of data, including clinical and illness outcome information, and laboratory test results from respiratory and serum specimens, with formal comparison between cases and controls with similar hospitalization dates. Furthermore, patients can be followed longitudinally over time. SUPERNOVA data will be useful to address several additional scientific questions related to COVID-19.

### COVID-19 Vaccine Effectiveness

Vaccine effectiveness (VE) against COVID-19 hospitalization among Veterans may be estimated using data obtained from this surveillance system by comparing vaccination status between hospitalized adults with and without laboratory-confirmed SARS-CoV-2 infection. Using a modified, prospective, test-negative case-control design (23, 24) to identify COVID-19 cases and controls with COVID-like signs or symptoms identified

through passive and active surveillance, VE can be calculated using multivariable logistic regression with case status as the outcome and vaccination status as the main predictor, adjusting for potential confounders (e.g., site, age, sex, race/ethnicity, and underlying health status), where estimated  $VE = (1 - \text{adjusted odds ratio}^4) \times 100$  (25). To address potential misclassification of controls, VE estimates will be calculated using both primary and secondary controls. SUPERNOVA is one of several surveillance platforms CDC is using to assess effectiveness of COVID-19 vaccines in various populations (26). SUPERNOVA data can be used to evaluate effectiveness of full or partial vaccination against COVID-19 as well as specific vaccine products, reflecting real-world use. Data from SUPERNOVA showed that, during February 1–August 6, 2021, VE of mRNA COVID-19 vaccines against COVID-19 hospitalization was 80% among adults aged  $\geq 65$  years compared with 95% among adults aged 18–64 years (27).

### Virus Variants

Genomic sequencing of specimens collected in SUPERNOVA may be used to identify emergence of novel respiratory pathogens such as SARS-CoV-2 variants, which are a cause of concern due to their potential to exacerbate the trajectory of the COVID-19 pandemic (28). Monitoring for variants, particularly among VA patients with multiple hospital admissions for COVID-19, may provide evidence regarding disease severity, potential reinfections, and variant influence on countermeasures including diagnostics, therapeutics, and vaccines. Among SUPERNOVA participants, Delta became the predominant SARS-CoV-2 variant in July 2021 (27).

### Immune Responses

SUPERNOVA data may be able to address whether antibodies to SARS-CoV-2 or other common coronaviruses might modulate COVID-19 illness severity, using serum representing a spectrum of disease from adults hospitalized with COVID-19.

### Multisystem Inflammatory Syndrome in Adults

Case series have been reported of Multisystem inflammatory syndrome in adults (MIS-A) associated with SARS-CoV-2 infection (29). Data on laboratory values and imaging studies from SUPERNOVA may be used to identify possible cases of MIS-A to target these cases for additional chart review and follow-up.

### Health Care Use

COVID-19 can result in late sequelae and prolonged illness (“long COVID,” or post-acute sequelae of SARS-CoV-2 infection), but relatively little is known about typical clinical course and health care use following hospital discharge for COVID-19 (30). SUPERNOVA data, which include information on disposition and health care use through at least 90 days

<sup>4</sup>Odds ratio for case status among vaccinated persons compared with unvaccinated persons.

following initial hospital discharge for both COVID-19 cases and controls, might help fill this knowledge gap.

Limitations to this surveillance approach include the reliance on current policy of universal screening for SARS-CoV-2 infection of inpatients at the participating sites to identify cases and controls; if these policies were to change, misclassification of COVID-19 cases and controls might be more likely. In addition, timeliness of reporting varies by pandemic phase and site; during pandemic surges in COVID-19 cases at respective sites, adjustments included prioritizing identification of cases rather than controls, and implementing flexible or extended deadlines for data entry and submission to CDC. Furthermore, although a test-negative design for assessing VE minimizes differences by healthcare seeking behavior, other COVID-19 risk mitigation measures could be relevant. Addition of an interview component could help identify differential behaviors associated with COVID-19 acquisition or transmission between cases and controls, such as compliance with non-pharmaceutical interventions (e.g., mask-wearing, physical distancing) or known close contact with a person with COVID-19 in the 14 days preceding symptom onset.

## CONCLUSION

In this methods paper, we describe the adaptation of an existing five-site sentinel surveillance platform for acute gastroenteritis and acute respiratory illness to monitor COVID-19 among hospitalized adult Veterans in the United States. The SUPERNOVA surveillance platform, comprising passive and active surveillance and including medical record reviews and clinical specimen collection, pivoted to address new public health priorities during the COVID-19 pandemic. Plans include dissemination of results of ongoing data analyses to inform program and policy decisions with continued attention and responsiveness to public health emergency needs.

## DATA AVAILABILITY STATEMENT

The original contributions presented in the study are included in the article/supplementary material; further inquiries can be directed to the corresponding author.

## ETHICS STATEMENT

The studies involving human participants were reviewed and approved by VAMC Research and Development Committee and Institutional Review Boards for each of the five sites; in addition, the activity was reviewed by CDC and conducted consistent with applicable federal law and policy (see e.g., 45 C.F.R. part 46.102(l) (2), 21 C.F.R. part 56; 42 U.S.C. §241(d); 5 U.S.C. §552a; 44 U.S.C. §3501 et seq.). The patients/participants

provided their written informed consent to participate in this study.

## SUPERNOVA COVID-19 SURVEILLANCE GROUP

Ghazal Ahmadi-Izadi, LaSara Bell, Joy Burnette, Rijalda Deovic, Lauren Epstein, Amy Hartley, Elena Morales, Taressa Sergeant, Tehquin Tanner, and Alexis Whitmire: Atlanta VA Medical Center, Atlanta, GA, United States. Katherine Elliot, Ilda Graham, Diki Lama, Awilda Mero, Ismael Pena, Adrienne Perea, Guerry Anabelle Perez, Johane Simelane, Sarah Smith, Gabriela Tallin, and Amelia Tisi: James J. Peters VA Medical Center, Bronx, NY, United States. Alonso Arellano Lopez, Miguel Covarrubias Gonzalez, Rosalba Gomez Morones, Bashir Lengi, Dena Mansouri, Gilberto Rivera Dominguez, Mariana Vanoye Tamez, and Blanca Vargas. Michael E. DeBakey VA Medical Center, Houston, TX, United States. Babak Aryanfar, Ian Lee-Chang, Karen Evangelista, Matthew Goetz, Evan Goldin, Chan Jeong, Anthony Matolek, Chad Mendoza, and Aleksandra Poteskhina: VA Greater Los Angeles Healthcare System, Los Angeles, CA, United States. Madhuri Agrawal, Jessica Lopez, Jude Lopez, and Theresa Peters: VA Palo Alto Health Care System, Palo Alto, CA, United States. Meredith McMorrow, Steve L. Evener, Rebecca Dahl, Daoling Bi, Lindsay Kim, and Aron J. Hall: Centers for Disease Control and Prevention, Atlanta, GA, United States.

## AUTHOR CONTRIBUTIONS

MP, CC, JC, EM, KB, and DS designed the study and drafted the protocol. VM, SB, MR-B, DB, MH, and CL-O revised and approved the final protocol and oversaw data collection. AK, MP, JC, EM, KB, and DS managed and analyzed the data. All authors contributed to the manuscript and approved the submitted version.

## FUNDING

This study was funded by the Centers for Disease Control and Prevention *via* a contract with the Foundation for Atlanta Veterans Education and Research, Inc. (contract number 75D30119C04211).

## ACKNOWLEDGMENTS

The authors thank the CDC COVID-19 Response Epidemiology & Surveillance Task Force, including Neha Balachandran, Mathew Esona, Fiona Havers, Miwako Kobayashi, Adam MacNeil, Sara Mirza, Umesh Parashar, Natalie Thornburg, Suxiang Tong, Chris Van Beneden, and Jennifer Verani for their expert advice and support of this work.

## REFERENCES

- Patel A, Jernigan DB, 2019-nCoV CDC Response Team. Initial public health response and interim clinical guidance for the 2019 novel coronavirus outbreak - United States, December 31, 2019-February 4, 2020. *MMWR Morb Mortal Wkly Rep.* (2020) 69:140–6. doi: 10.15585/mmwr.mm6908e1
- Veterans Health Administration. U.S. Department of Veterans Affairs. Available online at: <https://www.va.gov/health> (accessed March 30, 2021).
- Bagalman E. *The Number of Veterans That Use VA Health Care Services: A Fact Sheet*. Congressional Research Service, Contract No.: R43579 (2014).
- D'Avolio L, Ferguson R, Goryachev S, Woods P, Sabin T, O'Neil J, et al. Implementation of the Department of Veterans Affairs' first point-of-care clinical trial. *J Am Med Assoc.* (2012) 19:e170–e6. doi: 10.1136/amiajnl-2011-000623
- Rogers WH, Kazis LE, Miller DR, Skinner KM, Clark JA, Spiro A, et al. Comparing the health status of VA and non-VA ambulatory patients: the veterans' health and medical outcomes studies. *J Ambul Care Manage.* (2004) 27:249–62. doi: 10.1097/00004479-200407000-00009
- U.S. Department of Veterans Affairs. *Analysis of VA Health Care Utilization among Operation Enduring Freedom (OEF), Operation Iraqi Freedom (OIF), and Operation New Dawn (OND) Veterans* (2017).
- National Center for Veterans Analysis Statistics, U.S. Department of Veterans Affairs. VA Utilization Profile FY (2016). Available online at: [https://www.va.gov/vetdata/docs/QuickFacts/VA\\_Utilization\\_Profile.PDF](https://www.va.gov/vetdata/docs/QuickFacts/VA_Utilization_Profile.PDF) (accessed March 30, 2021).
- Garg S, Kim L, Whitaker M, O'Halloran A, Cummings C, Holstein R, et al. Hospitalization rates and characteristics of patients hospitalized with laboratory-confirmed coronavirus disease 2019 - COVID-NET, 14 States, March 1–30, 2020. *MMWR Morb Mortal Wkly Rep.* (2020) 69:458–64. doi: 10.15585/mmwr.mm6915e3
- Wu Z, McGoogan JM. Characteristics of and important lessons from the coronavirus disease 2019 (COVID-19) outbreak in China: summary of a report of 72314 cases from the Chinese Center for Disease Control and Prevention. *JAMA.* (2020) 323:1239–42. doi: 10.1001/jama.2020.2648
- Centers for Disease Control and Prevention, U.S. Department of Health and Human Services. *People at Increased Risk*. Available online at: <https://www.cdc.gov/coronavirus/2019-ncov/need-extra-precautions> (accessed April 28, 2021).
- Cates J, Lucero-Obusan C, Dahl RM, Schirmer P, Garg S, Oda G, et al. Risk for in-hospital complications associated with COVID-19 and influenza - Veterans Health Administration, United States, October 1, 2018–May 31 2020. *MMWR Morb Mortal Wkly Rep.* (2020) 69:1528–34. doi: 10.15585/mmwr.mm6942e3
- Rentsch CT, Kidwai-Khan F, Tate JP, Park LS, King JT Jr, Skanderson M, et al. Patterns of COVID-19 testing and mortality by race and ethnicity among United States veterans: a nationwide cohort study. *PLoS Med.* (2020) 17:e1003379. doi: 10.1371/journal.pmed.1003379
- Ioannou GN, Locke E, Green P, Berry K, O'Hare AM, Shah JA, et al. Risk Factors for hospitalization, mechanical ventilation, or death among 10131 US Veterans with SARS-CoV-2 infection. *JAMA Netw Open.* (2020) 3:e2022310. doi: 10.1001/jamanetworkopen.2020.22310
- Bravata DM, Perkins AJ, Myers LJ, Arling G, Zhang Y, Zillich AJ, et al. Association of intensive care unit patient load and demand with mortality rates in US Department of Veterans Affairs Hospitals during the COVID-19 pandemic. *JAMA Netw Open.* (2021) 4:e2034266. doi: 10.1001/jamanetworkopen.2020.34266
- Donnelly JP, Wang XQ, Iwashyna TJ, Prescott HC. Readmission and death after initial hospital discharge among patients with COVID-19 in a large multihospital system. *JAMA.* (2021) 325:304–6. doi: 10.1001/jama.2020.21465
- Grytdal S, Browne H, Collins N, Vargas B, Rodriguez-Barradas MC, Rimland D, et al. Trends in incidence of norovirus-associated acute gastroenteritis in 4 Veterans Affairs Medical Center Populations in the United States, 2011–2015. *Clin Infect Dis.* (2020) 70:40–8. doi: 10.1093/cid/ciz165
- Kambhampati AK, Vargas B, Mushtaq M, Browne H, Grytdal S, Atmar RL, et al. Active surveillance for norovirus in a US Veterans Affairs Patient Population, Houston, Texas, 2015–2016. *Open Forum Infect Dis.* (2019) 6:ofz115. doi: 10.1093/ofid/ofz115
- Cardemil CV, Balachandran N, Kambhampati A, Grytdal S, Dahl RM, Rodriguez-Barradas MC, et al. Incidence, etiology, and severity of acute gastroenteritis among prospectively enrolled patients in 4 Veterans Affairs hospitals and outpatient centers, 2016–18. *Clin Infect Dis.* (2021). doi: 10.1093/cid/ciaa806. [Epub ahead of print].
- Centers for Disease Control and Prevention. *CDC 2019–Novel Coronavirus (2019-nCoV) Real-Time RT-PCR Diagnostic Panel: for Emergency Use Only*. CDC-006-00019, Revision: 07. Available online at: <https://www.fda.gov/media/134922/download> (accessed July 21, 2021).
- Harris PA, Taylor R, Thielke R, Payne J, Gonzalez N, Conde JG. Research electronic data capture (REDCap)—a metadata-driven methodology and workflow process for providing translational research informatics support. *J Biomed Inform.* (2009) 42:377–81. doi: 10.1016/j.jbi.2008.08.010
- Harris PA, Taylor R, Minor BL, Elliott V, Fernandez M, O'Neal L, et al. The REDCap consortium: building an international community of software platform partners. *J Biomed Inform.* (2019) 95:103208. doi: 10.1016/j.jbi.2019.103208
- Cardemil CV, Dahl R, Prill MM, Cates J, Brown S, Perea A, et al. COVID-19-related hospitalization rates and severe outcomes among Veterans from 5 Veterans Affairs Medical Centers: Hospital-Based Surveillance Study. *JMIR Public Health Surveill.* (2021) 7:e24502. doi: 10.2196/24502
- Foppa IM, Haber M, Ferdinands JM, Shay DK. The case test-negative design for studies of the effectiveness of influenza vaccine. *Vaccine.* (2013) 31:3104–9. doi: 10.1016/j.vaccine.2013.04.026
- Chua H, Feng S, Lewnard JA, Sullivan SG, Blyth CC, Lipsitch M, et al. The use of test-negative controls to monitor vaccine effectiveness: a systematic review of methodology. *Epidemiology.* (2020) 31:43–64. doi: 10.1097/EDE.0000000000001116
- World Health Organization. *Evaluation of COVID-19 Vaccine Effectiveness*. Interim Guidance. Geneva: World Health Organization (2021). p. 1–70.
- Centers for Disease Control Prevention, U.S. Department of Health and Human Services. *COVID-19 Vaccine Effectiveness Research*. Available online at: <https://www.cdc.gov/vaccines/covid-19/effectiveness-research/protocols.html> (accessed March 30, 2021).
- Bajema KL, Dahl RM, Prill MP, Meites E, Rodriguez-Barradas MC, Marconi VC, et al. Effectiveness of COVID-19 mRNA vaccines against COVID-19-associated hospitalization - Five Veterans Affairs Medical Centers, United States, February 1–August 6, 2021. *MMWR.* (2021) 70:1294–9. doi: 10.15585/mmwr.mm7037e3
- Walensky RP, Walke HT, Fauci AS. SARS-CoV-2 variants of concern in the United States—challenges and opportunities. *JAMA.* (2021) 325:1037–8. doi: 10.1001/jama.2021.2294
- Morris SB, Schwartz NG, Patel P, Abbo L, Beauchamps L, Balan S, et al. Case series of multisystem inflammatory syndrome in adults associated with SARS-CoV-2 infection - United Kingdom and United States, March–August 2020. *MMWR Morb Mortal Wkly Rep.* (2020) 69:1450–6. doi: 10.15585/mmwr.mm6940e1
- Tenforde MW, Kim SS, Lindsell CJ, Billig Rose E, Shapiro NI, Files DC, et al. Symptom duration and risk factors for delayed return to usual health among outpatients with COVID-19 in a Multistate Health

Care Systems Network - United States, March-June 2020. *MMWR Morb Mortal Wkly Rep.* (2020) 69:993–8. doi: 10.15585/mmwr.mm6930e1

**Author Disclaimer:** The findings and conclusions in this report are those of the authors and do not necessarily represent the official position of the Centers for Disease Control and Prevention, Department of Veterans Affairs or United States Government.

**Conflict of Interest:** VM has received investigator-initiated research grants (to the institution) and consultation fees from Eli Lilly, Bayer, Gilead Sciences, and ViiV.

The remaining authors declare that the research was conducted in the absence of any commercial or financial relationships that could be construed as a potential conflict of interest.

**Publisher's Note:** All claims expressed in this article are solely those of the authors and do not necessarily represent those of their affiliated organizations, or those of the publisher, the editors and the reviewers. Any product that may be evaluated in this article, or claim that may be made by its manufacturer, is not guaranteed or endorsed by the publisher.

Copyright © 2021 Meites, Bajema, Kambhampati, Prill, Marconi, Brown, Rodriguez-Barradas, Beenhouwer, Holodniy, Lucero-Obusan, Cardemil, Cates, Surie and The SUPERNOVA COVID-19 Surveillance Group. This is an open-access article distributed under the terms of the Creative Commons Attribution License (CC BY). The use, distribution or reproduction in other forums is permitted, provided the original author(s) and the copyright owner(s) are credited and that the original publication in this journal is cited, in accordance with accepted academic practice. No use, distribution or reproduction is permitted which does not comply with these terms.



# Early Detection of COVID-19 Waves From Cases in a Neighboring Country With an Open Border

Anil Kamat<sup>1\*</sup> and Amrita Sah<sup>2</sup>

<sup>1</sup> Department of Mechanical, Aerospace and Nuclear Engineering, Rensselaer Polytechnic Institute, Troy, NY, United States,

<sup>2</sup> Nepalgunj Medical College, Nepalgunj, Nepal

## OPEN ACCESS

### Edited by:

Reza Lashgari,  
Shahid Beheshti University, Iran

### Reviewed by:

Uday Narayan Yadav,  
University of New South  
Wales, Australia  
Meghnath Dhimal,  
Nepal Health Research Council, Nepal  
Anil K. Giri,  
University of Helsinki, Finland

### \*Correspondence:

Anil Kamat  
anilkamat202@gmail.com

### Specialty section:

This article was submitted to  
Infectious Diseases—Surveillance,  
Prevention and Treatment,  
a section of the journal  
Frontiers in Public Health

**Received:** 11 July 2021

**Accepted:** 30 September 2021

**Published:** 29 October 2021

### Citation:

Kamat A and Sah A (2021) Early  
Detection of COVID-19 Waves From  
Cases in a Neighboring Country With  
an Open Border.  
Front. Public Health 9:739738.  
doi: 10.3389/fpubh.2021.739738

Border closure or travel restriction is a critical issue as closing the border early can badly affect the economy of the country, whereas substantial delay can put human lives at stake. While many papers discuss closing the border early in the pandemic, the question of when to close the border has not been addressed well. We have tried to estimate a date of closing the border by taking the reference of a neighboring country with a high correlation in Covid-19 incidence. Here we have used non-linear methods to probe the landscape of correlation between temporal COVID-19 incidences and deaths. We have tested our method on two neighboring countries, Nepal and India, with open borders, where closing the borders are among the top priorities to reduce the spread and spill-out of variants. We have selected these countries as they have close connectivity and intertwined socio-economic network with thousands of people crossing the border every day. We found the distance correlation for COVID-19 incidence between these countries to be statistically significant ( $p < 0.001$ ) and there is a lag of 6 days for maximum correlation. In addition, we analyzed the correlation for each wave and found the distance correlation for the first phase is 0.8145 ( $p < 0.001$ ) with a lag of 2 days, and the distance correlation for the second wave is 0.9685 ( $p < 0.001$ ) without any lag. This study can be a critical planning tool for policymakers and public health practitioners to make an informed decision on border closure in the early days as it is critically associated with the legal and diplomatic agreements and regulations between two countries.

**Keywords:** COVID-19, open border, wave detection, border closure, COVID-19 cases correlation

## INTRODUCTION

By the time World Health Organization (WHO) declared respiratory infectious disease (COVID-19) due to a novel coronavirus (SARS-CoV-2) as a pandemic (1) on March 11, 2020, the virus had already crossed the border of China and had spread into 114 countries due to its high reproduction number compared to other SARS coronaviruses (2). The globalization and ease of mobility from one country to another have highly contributed to the rapid and far spread of COVID-19 around the world (3). Greater connectedness and integration among countries naturally increase pathways for pathogens to cross borders and emerge in local populations. High-frequency trade and international travel facilitate global disease transmission while open borders and social networks have rendered neighboring countries more vulnerable to the emergence and spread of infectious diseases (4–6). When people from highly affected territories move to low



affected territories, it puts more pressure and challenge on the local public health system. It is well-established that a country with a low socioeconomic position suffers more (7). On the other hand, greater economic globalization leads to slower adaptation of policies due to legal bindings on travel and trade agreements (8). Countries with an open border and people working abroad may be less inclined to closing the border in order to minimize economic losses. Closing the border with some delay/lag and slowly reducing mobility is a common feature of most countries (9). In contrast, countries like China, Japan, and Korea which adopted stringent early travel restrictions, were successful in containing the virus whereas the countries with a porous border like Nepal and India faced worse conditions.

The relationship between Nepal and India is one of the oldest diplomatic relations in the world. These two countries are among the handful of countries that share open borders. People of either country can easily get into the other country without requiring any official documentation (10). Similar religions and social norms have created intense social-economic networks across the open border. The open border has greatly helped people of both countries to do trade and business which has created employment opportunities for the locals (11). Nevertheless, these benefits come with some risks, as the local people also share the potential vulnerability to disease transmission and outbreak. In fact, risk due to population outflow is higher than any other factors like geographical proximity and similarity in economic conditions. The open border and lack of documentation make it even harder to trace (12) and constrain the outbreak within one country. Thus, it is essential not only to know the strength of the relationship of COVID-19 incidence between these two countries but also to know the lead or the lag in the days for maximum similarity of the new cases.

A simple yet effective method to measure the relationship between the incidences is the correlation analysis. Depending upon the stationarity of the time series, the correlation method is selected to produce a meaningful relationship. As the traditional Pearson correlation can give a spurious relationship if the time series is not stationary, Distance Correlation is usually preferred to measure the dependencies of two time-series. Distance correlation is a new method to quantify the strength of dependences between two random vectors of arbitrary dimension (13). Distance correlation is the exact equivalence of Brownian correlation (14). Unlike the traditional Pearson product-moment correlation method, the distance correlation can measure the linear as well as the non-linear relationship between two variables (15). Further, 0 in distance correlation means absolute independencies, i.e., the distance correlation between two variables is zero if and only if they are statistically independent. The Distance Correlation has already been used for measuring dependencies in power-law growth of four countries (16). To the best of our knowledge, this is the first time anyone has analyzed the relationship between the COVID-19 incidence rate in Nepal and India to find out the number of days, it takes the effect to propagate from one country to another using cross-correlation. Given the complexity of pandemic decisions, governments face a dilemma about the beginning of travel restriction, and our analysis provides the lag in days, which may

help the policymakers of either country to prepare intervention measures and plan strategies to control transmission ahead of the pandemic in future to save thousands of lives.

## MATERIALS AND METHODS

### Data

All the data used in the study is taken from the Data Repository by the Center for Systems Science and Engineering (CSSE) at Johns Hopkins University (17). Individual-level data from the open-access datasets of COVID-19 cases for Nepal and India was considered from January 25, 2020 to May 18, 2021, and January 30, 2020, to May 18, 2021, respectively. All the data from the recorded first case till the date were selected for this study. The beginning dates of data are few months before the global pandemic declaration on March 11. The data from Nepal were reported by the ministry of health and population and the data from India were reported by the ministry of health and family welfare. All the analysis of data was carried out in Matlab® (18) (R2019b, <http://www.mathworks.com>). The Matlab® source code and the dataset used for this analysis can be found in the following GitHub repository: [https://github.com/anilkamat/Covid-19\\_NepIndCorrelation](https://github.com/anilkamat/Covid-19_NepIndCorrelation).

### Wave Detection

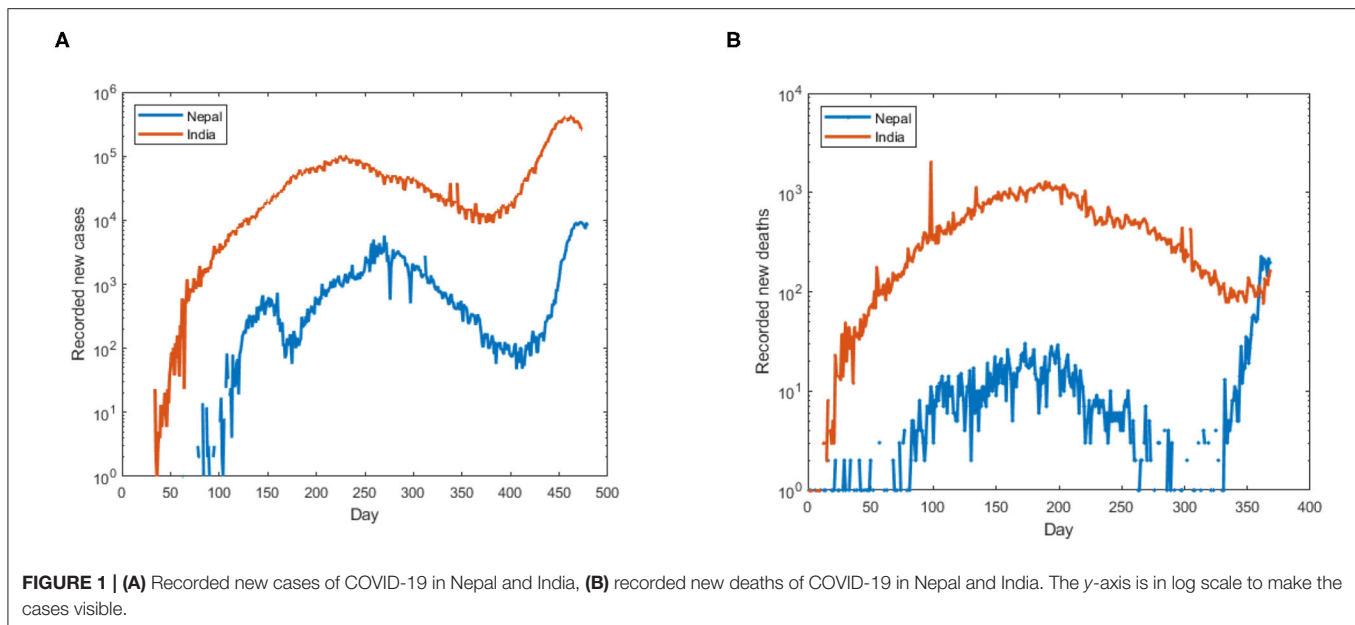
To detect the onset and end of the first and second waves of coronavirus, we have used the multiple change-point detection (CPD) method (19). The CPD method depends on the statistical properties of the time series. A change point is a sample or time instant at which some statistical property of a time series changes abruptly. We considered a change if the mean and slope of the time series have changed mostly abruptly. The approach of this method is to minimize a cost function over possible numbers and locations of change points. The whole time series is divided into  $n+1$  segments for the detection of  $n$  change points and the empirical property is estimated for each of the sections. Then, at each point, the deviation of the statistical property from the empirical estimates is computed. Similarly, the deviation of each section is calculated and added together to find the total residual error. The residual error for each of the division points along the time series is computed and compared to find the point with minimum residual error. Consider a time-series as:

$$y_{1:n} = (y_1, y_2, \dots, y_n)$$

The model can have  $m$  number of change points which will split the series into  $m+1$  segments:

$$t_{1:m} = (t_1, \dots, t_m)$$

Each change point position is an integer between 1 and  $n-1$  inclusive. Here, we have used the linear fit statistical property which uses the total deviation of the sum of squared differences between the time-series values and the predictions of the least-squares linear fit through the values of the line segment. The best



line through  $y_m, y_{m+1} \dots y_n$  is given by:

$$\hat{y} = \frac{S_{xt}|_m^n}{S_{tt}|_m^n} (t - \text{mean}([t_m \dots t_n])) + \text{mean}(y_m, y_{m+1} \dots y_n)$$

Where the sum of square  $S_{xy}$  is:

$$S_{xt}|_m^n = \sum_{r=m}^n (x - \text{mean}([x_m \dots x_n])) (y - \text{mean}([y_m \dots y_n]))$$

And the error sum of square (SSE):

$$\begin{aligned} SSE &= \sum_{i=m}^n (x_i - \hat{x}(t_i))^2 = S_{xx}|_m^n - \frac{S_{xt}^2|_m^n}{S_{tt}|_m^n} \\ &= (n - m + 1) \text{var}([x_m \dots x_n]) \\ &\quad - \frac{(\sum_{i=m}^n (x_i - \text{mean}([x_m \dots x_n]))(i - \text{mean}([m \dots n])))^2}{(n - m + 1) \text{var}([m \dots n])} \end{aligned}$$

If there are  $K$  change points the function minimizes:

$$J(K) = \sum_{k=0}^{K-1} \sum_{i=k_r}^{k_{r+1}-1} \Delta(x_i; \chi([x_{k_r} \dots x_{k_{r+1}-1}])) + \beta K$$

Where  $\beta$  is the proportionality constant which penalizes the function to minimize the residual error.

## Dependency Analysis

We first tested the stationarity of the data using Dickey-Fuller's test (20) to see if the time-series contains a unit root and found the time-series were not stationary, which requires non-linear correlation methods like distance correlation. Distance

measure takes the value of  $[0, 1]$ , where the 0, implies absolute independence and 1 implies the perfect correlation between the two vectors. It is free of matrix inversion and estimation of parameters and can be computed as below.

$$Cor_D(x, y) = \frac{Cov_D(x, y)}{\sigma_D(x)\sigma_D(y)}$$

Where,  $Cov_D(x, y)$  is the distance covariance between two variables and  $\sigma_D$  is the standard deviation.

Statistical significance was defined where  $p$ -values were  $< 0.01$ . Note: two countries can be considered to be dependent if the correlation of the confirmed new cases between them is  $> 0.5$  (21). To find the lag for optimal similarity of the cases, we have used cross-correlation (22). The value of the lag with the highest correlation coefficient represents the best fit between the two series.

## RESULTS

We first tested the presence of unit root in the data by employing Dickey-Fuller's test of stationarity. We found the time-series of incidence rate and mortality rate of Nepal and India (**Figures 1A,B**) were non-stationary ( $p > 0.05$ ), the presence of unit root suggests the use of distance correlation. Thus, to quantify the non-linear dependency, we used distance correlation, and a significant distance correlation coefficient of 0.6337 ( $p < 0.001$ ,  $N = 474$ ) was observed between the daily incidence of Nepal and India. We then performed cross-correlation for different lags of days which provides the difference in days for a maximum fit of both the incidence rates. Thus, to report the dependencies of incidence rate at each time lag, the normalized cross-correlation coefficients were calculated for a forward and backward lag of 500 days. We can observe (see **Figure 2A**) two peaks in the cross-correlation, first, a correlation

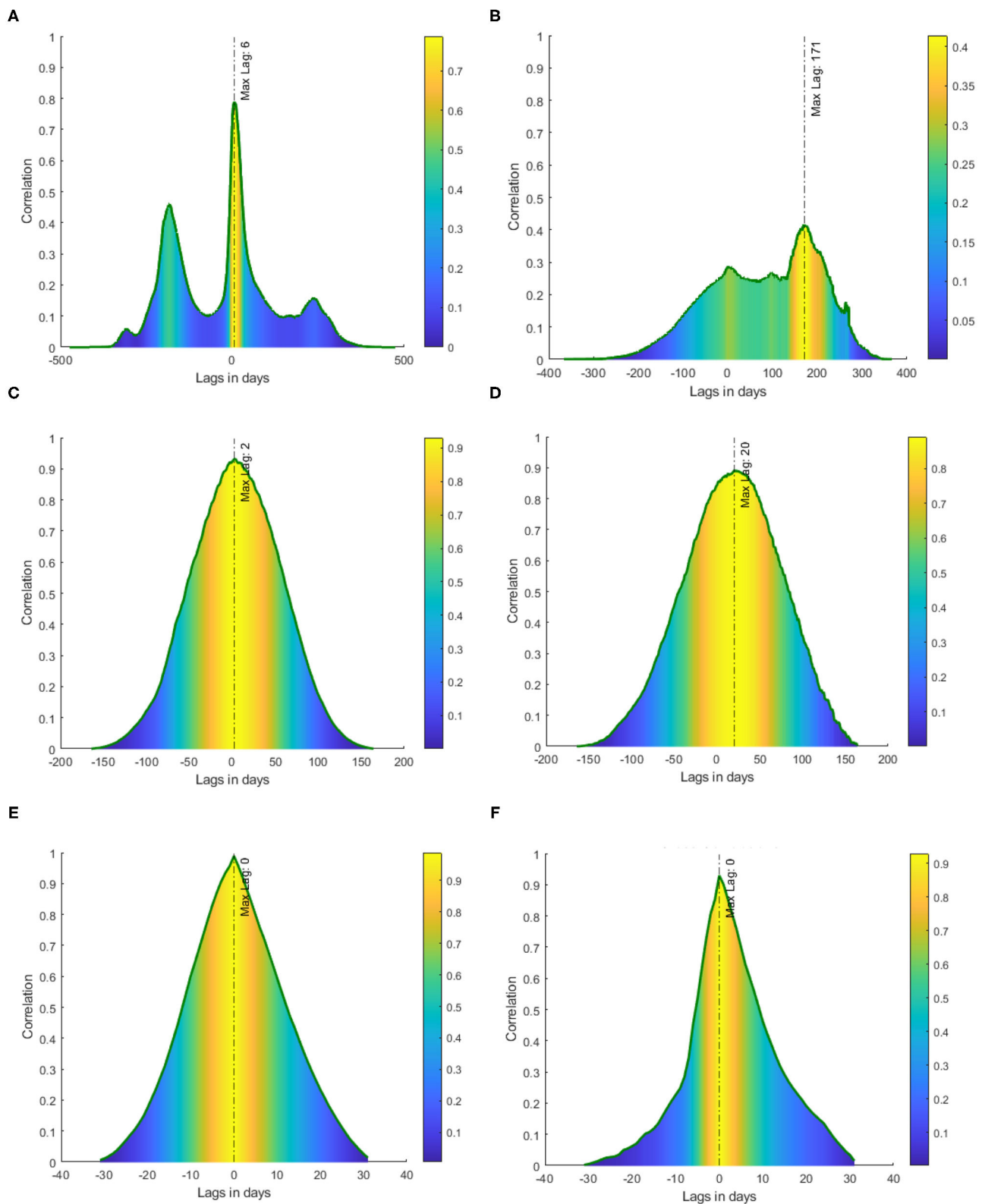
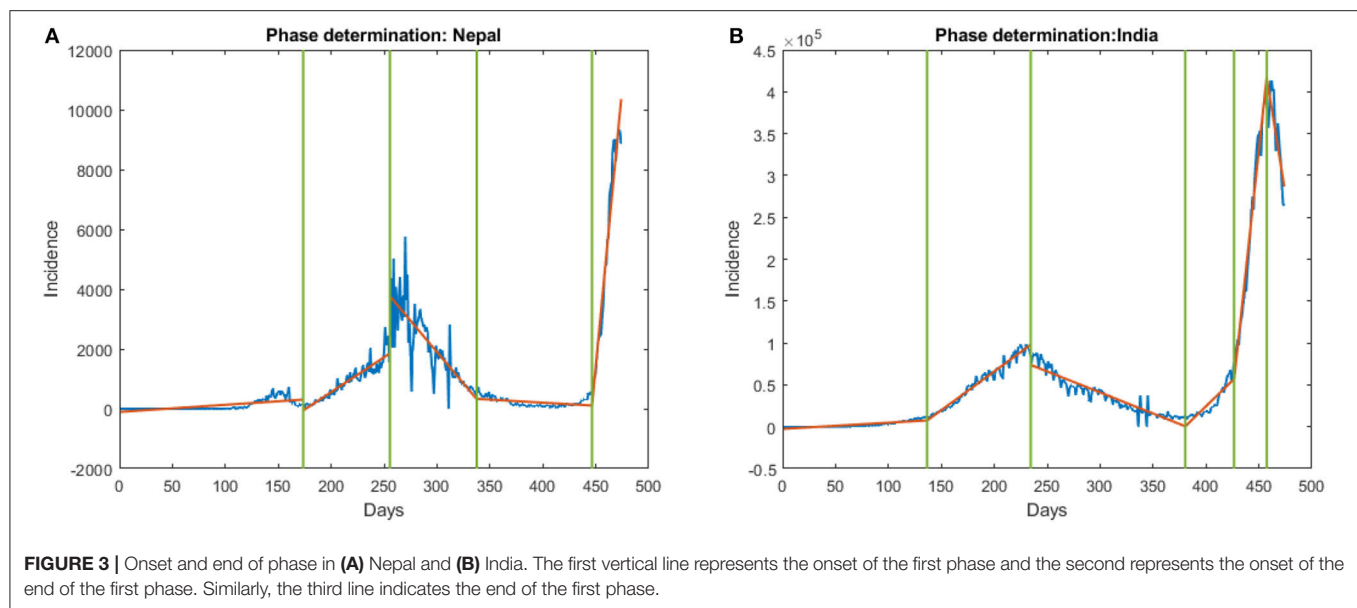


**FIGURE 2 |** Cross-correlation between Nepal and India with lags in days. The color represents the magnitude of cross-correlation at each lag. **(A)** Cross-correlation of incident cases, **(B)** cross-correlation of new deaths, **(C)** cross-correlation of incident cases in first wave, **(D)** cross-correlation of daily deaths in the first wave, **(E)** cross-correlation of incident cases in the second wave, and **(F)** cross-correlation of daily deaths in the second wave.



of 0.4602 occurs at the lag of 183 days, and the second of 0.78848 occurs at the lag of 6 days. Similarly, we found the distance correlation for the daily new deaths (see **Figure 2B**) to be non-linearly related with a correlation coefficient of 0.4702 ( $p < 0.001$ ,  $N = 368$ ), and the lag in days for the maximum correlation of 0.4144 in mortality rate was found to be 171 days.

We then studied the relationship in each COVID-19 wave separately. For which, we first detect the waves in the COVID-19 incident by observing the change in the statistical property of the data which indicates the different stages of the wave. To detect the change, we used the multiple change-point detections (CPD) (19) method which gave the start, inflection, duration, and end of each wave. Based on the multiple change-point detection methods, we observed the first wave in Nepal starts on July 16, 2020, and ends on December 27, 2020, (see **Figure 3A**). Similarly, the first phase in India starts on June 14, 2020, and ends on February 13, 2021, (see **Figure 3B**). We then computed the distance correlation between the two countries for the first wave and found it to be 0.8145 ( $p < 0.001$ ). The lag in the first wave for daily new cases and daily new deaths was found to be 2 and 20 days respectively (see **Figures 2C,D**). Similarly, we applied CPD to detect the second wave and observed the second wave in Nepal started on April 15, 2021, and it started on March 31, 2021, in India. The distance correlation between the incidence was found to be 0.9685 ( $p < 0.001$ ) for the second wave. The lag in the second wave for daily new cases and daily new deaths was found to be 0 and 0 days, respectively (see **Figures 2E,F**).

The reproducibility of the method was tested on other neighboring countries with open borders: the United Kingdom and Ireland, and Russia and Belarus. Between the UK and Ireland, the distance correlation for the daily new cases was found to be non-linearly dependent with a correlation coefficient of 0.568 ( $p < 0.01$ ,  $N = 445$ ), and the lag in days for the maximum correlation was found to be 23 days (see

**Supplementary Figure 1**). The distance correlation for the daily new death was found to be non-linearly dependent with a correlation coefficient of 0.615 ( $p < 0.01$ ,  $N = 434$ ), and the lag in days for the maximum correlation was found to be 2 days (see **Supplementary Figure 1**). Similarly, between Russia and Belarus, the distance correlation for the daily new cases was found to be non-linearly dependent with a correlation coefficient of 0.794 ( $p < 0.01$ ,  $N = 442$ ), and the lag in days for the maximum correlation was found to be 8 days (see **Supplementary Figure 2**). The distance correlation for the daily new death was found to be non-linearly dependent with a correlation coefficient of 0.853 ( $p < 0.01$ ,  $N = 414$ ), and the lag in days for the maximum correlation was found to be 0 days (see **Supplementary Figure 2**).

## DISCUSSION

For this study, we selected the two neighboring countries Nepal and India as both of them are fairly globalized (4) and share an open border. Our findings indicate that COVID-19 incidence in Nepal is significantly correlated with the incidence in India. It has been shown that the time to act is one of the most important measures for any health organization in curtailing the current COVID-19 pandemic (16, 23). While the timing of non-pharmaceutical interventions with respect to waves is fairly well-known, it is challenging to detect the wave itself and determine the optimal date prior to the start of the wave. The CPD can be used to detect the wave and the lag in days can be used to plan for pandemics in the future. The distance correlation in addition to cross-correlation can provide a way to estimate the timing to enact non-pharmaceutical measures. The high correlation observed in the second peak (**Figure 2A**) of incidence with a lag of 6 days can be attributed to the travelers crossing the open border between Nepal and India. It is not difficult to miss the



detection of COVID-19 cases at the border since the incubation period of the virus is 1 to 14 (24) days and people might be tested as false negative during this period. The maximum correlation detected by our method is for the days within the incubation periods, which means most of the cases might not have been detected in the early days of infection and could have easily crossed the border. The border quarantine centers were not effective as a few people fled the centers (25). The undetected or the false-negative tests can even give people a false sense of security to travel between the countries and be the root of the spread of the virus. The lag in daily new cases in the first wave is 2 days (**Figure 2C**) whereas the lag in the second wave is 0 days (**Figure 2E**). The difference in lags between the first and second waves may be due to the reopening of the border before the start of the second wave (21, 26, 27), unlike the first wave when the border was closed and border quarantine was mandatory for all the returning workers of both countries (28).

Our finding sheds light on the correlation of daily new cases in two neighboring countries with an open border and how the lag in correlation can be leveraged to help the countries plan and apply non-pharmaceutical measures to reduce the spread of the virus. The cross-border travel restriction in the early days can help the countries keep the pandemic under control (4, 29, 30), as it has been shown that closing the border after the introduction of the virus has very little effect in preventing within-country spread (31, 32). The knowledge about future waves is essential for policymakers to make an informed decision on border closure in the early days as it is critically associated with the legal and diplomatic agreements and regulations between two countries. This study can provide a beacon signal of an imminent COVID-19 wave by estimating the time of resurgence. The knowledge of lag in days of COVID-19 incidence can act as a precursor to the government and public to be vigilant and practice safety measures, learning from Vietnam (33), such as restricting people from crossing the country, the establishment of effective screening methods at the border, and maintaining on-site healthy and safe isolation centers as no fully proven and specific antiviral treatment for the coronavirus exists (34). The stringent travel restriction between countries like Nepal-India with a large and multilayered socio-economic network can have a great impact on the pandemic dynamics (35). Nevertheless, the gain from the border closures can only be appreciated by combining it with other preventive measures like social distancing, intensive surveillance, testing, and contact tracing as demonstrated by Vietnam (33, 36). The strict travel restriction, at the very least, can delay the arrival of the virus and permit some time to prepare the health infrastructure (32, 37).

In contrast to the high correlation seen in the incidence, the correlation for daily new death is lower. The lower correlation in death can be accounted for by the unequal health facilities available in these countries. It is well-known that the unequal distribution of health infrastructure between two countries plays a significant role in the impact on casualties and disease transmission (29). The difference in the strength of health infrastructure (**Table 1**), testing facilities, and public health policy and poverty rate within Nepal and India may explain the observed lower correlation in the daily deaths count whereas the

**TABLE 1** | Health care/facilities indicator [source: World Bank (38, 39)].

| S.N. | Indicator  | Nepal       | India       |
|------|--|-------------|-------------|
| (1)  | Number of doctors per 1,000                          | 0.7         | 0.9         |
| (2)  | Hospital beds per 1,000                              | 0.3         | 0.5         |
| (3)  | Current health expenditure per capita (current US\$) | 57.85       | 72.83       |
| (4)  | Nurses and midwives (per 1,000 people)               | 3.1         | 1.7         |
| (5)  | Poverty headcount ratio                              | 25.2 (2010) | 21.9 (2011) |

open border might be a contributing factor for high correlation in daily new cases. The lag in daily new death in the first wave is 20 days (**Figure 2D**) whereas the lag in the second wave is 0 days (**Figure 2F**) which may be due to the more lethal variant in the second wave, the lull in the travel restrictions (27), and the fact that border isolation centers were more effective in the first wave (40, 41).

The realization of containment, once the outbreak has occurred, depends on the adaptation time. The time window to apply containment intervention is very short and its efficiency decreases with the delay in the adaptation time (23). For the countries with a small population like Nepal, one of the efficient non-pharmaceutical measures to decrease COVID-19 spread is early isolation of asymptomatic individuals, and the effectiveness of the strategy demands the realization of a huge number of daily new tests in the early days of the infection (16, 29). The time to relax the lockdown should be carefully be studied as it can have positive as well as negative impacts depending upon the country (42). Likewise, social policy and programs based on social determinants of health must be enacted by policymakers, stakeholders, and researchers to embrace all sectors of society.

To test the reproducibility of our method, we have extended the analysis to four other countries with an open border. The analysis for United Kingdom-Ireland and Russia-Belarus suggests that the delay in closing the border should not be more than 23 days between the UK and Ireland, and should not be more than 8 days between Russia and Belarus. The maritime boundary between the United Kingdom and Ireland might be a reason for the larger lag in incidence between these countries as compared to Nepal-India and Russia-Belarus.

Despite the promising results, the analysis considered here has few limitations. This analysis uses data that is different from the true data on the ground due to less testing and inefficient counting of new and death cases by Nepal and India (43–46). Similarly, multivariate distance correlation can be used to determine the dependencies by including other factors of transmission and vaccination rate. In future study, local micro-events like public gatherings, which can affect the results, should be taken into account while analyzing the outbreak. This work can further be extended by incorporating other pandemic outbreaks to generalize the analysis and findings.

## CONCLUSION

In this paper, we analyzed the Covid-19 incidence and deaths between countries with an open border to approximate the



border closing data with respect to the beginning of waves seen in the neighboring country. We conclude that the non-linear correlation method, along with cross-correlation, can be applied to determine the dependencies and approximate the lead/lag in days of a Covid-19 wave between two neighboring countries with an open border. We tested the method on Nepal and India; one of the major findings of this analysis is that closing the border should not be delayed more than 6 days after detection of a Covid-19 wave in the neighboring country to stop/reduce the spillover.

## DATA AVAILABILITY STATEMENT

Publicly available datasets were analyzed in this study. This data can be found here: <https://github.com/owid/covid-19-data> COVID-19. Data Repository by the Center for Systems Science and Engineering (CSSE) at Johns Hopkins University (JHU).

## REFERENCES

- Cucinotta D, Vanelli M. WHO declares COVID-19 a pandemic. *Acta Biomed.* (2020) 91:157–60. doi: 10.23750/abm.v91i1.9397
- Liu Y, Gayle AA, Wilder-Smith A, Rocklöv J. The reproductive number of COVID-19 is higher compared to SARS coronavirus. *J. Travel Med.* (2020) 27:1–4. doi: 10.1093/jtm/taaa021
- Tatem J, Rogers DJ, Hay SI. Global transport networks and infectious disease spread. *Adv Parasitol.* (2006) 62:293–343. doi: 10.1016/S0065-308X(05)62009-X
- Zimmermann KE, Karabulut G, Bilgin MH, Doker AC. Inter-country distancing, globalisation and the coronavirus pandemic. *World Econ.* (2020) 43:1484–98. doi: 10.1111/twec.12969
- Gautret P, Botelho-Nevers E, Brouqui P, Parola P. The spread of vaccine-preventable diseases by international travellers: a public-health concern. *Clin Microbiol Infect.* (2012) 18(Suppl. 5):77–84. doi: 10.1111/j.1469-0691.2012.03940.x
- Farzanegan MR, Gholipour HE, Feizi M, Nunkoo R, Andargoli AE. International tourism and outbreak of coronavirus (COVID-19): a cross-country analysis. *J Travel Res.* (2021) 60:687–92. doi: 10.1177/0047287520931593
- Marmot M, Friel S, Bell R, Houweling TA, Taylor S. Closing the gap in a generation: health equity through action on the social determinants of health. *Lancet.* (2008) 372:1661–9. doi: 10.1016/S0140-6736(08)61690-6
- Weir L, Mykhalovskiy E. *Global Public Health Vigilance: Creating a World on Alert.* Oxfordshire: Routledge (2010).
- Milani F. COVID-19 outbreak, social response, and early economic effects: a global VAR analysis of cross-country interdependencies. *J Popul Econ.* (2021) 34:223–52. doi: 10.1007/s00148-020-00792-4
- Strategic Analysis: *Movement of Population Between India and Nepal.* Available online at: [https://ciaotest.cc.columbia.edu/olj/sa/sa\\_99ths02.html](https://ciaotest.cc.columbia.edu/olj/sa/sa_99ths02.html) (accessed July 04, 2021).
- Kumar R. India-Nepal open border: springboard for opportunities. *Int Stud.* (2016) 50:165–83. doi: 10.1177/0020881716654406
- Khanal L, Paudel BK, Acharya BK. *Community Vulnerability to Epidemics in Nepal: A High-Resolution Spatial Assessment Amidst COVID-19 Pandemic.* World Health Organization.
- Davis RA, Matsui M, Mikosch T, Wan P. Applications of distance correlation to time series. *Bernoulli.* (2018) 24:2429–60. doi: 10.3150/17-BEJ955
- Székel GJ, Rizzo ML. Brownian distance covariance. *Ann Appl Stat.* (2009) 3:1236–65. doi: 10.1214/09-AOAS312

## AUTHOR CONTRIBUTIONS

AS conceived and designed the concept and wrote the paper. AK and AS performed the literature review. AK contributed to analysis tools. Both authors have read and agreed to the published version of the manuscript.

## ACKNOWLEDGMENTS

We would like to express our highest gratitude to all health agents and individuals around the globe who were involved in reporting cases and making COVID-19 prevalence data available to the public.

## SUPPLEMENTARY MATERIAL

The Supplementary Material for this article can be found online at: <https://www.frontiersin.org/articles/10.3389/fpubh.2021.739738/full#supplementary-material>

- Mendes CFO, Beims MW. Distance correlation detecting Lyapunov instabilities, noise-induced escape times and mixing. *Phys A Stat Mech Appl.* (2018) 512:721–30. doi: 10.1016/j.physa.2018.08.028
- Brugnago EL, da Silva RM, Manchein C, Beims MW. How relevant is the decision of containment measures against COVID-19 applied ahead of time? *Chaos Solitons Fractals.* (2020) 140:110164. doi: 10.1016/j.chaos.2020.110164
- Dong E, Du H, Gardner L. An interactive web-based dashboard to track COVID-19 in real time. *Lancet Infect Dis.* (2020) 20:533–4. doi: 10.1016/S1473-3099(20)30120-1
- MathWorks - Makers of MATLAB and Simulink - MATLAB & Simulink. Available online at: [https://www.mathworks.com/?s\\_tid=gn\\_logo](https://www.mathworks.com/?s_tid=gn_logo) (accessed June 28, 2021).
- Killick R, Fearnhead P, Eckley IA. Optimal detection of changepoints with a linear computational cost. *J Am Stat Assoc.* (2012) 107:1590–8. doi: 10.1080/01621459.2012.737745
- Dickey DA, Fuller WA. Distribution of the estimators for autoregressive time series with a unit root. *J Am Stat Assoc.* (1979) 74:427–31. doi: 10.2307/2286348
- Coronavirus Cases Surge in Nepal - The Washington Post. Available online at: [https://www.washingtonpost.com/world/asia\\_pacific/nepal-coronavirus-cases/2021/05/13/5bff41c6-b36a-11eb-a980-a60af976ed44\\_story.html](https://www.washingtonpost.com/world/asia_pacific/nepal-coronavirus-cases/2021/05/13/5bff41c6-b36a-11eb-a980-a60af976ed44_story.html) (accessed July 11, 2021).
- Buck J, Daniel M, Singer A. *Computer Explorations in Signals and Systems Using MATLAB.* (1997). Available online at: <https://dl.acm.org/doi/abs/10.5555/248896> (accessed: July 05, 2021).
- Vasconcelos GL, Macêdo AMS, Ospina R, Almeida FAG, Duarte-Filho GC, Brum AA, et al. Modelling fatality curves of COVID-19 and the effectiveness of intervention strategies. *PeerJ.* (2020) 8:e9421. doi: 10.7717/peerj.9421
- Sharma S, Kumar V, Chawla A, Logani A. Rapid detection of SARS-CoV-2 in saliva: can an endodontist take the lead in point-of-care COVID-19 testing? *Int Endodontic J.* (2020) 53:1017–9. doi: 10.1111/iej.13317
- COVID-19: More Than 500 Migrant Workers in Nepal Escape Quarantine. Available online at: <https://www.downtoearth.org.in/news/health/covid-19-more-than-500-migrant-workers-in-nepal-escape-quarantine-70111> (accessed July 11, 2021).
- Nepal Opens Border for Indians, Registration and Covid-19 Report Must for Entry | Latest News India - Hindustan Times. Available online at: <https://www.hindustantimes.com/india-news/nepal-opens-border-for-indians-registration-and-covid-19-report-must-for-entry-101613998431681.html> (accessed July 10, 2021).

27. When Governance Took a Backseat, Second Wave Took Hold. Available online at: <https://kathmandupost.com/health/2021/04/23/when-governance-took-a-backseat-second-wave-took-hold> (accessed July 11, 2021).
28. Baniya J, Bhattarai S, Pradhan V, Thapa BJ. Visibility of invisible: Covid-19 and Nepal-India migration. *Tribhuvan Univ. J.* (2020) 34:101–14. doi: 10.3126/tuj.v34i0.31542
29. Qiu Y, Chen X, Shi W. Impacts of social and economic factors on the transmission of coronavirus disease (2019). (COVID-19) in China. *J Popul Econ.* (2020) 33:1–46. doi: 10.1101/2020.03.13.20035238
30. Eichner M, Schwehm M, Wilson N, Baker MG. Small islands and pandemic influenza: potential benefits and limitations of travel volume reduction as a border control measure. *BMC Infect Dis.* (2009) 9:160. doi: 10.1186/1471-2334-9-160
31. Mallapaty S. What the data say about border closures and COVID spread. *Nature.* (2021) 589:185. doi: 10.1038/d41586-020-03605-6
32. Grépin KA, Ho T-L, Liu Z, Marion S, Piper J, Worsnop CZ, et al. Evidence of the effectiveness of travel-related measures during the early phase of the COVID-19 pandemic: a rapid systematic review. *BMJ Global Health.* (2021) 6:e004537. doi: 10.1136/bmjgh-2020-004537
33. Dao TL, Nguyen TD, Hoang VT. Controlling the COVID-19 pandemic: useful lessons from Vietnam. *Travel Med Infect Dis.* (2020) 37:101822. doi: 10.1016/j.tmaid.2020.101822
34. Dolgin E. The race for antiviral drugs to beat COVID - and the next pandemic. *Nature.* (2021) 592:340–3. doi: 10.1038/d41586-021-00958-4
35. Russell TW, Wu JT, Clifford S, Edmunds WJ, Kucharski AJ, Jit M. Effect of internationally imported cases on internal spread of COVID-19: a mathematical modelling study. *Lancet Public Health.* (2021) 6:e12–e20. doi: 10.1016/S2468-2667(20)30263-2
36. Nguyen HV, Hoang MV, Dao ATM, Nguyen HL, Nguyen TV, Nguyen PT, et al. An adaptive model of health system organization and responses helped Vietnam to successfully halt the Covid-19 pandemic: what lessons can be learned from a resource-constrained country. *Int J Health Plann Manage.* (2020) 35:988–92. doi: 10.1002/hpm.3004
37. Chinazzi M, Davis JT, Ajelli M, Gioannini C, Litvinova M, Merler S, et al. The effect of travel restrictions on the spread of the 2019 novel coronavirus (COVID-19) outbreak. *Science.* (2020) 368:395–400. doi: 10.1126/science.aba9757
38. Nepal | Data. Available online at: <https://data.worldbank.org/country/nepal> (accessed July 10, 2021).
39. India | Data. Available online at: <https://data.worldbank.org/country/india> (accessed July 10, 2021).
40. Asrani P, Eapen MS, Hassan MI, Sohal SS. Implications of the second wave of COVID-19 in India. *Lancet Respir Med.* (2021) 9:E93–E4. doi: 10.1016/S2213-2600(21)00312-X
41. Ranjan R, Sharma A, Verma MK. Characterization of the second wave of COVID-19 in India. *medRxiv.* (2021) 121:85–93. doi: 10.1101/2021.04.17.21255665
42. Feroze N. Forecasting the patterns of COVID-19 and causal impacts of lockdown in top five affected countries using Bayesian Structural Time Series Models. *Chaos Solitons Fractals.* (2020) 140:110196. doi: 10.1016/j.chaos.2020.110196
43. Giri K, Rana DR. Charting the challenges behind the testing of COVID-19 in developing countries: Nepal as a case study. *Biosaf Health.* (2020) 2:53–6. doi: 10.1016/j.bshealth.2020.05.002
44. Vaidyanathan G. People power: how India is attempting to slow the coronavirus. *Nature.* (2020) 580:442. doi: 10.1038/d41586-020-01058-5
45. Roy MP. Doing more tests: next challenge for Covid 19 in India. *Virus Dis.* (2020) 31:249–50. doi: 10.1007/s13337-020-00606-x
46. Sharma K, Banstola A, Parajuli RR. Assessment of COVID-19 pandemic in Nepal: a Lockdown Scenario Analysis. *Front Public Health.* (2021) 9:599280. doi: 10.3389/fpubh.2021.599280

**Conflict of Interest:** The authors declare that the research was conducted in the absence of any commercial or financial relationships that could be construed as a potential conflict of interest.

**Publisher's Note:** All claims expressed in this article are solely those of the authors and do not necessarily represent those of their affiliated organizations, or those of the publisher, the editors and the reviewers. Any product that may be evaluated in this article, or claim that may be made by its manufacturer, is not guaranteed or endorsed by the publisher.

Copyright © 2021 Kamat and Sah. This is an open-access article distributed under the terms of the Creative Commons Attribution License (CC BY). The use, distribution or reproduction in other forums is permitted, provided the original author(s) and the copyright owner(s) are credited and that the original publication in this journal is cited, in accordance with accepted academic practice. No use, distribution or reproduction is permitted which does not comply with these terms.



# Leveraging of SARS-CoV-2 PCR Cycle Thresholds Values to Forecast COVID-19 Trends

Nicolas Yin<sup>1\*</sup>, Simon Dellicour<sup>2,3</sup>, Valéry Daubie<sup>1</sup>, Nicolas Franco<sup>4,5</sup>, Magali Wautier<sup>1</sup>, Christel Faes<sup>5</sup>, Dieter Van Cauteren<sup>6</sup>, Liv Nymark<sup>7,8</sup>, Niel Hens<sup>5,9</sup>, Marius Gilbert<sup>2</sup>, Marie Hallin<sup>1,10†</sup> and Olivier Vandenberg<sup>10,11,12†</sup>

<sup>1</sup> Department of Microbiology, Laboratoire Hospitalier Universitaire de Bruxelles – Universitair Laboratorium Brussel (LHUB-ULB), Université Libre de Bruxelles (ULB), Brussels, Belgium, <sup>2</sup> Spatial Epidemiology Lab (SpELL), Université Libre de Bruxelles, Bruxelles, Belgium, <sup>3</sup> Department of Microbiology, Immunology and Transplantation, Division of Clinical and Epidemiological Virology, Rega Institute, Katholieke Universiteit (KU) Leuven, Leuven, Belgium, <sup>4</sup> Department of Mathematics, Namur Centre for Complex Systems (Naxys), University of Namur, Namur, Belgium, <sup>5</sup> Interuniversity Institute for Biostatistics and Statistical Bioinformatics (I-BioStat), Data Science Institute, Hasselt University (UHasselt), Hasselt, Belgium, <sup>6</sup> Scientific Directorate of Epidemiology and Public Health, Sciensano, Brussels, Belgium, <sup>7</sup> Division of Infection Control and Environmental Health, Norwegian Institute of Public Health, Oslo, Norway, <sup>8</sup> Department of Health Management and Health Economics, University of Oslo, Oslo, Norway, <sup>9</sup> Centre for Health Economic Research and Modelling Infectious Diseases, Vaccine and Infectious Disease Institute, University of Antwerp, Antwerp, Belgium, <sup>10</sup> Centre for Environmental Health and Occupational Health, School of Public Health, Université Libre de Bruxelles (ULB), Brussels, Belgium, <sup>11</sup> Clinical Research and Innovation Unit, Laboratoire Hospitalier Universitaire de Bruxelles – Universitair Laboratorium Brussel (LHUB-ULB), Université Libre de Bruxelles (ULB), Brussels, Belgium, <sup>12</sup> Division of Infection and Immunity, Faculty of Medical Sciences, University College London, London, United Kingdom

## OPEN ACCESS

### Edited by:

Reza Lashgari,  
Shahid Beheshti University, Iran

### Reviewed by:

Zhen Luo,  
Jinan University, China  
Kristen Beck,  
IBM Research Almaden, United States

### \*Correspondence:

Nicolas Yin  
nicolas.yin@lhub-ulg.be

<sup>†</sup>These authors have contributed  
equally to this work and share senior  
authorship

### Specialty section:

This article was submitted to  
Infectious Diseases – Surveillance,  
Prevention and Treatment,  
a section of the journal  
Frontiers in Medicine

**Received:** 19 July 2021

**Accepted:** 05 October 2021

**Published:** 01 November 2021

### Citation:

Yin N, Dellicour S, Daubie V, Franco N,  
Wautier M, Faes C, Van Cauteren D,  
Nymark L, Hens N, Gilbert M, Hallin M  
and Vandenberg O (2021) Leveraging  
of SARS-CoV-2 PCR Cycle  
Thresholds Values to Forecast  
COVID-19 Trends.  
Front. Med. 8:743988.  
doi: 10.3389/fmed.2021.743988

**Introduction:** We assessed the usefulness of SARS-CoV-2 RT-PCR cycle thresholds (Ct) values trends produced by the LHUB-ULB (a consolidated microbiology laboratory located in Brussels, Belgium) for monitoring the epidemic's dynamics at local and national levels and for improving forecasting models.

**Methods:** SARS-CoV-2 RT-PCR Ct values produced from April 1, 2020, to May 15, 2021, were compared with national COVID-19 confirmed cases notifications according to their geographical and time distribution. These Ct values were evaluated against both a phase diagram predicting the number of COVID-19 patients requiring intensive care and an age-structured model estimating COVID-19 prevalence in Belgium.

**Results:** Over 155,811 RT-PCR performed, 12,799 were positive and 7,910 Ct values were available for analysis. The 14-day median Ct values were negatively correlated with the 14-day mean daily positive tests with a lag of 17 days. In addition, the 14-day mean daily positive tests in LHUB-ULB were strongly correlated with the 14-day mean confirmed cases in the Brussels-Capital and in Belgium with coinciding start, peak, and end of the different waves of the epidemic. Ct values decreased concurrently with the forecasted phase-shifts of the diagram. Similarly, the evolution of 14-day median Ct values was negatively correlated with daily estimated prevalence for all age-classes.

**Conclusion:** We provide preliminary evidence that trends of Ct values can help to both

follow and predict the epidemic's trajectory at local and national levels, underlining that consolidated microbiology laboratories can act as epidemic sensors as they gather data that are representative of the geographical area they serve.

**Keywords:** COVID-19, SARS-CoV-2, forecast, epidemic trend, cycle threshold (Ct) value

## INTRODUCTION

The coronavirus disease 2019 (COVID-19) pandemic dramatically highlighted the central position of diagnostic testing, not only for the clinical management of infected individuals but also for surveillance purposes (1). The use of clinical microbiology laboratories (CMLs) data to survey the presence of specific microorganisms in a given population represents one of the most established public health surveillance tools of infectious diseases. In a previous study, we proved that influenza trends in Belgium may be estimated using laboratory data provided by a CML serving the wider Brussels-Capital Region area (2). Since the start of the COVID-19 pandemic, several authors have demonstrated that CMLs could represent the first step toward a global set of sensor networks for infectious diseases surveillance, where each one of the CMLs can be seen as a real-time sensor in its area within an interconnected, complex network (1, 3, 4). In this perspective, CMLs have become a cornerstone in the fight against SARS-CoV-2 infections due to their ability to process large amounts of samples in large geographic areas while using highly specialised diagnostic tests (1, 5).

By reporting to Sciensano, the Belgian national public health research institute, the number of new positives among the tests conducted each day, CMLs share the data needed to estimate the effective reproduction number ( $R_t$ ) (6, 7). However, the data represent the growth rate of positive tests and not the incidence of infection, which requires adjustments to account for changes in testing capacity, delay between infection and test report date, and conversion from prevalence to incidence. We previously showed that SARS-CoV-2 RT-PCR cycle threshold (Ct) values are different between populations, with lower Ct values — thus higher viral loads — for outpatients, likely to be recently infected and higher Ct values for inpatients (8). In a recent article, Hay et al. used the SARS-CoV-2 RT-PCR Ct values in a model to forecast epidemic's trajectory (9). At the time of writing, RT-PCR assays are not standardised and the Ct values obtained using various PCR methods on various instruments in various laboratories using various sampling methods cannot be easily aggregated by surveillance systems. Sciensano recently encouraged laboratories to report their results using a semi-quantitative approach where a viral load below  $10^3$  RNA copies/mL is considered as “weak positive” (10). Sciensano's primary goal was to approach the actual infectiousness of patients with persistent positive RT-PCR. Therefore, the semi-quantitative dimension of positive test results is not used by surveillance systems yet.

Besides the difficulty of making use of all the data provided by CMLs in real time, public health authorities also face the challenge of making decisions, as the constantly evolving situation requires permanent adaptation (11). In this perspective,

various predictive models have been developed to support policy makers (12–15). To improve and facilitate the decision-making process, Hens *et al.* developed a phase portrait to monitor the epidemic allowing a real-time assessment of whether intervention measures are needed to keep hospital capacity under control (16). Nevertheless, such supportive decision tools are often designed at the national level instead of the hospital level where, during the pandemic, hospital managers needed support to forecast the cancellation and reintroduction of a series of medical activities, such as the surgical care program, or the number of COVID-related ICU beds (17). Thanks to the huge amount of data they collect on a daily basis, CMLs could also help the hospital structures they serve to anticipate the evolution of the epidemic and forecast their hospitalisation and medical activities.

The objectives of this study were: (1) to verify the accuracy of using of SARS-CoV-2 PCR Ct values trends in a single CML to monitor the dynamics of the epidemic; (2) to determine the added-value of using these data as an additional advanced information for scenario analysis, in relation to a phase diagram and an age-structured compartmental model, both developed to follow the path of the Belgian COVID-19 epidemic (14, 15).

## METHODS

The “Laboratoire Hospitalier Universitaire de Bruxelles - Universitair Laboratorium Brussel” (LHUB-ULB) is a merged clinical laboratory serving five university hospitals located in the Brussels-Capital region in Belgium (8). All the SARS-CoV-2 PCR results produced between April 1, 2020, and May 15, 2021, by the LHUB-ULB were extracted anonymously from its laboratory information system. The data collected were patients' postal code, age, qualitative PCR results, Ct values, instruments on which PCR were performed, and sampling dates. National Belgian data were extracted from the “total number of tests by date” and the “confirmed cases by date, province, age and sex” public dataset available on the Sciensano website on May 27, 2021. These datasets contain the total number of tests, the number of positive tests per day, and the confirmed number of cases per day and province. All Ct values were considered at their time of sampling regardless the days since symptoms onset or deduplication. To analyse trends and minimise day-to-day and holiday-related fluctuations, we computed mean daily positive tests and cases, and median and mean Ct values from May 1, 2020 to May 15, 2021, using a backward sliding window of 14 days (hereafter referred as “14-day mean positive tests/cases” and “14-day median/mean Ct values”).

To follow the trends of Ct values variation during the study period, only the SARS-CoV-2 PCR results on nasopharyngeal



swabs (NPS) obtained using the *m2000 RealTime SARS-CoV-2* assay (Abbott Molecular, USA) were considered, this assay being the only one used by our laboratory during the entire period of interest. As detection of both targeted genes (RdRp and N) was performed using the same fluorophore, the Ct values of this assay were observed up to 32 cycles and were not comparable with Ct values of other RT-PCR assays. Ct values were plotted against a standard calibration curve provided by the Belgian NRC to obtain the semi-quantitative results recommended by Sciensano (10). Accordingly, results with a  $Ct > 22.3$  were considered as “weak positive” (viral load  $< 10^3$  RNA copies/mL). Correlations between 14-day median/mean Ct values and daily mean positive tests were calculated using Spearman's  $r_s$  rank correlation coefficient. This correlation was performed with shifts of 0 to 30 days in the median and mean Ct values, to determine the shift with the highest  $r_s$  between the daily mean number of positive tests and Ct values. To test their validity as a source for COVID-19 surveillance, LHUB-ULB's data were also compared with all COVID-19 confirmed case notifications according to geographical coverage and time distribution.

We used phase diagrams depicting the evolution of COVID-19 hospitalisations in Belgium to compare these trends with the evolution of Ct values measures through time (16). These diagrams were developed to predict the number of COVID-19 patients requiring intensive care by considering the 7-day mean new hospitalisations and the daily ratio of the past 14-day new hospitalisations. For each combination, the total number of hospitalisations is projected for a horizon of 14 days, from which the number of patients requiring intensive care is predicted based on the distribution of the time spent in an intensive care unit (ICU). The hospital contingency plan in Belgium consists of five different phases (phases 0, 1A and 1B, 2A and 2B), incrementing COVID-19 related ICU beds capacities (18). Within this scheme, the total number of patients in ICU moves from 2001 to 2821, yielding a gradual decrease in non-COVID-19 ICU capacity (16). The hospital and future COVID-related ICU load is thus depicted from green to red: the green region can be considered a “safe zone” in which the number of new hospitalisations is limited with a decrease (growth  $< 1$ ) or a limited increase (growth  $> 1$ ) and associated with a limited number of COVID-19 patients at ICU (first part of Phase 0); the yellow region, a region of increased vigilance (second part of Phase 0). The orange (Phases 1A and 1B) and red (Phases 2A and 2B) regions are “high impact” and “no-go” zones, in which non-COVID-19 care decreases substantially and additional capacity for COVID-19 needs to be provided for.

A comparison between the evolution of 14-day median Ct values by age classes and the daily estimated Belgian COVID-19 prevalence for these age classes has been performed using a model of deterministic continuous age-structured compartmental model (extended SEIR-type) integrating social contact data and calibrated on hospitalisations and deaths incidence data as well as serological studies (15). The prevalence was estimated for the following age classes in years: 0–24, 25–44, 45–64, 65–74, and 75+ as the proportion of the sum of the infected compartments (exposed, asymptomatic, presymptomatic, symptomatic, and hospitalised individuals) compared to the total size of the age class, with a 90% confidence

interval estimated by Bayesian analysis. This method aims to provide a reliable comparison with the spreading of COVID-19 in Belgium among age classes since the number of RT-PCR positive tests are known to be biased over time due to testing policy changes (19).

Data from all sources were collected retrospectively and anonymously before analysis from a routine surveillance perspective without any additional intervention. Therefore, ethical review and approval was not required for the study on human participants in accordance with the local legislation and institutional requirements. Written informed consent from the participants' legal guardian/next of kin was not required to participate in this study in accordance with the national legislation and the institutional requirements.

## RESULTS

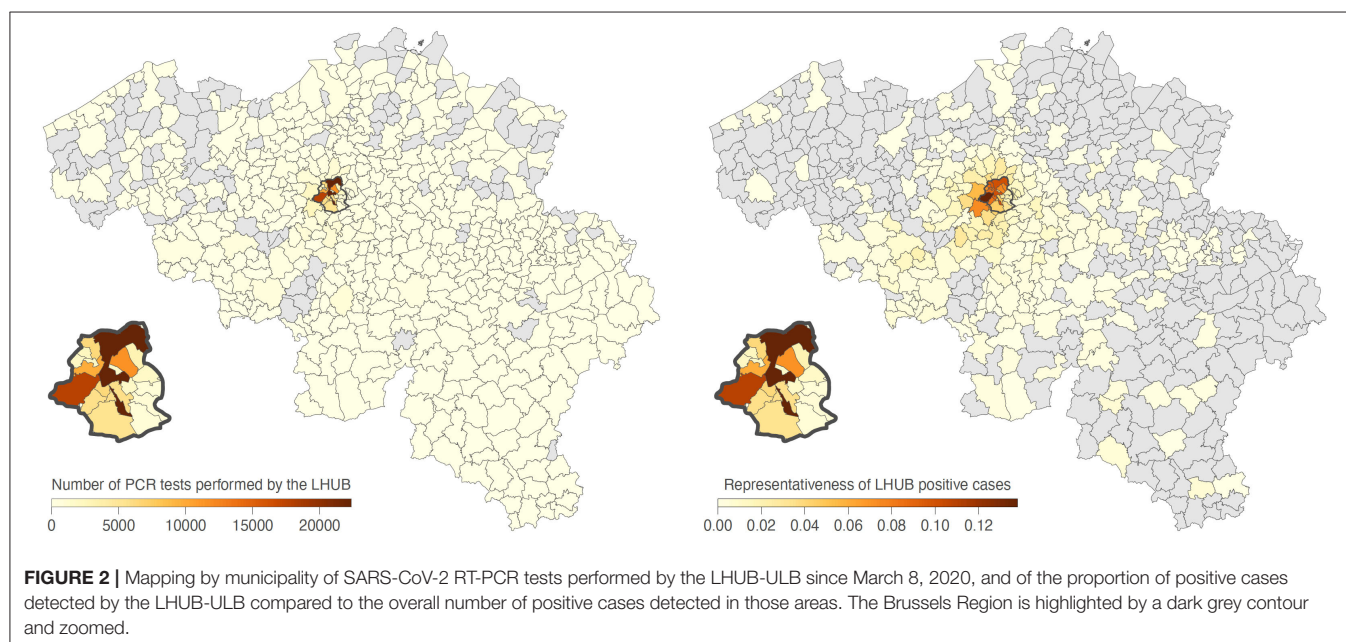
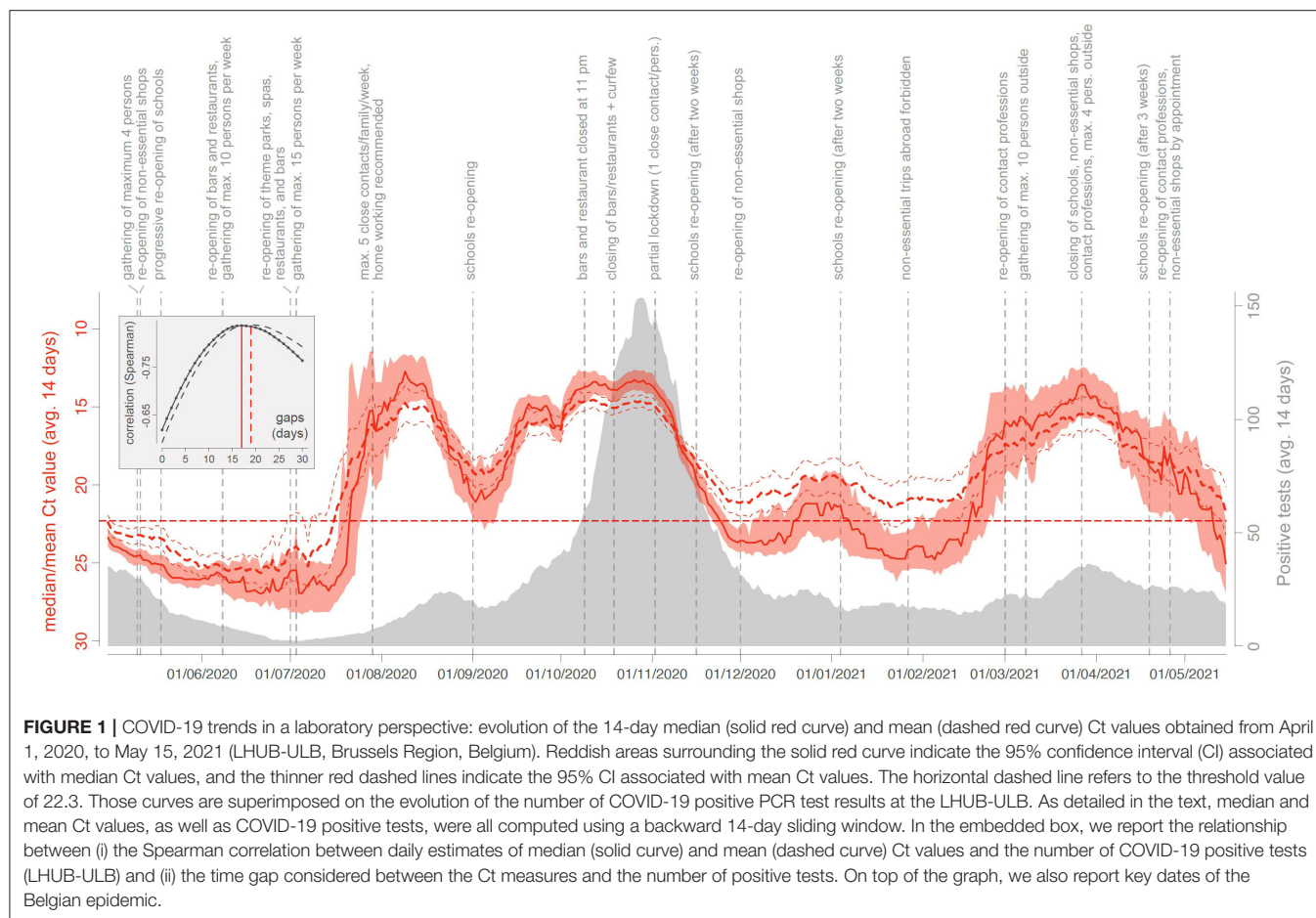
### Ct Values vs. Epidemic Trends

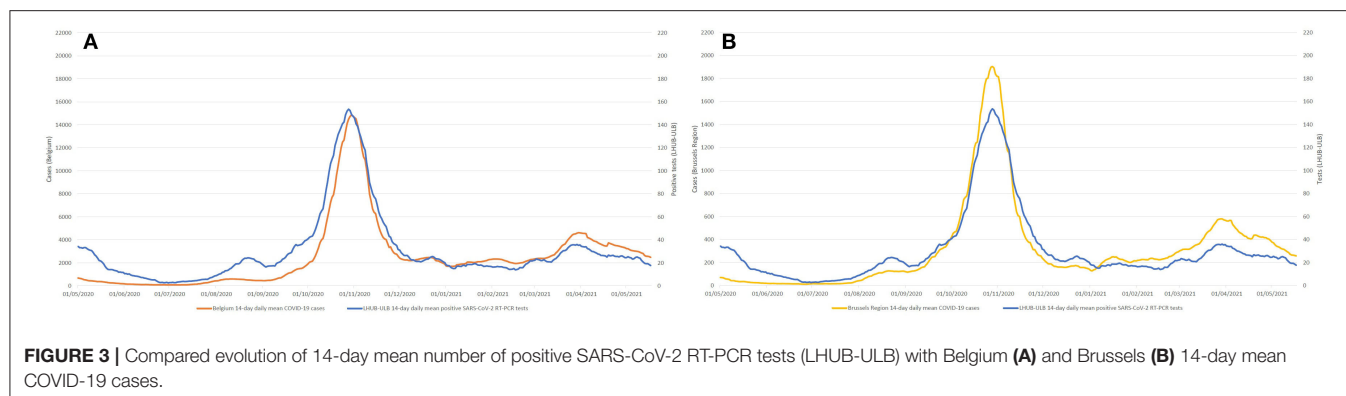
From April 1, 2020, to May 15, 2021, a total of 155,049 SARS-CoV-2 RT-PCR were performed in the LHUB-ULB and resulted in 12,771 positive results of which 7,906 Cts were analysed. A peak of LHUB-ULB 14-day mean daily positive tests was reached during the Belgian second wave on October 28, 2020 ( $n = 153.6$ , **Figure 1**). Beforehand, a lower peak was reached during the summer on August 22, 2020 ( $n = 24.4$ ). In both cases, these peaks were preceded by a drastic decrease in the 14-day median Ct values reaching local minima, respectively, 16 days before (13.12 on October 12, 2020) and 12 days before (12.76 on August 10, 2020). Ct values were negatively correlated with the number of LHUB-ULB positive tests, with a maximum reached for the correlation between the 14-day median Ct values with a lag of 17 days and the 14-day mean positive tests ( $r_s = -0.836$ ), as well as between the 14-day mean Ct values with a lag of 19 days and the 14-day mean positive tests ( $r_s = -0.834$ ).

### CML Data vs. Local and National Data

During the same period, a total of 1,381,393 tests were performed across the Brussels Region and 13,219,135 tests across the whole of Belgian territory, of which, respectively, 142,562 and 1,131,719 tests were positive. Overall, LHUB-ULB performed, respectively, 8.96% (12,771/142,562) and 1.13% (12,771/1,131,719) of all positive tests reported in the Brussels Region and at the national level. **Figure 2** shows the geographical distribution by postal code of the confirmed COVID-19 cases notified by the LHUB-ULB to Sciensano and the LHUB-ULB's representativeness in the COVID-19 notification (proportion of cases identified by the national surveillance network thank to the reporting of LHUB-ULB positive test results). Beside the Brussels Region, which concentrated most of the tests produced by the LHUB-ULB, its service area extended to several municipalities in Walloon and Flemish Region with, for some of them, about 5% of all notifications. Overall, the number of positive tests produced by the LHUB-ULB showed a high correlation with the regional and national trends of the incidence of COVID-19 notifications with coinciding start, peak and end of the different waves of the epidemic. The 14-day average number of positive tests in LHUB-ULB were strongly correlated with the 14-day average number of







positive tests in the Brussels Region ( $r_s = 0.843$ ) and in Belgium ( $r_s = 0.810$ ) but also with the 14-day average confirmed cases in the Brussels Region ( $r_s = 0.832$ ) and in the whole country ( $r_s = 0.804$ ) (Figure 3).

### Ct Values Trends vs. Epidemic's Dynamics

In Figure 4, the 14-days median estimates of daily Ct values are plotted in a white to blue colour scale on the phase diagram introduced above, showing how Ct values decrease when the situation worsens (and vice versa) in trends making clockwise movements. Figure 4A shows the downward trend of the end of the first epidemic wave during which the growth in new hospitalisations progressively decreased to reach below 0%, a moment at which the number of new hospitalisations started to decline: the Ct values, low at the peak, increase when the number of new hospitalisations starts to decline. In Figure 4B, an upward trend was observed, leading to a small summer wave. As soon as both growth and hospitalisations passed from the green “safe zone” to the yellow region of “increased vigilance,” the Ct values started to decrease, concurrently crossing the threshold value of 22.3. The opposite effect was observed when the points fell in the green region. The second wave is visualised in Figure 4C, with a clear decrease and increase of the Ct values. Finally, Figure 4D corresponds to the third wave, with again the same pattern observed in the evolution of Ct values.

### Ct Values Trends vs. Modelled Prevalence by Age Group

In Figure 5, the median of daily Ct values for different age groups are compared to the daily estimated prevalence of those age groups. The overall behaviour of Ct values was almost similar for all age classes and was negatively correlated to the estimated prevalence.

## DISCUSSION

Estimating the likely number of infected patients during epidemics but also the dynamics of spreading in the population is crucial to carry out adequate testing and infection control measures. As large and accurate data providers, CMLs can adequately support hospital capacity planning by providing valuable real-time information about the incidence trends of the

pandemic. This was already established by a previous study on influenza (2), but seems to be even more relevant in the context of a more severe disease like COVID-19, where hospital capacities are crucially challenged. Indeed, LHUB-ULB processed on its own 8.95% of the SARS-CoV-2 testing in the Brussels-Capital Region and was proved here to be representative not only of the region but to a certain extent, the whole country due its central geographic position in Belgium. A step further would be to capitalise on the ability of these CMLs to rapidly detect and communicate abnormal events such as sudden increase or emergence of variants of concern without the delay resulting from sending samples to central sequencing platforms. Thanks to the expertise gained in such data integration, UK scientists were able to rapidly share an early assessment of the variant Alpha's (lineage B.1.1.7) genomic characteristics and associated clinical outcomes (20).

Complementarily, and providing an adequate standardisation under appropriate management and regulatory structures, “virtual” CMLs consolidation can also adequately support ongoing COVID-19 surveillance by connecting some or all the produced data to national public health surveillance systems. In the frame of the COVID-19 pandemic, Sciensano started to monitor on a daily basis the epidemiological situation of SARS-CoV-2 in the country through multiple surveillance systems including the “healthdata.be” platform aggregating all information from all CMLs located in Belgium (21–23). The added value of such a combined structure was already demonstrated for monitoring viral infections by the Infection Response Through Virus Genomics-ICONIC consortium in London (24).

Beyond the variation of the infectiousness over time, our results suggest that following the trend of SARS-CoV-2 RT-PCR Ct values could predict the epidemic trends. Recently infected patients are known to have higher viral load, thus higher infectiousness (25). A decrease in Ct values, linked to an increase of recently infected people is likely to favour spreading, and goes hand in hand with an increase in the total number of cases. On the contrary, inpatients are known to have higher Ct values because of a longer evolution since the onset of the disease. Thus, the overall increase of Ct values can be observed before the decrease of hospitalisations at the decreasing phase of an epidemic wave. By gathering enough comparable data

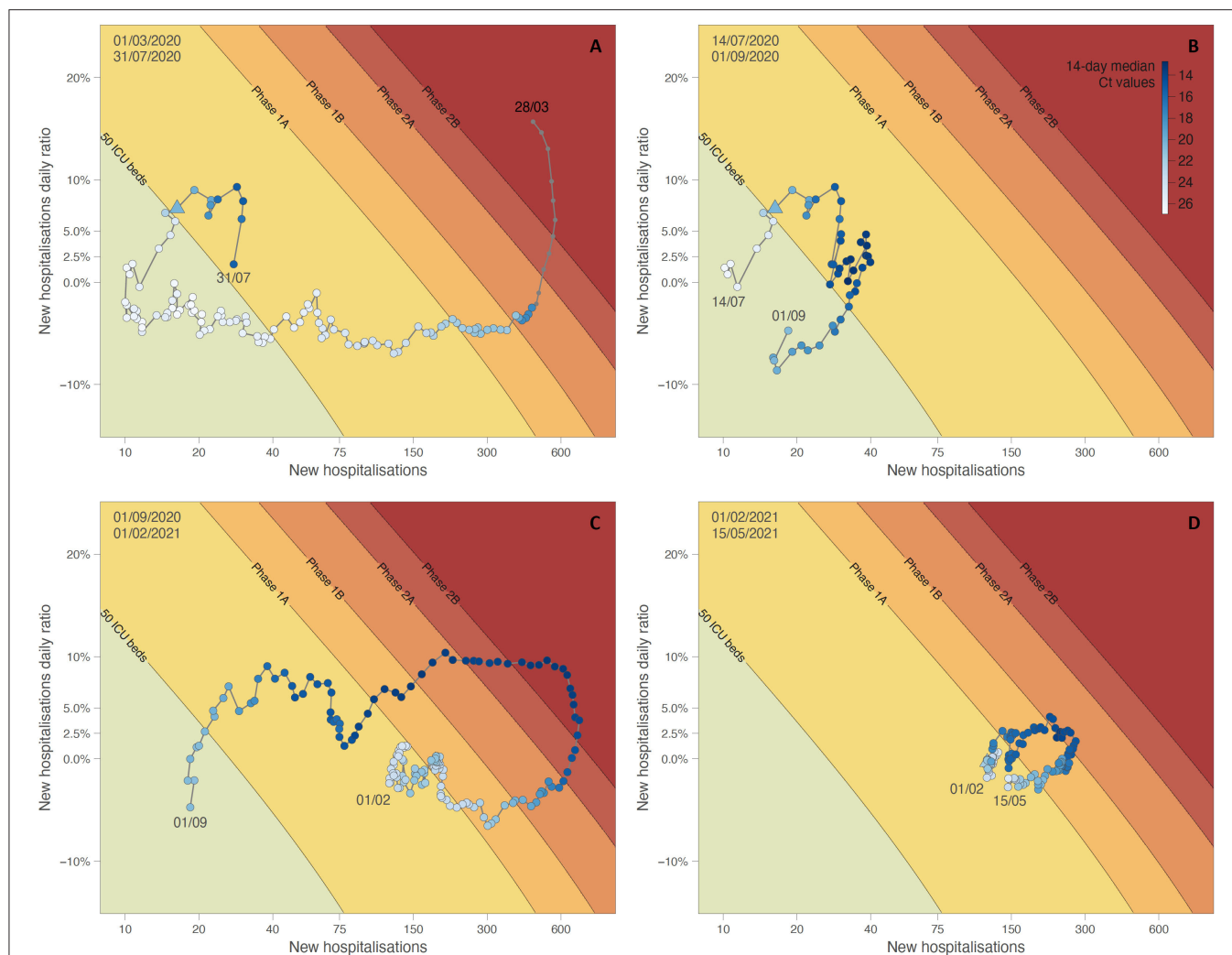
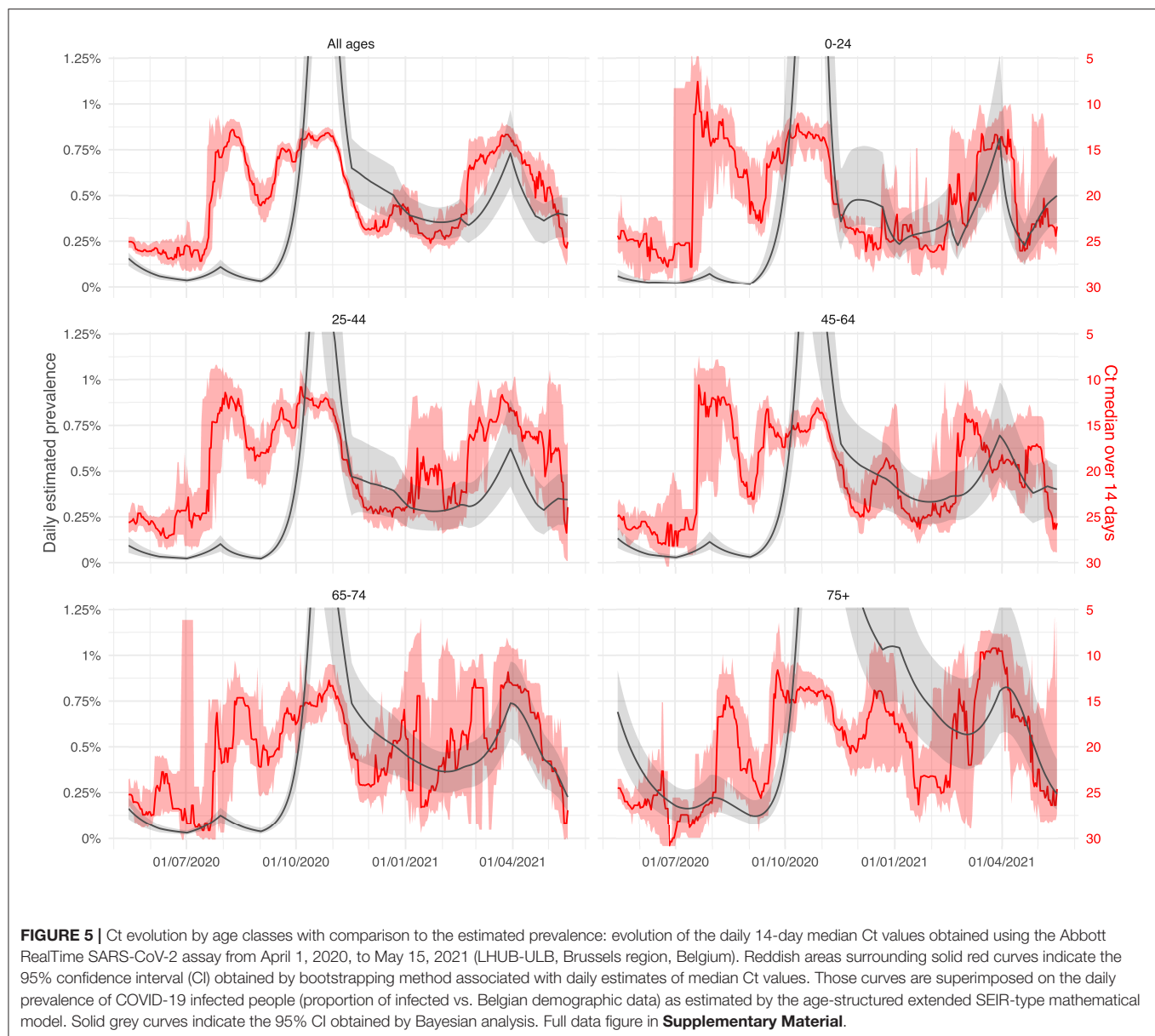


**FIGURE 4 |** Phase diagram generated for different time periods: situation from March 1 to July 14, 2020 **(A)**, situation from July 14 to September 1, 2020 **(B)**, and situation from September 1, 2020, to February 1, 2021 **(C)**, situation from February 1 until May 15, 2021 **(D)**. See the text for further detail on the principle of phase diagrams. Dots of the phase diagram are coloured according to 14-day median Ct values (thus computed using a backward sliding window of 14 days, from May 1, 2020). Triangle symbols indicate the dates when Ct values crossed down the threshold value of 22.3.

using semi-quantitative results, our Ct values based surveillance systems could approach in real time the average level of viral load in the population, hence approach the current spreading of the virus before the increase of cases becomes apparent, while avoiding the recurrent problem of normalisation. Predicting the shape and the size of the epidemic curve is not straightforward; and many parameters may influence it such as seasonality, infection control measures and population immunity level, to cite a few. The evolution of 14-day median Ct values was also tested against the daily estimated prevalence by age classes, and Ct values were similarly negatively correlated for all age classes, even we observed a shift by approximately half a month for the 75+ which might be due to intergenerational transmission. However, a starting divergence was observed in May 2021, with Ct values increasing for the oldest classes while remaining low for the youngest one. This was related to a period of

resumption of activities in Belgium such as reopening of schools, while older age-classes were progressively becoming protected through the vaccination campaign. The prevalence projections from the compartmental model followed the same trend. Hence, Ct values divergence by age classes could be a good indicator of a divergence in transmission in these age classes.

Following the trend of the Ct values might have helped the decision makers as demonstrated with the integration of the Ct values in a phase diagram predicting the number of COVID-19 patients requiring intensive care at a national level. For instance, in March 2021, after a long period of stagnation in the epidemic, the Belgian government decided to reopen close-contact professions and increased the number of people authorised to gather outside, at a time when Ct values were decreasing. This reopening was reversed a few weeks later due to the increase of cases underlining the untimely decision. During



the summer 2020, the evolution of Ct values accurately followed the dynamic of the epidemic with an increase accompanying each decrease of the pressure on hospitals. But the shift between the initial diagnosis, the admission, and the length of stay for COVID-19 inpatients makes it harder to anticipate the trends in hospitalisation between October 2020 and March 2021 when the epidemic had no real break between peaks and the tension in hospital beds remained stable. Only future evolution after a real epidemic reflux could confirm the added value of following the Ct values to anticipate the phase shifts.

At the hospital level, being able to foresee epidemic dynamics could allow a greater ability to anticipate measures such as pre-admission screenings, isolation, and postponement of non-urgent interventions, triage, and upscaling of human resources. In our study, each epidemic wave was preceded by a drastic

decrease of Ct values, the median crossing back the  $Ct = 22.3$  value threshold (i.e. the proportion of “weak positive” tests went below 50%), setting here an eventual easy-to-evaluate parameter at the local level. This threshold value of 22.3 was clearly crossed back concurrently with the passage of the number of new hospitalisations vs. the new hospitalisations’ daily ratio from the green “safe zone” to the yellow region of “increased vigilance” in the phase diagram. Even if the setting described here should likely be adjusted before being transposed to other laboratories to take account of the specificity of their own patients (ratios inpatients/outpatients and symptomatic/asymptomatic), repeating this exercise with their own data could allow them to set up their own alarm threshold. Likewise, local and national surveillance systems should track the difference in the proportion of strong vs. weak positive results to model the dynamics of the



epidemic and thus to provide guidance for prevention measures as suggested by Hay et al. (9).

A potential weakness of our data is that a limited part of the LHUB-ULB activity relies on ambulatory patients at the general practitioner level. Being able to reach this “non-hospitalised” population would likely increase the sensitivity of a surveillance system to weak signals when the epidemic begins in the community before affecting hospitals. However, the fact that overall behaviour of Ct values was almost similar for all age classes and was negatively correlated to the estimated prevalence in the compartment model indicates that our data capture the whole Belgian population to a sufficient extent. One could also argue that correlation between Ct value and actual viral load depends on many factors, such as sampling method, targeted genes, primers and probes, and possible mutations in targeted genes (26). Due to the absence of standardisation between SARS-CoV-2 RT-PCR assays, we only analysed Ct values obtained using one RT-PCR assay performed on nasopharyngeal swabs all along the studied period. We do believe that their number is sufficient to neutralise the effect of measurement bias. Furthermore, it has been discussed that some variants could exhibit an average higher viral load (20, 27, 28) which could directly impact observed trends in the overall evolution of Ct values. Nevertheless, this potentially higher viral load is likely to favour infectiousness and should not introduce a bias regarding epidemic surveillance.

In conclusion, this study established a correlation between the trends in the SARS-CoV-2 RT-PCR Ct values and the trends of the COVID-19 incidence a few days later. Following the dynamics of the average viral load could add a dimension in the surveillance of respiratory infectious diseases. Moreover, it underlines that the considerable amount of data daily collected by CMLs can play a key role at both local level and beyond, depending on the geographical area they serve. By gathering comparable laboratory data approaching the average viral load of respiratory viruses in the population, surveillance systems might be able to better follow epidemic dynamics, establish forecast models, capture weak signals, and thus anticipate uncontrolled spreading.

## DATA AVAILABILITY STATEMENT

The datasets presented in this study can be found in online repositories. The names of the repository/repositories and accession number(s) can be found at: [https://github.com/sdellicour/Ct\\_measures\\_LHUB](https://github.com/sdellicour/Ct_measures_LHUB).

## ETHICS STATEMENT

Data from all sources were collected retrospectively and anonymously before analysis from a routine surveillance

perspective without any additional intervention. Therefore, ethical review and approval was not required for the study on human participants in accordance with the local legislation and institutional requirements. Written informed consent from the participants' legal guardian/next of kin was not required to participate in this study in accordance with the national legislation and the institutional requirements.

## AUTHOR CONTRIBUTIONS

NY, SD, VD, LN, MH, and OV designed the study. NY and SD managed the database. NY, SD, DV, VD, and NF did the statistical analyses. NY, VD, MW, and MH validated the laboratory analyses on clinical samples. NY, SD, VD, NF, CF, MH, and OV accessed and verified the data. NY, SD, NF, MH, and OV wrote the paper. All authors had the opportunity to discuss the results, comment on the manuscript, full access to all the data in the study, and final responsibility for the decision to submit for publication.

## FUNDING

SD was supported by the Fonds National de la Recherche Scientifique (FNRS, Belgium). NF, CF, and NH acknowledge support from the European Union's Horizon 2020 research and innovation program (NF and NH: Grant Number: 682540—TransMID project; CF and NH: Grant Number: 101003688—EpiPose project).

## ACKNOWLEDGMENTS

We wish to thank the personnel of the LHUB-ULB for its daily technical assistance. The authors would like to thank Dirk Thielens for his appreciable assistance. This work is dedicated to the healthcare workers, the patients, and families affected by SARS-CoV-2.

## SUPPLEMENTARY MATERIAL

The Supplementary Material for this article can be found online at: <https://www.frontiersin.org/articles/10.3389/fmed.2021.743988/full#supplementary-material>

**Supplementary Figure 1** | Ct evolution by age classes with comparison to the estimated prevalence: evolution of the daily 14-day median Ct values obtained using the Abbott RealTime SARS-CoV-2 assay from April 1, 2020, to May 15, 2021 (LHUB-ULB, Brussels region, Belgium, full data figure). Reddish areas surrounding solid red curves indicate the 95% confidence interval (CI) obtained by bootstrapping method associated with daily estimates of median Ct values. Those curves are superimposed on the daily prevalence of COVID-19 infected people (proportion of infected vs. Belgian demographic data) as estimated by the age-structured extended SEIR-type mathematical model. Solid grey curves indicate the 95% CI obtained by Bayesian analysis.

## REFERENCES

- Vandenberg O, Martiny D, Rochas O, van Belkum A, Kozlakidis Z. Considerations for diagnostic COVID-19 tests. *Nat Rev Microbiol.* (2021) 19:171–83. doi: 10.1038/s41579-020-00461-z
- Van den Wijngaert S, Bossuyt N, Ferns B, Busson L, Serrano G, Wautier M, et al. Bigger and better? Representativeness of the influenza A surveillance using one consolidated clinical microbiology laboratory data set as compared to the Belgian sentinel network of laboratories. *Front Public Health.* (2019) 7:150. doi: 10.3389/fpubh.2019.00150



3. Vandenberg O, Durand G, Hallin M, Diefenbach A, Gant V, Murray P, et al. Consolidation of clinical microbiology laboratories and introduction of transformative technologies. *Clin Microbiol Rev.* (2020) 33:e00057–19. doi: 10.1128/CMR.00057-19
4. Albiger B, Revez J, Leitmeyer KC, Struelens MJ. Networking of public health microbiology laboratories bolsters Europe's defenses against infectious diseases. *Front Public Health.* (2018) 6:46. doi: 10.3389/fpubh.2018.00046
5. Vandenberg O, Kozlakidis Z, Schrenzel J, Struelens MJ, Breuer J. Control of infectious diseases in the era of European clinical microbiology laboratory consolidation: new challenges and opportunities for the patient and for public health surveillance. *Front Med.* (2018) 5:15. doi: 10.3389/fmed.2018.00015
6. Van Oyen H, De Cock J. Obligation de rapportage des résultats PCR/antigéniques et sérologiques dans le cadre de la pandémie COVID-19 (2020). Available online at: [https://covid-19.sciensano.be/sites/default/files/Covid19/COVID-19\\_communication\\_reporting\\_labs\\_to\\_contacttracing\\_20200720\\_FR.pdf](https://covid-19.sciensano.be/sites/default/files/Covid19/COVID-19_communication_reporting_labs_to_contacttracing_20200720_FR.pdf) (accessed May 14, 2021).
7. Cori A, Ferguson NM, Fraser C, Cauchemez S. A new framework and software to estimate time-varying reproduction numbers during epidemics. *Am J Epidemiol.* (2013) 178:1505–12. doi: 10.1093/aje/kwt133
8. Yin N, Debuysschere C, Decroly M, Bouazza FZ, Collot V, Martin C, et al. SARS-CoV-2 diagnostic tests: algorithm and field evaluation from the near patient testing to the automated diagnostic platform. *Front Med.* (2021) 8:650581. doi: 10.3389/fmed.2021.650581
9. Hay JA, Kennedy-Shaffer L, Kanjilal S, Lennon NJ, Gabriel SB, Lipsitch M, et al. Estimating epidemiologic dynamics from cross-sectional viral load distributions. *Science.* (2021) 373:eabh0635. doi: 10.1126/science.abh0635
10. Risk Assessment Group. *RAG Interpretation and Reporting of SARS-CoV-2 PCR Results.* (2020). Available online at: [https://covid-19.sciensano.be/sites/default/files/Covid19/20201208\\_Advice%20RAG%20Interpretation%20and%20reporting%20of%20COVID%20PCR%20results.pdf](https://covid-19.sciensano.be/sites/default/files/Covid19/20201208_Advice%20RAG%20Interpretation%20and%20reporting%20of%20COVID%20PCR%20results.pdf) (accessed May 14, 2021).
11. Rasmussen SA, Jamieson DJ. Public health decision making during Covid-19 — fulfilling the CDC pledge to the American people. *N Engl J Med.* (2020) 383:901–3. doi: 10.1056/NEJMp2026045
12. Willem L, Abrams S, Libin P, Coletti P, Kuylen E, Petrof O, et al. The impact of contact tracing and household bubbles on deconfinement strategies for COVID-19. *Nat Commun.* (2021) 12:1524. doi: 10.1038/s41467-021-21747-7
13. Abrams S, Wambua J, Santermans E, Willem L, Kuylen E, Coletti P, et al. Modelling the early phase of the Belgian COVID-19 epidemic using a stochastic compartmental model and studying its implied future trajectories. *Epidemics.* (2021) 35:100449. doi: 10.1016/j.epidem.2021.100449
14. Coletti P, Libin P, Petrof O, Willem L, Abrams S, Herzog SA, et al. A data-driven metapopulation model for the Belgian COVID-19 epidemic: assessing the impact of lockdown and exit strategies. *BMC Infect Dis.* (2021) 21:503. doi: 10.1186/s12879-021-06092-w
15. Franco, N. COVID-19 Belgium: extended SEIR-QD model with nursing homes and long-term scenarios-based forecasts. *Epidemics.* (2021) 37:100490. doi: 10.1016/j.epidem.2021.100490
16. Faes C, Hens N, Gilbert M. On the timing of interventions to preserve hospital capacity: lessons to be learned from the Belgian SARS-CoV-2 pandemic in 2020. *Arch Public Health.* (2021) 79:164. doi: 10.1186/s13690-021-00685-2
17. Fowler AJ, Dobbs TD, Wan YI, Laloo R, Hui S, Nepogodiev D, et al. Resource requirements for reintroducing elective surgery during the COVID-19 pandemic: modelling study. *Br J Surg.* (2021) 108:97–103. doi: 10.1093/bjs/znaa012
18. Hospital & Transport Surge Capacity Committee (HTSC). *Second Wave in Hospital V.1.9.* (2020). Available online at: [https://organesdeconcertation.sante.belgique.be/sites/default/files/documents/201029\\_htsc\\_second\\_wave\\_in\\_hospital.pdf](https://organesdeconcertation.sante.belgique.be/sites/default/files/documents/201029_htsc_second_wave_in_hospital.pdf) (accessed October 4, 2021).
19. Omori R, Mizumoto K, Chowell G. Changes in testing rates could mask the novel coronavirus disease (COVID-19) growth rate. *Int J Infect Dis.* (2020) 94:116–8. doi: 10.1016/j.ijid.2020.04.021
20. Frampton D, Rampling T, Cross A, Bailey H, Heaney J, Byott M, et al. Genomic characteristics and clinical effect of the emergent SARS-CoV-2 B.1.1.7 lineage in London, UK: a whole-genome sequencing and hospital-based cohort study. *Lancet Infect Dis.* (2021) 21:1246–56. doi: 10.1016/S1473-3099(21)00170-5
21. Muyltermans G, Ducoffre G, Leroy M, Dupont Y, Quolin S, Participating Sentinel Laboratories. Surveillance of infectious diseases by the sentinel laboratory network in Belgium: 30 years of continuous improvement. *PLoS ONE.* (2016) 11:e0160429. doi: 10.1371/journal.pone.0160429
22. Walckiers D, Stroobant A, Yourassowsky E, Lion J, Cornelis R. A sentinel network of microbiological laboratories as a tool for surveillance of infectious diseases in Belgium. *Epidemiol Infect.* (1991) 106:297–303. doi: 10.1017/S0950268800048445
23. Weemaes M, Martens S, Cuypers L, Van Elslande J, Hoet K, Welkenhuysen J, et al. Laboratory information system requirements to manage the COVID-19 pandemic: a report from the Belgian national reference testing center. *J Am Med Inform Assoc.* (2020) 27:1293–9. doi: 10.1093/jamia/ocaa081
24. Harvala H, Frampton D, Grant P, Raffle J, Ferns RB, Kozlakidis Z, et al. Emergence of a novel subclade of influenza A(H3N2) virus in London, December 2016 to January 2017. *Eurosurveillance.* (2017) 22:30466. doi: 10.2807/1560-7917.ES.2017.22.8.30466
25. Singanayagam A, Patel M, Charlett A, Bernal JL, Saliba V, Ellis J, et al. Duration of infectiousness and correlation with RT-PCR cycle threshold values in cases of COVID-19, England, January to May 2020. *Eurosurveillance.* (2020) 25:2001483. doi: 10.2807/1560-7917.ES.2020.25.32.2001483
26. Dahdouh E, Lázaro-Perona F, Romero-Gómez MP, Mingorance J, García-Rodríguez J. Ct values from SARS-CoV-2 diagnostic PCR assays should not be used as direct estimates of viral load. *J Infect.* (2021) 82:414–51. doi: 10.1016/j.jinf.2020.10.017
27. Cornelissen L, André E. Understanding the drivers of transmission of SARS-CoV-2. *Lancet Infect Dis.* (2021) 21:580–1. doi: 10.1016/S1473-3099(21)00005-0
28. Tom MR, Mina MJ. To interpret the SARS-CoV-2 test, consider the cycle threshold value. *Clin Infect Dis.* (2020) 71:2252–4. doi: 10.1093/cid/ci aa619

**Conflict of Interest:** The authors declare that the research was conducted in the absence of any commercial or financial relationships that could be construed as a potential conflict of interest.

**Publisher's Note:** All claims expressed in this article are solely those of the authors and do not necessarily represent those of their affiliated organizations, or those of the publisher, the editors and the reviewers. Any product that may be evaluated in this article, or claim that may be made by its manufacturer, is not guaranteed or endorsed by the publisher.

Copyright © 2021 Yin, Dellicour, Daubie, Franco, Wautier, Faes, Van Cauteren, Nymark, Hens, Gilbert, Hallin and Vandenberg. This is an open-access article distributed under the terms of the Creative Commons Attribution License (CC BY). The use, distribution or reproduction in other forums is permitted, provided the original author(s) and the copyright owner(s) are credited and that the original publication in this journal is cited, in accordance with accepted academic practice. No use, distribution or reproduction is permitted which does not comply with these terms.



OPEN ACCESS

**Edited by:**

Atefeh Abedini,  
Shahid Beheshti University of Medical  
Sciences, Iran

**Reviewed by:**

Sophie Massin,  
Université d'Artois, France  
Mustafa Kursat Sahin,  
Ondokuz Mayıs University, Turkey  
Bijaya Kumar Padhi,  
Post Graduate Institute of Medical  
Education and Research  
(PGIMER), India

**\*Correspondence:**

Lei Zhao  
leizhao@hust.edu.cn  
Jing Cheng  
chenjin1118@hotmail.com

<sup>†</sup>These authors have contributed  
equally to this work and share first  
authorship

**Specialty section:**

This article was submitted to  
Infectious Diseases – Surveillance,  
Prevention and Treatment,  
a section of the journal  
Frontiers in Medicine

**Received:** 29 July 2021

**Accepted:** 04 October 2021

**Published:** 03 November 2021

**Citation:**

Peng X, Gao P, Wang Q, Wu H-g,  
Yan Y-l, Xia Y, Wang J-y, Lu F, Pan H,  
Yang Y, Liang F, Zhao L and Cheng J  
(2021) Prevalence and Impact Factors  
of COVID-19 Vaccination Hesitancy  
Among Breast Cancer Survivors: A  
Multicenter Cross-Sectional Study in  
China. *Front. Med.* 8:741204.  
doi: 10.3389/fmed.2021.741204

# Prevalence and Impact Factors of COVID-19 Vaccination Hesitancy Among Breast Cancer Survivors: A Multicenter Cross-Sectional Study in China

Xin Peng<sup>1†</sup>, Ping Gao<sup>1†</sup>, Qiong Wang<sup>1</sup>, Hong-ge Wu<sup>1</sup>, Yun-li Yan<sup>2</sup>, Ying Xia<sup>3</sup>,  
Jian-ying Wang<sup>4</sup>, Fang Lu<sup>5</sup>, Hong Pan<sup>6</sup>, Yi Yang<sup>1</sup>, Fan Liang<sup>1</sup>, Lei Zhao<sup>7\*</sup> and Jing Cheng<sup>1\*</sup>

<sup>1</sup> Cancer Center, Union Hospital, Tongji Medical College, Huazhong University of Science and Technology, Wuhan, China,

<sup>2</sup> Department of Breast Center, Hebei Cancer Hospital, Wuhan, China, <sup>3</sup> Department of Thyroid Breast Surgery, Tongji

Hospital, Tongji Medical College, Huazhong University of Science and Technology, Wuhan, China, <sup>4</sup> Department of Thyroid

Breast Surgery, Renmin Hospital of Wuhan University, Wuhan, China, <sup>5</sup> Department of Thyroid and Breast Gland Surgery,

Zhongnan Hospital of Wuhan University, Wuhan, China, <sup>6</sup> Department of Thyroid Breast Surgery, Wuhan Central Hospital,

Wuhan, China, <sup>7</sup> Department of Infectious Diseases, Union Hospital, Tongji Medical College, Huazhong University of Science  
and Technology, Wuhan, China

Cancer patients are at a high risk of being infected with COVID-19 and have a poor prognosis after infection. Breast cancer is one of the most common cancers. Since vaccination is an effective measure to prevent the spread of COVID-19, we studied the vaccination rate among breast cancer survivors and analyzed their characteristics to provide evidence for boosting the vaccination rate. The researchers conducted a multicenter, cross-sectional study on 747 breast cancer survivors from six hospitals in Wuhan city between June 5, 2021, and June 12, 2021. The self-administrated questionnaires based on relevant studies were distributed. The researchers then compared differences in characteristics among vaccinated patients, hesitant patients, and non-vaccinated patients. Moreover, they performed univariable and multivariable logistic regression analyses to identify potential factors associated with vaccination hesitancy. The researchers assessed a total of 744 breast cancer survivors –94 cases in the vaccinated group, 103 in the planning group, 295 in the hesitancy group, and 252 in the refusal group. The vaccination rate was 12.63% (95% CI 10.25–15.02%) and 37.23% (95% CI 27.48–47.82%) patients reported adverse reactions. The vaccination hesitancy/refusal rate was 73.52% (95% CI 70.19–76.66%), which was independently associated with current endocrine or targeted therapy (odds ratio [OR] = 1.52, 95% CI 1.03–2.24), no notification from communities or units (OR = 2.46, 95% CI 1.69–3.59) and self-perceived feel (general vs. good, OR = 1.46, 95% CI 1.01–2.13; bad vs. good, OR = 4.75, 95% CI 1.85–12.16). In the hesitancy/refusal group, the primary reason was “I did not know who to ask whether I can get vaccinated” (46.07%), the person

who would most influence decisions of patients was the doctor in charge of treatment (35.83%). Effective interaction between doctors and patients, simple and consistent practical guidelines on vaccination, and timely and positive information from authoritative media could combat misinformation and greatly reduce vaccine hesitancy among breast cancer survivors.

**Keywords:** COVID-19, vaccination, breast cancer, vaccine hesitancy, vaccination rate

## INTRODUCTION

Since December 2019, Wuhan, China reported a cluster of novel COVID-19 cases that were caused by severe acute respiratory syndrome coronavirus 2 (SARS-CoV-2) (1, 2). COVID-19 rapidly spread worldwide with high contagion and has been officially declared a global pandemic (3). As of June 12, 2021, about 170 million cases of COVID-19 were confirmed worldwide, including about 3.8 million deaths (4). Cancer patients are a population of specific interest during the COVID-19 pandemic. Treatment-related side effects and other underlying diseases might present an immunosuppressive state and malnutrition in cancer patients. Two reviews suggested that cancer patients were highly vulnerable to SARS-CoV-2 and poor prognosis after infection, including high risk of mortality and intensive care unit admission (5, 6). Based on the global cancer statistics of 2020, female breast cancer has become the world's most prevalent cancer, and its incidence ranked higher than that of lung cancer (7). The statistics suggested that a large number of breast cancer patients had the risk of COVID-19 infection.

COVID-19 vaccines were touted as a promising preventive measure to mitigate the spread of COVID-19 (8). To accelerate its development, more than 200 vaccine candidates were studied for their efficacy against COVID-19, and the process of relevant clinical trials was accelerated. At present, a number of COVID-19 vaccines worldwide have received emergency use authorization. COVID-19 vaccination is facing insufficient confidence, changing acceptance, and preference heterogeneity from the public (9, 10). The delay in acceptance or refusal of vaccination despite the availability of vaccination services is known as vaccine hesitancy (11). Vaccine hesitancy caused by concerns about the safety of rapidly developed COVID-19 vaccines has been a great challenge in the fight against the COVID-19 pandemic (12). Targeting populations at risk of vaccine hesitancy with customized measures based on their characteristics is needed.

Cancer patients should be prioritized for COVID-19 vaccination (13) as they are a vulnerable population. A recent study showed that most patients with cancer should be recommended to receive vaccines when possible (14). However, many COVID-19 vaccine trials excluded cancer patients to limit the data on safety and tolerance. Meanwhile, ongoing cancer-related treatment would make their health condition unstable. Both situations made cancer patients hesitant about receiving a COVID-19 vaccine. One report suggested that as many as 30% of cancer patients were vaccine hesitant (15, 16). The number of breast cancer patients was huge. Meanwhile, following an intramuscular vaccine, axillary lymphadenopathy, which is easily

confused with the axillary lymph node enlargement caused by cancer, was observed (17).

Studying vaccine hesitancy among breast cancer patients had great significance. Recently, Villarreal-Garza et al. studied vaccine hesitancy among 540 breast cancer patients residing in Mexico by social media channels of non-governmental organizations and observed a 34% vaccine hesitancy rate (18). This study discussed the willingness to vaccination but did not report the vaccination rate and related side effects. In this cross-sectional study, we recruited breast cancer survivors admitted to six local tertiary hospitals in Wuhan city, China. We estimated the vaccination rate and related side effects, along with vaccine considerations and informative routine on vaccine hesitancy. The findings of this study would help target possible hesitant breast cancer survivors and provide evidence for customizing strategies to improve the vaccination rate.

## METHODS

### Study Design, Setting, and Participants

There are about 30 tertiary and graded A levels in Wuhan city, China. In this study, six major hospitals, which covered most cancer patients, were selected for this multicenter, cross-sectional survey. From June 5, 2021, to June 12, 2021, an anonymous web-based questionnaire was distributed through WeChat (a popular social media platform in China) to collect data; information confidentiality was guaranteed to each participant. The study had been approved by the Ethics Committee of Wuhan Union Hospital, Tongji Medical College, and Huazhong University of Science and Technology (20210580). We recruited patients who were diagnosed with breast cancer and were older than 18 years. Participants submitted an informed consent form before their enrollment. The exclusion criteria included (1) cognitive impairment, which might affect judgment and questionnaire filling; (2) taking <90 s to fill out the questionnaire; and (3) logical error in reported data.

### Data Collection

Healthcare professionals working in the field of breast cancer reviewed the questionnaire for content validity. Moreover, we conducted a pilot study for feasibility and recorded the average time required to fill out the questionnaire. The questionnaire consisted of five parts: (1) demographic characteristics; (2) status and willingness toward vaccination; (3) side effects among vaccinated participants; (4) reasons for non-vaccination and the person who would influence your decision and consideration in being vaccinated among non-vaccinated participants; and (5) channels and preference of vaccine promotion.

**TABLE 1** | Basic characteristics of breast cancer survivors.

| Characteristics                         | All patients<br>(N = 744) | Vaccinated<br>group<br>(N = 94) | Non-vaccinated group (N = 650)       |                              |                               | P                    |
|---|---------------------------|---------------------------------|--------------------------------------|------------------------------|-------------------------------|----------------------|
|   |                           |                                 | Planning<br>vaccination<br>(N = 103) | Hesitancy group<br>(N = 295) | Refusal<br>group<br>(N = 252) |                      |
| Sex                                     |                           |                                 |                                      |                              |                               | 1.000                |
| Male                                    | 3 (0.40%)                 | 0 (0.00%)                       | 0 (0.00%)                            | 2 (0.68%)                    | 1 (0.40%)                     |                      |
| Female                                  | 741 (99.60%)              | 94 (100.00%)                    | 103 (100.00%)                        | 293 (99.32%)                 | 251 (99.60%)                  |                      |
| Age, years                              | 48.00 (40.00,<br>54.00)   | 48.00 (42.00,<br>57.00)         | 50.00 (42.00,<br>57.00)              | 46.00 (40.00,<br>54.00)      | 47.00 (40.00,<br>53.00)       | 0.080                |
| <40                                     | 188 (25.27%)              | 18 (19.15%)                     | 20 (19.42%)                          | 79 (26.78%)                  | 71 (28.17%)                   | 0.459                |
| 40~60                                   | 477 (64.11%)              | 64 (68.09%)                     | 70 (67.96%)                          | 186 (63.05%)                 | 157 (62.30%)                  |                      |
| >60                                     | 79 (10.62%)               | 12 (12.77%)                     | 13 (12.62%)                          | 30 (10.17%)                  | 24 (9.52%)                    |                      |
| Marital status                          |                           |                                 |                                      |                              |                               | 0.912                |
| Unmarried                               | 19 (2.55%)                | 3 (3.19%)                       | 2 (1.94%)                            | 8 (2.71%)                    | 6 (2.38%)                     |                      |
| Married                                 | 672 (90.32%)              | 86 (91.49%)                     | 91 (88.35%)                          | 268 (90.85%)                 | 227 (90.08%)                  |                      |
| Others                                  | 53 (7.12%)                | 5 (5.32%)                       | 10 (9.71%)                           | 19 (6.44%)                   | 19 (7.54%)                    |                      |
| Educational level                       |                           |                                 |                                      |                              |                               | 0.144                |
| Middle school and below                 | 241 (32.39%)              | 26 (27.66%)                     | 38 (36.89%)                          | 88 (29.83%)                  | 89 (35.32%)                   |                      |
| High school                             | 142 (19.09%)              | 16 (17.02%)                     | 15 (14.56%)                          | 54 (18.31%)                  | 57 (22.62%)                   |                      |
| Junior college                          | 200 (26.88%)              | 32 (34.04%)                     | 29 (28.16%)                          | 89 (30.17%)                  | 50 (19.84%)                   |                      |
| Bachelor and above                      | 161 (21.64%)              | 20 (21.28%)                     | 21 (20.39%)                          | 64 (21.69%)                  | 56 (22.22%)                   |                      |
| Number of members in family             |                           |                                 |                                      |                              |                               | 0.388                |
| 1~2                                     | 152 (20.43%)              | 29 (30.85%)                     | 22 (21.36%)                          | 57 (19.32%)                  | 44 (17.46%)                   |                      |
| 3                                       | 275 (36.96%)              | 30 (31.91%)                     | 41 (39.81%)                          | 104 (35.25%)                 | 100 (39.68%)                  |                      |
| 4                                       | 156 (20.97%)              | 17 (18.09%)                     | 20 (19.42%)                          | 67 (22.71%)                  | 52 (20.63%)                   |                      |
| 5~                                      | 161 (21.64%)              | 18 (19.15%)                     | 20 (19.42%)                          | 67 (22.71%)                  | 56 (22.22%)                   |                      |
| Annual income, yuan                     |                           |                                 |                                      |                              |                               | 0.745                |
| <20,000                                 | 195 (26.21%)              | 20 (21.28%)                     | 25 (24.27%)                          | 78 (26.44%)                  | 72 (28.57%)                   |                      |
| 20,000~100,000                          | 371 (49.87%)              | 51 (54.26%)                     | 51 (49.51%)                          | 140 (47.46%)                 | 129 (51.19%)                  |                      |
| 110,000~200,000                         | 111 (14.92%)              | 12 (12.77%)                     | 18 (17.48%)                          | 49 (16.61%)                  | 32 (12.70%)                   |                      |
| >200,000                                | 67 (9.01%)                | 11 (11.70%)                     | 9 (8.74%)                            | 28 (9.49%)                   | 19 (7.54%)                    |                      |
| Medical cost                            |                           |                                 |                                      |                              |                               | 0.45                 |
| Self-paid                               | 39 (5.24%)                | 2 (2.13%)                       | 6 (5.83%)                            | 17 (5.76%)                   | 14 (5.56%)                    |                      |
| Insurance                               | 684 (91.94%)              | 87 (92.55%)                     | 94 (91.26%)                          | 269 (91.19%)                 | 234 (92.86%)                  |                      |
| Others                                  | 21 (2.82%)                | 5 (5.32%)                       | 3 (2.91%)                            | 9 (3.05%)                    | 4 (1.59%)                     |                      |
| Duration of cancer, year                |                           |                                 |                                      |                              |                               | 0.003 <sup>b,c</sup> |
| <1                                      | 275 (36.96%)              | 26 (27.66%)                     | 40 (38.83%)                          | 104 (35.25%)                 | 105 (41.67%)                  |                      |
| 1~3                                     | 326 (43.82%)              | 35 (37.23%)                     | 45 (43.69%)                          | 139 (47.12%)                 | 107 (42.46%)                  |                      |
| 4~5                                     | 77 (10.35%)               | 15 (15.96%)                     | 11 (10.68%)                          | 33 (11.19%)                  | 18 (7.14%)                    |                      |
| >5                                      | 66 (8.87%)                | 18 (19.15%)                     | 7 (6.80%)                            | 19 (6.44%)                   | 22 (8.73%)                    |                      |
| Self-perceived feel                     |                           |                                 |                                      |                              |                               | 0.024 <sup>d</sup>   |
| Good                                    | 231 (31.05%)              | 34 (36.17%)                     | 42 (40.78%)                          | 80 (27.12%)                  | 75 (29.76%)                   |                      |
| General                                 | 455 (61.16%)              | 57 (60.64%)                     | 58 (56.31%)                          | 189 (64.07%)                 | 151 (59.92%)                  |                      |
| Bad                                     | 58 (7.80%)                | 3 (3.19%)                       | 3 (2.91%)                            | 26 (8.81%)                   | 26 (10.32%)                   |                      |
| Recent breast cancer-related treatments | 483 (64.92%)              | 53 (56.38%)                     | 67 (65.05%)                          | 187 (63.39%)                 | 176 (69.84%)                  | 0.112                |
| Endocrine/targeted therapy              | 298 (40.05%)              | 25 (26.60%)                     | 36 (34.95%)                          | 130 (44.07%)                 | 107 (42.46%)                  | 0.013 <sup>b,c</sup> |

(Continued)

TABLE 1 | Continued

| Characteristics   | All patients<br>(N = 744) | Vaccinated<br>group<br>(N = 94) | Non-vaccinated group (N = 650)       |                              |                               | P                         |
|---|---------------------------|---------------------------------|--------------------------------------|------------------------------|-------------------------------|---------------------------|
|   |                           |                                 | Planning<br>vaccination<br>(N = 103) | Hesitancy group<br>(N = 295) | Refusal<br>group<br>(N = 252) |                           |
| Chemotherapy  | 134 (18.01%)              | 21 (22.34%)                     | 17 (16.50%)                          | 40 (13.56%)                  | 56 (22.22%)                   | 0.040 <sup>f</sup>        |
| Radiotherapy  | 51 (6.85%)                | 1 (1.06%)                       | 9 (8.74%)                            | 20 (6.78%)                   | 21 (8.33%)                    | 0.095                     |
| <b>COVID-19 related characteristics</b>   |                           |                                 |                                      |                              |                               |                           |
| Had been infected by COVID-19   | 6 (0.81%)                 | 0 (0.00%)                       | 2 (1.94%)                            | 2 (0.68%)                    | 2 (0.79%)                     | 0.496                     |
| Inform from communities or units  | 437 (58.74%)              | 78 (82.98%)                     | 67 (65.05%)                          | 170 (57.63%)                 | 122 (48.41%)                  | <0.001 <sup>a,b,c,e</sup> |
| Existence of no vaccination in family, friends and colleges who met vaccination condition | 361 (48.52%)              | 57 (60.64%)                     | 54 (52.43%)                          | 150 (50.85%)                 | 122 (48.41%)                  | 0.242                     |

Post-hoc comparison with Bonferroni adjustment: <sup>a</sup>Vaccinated group vs. planning group; <sup>b</sup>Vaccinated group vs. hesitancy group; <sup>c</sup>Vaccinated group vs. refusal group; <sup>d</sup>Planning group vs. hesitancy group; <sup>e</sup>Planning group vs. refusal group; <sup>f</sup>Hesitancy group vs. refusal group.

The demographic characteristics criteria included sex, age, marital status (unmarried/married/others), education level (middle school and below/high school/junior college/bachelor's and above), number of members in the family, annual family income (yuan), medical cost (self-paid/insurance/others), duration of cancer (years), and self-perceived feeling (good/general/bad). We also queried the participants about current breast cancer-related treatments, such as endocrine/targeted therapy, chemotherapy, and radiotherapy. COVID-19-related experience, including the infection history of participants and vaccination status of family, friends, and colleagues, was also enquired.

In section Methods, the participants were required to report vaccine status (Yes/No). If yes, they should report the number of vaccination (1/2) and vaccine-related adverse reactions. If their answer was no, participants were asked to report willingness to vaccination in the future (planning/hesitating/refusal). In sections Results and Discussion, we posed questions to participants who hesitated or refused vaccination in the future about reasons for non-vaccination and the person who would influence their decision and considerations in vaccination. Finally, all participants were asked about primary sources of information regarding COVID-19 (television media/mobile media/family and colleagues/medical institutions/communities/others) and their preference for vaccine promotion (70% efficacy rate for preventing infection/30% failure rate for preventing infection/7 out of 10 people can avoid infection).

## Statistical Analysis

We performed statistical description and group comparisons for basic characteristics among four groups: vaccinated group,

planning group, hesitating group, and refusal group. Categorical variables were described using frequencies and percentages. The age variable was categorized into three groups (<40, 40–60, and >60). We expressed continuous variables as means with SDs when normality was met or medians with interquartile ranges (IQRs) when normality was not met and tested the difference between groups in categorical variables using a chi-square test or Fisher's exact test. For differences in continuous variables, we applied Wilcoxon rank-sum test.

Based on the definition of vaccine hesitancy, the hesitancy group and refusal group were combined as the hesitancy/refusal group ( $Y = 1$ ), a combination of the vaccinated group and planning group was defined as the non-hesitancy group ( $Y = 0$ ). Both univariable and multivariable binary logistic regression analyses were performed to explore potential and independent factors associated with vaccine hesitancy, ordinal predictors were treated as nominal variables. We calculated the odds ratio (ORs) and corresponding 95% CI and  $p$ -value. And we used the Hosmer-Lemeshow test to check the goodness of fit for the multivariable logistic model with entering procession. Furthermore, reasons for un-vaccination, the persons who would influence their decision, and their considerations in the vaccine were plotted with a histogram among the defined vaccine hesitancy group (hesitating group and refusal group). Following this, we performed data analysis and visualization using IBM SPSS Statistics (version 22, IBM Corporation, Armonk, NY, USA) and Microsoft PowerPoint 2016. A two-sided  $p$ -value < 0.05 was considered statistical significant.

## RESULTS

A total of 747 participants signed the informed consent form and completed the questionnaire. Three participants were excluded



**TABLE 2 |** Univariable and multivariable logistic regression of characteristics for association with vaccine hesitancy.

| Characteristics                        | Univariable               |              | Multivariable <sup>a</sup> |              |
|--|---------------------------|--------------|----------------------------|--------------|
|  | OR<br>(95% CI)            | P            | OR<br>(95% CI)             | P            |
| <b>Age years</b>                       |                           |              |                            |              |
| 40~60                                  | <b>0.65 (0.43, 0.98)</b>  | <b>0.038</b> | 0.71 (0.44, 1.13)          | 0.152        |
| >60                                    | <b>0.55 (0.30, 0.99)</b>  | <b>0.046</b> | 0.58 (0.29, 1.17)          | 0.127        |
| <40                                    | 1.00                      |              | 1.00                       |              |
| <b>Marital status</b>                  |                           |              |                            |              |
| Unmarried                              | 1.00 (0.36, 2.82)         | 0.998        | 0.76 (0.24, 2.35)          | 0.628        |
| Others                                 | 0.91 (0.49, 1.69)         | 0.755        | 0.99 (0.49, 1.97)          | 0.972        |
| Married                                | 1.00                      |              | 1.00                       |              |
| <b>Educational level</b>               |                           |              |                            |              |
| High school                            | 1.29 (0.79, 2.11)         | 0.302        | 1.39 (0.81, 2.38)          | 0.231        |
| Junior college                         | 0.82 (0.54, 1.25)         | 0.36         | 0.97 (0.59, 1.57)          | 0.889        |
| Bachelor and above                     | 1.06 (0.67, 1.67)         | 0.807        | 1.21 (0.66, 2.21)          | 0.539        |
| Middle school and below                | 1.00                      |              | 1.00                       |              |
| <b>Number of family</b>                |                           |              |                            |              |
| 3                                      | 1.45 (0.94, 2.23)         | 0.091        | 1.29 (0.78, 2.14)          | 0.319        |
| 4                                      | 1.62 (0.99, 2.68)         | 0.057        | 1.45 (0.81, 2.58)          | 0.206        |
| 5~                                     | 1.63 (1.00, 2.68)         | 0.052        | 1.54 (0.87, 2.73)          | 0.142        |
| 1~2                                    | 1.00                      |              | 1.00                       |              |
| <b>Annual income, yuan</b>             |                           |              |                            |              |
| 20,000~100,000                         | 0.79 (0.53, 1.18)         | 0.255        | 0.86 (0.54, 1.35)          | 0.511        |
| 110,000~200,000                        | 0.81 (0.47, 1.38)         | 0.44         | 0.93 (0.48, 1.80)          | 0.827        |
| >200,000                               | 0.71 (0.38, 1.31)         | 0.269        | 0.87 (0.40, 1.87)          | 0.713        |
| <20,000                                | 1.00                      |              | 1.00                       |              |
| <b>Duration of cancer, year</b>        |                           |              |                            |              |
| 1~3                                    | 0.97 (0.67, 1.41)         | 0.878        | 1.02 (0.66, 1.59)          | 0.928        |
| 4~5                                    | 0.62 (0.36, 1.07)         | 0.086        | 0.76 (0.42, 1.40)          | 0.381        |
| >5                                     | <b>0.52 (0.29, 0.91)</b>  | <b>0.023</b> | 0.68 (0.36, 1.28)          | 0.228        |
| <1                                     | 1.00                      |              | 1.00                       |              |
| <b>Self-perceived feel<sup>a</sup></b> |                           |              |                            |              |
| General                                | <b>1.45 (1.03, 2.05)</b>  | <b>0.036</b> | <b>1.46 (1.01, 2.13)</b>   | <b>0.045</b> |
| Bad                                    | <b>4.25 (1.75, 10.33)</b> | <b>0.001</b> | <b>4.75 (1.85, 12.16)</b>  | <b>0.001</b> |
| Good                                   | 1.00                      |              | 1.00                       |              |
| Endocrine or targeted therapy          | <b>1.70 (1.21, 2.41)</b>  | <b>0.003</b> | <b>1.52 (1.03, 2.24)</b>   | <b>0.034</b> |
| Chemotherapy                           | 0.89 (0.59, 1.35)         | 0.586        | 0.85 (0.51, 1.42)          | 0.542        |
| Radiotherapy                           | 1.51 (0.74, 3.08)         | 0.253        | 1.28 (0.59, 2.80)          | 0.533        |
| <b>Medical cost</b>                    |                           |              |                            |              |
| Self-paid                              | 1.39 (0.63, 3.09)         | 0.413        | 1.41 (0.60, 3.27)          | 0.430        |
| Others                                 | 0.58 (0.24, 1.43)         | 0.241        | 0.61 (0.24, 1.58)          | 0.310        |
| Insurance                              | 1.00                      |              | 1.00                       |              |
| Had been infected by COVID-19          | 1.39 (0.25, 7.66)         | 0.704        | 1.38 (0.23, 8.48)          | 0.725        |

(Continued)

**TABLE 2 |** Continued

| Characteristics                           | Univariable              |                  | Multivariable <sup>a</sup> |                  |
|---|--------------------------|------------------|----------------------------|------------------|
|   | OR<br>(95% CI)           | P                | OR<br>(95% CI)             | P                |
| No notification from communities or units | <b>2.44 (1.70, 3.49)</b> | <b>&lt;0.001</b> | <b>2.46 (1.69, 3.59)</b>   | <b>&lt;0.001</b> |
| Existence of no vaccination               | 1.30 (0.94, 1.81)        | 0.111            | 1.27 (0.89, 1.81)          | 0.182            |

OR, odds ratio; CI, confidence interval.

<sup>a</sup>Intercept = -1.56 ( $p = 0.417$ ); Cox & Snellen  $r$  square = 0.08; Nagelkerke  $r$  square = 0.129; C statistics = 0.694. Bold values indicates that are statistically significant.

for taking <90 s; no logical error was found. Total of 744 participants were included in the final analysis. Out of the total, 99.60% of participants were female while the number of male participants was only three (Table 1). Their age ranged from 20 to 83, and the median age was 48 years old. In total, 90.32% of them were married, 67.61% had a high school and higher degree, and 79.47% lived with more than three family members. In total, 73.79% of participants reported an annual income of more than 20,000 yuan, while 91.94% stated that their medical cost was supported by insurance. About 80% of patients had lived with breast cancer for <3 years; only 58 (7.80%) reported bad self-perceived feel. In total, 64.92% of patients had recently undergone breast cancer-related treatments, mainly endocrine and targeted therapy (40.05%). About half of the patients learned about the COVID-19 vaccination from communities or units (58.74%) and found that family members, friends, and colleges who met the vaccination condition were not vaccinated (48.52%).

We divided the surveyed participants into four groups: 94 cases in the vaccinated group, 103 in the planning group, 295 in the hesitancy group, and 252 in the refusal group. The differences in the basic characteristics of the four groups are presented in Table 1. The coverage rate of COVID-19 vaccination was 12.63% (95% CI 10.25–15.02%). Of the 94 vaccinated participants, 35 reported adverse reactions after vaccination (rate was 37.23%, 95% CI 27.48–47.82%), such as 27 cases of local reaction (redness, pain at the site of injection), 2 cases of systematic reaction (fever, fatigue, and headache), and 13 cases of other reactions. Six participants had been infected by COVID-19 previously, but none of them received the vaccination.

The vaccine hesitancy/refusal rate among the sample group was 73.52% (547/744, 95% CI 70.19–76.66%). We used univariable and multivariable logistic regressions to assess the association between basic characteristics and vaccine hesitancy/refusal. In the univariable models, the prevalence of hesitancy/refusal rate was significantly associated with age, years with breast cancer, self-perceived feel, recent endocrine or targeted therapy, and notification from communities or units. In the multivariable model, the  $p$ -value for the Hosmer-Lemeshow test was 0.62, suggesting an acceptable fit. After adjustment,

age and years with breast cancer turned to be non-significant. Compared with good self-perceived feel, general and poor self-perceived feel increased the prevalence of hesitancy/refusal rate, OR = 1.46 (95% CI, 1.01–2.13,  $p = 0.045$ ) and OR = 4.75 (95% CI, 1.85–12.16,  $p = 0.001$ ), respectively. Current endocrine or targeted therapy and no notification from communities or units were also significantly associated with increased risk of hesitancy/refusal, OR = 1.52 (95% CI, 1.03–2.24,  $p = 0.034$ ) and OR = 2.46 (95% CI, 1.69–3.59), respectively (**Table 2**).

Furthermore, we explore the reasons influencing people and considerations regarding vaccines among 547 cases from the vaccine hesitancy/refusal group (**Figure 1**). The most common reason for vaccine hesitancy/refusal was lack of knowledge regarding the eligibility criteria (46.07%), followed by vaccine contraindications (14.81%), “think oneself can get rid of vaccine” (8.04%), and no confidence in the COVID-19 vaccine (0.73%), as can be seen in **Figure 1A**. Additionally, the opinion of doctors in charge of treatment (35.83%), family members (21.76%), and doctors in charge of vaccination (17.55%) influenced the decision of patients to vaccinate, as can be seen in **Figure 1B**. Regarding considerations of the COVID-19 vaccine (**Figure 1C**), 376 cases (68.74%) would get vaccinated if the doctor recommended and 176 (32.18%) would encourage others to get vaccinated, which suggested these cases were still waiting. In total, 31.63% of participants considered the vaccine unsafe for cancer patients, 23.22% were afraid of side effects, and 10.42% did not understand how the COVID-19 vaccine worked.

Finally, to promote COVID-19 vaccination, we collected channels of all participants for collecting vaccine-related information and preferred the wording for vaccine promotion. Mobile and television media were the primary sources for 67.88 and 51.75% of participants, respectively. The majority of participants (89.65%) preferred a “70% efficacy rate for preventing infection” for vaccine promotion.

## DISCUSSION

The COVID-19 pandemic was still widespread in the country, while patients with cancer were at high risk of infection and poor prognosis. Vaccination is an economical and effective measure to prevent and control the pandemic. Based on recommendations from the National Health Services, cancer patients were recommended to get vaccinated after being fully informed and weighing benefits over risks (19–21). To our knowledge, this was the first multicenter, cross-sectional study to assess both vaccination rate and vaccine hesitancy/refusal rate among breast cancer survivors.

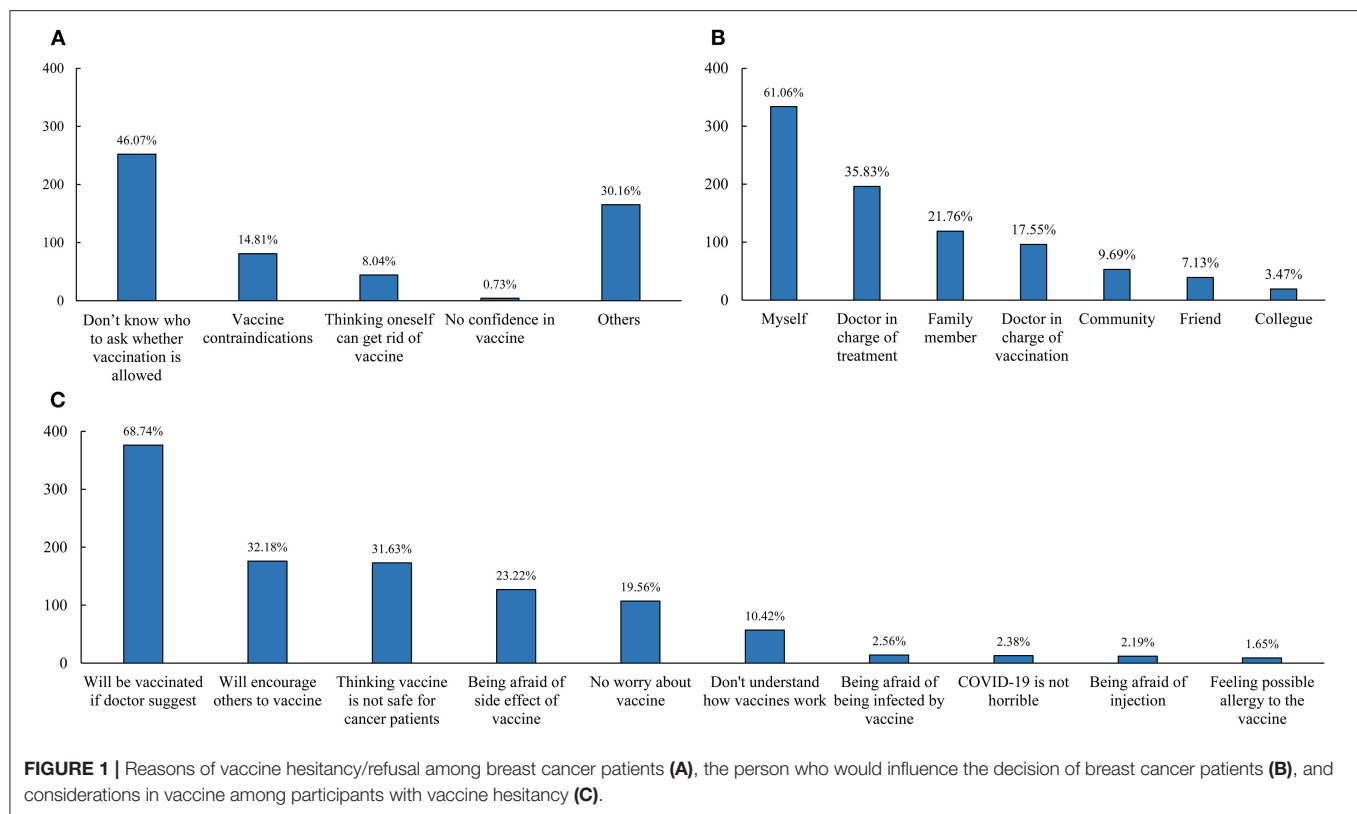
Various vaccines had been developed by different companies, such as Pfizer/BioNTech, Moderna, Johnson & Johnson’s Janssen, and Sinovac and Sinopharm (two Chinese companies). Various protective efficacies and adverse effects in these vaccines with different platforms were reported (22, 23). The Chinese government had initiated the vaccination process on December 15, 2020. As of June 12, 2021, about 800 million doses of the COVID-19 vaccine have been administered, which suggested at least a 30% vaccination rate. However, the vaccination rate

among breast cancer survivors was as low as 12.63%, which was similar to the vaccination rate worldwide (11.2%). In total, 37.23% adverse reactions were observed, and the common reaction was a local reaction at the injection site, which was slightly higher than the findings of two trials on the general population (24, 25). Meanwhile, no axillary adenopathy was observed even though a high rate of axillary adenopathy was reported after the administration of both the Moderna and Pfizer-BioNTech vaccines (21, 26). The low vaccination rate required effective and timely measures for improvement, and only high local reactions should be notified to reduce unavoidable anxiety and worries in vaccinators among breast cancer survivors.

Different levels of vaccine hesitancy had been found in the general public among 33 different countries (27). The nature of motives behind vaccine hesitancy could be complex, including such as policy and social factors, vaccine safety and effectiveness, and knowledge and experience of participants. In our study, researchers observed a high rate of COVID-19 vaccine hesitancy/refusal (73.52%) among breast cancer survivors, which was higher than previous studies on the subject in Mexico (34%) (18). The primary reason for vaccine hesitancy was that patients did not know whom to ask about the vaccination, which was different from concern about adverse effects in the study of Villarreal-Garza C et al. (18). Endocrine or targeted therapy, self-perceived feel, and notification from communities or units were identified as independent factors for vaccine hesitancy. Endocrine or targeted therapy is a long-term, complicated, and individualized treatment for breast cancer (28). The risk of adverse events related to the therapy was high, including the possibility of neutropenia and stomatitis (29). Both active treatment and adverse events would increase vaccine hesitancy in patients. Meanwhile, poor self-perception would decrease confidence of patients and willingness to receive the vaccination. It is notable that notifications about vaccines from communities or units were a powerful facilitator for vaccination. Communities and units were considered as communication centers to disseminate vaccine knowledge effectively.

The incidence of breast cancer varies greatly between male and female. Recently, significant differences between males and females in refusal of COVID-19 vaccination among general and cancer patients had been discussed (30–32). In our study, only three participants were male, and in the hesitant/refusal group, the influence of gender on hesitancy rate was not explored. To guarantee gender equality, the hesitancy rate and related factors in male breast cancer should be studied in the future. Moreover, dozens of COVID-19 vaccine candidates have been developed, and some vaccines with different protective efficacy were approved in an emergent way, potential and long-term side effects were not studied fully. The development of the COVID-19 virus might challenge the efficacy of existed vaccines. The unknown and variation could affect decisions of cancer patients and lead to varying degrees of vaccine hesitancy, which also required further studies.

In the hesitancy/refusal group, patients did not know whom to ask about the vaccination. Moreover, we found that opinions from doctors in charge of the treatment and vaccination could influence the decision of patients. A similar



study (18) highlighted the same in its findings. Doctors play a central role in strengthening the confidence and trust of the public in vaccination. Maintaining an effective interaction and communication between healthcare professionals in charge of either treatment or vaccination of cancer patients could relieve their concern and address the high hesitancy rate (33). Individuals with different social, cultural, and individual backgrounds (34) showed no clear considerations. It is imperative to arrange for professional doctors to establish expert consensus or practical guidelines on vaccination. More importantly, an extended, simple, and clear patient-centered vaccination guideline should be constructed and distributed. This should include guidelines about conditions, precautions, contraindications, and possible vaccination reactions.

We found that mobile media were the primary source of COVID-19 vaccine-related information. According to the WHO, media and disinformation played a vital role in the resurgence of vaccine hesitancy, which is a major threat to global health (35). New media, such as mobile media and social media, offers mixed and multifaceted information. Moreover, it allows individuals to create and share unverified content quickly. People who hesitate or refuse vaccines were more likely to search for vaccine-related information on the Internet. Exaggerated reports of adverse reactions to the COVID-19 vaccine could result in a lack of confidence and panic among the public. Confusing and biased information further fuels vaccine hesitancy. Authoritative media and regulatory platforms should report COVID-19 vaccination information in a timely, positive, and accurate manner. This would

guide patients toward learning and constructing verified knowledge about the vaccine and motivate suitable patients to be vaccinated.

## LIMITATIONS

Readers should consider the limitations of this study. Firstly, since it was a cross-sectional study, we restricted drawing any causal inferences. Secondly, due to resource limitations, breast cancer survivors from six tertiary grade A hospitals in Wuhan city were recruited. A large-scale survey is required to extend the generalization of our conclusion to other regions and countries. Finally, since the COVID-19 pandemic and vaccination are ongoing processes, attitudes of cancer patients to vaccines could change over time; a living survey system and updated guidelines for cancer patients should be developed and implemented to achieve this.

## CONCLUSION

Researchers observed suboptimal vaccination rates and high rates of vaccine hesitancy among breast cancer survivors in this study. It also concludes that endocrine or targeted therapy, poor self-perception, and no notification from communities or units can be used to identify the targeted population at high risk of vaccine hesitancy. Doctors in charge of treatment and vaccination can greatly influence these decisions of patients through effective interaction between

doctors and patients, and simple and consistent practical guidelines on vaccination, timely and positive information from authoritative media could combat the misinformation and greatly reduce the vaccine hesitancy among breast cancer survivors.

## DATA AVAILABILITY STATEMENT

The original contributions presented in the study are included in the article/supplementary material, further inquiries can be directed to the corresponding author/s.

## ETHICS STATEMENT

The studies involving human participants were reviewed and approved by Ethics Committee of Wuhan Union Hospital, Tongji Medical College, Huazhong University of Science and Technology. The patients/participants provided their written informed consent to participate in this study. Written informed

consent was obtained from the individual(s) for the publication of any potentially identifiable images or data included in this article.

## AUTHOR CONTRIBUTIONS

XP developed the idea, designed the study, and provided financial support for the study. XP and PG designed the questionnaires, drafted the manuscript, summarized the data, and contributed to data interpretation. QW, H-gW, Y-ly, YX, J-yW, FLu, HP, YY, and FLi were involved in the acquisition of the data. JC critically revised the manuscript for important intellectual content. The corresponding author had full access to all the data in the study and was responsible for submission for publication. All authors contributed to the article and approved the submitted version.

## FUNDING

The 2020 Huazhong University of Science and Technology Academic Projects (no. 2020kfyXGYJ001) supported this work.

## REFERENCES

- Jin Y, Cai L, Cheng Z, Cheng H, Deng T, Fan Y, et al. A rapid advice guideline for the diagnosis and treatment of 2019 novel coronavirus (2019-ncov) infected pneumonia (standard version). *Mil Med Res.* (2020) 7:4. doi: 10.1186/s40779-020-0233-6
- Jin Y, Zhan Q, Peng Z, Ren X, Yin X, Cai L, et al. Chemoprophylaxis, diagnosis, treatments, and discharge management of COVID-19: an evidence-based clinical practice guideline (updated version). *Mil Med Res.* (2020) 7:41. doi: 10.1186/s40779-020-00270-8
- Liu Y, Kuo R, Shih S. COVID-19: the first documented coronavirus pandemic in history. *Biomed J.* (2020) 43:328–33. doi: 10.1016/j.bj.2020.04.007
- WHO. WHO Coronavirus (COVID-19) Dashboard (2021). Available online at: <https://covid19.who.int/> (assessed June 12, 2021).
- Liu C, Zhao Y, Okwan-Duodu D, Basho R, Cui X. COVID-19 in cancer patients: risk, clinical features, and management. *Cancer Biol Med.* (2020) 17:519–27. doi: 10.20892/j.issn.2095-3941.2020.0289
- ElGohary GM, Hashmi S, Styczynski J, Kharfan-Dabaja MA, Alblooshi RM, de la Camara R, et al. The risk and prognosis of COVID-19 infection in cancer patients: a systematic review and meta-analysis. *Hematol Oncol Stem Cell Ther.* (2020). doi: 10.1016/j.hemonc.2020.07.005. [Epub ahead of print].
- Sung H, Ferlay J, Siegel RL, Laversanne M, Soerjomataram I, Jemal A, et al. Global cancer statistics 2020: globocan estimates of incidence and mortality worldwide for 36 cancers in 185 countries. *CA Cancer J Clin.* (2021) 71:209–49. doi: 10.3322/caac.21660
- Thanh LT, Andreadakis Z, Kumar A, Gómez Román R, Tollefsen S, Saville M, et al. The COVID-19 vaccine development landscape. *Nat Rev Drug Discov.* (2020) 19:305–6. doi: 10.1038/d41573-020-00073-5
- Wang J, Lu X, Lai X, Lyu Y, Zhang H, Fenghuang Y, et al. The changing acceptance of COVID-19 vaccination in different epidemic phases in china: a longitudinal study. *Vaccines.* (2021) 9:191. doi: 10.3390/vaccines9030191
- Leng A, Maitland E, Wang S, Nicholas S, Liu R, Wang J. Individual preferences for COVID-19 vaccination in china. *Vaccine.* (2021) 39:247–54. doi: 10.1016/j.vaccine.2020.12.009
- MacDonald NE. Vaccine hesitancy: definition, scope and determinants. *Vaccine.* (2015) 33:4161–4. doi: 10.1016/j.vaccine.2015.04.036
- Dror AA, Eisenbach N, Taiber S, Morozov NG, Mizrahi M, Zigran A, et al. Vaccine hesitancy: the next challenge in the fight against COVID-19. *Eur J Epidemiol.* (2020) 35:775–9. doi: 10.1007/s10654-020-00671-y
- Ribas A, Sengupta R, Locke T, Zaidi SK, Campbell KM, Carethers JM, et al. Priority COVID-19 vaccination for patients with cancer while vaccine supply is limited. *Cancer Discov.* (2021) 11:233–6. doi: 10.1158/2159-8290.CD-20-1817
- Hwang JK, Zhang T, Wang AZ, Li Z. COVID-19 vaccines for patients with cancer: benefits likely outweigh risks. *J Hematol Oncol.* (2021) 14:38. doi: 10.1186/s13045-021-01046-w
- Conti R, Akesson J, Weiss E, Sae-Hau M, Lee M, Gracia G, et al. COVID-19 Vaccine Safety Among Blood Cancer Patients. Available online at: <https://www.lls.org/news/covid-19-vaccine-safety-among-blood-cancer-patients> (accessed August 15, 2021).
- Kelkar AH, Blake JA, Cherabuddi K, Cornett H, McKee BL, Cogle CR. Vaccine enthusiasm and hesitancy in cancer patients and the impact of a webinar. *Healthcare.* (2021) 9:351. doi: 10.3390/healthcare9030351
- Adin ME, Isufi E, Kulon M, Pucar D. Association of COVID-19 mRNA vaccine with ipsilateral axillary lymph node reactivity on imaging. *JAMA Oncol.* (2021) 7:1241–2. doi: 10.1001/jamaoncol.2021.1794
- Villarreal-Garza C, Vaca-Cartagena BF, Becerril-Gaitan A, Ferrigno AS, Mesa-Chavez F, Platas A, et al. Attitudes and factors associated with COVID-19 vaccine hesitancy among patients with breast cancer. *JAMA Oncol.* (2021) 7:1242–4. doi: 10.1001/jamaoncol.2021.1962
- Fakonti G, Kyprianidou M, Toumbis G, Giannakou K. Attitudes and acceptance of COVID-19 vaccination among nurses and midwives in Cyprus: a cross-sectional survey. *Front Public Health.* (2021) 9:656138. doi: 10.3389/fpubh.2021.656138
- COVID-19 Vaccines and Cancer. Available online at: <https://www.singaporecancersociety.org.sg/covid-19-vaccines-and-cancer.html> (accessed August 15, 2021).
- COVID-19 Vaccines in People With Cancer. Available online at: <https://www.cancer.org/treatment/treatments-and-side-effects/physical-side-effects/low-blood-counts/infections/covid-19-vaccines-in-people-with-cancer.html> (accessed August 15, 2021).
- Xing K, Tu XY, Liu M, Liang ZW, Chen JN, Li JJ, et al. Efficacy and safety of COVID-19 vaccines: a systematic review. *Zhongguo Dang Dai Er Ke Za Zhi.* (2021) 23:221–8. doi: 10.7499/j.issn.1008-8830.2101133
- He Q, Mao Q, Zhang J, Bian L, Gao F, Wang J, et al. COVID-19 vaccines: current understanding on immunogenicity, safety, and further considerations. *Front Immunol.* (2021) 12:669339. doi: 10.3389/fimmu.2021.669339
- Xia S, Duan K, Zhang Y, Zhao D, Zhang H, Xie Z, et al. Effect of an inactivated vaccine against SARS-Cov-2 on safety and immunogenicity

- outcomes: interim analysis of 2 randomized clinical trials. *JAMA*. (2020) 324:951–60. doi: 10.1001/jama.2020.15543
25. Zhang Y, Zeng G, Pan H, Li C, Hu Y, Chu K, et al. Safety, tolerability, and immunogenicity of an inactivated SARS-Cov-2 vaccine in healthy adults aged 18–59 years: a randomised, double-blind, placebo-controlled, phase 1/2 clinical trial. *Lancet Infect Dis*. (2021) 21:181–92. doi: 10.1016/S1473-3099(20)30843-4
  26. Seely JM, Barry MH. The Canadian society of breast imaging/ Canadian association of radiologists' recommendations for the management of axillary adenopathy in patients with recent COVID-19 vaccination. *Can Assoc Radiol J*. (2021) 72:601–2. doi: 10.1177/0846537121998949
  27. Sallam M. COVID-19 vaccine hesitancy worldwide: a concise systematic review of vaccine acceptance rates. *Vaccines*. (2021) 9:160. doi: 10.3390/vaccines9020160
  28. Shen LS, Jin XY, Wang XM, Tou LZ, Huang J. Advances in endocrine and targeted therapy for hormone-receptor-positive, human epidermal growth factor receptor 2-negative advanced breast cancer. *Chin Med J*. (2020) 133:1099–108. doi: 10.1097/CM9.0000000000000745
  29. Martel S, Bruzzzone M, Ceppi M, Maurer C, Ponde NF, Ferreira AR, et al. Risk of adverse events with the addition of targeted agents to endocrine therapy in patients with hormone receptor-positive metastatic breast cancer: a systematic review and meta-analysis. *Cancer Treat Rev*. (2018) 62:123–32. doi: 10.1016/j.ctrv.2017.09.009
  30. Green MS, Abdullah R, Vered S, Nitzan D. A study of ethnic, gender and educational differences in attitudes toward COVID-19 vaccines in israel - implications for vaccination implementation policies. *Isr J Health Policy Res*. (2021) 10:26. doi: 10.1186/s13584-021-00458-w
  31. Corda V, Murgia F, Monni G. COVID-19 vaccine: the gender disparity. *J Perinat Med*. (2021) 49:723–4. doi: 10.1515/jpm-2021-0246
  32. Stoeklé H, Sekkate S, Angellier E, Hervé C, Beuzeboc P. Refusal of anti-coronavirus disease 2019 vaccination in cancer patients: is there a difference between the sexes? *Eur J Cancer*. (2021) 155:54–5. doi: 10.1016/j.ejca.2021.06.048
  33. Cooper LZ, Larson HJ, Katz SL. Protecting public trust in immunization. *Pediatrics*. (2008) 122:149–53. doi: 10.1542/peds.2008-0987
  34. Dube E, Bettinger JA, Halperin B, Bradet R, Lavoie F, Sauvageau C, et al. Determinants of parents' decision to vaccinate their children against rotavirus: results of a longitudinal study. *Health Educ Res*. (2012) 27:1069–80. doi: 10.1093/her/cys088
  35. Puri N, Coomes EA, Haghbayan H, Gunaratne K. Social media and vaccine hesitancy: new updates for the era of COVID-19 and globalized infectious diseases. *Hum Vaccin Immunother*. (2020) 16:2586–93. doi: 10.1080/21645515.2020.1780846
- Conflict of Interest:** The authors declare that the research was conducted in the absence of any commercial or financial relationships that could be construed as a potential conflict of interest.
- Publisher's Note:** All claims expressed in this article are solely those of the authors and do not necessarily represent those of their affiliated organizations, or those of the publisher, the editors and the reviewers. Any product that may be evaluated in this article, or claim that may be made by its manufacturer, is not guaranteed or endorsed by the publisher.

Copyright © 2021 Peng, Gao, Wang, Wu, Yan, Xia, Wang, Lu, Pan, Yang, Liang, Zhao and Cheng. This is an open-access article distributed under the terms of the Creative Commons Attribution License (CC BY). The use, distribution or reproduction in other forums is permitted, provided the original author(s) and the copyright owner(s) are credited and that the original publication in this journal is cited, in accordance with accepted academic practice. No use, distribution or reproduction is permitted which does not comply with these terms.





# Bibliometric Analysis and Systematic Review of Global Coronavirus Research Trends Before COVID-19: Prospects and Implications for COVID-19 Research

## OPEN ACCESS

### Edited by:

Reza Lashgari,  
Shahid Beheshti University, Iran

### Reviewed by:

Faris Hasan al Lami,  
University of Baghdad, Iraq  
Vasna Joshua,  
National Institute of Epidemiology  
(ICMR), India

### \*Correspondence:

Kehu Yang  
yangkh-ebm@lzu.edu.cn  
Shizhong Wang  
Wangshizhong-wuwe2021@163.com

†These authors have contributed  
equally to this work

### Specialty section:

This article was submitted to  
Infectious Diseases - Surveillance,  
Prevention and Treatment,  
a section of the journal  
Frontiers in Medicine

Received: 22 June 2021

Accepted: 04 October 2021

Published: 16 November 2021

### Citation:

Yan P, Li M, Li J, Lu Z, Hui X, Bai Y,  
Xun Y, Lao Y, Wang S and Yang K  
(2021) Bibliometric Analysis and  
Systematic Review of Global  
Coronavirus Research Trends Before  
COVID-19: Prospects and  
Implications for COVID-19 Research.  
Front. Med. 8:729138.  
doi: 10.3389/fmed.2021.729138

Peijing Yan<sup>1,2†</sup>, Meixuan Li<sup>2,3†</sup>, Jing Li<sup>3,2</sup>, Zhenxing Lu<sup>4</sup>, Xu Hui<sup>3,2</sup>, Yuping Bai<sup>5,6,7</sup>,  
Yangqin Xun<sup>2,8,9</sup>, Yongfeng Lao<sup>10</sup>, Shizhong Wang<sup>11\*</sup> and Kehu Yang<sup>2,3,8,9\*</sup>

<sup>1</sup> Department of Epidemiology and Health Statistics, West China School of Public Health and West China Fourth Hospital, Sichuan University, Chengdu, China, <sup>2</sup> Evidence-Based Medicine Center, School of Basic Medical Sciences, Lanzhou University, Lanzhou, China, <sup>3</sup> Evidence Based Social Science Research Center, School of Public Health, Lanzhou University, Lanzhou, China, <sup>4</sup> Institute of Medical Research, Northwestern Polytechnical University, Xi'an, China, <sup>5</sup> School of Basic Medicine, Gansu University of Chinese Medicine, Lanzhou, China, <sup>6</sup> Department of Scientific Research, Gansu Provincial Hospital, Lanzhou, China, <sup>7</sup> Department of Pathology, 940th Hospital of Joint Logistics Support Force of Chinese People's Liberation Army, Lanzhou, China, <sup>8</sup> Key Laboratory of Evidence Based Medicine and Knowledge Translation of Gansu Province, Lanzhou, China, <sup>9</sup> WHO Collaborating Centre for Guideline Implementation and Knowledge Translation, Lanzhou University, Lanzhou, China, <sup>10</sup> Department of Urology, Lanzhou University Second Hospital, Lanzhou, China, <sup>11</sup> Department of Orthopedics, Wuwei People's Hospital, Wuwei, China

Coronaviruses (CoV) cause respiratory and intestinal infections. We conducted this bibliometric analysis and systematical review to explore the CoV-related research trends from before COVID-19. We systematically searched the Ovid MEDLINE, Ovid Embase, and Web of Science (WOS) databases for published bibliometric analyses of CoV from database inception to January 24, 2021. The WOS Collection was searched from inception to January 31, 2020, to acquire the CoV-related publications before COVID-19. One-Way ANOVA and Bonferroni multiple-comparison tests were used to compare differences. Visualization mapping and keyword cluster graphs were made to illustrate the research topics and hotspots. We included 14,141 CoV-related publications for the bibliometric analysis and 16 (12 articles) CoV-related bibliometric analyses for the systematic review. Both the systematic review and bibliometric analysis showed (1) the number of publications showed two steep upward trajectories in 2003–2004 and in 2012–2014; (2) the research hotspots mainly focused on the mechanism, pathology, epidemiology, clinical diagnosis, and treatment of the coronavirus in MERS-CoV and SARS-CoV; (3) the USA, and China; the University of Hong Kong; and Yuen KY, came from the University of Hong Kong contributed most; (4) the *Journal of Virology* had the largest number of CoV related studies. More studies should focus on prevention, diagnosis, and treatment in the future.

**Keywords:** Coronaviruses, COVID-19, bibliometric analysis, systematic review, contribution, research topics

## INTRODUCTION

Coronaviruses (CoV) are a large family of positive-sense single-stranded RNA viruses that cause illnesses ranging from the common cold to more severe diseases (1, 2). Some CoV are zoonotic and can cause respiratory and intestinal infections in animals and humans (3), and have even resulted in lethal endemics, such as Middle East Respiratory Syndrome Coronaviruses (MERS-CoV), Severe Acute Respiratory Syndrome Coronaviruses (SARS-CoV), and Coronavirus Disease 2019 (COVID-19) (4).

With the outbreak and epidemic of CoV-related diseases, an increasing number of studies discussed the epidemic characteristics, diagnosis, infection mechanisms, and prevention of CoV (4–8). The appearance of COVID-19 was accelerating such research, which was certainly unique in the history of science and led to an explosion of research output. This output includes many meaningful approaches, but some appear to be excessive and not scientifically sound (9, 10). Against this background, it is very necessary to think about these compelling questions: Can we learn from previous research patterns regarding CoV? What influence do they have on future research? How can we use past efforts, their intensification, and the influences of research on CoV positively to better understand the needs for sustainable and appropriate research? (9). Therefore, it is very important to know about the global research on CoV in the time before COVID-19.

Systematically summarizing and analyzing the research of the CoV is helpful to understand the current state of research and provide references for future research. Bibliometric analysis is a statistical tool that is used to quantitatively and qualitatively measure and evaluate scientific publications (11–13). It consists of a review of the literature, and indicates the number, evaluation, and main trends of publications concerning a specific subject (14, 15).

To the best of our knowledge, there have been two bibliometric studies on CoV-related research in English before the COVID-19 pandemic (16, 17). One study published in 2016 assessed the characteristics of publications only focused on the MERS-CoV (18). Another study (19) analyzed the global research trends of the World Health Organization's top eight emerging infections including Ebola, Marburg, MERS, Severe Acute Respiratory Syndrome (SARS), and so on, but publications related to CoV were not systematically analyzed. A letter to the editor had simply investigated the publication characteristics of SARS-CoV, MERS-CoV, and COVID-19, but it only analyzed the number of publications and countries, which might not be enough to provide a reference for future research (20). In addition, several studies on coronavirus research trends were published in the time before the COVID-19 pandemic. However, some of the research focused on the specific periods, such as 2003 to March 2020. Therefore, we did a bibliometric analysis of all the publications before COVID-19. Additionally, these studies were based on various timespan and databases, and the findings did not well agree. We did this systematic review to summarize the findings of all the current bibliometric analyses in this topic to provide references for researchers focused on the emerging

human CoV, and to provide ideas for finding effective control measures, drugs, and vaccines.

## METHODS

This is a bibliometric analysis and systematic review, and the data we used were extracted from publications. Therefore, this study has no discernible ethical issues.

### Data Source and Search Strategy

We searched PubMed, Cochrane Library, and Embase databases using the Medical Subject Headings (MeSH) to acquire the CoV-related terms. For the bibliometric analysis, we searched publications using these terms in the Web of Science (WOS) Core Collection from its inception to January 31, 2020. In terms of the systematic review, we systematically searched the Ovid MEDLINE, Ovid Embase, and WOS databases using terms relating to CoV and bibliometric analysis, for published bibliometric analysis from database inception to January 24, 2021. The detailed search strategy is displayed in Appendix (Appendix, Supplementary Tables 1, 2). No limitation was used. As the metrics are changing over time, all the searches and data exports were completed on the same day to avoid the possible bias caused by frequent updates of the databases.

### Eligibility Criteria for Systematic Review

This systematic review included the bibliometric analyses of global CoV research trends. We excluded the bibliometric analyses without any indicators of publication and citation, journal, country or territory, affiliation and international cooperation, author, or subject/research topic. We also excluded conference abstracts, editorials, reviews, meta-analyses, and case reports or case series, as well as non-English and non-Chinese language publications and publications reporting duplicate data.

### Data Collection and Cleaning

In terms of bibliometric analysis, we obtained (1) the characteristics of all the retrieved publications; (2) the 2019 journal impact factor (JIF) (21), 5 year JIF (21), and publication counts of the journals; (3) publication count per year, h-index, various citation values [average citations per item (ACPI), sum of times cited (STC) and No. citations of most-cited item (NCMCI)] and top-5 most-publications research areas (top-5 research areas) of the top-10 most-publications countries (top-10 countries); and (4) institutes, h-index, various citation values, and top-5 research areas of the top-10 most-publications authors (top-10 authors). All documents were downloaded in tab separator format.

We standardized the keywords with the same meaning but in different styles. For example, “coronavirus” was replaced by “coronavirus (cov)”, “middle east respiratory syndrome coronavirus” was replaced by “MERS”, etc.

As for the systematic review, one researcher (Y-PB) extracted the information from the included studies using a pre-piloted, standardized extraction table, and the other researcher (P-JY) checked the extraction. Any discrepancies between the reviewers were resolved by discussion. We extracted the following

information: (1) study characteristics (first author, publication year, country, journal); (2) search strategies, and (3) indicators or findings on publication and citation, journal, country or territory, affiliation and international cooperation, author, subject/research topics, and keyword co-occurrence cluster.

Since there is no validated quality assessment tool that can be applied to bibliometric analyses, we did not assess the

risk of bias or the methodological quality for the included bibliometric analyses.

## Statistical Analysis

The data were entered into a spreadsheet program (Microsoft Excel 2016, Microsoft, Washington, USA). The statistical analyses and preparation of the figures were performed using

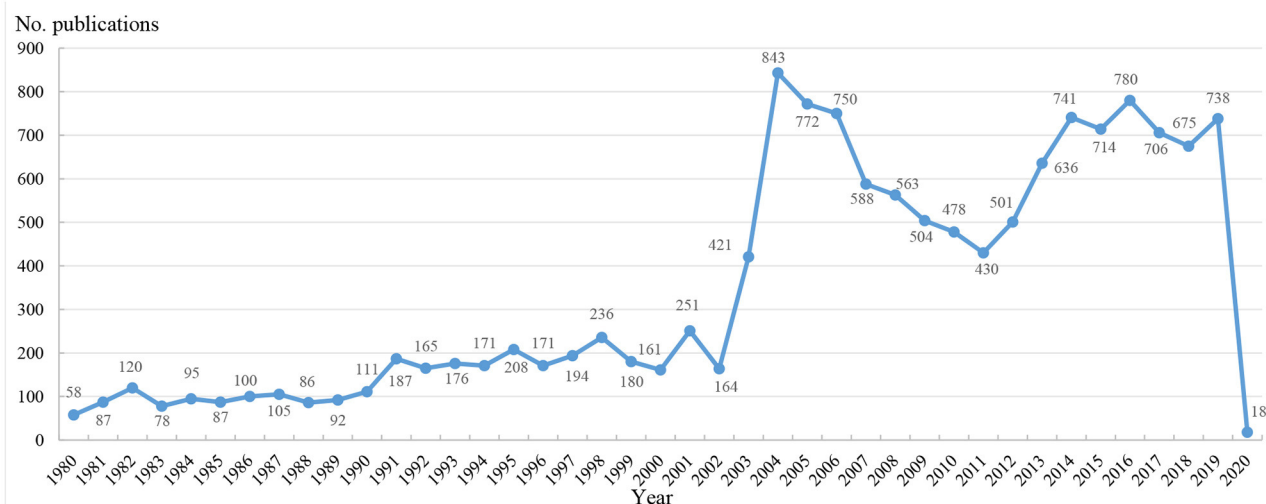


FIGURE 1 | Annual trends of CoV-related publications.

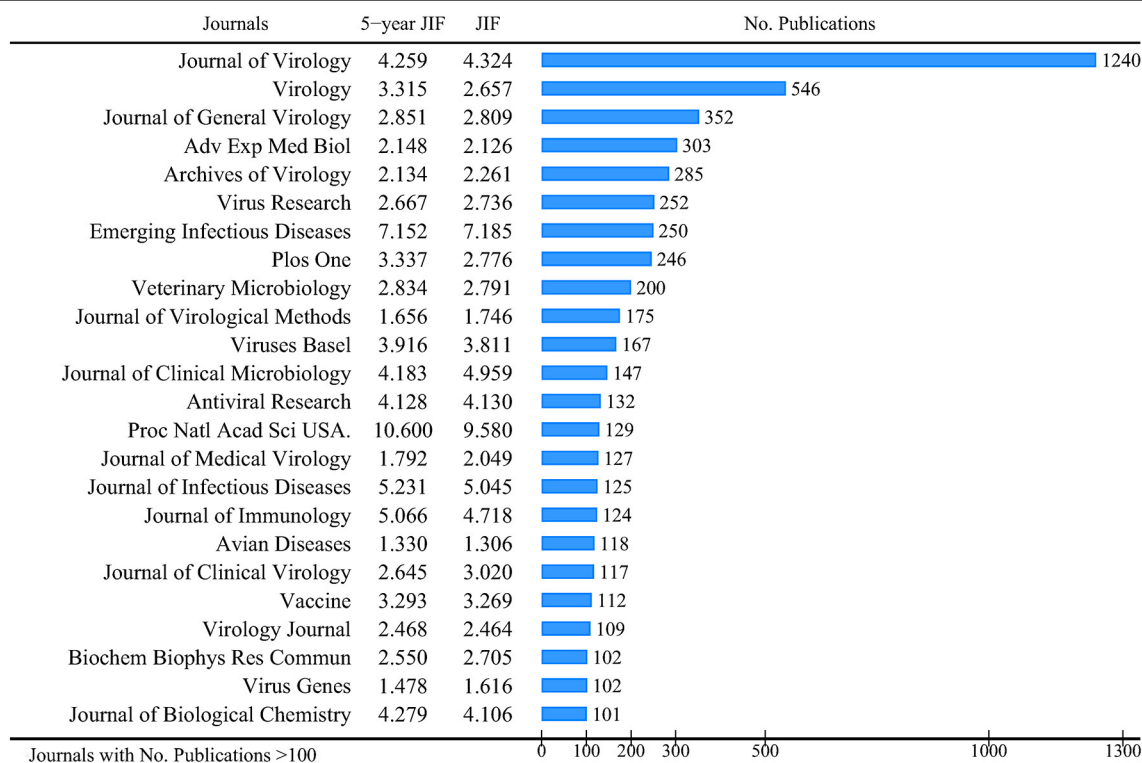


FIGURE 2 | Journals with more than 100 CoV-related publications.

Stata, version 15 (Stata Corp, College Station, TX, USA). For all statistical tests, a two-tailed  $\alpha$  level of 0.05 was used.

We used VOSviewer 1.6.1 (Centre for Science and Technology Studies, Leiden University, Leiden, The Netherlands) to analyze the publication characteristics (22, 23). Keywords co-occurrence can effectively reflect the research hotspots in the discipline fields, providing auxiliary support for scientific research (24). VOSviewer was also used for visualization mapping to present co-authorship and co-occurrence networks (25) and generate keywords clustering graph to present the research topic.

## RESULTS

### Basic Characteristics of CoV-Related Publications

A total of 14,141 publications were retrieved, of which around 77.27% were published as original articles, 8.36 % as reviews, 3.91% as proceedings papers, 3.13% as meeting abstracts, with the remaining being book chapters, etc., (Appendix, Supplementary Figure 1). For the book chapters, the Advances in Experimental Medicine and Biology (273), Advances in Virus Research (26), and Current Topics in Microbiology and

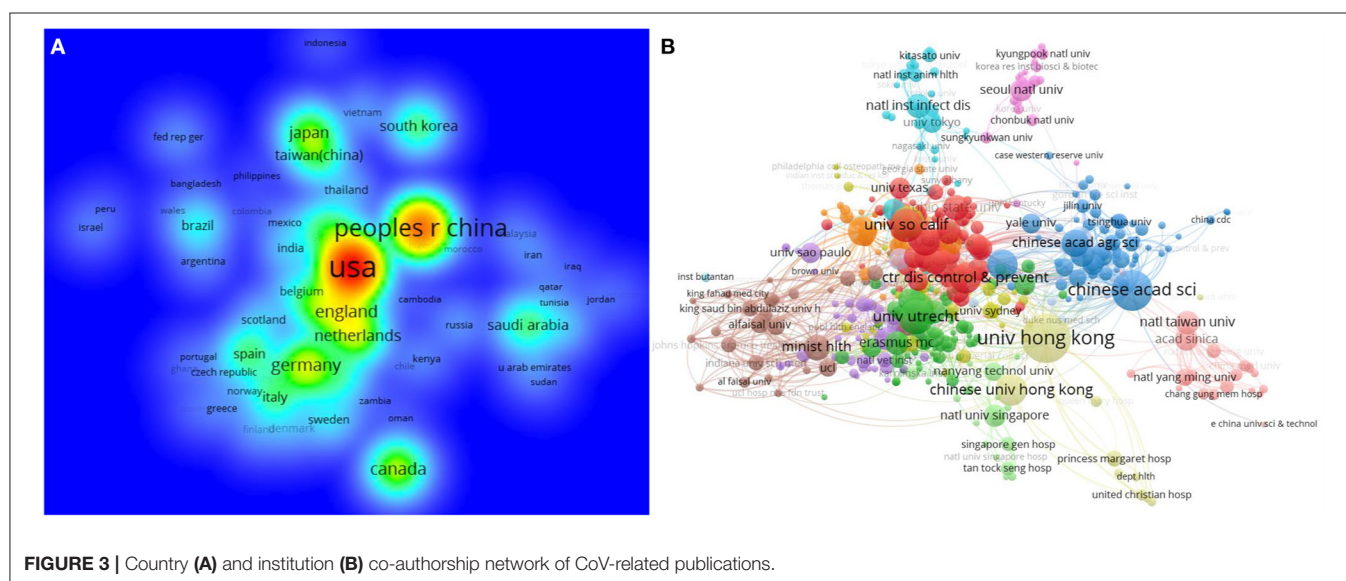


**TABLE 1 |** Characteristics of top-10 countries ( $N = 14,141$ ).

| ID | Country        | N (%)         | Region        | NCMCI | Top-5 Research areas   |
|----|----------------|---------------|---------------|-------|--|
| 1  | USA            | 5,142 (36.36) | North America | 1,823 | Virology; Immunology; Veterinary Sciences; Microbiology; Biochemistry Molecular Biology          |
| 2  | China          | 2,754 (19.48) | Asia          | 1,823 | Virology; Biochemistry Molecular Biology; Immunology; Infectious Diseases; Microbiology          |
| 3  | Germany        | 961 (6.80)    | Europe        | 1,732 | Virology; Immunology; Biochemistry Molecular Biology; Veterinary Sciences; Infectious Diseases   |
| 4  | Canada         | 887 (6.27)    | North America | 1,273 | Virology; Immunology; Veterinary Sciences; Biochemistry Molecular Biology; Infectious Diseases   |
| 5  | England        | 880 (6.22)    | Europe        | 1,328 | Virology; Veterinary Sciences; Infectious Diseases; Biochemistry; Molecular Biology Immunology   |
| 6  | Netherlands    | 788 (5.57)    | Europe        | 1,732 | Virology; Microbiology; Infectious Diseases; Immunology; Biochemistry Molecular Biology          |
| 7  | Japan          | 710 (5.02)    | Asia          | 794   | Virology; Veterinary Sciences; Immunology; Microbiology; Biochemistry Molecular Biology          |
| 8  | France         | 647 (4.58)    | Europe        | 1,732 | Virology; Infectious Diseases; Veterinary Sciences; Immunology; Microbiology                     |
| 9  | South Korea    | 438 (3.10)    | Asia          | 320   | Virology; Infectious Diseases; Veterinary Sciences; Microbiology; Immunology                     |
| 10 | Taiwan (China) | 422 (2.98)    | Asia          | 1,823 | Biochemistry Molecular Biology; Virology; Infectious Diseases; Pharmacology Pharmacy; Immunology |

NCMCI, No. citations of most-cited item.



Immunology (27) were the top-3 most-publications, others were less than 10 records.

Among these publications, 53.35% (7,544) records did not contain data in the funding agencies; 97.24 % (13,750) were published in English, 0.79 % (111) were in French, 0.75 % (106) were in German, and the remaining were in Spanish, Chinese, and 14 other languages.

## The Annual Trends of CoV-Related Publications

**Figure 1** plots the annual trends of CoV-related publications. Since the first literature was published in 1980, CoV-related research had a very slow increase in the following 20 years. The number of publications grew very sharply in 2003, hit a peak in 2004 (843), and then declined gradually until another sudden increase in 2012 (**Figure 1**).

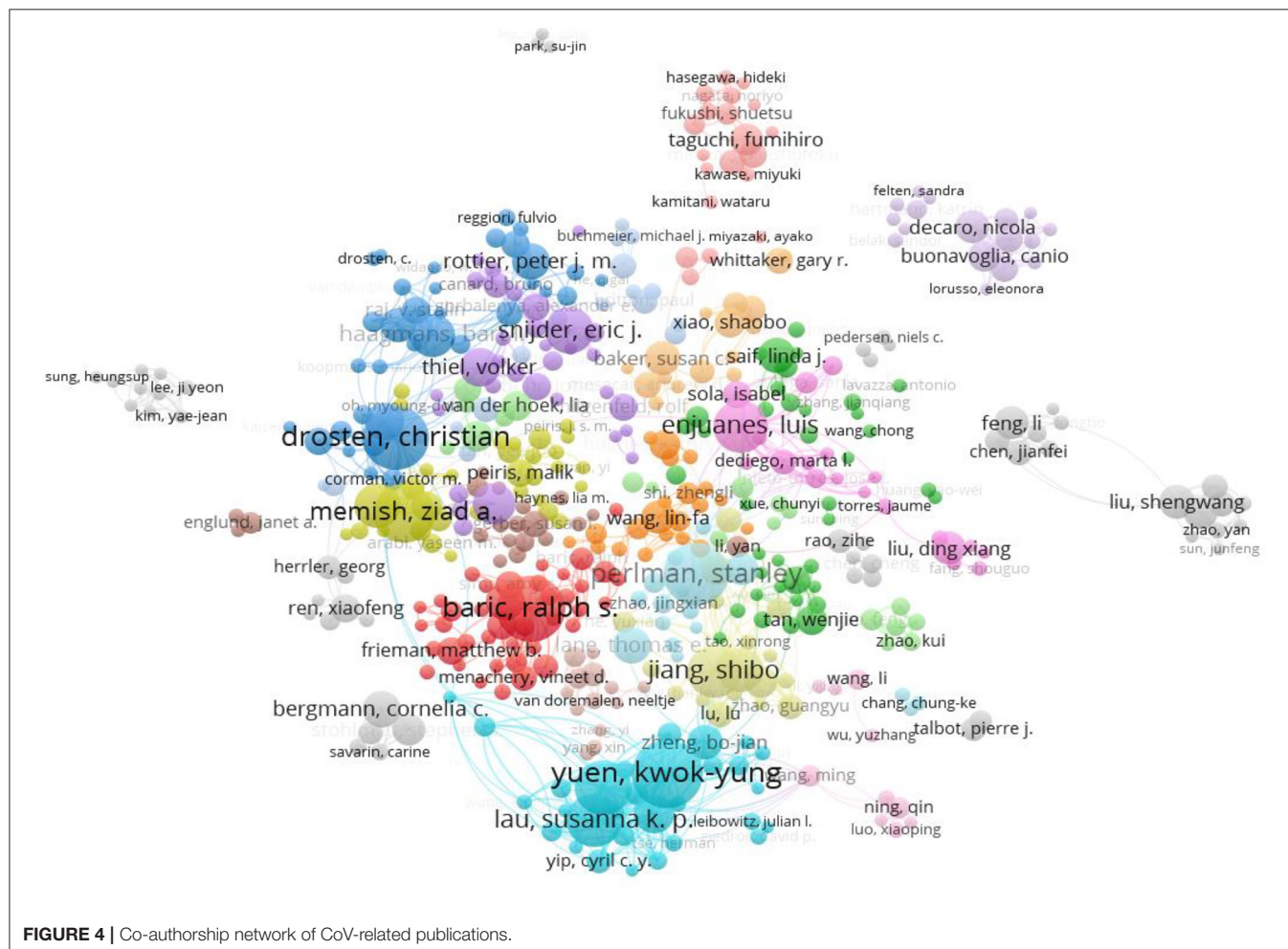
## Journals of CoV-Related Publications

The CoV-related publications were published in 500 journals. The 24 journals with more than 100 publications were listed. The journal with the most publications was the Journal of Virology (1,240), followed by Virology (546) and the Journal of General

Virology (352). The 2019 JIF ranged from 1.306 (Avian Disease) to 9.580 (Proceedings of The National Academy of Science of The United States of America), and the 5 year JIF ranged from 1.330 to 10.600 (**Figure 2**).

## Countries and Regions of CoV-Related Publications

A total of 134 countries published CoV-related studies. Around 32.49% of those publications were published in North America, 31.49% in Europe, 30.78% in Asia, and the remaining in Oceania, South America, and other regions (**Appendix, Supplementary Figure 2**). The cooperation network analysis included 88 countries, which with a frequency  $\geq 5$  times. The density map showed that the top-10 countries were the United States of America (USA) with 5,142, followed by China (2,754), Germany (961), Canada (887), England (880), Netherlands (788), Japan (710), France (647), South Korea (438), and Taiwan (China) (422) (**Figure 3A**). Among the top-10 countries, 1/5 were from North America, 2/5 from Asia, and the rest from Europe (**Table 1**). The CoV-related publication count of the top-10 countries over the 41 years is listed in **Appendix (Appendix, Supplementary Table 3)**.





Among these countries, a total of 6,753 institutions were involved in CoV-related publications. A network of 530 institutions with a frequency  $\geq 10$  was formed. The University of Hong Kong (China), the Chinese Academy of Sciences (China), Utrecht University (Netherlands), the University of Southern California (USA), and the University of Pennsylvania (USA) were at the center of the cooperation network and formed close cooperative relationships with other institutions (Figure 3B).

In terms of STC, h-index, and NCMCI of the top-10 countries, the USA was the most-contributed country with the highest h-index (156), STC (185,165), and NCMCI (1,823), followed by the Netherlands (107) and China (105) in h-index, China (73,101) and the Netherlands (47,486) in STC, and China (1,823) and Taiwan (1,823) in NCMCI (Table 1).

The CoV-related publications of the top-10 countries mainly focused on the following research areas: virology, veterinary

sciences, infectious diseases, immunology, biochemistry molecular biology, microbiology, and pharmacology (Table 1, Appendix, Supplementary Figure 3). The most-contributed research area of the top-10 countries was virology, except for Taiwan, which focused on biochemistry molecular biology. The Netherlands contributed more to the virology area than any of the other nine countries (Appendix, Supplementary Figure 3).

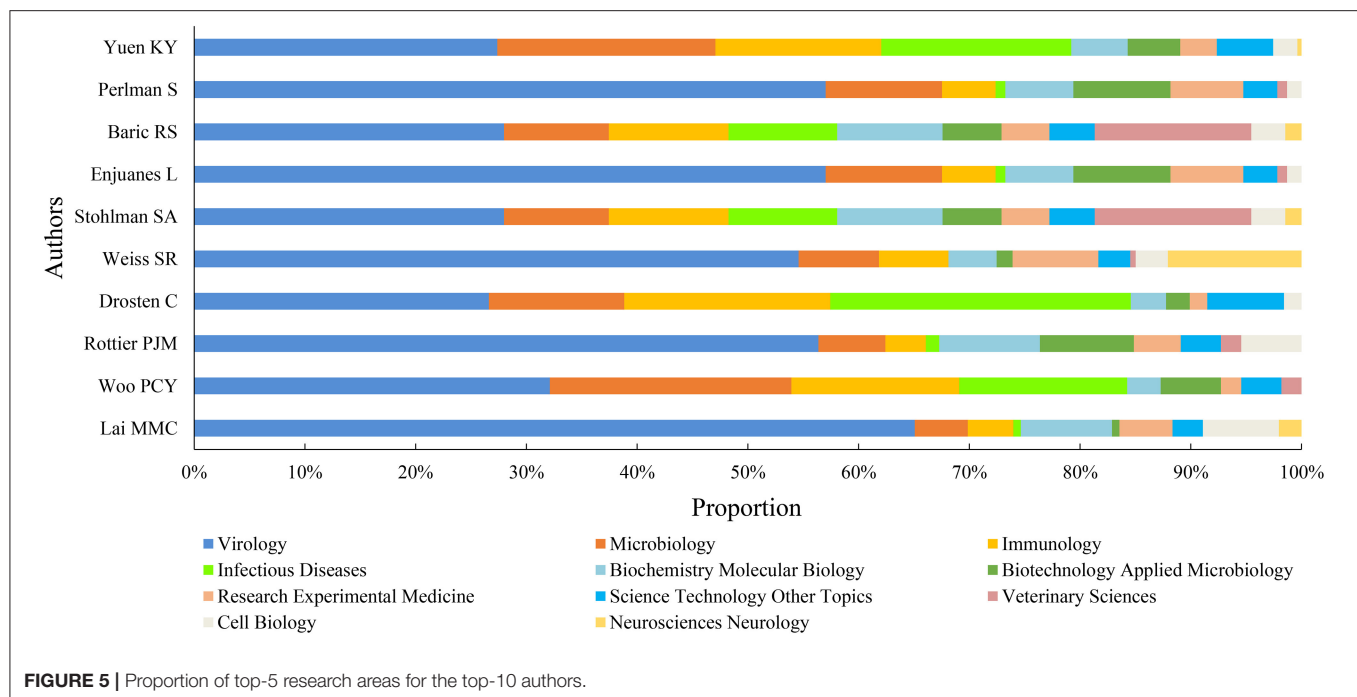
## Authors of CoV-Related Publications

A total of 43,476 authors were involved in the CoV-related publications, 402 authors with a frequency  $\geq 10$  times were included in the collaboration network analysis, and 27 cooperation networks were formed. Yuen KY (China), Baric RS (USA), and Drosten C (Germany) had the highest number of publications and were in the middle of the network diagram,

**TABLE 2 |** Characteristics of the top-10 authors.

| ID | Author      | N (%)      | Organization |  |   | H-Index | Citation |        |       | Top-5 Research areas   |
|----|-------------|------------|--------------|--|---|---------|----------|--------|-------|--|
|    |             |            | Country      | Institute  | Department  |         | ACPI     | STC    | NCMCI |  |
| 1  | Yuen KY     | 213 (1.51) | China        | University of Hong Kong                                    | Department of Microbiology and Pathology            | 67      | 76.10    | 16,210 | 1,436 | Virology; Microbiology; Infectious Diseases; Immunology; Biochemistry Molecular Biology                                    |
| 2  | Perlman S   | 187 (1.32) | USA          | University of Iowa   | Department of Microbiology                          | 44      | 32.13    | 6,008  | 321   | Virology; Microbiology; Biotechnology Applied Microbiology; Research Experimental Medicine; Biochemistry Molecular Biology |
| 3  | Baric RS    | 170 (1.20) | USA          | University of North Carolina                               | Department of Epidemiology                          | 53      | 43.61    | 7,413  | 321   | Virology; Veterinary Sciences; Immunology; Infectious Diseases; Biochemistry Molecular Biology                             |
| 4  | Enjuanes L  | 162 (1.15) | Spain        | Centro Nacional de Biotecnología                           | Department of Molecular and Cell Biology            | 48      | 40.62    | 6,580  | 350   | Virology; Microbiology; Biotechnology Applied Microbiology; Research Experimental Medicine; Biochemistry Molecular Biology |
| 5  | Stohlman SA | 156 (1.10) | USA          | University of Southern California                          | Departments of Microbiology and Neurology           | 52      | 48.13    | 7,508  | 266   | Virology; Veterinary Sciences; Immunology; Infectious Diseases; Biochemistry Molecular Biology                             |
| 6  | Weiss SR    | 156 (1.10) | USA          | University of Pennsylvania School of Medicine              | Department of Microbiology                          | 44      | 33.74    | 5,263  | 237   | Virology; Neurosciences Neurology; Research Experimental Medicine; Microbiology; Immunology                                |
| 7  | Drosten C   | 144 (1.02) | Germany      | National Reference Center for Tropical Infectious Diseases | Bernhard Nocht Institute for Tropical Medicine      | 48      | 76.30    | 10,987 | 1,732 | Infectious Diseases; Virology; Immunology; Microbiology; Science Technology Other Topics                                   |
| 8  | Rottier PJM | 134 (0.95) | Netherlands  | Utrecht University   | Department of Infectious Diseases & Immunology      | 50      | 56.95    | 7,631  | 459   | Virology; Biochemistry Molecular Biology; Biotechnology Applied Microbiology; Microbiology; Cell Biology                   |
| 9  | Woo PCY     | 127 (0.90) | China        | University of Hong Kong                                    | Department of Microbiology                          | 47      | 58.57    | 7,438  | 646   | Virology; Microbiology; Immunology; Infectious Diseases; Biotechnology Applied Microbiology                                |
| 10 | Lai MMC     | 123 (0.87) | USA          | University of Southern California                          | Department of Molecular Microbiology and Immunology | 56      | 67.42    | 8,293  | 545   | Virology; Biochemistry Molecular Biology; Cell Biology; Microbiology; Research Experimental Medicine                       |

ACPI, Average citations per item; STC, Sum of times cited; NCMCI, No. citations of most-cited item.



which shows that they formed close cooperative relationships with other authors (Figure 4).

The top-10 authors with the most CoV-related publications mainly came from the USA (1/2) and China (1/5), and were focused in the University of Southern California and the University of Hong Kong (Table 2). Most of the top-10 authors came from the departments of microbiology (Table 2) and mainly focused on virology, microbiology, infectious diseases, immunology, and seven other research areas (Figure 5, Table 2). The most-contributed research area of the top-10 authors was virology, except Drosten C who focused on infectious diseases (Figure 5).

Yuen KY had the highest number of publications, h-index, and STC, followed by Perlman S and Baric RS in number of publications, Lai MMC and Baric RS in h-index, and Drosten C and Lai MMC in STC. Drosten C had the highest NCMCI and ACPI, followed by Yuen KY and Woo PCY in NCMCI and Yuen KY and Lai MMC in ACPI (Table 2).

## Research Topics of CoV-Related Publications

A total of 23,732 keywords were included in the 14,141 publications, and 973 keywords with occurrence frequency  $\geq 20$  were clustered. In the cluster figure, one type of color represents one cluster, and a total of five main clusters were formed, indicating that the current CoV-related research concentrated on the following five topics: Topic 1 (red area, 239 items): the detection and identification of SARS-CoV by collecting nucleic acid and protein of virus *in vitro*; Topic 2 (green area, 211 items): research on the natural history, transmission, and diagnosis of CoV; Topic 3 (blue area, 166 items): research on SARS-CoV outbreaks in China, and the MERS-CoV outbreak

in Saudi Arabia; Topic 4 (yellow area, 138 items): research on the mechanisms of viral infection and expression in *in vitro* cells and lab mice; and Topic 5 (purple area, 133 items): research on pneumonia caused by human infection with CoV and the spread, prevalence, and burden of various diseases caused by infection with other viruses such as avian influenza (Figure 6).

The density map of 973 keywords is presented in the Appendix (Appendix, Supplementary Figure 4). “CoV (3,116 items),” “infection (1,413 items),” “identification” (1,393 items), etc. had the highest frequency in the red area, followed by “diagnosis (395 items),” and the “therapy (69 items)” in the yellow area and “treatment (35 items)” in the green area (Appendix, Supplementary Figure 4).

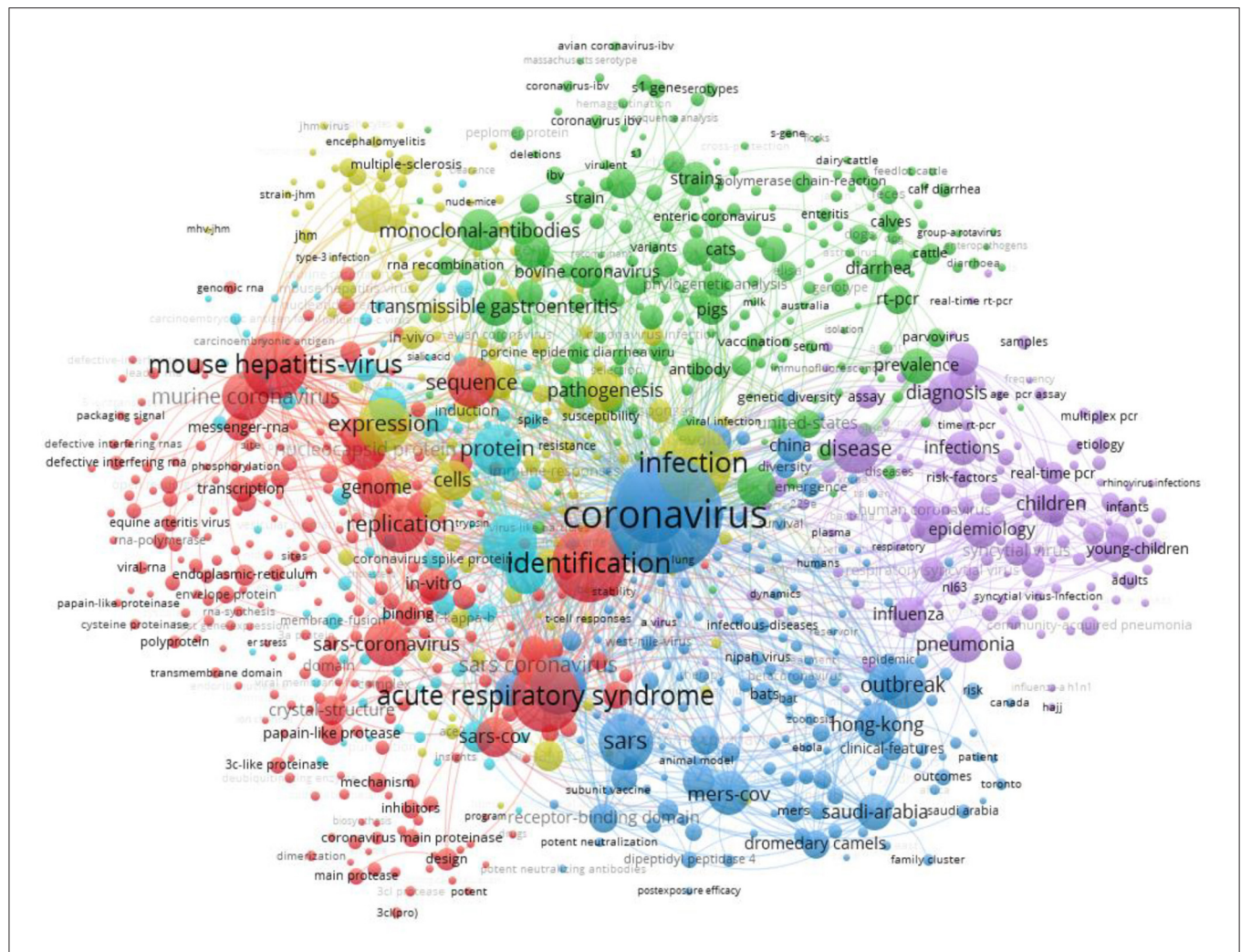
## High-Frequent Citation Articles

Most of the top-10 most-cited publications came from the USA and were in high impact-factor journals such as New England Journal of Medicine, British Medical Journal, and Science. The most frequently cited article (1,823 citations) was published by Ksiazek et al. (28), followed by Drosten et al. (29) (1,732 citations) (Table 3).

## Systematic Review of Published Bibliometric Analyses

### Study Characteristics of Published Bibliometric Analyses

A total of 17 (9, 11, 26, 27, 30–38) CoV-related bibliometric analyses from 13 articles were included, of which one study (27) conducted five bibliometric analyses. All 17 bibliometric analyses were published in 2020 and included between 641 and 15,207 primary studies (Table 4). Two included articles from India (26, 38), one from Spain (34), one from Turkey



(27), two from Israel (9, 31), and the remaining 7 reports were from China (**Appendix, Supplementary Table 4**). All the 13 included articles were published in journals with IF from 0 to 5.993 (**Appendix, Supplementary Table 4**). Most of the CoV-related bibliometric analyses (88.2%, 15/17) retrieved data from the WOS up to 2020, and the types of original studies included were mainly articles and reviews. A majority of the CoV-related bibliometric analyses indicated that the annual publication count increased due to three notable epidemic events in history.

# Journals, Countries, Institutions, and Authors of CoV-Related Publications in Published Bibliometric Analysis

Six (11, 26, 33, 36–38) of 17 included bibliometric analyses reported the total number of CoV-related research journals (100–3,443), 11 bibliometric analyses (8 articles) (11, 26, 27, 32–34, 36, 37) listed the top 1–20 journals, and all of them reported

that the *Journal of Virology* had the largest number of CoV-related studies (Table 4, Appendix, Supplementary Table 5).

In terms of countries, 6 bibliometric analyses (30, 32, 33, 36–38) reported the total number of CoV-related research by country (78–219), and nearly all of them listed the top 20 most-publications countries. In 16 of the 17 bibliometric analyses (9, 11, 26, 27, 30, 32–38) it was indicated that the USA had the largest number of CoV-related publications, followed by China, and their cooperative network diagram showed the most frequent cooperation occurred in the USA and China (Table 4, Appendix, Supplementary Table 5).

As for institutions, 4 bibliometric analyses (30, 33, 35, 38) reported the total number of CoV-related research institutions (147, 242, 333, 6,306 respectively), and 12 bibliometric analyses (9, 11, 26, 27, 30, 32–34, 36–38) indicated that the University of Hong Kong had the largest number of CoV-related publications. Only 5 bibliometric analyses (30, 32, 33, 35, 36) analyzed cooperation among institutions.

**TABLE 3 |** The top-10 most-cited publications.

| ID | Title   | Publication year | First author | Country      | Institution  | STC   | Journal |
|----|---|------------------|--------------|--------------|--|-------|---------|
| 1  | A novel coronavirus associated with severe acute respiratory syndrome                             | 2003             | Ksiazek TG   | USA          | CDC, the Special Pathogens Branch                                | 1,823 | NEJM    |
| 2  | Identification of a novel coronavirus in patients with severe acute respiratory syndrome          | 2003             | Drosten C    | Germany      | The Bernhard Nocht Institute for Tropical Medicine               | 1,732 | NEJM    |
| 3  | Characterization of a novel coronavirus associated with severe acute respiratory syndrome         | 2003             | Rota PA      | USA          | National Center for Infectious Diseases, CDC                     | 1,487 | Science |
| 4  | Coronavirus as a possible cause of severe acute respiratory syndrome                              | 2003             | Peiris JSM   | China        | University of Hong Kong, Queen Mary Hospital                     | 1,436 | Lancet  |
| 5  | Community study of role of viral infections in exacerbations of asthma in 9–11 years old children | 1995             | Johnston SL  | British      | University Medicine, Southampton General Hospital                | 1,328 | BMJ     |
| 6  | Isolation of a Novel Coronavirus from a Man with Pneumonia in Saudi Arabia                        | 2012             | Zaki AM      | Saudi Arabia | The Dr. Soliman Fakeeh Hospital                                  | 1,274 | NEJM    |
| 7  | The genome sequence of the SARS-associated coronavirus  | 2003             | Marra MA     | British      | BCCA, Genome Sciences Centre                                     | 1,273 | Science |
| 8  | Cloning of a human parvovirus by molecular screening of respiratory tract samples                 | 2005             | Allander N T | Sweden       | Karolinska University Hospital                                   | 1,011 | PNAS    |
| 9  | Psychological Stress and Susceptibility to the Common Cold  | 1991             | Cohen S      | USA          | Carnegie Mellon University                                       | 1,004 | NEJM    |
| 10 | Angiotensin-converting enzyme 2 is a functional receptor for the SARS coronavirus                 | 2003             | Li WH        | USA          | Division of Pulmonary Medicine and Ina Sue Perlmutter Laboratory | 968   | Nature  |

STC, Sum of times cited; CDC, Centers for Disease Control and Prevention; NEJM, New England Journal of Medicine; BMJ, British Medical Journal; PNAS, Proceedings of the National Academy of Sciences of the United States of America.

and their conclusions were inconsistent (Table 4, Appendix, Supplementary Table 5).

Regarding authors, 4 bibliometric analyses (30, 32, 33, 35) reported the total number of CoV-related research authors (121–29515), 12 bibliometric analyses listed top-20 authors (11, 27, 30, 32–36, 38), and 9 of them (11, 27, 30, 32–34, 36, 38) indicated that Yuen KY at the University of Hong Kong had the largest number of CoV-related publications. Collaboration between authors and highly cited authors were not fully analyzed in the included studies, and were only mentioned in 4 bibliometric analyses (30, 33, 35, 36) (Table 4, Appendix, Supplementary Table 5).

### Research Topics of CoV-Related Publications in Published Bibliometric Analysis

Four included bibliometric analyses (9, 27, 30, 31) reported the total number of CoV-related research keywords (132–216). Most of the included bibliometric analyses showed that the main research fields of the CoV-related research focused on basic medical sciences (virology, microbiology, biochemistry & molecular biology, immunology, pharmacology, and pharmacy), clinical medicine (infectious diseases, pediatrics, and the respiratory system), veterinary sciences, and public health (public, environmental, and occupational health). The research hotspots mainly focused on the mechanisms, pathology, epidemiology, clinical diagnosis, and treatment of the coronavirus in MERS-CoV and SARS-Cov (Table 5, Appendix, Supplementary Table 6).

## DISCUSSION

We found that CoV-related publications showed two steep upward trajectories in 2003–2004 and 2012–2014. The research hotspots mainly focused on the mechanisms, pathology, epidemiology, clinical diagnosis, and treatment of the coronavirus in MERS-CoV and SARS-Cov. The most contributions to CoV-related research were from the USA and China in terms of the country; the University of Hong Kong in terms of the institute; and Yuen KY from the University of Hong Kong, in terms of the author.

The outbreak of SARS and MERS had a vital impact on the number of CoV-related publications. This study and included bibliometric analyses indicated that the number of CoV-related publications showed two steep upward trajectories from 2003 to 2004 and from 2012 to 2014, separately. The trends were consistent with the outbreak of the life-threatening SARS and MERS. The first case of SARS was identified on November 16, 2002, in China (39). The MERS-CoV was first identified in Saudi Arabia in April 2012, and cases have been confirmed every year with some significant rises in 2014, 2015, and 2019 (40). Until 30 June 2019, the majority of cases (84%) had been reported in Saudi Arabia (41). Since they are the places where the virus first appeared, China (No. publications = 2,754) and Saudi Arabia (No. publications = 422) have extensively studied CoV, and their number of publications are ranked 2<sup>nd</sup> and 11<sup>th</sup> respectively.

Overall, the USA and China played an important role in CoV-related research, followed by the Netherlands and England. This



**TABLE 4 |** The characteristics and top-3 information of published bibliometric analyses.

| References | Search date-search deadline  | Dataset | No. publications | The Top-3 Journal                              | The Top-3 Countries or territories (n, %)   | The Top-3 Institutions (n)  | The Top-3 Authors  |
|------------|------------------------------|---------|------------------|--|---|---|--|
| (11)       | Database inception to Feb-20 | Scopus  | 15207            | 1. JVI;<br>2. EID;<br>3. Lancet                | 1. USA (4,225, 27.8%);<br>2. China (mainland) (2,720, 17.9%);<br>3. China (Hong Kong) (1,411, 9.3%) | 1. University of Hong Kong, China (703);<br>2. Chinese University of Hong Kong, China (499);<br>3. Chinese Academy of Sciences, China (407) | 1. Yuen KY, University of Hong Kong, China (180);<br>2. Drosten C, Charité-Universitätsmedizin Berlin, Germany (128);<br>3. Peiris JSM, University of Hong Kong, China (111) |
| (33)       | Jun-05 to Feb-20             | WOSCC   | 9760             | 1. JVI;<br>2. Virology;<br>3. PLoS One         | 1. USA (3,452, 35.4%);<br>2. China (2,402, 24.6%);<br>3. Germany (642, 6.6%)                        | 1. University of Hong Kong, China (959);<br>2. Chinese Academy of Sciences, China (469);<br>3. Chinese University of Hong Kong, China (411) | 1. Yuen KY, University of Hong Kong, China (200);<br>2. Baric RS, University of North Carolina, USA (134);<br>3. Perlman S, University of Iowa, USA (133)                    |
| (9)        | Database inception to Mar-20 | WOSCC   | 6905             | NR   | 1. USA (2,293, 33.2%);<br>2. China (1,707, 24.7%);<br>3. Germany (505, 7.3%)                        | 1. University Hong Kong, China (398);<br>2. Chinese University Hong Kong, China (217);<br>3. CDC, USA (155)                                 | NR   |
| (36)       | Jan-03 to Apr-20             | WOSCC   | 11036            | 1. JVI;<br>2. EID;<br>3. Virology              | 1. USA (3,606, 32.7%);<br>2. China (3,139, 28.4%);<br>3. Germany (669, 6.1%)                        | 1. University of Hong Kong (595); Chinese University of Hong Kong (311);<br>2. CDC (266)  | 1. Yuen, KY, University of Hong Kong, China (214);<br>2. Drosten C, University of Bonn, Germany (142);<br>3. Baric RS., University of North Carolina, USA (131)              |
| (37)       | Jan-00 to Mar 20             | WOSCC   | 9105             | 1. JVI;<br>2. Virology;<br>3. PLoS One         | 1. USA (3,101, 34.3%);<br>2. China (2,230, 24.7%);<br>3. Germany (584, 6.5%)                        | 1. University of Hong Kong, China (434);<br>2. Chinese Academy of Science, China (329);<br>3. University of California System, USA (246)    | NR   |
| (30)       | Jan-03 to Feb-20             | WOSCC   | 8433             | NR   | 1. USA (2,791, 33.1%);<br>2. China (2,231, 26.5%);<br>3. Germany (564, 6.7%)                        | 1. University of Hong Kong, China (399);<br>2. Chinese Academy of Sciences, China (298);<br>3. CDC, USA (184)                               | 1. Yuen KY, University of Hong Kong, China (178);<br>2. Drosten C, University of Bonn, Germany (118);<br>3. Baric RS, University of North Carolina, USA (114)                |
| (32)       | Jan-03 to Feb-20             | WOSCC   | 9294             | 1. JVI;<br>2. Virology;<br>3. Virus Research   | 1. USA (3,225, 34.7%);<br>2. China (2,410, 25.9%);<br>3. Germany (621, 6.7%)                        | 1. University of Hong Kong, China (452);<br>2. Chinese Academy of Sciences, China (323);<br>3. CDC, USA (197)                               | 1. Yuen KY, University of Hong Kong, China (TLS=598 times);<br>2. Chan KH, (TLS=411 times);<br>3. Woo PCY, University of Hong Kong, China (TLS=382 times)                    |
| (27)       | Jan-80 to Dec-19             | WOSCC   | 13833            | 1. JVI;<br>2. Virology;<br>3. ADV EXP MED BIOL | 1. USA (4,894, 35.4%);<br>2. China (16.7%);<br>3. Germany (6.7%)                                    | 1. University of Hong Kong, China (534);<br>2. Chinese Academy of Sciences, China (396);<br>3. Utrecht University, Netherlands (335)        | 1. Yuen KY, University of Hong Kong, China (218);<br>2. Perlman S, University of Iowa, USA (189);<br>3. Enjuanes L, Autonomous University of Madrid, Spain (176)             |
| (27)       | Jan-80 to Dec-19             | WOSCC   | 641              | JGV  | 1. USA (36.7%);<br>2. Germany (13.4%);<br>3. UK (12.2%)   | University of Würzburg, Germany   | Termeulen V  |
| (27)       | Jan-80 to Dec-19             | WOSCC   | 1674             | JVI  | 1. USA (44.3%);<br>2. Germany (9.0%);<br>3. Canada (8.3%)   | University of Southern California, USA (96)   | Lai MMC, University of Southern California, USA (70)   |

(Continued)



TABLE 4 | Continued

| References | Search date-search deadline  | Dataset                             | No. publications | The Top-3 Journal                              | The Top-3 Countries or territories (n, %)                                    | The Top-3 Institutions (n)  | The Top-3 Authors   |
|------------|------------------------------|-------------------------------------|------------------|--|--|---|---|
| (27)       | Jan-80 to Dec-19             | WOSCC                               | 4810             | 1. JVI;<br>2. Virology;<br>3. ADV EXP MED BIOL | 1. USA (1,679, 34.9%);<br>2. China (1,202, 25.0%);<br>3. Canada (324, 6.7%)  | 1. University of Hong Kong, China (284);<br>2. Chinese Academy of Sciences, China (221);<br>3. Chinese University of Hong Kong, China (172) | Yuen KY, University of Hong Kong, China (110)   |
| (27)       | Jan-80 to Dec-19             | WOSCC                               | 6601             | NR   | 1. USA (2,218, 33.6%);<br>2. China (1,479, 22.4%);<br>3. Germany (436, 6.6%) | 1. University of Hong Kong, China (243);<br>2. National Institutes of Health, USA (184);<br>3. Chinese Academy of Sciences, China (170)     | Drosten C, Charité – Universitätsmedizin, Germany (113)   |
| (26)       | Jan-68 to Mar-20             | WOS                                 | 6424             | 1. JVI;<br>2. JGV;<br>3. Virology              | 1. USA (2,345, 36.5%);<br>2. China (1,067, 16.6%);<br>3. Germany (480, 7.5%) | 1. University of Hong Kong, China (506);<br>2. University of North Carolina, USA (412);<br>3. Chinese Academy of Sciences, China (371)      | NR  |
| (34)       | Jan-70 to Apr-20             | WOS                                 | 12571            | 1. JVI;<br>2. Virology;<br>3. ADV EXP MED BIOL | 1. USA (4,513, 35.9%);<br>2. China (2,746, 21.8%);<br>3. UK (962, 7.7%)      | 1. University of Hong Kong, China (487);<br>2. Chinese Academy of Sciences, China (373);<br>3. University of California System, USA (321)   | 1. Yuen KY, University of Hong Kong, China (201);<br>2. Perlman S, University of Iowa, USA (169);<br>3. Baric RS, University of North Carolina (162);<br>Enjuanes L, Autonomous University of Madrid, Spain (162)   |
| (31)       | Jan-02 to NR                 | MAG;<br>PubMed;<br>SJR;<br>Wikidata | NR               | NR   | NR   | NR  | NR  |
| (35)       | Database inception to Feb-20 | WOSCC                               | 1747             | NR   | 1. USA (613, 35.4%);<br>2. China (582, 33.6%);<br>3. Germany (122, 7.1%)     | 1. Chinese Academy of Sciences, China (82);<br>2. University of Hong Kong, China (74);<br>3. Chinese University of Hong Kong, China (58)    | 1. Baric RS, University of North Carolina (21);<br>2. Yuen KY, University of Hong Kong, China (17); Snijder EJ, Netherlands (17); Kuochen Chou, USA (17);<br>3. Jiang Shibo, China (16)   |
| (38)       | Jan-00 to Dec-19             | WOS                                 | 10816            | 1. JVI;<br>2. Virology;<br>3. EID              | 1. USA (3,755, 34.6%);<br>2. China (2,618, 24.1%);<br>3. Germany (737, 6.8%) | 1. University of Hong Kong, China (511);<br>2. Chinese Academy of Sciences, China (385);<br>3. National Institute of Health, USA (270)      | 1. Yuen, KY, Pamela Youde Nethersole Eastern Hospital, Hong Kong (210);<br>2. Perlman, S, University of Iowa, USA (148);<br>3. Drosten, C, Bernhard Nocht Institute for Tropical Medicine, National Reference Center for Tropical Infectious Diseases, Hamburg, Germany (144) |

WOSCC, *The Web of Science Core Collection*; WOS, *Web of Science*; JVI, *Journal of Virology*; JGV, *Journal of General Virology*; EID, *Emerging Infectious Diseases*; CDC, *Center for Disease Control and Prevention*; NR, *not reported*; MAG, *Microsoft Academic Graph*; ADV EXP MED BIOL, *Advances in Experimental Medicine and Biology*; SJR, *Scientific Journal Rankings*; PNAS, *Proceedings of the National Academy of Sciences of the United States of America*; TLS, *total link strength*.

study found the USA and China were the most contributing countries in terms of STC, h-index, and NCMCI, which was supported by a previous study (20). This study showed that some institutes in the USA, China, and the Netherlands formed close cooperative relationships with other institutes. Because the USA

is leading global scientific production, and the effort of the USA to foster international cooperation on CoV-related disease.

Keywords cluster analyses showed that the main research fields of the CoV-related research focused on basic medical sciences (virology, microbiology, biochemistry & molecular

**TABLE 5 |** The findings of the main research topics in the published bibliometric analyses.

| References | Subject   | Main research topics  | Conclusions  |
|------------|---|---|--|
| (11)       | Focus on virology;<br>Public health;<br>Drugs and other hotspot fields;<br>Uncovers changes in the direction of coronavirus research.   | 1. Public health, preventive medicine and epidemiology;<br>2. Virus detection and clinical diagnosis;<br>3. Some immunological and pharmaceutical research.   | NR   |
| (33)       | NR  | 1. Clinical research;<br>2. Pathogenesis research;<br>3. Virological research;<br>4. Treatment;<br>5. Origin and transmission research.   | Notably, COVID-19 must become the research hotspot of coronavirus research, and clinical research on COVID-19 may be the key to defeating this epidemic.   |
| (9)        | The most frequently assigned research fields are virology (2140); Infectious diseases (899); Veterinary sciences (720); Microbiology (622); Immunology (558).   | 1. The molecular and biological topics;<br>2. outlines the articles dealing with the SARS epidemic;<br>3. Combines the articles dealing with the MERS epidemic;<br>4. Focuses on the spike protein that is characteristic of CoV, its pathogenesis, and its connection to the other clusters.   | The results underline the need for sustainable and forward-looking approaches that should not end with the containment of COVID-19.  |
| (36)       | The top six research areas were virology (2957); Infectious diseases (1594); Immunology (1306); Microbiology (1182); Veterinary sciences (1163); Biochemistry & molecular biology (1004).   | 1. Virology (including molecular, biology, and immunology);<br>2. Infectious diseases (including medicine, medical, and clinical);<br>3. Veterinary medicine.   | The international cooperation is an important way to accelerate research progress and achieve success. Developing corresponding vaccines and drugs are the current hotspots and research directions.   |
| (37)       | NR  | 1. The biological and virologic characteristics of coronavirus, including essential factors of infection and transmission routes during the outbreaks of SARS and MERS, as well as clinical features;<br>2. Some types of coronavirus spread among animals and humans;<br>3. Primary infection of coronavirus in mammals and birds is confined to the upper respiratory and gastrointestinal system;<br>4. The entrance into human body of SARS-CoV depends on the ACE2 receptor, while the spike protein functions as the adaptor;<br>5. The evolution based on the mutation of coronavirus RNA caused different symptoms to human kind. | More research on prevention and treatment is needed according to an analysis of term density.  |
| (30)       | Mainly involve basic medical sciences (virology, microbiology, biochemistry & molecular biology, immunology, pharmacology, & pharmacy); Clinical medicine (infectious diseases, pediatrics, respiratory system); Veterinary sciences; Public health (public, environmental, and occupational health). | 1. Mainly about respiratory viruses, which illustrated viral respiratory infections from the angle of the clinic;<br>2. Mostly about the genetic aspects of various coronaviruses;<br>3. Mainly about SARS-CoV;<br>4. Mainly about immunity;<br>5. Mostly about MERS-CoV.   | Bibliometric analysis of the literature shows the research on coronavirus boomed when a novel coronavirus triggered outbreaks in people. With the end of the epidemic, the research tended to be cooling. Virus identification, pathogenesis, and coronavirus-mediated diseases attracted much attention. We must continue studying the viruses after an outbreak ended.   |
| (32)       | Virology;<br>Veterinary sciences;<br>Infectious diseases.   | 1. "Pathological research;"<br>2. "Epidemiology research;"<br>3. "Clinical research;"<br>4. "Mechanism research."   | The outbreak of the epidemic could promote coronavirus research, meanwhile, coronavirus research contributes to overcoming the epidemic. Attention should be drawn to the latest popular research, including "Spike protein," "Receptor binding domain," and "Vaccine." Therefore, more and more efforts will be put into mechanism research and vaccine research and development, which can be helpful to deal with the epidemic. |
| (27)       | NR  | 1. The biological and virologic characteristics of coronavirus, including essential factors of infection and transmission routes during the outbreaks of SARS and MERS, as well as clinical features;   | While in the 1980s, USA and developed countries from Europe were major source countries and the virus was identified only as an animal disease in the literature and its biological and genetic structure was investigated, in   |

(Continued)

TABLE 5 | Continued

| References | Subject  | Main research topics   | Conclusions   |
|------------|--|--|---|
|            |  | 2. Some types of coronaviruses spread among animals and humans;<br>3. Primary infection of coronavirus in mammals and birds is confined to the upper respiratory and gastrointestinal system;<br>4. The entrance into human body of SARS-CoV depends on the ACE2 receptor, while the spike protein functions as the adaptor;<br>5. The evolution based on the mutation of coronavirus RNA caused different symptoms to human kind. | the 2000s, China became a major contributor of coronavirus literature because the SARS outbreak originated from southern China. Almost all most-cited publications in this period are related to SARS and the ACE2 protein.   |
| (27)       | NR   | NR   | NR  |
| (27)       | NR   | 1. Coronavirus;<br>2. Mouse hepatitis virus;<br>3. Transmissible gastroenteritis virus;<br>4. Rotavirus;<br>5. Cat.  | NR  |
| (27)       | NR   | 1. "Coronavirus;"<br>2. "SARS;"<br>3. "SARS coronavirus;"<br>4. "SARSCoV."   | NR  |
| (27)       | NR   | 1. "Saudi Arabia;"<br>2. "MERS-CoV;"<br>3. "Outbreak;"<br>4. "Vaccine;"<br>5. "Camel;"<br>6. "Zoonosis."   | NR  |
| (26)       | Infectious diseases (5341; 83.14%);<br>Microbiology (5034; 78.36%);<br>Virology (4956; 77.14%);<br>Biochemistry molecular biology (4195; 65.30%);<br>Genetics heredity (3191; 49.67%) etc. | The most commonly used keywords were "Coronavirus" followed by "Virus," "Sars," and "Infection."   | The results of the study showed that the growth pattern was not uniform, USA, and the University of Hong Kong have played a major role in the contribution of Coronavirus research. Even though this depicts a higher scientific growth, it is an alarming sign to the community for preparedness. Under the prevailing situation of seeking better prevention, treatment and vaccination for COVID-19, in-depth research in the above portrayed metrics would be an added knowledge for the researchers.                                     |
| (34)       | NR   | 1. Virus and coronavirus complementary research;<br>2. Virus and coronavirus types and strains.  | This research serves as a framework to strengthen existing research lines and develop new ones, establishing synergistic relationships that were not visible without the maps generated herein.   |
| (31)       | NR   | NR   | Independent of the outcome of the current COVID-19 outbreak, we believe that measures should be taken to encourage sustained research in the field.   |
| (35)       | The treatment hot spots focused on preventing virus adsorption, inhibiting the virus gene nucleic acid replication, transcription and translation.   | 1. CoVs epidemiology;<br>2. Basic research;<br>3. Drug development.  | Through the visualization analysis of knowledge graph, the development trend and hot spots of CoVs therapy research could be well observed. In this study, the degree of attention in the field of CoVs treatment showed periodic changes, related to the outbreak of new CoVs, and the country, institutions and the author were closely related. The treatment hot spots focused on preventing virus adsorption, inhibiting the virus gene nucleic acid replication, transcription and translation in order to develop new targets of drug. |
| (38)       | Virology (3205, 29.5);<br>Infectious Diseases (1442, 13.3);<br>Veterinary Science (1391, 12.8);<br>Immunology (1280, 11.8);<br>Biochemistry Molecular Biology (1270, 11.7) etc.            | NR   | Future studies need to include articles from other quality databases as well in order to achieve generalizations. Future researchers also need to focus their attention now on experimental studies on COV.   |

COVID-19, Coronavirus disease 2019; NR, not reported; SARS, severe acute respiratory syndrome; MERS, Middle East Respiratory Syndrome; CoV, coronavirus; ACE2, angiotensin-converting enzyme 2.

biology, immunology, pharmacology, and pharmacy), clinical medicine (infectious diseases, pediatrics, and the respiratory system), veterinary sciences, and public health (public, environmental, and occupational health). The research hotspots mainly focused on the mechanism, pathology, epidemiology, clinical diagnosis, and treatment of the coronavirus in MERS-CoV and SARS-CoV. These findings were in line with the findings of other published bibliometric analyses included in this study. However, the complete research process of virus includes the following: (1) studying the structure and function of the virus genome to fully understand the general morphology and structural characteristics of the virus; (2) exploring the replication, gene expression, and regulatory mechanism of the virus genome, to reveal the molecular nature of the virus infection and disease-causing; (3) researching and developing the virus genetic engineering vaccine and antiviral drugs; (4) studying the diagnosis, prevention, and treatment scheme of the virus infection disease (42, 43). This study showed the current research on CoV mainly focused on the first two stages of virus research. Therefore, there still was a lack of enough research on the related clinical, epidemiological, diagnostic, and therapeutic aspects (44). As the WHO recommended, drugs and vaccines were considered to need accelerated research and development (45), and research on the diagnosis, vaccines, and treatment options for CoV-related diseases should be strengthened (46).

Yuen KY from the University of Hong Kong contributed most to Cov-related research, especially in the fields of virology and microbiology. Followed by Baric RS and Drosten C, both of whom were members of the CoV Study Group (CSG) and assessed the novelty of the human pathogen tentatively named SARS-CoV-2 (47). The research of the CSG will improve understanding of virus-host interactions in an ever-changing environment and enhance our preparedness for future outbreaks (47). In the future, CoV-related researchers can collaborate to conquer the virus.

## STRENGTHS AND LIMITATIONS

To our best knowledge, this is the first systematic review of bibliometric analysis in global coronavirus research trends before COVID-19. We also explored the top-5 research areas of the top-10 countries and top-10 authors in this bibliometric analysis.

However, our study has some limitations. Firstly, for the bibliometric analysis, we only searched WOS, which may lead to

the omission of some important studies (48–50). Secondly, some of the data we analyzed were automatically extracted from the downloaded publications by the software, such as author names. Since the software could not distinguish between authors with the same name, this might affect the results of our analyses. Thirdly, for the systematic review, the assessment of the risk of bias for the included studies was important, but we did not conduct the risk of bias assessment for lack of a valid assessment tool.

## CONCLUSIONS

CoV-related publications before COVID-19 have shown a rapidly increasing trend. The USA and China have played a vital role in CoV-related researches. Yuen KY from the University of Hong Kong has made contributions. The research topics mainly involved the mechanisms, pathology, epidemiology, clinical diagnosis, and treatment of the coronavirus in MERS-CoV and SARS, and more researchers should focus on the prevention, diagnosis, and treatment in the future.

## AUTHOR CONTRIBUTIONS

KY, PY, SW, and ML were responsible for the conception and design of the study. PY was in charge of the literature search data acquisition. PY, ML, ZL, JL, XH, YB, and YX collected, analyzed, and interpreted the data and wrote the first draft of the manuscript. YL was responsible for the editing and standardization of the tables and figures and gave critical advice on the manuscript. All authors reviewed the manuscript for important intellectual content and approved the final version for publication.

## FUNDING

This work was supported by the Key Project of the Social Science Fund of Gansu Province: Social Research on the Response to COVID-19 in Gansu Province (Grant No. 20ZD016) and Fundamental Research Funds for the Central Universities (Grant No. lzujbky-2020-sp14).

## SUPPLEMENTARY MATERIAL

The Supplementary Material for this article can be found online at: <https://www.frontiersin.org/articles/10.3389/fmed.2021.729138/full#supplementary-material>

## REFERENCES

1. WHO. *Coronaviruses*. (2020). Available online at: <https://www.who.int/health-topics/coronavirus> (accessed February 10, 2020).
2. Yadav R, Chaudhary JK, Jain N, Chaudhary PK, Khanra S, Dhamija P, et al. Role of structural and non-structural proteins and therapeutic targets of SARS-CoV-2 for COVID-19. *Cells*. (2021) 10:821. doi: 10.3390/cells10040821
3. Cui J, Li F, Shi ZL. Origin and evolution of pathogenic coronaviruses. *Nat Rev Microbiol*. (2019) 17:181–92. doi: 10.1038/s41579-018-0118-9
4. Backer JA, Klinkenberg D, Wallinga J. Incubation period of 2019 novel coronavirus (2019-nCoV) infections among travellers from Wuhan, China, 20–28 January 2020. *Euro Surveill*. (2020) 25:1–6. doi: 10.2807/1560-7917.ES.2020.25.5.2000062
5. Liu P, Niu R, Chen J, Tang Y, Tang W, Xu L, et al. Epidemiological and clinical features in patients with coronavirus disease 2019 outside of Wuhan, China: special focus in asymptomatic patients. *PLoS Negl Trop Dis*. (2021) 15:e0009248. doi: 10.1371/journal.pntd.0009248

6. Tu H, Tu S, Gao S, Shao A, Sheng J. Current epidemiological and clinical features of COVID-19; a global perspective from China. *J Infect.* (2020) 81:1–9. doi: 10.1016/j.jinf.2020.04.011
7. Li Y, Cao L, Zhang Z, Hou L, Qin Y, Hui X, et al. Reporting and methodological quality of COVID-19 systematic reviews needs to be improved: an evidence mapping. *J Clin Epidemiol.* (2021) 135:17–28. doi: 10.1016/j.jclinepi.2021.02.021
8. Li J, Du W, Yan P, Yang K. [Subject topics and dissemination clustering of COVID-19 epidemic studies at home and abroad]. *Libr Inf.* (2021) 67–74. doi: 10.11968/tsyqb.1003-6938.2021025
9. Klingelhöfer D, Braun M, Brüggmann D, Groneberg DA. Coronavirus: an insight into global research until outbreak of COVID-19 and its implications for the future. *J Glob Health.* (2020) 10:020508. doi: 10.7189/jogh.10.020508
10. Goh S. Who will guard the guards? Covid-19 research may be incomplete, but experts are vital during this pandemic. *BMJ.* (2020) 370:m2658. doi: 10.1136/bmj.m2658
11. Deng Z, Chen J, Wang T. Bibliometric and visualization analysis of human coronaviruses: prospects and implications for COVID-19 research. *Front Cell Infect Microbiol.* (2020) 10:581404. doi: 10.3389/fcimb.2020.581404
12. Usman M, Ho YS. A bibliometric study of the fenton oxidation for soil and water remediation. *J Environ Manage.* (2020) 270:110886. doi: 10.1016/j.jenvman.2020.110886
13. Deng Z, Wang H, Chen Z, Wang T. Bibliometric analysis of dendritic epidermal T Cell (DETC) research from 1983 to 2019. *Front Immunol.* (2020) 11:259. doi: 10.3389/fimmu.2020.00259
14. Global I. *What is Bibliometric Analysis.* (2020). Available online at: <https://www.igi-global.com/dictionary/education-literature-development-responsibility/2406> (accessed March 1, 2020).
15. Blakeman K. Bibliometrics in a digital age: help or hindrance. *Sci Prog.* (2018) 101:293–310. doi: 10.3184/003685018X15337564592469
16. Zyoud SH. Global research trends of middle east respiratory syndrome coronavirus: a bibliometric analysis. *BMC Infect Dis.* (2016) 16:1–7. doi: 10.1186/s12879-016-1600-5
17. Wang Z, Chen Y, Cai G, Jiang Z, Liu K, Chen B, et al. A bibliometric analysis of pubmed literature on middle east respiratory syndrome. *Int J Environ Res Public Health.* (2016) 13:1–9. doi: 10.3390/ijerph13060583
18. Beal J, Mitchell T, Wyschogrod D, Manthey J, Clore A. Highly distinguished amino acid sequences of 2019-nCoV (Wuhan Coronavirus). *bioRxiv.* (2020). doi: 10.1101/2020.01.31.929497
19. Sweileh WM. Global research trends of World Health Organization's top eight emerging pathogens. *Global Health.* (2017) 13:9–29. doi: 10.1186/s12992-017-0233-9
20. Bonilla-Aldana DK, Quintero-Rada K, Montoya-Posada JP, Ramirez-Ocampo S, Paniz-Mondolfi A, Rabaan AA, et al. SARS-CoV, MERS-CoV and now the 2019-novel CoV: have we investigated enough about coronaviruses?—a bibliometric analysis. *Travel Med Infect Dis.* (2020) 33:101566. doi: 10.1016/j.tmaid.2020.101566
21. Thomson Reuters. *Journal Citation Reports.* (2020). Available online at: <https://jcr.clarivate.com/JCRJournalHomeAction.action> (accessed January 10, 2020).
22. Chen C, Hu Z, Liu S, Tseng H. Emerging trends in regenerative medicine: a scientometric analysis in citespace. *Expert Opin Biol Ther.* (2012) 12:593–608. doi: 10.1517/14712598.2012.674507
23. van Eck NJ, Waltman L. Software survey: VOSviewer, a computer program for bibliometric mapping. *Scientometrics.* (2010) 84:523–38. doi: 10.1007/s11192-009-0146-3
24. Shi J-g, Miao W, Si H. Visualization and analysis of mapping knowledge domain of urban vitality research. *Sustainability.* (2019) 11:988. doi: 10.3390/su11040988
25. Wrigley J, Carden V, von Isenburg M. Bibliometric mapping for current and potential collaboration detection. *J Med Libr Assoc.* (2019) 107:597–600. doi: 10.5195/jmla.2019.764
26. Joshua V, Sivaprakasam S. Coronavirus: bibliometric analysis of scientific publications from 1968 to 2020. *Med J Islam Repub Iran.* (2020) 34:64. doi: 10.47176/mjiri.34.64
27. Enel E, Topal FEJDM, Preparedness PH. Holistic Analysis of Coronavirus Literature: A Scientometric Study of the Global Publications Relevant to SARS-CoV-2 (COVID-19), MERS-CoV (MERS) and SARS-CoV (SARS). *Disaster Med Public Health Prep.* (2020) 1–15. doi: 10.1017/dmp.2020.300
28. Ksiazek TG, Erdman D, Goldsmith CS, Zaki SR, Peret T, Emery S, et al. A novel coronavirus associated with severe acute respiratory syndrome. *N Engl J Med.* (2003) 348:1953–66. doi: 10.1056/NEJMoa030781
29. Drosten C, Günther S, Preiser W, van der Werf S, Brodt HR, Becker S, et al. Identification of a novel coronavirus in patients with severe acute respiratory syndrome. *N Engl J Med.* (2003) 348:1967–76. doi: 10.1056/NEJMoa030747
30. Jia Q, Shi S, Yuan G, Shi J, Shi S, Hu Y. Analysis of knowledge bases and research hotspots of coronavirus from the perspective of mapping knowledge domain. *Medicine.* (2020) 99:e20378. doi: 10.1097/md.00000000000020378
31. Kagan D, Moran-Gilad J, Fire M. Scientometric trends for coronaviruses and other emerging viral infections. *Gigascience.* (2020) 9:1–17. doi: 10.1093/gigascience/giaa085
32. Mao XJ, Guo L, Fu PF, Xiang C. The status and trends of coronavirus research A global bibliometric and visualized analysis. *Medicine.* (2020) 99:e20137. doi: 10.1097/md.00000000000020137
33. Tao Z, Zhou S, Yao R, Wen K, Da W, Meng Y, et al. COVID-19 will stimulate a new coronavirus research breakthrough: a 20-year bibliometric analysis. *Ann Transl Med.* (2020) 8:528. doi: 10.21037/atm.2020.04.26
34. Herrera-Viedma E, Lopez-Robles JR, Guallar J, Cobo MJ. Global trends in coronavirus research at the time of Covid-19: a general bibliometric approach and content analysis using SciMAT. *Profesional De La Informacion.* (2020) 29:e290322. doi: 10.3145/epi.2020.may.22
35. Yi W, Wang Y, Tang J, Xiong X, Zhang Y, Yan S. [Visualization analysis on treatment of coronavirus based on knowledge graph]. *Zhonghua Wei Zhong Bing Ji Jiu Yi Xue.* (2020) 32:279–86. doi: 10.3760/cma.j.cn121430-20200225-00200
36. Zhai F, Zhai Y, Cong C, Song T, Xiang R, Feng T, et al. Research progress of coronavirus based on bibliometric analysis. *Int J Environ Res Public Health.* (2020) 17:3766. doi: 10.3390/ijerph17137666
37. Zhou Y, Chen L. Twenty-year span of global coronavirus research trends: a bibliometric analysis. *Int J Environ Res Public Health.* (2020) 17:3082. doi: 10.3390/ijerph17093082
38. Ali A, AhmadHakak I, Amin F. Assessing the coronavirus research output: a bibliometric analysis. *Glob Bus Rev.* (2020). doi: 10.1177/0972150920975116
39. Zhong NS, Zheng BJ, Li YM, Poon, Xie ZH, Chan KH, et al. Epidemiology and cause of severe acute respiratory syndrome (SARS) in Guangdong, people's republic of China, in February, 2003. *Lancet.* (2003) 362:1353–8. doi: 10.1016/S0140-6736(03)14630-2
40. CDC E. European Centre for Disease Prevention and Control. *Distribution of confirmed MERS-CoV cases.* (2019). Available online at: <https://www.ecdc.europa.eu/en/middle-east-respiratory-syndrome-coronavirus-mers-cov-situation-update> (accessed February 16, 2020).
41. WHO World Health Organization. *WHO MERS Global Summary and Assessment of Risk.* (2019). Available online at: <https://apps.who.int/iris/bitstream/handle/10665/326126/WHO-MERS-RA-19-1-eng.pdf?ua=1> (accessed February 17, 2020).
42. Solomon T, Lewthwaite P, Perera D, Cardoso MJ, Ooi MH. Virology, epidemiology, pathogenesis, and control of enterovirus 71. *Lancet Infect Dis.* (2010) 10:778–90. doi: 10.1016/S1473-3099(10)70194-8
43. Lau JY, Wright TL. Molecular virology and pathogenesis of hepatitis B. *Lancet.* (1993) 342:1335–40. doi: 10.1016/0140-6736(93)92249-S
44. Momattin H, Al-Ali AY, Al-Tawfiq JA. A systematic review of therapeutic agents for the treatment of the middle east respiratory syndrome coronavirus (MERS-CoV). *Travel Med Infect Dis.* (2019) 30:9–18. doi: 10.1016/j.tmaid.2019.06.012
45. WHO World Health Organization. *2018 Annual review of diseases prioritized under the Research andDevelopment Blueprint.* (2018). Available online at: <https://www.who.int/news-room/events/detail/2018/02/06/default-calendar/2018-annual-review-of-diseases-prioritized-under-the-research-anddevelopment-blueprint> (accessed March 1, 2020).
46. Zarocostas J. What next for the coronavirus response? *Lancet.* (2020) 395:401. doi: 10.1016/S0140-6736(20)30292-0



47. Gorbalenya AE, Baker SC, Baric RS, de Groot RJ, Drosten C, Gulyaeva AA, et al. The species Severe acute respiratory syndrome-related coronavirus: classifying 2019-nCoV and naming it SARS-CoV-2. *Nat Microbiol.* (2020) 5:536–44. doi: 10.1038/s41564-020-0695-z
48. Ge L, Tian J-h, Li Y-n, Pan J-x, Li G, Wei D, et al. Association between prospective registration and overall reporting and methodological quality of systematic reviews: a meta-epidemiological study. *J Clin Epidemiol.* (2018) 93:45–55. doi: 10.1016/j.jclinepi.2017.10.012
49. Lun Li, Jinhui, Tian, Hongliang, Tian, et al. Network meta-analyses could be improved by searching more sources and by involving a librarian. *J Clin Epidemiol.* (2014) 67:1001–7. doi: 10.1016/j.jclinepi.2014.04.003
50. Yao L, Sun R, Chen YL, Wang Q, Yang K. The quality of evidence in Chinese meta-analyses need to be Improved. *J Clin Epidemiol.* (2016) 74:73–9. doi: 10.1016/j.jclinepi.2016.01.003

**Conflict of Interest:** The authors declare that the research was conducted in the absence of any commercial or financial relationships that could be construed as a potential conflict of interest.

**Publisher's Note:** All claims expressed in this article are solely those of the authors and do not necessarily represent those of their affiliated organizations, or those of the publisher, the editors and the reviewers. Any product that may be evaluated in this article, or claim that may be made by its manufacturer, is not guaranteed or endorsed by the publisher.

Copyright © 2021 Yan, Li, Li, Lu, Hui, Bai, Xun, Lao, Wang and Yang. This is an open-access article distributed under the terms of the Creative Commons Attribution License (CC BY). The use, distribution or reproduction in other forums is permitted, provided the original author(s) and the copyright owner(s) are credited and that the original publication in this journal is cited, in accordance with accepted academic practice. No use, distribution or reproduction is permitted which does not comply with these terms.



# Chest-Related Imaging Investigations During Multiple Waves of COVID-19 Infection in Hong Kong

Kei Shing Ng and Varut Vardhanabhuti\*

Department of Diagnostic Radiology, Li Ka Shing Faculty of Medicine, The University of Hong Kong, Hong Kong, Hong Kong SAR, China

## OPEN ACCESS

### Edited by:

Reza Lashgari,  
Shahid Beheshti University, Iran

### Reviewed by:

Beatrice Ludovica Ritondo,  
University of Rome Tor Vergata, Italy  
Gigi Lam,  
Hong Kong Shue Yan University,  
Hong Kong SAR, China

### \*Correspondence:

Varut Vardhanabhuti  
varv@hku.hk

### Specialty section:

This article was submitted to  
Pulmonary Medicine,  
a section of the journal  
Frontiers in Medicine

**Received:** 03 May 2021

**Accepted:** 19 October 2021

**Published:** 17 November 2021

### Citation:

Ng KS and Vardhanabhuti V (2021)  
Chest-Related Imaging Investigations  
During Multiple Waves of COVID-19  
Infection in Hong Kong.  
Front. Med. 8:704515.  
doi: 10.3389/fmed.2021.704515

**Background:** The COVID-19 pandemic has caused significant disruption to healthcare worldwide. In this study, we aim to quantify its impact of chest related radiological procedures over the different waves of local infection in Hong Kong across the territory's public hospitals.

**Methods:** This was an observational study enrolling patients between January 2017 and December 2020. Consecutive population-based chest radiographs, CT, US, and interventional radiology (IR) procedures were obtained public hospitals across Hong Kong.

**Results:** A significant reduction of 10.0% ( $p < 0.001$ ) in the total number of chest radiographs was observed. Non-significant reduction of 2.5% ( $p = 0.0989$ ), 39.1% ( $p = 0.2135$ ), and 1.9% ( $p = 0.8446$ ) was observed for Chest CT, Chest US, and Chest IR procedures, respectively, in 2020 compared to the projected values.

**Conclusion:** Although, it was anticipated that there would be a significant impact to health services caused by the pandemic, for chest-related investigations in Hong Kong, the impact was not as severe. Quantitative analysis could help with future planning and public health decision making.

**Keywords:** COVID-19, X-ray, CT, chest ultrasound, interventional radiology

## INTRODUCTION

Significant impact of coronavirus disease 2019 (COVID-19) was observed in the year 2020. In particular, medical services have been reduced or have been redirected toward caring for patients with coronavirus disease 2019 (COVID-19) (1). The first local COVID-19 case in Hong Kong was reported on January 23, 2020. On October 18, 2021, 12,294 confirmed cases (2,952 imported cases and 9,342 local cases) and 213 deaths were reported in the territory. In terms of medical imaging, varying impacts on chest ultrasound (2) and interventional radiology (3–6) were reported globally, but few studies have examined the impact at a population level over a prolonged period. The effects

**TABLE 1** | The actual, predicted number using the time series method and percentage change of chest-related procedures in 2020.

| 2020                 | Chest X-rays |            |          | CT Chests |            |          | US Chests |            |          | Interventional Radiology |            |          |
|----------------------|--------------|------------|----------|-----------|------------|----------|-----------|------------|----------|--------------------------|------------|----------|
|                      | Actual       | Predicted* | % change | Actual    | Predicted* | % change | Actual    | Predicted* | % change | Actual                   | Predicted* | % change |
| Jan                  | 162,185      | 170,811    | −5.05    | 7,828     | 8,413      | −6.96    | 13        | 16         | −16.51   | 180                      | 211        | −14.65   |
| Feb                  | 129,066      | 154,692    | −16.57   | 5,429     | 7,668      | −29.20   | 12        | 16         | −26.11   | 147                      | 179        | −17.83   |
| Mar                  | 142,525      | 173,219    | −17.72   | 7,848     | 8,761      | −10.42   | 5         | 15         | −67.19   | 211                      | 224        | −5.61    |
| Apr                  | 129,669      | 159,359    | −18.63   | 7,182     | 7,739      | −7.20    | 9         | 10         | −12.11   | 207                      | 190        | 8.82     |
| May                  | 140,276      | 166,580    | −15.79   | 8,354     | 8,594      | −2.80    | 8         | 19         | −56.92   | 189                      | 212        | −10.94   |
| Jun                  | 146,924      | 158,344    | −7.21    | 9,065     | 8,361      | 8.43     | 14        | 18         | −20.32   | 219                      | 194        | 13.15    |
| Jul                  | 149,828      | 165,895    | −9.69    | 8,403     | 8,770      | −4.18    | 7         | 18         | −60.16   | 235                      | 224        | 5.12     |
| Aug                  | 141,393      | 162,393    | −12.93   | 8,372     | 9,195      | −8.96    | 12        | 15         | −17.64   | 240                      | 240        | 0.19     |
| Sep                  | 146,512      | 153,307    | −4.43    | 9,513     | 8,601      | 10.60    | 9         | 17         | −46.78   | 221                      | 224        | −1.44    |
| Oct                  | 147,334      | 158,694    | −7.16    | 8,624     | 8,587      | 0.43     | 6         | 16         | −62.29   | 165                      | 215        | −23.22   |
| Nov                  | 154,940      | 158,854    | −2.46    | 9,540     | 9,035      | 5.59     | 6         | 21         | −71.31   | 223                      | 218        | 2.35     |
| Dec                  | 161,229      | 165,331    | −2.48    | 9,534     | 8,535      | 11.70    | 20        | 20         | 2.20     | 235                      | 191        | 23.33    |
| Total                | 1,751,881    | 1,947,479  | −10.04   | 99,692    | 102,261    | −2.51    | 121       | 199        | −39.16   | 2,472                    | 2,520      | −1.90    |
| Stationary R-squared | 0.727        |            |          | 0.814     |            |          | 0.836     |            |          | 0.843                    |            |          |
| R-squared            | 0.650        |            |          | 0.742     |            |          | 0.446     |            |          | 0.684                    |            |          |
| RMSE                 | 5148.005     |            |          | 318.861   |            |          | 4.215     |            |          | 15.162                   |            |          |
| MAPE                 | 2.562        |            |          | 3.056     |            |          | 15.704    |            |          | 6.823                    |            |          |
| MAE                  | 3930.920     |            |          | 239.558   |            |          | 3.384     |            |          | 11.893                   |            |          |
| MaxAPE               | 10.175       |            |          | 8.505     |            |          | 49.340    |            |          | 17.637                   |            |          |
| MaxAE                | 14593.800    |            |          | 616.880   |            |          | 8.420     |            |          | 34.263                   |            |          |
| Normalised BIC       | 17.391       |            |          | 11.828    |            |          | 3.176     |            |          | 5.736                    |            |          |

RMSE, Root mean square error; MAE, Mean absolute error; MaxAPE, Maximum absolute percentage error; MaxAE, Maximum absolute error; Normalised BIC, Normalised Bayesian information criterion.

\*The predicted values were rounded to nearest integer, and the percentage change was based on the full digits of the predicted value.

of chest X-ray and chest CT have also not been quantitatively reported at a population scale. In this study, we systematically examined territory-wide chest-related imaging investigational data in the Hong Kong public hospitals database and compare the impact in 2020 with the prior 3 years.

## METHODS

The Hong Kong Hospital Authority Clinical Data Analysis and Reporting System (CDARS) was used to conduct a retrospective search of electronic records of patients using a national database. The study was approved by the institutional review board, and, due to the retrospective nature of the study, the patient consent was not required. The study retrieved data between January and December of the years 2017 and 2020, covering chest imaging investigations, specifically chest radiographs, chest computed tomography (CT), chest ultrasound (US), and chest interventional radiology (IR) procedures. The time series model was conducted on the data from the prior years of 2017–2019 to estimate the predicted number of procedures in 2020 (Time Series Modeller, SPSS, IBM Corp., Armonk, N.Y., USA). Differences in counts between the predicted and actual values were compared using a generalised linear model with the Poisson distribution. Statistical significance was set as  $p < 0.05$ . The

analysis was performed using R Studio version 1.3 (rstudio.com, Boston, Massachusetts, United States).

## RESULTS

In 2020, there were a total number of 1,751,881 chest radiographs, 99,692 chest CT, 121 chest US, and 2,472 chest IR procedures performed from 35, 19, 11, and 18 hospitals, respectively, across public hospitals in Hong Kong. A significant reduction of 10.0% ( $p < 0.001$ ) in the total number of chest radiographs was observed in 2020 compared to the predicted value based on the time series model. Non-significant reduction of 2.5% ( $p = 0.0989$ ), 39.1% ( $p = 0.2135$ ), and 1.9% ( $p = 0.8446$ ) was observed for Chest CT, Chest US, and Chest IR procedures in 2020 compared to the predicted values based on the time series model (see **Table 1**, **Figure 1**).

Monthly analysis revealed that there was an overall trend of a marked initial reduction in the early months at the start of pandemic. Cases were returned to almost a pre-pandemic level during the easing of social restrictions but reduced again in July 2020, coinciding with the reemergence of infection.

For chest radiograph, reduction was observed in all the months of 2020 compared to predicted numbers (with

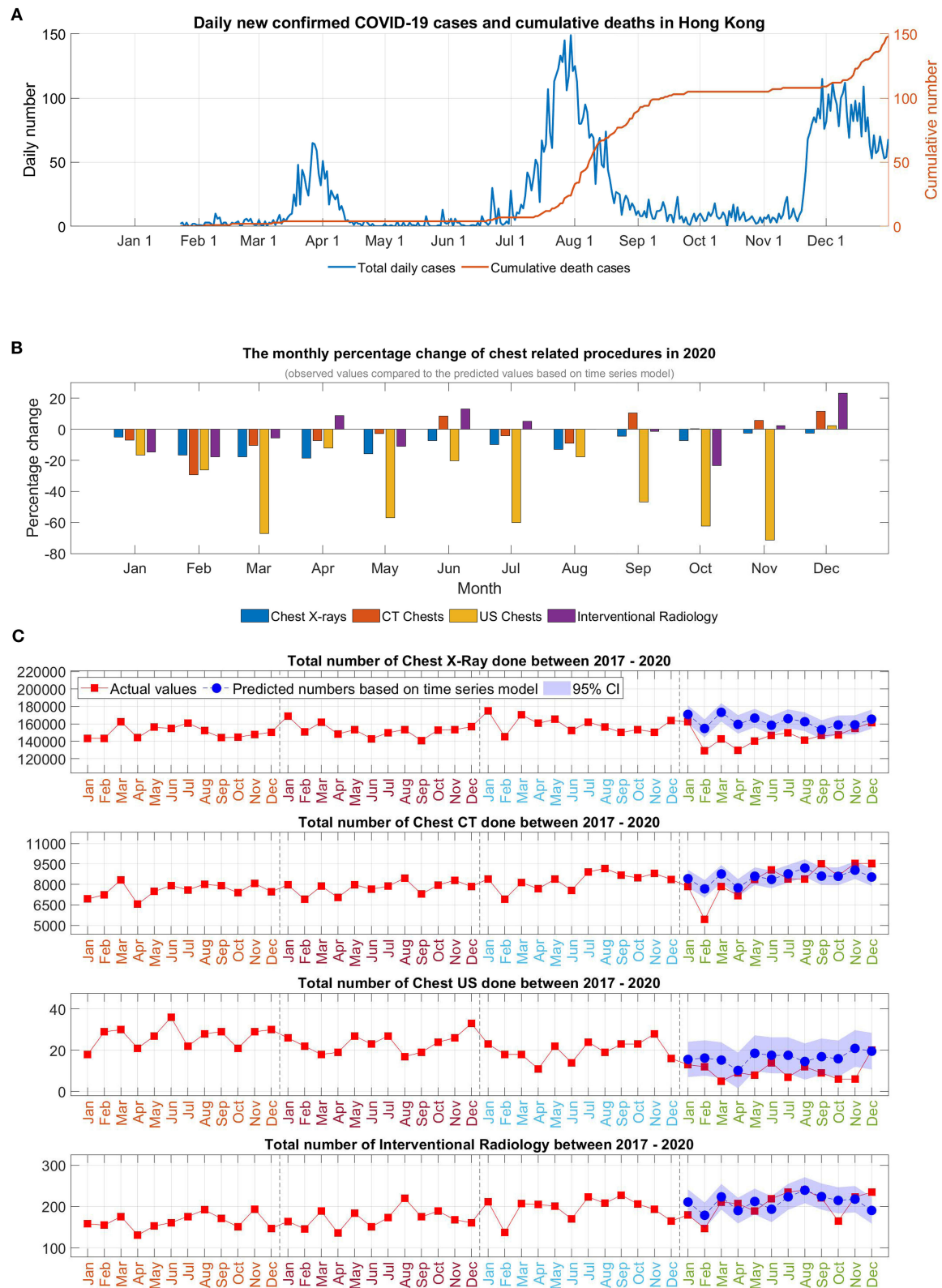
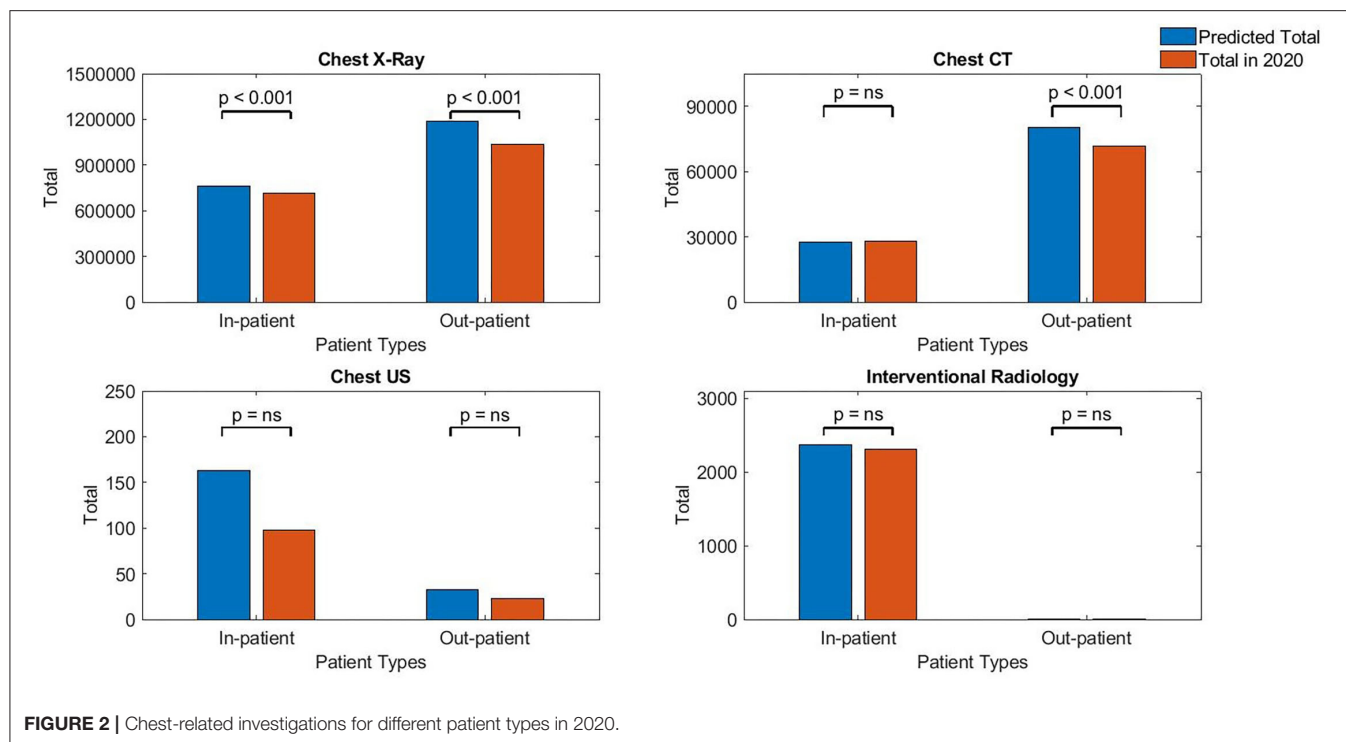


**FIGURE 1 | (A)** Daily newly confirmed COVID-19 cases and cumulative deaths in Hong Kong, **(B)** The monthly percentage change of chest-related procedures in 2020, **(C)** Time series analysis of the chest-related procedures in 2020.



negative % in all the months). For chest CT, although marked reduction was observed initially, there was an increase in number of investigations in the months of June, and September to December, and, by the year end, there was only minimal overall reduction of 2.5% for 2020. For chest US, the monthly changes showed a double-digit percentage reduction in January to November (−12.1 to −71.3%) in 2020 with only a mild catchup (2.2%) in December. For chest IR, monthly analysis showed a reduction in the period of January to March in 2020, and subsequently increased in the following months with another reduction in October, with increasing numbers again toward year end. As a result, the overall yearly reduction was mild (−1.9%,  $p = 0.8446$ ).

When analysis was done based on patient types, for chest radiographs, the impact was more for outpatient investigations (−12.45%,  $p < 0.001$ ) compared with inpatient (−6.40%,  $p < 0.001$ ). For Chest CT, outpatient investigations were more affected with overall reduction observed (−11.05%,  $p < 0.001$ ) compared to mild increase for inpatient investigations (+2.7%,  $p = 0.3716$ ). For Chest US, the inpatient contributed a marked reduction (−39.8%,  $p = 0.2516$ ) compared to a modest reduction for outpatient (−28.7%,  $p = 0.7210$ ). Finally, for chest IR, the reduction by type of a patient was mild for inpatient (−2.7%,  $p = 0.7882$ ) and large for outpatient (−50.7%,  $p = 0.7720$ ). However, the total chest IR done for outpatient was <10 procedures, which may be regarded negligibly small to draw firm conclusion (see **Figure 2**, **Table 2**).

## DISCUSSION

It was perceived that many radiology departments may observe up to a 50–70% reduction in imaging volume that may last for several months during the COVID-19 pandemic (7). In our study, during the initial waves, a more pronounced reduction was observed, which was most likely attributed to a tighter initial lockdown and cancellation of procedures, likely due to a more conservative stance taken due to a relative lack of knowledge about the new disease. The conservative stance may have stemmed from a previous encounter of Hong Kong with the SARS outbreak in 2003 (8), when the mortality rate in Hong Kong was 17.04%, which was about three times that of China (4.87%). Original findings of a high infection incidence and a mortality rate (2.97%) among healthcare staff in hospitals (9), as well as a lack of protective gear for hospitals and clinics (10), may have contributed to the extreme vigilance of the government and refusal of patients to attend hospital appointments (11). Anecdotally, this was often found at the local level, where some patients would phone to postpone or cancel appointments.

Despite of the confirmed case numbers being much higher for the subsequent waves of infection in December 2020, the opposite trend was observed with only a minor decline in Chest X-ray and a small increase in CT Chest, US Chest, and IR. This was more likely due to improved preparedness and increased precautions implemented in hospitals as well as more experience in coping with the COVID-19 pandemic in the months following the outbreak. During these times, precautions, such as wearing



**TABLE 2 |** The numbers of inpatient vs. outpatient vs. total number using the time series method for all four imaging investigations.

|                 | Chest X-rays |            |           | CT Chests |            |         | US Chests |            |        | Interventional radiology |            |       |
|-----------------|--------------|------------|-----------|-----------|------------|---------|-----------|------------|--------|--------------------------|------------|-------|
|                 | Inpatient    | Outpatient | Total     | Inpatient | Outpatient | Total   | Inpatient | Outpatient | Total  | Inpatient                | Outpatient | Total |
| 2020 Actual     | 713,161      | 1,038,720  | 1,751,881 | 28,177    | 71,515     | 99,692  | 98        | 23         | 121    | 2,312                    | 3          | 2,472 |
| 2020 Predicted* | 761,895      | 1,186,389  | 1,947,479 | 27,447    | 80,400     | 102,261 | 163       | 32         | 199    | 2,376                    | 6          | 2,520 |
| % change        | -6.40        | -12.45     | -10.04    | 2.66      | -11.05     | -2.51   | -39.82    | -28.66     | -39.20 | -2.68                    | -50.74     | -1.90 |

\*The predicted values were rounded to nearest integer, and the percentage change was based on the full digits of the predicted value.

masks, mandatory measurement of body temperature, protective covering for staffs, and frequent hand washing, were in place. The adoption of COVID-19 contact tracing apps for patients and anti-pandemic legislation Cap. 599 on home quarantine and social distancing, and compulsory testing for certain persons introduced by the Hong Kong SAR government were also routine procedures with a high adoption rate in Hong Kong.

There were likely multiple reasons for the reduction in radiological procedures observed. The reason for less impact on chest CT and chest IR procedures may be postulated to be due to the fact that more severely ill patients still required these crucial investigational procedures. In addition, we postulate that there were increasing needs of cross-sectional imaging and interventional procedure requirement for chest-related diseases during the pandemic. There may also have been preferential imaging practises, which caused a reduction of ultrasound procedure, for example, to try to minimise direct patient contact. This may be the reason why there was a reduction in chest US inpatient numbers (although not significantly reduced). It must be noted that the numbers were few, in general, to draw any firm conclusion. It was not possible to clearly identify the reasons (e.g., if this was due to change of practise or behaviour of physicians) due to retrospective nature of the study across multiple sites. Looking ahead, as we move toward living with COVID-19 as endemic infections, continued practises of enhanced precautions may become permanent. Health providers must, therefore, try to be more proactive and anticipate potential impact in the event of an outbreak, and minimise the impact of reduction in radiological investigations as far as possible. There are a few ways that one could do this. First, for urgent investigations, provisions must be put in place to be able to provide these services and minimise the cancellations as far as possible. Second, if cancellations were to occur for non-urgent cases, the healthcare providers should adopt a system that allows for a more rapid rearrangement and, for example, may increase the quota of non-emergency outpatient investigations to offset any reduction of services during the localised outbreaks. Radiologists should work closely with their referral doctors to review and reschedule such examinations.

In conclusion, despite relatively low case numbers in Hong Kong compared to other countries, a significant reduction in chest radiographs investigation was seen, but not for chest CT, chest US, or chest IR procedures when analysed at a population level based on yearly analysis.

## DATA AVAILABILITY STATEMENT

The raw data supporting the conclusions of this article will be made available by the authors, without undue reservation.

## ETHICS STATEMENT

The studies involving human participants were reviewed and approved by Cluster Research Ethics Committee/Institutional Review Board (REC/IRB). Written informed consent for participation was not required for this study in accordance with the national legislation and the institutional requirements.

## AUTHOR CONTRIBUTIONS

KN and VV were involved in study conception, statistical analysis, drafting of the initial version of the manuscript, data

collection, and statistical analysis. VV supervised the work and offered significant intellectual contribution. All the authors offered significant intellectual contribution for the last version of the manuscript and approved the final form.

## REFERENCES

- Vardhanabhuti V, Ng KS. Differential impact of COVID-19 on cancer diagnostic services based on body regions: a public facility-based study in Hong Kong. *Int J Radiat Oncol Biol Phys.* (2021) 111:331–6. doi: 10.1016/j.ijrobp.2021.05.010
- Vetrugno L, Baciarello M, Bignami E, Bonetti A, Saturno F, Orso D, et al. The “pandemic” increase in lung ultrasound use in response to Covid-19: can we complement computed tomography findings? A narrative review. *Ultrasound J.* (2020) 12:39. doi: 10.1186/s13089-020-00185-4
- Cahalane AM, Cui J, Sheridan RM, Thabet A, Sutphin PD, Palmer WE, et al. Changes in interventional radiology practice in a tertiary academic center in the United States during the coronavirus disease 2019 (COVID-19) pandemic. *J Am Coll Radiol.* (2020) 17:873–7. doi: 10.1016/j.jacr.2020.05.005
- Hashmi A, Parikh K, Al-Natour M, Azar N, Sutter C, Ramaiya N, et al. Interventional radiology procedural volume changes during COVID-19 initial phase: a tertiary level Midwest health system experience. *Clin Imaging.* (2021) 72:31–6. doi: 10.1016/j.clinimag.2020.10.039
- How GY, Pua U. Trends of interventional radiology procedures during the COVID-19 pandemic: the first 27 weeks in the eye of the storm. *Insights Imaging.* (2020) 11:131. doi: 10.1186/s13244-020-00938-8
- Zhong J, Datta A, Gordon T, Adams S, Guo T, Abdelaziz M, et al. The impact of COVID-19 on interventional radiology services in the UK. *CardioVasc Intervent Radiol.* (2021) 44:134–40. doi: 10.1007/s00270-020-02692-2
- Cavallo JJ, Forman HP. The economic impact of the COVID-19 pandemic on radiology practices. *Radiology.* (2020) 296:E141–4. doi: 10.1148/radiol.2020201495
- Leung GM, Ho LM, Lam TH, Hedley AJ. Epidemiology of SARS in the 2003. Hong Kong epidemic. *Hong Kong Med J.* (2009) 15(Suppl. 9):12–6.
- Razzak JA, Bhatti JA, Tahir MR, Pasha-Razzak O. Initial estimates of COVID-19 infections in hospital workers in the United States during the first wave of pandemic.(Research Article). *PLoS One.* (2020) 15:e0242589. doi: 10.1371/journal.pone.0242589
- Wu H, Huang J, Zhang CJP, He Z, Ming W-K. Facemask shortage and the coronavirus disease (COVID-19) outbreak: Reflection on public health measures. *medRxiv.* (2020). doi: 10.1101/2020.02.11.20020735
- LoGiudice SH, Liebhaber A, Schöder H. Overcoming the COVID-19 crisis and planning for the future. *J Nucl Med.* (2020) 61:1096–101. doi: 10.2967/jnumed.120.250522

**Conflict of Interest:** The authors declare that the research was conducted in the absence of any commercial or financial relationships that could be construed as a potential conflict of interest.

**Publisher’s Note:** All claims expressed in this article are solely those of the authors and do not necessarily represent those of their affiliated organizations, or those of the publisher, the editors and the reviewers. Any product that may be evaluated in this article, or claim that may be made by its manufacturer, is not guaranteed or endorsed by the publisher.

Copyright © 2021 Ng and Vardhanabhuti. This is an open-access article distributed under the terms of the Creative Commons Attribution License (CC BY). The use, distribution or reproduction in other forums is permitted, provided the original author(s) and the copyright owner(s) are credited and that the original publication in this journal is cited, in accordance with accepted academic practice. No use, distribution or reproduction is permitted which does not comply with these terms.



# Knowledge, Attitude, and Practice Toward COVID-19 Among Sherubtse College Students in Bhutan: A Web-Based Cross-Sectional Study

Thinley Dorji<sup>1\*</sup>, Karma Wangmo<sup>2</sup>, Yezer<sup>3</sup>, Tashi Wangchuk<sup>4</sup>, Tshokey<sup>5</sup> and Kinley Wangdi<sup>6</sup>

<sup>1</sup> Kanglung Hospital, Trashigang, Bhutan, <sup>2</sup> Regional Livestock Development Centre, Kanglung, Bhutan, <sup>3</sup> Sherubtse College, Royal University of Bhutan, Trashigang, Bhutan, <sup>4</sup> Mongar Higher Secondary School, Mongar, Bhutan, <sup>5</sup> Jigme Dorji Wangchuk National Referral Hospital, Thimphu, Bhutan, <sup>6</sup> Department of Global Health, Research School of Population Health, College of Health and Medicine, Australian National University, Canberra, ACT, Australia

## OPEN ACCESS

### Edited by:

Reza Lashgari,  
Shahid Beheshti University, Iran

### Reviewed by:

Susanta Kumar Ghosh,  
National Institute of Malaria Research  
(ICMR), India  
Morteza Arab-Zozani,  
Birjand University of Medical  
Sciences, Iran

### \*Correspondence:

Thinley Dorji  
thinleydorji2005@gmail.com

### Specialty section:

This article was submitted to  
Infectious Diseases - Surveillance,  
Prevention and Treatment,  
a section of the journal  
Frontiers in Public Health

**Received:** 07 June 2021

**Accepted:** 18 October 2021

**Published:** 17 November 2021

### Citation:

Dorji T, Wangmo K, Yezer,  
Wangchuk T, Tshokey and Wangdi K  
(2021) Knowledge, Attitude, and  
Practice Toward COVID-19 Among  
Sherubtse College Students in  
Bhutan: A Web-Based  
Cross-Sectional Study.  
Front. Public Health 9:721493.  
doi: 10.3389/fpubh.2021.721493

Bhutan has reopened schools and colleges after an initial closure to contain coronavirus disease 2019 (COVID-19) transmission. However, the risk of transmissions is higher in the schools and colleges due to crowding. Therefore, this study aimed to assess the level of knowledge, attitude, and practice (KAP) toward COVID-19 among the students of Sherubtse College in Bhutan. A cross-sectional study using a questionnaire was conducted in September 2020 among the students of Sherubtse College, Bhutan. The questionnaire was made in the Google Forms and administered through a social forum WeChat app. The KAP scores were calculated that include mean scores. The association between the KAP was assessed using the Pearson's correlation coefficient. A total of 613 students participated in the survey. The majority of the participants (57%) were female and 56% were from the third year. The mean knowledge score was 10.7 (SD = 1.7; range 0–14), mean attitude score of 3.67 (SD = 1.0; range: 0–5), and mean practice score of 5.19 (SD = range: 0–6). A majority of the students had good knowledge (98%) and practice (93.5%) scores, and a positive attitude (86.6%) toward COVID-19. A positive but weak correlation between good knowledge and practice ( $r = 0.1$ ,  $p = 0.0126$ ) was observed. Having a positive attitude led to practicing appropriately most of the time ( $r = 0.1866$ ,  $p < 0.001$ ). The students had good KAP scores and followed the COVID-19 prevention protocols advocated by the government. Good knowledge and a positive attitude were translated into good practice. Therefore, the education campaign of the Bhutan government seems to be effective in the students.

**Keywords:** knowledge, attitude, practice, COVID-19, Bhutan, coronavirus

## INTRODUCTION

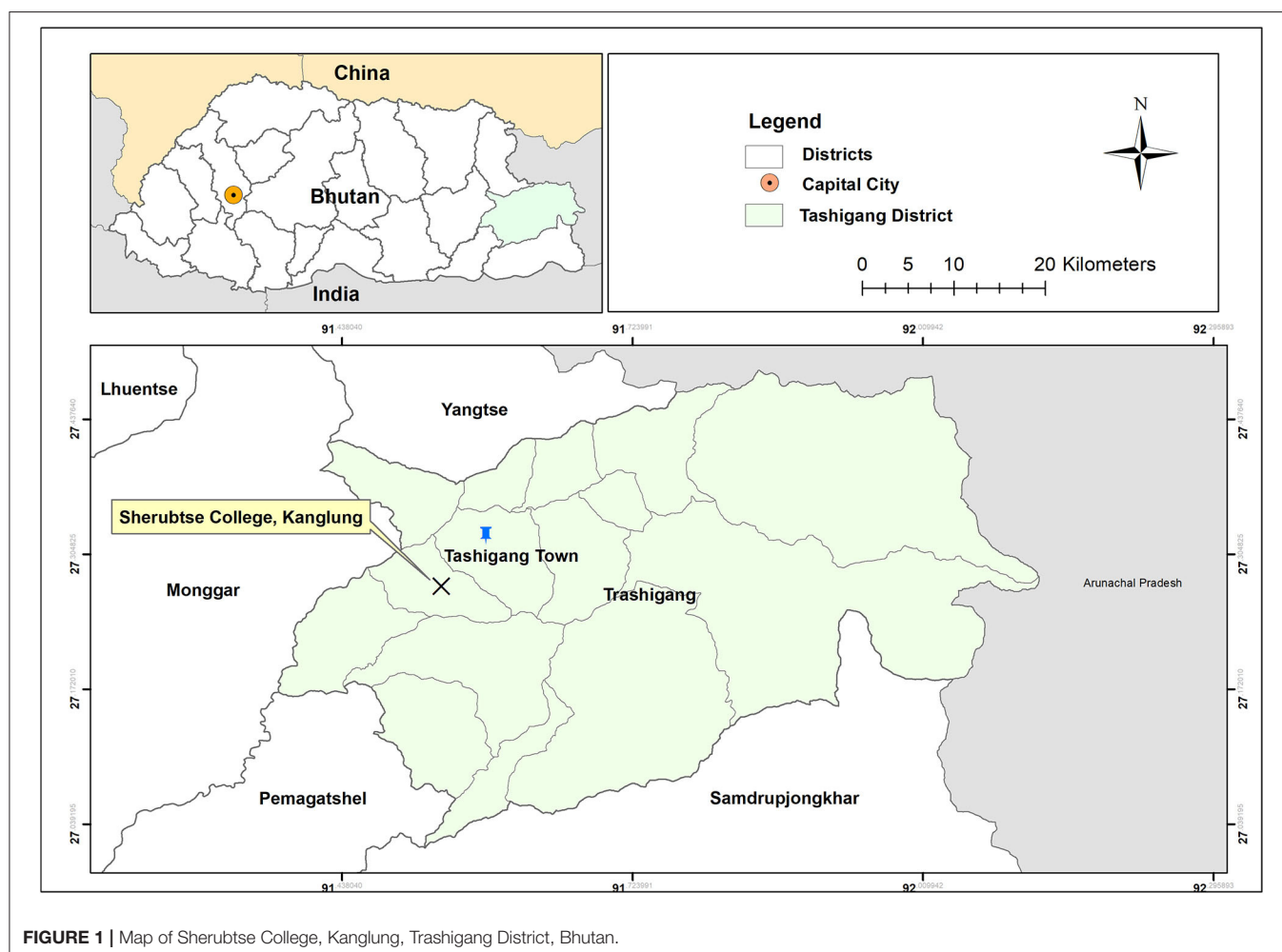
Coronavirus disease 2019 (COVID-19) pandemic, caused by the new coronavirus strain severe acute respiratory syndrome coronavirus 2 (SARS-CoV-2), has infected more than 172 million people as of June 7, 2021 (1) with 2.93 million deaths. As a result, it is one of the serious public health problems worldwide in the Twenty first century

(1, 2). The first case of COVID-19 in Bhutan was reported on March 5, 2020 (3, 4) and the current record stands (7 June 2021) at 1,687 cases with one death (5). As in other countries around the world, the COVID-19 pandemic has brought communities to a standstill due to the lockdowns to prevent outbreaks.

During the initial phase of the pandemic, each country adopted various responses to COVID-19 to slow transmission and to prevent oversaturation of the healthcare systems (6–9). Bhutan adopted proactive prevention methods to limit community transmission. This included a mandatory facility quarantine for returning traveler for 2 weeks from March 16, 2020 (10). It was later extended to 3 weeks upon the recommendation from the National COVID Task Force. In addition, the international borders were sealed from March 23, 2020 except for the supply of essential goods (3, 4), which was done under the strict COVID-19 prevention protocols, such as disinfection of vehicles and strict social distancing between delivery and trans-shipping personals. Further, the government has undertaken various preventive measures to stop the spread of the disease, such as hand washing, social distancing, and the use of face mask in public places (11). The public is encouraged to use the “Druk Trace” app, for contact tracing. Regular COVID-19

screenings were instituted among the frontline workers (police, foresters, and volunteers), students, and business community. All the patients undergo mandatory COVID-19 testing before admissions to the hospitals. The flu clinics for screening COVID-19 are set up to prevent the patients from visiting the hospitals. Moreover, the government has instituted enhanced COVID-19 surveillance whereby 10% of health workers, frontline workers, and school students need to be tested for COVID-19 fortnightly (12).

The schools and colleges have reopened after the initial lockdown with self-containment in place. The students are required to adhere to the normal prevention and control measures, such as social distancing, regular washing of hands and isolation, and testing for COVID-19 for any suspected signs and symptoms. Despite these safeguards against COVID-19, the colleges and schools are at risks for outbreaks due to the congregation of many people. This is evident by recent COVID 19 outbreak school (13) and college (14) in Bhutan. Therefore, knowledge, attitude, and practice (KAP) in the colleges and schools should be at the optimum in averting the outbreaks. The success of preventive measures initiated by the government depends on the uptake and adherence to these preventive



measures (15, 16), which is determined by the level of knowledge toward the disease (17, 18). The prior KAP studies on COVID-19 among the university students in other countries were variable (19–21). However, no such studies were done in Bhutan and this study aimed to assess the KAP on COVID-19 among the students of Sherubtse Colleges in Bhutan to inform the policymakers for making informed decisions in the future.

## METHODS

### Study Design and Setting

A cross-sectional study was conducted among the students of Sherubtse College in September 2020 using a web-based survey. A face-to-face survey was not feasible due to the social distance imposed by the Royal Government of Bhutan. Sherubtse College is the oldest college in Bhutan, located in Kanglung under Trashigang District in eastern Bhutan (Figure 1). For the 2020 academic year, there were 1,574 students of whom 52% were women. College offers five courses on Science, Mathematics, and Arts. Majority of the students reside in the college hostels and are allowed limited interaction with the general public.

### Sampling and Participant Recruitment

We calculated the sample size using the following formula:

$$N = \frac{z^2 pq}{d^2}$$

Where,

$N$  is the number of study participants;

$z$  is the value of the statistic in a normal distribution for a 95%

$CI$  (this value was 1.96 for this study);

$p$  is the prevalence estimate set at 0.5;

$q = (1-p)$ ;

$d$  is the precision of the prevalence estimate set at 0.05.

The required sample size was 384. However, we invited all the students to participate in this study.

The survey questionnaire was developed in the Google survey tool (Google Forms). The link generated from the Google Form was circulated to the students through social media groups via WeChat app. In addition, the link was shared with the students through the contact list of the researchers. The link led to the first page of the Google Form, which contained a summary of the survey, such as research background, aims, and expected outcomes. At the end of the first page, there was a declaration of confidentiality and an informed consent of the participants if they voluntarily agree to participate in the study.

### Questionnaire and Scoring

The data was collected using a pretested questionnaire adapted from a similar study in China by Zhong et al. (18). Moreover, the questionnaire was pre-tested among the 20 college students, and a questionnaire was modified accordingly. This group of students was asked not to participate in the main study. The questionnaire was divided into four parts: (i) socio-demographic characteristic; (ii) knowledge domain; (iii) attitude domain; and (iv) practice section. The demographic questions included age, sex, year of study, and the department. There were 14 knowledge questions,

such as four on clinical presentations, three on transmission routes, and four on the prevention and control of COVID-19. Five attitude questions were on insecurity, optimism, confidence, and responsibility. The six practice questions were on the use of the COVID-19 tracing app (Druk Trace), appropriate personal hygiene, such as hand washing, wearing a face mask, and avoiding going to public places.

For knowledge, the participants received one point for each correct answer and zero for an incorrect answer (range 0–14). Knowledge score of  $\leq 7$  (50%) and  $> 7$  was classified as poor and good knowledge, respectively. For practice, every correct answer was awarded one point while for a negative response was awarded zero points (range 0–6). A minimum of 3 (50%) of practice score was considered good practice. The attitude questions consisted of two questions with five responses and two questions into three responses. Total scores ranged from 0 to 5, and a score  $> 2.5$  indicating a positive attitude.

### Ethical Clearance

The ethical clearance was provided by the Research Committee of the Sherubtse College, Royal University of Bhutan [No.15 (3)-SC/Research/2020/11].

### Data Analysis

The data were downloaded from the Google Form into Microsoft Excel (Microsoft Corporation, WA, USA) for cleaning. The cleaned data were analyzed using STATA 13 (Stata Corporation, College Station, TX, USA). The descriptive data are presented in the frequencies and proportions with mean scores, SD, and

**TABLE 1 |** Sociodemographic characteristic of the study participants ( $n = 613$ ).

| Variables                      | Mean | SD  | Min | Max | Number | %    |
|--------------------------------|------|-----|-----|-----|--------|------|
| Knowledge score                | 16.7 | 1.7 | 0   | 14  |        |      |
| Attitude score                 | 3.7  | 1.0 | 0   | 5   |        |      |
| Practice score                 | 5.2  | 1.0 | 0   | 6   |        |      |
| <b>Gender</b>                  |      |     |     |     |        |      |
| Male                           |      |     |     |     | 260    | 42.4 |
| Female                         |      |     |     |     | 353    | 57.6 |
| <b>Age group (years)</b>       |      |     |     |     |        |      |
| <20                            |      |     |     |     | 47     | 7.7  |
| 20–24                          |      |     |     |     | 524    | 85.5 |
| 25+                            |      |     |     |     | 42     | 6.8  |
| <b>Year of study</b>           |      |     |     |     |        |      |
| First year                     |      |     |     |     | 114    | 18.6 |
| Second year                    |      |     |     |     | 139    | 22.7 |
| Third year                     |      |     |     |     | 345    | 56.3 |
| Fourth year                    |      |     |     |     | 15     | 2.5  |
| <b>Departments</b>             |      |     |     |     |        |      |
| Arts and humanities            |      |     |     |     | 200    | 32.6 |
| Computer science and maths     |      |     |     |     | 57     | 9.3  |
| Environmental and life science |      |     |     |     | 139    | 22.7 |
| Physical science               |      |     |     |     | 62     | 10.1 |
| Social science                 |      |     |     |     | 155    | 25.3 |



range. The distribution of the KAP of the participants based on their demographics was compared using the chi-square test. The association between the knowledge, attitude, and practices was assessed using the Pearson's correlation coefficient ( $r$ ).

## RESULTS

### Sociodemography

A total of 613 students completed the survey questionnaire with a mean age of 22 years (range 18–3). Majority of the respondents were female (57.6%, 353) and third-year students 56.5% (344). More than one-third (32.6%, 199) of participants were from the Department of Arts and Humanities (32.6%) (**Table 1**).

### Knowledge

The mean COVID-19 knowledge score was 10.7 ( $SD = 1.7$ ; range: 0–14). A good knowledge score (based on 50% of the total knowledge score) was reported by 98.4% of the students. However, 87% of the students had a misconception that COVID-19 was the name of the virus rather than a disease. The majority (93.6%) of the students knew the main symptoms of COVID-19 and 95% reported that there is no effective vaccine except a supportive treatment. About 84% of the respondents correctly

answered that people with COVID-19 can still transmit the disease in the absence of fever. The majority (87.5%) of the respondents knew that the virus spreads through the respiratory droplets and 88% believed that the face masks can prevent the transmission of the virus. Almost all the respondents noted that the disease can be prevented by avoidance of crowded places and large gatherings (**Table 2**).

### Attitude

The mean attitude score was 3.7 ( $SD = 1.0$ ; range: 0–5). A total of 531 (86.5%) students had a positive attitude while 83 (13.5%) had a poor attitude toward COVID-19. About 86% (527) of the respondents agreed or strongly agreed that COVID-19 was a very dangerous disease and over 60% (385) of them agreed or strongly agreed that COVID-19 could be successfully controlled. However, 11.3% (69) of them were unsure if COVID-19 was a dangerous disease and 30% (194) were unsure if the disease could be successfully controlled. The majority (81%) of the participants thought that Bhutan can win the battle against the virus and 97% of them were willing to help spread the preventive knowledge on COVID-19 to others. However, 42.6% reported that they were not at risk of getting the disease (**Table 3**).

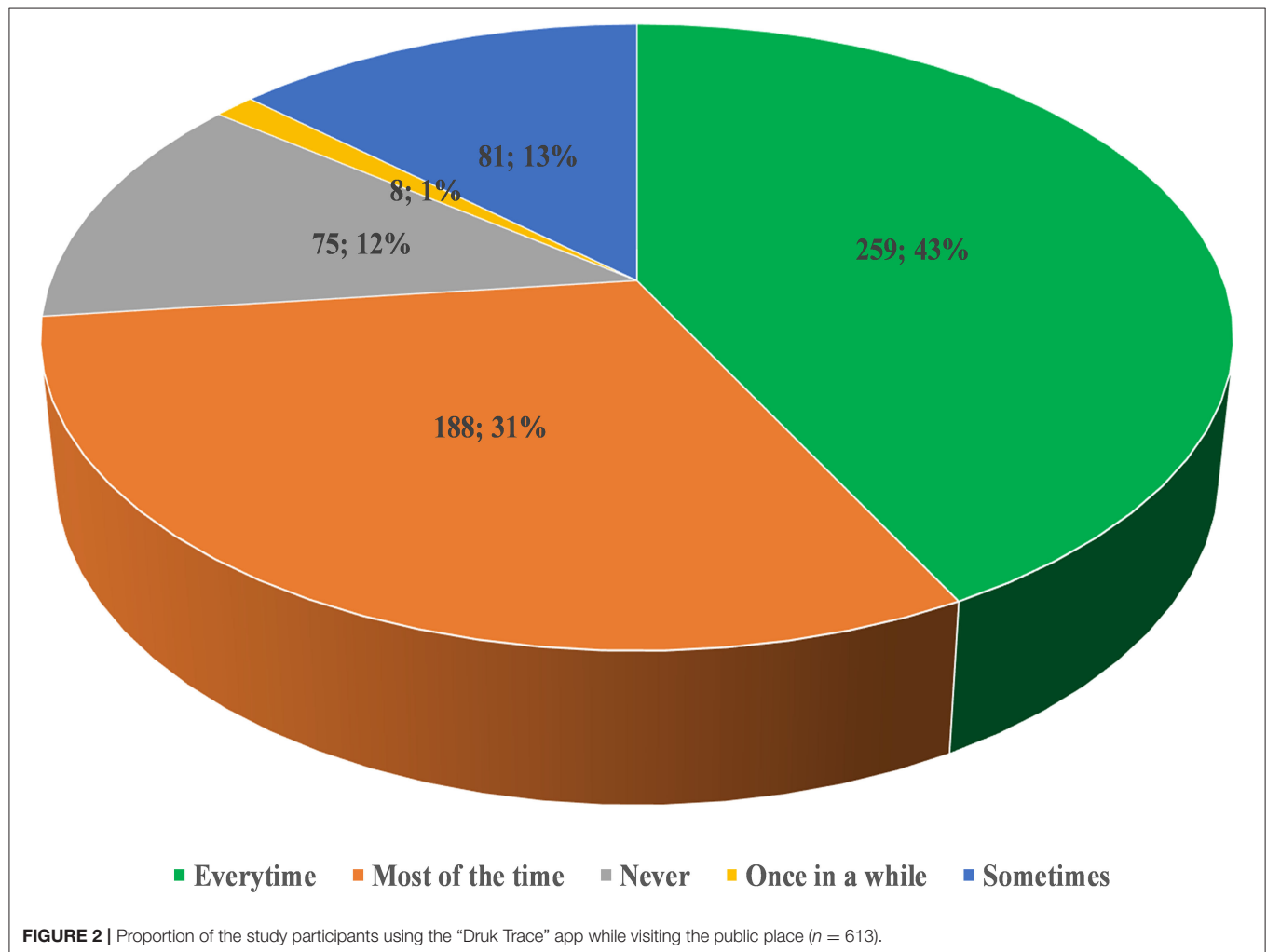
**TABLE 2 |** Knowledge on the coronavirus disease 2019 (COVID-19) among the Sherubtse College students.

| Knowledge on COVID-19   | No (%)             | Yes (%)             | Don't know (%) |
|---|--------------------|---------------------|----------------|
| K1. COVID-19 is the name of virus   | <b>79 (12.9)*</b>  | 532 (87.1)          | 0 (0.0)        |
| K2. The main clinical symptoms of COVID-19 are fever, fatigue, dry cough and body aches   | 15 (2.5)           | <b>573 (93.6)*</b>  | 24 (3.9)       |
| K3. Unlike the common cold, stuffy nose, runny nose, and sneezing are less common in persons infected with the COVID-19 virus                             | 189 (31)           | <b>266 (43.6)*</b>  | 155 (25.4)     |
| K4. Currently, there is no effective cure for COVID-19 but early detection and supporting treatment can help most patients recover from the infections    | 6 (1.0)            | <b>582 (95.1)*</b>  | 24 (3.9)       |
| K5. Not all persons with COVID-2019 will develop severe illness. Only those who are elderly and have chronic illnesses are more likely to be severe cases | 61 (10.0)          | <b>512 (83.6)</b>   | 39 (6.4)       |
| K6. Eating or touching wild animals would result in infection by the COVID-19 virus   | <b>273 (44.6)*</b> | 195 (31.9)          | 144 (23.5)     |
| K7. Persons with COVID-19 cannot transmit the virus to others if they do not have a fever   | <b>513 (83.8)*</b> | 13 (2.1)            | 86 (14.1)      |
| K8. The COVID-19 virus spreads via the respiratory droplets of infected individuals   | 23 (3.8)           | <b>533 (87.5)*</b>  | 53 (8.7)       |
| K9. Ordinary residents can wear face masks to prevent the infection by the COVID-19 virus   | 49 (8.0)           | <b>536 (87.9)*</b>  | 25 (4.1)       |
| K10. Children and young adults don't need to take measures to prevent the infection by the COVID-19 virus.  | <b>549 (89.7)*</b> | 52 (8.5)            | 11 (1.8)       |
| K11. To prevent the infection by COVID-19, individuals should avoid going to crowded places   | 1 (0.2)            | <b>605 (99.0) *</b> | 5 (0.8)        |
| K12. Isolation and treatment of people who are infected with the COVID-19 virus are effective ways to reduce the spread of the virus in the community.    | 2 (0.3)            | <b>607 (99.2)*</b>  | 3 (0.5)        |
| K13. People who have contracted with someone infected with the COVID-19 virus should be immediately isolated in a proper place.                           | 2 (0.3)            | <b>605 (98.9)</b>   | 5 (0.8)        |
| K14. Oral/nasopharyngeal swab is the mode of diagnosis of COVID-19  | 244 (40.9)         | <b>317 (53.2)*</b>  | 35 (5.9)       |

\*Correct response. The bold values indicates correct answers.

**TABLE 3** | Distribution of good knowledge, attitude, and practice based on the demographic characteristics of the participants.

| Questions  | Strongly disagree | Disagree | Neutral    | Agree      | Strongly agree |
|--|-------------------|----------|------------|------------|----------------|
| A1. Do you agree that COVID-19 will finally be controlled successfully?      | 8 (1.3)           | 24 (3.9) | 194 (31.8) | 250 (40.9) | 135 (22.1)     |
| A2. Is COVID 19 a very dangerous disease?                                    | 3 (0.5)           | 12 (2.0) | 69 (11.2)  | 192 (31.4) | 335 (54.8)     |
|  |                   |          | Yes        | No         | Don't Know     |
| A3. Are you confident that we can win the battle against the COVID-19 virus? |                   |          | 493 (80.8) | 20 (3.3)   | 97 (15.9)      |
| A4. Do you think that you are at risk of getting COVID-19?                   |                   |          | 246 (40.2) | 261 (42.7) | 105 (17.2)     |



## Practice

The mean COVID-19 practice score was 5.2 (SD = 1.0; range: 0–6), indicating good practices (98%). More than 80% of the respondents had the "Druk Trace" App installed on their mobile phones. While 43% of the participants used it every time while visiting a public place (**Figure 2**). Nearly all (98%) the participants followed the preventive measures of COVID-19 advocated by the Bhutan Ministry of Health. In addition, the majority (98%) of the participants were adhering to good hand hygiene using hand sanitizer or hand washing. The face masks

were worn in public places by 89% of the study participants (**Figure 3**).

## Association and Correlation of KAP on COVID-19

Age was associated with good knowledge ( $p = 0.023$ ). While the year of study was associated with a positive attitude ( $p = 0.026$ ) and good practice ( $p = 0.048$ ; **Table 4**). The correlation analysis indicated the presence of a positive but weak correlation between good knowledge and practice ( $r = 0.1$ ,  $p = 0.0126$ ), having a

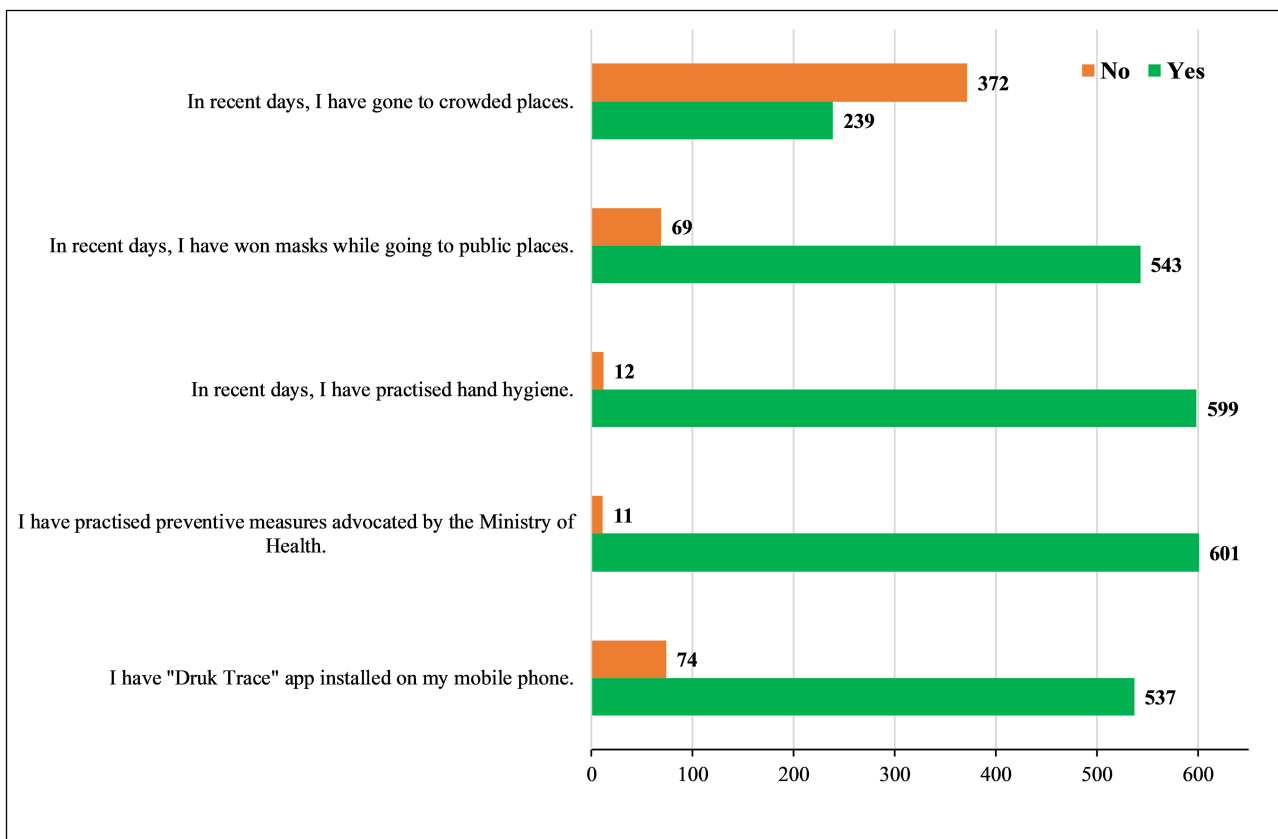


**FIGURE 3 |** The practices of the students toward coronavirus disease 2019 (COVID-19) ( $n = 613$ ).

positive attitude led to practicing appropriately most of the time ( $r = 0.1866$ ,  $p < 0.001$ ; **Table 5**).

## DISCUSSION

In the present study, we evaluated KAP toward COVID-19 among the students of Sherubtse College in Bhutan. This study showed 98% had a good level of knowledge, 87% had a positive attitude, and 98% reported good practice on COVID-19. There was a weak but positive correlation between the good knowledge and practice, and a positive attitude and practice.

The overall COVID-19 knowledge among the students in this study was good. Even though the study population was different, similar findings with good knowledge were reported in China (18, 22), Cameroon (23), Malaysia (24), Iran (25), and Egypt (26). While a poor level of knowledge toward COVID-19 was reported in Ethiopia (27) and Bangladesh (28). The high knowledge score in this study is not surprising due to the characteristics of the study sample being a college student. In addition, this study was conducted during massive public health education and awareness campaign by the government of Bhutan through all the available mass media, such as newspapers, television, radio, and various social media (Facebook). It would be important to evaluate the level of knowledge in the general population in Bhutan.

The study participants showed a positive and optimistic attitude toward COVID-19. The positive attitudes can be attributed to the response of the Bhutan government to the pandemic. After the first case of COVID-19 in Bhutan on March 5, 2020, Bhutan initiated 21 days mandatory quarantine for the returning travelers from a third country, 7 days quarantine for people moving from the border towns with India to interior districts, and snap lockdown of local areas when a community transmission is reported (3, 4). In addition, mandatory use of face mask in public places and restrictions to the mass gathering.

The overall practice score on the prevention of the COVID-19 in this study was much better than elsewhere (27). The majority of the respondents stated that they used a face mask in the public places and other mass gatherings. Similar findings were reported from China and Ethiopia (18, 27). The use of a face mask is known to prevent transmission of the virus (29). One of the reasons for the consistent use of the face mask by the students could be a result of a mandatory use imposed by the government. In addition, the compliance of the face mask is strictly monitored by police and other volunteers. The findings of this study were much better than among the university students in Bangladesh where only half of the students reported wearing face masks (21). The difference could be due to the study period because

**TABLE 4 |** Distribution of good knowledge, attitude, and practice based on the demographic characteristics of the participants.

| Variables          | Good knowledge |               | Positive attitude |               | Good practices |               |
|--------------------|----------------|---------------|-------------------|---------------|----------------|---------------|
|                    | N (%)          | P             | N (%)             | P             | N (%)          | P             |
| <b>Age (years)</b> |                |               |                   |               |                |               |
| <20                | 44 (93.6)      | <b>0.023*</b> | 39 (83.0)         | 0.580         | 45 (95.7)      | 0.475         |
| 20–24              | 518 (98.9)     |               | 457 (87.2)        |               | 515 (98.3)     |               |
| 25+                | 41 (97.6)      |               | 35 (83.3)         |               | 41 (97.6)      |               |
| <b>Sex</b>         |                |               |                   |               |                |               |
| Male               | 256 (98.5)     | 0.876         | 227 (87.3)        | 0.669         | 252 (96.9)     | 0.086         |
| Female             | 347 (98.3)     |               | 304 (86.1)        |               | 349 (98.9)     |               |
| <b>Year</b>        |                |               |                   |               |                |               |
| First year         | 111 (97.4)     | 0.642         | 90 (79)           | <b>0.026*</b> | 112 (98.3)     | <b>0.048*</b> |
| Second year        | 136 (97.8)     |               | 118 (84.9)        |               | 130 (95.6)     |               |
| Third year         | 341 (98.8)     |               | 310 (89.7)        |               | 341 (99.1)     |               |
| Fourth year        | 15 (100.0)     |               | 13 (86.7)         |               | 14 (93.3)      |               |
| <b>Department</b>  |                |               |                   |               |                |               |
| Arts & Humanities  | 197 (98.5)     | 0.806         | 168 (84)          | 0.103         | 192 (96.0)     | 0.130         |
| CSM**              | 56 (98.3)      |               | 53 (93)           |               | 57 (100.0)     |               |
| ELS <sup>†</sup>   | 138 (99.3)     |               | 123 (88.5)        |               | 137 (98.6)     |               |
| Physical science   | 61 (98.4)      |               | 58 (93.6)         |               | 61 (98.4)      | 61 (98.4)     |
| Social science     | 151 (97.4)     |               | 129 (83.2)        |               | 154 (99.4)     |               |

\*Significant at  $p < 0.05$ ; \*\*Computer science and mathematics; <sup>†</sup>Environmental and life science. The bold values indicate significant values ( $p$ -values  $< 0.05$ ).

**TABLE 5 |** Correlation between knowledge, attitude, and practices.

| Scales    |      | Knowledge                        |      | Attitude                           |           | Practice   |          |
|-----------|------|----------------------------------|------|------------------------------------|-----------|------------|----------|
|           |      | Good                             | Poor | Good                               | Poor      | Good       | Poor     |
| Knowledge | Good |                                  |      | 525 (87.1)                         | 78 (12.9) | 591 (98.0) | 12 (2.0) |
|           | Poor |                                  |      | 6 (60.0)                           | 4 (40.0)  | 10 (100.0) | 0 (0.0)  |
| Attitude  | Good | $r = -0.0182$                    |      |                                    |           | 526 (99.1) | 5 (0.94) |
|           | Poor | $p = 0.653$                      |      |                                    |           | 75 (91.5)  | 7 (8.5)  |
| Practice  | Good | $r = 0.1$                        |      | $r = 0.1866$                       |           |            |          |
|           | Poor | <b><math>p = 0.0126^*</math></b> |      | <b><math>p &lt; 0.001^*</math></b> |           |            |          |

\* $p < 0.05$ . The bold values indicate significant values ( $p$ -values  $< 0.05$ ).

the Bangladeshi study was conducted in the early phase of the pandemic. Furthermore, monitoring and implementation in the populated countries, such as Bangladesh might be difficult unlike in Bhutan.

There was a weak but positive correlation between knowledge and practice, and attitude and practice. A similar correlation between positive knowledge and practice (28, 30, 31), and attitude and practice (28, 30) were reported in other studies. A systematic review on KAP among the general population showed studies in Asia had comparatively good KAP compared with the Americans (32). This could be the reason that the preventive actions taken as a result of good knowledge led to a lesser number of cases in Asia compared with the United States. It has been shown that good knowledge can enhance the positive preventive behaviors through early identification of disease and better health-seeking behavior (33). In addition, knowledge affects the behavior of individual and a higher knowledge level reinforces

healthier behaviors (34), such as social distancing, avoiding mass gathering, and shaking hands (30). Such positive practices are important for breaking the transmission cycle of COVID-19 in the community.

The policy implication of this study is that the students had a high COVID-19 knowledge with a positive attitude and adhering to the recommended preventive measures. Therefore, reopening schools and colleges can be considered with minimal risk of COVID-19 transmission. Second, the current health education toward COVID-19 seems to be effective in this group of audience. Third, the students in Bhutan can be an important source of information for their immediate families because most of the older generation are illiterate.

## Conclusion

This is the first study to investigate KAP toward COVID-19 among the students in Bhutan. The students had good

KAP scores and followed COVID-19 protocols advocated by the government. Good knowledge and a positive attitude were translated into good practice. Therefore, the education campaign of Bhutan government seems to be effective in the students.

## Recommendations

Although the overall KAP score was good in this study, we recommend a similar study with a larger sample size, such as students from other schools. Further, a community-based KAP study in the general public needs to be undertaken to evaluate the effectiveness of the education program initiated by the Bhutan government in the general population. The study findings will be useful to inform the policymakers and healthcare professionals, on the future public health interventions, awareness-raising, policies, and health education programs.

## Limitations

The findings from this study need to be interpreted with the consideration of some limitations. First, causal inferences cannot be established due to a cross-sectional study design. Second, other socio-demographic characteristics could not be collected due to the similar characteristics of the student. Hence, future studies should use methods that will explore both the linear and non-linear relationships between socio-demographic characteristics and COVID-19. Third, due to the self-reporting of the survey questionnaire, there is a risk of reporting bias. This can be addressed in the future through a face-to-face interview. Fourth, some answers may not have been given honestly due to social desirability. In addition, this study was conducted among the

college students, who are educated, and therefore, the findings cannot be generalized.

## DATA AVAILABILITY STATEMENT

The raw data supporting the conclusions of this article will be made available by the authors, without undue reservation.

## ETHICS STATEMENT

The studies involving human participants were reviewed and approved by College Research Committee, Sherubtse College, Royal University of Bhutan. Written informed consent for participation was not required for this study in accordance with the national legislation and the institutional requirements.

## AUTHOR CONTRIBUTIONS

TD conceived, undertook the study, analysis, and drafted the manuscript. KWangmo helped in the statistical analysis and interpretation of results and revision of the manuscript. KWangdi assisted in data collection, analysis, and revision of the manuscript. Y, TW, and T assisted in the revision of the manuscript. All the authors read and approved the final draft.

## ACKNOWLEDGMENTS

The authors would like to thank students for responding to this study and the President of the Sherubtse College for allowing us to conduct this study.

## REFERENCES

1. World Health Organization. *WHO Coronavirus (COVID-19) Dashboard*. (2021). Available online at: <https://covid19.who.int/> (accessed April 13, 2021).
2. Pal M, Berhanu G, Desalegn C. Severe acute respiratory syndrome coronavirus-2 (SARS-CoV-2): an update. *Cureus*. (2020) 12:e7423. doi: 10.7759/cureus.7423
3. Penjor K, Tobgyal, Zangpo T, Clements ACA, Gray DJ, Wangdi K. Has COVID19 derailed Bhutan's national malaria elimination goal? A commentary. *Malar J*. (2021) 20:20. doi: 10.1186/s12936-020-03562-5
4. Tsheten T, Wangchuk S, Wangmo D, Clements ACA, Gray DJ. COVID-19 response and lessons learned on dengue control in Bhutan. *J Med Entomol*. (2021) 58:502–4. doi: 10.1093/jme/tjaa225
5. Ministry of Health. *National Situational Update On COVID-19*. (2021). Available online at: <http://www.moh.gov.bt/national-situational-update-on-covid-19-77/> (accessed July 6, 2021).
6. Haider N, Osman AY, Gadzekpo A, Akipede GO, Asogun D, Ansumana R, et al. Lockdown measures in response to COVID-19 in nine sub-Saharan African countries. *BMJ Glob Health*. (2020) 5:e003319. doi: 10.1136/bmjgh-2020-003319
7. Piryani RM, Piryani S. Nepal's response to contain COVID-19 infection. *J Nepal Health Res Counc*. (2020) 18:128–34. doi: 10.33314/jnhrc.v18i1.2608
8. Sharma K, Banstola A. Assessment of COVID-19 pandemic in nepal: a lockdown scenario analysis. *Front Public Health*. (2021) 9:599280. doi: 10.3389/fpubh.2021.599280
9. The Lancet. India under COVID-19 lockdown. *Lancet*. (2020) 395:1315. doi: 10.1016/S0140-6736(20)30938-7
10. Rinzin YC. *All Travellers Entering Bhutan Will be Quarantined*. Kuensel (2020). Available online at: <https://kuenselonline.com/all-travellers-entering-bhutan-will-be-quarantined/> (accessed April 13, 2021).
11. WHO. *Promote Hand Hygiene to Save Lives and Combat COVID-19*. (2020). Available online at: <https://www.who.int/southeastasia/news/detail/04-05-2020-promote-hand-hygiene-to-save-lives-and-combat-covid-19> (accessed April 13, 2021).
12. Ministry of Health. (2021). *Enhanced Surveillance Strategy for COVID-19*. Ministry of Health, Bhutan (2021).
13. Dem P. *Schools in Paro Reopen*. Kuensel (2021). Available online at: <https://kuenselonline.com/schools-in-paro-reopen/> (accessed July 6, 2021).
14. Rai R. *CST Compound Locked Down After Four Test Positive*. Kuensel (2021). Available online at: <https://kuenselonline.com/cst-compound-locked-down-after-four-test-positive/> (accessed July 6, 2021).
15. Girum T, Lentiro K, Geremew M, Migora B. Global strategies and effectiveness for COVID-19 prevention through contact tracing, screening, quarantine, and isolation: a systematic review. *Trop Med Health*. (2020) 48:91. doi: 10.1186/s41182-020-00285-w
16. Güner R, Hasanoglu I. COVID-19: Prevention and control measures in community. *Turk J Med Sci*. (2020) 50:571–7. doi: 10.3906/sag-2004-146
17. Zhang M, Zhou M, Tang F, Wang Y, Nie H, Zhang L. Knowledge, attitude, and practice regarding COVID-19 among healthcare workers in Henan, China. *J Hosp Infect*. (2020) 105:183–7. doi: 10.1016/j.jhin.2020.04.012
18. Zhong BL, Luo W, Li HM, Zhang QQ, Liu XG, Li WT. Knowledge, attitudes, and practices towards COVID-19 among Chinese residents during the rapid rise period of the COVID-19 outbreak: a quick online cross-sectional survey. *Int J Biol Sci*. (2020) 16:1745–52. doi: 10.7150/ijbs.45221



19. Angelo AT, Alemayehu DS. Knowledge, attitudes, and practices toward covid-19 and associated factors among university students in Mizan Tepi University, 2020. *Infect Drug Resist.* (2021) 14:349–60. doi: 10.2147/IDR.S299576
20. Singh JP, Sewda A. Assessing the knowledge, attitude and practices of students regarding the COVID-19 pandemic. *J Health Manage.* (2020) 22:281–290. doi: 10.1177/0972063420935669
21. Wadood MA, Mamun A, Rafi MA, Kamrul Islam M, Mohd S, Lee LL, et al. Knowledge, attitude, practice and perception regarding COVID-19 among students in Bangladesh: Survey in Rajshahi University. *medRxiv [Preprint]*. (2020). doi: 10.1101/2020.04.21.20074757
22. Gao H, Hu R, Yin L, Yuan X, Tang H, Luo L, et al. Knowledge, attitudes and practices of the Chinese public with respect to coronavirus disease (COVID-19): an online cross-sectional survey. *BMC Public Health.* (2020) 20:1816. doi: 10.1186/s12889-020-09961-2
23. Ngwewondo A, Nkengazong L, Ambe LA, Ebogo JT, Mba FM, Goni HO, et al. Knowledge, attitudes, practices of/towards COVID 19 preventive measures and symptoms: a cross-sectional study during the exponential rise of the outbreak in Cameroon. *PLoS Negl Trop Dis.* (2020) 14:e0008700. doi: 10.1371/journal.pntd.0008700
24. Azlan AA, Hamzah MR, Sern TJ, Ayub SH. Public knowledge, attitudes and practices towards COVID-19: a cross-sectional study in Malaysia. *PLoS ONE.* (2020) 15:e0233668. doi: 10.1371/journal.pone.0233668
25. Kakemam E, Ghoddoosi-Nejad D, Chegini Z, Momeni K, Salehiniya H, Hassanipour S, et al. Knowledge, attitudes, and practices among the general population during COVID-19 outbreak in iran: a national cross-sectional online survey. *Front Public Health.* (2020) 8:585302. doi: 10.3389/fpubh.2020.585302
26. Abdelhafiz AS, Mohammed Z, Ibrahim ME, Ziady HH, Alorabi M, Ayyad M. Knowledge, perceptions, and attitude of egyptians towards the novel coronavirus disease (COVID-19). *J Community Health.* (2020) 45:881–90. doi: 10.1007/s10900-020-00827-7
27. Akalu Y, Ayelign B. Knowledge, attitude and practice towards COVID-19 among chronic disease patients at addis zemen hospital, northwest Ethiopia. *Infect Drug Resist.* (2020) 13:1949–960. doi: 10.2147/IDR.S258736
28. Banik R, Rahman M, Sikder MT, Rahman QM. Knowledge, attitudes, and practices related to the COVID-19 pandemic among Bangladeshi youth: a web-based cross-sectional analysis. *Z Gesundh Wiss.* (2021) 1–11. doi: 10.1007/s10389-020-01432-7
29. Chu DK, Akl EA, Duda S, Solo K, Yaacoub S. Physical distancing, face masks, and eye protection to prevent person-to-person of SARS-CoV-2 and COVID-19: a systematic review and meta-analysis. *Lancet.* (2020) 395:1973–87. doi: 10.1016/S0140-6736(20)31142-9
30. Al-Hanawi MK, Angawi K, Alshareef N, Qattan AMN, Helmy HZY, Alsharqi O. Knowledge, attitude and practice toward COVID-19 among the public in the kingdom of Saudi Arabia: a cross-sectional study. *Front Public Health.* (2020) 8:217. doi: 10.3389/fpubh.2020.00217
31. Lee M, Kang BA. Knowledge, attitudes, and practices (KAP) toward COVID-19: a cross-sectional study in South Korea. *BMC Public Health.* (2021) 21:295. doi: 10.1186/s12889-021-10285-y
32. Saadatjoo S, Miri M, Hassanipour S, Ameri H. Knowledge, attitudes, and practices of the general population about coronavirus disease 2019 (COVID-19): a systematic review and meta-analysis with policy recommendations. *Public Health.* (2021) 194:185–95. doi: 10.1016/j.puhe.2021.03.005
33. Kanyangarara M, Hamapumbu H, Mamini E, Lupiya J, Stevenson JCS, Moss WJ. Malaria knowledge and bed net use in three transmission settings in southern Africa. *Malar J.* (2018) 17:41. doi: 10.1186/s12936-018-2178-8
34. Vandamme E. *Concepts and Challenges in the Use of Knowledge-Attitude-Practice Surveys: Literature Review*. Antwerp: Department of Animal Health. Institute of Tropical Medicine (2009).

**Conflict of Interest:** The authors declare that the research was conducted in the absence of any commercial or financial relationships that could be construed as a potential conflict of interest.

**Publisher's Note:** All claims expressed in this article are solely those of the authors and do not necessarily represent those of their affiliated organizations, or those of the publisher, the editors and the reviewers. Any product that may be evaluated in this article, or claim that may be made by its manufacturer, is not guaranteed or endorsed by the publisher.

Copyright © 2021 Dorji, Wangmo, Yezer, Wangchuk, Tshokey and Wangdi. This is an open-access article distributed under the terms of the Creative Commons Attribution License (CC BY). The use, distribution or reproduction in other forums is permitted, provided the original author(s) and the copyright owner(s) are credited and that the original publication in this journal is cited, in accordance with accepted academic practice. No use, distribution or reproduction is permitted which does not comply with these terms.



# Abnormal Respiratory Sounds Classification Using Deep CNN Through Artificial Noise Addition

Rizwana Zulfiqar<sup>1</sup>, Fiaz Majeed<sup>1</sup>, Rizwana Irfan<sup>2</sup>, Hafiz Tayyab Rauf<sup>3</sup>, Elhadj Benkhelifa<sup>4</sup> and Abdelkader Nasreddine Belkacem<sup>5\*</sup>

<sup>1</sup> Faculty of Computing and Information Technology, University of Gujrat, Gujrat, Pakistan, <sup>2</sup> Department of Information Technology, College of Computing and Information Technology at Khulais, University of Jeddah, Jeddah, Saudi Arabia, <sup>3</sup> Centre for Smart Systems, AI and Cybersecurity, Staffordshire University, Stoke-on-Trent, United Kingdom, <sup>4</sup> Cloud Computing and Applications Research Lab, Staffordshire University, Stoke-on-Trent, United Kingdom, <sup>5</sup> Department of Computer and Network Engineering, College of Information Technology, UAE University, Al Ain, United Arab Emirates

## OPEN ACCESS

### Edited by:

Reza Lashgari,  
Shahid Beheshti University, Iran

### Reviewed by:

Vasco Lopes,  
University of Beira Interior, Portugal  
Mohammed Chachan Younis,  
University of Mosul, Iraq  
Xing Yuan,  
Columbia University, United States

### \*Correspondence:

Abdelkader Nasreddine Belkacem  
belkacem@uaeu.ac.ae

### Specialty section:

This article was submitted to  
Pulmonary Medicine,  
a section of the journal  
Frontiers in Medicine

**Received:** 25 May 2021

**Accepted:** 07 October 2021

**Published:** 17 November 2021

### Citation:

Zulfiqar R, Majeed F, Irfan R, Rauf HT, Benkhelifa E and Belkacem AN (2021) Abnormal Respiratory Sounds Classification Using Deep CNN Through Artificial Noise Addition. *Front. Med.* 8:714811. doi: 10.3389/fmed.2021.714811

Respiratory sound (RS) attributes and their analyses structure a fundamental piece of pneumonic pathology, and it gives symptomatic data regarding a patient's lung. A couple of decades back, doctors depended on their hearing to distinguish symptomatic signs in lung audios by utilizing the typical stethoscope, which is usually considered a cheap and secure method for examining the patients. Lung disease is the third most ordinary cause of death worldwide, so; it is essential to classify the RS abnormality accurately to overcome the death rate. In this research, we have applied Fourier analysis for the visual inspection of abnormal respiratory sounds. Spectrum analysis was done through Artificial Noise Addition (ANA) in conjunction with different deep convolutional neural networks (CNN) to classify the seven abnormal respiratory sounds—both continuous (CAS) and discontinuous (DAS). The proposed framework contains an adaptive mechanism of adding a similar type of noise to unhealthy respiratory sounds. ANA makes sound features enough reach to be identified more accurately than the respiratory sounds without ANA. The obtained results using the proposed framework are superior to previous techniques since we simultaneously considered the seven different abnormal respiratory sound classes.

**Keywords:** respiratory sounds, abnormal respiratory sounds, continuous adventitious sounds (CAS), discontinuous adventitious sounds (DAS), deep CNN

## 1. INTRODUCTION

Respiratory sound (RS) attributes and their analyses structure a fundamental piece of pneumonic pathology such as COVID-19 pneumonia, and it gives symptomatic data about a patient's lung. Lung sound is produced when air flows during the process of respiration. A couple of decades back, doctors depended on their hearing to distinguish symptomatic signs in lung audios through utilizing the standard stethoscope equipment. The typical stethoscope is usually considered a cheap and secure method for examining the patients, other than setting aside less effort required for the conclusion. Furthermore, it gives much data about the respiratory organ and the indications of the sicknesses that influence it (1, 2).

Later on, the auscultation by stethoscope is whimsical because it relies upon the doctor's capacity and the low affectability of the human ear hearing. However, non-stationary signs are

hard to examine and challenging to recognize if not done by a well-prepared doctor; this may prompt wrong analysis. As of late, with the guide of electronic stethoscopes combined with pattern recognition and artificial intelligence, the mechanized respiratory sound examination has drawn much consideration since it conquers the confinements of normal auscultation and gives an effective technique to clinical conclusion (3). Machine Learning (4) and Deep learning approaches play an essential role in health care (5) and industrial applications (6, 7) for prediction and optimization.

## 1.1. Types of Respiratory Sounds

Since the classification criteria for respiratory sounds was defined in the 10th International Lung Sounds Association (ILSA) Conference, the respiratory audios classification step by step has become the focal point of audio respiratory examination. Respiratory sounds are partitioned into two different categories (normal and abnormal).

Normal respiratory sounds are those when a patient has no respiratory issue. Meanwhile, unordinary sounds when a patient is suffering from respiratory problems (8). As we talk about their further subtypes, they have “tracheal,” “bronchial,” and “broncho-vesicular” sounds. Audio of normal respiration is described through a commotion in the process of inspiration. Scarcely discernible clamor is in the process of termination/ expiration. In rough artery like “tracheal,” ordinary audios of respiration described through wide range noise, for example, the clamor has multiple parts of higher-frequency, these are capable of being heard in the process of inspiratory and expiratory period (1).

On the other hand, the second category of respiratory sounds is abnormal respiratory sound. They are different from the first one based on their natural and unique patterns in their behaviors. They appear when the patient has some respiratory issue and suffering from respiratory problem (8).

## 1.2. Subclasses of Abnormal Respiratory Sounds

Abnormal sounds are unwanted respiratory sounds that are excessively forced on ordinary breath sounds. Abnormal sounds have low power or strength during respiration. These sounds are classified based on some factors that help in the detection of each class separately. Unusual sounds are broadly categorized as continuous and discontinuous sounds, and that discrimination is due to the variance in their duration of occurrence while breathing (9). Continuous Adventitious Sounds are fallen in the category of unusual sounds, most of the time having 250 ms, but it is not valid for all the CAS, e.g., rhonchi. Based on the pitch, these sounds are classified as high pitch (Wheeze and Stridor) and low pitch (Rhonchi and Squawk) sound. On the other hand, Discontinuous Adventitious Sounds also fall in abnormal sounds, just like CAS. DAS is <25 ms in duration and is further categorized as fine crackle, coarse crackle, and pleural rub.

### 1.2.1. Wheeze

Wheezes are sharp, regular, and constant extrinsic audios having a pitch with a minimum of 400 Hz. They are usually caused by airway narrowing, which then causes an airflow limitation.

Wheeze sounds do not necessarily have durations of more than 250 ms. Some have reported that Wheeze can have minimum durations of around 80–100 ms (10). Diseases associated with Wheeze are asthma and COPD. If the Wheeze is localized, it may be caused by a foreign body blocking the airway, like a tumor (11).

### 1.2.2. Rhonchi

Rhonchi are low pitched and musical sounds of unusual RS. Rhonchi encountered continuous adventitious sounds, and they can be heard during the inspiration phase, mainly in expiration, or during both phases of respiration (8). They described a predominant frequency range of around 200 Hz with durations of around 80–100 and usually nonstop in nature. Rhonchi are observed on both phases (inspiration and expiration) and caused by airway thickness in large section (12).

### 1.2.3. Stridor

Stridor sounds are classified as hilarious inspiratory sounds, and it is a type of CAS. Stridor sounds are produced in the larynx or bronchial tree by turbulent airflow and are similar to airway obstruction (upper). They have their presence at the inspiration phase due to narrowing the upper airway, and it can be heard on expiration or even in both phases. Stridor has a pitch of more than 500 Hz and a duration of more than 250 ms. They are usually louder and harsher than wheeze sounds. The diseases associated with Stridor are epiglottitis, croup, and laryngeal edema because every disease is related to airway obstruction (13).

### 1.2.4. Squawk

Squawk sounds to DAS usually have short durations and are hearable at the phase of inspiration. These sounds are low in pitch (like wheezing sounds), and their frequency ranges from 200 to 300 Hz (8). Squawk observed when patient suffering from hypersensitive pneumonia or common pneumonia (14). Fine Crackle: Crackle sounds are the dangerous extrinsic sound of respiration. Crackles are irregular in their behavior patterns, described by explicit waveform, span, and position of sounds in the respiratory cycle. Crackles have two attributes and are portrayed through their span as “fine pops/ crackle” and “coarse pops.” Explosive openings of the small airways cause fine crackle sounds. They have a little span (around 5 ms) with high frequencies (650 Hz). Fine crackles can be heard on the phase of inspiration. They usually cause the diseases like pneumonia, congestive heart failure, and lung fibrosis (12).

### 1.2.5. Coarse Crackle

Air bubbles generate coarse crackle sounds in large bronchi. The Coarse sounds are audible when inspiration is in its early phase/ stage and hearable at the expiration phase. “Coarse pops/ crackle” are low pitch, around 350 Hz, and have a long span (about 15 ms). Coarse crackle sounds can be heard in patients with chronic bronchitis, bronchiectasis, as well as COPD (15).

### 1.2.6. Pleural Rub

Pleural rub is non-rhythmic and encounters in the category of DAS. When pleural aggravated surfaces rub each other in breathing, then “pleural rub” audio produced has a low pitch,

generally below 350 Hz, and only appears for 15 ms. The PR sounds are produced by the friction and audible during both phases of expiration and inspiration. The pleural rub is usually caused by inflammation of the pleural membrane, and it can also cause pleural tumor (8).

In the field of bioinformatics, respiratory sounds classification (RSC) has become the center of attention. Researchers worked in the past and still working on RSC (normal and abnormal) to get precise results. As research goes on and on, researchers face many difficulties in RS classification. As we talk about RS's previous classification research outcomes, the main concern was the misclassification of RS (specifically between the subclasses of adventitious RS). This was because they were not distinguishing the sounds with minor variance (change) in their behavioral patterns and did not encounter all abnormal respiratory sounds simultaneously. The study's goal was muddling the functions of examination/analysis and discrimination of ARS (those sounds showing minor differences in their frequencies and period) toward the appropriate classification of respiratory sound.

Respiratory sound examination/classification is a vital part of the Auscultation process. Doctors perform the auscultation process through typical techniques, leading them to wrong decisions due to the different dependencies. Research tells us that lung disease is the third most ordinary cause of death worldwide, so it is essential to classify the RS abnormality in an authentic way to overcome the death rate.

The proposed methodology based on Artificial Noise Addition technique (ANA) is used to enhance the features of ARS and helps in feature extraction through feature maps. Furthermore, "ANA" aid in differentiating the subclasses of abnormal/adventitious sounds more accurately. As far as we classified ARS using "ANA" phenomena, classification results boost, which ultimately smooth the doctor's progress flawlessly to carry out the auscultation process. It will support consultants in the auscultation process to identify the disorders or abnormalities related to the human respiratory system. When the doctors identify the disorder in the particular RS, they will diagnose the associated diseases caused by these sound abnormalities and prescribe the best treatment to a patient suffering from the syndrome.

The first thing is to focus on the number of classes of ARS. As per our knowledge, no such work with several lung sounds has been done so far; previous researchers classified few abnormal respiratory sounds, most common in patients' lungs that ultimately cause abnormality in them. So, we have incorporated the seven different classes of respiratory (lungs) sounds in our designed framework for the sake of classification.

The proposed framework based on the spectrogram of each respiratory sound by applying the Fourier transformation for the relative spectrogram of sound. Contribution for further enhancement after getting the required spectrograms, the framework makes the wave spectrogram more strengthen and clear through adding some artificial noise of the exact spectral nature. This process serves as constructive interference to augment/enhance the actual spectrogram of sounds. An "Artificial noise addition (ANA)" phenomenon helps prominent the pattern and aids feature extraction; make it more accessible

and fair. "ANA" does not mean that any traditional background noise. Finally, feature extraction is done through feature maps on spectral data and different classifiers (VGG, ResNet, InceptionNet, and AlexNet) used for classification purposes.

The rest of our manuscript is organized as follows: related work is discussed in section 2. Section 3 describes the complete overview of the applied framework and the steps involved in its deployment. Experimental setup and results are discussed in section 4, while the conclusion and recommendations have been discussed in section 5.

## 2. RELATED WORK

For normal and abnormal respiratory sound classification real-world dataset is designed to automate the process. By taking advantage of previous studies, researchers used "spectral" and "wavelet" techniques for feature extraction without enhancing the features of a particular sound (2). "Convolutional neural networks CNN," "Hidden Markov Models HMM," and "Gaussian Mixture Models GMM" were collaborated for decision level. Such a scheme could support the classification precision and outperform to distinguish respiratory sound with 66.7% precision. Other subclasses of respiratory sounds were not engaged, i.e., St, Sq, and Rh (16). As research tells us that lung disease is the third most ordinary cause of death worldwide, so it is important to classify the RS abnormality in a true way to overcome the death rate. Short-Time Fourier Transform (STFT) was used for feature extraction, and two other deep learning methods were used for classification from spectrogram after feature extraction. ICBHI database was put into consideration with different frequencies and noise. Two approaches were applied; the first used deep CNN for feature extraction and SVM for classification, whereas the second used a spectrogram. 65.5 and 63.09%, accuracies were recorded for first and second method respectively (17).

Chronic Obstructive Pulmonary Disease (COPD) and usual sound classification depend upon respiratory audios using different machine learning approaches. Twenty-five normal and thirty COPD sounds are collected and analyzed. Thirty-one features of audios were extracted and evaluated. COPD breath audios are categorized by using "Support vector machine (SVM)," "k-nearest neighbor (KNN)," "logistic regression (LR)," "decision tree," and "discriminant analysis (DA)" algorithms. After the study's evaluation results, the linear predictive coefficient and median frequency are best for classification tasks with an accuracy of almost 100%—the feature extraction process done without making them more strengthen. The multi-centered dataset can reduce the accuracy rate if encountered. Although they got the highest accuracy in terms of classification, this approach only classifies "normal" and "COPD" objects in RS. Other subclasses/subtypes of abnormal respiratory sounds were not considered, i.e., wheeze and crackle (18). When we look upon the medical diagnostic solutions for abnormalities, it took a lot of time and cost; a cheap solution was proposed. Patient internal sounds were recorded by Stethoscope, lungs, and heart sounds. These readings proved much and more significant to



assist the physicians. They determine the disease of the patient's lungs based on tagged audios through ML algorithms; through NN, they achieved the highest accuracy was 77.8%. However, only three types of sounds are considered (e.g., wheeze, bronchia). Other abnormal RS classes were not identified, and also accuracy can be affected due to the nature and size of the dataset, and multiple point classification is better to use (19).

A semi-supervised approach based on the graph is "one-class support vector machine (OCSVM)," which indicates the relationship between the entire sample and describes normal and abnormal lung sound (LS). "OCSVM" used a minimal amount of labeled samples for training purposes and tested the approach with a large number of unlabeled samples for testing purposes with an Accuracy of 60–80% by increasing the NLs. If a fair dataset is processed with this method, accuracy will decrease gradually because it supports artificial datasets. "OCSVM" was a detection technique for some classes of abnormal RS and was only suitable for the identification of ordinary, crackle, and wheeze sounds. The classification was not performed, and also, it had not encountered the other sounds, e.g., Stridor, Rhonchi, and squawk (20). Another method for LS classification introduced named "Multilevel Wavelet Packet Entropy (MWPE)" uses many entropy measurements. "MWPE" was a combination of two existing "Renyi" and "Tsallis" entropy. Feature extraction was done without making them more prominent. "MWPE" gained 97.98% accuracy during the classification of RS when decomposition levels are four (4) by using Shannon, whereas "MWPE" includes "Renyi entropy" and "Tsallis entropy" gained 93.94%, 57.58% accuracy, respectively. Five classes of RS were countered, i.e., normal, wheeze, crackle, stridor, and squawk. Discontinuous abnormal respiratory sound includes fine crackle, and coarse crackle was not considered (21).

In 2019, a Cancer diagnosis in its early growth stage was made with a 0.0212 error rate that assumed the least rate and 99.48% predictive rate recorded by applying soft Neural computing techniques like "Discrete AdaBoost optimized ensemble learning generalized neural networks." Data were taken from the "ELVIRA" source, mixed with noise and other anomalies. Removal of noise and anomalies were done with the help of the normalizing smoothing technique. After preprocessing, feature selection and dimension reduction to reduce the complexity of data were made through the Wolf heuristic features technique. When it considers how many classes were successfully detected by "Discrete AdaBoost," it only detects the normality and abnormality of a particular sound. The main focus of the "Discrete AdaBoost" was the detection of abnormality regardless of classification. Furthermore, subclasses of abnormal RS were not encountered. An optimized approach for capturing the data can have better outcomes if used in the future (22). A study was conducted in 2019 to find out the environmental factors that impact human health in many ways. Multiple types of data sources were involved, includes images of individuals and the information related to the social activities within a particular environment. Multiple techniques were introduced and tested to check the impact of environmental factors on human health. After characterizing many spatially correlated with deep convolutional neural networks, Deep CNN

has a strong effect on the human health of an individual. Deep CNN has more potential to do a better job (23). A review was conducted to check the multiple techniques for extracting the feature and classifying respiratory sounds. They discuss NN, ANN, CNN, KNN, and many other algorithms for abnormal RS analysis. In the end, it has been stated that the "CNN" consider as the latest approach for implication (24).

Fifty to two-hundred Hz is the fundamental frequency range found for features that are inputted by "Hidden Markov models (HMM)" and "Gaussian mixture models (GMM)" when they are joined together in a hybrid form. 39.56 ranking gain from spectral subtraction for unwanted sounds (noise) removal from multiple sounds directories in preprocessing. Features are extracted by removing noise without making them dense or strengthen. They direct the researcher to work on advanced noise suppression techniques that will improve the overall score. As it has cleared that the researcher did not encounter the further subclasses of abnormal RS, i.e., stridor, squawk, pleural rub, and rhonchi, only wheeze and undefined crackles (mixed fine and coarse crackle sounds) were considered (25). The feature extraction (FE) technique was introduced in 2018 when researchers altered the traditional Grey Level Difference Matrix (GLDM) in a new form. Texture analysis (TA) mixed with "GLDM." Texture analysis was done using signal ID or the value of a particular pixel. Performance checked through multilayer perceptron (MLP) in combination with SVM. 94.9% accuracy was recorded at sample distance  $d = 10$ . When the researcher used five features, "GLDM" and "cubic SVM." Taking a look at several classes that were considered in research was normal, wheeze, faint crackle, and stridor, other sound classes like squawk, fine crackle, coarse crackle, and rhonchi were not involved (26). The respiratory sound classification was done in the presence of multiple types of noise (includes 3–4 classes, e.g., speaking, coughing, heart sounds, and many more). An algorithm was proposed for feature extraction, and that was a fresh nonlinear approach for better representation and discrimination of RS. Later on, 49.86% accuracy was recorded when applied to classify the multiple RS sounds having a variety of noise in them, as mentioned above. However, here is an issue, only four classes (normal, wheeze and crackles, and crackle plus wheeze) are considered, and the noise in sounds may confuse its nature with crackle sounds as well as the other abnormal RS classes were not considered, i.e., stridor, squawk, pleural rub, and rhonchi (27).

When researchers examined the asthmatic patients through ENS, SVM, and Spectral integrated (SI) features, they categorized patients based on their illness degree (first stage, moderate stage, or last stage). Fifty-five patient samples were taken for examination, and multiple Statistical analyses were performed to check the different patterns/manners of features with relentlessness stage of different groups. Overall best results gained by these methods for the first, moderate, and the last stage were 95, 88, and 90%, respectively. Still, that method identifies only the wheezing sounds (not other abnormal RS subclasses) and lacks focus on better representation of patterns, e.g., frequency and phase (28). An Overview of deep learning was done for radiology for disease detection, classification, quantification,



and segmentation. Radiology is an intrinsically information-driven approach. It is beneficial for using information handling strategies. In this work, the Association of University Radiologists Radiology Research Alliance Task Force on Deep Learning reviews deep learning to the radiologist. The article introduces a review of deep learning in an understandable way to radiologists to analyze past, present, and future applications, just as to assess how radiologists may profit from this new tool. These researches portray a few regions inside radiology wherein deep learning methods have the most critical effect: malady recognition, classification, evaluation, and division (29).

COPD is a respiratory illness that is caused by smoking. Respiratory Database @TR was used to analyze the “COPD” patients. The second Order difference plot (SODP) method was introduced for analysis. Performance gain recorded 95.84% (accuracy), 93.34% (sensitivity), and 93.65% (specificity) when “Second-Order difference plot (SODP)” designed for examination levels of COPD sounds. Overall gain is high because SODP is based on many factors related to sound’s three-dimensional quantization. Deep belief networks (DBN) were used for classification and training purposes (30). Three approaches (Approach 1: KNN, SVM, and GMD, Approach 2: local binary pattern (LBP), and Approach 3: CNN designs) perform the critical task of analysis, recognition, and distinction of LS with 95.50% accuracy. The highest numbers of adventitious respiratory sounds classes were used in that method till now. Wheeze, fine crackle, coarse crackle, stridor, and squawk were involved; only pleural rub was compromised and not countered. However, the fact is, the researcher used a dataset of 7–8 sounds/recordings to classify the sounds, which is very small from a research perspective. More consideration is required for better pattern recognition, and this may be done when we involve spectrums of sounds and enhance their features through adding artificial noise in them for further research (1).

Another problem is when a doctor/specialist sees the ECG waves; there is the possibility of error in the vision of humans (doctor itself) during reading because of the petite/short wavelength, tiny span, and arbitrary/random phase shift of ECG signals. Convolution networks were used and tried to sort out the particular problem as mentioned above. Eventually, two approaches were adopted with multiple different factors to check the maximum accuracy rate of the problem. De-noising was involved in checking the difference of accuracies between noised and de-noised data. The first approach gained the 93.53% accuracy rate when CNN was applied on data with noise and the second one gained a 95.22% accuracy rate when ECG waves are free of noise (31).

Researchers designed a low-cost stethoscope for examining lung sounds and classify them into different classes. Two algorithm approaches were used to classify LS (MFCC & spectrogram). A method of “Mel Frequency Cepstral Coefficient (MFCC),” with the help of an image spectrogram, classifies the data of 17,930 sounds. The classification was the main objective of this work. CNN and the traditional SVM algorithm classify the four different breathing audio sounds. Normal, Rale, and Rhonchi audios were classified with different precision results. Other classes such as stridor, squawk, and pleural rub were

not considered. As we talk about results, “MFCC” gain results in a range for four classes; first-class CNN 86%, SVM 86%, second class CNN 76%, SVM 75%, third class CNN 80%, SVM 80%, and last class have CNN 62%, SVM 62% accuracy rate, respectively (15). The machine learning approach was used in the next research, and the researcher classifies the normal and wheezing sounds from the data, which consist of 43 samples of recordings. They got minimum samples to detect wheezes; they did a data augmentation step on the sample for data enlargement. WD CNN architecture used minimal steps and took no time to preprocess the data to remove the anomalies. It is also an insensitive method to shifting lung sound, and noise observed externally from environmental factors. As a result, automatic wheeze detection in lung sounds through CNN Achieved an accuracy of 99%, but only Wheezing sounds are detected here. Low pitched sounds are not detected through this mechanism (32). For pulmonary issues detection, different methods and techniques are used to analyze the spectrum of RS. Fast Fourier Transform (FFT), AutoRegressive (AR), and the AutoRegressive Moving Average (ARMA) were used for calculating the densities of the spectrum of RS. Feature vectors were given as input to ANN. Spectrum analysis performance was recorded in classification accuracy (CA) as 85.67% for AR, 84.67% for ARMA, and 80.33% for FFT, but that accuracy is only for limited data points new or large test data inputted, then accuracy is not guaranteed. It only checks the normal and COPD individuals, not identifying the other abnormal RS classes such as wheeze, rhonchi, and stridor (33).

Lung sound classification is often done by applying the technique of signal processing (SP). Multiple “SP” methods were applied to RS/LS and classified them based on their nature and behavior. “Multi-scale Hjorth descriptor (MHD)” was introduced to classify RS in a particular class. “MHD” measured LS signal complexity. Signal complexity and accuracy were measured based on scale 1–5 and “Multi-scale Hjorth descriptor” measurements took with 96.06% accuracy, but the accuracy will not improve by enlarging the scale (34). Radiographs are usually very tiny in size; used for reliable classification of different most relevant images to medical science. Here the approach adapted where the techniques in computer visions and deep learning were bridged. It was a challenge for developers and researchers, which was tackle through deep-CC. The researcher divided the dataset into three groups for training, testing, and validation purposes. They applied the data augmentation technique for data enlargement as deep CC needs massive data for their processing. After experimentation, Deep Convolution Network (DCN) gained 97.73% accuracy when it is integrated with different GoogleNet and ImageNet (35). The following study examined the three different classes of respiratory sounds and evaluated them based on their distinctive nature and exclusive patterns. Experiments were conducted on thirty (30) dataset items with the help of an artificial neural network (ANN). “ANN” worked as a classifier in experimentation. Mel-frequency Cepstral coefficients (MFCC) pull out the statistical features from a dataset of RS. Further, the attributes for impure lung sound were acknowledged. They have discovered that their recently examined attributes were stronger than existing ones and showed better precision. Every single

class of adventitious RS was not occupied here. The considered classes of RS were normal, wheeze, and faint crackle. CNN with wavelet-based features and MFCCs classify the sound and got an accuracy of 94.98, 97.83, and 97.6% for normal, wheeze, and crackle, respectively (36).

Pattern recognition classifies LS through “Genetic Algorithm (GA),” “Fisher’s Discriminant Ratio (FDR)” was used to overcome the dimensionality of LS, and “Higher-order statistics (HOS)” used for feature extraction in this research. “k-nearest neighbor” algorithm used for pattern event recognition with an accuracy of 94.6% invalidation. Pattern recognition can be enhanced for more classes of respiratory sounds to improve classification performance. Four classes such as “normal,” “coarse crackle,” “fine crackle,” and “wheeze” were considered and recognized whereas, St, Sq, Rh, and PR were omitted (37). Identification of crackle in respiratory sound causes pulmonary abnormalities in the human body. PC has a minimal period and discontinuity, which usually appear at the inspiration and expiration phases. Multiple entropies did detect these PC. However, the “Tsallis entropy” was utilized as a feature extraction technique and achieved 95.35% accuracy for pulmonary crackle sound detection. The significant edge of using the Tsallis entropy was that it produces fewer features, but it took a minute dataset. Plus, it had not encountered all classes for abnormal sounds (just functional for faint crackle sound) (38).

Rational Dilation Wavelet Transform (RDWT) Discriminate the crackle, normal and wheeze sounds gained the accuracy of 95.17% for the total sound signal type. Q-factors were excluded in this approach because they cannot cope with the oscillatory signals (rapidly changing). Lung sounds were classified, and the feature was extracted without enhancing them, and while taking a look at several classes that were put in approach, were only three as mentioned above. The approach was suitable for high-pitched RS because low-pitch RS was not well-thought-out and performance reduced due to superimposed (cover-up) crackle and wheezes. So researchers still need a method and more consideration to tackle the issue if they overlapped to each other (39).

In 2015, automatic analysis of lung sound recordings (captured through electronic gadgets) involves and classification was done with the help of characteristics of LS signals. Feature extraction was done on a tool named “MATLAB” and classification through a combination of “artificial neural networks (ANN)” with “neuro-fuzzy inference systems (ANFIS).” The system successfully classified different RS/LS and gave 98.6% of accuracy. Results can be enhanced if correlation involves order, let alone the complexities in the feature extraction process (40). Pulmonary chaos/issues analysis based on auscultation to classify respiratory sound. The classification was done on normal and continuous RS includes Wh, Rh, St, and Sq. Discontinuous sounds like FC, CC, and PR were not put into the study. Features extraction was done on time-frequency based with an average set of frequencies. Spectro-temporal features extraction was used and got classification results for inspiratory and expiratory parts separately though “Support Vector Machine.” When SVM was applied on actual recordings, the

accuracy recorded for inspiration is 97.7% and for expiration 98.8% (41).

The main objective of this study was to detect pneumonia inpatient which is already suffering in “COPD.” Almost 50 patients were examined in the study as an initial dataset. A hybrid approach was adopted to detect contemporaneous pneumonia. The approach was a combination of “principal component analysis (PCA)” and “probabilistic neural networks (PNNs).” Short-time Fourier transform (STFT) is used to extract features from the dataset. Dimensions were reduced through “PCA” and “PNN” used for training classifiers. Results show 72% of sensitivity and 81.8% of specificity on cross-validation (42). The empirical classification (EC) method was introduced for respiratory sound analysis. Undefined normal and abnormal respiratory sounds come across for classification purposes, excluding their subclasses. The principle of multi-scaling was applied for signal enhancement and helped feature extraction while combined to imprison the inconsistency of sound signal. The empirical classification was dependent upon the principle of multi-scaling dimension reduction to boost the actual signal. EC applied on 689 recorded segments and gained 98.34% for classification (43).

In their research work, the researcher presented the “pattern recognition (PR)” scheme for the classification of RS. As a dataset, they took only normal and wheezing sounds for classification. Post-pre-processing was applied to raw data to enhance the process of classification. Feature extraction schemes were evaluated and compared with each other includes FT, LP coding, and MFCC. “GMM” with “ANN” was applied, and they used a “threshold” value for differentiating the wheezing sounds from normal ones. Their experiment results showed better performance from previous work (44). Texture-based classification named “LAC” was done on discontinuous sounds, i.e., fine crackle, coarse crackle, and squawk, to capture the changes in pulmonary acoustic, which is helpful in pathology. De-noising was applied to remove the background noise effect from discontinuous sounds. Four lung sound databases were used in studies includes 25 cases with 365 sounds. LAC was so simple because it introduced “texture” analysis for DAS. As talk about results of this approach, three databases out of four successfully classify the FC < CC and SQ. 100% accuracy for FC-SQ, 99.62% accuracy for CC-SQ, and 99.77% accuracy for FC-CC-SQ achieved, but only three classes were captured for “LAC” texture-based classification (45).

The analysis was drawn for respiratory sounds RS to check the ongoing RS methods and research. The researcher reviewed different technological and therapeutic experiences. The analysis involved a range of trends and techniques used to gather respiratory sounds RS for involuntary recognition gear development. Current tools are based on “fuzzy system (FS),” “artificial intelligence (AI),” “genetic algorithms (GA),” and “artificial neural networks (ANN).” Finally, they tried to find out some gaps in previous trends to facilitate the researchers for further enhancement in this area of RS identification, recognition, classification, and tool development for their analysis (46). Furthermore, researchers introduced a new technique or method for lung audios analysis by combining

**TABLE 1** | Comparison and overview of exiting “ARS” classes.

| References                           | Abnormal respiratory sounds    |    |    |    |                                   |    |    |    | Approach |    |
|--------------------------------------|--------------------------------|----|----|----|-----------------------------------|----|----|----|----------|----|
|                                      | Continuous adventitious sounds |    |    |    | Discontinuous adventitious sounds |    |    |    | De       | CI |
|                                      | Wh                             | Rh | St | Sq | UC                                | FC | CC | PR |          |    |
| Ntalampiras (16)                     | ✓                              |    |    |    |                                   |    |    |    |          | ✓  |
| Haider et al. (18)                   | ✓                              |    |    |    |                                   |    |    |    |          | ✓  |
| Lang et al. (20)                     | ✓                              |    |    |    | ✓                                 |    |    |    | ✓        |    |
| Rizal et al. (21)                    | ✓                              |    | ✓  |    | ✓                                 |    |    | ✓  |          | ✓  |
| Jakovljević and Lončar-Turukalo (25) | ✓                              |    |    |    | ✓                                 |    |    |    |          | ✓  |
| Rizal et al. (26)                    |                                |    |    |    |                                   |    |    |    |          | ✓  |
| Serbes et al. (27)                   | ✓                              |    |    |    | ✓                                 |    |    |    |          | ✓  |
| Nabi et al. (28)                     | ✓                              |    |    |    |                                   |    |    |    |          | ✓  |
| Altan et al. (30)                    | ✓                              |    |    |    | ✓                                 |    |    |    |          | ✓  |
| Aykanat et al. (15)                  | ✓                              | ✓  |    |    |                                   |    |    |    |          | ✓  |
| Bardou et al. (1)                    | ✓                              |    | ✓  | ✓  |                                   | ✓  | ✓  |    |          | ✓  |
| Kochetov et al. (32)                 | ✓                              |    |    |    |                                   |    |    |    | ✓        |    |
| Göğüş et al. (33)                    | ✓                              |    |    |    | ✓                                 |    |    |    | ✓        |    |
| Sengupta et al. (36)                 | ✓                              |    |    |    | ✓                                 |    |    |    |          | ✓  |
| Naves et al. (37)                    | ✓                              |    |    |    |                                   | ✓  | ✓  |    |          | ✓  |
| Rizal et al. (14, 34)                |                                |    |    |    |                                   | ✓  | ✓  |    | ✓        |    |
| Ulukaya et al. (39)                  | ✓                              |    |    |    | ✓                                 |    |    |    |          | ✓  |
| Rajkomar et al. (35)                 |                                |    |    |    |                                   |    |    |    |          | ✓  |
| Jin et al. (41)                      | ✓                              | ✓  |    |    |                                   |    |    |    | ✓        |    |
| Xie et al. (43)                      |                                |    |    |    |                                   |    |    |    |          | ✓  |
| Hadjileontiadis (45)                 |                                |    |    | ✓  |                                   | ✓  | ✓  |    |          | ✓  |
| Bahoura (44)                         | ✓                              |    |    |    |                                   |    |    |    |          | ✓  |
| Kandaswamy et al. (47)               | ✓                              |    | ✓  | ✓  |                                   |    |    |    |          | ✓  |
| Research methodology                 | ✓                              | ✓  | ✓  | ✓  |                                   | ✓  | ✓  | ✓  |          | ✓  |

the two previous frameworks to maximize results. ANN joint with wavelet transforms in this approach. The procedure was simple; with the help of wavelet transform, they divided the audio dataset of lungs into its multiple sub-spectrums and learn the features of sounds from those spectrums. Researchers built a standard 19-40-6 for this framework. 91.67% accuracy was recorded through distribution WC-ANN architecture, but all types of abnormal RS are not identified and considered here, e.g., fine crackles, coarse crackles. Moreover, only ANN is used here (47). A comparative study was conducted to analyze and built libraries for normal and pathological. Feature extraction for healthy and pathological recordings was done through autoregressive (AR) schemes. By “AR,” a Quadratic classifier and KNN (two classifiers) were designed and analyzed. The performance was evaluated on multiple models (48).

As we talk about the phenomena of “Artificial Noise Addition ANA” used for training neural networks. Training of ANN with noise injection done to avoid over-fitting of curves and in results this phenomena gives better outcomes for resolving the over-fitting issues (49). On the other hand, the problem arises with labeling features, a layered design that adapts the “Noise” as a positive factor, named “Noise adaptation layer.” Features enhanced by “noise adaptation layer” and correct labels

which make the training process of NN easier (50). Also, to increase the resilience of NN, the ANA method was applied to the patterns of particular objects (51). Another research shows how the artificial noise adding to the signal (input) positively impacts NN performance. This technique improves the measurements that are needed for secret keys (52). The detail comparison and overview of exiting “ARS” classes are given in **Table 1**.

### 3. MATERIALS AND METHODS

In research methodology, the classification of adventitious respiratory sounds was done using the respiratory sound data set from multiple sources. Sequence and detail of all leading points are given below.

#### 3.1. Preprocessing of Sounds

The practice begins with audio dataset loading—raw data taken from multiple sources and preprocessing. In preprocessing phase, all audio files were converted into “wav.” format. The motivation behind this conversion is to perform further modification on sound samples. Redundancies were also removed and bring the data in normalized form.

### 3.2. Sound Signaling

The variation in the air produces sound. As “RS” are produced during the respiration cycle of a human being. When these sounds have represented the variation concerning time ( $t$ ), it forms a sound signal. The extraction of information from a complex sound was done by converting the sound into analog or digital signals form. RS conversion into its first spectrogram (waveform representation) was done through the sound signaling process. Here the RS were converted into sound waves/signals having the information about their amplitude and time. Each respiratory sound has a different period and amplitude as they belong to a different category and show their unique spectrogram, which discriminates them from one another in terms of their pattern and behavior. For a basic understanding, take a look at the following equations. Wave period ( $t$ ), frequency ( $f$ ) as following;

$$\text{Frequency}(f) = 1/\text{timeperiodorf} = \frac{1}{t} \quad (1)$$

$$\text{Timeperiod} = 1/\text{frequencyort} = \frac{1}{f} \quad (2)$$

Whereas, the velocity is defined as following;

$$\text{Velocity} = \text{frequency} * \text{wavelengthorv} = f \times \lambda \quad (3)$$

Rearranging the equation (3);

$$\text{Frequency}(f) = \text{velocity}/\text{wavelengthorf} = \frac{v}{\lambda} \quad (4)$$

From equation (2) and (4), we'll get the value of time period in terms of velocity and wavelength;

$$\text{Timeperiod} = \text{wavelength}/\text{velocityort} = \frac{\lambda}{v} \quad (5)$$

Relationship between the ( $t$ ), ( $v$ ), ( $\lambda$ ) and ( $f$ ) defined as above.

### 3.3. Fourier Transform

Fourier transform (FT) is a mathematical transform that decomposes a function (often a function of time, or a signal) into its constituent frequencies, such as the expression of RS represents in terms of the frequencies. Fourier transformation was applied on data (Python 3.7 with scipy library) to generate the spectrograms (sounds into its waveform representation) for unhealthy sounds and visualize their behavior. The motivation was to capture the discriminative frequency characteristics of lung sounds for better representation of different classes. Two approaches are applied, named “positive” and “complete” Fourier transformations, which enabled us to get the information about the respiratory sound frequency and its proportion in a particular signal.

**Complete Fast Fourier Transformation:** Complete FFT count the double side frequencies for positive and negative values simultaneously.

$$F_{ft} = \frac{f(t)e^{os} + S(f(t)e^{os})}{|f_{one}|} \quad (6)$$

Where  $S(f(t)e^{os})$  indicates the size of sound signal and  $|f_{one}|$  represents the both side frequencies in one transform.

**Positive Fast Fourier Transformation:** Positive FFT count one side frequency of sound signal

$$P_{ft} = \frac{F_{ft} + S(F_{ft})}{|N/2|} \quad (7)$$

Where  $S(F_{ft})$  indicates the size of Fast Fourier Transformation and  $|N/2|$  represents the half frequency range for each input bit. We get the spectrogram of respiratory sound with relevant frequency ( $f$ ) according to the time ( $t$ ) and amplitude ( $A$ ) of sound. FT is employed to increase the performance of the proposed system. Another mathematical representation of Fourier Transform in sine wave is described in Equation (8).

$$G(\omega) = \int_{-\infty}^{\infty} (f(t) e^{os} f(t) e^{as})^{-j\omega t} dt \quad (8)$$

In above equation  $f(t)$  represents the input sound signal of RS and  $G(\omega)/F(\omega)$  represent the fourier transform. Integral of Fourier transform is over  $-\infty < t < \infty$ . It's a time domain representation of input sound signal. Here is the input signal  $f(t)$  is multiplied with composite exponential function. The complex exponential function broken into component according “Euler's formula”:

$$e. -j\omega t = \cos(\omega t) + j\sin(\omega t) \quad (9)$$

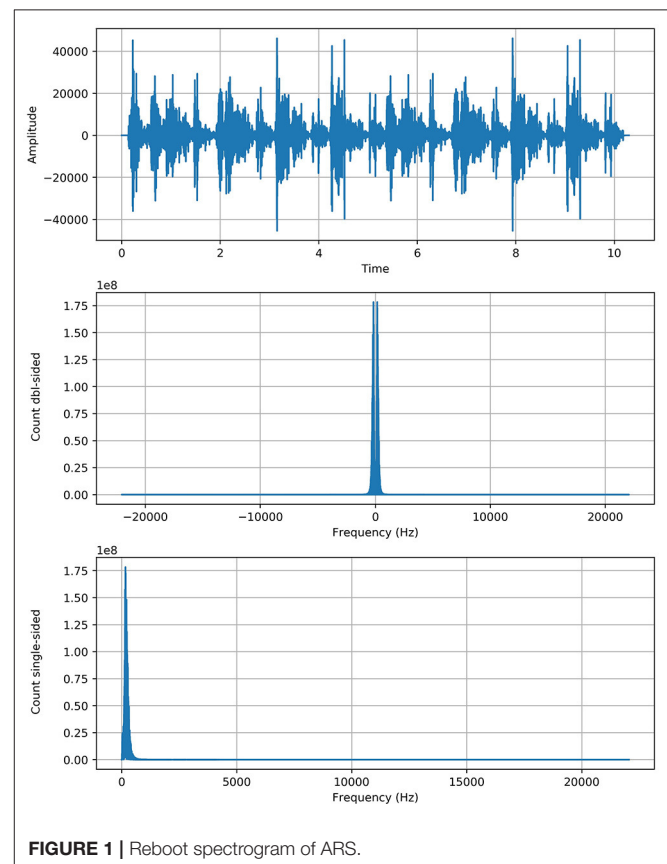


FIGURE 1 | Reboot spectrogram of ARS.



The similarity of input signal  $f(t)$  with complex exponential is described by a set of coefficients obtained through this equation. In other words, it tells how the input signal is similar to series of frequencies.

### 3.4. Spectrogram Robustness

Contribution for further enhancement, the spectrogram of RS with the gradual (minor) change, we added the artificial noise of exact spectral nature to enhance the actual spectrogram of faded sounds to make them more strengthen and enhance their robustness. As we applied the “noise addition” on respiratory sounds, neither the approach has changed the actual behavior of the spectrum nor produced any abnormality in the sound spectrogram. An “Artificial noise addition (ANA)” phenomenon only helped prominent the pattern and made feature extraction easy and fair. “ANA” does not mean that any traditional background noise in RS. References to “ANA” are given in the previous section of the literature review. The following equation does artificial noise addition.

$$F_{ft}^{Noise} = F_{ft} + F_{ft} \quad (10)$$

As  $F_{ft}$  represented the actual signal of RS and added twice to boost the potency/strength of a particular signal without shifting its circumstances as we see that the y-axis of the signal graph extended from  $1e7$  to  $1e8$  scale through the above equation. The **Figure 1** shows the graph of each class with more strength without any alteration in genuine behavior.

### 3.5. Texture Analysis

An image texture is a set of metrics calculated in spectral processing designed to quantify the perceived texture of the spectrogram. The texture of any spectrum gives us information about the spatial arrangement of color or intensities in an image or selected spectrum region. We present a set of textural measures derived from the texture spectrum. The proposed features extract textural information of an RS spectrum with complete respect to texture characteristics. Different classes of adventitious respiratory sounds get through the textural analysis and assigned different colors to enhance the performance of the features extraction in the characterization and discrimination of the texture aspects of spectrograms. Texture analysis of ARS for each target class is visualized in **Figure 2**.

### 3.6. Feature Extraction

Feature extraction is an attribute reduction process. Unlike feature selection, which ranks the existing attributes according to their predictive significance, feature extraction transforms them. The feature is an individual measurable property or characteristic of a phenomenon being observed. Feature extraction is an attribute reduction process; unlike feature selection, which ranks the existing attributes according to their predictive significance, FE transforms them. Choosing informative and discriminating is a crucial step for practical algorithms in pattern recognition and classification. FE is done to enhance the effectiveness of classification. In the case of respiratory sounds, feature extraction is done through feature mapping. Feature mapping was applied to extract the patterns or maps of RS features. We applied a filter on the input spectrum and got the map of the spectrum as output. The output of the feature map gave us a visual understanding of the RS feature.

### 3.7. Data Augmentation

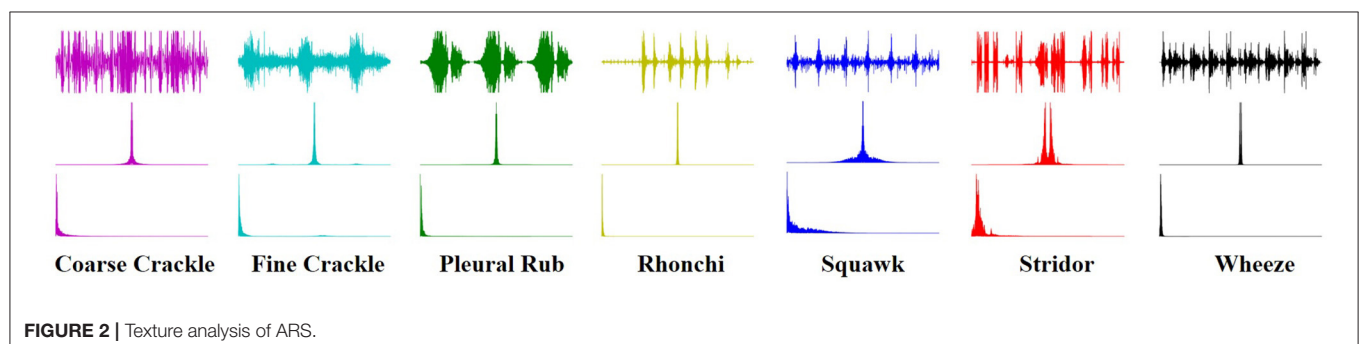
Data augmentation techniques are used to normalize the data and increase the number of dataset elements into multiples, e.g., padding, cropping, flipping, and removing all those factors that may be considered errors. The augmentation techniques have been tested to increase the cardinality of the training set for all the classes and overcome the problem of over-fitting. One augmentation technique applied to the spectrograms and is horizontal flipping.

**Horizontal Flip:** A simple idea for data augmentation is “horizontal flipping,” which was applied on spectrograms. Each spectrogram was randomly flipped from left to right.

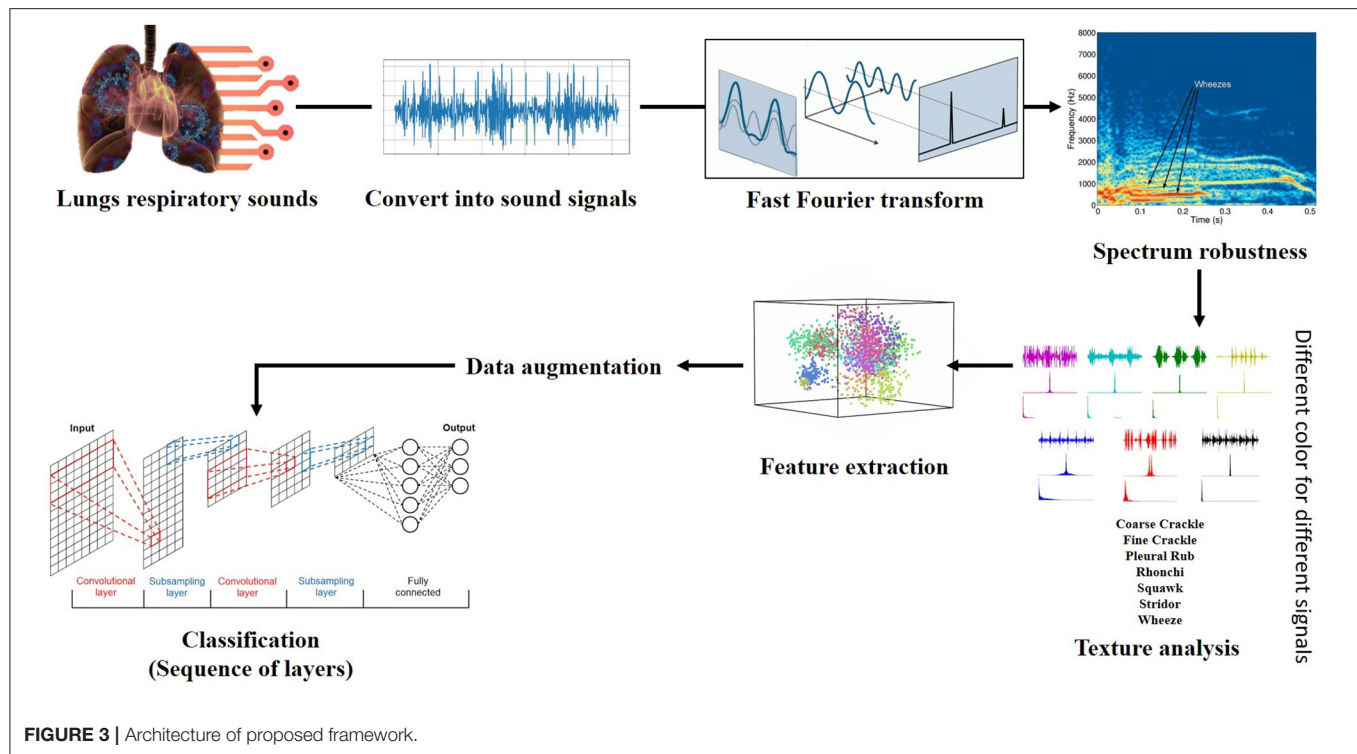
### 3.8. Classification

Finally, multiple classifiers were applied to check which of them gave the best results in terms of accuracy, which was considered a primary performance measure of research. Deep learning algorithms implemented such as VGG (VGG-B1, VGG-B3, VGG-V1, VGG-V2, and VGG-D1), AlexNet, ResNet, InceptionNet, and LeNet, on the spectral data for classification purposes and analyze the results and compare it with each other for better classification of abnormal respiratory sounds.

- VGG: VGG stands for Visual Geometry Group. In 2014, Simonyan and Zisserman launched VGG network







architecture. Now it has numerous variants like VGG-B1, VGG-B3, VGG-V1, VGG-V2, and VGG-D1.

- AlexNet: Its convolutional neural network was developed by Alex Krizhevsky, Geoffrey Hinton, and Ilya Sutskever in 2012. Sixty million parameters are involved in its architecture.
- ResNet: often known as Residual Neural Networks designed in 2015 by Kaiming He, having 3.6% error rate.
- InceptionNet: Google designed the CNN known as GoogleNet or InceptionNet in 2014. Four million parameters were incorporated with a 6.67% error rate.
- LeNet: Develop by Yann LeCun et al. Number of parameters are 60,000 involved in processing. Error rates were also not defined because it was designed in 1998.

“AlexNet” is an effective model for attaining excessive accuracies on complicated data units. It is a leading structural design for any object recognition challenge. AlexNet consists of five convolutional layers and three fully connected layers.

- First Convolutional Layer (CL1) has 96 filters with kernel size (11x11) for extracting features for a particular spectrogram of RS. The Stride for CL1 is four for compressing the spectrogram, which moves the filter to four pixels at a time. Max-Pooling (MP1) overlapped CL1 kept padding valid the same as CL1. Filters are the same, but the kernel size is (2x2), different from CL1. As we talk about Stride, it is two for Max-pooling.
- The second Convolutional Layer (CL2) of the network has 256 filters with the same kernel size (CL1). Stride is two for compressing the spectrogram, which moves the filter to two

pixels at a time. Max-Pooling (MP2) overlapped CL2 kept padding valid the same as CL2. Filters of MP2 are equal to CL2 filters. Kernel size and strides are the same as the MP1 layer.

- The third and fourth convolutional layers (CL3 & CL4) have 384 filters with the same kernel size (3 × 3). Both of them have one Stride for moving filter to 1 pixel with valid padding. Any pooling layer does not follow CL3 & CL4. The fifth Convolutional Layer (CL5) has 256 filters with the same kernel size (3 × 3). Stride is (1) for compressing the spectrogram, which moves the filter to 1 pixel at a time.
- Max-Pooling (MP3) overlapped to CL5 kept padding valid. Filters of MP3 are equal to CL5 filters. Kernel size and Stride are (2 × 2) and (2), respectively. Three fully connected layers (FCL1, FCL2, & FCL3) are involved at the end of convolutional layers, altering data in 1-dimension and finally classification performed on that single long array of data.

The flow chart of proposed framework is given in **Figure 3**.

## 4. RESULTS AND DISCUSSION

### 4.1. Dataset Collection

Mainly researchers use datasets from multiple repositories for research purposes, and all of them were primarily generated for academic aspire. Every catalog contains a different amount of mock-ups. Unluckily, most of these repositories have limited classes of respiratory/ lung sounds. If someone wants to examine all respiratory sounds (abnormal), he/ she will not discover any solo platform from where they can get the desired/ preferred dataset.

**TABLE 2** | Comparative results obtained (Precision and Recall) for VGG-B1.

|                | Precision | Recall | F1-score |
|----------------|-----------|--------|----------|
| Coarse crackle | 1.00      | 1.00   | 1.00     |
| Fine crackle   | 0.67      | 1.00   | 0.80     |
| Pleural rub    | 1.00      | 0.50   | 0.67     |
| Rhonchi        | 1.00      | 1.00   | 1.00     |
| Squawk         | 1.00      | 1.00   | 1.00     |
| Stridor        | 1.00      | 1.00   | 1.00     |
| Wheeze         | 1.00      | 1.00   | 1.00     |
| Accuracy       |           |        | 0.95     |
| Macro avg      | 0.95      | 0.93   | 0.92     |
| Weighted avg   | 0.96      | 0.95   | 0.94     |

In this research work, we assemble datasets from multiple internet sources [e.g., “(R.A.L.E. Lung Sounds 3.2),” “Thinklabs One (digital stethoscope),” and “Easy Auscultation”] used in prior research work. Founded respiratory sounds were not in symmetry, some of these sources contain hundreds of samples, and some of them hardly have few entities for particular classes. So we took a small number of entities from the above-cited foundations for purposed research. The number of target instances corresponds to each class are: Wheeze (12), Rhonchi (9), Stridor (10), Squawk (8), Fine Crackle (11), Coarse Crackle (11), and Pleural Rub (9).

## 4.2. Evaluation Metrics

We divided the dataset into two sets of classes. We train a classifier on 70% data and test on 30% to apply different classifiers to perform the analysis. The ratio of training and testing sets was decided based on random selection.

The performance of the system evaluated using Percision, Recall, F1-Score, and Accuracy.

## 4.3. Results

### 4.3.1. VGG-B1

**Table 2** shows, “VGG-B1” has a precision of 0.67 for fine crackle sounds, and recall for a plural rub is recorded as 0.50. F1-score recorded as 0.80 and 0.67 for fine crackle and plural rub, respectively. Other results of precision and recall reached a 1.00 score for all classes of ARS. As we talk about the accuracy results, the overall accuracy of VGG-B1 for all abnormal RS classes is traced as 0.95%.

### 4.3.2. VGG-B3

From the accuracy plot of VGG-B3 (referred to **Figure 4**), the model was trained for 500 iterations (epoch). The training curve remains stable during iterations because it learns speedily as the training dataset given to it. On the other side, the validation/accuracy curve in the accuracy model shows that in the start, it underlines, but when the epoch is exceeded, the curve rises slowly, and in the last few epochs, it shows consistency with the training curve.

The model has the same iteration as the inaccuracy model from the loss plot of VGG-B3 (referred to **Figure 4**). The loss of the model is far above the ground at the starting stage of the

iterations invalidation process. However, when epochs increase, a reduced amount of loss is observed compared to the earlier testing stage.

### 4.3.3. VGG-V1

**Table 3** shows that “VGG-V1” has unique and poor results compared to other algorithms. “VGG-V1” has a precision of 0.67 for coarse and fine crackle and 0.00 for the pleural rub. On the other side, the recall is recorded as 0.67, 0.00 for stridor and pleural rub, respectively. F1-score was captured as 0.80 for CC, FC, and stridor, whereas 0.00 is for the pleural rub. Other results of precision and recall hit a 1.00 score for all ARS. In VGG-V1, the overall accuracy for all abnormal RS classes is achieved as 0.84%.

### 4.3.4. VGG-V2

**Table 4** shows that “VGG-V2” has similar results with “VGG-V1” in terms of accuracy. “VGG-V2” has a precision of 0.00 for the pleural rub. 0.75, 0.67 precision is also recorded for stridor and wheeze, respectively. The recall is recorded as 0.00 for a pleural rub and 0.50 for rhonchi. F1-score captured as 0.00 for pleural rub, 0.67 for rhonchi, 0.86 for stridor, and 0.80 for wheeze. In VGG-V2, the concerning outcome of overall accuracy for all classes is achieved as 0.84%.

### 4.3.5. VGG-D1

**Table 5** shows that “VGG-D1” has similar results as “VGG-B1” and “VGG-B3.” VGG-D1 has a precision of 0.67 for fine crackle sounds, and recall for a pleural rub is recorded as 0.50. F1-score captured as 0.80 and 0.67 for fine crackle and plural rub, respectively. Other results of precision and recall reached a 1.00 score for all classes of ARS. While taking a look at the accuracy results, the overall accuracy of VGG-D1 for all abnormal RS classes is achieved as 0.95%.

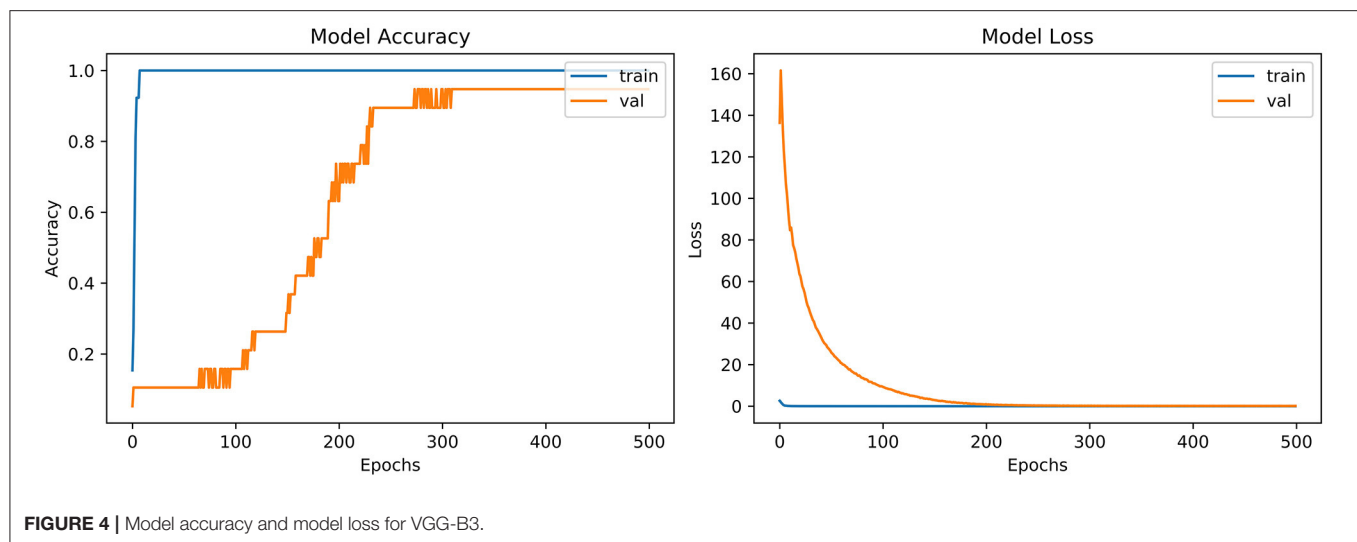
### 4.3.6. AlexNet

From the accuracy plot of AlexNet (referred to **Figure 5**), the model was trained for 500 iterations (epoch). At the start of the training process model, it becomes skilled fast on the training dataset, so it remains regular after further iterations. On the other hand, the validation accuracy curve in the accuracy model remains straight and contradicts the training curve to 150 epochs. After 150–300 epochs, it gradually increases and meets the training curve till the end of epochs.

From loss plot of AlexNet (referred to in **Figure 5**) has the same iteration as did in the accuracy model. A significant loss was observed in the model at the early stages of validation. Then suddenly, the loss reduces after 100 iterations and meets with the training curve after 300 epochs.

### 4.3.7. InceptionNet

**Table 6** shows that “InceptionNet” has a precision of 0.67 for rhonchi sounds, and recall for stridor is recorded as 0.67. F1-score was captured as 0.80 for both rhonchi and stridor. Other results of precision and recall reached a 1.00 score for all classes of ARS. While looking at the accuracy results, the overall accuracy of “InceptionNet” for all abnormal RS classes is achieved as 0.95%.

**TABLE 3 |** Comparative results obtained (Precision and Recall) for VGG-V1.

|                | Precision | Recall | F1-score |
|----------------|-----------|--------|----------|
| Coarse crackle | 0.67      | 1.00   | 0.80     |
| Fine crackle   | 0.67      | 1.00   | 0.80     |
| Pleural rub    | 0.00      | 0.00   | 0.00     |
| Rhonchi        | 1.00      | 1.00   | 1.00     |
| Squawk         | 1.00      | 1.00   | 1.00     |
| Stridor        | 1.00      | 0.67   | 0.80     |
| Wheeze         | 1.00      | 1.00   | 1.00     |
| Accuracy       |           |        | 0.84     |
| Macro avg      | 0.76      | 0.81   | 0.77     |
| Weighted avg   | 0.79      | 0.84   | 0.80     |

**TABLE 4 |** Comparative results obtained (Precision and Recall) for VGG-V2.

|                | Precision | Recall | F1-score |
|----------------|-----------|--------|----------|
| Coarse crackle | 1.00      | 1.00   | 1.00     |
| Fine crackle   | 1.00      | 1.00   | 1.00     |
| Pleural rub    | 0.00      | 0.00   | 0.00     |
| Rhonchi        | 1.00      | 0.50   | 0.67     |
| Squawk         | 1.00      | 1.00   | 1.00     |
| Stridor        | 0.75      | 1.00   | 0.86     |
| Wheeze         | 0.67      | 1.00   | 0.80     |
| Accuracy       |           |        | 0.84     |
| Macro avg      | 0.77      | 0.79   | 0.76     |
| Weighted avg   | 0.79      | 0.84   | 0.79     |

#### 4.3.8. LeNet-5

From the accuracy plot of LeNet-5 (referred to **Figure 6**), the model was trained for 500 iterations (epoch). At the early stages of the process, the model shows high inflection in many curve points and rises with unrepresentative manners. It shows

a steady curve after 350 iterations of training. On the other side, the Val-acc curve shows a considerable divergence from the start to the end of the model. Val-curve rising in random manners from the start of the model and shows vulnerability in behavior.

The loss plot of LeNet-5 (referred to **Figure 6**) has the same iteration as did in the accuracy model. The validation curve shows “unrepresentative” in the model. High loss between training and validation curves at the starting stage was observed. When iterations were performed in the testing process, loss reduces in contrast with the earlier validation stage.

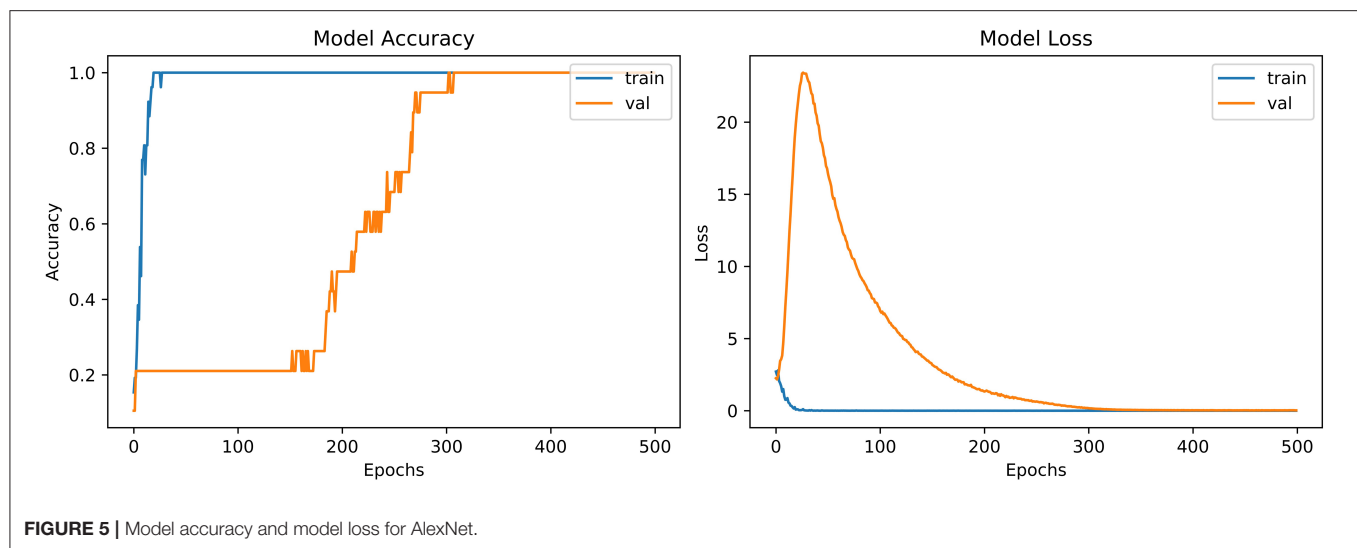
#### 4.3.9. ResNet

From the accuracy plot of ResNet (referred to **Figure 7**), the model was trained for 500 iterations (epoch). At the start of the training, the process model is trained swiftly, showing a steady curve during further iterations for training. Before obtaining steadiness, it shows the variation in multiple points. While seeing at the Val-acc curve, the significant deviation was noticed, but after few epochs, it suddenly arises to meet the training curve. Then again Val-acc curve became steady from 200 epochs and onward.

From the loss plot of ResNet (referred to **Figure 7**), the model shows deviation and high loss between training and validation curves at the early stage. However, after 100 epochs, the reduced amount of loss was observed in contrast with an earlier validation stage, and the Val curve meets with the training curve.

## 4.4. Discussion

“VGG-B1,” “VGG-B3,” “VGG-D1,” and “ResNet” have similar results in terms of accuracy which is recorded as 0.95%. **Figure 4** shows similar curves as the model accuracy curve shows that model trained fits well. The validation curve is a little dissatisfactory due to underfitting, which enhances

**TABLE 5 |** Comparative results obtained (Precision and Recall) for VGG-D1.

|                | Precision | Recall | F1-score |
|----------------|-----------|--------|----------|
| Coarse crackle | 1.00      | 1.00   | 1.00     |
| Fine crackle   | 0.67      | 1.00   | 0.80     |
| Pleural rub    | 1.00      | 0.50   | 0.67     |
| Rhonchi        | 1.00      | 1.00   | 1.00     |
| Squawk         | 1.00      | 1.00   | 1.00     |
| Stridor        | 1.00      | 1.00   | 1.00     |
| Wheeze         | 1.00      | 1.00   | 1.00     |
| Accuracy       |           |        | 0.95     |
| Macro avg      | 0.95      | 0.93   | 0.92     |
| Weighted avg   | 0.96      | 0.95   | 0.94     |

**TABLE 6 |** Comparative results obtained (Precision and Recall) for InceptionNet.

|                | Precision | Recall | F1-score |
|----------------|-----------|--------|----------|
| Coarse crackle | 1.00      | 1.00   | 1.00     |
| Fine crackle   | 1.00      | 1.00   | 1.00     |
| Pleural rub    | 1.00      | 1.00   | 1.00     |
| Rhonchi        | 0.67      | 1.00   | 0.80     |
| Squawk         | 1.00      | 1.00   | 1.00     |
| Stridor        | 1.00      | 0.67   | 0.80     |
| Wheeze         | 1.00      | 1.00   | 1.00     |
| Accuracy       |           |        | 0.95     |
| Macro avg      | 0.95      | 0.95   | 0.94     |
| Weighted avg   | 0.96      | 0.95   | 0.95     |

the model's training. In the model loss, the curve outcome represents that training reduces the loss. In **Figure 7**, the accuracy model curve indicates that the model could be trained more to avoid the underfitting and inflection in some points because the model has not been overlearned for the training set. Model loss shows a divergence from the training curve due to less training, which is why the loss is high from starting epochs.

Accuracy is captured as 0.84% for VGG-V1 and VGG-V2 (**Tables 3, 4**), which is relatively low compared to other classifiers. The reason is that both classifiers need more iteration or data samples for training to enhance the accuracy.

Refer to **Table 6**, which represent that InceptionNet has accuracy of 0.95%. **Figure 6** point toward the accuracy model curve indicates that the model can be trained further to avoid the underfitting and dissimilarity between training and validation because the model has not learned enough for the validation set. Model loss shows a divergence from the training curve due to less training, which is why the loss is high from the start to the end of epochs.

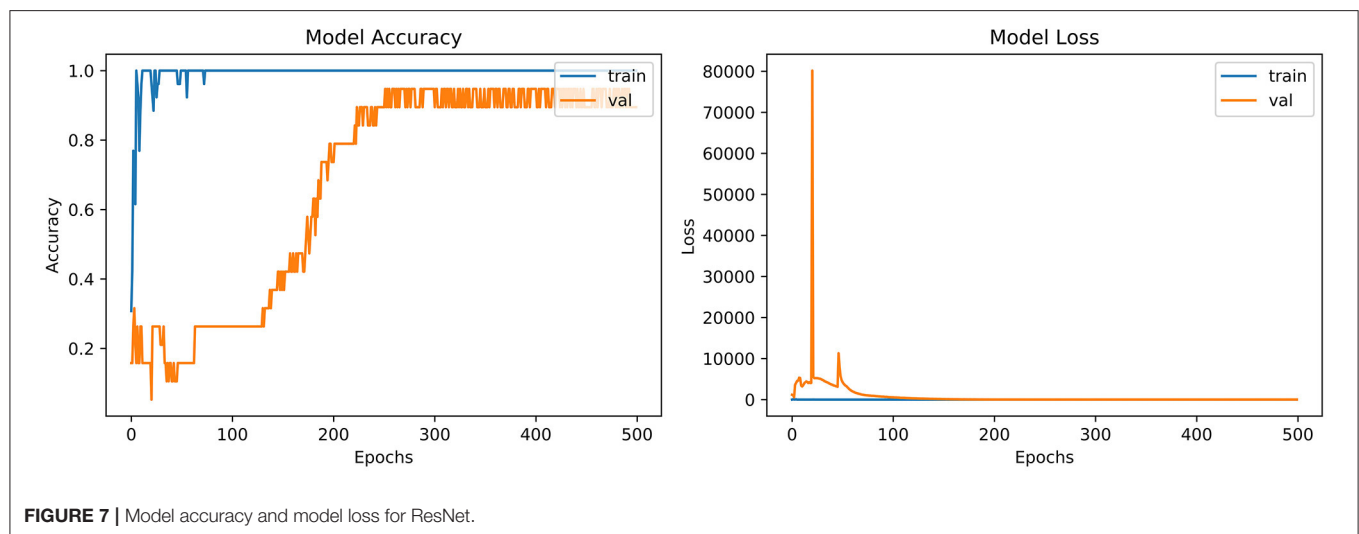
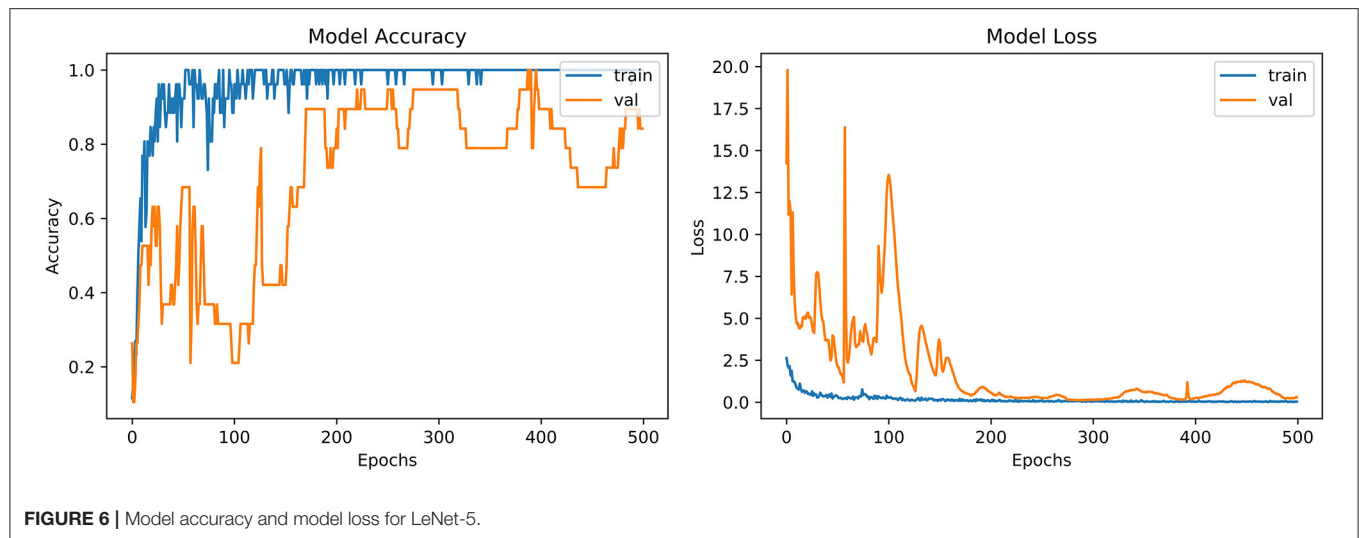
## 4.5. Comparative Analysis

For comparison, the analysis was performed based on mean precision, recall, f1-score, and accuracy for all algorithms. Overall results from the classifiers used for ARS classification are shown in **Table 7**.

The above table shows that the “AlexNet” algorithm has the highest accuracy rate than other classifiers. 1.00% classification accuracy is captured for AlexNet, other algorithms mostly have 0.95% accuracy, and some have below 0.95%. Graphical representation of the above results is as following in **Figure 8**.

## 5. CONCLUSION

The possible concern with the neural network approach is that barely a few units can be employed for classification. If further research is conducted on this domain, researchers can consider more sounds or build their dataset for the classification task, especially for COVID-19. Researchers may integrate more features such as sound quality (timbre) for classification in a new-fangled way, train the neural network for a healthier



consequence, and upgrade the classification scheme. RS attributes and their analysis gives symptomatic data about a patient's lung. A couple of decades back, doctors distinguish symptomatic signs in lung sounds through a typical stethoscope, usually considered as a cheap and secure method for examining. Lung diseases are the third most common cause of death worldwide, so it is essential to classify RS abnormality to overcome the death rate accurately.

In this research, ANA methods are used in conjunction with different deep convolutional networks to classify the various abnormal respiratory sounds—both continuous and discontinuous. Visual inspection of abnormal respiratory sound was done by Fourier analysis. The presence of abnormal sounds like a wheeze, stridor, fine crackle, and coarse crackle was revealed when Fourier Transform was applied over a short time duration and frequency. Texture analysis was performed for better feature extraction through feature maps and data augmentation executed for enlarging the

**TABLE 7 |** Comparative results obtained (Precision, Recall, F1-score, and Accuracy) for all algorithms employed.

|              | Precision | Recall | F1-score | Accuracy (%) |
|--------------|-----------|--------|----------|--------------|
| VGG-B1       | 0.95      | 0.93   | 0.92     | 0.95         |
| VGG-B3       | 0.95      | 0.93   | 0.92     | 0.95         |
| VGG_Drop     | 0.95      | 0.93   | 0.92     | 0.95         |
| VGG-V1       | 0.76      | 0.81   | 0.77     | 0.84         |
| VGG-V2       | 0.77      | 0.79   | 0.76     | 0.84         |
| AlexNet      | 1.00      | 1.00   | 1.00     | 1.00         |
| InceptionNet | 0.95      | 0.95   | 0.94     | 0.95         |
| ResNet       | 0.95      | 0.93   | 0.92     | 0.95         |
| LeNet5       | 0.95      | 0.90   | 0.90     | 0.89         |

number of entities. Numerous algorithms were applied on a range of spectrograms, and results obtained from this method were satisfactory as it considered the seven classes of



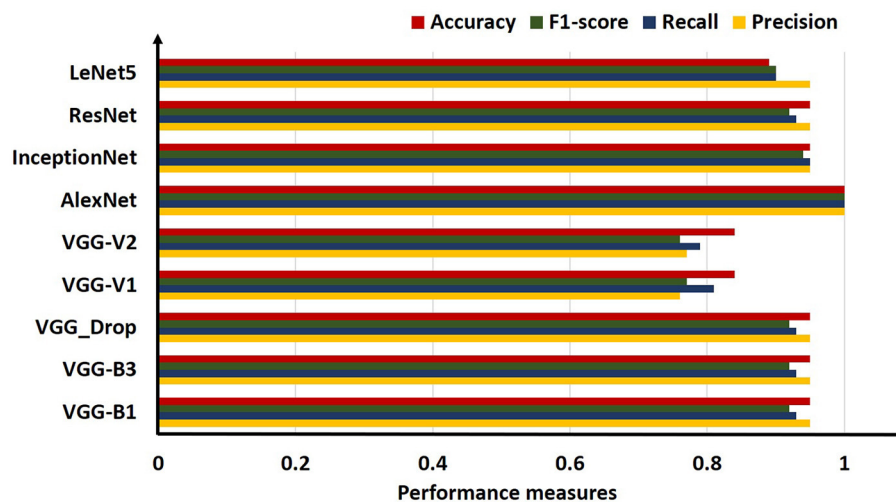


**FIGURE 8 |** Comparative bar chart visualization obtained for all algorithms employed.

abnormal RS concurrently 1.00% accuracy gained through the AlexNet algorithm.

## DATA AVAILABILITY STATEMENT

The original contributions presented in the study are included in the article/supplementary material, further inquiries can be directed to the corresponding author/s.

## REFERENCES

- Bardou D, Zhang K, Ahmad SM. Lung sounds classification using convolutional neural networks. *Artif Intell Med.* (2018) 88:58–69. doi: 10.1016/j.artmed.2018.04.008
- Belkacem AN, Ouhbi S, Lakas A, Benkhalifa E, Chen C. End-to-end AI-based point-of-care diagnosis system for classifying respiratory illnesses and early detection of COVID-19: a theoretical framework. *Front Med.* (2021) 8:372. doi: 10.3389/fmed.2021.585578
- Iccer S, Genge S. Classification and analysis of non-stationary characteristics of crackle and rhonchus lung adventitious sounds. *Digital Signal Process.* (2014) 28:18–27. doi: 10.1016/j.dsp.2014.02.001
- Gao J, Wang H, Shen H. Machine learning based workload prediction in cloud computing. In: *2020 29th International Conference on Computer Communications and Networks (ICCCN)*. (2020). p. 1–9. doi: 10.1109/ICCCN49398.2020.9209730
- Rauf HT, Gao J, Almadhor A, Arif M, Nafis MT. Enhanced bat algorithm for COVID-19 short-term forecasting using optimized LSTM. *Soft Comput.* (2021) 25:1–11. doi: 10.1007/s00500-021-06075-8
- Gao J, Wang H, Shen H. Smartly handling renewable energy instability in supporting a cloud datacenter. In: *2020 IEEE International Parallel and Distributed Processing Symposium (IPDPS)*. New Orleans, LA (2020). p. 769–78. doi: 10.1109/IPDPS47924.2020.00084
- Gao J, Wang H, Shen H. Task failure prediction in cloud data centers using deep learning. *IEEE Trans Services Comput.* (2020). doi: 10.1109/TSC.2020.2993728
- Gurung A, Scraftford CG, Tielsch JM, Levine OS, Checkley W. Computerized lung sound analysis as diagnostic aid for the detection of abnormal lung sounds: a systematic review and meta-analysis. *Respir Med.* (2011) 105:1396–403. doi: 10.1016/j.rmed.2011.05.007
- Sarkar M, Madabhavi I, Niranjana N, Dogra M. Auscultation of the respiratory system. *Ann Thorac Med.* (2015) 10:158. doi: 10.4103/1817-1737.160831
- Weisman I. Erratum: ATS/ACCP statement on cardiopulmonary exercise testing. *Am J Respir Crit Care Med.* (2003) 167:1451–2. doi: 10.1164/ajrccm.167.10.952
- Dokur Z. Respiratory sound classification by using an incremental supervised neural network. *Pattern Anal Appl.* (2009) 12:309–19. doi: 10.1007/s10044-008-0125-y
- Munakata M, Ukita H, Doi I, Ohtsuka Y, Masaki Y, Homma Y, et al. Spectral and waveform characteristics of fine and coarse crackles. *Thorax.* (1991) 46:651–7. doi: 10.1136/thx.46.9.651
- Baughman RP, Loudon RG. Stridor: Differentiation from asthma or upper airway Noise1-3. *Am Rev Respir Dis.* (1989) 139:1407–9. doi: 10.1164/ajrccm/139.6.1407
- Rizal A, Hidayat R, Nugroho HA. Lung sounds classification using spectrogram's first order statistics features. In: *2016 6th International Annual Engineering Seminar (InAES)*. Yogyakarta (2016). p. 96–100. doi: 10.1109/INAES.2016.7821914
- Aykanat M, Kılıç, Kurt B, Saryal S. Classification of lung sounds using convolutional neural networks. *EURASIP J Image Video Process.* (2017) 2017:1–9. doi: 10.1186/s13640-017-0213-2
- Ntalampiras S. Collaborative framework for automatic classification of respiratory sounds. *IET Signal Process.* (2020) 14:223–8. doi: 10.1049/iet-spr.2019.0487
- Demir F, Sengur A, Bajaj V. Convolutional neural networks based efficient approach for classification of lung diseases. *Health Inform Sci Syst.* (2020) 8:1–8. doi: 10.1007/s13755-019-0091-3
- Haider NS, Singh BK, Periyasamy R, Behera AK. Respiratory sound based classification of chronic obstructive pulmonary disease: a risk stratification

## AUTHOR CONTRIBUTIONS

All authors listed have made a substantial, direct and intellectual contribution to the work, and approved it for publication.

## FUNDING

This work was supported by the United Arab Emirates University (UAEU Grant No. G00003270 31T130).

- approach in machine learning paradigm. *J Med Syst.* (2019) 43:1–13. doi: 10.1007/s10916-019-1388-0
19. Patil S, Saxena A, Talreja T, Bhatti V. Medical diagnosis of ailments through supervised learning techniques on sounds of the heart and lungs. In: Wang J, Ram Mohana Reddy G, Kamakshi Prasad V, Sivakumar Reddy V, editors. *Soft Computing and Signal Processing*. New Delhi: Springer (2019). p. 253–62. doi: 10.1007/978-981-13-3393-4\_26
  20. Lang R, Lu R, Zhao C, Qin H, Liu G. Graph-based semi-supervised one class support vector machine for detecting abnormal lung sounds. *Appl Math Comput.* (2020) 364:124487. doi: 10.1016/j.amc.2019.06.001
  21. Rizal A, Hidayat R, Nugroho HA. Comparison of multilevel wavelet packet entropy using various entropy measurement for lung sound classification. *Int J Adv Comput Sci Appl.* (2019) 10:77–82. doi: 10.14569/IJACSA.2019.0100211
  22. Shakeel PM, Tolba A, Al-Makhadmeh Z, Jaber MM. Automatic detection of lung cancer from biomedical data set using discrete AdaBoost optimized ensemble learning generalized neural networks. *Neural Comput Appl.* (2020) 32:777–90. doi: 10.1007/s00521-018-03972-2
  23. Weichenthal S, Hatzopoulou M, Brauer M. A picture tells a thousand-exposures: opportunities and challenges of deep learning image analyses in exposure science and environmental epidemiology. *Environ Int.* (2019) 122:3–10. doi: 10.1016/j.envint.2018.11.042
  24. Dubey R, M Bodade R. A review of classification techniques based on neural networks for pulmonary obstructive diseases. In: *Proceedings of Recent Advances in Interdisciplinary Trends in Engineering & Applications (RAITEA)*. (2019). doi: 10.2139/ssrn.3363485
  25. Jakovljević N, Lončar-Turukalo T. Hidden markov model based respiratory sound classification. In: Maglaveras N, Chouvarda I, de Carvalho P, editors. *Precision Medicine Powered by pHealth and Connected Health, IFMBE Proceedings*. Singapore: Springer (2018). p. 39–43. doi: 10.1007/978-981-10-7419-6\_7
  26. Rizal A, Hidayat R, Nugroho HA. Modification of grey level difference matrix (GLDM) for lung sound classification. In: *2018 4th International Conference on Science and Technology (ICST)*. Bandung (2018). p. 1–5. doi: 10.1109/ICSTC.2018.8528650
  27. Serbes G, Ulukaya S, Kahya YP. An automated lung sound preprocessing and classification system based on spectral analysis methods. In: *International Conference on Biomedical and Health Informatics*. Yogyakarta: Springer (2017). p. 45–9. doi: 10.1007/978-981-10-7419-6\_8
  28. Nabi FG, Sundaraj K, Lam CK, Palaniappan R. Characterization and classification of asthmatic wheeze sounds according to severity level using spectral integrated features. *Comput Biol Med.* (2019) 104:52–61. doi: 10.1016/j.compbiomed.2018.10.035
  29. McBee MP, Awan OA, Colucci AT, Ghobadi CW, Kadom N, Kansagra AP, et al. Deep learning in radiology. *Acad Radiol.* (2018) 25:1472–80. doi: 10.1016/j.acra.2018.02.018
  30. Altan G, Kutlu Y, Pekmezci AO, Nural S. Deep learning with 3D-second order difference plot on respiratory sounds. *Biomed Signal Process Control.* (2018) 45:58–69. doi: 10.1016/j.bspc.2018.05.014
  31. Acharya UR, Fujita H, Oh SL, Hagiwara Y, Tan JH, Adam M. Application of deep convolutional neural network for automated detection of myocardial infarction using ECG signals. *Information Sci.* (2017) 415:190–8. doi: 10.1016/j.ins.2017.06.027
  32. Kochetov K, Putin E, Azizov S, Skorobogatov I, Filchenkov A. Wheeze detection using convolutional neural networks. In: *EPIA Conference on Artificial Intelligence*. Springer (2017). p. 162–73. doi: 10.1007/978-3-319-65340-2\_14
  33. Göğüş F, Karlık B, Harman G. Identification of pulmonary disorders by using different spectral analysis methods. *Int J Comput Intell Syst.* (2016) 9:595–611. doi: 10.1080/18756891.2016.1204110
  34. Rizal A, Hidayat R, Nugroho HA. Multiscale Hjorth descriptor for lung sound classification. In: *AIP Conference Proceedings*. Vol. 1755. Yogyakarta: AIP Publishing LLC (2016). p. 160008. doi: 10.1063/1.4958601
  35. Rajkomar A, Lingam S, Taylor AG, Blum M, Mongan J. High-throughput classification of radiographs using deep convolutional neural networks. *J Digit Imaging.* (2017) 30:95–101. doi: 10.1007/s10278-016-9914-9
  36. Sengupta N, Sahidullah M, Saha G. Lung sound classification using cepstral-based statistical features. *Comput Biol Med.* (2016) 75:118–29. doi: 10.1016/j.compbiomed.2016.05.013
  37. Naves R, Barbosa BH, Ferreira DD. Classification of lung sounds using higher-order statistics: a divide-and-conquer approach. *Comput Methods Prog Biomed.* (2016) 129:12–20. doi: 10.1016/j.cmpb.2016.02.013
  38. Rizal A, Hidayat R, Nugroho HA. Pulmonary crackle feature extraction using tsallis entropy for automatic lung sound classification. In: *2016 1st International Conference on Biomedical Engineering (IBIOMED)*. Yogyakarta (2016). p. 1–4. doi: 10.1109/IBIOMED.2016.7869823
  39. Ulukaya S, Serbes G, Sen I, Kahya YP. A lung sound classification system based on the rational dilation wavelet transform. In: *2016 38th Annual International Conference of the IEEE Engineering in Medicine and Biology Society (EMBC)*. Orlando, FL (2016). p. 3745–8. doi: 10.1109/EMBC.2016.7591542
  40. Oweis RJ, Abdulhay EW, Khayal A, Awad A, et al. An alternative respiratory sounds classification system utilizing artificial neural networks. *Biomed J.* (2015) 38:e61. doi: 10.4103/2319-4170.137773
  41. Jin F, Sattar F, Goh DY. New approaches for spectro-temporal feature extraction with applications to respiratory sound classification. *Neurocomputing.* (2014) 123:362–71. doi: 10.1016/j.neucom.2013.07.033
  42. Sánchez Morillo D, Leon Jimenez A, Moreno SA. Computer-aided diagnosis of pneumonia in patients with chronic obstructive pulmonary disease. *J Am Med Inform Assoc.* (2013) 20:e111–7. doi: 10.1136/amiajnl-2012-001171
  43. Xie S, Jin F, Krishnan S, Sattar F. Signal feature extraction by multi-scale PCA and its application to respiratory sound classification. *Med Biol Eng Comput.* (2012) 50:759–68. doi: 10.1007/s11517-012-0903-y
  44. Bahoura M. Pattern recognition methods applied to respiratory sounds classification into normal and wheeze classes. *Comput Biol Med.* (2009) 39:824–43. doi: 10.1016/j.compbiomed.2009.06.011
  45. Hadjileontiadis LJ. A texture-based classification of crackles and squawks using lacunarity. *IEEE Trans Biomed Eng.* (2009) 56:718–32. doi: 10.1109/TBME.2008.2011747
  46. Reichert S, Gass R, Brandt C, Andrés E. Analysis of respiratory sounds: state of the art. *Clin Med Circul Respir Pulm Med.* (2008) 2:CCRPM-S530. doi: 10.4137/CCRPM.S530
  47. Kandaswamy A, Kumar CS, Ramanathan RP, Jayaraman S, Malmurugan N. Neural classification of lung sounds using wavelet coefficients. *Comput Biol Med.* (2004) 34:523–37. doi: 10.1016/S0010-4825(03)00092-1
  48. Sankur B, Kahya YP, Güler E, Engin T. Comparison of AR-based algorithms for respiratory sounds classification. *Comput Biol Med.* (1994) 24:67–76. doi: 10.1016/0010-4825(94)90038-8
  49. Zur RM, Jiang Y, Pesce LL, Drukker K. Noise injection for training artificial neural networks: a comparison with weight decay and early stopping. *Med Phys.* (2009) 36:4810–8. doi: 10.1118/1.3213517
  50. Goldberger J, Ben-Reuven E. Training deep neural-networks using a noise adaptation layer (2016). Available online at: <https://openreview.net/forum?id=H12GRgcxg>
  51. Isaev I, Dolenko S. Training with noise addition in neural network solution of inverse problems: Procedures for selection of the optimal network. *Proc Comput Sci.* (2018) 123:171–6. doi: 10.1016/j.procs.2018.01.028
  52. Kim J, Picek S, Heuser A, Bhasin S, Hanjalic A. Make some noise. Unleashing the power of convolutional neural networks for profiled side-channel analysis. *IACR Transactions on Cryptographic Hardware and Embedded Systems.* (2019) p. 148–79. doi: 10.46586/tches.v2019.i3.148-179

**Conflict of Interest:** The authors declare that the research was conducted in the absence of any commercial or financial relationships that could be construed as a potential conflict of interest.

**Publisher's Note:** All claims expressed in this article are solely those of the authors and do not necessarily represent those of their affiliated organizations, or those of the publisher, the editors and the reviewers. Any product that may be evaluated in this article, or claim that may be made by its manufacturer, is not guaranteed or endorsed by the publisher.

Copyright © 2021 Zulfiqar, Majeed, Irfan, Rauf, Benkhelefa and Belkacem. This is an open-access article distributed under the terms of the Creative Commons Attribution License (CC BY). The use, distribution or reproduction in other forums is permitted, provided the original author(s) and the copyright owner(s) are credited and that the original publication in this journal is cited, in accordance with accepted academic practice. No use, distribution or reproduction is permitted which does not comply with these terms.



# Automatic Classification Between COVID-19 and Non-COVID-19 Pneumonia Using Symptoms, Comorbidities, and Laboratory Findings: The Khorshid COVID Cohort Study

## OPEN ACCESS

### Edited by:

Reza Lashgari,  
Shahid Beheshti University, Iran

### Reviewed by:

Varun Bajaj,  
PDPM Indian Institute of Information  
Technology, Design and  
Manufacturing, India  
Alberto Botter,  
Politecnico di Torino, Italy

### \*Correspondence:

Marjan Mansourian  
marjan.mansourian@upc.edu  
Hamid Reza Marateb  
h.marateb@eng.ui.ac.ir

<sup>†</sup>These authors have contributed  
equally to this work and share first  
authorship

<sup>‡</sup>These authors have contributed  
equally to this work and share last  
authorship

### Specialty section:

This article was submitted to  
Infectious Diseases - Surveillance,  
Prevention and Treatment,  
a section of the journal  
Frontiers in Medicine

**Received:** 31 August 2021

**Accepted:** 06 October 2021

**Published:** 18 November 2021

### Citation:

Marateb HR, Ziaie Nezhad F,  
Mohebian MR, Sami R, Haghooy  
Javanmard S, Dehghan Niri F,  
Akafzadeh-Savari M, Mansourian M,  
Mañanas MA, Wolkewitz M and  
Binder H (2021) Automatic  
Classification Between COVID-19 and  
Non-COVID-19 Pneumonia Using  
Symptoms, Comorbidities, and  
Laboratory Findings: The Khorshid  
COVID Cohort Study.  
Front. Med. 8:768467.  
doi: 10.3389/fmed.2021.768467

Hamid Reza Marateb <sup>1\*†</sup>, Farzad Ziaie Nezhad <sup>1†</sup>, Mohammad Reza Mohebian <sup>2</sup>,  
Ramin Sami <sup>3</sup>, Shaghayegh Haghooy Javanmard <sup>4</sup>, Fatemeh Dehghan Niri <sup>5</sup>,  
Mahsa Akafzadeh-Savari <sup>6</sup>, Marjan Mansourian <sup>7,8\*‡</sup>, Miquel Angel Mañanas <sup>7,9‡</sup>,  
Martin Wolkewitz <sup>10‡</sup> and Harald Binder <sup>10‡</sup>

<sup>1</sup> The Biomedical Engineering Department, Engineering Faculty, University of Isfahan, Isfahan, Iran, <sup>2</sup> Department of Electrical and Computer Engineering, University of Saskatchewan, Saskatoon, SK, Canada, <sup>3</sup> Department of Internal Medicine, School of Medicine, Isfahan University of Medical Sciences, Isfahan, Iran, <sup>4</sup> Department of Physiology, Applied Physiology Research Center, School of Medicine, Cardiovascular Research Institute, Isfahan University of Medical Sciences, Isfahan, Iran, <sup>5</sup> School of Medicine, Isfahan University of Medical Sciences, Isfahan, Iran, <sup>6</sup> Isfahan Clinical Toxicology Research Center, Isfahan University of Medical Sciences, Isfahan, Iran, <sup>7</sup> Automatic Control Department (ESAI), Biomedical Engineering Research Centre (CREB), Universitat Politècnica de Catalunya-Barcelona Tech (UPC), Barcelona, Spain, <sup>8</sup> Department of Epidemiology and Biostatistics, School of Health, Isfahan University of Medical Sciences, Isfahan, Iran, <sup>9</sup> Biomedical Research Networking Center in Bioengineering, Biomaterials, and Nanomedicine (CIBER-BBN), Madrid, Spain, <sup>10</sup> Faculty of Medicine and Medical Center, Institute of Medical Biometry and Statistics, University of Freiburg, Freiburg, Germany

Coronavirus disease-2019, also known as severe acute respiratory syndrome coronavirus 2 (SARS-CoV-2), was a disaster in 2020. Accurate and early diagnosis of coronavirus disease-2019 (COVID-19) is still essential for health policymaking. Reverse transcriptase-polymerase chain reaction (RT-PCR) has been performed as the operational gold standard for COVID-19 diagnosis. We aimed to design and implement a reliable COVID-19 diagnosis method to provide the risk of infection using demographics, symptoms and signs, blood markers, and family history of diseases to have excellent agreement with the results obtained by the RT-PCR and CT-scan. Our study primarily used sample data from a 1-year hospital-based prospective COVID-19 open-cohort, the Khorshid COVID Cohort (KCC) study. A sample of 634 patients with COVID-19 and 118 patients with pneumonia with similar characteristics whose RT-PCR and chest CT scan were negative (as the control group) (dataset 1) was used to design the system and for internal validation. Two other online datasets, namely, some symptoms (dataset 2) and blood tests (dataset 3), were also analyzed. A combination of one-hot encoding, stability feature selection, over-sampling, and an ensemble classifier was used. Ten-fold stratified cross-validation was performed. In addition to gender and symptom duration, signs and symptoms, blood biomarkers, and comorbidities were selected. Performance indices of the cross-validated confusion matrix for dataset 1 were as follows: sensitivity of 96% [confidence interval, CI, 95%: 94–98], specificity of 95% [90–99], positive predictive

value (PPV) of 99% [98–100], negative predictive value (NPV) of 82% [76–89], diagnostic odds ratio (DOR) of 496 [198–1,245], area under the ROC (AUC) of 0.96 [0.94–0.97], Matthews Correlation Coefficient (MCC) of 0.87 [0.85–0.88], accuracy of 96% [94–98], and Cohen's Kappa of 0.86 [0.81–0.91]. The proposed algorithm showed excellent diagnosis accuracy and class-labeling agreement, and fair discriminant power. The AUC on the datasets 2 and 3 was 0.97 [0.96–0.98] and 0.92 [0.91–0.94], respectively. The most important feature was white blood cell count, shortness of breath, and C-reactive protein for datasets 1, 2, and 3, respectively. The proposed algorithm is, thus, a promising COVID-19 diagnosis method, which could be an amendment to simple blood tests and screening of symptoms. However, the RT-PCR and chest CT-scan, performed as the gold standard, are not 100% accurate.

**Keywords:** COVID-19, computer-aided diagnosis, screening, validation studies, machine learning

## INTRODUCTION

Among all infectious diseases known to humankind that caused massive pandemics, certainly, COVID-19 has been the most recognized one. Despite all the efforts and experiences in fighting these contagious diseases in the past, we are still struggling to control the situation globally. Almost all epidemics were resolved in the past, but their damages were long-standing (1). According to the World Health Organization (WHO), more than 180 million people have been diagnosed, and nearly 4 million souls have been lost since the outbreak of COVID-19 in December 2019 until June 2021. The spread of the virus has not been consistent, and it is mutating rapidly, making it even harder to confront. Fortunately, vaccines came to our aid to eradicate the virus at once. However, only 2.5 billion doses have been administered. Therefore, this pandemic is still ravaging some parts of the world. Also, lockdowns and restrictions have reviled or created fundamental problems in our daily lives, such as undiscovered market patterns and transitions in short-term economic strategies (2). On the whole, an increase in the number of mental health problems was reported in some countries during the COVID-19 pandemic (3). In the future, to prevent

the widespread of such contagious airborne diseases, an agile diagnosis will be crucial.

Coronavirus disease-2019 is a severe type of pneumonia (4); symptoms of various types of pneumonia infections are very similar, and it is almost impossible for physicians to diagnose COVID-19 without proper means of examination. There are two viral methods to determine whether the virus infects someone or not; the first is using chest computerized tomography (CT) images (4), and the second is reverse-transcription polymerase chain reaction (RT-PCR) test (5), which is based on respiratory samples of a patient, like nasal mucus. The CT scan is not mobile, and multiple scans magnify any risk of getting cancer, although currently, RT-PCR kits are much more available publicly. Thus, the gold standard for COVID-19 diagnosis is RT-PCR. However, viral RT-PCR has limited sensitivity and may need up to 48 h because of technical dilemmas (6).

Many blood factors, along with body symptoms, can expose the illness. These factors are significantly differentiable between healthy and hospitalized individuals, like D-dimer, alanine transaminase (ALT), C-reactive protein (CRP), bilirubin, lymphocytes, platelets, albumin, neutrophils, diastolic blood pressure, heart rate levels, and Charlson Comorbidity Index (7–14). Furthermore, lactate dehydrogenase (LDH) and  $\alpha$ -hydroxybutyrate dehydrogenase ( $\alpha$ -HBDH) levels were two noticed markers that discriminate COVID-19 from other kinds of pneumonia. Also, liver functionality was altered considerably (4).

It is worth mentioning that RT-PCR is not always reliable, and that it has its limitations. Long et al. demonstrated that the sensitivity of the RT-PCR test is only 83.3% (15); in addition, RT-PCR standalone diagnosis showed false positive outcomes (16, 17). Interpretation of blood test results does not require dedicated testing kits, and it can be performed in any laboratory. Therefore, a method that can accurately detect COVID-19 would be more favorable, especially in countries with a shortage of RT-PCR reagents and proper laboratories. In this scenario, machine learning and automatic diagnosis combined with blood test results play a vital role. Accordingly, routine blood exams, with symptoms of patients, could diagnose the SARS-CoV-2 infection

**Abbreviations:** ACC, Accuracy; ALT, Alanine Transaminase; ALP, Alkaline Phosphatase; AUC, The area under the receiver operating characteristic; AST, Aspartate Aminotransferase; Ca, Blood Calcium; Cr, Blood Creatinine; BUN, Blood Urea Nitrogen; CCI, Charlson Comorbidity Index; HRCT, Chest computed High-resolution CT; CT, Computerized Tomography; CI, Confidence Interval; CRP, C-Reactive Protein; DOR, diagnosis odds ratio; DP, discriminant power; F1S, F1-score; FN, False Negative; FP, False Positive; GMDH, Group method of data handling; K(c), Kappa; KCC, Khorshid COVID Cohort; LDH, Lactate Dehydrogenase; WBC, Leukocytes; LightGBM, light gradient-boosting machine learning algorithm based on decision-tree; Lymph, Lymphocytes; LDA, Linear Discriminant Analysis; Mg, Magnesium; MCC, Mathew Correlation Coefficient; MLP, Multi-level Perceptron neural network; Neut, Neutrophils; PLT, Platelets; K or P, Potassium; RT-PCR, reverse-transcription polymerase chain reaction; RBF, Radial Basis Function; SES, socioeconomic status; Na, Sodium; STARD, Standards for Reporting Diagnostic Accuracy; XGBOOST, Stochastic Gradient Descent; SVM, Support Vector Machine; TRIPOD, Transparent Reporting of a multivariable prediction model for Individual Prognosis or Diagnosis; TN, True Negative; TP, True Positive; WHO, World Health Organization;  $\alpha$ -HBDH,  $\alpha$ -Hydroxybutyrate Dehydrogenase.



with an accuracy of above 82%; these factors can, in fact, separate COVID-19 from other kinds of pneumonia (18).

Most computer-aided diagnosis (CAD) studies with blood examinations only considered COVID-19 cases vs. healthy ones and ignored other pneumonia types (11, 19–21). Further studies illustrated that various kinds of pneumonia diseases had similar characteristics (4); hence, without considering this fact, automatic COVID-19 detection algorithms may have a substantial pragmatic bias, and the number of misclassified cases rises. On the other hand, a few CT and x-ray CAD systems distinguished COVID-19 from other types of pneumonia (5, 20, 22–27).

## Related Studies

Several studies analyzed the possibility of diagnosing COVID-19 from blood tests by combining blood tests and symptoms. Goodman-Meza et al. (19) used the UCLA electronic health record data and developed a CAD system for hospital settings. They included complete blood counts and an inflammatory marker (LDH) with the gold standard PCR test. They used an ensemble learning method with several renowned machine learning algorithms [e.g., support vector machine (SVM), logistic regression, multi-level perceptron (MLP) neural network, stochastic gradient descent, and extreme gradient boosting (XGBOOST)], along with hold-out validation method (1,455 and 392 samples for training and test sets), and achieved an area under ROC (AUC) of 0.83.

Zoabi et al. (21) investigated the nationwide public data reported by the Israeli Ministry of Health, in which eight binary symptomatic features (the appearance of five initial clinical symptoms, known contact with an infected individual, sex, and age  $\geq 60$ ) were presented along with the result of the RT-PCR test (nasopharyngeal swab11) as the ground truth. With the hold-out evaluation method (51,831 and 47,401 samples for training and test sets), they achieved an AUC of 0.86 using a light gradient-boosting machine (LightGBM) learning algorithm based on a decision tree (28). Their dataset contained healthy control and patients with COVID-19.

Banerjee et al. (29) obtained the AUC of 0.94 by stratified 10-fold cross-validation on 598 individuals diagnosed with different kinds of pneumonia, despite others, without symptoms or history of the patients. They utterly relied on blood test results and the gold standard RT-PCR test. Their approach was based on three classifiers: random forest decision tree, MLP neural network, and Lasso-elastic-net regularized generalized linear models.

Feng et al. (30) investigated the data of 132 healthy individuals and patients with COVID-19 containing information like vital signs, epidemiological history of exposure, comorbidities, blood routine values, and clinical symptoms. They used Adaboost, LASSO, logistic regression with ridge regularization decision Tree, and 10-fold cross-validation, and achieved an AUC of 0.84.

Wu et al. (31) examined 169 patients from multiple sources (originally from Lanzhou city), from which 27 subjects had COVID-19. Moreover, these patients were diagnosed with different kinds of respiratory-related diseases (e.g., tuberculosis and lung cancer). Based on the hematological and biochemical

parameters of their patients and a random forest decision tree with 10-fold cross-validation, an AUC of 0.99 was obtained.

While CT scan machines and RT-PCR kits are not available everywhere, blood tests are widely available and faster. Most of the previous studies have ignored other types of pneumonia infections even though not all patients with COVID-19 symptoms are infected; therefore, presumably, patients may receive wrong medications based on previous methods. Our goal here is to propose a reliable and practical method with a suitable dataset.

This study described a clinically reliable CAD system for distinguishing COVID-19 pneumonia from other types of pneumonia and healthy individuals using blood tests, symptoms, and comorbidities. The discrimination between COVID-19 and distinct types of pneumonia is not a trivial task, as these airborne diseases show similar symptoms (4). Hence, our research was based on the Khorshid COVID Cohort (KCC) study (32), which covered different kinds of pneumonia. Additionally, we used the dataset from the studies presented by Zoabi et al. (21, 33) and Banerjee et al. (29) for cross-validation and discrimination between COVID-19 and healthy controls. Such datasets were also used to compare our method with the state-of-the-art.

## MATERIALS AND METHODS

This study presented a rapid COVID-19 detection system, which is a clinically reliable model to be used in non-clinical settings, based on blood test results and symptoms. Our methodology consisted of feature selection, over-sampling, and ensemble machine learning techniques. The model was developed and evaluated on three datasets, described in the following section.

### Datasets

We used three different sets of data, one containing a national dataset including patients with COVID-19 and non-COVID-19 pneumonia [KCC study (32)], and its combinations with two other public datasets (33, 34).

The first dataset was from the Khorshid COVID-19 Cohort (KCC) study (32, 35, 36). KCC is a hospital-based surveillance study to investigate COVID-19 and non-COVID pneumonia patients since February 2020. Patient recruitment ended in late August 2020. During this period, Khorshid Hospital in Isfahan was the hot outbreak zone in central Iran.

Patients were diagnosed according to the WHO provisional advice (37). Then, those with positive PCR or compatible chest computed high-resolution CT (HRCT) were enrolled as the case group, while patients with non-COVID pneumonia were recruited as the control group. The study was conducted in two parts: admission until discharge or death and follow-ups after hospital discharge.

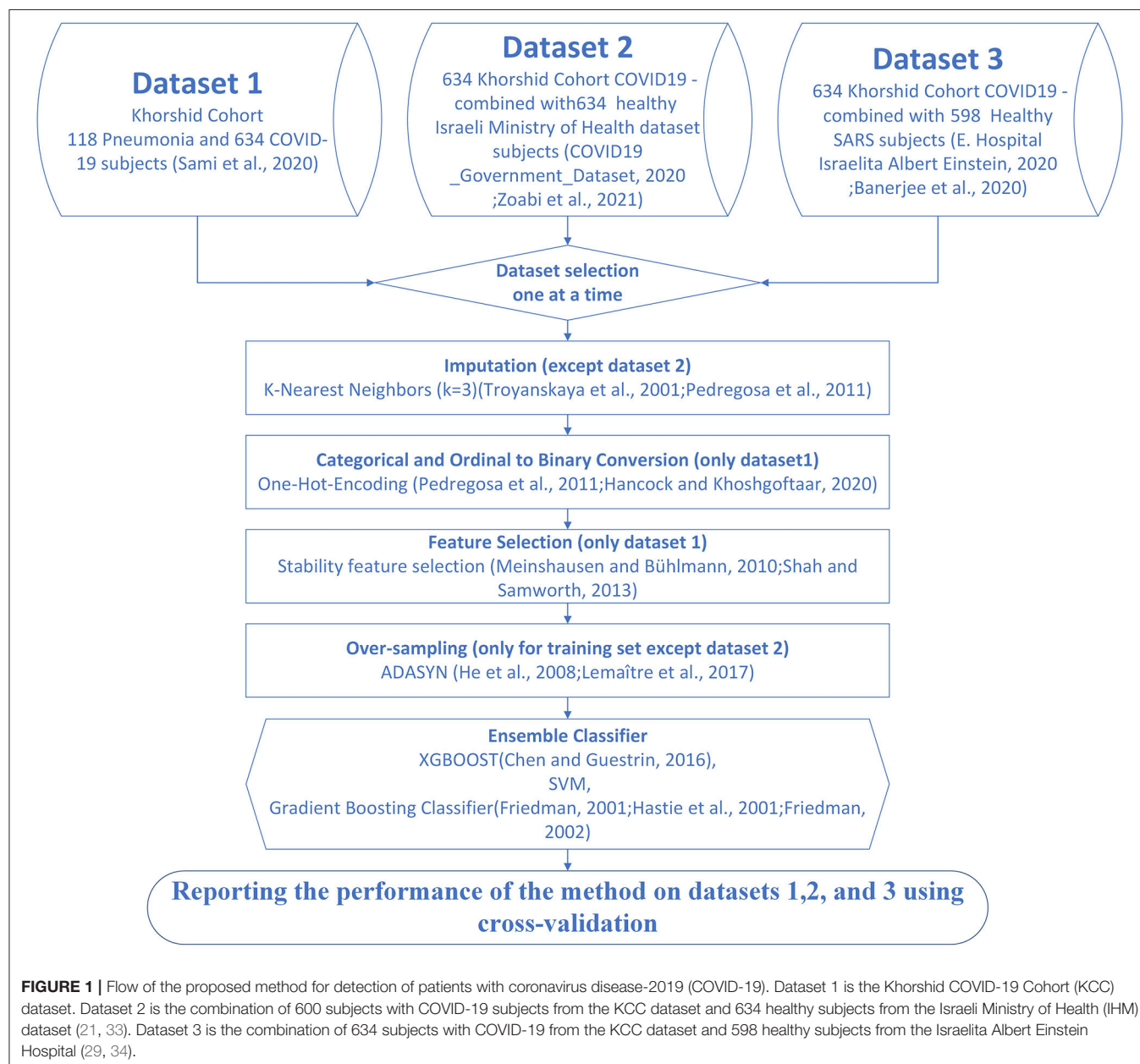
Demographics, medical history, underlying chronic diseases, socioeconomic status (SES), Charlson Comorbidity Index (CCI), signs, symptoms, chest computed tomographic (CT) scans, laboratory findings, and treatments in the hospital were collected for the control and case groups. On the whole, 55% of all 630 closely observed patients with COVID-19 died (36).



The ethics committee of the Isfahan University of Medical Sciences (IUMS) and other national authorities approved the experimental protocol conforming to the Declaration of Helsinki: [longitudinal epidemiologic investigation of the characteristics of patients with coronavirus infection referring to Isfahan Khorshid Hospital: IR.MUI.MED.REC.1399.029 (<https://ethics.research.ac.ir/EthicsProposalViewEn.php?id=127640>), and modeling of incidence and outcomes of COVID-19: IR.MUI.RESEARCH.REC.1399.479 (<https://ethics.research.ac.ir/EthicsProposalViewEn.php?id=158927>)]. The entire subjects gave written informed consent to the experimental procedure. It was given by the first relative family of patients with severe conditions. No minors participated in our study. The sample

dataset was provided as follows on <https://figshare.com/s/fe311d566d580197cdf1>.

The following blood markers were recorded: alanine aminotransferase (ALT), alkaline phosphatase (ALP), aspartate aminotransferase (AST), lactic dehydrogenase (LDH), C-reactive protein (CRP), urea, platelet (PLT), neutrophils (Neut), lymphocytes (Lymph), and white blood cell (WBC) counts, Sodium (Na), hemoglobin, blood urea nitrogen (BUN), potassium (K), blood creatinine (Cr), potassium (P), blood calcium (Ca), and magnesium (Mg). In dataset 1, baseline blood tests for patient with COVID-19 (case) and non-COVID-19 pneumonia (control) were used, in addition to demographics, SES, medical history, and underlying chronic diseases.



We created the second dataset by mixing the 634 subjects with COVID-19 to KCC with randomly selected 634 healthy subjects from the Israeli Ministry of Health dataset (21, 33). The following similar features were used: gender, age category (above 60 counted as 1 and below 60 as zero), cough details (dry cough counted as 1 and others as zero), shortness of breath, headache, sore throat, and body temperature (considered as positive if fever was above 37.5°), making it possible to compare our results with the study presented by Zoabi et al. (21).

We also prepared the third dataset by mixing 634 subjects with COVID-19 to KCC with 598 healthy subjects from the Israelita Albert Einstein Hospital (29, 34). The following similar features were used: WBC, PLT, CRP, LDH, Neut, and Lymph, making it possible to compare our results with the study presented by Banerjee et al. (29). **Figure 1** illustrates the analyzed datasets and the proposed algorithm.

## Method

The first step toward processing data is either removing samples with missing values or imputing the missing values. For datasets 1 and 3, imputation was necessary because dropping samples with few missing values could dramatically decrease the size of the sample. The randomness of the missing data was analyzed before imputation. One of the most common imputation methods is the k-Nearest Neighbors algorithm (38, 39). The neighboring samples were set to 3 to restrict copying to the closest similarity (**Figure 1**). The mean, median, and mode of the features of neighboring samples were used to impute missing values in the interval, ordinal, and nominal features (40).

To make each category more comparable and avoid prioritization, we replaced each categorical or ordinal column with its binary encoded feature matrix known as one-hot encoding (39, 41). The categorical features were then converted into numerical variables by label encoding to perform standard pattern recognition techniques.

Taking informative, discriminating, and stable features is vital for devising a classification model (42). The stability selection algorithm (42, 43), which we used in this study, provided bootstrap data batches and used a baseline feature selection algorithm. Then, the stability score for each feature was calculated using the results of each bootstrap sample. In each bootstrap step, we used logistic regression (44) to analyze feature importance. In the end, features that improved the classification accuracy in most of the iterations were selected as stable features.

Datasets 1 and 3 had imbalance, and minority classes needed to be over-sampled only for the training procedure. We used the ADASYN (45, 46) over-sampling method that uses weighted distribution base on their learning difficulty. Without over-sampling, the classifiers tend to ignore the minority class, and this means that the cost function gets smaller only by fitting to the majority class.

The ensemble model consisted of three voter classifiers, XGBOOST, SVM, and gradient boosting classifier (47–49) (**Figure 1**). Ensemble learning is a common way of looking at a problem from different perspectives, predicting an outcome from different approaches, and combining their predictions. In some machine learning cases, only one method might have a significant error in parts of the dataset (50); ensemble learning brings

more generality and robustness to the mechanism of prediction. XGBOOST (51) is an enhanced version of gradient boosted decision trees (52), designed to increase speed and performance by adding multiple regression trees and a stochastic gradient boosting mechanism. SVM (53) maps data to higher dimensions to find a hyperplane to classify samples.

We trained each model independently on the training set during cross-validation. Thus, for every single test input, we had three outputs from the classifiers. Consequently, the class with the majority of the votes was the output of the ensemble model. The hyperparameters of the models were tuned with the grid search method in Scikit-Learn (39) on the training set. The training set was split into estimation and validation with internal 5-fold cross-validation to tune the free parameters. The number of gradient boosting trees ranged between 200 and 1,200, and the objective binary logistic function and AUC evaluation metric were used for XGBOOST. The deviance loss function and the Friedman Mean Square Error metric were used for the gradient boost classifier, while the number of gradient boosting trees ranged between 200 and 1,600. For the non-linear SVM classifier, the radial basis function (RBF) kernel was used, and the penalty and kernel parameters were tuned during internal cross-validation. Noted that the objective or cost functions were minimized for the XGBOOST or gradient boost classifier, and the evaluation metric was used as the early stopping criterion.

## Evaluation

We evaluated all the models with the 10-fold stratified cross-validation method using the stratified K-fold (39). We performed linear discriminant analysis (LDA) as a base classifier and compared the performance of the proposed method with that of the LDA classifier on different datasets. We used the cross-validated confusion matrix instead of the confusion matrix of each fold to ensure that all the results were without systematic bias and error with the small dispersion index. In this study, we reported the following indices to analyze the performance of the classifiers: true positive (TP), subjects with COVID-19 correctly identified; true negative (TN), subjects without COVID-19 correctly identified; false positive (FP), subjects without COVID-19 incorrectly identified; and false negative (FN), COVID-19 incorrectly identified;

The following performance indices were then calculated:

Sensitivity or recall (Se or Rl, Equation 1); specificity (Sp, Equation 2); precision (Pr, Equation 3); area under the receiver operating characteristic (AUC, Equation 4) (54); accuracy (ACC, Equation 5); Mathew Correlation Coefficient (MCC, Equation 6; a.k.a., phi coefficient) (55), the association between the ground truth and the predicted class labels; F<sub>1</sub>S (F<sub>1</sub> score) as the harmonic mean of the sensitivity and precision (Equation 7); Kappa [K(c)] (56), agreement rate between the ground truth and the predicted class labels (Equation 8); diagnosis odds ratio (DOR; Equation 9); and discriminant power (DP; Equation 10) (57, 58). The reference intervals of the indices AUC, Kappa, MCC, and DP were provided by Marateb et al. (59) (Supplementary Material S3).

$$Se = \frac{TP}{TP + FN} \quad (1)$$

$$Sp = \frac{TN}{TN + FP} \quad (2)$$

$$Pr = \frac{TP}{TP + FP} \quad (3)$$

$$AUC = \frac{Se + Sp}{2} \quad (4)$$

$$ACC = \frac{TP + TN}{TP + TN + FP + FN} \quad (5)$$

$$MCC = \frac{TP \times TN - FP \times FN}{\sqrt{(TP + FP) \times (TP + FN) \times (TN + FP) \times (TN + FN)}} \quad (6)$$

$$F_1S = \frac{2 \times Pr \times Se}{Pr + Se} \quad (7)$$

$$K(c) = \frac{2 \times (TP \times TN - FP \times FN)}{(TP + FP) \times (FP + TN) + (TP + FN) \times (FN + TN)} \quad (8)$$

$$DOR = \frac{TP \times TN}{FP \times FN} \quad (9)$$

$$DP = \left( \sqrt{\frac{3}{\pi}} \right) \times \log(DOR) \quad (10)$$

Following the Standards for Reporting Diagnostic Accuracy (STARD) (60) and Transparent Reporting of a multivariable prediction model for Individual Prognosis or Diagnosis (TRIPOD) (61) guidelines, the Confidence Interval (CI) 95% of the performance indices were provided. It showed the precision of the indices and indicated how the prediction from the analyzed samples could be generalized to the entire population. Moreover, a diagnosis system was considered clinically reliable (59, 62) if the entire following conditions were met: The sensitivity higher than 80%, the specificity, and precision higher than 95% (63, 64), and DOR higher than 100 (65).

## Statistical Analysis

Results were reported as frequencies (for categorical variables) and mean  $\pm$  standard deviation (for interval variables). For interval features, those normally distributed in analyzed two classes, Independent Samples *t*-test was performed. Otherwise, and in ordinal features, the Mann–Whitney *U*-test was utilized. The pairwise  $\chi^2$  analysis was performed for nominal features, and when the Cochran conditions were not met, the Fisher exact test was performed. The McNemar's test (66, 67) was performed to compare the performance of the proposed and the LDA classifiers on different datasets. *P*-values  $<0.05$  were considered significant. The statistical analysis was performed using the IBM SPSS® Statistics for Windows, version 22.0, which was released in 2013 (IBM Corp., Armonk, NY, United States). The classification was performed offline using Python version 3.8.8 (Python Software Foundation, 501(c) (3) non-profit organization).

## RESULTS

The descriptive statistics of dataset 1 are provided in **Table 1** for the patients with COVID and non-COVID pneumonia. Overall, 41% of the patients were female, and the average age of the patients was  $57 \pm 17$  (years). Fourteen percent of the patients were smoker, 36% were hypertensive, and 27% had diabetes. Based on the univariate analysis (**Table 1**), significant differences

**TABLE 1 |** Descriptive statistics of dataset 1.

|                                       | Non-COVID pneumonia<br>(N = 118) | COVID-19 pneumonia<br>(N = 634) | P-value  | OR<br>(CI 95%)     |
|---------------------------------------|----------------------------------|---------------------------------|----------|--------------------|
| Age (years)                           |                                  |                                 |          |                    |
| Mean (SD)                             | 61.7 (18.3)                      | 57.0 (15.4)                     | 0.009    | –                  |
| Gender                                |                                  |                                 |          |                    |
| Male                                  | 56 (47.5%)                       | 389 (61.4%)                     | 0.007    | 1.76<br>1.18–2.61  |
| Female                                | 62 (52.5%)                       | 245 (38.6%)                     |          |                    |
| Occupation                            |                                  |                                 |          |                    |
| Yes                                   | 41 (34.7%)                       | 326 (51.4%)                     | 0.001    | 1.99<br>1.32–2.99  |
| No                                    | 77 (65.3%)                       | 308 (48.6%)                     |          |                    |
| Marriage status                       |                                  |                                 |          |                    |
| Single                                | 10 (8.5%)                        | 21 (3.3%)                       | 0.035    | –                  |
| Married                               | 107 (90.7%)                      | 608 (95.9%)                     |          | –                  |
| Divorced or widowed                   | 1 (0.8%)                         | 5 (0.8%)                        |          | –                  |
| Symptom's duration (day)              |                                  |                                 |          |                    |
| Mean (SD)                             | 6.11 (6.04)                      | 7.97 (5.71)                     | 0.002    | –                  |
| Smoking status                        |                                  |                                 |          |                    |
| Yes                                   | 23 (19.5%)                       | 82 (12.9%)                      | 0.081    | 0.61<br>0.37–1.02  |
| No                                    | 95 (80.5%)                       | 552 (87.1%)                     |          |                    |
| Contact with confirmed COVID-19 cases |                                  |                                 |          |                    |
| Yes                                   | 4 (3.4%)                         | 95 (15.0%)                      | 0.001    | 5.02<br>1.81–13.94 |
| No                                    | 114 (96.6%)                      | 539 (85.0%)                     |          |                    |
| Quarantine before admission           |                                  |                                 |          |                    |
| Yes                                   | 110 (93.2%)                      | 589 (92.9%)                     | 1        | 0.95<br>0.44–2.07  |
| No                                    | 8 (6.8%)                         | 45 (7.1%)                       |          |                    |
| <b>Comorbidities</b>                  |                                  |                                 |          |                    |
| Ischemic heart disease                |                                  |                                 |          |                    |
| Yes                                   | 27 (22.9%)                       | 91 (14.4%)                      | 0.028    | 0.56<br>0.35–0.92  |
| No                                    | 91 (77.1%)                       | 543 (85.6%)                     |          |                    |
| Hypertension                          |                                  |                                 |          |                    |
| Yes                                   | 53 (44.9%)                       | 221 (34.9%)                     | 0.048    | 0.66<br>0.44–0.98  |
| No                                    | 65 (55.1%)                       | 413 (65.1%)                     |          |                    |
| Chronic kidney disease                |                                  |                                 |          |                    |
| Yes                                   | 5 (4.2%)                         | 18 (2.8%)                       | 0.604    | 0.66<br>0.24–1.81  |
| No                                    | 113 (95.8%)                      | 616 (97.2%)                     |          |                    |
| COPD                                  |                                  |                                 |          |                    |
| Yes                                   | 10 (8.5%)                        | 13 (2.1%)                       | $<0.001$ | 0.23<br>0.10–0.53  |
| No                                    | 108 (91.5%)                      | 621 (97.9%)                     |          |                    |
| Cancer                                |                                  |                                 |          |                    |
| Yes                                   | 3 (2.5%)                         | 15 (2.4%)                       | 1        | 0.93<br>0.26–3.26  |
| No                                    | 115 (97.5%)                      | 619 (97.6%)                     |          |                    |

(Continued)

TABLE 1 | Continued

|                             | Non-COVID<br>pneumonia<br>(N = 118) | COVID-19<br>pneumonia<br>(N = 634) | P-value | OR<br>(CI 95%)    |
|-----------------------------|-------------------------------------|------------------------------------|---------|-------------------|
| Chronic respiratory disease |                                     |                                    |         |                   |
| Yes                         | 27 (22.9%)                          | 56 (8.8%)                          | <0.001  | 0.33<br>0.20–0.54 |
| No                          | 91 (77.1%)                          | 578 (91.2%)                        |         |                   |
| Other comorbidities         |                                     |                                    |         |                   |
| Yes                         | 47 (39.8%)                          | 143 (22.6%)                        | <0.001  | 0.44<br>0.29–0.66 |
| No                          | 71 (60.2%)                          | 491 (77.4%)                        |         |                   |
| CCI                         |                                     |                                    |         |                   |
| Mean (SD)                   | –                                   | 2.25 (2.10)                        | –       | –                 |
| <b>Signs and symptoms</b>   |                                     |                                    |         |                   |
| Sneeze                      |                                     |                                    |         |                   |
| Yes                         | 4 (3.4%)                            | 56 (8.8%)                          | 0.069   | 2.76<br>0.98–7.77 |
| No                          | 114 (96.6%)                         | 578 (91.2%)                        |         |                   |
| Runny nose                  |                                     |                                    |         |                   |
| Yes                         | 10 (8.5%)                           | 73 (11.5%)                         | 0.419   | 1.41<br>0.70–2.81 |
| No                          | 108 (91.5%)                         | 561 (88.5%)                        |         |                   |
| Body temperature (°C)       |                                     |                                    |         |                   |
| Mean (SD)                   | 37.1 (1.10)                         | 37.5 (1.10)                        | <0.001  | –                 |
| Fatigue                     |                                     |                                    |         |                   |
| Yes                         | 73 (61.9%)                          | 482 (76.0%)                        | 0.002   | 1.95<br>1.29–2.96 |
| No                          | 45 (38.1%)                          | 152 (24.0%)                        |         |                   |
| Cough details               |                                     |                                    |         |                   |
| Other                       | 41 (34.7%)                          | 117 (18.5%)                        | <0.001  | 0.43<br>0.28–0.65 |
| Dry                         | 77 (65.3%)                          | 517 (81.5%)                        |         |                   |
| Nausea                      |                                     |                                    |         |                   |
| Yes                         | 43 (36.4%)                          | 269 (42.4%)                        | 0.267   | 1.29<br>0.86–1.93 |
| No                          | 75 (63.6%)                          | 365 (57.6%)                        |         |                   |
| Decreased appetite          |                                     |                                    |         |                   |
| Yes                         | 70 (59.3%)                          | 508 (80.1%)                        | <0.001  | 2.76<br>1.82–4.19 |
| No                          | 48 (40.7%)                          | 126 (19.9%)                        |         |                   |
| Weight loss                 |                                     |                                    |         |                   |
| Yes                         | 27 (22.9%)                          | 268 (42.3%)                        | <0.001  | 2.47<br>1.56–3.90 |
| No                          | 91 (77.1%)                          | 366 (57.7%)                        |         |                   |
| Chills                      |                                     |                                    |         |                   |
| Yes                         | 64 (54.2%)                          | 457 (72.1%)                        | <0.001  | 2.18<br>1.46–3.26 |
| No                          | 54 (45.8%)                          | 177 (27.9%)                        |         |                   |
| Headache                    |                                     |                                    |         |                   |
| Yes                         | 39 (33.1%)                          | 306 (48.3%)                        | 0.003   | 1.89<br>1.25–2.86 |
| No                          | 79 (66.9%)                          | 328 (51.7%)                        |         |                   |
| Shortness of breath         |                                     |                                    |         |                   |
| Yes                         | 83 (70.3%)                          | 440 (69.4%)                        | 0.925   | 0.96<br>0.62–1.47 |

(Continued)

TABLE 1 | Continued

|                                   | Non-COVID<br>pneumonia<br>(N = 118) | COVID-19<br>pneumonia<br>(N = 634) | P-value | OR<br>(CI 95%)    |
|-----------------------------------|-------------------------------------|------------------------------------|---------|-------------------|
| No                                | 35 (29.7%)                          | 194 (30.6%)                        |         |                   |
| Influenza vaccine                 |                                     |                                    |         |                   |
| Yes                               | 8 (6.8%)                            | 22 (3.5%)                          | 0.153   | 0.49<br>0.21–1.14 |
| No                                | 110 (93.2%)                         | 612 (96.5%)                        |         |                   |
| Diabetes                          |                                     |                                    |         |                   |
| Yes                               | 32 (27.1%)                          | 172 (27.1%)                        | 1       | 1.00<br>0.64–1.56 |
| No                                | 86 (72.9%)                          | 462 (72.9%)                        |         |                   |
| Diarrhea                          |                                     |                                    |         |                   |
| Yes                               | 21 (17.8%)                          | 200 (31.5%)                        | 0.004   | 2.13<br>1.29–3.51 |
| No                                | 97 (82.2%)                          | 434 (68.5%)                        |         |                   |
| Sore throat                       |                                     |                                    |         |                   |
| Yes                               | 21 (17.8%)                          | 134 (21.1%)                        | 0.484   | 1.24<br>0.74–2.06 |
| No                                | 97 (82.2%)                          | 500 (78.9%)                        |         |                   |
| Vomiting                          |                                     |                                    |         |                   |
| Yes                               | 27 (22.9%)                          | 178 (28.1%)                        | 0.293   | 1.32<br>0.83–2.09 |
| No                                | 91 (77.1%)                          | 456 (71.9%)                        |         |                   |
| Abdominal pain                    |                                     |                                    |         |                   |
| Yes                               | 19 (16.1%)                          | 123 (19.4%)                        | 0.476   | 1.25<br>0.74–2.13 |
| No                                | 99 (83.9%)                          | 511 (80.6%)                        |         |                   |
| Body pain                         |                                     |                                    |         |                   |
| Yes                               | 59 (50.0%)                          | 446 (70.3%)                        | <0.001  | 2.37<br>1.59–3.54 |
| No                                | 59 (50.0%)                          | 188 (29.7%)                        |         |                   |
| <b>Vital symptoms</b>             |                                     |                                    |         |                   |
| Pulse rate (per min)              |                                     |                                    |         |                   |
| Mean (SD)                         | 98.1 (20.3)                         | 96.0 (16.4)                        | 0.294   | –                 |
| Respiratory rate (per min)        |                                     |                                    |         |                   |
| Mean (SD)                         | 23.2 (5.48)                         | 21.9 (5.19)                        | 0.019   | –                 |
| Oxygen saturation (%)             |                                     |                                    |         |                   |
| Mean (SD)                         | 86.8 (8.39)                         | 89.3 (7.19)                        | 0.003   | –                 |
| Systolic blood pressure (mmHg)    |                                     |                                    |         |                   |
| Mean (SD)                         | 139 (24.4)                          | 133 (19.5)                         | 0.016   | –                 |
| Diastolic blood pressure (mmHg)   |                                     |                                    |         |                   |
| Mean (SD)                         | 83.1 (15.3)                         | 82.0 (28.5)                        | 0.559   | –                 |
| <b>Laboratory findings</b>        |                                     |                                    |         |                   |
| White blood cell count (× 10e9/L) |                                     |                                    |         |                   |
| Mean (SD)                         | 9.71 (8.16)                         | 6.13 (3.01)                        | <0.001  | –                 |
| Neutrophil count (× 10e9/L)       |                                     |                                    |         |                   |
| Mean (SD)                         | 7.51 (14.5)                         | 7.35 (11.2)                        | 0.247   | –                 |
| Lymphocyte count (× 10e9/L)       |                                     |                                    |         |                   |
| Mean (SD)                         | 1.76 (11.10)                        | 2.07 (9.65)                        | 0.006   | –                 |
| Platelet count (× 10e9/L)         |                                     |                                    |         |                   |
| Mean (SD)                         | 203 (91.7)                          | 191 (70.9)                         | 0.186   | –                 |

(Continued)

**TABLE 1 |** Continued

|                   | Non-COVID<br>pneumonia<br>(N = 118) | COVID-19<br>pneumonia<br>(N = 634) | P-value | OR<br>(CI 95%) |
|-------------------|-------------------------------------|------------------------------------|---------|----------------|
| Hemoglobin (g/dL) |                                     |                                    |         |                |
| Mean (SD)         | 12.7 (2.48)                         | 13.3 (1.75)                        | 0.018   | –              |
| CRP (mg/L)        |                                     |                                    |         |                |
| Mean (SD)         | 35.2 (21.9)                         | 35.3 (17.4)                        | 0.978   | –              |
| LDH (U/L)         |                                     |                                    |         |                |
| Mean (SD)         | 1,100<br>(1,050)                    | 886 (592)                          | 0.035   | –              |
| AST (U/L)         |                                     |                                    |         |                |
| Mean (SD)         | 60.4 (171)                          | 46.6 (46.3)                        | 0.386   | –              |
| ALT (U/L)         |                                     |                                    |         |                |
| Mean (SD)         | 60.1 (290)                          | 33.9 (44.5)                        | 0.328   | –              |
| ALP (U/L)         |                                     |                                    |         |                |
| Mean (SD)         | 192 (88.7)                          | 177 (96.0)                         | 0.101   | –              |
| Na (meq/L)        |                                     |                                    |         |                |
| Mean (SD)         | 136 (4.13)                          | 135 (3.38)                         | 0.011   | –              |
| K (mmol/L)        |                                     |                                    |         |                |
| Mean (SD)         | 3.92 (0.59)                         | 3.78 (0.42)                        | 0.019   | –              |
| Ca (mg/dL)        |                                     |                                    |         |                |
| Mean (SD)         | 8.72 (0.88)                         | 8.53 (0.70)                        | 0.030   | –              |
| P (mg/dL)         |                                     |                                    |         |                |
| Mean (SD)         | 3.35 (1.21)                         | 2.94 (0.73)                        | <0.001  | –              |
| Mg (mg/dL)        |                                     |                                    |         |                |
| Mean (SD)         | 1.94 (0.22)                         | 1.95 (0.24)                        | 0.914   | –              |
| BUN (mg/dL)       |                                     |                                    |         |                |
| Mean (SD)         | 23.80<br>(18.00)                    | 19.50<br>(13.60)                   | 0.016   | –              |
| Cr (mg/dL)        |                                     |                                    |         |                |
| Mean (SD)         | 1.43 (1.43)                         | 1.20 (0.99)                        | 0.093   | –              |
| PH                |                                     |                                    |         |                |
| Mean (SD)         | 7.33 (0.09)                         | 7.36 (0.06)                        | <0.001  | –              |
| PCO2 (mmHg)       |                                     |                                    |         |                |
| Mean (SD)         | 50.6 (15.8)                         | 44.4 (9.38)                        | <0.001  | –              |
| ESR (mm/h)        |                                     |                                    |         |                |
| Mean (SD)         | 42.3 (28.1)                         | 48.0 (26.4)                        | 0.045   | –              |

OR, odds ratio; CI, confidence interval.

were found in the variables age, gender, occupation, marriage status, symptom duration, contact with confirmed COVID-19 cases, history of ischemic heart disease, hypertension, chronic obstructive pulmonary disease (COPD), chronic respiratory disease, other comorbidities, body temperature, nausea, decreased appetite, weight loss, chills, headache, diarrhea, body pain, respiratory rate, oxygen saturation, systolic blood pressure, white blood cell count, lymphocyte count, hemoglobin, LDH, Na, K, Ca, P, BUN, PH, PCO2, and ESR among the patients with COVID and non-COVID pneumonia. Other comorbidities were defined as having comorbidities except for hypertension, diabetes, heart failure, percutaneous coronary intervention (PCI), coronary artery bypass graft (CABG), ischemic heart

**TABLE 2 |** Descriptive statistics of the dataset 2.

|                                      | Non-COVID<br>(N = 634) | COVID-19<br>(N = 634) | P-value | OR (CI 95%)           |
|--------------------------------------|------------------------|-----------------------|---------|-----------------------|
| Age category (years)                 |                        |                       |         |                       |
| >60                                  | 89 (14.0%)             | 276 (43.5%)           | <0.001  | 4.72<br>3.59–6.21     |
| ≤60                                  | 545 (86.0%)            | 358 (56.5%)           |         |                       |
| Gender                               |                        |                       |         |                       |
| Male                                 | 291 (45.9%)            | 389 (61.4%)           | <0.001  | 1.87<br>1.50–2.34     |
| Female                               | 343 (54.1%)            | 245 (38.6%)           |         |                       |
| Cough category                       |                        |                       |         |                       |
| Other                                | 600 (94.6%)            | 117 (18.5%)           | <0.001  | 0.01<br>0.01–0.02     |
| Dry                                  | 34 (5.4%)              | 517 (81.5%)           |         |                       |
| Shortness of breath                  |                        |                       |         |                       |
| Yes                                  | 1 (0.2%)               | 440 (69.4%)           | <0.001  | –                     |
| No                                   | 633 (99.8%)            | 194 (30.6%)           |         |                       |
| Headache                             |                        |                       |         |                       |
| Yes                                  | 1 (0.2%)               | 306 (48.3%)           | <0.001  | –                     |
| No                                   | 633 (99.8%)            | 328 (51.7%)           |         |                       |
| Sore throat                          |                        |                       |         |                       |
| Yes                                  | 3 (0.5%)               | 134 (21.1%)           | <0.001  | 56.37<br>17.84–178.06 |
| No                                   | 631 (99.5%)            | 500 (78.9%)           |         |                       |
| Fever (body temperature<br>> 37.5°C) |                        |                       |         |                       |
| Yes                                  | 14 (2.2%)              | 308 (48.6%)           | <0.001  | 41.84<br>24.09–72.68  |
| No                                   | 620 (97.8%)            | 326 (51.4%)           |         |                       |

disease (IHD), cardiovascular disease (CVD), chronic respiratory diseases (CRDs), COPD, being immunocompromised, cancer, chronic kidney disease (CKD), having organ transplantation, hyperkeratosis lenticularis perstans (HLP), end-stage renal disease (ESRD), and hypothyroidism.

The descriptive statistics of dataset 2 are provided in **Table 2** for the patients with COVID-19 and control subjects. All the variables had significant differences between the patients with COVID-19 and control subjects. Since the variables of the control group of dataset 3 were normalized (29, 34) and the original values were not available, a descriptive table was not provided for dataset 3.

The selected features of datasets 1, 2, and 3, and their importance (weights between zero and 1) by the proposed algorithm are listed in **Table 3**. The most important features were WBC, shortness of breath, and CRP in datasets 1, 2, and 3, respectively.

The performance of the proposed algorithm and the LDA classifier on datasets 1, 2, and 3 is shown in **Table 4**. Such indices were provided in the cross-validated confusion matrix. The system is clinically reliable on datasets 1 and 2, while it is not reliable on dataset 3 because of a Type I error of 0.1, false discovery rate (FDR) of 0.09, and DOR of 67.8. It showed



excellent balanced diagnosis accuracy ( $AUC \geq 0.9$ ), excellent class labeling agreement rate with the PCR test [ $K(c) \geq 0.75$ ], high/very high correlation between predicted and observed class

**TABLE 3 |** Selected features of datasets 1, 2, and 3, along with their importance (shown as weights between zero and 1) using the proposed algorithm.

| Dataset 1                                |        | Dataset 2           |        | Dataset 3   |        |
|--|--------|---------------------|--------|-------------|--------|
| Feature                                  | Weight | Feature             | Weight | Feature     | Weight |
| WBC                                      | 1.000  | Shortness of breath | 1.000  | CRP         | 1.000  |
| PCO2                                     | 0.995  | Cough details       | 0.539  | WBC         | 0.322  |
| Decreased appetite                       | 0.957  | Headache            | 0.111  | LDH         | 0.215  |
| Contact with conformed COVID-19 patients | 0.947  | Body temperature    | 0.034  | Neutrophils | 0.158  |
| Cough details                            | 0.914  | Age                 | 0.026  | PLT         | 0.157  |
| Other comorbidities                      | 0.901  | Sore throat         | 0.025  | Lymphocytes | 0.127  |
| <i>P</i>                                 | 0.882  | Gender              | 0.004  |             |        |
| Myalgia                                  | 0.862  |                     |        |             |        |
| Body temperature                         | 0.846  |                     |        |             |        |
| Chronic respiratory disease              | 0.825  |                     |        |             |        |
| Symptom duration                         | 0.819  |                     |        |             |        |
| COPD                                     | 0.782  |                     |        |             |        |
| Occupation                               | 0.780  |                     |        |             |        |
| Gender                                   | 0.777  |                     |        |             |        |
| Na                                       | 0.775  |                     |        |             |        |
| LDH                                      | 0.772  |                     |        |             |        |
| HB                                       | 0.748  |                     |        |             |        |
| Weight loss                              | 0.747  |                     |        |             |        |
| Chills                                   | 0.709  |                     |        |             |        |
| Diarrhea                                 | 0.674  |                     |        |             |        |
| ESR                                      | 0.625  |                     |        |             |        |
| SatO2                                    | 0.5928 |                     |        |             |        |

labels ( $MCC \geq 0.7$ ), and fair discriminant power ( $3 > DP \geq 2$ ) for datasets 1 and 2. Note that the performance of the proposed algorithm was significantly better than that of the LDA classifier on datasets 1 ( $P < 0.001$ ), 2 ( $P < 0.01$ ), and 3 ( $P < 0.001$ ). Moreover, the average performance of the proposed algorithm and the LDA classifier on the test folds is provided in **Table 5**, showing the reproducibility of the results.

Also, the random accuracy of the datasets was estimated by random assignment of classes, considering the prevalence of the minority class. Ten thousand simulations were performed. The range (mean) of the obtained random accuracies was 68–79 (74%), 43–56 (50%), and 44–56% (50%) for datasets 1, 2, and 3, respectively. The obtained accuracy of the proposed method and the LDA classifier was 96, 78 (dataset 1), 97, 96 (dataset 2), and 93, 56% (dataset 3) on the cross-validated confusion matrix. Except for the results of the LDA classifier on datasets 1 and 3, the other results were higher than the random classification thresholds.

## DISCUSSION

During the pandemic, morbidity and mortality can be reduced by early prediction of population infection risks, ensuring efficient treatment planning and resource allocation. A high patient load is prevented by rapid disease diagnosis. Higher mortality rates are an essential consequence of an overloaded medical system due to inefficient management of limited medical resources.

This study constructed a prediction model trained using the cohort in KCC. It accurately forecasted infection cases in comparison with both pneumonia (dataset 1) and healthy subjects (datasets 2 and 3) (**Table 4**). There are some studies in the literature for COVID-19 diagnosis (68). However, to the best of our knowledge, no similar study was performed to classify COVID-19 and non-COVID pneumonia, without using image processing methods on CT-scan results. Moreover, the cross-validation method used in our study guarded

**TABLE 4 |** Performance of the proposed algorithm and linear discriminant analysis (LDA) classifier on datasets 1, 2, and 3, based on the results of cross-validated confusion matrix.

| Dataset   | Classifier | Indices | Se        | Sp        | PPV       | NPV       | AUC       | MCC       | F <sub>1</sub> S | DOR            | DP        | K(c)      |
|-----------|------------|---------|-----------|-----------|-----------|-----------|-----------|-----------|------------------|----------------|-----------|-----------|
| Dataset 1 | Proposed   | Value   | 0.96      | 0.95      | 0.99      | 0.82      | 0.96      | 0.87      | 0.98             | 495.88         | 2.63      | 0.86      |
|           |            | CI 95%  | 0.94–0.98 | 0.90–0.99 | 0.98–1    | 0.76–0.89 | 0.94–0.97 | 0.85–0.88 | 0.95–1           | 197.46–1245.30 | 2.24–3.02 | 0.81–0.91 |
|           | LDA        | Value   | 0.81      | 0.61      | 0.92      | 0.37      | 0.71      | 0.35      | 0.86             | 6.57           | 0.80      | 0.33      |
|           |            | CI 95%  | 0.78–0.84 | 0.52–0.70 | 0.89–0.94 | 0.30–0.44 | 0.66–0.75 | 0.28–0.41 | 0.83–0.89        | 4.32–9.99      | 0.62–0.98 | 0.24–0.42 |
| Dataset 2 | Proposed   | Value   | 0.96      | 0.97      | 0.97      | 0.97      | 0.97      | 0.94      | 0.97             | 952.00         | 2.91      | 0.94      |
|           |            | CI 95%  | 0.95–0.98 | 0.96–0.98 | 0.96–0.98 | 0.95–0.98 | 0.96–0.98 | 0.93–0.94 | 0.96–0.98        | 505.57–1792.64 | 2.64–3.18 | 0.91–0.96 |
|           | LDA        | Value   | 0.94      | 0.97      | 0.97      | 0.94      | 0.95      | 0.90      | 0.95             | 422.20         | 2.57      | 0.90      |
|           |            | CI 95%  | 0.92–0.96 | 0.95–0.98 | 0.95–0.98 | 0.92–0.95 | 0.94–0.96 | 0.90–0.91 | 0.94–0.97        | 246.54–722.99  | 2.34–2.80 | 0.88–0.93 |
| Dataset 3 | Proposed   | Value   | 0.94      | 0.91      | 0.90      | 0.94      | 0.92      | 0.85      | 0.92             | 156.35         | 2.14      | 0.85      |
|           |            | 95% CI  | 0.92–0.96 | 0.89–0.93 | 0.88–0.93 | 0.93–0.96 | 0.91–0.94 | 0.83–0.86 | 0.90–0.94        | 101.03–241.33  | 1.96–2.33 | 0.82–0.88 |
|           | LDA        | Value   | 0.56      | 0.55      | 0.39      | 0.71      | 0.56      | 0.11      | 0.46             | 1.60           | 0.20      | 0.10      |
|           |            | CI 95%  | 0.51–0.61 | 0.52–0.59 | 0.35–0.43 | 0.68–0.75 | 0.52–0.60 | 0.01–0.17 | 0.42–0.50        | 1.26–2.02      | 0.10–0.30 | 0.05–0.16 |

CI, confidence interval; Se, sensitivity; Sp, specificity; PPV, positive predictive value; NPV, negative predictive value; AUC, area under the ROC; MCC, Matthews Correlation Coefficient; F<sub>1</sub>S, F<sub>1</sub> score; DOR, diagnostic odds ratio; DP, discriminant power; K(c), Cohen's Kappa.

**TABLE 5 |** Performance of the proposed algorithm and LDA classifier on datasets 1, 2, and 3 over the test folds during cross-validation in mean  $\pm$  standard deviation (SD).

| Dataset   | Indices classifier | Se              | Sp              | PPV             | NPV             | AUC             | MCC             | F <sub>1</sub> S | DOR                 | DP              | K(c)            |
|-----------|--------------------|-----------------|-----------------|-----------------|-----------------|-----------------|-----------------|------------------|---------------------|-----------------|-----------------|
| Dataset 1 | Proposed           | 0.96 $\pm$ 0.02 | 0.95 $\pm$ 0.04 | 0.99 $\pm$ 0.01 | 0.83 $\pm$ 0.06 | 0.96 $\pm$ 0.02 | 0.87 $\pm$ 0.05 | 0.98 $\pm$ 0.01  | 423.18 $\pm$ 279.76 | 2.51 $\pm$ 0.30 | 0.86 $\pm$ 0.05 |
|           | LDA                | 0.79 $\pm$ 0.02 | 0.62 $\pm$ 0.03 | 0.92 $\pm$ 0.01 | 0.35 $\pm$ 0.03 | 0.70 $\pm$ 0.02 | 0.33 $\pm$ 0.04 | 0.85 $\pm$ 0.01  | 6.17 $\pm$ 1.35     | 0.77 $\pm$ 0.09 | 0.31 $\pm$ 0.04 |
| Dataset 2 | Proposed           | 0.96 $\pm$ 0.02 | 0.97 $\pm$ 0.02 | 0.97 $\pm$ 0.02 | 0.96 $\pm$ 0.02 | 0.97 $\pm$ 0.01 | 0.94 $\pm$ 0.02 | 0.97 $\pm$ 0.01  | 1050.30             | 2.95 $\pm$ 0.07 | 0.94 $\pm$ 0.02 |
|           | LDA                | 0.97 $\pm$ 0.02 | 0.94 $\pm$ 0.03 | 0.94 $\pm$ 0.02 | 0.97 $\pm$ 0.02 | 0.95 $\pm$ 0.01 | 0.90 $\pm$ 0.03 | 0.95 $\pm$ 0.01  | 440.60 $\pm$ 29.35  | 2.58 $\pm$ 0.03 | 0.90 $\pm$ 0.03 |
| Dataset 3 | Proposed           | 0.90 $\pm$ 0.04 | 0.94 $\pm$ 0.02 | 0.94 $\pm$ 0.02 | 0.91 $\pm$ 0.03 | 0.92 $\pm$ 0.02 | 0.85 $\pm$ 0.04 | 0.92 $\pm$ 0.2   | 258.38 $\pm$ 328.30 | 2.20 $\pm$ 0.31 | 0.85 $\pm$ 0.04 |
|           | LDA                | 0.39 $\pm$ 0.06 | 0.71 $\pm$ 0.08 | 0.57 $\pm$ 0.07 | 0.55 $\pm$ 0.03 | 0.55 $\pm$ 0.04 | 0.11 $\pm$ 0.09 | 0.46 $\pm$ 0.6   | 1.78 $\pm$ 0.82     | 0.20 $\pm$ 0.18 | 0.11 $\pm$ 0.09 |

CI, confidence interval; Se, sensitivity; Sp, specificity; PPV, positive predictive value; NPV, negative predictive value; AUC, area under the ROC; MCC, Matthews Correlation Coefficient; F<sub>1</sub>S, F<sub>1</sub> score; DOR, diagnostic odds ratio; DP, discriminant power; K(c), Cohen's Kappa.

against testing hypotheses suggested by the data [type III errors (69)].

The combination of the PCR and CT-scan results was used as the ground truth in our study. It was shown that the PCR test is not 100% correct to be considered as gold standard (70). Mainly, it was shown to have a false negative rate (FNR) ranging from 0.018 to 0.58, with a median of 0.11 (71), in addition to a sensitivity of 83.3% (15). It was recommended to combine the results of PCR and CT-scan with improving the ground truth for COVID-19, mainly to improve the FNR of the PCR test (72, 73).

Notably, three different datasets related to control individuals in comparison with our COVID-19 dataset were observed in this analysis.

In the first round, COVID-19 diagnosis compared with pneumonia model performance showed very good results using 22 pre-admission and hospital-based characteristics (Table 4). The analyses of this study highlighted three non-invasive features: WBC (weight of 1), PCO<sub>2</sub> (0.99), and contact with confirmed COVID-19 cases (0.95).

However, CT scan has become the primary gold standard for screening COVID-19 cases; however, it cannot be used to identify specific viral infections (74). Furthermore, some patients with COVID-19 can also present with standard CT imaging in the early stage (74). Thus, clinical symptoms, pre-admission variables, and laboratory tests can be more specific for early COVID-19 infection. According to studies, the most common early symptoms of COVID-19 were cough, fever, myalgia, and diarrhea (75). The results of weighted features in our study presented that cough ( $w = 0.91$ ) and myalgia ( $w = 0.86$ ) were the two most essential symptom predictors after decreased appetite.

There are some studies in the literature that used similar features for COVID-19 diagnosis. Long et al. (6) reported that WBC and body temperature were good factors in uncovering the COVID-19 infection. Another study by Brinati et al. (18) also showed that LDH and WBC were essential features. Moreover, Gongj and Qiu (76) illustrated that LDH was one of the good features for predicting severe COVID-19. Likewise, Goodman-Meza et al. (19) reported gender, HB, and LDH as essential features related to COVID-19 infection.

In the second round, we developed our predictive models for diagnosing patients with COVID-19 and healthy control subjects with the eight standard non-invasive features used in Zoabi et al.

(21). Our joint model provides rapid and accurate predictions using seven features. While shortness of breath ( $w = 1$ ) and cough details ( $w = 0.54$ ), were the most critical features in our analysis for dataset 2 (Table 3), cough details and fever were the essential features in Zoabi et al. (21). In fact, the performance of the proposed method was higher in dataset two compared with dataset 1 in almost all the indices (Table 4), knowing that only eight demographic and symptom features were used in dataset 2 compared with the 22 selected features in dataset 1 (Table 3). It primarily showed that the classification of COVID-19 was more difficult with non-COVID pneumonia (dataset 1) compared with healthy control subjects (dataset 2). In fact, when we used reduced feature sets for dataset 1, the performance significantly dropped. Also, comparing datasets 1 and 2, shortness of breath and sore throat were not statistically significant between COVID-19 and non-COVID-19 pneumonia (Table 1), while they were statistically significant between COVID-19 and healthy control subjects (Table 2). It showed the similarity of the characteristics of dataset 1 compared with dataset 2 for standard features.

In the last round, using another dataset related to six invasive laboratory variables (29, 34), our results revealed that invasive features showed an overall good prediction capacity between COVID-19 patients and healthy people (Table 4). However, the results were not as good as those obtained on datasets 1 and 2, showing that symptoms added valuable information to blood tests for screening. Moreover, among the six variables, neutrophil, platelet counts, and CRP were not statistically significant in dataset 1 (Table 1), showing that patients with COVID-19 and non-COVID-19 pneumonia showed similar features based on 50% of the laboratory variables used in dataset 3. This difference in prediction criteria reached lower sensitivity, specificity, and AUC using invasive characteristics compared with the model using non-invasive variables. It might be because invasive biomarkers have a distinct temporal dynamic behavior (13).

Both CT-scan and laboratory-based methods share the main limitation when applied to the population. For cases such as COVID-19 infection, where the prevalence of the disease (i.e., the minority class) is low in the population, the performance of the diagnosis methods drops. It happens especially when the analyzed imbalanced test datasets are balanced. For example, Sun et al. designed a diagnosis method based on CT-scan image

processing and reached 93 and 90% sensitivity and specificity, respectively, to discriminate between COVID and non-COVID pneumonia (25). Considering the prevalence of 14% of COVID-19 (77), it is possible to use Bayes' theorem to predict the true PPV and NPV of the diagnosis method when applied to the population (Equations 11, 12) (78):

$$PPV = \frac{Se \times P}{Se \times P + (1 - Sp) \times (1 - P)} \quad (11)$$

$$NPV = \frac{Sp \times (1 - P)}{Sp \times (1 - P) + (1 - Se) \times P} \quad (12)$$

where  $P$  is the prevalence of COVID-19. The parameter PPV is also the probability of having COVID-19 when the proposed diagnosis test is positive. Similarly, NPV is the probability of not having COVID-19 when the proposed diagnosis test is negative. For this example, the estimated PPV and NPV were 60 and 99%. When examining our proposed method, the true PPV and NPV were 75 and 99%. Thus, the performance of the proposed method must be improved to be used in clinical practice. Noted that such a problem is similar to many other areas in which the prevalence of the minority class is very low (79).

Indeed, key laboratory features, such as LDH, CRP, WBC, and PLT, have high temporal dynamicity, and in a relatively short time, they rise and return to their normal range (80). Additionally, laboratory variable abnormalities only show disruptions in body systems linked to many infectious diseases. In contrast, many non-invasive features, such as symptoms and age, contain a substantial amount of less dynamic data.

We proposed that a prediction model can be used for risk assessment to notify high-risk subjects for receiving the complementary RT-PCR test. A promising area for future research is to analyze the combined performance of the new rapid clinical application diagnosis system, machine learning algorithms, and new biomarkers (81).

Nevertheless, this study still had several limitations. First, the major participants were from Isfahan province. Furthermore, nationwide studies are needed to access the best generality of the suggested model. Moreover, because of the inaccessibility of the data of healthy control subjects, control subjects from other studies (21, 29) were also used in datasets 2 and 3. The KCC dataset was mainly limited to alpha variants of COVID-19 (32), and it is necessary to perform extra validation on other mutants to assess its performance (82). Also, preparing the COVID-19 diagnosis risk chart, which is a valuable tool, is the focus of our feature study. Finally, the RT-PCR and chest CT-scan used as gold standard are not 100% accurate, and the agreement rate (Cohen's Kappa) reported in the study is, thus, a better index than traditional predictive indices (83).

## CONCLUSION

In conclusion, we designed a reliable computer-aided diagnosis system to classify patients with COVID-19 from non-COVID

pneumonia. Demographics, symptoms, and blood tests were used in the proposed system. The proposed system is a promising screening tool for COVID-19.

## DATA AVAILABILITY STATEMENT

The datasets presented in this study can be found in online repositories. The names of the repository/repositories and accession number(s) can be found at: <https://doi.org/10.6084/m9.figshare.16682422>.

## ETHICS STATEMENT

The studies involving human participants were reviewed and approved by the Ethics Committee of the Isfahan University of Medical Sciences (IUMS). The patients/participants provided their written informed consent to participate in this study.

## AUTHOR CONTRIBUTIONS

HM, FZ, MRM, RS, MM, MAM, MW, and HB participated in conceptualization, investigation, and methodology. HM, FZ, and MRM participated in visualization, software, and validation. RS, SHJ, MM, MAM, MW, and HB participated in project administration. HM, FZN, MRM, and MM participated in formal analysis. RS, SHJ, MM, FDN, and MA-S participated in data acquisition. FDN, MA-S, and RS participated in data curation. RS, SHJ, MM, and MAM participated in funding acquisition. MM, MAM, and RS participated in supervision. MM, RS, HB, MAM, and MW participated in the interpretation of the results. HM, FZN, MRM, MM, and MW participated in writing—original draft, while RS, SHJ, FDN, MA-S, MAM, and HB participated in writing—review and editing. All authors read and approved the final manuscript and agreed to be accountable for all aspects of this study.

## FUNDING

The research that led these results has received funding from the European Union's Horizon 2020 Research and Innovation Programme under the Marie Skłodowska-Curie Grant Agreement No. 712949 (TECNIOspring PLUS), and from the Agency for Business Competitiveness of the Government of Catalonia (TECSPR18-1-0017). The TECSPR18-1-0017 project provided the APC. These funders had no role in study design, data collection, analysis, decision to publish, or manuscript preparation.

## ACKNOWLEDGMENTS

We would like to acknowledge the Khorshid Hospital nurses and interns for this study, who recruited patients and collected follow-up data. Most importantly, we would like to acknowledge all the patients who consented to participate in this study.

## REFERENCES

- Jones DS. History in a crisis—lessons for Covid-19. *N Engl J Med.* (2020) 382:1681–3. doi: 10.1056/NEJMp2004361
- He H, Harris L. The impact of Covid-19 pandemic on corporate social responsibility and marketing philosophy. *J Bus Res.* (2020) 116:176–82. doi: 10.1016/j.jbusres.2020.05.030
- Xiong J, Lipsitz O, Nasri F, Lui LMW, Gill H, Phan L, et al. Impact of COVID-19 pandemic on mental health in the general population: a systematic review. *J Affect Disord.* (2020) 277:55–64. doi: 10.1016/j.jad.2020.08.001
- Zhao D, Yao F, Wang L, Zheng L, Gao Y, Ye J, et al. A comparative study on the clinical features of coronavirus 2019 (COVID-19) pneumonia with other pneumonias. *Clin Infect Dis.* (2020) 71:756–61. doi: 10.1093/cid/ciaa247
- Fang Y, Zhang H, Xie J, Lin M, Ying L, Pang P, et al. Sensitivity of chest CT for COVID-19: comparison to RT-PCR. *Radiology.* (2020) 296:E115–7. doi: 10.1148/radiol.202000432
- Long DR, Gombor S, Hogan CA, Greninger AL, O'reilly-Shah V, Bryson-Cahn C, et al. Occurrence and timing of subsequent severe acute respiratory syndrome coronavirus 2 reverse-transcription polymerase chain reaction positivity among initially negative patients. *Clin Infect Dis.* (2021) 72:323–326.
- Charlson ME, Pompei P, Ales KL, Mackenzie CR. A new method of classifying prognostic comorbidity in longitudinal studies: development and validation. *J Chronic Dis.* (1987) 40:373–83. doi: 10.1016/0021-9681(87)90171-8
- Docherty AB, Harrison EM, Green CA, Hardwick HE, Pius R, Norman L, et al. Features of 20 133 UK patients in hospital with covid-19 using the ISARIC WHO clinical characterisation protocol: prospective observational cohort study. *BMJ.* (2020) 369:m1985. doi: 10.1101/2020.04.23.20076042
- Guan WJ, Ni ZY, Hu Y, Liang WH, Ou CQ, He JX, et al. Clinical characteristics of coronavirus disease 2019 in China. *N Engl J Med.* (2020) 382:1708–20. doi: 10.1056/NEJMoa2002032
- Kermali M, Khalsa RK, Pillai K, Ismail Z, Harky A. The role of biomarkers in diagnosis of COVID-19—a systematic review. *Life Sci.* (2020) 254:117788. doi: 10.1016/j.lfs.2020.117788
- Sun L, Song F, Shi N, Liu F, Li S, Li P, et al. Combination of four clinical indicators predicts the severe/critical symptom of patients infected COVID-19. *J Clin Virol.* (2020) 128:104431. doi: 10.1016/j.jcv.2020.104431
- Wang D, Hu B, Hu C, Zhu F, Liu X, Zhang J, et al. Clinical characteristics of 138 hospitalized patients with 2019 novel coronavirus-infected pneumonia in Wuhan, China. *JAMA.* (2020) 323:1061–9. doi: 10.1001/jama.2020.1585
- Cerdà P, Ribas J, Iriarte A, Mora-Luján JM, Torres R, Del Río B, et al. Blood test dynamics in hospitalized COVID-19 patients: potential utility of D-dimer for pulmonary embolism diagnosis. *PLoS ONE.* (2021) 15:e0243533. doi: 10.1371/journal.pone.0243533
- Petrone L, Petruccioli E, Vanini V, Cuzzi G, Najafi Fard S, Alonzi T, et al. A whole blood test to measure SARS-CoV-2-specific response in COVID-19 patients. *Clin Microbiol Infect.* (2021) 27:286.e287–213. doi: 10.1016/j.cmi.2020.09.051
- Long C, Xu H, Shen Q, Zhang X, Fan B, Wang C, et al. Diagnosis of the coronavirus disease (COVID-19): rRT-PCR or CT? *Eur J Radiol.* (2020) 126:108961. doi: 10.1016/j.ejrad.2020.108961
- Chen Z, Li Y, Wu B, Hou Y, Bao J, Deng X. A patient with COVID-19 presenting a false-negative reverse transcriptase polymerase chain reaction result. *Korean J Radiol.* (2020) 21:623. doi: 10.3348/kjr.2020.0195
- Winichakoon P, Chaiwarith R, Liwsrisakun C, Salee P, Goonna A, Limsukon A, et al. Negative nasopharyngeal and oropharyngeal swabs do not rule out COVID-19. *J Clin Microbiol.* (2020) 58:e00297–20. doi: 10.1128/JCM.00297-20
- Brinati D, Campagner A, Ferrari D, Locatelli M, Banfi G, Cabitza F. Detection of COVID-19 infection from routine blood exams with machine learning: a feasibility study. *J Med Syst.* (2020) 44:1–12. doi: 10.1007/s10916-020-01597-4
- Goodman-Meza D, Rudas A, Chiang JN, Adamson PC, Ebinger J, Sun N, et al. A machine learning algorithm to increase COVID-19 inpatient diagnostic capacity. *PLoS ONE.* (2020) 15:e0239474. doi: 10.1371/journal.pone.0239474
- Kamalov F, Cherukuri A, Sulieman H, Thabtah F, Hossain A. Machine learning applications for COVID-19: a state-of-the-art review. *arXiv [preprint] arXiv:2101.07824v1* (2021).
- Zoabi Y, Deri-Rozov S, Shomron N. Machine learning-based prediction of COVID-19 diagnosis based on symptoms. *NPJ Digital Med.* (2021) 4:1–5. doi: 10.1038/s41746-020-00372-6
- Apostolopoulos ID, Mpesiana TA. Covid-19: automatic detection from x-ray images utilizing transfer learning with convolutional neural networks. *Phys Eng Sci Med.* (2020) 43:635–40. doi: 10.1007/s13246-020-00865-4
- Li L, Qin L, Xu Z, Yin Y, Wang X, Kong B, et al. Using artificial intelligence to detect COVID-19 and community-acquired pneumonia based on pulmonary CT: evaluation of the diagnostic accuracy. *Radiology.* (2020) 296:E65–71. doi: 10.1148/radiol.202000905
- Nour M, Cömert Z, Polat K. A novel medical diagnosis model for COVID-19 infection detection based on deep features and Bayesian optimization. *Appl Soft Comput.* (2020) 97:106580. doi: 10.1016/j.asoc.2020.106580
- Sun L, Mo Z, Yan F, Xia L, Shan F, Ding Z, et al. Adaptive feature selection guided deep forest for covid-19 classification with chest ct. *IEEE J Biomed Health Informatics.* (2020) 24:2798–805. doi: 10.1109/JBHI.2020.3019505
- Zhang K, Liu X, Shen J, Li Z, Sang Y, Wu X, et al. Clinically applicable AI system for accurate diagnosis, quantitative measurements, and prognosis of COVID-19 pneumonia using computed tomography. *Cell.* (2020) 181:1423–33. e1411. doi: 10.1016/j.cell.2020.04.045
- Liang X, Zhang Y, Wang J, Ye Q, Liu Y, Tong J. Diagnosis of COVID-19 pneumonia based on graph convolutional network. *Front Med.* (2021) 7:612962. doi: 10.3389/fmed.2020.612962
- Ke G, Meng Q, Finley T, Wang T, Chen W, Ma W, et al. Lightgbm: a highly efficient gradient boosting decision tree. *Adv Neural Inf Process Syst.* (2017) 30:3146–54. doi: 10.5555/3294996.3295074
- Banerjee A, Ray S, Vorselaars B, Kitson J, Mamalakakis M, Weeks S, et al. Use of machine learning and artificial intelligence to predict SARS-CoV-2 infection from full blood counts in a population. *Int Immunopharmacol.* (2020) 86:106705. doi: 10.1016/j.intimp.2020.106705
- Feng C, Wang L, Chen X, Zhai Y, Zhu F, Chen H, et al. A novel triage tool of artificial intelligence-assisted diagnosis aid system for suspected COVID-19 pneumonia in fever clinics. *medRxiv.* (2021) 9:201. doi: 10.2139/ssrn.3551355
- Wu J, Zhang P, Zhang L, Meng W, Li J, Tong C, et al. Rapid and accurate identification of COVID-19 infection through machine learning based on clinical available blood test results. *medRxiv.* (2020). doi: 10.1101/2020.04.02.20051136
- Sami R, Soltaninejad F, Amra B, Naderi Z, Haghighi Javanmard S, Iraj B, et al. A one-year hospital-based prospective COVID-19 open-cohort in the Eastern Mediterranean region: the Khorshid COVID Cohort (KCC) study. *PLoS ONE.* (2020) 15:e0241537. doi: 10.1371/journal.pone.0241537
- Covid19\_Government\_Dataset. *Covid-19 Government Data, Tested by PCR and Case Symptoms.* Israeli Ministry of Health (2020). Available online at: <https://data.gov.il/dataset/covid-19> (accessed October 26, 2021).
- Diagnosis of Covid-19 and Its Clinical Spectrum. (2020). Available online at: <https://www.kaggle.com/einsteindata4u/covid19> (accessed October 26, 2021).
- Vedaei SS, Fotovat A, Mohebbian MR, Rahman GME, Wahid KA, Babyn P, et al. COVID-SAFE: an IoT-based system for automated health monitoring and surveillance in post-pandemic Life. *IEEE Access.* (2020) 8:188538–51. doi: 10.1109/ACCESS.2020.3030194
- Marateb HR, Von Cube M, Sami R, Javanmard SH, Mansourian M, Amra B, et al. Absolute mortality risk assessment of COVID-19 patients: the Khorshid COVID Cohort (KCC) Study. *BMC Med Res Methodol.* (2021) 21:146. doi: 10.1186/s12874-021-01340-8
- Jernigan DB, CDC COVID-19 Response Team. Update: public health response to the coronavirus disease 2019 outbreak—United States, February 24, 2020. *Morbidity Mortal Wkly Rep.* (2020) 69:216. doi: 10.15585/mmwr.mm6908e1
- Troyanskaya O, Cantor M, Sherlock G, Brown P, Hastie T, Tibshirani R, et al. Missing value estimation methods for DNA microarrays. *Bioinformatics.* (2001) 17:520–5. doi: 10.1093/bioinformatics/17.6.520
- Pedregosa F, Varoquaux G, Gramfort A, Michel V, Thirion B, Grisel O, et al. Scikit-learn: machine learning in Python. *J Machine Learn Res.* (2011) 12:2825–30.



40. Marateb HR, Mansourian M, Adibi P, Farina D. Manipulating measurement scales in medical statistical analysis and data mining: a review of methodologies. *J Res Med Sci.* (2014) 19:47.
41. Hancock JT, Khoshgoftaar TM. Survey on categorical data for neural networks. *J Big Data.* (2020) 7:28. doi: 10.1186/s40537-020-00305-w
42. Meinshausen N, Bühlmann P. Stability selection. *J R Stat Soc Ser B.* (2010) 72:417–73. doi: 10.1111/j.1467-9868.2010.00740.x
43. Shah RD, Samworth RJ. Variable selection with error control: another look at stability selection. *J R Stat Soc Ser B.* (2013) 75:55–80. doi: 10.1111/j.1467-9868.2011.01034.x
44. Pregibon D. Logistic regression diagnostics. *Ann Stat.* (1981) 9:705–24. doi: 10.1214/aos/1176345513
45. He H, Bai Y, Garcia EA, Li S. ADASYN: adaptive synthetic sampling approach for imbalanced learning. In: *2008 IEEE International Joint Conference on Neural Networks (IEEE World Congress on Computational Intelligence)*. Hong Kong: IEEE (2008). p. 1322–8.
46. Lemaitre G, Nogueira F, Aridas CK. Imbalanced-learn: a python toolbox to tackle the curse of imbalanced datasets in machine learning. *J Machine Learn Res.* (2017) 18:559–63.
47. Friedman JH. Greedy function approximation: a gradient boosting machine. *Ann Stat.* (2001) 29:1189–232. doi: 10.1214/aos/1013203451
48. Hastie T, Tibshirani R, Friedman J, editors. Boosting and additive trees. In: *The Elements of Statistical Learning: Data Mining, Inference, and Prediction*. New York, NY: Springer New York (2009). p. 337–87.
49. Friedman JH. Stochastic gradient boosting. *Comput Stat Data Anal.* (2002) 38:367–78. doi: 10.1016/S0167-9473(01)00065-2
50. Seni G, Elder JF. Ensemble methods in data mining: improving accuracy through combining predictions. *Synthesis Lectures Data Mining Knowl Discov.* (2010) 2:1–126. doi: 10.2200/S00240ED1V01Y200912DMK002
51. Chen T, Guestrin C. Xgboost: a scalable tree boosting system. In: *Proceedings of the 22nd ACM SIGKDD International Conference on Knowledge Discovery and Data Mining*. San Francisco, CA (2016). p. 785–94.
52. Friedman J, Hastie T, Tibshirani R. Additive logistic regression: a statistical view of boosting (with discussion and a rejoinder by the authors). *Ann Stat.* (2000) 28:337–407; 371. doi: 10.1214/aos/1016218223
53. Platt J. Probabilistic outputs for support vector machines and comparisons to regularized likelihood methods. *Adv Large Margin Classifiers.* (1999) 10:61–74.
54. Šimundić A-M. Measures of diagnostic accuracy: basic definitions. *Ejifcc.* (2009) 19:203.
55. Boughorbel S, Jarray F, El-Anbari M. Optimal classifier for imbalanced data using Matthews Correlation Coefficient metric. *PLoS ONE.* (2017) 12:e0177678. doi: 10.1371/journal.pone.0177678
56. Fleiss JL, Levin B, Paik MC. *Statistical Methods for Rates and Proportions*. West Sussex: John Wiley & Sons (2013).
57. Sokolova M, Japkowicz N, Szpakowicz S. Beyond accuracy, F-score and ROC: a family of discriminant measures for performance evaluation. In: *Australasian Joint Conference on Artificial Intelligence*. Hobart, TAS: Springer (2006). p. 1015–21.
58. Mert A, Kiliç N, Bilgili E, Akan A. Breast cancer detection with reduced feature set. *Comput Math Methods Med.* (2015) 2015:265138. doi: 10.1155/2015/265138
59. Marateb HR, Mohebian MR, Javanmard SH, Tavallaei AA, Tajadini MH, Heidari-Beni M, et al. Prediction of dyslipidemia using gene mutations, family history of diseases and anthropometric indicators in children and adolescents: the CASPIAN-III study. *Comput Struct Biotechnol J.* (2018) 16:121–30. doi: 10.1016/j.csbj.2018.02.009
60. Bossuyt PM, Reitsma JB, Bruns DE, Gatsonis CA, Glasziou PP, Irwig L, et al. STARD 2015: an updated list of essential items for reporting diagnostic accuracy studies. *Clin Chem.* (2015) 61:1446–52. doi: 10.1373/clinchem.2015.246280
61. Collins GS, Reitsma JB, Altman DG, Moons KG. Transparent reporting of a multivariable prediction model for individual prognosis or diagnosis (TRIPOD): the TRIPOD statement. *J Br Surg.* (2015) 102:148–58. doi: 10.1002/bjs.9736
62. Mansourian M, Marateb HR, Mansourian M, Mohebbian MR, Binder H, Mañanas MÁ. Rigorous performance assessment of computer-aided medical diagnosis and prognosis systems: a biostatistical perspective on data mining. In: Bajaj V, Sinha GR, editors. *Modelling and Analysis of Active Biopotential Signals in Healthcare*, Vol. 2. IOP Publishing (2020). p. 17–24.
63. Ellis PD. *The Essential Guide to Effect Sizes: Statistical Power, Meta-Analysis, and the Interpretation of Research Results*. Cambridge: Cambridge University Press (2010).
64. Colquhoun D. An investigation of the false discovery rate and the misinterpretation of p-values. *R Soc Open Sci.* (2014) 1:140216. doi: 10.1098/rsos.140216
65. Ghosh AK. *Mayo Clinic Internal Medicine Review*. Boca Raton, FL: CRC Press (2008).
66. Dietterich TG. Approximate statistical tests for comparing supervised classification learning algorithms. *Neural Comput.* (1998) 10:1895–923. doi: 10.1162/089976698300017197
67. Webb AR, Copsey KD, editors. Performance assessment. In: *Statistical Pattern Recognition*. West Sussex: John Wiley & Sons, Ltd (2011). p. 404–32.
68. Marateb HR, Mohebbian MR, Shirzadi M, Mirshamsi A, Zamani S, Abrisham Chi A, et al. Reliability of machine learning methods for diagnosis and prognosis during the COVID-19 pandemic: a comprehensive critical review. In: Bajaj V, Ansari IA, editors. *High Performance Computing for Intelligent Medical Systems*. IOP Publishing (2021). p. 5–25.
69. Mosteller F. A k-sample slippage test for an extreme population. In: Fienberg SE, Hoaglin DC, editors. *Selected Papers of Frederick Mosteller*. New York, NY: Springer New York (2006). p. 101–9.
70. Mansourian M, Marateb HR, Von Cube M, Khademi S, Jordanic M, Mañanas MÁ, et al. Reliable diagnosis and prognosis of COVID-19. In: Bajaj V, Sinha GR, editors. *Computer-Aided Design and Diagnosis Methods for Biomedical Applications*. Boca Raton, FL: CRC Press (2021). p. 319–40.
71. Arevalo-Rodriguez I, Buitrago-García D, Simancas-Racines D, Zambrano-Achig P, Del Campo R, Ciapponi A, et al. False-negative results of initial RT-PCR assays for COVID-19: a systematic review. *PLoS ONE.* (2020) 15:e0242958. doi: 10.1371/journal.pone.0242958
72. Hossein H, Ali KM, Hosseini M, Sarveazad A, Safari S, Yousefifard M. Value of chest computed tomography scan in diagnosis of COVID-19; a systematic review and meta-analysis. *Clin Transl Imaging.* (2020) 8:469–81. doi: 10.1007/s40336-020-00387-9
73. Kovács A, Palásti P, Veréb D, Bozsik B, Palkó A, Kincses ZT. The sensitivity and specificity of chest CT in the diagnosis of COVID-19. *Eur Radiol.* (2021) 31:2819–24. doi: 10.1007/s00330-020-07347-x
74. Chung M, Bernheim A, Mei X, Zhang N, Huang M, Zeng X, et al. CT imaging features of 2019 novel coronavirus (2019-nCoV). *Radiology.* (2020) 295:202–7. doi: 10.1148/radiol.2020200230
75. Han C, Duan C, Zhang S, Zhang S, Spiegel B, Shi H, Wang W, et al. Digestive symptoms in COVID-19 patients with mild disease severity: clinical presentation, stool viral RNA testing, and outcomes. *Am J Gastroenterol.* (2020) 115:916–23. doi: 10.14309/ajg.0000000000000664
76. Gongji OJ, Qiu X. A tool to early predict severe corona virus disease 2019 (COVID-19): a multicenter study using the risk nomogram in Wuhan and Guangdong, China. *Clin Infect Dis.* (2020) 71:833–40. doi: 10.1093/cid/cia443
77. Jia Z, Yan X, Gao L, Ding S, Bai Y, Zheng Y, et al. Comparison of clinical characteristics among COVID-19 and non-COVID-19 pediatric pneumonias: a multicenter cross-sectional study. *Front Cell Infect Microbiol.* (2021) 11:663884. doi: 10.3389/fcimb.2021.663884
78. Mohebian MR, Marateb HR, Mansourian M, Mañanas MA, Mokarian F. A hybrid computer-aided-diagnosis system for prediction of breast cancer recurrence (HPBCR) using optimized ensemble learning. *Comput Struct Biotechnol J.* (2017) 15:75–85. doi: 10.1016/j.csbj.2016.11.004
79. Mansourian M, Khademi S, Marateb HR. A comprehensive review of computer-aided diagnosis of major mental and neurological disorders and suicide: a biostatistical perspective on data mining. *Diagnostics.* (2021) 11:393. doi: 10.3390/diagnostics11030393
80. Kotas ME, Medzhitov R. Homeostasis, inflammation, disease susceptibility. *Cell.* (2015) 160:816–27. doi: 10.1016/j.cell.2015.02.010
81. Kukar M, Gunčar G, Vovko T, Podnar S, Cernelc P, Brvar M, et al. COVID-19 diagnosis by routine blood tests using machine learning. *Sci Rep.* (2021) 11:10738. doi: 10.1038/s41598-021-90265-9



82. Twohig KA, Nyberg T, Zaidi A, Thelwall S, Sinnathamby MA, Aliabadi S, et al. Hospital admission and emergency care attendance risk for SARS-CoV-2 delta (B. 1.617. 2) compared with alpha (B. 1.1. 7) variants of concern: a cohort study. *Lancet Infect Dis.* (2021) 27:S1473–3099. doi: 10.1016/S1473-3099(21)00475-8
83. Mansourian M, Marateb HR, Cube MV, Khademi S, Jordanic M, Mañanas MÁ, et al. Reliable diagnosis and prognosis of COVID-19. In: Bajaj V, Sinha GR, editors. *Computer-Aided Design and Diagnosis Methods for Biomedical Applications*. 1st ed. Boca Raton, FL: CRC Press (2021). p. 22.

**Conflict of Interest:** The authors declare that the research was conducted in the absence of any commercial or financial relationships that could be construed as a potential conflict of interest.

**Publisher's Note:** All claims expressed in this article are solely those of the authors and do not necessarily represent those of their affiliated organizations, or those of the publisher, the editors and the reviewers. Any product that may be evaluated in this article, or claim that may be made by its manufacturer, is not guaranteed or endorsed by the publisher.

Copyright © 2021 Marateb, Ziaie Nezhad, Mohebian, Sami, Haghooy Javanmard, Dehghan Niri, Akafzadeh-Savari, Mansourian, Mañanas, Wolkewitz and Binder. This is an open-access article distributed under the terms of the Creative Commons Attribution License (CC BY). The use, distribution or reproduction in other forums is permitted, provided the original author(s) and the copyright owner(s) are credited and that the original publication in this journal is cited, in accordance with accepted academic practice. No use, distribution or reproduction is permitted which does not comply with these terms.



# Assessment of Sequelae of COVID-19 Nearly 1 Year After Diagnosis

Fangyuan Zhou<sup>1†</sup>, Meihui Tao<sup>2†</sup>, Luorui Shang<sup>1†</sup>, Yuhao Liu<sup>1</sup>, Guangtao Pan<sup>1</sup>, Yan Jin<sup>3</sup>, Li Wang<sup>3</sup>, Shaokun Hu<sup>4</sup>, Jinxiao Li<sup>1</sup>, Mengqi Zhang<sup>1</sup>, Yu Fu<sup>2\*</sup> and Shenglan Yang<sup>1\*</sup>

<sup>1</sup> Department of Traditional Chinese Medicine, Union Hospital, Tongji Medical College, Huazhong University of Science and Technology, Wuhan, China, <sup>2</sup> Department of Gastroenterology, Union Hospital, Tongji Medical College, Huazhong University of Science and Technology, Wuhan, China, <sup>3</sup> Department of Emergency, Union Hospital, Tongji Medical College, Huazhong University of Science and Technology, Wuhan, China, <sup>4</sup> Department of Medical Engineering, Union Hospital, Tongji Medical College, Huazhong University of Science and Technology, Wuhan, China

## OPEN ACCESS

### Edited by:

Reza Lashgari,  
Shahid Beheshti University, Iran

### Reviewed by:

Marc Emmenegger,  
University Hospital Zürich, Switzerland  
Talat Kilic,  
İnönü University, Turkey

### \*Correspondence:

Shenglan Yang  
yangshenglan@126.com  
Yu Fu  
futureyu@hust.edu.cn

<sup>†</sup>These authors have contributed  
equally to this work and share first  
authorship

### Specialty section:

This article was submitted to  
Pulmonary Medicine,  
a section of the journal  
Frontiers in Medicine

Received: 30 May 2021

Accepted: 25 October 2021

Published: 23 November 2021

### Citation:

Zhou F, Tao M, Shang L, Liu Y, Pan G,  
Jin Y, Wang L, Hu S, Li J, Zhang M,  
Fu Y and Yang S (2021) Assessment  
of Sequelae of COVID-19 Nearly 1  
Year After Diagnosis.  
Front. Med. 8:717194.  
doi: 10.3389/fmed.2021.717194

**Background:** A previous study has shown that 81% of the COVID-19 patients had mild or moderate symptoms. However, most studies on the sequelae in COVID-19 patients focused on severe cases and the long-term follow-up studies on the health consequences in non-severe cases are limited. The current study aimed to assess the sequelae of COVID-19 in patients nearly 1 year after diagnosis with a particular focus on the recovery of patients with non-severe COVID-19.

**Methods:** We enrolled 120 patients infected with SARS-CoV-2 discharged from Wuhan Union hospital west district (designated hospital for COVID-19) and Fangcang shelter hospitals between January 29, 2020 and April 1, 2020. All participants were asked to complete a series of questionnaires to assess their symptoms and quality of life and for psychological evaluation. Also, pulmonary function test, chest CT, 6-min walking test (6MWT), routine blood test, liver and kidney function tests, fasting blood glucose test, lipid test, and immunoglobulin G antibody test were performed to evaluate their health.

**Results:** The mean age of the study population was  $51.6 \pm 10.8$  years. Of the 120 patients, 104 (86.7%) were cases of non-severe COVID-19. The follow-up study was performed between November 23, 2020 and January 11, 2021, and the median time between the diagnosis and the follow-up was 314.5 (IQR, 296–338) days. Sleep difficulties, shortness of breath, fatigue, and joint pain were common symptoms observed during follow-up and nearly one-third of the non-severe cases had these symptoms. A total of 50 (41.7%) and 45 (37.5%) patients reported anxiety and depression, respectively. And 18.3% of the patients showed negative results in the IgG test at the follow-up, which correlated with the severity of the infection ( $R = 0.203$ ,  $p = 0.026$ ), and the proportion of IgG negative cases in non-severe COVID-19 patients was higher than that in the severe cases (20.2 vs. 6.3%). Pulmonary diffusion impairment was reported in 30 (26.1%) out of 115 patients, and 24 (24.2%) out of the 99 non-severe cases. The values of forced vital capacity (FVC), forced expiratory volume in 1 s (FEV1), FVC/FEV1, vital capacity (VC), total lung capacity (TLC), and residual volume (RV) were less than the normal range in 1.7, 8.6, 0.9, 11.2, 7.0, and 0.9% of the patients, respectively. A total of 55 (56.7%)

out of the 97 patients showed abnormal CT findings, including ground-glass opacities (GGO), bronchiectasis, nodules, lines and bands, and fibrosis. Furthermore, there was a correlation between all the SF-36-domain scores and the duration of hospitalization, pulmonary function, and a 6MWT.

**Conclusions:** At the nearly 1-year follow-up, COVID-19 survivors still had multi-system issues, including those in the respiratory functioning, radiography, quality of life, and anxiety and depression. Moreover, non-severe cases also showed some sequelae and the proportion of IgG negative cases in the non-severe patients was higher than that in severe cases. Therefore, conducting follow-ups and preventing the reinfection of SARS-CoV-2 in this group is necessary.

**Keywords:** long-term COVID-19, SARS-CoV-2, follow-up, sequelae, multi-system assessment

## INTRODUCTION

Since December 2019, Coronavirus Disease 2019 (COVID-19) has been spreading around the world. On March 11, 2020, the World Health Organization (WHO) declared the outbreak of COVID-19 a pandemic (1). As of July 7, 2021, there were more than 180 million COVID-19 cases and over 3 million deaths worldwide, posing a tremendous burden on the health care systems (2). Despite the high mortality rate of COVID-19, most patients recovered from acute infection. Therefore, long-term follow-up studies to assess the sequelae in COVID-19 survivors are urgently needed to improve the prognosis and survival (3).

Previous studies reported that discharged COVID-19 patients had multiple health issues, such as persistent symptoms, impaired pulmonary function, chest CT abnormalities, anxiety, depression, and a decreased quality of life (4–6). The previous follow-up studies on the sequelae in COVID-19 survivors were mostly performed 1–6 months after recovery (5, 7, 8). However, a 1-year follow-up study on patients recovered from 2003 SARS showed that one-third of the patients had persistent pulmonary function impairment, and poorer health, in general, than the healthy population (9). So far, there are few follow-up studies over 1 year assessing the sequelae in the patients recovered from COVID-19 infection (10–13). Furthermore, the studies on multi-system assessment of long-term consequences in COVID-19 survivors are limited. A previous study reported that 81% of the patients with COVID-19 showed mild to moderate disease (14). However, most studies focused on the sequelae in severe cases, and the data on non-severe cases is limited, especially on those treated at the Fangcang Hospital (5, 15). In the current study, we aimed to evaluate the health status of COVID-19 patients nearly 1 year after diagnosis, with a particular focus on the recovery of patients with non-severe COVID-19.

## METHODS

### Study Design and Participants

In the current cohort study, we enrolled laboratory-confirmed COVID-19 patients discharged from the Wuhan Union hospital west district (designated hospital for COVID-19) and Fangcang shelter hospitals between January 29, 2020 and April 1,

2020. After excluding patients without considerable data due to physiological or subjective rejection tests, data on 120 patients were considered for the analyses. The patients were classified as severe based on the guidelines for the severity of infection provided in the “Diagnosis and Treatment Protocol for Novel Coronavirus Pneumonia” issued by the National Health Commission, which were—shortness of breath, respiratory rate (RR)  $\geq 30$  /min, oxygen saturation  $\leq 93\%$  at rest, and arterial oxygen pressure (PaO<sub>2</sub>)/fraction of inspiration of O<sub>2</sub> (FiO<sub>2</sub>)  $\leq 300$  mm Hg; and the rest of the patients were considered as non-severe cases (16). All enrolled patients met the discharge standards as indicated in the Diagnosis and Treatment Protocol issued by the National Health Commission, including no fever for three consecutive days, obvious improvement in the respiratory symptoms, acute lesions on imaging, and two consecutive negative results of the SARS-CoV-2 RNA tested using real-time reverse-transcriptase-polymerase-chain-reaction (RT-PCR) with an interval of 24 h.

The study was approved by the ethics committee of the Wuhan Union Hospital (UHCT-IEC-SOP-016-02-01) and the Chinese Clinical Trial Registry (ChiCTR2100049283). We obtained written informed consent from all the participants during enrollment.

### Follow-Up Assessment

Follow-up was performed nearly 1 year after being diagnosed with COVID-19. All patients were asked to complete a series of questionnaires to assess their symptoms and quality of life and for psychological evaluation. The modified British Medical Research Council (mMRC) dyspnea scale and Brog scale were used to assess self-reported dyspnea (17). Anxiety and depression were measured using the Hamilton Anxiety Scale (HAMA) and Hamilton Depression Scale (HAMD), respectively (18, 19). The MOS item short-form health survey (SF-36), which assessed the Physical Functioning (PF), Role-Physical (RP), Bodily Pain (BP), General Health (GH), Vitality (VT), Social Functioning (SF), Role-Emotional (RE), and Mental Health (MH), was used to evaluate the Health-Related Quality of Life (HRQoL) (20). Furthermore, the patients underwent a series of laboratory examinations to evaluate their health, including routine blood test, liver and kidney function tests, fasting blood glucose

test, lipid test, and immunoglobulin (Ig) G antibody test. The IgG antibodies against the nucleoprotein of SARS-CoV-2 were measured using enzyme-linked immunosorbent assay (ELISA) kits (Beijing Wantai Biological Pharmacy Enterprise Co., Ltd.) as reported previously (21).

### Pulmonary Function Test

The pulmonary function test was performed in the Lung Function Laboratory of the Wuhan Union Hospital according to the current guidelines by the American Thoracic Society (22). Pulmonary function parameters included FVC, FEV<sub>1</sub>, FEV<sub>1</sub>/FVC, VC, TLC, RV, Diffusing capacity for carbon monoxide (DLCO), and DLCO/VA. In the light of the guidelines by the European Community Lung Health Survey, the results are shown as a percentage of the predicted value (23). The 6MWT was performed based on the guidelines by the American Thoracic Society (24). The blood oxygen saturation of the participants was also measured before and after the 6MWT.

### Radiographic Assessment

The radiographic images were evaluated by experienced radiologists who were blinded to the clinical data. We assessed 97 patients' chest CT images for the presence of ground-glass opacities, bronchiectasis, nodules, lines and bands, and fibrosis. The percentage of involvement of each of the five lobes was transformed into a corresponding score as following: 0, no involvement; 1, 1–25% involvement; 2, 26–50% involvement; 3, 51–75% involvement; and 4, 75–100% involvement. The “total severity score (TSS)” was the sum of the scores of the five lobes (range 0–20) (25). In addition, the artificial intelligence software (YT-CT-Lung, YITU Healthcare Technology Co., Ltd., China) was used to quantify and analyze the chest CT images of the patients (26).

### Statistical Analysis

Continuous variables are expressed as means (standard deviations, SD) or medians (interquartile ranges, IQR). The normality of the distribution was estimated using the Kolmogorov–Smirnov test. Categorical variables were described as numbers (percentages, %). We appropriately adopted the *t*-test, Mann–Whitney *U*-test,  $\chi^2$  test, and Fisher's exact test to compare the characteristics of the COVID-19 survivors of different severities according to variable types and distribution characteristics. The correlations of SF-36 scores across the eight domains with the length of hospitalization, 6-min walking distance (6MWD), and pulmonary function were measured using Spearman's correlation test. All statistical analyses were performed using SPSS (Statistical Package for the Social Sciences) version 21.0. Statistical tests were two-tailed, and a *P* < 0.05 was considered statistically significant.

## RESULTS

### Characteristics of Enrolled COVID-19 Patients

The clinical characteristics of 120 participants are shown in **Table 1**. There were 104 (86.7%) non-severe cases and 16 (13.3%)

severe cases. The mean age was 51.6 ( $\pm 10.8$ ) years, and 49 (40.8%) of them were men. A total of 16 (13.3%) patients had a history of smoking. The most common comorbidities observed were hypertension (20 [16.7%]), followed by diabetes (6 [5%]). Compared to non-severe cases, diabetes accounted for a larger proportion in severe cases (*p* = 0.031). The median duration of hospital stay was 25.5 (IQR, 18–33.8) days and the median time from discharge to follow-up was 284.5 (270–309) days. The median time from diagnosis to follow-up was 314.5 (296–338) days, ranging from 274 to 379 days.

### Symptoms and the Results of the Laboratory Tests at the Nearly 1-Year Follow-Up

**Table 2** shows the body mass index (BMI), symptoms, and the results of the laboratory tests during follow-up. The mean BMI was 24.6 ( $\pm 2.8$ ) kg/m<sup>2</sup>, and the severe cases showed a significantly higher BMI than the non-severe ones (*p* = 0.02). The most common symptoms in COVID-19 survivors at the nearly 1-year follow-up were sleep difficulties (52 [43.3%]), shortness of breath (49 [40.8%]), fatigue (43 [35.8%]), and joint pain (39 [32.5%]), and nearly one-third of the non-severe cases had these symptoms. At follow-up, all participants showed healthy levels of white blood cells, lymphocytes, hemoglobin, and platelets. In addition, the proportions of patients with levels of alanine aminotransferase (ALT), aspartate aminotransferase (AST), creatinine, triglyceride, total cholesterol, and fasting blood glucose above the normal range were 21/119 (17.6%), 8/119 (6.7%), 20/119 (16.8%), 51/119 (42.9%), 71/119 (59.7%), and 20/118 (16.9%), respectively. Compared to the non-severe cases, severe cases showed significantly higher lymphocytes (*p* = 0.041), hemoglobin (*p* = 0.013), ALT (*p* = 0.011), triglyceride (*p* = 0.049), and fasting blood glucose (*p* = 0.033). The results of the IgG test were negative in 22 (18.3%) patients, and the proportion of IgG negative patients in non-severe cases was higher than that in severe cases (20.2 vs. 6.3%), but the difference was not statistically significant (*p* = 0.075). At the nearly 1-year follow-up, IgG test results correlated with the severity of the disease (*R* = 0.203, *p* = 0.026).

### Results of the Psychological Assessment and Quality of Life at the Nearly 1-Year Follow-Up

At the nearly 1-year follow-up, 50 (41.7%) and 45 (37.5%) patients showed greater-than-normal HAMA and HAMD scores, respectively, while in the non-severe cases, 41 (39.4%) reported anxiety and 39 (37.5%) reported depression (**Table 2**). **Figure 1** shows the average scores across the 8 domains of SF-36 used for assessing HRQoL. All SF-36-domain scores significantly decreased. Patients with the severe disease had significantly lower levels of PF and GH than the non-severe cases (*p* = 0.049 and 0.045, respectively). **Table 3** shows the correlations between all the SF-36-domain scores and the length of hospitalization, pulmonary function, and the 6MWD. Except for SF, other domains of SF-36 negatively correlated with length of hospitalization, among which the correlations with RP and

**TABLE 1** | Demographic and clinical characteristics of the enrolled COVID-19 patients.

|  | Total (N = 120) | Non-severe (n = 104) | Severe (n = 16)     | P-value |
|--|-----------------|----------------------|---------------------|---------|
| Demographic characteristics            |                 |                      |                     |         |
| Age, years                             | 51.6 ± 10.8     | 51.4 ± 10.9          | 52.6 ± 10.1         | 0.67    |
| Sex                                    |                 |                      |                     |         |
| Men                                    | 49 (40.8)       | 41 (39.4)            | 8 (50)              | 0.423   |
| Women                                  | 71 (59.2)       | 63 (60.6)            | 8 (50)              |         |
| Cigarette smoking                      |                 |                      |                     |         |
| Yes                                    | 16 (13.3)       | 14 (13.5)            | 2 (12.5)            | 1       |
| No                                     | 104 (86.7)      | 90 (86.5)            | 14 (87.5)           |         |
| Comorbidities                          |                 |                      |                     |         |
| Diabetes                               | 6 (5)           | 3 (2.9)              | 3 (18.8)            | 0.031   |
| Hypertension                           | 20 (16.7)       | 16 (15.4)            | 4 (25)              | 0.548   |
| Hyperlipidemia                         | 4 (3.3)         | 3 (2.9)              | 1 (6.3)             | 0.44    |
| Coronary heart disease                 | 3 (2.5)         | 3 (2.9)              | 0 (0)               | 1       |
| Length of hospitalization, days        | 25.5 (18–33.8)  | 24.5 (18–32.8)       | 31 (17.5–41.5)      | 0.114   |
| Days from diagnosis to follow-up, days | 314.5 (296–338) | 315.5 (296–338.8)    | 307.5 (296.3–327.3) | 0.671   |
| Days from discharge to follow-up, days | 284.5 (270–309) | 288.5 (270.5–309.8)  | 274.5 (256–294)     | 0.066   |

Data are presented as mean ± SD, median (interquartile range), and n (%).

Continuous variables were tested using the t-test, while categorical variables were compared using the  $\chi^2$  test or Fisher's exact test.

GH were statistically significant. FEV1/FVC, DLCO, and FEV1 showed significant positive correlations with PF, RP, and GH, respectively. Furthermore, 6MWD was positively associated with PF, GH, VT, and RE.

## Results of the Pulmonary Function Test, 6MWT, and Chest CT Assessment at the Nearly 1-Year Follow-Up

As shown in Table 4, the proportions of mMRC  $\geq 1$  and Brog  $\geq 1$  were significantly higher in the severe cases than the non-severe cases, and these proportions were 32.7 and 34.6% in the non-severe cases, respectively. The mean 6MWD of participants was 514.1 ( $\pm 73$ ) m, and there was no significant decrease in the oxygen saturation after the walk. The walk distance was below 80% of the predicted value in 18.5% of the total patients and 18.4% of the non-severe cases. Pulmonary diffusion impairment was found in 30/115 (26.1%) participants and 24 (24.2%) of the 99 non-severe cases. The proportions of patients with FVC, FEV1, FVC/FEV1, VC, TLC, and RV were lower than the lower limit of the normal range were 2/116 (1.7%), 10/116 (8.6%), 1/116 (0.9%), 13/116 (11.2%), 8/115 (7.0%), and 1/114 (0.9%), respectively. The differences in FVC, FEV1, VC, TLC, RV, and DLCO/VA were significant between the severe and non-severe cases. Follow-up chest CT evaluation showed that 55/97 (56.7%) patients showed abnormal CT findings, including 47 (56.6%) non-severe cases and 8 (57.1%) severe cases. The most common abnormal CT manifestations were nodules (55.7%), followed by lines and bands (47.4%), fibrosis (17.5%), GGO (16.5%), and bronchiectasis (14.4%). TSS  $\geq 1$  was found in 15/97 (15.5%) patients, and the maximum TSS score was 13. Besides, quantitative assessment of CT showed that the volume of the residual lesions, GGO,

and consolidation of bilateral lung were 0.03 (0–0.58) cm<sup>3</sup>, 0.02 (0–0.45) cm<sup>3</sup>, and 0.01 (0–0.07) cm<sup>3</sup>, respectively.

## DISCUSSION

To the best of our knowledge, to date, there are few studies assessing the health outcomes of COVID-19 patients 1 year after diagnosis (10–13). In the current cohort study, we evaluated the health status of COVID-19 survivors nearly 1 year after diagnosis. We found that participants showed certain symptoms like anxiety, depression, and impaired HRQoL, as well as residual chest CT abnormalities, accompanied by pulmonary diffusion impairment. Also, the levels of the indicators for liver and kidney functions were found to be higher than the normal range.

In the current study, we found that COVID-19 survivors showed sleep difficulties, shortness of breath, fatigue, and abnormal anxiety and depression at the nearly 1-year follow-up, and more than one-third of the non-severe cases showed these symptoms. These observations were consistent with those of the previous studies. It was shown that several COVID-19 survivors reported fatigue, sleep difficulties, anxiety, and depression 6 months after the onset of the illness (5). A 4-year follow-up study of 2003 SARS reported that 40% of the survivors had persistent fatigue and psychological sequelae (27). In addition, participants suffered from impaired HRQoL, as assessed using the Chinese version of the SF-36 questionnaire. These psychological sequelae and impaired HRQoL may be associated with a variety of factors, including direct lung injury and neurological involvement caused by the viral infection, the long period of isolation, and the anxiety caused by the pandemic (28).

Our study showed that more than one-third of the subjects reported abnormal mMRC and Brog scores. Some participants



**TABLE 2 |** Symptoms, laboratory findings, and mental and cognitive status at the nearly 1-year follow-up.

|   | Total (N = 120) | Non-severe (n = 104) | Severe (n = 16) | P-value |
|---|-----------------|----------------------|-----------------|---------|
| BMI, kg/m <sup>2</sup>                      | 24.6 ± 2.8      | 24.3 ± 2.8           | 26.1 ± 2.9      | 0.02    |
| <b>Symptoms</b>                             |                 |                      |                 |         |
| Shortness of breath                         | 49 (40.8)       | 40 (38.5)            | 9 (56.3)        | 0.178   |
| Fatigue                                     | 43 (35.8)       | 34 (32.7)            | 9 (56.3)        | 0.067   |
| Sleep difficulties                          | 52 (43.3)       | 44 (42.3)            | 8 (50)          | 0.563   |
| Joint pain                                  | 39 (32.5)       | 33 (31.7)            | 6 (37.5)        | 0.646   |
| Loss of Smell                               | 9 (7.5)         | 7 (6.7)              | 2 (12.5)        | 0.76    |
| Constipation                                | 21 (17.5)       | 18 (17.3)            | 3 (18.8)        | 1       |
| Diarrhea                                    | 4 (3.3)         | 3 (2.9)              | 1 (6.3)         | 0.44    |
| <b>Laboratory findings</b>                  |                 |                      |                 |         |
| White blood cell count, ×10 <sup>9</sup> /L | 5.9 ± 1.6       | 5.8 ± 1.6            | 6.5 ± 1.6       | 0.16    |
| Lymphocytes count, ×10 <sup>9</sup> /L      | 1.9 ± 0.5       | 1.8 ± 0.4            | 2.1 ± 0.5       | 0.041   |
| Hemoglobin, g/L                             | 146.8 ± 15.8    | 145.3 ± 16.1         | 156.1 ± 10.2    | 0.013   |
| Platelet count, ×10 <sup>9</sup> /L         | 221.7 ± 59.9    | 220.4 ± 58.7         | 229.5 ± 68.6    | 0.586   |
| ALT, U/L                                    | 23 (18–31)      | 22 (17–30)           | 28.5 (25–66.3)  | 0.011   |
| >35   | 21/119 (17.6)   | 16 (15.5)            | 5 (31.3)        | 0.237   |
| AST, U/L                                    | 23 (20–29)      | 23 (19–29)           | 26 (22.3–29.5)  | 0.178   |
| >40   | 8/119 (6.7)     | 5 (4.9)              | 3 (18.8)        | 0.126   |
| Creatinine, μmol/L                          | 62.4 ± 15.4     | 62.5 ± 15.9          | 61 ± 11.7       | 0.627   |
| >81   | 20/119 (16.8)   | 19 (18.4)            | 1 (6.3)         | 0.225   |
| Triglyceride, mmol/L                        | 1.8 ± 0.9       | 1.7 ± 0.9            | 2.2 ± 1         | 0.049   |
| >1.7  | 51/119 (42.9)   | 42 (40.8)            | 9 (56.3)        | 0.245   |
| Total cholesterol, mmol/L                   | 5.5 ± 0.9       | 5.4 ± 0.9            | 5.7 ± 1         | 0.146   |
| >5.2  | 71/119 (59.7)   | 61 (59.2)            | 10 (62.5)       | 0.804   |
| Fasting blood glucose, mmol/L               | 5.5 (5.1–5.9)   | 5.5 (5.1–5.9)        | 5.9 (5.5–6.2)   | 0.033   |
| >6.1  | 20/118 (16.9)   | 16 (15.7)            | 4 (25)          | 0.572   |
| <b>IgG</b>                                  |                 |                      |                 |         |
| Negative                                    | 22 (18.3)       | 21 (20.2)            | 1 (6.3)         | 0.075   |
| Weakly positive                             | 32 (26.7)       | 30 (28.8)            | 2 (12.5)        |         |
| Positive                                    | 66 (55)         | 53 (51)              | 13 (81.3)       |         |
| <b>Mental status</b>                        |                 |                      |                 |         |
| HAMA  | 5 (2–11.5)      | 5 (2–9)              | 7.5 (1.5–13)    | 0.496   |
| 0–6 (no)                                    | 70 (58.3)       | 63 (60.6)            | 7 (43.8)        | 0.317   |
| 7–13 (mild/moderate)                        | 29 (24.2)       | 23 (22.1)            | 6 (37.5)        |         |
| ≥14 (severe/extreme)                        | 21 (17.5)       | 18 (17.3)            | 3 (18.8)        |         |
| HAMD  | 4.0 (2–9)       | 4 (2–9)              | 6 (3.3–10.8)    | 0.405   |
| 0–6 (no)                                    | 75 (62.5)       | 65 (62.5)            | 10 (62.5)       | 0.817   |
| 7–23 (mild/moderate)                        | 39 (32.5)       | 33 (31.7)            | 6 (37.5)        |         |
| ≥24 (severe/extreme)                        | 6 (5)           | 6 (5.8)              | 0 (0)           |         |

Data are presented as mean ± SD, median (interquartile range), and n (%).

Continuous variables were tested using the t-test or Mann–Whitney U-test, while categorical variables were compared using the  $\chi^2$  test or Fisher's exact test.

BMI, body mass index; ALT, alanine aminotransferase; AST, aspartate aminotransferase; HAMA, Hamilton Anxiety Scale; HAMD, Hamilton Depression Scale.

had impaired pulmonary function during follow-up, the most common of which was DLCO abnormalities (26.1%). This was consistent with another follow-up study on 2003 SARS, where 23.7% of the survivors developed diffusing-capacity impairment 1 year after the onset of the symptoms (29). We found that a considerable proportion (56.7%) of the patients showed abnormalities in their corresponding radiographic images, and the major findings were nodules, lines and bands, and fibrosis. Previous studies showed interstitial changes in the lungs as the

most common long-term pulmonary abnormality in COVID-19 and 2003 SARS survivors (5, 30). It was shown that even at 12 months after discharge, 24% of the COVID-19 survivors had persistent abnormalities in their radiographical images, which included GGO, interlobular septal thickening, reticular opacity, and mosaic attenuation (10). The proportions of residual pulmonary abnormalities were higher in our study, which may be due to the use of artificial intelligence for the evaluation and detection of more subtle changes. Moreover,

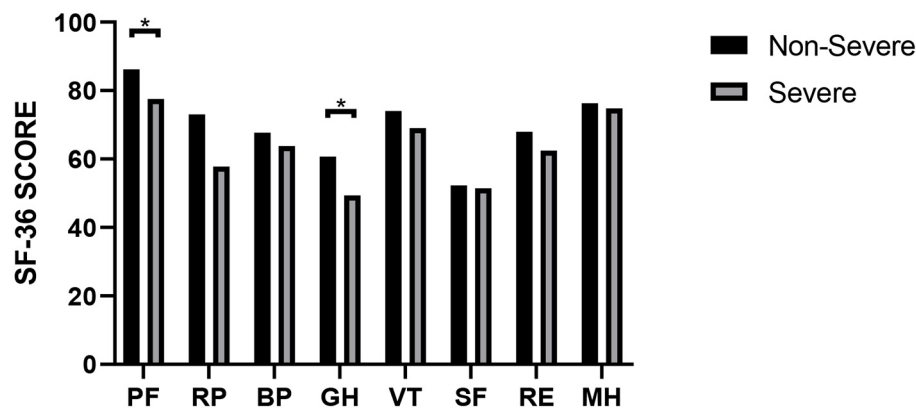


**FIGURE 1** | SF-36 scores of COVID-19 patients with different severities. \* $P < 0.05$ .  $P$ -values were calculated using the  $t$ -test.

**TABLE 3** | Correlations among HRQoL, length of hospitalization, pulmonary function, and 6MWD at the nearly 1-year follow-up.

| SF-36 | LOH    | FVC   | FEV1  | FEV1/FVC | VC    | TLC   | DLCO   | 6MWD  |
|-------|--------|-------|-------|----------|-------|-------|--------|-------|
| PF    | -0.16  | 0.03  | 0.11  | 0.19*    | 0.01  | 0.07  | 0.16   | 0.22* |
| RP    | -0.25† | 0.16  | 0.16  | 0.02     | 0.14  | 0.14  | 0.219* | 0.15  |
| BP    | -0.14  | 0.04  | 0.06  | 0.08     | 0.05  | 0.07  | -0.01  | -0.11 |
| GH    | -0.18* | 0.1   | 0.21* | 0.15     | 0.07  | 0.1   | 0.15   | 0.2*  |
| VT    | -0.16  | -0.04 | 0.05  | 0.22*    | -0.06 | -0.03 | 0.12   | 0.22* |
| SF    | 0.02   | -0.02 | 0.02  | 0.08     | 0     | 0.02  | 0.15   | 0.08  |
| RE    | -0.01  | 0.15  | 0.17  | 0.09     | 0.12  | 0.09  | 0.14   | 0.21* |
| MH    | -0.14  | -0.01 | 0.07  | 0.17     | -0.04 | -0.03 | 0.03   | 0.14  |

Values shown are Spearman correlation coefficients ( $r$ ). \* $P < 0.05$ ; † $P < 0.01$ .

LOH, length of hospitalization; 6MWD, 6-minute walk distance; PF, Physical Functioning; RP, Role-Physical; BP, Bodily Pain; GH, General Health; VT, Vitality; SF, Social Functioning; RE, Role-Emotional; MH, Mental Health.

compared to the residual lung lesion volume in a previous study performed 6 months after the onset of the symptoms, the volume of bilateral pulmonary lesions was significantly lesser in our study (5). It suggested that although some patients showed abnormalities in their radiographic images, the intensity of impairment was small and the lesions were continuously resolved. A 15-year follow-up study showed that the interstitial changes in the lungs and the decline in the lung function caused by 2003 SARS may be successfully treated, and significant recovery can be achieved within 2 years (31). Whether recovery in pulmonary function and abnormalities observed in the radiographic images is possible remains to be further investigated.

The inflammatory indicators in the current study were within the normal range but abnormal ALT, AST, and creatinine values were observed in a few COVID-19 survivors. As reported previously, a proportion of COVID-19 survivors showed abnormal liver function test results during follow-up (32). Furthermore, 35% of the COVID-19 survivors had an eGFR  $< 90$  mL/min per  $1.73 \text{ m}^2$  but 13% of these patients presented normal eGFR at the acute phase (5). This indicated that abnormal indicators in COVID-19 survivors were not necessarily a persistent impairment after acute injury. This may

also be caused by factors during the post-acute phase, such as drugs and fatty liver caused by overnutrition and other factors. However, since the liver and kidney function test results of the subjects before viral infection were unavailable, the liver and kidney function abnormalities could not be completely attributed to COVID-19 and long-term follow-up studies are necessary. Besides, 18.3% of the patients had negative results in the IgG test, and a higher proportion of the non-severe cases showed negative results in the IgG test. There was a correlation between IgG conversion and the severity of infection. A study of COVID-19 immune response 8 weeks after discharge found that the proportions of IgG negative patients in the asymptomatic and symptomatic cases were 40 and 12.9%, respectively (33). As reported previously, patients with severe disease had higher levels of IgG than asymptomatic individuals and mild cases (34), suggesting that the severity of the disease is associated with the immune response to the viral infection. A previous study on 2003 SARS survivors demonstrated that IgG was still detectable in the patients 16 months after the onset of the illness (35). Hence, the immune response to SARS-CoV-2 needs to be investigated in further long-term studies.

There were some limitations to the current study. Firstly, it was a small cohort study. We did not study the longitudinal

**TABLE 4 |** Dyspnea, pulmonary function, 6MWD, and chest CT assessment at the nearly 1-year follow-up.

|  | Total (N = 120)   | Non-severe (n = 104) | Severe (n = 16) | P-value |
|--|-------------------|----------------------|-----------------|---------|
| <b>Dyspnea</b>   |                   |                      |                 |         |
| <b>mMRC score</b>  |                   |                      |                 |         |
| ≥1   | 46 (38.3)         | 34 (32.7)            | 12 (75)         | 0.001   |
| <b>Brog score</b>  |                   |                      |                 |         |
| ≥1   | 47 (39.2)         | 36 (34.6)            | 11 (68.8)       | 0.009   |
| <b>Pulmonary function</b>  |                   |                      |                 |         |
| FVC, % of predicted  | 108.6 ± 17.5      | 110 ± 17.7           | 100.2 ± 14.4    | 0.037   |
| FVC < 80%, No. (%)   | 2/116 (1.7)       | 1/100 (1)            | 1/16 (6.3)      | 0.258   |
| FEV1, % of predicted   | 99.8 ± 13.5       | 101 ± 13.3           | 92.3 ± 12.7     | 0.016   |
| FEV1 < 80%, No. (%)  | 10/116 (8.6)      | 6/100 (6)            | 4/16 (25)       | 0.042   |
| FEV1/FVC, % of predicted   | 92 ± 7.4          | 91.6 ± 7.4           | 94.3 ± 7.2      | 0.186   |
| FEV1/FVC < 70%, No. (%)  | 1/116 (0.9)       | 1/100 (1)            | 0/16 (0)        | 1       |
| VC, % of predicted   | 107.1 ± 14.5      | 108.5 ± 14.3         | 98.7 ± 13.6     | 0.012   |
| VC < 90%, No. (%)  | 13/116 (11.2)     | 9/100 (9)            | 4/16 (25)       | 0.145   |
| TLC, % of predicted  | 95.1 ± 10.8       | 96.2 ± 10.2          | 88 ± 12.5       | 0.005   |
| TLC < 80%, No. (%)   | 8/115 (7.0)       | 4/99 (4)             | 4/16 (25)       | 0.011   |
| RV, % of predicted   | 90.2 ± 13.6       | 91.6 ± 13.3          | 81.9 ± 12.4     | 0.007   |
| RV < 60%, No. (%)  | 1/114 (0.9)       | 0/98 (0)             | 1/16 (6.3)      | 0.14    |
| DLCO, % of predicted   | 88.4 ± 12.5       | 88.6 ± 12.5          | 87.3 ± 12.7     | 0.697   |
| DLCO < 80%, No. (%)  | 30/115 (26.1)     | 24/99 (24.2)         | 6/16 (37.5)     | 0.416   |
| DLCO/VA, % of predicted  | 96.2 ± 13.7       | 95 ± 13.6            | 103.1 ± 12.1    | 0.027   |
| <b>6MWD</b>  |                   |                      |                 |         |
| Distance, m  | 514.1 ± 73        | 517.3 ± 72.2         | 493.5 ± 77.3    | 0.225   |
| % of predicted   | 92.4 (84.1–101.1) | 92.6 (84.4–103.1)    | 91 (81.3–97.6)  | 0.445   |
| <80% predicted value, No. (%)  | 22/119 (18.5)     | 19/103 (18.4)        | 3/16 (18.8)     | 1       |
| SpO <sub>2</sub> before exercise, %                                    | 98 (97–99)        | 98 (97–99)           | 97 (97–98.8)    | 0.029   |
| SpO <sub>2</sub> after exercise, %                                     | 98 (98–99)        | 99 (98–99)           | 98 (97–99)      | 0.103   |
| <b>Chest CT</b>  |                   |                      |                 |         |
| <b>Abnormal CT findings, No. (%)</b>                                   |                   |                      |                 |         |
| TSS  | 0 (0–0)           | 0 (0–0)              | 0 (0–0.5)       | 0.535   |
| ≥1, No. (%)  | 15/97 (15.5)      | 12/83 (14.5)         | 3/14 (21.4)     | 0.789   |
| <b>Type of chest CT abnormalities present, No. (%)</b>                 |                   |                      |                 |         |
| GGO  | 16/97 (16.5)      | 11/83 (13.3)         | 5/14 (35.7)     | 0.088   |
| Bronchiectasis   | 14/97 (14.4)      | 13/83 (15.7)         | 1/14 (7.1)      | 0.738   |
| nodules  | 54/97 (55.7)      | 47/83 (56.6)         | 7/14 (50)       | 0.644   |
| Lines and bands  | 46/97 (47.4)      | 41/83 (49.4)         | 5/14 (35.7)     | 0.343   |
| Fibrosis   | 17/97 (17.5)      | 14/83 (16.9)         | 3/14 (21.4)     | 0.972   |
| <b>Quantitative assessment</b>   |                   |                      |                 |         |
| Volume of bilateral pulmonary lesions (cm <sup>3</sup> )               | 0.03 (0–0.58)     | 0.03 (0–0.6)         | 0.03 (0–0.73)   | 0.81    |
| Volume of bilateral pulmonary GGO lesions (cm <sup>3</sup> )           | 0.02 (0–0.45)     | 0.01 (0–0.54)        | 0.03 (0–0.67)   | 0.896   |
| Volume of bilateral pulmonary consolidation lesions (cm <sup>3</sup> ) | 0.01 (0–0.07)     | 0.01 (0–0.07)        | 0.01 (0–0.06)   | 0.597   |
| Percent of bilateral pulmonary lesions (%)                             | 0 (0–0.01)        | 0 (0–0.01)           | 0 (0–0.02)      | 0.763   |
| Percent of bilateral pulmonary GGO lesions (%)                         | 0 (0–0.01)        | 0 (0–0.01)           | 0 (0–0.02)      | 0.99    |
| Percent of bilateral pulmonary consolidation lesions (%)               | 0 (0–0)           | 0 (0–0)              | 0 (0–0)         | 0.1     |

Data are presented as mean ± SD, median (interquartile range), and n (%). Continuous variables were tested using the t-test or Mann–Whitney U-test, while categorical variables were compared using the  $\chi^2$  test or Fisher's exact test. mMRC, modified British Medical Research Council; 6MWD, 6-minute walk distance; TSS, total severity score; GGO, ground-glass opacities.

physical and psychological changes in the COVID-19 survivors with a prolonged recovery time. In the future, we will continue to follow the COVID-19 patients and observe changes in the

sequelae. Secondly, our study sampled a small population. However, our results provided further insights into the understanding of COVID-19. Larger sample size is needed to

investigate the sequelae in COVID-19 patients with differing severities. Thirdly, the baseline data before the SARS-CoV-2 infection and during the acute phase were not available. Therefore, the abnormal health status of COVID-19 survivors cannot be attributed exclusively to the viral infection. However, although it may be underestimated since it was self-reported by the patients, the proportion of patients with underlying diseases was low. Finally, due to the lack of a control group that had not contracted SARS-CoV-2, the sequelae of COVID-19 could not be better evaluated.

In conclusion, the discharged patients suffered from multi-system issues nearly 1 year after being diagnosed with COVID-19, even the non-severe cases. Moreover, the proportion of IgG negative cases was higher in the non-severe cases than the severe ones. Our results complemented the current limitations of research on the long-term effects in COVID-19 patients with the non-severe disease and enabled us to have a more comprehensive understanding of COVID-19. The results suggested that physicians should also pay attention to post-discharge care in non-severe cases, and the non-severe cases should also be studied to fully understand the health consequences after viral infection and prevent the reinfection of SARS-CoV-2.

## DATA AVAILABILITY STATEMENT

The raw data supporting the conclusions of this article will be made available by the authors, without undue reservation.

## REFERENCES

1. WHO. *Director-General's Opening Remarks at the Media Briefing on COVID-19*. (2020). Available online at: <https://www.who.int/dg/speeches/detail/who-director-general-s-opening-remarks-at-the-media-briefing-on-covid-19--11-march-2020> (accessed January 29, 2021).
2. WHO. *Coronavirus Disease (COVID-19) Outbreak Situation*. Available online at: <https://www.who.int/emergencies/diseases/novel-coronavirus-2019> (accessed July 7, 2021).
3. Yelin D, Wirtheim E, Vetter P, Kalil AC, Bruchfeld J, Runold M, et al. Long-term consequences of COVID-19: research needs. *Lancet Infect Dis*. (2020) 20:1115–7. doi: 10.1016/S1473-3099(20)30701-5
4. Lerum TV, Aalokken TM, Bronstad E, Aarli B, Ikdahl E, Lund KMA, et al. Dyspnoea, lung function and CT findings 3 months after hospital admission for COVID-19. *Eur Respir J*. (2021) 57:2003448. doi: 10.1183/13993003.03448-2020
5. Huang C, Huang L, Wang Y, Li X, Ren L, Gu X, et al. 6-month consequences of COVID-19 in patients discharged from hospital: a cohort study. *Lancet*. (2021) 397:220–32. doi: 10.1016/S0140-6736(20)32656-8
6. van den Borst B, Peters JB, Brink M, Schoon Y, Bleeker-Rovers CP, Schers H, et al. Comprehensive health assessment three months after recovery from acute COVID-19. *Clin Infect Dis*. (2021) 73:e1089–e1098. doi: 10.1093/cid/ciaa1750
7. Bellan M, Soddu D, Balbo PE, Baricich A, Zeppegno P, Avanzi GC, et al. Respiratory and psychophysical sequelae among patients with COVID-19 four months after hospital discharge. *JAMA Netw Open*. (2021) 4:e2036142. doi: 10.1001/jamanetworkopen.2020.36142
8. Huang Y, Tan C, Wu J, Chen M, Wang Z, Luo L, et al. Impact of coronavirus disease 2019 on pulmonary function in early convalescence phase. *Respir Res*. (2020) 21:163. doi: 10.1186/s12931-020-01429-6

## ETHICS STATEMENT

The study was approved by the Ethics Committee of the Wuhan Union Hospital. Written informed consent was obtained from all the participants during enrollment.

## AUTHOR CONTRIBUTIONS

SY conceptualized and designed the study and had full access to all of the data in the study. SY and YF took responsibility for the integrity of the data and the accuracy of the data analysis. LS, YL, MZ, GP, and JL summarized the data. FZ and MT contributed to data analysis and drafted the manuscript. SH contributed to data platform establishment and artificial intelligence analysis. LW took the responsibility of project contact. YJ was responsible for patient care and communication. All authors contributed to data acquisition or data interpretation, reviewed the manuscript, and approved the final version.

## FUNDING

This study was funded by Key R&D Program of Hubei Province (Grant Number: 2020BCA065).

## ACKNOWLEDGMENTS

We would like to thank all the patients involved in this study.

9. Ong KC, Ng AW, Lee LS, Kaw G, Kwek SK, Leow MK, et al. 1-year pulmonary function and health status in survivors of severe acute respiratory syndrome. *Chest*. (2005) 128:1393–400. doi: 10.1378/chest.128.3.1393
10. Wu X, Liu X, Zhou Y, Yu H, Li R, Zhan Q, et al. 3-month, 6-month, 9-month, and 12-month respiratory outcomes in patients following COVID-19-related hospitalisation: a prospective study. *Lancet Respir Med*. (2021) 9:747–54. doi: 10.1016/S2213-2600(21)00174-0
11. Xiao K, Yang H, Liu B, Pang X, Du J, Liu M, et al. Antibodies can last for more than 1 year after SARS-CoV-2 infection: a follow-up study from survivors of COVID-19. *Front Med (Lausanne)*. (2021) 8:684864. doi: 10.3389/fmed.2021.684864
12. Han X, Fan Y, Alwalid O, Zhang X, Jia X, Zheng Y, et al. Fibrotic interstitial lung abnormalities at 1-year follow-up CT after severe COVID-19. *Radiology*. (2021) 210972. doi: 10.1148/radiol.2021210972
13. Yan X, Huang H, Wang C, Jin Z, Zhang Z, He J, et al. Follow-up study of pulmonary function among COVID-19 survivors 1 year after recovery. *J Infect*. (2021) 83:381–412. doi: 10.1016/j.jinf.2021.05.034
14. Wu Z, McGoogan JM. Characteristics of and important lessons from the coronavirus disease 2019 (COVID-19) outbreak in China: summary of a report of 72314 cases from the chinese center for disease control and prevention. *JAMA*. (2020) 323:1239–42. doi: 10.1001/jama.2020.2648
15. Gonzalez J, Benitez ID, Carmona P, Santistevan S, Monge A, Moncusi-Moix A, et al. Pulmonary function and radiologic features in survivors of critical COVID-19: a 3-month prospective cohort. *Chest*. (2021) 160:187–98. doi: 10.1016/j.chest.2021.02.062
16. Commission, C. N. H. *Chinese Clinical Guidance for COVID-19 Pneumonia Diagnosis and Treatment*. Available online at: <http://kjfy.meetingchina.org/msite/news/show/cn/3337.html> (accessed March 4, 2020).
17. Mahler DA, Wells CK. Evaluation of clinical methods for rating dyspnea. *Chest*. (1988) 93:580–6. doi: 10.1378/chest.93.3.580

18. Hamilton M. A rating scale for depression. *J Neurol Neurosurg Psychiatry*. (1960) 23:56–62. doi: 10.1136/jnnp.23.1.56
19. Hamilton, M. The assessment of anxiety states by rating. *Br J Med Psychol*. (1959) 32:50–5. doi: 10.1111/j.2044-8341.1959.tb00467.x
20. Li L, Wang H, Shen Y. Development and psychometric tests of a Chinese version of the SF-36 Health Survey Scales. *Zhonghua Yu Fang Yi Xue Za Zhi*. (2002) 36:109–13. doi: 10.3760/j.issn:0253-9624.2002.02.011
21. Zhao J, Yuan Q, Wang H, Liu W, Liao X, Su Y, et al. Antibody responses to SARS-CoV-2 in patients with novel coronavirus disease 2019. *Clin Infect Dis*. (2020) 71:2027–34. doi: 10.1093/cid/ciaa344
22. Standardization of Spirometry, 1994 Update. American Thoracic Society. *Am J Respir Crit Care Med*. (1995) 152:1107–36. doi: 10.1164/ajrccm.152.3.7663792
23. Roca J, Burgos F, Sunyer J, Saez M, Chinn S, Anto JM, et al. Reference values for forced spirometry. Group of the European Community Respiratory Health Survey. *Eur Respir J*. (1998) 11:1354–62. doi: 10.1183/09031936.98.11061354
24. ATS Committee on Proficiency Standards for Clinical Pulmonary Function Laboratories. ATS statement: guidelines for the six-minute walk test. *Am J Respir Crit Care Med*. (2002) 166:111–7. doi: 10.1164/ajrccm.166.1.at1102
25. Li K, Fang Y, Li W, Pan C, Qin P, Zhong Y, et al. CT image visual quantitative evaluation and clinical classification of coronavirus disease (COVID-19). *Eur Radiol*. (2020) 30:4407–16. doi: 10.1007/s00330-020-06817-6
26. Pan F, Li L, Liu B, Ye T, Li L, Liu D, et al. A novel deep learning-based quantification of serial chest computed tomography in Coronavirus Disease 2019 (COVID-19). *Sci Rep*. (2021) 11:417. doi: 10.1038/s41598-020-80261-w
27. Lam MH, Wing YK, Yu MW, Leung CM, Ma RC, Kong AP, et al. Mental morbidities and chronic fatigue in severe acute respiratory syndrome survivors: long-term follow-up. *Arch Intern Med*. (2009) 169:2142–7. doi: 10.1001/archinternmed.2009.384
28. Baig AM, Khaleeq A, Ali U, Syeda H. Evidence of the COVID-19 virus targeting the CNS: tissue distribution, host-virus interaction, and proposed neurotropic mechanisms. *ACS Chem Neurosci*. (2020) 11:995–8. doi: 10.1021/acscchemneuro.0c00122
29. Hui DS, Wong KT, Ko FW, Tam LS, Chan DP, Woo J, et al. The 1-year impact of severe acute respiratory syndrome on pulmonary function, exercise capacity, and quality of life in a cohort of survivors. *Chest*. (2005) 128:2247–61. doi: 10.1378/chest.128.4.2247
30. Xie L, Liu Y, Xiao Y, Tian Q, Fan B, Zhao H, et al. Follow-up study on pulmonary function and lung radiographic changes in rehabilitating severe acute respiratory syndrome patients after discharge. *Chest*. (2005) 127:2119–24. doi: 10.1378/chest.127.6.2119
31. Zhang P, Li J, Liu H, Han N, Ju J, Kou Y, et al. Long-term bone and lung consequences associated with hospital-acquired severe acute respiratory syndrome: a 15-year follow-up from a prospective cohort study. *Bone Res*. (2020) 8:8. doi: 10.1038/s41413-020-00113-1
32. Nayagam JS, Jeyaraj R, Mitchell T, Walder DP, Al-Agil M, Shek A, et al. Patterns and prediction of liver injury with persistent cholestasis in survivors of severe SARS-CoV-2 infection. *J Infect*. (2021) 82:e11–e3. doi: 10.1016/j.jinf.2021.03.029
33. Long QX, Tang XJ, Shi QL, Li Q, Deng HJ, Yuan J, et al. Clinical and immunological assessment of asymptomatic SARS-CoV-2 infections. *Nat Med*. (2020) 26:1200–4. doi: 10.1038/s41591-020-0965-6
34. Carsetti R, Zaffina S, Piano Mortari E, Terreri S, Corrente F, Capponi C, et al. Different innate and adaptive immune responses to SARS-CoV-2 infection of asymptomatic, mild, and severe cases. *Front Immunol*. (2020) 11:610300. doi: 10.3389/fimmu.2020.610300
35. Liu W, Fontanet A, Zhang PH, Zhan L, Xin ZT, Baril L, et al. Two-year prospective study of the humoral immune response of patients with severe acute respiratory syndrome. *J Infect Dis*. (2006) 193:792–5. doi: 10.1086/500469

**Conflict of Interest:** The authors declare that the research was conducted in the absence of any commercial or financial relationships that could be construed as a potential conflict of interest.

**Publisher's Note:** All claims expressed in this article are solely those of the authors and do not necessarily represent those of their affiliated organizations, or those of the publisher, the editors and the reviewers. Any product that may be evaluated in this article, or claim that may be made by its manufacturer, is not guaranteed or endorsed by the publisher.

Copyright © 2021 Zhou, Tao, Shang, Liu, Pan, Jin, Wang, Hu, Li, Zhang, Fu and Yang. This is an open-access article distributed under the terms of the Creative Commons Attribution License (CC BY). The use, distribution or reproduction in other forums is permitted, provided the original author(s) and the copyright owner(s) are credited and that the original publication in this journal is cited, in accordance with accepted academic practice. No use, distribution or reproduction is permitted which does not comply with these terms.





# Clinical Applicable AI System Based on Deep Learning Algorithm for Differentiation of Pulmonary Infectious Disease

Yu-han Zhang<sup>1†</sup>, Xiao-fei Hu<sup>1†</sup>, Jie-chao Ma<sup>2</sup>, Xian-qi Wang<sup>1</sup>, Hao-ran Luo<sup>1</sup>, Zi-feng Wu<sup>2</sup>, Shu Zhang<sup>2</sup>, De-jun Shi<sup>2</sup>, Yi-zhou Yu<sup>2</sup>, Xiao-ming Qiu<sup>3</sup>, Wen-bing Zeng<sup>4,5</sup>, Wei Chen<sup>1\*</sup> and Jian Wang<sup>1\*</sup>

## OPEN ACCESS

### Edited by:

Reza Lashgari,  
Shahid Beheshti University, Iran

### Reviewed by:

Giulia Besutti,  
AUSL Reggio Emilia, Italy  
Bertrand De Meulder,  
European Institute for Systems  
Biology and Medicine (EISBM), France

### \*Correspondence:

Wei Chen  
cwjxl\_2006@163.com  
Jian Wang  
wangjian\_811@yahoo.com

<sup>†</sup>These authors have contributed  
equally to this work and share first  
authorship

### Specialty section:

This article was submitted to  
Infectious Diseases - Surveillance,  
Prevention and Treatment,  
a section of the journal  
Frontiers in Medicine

Received: 04 August 2021

Accepted: 03 November 2021

Published: 03 December 2021

### Citation:

Zhang Y-h, Hu X-f, Ma J-c, Wang X-q,  
Luo H-r, Wu Z-f, Zhang S, Shi D-j,  
Yu Y-z, Qiu X-m, Zeng W-b, Chen W  
and Wang J (2021) Clinical Applicable  
AI System Based on Deep Learning  
Algorithm for Differentiation of  
Pulmonary Infectious Disease.  
Front. Med. 8:753055.  
doi: 10.3389/fmed.2021.753055

<sup>1</sup> Department of Radiology, The First Affiliated Hospital of the Army Medical University (Southwest Hospital), Chongqing, China, <sup>2</sup> Deepwise Artificial Intelligence (AI) Lab, Deepwise Inc., Beijing, China, <sup>3</sup> Department of Radiology, Huangshi Central Hospital, Affiliated Hospital of Hubei Polytechnic University, Edong Healthcare Group, Huangshi, China, <sup>4</sup> Department of Radiology, Chongqing University Three Gorges Hospital, Chongqing, China, <sup>5</sup> Department of Radiology, Chongqing Three Gorges Central Hospital, Chongqing, China

**Objective:** To assess the performance of a novel deep learning (DL)-based artificial intelligence (AI) system in classifying computed tomography (CT) scans of pneumonia patients into different groups, as well as to present an effective clinically relevant machine learning (ML) system based on medical image identification and clinical feature interpretation to assist radiologists in triage and diagnosis.

**Methods:** The 3,463 CT images of pneumonia used in this multi-center retrospective study were divided into four categories: bacterial pneumonia ( $n = 507$ ), fungal pneumonia ( $n = 126$ ), common viral pneumonia ( $n = 777$ ), and COVID-19 ( $n = 2,053$ ). We used DL methods based on images to distinguish pulmonary infections. A machine learning (ML) model for risk interpretation was developed using key imaging (learned from the DL methods) and clinical features. The algorithms were evaluated using the areas under the receiver operating characteristic curves (AUCs).

**Results:** The median AUC of DL models for differentiating pulmonary infection was 99.5% (COVID-19), 98.6% (viral pneumonia), 98.4% (bacterial pneumonia), 99.1% (fungal pneumonia), respectively. By combining chest CT results and clinical symptoms, the ML model performed well, with an AUC of 99.7% for SARS-CoV-2, 99.4% for common virus, 98.9% for bacteria, and 99.6% for fungus. Regarding clinical features interpreting, the model revealed distinctive CT characteristics associated with specific pneumonia: in COVID-19, ground-glass opacity (GGO) [92.5%; odds ratio (OR), 1.76; 95% confidence interval (CI): 1.71–1.86]; larger lesions in the right upper lung (75.0%; OR, 1.12; 95% CI: 1.03–1.25) with viral pneumonia; older age ( $57.0 \text{ years} \pm 14.2$ , OR, 1.84; 95% CI: 1.73–1.99) with bacterial pneumonia; and consolidation (95.8%, OR, 1.29; 95% CI: 1.05–1.40) with fungal pneumonia.

**Conclusion:** For classifying common types of pneumonia and assessing the influential factors for triage, our AI system has shown promising results. Our ultimate goal is to assist clinicians in making quick and accurate diagnoses, resulting in the potential for early therapeutic intervention.

**Keywords:** pulmonary infectious disease, COVID-19, deep learning, computed tomography, pneumonia

## INTRODUCTION

Pneumonia is a leading cause of death, with mortality among older individuals (70 years) increasing by 33.6 percent between 2007 and 2017 (1). Bacterial pneumonia, viral pneumonia, fungal pneumonia, and parasitic pneumonia are the four types of pneumonia (2), each of which requires different treatment and has a varied prognosis. Rapid pathogen detection and identification are critical for guiding prompt and successful pneumonia therapies, resulting in faster clinical benefits, fewer problems, and lower hospital costs. The existing pneumonia pathogen testing method has various flaws, including low sensitivity and accuracy, long wait times, and high labor expenses. Non-specific medications, such as broad-spectrum antibiotics, might worsen sickness, and raise hospital expenses (3). More effective diagnostic methods with improved accuracy are required to reduce over-treatment.

Computed tomography (CT) plays an important role in the diagnosis of pneumonia. In the lack of a specific image clinical presentation, identifying pneumonia pathogens early and precisely is a major issue (4). Because the imaging signs of different types of pneumonia are similar, making it difficult for radiologists to identify and distinguish them with the naked eye. Furthermore, radiologists' inter-rater variability may result in conflicting outcomes. Artificial intelligence (AI) technologies, particularly deep learning (DL), offer a promising solution for such medical image interpretation, rapid identification, and classification, which can not only avoid doctor heterogeneity but also rapidly and automatically achieve higher diagnostic accuracy. Recent work using AI for the automated diagnosis of pneumonia has also yielded promising results (5–8). In pediatric chest X-rays, DL was used to identify and discriminate between bacterial and viral pneumonia (9, 10). Other studies (5, 11) used CT images to build DL models to identify COVID-19 and distinguish it from community-acquired pneumonia (CAP) and other lung diseases. However, because these studies were designed to focus solely on COVID-19 and normal CT, additional pneumonia manifestations such as bacterial pneumonia were not examined. The real-world situation, on the other hand, would not be similar to this setting. Furthermore, these studies only looked at the image manifestations of pneumonia and ignored the accompanying clinical factors. CT, in conjunction with clinical presentation, can produce a high detection result. Moreover, these approaches do not provide an interpretative study of the model's learning factors, and the prediction models that arise may not be useful in guiding early and quick identification of various pulmonary infections. Some studies (5, 9–11) utilized class activation maps (12), a sort of heat map that overlays CT

scans to indicate the important areas for model predictions. Although intuitive, these heat maps do not offer radiologists useful information for describing features or interpreting for fundamental clinical indications.

CT characteristics, also referred to as key imaging features or clinical indicators, include the number, location, and extents of different pulmonary lesions, such as ground-glass opacity (GGO) and consolidation. In recent studies of COVID-19 pneumonia, some of these CT characteristics, like lesions, have been exploited to monitor the progress of diseases (13). In contrast, others, like lesion location, were found to be risk factors for poor outcome (14). Although such accurate and automated quantification of these CT characteristics has already been made possible by machine learning-based algorithms, few studies have made efforts to assist radiologists in understanding the predicted results produced by the systems.

In this retrospective study, we aimed to develop and validate a CT-based DL system to classify pneumonia patients into four pathogenic types: common virus, bacteria, fungus, and SARS-CoV-2. This method will facilitate faster diagnosis and subsequently, more suitable treatment for pneumonia patients. Furthermore, we retrieved a slew of quantitative CT features or clinical indications, such as lesion numbers and location. In order to help radiologists in interpreting CT scans of pneumonia patients, we evaluated the relative relevance of each imaging feature in determining the pathogenic sources of pneumonia in a standard machine learning (ML) model/classifier.

## METHODS

### Patient Cohort and Data Collection

The ethics committees approved this multi-center retrospective study and written informed consent was waived because the data used for system development were de-identified by removing personal information. Patients with respiratory symptoms suggestive of pulmonary infection (fever, cough, and sputum production) were enrolled in this research, who underwent chest CT scanning and received laboratory confirmation of the underlying pathology of pneumonia: SARS-CoV-2, common virus, bacterium, or fungus. The four pathogens of pneumonia were identified using reverse transcriptase-polymerase chain reaction (RT-PCR) and culture and microscopic inspection of sputum, blood, or lung tissue samples. From January 2011 to February 2020, we gathered 7,487 anonymous lung CT images from 2,195 individuals using these first criteria. Then, individuals who had previously undergone thoracic surgery, had severe TB, or had no radiological indications of pneumonia were eliminated.

We also eliminated individuals with respiratory artifacts, less than three slices, or a thickness more than 3 mm on their CT images.

Finally, a total of 1,431 patients from three institutions were employed in this study to establish the classification system. **Figure 1** has more information on the inclusion and exclusion criteria, as well as a flowchart. To evaluate the robustness of our AI system in various clinical settings, the CT data obtained in this study came from a range of vendors, including Toshiba Medical Systems, Japan; GE Healthcare, USA; United Imaging, China; and Siemens Healthineers, Germany. All CT scans were obtained with a resolution of 512\*512 with slice spacing ranging from 0.625 to 3 mm in the axial direction. A tube voltage of 120 kVp was used for CT examinations. The automated tube current modulation approach was utilized to control the tube current (30–70 mAs). The examinations were carried out in helical mode with a helical pitch of 0.8125–0.984 mm.

## Overview of the AI System

We proposed a four pathogenic classification AI system for pneumonia that uses CT images as input and explains the interactions between the factors learned by the model (image and

clinical records) to help clinicians make accurate and efficient predictions (**Figure 2**). The suggested classifier consists of three tasks, the first two of which were trained using a deep learning model (DL system) with a convolution neural network based on the PyTorch frame [(15); **Figure 2B**], and the third by a machine learning method (ML system) (**Figure 2D**). Based on radiologists' recommendations, the first two CNN classifiers were developed: a bi-classifier for differentiating viral from non-viral pneumonia and a quad-classifier for the four pathogenic types. The given data was split into three sets with an 8:1:1 ratio for training, validation, and testing, while the third task combining images and medical records information to explain the clinical indicators.

## Construction of the Deep Learning System

The pipeline of our deep learning-based system included four key components: (a) an abnormal-slice identification model (normal or abnormal), (b) a segmentation model that segmented the lung lobe and the contour of the lesions, (c) a classification model that investigated multiple indicators of pneumonia and differentiated the types (bi-classifier or quad-classifier), and (d) a voting model that merged the CT slices-wise scores to generate a patient-level CT volume prediction. The abnormal

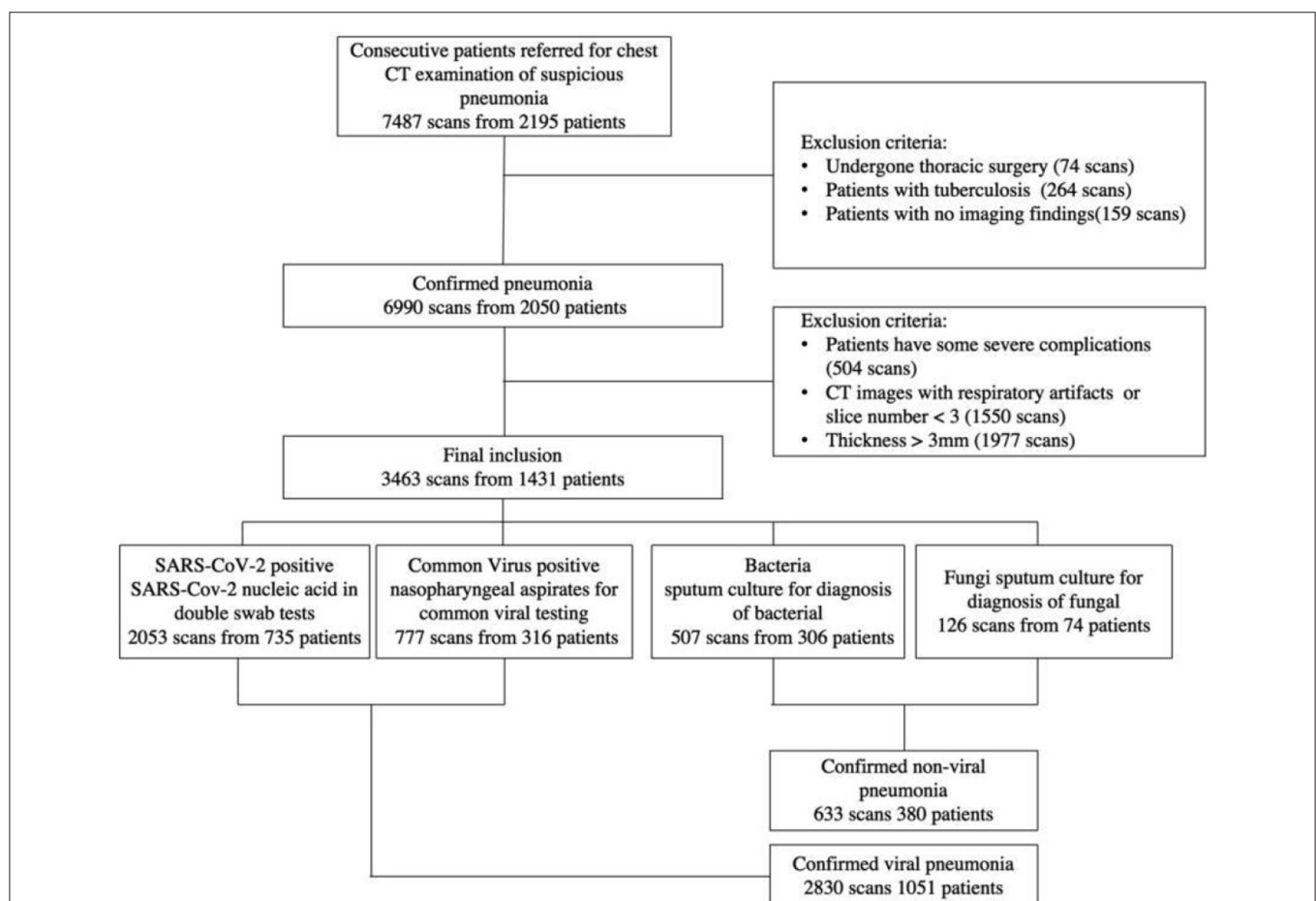
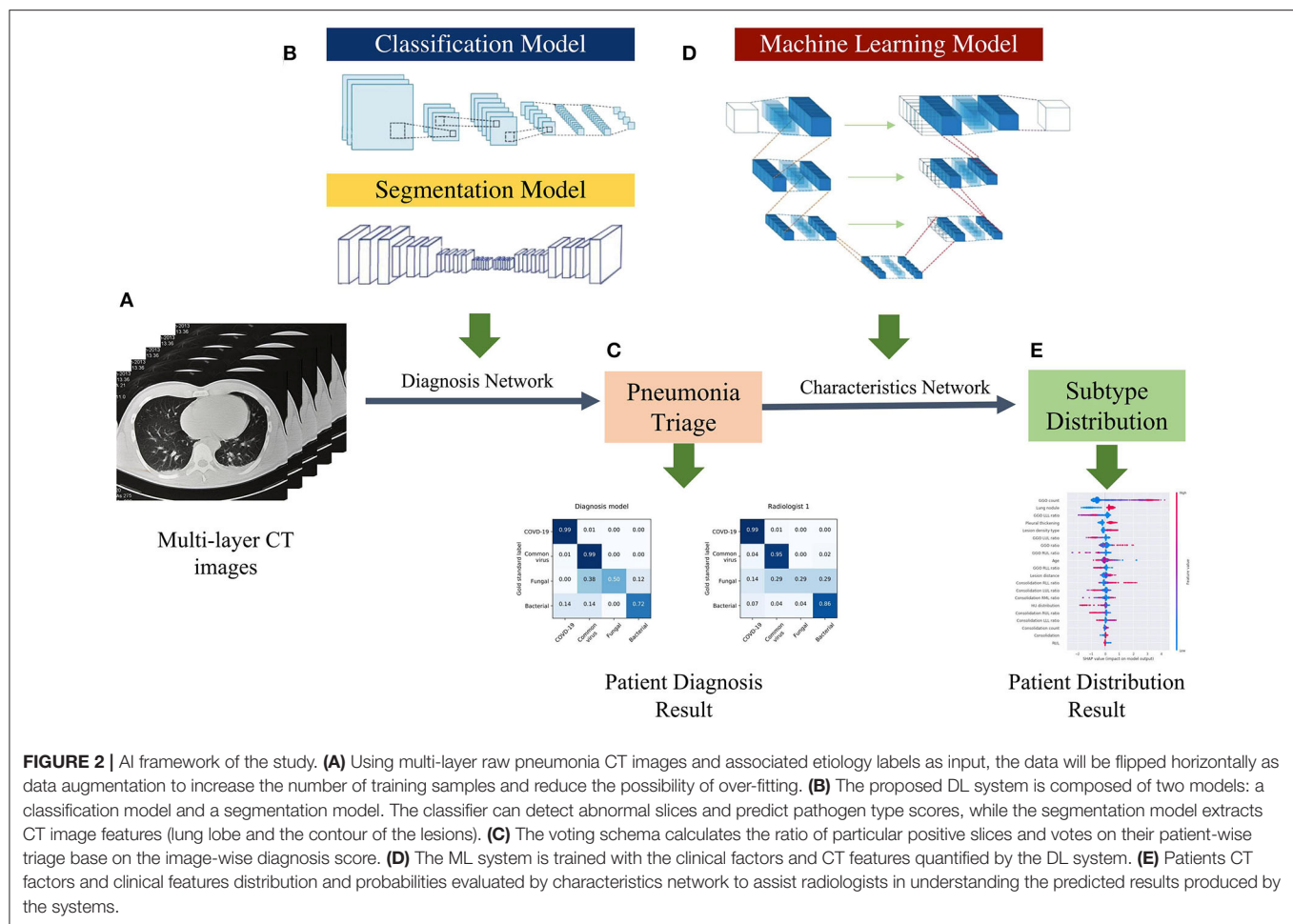


**FIGURE 1** | A flow diagram of the patient selection process with inclusion and exclusion criteria is shown. Between January 2011 and February 2020, this study included 2,195 patients from three institutions, 1,431 of whom were finally used to construct the classification system.



CT slices with pneumonia-related lesions were used to train a convolutional neural network (CNN)-based classifier for the pneumonia pathogens. Specifically, for CT volumes, we have developed modified ResNet-50 networks (16) for radiological abnormality identification. We also developed a novel lesion segment network architecture for contour extraction of lesions and lobes, based on the trained backbone parameters and further fusing the extracted feature (lesion size, counts) to imitate physician diagnostic practice. In order to extract 3D context information based on a given lesion slice, this module used continuous multi-slice CT images as input to learning the weights of different layers and adaptive modifies network learning parameters depending on spatial changes in lesions. Furthermore, the model was designed for multi-resolutions, and the information gathered at various resolutions is adaptable in order to provide a more complete information basis on lesions of varying sizes. The high cost of data collection and labeling influences the difficulty of modeling pneumonia framework. As a result, transfer learning was used to solve the problem of insufficient training data by first learning the specific weights of the neural network on the source data set such as ImageNet (17) and then re-learning the appropriate weights for some of the different instances of the target data set. By majority voting, the final score of the CNN classifier's prediction for all abnormal CT slices was merged to generate a patient-level CT

volume prediction. In the validation cohort, we preprocessed the given CT scan in the same way that we did in the training cohort. After that, the preprocessed image is sent to the backbone for predictions and majority voting. The code for reproducing the study's findings is available at <https://github.com/chiehchiu/CAAS>.

### Construction of the Machine Learning System

The DL system was built just to evaluate medical images, neglecting the complementary nature of medical records and visuals, as well as the need to see and comprehend the issue from several viewpoints. A written medical record reflects on the patient's health, and the image of the patient depicts the condition using the pathogenesis idea. The combination of both improves the patient's overall condition and reduces misdiagnosis.

To provide a comprehensive diagnosis of the image's clinical and case information, our machine learning-based system analyzes all data samples obtained from image and quantitative CT characteristics such as GGO count and location, as well as other clinical indicators such as sex and age, and to explain the interactions between the factors learned by the model. We utilized Shapley Additive exPlanation (SHAP) (18) on the XGBoost classifier (19) to analyze the contribution of each feature in detecting pneumonia pathogens (Figure 2D). The most important step in this model is the filtering of key features.



We need to filter several of the features obtained in the previous step (quantitative CT characteristics) to remove those that may cause model deviation and those with low correlation. The specific methods are as follows: (a) screening based on statistical features such as variance; (b) using the maximum correlation and minimum redundancy feature selection methods and the lasso feature selection method to regress the highly correlated features of the predicted target and obtain the key features with high stability, discrimination, and independence; and (c) based on the lasso feature selection method to get the best K features for preservation. To counteract the class imbalance in our dataset during model training, we also used down-sampling and over-sampling as needed.

## Expert Performance Assessment

Two groups of doctors with varying levels of experience (three junior radiologists [3–4 years of experience] and three senior radiologists [7–8 years of experience]) were asked to evaluate pneumonia cases solely on CT scans independently and blindly to establish a comparative baseline for our AI system. In group examinations of three physicians, annotated lesions were identified as positive samples whereas the lesions viewed by two or more radiologists were considered as true lesions.

## Statistical Analysis

The following measures were used to assess the performance of our classifiers: area under the receiver operating characteristic curve (AUC), accuracy, sensitivity, and specificity (20). The DeLong technique (21) was used to calculate the 95% confidence intervals (CIs) for the AUC. The median and interquartile range (IQR) with a 95% confidence interval (CI) are used to represent continuous variables. The ANOVA test was used to determine whether there was a difference between the two or four pathogenic categories of pneumonia patients (22). For categorical characteristics, the  $\chi^2$  or Fisher exact test (23) was employed to compare the pathogenic groups. All statistical tests were two-tailed, with statistical significance set at  $p < 0.05$ .

## RESULTS

### Study Population Characteristics

The study cohort included 1,431 laboratory-confirmed pneumonia patients with 3,463 chest CT scans, with 316

patients with 777 scans having viral pneumonia, 306 patients with 507 scans having bacterial pneumonia, 74 patients with 126 scans having fungus pneumonia, and 735 patients with 2,053 scans having COVID-19. The study comprised 779 men ( $49.6 \pm 15.6$ ; 14–94 years) and 652 women ( $48.9 \pm 14.8$ ; range, 15–90 years). According to the data split strategy, 2,990 CT series with 492,346 slices were utilized for training, 255 CT series with 41,825 slices were used for validation, and 218 CT series were used for testing (Table 1).

## Deep Learning-Based Pathogen Identification

The performance of our pneumonia pathogens classification system was assessed on test data and described in Table 2. The first level of the diagnostic system categorized the virus pneumonia (SARS-CoV-2, common virus) and non-virus pneumonia (bacterium, fungus). The proposed bi-classifier achieved an average AUROC of 0.984 (95% CI, 0.983–0.985) on slice-level and 0.988 (95% CI, 0.977–0.997) on patient-level, respectively. The performance results (cut-point yield maximum specificity plus specificity) showed a sensitivity of 0.931 (95% CI, 0.926–0.937), specific of 0.945 (95% CI, 0.943–0.947), accuracy of 0.939 (95% CI, 0.937–0.941) for slice-level and sensitivity of 0.959 (95% CI, 0.899–0.988), specific of 0.965 (95% CI, 0.938–0.992), accuracy of 0.961 (95% CI, 0.937–0.941) for patient-level. Then, within each categorized system, further sub-classifications and hierarchical layers were made, where applicable. Our quad-classifier also performed better on classifying SARS-CoV-2 and common virus [AUROC: 0.995 (0.990–0.998) and 0.986 (0.977–0.995)] than bacteria and fungus [AUROC: 0.984 (0.970–0.995) and 0.991 (0.978–1.000)], especially in terms of sensitivity of 0.978 (95% CI, 0.946–1.000) and specificity of 0.947 (95% CI, 0.915–0.977), which included both common non-viral pneumonia and viral pneumonia cases as binary distracters.

To identify positive cases, we also established cutoff values of the output probability value based on the findings, resulting in a high-sensitivity cutoff of 98% sensitivity for patient-wise classification and a high-specificity cutoff of 98% specificity. From this result, operating thresholds were defined as a probability of 0.15 [high sensitivity threshold; sensitivity, 0.979 (95% CI, 0.977–0.981); specificity, 0.795 (95% CI, 0.790–0.801)] and 0.91 [high specificity threshold; sensitivity, 0.836 (95%

**TABLE 1** | Summary of training + validation and testing datasets by four pathogenic types.

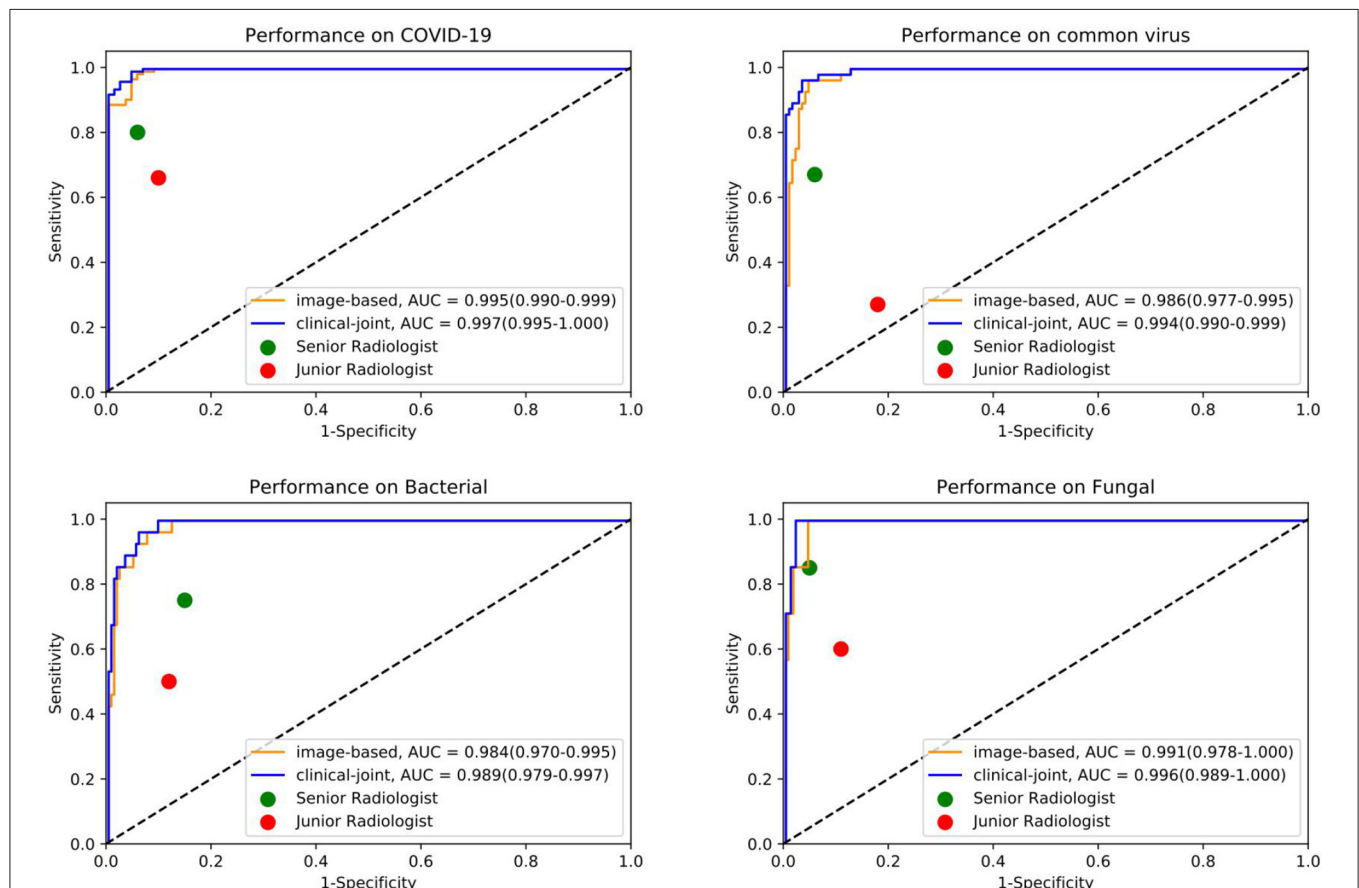
|                         | Training + validation |                 |                 |                 |           | Testing         |                 |                 |                 |           |
|-------------------------|-----------------------|-----------------|-----------------|-----------------|-----------|-----------------|-----------------|-----------------|-----------------|-----------|
|                         | COV-19                | Common          | Bacterial       | Fungal          | P-value   | COV-19          | Common          | Bacterial       | Fungal          | P-value   |
| Patients                | 688 (51.4%)           | 293 (21.9%)     | 287 (21.4%)     | 70 (5.2%)       | –         | 47 (50.5%)      | 23 (24.7%)      | 19 (20.4%)      | 4 (4.3%)        | –         |
| Scans                   | 1,925 (59.3%)         | 722 (22.2%)     | 480 (14.8%)     | 118 (3.6%)      | –         | 128 (58.9%)     | 55 (25.1%)      | 27 (12.3%)      | 8 (3.7%)        | –         |
| Slices                  | 374,862               | 89,310          | 55,328          | 14,671          | –         | 40,446          | 7,630           | 3,159           | 1,216           | –         |
| Male                    | 386 (56.1%)           | 154 (52.5%)     | 152 (52.9%)     | 37 (52.8%)      | 0.75      | 24 (51.1%)      | 13 (56.5%)      | 11 (57.9%)      | 2 (50.0%)       | 0.17      |
| Age $\geq 60$ years old | 144 (20.9%)           | 129 (44.0%)     | 122 (42.5%)     | 27 (38.6%)      | –         | 9 (19.1%)       | 9 (39.1%)       | 8 (42.1%)       | 2 (50.0%)       | –         |
| Age $< 60$ years old    | 544 (79.1%)           | 173 (56.0%)     | 165 (57.5%)     | 43 (61.4%)      | –         | 38 (80.9%)      | 14 (60.9%)      | 11 (57.9%)      | 2 (50.0%)       | –         |
| Mean age                | $47.6 \pm 14.7$       | $55.2 \pm 16.2$ | $56.6 \pm 14.3$ | $52.8 \pm 18.8$ | $< 0.001$ | $45.8 \pm 14.6$ | $57.9 \pm 15.0$ | $58.9 \pm 13.8$ | $52.1 \pm 21.4$ | $< 0.001$ |

Data presented as n (%) unless otherwise indicated. Mean ages are reported as mean  $\pm$  standard deviation. COV-19, COVID-19 pneumonia; common, common virus pneumonia.



**TABLE 2 |** The performance of the DL system in making multi-pathogenic types classification based on the CT cohort.

|         | Metric          | Bi-classifier           |                         |                         | Quad-classifier                            |                         |                         |                         |                         |
|---------|-----------------|-------------------------|-------------------------|-------------------------|--|-------------------------|-------------------------|-------------------------|-------------------------|
|         |                 | Mean                    | Viral                   | Non-viral               | Mean                                       | COV-19                  | Common                  | Bacterial               | Fungal                  |
| Testing | AUC (95%CI)     | 0.984<br>(0.983, 0.985) | 0.980<br>(0.979, 0.981) | 0.988<br>(0.987, 0.989) | 0.985<br>(0.983, 0.987)<br>(slice-level)   | 0.983<br>(0.982, 0.984) | 0.987<br>(0.986, 0.988) | 0.990<br>(0.989, 0.991) | 0.979<br>(0.974, 0.984) |
|         | Accuracy (%)    | 0.939<br>(0.937, 0.941) | 0.926<br>(0.924, 0.928) | 0.953<br>(0.951, 0.954) | 0.937<br>(0.934, 0.938)                    | 0.931<br>(0.929, 0.933) | 0.932<br>(0.930, 0.934) | 0.938<br>(0.936, 0.940) | 0.944<br>(0.942, 0.946) |
|         | Sensitivity (%) | 0.931<br>(0.926, 0.937) | 0.916<br>(0.914, 0.920) | 0.945<br>(0.938, 0.954) | 0.961<br>(0.955, 0.968)                    | 0.918<br>(0.915, 0.922) | 0.989<br>(0.985, 0.993) | 0.981<br>(0.975, 0.987) | 0.957<br>(0.943, 0.971) |
|         | Specificity (%) | 0.945<br>(0.943, 0.947) | 0.937<br>(0.934, 0.940) | 0.953<br>(0.951, 0.955) | 0.938<br>(0.936, 0.941)                    | 0.946<br>(0.943, 0.949) | 0.927<br>(0.925, 0.929) | 0.936<br>(0.934, 0.938) | 0.943<br>(0.941, 0.946) |
| Testing | AUC (95%CI)     | 0.988<br>(0.977, 0.997) | 0.993<br>(0.986, 0.998) | 0.983<br>(0.968, 0.996) | 0.989<br>(0.978, 0.997)<br>(patient-level) | 0.995<br>(0.990, 0.998) | 0.986<br>(0.977, 0.995) | 0.984<br>(0.970, 0.995) | 0.991<br>(0.978, 1.000) |
|         | Accuracy (%)    | 0.961<br>(0.936, 0.979) | 0.959<br>(0.932, 0.977) | 0.963<br>(0.941, 0.982) | 0.954<br>(0.933, 0.977)                    | 0.968<br>(0.954, 0.991) | 0.959<br>(0.941, 0.982) | 0.932<br>(0.900, 0.959) | 0.959<br>(0.936, 0.977) |
|         | Sensitivity (%) | 0.959<br>(0.899, 0.988) | 0.952<br>(0.924, 0.977) | 0.964<br>(0.875, 0.999) | 0.978<br>(0.946, 1.000)                    | 0.984<br>(0.969, 1.000) | 0.965<br>(0.919, 1.000) | 0.964<br>(0.897, 1.000) | 1.000<br>(1.000, 1.000) |
|         | Specificity (%) | 0.965<br>(0.938, 0.992) | 0.967<br>(0.937, 0.999) | 0.963<br>(0.937, 0.984) | 0.947<br>(0.915, 0.977)                    | 0.946<br>(0.900, 0.988) | 0.957<br>(0.933, 0.981) | 0.927<br>(0.892, 0.962) | 0.958<br>(0.933, 0.976) |

**FIGURE 3 |** The individual ROC curves of our image-based DL system and clinical-joint ML system in classifying the four pathogens of pneumonia on testing dataset. In the observer performance test, the AI system performed much better than all reader groups in terms of four type classification.

CI, 0.828–0.846); specificity, 0.980 (95% CI, 0.980–0.982)]. We plotted the AUC curves of our quad-classifier on each pathogenic category, as shown in **Figure 3**, which also showed a similar trend.

## Machine Learning-Based Feature Analysis

In this study, we utilized machine learning (ML) algorithms to integrate chest CT results (quantified by a DL system) with clinical symptoms in order to promptly diagnose patients who tested positive for four forms of pneumonia (**Table 3**). Then, using these features, determining the contribution of outcome to the prediction of pneumonia types. On the test set, we assessed the ML models and compared their performance to that of a DL system and two groups of radiologists with varying levels of expertise. The AUROC were calculated for both human readers and the two models in **Figure 3** and **Table 4**. The ML algorithm showed a satisfactory performance with an AUC of 0.997 (95% CI, 0.995–1.000) for SARS-CoV-2, 0.994 (0.990–0.999) for common virus, 0.989 (0.979–0.997) for bacteria, and 0.996 (0.989–1.000) for fungus. The senior radiologist using both the CT and corresponding clinical data achieved a 80.6% sensitivity (95% CI 76.4%, 84.7%;  $P = 0.0510$ ), 93.8% specificity (95% CI 88.5%, 97.1%;  $P = 0.005$ ) for Covid-19. The junior radiologist fellow using both the CT and clinical data achieved a 66.0% sensitivity (95% CI 57.1%, 74.5%;  $P < 1 \times 10^{-4}$ ), 90.3% specificity (95% CI 84.3%, 94.6%,  $P = 0.090$ ).  $P$ -values indicate the significance of difference in performance metric compared with respect to the joint model.

Regarding clinical features interpreting (**Table 3**), there are no significant difference in terms of sex ( $p = 0.80$ ) and age

( $P = 0.6$ ). The four pathogenic groups differed in most of the CT characteristics ( $p < 0.001$ ; **Figure 4**). Patient's age, lesion features such as GGO count, presence of lung nodule, and lesion density type, were significant features associated with SARS-CoV-2 status. The GGO features were identified as the most significant contributor to the evaluation of identifying COVID-19 from the four pneumonia types [odds ratio (OR), 1.76; 95% CI: 1.71–1.86;  $P = 0.003$ ]. Clinical parameters relating to the lesion location (right upper lung or, 1.12; 95% CI: 1.03–1.25,  $P = 0.01$ ) contributed to the prediction of viral pneumonia patients.

## DISCUSSION

In this study, we presented an effective clinically relevant AI system based on medical image identification and clinical feature interpretation system based on real-world datasets. The accuracy of our AI system for distinguishing the four common types of pneumonia were relatively high [COVID-19 (99.7%), common viral pneumonia (99.4%), bacterial pneumonia (98.9%), and

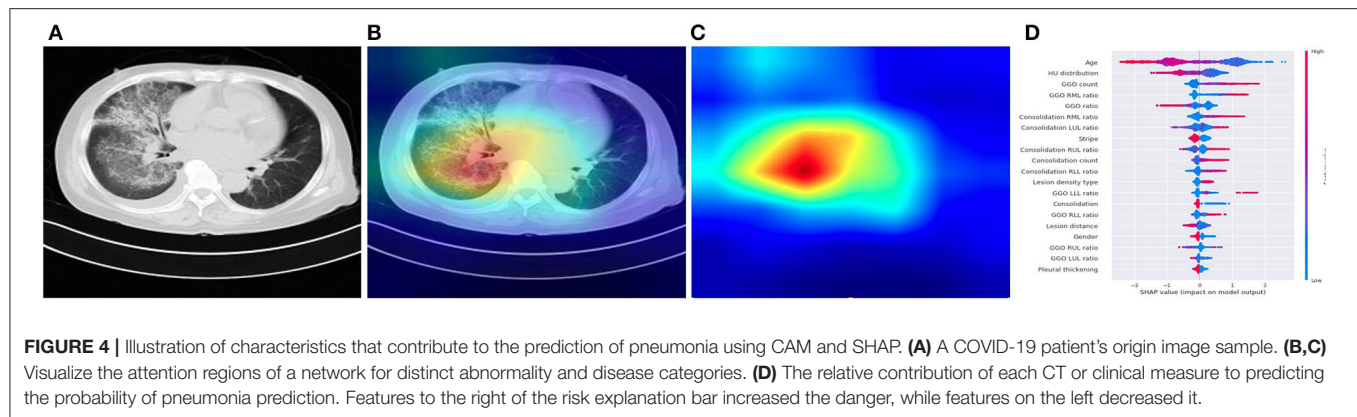
**TABLE 4 |** Receiver operating characteristic (ROC) of the Image-based model and Clinical-joint model.

|           | Image-based model    | Clinical-joint model | P-value |
|-----------|----------------------|----------------------|---------|
| COV-19    | 0.995 (0.990, 0.998) | 0.997 (0.995, 1.000) | 0.032   |
| Common    | 0.986 (0.977, 0.995) | 0.994 (0.990, 0.995) | 0.018   |
| Bacterial | 0.984 (0.970, 0.995) | 0.989 (0.979, 0.997) | <0.001  |
| Fungal    | 0.991 (0.978, 1.000) | 0.996 (0.989, 1.000) | <0.001  |

**TABLE 3 |** Lesion characteristics in CT image of different types of pneumonia.

|   | Metric               | COV-19        | Common       | Bacterial    | Fungal       | P-value |
|---|----------------------|---------------|--------------|--------------|--------------|---------|
| Characteristics                                     | Patients             | 670           | 268          | 241          | 70           | –       |
|   | Age (year)           | 47.5 + 14.7   | 55.7 + 15.0  | 57.0 + 14.2  | 52.8 + 18.9  | 0.6     |
|   | Sex (male)           | 371 (55.4%)   | 142 (53.0%)  | 126 (52.3%)  | 37 (52.1%)   | 0.80    |
| Total lesion percent (%)                            | –                    | 3.5 (7.9%)    | 15.7 (24.1%) | 5.7 (11.4%)  | 7.2 (17.0%)  | <0.001  |
| GGO percentage in each lung lobe (%)                | LUL (%)              | 3.4 (9.2%)    | 12.1 (20.5%) | 3.3 (9.2%)   | 4.8 (13.1%)  | <0.001  |
|   | LLL (%)              | 2.7 (9.2%)    | 16.2 (23.8%) | 4.6 (12.7%)  | 4.8 (13.8%)  | <0.001  |
|   | RUL (%)              | 1.7 (7.3%)    | 10.6 (19.8%) | 2.4 (6.6%)   | 3.8 (12.5%)  | <0.001  |
|   | RML (%)              | 1.3 (6.7%)    | 8.4 (17.6%)  | 0.5 (2.9%)   | 2.7 (10.6%)  | <0.001  |
|   | RLL (%)              | 2.7 (9.4%)    | 14.0 (21.7%) | 2.8 (8.8%)   | 3.3 (10.8%)  | <0.001  |
| Consolidation percentage in each lung lobe (%)      | LUL (%)              | 6.8 (14.5%)   | 9.4 (21.5%)  | 4.3 (9.4%)   | 12.1 (19.2%) | <0.001  |
|   | LLL (%)              | 13.9 (21.1%)  | 13.8 (26.7%) | 16.0 (20.0%) | 12.9 (21.5%) | 0.33    |
|   | RUL (%)              | 8.7 (16.8%)   | 11.2 (23.6%) | 6.2 (10.0%)  | 13.9 (21.5%) | <0.001  |
|   | RML (%)              | 8.6 (18.3%)   | 9.1 (20.6%)  | 3.1 (10.2%)  | 11.1 (21.5%) | <0.001  |
|   | RLL (%)              | 16.3 (22.8%)  | 14.4 (25.6%) | 14.9 (18.1%) | 17.4 (25.5%) | 0.17    |
| Density: HU distribution within lesions             | > –200 HU (%)        | 9 (0.4%)      | 43 (6.5%)    | 14 (4.0%)    | 9 (4.8%)     | 0.12    |
|   | –400~–200 HU (%)     | 96 (4.8%)     | 65 (9.8%)    | 68 (19.3%)   | 44 (23.4%)   | 0.25    |
|   | –600~–400 HU (%)     | 678 (34.0%)   | 264 (40.0%)  | 171 (48.4%)  | 84 (44.7%)   | <0.001  |
|   | < –600 HU (%)        | 1,209 (60.7%) | 287 (43.5%)  | 100 (28.3%)  | 51 (27.1%)   | <0.001  |
| Location: distance from lesion to pulmonary pleurae | Lesion distance (mm) | 4.8 ± 4.3     | 1.3 ± 2.6    | 2.2 ± 3.4    | 3.0 ± 3.3    | <0.001  |

GGO, ground glass opacity; RUL, right upper lobe; RML, right middle lobe; RLL, right lower lobe; LUL, left upper lobe; LLL, left lower lobe; HU, hounsfield unit. Data presented as n (%) unless otherwise indicated. Lesion distance are reported as mean ± standard deviation.



fungal pneumonia (99.6%)). Furthermore, using a specialized CT analysis, we retrieved dozens of quantitative CT features from the study cohort as CT findings or clinical indications. The GGO characteristics were found as the most important contributors in identifying the four pneumonia types. Notably, the COVID-19 patients had more GGO lesions; patients with common viral pneumonia were less likely to have bilateral lung infection; and patients with fungal pneumonia had a modest number of consolidation lesions. In this study, we present an AI system that outperforms immediate-level radiologists on differentiating the pulmonary infection based on CT scans. This fast imaging-based triaging system has the potential to be a non-culture technique for identifying common pneumonia, which would promote timely targeted antibiotic treatment for pneumonia patients and thus help reduce antimicrobial resistance, treatment side effects, and costs. During the COVID-19 pandemic, this system can also help stratify pneumonia patients for proper care or quarantine and thus lessen the burden of diagnosing numerous potentially infected patients. With the availability of more fine-grained pneumonia data, this system can easily be extended to recognize new strains or sub-strains of pulmonary infections.

Our DL system performed well in differentiating the four major kinds of pneumonia, and our results are somewhat more accurate than the prior AI study-based CT for COVID-19 diagnosis (24). Although CT is an essential tool for early detection of pneumonia, it is not as accurate in identifying the virus in the absence of clinical symptoms. In ML system, our joint AI model incorporates CT and clinical data, demonstrating that clinical information played a role in the accurate diagnosis of pneumonia in individuals in the early stage. Compared with radiologists, our CT image-based AI system can identify the possible pathogenic infectious pneumonia more quickly, and the accuracy is much improved, to timely guide clinical medication to maximize the patients' benefits. The timeliness and accuracy of AI can not only enable patients to get correct treatment decisions at an early stage, reduce hospitalization duration, and save treatment costs, but also significantly reduce the incidence of complications caused by delayed diagnosis and treatment decisions because of waiting for pathogen detection (25). The quantitative CT characteristics extracted from the study cohort by a dedicated CT analysis can help physicians to interpret

better the CT scan and the prediction made by our system, such as more GGO lesions in the COVID-19, less bilateral lung infection in common viral pneumonia, fungal pneumonia had a moderate amount of consolidation lesions. The SHAP explainer also supported this statistical observation on the XGBoost classifier built from these CT features, which revealed the top 20 most important CT characteristics for predicting the pathogens of pneumonia, including age, GGO ratio, lesion position, and consolidation. The listing of these CT features together with their relative importance to the pathogen classification provides a clinician instant valuable information, instead of a straight diagnosis suggestion, of a chest CT scan that can help them make an informed decision on the final diagnosis and treatment. It can also serve as a training tool for junior radiologists to interpret CT scans and make a better judgement.

The GGO features were identified as the most significant contributor in identifying the four pneumonia types. GGO has traditionally been non-specific and can be seen in all types of pneumonia (26, 27), but a recent study has found subtle differences in GGO between different diseases (28). Our study found that there were statistically significant differences in the distribution of GGO among the four pneumonia types, showing that our AI system could distinguish subtle differences in GGO from the four pneumonia types.

Our AI system combines the clinical advantages of CT and the intelligent advantages of AI, and has a good application prospect in clinical practice. In contrast to etiological tests such as RT-PCR, CT has some advantages. Although RT-PCR is the gold standard, but it also has certain instability. RT-PCR and other etiological tests can only make exclusive and definite diagnosis in the diagnosis of pneumonia, that is, RT-PCR can only detect covid-19 infection; CT, on the other hand, can simultaneously identify a variety of pathogens in the diagnosis process. And the detection rate of RT-PCR and other etiological tests is susceptible to some factors, such as variation in detection rate from different manufacturers, low patient viral load, or vulnerable clinical sampling (29), and so on. RT-PCR is prone to false negative results and may require repeated testing (30). So, compared with RT-PCR, CT is more economical and faster, and the CT scan showed more stable results and higher sensitivity (31).

Although our AI system was more accurate than human experts in this aspect, and have many advantages, it cannot completely replace the gold standard set by laboratory tests. Future research could be conducted to address the issues as mentioned earlier. For instance, our AI system can benefit from more data samples in the bacteria and fungus groups. Clinical or laboratory information (such as exposure history and blood biochemical examination) may be incorporated as an additional information source into our CT-based AI system to boost the classification accuracy.

There are some limitations in our research. Firstly, the incidence of fungal pneumonia is much lower than that of other pneumonia, so the data volume of fungal pneumonia is much smaller than that of other pneumonia, in subsequent studies, we will further expand the data of fungal pneumonia. Secondly, our data contains different examinations of the same patient at one admission, but there is no different scan reconstruction of the same examination. The reasons for this are as follows: (1) The amount of data is small; (2) For a certain patient, examinations that took place at different time were included in our study. For different examinations of the same admission, CT findings will present different characteristics according to different phases of the course of the disease. Therefore, training and testing with CT images of the same pathogen infection at different periods (progression/improvement) can improve the performance and robustness of the model. This approach might have some limitations regarding to metric calculation, but other studies (5) have also adopted a similar approach. Moreover, compared to their method, our data have broader inclusion criteria and are more in line with real clinical scenarios. When we built the model, the data of training set and test set were randomly selected, which would not have a great influence on the final result. And thirdly, due to geographical and other factors, we cannot obtain data from other countries, so we only conduct data analysis on Chinese patients. This does have some limitations. But we are willing to disclose the code release: (<https://github.com/chiehchiu/CAAS>), and very welcome more countries researchers use more diversified data for research.

In conclusion, we proposed a CT-based AI system that can assist clinicians in classifying patients into four pathogenic types efficiently and accurately by listing quantitative CT characteristics and their importance for making the prediction. This study takes the first step in developing a rapid, CT-based, non-culture diagnostic method to triage pneumonia patients for timely targeted treatment. The proposed classifier may be used in

pre-screening patients to conduct triage and fast-track decision making before RT-PCR.

## DATA AVAILABILITY STATEMENT

The data used in this work is subject to the following licenses/restrictions: data sets cannot be made public. Access to these datasets should be requested through Wei Chen at [cwjxl\\_2006@163.com](mailto:cwjxl_2006@163.com) or Jian Wang at [wangjian\\_811@yahoo.com](mailto:wangjian_811@yahoo.com).

## ETHICS STATEMENT

The studies involving human participants were reviewed and approved by the Ethics Committees of the First Affiliated Hospital of Army Medical University, PLA (Approval Number: KY2020036). Written informed consent for participation was not required for this study in accordance with the national legislation and the institutional requirements.

## AUTHOR CONTRIBUTIONS

JW, WC, Y-hZ, and X-fH all helped to conceptualize and design the study. X-mQ and W-bZ recruited patients. X-qW and H-rL sorted out the data. This manuscript was primarily written by Y-hZ, X-fH, and J-cM. Y-hZ, X-fH, J-cM, Y-zY, Z-fW, SZ, D-jS, WC, and JW analyzed the data. Y-hZ, X-fH, J-cM, SZ, WC, and JW provided feedback on prior drafts of the work. The final manuscript was read and approved by all writers.

## FUNDING

This work was supported in part by the Central Government Guided, the local special fund for Science and Technology Development, the local Science and Technology Innovation Projects (WX2017-07-05), the National Innovation Talent Promotion Program (4139Z2399), and the Beijing Municipal Science and Technology Planning Project (Grant No. Z211100003521009).

## ACKNOWLEDGMENTS

We would like to thank Editage ([www.editage.cn](http://www.editage.cn)) for English language editing.

## REFERENCES

- Roth GA, Abate D, Abate KH, Abay SM, Abbafati C, Abbasi N, et al. Global, regional, and national age-sex-specific mortality for 282 causes of death in 195 countries and territories, 1980–2017: a systematic analysis for the Global Burden of Disease Study 2017. *Lancet*. (2018) 392:1736–88. doi: 10.1016/S0140-6736(18)32203-7
- Templeton KE, Scheltinga SA, van den Eeden WCJFM, Graffelman AW, van den Broek PJ, Claas EC. Improved diagnosis of the etiology of community-acquired pneumonia with real-time polymerase chain reaction. *Clin Infect Dis*. (2005) 41:345–51. doi: 10.1086/431588
- Ho C-S, Jean N, Hogan CA, Blackmon L, Jeffrey SS, Holodniy M, et al. Rapid identification of pathogenic bacteria using Raman spectroscopy and deep learning. *Nat Commun*. (2019) 10:4927. doi: 10.1038/s41467-019-12898-9
- Garin N, Marti C, Carballo S, Darbellay Farhoumand P, Montet X, Roux X, et al. Rational use of CT-scan for the diagnosis of pneumonia: comparative accuracy of different strategies. *J Clin Med*. (2019) 8:514. doi: 10.3390/jcm8040514
- Li L, Qin L, Xu Z, Yin Y, Wang X, Kong B, et al. Using artificial intelligence to detect COVID-19 and community-acquired pneumonia based on pulmonary CT: evaluation of the diagnostic accuracy. *Radiology*. (2020) 296:E65–71. doi: 10.1148/radiol.2020200905



6. Huang L, Han R, Ai T, Yu P, Kang H, Tao Q, et al. Serial quantitative chest CT assessment of COVID-19: a deep-learning approach. *Radiol Cardiothor Imaging*. (2020) 2:e200075. doi: 10.1148/ryct.2020200075
7. Wang J, Bao Y, Wen Y, Lu H, Luo H, Xiang Y, et al. Prior-attention residual learning for more discriminative COVID-19 screening in CT images. *IEEE Trans Med Imaging*. (2020) 39:2572–83. doi: 10.1109/TMI.2020.2994908
8. Kanne JP, Bai H, Bernheim A, Chung M, Haramati LB, Kallmes DF, et al. COVID-19 imaging: what we know now and what remains unknown. *Radiology*. (2021) 299:E262–79. doi: 10.1148/radiol.2021204522
9. Kermayn DS, Goldbaum M, Cai W, Valentim CCS, Liang H, Baxter SL, et al. Identifying medical diagnoses and treatable diseases by image-based deep learning. *Cell*. (2020) 172:1122–31.e9. doi: 10.1016/j.cell.2018.02.010
10. Rajaraman S, Candemir S, Kim I, Thoma G, Antani S. Visualization and interpretation of convolutional neural network predictions in detecting pneumonia in pediatric chest radiographs. *Appl Sci*. (2018) 8:1715. doi: 10.3390/app8101715
11. Wang L, Gao YH, Lou LL, Zhang GJ. The clinical dynamics of 18 cases of COVID-19 outside of Wuhan, China. *Eur Respir J*. (2020) 55:2000398. doi: 10.1183/13993003.00398-2020
12. Bolei Z, Khosla A, Lapedriza A, Oliva A, Torralba A. Learning deep features for discriminative localization. In: *Proceedings of the IEEE Conference on Computer Vision and Pattern Recognition*. Las Vegas (2016). p. 2921–9.
13. Zhang K, Liu X, Shen J, Li Z, Sang Y, Wu X, et al. Clinically applicable AI system for accurate diagnosis, quantitative measurements, and prognosis of COVID-19 pneumonia using computed tomography. *Cell*. (2020) 181:1423–33.e11. doi: 10.1016/j.cell.2020.04.045
14. Yu Q, Wang Y, Huang S, Liu S, Zhou Z, Zhang S, et al. Multicenter cohort study demonstrates more consolidation in upper lungs on initial CT increases the risk of adverse clinical outcome in COVID-19 patients. *Theranostics*. (2020) 10:5641–8. doi: 10.7150/thno.46465
15. Paszke A, Gross S, Massa F, Lerer A, Bradbury J, Chanan G, et al. Pytorch: an imperative style, high-performance deep learning library. In: *Advances in Neural Information Processing Systems*. Vol. 32. Vancouver, CA (2019). p. 8026–37.
16. He K, Zhang X, Ren S, Sun J. Identity mappings in deep residual networks. In: *European Conference on Computer Vision*. Cham: Springer (2016). p. 630–45.
17. Krizhevsky A, Sutskever I, Hinton GE. ImageNet classification with deep convolutional neural networks. In: *Advances in Neural Information Processing Systems*. Vol. 25. Lake Tahoe (2012). p. 1097–105.
18. Lundberg SM, Nair B, Vavilala MS, Horibe M, Eisses MJ, Adams T, et al. Explainable machine-learning predictions for the prevention of hypoxaemia during surgery. *Nat Biomed Eng*. (2020) 2:749–60. doi: 10.1038/s41551-018-0304-0
19. Chen T, Guestrin C. XGBoost: a scalable tree boosting system. In: *Proceedings of the 22nd ACM SIGKDD International Conference on Knowledge Discovery and Data*. San Francisco, CA (2016). p. 785–94. doi: 10.1145/2939672.2939785
20. Puza B, O'Neill T. Generalised Clopper–Pearson confidence intervals for the binomial proportion. *J Stat Comput Simul*. (2020) 76:489–508. doi: 10.1080/10629360500107527
21. McHugh ML. The Chi-square test of independence. *Biochem Medica*. (2013) 23:143–9. doi: 10.11613/BM.2013.018
22. Raymond M, Rousset F. An exact test for population differentiation. *Evolution*. (1995) 49:1280–3. doi: 10.1111/j.1558-5646.1995.tb04456.x
23. Warman A, Warman P, Sharma A, Parikh P, Warman R, Viswanadhan N, et al. Interpretable artificial intelligence for COVID-19 diagnosis from chest CT reveals specificity of ground-glass opacities. *medRxiv [Preprint]*. (2020) 18. doi: 10.1101/2020.05.16.20103408
24. Chumbita M, Cillóniz C, Puerta-Alcalde P, Moreno-García E, Sanjuan G, García-Pouton N, et al. Can artificial intelligence improve the management of pneumonia. *J Clin Med*. (2020) 9:248. doi: 10.3390/jcm9010248
25. Chung M, Bernheim A, Mei X, Zhang N, Huang M, Zeng X, et al. CT imaging features of 2019 novel coronavirus (2019-nCoV). *Radiology*. (2020) 295:202–7. doi: 10.1148/radiol.2020200230
26. Bernheim A, Mei X, Huang M, Yang Y, Fayad ZA, Zhang N, et al. Chest CT findings in coronavirus disease-19 (COVID-19): relationship to duration of infection. *Radiology*. (2020) 295:200463. doi: 10.1148/radiol.2020200463
27. Li M, Narayan V, Gill RR, Jagannathan JP, Barile MF, Gao F, et al. Computer-aided diagnosis of ground-glass opacity nodules using open-source software for quantifying tumor heterogeneity. *AJR Am J Roentgenol*. (2017) 209:1216–27. doi: 10.2214/AJR.17.17857
28. Fang Y, Zhang H, Xie J, Lin M, Ying L, Pang P, et al. Sensitivity of chest CT for COVID-19: comparison to RT-PCR. *Radiology*. (2020) 296:E115–7. doi: 10.1148/radiol.2020200432
29. Khatami F, Saatchi M, Zadeh SST, Aghamir ZS, Shabestari AN, Reis LO, et al. A meta-analysis of accuracy and sensitivity of chest CT and RT-PCR in COVID-19 diagnosis. *Sci Rep*. (2020) 10:22402. doi: 10.1038/s41598-020-80061-2
30. Long C, Xu H, Shen Q, Zhang X, Fan B, Wang C, et al. Diagnosis of the coronavirus disease (COVID-19): rRT-PCR or CT? *Eur J Radiol*. (2020) 126:108961. doi: 10.1016/j.ejrad.2020.108961
31. Demler OV, Pencina MJ, D'Agostino RB. Misuse of DeLong test to compare AUCs for nested models. *Stat Med*. (2012) 31:2577–87. doi: 10.1002/sim.5328

**Conflict of Interest:** J-cM, Z-fW, SZ, D-jS, and Y-zY were employed by company Deepwise Inc.

The remaining authors declare that the research was conducted in the absence of any commercial or financial relationships that could be construed as a potential conflict of interest.

**Publisher's Note:** All claims expressed in this article are solely those of the authors and do not necessarily represent those of their affiliated organizations, or those of the publisher, the editors and the reviewers. Any product that may be evaluated in this article, or claim that may be made by its manufacturer, is not guaranteed or endorsed by the publisher.

Copyright © 2021 Zhang, Hu, Ma, Wang, Luo, Wu, Zhang, Shi, Yu, Qiu, Zeng, Chen and Wang. This is an open-access article distributed under the terms of the Creative Commons Attribution License (CC BY). The use, distribution or reproduction in other forums is permitted, provided the original author(s) and the copyright owner(s) are credited and that the original publication in this journal is cited, in accordance with accepted academic practice. No use, distribution or reproduction is permitted which does not comply with these terms.





# The Second Wave of COVID-19 in South and Southeast Asia and the Effects of Vaccination

Haitao Song<sup>1</sup>, Guihong Fan<sup>2</sup>, Yuan Liu<sup>3</sup>, Xueying Wang<sup>4</sup> and Daihai He<sup>3\*</sup>

<sup>1</sup> Complex Systems Research Center, Shanxi University, Taiyuan, China, <sup>2</sup> Department of Mathematics, Columbus State University, Columbus, OH, United States, <sup>3</sup> Department of Applied Mathematics, Hong Kong Polytechnic University, Kowloon, Hong Kong SAR, China, <sup>4</sup> Department of Mathematics and Statistics, Washington State University, Pullman, WA, United States

**Background:** By February 2021, the overall impact of coronavirus disease 2019 (COVID-19) in South and Southeast Asia was relatively mild. Surprisingly, in early April 2021, the second wave significantly impacted the population and garnered widespread international attention.

**Methods:** This study focused on the nine countries with the highest cumulative deaths from the disease as of August 17, 2021. We look at COVID-19 transmission dynamics in South and Southeast Asia using the reported death data, which fits a mathematical model with a time-varying transmission rate.

**Results:** We estimated the transmission rate, infection fatality rate (IFR), infection attack rate (IAR), and the effects of vaccination in the nine countries in South and Southeast Asia. Our study suggested that the IAR is still low in most countries, and increased vaccination is required to prevent future waves.

**Conclusion:** Implementing non-pharmacological interventions (NPIs) could have helped South and Southeast Asia keep COVID-19 under control in 2020, as demonstrated in our estimated low-transmission rate. We believe that the emergence of the new Delta variant, social unrest, and migrant workers could have triggered the second wave of COVID-19.

**Keywords:** COVID-19, Southeast Asia, South Asia, mathematical modeling, Delta variants, vaccination, infection attack rate, infection fatality rate

## OPEN ACCESS

### Edited by:

Reza Lashgari,  
Shahid Beheshti University, Iran

### Reviewed by:

Andree Kurniawan,  
University of Pelita Harapan, Indonesia  
Yang Xiang,  
Peng Cheng Laboratory, China

### \*Correspondence:

Daihai He  
daihai.he@gmail.com

### Specialty section:

This article was submitted to  
Infectious Diseases—Surveillance,  
Prevention and Treatment,  
a section of the journal  
Frontiers in Medicine

**Received:** 09 September 2021

**Accepted:** 11 November 2021

**Published:** 14 December 2021

### Citation:

Song H, Fan G, Liu Y, Wang X and  
He D (2021) The Second Wave of  
COVID-19 in South and Southeast  
Asia and the Effects of Vaccination.  
Front. Med. 8:773110.  
doi: 10.3389/fmed.2021.773110

## INTRODUCTION

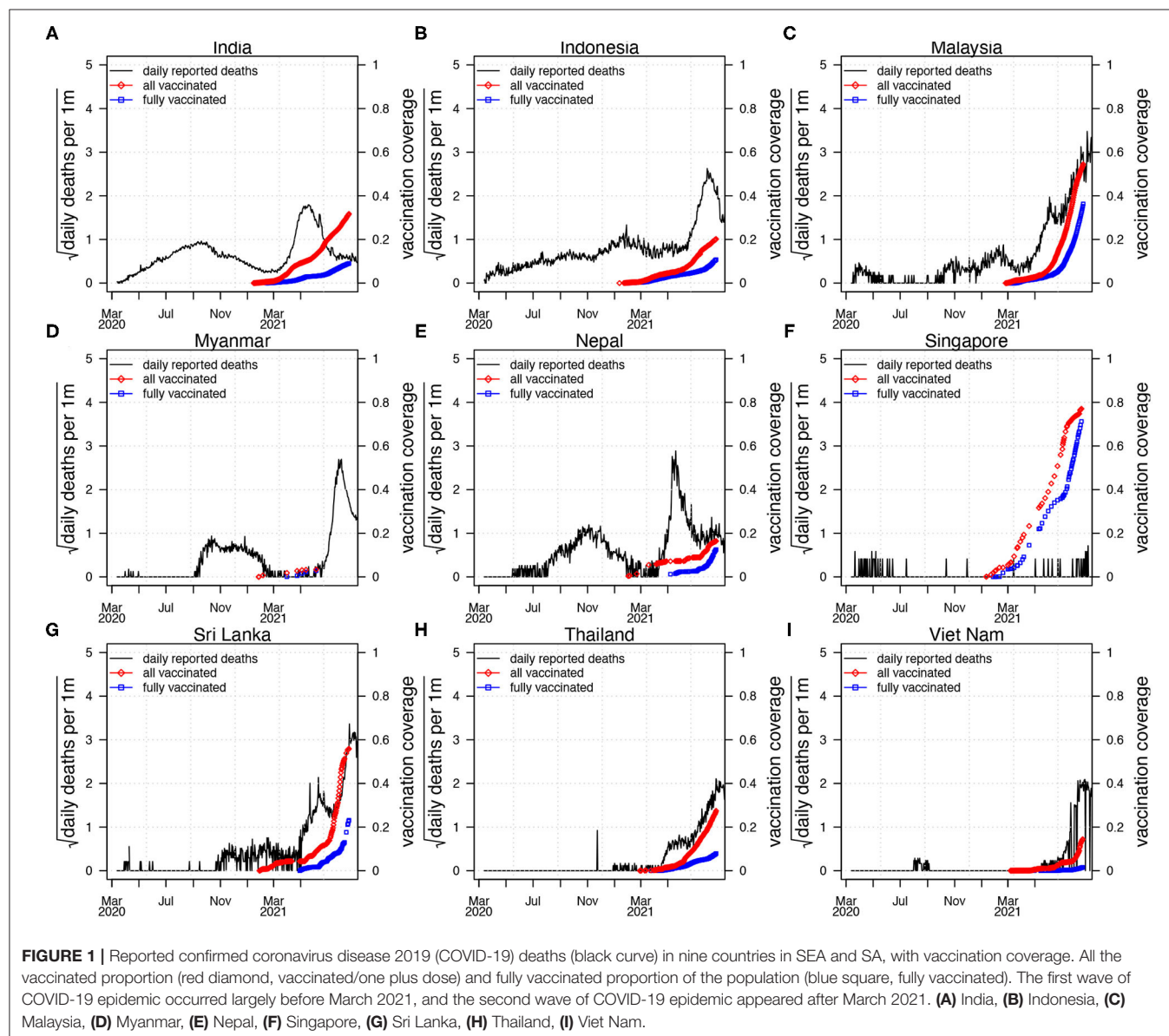
Coronavirus disease 2019 (COVID-2019) (caused by SARS-CoV-2) invaded the world unexpectedly in 2019 and changed human life tremendously (1). The SARS-CoV-2 virus is transmitted *via* respiratory droplets with an incubation period of 2–14 days (2). Common symptoms of light infection include fever, cough, and shortness of breath, while severe infections may require intensive care or ventilator support (2). Ever since the WHO declared the disease a pandemic on March 11, 2020 (3), there have been 199.67 million confirmed cases worldwide, and more than 4 million deaths were reported (4) as of August 4, 2021.

Coronavirus disease 2019 pandemic in South Asia (SA) and Southeast Asia (SEA) was mild in 2020 compared with other hot spots such as Europe or North America (see **Figure 1**). **Figure 1** shows the reported COVID-19 deaths in nine countries of SA and SEA, with the vaccination

coverage. However, the appearance of the new variants of concern (VOC) changed the nature of the pandemic dramatically in SA and SEA with a sudden increase of cases in many countries in this region (5). In Singapore, Vietnam, and Malaysia, COVID-19 was well-controlled at the earlier pandemic stages with both non-pharmacological interventions (NPI) (5), social media (6, 7), and vaccination. The emergence of new VOC has reversed this trend and caused a new wave of infection. Since April 2021, SA and SEA have been plagued by a new, more contagious Delta variant of COVID-19, which was the first reported in India in October 2020 (6) (see **Figure 2**). According to (6), the new variant was one of the main factors that accounted for the ongoing wave of COVID-19 in SA and SEA. In **Figure 2**, we show the strain (pre-Alpha strain and new variants) percentage sequenced in seven countries of SA and SEA where such data are available. We only show strain which

had a maximum percentage > 20%. The main picture is that the Delta variant replaced the pre-Alpha strain directly, while Alpha and Beta strains only dominated shortly in some of the seven countries.

The Delta variant caused an increasing crisis in Indonesia and other nearby regions (7, 9) (see **Figures 1, 2**). By August 18, 2021, SEA has been fighting with the highest COVID-19 death toll of the world caused by VOC, but enhanced by the relatively low coverage of vaccines (10). Based on the survey (11) by the Indian Council of Medical Research (ICMR), around 21.4% of 28,589 adolescent participants had been infected as of February 4, 2021. Another serological study (12) found that the prevalence of IgG antibody (indication of past infection) to SARS-CoV-2 was 11.4% in East Java, Indonesia. A serological study (13) among healthcare workers in the Kathmandu valley, Nepal, showed a 23% positivity



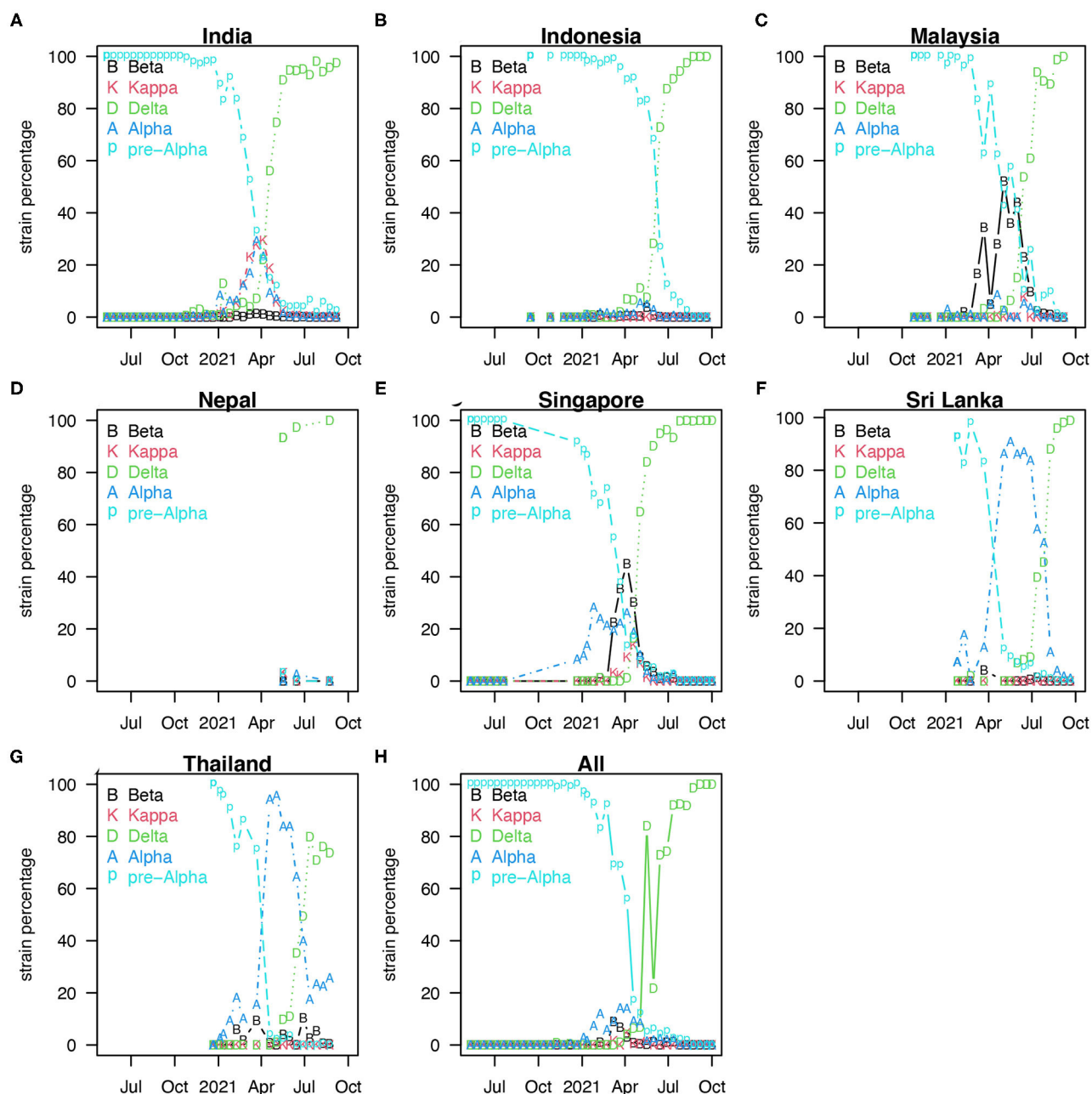


**FIGURE 2 |** Percentage of strains sequenced biweekly [strain percentage in seven countries of SA and SEA (A–G)] where variants sequenced data are available (8). We only show these strains with a maximum percentage > 20%. (H) Showed the median of strain percentage for each strain sequenced in the seven countries.

for polymerase chain reaction (PCR) testing. SARS-CoV-2 seroprevalence study (14) indicated that a symptom-based PCR-testing strategy missed 62% of COVID-19 diagnoses, and ~36% of individuals with SARS-CoV-2 infection were asymptomatic. These serological studies found a much higher infection attack rate (IAR, proportion of the infected population) than the estimated IAR based on reported cases. Therefore,

these serological studies should be considered in modeling if a reasonable IAR estimation and useful forecast for the pandemic is expected.

In Table 1, the survey in India involved 70 districts across India. Each district recruited 400 members of the general population (over 10 years old) and 100 healthcare workers. After adjustment for weighting and assay characteristics, for 28,598

**TABLE 1** | Coronavirus disease 2019 (COVID-19) serum survey conducted in three places.

| Time                  | Place                | People   | Blood serum   |
|-----------------------|----------------------|--|---|
| 2020/12–2021/01       | India                | 28,598(general population and healthcare workers (HCWs)) | Antibodies 24.1% with 23.0%–25.3% (95% CI)  |
| 2020/06–2020/12       | East Java, Indonesia | 1,819  | IgG antibody to SARS-CoV-2 was 11.4% (207/1,819)  |
| 2020/03/25–2020/07/25 | Singapore            | 198,320<br>migrant workers                               | 111,280 residents with a positive PCR or serology result, for an overall infection prevalence of 56.1% with 55.9–56.3% (95% CI) |

serum samples, the seropositive rate of antibodies against either N protein or S1 receptor-binding domain protein was 24.1% (15).

Because of the limited data on COVID-19 prevalence in Indonesia, there was an investigation into SARS-COV-2, which causes COVID-19 disease. From June to December 2020, 1,819 participants aged 16 years or older were recruited from Surabaya city. An overall 11.4% prevalence of IgG antibodies against SARS-COV-2 was observed in the subjects (see **Table 1**). Using a chi-squared test of categorical variables, there is a significant difference in the prevalence of SARS-COV-2 antibodies between working and occupational groups. A higher prevalence of IgG was detected in laboratory technicians (22.2%) compared with healthcare workers (6.0%) directly treating patients with COVID-19 and other healthcare workers (2.9%) (12).

As a part of the national public health response to COVID-19, PCR and serum tests were conducted on migrant workers residing in all dedicated hostels in Singapore between March 25 and July 25, 2020. This included 43 dormitories with a total population of 198,320 (63.6% underwent PCR testing, and 68.4% underwent serological testing). PCR or serological results were positive in 111,280 inhabitants, with an overall infection rate of 56.1% (and 55.9–56.3% of 95% CI) (16) (see **Table 1**).

## MATERIALS AND METHODS

Mathematical modeling has been successfully used to forecast COVID-19 trends and has assisted public health organizations in policy making. This article uses a simple compartmental epidemic model. Our model considers a time-dependent transmission rate since both changes in human behavior, and the use of control measures can alter the transmission rate of the disease. Other epidemiological parameters such as the latency period and the infection fatality rate (IFR) may vary as well. To simplify the model, we focus only on the time-varying transmission rate and assume that other parameters are constant.

The population is divided into susceptible (*S*), exposed (*E*), infectious (*I*), hospitalized or delayed (*T*), death (*D*), and recovered/immunized classes (*R*), respectively. Susceptible individuals can become exposed after getting contact with an infectious person. Exposed individuals can become infectious after the latency period. Infectious individuals can move to the hospitalized (or delayed) classes and recovered/immunized classes. Hospitalized (or delayed) individuals may die or survive and recover/be immunized. In addition, recovered/immunized individuals become susceptible after vaccine immunization failure. We choose the model and parameter values from (11, 17,

18), with the addition of vaccination.

$$\dot{S} = -\beta SI - \eta \tilde{v}(t - \tau)S$$

$$\dot{E} = \beta SI - \sigma E$$

$$\dot{I} = \sigma E - \gamma I$$

$$\dot{T} = \phi \gamma I - \kappa T$$

$$\dot{D} = \theta \kappa T$$

$$\dot{R} = (1 - \phi) \gamma I + (1 - \theta) \kappa T + \eta \tilde{v}(t - \tau)S$$

Here, *S*, *E*, *I*, and *R* are susceptible, exposed, infectious, and recovered/immunized classes, respectively. *T* denotes a delay class between infectious and death classes, while *D* denotes death class.  $\beta$  denotes a time-varying transmission rate which is modeled using an exponential cubic spline (19–21) with a fixed number of nodes ( $n_\beta = 9$ ) evenly cover the study period. Parameters  $\sigma$ ,  $\gamma$ , and  $\kappa$  are rates at which the individual loses exposed status and infectious status,  $\sigma = 0.5$  days,  $\gamma = 1/3$  days, and  $\kappa = 1/12$  days. Thus, we have a mean generation time ( $\sigma^{-1} + \gamma^{-1}$ ) of 5 days and a mean delay between loss of infectiousness to death 12 days that are well in line with estimates in previous studies (22). The IFR is  $\phi\theta$ . One cannot estimate simultaneously  $\phi$  and  $\theta$  with only the death data. Thus, we choose to fix  $\phi$  and estimate  $\theta$ . Parameter  $\tilde{v}$  is the vaccination rate per capita among unvaccinated. The rate at which susceptible individuals get vaccinated is  $\tilde{v}(t) = v(t)/(1 - \int_0^{t-1} v(s)ds)$ , where  $v(s)$  represent the vaccination rate per capita among all population per day. When we incorporated this effective vaccination rate, we considered a delay of 2 weeks ( $\tau$ ) for the vaccine to take effect and uniform vaccine efficacy of  $\eta = 85\%$ . We note that this is the simplest model for this situation. Given that seven of the nine countries have a vaccination coverage (fully vaccinated) of less than 20%, the effect of the vaccination in these seven countries would be mild. In Malaysia and Singapore, especially in Singapore, the vaccination coverage is high, and we first fit the model with the vaccination, then we simulated our fitted model without vaccination. Thus, we showed the effects of the vaccination campaign. We used the famous R package POMP. A detailed description of the usage of this package on epidemiological models can be found here (23–25). We provide sensitivity analyses in the **Supplementary Material**, where we consider different number of nodes in the transmission rate ( $n_\beta = 8$ ), a lower vaccine efficacy ( $\eta = 75\%$ ), and different model structure (i.e., with an explicitly vaccinated class with a reduced susceptibility) and reduced IFR due to vaccination.

We fit a unified model to the reported COVID-19 deaths in nine countries in this region. Our study period is from March 11,



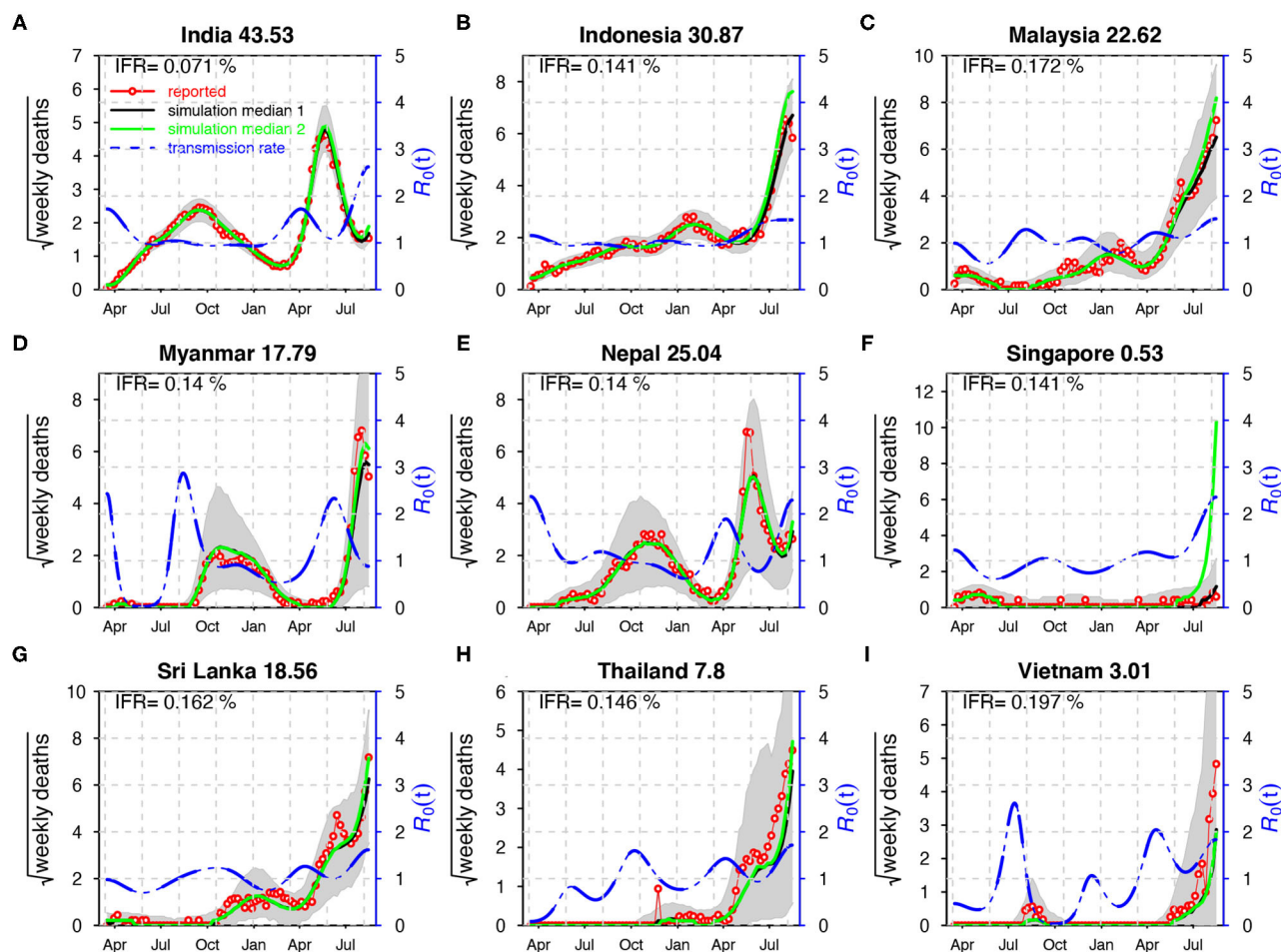


**FIGURE 3 |** Fitting the model to the reported deaths in India (A), Indonesia (B), Malaysia (C), Myanmar (D), Nepal (E), Singapore (F), Sri Lanka (G), Thailand (H), and Viet Nam (I) with a time-varying transmission rate. The red circles denote the daily reported COVID-19 deaths. The black curve denotes the median of 1,000 model simulations with vaccination, while the green curve shows the simulation median without vaccination. The shaded region denotes the 95% CI of the 1,000 model simulations. The blue-dashed curve denotes the reconstructed transmission rate.  $\phi = 0.008$  for India;  $\phi = 0.03$  for other countries. Here,  $R_0 = \beta(t)/\gamma$ . The IFR is shown in each panel and the IAR is shown above each panel.

2020 to August 17, 2021. We assume the transmission rate to be an exponential cubic spline function spanning the whole time series. This semi mechanistic approach of modeling multiple waves of infections has been successfully used in the previous epidemics and pandemics.

## RESULTS

Using data from the WHO dashboard, **Figure 1** shows the confirmed COVID-19 deaths and vaccination coverage (including partly vaccinated and fully vaccinated) of the nine countries (India, Indonesia, Malaysia, Myanmar, Nepal, Singapore, Sri Lanka, Thailand, and Vietnam). These nine countries account for most deaths in SA and SEA (26). **Figure 1** shows that the first wave of COVID-19 epidemic remains relatively low, while the second wave causes a much higher

level of COVID-19 pandemic when specific vaccine coverage is achieved.

**Figure 2** shows the percentage of strains sequenced biweekly (strain percentage) in the seven countries of SA and SEA where variants sequenced data are available (8). Panel h shows the median of strain percentage for each strain sequenced in the seven countries. The overall strain-dominance pattern in SA and SEA is that Delta strain replaced pre-Alpha directly, while Alpha and Beta strains only dominated in some among the seven countries but not all.

In **Figure 3**, the SEITDR (Susceptible-Exposed-Infectious-Hospitalized-Death-Recovered/immunized) model simulated the reported deaths from COVID-19 for the nine countries in SA and SEA and investigated the dynamics of COVID-19 in this region. The fitting results were used to evaluate the time-varying transmission rate [in terms of reproduction number  $R_0(t)$ ] for each country. From **Figure 3**, except for Singapore, all other



eight countries shared a similar pattern: a lower level of the first wave and a higher level of the second wave of infection of COVID-19. Our model simulation well-matched the reported deaths in the nine countries. The IFR is similar in most of the countries at a level of 0.21% except for India at a level of 0.071%. The transmission rate varied dramatically in some countries, likely due to invasion of new variants and on-off of control measures. The red circles are the daily reported deaths; the black curve denotes the median of 1,000 model simulations; the shaded region denotes the 95% CI of the 1,000 simulations. The green curve shows the simulation median without vaccination while other parameters were kept. The blue-dashed curve denotes the reconstructed time-varying transmission rate. The deviation of the green and the black curves illustrates the effects of the vaccination. Results of sensitivity analyses are provided in **Supplementary Figures S1–S4**. We found that our results in the main text are robust to a variety of parameter and model modifications.

## DISCUSSION AND CONCLUSION

Ever since the emergence of COVID-19 in 2019, it has spread worldwide (more than 200 countries and territories) rapidly. Countries in SA and SEA have implemented prevention and mitigation strategies to combat COVID-19 pandemic, including testing, contact tracing, and border control (5). In **Table 1**, we compare three serum surveys in the three locations. The Indian government-initiated serum surveys indicate a 24.1% positivity of serum antibody (15). An 11.4% overall prevalence of IgG antibodies is demonstrated, but the prevalence of IgG in laboratory technicians was much higher than in other professions in East Java, Indonesia (12). The Singapore government tested all the migrant workers in dedicated hostels through PCR and serological methods within 4 months and obtained an overall infection rate of 56.1% (16).

**Figure 1** shows COVID-19 death and vaccination coverage trends in SA and SEA, and demonstrates that COVID-19 epidemic first wave infections remain relatively low without vaccination coverage. In contrast, COVID-19 epidemic second wave infections attained a much higher level, likely due to invasion of the Delta strain (see **Figure 2**) and possibly relaxing of control measures.

It is well-recognized that because of the implementation of NPIs, COVID-19 pandemic in SA and SEA was kept under control in 2020 (5). Subsequently, a new wave of COVID-19 pandemic has appeared in 2021. The emergence of VOC was believed to be one of the key driving factors for the second wave of COVID-19 in SA and SEA (6). Except for this common factor, the second wave of COVID-19 demonstrates some unique features that vary between countries. Multiple factors (including a lack of nationwide preparations and poorly implemented or enforced health and safety precautions during festivals, sporting events, and state/local elections) could have caused the rapid expansion of the epidemic in India and resulted in a large number of deaths. The test positivity rate increased dramatically

from 2% on March 1 to 22% on May 1 during the second wave in India. In Myanmar, a series of events in February 2021 possibly treated national health and favored the spread of the virus (27). The second wave in Nepal worsened possibly due to the returning of many migrant workers from neighboring countries (23). In Thailand, a group of young, urban, upper-middle class individuals got infected after visiting nightclubs and restaurants in Bangkok during the long weekend. Then, the disease spread to their families and relatives and across the whole country quickly (28). All these particular reasons could have caused the second wave of COVID-19 to worsening SA and SEA. The reasons for low IFR estimated here include that we assume that COVID-19 death data were accurate. In reality, deaths were under reported. While the serological studies in these countries suggested that a large proportion of the population had been infected. The IFR may be regarded as a ratio of infection to reported death rather than the true IFR in these countries.

This work has several limitations, including the assumption that all parameters are constant except for the transmission rate and that the model is for the whole country while we ignored the heterogeneity across age groups and regions. This study relies on the reported death data and adopted a non-mechanistic cubic spline type of transmission rate. Alternatively, one could consider explicitly incorporating all kinds of control measures (such as the Google mobility matrix) into their model and expect to get more insightful observations on the transmission status of COVID-19 in SA and SEA. This work should be treated as a simple conceptual modeling attempt to estimate the size of the epidemic (IAR) in this region and the associated large-scale trends. Our estimated IAR is essentially in line with serological studies, and we illustrate the effects of vaccination *via* a straightforward approach. The actual IFR and vaccination effect are much more challenging to model. Nevertheless, we have laid the groundwork for further improvement.

Before the vaccine coverage reaches sufficiently high level, public health department must establish and maintain strong public health infrastructure and NPI to respond effectively to combat COVID-19 pandemic in places where the IAR was low and vaccination coverage was high, vaccination saved a lot of lives.

## DATA AVAILABILITY STATEMENT

Publicly available datasets were analyzed in this study. The data are from World Health Organization website.

## AUTHOR CONTRIBUTIONS

DH, HS, and GF conceived the study, performed data analysis, and wrote the draft. DH, HS, YL, XW, and GF discussed the results, revised the manuscript critically, and approved it for publishing. All authors contributed to the article and approved the submitted version.

## FUNDING

This study described in this article was partially supported by a grant from the Research Grants Council of the Hong Kong Special Administrative Region, China (HKU C7123-20G), the Fund Program for the Scientific Activities of Selected Returned Overseas Professionals in Shanxi Province (20200001), the National Natural Science Foundation of China (12171291),

and the Key Research and Development Project in Shanxi Province (202003D31011/GZ).

## SUPPLEMENTARY MATERIAL

The Supplementary Material for this article can be found online at: <https://www.frontiersin.org/articles/10.3389/fmed.2021.773110/full#supplementary-material>

## REFERENCES

- Niu Y, Rui J, Wang Q, Zhang W, Chen Z, Xie F, et al. Containing the transmission of COVID-19: a modeling study in 160 countries. *Front Med.* (2021) 2021:1322. doi: 10.3389/fmed.2021.701836
- CDC. Centers for Disease Control and Prevention Coronavirus Disease 2019 (COVID-19). (2020). Available online at: <https://www.cdc.gov/coronavirus/2019-ncov/index.html> (accessed September 9, 2021).
- WHO. WHO Director-General's Opening Remarks at the Media Briefing on COVID-19-11 March 2020. (2020). Available online at: <https://www.who.int/director-general/speeches/detail/who-director-general-s-opening-remarks-at-the-media-briefing-on-covid-19--11-march-2020> (accessed September 9, 2021)
- Hopkins J. Coronavirus Resource Center, Johns Hopkins University. Available online at: <https://coronavirus.jhu.edu/data>; <https://coronavirus.jhu.edu/map.html> (accessed September 9, 2021).
- Fauzi MA, Paiman N. COVID-19 pandemic in Southeast Asia: intervention and mitigation efforts. *Asian Educ Dev Stud.* (2020) 10:176–84. doi: 10.1108/AEDS-04-2020-0064
- Rambaut A, Holmes EC, O'Toole A, Hill V, McCrone JT, Ruis C, et al. A dynamic nomenclature proposal for SARS-CoV-2 lineages to assist genomic epidemiology. *Nat Microbiol.* (2020) 5:1403–7. doi: 10.1038/s41564-020-0770-5
- Chookajorn T, Kochakarn T, Wilasang C, Kotanan N, Modchang C. Southeast Asia is an emerging hotspot for COVID-19. *Nat Med.* 27:1495–6. doi: 10.1038/s41591-021-01471-x
- Our World in Data. Variant of Concern Sequenced Proportion. (2021). Available online at: <https://ourworldindata.org/grapher/covid-variants-area> (accessed November 1, 2021).
- Dyer O. Covid-19: Indonesia becomes Asia's new pandemic epicentre as delta variant spreads. *BMJ.* (2021) 374:n1815. doi: 10.1136/bmj.n1815
- IFRC. COVID-19: Southeast Asia Battles World's Highest Deaths. (2021). Available online at: <https://reliefweb.int/report/indonesia/covid-19-southeast-asia-battles-world-s-highest-deaths> (accessed August 18, 2021).
- Song H, Fan G, Zhao S, Li H, Huang Q, He D. Forecast of the COVID-19 trend in India: A simple modelling approach[J]. *Math Biosci Eng.* (2021) 18:9775–86. doi: 10.3934/mbe.2021479
- Megasari NL, Utsumi T, Yamani LN, Gunawan E, Furukawa K, Nishimura M, et al. Seroepidemiological study of SARS-CoV-2 infection in East Java, Indonesia. *PLoS ONE.* (2021) 16:e0251234. doi: 10.1371/journal.pone.0251234
- Pandey KR, Bhattarai A, Pant S, Barakoti R, Pandey J, Subedee A, et al. Seroprevalence of COVID-19 among health workers in the Kathmandu valley, Nepal (SEVID-KaV): a longitudinal cohort study. *Res Square.* (2021). doi: 10.21203/rs.3.rs-626260/v1
- Ng OT, Marimuthu K, Koh V, Pang J, Linn KZ, Sun J, et al. SARS-CoV-2 seroprevalence and transmission risk factors among high-risk close contacts: a retrospective cohort study. *Lancet Infect Dis.* (2021) 21:333–43. doi: 10.1016/S1473-3099(20)30833-1
- Murhekar MV, Bhatnagar T, Thangaraj JW, Saravanakumar V, Kumar MS, Selvaraju S, et al. SARS-CoV-2 seroprevalence among the general population and healthcare workers in India, December 2020–January 2021. *Int J Infect Dis.* (2021) 108:145–55.
- Tan IB, Tan C, Hsu LY, Dan YY, Aw A, Cook AR, et al. Prevalence and outcomes of SARS-CoV-2 infection among migrant workers in Singapore. *JAMA.* (2021) 325:584–5. doi: 10.1001/jama.2020.24071
- He D, Artzy-Randrup Y, Musa SS, Stone L. The unexpected dynamics of COVID-19 in Manaus, Brazil: herd immunity versus interventions. *medRxiv [Preprint].* (2021). doi: 10.1101/2021.02.18.21251809
- Musa SS, Wang X, Zhao S, Li S, Hussaini N, Wang W, He D. The heterogeneous severity of COVID-19 in African countries: a modeling approach. *Res Square.* (2021). doi: 10.21203/rs.3.rs-316589/v1
- Burden RL, Faires JD. *Numerical Analysis 8th ed.* Boston, MA: Thomson Brooks/Cole (2005).
- Bartels RH, Beatty JC, Barsky BA. *An Introduction to Splines for Use in Computer Graphics and Geometric Modeling.* Burlington, MA: Morgan Kaufmann (1995).
- Vetterling WT, Press WH, Teukolsky SA, Flannery BP. *Numerical Recipes: Example Book C (The Art of Scientific Computing).* Cambridge: Press Syndicate of the University of Cambridge (1992).
- Tang X, Musa SS, Zhao S, Mei S, He D. Using proper mean generation intervals in modeling of COVID-19. *Front Public Health.* (2021) 9:691262. doi: 10.3389/fpubh.2021.691262
- King AA, Nguyen D, Ionides EL. Statistical inference for partially observed Markov processes via the R package pomp. *arXiv preprint arXiv:1509.00503* (2015). doi: 10.18637/jss.v069.i12
- King AA. *Working With Ordinary Differential Equations in Pomp.* (2017). Available online at: <https://kingaa.github.io/clim-dis/parest/odes.html> (accessed November 1, 2021).
- King AA, Ionides EL, Lin Q. *Simulation-Based Inference for Epidemiological Dynamics.* (2019). Available online at: <https://kingaa.github.io/sbied/> (accessed November 1, 2021).
- WHO. WHO Coronavirus (COVID-19) Dashboard. (2021). Available online at: <https://covid19.who.int/> (accessed September 9, 2021).
- Han SM, Lwin KS, Swe KT, Gilmour S, Nomura S. Military coup during COVID-19 pandemic and health crisis in Myanmar. *BMJ Global Health.* (2021) 6:e005801. doi: 10.1136/bmjgh-2021-005801
- Tanomkiat W. The third COVID-19 wave in Thailand. *ASEAN J Radiol.* (2021) 22:03–4. doi: 10.46475/aseanjr.v22i1.125

**Conflict of Interest:** The authors declare that the research was conducted in the absence of any commercial or financial relationships that could be construed as a potential conflict of interest.

**Publisher's Note:** All claims expressed in this article are solely those of the authors and do not necessarily represent those of their affiliated organizations, or those of the publisher, the editors and the reviewers. Any product that may be evaluated in this article, or claim that may be made by its manufacturer, is not guaranteed or endorsed by the publisher.

Copyright © 2021 Song, Fan, Liu, Wang and He. This is an open-access article distributed under the terms of the Creative Commons Attribution License (CC BY). The use, distribution or reproduction in other forums is permitted, provided the original author(s) and the copyright owner(s) are credited and that the original publication in this journal is cited, in accordance with accepted academic practice. No use, distribution or reproduction is permitted which does not comply with these terms.



# Modeling COVID-19 Transmission Dynamics With Self-Learning Population Behavioral Change

Tsz-Lik Chan<sup>1</sup>, Hsiang-Yu Yuan<sup>2</sup> and Wing-Cheong Lo<sup>1\*</sup>

<sup>1</sup> Department of Mathematics, City University of Hong Kong, Kowloon, Hong Kong SAR, China, <sup>2</sup> Department of Biomedical Sciences, City University of Hong Kong, Kowloon, Hong Kong SAR, China

Many regions observed recurrent outbreaks of COVID-19 cases after relaxing social distancing measures. It suggests that maintaining sufficient social distancing is important for limiting the spread of COVID-19. The change of population behavior responding to the social distancing measures becomes an important factor for the pandemic prediction. In this paper, we develop a SEAIR model for studying the dynamics of COVID-19 transmission with population behavioral change. In our model, the population is divided into several groups with their own social behavior in response to the delayed information about the number of the infected population. The transmission rate depends on the behavioral changes of all the population groups, forming a feedback loop to affect the COVID-19 dynamics. Based on the data of Hong Kong, our simulations demonstrate how the perceived cost after infection and the information delay affect the level and the time period of the COVID-19 waves.

**Keywords:** COVID-19, mathematical modeling, population behavioral change, pandemic in Hong Kong, delay differential equation

## OPEN ACCESS

### Edited by:

Reza Lashgari,  
Shahid Beheshti University, Iran

### Reviewed by:

Wenrui Hao,  
Penn State York, United States  
Tzai-Hung Wen,  
National Taiwan University, Taiwan

### \*Correspondence:

Wing-Cheong Lo  
wingclo@cityu.edu.hk

### Specialty section:

This article was submitted to  
Infectious Diseases - Surveillance,  
Prevention and Treatment,  
a section of the journal  
Frontiers in Public Health

**Received:** 01 September 2021

**Accepted:** 30 November 2021

**Published:** 22 December 2021

### Citation:

Chan T-L, Yuan H-Y and Lo W-C  
(2021) Modeling COVID-19  
Transmission Dynamics With  
Self-Learning Population Behavioral  
Change.  
Front. Public Health 9:768852.  
doi: 10.3389/fpubh.2021.768852

## 1. INTRODUCTION

Coronavirus disease (COVID-19) is an infectious disease caused by a newly discovered coronavirus known as SARS-CoV-2 (1). According to the report of WHO in April 2021, over 132 million people were reported to be infected with COVID-19 and there were over 2.8 million deaths (2). As such, COVID-19 has been declared as a public health emergency of international concern on July 30, 2020. Since the beginning of the pandemic, many efforts were put into predicting the disease dynamics and suggesting optimal disease control strategies. Mathematical modeling is a major tool for COVID-19 prediction, for example using SIR (susceptible-infected-recovered) or SEIR (susceptible-exposed-infected-recovered) model to describe the dynamics of COVID-19 (3–5). Different variations of the SIR model were also studied, such as COVID-19 network models (6, 7) and a model with spatial impact on COVID-19 transmission (8).

Recurrent outbreaks of COVID-19 cases were observed in many locations. The existence of asymptomatic patients and the change of population behavior responding to the social distancing measures may be the factors for these recurrent outbreaks. Asymptomatic patients are individuals who are infectious but are not reported and show no symptoms. Because of the unawareness of infection status, asymptomatic infectious is not defined in SIR models. Recent research showed that the incubation period of COVID-19 could be as long as 12 days while the latent period is about 4 days (9). This result emphasizes the importance of the consideration of asymptomatic patients. For including the COVID-19 transmission with asymptomatic patients, some recent studies (10, 11)

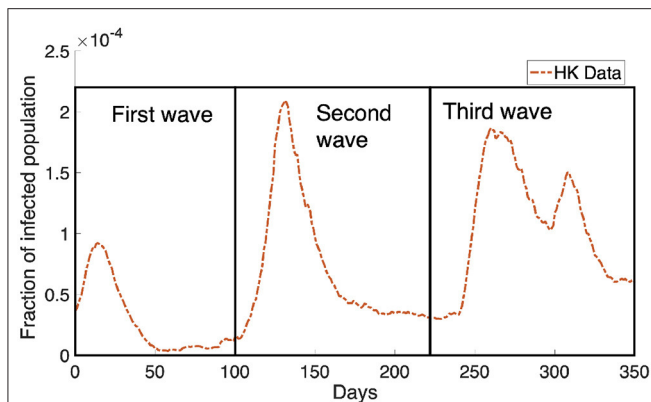


**FIGURE 1 |** The Hong Kong infected population obtained from Department of Health, Government of HKSAR (20) is shown in the orange dotted curve. We can see the infected population rebound multiple times in the data, causing the dynamics of the infected population to look like waves. There are three waves where we have boxed them and marked them as the first wave, the second wave and the third wave as shown in the figure.

considered the extension of SIR model to SAIR model, incorporating a new compartment for asymptomatic patients.

Another significant factor affecting COVID-19 transmission is related to the behavioral change of individuals. Policymakers enforced social distancing measures that aim to reduce the contact in a population. It is observed that 139 countries have implemented social distancing measures (12). Regulating social distancing has been shown to be an effective strategy in controlling the COVID-19 transmission (13–15) as it implies a behavioral change in population which will reduce the rate of COVID-19 transmission. In (16, 17), it was shown that individual behavior has a huge impact on the disease dynamics and sometimes leads to different predictions when comparing to a standard SIR model (18). Besides the intervention by the policymaker, individuals' decisions can be based on the perceived risk of infection (19) and the demands of a social environment (6). In general, the behavior change depends on the individual's utility which measures the balance between the risk of infection and the normal lifestyle. This adaptive behavior change may lead to the recurrent outbreaks of COVID-19 cases observed in many cities, such as Hong Kong (Figure 1).

The population decides the activity using the information about the infected population and the perceived cost after infection, including treatment fee and loss in economic productivity. How do the dynamics of COVID-19 transmission depend on the cost after infection and the time delay for receiving the information? In this paper, we will apply the data of Hong Kong to study how self-learning behavioral change affects the level and the time period of the COVID-19 waves. First, we will develop a SEAIR compartmental model for simulating the dynamics of COVID-19 transmission, in which the population can decide to reduce their activity outside or to have a normal lifestyle based on the evaluation of the utility functions. Then we will discuss the parameter estimation and perform numerical simulations

to study the role of self-learning behavioral change in disease transmission.

## 2. METHODS

In this section, we will develop a mathematical model for studying COVID-19 transmission. We first discuss an existing model from a recent study and then develop a novel model with a consideration of population behavioral change and asymptomatic patients.

Here we will define some terminologies and notations used in the paper. We separate the population into five compartments: susceptible compartment  $S$ , exposed compartment  $E$ , asymptomatic compartment  $A$ , infected compartment  $I$ , recovered compartment  $R$ . The susceptible compartment, the exposed compartment and the asymptomatic compartment are further divided into two types. We define the population who behaves normally as “normal activity type” and the population who reduces the frequency of outside activities as “reduced activity type.” In our model, the normal activity type is labeled by a superscript “ $n$ ” and the reduced activity type is labeled by “ $r$ .” For example,  $S^n$  represents the susceptible compartment that has normal activity and  $A^r$  represents the asymptomatic compartment that has reduced activity. We define that  $S^n$ ,  $S^r$ ,  $E^n$ ,  $E^r$ ,  $A^n$ ,  $A^r$ ,  $I$ , and  $R$  are the population numbers for the corresponding compartments and types, which are the functions of time  $t$ . The dot notation represents the derivative with respect to  $t$ , for example,  $\dot{S}^n$  represents the derivative of  $S^n$  with respect to  $t$ .

### 2.1. Mathematical Model

In (19), based on the variables  $S$ ,  $I$ , and  $R$  defined before, Amaral et al. studied the behavioral change in a SIR model:

$$\begin{cases} \dot{S}^n = -\beta_N I^n S^n - \beta_a I^r S^n + \rho \Phi_S, \\ \dot{S}^r = -\beta_N I^n S^r - \beta_Q I^r S^r - \rho \Phi_S, \\ \dot{I}^n = \beta_N I^n S^n + \beta_a I^r S^n + \rho \Phi_I - \gamma I^n, \\ \dot{I}^r = \beta_N I^n S^r + \beta_Q I^r S^r - \rho \Phi_I - \gamma I^r, \\ \dot{R} = \gamma (I^n + I^r), \end{cases} \quad (1)$$

where  $\beta_a$ ,  $\beta_N$ ,  $\beta_Q$  are the transmission rate, and  $\gamma$  is the recovery rate. The functions  $\Phi_S$  and  $\Phi_I$  are the rates that the population changes the behavior (normal activity or reduced activity), defined as

$$\Phi_S = S^r (S^n + I^n) \theta(p_r, p_n) - S^n (S^r + I^r) \theta(p_n, p_r), \quad (2)$$

$$\Phi_I = I^r (S^n + I^n) \theta(p_r, p_n) - I^n (S^r + I^r) \theta(p_n, p_r), \quad (3)$$

where  $p_n$  and  $p_r$  are the payoffs for the normal and reduced activity population, respectively. The payoffs depend on the perceived cost after infection and the infection probability under different types of activities. The function  $\theta$  is the Fermi rule

$$\theta(p_1, p_2) = \frac{1}{1 + e^{-(p_2 - p_1)/k}}, \quad (4)$$



which gives the probability of population to change from the strategy with payoff  $p_1$  to the strategy with payoff  $p_2$ . This rule is used in many literature (19, 21–24). The term  $\frac{1}{k}$  gives the intensity of selection. Equations (2) and (3) depend on the probability (4) and the interaction rate among populations, which is based on the *social learning* in the behavioral game theory (25).

Based on (19), we develop a new mathematical model for capturing the spreading of COVID-19 with self-learning behavioral change. Here, we consider two more compartments: exposed patients  $E$  and asymptomatic patients  $A$ . So we will add four new variables,  $E^r$  and  $E^n$ ,  $A^r$  and  $A^n$ , to system (1). Here the asymptomatic patients refer to some patients who are in their pre-symptomatic transmission period and will become infectious in next stage. In our model, the rate of the behavior change is based on the *self-learning* (25). This assumption is different from the model in (19) that is based on the *social learning*. We assume that, based on the information of the spreading of disease, each individual can unilaterally decide his/her own strategy which will affect the population distribution of the two activity types, normal activity type and reduced activity type. Other than these two types, we also consider that there are  $M$  different groups in the population. Each compartment that belongs to the  $i$ -th group is labeled by subscript “ $i$ .” For example, we can decide the groups according to the age groups of the population. The total number of the whole population is constant during the time interval  $[0, T]$  of the model where  $T$  denotes the final time of the simulation. The model considered in this paper is

$$\begin{cases} \dot{S}_i^n = a_i S_i^n - b_i S_i^n - \beta_i^n S_i^n, \\ \dot{S}_i^r = -a_i S_i^n + b_i S_i^n - \beta_i^r S_i^n, \\ \dot{E}_i^n = a_i E_i^n - b_i E_i^n - (1 - \mu)\sigma E_i^n - \mu\sigma E_i^n + \beta_i^n S_i^n, \\ \dot{E}_i^r = -a_i E_i^n + b_i E_i^n - (1 - \mu)\sigma E_i^n - \mu\sigma E_i^n + \beta_i^r S_i^n, \\ \dot{A}_i^n = a_i A_i^n - b_i A_i^n + (1 - \mu)\sigma E_i^n - \lambda A_i^n, \\ \dot{A}_i^r = -a_i A_i^n + b_i A_i^n + (1 - \mu)\sigma E_i^n - \lambda A_i^n, \\ \dot{I}_i = \lambda(A_i^n + A_i^r) + \mu\sigma E_i^n + \mu\sigma E_i^r - \gamma_i I_i, \\ \dot{R} = \sum_{i=1}^M \gamma_i I_i. \end{cases} \quad (5)$$

A schematic diagram of our model is given in **Figure 2**. The meanings of the functions and parameters used in Model (5) are listed in **Table 1**.

The populations can interchange between normal activity type ( $S_i^n$ ,  $E_i^n$ , and  $A_i^n$ ) and the reduced activity type ( $S_i^r$ ,  $E_i^r$ , and  $A_i^r$ ) with rates  $a_i$  and  $b_i$ . The two rates  $a_i$  and  $b_i$  will be defined in the later subsection. Susceptible populations  $S_i^n$  and  $S_i^r$  are infected at rates  $\beta_i^n$  and  $\beta_i^r$ , respectively. The two rates  $\beta_i^n$  and  $\beta_i^r$  depend on the numbers of infected populations and will be explained later. After infection, the susceptible populations will become corresponding exposed populations  $E_i^n$  or  $E_i^r$ . After the latent period  $\frac{1}{\sigma}$  days, the exposed populations will show symptoms with probability  $\mu$  and enter the infected population. Otherwise, if they show no symptoms with probability  $1 - \mu$ , they will enter the asymptomatic populations. When the asymptomatic populations are reported through testing, contact tracing or developing symptoms after some time, they will become infected population. The report rate is denoted by  $\lambda$ . The infected population  $I_i$  is recovered at rate  $\gamma_i$  to the recovered population  $R$  which is

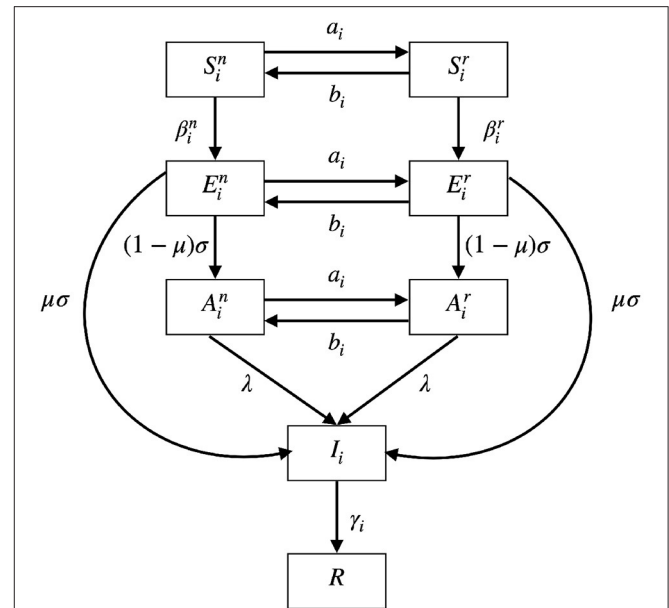


**FIGURE 2** | A schematic diagram of Model (5).  $S$  represents susceptible compartment;  $E$  represents exposed compartment;  $A$  represents asymptomatic compartment;  $I$  represents infected compartment;  $R$  represents recovered compartment. The populations can interchange between normal activity type ( $S_i^n$ ,  $E_i^n$ , and  $A_i^n$ ) and the reduced activity type ( $S_i^r$ ,  $E_i^r$ , and  $A_i^r$ ). The biological meaning of the parameters can be found in **Table 1**.

**TABLE 1** | Biological meaning of the function and the parameters used in Model (5).

| Variables  | Biological meanings  |
|------------|--|
| $S_i^n$    | The $i$ -th susceptible compartment with normal activity                                 |
| $E_i^n$    | The $i$ -th exposed compartment with normal activity                                     |
| $E_i^r$    | The $i$ -th exposed compartment with reduced activity                                    |
| $A_i^n$    | The $i$ -th asymptomatic compartment with normal activity                                |
| $A_i^r$    | The $i$ -th asymptomatic compartment with reduced activity                               |
| $I_i$      | The $i$ -th infected compartment   |
| $R$        | The recovered compartment  |
| Parameters | Biological meanings  |
| $a_i$      | Rates at which $S_i^n$ , $E_i^n$ , and $A_i^n$ goes to $S_i^r$ , $E_i^r$ , and $A_i^r$ . |
| $b_i$      | Rates at which $S_i^r$ , $E_i^r$ , and $A_i^r$ goes to $S_i^n$ , $E_i^n$ , and $A_i^n$ . |
| $\mu$      | Probability that individuals show symptoms after exposed.                                |
| $\lambda$  | Report rate of asymptomatic populations.   |
| $\gamma$   | Recovery rate of infected population.  |
| $\sigma$   | Rate at which exposed population become infectious.                                      |

immune to further infection as the reinfection rate is not high during the time period we considered.

## 2.2. Rate of Behavioral Change

Here we will introduce how the population decides to behave normally or reduce the frequency of their outside activities. There are two types of population, normal activity type and reduced



activity type, in the  $S$ ,  $E$ , and  $A$  compartments. The populations choose to alter their types, based on a self-learning process which depends on the utility functions.

The utility function of the individual in the  $i$ -th normal activity type at time  $t$  is defined as  $v_i^n(z^n, e(t))$  which depends on the response function  $z^n$  and the environment vector  $e = [I_1(t - \tau), \dots, I_M(t - \tau)]$ , where  $\tau$  is the information delay. The individuals will select the optimal response function  $z_i^{n*} : [0, T] \rightarrow [0, 1]$  to maximize their own utility:

$$u_i^n(t) := \max_{z_i^n} v_i^n(z_i^n, e(t)), \quad (6)$$

where  $z_i^{n*}(t) = \operatorname{argmax}_{z_i^n} v_i^n(z_i^n, e(t))$ .

The instantaneous optimization problem was applied in the discrete SIR model of the study (18). Here we consider it in the continuous model (5). Similarly we can define the utility for the reduced activity type. The individuals in the reduced activity type will select the optimal response function  $z_i^{r*} : [0, T] \rightarrow [0, r_{\max}]$  to maximize their own utility:

$$u_i^r(t) := \max_{z_i^r} v_i^r(z_i^r, e(t)), \quad (7)$$

where  $z_i^{r*} = \operatorname{argmax}_{z_i^r} v_i^r(z_i^r, e(t))$ . The feasible set for the reduced activity type is bounded above by a constant  $0 < r_{\max} < 1$  to reflect the reduced activity.

For the whole time interval  $[0, T]$ , the function  $z^{n*} : [0, T] \rightarrow [0, 1]$  which represents the optimal activity outside for  $S_i^n$ ,  $E_i^n$ , and  $A_i^n$ ;  $z^{r*} : [0, T] \rightarrow [0, r_{\max}]$  which represents the optimal activity outside for  $S_i^r$ ,  $E_i^r$  and  $A_i^r$ .

The normal activity populations can choose to reduce their activity and enter the reduced activity populations at rate  $a_i$ . Similarly the reduced activity populations can choose to become the normal activity populations at rate  $b_i$ . The rates  $a_i$  and  $b_i$  are given as

$$a_i = \omega_1 \theta(u_i^n(t), u_i^r(t)), \quad (8)$$

$$b_i = \omega_1 \theta(u_i^r(t), u_i^n(t)), \quad (9)$$

where  $\omega_1$  is a positive constant and  $\theta$  is the Fermi Rule defined before. Here,  $a_i$  and  $b_i$  depend only on the utility function  $u_i^n$  and  $u_i^r$ . They are different from the rates in Model (1).

## 2.3. Transmission Rate

In this subsection, we will discuss the transmission rates  $\beta_i^r$  and  $\beta_i^n$  in Model (5). Since there are two different strategies in the model, the population either can be a normal activity type or reduce the frequency of their activities. Thus we formulate two kinds of transmission rates,  $\beta_i^n$  for the populations in the normal activity type, and  $\beta_i^r$  for the populations in the reduced activity type. The transmission rates depend on the optimal function  $z^{n*}$  and  $z^{r*}$ . Let  $m(z)$  represent the rate of contact made outside with the response function  $z$ . We assume that  $m$  is an increasing function of  $z$ .

Infection occurs when susceptible individuals make contact with the infectious compartment  $[A_i^n, A_i^r$  and  $I_i$  in Model (5)]

and that contact may lead to successful infection. The number of infection increases when the number of contact increases. From this assumption, we define that

$$\beta_i^r(z^{r*}, t) = m(z^{r*}) \sum_{j=1}^M k_n A_j^n + k_r A_j^r + k_I I_j, \quad (10)$$

$$\beta_i^n(z^{n*}, t) = m(z^{n*}) \sum_{j=1}^M k_n A_j^n + k_r A_j^r + k_I I_j, \quad (11)$$

where  $k_n$ ,  $k_r$  and  $k_I$  are the infection rates.

## 2.4. Value Functions

Now, we define the utility function in (6). The function  $v_i^n$  models the internal decision process of behavioral change of individuals. It depends on the optimal value of  $z^{n*}$ , the environment vector  $e(t - \tau)$ , and includes the present value and the expected cost in the future. This form is similar to the Bellman equation and has been used by other studies (18, 26, 27). Here,  $v_i^n$  is defined as

$$v_i^n(t, e) = \underbrace{\bar{v}(z_i^{n*}(t))}_{\text{Present value}} - \underbrace{c\omega_2 m(z^{n*}) \sum_{j=1}^M k_I I_j(t - \tau)}_{\text{Expected cost after infection}} - \underbrace{\left(1 - \omega_2 m(z^{n*}) \sum_{j=1}^M k_I I_j(t - \tau)\right)}_{\text{Expected cost of susceptible}}, \quad (12)$$

where  $\omega_2$  is a positive constant. In Equation (12), the present value is given by  $\bar{v}(z_i^{n*}(t))$ . The perceived cost after infection is a product of the perceived cost  $c$  and the transmission rate without asymptomatic infection  $m(z^{n*}) \sum_{j=1}^M k_I I_j(t - \tau)$ . The transmission rate is different from Equation (11). Equation (12) does not depend on  $A_i^r$  nor  $A_i^n$  as we assume that individuals do not have any information about the asymptomatic population when making decision. We also assume that there is a time delay  $\tau$  for the information. The delay  $\tau$  is the time period that an individual becomes infected and this information reaches the decision-maker. The perceived cost after infection is related to treatment fee or loss in economic productivity but is not meant to be the exact measurement of the monetary value of the economical loss. It should be considered as the generic measurement and is relative to the cost of susceptible.

Similarly, we can define the value function for the reduced activity type as in (12) but  $z^{n*}$  is replaced by  $z^{r*}$ :

$$v_i^r(t, e) = \underbrace{\bar{v}(z_i^{r*}(t))}_{\text{Present value}} - \underbrace{c\omega_2 m(z^{r*}) \sum_{j=1}^M k_I I_j(t - \tau)}_{\text{Expected cost after infection}} - \underbrace{\left(1 - \omega_2 m(z^{r*}) \sum_{j=1}^M k_I I_j(t - \tau)\right)}_{\text{Expected cost of susceptible}}. \quad (13)$$

**TABLE 2** | Parameters used in numerical simulations and the references.

| Parameters | Values  | References |
|------------|---|------------|
| $\mu$      | 0.21  | (20)       |
| $\lambda$  | $\frac{1}{5.7 \text{ days}} = 0.1754 \text{ days}^{-1}$ | (28)       |
| $\gamma$   | $\frac{1}{10 \text{ days}} = 0.1 \text{ days}^{-1}$     | (29)       |
| $\sigma$   | $\frac{1}{3 \text{ days}} = 0.3333 \text{ days}^{-1}$   | (30)       |
| $k$        | 0.1   | (19)       |

## 2.5. Parameter Estimation

First we provide the estimation of the parameters used in the numerical simulations. For the contact rate  $m(x)$ , we set it as

$$m(x) = 2.2x, \quad (14)$$

which is based on (18). We define the present value  $\bar{v}(x)$  as in (18),

$$\bar{v}(x) = x - \frac{x^2}{2}. \quad (15)$$

The fraction of asymptomatic patient is based on the data from Department of Health, Government of HKSAR (20):

$$\frac{\text{number of reported asymptomatic patients}}{\text{number of reported infected patients}} = 0.21. \quad (16)$$

We assume that the probability of showing symptoms after infection is 0.79. We take  $\lambda = \frac{1}{5.7 \text{ days}}$ ,  $\gamma = \frac{1}{10 \text{ days}}$ ,  $\sigma = \frac{1}{3 \text{ days}}$ . Here,  $\lambda^{-1}$  is the mean time period of contact to illness onset, which is estimated from the study (28);  $\gamma^{-1}$  is the median recovery time of Remdesivir treatment, which is estimated from the study (29); the mean latent period,  $\sigma^{-1}$ , is based on (30). We set  $k = 0.1$  in the intensity of selection in the Fermi Rule as in (19). We summarize the parameter values mentioned above in **Table 2**.

The reduced activity type is assumed to have a maximum activity at  $r_{\max} = 0.8$ . The impact of other  $r_{\max}$  will be studied in section 3. We assumed that  $k_n = 2k_r = 2k_l$ . The cost after infection is assumed to be  $c = 10^6$  and the impact of varying the value of  $c$  will be discussed in the next section. The constants  $\omega_1$  and  $\omega_2$  are both set to be 1 in the simulations.

The initial condition used for the case of Hong Kong is based on the data from The Department of Health, Government of HKSAR (20). The simulation starts on March 25, 2020 which is the day that HK Government announced that border closures measure and all returning residents are subjected to Compulsory Quarantine Order (31). We consider all infected cases after this day are local cases. The final time for the simulation is  $T = 350$  days. We assumed that initially the normal activity and reduced activity populations are both halves of the susceptible, asymptomatic and infected population. In the case of the simulations with more than one group, the population is distributed equally among the groups.

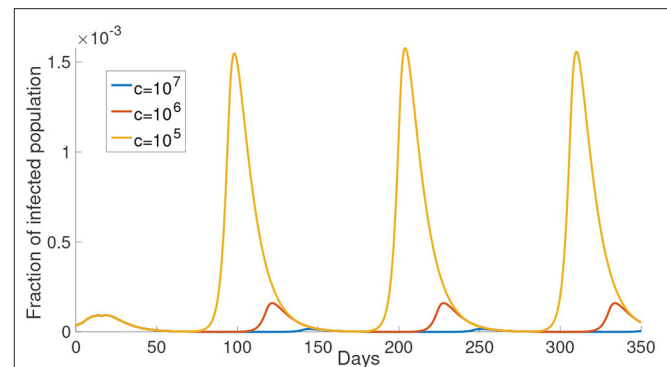


**FIGURE 3** | The effect of varying the cost after infection. The cost after infection is the scalar  $c$  in Equations (12) and (13). The infected population with different cost after infection is shown in different color. The corresponding  $c$  is shown in the legend.

## 3. RESULTS

For the long-term dynamics, the infected population will go to zero and the outcome will reach the disease-free equilibrium at the end. The intermediate dynamics of Model (5) is not trivial and we will apply numerical simulations to investigate the intermediate dynamics of Model (5). The detailed numerical scheme is discussed in Supporting Information.

### 3.1. Impact of Key Parameters

Based on the parameter setting before, we study the impact of some key parameters including the perceived cost after infection  $c$ , the time delay constant  $\tau$  and the upper bound of reduced activity  $r_{\max}$ .

#### 3.1.1. Perceived Cost After Infection $c$

In this subsection, we investigate the impact of varying the cost after infection. We consider the case that  $M = 1$ , that is, for example, the susceptible population is divided into  $S_1^r$  and  $S_1^n$ . The perceived cost after infection,  $c$ , in Equations (12) and (13), is the perceived cost that the individuals need to pay if they are infected, which is related to the treatment fee or the loss in economic productivity due to sick leave. In **Figure 3**, we can see the simulations of the infected population with different values of  $c$ . As shown in **Figure 3**, the infected population is the least when  $c$  is the largest ( $c = 10^7$ , yellow curve). When  $c$  decreases, the infected population increases. When the perceived cost  $c$  is small, such population may not choose to reduce their activity to prevent infection. In Equations (12) and (13), the second part is the expected cost, which depends on the perceived cost  $c$ . Thus, the lower the perceived cost after infection, the more the population will increase their activity to gain the optimal utility. Ultimately, this kind of response will contribute to more infections.

#### 3.1.2. Time Delay $\tau$

In this subsection, we study the dynamics of Model (5) under different values of time delay  $\tau$ . The parameter  $\tau$  represents

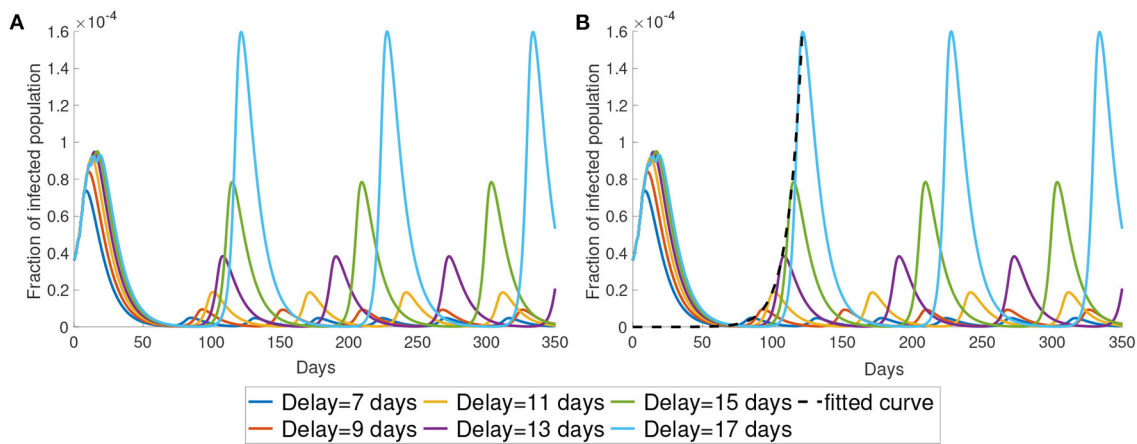


**FIGURE 4 |** The impact of time delay. **(A)** We present the simulation with different delays. **(B)** We use exponential curve to fit the maximum in the first wave of the simulation. The fitted exponential curves are the black dotted line.

the time lag between infected time and the moment that the information of the infected individuals reaches the decision-maker. This time delay is the sum of the latent period, the time period for testing and the delay of reporting. As shown in **Figure 4**, the time period between the maxima increases as the time delay increases. Also, a longer time delay will lead to a larger outbreak. The maximum of the infected population for each wave increases exponentially as the time delay increases. In **Figure 4B**, we plot the maximum of the first waves using the exponential form  $ae^{b \times \text{days}}$ . The fitted curve has the formula  $5.61 \times 10^{-12} e^{0.1335t}$ .

### 3.1.3. Upper Bound of Reduced Activity $r_{\max}$

Now, we study the dynamics of Model (5) with varying the upper bound of reduced activity  $r_{\max}$ . The simulations of the infected population with different  $r_{\max}$  are shown in **Figure 5**. The infected population decreases as  $r_{\max}$  decreases from 1 to 0.6. But the infected population increases as  $r_{\max}$  decreases from 0.4 to 0.2. The local maximum in each wave of the infected population is the highest when  $r_{\max} = 0.2$  and the lowest when  $r_{\max} = 0.6$ . This result shows that the infected population is not monotonically decreasing with  $r_{\max}$ . In the subsequent simulations we will use  $r_{\max} = 0.8$ .

## 3.2. Simulation With the Data of Hong Kong

In this section, we present the simulation of our model comparing with the data of the infected population in Hong Kong. We first start with the case of  $M = 1$ . We set the parameters  $k_n = 0.595$  and  $\tau = 21$  days. As seen in **Figure 6**, the simulation can produce several waves of infection. The number of infections reaches the local maximum point between day 100 and day 150 and decreases to a low level on around day 200. After day 200, the infected population starts to rise and reaches another local maximum on around day 250 before the infected population decreases to a low level again.

The infection waves are due to the change in the optimal activity as shown in **Figure 6**. As we can see in **Figure 6** that when

the infected population is at a low level, the optimal activity will increase and lead to a higher transmission rate; when the infected population is at a high level, the optimal activity will decrease and lead to a lower transmission rate. The third wave in **Figure 6A**, that is the wave between day 200 and day 250, is higher than the observed third wave in the data. As our simulation consider a long time horizon, many parameters may change along with time, such as the report rate  $\lambda$ . The Government in Hong Kong aims to improve the surveillance strategy by increasing the number of COVID-19 tests continuously (13). It would be reasonable to assume that the report rate will increase over time. In **Figure 6C**, we set the report rate  $\lambda$  to be  $\frac{1}{3.7 \text{ days}} = 0.2702 \text{ days}^{-1}$  after day 200 and observe a lower local maximum of the third wave which is similar to the one observed in the data.

## 3.3. The System With Bipartite Transmission Rates

In the previous simulation, we observe that the difference between the data and the simulation in the third wave of infection. To improve the accuracy of the simulation, we will investigate the situation where the transmission rate is modified to be the following form

$$\beta_i^n = \underbrace{m(z_i^{n*})}_{\text{First part}} \left[ \underbrace{k_n}_{\text{Second part}} \underbrace{m(z_i^{n*})}_{\text{Second part}} \sum_{j=1}^M A_j^n + k_r \underbrace{m(z_i^{r*})}_{\text{Second part}} \sum_{j=1}^M A_j^r \right], \quad (17)$$

$$\beta_i^r = \underbrace{m(z_i^{r*})}_{\text{First part}} \left[ \underbrace{k_n}_{\text{Second part}} \underbrace{m(z_i^{n*})}_{\text{Second part}} \sum_{j=1}^M A_j^n + k_r \underbrace{m(z_i^{r*})}_{\text{Second part}} \sum_{j=1}^M A_j^r \right], \quad (18)$$

where  $k_n = k_r$  is the infection rate. The biological meaning of this transmission rate is that the asymptomatic population has no symptoms and behaves like the susceptible population.

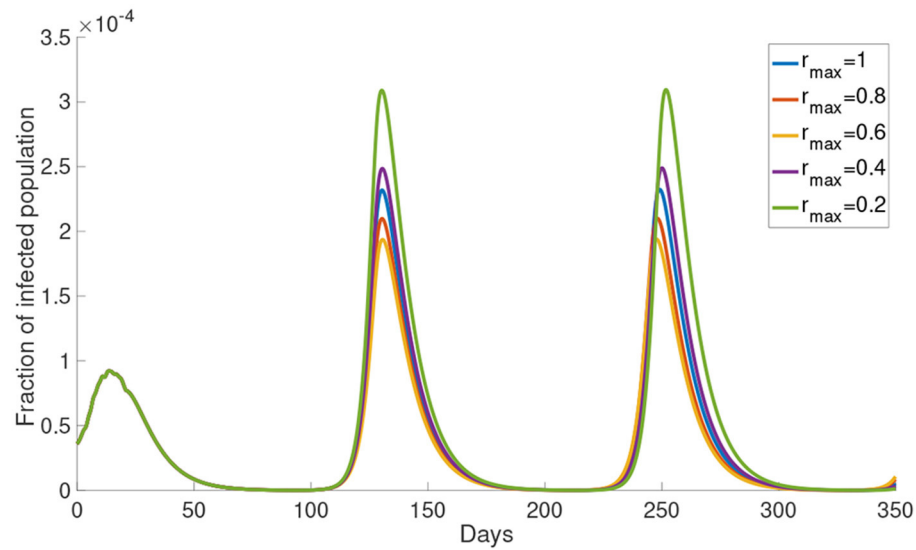


**FIGURE 5 |** The simulation of the infected population with different  $r_{\max}$ .

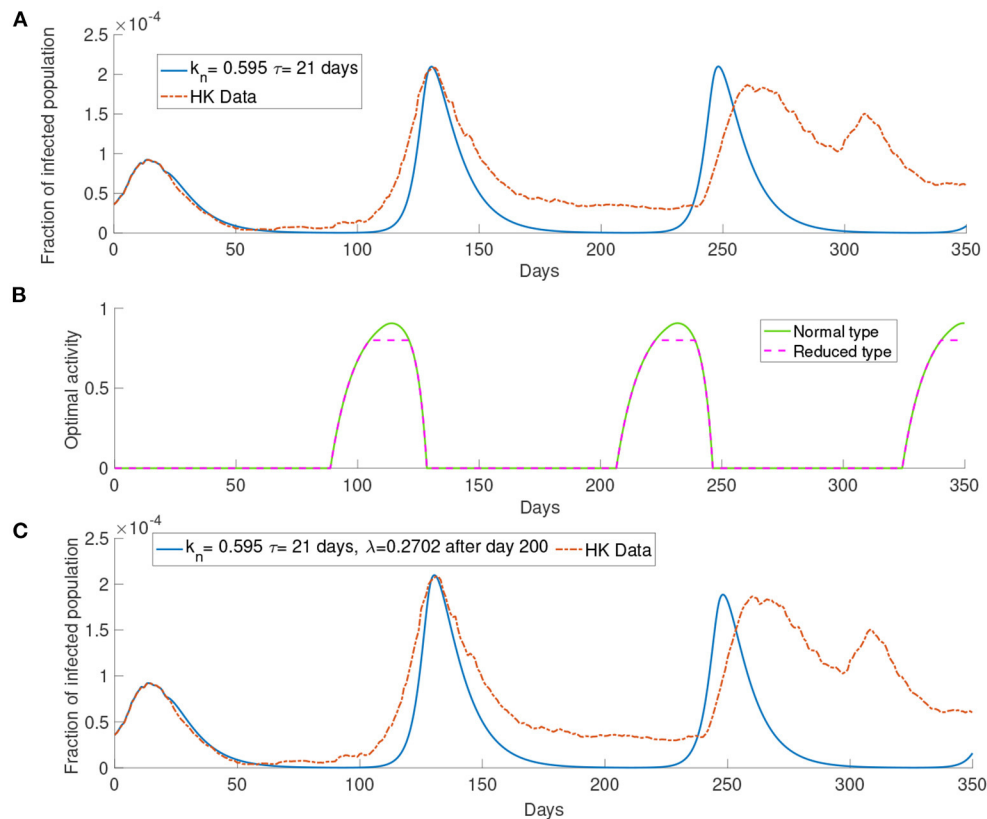


**FIGURE 6 |** The simulation with the data of Hong Kong. **(A)** The comparison between the simulated and observed data. **(B)** The optimal activity. **(C)** The comparison of the infected population from the data and the simulation of our model with report rate  $\lambda$  increase to 0.2702 after day 200.

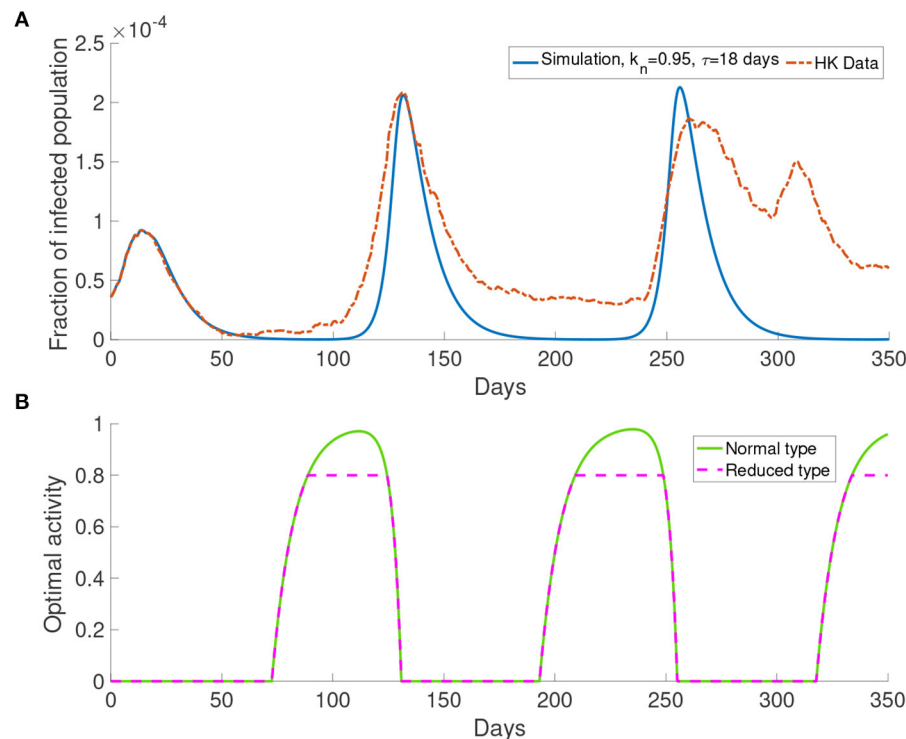


**FIGURE 7 |** The simulation result with  $M = 1$  and transmission rates in the form of Equations (17) and (18). **(A)** The comparison of data and the simulation. **(B)** The corresponding optimal activity for different types. Normal activity type and reduced activity type are the same except in the three intervals of behavioral change. They are from around day 75 to day 175, from around day 180 to day 250 and from around day 320 to day 350.

For the normal activity type and the reduced activity type asymptomatic populations, similar to the susceptible population, we solve (6) and (7) to find out their optimal activity. The asymptomatic population contributes to less transmission if the population has a smaller optimal activity because a smaller optimal activity means less contact with other populations. The contact function in the first part models the contact made by the susceptible population. The contact function in the second part models the contact made by the asymptomatic population of the normal activity type and the reduced activity type. Thus, Equations (17) and (18) are bipartite transmission rates which involves the activity of the susceptible population and the asymptomatic population.

### 3.3.1. Simulation With Single Group $M = 1$

Here we present the simulation with  $M = 1$  for the system with bipartite transmission rates. In the simulations, we set  $k_n = 0.95$  and  $\tau = 18$  days. The cost after infection is  $10^6$ . The result shown in **Figure 7** provides a better agreement with the third wave observed in the data.

**Figure 7B** shows the optimal activity for the normal activity type and the reduced activity type. We refer to the interval that shows different behavior for the normal activity type and the reduced activity type as *interval of behavioral change*. The optimal activity for the normal activity type and the reduced activity type is the same except in three intervals of behavioral change as

depicted by **Figure 7**. The intervals of behavioral change are from day 75 to day 125, from day 180 to day 250 and from day 320 to day 350. On day 100, the population receives information about the infected population with 18 days delay, which corresponds to a moment with a small infected population (**Figure 7A**). On day 100, the normal activity type population perceives the risk of infection to be low and their optimal activity will be higher than the reduced activity type. Due to the definition of the reduced activity type, the reduced activity type will not increase their optimal activity despite having more utility. Finally, it causes the difference in the optimal activity in the intervals of behavioral change.

### 3.3.2. Simulation With Multiple Groups $M > 1$

Here we present the simulation when there are two groups,  $M = 2$ , for the population. We investigate the situation where the older people perceive the cost after infection to be higher than the young people as older people have longer recovery time (32) which will cost more in treatment fee. According to the discussion before, the behavioral change depends on the perceived cost after infection. Thus we define the first group corresponding to the older people who have higher perceived cost after infection  $c = 10^6$ , and the second group corresponding to the middle-aged and young people who have lower perceived cost after infection  $c = 10^5$ . We set the time delay  $\tau = 15$  days and  $k_n = 1.81$ . All other parameters are the same as those used before.



In **Figure 8A**, this simulation with two groups still produces wave-form dynamics of the infected population. By observing the susceptible population, the reduced activity type susceptible population decreases and the normal activity type susceptible population increases in the intervals of behavioral change. We can observe that there are three intervals of behavioral change shown in **Figure 8**. In these intervals of behavioral change, the utility will be larger for being the normal activity type. **Figure 8** shows that the intervals of behavioral change are different for group 1 and group 2. Each interval of behavioral change of group 2 is longer than the interval of behavioral change of group 1. It means that the individuals in group 2, which have a smaller perceived cost after infection, increase their activity faster and remain their activity level longer than the individuals in group 1 which have a higher perceived cost after infection.

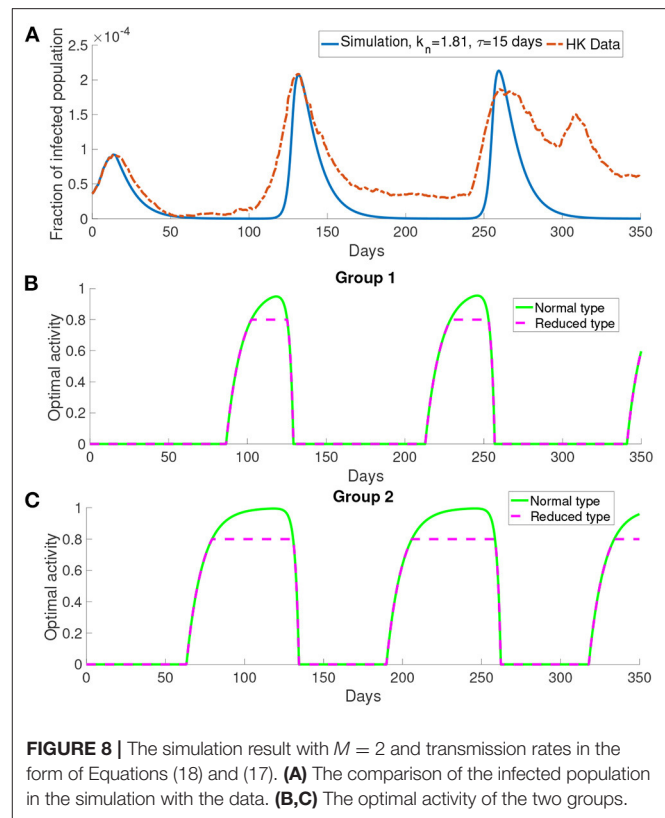
**Figures 9A,B** show the difference in the utility of the normal activity type and the reduced activity type. The utility of the normal activity type is always bigger than or equal to the reduced activity type since the activity of the reduced activity type is bounded by  $r_{\max}$ . **Figures 9A,B** show that the difference in the utility for group 2 forms a valley in each interval of behavioral change. The difference in the utilities controls the exchange rates  $a_i$  and  $b_i$ . The two rates  $a_i$  and  $b_i$  are shown in **Figures 9B,C**. The normal activity type will gain more utility than the reduced activity type when the number of the infected population is small. As a result, the population in the reduced activity type will move to the normal activity type according to the Fermi Rule in the intervals of behavioral change.

After day 125, the activity of the normal activity type begins to decrease due to the delayed information of a large infected population has reached the normal activity type. Thus, the optimal responses of the two types are the same again as both of them are now below  $r_{\max}$ .  $S^n$  decreases to the initial level and then the normal activity type moves to the reduced activity type as the infected population becomes larger.  $S'$  and  $S^n$  remain constant outside the intervals of behavioral change. Also, the rates  $a_i$ ,  $b_i$  and the utility are the same outside the intervals of behavioral change.

**Figure 10** shows the dynamics of different compartments. We can observe that the local maximum in each wave in the asymptomatic population (**Figures 10B,C**) constituted roughly 68% of all infected population. The asymptomatic population in group 1 is roughly 41% of the asymptomatic population in group 2 in both the normal activity type and the reduced activity type. But the infected population (**Figure 10A**) of group 1 and group 2 are the same.

Similar to **Figure 6A**, **Figure 11** shows a simulation with the report rate  $\lambda$  increased to  $0.195 \text{ days}^{-1}$  after day 200. We observe a lower local maximum of the third wave which is similar to the one observed in the data.

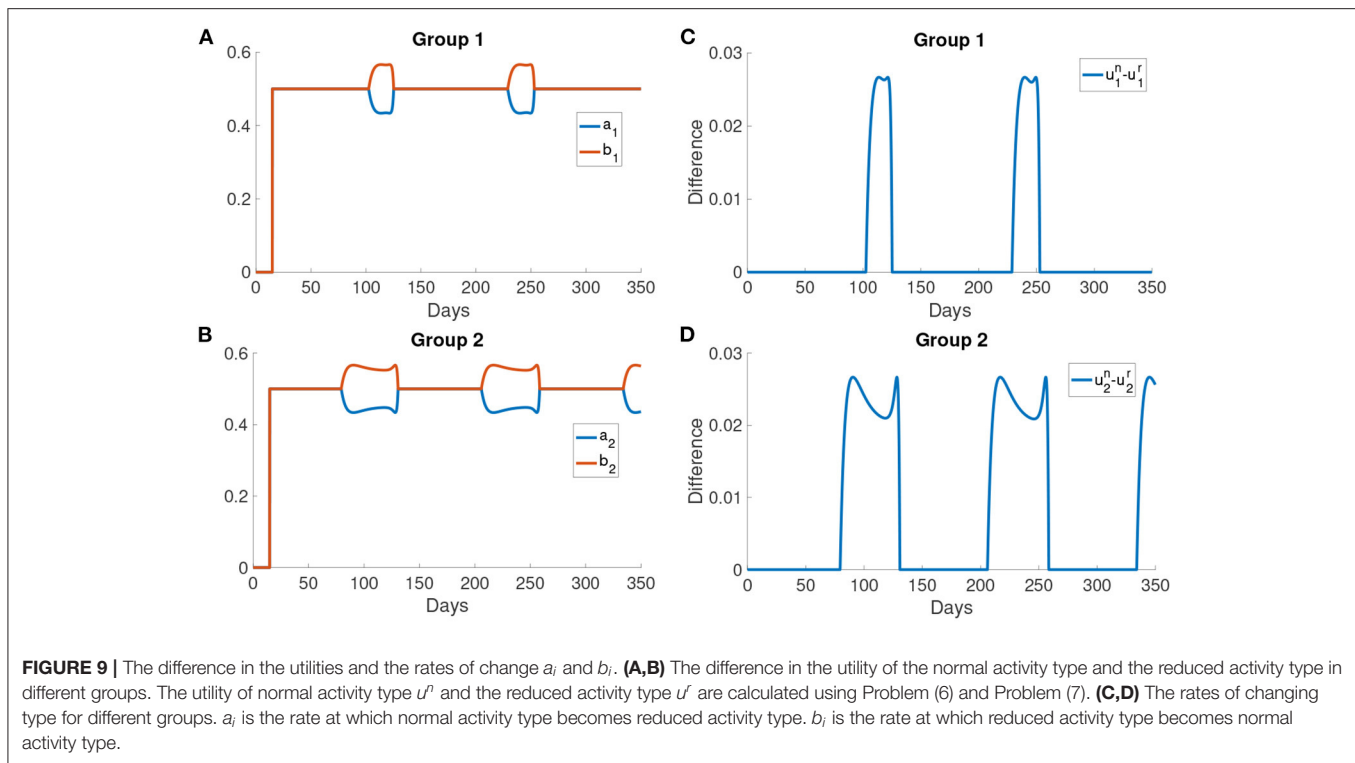
Now, we consider more groups  $M = 3$  for the population. We assume that the population is divided into three groups: young people, middle-aged people, and old people. In this case, we set the young people having  $c = 10^4$ , the middle-aged people having  $c = 10^5$ , the old people having  $c = 10^6$ . This reflects a finer group division scheme for age-specific perceived cost after infection. We model the old people to have



the highest cost after infection due to the highest treatment fee and longest recovery time (32), followed by the middle-aged people who have a medium cost after infection and the young people who have the lowest cost after infection since they often have a less economic burden and short recovery time. The cost after infection for group 1, group 2 and group 3 are  $10^6$ ,  $10^5$  and  $10^4$ , respectively. We set  $k_n = 0.865$  and  $\tau = 19$  days. In our simulations, we observe that the properties of the system with more groups are similar to what we observed in the system with two groups. **Figure 11** shows that the simulation with more groups can provide a better agreement with the real data.

## 4. DISCUSSION

Many surveys suggest that different individuals in the population behave differently to COVID-19 due to various reasons, for example, age (33), gender (34, 35), political orientation (36–39), and education level (40). The aim of this study is to formulate a mathematical model for COVID-19 transmission with self-learning behavioral change in multiple population groups. In this paper, we have introduced a SEAIR compartmental model in which the transmission rates depend on the population's optimal activity. The population decides the optimal activity using the information about the infected population and the perceived cost after infection. We investigated the simulation with varying the cost after infection ( $c$ ),



the time delay for receiving the information ( $\tau$ ) and the upper bound for the optimal activity in the reduced activity type population ( $r_{\max}$ ). The cost after infection is high in our model.

The model developed in our paper incorporated population behavior change which was discussed in some recent papers (18, 19, 41, 42). In (19), the authors consider the population dynamics as an evolutionary process. In their model, the population needs to learn from another population to make new decisions. One of the fundamental differences between our model and the model by Amaral et al. (19) is that we have relaxed their evolutionary assumption by allowing the population to change their strategy without contacting another population. Instead, the population changes their strategy based on what kind of information they received. We made this change in a way that is closely related to the daily life of people nowadays since people make their decision based on the information they receive from, for example, TV and newspapers. Nardin et al. (41) also studied the case where the population can change their strategy without meeting other populations. In their model, the rate of behavioral change is based on a discrete mechanism, unlike in our model where we used the Fermi rule for behavioral change. This also affects the dynamics of the infected population in which the waves of the infected population are less prominent in (41) than the waves in the models with a continuous rate of behavioral change in our study. In (42), the behavioral change with reduced activity is modeled as a percentage reduction in the transmission rate for the behavioral changed individual. This method works well for a relatively small time window of 5 months. In our study, the activity rate can vary with the

utility function and be predicted in a longer time window of about 12 months.

We presented numerical simulations with unipartite transmission rates and bipartite transmission rates. Through the numerical simulations, we found that the mathematical model reproduces the observed waves of infection in Hong Kong. One main mechanism in our model that leads to the waves is the self-learning behavioral change. The population will choose an optimal response that balances the infection risk and the benefit from the outside activity. Our results suggest that the different waves of the infected population appear in the intervals of behavioral change. The interval of behavioral change is the time interval where the normal activity type population can obtain a higher utility by choosing a higher activity. A higher activity will lead to a higher transmission rate and more infections. Social distancing measures will alter the population behavior by lowering the population activity over a period of time, thus social distancing measure is an effective strategy in COVID-19 control. This supports the observed effectiveness of social distancing as a disease control measure (13–15).

In this paper, we investigated an alternate disease control measure that is in the absence of centralized agencies like the government. Instead, the disease control measure is initiated by individuals. In the model, the populations make a decision of reducing activity or not mainly based on the delayed information and their utility functions. Our simulations explained that different waves of the infected population are due to the individuals trying to balance the risk of infection and normal lifestyle. The perceived cost after infection and the delayed

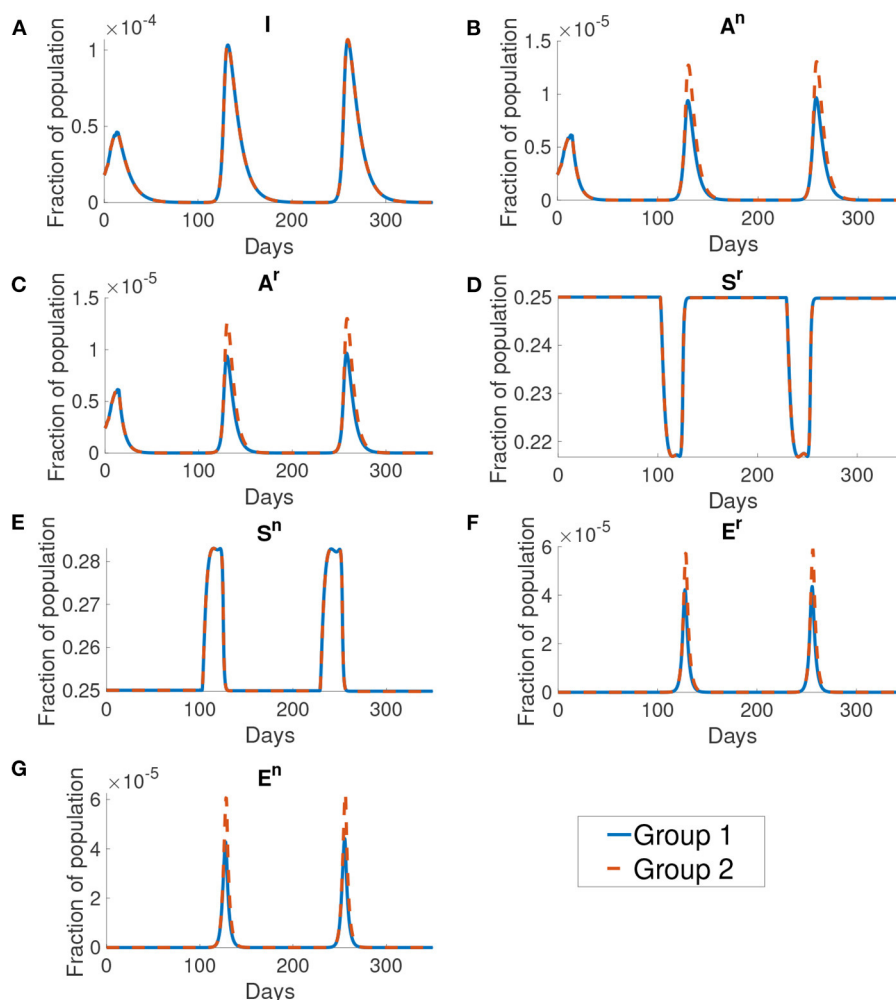


**FIGURE 10 |** The dynamics of different compartments in the simulation. From figures (A–G) shows the infected population, the normal asymptomatic population, the reduced asymptomatic population, the reduced susceptible population, the normal susceptible population, the reduced exposed population and the normal exposed population. The blue curve shows the fraction of population for group 1 and the orange curve shows the fraction of population of group 2. We can see that the group 1 and group 2 are the same except at the normal asymptomatic and the normal exposed population.

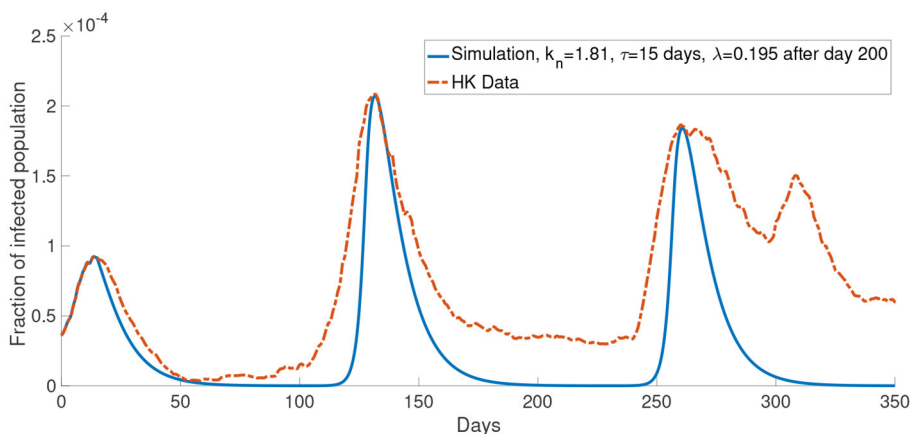


**FIGURE 11 |** The comparison of the data and the simulation for the system with  $M = 2$  with  $\lambda$  increased to 0.195 after day 200.

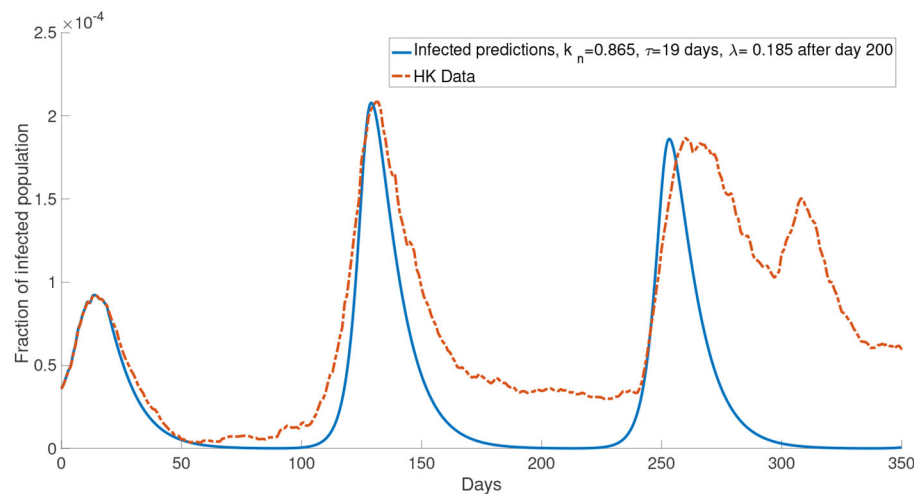


**FIGURE 12 |** The comparison of the data and the simulation for the system with  $M = 3$  with  $\lambda$  increased to 0.185 after day 200.

information are two determining aspects when individuals make a decision. As shown in **Figure 3**, for a smaller cost after infection, the infected population is larger. When the perceived cost  $c$  is small, the population will not reduce the chance of being infected by reducing the frequency of their activity. It will contribute to more infections. Another significant factor is the time delay  $\tau$ . Long time-delayed information causes a larger outbreak. To effectively prevent an outbreak, we should decrease the time delay. This conclusion is consistent with the result in (43) which shows that the short time delay will reduce the number of the infected population. The numerical simulations suggest that information about the infected population should be disclosed as fast as possible to minimize the delay. Individuals with the latest information can make the best decision as a response to the disease. This implies that policymakers should let the population have full information about the consequence of infection.

Although in our simulations, the local maximum in the second wave is similar to the data, the number of the infected population is less than the data in other times (for example, between day 100 and day 175 in **Figure 6**). One possible reason for this is that the mean-field assumption of a well-mixed population is not valid. It can be seen that our simulations reach the local maximum in a shorter time than the data from zero. This means that our simulations increase faster than the data. It is well-known that the infected population in a SIR model has exponential growth. Thus the data has a growth rate slower than exponential growth. It was shown that the population could be in the so-called small-world network, and this network leads to linear growth of the pandemic (44). We did not opt for a network model, but we used a continuous model because the network model is limited by computational power and speed, which is not feasible in simulating a large population. Apart from the underestimation of the infected population in some times, it can be seen that our model agrees quite well with the COVID-19 dynamics in Hong Kong for the first 150 days.

But the numerical simulations appear to be inaccurate after 150 days. Specifically it seems that in most of our simulations (**Figures 6–8**), we overestimated the local maximum in the third wave. This inaccuracy is possibly due to our long prediction interval of 350 days. As the pandemic radically evolves, many of the parameters will change over these 350 days. For example, better disease control measures and increased usage of face masks could lower the transmission rate, a different variant of COVID-19 could increase the transmission rate and, better treatment methods could increase the recovery rate. In **Figure 11**, we investigated one such possible scenario in which the report rate increased over time. By introducing a time-dependent report rate, the numerical simulations, and the observed data showed a better agreement. The increase in report rate can lower the local maximum of the infected population as seen from the height in the third wave of the infected population in **Figures 11, 12**. This result suggests that increasing the report rate is a feasible COVID-19 control measure which is also noticed by the study in (45). One way to increase the report rate is by increasing the number of tests done, which was shown to be effective in practice (13, 46).

## DATA AVAILABILITY STATEMENT

The original contributions presented in the study are included in the article/supplementary material, further inquiries can be directed to the corresponding author/s.

## AUTHOR CONTRIBUTIONS

T-LC, H-YY, and W-CL: conceptualization and writing—review and editing. T-LC: formal analysis, methodology, and writing—original draft. T-LC and W-CL: investigation. W-CL: supervision. All authors contributed to the article and approved the submitted version.

## FUNDING

In this study, H-YY was supported by the Health and Medical Research Fund (COVID190215) and W-CL are partially supported by the CityU Strategic Research Grant (CityU 11301520).

## REFERENCES

- Guo YR, Cao QD, Hong ZS, Tan YY, Chen SD, Jin HJ, et al. The origin, transmission and clinical therapies on coronavirus disease 2019 (COVID-19) outbreak-an update on the status. *Mil Med Res.* (2020) 7:1–10. doi: 10.1186/s40779-020-00240-0
- World Health Organization. *WHO Coronavirus (COVID-19) Dashboard.* (2021). Retrieved from: <https://covid19.who.int>
- Cooper I, Mondal A, Antonopoulos CG. A SIR model assumption for the spread of COVID-19 in different communities. *Chaos Solitons Fractals.* (2020) 139:110057. doi: 10.1016/j.chaos.2020.110057
- Chen YC, Lu PE, Chang CS, Liu TH. A Time-dependent SIR model for COVID-19 with undetectable infected persons. *IEEE Trans Netw Sci Eng.* (2020) 7:3279–94. doi: 10.1109/TNSE.2020.3024723
- Calafiore GC, Novara C, Possieri C. A modified SIR model for the COVID-19 contagion in Italy. *arXiv [Preprint] arXiv:200314391.* (2020). doi: 10.1109/CDC42340.2020.9304142
- Ye Y, Zhang Q, Ruan Z, Cao Z, Xuan Q, Zeng DD. Effect of heterogeneous risk perception on information diffusion, behavior change, and disease transmission. *Phys Rev E.* (2020) 102:042314. doi: 10.1103/PhysRevE.102.042314
- Chang S, Pierson E, Koh PW, Gerardin J, Redbird B, Grusky D, et al. Mobility network models of COVID-19 explain inequities and inform reopening. *Nature.* (2021) 589:82–7. doi: 10.1038/s41586-020-2923-3
- Gatto M, Bertuzzo E, Mari L, Miccoli S, Carraro L, Casagrandi R, et al. Spread and dynamics of the COVID-19 epidemic in Italy: effects of emergency containment measures. *Proc Natl Acad Sci USA.* (2020) 117:10484–91. doi: 10.1073/pnas.2004978117
- Ma S, Zhang J, Zeng M, Yun Q, Guo W, Zheng Y, et al. Epidemiological parameters of coronavirus disease 2019: a pooled analysis of publicly reported individual data of 1155 cases from seven countries. *medRxiv [Preprint].* (2020). doi: 10.1101/2020.03.21.20040329
- Liu Z, Magal P, Seydi O, Webb G. Understanding unreported cases in the COVID-19 epidemic outbreak in Wuhan, China, and the importance of major public health interventions. *Biology.* (2020) 9:50. doi: 10.3390/biology9030050
- Gaeta G. A simple SIR model with a large set of asymptomatic infectives. *arXiv [Preprint] arXiv:200308720.* (2020). doi: 10.3934/mine.2021013
- Cheng C, Barceló J, Hartnett AS, Kubinec R, Messerschmidt L. COVID-19 government response event dataset (CoronaNet v. 1.0). *Nat Hum Behav.* (2020) 4:756–68. doi: 10.1038/s41562-020-0909-7
- Lam HY, Lam TS, Wong CH, Lam WH, Leung CME, Au KWA, et al. The epidemiology of COVID-19 cases and the successful containment strategy in Hong Kong-January to May 2020. *Int J Infect Dis.* (2020) 98:51–8. doi: 10.1016/j.ijid.2020.06.057
- Inoue H. Japanese strategy to COVID-19: How does it work? *Glob Health Med.* (2020) 2:131–2. doi: 10.35772/ghm.2020.01043
- Milne GJ, Xie S. The effectiveness of social distancing in mitigating COVID-19 spread: a modelling analysis. *medRxiv [Preprint].* (2020). doi: 10.1101/2020.03.20.20040055
- Chen FH. Rational behavioral response and the transmission of STDs. *Theoret Popul Biol.* (2004) 66:307–16. doi: 10.1016/j.tpb.2004.07.004
- Matrajt L, Leung T. Evaluating the effectiveness of social distancing interventions to delay or flatten the epidemic curve of coronavirus disease. *Emerg Infect Dis.* (2020) 26:1740. doi: 10.3201/eid2608.201093
- Garibaldi P, Moen ER, Pissarides CA. *Modelling Contacts and Transitions in the SIR Epidemics Model. Covid Economics Vetted and Real-Time Papers.* CEPR Press (2020).
- Amaral MA, de Oliveira MM, Javarone MA. An epidemiological model with voluntary quarantine strategies governed by evolutionary game dynamics. *arXiv [Preprint] arXiv:200805979.* (2020). doi: 10.1016/j.chaos.2020.110616
- The Government of HKSAR, Department of Health. *Data in Coronavirus Disease (COVID-19).* (2021). Retrieved from: <https://data.gov.hk/en-data/dataset/hk-dh-chpsebcdrr-novel-infectious-agent>
- Xia S, Liu J. A computational approach to characterizing the impact of social influence on individuals' vaccination decision making. *PLoS ONE.* (2013) 8:e60373. doi: 10.1371/journal.pone.0060373
- Fu F, Rosenbloom DI, Wang L, Nowak MA. Imitation dynamics of vaccination behaviour on social networks. *Proc R Soc B Biol Sci.* (2011) 278:42–9. doi: 10.1098/rspb.2010.1107
- Ndeffo Mbah ML, Liu J, Bauch CT, Tekel YI, Medlock J, Meyers LA, et al. The impact of imitation on vaccination behavior in social contact networks. *PLoS Comput Biol.* (2012) 8:e1002469. doi: 10.1371/journal.pcbi.1002469
- Szabó G, Tóke C. Evolutionary prisoner's dilemma game on a square lattice. *Phys Rev E.* (1998) 58:69. doi: 10.1103/PhysRevE.58.69
- Chang SL, Piraveenan M, Pattison P, Prokopenko M. Game theoretic modelling of infectious disease dynamics and intervention methods: a review. *J Biol Dyn.* (2020) 14:57–89. doi: 10.1080/17513758.2020.1720322
- Fenichel EP, Castillo-Chavez C, Ceddia MG, Chowell G, Parra PAG, Hickling GJ, et al. Adaptive human behavior in epidemiological models. *Proc Natl Acad Sci USA.* (2011) 108:6306–11. doi: 10.1073/pnas.1011250108
- Cho S. Mean-field game analysis of SIR model with social distancing. *arXiv [Preprint] arXiv:200506758.* (2020).
- Tian S, Hu N, Lou J, Chen K, Kang X, Xiang Z, et al. Characteristics of COVID-19 infection in Beijing. *J Infect.* (2020) 80:401–6. doi: 10.1013/ssrn.3541134
- Beigel JH, Tomashek KM, Dodd LE, Mehta AK, Zingman BS, Kalil AC, et al. Remdesivir for the treatment of COVID-19. *N Engl J Med.* (2020) 383:1813–26. doi: 10.1056/NEJMoa2007764
- Lin Q, Zhao S, Gao D, Lou Y, Yang S, Musa SS, et al. A conceptual model for the coronavirus disease 2019 (COVID-19) outbreak in Wuhan, China with individual reaction and governmental action. *Int J Infect Dis.* (2020) 93:211–6. doi: 10.1016/j.ijid.2020.02.058
- The Government of HKSAR. *Government Announces Enhancements to Anti-Epidemic Measures in Four Aspects.* (2020). Retrieved from: <https://www.info.gov.hk/gia/general/202003/24/P2020032400050.htm?fontSize=1>
- Pan A, Liu L, Wang C, Guo H, Hao X, Wang Q, et al. Association of public health interventions with the epidemiology of the COVID-19 outbreak in Wuhan, China. *JAMA.* (2020) 323:1915–23. doi: 10.1001/jama.2020.6130
- Barber SJ, Kim H. COVID-19 worries and behavior changes in older and younger men and women. *J Gerontol Ser B.* (2021) 76:e17–23. doi: 10.1093/geronb/gbaa068
- Galasso V, Pons V, Profeta P, Becher M, Brouard S, Foucault M. Gender differences in COVID-19 attitudes and behavior: panel evidence from eight countries. *Proc Natl Acad Sci USA.* (2020) 117:27285–91. doi: 10.1073/pnas.2012520117
- Clark C, Davila A, Regis M, Kraus S. Predictors of COVID-19 voluntary compliance behaviors: an international investigation. *Global Trans.* (2020) 2:76–82. doi: 10.1016/j.glt.2020.06.003
- Harper CA, Satchell LP, Fido D, Latzman RD. Functional fear predicts public health compliance in the COVID-19 pandemic. *Int J Mental Health Addict.* (2020) 9:1–14. doi: 10.31234/osf.io/jkfu3
- Syon B, Daniel HJ. *Partisan Polarization and Resistance to Elite Messages: Results from a Survey Experiment on Social Distancing.* Retrieved from: <https://ssrn.com/abstract=3593450> (accessed May 5, 2020).

## ACKNOWLEDGMENTS

The authors would like to express very great appreciation to Kendra M. Wu for her valuable and constructive suggestions for editing the writing.



38. Van Bavel JJ, Baicker K, Boggio PS, Capraro V, Cichocka A, Cikara M, et al. Using social and behavioural science to support COVID-19 pandemic response. *Nat Hum Behav.* (2020) 4:460–71. doi: 10.1038/s41562-020-0884-z
39. Green J, Edgerton J, Naftel D, Shoub K, Cranmer SJ. Elusive consensus: polarization in elite communication on the COVID-19 pandemic. *Sci Adv.* (2020) 6:eabc2717. doi: 10.1126/sciadv.abc2717
40. Lüdecke D, von dem Knesebeck O. Protective behavior in course of the COVID-19 outbreak—survey results from Germany. *Front Public Health.* (2020) 8:567. doi: 10.3389/fpubh.2020.572561
41. Nardin LG, Miller CR, Ridenhour BJ, Krone SM, Joyce P, Baumgaertner BO. Planning horizon affects prophylactic decision-making and epidemic dynamics. *PeerJ.* (2016) 4:e2678. doi: 10.7717/peerj.2678
42. Kim S, Seo YB, Jung E. Prediction of COVID-19 transmission dynamics using a mathematical model considering behavior changes in Korea. *Epidemiol Health.* (2020) 42:e2020026. doi: 10.4178/epih.e2020026
43. Rong X, Yang L, Chu H, Fan M. Effect of delay in diagnosis on transmission of COVID-19. *Math Biosci Eng.* (2020) 17:2725–40. doi: 10.3934/mbe.2020149
44. Thurner S, Klimek P, Hanel R. A network-based explanation of why most COVID-19 infection curves are linear. *Proc Natl Acad Sci USA.* (2020) 117:22684–9. doi: 10.1073/pnas.2010398117
45. Moghadas SM, Fitzpatrick MC, Sah P, Pandey A, Shoukat A, Singer BH, et al. The implications of silent transmission for the control of COVID-19 outbreaks. *Proc Natl Acad Sci USA.* (2020) 117:17513–5. doi: 10.1073/pnas.2008373117
46. Balilla J. *Assessment of COVID-19 Mass Testing: The Case of South Korea* (March 18, 2020). Retrieved from: <https://ssrn.com/abstract=3556346> (accessed March 18, 2020).

**Conflict of Interest:** The authors declare that the research was conducted in the absence of any commercial or financial relationships that could be construed as a potential conflict of interest.

**Publisher's Note:** All claims expressed in this article are solely those of the authors and do not necessarily represent those of their affiliated organizations, or those of the publisher, the editors and the reviewers. Any product that may be evaluated in this article, or claim that may be made by its manufacturer, is not guaranteed or endorsed by the publisher.

Copyright © 2021 Chan, Yuan and Lo. This is an open-access article distributed under the terms of the Creative Commons Attribution License (CC BY). The use, distribution or reproduction in other forums is permitted, provided the original author(s) and the copyright owner(s) are credited and that the original publication in this journal is cited, in accordance with accepted academic practice. No use, distribution or reproduction is permitted which does not comply with these terms.



# Developing a Screening Procedure During the COVID-19 Pandemic: Process and Challenges Faced by a Low-Incidence Area

Wei Tang<sup>1</sup>, Fei Wang<sup>2</sup>, Jian-Wei Wang<sup>1\*</sup>, Yao Huang<sup>1</sup>, Li Liu<sup>1</sup>, Shi-Jun Zhao<sup>1</sup>, Xin-Ming Zhao<sup>1</sup> and Ning Wu<sup>1,3</sup>

<sup>1</sup> Department of Diagnostic Radiology, National Cancer Center, National Clinical Research Center for Cancer, Cancer Hospital, Chinese Academy of Medical Sciences and Peking Union Medical College, Beijing, China, <sup>2</sup> Office of Cancer Screening, National Cancer Center, National Clinical Research Center for Cancer, Cancer Hospital, Chinese Academy of Medical Sciences and Peking Union Medical College, Beijing, China, <sup>3</sup> Department of PET-CT Center, National Cancer Center, National Clinical Research Center for Cancer, Cancer Hospital, Chinese Academy of Medical Sciences and Peking Union Medical College, Beijing, China

**Purpose:** To summarize the imaging results of COVID-19 pneumonia and develop a computerized tomography (CT) screening procedure for patients at our institution with malignant tumors.

**Methods:** Following epidemiological investigation, 1,429 patients preparing to undergo anti-tumor-treatment underwent CT scans between February 17 and April 16, 2020. When CT findings showed suspected COVID-19 pneumonia after the supervisor radiologist and the thoracic experience radiologist had double-read the initial CT images, radiologists would report the result to our hospital infection control staff. Further necessary examinations, including the RT-PCR test, in the assigned hospital was strongly recommended for patients with positive CT results. The CT examination room would perform sterilization for 30 min to 1 h. If the negative results of any suspected COVID-19 pneumonia CT findings were identified, the radiologists would upload the results to our Hospital Information Systems and inform clinicians within 2 h.

**Results:** Fifty (0.35%, 50/1,429) suspected pneumonia cases, including 29 males and 21 females (median age: 59.5 years old; age range 27–79 years), were identified. A total of 34.0% (17/50) of the patients had a history of lung cancer and 54.0 (27/50) underwent chemotherapy or targeted therapy. Forty-six patients (92.0%) had prior CT scans, and 35 patients (76.1%) with suspected pneumonia were newly seen (median interval time: 62 days). Sub-pleura small patchy or strip-like lesions most likely due to fibrosis or hypostatic pneumonia and cluster of nodular lesions were the two main signs of suspected cases on CT images (34, 68.0%). Twenty-seven patients (54.0%) had, at least once, follow-up CT scan (median interval time: 18.0 days). Only one patient had an increase in size (interval time: 8 days), the immediately RT-PCR test result was negative.

**Conclusion:** CT may be useful as a screening tool for COVID-19 based on imaging features. But the differential diagnosis between COVID-19 and other pulmonary infection and/or non-infectious disease is very difficult due to its overlapping imaging features. The confirmed diagnosis of the COVID-19 infection should be based on the etiologic

## OPEN ACCESS

### Edited by:

Reza Lashgari,  
Shahid Beheshti University, Iran

### Reviewed by:

Bin Lin,  
Zhejiang University, China  
Guang Yang,  
Imperial College London,  
United Kingdom

### \*Correspondence:

Jian-Wei Wang  
dr\_jianweiwang@sina.com

### Specialty section:

This article was submitted to  
Pulmonary Medicine,  
a section of the journal  
Frontiers in Medicine

**Received:** 17 January 2021

**Accepted:** 20 October 2021

**Published:** 24 December 2021

### Citation:

Tang W, Wang F, Wang J-W, Huang Y,  
Liu L, Zhao S-J, Zhao X-M and Wu N  
(2021) Developing a Screening  
Procedure During the COVID-19  
Pandemic: Process and Challenges  
Faced by a Low-Incidence Area.  
Front. Med. 8:654754.  
doi: 10.3389/fmed.2021.654754

eventually. The cancer patients at a low-incidence area would continue treatment by screening carefully before admission.

**Keywords:** COVID-19, screening, computerized tomography (CT), healthcare [MeSH], hospital (clinic)-clinic corporation

## INTRODUCTION

Since December 2019, the Novel Coronavirus (COVID-19) has caused an outbreak of pneumonia and has rapidly spread across the globe. On 11 March 2020, the WHO, declared COVID-19 to be a pandemic (1). Globally, as of 2:10 p.m. CET, 13 March 2021, there have been 118,754,336 confirmed cases of COVID-19, including 2,634,370 deaths, reported to WHO. While the number of confirmed and suspected cases continues to grow, the rate of increase is now gradually declining in some areas. On March 19, China reported no new domestic cases for the first time, and the first prevailing peak period of the pandemic was over. Thanks to the efforts of the Chinese government, numerous measures such as preventing the spread and import of the infection, strict restrictions on the gathering of large numbers of people, disinfecting public areas, and taking charge of symptomatic people (such as those with fever and/or cough) has led to Beijing, the capital of China, maintaining its status up until mid-April, 2020 as a low-incidence area of COVID-19 infections during the period of outbreak in China.

The epidemiologic, laboratory, and clinical features of COVID-19 pneumonia have been described (2–5). Because a curative vaccine has not yet been developed, early detection and efficient control of the route of transmission (i.e., isolation of suspected cases, and disinfection) remain the most effective ways to fight the outbreak. The WHO recommends suspected cases be screened for the virus with nucleic acid amplification tests (NAAT) (6), such as reverse-transcriptase polymerase chain reaction (RT-PCR). Laboratory detection is time-consuming and may not be available for all those with a suspected infection owing to the shortage of test kits for SARS-CoV-2. These challenges increase the risk of spread by free movement of people highly suspected of carrying the disease. In addition, the laboratory test can give false negative results. CT is considered the first-line imaging modality in highly suspected cases and is helpful in monitoring imaging changes during treatment. Therefore, CT has been identified as an efficient clinical diagnostic tool for people with suspected COVID-19 (7).

Sensitivity and specificity of chest CT for COVID-19 are reported to range from 80 to 90% and 60 to 70%, respectively (8, 9). The diagnosis and treatment program (6th version), published by the National Health Commission of the People's Republic of China (10), defined the diagnosis of viral pneumonia based on radiologic features by radiologists as one of the diagnostic criteria for COVID-19.

The Cancer Hospital Chinese Academy of Medical Sciences (CHCAMS) & National Cancer Center of China (NCC) is one of the leading specialist cancer hospitals of China. NCC has over 1,000,000-patient output annually. In 2019, 79,398 X-ray, 210,503 CT, and 49,988 MRI examinations were performed

in the center. Patients with cancer have an increased risk of complication and death during or after treatment related to COVID-19 infection (11, 12). During the outbreak period, a large proportion of the examinations, diagnosis, treatments and curative effect evaluations of patients were delayed. It is very important for the patients with malignant tumor that the prevention and control of COVID-19 infection, especially when they undergo therapies such as chemotherapy, radiotherapy, targeted therapy or immunotherapy. Our hospital has made any efforts to minimize any possibilities of in-hospital transmission to ensure a safe environment for both patients and staff. In order to make the patients with malignant tumor get the necessary treatment on time, the infection control committee of NCC/CHCAMS decided to use CT to screen the COVID-19 pneumonia for pre-treatment patients as a necessary examination on February 16, 2019.

To our knowledge, few articles which focuses on the COVID-19 CT screening for cancer patients had been published (13). Now, we will want to share our experience and understanding with medical peers, which will contribute directly to the accumulation of experience in other medical facilities.

## MATERIALS AND METHODS STUDY

### Design and Patients

The questionnaire survey which designed by our hospital infection control team were written by each pre-anti-tumor treatment patients. This questionnaire included personal information (gender, age, telephone number, home or permanent address, exact date of arrival Beijing, and duration from arrival in Beijing to the current date) and epidemiological investigation. The epidemiological investigation included (10): (i) whether the patient had been to Hubei Province within the past 2 weeks; (ii) whether the patient had taken public transport which passed through Hubei Province within the past 2 weeks; (iii) whether the patient had had contact with anybody from Hubei Province within the past 2 weeks; (iv) whether the patient had been abroad or had had contact with anybody who coming overseas; (v) whether the patient had had contact with COVID-19 confirmed or suspected cases; (vi) appearance or worsening of symptoms such as fever and body temperature; (vii) whether the patient had taken any antipyretics during the fever; and (viii) whether the patient displayed typical symptoms such as fever, sore throat, nasal congestion, malaise, headache, myalgia, or dyspnea. Given that our hospital was not a designated hospital for COVID-19 infection patients, if patients or those accompanying them gave any positive responses, they would be declined entry. If the patients or those accompanying them had a fever higher than 37.3°C, and had no alternative explanation for these symptoms, COVID-19 testing via a SARS-CoV-2 quantitative

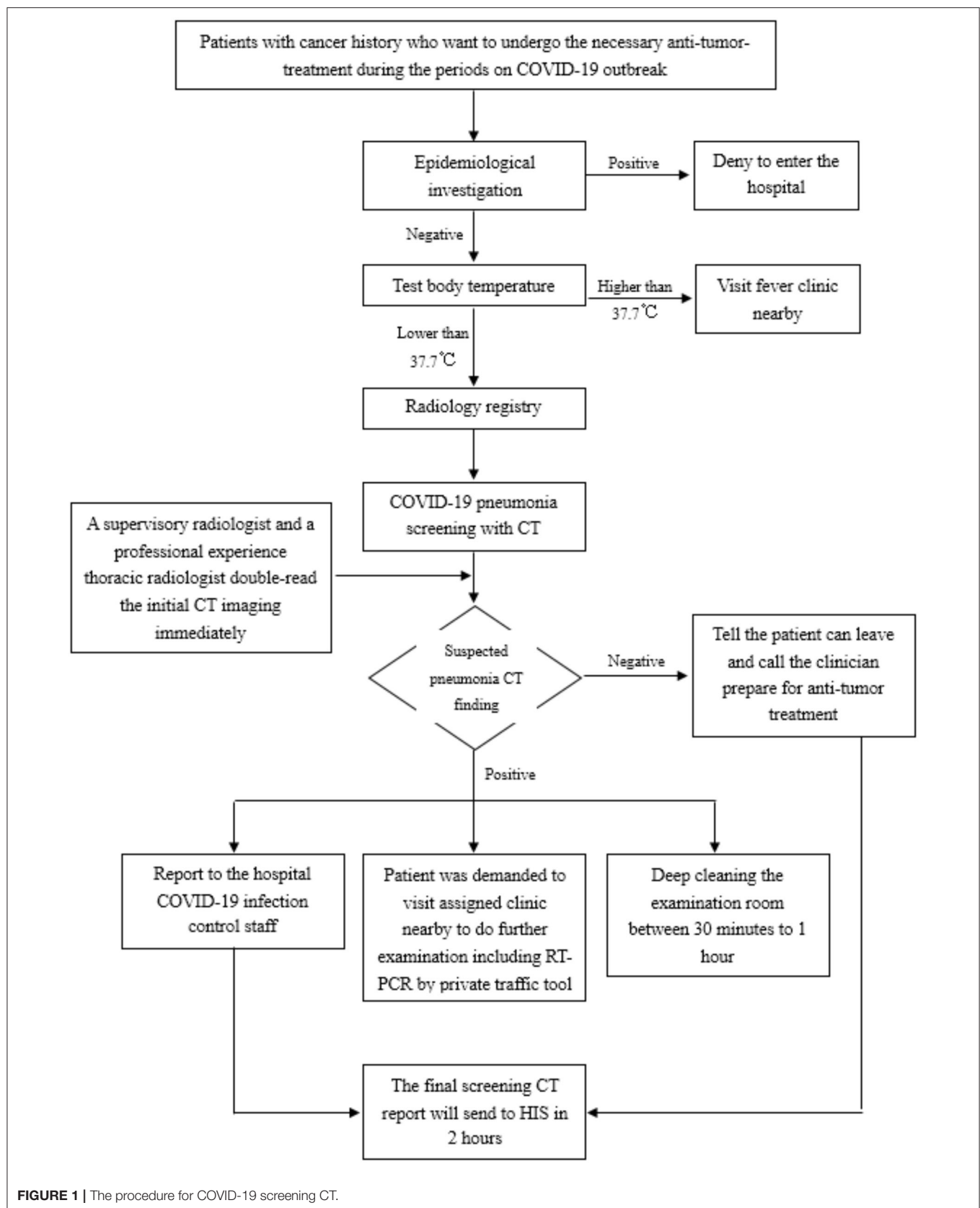


**FIGURE 1 |** The procedure for COVID-19 screening CT.

PCR nasopharyngeal swab was sent in addition to a respiratory pathogen panel PCR at the nearby fever clinic.

Finally, in this center, a total of 1,429 patients with cancer history underwent the CT procedure and routine blood test between February 17 and April 16, 2020. All patients denied any direct exposure history to Wuhan or to people who had a direct exposure history to Wuhan (i.e., long-term exposure history to Wuhan, or travel to Wuhan before diagnosis) and no one showed any symptoms associated with COVID-19.

## Imaging Technique

All patients underwent scanning with the following four scanners: Optima 660, LightSpeed VCT, Discovery 750 HD (GE Healthcare, Milwaukee, USA), and Somatom Edge (Siemens Healthcare, Erlangen, Germany). Instead, the routine CT scan of Low-dose CT scan was used. The acquisition parameters were set at 120 kVp; 150–250 mAs; pitch, 0.938–1.0; and collimation, 0.625 mm. All imaging data were reconstructed by use of a standard reconstruction algorithm with a slice thickness of 0.625–1.0 mm. All patients were scanned in the supine position while holding their breath at the end of inspiration. The field of view was set from the apex to the base of the lungs. Images were sent to the Picture Archiving and Communication System (PACS) system to be read by the radiologists.

## Computed Tomography Scan Procedure and Imaging Interpretation

To detect suspected COVID-19 on CT imaging, we arranged for several Supervisory Radiologists (SR) to read the CT images immediately after completion of the scan. The SR confirmed whether the CT images showed signs of any type of pneumonia, including bacterial pneumonia, viral pneumonia, and other types, including suspected COVID-19. Comparison was made with prior CT images, in order to confirm whether the lesion was newly seen, persistently existed, or had changed in size or density. All images were viewed with both lung (width, 1,500 HU; level, –700 HU) and mediastinal (width, 350 HU; level, 40 HU) settings. The patient was not permitted to leave the scan room until the technologist of radiology (TR) had obtained permission from the SR. If any CT images showed suspected pneumonia, the SR would ask one of the Professor Radiologists (PR, Y. Huang, JW. Wang, SJ. Zhao, and L. Liu, each of whom have over 10 years of thoracic-imaging diagnosis experience) to immediately read the images again. If the PR confirmed the suspected diagnosis of viral pneumonia, the SR would immediately report the details, including the CT findings and blood test results, to the clinician and the hospital infection control staff. The clinician would then order immediate isolation of the patient for clinical monitoring and treatment. The TR would request the patients attend the nearby fever clinic (given that our center does not have a fever clinic) while avoiding use of public transportation to do the further examination including RT-PCR. The hospital infection control staff would document the information to follow up the results of the patient. Sterilization would be performed: room downtime was typically 30 min to 1 h for room decontamination and passive air exchange. In addition, the final CT report would be double-read by a further two radiologists. The

**TABLE 1 |** Malignant tumor and the treatment history of the patients.

|  | <b>Surgical resection<br/>(n = 26)</b> | <b>Chemotherapy/<br/>Target therapy<br/>(n = 27)</b> | <b>Radiotherapy<br/>(n = 8)</b> | <b>Interventional<br/>therapy<br/>(n = 1)</b> |
|--|--|--|---------------------------------|---|
| Lung cancer<br>(n = 17)                      | 6                                      | 12   | 1                               | 0   |
| Breast cancer<br>(n = 9)                     | 8                                      | 1  | 1                               | 0   |
| Esophagus cancer<br>(n = 4)                  | 2                                      | 2  | 2                               | 0   |
| Gastric cancer<br>(n = 3)                    | 2                                      | 1  | 0                               | 0   |
| Ovarian cancer<br>(n = 3)                    | 2                                      | 3  | 0                               | 0   |
| Endometrial<br>cancer (n = 2)                | 1                                      | 1  | 1                               | 0   |
| Hepatocellular<br>carcinoma (n = 2)          | 1                                      | 0  | 0                               | 1   |
| Non-Hodgkin<br>Lymphoma<br>(n = 2)           | 0                                      | 2  | 0                               | 0   |
| Gallbladder<br>carcinoma (n = 1)             | 1                                      | 1  | 0                               | 0   |
| Colon cancer<br>(n = 1)                      | 1                                      | 0  | 0                               | 0   |
| Hodgkin<br>lymphoma (n = 1)                  | 0                                      | 1  | 0                               | 0   |
| Cervical cancer<br>(n = 1)                   | 0                                      | 1  | 1                               | 0   |
| Thymic carcinoma<br>(n = 1)                  | 0                                      | 1  | 1                               | 0   |
| Clear cell<br>carcinoma of<br>kidney (n = 1) | 1                                      | 0  | 0                               | 0   |
| Nasopharyngeal<br>carcinoma (n = 1)          | 0                                      | 1  | 1                               | 0   |
| Olfactory<br>neuroblastoma<br>(n = 1)        | 1                                      | 0  | 0                               | 0   |

imaging features defined in a previous study (14): ground-glass opacities (GGO), consolidation, mixed GGO and consolidation, centrilobular nodules, architectural distortion, cavitation, tree-in-bud, bronchial wall thickening, reticulation, subpleural bands, traction bronchiectasis, intrathoracic lymph node enlargement, vascular enlargement in the lesion, and pleural effusions (**Figure 1** refers to the procedure for COVID-19 screening CT).

## Follow-Up CT Scan

We defined three types of imaging changes: no change, progressive change, and improvement change. No change referred to no obvious changes presented in the chest CT progressive change referred to the presence of new lesions or the presence of extent involvement area during treatment; and improvement change referred to the continually absorbed abnormalities. We also evaluated the duration of imaging progress, which was calculated from the time of baseline CT or the time



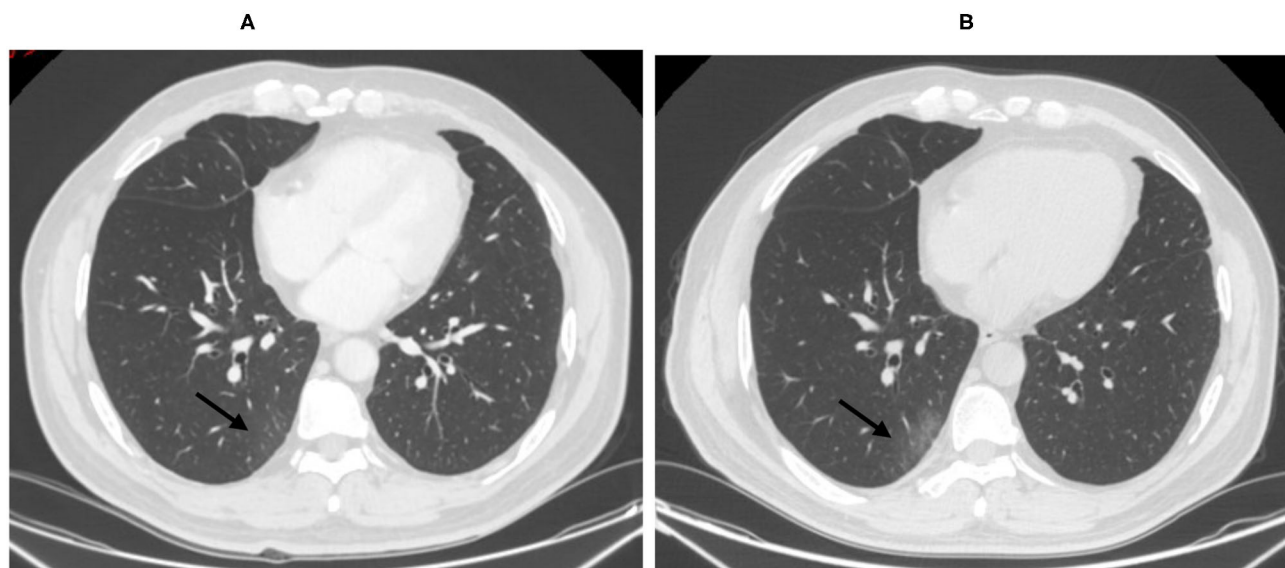


**FIGURE 2 |** Fifty-six-year-old male with lung adenocarcinoma history. Screening CT images (B) showed subpleural bandlike areas of ground glass opacity (GGO) had been increased in size compare to the prior CT scan (A) (arrow).

of CT showing new lesions to that of the CT showing abnormal imaging findings.

## RESULTS

### Patients

Among the 1,429 COVID-19 infection screening cases for pre-inpatients, 50 cases (0.35%, 50/1,429) of suspected virus pneumonia in CT imaging, which had been double-read by SR and PR, were reported to the hospital infection control staff. The total of 50 suspected virus pneumonia patients (29 males, 21 females; median 59.5 years old; age range 27–79 years) were included in analysis and the cancer history. Treatment history before CT scan were listed in **Table 1**. A total of 34.0% (17/50) of the patients had a history of lung cancer, 18.0% (9/50) had a history of breast cancer. Fifty-two percentage (26/50) patients underwent surgical resection, 54.0% (27/50) underwent chemotherapy or targeted therapy, 16.0% (8/50) underwent radiotherapy, and one patient (4.0%) with hepatocellular carcinoma underwent interventional therapy. Thirty-six patients (72.0%) were natives of Beijing and 14 patients (28.0%) were from outside of Beijing, including one patient from Hubei Province. They had complied with 2-week home quarantine requirements before the CT scan. All available clinical, laboratory examinations, and epidemic characteristics were collected.

### Initial COVID-19 Screening CT Scan

In our retrospective cohort of 50 patients, 46 patients (92.0%) had prior CT scans. Thirty-five patients (76.1%, 35/46) with suspected pneumonia were newly seen (interval time: 26–145 days, median: 62 days), eight patients (17.4%, 8/46) had slightly increased in size or density (interval time: 13–144 days, median:

74 days), two patients (4.3%, 2/46) had no change, and one (2.2%, 1/46) had increased in size when compared with the recent examination.

In COVID-19 screening CT, all lung segments may be involved; there was a slight predilection for the left lower lobe (30 (33.0%) of 91 affected segments among all patients). Involvement of lower lobes (right 48.0 vs. left 60.0%) was more than that of the upper lobes (right 20.0 vs. left 40.0%). Twenty-nine (58.0%) patients had single lobe involvement, 10 (20.0%) patients had involvement of two lobes, and 11 (22.0%) patients had three or more lobes involved. The lesions were predominantly peripheral and subpleural in 29 (58.0%) patients. Sub-pleura small patchy (**Figure 2**) or strip-like lesions most likely due to fibrosis or hypostatic pneumonia and cluster of nodular lesions (**Figure 3**) were two main signs of suspected cases on CT images (34, 68.0%). Fourteen cases (28.0%, 14/50) manifested GGO (**Figure 4**) and consolidation (**Figure 5**). One case (2.0%, 1/50) manifested interstitial inflammation (**Figure 6**) and another case (2.0%, 1/50) manifested diffuse small airway lesions most likely due to respiratory bronchiolitis. No patients had mediastinal lymphadenopathy or pleural effusion. Cavitation and tree-in-bud were absent in our cohort. In addition, a part-solid pulmonary nodule with a primary lung cancer imaging feature was identified in a patient with a history of esophagus cancer.

### Follow Up COVID-Screening CT Scan

A total of 85 chest CT examinations on 27 patients had been performed with at least once follow up CT scan as of April 16, 2020. The mean number of CT examinations per patient was 1.7 (85/50). The mean time between the initial and follow up CT studies was 18.0 days (range, 6–53 days). Only one patient

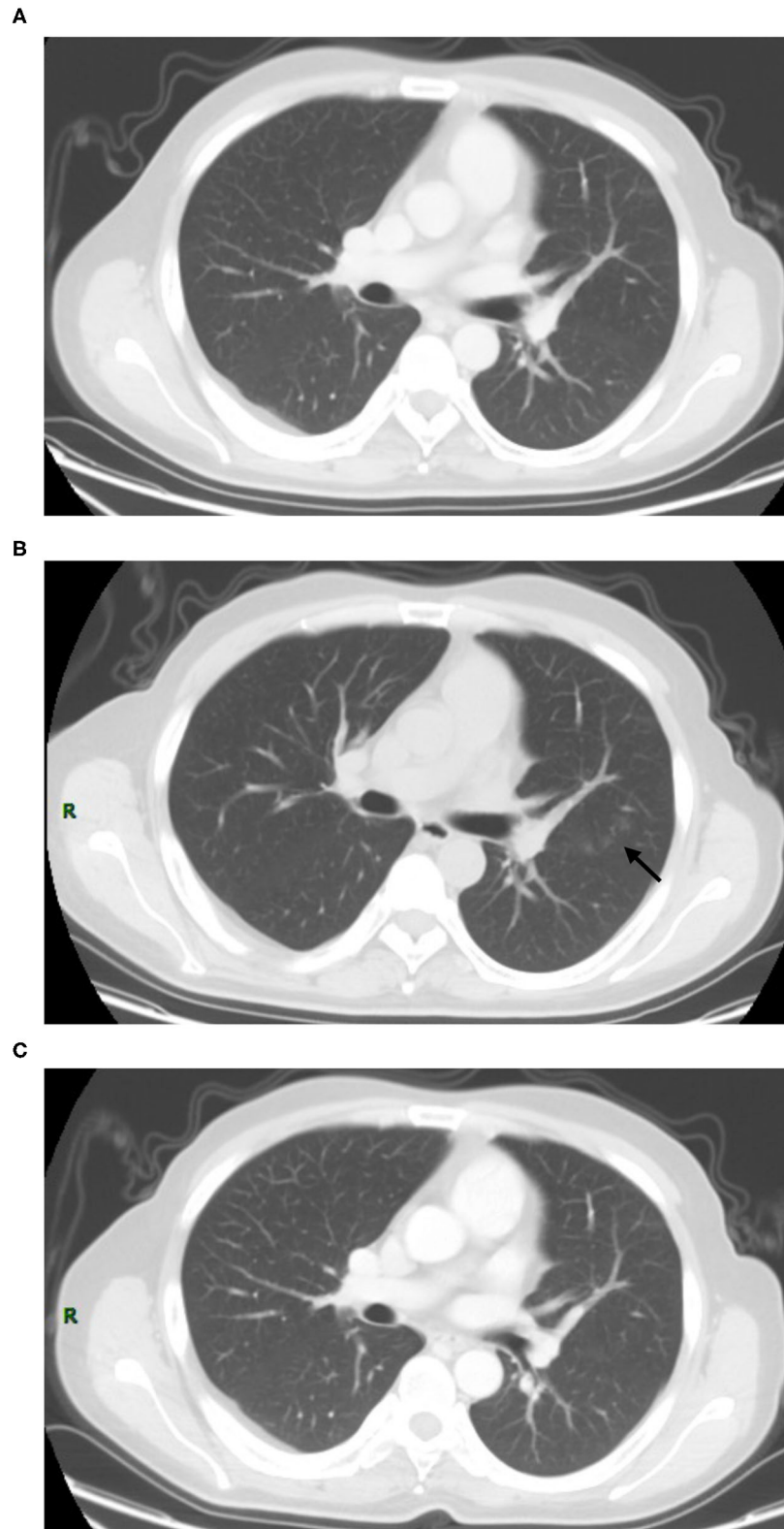


**FIGURE 3 |** Thirty-seven-year-old male with nasopharynx cancer. Patchy ground glass opacities affecting the left upper lobe had been newly seen **(B)** (arrow) when compared to the prior CT which performed at 2 months ago **(A)**. The short-term CT scan **(C)** showed the lesion had been completely resolved.

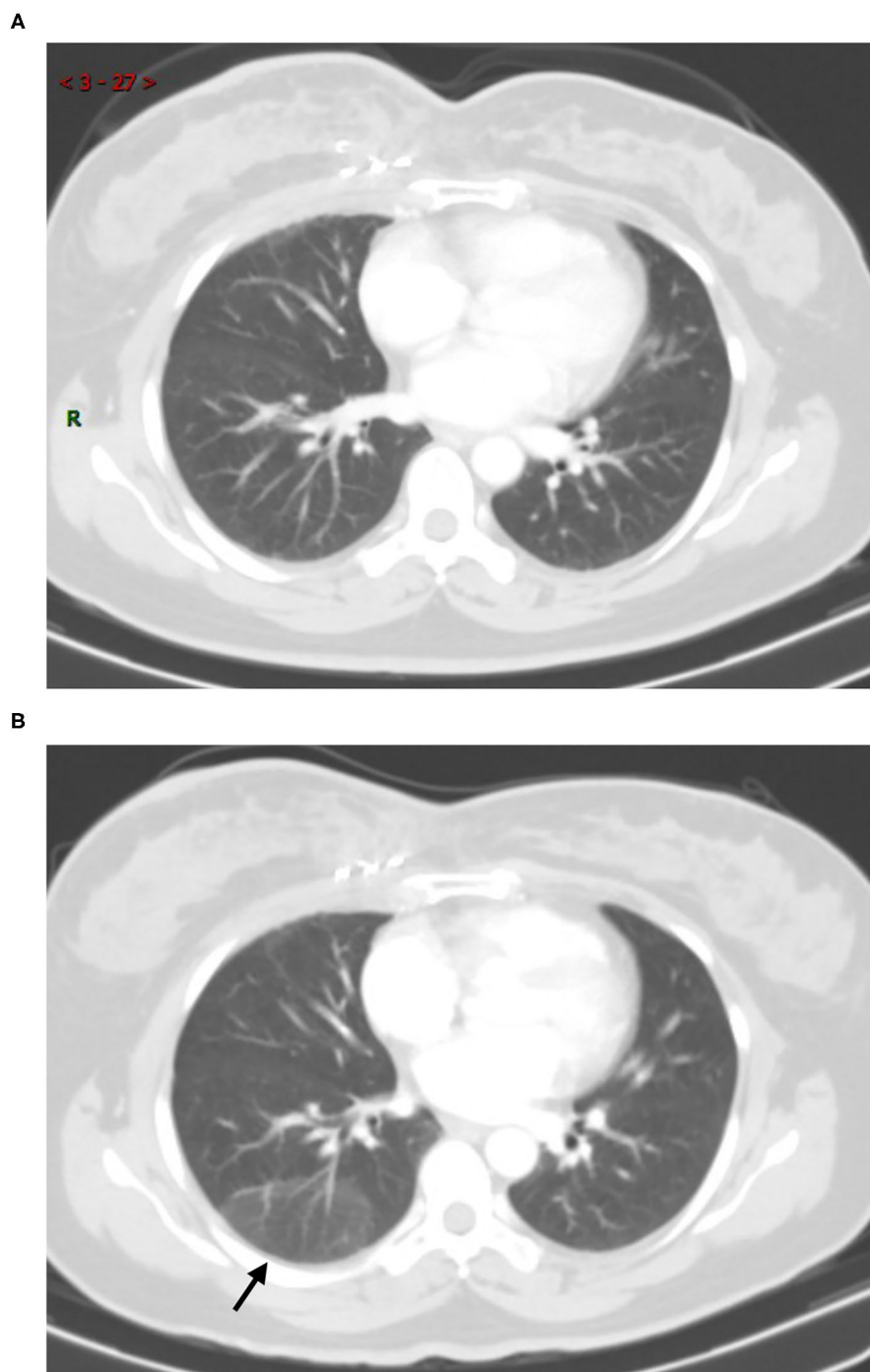


**FIGURE 4 |** Forty-two-year-old female with breast cancer history. Screening CT scan showed a focal peripheral rounded and ill-defined GGOs in the right lower lobe [(B), arrow]. Comparison to the prior CT scan (A), it has been newly seen.

had increased in size (interval time: 8 days) compared with the previous CT scan.

Immediate RT-PCR was strongly recommended by the clinician for the patient, and the final test result was negative (Figure 7). Thirteen patients (26.0%, 13/50) had no change

(median: 19 days, range: 6–42 days). Among these, five patients (18.5%, 5/27) showed cluster nodular lesion, three (11.1%, 3/27) showed patchy shadow, most likely due to the inflammatory, three (11.1%, 3/27) showed consolidation, most likely due to the inflammatory or atelectasis, one (3.7%, 1/27) showed sub-pleural

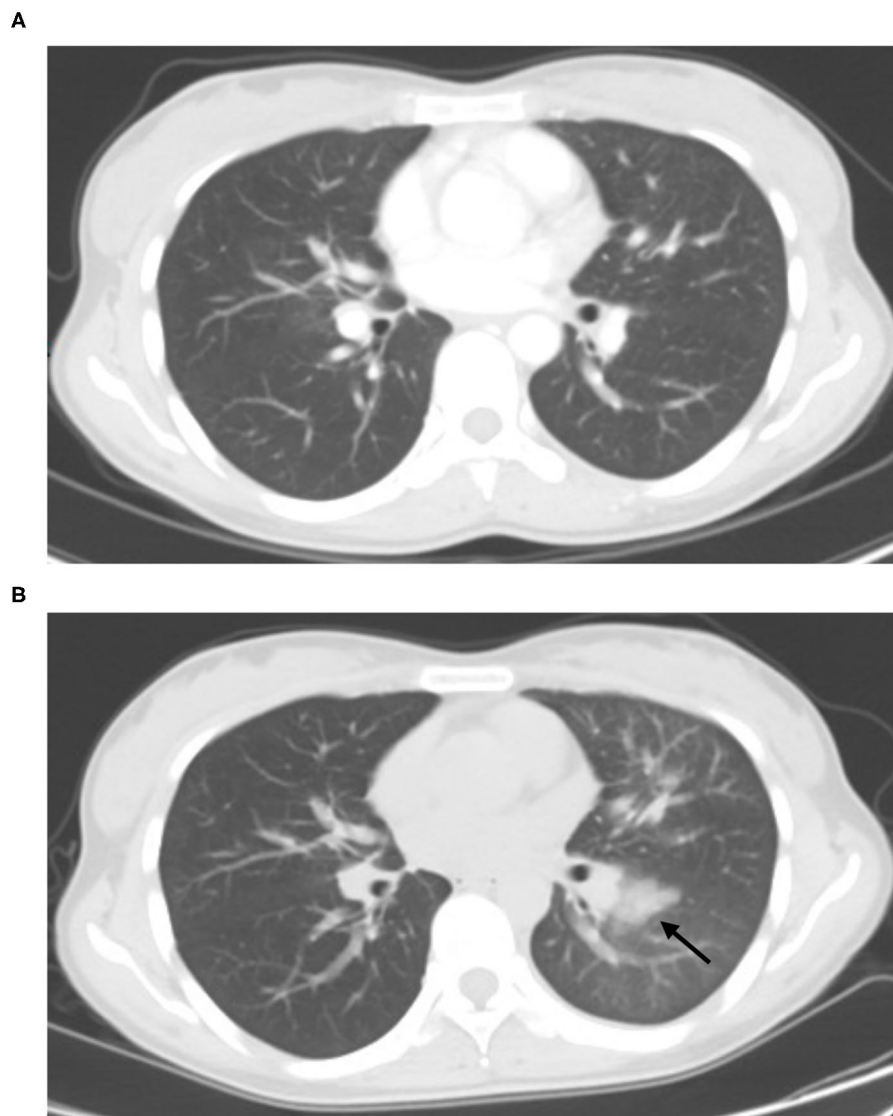


**FIGURE 5 |** Twenty-seven-year-old female with post-chemotherapy of lung cancer history. Comparison to the prior CT scan **(A)** which performed at 2 months ago, the focal left lower lobe subpleural consolidations was identified **[(B), arrow]**.

interstitial inflammation change, and one (3.7%, 1/27) manifested multiple GGO on bilateral lung parenchyma (**Figure 8**). Thirteen patients (26.0%, 13/50) had resolved or partly resolved (median: 19 days, range: 6–53 days).

Among the 23 patients who had no further follow up CT scan, nine patients (39.1%, 9/23) showed patchy shadow on sub-pleural due to atelectasis or hypostatic pneumonia, seven patients (30.4%, 7/23) manifested consolidation due to chronic inflammation or atelectasis, four patients (17.4%, 4/23) manifested cluster of nodular lesion, most likely due to inflammatory, one (4.3%, 1/23) manifested focal GGO, most likely due to Atypical adenomatous hyperplasia (AAH) of lung, one (4.3%, 1/23) manifested segmental GGO, most likely due to inflammatory or AAH, and another one (4.3%, 1/23) manifested

diffuse small airway lesions or respiratory bronchiolitis (All the COVID-19 screening CT finding were showed in **Table 2**).

## DISCUSSION

At the time of writing, although COVID-19 is still spreading rapidly overseas, all COVID-19 patients in Wuhan, where the first case was reported in the city in December 2019, had been discharged, and hospitalized COVID-19 cases had dropped to zero on April 26, 2020. A new issue is that asymptomatic patients may add a new and worrying dimension to the spread of the pandemic. Besides Wuhan city, the medical institutions of all other Chinese cities have now switched back to their normal work status to serve the medical needs of the public. Because



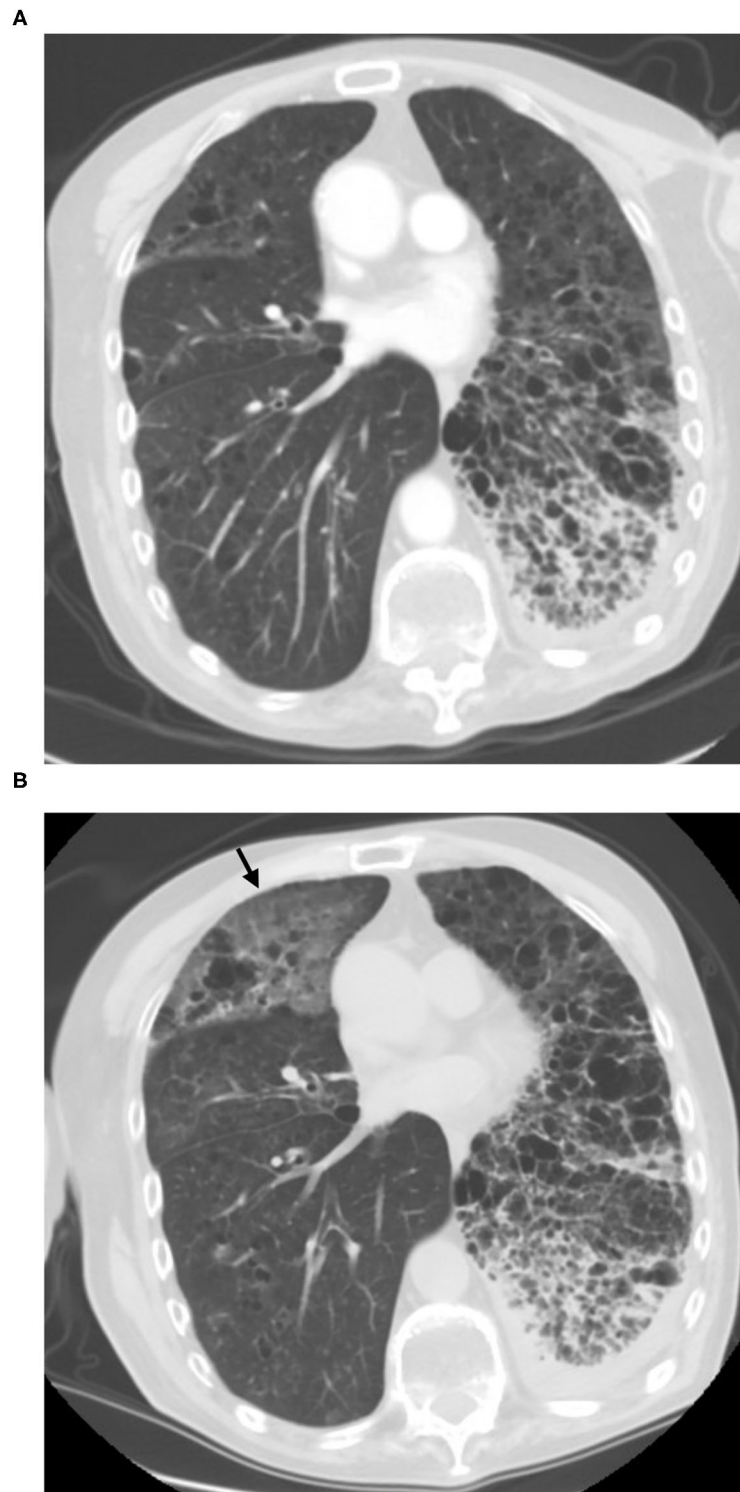
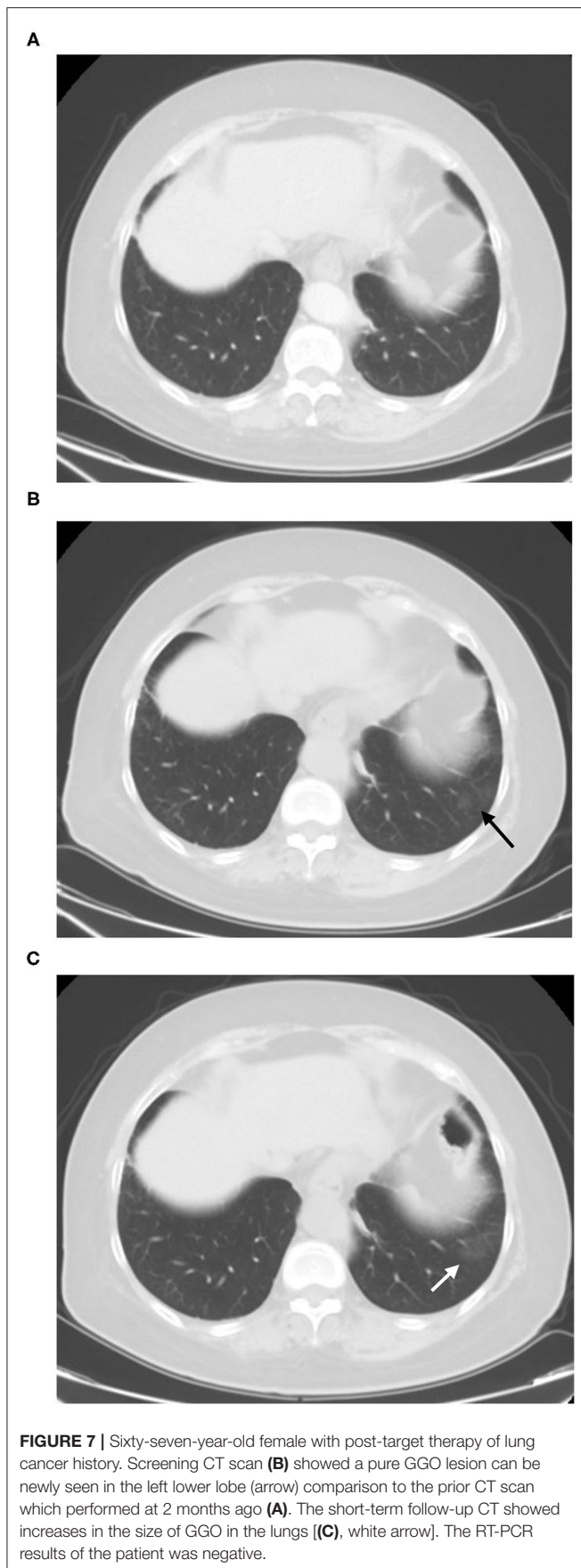


**FIGURE 6 |** Sixty-six-years-old male with post-target therapy of lung adenocarcinoma history. Comparison with the transverse CT scan (A), the screening CT (B) shows new bilateral, peripheral GGO associated with smooth interlobular and intralobular septal thickening (crazy-paving pattern) (arrow).

SARS-Cov-2 has proved to have the ability for efficient human-to human transmission, hospitals are not only gathering places for suspected COVID-19 patients but also remain high-risk areas

for infection. From February 1, all patients, except emergencies, were denied access to our hospital. All the patients should make an appointment by telephone, internet, or hospital appointment





system. This minimized the risks to both patients and the healthcare team while reducing the utilization of unnecessary resources. All elective surgical and other anti-tumor treatments were postponed during the pandemic. In addition, postponing these services also minimized potential exposure of the COVID-19 to unsuspecting healthcare providers and patients (15). The National Cancer Center of China, also known as the Cancer Hospital, is the largest cancer-specialist hospital and research institution in Asia. Nearly 1.3 million outpatients visit it, and nine thousand inpatients receive various anti-tumor-treatment. Therefore, to minimize the effect of the epidemic on cancer patients, providing recommendations of scientific and reasonable treatment and preventive measures for cancer patients in the global epidemic scenario is an urgent requirement. Given the occurrence of recurrent waves and outbreaks of COVID-19, it is of paramount importance to resume medical services in specialized hospitals in the long run while controlling the epidemic. Nowadays, patients were required to take the nucleic acid testing before receiving treatments or examinations in all specialized hospitals in China. However, this is not practical to be included as a clinical routine procedure. Accordingly, our experiences provided a feasible pathway for the specialized hospitals to deal with the potential threat of COVID-19 in the post-COVID 19 period. We recommend those who are suspect of COVID-19 from CT images to be referred to take the nucleic acid testing or other investigations. In this context, CT scans could serve as a timely alarm for further testing and intense follow-up so that we could provide the right care, to the right patients, at the right time.

When we decided to re-admit cancer patients, the most important consideration was identification of suspected cases of COVID-19 including patients and the accompanying persons at the earliest possible stage.

Although SARS-CoV-2 nucleic acid testing remains the golden standard for the diagnosis of COVID-19, due to qualification of the specimen sampling from nasopharyngeal swab and the detection kit, the positive rate of SARS-CoV-2 nucleic acid testing is only around 30–50% (16). High-resolution CT is the optimum choice to detect possible pulmonary opacities in COVID-19 suspicious patient. At present, low dose CT is not recommended for the screening of COVID-19 due to the low imaging quality and possibility of false negative GGO detection.

In order to detect suspected viral pneumonia even COVID-19 on CT imaging, we have set up an effective mechanism of the supervisory radiologist reading system. The SR reads the initial CT images immediately after completion of the scan for each patient to determined suspected pneumonia CT characteristics. If the SR is unable to determine the pneumonia CT diagnosis, our procedure is to seek consultation from the PR. Fortunately, all the 50 cases we reported were false positive results which could be diagnosed by our thoracic-experience radiologists. To date, we have had no confirmed cases of COVID-19.

CT imaging characteristics are non-specific (14, 17). Although definitive diagnosis cannot be made on the basis of imaging features alone, especially in the COVID-19 low incidence area, in our cohort, the pneumonia lesions were predominantly peripheral and subpleural in 29 (58.0%) patients, much less than other reports (16, 18–24). GGO and consolidation were

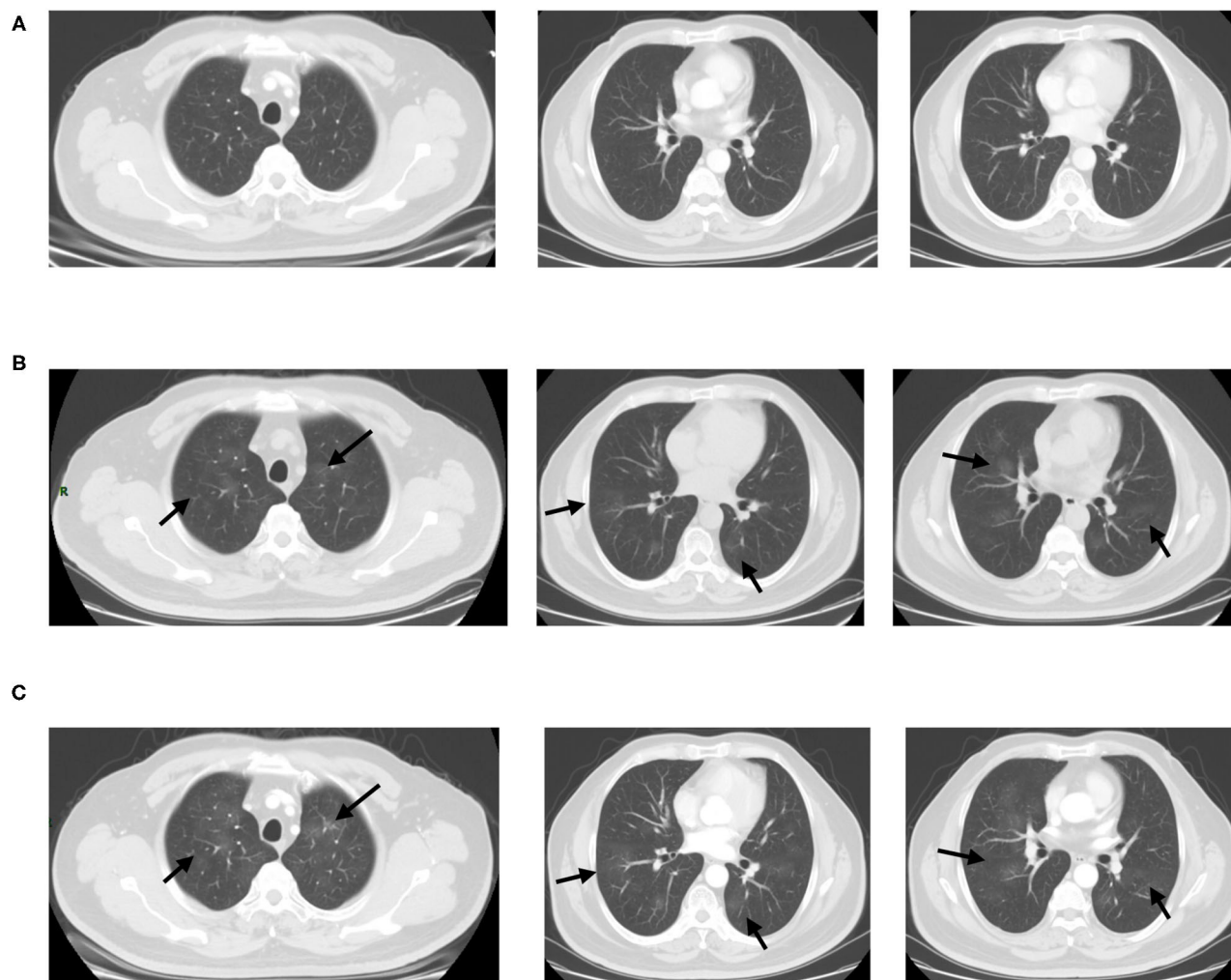


**FIGURE 8 |** Fifty-six-year-old male with post-operation of ascending colon carcinoma history. Comparison with the prior CT which performed 1 month ago (A), screening CT scans of the chest (B) show bilateral multiple GGOs without vascular enlargement (arrows). Most of lesions were identified in the centrally distributed. The short-term follow-up CT scan (C) showed unchanged (arrows). The RT-PCR results of the patient was negative.

manifested only in 14 cases, much lower than the typical COVID-19 CT finding on previously reports (16, 18–23). On the contrary, sub-pleura small patchy or strip-like lesions most likely due to fibrosis or hypostatic pneumonia and cluster of nodular lesions were two main signs of suspected cases on CT images (34, 68.0%). Therefore, we could distinguish these cases as the other type of pneumonia, like other viral pneumonia, bacterial pneumonia, mycoplasma pneumonia, and many non-infectious diseases preliminarily from the COVID-19 cases. Machine-learning based methods are emerging rapidly in recent years focusing on COVID detection or disease diagnosis (24, 25). These methods may be helpful to differentiate COVID-19 from other pulmonary infection and/or non-infectious diseases (26, 27). However, our experience would provide a practical tool for health providers where machine learning is not accessible, especially in hospitals with limited medical resources.

**TABLE 2 |** Morphological feature of screening CT and the results of follow-up CT scan.

|                           | Patients had further CT scan (n = 27) |                                    |                          | Patients had no further CT scan (n = 23) |
|---------------------------|---------------------------------------|------------------------------------|--------------------------|--|
|                           | Unchanged (n = 13)                    | Resolve or partly resolve (n = 13) | Increase in size (n = 1) |  |
| Cluster nodular lesion    | 5                                     | 7                                  | 1                        | 4  |
| GGO                       | 1                                     | 0                                  | 0                        | 2  |
| Interstitial inflammation | 1                                     | 0                                  | 0                        | 0  |
| Consolidation             | 3                                     | 1                                  | 0                        | 7  |
| Sub-pleural patchy shadow | 3                                     | 5                                  | 0                        | 9  |
| Respiratory bronchiolitis | 0                                     | 0                                  | 0                        | 1  |

Some patients with COVID-19 who do not receive effective therapy will demonstrate deterioration and changes will be relatively rapid. The lesions on CT will become more diffuse distributed in a truly short term (28, 29). Therefore, serial CT imaging of patients could help to diagnosis, or continuously monitor disease changes. In our cohort, 13 patients (26.0%) had no change, while 13 patients (26.0%) had resolved or partly resolved. These cases were subsequently excluded by the diagnosis of COVID-19 because of persistent existence pulmonary lesions or resolved in a short-period. Only one patient had increased in size (interval time: 8 days) compared with the further CT scan and the final RT-PCR test result was negative.

## LIMITATIONS

The study has several limitations. First, this was a single-center study, and a multicenter study and/or including more cases, especially more confirmed COVID-19 cases, are needed.

Second, we did not take throat swab samples and the blood routine examination of WBC, Neutrophil, and Lymphocyte are more suitable for finding cancer patients with asymptomatic suspected COVID-19 infection. Third, 23 (46.0%) patients had no further CT examination to evaluate the change of the CT feature. Therefore, long-term radiological follow-up is needed to confirm our findings.

## CONCLUSION

In conclusion, CT may be useful as a screening tool for COVID-19 based on imaging features. Confirmed diagnosis should,

however, ultimately be based on the etiology. The cancer patients in low-incidence areas should continue treatment after careful screening before admission.

## DATA AVAILABILITY STATEMENT

The raw data supporting the conclusions of this article will be made available by the authors, without undue reservation.

## AUTHOR CONTRIBUTIONS

WT: conceptualization, data curation, formal analysis, investigation, methodology, writing-original draft, and writing-review and editing. NW and J-WW: conceptualization, formal analysis, investigation, methodology, supervision, funding acquisition, project administration, writing-original draft, and writing-review and editing. XZ, S-JZ, LL, and YH: formal analysis, investigation, and writing-review and editing. All authors contributed to the article and approved the submitted version.

## FUNDING

This study was supported by the National Key Research and Development Program of China (No. 2017YFC1308700), National Natural Sciences Foundation of China (No. 81971616), Beijing Nova Program (Z202200006820070), and Chinese Academy of Medical Sciences Initiative for Innovative Medicine (No. 2017-I2M-1-005).

## REFERENCES

- World Health Organization. *WHO Director-General's opening remarks at the media briefing on COVID-19- 11 March*. (2020). Available online at: <https://www.who.int/dg/speeches/detail/who-director-general-s-opening-remarks-at-the-media-briefing-on-covid-19-11-march-2020>
- Ren L, Wang Y, Wu Z, Xiang Z, Guo L, Xu T, et al. Identification of a novel coronavirus causing severe pneumonia in human: a descriptive study. *Chin Med J*. (2020) 133:1015–24. doi: 10.1097/CM9.0000000000000722
- Chan JF, Yuan S, Kok KH, To KK, Chu H, Yang J, et al. A familial cluster of pneumonia associated with the 2019 novel coronavirus indicating person-to-person transmission: a study of a family cluster. *Lancet*. (2020) 395:514–23. doi: 10.1016/S0140-6736(20)30154-9
- Wang C, Horby PW, Hayden FG, Gao GF, A. novel coronavirus outbreak of global health concern. *Lancet*. (2020) 395:470–3. doi: 10.1016/S0140-6736(20)30185-9
- Huang C, Wang Y, Li X, Ren L, Zhao J, Hu Y, et al. Clinical features of patients infected with 2019 novel coronavirus in Wuhan, China. *Lancet*. (2020) 395:497–506. doi: 10.1016/S0140-6736(20)30183-5
- World Health Organization. *Global Surveillance for COVID-19 Caused by Human Infection With COVID-19 Virus: Interim Guidance*. Geneva: World Health Organization (2020). Available online at: <http://apps.who.int/iris/rest/bitstreams/1272502/retrieve>
- China National Health Commission website. *Notice on issuing a new coronavirus infected pneumonia diagnosis and treatment plan*. Available online at: (trial version 5) [bgs.satcm.gov.cn/zhengcewenjian/2020-02-06/12847.html](http://www.bgs.satcm.gov.cn/zhengcewenjian/2020-02-06/12847.html) (accessed February 18, 2020).
- Ai T, Yang Z, Hou H, Zhan C, Chen C, Lv W, et al. Correlation of chest CT and RT-PCR testing in coronavirus disease 2019 (COVID-19) in China: a report of 1014 cases. *Radiology*. (2020) 26:200642. doi: 10.1148/radiol.2020200642
- Bai HX, Hsieh B, Xiong Z, Halsey K, Choi JW, Tran TML, et al. Performance of radiologists in differentiating COVID-19 from viral pneumonia on chest CT. *Radiology*. (2020) 10:200823. doi: 10.1148/radiol.2020200823
- National Health Commission of the People's Republic of China website. *Diagnosis and treatment of novel coronavirus infection*. Available online at: <http://www.nhc.gov.cn/yzygj/s7653p/202002/8334a8326dd94d329df351d7da8aefc2.shtml> (accessed February 19, 2020).
- Guan W-J, Ni Z-Y, Hu Y, Liang W-H, Ou C-Q, He J-X, et al. Clinical characteristics of coronavirus disease 2019 in China. *N Engl J Med*. (2020) 382:1708–20. doi: 10.1056/NEJMoa2002032
- Liang W, Guan W, Chen R, Wang W, Li J, Xu K, et al. Cancer patients in SARS-CoV-2 infection: a nationwide analysis in China. *Lancet Oncol*. (2020) 21:335–7. doi: 10.1016/S1470-2045(20)30096-6
- Ajlan AM, Ahayd RA, Jamjoom LG, Alharthy A, Madani TA. Middle East respiratory syndrome coronavirus (MERS-CoV) infection: chest CT findings. *AJR Am J Roentgenol*. (2014) 203:782–7. doi: 10.2214/AJR.14.13021
- Joint GI Society Message: *COVID-19 clinical insights for our community of gastroenterologists and gastroenterology care providers*. Available online at: <https://www.asge.org/home/joint-gi-society-message-covid-19> (accessed March 23, 2020).
- Xie X, Zhong Z, Zhao W, Zheng C, Wang F, Liu J. Chest CT for typical 2019-nCoV pneumonia: relationship to negative RT-PCR testing. *Radiology*. (2020) 296:200343. doi: 10.1148/radiol.2020200343
- Das KM, Lee EY, Enani MA, AlJawder SE, Singh R, Bashir S, et al. CT correlation with outcomes in 15 patients with acute Middle East

- respiratory syndrome coronavirus. *AJR Am J Roentgenol.* (2015) 204:736–42. doi: 10.2214/AJR.14.13671
17. Shi H, Han X, Fan Y, et al. Radiologic features of patients with 2019-nCoV infection. *J Clin Radiol.* (2020) 39:8–11. doi: 10.13437/j.cnki.jcr.20200206.002
  18. Huang L, Han R, Yu P-X, Wang S-K, Xia L-M. A correlation study of CT and clinical features of different clinical types of COVID-19. *Chin J Radiol.* (2020) 54:300–4.
  19. Liu P, Tan X. Novel coronavirus (2019-nCoV) pneumonia. *Radiology.* (2020) 295:19. doi: 10.1148/radiol.2020020257
  20. Kanne JP. Chest CT findings in 2019 novel coronavirus. (2019-nCoV) infections from Wuhan. China: key points for the radiologist. *Radiology.* (2020) 295:16–7. doi: 10.1148/radiol.2020020241
  21. Shi H, Han X, Zheng C. Evolution of CT manifestations in a patient recovered from 2019 novel coronavirus. (2019-nCoV) pneumonia in Wuhan. *China Radiology.* (2020) 295:20. doi: 10.1148/radiol.2020020269
  22. Qian L, Yu J, Shi H. Severe acute respiratory disease in a Huanan seafood market worker: images of an early casualty. *Radiol Cardiothorac Imaging.* (2020) 2:e200025. doi: 10.1148/ryct.2020020033
  23. Huang P, Liu T, Huang L, Liu H, Lei M, Xu W, et al. Use of chest CT in combination with negative RT-PCR assay for the 2019 novel coronavirus but high clinical suspicion. *Radiology.* (2020) 295:22–3. doi: 10.1148/radiol.2020020330
  24. Roberts M, Driggs D, Thorpe M, Gilbey J, Schnlieb CB. Common pitfalls and recommendations for using machine learning to detect and prognosticate for COVID-19 using chest radiographs and CT scans. *Nature Machine Intelligence.* (2021) 3:199–217. doi: 10.1038/s42256-021-00307-0
  25. Driggs D, Selby I, Roberts M, Gkrania-Klotsas E, Schnlieb C. Machine learning for COVID-19 diagnosis and prognostication: lessons for amplifying the signal while reducing the noise. *Radiology.* (2021) 3:e210011. doi: 10.1148/ryai.2021210011
  26. Hu, S, Gao Y, Niu Z, Jiang Y, Yang G. Weakly supervised deep learning for covid-19 infection detection and classification from CT images. *IEEE Access.* (2020) 8:118869–83. doi: 10.1109/ACCESS.2020.3005510
  27. Ma H, Ye Q, Ding W, Jiang Y, Yang G. Can clinical symptoms and laboratory results predict CT abnormality? initial findings using novel machine learning techniques in children with COVID-19 infections. *Front Med.* (2021) 8:855. doi: 10.3389/fmed.2021.699984
  28. Jiang N-C, Zheng C-S, Fan Y-Q, Han X-Y, Chen Y, Cheng Q-G, et al. CT appearances and short-term, changes of COVID-19 in subclinical period. *Chin J Radiol.* (2020) 54:305–9.
  29. Shohei N, Yusuke K, Yuya A, Sho F, Masaru T, Kazuaki F, et al. Characteristics and outcomes of c coronavirus disease 2019(COVID-19) patients with cancer: a single-center retrospective observational study in Tokyo, Japan. *Int J Clin Oncol.* (2021) 23:485–93 doi: 10.1007/s10147-020-01837-0

**Conflict of Interest:** The authors declare that the research was conducted in the absence of any commercial or financial relationships that could be construed as a potential conflict of interest.

**Publisher's Note:** All claims expressed in this article are solely those of the authors and do not necessarily represent those of their affiliated organizations, or those of the publisher, the editors and the reviewers. Any product that may be evaluated in this article, or claim that may be made by its manufacturer, is not guaranteed or endorsed by the publisher.

Copyright © 2021 Tang, Wang, Wang, Huang, Liu, Zhao, Zhao and Wu. This is an open-access article distributed under the terms of the Creative Commons Attribution License (CC BY). The use, distribution or reproduction in other forums is permitted, provided the original author(s) and the copyright owner(s) are credited and that the original publication in this journal is cited, in accordance with accepted academic practice. No use, distribution or reproduction is permitted which does not comply with these terms.





# Impact of Workplace on the Risk of Severe COVID-19

Tsuyoshi Nakamura<sup>1\*</sup>, Hiroyuki Mori<sup>2</sup>, Todd Saunders<sup>3</sup>, Hiroaki Chishaki<sup>4</sup> and Yoshiaki Nose<sup>5</sup>

<sup>1</sup> Faculty of Environmental Science, Nagasaki University, Nagasaki, Japan, <sup>2</sup> Department of Life Creation, Nagasaki Women's College, Nagasaki, Japan, <sup>3</sup> Graduate School of Biomedical Science, Nagasaki University, Nagasaki, Japan, <sup>4</sup> Department of Family Practice, National Health Insurance Clinic, Nakatsu, Oita, Japan, <sup>5</sup> Graduate School of Medical Sciences, Kyushu University, Fukuoka, Japan

## OPEN ACCESS

### Edited by:

Reza Lashgari,  
Shahid Beheshti University, Iran

### Reviewed by:

Eirini Christaki,  
University of Cyprus, Cyprus  
Vincent Hooper,  
Xiamen University, China

### \*Correspondence:

Tsuyoshi Nakamura  
Naka@Nagasaki-U.ac.jp

### Specialty section:

This article was submitted to  
Infectious Diseases - Surveillance,  
Prevention and Treatment,  
a section of the journal  
Frontiers in Public Health

**Received:** 26 June 2021

**Accepted:** 15 October 2021

**Published:** 05 January 2022

### Citation:

Nakamura T, Mori H, Saunders T,  
Chishaki H and Nose Y (2022) Impact  
of Workplace on the Risk of Severe  
COVID-19.  
Front. Public Health 9:731239.  
doi: 10.3389/fpubh.2021.731239

Indiscriminate regional lockdowns aim to prevent the coronavirus disease 2019 (COVID-19) infection by restricting the movement of people; however, this comes with psychological, social, and economic costs. Measures are needed that complement lockdowns and reduce adverse effects. Epidemiological studies, to date, have identified high-risk populations, but not workplaces appropriate for closure. This study was conducted to provide evidence-based measures that used exact and reliable follow-up data of the PCR-positive COVID-19 cases to complement lockdowns. The data are not subjected to selection or follow-up biases, since the Japanese government, by law, must register and follow all the PCR-positive cases until either recovery or death. Direct customer exposure may affect the quantity of viral inoculum received, which, in turn, may affect the risk of the severity of disease at infection. Therefore, the professions of the cases were grouped according to their frequency of direct customer exposure (FDCE) based on subjective observations, which resulted in five workplaces; hospital, school, food service, outdoor service, and indoor office being identified. Analyzing the follow-up data, we obtained precise estimates for the risk of severe disease, defined as intensive care unit (ICU) hospitalization or death, for the workplaces adjusted for age, sex, family status, and comorbidity. Major findings are as follows: hospital and school are the lowest risk, food and outdoor services are, despite higher FDCE, safer than indoor office. Unemployed and unclear are the highest risk, despite low FDCE. These results suggest the following workplace-specific measures complementing the lockdown: school should not be closed and indiscriminate closing of food and outdoor service industries should be avoided, since it would be more effective to reinforce their efforts to promote adherence to public health guidelines among students and customers. These actions would also reduce the adverse effects of the lockdown. This study is the first to address the causality between the workplaces and severe disease. We introduce FDCE and adherence to public health guidelines (APHGs) to associate the workplace characteristics with the risk of COVID-19 severity, which provided the basis for the measures complementing lockdowns.

**Keywords:** COVID-19, severe disease, workplace, occupation, cohort study, relative risk, lockdown, direct customer exposure



## INTRODUCTION

The novel coronavirus disease 2019 (COVID-19), first appeared in Wuhan, China at the end of 2019, spread globally and as of March 11, 2021 has resulted in 2,624,677 deaths worldwide (1). In addition to this loss of life, measures to control the spread of the disease have resulted in the severe economic consequences for citizens and countries around the world (2).

Different efforts of the countries to control its spread include a variety of management techniques such as travel bans, quarantines, lockdowns, and mask mandates (3). Versions of these include restrictions, both total and partial on those entering countries from the high COVID-19 rate countries, domestic quarantines for arriving individuals, total and partial lockdowns based on the current situation at the moment, and federal, state, city, town, and private business mask rules (3–11). By April 2020, more than 90 countries were under various forms of lockdowns, resulting in about half of the population of world having been asked or ordered to stay at home by their governments (4). Nevertheless, the pandemic had not abated and the prevalence and mortality due to the COVID-19 in 27 countries failed to show a significant decline 15 days after the lockdown compared to the 15 days before the lockdown (2).

Although lockdowns have, despite other consequences, been effective in reducing the COVID-19 cases in many countries and/or regions during periods of rapid spread of the virus, they have caused mental health issues (5, 6), disrupted social lives (7, 8), decreased access to food and healthcare (9), and resulted in business closures and loss of employment and income (10). School closures have led to an unprecedented negative impact on education (11) with over 200 million students enrolled at primary, secondary, and higher levels of education being affected as of February, 2021 (12). In Japan, as a result of the suspension of operations in much of the service industry, many workers lost their jobs. There has also been an important psychological toll with 6,976 women in Japan taking their lives last year, a nearly 15% increase from 2019 which was the first year-over-year increase in more than a decade (13). While social distancing measures have decreased the transmission rate, they have failed to decrease the number of cases infected with the COVID-19 (14).

Since global deaths from the COVID-19 continue to increase, world governments and agencies are still working toward understanding who is most at risk of death (15). In Sweden, income and education levels were significantly associated with the COVID-19-related deaths (16), while in England, deprivation (essentially a measure of poverty) was positively associated with the COVID-19-related deaths (17). The risk of death for essential workers and healthcare workers (HCWs) has been well documented (18–20). In Britain, the risk of the COVID-19 deaths or intensive care unit (ICU) hospitalization for HCW is estimated to be 7.4 times that of non-essential workers (21). However, since the agreement between job at baseline 2006–2010 and the follow-up period 2014–2019 for a subsample of the cohort was substantially lower, 67% to 92%, their risk estimates would be subjected to biases due to the misclassifications (22).

While these previous findings can help to determine high-risk groups in need of administrative assistance, they are not immediately tied to any effective public health measures reducing the risk of severity of the COVID-19. More detailed results and some insight into the causality between the disease severity and biosocial factors are needed to generalize the results to find the cost-effective preventive measures.

The viral pathogenesis theory states that the severity of disease is proportionate to the viral inoculum received (23) and Gandhi and Rutherford (23) argued that universal masking could become a form of “variation” that would generate immunity thereby helping reduce the severity of disease and ensuring that a greater proportion of new infections are asymptomatic. The quantity of viral inoculum received is also possibly affected by such measures as the disinfecting of hands and adequate ventilation. Importantly, contact frequency (CF) with others inside of the minimum centers for disease control and prevention (CDC) recommended social distance of 6 feet (24) and the degree of adherence to public health guidelines (APHG), which the CDC defines as wearing a mask that covers the mouth and nose, staying at least 6 feet apart, washing the hands often, and getting vaccinated where possible (25), may affect the quantity of viral inoculum received, which, in turn, may affect the risk of the severity of disease at infection. Lockdowns that restrict the movement of people or business operations reduce CF, but do not necessarily promote APHG.

Research with the objective of estimating the occupational risk related to the COVID-19 severity is rare and more data are needed to further elucidate the occupation-specific risks to ensure workplace safety (26). Since the COVID-19 is designated a type II infectious disease, Japanese public health centers, by law, must register all the PCR-positive cases and follow them until recovery or death without exception. This follow-up data comprises an ideal cohort with no selection and no follow-up biases. The objectives of this study are to precisely estimate the risk of the severity of the COVID-19 intrinsic to workplaces by using these ideal cohort data and address workplace-specific interventions complementing the lockdowns.

## MATERIALS AND METHODS

### Subjects

Doctors identifying the COVID-19 PCR test positive cases must fill out a “Notification of Outbreak” form, specified by the Japanese Ministry of Health, Labor and Welfare, and send it to a city public health center. These centers register patient information to share with the government office and the other public health centers, assign patients to home or hotel quarantine, or hospitals, and track them until either recovery or death. With the exception of personal identification such as name and address, these centers publicize all the case information on the internet. For this study, we downloaded this case information for all the patients, regardless of age, registered in Osaka prefecture, population 8.8 million, between February 20th and September 15th, 2020. The data comprise ideal cohort data with no selection and no follow-up biases. Excluding 14 cases whose PCR samples

were collected after death, we have 9,690 COVID-19 cases for analysis. Ten cases of those who died of other diseases while hospitalized for COVID-19 treatment were categorized as the COVID-19 deaths, since the COVID-19 was considered to have aggravated the diseases. Provided material in the Supplement, it describes the method for access to the original data and transformation to an EXCEL file.

## Outcome

In the COVID-19 follow-up reports, disease severity is classified as asymptomatic and symptomatic but mild or ICU hospitalized and cases are either recovered or deceased at discharge. Our outcome of interest is “the severe COVID-19” defined as either died or hospitalized in the ICU. The proportion of severe cases will be termed as severe rate.

## Workplace

Since the risk of the COVID-19 infection increases with the entry of others inside a critical social distance (24), the risk of infection should be different among workplaces where the frequency of direct customer exposure (FDCE) is different. Since it is difficult to obtain a representative value of FDCE for each workplace, we will consider the difference in FDCE between workplaces according to the characteristics of each workplace specialty. We classified the professions of the COVID-19 cases in consideration of FDCE into the following five workplace categories: hospital, school, indoor office (private companies and government offices), food service (restaurants, bars, and supermarkets), and outdoor services (e.g., construction, transportation, and security). Outdoor service is comprised of a profession whose work is conducted mostly outside or interactively with unspecified customers.

Hospitals engulf a greater risk than schools due to higher exposure to symptomatic people with the COVID-19 and due to increased density of exposure. However, hospitals and schools have the following features in common. Hospital and school staff often interact with patients and students inside a critical social distance, respectively. In hospitals, healthcare professionals such as doctors and nurses set an example for observing health regulations to prevent nosocomial infections and hospital staff and patients have regular physically close contact. Schools are similar to hospitals in that faculty and staff set an example for observing health regulations to prevent interstudent transmission and students follow this example. FDCE for food service and outdoor service is relatively higher compared to indoor office.

**Table 1** shows the professions, described in the Notification of Outbreak form, grouped by workplace and the frequency of cases. Unemployed in **Table 1** includes housewives, pensioners, and those looking for jobs, while unclear consists of those who declined or failed to identify their professions. Unemployed individuals have virtually no customers and, therefore, a relatively lower FDCE than indoor office individuals. FDCE in the unclear workplace is not known because their professions are not clearly specified. FDCE assigned to the workplaces is summarized in **Table 1**. While FDCE may differ according to country, the data here references Japan.

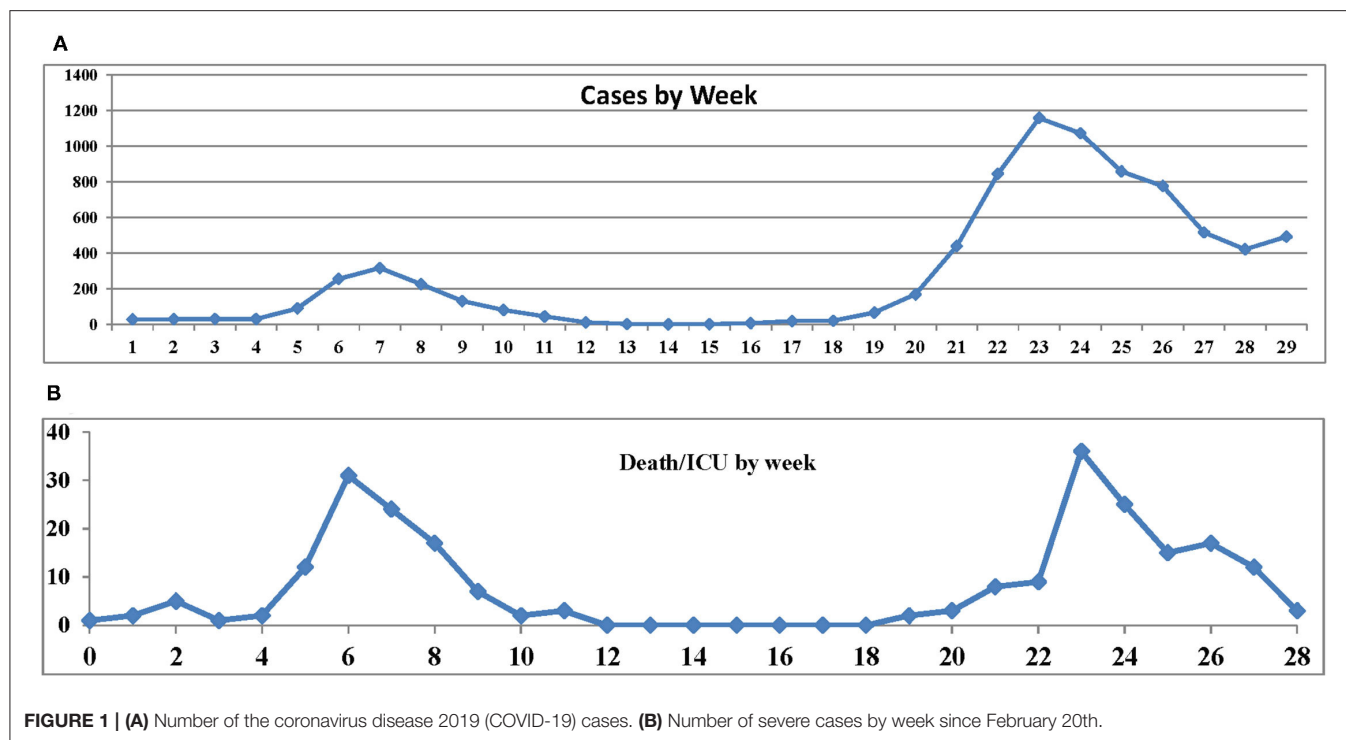
**TABLE 1 |** Professions classified according to workplace.

| Workplace       | Profession                  | Freq. | Total | FDCE    |
|-----------------|-----------------------------|-------|-------|---------|
| Hospital        | Medical staff               | 539   | 786   | High    |
|                 | Nursing care staff          | 168   |       |         |
|                 | Elderly care staff          | 49    |       |         |
|                 | Hospital chef               | 22    |       |         |
|                 | Welfare staff               | 7     |       |         |
| School          | Nutritionist                | 1     | 992   | High    |
|                 | Student                     | 838   |       |         |
|                 | Teacher                     | 153   |       |         |
| Indoor Office   | Monk                        | 1     | 2,181 | Medium  |
|                 | Private company employee    | 2,036 |       |         |
| Food Service    | Government employee         | 145   | 1,254 | High    |
|                 | Restaurant and bar employee | 1,250 |       |         |
| Outdoor Service | Supermarket employee        | 4     | 1,188 | High    |
|                 | Self-employed               | 539   |       |         |
|                 | Day Laborer                 | 180   |       |         |
|                 | Construction worker         | 113   |       |         |
|                 | Retail sales                | 87    |       |         |
|                 | Salesperson                 | 76    |       |         |
|                 | Factory worker              | 49    |       |         |
|                 | Driver                      | 33    |       |         |
|                 | Transporter                 | 25    |       |         |
|                 | Delivery                    | 17    |       |         |
|                 | Real estate employee        | 13    |       |         |
|                 | Security guard              | 13    |       |         |
|                 | Instructor                  | 12    |       |         |
|                 | Cleaning                    | 10    |       |         |
|                 | Demolition                  | 8     |       |         |
|                 | Painter                     | 5     |       |         |
|                 | Home helper                 | 3     |       |         |
|                 | Contractor                  | 3     |       |         |
|                 | Advertising                 | 1     |       |         |
|                 | Welding                     | 1     |       |         |
| Unemployed      | Unemployed                  | 1,730 | 1,730 | Low     |
| Unclear         | No description              | 1,559 | 1,559 | Unknown |

## Stage 0 and 1

**Figure 1** shows the number of the COVID-19 cases (A) and severe cases (B) by week since February 20th, 2020. **Table 2** shows the date of the first day of each week. The first wave ended at week 12, but began to spread again at week 18. Weeks 0–15 will be denoted by stage 0 and weeks 16–28 by stage 1.

The objective of this study is to assess the impact of workplace on the severity of disease adjusted for background biosocial factors such as age, sex, family (family members living together), and comorbidity. **Table 3** presents the levels and codes of the variables. The frequencies of cases, the number of severe cases, and the proportion of severe cases (rate) are shown by stage. Hereafter, the rate will be referred to as severe rate. Since professions in hospital and school categories rarely developed severe disease, these were combined to create a level termed as hospital/school food and outdoor services were combined to create a level termed as service.

**TABLE 2 |** Date of the first day of each week.

| Week    | 0    | 1    | 2    | 3    | 4    | 5    | 6    | 7    | 8    | 9    |
|---------|------|------|------|------|------|------|------|------|------|------|
| 1st Day | 2/20 | 2/27 | 3/5  | 3/12 | 3/19 | 3/26 | 4/2  | 4/9  | 4/16 | 4/23 |
| Week    | 10   | 11   | 12   | 13   | 14   | 15   | 16   | 17   | 18   | 19   |
| 1st Day | 4/30 | 5/7  | 5/14 | 5/21 | 5/28 | 6/4  | 6/11 | 6/18 | 6/25 | 7/2  |
| Week    | 20   | 21   | 22   | 23   | 24   | 25   | 26   | 27   | 28   | 29   |
| 1st Day | 7/9  | 7/16 | 7/23 | 7/30 | 8/6  | 8/13 | 8/20 | 8/27 | 9/3  | 9/10 |

## Statistical Analysis

First, we define the endpoint D/I as  $D/I = 1$  for severe cases and  $D/I = 0$  for otherwise cases. We also define the binary variable stage as stage = 0 for cases in stage 0 and stage = 1 for cases in stage 1. Then, we define  $\text{age}_{50} = \text{Max}(\text{age}-50, 0)$ . In other words,  $\text{age}_{50} = 0$  while  $\text{age} \leq 50$  and  $\text{age}_{50} = \text{age}-50$  for  $\text{age} > 50$ . This is a piecewise linear function with one change point at  $\text{age} = 50$ .  $\text{Age}_{60}$  and  $\text{age}_{70}$  are similarly defined. These functions fit the data better than age only with the least loss of efficiency (27).

Since family has three levels 0, 1, and 2, we define one piecewise linear function  $\text{family}_1 = \text{Max}(\text{family}-1, 0)$ . That is,  $\text{family}_1 = 0$  if  $\text{family} = 0$  or 1 and  $\text{family}_1 = 1$  if  $\text{family}_2 = 2$ . The binary variables such as sex, comorbidity, and stage are used. An interaction term  $\text{age}_{60} \times \text{comorbidity}$ , defined as a multiplication of two variables  $\text{age}_{60}$  and comorbidity, is used to deal with age-dependent effect of comorbidity.

For workplace, we define an indication function  $\text{Job} * k$  for each level  $k$  as follows:  $\text{Job} * k = 1$  if  $\text{level} = k$  and  $\text{Job} * k = 0$

**TABLE 3 |** Frequency of severe cases and severe rate (%) by stage.

| Variable      | Code: level      | Stage 0 |        |          | Stage 1 |        |          |
|---------------|------------------|---------|--------|----------|---------|--------|----------|
|               |                  | Freq.   | Severe | Rate (%) | Freq.   | Severe | Rate (%) |
| Age           | 20: 0–29         | 351     | 0      | 0        | 3,460   | 0      | 0        |
|               | 40: 30–49        | 511     | 8      | 1.57     | 2,252   | 1      | 0.04     |
|               | 60: 50–69        | 364     | 30     | 8.24     | 1,445   | 31     | 2.15     |
|               | 80: 70–99        | 268     | 78     | 29.1     | 1,039   | 106    | 10.2     |
| Sex           | 0: Female        | 674     | 41     | 6.08     | 3,555   | 42     | 1.18     |
|               | 1: Male          | 820     | 75     | 9.15     | 4,639   | 96     | 2.07     |
| Family status | 0: With          | 879     | 51     | 5.8      | 5,228   | 56     | 1.07     |
|               | 1: No            | 249     | 19     | 7.63     | 2,427   | 58     | 2.39     |
| Workplace     | 2: Unclear       | 366     | 46     | 12.57    | 541     | 24     | 4.44     |
|               | 0: Hosp./Sch.    | 240     | 2      | 0.833    | 1,538   | 1      | 0.065    |
|               | 1: Service       | 235     | 11     | 4.681    | 2,207   | 9      | 0.408    |
|               | 2: Indoor Office | 343     | 15     | 4.373    | 1,838   | 7      | 0.381    |
|               | 3: Unemployed    | 210     | 30     | 14.29    | 1,520   | 86     | 5.66     |
| Comorbidity   | 4: Unclear       | 466     | 58     | 12.45    | 1,093   | 35     | 3.2      |
|               | 0: No            | 1,329   | 83     | 6.25     | 7,387   | 81     | 1.1      |
|               | 1: With          | 165     | 33     | 20       | 809     | 57     | 7.05     |
| D/I           | 0: No            | 1,378   |        | 0.92     | 8,058   |        | 0.98     |
|               | 1: Yes           | 116     |        | 0.08     | 138     |        | 0.02     |

otherwise ( $k = 1, 2, 3, 4$ ). It follows that  $\text{Job} * 1 = \text{Job} * 2 = \text{Job} * 3 = \text{Job} * 4 = 0$  if and only if  $\text{level} = 0$ .

We examined associations between D/I and workplace, age, sex, family, and comorbidity by using a logistic model. It is

**TABLE 4 |** Frequency of cases and severe cases by workplace: (A) By stage. (B) Pooled.

| (A)        |         |        |          |         |        |          |
|------------|---------|--------|----------|---------|--------|----------|
| Workplace  | Stage 0 |        |          | Stage 1 |        |          |
|            | Freq.   | Severe | Rate (%) | Freq.   | Severe | Rate (%) |
| Hospital   | 157     | 1      | 0.64     | 629     | 1      | 0.16     |
| School     | 83      | 1      | 1.2      | 909     | 0      | 0        |
| Food       | 97      | 3      | 3.09     | 1,157   | 2      | 0.17     |
| Outdoor    | 138     | 8      | 5.8      | 1,050   | 7      | 0.67     |
| Company    | 313     | 13     | 4.15     | 1,723   | 7      | 0.41     |
| Government | 30      | 2      | 6.67     | 115     | 0      | 0        |
| Unemployed | 210     | 30     | 14.29    | 1,520   | 86     | 5.66     |
| Unclear    | 466     | 58     | 12.45    | 1,093   | 35     | 3.2      |

| (B)        |        |        |        |      |        |      |
|------------|--------|--------|--------|------|--------|------|
| Workplace  | Pooled |        |        |      |        |      |
|            | Freq.  | Severe | Odds   | OR   | Risk   | RR   |
| Hospital   | 786    | 2      | 0.0026 | 1    | 0.0025 | 1    |
| School     | 992    | 1      | 0.001  | 0.4  | 0.001  | 0.4  |
| Food       | 1,254  | 5      | 0.004  | 1.57 | 0.004  | 1.6  |
| Outdoor    | 1,188  | 15     | 0.0128 | 5.01 | 0.0126 | 5.04 |
| Company    | 2,036  | 20     | 0.0099 | 3.89 | 0.0098 | 3.92 |
| Government | 145    | 2      | 0.014  | 5.48 | 0.0138 | 5.52 |
| Unemployed | 1,730  | 116    | 0.0719 | 28.2 | 0.0671 | 26.8 |
| Unclear    | 1,559  | 93     | 0.0634 | 24.9 | 0.0597 | 23.9 |

disadvantageous that the logistic model presents the odds ratio (OR) but not the relative risk (RR), since RR is straightforward to interpret. Therefore, we apply a modified logistic model (28) to obtain a precise estimate of RR as follows: First, an ordinary stepwise logistic model is applied to select significant variables and then a modified logistic model by using the selected variables is applied. The results present precise estimates of RR for the levels of each variable, but do not provide their SDs.

To investigate relationships between the severe rates in 1st stage and 2nd stage, a simple linear regression model  $y = \alpha + \beta x + \varepsilon$ ,  $\varepsilon \sim N(0, \sigma^2)$  was applied, where  $\alpha$  is a constant,  $\beta$  is a regression coefficient, and  $x$  and  $y$  take values  $\log(\text{severe rate})$  in stage 0 and stage 1, respectively.

## RESULTS

### Severe Rates by Stage

Table 4A shows the frequencies of cases and severe cases and severe rates by workplace and stage. Table 4B shows the frequency of cases and severe cases, odds, OR, risk, and RR for the pooled data.

Figure 2 shows a scatter plot between  $\log(\text{severe rate})$  in stage 0 and stage 1 in Table 4A. Applying a linear regression model  $y = \alpha + \beta x + \varepsilon$ , we have  $\hat{\beta} = 1.705$  ( $SE = 0.114$ ,  $p < 0.001$ ),  $\hat{\alpha} = 0.18$  ( $SE = 0.321$ ,  $p = 0.59$ ), and  $R^2$ , the coefficient of determination adjusted for the degree of freedom, is 0.94. The test

for the normality of residuals was 0.208 ( $p = 0.84$ ). The results suggest it approximately holds that  $y = 1.7x + \varepsilon$ . Briefly, severe rates in stage 1 are approximately determined by corresponding severe rates in stage 0 plus random errors, irrespective of the levels of the variables. These finding prompted us to pool stage 0 and stage 1 in estimating the risk of severe disease associated with the levels of the variables.

### Naïve OR and RR

Table 5 shows the frequency of severe cases, OR, and RR. RR for age 70–99 years compared to age 30–49 years is extremely high: about 43. RR of unemployed and unclear compared to hospital/school is also remarkably high: about 41 and 36, respectively.

Figure 3A displays large imbalances in age among workplaces. On average, hospital/school is the youngest, service is similar to indoor office; unclear is older than indoor office and unemployed the oldest. Figure 3B shows the proportion of comorbidity by workplace: unemployed is by far the highest and hospital/school the lowest, while service, indoor office, and unclear are similar to each other. These figures indicate that the OR and RR in Table 5 are misleading, since they are obtained ignoring the biases due to those imbalances in age and comorbidity. Hereafter, they will be termed as naïve OR and RR.

Table 6 obtained from stratifying by age shows the risks for the workplaces by age. Risks for unemployed and unclear are drastically reduced to 3.51 and 9.34 and 3.07 and 6.9 for age 50–69 and 70–99 years, respectively. The risks though may still be biased due to imbalances in sex, family status, and comorbidity. Since the stratifying method is not applicable to adjust for those confounders simultaneously, we had to resort to a logistic model. We estimate RR adjusted for those confounders by using a modified logistic model (27).

### Naïve OR and RR for Workplace by Using a Logistic Model

First, an ordinary logistic model with one covariate, workplace, is applied. The OR obtained from the model correspond to the naïve OR in Table 5. “Logistic for Odds” in Table 7 shows the results where  $OR = \exp(\text{Estimate})$ . The ORs in Table 7 coincide well with the corresponding ORs in Table 5. A modified logistic model (28) resulted in “Logistic for RR” in Table 7, where  $RR = \exp(\text{Estimate})$ . The naïve RR in Table 5 coincides exactly with the RR in Table 7, indicating a high accuracy of the estimates obtained from the modified logistic model.

### RR Adjusted for Confounders

First, we applied an ordinary stepwise logistic model by using all the variables and stage as covariates to determine a best fit model. The selected variables are shown in “Logistic for Odds” in Table 8, where  $OR = \exp(\text{Estimate})$ . The term  $\text{age}_{60} \times \text{comorbidity}$  is significant, indicating an age-dependent effect of comorbidity. Then, the modified logistic model (28), by using the selected variables as covariates, was applied. The results are shown in “Logistic for RR” in Table 8 where  $RR = \exp(\text{Estimate})$ . RR for age is calculated by using the estimates  $\exp$

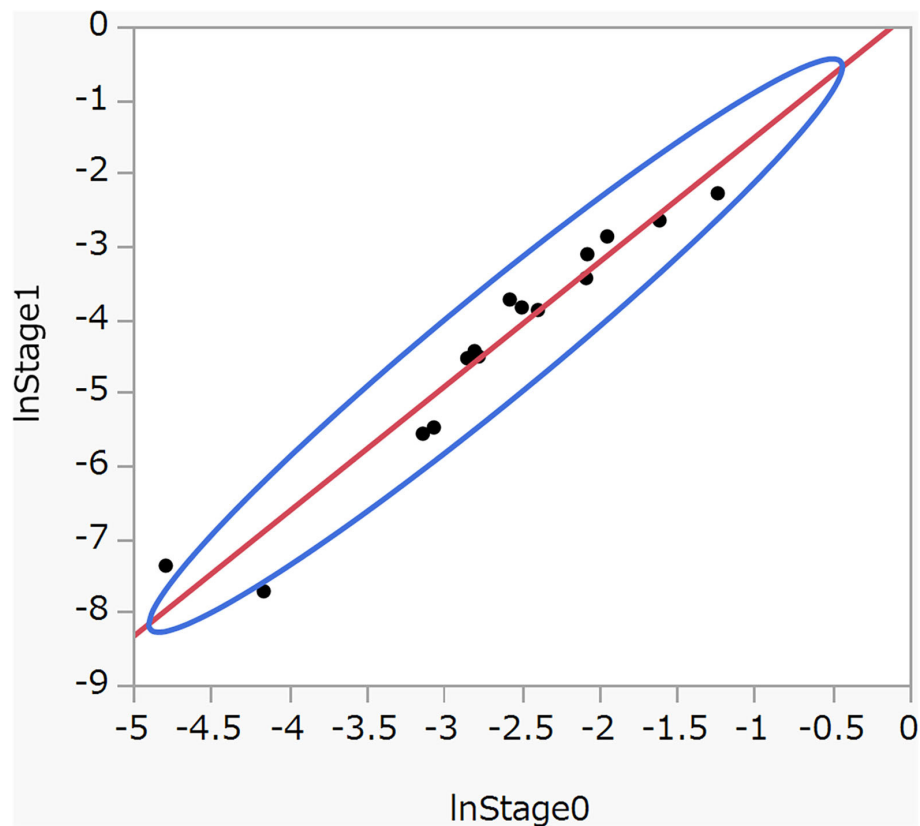


**FIGURE 2 |** Scatter plot between log (severe rate) in stage 0 and stage 1 with 95% density ellipse.

**TABLE 5 |** Frequency of severe cases and odds ratio (OR) and relative risk (RR).

| Variable    | Code | Level         | Severe | Freq. | Odds    | Risk  | OR   | RR   |
|-------------|------|---------------|--------|-------|---------|-------|------|------|
| Age         | 20   | 0–29          | 0      | 3,811 | 0       | 0     | 0    | 0    |
|             | 40   | 30–49         | 9      | 2,763 | 0.0033  | 0.003 | 1    | 1    |
|             | 60   | 50–69         | 61     | 1,809 | 0.0349  | 0.034 | 10.7 | 10.4 |
|             | 80   | 70–99         | 184    | 1,307 | 0.1,638 | 0.141 | 50.1 | 43.2 |
| Sex         | 0    | Female        | 83     | 4,229 | 0.02    | 0.02  | 1    | 1    |
|             | 1    | Male          | 171    | 5,459 | 0.0323  | 0.031 | 1.62 | 1.6  |
| Family      | 0    | With          | 107    | 6,107 | 0.0178  | 0.018 | 1    | 1    |
|             | 1    | No            | 77     | 2,676 | 0.0296  | 0.029 | 1.66 | 1.64 |
|             | 2    | Unclear       | 70     | 907   | 0.0836  | 0.077 | 4.69 | 4.4  |
| Workplace   | 0    | Hosp./Sch.    | 3      | 1,828 | 0.0016  | 0.002 | 1    | 1    |
|             | 1    | Service       | 20     | 2,398 | 0.0084  | 0.008 | 5.12 | 5.08 |
|             | 2    | Indoor Office | 22     | 2,176 | 0.0102  | 0.01  | 6.21 | 6.16 |
|             | 3    | Unemployed    | 116    | 1,730 | 0.0719  | 0.067 | 43.7 | 40.9 |
|             | 4    | Unclear       | 93     | 1,558 | 0.0635  | 0.06  | 38.6 | 36.4 |
| Comorbidity | 0    | No            | 164    | 8,716 | 0.0192  | 0.019 | 1    | 1    |
|             | 1    | With          | 90     | 974   | 0.1018  | 0.092 | 5.31 | 4.91 |

(0.257 age<sub>50</sub>–0.211 age<sub>60</sub>) and that for comorbidity is  $\exp(0.874 \text{ comorbidity} - 0.033 \text{ age}_{60} \times \text{comorbidity})$ .

The estimates for service and indoor office are not significant due to low frequencies of severe cases. The risk for each case is calculated from the estimates and the levels of the case according

to the model equation. A receiver operating characteristic (ROC) curve obtained from the model shows a sensitivity of 0.85 and specificity of 0.9 (**Figure 4**), indicating a high discrimination ability between the severe and non-severe cases. The adjusted RRs for the workplaces are illustrated in **Figure 5**. Since the



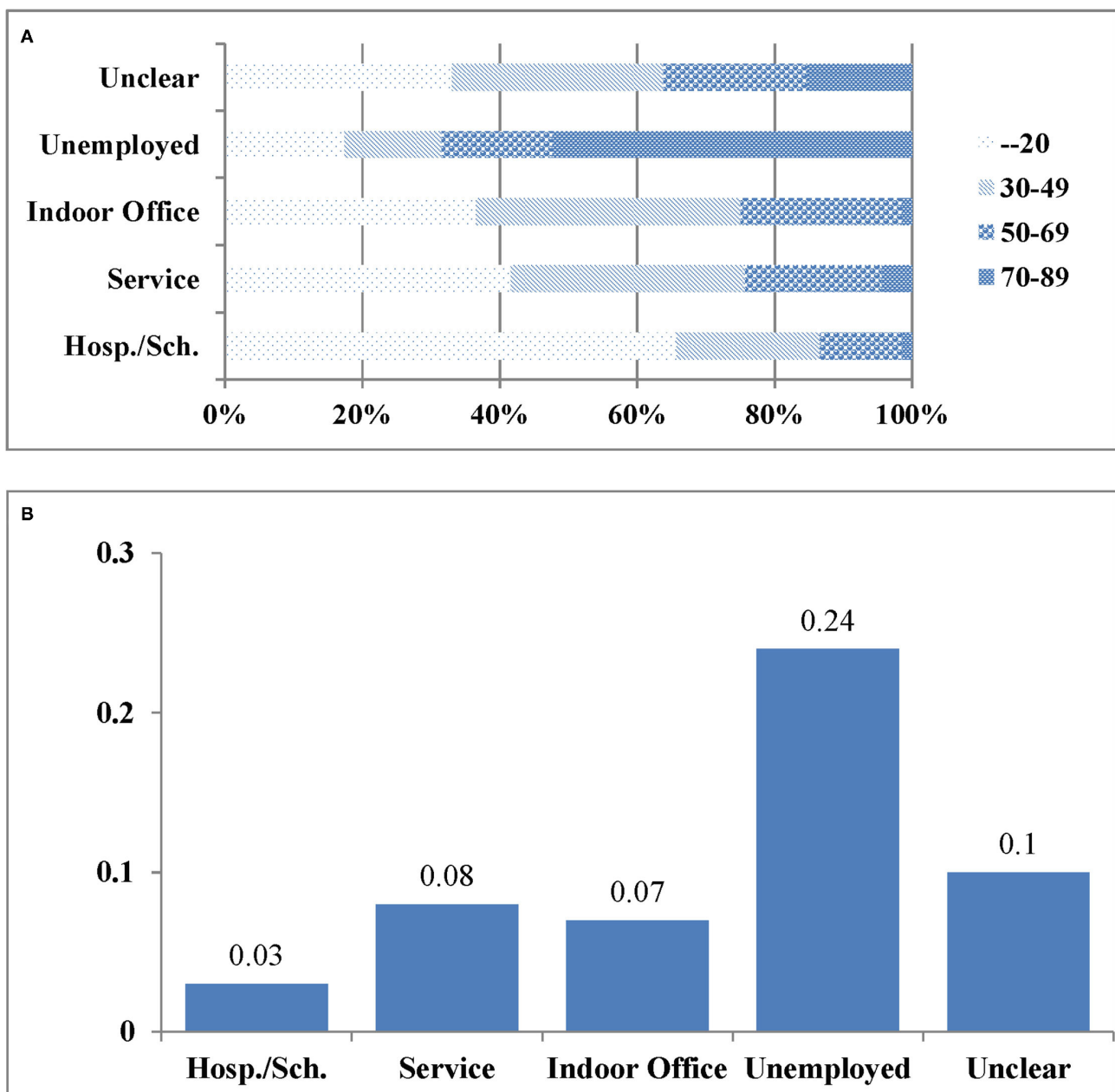


**FIGURE 3 | (A)** The distributions of age by workplace. **(B)** The proportion of comorbidity by workplace.

adjusted RRs still vary considerably, there should be unobserved, substantial risk factors intrinsic to workplaces.

## DISCUSSION

### Prioritizing Cases According to the Risk of Disease Severity

The rapidly rising number of the COVID-19 cases in Japan and around the world has led to a shortage of ICU beds, medical staff, and the need to build emergency field hospitals (29). This shortage of ICU beds to treat the severe COVID-19 cases required

the prioritization of patients to be hospitalized in ICU (30). The model described in **Table 8** was obtained by using the ideal cohort data free from follow-up and selection biases and the ROC curve (**Figure 4**) demonstrates the high accuracy of the model to predict severe cases. Hence, the model could help to determine the COVID-19 cases at high risk of becoming severe at the initial diagnosis.

### Adjusted RR for Workplace

The large variations in the adjusted RR across the workplaces (**Figure 5**) suggest the existence of substantial, unobserved risk

**TABLE 6 |** The risk for workplace stratified by age.

| Age       | Workplace        | Freq. | Severe | Rate (%) | RR   |
|-----------|------------------|-------|--------|----------|------|
| 20: 0–29  | 0: Hosp./Sch.    | 1,202 | 0      | 0        | –    |
|           | 1: Service       | 998   | 0      | 0        | –    |
|           | 2: Indoor Office | 796   | 0      | 0        | –    |
|           | 3: Unemployed    | 301   | 0      | 0        | –    |
|           | 4: Unclear       | 514   | 0      | 0        | –    |
| 40: 30–49 | 0: Hosp./Sch.    | 382   | 0      | 0        | –    |
|           | 1: Service       | 818   | 2      | 0.24     | 1    |
|           | 2: Indoor Office | 837   | 5      | 0.6      | 2.5  |
|           | 3: Unemployed    | 245   | 0      | 0        | 0    |
|           | 4: Unclear       | 481   | 2      | 0.42     | 1.75 |
| 60: 50–69 | 0: Hosp./Sch.    | 218   | 2      | 0.92     | 1    |
|           | 1: Service       | 476   | 9      | 1.89     | 2.05 |
|           | 2: Indoor Office | 510   | 13     | 2.55     | 2.77 |
|           | 3: Unemployed    | 279   | 9      | 3.23     | 3.51 |
|           | 4: Unclear       | 326   | 28     | 8.59     | 9.34 |
| 80: 70–99 | 0: Hosp./Sch.    | 26    | 1      | 3.85     | 1    |
|           | 1: Service       | 106   | 9      | 8.49     | 2.21 |
|           | 2: Indoor Office | 33    | 4      | 12.12    | 3.15 |
|           | 3: Unemployed    | 905   | 107    | 11.82    | 3.07 |
|           | 4: Unclear       | 237   | 63     | 26.58    | 6.9  |

**TABLE 7 |** OR and RR estimated by using logistic models.

| Workplace     | Level | Logistic model for Odds |         |      | Model for RR |      |
|---------------|-------|-------------------------|---------|------|--------------|------|
|               |       | Estimate                | P-value | OR   | Estimate     | RR   |
| Hosp./Sch.    | –     | –                       | –       | 1    | –            | 1    |
| Service       | Job*1 | 1.63                    | 0.0085  | 5.11 | 1.626        | 5.08 |
| Indoor Office | Job*2 | 1.83                    | 0.003   | 6.22 | 1.818        | 6.16 |
| Unemployed    | Job*3 | 3.78                    | <0.0001 | 43.7 | 3.71         | 40.9 |
| Unclear       | Job*4 | 3.65                    | <0.0001 | 38.6 | 3.594        | 36.4 |

factors intrinsic to workplaces. Here, we consider two possible factors APHG and FDCE in the following discussion.

Adherence to public health guidelines (31) reduced hospitalization by 88% and mortality by 100% in Delaware (32). Since January 2020 in Japan, over 2,000 nurses and doctors of the self-defense forces (33) have supported healthcare efforts for patients with the COVID-19, yet none of them have been infected with the COVID-19. This demonstrates that the COVID-19 infections could be completely prevented or at least greatly reduced by strict APHG. With respect to the association between APHG and the severity of disease, Gandhi and Rutherford (23) argued that facial masking could become a form of “variolation” that may reduce the severity of disease among people who do become infected. As described in the introduction, their theory implies “following the appropriate public health guidelines might help to reduce the severity of disease among the infected cases.” The “variolation hypothesis” well explains the RRs for workplaces in **Figure 5**.

The risk of severe cases increases in the following order: hospital/school, service, indoor office, unemployed, and unclear. The lowest risk is hospital/school, despite high FDCE. In hospitals, healthcare professions, by virtue of their responsibilities to prevent nosocomial infections, demonstrate the public health guidelines for hospital staff and patients to follow. Schools are similar to hospitals in that faculty and staff set an example for observing health regulations to prevent interstudent transmission for students to follow. The results suggest that school is the safest place for students.

According to the data for the infection status of students summarized by the national government (**Supplementary Material 3**), school is the lowest risk place (5–7%) for primary and junior high students as compared to home (78–64%) and the other or unclear places (18–28%). The facts suggest that school is the safest place and students would visit higher risk places if schools were closed. This is in line with the above interpretation of the risks based on the variolation hypothesis.

The second lowest risk is, again despite high FDCE, the service industry. Service is not statistically significant (**Table 8**), since the frequency of severe cases is too low. These data do appear to provide evidence of high APHG usage within the service industry. Incentives for the high APHG in service include: professional courtesy to customers, deep-seated social customs, and the fact that infection would require quarantine or hospitalization without pay.

The risk in service industry is lower than that of indoor office. Indoor office employees have similar incentives to service industry regarding APHG, but with the addition that they are allowed to take paid leave. This paid leave system might have resulted in a lower APHG for indoor office, which, in turn, resulted in a higher risk than service industry. All the Japanese citizens receive benefits from the universal health insurance system regardless of income and income disparities are not very large among regular employees in Japan. Hence, differences in APHG should have a greater impact on risk than income disparity among regular employees. This might explain why service carries a lower risk than indoor office despite service having lower incomes on average than indoor office.

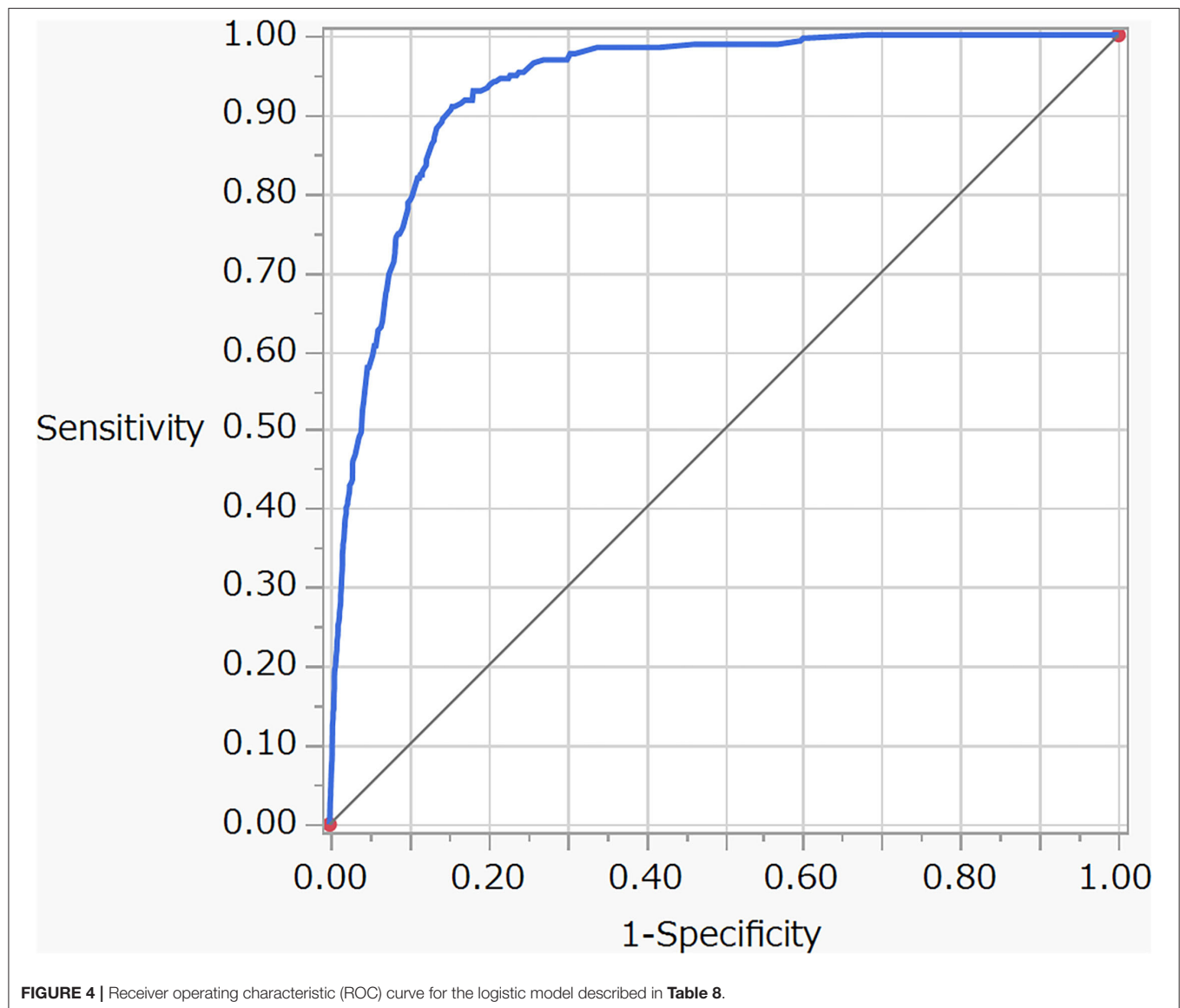
High FDCE should normally result in a potentially higher risk of infection; in fact, a high FDCE associated with a high risk of infection was observed in a cross-sectional study on 104 retail workers in Massachusetts (34). According to the “variolation” hypothesis (23), however, a high FDCE combined with a high APHG, such as in the service industry, should result in generating immunity and helping to reduce the severity of disease among people who do become infected, which it does in our case. This hypothesis may also apply to the low risk in hospital/school.

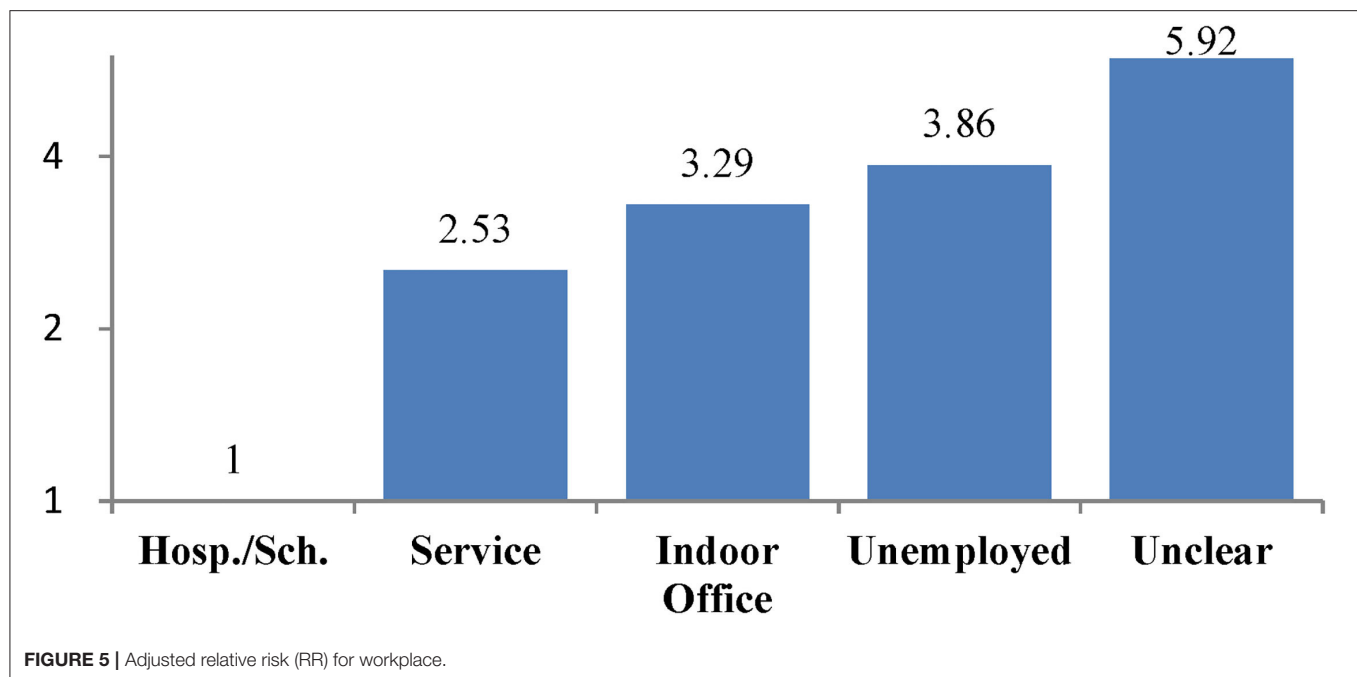
“Unemployed” has a higher risk than indoor office. This could be because those in unemployed may be less motivated to follow APHG than indoor office. Research to ensure exact reasons and to promote effective measures among any high-risk group is urgent for reducing severe future infections.

Unclear shows the highest severity risk. To the best of our knowledge, no studies have investigated the risk of the severity of the COVID-19 for the unclear category. Normally, requesting

**TABLE 8** | Results from ordinary stepwise and modified logistic models.

| Variable        | Logistic for Odds |        |       |        | Logistic for RR |      |        |      |
|-----------------|-------------------|--------|-------|--------|-----------------|------|--------|------|
|                 | Estimate          | 95% CI | OR    | 95% CI | Estimate        | RR   |        |      |
| Stage 0         | −1.24             | −1.54  | −0.94 | 0.29   | 0.21            | 0.39 | −1.059 | 0.35 |
| Age_50          | 0.273             | 0.22   | 0.32  |        |                 |      |        |      |
| Age_60          | −0.218            | −0.28  | −0.16 |        |                 |      |        |      |
| Sex             | 0.878             | 0.57   | 1.18  | 2.41   | 1.77            | 3.25 | 0.778  | 2.18 |
| Family_1        | 0.488             | 0.31   | 0.67  | 1.63   | 1.36            | 1.95 | 0.396  | 1.49 |
| Service         | 0.896             | −0.34  | 2.14  | 2.45   | 0.71            | 8.5  | 0.928  | 2.53 |
| Office/Gov.     | 1.133             | −0.1   | 2.37  | 3.11   | 0.9             | 10.7 | 1.192  | 3.29 |
| Unemployed      | 1.265             | 0.07   | 2.46  | 3.54   | 1.07            | 11.7 | 1.351  | 3.86 |
| Unclear         | 1.886             | 0.7    | 3.07  | 6.59   | 2.01            | 21.5 | 1.779  | 5.92 |
| Comorbidity     | 0.935             | 0.45   | 1.42  |        |                 |      |        |      |
| Age_60 × Comorb | −0.035            | −0.07  | 0     |        |                 |      |        |      |





occupation when recruiting volunteer participants can result in eliminating or ignoring this category (20, 21), making it generally difficult to study its characteristics. In this study, however, data on the cases of unclear were collected in the same way as the other occupations, since it was obligatory by law.

While age, sex, family status, and comorbidity are confounders that should be adjusted for estimating the risk, income is a so-called “intermediate factor” in epidemiology that should not be adjusted in eliminating risk. Professions affect income and, in turn, income affects the risk. The higher risk for unemployed and unclear might be partly due to low APHG caused by low income. Nevertheless, we should consider effective measures to promote APHG for unemployed and unclear because low income is intrinsically associated with unemployed and unclear.

The results of this study suggest that promoting APHG would be the most effective measure in preventing the disease severity irrespective of FDCE. Therefore, we conclude that measures for promoting APHG should be coupled with lockdowns to mitigate both the disease severity and the negative impact of lockdowns. In addition, since the food industry seems to be taking effective measures to promote APHG, it should not be targeted indiscriminately by lockdowns. Rather, it would be more effective to help reinforce their efforts to prevent infection; for example, by installing CO<sub>2</sub> concentration measuring devices (35) for assessing their efforts to prevent droplets infections or by providing financial reinforcement so that they can advance their own measures for prompting customers to follow APHG. In addition, the higher likelihood that lower ventilation rates are associated with higher infection risks (36) could help explain higher risk for indoor office than service, since many high-rise offices cannot open windows and the air is only filtered for quality and not pathogens; therefore, providing adequate

ventilation would be in many cases a low technology, low cost way to reduce transmission rates. The evidence-based workplace-specific measures should be tested and corroborated in order to effectively control the infection with fewer negative effects.

### Study Limitations

Our data is not subjected to the biases that are usually associated with cohort studies such as follow-up biases, selection biases, and biases due to misclassifications in outcome or covariates. However, since our data were published by the Osaka Prefecture, which strictly follows the common privacy rules, there are limitations in available information. To gather information on the background of individuals in unclear, we must submit a study protocol based on the results of this study to the Institutional Review Board. If approved, the Osaka Prefecture government will help us conduct the study.

Frequency of direct customer exposure and APHG are assumed to be the major variables causing the large differences in the workplace-specific risks. FDCE for a workplace is evaluated based on the subjective observations. It is a study limitation for FDCE to be currently assessed subjectively, not objectively. For example, the questionnaire used by Lan et al. to evaluate FDCE of employees is also based on the subjective evaluation of the employees. Nevertheless, we feel that FDCE is a key concept to understand the relationship between the risk and workplaces. Mission of epidemiology is to discover effective countermeasures based on uncertain observational information. We hope that this research will recognize the importance of FDCE and devise future objective measurement methods.

While the workplace-specific severe disease risks that we have obtained might not be in line with the beliefs of some policymaking, lockdown planners, these risks are facts obtained by applying standard statistical methods to cohort data of the

PCR-positive COVID-19 infected cases of Osaka, which were, without exception, confirmed as either recovered or dead on the day of discharge.

## DATA AVAILABILITY STATEMENT

The original contributions presented in the study are included in the article/**Supplementary Material**, further inquiries can be directed to the corresponding author/s.

## AUTHOR CONTRIBUTIONS

YN and TN designed the cohort study. HM organized a team for collecting data for analysis as described in **Supplementary Material**. TN and HM performed statistical analysis. TN and TS wrote the draft and HM elaborated tables and figures. HC reviewed literature and discussed the results from a medical

point of view. All authors approved the final manuscript for submission.

## ACKNOWLEDGMENTS

We are grateful to Toshio Makie, Kohei Akazawa, Koshi Kataoka, and Tomoko Maeda for help in collecting and organizing the data. We also thank the Osaka Prefecture for helping us understand the treatment procedure and the data publication policy for the COVID-19 cases.

## SUPPLEMENTARY MATERIAL

The Supplementary Material for this article can be found online at: <https://www.frontiersin.org/articles/10.3389/fpubh.2021.731239/full#supplementary-material>

## REFERENCES

1. WHO. *Coronavirus Disease (COVID-19) Dashboard*. Available online at: <https://covid19.who.int/Table>
2. Meo SA, Abukhalaf AA, Alomar AA, AlMutairi FJ, Usmani AM, Klonoff DC. Impact of Lockdown on COVID-19 prevalence and mortality during 2020 pandemic: observational analysis of 27 countries. *Eur J Med Res*. (2020) 25:56. doi: 10.1186/s40001-020-00456-9
3. Li W, Gong J, Zhou J, Zhang L, Wang D, Li J, et al. An evaluation of COVID-19 transmission control in Wenzhou using a modified SEIR model. *Epidemiol Infect*. (2021) 149:e2. doi: 10.1017/S0950268820003064
4. Euronews. *Coronavirus: Half of Humanity now on Lockdown as 90 Countries Call for Confinement*. (2020). Available online at: <https://www.Euronews.com/2020/04/02/Coronavirus-in-Europe-Spain-S-Death-Toll-Hits-10-000-After-Record-950-New-Deaths-in-24-Hou> (accessed May 19, 2020).
5. Pandey D, Bansal S, Goyal S, Garg A, Sethi N, Pothiyill DI, et al. Psychological impact of mass quarantine on population during pandemics—the COVID-19 Lock-Down (COLD) Study. *PLoS ONE*. (2020) 15:E0240501. doi: 10.1371/journal.pone.0240501
6. Fiorillo A, Sampogna G, Giallonardo V, Del Vecchio V, Luciano M, Albert U, et al. Effects of the lockdown on the mental health of the general population during the COVID-19 pandemic in Italy: results from the COMET Collaborative Network. *Euro Psychiatr*. (2020). 63:1–11. doi: 10.1192/j.eurpsy.2020.89
7. Arenas-Arroyo E, Fernandez-Kranz D, Nollenberger N. Intimate partner violence under forced cohabitation and economic stress: evidence from the COVID-19 pandemic. *J Public Econ*. (2021) 194:350. doi: 10.1016/j.jpubeco.2020.104350
8. Wright L, Steptoe A, Fancourt D. Are we all in this together? Longitudinal assessment of cumulative adversities by socioeconomic position in the first 3 weeks of lockdown in the UK. *J Epidemiol Commun Health*. (2020) 74:683–88. doi: 10.1016/S2468-2667(20)30288-7
9. Yocum AK, ZhaiY,McInnis MG, Han P. Covid-19 pandemic and lockdown impacts: a description in a longitudinal study of bipolar disorder. *J Affect Disorders*. (2021) 28:1226–33. doi: 10.1016/j.jad.2021.01.028
10. Prochazka J, Scheel T, Pirozek P, Kratochvil T, Civilotti C, Bollo M, et al. Data on work-related consequences of COVID-19 pandemic for employees across Europe. *Data Brief*. (2020) 32:74. doi: 10.1016/j.dib.2020.106174
11. Kapasia N, Paul P, Royc A, Sahac J, Zaveric A, Mallick R, et al. Impact of lockdown on learning status of undergraduate and postgraduate students during COVID-19 Pandemic in West Bengal, India. *Child Youth Serv Rev*. (2020) 116:194. doi: 10.1016/j.childyouth.2020.105194
12. UNESCO. *COVID-19 Impact on Education. Global Monitoring of School Closures Caused by COVID-19*. (2019). Available online at: <https://en.Unesco.org/Covid19/Educationresponse>
13. The New York Times. *As Pandemic Took Hold, Suicide Rose Among Japanese Women*. (2021). Available online at: <https://www.Nytimes.com/2021/02/22/World/Asia/Japan-Women-Suicide-Coronavirus.Html>
14. Wagner AB, Hill EL, Ryan SE, Sun Z, Deng G, Bhadane S, et al. Social distancing merely stabilized COVID-19 in the United States. *Stat Newslett*. (2021) 4:32. doi: 10.1101/2020.04.27.20081836
15. University of Minnesota Center for Infectious Disease Research and Policy. *Global Cases Stabilizing, but COVID Deaths Continue to Climb*. (2020). Available online at: <https://www.Cidrap.umn.edu/News-Perspective/2020/12/Global-Cases-Stabilizing-Covid-Deaths-Continue-Climb>
16. Drefahl S, Wallace M, Mussino E. A population-based cohort study of socio-demographic risk factors for COVID-19 deaths in Sweden. *Nat Commun*. (2020) 11:5097. doi: 10.1038/s41467-020-18926-3
17. Williamson EJ, Walker AJ, Bhaskaran K. Factors associated with COVID-19-related death using open safely. *Nature*. (2020) 584:430–6. doi: 10.1038/s41586-020-2521-4
18. Patelarou A, Mechili EA, Galanis P, Zografakis-Sfakianakis M, Konstantinidis T, Saliaget A, et al. Nursing students, mental health status during COVID-19 quarantine: evidence from three European countries. *J Ment Health*. (2021) 18:75420.
19. Kim R, Nachman S, Fernandes R, Meyers K, Taylor M, LeBlanc D, et al. Comparison of COVID-19 Infections among healthcare workers and non-healthcare workers. *PLoS ONE*. (2020) 15:241956. doi: 10.1101/2020.08.13.20174482
20. Nguyen LH, Drew DA, Graham MS, Colaneri M, Novelli V, Cutti S, et al. Risk of COVID-19 among front-line health-care workers and the general community: a prospective cohort study. *Lancet Public Health*. (2020) 5:E475–83. doi: 10.1016/S2468-2667(20)30164-X
21. Mutambudzi M, Claire N, Ewan Beaton M, Alastair L, Frances M, Anderson J, et al. Occupation and risk of severe COVID-19: prospective cohort study of 120 075 UK biobank participants. *Occup Environ Med*. (2020) 0:1–8. doi: 10.1136/oemed-2020-106731
22. Nakamura T, Yamada T, Kataoka K, Sera K, Saunders T, Takatsuji T, Makie T, Nose Y. Statistical resolutions for large variabilities in hair mineral analysis. *PLoS ONE* (2018) 20:8816. doi: 10.1371/journal.pone.0208816
23. Gandhi M, Rutherford GW. Facial Masking for Covid-19 — Potential for “Variolation” as We Await a Vaccine. *N Engl J Med*. (2020) 383:E101. doi: 10.1056/NEJMp2026913
24. Centers for Disease Control and Prevention. *Social Distancing. Centers for Disease Control and Prevention* (2021). Available online at: <https://www.cdc.gov/Coronavirus/2019-Ncov/Prevent-Getting-Sick/Social-Distancing.Html>
25. Centers for Disease Control and Prevention. *How to Protect Yourself & Others. Centers for Disease Control and Prevention* (2021). Available online



- at: <https://www.cdc.gov/Coronavirus/2019-Ncov/Prevent-Getting-Sick/Prevention.Html>
26. Larochelle MR. "Is It Safe for Me to Go to Work?" risk stratification for workers during the Covid-19 pandemic. *N Engl J Med.* (2020) 383:e28. doi: 10.1056/NEJMp2013413
  27. Akazawa K, Nakamura T, Palesch Y. Power of logrank test and cox regression model in clinical trials with heterogeneous samples. *Statistics Med.* (1997) 16: 583–597. doi: 10.1002/(SICI)1097-0258(19970315)16:5<583::AID-SIM433>3.0.CO;2-Z
  28. Diaz-Quijano FA. A simple method for estimating relative risk. *BMC Med Res Methodol.* (2012) 12:14. doi: 10.1186/1471-2288-12-14
  29. The New York Times. *Covid Overload: U.S. Hospitals Are Running Out of Beds for Patients.* Available online at: <https://www.nytimes.com/2020/11/27/Health/Covid-Hospitals-Overload.Html>
  30. Los Angeles Times. *Paramedics Having Some Patients Stay Home as Hospitals Struggle With COVID-19 Wave.* (2020). Available online at: <https://www.latimes.com/California/Story/2020-12-30/Paramedics-Patients-Stay-Home-Hospitals-Covid-19>
  31. WHO Coronavirus Disease (COVID-19) Advice for the Public. (2020). Available online at: <https://www.who.int/emergencies/diseases/novel-coronavirus-2019/advice-for-public> (accessed 8 December 2020).
  32. Kanu FA, Smith EE, Offutt-Powell T, Hong R. Declines in SARS-CoV-2 transmission, hospitalizations, and mortality after implementation of mitigation measures-delaware. *MMWR.* (2020) 69:1691–4. doi: 10.15585/mmwr.mm6945e1
  33. Self-Defense Forces in Japan. *Self-Defense Forces Engagement in Response to COVID-19.* (2019). Available online at: [https://www.mod.go.jp/en/d\\_act/Disaster/Covid/Siryō2.pdf](https://www.mod.go.jp/en/d_act/Disaster/Covid/Siryō2.pdf)
  34. Lan F-Y, Suharlim C, Kales SN, Young J. Association between SARS-CoV-2 infection, exposure risk and mental health among a cohort of essential retail workers in the USA. *Occupation Environ Med.* (2020) 78:106774. doi: 10.1136/oemed-2020-106774
  35. Dietrich F, Chen J, Voggenreiter B, Aigner B, Nachtigall N, Reg B. MUCCnet: munich urban carbon column network. *Atmos Meas Tech.* (2021) 14:1111–26. doi: 10.5194/amt-14-1111-2021
  36. Julian LM, Tang W, Bahnfleth W, Bluysen PM, Boerstra A, Buonanno G, et al. How can airborne transmission of COVID-19 indoors be minimised? *Environ Int.* (2020). 142:105832. doi: 10.1016/j.envint.2020.105832

**Conflict of Interest:** The authors declare that the research was conducted in the absence of any commercial or financial relationships that could be construed as a potential conflict of interest.

**Publisher's Note:** All claims expressed in this article are solely those of the authors and do not necessarily represent those of their affiliated organizations, or those of the publisher, the editors and the reviewers. Any product that may be evaluated in this article, or claim that may be made by its manufacturer, is not guaranteed or endorsed by the publisher.

Copyright © 2022 Nakamura, Mori, Saunders, Chishaki and Nose. This is an open-access article distributed under the terms of the Creative Commons Attribution License (CC BY). The use, distribution or reproduction in other forums is permitted, provided the original author(s) and the copyright owner(s) are credited and that the original publication in this journal is cited, in accordance with accepted academic practice. No use, distribution or reproduction is permitted which does not comply with these terms.



# Differential COVID-19 Symptoms Given Pandemic Locations, Time, and Comorbidities During the Early Pandemic

Yang Wang<sup>1,2</sup>, Fengwei Zhang<sup>1</sup>, J. Brian Byrd<sup>3</sup>, Hong Yu<sup>1,2</sup>, Xianwei Ye<sup>1,2\*</sup> and Yongqun He<sup>4\*</sup>

<sup>1</sup> Guizhou University School of Medicine, Guiyang, China, <sup>2</sup> NHC Key Laboratory of Immunological Diseases, Department of Pulmonary and Critical Care Medicine, Guizhou Provincial People's Hospital and People's Hospital of Guizhou University, Guiyang, China, <sup>3</sup> Division of Cardiovascular Medicine, Department of Internal Medicine, University of Michigan Medical School, Ann Arbor, MI, United States, <sup>4</sup> Unit for Laboratory Animal Medicine, Department of Microbiology and Immunology, Center for Computational Medicine and Bioinformatics, University of Michigan Medical School, Ann Arbor, MI, United States

## OPEN ACCESS

### Edited by:

Reza Lashgari,  
Shahid Beheshti University, Iran

### Reviewed by:

Nirmal Kumar Ganguly,  
Indraprastha Apollo Hospitals, India  
Liwei Wang,  
Mayo Clinic, United States

### \*Correspondence:

Xianwei Ye  
yxw1205@163.com  
Yongqun He  
yongqunh@med.umich.edu

### Specialty section:

This article was submitted to  
Infectious Diseases – Surveillance,  
Prevention and Treatment,  
a section of the journal  
Frontiers in Medicine

**Received:** 03 September 2021

**Accepted:** 04 January 2022

**Published:** 28 January 2022

### Citation:

Wang Y, Zhang F, Byrd JB, Yu H, Ye X  
and He Y (2022) Differential COVID-19  
Symptoms Given Pandemic  
Locations, Time, and Comorbidities  
During the Early Pandemic.  
Front. Med. 9:770031.  
doi: 10.3389/fmed.2022.770031

**Background:** COVID-19 pandemic is disaster to public health worldwide. Better perspective on COVID's features early in its course—prior to the development of vaccines and widespread variants—may prove useful in the understanding of future pandemics. Ontology provides a standardized integrative method for knowledge modeling and computer-assisted reasoning. In this study, we systematically extracted and analyzed clinical phenotypes and comorbidities in COVID-19 patients found at different countries and regions during the early pandemic using an ontology-based bioinformatics approach, with the aim to identify new insights and hidden patterns of the COVID-19 symptoms.

**Results:** A total of 48 research articles reporting analysis of first-hand clinical data from over 40,000 COVID-19 patients were surveyed. The patients studied therein were diagnosed with COVID-19 before May 2020. A total of 18 commonly-occurring phenotypes in these COVID-19 patients were first identified and then classified into different hierarchical groups based on the Human Phenotype Ontology (HPO). This meta-analytic approach revealed that fever, cough, and the loss of smell and taste were ranked as the most commonly-occurring phenotype in China, the US, and Italy, respectively. We also found that the patients from Europe and the US appeared to have more frequent occurrence of many nervous and abdominal symptom phenotypes (e.g., loss of smell, loss of taste, and diarrhea) than patients from China during the early pandemic. A total of 22 comorbidities, such as diabetes and kidney failure, were found to commonly exist in COVID-19 patients and positively correlated with the severity of the disease. The knowledge learned from the study was further modeled and represented in the Coronavirus Infectious Disease Ontology (CIDO), supporting semantic queries and analysis. Furthermore, also considering the symptoms caused by new viral variants at the later stages, a spiral model hypothesis was proposed to address the changes of specific symptoms during different stages of the pandemic.

**Conclusions:** Differential patterns of symptoms in COVID-19 patients were found given different locations, time, and comorbidity types during the early pandemic. The ontology-based informatics provides a unique approach to systematically model, represent, and analyze COVID-19 symptoms, comorbidities, and the factors that influence the disease outcomes.

**Keywords:** COVID-19, symptom, phenotype, comorbidity, early pandemic, ontology, Human Phenotype Ontology (HPO), Coronavirus Infectious Disease Ontology (CIDO)

## INTRODUCTION

Since December 2019, the COVID-19 pandemic has caused an unpredictable and catastrophic disaster worldwide. COVID-19 is caused by SARS-CoV-2, a human coronavirus that was first found in Wuhan, China, and now worldwide. Other than the Wuhan strain, different variants of the SARS-CoV-2 virus, such as Alpha and Delta variants, have been identified. As of December 27, 2021, the pandemic has caused ~280 million confirmed cases and more than 5.4 million deaths globally. To better understand and control COVID-19, it is critical to study the host-coronavirus interactions, including the various symptoms or phenotypes occurring in COVID-19 patients.

While the common symptoms of COVID-19 patients are generally similar between studies, differences have also been found (1–4). The common symptoms include fever, cough, myalgia and fatigue; some patients also develop digestive symptoms such as nausea, vomiting, abdominal pain and diarrhea. Some patients have suffered the new loss of smell or taste as a symptom of COVID-19. However, these symptoms appeared to have varied over time, viral variant, patient condition, and geographically. COVID-19 patients with comorbidities tend to have poorer outcomes and higher mortality. Comorbidities here refers to the simultaneous presence of some disease(s) or condition(s) in a patient when COVID-19 occurs in the patient. Hypertension, diabetes, and cardiovascular diseases are a few examples of the most common comorbidities commonly reported in patients infected with COVID-19 (5). To better understand and control the pandemic, it is important to systematically investigate various types of COVID-19 disease symptoms and comorbidities under different conditions and at different stages. The ignorance of the patterns hidden in these phenomena would pose us some huge risks without prompt actions.

Given the extensive reports and complexity of the COVID-19 symptoms in patients with different backgrounds, it is crucial to standardize the results and conditions of these studies in order to achieve consistent and integrative results. Ontology has emerged to play a significant role in standard data representation, classification, integration, and analysis. Basically, an ontology is a human- and computer-interpretable vocabulary of terms and relations that represents entities and how they interact in a specific domain. The Human Phenotype Ontology (HPO) is a standardized vocabulary for phenotypic abnormalities and clinical features encountered in human disease. Each term in the HPO describes a phenotypic abnormality, such

as fever, cough, pneumonia, etc. HPO currently contains over 13,000 terms (6). The Coronavirus Infectious Disease Ontology (CIDO) is a newly developed community-based ontology in the domain of coronavirus infectious diseases, including SARS, MERS, and COVID-19 (7). CIDO systematically represents and interlink these diseases with phenotypes, disease etiology, transmission, drugs, vaccines, etc. CIDO has been proven to be effective in modeling and representation of anti-coronavirus drugs (8). CIDO reuses HPO terms for classifying the phenotypes and symptoms associated with coronavirus diseases including COVID-19.

In this study, we focused on systematic annotation, integration, and analysis of various COVID-19 symptoms that were identified in the early stage of the COVID-19 pandemic. Specifically, we systematically collected, annotated, and analyzed COVID-19 clinical phenotypes and comorbidities that occurred in patients infected with COVID-19 during the early stage of the pandemic. Our study used the data primarily extracted from journal and preprint articles published by August 2020. The data reported in these publications were collected by early May 2020.

Our study considers May 2020 as an important time cutoff of the early pandemic development. Historically, it had been approximately half a year from the first case report in December 2019–May 2020. On May 2, the WHO renewed its previous emergency declaration calling the pandemic a global health crisis. The COVID-19 death toll in the U.S. surpassed 100,000 in May 2020, a critical milestone in the pandemic history. Meanwhile, while many variants of SARS-CoV-2 appeared to exist by early May 2020 (9), the major variants of concern (e.g., Alpha, Beta, Delta strains) of SARS-CoV-2 defined by the WHO (10) were not yet reported. For example, the virus variant lineage B.1.1.7 was first detected in October 2020 in UK, and it was later labeled as the Alpha strain and became the first variant under investigation in December 2020 by the WHO. The Alpha variant was reported to have 40–90% increased transmissibility (11) and lethality (12). The Beta variant was first identified at South Africa in October 2020 and likely first emerged in July or August 2020 (13). No COVID-19 vaccine was licensed or provided at the early stage. By selecting the early stage of pandemic, we were able to focus on the other variables on the symptoms than major highly transmissible viral variants and vaccination. Targeting our study on the early stage, we could also focus on the relatively less but more manageable number of publications, with the aim to find distinct patterns at the early stage, permitting useful and relevant discovery.

In addition, to systematically understand the changing trend of the occurrence and development of patients' symptoms, we applied the HPO and CIDO ontologies to classify these phenotypes, comorbidities, and the relations between each of them and the disease. Our study identified many shared and differential phenotype patterns in COVID-19 patients from countries in different regions of the world. Since all the symptoms are included in HPO and the term "symptom" is more naturally and medically used, in this paper we have prioritized the usage of the term "symptom" later in this paper.

## METHODS

### Related Article Search and Collection

Peer-reviewed journal articles from December 2019 to August 2020 in PubMed and preprint bioRxiv and medRxiv articles were searched to identify relevant articles. The keywords used to identify the COVID-19 disease included "COVID-19," "2019-nCoV," and "SARS-CoV-2." The keywords used to identify symptoms included "Clinical," "Phenotype," "Symptom," "Character," and specific symptoms such as "loss of smell" and "loss of taste." The countries searched in our study included "China," "the United States," "Iran," and many European Countries including "United Kingdom," "Italy," "France," and "Germany," etc.

Inclusion and exclusion criteria were preset in our study. Studies were included when the following inclusion criteria were met: (1) articles were original English-language reports; (2) COVID-19 patient cases were laboratory-confirmed; (3) the clinical data of COVID-19 patients were first-handed data; (4) detailed information about clinical phenotypes was provided; and (5) articles were published before August 2020. Our study showed that the clinical data covered in all our identified articles were collected by early May 2020, which represented the cutoff of the early stage of the pandemic. The reasons of this selection are described in the Introduction.

As an exclusion criterion, case reports of individual cases were excluded in this study. In one specific three-country (China, Italy, and USA) comparison, the infection cases in children and pregnant women were not included, and those articles with <50 patients each were excluded. However, for a more general scope study, these two exclusion criteria were not applied due to the complexity of the datasets covered in various articles.

Although the data from related bioRxiv and medRxiv papers were initially extracted and used, we later found that all the bioRxiv and medRxiv preprint papers used in our study had their corresponding journal articles, and sometimes the data in the formal journal articles were updated compared to their preprint versions. In this case, we updated our data records at a later stage to use the newly reported data in the formal journal articles. We also ensured that no double counting occurred in our study.

### Symptom Extraction, Mapping to HPO, and Hierarchical Classification

COVID-19-related symptoms and comorbidities were manually identified from the articles. The main source of the information came from the tables and **Supplementary Materials** provided

in the articles. The extracted data were initially organized in a pre-defined Excel worksheet (See **Supplementary Files 1–3**). The extracted results were peer-reviewed by two members in the project.

The identified symptoms and comorbidities were mapped to the terms in the Human Phenotype Ontology (HPO) (14). The Ontobee ontology browser (<http://www.ontobee.org>) (15) was primarily used to search the phenotype and symptom terms from the HPO. Synonyms (such as fever and pyrexia) might be used in different articles. We ensured that these synonyms were mapped to the same HPO IDs (e.g., HPO\_0001945).

To identify the hierarchical relations among the COVID-19 related symptoms and comorbidities detected in our literature mining, the Ontofox ontology term extraction tool (<http://ontofox.hegroup.org>) (16) was used. The settings of "includeComputedIntermediates" and "includeAllAxioms" were used in the Ontofox execution, leading to the extraction of additional high level HPO terms that are the ancestral terms of our identified specific symptoms and comorbidities. To display and analyze the extracted terms out of the Ontofox execution, the Protégé-OWL editor (17) was used.

### CIDO Ontology Modeling, Representation, and Analysis

The Coronavirus Infectious Disease Ontology (CIDO) was used as a platform for further COVID-19 symptom knowledge representation and analysis. Specifically, the Ontofox output described above, which included our identified HPO terms, was first imported to the CIDO to become a part of the CIDO. Further ontology modeling and representation were performed in the CIDO to add new relations that semantically link the phenotypes with other entities in CIDO.

The Protégé-OWL editor was used for ontology term display, classification, editing, and analysis.

CIDO is formatted using the Web Ontology Language (OWL; <https://www.w3.org/OWL/>) format, which is computer interpretable. Computational programs can be developed to automatically query the knowledge stored in the CIDO. For example, the CIDO knowledge represented in OWL can be queried using Description Logic (DL)-query or SPARQL Protocol and RDF Query Language (SPARQL). SPARQL scripts were developed to automatically query the CIDO knowledge using the Ontobee SPARQL program (<http://www.ontobee.org/sparql>) (15).

## RESULTS

### Statistics of Surveyed and Analyzed Studies in the Literature

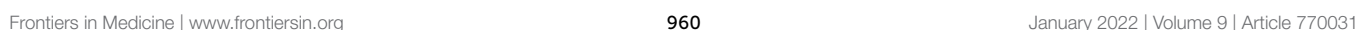
This study aimed to collect, annotate, and compare the clinical phenotype data across a range of studies of patients who were diagnosed with COVID-19 during the early stage of the pandemic, specifically, before August 2020. The early stage of the disease outbreak and pandemic is an important time period since there were no major viral variants spreading during the time, and vaccination had not started so that we do not



Our literature search found that clinical phenotypes of COVID-19 patients were first reported early in Asian countries such as China, South Korea, Japan, Singapore, and Iran, followed by European countries such as Italy, France, Germany, and the United States. We collected the data based on the chronological order and geographical characteristics of the emergence of the COVID-19 epidemic. For concise and focused reporting, we have chosen two strategies for presentation: one is to focus on representative countries, the other is to focus on specific regions.

Using the methods detailed in the Methods section, a total of 18 common clinical symptoms were identified, including fever, cough, dyspnea, myalgia, arthralgia, chills, sore throat, headache,

Based on the categorization of pathophysiology, Ageusia (i.e., loss of taste) and Anosmia (i.e., loss of smell) belong to the abnormal nervous system physiology. Based on anatomic





location, they belong to the category of abnormality of the face. The synonyms of ageusia include impaired taste sensation, absent sense of taste, and lost taste (**Figure 1A**). Anosmia's synonyms in HPO include lost smell and loss of smell. These symptoms newly arising within a patient are critical signs for diagnosing COVID-19 patients. The other abnormality of the face identified as a frequently occurring symptom was nasal obstruction. These categories defined by the pathophysiology and anatomic locations provide a hierarchical and more systematic view of the phenotypes of COVID-19. These classifications facilitate prompt disease location and identification of etiology.

Our literature survey identified 22 common comorbidities. Hypertension, diabetes, cardiovascular diseases, chronic pulmonary diseases are the most common comorbidities in COVID-19 patients. Other common comorbidities include obesity, chronic kidney, hepatitis B/C infection, chronic hepatic failure, cirrhosis, chronic neurological disease (e.g., seizures and dementia), and hematological system disease (e.g., abnormality of blood and blood-forming tissues) (22, 23). These comorbidities were classified to different hierarchical groups (**Figure 1B**). Specifically, these comorbidities were found to occur in various systems such as the cardiovascular system, blood, immune system, metabolism, digestive system, nervous system, kidney, respiratory system. Cirrhosis, viral hepatitis, and chronic hepatic failure belong to the digestive system. Dementia, seizure is the subclass of abnormal nervous system. Obesity and autoimmune deficiency comorbidities are also important markers for poor prognosis (**Figure 1B**).

## Differential Profiles of Symptoms in Early COVID-19 Patients

### Differential Profiles of Symptoms in Early COVID-19 Patients in China, Italy, and the USA

To examine how the COVID-19 symptoms varies depending on countries, we focused our study on the set of rich clinical data from China, Italy and the United States of America (USA). These three countries were first chosen because of the many reports on the clinical results from these three countries, and there appeared to be differences in clinical phenotypes in patients reported in these three countries as well. A total of 17 articles included 5 articles from China (1, 2, 24–26), 7 from Italy (27–33), and 5 from the US (34–38). As summarized in **Table 1**, these 17 papers annotated in our study covered 3,630 patients from different countries. The commonly reported 12 symptoms in these papers were listed in **Table 1** and plotted in **Figure 2** and **Table 1**.

Our comparative study showed that the incidence of fever of COVID-19 patients was 85% in China, higher than in the other two countries (**Figure 2**). In contrast, 70 and 50% of the patients in Italy and the US had fever as a symptom. With an incidence of 43%, fatigue was also common in COVID-19 patients in China. Beyond fever, cough, and fatigue, the incidence of other symptoms (i.e., headache, diarrhea, nausea and vomiting etc.) in China was relatively lower, all below 20%. This finding accords with the results published in a paper (also included in our study) by Guan et al. (2), which summarized the clinical data from 1,099 COVID-19 patients from 552 hospitals in 30 provinces in

**TABLE 1** | Comparison of common COVID-19 phenotypes in China, Italy and USA from December 2019 to May 2020.

|                           | China               | Italy            | USA            |
|---------------------------|---------------------|------------------|----------------|
| Fever                     | 1,406/1,651 (0.85)* | 940/1,337 (0.7)  | 282/565 (0.50) |
| Cough                     | 1,058/1,651 (0.64)  | 665/1,337 (0.5)  | 399/565 (0.71) |
| Dyspnea                   | 252/1,377 (0.18)    | 236/665 (0.35)   | 252/565 (0.45) |
| Myalgia or/and Arthralgia | 221/1,297 (0.17)    | 486/910 (0.53)   | 123/318 (0.39) |
| Sore throat               | 208/1,451 (0.14)    | 139/382 (0.36)   | 219/565 (0.39) |
| Headache                  | 202/1,511 (0.13)    | 368/982 (0.37)   | 310/565 (0.55) |
| Loss of smell             | 13/274 (0.05)       | 699/1,337 (0.52) | 229/565 (0.41) |
| Loss of taste             | 16/274 (0.06)       | 573/1,135 (0.5)  | 133/420 (0.32) |
| Nasal congestion          | 53/1,099 (0.05)     | 130/874 (0.15)   | 152/565 (0.27) |
| Diarrhea                  | 115/1,591 (0.07)    | 328/1,265 (0.26) | 153/420 (0.36) |
| Nausea or/and vomiting    | 105/1,377 (0.08)    | 110/802 (0.14)   | 154/335 (0.46) |
| Fatigue                   | 621/1,437 (0.43)    | 542/1,157 (0.47) | 156/548 (0.28) |

The data were obtained by summarizing the results reported in 17 papers (see **Supplementary Files 1, 2**). \*Represents 1,406 out of 1,651 (85%) COVID-19 patients who had the fever symptom.

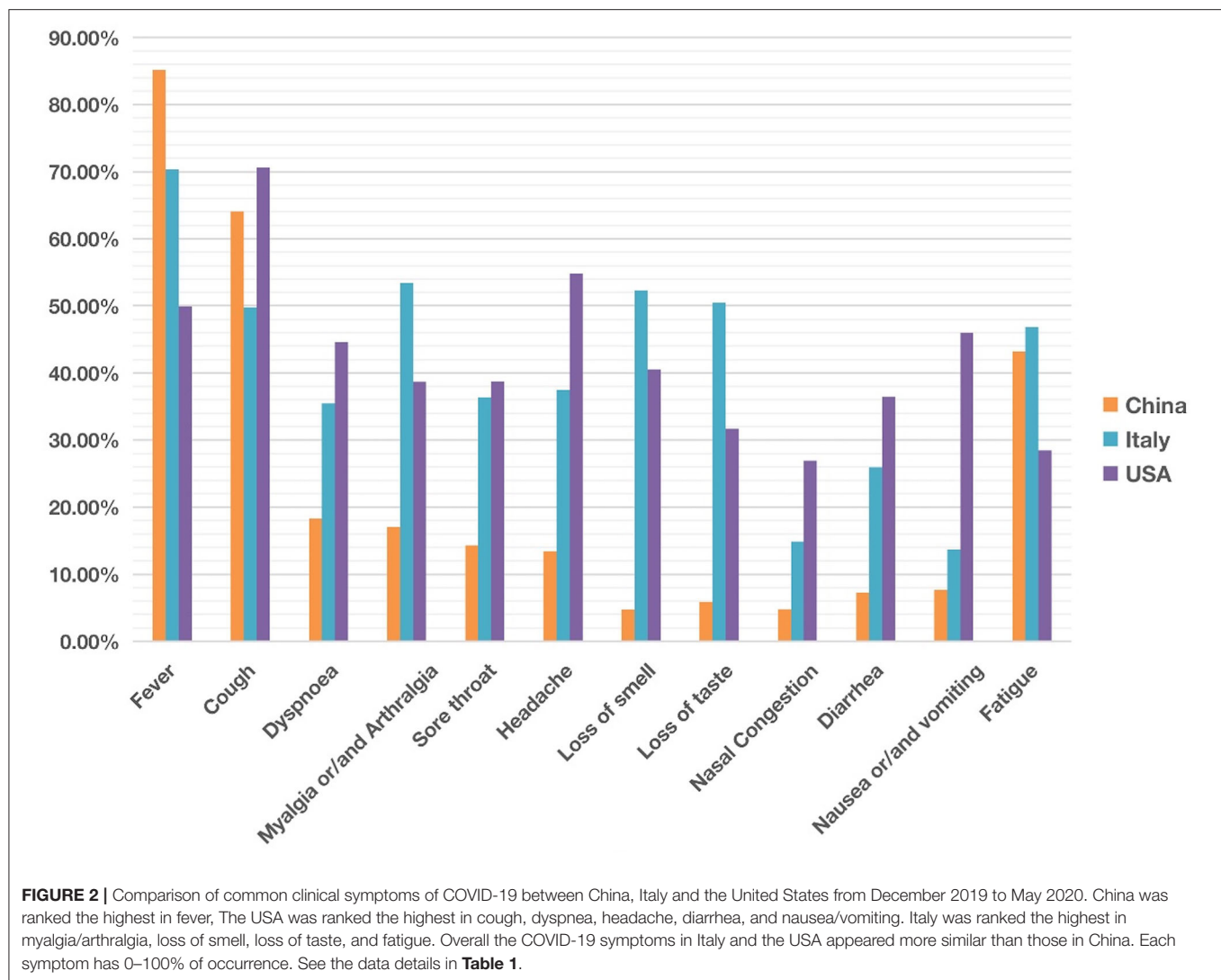
China and found that the most common symptoms of COVID-19 in China were fever (88.7% during hospitalization) and cough (67.8%), whereas diarrhea was uncommon (3.8%).

COVID-19 patients in the US had 7 symptoms ranked most frequently reported out of the three countries: cough, dyspnea, sore throat, headache, nasal congestion, diarrhea, and nausea/vomiting. A total of 71% of patients in the US reported cough, and the numbers were 64 and 50% in China and Italy, respectively. The most dramatic difference appeared to be nausea/vomiting, with 46% in the US, 14% in Italy, and 8% in China. The incidence of headache also differed substantially among the three countries, with 55% in the US, 37% in Italy, and 13% in China.

COVID-19 patients in Italy showed four symptoms at a higher frequency compared with the other two countries: myalgia/arthralgia, loss of smell, loss of taste, and fatigue. A total of 52% of the patients in Italy reported loss of smell, and 51% reported loss of taste. In the US, 32 and 41% of patients reported loss of smell and taste, respectively. In contrast, in China, only 5% of the patients reported loss of smell, and 6% reported loss of taste (**Table 1**).

### Differential Profiles of Nervous Symptoms in Early COVID-19 Patients From Different Countries and Regions

Instead of focusing on individual symptoms, we hypothesized that the analysis of symptoms as groups would identify new scientific insights. First, we analyzed the group of COVID-19-related nervous system symptoms, which includes loss of smell (anosmia), loss of taste (ageusia), and headache as shown in the HPO classification. Our combined analysis of all three symptoms, at the study/paper level instead of individual patient level, provided us with a unique approach to studying how the disease affects the nervous system.



In studies of patients in East Asian countries including China, South Korea, and Japan, all three nervous system symptoms were uncommon (**Figure 3; Supplementary Files 1, 2**). Among the three symptoms, headache was relatively common in these countries, with incidences ranging from 6 to 31.4%. However, except one article in China reporting hyposmia (i.e., reduced ability to smell) and hypogeusia (i.e., reduced ability to taste) (39), the other 9 Chinese articles did not report any cases of loss of smell and loss of taste. All these 10 Chinese articles covered patients with COVID-19 from December 2019 to February 2020. Another retrospective cohort study published in February 2021, which followed 1,172 COVID-19 patients discharged from Tongji Hospital in Wuhan between January and March 2020. The result was that 20.6% patients had loss of taste and 11.4% had loss of smell (40). The reduced or lost ability of smell or taste was not reported in a paper that collected the clinical data with the early six patients in Japan in 13–25 February 2020 (41) (**Figure 3**). However, an analysis of 213 patients in South Korea with mild COVID-19 during 12–16 March 2020 and assigned to specialized

isolation facilities found that 39.5% of these patients reported hyposmia and 33.7% reported hypogeusia (42). It is still unclear whether the difference in smell and taste related symptoms was due to an issue of reporting instead of the reality. However, it appears that the report of smell and taste related symptoms became common after early March.

The nervous system symptom patterns in Iran, European countries (including Italy, France, Germany, and Spain) and USA appeared to overlap and differ in many ways from China according to the reports during the first stage of infection (**Figure 3; Supplementary Files 1, 2**). The major differences existed in the loss of smell and taste. The incidence of loss of smell in Iran ranged from 58 to 60.9% (3, 43). Two large European investigations (44, 45) identified the loss of smell as a key symptom in mild-to-moderate COVID-19 patients, and they noticed that the loss of smell was not associated with nasal obstruction and rhinorrhea. Females and young patients were more susceptible to having the symptoms of smell and taste losses. Five Italian articles reported nervous system symptoms

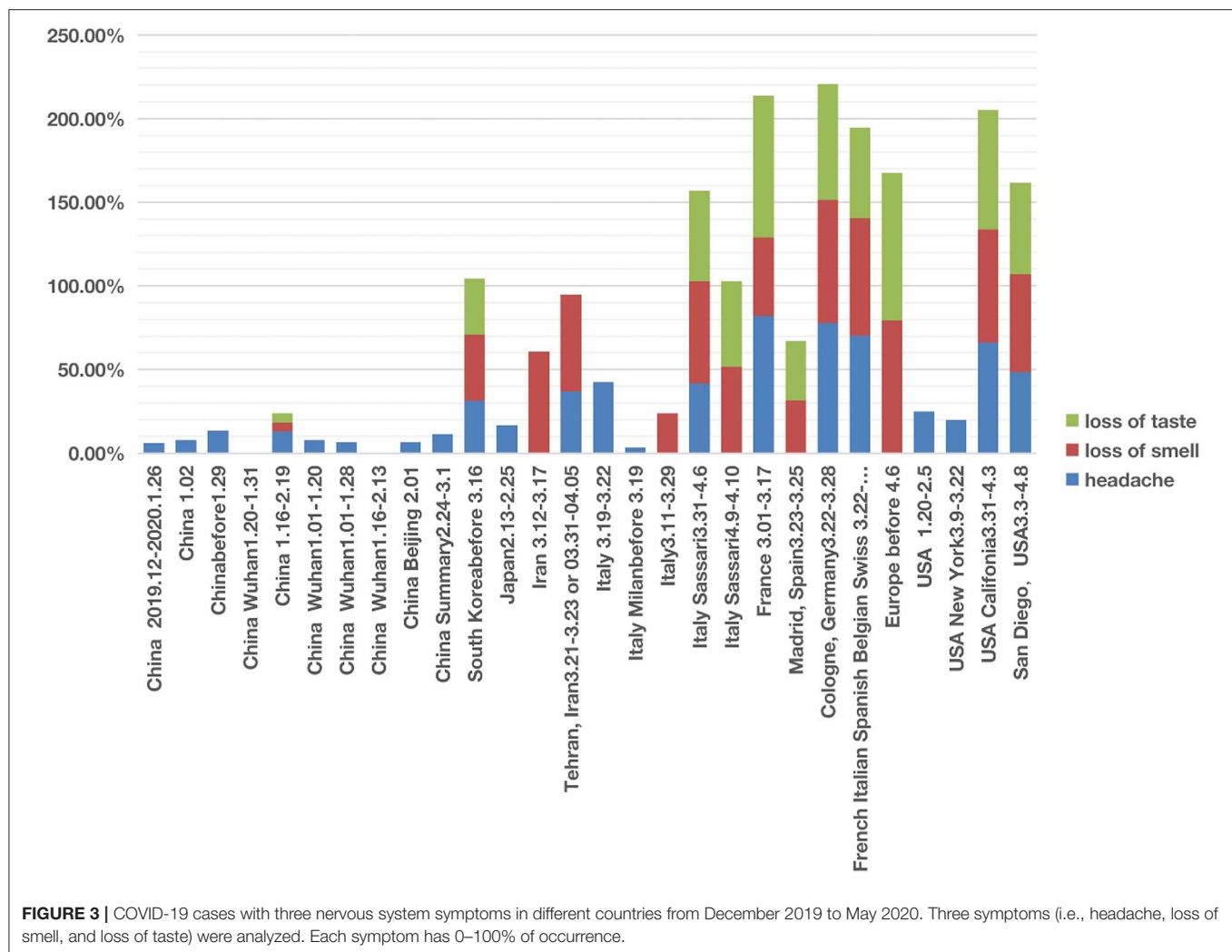


(Figure 3). Two of these five studies only reported headache but not loss of smell or taste (1, 41). However, loss of smell (24–61%) was the major nervous system symptoms among the three other studies (26, 42, 43), and loss of taste (51–54%) was reported in two studies (30, 46). In addition, loss of taste and smell were widely reported in COVID-19 cases in France, Spain, Germany, Belgium, and Switzerland (47). A systematic study published in April 2020 concluded 80% loss of smell and 88% loss of taste in Europe (44).

The three nervous system symptoms (i.e., headache, loss of taste, and loss of smell) in four US studies were collected and analyzed (34, 48–50) (Figure 3). Two studies with hospitalized COVID-19 patients reported the incidence of headache ranging from 20 to 25%, but not loss of smell or taste (48, 49). Based on self-reported symptoms (34, 50), the other two studies reported high incidences of all the three symptoms, with headache ranging from 48 to 66%, loss of taste from 55 to 71%, and loss of smell from 59 to 68%. These two survey-based studies found that COVID-19 patients with general mild-to-moderate symptoms more likely had the loss of smell and taste symptoms.

### Differential Profiles of Gastrointestinal Phenotypes in Early COVID-19 Patients From Different Countries and Regions

The primary abdominal symptoms included diarrhea, abdominal pain, nausea, and vomiting. With the help of the HPO classification (Figure 1), we analyzed these four abdominal symptoms together and compared the cases from different countries and regions.

We found that of the four digestive symptoms, diarrhea occurred in almost all countries, but the incidence in East Asian countries, including China, Singapore, South Korea, Japan, etc. was lower than 20%. In contrast, the incidence in Italy, the UK, France, Germany, USA generally ranged from 20 to 40%, and the highest proportion in one report of New York reached 61% (Figure 4; Supplementary Files 1, 2). The highest proportion of nausea and vomiting reported in China was 22.3% (24). However, the incidence in one report in New York reached 58% (51); the authors found that the patients with gastrointestinal symptoms (defined as diarrhea or nausea/vomiting) were significantly more likely to test positive than to test negative for COVID-19 (61

vs. 39%,  $P = 0.04$ ). Among 393 COVID-19 patients in two New York hospitals (4), gastrointestinal symptoms seemed to be more common than in China.

After screening, we documented three articles that specifically reported abdominal pain of COVID-19 patients. One study in Japan reported an incidence of 16.67% (41). Another study conducted in France found the incidence of abdominal pain was 28.00% among 54 patients with anosmia (20). In the UK, the incidence of abdominal pain was 10.20% of 20,133 patients between 6 February and 19 April 2020 in 208 acute care hospitals (52).

The time appeared to be another factor related to the presence of abdominal symptom phenotypes. The different abdominal symptoms were infrequently reported in studies in January and February 2020. However, more digestive symptoms were shown in the middle-late of March and early April 2020 (Figure 4).

## Correlation Between Comorbidities and Severe Disease Outcomes

To further study the relation between different comorbid phenotypes and disease outcomes, we reviewed the literature and compared the incidences of specific comorbid phenotypes in severe or non-severe COVID-19 patients. From the long list of comorbidities (Figure 1B), we chose diabetes and kidney disease for our further analysis (Figure 5). Zaki et al. showed that diabetes, hypertension, and cholesterol levels were significantly associated with COVID-19 severity, and kidney disease was strongly linked to the viral infection (53). Cheng et al. found that COVID-19 patients had a high prevalence of renal disease on admission and the development of acute kidney injury during hospitalization, and the kidney disease comorbidity was associated with increased in-hospital mortality (54). Therefore, diabetes and kidney disease appeared to be two independent risk factors for poor prognosis and intensive care unit admission in patients with COVID-19.

Given the poor prognosis of COVID-19 in patients with diabetes and kidney disease, we made a more systematic comparison of how the two diseases were related to the prognosis (i.e., severe or non-severe) of COVID-19 patients. The results from a total of 7 papers were summarized and analyzed (Figure 5). These 7 papers were selected since they met our inclusion criteria and included the incidences of COVID-19 comorbidities in both severe and non-severe patients (1, 2, 4, 19, 55–57).

As shown in Figure 5, the percentage of severe COVID-19 patients with diabetes was generally higher than that in non-severe patients. In all regions except California, the percentage of kidney disease of COVID-19 patients was also higher in severe patients than in non-severe patients. Specifically, the incidence of diabetes with severe or non-severe outcomes ranged from 16.20 to 39.8% or 5.7 to 27.7%, respectively (Figure 5). For each study, the fold change between severe and non-severe diabetes was usually over 2.0; even in California it was 1.15. The incidence of kidney disease of COVID-19 in the severe group ranged from 1.7 to 37.5%, in the non-severe group ranged from 2.0 to 15.0% (Figure 5). The average fold change between these patients was

2.7. In summary, the above results indicated that the patients with diabetes and kidney failure had worse outcomes compared with those without these comorbidities. It was reported that cytokine storm might be activated in diabetic patients, leading to poor prognosis and death (58). The exact mechanism deserves further investigation.

## CIDO Modeling, Query and Analysis of the COVID-19 Phenotypes and Comorbidities

As a foundation of AI, ontology is computer-interpretable. To allow users, including bioinformaticians, to develop and use computational programs to automatically access our annotated data, we represented our annotated knowledge in the Coronavirus Infectious Disease Ontology (7). Different diseases have the potential or susceptibility to induce specific phenotypes in patients. To differentiate the relations between diseases and phenotypes, in CIDO we generated a new ontology relation called “disease susceptibly has phenotype.” With this relation, we can define the disease-phenotype relation such as the following (Figure 6A):

*COVID-19 disease (process): “disease susceptibly has phenotype” some Fever.*

This means that COVID-19 patients are prone to fever. Such representation semantically links the disease to various phenotypes.

Similarly, to link a coronavirus disease such as COVID-19 with a comorbidity with which the disease is likely to have a more severe outcome, we also generated a new relation named “disease susceptibly severe with comorbidity.” With this relation in CIDO, we can define the disease-comorbidity relation such as the following (Figure 6A):

*COVID-19 disease (process): “disease susceptibly severe with comorbidity” some hypertension.*

This relation indicates that COVID-19 patients with hypertension and other comorbidities are prone to poor disease outcomes and prognosis. Such axioms allow us to semantically separate those phenotypes that are new symptoms in COVID-19 patients and the other phenotypes that are comorbidities present in COVID-19 patients when they were infected with the SARS-CoV-2 virus.

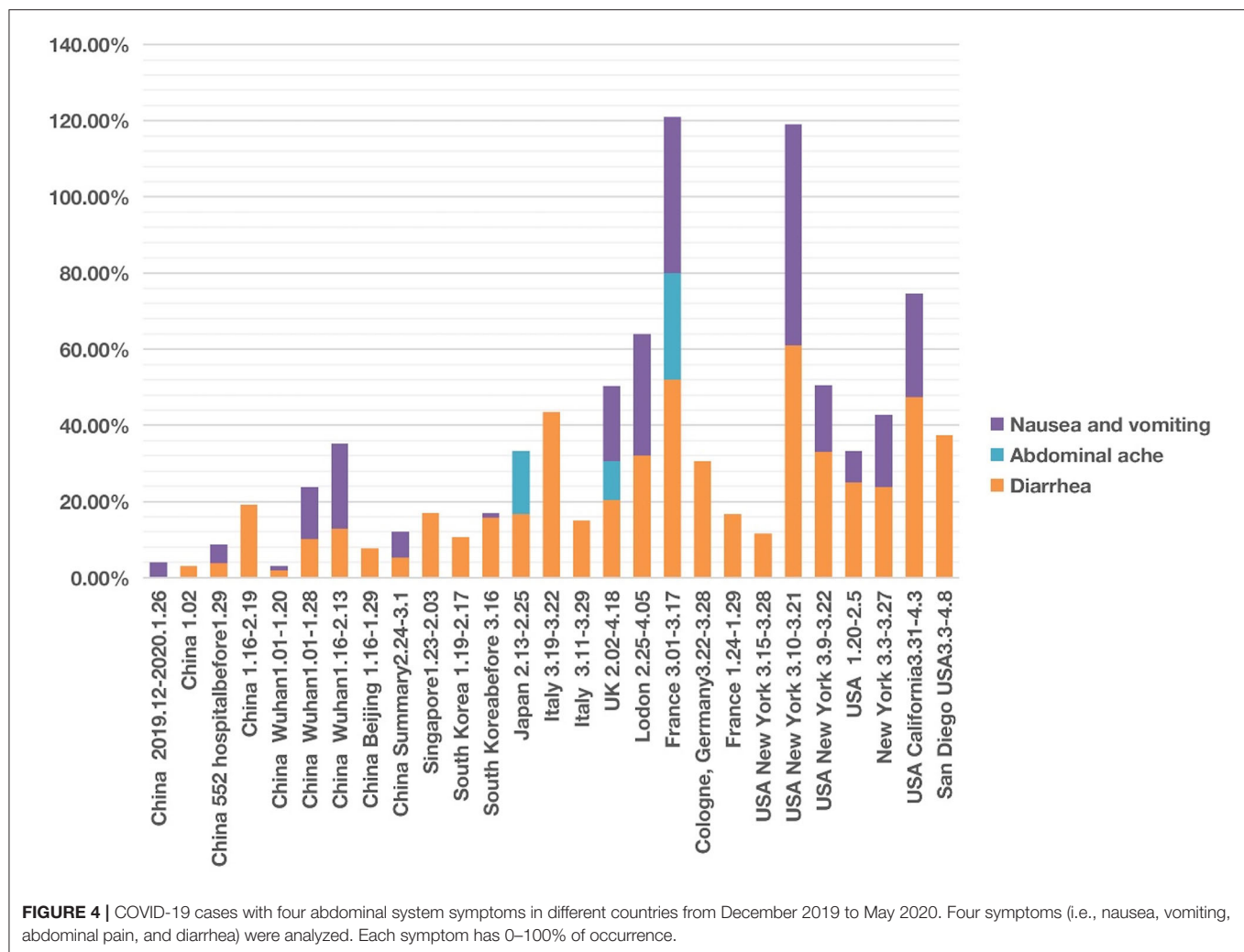
With CIDO modeling and representation of the COVID-19 disease, symptoms of COVID-19, and comorbidities in COVID-19 patients, and the semantic relations among these terms, we are able to develop new methods to query and analyze the knowledge represented in the CIDO using ontology-based semantic tools.

Figure 6B demonstrates how we can generate a SPARQL query to identify the four COVID-19-associated digestive symptoms including vomiting, diarrhea, nausea, and abdominal pain.

## DISCUSSION

The contributions of our paper are multi-faceted. First, we performed a systematic survey on the phenotypes/symptoms on COVID-19 patients who got infected at the early stage of the pandemic (before early May 2020), from the publications reported before August 2020. Our study focused on the





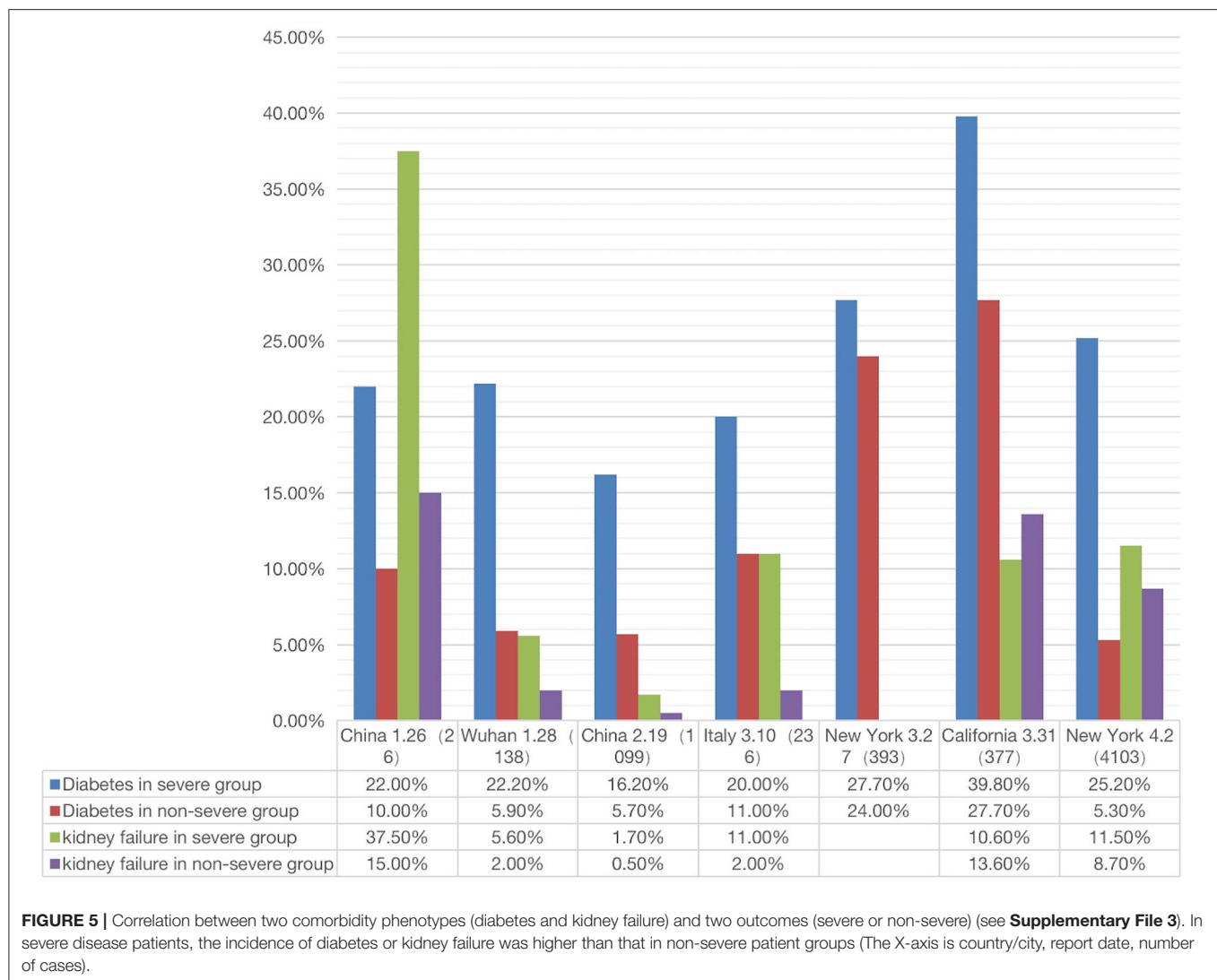
influence of three variables on the symptom outcomes: location of incidence, time of incidence, and comorbidity type. The ontology analysis allowed us to focus on groups of symptoms or comorbidities. Second, differential COVID-19 symptom patterns given different conditions were identified and analyzed. Our survey identified and classified 18 common symptoms. Furthermore, we found that these symptoms (e.g., loss of smell and taste) often differed significantly given specific regions, time, and comorbidities. Third, we showed how Coronavirus Infectious Disease Ontology (CIDO) can be applied to support modeling and linkage between COVID-19, viruses, symptoms, and comorbidities. Fourth, we propose a “Spiral Symptom Occurrence Hypothesis” to explain the spiral occurrence of certain symptoms that have occurred during the COVID-19 pandemic, as further discussed below. The first and third contributions listed here focus on method novelty, and the second and fourth contributions are scientifically more important.

It is generally considered that different SARS-CoV-19 variants induced similar symptoms, as demonstrated by the 18 common

symptoms classified under different categories (**Figure 1**). However, symptoms might significantly differ given conditions. Many infected patients had no symptoms, but many died with severe symptoms, indicating human conditions significantly affected the disease outcome. On the other hand, virus variations might significantly change the disease outcome. Some variants, including Alpha variant (12) and Delta variant (59), cause more severe illness and death than the other variants. However, the more recent Omicron variant appears to cause milder symptoms in general (60, 61). Since our study focused on the early pandemic stage, we did not need to consider the influence of the highly transmissible virus variants reported at the later stage. To the best of our knowledge, our study provided the first systematic analysis of the influence and co-influence of three specific variations (i.e., location, time, and comorbidity type) on various COVID-19 symptoms. While the time variable is mainly reflected in the time when the data were collected, we focused on the variables of the location and comorbidity type.

The location of incidence at the early stage of pandemic appeared to significantly influence the disease symptoms. Many



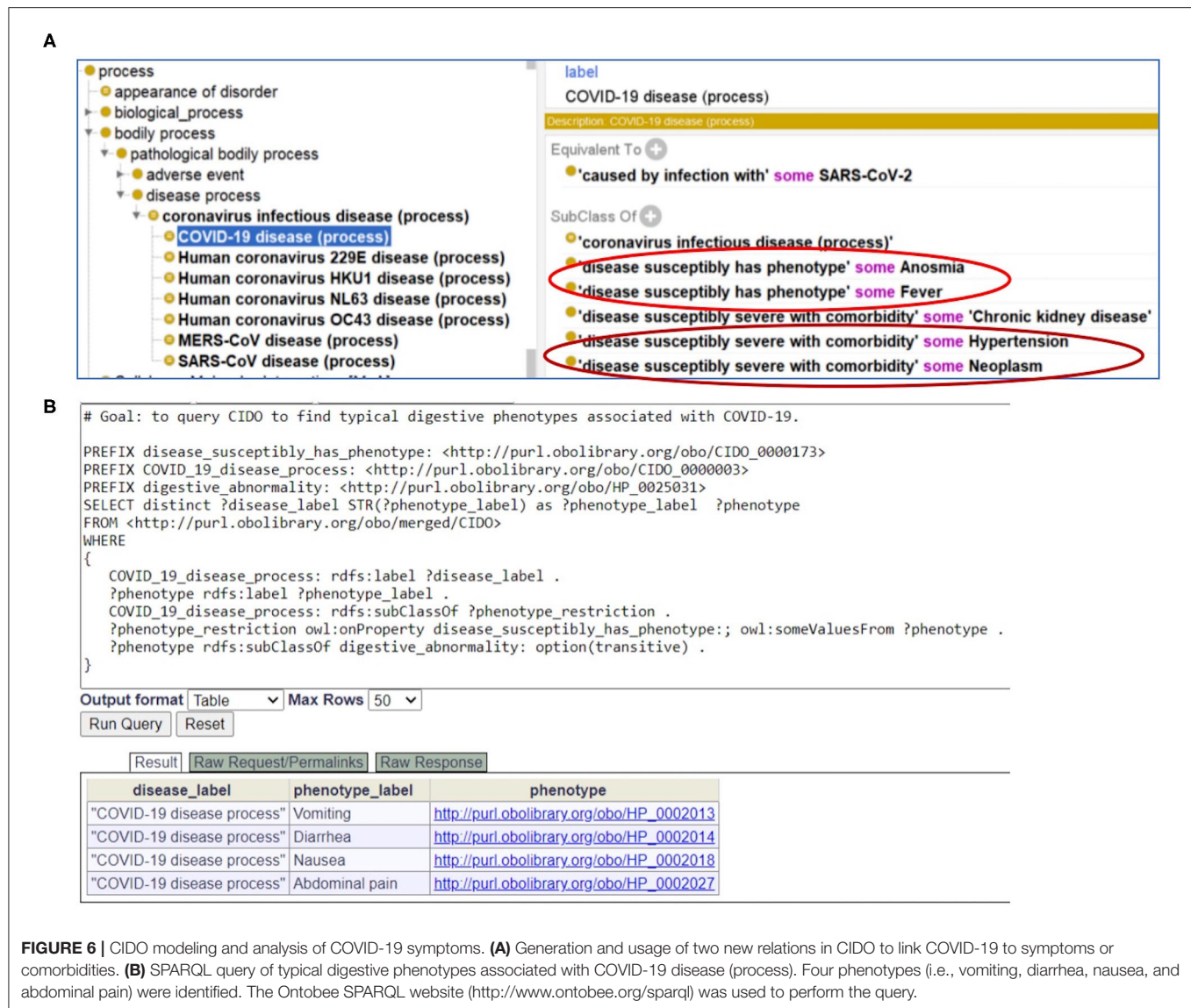


distinct and differential COVID-19 symptoms among different regions before the summer of 2020 were identified using our ontology-based literature meta-analysis (**Table 1**; **Figures 2–4**). From our comparison of individual symptoms in China, Italy, and the US, we found that COVID-19 patients in China frequently exhibited fever, whereas the USA ranked high in symptoms of cough, dyspnea, and sore throat, etc. And Italy was ranked high in myalgia/arthralgia, loss of smell, loss of taste, and fatigue (**Figure 2**). Overall, the patients in Italy and the USA had more similar symptoms than those in China. A possible reason for the difference could be different reporting styles of the disease between China and Italy/USA. However, it was likely not the case due to the fairly similar nature of professional investigations across different regions. The other possible reasons include viral variation, time of occurrence, host variation, non-pharmaceutical intervention policy, etc. (see more discussion below).

Grouped symptoms in the nervous system (including loss of smell, loss of taste, and headache) (**Figure 3**) and the abdominal symptom (including nausea, vomiting, abdominal

pain, and diarrhea) (**Figure 4**) with more countries included were then further analyzed with the help of the HPO ontology classification. Our study found that more of the COVID-19 patients from Europe and USA had nervous symptoms and abdominal symptoms compared with patients from Asia (**Figures 3, 4**). For example, during the early pandemic stage, 51–52% of patients in Italy and 32–41% of patients in US reported the losses of smell or taste, and the numbers came below 6% in China. Diarrhea occurred in East Asian countries was lower than 20%. In contrast, the incidence in European countries and the USA generally ranged from 20 to 61% (**Figure 4**; **Supplementary Files 1, 2**).

Comorbidities have been strongly associated with COVID-19 patients' clinical outcomes (**Figures 1B, 5**). A total of 22 comorbidities (**Figure 1B**) were found to commonly exist among COVID-19 patients, and usually COVID-19 patients with comorbidities had worse outcomes. Patients with these comorbidities such as diabetes and kidney failure were found to have worse outcomes compared with those without these



comorbidities (Figure 5). Specifically, the percentage of severe COVID-19 patients with diabetes was generally higher than that in non-severe patients (Figure 5). Our collected data also showed that in most regions, the percentage of kidney disease of COVID-19 patients was higher in severe patients than in non-severe patients (Figure 5). The incidence of acute kidney injury (AKI) in hospitalized patients varies from 0.5 to 40% due to factors such as race, region, and disease severity, and the mortality rate is significantly higher than the general infected population (1, 2, 54, 62–65). A recent study identified two clinical phenotypes of AKI (AKI-early and AKI-late) based on whether the kidney is the first dysfunctional organ (66). Such a distinction is likely due to whether the kidney is directly infected or indirectly affected through the failure of other infected organs. How the kidney disease as a comorbidity affects the host-coronavirus interaction and disease outcomes appears very complex and requires further investigation.

Many reasons may explain the symptom differences identified in the early stage of COVID-19 pandemic. First, data biases in the literature report may exist. For example, cases of some specific symptoms might have been reported more in some regions than the others. We know that such biases might have existed. However, given the impact and scope of the pandemic, there had been a lot of high impact and professional case reports, and we managed to collect all we could have found. Therefore, the data biases were likely low. Second, different predominant viral strains and viral variation in different regions may be combined to affect the outcomes. As per Forster et al. (March 30, 2020), novel coronavirus strains can be divided into three types: A, B and C (9). Although the original version of “A type” appeared in Wuhan, there were more mutated “B type” strains in Wuhan samples. B type is more common in East Asia. Type C, a variant of type B, is mainly present in Europe and has been found in early French, Italian, Swedish and British patients. The type A strain

was more common in the US and Australian study samples (9). However, there has been skepticism about the claim reported in the paper (9), considering that the sample size they collected was too small, only 160 cases. An examination of strains collected from Northern California in early February and mid-March 2020 indicated that international travel (from China and Europe) and interstate travel caused multiple transmissions. Sequencing of strains collected in the New York metropolitan area in March 2020 also suggested that the viral strains found in New York originated from Europe and other parts of the US (67). The results may explain the similarities of COVID-19 symptoms among European countries and the USA.

Our early-pandemic phenotypic analysis does not cover the potential influences of major genetic variants of concern or interest of COVID-19 after the first stage of pandemic. The WHO defined many variants of concern (VOCs) and variants of interest (VOIs) of SARS-CoV-2 worldwide (68). The comparison of our collected findings with the new reports of symptoms associated with the infection of the VOCs and VOIs suggests that the symptoms associated with these VOCs and VOIs are generally similar but may differ in specific scenarios. There is evidence that variants with the D614G mutation spread more quickly than viruses without this mutation (69). Variants containing the D614G mutation are found in the B.1 clade by the PANGOLIN tool. The Alpha variant (lineage B.1.1.7), first detected in September 2020 in United Kingdom, shows ~50% increased transmission (11). The Beta strain (lineage B.1.351) was first identified at South Africa in October 2020 and likely first emerged in July or August 2020 (13). The Delta variant (lineage B.1.617), first discovered in October 2020 in India, strain was dominant in many countries (70) for a long period of time in 2021. The most recent Omicron variant (lineage B.1.1.529) is more transmissible but likely less virulent (60, 61). The last day of the data collection for the papers included in our study was May 2, and those data came from Italy (31). Therefore, our study does not describe the specific impact of these VOCs and VOIs. Such a limitation can be filled up with more specific studies. However, our study design also offers us an advantage in that we could focus on the impact of other factors.

Our study did not specifically analyze the influence of many factors, such as host genetic variations, age, gender, vaccination, and non-pharmaceutical interventions, on the symptom outcomes in COVID-19 patients. More specific investigations are required to overcome these limitations. The host genetic variations may be reflected in the factor of different regions or countries. The FDA issues the emergency use authorization for the first COVID-19 vaccine, i.e., Pfizer-BioNTech COVID-19 Vaccine, in December 2020. Considering our study used the clinical data during the early stage of the pandemic, the impact of vaccination was not shown in our study. Different from vaccination and drug treatment, many non-pharmaceutical interventions (NPIs), such as social distancing, travel restriction, and resource allocation, are very effective against COVID-19 pandemic (71). During the pandemic, China took very strict NPI measures, but the levels of NPIs in other countries varied in time and location. The specific influence of

the NPIs on the symptoms of COVID-19 was not analyzed in this study.

Instead of providing direct guidance on the COVID-19 disease management in the post-vaccination period, our study provides a more historical perspective of the disease symptoms and evolutions at the early stage of the COVID-19 outbreak and then pandemic. Such results can also be used to compare with the symptom data obtained during the later stages of the pandemic, leading to more scientific insights and hypotheses. As a demonstration, after putting together our early stage findings and the symptoms observed with the COVID-19 variants coming out at later stages, we have identified and are proposing here a new hypothesis to address the dynamic symptom changes given different conditions:

Our *Spiral Symptom Occurrence Model Hypothesis* proposes that while non-specific symptoms (e.g., fever and fatigue) are conserved and transmission rate is increasing, specific COVID-19 symptoms (e.g., loss of smell and taste) may spirally be absent, appear, and then disappear in patients, primarily through viral genetic variations and host responses under various conditions.

Aligned with this hypothesis, initially the loss of smell and loss of taste did not occur frequently in the very early stage of infection in China, then occurred a lot in the European and Mideast countries and U.S., and now they have apparently disappeared or at a much less frequency in patients infected with the Omicron variant (60, 61). More specifically, these two symptoms were below 6% in early 2020 in China, then they were significantly changed to the range of 32–75% at later time in the first half of 2020 in US and Europe (**Table 1; Figure 4**), and now both symptoms have not generally been reported from the COVID-19 patients infected with the Omicron variant (60, 61). Our proposed spiral model suggests that the viruses might have first randomly mutated into more virulent and transmissible variants leading to the appearance of the loss of smell and taste; however, given various human responses including vaccination and non-pharmaceutical interventions, the viruses further mutated to form genetic variants such as Omicron that failed to generate the same symptoms. Based on this hypothesis, it is possible to identify some specific genetic mutations responsible for the loss of smell and tastes, which may be present in strains like Alpha and Delta variants but be absent or disappear in the Wuhan and Omicron genomes.

In the future, we plan to perform more systematic monitoring and analysis of the symptoms and comorbidities in COVID-19 patients of dominant variants (e.g., Alpha, Delta, and Omicron) given various conditions. We also plan to further compare our results found at the early stage of the pandemic with the later stages of the pandemic. Our integrative ontology-based analysis approaches as demonstrated in this paper provide a new strategy for data standardization, normalization, and systematic comparison. Our two newly generated relations (**Figure 6**) allowed semantic and accurate presentation of the relations between COVID-19 and its associated 18 symptoms and 22 comorbidities. Such representations then allow the development of new computer queries and software programs, which further advance our opportunities for more advanced analyses. To better understand the contributions of different factors, we will also

require deep modeling and representation of intricate molecular and cellular host-coronavirus interactions and understanding the fundamental interaction mechanisms.

## CONCLUSIONS

The clinical data of COVID-19 phenotypes found in 43,567 COVID-19 patients, as reported in 48 articles, were systematically surveyed and analyzed. The 18 commonly occurring symptoms and 22 comorbidities in COVID-19 patients were ontologically categorized and grouped using the Human Phenotype Ontology (HPO). Differential patterns were detected in different countries and regions. Fever, cough, and the new loss of smell/taste were ranked as the most frequent phenotypes in China, the US, and Italy, respectively. Using data reported from 12 countries, we found that the patients from Europe and USA more frequently had nervous system phenotypes and abdominal phenotypes than patients from Asia during the first half of 2020. The Coronavirus Infectious Disease Ontology (CIDO) was used to model and interlink the COVID-19 disease, 18 symptoms, and 22 comorbidities together, and CIDO-based semantic queries were performed to demonstrate the advantages of computer-assisted reasoning and analysis. In addition to our method novelty, these findings discovered in this study provide historic views of COVID-19 symptoms in terms of our long-term COVID-19 disease study.

## DATA AVAILABILITY STATEMENT

The original contributions presented in the study are included in the article/**Supplementary Material**, further inquiries can be directed to the corresponding author/s.

## AUTHOR CONTRIBUTIONS

YW, XY, and HY contributed to the overall study design. YW, FZ, and HY contributed to data collection and data analysis. YW and YH provided manual data/result verification and ontology editing. JB, HY, and XY who are COVID-19 medical doctors,

served as domain experts to perform data/result interpretation, and discussion. YW and YH prepared the initial complete manuscript and all authors contributed to the manuscript writing and reviews. All authors contributed to the article and approved the submitted version.

## FUNDING

YW was supported by a scholarship offered by the China Scholarship Council with the University of Michigan as a Visiting Ph.D. Student (File No. 202006670006). The research was also supported by the Youth Found of Guizhou Provincial People's Hospital of China, GZSYQN[2019]09, a non-profit Central Research Institute Fund of the Chinese Academy of Medical Sciences (2019PT320003), a NIH NIAID grants 1UH2AI132931 (to YH), a COVID-19 pilot award from Michigan Medicine-Peking University Health Sciences Center Joint Institute for Clinical and Translational Research (to YH), and a Fast Grants award for a clinical trial related to COVID-19 (to JB).

## ACKNOWLEDGMENTS

A preprint of this paper was published earlier in arXiv with the title Ontology-based annotation and analysis of COVID-19 phenotypes (<https://arxiv.org/abs/2008.02241>). Our preliminary ontology-focused work was also presented in the 19th International Conference on Bioinformatics (InCoB 2020) held virtually on Nov 25–29, 2020, and we appreciate the constructive discussions and feedback from the attendees of the conference. We also appreciate the development and open availability of HPO and CIDO.

## SUPPLEMENTARY MATERIAL

The Supplementary Material for this article can be found online at: <https://www.frontiersin.org/articles/10.3389/fmed.2022.770031/full#supplementary-material>

## REFERENCES

- Wang D, Hu B, Hu C, Zhu F, Liu X, Zhang J, et al. Clinical characteristics of 138 hospitalized patients with 2019 novel coronavirus-infected pneumonia in Wuhan, China. *JAMA*. (2020) 323:1061–9. doi: 10.1001/jama.2020.1585
- Guan WJ, Ni ZY, Hu Y, Liang WH, Ou CQ, He JX, et al. Clinical characteristics of coronavirus disease 2019 in China. *N Engl J Med*. (2020) 382:1708–20. doi: 10.1056/NEJMoa2002032
- Moein ST, Hashemian SM, Mansourafshar B, Khorram-Tousi A, Tabarsi P, Doty RL. Smell dysfunction: a biomarker for COVID-19. *Int Forum Allergy Rhinol*. (2020) 10:944–50. doi: 10.1002/alr.22587
- Goyal P, Choi JJ, Pinheiro LC, Schenck EJ, Chen R, Jabri A, et al. Clinical characteristics of Covid-19 in New York City. *N Engl J Med*. (2020) 382:2372–4. doi: 10.1056/NEJMc2010419
- Chen C, Chen C, Yan JT, Zhou N, Zhao JP, Wang DW. [Analysis of myocardial injury in patients with COVID-19 and association between concomitant cardiovascular diseases and severity of COVID-19]. *Zhonghua Xin Xue Guan Bing Za Zhi*. (2020) 48:E008. doi: 10.3760/cma.j.cn112148-20200225-00123
- Groza T, Kohler S, Moldenhauer D, Vasilevsky N, Baynam G, Zemojtel T, et al. The human phenotype ontology: semantic unification of common and rare disease. *Am J Human Gen*. (2015) 97:111–24. doi: 10.1016/j.ajhg.2015.05.020
- He Y, Yu H, Ong E, Wang Y, Liu Y, Huffman A, et al. CIDO, a community-based ontology for coronavirus disease knowledge and data integration, sharing, and analysis. *Sci data*. (2020) 7:181. doi: 10.1038/s41597-020-0523-6
- Liu Y, Hur J, Chan WKB, Wang Z, Xie J, Sun D, et al. Ontological modeling and analysis of experimentally or clinically verified drugs against coronavirus infection. *Sci Data*. (2021) 8:16. doi: 10.1038/s41597-021-00799-w
- Forster P, Forster L, Renfrew C, Forster M. Phylogenetic network analysis of SARS-CoV-2 genomes. *Proc Natl Acad Sci USA*. (2020) 117:9241–3. doi: 10.1073/pnas.2004999117
- Baldwin CL, Verstrete DR, Winter AJ. Immune response of cattle to *Brucella abortus* outer membrane proteins measured by



- lymphocyte blastogenesis. *Vet Immunol Immunopathol.* (1985) 9:383–96. doi: 10.1016/0165-2427(85)90067-4
11. Davies NG, Abbott S, Barnard RC, Jarvis CI, Kucharski AJ, Munday JD, et al. Estimated transmissibility and impact of SARS-CoV-2 lineage B.1.1.7 in England. *Science.* (2021) 372:eabg3055. doi: 10.1126/science.abg3055
  12. Davies NG, Jarvis CI, Group CC-W, Edmunds WJ, Jewell NP, Diaz-Ordaz K, et al. Increased mortality in community-tested cases of SARS-CoV-2 lineage B.1.1.7. *Nature.* (2021) 593:270–4. doi: 10.1038/s41586-021-03426-1
  13. Tegally H, Wilkinson E, Giovanetti M, Iranzadeh A, Fonseca V, Giandhari J, et al. Emergence and rapid spread of a new severe acute respiratory syndrome-related coronavirus 2 (SARS-CoV-2) lineage with multiple spike mutations in South Africa. *MedRxiv.* (2020). doi: 10.1101/2020.12.21.20248640
  14. Köhler S, Vasilevsky NA, Engelstad M, Foster E, McMurry J, Aymé S, et al. The human phenotype ontology in 2017. *Nucleic Acids Res.* (2016) 45:D865–76. doi: 10.1093/nar/gkw1039
  15. Ong E, Xiang Z, Zhao B, Liu Y, Lin Y, Zheng J, et al. Ontobee: a linked ontology data server to support ontology term dereferencing, linkage, query and integration. *Nucleic Acids Res.* (2017) 45:D347–52. doi: 10.1093/nar/gkw918
  16. Xiang Z, Courtot M, Brinkman RR, Ruttenberg A, He Y. OntoFox: web-based support for ontology reuse. *BMC Res Notes.* (2010) 3:175:1–12. doi: 10.1186/1756-0500-3-175
  17. Rubin DL, Noy NF, Musen MA. Protege: a tool for managing and using terminology in radiology applications. *J Digital Imag.* (2007) 20(Suppl. 1):34–46. doi: 10.1007/s10278-007-9065-0
  18. Bagheri SH, Asghari A, Farhadi M, Shamshiri AR, Kabir A, Kamrava SK, et al. “Coincidence of COVID-19 epidemic and olfactory dysfunction outbreak in Iran.” *Med J Islam Repub Iran.* (2020) 34:62. doi: 10.34171/mjiri.34.62
  19. Yang X, Yu Y, Xu J, Shu H, Xia J, Liu H, et al. Clinical course and outcomes of critically ill patients with SARS-CoV-2 pneumonia in Wuhan, China: a single-centered, retrospective, observational study. *Lancet Respir Med.* (2020) 8:475–81. doi: 10.1016/S2213-2600(20)30079-5
  20. Klopfenstein T, Kadiane-Oussou NJ, Toko L, Royer PY, Lepiller Q, Gendrin V, et al. Features of anosmia in COVID-19. *Méd Maladies Infect.* (2020) 50:436–9. doi: 10.1016/j.medmal.2020.04.006
  21. Lee SG, Fralick M, Sholzberg M. Coagulopathy associated with COVID-19. *CMAJ.* (2020) 192:E583. doi: 10.1503/cmaj.200685-f
  22. Perez-Guzman PN, Daunt A, Mukherjee S, Crook P, Forlano R, Kont MD, et al. Clinical characteristics and predictors of outcomes of hospitalized patients with COVID-19 in a multi-ethnic London NHS trust: a retrospective cohort study. *Clin Infect Dis.* (2020) 73:e4047–e4057. doi: 10.1093/cid/ciaa1091
  23. Richardson S, Hirsch JS, Narasimhan M, Crawford JM, McGinn T, Davidson KW, et al. Presenting characteristics, comorbidities, and outcomes among 5700 patients hospitalized with COVID-19 in the New York City area. *JAMA.* (2020) 323:2052–9. doi: 10.1001/jama.2020.6775
  24. Zhang JJ, Dong X, Cao YY, Yuan YD, Yang YB, Yan YQ, et al. Clinical characteristics of 140 patients infected with SARS-CoV-2 in Wuhan, China. *Allergy.* (2020) 75:1730–41. doi: 10.1111/all.14238
  25. Mao L, Jin H, Wang M, Hu Y, Chen S, He Q, et al. Neurologic manifestations of hospitalized patients with coronavirus disease 2019 in Wuhan, China. *JAMA Neurol.* (2020) 77:683–90. doi: 10.1001/jamaneurol.2020.1127
  26. Lu Y, Li X, Geng D, Mei N, Wu PY, Huang CC, et al. Cerebral micro-structural changes in COVID-19 patients - an mri-based 3-month follow-up study. *EClin Med.* (2020) 2020:100484. doi: 10.1016/j.eclinm.2020.100484
  27. Spinato G, Fabbris C, Polesel J, Cazzador D, Borsetto D, Hopkins C, et al. Alterations in smell or taste in mildly symptomatic outpatients with SARS-CoV-2 infection. *JAMA.* (2020) 323:2089–90. doi: 10.1001/jama.2020.6771
  28. Dell’Era V, Farri F, Garzaro G, Gatto M, Aluffi Valletti P, Garzaro M. Smell and taste disorders during COVID-19 outbreak: cross-sectional study on 355 patients. *Head Neck.* (2020) 42:1591–6. doi: 10.1002/hed.26288
  29. Vacchiano V, Riguzzi P, Volpi L, Tappatà M, Avoni P, Rizzo G, et al. Early neurological manifestations of hospitalized COVID-19 patients. *Neurol Sci.* (2020) 41:2029–31. doi: 10.1007/s10072-020-04525-z
  30. Vaira LA, Deiana G, Fois AG, Pirina P, Madeddu G, De Vito A, et al. Objective evaluation of anosmia and ageusia in COVID-19 patients: single-center experience on 72 cases. *Head Neck.* (2020) 42:1252–8. doi: 10.1002/hed.26204
  31. Petrocilli M, Ruggiero F, Baietti AM, Pandolfi P, Salzano G, Salzano FA, et al. Remote psychophysical evaluation of olfactory and gustatory functions in early-stage coronavirus disease 2019 patients: the Bologna experience of 300 cases. *J Laryngol Otol.* (2020) 134:571–6. doi: 10.1017/S0022215120001358
  32. Lovato A, Galletti C, Galletti B, de Filippis C. Clinical characteristics associated with persistent olfactory and taste alterations in COVID-19: a preliminary report on 121 patients. *Am J Otolaryngol.* (2020) 41:102548. doi: 10.1016/j.amjoto.2020.102548
  33. Barillari MR, Bastiani L, Lechien JR, Mannelli G, Molteni G, Cantarella G, et al. A structural equation model to examine the clinical features of mild-to-moderate COVID-19: a multicenter Italian study. *J Med Virol.* (2020) 93:983–94. doi: 10.1002/jmv.26354
  34. Yan CH, Faraji F, Prajapati DP, Ostrander BT, DeConde AS. Self-reported olfactory loss associates with outpatient clinical course in COVID-19. *Int Forum Allergy Rhinol.* (2020) 10:821–31. doi: 10.1002/alr.22592
  35. Roland LT, Gurrola JG, 2nd, Loftus PA, Cheung SW, Chang JL. Smell and taste symptom-based predictive model for COVID-19 diagnosis. *Int Forum Allergy Rhinol.* (2020) 10:832–8. doi: 10.1002/alr.22602
  36. Bergquist SH, Partin C, Roberts DL, O’Keefe JB, Tong EJ, Zreloff J, et al. Non-hospitalized adults with COVID-19 differ noticeably from hospitalized adults in their demographic, clinical, and social characteristics. *SN Compr Clin Med.* (2020) 2020:1–9. doi: 10.1007/s42399-020-00453-3
  37. Kempker RR, Kempker JA, Peters M, Rebolledo PA, Carroll K, Toomer L, et al. Loss of smell and taste among healthcare personnel screened for coronavirus 2019. *Clin Infect Dis.* (2021) 72:1244–1246. doi: 10.1093/cid/ciaa877
  38. Yan CH, Faraji F, Prajapati DP, Boone CE, DeConde AS. Association of chemosensory dysfunction and COVID-19 in patients presenting with influenza-like symptoms. *Int Forum Allergy Rhinol.* (2020) 10:806–13. doi: 10.1002/alr.22579
  39. Roe K. Explanation for COVID-19 infection neurological damage and reactivations. *Transbound Emerg Dis.* (2020) 67:1414–5. doi: 10.1111/tbed.13594
  40. Song J, Deng YK, Wang H, Wang ZC, Liao B, Ma J, et al. Self-reported taste and smell disorders in patients with COVID-19: distinct features in China. *Curr Med Sci.* (2021) 41:14–23. doi: 10.1007/s11596-021-2312-7
  41. Kobayashi KI, Kaki T, Mizuno S, Kubo K, Komiya N, Otsu S. Clinical characteristics of patients with coronavirus disease 2019 in Japan: a single-center case series. *J Infect Dis.* (2020) 222:194–7. doi: 10.1093/infdis/jiaa244
  42. Kim GU, Kim MJ, Ra SH, Lee J, Bae S, Jung J, et al. Clinical characteristics of asymptomatic and symptomatic patients with mild COVID-19. *Clin Microbiol Infect.* (2020) 26:948 e1–3. doi: 10.1016/j.cmi.2020.04.040
  43. Cetinkaya EA. Coincidence of COVID-19 infection and smell-taste perception disorders. *J Craniofac Surg.* (2020) 31:e625–6. doi: 10.1097/SCS.00000000000006601
  44. Lechien JR, Chiesa-Estomba CM, De Siati DR, Horoi M, Le Bon SD, Rodriguez A, et al. Olfactory and gustatory dysfunctions as a clinical presentation of mild-to-moderate forms of the coronavirus disease (COVID-19): a multicenter European study. *Eur Arch Otorhinolaryngol.* (2020) 277:2251–61. doi: 10.1007/s00405-020-05965-1
  45. Lechien JR, Cabaraux P, Chiesa-Estomba CM, Khalife M, Plzak J, Hans S, et al. Objective olfactory testing in patients presenting with sudden onset olfactory dysfunction as the first manifestation of confirmed COVID-19 infection. *Medrxiv.* (2020). doi: 10.1101/2020.04.15.20066472
  46. Vaira LA, Salzano G, Petrocelli M, Deiana G, Salzano FA, De Riu G. Validation of a self-administered olfactory and gustatory test for the remotely evaluation of COVID-19 patients in home quarantine. *Head Neck.* (2020) 42:1570–6. doi: 10.1002/hed.26228
  47. Lechien JR, Chiesa-Estomba CM, Place S, Van Laethem Y, Cabaraux P, Mat Q, et al. Clinical and epidemiological characteristics of 1420 European patients with mild-to-moderate coronavirus disease 2019. *J Intern Med.* (2020) 288:335–44. doi: 10.1111/joim.13089
  48. Team C-I. Clinical and virologic characteristics of the first 12 patients with coronavirus disease 2019 (COVID-19) in the United States. *Nat Med.* (2020) 26:861–8. doi: 10.1038/s41591-020-0877-5
  49. Palaiodimos L, Kokkinidis DG, Li W, Karamanis D, Ognibene J, Arora S, et al. Severe obesity, increasing age and male sex are independently associated with worse in-hospital outcomes, and higher in-hospital mortality, in a cohort of patients with COVID-19 in the Bronx, New York. *Metabolism.* (2020) 108:154262. doi: 10.1016/j.metabol.2020.154262



50. Petrilli CM, Jones SA, Yang J, Rajagopalan H, O'Donnell L, Chernyak Y, et al. Factors associated with hospital admission and critical illness among 5279 people with coronavirus disease 2019 in New York City: prospective cohort study. *BMJ*. (2020) 369:m1966. doi: 10.1136/bmj.m1966
51. Nobel YR, Phipps M, Zucker J, Lebowitz B, Wang TC, Sobieszczyk ME, et al. Gastrointestinal symptoms and coronavirus disease 2019: a case-control study from the United States. *Gastroenterology*. (2020) 159:373–5 e2. doi: 10.1053/j.gastro.2020.04.017
52. Docherty AB, Harrison EM, Green CA, Hardwick HE, Pius R, Norman L, et al. Features of 20 133 UK patients in hospital with covid-19 using the ISARIC WHO clinical characterisation protocol: prospective observational cohort study. *BMJ*. (2020) 2020:369. doi: 10.1136/bmj.m1985
53. Zaki N, Alashwal H, Ibrahim S. Association of hypertension, diabetes, stroke, cancer, kidney disease, and high-cholesterol with COVID-19 disease severity and fatality: a systematic review. *Diabetes Metab Syndr*. (2020) 14:1133–42. doi: 10.1016/j.dsx.2020.07.005
54. Cheng Y, Luo R, Wang K, Zhang M, Wang Z, Dong L, et al. Kidney disease is associated with in-hospital death of patients with COVID-19. *Kidney Int*. (2020) 97:829–38. doi: 10.1016/j.kint.2020.03.005
55. Colombi D, Bodini FC, Petrini M, Maffi G, Morelli N, Milanese G, et al. Well-aerated lung on admitting chest CT to predict adverse outcome in COVID-19 pneumonia. *Radiology*. (2020) 296:E86–96. doi: 10.1148/radiol.2020.01433
56. Myers LC, Parodi SM, Escobar GJ, Liu VX. Characteristics of hospitalized adults with COVID-19 in an integrated health care system in California. *JAMA*. (2020) 323:2195–8. doi: 10.1001/jama.2020.7202
57. Petrilli CM, Jones SA, Yang J, Rajagopalan H, O'Donnell LF, Chernyak Y, et al. Factors associated with hospitalization and critical illness among 4,103 patients with COVID-19 disease in New York City. *Medrxiv*. (2020) 2020:20057794. doi: 10.1101/2020.04.08.20057794
58. Cole SA, Laviada-Molina HA, Serres-Perales JM, Rodriguez-Ayala E, Bastarrachea RA. The COVID-19 pandemic during the time of the diabetes pandemic: likely fraternal twins? *Pathogens*. (2020) 9:389. doi: 10.3390/pathogens9050389
59. Twohig KA, Nyberg T, Zaidi A, Thelwall S, Sinnathamby MA, Aliabadi S, et al. Hospital admission and emergency care attendance risk for SARS-CoV-2 delta (B.1.617.2) compared with alpha (B.1.1.7) variants of concern: a cohort study. *Lancet Infect Dis*. (2022) 22:35–42. doi: 10.1016/S1473-3099(21)00475-8
60. Iacobucci G. Covid-19: runny nose, headache, and fatigue are commonest symptoms of omicron, early data show. *BMJ*. (2021) 375:n3103. doi: 10.1136/bmj.n3103
61. Christie B. Covid-19: early studies give hope omicron is milder than other variants. *BMJ*. (2021) 375:n3144. doi: 10.1136/bmj.n3144
62. Naicker S, Yang CW, Hwang SJ, Liu BC, Chen JH, Jha V. The novel coronavirus 2019 epidemic and kidneys. *Kidney Int*. (2020) 97:824–8. doi: 10.1016/j.kint.2020.03.001
63. Zhou F, Yu T, Du R, Fan G, Liu Y, Liu Z, et al. Clinical course and risk factors for mortality of adult inpatients with COVID-19 in Wuhan, China: a retrospective cohort study. *Lancet*. (2020) 395:1054–62. doi: 10.1016/S0140-6736(20)30566-3
64. Arentz M, Yim E, Klaff L, Lokhandwala S, Riedo FX, Chong M, et al. Characteristics and outcomes of 21 critically ill patients with COVID-19 in Washington State. *JAMA*. (2020) 323:1612–1614. doi: 10.1001/jama.2020.4326
65. Hirsch JS, Ng JH, Ross DW, Sharma P, Shah HH, Barnett RL, et al. Acute kidney injury in patients hospitalized with COVID-19. *Kidney Int*. (2020) 98:209–18. doi: 10.1016/j.kint.2020.05.006
66. Peng S, Wang HY, Sun X, Li P, Ye Z, Li Q, et al. Early versus late acute kidney injury among patients with COVID-19—a multicenter study from Wuhan, China. *Nephrol Dialysis Transpl*. (2020) 35:2095–102. doi: 10.1093/ndt/gfaa288
67. Schuchat A, Team CC-R. Public health response to the initiation and spread of pandemic COVID-19 in the United States, February 24–April 21, 2020. *MMWR Morb Mortal Wkly Rep*. (2020) 69:551–6. doi: 10.15585/mmwr.mm6918e2
68. Baldwin CL, Antczak DF, Winter AJ. Cell titration assay for measuring blastogenesis of bovine lymphocytes. *Vet Immunol Immunopathol*. (1985) 9:319–33. doi: 10.1016/0165-2427(85)90062-5
69. Korber B, Fischer WM, Gnanakaran S, Yoon H, Theiler J, Abfalterer W, et al. Tracking changes in SARS-CoV-2 spike: evidence that D614G increases infectivity of the COVID-19 virus. *Cell*. (2020) 182:812–27 e19. doi: 10.1016/j.cell.2020.06.043
70. Planas D, Veyer D, Baidaliuk A, Staropoli I, Guivel-Benhassine F, Rajah MM, et al. Reduced sensitivity of SARS-CoV-2 variant delta to antibody neutralization. *Nature*. (2021) 596:276–80. doi: 10.1038/s41586-021-03777-9
71. Chan LYH, Yuan B, Convertino M. COVID-19 non-pharmaceutical intervention portfolio effectiveness and risk communication predominance. *Sci Rep*. (2021) 11:10605. doi: 10.1038/s41598-021-88309-1

**Conflict of Interest:** The authors declare that the research was conducted in the absence of any commercial or financial relationships that could be construed as a potential conflict of interest.

**Publisher's Note:** All claims expressed in this article are solely those of the authors and do not necessarily represent those of their affiliated organizations, or those of the publisher, the editors and the reviewers. Any product that may be evaluated in this article, or claim that may be made by its manufacturer, is not guaranteed or endorsed by the publisher.

Copyright © 2022 Wang, Zhang, Byrd, Yu, Ye and He. This is an open-access article distributed under the terms of the Creative Commons Attribution License (CC BY). The use, distribution or reproduction in other forums is permitted, provided the original author(s) and the copyright owner(s) are credited and that the original publication in this journal is cited, in accordance with accepted academic practice. No use, distribution or reproduction is permitted which does not comply with these terms.



# Staffing and Capacity Planning for SARS-CoV-2 Monoclonal Antibody Infusion Facilities: A Performance Estimation Calculator Based on Discrete-Event Simulations

Çaglar Çaglayan<sup>1\*</sup>, Jonathan Thornhill<sup>1</sup>, Miles A. Stewart<sup>1</sup>, Anastasia S. Lambrou<sup>1</sup>, Donald Richardson<sup>1</sup>, Kaitlin Rainwater-Lovett<sup>1</sup>, Jeffrey D. Freeman<sup>1</sup>, Tiffany Pfundt<sup>2</sup> and John T. Redd<sup>2</sup>

<sup>1</sup> Asymmetric Operations Sector, Johns Hopkins University Applied Physics Laboratory, Laurel, MD, United States, <sup>2</sup> Office of the Assistant Secretary for Preparedness and Response, United States Department of Health and Human Services, Washington, DC, United States

## OPEN ACCESS

### Edited by:

Reza Lashgari,  
Shahid Beheshti University, Iran

### Reviewed by:

Yixin Xie,  
The University of Texas at El Paso,  
United States  
Melike Yildirim,  
Harvard University, United States

### \*Correspondence:

Çaglar Çaglayan  
Caglar.Caglayan@jhuapl.edu

### Specialty section:

This article was submitted to  
Infectious Diseases - Surveillance,  
Prevention and Treatment,  
a section of the journal  
Frontiers in Public Health

**Received:** 03 September 2021

**Accepted:** 29 December 2021

**Published:** 28 January 2022

### Citation:

Çaglayan Ç, Thornhill J, Stewart MA, Lambrou AS, Richardson D, Rainwater-Lovett K, Freeman JD, Pfundt T and Redd JT (2022) Staffing and Capacity Planning for SARS-CoV-2 Monoclonal Antibody Infusion Facilities: A Performance Estimation Calculator Based on Discrete-Event Simulations. *Front. Public Health* 9:770039. doi: 10.3389/fpubh.2021.770039

**Background:** The COVID-19 pandemic has significantly stressed healthcare systems. The addition of monoclonal antibody (mAb) infusions, which prevent severe disease and reduce hospitalizations, to the repertoire of COVID-19 countermeasures offers the opportunity to reduce system stress but requires strategic planning and use of novel approaches. Our objective was to develop a web-based decision-support tool to help existing and future mAb infusion facilities make better and more informed staffing and capacity decisions.

**Materials and Methods:** Using real-world observations from three medical centers operating with federal field team support, we developed a discrete-event simulation model and performed simulation experiments to assess performance of mAb infusion sites under different conditions.

**Results:** 162,000 scenarios were evaluated by simulations. Our analyses revealed that it was more effective to add check-in staff than to add additional nurses for middle-to-large size sites with  $\geq 2$  infusion nurses; that scheduled appointments performed better than walk-ins when patient load was not high; and that reducing infusion time was particularly impactful when load on resources was only slightly above manageable levels.

**Discussion:** Physical capacity, check-in staff, and infusion time were as important as nurses for mAb sites. Health systems can effectively operate an infusion center under different conditions to provide mAb therapeutics even with relatively low investments in physical resources and staff.

**Conclusion:** Simulations of mAb infusion sites were used to create a capacity planning tool to optimize resource utility and allocation in constrained pandemic conditions, and more efficiently treat COVID-19 patients at existing and future mAb infusion sites.

**Keywords:** coronavirus disease 2019 (COVID-19), capacity-planning, staffing, discrete-event simulation, monoclonal antibody treatment, decision-support tool, disaster preparedness and response

## INTRODUCTION: BACKGROUND AND SIGNIFICANCE

Spreading rapidly, Coronavirus disease 2019 (COVID-19) became a global pandemic in early 2020 (1). Caused by severe acute respiratory syndrome coronavirus 2 (SARS-CoV-2), COVID-19 is a highly contagious disease that can result in mild to severe symptoms, hospitalization, need for intensive care or ventilator treatment, and mortality (2). By July 2021, SARS-CoV-2 had infected more than 33 million Americans, caused over 600,000 deaths in the United States (U.S.) (3), and killed more than 3,900,000 people worldwide (4).

In November 2020, the Food and Drug Administration issued emergency use authorizations for monoclonal antibody (mAb) monotherapy bamlanivimab and combination therapy casirivimab/imdevimab to treat COVID-19 among individuals at high risk for progressing to severe disease (5). These mAb treatments were shown to be effective for preventing progression of disease and COVID-19-associated hospitalizations (6, 7). Given that a significant number of individuals remain at risk for COVID-19 in the U.S. (8), mAb treatments will continue to be critical for saving lives and reducing COVID-19 morbidity and mortality (9, 10).

In the context of capacity and staffing shortages, mAb therapies are especially important to reduce burdens on the U.S. healthcare system. However, these treatments have administration challenges, including authorized use only in confirmed COVID-19 outpatients; the need to treat patients as early as possible; and the messaging required to introduce mAb products to providers and patients in an already-stressed system (11). Moreover, an outpatient mAb treatment requires the allocation of staff, physical space, equipment, and supplies, and involves several sequential treatment procedures necessitating synchronization. Thorough analysis and careful planning are needed to decrease barriers to implementation and ensure efficient service.

As of October 14, 2021, there are thousands of healthcare facilities in the U.S. that periodically receive and offer mAb treatments (12). In those healthcare facilities, mAb administrations occur across a wide variety of settings including hospitals, hospital-based infusion sites, emergency departments, urgent care clinics, and stand-alone infusion centers (13). These infusion sites have diverse physical capacity and staffing limitations, requirements, and service features, including differences in the patterns and volumes of daily patient demand, appointment scheduling regimes, service hours, service and performance targets, and state and local regulations. Accordingly, critical planning and resource allocation decisions for these mAb infusion sites must be made locally to ensure the best service quality and optimal performance. Developed upon the request of (and now administered by) the U.S. Assistant Secretary for Preparedness and Response (ASPR), the decision-support tool that we present in this paper serves this exact purpose by helping infusion sites tailor their capacity and staffing decisions, and has highly valuable utility in the face of a surge of COVID-19 cases and increased demand

for mAb treatments fueled by the highly contagious Delta variant (14, 15).

The objective of this study was to create a capacity and staffing planning tool to support the implementation of mAb drug products at U.S. healthcare facilities. Taking a simulation approach, we developed a web-based calculator to investigate the operational performance of mAb infusion sites as a function of staffing, capacity, and other key factors. The decision-support tool can be used to identify bottlenecks in the mAb infusion process, and help decision-makers make informed resource allocation decisions for mAb treatment service.

## MATERIALS AND METHODS

Discrete-event simulation (DES) experiments were conducted for 162,000 alternative scenarios considering different staffing and capacity levels, scheduling protocols, patient demand, facility service hours, and infusion durations. To inform the model structure and collect data for simulation experiments, the mAb treatment process was observed at three U.S. medical centers implementing mAb infusions in collaboration with Disaster Medical Assistance Teams deployed by the US Department of Health and Human Services under the direction of the Assistant Secretary for Preparedness and Response's National Disaster Medical System. To make simulation results accessible, a web-based decision-support tool was developed, which displays estimated performance outputs for the scenarios associated with user-selected inputs. These inputs are described in Web-based decision-support tool: mAb infusion process calculator. The DES model and simulation experiments were programmed using Matlab version R2020a.

### Patient Arrival Process

Infusion facilities either had walk-in encounters, where patients were admitted to check-in area on a first-come-first-served basis, or utilized scheduled appointments of three different types: (i) block, (ii) spread-out, and (iii) mixed (**Table 1**). A block schedule uses only a few scheduling points (e.g., 9 AM, 1 PM, 4 PM) and books a batch of patients for each time block. Spread-out scheduling uses numerous scheduling points and books a small number of patients for the same time point to more evenly distribute patient load on resources. Lastly, mixed scheduling strikes a balance between block and spread-out scheduling by being more dispersed than block and more condensed than spread-out scheduling. Delays and early arrivals were accounted for via a delay function that adjusts patient arrival times by adding (or subtracting) some random amount of time to (from) appointment times.

### Monoclonal Antibody Treatment Process

The mAb treatment process in the decision-support tool starts with pre-infusion check-in (**Figure 1**). There are no capacity restrictions in the check-in area, as arriving patients are directed to wait outside when this area is fully occupied. Each check-in area staff serves a single patient at a time and performs clerical and clinical duties such as obtaining patient information and signatures for consent forms, verifying patient identification and

**TABLE 1 |** Different appointment types considered in our analysis.

| Appointment type            | Brief description  | An example with 15 patients                      |
|-----------------------------|--|--|
| Walk-in only                | Unscheduled appointments with random arrivals  | 1 111 11 11 11 1 1 11<br>▲▲▲▲▲▲▲▲▲▲▲▲▲▲▲         |
| Scheduled only - Block      | Schedules with few appointment blocks, where a large group of patients are scheduled for each block  | 5 5 5<br>▲▲▲▲▲▲▲▲▲▲▲▲▲▲▲                         |
| Scheduled only - Spread-Out | Schedules with a large number of appointment times throughout the operating hours, where only a single or a few individual(s) are scheduled for each | 1 1 1 1 1 1 1 1 1 1 1 1 1 1 1<br>▲▲▲▲▲▲▲▲▲▲▲▲▲▲▲ |
| Scheduled only -Mixed       | Schedules with relatively few appointment blocks, where appointment times are dispersed within each block to balance patient load                    | 2 2 1 2 2 1 2 2 1<br>▲▲▲▲▲▲▲▲▲▲▲▲▲▲▲             |

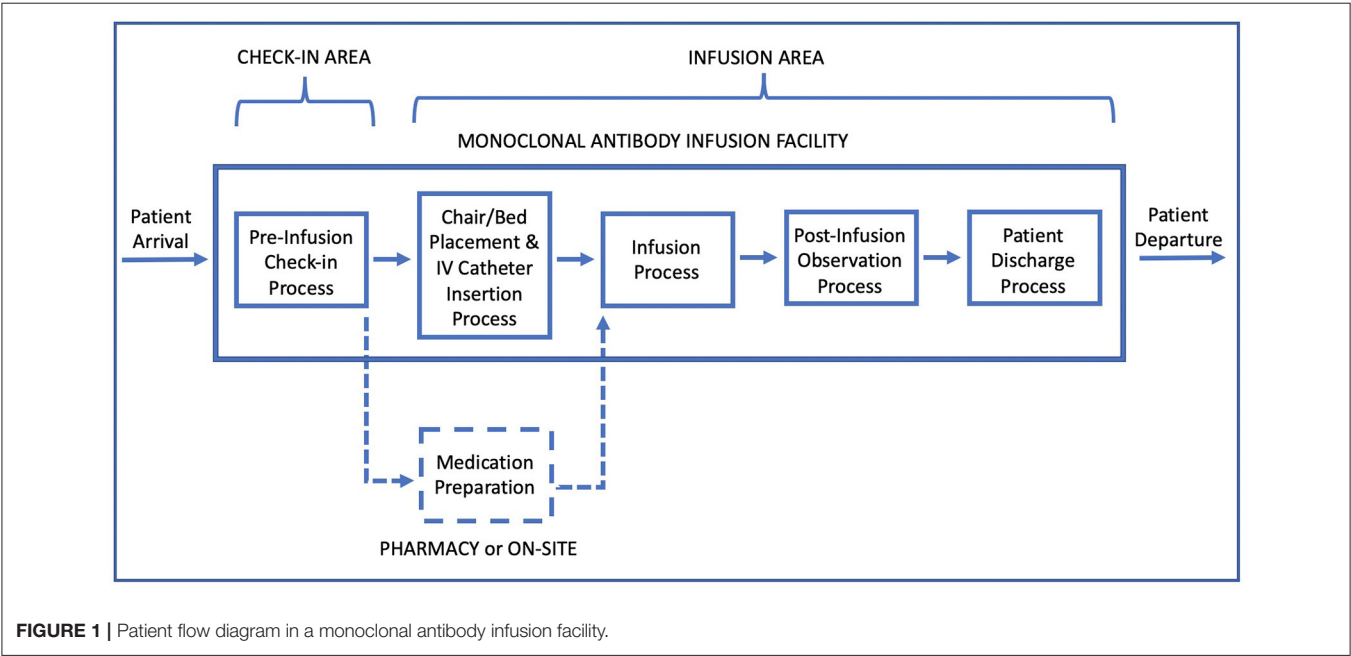


**FIGURE 1 |** Patient flow diagram in a monoclonal antibody infusion facility.

health insurance, providing information about the treatment, and checking vitals. At the end of this process, clinical staff in walk-in facilities inform the pharmacy to initiate medication preparation. This step is bypassed for scheduled appointments, as medications are assumed to be prepared in advance for scheduled visits.

Following the waiting time after check-in, patients enter the infusion area and are directed to a treatment chair/bed. Consisting of nurses and allied health professionals (e.g., paramedics), the medical team in the infusion area prepare patients for infusion by conducting a medical examination, and inserting a peripheral intravenous (IV) catheter for drug administration. “Chair/Bed placement and IV catheter insertion” is followed by the infusion process. Infusion therapy requires a fixed amount of time, depending on medication, and is delayed when there is no medication readily available or if the medical care team is busy attending other patients.

The infusion process is followed by an observation period, during which patients remain seated and are monitored. Post-infusion observation period takes an hour but might be prolonged by concerns about a patient’s health status. Following the observation, the IV is removed and each patient goes through a discharge process, waiting for the final paperwork and the discharge consent from the physician in charge. Subsequently, patients depart the mAb infusion facility.

Data Sources, Data Collection, and Simulation Parameters

The parameters and probability distributions used in simulation experiments reflect the data collected during observation of three U.S. medical centers implementing mAb infusions (Table 2). These parameters correspond to service durations and do not include preceding or succeeding waiting times. Data and



**TABLE 2 |** Probability distributions and parameters for mAb treatment sub-processes.

| Process                       | Probability distribution         | Parameters (minutes)   |
|-------------------------------|----------------------------------|--|
| Pre-infusion check-in         | Exponential                      | Mean = 20  |
| Chair placement & IV catheter | Exponential                      | Mean = 10  |
| Infusion                      | Deterministic                    | Duration = 20, 30, or 60                                     |
| Post-infusion observation     | Deterministic                    | Duration = 60  |
| Discharge                     | Normal                           | Mean = 5, Standard Deviation = 1                             |
| Medication preparation        | Uniform, NA – if scheduled appt. | Minimum = 15, Maximum = 30<br>NA – if scheduled appointments |

**TABLE 3 |** Model inputs for discrete event simulation model.

| Model variables  | Alternative input values  | Number of alternatives |
|--|---|------------------------|
| Physical capacity – number of treatment beds/chairs        | 3, 5, 6, 9, 10, 12, 15, 20, 30  | 9                      |
| Appointment type   | Walk-in, Scheduled – Block, Scheduled – Mixed, Scheduled – Spread-Out | 4                      |
| Operating hours  | 6, 8, 10, 12, 24  | 5                      |
| Daily patient demand                                       | 10, 15, 20, 25, 30  | 5                      |
| Infusion duration  | 20, 30, 60 minutes  | 3                      |
| Check-in area staffing levels                              | 1, 2, 3   | 3                      |
| Infusion area staffing levels (Nurse)                      | 1, 2, 3, 4  | 4                      |
| Infusion area staffing levels (Allied Health Professional) | 0, 1, 2, 3, 4   | 5                      |

descriptions for the generation of scheduled and walk-in arrivals and delays during the observation process are provided in the **Supplementary Material—Appendix A**.

## Discrete-Event Simulation (DES) Model

A simulation model was developed to analyze the COVID-19 mAb infusion therapy process and assess the performance of mAb infusion sites under various scenarios. The model inputs and outputs were identified based on our discussions with clinical experts and partner mAb sites. Model inputs were (i) treatment bed/chair capacity, (ii) type of appointments, (iii) service hours, (iv) daily patient demand, (v) infusion duration, and (vi) staffing levels at check-in and infusion areas (**Table 3**). Model outputs were (i) average patient length of stay (LoS) with 95% confidence intervals, (ii) number and percentage of patients treated during service hours, and (iii) percentages of patients treated within 3 and 4 h.

Inputs for staffing levels were concentrated on the number of nurses and allied health professionals. Other roles, such as physicians or pharmacists, are also critical for infusion facilities, but were not observed to directly limit the capacity and patient

flow. Based on on-site observations, a nurse was assumed to deliver concurrent care for up to five patients, whereas an allied health professional was assumed to simultaneously care for up to three patients. Model assumptions required at least one nurse to be present in infusion area. The type of clinical staff was assumed not to impact check-in tasks, where a single employee serves one patient at a time.

The simulated events for mAb infusion process were (i) patient arrivals, (ii) check-in service completion, (iii) service completion for chair/bed placement and IV catheter insertion, (iv) completion of infusion therapy, (v) end of post-infusion observation, (vi) patient departure following discharge process, and (vii) closure of the infusion clinic. Walk-in clinics required an additional event of medication preparation since they do not start preparing infusion medication before patient arrival and check-in. The model structure and status updates performed for these events are described in the **Supplementary Material—Appendix B**.

In this study, our goal was to focus on provision of efficient treatment. Variables that may affect provision of treatment include, but are not limited to, the effectiveness of treatments, human and physical resources of a treatment facility, patient load on an individual treatment site or the general healthcare delivery system, and the duration of sequential sub-processes that constitute the overall treatment process. Accordingly, we concentrated on capturing these factors in our discrete event simulation model, rather than the ones that are considered in epidemiology models for the spread of an infectious disease over time, as our focus was on the treatment process and our objective was to develop a decision-support tool to help mAb infusion sites with their staffing and capacity planning decisions.

## Model Verification and Validation

A verification analysis was conducted to confirm that the simulation model was consistent with the mAb therapy process and experiments were correctly implemented. Examining 162,000 simulated scenarios, we observed that patient LoS and other output metrics either improved or remained constant but never worsened when staffing or capacity levels were increased while other inputs were kept constant. Similarly, all output metrics improved, though not at the same magnitude, when infusion time was reduced from 60 to 30 min and from 30 to 20 min. Finally, all output measures in 40,500 walk-in scenarios worsened when medication preparation time range was increased from 15–30 to 30–60 min. These verification analyses confirmed logical outcomes and that the simulation experiments were performed correctly.

Since mAb infusion for COVID-19 is a novel therapy, there are insufficient data to perform a comprehensive validation analysis. However, the accuracy of the generated estimates was assessed using expert face validation. Several feedback and pilot sessions were conducted with partner mAb sites and experts were asked to validate estimates for performance metrics. Using the web-based decision-support tool, they evaluated multiple different scenarios, and affirmed that estimated outputs were in line with their observations and expectations.

## Web-Based Decision-Support Tool: mAb Infusion Process Calculator

Utilizing simulation results, a web-based calculator (Figure 2) was created to assist capacity planning and resource allocation decisions for mAb infusion sites. At the website, users provide inputs for the main variables of a mAb infusion process (Table 3) and the outputs of the corresponding scenario are displayed to the user. There are 162,000 scenarios that users can investigate. All simulation experiments were performed in advance and saved on the website to provide instant feedback to users.

In addition to simulation outputs, the web-based calculator also displays two plots for each selected scenario (Figure 3). The first plot depicts the impact of increasing or decreasing the number of infusion nurses on the total number of patients that can be served throughout a day. The second plot shows the effect of any two variables chosen by the user (e.g., number of infusion nurses and bed capacity) on the number of patients treated. Together, the graphs help users assess the value of changing staffing levels for a given scenario, examine how added resources lead to improvements or diminishing returns, and identify the bottlenecks of the simulated scenario. Further, these graphs could be used to determine the minimum number of resources required to meet desired targets in terms of daily patient throughput.

As a programming language, Matlab version R2020a was employed to develop and code the simulation model and perform the simulation experiments. Twenty virtual machines, belonging to the Johns Hopkins University Applied Physics Laboratory, were utilized to expedite simulation experiments and processing of 162,000 scenarios. To translate the simulation results into a web-based calculator, a single-page application (SPA), the current standard for creating modern web applications, was produced. The use of SPA enabled the online calculator to be compiled into a simple HTML/JavaScript bundle. This bundle contained the outputs of the 162,000 scenarios, embedded into a page or run by a basic web server without the need for additional computational capabilities. Overall, the core frameworks used to develop the web-based platform were *Vue.js*, *Vuetify*, *Plotly.js*, and *Bootstrap*. In particular, the JavaScript framework “Vue.js” was used jointly with “Vuetify” to construct user interfaces and SPA, the data visualization library “Plotly.js” was utilized to create two interactive graphs (Figure 3) for each scenario, and “Bootstrap” was employed to enforce a uniform appearance to the website in terms of color, size, font and layout.

## RESULTS

A total number of 162,000 different scenarios were evaluated by simulation experiments. Each infusion duration considered in the analysis (namely, 20-, 30-, and 60-min) corresponded to 54,000 different cases, where walk-in scenarios and different scheduling protocols each made up one fourth (i.e., 13,500) of these cases (Supplementary Material—Appendix C). All results can be accessed via the web-based calculator hosted at <https://www.phe.gov/emergency/mAbs-calculator/Pages/default.aspx>.

Based on 162,000 scenarios considered, various analyses can be performed to generate insights about different aspects of

the mAb infusion process. To demonstrate the utility of the web-based calculator and shed light onto important planning and research questions for mAb infusion sites, we focused on four main areas: (i) the impact of scheduling on performance metrics, (ii) the effect of infusion duration on patient LoS, (iii) the role of medication preparation duration for walk-in encounters, and (iv) when and where to add additional staff to improve overall performance.

## Impact of Scheduling on Performance Metrics

To assess the impact of scheduling, we compared 13,500 walk-in scenarios with 60-min infusion times to their 13,500 spread-out scheduling counterparts. Excluding 3,457 scenarios having <10 min gap in LoS difference, we analyzed 10,043 scenarios with a non-negligible difference (i.e.,  $\geq 10$  min gap) between LoS durations when spread-out scheduling was compared to walk-ins. Among these 10,043 scenarios, where the LoS difference were non-negligible, scheduled appointments had shorter LoS averages in 7,286 (72.5%) scenarios, and walk-in clinics achieved lower patient LoS in 2,757 (27.5%) cases.

Our analysis revealed that *traffic intensity*, a measure of the average occupancy of a service area, could play a key role in identifying when scheduling is the most and least beneficial. Traffic intensity estimates the average patient load on each resource (treatment bed or staff member) per hour by multiplying mean service duration (e.g., check-in time) with the average number of arrivals to the work station of interest per hour divided by the maximum resource capacity (beds or staff) available there. We observed that when the traffic intensity level was low to medium in infusion and check-in areas, indicating that the patient load on the mAb infusion site was manageable, scheduling yielded better outcomes and was an effective means for providing timely mAb treatments. In particular, there were 7,916 scenarios when the traffic intensity of the check-in process was <2.94 (i.e., medium), and scheduling resulted in lower LoS in 7,247 (91.5%) of these cases. Similarly, LoS averages were shorter with scheduling in 7,068 (90.2%) out of 7,839 scenarios when the traffic intensity in the infusion area was below 0.35 (i.e., low). However, scheduling had a limited impact on reducing LoS when the traffic intensity was high in either service area (Table 4). Compared to walk-in clinics, implementation of scheduled appointments achieved no improvement on LoS durations when traffic intensity was  $\geq 3.86$  in the check-in and  $\geq 0.43$  in the infusion area.

## Effect of Infusion Time on Patient Length of Stay

Infusion times ranged from approximately 20–60 min. To investigate the effect of infusion time on patient LoS, we compared the average LoS outputs of 54,000 scenarios that had 30-min infusion time to their 108,000 counterparts with 20- and 60-min-long infusions. The distributions of LoS difference

U.S. Department of Health & Human Services  
Office of the Assistant Secretary for Preparedness and Response

Preparedness Emergency About ASPR

**Public Health Emergency**  
Public Health and Medical Emergency Support for a Nation Prepared

PHE Home > Preparedness Search...

## Monoclonal Antibody Infusion Calculator

**Physical Capacity**  
How many infusion beds or bays will be operational? 12

**Patient Arrival Process**  
Will infusion encounters be scheduled or walk-in? Scheduled-Sp  
On a typical day, how many hours will the infusion center be open? 10  
On a typical day, what is the expected patient demand? 20

**Check-in Process**  
How many staff will support the check-in process (including checking vital signs and confirming patient eligibility for infusion)? 1

**Infusion Area**  
What is the infusion time in minutes? 30  
How many nursing professionals will support the infusion process? 1  
How many other non-nurse clinical staff (e.g., paramedics) will support the infusion process? 1

**Outputs Table**

| Metric  | Value   |
|---|---|
| Number of patients seen during infusion center hours:   | 19.0  |
| Average patient time (hours) for an infusion session to be completed (check-in to departure): | Avg. Time 2 hr 39 min 95% CI ( 2 hr 35 min, 2 hr 44 min ) |
| Percent of infusions completed within 3 hours:  | 72.7%   |
| Percent of infusions completed within 4 hours:  | 94.1%   |

**FIGURE 2 |** User Interface of the web-based mAb infusion process calculator (<https://www.phe.gov/Preparedness/Pages/mabcalctool.aspx>).

when 30-min infusions compared to other two alternatives are presented in **Figure 4**.

The differences in LoS averages centered around the amount of change in infusion times, which was a 10-min decrease and a 30-min increase for 20- and 60-min infusions, respectively (**Figure 4**). Yet, noticeably higher/lower changes in patient LoS were observed for a fair number of comparisons. In particular, 4,000 (7.4%) scenarios achieved > 45 min reduction in LoS when infusions took 30 min instead of 60 min. Similarly, 4,530 (8.4%) scenarios had >15 min difference in LoS when 20-min infusions were compared to 30 min infusions.

For the comparisons having significantly higher/lower change in LoS, queueing theory concepts “traffic intensity,” measuring the average occupancy of a service system, and “stability,” indicating whether its traffic intensity is at manageable levels or not, were helpful to explain this phenomenon (16, 17). The improvements observed in LoS were noticeably higher when reducing infusion duration led an unstable infusion site to experience manageable traffic intensity and become stable. This was because, by achieving stability, the whole service system functioned more efficiently, waiting times between consecutive

services were reduced, and as a result, total reductions in LoS were higher than the change in infusion time. Similarly, the performance of a stable infusion site significantly worsened following an increase in infusion time when this change caused its traffic intensity to rise above manageable levels.

### Role of Medication Preparation Duration for Walk-In mAb Clinics

At walk-in clinics, the preparation of mAb solution was performed after patient check-in rather than beforehand. In general, this might cause delays in infusion therapy. To quantify the effect of medication preparation on patient LoS, we conducted additional experiments, where medications were prepared within 30–60 min, and compared them to the baseline scenarios of 15–30-min-long medication preparation time. The difference between LoS averages mostly accumulated near 22.5 min, which was the average difference between 15–30 (mean time 22.5) and 30–60 (mean time 45.0) min preparation times (**Figure 5**). Changing the duration made less impact on LoS when physical capacity was low (i.e., number of beds  $\leq 6$ ) or patient load was high (i.e.,  $\geq 15$  patients in  $\leq 12$  service hours). For those

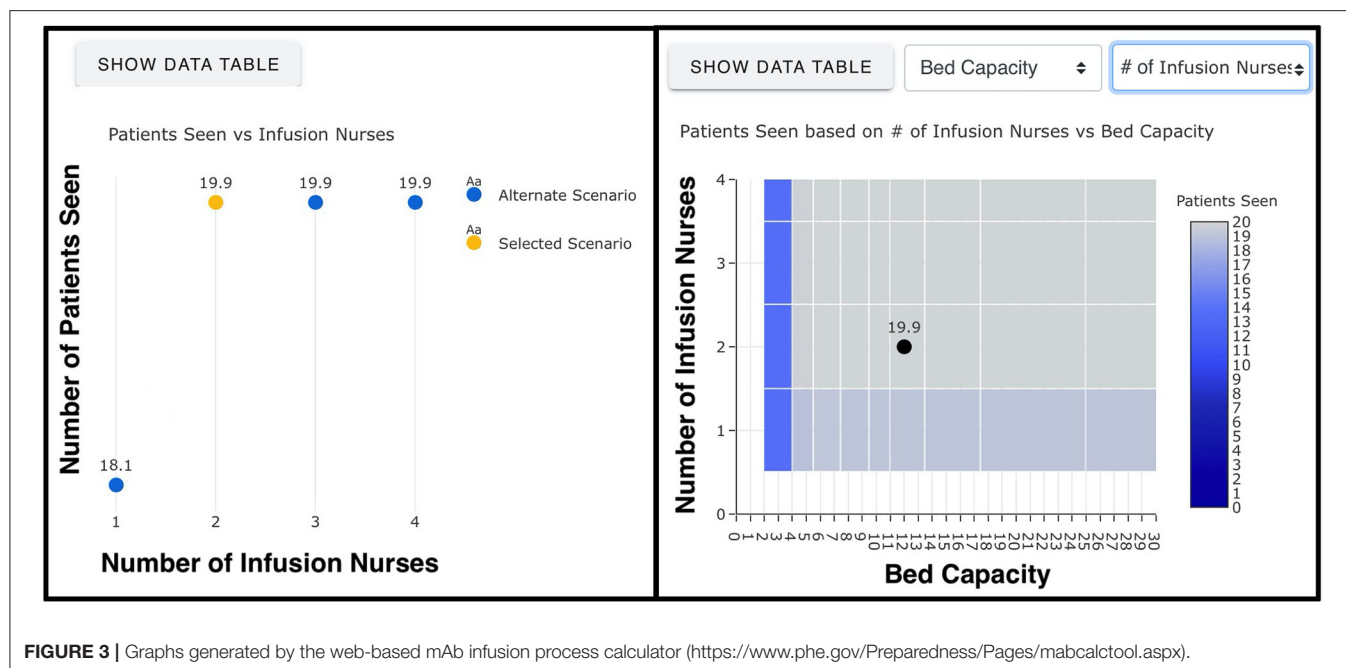


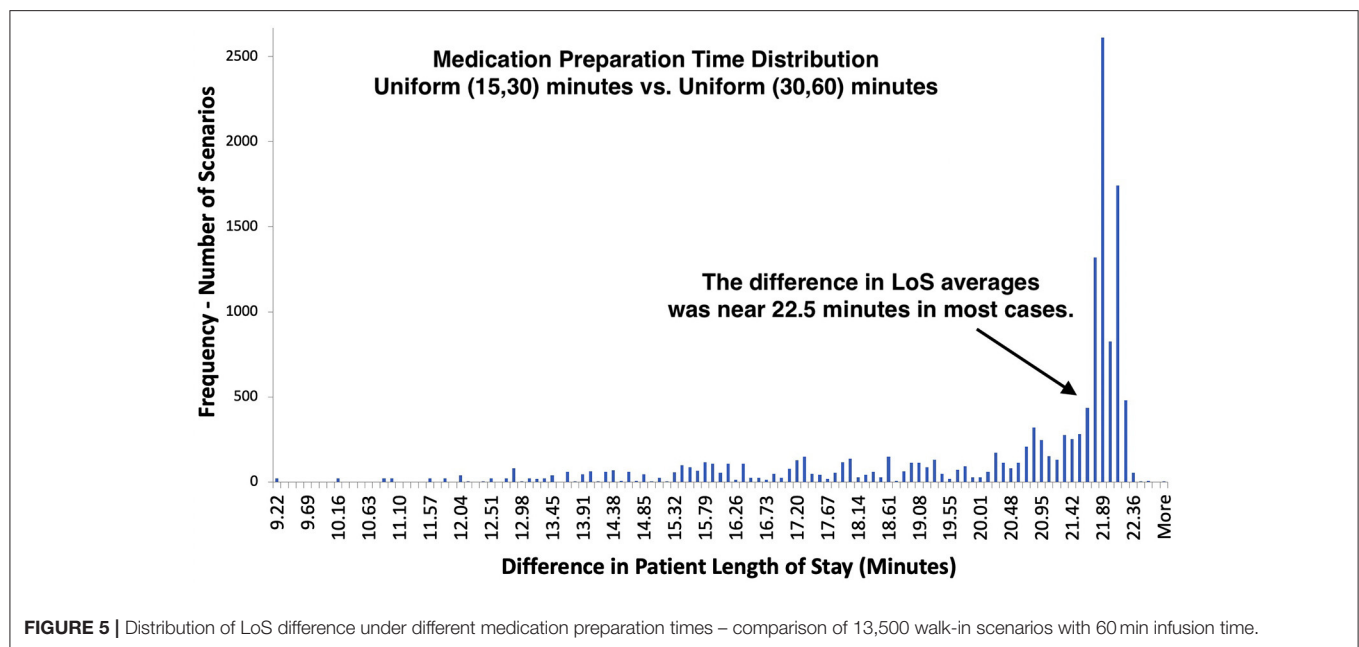
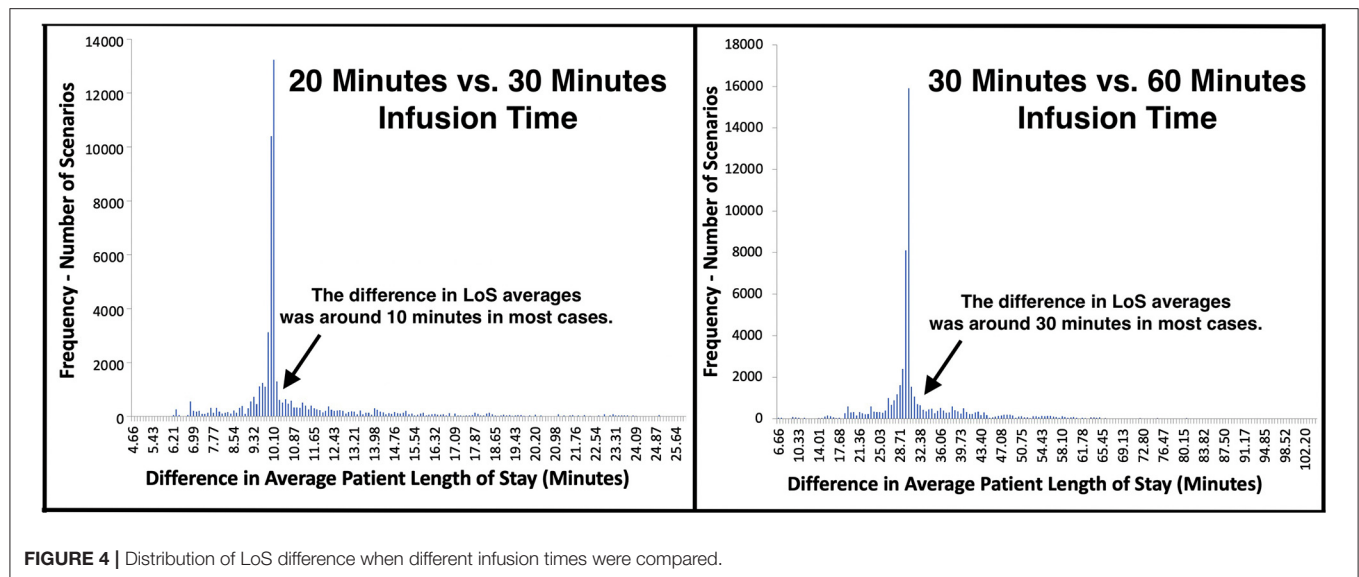
**FIGURE 3 |** Graphs generated by the web-based mAb infusion process calculator (<https://www.phe.gov/Preparedness/Pages/mabcalctool.aspx>).

**TABLE 4 |** Number of scenarios with shorter LoS under walk-ins and spread-out schedules.

| Location: check-in area       |              |         | Number of scenarios with shorter patient LoS |            | Location: Infusion area       |              |         | Number of scenarios with shorter patient LoS |            |
|-------------------------------|--------------|---------|--|------------|-------------------------------|--------------|---------|--|------------|
| Metric = TI                   | Cut-off (CO) | TI < CO | Walk-in                                      | Spread-out | Metric = TI                   | Cut-off (CO) | TI < CO | Walk-in                                      | Spread-out |
| <b>Check-in area</b>          | 0.64         | 1080    | 0  | 1080       | <b>Infusion area</b>          | 0.10         | 2491    | 3  | 2488       |
| <b>traffic intensity (TI)</b> | 0.87         | 2160    | 0  | 2160       | <b>traffic intensity (TI)</b> | 0.18         | 5218    | 109  | 5109       |
|                               | 1.10         | 3220    | 0  | 3220       |                               | 0.26         | 6888    | 354  | 6534       |
|                               | 1.33         | 4624    | 20   | 4604       |                               | 0.35         | 7839    | 771  | 7068       |
|                               | 1.56         | 5156    | 80   | 5076       |                               | 0.43         | 8490    | 1204   | 7286       |
|                               | 1.79         | 5886    | 246  | 5640       |                               | 0.51         | 8903    | 1617   | 7286       |
|                               | 2.02         | 6500    | 367  | 6133       |                               | 0.59         | 9149    | 1863   | 7286       |
|                               | 2.25         | 6834    | 435  | 6399       |                               | 0.68         | 9565    | 2279   | 7286       |
|                               | 2.48         | 6834    | 435  | 6399       |                               | 0.76         | 9739    | 2453   | 7286       |
|                               | 2.71         | 7916    | 907  | 7009       |                               | 0.84         | 9918    | 2632   | 7286       |
|                               | 2.94         | 7916    | 907  | 7009       |                               | 0.93         | 9918    | 2632   | 7286       |
|                               | 3.17         | 8602    | 1355   | 7247       |                               | 1.01         | 9983    | 2697   | 7286       |
|                               | 3.40         | 8996    | 1749   | 7247       |                               | 1.09         | 10023   | 2737   | 7286       |
|                               | 3.63         | 8996    | 1749   | 7247       |                               | 1.18         | 10043   | 2757   | 7286       |
|                               | 3.86         | 9282    | 1996   | 7286       |                               | 1.26         | 10043   | 2757   | 7286       |
|                               | 4.09         | 9282    | 1996   | 7286       |                               | 1.34         | 10043   | 2757   | 7286       |
|                               | 4.32         | 9717    | 2431   | 7286       |                               | 1.42         | 10043   | 2757   | 7286       |
|                               | 4.55         | 9717    | 2431   | 7286       |                               | 1.51         | 10043   | 2757   | 7286       |
|                               | 4.78         | 9717    | 2431   | 7286       |                               | 1.59         | 10043   | 2757   | 7286       |
|                               | 5.00         | 10043   | 2757   | 7286       |                               | 1.67         | 10043   | 2757   | 7286       |

CO, Cut-off value for traffic intensity levels; Traffic Intensity (TI), Average patient load over a single unit of limiting resource (staff or bed) per hour.





infusion sites, increasing bed capacity or staffing could be more beneficial than preparing infusion medications faster.

### Staff Adjustments to Improve Overall Performance of a mAb Infusion Site

Simulated scenarios with 60-min infusion times ( $n = 54,000$ ) were examined separately for each scheduling type ( $n = 13,500$ ) to assess the impact of adding staff members under different roles (Figure 6). To simplify the analysis, the scenarios, where infusion teams consisted of only nurses ( $n = 2,700$ ), were considered. The cases for which the limiting factor was physical capacity rather than staffing were excluded. Consequently, a total of 650 scenarios were identified, for

which staffing levels in check-in and infusion areas could both be increased. For these 650 scenarios, a staff was exclusively added to only one area and then, LoS averages were compared.

In 344 scenarios, the reduction in LoS achieved by adding a staff to an area were  $>5$  min shorter than the other alternative (Figure 6). In 212 (62%) scenarios, adding an infusion nurse resulted in a larger decrease to LoS (mean 34 min). In the remaining 132 (38%) scenarios, where adding a check-in staff member was more beneficial (mean 24 min), physical capacity was  $\geq 12$  beds, the number of infusion area nurses was  $\geq 2$ , and check-in staff were always originally fewer. These similarities in 132 scenarios suggest that, for medium-to-large size infusion sites having more than 10 or 11 beds, providing support to check-in

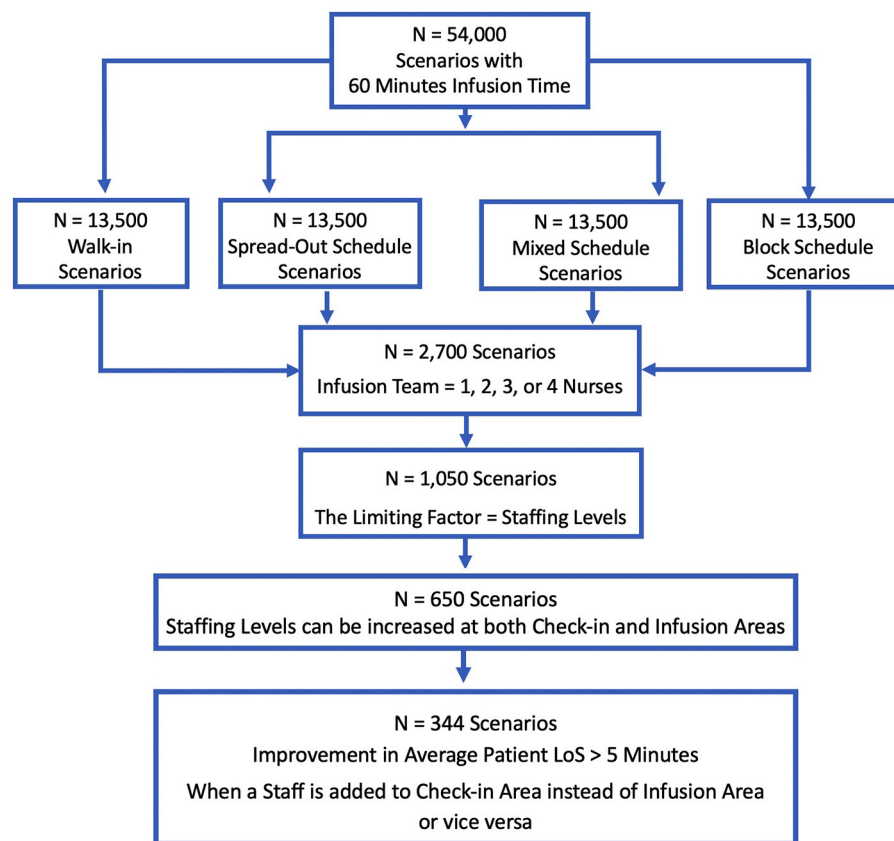


**FIGURE 6** | CONSORT diagram - the number of scenarios included in staff adjustment analysis.

area might be more beneficial when there is a single check-in staff member and more than one infusion nurse.

## DISCUSSION

Based on data collected from three U.S. COVID-19 mAb infusion centers, we conducted simulations allocating personnel and other resources in mAb infusion sites and translated the results into a web-based decision-support tool. The simulation experiment results and our analyses led to several important findings. In particular, despite nursing staff shortages often being perceived as the main barrier, this study identified that other factors were equally important for the overall performance of a mAb site. Frequently, patient LoS was extended due to other factors such as physical capacity, staffing levels at check-in, or the duration of infusion process, even with low nursing levels. These findings suggest that decisions should be made carefully for all key components of a mAb infusion process to provide timely service and improve staffing and capacity efficiency.

Regarding the value of appointment scheduling, it is common to assume scheduling would yield better performance as it allows planning and preparation for upcoming patients beforehand. Yet, this analysis revealed that scheduling appointments was not

necessarily beneficial when daily patient volumes were above a level that a mAb site can effectively manage. In those situations, patient load on resources should be reduced by either extending business hours or increasing the levels of the limiting resource.

Achieving a reduction in the duration of a critical service, such as infusion or medication preparation time, did not always lead to significant improvements. In particular, when an infusion site continued to experience high traffic intensity resulting from high patient volumes, short business hours, or low capacity and staffing levels, improvements in patient LoS were minimal. However, when traffic intensity was only slightly above manageable levels, shortening the duration of a medical service (e.g., infusion time) achieved stability and made a significant impact for the operational performance of mAb sites. These results suggest that the infusion sites experiencing patient traffic that is only marginally higher than their physical and staff capacity could benefit the most from shortened service durations, which, for instance, can be achieved by using subcutaneous route for mAb administration instead of IV route.

The demand and need for mAb infusions will vary across communities and over time. Overall, the results from this study suggest that health systems in the U.S. can effectively provide mAb treatments under different settings even with relatively

low investments for physical resources and staff. This is not to say that the launch of a mAb site is without barriers, but that this service can be made available to a community and reduce hospitalizations and COVID-19 deaths without a heavy burden on resources. The key, here, is to correctly identify the bottlenecks of the mAb infusion process in the corresponding setting and make the right adjustments to efficiently use limited resources. By analyzing mAb infusions under different conditions and resource allocations, this study can offer guidance for the optimal planning and implementation of mAb infusion sites, which can have a considerable impact in regional COVID-19 response efforts.

This study was not free of limitations. First, the process model aligned with field observations for several sites and was validated by focus groups with those same sites. Hospitals may choose to implement mAb infusions in a different setting. Second, simulations relied on several assumptions for service times, nurse-to-patient ratio in infusion area, and arrival patterns under different scheduling protocols. Differences in these assumptions could impact simulation results. Third, despite considering the majority of the practical scenarios, the web-based decision-support tool is not exhaustive of all possible cases. Accordingly, users will not always be able to select the exact model input values corresponding to the scenario(s) they desire to investigate. Fourth, the data collected from three U.S. COVID-19 mAb infusion centers for our study might not exactly match particular mAb sites especially if patient demographics or geographical conditions are significantly different. Finally, in addition to IV infusions, mAb treatments have also been approved as subcutaneous injections, which were not the focus of our study.

## CONCLUSION

During his speech addressing the nation on September 9, 2021, President Biden emphasized the importance of mAb treatments for saving lives and reducing the strain on the U.S. healthcare system by preventing severe disease and reducing hospitalizations and reiterated his administration's commitment to making mAb treatments available (18). Following the president's speech, the U.S. government agreed to purchase 1.4 million doses of additional mAb medications casirivimab and imdevimab, as declared by President Biden (18) and announced by Regeneron Pharmaceuticals (19). Concurrently, the Department of Health and Human Services' (HHS) Assistant Secretary for Preparedness and Response (ASPR) took over the distribution of COVID-19 mAb therapies over the country to ensure the availability of this critical COVID-19 treatment across all states and territories (20). Since undertaking the distribution of mAb therapies, ASPR has been in coordination with thousands of individual healthcare facilities and regional leaders to allocate mAb supplies to 4,280 separate healthcare sites throughout the nation (<https://protect-public.hhs.gov/pages/therapeutics-distribution>), as of October 14 2021, on a weekly basis (12). In parallel with these efforts, the federal government has also initiated to deploy "mAb strike teams"

through HHS, Federal Emergency Management Agency, and Department of Defense to support the staffing needs of mAb infusion sites and increase the public access to COVID-19 mAb therapeutics, as declared in Biden Administration's COVID-19 action plan (21). Overall, the active engagement of the federal government and agencies in leading all of these recent efforts and establishing cooperation with local governments and individual healthcare facilities, has been very critical to leverage the maximum use of COVID-19 mAb therapies. These efforts secured the continued availability of mAb injections for the Americans infected with COVID-19, played a fundamental role for achieving an organized and effective implementation of mAb treatments throughout the country, and prevented further burdening of the U.S. healthcare system during its fight against a pandemic. By developing an online decision-support tool for COVID-19 mAb treatment process, we seek to complement these efforts and facilitate complex resource allocation and planning decisions that are needed to be made for each mAb infusion site.

This effort used a simulation approach to create a capacity and staffing planning tool to support adoption and spread of mAb therapy for COVID-19. The objective was to better understand staffing, physical resources, and other requirements for providing timely mAb infusion services with efficient resource use. Considering different staffing and capacity levels, scheduling protocols, patient demand, service hours, and infusion durations, 162,000 scenarios were evaluated via simulation experiments. A web-based decision-support tool was created to allow decision-makers, researchers, and other users to easily access the results, investigate operational performance of mAb infusion sites under different conditions, and generate managerial insights for existing and future infusion sites. Given that mAb treatments are expected to continue being an important instrument for the management of COVID-19, the web-based calculator introduced in this study could significantly contribute to pandemic control, planning, and preparation efforts.

## DATA AVAILABILITY STATEMENT

Data were collected from three monoclonal infusion sites, operating with federal field team support from the U.S. Department of Health and Human Services' Office of the Assistant Secretary for preparedness and response. Requests to access the datasets should be directed to Dr. Çağlar Çaglayan via his email [Caglar.Caglayan@jhuapl.edu](mailto:Caglar.Caglayan@jhuapl.edu).

## AUTHOR CONTRIBUTIONS

ÇÇ and AL designed the conceptual model. ÇÇ performed data and statistical analysis, developed the simulation model, conducted simulation experiments, and wrote the first draft of the manuscript. MS designed and programmed the user interface for the online calculator. ÇÇ and DR performed verification and validation analysis. KR-L performed major edits on the manuscript. JT managed the overall project. TP and JR served

as subject-matter experts. JR supervised the project and provided mentorship. All authors contributed to conception and design of the study, contributed to manuscript revision, read, and approved the submitted version.

## FUNDING

This study was supported by the U.S. Department of Health and Human Services' Office of the Assistant Secretary for Preparedness and Response. Virtual machines belonging to the Johns Hopkins University Applied Physics Laboratory were utilized to perform the simulation experiments. The findings and conclusions in this paper are those of the authors and

do not represent the official position of any government or private organization.

## ACKNOWLEDGMENTS

We thank our partner mAb infusion sites for their valuable inputs in various stages of this study.

## SUPPLEMENTARY MATERIAL

The Supplementary Material for this article can be found online at: <https://www.frontiersin.org/articles/10.3389/fpubh.2021.770039/full#supplementary-material>

## REFERENCES

- World Health Organization (2021). Available online at: <https://www.who.int/director-general/speeches/detail/who-director-general-s-opening-remarks-at-the-media-briefing-on-covid-19--11-march-2020> (accessed June 28, 2021).
- Ou M, Zhu J, Ji P, Li H, Zhong Z, Li B, et al. Risk factors of severe cases with COVID-19: a meta-analysis. *Epidemiol Infect.* (2020) 148:e175. doi: 10.1017/S095026882000179X
- Centers for Disease Control and Prevention. *Covid Data Tracker Weekly Review.* (2021). Available online at: <https://www.cdc.gov/coronavirus/2019-ncov/covid-data/covidview/index.html> (accessed June 28, 2021).
- The New York Times. *Coronavirus World Map: Tracking the Global Outbreak.* (2021). Available online at: <https://www.nytimes.com/interactive/2021/world/covid-cases.html> (accessed June 28, 2021).
- Food and Drug Administration (2020). Available online at: <https://www.fda.gov/emergency-preparedness-and-response/mcm-legal-regulatory-and-policy-framework/emergency-use-authorization#coviddrugs> (accessed June 28, 2021).
- Bariola JR, McCreary EK, Wadas RJ, Kip KE, Marroquin OC, Minnier T, et al. Impact of bamlanivimab monoclonal antibody treatment on hospitalization and mortality among nonhospitalized adults with SARS-CoV-2 infection. *Open Forum Infect Dis.* (2021) 8. doi: 10.1093/ofid/ofab254
- Jahanshahlu L, Rezaei N. Monoclonal antibody as a potential anti-COVID-19. *Biomed Pharmacother.* (2020) 129:110337. doi: 10.1016/j.biopha.2020.110337
- Charumilind S, Craven M, Lamb J, Sabow A, Wilson M. *When Will the COVID-19 Pandemic End?* (2021). Available online at: <https://www.mckinsey.com/industries/healthcare-systems-and-services/our-insights/when-will-the-covid-19-pandemic-end> (accessed June 28, 2021).
- Cascella M, Rajnik M, Aleem A, Dulebohn S, Di Napoli R. *Features, Evaluation, and Treatment of Coronavirus (COVID-19).* StatPearls (2021).
- Weinreich DM, Sivapalasingam S, Norton T, Ali S, Gao H, Bhore R, et al. REGN-COV2, a neutralizing antibody cocktail, in outpatients with Covid-19. *New Engl J Med.* (2021) 384:238–51. doi: 10.1056/NEJMoa2035002
- Lambrou AS, Redd JT, Stewart MA, Rainwater-Lovett K, Thornhill JK, Hayes L, et al. Implementation of SARS-CoV-2 monoclonal antibody infusion sites at three medical centers in the United States: Strengths and challenges assessment to inform COVID-19 pandemic and future public health emergency use. *medRxiv.* (2021). Available online at: <https://www.medrxiv.org/content/10.1101/2021.04.05.21254707v1.full.pdf>
- U.S. Department of Health & Human Services, HHS Protect Public Data Hub - Therapeutic Distribution Location (2021). Available online at: <https://www.arcgis.com/home/item.html?id=c0371324e1a44ad0aa77b6d301a7e262#data> (accessed October 15, 2021).
- U.S. Department of Health & Human Services, Federal Response to COVID-19: Monoclonal Antibody Clinical Implementation Guide (2021). Available online at: <https://www.phe.gov/emergency/events/COVID19/investigation-MCM/Documents/USG-COVID19-Tx-Playbook.pdf> (accessed October 15, 2021).
- Kennedy, Kelli and Perrone, Matthew. *Demand for COVID Antibody Drugs Soars in Hard-Hit States, the Associated Press.* (2021). Available online at: <https://apnews.com/article/health-coronavirus-pandemic-ad87808ad28f29c6cb5f1b98e478c6db> (accessed October 15, 2021).
- Schreiber, Melody, Demand soars for monoclonal antibody treatments in states with low vaccination rates, *The Guardian* (2021). Available online at: <https://www.theguardian.com/us-news/2021/sep/21/monoclonal-antibodies-covid-treatment-vaccines> (accessed October 15, 2021).
- Bramson M. *Stability of Queueing Networks.* Berlin: Springer (2008).
- Alexopoulos C, Goldsman D (2017). Available online at: [https://www2.isye.gatech.edu/~sman/courses/6644/Module05Q-QueueingSlides\\_171025.pdf](https://www2.isye.gatech.edu/~sman/courses/6644/Module05Q-QueueingSlides_171025.pdf) (accessed June 28, 2021).
- The White House, Briefing Room. *Speeches and Remarks, Remarks by President Biden on Fighting the COVID-19 Pandemic.* (2021). Available online at: <https://www.whitehouse.gov/briefing-room/speeches-remarks/2021/09/09/remarks-by-president-biden-on-fighting-the-covid-19-pandemic-3/> <https://www.whitehouse.gov/briefing-room/speeches-remarks/2021/09/09/remarks-by-president-biden-on-fighting-the-covid-19-pandemic-3/> (accessed October 15, 2021).
- Regeneron Pharmaceuticals, Inc., News Release – Press Releases. *Regeneron Announces New U.S. Government Agreement to Purchase Additional Doses of Regeneron's Regeneron-COV™ (Casirivimab And Imdevimab) Antibody Cocktail.* (2021). Available online at: [https://investor.regeneron.com/news-releases/news-release-details/regeneron-announces-new-us-government-agreement-purchase#:\\$sim\\$.text=Under%20the%20new%20agreement%2C%20Regeneron,July%202020%20and%20January%202021%20](https://investor.regeneron.com/news-releases/news-release-details/regeneron-announces-new-us-government-agreement-purchase#:$sim$.text=Under%20the%20new%20agreement%2C%20Regeneron,July%202020%20and%20January%202021%20) (accessed October 15, 2021).
- U.S. Department of Health and Human Services (HHS) Office of Assistant Secretary for Preparedness and Response (ASPR). *HHS Announces State/territory-coordinated Distribution System for Monoclonal Antibody Therapeutics.* (2021). Available online at: <https://www.phe.gov/emergency/events/COVID19/investigation-MCM/Bamlanivimab-etesevimab/Pages/Update-13Sept21.aspx> (accessed October 15, 2021).
- The White House. *Path Out of The Pandemic - President Biden's Covid-19 Action Plan.* (2021). Available online at:



<https://www.whitehouse.gov/covidplan/> (accessed October 15, 2021).

**Conflict of Interest:** The authors declare that the research was conducted in the absence of any commercial or financial relationships that could be construed as a potential conflict of interest.

**Publisher's Note:** All claims expressed in this article are solely those of the authors and do not necessarily represent those of their affiliated organizations, or those of the publisher, the editors and the reviewers. Any product that may be evaluated in

this article, or claim that may be made by its manufacturer, is not guaranteed or endorsed by the publisher.

*Copyright © 2022 Çaglayan, Thornhill, Stewart, Lambrou, Richardson, Rainwater-Lovett, Freeman, Pfundt and Redd. This is an open-access article distributed under the terms of the Creative Commons Attribution License (CC BY). The use, distribution or reproduction in other forums is permitted, provided the original author(s) and the copyright owner(s) are credited and that the original publication in this journal is cited, in accordance with accepted academic practice. No use, distribution or reproduction is permitted which does not comply with these terms.*



# Understanding the Geography of COVID-19 Case Fatality Rates in China: A Spatial Autoregressive Probit-Log Linear Hurdle Analysis

Hanchen Yu<sup>1</sup>, Xin Lao<sup>2\*</sup>, Hengyu Gu<sup>3</sup>, Zhihao Zhao<sup>2</sup> and Honghao He<sup>4</sup>

<sup>1</sup> Center for Geographic Analysis, Harvard University, Cambridge, MA, United States, <sup>2</sup> School of Economics and Management, China University of Geosciences, Beijing, China, <sup>3</sup> Department of Geography and Resource Management, The Chinese University of Hong Kong, Hong Kong, China, <sup>4</sup> School of Software and Microelectronics, Peking University, Beijing, China

## OPEN ACCESS

### Edited by:

Reza Lashgari,  
Shahid Beheshti University, Iran

### Reviewed by:

Rajvi Jayant Wani,  
Amgen, Canada  
John Thomas Manning,  
Swansea University, United Kingdom

### \*Correspondence:

Xin Lao  
laoxin2017@cugb.edu.cn

### Specialty section:

This article was submitted to  
Infectious Diseases - Surveillance,  
Prevention and Treatment,  
a section of the journal  
Frontiers in Public Health

**Received:** 02 August 2021

**Accepted:** 10 January 2022

**Published:** 15 February 2022

### Citation:

Yu H, Lao X, Gu H, Zhao Z and He H  
(2022) Understanding the Geography  
of COVID-19 Case Fatality Rates in  
China: A Spatial Autoregressive  
Probit-Log Linear Hurdle Analysis.  
*Front. Public Health* 10:751768.  
doi: 10.3389/fpubh.2022.751768

This study employs a spatial autoregressive probit-log linear (SAP-Log) hurdle model to investigate the influencing factors on the probability of death and case fatality rate (CFR) of coronavirus disease 2019 (COVID-19) at the city level in China. The results demonstrate that the probability of death from COVID-19 and the CFR level are 2 different processes with different determinants. The number of confirmed cases and the number of doctors are closely associated with the death probability and CFR, and there exist differences in the CFR and its determinants between cities within Hubei Province and outside Hubei Province. The spatial probit model also presents positive spatial autocorrelation in death probabilities. It is worth noting that the medical resource sharing among cities and enjoyment of free medical treatment services of citizens makes China different from other countries. This study contributes to the growing literature on determinants of CFR with COVID-19 and has significant practical implications.

**Keywords:** COVID-19, case fatality rate, spatial autocorrelation, spatial heterogeneity, hurdle model

## INTRODUCTION

The ongoing coronavirus disease 2019 (COVID-19), as a rapidly spreading global pandemic, comes as a big blow to the economic and social development of the world and has become a global health concern. Case fatality rate (CFR), known as the proportion of deaths from a kind of disease to the number of confirmed cases of this disease (the proportion of infected people who die), is an important indicator to measure the severity degree of the epidemic (1), as well as a reflection of the government capacity to prevent and control the epidemic (2). Outbreaking in Wuhan, China, in January 2020, the virus rapidly spreads through Hubei Province and the rest of China. It then became under control within 2 months through stringent prevention and control measures taken by Chinese governments such as lockdown, wearing face masks, self-quarantine, the detection and isolation of infected individuals, contact-tracing, social distancing, traffic restrictions, and community containment (3). COVID-19, however, is now affecting countries all over the world. As of January 25, 2021, there are 98,977,480 confirmed cases and 2,126,232 deaths worldwide, covering 224 countries and regions. Therefore, it is quite necessary to investigate determinants on COVID-19 CFRs of cities in China. The experience of China in controlling the spread of the virus and reducing mortality

can help to inform other countries to better cope with the local epidemic outbreaks.

The fatality rate of COVID-19 is affected by multiple factors, including air pollution, climatic conditions, demographic characteristics, socioeconomic factors, and the controlling measures. Many scholars focus on the close association between air pollution and COVID-19 cases and mortality rates (4–10). As an essential environmental factor, climatic conditions also influence the death rates of COVID-19 (11), mainly measured by temperature and air humidity (12–14). Demographic characteristics have remarkable effects on the mortality of patients with COVID-19: age is the dominant factor; besides, gender, race, ethnicity, medical history (such as comorbidity and obesity), and neighborhood characteristics also play a significant role in determining the CFR (15–19). The socioeconomic factors exert specific impacts on COVID-19 spread, including income, unemployment, inequality, poverty, total population, population density, human mobility, and medical resources (17, 19–22). Finally, the government actions (such as containment measures, travel restrictions, and social distancing policies) prove to be effective in mitigating the spread of the disease and reducing the confirmed cases and deaths (23–25).

Scholars employ traditional statistical methods (such as multivariate and panel regression) to reveal the effects of demographic and clinical characteristics on the mortality of patients with COVID-19 (26–29). At the regional level, scholars use GIS (Geographic information system)-based spatial analysis methods and spatial regression models to evaluate the impacts of environmental conditions, socioeconomic factors, demographic features (age, sexual, racial, and ethnic structure) on the spatial distribution of COVID-19 cases and deaths, based on the data of country level, state level, county level, or city level (16, 17, 21, 23, 30, 31).

The CFR of COVID-19 in China (4.79% on January 25, 2021) is more than the double of the worldwide CFR (2.15% on January 25, 2021). One of the reasons why CFR of China is so high may be that people knew little about the virus early in the epidemic. The studies on the determinants of COVID-19 mortality of China focus more on the individual level from the perspective of patients in Wuhan of Hubei Province (29, 32–34). There are relatively few studies at the city level in China, which mainly concern the impacts of air pollution, climatic factors, and medical resources (35–37). It is significant to analyze the influence factors at the city level, as Chinese city governments have played an important role in taking timely measures to mitigate the spread of the epidemic. Besides environmental factors and medical factors, demographic characteristics and socioeconomic factors also need to be considered. Since China has successfully controlled the spread of the virus by March 13, 2020, the CFRs of COVID-19 in many cities outside Hubei Province are zero, and the zero-inflated models will better fit the data (38, 39). As China is a large country with a vast territory, there inevitably exist spatial heterogeneity and spatial spillover effects among cities. Therefore, this study employs a spatial autoregressive probit-log (SAP-Log) linear hurdle model, a combination of zero-inflated models and spatial effects, to examine the determinants on COVID-19 CFRs of cities in

China and thus provides evidence for responding to the public health crisis in the future. Specifically, we will address the following questions:

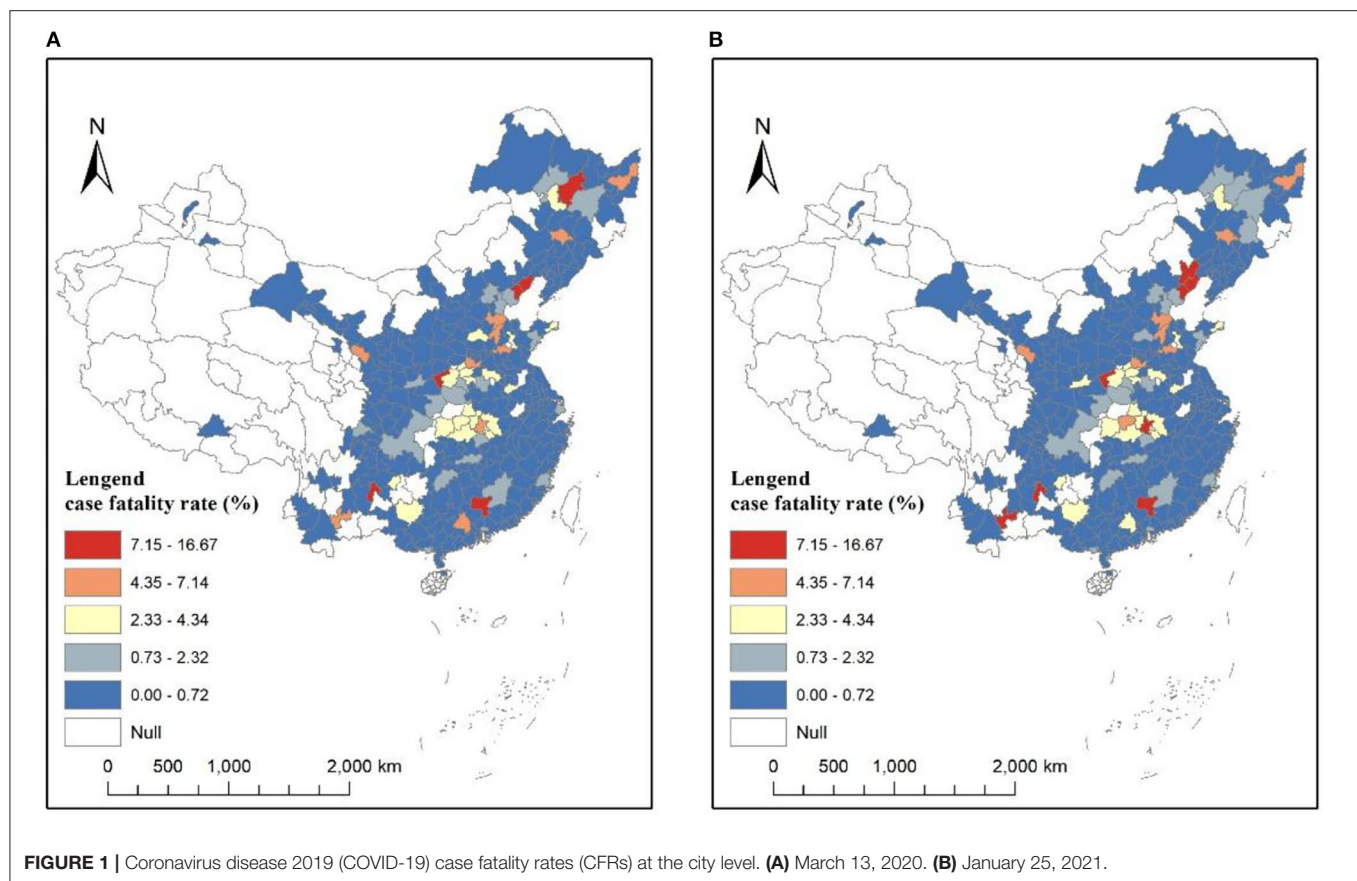
- (1) Do the probability of death from COVID-19 and the CFR level belong to two different processes?
- (2) If they are different processes, what are the respective determinants on them?
- (3) Is there a significant spatial spillover effect in the CFR?
- (4) Are there differences in the determinants of the CFR between cities within and outside Hubei Province?

## METHODOLOGY AND DATA

### Data Collection

The data of COVID-19 cumulative confirmed cases and deaths are collected from the China National Health Commissions (CNHCs) (<http://www.nhc.gov.cn>) and the provincial Health Commissions by March 13, 2020 and January 25, 2021. The dataset covered 280 prefecture-level cities that have public data online. The CFR (CFR-spring and CFR-2021) of COVID-19, as the dependent variable in this study, is measured by the number of deaths per 100 confirmed COVID-19 cases by March 13, 2020 and January 25, 2021, respectively. The cumulative CFR on March 13, 2020 and January 25, 2021, respectively, represents the first and second waves of COVID-19 spread. In the first wave of a massive disease outbreak, Chinese governments have no experience in dealing with this epidemic, and it takes 2 months to control the spread of the virus; while in the second wave, Chinese governments have enough experience in prevention and control measures, contributing to the rapid containment of sporadic outbreaks. The comparison of the confirmed cases and CFR between these 2 research periods can better reveal the influence factors on CFR in the whole process of responding to COVID-19 and the effect of disease controlling experience. When the pandemic is still ongoing, the current CFR will not reflect the real situation because the infected people are likely to die in the future. Until March 13, 2020, however, the first wave of epidemic spread has been curbed in China, and the confirmed cases and deaths do not grow considerably. Between March 13, 2020 and January 25, 2021, the confirmed cases with COVID-19 have grown very slowly, not to mention the CFR. Therefore, the CFR is a reasonable indicator to measure the developing state of the epidemic. The CFR by March 13, 2020 varies significantly from city to city, with 65 non-zero CFR and 215 zero CFR. By January 25, 2021, the number of cities with non-zero CFR has increased to 68.

The spatial distributions of COVID-19 CFRs are shown in **Figure 1**. As shown in **Figures 1A,B**, the distributions at both the times are similar. There exists significant spatial autocorrelation in CFR. The highest CFR values are mainly concentrated in Hubei Province cities, ranging from 2 to 7% on March 13, 2020. The spatial distribution of CFR in cities outside Hubei Province is relatively random and fluctuates considerably, ranging from 0 to 15%, due to a greater uncertainty of statistical inference caused by a smaller number of deaths. The confirmed cases in those cities are relatively smaller (even single digits), easily



leading to extremely high CFR values (as shown in several spots of red color in **Figure 1**). COVID-19 cases vs. deaths in Hubei Province and other provinces are shown in **Figure 2**. The slope in **Figure 2** represents the average CFR. The average CFR in Hubei Province has increased from 4.9 to 8.0%, while it decreased from 0.83 to 0.4% in other provinces. Cities in Hubei Province had much more cases and much higher CFR than other cities. There exists a significant linear relationship between the number of confirmed cases and death cases with a high value of  $R^2$  in Hubei Province (**Figure 2A**), illustrating that the CFR of each city in Hubei Province is consistent. The scatterplot of cities outside Hubei Province presents a roughly linear relationship, whereas a great disturbance on CFR emerges, resulting from the death cases ranging from 0 to 6.

## Statistical Analysis

Since the numbers of deaths in 215 out of 280 Chinese cities are zero in 2020, there exists an obvious zero-inflation problem in the regression of the CFR. However, extant studies on the CFR often ignored the zero-inflation problem, which led to statistical biases (38, 39). There are two reasons for the zero-inflation problem:

(1) The epidemic in China was under control. In total, 84% of the cases occurred in Hubei Province until March 13, 2020. The average confirmed cases inside and outside Hubei Province were 5,916.6 and 46.3, respectively. In contrast, there were fewer cases distributed in other regions. The slope in **Figure 2B** represents

the CFR, which is 0.83%. Hence, the average number of deaths in those cities was  $46.3 \times 0.83\% = 0.38$ . The average number of deaths was  $<1$ , resulting in no deaths in most cities.

(2) Some cities did not have the medical conditions to receive critically ill patients. Many critically ill patients were sent to surrounding cities with better medical resources.

A hurdle model is employed in this research to deal with the zero-inflation problem. It is a two-part model that specifies one process for zero counts and another process for positive counts.

The first part we used is a SAP model, which estimates the probability of attaining non-zero CFR predictors. The second part we used is a log-linear model, which estimates the predictors of the non-zero CFR values. Therefore, the SAP-Log hurdle model employed in this study is demonstrated as follows:

The SAP model part:

$$Y^* = \rho WY^* + X\beta + \epsilon \quad (1)$$

The log-linear part:

$$\ln(Y) = X\beta + \epsilon \quad (2)$$

where  $Y^*$  signifies the probability of whether there is a death case in a city, assigned as 1 when the answer is yes, otherwise 0;  $Y$  denotes the CFR  $>0$ ;  $X$  is the matrix of predictor variables,  $\beta$  is the parameter vector,  $\epsilon$  is the error term. Medical, environmental,



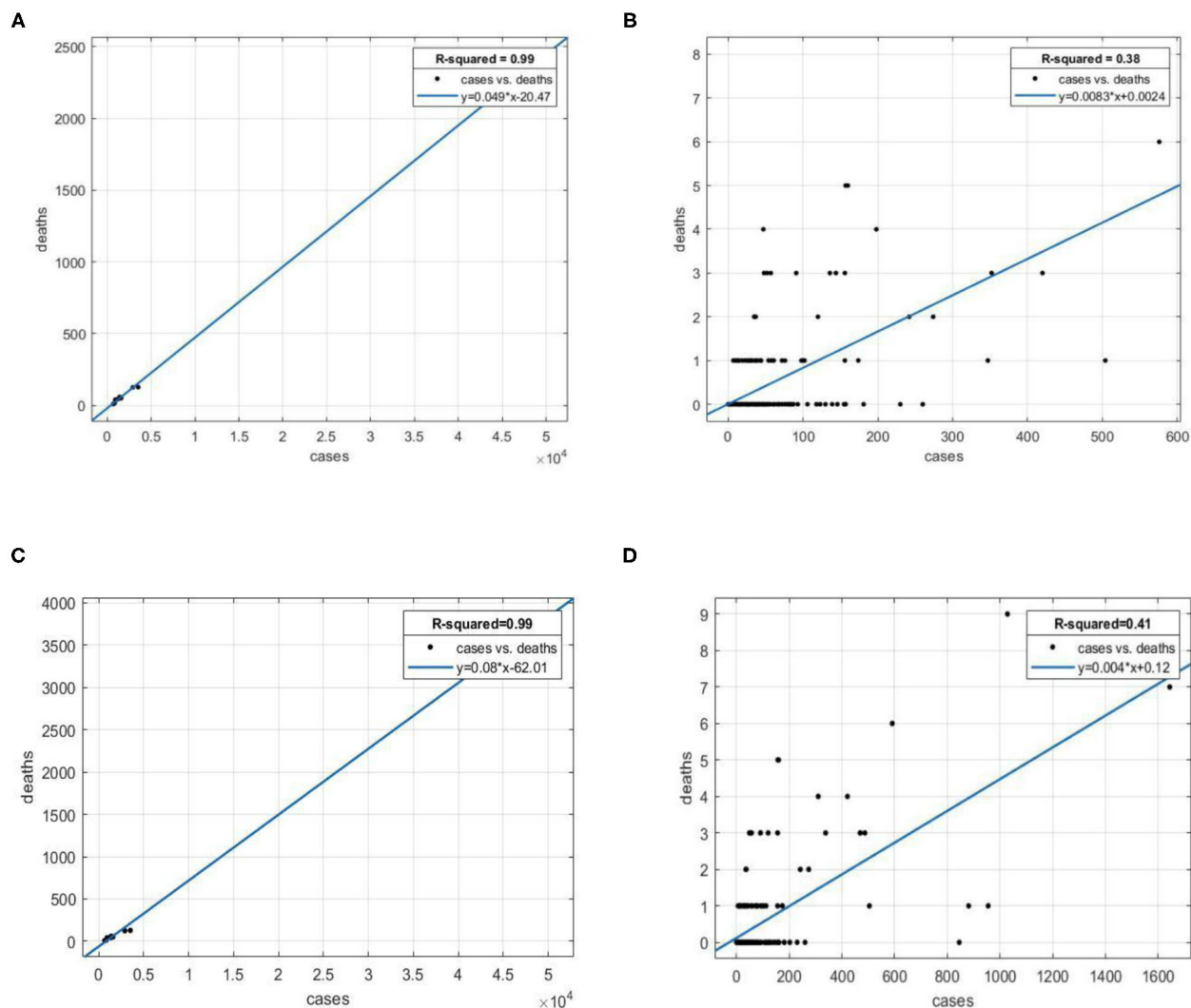


**FIGURE 2 |** Scatterplot of COVID-19 deaths against cases. **(A)** Hubei Province, March 13, 2020. **(B)** Outside Hubei Province, March 13, 2020. **(C)** Hubei Province, January 25, 2021. **(D)** Outside Hubei Province, January 25, 2021.

demographic, socioeconomic, and time factors were compiled and considered explanatory variables in **Table 1**.

Based on the extant literature, the influence factors on the CFR with COVID-19 consist of medical factors, environmental factors, demographic characteristics, and socioeconomic factors. The medical factors are directly connected with the CFR, including the number of confirmed COVID-19 cases and the number of doctors. The former indicator is gathered from the National Health Commission and the Provincial Health Commissions, closely associated with the CFR as shown in **Figure 2**. The latter indicator is a good proxy to assess the healthcare capacity (medical resource availability and accessibility), explaining different mortality rates in different regions (40). The environmental factors are very important in determining the transmission capacity and pathogenicity of the virus, thus affecting the CFR (4–14), which consist of air quality (or pollution), humidity, and temperature. First, the

particles of air pollution act as carriers for virus transmission (41), which aggravates the epidemic spread; second, people exposed to the ambient air pollution are often in a state of subhealth and easy to be infected with the virus (42); third, the air pollution will make the diseases of infected patients deteriorate, thus increasing the CFR (43). Air quality index (AQI) measures the degree of air pollution, including the contents of sulfur dioxide, nitrogen dioxide, carbon monoxide, ozone and particle matters, and it is commonly believed that air pollution emerges when the AQI is higher than 100. The demographic characteristics are composed of age, ethnicity, gender structures, average years of education, the average number of persons per household, and rurality, which signify different health conditions, living conditions, and capacities to respond to COVID-19 of the susceptible population, thus directly influencing COVID-19 mortality (15–19). The socioeconomic factors also matter in affecting the CFR, which incorporate the insurance coverage,

**TABLE 1** | Description of explanatory variables.

| Category                    | Variable name         | Description  | Data sources  |
|-----------------------------|-----------------------|--|---|
| Medical factors             | Cases-spring          | Cumulative number of confirmed COVID-19 cases by 13 March 2020                     | National Health Commission and the Provincial Health Commissions  |
|                             | Cases-2021            | Cumulative number of confirmed COVID-19 cases by 25 January 2021                   | National Health Commission and the Provincial Health Commissions  |
|                             | Doctors               | Number of doctors (10,000 doctors)   | China City Statistical Yearbook 2019                              |
| Environmental factors       | AQI-spring            | Average Air Quality Index from 1 January 2020 to 13 March 2020                     | Ministry of Ecology and Environment of People's Republic of China |
|                             | AQI-2020              | Average Air Quality Index in 2020  | Ministry of Ecology and Environment of People's Republic of China |
|                             | Humidity-spring       | Average humidity from 1 January 2020 to 13 March 2020 (%)                          | China Meteorological Administration                               |
|                             | Humidity-2020         | Average humidity in 2020 (%)   | China Meteorological Administration                               |
|                             | Temperature-spring    | Average temperature from 1 January 2020 to 13 March 2020 (Celsius)                 | China Meteorological Administration                               |
|                             | Temperature-2020      | Average temperature in 2020 (Celsius)  | China Meteorological Administration                               |
| Demographic characteristics | Age                   | Average age of residents   | Sixth National Population Census of China                         |
|                             | Ethnicity             | Proportion of ethnic minorities (%)  | Sixth National Population Census of China                         |
|                             | Gender                | Percentage of males (%)  | Sixth National Population Census of China                         |
|                             | Education             | Average years of education (years)   | Sixth National Population Census of China                         |
|                             | Household             | Average number of persons per household  | Sixth National Population Census of China                         |
|                             | Rurality              | Percentage of rural population(%)  | Sixth National Population Census of China                         |
| Socioeconomic factors       | Insurance             | Percentage of employees joining the urban basic medical care system (%)            | China City Statistical Yearbook 2019                              |
|                             | Unemployment          | Percentage of unemployment (%)   | China City Statistical Yearbook 2019                              |
|                             | Wage                  | Average wage of employed staff and workers (10,000 yuan)                           | China City Statistical Yearbook 2019                              |
|                             | Poverty               | Percentage of the population below poverty level (%)                               | China Rural Poverty Monitoring Report 2020                        |
|                             | Public transportation | Bus passenger volume per capita(Number of times)                                   | China City Statistical Yearbook 2019                              |
| Time factor                 | First case            | The number of days from the beginning of the epidemic to the first confirmed case. | National Health Commission and the Provincial Health Commissions  |

the percentage of unemployment, the average wage of employed staff and workers, poverty, and public transportation. This kind of factors reflect the socioeconomic status of people and concern the living standards, sanitary conditions, and capacities to afford healthcare, thus exerting impacts on their health outcomes (17, 19–22). Regarding the specific data sources, the number of doctors (doctors), the percentage of unemployment (unemployment), the average wage of employed staff and workers (wage), the percentage of employees joining the urban basic medical care system (insurance), and the bus passenger volume per capita (public transportation) are collected from China City Statistical Yearbook 2019, which records the newest available data of cities in 2018. The percentage of the population below the poverty level (Poverty) is gathered from China Rural Poverty Monitoring Report 2020. The AQI daily observation data are acquired from the Ministry of Ecology and Environment of the People's Republic of China, and the average daily values of each city during the 2 research periods (from January 1, 2020 to March 13, 2020, and from January 1, 2020 to January 1, 2021) are calculated. Similarly, the average humidity (humidity) and the average temperature (temperature) during the research period are gathered from the China Meteorological Administration.

The average age of residents (age), the proportion of ethnic minorities (ethnicity), the percentage of males (gender), the average years of education (education), the average number of persons per household (household), and the percentage of the rural population (rurality) come from the Sixth National Population Census of China, which records the demographic data of 2010 and is the latest data available in public because China conducts national population census every 10 years. As the time of the event may affect the mortality rate, we also collected the number of days from the beginning of the epidemic to the first confirmed case (First case) in the city.

## ANALYSIS OF RESULTS

To test the multicollinearity in the regression model, we calculated the variance inflation factor (VIF) and found that the VIF value of each variable is <4, indicating that there is no multicollinearity in our model. A series of control variables have been incorporated into the model, and the dependent variable is lagged from the independent and control variables, thus reducing the possible endogeneity problem to some extent. The descriptive statistical analysis of all variables is shown in **Table 2**. In both

**TABLE 2 |** Descriptive statistical analysis.

| Variables             | Mean   | Min   | Max       | SD       |
|-----------------------|--------|-------|-----------|----------|
| CFR-spring            | 0.81   | 0.00  | 14.29     | 1.99     |
| CFR-2021              | 0.83   | 0.00  | 16.67     | 2.16     |
| Cases-spring          | 276.91 | 0.00  | 49,995.00 | 3,000.03 |
| Cases-2021            | 299.74 | 0.00  | 50,355.00 | 3,023.17 |
| Doctors               | 1.20   | 0.10  | 10.94     | 1.21     |
| AQI-spring            | 57.23  | 23.24 | 105.52    | 17.73    |
| Humidity-spring       | 66.14  | 31.66 | 90.60     | 14.16    |
| Temperature-spring    | 7.13   | −7.82 | 23.48     | 6.58     |
| AQI-2020              | 56.62  | 23.73 | 99.94     | 16.18    |
| Humidity-2020         | 65.49  | 30.15 | 85.46     | 13.10    |
| Temperature-2020      | 16.56  | 2.01  | 27.89     | 5.30     |
| Age                   | 35.87  | 29.92 | 43.13     | 2.48     |
| Ethnicity             | 92.20  | 11.89 | 99.99     | 16.07    |
| Gender                | 51.38  | 47.27 | 99.10     | 3.00     |
| Education             | 8.96   | 11.71 | 6.55      | 0.83     |
| Household             | 3.07   | 4.75  | 2.04      | 0.46     |
| Rurality              | 71.82  | 39.11 | 91.79     | 12.01    |
| Poverty               | 1.74   | 0.00  | 5.8       | 1.57     |
| Insurance             | 0.73   | 0.17  | 10.32     | 0.65     |
| Unemployment          | 2.38   | 0.19  | 12.42     | 1.45     |
| Wage                  | 7.14   | 14.98 | 3.89      | 1.45     |
| Public transportation | 49.00  | 0.00  | 582.24    | 67.75    |
| First case            | 4.03   | 50.00 | 1.00      | 8.80     |

parts of the hurdle models, we established the models with CFR in 2020 and 2021 as the dependent variables. The cases, AQI, humidity, and temperature variables are different in the 2 research periods, while others are constant. We employed the average AQI, humidity, and temperature from January 1, 2020 to March 13, 2020 (AQI-spring, humidity-spring, and temperature-spring) to model CFR-2020 and the yearly average AQI, humidity, and temperature in 2020 (AQI-2020, humidity-2020, and temperature-2020) to model CFR-2021.

In the first part of the hurdle model, we established a SAP model and a traditional probit model to regress the death probability of March 13, 2020 and January 25, 2021, respectively, with the results displayed in **Table 3**. It explains whether a city has a death case with COVID-19.

By comparing the spatial and the non-spatial models, it is evident that the value of pseudo  $R^2$  of the spatial model is higher than that of the non-spatial model, indicating better goodness of fit. The regression coefficient of the spatially lagged term  $\rho$  is also significant. Therefore, the SAP model is more suitable, because the neglect of the spatial effect will cause omitted variable bias.

In the 2 spatial models of different research periods, the regression coefficients of cases, doctors, education, wage, first case, and  $\rho$  are all significant. The number of confirmed cases (cases) with COVID-19 is an important determinant of the appearance of death, which often emerges after the number of death cases reaches a certain level. The regression coefficient of cases is 0.001 and 0.003 at different times, demonstrating that

**TABLE 3 |** First part: Regression estimates of the probit models.

| Explanatory variables  | Probit model (CFR-2020) | Spatial probit model (CFR-2020) | Probit model (CFR-2021) | Spatial probit model (CFR-2021) |
|------------------------|-------------------------|---------------------------------|-------------------------|---------------------------------|
|                        | Coefficients            |                                 |                         |                                 |
| Cases-2020             | 0.008***                | 0.001***                        |                         |                                 |
| Cases-2021             |                         |                                 | 0.004***                | 0.003***                        |
| Doctors                | 0.178                   | 0.473***                        | 0.375**                 | 0.408***                        |
| AQI-spring             | 0.013                   | 0.012                           |                         |                                 |
| Humidity-spring        | 0.020*                  | 0.002**                         |                         |                                 |
| Temperature-spring     | −0.015                  | −0.012                          |                         |                                 |
| AQI-2020               |                         |                                 | 0.001                   | −0.001                          |
| Humidity-2020          |                         |                                 | 0.002                   | 0.007                           |
| Temperature-2020       |                         |                                 | −0.048                  | −0.057**                        |
| Age                    | −0.154                  | −0.12                           | −0.124                  | −0.088                          |
| Ethnicity              | −0.010                  | 0.007                           | −0.007                  | 0.008                           |
| Gender                 | −0.165                  | −0.010                          | −0.097                  | −0.034                          |
| Education              | 0.517**                 | 0.371***                        | 0.443*                  | 0.494***                        |
| Household              | 0.073                   | 0.136                           | 0.456                   | 0.627**                         |
| Rurality               | −0.004                  | −0.009                          | −0.012                  | −0.009                          |
| Poverty                | −0.095                  | −0.080                          | 0.043                   | 0.053                           |
| Insurance              | 0.912                   | 0.598                           | 0.718                   | 0.594                           |
| Unemployment           | −0.075                  | −0.076                          | −0.061                  | 0.049                           |
| Wage                   | −0.106                  | −0.188*                         | −0.177                  | −0.173*                         |
| Public transportation  | −0.004                  | −0.001                          | −0.005                  | −0.004                          |
| First case             | −0.048                  | −0.065***                       | −0.081                  | −0.073***                       |
| $\rho$                 |                         | 0.168**                         |                         | 0.114**                         |
| Pseudo $R^2$           | 0.363                   | 0.365                           | 0.358                   | 0.363                           |
| Number of observations | 280                     | 280                             | 280                     | 280                             |

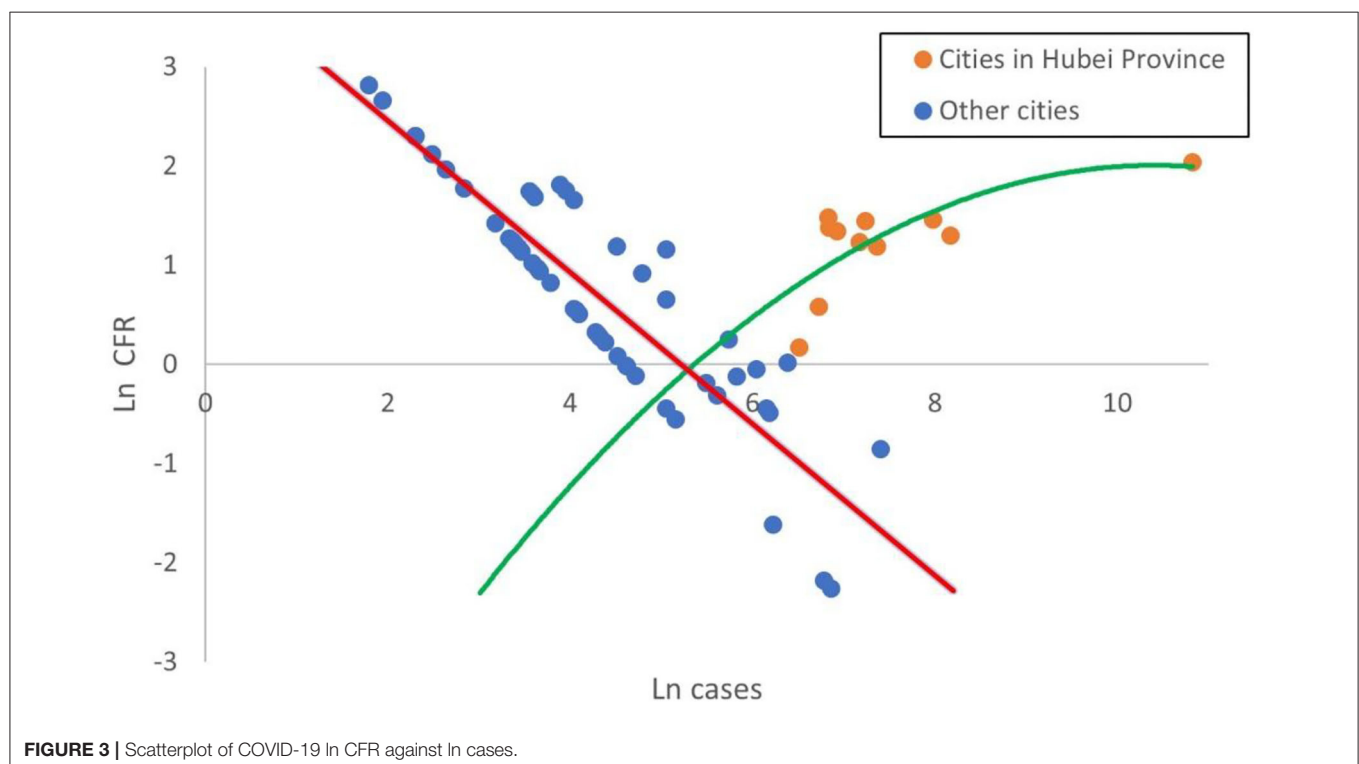
\* $p < 0.1$ ; \*\* $p < 0.05$ ; \*\*\* $p < 0.01$ .

the probability of death will increase by 0.1 and 0.3% with 1 newly increased confirmed case. The number of confirmed cases (cases) reflects the demand for treatment of COVID-19. During the period of epidemic outbreak, as the number of confirmed cases increases, there are limited medical resources (experienced doctors, medical facilities, and medicines) in most cities, which cannot satisfy the increasing demand for treatment and thus lead to a growth in CFR. Since doctors are an indicator to measure the medical resource availability and accessibility, its relation with the death probability should be negative. However, the results of the spatial probit models show that better medical resources will cause a higher possibility of death. Such a seemingly contradictory phenomenon is due to the uneven distribution of medical resources in China, there is a lack of necessary medical facilities in most cities. When severe cases happen in the cities with fewer medical resources, the governments tend

to transfer the patients to the surrounding cities with more medical resources. At the same time, the patients with serious conditions will also choose to seek treatment in a city with more medical resources. Consequently, the cities with more medical resources will have higher death probabilities, as they gather the severe patients from surrounding cities, while the cities with fewer medical resources will have lower death probabilities. The regression coefficient of doctors displays that the death probability will increase by 40.8–47.3% with the augment of 10,000 doctors. The variable education measures the average education attainment level, which determines the type of job mainly based on physical labor or mental labor. People engaged in physical labor often have a higher health level than those of mental labor, owing to the fact that the former group has more physical exercise than the latter. Hence, people in the region of higher education level tend to have poorer health than the region with lower education level, thus causing worse disease conditions and increasing the risk of death from COVID-19. The death probability will grow by 37.1–49.4% with the increase of 1 year of education. Wage exerts negative impacts on the appearance of death: the new odds of death will decrease by 17.3–18.8% compared with the original odds, in response to a rise of 1 unit in wage. People with a higher wage level are inclined to receive early medical treatment and choose better medical treatment, and the prompt treatment and high-quality medical care both decrease the possibility of death. The first case shows the time of discovering the first confirmed case in a city. The later the first case appears, the better preparation the city will have for responding to the epidemic, thus leading to a lower possibility of death. It is because a city where the first confirmed case emerges late can learn experience from other cities.

The spatial effect coefficient  $\rho$  in the 2 spatial models of different research periods is significantly positive, indicating an evident spatial autocorrelation in CFR: on one hand, the high–high agglomeration signifies that a city with a high death probability is surrounded by cities that also have a high possibility of death; on the other hand, the low–low agglomeration represents that a city with a low death probability is surrounded by cities that also have a low possibility of death. The former phenomenon is caused by the transfer of critical patients among cities. When the medical resources of a city are not enough for the critical patients, part of critical patients will be transferred to surrounding cities for treatment. The relative shortage of medical resources in the city and the number of critical patients exceeding the medical care capacity will both require the support of medical resources from surrounding cities. The latter phenomenon results from the distance decay effect of medical knowledge and experience. A city with rich medical care experience in COVID-19 treatment will benefit surrounding cities, thus reducing the likelihood of death from COVID-19, which will be further verified in the second part model. The medical resource sharing among neighboring cities also contributes to this.

In the spatial model of the first research period, Humidity is significantly positive at the 5% level, indicating that a higher humidity increases the likelihood of death occurring in the early days of the outbreaks. A higher humidity may contribute to the survival and transmission of the virus. In the spatial model of the second research period, Humidity no longer influences CFR, but temperature and household have a marked impact on CFR, stating that lower temperature and larger family size will lead to a higher death possibility with COVID-19.





The probable reason is that lower temperature is favorable for the survival and transmission of the virus, and a larger family size indicates a higher chance of transmission between family members.

In the probit part of the hurdle model, the regression result of the first research period is very similar to that of the second research period, which proves the robustness of our results.

Before the second part of the hurdle model, we first consider the relationship between Cases and CFR. Since the emergence of death has been explained by the first part model, we only analyze the cities that have death cases. Given the fact that the difference between cities is large, we take the logarithm of Cases and CFR and create a scatterplot in **Figure 3**.

**Figure 3** demonstrates that there exist marked differences in the relationship between cities in Hubei Province and outside Hubei Province. There exists a negative linear relationship between  $\ln$  CFR and  $\ln$  cases in cities outside Hubei Province. This indicates that the medical treatment experience has a great impact on CFR in cities outside Hubei Province and the medical experience accumulation with the increasing confirmed cases will result in the CFR reduction. It is worth noting that some cities with relatively few confirmed cases even have higher CFR than Wuhan due to the lack of the medical experience. On the contrary, there exists a positive nonlinear relationship between  $\ln$  CFR and  $\ln$  Cases in cities within Hubei Province. This is mainly because the first outbreak of COVID-19 in Hubei Province in January 2020 caused an explosive growth in the number of confirmed cases. The limited medical resources in Hubei Province were overwhelmed and some critical patients could not get adequate treatment, giving rise to the increase of CFR along with cases. As cases grew, the CFR of Hubei Province reached a peak ( $e^2$ ) and then no longer increased anymore. Considering that there exist significant differences between the cities within and outside Hubei Province, i.e., spatial heterogeneity, we will build the regression models of cities within Hubei Province and outside Hubei Province, respectively.

The second part of the hurdle model also includes 2 cross-sections and considers the spatial heterogeneity of cities within and outside Hubei Province. The value of Moran's  $I$  is not significant, indicating no spatial effects. The regression results are shown in **Table 4**, with a relatively higher fitting degree (adj  $R^2 > 0.7$ ). First, we analyze the cities outside Hubei Province. The increase of 1% in the number of  $\ln$  Cases will cause CFR to decrease by 0.816 and 0.896% in 2020 and 2021, respectively, which implies that the accumulation of medical experience significantly reduces the CFR. Regarding the 11 cities within Hubei Province and considering the degree of freedom and multicollinearity of the model, we employ the stepwise regression method to select the variables. Cases, AQI and Humidity all have significant positive effects on CFR, while the other variables are non-significant in the model. The growth of the number of Cases quickly strains medical capacity and increases mortality. The environment also affects the CFR, with higher AQI and Humidity leading to higher CFR. A higher AQI means higher air pollution, which will contribute to the transmission of the virus and lower the resistance of people to diseases.

**TABLE 4 |** Second part: Log-linear regression estimates for cities with nonzero case fatality rate (CFR).

| Explanatory variables  | Cities outside Hubei province: CFR-2020 | Cities outside Hubei province: CFR-2021 | Cities in Hubei province: CFR-2020 | Cities in Hubei province: CFR-2021 |
|------------------------|---|---|------------------------------------|------------------------------------|
|                        | Coefficients                            |   |                                    |                                    |
| $\ln$ Cases-2020       | −0.816***                               |   | 0.250***                           |                                    |
| $\ln$ Cases-2021       |   | −0.896***                               |                                    | 0.347***                           |
| Doctors                | 0.125                                   | 0.147                                   |                                    |                                    |
| AQI-spring             | 0.009                                   |   | 0.056***                           |                                    |
| Humidity-spring        | −0.007                                  |   | 0.079***                           |                                    |
| Temperature-spring     | −0.021                                  |   |                                    |                                    |
| AQI-2020               |   | 0.016                                   |                                    | 0.077***                           |
| Humidity-2020          |   | 0.006                                   |                                    | 0.065***                           |
| Temperature-2020       |   | −0.016                                  |                                    |                                    |
| Age                    | −0.015                                  | −0.001                                  |                                    |                                    |
| Ethnicity              | −0.004                                  | 0.001                                   |                                    |                                    |
| Gender                 | −0.004                                  | 0.060                                   |                                    |                                    |
| Education              | −0.252                                  | −0.287                                  |                                    |                                    |
| Household              | −0.081                                  | −0.129                                  |                                    |                                    |
| Rurality               | −0.012                                  | −0.014                                  |                                    |                                    |
| Poverty                | −0.032                                  | −0.019                                  |                                    |                                    |
| Insurance              | −0.224                                  | −0.346                                  |                                    |                                    |
| Unemployment           | −0.056                                  | −0.072                                  |                                    |                                    |
| Wage                   | −0.076                                  | −0.031                                  |                                    |                                    |
| Public transportation  | 0.001                                   | 0.002                                   |                                    |                                    |
| First case             | −0.007                                  | −0.017                                  |                                    |                                    |
| Constant               | 8.965                                   | 4.756                                   | −9.264***                          | −10.396***                         |
| Adj $R^2$              | 0.714                                   | 0.771                                   | 0.717                              | 0.885                              |
| Number of observations | 54                                      | 57                                      | 11                                 | 11                                 |

\* $p < 0.1$ ; \*\* $p < 0.05$ ; \*\*\* $p < 0.01$ .

## CONCLUSION AND DISCUSSION

Given the enormous damages to human society caused by the spread of COVID-19, robust scientific evidence will significantly contribute to the epidemic responses, especially the successful disease prevention and control experiences in China. Therefore, it is crucial to clarify the influence factors that significantly affect the CFR with COVID-19 by conducting a multicity study in China.

In this study, a SAP-Log hurdle model is employed to deal with the zero-inflation problem since nearly three quarters of cities have zero-value CFR, which dramatically reduces the estimation bias and improves the explanatory power and goodness of fit

of the model. The hurdle model also reflects the two different processes: whether there is a death from COVID-19 in a city and how high the nonzero value of CFR in a city is. During these two different processes, the influence factors are different. The application of the hurdle model in the research on the CFR with COVID-19 will provide methodological guidance for epidemic response.

The main conclusions of this study are shown as follows:

First, the influencing factors on the death occurrence probability include the number of confirmed cases, the number of doctors, average humidity, average temperature, average years of education, the average wage of employed staff and workers, the average number of persons per household, the number of days from the beginning of the epidemic to the first confirmed case. The determinants of the CFR level include the number of confirmed cases, AQI, and average humidity. Regarding the determinants, the number of confirmed cases is the most significant variable in both the two parts of the hurdle model, which is much in evidence since it is the denominator of CFR. Cases have a positive impact on the death occurrence probability and the CFR level of cities within Hubei Province, but have a negative impact on the CFR level of cities outside Hubei Province, displaying a remarkable spatial heterogeneity. The former mechanism is that a larger number of confirmed cases will cause a higher death probability under a certain level of CFR. The latter mechanism is shown as below: In cities outside Hubei Province with relatively fewer confirmed cases, a larger number of confirmed cases will result in more abundant medical treatment experience and a lower CFR level; in cities within Hubei Province with relatively numerous confirmed cases, a larger number of confirmed cases will exert huge pressure on limited medical resources and cause higher CFR. Besides the number of confirmed cases, the number of doctors also exerts significant influences. Though cities with rich medical resources can provide better treatment, the transfer of critical patients from surrounding cities to these cities will drive up death probability. As it is known to all, air quality plays a vital role in the spread of COVID-19 because aerosol is a potential transmission route for COVID-19, embodied in the effects of AQI, humidity and temperature on CFR (44, 45). However, the other socioeconomic factors and demographic characteristics do not affect the CFR levels dramatically. The fact that people in China all enjoy free medical treatment services for COVID-19 significantly contributes to reduce CFR, no matter which levels of cities they are in and which kinds of groups they belong to.

Second, there exist significant spatial spillover effects in the death occurrence probabilities, i.e., a city where death from COVID-19 is likely to happen is surrounded by cities with higher death possibilities. The reasons for this are the transfer of critical patients among cities, the sharing of medical resources among cities, and the spatial spillover effects of medical knowledge dissemination.

The main findings of this study have certain policy implications: To begin with, given the importance of the number of confirmed cases in determining CFR, the proposal of “flatten the curve” (46) is still vital to help save lives and decrease CFR, by taking lockdown and social distancing measures to reduce the number of infected people in countries

most affected by COVID-19, when limited by the current medical resources. Furthermore, the availability and accessibility of medical resources are very vital to control the spread of an epidemic, since the critical patients can be transferred to the large cities with better medical conditions in China, the medical treatment level of these large cities should be further improved. Considering the two different processes in the hurdle model, the governments should attach importance to the socioeconomic factors when preventing the emergence of death from this disease and lay much stress on the air quality when the aim is to reduce the CFR. In addition, the generally greater effects of the estimators in the model of the second research period than those in the first research period, as well as the significant effect of the number of days from the beginning of the epidemic to the first confirmed case on the death probability and CFR, have signified the influence of accumulated experiences in the response to COVID-19. The containment policies in China, including the immediate lockdown, community containment, self-quarantine, contact-tracing, as well as the free detection and medical treatment of this infectious disease for all residents, prove to be very effective in controlling the spread of the virus and reducing the CFR (47), which can also provide valuable references for other countries in the fight against the pandemic. Finally, the spatial probit models reveal the spatial spillover effects in the death probabilities, demonstrating that the popularization of medical knowledge and experience is very important to effectively control the spread of COVID-19. Hence, it is suggested that the city governments offer specialized training for the response to COVID-19.

Consistent with extant studies on COVID-19-related cases and deaths using spatial regression models in different countries (17, 19, 21, 48–51), this study also discovers that spatial regression models, with better goodness of fit than aspatial regression models, can partially explain the spatial heterogeneity in the CFR with COVID-19 and significantly reveal the spatial spillover effects on the CFR of neighboring cities and its various determinants (medical, environmental, demographic, and socioeconomic indicators). In addition, this study contributes to the existing literature by introducing a hurdle model into the spatial autoregressive model to deal with the zero-inflation problem, thus discovering two different processes influencing COVID-19 related deaths: whether there is a death from COVID-19 in a city and how high the non-zero value of CFR in a city is. There are relatively few studies on the determinants of COVID-19 confirmed cases and deaths in China employing spatial regression models, which focus more on COVID-19 transmission and the influencing factors on the number of COVID-19 cases (52–54), while this study considers the determinants on CFR with COVID-19 from different perspectives.

Despite its methodological contributions and practical implications, there still exist some deficiencies in this study. The dependent variable reflects the confirmed cases and CFR on March 13, 2020 and January 25, 2021, while some explanatory variables only reflect the annual averages limited by the data accessibility. What is more, among explanatory variables, the city-level socioeconomic data from *China City Statistical Yearbook 2019* records the situation of 2018, and the

demographic data of Sixth National Population Census's record the conditions of 2010, which are all the most recent data available publicly in China. The policy-related variables (such as lockdowns, containment measures, travel restrictions, and social distancing policies) and hospitalization variables also play an important role in affecting CFR. However, the related data of each city is not available in China, so we cannot consider the effects of them in the model. Finally, the biological differences of residents among different cities can be taken into consideration in the future studies on determinants on the CFR with COVID-19 at the city level, including the effects of digit ratio (2D:4D) and ACE (Angiotensin-Converting Enzyme) I/D polymorphism on the CFR (55–58).

## DATA AVAILABILITY STATEMENT

Publicly available datasets were analyzed in this study. This data can be found here: <https://figshare.com/s/853348383d39f65bb6a6>.

## REFERENCES

- Mi YN, Huang TT, Zhang JX, Qin Q, Gong YX, Liu SY, et al. Estimating the instant case fatality rate of COVID-19 in China. *Int J Infect Dis.* (2020) 97:1–6. doi: 10.1016/j.ijid.2020.04.055
- Staaedegaard L, Taylor RJ, Spreeuwenberg P, Caini S, Simonsen L, Paget J. Monitoring the mortality impact of COVID-19 in Europe: What can be learned from 2009 influenza H1N1p mortality studies? *Int J Infect Dis.* (2021) 102:115–7. doi: 10.1016/j.ijid.2020.10.037
- Zhang X, Tang M, Guo F, Wei F, Yu Z, Gao K, et al. Associations between air pollution and COVID-19 epidemic during quarantine period in China. *Environ Pollut.* (2021) 268:115897. doi: 10.1016/j.envpol.2020.115897
- Ali SM, Malik F, Anjum MS, Siddiqui GF, Anwar MN, Lam SS, et al. Exploring the linkage between PM25 levels and COVID-19 spread and its implications for socio-economic circles. *Environ Res.* (2021) 193:110421. doi: 10.1016/j.envres.2020.110421
- Bashir MF, Ma BJ, Bilal, Komal B, Bashir MA, Farooq TH, Bashir M. Correlation between environmental pollution indicators and COVID-19 pandemic: a brief study in Californian context. *Environ Res.* (2020) 187:109652. doi: 10.1016/j.envres.2020.109652
- Filippini T, Rothman KJ, Cocchio S, Narne E, Mantoan D, Saia M, et al. Associations between mortality from COVID-19 in two Italian regions and outdoor air pollution as assessed through tropospheric nitrogen dioxide. *Sci Total Environ.* (2021) 760:143355. doi: 10.1016/j.scitotenv.2020.143355
- Frontera A, Cianfanelli L, Vlachos K, Landoni G, Cremona G. Severe air pollution links to higher mortality in COVID-19 patients: The “double-hit” hypothesis. *J Infect.* (2020) 81:255–9. doi: 10.1016/j.jinf.2020.05.031
- Marquès M, Rovira J, Nadal M, Domingo JL. Effects of air pollution on the potential transmission and mortality of COVID-19: a preliminary case-study in Tarragona Province (Catalonia, Spain). *Environ Res.* (2021) 192:110315. doi: 10.1016/j.envres.2020.110315
- Saez M, Tobias A, Barceló MA. Effects of long-term exposure to air pollutants on the spatial spread of COVID-19 in Catalonia, Spain. *Environ Res.* (2020) 191:110177. doi: 10.1016/j.envres.2020.110177
- Sasidharan M, Singh A, Torbaghan ME, Parlikad AK. A vulnerability-based approach to human-mobility reduction for countering COVID-19 transmission in London while considering local air quality. *Sci Total Environ.* (2020) 741:140515. doi: 10.1016/j.scitotenv.2020.140515
- Bashir MF, Ma B, Bilal, Komal B, Bashir MA, Tan D, et al. Correlation between climate indicators and COVID-19 pandemic in New York, USA. *Sci Total Environ.* (2020) 728:138835. doi: 10.1016/j.scitotenv.2020.138835

## AUTHOR CONTRIBUTIONS

HY contributed to idea formulation, study design, methodology, data collection, and analysis. XL contributed to data interpretation and manuscript writing. HG contributed to discussion, review, and editing of writing. ZZ contributed to the collection of literature and data. HH contributed to the data collection. All authors contributed to the article and approved the submitted version.

## FUNDING

The corresponding author would like to acknowledge the financial support from the grants of National Natural Science Foundation of China (No. 42101226). HY would like to acknowledge the financial support for the grants of US National Science Foundation (Nos. 1841403, 1758786, and 2117455), the China Data Institute, and the Future Data Lab.

- Ma Y, Zhao Y, Liu J, He X, Wang B, Fu S, et al. Effects of temperature variation and humidity on the death of COVID-19 in Wuhan, China. *Sci Total Environ.* (2020) 724:138226. doi: 10.1016/j.scitotenv.2020.138226
- Biktasheva IV. Role of a habitat's air humidity in Covid-19 mortality. *Sci Total Environ.* (2020) 736:138763. doi: 10.1016/j.scitotenv.2020.138763
- Meo SA, Abukhalaf AA, Alomar AA, Al-Beeshi IZ, Akram J. Climate and covid-19 pandemic: effect of heat and humidity on the incidence and mortality in world's top ten hottest and top ten coldest countries. *Eur Rev Med Pharmacol Sci.* (2020) 24:8232–8. doi: 10.26355/eurrev\_202008\_22513
- Bryan MS, Sun J, Jagai J, Horton DE, Montgomery A, Sargis R, et al. Coronavirus disease 2019 (COVID-19) mortality and neighborhood characteristics in Chicago. *Ann Epidemiol.* (2021) 56:47–54.e45. doi: 10.1016/j.annepidem.2020.10.011
- Mollalo A, Vahedi B, Rivera KM. GIS-based spatial modeling of COVID-19 incidence rate in the continental United States. *Sci Total Environ.* (2020) 728:138884. doi: 10.1016/j.scitotenv.2020.138884
- Sannigrahi S, Pilla F, Basu B, Basu AS, Molter A. Examining the association between socio-demographic composition and COVID-19 fatalities in the European region using spatial regression approach. *Sustain Cities Soc.* (2020) 62:102418. doi: 10.1016/j.scs.2020.102418
- Wang K, Wu C, Xu J, Zhang B, Zhang X, Gao Z, et al. Factors affecting the mortality of patients with COVID-19 undergoing surgery and the safety of medical staff: a systematic review and meta-analysis. *EClinicalMedicine.* (2020) 29–30:100612. doi: 10.1016/j.eclim.2020.100612
- Kathe NJ, Wani RJ. Determinants of COVID-19 Case Fatality Rate in the United States: spatial analysis over one year of the pandemic. *J Health Econ Outcomes Res.* (2021) 8:51. doi: 10.36469/jheor.2021.22978
- Goutte S, Péran T, Porcher T. The role of economic structural factors in determining pandemic mortality rates: evidence from the COVID-19 outbreak in France. *Res Int Bus Finance.* (2020) 54:101281. doi: 10.1016/j.ribaf.2020.101281
- Sun Y, Hu X, Xie J. Spatial inequalities of COVID-19 mortality rate in relation to socioeconomic and environmental factors across England. *Sci Total Environ.* (2021) 758:143595. doi: 10.1016/j.scitotenv.2020.143595
- Whittle RS, Diaz-Artiles A. An ecological study of socioeconomic predictors in detection of COVID-19 cases across neighborhoods in New York City. *BMC Med.* (2020) 18:17. doi: 10.1186/s12916-020-01731-6
- Chaudhry R, Dranitsaris G, Mubashir T, Bartoszko J, Riaz S. A country level analysis measuring the impact of government actions, country preparedness and socioeconomic factors on COVID-19 mortality and related

- health outcomes. *EClinicalMedicine*. (2020) 25:8. doi: 10.1016/j.eclinm.2020.100464
24. Sun ZB, Zhang H, Yang YF, Wan H, Wang YX. Impacts of geographic factors and population density on the COVID-19 spreading under the lockdown policies of China. *Sci Total Environ*. (2020) 746:7. doi: 10.1016/j.scitotenv.2020.141347
  25. Figueiredo AM, Daponte CA, Figueiredo M, Saez M, Cabrera León A. Impact of lockdown on COVID-19 incidence and mortality in China: an interrupted time series study. *Bull World Health Organ*. (2020) 98:150. doi: 10.2471/BLT.20.256701
  26. Branden M, Aradhya S, Kolk M, Harkonen J, Drefahl S, Malmberg B, et al. Residential context and COVID-19 mortality among adults aged 70 years and older in Stockholm: a population-based, observational study using individual-level data. *Lancet Healthy Longev*. (2020) 1:e80–8. doi: 10.1016/S2666-7568(20)30016-7
  27. Skrip L, Derra K, Kaboré M, Noori N, Gansané A, Valéa I, et al. Clinical management and mortality among COVID-19 cases in sub-Saharan Africa: a retrospective study from Burkina Faso and simulated case analysis. *Int J Infect Dis*. (2020) 101:194–200. doi: 10.1016/j.ijid.2020.09.1432
  28. Rodriguez-Nava G, Yanez-Bello MA, Trelles-Garcia DP, Chung CW, Chaudry S, Khan AS, et al. Clinical characteristics and risk factors for death of hospitalized patients with COVID-19 in a community hospital: a retrospective cohort study. *Mayo Clinic Proc Innov Qual Outcomes*. (2021) 5:1–10. doi: 10.1016/j.mayocpiqo.2020.10.007
  29. Yu CZ, Lei Q, Li WK, Wang X, Liu W, Fan XL, et al. Clinical characteristics, associated factors, and predicting COVID-19 mortality risk: a retrospective study in Wuhan, China. *Am J Prev Med*. (2020) 59:168–75. doi: 10.1016/j.amepre.2020.05.002
  30. Fielding-Miller RK, Sundaram ME, Brouwer K. Social determinants of COVID-19 mortality at the county level. *PLoS ONE*. (2020) 15:11. doi: 10.1371/journal.pone.0240151
  31. Andersen LM, Harden SR, Sugg MM, Runkle JD, Lundquist TE. Analyzing the spatial determinants of local Covid-19 transmission in the United States. *Sci Total Environ*. (2021) 754:10. doi: 10.1016/j.scitotenv.2020.142396
  32. Chen L, Liu S, Tian JC, Pan HS, Liu Y, Hu J, et al. Disease progression patterns and risk factors associated with mortality in deceased patients with COVID-19 in Hubei Province, China. *Immun Inflamm Dis*. (2020) 8:584–94. doi: 10.1002/iid3.343
  33. Wang K, Zuo P, Liu Y, Zhang M, Zhao X, Xie S, et al. Clinical and laboratory predictors of in-hospital mortality in patients with COVID-19: a cohort study in Wuhan, China. *Clin Infect Dis*. (2020) 71:2079–88. doi: 10.2139/ssrn.3546115
  34. Zhu GP, Zhu YH, Wang ZL, Meng WJ, Wang XX, Feng JN, et al. The association between ambient temperature and mortality of the coronavirus disease 2019 (COVID-19) in Wuhan, China: a time-series analysis. *BMC Public Health*. (2021) 21:10. doi: 10.1186/s12889-020-10131-7
  35. Wang B, Liu JT, Li YL, Fu SH, Xu XC, Li LY, et al. Airborne particulate matter, population mobility and COVID-19: a multi-city study in China. *BMC Public Health*. (2020) 20:10. doi: 10.1186/s12889-020-09669-3
  36. Xie JG, Zhu YJ. Association between ambient temperature and COVID-19 infection in 122 cities from China. *Sci Total Environ*. (2020) 724:5. doi: 10.1016/j.scitotenv.2020.138201
  37. Yao Y, Pan JH, Wang WD, Liu ZX, Kan HD, Qiu Y, et al. Association of particulate matter pollution and case fatality rate of COVID-19 in 49 Chinese cities. *Sci Total Environ*. (2020) 741:5. doi: 10.1016/j.scitotenv.2020.140396
  38. Mukherji N. The social and economic factors underlying the impact of COVID-19 Cases and deaths in US Counties. *medRxiv*. [Preprint]. (2020). doi: 10.1101/2020.05.04.20091041.
  39. Wang L, Wang G, Gao L, Li X, Yu S, Kim S, et al. Spatiotemporal dynamics, nowcasting and forecasting of COVID-19 in the United States. *arXiv:2004.14103*. (2020). Available online at: <https://arxiv.org/abs/2004.14103>
  40. Ji YP, Ma ZR, Peppelenbosch MP, Pan QW. Potential association between COVID-19 mortality and healthcare resource availability. *Lancet Glob Health*. (2020) 8:E480–E480. doi: 10.1016/S2214-109X(20)30068-1
  41. Setti L, Passarini F, De Gennaro G, Barbieri P, Perrone MG, Borelli M, et al. SARS-Cov-2RNA found on particulate matter of Bergamo in Northern Italy: first evidence. *Environ Res*. (2020) 188:109754. doi: 10.1016/j.envres.2020.109754
  42. Block ML, Calderón-Garcidueñas L. Air pollution: mechanisms of neuroinflammation and CNS disease. *Trends Neurosci*. (2009) 32:506–16. doi: 10.1016/j.tins.2009.05.009
  43. Conticini E, Frediani B, Caro D. Can atmospheric pollution be considered a co-factor in extremely high level of SARS-CoV-2 lethality in Northern Italy? *Environ Pollut*. (2020) 261:114465. doi: 10.1016/j.envpol.2020.114465
  44. Fareed Z, Iqbal N, Shahzad F, Shah SGM, Zulfikar B, Shahzad K, et al. Co-variance nexus between COVID-19 mortality, humidity, and air quality index in Wuhan, China: New insights from partial and multiple wavelet coherence. *Air Qual Atmos Health*. (2020) 13:673–82. doi: 10.1007/s11869-020-00847-1
  45. Pansini R, Fornacca D. COVID-19 higher mortality in chinese regions with chronic exposure to lower air quality. *Front. Public Health* 8:597753. doi: 10.3389/fpubh.2020.597753
  46. Godoy M. *Flattening A Pandemic's Curve: Why Staying Home Now Can Save Lives*. National Public Radio (2020).
  47. Maier BF, Brockmann D. Effective containment explains subexponential growth in recent confirmed COVID-19 cases in China. *Science*. (2020) 368:742. doi: 10.1126/science.abb4557
  48. Sun F, Matthews SA, Yang TC, Hu MH. A spatial analysis of the COVID-19 period prevalence in US counties through June 28, 2020: where geography matters? *Ann Epidemiol*. (2020) 52:54–9. doi: 10.1016/j.annepidem.2020.07.014
  49. Breen R, Ermisch J. The distributional impact of Covid-19: Geographic variation in mortality in England. *Demogr Res*. (2021) 44:397–414. doi: 10.4054/DemRes.2021.44.17
  50. Ehler A. The socio-economic determinants of COVID-19: a spatial analysis of German county level data. *Socioecon Plann Sci*. (2021) 78:101083. doi: 10.1016/j.seps.2021.101083
  51. Kandula S, Shaman J. Investigating associations between COVID-19 mortality and population-level health and socioeconomic indicators in the United States: a modeling study. *PLoS Med*. (2021) 18:e1003693. doi: 10.1371/journal.pmed.1003693
  52. Xi W, Pei T, Liu Q, Song C, Liu Y, Chen X, et al. Quantifying the time-lag effects of human mobility on the COVID-19 transmission: a multi-city study in China. *IEEE Access*. (2020) 8:216752–61. doi: 10.1109/ACCESS.2020.3038995
  53. Yu H, Li J, Bardin S, Gu H, Fan C. Spatiotemporal Dynamic of COVID-19 diffusion in China: a dynamic spatial autoregressive model analysis. *ISPRS Int J Geo-Inform*. (2021) 10:510. doi: 10.3390/ijgi10080510
  54. Zhang Y, Deng Z, Supriyadi A, Song R, Wang T. Spatiotemporal spread characteristics and influencing factors of COVID-19 cases: Based on big data of population migration in China. *Growth and Change*. (2021) 00:1–22. doi: 10.1111/grow.12604
  55. Li X, Sun X, Jin L, Xue F. Worldwide spatial genetic structure of angiotensin-converting enzyme gene: a new evolutionary ecological evidence for the thrifty genotype hypothesis. *Eur J Hum Gene*. (2011) 19:1002–8. doi: 10.1038/ejhg.2011.66
  56. Xu Y, Zheng Y. The digit ratio (2D: 4D) in China: a meta-analysis. *Am J Hum Biol*. (2015) 27:304–9. doi: 10.1002/ajhb.22639
  57. Manning JT, Fink B. Understanding COVID-19: Digit ratio (2D: 4D) and sex differences in national case fatality rates. *Early Hum Dev*. (2020) 146:105074. doi: 10.1016/j.earlhumdev.2020.105074
  58. Manning JT, Fink B. Understanding COVID-19: a hypothesis regarding digit ratio (2D: 4D), ACE I/D polymorphism, oxygen metabolism and national case fatality rates. *Early Hum Dev*. (2020) 151:105161. doi: 10.1016/j.earlhumdev.2020.105161

**Conflict of Interest:** The authors declare that the research was conducted in the absence of any commercial or financial relationships that could be construed as a potential conflict of interest.

**Publisher's Note:** All claims expressed in this article are solely those of the authors and do not necessarily represent those of their affiliated organizations, or those of the publisher, the editors and the reviewers. Any product that may be evaluated in this article, or claim that may



be made by its manufacturer, is not guaranteed or endorsed by the publisher.

Copyright © 2022 Yu, Lao, Gu, Zhao and He. This is an open-access article distributed under the terms of the Creative Commons Attribution License (CC BY).

*The use, distribution or reproduction in other forums is permitted, provided the original author(s) and the copyright owner(s) are credited and that the original publication in this journal is cited, in accordance with accepted academic practice. No use, distribution or reproduction is permitted which does not comply with these terms.*



# An Unsupervised Machine Learning Clustering and Prediction of Differential Clinical Phenotypes of COVID-19 Patients Based on Blood Tests—A Hong Kong Population Study

Kitty Yu-Yeung Lau<sup>1</sup>, Kei-Shing Ng<sup>2</sup>, Ka-Wai Kwok<sup>3</sup>, Kevin Kin-Man Tsia<sup>4</sup>, Chun-Fung Sin<sup>5</sup>, Ching-Wan Lam<sup>5</sup> and Varut Vardhanabhuti<sup>2\*</sup>

## OPEN ACCESS

### Edited by:

Reza Lashgari,  
Shahid Beheshti University, Iran

### Reviewed by:

Antonio Lalueza,  
Hospital Universitario 12 de  
Octubre, Spain  
Mohsen Rokni,  
Tehran University of Medical  
Sciences, Iran

### \*Correspondence:

Varut Vardhanabhuti  
varv@hku.hk

### Specialty section:

This article was submitted to  
Pulmonary Medicine,  
a section of the journal  
Frontiers in Medicine

**Received:** 26 August 2021

**Accepted:** 27 December 2021

**Published:** 24 February 2022

### Citation:

Lau K-Y, Ng K-S, Kwok K-W,  
Tsia K-M, Sin C-F, Lam C-W and  
Vardhanabhuti V (2022) An  
Unsupervised Machine Learning  
Clustering and Prediction of  
Differential Clinical Phenotypes of  
COVID-19 Patients Based on Blood  
Tests—A Hong Kong Population  
Study. *Front. Med.* 8:764934.  
doi: 10.3389/fmed.2021.764934

<sup>1</sup> Biomedical Engineering Programme, The University of Hong Kong, Hong Kong, Hong Kong SAR, China, <sup>2</sup> Department of Diagnostic Radiology, Li Ka Shing Faculty of Medicine, The University of Hong Kong, Hong Kong, Hong Kong SAR, China, <sup>3</sup> Department of Mechanical Engineering, The University of Hong Kong, Hong Kong, Hong Kong SAR, China, <sup>4</sup> Department of Electrical and Electronic Engineering, The University of Hong Kong, Hong Kong, Hong Kong SAR, China, <sup>5</sup> Department of Pathology, Li Ka Shing Faculty of Medicine, The University of Hong Kong, Hong Kong, Hong Kong SAR, China

**Background:** To better understand the different clinical phenotypes across the disease spectrum in patients with COVID-19 using an unsupervised machine learning clustering approach.

**Materials and Methods:** A population-based retrospective study was conducted utilizing demographics, clinical characteristics, comorbidities, and clinical outcomes of 7,606 COVID-19-positive patients on admission to public hospitals in Hong Kong in the year 2020. An unsupervised machine learning clustering was used to explore this large cohort.

**Results:** Four clusters of differing clinical phenotypes based on data at initial admission was derived in which 86.6% of the deceased cases were aggregated in one of the clusters without prior knowledge of their clinical outcomes. Other distinctive clinical characteristics of this cluster were old age and high concurrent comorbidities as well as laboratory characteristics of lower hemoglobin/hematocrit levels, higher neutrophil, C-reactive protein, lactate dehydrogenase, and creatinine levels. The clinical patterns captured by the cluster analysis was validated on other temporally distinct cohorts in 2021. The phenotypes aligned with existing literature.

**Conclusion:** The study demonstrated the usefulness of unsupervised machine learning techniques with the potential to uncover latent clinical phenotypes. It could serve as a more robust classification for patient triaging and patient-tailored treatment strategies.

**Keywords:** COVID-19, clinical phenotypes, laboratory test, machine learning, clustering

## INTRODUCTION

Coronavirus disease 2019 (COVID-19) is a respiratory disease caused by severe acute respiratory syndrome coronavirus (SARS-CoV-2). This novel coronavirus was first reported in Wuhan, China, in December 2019 and quickly spread worldwide (1). Belonging to the same coronavirus family as SARS-CoV and MERS-CoV, SARS-CoV-2 also exhibits a remarkable infectivity power (2). Immediate practices have been taken to allocate medical resources and plan for treatments. However, they might not be as effective as expected due to a lack of knowledge about SARS-CoV-2. A better understanding of the pathogenesis of COVID-19 and its different clinical phenotypes and risk groups is essential to address the immunopathology of the infection. The accumulated observational data on COVID-19 positive patients available to date serve as valuable resources. To probe this large amount of clinical data, supervised machine learning approaches have been applied to the diagnosis and prognosis of COVID-19, risk stratification, and the prediction of different outcomes (3–9). Unsupervised machine learning is an alternative approach that does not require specific labels. It avoids using preconceived knowledge or assumptions that may be subjected to biases and unknown confounders. To this end, unsupervised clustering techniques are often used for exploratory analysis to probe the underlying patterns within big data sets, enabling identification of latent clinical phenotypes and potentially deriving novel insights from the associated correlations. For example, it has been applied to derive the phenotypes of COVID-19 patients using electronic health record (EHR) data on admission of 6,000 COVID-19-positive adults at the Mount Sinai Health System in New York in the United States (10), 413 patients from an individual-level published study (11), and 213 patients in Wuhan Pulmonary Hospital (12). Hong Kong's health system is unique when dealing with the COVID-19 pandemic. Due to a government-wide policy, all COVID-19-positive patients were admitted to public hospitals regardless of their disease severity or symptoms. Therefore, the data in Hong Kong can capture the varying presentations of COVID-19. This study aims to use unsupervised clustering analysis to discover different phenotypic presentations across the disease spectrum of COVID-19 in Hong Kong based on demographics and laboratory information on admission to hospital.

## MATERIALS AND METHODS

### Study Design and Participants

This study protocol was approved by institutional review boards in multiple hospitals across Hong Kong (see **Supplementary Material** for further details). Patient-informed consent was waived owing to the retrospective nature.

A retrospective search of patients' electronic records was conducted using the Hong Kong Hospital Authority Clinical Data Analysis and Reporting System (CDARS). It covered 42 hospitals across the territory in Hong Kong. Patients who were retrieved had a positive diagnosis of COVID-19 based on a reverse-transcriptase polymerase chain reaction (RT-PCR) test for SARS-CoV-2 fulfilling the testing criteria set by the Center

for Health Protection, Department of Health, Government of Hong Kong SAR. The first cohort was retrieved from January 23 to December 31, 2020. The second cohort (used as a temporal validation set) was retrieved from January 1 to February 15, 2021.

Observational data, including demographics (age and sex), and 20 basic laboratory tests [white blood cell count (WBC), neutrophil count (NEUT), lymphocyte count (LYM), monocyte count (MON), hemoglobin (HGB), hematocrit (HCT), platelet (PLT), albumin (Alb), total bilirubin (TBIL), alanine aminotransferase (ALT), alkaline phosphatase (ALP), lactate dehydrogenase (LDH), creatine kinase (CK), urea, creatinine (Cr), C-reactive protein (CRP), sodium (Na), potassium (K), phosphate (P), and calcium (Ca)] were retrieved on the first day of admission (see **Table 1**). Blood tests with <50% of available data were excluded (13). Patients' comorbidities (19 systems) as specified by the international classification of disease (ICD-9) (14) were retrieved up to 3 days before that individual's admission to avoid including input of coding for the current admission. Mortality data was retrieved and set at 45 days after discharge for each patient to ensure that death, if it occurred, was likely related to COVID-19 and not from other causes. For more detailed information, please refer to **Supplementary Table 1**.

### Data Preparation and Preprocessing

Yeo–Johnson transformation was applied to provide multivariate normal distributions (15). Patients with more than 40% missing variables and inconsistent data were excluded (13). Multiple imputation *via* chained equations (MICE) (16) was adopted to handle missing data and produced the least biased estimation under the verified assumption missing at random (MAR) (17). Bayesian ridge regression was used to introduce variations. Ten iterations and ascending order of imputations were set and deemed to be sufficient (18).

Principal components analysis (PCA) was used to compress intrinsically correlated and dependent numerical variables and project them to low-dimension representations (see **Supplementary Figures 1, 2**). Ten principal components (PCs) were kept to preserve 80% of the variance (see **Supplementary Figure 3**).

### Model Training

*k*-prototype clustering (19) accounted for numerical data, and categorical data were used to probe the underlying clinical patterns of COVID-19-positive patients on admission. To select the number of clusters, the within-cluster sum of squared error (WCSS) was plotted from 1 to 10 clusters (see **Supplementary Figure 4**). According to the elbow method, four clusters were selected for the *k*-prototype model. The partitioning of three and five clusters was also examined (see **Supplementary Figure 5**).

### Model Evaluation

To evaluate the generated clusters, a surrogate prediction model was built to check if partitioning found by the *k*-prototype model was still preserved. A gradient-boosting decision tree model named LightGBM (20) was used to build the prediction model. It predicted COVID-19 prognosis based on electronic

**TABLE 1** | Demographics and clinical characteristics of 7,606 COVID-19 positive patients.

| Patients characteristics<br>( <i>n</i> = 7,606) | Median (IQR)<br>or count (%) <sup>*</sup> | Missing<br>count (%) |
|---|---|----------------------|
| <b>I. Demographics</b>                          |   |                      |
| Age (years)                                     | 47 (32–61)                                | 0 (0%)               |
| Sex (Males)                                     | 3,697 (48.6%)                             | 0 (0%)               |
| <b>II. Complete blood count</b>                 |   |                      |
| White blood cell count (*10 <sup>9</sup> /L)    | 5.3 (4.3–6.6)                             | 0 (0%)               |
| Neutrophil count (*10 <sup>9</sup> /L)          | 3.2 (2.4–4.3)                             | 110 (1.4%)           |
| Lymphocyte count (*10 <sup>9</sup> /L)          | 1.3 (1.0–1.8)                             | 110 (1.4%)           |
| Monocyte count (*10 <sup>9</sup> /L)            | 0.5 (0.4–0.7)                             | 110 (1.4%)           |
| Hemoglobin (g/dL)                               | 13.7 (12.6–14.7)                          | 0 (0%)               |
| Hematocrit (L/L)                                | 0.40 (0.37–0.43)                          | 1 (<0.1%)            |
| Platelet (*10 <sup>9</sup> /L)                  | 214 (173–264)                             | 5 (<0.1%)            |
| <b>III. Liver function</b>                      |   |                      |
| Albumin (g/L)                                   | 40.0 (37.2–43.5)                          | 3 (<0.1%)            |
| Total bilirubin (μmol/L)                        | 7.9 (5.8–10.9)                            | 8 (<0.1%)            |
| Alanine aminotransferase (μ/L)                  | 23.4 (16.0–36.0)                          | 8 (<0.1%)            |
| Alkaline phosphatase (μ/L)                      | 66 (54–81)                                | 8 (<0.1%)            |
| <b>IV. Kidney function</b>                      |   |                      |
| Urea (mmol/L)                                   | 3.9 (3.1–4.8)                             | 5 (<0.1%)            |
| Creatinine (μmol/L)                             | 69.1 (58.0–83.0)                          | 5 (<0.1%)            |
| <b>V. Inflammatory marker</b>                   |   |                      |
| C-reactive protein                              | 0.4 (0.1–1.5)                             | 872 (11.5%)          |
| <b>VI. Electrolyte</b>                          |   |                      |
| Sodium (mmol/L)                                 | 138 (137–140)                             | 5 (<0.1%)            |
| Potassium (mmol/L)                              | 3.8 (3.5–4.1)                             | 31 (0.4%)            |
| Phosphate (mmol/L)                              | 1.04 (0.90–1.18)                          | 2,778 (36.5%)        |
| Calcium (mmol/L)                                | 2.26 (2.18–2.34)                          | 2,720 (35.8%)        |
| <b>VII. Others</b>                              |   |                      |
| Lactate dehydrogenase (μ/L)                     | 193.0 (165.0–235.0)                       | 238 (3.1%)           |
| Creatine kinase (μ/L)                           | 91 (63–143)                               | 818 (10.8%)          |

<sup>\*</sup>Decimal places were kept according to normal reference range.

patient record data, and the performance was demonstrated (8). Eighty percent of features were used before training each decision tree to prevent overfitting. Missing data were ignored in the training. A separate cohort of 722 COVID-19 positive patients admitted from January 1 to February 15, 2021, were retrieved as a separate temporal validation set to assess the prediction (see **Supplementary Table 2**). Shapley additive explanation (SHAP) (21) was used to explain the feature importance of the prediction model. The data processing was conducted using Python version 3.8.5 (Python Software Foundation, Beaverton, USA) and available libraries.

## Statistical Analysis

Descriptive statistics were generated using SPSS version 26 (IBM Corp, Armonk, NY). Because the numerical data were not normally distributed, medians and interquartile ranges were reported. For categorical data, counts and percentages were reported. The level of missing data was also reported.

To compare the intercluster dissimilarity of numerical data, the central limit theorem (CLT) was applied, and

parametric ANOVA was conducted. A  $p < 0.05$  equates to statistical significance. Because the Levene's test of equality of error variances was statistically significant, equal variance across clusters was not assumed. Games–Howell *post-hoc* tests were performed for multiple comparisons. To compare the intercluster dissimilarity of categorical data, a chi-square test was conducted. Bonferroni *post-hoc* tests were performed for multiple comparisons. Interquartile range (IQR) and charts were reported and used for interpretation (22).

## RESULTS

Initial data retrieval yielded a total of 8,562 patients. After data preparation to deal with missing variables and inconsistent data, a final number of 7,606 patients was kept (see **Figure 1**). The demographics and clinical characteristics are shown in **Table 1**.

Four clusters were identified using demographics and laboratory variables on admission. A separate analysis was done on the deceased cohort (see **Table 2**). The clusters were compared with one another. Each cluster was compared with the derived population and the most used normal reference range in the cohort. Each cluster was also compared with the deceased cases. A value was marked “high/low” if still within the reference range but considered close to the cutoff values. A value was marked “elevated/reduced” if it was outside the normal reference range (see **Table 2**, **Figure 2**; **Supplementary Table 3**).

## General Characteristics

The size of the four clusters were cluster 1:  $n = 1,959$ , cluster 2:  $n = 2,224$ , cluster 3:  $n = 1,850$ , and cluster 4:  $n = 1,573$ . Clusters 1 and 2 had the youngest median age [cluster 1: 36 (IQR: 24–50), cluster 2: 38 (IQR: 27–53)]. Increasing median age was observed from cluster 1 to 4. Clusters 2 and 4 had a greater proportion of males [cluster 2:  $n = 1,947$  (87.5%), cluster 4:  $n = 1,023$  (65.0%)]. The lymphocyte count was in the low value of the reference range in four clusters [cluster 1: 1.7 (IQR: 1.3–2.2), cluster 2: 1.5 (IQR: 1.2–2.0), cluster 3: 1.1 (IQR: 0.8–1.3), cluster 4: 1.0 (IQR: 0.7–1.3), normal reference range: 1.0–3.1]. Most of the indicators for liver function, including total bilirubin and alanine phosphatase levels, and for electrolytes, including sodium and potassium, were in the normal reference range for four clusters. Specific cluster analysis was discussed as follows.

## Cluster 1

Of COVID-19-positive patients, 25.4% ( $n = 1,959$ ) were aggregated in cluster 1. Cluster 1 was characterized by the youngest median age and the highest proportion of females (85.5%) within the cluster. The laboratory test results were unremarkable.

## Cluster 2

Of COVID-19-positive patients, 28.9% ( $n = 2,224$ ) were aggregated in cluster 2. Cluster 2 was characterized as the largest cluster with the highest proportion of males (87.5%) within the cluster. Hemoglobin, hematocrit, and creatinine levels were observed in the higher range of the reference values.



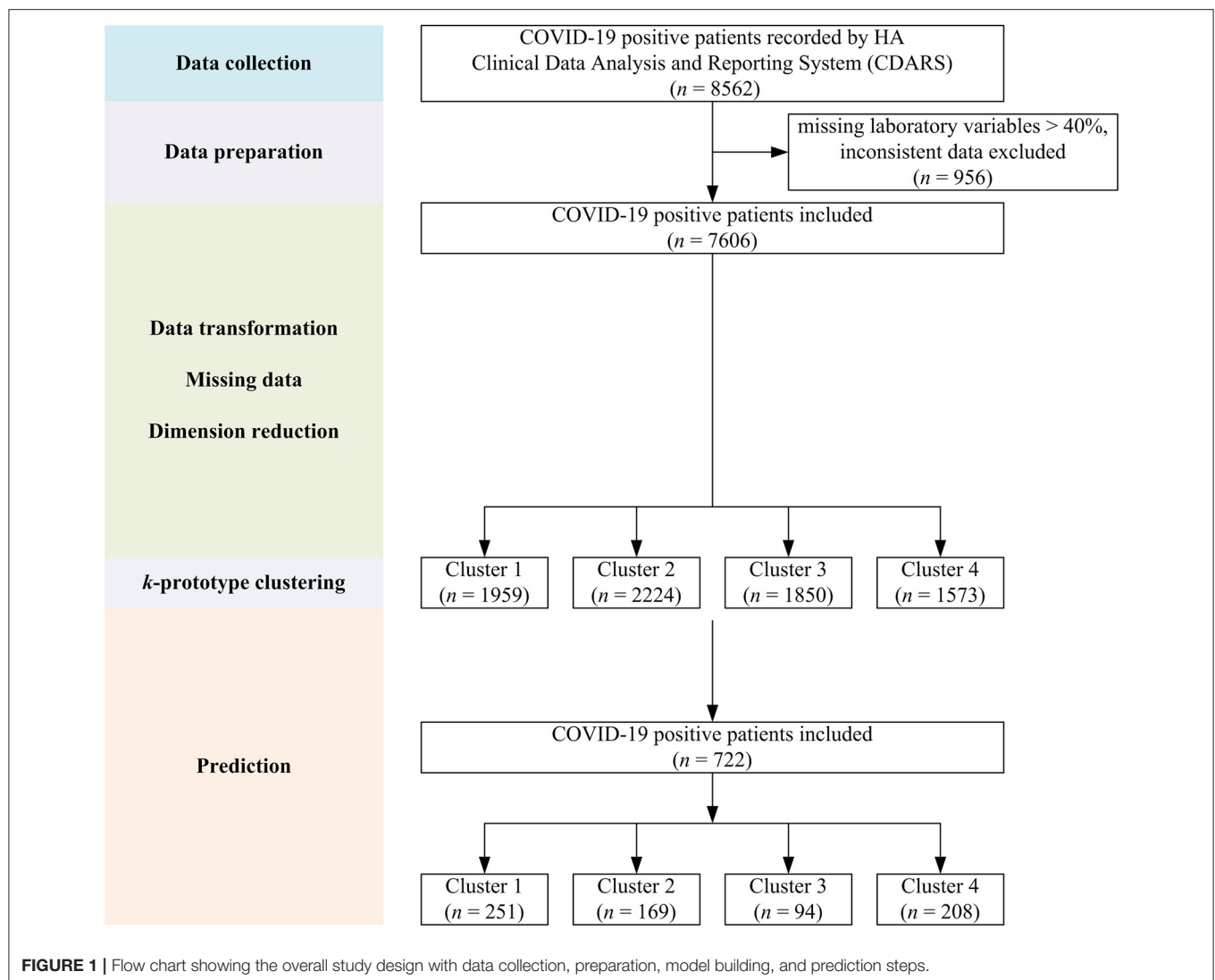


**FIGURE 1 |** Flow chart showing the overall study design with data collection, preparation, model building, and prediction steps.

### Cluster 3

Of COVID-19-positive patients, 24.0% ( $n = 1,850$ ) were aggregated in cluster 3. Cluster 3 was characterized by a higher proportion of females (76.1%) within the cluster. White blood cell counts were observed in the lower range of the reference values.

### Cluster 4

Of COVID-19-positive patients, 20.4% ( $n = 1,573$ ) were grouped in cluster 4. Significantly, cluster 4 captured 123 out of 142 (86.6%) deceased cases. Cluster 4 was characterized by being the smallest cluster with the oldest median age and a higher proportion of males. In terms of blood tests, hemoglobin, hematocrit, lymphocyte, and albumin levels were observed in the lower range. Neutrophil, urea, and C-reactive protein were observed in the higher range of the reference values. Lactate dehydrogenase was elevated. Cluster 4 also had the highest comorbidity scores with triple the rate of immunity disorders and diseases of the circulatory systems; double the rate of diseases of the nervous systems; and a higher proportion of

disease of the digestive system, genitourinary system, skin and subcutaneous tissue musculoskeletal system, other symptoms, injuries, and morphology of neoplasms compared with the other clusters. Cluster 4 captured almost all clinical characteristics of the deceased cases with the deceased cases having an even older median age and higher comorbidity scores.

### Deceased Cohort

There were 142 deceased cases in 7,606 censored COVID-19-positive patients. The deceased cohort was characterized by an old median age and a higher proportion of males. In terms of blood tests, lymphocyte, platelet, and albumin were observed in the lower range of the reference values. Urea and creatinine were observed in the higher range of the reference value. C-reactive protein and lactate dehydrogenase, although still in the reference range, were comparable to that of cluster 4 appearing higher than the other clusters. The comorbidity scores of the deceased cohort were high. There was a high degree of concordance with cluster 4.

**TABLE 2 |** Demographics and clinical characteristics of four clusters and deceased cohort for comparison.

| Characteristics<br>(unit; normal reference range**)      | Cluster 1<br>(n = 1,959) | Cluster 2<br>(n = 2,224) | Cluster 3<br>(n = 1,850) | Cluster 4<br>(n = 1,573) | p-value | Deceased<br>cohort     |
|--|--------------------------|--------------------------|--------------------------|--------------------------|---------|------------------------|
| Median (IQR) or count (within cluster %)                 |                          |                          |                          |                          |         |                        |
| <b>I. Demographics</b>                                   |                          |                          |                          |                          |         |                        |
| Age<br>(years)   | 36a***<br>(24–50)        | 38b<br>(27–53)           | 51c<br>(38–61)           | 65d<br>(57–75)           | <0.001  | 81<br>(74–87)          |
| Sex<br>(Males)   | 285a<br>(14.5%)          | 1947b<br>(87.5%)         | 442c<br>(23.9%)          | 1023d<br>(65.0%)         |         | 87<br>(61.3%)          |
| <b>II. Complete blood count</b>                          |                          |                          |                          |                          |         |                        |
| White blood Cell count<br>(*10 <sup>9</sup> /L; 3.7–9.2) | 6.2a<br>(5.2–7.5)        | 5.6b<br>(4.7–6.8)        | 3.8c<br>(3.2–4.3)        | 5.8d<br>(4.8–7.1)        | <0.001  | 6.9<br>(5.1–9.0)       |
| Neutrophil count<br>(*10 <sup>9</sup> /L; 1.7–5.8)       | 3.7a<br>(2.9–4.8)        | 3.3b<br>(2.6–4.2)        | 2.2c<br>(1.7–2.7)        | 4.0d<br>(3.2–5.3)        | <0.001  | 4.9<br>(3.5–7.4)       |
| Lymphocyte count<br>(*10 <sup>9</sup> /L; 1.0–3.1)       | 1.7a<br>(1.3–2.2)        | 1.5b<br>(1.2–2.0)        | 1.1c<br>(0.8–1.3)        | 1.0d<br>(0.7–1.3)        | <0.001  | 1.0<br>(0.7–1.3)       |
| Monocyte count<br>(*10 <sup>9</sup> /L; 0.1–0.8)         | 0.5a<br>(0.4–0.7)        | 0.6b<br>(0.4–0.7)        | 0.4c<br>(0.3–0.5)        | 0.5a<br>(0.4–0.7)        | <0.001  | 0.6<br>(0.3–0.8)       |
| Hemoglobin<br>(g/dL; 11.7–14.9)                          | 13.0a<br>(12.1–13.6)     | 15.1b<br>(14.5–15.7)     | 13.2c<br>(12.3–13.9)     | 13.3c<br>(12.1–14.2)     | <0.001  | 12.2<br>(10.7–13.4)    |
| Hematocrit<br>(L/L; 0.35–0.45)                           | 0.38a<br>(0.36–0.40)     | 0.44b<br>(0.43–0.46)     | 0.39c<br>(0.37–0.41)     | 0.39c<br>(0.36–0.42)     | <0.001  | 0.36<br>(0.32–0.40)    |
| <b>III. Liver function</b>                               |                          |                          |                          |                          |         |                        |
| Albumin<br>(g/L; 35.0–52.0)                              | 41.2a<br>(38.8–43.9)     | 43.0b<br>(40.9–45.5)     | 40.0c<br>(37.0–42.0)     | 36.0d<br>(32.0–39.0)     | <0.001  | 34.0<br>(29.0–38.1)    |
| Total bilirubin<br>(μmol/L; 5.0–21.0)                    | 7.0a<br>(5.0–9.7)        | 9.5b<br>(7.0–12.9)       | 6.6c<br>(5.0–9.0)        | 8.2d<br>(6.2–11.3)       | <0.001  | 8.2<br>(6.0–11.6)      |
| Alanine aminotransferase<br>(μ/L; 0.0–34.4)              | 18.0a<br>(13.1–27.0)     | 29.0b<br>(20.0–45.0)     | 20.0a<br>(14.0–28.5)     | 29.0b<br>(20.0–44.0)     | <0.001  | 20.8<br>(14.0–33.2)    |
| Alkaline phosphatase<br>(μ/L; 30–120)                    | 67a<br>(54–87)           | 69b<br>(58–82)           | 60c<br>(50–73)           | 67b<br>(56–84)           | <0.001  | 72<br>(59–103)         |
| <b>IV. Kidney function</b>                               |                          |                          |                          |                          |         |                        |
| Urea<br>(mmol/L; 2.8–8.1)                                | 3.4a<br>(2.7–4.1)        | 4.2b<br>(3.6–5.0)        | 3.6c<br>(2.9–4.3)        | 4.9d<br>(3.9–6.6)        | <0.001  | 7.0<br>(5.3–10.0)      |
| Creatinine<br>(μmol/L; 49.0–90.0)                        | 57.0a<br>(50.8–64.0)     | 80.0b<br>(72.0–90.0)     | 72.0c<br>(62.8–84.0)     | 82.0d<br>(69.0–101.0)    | <0.001  | 101.1<br>(73.0–137.7)  |
| <b>V. Inflammatory marker</b>                            |                          |                          |                          |                          |         |                        |
| C-reactive protein<br>(mg/dL; 0.0–5.0)                   | 0.2a<br>(0.1–0.4)        | 0.3b<br>(0.1–0.7)        | 0.5c<br>(0.2–1.2)        | 3.6d<br>(1.6–7.2)        | <0.001  | 3.6<br>(1.3–8.6)       |
| <b>VI. Electrolyte</b>                                   |                          |                          |                          |                          |         |                        |
| Sodium<br>(mmol/L; 136–145)                              | 139a<br>(137–140)        | 139a<br>(138–140)        | 139b<br>(137–140)        | 136c<br>(133–138)        | <0.001  | 136<br>(133–140)       |
| Potassium<br>(mmol/L; 3.4–4.8)                           | 3.8a<br>(3.5–4.0)        | 3.9b<br>(3.6–4.1)        | 3.7c<br>(3.4–3.9)        | 3.8a<br>(3.5–4.1)        | <0.001  | 4.0<br>(3.7–4.3)       |
| Phosphate<br>(mmol/L; 0.88–1.45)                         | 1.11a<br>(0.98–1.27)     | 1.07b<br>(0.95–1.20)     | 1.02c<br>(0.89–1.15)     | 0.95d<br>(0.83–1.09)     | <0.001  | 1.08<br>(0.90–1.23)    |
| Calcium<br>(mmol/L; 2.15–2.55)                           | 2.31a<br>(2.25–2.38)     | 2.33a<br>(2.26–2.39)     | 2.22b<br>(2.16–2.28)     | 2.17c<br>(2.10–2.24)     | <0.001  | 2.14<br>(2.06–2.25)    |
| <b>VII. Others</b>                                       |                          |                          |                          |                          |         |                        |
| Lactate dehydrogenase<br>(μ/L; 0.0–246.4)                | 176.5a<br>(154.0–208.0)  | 182.2b<br>(161.0–210.0)  | 191.0c<br>(164.0–220.0)  | 263.0d<br>(212.0–350.0)  | <0.001  | 249.0<br>(199.1–378.8) |
| Creatine kinase<br>(μ/L; 39–308)                         | 67a<br>(49–91)           | 104b<br>(76–151)         | 82c<br>(59–120)          | 141d<br>(85–258)         | <0.001  | 131<br>(71–250)        |

\*\*Most used normal reference range.

\*\*\*Each subscript letter denotes a cluster whose column proportions do not differ significantly from each other at the 0.05 significance level. The clusters with different letter are significantly different from each other at the 0.05 significance level.

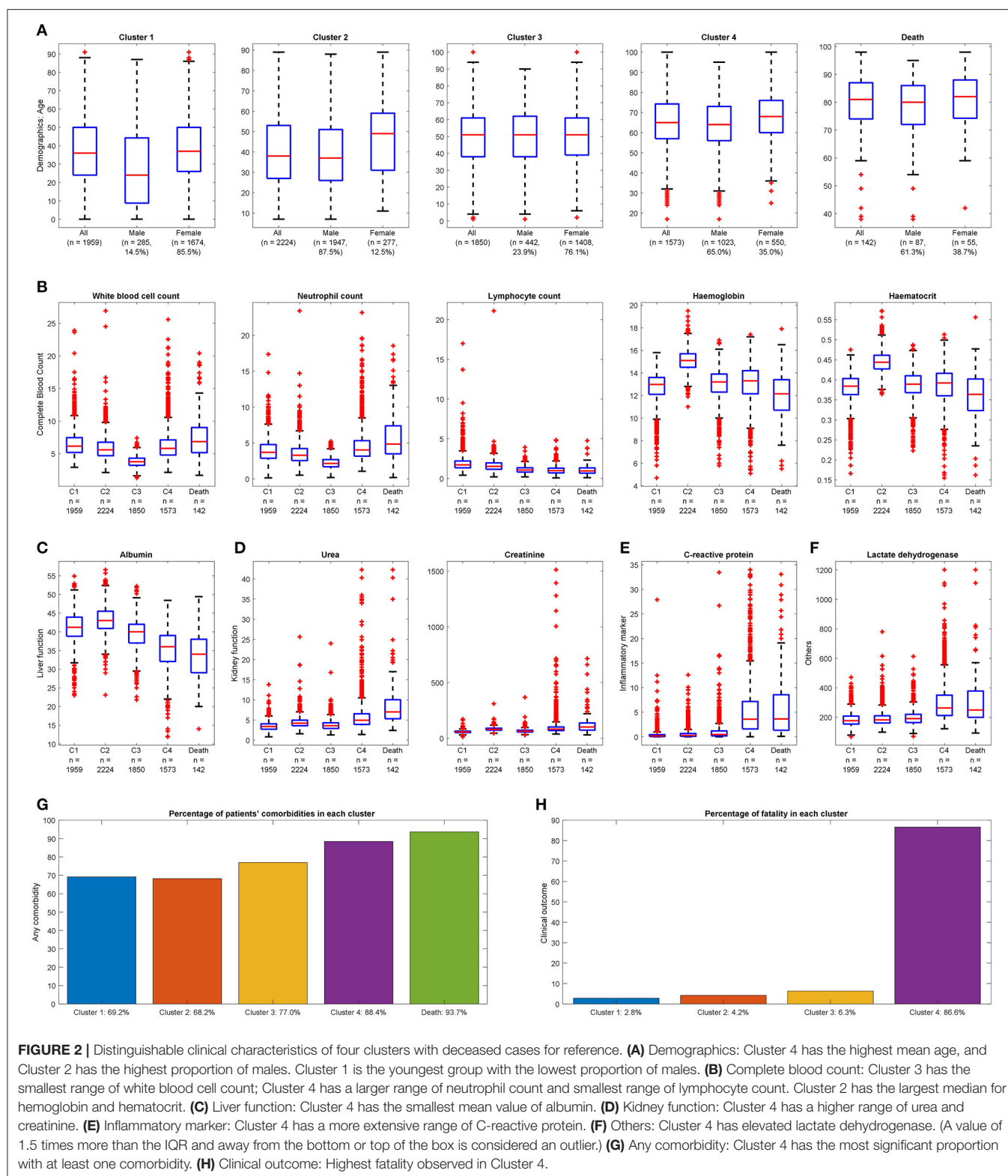


**FIGURE 2 |** Distinguishable clinical characteristics of four clusters with deceased cases for reference. **(A)** Demographics: Cluster 4 has the highest mean age, and Cluster 2 has the highest proportion of males. Cluster 1 is the youngest group with the lowest proportion of males. **(B)** Complete blood count: Cluster 3 has the smallest range of white blood cell count; Cluster 4 has a larger range of neutrophil count and smallest range of lymphocyte count. Cluster 2 has the largest median for hemoglobin and hematocrit. **(C)** Liver function: Cluster 4 has the smallest mean value of albumin. **(D)** Kidney function: Cluster 4 has a higher range of urea and creatinine. **(E)** Inflammatory marker: Cluster 4 has a more extensive range of C-reactive protein. **(F)** Others: Cluster 4 has elevated lactate dehydrogenase. (A value of 1.5 times more than the IQR and away from the bottom or top of the box is considered an outlier.) **(G)** Any comorbidity: Cluster 4 has the most significant proportion with at least one comorbidity. **(H)** Clinical outcome: Highest fatality observed in Cluster 4.

## Evaluation

Cluster analysis was also applied to a separate temporal validation set with the results of seven out of eight (87.5%) deceased cases being captured by cluster 4.

To further verify if criteria generated by *k*-prototype clustering were properly followed, SHAP was used to determine the feature importance used in the classification (see **Figure 3**). Overall, white blood count has the highest mean SHAP value for the

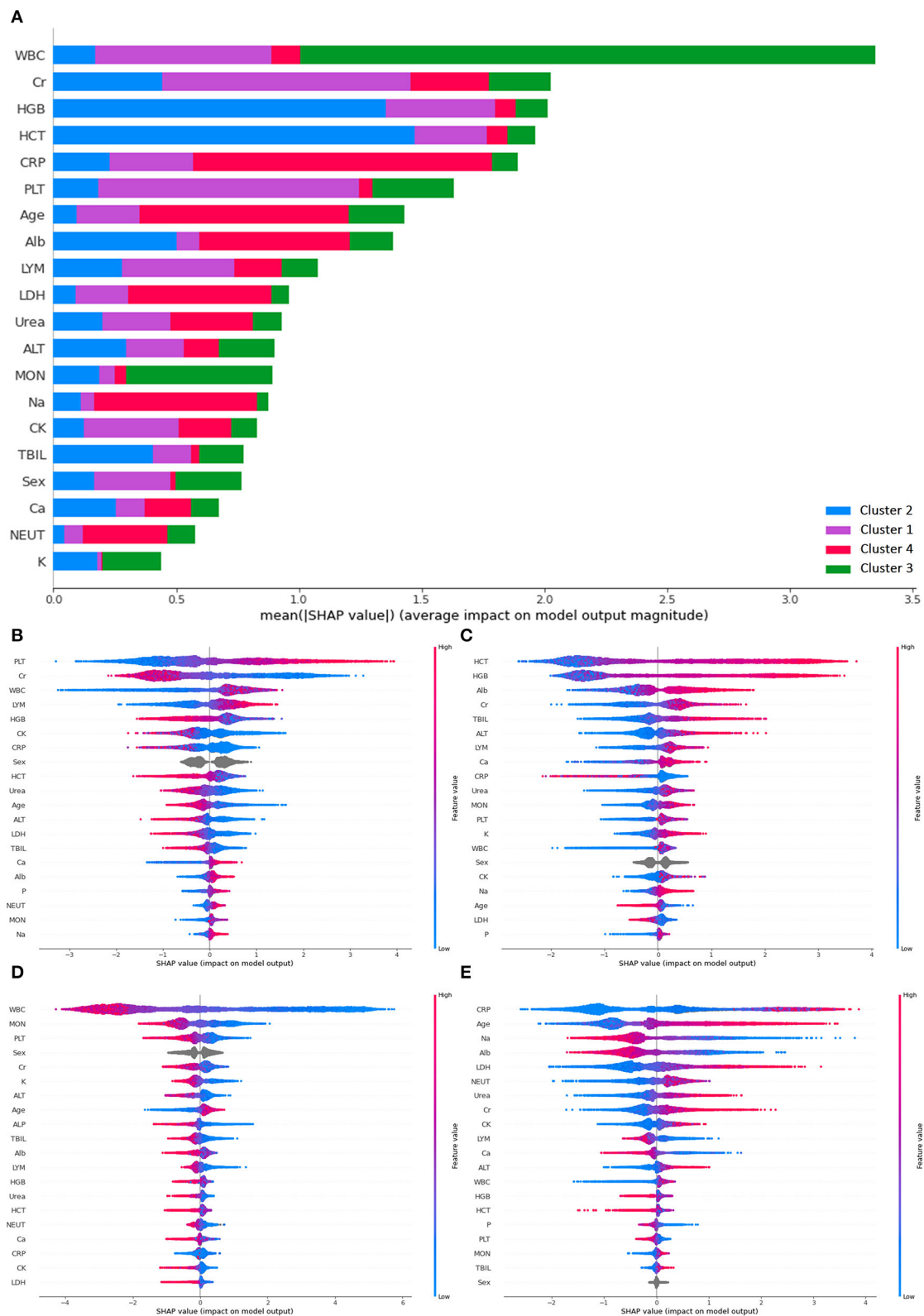


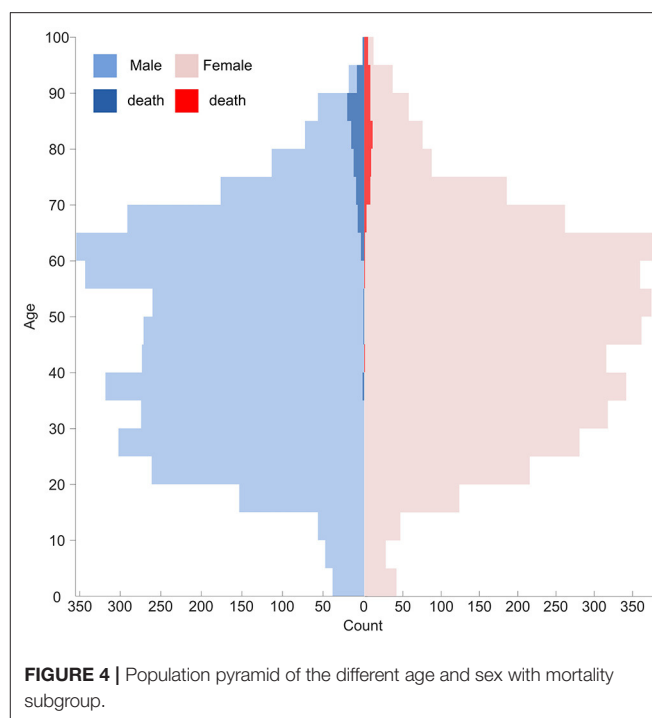
**FIGURE 3 |** SHAP plots demonstrating differential importance of different features and clusters. **(A)** Mean SHAP value of the prediction, **(B)** SHAP value for cluster 1, **(C)** SHAP value for cluster 2, **(D)** SHAP value for cluster 3, **(E)** SHAP value for cluster 4. ALT, Alanine aminotransferase; Alb, albumin; ALP, alkaline phosphatase; Ca, calcium; CRP, C-reactive protein; CK, creatine kinase; Cr, creatinine; HCT, hematocrit; HGB, hemoglobin; LDH, lactate dehydrogenase; LYM, lymphocyte count; MON, monocyte count; NEUT, neutrophil count; P, phosphate; PLT, platelet; K, potassium; Na, sodium; TBIL, total bilirubin; WBC, white blood cell.

prediction, followed by creatinine, hemoglobin, hematocrit, C-reactive protein, and platelet. High platelet and low creatinine were most important in classifying patients into cluster 1. Elevated hemoglobin and hematocrit were most important in classifying patients into cluster 2. Reduced white blood cell count was the most important in classifying patients into cluster 3. High C-reactive protein and old age were most important in classifying patients into cluster 4.

## DISCUSSION

Unsupervised clustering was used to probe the latent phenotypes of 7,606 COVID-19-positive patients in Hong Kong across 2020. Based on age, sex, and 20 laboratory blood tests on admission, one of the four generated clusters aggregated 86.6% of deceased cases without prior information of their clinical outcomes. The clinical characteristics of this cluster, including the oldest median age; highest aggregated comorbidity; and the laboratory tests of hemoglobin, hematocrit, and lymphocyte were observed to be in the lower range of normal, whereas neutrophil, C-reactive protein, and lactate dehydrogenase were observed to be in the higher range of normal. Findings are comparable with poor prognostic features based on contemporaneous literature. Notably, when applied to a separate validation cohort, cluster 4 was still able to identify seven out of eight (87.5%) deceased cases. A potential clinical utility may be to call for early medical attention and resource to patients that belong to cluster 4 at the initial diagnosis at hospitalization. The clinical characteristics of cluster 4 and deceased cases in this study aligned with previous findings (23–25). First, old age reflects a weaker immune system to fight against pathogens, including pneumonia (26). It is a well-established risk factor correlated with chronicity and comorbidity in COVID-19 prognosis (10, 27). On the other hand, increased neutrophil count and high neutrophil-to-lymphocyte ratio can be elicited by deep airway and alveolar damage. They represent an acute inflammatory response and are indicators of a poor prognosis and higher disease severity for COVID-19 (28–31). In line with cluster 4 and the deceased cases in this study, at an early stage of COVID-19, lymphocyte counts typically decrease, whereas white blood cell count may or may not decrease (32). In addition, patients with severe COVID-19 outcomes have exhibited abnormally high C-reactive protein levels, lactate dehydrogenase, and neutrophils, implying an inflammatory response and severe pneumonia (33). Although C-reactive protein level is not affected by physical status, age, and sex (34), it may be used to early diagnose severe pulmonary disease secondary to bacterial infection (35).

A greater proportion of males than females were infected with COVID-19 in contemporary literatures as well as MERS-CoV and SARS-CoV infection (24, 36, 37). It can be a cofounder in evaluating the sex-based difference in the susceptibility of COVID-19 (38). In this retrospective study, the proportion of males and females was roughly equal across all age groups (see **Figure 4**) on admission. No significant difference in disease prevalence existed between males and females. Under this condition, a higher proportion of males was still observed in



cluster 4 (65.0%) and deceased cases (61.3%). It indicates being male as a risk factor for mortality (37, 39, 40). This reduced disease susceptibility of females is hypothesized to be related to the major roles of the X chromosome and sex hormones in innate and adaptive immunity (41). Nonetheless, this correlation needs further exploration and investigation.

The complications of COVID-19 include severe pneumonia, septic shock, acute respiratory distress syndrome (ARDS), and multiple organ failure (31, 42). Although lung has been the primary organ involved in the infection, elevated creatinine and urea levels were also detected in cluster 4 and in the deceased cases, which implies that impaired renal function was a potential early indicator of poor prognosis. Additionally, a low albumin level, reflective of liver synthetic function, was also observed. These abnormal laboratory variables imply that indicators for early multiorgan failure were important and is likely a reflection of systemic inflammatory response. For the reduced hemoglobin and hematocrit levels detected in cluster 4 and the deceased, a prior study suggests that SARS-CoV-2 may attack the heme on 1-beta chain of hemoglobin through CD147, and CD26, ACE2 receptors or by simulating hepcidin to increase tissue ferritin, block ferroprotein, causing the iron deficiency, and thus lower hemoglobin level (43).

In previous clustering analysis (10–12), both three and four clusters have been identified, which were similar to the number chosen by this study. Previous clusters have also found some correlations for a poor prognosis, such as old age and high comorbidity scores (12, 28), being male, high lymphocytes high neutrophil count (11), and albumin level (12). In respect to the clinical outcomes, our study shows the greatest power to differentiate a cluster by aggregating 86.6%



deceased cases and capturing most of their clinical characteristics and correlations.

There were several key strengths to our study. First, a large sample size of 7,606 COVID-19-positive patients was included. This adds to greater statistical power and generalizability. The data were collected from a single integrated EHR system fully covering the Hong Kong population, meaning the clinical data set is representative of this cohort. Second, all patients that were tested positive despite mild or no symptoms were nevertheless hospitalized in Hong Kong. Our study is unique capturing a wide spectrum of clinical severity. On the contrary, most other countries only tend to admit patients with severe symptoms to the hospitals. Third, we validated our clusters on a separate temporal validation with further feature explanation using SHAP. It was demonstrated that criteria from PCA-based  $k$ -prototype clustering were correctly captured, used, and inferred. Granular analysis of these distinct clusters should give a better understanding of different clinical representations of COVID-19 on admission. Besides this, delineating interactions between specific chronicity and poor prognosis regarding different clinical groups can help understand the mechanism of COVID-19.

There were a few limitations to our study. First, for a retrospective study using observational data, the sampling was not random. There may be the potential of selection and recall bias. Although all age groups were represented, they were not evenly distributed. The results and interpretations will be best applied to the Hong Kong cohort with race dominated by patients of Chinese ethnicity although there were several imported cases of different ethnic origins. Owing to a lack of accurate data on ethnicity, we could not perform further sub-analysis. Second, as with any large-scale studies covering multiple hospitals, there may be different standards and measurement protocols. It was observed that the normal reference ranges of laboratory variables varied mildly across institutions and according to age and sex. Because no significant discrepancy was detected, the data were put together directly using their original values. Although a linear mapping could have been used to reduce the systematic noise, variations due to age and sex need to be further distinguished. Finally, some potential important clinical and laboratory data with more than 50% of missing data were excluded from the study. They include BMI, blood pressure, oxygen saturation, D-Dimer, need for assisted ventilation, ITU admission, etc., which are potentially useful for severity assessment and prognostication. These may additionally aid prediction and more accurate allocation of medical resources in the future. Owing to a lack of testing or

accurate documentations, these were not able to be included in this large scale multi-institutional study. These variables are recommended to be documented or performed in the future. However, they were not routinely recorded nor taken in usual clinical practice in Hong Kong at the time of the study period.

## CONCLUSION

Unsupervised clustering was used to probe the latent phenotypes of 7,606 COVID-19-positive patients in Hong Kong across the year 2020. Based on age, sex, and 20 laboratory variables on admission, one of the four generated clusters aggregated 86.6% deceased cases without prior knowledge of their clinical outcomes. Further understanding of the different COVID-19 clinical phenotypes may pave the way for more individualized patient risk stratification and treatment.

## DATA AVAILABILITY STATEMENT

Data can be provided upon reasonable request and inquiries can be directed to the corresponding author

## ETHICS STATEMENT

The studies involving human participants were reviewed and approved by Cluster Research Ethics Committee/Institutional Review Board (REC/IRB). Written informed consent for participation was not required for this study in accordance with the national legislation and the institutional requirements.

## AUTHOR CONTRIBUTIONS

KL, K-SN, and VV were involved in study conception, statistical analysis, and drafting of the initial version of the manuscript. K-SN and VV were involved in data collection. K-WK, KT, C-FS, C-WL, and VV supervised the work and offered significant intellectual contribution. All authors discussed the data analysis, results, and approved the final version.

## SUPPLEMENTARY MATERIAL

The Supplementary Material for this article can be found online at: <https://www.frontiersin.org/articles/10.3389/fmed.2021.764934/full#supplementary-material>

## REFERENCES

- Zhu N, Zhang D, Wang W, Li X, Yang B, Song J, et al. A Novel Coronavirus from Patients with Pneumonia in China, 2019. *N Engl J Med.* (2020) 382:727–33. doi: 10.1056/NEJMoa2001017
- Li Q, Guan X, Wu P, Wang X, Zhou L, Tong Y, et al. Early transmission dynamics in Wuhan, China, of novel coronavirus-infected pneumonia. *N Engl J Med.* (2020) 382:1199–207. doi: 10.1056/NEJMoa2001316
- Yan L, Zhang H-T, Goncalves J, Xiao Y, Wang M, Guo Y, et al. A machine learning-based model for survival prediction in patients with severe COVID-19 infection. *medRxiv.* (2020) 7:1–7. doi: 10.1101/2020.02.27.20028027
- Wynants L, Van Calster B, Collins GS, Riley RD, Heinze G, Schuit E, et al. Prediction models for diagnosis and prognosis of covid-19: systematic review and critical appraisal. *BMJ.* (2020) 369:m1328. doi: 10.1136/bmj.m1328

5. Vaid A, Somani S, Russak AJ, De Freitas JK, Chaudhry FF, Paranjpe I, et al. Machine learning to predict mortality and critical events in a cohort of patients with COVID-19 in New York City: model development and validation. *J Med Internet Res.* (2020) 22:e24018. doi: 10.2196/24018
6. Alakus TB, Turkoglu I. Comparison of deep learning approaches to predict COVID-19 infection. *Chaos Soliton Fract.* (2020) 140:110120. doi: 10.1016/j.chaos.2020.110120
7. An C, Lim H, Kim D-W, Chang JH, Choi YJ, Kim SW. Machine learning prediction for mortality of patients diagnosed with COVID-19: a nationwide Korean cohort study. *Sci Rep.* (2020) 10:18716. doi: 10.1038/s41598-020-75767-2
8. Ferrari D, Milic J, Tonelli R, Ghinelli F, Meschiari M, Volpi S, et al. Machine learning in predicting respiratory failure in patients with COVID-19 pneumonia—Challenges, strengths, and opportunities in a global health emergency. *PLoS ONE.* (2020) 15:e0239172. doi: 10.1371/journal.pone.0239172
9. Du R, Tsougenis ED, Ho JWK, Chan JKY, Chiu KWH, Fang BXH, et al. Machine learning application for the prediction of SARS-CoV-2 infection using blood tests and chest radiograph. *Sci Rep.* (2021) 11:14250. doi: 10.1038/s41598-021-93719-2
10. Cui W, Robins D, Finkelstein J. Unsupervised machine learning for the discovery of latent clusters in COVID-19 patients using electronic health records. *Stud Health Technol Inform.* (2020) 272:1–4. doi: 10.3233/SHTI200478
11. Li WT, Ma J, Shende N, Castaneda G, Chakladar J, Tsai JC, et al. Using machine learning of clinical data to diagnose COVID-19: a systematic review and meta-analysis. *BMC Med Inform Decis Mak.* (2020) 20:247. doi: 10.1186/s12911-020-01266-z
12. Ye W, Lu W, Tang Y, Chen G, Li X, Ji C, et al. Identification of COVID-19 clinical phenotypes by principal component analysis-based cluster analysis. *Front Med.* (2020) 7:570614. doi: 10.3389/fmed.2020.570614
13. Jakobsen JC, Gluud C, Wetterslev J, Winkel P. When and how should multiple imputation be used for handling missing data in randomised clinical trials – a practical guide with flowcharts. *BMC Med Res Methodol.* (2017) 17:162. doi: 10.1186/s12874-017-0442-1
14. World Health Organisation. *International Classification of Diseases: [9th] Ninth Revision, Basic Tabulation List With Alphabetic Index.* Geneva: World Health Organization (1978).
15. Yeo IK, Johnson RA. A new family of power transformations to improve normality or symmetry. *Biometrika.* (2000) 87:954–9. doi: 10.1093/biomet/87.4.954
16. Raghunathan TE, Lepkowski JM, Van Hoewyk J, Solenberger P. A multivariate technique for multiply imputing missing values using a sequence of regression models. *Surv Methodol.* (2001) 27:85–96.
17. Carpenter JR, Kenward MG. *Missing Data in Randomised Controlled Trials: A Practical Guide.* Birmingham: Health Technology Assessment Methodology Programme (2007). p. 199.
18. Papageorgiou G, Grant SW, Takkenberg JJM, Mokhles MM. Statistical primer: how to deal with missing data in scientific research? *Interact CardioVasc Thoracic Surg.* (2018) 27:153–8. doi: 10.1093/icvts/ivy102
19. Huang Z. Extensions to the k-means algorithm for clustering large data sets with categorical values. *Data Min Knowl Discov.* (1998) 2:283–304.
20. Ke G, Meng Q, Finley T, Wang T, Chen W, Ma W, et al. (editors). *LightGBM: A Highly Efficient Gradient Boosting Decision Tree.* Long Beach, CA: NIPS (2017).
21. Lundberg SM, Erion G, Chen H, DeGrave A, Prutkin JM, Nair B, et al. From local explanations to global understanding with explainable AI for trees. *Nat Machine Intell.* (2020) 2:56–67. doi: 10.1038/s42256-019-0138-9
22. Kaplan RM, Chambers DA, Glasgow RE. Big data and large sample size: a cautionary note on the potential for bias. *Clin Transl Sci.* (2014) 7:342–6. doi: 10.1111/cts.12178
23. Wang D, Hu B, Hu C, Zhu F, Liu X, Zhang J, et al. Clinical characteristics of 138 hospitalized patients with 2019 novel coronavirus-infected pneumonia in Wuhan, China. *JAMA.* (2020) 323:1061–9. doi: 10.1001/jama.2020.1585
24. Chen N, Zhou M, Dong X, Qu J, Gong F, Han Y, et al. Epidemiological and clinical characteristics of 99 cases of 2019 novel coronavirus pneumonia in Wuhan, China: a descriptive study. *Lancet.* (2020) 395:507–13. doi: 10.1016/S0140-6736(20)30211-7
25. Guan W-j, Ni Z-y, Hu Y, Liang W-h, Ou C-q, He J-x, et al. Clinical characteristics of coronavirus disease 2019 in China. *N Engl J Med.* (2020) 382:1708–20. doi: 10.1056/NEJMoa2002032
26. Yang J, Zheng Y, Gou X, Pu K, Chen Z, Guo Q, et al. Prevalence of comorbidities and its effects in patients infected with SARS-CoV-2: a systematic review and meta-analysis. *Int J Infect Dis.* (2020) 94:91–5. doi: 10.1016/j.ijid.2020.03.017
27. Lee K-Y. Pneumonia, acute respiratory distress syndrome, and early immune-modulator therapy. *Int J Mol Sci.* (2017) 18:388. doi: 10.3390/ijms18020388
28. Zhang B, Zhou X, Zhu C, Feng F, Qiu Y, Feng J, et al. Immune phenotyping based on neutrophil-to-lymphocyte ratio and IgG predicts disease severity and outcome for patients with COVID-19. *medRxiv.* (2020). doi: 10.1101/2020.03.12.20035048
29. Ye W, Chen G, Li X, Lan X, Ji C, Hou M, et al. Dynamic changes of D-dimer and neutrophil-lymphocyte count ratio as prognostic biomarkers in COVID-19. *Respir Res.* (2020) 21:169. doi: 10.1186/s12931-020-01428-7
30. Celikbilek M, Dogan S, Ozbakir O, Zarsarsiz G, Küçük H, Gürsoy S, et al. Neutrophil-lymphocyte ratio as a predictor of disease severity in ulcerative colitis. *J Clin Lab Anal.* (2013) 27:72–6. doi: 10.1002/jcla.21564
31. Huang C, Wang Y, Li X, Ren L, Zhao J, Hu Y, et al. Clinical features of patients infected with 2019 novel coronavirus in Wuhan, China. *Lancet.* (2020) 395:497–506. doi: 10.1016/S0140-6736(20)30183-5
32. Jin Y-H, Cai L, Cheng Z-S, Cheng H, Deng T, Fan Y-P, et al. A rapid advice guideline for the diagnosis and treatment of 2019 novel coronavirus (2019-nCoV) infected pneumonia (standard version). *Military Med Res.* (2020) 7:4. doi: 10.1186/s40779-020-0233-6
33. Wang L. C-reactive protein levels in the early stage of COVID-19. *Méd Maladies Infect.* (2020) 50:332–4. doi: 10.1016/j.medmal.2020.03.007
34. Bilgir O, Bilgir F, Calan M, Calan OG, Yuksel A. Comparison of pre- and post-levothyroxine high-sensitivity c-reactive protein and fetuin-a levels in subclinical hypothyroidism. *Clinics.* (2015) 70:97–101. doi: 10.6061/clinics/2015(02)05
35. Warusevitane A, Karunatilake D, Sim J, Smith C, Roffe C. Early diagnosis of pneumonia in severe stroke: clinical features and the diagnostic role of C-reactive protein. *PLoS ONE.* (2016) 11:e0150269. doi: 10.1371/journal.pone.0150269
36. Badawi A, Ryoo SG. Prevalence of comorbidities in the Middle East respiratory syndrome coronavirus (MERS-CoV): a systematic review and meta-analysis. *Int J Infect Dis.* (2016) 49:129–33. doi: 10.1016/j.ijid.2016.06.015
37. Channappanavar R, Fett C, Mack M, Ten Eyck PP, Meyerholz DK, Perlman S. Sex-based differences in susceptibility to severe acute respiratory syndrome coronavirus infection. *J Immunol.* (2017) 198:4046–53. doi: 10.4049/jimmunol.1601896
38. Docherty A, Harrison E, Green C, Hardwick H, Pius R, Norman L, et al. Features of 16,749 hospitalised UK patients with COVID-19 using the ISARIC WHO Clinical Characterisation Protocol. *medRxiv.* (2020). doi: 10.1101/2020.04.23.20076042
39. Deng G, Yin M, Chen X, Zeng F. Clinical determinants for fatality of 44,672 patients with COVID-19. *Crit Care.* (2020) 24:179. doi: 10.1186/s13054-020-02902-w
40. Williamson EJ, Walker AJ, Bhaskaran K, Bacon S, Bates C, Morton CE, et al. Factors associated with COVID-19-related death using OpenSAFELY. *Nature.* (2020) 584:430–6. doi: 10.1038/s41586-020-2521-4
41. Jaillon S, Berthenet K, Garlanda C. Sexual dimorphism in innate immunity. *Clin Rev Allergy Immunol.* (2019) 56:308–21. doi: 10.1007/s12016-017-8648-x
42. Xu Z, Shi L, Wang Y, Zhang J, Huang L, Zhang C, et al. Pathological findings of COVID-19 associated with acute respiratory distress syndrome. *Lancet Respir Med.* (2020) 8:420–2. doi: 10.1016/S2213-2600(20)30076-X

43. Cavezzi A, Troiani E, Corrao S. COVID-19: hemoglobin, iron, and hypoxia beyond inflammation. A narrative review. *Clin Pract.* (2020) 10:1271. doi: 10.4081/cp.2020.1271

**Conflict of Interest:** The authors declare that the research was conducted in the absence of any commercial or financial relationships that could be construed as a potential conflict of interest.

**Publisher's Note:** All claims expressed in this article are solely those of the authors and do not necessarily represent those of their affiliated organizations, or those of

the publisher, the editors and the reviewers. Any product that may be evaluated in this article, or claim that may be made by its manufacturer, is not guaranteed or endorsed by the publisher.

*Copyright © 2022 Lau, Ng, Kwok, Tsia, Sin, Lam and Vardhanabhuti. This is an open-access article distributed under the terms of the Creative Commons Attribution License (CC BY). The use, distribution or reproduction in other forums is permitted, provided the original author(s) and the copyright owner(s) are credited and that the original publication in this journal is cited, in accordance with accepted academic practice. No use, distribution or reproduction is permitted which does not comply with these terms.*



# Research on Spatial-temporal Spread and Risk Profile of the COVID-19 Epidemic Based on Mobile Phone Trajectory Data

Qi Zuo<sup>1\*</sup>, Jiaman Du<sup>2</sup>, Baofeng Di<sup>1</sup>, Junrong Zhou<sup>3</sup>, Lixia Zhang<sup>4</sup>, Hongxia Liu<sup>5</sup> and Xiaoyu Hou<sup>6</sup>

<sup>1</sup> Institute for Disaster Management and Reconstruction, Sichuan University, Chengdu, China, <sup>2</sup> The School of International Studies, Sichuan University, Chengdu, China, <sup>3</sup> Chengdu Fangwei Technology Co., Ltd., Chengdu, China, <sup>4</sup> Sichuan Wisisoft System Integration Co., Ltd., Chengdu, China, <sup>5</sup> West China Hospital, Sichuan University, Chengdu, China, <sup>6</sup> SinoMaps Press Co., Ltd., Beijing, China

## OPEN ACCESS

### Edited by:

Reza Lashgari,  
Shahid Beheshti University, Iran

### Reviewed by:

Ariful Islam,  
EcoHealth Alliance, United States  
Gregory R. Hart,  
Yale University, United States

### \*Correspondence:

Qi Zuo  
1818688@qq.com

### Specialty section:

This article was submitted to  
Medicine and Public Health,  
a section of the journal  
Frontiers in Big Data

Received: 06 May 2021

Accepted: 23 March 2022

Published: 27 April 2022

### Citation:

Zuo Q, Du J, Di B, Zhou J, Zhang L,  
Liu H and Hou X (2022) Research on  
Spatial-temporal Spread and Risk  
Profile of the COVID-19 Epidemic  
Based on Mobile Phone Trajectory  
Data. *Front. Big Data* 5:705698.  
doi: 10.3389/fdata.2022.705698

The COVID-19 epidemic poses a significant challenge to the operation of society and the resumption of work and production. How to quickly track the resident location and activity trajectory of the population, and identify the spread risk of the COVID-19 in geospatial space has important theoretical and practical significance for controlling the spread of the virus on a large scale. In this study, we take the geographical community as the research object, and use the mobile phone trajectory data to construct the spatiotemporal profile of the potential high-risk population. First, by using the spatiotemporal data collision method, identify, and recover the trajectories of the people who were in the same area with the confirmed patients during the same time. Then, based on the range of activities of both cohorts (the confirmed cases and the potentially infected groups), we analyze the risk level of the relevant places and evaluate the scale of potential spread. Finally, we calculate the probability of infection for different communities and construct the spatiotemporal profile for the transmission to help guide the distribution of preventive materials and human resources. The proposed method is verified using survey data of 10 confirmed cases and statistical data of 96 high-risk neighborhoods in Chengdu, China, between 15 January 2020 and 15 February 2020. The analysis finds that the method accurately simulates the spatiotemporal spread of the epidemic in Chengdu and measures the risk level in specific areas, which provides an objective basis for the government and relevant parties to plan and manage the prevention and control of the epidemic.

**Keywords:** COVID-19, community, risk profiling, mobile phone trajectory data, the spatiotemporal spread

## INTRODUCTION

Since the first reported case of COVID-19 in the world in December 2019, and until 30 September 2020, 208 countries and regions on six continents have successively reported confirmed cases. The mortality rate of the European countries is peaking at more than 10% at the end of March 2020 (Niu et al., 2020). Studies have found that the spread of the COVID-19 virus is affected by population density and population mobility, and has obvious temporal and spatial aggregation

(Huang and He, 2010; Ahmadi et al., 2020). Therefore, tracking and isolation of close contacts and suspected cases is the key to epidemic prevention and control.

Mobile phone trajectory data is a kind of spatiotemporal trajectory big data. Based on the position of the cellular base stations, the data can be extrapolated into the spatiotemporal distribution and flow matrix of the entire population in a highly anonymized manner. The rapid development and popularization of information technology make mobile phone trajectory data analysis become one of the most effective ways to quickly track the movement of the population. However, mobile phone trajectory data is complex and diverse, and the analysis workload is heavy. Fortunately, the rapid collision method based on time-space trajectory greatly improves the analysis efficiency. In the scene of large data volume and sizeable crowd, this method can still quickly analyze the data with high performance and obtain information about the number of encounters or contacts between individuals and the location of the contacts (Tang et al., 2017; Wang, 2017). Therefore, based on the characteristics of mobile phone trajectory data, by combining the communication signaling and geographic information, we simulate the full trajectory data of more than 16 million people in Chengdu to form the trajectory basis for spatiotemporal collisions. Process continuous trajectory data, find out potential high-risk populations and their distribution, classify and evaluate the activity area and risk size formed by the re-diffusion of potential high-risk populations, and analyze the spatial activity and spatial relationship of potential high-risk populations. Finally, through the risk assessment of these regions, the spatiotemporal spread and risk profiles of the epidemic are constructed, in order to provide a methodological basis for guiding the allocation of anti-epidemic resources and manpower in specific geographic regions and the formulation of epidemic prevention and control policies.

The potential risk population referred to in this article is the group of people who have had “time and space” intersections with the confirmed patients within 14 days.

## LITERATURE REVIEW

Studies have found that the spread of the COVID-19 virus, affected by population density and population mobility, displays obvious Space-time aggregation (Huang and He, 2010; Ahmadi et al., 2020; Laborde et al., 2020; Li et al., 2020). At present, the research on the prevention and control measures of COVID-19 mainly focuses on: rapidly tracing the movement of contacts within 4 days of the onset of the COVID-19 symptoms is critical for epidemic prevention and control (Willem et al., 2020), but the ultimate success of epidemic prevention and control depends on the speed and effectiveness of controlling suspected infected persons. Only when the time from primary case infection to contact tracing is shorter than the incubation period can the spread of the outbreak be prevented to the greatest extent possible (Hsiang et al., 2020; Keeling et al., 2020). Besides appropriate social isolation can reduce the COVID-19 infection rate, mortality rate, and the need for medical resources (Aaa, 2021). For example, in socially intensive environments such as schools or workplaces (Ahmed et al., 2018). However, with the advancement of current vaccine research and development

technology, contact tracing and follow-up control measures have become particularly important in the early stages of epidemic control (Müller et al., 2000; Kwok et al., 2019; Read et al., 2020; Walker et al., 2020). Rapid and effective contact tracing can reduce the initial number of cases, which would make the outbreak easier to control overall (Jin et al., 2020). Effective contact tracing and isolation could contribute to reducing the overall size of an outbreak or bringing it under control over a longer period (Hellewell et al., 2020; Xu et al., 2020).

They used mobile-phone-data to develop a spatio-temporal “risk source” model that leverages population flow data to forecast confirmed cases, and identify high-transmission-risk locales at an early stage (Jia et al., 2020). Or they used the location data of the subscriber identity module (SIM) card from the largest mobile phone company in Haiti, to predict the scale and trend of population migration in Haiti following the 2010 earthquake and cholera outbreak. His studies have shown that it is potentially efficient to use this method to estimate population mobility in areas with high mobile phone usage (Bengtsson et al., 2011). Since the outbreak of the COVID-19 epidemic, many scholars have also done relevant theoretical and applied research on the protection of the epidemic and the resumption of work and production based on mobile phone signaling and spatiotemporal data. For example, based on epidemiological survey data of COVID-19 infection cases and mobile phone trajectory data of 15 million users during the epidemic, the spatiotemporal characteristics of COVID-19 and changes in personnel mobility were analyzed (Li et al., 2020; Liu et al., 2021). By aggregating and analyzing the big data and the epidemic data, it suggests cutting off the connection between different human mobility network communities and blocking the local transmission inside the community (Dong et al., 2020). The Johns Hopkins University in the United States has developed a real-time updated global spatiotemporal database of COVID-19 for epidemic prevention and research. The Chongqing has also formed a COVID-19 epidemic query system based on natural resources, a spatiotemporal geographic database, and a spatiotemporal big data service platform, and developed a COVID-19 epidemics map to report the progress of the epidemic in real-time. In addition, the research also builds a population mobile network model based on mobile phone location data to assess the possibility of infection in different regions. And with the support of spatiotemporal data, a comprehensive analysis of the spatiotemporal distribution of patient behavior trajectories was carried out. In addition, combining official data onto city, district, and county governments. Based on official case data, explore the temporal and spatial evolution of the COVID-19 epidemic and assess the epidemic risk level of key cities (Liu et al., 2020; Wang et al., 2020).

Previous research results have effectively supported COVID-19 epidemic protection and control of the epidemic at the national, social, and urban levels, but it needs to be in-depth, which has played an important role in blocking the spread of the epidemic, ensuring the needs of residents, and maintaining social stability community's research. In addition, most of the discussions on COVID-19 epidemic protection and control measures focus on the isolation and control of two types of people, confirmed patients and contacts, and how



to quickly identify and locate the activity trajectories of these two groups of people, and take accurate and timely follow-up prevention and control measures. There are some shortcomings, and these two points are the main content that this article wants to explore.

## METHODS

### The Research Data

The data used in this article come from the epidemic community data released by the Sichuan Provincial Health and Health Commission from 15 January to 15 February 2020, and questionnaire data of 10 confirmed cases in a hospital in Chengdu. Interviews include age, gender, residence, working place, time of diagnosis, time of isolation, travel, transportation, and relationship with other existing confirmed cases, etc. It also includes statistics on the population of more than 16 million in Chengdu.

### The Research Methods

#### Method to Generate the Population Activities

- 1) Signaling location data integration: According to the time and space distribution characteristics of the signaling trajectory data of a single user entity, integrate the adjacent signaling data in time and space to correct the error data and eliminate invalid data. Determine the characteristics of the signaling trace data of the user in a behavior scenario;
- 2) Space block entity feature trajectory calculation: According to the base station cell engineering parameters, including network standard, coverage type, coverage scene, direction angle, latitude and longitude coordinate position, etc., combined with the base station coverage gravity model and cluster analysis in the actual scene, the trajectory data is processed. Calculate the user's actual geographic location; use the actual location and coverage coordinate distribution of the space block provided by China Map Publishing Group to calculate the user's characteristic trajectory on the space block entity;
- 3) User space behavior recognition: According to the user's behavior characteristic trajectory on the spatial entity, combined with the attribute characteristics of the context space block entity in the trajectory, a user behavior trajectory chain is formed;
- 4) User base location tags and behavior feature tags: According to the user behavior tag trajectory chain, the multi-dimensional statistical results of user behavior characteristics are formed, such as users, blocks, behavior frequency within a period, average residence time, number of days of stay in working days, non-work analysis indicators such as the number of days of stay in a day, the number of similar behavior blocks; At the same time, a variety of model algorithms including Monte Carlo tree search are introduced to label users with basic location—workplace, residence, etc.; combined with analysis indicators to characterize Various feature tags form a clear user portrait.

### Model Structure

We suppose the operator's population trajectory data:  $P_i$ ,  $\{l_x \dots l_i\}$ , where " $P_i$ " is a person, " $l_i$ " is a location, " $t$ " is time and time span. Finally, the spatial-temporal collision forms the population trajectory data.

#### Step 1: Conduct basic evaluation of location-based on population spatial activity behavior.

- 1) Based on the trajectory of human activities, the stationary points of people is deduced, where " $p_i$ " is a person, " $p_i, \{l_x \dots l_i\}$ " is the trajectory of " $p_i$ ". The effective stationary position of " $p_i$ " is " $p_i, \{L_1 \dots L_i\}$ ", where " $L_i$ " represents the effective lingering position obtained based on the statistical cycle of " $\{l_x \dots l_i\}$ ", and the lingering time is more than 30 min.
- 2) According to " $p_i, \{L_{live} \dots L_i\}$ ", " $p_i$ " is deduced, where " $a_i$ " is the activity of " $p_i$ " and " $d_i$ " is the dispersion of lingering position of " $p_i$ " (" $a_i$ " is the locations that people have visited and lingered in the target cycle; " $d_i$ " is the calculation of the degree of location dispersion involved in " $p_i, \{L_{live} \dots L_i\}$ ", i.e., the degree of lingering points dispersion of " $p_i$ ").
- 3) Table of spatial behavior data of a new person —TAB1;
- 4) Taking " $L_i$ " as the statistical objective, " $L_i, P, P_{live}, A, D, F$ —TAB2" is derived, where " $P$ " is the population size: the number of people effectively linger at " $P_{all}$ " is the de-duplication count of " $p_i$ ", and " $P_{live}$ " is the resident population: when the number of people effectively resident in " $L_{live}$ " is the de-duplication count " $p_i$ " etc.; " $A$ " is population activity:  $\bar{a} = \frac{1}{n} \sum_{i=1}^n a_i$ , " $D$ " is the diffusance: what other locations have been visited by people who has stayed at this location, and then set this location as the center to calculate the dispersion of the two locations, " $F$ " is fluidity: " $\frac{P_{live}}{P_{all}} * 100\%$ ".

#### Step 2: Assuming that the specific patient is known, the risk factor is determined at the increased position.

Define " $S$ " as the identified risk, " $s_i$ " as the specific patient, and

$$TAB1 = p'_i = p'_i, \{l_x \dots l_i\}, \text{ based on } "s_i".$$

- 1) In TAB1, based on " $S(p'_i)$ ", get " $p'_i, \{L_{live} \dots L_i\}, a'_i, d'_i$ —TAB3."
- 2) " $\{L_{live} \dots L_i\}$ " in TAB3, use " $L_i$ " as the statistical target to calculate " $L_i, P', P'_{live}, A', D'$ —TAB4", where " $P'$ " is the total number of patients living in this location, " $A'$ " is the patient's spatial activity, and " $D'$ " is the patient's spatial spread.

#### Step 3: By the rapid collision method based on the trajectory of patients passing by at the same time, increase the potential risk factors at the location.

- 1) Based on " $t$ " and " $l_i$ " in " $p'_i, \{l_x \dots l_i\}$ " of " $s_i$ ", map " $p_i, \{l_x \dots l_i\}$ " to get " $p''_i$ " (excluding " $p'_i$ ").
- 2) In TAB1, get " $p''_i, \{L_{live} \dots L_i\}, a''_i, d''_i$  —TAB5" based on " $B(p''_i)$ ".

**TABLE 1** | Risk categories for a specific location.

| Category 1        | Condition 1       | Category 2       | Condition 2                      | Instructions  |
|-------------------|-------------------|------------------|----------------------------------|---|
| A Identified risk | $P' > 0$          | Steady           | $P'_{live} > 0$                  | The location of the confirmed cases can be identified by the people who live or linger here |
|                   |                   | Fluctuation      | $P' > 0, P'_{live} = 0$          |   |
| B Potential risk  | $P' = 0$          | Steady           | $P'' > 0, P'_{live} > 0$         | People who have been at the same time and space with the confirmed case, live here          |
|                   |                   | Fluctuation      | $P' = 0, P'' > 0, P'_{live} = 0$ | People who have been at the same time and space with the confirmed case, do not live here   |
| C Normal areas    | $P' = 0, P'' = 0$ | Susceptible area | The A,D,F index is high          | People in these areas move to many places and in a large range                              |
|                   |                   | Other areas      | The A,D,F index is low           | People in these areas move to fewer places and in a small range                             |

**TABLE 2** | Spatial autocorrelation instruction.

| Z(I)            | Spatial distribution correlation |
|-----------------|----------------------------------|
| $> 1.96$        | Positive spatial autocorrelation |
| $[-1.96, 1.96]$ | Weak spatial correlation         |
| $< -1.96$       | Negative spatial autocorrelation |

3) In TAB5, “ $\{L_{live} \dots L_i\}$ ” takes “ $L_i$ ” as the statistical target to get “ $L_i, P'', A'', D''$ –TAB6”, where “ $\{L_{live} \dots L_i\}$ ” (excluding “ $\{L_{live} \dots L_i\}$ ” in TAB3), “ $P''$ ” are the number of people who have been at the same time and space, “ $P'_{live}$ ” are the number of people who have been at the same time and space living here, “ $A''$ ” is the spatial activity of people who have been at the same time and space, and “ $D''$ ” is the spatial diffusion of people who have been the same time and space.

**Step4: Combine TAB2, TAB4, TAB6 to get TAB7, and comprehensively evaluate the risk category of the specific location based on TAB7.**

The location risk is preliminarily classified by using the numerical value, as shown in Table 1.

**Step 5: Based on Moran's I Statistics, conduct an overall evaluation of the risk distribution in the target area.**

Moran's I was used to measure the degree of Spatial autocorrelation (similar dimensional attributes), it means to evaluate whether the distribution of elements was aggregated, discrete or random. Moran's I index closer to “1” indicates aggregation, and closer to “-1” indicates dispersion. As shown in Table 2.

**Step 6: Based on “ $P_i\{L_1 \dots L_i\}$ ”, get the specific spatial field correlation.**

Information entropy is used to measure the correlation of spatial fields. The conditions for defining the correlation index “ $r$ ” between two discrete space fields are as follows: when the two space fields are independent of each other, there is “ $r_{min} = 0$ ”. When the correlation degree of the two spatial fields increases gradually, “ $r$ ” also increases gradually. There is “ $r_{max} = 1$ ” when the two space fields are completely correlated. According to the nature of information entropy, the expression of “ $r$ ” can be established.

When the discrete state sets “A” and “B” are completely related, each type area of the two layers must have a one-to-one mapping relationship in space. According to the layer properties of the index “A” space, it is divided into “m” types. The proportion

of the area of the type “ $a_i$ ” to the total area of the area is  $P(a_i)$ , and the layer properties of the index “B” space are divided into “n” types, and the proportion of the area of the type “ $b_j$ ” to the total area of the area is “ $P(b_j)$ .” “ $a_i b_j$ ” represents the category after the type “ $a_i$ ” in the “A” layer and the space “ $b_j$ ” in the “B” layer are superimposed (up to “m\*n” categories appear after the two layers are superimposed), and the area ratio is “ $P(a_i b_j)$ ,” and the information entropy is  $H(A)$ ,  $H(B)$  and  $H(A, B)$ . Finally, the correlation index between thematic layers “A” and “B” is calculated. The higher the entropy is, the more information can be transmitted; the lower the entropy is, the less information can be transmitted. Thereby, the linkage cascading relationships among indicators of different dimensions can be classified. As shown in Figure 1.

## RESULTS

### Conduct Basic Location Evaluation Based on Population Spatial Activity Behavior Analysis of the Number of Population Resident Places

By using the trajectory activity data of 10 confirmed patients collected, the random distribution and activity spaces of more than 16 million Chengdu are simulated based on the model, and the number of residents places in Chengdu within 14 days is obtained. Whether it is a transient population or temporary population, the more effective residences there are, the higher the transmission of infection will be. As shown in Table 3.

To classify the temporal and spatial activity of the population and set the risk coefficient. As shown in Table 4.

### Analysis of the Scope of Population Activities

The analysis of the scope of activity is mainly aimed at the spatial distance of the “location,” that is, the description and analysis of the dispersion of the stationary points of people, which represents the direction of spatial diffusion. Combined with the number of resident positions, the spatial dispersion can be measured as whether it is concentrated or dispersed. The higher the value is, the higher its spatial propagation is. The setting of each propagation coefficient is shown in Table 5.

### Distribution of Track Resident Point of People-Based on Resident Places

Based on the simulation data of population activity trajectory, the distribution of resident heat, residential heat, activity, and

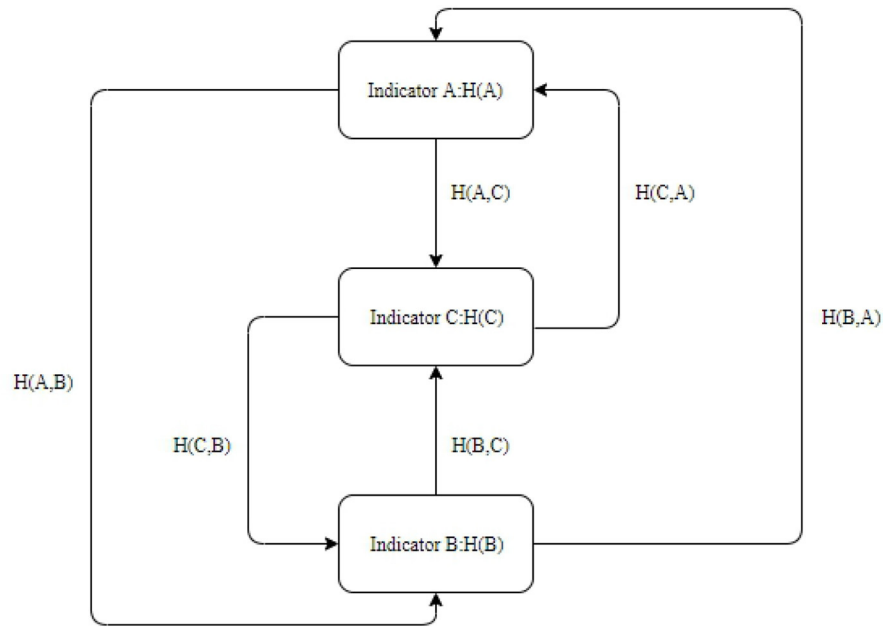


**FIGURE 1 |** Information entropy relationship.

**TABLE 3 |** The number of effective population resident places.

| Classification (places)  | 1     | 2     | 3-4   | 4-5  | 6-10 | >10  |
|--------------------------|-------|-------|-------|------|------|------|
| Transient population (%) | 17.30 | 9.13  | 5.61  | 3.12 | 2.66 | 0.01 |
| Permanent population (%) | 7.69  | 21.33 | 19.22 | 9.29 | 4.64 | 0.00 |
| Total (%)                | 55.45 |       | 37.24 |      | 7.31 |      |

*Transient population refers to the non-permanent population that appears during the monitoring period (14 days) and has effectively resided at least one place in the city.*

spatial diffusion of the population can be obtained. As shown in **Figure 2**.

It can be seen from the Population Resident Heat Distribution Map that the darker color presents more people stay in the place, and the lighter color presents less people stay in the place, and the resident heat are lower. Residential heat distribution is different from resident heat distribution, once a confirmed case is found in the place of residence, the size of the population at that location can be quickly known and the epidemic situation in the place can be protected in time. In addition, combining with “P,” location “ $P/P_{live}$ ” with high-population mobility can be quickly obtained. With high mobility (the greater the ratio), the higher the risk coefficient of transmission or infection in this location will be. In the Population Activity Distribution Map, the darker the color, the greater the number of related locations between this location and other locations. From the Distribution of Population Spatial Diffusion Map, the spatial diffusion of a single person is mainly spread out in the way of one point and more lines.

**TABLE 4 |** Classify the temporal and spatial activity of the population and the risk factor.

| Spatial activity | Risk coefficient | Definition   | Instruction                                  |                            |
|------------------|------------------|--|--|----------------------------|
|                  |                  |  | Normal people: Possibility of being infected | Patients: Transmissibility |
| Low              | 1                | Effective Resident Positions $\leq 2$ places           | Low  | Low                        |
| Medium           | 5                | 3 places $<$ Effective Resident Positions $< 5$ places | Medium                                       | Medium                     |
| High             | 10               | Effective Resident Positions $> 5$ places              | High   | High                       |

## Analysis of Spatial Activity of Confirmed Patients

### Distribution of Residence and Track Resident Point of Confirmed Patients

According to the specific locations of the 94 closed communities with confirmed cases as of 14 February 2020 issued by the Health Commission of Sichuan Province, the specific location distribution map of the confirmed patients can be drawn, as shown in **Figure 3**.

As can be seen from the figure, the residents of the confirmed patients are mainly distributed downtown. Resident location distribution is related to regional population density

and socio-economic vitality. The downtown or places with convenient transportation (subway, bus) lines, large shopping

TABLE 5 | The degree of spatial transmission of people.

| Number of position              | Concentration (<1 km) | Dispersion (>1 km or negative spatial autocorrelation) | Random |
|---------------------------------|-----------------------|--|--------|
| Number of position 1-2 (places) | 1                     | 2  | Null   |
| Number of position 3-5 (places) | 3                     | 4  | 4      |
| Number of position >5 (places)  | 5                     | 6  | 6      |

TABLE 6 | Calculation methods for different risk categories.

| Category 1        | Color  | Value at risk  |
|-------------------|--------|--|
| A Identified risk | Red    | Number of people * Space Activity Coefficient * Propagation Coefficient            |
| B Potential risk  | Yellow | Number of people * Space Activity Coefficient * Propagation Coefficient            |
| C Normal region   | Green  | Number of people * Space Activity Coefficient * Propagation Coefficient * Mobility |

malls, and shopping centers are places where confirmed patients stay frequently.

Analysis of Activity and Spatial Diffusion of Confirmed Patients

The spatial information such as the patient’s address and activity location is converted into spatial and temporal data to form the spatial transmission trajectory of the confirmed cases. According to the second step of the analysis method, the activity and spatial diffusion of the confirmed patients can be analyzed. However, in order to protect personal privacy, the trajectory of confirmed patients will not be analyzed graphically.

Distribution of Track Resident Point of Trajectories of People, Who Have Been at the Same Time and Space With the Confirmed Patient

According to Figure 4 the trajectories of people who have been at the same time and space with the confirmed patient, it can conclude that the trajectories of such people are almost all over the districts and counties of Chengdu. Among them, the densest track resident points are the downtown.

Risk Profiling of COVID-19 Epidemic for Specific Location

As shown in Table 6.

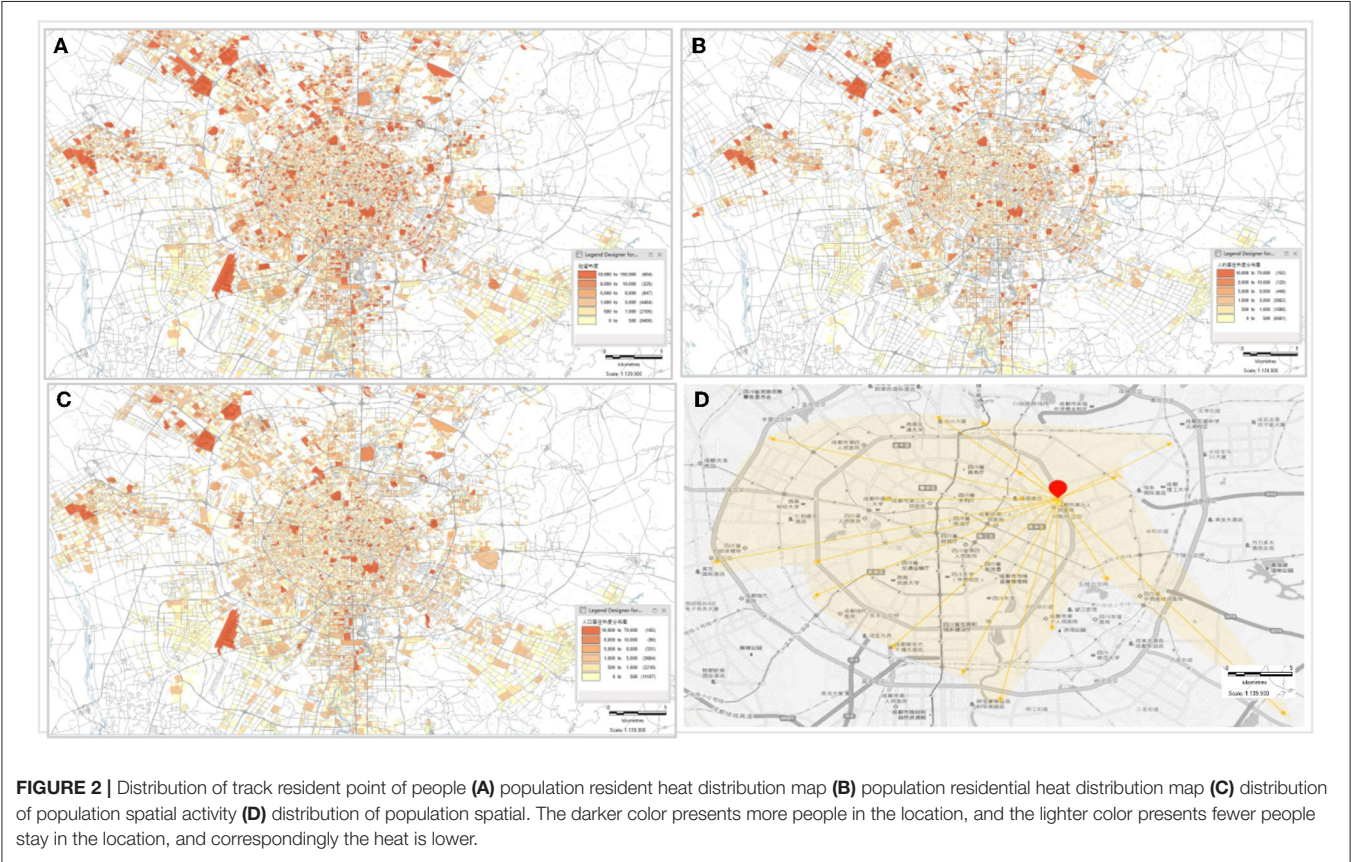






**FIGURE 3 |** Distribution of residence and track resident point of confirmed patients **(A)** stationary place distribution **(B)** trajectory distribution.

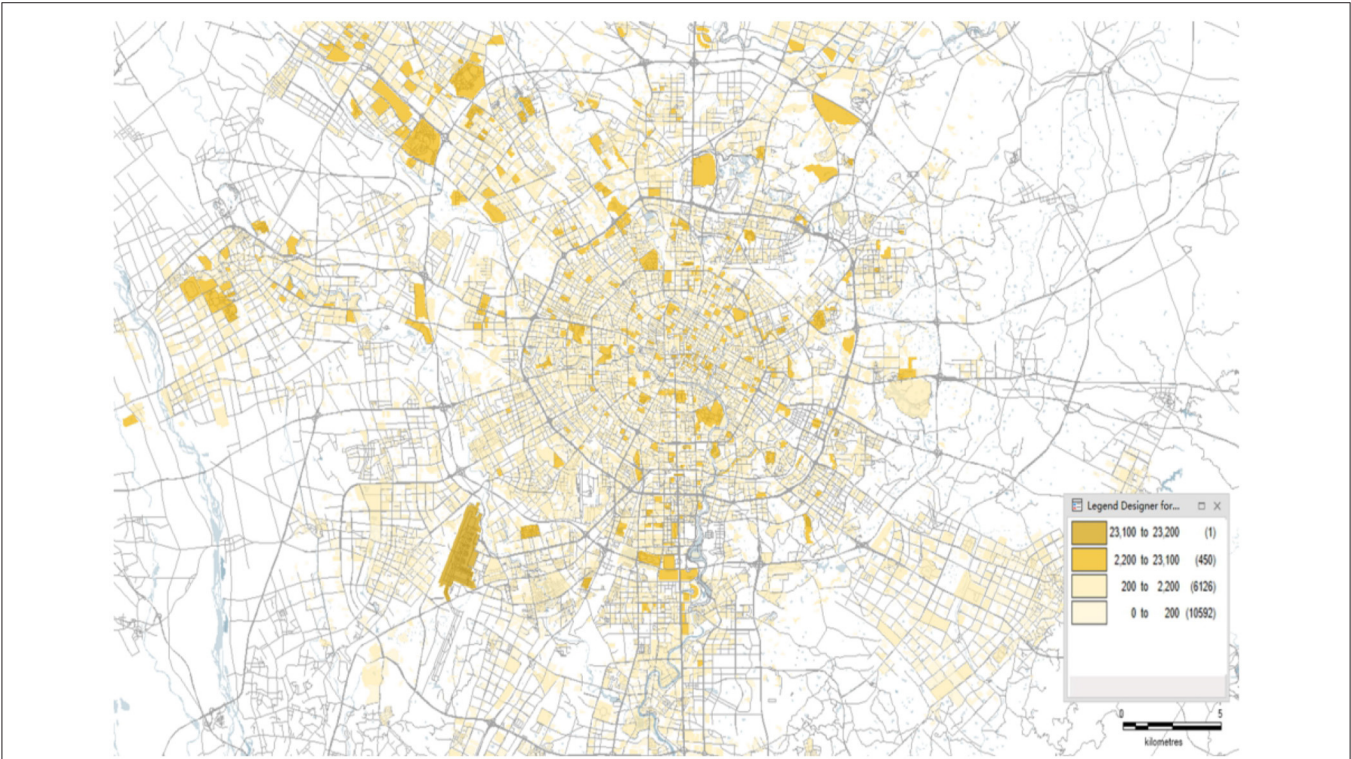


**FIGURE 4 |** Distribution of track resident point.

| TABLE 7   Description of the spatial correlation distribution of different risk categories. |             |                                  |               |
|---|-------------|----------------------------------|---------------|
| Category 1  | Correlation | Value specification              | Result        |
| A Identified risk   | 1.12        | Positive spatial autocorrelation | Concentration |
| B Potential risk  | 1.28        | Negative spatial autocorrelation | Dispersion    |
| C Normal region   | −1.2        | Weak spatial correlation         | Random        |

**Calculation of Risk Factors for a Specific Location**  
Assuming that the risk value of each category is the same, the risk value of epidemic transmission is divided into segments, and the level is set. As shown in Table 5.

**Analysis of Risk Categories at Specific Locations**  
From 0:00 to 6:00 on 8 December 2020, 3 new cases of new coronary pneumonia were confirmed in Chengdu. The students of the Chengdu University of Technology have had contact



with this confirmed case. Therefore, this article taking the Chengdu University of Technology as an example analyzes the

comprehensive information of its location according to the aforementioned method as shown in **Figure 5**.

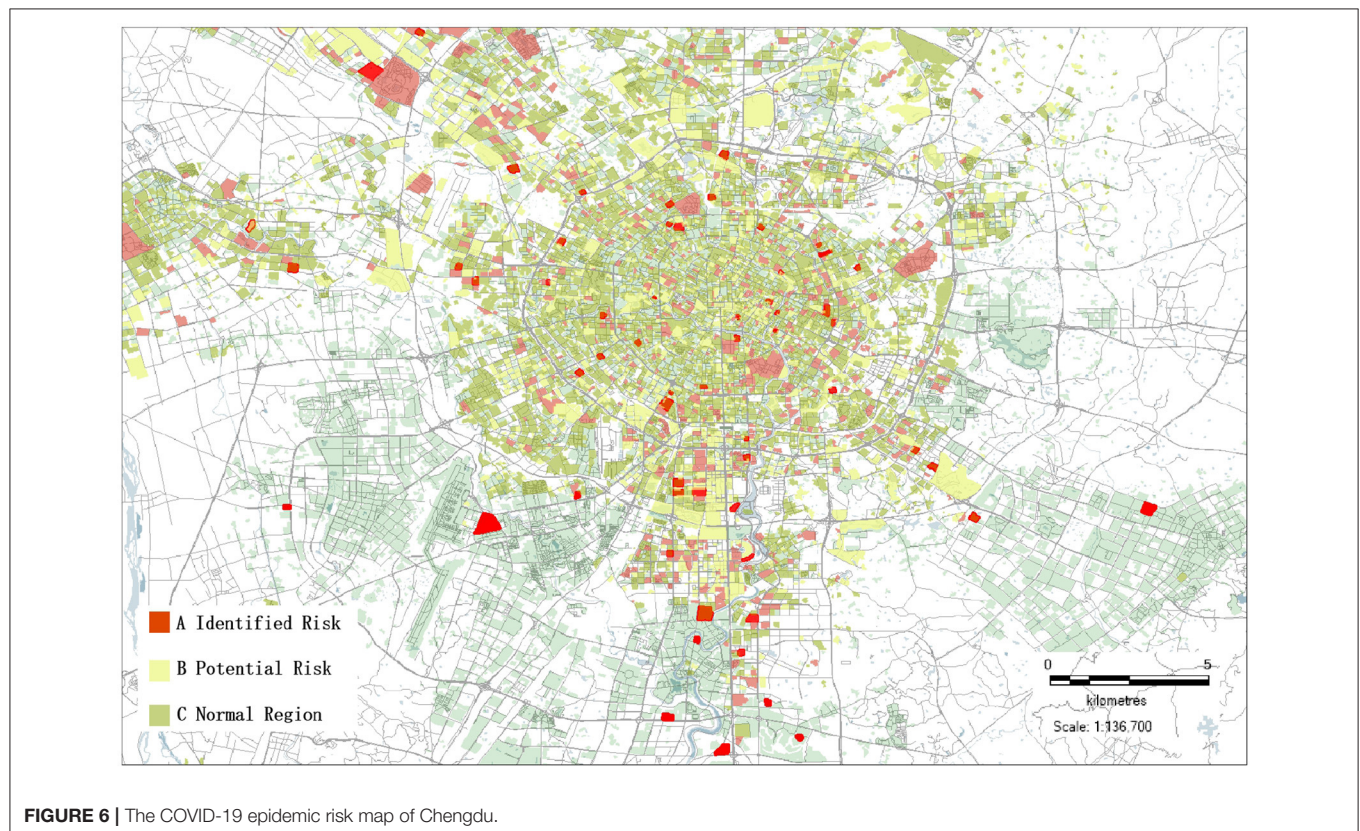
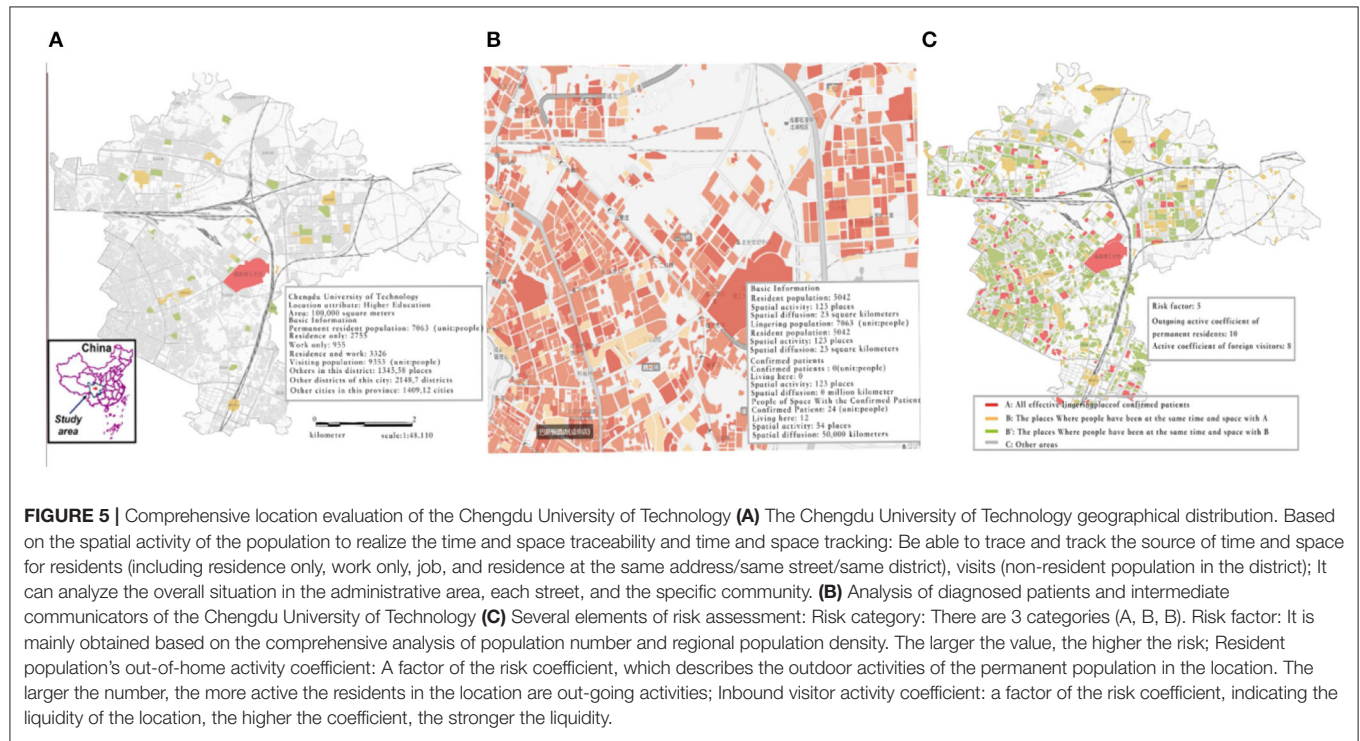


**TABLE 8 |** Specific distribution characteristics of the affected communities.

| Distribution characteristics                              | Specific communities  | Distance  |
|---|---|---|
| A-B-C-A<br>triangular shape<br>Distance <1,000 m          | Zhonghai No. 9 Residence, Jinxi Hotel,<br>Zhonghai Chengnan No. 1   | 445; 941;<br>835  |
| A-B-C<br>broken line<br>Each section Distance<br><1,000 m | Lloyds Garden-Chaoyang Langxiang<br>Plaza-Tianxin Garden<br>Hua Min Yiyuan-Siji Kang Cheng<br>Hotel-Shidai Haoting<br>Zhongliang Xiangyun-Wuhou<br>Villa-Wuhou International Garden   | 388; 921<br>604; 850<br>521; 769  |
| A-B, segment type<br>Distance <1,000 m                    | Shuangnan Mansion-Shuangnan<br>Garden Community<br>Bali Yangguang-Xiangmulin Garden<br>Jia Zhao Ye Li Jing Mansion-Ruijing<br>Lanting<br>Shenxianshu Courtyard Phase 4-Vienna<br>International Hotel<br>Fengjing Yaju-Gaoyi Hotel<br>Tianfu Changcheng Bainanjun-Shidai<br>Jincheng Hotel<br>The Holy Birch City-Guandu East Road<br>Alley<br>Tianfu Oucheng-Qingjiang Huatng<br>Wanke Golden Area-Junfa Shidai<br>Junyuan<br>Linjiang Road, Yard 8-Roland Hotel<br>Jinsha Guoji-Shiji Jinsha | 368<br>468<br>531<br>536<br>596<br>849<br>912<br>922<br>936<br>974<br>999 |

Combining calculations with specific models can be obtained, the Chengdu University of Technology, epidemic risk category: A, epidemic risk coefficient: 5, of which, the resident population's active coefficient of going out: 10, and the active coefficient of foreign visitors: 8.

## RISK PROFILING OF COVID-19 EPIDEMIC IN CHENGDU

### Distribution of Regional Risks in Chengdu

According to the standardized statistics of the Local Moran's I index test, the spatial correlation values of different risk categories can be calculated, and the overall spatial distribution type can be determined based on this correlation, as shown in Table 7.

According to the aforementioned formula, the spatial correlation distribution value of the identified risk area can be calculated. For areas with positive spatial autocorrelation, centralized protection deployment can be adopted. For areas with negative spatial autocorrelation, decentralized protection methods can be implemented. In areas with weak spatial correlation, the distribution among communities is generally random and the COVID-19 epidemic protection is complex. Therefore, the actual situation of the epidemic in the community should be investigated and corresponding protection measures can be taken.

## Portrait of Epidemic Risk in Chengdu

The risk value is segmented and the risk level is set. Assuming that the risk value of each category is the same, based on the comprehensive distribution, a geographic profile of the risk of the epidemic community in Chengdu can be obtained, as shown in Figure 6.

According to the different colors shown in the figure aforementioned, the risk of the COVID-19 epidemics in Chengdu can be clearly identified, and the sequence of nucleic acid testing for COVID-19 can also be accurately guided in each region. For example, in areas with high-spatial population activity, high diffusion, and high-transmission coefficient, priority will be given to arranging local professional epidemic prevention forces to the station in the community, and residents in the whole region should conduct nucleic acid testing. In the potential risk areas, nucleic acid testing and identification of suspected cases should be strengthened, and the movement of suspected cases should be closely tracked, which can help to cut off the transmission chain of the epidemic in the shortest time. In areas where the risk assessment shows normal, nucleic acid testing can be done voluntarily by residents, in order to promptly guide and relieve residents' nervousness.

## Analysis of COVID-19 Epidemic Spread in Chengdu

The analysis shows that 36% of the affected communities in Chengdu are within 1 km next to each other, and 9% of the communities are within 500 m. There are four main distribution characteristics: "A-B-C-A" triangular shape, "A-B-C" broken line, "A-B" segment type and scatter type, as shown in Table 8.

The distribution characteristics of the affected communities aforementioned in Chengdu: "triangle," "broken line" and "line segment." The causes and rules of the spread of the COVID-19 epidemic can be preliminarily summarized, so that different protection measures can be taken according to the distribution shape among communities.

## Spatial Distribution of Epidemic Communities in Chengdu

Based on the confirmed cases published by the Health Commission of Sichuan Province, the spatial distribution of the outbreak communities in Chengdu is described, as shown in Figure 7.

The aforementioned picture depicts the spatial distribution of the epidemic communities in Chengdu, which can guide relevant government departments to formulate appropriate plans to block the spread of the COVID-19 epidemics. In areas where epidemic communities are densely distributed, protection departments must implement strict epidemic surveillance to ensure early detection, quarantine, and treatment of infected people to reduce the spread of the COVID-19 epidemic. For non-infected communities that are far away from the affected communities, the protection strategy should be adjusted to prevent the importation of outbreaks from other places, so that the resumption of work and production can be carried out to the maximum extent.



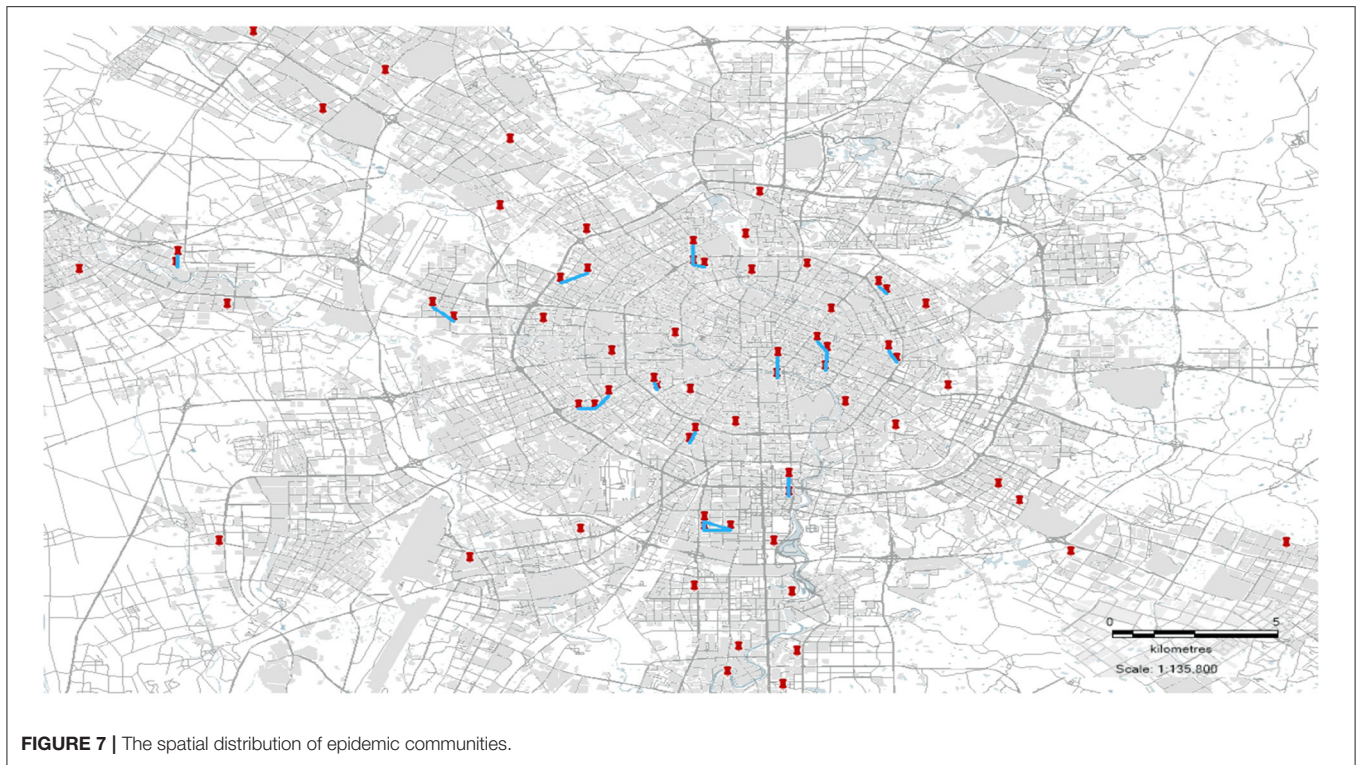


**FIGURE 7 |** The spatial distribution of epidemic communities.

## DISCUSSION

Based on the mobile phone trajectory data, using the research methods and steps in this article, combined with the relevant data of the epidemic in Chengdu, the verification found that: according to the established model, based on basic population data and spatiotemporal collision methods, it accurately described people who have close contacts. The epidemic risk coefficient and risk level of the Chengdu University of Technology, and also the epidemic risk map of the entire area of Chengdu and the overall distribution characteristics of the epidemic community. This distribution feature can effectively guide different urban areas and risk communities to carry out nucleic acid inspections, putting anti-epidemic supplies, and formulating plans for resuming work and production.

In addition, this method can also be used for the research on spatial-temporal diffusion and profiling of various risks in the future. There are also aspects that need to be improved and optimized in the research: first, the activity trajectory of confirmed cases, medical information, and other data are relatively fragmented and not detailed enough. The overall profiling of the development of the COVID-19 epidemic in Chengdu may be biased. Future analysis of similar disaster events still needs to rely on more detailed spatial-temporal trajectory data and further study the micro-scale population activities and risk communication. Second, considering personal privacy and the difficulty of obtaining certain data, the analysis of the spatial diffusion of risk factors and the overall diffusion situation of the region is relatively rough. Therefore, the analysis method should

be improved in the future, which requires a higher requirement for desensitization of spatial-temporal data.

## DATA AVAILABILITY STATEMENT

The original contributions presented in the study are included in the article/supplementary material, further inquiries can be directed to the corresponding author/s.

## ETHICS STATEMENT

Ethical review and approval was not required for the study on human participants in accordance with the local legislation and institutional requirements. Written informed consent for participation was not required for this study in accordance with the national legislation and the institutional requirements.

## AUTHOR CONTRIBUTIONS

QZ, BD, and JZ substantial contributions to the conception or design of the work and the acquisition and analysis. JZ, XH, HL, and LZ contributions to the acquisition and analysis of data for the work. JZ, LZ, and JD drafting the work or revising it critically for important intellectual content. QZ and BD final approval of the version to be published. LZ and JD agreement to be accountable for all aspects of the work in ensuring that questions related to the accuracy or integrity of any part of the work are appropriately investigated and

resolved. All authors contributed to the article and approved the submitted version.

## FUNDING

National Key Research and Development Program of China, No. 2020YFD1100701.

## REFERENCES

- Aaa, B. (2021). Role of social distancing in tackling covid-19 during the first wave of pandemic in nordic region: evidence from daily deaths, infections and needed hospital resources. *Int. J. Nurs. Sci.* 8, 145–151. doi: 10.1016/j.ijnss.2021.03.010
- Ahmadi, M., Sharifi, A., Dorosti, S., Ghouschi, S. J., and Ghanbari, N. (2020). Investigation of effective climatology parameters on covid-19 outbreak in Iran. *Sci. Total Environ.* 729, 138705. doi: 10.1016/j.scitotenv.2020.138705
- Ahmed, F., Zviedrite, N., and Uzicanin, A. (2018). Effectiveness of workplace social distancing measures in reducing influenza transmission: a systematic review. *BMC Public Health* 18, 518. doi: 10.1186/s12889-018-5446-1
- Bengtsson, L., Lu, X., Thorson, A., Garfield, R., Schreeb, J. V., and Gething, P. W. (2011). Improved response to disasters and outbreaks by tracking population movements with mobile phone network data: a post-earthquake geospatial study in haiti. *PLoS Med.* 8, e1001083. doi: 10.1371/journal.pmed.1001083
- Dong, E., Du, H., and Gardner, L. M. (2020). An interactive web-based dashboard to track covid-19 in real time. *Lancet Infect. Dis.* 20, 533–534. doi: 10.1016/S1473-3099(20)30120-1
- Hellewell, J., Abbott, S., Gimma, A., Bosse, N. I., and Zandvoort, K. V. (2020). Feasibility of controlling covid-19 outbreaks by isolation of cases and contacts. *Lancet Global Health* 8, 4. doi: 10.1016/S2214-109X(20)30074-7
- Hsiang, S., Allen, D., Annan-Phan, S., Bell, K., and Wu, T. (2020). The effect of large-scale anti-contagion policies on the covid-19 pandemic. *Nature* 584, 262–267. doi: 10.1038/s41586-020-2404-8
- Huang, K. S., and He, D. (2010). Research on population flow trajectory based on big data. *Population Health Sci.* 2, 14–17.
- Jia, J. S., Lu, X., Yuan, Y., Xu, G., and Christakis, N. A. (2020). Population flow drives spatio-temporal distribution of covid-19 in china. *Nature* 582, 1–11. doi: 10.1038/s41586-020-2284-y
- Jin, A. N., Li, G., and Wang, J. B. (2020). Spatio-temporal evolution and control strategies of COVID-19 epidemic in Shenzhen China. *J. Shaanxi Normal University* 48, 18–32. doi: 10.15983/j.cnki.jsnu.2020.03.017
- Keeling, M. J., Hollingsworth, T. D., and Read, J. M. (2020). The efficacy of contact tracing for the containment of the 2019 novel coronavirus (COVID-19). *J. Epidemiol. Community Health* 74, 861–866. doi: 10.1101/2020.02.14.20023036
- Kwok, K. O., Tang, A., Wei, V., Park, W. H., Yeoh, E. K., and Riley, S. (2019). Epidemic models of contact tracing: systematic review of transmission studies of severe acute respiratory syndrome and middle east respiratory syndrome. *Comput. Struct. Biotechnol. J.* 17, 186–194. doi: 10.1016/j.csbj.2019.01.003
- Laborde, D., Martin, W., Swinnen, J., and Vos, R. (2020). Covid-19 risks to global food security. *Science* 369, 500–502. doi: 10.1126/science.abc4765
- Li, D. R., Shao, Z. F., and Yu, W. B. (2020). Public epidemic prevention and control services based on big data of spatiotemporal location make cities more smart. *Geomatics Inform. Sci. Wuhan University* 45, 475–487. doi: 10.13203/j.whugis20200145
- Liu, Y. X., Song, C., Liu, Q. Y., Zhang, Z. X., Wang, X., Ma, J., et al. (2021). Spatial-temporal characteristics of COVID-19 in Chongqing and its relationship with human mobility. *J. Geo-inform. Sci.* 2, 222–235. doi: 10.13284/j.cnki.rddl.003228

## ACKNOWLEDGMENTS

We gratefully appreciate the Foundation item: National Key Research and Development Program of China, No.2020YFD1100701 and Novel Coronavirus (2019-nCoV) Emergency Project of Sichuan University.

- Liu, Z. Q., Ye, Y. Y., Zhang, H. O., Guo, H. X., Yang, J., and Wang, C. J. (2020). Spatio-temporal characteristics and transmission path of COVID-19 cluster cases in Zhuhai. *Trop. Geography* 40, 422–431.
- Müller, J., Kretzschmar, M., and Dietz, K. (2000). Contact tracing in stochastic and deterministic epidemic models. *Health Care Manag. Sci.* 10, 341–355. doi: 10.1016/S0025-5564(99)00061-9
- Niu, B., Liang, R., Zhang, S., Zhang, H., and Chen, Q. (2020). Epidemic analysis of covid in italy based on spatiotemporal geographic information and google trends. *Transboundary Emerg. Dis.* 68, 2384–2400. doi: 10.1111/tbed.13902
- Read, J. M., Bridgen, J. R., Cummings, D. A., Ho, A., and Jewell, C. P. (2020). Novel coronavirus 2019-nCoV: early estimation of epidemiological parameters and epidemic predictions. *Philos. Transact. R. Soc. B: Biol. Sci.* 2020, 18549. doi: 10.1101/2020.01.23.20018549
- Tang, X. Y., Zhou, T., and Lu, B. C. (2017). Analysis of wide range population flow analysis based on mobile phone signaling. *J. Chongqing Jiaotong University* 36, 87.
- Walker, P., Whittaker, C., Watson, O. J., Baguelin, M., Winskill, P., and Hamlet, A., et al. (2020). The impact of covid-19 and strategies for mitigation and suppression in low- and middle-income countries. *Science* 369, eabc0035. doi: 10.1126/science.abc0035
- Wang, J. B., Li, G., Wang, J. P., Qiang, J. Q., and Zhu, D. D. (2020). Spatiotemporal evolution and risk profiling of the COVID-19 epidemic in Shaanxi Province. *Trop. Geography* 40, 432–445.
- Wang, R. (2017). *Big Data Investigation*. Tsinghua: Tsinghua University Press.
- Willem, L., Abrams, S., Petrof, O., Coletti, P., and Hens, N. (2020). The impact of contact tracing and household bubbles on deconfinement strategies for COVID-19: an individual-based modelling study. *Nat. Commun.* 12, 1524. doi: 10.1101/2020.07.01.20144444
- Xu, X. K., Wen, C., Zhang, G. Y., Sun, H. C., Liu, B., and Wang, X. W. (2020). The geographical destination distribution and effect of outflow population of wuhan when the outbreak of COVID-19. *J. University Electr. Sci. Technol. China* 49, 324–329.

**Conflict of Interest:** JZ was employed by Chengdu Fangwei Technology Co., Ltd. LZ was employed by Sichuan Chuanda Zhisheng System Integration Co., Ltd. XH was employed by SinoMaps Press Co., Ltd.

The remaining authors declare that the research was conducted in the absence of any commercial or financial relationships that could be construed as a potential conflict of interest.

**Publisher's Note:** All claims expressed in this article are solely those of the authors and do not necessarily represent those of their affiliated organizations, or those of the publisher, the editors and the reviewers. Any product that may be evaluated in this article, or claim that may be made by its manufacturer, is not guaranteed or endorsed by the publisher.

Copyright © 2022 Zuo, Du, Di, Zhou, Zhang, Liu and Hou. This is an open-access article distributed under the terms of the Creative Commons Attribution License (CC BY). The use, distribution or reproduction in other forums is permitted, provided the original author(s) and the copyright owner(s) are credited and that the original publication in this journal is cited, in accordance with accepted academic practice. No use, distribution or reproduction is permitted which does not comply with these terms.



## OPEN ACCESS

## Edited by:

Reza Lashgari,  
Shahid Beheshti University, Iran

## Reviewed by:

Kuldeep Singh,  
National Institute of Malaria Research  
(ICMR), India  
Gengfeng Fu,  
Jiangsu Provincial Center for Disease  
Control and Prevention, China  
Junjie Wang,  
Chinese Center for Disease Control  
and Prevention, China

## \*Correspondence:

Hong Shang  
hongshang100@hotmail.com  
Junjie Xu  
xjcmu@163.com

†These authors have contributed  
equally to this work

## Specialty section:

This article was submitted to  
Infectious Diseases—Surveillance,  
Prevention and Treatment,  
a section of the journal  
Frontiers in Medicine

Received: 09 July 2021

Accepted: 28 March 2022

Published: 29 April 2022

## Citation:

Gao Y, Hu Q, Leuba SI, Jia L, Wang H,  
Huang X, Chen Y, Wang H, Zhang J,  
Chu Z, Zhang L, Wang Z, Shang H,  
Xu J and CROPrEP Study Team  
(2022) Medication Non-adherence  
and Condomless Anal Intercourse  
Increased Substantially During the  
COVID-19 Pandemic Among MSM  
PrEP Users: A Retrospective Cohort  
Study in Four Chinese Metropolises.  
Front. Med. 9:738541.  
doi: 10.3389/fmed.2022.738541

# Medication Non-adherence and Condomless Anal Intercourse Increased Substantially During the COVID-19 Pandemic Among MSM PrEP Users: A Retrospective Cohort Study in Four Chinese Metropolises

Yangyang Gao<sup>1,2,3,4†</sup>, Qinghai Hu<sup>1,2,3,4†</sup>, Sequoia I. Leuba<sup>5</sup>, Le Jia<sup>1,2,3,4</sup>, Hongyi Wang<sup>1,2,3,4</sup>, Xiaojie Huang<sup>6</sup>, Yaokai Chen<sup>7</sup>, Hui Wang<sup>8</sup>, Jing Zhang<sup>1,2,3,4</sup>, Zhenxing Chu<sup>1,2,3,4</sup>, Lukun Zhang<sup>8</sup>, Zixin Wang<sup>9</sup>, Hong Shang<sup>1,2,3,4\*</sup>, Junjie Xu<sup>1,2,3,4\*</sup> and CROPrEP Study Team

<sup>1</sup> National Health Commission Key Laboratory of Acquired Immunodeficiency Syndrome (AIDS) Immunology (China Medical University), National Clinical Research Center for Laboratory Medicine, The First Affiliated Hospital of China Medical University, Shenyang, China, <sup>2</sup> Key Laboratory of AIDS Immunology, Chinese Academy of Medical Sciences, Shenyang, China, <sup>3</sup> Key Laboratory of AIDS Immunology of Liaoning Province, Shenyang, China, <sup>4</sup> Collaborative Innovation Center for Diagnosis and Treatment of Infectious Diseases, Hangzhou, China, <sup>5</sup> Department of Epidemiology, University of North Carolina at Chapel Hill, Chapel Hill, NC, United States, <sup>6</sup> Center for Infectious Diseases, Beijing Youan Hospital, Capital Medical University, Beijing, China, <sup>7</sup> Chongqing Public Health Medical Center, Chongqing, China, <sup>8</sup> Department of Infectious Diseases, National Clinical Center for Infectious Diseases, Third People's Hospital of Shenzhen, Second Affiliated Hospital of Southern University of Science and Technology, Shenzhen, China, <sup>9</sup> Faculty of Medicine, The Jockey Club School of Public Health and Primary Care, The Chinese University of Hong Kong, Hong Kong, Hong Kong SAR, China

**Background:** The coronavirus disease (COVID-19) pandemic has impacted HIV prevention strategies globally. However, changes in pre-exposure prophylaxis (PrEP) adherence and HIV-related behaviors, and their associations with medication adherence among men who have sex with men (MSM) PrEP users remain unclear since the onset of the COVID-19 pandemic.

**Methods:** A Retrospective Cohort Study of HIV-negative MSM PrEP users was conducted in four Chinese metropolises from December 2018 to March 2020, assessing the changes in PrEP adherence and HIV-related behaviors before and during the COVID-19. The primary outcome was poor PrEP adherence determined from self-reported missing at least one PrEP dose in the previous month. We used multivariable logistic regression to determine factors correlated with poor adherence during COVID-19.

**Results:** We enrolled 791 eligible participants (418 [52.8%] in daily PrEP and 373 [47.2%] in event-driven PrEP). Compared with the data conducted before the COVID-19, the proportion of PrEP users decreased from 97.9 to 64.3%, and the proportion of poor PrEP adherence increased from 23.6 to 50.1% during the COVID-19 [odds ratio (OR) 3.24, 95% confidence interval (CI) 2.62–4.02]. While the percentage of condomless anal intercourse (CAI) with regular partners (11.8 vs. 25.7%) and with casual partners (4.4



vs. 9.0%) both significantly increased. The proportion of those who were tested for HIV decreased from 50.1 to 25.9%. Factors correlated with poor PrEP adherence during the COVID-19 included not being tested for HIV (adjusted odds ratio [aOR] = 1.38 [95% CI: 1.00, 1.91]), using condoms consistently with regular partners (vs. never, aOR = 2.19 [95% CI: 1.16, 4.13]), and being married or cohabitating with a woman (vs. not married, aOR = 3.08 [95% CI: 1.60, 5.95]).

**Conclusions:** Increased poor PrEP adherence and CAI along with the decrease in HIV testing can lead to an increase in HIV acquisition and drug resistance to PrEP. Targeted interventions are needed to improve PrEP adherence and HIV prevention strategies.

**Keywords:** COVID-19, pre-exposure prophylaxis (PrEP), adherence–compliance–persistence, men who have sex with men (MSM), condomless anal intercourse (CAI)

## INTRODUCTION

Since the declaration of the coronavirus disease 2019 (COVID-19) pandemic by the World Health Organization (WHO) on 11 March 2020, social distancing has interrupted hospital-based HIV prevention methods, HIV care, and testing services, particularly among men who have sex with men (MSM) (1, 2). Almost one quarter (23%) of new HIV infections globally in 2019 were among MSM, and the percentage of incident HIV infections among MSM was even higher in the Asia-Pacific region (3). The HIV incidence among Chinese MSM has increased from 3.24/100 PY (95% CI: 2.81–3.74) in 2005–2008 to 5.95/100 PY (95% CI: 5.37–6.56) in 2012–2018 (4). New strategies to prevent HIV transmission, especially those that are effective despite social distancing, are needed to address the increasing HIV epidemic among Chinese MSM.

Pre-exposure prophylaxis (PrEP) is an innovative and effective biomedical HIV prevention strategy for people at high risk of HIV infection (5). PrEP is a medication that is usually taken daily or event-driven to prevent HIV transmission and is frequently tenofovir/emtricitabine (TDF/FTC). If used with optimal adherence, PrEP is highly effective at preventing HIV transmission (6, 7). However, if adherence is <40%, PrEP is no longer protective against HIV transmission (8). Since the onset of the COVID-19 pandemic, few studies have assessed PrEP adherence but several have reported that the number of PrEP users has decreased significantly (9, 10). In the United Kingdom, Belgium, and Australia, there have been 80.0, 47.0, and 41.8% reductions in HIV PrEP users after the outbreak of COVID-19, respectively (11–13). In addition to decreasing the use of PrEP, changes in HIV-related sexual behaviors and increased barriers to accessing HIV prevention and testing services during the COVID-19 pandemic could lead to an increase in HIV acquisition (9, 11, 14). Little is known about possible changes

in PrEP adherence and HIV-related sexual and testing behaviors from before to during the COVID-19 pandemic.

This study was based on the China Real-world Oral Intake of PrEP (CROPrEP) project, which is an ongoing multi-center, real-world trial of HIV PrEP among Chinese MSM to assess the effectiveness and adherence of daily or event-driven PrEP (15). Participants would complete five follow-up visits that included an online questionnaire and a clinic visit at 4, 12, 24, 36, and 48 weeks after enrollment. After clinical evaluations and HIV laboratory testing, participants received TDF/FTC tablets to use as PrEP. We, thus, investigated PrEP adherence and HIV-related sexual and testing behaviors among Chinese MSM PrEP users and determining factors correlated with poor adherence before and during the COVID-19 outbreak. Our findings will help researchers develop interventions to maintain and support PrEP use during the pandemic.

## METHODS

### Study Design

The study recruited 791 MSM aged 16–65 years from four major Chinese cities (Shenyang, Beijing, Shenzhen, and Chongqing) from December 2018 to March 2020. In this study, we invited participants to complete two online self-administered surveys. The aim of this study was to determine changes in PrEP adherence and HIV-related and testing behaviors among PrEP-using Chinese MSM from before to during the COVID-19 outbreak. The median interval between the 4-week visit and this additional online survey was 28 weeks, and the interquartile range (IQR) was 24–36 weeks.

### Participants

The inclusion criteria for this additional online survey were the following: (1) participants of the CROPrEP project, (2) screened to be HIV-negative at the most recent follow-up visit, and (3) had not yet completed the final follow-up visit at Week 48. We excluded those who did not complete a Week 4 follow-up visit as data from this visit were used to provide information from before the COVID-19 outbreak.

**Abbreviations:** COVID-19, coronavirus disease 2019; PrEP, pre-exposure prophylaxis; MSM, men who have sex with men; OR, odds ratio; CI, confidence interval; CAI, condomless anal intercourse; WHO, World Health Organization; PY, person-years; TDF/FTC, tenofovir/emtricitabine; CROPrEP, the China Real-world Oral Intake of PrEP; IQR, interquartile range; HIVST, HIV self-testing; aOR, adjusted odds ratio.

## Data Collection

This additional online survey assessing changes in PrEP adherence and HIV-related sexual and testing behaviors due to the COVID-19 pandemic was developed by a panel consisting of HIV epidemiologists, clinicians, and MSM-serving community-based organization members. This questionnaire was then pilot-tested among 15 MSM volunteers who were not *CROPrEP* participants and was revised based on their comments. A link to this additional online questionnaire was shared among all participants in *CROPrEP* by using the WeChat (i.e., a popular social media platform) group. If participants did not complete the survey within 24 h, project staff reminded them of the invitation *via* a phone call or a text message. Participation in this additional online survey was voluntary, refusal to participate had no effect on their participation in the *CROPrEP* project, and data were confidential and used only for research purposes. Each individual account was allowed to access the online questionnaire only once to avoid duplicate responses (refer to **Supplementary Appendix 1**).

## Measures

Before the COVID-19, measures were determined from the 4-week follow-up visit for *CROPrEP*, conducted between October 2018 and November 2019, and during the COVID-19, measures were determined from the additional online survey conducted between February and March 2020. Baseline background characteristics assessed included type of PrEP regimen, age, education, monthly income, marital status, sexual identity, and lockdown restrictions experience (during the COVID-19 survey only). We asked about HIV-related sexual behaviors, such as primary locations to seek male sexual partners, the number and types of male sexual partners, frequency of sexual acts, frequency of condomless anal intercourse (CAI) with specific types of male sexual partners, and sexualized drug use. For HIV testing behavior, we asked about the self-perceived risk of HIV infection, HIV test behavior in the past month, location of the HIV test [i.e., facility-based HIV testing or HIV self-testing (HIVST)], and self-assessment of the frequency of HIV testing compared with pre-COVID-19 (during the COVID-19 survey only). To assess changes, we also asked whether they had experienced lockdown restrictions due to COVID-19, how frequently were they concerned about the COVID-19 pandemic (i.e., never, sometimes, often, and always), or whether they had delayed a scheduled follow-up visit for the *CROPrEP* project (refer to **Supplementary Appendix 2**).

Male sexual partners were defined as regular (i.e., those who were in a stable relationship and did not involve transactional sex) or casual (i.e., those who were not in a stable relationship and did not involve transactional sex). Sexualized drug use was defined as using any of the following drugs during sexual relations in the previous month: rush poppers (alkyl nitrites), cocaine, methamphetamine, ketamine, and bath salts. Having delayed a scheduled follow-up visit for the *CROPrEP* project was defined as attending a follow-up visit after the previously scheduled appointment date by 7 days or more.

## Outcome

Self-reported PrEP adherence was defined based on a comprehensive evaluation of the self-reported missed PrEP doses and sexual behaviors. Poor adherence was defined as the following: (1) missing doses among daily PrEP users in the past month and (2) missing doses among event-driven PrEP users if they had sexual behaviors in the past month. If not defined as having poor adherence, participants were defined as having good adherence during the COVID-19 (16).

## Statistical Analysis

We analyzed the demographics and HIV-related behaviors of Chinese MSM PrEP users using frequencies and percentages. We then used the generalized estimating equation (GEE model-Binary logistic regression) to analyze the changes in adherence and HIV-related behaviors sexual and testing behaviors, and PrEP use in the past month from before (using data from the 4-week follow-up visit from *CROPrEP*) and during the COVID-19 outbreak (using data collected from the additional online survey during COVID-19). We then assessed factors correlated with poor adherence using univariable and multivariable logistic regression models adjusted for age, education, and monthly income. A two-tailed value of *p* below 0.05 and between 0.05 and 0.10 was considered statistically significant and marginally significant, respectively. All statistical analyses were performed using SPSS<sup>TM</sup> software version 25.0 (IBM Corp, Armonk, NY, US).

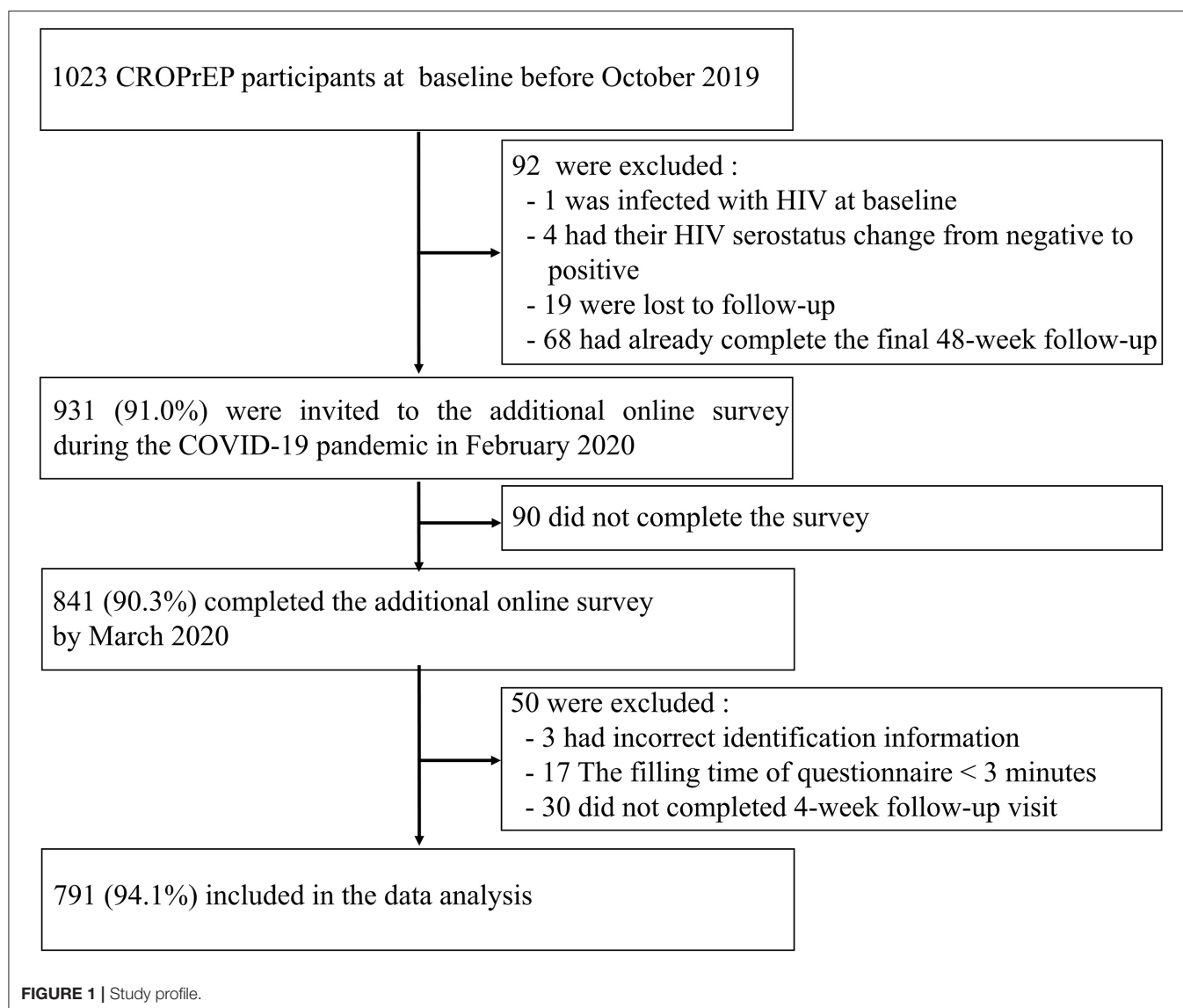
## Ethical Review

This study was reviewed and approved by the Medical Science Research Ethics Committee of the First Affiliated Hospital of China Medical University ([2018]2015-139-5) and was registered with the Chinese Clinical Trial Registry (ChiCTR-IIN-17013762). After providing online informed consent, eligible participants were asked to complete the additional questionnaire and had the opportunity to review and modify their responses. All data and informed consent were password-protected and stored in a secure server, and only the principal investigator had access to the database. Each participant was compensated \$4.20 (30 Yuan) after completing the additional online survey (refer to **Supplementary Appendix 3**).

## RESULTS

### Baseline Characteristics

Before the COVID-19 outbreak, 1,023 MSM were enrolled in the *CROPrEP* trial, and 931 (91.0%) were invited to participate in this survey. During the COVID-19 pandemic, 841 (90.3%) invited participants completed the online survey, and of these participants, 791 (94.1%) were included in the data analysis (300 in Shenyang, 362 in Beijing, 61 in Shenzhen, and 68 in Chongqing) (refer to **Figure 1**). The median age of participants was 30 years (IQR: 26–36 years), 79.6% (630/791) had an education level of college and above, 38.1% (301/791) had a monthly income of 2,001–6,000 Yuan (~\$310–929), and 81.0% (641/791) self-described their sexual identity as a homosexual. In response to COVID-19, 93.6% (740/791) of participants reported



experiencing COVID-19 lockdown restrictions, such as physical distancing, community restrictions, and the banning of indoor gatherings (refer to **Table 1**).

### Changes in HIV-Related Sexual Behavior, HIV Testing, and PrEP Adherence From Before to During the COVID-19 Pandemic

Sexual acts, sexualized drug use, HIV testing, and PrEP use and adherence sharply decreased as more participants had no partner during the pandemic. The percentage of participants who had regular or no male sexual partners in the past month greatly increased from 33.4% (264/791) before to 74.0% (585/791) during COVID-19, and the percentage of those who used the internet as their primary location to seek male sexual partners dropped from 60.4% (478/791) before to 25.3% (200/791) during COVID-19. In addition, sexual activity, such as frequency of sexual acts, having 2 or more male sexual partners and having

either a regular or casual male sexual partner greatly decreased from before to during COVID-19. However, the proportion of CAI with regular (11.8–25.7%) and casual (4.4–9.0%) male sexual partners increased during COVID-19. Sexualized drug use sharply decreased from 39.8% (315/791) before to 24.1% (191/791) during COVID-19. HIV testing behaviors sharply decreased from 50.1% (396/791) of participants having been tested for HIV in the past month before COVID-19 to 25.9% (205/791) during COVID-19, including HIVST (34.5% (273/791) before to 20.7% (164/791) during COVID-19) or through a facility [26.9% (213/791) before to 6.4% (51/791) during COVID-19]. Prevention of HIV also decreased as PrEP use dropped from 97.9% (774/791) before to 64.5% (510/791) and poor PrEP adherence increased from 23.6% (187/791) before to 50.1% (396/791) during COVID-19. Participants also delayed a scheduled follow-up visit for the CROPrEP trial more during COVID-19 (14.5%, 115/791) than before (10.0%, 79/791) (refer to **Table 2**).

**TABLE 1** | Characteristics of Chinese MSM PrEP users during the COVID-19 pandemic ( $N = 791$ ).

| Characteristic  | Participants ( $n$ , %) |
|---|-------------------------|
| <b>PrEP regimen</b>   |                         |
| Daily   | 418 (52.8)              |
| Event-driven  | 373 (47.2)              |
| <b>Age (years)</b>  |                         |
| 18–24   | 130 (16.4)              |
| 25–39   | 534 (67.5)              |
| 40–65   | 127 (16.1)              |
| <b>Education</b>  |                         |
| High school and below   | 161 (20.4)              |
| College and above   | 630 (79.6)              |
| <b>Average monthly income (RMB, Yuan)</b>                         |                         |
| <2,000  | 129 (16.3)              |
| 2,001–6,000   | 301 (38.1)              |
| 6,001–10,000  | 153 (19.3)              |
| More than 10,000  | 208 (26.3)              |
| <b>Marital status</b>   |                         |
| Not married   | 499 (63.1)              |
| Married or cohabitating with a woman                              | 61 (7.7)                |
| Cohabitating with a male  | 203 (25.7)              |
| Divorced, separated, or widowed                                   | 28 (3.5)                |
| <b>Sexual identity</b>  |                         |
| Homosexual  | 641 (81.0)              |
| Bisexual  | 126 (15.9)              |
| Heterosexual  | 3 (0.4)                 |
| Not sure  | 21 (2.7)                |
| <b>Experienced lockdown restrictions in response to COVID-19*</b> |                         |
| Yes   | 740 (93.6)              |
| No  | 51 (6.4)                |

Data are from the additional online survey administered during the COVID-19 pandemic. MSM, men who have sex with men; PrEP, pre-exposure prophylaxis; COVID-19, Coronavirus disease 2019.

\*Lockdown restrictions include physical distancing of two meters when individuals have to leave their homes, community restrictions, and the banning of indoor gatherings.

In the generalized estimating equations model, there was a significant decrease in the odds of using PrEP (odds ratio ( $OR$ ) = 0.04 [95%  $CI$ : 0.02, 0.07],  $p < 0.001$ ) and a significant increase in the odds of self-reporting missing at least one PrEP dose ( $OR$  = 3.24 [95%  $CI$ : 2.62, 4.02],  $p < 0.001$ ) and in the odds of delaying a scheduled CROPrEP follow-up visit ( $OR$  = 1.54 [95%  $CI$ : 1.13, 2.08],  $p = 0.006$ ) compared during to before the COVID-19 pandemic. Additionally, there were significant reductions in the odds of having been tested for HIV in the past month ( $OR$  = 0.35 [95%  $CI$ : 0.28, 0.43],  $p < 0.001$ ). In concordance with the decrease in HIV-related sexual behavior, there was a significant increase in the odds of self-perceiving risk of HIV infection as compared with no risk ( $OR$  = 3.41 [95%  $CI$ : 2.72, 4.28],  $p < 0.001$ ). By contrast, among those still having sexual behavior during the COVID-19, there were significant increases in the odds of having CAI with regular male sexual partners ( $OR$  = 2.61 [95%  $CI$ : 1.76, 2.87],  $p < 0.001$ ) and marginal increases in the odds of having

CAI with casual male sexual partners ( $OR$  = 2.09, 95%  $CI$ : 0.92, 4.72,  $p = 0.077$ ) compared to before COVID-19 (refer to **Table 2**).

## Factors Correlated With Poor PrEP Adherence During the COVID-19 Pandemic

About half of the participants (396/791, 50.1%) were defined as having poor PrEP adherence during the COVID-19. After adjusting for age, education, and income, the following factors over the past month were associated with increased odds of poor PrEP adherence during the COVID-19 pandemic: being married or cohabitating with a woman (compared with not married:  $aOR$  = 3.08 [95%  $CI$ : 1.60, 5.95],  $p < 0.001$ ), using condoms consistently with regular male sexual partners (compared with never using condoms:  $aOR$  = 2.19 [95%  $CI$ : 1.16, 4.13],  $p = 0.016$ ), and often concerned about the COVID-19 pandemic (compared with always concerned:  $aOR$  = 1.45 [95%  $CI$ : 1.07, 1.97],  $p = 0.017$ ). Knowing the HIV status of regular male sexual partners ( $aOR$  = 1.44 [95%  $CI$ : 0.98, 2.11],  $p = 0.065$ ) and not having been tested for HIV in the previous month (compared with have been tested for HIV:  $aOR$  = 1.38 [95%  $CI$ : 1.00–1.91],  $p = 0.050$ ) were associated with marginally higher odds of poor PrEP adherence. There was no difference in the odds of poor or good PrEP adherence based on the PrEP dosing regimen (event-driven vs. daily:  $aOR$  = 1.09 [95%  $CI$ : 0.82, 1.45],  $p = 0.560$ ) (refer to **Table 3**).

## DISCUSSION

In this retrospective cohort study in China, we found a dramatic increase in poor PrEP adherence along with decreases in HIV testing, the number of male sexual partners, and sexual acts during the COVID-19 pandemic. Factors correlated with the increased odds of poor PrEP adherence during COVID-19 included not having an HIV test conducted in the last month, using condoms consistently with regular male sexual partners, and being married or cohabitating with a woman. Among those who had regular or casual male sexual partners, the percentage of those who had CAI substantially increased during COVID-19 compared with the percentage before the pandemic. This may result in an increased risk of HIV infection and drug resistance in this sexually active group during the pandemic. Thus, public health officials should promote safer sex behaviors among those who are sexually active during COVID-19. In addition, poor PrEP adherence during the pandemic was found among participants with likely less access to MSM-specific HIV care, such as MSM married or cohabitating with a woman and MSM who had not been tested for HIV in the last month. To improve PrEP adherence, public health officials must improve outreach to these subpopulations, such as sending at-home HIV tests, re-enforcing risks for HIV acquisition if poor adherence to PrEP, and if poor adherence is likely to continue, suggesting stopping PrEP use to prevent drug resistance. Knowledge about challenges to PrEP use due to COVID-19 provides first-hand real-world evidence of issues that must be addressed prior to wide-spread PrEP implementation globally.



**TABLE 2 |** Changes in sexual behaviors, HIV testing, and PrEP adherence among during compared to before the COVID-19 ( $N = 791$ ).

|   | Before COVID–19 <sup>a</sup><br><i>n</i> (%) | During COVID–19<br><i>n</i> (%) | Odds ratio<br>(95% CI) | <i>P</i> -value |
|---|--|---------------------------------|------------------------|-----------------|
| <b>HIV-related sexual behaviors in the past month</b>           |  |                                 |                        |                 |
| <b>Primary location to seek male sexual partners</b>            |  |                                 |                        |                 |
| Internet  | 478 (60.4)                                   | 200 (25.3)                      | 0.22 (0.18, 0.27)      | <0.001          |
| Park/Bathroom/Club  | 49 (6.2)                                     | 6 (0.8)                         | 0.12 (0.05, 0.27)      | <0.001          |
| Had regular or no male sexual partners                          | 264 (33.4)                                   | 585 (74.0)                      | 5.68 (4.60, 701)       | <0.001          |
| <b>Frequency of sexual acts<sup>b</sup></b>                     |  |                                 |                        |                 |
| More than once a week   | 413 (52.2)                                   | 125 (15.8)                      | 0.17 (0.14, 0.21)      | <0.001          |
| Once a week or less than once a week                            | 321 (40.6)                                   | 224 (28.3)                      | 0.58 (0.47, 0.72)      | <0.001          |
| No sex  | 57 (7.2)                                     | 442 (55.9)                      | 16.31 (12.04, 22.10)   | <0.001          |
| <b>Sexual partners in the past month</b>                        |  |                                 |                        |                 |
| Had two or more male sexual partners                            | 536 (67.8)                                   | 136 (17.2)                      | 0.10 (0.08, 0.12)      | <0.001          |
| Had regular male sexual partners                                | 467 (59.0)                                   | 249 (31.5)                      | 0.32 (0.26, 0.39)      | <0.001          |
| Had casual male sexual partners                                 | 317 (40.1)                                   | 134 (16.9)                      | 0.30 (0.24, 0.38)      | <0.001          |
| <b>Condom use with regular male sexual partners<sup>c</sup></b> |  |                                 |                        |                 |
| Consistently  | 220 (47.1)                                   | 121 (48.6)                      | 1.05 (0.79, 1.44)      | 0.745           |
| Most or sometimes   | 192 (41.1)                                   | 64 (25.7)                       | 0.05 (0.36, 0.70)      | <0.001          |
| Never   | 55 (11.8)                                    | 64 (25.7)                       | 2.61 (1.76, 2.87)      | <0.001          |
| <b>Condom use with casual male sexual partners<sup>c</sup></b>  |  |                                 |                        |                 |
| Consistently  | 167 (52.7)                                   | 74 (55.2)                       | 1.13 (0.75, 1.71)      | 0.566           |
| Most or sometimes   | 136 (42.9)                                   | 48 (35.8)                       | 0.73 (0.348, 1.11)     | 0.143           |
| Never   | 14 (4.4)                                     | 12 (9.0)                        | 2.09 (0.92, 4.72)      | 0.077           |
| <b>Sexualized drug use<sup>d</sup></b>                          | 315 (39.8)                                   | 191 (24.1)                      | 0.21(0.17, 0.26)       | <0.001          |
| <b>HIV testing behaviors in the past month</b>                  |  |                                 |                        |                 |
| Had HIV test  | 396 (50.1)                                   | 205 (25.9)                      | 0.35 (0.28, 0.43)      | <0.001          |
| Had HIV test through HIVST                                      | 273 (34.5)                                   | 164 (20.7)                      | 0.50 (0.40, 0.61)      | <0.001          |
| Had facility-based HIV testing                                  | 213 (26.9)                                   | 51 (6.4)                        | 0.19 (0.13, 0.26)      | <0.001          |
| <b>PrEP status in the past month</b>                            |  |                                 |                        |                 |
| <b>PrEP regimen</b>   |  |                                 |                        |                 |
| Daily   | 410 (51.8)                                   | 418 (52.8)                      | 1.04 (0.86, 1.26)      | 0.682           |
| Event-driven  | 381 (48.2)                                   | 373 (47.2)                      | 0.96 (0.79, 1.17)      | 0.682           |
| <b>Used PrEP</b>  | 774 (97.9)                                   | 510 (64.5)                      | 0.04 (0.02, 0.07)      | <0.001          |
| <b>Poor PrEP adherence</b>                                      | 187 (23.6)                                   | 396 (50.1)                      | 3.24 (2.62, 4.02)      | <0.001          |
| <b>Delayed scheduled CROPrEP follow-up visit</b>                | 79 (10.0)                                    | 115 (14.5)                      | 1.54 (1.13, 2.08)      | 0.006           |
| <b>Self-perceived risk of HIV infection</b>                     |  |                                 |                        |                 |
| No risk   | 160 (20.2)                                   | 367 (46.4)                      | 3.41 (2.72, 4.28)      | <0.001          |
| Low risk (<25%)   | 419 (53.0)                                   | 315 (39.8)                      | 0.59 (0.48, 0.72)      | <0.001          |
| Moderate risk (25–49%)  | 142 (18.0)                                   | 68 (8.6)                        | 0.43 (0.32, 0.58)      | <0.001          |
| High risk (50–75%)  | 52 (6.6)                                     | 24 (3.0)                        | 0.45 (0.27, 0.72)      | 0.001           |
| Very high risk (>75%)   | 18 (2.3)                                     | 17 (2.1)                        | 0.94 (0.49, 1.82)      | 0.862           |

ALL data are among Chinese MSM PrEP users.

COVID-19, coronavirus disease 2019; MSM, men who have sex with men; PrEP, pre-exposure prophylaxis; HIVST, HIV self-testing.

CROPrEP, China Real-world Oral Intake of PrEP.

<sup>a</sup>Before COVID-19 estimates were determined from the 4th week follow-up visit of the China Real-world Oral Intake of PrEP (CROPrEP) project conducted between October 2018 to November 2019.

<sup>b</sup>Sexual acts included receptive anal intercourse, insertive anal intercourse, and oral intercourse.

<sup>c</sup>Only people with regular or casual partners answered the question.

<sup>d</sup>Sexualized drug use in the past month included use of rush poppers (alkyl nitrites), cocaine, methamphetamine, ketamine, and bath salts before or during sexual activity.

In this study, similar to peer studies finding decreases in the number of sexual partners and sexual practices since the onset of COVID-19 (10, 14, 17), we observed that 93.5% of Chinese MSM PrEP users were impacted by lockdown restrictions and

had fewer sexual partners and fewer sexual acts. These decreases may suggest that our participants overall may have temporarily lower risks of HIV infection. Nevertheless, no excess risks among MSM PrEP users were found in developing countries before.



**TABLE 3 |** Factors correlated with poor adherence to PrEP among Chinese MSM PrEP users during the COVID-19 ( $N = 791$ ).

|  | Poor adherence<br>$n = 396, n (\%)$ | Good adherence<br>$n = 395, n (\%)$ | Odds ratio<br>(95% CI) | Adjusted odds ratio<br>(95% CI) <sup>a</sup> | P-value |
|--|-------------------------------------|-------------------------------------|------------------------|--|---------|
| <b>PrEP regimen</b>  |                                     |                                     |                        |  |         |
| Event-driven   | 192 (48.5)                          | 181 (45.8)                          | 1.11 (0.84, 1.47)      | 1.09 (0.82, 1.45)                            | 0.560   |
| Daily  | 204 (51.5)                          | 214 (54.2)                          | Reference              | Reference                                    |         |
| <b>Marital status</b>  |                                     |                                     |                        |  |         |
| Married or cohabitating with a woman   | 45 (11.4)                           | 16 (4.1)                            | 3.10 (1.70, 5.63)      | 3.08 (1.60, 5.95)                            | 0.001   |
| Cohabitating with male   | 98 (24.7)                           | 105 (26.6)                          | 1.03 (0.74, 1.43)      | 1.00 (0.72, 1.40)                            | 0.973   |
| Divorced, separated, or widowed  | 15 (3.8)                            | 13 (3.3)                            | 1.36 (0.64, 2.88)      | 1.43 (0.64, 3.18)                            | 0.382   |
| Not married  | 238 (60.1)                          | 261 (66.1)                          | Reference              | Reference                                    |         |
| <b>Primary location to seek male sexual partners</b>                           |                                     |                                     |                        |  |         |
| No male sexual partner   | 197 (49.7)                          | 173 (43.8)                          | 1.48 (1.05, 2.09)      | 1.47 (1.04, 2.09)                            | 0.030   |
| Park/Bathroom/Club   | 3 (0.8)                             | 3 (0.8)                             | 1.30 (0.26, 6.59)      | 1.02 (0.20, 5.26)                            | 0.985   |
| Had regular male sexual partners   | 109 (27.5)                          | 106 (26.8)                          | 1.34 (0.91, 1.97)      | 1.27 (0.86, 1.88)                            | 0.224   |
| Internet <sup>b</sup>  | 87 (22.0)                           | 113 (28.6)                          | Reference              | Reference                                    |         |
| <b>HIV-related sexual behaviors in the past month</b>                          |                                     |                                     |                        |  |         |
| <b>Had two or more male sexual partners</b>                                    |                                     |                                     |                        |  |         |
| Yes  | 65 (16.4)                           | 71 (18.0)                           | 0.90 (0.62, 1.30)      | 0.83 (0.57, 1.20)                            | 0.333   |
| No   | 331 (83.6)                          | 324 (82.0)                          | Reference              | Reference                                    |         |
| <b>Had regular male sexual partners</b>  |                                     |                                     |                        |  |         |
| Yes  | 130 (32.8)                          | 119 (30.1)                          | 1.13 (0.84, 1.53)      | 1.07 (0.79, 1.45)                            | 0.665   |
| No   | 266 (67.2)                          | 276 (69.9)                          | Reference              | Reference                                    |         |
| <b>Had casual male sexual partners</b>   |                                     |                                     |                        |  |         |
| Yes  | 61 (15.4)                           | 73 (18.5)                           | 0.80 (0.55, 1.17)      | 0.79 (0.55, 1.15)                            | 0.224   |
| No   | 335 (84.6)                          | 322 (81.5)                          | Reference              | Reference                                    |         |
| <b>Condom use with regular male sexual partners</b>                            |                                     |                                     |                        |  |         |
| Consistently   | 71 (54.6)                           | 50 (42.0)                           | 2.22 (1.19, 4.11)      | 2.19 (1.16, 4.13)                            | 0.016   |
| Most or sometimes  | 34 (26.2)                           | 30 (25.2)                           | 1.77 (0.88, 3.57)      | 1.74 (0.84, 3.61)                            | 0.135   |
| Never  | 25 (19.2)                           | 39 (32.8)                           | Reference              | Reference                                    |         |
| <b>Condom use with casual male sexual partners</b>                             |                                     |                                     |                        |  |         |
| Consistently   | 34 (55.7)                           | 40 (54.8)                           | 0.85 (0.25, 2.88)      | 0.96 (0.28, 3.35)                            | 0.951   |
| Most or sometimes  | 21 (34.4)                           | 27 (37.0)                           | 0.78 (0.22, 2.76)      | 0.82 (0.23, 3.00)                            | 0.769   |
| Never  | 6 (9.8)                             | 6 (8.2)                             | Reference              | Reference                                    |         |
| <b>Know the HIV status of regular male sexual partners</b>                     |                                     |                                     |                        |  |         |
| Yes  | 95 (39.4)                           | 72 (30.9)                           | 1.46 (1.00, 2.13)      | 1.44 (0.98, 2.11)                            | 0.065   |
| No   | 146 (60.6)                          | 161 (69.1)                          | Reference              | Reference                                    |         |
| <b>HIV testing behaviors in the past month</b>                                 |                                     |                                     |                        |  |         |
| <b>Had HIV test</b>  |                                     |                                     |                        |  |         |
| No   | 304 (76.8)                          | 282 (71.4)                          | 1.32 (0.96, 1.82)      | 1.38 (1.00, 1.91)                            | 0.050   |
| Yes  | 92 (23.2)                           | 113 (28.6)                          | Reference              | Reference                                    |         |
| <b>Self-assessment of the frequency of HIV testing compare to pre-COVID-19</b> |                                     |                                     |                        |  |         |
| Increase   | 6 (1.5)                             | 7 (1.8)                             | 0.93 (0.31, 2.79)      | 0.87 (0.29, 2.66)                            | 0.809   |
| Decrease   | 111 (28.0)                          | 86 (21.8)                           | 1.40 (1.00, 1.93)      | 1.46 (1.05, 2.03)                            | 0.026   |
| No change  | 279 (70.5)                          | 302 (76.5)                          | Reference              | Reference                                    |         |
| <b>Concerned about the COVID-19 pandemic<sup>c</sup></b>                       |                                     |                                     |                        |  |         |
| Never  | 2 (0.5)                             | 1 (0.3)                             | 2.52 (0.23, 28.09)     | 2.90 (0.25, 33.44)                           | 0.393   |
| Sometimes  | 59 (14.9)                           | 44 (11.1)                           | 1.69 (1.08, 2.65)      | 1.74 (1.11, 2.75)                            | 0.017   |
| Often  | 193 (48.7)                          | 171 (43.3)                          | 1.42 (1.05, 1.92)      | 1.45 (1.07, 1.97)                            | 0.017   |
| Always   | 142 (35.9)                          | 179 (45.3)                          | Reference              | Reference                                    |         |

COVID-19, coronavirus disease 2019; MSM, men who have sex with men; PrEP, pre-exposure prophylaxis.

<sup>a</sup>Adjusted odds ratios were obtained through multivariable analysis and were adjusted for age, education, and monthly income.

<sup>b</sup>Internet include geosocial networking applications including WeChat, QQ, Blued or Jacked.

<sup>c</sup>Concerned about the COVID-19 pandemic was defined as how often obtaining information about COVID-19 through social media and other material proactively.

However, compared with those sexually active individuals before the pandemic, among those who were sexually active during the pandemic, a much higher percentage had CAI with sexual partners. PrEP cannot be used to replace condoms completely and is a part of a comprehensive prevention strategy that includes counseling and behavioral interventions promoting condom use, abstinence, and monogamy (18, 19). An online survey among MSM from the United States found conflicting results and did not find an effect on condom use during COVID-19 (20). A possible explanation is that China was the first country impacted by COVID-19 and quickly introduced physical distancing restrictions and lockdowns, leading to sudden significant changes in lifestyle and sexual practices, while other countries could have anticipated potential restrictions based on news from China. In the future, public health officials must target individuals who are likely to maintain sexual activity during times where general sexual activity drops and promote safer sex, such as high PrEP adherence and condom use. In addition, we strongly recommend that medical staff and community volunteers popularize safety knowledge regularly and emphasize the significance of PrEP good adherence.

As suboptimal PrEP adherence will decrease the effectiveness of PrEP (21), hence, all global public health sections highlight the importance of maintaining high medication adherence among subjects who take oral PrEP pills before or after the COVID-19 era. We found worse adherence during COVID-19 as more than one-third (35.7%) of participants did not obtain PrEP refills, and a half (50.1%) self-reported missing at least one PrEP dose in the previous month. Our findings are similar to the increase in the proportion who discontinued PrEP use and the increase in the mean number of missed PrEP doses found among MSM in the Southern United States (22). Individuals may have discontinued PrEP use because they were no longer engaging in sexual activity since COVID-19. Among those still engaging in sexual activity, they could have been unable to access PrEP and thus had worse adherence because they could not access PrEP or PrEP support when facilities were closed due to lockdowns. If users discontinued using PrEP, public health officials should reach out frequently to see if they would like to begin using PrEP again, and if users had worse adherence to PrEP, practitioners should ensure access to medication through a no-contact method, such as the mail and counsel users on the importance of adherence to prevent HIV transmission.

Frequent HIV testing can also help prevent HIV transmission, but during the COVID-19 pandemic, the rate of HIV testing was substantially reduced and correlated with poor PrEP adherence among Chinese MSM PrEP users. Our finding of less HIV testing, both HIVST and facility-based HIV-testing, was similar to results from other studies (23, 24). An online survey from the Southern United States also found that one-quarter of MSM PrEP users encountered obstacles to HIV testing (22). These difficulties in accessing HIV testing could have been caused by the physical distancing restrictions in response to COVID-19 and thus restricting access to facility-based HIV testing. However, continuous use of PrEP pills when infected with HIV can lead to HIV drug resistance events (25, 26), and PrEP users must be tested for HIV at frequent intervals. More web-based health

promotion (e.g., text messaging) and home-based HIV-testing (e.g., oral self-tests) were practical tools for raising awareness of sexual health and HIV-testing in the United Kingdom and Africa (27, 28). Thus, to flatten the curve of the COVID-19 pandemic, we suggest providing counseling and HIVST through a no-contact method to PrEP users to ensure timely knowledge of HIV serostatus and prevent HIV drug resistance.

Along with decreased HIV testing, using condoms consistently with regular male sexual partners was significantly correlated with increased odds of poor PrEP adherence during COVID-19. Consistent with our results, low PrEP adherence in East Africa was associated with using condoms with all types of partners (29). We additionally found a decrease in self-perceived risk of HIV acquisition among PrEP users during COVID-19, which may be from decreased sexual activity or using condoms consistently with regular male sexual partners.

In addition to consistent condom use with regular male sexual partners, being married or cohabitating with a woman was also correlated with poor PrEP adherence during COVID-19. Due to traditional Chinese culture and attitudes toward homosexuality, up to 25–35% of Chinese MSM have already been in a heterosexual marriage and more than 70% of MSM may eventually form a family with a woman to have children and help conceal their homosexuality (30). Similarly, MSM partnering with a woman for cultural reasons also occurs in Nigeria and India (31, 32). However, despite this common practice, little is known about MSM who are married or cohabitating with a woman and their adherence to PrEP. It is possible that these partnered MSM feared disclosure of their PrEP use and, thus, sexual orientation, leading to poor PrEP adherence. Discrete yet effective strategies are needed to improve PrEP adherence among MSM married or cohabitating with a woman.

## Strengths and Limitations

By surveying changes in PrEP adherence and HIV-related behaviors from before to during the COVID-19 pandemic from a large population of Chinese MSM who used PrEP in four Chinese cities, our results were more representative. We were additionally able to stratify differences in adherence during the COVID-19 by PrEP regimen and found no difference in adherence between them. By being the first study to identify changes in PrEP adherence and HIV-related behaviors among Chinese MSM from before to during the COVID-19 pandemic, we were able to determine obstacles to PrEP adherence due to lockdown that must be addressed in possible future societal restrictions. A limitation of this study was that it used self-reported measures to define PrEP adherence. Another limitation was that we asked sensitive questions about sexual activities and our data may have been influenced by social desirability bias. To address this issue, the survey was conducted online, was self-reported, and was anonymous.

## CONCLUSION

We demonstrated a substantial increase in poor adherence and CAI among those sexually active, and a decrease in HIV testing among Chinese MSM who used PrEP from before to during

the COVID-19 pandemic. Our results suggest that some MSM PrEP users have a likely increased risk of HIV acquisition during COVID-19, and health workers should develop online targeted interventions, such as adding online follow-up, promoting safer sex, PrEP adherence, and condom use, providing no-contact counseling and HIVST to increase knowledge of HIV serostatus, and prevent drug resistance event to PrEP, and discrete strategies to reach out to MSM married or living with a woman to promote PrEP adherence.

## DATA AVAILABILITY STATEMENT

The datasets presented in this study can be found in online repositories. The names of the repository/repositories and accession number(s) can be found in the article/**Supplementary Material**.

## ETHICS STATEMENT

This study was reviewed and approved by the Medical Science Research Ethics Committee of the First Affiliated Hospital of China Medical University ([2018]2015-139-5) and was registered with the Chinese Clinical Trial Registry (ChiCTR-IIN-17013762). The patients/participants provided their written informed consent to participate in this study.

## CROPrEP STUDY TEAM

Members of the CROPrEP study team not included in the authors' list include, Xiaoqing He, Yao Li, Fang Zhao, Yijun Duan,

Rui Li, Shangcao Li, Hang Li, Zhili Hu, Rantong Bao, Sitong Cui, Zhaozhen Liu, Zehao Ye, and Xiaoyun Shi.

## AUTHOR CONTRIBUTIONS

YG conceived and designed the study and analyzed the data. LJ, QH, HoW, XH, YC, HuW, LZ and ZC performed the study. YG, QH, and SL draw the figures and tables. YG, QH, ZW, and SL wrote and revised the manuscript. All authors reviewed and approved the final manuscript.

## FUNDING

This study was supported by the Mega-Projects of National Science Research for the 13th Five-Year Plan [2017ZX10201101], the National Natural Science Foundation of China [81872674], and the National Science and Technology Major Project [2018ZX10101001-001-003].

## ACKNOWLEDGMENTS

We thank the MSM who participated in this study and the staff of community-based organizations who contributed to its success.

## SUPPLEMENTARY MATERIAL

The Supplementary Material for this article can be found online at: <https://www.frontiersin.org/articles/10.3389/fmed.2022.738541/full#supplementary-material>

## REFERENCES

- World Health Organization. *WHO Announces the COVID-19 Outbreak a Pandemic*. (2020). Available online at: [http://www.euro.who.int/en/health-topics/health-emergencies/coronavirus-covid-19/news/news/2020/3/who-announces-covid-19-outbreak-a-relax\\$@@@underlinedbox{pandemic}\mathsurround{z@\\$relax,2020](http://www.euro.who.int/en/health-topics/health-emergencies/coronavirus-covid-19/news/news/2020/3/who-announces-covid-19-outbreak-a-relax$@@@underlinedbox{pandemic}\mathsurround{z@$relax,2020) (accessed November 26, 2020).
- Jiang H, Zhou Y, Tang W. Maintaining HIV care during the COVID-19 pandemic. *Lancet HIV*. (2020) 7:e308-9. doi: 10.1016/S2352-3018(20)30105-3
- Joint United Nations Programme on HIV/AIDS, 2020 DATA. (2020). Available online at: <https://aidsinfo.unaids.org/> (accessed November 26, 2020).
- Joint United Nations Programme on HIV/AIDS, UNAIDS Epidemiological Estimates. (2020). Available online at: <https://aidsinfo.unaids.org/> (accessed September 29, 2020).
- McCormack S, Dunn DT, Desai M, Dolling DI, Gafos M, Gilson R, et al. Pre-exposure prophylaxis to prevent the acquisition of HIV-1 infection (PROUD): effectiveness results from the pilot phase of a pragmatic open-label randomised trial. *Lancet*. (2016) 387:53-60. doi: 10.1016/S0140-6736(15)00056-2
- Molina JM, Capitán C, Spire B, Pialoux G, Cotte L, Charreau I, et al. On-demand preexposure prophylaxis in men at high risk for HIV-1 infection. *N Engl J Med*. (2015) 373:2237-46. doi: 10.1056/NEJMoa1506273
- Molina JM, Charreau I, Spire B, Cotte L, Chas J, Capitán C, et al. Efficacy, safety, and effect on sexual behaviour of on-demand pre-exposure prophylaxis for HIV in men who have sex with men: an observational cohort study. *Lancet HIV*. (2020) 4:e402-10. doi: 10.1016/S2352-3018(17)30089-9
- Marrazzo JM, Ramjee G, Richardson BA, Gomez K, Mgodi N, Nair G, et al. Tenofovir-based preexposure prophylaxis for HIV infection among African women. *N Engl J Med*. (2015) 372: 509-18. doi: 10.1056/NEJMoa1402269
- Hammoud MA, Grulich A, Holt M, Maher L, Murphy D, Jin F, et al. Substantial decline in use of HIV preexposure prophylaxis following introduction of COVID-19 physical distancing restrictions in Australia: results from a prospective observational study of gay and bisexual men. *J Acquir Immune Defic Syndr*. (2021) 86:22-30. doi: 10.1097/QAI.0000000000002514
- Davey DLJ, Bekker LG, Mashele N, Gorbach P, Coates TJ, Myer L. PrEP retention and prescriptions for pregnant women during COVID-19 lockdown in South Africa. *Lancet HIV*. (2020) 7:e735. doi: 10.1016/S2352-3018(20)30226-5
- Junejo M, Girometti N, McOwan A, Whitlock G. HIV postexposure prophylaxis during COVID-19. *Lancet HIV*. (2020) 7:e460. doi: 10.1016/S2352-3018(20)30146-6
- Reyniers T, Rotsaert A, Thunissen E, Buffel V, Masquillier C, Van Landeghem E, et al. Reduced sexual contacts with non-steady partners and less PrEP use among MSM in Belgium during the first weeks of the COVID-19 lockdown: results of an online survey. *Sex Transm Infect*. (2020) 97:414-9. doi: 10.1136/sextrans-2020-054756
- Charre C, Icard V, Pradat P, Brochier C, Lina B, Chidiac C, et al. Coronavirus disease 2019 attack rate in HIV-infected patients and in preexposure prophylaxis users. *AIDS*. (2020) 34:1765-70. doi: 10.1097/QAD.0000000000002639
- Chow EPF, Hocking JS, Ong JJ, Schmidt T, Buchanan A, Rodriguez E, et al. Changing the use of HIV pre-exposure prophylaxis among men who have sex with men during the COVID-19 pandemic in Melbourne, Australia. *Open Forum Infect Dis*. (2020) 7:ofaa275. doi: 10.1093/ofid/ofaa275

15. Wang H, Zhang Y, Mei Z, Jia Y, Leuba SI, Zhang J, et al. Protocol for a multicenter, real-world study of HIV pre-exposure prophylaxis among men who have sex with men in China (CROPrEP). *BMC Infect Dis.* (2019) 19:721. doi: 10.1186/s12879-019-4355-y
16. Riddell J, Amico KR, Mayer KH. HIV preexposure prophylaxis: a review. *JAMA.* (2018) 319:1261–8. doi: 10.1001/jama.2018.1917
17. Stephenson R, Chavanduka T, Rosso M, Sullivan SP, Pitter RA, Hunter AS, et al. Sex in the time of COVID-19: results of an online survey of gay, bisexual and other men who have sex with men's experience of sex and HIV prevention during the US COVID-19 epidemic. *AIDS Behav.* (2021) 25:40–8. doi: 10.1007/s10461-020-03024-8
18. Saag MS, Gandhi RT, Hoy JF, Landovitz RJ, Thompson MA, Sax PE, et al. Antiretroviral drugs for treatment and prevention of HIV infection in adults: 2020 recommendations of the International Antiviral Society-USA Panel. *JAMA.* (2020) 324:1651–69. doi: 10.1001/jama.2020.17025
19. Smith D, Herbst J, Zhang X, Rose C. Condom effectiveness for HIV prevention by consistency of use among men who have sex with men in the United States. *J Acquir Immune Defic Syndr.* (2015) 68:337–44. doi: 10.1097/QAI.0000000000000461
20. Sanchez TH, Zlotorzynska M, Rai M, Baral SD. Characterizing the impact of COVID-19 on men who have sex with men across the United States in April 2020. *AIDS Behav.* (2020) 24:2024–32. doi: 10.1007/s10461-020-02894-2
21. Buchbinder SP, Glidden DV, Liu AY, McMahan V, Guanira JV, Mayer KH, et al. HIV pre-exposure prophylaxis in men who have sex with men and transgender women: a secondary analysis of a phase 3 randomised controlled efficacy trial. *Lancet Infect Dis.* (2014) 14:468–75. doi: 10.1016/S1473-3099(14)70025-8
22. Pampati S, Emrick K, Siegler A, Jones J. Changes in sexual behavior, PrEP adherence, and access to sexual health services because of the COVID-19 pandemic among a cohort of PrEP-using MSM in the South. *J Acquir Immune Defic Syndr.* (2021) 87:639–43. doi: 10.1097/QAI.0000000000002640
23. Jewell BL, Mudimu E, Stover J, Ten Brink D, Phillips AN, Smith JA, et al. Potential effects of disruption to HIV programmes in sub-Saharan Africa caused by COVID-19: results from multiple mathematical models. *Lancet HIV.* (2020) 7:e629–40. doi: 10.1016/S2352-3018(20)30211-3
24. Anderson L, Caniza M. COVID-19 and preventative medicine for HIV infected children. *Clin Infect Dis.* (2020) 73:e2834–5. doi: 10.1093/cid/ciaa1626
25. Rocheleau G, Brumme CJ, Shoveller J, Lima VD, Harrigan PR. Longitudinal trends of HIV drug resistance in a large Canadian cohort, 1996–2016. *Clin Microbiol Infect.* (2018) 24:185–91. doi: 10.1016/j.cmi.2017.06.014
26. McClung RP, Oster AM, Ocfemia MCB. Transmitted drug resistance among HIV-1 diagnoses in the United States, 2014–2018. *Clin Infect Dis.* (2021) 74:1055–62. doi: 10.1093/cid/ciab583
27. Middleton M, Somerset S, Evans C, Blake H. Test@Work texts: mobile phone messaging to increase awareness of HIV and HIV testing in UK construction employees during the COVID-19 pandemic. *Int J Environ Res Public Health.* (2020) 17:7819. doi: 10.3390/ijerph17217819
28. Amstutz A, Kopo M, Lejone TI, Khesa L, Kao M, Muhairwe J, et al. “If it is left, it becomes easy for me to get tested”: use of oral self-tests and community health workers to maximize the potential of home-based HIV testing among adolescents in Lesotho. *J Int AIDS Soc.* (2020) 23(Suppl 5):e25127. doi: 10.1002/jia2.25563
29. Haberer JE, Baeten JM, Campbell J, Wangisi J, Katabira E, Ronald A, et al. Adherence to antiretroviral prophylaxis for HIV prevention: a substudy cohort within a clinical trial of serodiscordant couples in East Africa. *PLoS Med.* (2013) 10:e1001511. doi: 10.1371/journal.pmed.1001511
30. Luo D, Yan X, Xu R, Zhang J, Shi X, Ma J, et al. Chinese trends in adolescent marriage and fertility between 1990 and 2015: a systematic synthesis of national and subnational population data. *Lancet Glob Health.* (2020) 8:e954–64. doi: 10.1016/S2214-109X(20)30130-3
31. Schwartz SR, Nowak RG, Orazulike I, Keshinro B, Ake J, Kennedy S, et al. The immediate effect of the Same-Sex Marriage Prohibition Act on stigma, discrimination, and engagement on HIV prevention and treatment services in men who have sex with men in Nigeria: analysis of prospective data from the TRUST cohort. *Lancet HIV.* (2015) 2:e299–306. doi: 10.1016/S2352-3018(15)00078-8
32. Campion EW, Morrissey S, Drazen JM. In support of same-sex marriage. *N Engl J Med.* (2015) 372:1852–3. doi: 10.1056/NEJMe1505179

**Conflict of Interest:** Gilead sciences inc. donated all the PrEP drugs for the CROPrEP.

The authors declare that the research was conducted in the absence of any commercial or financial relationships that could be construed as a potential conflict of interest.

**Publisher's Note:** All claims expressed in this article are solely those of the authors and do not necessarily represent those of their affiliated organizations, or those of the publisher, the editors and the reviewers. Any product that may be evaluated in this article, or claim that may be made by its manufacturer, is not guaranteed or endorsed by the publisher.

Copyright © 2022 Gao, Hu, Leuba, Jia, Wang, Huang, Chen, Wang, Zhang, Chu, Zhang, Wang, Shang, Xu and CROPrEP Study Team. This is an open-access article distributed under the terms of the Creative Commons Attribution License (CC BY). The use, distribution or reproduction in other forums is permitted, provided the original author(s) and the copyright owner(s) are credited and that the original publication in this journal is cited, in accordance with accepted academic practice. No use, distribution or reproduction is permitted which does not comply with these terms.



# Frontiers in Medicine

Translating medical research and innovation into  
improved patient care

A multidisciplinary journal which advances our  
medical knowledge. It supports the translation  
of scientific advances into new therapies and  
diagnostic tools that will improve patient care.

## Discover the latest Research Topics

[See more →](#)

### Frontiers

Avenue du Tribunal-Fédéral 34  
1005 Lausanne, Switzerland  
[frontiersin.org](https://frontiersin.org)

### Contact us

+41 (0)21 510 17 00  
[frontiersin.org/about/contact](https://frontiersin.org/about/contact)



### Frontiers in Medicine

